In the name of God

Proceeding of the 14th Iranian Physical Chemistry Conference

University of Tehran, Kish, Iran

Feb 25-28, 2011

Organizer:

University of Tehran

Iranian Chemical Society

Scientific Chairman: Dr. Ali Maghari

Executive Chairman: Dr. Hassan Behnejad

Scientific Committee:

Dr. A. Maghari
Dr. Gh. Islampour
Dr. H. Islami
Dr. H. Behnejad
Dr. Gh. Parsafar
Dr. A. H. Pakiari
Dr. M. Tafazzoli
Dr. S. Jalili
Dr. A. Rostami
Dr. P. Rashidi Ranjbar
Dr. a. Zeini Esfahani
Dr. H. Sabzian
Dr. N. Zargham
Dr. H. Ghatee
Dr. E. Goharshadi
Dr. A. Mohajeri
Dr. S. H. Mousavipour
Dr. B. Najafi

Organizing Committee:

Dr. H. Behnejad
Dr. A. Shayesteh
Dr. N. Zargham
Dr. M. Foroutan
Mr. A. Rafi Dargahi

List of Referees:

Dr. Ashasi, H.
Dr. Azizi, Kh.
Dr. Behnejad, H.
Dr. Bordbar, A.
Dr. Bordbar, M. M.
Dr. Dahestani, M.
Dr. Ebrahimi, A.
Dr. Eslami, H.
Dr. Fakhraei, S.
Dr. Farrokhnia, M.
Dr. Farzi, N.
Dr. Foroutan, M.
Dr. Ghannadzadeh, A.
Dr. Gharibi, H.
Dr. Ghatee, H.
Dr. Gholami, M. R.
Dr. Goharshadi, E.
Dr. Habibi, A.
Dr. Habibi, M. H.
Dr. Habibi, S. M.
Dr. Hadipour, N.
Dr. Hashemianzadeh, M.
Dr. Hamedanian, M.
Dr. Illukhani, H.
Dr. Islampour, Gh.
Dr. Jafarian, M.
Dr. Jalili, A. H.
Dr. Jamshidi, Z.
Dr. Karimi, M. H.
Dr. Keshavarzi, E.
Dr. Maghari, A.
Dr. Mahjani, M. Gh.
Dr. Mohajeri, A.
Dr. Mousavipour, S. H.
Dr. Najafi, b.
Dr. Nasehzadeh, A.
Dr. Nourizadeh, S.
Dr. Pakiari, H. A.
Dr. Parsafar, Gh.
Dr. Rashidi Ranjbar, P.
Dr. Refati, A. A.
Dr. Rezaei, M.
Dr. Rostami, A.
Dr. Sabet, A.
Dr. Sabouri, A. A.
Dr. Sabzian, H.
Dr. Sadeghi, R.
Dr. Shayesteh, A.
Dr. Soleyman Nejad, M.
Dr. Tabrizchi, M.
Dr. Tafazzoli, M.
Dr. Yeganegi, S.
Dr. Zafarani, M. T.
Dr. Zargam, N.
Dr. Zeini, A.

Table of Content

Invited Lecturer

Computational Modelling of Biological Nano-motors

H. Rafii-Tabar

Department of Nano-Science, Institute for Research in Fundamental Sciences (IPM), P.O. Box 19395-5531 Tehran

&

Department of Medical Physics and Biomedical Engineering, and Research Centre for Medical Nanotechnology and Tissue Engineering, Shahid Beheshti University of Medical Sciences , Evin Tehran

Abstract

A significant part of the intracellular activities is carried out by the biological nano-scale protein motors. These nanoscopic machines perform directed motion along microtubule protofilaments , and are responsible for some of the most intricate cellular activities, such as cargo transport within the cell, cell mitosis, and cell motility. Biological nano-motors are manifestations of the actually existing nanotechnology in nature, and some of the most fundamental ideas of physical and medical nanotechnology have been inspired by studying the structure and function of these machines. Examples of such machines include, kinesins, myosins and dyenins that perform processive movement inside the cell. Investigation into the stochastic dynamics of these machines forms one of the leading areas of research in nanotechnology internationally. In this talk, we will first give a brief introduction into the topic of biological nano-motors, and then report on the current research in this field .

Introducing some latest researches on nonporous and their applications

M Moradi[1, 2]

[1]Department of Physics, Shiraz University, Shiraz 71454, Iran

[2]Institute of Nanotechnology, Shiraz University, Shiraz 71454, Iran

E-mail: moradi@susc.ac.ir

Self-organized porous anodic alumina (PAA) nanostructural films have attracted considerable attention due to technological applications for nanometric device fabrication. Recently PAA films have been extensively used in fields of optoelectronics [1], photonics [2], photocatalysis [3], biosensors [4] and magnetics [5, 6]. Self–ordered PAA films have been obtained by the mild anodization (MA) within three limited growth regimes in H_2SO_4, $H_2C_2O_4$, and H_3PO_4 [7-11]. MA procedure is a slow process to obtain PAA films suitable for fabrication of nanodevices. To solve the problem of very slow anodization, a new method based on the hard anodization (HA) process, was reported [12]. HA considerably speeds up the process with various range of pore sizes and interpore distances. More recently, several new approaches, based on MA and HA anodization techniques for engineering of various nanostructures, have been reported. This method provides new degree of freedom to fabricate three-dimensional ordered porous nanostructures. Recently fabrication of PAA films with periodically modulated diameters of nanopores has been achieved by several methods such as combining conventional mild anodization and new hard anodization processes, pulse anodization and cyclic anodization [12-15]. In all these processes changing of the anodization voltage or anodization current is an important factor in engineering of alumina nanostructures. The morphology of AAO contains hexagonal array of straight long cylindrical nanopores oriented perpendicular to the metal/oxide interface and at the bottom of each pore, there is a thin barrier oxide layer with hemispherical geometry. Here we introduce some of the nanopores applications.

We mixed two kinds of anodization process (hard and mild anodization) to fabricate AAO nanotemplates suitable for producing nanocapacitores. We investigate the capacitance of capacitors in terms of the voltage and anodization time which control the pore diameter and thickness of the template. *Porous anodic alumina (PAA) with high aspect ratio is fabricated by mild and then hard anodizing process is used to produce Sn nanowires by electrodeposition process where the nanopores in PAA are filled with Sn. These nanowires are used for many industrial applications.* Self-organized porous anodic alumina (PAA) nanostructural films *employed here to fabricate a superhydrophobic. According to our experiment, the optimum anodization process is used to achieve the water contact angle (CA) to be about 160°.*

References

[1] Tonucc R J, Justus B L, Campillo A J and Ford C E, Science **258,** 783 (1992)

[2] Nishio K and Masuda H, Electrochem. Solid-State Let. 7 H, 27(2004)

[3] Chu S Z, Inoue S, Wada K, Li D, Haneda H, J. Mater. Chem. **13,** 866(2003)

[4] Matsumoto F, Nishio K and Masuda H, Adv. Mater. **16,** 2105 (2004)

[5] Whitney T W, Jiang J S, Searson P C and Chien C L, Science **261,** 1316 (1993)

[6] Nielsch K, Müller F, Li A. P and Gösele U, Adv. Mater. **12,** 582 (2000).

[7] Jessensky O, Muller F and Gosele U J Electrochem. Soc. **145,** 3735(1998)

[8] Li F Y, Zhang L and Metzger R M, Chem. Mater. **10,** 2470 (1998).

[9] Masuda H and Fukuda K, Science **268** 1466(1995).

[10] Ono S, Saito M, Ishiguro M and Asoh H, J. Electrochem. Soc. **151,** 473 (2004).

[11] Nielsch K, Choi J, Schwirn K, Wehrspohn R B and Gosele U, NanoLet. **2,** 677 (2002).

[12] Lee W, Ji R, Gosele U and Nielsch K, *Nature Matter* **5,** 741 (2006).

[13] Lee W, Schwirn K, Steinhart M, Pippel E, Scholz R and Gosele U, Nat. Nanotechnol. **3,** 234 (2008).

[14] Lee W, Scholz R and Gosele U, NANO LETTERS Vol **8** No. 8 2155(2008).

[15] Losic D, and Losic Jr D, Langmuir **25**(10), 5426 (2009).

Nano-sono degradation and kinetic study of an azo dye using core-shell nanocrystals of CdS-TiO_2 fabricated by ultrasound

Mohammad H. Entezari* and Narjes Ghows
Department of Chemistry, Ferdowsi University of Mashhad, 91775, Mashhad, Iran
*Corresponding author: moh_entezari@yahoo.com

Abstract

A novel composite with a core-shell structure was prepared through the combination of microemulsion and ultrasound. The composite with a proper ratio has shown exceptional sonocatalytic activity in comparison to the pure nano-sized TiO_2 and CdS. This method was simultaneously able to decolorize and oxidize the dye with a complete mineralization due to the enhancement of mass transfer, cleaning the catalyst surface, and preventing the aggregation of particles. In this paper, two kinetic models of Langmuir–Hinshelwood and consecutive first-order reaction were investigated. The rate constants of sonocatalytic were higher than what obtained in the absence of the catalysts, solar and UV irradiation.

Keywords: Core-shell, Kinetic, Reactive black 5, Mineralization, Sonocatalytic degradation

Introduction

TiO_2 has some drawbacks [1]: (a) not applicable in visible light (b) fast recombination of the hole and electron pairs (c) low efficiency of UV light. Due to these limitations, significant efforts have been made over the last two decades for handling these problems [2]. Ultrasound is an easy and effective method under the mild conditions for preparing nonmaterials [3, 4]. It can improve the contact of the two components, crystallinity, and the formation of uniform coating [5, 6]. In this study, CdS/TiO_2 couples have been prepared by a combination of ultrasound and microemulsion in order to: (i) exploit the maximum optical absorption in the visible range, (ii) increase the surface contact between the two components (iii) facilitate the crystallization. Then the degradation of RB5 as a model pollutant is investigated under different conditions.

Experimental

A microemulsion with weight ratio between oil, CTAB, water, and co-surfactant was devided in two separate parts (A= contained sulfur in oil phase and B= cadmium chloride and ethylenediamine in aqueous phase) for preparing CdS. The synthesis of core-shell nanoparticles has carried out with combination of ultrasound and microemulsion by adding TTIP to the mixture. The precipitate was separated, washed and then dried. Then 50 mL of RB5 solution containing catalyst was sonicated for removal of dye. The other experiments were carried out under the same conditions by UV lamp and sunlight.

Results and discussion

The XRD peaks and the HRTEM for the composite confirm a core-shell structure. The results show that the sonocatalytic removal is more effective than UV light or sunlight in the presence of catalyst. This is due to the synergetic effect of ultrasound and semiconductor that may promote the formation of reactive oxygen species on the surface of catalyst and fast charge separation and transportation throughout the particles [1, 2]. In addition, the light and high temperature caused by cavitation effect can activate the electronic excitation. The TOC was fast, and then decreased slowly due to a detrimental effect of the adsorbed SO_4^{2-} ions on the catalyst surface [7]. The ultrasonic degradation follows L-H rate kinetics, but this model may not be valid at longer periods. Then, we examine a kinetic model of consecutive first-order reaction.

Conclusion

Ultrasound has a key role in the synthesis of the core-shell nanocomposites. The contact between the two nanoparticles is very important for electron transfer through the crystal interphase between TiO_2 and CdS. It results in separation of electron–hole pairs. In addition, for the removal of RB5, ultrasound has a pronounce effect on the de-aggregation of the nanocomposite particles, cleaning and sweeping the catalyst surface by acoustic micro-streaming. The sonocatalytic rate with the TiO_2/CdS is very fast compared to “only ultrasound” state, solar and UV.

Acknowledgment

This work has been supported by the "Iranian National Science Foundation: INSF" (No. 85103/31).

References

[1] J. Wang, et al., Ultrason. Sonochem. 16 (2009) 225–231.

[2] A. Kongkanand, et al., J. Am. Chem. Soc. 130 (2008) 4007–4015.

[3] M. H. Entezari, N. Ghows Ultrason. Sonochem. 18 (2011) 127–134.

[4] N. Ghows, M.H. Entezari, Ultrason. Sonochem 18 (2011) 629–634.

[5] S. Anandan, F. Grieser, M. Ashokkumar, J. Phys. Chem. C 112 (2008) 15102–15105.

[6] A.L. Morel, et al., acs nano 2 (2008) 847.

[7] C. Gomes da Silva, J. L. Faria, J. Photochem. Photobiol. A: Chem.155 (2003) 133.

Theory of Intramolecular Non-radiative processes

R.Islampour[a*], M.Mirahnaghi[b]

[a] Department of chemistry, Tarbiat. Moalem University, 49 Mofateh Avenue, Tehran, Iran

islampour @ tmu.ac.ir

[b] Department of chemistry, Varamin-Pishva branch, Islamic Azad Univeristy, Tehran, Iran

Abstract

Molecules in their excited electronic states possess excess energy due to their formation by photon absorption. These excited states are short-lived, and there by lose their excess energy within a short period of time through a variety of in tramolecular processes, consisting of radiative and nonradiative transition, and intermolecular processes, such as vibrational relaxation, energy transfer, electron transfer, etc.

Intramolecular nonradiative processes, which are of our concern here, was first experimentally revealed by Kasha(1) in 1950, which has been known as kasha rule ever since. With rare exceptions, polyatomic molecular luminescence was observed only from the lowest excited electronic state of a given multipilicity, no matter which stable electronic state and phosphorescence occurred from the lowest triplet state. Kasha discriminated between two types of radiationless transitions, the one occurring between states of the same multipilicty, which he called internal conversion, and the one occurring between states of different multiplicity, called inter system crossing. Such processes are necessarily energy – conserving in an isolated molecule, so the energy difference is converted into excess vibrational energy.

The formal thory of the intramolecular nonradiative transitions in isolated (collision-free) polyatomic molecules of sufficient size was put forward by Lin(2,3) and by Bioxon and Jortner(4), who attempted to formulate the entire problem of radiationless transitions by being more explicit about the coupling mechanism that was responsible for the radiationless process and to establish the criteria that malce an irreversible radiativuless relaxation process possible. They bava attributed the nonstationary character of the excited electronic states to a concerling between vibrational and electronic motion brought about by a breakdown ant he Born-

Oppenhencr approximation (in case of internal conversion) plue the state exprossions we have recently derived for the internal conversion deose stanc between two adiabatic and between two diabetic potential energy such rotational normal modes), the prornoting modes, and the temperature (5). Finally the application of the expressions will be discussed.

Refrences:

1. M. Kasha, *Discuss. Faraday Soc.*, **9**, 14 (1950).
2. S. H. Lin, *J. Chem. Phys.* **44**, 3759 (1966).
3. S. H. Lin and R. Bersohn, *J. Chem. Phys.*, **48**, 2732 (1968).
4. M. Bixon and J. Jortner, *J. Chem Phys.*, 48, 715 (1968), ibid, 50, 4061 (1969).
5. R. Islampourand M. Miralinaghi, *J. Phys. Chem. A*, **113**, 2340 (2009).

Faddeev Equations in Momentum Space

Hamidreza Moshfegh
Department of Physics, University of Tehran, Tehran-Iran

Scattering problem and calculating of the scattering cross sections is crucial key to understanding the nature of interactions of systems from elementary particles to macro molecules.

Traditionally the two-body interactions are the dominate term in interaction part of Hamiltonian of systems. So it seems that the Lippman-Shcwinger equation and its approximations are enough to solve the problem. Recent progress both in computers and computational techniques shows the importance of three-body forces to obtain more accurate results for scattering and bound state problems.

Faddeev formalism is among the methods that could help us to done calculation of three-body scattering problems. Generalized Faddeev-Yakubovsky theory is used for four-body scattering problem as well as bound states.

Usually Faddeev equations are represented in partial wave decomposition as a 2l+1 component of angular momentum space. Recently, by representing of these equations in linear momentum space as a three dimensional integral equations , open a new window to apply the Faddeev formalism to bound states three-body systems. . Advantages of this new representation encourage us to replace the discrete angular momentum variables by continuum spectrum of linear momentum space.

In this talk we introduce the Faddeev equations in its traditional fashion, and then the new representation in linear momentum space is presented. Finally by employing a simple two-body interaction, the results for elastic scattering of a three-body system as well as a three body bound state system are discussed.

Oral Session

Critical behavior of thermalized bond Ising model in two and three dimensions

S. Davatolhagh, M. Moshfeghian and L. Separdar
Department of Physics, College of Sciences, Shiraz University, Shiraz 71454

Keywords: Critical phenomena, Monte Carlo Method, Annealed impurity, Finite-size scaling

Introduction

Thermalized Bond Ising Model (TBIM) is a lattice Ising model with annealed bond dilution in which every covalent bond linking a nearest-neighbor pair of atoms is allowed thermally induced electronic transitions between bonding and anti bonding electronic states [1]. Hence, it can be regarded as containing annealed bond defects with a temperature-dependent concentration. In TBIM, each bond at every instant is characterized by a coupling constant J=0, J_0 such that J = 0 corresponds to a broken bond (anti bonding electronic state), while J = J_0 means an attractive coupling between the two atoms (bonding electronic state). This provides for a natural bond breaking mechanism that may be suitably incorporated in the lattice models of covalently bonded structures. We denote the thermally averaged bond concentration by p. The ratio of the bonds to the broken bonds in equilibrium is given by the ratio of the corresponding Boltzmann factors:

$$p = \frac{1}{(1+e^{-\beta J_0})} \qquad (1)$$

The bond distribution function for the bond diluted TBIM is of the form

$$P_{J_{ij}}(\beta) = p\delta_{J_{ij},J_0} + (1-p)\delta_{J_{ij},0} \qquad (2)$$

where p is given by Eq. (1) and δ denotes the Kronecker delta. The microscopic Hamiltonian of the system under consideration can be formally defined by

$$H = -\sum_{\langle ij \rangle} J_{ij}\sigma_i\sigma_j \qquad (3)$$

where $\sigma_i = \pm 1$ is the structural (Ising) variable at the site i of the underlying lattice, and $J_{ij}=0$, J_0 represents the annealed bond variable associated with the nearest-neighbor sites <ij>.

Methods

The critical behavior of 3D TBIM has been investigated analytically using the method of chemical potentials and the grand canonical ensemble [1]. Furthermore, the 2D TBIM was studied numerically by performing a suitably modified Wolff single-cluster Monte Carlo simulation [2]. In our simulations, the order parameter and the corresponding susceptibility for a lattice of linear size L, are given by

$$\langle m \rangle = \left\langle \left| \sum_{i=1}^{N} \sigma_i \right| \right\rangle / N \qquad (4)$$

$$\chi_L = \frac{N}{k_B T} (\langle m^2 \rangle - \langle m \rangle^2) \qquad (5)$$

The susceptibility is known to obey the finite-size scaling form

$$\chi_L(T) = L^{\gamma/\nu} \, \tilde{\chi}(L^{1/\nu}(T - T_c)) \qquad (6)$$

By performing a finite-size scaling analysis of the susceptibility and the fourth-order cumulant, defined by Eq. (7) below, the critical behavior of the system in thermodynamic limit is obtained:

$$U_L = 1 - \frac{\langle m^4 \rangle}{3\langle m^2 \rangle^2} \qquad (7)$$

The cumulant is believed to obey the finite-size scaling ansatz

$$U_L(T) = \tilde{U}(L^{1/\nu}(T - T_c)) \qquad (8)$$

that is independent of L at the critical point T_c [3].

Results and Discussion

In order to locate the critical temperatures of 2d TBIM and 3d TBIM, we have relied on the cumulant crossing method [3]. The result for 2d TBIM is T_c=1.4897(3), and for 3d TBIM T_c= 2.557(1). The lowering of the transition points compared to the

pure systems, is due to the presence of annealed bond disorder. Furthermore, the correlation length exponent ν, defined by $\xi \sim |T-Tc|^{-\nu}$, is estimated from the scaling plot of $U_L(x)$ against $x=L^{1/\nu}(T-T_c)$. Our best estimate of the correlation length exponent for 2d TBIM is ν=1.006(8), and for 3d TBIM is ν =0.70(1). We have also carried out a finite-size scaling of the susceptibility χ_L, which gives the susceptibility exponent γ defined by $\chi \sim |T-Tc|^{-\gamma}$. The results are γ= 1.755(5) for 2d TBIM and γ=1.40(1) for 3d TBIM. Having estimated two of the critical exponents, the rest can be obtained from a variety of scaling laws relating the exponents. The hyperscaling law α=2-dν, where d is the space dimensions, is used to estimate the specific heat exponent α, and the order parameter exponent β can be obtained from the scaling law 2β+α+γ=2, thus giving α=0.000(16) and β=0.122(11) for 2d TBIM, and α=0.10(3) and β=0.35(2) for 3d TBIM.

Conclusion

The results are in excellent agreement with certain phenomenological relations due to Fisher [4], which describe the renormalization of the critical exponents by the so called 'hidden variables' in terms of the known exponents of the pure model system. Physically, this consistency should be interpreted in the light of the fact that the minute details of the microscopic interactions of a physical system, in this case the temperature dependence of the bond dilution, may not alter the large-scale behavior at a critical point, thus preserving the renormalized Fisher exponents and their universality.

References

[1] S. Davatolhagh, L. Separdar and M. Barati, Phys. Rev. E **78**, 021138 (2008)

[2] S. Davatolhagh and M. Moshfeghian, Physica A **389**, 3349 (2010)

[3] K. Binder, Phys. Rev. Lett. **47**, 693 (1981)

[4] M. E. Fisher, Phys. Rev. **176**, 257 (1968)

How the Nonextensivity Parameter Affects Energy Fluctuations

Ezat Keshavarzi *,[1], Abbas Helmi[1], and Mohammad Kamalvand[2]

[1]Physical chemistry group, Department of Chemistry, Isfahan University of Technology, Isfahan, Iran, 8415683111

[2]Department of Chemistry, Faculty of Science, Yazd University, Yazd, Iran, 89195741

E-mail: keshavrz@cc.iut.ac.ir

Introduction

In the recent years the generalized Tsallis statistical mechanics has been of interest for many researchers in different fields. They have applied it to predict the phenomena in different nonextensive systems for which Boltzmann Gibbs statistics fails [1-3]. In this statistical mechanics the entropy is defined as [3]:

$$S = \frac{k}{q-1}(1 - \sum_i^w P_i{}^q) \quad (1)$$

where P_i is the probability function of finding the system in *i'th* state, k is a positive constant, and q is the entropic index related to the degree of the nonextensivity. So far four different energy constraints have been used with only one of them (known as 2nd version) being un-normalized. In this article, the effect of the nonextensivity parameter on the energy fluctuations of nonextensive systems has been studied in two different versions of the Tsallis statistical mechanics.

The energy fluctuations in the second version of the Tsallis statistical mechanics

The different energy constrains, un-normalized and normalized, in the second and fourth versions have been used to obtain the probability function in canonical ensemble in the Tsallis statistical mechanics. The different partition functions in these two versions have been obtained corresponding to these different constraints as:

$$\sum_1^w \varepsilon_i \; P_i{}^q - \overline{E_q} = 0 \qquad ; \qquad Z_q^{(2)} = \sum_i^w [1 - (1-q)\beta\varepsilon_i]^{\frac{1}{(1-q)}} \quad (2)$$

$$\sum_i^w (\varepsilon_i - \overline{E_q}) {P_i}^q = 0 \qquad ; \qquad Z_q^{(4)} = \sum_i^w [1 - (1-q)\beta'(\varepsilon_i - \overline{E_q})]^{\frac{1}{(1-q)}}$$

In the second version, $\overline{\Delta E^2} = \overline{(\bar{E} - E)^2}$ can be calculated as follows:

$$\overline{\Delta E^2} = \overline{E^2} + \bar{E}^2 \left[{Z_q}^{1-q} - 2 + (1-q)\beta \overline{E_q} \right] \tag{3}$$

$\overline{{E_q}^2}$ in the second version of the Tsallis statistical mechanics is defined as:

$$\overline{{E_q}^2} = \sum_i^w {\varepsilon_i}^2 \ {P_i}^q = -\frac{1}{{Z_q}^q} \frac{\partial}{\partial \beta} \left[\sum_i^w \varepsilon_i [1 - (1-q)\beta\varepsilon_i]^{\frac{1}{(1-q)}} \right] \tag{4}$$

The term in the bracket may be written as $Z_q \sum_i^w \varepsilon_i \ P_i$. We have obtained the following equation for energy fluctuations after some mathematical calculations as:

$$\overline{\Delta {E_q}^2} = -\frac{1}{1-A} \frac{\partial \overline{E_q}}{\partial \beta} + \frac{1-q}{1-A} \beta \frac{\partial \overline{{E_q}^2}}{\partial \beta} + \frac{A-B}{1-A} \overline{E_q}^2 \tag{5}$$

where *A* and *B* coefficients are as follow:

$$A = (1-q) + \frac{(q^2 - q)\beta \overline{E_q}}{{Z_q}^{(1-q)}} \ , \ B = \left(2 + \beta(q-1)\overline{E_q} - {Z_q}^{(1-q)} - \frac{q}{{Z_q}^{(1-q)}} \right) \tag{6}$$

It should be noted that Eq. (6) in the limit of $q \rightarrow 1$, tends to that corresponding equation in the Boltzmann Gibbs statistics.

Energy fluctuations for generalized ideal gas and harmonic oscillator in 2nd and 4th versions of Tsallis statistics

In Fig. 1 the relative energy fluctuation and its three parts have been plotted according to Eq. 6 for an ideal gas, Argon at *T*=300K. According to this Figure, the relative energy fluctuations are usually greater than BG ones. In fact, only for a very small region around unity, when q is smaller than unity, the square of relative energy fluctuation (SREF) is less than the BG. In figure 2. the SREF and its three parts according to Eq.(6) have been plotted for quantum harmonic oscillator band compared with the corresponding value in the BG statistics for $\beta h\nu = 1$. Clearly, the SREF is less than BG when q is smaller than unity and will be greater than BG when q>1. This behavior is related to the number of accessible states which increases with q. The results related to relative energy fluctuation for Argon atom at *T*=300K have been

shown in Fig. 4 for 4th version of the Tsallis statistics. As it has been shown in this figure, when entropic index q is smaller than unity, relative energy fluctuation is smaller than BG value, $\sqrt{2/3}$, and when q is greater than 1, relative energy fluctuation is greater than $\sqrt{2/3}$. Also, the relative energy fluctuation for a quantum harmonic oscillator in 4th version of the Tsallis statistics has been shown in this figure. In Fig. 5 the relative energy fluctuation for an ideal gas with a different number of particles has been shown in the fourth version. According to Fig. 5 this result is correct only for q<1, and as we have shown for q>1, like one particle system, the relative energy fluctuation of a nonextensive system is always greater than extensive one.

Conclusion

The energy fluctuation in the second version for ideal gas is larger than BG in nearly all the values of q, it is because of the un-normalized picture of this version. Our study in the forth version reveals that the energy fluctuation is strongly dependent on the accessible states via the nonextensivity parameter. In this manner when q is less than unity, the relative energy fluctuation is less than BG and when q is more than unity, the energy fluctuations will be more.

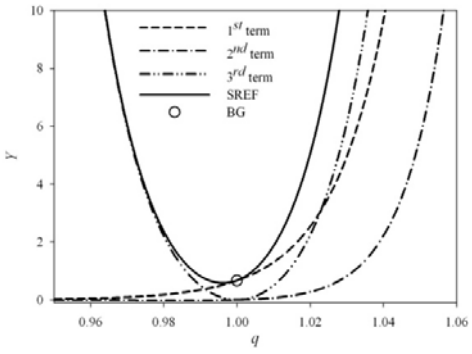

Fig. 1

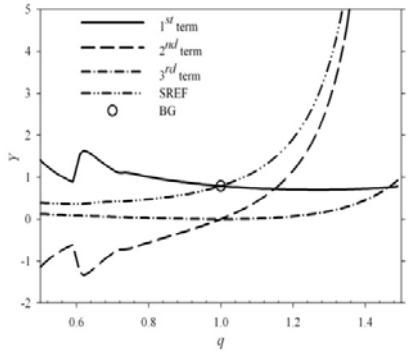

fig.2

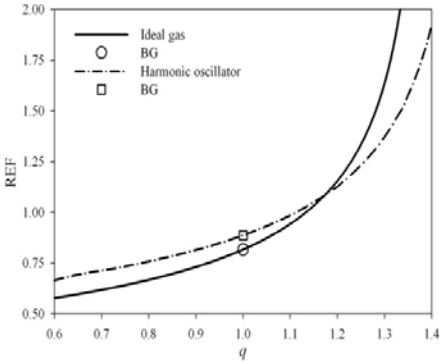

Fig. 3

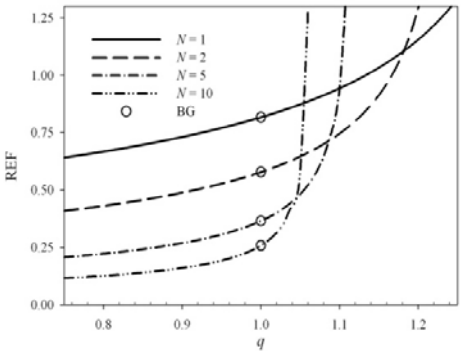

fig.4

References

[1] H. Hasegawa, phys review E, 80 (2009) 011126.

[2] Z.H. Feng, L. Y. Liu, Physica A 389 (2010) 237.

[3] C. Tsallis, J. Stat. Phys. 52 (1988) 479.

Calculation of radial distribution functions for methane by wavelets

M. Moradi* and M. Katiraee

Department of Physics, Shiraz University, Shiraz, Iran

(Email:moradi@susc.ac.ir)

(Email:mm_katiraee@yahoo.com)

Keywords: Radial distribution function, Molecular liquid, Ornstein-Zernike equation, Wavelets

1. Introduction

As we know, the radial distribution function has an important role in acquiring thermodynamics and properties of different kind of fluids such as molecular liquids. Up to now, several methods have been presented in order to calculate these properties [1-2]. In the last decades integral equations approach accompany with the Ornstein-Zernike (OZ) equation is one of the successful methods that has been used [3]. In conventional methods of solution of OZ equation, there are many difficulties such as high dimension of the Jacobian matrix, relatively slow convergence and etc. For these reasons, here we have used wavelets analysis that is a modern numerical tool that is an extension of the Fourier analysis [5]. In this article we have efforted to solve OZ equation for methane by using wavelets and their properties and compare the results with acquired results from the molecular dynamics (MD) simulations.

2. Methods

In this article we calculate the radial distribution function (RDF) using the referenced interaction site model of molecular liquids. As we know, in this theory, it is purposed to calculate the RDFs by solving the set formed by the OZ equation and a closure relation. For a molecular liquid consisting of N-site molecules, the site-site OZ (SSOZ) equation has the following form [4]:

nHn=nW*C*(nW+nHn)

(1)

Where H and C are the site-site intermolecular pair correlation functions and the direct correlation functions respectively, n is the diagonal matrix whose elements are number densities of each molecular species and W is the intramolecular correlation

matrix. In order to solve OZ equation, for molecular liquids, a secondary relation as closure relation and knowing of intermolecular interactions is required. In this article the site-site interactions between molecules are represented by the Lennard-Jones (L-J) potential plus coulomb terms. Most of the numerical algorithms for solving relation (1) impose the Fourier representation of (1) written as:

$$\hat{G}(k)=\hat{H}(k)-\hat{C}(k)=\hat{W}(k)(I-n\hat{W}(k)\hat{C}(k))^{-1}\hat{C}(k)\hat{W}(k)-\hat{C}(k)\hat{W}(k)-\hat{C}(k) \quad (2)$$

Where $\hat{G}(k)$ is the Fourier transformed of indirect correlation functions, $\hat{W}(k)$ is the Fourier transformed of intramolecular correlation functions and I is the unity matrix. Tilde notation used above means 3D Fourier transform (FT) of the corresponding matrices. To solve equation (2) by wavelets, we expand matrices G and C in an arbitrary orthonormal basis set and by substituting in relation (1), we obtain the basis representation of the SSOZ equation and calculate the approximating coefficients[5].

3. Results and discussion:

By using of the wavelet and the method of applying it in pervious relations, we can calculate pair correlation function in Fourier space and then by inverting it, we can obtain correlation function in real space and some thermodynamics properties. For this purpose, we have applied the hybrid scheme in which the coarse part of the solution is calculated by wavelets with the use of the Newton-Raphson procedure, while the fine part is evaluated by the direct iterations. The Coifman 2 basis set is employed for the wavelet treatment of the coarse solution. The methane density n is assumed $0.00347 gr/cm^3$ in 298K and the L-J parameters are chosen: ε_{cc}=0.397kj/mol, ε_{ch}=0.168kj/mol, ε_{hh}=0.0711kj/mol, $\sigma_{cc}=3.357A^0$, $\sigma_{ch}=2.741A^0$, $\sigma_{hh}=2.134A^0$ [6].

4. Conclusions

We have calculated RDFs of methane. The calculated RDFs are in fairly agreement with those obtained by discontinues molecular dynamics (DMD) and standard molecular dynamics (SMD) computer simulation. These agreements between the results show that the using of wavelets is useful and powerful method to study the fluids structure. In figure (1), the results of solution of SSOZ equation for RDF of

carbon-carbon interaction sites are compared with results from DMD and SMD computer simulation [6].

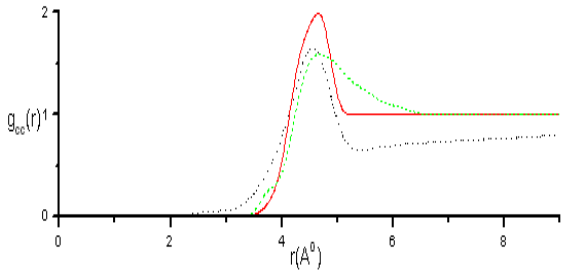

Figure (1). Carbon-carbon RDF in methane: the solid line represents DMD and the dashed line represents SMD computer simulation and the dotted line represents this work.

Reference

[1] M . Moradi , J . Sci . I . R . 2 (1991) 74.

[2] M . Moradi and F. Taghizadeh, Int . J . Mod . Phys . C. 20 (2009) 337.

[3] H. Frisch and J. L. Lebowitz,The Equilibriu,Theory of classical Fluids , New York , Benjammi (1964).

[4] D. Chandler and H. C. Andersen, J. Chem Phys. 57 (1972) 1930.

[5] G. N. Chuev and M. V. Fedorov: J. Comput. Chem. 5 (11) (2004) 1369-1377.

[6] Herna ´ndez de la Pen~a, Lisandro, van Zon, Rams es, Schofield, Je remy, Opps, Sheldon B, J Chem Phys 126,(2007)

Investigation for Validity of a New Equation of State for Nanosystems

N. Masoumi , G. A. Parsafar*
Department of Chemistry, Sharif University of Technology, Tehran, Iran
(Parsafar@sharif.edu)

Key words : Equation of State, Effective pair potential, Nanosystems, Molecular Dynamic

Introduction

Equations of state have an important role in study of systems, from which thermodynamic properties can be calculated. In 1993, Parsafar and Mason derived an equation of state (EoS) for compressed liquids and dense supercritical fluids [1], EoS I. However, this EoS is not accurate for the liquid alkali metals like cesium and rubidium, so Ghatee and Bahadori derived an EoS for liquid alkali metals [2], EoS II. In a later investigation, it was shown that EoS I can be applied for non-ionic and non-metallic (molecular) solids and EoS II for ionic and metallic solids [3], respectively. Recently, Parsafar et al. [4] derived another EoS which gives a good description for all types of solids and fluids, except near the critical temperature, EoS III. The validity of EoS III will be investigated for nanosystems.

Method

An extended Lennard – Jones (ELJ) (12,6,3) potential function was introduced as an effective near – neighbor pair potential in liquids and solids (in bulk). Based on such a function, the potential energy, *U,* may be given as equation (1).

$$U = \frac{N}{2} z \left(\frac{C_{12}(T)}{r^{12}} + \frac{C_6(T)}{r^6} + \frac{C_3(T)}{r^3}\right) \qquad (1)$$

where r is taken to be a mean near – neighbor distance, N is number of particles of system, C_i is a temperature dependent parameter and z is the mean coordination number. The r^{-6} and r^{-12} terms represent the long and short range interactions respectively.

Based on ELJ, the EoS III has been derived as is shown in equation (2).

$$(Z-1)v^2 = e + \frac{f}{\rho} + g\rho^2 \qquad (2)$$

where e, f and g are nontrivial functions of temperature, $Z = \frac{Pv}{k_B T}$ is the compressibility factor, $\rho = \frac{1}{v}$ is the molar density and k_B is the Boltzmann constant. The validity of this equation of state for

nanosystems will be studied using experimental data as well as molecular dynamic simulation of such systems.

Results and Discussion

We have evaluated EoS III for different solids and liquids and found that it has high accuracy for various types of them. Therefore, we try to consider this EoS for systems like metallic and ionic solids at nanoscale, similar those we obtained for bulk data (see table 1). Because of inadequate experimental *PVT* data for these systems we use molecular dynamic (MD) simulation for obtaining the *PVT* data. The experimental data for nanosystems will be used for approving the validity of the EoS III. Then we will use MD simulations for some other nanosystems without any experimental data. It could also help us to find the way for validating the MD simulations for obtaining the thermodynamic properties of nanosystems.

Table 1: The coefficients of EoS III for give isotherm of give fluids along the correlation coefficient

Fluid	*T,K*	*e*	*f*	*G*	R^2
Ar	120	-0.00924	0.0839	6.17E-06	1.000
Ar	308.15	-0.00032	0.008526	2.01E-06	1.000
Ne	298	-0.00032	0.008526	2.01E-06	1.000
N_2	308.15	-0.00032	0.008526	2.01E-06	1.000
CO	308.15				
CH_4	150	-0.01569	0.09898	1.87E-05	1.000
	308.15	-0.01569	0.09898	1.87E-05	1.000
	500	-0.01569	0.09898	1.87E-05	1.000
C_3H_8	308.15				
n-C_9H_{20}	303.15	-3.981	11.02	0.06387	1.000
n-$C_{19}H_{40}$	343.15	-34.78	50.65	2.109	1.000
CH_3OH	300	-0.0297	0.2547	2.94E-05	1.000
H_2O	298.15	0.000711	-0.1435	5.09E-07	1.000
Hg	303.15	-0.01819	0.09038	3.64E-06	1.000

References

[1] G. A. Parsafar and E. A. Mason, J. Phys. Chem. 97 (**1993**) 9048.

[2] M. H. Ghatee and M. Bahadori, J. Phys. Chem. B 105 (**2001**) 11256.

[3] M. Shokouhi et al., Fluid Phase Equilibria 271 (**2008**) 94.

[4] G. A. Parsafar and H. V. Spohr and G. N. Patey, J. Phys. Chem. B 113 (**2009**) 11977.

Fabrication, characterization,and measurement of some transport properties of α-fe_2o_3 and fe_3o_4 magnetic nanofluids

Sayyed Hashem Sajjadi,*[a] Elaheh K. Goharshadi,[b] Maryam Abareshi,[b] and, Seyed Mojtaba Zebarjad[c]

Email: shsajjadi@mehr.sharif.ir

[a]Department of Chemistry, Sharif University of Technology, Tehran , Iran

[b]Department of Chemistry, Ferdowsi University of Mashhad, Mashhad 91779, Iran

[c]Center of Nano Research, Ferdowsi University of Mashhad, Mashhad 91775-1436, Iran

Keywords: Magnetic nanoparticles, Nanofluid, Thermal conductivity, Viscosity.

Introduction

Nanosized iron oxide particles have multiple practical applications, for example, in drug delivery, magnetic hyperthermia, magnetic resonance imaging, pigments, and photocatalysis [1]. The magnetic nanofluid, ferrofluid, behaves as a smart fluid due to some of its unique features. They have some applications in a variety of fields such as electronic packing, mechanical engineering, aerospace, and bioengineering [2,3].

Although the magnetic properties of the magnetic nanofluids are the subject of intensive studies , there are few data in the literature concerning their thermal and rheolegical properties. The first goal of the present study is to investigate the effect of both temperature and volume fraction on the thermal conductivity of Fe_3O_4-water nanofluids. For this purpose, we were synthesized Fe_3O_4 nanoparticles by co-precipitation method. The second aim of this work is to measure the viscosity of α-Fe_2O_3-glycerol nanofluids as a function of temperature, volume fraction, and shear rate. For this purpose, we were synthesized α-Fe_2O_3 nanoparticles with solvothermal route

Results and discussion

Superparamagnetic Fe_3O_4 nanoparticles were successfully synthesized by a simple and cost-effective co-precipitation method in different conditions. The XRD, TEM, FTIR, and VSM techniques were used to characterize the structure, size, purity, and magnetic properties of the nanoparticles. The best crystallinity was observed for pH initial=1.5 and pH final = 9.5. Fe_3O_4 nanofluids were prepared by dispersing Fe_3O_4 nanoparticles in distilled water as the base fluid. Tetramethyl ammonium hydroxide was used to improve the dispersion of Fe_3O_4 in distilled water. Measurement of zeta potential of nanofluids shows that Fe_3O_4 nanofluids have good stability.

The effective thermal conductivity of Fe_3O_4 nanofluids with different volume fractions was investigated experimentally at 10, 20, 30, and 40 ^oC. The experimental results were also compared with some different theoretical models. Among the models, the Murshed model gives better predictions of the thermal conductivity of these nanofluids compared with the classical models.

α-Fe_2O_3 nanoparticles were prepared by solvothermal method. The nanoparticles were characterized by XRD and TEM. The α-Fe_2O_3 nanoparticles were dispersed in a glycerol as the base fluid. Both experimental and theoretical work was performed on the rheological behavior of α-Fe_2O_3-glycerol nanofluids. The experiments were done at different temperatures, shear rates, and volume fractions.

Conclusions

The measurement of thermal conductivity and viscosity of Fe_3O_4 and α-Fe_2O_3 nanofluids contains the following conclusions:

1. The relative thermal conductivity of nanofluids increases with increasing volume fraction and temperature.
2. Thermal conductivity of Fe_3O_4 nanofluids increases up to 11.5% as the volume fraction of nanoparticles increase up to 3 vol. % at 40 ^oC.
3. α-Fe_2O_3-glycerol nanofluids are non-Newtonian fluids with shear-thinning. The viscosity of nanofluids significantly decreases with increasing temperature and increases with increasing particle volume concentration.

4. The rheological behavior of α-Fe_2O_3-glycerol nanofluids can not be predicted by Einstein, Brinkman, and Batchelor models.

References

[1] S. W. Cao and Y. J. Phys. Chem. C 112 (2008) 6253.

[2] J. Li, Y. Huang, X. Liu, Y. Lin, L. Bai, and Q. Li, Sci. Tech. Adv. Mater. 8 (2007) 448.

[3] R. Tackett, C. Sudakar, R. Naik, G. Lawes, C. Rablau, and P. P. Vaishnava, J. Magn. Magn. Mater. 320 (2008) 2755.

Coarse Graining in Polymers

Hossein Eslami

Department of Chemistry, College of Sciences, Persian Gulf University, Boushehr 75168, Iran

email: heslami@hotmail.com

Introduction

In studying polymer systems one is confronted with a variety of time and length scales. The range of length scales varies from about 0.1 nm, which is a typical bond length, to, for example, the radius of gyration of polymers, which is around 10 nm. The time scales also span from about <1 fs, the period of vibration of chemical bonds, to typical relaxation times of polymers (around a few miliseconds). The practical limitation of atomistic simulation methods in simulating such systems as polymers stems from handling a large number of particles and using hard atomistic potentials, which limits the largest time steps that can be used to perform a stable simulation. In practice, one can construct models with less computational effort by integrating out the fast motions in confined polymers, or averaging over their steep potentials. One way to do this is through the concept of coarse-grained models.

Method

Mapping a group of atoms onto a substantially smaller number of beads, connected by effective bonds and a soft effective potential acting between nonbonded beads, the coarse-grained models are constructed. Performing reference atomistic simulations, one can invert the resulting probability distributions to obtain the effective intra- and inter-molecular potentials among the beads. The resulting effective pair potentials obtained using this procedure reproduce well the structural properties.

Coarse-Grained Force Field

To match all the distributions, derived from atomistic simulations, a preferential order is taken into account. Normally, the stiffest interactions in the system correspond to the potential energies of interaction between closely spaced beads (bond lengths and bond angles). Having matched the distributions of bond lengths and bond angles, one

goes ahead with matching the distributions of nonbonded degrees of freedom. Fitting the target distributions, the force-field is obtained, which can well reproduce the structural properties of them atomistic sample. The force-field obtained in this way does not have the limitations of atomistic force fields; one can perform the coarse-grained simulation with a much bigger time step than the corresponding atomistic ones. Therefore, one can do simulations of bigger chains for a longer time, compared to atomistic simulations.

Results and Discussion

Here we report the simulation results on a sample of confined polyamide-6,6, as a typical example. Adopting a proper mapping scheme, we have compared in Figure 1 the density profiles of all beads, derived from atomistic simulations, and compared them with the same distributions, calculated in our coarse-grained model. As it is seen, a nice matching is seen. We have used the coarse-grained force-field to simulate long chains of confined polyamide (100-mer). The results show that the polymer forms layers in contact with surfaces. We have also computed the chain orientation, as well the relaxation time for end-to-end vectors. The results (not shown here) indicate that the coarse-grained model relaxes much faster than the corresponding atomistic model.

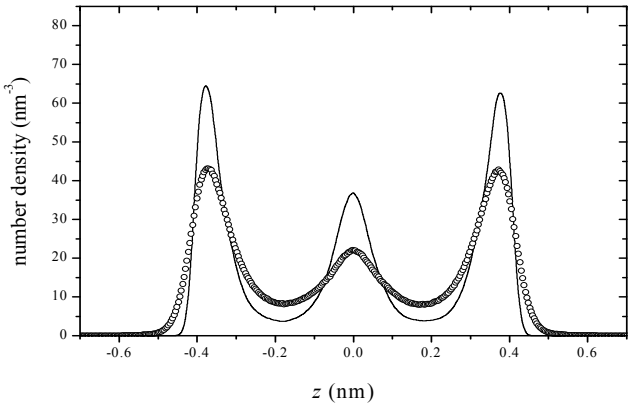

Figure 1. Comparison of the calculated density profiles for all beads in atomistic (full curve) and in coarse-grained models (dots).

Dependence of Surface Tension on Temperature And Density Along The Coexistence Curve

Z.Khorsandi*, G.A.Parsafar*

*Department of Chemistry, Sharif University of Technology, Tehran, Iran

Khorsandy_z@yahoo.com

Keyword: Surface Tension, Density, Coexistence curve, Effective pair interaction potential.

Introduction:

Using the Lennard-Jones (12,6) potential , as an effective pair interaction potential, dependence of surface tension , γ , of some isotherms on density, ρ, for fluids was derived as $\frac{\gamma}{\rho^2} = C\rho^2 + D$ [1].The accuracy of this equation was confirmed for 20 different fluids such as monatomic ,diatomic atomic and fluids with strong hydrogen bonding.

In this study the dependence of surface tension to temperature ,*T*, and density is obtained along the coexistence curve.

Method:

May use the effective pair interaction potential to obtain an expression for the fluid potential ,E_p, as:

$E_p = 4\varepsilon\sigma^{12}\rho^4 - 4\varepsilon\sigma^6\rho^2$; where $C_{12} = 4\varepsilon\sigma^{12}$ and $C_6 = 4\varepsilon\sigma^6$ *(1)*

where σ and ε are the potential parameters.

Since the pressure may be given as:

$$p = -\left(\frac{\partial E_P}{\partial V}\right)_T + T\left(\frac{\partial P}{\partial T}\right)_P = \rho^2\left(\frac{\partial E_P}{\partial \rho}\right) + T\left(\frac{\partial P}{\partial T}\right)_P \quad (2)$$

hence,

$$p = \rho^2[4c_{12}\rho^3 - 2c_6\rho] + T\left(\frac{\partial P}{\partial T}\right)_P \quad (3)$$

Equation (3) may be simply written as, $\frac{p-p_0}{\rho^3} = 4C_{12}\rho^2 + A_2RT - 2C_6$ (4)

where p_0 is the ideal gas pressure.

If we plot $\frac{p-p_0}{\rho^3}$ versus ρ^2we may obtain the parameters C_6 and C_{12} at any temperature. on the bases at linear isotherm regularity ,LIR, we can show that both parameters are linear in terms of *T*.

On the other hand , it is shown that the liquid surface tension varies with density as [1]

$$\gamma = -\frac{Zu(r)}{4\pi\sigma^2} = \frac{C_{12}}{4\pi\sigma^2}\rho^4 - \frac{C_6}{4\pi\sigma^2}\rho^2 = C\rho^4 + D\rho^2 \qquad (Z = \text{coordination number}) \tag{5}$$

There for, we may conclude the parameters *C* and *D* in equation (5) vary with *T* ,linearly. we have use the experimental data along the coexistence curve to check the validity of equation (5),for some fluids.

Result:

It can easily shown that the dependencies of *C* and *D* are related to the LIR parameters. We have used experimental data of Argon to find temperature dependencies of *C* and *D* (shown in (fig 1) [3].

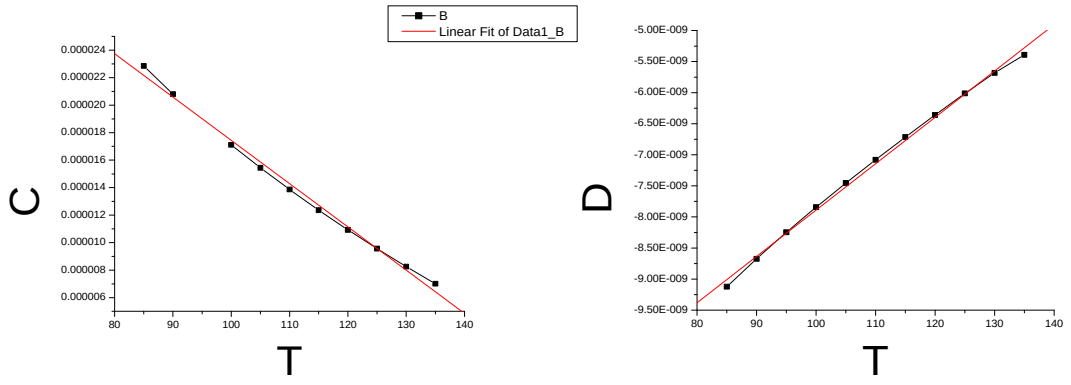

(a) (b)

Fig(1): Temperature dependency of (a)*C* and (b)*D*

The linear dependencies of *C* and *D* are used to calculate the surface tension along the coexistence curve ,see (Table I) [3].

T(K)	ρ(mole/L)	$100((\gamma_{calculate} - \gamma_{exp})/\gamma_{calculate})$
91.4	34.29	4
101.2	32.68	5
113.4	30.46	5.1
121.1	28.86	5.4
125.6	27.84	6.8
133.8	25.68	8
140.7	23.32	17

Table(I):percent deviation of surface tension of Argon at given states along the coexistence cure.

Conclusion

A simple model used to calculate surface tension of a liquid along the coexistence curve , gives a good agreement with experiment, except nearly the critical point (see table I).

Reference:

[1]H. Alizadeh; *Investigation of dependence of the surface tension to density and temperature in dense systems,*M.S. thesis (1388);sharif university of Technology

[2]G.A.Parsafar and E.A.Mason,J.Phys.Chem.97(1993)9048

[3] Tegeler, Ch.; Span, R.; Wagner, W., **J. Phys. Chem.**1999, 28, 3, 779-850.

Extended UNIQUAC model for modeling of liquid-liquid equilibria in mixed solvent electrolyte systems

F.Pirahmadi, M.R.Dehghani*[a], B.Behzadi

[a] *Department of Chemical Engineering, Iran University of Science and Technology, Narmak,Tehran, Iran,(m_dehghani@iust.ac.ir)*

Keywords: Mixed solvent; Liquid-liquid equilibria; Extended UNIQUAC model; Modeling

Introduction

The modeling of mixed solvent-electrolyte systems is important due to their applications in separation technologies. Iliuta [1] and Thomsen [2] presented the extended UNIQUAC model for correlation of phase equilibria in aqueous salt systems containing non-electrolytes. During recent years a lot of works have been done on liquid-liquid equilibria in mixed solvent electrolyte solution, in this work, we have utilized the extended UNIQUAC model for modeling of the large amount of experimental LLE data in the aqueous salt systems containing alcohols to recognize the capability of this model.

Methods

The extended UNIQUAC model for the excess Gibbs energy consists of two contributions; the first contribution is the UNIQUAC term as given by Abrams et al. [3] accounting for short-range effects in the mixture. A Debye-Hückel contribution has also been used to account for the long-range interaction effects. In this model, water is considered as the solvent and alcohols (non-electrolytes) and ions are considered to be solutes. The only parameters for the model are the UNIQUAC interaction parameters and volume and surface area parameters. The volume and surface area parameters for water, ions, and also all the binary interaction parameters for aqueous systems containing electrolytes have been extracted from the work of Thomsen et al.[4].The remaining parameters have been obtained by fitting the model to experimental data.

Results and discussion

We have used this model for 31 liquid-liquid equilibrium systems and 421 data points. The accuracy of the results in average deviation in mass percent ($\%\Delta w$) are given in Table1.

Conclusion

The extended UNIQUAC model has been shown good performance for modeling of liquid-liquid equilibria in most aqueous salt systems containing alcohols. All model parameters have been presented in this work.

Table 1. Average deviation in mass percent of liquid-liquid equilibrium of ternary systems

Alcohol	Salt	Temperature(◦C)	Data Point	%Δw
Ethanol	K_2CO_3	25-45	18	6.1
1-Propanol	NaCl	25	8	3.23
1-Propanol	KCl	25	8	4.32
2-Propanol	NaCl	25	8	7.77
2-Propanol	NaCl	25	10	5.13
1-Butanol	NaCl	20-40	96	0.89
1-Butanol	NaCl	25	10	0.51
1-Butanol	KCl	20-40	29	0.38
1-Butanol	KCl	25	8	0.85
1-Butanol	$NaNO_3$	25-35	24	1.96
2-Butanol	NaCl	25	8	1.52
2-Butanol	NaCl	25	20	2.52
2-Butanol	KCl	25	8	2.7
2-methyl1-propanol	NaCl	25	8	0.6
2-methyl1-propanol	NaCl	25	20	1.04
2-methyl1-propanol	KCl	25	8	0.78
2-methyl2-propanol	NaCl	25	7	3.03
2-methyl2-propanol	NaCl	25	14	4.36
2-methyl2-propanol	KCl	25	6	6.22
2-methyl2-propanol	Na_2SO_4	23-80	13	6.37
2-methyl2-propanol	K_2CO_3	25-45	16	2.73
1-Pentanol	NaCl	25	9	0.056
1-Pentanol	KCl	25	8	0.088
2-Pentanol	NaCl	25	9	0.046
2-Pentanol	KCl	25	8	0.058
3-Pentanol	NaCl	25	9	0. 15
3-Pentanol	KCl	25	8	0. 18
2-methyl1-butanol	NaCl	25	9	0.22
2-methyl1-butanol	KCl	25	8	0.16
2-methyl2-butanol	NaCl	25	8	0.24
2-methyl2-butanol	KCl	25	8	0.19

References

[1] M.C. Iliuta, K. Thomsen, P. Rasmussen, Chem. Eng. Sci. 55 (2000) 2673-2686.

[2] K. Thomsen, M.C. Iliuta, P. Rasmussen, Chem. Eng. Sci. 59 (2004) 3631-3647.

[3] D.S. Abrams, J.M. Prausnitz, AIChE J. 21 (1975) 116-128.

[4] K.Thomsen, aqueous electrolytes: model parameters and process simulation, PH.D. Thesis, Department of chemical engineering, Technical University of Denmark,1997

Description of Hydrogen Adsorption on Graphitic Nitrogen Doped Graphene Sheet

S.Jalili, A.Vahidi Ferdowsi*

Department of Chemistry, K. N. Toosi University of Technology, P.O. Box 15875-4416, Tehran, Iran

*(E-mail: a.v.ferdowsi@gmail.com)

Keywords: Molecular Dynamics, Graphitic N-doped Graphene Sheet (GNDG), Excess Adsorption , Adsorbent Sites, Data Fitting, Adsorption Models.

Introduction

Increasingly process in applying fossil fuels and producing greenhouse gases have been turned into one of the most important challenges in the environment. Recently, replacing and applying hydrogen as a suitable energy carrier and clean fuel have been taken in to account [1].

Currently, researchers interest in apply solid adsorbent surface, particularly, carbon-based materials because of their advantages. In this research, also, hydrogen adsorption on graphene surface with nitrogen graphitic defects has been studied by Molecular Dynamics method.

Methods

At first, a primary structure with respect to a synthetic sample [2] has been optimized by a semi-empirical method (PM3). Then, adsorption on its surface has been simulated by NVT ensemble with pressure 1-25MPa and temperature 77-400K. Interaction between gas molecules, gas molecules and the surface has been described by simple Lennard-Jones (6-12) potential. The periodic boundary conditions were applied in all three directions. The cutoff was chosen 16 Å. Temperature was controlled by using the Nose-Hoover thermostat. For the numerical integration of motion equations, a time step of 1 fs was utilized in all the simulations. To achieve reliable results for the hydrogen adsorption characteristics, all the simulations were performed for 1 ns. MD simulations were performed by the GROMACS 4.0.6 package.

Results and Discussion

With doping nitrogen to graphene sheet, the strength and capability of hydrogen– surface interaction will be increased. The other layers, also, will be formed under the 100K. The kind of defect has not too much effect on weight ratio of adsorption and increasing of layers in

synthesized sample caused weight ratio to be decreased. Adjustment of distance between produced layers is an important point in production of adsorption systems. Geometrical effects and overlap potential of layers in this state cause the adsorption and the amount of isosteric heat of adsorption in the interlayer space to be increased. In low temperature with increasing the pressure the excess adsorption after a certain pressure, because of the presence of adsorbent surface and van der Waals interactions, will be decreased. For example, excess adsorption in 85K after 7MPa and in 100K after 8MPa, will be decreased. The relationship between temperature and pressure can be described through the mathematical equations$\{\theta = f(P,T)\}$. Power of temperature and pressure in these equations indicate the level of importance and effect of temperature and pressure on the amount of adsorption. Using the mathematical derivation of these expressions, the minimum temperature and pressure of saturation for different kinds of adsorption will be obtained. For the system studied, by increasing the pressure, the saturation state is observed firstly in excess adsorption, consequently for monolayer adsorption and finally for multi layer adsorption. From another hand, saturation state can be observed in multi layer adsorption, consequently in excess adsorption and finally in monolayer adsorption, through decreasing of temperature. The absolute amount of q_{st} is affected by availability of surface, amount and arrangement of existed materials in the surface and interaction of adsorbed molecules with each other. Also, a higher amount of binding energy indicates a stronger interaction of hydrogen with defected surface than non-defective sample. Using the process of changes in the molecules' distances from surface than the changes in temperature and pressure, different adsorption phases can be observed in different amounts of coverage. It became clear that in low coverage, empty sites in surface (hexagonal centers) and in high coverage, surface atoms and bond distances, will include adsorption sites. Using data fitting of simulated result on different mathematical models of adsorption, a description of hydrogen adsorption on this structure is obtained. In this research non-linear fitting using error function of minimum Squares is applied. Then adjusted-R squares are used in order to compare different relationships of models. Among these eight models studied, 3-parameter model of Redlich–Peterson shows the best agreement with data. Multilayer adsorption by Temkin Isotherm and monolayer adsorption through Hill De-Boer can be described well. By Increasing the temperature, Fowler-Guggenheim isotherm shows a good agreement with the data too. Considering these data we can say that in temperatures lower than 130K, the interaction of adsorbed molecules with each other and their mobility is more. In temperatures higher than 180K the effects of mobility is not observed and

the adsorption is local. In this range, the coverage of monolayer adsorption is defected and adsorption energy in most of the adsorption sites is less than its mean value in the whole sample. From one other hand, in temperatures lower than 100K, heat loss in adsorption is more linear than logarithmic curves of other models and its amount is independent of temperature.

References

[1] Jalili, S. et al. Int. J. Nano. Sci. 8 (2009) 425

[2] Wei, D. Liu, Y. Wang, Y. Zhang, H. Huang, L. Gui, Y. Nano. Lett. 9 (2009) 1752

Theoretical study of electronic structure of small bimetallic cluster and its interaction with C_2H_4

AH Pakiari* and M. Mousavi

pakiariah@gmail.com

Chemistry department, College of Sciences, Shiraz University, Shiraz, Iran, 71454

Introduction

The advantage of using bimetallic clusters (alloy) for a variety of reactions has been the source of extensively experimental research for many years (1-3). The modification of the catalytic behavior of a metal by addition of controlled amount of other metals gives a novel electronic structure which might be responsible for the unique catalytic behavior of the bimetallic clusters. In fact, the mutual influence of different neighboring atoms leads to catalytic behavior which is often considerably different that of monometallic species. We will present here some results of Fe_nCu_m ($2 \leq m+n \leq 3$).

Computational Method

DFT procedure with functional BPW91 basis set 6-311G* in Gaussian 03 (4) is applied in this research. Binding energy E_{bind} (or adsorption energy) as the function of bond strength between metallic substrate and adsorbate describes the thermodynamic stability of the system and is computed by;

$$E_{bind} = E_{complex} - \left(E_{metal} + E_{ethylene}\right) \qquad 1$$

In this definition E_{metal} and $E_{ethylene}$ refer to electronic energy of free spices. We also present define interaction energy, E_{int}, as a function of interaction strength between metallic cluster and C_2H_4 in their deformed geometries;

$$E_{int} = E_{bind} - \left(\Delta E_{metal} + \Delta E_{ethylene}\right) \qquad 2$$

where ΔE_{metal} and $\Delta E_{ethylene}$ are the deformation energies of metallic cluster and ethylene molecule in the fully relaxed adsorption system. The zero-point vibrational energy are included energy.

Results and Discussion

We are presenting only the results of Fe_nCu_m ($2 \leq m+n \leq 3$) and reaction with C_2H_4. Therefore, C_2H_4 adsorption behaviors on this alloy cluster, such as binding sites and adsorption energies are examined and compared with those of pure species. For interaction of C_2H_4 on whole of the clusters, we have studied π bonding (ethylene is placed on top of an iron atom) and di-σ bonding (C_2H_4 bridging over two metal atoms with the C-C axis parallel to the metal-metal axis), as shown in Fig 1. In order to find the most stable multiplicity, we have tried to calculate several multiplicities for each species.

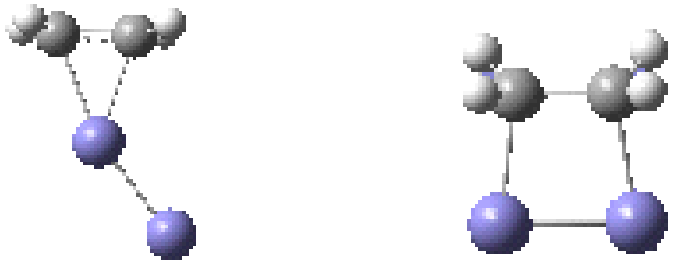

π- C_2H_4 **di-σ- C_2H_4**

Fig. 1 Interaction of Fe_2 and C_2H_4 in the form of π- C_2H_4 and di-σ- C_2H_4

Table 1 shows the π and di-σ coordinations of ethylene on a range of Fe/Cu clusters with different sizes, compositions, and structures. DFT results, including optimized geometries of the lowest energy isomers of Fe_nCu_m/C_2H_4 complexes with their corresponding spin multiplicities, binding energies (E_{bind}), and interaction energies ($E_{int.}$) between the distorted adsorbate and distorted metal cluster are listed in this table. All the energies are in kcal/mol and include the zero-point vibrational energy.

Table 1. The most stable adsorption configurations of ethylene on pure and bimetallic of Fe and Cu clusters, (All the energies are in kcal/mol)

Species	Mult.	$E_{int.}$	E_{bind}	Species	Mult.	$E_{int.}$	E_{bind}
π- C_2H_4							
Fe_2/C_2H_4	7	-30.4	-22.4	Fe_3/C_2H_4	11	-35.8	-22.4
$FeCu/C_2H_4$	4	-41.4	-35.9	Fe_2Cu/C_2H_4	6	-40.2	-35.9
Cu_2/C_2H_4	1	-20.5	-18.3	$FeCu_2/C_2H_4$	3	-46.3	-18.3
-	-	-	-	Cu_3/C_2H_4	2	-20.5	-18.3
di-σ- C_2H_4							
Fe_2/C_2H_4	7	-38.8	-16.7	Fe_3/C_2H_4	11	-55.5	-29.1
$FeCu/C_2H_4$	-	-	-	Fe_2Cu-$/C_2H_4$	8	-65.9	-34.3
Cu_2/C_2H_4	1	-88.22	+8.3	$FeCu_2$-$/C_2H_4$	-	-	-
-	-	-	-	Cu_3/C_2H_4	2	-42.0	-23.7

Conclusion

Through the range of our studies, many evidences confirm that di–σ–C_2H_4 interacts more strongly with metallic substrate than π–C_2H_4. Another important outcome of this part of our studies is that there is no always a direct relation between the interaction energy and final adsorption binding energy.

References

[1] Bengaard, H. S.; Norskov, J. K.; Sehested, J.; Clausen, B. S.; Nielsen, L. P.;Molenbroek, A. M.; Rostrup-Nielsen, J. R. *J. Catal.* **2002**, *209*, 365.

[2] Rodriguez, N.M.; Kim, M. S.; Baker, R. T. K. *J. Catal* **1993**, *144*, 93.

[3] Lo, J. M. H.; Ziegler, T. *J. Phys.Chem.C.* **2008,** *112*, 3679.

[4] Frisch M.J. et al., Gaussian, Inc., Pittsburgh, PA, 2003.

Investigating the Nature of Noble Metal – Nobel Gas Interaction

Z. Jamshidi

Chemistry and Chemical Engineering Research Center of Iran

P.O. Box 14335-186, Tehran, Iran

(jamshidi@ccerci.ac.ir)

Introduction

In resent years great effort has been expended to prepare and characterize systems in which a noble metal like Cu, Ag, or Au is bound to a noble gas.[1-4] Because of their respective noble characters, noble metals and gases were considered unable to form any chemical bonds. Contrary to this suggestion, the chemistry of noble metals is nowadays recognized to be board and rich, for instance, Au has a very high chemical activity because of its exceptional relativistic effects, and the nobleness of noble gases was challenged by the discovery of the first Xe compound in 1962.In 1995, Pyykkö predicted the existence of Au–Ng (noble gas) compounds based on theoretical studies on Au^+–Ng (Ng = He – Xe) systems and concluded that, of all of the stable noble gases, Xe would form the strongest bond with Au^+. Indeed, the $AuXe^+$ ion was detected by mass spectrometer in 1998. Recently Zeng et al.[5] reported a joint experimental (used photoelectron spectroscopy (PES)) and theoretical study of the interaction between gold anion, Au^- and an Ng atom and observed the spectra for $AuAr^-$.These findings encouraged us to probe the nature of the interaction between noble metal and noble gas. Pyykkö suggested the covalent character for Au^+–Ng interaction with the significant charge transfer from Xe to Au^+.

Method of Calculation

The interaction potential energy surface of the cationic (CM^+), anionic (CM^-) and neutral (CM°) coinage metal (CM= Cu, Ag and Au) complexes with rare gas (RG= Kr, Xe and Rn) are calculated by MP2 and CCSD(T)methods.We employed two different density functional methods that recently have been used for weak and noncovalent interaction. These methods are M06-2X “Minnesota 2006 functional with double Hartree-Fock exchange” developed by Truhlar et al. and the CAM-B3LYP, hybrid exchange-correlation functional presented by Yanai et al. who combine B3LYP at short-range with an increasing amount of exact HF

exchange at long-range. These calculations have been done using Gaussian 09 suite of programs.

The quasirelativistic pseudopotential augmented correlation-consistent polarized valence triple-ζ (aug-cc-pVTZ-PP) basis sets based on the small core relativistic pseudopotentials (PPs) of Figgen et al., were employed for RG and CM. The bond length, interaction energy and spectroscopic constants were obtained and to reveal the nature of bonds, the NBO, QTAIM, and EDA analyses were carried out on the optimized structures.

Results and Discussions

We used CCSD(T) method and basis sets described above to perform single-point calculations for 30 internuclear distances ranging from 2.00 to 5.00 Å. After that we run geometry optimization and frequency calculation around the minimum point of potential energy surface and obtained the bond length (R_e) and dissociation energy (D_e).

For CM^- and CM° metal there are highly unintuitive trends in $R_e$as Ng is changed, in that for each CM the equilibrium bond length decrease from Kr through to Rn, despite the concomitant increase in van der Waals radius with increasing atomic mass of RG. Such surprising trends have been previously observed for the complexes of CM with He, Ne and Ar. However for cationic metal (CM^+) the expected trend of an increasing in R_e with increasing atomic number in Ng is observed. The expected trend of an increase in D_e with increasing atomic number in Ng is observed for each metal, in the line with the trend of increasing polarizability of Ng atom and hence the increasing attractive dispersion forces.

The nature of CM–Ng bonds have been investigated by means of energy decomposition analysis (EDA) and NBO method. There are a number of effects that should be considered to discussed the nature of bond, dispersion interaction, *sp* hybridization and charge transfer.

References

[1]Belpassi, L.;Infante, I.; Tarantelli, F. Visscher, L.*J. Am. Chem. Soc.***2008**, *130*, 1048.

[2] Zeng, T.; Klobukowski, M. *J. Phys. Chem. A* **2008**, *112*, 5236.

[3]Gardner, A. M.; Plowright, R. J.; Watkins, M. J.; Breckenridge, W. H.; Wright, T. G.*J. Chem. Phys.***2010**, *132,* 184301.

[4] Breckenridge, W. H.; Ayles, V. L.; Wright, T. G. *J. Phys. Chem. A* **2008**, *112,* 4209.

[5] Gao, Y.; Huang, W.; Woodford, J.; Wang, L. S.; Cheng Zeng, X.*J. Am. Chem. Soc.***2009**, *131*, 9484.

Unconventional Interactions: Review of Recent Investigations

Mohammad Solimannejad*

Quantum Chemistry Group, Department of Chemistry, Faculty of Sciences, Arak University, Arak 38156-8-8349, Iran

(m-solimannejad@araku.ac.ir)

Keywords: Unconventional interactions, SH···N, SH···P, Halogen-hydride, σ-hole, Ab initio.

Very recently new types of unconventional interactions reported in our research group [1-3]. The goal of the present review is presentation of important aspects of our achievements.

Project 1: Unconventional H-bonds: SH···N Interaction [1].

Quantum calculations at the MP2/aug-cc-pVDZ level are used to analyze the SH…N H-bond in complexes pairing H_2S and SH radical with NH_3, $N(CH_3)_3$, NH_2NH_2, and $NH_2N(CH_3)_2$. Complexes form nearly linear H-bonds in which the SH covalent bond elongates and shifts its stretching frequency to the red. Binding energies vary from 14 kJ/mol for acceptor NH_3 to a maximum of 22 kJ/mol for $N(CH_3)_3$ and $N(CH_3)_2NH_2$. Analysis of geometric, vibrational, and electronic data indicate that the SH…N interaction involving SH is slightly stronger than that in which the closed-shell H_2S serves as donor.

Project 2: SH···N and SH···P Blue-Shifting H-Bonds and N···P Interactions in Complexes Pairing

HSN with Amines and Phosphines [2].

Quantum calculations at the MP2/aug-cc-pVDZ level examine complexes pairing HSN with aliphatic amines and phosphines. Complexes are cyclic and contain two attractive interactions. The first is a SH···N/P H-bond in which the S-H covalent bond contracts and shifts its stretching frequency to the blue, more so for amines than for phosphines. The second interaction is different for the amines and phosphines. The amines engage in a NH··N H-bond comparable in strength to the aforementioned SH··N interaction. In contrast, the second interaction in the phosphine complexes is a direct N··P attraction without an intervening H. This interaction is due in part to opposite partial charges on the N and P atoms, as well as covalent forces generated by charge transfer effects.

Project 3: Cooperative and Diminutive Unusual Weak Bonding In $F_3CX\cdot\cdot\cdot HMgH\cdot\cdot\cdot Y$ and

$F_3CX\cdot\cdot\cdot Y\cdot\cdot\cdot HMgH$ Trimers (X = Cl, Br; Y = HCN, and HNC)[3].

MP2 calculations with cc-pVTZ basis set were used to analyze intermolecular interactions in $F_3CX\cdot\cdot\cdot HMgH\cdot\cdot\cdot Y$ and $F_3CX\cdot\cdot\cdot Y\cdot\cdot\cdot HMgH$ triads (X = Cl, Br; Y = HCN, and HNC) which are connecting with three kinds of unusual weak interactions, namely halogen-hydride, dihydrogen, and σ-hole. To understand the properties of the systems better, the corresponding dyads are also studied. Molecular geometries, binding energies, and infrared spectra of monomers, dyads, and triads were investigated at the MP2/cc-pVTZ computational level. Particular attention is given to parameters such as cooperative energies, cooperative dipole moments, and many-body interaction energies. Those complexes with simultaneous presence of a σ-hole bond and a dihydrogen bond show cooperativity energy ranging between -1.02 and -2.31 kJ mol^{-1}, whereas those with a halogen-hydride bond and a dihydrogen bond are diminutive, with this energetic effect between 0.1 and 0.63 kJ mol^{-1}. The electronic properties of the complexes have been analyzed using the molecular electrostatic potential (MEP), the electron density shift maps, and the parameters derived from the atoms in molecules (AIM) methodology.

Acknowledgments: Thanks are given to Prof. I. Alkorta and Prof. S. Scheiner for collaboration with us.

References

[1] M. Solimannejad, S. Scheiner Int. J. Quantum. Chem (2011) in press.

[2] M. Solimannejad, M. Gharabaghi, S. Scheiner J. Chem. Phys (2011) in press.

[3] M. Solimannejad, M. Malekani, I. Alkorta, J. Phys. Chem. A 114 (2010) 12106.

Ab initio potential energy surface for He-F2 complex

M. Dehestani[a], M. Amiri[a], M. Efthekhari[b]

[a]Department of Chemistry, Shahid Bahonar University of Kerman, Kerman, Iran

[b]Department of Computer Engineering, Shahid Bahonar University of Kerman, Kerman, Iran

dehestani2002@yahoo.com

Keywords: He-F2, potential energy surface, SAPT, second second virial coefficient

Introduction

Intermolecular interaction plays a significant role in realizing the reaction selectivity, drug- receptor interaction [1]. Experimental studies of F_2-rare gas are very limited because of spectroscopic technique are more difficult to apply to compound of F_2 [2]. Symmetry adapted perturbation theory (SAPT) has been applied to compute the intermolecular potential energy surface (PES) of the He-F_2 dimer. Ab initio calculations have been performed with the cc-pVQZ-F12 basis set. Our SAPT results indicate that the linear configuration is more stable than T-shaped form. The model which created by fuzzy method has been used to compute second virial coefficient.

Computational method

The SAPT interaction energy $(E_{int}^{SAPT})$is calculated as follows: $E_{int}^{SAPT}=E_{int}^{HF}+E_{int}^{CORR}$ We used the SAPT2 method in this study. For further information about SAPT, the reader is referred to the Refs. [4, 5, 6]. The coordinate system of He-F_2 is indicated in figure(1) .We used 714 points to modeling PES which consist of 21 and 34 for θ and R, respectively in r =1.412 Å.

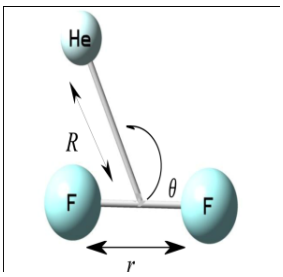

Fig (1) The coordinate system of He-F_2

Results and discussion

The resulted energies in this research and in two previous researches are compared in Table (1). Fuzzy method applied to create our model in MATLAB (2009a) program which expansion as:

$$E_{\text{int}} = \sum_{i=1}^{5} w_i E_i / \sum_{i=1}^{5} w_i \quad \text{which} \quad w_i = A_{1i}(\theta) A_{2i}(R) \quad E_i = a_i \theta + b_i R + c_i$$

Where the angle dependence of the $A_{1i}(\theta)$ and radial dependence of the $A_{2i}(R)$ are given by

$$A_{1i}(\theta) = \exp[-(\theta - \mu_{\theta_i})^2 / 2\sigma_{\theta_i}^2] \qquad A_{2i}(R) = \exp[-(R - \mu_{R_i})^2 / 2\sigma_{R_i}^2]$$

Table(1) Interaction energies (μHa) of our works vs others

R(Å)	=0			=90		
	Our work	Ref. (2)	Ref. (3)	Our work	Ref. (2)	Ref. (3)
1.60	3011688.28	------	352112.71	31008.62	------	30707.71
2.00	72115.92	------	75677.47	5693.13	------	5174.66
2.40	12443.73	------	12427.87	737.20	------	423.35
2.80	1505.57	------	1256.82	-37.03	------	-219.39
3.00	347.80	314.80	123.11	-91.15	-151.40	-228.94
3.25	-75.47	-108.00	------	-89.83	-125.60	------
3.50	-137.38	-162.30	------	-67.65	-91.00	------
3.75	-114.23	-131.40	------	-47.75	-63.10	------
4.00	-82.04	-92.80	-147.36	-33.20	-43.50	-79.74
4.50	-38.53	-42.80	------	-17.09	-21.90	------
5.00	-18.79	-20.60	------	-9.03	-11.50	------
6.00	-5.48	-6.00	------	-2.98	-3.70	------

Our model has a good coefficient correlation (0.99998). The second virial coefficient at temperature T calculated by following formula $B_{12}(T) = \pi N_A \int_0^{\infty} \int_0^{\pi} \{1 - \exp[-V(R,\theta)/kT]\}$ The result of second virial coefficient which report for first time is shown in Fig(2).

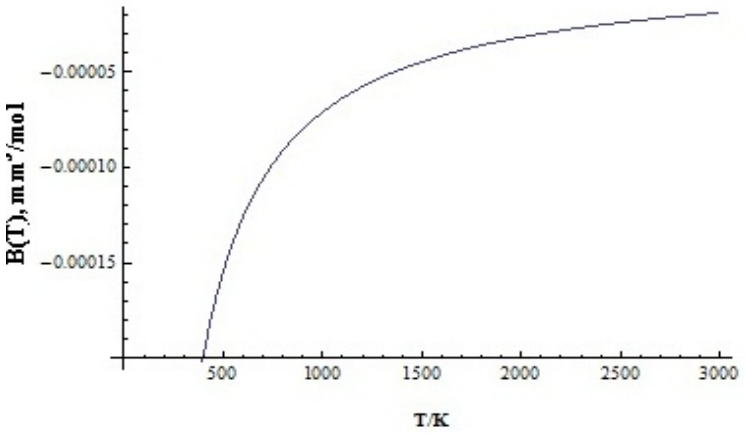

References

[1] J .Wu, J .Zhang, Z .Wang, and W .Cao, Int .J .Quantum Chem. **107,** (2007)1897 **.**

[2] K.W .Chan, T. D. Power, J. Jainhuknan, and S. M. Cybulski, J. Chem. Phys. **110**, (1999) 860.

[3] U. Lourderaj, and N .Sathyamurthy, Chem. Phys .**308**, (2004) 277.

[4] B .Jeziorski, R .Moszynski, K .Szalewicz, Chem. Rev. **94**, (1994) 1887.

[5] B. Jeziorski, K. Szalewicz, P .von Rague Schleyer (*Ed.*), Encyclopedia of Computational Chemistry, Wiley, New York, 1998, p .1376.

[6] J. Wu, J. Zhang, Z. Wang, and W .Cao, Int. J. Quantum Chem., **107,** (2007) 1897.

Theoretical detection of π-type bonding critical points

S. M. Azami

Department of Chemistry, College of Sciences, Yasouj University, Yasouj 75914, Iran.

(Email: azami@mail.yu.ac.ir)

Keywords: QTAIM, bond critical point, π bond.

Introduction

Electron density based characterization of chemical bonds is one of the most accepted methods in electronic structure analysis, such as quantum theory of atoms in molecules (QTAIM) [1,2]. Critical points (CPs), points at which the first derivatives of electron density vanish, play important role in the characterization of electron density topology in QTAIM.

According to QTAIM, an interatomic interaction can be characterized via the corresponding bond critical point (BCP). In the present work we wish to explore properties of the electron density topology provided by the molecular π system and show how it can be useful for characterization of π bonds in planar molecules.

Methods

The molecular geometries and electronic wave functions are optimized using HF/6-311++G** theoretical level, utilizing Gaussian 03 suite of programs [3]. Frequency analysis is also performed to make sure that the geometries are minimum structures. AIM2000 package [4] is also employed in order to detect and visualize the CPs and BPs corresponding to molecular π systems.

Results and discussion

Fig. 1 compares the bond paths of ethylene due to σ molecular graph as conventional QTAIM, with π bond paths according to the present work which only considers the electron density originated from π orbitals.

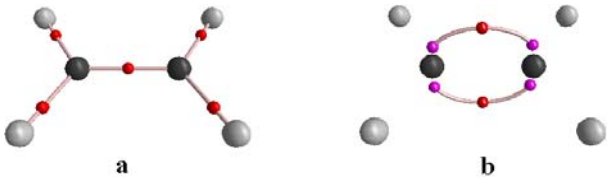

Fig. 1. a. Conventional QTAIM molecular graph for ethylene representing σ-skeleton. **b.** π molecular graph (the present work).

According to Fig. 1b, the C-C π bond for ethylene, is composed of four attractors on the top and bottom of either nuclei, two BCPs at the middle of π bond, and two curved bond paths. The two attractors on either side of the nuclei are a result of two local maxima in the density of *p* atomic orbitals perpendicular to the molecular plane.

Table 1. Chemical Structure of the molecules and the corresponding values of ρ_{BCP} and $\nabla^2\rho_{BCP}$ for the illustrated BCP.

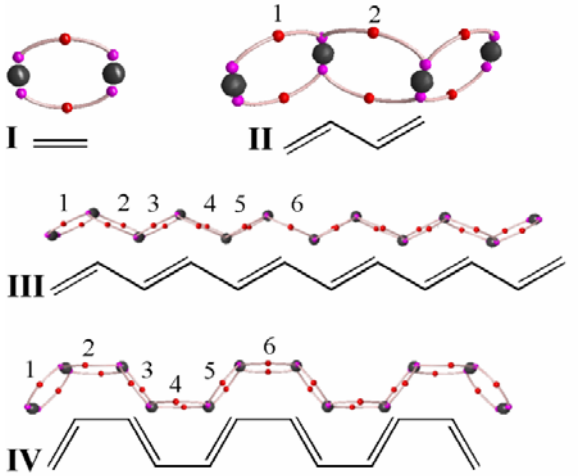

	ρ_{BCP}	$\nabla^2\rho_{BCP}$
I	0.060	– 0.184
II	0.059	– 0.180
	0.023	– 0.004
III	0.059	– 0.176
	0.024	– 0.008
	0.058	– 0.168
	0.025	– 0.012
	0.057	– 0.164
	0.025	– 0.012
IV	0.059	– 0.176
	0.023	– 0.008
	0.058	– 0.168
	0.024	– 0.008
	0.057	– 0.164
	0.024	– 0.012

Table 1 shows the BCPs of π system of 1,3-butadiene (**II**); and their corresponding electron density (ρ_{BCP}) and Laplacian ($\nabla^2\rho_{BCP}$) values. Although the bond connecting second and third carbons is formally a single bond, the π graph shows a continuous π bonding which is in agreement with π delocalization in this and similar conjugated molecules. According to Table 1, $\nabla^2\rho_{BCP}$ is positive for formally single bonds in **V**

while they are negative in **II-IV**, which shows that the π bonds in **V** are less delocalized than the other two types of polyenes.

Summary and concluding remarks

The electron density due to π system can be characterized via QTAIM concepts and definitions. To accomplish this, BCP can be generalized to π electron density; and π delocalization/localization phenomena could be obviously detected on the basis of π electron density and its Laplacian at the BCPs.

References

[1] R.F.W. Bader, Atoms in molecules: a quantum theory; Oxford University Press: Oxford, U.K., 1990.

[2] R.F.W. Bader, Chem. Rev. 91 (1991) 893.

[3] Frisch, M. J.; et al. GAUSSIAN 03, Gaussian, Pittsburgh, PA, 2003.

[4] Biegler-König, F.; Schönbohm, J. AIM2000 2.0, 2002.

Investigation on dihedral angle dependency of ^{1}H and ^{13}C NMR chemical shifts calculation

Hoora Shaghaghi*[a], Mohsen Tafazzoli[b]

[a]Department of Chemistry, Payame Noor University, 31578-36899, Karaj, Iran

(hoora.shaghaghi@gmail.com)

[b]Department of Chemistry, Sharif University of Technology, P. O. Box 11155-9516, Tehran, Iran

Introduction

Measurement of dihedral angles is essential in many investigations such as secondary structure determination of proteins. Using Karplus relation and empirical J-coupling constant values is common approach in the estimation of dihedral angles but determination of the adjustable parameters of the Karplus curve is complicated by serious difficulties especially for macromolecules [1]. Theoretical calculations can be a reasonable alternative when experiment is not able to solve the problem. Calculated NMR chemical shift values directly depend on geometrical structure [2,3] then they rely on dihedral angles. The main aim of the present contribution is to obtain a new approach in determination of dihedral angles. Accordingly, dependency of calculated ^{1}H and ^{13}C NMR chemical shifts to dihedral angles were considered for alkanes and amines as model compounds and the optimum dihedral angles were determined. The results of this work are promising and indicate that this approach can pave the way for subsequent investigations.

Methods

Ten various molecules of alkanes and amines were selected and 37 conformations of each compound were considered using different C-C-C-C and C-C-N-C dihedral angles (-180 to 180) for alkanes and amines respectively. ^{1}H and ^{13}C nuclear magnetic shielding constants were calculated using gauge-independent atomic orbital (GIAO) method and different level of theory. ^{1}H and ^{13}C chemical shifts δ, were referred to TMS, using corresponding shielding calculated at the same theoretical levels. Chemical shifts were calculated and their differences with the experimental

ones were obtained. Chemical shifts deviation values Δδ (theoretical- experimental) were plotted to the dihedral angles. The structures of all compounds selected for this work were optimized using density functional theory (B3LYP) and a diffuse wave function (6-311+G(d,p)). The polarizable continuum model (PCM) was also applied to optimize structure and to calculate ^{1}H and ^{13}C chemical shifts in solution phase. The Gaussian 98 package [4] was used to perform all the calculations, and the experimental values of gas and solution phase chemical shifts were reported in reference 5 and 6 respectively.

Results and discussion

Figure 1 demonstrates the variation of Δδ to the dihedral angles for pentane and N,N-dimethylethylamine as sample molecules. Gas phase ^{13}CNMR chemical shifts of pentane were computed at B3LYP/6-311+G(d,p) and B3LYP/6-311G levels of theory. Deviations of calculated chemical shifts were plotted to the variation of dihedral angels (-180 to 180). As it can be observed in figure 1-A, the curves appear with some minimum and maximum points that the minimum ones belong to the best dihedral angles. Using B3LYP/6-311+G(d,p) and B3LYP/6-311G to calculate chemical shifts results in similar plots and the minimums of two plots appear exactly at the same points (dihedral angles). It means variations of Δδ are independent of calculation level of theory and this characteristic makes using the method for large molecules possible. Accordingly, to find the optimum structure, high calculation level of theory is not required and the increase of calculation level of theory improves only the results.

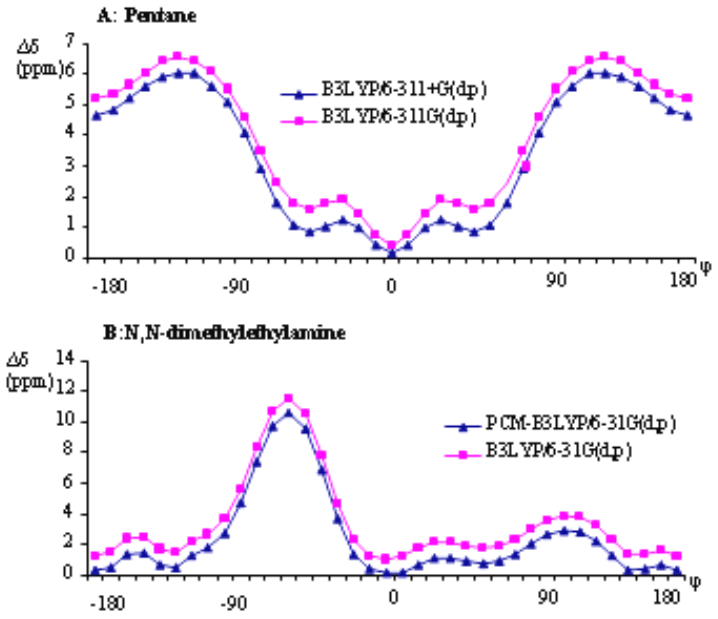

Figure 1 Comparison of variation of Δδ to the dihedral angles at two levels of theory for A: pentane, B: N,N-dimethylethylamine

The same procedure was utilized to compare chemical shifts calculation in solution phase with gas phase. Therefore, ^{13}CNMR chemical shifts of N,N-dimethylethylamine were calculated using PCM method at B3LYP/6-31G(d,p) level of theory in CDCl3 solution. Figure 1-B shows using PCM method to calculate ^{13}C chemical shifts only improves the results, and the minimum and maximum points of two plots appear exactly at the same points (dihedral angles). The same results in calculation of chemical shifts of all 10 compounds were observed and this indicates reliability of the method. Moreover, based on the above method, the optimum dihedral angles were found for 10 alkanes and amines; ^{1}H and ^{13}CNMR chemical shifts were calculated using the optimum structure and B3LYP/6-311+G(d,p) level of theory. The calculated chemical shifts have excellent agreement with experimental values. The Root Mean Square deviations, RMS, and correlation coefficient for ^{1}HNMR chemical shifts calculation are 0.09 and 0.9974, and for ^{13}CNMR chemical shifts calculation are 1.01 and 0.9999 respectively. These statistical data also confirm this presented method is reliable for dihedral angles determination.

Conclusion

The main aim of the present work is developing a theoretical method for the determination of dihedral angels. Accordingly, variations of Δδ to the dihedral angles were considered and optimum dihedral angles were determined for different molecules. Variations of Δδ are independent of calculation level of theory and this characteristic makes using the method for large molecules possible.

References

[1]. A.C. Wang, A. Bax, *J. Am. Chem. Soc.* **1996**, *118*, 2483.

[2]. R. J. Abraham, J. J. Byrne, L. Griffiths, R. Koniotou. *Magn. Reson. Chem*. **2005**, *4*, 611.

[3]. R. J. Abraham, J. J. Byrne, L. Griffiths, M. Perez. *Magn. Reson. Chem*. **2006**, *44*, 491.

[4]. M. J. Frisch, et al. Gaussian 98W. **1998**, Pittsburgh, PA: Gaussian Inc.

[5]. J. P. Chauvel, M. M. Folkendt, N. S. True. *Magn. Reson. Chem*. **1987,** *25* 101.

[6]. H. E. Gottlieb, V. Kotlyar, A. Nudelman, *J. Org. Chem*. **1997**, *62*, 7512.

Reverse Nonequilibrium Molecular Dynamics Simulation of Thermal Conductivity of Nanoconfined Polyamid-66

H. Eslami and L. Mohammadzadeh

Department of Chemistry, College of Sciences, Persian Gulf University, Boushehr 75168, Iran.

E-mail: liela.mohammadzadeh@gmail.com

Keywords: Polyamid-66, Molecular Dynamics, Nanothecnology, Thermal Conductivity.

Introduction

Reverse nonequilibrium molecular dynamics (RNEMD) simulation technique has been applied to study the thermal conductivity of polyamide-6,6 (PA-6,6) confined between graphite surfaces. For this purpose, equilibrium MD simulations are performed in the isosurface- isothermal-isobaric ensemble (NAPT) [1]. According to this approach coupling of the system to a heat bath with a fixed temperature T_0 is done by scaling of velocities. Coupling to a constant pressure bath can also be accomplished according to the similar method. The pressure change can be accomplished by scaling the z-coordinates of all particles per time step.

In this work, this method has been employed to perform equilibrium MD simulations of PA-6,6, in equilibrium with the bulk sample.

Method

To calculate the thermal conductivity of nanoconfined polymer, the simulation box in the direction of confinement is divided into a number of slabs and energy is transferred unphysically between the first (coldest) and the last (hottest) slabs [2]. The heat flux is generated by exchanging the velocity vectors of an atom in the cool slab and one in the hot slab. According to this method energy is transferred unphysically between coldest and the hottest slabs. The thermal conductivity can be calculated as:

$$\lambda = -\frac{\sum_{transfers} \frac{m}{2}\left(v_h^2 - v_c^2\right)}{2tL_xL_y\left\langle \partial T / \partial z \right\rangle}$$

Where t is simulation time, the subscripts h and c refer to the hot and the cold particle of identical mass m whose velocities are interchanged. L_x and L_y , are the box lengths in x and y directions respectively, the factor of 2 in the denominator arises from the periodicity of the arrangement.

Results

In the steady state, the energy transfer imposed by the unphysical velocity exchange is exactly balanced by the heat flux in the opposite direction effected by the thermal conductivity of the system. Therefore, linear temperature profiles are expected in the steady state. Shown in Figure 1 is a typical linear temperature profile (at a velocity exchange period of 50) across the pore.

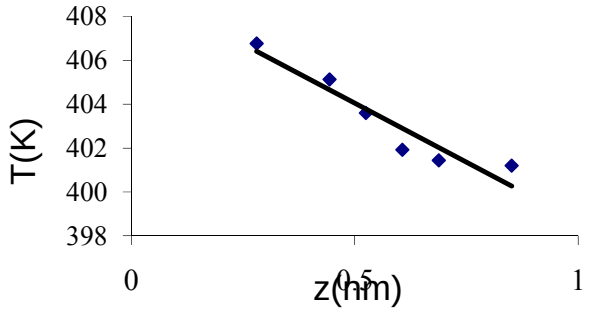

Figure 1. Temperature profiles in the RNEMD simulation of PA-6,6.

The results of this study show an increase (by a factor of 2) in the thermal conductivity in the pore with respect to the bulk polymer.

Conclusion

The RNEMD technique is employed to calculate the thermal conductivity of nanoconfined PA-6,6 oligomers, confined between graphene surfaces. For this purpose, equilibrium molecular dynamics simulations are performed in NAPT ensemble. Our results show that by applying RNEMD method to exchange the velocities, linear temperature profiles are obtained. The thermal conductivity can be

calculated by knowing the amount of energy transferred and the slope of linear velocity profiles. Our results show that the thermal conductivity increases with decreasing the pore size.

References

[1] H. Eslami, F. Mozaffari, J. Moghadasi, F. Müller-Plathe, *J. Chem. Phys*. 129, 194702. (**2008**).

[2] H. Eslami; F. Müller-Plathe, *J. Phys. Chem. B*, 113, 5568. (**2009**).

Modeling and simulation of ionic transport in electrolyte of Li - ion battery by MATLAB

N. Hamze [a], L. Karimi [b]

[a] Department of Engineering Chemistry, Amirkabir University of Technology, Tehran, Iran (n.hamze@aut.ac.ir)

[b] Saba battery company, Taban research center, Tehran, Iran (lkarimi_52@yahoo.com)

Keywords: Li - ion battery, Ion transport, Nernst - Plank equations, Organic electrolytes

Abstract

In this paper ionic conductivity of electrolyte in Li-ion batteries has been modeled. According to the classical one dimensional Nernst-Planck method, under neutrality condition, it is possible to simplify the complicated system of equation to simpler diffusion equations. At the end, complete information about electrolyte behavior in steady and transient state, like potential gradients and diffusion/ migration fluxes of Li^+, PF_6^- is given.

Introduction

Light Li-ion batteries are used for high power applications, because they have combined high energy density with low discharge rate and long cycle life.

Simulating discharge curves of Li-ion batteries was first done on the basis of Newman theory of porous electrode, at 1980. According to microscopic description of physical and electrochemical process occurring in the system, equivalent electronic network models have been presented [1].

Simulation results agree completely with the experimental results. Properties of ion transfer in organic electrolyte like migration and diffusion processes has been described in detail [2, 3].New experimental results have shown that energy loss in Li-ion batteries is because of limited ionic conductivity and it has negative effect on batteries performance. Up to now, exact information about limitations of electrolytes in batteries has not yet been achieved.

Theoretical Model:

Nernst-Plank equation states the fluxes of ions in the electrolyte according to:

$$J_j = -D_j \frac{\partial c_j}{\partial y} - \frac{z_j F}{RT} D_j \, c_j \, \frac{\partial \varphi}{\partial y}$$

And by using Maxwell equation and considering these assumptions:

- $I(t) = I_{LiCoO_2}(t) = -I_{LiC_6}(t)$
- $c(y,t) = c_{Li^+}(y,t) = c_{PF_6^-}(y,t)$
- $\frac{2}{D} = \frac{1}{D_{Li^+}} + \frac{1}{D_{PF_6^-}}$

At the end, by simplifying and solving the equations we will reach the following equation:

- $\frac{\partial c}{\partial t} = \frac{2D_{Li^+} D_{PF_6^-}}{D_{Li^+} + D_{PF_6^-}} \frac{\partial^2 c}{\partial y^2}$
- $E(y,t) = \frac{RT}{F} \frac{1}{c} \left\{ \frac{I(t)}{2FAD_{Li^+}} + \left(t_{Li^+} - t_{PF_6^-}\right) \times \left[\frac{\partial c}{\partial y} - \frac{I(t)}{2FAD_{Li^+}} \right] \right\}$
- $J_i^{tot}(y,t) = J_i^{mig} + J_i^{dif} = -D_i \frac{\partial c}{\partial y} + \frac{F}{RT} D_i c. E$
- $\eta(t) = \frac{RT}{F} Ln\left(\frac{c(L,t)}{c(0,t)}\right) - \int_0^L E(y,t)dy$

Concentration, electric field, ionic fluxes and over potentials profiles calculated by

MATLAB:

Development of concentration profile by MATLAB, and difference steps by changing position to $\frac{L}{200}$ and time steps are all calculated for Sony Li-ion battery (CGR17500) [3] with capacity of 720mAh and using $LiPF_6$ as conductive ionic salt.

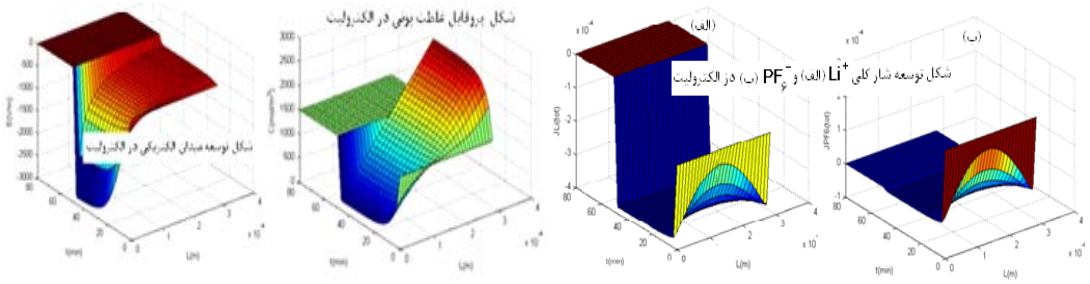

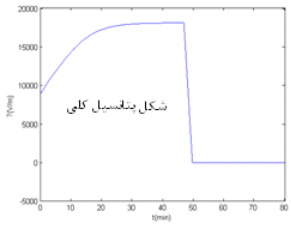

References

[1] M. Doyle, T.F. Fuller, J. Newman, J. Electro chem. Soc. 140 (1993) 1526.

[2] W.S. Kruijt, P.H.L. Notten and H.J. Bergveld, J. Electro chem. Soc. **145** (1998) 3764.

[3] H.J. Bergveld, W.S. Kruijt and P.H.L. Notten, Battery Management Systems, Design by Modelling Philips Research Book Series, vol.1, Kluwer Academic Publishers, Boston (2002).

Molecular Dynamic Simulation of Bulk and Surface Structure of the Ionic Liquids 1-Alkyl-3-Methylimidazolium Iodides

M. H. Ghatee*, A. R. Zolghadr, and F. Moosavi
Department of Chemistry, Shiraz University, Shiraz 71454, Iran
(E-mail: ghatee@susc.ac.ir)

Keyword: Molecular dynamics, orientation, density profile, ionic liquids.

Introduction

Room temperature ionic liquids (RTILs) are molten salts whose normal melting points are below 100 °C. These substances have received a lot of attention within the past decade due to their unusual properties, which open up new applications as solvents and catalysts in synthesis, extraction, and electrochemical processes. [1,2]

The purpose of present study is the simulation of bulk and liquid/vapor interface of 1-alkyl-3-methylimidazolium iodides [$C_n$mim]I by classical molecular dynamics to demonstrate the molecular orientation in bulk and at the surface, where n=4,6 and 8.

Methods

The intramolecular force used for the simulation of [$C_n$mim]I is in from of systematic all atom force field developed by Lopes et al. [3]. For each liquid system, a single ion pair was replicated 8×8×12 to obtain a simulation box containing 768 ion pairs. Relaxation of the geometry through energy minimization was carried out, followed by MD simulations under constant NPT and NVT conditions respectively, for the bulk and liquid/vapor interface. The equations of motion were solved using Verlet-Leapfrog integration algorithm. The temperature of the system was increased up to a final value of 358 K and the system was equilibrated for 1 ns. Then the temperature of the system was decreased to 298 K in the interval of 10 K. The duration of simulation at each temperature was 500 ps.

The density profiles are calculated using the average density of constituting atoms at any point along the axis of the normal to the slab surface, the z-direction. Radial

Distribution Functions (RDF) between different atoms have been used to characterized the bulk structure of these ILs.

Results and Discussion

The differences in physical and chemical properties of ILs arise from their structural details. Therefore, the characteristics of the 1-Alkyl-3-methylimidazolium iodides have been studied by MD simulation. Figure 1 typically shows atomistic RDFs between different atoms of the cation and the anion of [C_4mim]I. The height of the first peak in the case of C6-I interaction is relatively higher than other peaks. The correlation of interaction between C2 and anion is relatively high. From further comparison of other peaks, the proposed relative position of the anion and cation in the bulk of [C_4mim]I is shown in Figure 1. This structure is comparable with the results of gas phase *ab initio* calculations (Figure 2). Hydrogen bond formation between the hydrogen of the ring and iodide anion could be predicted from the height of RDFs in Figure 3.

Values of equilibrium distances according to the $g(r)$'s first peak position r_1 are listed in Table 1 and compared with the results of *ab initio* molecular dynamic simulation, CPMD [4].

Table 1: The average equilibrium distance r_1 between the anion and particular atom on the [C_4mim] imidazolium ring compared with Ref [4].

atom	C2	C4	C5	C6	C7	C8	C9	C10
r_1 (Å)	3.82	3.93	3.93	3.98	3.98	4.08	4.19	4.29
r_1 (Å)[4]	3.25	3.78	3.85	3.63	3.56			

The sketch of the density profiles of atoms are shown in Figure 4. It can be seen that the butyl group tends to stick out into the vacuum phase, and the methyl group is, on average, on the liquid side of the interface. In particular the relative position of the molecule can be understood based on the understanding of alkyl and methyl group positions. In the vapor side of the Gibbs dividing surface the anion bears a negatively in excess. Conversely in the liquid side, the anion distinctively is positively in excess.

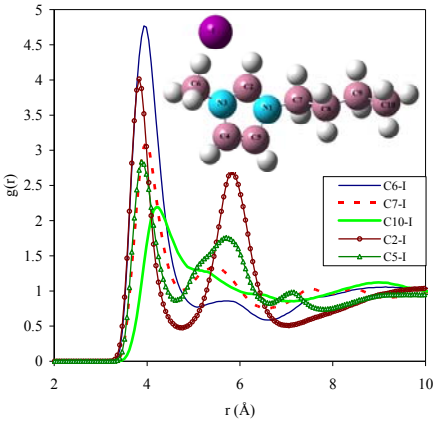

Figure 1: RDFs for [C_4mim]I molecules.

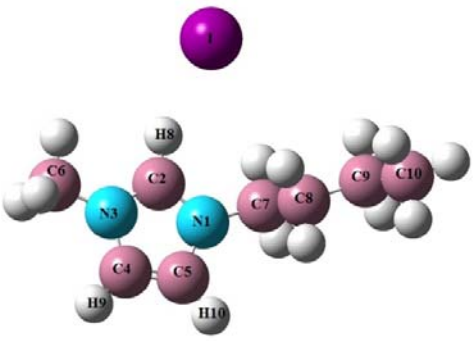

Figure 2: The optimized gas phase structure of the [C_4mim]I ILs obtained at B3LYP/6-311++G** level of theory.

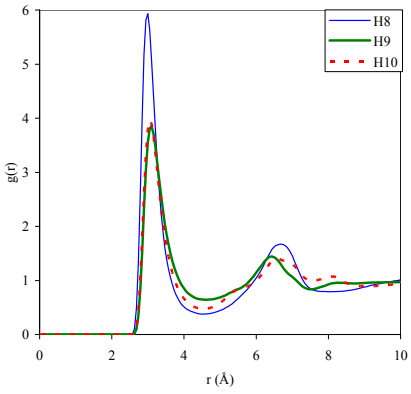

hydrogen of the ring.

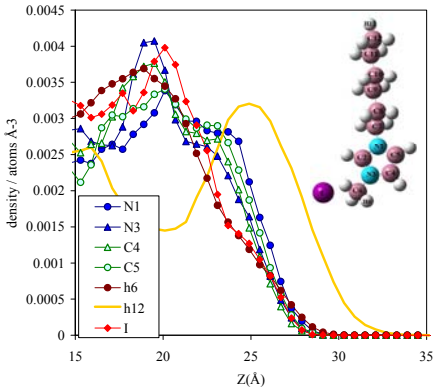

region for [C_4mim]I.

Figure 3: RDFs betw

Conclusions

From these and more detailed considerations it can be concluded that in the vapor side, the alkyl group is pointing to the surface, and the imidazolium ring and the anion tend to the liquid side of the interface.

References

[1] Earle, M. J.; Seddon, K. R.; Pure Appl. Chem. 72 (2000)1391.

[2] Wasserscheid, P.; Keim, W.; Angew. Chem., Int. Ed. 39 (2000) 3772.

[3] Lopes, J. N. C.; Deschamps J. and Pádua, A. A. H.; J. Phys. Chem. B 108 (2004) 2038.

[4] Ghatee, M. H.; and Ansari, Y.; J. Chem. Phys. 126 (2007) 154502.

Molecular dynamics simulation of self-diffusion of benzene in Beta-zeolite

*S. Tashakor[a], H. Mohammadimanesh[a] and S. Alavi[b]

[a]Department of Chemistry, Yazd University, Yazd, Iran

[b]Department of Chemistry, University of Ottawa, Ottawa, Canada

(Email:saeedeh_tashakor@yahoo.com)

Introduction

The diffusion of guest molecules inside the nanometer-scale pores of zeolite controls the performance of zeolites in many applications of these materials for chemical separations and catalysis.[1] Beta-zeolite represented the first high silica zeolite (Si/Al=10-100) synthesized and it has superior thermal and acid stability. The structure of Beta-zeolite consists of intersecting 6.5×5.6 and 7.5×5.7 $Å^2$ channels. The most straightforward way is to compute a diffusion coefficient of an adsorbed molecule directly from a MD simulation.[1] The aim of this study is to understand the effects of the temperature and loading on the dynamics behavior and the guest diffusion in Beta-zeolites. In this study, self-diffusion coefficients, adsorption energies, and activation energies of benzene gases molecules in Beta-zeolite with BEA code and $Si_{64}O_{128}$ chemical formula has been studied by MD simulations.

Keywords: MD simulation, Beta-zeolite, Benzene, Diffusion, Adsorption energy.

Computational and Methodology

The nine-site benzene model of Zhao et al. has been used to study the adsorption of benzene in Beta-zeolite[2] The intermolecular van der Waals potentials between atoms *i* and *j* on different molecules are considered to be the sum of Lennard-Jones (LJ) 12-6 and electrostatic point charge potentials centered on the atoms. To equilibrate the initial configurations, NVT MD simulations with the Nosé-Hoover thermostat-barostat algorithm have been performed on a periodic 3×3×3 (a = 12.6 Å, c = 26.2 Å) replica of the tetragonal unit cell with the DL_POLY molecular dynamics program version 2.15. The simulations have done at a range of temperatures between 300 and 1000 K, at ambient pressure and at a loading 1, 2 and

3 of guest molecules per unit cell. To obtain the mean-square displacement and diffusion coefficient, NVE simulations were performed for a minimum total simulation time of 500 ps, starting with configurations equilibrated by the previous NVT runs. The self-diffusion coefficient values of benzene in BEA zeolite are obtained from the slopes of the mean square displacement (MSD) versus time plots at different temperatures using the Einstein relation, [3]

$$D_\alpha = \frac{1}{6N_\alpha} \lim_{t\to\infty} \frac{d}{dt} \sum_{i=1}^{N_\alpha} \left\langle \left| r_i(t) - r_i(0) \right|^2 \right\rangle$$

where N_α is the number of diffusing molecules of type α, $r_i(0)$ and $r_i(t)$ are the location of the center of mass of molecule *i* at time zero and *t*, respectively. The adsorption energy for the BEAs with *n* benzenes molecules per unit cell is defined as,

$$E_{adsorption} = E_{(BEA+guests)} - E_{(BEA)} - nE_{(guests)}$$

where $E_{(BEA+guests)}$ and $E_{(BEA)}$ have been obtained from MD simulations and E_{gas} has been calculated by $E_{gas} = 3nRT/2$. The activation energies corresponding to the self-diffusion processes have been evaluated from the Arrhenius relation.

Results and discussion

The MSDs for center of mass of benzene in BEA were calculated at different loadings and at different temperatures in the range of 0–500 ps. At all of these loadings, the MSDs increase with temperature. The diffusion coefficients have been calculated from the Eq.(1) and given in the Table 1. As can be seen from the table, the diffusion coefficients increase as the temperature is increased, due to the increase of mobility of particles by increasing of temperature. The adsorption energies of guest molecule at different temperatures have been calculated from the Eq.(2) and given in the Table 1. The adsorption energies decrease with temperature for the increase of kinetic energy of the molecules.

T (K)	300	400	500	600	700	800	900	1000
$D\times10^{-8}(m^2\cdot s^{-1})$	0.54	0.83	1.18	2.73	2.91	3.07	4.65	5.12
$E_{adsorption}(kJ/mol)$	-40.7	-38.3	-35.8	-33.4	-30.9	-28.5	-26.0	-23.6

Table 1: Diffusion coefficients and adsorption energies calculated for benzene in Beta-zeolite at loading 1 and at different temperatures.

References

[1] Smit, B.; Maesen and T.L.M. *Chem. Rev*. **2008**, *108*, 4125-4184**.**
[2] Ban, S.; Laak, A.N.C.van.; Jongh, P.E.de.; Eerden, J.P.J.M.van der.; Vlugt, T.J.H. *J. Phys. Chem. C* **2007**, *111*, 17241–17248.
[3] Yazaydin, O.A.; Thompson, R.W. Microporous and Mesoporous Materials **2009**, *123*, 169–176.

Investigation on pressure dependence of wilson parameters in vapour liquid equilibrium study of binary Ethylenediamine + Water system at some subatmospheric pressures

S.A. Nabavi-Amri [a] , A. Haghighi-Asl [a] , N. Mirbolooki-Moghaddam* [a] , N. Saadatmand [a]

a Thermodynamic research lab, School of Chemistry, University of Damghan, Damghan ,Iran

(Email:nedamirbolookimoghaddam@yahoo.com)

Abstract

Isobaric vapor-liquid equilibrium (VLE) measurements are reported for binary mixtures of Ethylenediamine (EDA) + Water at some subatmospheric pressures from 37.75 to 71.08 kPas. The data were obtained using an ebulliometer (modified Kojima's) equilibrium still. The mixtures, which deviate negatively from ideal behavior do form any azeotrope. The values of activity coefficients and excess Gibbs free energy has been calculated from the experimental data. The values of Wilson parameters (A_{ij}) have obtained by the Wilson model that satisfy to pressure changes.

Keywords: Ethylenediamine, VLE, Wilson parameters, Azeotrope, Excess functions.

Introduction

The distillation is a process very used in the separation and purification of organic compounds. To be able to design the distillation columns appropriately is essential to have the information on the VLE of the systems implied. This information involves isobaric equilibrium data as well their variation with the pressure. Unfortunately, VLE data frequently are not available at different pressures. Determination of these VLE data constitutes an interesting investigation work. In this work we studied EDA + water binary system; among to industrial usage of EDA. We correlate wilson parameters (A_{ij}) [1] to pressure.

Experimental section

1. Chemicals

Analytical-grade EDA, supplied by the Merck chemical company.

*2. Experimental apparatus and procedur*e

An ebulliometer (modified Kojima's), shown in figure 1 was used to measure the equilibrium temperatures and pressures. A standard electronic thermometer was employed to measure the equilibrium temperature of the system. About 60 cm^3 of a liquid mixture of known composition was put into the ebulliometer. The ebulliometer was connected to a vacuum system and was sealed. After several times, the pressure was first reduced to the desired point with the help of a vacuum pump. Then the pressure was kept constant and the mixture in the ebulliometer was heated slowly. When the temperature and the amount of reflux drops reached stability for more than 5 min, the corresponding temperature and justified pressure were recorded. Samples of vapour and liquid phases analyzed by refractometer to determining mole fraction of mixture. Figur 2 shows the calibration curve for binary system of EDA + water.

3. Results and discussion

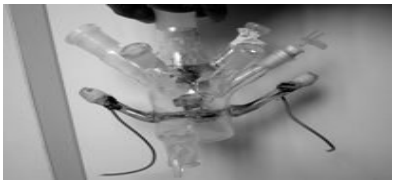

Fig. 1- Ebulliometer

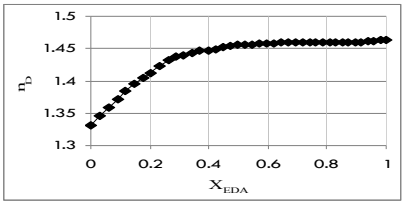

Fig. 2- Calibration curve for nD=f(x). Refractivity index determines mole fraction.

Fig. 3 shows that we have no conflict to y=f(x) curve; this means EDA + water binary system has no azeotrope.

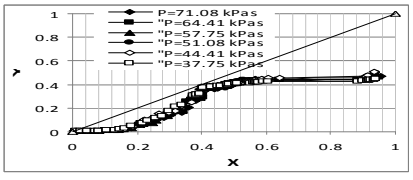

Fig. 3- Mole fractions of vapour vs. liquid of EDA.

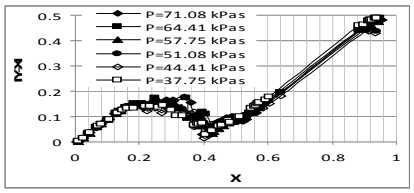

Fig. 4- |y-x| vs. x curve.

We calculate activity coefficient by Antoine eq.[2] logp=A+B/(T-C) and γ1=y1 We calculate activity coefficient by Antoine eq.[2] logp=A+B/(T-C) and γ1=y1 psat/x1p and so on for γ2. We will have GE/RT=-x1ln(x1 +A12x2)-x2ln(x2+A21x1), lnγ1 =-ln(x1+A12x2)+x2 (A12/ (x1+A12x2)-A21/(x2+A21x1); lnγ2=-ln(x2+A21x1)+x1(A12/(x1+A12x2)-A21/ (x2+A21x1). The samples, deviate negatively from ideal behavior.

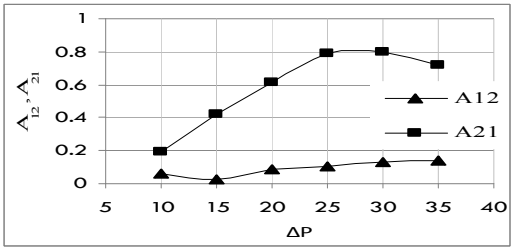

Fig. 5- Wilson parameters (Aij) vs. pressure changes.

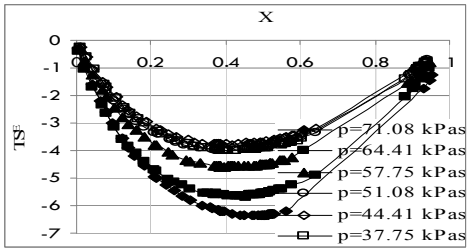

Fig. 6- TSE vs. mole fraction.

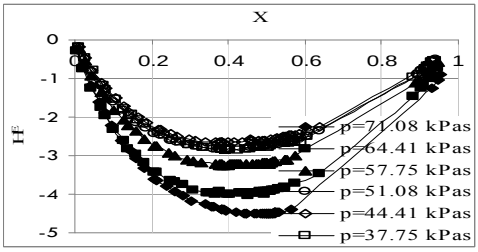

Fig. 7- HE vs. mole fraction.

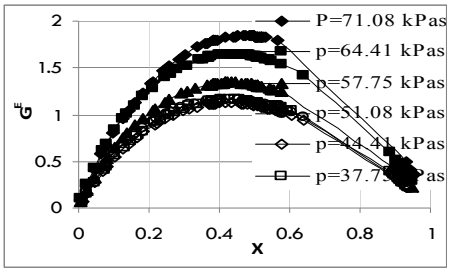

Fig. 8- GE vs. mole fraction

References:

[1] Grant M. Wilson," A New Expression for the Excess Free Energy of Mixing", J. Am. Chem. Soc., 1964, 86 (2), 127-130.

[2] V. K. Rattan, Baljinder K. Gill, Seema Kapoor,"Isobaric Vapor-Liquid Equilibrium Data for Binary Mixture of 2-Methyltetrahydrofuran and Cumene" Proceedings of world academy of science, engineering and technology, vol. 30, 2008 ISSN 1307-6884.

Growth of carbon nanostructures upon different substrates by thermal chemical vapor deposition method

Z. Haghparast*[a], F. Bisepar[a] and Sh. Moradi[b]

[a] *Department of Chemistry, Science and Research Branch, Islamic Azad University, Tehran, Iran*
(Email:zhaghparast_tmu@yahoo.com)

[b] *Department of Chemistry, Tehran North Branch, Islamic Azad University, Tehran, Iran*

INTRODUCTION

High yield CNTs synthesis is desired for many composite materials and mechanical applications due to their high strength and light weight [1-3], that also have very promising applications in electronics, such as super-capacitor electrodes [2, 4].

Various methods have been used to grow both SWCNTs and MWCNTs, in clouding arc-discharge [5, 6], laser vaporization [7], and CVD [8]. The CVD method has many advantages over other methods, since the CNTs can be synthesized with high purity and yield, selective growth and well-alignment [9, 10].

TCVD is preferred due to its simplicity and low cost production of nanomaterials for future industrial applications [11]. However, most of these studies are based on an empirical optimization of growth conditions and a systematic investigation is still needed for a better understanding about the effect of different experimental parameters (e.g. substrate, catalyst and gas composition) on the extended of growing [12]. Among the growth methods, TCVD allows the production of CNTs film vertically aligned on predeposited catalyst pads on large scale and good uniformity. In general the synthesis of aligned CNTs via TCVD is based on the decomposition of hydrocarbon gas molecules (CH_4, C_2H_2, CF_4, …), at relatively low temperatures (500-1000 $^{\circ}$C), on the surfaces catalyzed by transition metals, like Fe, Ni, Co and Cu followed by bulk or surface diffusion of carbon on the catalyst particles [13, 14]. Many researchers have also found that the substrate could affect the growth of CNTs in TCVD process [15-18].

In the present study, we try to grow the carbon nanostructures such as MWCNTs, nanofibers, nano crystalline diamond on the stainless steel, brass, Cu and Al as substrates by TCVD method.

EXPERIMENTAL

Substrate preparation

Stainless steel, brass, Cu and Al plates were prepared into 20 × 25 mm^2 rectangular pieces and used as substrates for growing CNTs. Polishing of substrates was done mechanically with sandpaper in order to remove contaminants and stains of the surface. By emission spectroscopy (ARL 3460/451) image, the elementary analysis of stainless steel as Fe alloy, brass as Cu alloy, Cu and Al can be achieved. The results are shown in Table 1.

Table 1. Elementary analysis of Stainless Steel, Brass, Cupper and Aluminum by emission spectroscopy method

Stainless steel		**Brass**		**Cupper**		**Aluminum**	
Component	Percentage	Component	Percentage	Component	Percentage	Component	Percentage
C	0.014	Pb	0.018	Sn	0.002	Si	0.133
P	0.027	Fe	0.029	Zn	0.009	Fe	0.372
Mn	1.394	Ni	0.058	Pb	0.014	Cu	0.077
Ni	7.951	Al	0.001	Fe	0.001	Mn	0.038
Cr	18.174	P	0.002	Ni	0.032	Mg	0.022
Mo	0.235	Si	0.001	Al	0.003	Zn	0.012
Sn	0.011	Zn	32.378	P	0.001	Ti	0.003
Co	0.163	Sn	0.001	Si	0.001	Cr	0.002
Al	0.011	Mn	0.003	Mn	0.005	Ni	0.002
B	0.000	Bi	0.001	Cr	0.004	Pb	0.001
Si	0.491	As	0.002	Mg	0.001	Sn	0.002
S	0.007	Cu	67.51	As	0.00	Na	0.000
Nb	0.005			Cu	99.92	B	0.001
Fe	71.10					V	0.002
V	0.069					Be	0.000
Cu	0.278					Cd	0.002
W	0.067					Li	0.000
Ti	0.006					Al	99.33

Substrate activation

All of prepared substrates were cleaned under ultrasonic irradiation in three-consecutive steps by deionized water, ethanol and acetone for 10 minutes that followed by rinsing with deionized water.

Substrate etching

Prepared stainless steel were etched by fresh etchant of 15 ml HNO_3 (64%), 15 ml HCl (37%) and 7 ml CH_3OH (99%). It was immersed in the etchant up to 40 seconds. The etchant of 50 ml H_2O and 50 ml HNO_3 (64%) was used for etching of the brass and Cu samples up to 5 seconds. The etchant of HF solution (30%) was used for etching of Al samples up to 8 seconds. HNO_3, HCl, HF and CH_3OH were purchased from Merck's company and use without further purification.

Substrate Sputtering

A thin film of Cu as catalyst was deposited on the prepared stainless steel, brass, Cu and Al as substrates. All deposition was performed by a DC magnetron sputtering system under 4×10^{-2} Torr pressure at room temperature for 15 second.

TCVD method

After Cu deposition, the samples were placed on a ceramic boat and loaded into a quartz tube of 100 mm inner diameter with heating furnace at atmospheric pressure. Temperature of the samples was ramped up to 150 $^{\circ}$C for 15 min with a flow of Argon gas (80 sccm) for 10 min, then from 150 $^{\circ}$C to 350 $^{\circ}$C with mixed flow Argon gas (80 sccm) and H_2 (20 sccm) for 20 min. After stabilizing the temperature at 350 $^{\circ}$C for 30 min, then, the furnace temperature was reramped to 550 $^{\circ}$C with a flow of Argon gas (80 sccm) and H_2 (20 sccm) for 30 min. After

stabilizing the temperature at 550 °C, C_2H_2 gas (20 sccm) was introduced into the quartz tube for 45 min for CNTs growth. Finally, Argon gas (80 sccm) was introduced to cool the samples to the room temperature.
The morphology and structure of the as-prepared samples were examined by SEM (Philips XL30).

RESULTS AND DISCUSSIONS

Fig. 1 The AFM images show 3D projection of different substrates surfaces after sputtered nano thin layer of Cu on stainless steel (Fig. 1a) with 8.97Å roughness, brass alloy (Fig. 1b) with 35.14Å roughness, Cu (Fig. 1c) with 10.39Å roughness and Al (Fig. 1d) with 18.83Å roughness.

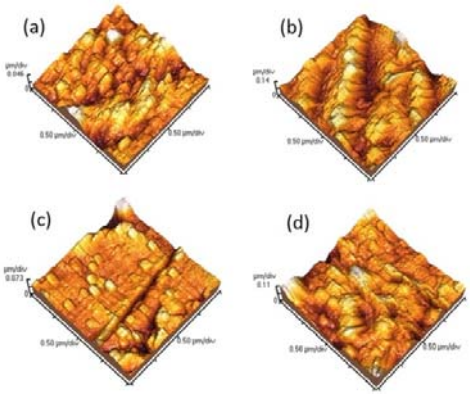

Fig. 1. 3D projections of stainless steel/Cu (a), brass/Cu substrate (b).Cu/Cu (c) and Al/Cu (d) after sputtering.

Fig. 2 represents the SEM photographs of carbon nanostructures grew on the stainless steel, brass, Cu and Al substrates. Fig. 2 (a) shows some nanostructures such as MWCNTs, SWCNTs, bundle, nano wall and amorphous carbon that formed on stainless steel as substrate. The diameters of MWCNTs are about 24 nm and SWCNTs are about10 nm. Fig. 2 (b) reveals that different kind of CNTs such as MWCNTs (30-50 nm), nano crystalline diamond (10-30 nm), amorphous carbon, roped (70-80 nm) structures with different sizes have grown on brass substrate. Fig. 2 (c) shows some nanostructures such as nano wall, MWCNTs, bundle, nano sheet and amorphous carbon that formed on Cu as substrate. Fig. 2 (d) shows some nanostructures such as SWCNTs and nano sheet that formed on Al as substrate.

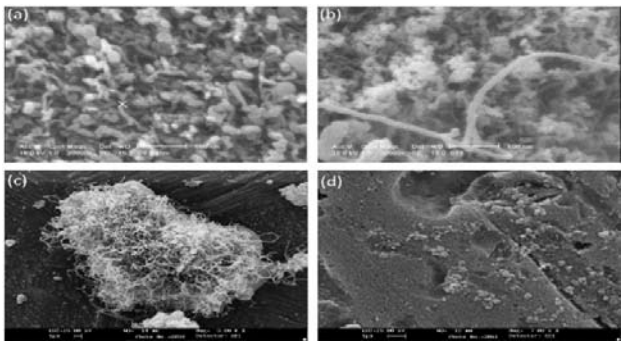

Fig. 2. SEM images of grew carbon nanostructures: (a) on the stainless steel/Cu, (b) on the brass/Cu, (c)on the Cu/Cu, (d) on the Al/Cu substrate.

It seems, the above different behavior comes from may be due to the kind of the substrates (stainless steel, brass, Cu and Al), and also, from etching effect and interaction between substrate and catalyst (Cu). Ward et al. Indicated that the ideal substrate for SWNT growth is a spun-on alumina film, while, single crystal substrates promoted the growth of mixed SWNTs and MWNTs [19]. On the other hand, some previous reports have been shown that etching time and species have important roles in some growth characteristics of CNTs such as density (yield) and diameters [20, 21].

CONCLUSION

Carbon nanostructures were synthesized from acetylene and hydrogen directly on the prepared stainless steel, brass, Cu and Al substrates by TCVD method. It was found that pretreatment of the substrate surface is very important for successful nanostructures synthesis. We observed different kind of morphologies and nanostructures, with different yield and length of CNTs using SEM. SEM observations conformed that there are a very kind of nanostructures on to these substrates but not the same. In addition MWCNTs yields and lengths respect to four these substrates. It seems that the stainless steel, brass and Cu substrates are better than the Al substrate for growing the nanostructures. Never the less, we suggest that Si/SiO_2 can be replaced with stainless steel and brass as substrate in practical applications.

REFERENCES

[1] H.W. Zhu, C.L. Xu, D.H. Wu, B.Q. Wei, R. Vajtai, P.M. Ajayan, Science 296 (2004) 884.

[2] J. Robertson, Materials Today 7 (2004) 46.

[3] Q. Li, X. Zhang, R.F. Depaula, L. Zheng, Y. Zhao, L. Stan, T.G. Holesinger, P.N. Arendt, D.E. Peterson, Y.T. Zhu, Adv. Mater. 18 (2006) 3160.

[4] D.N. Futaba, K. Hata, T. Yamada, T. Hiraoka, Y. Hayamizu, Y. Kakudate, O. Tanaike, H. Hatori, M. Yumura, S. Iijima, Nature Materials 5 (2006) 987.

[5] S. Iijima, Nature 354 (1991) 56.

[6] S. Iijima, T. Ichihashi, Nature 363 (1993) 603.

[7] T. Guo, P. Nikolaev, A. Thess, D.T. Colbert, R.E. Smalley, Chem. Phys. Lett. 243 (1-2) (1995) 49.

[8] J. Liu, H. Dai, J.H. Hafner, D.T. Colbert, S.J. Tans, C. Dekker, R.E. Smalley, Nature 385 (1997) 780.

[9] Y.Y. Wei, G. Eres, V. I. Merkulov, D.H. Lowndes, Appl. Phys. Lett. 78 (10) (2001) 1394.

[10] J.H. Hafner, M.J. Bronikowski, B.R. Azamian, P. Nikolaev, A.G. Rinzler, D.T. Colbert, K.A. Smith, R.E. Smalley, Chem. Phys. Lett. 296 (1998) 195.

[11] S.Z. Mortazavi, A. Reyhani, A. Irajizad, Applied Surface Science 254 (2008) 6416.

[12] C. Zhang, S. Pisana, C.T. Wirth, A. Parvez, C. Ducati, S. Hofmann, J. Robertson, Diamond & Related Materials 17 (2008) 1447.

[13] A. Rizzo, R. Rossi, M.A. Signore, E. Piscopiello, L. Capodicei, R. Pentassuglia, T. Dikonimos, R. Giorgi, Diamond & Related Materials 17 (2008) 1502.

[14] R.Z. Ma, J. Liang, B.Q. Wei, B. Zhang, C.L. Xu, D.H. Wu, Power Sources 84 (1) (1999) 126.

[15] I. Gordon, L. Carnel, D. Van Gestel, G. Beaucarne, J. Poortmans, Thin Solid Films 516 (2008) 6984.

[16] Y. Ando, S. Tobe, H. Tahara, Vacuum 83 (2009) 102.

[17] A.R. Beaber, J. Hafiz, J.V.R. Heberlein, W.W. Gerberich, S.L. Girshick, Surface & Coatings Technology 203 (2008) 771.

[18] S. Hermann, R. Ecke, S. Schulz, T. Gessner, Microelectronic Engineering 85 (2008) 1979.

[19] J.W. Ward, B.Q. Wei, P.M. Ajayan, Chemical Physics Letters 376 (5-6) (2003) 717.

[20] J.H. Han, B.S. Moon, W.S. Yang, J.B. Yoo, C.Y. Park, Surface and Coating Technology 131 (1-3) (2000) 93.

[21] T. Ono, N. Orimoto, S. Lee, T. Simizu, M. Esashi, Jpn. J. Appl. Phys. 39 (2000) 6976.

VTST Study of the Reactions of CH_3CH_3+H, CH_3CD_3+D and CH_3D+CD_3

Sh. Ramazani

Department of Chemistry, College of Sciences, Yasouj University, Yasouj, Iran

ramazani@mail.yu.ac.ir

Introduction

The study of reactions of radicals is very important because there are a lot of kinds of radicals in atmosphere and installer, so in this investigation we are studied reactions of some hydrocarbons with H, D and CD_3 radicals. The kinetics and mechanism of these reactions have been investigated theoretically on adiabatic surfaces. Considering to, radicals approached to which direction and atom of molecules, there are 10 possible channels for these reactions. The possible mechanisms which are studied in this article are shown below.

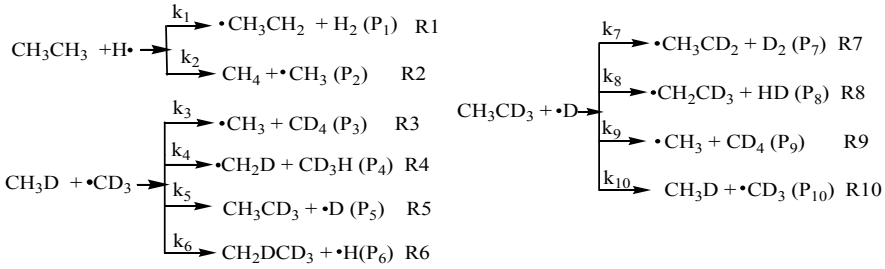

Computational Details

Ab initio calculations were carried out using the Gaussian 03 program. The geometries of all the stationary points were optimized at the MP2 [1] and MPWB1K [2] levels, and single point calculations on the optimized MP2 geometries at the CCSD(T) level with the 6-311++G(d,p) basis set were carried out. All dynamics calculation were performed by VTST/MT using the MPWB1K level with the 6-311++G(d,p) basis set to build the potential energy surface, calculations were performed using GAUSSRATE9.program. The minimum energy paths were searched from 4.0 bohr inside the reactants valley up to 4.0 bohr inside the product valley using the step size

of 0.02 bohr. The Hessian calculations were performed at 0.2 bohr intervals. Page-McIver algorithm was used to follow minimum energy path (MEP), it has performed a generalized normal mode analysis projecting out frequencies at each point along the path. With this information, we can calculate both the vibrational partition function along the MEP and the ground state vibrationally adiabatic potential curve. It was used a method based on VTST [3] method to calculate the rate constants for reactions R1 to R10. Variational effects were incorporated by the canonical variational transition-state theory (CVT), in which the flux is minimized for a canonical ensemble. The CVT rate constant, $k^{\mathrm{CVT}}(T)$, at temperature T, can be obtained as the minimum of the generalized transition-state theory rate constant, $k^{\mathrm{GT}}(T, s)$, as a function of s, that is, $k^{CVT}(T) = \min_{s} k^{GT}(T,s) = \sigma \frac{1}{\beta h} \frac{Q^{GT}(T, s_*^{CVT})}{Q^{R}(T)} \exp\left[-\beta V_{MEP}(s_*^{CVT})\right]$ [4] where s is the arc along the MEP measured from the saddle point; s_*^{CVT} is the value of s at which $k^{GT}(T,s)$ has a minimum: σ is the symmetry number, $V_{MEP}(s_*^{CVT})$ is the classical MEP potential at $s = s_*^{CVT}$; and $Q^{GT}(T, s_*^{CVT})$ and $Q^{R}(T)$ are the internal partition functions of the generalized transition state at $s = s_*^{CVT}$ and reactants, respectively.

Results and discussions

Variation of the vibrationaly adiabatic ground state potential ($V_a^G(s)$), minimum energy path potential, V_{MEP} and Zero Point Energy (ZPE)(see figure 1) for all reactions have calculated. We have also monitored variations of the normal mode vibrational frequencies along the MEPs and curvature parameter of the reaction paths $B_{mF}(s)$ for these channels. All of the result will be reported in the conference, including rate constants, preliminary investigations of tunnelling effect, kinetic isotope effect, and thermally averaged transmission probability.

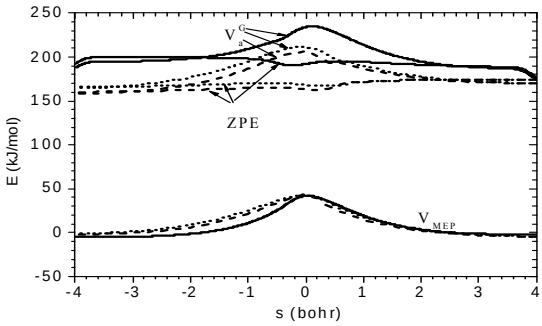

Figure 1. Ground-state vibrationally adiabatic potential (V_a^G), potential minimum energy path (V_{MEP}) and zero point energy (ZPE), for the R1 reaction (solid line), R7 reaction (dash line) and R8 reaction (dot line).

Keywords: Tunneling, Isotope Effects, Minimum Energy Path, Adiabatic Surfaces

References

[1] C. Møller, M.S. Plesset, Phys. Rev. 46 (1934) 618.

[2] Y. Zhao, D.G. Truhlar, J. Phys. Chem. A. 108 (2004) 6908.

[3] D.G. Truhlar, A. Kuppermann, J. Am. Chem. Soc. 93 (1971) 1840.

[4] S. H. Mousavipour, A. F. Ramos, R. M. Pan, E. M. Nu´n˜ ez, S. A. Va´zquez and M. A. R1´os, *J. Phys. Chem. A 111(*2007**)** 719.

Solubility of H_2S in imidazolium – based ionic liquids

Amir Hossein Jalili[a*], Hossein Sakhaeinia[b], Mohammadali Safavi[c], Rozhin Fatehi[d], Mohammad Shokouhi[a], Vahid Taghikhani[c], Cyrus Ghotbi[c], Behrooz Adib[d]

[a] *Gas Science Department, Research Institute of Petroleum Industry (RIPI), National Iranian Oil Company (NIOC), P.O. Box: 14665 – 137, Tehran, Iran (Email: jaliliah@ripi.ir)*

[b] *Department of Chemical Engineering, Faculty of Engineering, Islamic Azad University – Semnan Branch, Semnan, Iran*

[c] *Department of Chemical and Petroleum Engineering, Sharif University of Technology, Tehran, Iran*

[d] *Department of Chemistry, Islamic Azad University – North Tehran Branch, Tehran, Iran*

Given the capital demands for environmentally favorable processes as well as industrial tendency for sustainable technology, one of the active research areas nowadays is exploring ionic liquids (IL) as green solvents for removal of CO_2 and H_2S acid gases in the course of natural gas sweetening processes [1]. In this lecture the results of the measurement of the solubility of H_2S in a series of 1-alkyl-3-methylimidazolium–based ionic liquids ([$C_n$mim][X]) with methylimidazolium cation containing a simple alkyl group of different chain lengths (n = 2 – 8) or a 2-hydroxyethyl substituent and simple anions as well as those containing fluorine, at temperatures ranging from (303.15 to 353.15) K and pressures under 2.0 MPa is presented [2-7]. The solubility data were correlated using two models: the Pitzer's model ($\gamma - \varphi$ approach), and a generic Redlich–Kwong equation of state ($\varphi - \varphi$ approach) [8]. Henry's law constants and the partial molar thermodynamic functions of solution were estimated at different temperatures from the obtained experimental data. The results were compared with previously reported experimental data for other H_2S/IL and also CO_2/IL systems [4,9], which shows that the solubility of H_2S is higher than that of CO_2 in the corresponding ILs. Also the solubility of H_2S in imidazolium – based ILs increases as the number of $-CF_3$ groups in the anion and/or the alkyl chain length in the cation increases. The results were interpreted from molecular point of view using extensive *ab initio* quantum chemical calculations of the energies and

geometries of interaction between cations and anions in pure ILs as well as those of H_2S with cation and anion of the ILs. In addition the complexes were characterized and analyzed by using the Bader's theory of atoms-in-molecules (AIM).

Keywords: Ionic liquid, Gas solubility, H_2S, Henry's constant, Modeling, *Ab initio* calculation

Acknowledgements

We are thankful to the research council of the Research and Development of the National Iranian Oil Company (NIOC) for their support of this work.

References:

[1] E. D. Bates, R. D. Mayton, I. Ntai, J. H. Davis, *J. Am. Chem. Soc.* **124**, 926 (2002).

[2] A. H. Jalili, M. Rahmati-Rostami, C. Ghotbi, M. Hosseini-Jenab, A. N. Ahmadi, *J. Chem. Eng. Data* **54**, 1844 (2009).

[3] M. Rahmati-Rostami, C. Ghotbi, M. Hosseini-Jenab, A. N. Ahmadi, A. H. Jalili, *J. Chem. Thermodyn.* **41**, 1052 (2009).

[4] M. Shokouhi, M. Adibi, A. H. Jalili, M. Hosseini-Jenab, A. Mehdizadeh, *J. Chem. Eng. Data* **55**, 1663 (2010).

[5] A. H. Jalili, A. N. Ahmadi, A. Mehdizadeh, M. Shokouhi, M. Hosseini-Jenab, F. Fateminasab, *J. Chem. Thermodyn.* **42**, 1298 (2010).

[6] H. Sakhaeinia, V. Taghikhani, A. H. Jalili, A. Mehdizadeh, A. A. Safekordi, *Fluid Phase Equilib.* **298**, 303 (2010).

[7] H. Sakhaeinia, A. H. Jalili, V. Taghikhani, A. A. Safekordi, *J. Chem. Eng. Data* (accepted).

[8] Shiflett, M. B.; Yokozeki, A. *Fluid Phase Equilib.* **294**, 105 (2010).

[9] A. H. Jalili, A. Mehdizadeh, M. Shokouhi, H. Sakhaeinia, V. Taghikhani, *J. Chem. Thermodyn.* **42**, 787 (2010).

Experimental Kinetics of 2-Pyridylacetic acid Pyrolysis

M. Izadyar

Department of Chemistry, Faculty of Sciences, Ferdowsi University of Mashhad, Mashhad, Iran

Izadyar @um.ac.ir

Keywords: 2-Pyridylacetic acid; Asynchronous concerted mechanism; Homogeneous.

Introduction

Recent studies on the gas phase pyrolysis reactions of 2-substituted chloro, hydroxyl, alkoxy, phenoxy and acetoxy carboxylic acids [1-2] show that the acidic H of the COOH group assists as the leaving group for the elimination. Through these reactions the unstable α-lacton has been formed. The α-lactone decomposes rapidly, yielding carbon monoxide and the corresponding carbonyl compound. If an amino or nitrogen derivative is considered as a leaving group L in organic compounds, the reaction proceeding will be changed. In view of the scare information on the gas phase pyrolysis of amino acids including mechanistic consideration, an experimental study aimed at investigation of 2-pyridylacetic acid pyrolysis in the gas phase (Fig.1).

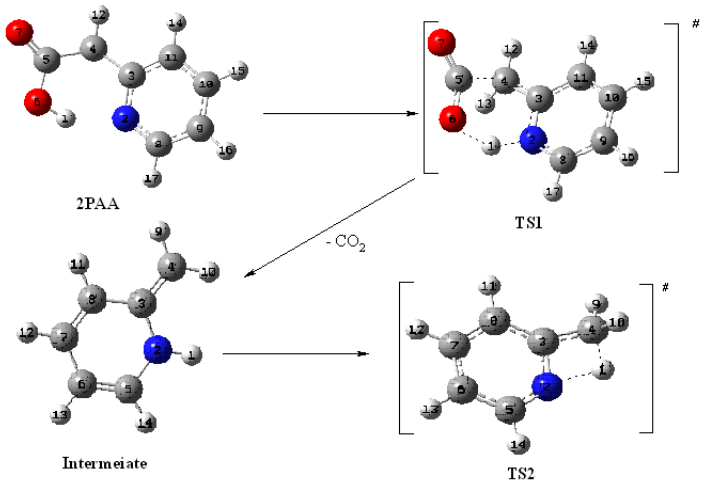

Fig. 1. Suggested concerted mechanism for the pyrolysis of 2PAA in the gas phase.

Experimental

2-pyridylacetic acid hydrochloride was purchased from Aldrich. The hydrochloride was converted to free acids by treatment with fresh Ag_2CO_3, filtration of the resultant AgCl precipitate, precipitation of dissolved Ag with H_2S and evaporation to dryness. The pyrolysis experiments were performed in a static system over 10 half-lives in the presence of the free radical scavenger (cyclohexene). 2-Pyridyl acetic acid (2PAA) was dissolved in glacial acetic acid and injected directly into the reaction vessel (~20μL), using a microsyring. The reaction mixture was injected into the GC instrument equipped with a thermal conductivity detector (TCD) in each kinetic run.

Gaseous mixture at the definite interval times by a gas-tight syringe (PS, A-2) was injected into the GC capillary column (HP-5, 30 m* 0.32 mm i.d.). The experimental techniques have been described elsewhere [3-5].

Results and discussion

According to scheme 3, pyrolysis reaction of 2PAA demands $P_f/P_0=2.0$, where P_f and P_0 are the final to initial pressures, respectively. The average experimental P_f/P_0 value at five different temperatures between 541.2-583.4 K and 10 half-lives is 1.87.

The homogeneity of this process was studied using the vessels with a surface-to-volume ratio of 3.0 and 6.0 times greater than the unpacked vessel. The effect of different proportions of cyclohexene indicate that the reaction is molecular and not free radical in nature.

The first-order rate coefficients for the reaction calculated from $k= (2.303/t) \log [P_0/ (2P_0-P_t)]$ were found to be independent of the initial pressure. The average k value is estimated within ±5% standard deviation. A good straight line up to 82% decomposition was achieved by means of plotting the $\log (2P_0-P_t)$ vs. time t. A least square fit of the rate coefficients in the form of the Arrhenious equation produced the following relationship;

$$\log k = (10.90\pm0.32)-(152.74\pm2.02\ kJmol^{-1})(2.303RT)^{-1}$$

Activation parameter values for 2PAA are listed in table 1. Activation energy for the pyrolysis reaction of 2PAA is nearly small relative to similar amino acids such as picolinic acid. This small difference may be attributed to the facile formation of six-center TS for 2PAA rather than five-member TS for picolinic acid. The concerted nature of the reaction could be confirmed by negative values for the activation entropy, too.

Table 1
Experimental kinetic and activation parameters for the pyrolysis reaction in the gas phase

Ea (kJmol^{-1})	**log A**	**$\Delta H^{\neq}$**(kJmol^{-1})	**$\Delta G^{\neq}$**(kJmol^{-1})	**$-\Delta S^{\neq}$**(Jmol^{-1}K^{-1})
152.74	10.90	148.07	176.06	49.82

References:

[1] V.S. Safont, V. Moliner, J. Anders, L.R. Domingo, J. Phys. Chem. 101 (1997) 1659.

[2] L.R. Domingo, J. Anders, V. Moliner, V.S. Safont, J. Am. Chem. Soc. 119 (1997) 6415.

[3] M.R. Gholami, M. Izadyar, J. Phys. Org. Chem. 16 (2003)153.

[4] M.R. Gholami, M. Izadyar, Chem. Phys. 301 (2004) 45.

[5] M. Izadyar, N. Zamani, M.R. Gholami, Chem. Phys. 330(2006) 394.

Study of the kinetics and mechanism of the electrodeposition of Bi, Bi_2Se_3 and Sb_2Se_3 semiconductors

F.Gobal, S .Jafarzadeh*

Department of Chemistry, Sharif University of Technology, P.O. Box 11365-9516, Tehran, Iran

(E-mail: sanaz.jafarzadeh@yahoo.com)

Introduction:

In this study a systematic effort is made to clarify some controversies about the mechanism and kinetics of the electrodeposition of Bismuth, Bismuth Selenide and Antimony Selenide in aqueous solutions.

Methods:

Electrochemical techniques consisting Chronoamperometry (CA) and Cyclic Voltammetry (CV) were applied .Characterization of the electrodeposition process is based on quantitive analysis of the potentiostatic current-time curves recorded during semiconductors deposition.

Results and discussion:

Nucleation and growth rate constants obtained from the fit of recorded transients to the generalized equations derived based on Abyaneh and Fleischmann model. The conditions that justify the use of the limiting forms of the transient equations for the so-called "instantaneous" and "progressive" nucleation processes were evaluated. Effect of potential, temperature and concentration on the kinetics and mechanism of this process were investigated. The electrochemical cell used in this study is a conventional three electrode cell having provisions for a working electrode, a reference electrode and an auxiliary electrode. A Pt sheet (0.5×1 cm2) was used as auxiliary electrode and a saturated calomel electrode (SCE) was used as reference electrode and all potentials in the present study are reported against the SCE. The deposited electrodes were washed in distilled water and dried in room temperature. All

electrochemical depositions and capacitive measurements were performed by means of a galvanostat-potentiostat (Behpajoo 2063+).

It was found that the deposition process for Bi_2Se_3 with 9:2 and 5:1 molar proportion of Bi:Se could be well described by a model that involves four contributions: (1) a double layer charging process(I_{DL}) Two different kinds of two-dimensional nucleation mechanisms, (2) an instantaneous(I_{2DI}) and (3) a progressive(I_{2DP}). Finally, (4) a progressive three-dimensional nucleation and growth(I_{3DP}). For Bi_2Se_3 with 7.5:2 molar proportion, the deposition process changed to other contributions that involved: (I_{DL}), (I_{2DI}), (I_{3DI}) and (I_{3DP}) nucleation and growth. Electrodeposition of Antimony Selenide hasn't shown any nucleation and growth process and has a monolayer deposition.

Conclusion:

Bi electrodeposition on Pt substrate, was a process with two and three-dimensional nucleation and growth that current equation was: $I= I_{DL}+I_{2DI}+I_{2DP}+I_{3DP}$. Equivalent current for Bi_2Se_3 with 7.5:2 molar proportion was : $I=I_{DL}+I_{2DI}+I_{3DI}+I_{3DP}$ and finally Sd_2Se_3 showed no nucleation in deposition process and its Catrel curve corresponds to a monolayer deposition.

Keyword: 1-Electrodeposition 2- Nucleation and growth 3- Cyclic Voltammetry 4- Chronoamperometry

References:

[1].M.S.Gonzalez, A.L.Prieto, J.of Electrochemical Society, 149(2002)11.

[2].M.Stozler, M.Strodeur, H.Sobtta, Phy.Status.Solid 138(1986)259.

[3].N.S.Yesugade, C.D. Lokhande, C.H.Bhosale, Thin Solid Films 263(1995)145.

[4].P.C.Searson, T.P.Moffat, Crit. Rev.Surf.Chem. 3(1994)171.

L.Li.Y.Zhange, G.Li.L.Zhange, Chem.Phys.Lett.378(2003)244.

New Local Composition Model for Modeling of Thermodynamic Properties of Binary Aqueous Electrolyte Solutions

Mohammed Taghi Zafarani-Moattar and Roghayeh Majdan-Cegincara*
Email: majdan_26@yahoo.com
Physical Chemistry Department, University of Tabriz, Tabriz, Iran

Introduction: The design and operation of industrial process that involve electrolyte solution require knowledge of rigorous models or experimental data to represent the nonideality of the mixtures. The local composition models are frequently used in engineering thermodynamics for the prediction of multi-component electrolyte systems [1-3]. In this work, a new local composition model is applied to correlate the mean ionic activity coefficients of aqueous electrolyte solutions at 25 °C. In this model for excess Gibbs energy sum of a long-range and a short-range terms is used. The contribution of the long-range excess Gibbs energy is represented by the Pitzer-Debye-Hückel model. A new expression based on the local composition concept, which is a NRF-modified-NRTL (NRF-mNRTL) model, has been developed to account for the contribution of the short range excess Gibbs energy. Fitting quality of proposed model has favorably been compared with other local composition models.

Theoretical framework: The promising features of the NRTL-NRF and mNRTL models led us to develop a new local composition model (NRF-mNRTL) for excess Gibbs energy of electrolyte solution using Chen's local cell theory and considering different reference state assumptions and correction terms. To express the short-range contribution, the assumption of existence of three types of cells depending on the central species in the microstructure of a solution of single electrolyte has been used. The excess molar Gibbs energy of NRF-mNRTL model was derived as

$$(\frac{g^{ex}}{RT})^{*}_{NRF-mNRTL} = (z_c^2 z_a + z_a^2 z_c)x_s^2 \frac{\frac{z_c z_a x_s \lambda_E (\frac{\beta_E}{z_c z_a x_s \beta_E + x_m}) + x_m \lambda_E (\frac{\beta_E}{z_c z_a x_s \beta_E + x_m}) - \lambda_E}{z_c z_a x_s + x_m} -$$

$$x_m^2 \lambda_m (1 - \frac{1}{2 z_c z_a x_s \beta_m + x_m}) - \lambda_m x_s (\nu - 2 z_c z_a \beta_m), \qquad \beta_E = \exp(-\frac{\lambda_E}{ZRT} + \frac{\omega_E}{RT}), \qquad \beta_m = \exp(-\frac{\lambda_m}{ZRT} + \frac{\omega_m}{RT}) \qquad (1)$$

where λ_E, λ_m, ω_E and ω_m are the adjustable parameters of NRF-mNRTL model. $x_s = \frac{vmM_1}{1+vmM_1}$ where m and M_1 are respectively molality of solution and molar mass of solvent in the unit of kg.mol^{-1}; $x_m = 1 - x_s$; $\nu = \nu_c + \nu_a$, where ν_c and ν_a are the stochiometric coefficients of cation and anion, respectively. The mean ionic activity coefficient ($\gamma_\pm$) of an electrolyte in aqueous solution was obtained from $\nu \ln \gamma_\pm = \frac{\partial}{\partial n_s}(\frac{ng^{ex}}{RT})_{n_m}$. Here, n is the total mole number, n_s and n_m are the mole number of solute and solvent.

Result and discussion: The mean ionic activity coefficients of binary aqueous electrolyte solutions from dilute to concentrated ranges were correlated with the proposed NRF-mNRTL model. Applicability of NRF-mNRTL model in the fitting of $\ln \gamma_\pm^*$ of binary aqueous electrolyte solutions has been compared with other local composition models. The standard deviations for activity coefficients obtained from different local composition models are reported in Table 1.

Table 1. Comparison of standard deviations ($\sigma(\ln \gamma_\pm^*)$) of different local composition models in the correlation of the logarithm of mean ionic activity coefficients ($\ln \gamma_\pm^*$) of binary aqueous electrolyte solutions at 298.15 K

electrolyte	Maximum molality	NRTL	Wilson	mNRTL	NRTL-NRF	NRF-Wilson	UNIQUAC-NRF	NRF-mNRTL
KOH	20.0	0.274	0.0540	۰,۰۲۵۶	0.039	0.0370	0.022	0.0162
$LiNO_3$	20.0	0.039	0.0202	۰,۰۱۴۳	0.016	0.0284	0.082	0.0136
NaCNS	18.0	0.065	0.0460	0.0419	0.039	0.0512	0.044	0.0360
K_2CrO_4	3.5	0.022	0.0140	0.0156	0.017	0.0136	0.016	0.0034
$CaCl_2$	6.0	0.205	0.1815	۰,۰۱47	0.021	0.0491	0.072	0.0090
$Zn(NO_3)_2$	6.0	0.148	0.0507	۰,۰۱۵۸	0.021	0.0497	0.053	0.0045
$MgSO_4$	۳,۵	۰,۰۳۶	۰,۰۵۱۴	۰,۰۱۹۵	۰,۰۷۴	۰,۰۵۷۱	0.051	0.0175
UO_2SO_4	۶,۰	۰,۰۵۰	۰,۰۸۸۹	۰,۰۰۷۷	۰,۰۵۴	۰,۰۹۴۵	0.053	0.0119
$AlCl_3$	۱,۸	۰,۱۱۵	۰,۰۸۰۲	۰,۰۲۱۳	۰,۰۸۰	۰,۰۷۶۶	0.084	0.0066
$NdCl_3$	۲,۰	۰,۰۸۳	۰,۰۸۳۰	۰,۰۱۷۵	۰,۰۶۱	۰,۰۵۹۵	0.078	0.0018
$Cr_2(SO_4)_3$	۱,۲	۰,۱۲۹	۰,۱۳۷۴	۰,۰۳۱6	۰,۱۳۲	۰,۱۳۶۳	0.133	0.0036

Conclusion: New excess Gibbs energy model, NRF-mNRTL, has been developed based on the local cells theory. The corresponding activity coefficient equations have been derived from the proposed model. It is found that the performance of NRF-mNRTL model in the correlation of $\ln\gamma_{\pm}^{*}$ values is better than the other local composition models, especially for multivalent electrolytes.

Keywords: Formulation; Mathematical modeling; New local composition model; Aqueous electrolyte solutions; Mean ionic activity coefficient

References

[1]. C.C. Chen, H.I. Britt, J.F. Bostom, L.B. Evans, AIChE J. 28 (1982) 588-596.

[2]. A. Haghtalab, J.H. Vera, AIChE J. 34 (1988) 803-813.

[3]. A. Jaretun, G. Aly, Fluid Phase Equilib. 175 (2000) 213-228.

Thermodynamic investigation of tetrakis (N, N′, N′′, N′′′-tetramethyl tetra-2, 3-pridino) porphyrazine Cu(II) and cationic surfactants with different alkyl chain length studied by the method of continuous variations

H. Dezhampanah [a*], B. Ghalami[a], E. Alizade[a], and E. Shams

[a] Department of Chemistry, Faculty of Science, University of Guilan P.O. Box 1914, Rasht 0098, Iran.

(***e-mail**: h.dpanah@guilan.ac.ir)

Key word: porphyrazine, anionic surfactant, job method, aggregation

1. Introduction:

Porphyrins and related macrocyclic compounds have been studied in recent decades for a wide variety of applications such as therapeutic drugs and targeting agents, energy converters in photovoltaic cells and catalysts in many chemical reactions, such as for oxygen reduction in fuel cells [1]. Cationic tetraazaporphyrins, or porphyrazines, represent an alternative and highly developed class of cationic porphyrinic compounds. Macrocycles hasted on the porphyrazine core, including phthalocyanins, but the replacement of the meso methylene carbons of porphyrins with nitrogen in porphyrazines creates profound differences [2].

In the present paper we have investigated interactions of a series of anionic surfactants with different alkyl chain length; sodium dodecyl sulfate (SDS), sodium tetra decyl sulfonate (STS), sodium hexa decyl sulfonate (SHS) with tetrakis (N, N′, N′′, N′′′-tetramethyl tetra-2, 3-pridino) porphyrazine cupper(II) ([Cu (II) 2, 3-tmtppa] $^{4+}$) (scheme 1) in aqueous submicellar solutions by using optical absorption spectroscopy at different temperatures. In order to explain the nature of porphyrazine-surfactant interaction, the standard free energy, enthalpy and entropy for this binding were determined and compared.

2. Methods: The [Cu (II) 2, 3-tmtppa] $^{4+}$ was prepared and purified according to literature methods [2]. Sodium do decyl sulfate (SDS), sodium tetra decyl sulfonate (STS), sodium hexa decyl sulfonate (SHS) were Sigma chemicals and were used without further purification All experiments were run in phosphate buffer of pH=7.2. The initial concentration of the Porphyrazine and surfactant solutions was 2.0×10^{-5} mol^{-1}. At this concentration, the Porphyrazine used do not spontaneously aggregate and the surfactants used do not form

micelles. The absorbances were measured on the double beam absorbance spectrophotometer Cary 500 scan UV-vis, with thermostated cells. The measurements were taken at 25, 30, 40, and 50 °C. The mixed solutions were prepared instantly and the absorbances were measured after thermostation. The absorbance was read at the absorption maximum at 638 nm for [Cu (II) 2, 3-tmtppa] $^{4+}$.

3. Results and discussion: Figure 1 shows the equimolar Job's plots for binding of the porphyrazine and the surfactant SDS at 25, 30, 40, and 50 °C in buffer solutions. The minimum is at x= 0.5 on all plots. At this point the concentration of the porphyrazine and the surfactant ions is equal and in such a mixed solution the highest amount of the associate is formed. This means that 1:1 associates are formed between the porphyrazine and the surfactant SDS ions. The binding ratio remains the same at different temperatures. The same results obtained for other surfactants. The calculated values of the thermodynamic functions are collected in table 1. Equilibrium constants and standard free enthalpy change also show that [Cu (II) 2, 3-tmtppa] $^{4+}$ interacts with SDS more easily and strongly than with STS and SHS at the same conditions. Because the only difference between the systems is in the length of the alkyl chain of both surfactants, it implies that the hydrophobicity of the alkyl chain, which is responsible for hydrophobic interactions, plays an important role in porphyrazine–surfactant interactions. The binding energy increases with increase of the hydrophobicity of the alkyl chain and the results indicate that the process is entropy driven.

Table 1: Thermodynamic parameters and affinity constants for binding of [Cu(II)2,3-tmtppa]$^{4+}$ to surfactant at 1mM phosphate buffer pH 7.2 at 30°C.

surfactant	ln K	$\Delta G^{\circ}(kJmol^{-1})$	$\Delta H^{\circ}(kJmol^{-1})$	$\Delta S^{\circ}(Jmol^{-1})$
SDS	16.82	-42.37	36.50	260.31
STS	19.34	-48.73	16.30	214.49
SHS	20.82	-52.46	102.78	512.38

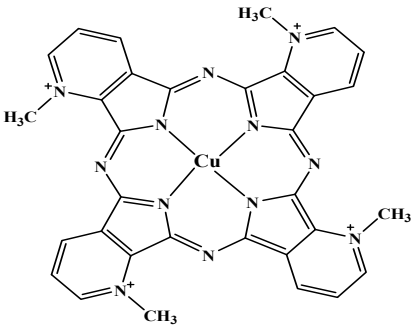

Scheme1: Chemical structures of [Cu (II) 2, 3-tmtppa] $^{4+}$.

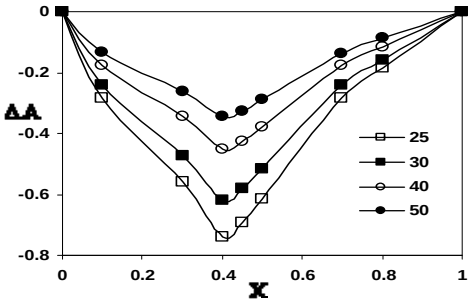

Figure 1. Job's plots of SDS and [Cu (II) 2, 3-tmtppa] $^{4+}$ in buffer solutions at different temperatures.

References

[1] Yaffe, O. Korin, E. and Bettelheim, A. *Langmuir* **2008,** *24,* 11514-11517

[2] Dezhampanah, H. Bordbar, A. K., Salimian, Z. and Safa, E. *J. Porphyrins Phthalocyanines* **2010**, 14: 354–360.

Kinetics, thermodynamic and equilibrium isotherms of Reactive Oreange 12 adsorption on cadmium sulfide nano particle loaded on activated carbon

M. Ghaedi[a]*, A. Amiri. Pebdani[a], B. Sadeghian[a], R. Sahraei[b], A. Daneshfar[b], N. Shokri[b]

[a] Chemistry Department, Yasouj University Yasouj, 75914-35, Iran

[b] Chemistry Department, Ilam University, 65315-516, Iran

*E-mail: m_ghaedi@mail.yu.ac.ir

Abstract

The objective of this study was to assess the adsorption potential of cadmium sulfide nanoparticle loaded on activated carbon (CSN-AC) for the removal of Reactive orange 12 (RO-12) molecules from aqueous solutions. Adsorption studies were conducted in a batch system as a function of solution pH, contact time, initial dye concentration, amount of adsorbent, temperature, etc. In order to investigate the adsorption processes, pseudo-first-order, pseudo-second-order, Elovich and intra-particle diffusion kinetic models were studied and it followed the pseudo-second-order kinetic model with good correlation. Equilibrium data fitted well with the Langmuir models. Thermodynamic parameters such as enthalpy, entropy and Gibb's free energy changes were also calculated. It was found from thermodynamic parameters, that the sorption of dye by CSN-AC was feasible, spontaneous and endothermic process.

Keywords: Adsorption; Reactive orange 12; CdS nanoparticle loaded on activated carbon; Adsorption isotherm; Thermodynamics and kinetic of adsorption.

Introduction

Nano particle have very interesting physicochemical properties, such as ordered structure with high aspect ratio, ultra-light weight, high mechanical strength, high electrical conductivity, high thermal conductivity, metallic or semi-metallic behavior and high surface area [1, 2]. The objective of the present work is to

investigate the potential feasibility of CSN-AC for the adsorption of RO-12. Reactive dyes in both ordinary and hydrolyzed forms are not easily biodegradable, and thus, even after extensive treatment, colour may still remain in the effluent.

Experimental and results

In the first CdS Nanoparticles were synthesized from solution containing $Cd(ClO_4)_2.6H_2O$ (0.02 $molL^{-1}$), urea (0.25 $molL^{-1}$), and thioacetamide (0.02 $molL^{-1}$) to obtain 100 ml solution. Finally, the pH of solution was adjusted to 4.0 by dropwise addition of 2 mol L^{-1} HCl solution. The solution was maintained for 5 h at room temperature (25 ºC). The solution turned light yellow after 30 minutes, visually manifesting the initial formation of CdS nanoparticles and remained optically clear.
The influence of variables including pH, contact time, initial dye concentration, amount of adsorbent, temperature required for efficient removal of RO-12 from 50 mL of 50 µg mL^{-1} sample has been investigated. The system is suitable for quantitative removal of this dye from such solution at pH 1 using 0.035 g CSN-AC, equilibrium time 7 min even temperature of 50 ºC. The graphical correlation of various adsorption isotherm models like, Langmuir, Freundlich and Tempkin have been carried out for this adsorbent. Calculation of various thermodynamic parameters such as, Gibb's free energy, entropy and enthalpy of the on-going adsorption process indicate feasibility and endothermic nature or RO-12 adsorption on all adsorbent. The kinetic studies suggest the following pseudo second order kinetics and involvement of particle diffusion mechanism.

Conclusion

The CSN-AC is identified to be an effective adsorbent for the removal of RO-12 from aqueous solutions. It was observed that batch sorption using CSN-AC was dependent on parameters such as initial concentration of dye, time, pH, dose of adsorbent and type of dye. The equilibrium and kinetic studies were made for the adsorption of dyes from aqueous solutions onto CSN-AC. Adsorption parameters for the

Langmuir, Freundlich and Tempkin isotherms were determined and the equilibrium data were best described by the Langmuir model. The process is endothermic in nature and its kinetics can be successfully fitted to pseudo-second-order kinetic model. The results of the intraparticle diffusion model suggested that intraparticle diffusion was not the only rate controlling step.

References

[1] M. Arami, N. Y. Limaee, N. M. Mahmoodi, N.S. Tabrizi, J. Colloid Interface Sci. 288 (2005) 371–376.

[2] F. D. Ardejani, K. H. Badii, N.Y. Limaee, N.M. Mahmoodi, M. Arami, S.Z. Shafaei, A.R. Mirhabibi, Dye Pigm. 73 (2007) 178–185.

A Theoretical Study on the Effect of Dimethylzinc Catalysis on the Kinetics of Addition Reactions

S. Hosein Mousavipour* and Maryam Dehdashti-Jahromi
Email: mousavi@susc.ac.ir
Department of Chemistry, College of Sciences, Shiraz University, Shiraz, Iran

Introduction

The generation of radical species for the efficient construction of chemical bonds is a well-recognized strategy in organic synthesis.[1] In 2001 it has been observed that the rate of addition of tetrahydrofuran to imine in the presence of $Zn(CH_3)_2$ unexpectedly increases.[2] It has been suggested the reaction proceeds via a radical mechanism and dimethylzinc is used as an efficient radical initiator.[3] In the present study the mechanism and kinetics of reaction R1 is theoretically studied in the presence or absence of dimethylzinc in gas phase and in tetrahydrofuran.

R1

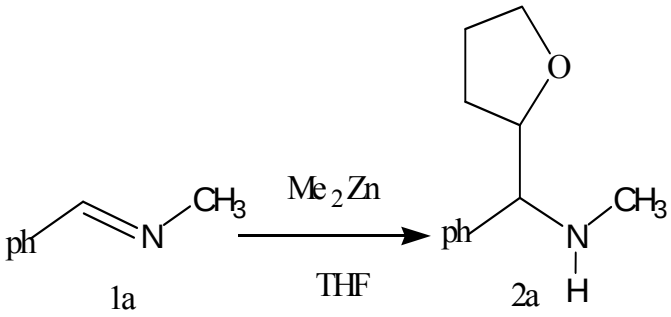

Method

The ab initio calculations were performed by means of Gaussian03 program. The geometry of all the stationary points were optimized at the B3LYP level of theory along with the lanl2dz for zinc and 6-31+G basis set for the other elements. The IRC calculations carried out to correlate each transition state structure to the corresponding minima. Polarizable Continuum Model (PMC) was used to calculate the geometry and energy of the stationary points in liquid phase. Frequency calculations at the same level of theory were carried out to determine the structure of each saddle point and also to calculate the free energy of activation for each elementary step. The thermodynamic expression for the transition state theory was used to calculate the rate constant of the reaction in the presence or absence of the catalyst.

Results and Discussion

Our results indicated the addition of THF to imine in the presence of $Zn(CH_3)_2$ as catalyst decreases the activation free energy of the reaction by 34 percent and causes to increase the rate of the reaction. Figure 1 shows the free energy changes of the reaction in the presence of dimethylzinc at the B3LYP/6-31+G(d,p) level of theory.

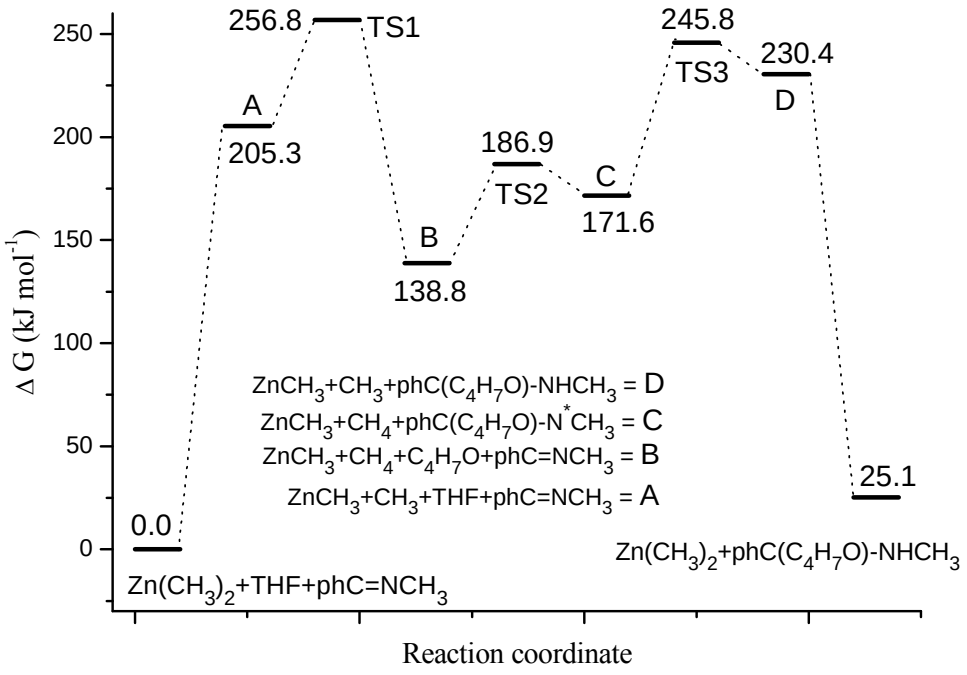

Figure 1

The rate constant for this reaction in the presence and absence of the catalyst has been calculated and will be discussed.

References

[1] Renaud, P.; Sibi, M.P. eds.; *Radicals in Organic Synthesis*, Wiley-VCH: Weinheim, Germany, **2001**; Vols. 1 and 2.

[2] Akindele, T.; Yamada, K-I.; Tomioka, K. *Acc. Chem. Res*. **2009**, *42*, 345.

[3] Skatova, A. A.; Ignatov, S. K.; Dodonov, V. A.; Razuvaev, A. G.; Druzhkov, O. N. Rus. Chem. Bul. **1995**, 44.

A new theoretical description by statistical rate theory for close to equilibrium desorption systems

Hadis Bashiri

Department of Physical Chemistry, Faculty of Chemistry, University of Kashan, Kashan, Iran

Abstract

In present work kinetics of solute desorption at solid/solution interface has been studied by statistical rate theory (SRT) when the system is close to equilibrium. A new and simple equation was derived for close to equilibrium desorption systems. Based on numerically generated points (t; q) by the SRT equation and also by analysis of two experimental systems, the results of present theoretical study were confirmed.

Keywords: Desorption kinetics, Solid/solution interface, Statistical rate theory

Introduction

The adsorption and desorption processes are the most common methods for removal of pollutants from waste waters. Desorption kinetic and equilibrium are important in understanding desorption characteristics from adsorbent.

There are different models to describe desorption kinetics but most of these models were presented experimentally and there are no theoretical basic for them. This article is intent to derive desorption rate equation on the basis of statistical rate theory at close to equilibrium condition.

Theory

The statistical rate theory (SRT) approach, which is based on quantum mechanics and thermodynamics, has been provided by Ward[1] and generalized by Rudzinski[2]. Our recent studies have concerned the description of desorption kinetics at the solid/solution interfaces by using the SRT approach.[3] Basic equation of SRT for kinetics of desorption at solid/solution interface is expressed as[3]:

$$\frac{d\theta}{dt} = K'_{ls}[K_L \frac{\beta(\theta_i - \theta)(1-\theta)}{\theta} - \frac{\theta}{K_L \beta(\theta_i - \theta)(1-\theta)}] \qquad (1)$$

Recently, we have derived the following simple equation for description of desorption kinetics at initial times of process based on the above equation.[3] The aim of this paper is to derive a new and simple equation from eq 1 for desorption kinetics when system is close to equilibrium. By simplification of above equation one arrives at

$$\frac{d\theta}{dt} = \frac{K'_{ls}K_L\beta}{\theta\theta_e^2}(\theta_e - \theta)(\theta_i - \theta\theta_e)\left(\frac{[(\theta_e + \theta)(\theta_i + \theta\theta_e)] - 2\theta\theta_e(1+\theta_i)}{(1-\theta)(\theta_i - \theta)}\right) \qquad (2)$$

Since the system is close to equilibrium, the assumptions $\theta_e + \theta \approx 2\theta_e$, $\frac{1-\theta_e}{1-\theta} \approx 1$ and $\frac{\theta_i - \theta_e}{\theta_i - \theta} \approx 1$ are acceptable. Based on these assumptions eq 2 simplifies to

$$\frac{d\theta}{dt} = \frac{2K'_{ls}K_L\beta}{\theta_e^2}(\theta_e - \theta)(\theta_i - \theta\theta_e) \qquad (3)$$

Based on the present derivation, the integration of the mentioned kinetic model should be done with the boundary condition □(*t*1)=□□1. Therefore integration of eq 3 with the boundary condition □(*t*1)=□□1 yields

$$\ln\frac{\theta_i - \theta\theta_e}{\theta_e - \theta} = \alpha + Kt \qquad (\text{for } t \geq t_1) \qquad (4)$$

where□□□and *K* are constants. As shown in eq 4, it is expected that the plot of $\ln\frac{\theta_i - \theta\theta_e}{\theta_e - \theta}$ is a linear function of time (for $t \geq t_1$). The intercept of this plot is □□and the tangent is *K*.

Result and Discussion

In this section, we are going to analyze the applicability of the derived equation (eq 4). For this purpose three sets of hypothetical kinetic data points (*q*; *t*) were generated based on SRT rate equation for desorption at solid/solution interface (eq 1). Also two different sets of experimental have been selected from the literatures to be analyzed by SRT approach.

The comparison between the obtained K_{ls} values and the original ones (calculated by SRT rate equation) proves the accuracy of the above derivation again. Both experimental and theoretical (SRT) data are in perfect agreement with our theoretical derivation.

References

1) Ward, C. A. *J. Chem. Phys*. 1977, *67*, 229.
2) Rudzinski, W.; Plazinski, W. *J. Phys. Chem. B* 2006, *110*, 16514.
3) Azizian, S.; Bashiri, H. *Langmuir*, 2008, *24*, 13013.

Enhancement of the photocatalytic performance of TiO_2 photocatalysts via transition metal modification

Masood Hamadanian[1,2]*, Ali Mohammadi Mehra[2], Vahid Jabbari[1]

[1] Institute of Nanosciences and Nanotechnology, University of Kashan, Kashan, I. R. Iran

[2] Department of Physical Chemistry, Faculty of Chemistry, University of Kashan, Kashan, I. R. Iran

Tel: +98 361 5512828, Fax: +98 361 5514005 (Email: hamadani@kashanu.ac.ir)

Keywords: TiO_2, Nanoparticle, Cr-S co-doped TiO_2, Photocatalyst

Introduction

Photocatalytic degradation and complete mineralization of toxic organic compounds in water, soil, and air in the presence of semiconductor powders have received much attention over the last two decades [1,2]. TiO_2 is considered the most promising photocatalyst due to its high efficiency, chemical stability, nontoxicity, and relative cost. The TiO_2 have a band gap around 3.20 eV, that corresponds to 388 nm, and many efforts have been made to decrease the band gap energy. The doping process with transition metals seems to be efficient in reducing the energy necessary for these transitions. TiO_2 photocatalysts doped with either anions (N, C, S, F, P, I, etc.) or cations (Fe, Co, Pt, Cu, etc.) or codoped with several ions [3,4] have been reported to show their absorption edge red-shifted to lower energies and enhance the photocatalytic performance to the visible light range. However, little work has been reported to prepare Cr-S co-doped TiO_2 nanoparticles. The sol–gel process has been widely used to synthesize TiO_2-based photocatalysts. The incorporation of active ions (dopants) in the sol during the gelation stage allows the ions to have direct interaction with TiO_2; therefore, active ions could be doped into the lattice of TiO_2, resulting in materials with special optical and catalytic properties. In the present research, we prepared Cr-S co-doped anatase TiO_2 photocatalysts by a sol–gel process.

Experimental

All the chemicals were purchaced from Merck and were used without any further purification. The typical synthesis procedure of TiO_2 and Cr-S co-doped TiO_2 nanoparticles is as follows: Titanium (IV) isopropoxide (4.7 ml) , glacial acetic acid, and deionized water (1:2:20). The gel was dried at 100 ºC and subsequently the resulting material was powdered and then calcined in a muffle furnace at 500 ºC for 2h. The preparation of Cr-S co-doped TiO_2 nanoparticles was the same as that of TiO_2, except that the water used for the synthesis, 98.8 ml, contained the required amount of chromium nitrate (corresponding to 5 mol% compared with TiO_2) and thiourea (corresponding to 1, 2, 5, 7, and 10 mol% compared with TiO_2).

Results and discussion

The FT-IR spectra of samples (Fig. 1) show peaks corresponding to stretching vibrations of the O–H and bending vibrations of the adsorbed water molecules about 3350–3450 and 1620–1635 cm^{-1}, respectively. These results strongly confirm the presence of hydroxyl ions in the structure of the samples. In the region below 1000 cm^{-1}, several peaks were ascribed to absorption bands of Ti–O (653–550 cm^{-1}) and O–Ti–O flexion vibration (495–436 cm^{-1}). The X-ray diffraction patterns of the samples have been showed, the nanocrystalline anatase structure was confirmed by (101), (004), (200), (105) and (211) diffraction peaks [5]. In the region of 10–80 $^0\theta$, the shape of diffractive peaks of the pure TiO_2 crystal planes is quite similar to that of Cr-S co-doped TiO_2 with different concentration of S. The XRD pattern did not show any chromium or sulfur phase and may be concluded that Cr and S ions uniformly dispersed among the anatase crystallites. The average size of nanoparticles was estimated from the Scherrer equation on the anatase diffraction peak (101) and for pure TiO_2 and Cr (5%)-S (5%)) co-doped TiO_2 are around 13–15 and 10–16 nm, respectively. Fig. 2 shows SEM micrographs of the calcinated samples at 500 ^{0}C. Images show that nanoparticles are uniform, global and slightly agglomerated. Further observation indicates that the morphology of samples is very rough and may be beneficial to enhancing the adsorption of reactants due to its great surface roughness

and high surface area. Fig. 2 also reveals that the doping of Cr and S does not leave any change in morphology of the catalyst surface. The EDX data of Cr (5%)-S (5%)) co-doped TiO_2 sample are shown in Fig. 2. Nano-TiO_2 shows a peak around 0.4 keV and another intense peak appears at 4.5, 4.9 keV. The intense peak is assigned to the balk TiO2 and the less intense peak to the surface TiO_2. The peaks due to sulfur are clearly distinct at 2.3 and 2.4 keV and due to chromium are clearly distinct at 0.6, 0.7, 5.5 and 6 keV. These results confirm that Ti, O, S and Cr exist in the catalyst structure. Also, degradation of MO in the presence of Cr-S co-doped TiO_2 photocatalyst with 5% Cr and various amount of S under UV and visible irradiation are investigated.

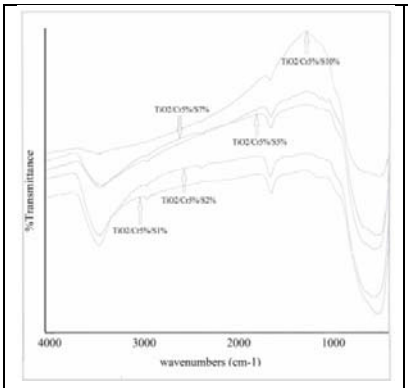

Fig. 1. FT-IR spectrum of Cr-S co-doped TiO_2 nanoparticles: (a) 5% Cr,1% S (b) 5% Cr,2% S (c) 5% Cr,5% S (d) 5% Cr,7% S and (e) 5% Cr,10% S

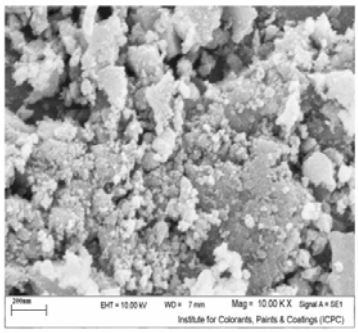

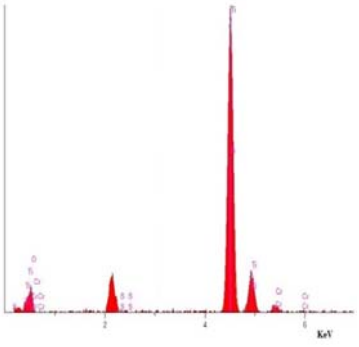

(a) (b)

Fig. 2. SEM images of Cr (5%)-S (5%)) co-doped TiO2 nanoparticles (a) and its EDX spectrum (b).

Conclusion

Visible-light active Cr-S co-doped TiO_2 nanoparticles were synthesized through a sol-gel method. All of the as-synthesized spherical powders are composed of anatase, the grain size ranged from 10-16 nm. The prepared Cr-S co-doped TiO_2 powders have good visible-light response and show good visible-light photocatalytic activities in the degradation of MO.

References

[1] Anpo M., Takeuchi M., *J. Catal.,* 216 (2003) 505.

[2] Behrend O.P., Odoni L., Loubet J.L., and Burnham N.A., *App. Phys. Lett.,* 75 (1999) 2551.

[3] Ramalho T.C., Carvalho H.W.P., Batista A.P.L., Perez C.A., and Gobbi A.L. *J. Mater. Sci.,* 44 (2009) 1029.

[4] Martı´nez-Ferrero E., Sakatani Y., Boissie`re C., and Grosso D., *Adv. Funct. Mater.,* 17 (2007) 3348.

[5] Djaoued Y., Badilescu S., Ashrit P.V., and Bersani D., *J. Sol–Gel Sci. Technol.,* 24 (2002) 255.

[6] Dvoranová D., Brezová V., Mazúr M., and Malati M. A., *Appl. Catal. B,* 37 (2002) 91.

Fabrication of Novel Metallic Nanostructured Substrates via Electroless Deposition for Surface-Enhanced Raman Scattering (SERS)

M.Reza Hormozi Nezhad* and Amir Radmand

Chemistry Department and Institute for Nanoscience and Nanotechnology(INST), Sharif University of Technology,Tehran, Iran. E-mail : hormozi@sharif.edu

Introduction:

Noble metallic nanostructures exhibit a phenomenon known as surface-enhanced Raman scattering (SERS) in which the scattering cross sections are dramatically enhanced for molecules adsorbed thereon. In recent years, it has been reported that even single-molecule spectroscopy is possible by SERS, suggesting that the enhancement factor (EF) can reach as much as 10^{14}-10^{15}[1]. According to theoretical studies, at least 8-10 orders of magnitude can arise from electromagnetic surface plasmon excitation, in addition to the chemical enhancement associated with either the metal-to-molecule or the moleculeto-metal charge-transfer transition. SERS is a powerful analytical tool for chemical and biological sensing applications. However, one feature which has limited its use in sensing and biosensing applications is the difficulty involved in producing uniform, highly sensitive, and reproducible SERS substrates[1]. Many substrate preparation techniques exist that can form roughened metal surfaces of the types required for ideal SERS enhancements. Currently, there are five fabrication techniques that could potentially produce the desired SERS substrates to meet these requirements: electron beam lithography, nanosphere lithography, the template method, the hybrid method, and an oblique angle vapor deposition method. Unfortunately, many of them are very expensive to produce large area substrates. In this article, we report a simple method to synthesize nanostructure of Ag and Au on semiconducting GaAs and metallic wafers through the galvanic reaction (Scheme 1) [2] between an aqueous solution of metallic salts and wafers. This kind of reaction has been demonstrated to deposit metal nanstructures (in most cases with random morphologies), thin films, and other structures on wafers . The metallic nanostructures

have rough and clean surfaces and large areas, which enable them to function as a new class of promising structures for surface-enhanced spectroscopy applications [3].

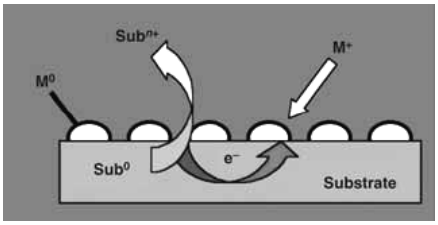

Scheme 1: Outline of galvanic displacement

General procedure:

To carry out galvanic displacement, the cleaned copper or GaAs wafers was placed in a 10 mL of $HAuCl_4$ or $AgNO_3$ in a glass vial and kept in the dark for the required length of time. The wafer was then removed from the solution and dipped in water and then ethanol and dried under a nitrogen stream.

Results and Disscussion:

1.Growth of Ag nanoplates and gold nanoparticles:

Immersion of wafer in an aqueous $HAuCl_4$ and $AgNO_3$ (1 mm) solution in the presence of dilute acid at room temperature results in rapid deposition of silver nanoplates on GaAs and gold nanoparticles on the copper surface. The reaction proceeds because the standard reduction potential of the Ag^{+}/Ag pair (0.799 V versus a normal hydrogen electrode (NHE)) and Au^{3+} /Au(1.002V versus NHE) is higher than those of the Ga^{3+}/Ga (-0.56 V versus NHE) , the As_2O_3/As (0.234 V versus NHE) and Cu^{2+}/Cu(0.34 V versus NHE) pairs. Fig. 1(a,b) present the scanning electron microscopy (SEM) images of silver nanoplates and gold nanoparticles on GaAs and copper surfaces, respectively. Morphological evolution of the Ag plates and gold nanoparticles was monitored by examining the structures formed at different reaction times (Data not shown).

(a) 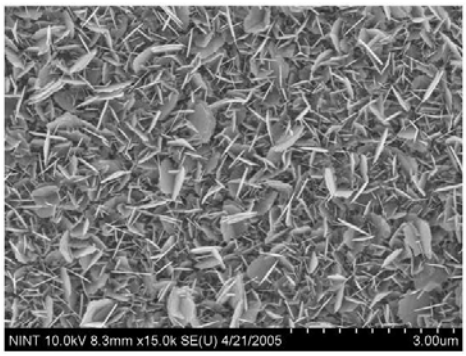

b) 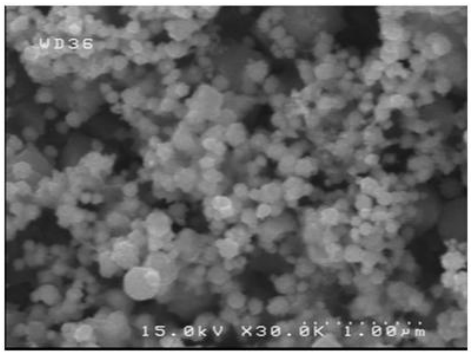

Figure 1. a) SEM images of Ag nanoplates interfaced with GaAs produced in the presence of 1 mM of $AgNO_3$ for 10min. and b) SEM images of Au nanoparticles interfaced with copper in the presence of 1 mM of $HAuCl_4$ for 4h.

2. SERS of Thiophene-2-carbaldehyde Molecules Adsorbed on Ag Nanoplates

The chemical cleanliness and surface roughness associated with the as-grown Ag nanoplates and Au nanoparticles enable them to be easily modified and have large surface areas, which are beneficial to SERS. Thiophene-2-carbaldehyde was chosen as an analyte in the present study. A typical sample of Au nanoparticles as shown in Fig. 1b was used to evaluate SERS activity with the use of thiophene-2-carbaldehyde as a probing molecule. The SERS spectra of Thiophene-2-carbaldehyde at 5% concentration are shown in Figure 2. Au nanoparticles covered with analyte results in a strong Raman signal. As a contrast, the analyte molecules on the surface of the bare Cu do not generate detectable Raman signals (dashed curve , Fig. 2) when they are excited under the same conditions. In conclusion, the cleanliness, surface roughness and high surface area associated with the Au nanoparticles represent a new class of promising structures for possible applications in surface-enhanced spectroscopies.

A 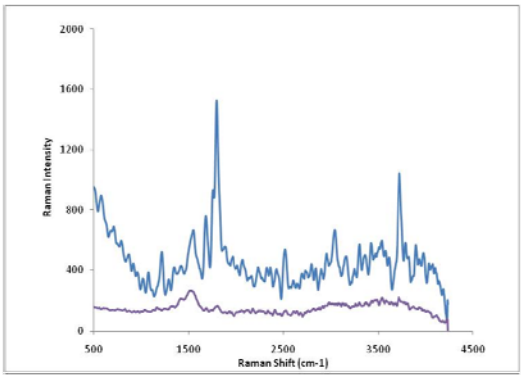

Figure 2. Raman spectra thiophene-2-carbaldehyde self-assembled on Au nanoparticles deposited on Cu foil (curve A) and on the bare Cu foil (curve B).

References

[1] Ralph A. Tripp, Richard A. Dluhy and Yiping Zhao, *Nano Today 2008 (3), 31.*

[2] M.R. Hormozi nezhad, M.Aizawa,A. Ribbe, L.Porter J. Buriak, *Small*, 2005 (11), 1076.

[3] H. Lin, J. Mock, D. Smith,T. Gao, and M. J. Sailor, *J. Phys. Chem. B* 2004, 108, 11654.

A New Perturbation Expansion for Short-Ranged Hard Core Potentials

Mehrdad Khanpour

Department of Chemistry, Islamic Azad University, Amol Branch, Amol, Iran.

E-Mail: mtankhanpour@yahoo.com

Keywords: Thermodynamic Perturbation Theory and Short-Ranged Hard Core Potentials.

Introduction

Thermodynamic perturbation theories are among the most successful theories to describe the properties of liquids. They describe successfully the thermodynamic properties of simple liquids and to some extent their structure [1]. But their success is limited to potentials with attractive tail and with long to moderate range [2]. When the tail of the pair potential of the system under study is short-ranged or very deep, the present perturbation theories are no longer so confident to represent even their thermodynamics properties [2]. So in recent years there have been many attempts to modify thermodynamic perturbation theories in such a way that they can become suitable for short-ranged potentials. We intend in this work to derive a thermodynamic perturbation theory which is in fact a simple generalization of random phase approximation (RPA) and its optimized form (ORPA) to include wider temperature range and hence is somehow appropriate for short-ranged potentials.

The Perturbation Expansion

Like all perturbation theories we will suppose that the pair potential of the system is as follows $u(r)=u_0(r)+\lambda w(r)$ where u_0 stands for the hard sphere fluid with known structure and thermodynamics, λ is a coupling parameter, and $w(r)$ represents the perturbation potential. We start out with the following exact relation [1]:

$$\frac{\beta F}{N}=\frac{\beta F_0}{N}+\frac{1}{2}\beta\rho\int_0^1 d\lambda\int_0^\infty w(r)g(r,\lambda)d^3r \qquad (1)$$

where the F indicates the Helmholtz free energy, N the number of particles, the subscript zero refers to hard sphere liquid, $\beta=\frac{1}{kT}$ where k is the Boltzmann

constant, and T and ρ are the absolute temperature and number density, respectively. Clearly, if we put $g(r,\lambda)=g(r,0)$, the simplest perturbation theory will be reached. In order to get a better expansion we should find a reasonable approximation for $g(r,\lambda)$. This can be achieved by an approximate direct correlation function with the following form:

$$c(r,\lambda)=\begin{cases} c_{HS}(r) & \text{for} \quad r\le 1 \\ c_{HS}(r)+e^{-\lambda\beta w(r)}-1 & \text{for} \quad r>1 \end{cases} \qquad (2)$$

If we expand Eq. (1) with respect to λ and use of the Parseval theorem in Fourier transform theory, we will obtain the following expansion:

$$\frac{\beta F}{N}=\frac{\beta F_0}{N}+\frac{1}{2}\beta\rho\int_0^\infty w(r)g(r,0)d^3r+\frac{1}{2(2\pi)^3}\beta\rho\int_0^\infty w(k)\sum_{n=1}^\infty\frac{h^{(n)}(k,0)}{(n+1)!}d^3k \qquad (3)$$

where $w(k)$ is the Fourier transforms of $w(r)$ and $h^{(n)}(k,0)$ are the Fourier transforms of the successive derivatives of $g(r,\lambda)$ with respect to λ evaluated at $\lambda=0$. Combination of the direct correlation function given by Eq. (2) and its derivatives with respect to λ with the Ornstein-Zernike equation in the Fourier Transformed form enable us to find $h^{(n)}(k,0)$. Up to five terms they are found to be:

$$\begin{aligned} &h'(k,0)=c_1S_0^2\ ,\ \ h''(k,0)=c_2S_0^2+2\rho c_1^2S_0^3\ ,\ h^{(3)}(k,0)=c_3S_0^2+6\rho c_1c_2S_0^3+6\rho^2c_1^3S_0^4 \\ &h^{(4)}(k,0)=c_4S_0^2+8\rho c_1c_3S_0^3+36\rho^2c_1^2c_2S_0^4+6\rho c_2^2S_0^3+24\rho^3c_1^4S_0^5 \\ &h^{(5)}(k,0)=c_5S_0^2+10\rho c_1c_4S_0^3+60\rho^2c_1^2c_3S_0^4+20\rho c_2c_3S_0^3+240\rho^3c_1^3c_2S_0^5+ \\ &90\rho^2c_1c_2^2S_0^4+120\rho^4c_1^5S_0^6 \end{aligned} \qquad (4)$$

where $c_n(k,0)=\int(-\beta w(r))^n e^{-i\mathbf{k}.\mathbf{r}}d^3r$ and S_0 is the static structure factor of hard spheres. In this way the Helmholtz free energy may be computed to every desired degree through Eqs. (3-4). We can also find the radial distribution function of the system. It is given by $g(r)=g(r,0)+\frac{1}{(2\pi)^3}\int_0^\infty e^{i\mathbf{k}.\mathbf{r}}(H(k)+c_1\frac{\delta H}{\delta c_1})d^3k$ where $H(k)=\sum_{n=1}^\infty\frac{h^{(n)}(k,0)}{(n+1)!}$ and $\frac{\delta H}{\delta c_1}=\sum_{n=1}^\infty\frac{\delta h^{(n)}(k,0)}{\delta c_1}/(n+1)!$. Use of Eqs. (3-4) leads to:

$$\frac{\delta h^{'}(k,0)}{\delta c_1} = S_0^2 \ , \ \frac{\delta h^{(2)}(k,0)}{\delta c_1} = 2c_1 S_0^2 + 4\rho c_1 S_0^3 \ , \ \frac{\delta h^{(3)}(k,0)}{\delta c_1} = 3c_2 S_0^2 + 6\rho(c_2 + 2c_1^2)S_0^3 + 18\rho^2 c_1^{\ 2} S_0^4$$
$$\frac{\delta h^{(4)}(k,0)}{\delta c_1} = 4c_3 S_0^2 + 8\rho(c_3 + 3c_2 c_1)S_0^3 + 72\rho^2(c_2 c_1 + c_1^3)S_0^4 + 24\rho c_1 c_2 S_0^3 + 96\rho^3 c_1^{\ 3} S_0^5 \qquad (5)$$
$$\frac{\delta h^{(5)}(k,0)}{\delta c_1} = 5c_4 S_0^2 + 10\rho(c_4 + 4c_1 c_3)S_0^3 + 60\rho^2(2c_1 c_3 + 3c_2 c_1^2)S_0^4 + 20\rho(2c_1 c_3 + 3c_2^2)S_0^3 +$$
$$240\rho^3(3c_1^{\ 2} c_2 + 2c_1^4)S_0^5 + 90\rho^2(c_2^2 + 4c_2 c_1^2)S_0^4 + 600\rho^4 c_1^{\ 4} S_0^6$$

This is our perturbation expansion. It can be shown that this general expansion contains the Optimized Random Phase Approximation (ORPA) as a special case. Now we can use this perturbation expansion to find the structure and thermodynamics of hard-core potentials especially when they are short-ranged. We have done such calculations for square-well potentials with some typical results shown in the following figures. One can simply see the superiority of our perturbation expansion over ORPA and Barker-Henderson's in their Macroscopic Approximation (MC-BH).

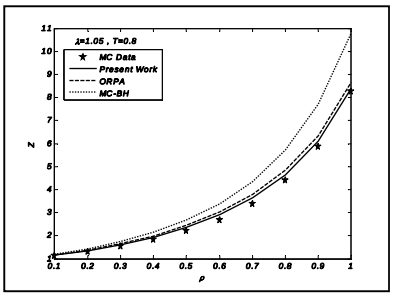

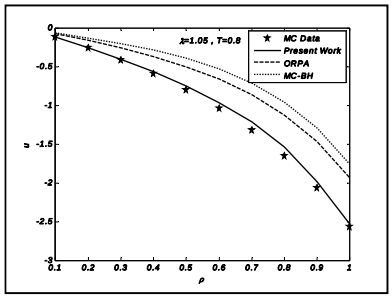

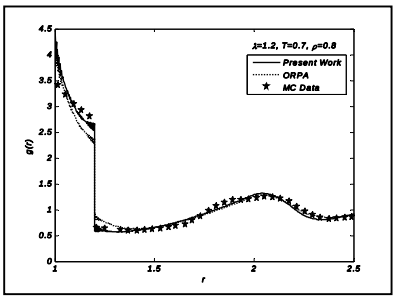

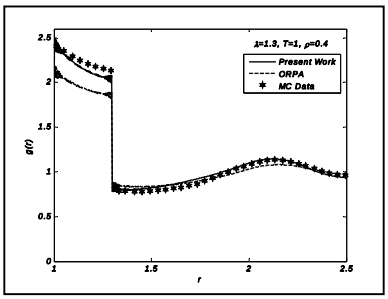

References

[1] J. -P. Hansen and I. R. McDonald, *Theory of Simple Liquids*, (Academic, London, **(2006)**.

[2] S. Zhou, *J. Chem. Phys*, **130**, 054103, (**2009**).

A comparative study of the molecular interactions of polystyrene-CNT composite with polystyrene-BNNT composite

M. Foroutan and A. Taghavi Nasrabadi*

Department of Physical Chemistry, School of Chemistry, College of Science, University of Tehran, Tehran, Iran.

Email: amirtaghavi@khayam.ut.ac.ir

Keywords: Density functional theory, Simulation, Boron nitride nanotube, Polystyrene

Introduction

Boron nitride nanotubes (BNNTs) are structural analogs of carbon nanotubes (CNTs), where C atoms are substituted by alternating B and N atoms. According to the recent experimental studies on BNNT composites [1], it seems that BNNTs have much stronger interactions with polymers, as compared with CNTs. However, the detailed features of the present strong interactions between BNNTs and polymers, and electrical polarization in BNNTs really require further studies which form the goal of this research.

Methods

Single-walled (10,10) BNNT and (10,10) CNT with a length of about 50 Å and nearly the same diameter (13.5 Å) were considered. The tubes are saturated at the ends with hydrogen atoms. Polystyrene (PS) molecule was selected with 5 monomer units. In order to investigate the effect of the polarization of BNNT on polymer adhesion, we have to consider the partial charges of polymer and BNNT. Density functional theory (DFT) calculations with B3LYP/6-31+G** method were performed on polymer structure to get the final geometry-optimized structure and then electrical partial charges was computed and included in the following molecular dynamics (MD) simulations. Partial charges of (10,10) BNNT was also taken from Ref. [2]. All MD simulations were performed in Tinker molecular modeling package (version 5.0) [3]

using the MM3 force field [4]. The simulations are carried out in the NVT ensemble. The Nose-Hoover thermostat was employed to regulate the temperature at 300 K. A cutoff distance of 10.0 Å was used for the van der Waals potentials and the particle mesh Ewald method was implemented to compute the electrostatic interactions. The equations of motion were integrated by using the velocity form of Verlet algorithm. After 500 ps of equilibration time; the simulations were continued for another 1 ns to obtain enough statistical sampling to do calculations.

Results and Discussion

The dynamic behavior of the polymer molecule can be illustrated by tracking the interaction energy of the nanotube–polymer molecule. The interaction energy (E_{inter}) is estimated from the difference between the potential energy of the composite (E_{total}) and the potential energies of the polymer molecule ($E_{polymer}$) and the corresponding nanotube ($E_{nanotube}$) as follows:

$$E_{inter} = E_{total} - (E_{nanotube} + E_{polymer}) \quad (1)$$

Table 1 contains the time-averaged interaction energies of (10,10) CNT and (10,10) BNNT with polystyrene at constant temperature of 300 K, as well as their respective standard deviations.

Table 1: Interaction energies (kcal/mol) of BNNT/CNT-PS composites at T = 300 K.

Nanotube	Diameter (Å)	Interaction with PS
(10,10) CNT	13.59	-26.80±5.45
(10,10) BNNT	13.83	-154.41±6.44

As table 1 show, the amounts of interaction energy of BNNT–PS composite is much higher than its corresponding CNT–PS, which purely demonstrates a much stronger adhesion in the interface of BNNT–polymer composite compared to the similar CNT–based composite. In fact, in addition to the well-known van der Waals interactions of BNNT with polymer, the electrostatic interactions influence markedly its interaction energy; while, only van der Waals interactions govern the interface of CNT–polymer.

Conclusions

On the basis of our calculations, the BNNTs are suggested as better candidates compared to same CNTs for nanocomposite reinforcement applications. This consequence is in good agreement with the recent experimental observations [5].

References

[1] C.Y. Zhi, Y. Bando, C.C. Tang, R.G. Xie, T. Sekiguchi, D. Golberg, J. Am. Chem. Soc. 127 (2005) 15996.

[2] C.Y. Won, N.R. Aluru, J. Phys. Chem. C 112 (2008) 1812.

[3] P. Ren, J.W. Ponder, J. Phys. Chem. B 107 (2003) 5933.

[4] N.L. Allinger, Y.H. Yuh, J.H. Lii, J. Am. Chem. Soc. 111 (1989) 8551.

[5] S. Velayudham, C.H. Lee, M. Xie, D. Blair, N. Bauman, Y.K. Yap, S.A. Green, H. Liu, ACS Appl. Mater. Interfaces. 2 (2010) 104.

Modeling Vapor-Liquid Equilibrium of Mixtures with Tao-Mason Equation of State

Mohammad Mehdi Papari[1,*], Jalil Moghadasi[2], and Fatemeh Fadaei[2]

[1]Department of Chemistry, Shiraz University of Technology, Shiraz, 71555-313, Iran

Email: papari@sutech.ac.ir

Fatima_fadaei_84@yahoo.com

[2]Department of Chemistry, Shiraz University, Shiraz, 71454, Iran

Keywords: Equation of state, Thermodynamic properties, phase equilibria, mixtures

1. Introduction

The need for a reliable model for predicting phase equilibria of pure fluids and fluids mixtures is one of major industrial problems. Measurements are costly and time-consuming. Therefore, it is of vital to have predicative methods to describe thermodynamic properties of fluids and fluid mixtures. Equations of state constitute an important tool in equipment design and have assumed an expanding role in correlating of phase equilibria of pure fluid and mixture fluid. In general, the equations of state in common use can be classified as belonging to the van der Waals family of cubic equations, the extended family of virial equations, or equations based more closely on the results from statistical mechanics and computer simulations.[1]. The Tao-Mason (TM) equation of state (EOS) [2] falls in the latter category. In the case of mixtures, it is mixing and combining rules that allow an EOS developed for pure fluids to be used for mixtures. Accuracy in the prediction of properties of mixtures is one of the major concerns in scientific research and engineering calculations

2. Results and Discussion

In our previous work we extended the Tao-Mason EOS to predict volumetric properties of fluid mixtures [3]. Our objective in the present work is to examine the ability of the TM EOS in modeling vapor-liquid equilibria of mixtures. In this regard, several thermodynamic properties of mixtures consisting of molar densities, vapor pressure, and also excess molar volumes, Gibbs free energy, and thermal expansitivity at constant pressure were calculated. The studied mixtures are

binary noble gas mixtures, refrigerant mixtures, the mixture of noble gases and n-alkanes, the mixtures of ethane or propane with refrigerants, and finally ionic liquid mixtures.

Typically Table 1 contains the predicted and experimental values [4] of vapor pressure of propane-C32 binary mixture at different mole fractions. The harmony between the calculated and experimental values is remarkable.

3. Conclusion

The results demonstrate that the modified TM EOS is able to predict fluid phase equilibria of mixtures in comparison to experimental results.

Propane+C32	Vapoe pressure		
x	ex	cal	dev
0.566	69.8	67.9	2.722063
0.511	77.2	75.9	1.683938
0.451	80.9	80.1	0.988875
0.431	84.5	84.8	-0.35503
0.381	88.3	87.9	0.453001
0.316	90.7	91.2	-0.55127
0.275	93.1	91.8	1.396348
0.22	93.3	93.1	0.214362
0.145	91.3	90.9	0.438116
0.0915	89.6	89.4	0.223214
0.0536	86.3	86.8	-0.57937
0.0428	84.7	84.3	0.472255
0.0401	82.4	81.9	0.606796
0.0286	79.8	79.6	0.250627
0.02	77.4	77.3	0.129199
0.015	75.2	75.7	-0.66489

Table1:phase equilibrium data for propane-nC32 .

4. Reference

(1) Susan F.Barrelros,Jorge C.G.Calado*,Paulette Ciancy.J.Phys.Chem.1982.86.1722-1729

[2] Tao, F. M. and E. A. Mason; “Statistical-Mechanical Equation of State for Nonpolar Fluids: Prediction of Phase Boundaries,” J. Chem. Phys., 100, 9075–9084(1994).

[3] F. Yousefi, J. Moghadasi, M. M. Papari, and A. Campo, Ind. Eng. Chem. Res. 48 (2009) 5079-5084.

[4] C. E. Schwarz, Izak Nieuwoudt, J. Supercritc. Fluids 27 (2003) 133-144.

Surface and Bulk Properties of New Fluid ; SW-HCB Fluid

Mohsen Najafi[1,2] and Ali Maghari[3]

1-Nuclear Science and Technology Institute, AEOI, Tehran, Iran

2-Department of Chemistry, Faculty of Science ,Tarbiat Modares University,Tehran,Iran

mnajafi@aeoi.org.ir , msnnajafi@gmail.com

2-Department of Physical Chemistry , University College of Science ,University of Tehran,Tehran,Iran

maghari@khayam.ut.ac.ir

Abstract

In this paper, we introduce a new fluid called Square Well-Hard Convex Body Fluid (SW-HCB Fluid) and investigate many of the thermodynamic and surface properties of it. In this respect, some of the regularities, phase diagrams, critical behaviors, surface tensions of this fluid are studied. Density functional theory is applied to study the properties of planar liquid–vapor interfaces. We have also optimized potential parameters using experimental surface tension data for several pure fluids.

Keywords : Bulk properties; surface properties; regularities; square- well potential; hard convex body; density functional theory

Introduction

Square-Well (SW) model has been studied for decades. It is a simple fluid that captures the phase behavior of real molecular systems and has analytic representation which makes it more tractable analytically than continuous molecular potentials. In this paper, the term for hard sphere is replaced by the equation for hard convex body and introduced a new fluid called SW-HCB fluid. It contains the essential features of repulsion and attraction. Some of the regularities, phase diagrams, critical behaviors and surface tensions of this fluid are studied in this paper,. Because the vapor-liquid interfacial region is an inhomogeneous one, we apply a density functional approach in order to predict surface properties.

Theory

In this work, we investigate the surface and bulk properties of SW-HCB fluids. It is clear that thermodynamic properties of the system in the bulk, like free energy F, are isotropic

functions. But the surface region is an inhomogeneous one and there is the density gradient in it. A description of interfacial phenomena of fluids at the molecular level is a challenging problem especially inside the critical region. However, the Density Functional Theory (DFT) is the most popular approach to the statistical mechanics of inhomogeneous fluids. The density gradient and the heterogeneity are taken into account in this theory [1]. In DFT, for a free surface, the grand potential functional $\Omega[\rho(\boldsymbol{r})]$ is given by [1-2]:

$$\Omega[\rho(\boldsymbol{r})] = F[\rho(\boldsymbol{r})] - \mu \int \rho(\boldsymbol{r}) d\boldsymbol{r} \qquad (1)$$

We consider a simple fluid in which the intermolecular potential consists of a short-ranged repulsion and long-ranged attraction. In this fluid, the free energy functional $F[\rho(\boldsymbol{r})]$ can be formally expressed as

$$F[\rho(\boldsymbol{r})] = F^{\mathrm{id}}[\rho(\boldsymbol{r})] + F^{\mathrm{hcb}}[\rho(\boldsymbol{r})] + F_{att}^{SW}[\rho(\boldsymbol{r})] \qquad (2)$$

where $F^{id}[\rho(\boldsymbol{r})]$ corresponds to that for an ideal gas and $F^{hcb}[\rho(\boldsymbol{r})]$ and $F_{att}^{SW}[\rho(\boldsymbol{r})]$ stand for the contributions due to the repulsion and attraction respectively. At equilibrium, $\Omega[\rho(r)]$ is a minimum and the corresponding density profile $\rho(r)$ is obtained by a minimization with respect to $\rho(r)$, i.e. $\delta\Omega[\rho(r)]/\delta\rho(r) = 0$

Since we are dealing with planer vapor-liquid interface, the density profile is a function of z only. Once the equilibrium density $\rho_{\mathrm{eq}}(z)$ is obtained by solving the Euler-Lagrange equation, the surface tension can be calculated from [1-2]

$$\gamma = \int_{-\infty}^{+\infty} \{ f[\rho_{\mathrm{eq}}(z)] - \mu\rho_{\mathrm{eq}}(z) + p \} dz \qquad (3)$$

in which $f[\rho_{\mathrm{eq}}(z)] = \rho_{\mathrm{eq}}(z) F[\rho_{\mathrm{eq}}(z)]$ and p is bulk pressure or vapor pressure.

Before studying the interfacial behavior of SW-HCB fluids, it should be calculated vapor pressure, chemical potential and the co-existing bulk densities (ρ^{l} and ρ^{v}). In bulk phases, there are isotropic systems and thermodynamic functions like energy, pressure and entropy are independent of position and the fluid is considered as a homogenous one. In this respect, the above mentioned thermodynamic system is not a functional and therefore,

phase diagram, vapor pressure, Clausius-Clapeyron plot and other thermodynamic properties of homogeneous system can be calculated.

Results and discussion

Calculation of surface properties such as the density profile and surface tension needs accurate values of bulk densities, bulk chemical potential and bulk pressure and therefore, it is better to be investigated bulk properties at first.

1.Bulk properties

In this work, different values of the SW attractive well range parameter (λ) and the non-spherical degree parameter (α) were studied: $1.1 \le \lambda \le 3$ and $1.0 \le \alpha \le 1.2$. For example, phase diagrams of SW-HCB fluids are shown in Fig. 1 for $\lambda = 2.0$ and different αs. It is clear that in liquid-vapor equilibrium, the critical temperature is decreased with increasing α.

2.Surface properties

As it is said before, at equilibrium, $\Omega[\rho(z)]$ is a minimum and the corresponding density profile $\rho(z)$ is obtained from the solution of the Euler-Lagrange equation. Figure 2 presents results using method discussed above for the surface tension of the SW-HCB model for $\lambda = 2.0$ and different αs, as a function of reduced temperature. Generally, as expected, the surface tension decreases monotonically with increasing temperature and vanishes at the critical point. For a given reduced temperature, the reduced surface tension is seen to decrease with increasing the non-spherical degree parameter.

We now use the DFT represented in this work to examine surface tension of several pure fluids such as argon, nitrogen, methane and ammonia. All molecules are modeled as a SW-HCB fluid. In this respect, we optimize the parameters of SW-HCB i.e. $\sigma, \varepsilon, \alpha$ and λ using experimental surface tension data for those molecules. In order to do it, these parameters are regressed with the minimization of the objective function

$$O.F. = \frac{1}{n}\sum_{i=1}^{n} \frac{\left|\gamma_{\text{sw-hcb}} - \gamma_{\text{exp}}\right|}{\gamma_{\text{exp}}} \times 100 \qquad (4)$$

Figure 3 shows the DFT predictions with optimized parameters for the temperature dependence of the surface tension of ammonia. As can be seen, the theoretical descriptions of the surface tension are found to be in a very good agreement with experimental values of the surface tension over the whole range of the temperatures. The experimental data has been taken from the NIST Chemistry WebBook [3].

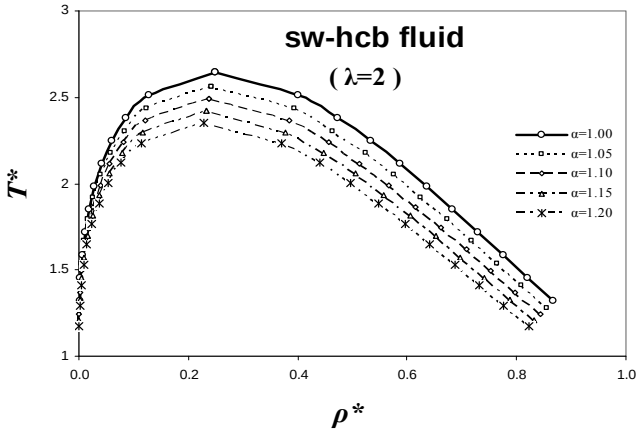

Fig. 1. Liquid-vapor coexistence curve of SW-HCB fluid with the range of potential λ=2.0 and α = 1.0 to 1.2

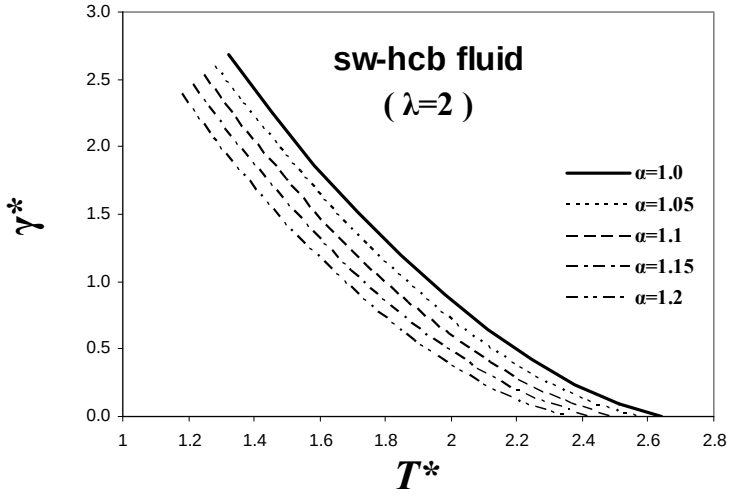

Fig. 2. The reduced surface tension of SW-HCB fluid with $\lambda = 2.0$ and α = 1.0 to 1.2 versus T^*.

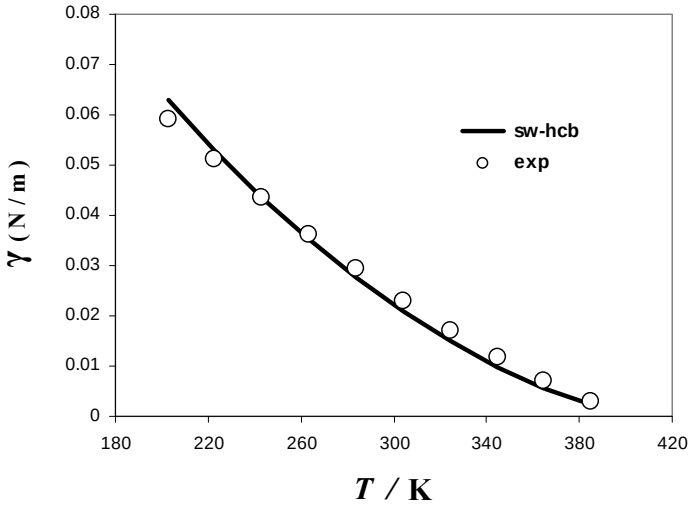

Fig. 3. Surface tension as a function of temperature for ammonia

References

[1] R. Evans , *Advanced in Physics* , **28**(1979)143

[2] Bo Q. Lu, R. Evans and M. M. Telo Da Gama, *Mol. Phys*., **55**(1985)1319

[3] NIST Chemistry Webbook, NIST Standard Reference Database Number 69. National Institute of Standards and Technology, http:www.webbook.nist.gov.

Prediction thermal properties of dense argon using Ihm- Song- Mason Equation of state

F. Kermanpour*

*Faculty of Chemistry, Bu- Ali Sina University, Hamadan, 65178-38695, Iran

In this work, the concept of effective pair potential (EPP) [1] has been applied for calculating thermal properties of liquid argon via ISM equation of state [2]. In such a pair potential, we assume that all of the non additive interaction effects are included in the state dependency of the pair potential parameters. It is indicated that using such an EPP we can obtain more accurate results for both thermodynamic properties of dense fluids.

By using the reported effective potential depth values (ε_{eff}) for dense argon [3], we have obtained the following correlation for this quantity in the temperature range between 130-220 K, and density between 6- 25 mol L^{-1} as,

$$\varepsilon_{eff} = \varepsilon_0 \left(-2.71415 + \left(-0.01877T^* + 0.01362T^{*2}\right)\rho^* + \left(3.30554e-5T^* - 2.37164e-5T*2\rho*2+-1.64871e-8T*+1.20671e-8T*2\rho*3+5.1863T*e-3.04011e-7\rho*2 \right. \right. \quad (1)$$

where ε_0 is the isolated potential depth value, and $T^*$and ρ^* are the reduced temperature and density, respectively. Applying Eq. (1) for ε_{eff} and using ISM equation of state, we have obtained a correlation function for effective intermolecular distance (σ_{eff}), by fitting calculated and experimental data of argon [4] for predicting a given thermodynamic function like internal energy as,

$$\sigma_{eff} = \sigma_0 \left(-2.563503 + 6.098529T^* - 2.14524T^{*2} + \left(-3.808868e-3T^* + 6.440897e-4T*2\rho*+4.49813e-7T*+1.019471e-6T*2\rho*2+1.603428T*e-156739.3\rho*2 \right. \right. \quad (2)$$

Then by having in hand the effective equation of state and using thermodynamic relations, one can calculate other thermodynamic properties of argon, in example heat capacity. The results of such calculations have been shown in the Fig. 1 and 2 for liquid argon. In these figures the symbols indicate the experimental data, solid lines are calculated values using EPP, and dashed lines are calculated values via isolated pair potential parameters. As one

can see, the EPP can predict the thermodynamic properties more accurate than isolated ones. This result is reasonable, because in the dense fluid the interaction potential is different from isolated one, and the non ideality contributions in the interaction energy can be attributed to the state dependencies of the potential parameters interaction. The obtained correlations for potential parameters have also examined for prediction of viscosity and the same conclusion can be gained. All of the figures are for T= 160 K.

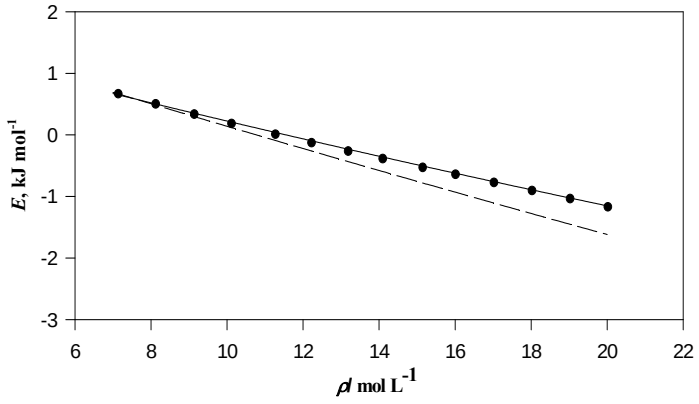

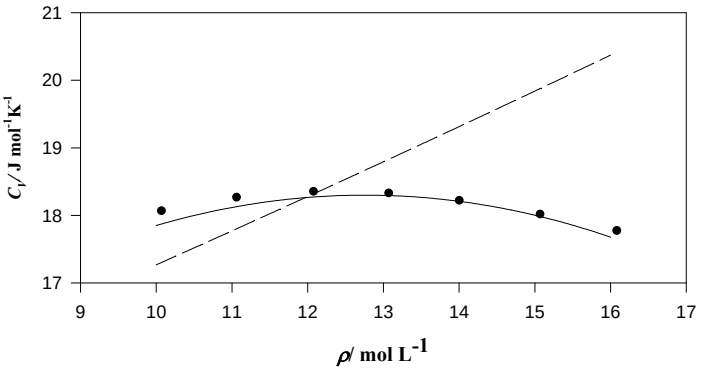

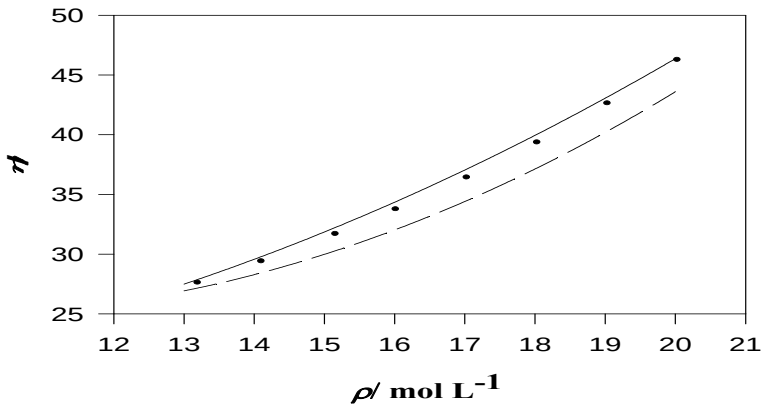

References

[1] G. A. Parsafar, F. Kermanpour, B. Najafi, Phys. Chem. B, 103 (1999) 7287.

[2] G. Ihm, Y. Song, E.A.Mason, J. Chem. Phys., 94 (1991) 3839.

[3] P.G. Mikola & C.J. Pings, Chem.Phys., 46 (1967) 1412.

[4] webbook.nist.gov/fluids/

Direct-potential-fit analysis of the $A\ ^1\Pi$ - $X\ ^1\Sigma^+$ spectra of CH^+

A. Shayesteh* and E. Masoumi

School of Chemistry, College of Science, University of Tehran, Tehran, Iran

E-mail: shayesteh@khayam.ut.ac.ir

Keywords: CH^+ ion, Electronic spectroscopy, Direct-potential-fit

Introduction

The CH^+ ion is a major constituent of the interstellar medium, and is believed to be important in formation of other carbon-containing molecules [1]. There have been numerous studies on the formation, destruction, and abundance of CH^+ ion in the interstellar space [2]. The first laboratory spectra of CH^+ ion were recorded by Douglas and Herzberg [3,4] in the 1940s, and four emission bands (0–0, 1–0, 2–0, and 0–1) were observed in the $A\ ^1\Pi - X\ ^1\Sigma^+$ electronic transition. Douglas and Morton [5] extended the earlier work by observing the $v'' = 0$ and $v'' = 1$ progressions in the $A\ ^1\Pi - X\ ^1\Sigma^+$ system up to $v' = 4$. They also confirmed the occurrence of $R(0)$ lines of the 0–0, 1–0, 2–0 and 3–0 bands of CH^+ ion in the interstellar absorption spectrum at 4233, 3958, 3745 and 3579 Å, respectively. The $A\ ^1\Pi - X\ ^1\Sigma^+$ spectrum of CH^+ has been studied by several research groups since then, [6-11] and spectroscopic data have been obtained for the four isotopologues $^{12}CH^+$, $^{13}CH^+$, $^{12}CD^+$ and $^{13}CD^+$.

Overview of data

We used all the $A\ ^1\Pi - X\ ^1\Sigma^+$ data available in the literature [3-12] in our analysis. The data set includes absorption and emission spectra of all four isotopologues $^{12}CH^+$, $^{13}CH^+$, $^{12}CD^+$ and $^{13}CD^+$. We also included several rotational lines of the $A\ ^1\Pi - X\ ^1\Sigma^+$ system (high J) that were observed using high-resolution laser photofragment spectroscopy [13,14]. The data span up to $v' = 13$ of the $A\ ^1\Pi$ state.

Results

The observed transition wavenumbers were first fitted using the Dunham expression:

$$E(v,J) = \sum_{m=0}\sum_{l=0} Y_{l,m}\left(v+\tfrac{1}{2}\right)^l \left(J(J+1)-\Lambda^2\right)^m .$$

The Λ-doubling in the $^1\Pi$ state was taken into account by adding the following expression to the Dunham formula:

$$\delta E_\Lambda = \pm\frac{1}{2}\sum_{m=1}\sum_{l=0} q_{l,m}\left(v+\tfrac{1}{2}\right)^l \left(J(J+1)-\Lambda^2\right)^m .$$

Using the Dunham constants, we constructed RKR potential curves for the $X\ ^1\Sigma^+$ and $A\ ^1\Pi$ states. The RKR potential curves were then used as trial potentials for the direct-potential-fit (DPF) procedure. In the DPF analysis, the potential energy curves of the $X\ ^1\Sigma^+$ and $A\ ^1\Pi$ states are described by analytic potential energy functions whose parameters are adjusted until the eigenvalues of the following radial Schrödinger equation match the observed rovibronic energy levels [15]:

$$\left\{\frac{-\hbar^2}{2\mu}\frac{\mathrm{d}^2}{\mathrm{d}r^2}+V_{\mathrm{ad}}(r)+\frac{\hbar^2 J(J+1)}{2\mu r^2}\left[1+g(r)\right]+s(e/f;J)\,\Delta V_{\Sigma}(r)\right\}\psi_{\mathrm{v},J}(r)=E_{\mathrm{v},J}\psi_{\mathrm{v},J}(r).$$

Some preliminary results are shown in the following table and figure.

Table 1. RKR turning points for the $A\ ^1\Pi$ state of $^{12}CH^+$

v	E(v) / cm^{-1}	$r_{\min}$ (Å)	$r_{\max}$ (Å)
0	25021.03	1.1161	1.4027
1	26662.32	1.0516	1.5752
2	28095.59	1.0161	1.7321
3	29336.69	0.9921	1.8918
4	30406.70	0.9746	2.0594
5	31326.29	0.9610	2.2381
6	32112.09	0.9502	2.4320
7	32775.03	0.9415	2.6486
8	33320.40	0.9346	2.9016
9	33749.61	0.9293	3.2158
10	34063.35	0.9256	3.6389
11	34266.08	0.9232	4.2767
12	34371.70	0.9220	5.4156
13	34410.24	0.9215	7.7930

Figure 1. Potential energy curves for the X and A states of CH^+

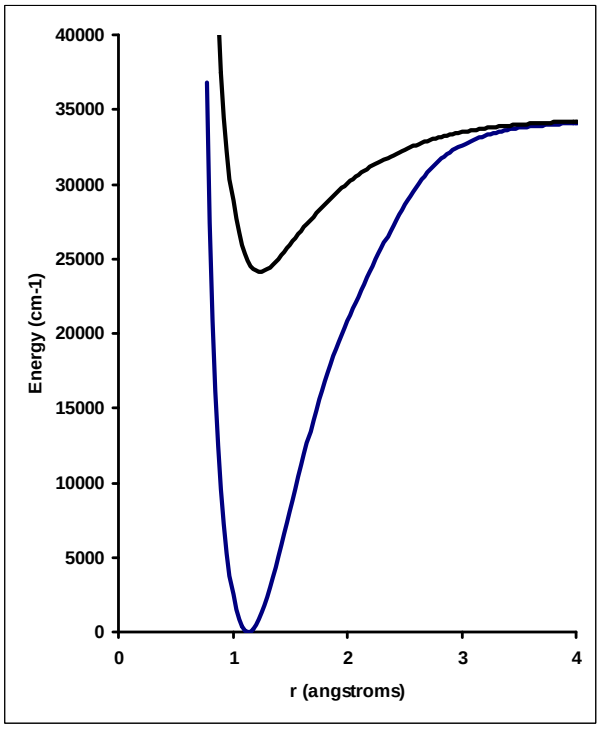

Work in progress

The v′ = 13 of the $A\ ^1\Pi$ state has its $r_{\max}$ turning point at about 7.8 Å, and is likely to be the highest bound vibrational level of the $A\ ^1\Pi$ state. The direct-potential-fit (DPF) analysis will yield accurate potential energy curves for the $X\ ^1\Sigma^+$ and $A\ ^1\Pi$ states of CH^+. In these electronic states, the CH^+ ion dissociates into the C^+ (^{2}P) + H (^{2}S) channel, and our DPF analysis may lead to an improvement in the accuracy of the dissociation energy of CH^+ ion.

References

[1] W. Klemperer and P. M. Solomon, *Astrophys. J.* 178 (1972) 389.

[2] J. Cernicharo, X. -W. Liu, E. Gonzalez-Alfonso, P. Cox, M. J. Barlow, T. Lim and B. M. Swinyard, *Astrophys. J.* 483 (1997) L65.

[3] E. A. Douglas and G. Herzberg, *Astrophys. J.* 94 (1941) 381.

[4] E. A. Douglas and G. Herzberg, *Canad. J. Res. A* 20 (1942) 71.

[5] E. A. Douglas and J. R. Morton, *Astrophys. J.* 131 (1960) 1.

[6] A. Carrington and D. A. Ramsay, *Phys. Scr.* 25 (1982) 272.

[7] Z. Bembenek et al. *J. Phys. B: At., Mol. Opt. Phys.* 20 (1987) 6197.

[8] Z. Bembenek, *J. Mol. Spectrosc.* 181 (1997) 136.

[9] Z. Bembenek, *J. Mol. Spectrosc.* 182 (1997) 439.

[10] U. Hechtfischer et al. *J. Chem. Phys*. 117 (2002) 8754.

[11] R. Hakalla, R.Kepa, W. Szajna and M. Zachwieja, *Eur. Phys. J. D* 38 (2006) 481.

[12] T. Amano, *Astrophys. J.* 716 (2010) L1.

[13] P. J. Sarre, J. M. Walmsley and C. J. Whitham, *J. Chem. Sos., Faraday Trans. 2*, 82 (1986) 1243.

[14] P. J. Sarre, C. J. Whitham and M. M. Graff, *J. Chem. Phys.* 90 (1989) 6061.

[15] A. Shayesteh, R.D.E. Henderson, R.J. Le Roy and P.F. Bernath, *J. Phys. Chem. A* 111 (2007) 12495.

Calculation of rovibrational energy levels of rare gas dimmers with Ogilvie-Wang potential function

Nasim Vahdatpour*[a], M.Gharibi[a], and R.Islampour[a]

[a]Department of Chemistry, Tarbiat Moallem University, Tehran, Iran

nvahdatpour@yahoo.com

Keywords: Numerov, DVR, Rare gas, Ogilvie-Wang Potential energy function

Introduction

This work uses the "Numerov and discrete variable representation (DVR) methods" to find rovibrational energy levels of homonuclear and heteronuclear rare gas dimers. By solving the related nuclear Schrödinger equation with Ogilvie-Wang potential energy function, rovibrational energy levels of the ground electronic state of the dimers are calculated. The results are compared with the semi-empirical data calculated by Ogilvie-Wang using fitting method. The results show that the proposed methods lead to highly accurate rovibrational levels.

The vibrational Schrödinger equation for diatomic molecules has the following form

$$-\frac{\hbar^2}{2\mu}F''(R)+\left[U(R)+\frac{J(J+1)\hbar^2}{2\mu R^2}\right]F(R)=E_{int}F(R) \quad (1)$$

where the $U(R)$ is the potential energy function and is taken to be the Ogilvie-wang semi-empirical potential function given by

$$U(R)=c_0 z^2\left(1+\sum_{j=1} c_j\, z^j\right) \quad (2)$$

Where $z=\frac{2(R-R_e)}{(R+R_e)}$. R_e is the equilibrium internuclear distance [1].

There are several methods for solving eq.(1) numerically, as Numerov, DVR and log derivative methods.

The Calculation Method

1. Numerov Method

The Numerov method presents a numerical method for computer solution of the one – particle, one-dimensional Schrödinger equation that allows one to get accurate bound – state eigenvalues and eigenfunctions for an arbitrary $V(x)$. Using Taylor series expansion we obtain the following formula[2]

$$\psi_{n+1} \approx \frac{2\psi_n - \psi_{n-1} + \frac{5}{6}Q_n\psi_n s^2 + \frac{1}{12}Q_{n-1}\psi_{n-1}s^2}{1 - \frac{1}{12}Q_{n+1}s^2} \quad (3)$$

where $G = m\hbar^2(2V - 2E)$ and s is the interval length.

Equation (3) allows us to calculate ψ_{n+1}, the value of ψ at point $x_n + s$, if we know $\psi_n$and ψ_{n-1}, the values of ψ at the preceding two points x_n and $x_n - s$.

In Numerov method we start the solution at a point x_0 well into the left-hand classically forbidden region, where $\psi(x_0)$ is very smal, and end the solution at a point x_{max} well into the right-hand classically forbidden region, where $\psi(x_{max})$ is also close to zero[2].

2. DVR method

The discrete variable representation (DVR) offers an alternative approach widely used in atomic and molecular systems. This method was introduced and developed by Light and et al. [3]. The attractive features of the DVR are that the potential matrix elements are diagonal and equal to the values of the potential operator at the DVR points, while the kinetic energy T can be evaluated analytically [4].

DVR method is based on the variation method. The advantage of this method over numerov method is its simplicity. While the numerov method is applicable only for solving one-dimensional Schrödinger equation, DVR method is widely used to solve multi-dimensional problems.

Results

Tables 1 and 2 represent the DVR- and Numerov- calculated vibrational and rotational spacings forAr_2, Ne_2 and NeAr dimers with Ogilvie-Wang potential function. It is seen that the results of both numerov and DVR methods are identical. So, both methods have high accuracy and can be applied for calculating rovibrational energy levels of rare gas dimers.

Table 1: Comparison of experimental and calculated vibrational spacings (cm^{-1})

Molecule	v'-v''	DVR	Numerov	experimental
Ne_2	1-0	13.8429	13.8429	13.70±0.5
Kr_2	1-0	21.4330	21.4330	21.4137±0.00007
	2-1	19.2863	19.2863	19.2714±0.0003
	3-2	17.1531	17.1531	17.1410±0.0009
NeKr	1-0	18.347	18.3477	18.384±0.028
	2-1	11.445	11.4267	11.52±0.18
	3-2	6.8468	6.0501	6.81±0.64

Table 2: Comparison of experimental and calculated rotational spacings in the ground vibrational state (cm^{-1})

Molecule	J'-J''	DVR	Numerov	experimental
Ne_2	1-0	0.306	0.306	0.34
	2-1	0.612	0.612	-
	3-2	0.916	0.916	-
Ar_2	1-0	0.115	0.115	0.115
	2-1	0.231	0.2311	0.2310
	3-2	0.346	0.3467	0.3464
NeKr	1-0	0.1489	0.1488	0.1498±0.0014
	2-1	0.2977	0.2977	0.2996±0.0014
	3-2	0.4464	0.4465	0.4491±0.0014

References:

[1] J.F. Ogilvie, Y.H. Wang, J. Molec. Struct., 273 (1992), pp. 277-290

[2] I.N. Levine, *Quantum Chemistry*, 5 th ed., Prentice-Hall, 2002

[3] Light, J. C., Hamilton, I. P., Lill, J. V.: J. Chem. Phys. 82, 1400 (1984)

[4] Barletta, P., Lombardi, M., Kievsky, A., Few-Body Systems 34, 11–14 (2004)

Measurement problem and a Critical approach on Decoherence theory

Arash Tirandaz[‡] and Afshin Shafiee[†]

Research Group on Foundation of Quantum Theory and Information,
Department of Chemistry, Sharif University of Technology,
P.O.Box 11365-9516, Tehran, Iran

Abstract: Considering the decoherence theory we try to mention some conceptual problems of this theory in tackling the measurement problem The quantum to classical transition discussed in the framework of decoherence theory in section I. At the end, we survey some defects of the decoherence approach on measurement problem in the framework of *gedanken* experiments.

Introduction:

The main stream in quantum mechanics is the Copenhagen interpretation mechanics routed in the beliefs of Bohr that the quantum phenomena is a black box and it is impossible to represent a lucid description of its nature. Considering Copenhagen hegemony, quantum domain is not in the access of experimenter. Then, his knowledge about the micro world is based on the measurement results. What is happened in the black box, consisting of quantum system and apparatus, must be consider as a metaphysical and mysterious phenomena that has not any physical description in the theory.

I. Decoherene approach on measurement problem

Decoherence theory tries to explain the so-called transition from quantum to classical by considering the openness of quantum systems. Decoherence demands that realistic quantum systems are not isolated from their environment.

In spite of the classical physics, the environment has a crucial effect on the evolution of the system. The role of the environment is twofold: First the interaction with environment leads to the suppression of interference terms between quantum states of the system. It corresponds with the suppression of the off-diagonal elements of the reduced density matrix of the system under its interaction with surrounding. Then by the means of a non-unitary evolution which results from the trace operation on the environment degrees of freedom decoherence shows that why interference terms due to the quantumness of the system, removes through the interaction with the environment. Second: during the ubiquitous interaction of system-environment, some preferred states of the system are selected known as pointer states. These are states which preserve their correlation under the decoherence phenomena.

Discussion: Critical approach on Deceherence

[‡] tirandaz@mehr.sharif.ir
[†] shafiee@sharif.edu

In the theory of the classical statistics, mixed states are in relation with ignorance interpretation of probability. It means, the experimenter knows that every subsystem of the an ensemble is in definite states but she does not know exactly that which one is in which state. Then, it seems that mixed density matrix of the system results from decoherence phenomena, could be interpreted as classical ones. One should keep in mind that the improper mixed states results from trace operation on a pure density matrix of the system-environment. The whole is in a pure state and all of the possibilities exist simultaneously. Proper mixed state, in its classical sense, does not results from a pure density matrix. So, it is not accurate to say that improper mixed states could be considered as their classical counterparts. In addition, the interpretation of the proper mixed states is dependent on the interpretation of the quantum states. Before going further, suppose that we have an ensemble of a proper mixture with 30% of quantum systems in the state$|0_z\rangle$, 50% in $|0_x\rangle$ and 20% in the state$|1_y\rangle$. Where $|0\ \rangle and\ |1\ \rangle$ represents spin up and down respectively. If one carries out the spin measurement in the Z-direction what will be the results? One may think that the answer is that 20% of quantum particles in the ensemble reflected by the measuring apparatus in positive direction of the Z axis . However one can easily show that it is not correct! Since $|0_x\rangle and\ |1_y\rangle$ are in relation with $|0_z\rangle$ according to following relations:

$$|0_x\rangle = \frac{1}{\sqrt{2}}(|0_z\rangle + |1_z\rangle) \qquad .2$$

$$|1_y\rangle = \frac{1}{\sqrt{2}}(|0_z\rangle - i|1_z\rangle) \qquad .3$$

So, even if we have a proper mixture of states, still its interpretation is dependent rigorously on the interpretation of the isolated quantum states or the wave function. Obviously, the two description results from the formalism of standard quantum mechanics and the density matrix approach are not in agreement. There is no evidence if the mixed state 3 could be results from the $|\psi\rangle$ in relation 4. As it is not possible to have a theory with two incompatible descriptions decoherence demands that if one takes the effect of the environment into account to describe the evolution of $|\psi\rangle$ and trace over the degrees of the environment the reduced density matrix 4 could be retrieved.

References:

1.M. Schlosshauer, Decoherence, "the measurement problem, and interpretations of quantum mechanics", *Review Of Modern Physics* **76**, 1267–1305 (2004).

2. W. H. Zurek, "Pointer basis of quantum apparatus: Into what mixture does the wave packet collapse?", *Physical Review.D* **24**, 1516–1525 (1981).

3.W. H. Zurek, “Environment-induced superselection rules”, *Phyical Reiewv.D* **26**, 1862–1880 (1982).

Conceptual density functional theory description of etherification rate constant

Mojtaba Alipour* and Afshan Mohajeri

Department of Chemistry, College of Sciences, Shiraz University, Shiraz, 71454, Iran

(*Email: malipour@shirazu.ac.ir)

Keywords: CDFT, Electrostatic potential, Etherification rate constant, Phenol derivatives.

Introduction

Conceptual Density Functional Theory (CDFT) [1] plays an emerging role to get a simple picture of chemical phenomena and rationalizing the experimental data by using reactivity descriptors. Among various descriptors, the molecular electrostatic potential (MEP) [2] is a real physical property which can be determined either computationally or experimentally. The MEP, $\Phi(r)$, that the *electrons* and *nuclei* of a molecule create in the surrounding space is given by

$$\Phi(r)=\sum_{\alpha}\frac{Z_{\alpha}}{|R_{\alpha}-r|}-\int\frac{\rho(r')}{|r'-r|}dr' \qquad (1)$$

in which Z_{α} is the charge on nucleus α, located at R_{α}, and $\rho(r)$ is the electronic density. In this work the MEP at the nucleus is applied as an effective approach in describing the influence of substituent on the rate constant of etherification reaction of phenol derivative

Theory and method

According to the DFT framework, the total energy of a given system is a functional of the number of electrons, N, and of the external potential, $\upsilon(r)$, i.e. $E=E[N,\upsilon(r)]$. The energy can be perturbed by changing N and/or $\upsilon(r)$ as ΔN and/or $\Delta\upsilon(r)$. With the Taylor expansion up to the second order, the subsequent change in the total energy reads

$$\Delta E=\left[\left(\frac{\partial E}{\partial N}\right)_{\upsilon(r)}\Delta N+\int\left(\frac{\delta E}{\delta\upsilon(r)}\right)_{N}\Delta\upsilon(r)dr\right]+\frac{1}{2!}\left[\left(\frac{\partial^2 E}{\partial N^2}\right)_{\upsilon(r)}(\Delta N)^2+2\,\Delta N\int\left(\frac{\delta\partial E}{\delta\upsilon(r)\partial N}\right)\Delta\upsilon(r)dr+\iint\left(\frac{\delta^2 E}{\delta\upsilon(r')\delta\upsilon(r)}\right)_{N}\Delta\upsilon(r)\Delta\upsilon(r')\,dr\,dr'\right] \qquad (2)$$

We consider proton dissociation of phenol as a special case of the general consideration in Eq. (2) leading to the change in external potential, $\Delta\upsilon(r)$, but the number of electrons

remains unchanged ($\Delta N = 0$). Accordingly, under the hypothesis that oxygen is the center of the etherification and that the change in the electronic feature of the phenol derivatives through the substituent influence can be well reflected by the local property of either oxygen or hydrogen of phenolic hydroxyl group, in our recent work we have proposed a quantitative prediction of etherification rate constant through the MEP at the nuclei of hydroxyl moiety [3]

$$\log k_X / k_H \propto \sum_{i \neq H} \frac{Z_i}{|R_i - R_H|} - \int \frac{\rho(r)}{|r - R_H|} d\tau \qquad (3)$$

where k_X is the first order rate constant of substituted phenol and k_H is the corresponding value for phenol. In this equation R_H is the coordinate of the leaving proton in etherification and $\{R_i\}$ are the coordinates of the other nuclei in the phenol molecule. As an illustrative example for etherification and validation of Eq. (3), 30 mono- and di-substituted phenol derivatives including electron-donating and electron-withdrawing substituents have been investigated. All geometry optimization and frequency calculation at B3LYP/6-311++G(d,p) level of theory have been performed with the Gaussian 03 suite of programs.

Results and discussion

In Figures 1(a) and 1(b) we presented the experimental rate constant data versus MEP at oxygen and hydrogen nuclei of phenolic hydroxyl group, respectively. As can be seen from this figures, the changes in the MEP at oxygen (R^2=0.920) and at hydrogen (R^2=0.884) were strongly correlated with the variation of experimental rate constant data. The oxygen atom, however, is in direct contact with the phenolic ring and consequently it is more influenced by the substituent effect. Therefore, we can deduce that the MEP on the oxygen is a more sensitive descriptor for rate constant prediction. In conclusion, the proposed method provides a simple route to predict rate constant of etherification reaction of

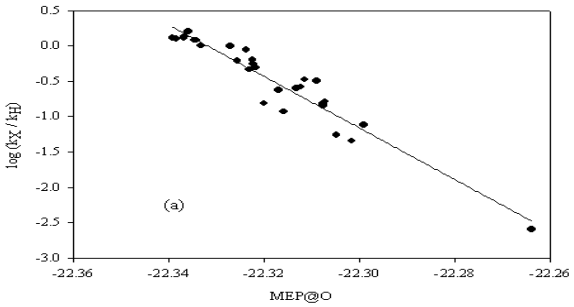

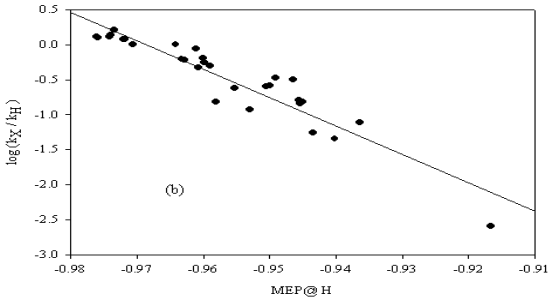

substituted phenols from a simple density functional calculation.

Figure 1. Etherification rate constants versus MEP@O (a) and MEP@H (b) for a series of mono- and di- substituted phenols.

References

[1] Parr, R.G.;Yang, W. *Density-functional theory of atoms and molecules*; Oxford University Press: New York, 1989.

[2] Politzer, P.; Truhlar, D.G. Eds. *Chemical Applications of Atomic and Molecular Electrostatic Potentials*; Plenum Press: New York, 1981.

[3] Alipour, M.; Mohajeri, A. *J. Phys. Chem. A* 114 (2010) 7417.

Peltier and Seebeck Effects in Molecular Electrode Junction Systems

H. Sabzyan*, R. Safari

Department of Chemistry, University of Isfahan, Isfahan 81746-73441, I. R. Iran,
Email: sabzyan@sci.ui.ac.ir & safari_physicalchemistry@yahoo.com

Abstract

Molecular Peltier coefficients (MPCs) and molecular Seebeck coefficients (MSCs) are introduced and computed, based on the density and energy transfers between different parts (as intramolecular sectional junctions, ISJs) of a single molecule nanoelectronic device using quantum theory of atoms in molecule. The MPCs and MSCs, calculated for a typical single molecule electrode junction (E-M-E), show non-linear dependence on the electric field strength. Analysis of these proposed coefficients can discriminate and rank the electrothermal or thermoelectric performance of molecular devices. In E-M-E system, electrons of the gold electrodes contribute to the electron transfer mechanism between ISJs, via coupling between the molecule and electrode, and so the EF dependences of the MPCs and MSCs are sizeable.

Keyword: Peltier effect, Seebeck effect, thermoelectric, Nanoelectronic

Introduction

The temperature difference induced by a voltage gradient is known as Peltier effect [1]. The Seebeck effect is the reverse of Peltier effect. Calculation of molecular Peltier coefficients (MPCs) for isolated molecule in EF has been reported previously [2]. In this work, MPCs and molecular Seebeck coefficients (MSCs) are calculated for a molecule sandwiched between two gold electrodes (E-M-E). We divided the E-M-E system into four sections, Fig. 1, as intramolecular sectional junction (ISJ). In a nanoelectronic circuit, the charge and energy transfer occur between ISJs due to electric field (EF). Then, the reduced

sectional Peltier and Seebeck coefficients, $\bar{\pi}_M(S_U,S_D)$ & $\bar{\pi}_M(S_L,S_R)$ and $\bar{S}_M(S_U,S_D)$ & $\bar{S}_M(S_L,S_R)$, are calculated based on the energy transfers between different ISJs, within the quantum theory of atoms in molecule (QT-AIM) [3]. These coefficients are respectively related to (up↔down) and (left↔right) energy transfer in the single molecule device.

Methodology

We assumed that the redistribution of energy between ISJ and flow of heat (heat in ↔heat out) between macroscopic Peltier junctions are similar. Based on the linear law of thermoelectric phenomenological equation, the reduce molecular Peltier coefficient ($\bar{\pi}_M$) can be introduced and computed via

$$\vec{\nabla}\bar{E} = \bar{\pi}_M \cdot \vec{F}_{elec} \quad (\vec{F}_{elec} = \varepsilon_F L) \tag{1}$$

where $\vec{\nabla}\bar{E}$, $\vec{F}_{elec}$, ε_F and L are the reduce energy transferred between ISJ due to the EF, electric field (EF) voltage, electrical field intensity and distance between the two ends (ISJs) of the single molecule. Values of the kinetic energy ($K(\Omega)$), total atomic virial ($\nu(\Omega)$) and total atomic energy ($E(\Omega)$) can be calculated for atomic basin Ω using QT-AIM via

$$E(\Omega) = K(\Omega) + \nu(\Omega), \quad K(\Omega) = \frac{-\hbar^2}{2m} N \int_{\Omega} dr \int d\tau \left[\psi \nabla^2 \psi^* + \psi^* \nabla^2 \psi\right] \tag{2}$$

For a system in electrostatic equilibrium, $\nu(\Omega) = V(\Omega)$ [3]. Based on the Onsager reciprocal relation, the reduce molecular Seebeck coefficient, $\bar{\sigma}_M$, becomes

$$(\bar{\sigma}_M)_{J_I,J_{II}} = \frac{(\bar{\pi}_M)_{J_I,J_{II}}}{T_{eq}}, \quad T_e(J,\varepsilon_F) \equiv \frac{2}{3k_B}\left\{\sum_{N_J}^{All\ atoms} (< K(J,\varepsilon_F) > - < \overset{\circ}{K}(J,0) >)\right\}_J + \overset{\circ}{T}_e \tag{3}$$

where ($T_e(J,\varepsilon_F)$, $< K(J,\varepsilon_F) >$) and ($T_e(J,0)$, $< \overset{\circ}{K}(J,0) >$) are respectively the electronic temperature and kinetic energy in the absence and presence of EF. In the Eq.(3), T_{eq} and $\overset{\circ}{T}_e$ are the equilibrium and the reference temperatures, respectively. Geometry optimization and calculation of the structural and electronic properties have been carried out under different

EF intensities applied in the *x* direction, at the UB3LYP/6-311G* level of theory using LANL2DZ pseudopotential for the gold atoms.

Results and Discussion

The results are shown in Fig. 2. The calculated MPCs and MSCs show non-linear dependence on the EF strength. In comparison with the response of the isolated molecule, response of the E-M-E is intensified due to the coupling of the gold atoms electrons with the molecule electronic system. Based on the method proposed in this work, it is possible to predict and analyze details of the thermoelectric effect in all E-M-E nanoelectronic systems.

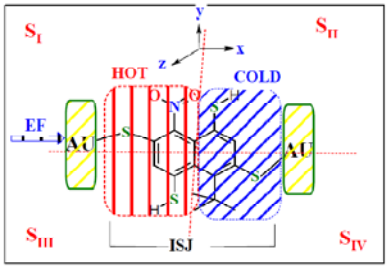

Fig.1. Single molecule electrode junctions.

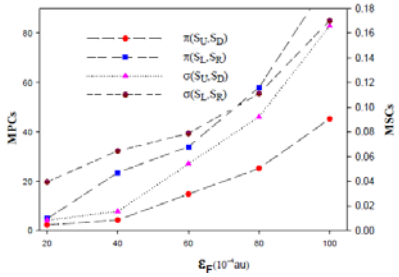

Fig. 2. EF effect on the MPCs and MSCs.

References:

[1] Rowe, D.M., *Thermoelectric Handbook, Macro to Nano*, CRC Press, Boca Raton, **2006**.

[2] Sabzyan , H. ; Safari, R., ICNN- **2010**, 9-11 November, Shiraz, Iran.

[3] Matta C. F., *Quantum Biochemistry, Wiley:* Weinheim**, 2010**.

Computational Approach for Evaluating of Anti-Cancer Activity of Chalcones from Their Molecular Structure

Z. Rostami*[a], H. Iloukhani[b], A. Najafi[a], N. Afshari[a], and M. Frouzandeh[a]

[a]*Department of Chemistry, University of Payame Noor, Hamedan, Iran*

(Email: P_Rostami1978@yahoo.com)

[b]*Department of Physical Chemistry, Faculty of Chemistry, Bu-ali Sina University, Hamedan, Iran*

Keywords: QSAR, MLR analysis, Chalcones derivatives, Anti cancer activity

Introduction:

Cancer is a terrible disease which is the leading death of the human population in some areas of the world [1]. Halcone (and related compounds "chalconoids") is an aromatic ketone that forms the central core for a variety of important biological compounds, which are known collectively as chalcones. They show antibacterial, antifungal, anticancer and anti-inflammatory properties. Some chalcones demonstrated the ability to block voltage-dependent potassium channels. Methyl hydroxychalcone, found in cinnamon, was thought to be insulin mimetic, improving insulin response of diabetics. A data set containing 36 chalcones derivatives was used in this study. These compounds synthesized first by Hui Wua et al. [2]. The biological evaluation of these compounds was made by cytotoxicity in LNCaP cell line, IC50, and presented in Table 1.

Table 1. Chemical structure and cytotoxicity of chalcones derivatives.

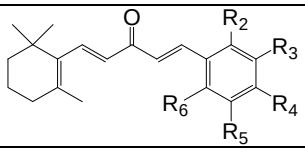

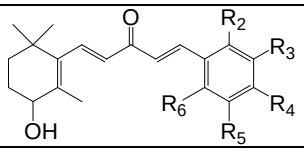

Compound	R_2	R_3	R_4	R_5	R_6	IC50	Compound	R_2	R_3	R_4	R_5	R_6	IC50
1	H	OCH_3	OH	H	H	9.5	19	H	H	H	H	H	5.8
2	H	OH	OCH_3	H	H	9.9	20	CF_3	H	H	H	H	2.9
3	H	CF_3	H	H	H	2.8	21	H	CF_3	H	H	H	0.74
4	H	H	CF_3	H	H	9.1	22	H	H	CF_3	H	H	3.0
5	F	H	H	H	H	10.7	23	F	H	H	H	H	2.9
6	H	F	H	H	H	12.9	24	H	F	H	H	H	4.4
7	H	H	F	H	H	7.3	25	H	H	F	H	H	3.9
8	H	NO_2	H	H	H	2.7	26	H	CF_3	F	H	H	2.2
9	H	NO_2	OH	H	H	26.8	27	H	CF_3	H	F	H	1.1
10	H	NO_2	H	H	Cl	4.2	28	F	CF_3	H	H	H	1.1
11	H	CH_3	H	H	H	17.8	29	F	H	CF_3	H	H	2.6
12	CF_3	H	H	H	H	22.6	30	F	H	H	CF_3	H	1.7
13	H	CF_3	H	H	H	1.0	31	F	H	H	H	CF_3	4.9
14	H	H	CF_3	H	H	4.7	32	H	CH_3	H	H	H	4.1
15	F	H	H	H	H	1.6	33	H	CN	H	H	H	1.8
16	F	H	H	CF_3	H	1.7	34	H	NO_2	H	H	H	2.0
17	H	NO_2	H	H	H	3.3	35	H	H	NO_2	H	H	4.2
18	H	CH_3	H	H	H	12.2	36	H	OCH_3	H	H	H	4.9

Methods:

In the present study we aimed to develop Quantitative Structure Activity Relationship (QSAR) method for the anticancer activity of chalcones derivatives. AM1 semi-empirical quantum-chemical calculation was used to optimize the 3D geometry of the molecules using the HyperChem software. Dragon computer software was employed to calculate the molecular descriptors. Genetic algorithms (GA) were used as a variable selection method. Table 2 presents the molecular descriptors used in this study.

Table 2. 2D Autocorrelations descriptors used in this study.

No.	Symbol	Description
1	Eeig04r	Eigenvalue 04 from edge adj. matrix weighted by resonance integrals
2	PJI2	2D Petitjean shape index
3	C-038	Al □ C (=X) □- Al
4	HATS7p	leverage-weighted autocorrelation of lag 7 / weighted by atomic polarizabilities
5	H8m	H autocorrelation of lag 8 / weighted by atomic masses
6	Mor31m	3D-MoRSE - signal 31 / weighted by atomic masses
7	Mor02p	3D-MoRSE - signal 02 / weighted by atomic polarizabilities

Results and Discussion:

Multiple linear regressions (MLR) were used to derive the QSAR equation. The best QSAR model obtained with the descriptors (Table 2) is given below together with the statistical parameters of the regression:

Log (IC50) = 2.0175 -2.1058 (Eeig04r) + 0.9878 (PJI2) -0.9933 (C-038) –1.5304 (HATS7p) - 2.4676 (H8m) - 1.1573 (Mor31m) + 0.2164 (Mor02p)

N = 36, R^2 = 0.922, RMS = 0.108, F= 51.662, Q^2 = 0.8371

Where N is the number of compounds, R^2 is the correlation coefficient, RMS is the root mean square deviation, F is the Fisher ration, and Q^2 is the correlation coefficient of the cross-validation.

Conclusion:

As can be seen, the MLR model has good statistical quality with low prediction error. The plot of the experimental versus predicted values for the above presented model is shown in Figure 1.

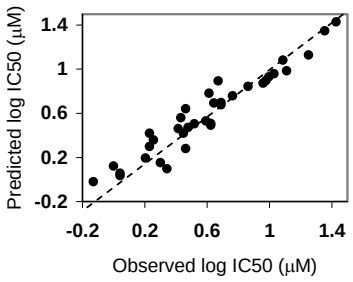

Figure 1. Plot of the calculated from MLR *vs.* observed log (IC50).

References:

[1] Gibbs. J. B., *Science*, **2000**, 287, 1969.

[2] Zhou. J, Geng. G, Batis. G, Huiwu., *Bioorg. Med. Chem. Lett.* , **2009**, 19, 1184.

Study of a Cytosine-Assisted Carbon Nanotubes Hybrid

Mahmoud Mirzaei and Nasser L. Hadipour *

Department of Chemistry, Tarbiat Modares University, Tehran, Iran

* *E-mail address:* hadipour.n@gmail.com

Keywords: Carbon nanotube; Cytosine; Hybrid; Density functional theory

Introduction

Considerable efforts after the carbon nanotube (CNT) discovery have indicated that the CNTs are capable to be chemically or physically functionalized by other atoms or molecules in which new properties could be generated for the new hybrid compounds [1,2]. Moreover, functionalization of CNTs by biological molecules such as nucleobases could make them important materials for medicinal processes like gene therapy and drug delivery [3,4]. In current research, we have investigated the hybrid of a pair of (6,0) zigzag CNTs through a bridging cytosine linkage (Fig. 1) by performing density functional theory (DFT) calculations. N_1 and C_5 are two atomic sites of pyrimidine ring of cytosine in which we have employed as binding sites for the CNTs. It is noted that the CNTs are covalently bound to N_1 and C_5 sites of cytosine to make possible the junction through this bridging linkage.

Computational aspects

The B3LYP exchange-functional and the 6-31G* standard basis set as implemented in the Gaussian 98 package [5] have been employed to optimize the investigated model. The optimization process yielded the properties such as dipole moment, band gap, binding energy, and binding length. The nuclear quadrupole resonance (NQR) properties including quadrupole coupling constant (C_Q) have also been evaluated for the optimized structures.

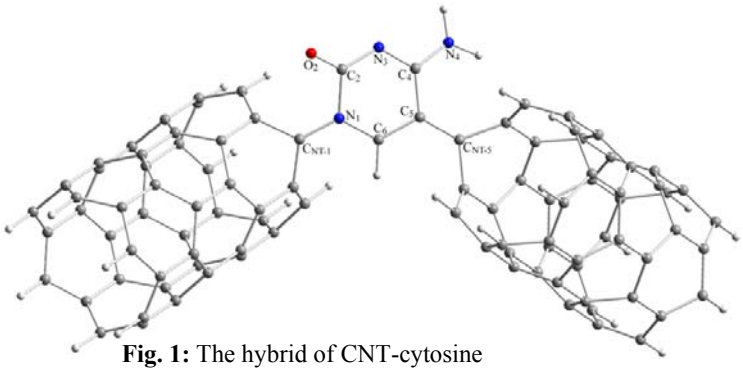

Fig. 1: The hybrid of CNT-cytosine

Table 1: The calculated properties for the investigated CNT-cytosine hybrid *

Structural Property	CNT-Cytosine	NQR Property	CNT-Cytosine
Stoichiometry	$C_{100}H_{25}N_3O$	C_Q [N_1] /MHz	1.10
Dipole Moment /Debye	2.28	C_Q [N_3] /MHz	3.28
Band Gap /eV	0.16	C_Q [N_4] /MHz	3.91
Binding Energy /eV	9.21	C_Q [O_2] /MHz	9.30
C_{NT-1}-N_1 Length /Å	1.35		
C_{NT-5}-C_5 Length /Å	1.39		

* See Fig. 1 for details.

Results and discussion

The calculated properties including the structural and NQR properties for the investigated hybrid of CNT-cytosine (Fig. 1) are listed in Table 1. Values of dipole moment, band gap, binding energy, and the covalently attached bond lengths for the counterparts are listed for the investigated structure. The values of NQR properties indicate that the two N atoms of the investigated models which belong to the cytosine-linkage part indicate that the N atoms detect different electronic environments in the structure of hybrid. Due to the covalent attachment of N_1 by CNT, the magnitude of C_Q for this atom is smaller than the other two N atoms. It is important to note that the NQR parameters are originated at the electronic sites of atoms; therefore, they could reveal insightful trends about the chemical environments of matters.

Conclusions

In this work, we have studied the properties of a cytosine-assisted CNT hybrid through computations. The stabilized structures have been achieved through optimization and the NQR properties have been calculated for the optimized structures. The NQR

properties indicate that the chemical environments of N atoms of cytosine are different in the structure of hybrid in which the most difference is observed for N_1.

References

[1] S. Iijima, Nature 354 (1991) 56.

[2] A.A. Farajian, H. Mizuseki, Y. Kawazoe, Physica E 22 (2004) 675.

[3] P. Kohli, C. Harrel, Z. Cao, R. Gasparac, W. Tan, C.R. Martin, Science 305 (2004) 984.

[4] M. Mirzaei, H.R. Kalhor, N.L. Hadipour, J. Mol. Mod., in press.

[5] M.J. Frisch, et al., GAUSSIAN 98, Gaussian, Inc., Pittsburgh, PA, 1998.

The effect of the electrode/Molecule coupling on the I-V characteristics of Metal/trans-polyacetylene/Metal molecular wire in the presence of solitons

Hossain Milani Moghaddam

Physics department, Mazandaran University, Babolsar, Mazandaran,Iran

(Email: milani@umz.ac.ir), (Tel: 01125342486)

Abstract:

Using a tight-binding model and methods based on Green's function theory, we numerically investigate the effects of the coupling strength and the role of the soliton on the current-voltage (I-V) characteristics of the Metal/trans-polyacetylene/Metal (M-PA-M) molecular wire. Our calculations show that the solitons play an important role in the response of this system causing a large enhancement in the wire current. Our results suggest that the I-V characteristic is sensitive to the Metal/molecule coupling strength.

Keywords: molecular wire, trans-polyacetylene, Green's function theory, I-V characteristics

Introduction:

The progress of molecular wires attracts much attention on their transport behaviors [1]. The typical systems considered are usually organic or polymer molecules sandwiched between two electrodes. Doping of conjucated polymers give rise to creation of the geometrical defects in the structure of them. In PA, these defects are 'solitons' and may effectively affect the electronic conduction through the polymer [2]. As a model, we numerically investigate the effects of the coupling strength and the role of the soliton on the current-voltage (I-V) characteristics of the M-PA-M structure (Fig. 1), where the metal nanocontacts are considered as the Newns-Anderson model.

Methodology:

$I(V) = (2e/h)\int_{-\infty}^{+\infty} d\varepsilon\ T(\varepsilon)[f_L(\varepsilon) - f_R(\varepsilon)]$ and $T(E) = Tr[\Delta_L(E)G^+(E)\Delta_R(E)G(E)]$ where $f_{L/R}(\varepsilon)$ is the Fermi-Dirac distribution function [3]. $\Delta_L(E) = \Delta_R(E) = \Delta(E)$ is minus the imaginary part of the electrodes' self-energy. E and $G(E) = (E\,I - H_{SSH} - \Sigma_L(E) - \Sigma_R(E))^{-1}$ are the electron energy and the modified Green's function of the extended molecule, respectively. I, H and $\Sigma_L(E) = \Sigma_R(E) = \Sigma(E)$ are respectively the unit matrix, the molecule's Hamiltonian and the electrodes' self-energy via the Newns-Anderson model [3]. The electronic part of H_{SSH} is given as [2], $H_{SSH} = -\sum_n t_{n+1,n}(c_{n+1}^+ c_n + c_n^+ c_{n+1})$, $t_{n+1,n} = t_0 + \alpha(u_n - u_{n+1})$, $t_0 = 2.5\,eV$, $\alpha = 4.1\,eV/\AA$. In the presence of solitons $u_n = (-1)^n u_0 \prod_m \tanh[\frac{(n-m)}{7}]$, $u_0 \approx 0.04\,\AA$ [2]. m shows the location of the soliton center on the chain which we choose in the center of the PA chain.

Results and discussion:

Our calculations are done for 56 carbon atoms in the PA chain. According to Fig. 2, the solitons play an important role in the response of this system causing a large enhancement in the wire current. Our results also suggest that the I-V characteristic is sensitive to the Metal/molecule coupling strength (as shown in Fig. 3 and 4).

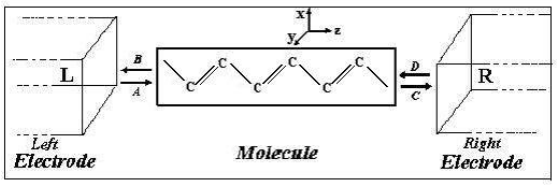

Fig. 1. A schematic representation of the M-PA-M structure.

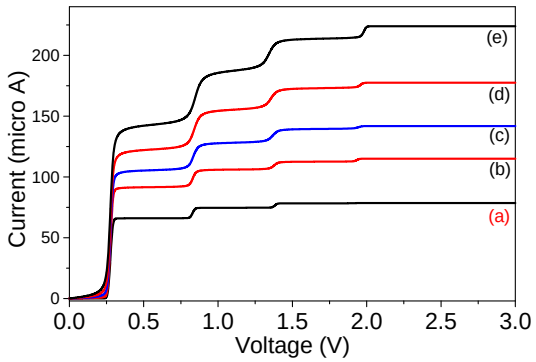

Fig. 3. the I-V curves for the different t_c s . (a)-(e) t_c s are 0.1, 0.3, 0.5, 0.7 and 0.9, respectively.

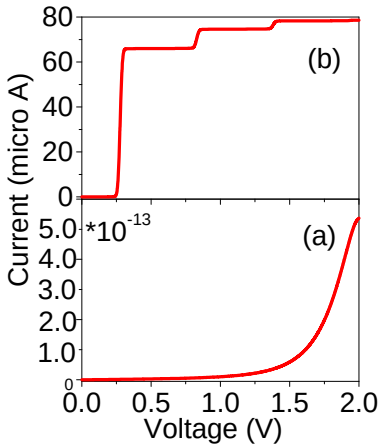

Fig. 2. (a) and (b) show the I-V curve of the M-PA-M molecular wire in the absence and presence of solitons, respectively.

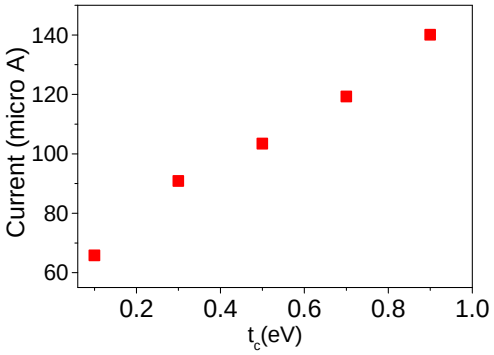

Fig. 4. current vs. t_c at $V = 2.5$ Volt .

References:

[1] R. F. Service, Science **295** (2002) 2398.

[2] W. P. Su, J. R. Schrieffer and A. J. Heeger, *Phys. Rev. B* **22** (1980) 2099.

[3] V. Mujica, M. Kemp and M. A. Ratner, *J. Chem. Phys.* **101** (1994) 6856.

Formation of Proton-bound Dimers in Atmospheric Pressure, A Thermodynamics Study

Z. Izadi, M. Tabrizchi*and H. Farrokhpour

E-mail: z.izadinajafabadi@ch.iut.ac.ir, m-tabriz@cc.iut.ac.ir

Chemistry Department, Isfahan University of Technology, Isfahan, 84156-83111, Iran

Keyword: Ion Mobility Spectrometry, Proton Bound Dimer, Vant's Hoff equation

Introduction

Proton-bound dimers, in the form of A-H^+-B, are formed via a reaction between protonated molecules and a second molecule with high proton affinity. Such dimers are regularly observed in atmospheric pressure chemical ionization techniques such as ion mobility spectrometry (IMS) [1]. They also have a major role in the chemistry of the hydrogen bond. Thermodynamic properties of those dimers have been experimentally studied by various techniques such as; ion cyclotron resonance, pulsed electron beam, high pressure mass spectrometry [2]. In this work, an ion mobility spectrometer was used to experimentally study the thermodynamics of proton bond dimer formation at atmospheric pressure. Based on ab initio calculation, it was assumed that the monomer ion is hydrated and it is in equilibrium with the unhydrated dimer such that;

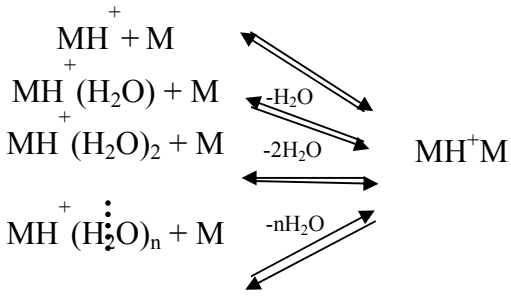

Fig. 1. Multi equilibrium reaction for hydrated protonated ions happening in atmospheric pressure.

Experimental and Method

The ion mobility spectrometer was constructed in our lab and described elsewhere[3]. IMS cell was installed in a thermostat oven where temperature could be adjusted from room temperature to 500 K. The sample was injected into the carrier gas using a syringe pump at flow rates in the range of from 5-40 μL min^{-1}. Protonated ions were produced by a corona discharge ionization source. The reaction was established in the ionization region of IMS as; $MH^+ + M \rightleftharpoons MHM^+$ $\qquad Q = \frac{[M_2H^+]}{[MH^+][M]}$ (1)

To ensure the equilibrium condition, the reaction quotient (Q) of Reaction 1 was measured while the pump flow rate was increased. At equilibrium, Q was independent of the flow rate. Then the relative abundances of the monomer and dimer were obtained from the intensity of their corresponding peaks in the mobility spectrum. The equilibrium constant, K_{eq}, was then calculated from the relative intensities at different temperatures.

Calculation

First, the geometry of the reactants and products for methyl-isobutyl-keton, (MIBK) was optimized using Gaussian 98. Then the enthalpies and Gibbs free energies were calculated using Hartrree-Fock method with 6-311++G** basis set. The calculation was then carried out using B_3LYP method to obtain more accurate results. The enthalpy change of reaction $MH^+(H_2O)_n + M \rightarrow MH^+M$ for different hydrated protonated monomers are -28.5, -7.9 ,6.53, 18.6, 29.2, 38.7 for n = 0-5, respectively.

Results and Discussion

The experimentally measured equilibrium constant at different temperatures are shown in Fig.2. As shown, the equilibrium constant goes up with temperature at low temperatures but decreases at high temperatures. This means that the reaction is endothermic at low temperatures and exothermic at high temperatures. This relates that it is a complicated reaction that its nature changes with temperature. In fact, a series of multiequilibrium reactions, rather than a simple reaction happens in atmospheric pressure. The Van't Hoff plot of $\ln(K_{eq})$ versus the reciprocal temperature yielded an enthalpy change for reaction 1

to be -5kcal/mol. This is far from the expected value of about -28 kcal/mol for typical hydrogen bonding.

A model was proposed to solve this complicated system. Based on the results obtained from the calculation, a mixture of protonated monomers, $MH^+(H_2O)_n$ were assumed to be in equilibrium with dimer. For the complicated reaction shown in Fig.1, we define here a general equilibrium constant, as;

$$K = \frac{[MH^+M]}{[M].\sum_n [MH^+(H_2O)_n]} \qquad (2)$$

The new equilibrium constant can be expressed in terms of the equilibrium constants for the individual reactions as;

$$\frac{1}{K_{red}} = \frac{1}{K_0} + \frac{p_{H_2O}}{K_1} + \frac{(p_{H_2O})^2}{K_2} + \ldots + \frac{(p_{H_2O})^n}{K_n} \qquad (3)$$

We call this constant as the reduced equilibrium constant. K_o, K_1 to K_5 where determined using the results obtained from the ab inito calculation. The defined equilibrium constant calculated at different temperatures for different water vapor pressure along with the experimental results are shown in Fig.2. The model well describes the behavior of the equilibrium constant as a function of temperature.

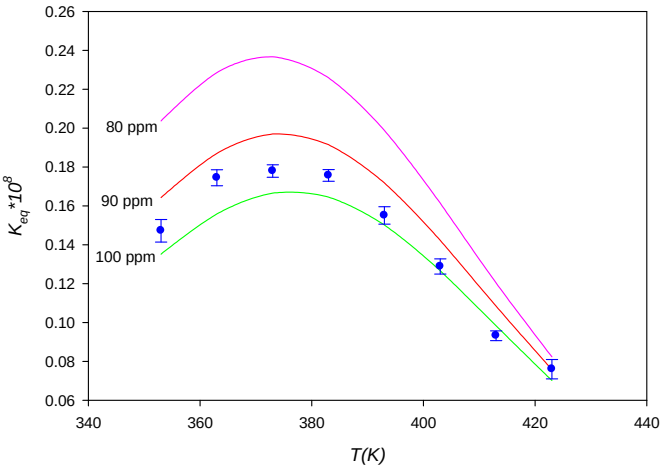

Fig. 2. Experimental (dots) and theoretical (lines) equilibrium constant, defined in Eq. 2 as a function of temperatures for different water vapor pressure.

References

[1] C. L. Perrin and J. B. Nielson, Annu. Rev. Phys. Chem. 48 (1997) 511.

[2] R. G. Ewing, G. A. Eiceman and J. A. Stone, Int. J. Mass. Spectros. 193 (1999) 57.

[3] H.R.Shamlouei and M,Tabrizchi, Int. J. Mass. Spectros.273(2008) 78.

Using Electrochemical Impedance Spectroscopy (EIS) in Evaluation of Polyurethane Coatings Thickness for Pipeline

F.Akvan [*, a], J. Neshati [b], J. Mofidi [c]

[a] Faculty of Chemistry, North Tehran Branch, Islamic Azad University,
Young Researchers Club, Tehran, Iran
(Email: f.akvan@gmail.com)

[b] Corrosion Department, Research Institute of Petroleum Industry (RIPI) ,
P.o.Box 18745-4163, Tehran, Iran

[c] Faculty of Chemistry ,North Tehran Branch ,Islamic Azad University, Tehran , Iran

Keywords: Cathodic disbonding, Polyurethane, Electrochemical impedance spectroscopy (EIS), Pipeline.

Introduction

Cathodic disbonding is one of the main causes that results in the loss of adhesiveness and degradation, which has a great impact on the service life of gas and oil buried pipelines under cathodic protection [1] .

Cathodic disbonding tests were developed in the 1960s and leading to the publication of ASTM G8 in which an artificial defect was introduced to simulated the damaged area of a coating[2]. Many studies have been dedicated to this subject regarding the mechanisms of cathodic disbonding of organic coatings on steel[3-4] .

Method

In this research three coating thickness were investigated according to ASTM G8 using EIS. Electrochemical cells were designed to separate the measurements of cathodic disbonding process from influence of impedance in artificial holiday. Experiments were done in 3.5% NaCl solutions at room temperature with different coating thicknesses (354, 483 and 1014 μm). Artificial holiday diameter was 6 mm. Immersion time was 28 day and during the immersion, cathodic potential of -1.5 V (vs. SCE) was applied, but the EIS measurements were done in open circuit potential (OCP).

Results and Discussion

In evaluation of coating thickness effect, based on table 1, analysis of EIS curves in break point frequency (θ=-45) showed that several parameter under over protection conditions were efficacious in cathodic disbonding coating process, but with no logical correlations between each parameter and any disbonded area individually.

Table 1- Evaluation of coating thickness effect after 28 days immersion

Sample	Thickness of Coating (µm)	Equivalent circuit diameter (mm)	Disbonded area (mm^2)	Frequency in θ= -45 High frequency (Hz)	Frequency in θ= -45 Low frequency (Hz)
A	483	19.02	284.07	0.0136	0.0136
B	354	22.94	413.50	3.3386	0.036989
D	1014	10.91	93.49	0.005	0.005

According to figures 1-3 evaluation of samples showed that the behavior of coatings is like a metal with no coating. .

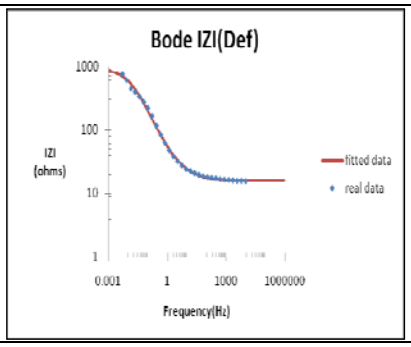

Fig.1– IZI versus frequency

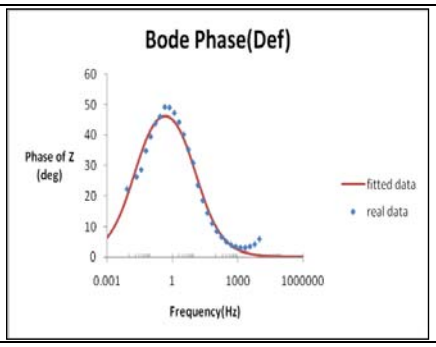

Fig.2–Phase of Z versus frequency

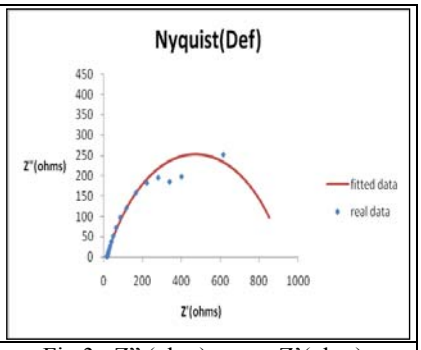

Fig.3 –Z" (ohm)versus Z'(ohm)

Fluctuations of open circuit potential (E_{ocp}) during time indicated the negative trend ,it seems that diffusion of ions corrosive and water absorption under healthy area was increasing ,so reactions of carbon steel corrosion was increased too[5]. The fluctuation of open circuit potential were given in fig.4 .

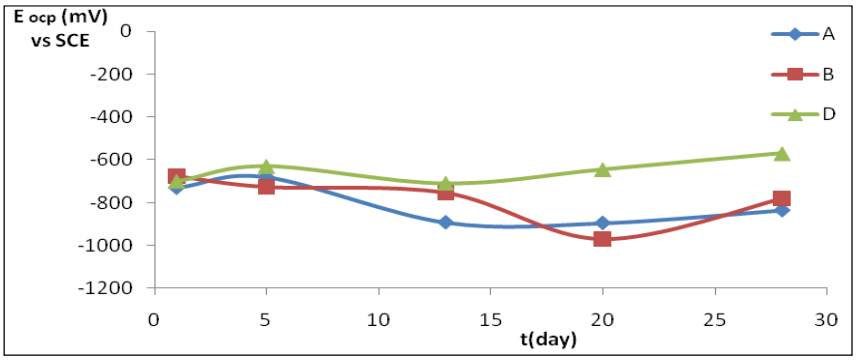

Fig.4- Fluctuations of measured potential (E_{ocp}) during time

Conclusions

The most influence was observed between the fifth and thirteenth days based on EIS plots. It seems that diffusion of electrolyte is dependence on the coatings thickness and on the defects in coatings and environmental factors.

There is no accurate logical correlation between thickness of coating and disbonded area but it can resulted thickness of coating has reverse relation versus disbanded area.

References

[1] F. Deflorian, S. Rossi, Electrochimica Acta, 51 (2006) 1736-1744.

[2] J. Zhang, J. Hu, J. Zhang, C. Cao, Progress in Organic Coatings, 49 (2004) 293-301.

[3] J. Neshati, F. Rezaei, E. Akbarinezhad, Surface Engineering, 24 (2008) 470-474.

[4] D. Flavio, R. Stefano, Electrochim. Acta, 5 (2006) 1736.

[5] V. Afshari, C. Dehghanian, Anti-Corrosion Methods and Materials, 57 (2010) 142-147.

Poster Session:

- Applied Chemistry
- Computational Chemistry
- Classical Thermodynamics
- Electrochemistry
- Chemical Kinetics
- Nanotechnology
- Quantum Mechanics & Spectroscopy
- Surface Chemistry
- Statistical
- Thermodynamics

Applied Chemistry

Complete basis set, hybrid-DFT study and NBO interpretations of conformational behaviours of trans-2,3- and trans-2,5-dihalo-1,4-diselenanes

Pirahan-Siah [a] .R,Mousavi [a].S.N , Yahyayi[b] .H and Nori-Shargh[a] .D

a) *Chemistry Department, Science Faculty, Arak Branch, Islamic Azad University, Arak, Iran*

b)*Chemistry Department, Zanjan Branch, Islamic Azad University, P.O.Box: 49195-467, Zanjan, Iran*

Abstract:

The conformational behaviours of trans-2,3-dihalo-1,4-diselenanes [halo = F (**1**), Cl (**2**), Br (**3**)] and trans-2,5-dihalo-1,4- diselenanes [halo = F (**4**), Cl (**5**), Br (**6**)] have been analyzed by means of complete basis set CBS-4, hybrid-density functional theory (B3LYP/6-311+G**//B3LYP/6-311+G**) based methods and NBO interpretation. Both methods showed that the axial conformations of compounds **1** and **4** are more stable than their equatorial conformation*s* but resulted in equatorial preferences for compounds **2**, **3**, **5** and **6**. The Gibbs free energy difference (G_{eq}–G_{ax}) values (i.e. $\Delta G_{eq\text{-}ax}$) at 298.15 K and 1 atm between the axial and equatorial conformations decrease from compound **1** to compound **3**. Also, the calculated $\Delta G_{eq\text{-}ax}$ values decrease from compound **4** to compound **6**. The NBO analysis of donor-acceptor (LP→σ*) interactions showed that the *anomeric effects* (*AE*)[1,2] decrease from compound **1** to compound **3** and also from compound **4** to compound **6**. Also, the calculated dipole moment values between the axial and equatorial conformations [$\Delta(\mu_{eq} - \mu_{ax})$] decrease from compound **1** to compound **3**. There is no conflict between the increase of *AE* and the decrease of $\Delta(\mu_{eq} - \mu_{ax})$ values. The calculated AE and $\Delta(\mu_{eq} - \mu_{ax})$ values reasonably explain the decrease of the axial conformation stability from compound 1 to compound 3 and also from compound 4 to compound 6 compared to their corresponding equatorial conformations. The Gibbs free energy difference values between the axial and equatorial conformations (i.e. $\Delta G_{ax\text{-}ax}$ and $\Delta G_{eq\text{-}eq}$) of compounds **1** and **4**, **2** and **5** and also **3** and **6** have been calculated. The correlations between the *AE*, bond orders, pairwise steric exchange energies (*PSEE*), $\Delta G_{eq\text{-}ax}$, $\Delta G_{ax\text{-}ax}$, $\Delta G_{eq\text{-}eq}$, dipole-dipole interactions, structural parameters and conformational behaviors of compounds **1-6** have been investigated.

Keywords: anomeric effects, stereoelectronic interactions, molecular modeling, ab initio, NBO, dihalo-1,4-diselenane

Refrences:

[1] D. Nori-Shargh, H. Yahyaei, J .E. Boggs, *J. Mol. Graph. Model.* **2010**, *28*, 807.

[2] D. Nori-Shargh, J.E Boggs, *J. Phys. Org. Chem*. **2010**, doi:10.1002/poc.1728

Adsorption of C.I. Basic Violet 2 from aqueous solution onto sawdust

Mehdi pirniya*, Nasser Modirshahla, Nilofar Ghalebsaz-Jeddi, Behrouz Vahid

Department of Chemistry, Islamic Azad University, Tabriz Branch, Islamic Republic of Iran(Email: Mehdi.pirniya@gmail.com)

Abstract:

The aim of the present study is to investigate the adsorption of Basic Violet 2 onto sawdust in aqueous solution. The effect of different operational parameters such as pH, agitation speed, contact time, mesh size, adsorbent dose and initial dye concentration was studied in a batch mode reactor.

Keywords: Sawdust, Adsorption models, C.I. Basic Violet 2, Operational parameters

Introduction

Dyes are widely used in paper, plastic, food, cosmetics, textile, and printing industries .Waste water containing dyes presents a serious environmental problem because it contains a variety of organic compound and toxic substances which are harmful to fish and other aquatic organisms [1]. These dyes are stable to light and oxidizing agents, and are resistant to aerobic digestion, which make it difficult to treat such effluents using conventional wastewater treatment methods[2].In the percent study , the removal of chemical grade Basic Violet 2 by wood sawdust was studied .The results show that the removal efficiency depends on operational parameters.

Experimental

In order to study the adsorption of BV2 50 mL of adsorbate solution with known concentration was prepared. These adsorbent with amount and particle size was added into the above solution and in 10 min time intervals the samples were withdrawn, centrifuged and absorbance was measured by spectrophotometer to calculate the removal efficiency and also a mechanical stirrer (GFL, 30006, Germany) were used to agitate the solution.

1.The effect of particle size

The different particle size of the adsorbent were sieved using 60-325 mesh sieves. Then 0.5 g of adsorbent was added into 50 mL of 15 mg L^{-1} BV2 and agitated for 1 hour with 125 stroke per minute. Results showed that removal of 97.7% occurs with 200 – mesh size and above that remains unchanged. Increasing mesh size produces smaller particle size resulting enhanced surface area of the adsorbent, hence active sites increases which causes higher removal percent [3]. But reducing the particle size to a critical size agglomeration of the adsorbent particles increases, therefore pores and active sites are covered and the removal percent decreases.

2. The effect of adsorbate dosage

Various amounts of adsorbent ranging from (0.1-3) g with 200-mesh size were taken and the same conditions as previous section were applied. Results revealed that the removal efficiency increases (95.4%) up to o.5 g of adsorbent. Due to the increases in the surface of the adsorbent and above that the removal percent remains almost constant since the solution becomes saturated with adsorbent and adsorption- desorption phenomenon takes place[4].

3. The effect of contact time

Using 0.5 g of adsorbent with 200-mesh size with similar conditions as expressed in section 2.1, different contact times from (5-120) min were investigated. It is observed that in the first 30 min the removal percent increases up to (99.3%) and remains almost constant after that .This is due to the occupation of the available active sites on the adsorbent surface during the process.

4. The effect of stirring rate

Using the optimum conditions which were obtained in previous sections, agitation speeds of (25-215) stroke per minute were employed. Findings showed that removal of (99.5%) occurs up to 125 s/m and after that no change could be observed which can be explained due to sedimentation of adsorbent particles, and also increasing the agitation rate decreases boundary layer of the adsorbent and consequently diffuses the adsorbent molecules into adsorbent pores easily[5].

5. The effect of pH

The effect of pH was investigated in the same conditions as mentioned. The pH was in the range (3-9).Since there was no charge on the adsorbent surface hence the variation of pH does not influence the adsorption rate, therefore the initial pH of the solution was taken in whole experiments.

6. The effect initial dye concentration

Employing the optimum conditions, the concentration of dyes (5-35)mg L^{-1} were investigated . Results showed that removal percent decreases from 97.4% to 87.4% , because as the number of molecules per unit of volume increases, the electrostatic repulsion takes place on the adsorbent surface.

Conclusion

The present study shows that wood sawdust is an effective adsorbent for the removal of Basic Violet 2 from aqueous solution . The results would be useful for the design of wastewater treatment plants for the removal of dyes .

References

[1] E. Demirbas, M. Kobya, M. T. Sulak: Bio. Tech 99 (2008) 5368-5373

[2] Q. Sun, L. Yang: Water . Res.37(2003)1535

[3] H. Metivier-Piganon, C. Faur-Brasquet, P. L. Cloriec: sep. purif. Tech. 31(2003)3-11

[4] B. Royer, N. F. Cradoso, E. C. Lima, V. S. O. Ruiz, T. R. Macedo, C. Airoldi: J. Collid Interface sci.336(2009)398-405

[5] R. Dhodapkar, N. N. Rao, S. P. Pando, S. N. Kaul: Eng. Res. Ins. 97(2006)885-887

A physical properties and phase diagram investigation of clay-sand system

A. Aminifar[a*], F.Khosravi [b], M.S.Abazari [a], E.Tavakoli [a]

a Department of chemistry, Faculty of sciences, Imam hossein comprehensive university, Tehran, Iran

b Department of civil engineering, Faculty of engineering, Imam hossein comprehensive university, Tehran, Iran

Email: aaminifar@hotmail.com

Key words: Phase diagram, Physical properties, Sand soil, Clay soil.

Introduction:

Many researchers are interested to study physical properties and phase diagram of metallic oxides which are constituent the soils. In our research we decided to use the prevalent clay and sand which available and manufactured in Iran to use directly. It may improve and open new view in the field of applied physical chemistry and soil science. Clay soil is hardened when fired or dried. They may also have contained variable common of water trapped in the mineral structure which is cause polar attraction. In a view of soil scientist and colloid chemist are usually preferred the size of clay between 1-2 μm respectively.

Sieving ventilation of air during of kiln it has an important rule for improving the physical properties of the clay. The melting point of clay, depend to their compositions. It seems presents of potassium oxide can lower the melting point temperature. The main composition of sand is SiO_2 , which make an unique tightness of it and enhance the melting point of sand. The microstructure of different metal oxides by variation temperatures have been studied so far and their phase diagrams CaO- MgO,CaO- MgO-SiO_2 and so on, have been reported, in condition of desification, sinteration and crystallization have also been investigated but there is not any report of this view that to measure clay and sand system so far [1-7].

Materials and methods:

Clay soil had grain size less than 0.75 mm and their liquid limit(LL) and plastic limit are equal to 40% and 14% respectively it has a density equal to 2.7 $g.cm^{-3}$. Sand soil has approximately size of 0.08-4.75 mm. In this case angle of fraction for sand is equal to 32^0 and there is no cohesive coefficient ,also sand density is equal to $2.6g.cm^{-3}$.

Apparatus:

The Casagranda tool has been applied for determining the liquid limit and direct shear test has been applied for determining shear resistant of the sand soil ,on the other hand the triaxial test is suitable for clay soil. Clay and soil are dried in oven made by Yamato Company, for high temperature a special design oven made by Exciton Company had been used. [Model: EX.1200-30-6 STH, this oven is made by Iran].

Result and discussion:

The physical property of sand and clay had been report in previous section melting point of sand and clay was 1590 ^{0C} and 650 ^{0C} respectively. It seems the main compositions of clay soil are potassium oxide and calcium oxide as can observe in EDAX diagram. There is two eutectic point one eutectic point at molar concentration 65% of clay is equal to 850 ^{0C} and the eutectic point in molar concentration equal to 72% of sand is equal to 1220 ^{0C}. The lowering melting point of the clay and sand on addition of the clay and sand are on investigations.

Conclusion:

Eutectic points of clay-sand system has been measured, most of researches have been concerned diagram phase of metallic oxides of constituents of clay and sand but they haven't directly investigated clay and sand soil which we have done in this paper. It has also concluded melting point of clay is increased on adding sand soil, definitely resistance of clay in this manner is improved. By addition of clay to sand soil its melting point is decrease it my caused decreasing uses of energy in the concern industrial.

Reference:

[1] R.Krishna and etal; "CME315 Soil Mechanics Laboratory ; University of Illinois;2010

[2] www.msds.chem.ox.ac.uk,our Sand molecular formula SiO_2 silicon dioxide with Cas, No:14808-60-7 .

[3] E.Wemer etal . ; "A review of mechanical assisted equilibrium technique and nanonugget issue" ; Chemical Geology ; 248,119-139,2008.

[4] I.M.Ranieri etal ;"The phase diagram studies …" ; Journal of Solid State Chemistry; 181, 1070-1074 ,2008 .

[5] K.R.Moore etal. ;" The transition from carbonate to silicate melts in the CaO-MgO-SiO2 –CO2 system " ; Journal of petrology(Oxford university press) ;1943-1951,1998.

[6] D.U.Tulyaganov etal ."synthesis of glass-ceramics in the CaO-MgO-SiO_2 system with B_2O_3 , P_2O_3, Na_2O and CaF_2 additive" Journal of European ceramic society 26,1463-1471,2006.

[7] A.Karamanov; A kinetics of phase formation in jarosite glass-ceramics, J.Eur.Ceram. Soc;19,527-533, 1999.

Equilibrium and Thermodynamic Study platanus as biosorbent for removal of Rhodamine dye from industrial Waste water"

[a] S. Chagervand , [b] M. Rahimi

[a] Department of Chemistry, Science Faculty, Islamic Azad University, Khorramabad Branch, Khorramabad, Iran.

(schagervand@yahoo.com)

[b] Department of mechanic,, University of Imam hossain, Loresatan Branch, Khorramabad, Iran.

Introduction

Many industries which used dyes and pigments generated waste water. Dyes are widely used in industries such as textile, plastic, cosmetic, rubber, paper, etc. The adsorption process is on of the effective methods for removal dyes from the waste effluent [1]. In recent years, agricultural by-products have been widely studied for metal and dye removal from water. These include pine bark, tree tern, wheat shell, rice hush, saw dust, etc [2]. platanus Leaf was chosen as biosorbent in this experiment. The aim of this work was to study the possibility of the utilization of platanus Leaf For biosorption of dye from aqueous solutions. The system variables studied include biosorptive time, PH and temperature. The isotherm constants for Langmuir, Freundlich, Temkin, Halsey, Henderson and Harkins-jura isotherm have been determined.

Materials and methods

For this study, rhodamine was used and it was obtained from Merck co. An accurate weighed quantity of the dye was dissolved in double distilled water to prepared stock solution ($1000\ {}^{mg}/_{l}$). experimental solution of the desired concentration was obtained by successively dilutions. The platanus Leaf were rinsed with distilled water and dried in room temprature for the time. Of necessary the leaves ground and screened through a set of sieves $60\ \mu m$. The leaf sample was kept dry till the time of usage.

The results of different PH for dye biosorption was shown an increase in dye adsorption per PH 5. then solutions were supplied in this PH. The concentration of colouring matter in each sample was determined by calibration plots drawn by recording the absorbance of dye at

different concentration, all measurement were made at $\lambda_{Max} = 550$. Batch adsorption tests were performed to study the adsorptive removal of dye from aqueous solution by biomass, where 20 ml of dye solution of known initial concentration (C_0) and a known amount of the biomass were taken in the 50 ml flasks. The flasks were shaken at 150 rpm for 60 minutes to ensure the adsorption equilibrium. The equilibrium concentration (C_0) of dye was determined using uv/vis spectrometer. The amount of solute adsorbed (q_e) per gram of biomass was calculated by C_0 and C_e.

$$q_e(\frac{mg}{g}) = \frac{(C_i - C_e)V}{m}$$

Where V is the volume of solution and m is the mass of adsorbent.

Result and discussion

This study shows that the platanus leaf is an effective adsorbent for removal of rhodamine From aqueous solution because each 0.1 gram of biomass have adsorption efficiency about %91.75.

Biosorption equilibrium data were correlated with the Langmuir and Frundlich isotherms. The linearized from of the Langmuir and Frundlich isotherms are:

$$\frac{C_e}{q_e} = \frac{1}{bq_{Max}} + \frac{C_e}{q_{Max}}$$

$$Lnq_e = \frac{1}{n} LnC_e + Lnk_f$$

Where q_{Max} is the Maximum amount of solute adsorbed and b, n, k_f are constants [3]. The results of langmuir isotherm are shown in fig.1 and the calculated values from lang muir and frundlich isotherms at 30 and $35°c$ are shown in tab.1.

The essential characteristics of the Langmuir isotherm can be expressed in terms of either a dimensionless constant separation factor or equilibrium parameter,

$R_L = \frac{1}{1+bC_i}$.

where R_L is a dimensionless separation factor C_i the initial concentration of dye (mgL^{-1}) and b is the Langmuir constant. The parameter R_L indicates the shape of isotherm accordingly $R_L \succ 1$ un favourable $R_L = 1$ linear, $R_L = 0$ irreresible $0 \prec R_L \prec 1$ favourable

In this study R_L is between 0and1, therefore ,biosorption process is favourable adsorption[4].

Tab.1: values from Langmuir and Frundlich isotherms at 30 and 35 $^{\circ}C$

biosorbent	$q_{\max})_{\exp er.}(\frac{mg}{g})$	$\max(\frac{mg}{g})$	$b(\frac{l}{mg})$	r^2
platanus Leaf	277.798	243.9	0.0048	0.963

biosorbent	K_F	1/n	r^2
platanus Leaf	4.21	0.555	0.832

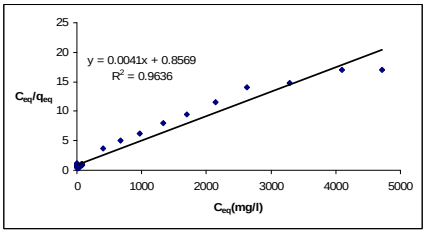

Fig1: results of Langmuir isotherm

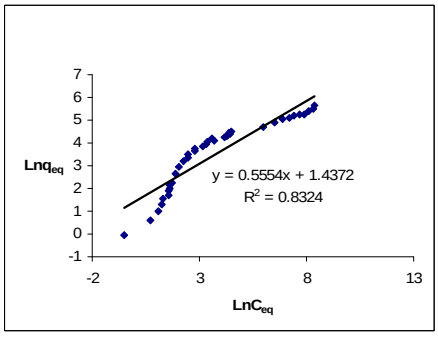

Fig2: results of Frundlich isotherm

Refrence

[1]Shaobin wang, Y. Boyjoo, A .Choueib and Z.H. Zhu , 2005. "Removal of dyes from aqueus solution using fly ash and red mud", Water Res.,39:129-138.

[2]Runping Han, etal, "Equilibrium biosorption isotherm for lead ion on chaff", Hazaradous materials. B125(2005)266-271.

[3]S.Qaiser,A.R.Saleemi,M.M.Ahmad,Heavy metal uptake by agro based waste materials, Electronic journal of Biotechnology, 10(2007)409-416.

Modified ISM equation of state for second thermodynamic derivative properties and interfacial surface tension

A. Maghari and A. Haj seyed javadi
Department of chemistry, University College of Science, University of Tehran, Tehran, Iran
E-mail: maghari@khayam.ut.ac.ir; alireza.seyedjavadi@khayam.ut.ac.ir

Keywords: ISM equation of state, Speed of sound.

Introduction

In the present work, second derivative thermodynamic properties as well as surface tension are studied by using the ISM equation of state (EOS). Song and Mason presented an analytical EOS, called ISM, based on statistical-mechanical perturbation theory for real molecular fluids [1]. The equation has two temperature-dependent quantities, i.e. effective hard-sphere diameter and a scaling factor as well as the second virial coefficient, which can be written as follow:

$$\frac{p}{\rho kT} = 1 + B_2(T)\rho + \bar{\alpha}(T)\rho[G(\eta) - 1] \quad (1)$$

where $B_2(T)$ is the second virial coefficient and $\alpha(T)$ is scaling factor, which can written as:

$$\alpha(T) = 2\pi \int_0^{\mathrm{rm}} \left(1 - e^{-\frac{u(r)}{kT}}\right) r^2\, dr \quad (2)$$

In this work, we have suggested the following pair distribution function, appeared in Eq. (1):

$$G(\eta) = \frac{1}{1-\eta} + \frac{3\alpha(1+\alpha)\eta}{(1-\eta)^2(1+3\alpha)} + \frac{2\eta^2\alpha^2}{(1-\eta)^3(1+3\alpha)} \quad (3)$$

Where η is the packing fraction $= \frac{b(T)\rho}{4F}$, in which $b(T)$ is co-volume, obtained as:

$$b(T) = 2\pi \int_0^{\bar{r}_m} (1 - (1 + \frac{\overline{u_0}(r)}{kT}) e^{-\overline{u_0}(r)/kT}) r^2\, dr \quad (5)$$

Thermophysical properties

A most important derivative property is the speed of sound, defined as:

$$v_s = [\left(\frac{\gamma}{M}\right)\left(\frac{\partial p}{\partial \rho}\right)]^{1/2} \quad (6)$$

where M is the molecular mass and $\gamma \equiv \frac{C_p}{C_v}$, which is determined by C_p and C_v, given by:

$$C_p = T\int_{\infty}^{V}\left(\frac{\partial^2 p}{\partial T^2}\right) dV - T\frac{(\frac{\partial p}{\partial T})_v^2}{(\frac{\partial p}{\partial v})_T} - R + C_{pi}\ ,\ C_v = C_p + T\frac{(\frac{\partial p}{\partial T})_v^2}{(\frac{\partial p}{\partial v})_T} \quad (7)$$

Further, in our continuing work, the interfacial properties, such as surface tension and surface thickness, will be studied. For this purpose, we calculate the surface tension and its corresponding surface thickness by using density functional approach and ISM EOS [2].

Result and discussion

Figures 1 and 2 are shown the VLE of N_2 and H_2O. Figures 3 and 4 have shown the calculated C_p and speed of sound versus density, respectively, for N_2 and the agreement with correlated data is generally satisfactory. The experimental data were taken from NIST Chemistry Web Book [3]. The solid curves represent the ISM EOS and symbols represent experimental data.

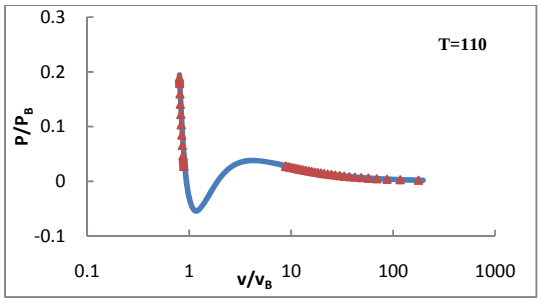

Fig. 1. Reduced $\mathbf{p-v}$ isotherm for $\mathbf{N_2}$

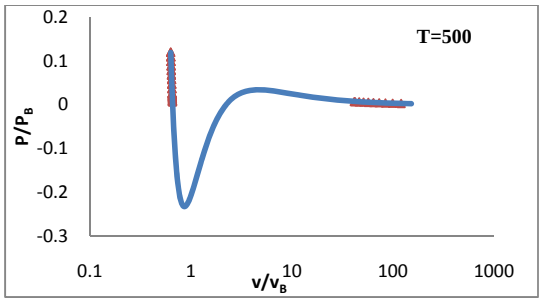

Fig. 2. Reduced $\mathbf{p-v}$ isotherm for $\mathbf{H_2O}$

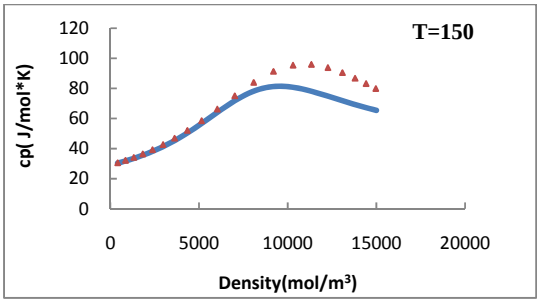

Fig. 3. Prediction of C_p for N_2

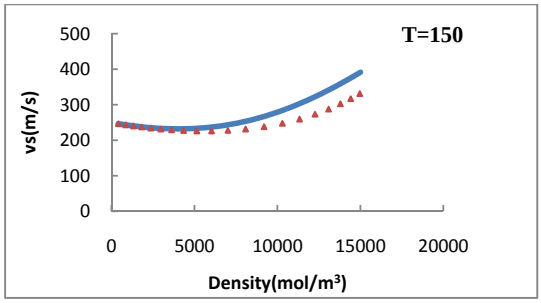

Fig. 4. Prediction of speed of sound for N_2

References

[1] Song Y and Mason E. A, 1989 J. Chem. Phys. 91, 7840; 1990, Phys. Rev. A 42, 4749.

[2] Najafi M and Maghari A, 2009 J. Stat. Mech. P05003.

[3] NIST Chemistry Web Book, NIST Standard Reference Database Number 69.

Evaluating the possibility of wrapping carbon nanotube bundle by polymers

M. Foroutan, R. Hadidi M.
Department of Physical Chemistry, School of Chemistry, College of Science, University of Tehran, Tehran ,Iran,
R.Hadidi@khayam.ut.ac.ir

Keywords: Carbon Nanotubes, Polymer, Molecular dynamics simulation, Wrapping.

Introduction

Polymer-based nanocomposite materials are being increasingly used as structural components in aerospace and automobile industry due to their excellent high adhesion, low-weight, and good chemical/corrosion-resistance [1]. However, the relatively weak mechanical properties of polymers have prevented their application in components that demand high mechanical strength and stability. In recent years, single-walled carbon nanotubes (SWNTs) as fliers in polymer matrix attracted considerable interest due to their unique carbon structure and extraordinary mechanical, thermal, and electrical properties. In general, products obtained from experiments often aggregate together to form SWNTs bundles [2]. Therefore, it is important to investigate behavior of polymer near bundles.

In this paper we display our observations from molecular dynamics (MD) simulation of wrapping nanotube bundle by polymer.

Simulation Details

MD simulations were performed in Tinker molecular modeling package (version 5.0) using the MM3 force field. The velocity form of Verlet algorithm method and the Nose-Hoover thermostat algorithm were used to integrate the equations of motion with a time step of 1.0 fs. Our simulated systems contain seven (5,5) SWCNTs as a bundle with the same length 40 Å accompany with epoxy polymer containing 213 atoms.

Result and Discussion

Figure 1 shows MD simulation snapshot of the wrapping of bundle by polymer epoxy.

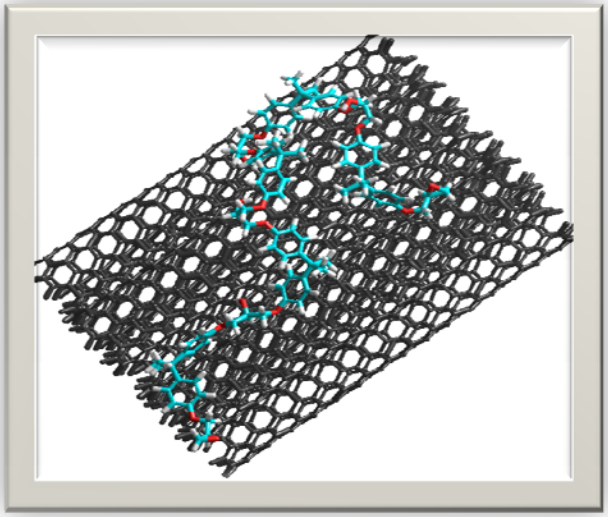

Figure 1- MD simulation snapshot of the wrapping of bundle by polymer epoxy

In the preset work, using the radial distribution functions for different atoms of polymer respect to carbon atoms of nanotube, interction energy between naotube bundle and polymer and also the radius of gyration of wrraped polymers, the possibility of wrapping carbon nanotube bundle by polymers is evaluated.

References

[1] Frisch, H.L.; Mark, J.E. Chem. Mater. 1996; 8: 1735–8.

[2] Dillon, A.C.; Jones, K.M.; Bekkedahl, T.A.; Kiang, C.H.; Bethune, D.S.; Heben, M.J., Nature 1997; 386: 377–379.

Conformational behavior of polymers adsorbed on carbon nanotubes

M. Foroutan, R. Hadidi M.

Department of Physical Chemistry, School of Chemistry, College of Science, University of Tehran, Tehran ,Iran,
R.Hadidi@khayam.ut.ac.ir

Keywords: Carbon Nanotubes, Polymer, Molecular Dynamics Simulation, Wrapping.

Introduction

Carbon nanotubes (CNTs) are materials of interest in wide fields of science and technology due to their remarkable electronic, optical, and mechanical properties [1]. Various methods have been developed to disperse nanotube aggregates into individual CNTs [2], including solubilization using a polymer coating via a tightly bound association ('wrapping') of polymers [3]. These findings suggest that polymer conformational behavior might be strongly influenced by geometric constraints of the cylindrical surface and not specific interactions between the polymer and CNTs. In the present work, we study the behavior of epoxy polymers adsorbed on single wall carbon nanotube with two different lengths using molecular dynamic (MD) simulation.

Simulation Details

MD simulations were performed in Tinker molecular modeling package (version 5.0) using the MM3 force field. The velocity form of Verlet algorithm method and the Nose-Hoover thermostat algorithm were used to integrate the equations of motion with a time step of 1.0 fs and temperature control of 300 K, respectively. A cutoff distance of 10 Å was used for the van der Waals potentials and Lorentz–Berthelot mixing rules were used for cross interactions. The CNT atoms to their initial positions have been fixed. Our simulated systems contains (5, 5) single-walled CNTs with two different lengths of 30 and 40 Å and epoxy polymer containing 213 atoms as shown in figure 1.

Result and Discussion

The behavior of adsorbed epoxy polymer on CNTs with two different lengths was studied using molecular dynamic simulation. In order to keep the text concise as possible as, just the plot for radius of gyration evolution of adsorbed polymers on (5,5) CNT with different lengths is

presented. Fig. 3 shows the radius of gyration evolution for polymer and adsorbed polymers on (5,5) CNTs with different lengths of 30 and 40 Å. As Fig. 3 shows with increasing the length of CNT, the radius of gyration decreases which it can be assigned to high intermolecular interaction between polymers and CNTs with length of 40 Å.

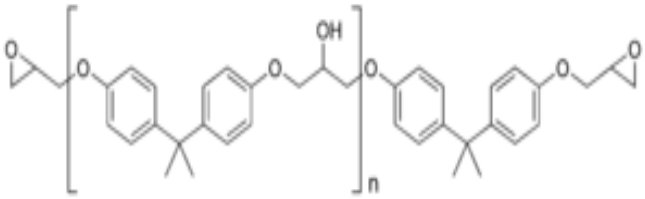

Fig. 1- Chemical structure of the epoxy polymer, n=3.

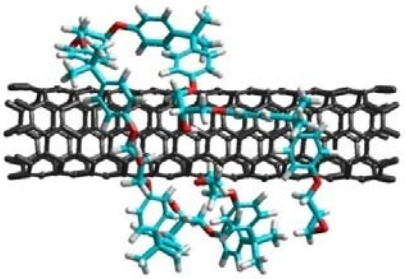

Fig. 2- MD simulation snapshot of the wrapping of CNT by polymer epoxy.

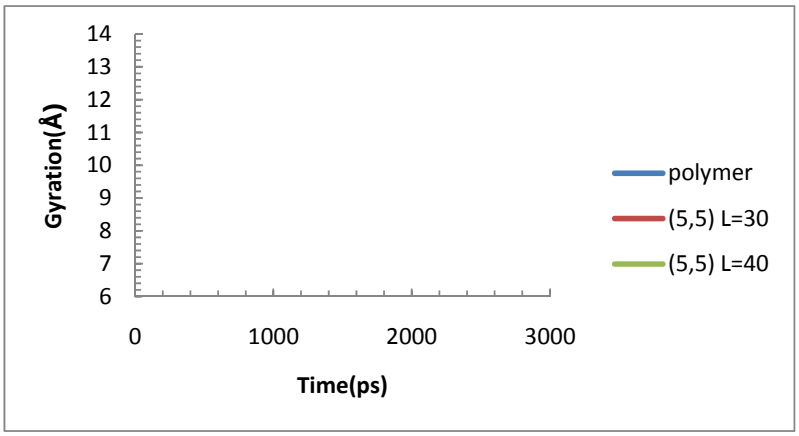

Fig. 3- Radius of gyration evolution for polymer and adsorbed polymer on (5,5) CNT with different lengths.

References

[1] S. E. Moulton, A.I. Minett, G.G. Wallace, Sensor Letters 3 (2005) 183.

[2] A. Hirsch, O. Vostrowsky, Topics in Current Chemistry 245 (2005) 193.

[3] M.J. O'Connell et al., Chemical Physics Letters 342 (2001) 265.

COMPARISON OF MULTIWALLED CARBON NANOTUBES AND ACTIVATED CARBON FOR EFFICIENT REMOVAL OF METHYL ORANGE: KINETIC AND THERMODYNAMIC INVESTIGATION

S. Javad Hosseini*[1], Syamak Nasiri Kokhdan, A. M. Ghaedi, S. Saman Moosavian

[1] Chemistry Department, Gachsaran Azad University, Gachsaran Branch- Iran

Corresponding author, Telefax 0098-7423332003, email: j.hosseini@iaug.ac.ir or javadchem2003@yahoo.com

Summary

The commercially powdered activated carbon and multiwalled carbon Nanotubes were used for the removal of methyl orange (MO) from aqueous solutions. The effect of solution pH, initial dye concentration, temperature and sorption time on MO removal was studied. The equilibrium sorption isotherms have been analysed by the, Langmuir, Freundlich, Dubinin and Radushkevich (D-R), and Harkins-Jura (H-J) models and the Langmuir isotherms has the high correlation coefficients. The apparent thermodynamic parameters were calculated and the obtained values support the conclusion that the MO molecules sorbs by entropy-driven, endothermic process. The kinetic of the sorption was analysed using the pseudo-first order, pseudo-second order, Elovich and Intraparticle diffusion kinetic models. The data showed that the second-order equation was the more appropriate although the intraparticle diffusion is the rate limiting factor.

Key words: Multiwalled carbon nanotubes (MWCNT), carbon nanotubes (CNTs), activated carbon (AC), methyl orange (MO), sorption, kinetic, thermodynamic, isotherm

Introduction

Due to high consumption of dyes in various process and industries such as food, paper, carpets, rubbers, plastics, cosmetics, and textiles, the discharge of colored wastewater from these industries causes many significant environmental problems [1]. Methyl Orange (a water-soluble azo dye) as well known carcinogenic organic substance is widely used in the textile, printing, paper manufacturing, pharmaceutical food industries and also in research

laboratories as an acid base indicator due to its ability to function as weak acid [2]. Methyl orange is a representative contamination in industrial wastewater and shows poor biodegradability [1]. AC and MWCNTs as adsorbents have been widely used due to their large surface area, micro porous character, and adequate porous and chemical features. CNTs have been considered useful in pollution prevention strategies and are known to have widespread applications as environmental adsorbents and high flux membranes [3], and are also potentially important for in situ environmental remediation due to their unique properties and high reactivity [4,5].

Methods

Measurements of dye uptake

Concentrations of MO in solution were estimated quantitatively using calibration curve over investigated concentration range. The dye adsorption capacities of adsorbent were determined at a certain time intervals (5-90 min for AC and 1-35 min for MWCNT) and the equilibrium was established after 22 min for MWCNT and 90 min for AC. The effect of pH on adsorption was studied by adjusting dye solutions (100 mgL^{-1}) to different pH values (2.0–9.0 and/or 1-8) and agitated with 1.4 g of activated carbon and/or 0.04 g MWCNT for desired time, while the dye solutions pH were adjusted to the required initial pH values with the addition of HCl or KOH. Dye adsorption experiments were also accomplished to obtain isotherms at various temperatures (25–60 °C) and to a range of 50–200 mg L^{-1} MO concentrations. The amount of MO adsorbed by adsorbent, q_e (mg g^{-1}), was calculated by the following mass balance relationship:

$$q_e = (C_0 - C_e)\, V/W \qquad (1)$$

Where C_0 and C_e are the initial and equilibrium dye concentrations in solution, respectively (mg L^{-1}), V the volume of the solution (l) and W is the mass (g) of the adsorbent used.

Results and discussion

Effect pH on MO adsorption efficiency

To study the effect of solution pH on MO adsorption, 50 mg/L^{-1} of solution was agitated with 1.2 g AC after 90 min or 0.04 g MWCNT at after 25 min at different pH values (1.0–8.0 or 2.0-9.0) in a water bath shaker at 25 °C and the results are shown in Fig. 1. The initial pH

value was written as pH_i and the solution pH after adsorption was also measured and written as pH_f

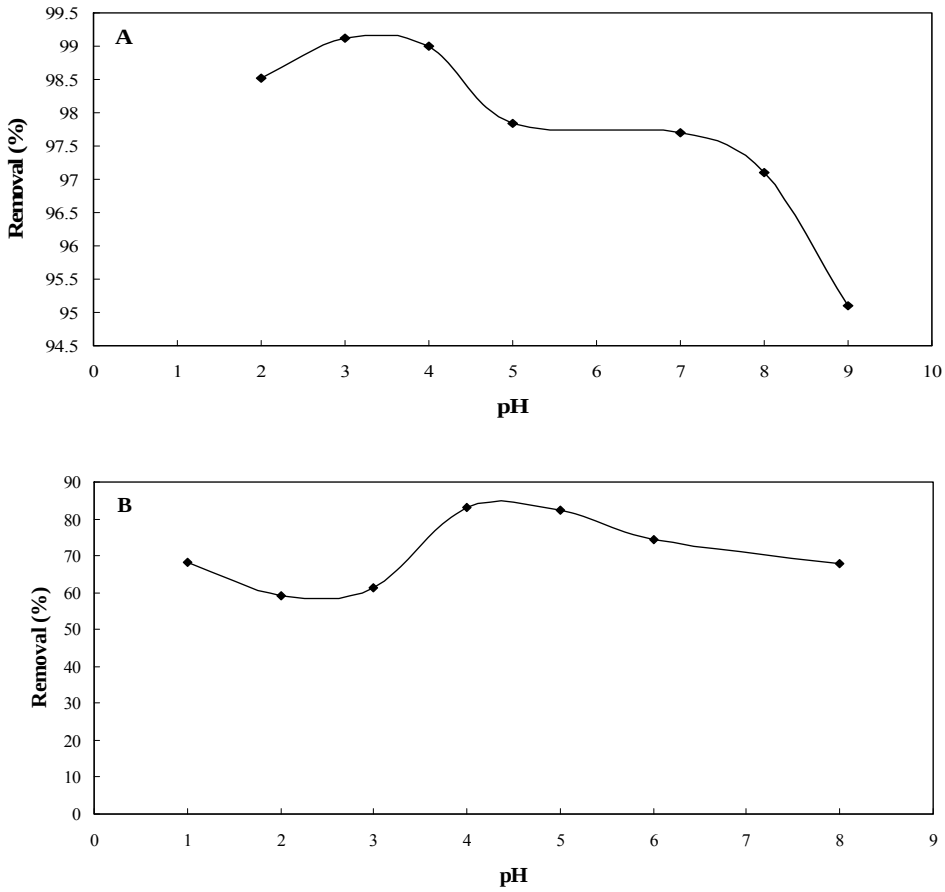

References:

[1] El Qada, E.N., Allena, S.J. and Walker, G.M. (2008) Adsorption of basic dyes from aqueous solution onto activated carbons. Chem. Eng. J. 135 (3), 174-184.

[2] Kucukosmanoglu, M., Gezici, O. and Ayar, A. (2006) The adsorption behaviors of methylene blue and methyl orange in a diaminoethane sporopolleninmediated column system. Sep. Purif. Technol. 52 (2), 280–287.

[3] Mauter, M.S. and Elimelech, M. (2008) Environmental applications of carbon-based nanomaterials. Environ. Sci. Technol, 42 (16), 5843–5859.

[4] Fugetsu, B., Satoh, S., Shiba, T., Mizutani, T., Lin, Y., Terui, N., Nodasaka, Y., Sasa, K., Shimizu, K. and Akasaka, T. (2004) Caged multiwalled carbon nanotubes as the adsorbents for affinity-based elimination of ionic dyes. Environ. Sci. Technol. 38 (24), 6890–6896.

[5] Chen, G.C., Shan, X.Q., Zhou, Y.Q., Shen, X.e., Huang, H.L. and Khan, S.U. (2009) Adsorption kinetics, isotherms and thermodynamics of atrazine on surface oxidized multiwalled carbon nanotubes. J. Hazard. Mater. 169 (1-3), 912–918.

Fluorescence spectroscopy investigation of the simultaneous interaction of two different drugs to human serum albumin

E. Hamidipor[1], M.R. Saberi[2], M. Vahidzadeh[1], M. Gharanfoli[3] and J. Chamani[1]

1. Department of Biology, Faculty of Sciences, Islamic Azad university–Mashhad Branch, Mashhad, Iran
2. School of Pharmacy, Mashhad University of Medical Sciences, Mashhad, Iran
3. Department of Development of Biology University of Science and Culture, Tehran, Iran

Abstract:

The interaction of ASA and COL with human serum albumin (HSA) has been studied using fluorescence techniques. Fluorescence spectrum of HSA in the presence of drugs clearly shows that drugs acts as a quencher. The interaction between drugs and HSA is consistent with static quenching. The thermodynamic parameters of HSA-drug bindings in binary and ternary systems have been calculated from fluorescence quenching

Introduction:

Serum albumin, the most abundant protein in the blood circulatory system, plays an important role in the transport and deposition of a variety of endogenous and exogenous. Acetylsalicylic acid (Aspirin) was one of the earliest agents to show promise for the treatment of sickle cell disease. Colchicine has been proposed as a treatment to alleviate chronic lung inflammation in cystic fibrosis patients and clinical trials are ongoing.

Method:

For macromolecules, the fluorescence measurements can give some information of the binding of small molecule substances to protein at the molecular level.

Results and discussion:

The fluorescence quenching of HSA induced by ASA and COL as binary systems showed in Fig. 1 (A,B). Obviously, in binary systems, the fluorescence intensities of HSA decreased remarkably with increasing concentration of ASA and COL and the emission maximum undergoes a blue shift with increasing transition ASA and COL concentration. It is noted that complex was formed between ASA and COL to HSA and which blue shift suggests a less polar (more hydrophobic) environment of tryptophan and/or tyrosine residue [1]. Quenching

can be classified as either dynamic or static quenching by different mechanisms. Dynamic quenching results from collision between fluorophore and quencher, and static quenching is due to the formation of ground-state complex between fluorophore and quencher [2]. The values of the quenching constants K_Q and the fractional accessible protein fluorescence f_a from modify Stern-Volmer equation were determined for the binary and ternary systems compared at excitation wavelength of 280 nm (Table. 1). It can be observed that quenching constants for the ternary system (HSA-COL)ASA and (HSA-ASA)COL at 280 nm are lower than that for the binary system of HSA-ASA, HSA-COL, respectively. It can be concluded that the presence of the second drug in the ternary system make difficult the formation of HSA-ASA and HSA-COL complex. Our results showed that quenching constants in (HSA-ASA)COL complex decreased (Table 1). Subsequently a larger distance between chromophore of COL and the excited fluorophores Trp-214 is noted. The values of f_a calculated for the fluorophores located in the corresponding binding sites for the binary and ternary systems in Table 1. Data shows that in presence of COL at in the first type of binding site in HSA-ASA and f_a increased but in the second type of binding sites f_a decreased. Also in the presence of ASA, f_a values decreased. The f_a values show that fluorophore exposition to the aqueous solution and the affinity between fluorophores and the protein increases and vise versa. When the distance between excited fluorophore is small, the rise of accessibility of fluorophore was observed.

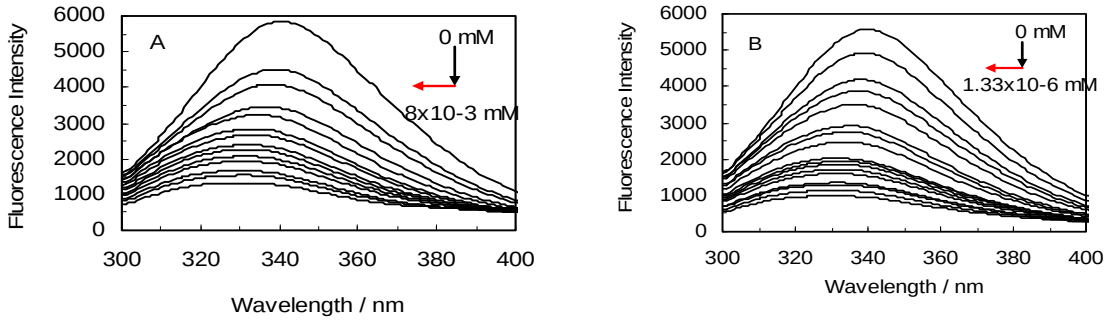

Fig. 1. Emission fluorescence spectra of HSA in interaction by HSA-ASA (A) and HSA-COL (B) at λ_{exi}=280 nm.

Table. 1. Quenching constant and the fractional accessibility of the fluorophore for the ligand for independent class of drug binding sites in HSA molecule determined for binary and ternary systems.

System	K_{QI} /M^{-1}	K_{QII} / M^{-1}	faI	faII
HSA-ASA	8.3×10^5	0.2×10^3	0.9	0.6
HSA-[COL]-ASA	7.6×10^2	11.6×10^3	2.1	-----
HSA-COL	2×10^6	-----	2.1	-----
HSA-[ASA]-COL	1×10^6	-----	1.1	-----

Conclusion

The interaction between ASA and COL with HSA has been studied by the fluorescence method. The results presented clearly indicated that drugs quenches the fluorescence of HSA through static quenching procedure. The quenching constant and fractional accessibility of the fluorophore for the ligand were calculated according to the relevant fluorescence data. The binding study of drugs with HSA is of great important in pharmacy, pharmacology and biochemistry.

References:

[1] P.B. Kandagal, S.S. Kalanur, D.H. Manjunatha, J. Seetharamappa. Journal of Pharmaceutical and Biomedical Analysis 47(2) (2008) 260–7.

[2] F. Ding, J.Huang, J. Lin, Z. Li, F. Liu, Z. Jiang, Y. Sun, Dyes and Pigments. 82 (2009) 65–70.

Separation of two amino acids by reversed micelle liquid membrane

A. Salabat*[a], F. Dehghani Sanij[a]

(Email:a-salabat@araku.ac.ir)

[a]*Chemistry Department, Arak University, P.O. Box 38156-879, Arak, Iran.*

Abstract

The transport of two amino acids L-tryptophan and L-tyrosine through the bulk liquid membrane system was investigated at 298.15 K. Reversed micelle formed by sodium bis (2-ethylhexyl) sulfosuccinate (AOT) were used as mobile carriers to transport amino acids across liquid membrane. The influence of some different parameters on the extraction was studied: pH of the source phase, surfactant concentration and initial amino acid concentration in the source phase. It is verified that for a mixtures of two amino acids, L-Trp can be extracted selectively in this type of the liquid membrane.

Keywords: Amino acids, AOT, Liquid membrane, Reversed micelle, Microemulsion.

Introduction

Recently, liquid membranes have been developed owing to several advantages such as ease of operation, low energy consumption and high selectivity factors [1]. Liquid membranes may be classified into three types: bulk liquid Membranes, emulsion liquid membranes and support liquid membranes. In general, the BLM system can be defined as a water-immiscible liquid (membrane phase) and a carrier molecule between two liquid phases (source and receiving phases) [2,3]. In recent years, there have been several reports that involving a new type of mobile carrier, namely micelles or microemulsion globules. Amino acids can be solubilized in the water core, or the interface between water and surfactant layer, depending on their electric charge [4].

Methods

Materials. 1,2-Dichloroethane was brought from Merck. AOT was obtained from Acrose Company with purity of 96%. L-tryptophan (>99%) and L-tyrosine (>99%) were also purchased from Merck. **Methods.** In the extraction experiments 25 mL of the liquid membrane, were placed in a thermostated U-tube (298.1±0.1 K). The source phase contains

10 mL of amino acid aqueous solution with pH between 1.8-5, present in one arm. The aqueous receiving phase contain 10 mL of a sodium tetraborate buffer solution at pH=10, which is present in the other arm. The liquid membrane was magnetically stirred at 200 rpm. The concentration of amino acids was determined by a double beam Perkin Elmer Lambda 15 UV-Vis spectrophotometer. The pH was measured by a digital Metrohm 691 pH-meter. The water content of the microemulsion liquid membrane was determined by Karl-Fisher titration. The molar ratio ($W=[H_2O]/[AOT]$) is increased with increasing AOT concentration.

Result and discussion

The results showed that, at the interface between the aqueous source phase and the membrane phase, an anionic surfactant (AOT) binds the cationic form of an amino acid via electrostatic interaction. The cationic form of an amino acid, from reversed micelles, were exrtacted to the receiving phase by an exchang reaction with Na^+.

1. Effect of pH in the source phase and surfactant concentration

The extraction efficiency and flux of L-Trp and L-Tyr is affected obviously by the pH of the source phase and concentration of AOT. For example as shown in Fig. 1, the extraction efficiency and flux of L-Trp decreases with increasing of the pH.

2. Effect of initial amino acid concentration

The experimental results show that the extraction efficiency, for two amino acids, is increased by decreasing in initial amino acids concentration.

3. Separation of two amino acids

For the final step, we performed separation of two amino acids by the microemulsion liquid membrane at the optimized condition. The results showed that for a mixture of amino acids (L-Trp and L-Tyr) in the following condition: pH=1.8 and [AOT]=0.005 mol L^{-1}, L-Trp was extracted selectively with liquid membrane.

Conclusions

In this research we have examined the specific ability of AOT reversed micelles to separate two amino acids L-Trp and L-Tyr. It is verified that the suitable parameters for extraction of

L-Trp would be pH of 1.8 and AOT concentration of 0.005 mol L^{-1} and for L-Tyr, pH of 5 and AOT concentration of 0.05 mol L^{-1}.

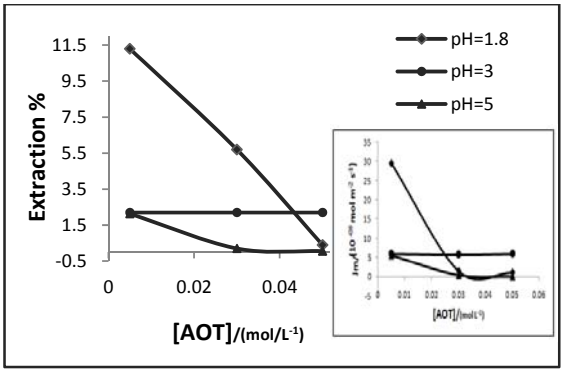

Fig. 1. Effect of pH in the source phase and surfactant concentration on the extraction efficiency and flux of L-Trp.

References

[1] E. Bringas, M. F San Roman, J.A. Irabien, I. Ortiz, J. Chem. Technol. Biotechnol. 84 (2009) 1583.

[2] S. Gong, J. Xing, P. Fang, X. Lu, Y. Chen, J. Membr. Sci. 205 (2002) 265.

[3] T. Araki, H. Tsukube, Liquid membranes: Chemical Applications, CRC Press, Boca Raton, FL, 1990.

[4] H. Stobbe, X. Yunguang, W. Zihao, F. Jufu, Biotechnol. Bioeng. 53 (1997) 267.

Activity Coefficients of Major Ions in Urmia Sea Water

N.Heidari[a], M.Rezaei[* b]

[a]Assistant Professor, Depatment of Chemistry, University of Urmia, Urmia, Iran

[b]Msc Graduate, Depatment of Chemistry, University of Urmia,Urmia,Iran

(Email: maryam.razaei87@gmail.com)

Key words: Pitzer aqueous, Activity coefficients, Water activity

Introduction

Lake Urmia (Orumiyeh),is one of the largest permanent hypersaline lake in the world and resembles the Great Salt Lakes in the western USA in many respects of morphology ,chemistry and sediments.

The purpose of this paper, the first paper of a series of papers devoted to the physic-chemical investigation of the Urmia Sea water body ,is to study the conventional single-ion activity coefficients of major ions and water activity in the Urmia Sea water body under different ionic compositions.

In this article we have tested the accuracy of the Pitzer equations in modeling mineral solubilities for the system H_2O-Na-K-Mg-Ca-Cl-HCO_3-SO_4. Parameterization of this models is completely defined by data from the experimentally simple binary and ternary systems. We have found that calculated results of this theory are within the experimental errors of the solubility measurements available.

experimental

Preparation of end-member solutions—The experiments involved sampling from Urmia Sea and analyze concentration of different ions at 25°C.

Table I, The composition of Urmia Sea waters and their ionic strength at different periods of time (ion concentrations are in molality units at 25°C)

Ions	Na^+	K^+	Mg^{+2}	Ca^{+2}	Cl^-	HCO_3^-	SO_4^{2-}	**Ionic strength**
2007	4.9000	0.0050	0.4613	0.0156	5.400	0.0098	0.1813	6.4736
2009	5.3900	0.0700	0.5000	0.0140	6.1800	0.0220	0.2240	7.3070
2010	4.1050	0.0510	0.7610	0.0405	4.7800	0.0160	0.2990	6.6770

Procedures- Appropriate volumes of the end-member solutions were estimated of ionic activity coefficient and the osmotic coefficient and water activity by used from the Pitzer model in Urmia Sea brains.

The general approach for the calculation of ionic activity and osmotic coefficients for multiple component electrolyte solutions was developed by Pitzere s equations. This approach was based on a set of theoretically and empirically derived equations that account for the interactions between the particular ions present in the solution and for indirect forces arising from the ion-solvent interactions. The up-to data and complete equations for conventional single ion activity, the osmotic coefficients and water activity are:

$$Ln\,\gamma_M = Z_M^2 (f^\gamma + \sum_c \sum_a m_c m_a B'_{c,a} + \sum_{c<} \sum_{c'} m_c m_{c'} \phi'_{c,c'} + \sum_{c<} \sum_{c'} m_a m_{a'} \phi'_{a,a'} + 2\sum_a m_a (B_{M,a} + \frac{\sum_i m_i |Z_i|}{2} C_{M,a}) + \sum_{a<} \sum_{a'} m_a m_{a'} \psi_{a,a',M} + Z_M \sum_c \sum_a m_c m_a C_{c,a} \quad (A_1)$$

$$Ln\,\gamma_X = Z_X^2 (f^\gamma + \sum_c \sum_a m_c m_a B'_{c,a} + \sum_{c<} \sum_{c'} m_c m_{c'} \phi'_{c,c'} + \sum_{a<} \sum_{a'} m_a m_{a'} \phi'_{a,a'}) + 2\sum_c m_c (B_{c,X} + \frac{\sum_i m_i |Z_i|}{2} C_{c,X}) + \sum_{c<} \sum_{c'} m_c m_{c'} \psi_{c,c',X} + |Z_X| \sum_c \sum_a m_c m_a C_{c,a} \quad (A_2)$$

$$\phi = 1 + 2(\Sigma_i m_i)^{-1} [f^\phi + \sum_c \sum_a m_c m_a (B^\varphi_{c,a} + E C_{c,a}) + \sum_{a<} \sum_{a'} (\phi^\varphi_{a,a'} + \sum_c m_c \psi_{a,a'c})] + \sum_{c<} \sum_{c'} (\phi^\varphi_{c,c'} + \sum_a m_a \psi_{c,c'a}) \quad (A_3)$$

$$a_{H_2O} = \exp(-\frac{\phi}{55.51} \sum_i m_i) \quad (A_4)$$

The meanings and calculations of all parameters in Ege. (A_1), (A_2), (A_3) and (A_4) can be found in Krumgalz and Millero (1982).

Result

The final results of the conventional single-ion activity coefficients (γ_M and γ_X) of major ions in Urmia Sea water, calculated by equations (A_1) and (A_2), are presented in Table II.

activity coefficients	Na^+	K^+	Mg^{+2}	Ca^{+2}	Cl^-	HCO_3^-	SO_4^{2-}	Ionic strength
2007	0.8371	0.4967	1.3432	0.7688	1.1332	0.4082	0.0309	6.4736
2009	0.9351	0.5180	2.3943	1.1840	1.2266	0.4036	0.0288	7.3070
2010	0.7330	0.4330	0.8180	0.4580	1.3030	0.4010	0.0352	6.6770

And the result of the calculation of the osmotic coefficients, water activity of Urmia Sea brines by equations (A_3) and (A_4) are summarized in Table III.

Parameter	Ionic strength		
	I=6.4736	I=7.3070	I=6.6670
ϕ	1.3000	1.3070	1.3011
α H2O	0.7733	0.7343	0.7900

References:

[1] .Krumgalz, B.S and Millero, F.J. 1982. Physico-chemical study of the Dead Sea waters. I. Activity coefficients of major ions in Dead Sea water. Mar. Chem.,11: 209-222.

[2] .Pitzer, K.S. 1991. Ion interaction approach: theory and data correlation. In: Activity Coefficients in Electrolyte Solutions. 2 ed .K.S. Pitzer (ed). CRC Press, pp. 75-153.

Wave rotating approximation in Atom-field interaction semiclassical theory

F. rahnamai*[a]

[a]Department of physics, University of Islamic Azad University-shahreza Branch, shahreza, Iran

(Email:rahnamai@iaush.ac.ir)

Abstract:

One of the simplest nontrivial problems involving the atom-field in-teraction is the coupling of a two-level atom with a single mode of the electromagnetic field. A two-level atom description is valid if the two atomic levels involved are resonant or nearly resonant with the driving field, while all other levels are highly detuned. we present semiclassical theory of the interaction of a single two-level atom with a single mode of the field in which the atom is treated as a quantum two-level system and the field is treated classically. Just as the spin-1/2 system undergoes the so-called Rabi oscillations between the spin-up and spin-down states under the action of an oscillating magnetic field, the two-level atom also undergoes optical Rabi oscillations under the action of the driving electromagnetic field.

keywords: Wave rotating, approximation , field interaction

Introduction:

electromagnetic field is described by a minimal-coupling Hamiltonian

$H = \frac{1}{2m}\left[P - e\ A(r,t)\right]^2 + eu\ (r,t) + V(r)(1)$ we first derive this Hamiltonian from a gauge invariance point of view, HamiltonianThe motion of a free electron is described by the Schrodinger equation such that

$$ih\left[\frac{ie}{h}A^0.r\phi_{(r,t)} + \phi^0(r,t)\right]\exp(\frac{ie}{h}A.r) = \exp(\frac{ie}{h}A.r)\left[\frac{P^2}{2m} + V(r)\right]\phi_{(r,t)} \quad (2)$$

If we want to satisfy local gauge (phase) invariance, then the Schrodinger equation must be modified by adding new terms where A(r, t) and U(t, t) are functions

$ih\phi_{(r,t))} = [(H_0 - er.E_{(r_0,t)})]\phi_{(r,t)}, H = H_0 + H_1, H_1 = -er_1 E(r_0,t)$ (3). The electrons are described by the wave function $X_{(r,t)} = -\frac{e}{h}A(r_0,t).r$ (4). The minimal-coupling Hamiltonian for an interaction between an atom and the radiation field can be reduced to a simple form by using the dipole approximation. The Schrodinger equation for this problem (in the dipole approximation) is given by Eq.

$$ih\left[\frac{ie}{h}A^0.r\phi_{(r,t)} + \phi^0(r,t)\right]\exp(\frac{ie}{h}A.r) = \exp(\frac{ie}{h}A.r)\left[\frac{P^2}{2m} + V(r)\right]\phi_{(r,t)} \quad (5)$$

We have added the term V(r) in the Hamiltonian which arises from the electrostatic potential that binds the electron to the nucleus.. We again choose a radiation gauge in which U(r, t) = 0 and $H_2 = -\frac{e}{m}[P.A(r_0,t)] + \frac{e^2}{2m}A^2(r_0,t)$. (6)

Results and disscution:

The electric field then takes the form and the corresponding vector potential in the radiation gauge is $E(t) = \varepsilon \cos vt$

Consider now the time-independent amplitudes associated with

$$|\Psi_{(t)}>= C_a(t)|a> + C_b(t)|b>$$

$$|\Psi^0(t)>= -i/h\, H|\Psi_{(t)}> \quad (7)$$

$$H = H_0 + H_1 \quad (8)$$

$$H_0 = (|a><a| + |b><b|)H_0(|a><a| + |b><b| = hw_a|a><a| + hw_b|b><b|$$
$$H_0|a>= hw_a|a> \quad , H_0|b>= hw_b|b> \quad (9)$$

$$= -e(|a><a| + |b><b|)x(|a><a| + |b><b|)E(z,t)$$
$$= -(\delta_{ab}(|a><a| + |b><b|) + \delta_{ba}(|b><a|)E(t) \quad (10)$$

$$\delta_{ab} = \delta_{ba} = e < a|x|b > \qquad \Omega_R = \frac{|\delta_{ab}|\varepsilon}{h} \quad (11)$$

$$C_a^{\cdot} = -iw_a C_a + i\Omega R_e^{-i\phi} Cos(v_t) C_b$$
$$C_b^{\cdot} = -iw_b C_b + i\Omega \mathrm{Re}^{i\phi} Cos(v_t) C_a \quad (12)$$

$$C_a^{\cdot} = -iw_a C_a + i\Omega R_e^{-i\phi} Cos(v_t) C_b \quad , C_b^{\cdot} = -iw_b C_b + i\Omega \mathrm{Re}^{i\phi} Cos(v_t) C_a \quad (13)$$

we can use $Cos(v_t) =$ $e^{i(w-v)t}$ then

$$C_b^{\cdot} = \frac{i\Omega R}{2} e^{-i\phi} C_b \left[e^{i(w-v)_t} + e^{i(v+w)t} \right], C_a^{\cdot} = \frac{i\Omega R}{2} e^{-i\phi} C_a \left[e^{i(w-v)_t} + e^{-i(v+w)t} \right] \quad (14)$$

Conclusion:

if $ex_p[\pm i(w+v)t]$=0 at $v \cong w$ we use approximation in wave rotating and we have

$P_{(t)} = (C_a < a| + C_b < b|r|C_a|a > + C_b|b >$ (10) using this approximation

$$P_{(t)} = 2\mathrm{Re}\left[\frac{i\Omega R}{\Omega} \delta_{ab} \left[Cos(\frac{\Omega_t}{2}) + \frac{i\Delta}{\Omega} \sin(\frac{\Omega_t}{2}) \right] \sin(\frac{\Omega_t}{2}) e^{i\phi} e^{ivt} \right] \quad \textbf{(15)}$$

References:

[1].W. E. Lamb and R. C Retherford, Phys. Rev. 72, 339 A947).

[2].R. P. Feynman, F. L. Vernon, and R. W. Hellworth, J. Appl. Phys. 28, 49 A957).

[3].E. T. Jaynes and F. W. Cummings, Proc. IEEE 51, 89 A963).

[4].L Allen and J. Eberly, Optical Resonance, (Wiley, New York 1975).

Electronic properties of titanium dioxide by using ab intio calculations

zare, s*[a] ; Mirzaei , R[b] ; Hosaini , B[c]

[a]Islamic Azad University Branch,sama shiraz,Iran

[b]University of Applied Science,dehloran,Iran

[c]Islamic Azad University Kazerun Branch,Iran

email:samadzare@gmail.com

Keywords; TiO_2 , rutile structure, anatas , Charge density

Introduction

Titanium dioxide (TiO_2) forms three distinct polymorphs : rutile , anatase, and brookite.for the past several decades TiO_2 has been extensively studied for its interesting electric, magnetic ,catalytic and electrochemical properties[1-4].based upon these properties,a variety of technological applications are possible. TiO_2 has been widely used in catalysis, in electrochromism,and as sensors[5]. TiO_2 is a direct transition compound semiconductor whose bandgap is 3 ev. This compound is crystallized in the rutile and anatase is tetragonal structure and The lattice constant parameters used in this work a=5.409 A° , c=2.958 A° for Rutile structure,a=3.784 A°,c=9.515 A° for Anatas structure.

Method

The calculations have been performed by using soft–core ab initio pseudpotential constructed augmented with in Density Functional Theory (DFT) with using pwscf package.

In this study, for making pseudopotential elements Ti and O, we select the norm conserving pseudopotential method. The Monkhorst-Pack k-point meshes of 5×5×5 for the rutile andanatase structure were employed.

Results and Discussion

In fact , e lectronic charge density is the charge density that shows the electronic charge distribution around atoms . amount of charge distribution around the atoms indicates type bondings between the atoms. High electron density between two atoms indicates a

strong bonding and lower electron density shows the weaker bonding between the atoms. electronic density plot shows the density in different positions and indicates where the more electron density points are and so are the less.Figures 1 and 2 shows the electronic charge density plot in the (110) plane of TiO_2 for rutile and anatase structures. the figures indicate the highest electron charge density on oxygen atoms precisely, due to the high electronegativity oxygen in this compound. lower electron charge density in Ti atoms shows that the Ti atoms have lost the electron.

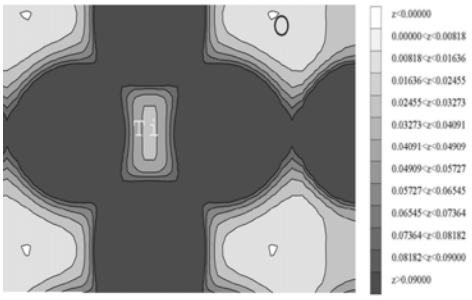

Fi g. 1. Electronic charge density plot in the plan e (110) of rutile structure

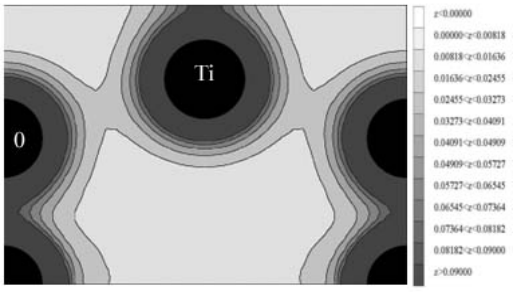

Fi g. 2. Electronic charge density plot in the plan e (110) of anatase structure

There is a strong covalent bonding between the Ti and O atoms due to Ti^{+4} cations and O^{-2} anions in this compound. the calculated charge distribution shows a polar covalent feature in bonding Ti-O. It can be seen that the O ions is larger than Ti, and there is a charge transfer from Ti to O. This is because of higher electronegativity of O than Ti. If the electronic charge density is drawn considering spin coupling, it does not change the obtained results. It can be concluded that the spin does not effect on charge density in this compound. This is highly excellent agreed with experimental results.

Conclusion

According to the electronic charge density plot in the (110) plane of TiO_2, the electronic charge density on O atoms is higher than Ti atoms, this is due to the higher electronegativity of O than Ti. The lower electronic charge density around Ti atoms shows that the Ti atoms have lost the electron. high electronic charge density between Ti and O atoms indicates a

covalent bonding between Ti and O atoms This is highly excellent agreed with available experimental results.

Refrences:

[1] M. F. Yan and W. W. Rhodes, in Grain Boundaries in Semiconductors,
edited by H. J. Leamy, G. E. Pike, and C. H. Seager North-Holland, New York, (198 1).
[2] J. Reintjes and M. B. Schultz, J. Appl. Phys. 39, 5254 (1968).
[3] J. B. Goodenough and J. M. Longo, in Landolt-B|rnstein Tabellen,edited by K. H. Hellwege and A. M. Hellwege ,Springer-verlag, Berlin,(1970).
[4] s. J. Tauster, S. C. Fung, and R. L. marten, J. Am. Chem. Soc.1, 170 (1978).
[5] 6B. Poumellec, PhD. thesis, university d'Orsay. 1986.

Sorption study of C. I. Basic Violet 2 from aqueous solutions on perlite

N. Modirshahla[a], M. A. Behnajady[a], H. Sadeghzadeh[b], R. Sadeghzadeh[a]

[a]Faculty of science, Department of Chemistry, Islamic Azad University – Tabriz Branch, Tabriz, Iran

(Email: sadegzade.samie@yahoo.com)

[b]Academic member of Islamic Azad University – Bonab Branch

Keywords: Adsorption, C. I. Basic Violet 2, Perlite, Kinetic models

Introduction

Many industries, such as dyestuffs, textile, paper and plastics, use dyes in order to color their products and also consume substantial volumes of water. As a result, they generate a considerable amount of colored wastewater. Amongst the numerous techniques of dye removal, adsorption is the procedure of choice and gives the best results as it can be used to remove different types of coloring materials[1].

The present study deals with the removal of C. I. Basic Violet 2 from aqueous solutions by adsorption method using expanded perlite as an adsorbent. The effect of operational parameters such as adsorbent dose, contact time, agitation speed and pH were examined in a batch system. Three Kinetic models, pseudo first-order kinetic model, pseudo second-order kinetic model and intra particle diffusion model were studied.

Materials and methods

Basic Violet 2 (BV2), (C. I. 42520, FW: 365.90, λ_{max}: 543 nm, supplied by ACROS ORGANICS, USA) was used as adsorbate, and the adsorbent was purchased from Azarbaijan expanded perlite company (Tabriz, Iran). It was sieved through 100-mesh sieve, and washed with distilled water. Then it was filtered and dried at 120^0C for 15 hr in an oven.

The experiments were performed on BV2 solutions with concentrations of 15 mgL^{-1}.

Results and discussion

The effect of adsorbent dose on the dye uptake showed at the amount of 4 g of perlite the removal percent is maximum. The dependence of BV2 adsorption on contact time and

agitation speed were studied. The results showed that the removal of dye increases with increase in time up to 30 min and after that the dye uptake decreases due to deposition of dye molecules on the available adsorption sites on the adsorbent[2]. It was also found that increasing agitation speed (up to 125 stroke/min) reduced the film boundary layer surrounding particles, thus increasing the external film transfer coefficient and hence the percentage dye removal[3].

In order to study the adsorption mechanism, it is necessary to determine the point of zero charge (pH_{ZPC}) of the adsorbent. In this study pH_{ZPC} of the perlite was found to be 7.6. The results revealed that the adsorption process is favored at $pH > pH_{ZPC}$. This behavior may be due to the development of negative charge of the perlite. At a higher pH above the pH_{ZPC}, the surface of the adsorbent gets negatively charged, wich enhances the adsorption of positively charged dye cations (BV2) through electrostatic force of attraction[2].

In the present study, three kinetic equations were examined to evaluate the kinetic mechanism. It was obtained that the adsorption process obeys the pseudo second-order kinetic model with a high value of correlation coefficient ($r^2 = 0.99$), that is shown in Fig. 1. The r^2 values were 0.42 and 0.61 for the pseudo first-order kinetic model and intra particle diffusion model, respectively.

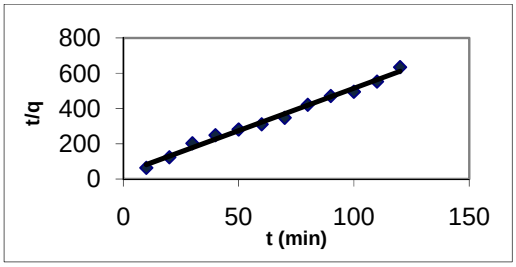

Fig. 1. pseudo-second order kinetic model for the adsorption of BV2 dye on perlite

Conclusion

The removal of BV2 using expanded perlite was investigated under different experimental conditions in a batch mode. The adsorption of BV2 was dependent on adsorbent dose, contact time, agitation speed and pH of aqueous solution. Furthermore, kinetic studies showed that the adsorption process followed the pseudo second-order kinetic model.

References

[1] Crini, G., 2006. Non-conventional low-cost adsorbents for dye removal: A review, Bioresour. Technol., 97, 1061-1085.

[2] Govindasamy, V., Sahadevan, R., Subramanian, S., Mahendradas, D. K., 2009. Removal of Malachite Green from Aqueous Solutions by Perlite, Int. J. Chem. React. Eng., Article A43.

[3] Nandi, B. K., Goswami, A., Purkait, M. K., 2009. Adsorption characteristics of brilliant green dye on kaolin, J. Hazard. Mater., 161, 387-395.

DFT study on a selective BN- doped graphene

Tina Tayebi[a*], Zahra Alipanah[a] ,Azita Nouri[b], Mahmoud Mirzaei[c] , Ehsan zahedi[a]

[a]*Chemistry Department, Shahrood Branch, Islamic Azad University, Shahrood, Iran*

[b]*Chemistry Department ,Shahreghods Branch, Islamic Azad University, Shahre-ghods, Iran*

[c]*Department of Chemistry, Tarbiat Modares University (TMU), P.O. Box 14115-175, Tehran, Iran*

Corresponding Author E-mail: tinatayebi@gmail.com

Keywords: Graphene, Boron-Nitride doping, Density functional theory, chemical shielding.

Introduction:

In a graphene sheet, each carbon atom forms bonds with three other carbon atoms to produce a two-dimensional honeycomb structure . These carbon–carbon bonds are very strong, which renders graphene stable, even when it has been cut into nano scale structures. Graphene is a zero-gap semiconductor, an electronic state of matter that is precisely in between a semiconductor and a metal [1].

Theoretical section:

In this computational study we considered the pristine model of eight-ring graphene consisted of 28 carbon atoms (C28H14)(figure 1).The BN-doped (figure 2) consisted of 26 carbon atoms ، one boron and one nitride atom(BNC26H14). All of the models are optimized at the BLYP/6-31G* level of theory. Subsequently, the CS parameters have been calculated in the optimized structures using the same level of theory. The results are presented in Table1. Eqs. (1) and (2) are used to convert the calculated CS tensors to the isotropic (CS^I) and anisotropic (CS^A) parameters [2].

$CS^I(ppm) = \frac{1}{3}(\sigma_{11} + \sigma_{22} + \sigma_{33})$ (1) $CS^A(ppm) = \sigma_{33} - \frac{1}{2}(\sigma_{11} + \sigma_{22})$ (2)

All calculations are performed using guassian 98 software.

Results:

In double doped graphene, C42 and C43 are respectively doped by B and N atoms (Fig1,2).The results of geometry optimization (Table1) revealed similar bond lengths for equivalent positions in the BN-doped and also in the pristine model. The value of bond length

of the B-N is larger than the C-C one that is 1.45 A^0, in pristine model. The B-N one is 1.48 A^0 and the C-N one is 1.40 A^0 and the B-C one is 1.49 A^0. Furthermore the calculated total energies indicated that the structure of the pristine model of graphene,was 92 ev less stable than BN-doped structure. The calculated band gap energies of this study showed that pristine model was calculated 0.4982 larger than the BN-doped. The value of dipole moment changed from 0.0044 Debye in the pristine model to 2.4 Debye in the B-N doped model. Also Table 1 presents NMR parameters (CS^I and CS^A). The chemical shielding parameters of C atoms which are directly bonded to B atom (C32 and C52), are changed smaller than C atoms which are directly bonded to N atom (C33 and C53) in double doped graphene .

Conclusions:

We performed this computational work to study double doping effects on the electronic structure properties of the pristine model of graphene. In doping effects, the calculated total energies indicated that BN-doped structure was more stable than the pristine model. The calculated band gap energies indicated that the value was smaller for the BN-doped structure. The calculated dipole moments elucidated that the polarizabilty of the BN-doped model was more than the pristine one. The calculated CS^I and CS^A values revealed that these parameters belong to C atoms near to N nuclei are more sensitive than N nuclei.

*** Table 1**

	Pristine		BN-doped	
	σ_{iso}	σ_{aniso}	σ_{iso}	σ_{aniso}
C_{11}	66.15	149.99	64.88	149.34
C_{12}	72.33	144.56	73.88	144.72
C_{13}	72.12	144.66	69.56	144.01
C_{14}	66.19	150.04	65.81	150.74
C_{21}	64.67	132.35	61.35	140.28
C_{22}	58.97	158.84	56.68	165.12
C_{23}	58.82	159.02	57.29	145.09
C_{24}	64.82	132.36	68.40	125.05
C_{31}	59.14	17857	53.42	182.29
C_{32}	64.87	172.13	61.93	198.55
C_{33}	64.86	172.19	51.64	131.71
C_{34}	59.24	178.59	59.77	165.06
C_{41}	65.43	110.34	67.45	100.96
C_{42}	63.28	157.89	79.17	50.23
C_{43}	63.31	157.84	54.73	258.68
C_{44}	65.32	110.41	63.53	109.87
C_{51}	59.24	178.53	53.42	182.29
C_{52}	64.86	172.16	61.93	198.55
C_{53}	64.85	172.17	51.64	131.71
C_{54}	59.13	178.56	59.77	165.06
C_{61}	64.67	132.25	61.35	140.28
C_{62}	58.85	158.94	56.68	165.12
C_{63}	58.92	158.89	57.29	145.09
C_{64}	64.69	132.34	68.40	125.05
C_{71}	66.17	150.02	64.88	149.34
C_{72}	72.16	144.70	73.88	144.72
C_{73}	72.34	144.50	69.56	144.01
C_{74}	66.26	149.90	65.81	150.73
Total energy	-29254		-29346	
Band gap	0.9363		0.4381	
Dipole moment	0.0044		2.4	

*The units of energy and dipole moment are eV and Debye respectively.

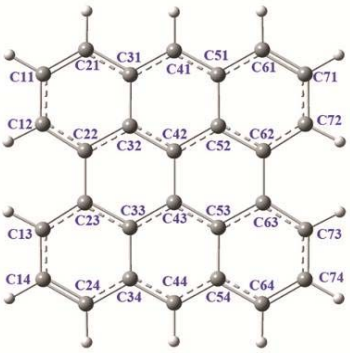

Figure 1

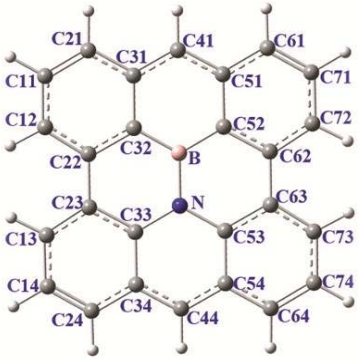

Figure 2

References:

[1] Meyer, J. et al. Nature **446,** 60–63 (2007).

[2] A. Seif, A. Boshra, J. Mol. Struct. (THEOCHEM) 895 (2009) 82.

Resonance Rayleigh scattering and Fluorescence quenching investigation of human serum albumin upon interaction with aspirin and amlodipine as binary and ternary systems

N. Abdollahpour[1], A. Asoodeh[2], M.R. Saberi[3], V. Soheili[3], J. Chamani[4]

1. Department of Biology, Faculty of Sciences, Islamic Azad University- Mashhad Branch,Young Researchers Club, Nooshin.ap@gmail.com

2. Department of Chemistry, Faculty of Sciences, Ferdowsi University of Mashhad, Mashhad, Iran

3. School of Pharmacy, Mashhad University of Medical Sciences, Mashhad, Iran

4. Department of Biology, Faculty of Sciences, Islamic Azad University- Mashhad Branch, Mashhad, Iran

Keywords: Aspirin, Amloipine, Human Serum Albumin, Resonance Rayleigh scattering, Fluorescence Quenching

Introduction:

Among the four aspects of pharmacokinetics (absorption, distribution, metabolism, and excretion), distribution is the one that this protein controls because most drugs that travel in plasma bind to HSA [1]. Resonance Rayleigh Scattering (RRS) is a special elastic scattering produced when the wavelength of Rayleigh Scattering (RS) is located at or close to the molecular absorption band [2]. Fluorescence spectroscopy has found wide use in studying the physico–chemical properties of proteins, proteins–ligand interactions, and protein dynamics. Fluorescence spectroscopy is often the method of choice for studying properties such as stability, hydrodynamics, kinetics, or ligand binding, because of its exquisite sensitivity [3].

Methods:

Fluorescence quenching spectra of HSA were obtained at excitation and emission wavelength of λ_{ex}=280, 295 nm and λ_{em} =300-600 nm and for a RRS spectrum can be developed by scanning both the excitation and emission monochromators of a common spectrofluorometer, with $\Delta\lambda$=0 nm ,from 220nm to 600 nm .

Results and discussion:

Fig.1 shows that the RLS spectrum of HSA-ASA in present of AML that has a sharp and maximum peak at 300 nm. when AML was added to HSA, the RLS intensity was increased.

Then an increase of drug concentration led to a reduction of the RLS intensity .It can be seen that when both AML and ASA is added to HSA , the RLS intensity of this ternary system is much stronger than those binary system, which indicating the formation of the larger ternary complex with HSA in the system. It can be seen from Fig. 1 that the intensities of the fluorescence emission of HSA in the binary and ternary systems decreased gradually when increasing the drug concentrations, this suggests that the chromophore of the protein was positioned in a more hydrophobic environment after addition of ASA and AML. The fluorescence quenching behavior could be analyzed using the Stern-Volmer and Lehrer

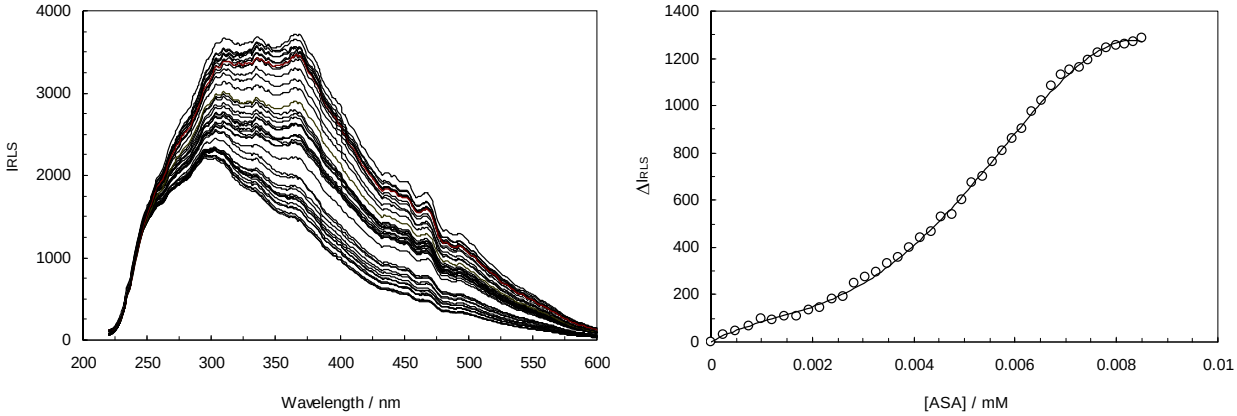

equations.

Figure 1: Resonance light scattering of HSA-ASA complex in the presence of AML.

Conclusions:

The analysis of the fluorescence quenching of HSA in binary and ternary systems pointed at ASA and AML having an effect on the HSA-AML and HSA-ASA complexes. Furthermore, the results of resonance light scattering and of the binary and ternary systems showed that the binding of AML and ASA to HSA could induce conformational changes in HSA. Moreover, the simultaneous presence of ANL and ASA during binding to HSA should be taken into account in multi-drug therapy.

Reference:

[1]Feng Yang ,Chuanbing Bian ,Lili Zhu,Gengxiang Zhao ,Zixiang Huang ,Mingdong Huang , *J. structural Biology.* **157** (2007)348-355.

[2] Nian Bing Li .Hong Qun Luo ,Shao Pu Liu ,*J.Talanta* **66** (2006) 495-500

Binding analysis of amlodipine to human serum albumin in pH different condition: fluorescence spectroscopy

P. Atarodi-Shahri[1], N. Abdollahpour[1], M.R. Saberi[2] and J. Chamani[1]

1. Department of Biology, Faculty of Sciences, Islamic Azad University-Mashhad Branch, Mashhad, Iran
2. Medical Chemistry Department, School of Pharmacy, Mashhad University of Medical Sciences, Mashhad, Iran

Keywords: Human Serum Albumin, Amlodipine, Spectroscopy methods

Introduction.

AmlodipineR, S-2 [(2-aminoethoxy)methyl] -4- (2-chlorophenyl) -ethoxycarbonyl-5-methoxycarbonyl-6-methyl-1,4-dihydropyridine [1] belongs to the pharmacological family of calcium channel blockers[2]. Drugs are mainly transported by human serum albumin (HSA),a1-asidicglycoprotein (a1-AGP),and lipoproteins in blood's is the most abundant plasma protein. Investigation the interaction of drug-protein complex, as it may provide useful information of the structural features that determine the therapeutic effectiveness of drug. There are some works to study the interaction of drug with protein by fluorescence spectroscopy.

Materials and methods

All reagents were of analytical grade and purchased from sigma-Aldrich Co. (St Louis, MO. USA). The solutions of HSA were prepared under physiological conditions. The fluorescence spectra were then measured (the excitation wavelength at 280 nm) at room temperature.

Results and discussion

The fluorescence of HSA comes from the tryptophan, tyrosine, and phenylanine residues. Actually, the intrinsic fluorescence of HSA is almost contributed by tryptophan alone located in sub-domain IIA. In the fluorescence quenching experiments the excitation wavelength used was 280 nm in order to reduce the quantum yield by AML. Fig.1 shows fluorescence emission spectra for HSA in the presence of increasing of AML in pH 7.4.AML causes a

decrease in the protein tryptophan fluorescence quantum yield. The influence of pH was studied in the range of 6.4-8.4.The pH dependence of the HSA Stern-Volmer`s plot in the presence of AML shows in Fig.2. The Stern-Volmer`s plots are linear ,indicating that only one type of quenching process occurs [4]and values of Ksv and correlation coefficient listed in Table 1.The most binding AML to HSA indicate in pH 8.4.

Fig. 1. Trp fluorescence of HSA at pH 7.4 in different concentration of AML. Stern-Volmer plots of the quenching of fluorescence of HSA by AML at different pH. The pH values Were 6.4(Δ) 7.4(◊), 8.4(□)

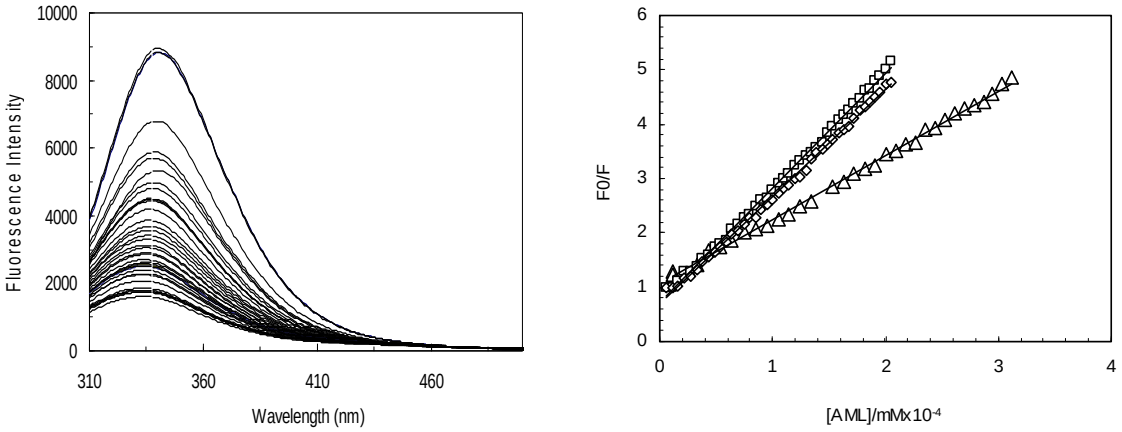

Table1. The values of Stern-Volmer constants and correlation coefficient in different pH.

pH	K_{SV}(x 10^6 M^{-1})	R^2
6.4	1.1	0.097
7.4	1.9	0.997
8.4	2.1	0.998

Refrences

[1] A.Zarghi, S.M.Farouton, A.Shofaati, A.Khoddam, ValidatedHPLC method for determination of amlodipine in human plasma and its application to pharmacokinetic studies ,II Farmaco 60 (2005)789-792.

[2] Renaud Tissier, DVM, PhD, Sebastien Petrrot, Pharm D, PhD, Brigitte Enriques, DVM,PhD, Dipl ECVPT, Amlodipine:One of the main anti-hypertensive drugs in vesterinary therapeutics, Journal of veterinary Cardiology (2005)7.53-58.

A computational study of the behavior of the of the 1-*n*- butyl-4-amino-1, 2, 4-triazoliumn bromide ionic liquid confined inside single walled carbon nanotube

M. Foroutan, M. A. Balazadeh
Department of Physical Chemistry, College of Science, University of Tehran,
Tehran, Iran
balazadeh@khayam.ut.ac.ir

Keywords: Ionic Liquids, Single walled carbon nanotube, Molecular dynamic simulation

Introduction

Uses of ionic liquids (ILs), because of specific properties have been increased in many different science fields [1]. In this research we have performed molecular dynamic (MD) simulation to study the properties of the 1-*n*- butyl-4-amino-1, 2, 4-triazoliumn bromide ionic liquid confined inside single walled carbon nanotube (SWCNT). In previous papers simulation of melting this IL has performed [2]. Atomic labels of the IL are shown in figure 1.

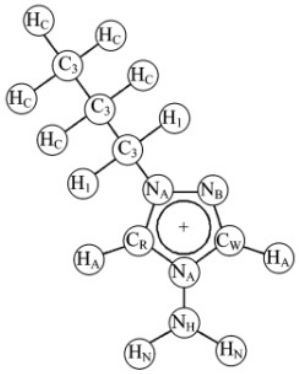

Figure 1- Schematic representation of cation of IL 1-*n*- butyl-4-amino-1, 2, 4-triazoliumn

Simulation details

Simulations have been performed with the tinker program in ensemble NVT. SWCNT was kept in fixed position. The force field used was based on the OPLS all–atom. Intermolecular

parameters such as harmonic and dihedral angles for IL were obtained from reference no. 2. We placed 4 ILs inside SWCNT at temperature 400K. Cut off distance was 12A° and simulation time step was 1.0 fs. SWCNT is used in this work is (15,15) having a length of L=27.06A° with internal pore diameter equal to 26 nm.

Results and Discussion

Representative simulation snapshot of system is depicted in figure 2.

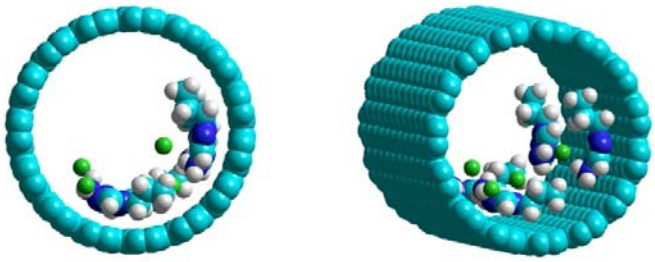

Fig. 2- Representative simulation snapshots of IL confined inside SWCNT, at initial simulation time (Left), the last simulation time (Right).

For study the behavior of IL confined in SWCN we presented the radial distribution functions (RDFs) between atoms of cation with carbon nanotube, plotted in figure 3. As figure 3 shows, one sharp peak can be seen at distance 3A°, for NA, NB, CB, CW and CR atoms of IL. Therefore, the probability of finding these atoms surrounding the CNT is higher than that of other atoms of cation.

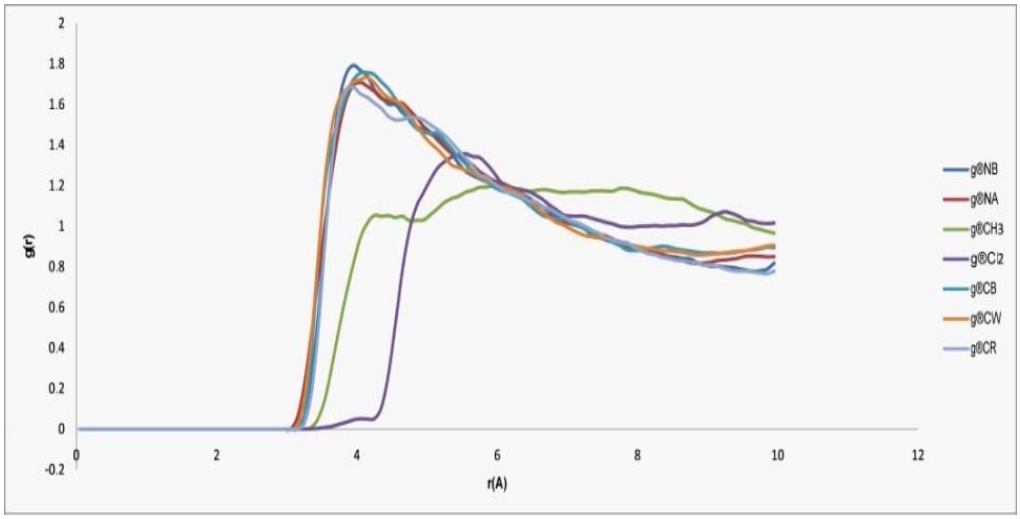

Fig.3- RDFs profiles for different atoms of cation and carbon nanotube.

References

[1] A. Heintz, J. Chem. Thermody. 37 (2005) 525.

[2] S. Alavi, D.L. Thompson, J. Phys. Chem. B 2005 (109) 18127.

Effect of B and Al functional groups on a selective graphene: A computational study

Zahra Alipanah[a*], Tina Tayebi[a] , Azita Nouri[b], Mahmoud Mirzaei[c] ,Ehsan zahedi[a]

[a]*Chemistry Department, Shahrood Branch, Islamic Azad University, Shahrood, Iran*

[b]*Chemistry Department ,Shahreghods Branch, Islamic Azad University, Shahre-ghods, Iran*

[c]*Department of Chemistry, Tarbiat Modares University (TMU), P.O. Box 14115-175, Tehran, Iran*

Corresponding Author E-mail: shadialipanah@gmail.com

Keywords: Graphene, functionalization effect, Density functional theory, chemical shielding.

Introduction:

Graphene is the ideal material for many dream applications, such as single electron transistors, field emission sources [1], The edges of graphene, in particular the zigzag edges, play the most important role in defining the electronic properties of graphene [2]. Any changes in the edge geometry such as termination, reconstruction, distortion would modify the electronic properties of graphene.In this work we studied electronic properties and NMR parameters of some structures of a selective graphene.

Theoretical methods:

The considered models of this study are selected models of geaphene. These models are pristine, graphene with B functional group and graphene with Al functional group instead of an edge's H atom. All models are individually optimized and then the CS tensors at the sites of ^{4}C , ^{27}Al and ^{5}B nuclei are calculated based on the gauge included atomic orbital (GIAO) approach. The calculated CS tensors in principal axes system (PAS) ($\delta 33 > \delta 22 > \delta 11$) are converted to measurable NMR parameters, chemical shielding isotropic (CSI) and chemical shielding anisotropic (CSA) using (1) and (2), respectively .

$$CS^{I}(ppm) = \tfrac{1}{3}(\sigma_{11} + \sigma_{22} + \sigma_{33}) \quad (1)$$

$$CS^{A}(ppm) = \sigma_{33} - \tfrac{1}{2}(\sigma_{11} + \sigma_{22}) \quad (2)$$

Results:

The three structures had the same number of atoms, the functional groups were members at the top of the graphene instead of H atom (fig.2, 3).Values of band gap detect significant changes in which the values of band gaps for the pristine, with B functional group and with Al functional group are 0.9363, 0.8473 and 0.8952 ev respectively. This trend means that B functional group has more influence on the band gap of pristine model .The results of NMR calculations indicated that the CS parameters of the pristine models can be divided into some layers with the same values in each layer; however, different values are observed in atoms near functional group atoms. The highest changes of CS tensors are observed at the sites of C41, C42, C43, C44, C31 and C51 nucleuses whereas the changes of those of the other C atom negligible. Furthermore, we studied the B-C and Al –C bond length and B-C-C and AL-C-C angles in this work.

Conclusions:

We carried out this computational work to study functionalization effects on the electronic structure properties of the pristine model of graphene . In functionalization effects, the calculated total energies indicated graphene functionalized with Al is the most stable model. The calculated dipole moment indicated that the polarizibility of graphene with the B functional group was more than Al functional group. The changes of the calculated CS tensors in two different functional group regarding to the pristine models are also shown by changes of the structural properties.

Table 1

Nuclei	**CSI/PPM**			**CSA/PPM**		
	Pristine	B	Al	Pristine	B	Al
C_{11}	66.15	65.27	65.80	149.99	151.73	151.33
C_{12}	72.33	71.88	72.03	144.56	147.39	147.01
C_{13}	72.12	70.44	72.02	144.66	147.45	145.94
C_{14}	66.19	65.63	66.01	150.04	151.41	150.65
C_{21}	64.67	62.80	69.11	132.35	152.81	139.25
C_{22}	58.97	60.10	58.33	158.84	158.70	160.34
C_{23}	58.82	58.70	58.93	159.02	161.26	159.32
C_{24}	64.82	64.14	64.61	132.36	133.42	132.73
C_{31}	59.14	49.96	49.16	178.57	185.51	169.91
C_{32}	64.87	64.66	66.00	172.13	172.37	171.96
C_{33}	64.86	64.47	64.59	172.19	174.86	173.19
C_{34}	59.24	59.63	59.25	178.59	179.20	178.54
C_{41}	65.43	53.49	22.98	110.34	177.35	206.26
C_{42}	63.28	54.64	61.13	157.89	168.28	159.48
C_{43}	63.31	64.33	63.54	157.84	159.93	158.65
C_{44}	65.22	60.39	63.97	110.41	117.18	112.29
C_{51}	59.24	49.96	49.16	178.53	185.51	169.91
C_{52}	64.86	64.66	66.00	172.16	172.37	171.96
C_{53}	64.85	64.47	64.59	172.17	174.86	173.19
C_{54}	59.13	59.63	59.25	178.56	179.20	178.54
C_{61}	64.67	62.79	69.11	132.25	152.82	139.25
C_{62}	58.85	60.10	58.33	158.94	158.70	160.34
C_{63}	58.92	58.70	58.93	158.89	161.26	159.32
C_{64}	64.69	64.14	64.61	132.34	133.42	132.73
C_{71}	66.17	65.27	65.80	150.02	151.73	151.33
C_{72}	72.16	71.88	72.03	144.70	147.39	147.01
C_{73}	72.34	70.44	72.02	144.50	147.45	145.94
C_{74}	66.26	65.63	66.01	149.00	151.41	150.65

	Pristine	B	Al
Total energy	-29254	-29945	-35833
Band gap energy	0.9363	0.8473	0.8952
Dipol moment	0.0044	3.761	2.1055

The units of energy and dipole moment are ev and Debye.

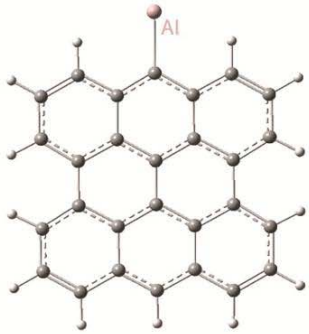

Figure3

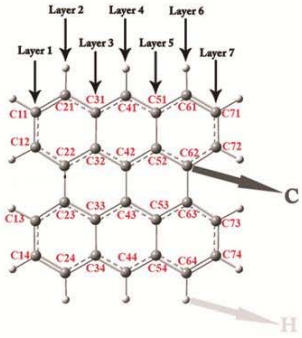

Figure 1

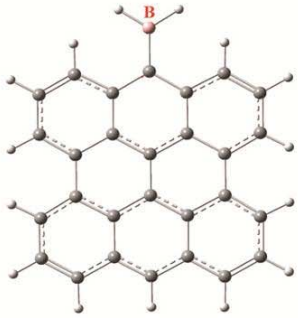

Figure2

Refrence:

[1] K.S. Novoselov, A.K. Geim, S.V. Morozov, D. Jiang, Y. Zhang, S.V. Dubonos, I.V.Grigorieva, A.A. Firsov, Science 306 (2004) 666.

[2] A.K. Geim, K.S. Novoselov, Nature Mater. 6 (2007) 183.

Ab initio And DFT Studies of Huisgen 1,3-Dipolar Cycloaddition Mechanism

R.Soleymani*[a,c] ,S.Farsi-Madan [b],Soleyman-Abadi [a] ,M.karimi [d]

[a]*chesmistry Department,Faculty of Sciences,Islamic Azad University,Touyerkan Branch,Young researchers Club,Touyserkan , Iran*

(Email:nima_Soleimany @ yahoo.com)

[b]*Chemistry Department,Faculty of Sciences , Payame-Noor University (PNU) Shiraz Branch , Shiraz,Iran*

[c]*Chemistry Department,Faculty of Sciences , Islamic Azad University Shahre-rey Branch Tehran,Iran*

[d]*Chemistry Department , Faculty of Sciences,Islamic Azad University of Omidieh Branch,Omidieh,Iran*

Keywords: Abinitio ؛ Cycloaddition ؛ DFT ؛ Transition State

Inrtoduction

Process of this mechanism , is a dipolereaction with a compound (1,3-dipole)that cause to formation of heterocycle with 5elements. Dipoles are consist of Alkenes , Alkines and molecules with functional groups such as carbonyl and nitryl.

Mechanism of this reaction is affected by heat and addition is performed by reaction of conformation . That this reaction isn,t required to more activation energy till reached to transition state . This reaction is synthesized experimenally [1,2] that is show below:

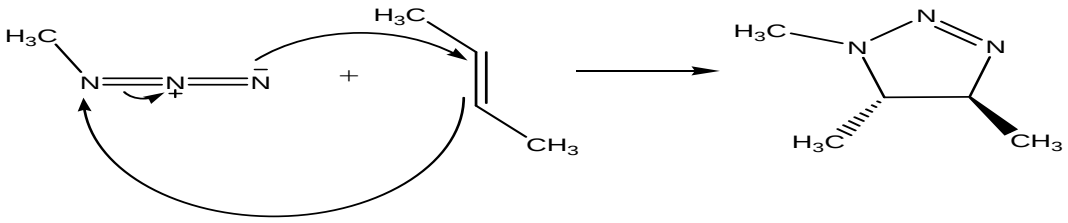

A **B**

Methods

For Ab initio calculation in theory of the levels b3Lyp/6-311+g** and hf/6-311+g** using Gaussian 03w package program[3].The firstly A and B structures designed by chemoffice 2010 software and transition state obtained by QST2 keyword in Gaussian 03w software. Also for total calculation used by pentum-pc computer with Intel core 2 Quad cpu Q95502.83GHZ processor (4cpus) and 4GB RAM.Under windows xp operating system.

Result and discussion

Result of obtained energetic constants by theoretical methods are reported In table 1,2 :

Table 1: Results geometrical energy for top reaction by theoretical methods

Method	Structure	ZPE	Eele	E_0	ΔE_0
HF 6-311+G**	[A]	0.176355	-359.1196459	-358.943291	0.007423 (4.6579325)[a]
	[A-B]#	0.176015	-359.126729	-358.950714	
	B	0.176357	-3591196458	-358.943288	
B3LYP 6-311+G**	A	0.164297	-361.4595197	-361.295223	0.003655 (2.293512)[a]
	[A-B]#	0.164002	-361.4555706	-361.291568	
	B	0.164297	-361.4595196	-361.295222	

[a] (in kcal/mol)

Table 2: Obtained result by B3LYP/6-311+G**

Geometry / Structure	Sum of electronic and thermal Enthalpies[a]	Sum of electronic and thermal Free Energies[a]
A	-361.285643	-361.328136
[A-B]#	-361.282607	-361.323901
B	-361.285642	-361.328136

[a](in Hartree)

Conclusion

Mechanism of formation hetrocyclic with five elements is considered by theoretical methods and resulted that dipole electrons and four electronses in dipole compounds are in this reaction and is accomplished by retention of steric conformation. So, Cyclo addition of [2S,4S]is similar to Diles Alder reaction ,that is required to 2.293512 kcal/mol to transformation of reactant to transition state , That specific is depend on pressure and electronical effects.

References

[1]Taylor,E.C.;WIPF,P.*In The chemistry of Hetrocyclic compounds,*Vol.59:synthesic Application of 1,3-Dipolar cycloaddition chemistry Toward Hetrocycles and Natural products A:person,W.H.Eds.;Wiely&sons,Newyork ***2002***

[2]Huisgen 1,3-DipolarCycloaddition,Huisgen,*Rproc.chem.soc.***1961**,3511

[3]M.j.Frisch et al.*GUSSIAN 03,Revision C.01*,Gussian Inc.,Wallingford.CT,**2004**

Preparation of Mn-Cr/TiO_2 catalyst from a novel precursor, $[Mn(OH_2)_6]_3[Cr(NCS)_6]_2.4H_2O/TiO_2$, for carbon monoxide hydrogenation and water gas shift reaction

Ali Reza Rezvani* and javad farzanfar

Department of Chemistry, Universityof Sistan and Baluchestan, Zahedan, IRAN

(E-mail: rezvani2001ir@yahoo.ca)

Abstract

The Fischer-Tropsch synthesis can be simplified as a combination of the carbon monoxide hydrogenation (FT reaction) (1) and the water gas shift reaction (2):

$$CO + (1 + m/2n)\ H_2 \rightarrow 1/n\ C_nH_m + H_2O \quad (1)$$

$$CO + H_2O \leftrightarrow CO_2 + H_2 \quad (2)$$

Water is a primary product of the CO hydrogenation, and CO_2 can only be produced by the water gas shift reaction. Water gas shift reaction (WGSR) is used to generate hydrogen and CO_2 from the reaction between carbon monoxide and water. WGSR has been employed in industrial catalytic processes to control H_2/CO ratio in syngas. Mn based-catalyst has been investigated to ascertain its suitability for the WGSR[1]. In previous researches, Mn-based catalysts were prepared by precipitation[2], urea-nitrat combustion[3] and sol-gel[4] methods.

In this work, the Mn-Cr/TiO_2 catalyst was prepared from calcination of titania-supported $[Mn(OH_2)_6]_3[Cr(NCS)_6]_2.4H_2O$ precursor. The cationic-anionic complex, has been prepared from the reaction of $(NH_4)_3[Cr(NCS)_6]$ with $Mn(NO_3)_2.4H_2O$ in water. The catalyst was evaluated for CO hydrogenation and water gas shift reaction. The carbon monoxide hydrogenation was studied over prepared catalyst in the temperature range of 553-653 K, gas hourly space velocity (GHSV) of 3600 h^{-1}, H_2/CO molar ratio 2, and at atmospheric pressure. In the proposed structure of the bimetallic complex, $[Mn(OH_2)_6]_3[Cr(NCS)_6]_2.4H_2O$, the Cr(III) ion is coordinated by six isothiocyanate ligands via their nitrogen donor resulting in the formation of a $[Cr(NCS)_6]^{3-}$ trivalent anion. The $[Cr(NCS)_6]_2^{3-}$ trivalent anion is chargebalanced by the $[Mn(OH_2)_6]_3^{2+}$ divalent cation. The IR spectrum of complex displays all the characteristic bands of the aqua and isothiocyanate ligands. The FT-IR spectra of

calcined catalyst shows the typical absorption bands of pure TiO_2. The XRD pattern of calcined catalyst contains characteristic diffraction peaks of CrS, $MnSO_4$, $MnSO_4.H_2O$, Cr_2O_3 and CS_2. TGA curve for precursor shows first weight loss over 80-180°C corresponding to the loss of adsorbed and lattice water molecules. One further heating, weight loss were observed in 270-320°C and 380-450°C ranges with the loss of the coordinated water molecules and the isothiocyanate ligands, respectively. The final decomposition products were the stable oxides and Sulfates forms, identified by XRD. DSC for the precursor exhibits three main changes in agreement with TGA result. SEM observations have shown differences in morphology of both precursor and calcined catalyst. The effect of temperature on CO hydrogenation in terms of CO conversion, hydrocarbon selectivity and CO_2 selectivity have shown in below. The catalytic tests at 553-653 K (P=1 atm, H_2/CO=2:1) showed that the catalyst has the high catalytic activity for methanation and water gas shift (WGS) reactions.

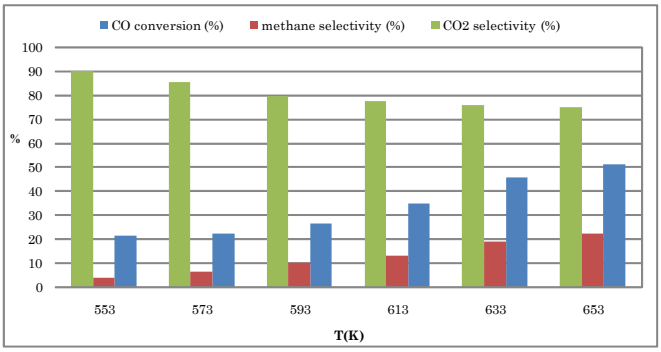

Keywords: Manganese-based catalysts, Calcined catalysts, Catalytic activity, Water gas shift.

References

[1]. Y. Tanaka, T. Utaka, R. Kikuchi, T. Takeguchi, K. Sasaki, K. Eguchi, Journal of catalysis, 215 (2003) 271.

[2]. M. Kang, E. D. Park, J. M. Kim, J. E. Yie, Catal. Today 111 (2006) 236.

[3]. J. Papavasiliou, G. Avgouropoulos, T. Ioannides, Catalysis Communications 6 (2005)497

[4]. L. Guczi, Catal. Lett. 7 (1990) 205.

Measurement and correlation of tie-line data for ternary aqueous mixture of butyric acid with isobutyl acetate at T = (298.2, 303.2, and 308.2) K.

Hossein Ghanadzadeh [a,b] *, Ali Ghanadzadeh [b] and Nastaran Dastmoozeh [b]

[a] *Department of Chemical Engineering , University of Guilan, Rasht , Iran*

(*Email: hggilani@guilan.ac.ir*)

[b] *Department of Chemistry, University of Guilan,41335 Rasht, Iran*

*(Email: aggilani@guilan.ac.ir ; ndastmoozeh@yahoo.com)***Keyword:** NRTL model; UNIQUAC model; Extraction processes; Tie-line data

Abstract

The short-chain carboxylic acid used in the current study was butyric acid (BA). It has many scientific and industrial applications. Therefore, the extraction of this acid from aqueous mixtures using the liquid-liquid extraction technique is still an important problem.

In this research, isobutyl acetate was tested as organic solvent for recovery of BA from water. For this system, three different temperatures were chosen to study the ternary equilibrium system in order to observe the change of the tie-lines and equilibrium characteristics. At each temperature, T = (298.2, 303.2 and 308.2) K, the phase compositions were measured.

The solubility curves for the ternary mixtures were determined by the cloud point method in an equilibrium glass cell [1-2]. The prepared binary mixtures of known compositions were introduced to the glass cell. The temperature of the cell was controlled by a water jacket and maintained with an accuracy of within ± 0.1 K. At each temperature, the third component was progressively added using a microburet. The end point was determined by observing the transition from an appearance to a disappearance mixture. The tie-line data were determined by karl-fisher method, too.

The experimental tie-line data for the ternary system (water + BA + isobutyl acetate) were determined at T = (298.2, 303.2, and 308.2) K and atmospheric pressure. The LLE diagrams as a function of temperature for the ternary system of (water + BA + isobutyl acetate) are plotted in Figures 1 to 3.

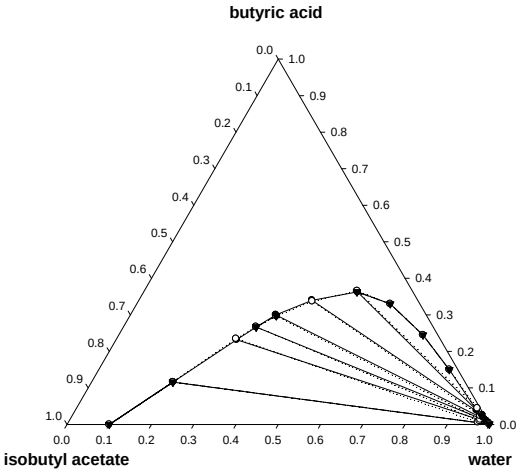

Fig.1

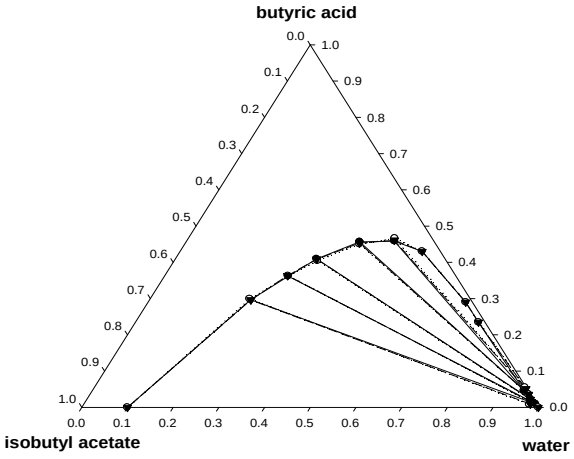

Fig.2

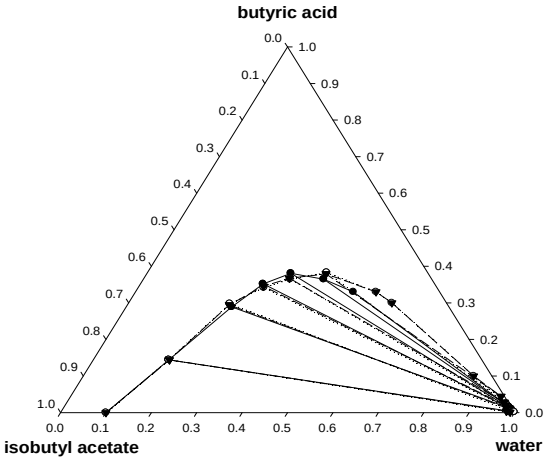

Fig.3

The experimental results indicated that the organic solvent, isobutyl acetate, has high separation factors and distribution coefficients, which shows the ability of the solvent to extract butyric acid from water. It can be concluded that this solvent, may be considered to be reliable organic solvent for the extraction of the acid from aqueous solutions and this solvent has better ability for extraction of butyric acid at 308.2K.

References

[1] A. Arce; A. Blanco; J. Martínez -Ageitos .Fluid Phase Equilib. 109, (1995), 291–297.

[2] A.Senol. Fluid Phase Equilib. 243, (2006), 51–56.

Study of phase equilibria of (water +butyric acid + dibasic esters) ternary system and Correlation by UNIQUAC model at 298.2 K

Hossein Ghanadzadeh [a,b] *, Ali Ghanadzadeh [b] and Nastaran Dastmoozeh [b]

[a] *Department of Chemical Engineering , University of Guilan, Rasht , Iran*

(*Email: hggilani@guilan.ac.ir*)

[b] *Department of Chemistry, University of Guilan,41335 Rasht, Iran*

(Email: aggilani@guilan.ac.ir ; ndastmoozeh@yahoo.com)

Keywords: LLE data; Ternary systems; UNIQUAC model**;** Extraction process

Abstract

Liquid–liquid equilibrium (LLE) investigations for ternary mixtures are important in the evaluation of industrial units for solvent extraction processes. The type of solvent is one of the most important factors which Influence the equilibrium characteristics of extraction of the acid from aqueous solutions. This work presents a useful LLE data for the extraction of butyric acid from aqueous solution [1–3].The experimental tie-line data for the ternary systems {water+ butyric acid +organic solvents (diethyl adipate, diethyl succinate and diethyl glutarate)} were determined at T=298.2K (fig.1).

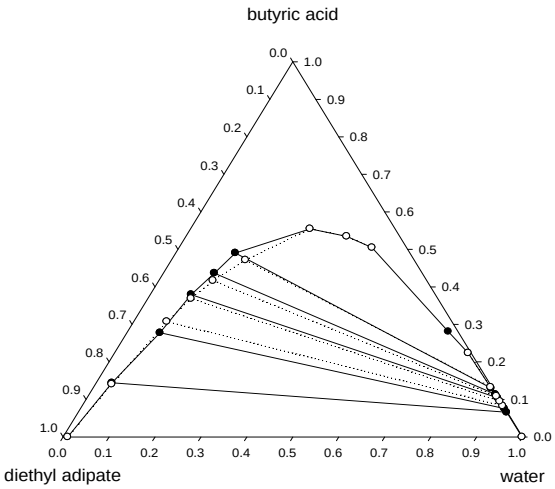

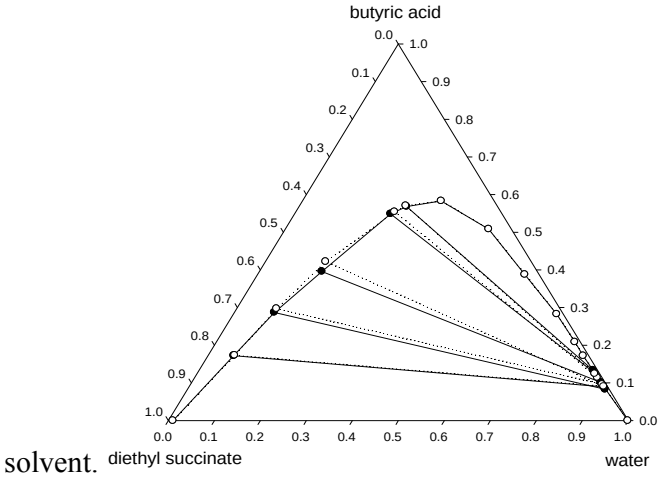

solvent.

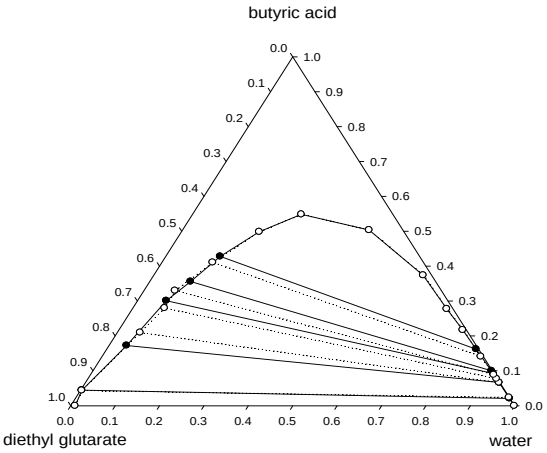

Fig.1. Ternary phase diagram; (●) Experimental points; (○) UNIQUAC calculated points.

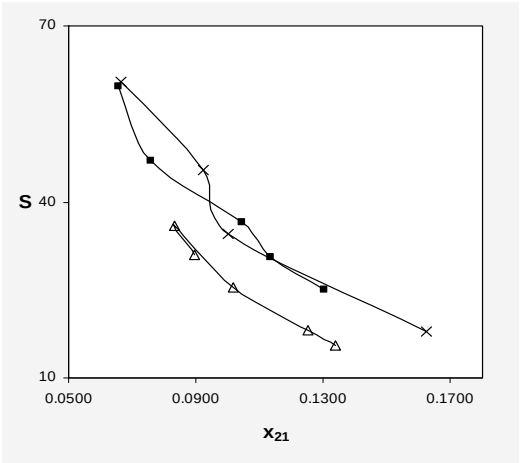

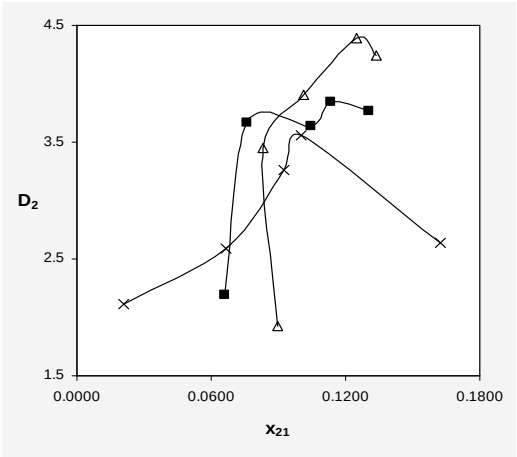

Fig.2. diethyl adipate, (△) diethyl succinate and (✕) diethyl glutarate.

The observed results were also used to determine the optimum UNIQUAC between an i–j pair of molecules or between each pair of compounds. The quality of the correlation is measured by the root-mean square deviation (RMSD). These results show that the diethyl glutarate is better solvent for the extraction of the butyric acid from the aqueous solution.

References

[1]A. Senol, Fluid Phase Equilib. 243 (2006) 51–56.

[2]D. Özmen, Fluid Phase Equilib. 250 (2006) 70–75.

[3]H. Ghanadzadeh, A. Ghanadzadeh, Z. Aghajani, S. Abbasnejad, S. Shekarsaraee, J. Chem. Thermodyn. 42 (2010) 695–699.

Photocatalytic degradation of Triton X-100 by zinc oxide nanoparticles

M. Giahi[a], F. Ghanbari[a], M.A. Bagherinia[a]

[a]Department of Chemistry, Islamic Azad University, Lahijan Branch, Lahijan, Iran.

(E-mail: giahi_m@yahoo.com)

Introduction:

Non-ionic surfactants in aqueous solutions are excessively used in many formulations applied in various industrial areas such as detergent industry, textiles and metallurgy. In contrast, ZnO a kind of semiconductor has the similar band gap as TiO_2, is not thoroughly investigated. However, the most advantage of ZnO in comparison with TiO_2 is that it absorbs over a larger fraction of UV spectrum [1-3]. In this paper, we selected a non-ionic surfactant as a model compound of organic pollutants and ZnO nanoparticles as a photocatalyst. The effects of various parameters on the photocatalytic degradation of Triton X-100 were studied.

Methods:

The conditions used in the present study was a batch reactor(a cylindrical pyrex vessel of 2 cm diameter with capacity of 50 mL), 20 cm distance between UV source (high pressure mercury vapour lamp 400 W) and solution with a stirring speed of 80 rpm and 30 min for adsorption equilibrium. The quantitative estimation of the surfactant was carried out using a UV-Vis spectrophotometer (model Jenway 6405) at λ_{mAX}=223 nm.

To estimate the kinetic parameters (k and n) and n^{th}-order rate, an equation of from $-r_{surfactant} = -dC/dt = k.C^n$, was used where k is the degradation rate constant, 1/min. the first – order kinetic model (n=1) was shown as follows: $-Ln= C/C_0= kt$. Fig.1 shows $-\ln C/C_0$ of TX-100 versus irradiation time. As it is clear from Fig.2 decreasing of the surfactant concentration obeys a linear pattern towards the elapse of irradiation time. It means that the pseudo-first-order kinetics in relation to surfactant is operative.

Results and discussion:

Results are shown in Fig. 2 that ZnO exhibits higher photocatalytic activity than TiO_2 and this was explained as ZnO having greater quantum efficiency than TiO_2. The low cost is another important advantage of ZnO.

Comparison of catalytic activities of ZnO powders and nano particles has shown in Fig. 3. It shows that decomposition of Trition X-100 is increased in the reaction catalyzed by ZnO commercial oxide. Thus, subsequent experiments were carried out with Merck ZnO.

The effect of sulfate radical ($SO_4^{\cdot-}$) as an oxidant on the degradation of TX - 100 was investigated and compared with the ZnO (only), $S_2O_8^{2-}$ (only), UV / $S_2O_8^{2-}$, UV /ZnO and

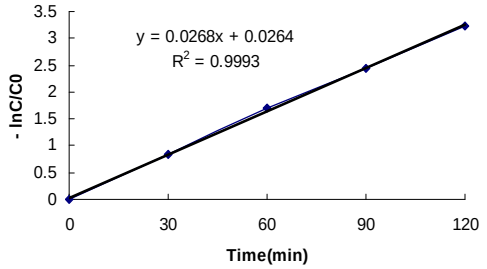

Fig .1 .Pseudo-first-order degradation rate of TX-100
Conditions: [TX-100]=40 mg/L ,ZnO =0.36 g/L, [$K_2S_2O_8$]=3 mM, reaction time=120 min l pH =6.

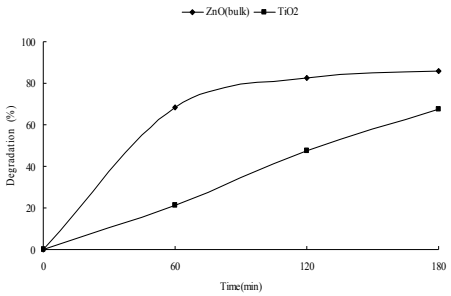

Fig. 2. The effect of the catalyst type on the degradation efficiency

UV/ZnO/ $S_2O_8^{2-}$ systems. As shown in Fig. 4 UV/ZnO system had more significant effect on the degradation of surfactant than the UV/ $S_2O_8^{2-}$ system. When potassium peroxydisulfate was added to the UV/ ZnO system, surfactant degradation increased from 82.7% to 96.1% after 120 min (Fig. 4).

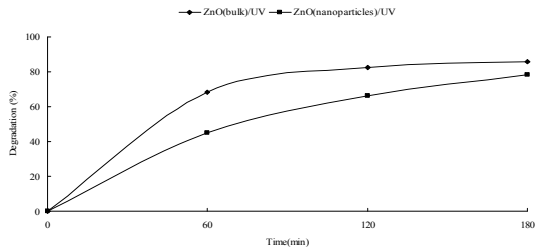

Fig.3. The effect of the catalyst size on the degradation efficiency

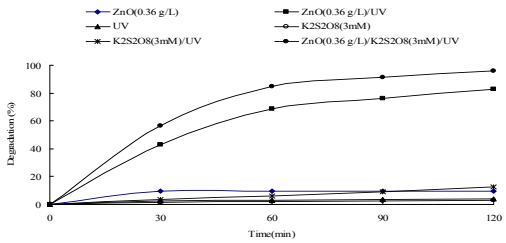

Fig .4 Degradation of Triton X- 100

Conclusion:

The optimal degradation conditions of TX-100 obtained from the present research were:the dosage of catalyst 0.36 g/L, pH 6 ,the amount of $K_2S_2O_8$ 3mM.Under optimal degradation

conditions of TX-100, the photodegradation percent of TX-100 was 96.1% when the solution was irradiated by the 400w high pressure mercury –vapour lamp for 2h. Degradation of TX-100 was accelerated remarkably by adding proxydisulfate. Therefore, when peroxydisulfate was added to the UV/ZnO system, surfactant degradation increased from 82.7% to 96.1% after 120 min.The kinetics of photocatalytic degradation for surfactant TX-100 follows a pseudo-first-order equation.

References

[1] C. A. K. Gouvea, F. Wypych, S. G. Moraes, N. Duran, N. Nagata, P. Peralta Zamora, Chemosphere 40 (2000) 433- 440.

[2] C. Lizama, J. Freer, J. Baeza, H. D. Mansilla, Catal.Today 76(2002) 235-246.

[3] Y.T. Kown, K.Y. Song, W.I. Lee, G.J. Choi, Y.R. Do, J. Catal. 191 (2000) 192.

The comparison between binary and ternary systems of interaction between human serum albumin to anti-parkinson drugs by fluorescence spectroscopy

H. Mahaki [1*], M. Vahidzadeh[1], N. Abdollahpour[1], M.R. Saberi[2], J. Chamani[1]

1. Department of Biology, Faculty of Sciences, Islamic Azad University-Mashhad Branch, Mashhad, Iran,
2. School of Pharmacy, Mashhad University of Medical Sciences, Mashhad, Iran

Abstract

The mechanism of interaction of an anti-parkinson, aspirin and Ropinirole hydrochloride with human serum albumin has been studied by fluorescence spectroscopic and Resonance light scattering techniques under physiological conditions. Both two drugs were found to quench the intrinsic fluorescence of protein by static quenching mechanism. The quenching constant and fractional maximum fluorescence intensity of the protein calculated for binary and ternary systems. The n and K values of binary and ternary systems have been calculated for comparing of the second drug role in the number of binding site and binding affinity of first drug on the HSA.

Keywords: Fluorescence spectroscopy, HSA, ASA, RP, binary and ternary systems

Introduction

Human serum albumin (HSA) is the most abundant protein in blood plasma and plays an important role in the regulation of plasmatic concentrations of several drugs, including endogens and exogens [1]. Acetylsalicylic acid (ASA) has been shown to reduce the risk for colorectal cancer by as much as approximately 40%, a property that is shared by other non-steroidal anti-inflammatory drugs [2].

Materials and Apparatus

RP, ASA and HSA was purchased from Sigma (St. Louis, MO, USA). Fluorescence measurements were carried out on a F-2500 (Hitachi, Japan) with a 150W Xenon lamp spectrofluorimeter.

Results and discussion

Fluorescence quenching of HSA by drugs has been studied. The fluorescence spectroscopy was used to determine the nature of interaction between HSA by ASA and RP. In HSA, tryptophan and tyrosine residues contribute to fluorescence spectra. The decrease in fluorescence intensity of a compound by a variety of molecular reactions viz., energy transfer, ground state complex formation, excited state reactions, collision quenching and molecular rearrangements is called quenching. In order to know the binding of ASA and RP to HSA, the fluorescence spectra were recorded upon excitation at 280nm (Fig. 1 A,B). The fluorescence intensity of HSA decreased regularly with a blue shift in presence of increasing concentrations of ASA and RP. This suggested that a complex was possibly formed between drugs and HSA [4]. Quenching can be induced by different mechanisms, which were usually classified into dynamic quenching and static quenching. When secondary drug is added to the binary system at excitation wavelength of 280 nm according to the Fig. 2A,B and Table. 1, the quenching constant (K_Q) increases. Subsequently a larger distance between chromophore of primary drugs and the excited fluorophores Trp-214 is noted. Also the values of f_a calculated for the fluorophores located in the corresponding binding sites for the binary and ternary systems in Table 1 and Fig. 2A,B, in the presence of secondary drug at $\lambda_{exi} = 280$ nm, f_a values decreased. The f_a values show that fluorophore inside to the aqueous solution and the affinity between fluorophores and the protein decreases [6].

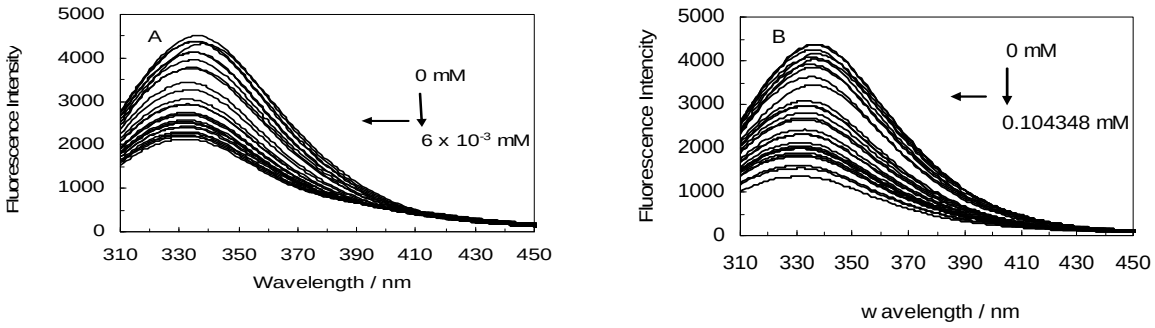

Fig. 1: Fluorescence spectra of HSA in presence of ASA (A) and RP (B) in pH=7.4

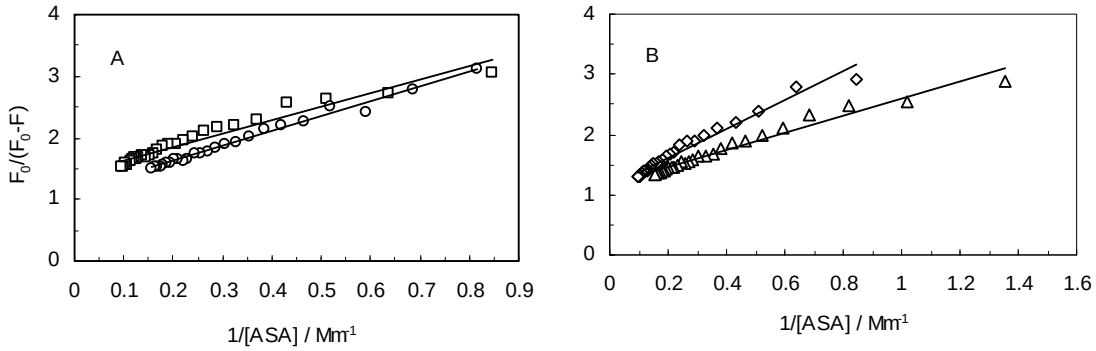

Fig. 2: The modified Stern-Volmer plot of binary and ternary systems of HSA-ASA and (HSA-RP)ASA ○, Δ in Fig. A receptively, Also HSA-RP and (HSA-ASA)RP □, ◊ in Fig. B respectively at excitation wavelength 280 nm.

References

[33] Klajnert, B.; Bryszewska, M. Fluorescence studies on PAMAM dendrimers interactions with bovine serum albumin. *Bioelectrochemistry*, **2002**, 55, 33-35.

[34] Ding, F.; Liu, W.; Zhang, L.; Yin, B.; Sun, Y. Sulfometuron-methyl binding to human serum albumin: Evidence that sulfometuron-methyl binds at the Sudlow's site I. *J. Mol. Struct*., **2010**, 968, 59-66

Molecular Docking of 15- lipoxygenase with pyrimido[4,5-*b*][1,4]benzothiazine derivatives, theoretical study of enzyme inhibition

M. K. Mohammadi, *,a M. Nikpour[a] ,M. R. Bozorgmehr[b] and S. Atashi[b]

[a] Faculty of Sciences, Islamic Azad University, Ahvaz Branch, 6134968875, Iran

Email:mohammadi@iauahvaz.ac.ir

[b] Department of Chemistry, Faculty of Sciences, Islamic Azad University, Mashhad Branch, Iran

Keywords: Molecular Docking , 15- lipoxygenase , theoretical study , enzyme inhibition

Introduction:

It is well documented that mammalian lipoxygenases (LO's) are nonheme ironcontaining enzymes responsible for the oxidation of polyunsaturated fatty acids and esters to hydroperoxy derivatives [1]. Among the mammalian lipoxygenases involved in the etiology of human disease, 5-lipoxygenase (5-LO) is now well established as a target for inhibiting the production of leukotrienes involved in the progression of inflammatory diseases, in particular asthma [2]. More recently, 15-lipoxygenase (15-LO) has emerged as an attractive target for therapeutic intervention [3].

Methods:

15-LO has been implicated in the progression of certain cancers [4] and chronic obstructive pulmonary disease (COPD) [5]. Both transgenic and knockout studies implicate a role for 15-LO in atherogenesis [6]. The enzyme is abundantly expressed in macrophages residing within the atherosclerotic lesion [3].

Results:

the immediate products of 15-LO oxidation of AA and linoleic acid (LA) have been shown to be pro-inflammatory [7] and pro-thrombotic [8]. It is also found that 15-LO is linked to cardiovascular complications since it is known to participate in oxidative modification of low-density lipoproteins (LDL) leading to the development of atherosclerosis [9].

In the present study, we report the energy minimization of eight new 2-substituted pyrimido[4,5-*b*][1,4]benzothiazines **1a-h** as potential lipoxygenase inhibitors.

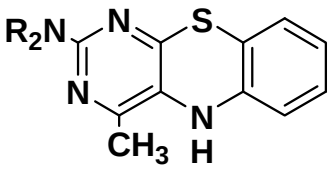

1a-h

R = Me, Et, Pr, Bu, Iso-pr, Pentyl , Pyrazin , Piperazin

These analogues after energy minimization were docked to the binding site of the 15-lipoxygenase. The results of docking processing (ΔG_b: Estimated Free Energy of Bonding, E_d: Final Docked Energy and K_i: Estimated Inhibition Constant) are outlined in table 1.

References:

[1] Brash, A. R. *J. Biol. Chem.* **1999**, *274*, 23679.

[2] (a) Larsen, J. S.; Acosta, E. P. *Ann. Pharmacother.* **1993**, *27*, 898; (b) Ford-Hutchinson, A. W. *New Drugs Asthma* **1992**, *2*, 94.

[3] Schewe, T. *Biol. Chem.* **2002**, *383*, 365.

[4] (a) Kelavkar, U.; Glasgow, W.; Eling, T. E. *Curr. Urol. Rep.* **2002**, *3*, 207; (b) Kelavkar, U. P.; Cohen, C.; Kamitani, H.; Eling, T. E.; Badr, K. F. *Carcinogenesis* **2000**, *21*, 1777.

[5] Zhu, J.; Kilty, I.; Granger, H.; Gamble, E.; Qiu, Y. S.; Hattotuwa, K.; Elston, W.; Liu, W. L.; Liva, A.; Pauwels, R. A.; Kis, J. C.; De Rose, V.; Barnes, N.; Yeadon, M.; Jenkinson, S.; Jeffery, P. K. *Am. J. Respir. Cell Mol. Biol.* **2002.**

[6] Harats, D.; Shaish, A.; George, J.; Mulkins, M.; Kurihara, H.; Levkovitz, H.; Sigal, E. *Arteriosler. Thromb. Vasc. Biol.* **2000**, *20*, 2100.

[7] Sultana, C.; Shen, Y.; Rattan, V.; Kalra, V. J. *J. Cell. Phys.* **1996**, *167*, 467.

[8] Setty, B. N.; Werner, M. H.; annun, Y. A.; Stuart, M. *J. Blood* **1992**, *80*, 2765.

[9] Zhao, L.; Funk, C. D. *Trends CardioVasc. Med.* **2004**, *14*, 191.

Dispersion of aggregated carbon nanotubes by ionic liquids

M. Foroutan, M. Mohammadi
Department of Physical Chemistry, School of chemistry, Collage of Science, University of Tehran, Tehran, Iran
Mohammadi_morteza@khayam.ut.ac.ir

Keywords: Ionic liquid, Carbon nanotube, Molecular dynamics simulations, Dispersion

Introduction

Ionic liquids (ILs) have numerous advantages, such as negligible vapor pressures, high thermal stability, superiority in electrochemistry, and environmentally friendly properties [1]. The applicability of carbon nanotubes (CNT) as sensory and manipulating devices in biological systems is critically related to their solubility and wet ability in aqueous environments, or in general with their hydrophobic–hydrophilic behavior [2].

Simulation Details

Using NVT ensemble, molecular dynamics simulations for ionic liquid 1-*n*-propyl-4-amino-1, 2, 4-triazolium bromide have been performed. The equations of motion are integrated using the Verlet leapfrog scheme. All interatomic interactions between the atoms in the simulation box and the nearest image sites were calculated within a cutoff distance equal to 12 Å. The columbic long-range interactions were calculated using Ewald's method, with a precision of 1×10^{6}. The time step for the simulations was 1.0 fs and temperature was equal to 400K.

Results and Discussion

Figure 1 shows snapshots of simulated system at initial and the last simulation time. These figures show us how ionic liquid can separate the aggregated nanotubes. We follow-up the result with plots of radial distribution functions, total energy evolution and especially, the time history of distance between the center of mass of the carbon nanotubes during equilibration.

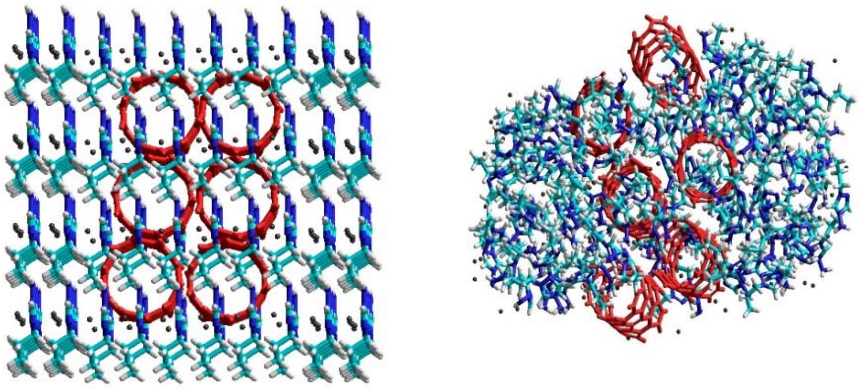

Figure 1- Snapshots of the simulated system at initial simulation time (left side) and at the last simulation time (right side).

References

[1]B. Sun, P .Wu, J. Phys. Chem. B, 114(2010) 9209-9219.

[2]J.H. Walther, R.L. Jaffe, E.M. Kotsalis, T. Werder, T. Halicioglu, P. Koumoutsakos Carbon 42 (2004) 1185–1194.

The study of intramolecular hetero-Diels-Alder reaction of ABT-773: quantum mechanic approach

M. Nikpour*,[a] M. R. Bozorgmehr[b] and S. Atashi[b]

[a] Department of Chemistry, School of Sciences, Islamic Azad University, Ahvaz Branch, Ahvaz 6134968875, Iran

[b] Department of Chemistry, School of Sciences, Islamic Azad University, Mashhad Branch, Mashhad, Iran

ABT-773 is a ketolide effective against antimicrobial-resistant respiratory tract phatogens [1]. Stoner et al. have reported a Diels-Alder reaction in which ABT-773 **1** and its cis isomer **3** are converted into two different adducts [2]. The experiments performed by Stoner et al. are subject of theoretical study in this project. Based on experimental data an appropriate mechanism proposed for this reaction in which contain the initial enolization of the dien system that causes β-elimination of the desosamine suger, culminating in the production of the presumed transitional enone **5**, in subsequent stage after the transition stae react with 6-o-quinolin during Diel-Alder reaction, adducts **2** and **4** are formed. The proposed mechanism represented schematically as follow:

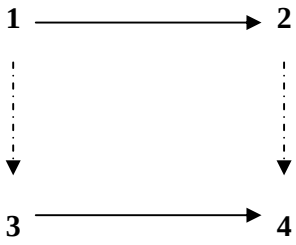

The optimized structure of these compounds showed as a follow:

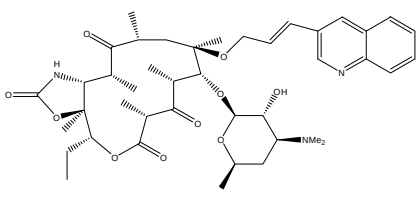

1

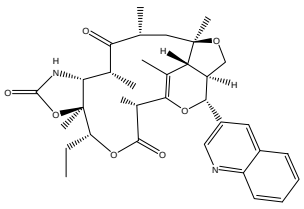

2

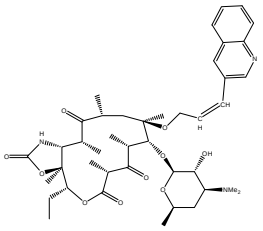

3

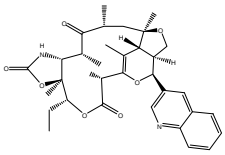

4

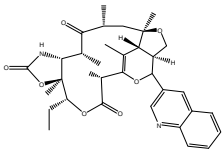

5

The Gibbs free energy values of each structure and its variations for different conversions shown in above figure have been obtained with regard to frequency calculations as well as by considering the Zero Point Energy corrections. it is observed that values of Gibbs free energy variations for conversions of **1** to **2** and **3** to **4** is negative and for conversion of **1** to **3** and **2** to **4** is positive, therefore there is no possibility of conversion of **1** into cis isomer and no possibility for internal conversion of their corresponding products. In other words, the process of cycloaddition relative to geometry of double bond is stereoselective. For this reason, in the above diagram the conversions of **1** into **3** and **2** into **4** have been shown with dotted arrow.

References

[1] M. J. Mitten, J. Meulbroek, M. Nukkala, L. Paige, K. Jarvis, A. Oleksijew, A. Tovcimak, L. Hernandez, J. D. Alder, P. Ewing, Y. S. Or, Z. Ma, A. M. Nilius, K. Mollison, and R. K. Flamm. *Antimicrob Agents Chemother.*, **45**(9) (2001) 2585.

[2] E. J. Stoner, M. S. Allen, A. C. Christesen, R. F. Henry, L. S. Hollis, R. Keyes, I. Marsden, T. C. Rehm, S. G. Shiroor, N. B. Soni, and K. D. Stewart*, J. Org. Chem.,* 70 (8), (2005), 3332.

Molecular Docking of phosphodiesterase3B with 6-hydroxy-4-methylquinolin-2(1H)-one derivatives, theoretical study of enzyme inhibition.

M. Nikpour[*,a] M. R. Bozorgmehr[b], Hamid Sadeghian[c] and S. Atashi[b]

[a] Department of Chemistry, School of Sciences, Islamic Azad University, Ahvaz Branch, Ahvaz 6134968875, Iran

[b] Department of Chemistry, School of Sciences, Islamic Azad University, Mashhad Branch, Mashhad, Iran

[c] Department of Laboratory Sciences, School of Health and Paramedical Sciences, Mashhad University of Medical Sciences, Mashhad, I. R. Iran

Introduction

Congestive heart failure (CHF) is a major cause of death in patients with heart disease. For many years, digitalis glycosides have been used for the treatment of CHF. However, the application of these agents is limited because of their narrow therapeutic window and their propensity to cause life-threatening arrhythmias (arrhythmogenic lability). The search for orally active 'non-glycoside' cardiotonic drugs displaying a greater safety profile and improved efficacy on patient survival resulted in establishing the selective inhibitors of cyclic nucleotide phosphodiesterase (PDE) enzymes as a new class of cardiotonic agents. PDE3B enzyme specifically hydrolyze cAMP (cyclic adenosine monophosphate) in heart cells. The inhibition of PDE3 activity in cardiovascular tissues results in increased levels of cAMP with consequent reduction in platelet aggregation and smooth muscle cell proliferation *in vitro*, and induction of a cardiotonic effect [1,2].

Results and Discussion

In the present research we investigate the inhibition of PDE3a by 6-hydroxy-4-methylquinolin-2(1H)-one derivatives **1a-j** by theoretical method**.**

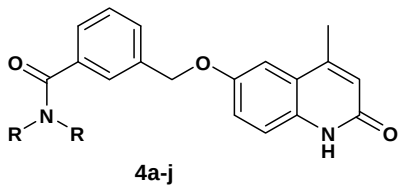

4a-j

Structures **1a-j** were simulated in chem3D professional; Cambridge software; using MM2 method (RMS gradient = 0.05 kcal/mol). Output files were minimized under semi-empirical AM1 method in the second optimization (Convergence limit = 0.01; Iteration limit = 50; RMS gradient = 0.05 kcal/mol; Fletcher-Reeves optimizer algorithm) in HyperChem7.5. Automated docking simulation was implemented to dock **1a-j** into the active site of PDE3B with AutoDockTools 4.0 (ADT4) version 1.5.2 using Lamarckian genetic algorithm. The results of docking processing (ΔG_b: Estimated Free Energy of Bonding, E_d: Final Docked Energy and K_i: Estimated Inhibition Constant) are outlined in Table 1.

Table 1

Compound	K_i	ΔG_b	E_d
4a	3.72e-8	-10.14	-11.69
4b	8.64e-9	-11.00	-12.62
4c	2.37e-8	-10.40	-11.30
4d	4.50e-8	-10.04	-11.90
4e	3.50e-8	-10.17	-12.09
4f	5.24e-8	-9.93	-11.73
4g	5.05e-9	-11.32	-13.01
4h	1.43e-9	-12.07	-13.92
4i	5.68e-10	-12.61	-14.61
4j	7.64e-8	-9.71	-11.01

Acknowledgement

Financial support of this research by Islamic Azad University, Ahvaz Branch is gratefully acknowledged.

References

[1] Hidaka, H.; Hayashi, H.; Kohri, H.; Kimur, H.; Hosokawa, T.; Igawa, T.; Saitoh Y. *J. Pharmacol. Exp. Ther.* **1979**, *211*, 26.

[2] E. J. Stoner, M. S. Allen, A. C. Christesen, R. F. Henry, L. S. Hollis, R. Keyes, I. Marsden, T. C. Rehm, S. G. Shiroor, N. B. Soni, and K. D. Stewart, *J. Org. Chem.,* **70**, 2005, 3332.

Determination of the conductivity of [N6$_3$14][Cl] and [C$_4$MI][PF$_6$] on the basis of Viscosity

B. najafi[*a], M. H. Hadizadeh[b] and S.Naseh [b]

[a]Department of chemistry, Isfahan University of Technology, Isfahan, Iran

[b]Department of chemistry, University of Kashan, Kashan, Iran

*E-mail: najafi@cc.iut.ac.ir

Keywords: Ionic liquids, Conductivity

Introduction

In comparison with standard solvents such as water, alcohols, alkanes or classical molten salts, up-coming ionic liquids (ILs) exhibit a very unusual combination of properties [1]. Namely, they are liquid with a wide range (from -50^{o}C to +400^{0}C), an excellent thermal stability (up 400^{o}C) and a wide electrochemical window (from -40eV to +4eV). Ionic liquids (ILs) are receiving more attention as alternative to volatile organic solvents due to their negligible vapor pressure. Moreover, ILs possess intriguing properties such as hight thermal and electrochemical stability and high ionic conductivity [2,3]. Although reaching to high conductivity by ILs is possible, and it is very important in electrochemical researches, but there are some barriers to synthetize of these substances such as using commercial and accessible primary materials, econemic benefits, time of experiment and sensitivity of substances to humidity and so on. In this paper we gained a simple theoritical methods in synthetizing ionic liquids with high conductivity to prevent existing these circumstances.

Determination of the conductivity of [C4MI][PF6] and [N6314][Cl]

Higher conductivity is generally associated with lower viscosity and the order of conductivity values (from high to low) for the imide salts is concordant with the order of the T_g data (from low to high) [4,5]. Bonhote et al. has derived the relation between specific conductivity and anion, cation hydrodynamic radii as well as other physical parameters:

$$\sigma = yF^2 d/(6\pi N_A FW\eta)\left[(\xi_a r_a)^{-1} + (\xi_c r_c)^{-1}\right] \qquad (1)$$

This includes the 'correction' factor ξ taking into account the specific interactions between the mobile ions in the melting state, their viscosities η, formula weight *FW*, densities *d*, and the radii of their ions (r_a and r_c) . Furthermore, vogel-Tammann-Fulcher equation provides a good description of molten salt electrolyte behavior change with temperature:

$$\sigma(T) = \frac{A}{\sqrt{T}} \exp(\frac{-B}{T - T_0}) \qquad (2)$$

Where A, B, and T are the frequency factors related to the activation energy and deal glass transition temperature, respectively [6,7]. According to equation(2) we can not determine favourite conductivities in electrochemical researches. Therefore, we found simple relations between viscosity and temprature based on viscosity data and statistical calculations of 1-butyl-3-methylimidazolium hexafluorophosphate [C4MI][PF6] and trihexyl-tetradecylammonium chloride [N6314][Cl] compounds. Based on statistical calculation ,we have reached simple relations between viscosity and temperature (3) which according to these relations, with use of equation (1), and only change in temperature ,conductivity in various electrochemical research can be determined easily.

If $0.4 \leq \eta \leq 11.85 \Leftrightarrow \eta = -0.138T + 12.281$ & if $28.5 \leq \eta \leq 207 \Leftrightarrow \eta = -2.946T + 219.21$ (3)

Conclusion

We need high conductivity in many Electrochemical researches, which requires its specific conditions in different tempratures. Sometimes creating such conditions need to spend a long time and great expenses. Using statistical calculation among different ionic liquids, we reached to this conclusion that [N6314][Cl] and [C4MI][PF6] salts can provide broad range of high conductivities for performing Electrochemical activities. Therefore, using statistical calculations and on the basis of gained relations in this research, we can easily obtain needed conductivities in variety tempreture.

Reference

[1] P. Wasserscheid, T. Welton (Eds.), Ionic Liquids in Synthesis, Wiley- VCH, Weinheim, 2002.

[2] P. Bonhôte, A.-P. Dias, N. Papageorgiu, K. Kalyanasundaram, M. Grätzel, Inorg. Chem. 36 (1996) 1168.

[3] H. Ohno (Ed.), Electrochemical Aspects of Ionic Liquids, Wiley-Interscience, New York, 2005.

[4] J. Sun, M. Forsyth, and D. R. MacFarlane, J. Phys. Chem. B 102 (1998) 8858.

[5] J. Sun, D. R. MacFarlane, and M. Forsyth, Electrochim. Acta 48 (2003) 1707.

[6] D. R. MacFarlane, J. Sun, J. Golding, P. Meakin, and M. Forsyth, Electrochim. Acta 45 (2000) 1271.

[7] H. Ohno and M. Yoshizawa, Solid State Ionics 154 (2002) 303.

Foreseeing and relationship between the degree of [EMI][BF_4] conductivity and temprature

B. najafi*[a], M. H. Hadizadeh[b] and S.Naseh[b]

[a]Department of chemistry, Isfahan University of Technology, Isfahan, Iran

[b]Department of chemistry, University of kashan, Kashan, Iran

*E-mail: najafi@cc.iut.ac.ir

Keywords: Ionic liquids,Conductivity

Introduction

An ionic liquid (IL) is a salt in the liquid state. In some contexts, the term has been restricted to salts whose melting point is below some arbitrary temperature, such as 100 °C (212 °F). While ordinary liquids such as water and gasoline are predominantly made of electrically neutral molecules, ILs are largely made of ions and short-lived ion pairs. Because ionic liquids are composed of only ions, they show very high ionic conductivity, non-volatility, and non-flammability, the nonflammable liquids with high ionic conductivity are practical materials for use in electrochemistry [1-3]. There are some elements which make the act of gaining access to needed conductivity for carrying out Electrochemical activities difficult such as: using commercial and accessible primary materials, economical profit, observing high accuracy, spending long time, and so on.

Experimental method and its difficulty

There are two main stage in synthetizing of ion liquids with imidazol base and different anions: (1) quadruple the nitrogen of imidazol ring (2) anionic exchangment. The first stage extremly depend on temprature and most of researches are about preparing chemicaphysics or systematic conditions and increasing the efficiency of this step. To preparing various derivatives of 1-alkyl imidazol, imidazole become deprotonated with metalic sodium or sodium ethoccylate and then the product is obtained in ethanol or acetonitryl solvents attending an alkylation indicator (Fig. 1).

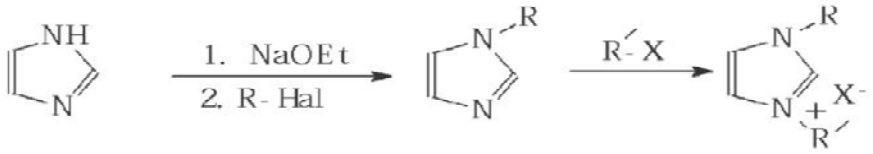

Figure 1. total stages of synthetizing imidazol salt

synthetizing these material in lab needs the high precision because ion liquids are extremly sensitive to humidity [4-7].this problem and what have mentioned before make creat a theory method.

Theoretical method

We considered two important points: first obtained equation apply for wide range of density of ionic liquids and second used cations and anions would have been favourite conditions for statistical tests. Statistical calculations showed that the conductivity of 1-ethyl-3-methylimidazoliumfluoroborate [EMI][BF_4] enhanced with gradual increasing of temprature. This molecule has been selected from 276 type of cations and 55 type of anions. On the other hand 15180 type of ion liquids have been investigated. After passing various statistical stage and applying F (comparison between relative precision Of datas) and Q (deleteing doubtful datas) tests, we came to conclusion that there is a simple relation between conductivity and temprature: $\sigma_c = 0.0425T + 0.1889$

Using this relations facilate obtaining both high and low conductivities in electrochemical researches.

Conclusion

We reach to interesting relations between 1-ethyl-3-methylimidazolium tetrafluoroborate ([EMI][BF_4]) salts and temperature, after making different statistical calculations among the data of conducting numerous group of ionic liquid (including 276 different type cation and 55 different type anion) which satisfy the need of performing different experiments for accessing ideal conductivity of Electrochemical activities.

References

[1] K. R. Seddon, J. Chem. Tech. Biotechnol. 68 (1997) 351.

[2] T. Welton, Chem. Rev. 99 (1999) 2071

[3] P.Wasserscheid,; T.Welton, Ionic Liquids In Synthesis; Wiley-VCH: Weinheim,2003.
[4] C.P.Mehnert, N.C. Dispenziere & R.A. Cook"Method for preparating highpurity ionic liquids", US Patent App. 0074842A1, 2004.
[5] P.A.Z. Suarez & J.Dupont, J. Chim. Phys. 95 (1998) 1626.
[6] P.Bonhote & A.Dias "Hydrophobic, highly conductive ambient–temperature molten salts", Inorganic Chemistry. 35 (1996) 1168.
[7] P.J.Dyson, M.C.Grossel, N.Srinivasan, Tr.Vine, T.Welton, D.J.Williams, A.J.P. White & T. Zigras, J. Chem. Soc.Datlon Trans. (1997) 3465.

Determination of the density of the liquid ions based on statistical calculations

B. najafi[*a], M. H. Hadizadeh[b] and S.Naseh[b]
[a]Department of chemistry, Isfahan University of Technology, Isfahan, Iran
[b]Department of chemistry, University of Kashan, Kashan, Iran
*E-mail: najafi@cc.iut.ac.ir

Keywords: Ionic liquids,Density

Introduction

Ionic liquids as green solvents are a new group of salts which can be liquid in lower than 100 ^{o}C. they are consist of large non-symmetric organo cations like: imidazolium, phosphonium, pyridenium, thiazolium, pyrazolium, solfunium, thriazolium derivatives and so on and smaller organic or inorganic anions. The low symmetry and the weak concentration of the possitive charge are the most important of specefications of cationic part of these compounds which prevent from formation of a new regular crystalline lattice and therefore it reduces melting point. Some features of ionic liquids are: high density, low vapour pressure, non-flammable, high conductivity, wide electrochemical window, mix ability with many common organic solvents and its efficiency in analysis processes in multiphase systems [1-5]. There is more attention to Imidazolium salts in order to facilate research on ion liquids, because these cations have two substituted groups that substituting them make different solvent properties. In spite of this specefication, there are some obstacles like spending much time and money along with experimental and instrumental errors. This was why we created a theoritical method based on statistical calculation to measure density of ion liquids.

statistical methods

Two important points have been considered: first obtained equation apply for wide range of density of ionic liquids and second used cations and anions would have been favourite conditions for statistical tests. Therefore imidazolium derivatives were used for cationic parts. After passing various statistical stage and applying F (comparison between relative precision of datas) and Q (deleteing doubtful datas) tests, we came to conclusion that

bis((threefloromethyl)solfunyl)imid, (TFSI) with chemical formula $C_2F_6NO_4S_2$ obeyed from determined conditions. On the other hand, this anion in combination with imidazolium cations produced a wide range of densities. In the next step with constanting anionic base, we felt the need of a relation between alkylic group of cationic part and density. Then we ploted density base on incresing the number of carbon atoms of alkyl group of imidazolium salts having total formula 1-alkyl3-methyl imidazolium $[C_nMI]$ along with [TFSI] anion in 25 ^oC. We found following equation with regration coefficient 0.99 that showed good agreement between presented data and this equation: $\rho = (-0.0308[n] + 1.5676)$ (1)

this statistical metod has gained among 276 cations and 55 anions in different experimental conditions. It is clearly The reason behind the use of TFSI anion in following samples and density data (Fig. 1)

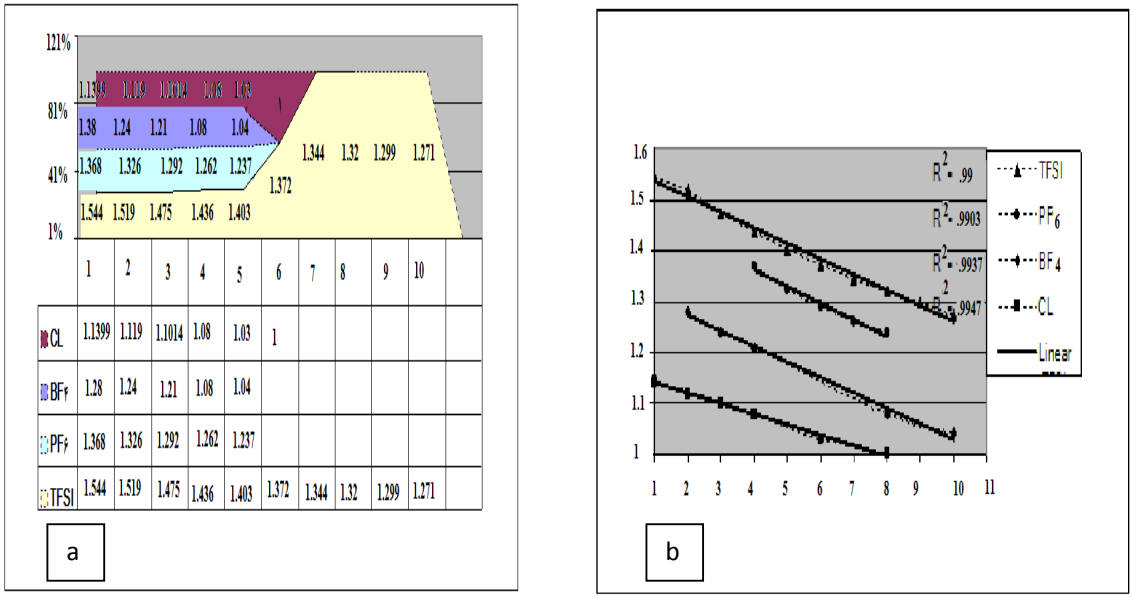

Figure 1.percentage of accumulation diagrams (a) and density-number of carbon atoms [C_nMI] (b).

Conclusion

To prevent the problems during synthetizing an ion liquid with favourite properties, we investigated a statistical method and a simple equation between density values and the number of carbon atoms of alkyl group.

References

[1] J. F. Brennecke, E. J. Maginn, AIChE J. 47 (2001) 2384.

[2] K. N. Marsh, A. Deev, A. Wu, E. Tran, A. Klamt, Korean J. Chem. Eng. 19 (2002) 357.

[3] C. P. Fredlake, J. M. Crosthwaite, D. G. Hert, S. N. V. K.Aki, J. F. Brennecke, J. Chem. Eng. Data 49 (2004) 954.

[4] J. G. Huddleston, A. E.Visser, W. M. Reichert, H. D. Willauer, G. A.Broker, R. D. Rogers, Green Chem. 3 (2001) 156.

[5] H. Xue, R.Verma, J. M. Shreeve, J. Fluorine Chem. 127 (2006) 159.

The investigation critical aggregation point of colchicine and aspirin on the human serum albumin: Resonance light scattering and synchronous fluorescence techniques

M. Vahidzadeh[1], H. Saneii[1], M. Gharanfoli[2] and J. Chamani[1]

1. Department of Biology, Faculty of Sciences, Islamic Azad University–Mashhad Branch, Mashhad, Iran.
2. Department of Development of Biology, University of Science and Culture, Tehran, Iran.

Abstract

The interaction of colchicin (COL) and aspirin (ASA) to HSA was studied using resonance Rayleigh scattering technology; the resonance light scattering method can be used as a new technology for the determination of the aggregation point of drugs at interaction of proteins. The participation of tyrosyl and tryptophan residues of protein was also estimated in the drug–HSA complex by synchronous fluorescence.

Keywords: RLS, synchronous fluorescence, aggregation point, HSA, ASA and COL

Introduction

HSA plays an important role on transportation of drug and other exogenous and endogenous compounds to their targets. Colchicine is a naturally occurring alkaloid used in human and veterinary medicine. ASA is used as analgesic against less intense pains; it is a soft and excellent antipyretic sedative. The aim of this study is to analyze the interaction of COL and ASA with HSA.

Methods:

The resonance light scattering analysis is attractive for the determination of biomacromolecules, and the synchronous fluorescence spectra only shows the tyrosine residues and the tryptophan residue of HSA when the wavelength interval $\Delta\lambda$ is 15 nm and $\Delta\lambda$ is 60 nm, respectively.

Results and discussion

The resonance light scattering spectroscopy (RLS) spectra of the HSA-ASA and HSA-COL complexs is shown in Fig. 1(A,B). The enhanced RLS intensity increases with the increasing druga concentration. It can be consequently concluded that drugs reacted with HSA and produced a complex [1]. It has been also shown in Fig. 2A that the slope of HSA-ASA was higher when $\Delta\lambda$ was 15 nm, indicating that in presence of COL interaction of ASA to tryptophan residues, decrease, and Fig. 2B show the slope was higher when $\Delta\lambda$ was 60 nm, indicating that in the presence of COL interaction of ASA to tyrosine residues, increase [2]. According to the Fig. 2C in $\Delta\lambda = 15$ nm curve of both binary and ternary systems have overlap below the concentration of COL:HSA, 7×10^{-7} mM, therefore fewer than 7×10^{-7} in binary and ternary systems, tyrosine has influence similar in interaction of COL to HSA, whereas above this concentration, the interaction between COL and tyrosine residues, increase. Also Fig. 2D shows the slope was higher when $\Delta\lambda = 60$ nm, indicating that in the presence of ASA, interaction of COL to tryptophan residues, increase.

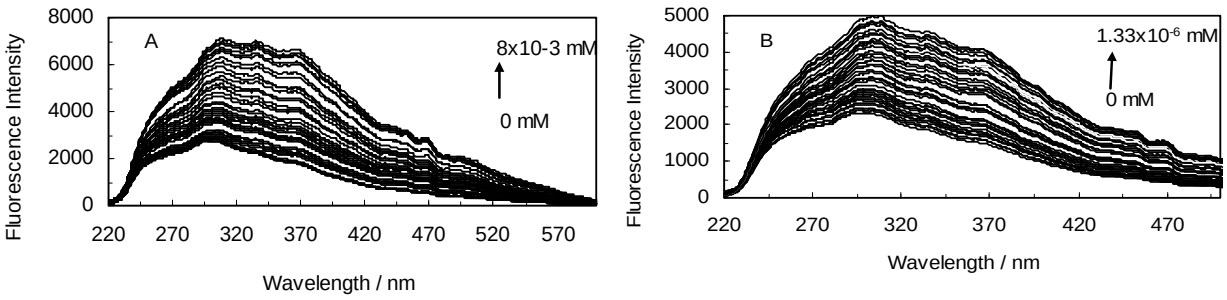

Fig. 1: Resonance light scattering spectra of HSA in the presence of different concentration of ASA (A) and COL (B), T=310 K, pH=7.4.

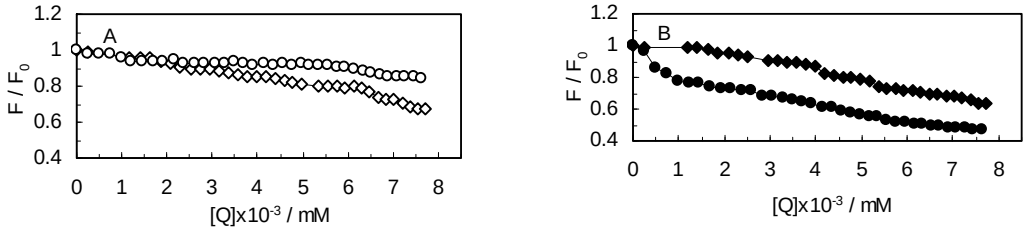

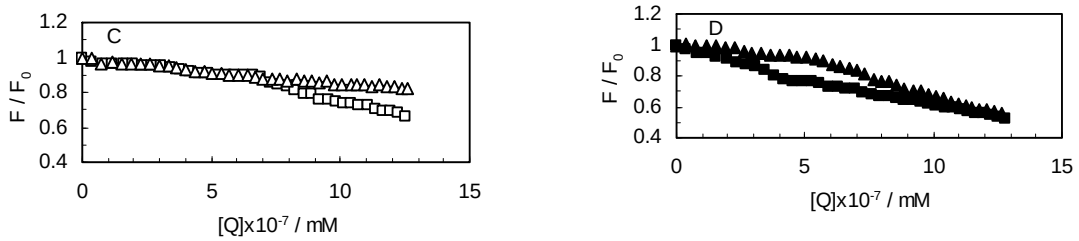

Fig. 2: The quenching of HSA synchronous fluorescence by ASA (○), (COL)ASA (◊) and COL (□), (ASA)COL (Δ) at $\Delta\lambda$ =15 (open symbols), 60 nm (closed symbols).

Conclusions

In this work, resonance Rayleigh scattering method is applied to study the interaction of drug with protein, results show that the enhanced RLS intensity increases with the increasing drugs concentration. Changes in the environment of the aromatic residues are also observed by synchronous fluorescence.

References:

[1] Z. Chen, J. Liu, Y. Han, Talanta, 71 (2007) 1246–1251.

[2] L. Wang, R. Liu, Z. Chi, B. Yang, P. Zhang, M. Wang, Spectrochimica Acta Part A, 76 (2010) 155–160.

Novel Autocorrelation Descriptors Based on Quantum Topological Molecular Similarity to Construct Quantitative Sequence- Activity Models for Peptides

Bahram Hemmateenejad* and Saeed Yousefinejad
(Email: hemmatb@sums.ac.ir)
Department of Chemistry, Shiraz University, Shiraz, Iran

Key words: Amino acid indices, QTMS, Auto correlation, QSAM, Peptide, Active site analysis

Introduction:

Description of amino acids (AAs) is important for many reasons. Peptides play significant roles in biological world especially in human life and also as pharmaceutical targets. Since the subject of quantitative sequence-activity model (QSAM) that employs quantitative structure-activity relationship (QSAR) strategies to quantify biosequence-activity/function relationship for the peptides, proteins and nucleic acids has proposed, this field becomes an attractive and active area in computational study of peptides.

In the recent years, merging quantum mechanical data with the topological approach, according the theory of atoms in molecules (AIM), led to a novel category of descriptors, called quantum topological molecular similarity (QTMS) indices [1] .Over the last several years QTMS methods have produced excellent results of relevance to different fields [2].

Very recently a new source of AA indices based on quantum topological molecular similarity (QTMS) descriptors has been proposed by us for use in QSAR study of peptides, contain topological and quantum information of AAs [3]. These indices showed multiple advantages, such as definite physical and chemical meaning, good structural characterization ability and producing statistically significant QSAR models.

In this work autocorrelation function was applied on the QTMS descriptors of amino acids to extract a new source of AA descriptors with additional advantages related to our previous work. This proposed group of descriptors has used for construction of quantitative sequence-

activity (QSAM) model for 3 set of biologically and pharmaceutically important peptides with different chain size and also their active site analysis successfully.

Materials and methods

***Data set**:* In order to validate properly the new QTMS-based autocorrelation scales, it is important that the example data sets used are representative and have well-understood structures. 58 dipeptides inhibiting the angiotensin converting enzyme (ACE), 177 nonameric binding peptides of HLA-A*0201 molecule and 48 di-peptides bitter tasting thresholds (BTT) were the 3 data sets which was studied.

Calculation procedure: After optimization of the three-dimensional geometry of the AAs molecules at the RHF/6-31+G* level of theory, the nine QTMS descriptors was calculated for each AA bond using AIM software. Then, these parameters were transformed into a novel set of descriptive parameters (named as ATSQ) using the autocorrelation approaches (The obtained index is not shown). Some chemometrics approaches was used to model construction, model validation and active site analysis of the under study peptides.

Result and discussion

However the detail of obtaining our proposed index, model making and validation are not discussed and their data are not shown here, the final results for the under study peptides data sets are abstracted in Table 1. The constructed models exhibited not only good self-prediction power (internal validation) but also had sufficient prediction ability for activity of the test set samples and showed the power of proposed index to use in QSAM of peptides. The models which were made based on ATSQ indices, had better results in most cases related to previous indices which had been reported in literatures for AAs (comparison data has large volume and are not shown). Active site analysis of peptides in the under study data sets was also done using variable importance in the projection (VIP) of models coefficients. Most sequence which was selected as the active site in the peptides was in agreement with literature and indicated the good descriptive ability of proposed indices (data and related figures are not shown).

Table 1 QSAM models of the ACE, HLA and BTT data sets using ATSQ index.

Data set	n_{SV}	n_{LV}	R^2_{cal}	Q^2_{LOO}	Q^2_{LMO}	R^2_P	RMSE cal	RMSE p	Q^2_{MP}
ACE	7	3	0.868	0.812	0.800	0.702	0.36	0.55	0.061
HLA	20	6	0.782	0.682	0.651	0.500	0.47	0.73	0.031
BTT	5	2	0.809	0.761	0.762	0.770	0.437	0.550	0.124

References:

[1] O'Brien SE, Popelier PLA (2002) J Chem Soc Perkin Trans 2: 478-483.

[2] Hemmateenejad B, Mohajeri A (2007) J Comput Chem 29:266–274.

[3] Hemmateenejad B, Yousefinejad S, Mehdipour AR (2010). Amino Acids, in press

Computational Chemistry

QSAR studies of some cyclic nitrogen compounds Using multiple linear regression analysis

Zahra Hoseyni[*,1], Mina Ebrahimy[1] & Hossein daj[1]

1.Islamic Azad University of Omidieh

e-mail: Mina.Ebrahimy@yahoo.com

Abstract:

According to laboratory work hard, this study will try to obtain some cyclic nitrogen compounds QSAR (Quantitative Structure-Activity Relationship) with a group of them; to face of computational methods the kinds of descriptors molecules obtained using statistical techniques MLR, the best relationship between biological activity and descriptors obtain and to use this relationship to predict and interpret the families molecules of this group was discussed. Model obtained was tested on 10 molecules and their biological activity values obtained.

Key words:MLR analysis, cyclic nitrogen compounds, Quantitative Structure-Activity Relationship, QSAR.

Introduction:

One of the main objects of scientists to predict the behavior of a new molecule, based on analysis of the behavior of similar molecules that have previously been investigated .Problems and risks associated with chemical measurements has caused some of today's computing molecular properties using computational methods or parameter, is actually welcomed by many. In parameter methods between the describing the procedures and communicate desired are behaviors [1].

Methods:

Table (1): molecules used in this study

num	Com. name	num	Com. name	num	Com. name
١	Diglycol Dinitrate	٧	Ethylene glycol dinitrate	١٣	Nitrobenzene
٢	1.2 - Dinitroglycerol	٨	Nitroguanidine	١٤	Picric acid
٣	1.3 - Dinitroglycerol	٩	Octahydro – 1.3.5.7 trtranitro – 1.3.5.7 tetrazocine	١٥	Hex hydro – 1.3.5 trinitro – 1.3.5 trizine
٤	Meta Dinitrobenzene	١٠	Losorbide dinitrate	١٦	1.3 – Dlhydroxy 2.4.6 - trinitrobenzene
٥	2.4 - Dinitrotoluene	١١	Ortho Nitro toluene	١٧	N – methyl-N.2.4.6 tetranitroaniline
٦	2.6 – Dinitrotoluene	١٢	Meta Nitro toluene	١٨	Trinitrotoluene

Object in this study to gain respect QSAR for some of cyclic nitrogen compounds and predictions biological activities of other families' compounds with relationship obtained. Civil code further studied the biological activity in Log k research and reference number [3] are obtained. Compounds named in this study have been reviewed in Table (1) you can see.
QSAR modeling step is a process that are includes five main steps:
1. Entre structure and optimization and selection of data series.
2. Selected and calculated describes.
3. Analysis and resolution and valuation describe (trait selection).
4. Analysis Statistical model and selection and construction of suitable models.
5. Evaluate the validity of the model chosen (or model predictions and validation)

1. Entre structure and optimization and selection of data series:

In the first step, after entering the structure and optimization of molecules, different descriptors (Table (2)) were obtained for the molecules.

Table (2): names of different descriptors for molecules obtained

Descriptors obtained for molecules					
H.E	**ω**	**μ**	**η**	**ε_L**	**ε_H**
ΔN	**Mass**	**Pol**	**Ref**	**Vol**	**Log P**

2. Select and calculate molecular describing:

At this stage, before the formation of statistical models for modeling of communication, first calculated the numbers of descriptors, which provide little information or put in close contact with each other were excluded.

3. Analysis and resolution and valuation describe:

In next for the selection of variables and selecting the best subset of descriptors remaining techniques MLR (multiple linear regressions) and forward step method was used. So the molecules of biological activity as dependent variable and molecular descriptors as independent variables were used and were trying to best the relationship between biological activity and molecular quantum mechanics descriptors obtained, which is usually the best state, for the relationship is linear state.

4. Analysis Statistical model and selection and construction of suitable models:

Must have the best relationship that amounts R^2 as possible to 1 , to be obtained. In this study tray the MLR techniques, first for each model were considered independent variables, then selected the best model and because correlation coefficient is still lower and the model was not appropriate; models varying from 2 to 7, which subset best linear model For

molecules were created. The best results related to model variables in Table 1 to 7 (3) is given.

Table (3): Find the best regression equations obtained in 1 to 7 variable

variables	equations	R^2
1	Log k= a + b(Ref)	0.2626
2	Log k= a + b(Ref) + d(H.E)	0.7918
3	***Log k=a + b(Ref) + d(Pol)+ e(H.E)***	***0.9061***
4	Log k= a + b(ΔN) + d(Ref)+ e(Pol) + f(H.E)	0.9388
5	Log k= a + b(ΔN) + d(ω) + e(Ref) + f(Pol) + g(H.E)	0.9371
6	Logk= a + b(μ) + d(ΔN) + e(ω) + f(Red) + g(Pol) + h(H.E)	0.9404
7	Logk= a + b(μ) + d(ΔN) + e(ω) + f(Ref) + g(Pol) + h(H.E) + i(Vol)	0.94

According to the regression rates obtained for different models and considering the best model, is the model that the correlation coefficient is high, have less the number of independent variables and also considering the increase models of 3 variable to…by increase less than 0.03% regression attendant which is partial and is negligible, so we can say the best model among these models, model 3 variable. In table (4) the profile and the final model coefficients given.

Table (4): final model profile

equation	graph
Log k = a +b(Ref)+d(Pol)+e(H.E)	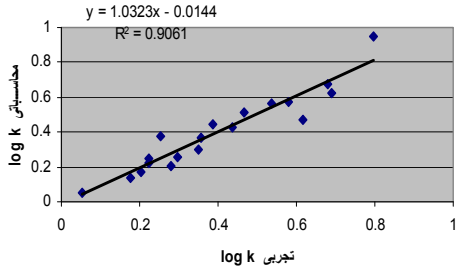

coefficient	symbol	variable
b = 0.0292	**Ref**	**Refractivity**
d = -0.072	**Pol**	**Polarizability**
e = 0.0351	**H.E**	**Hydration Energy**
a = 0.8034		Constant coefficient

5. Evaluate the validity of the model chosen (or model predictions and validation):

Series are expected to help extend functionality related quality of QSAR is obtained. For this first time the number of families of molecules with molecules selected reference series and then considering the relationship QSAR obtained, the biological activity of these compounds were predicted (Table (5)).

Table (5): descriptors are calculated and predicted biological activity for molecules Series predictions

:Tests	H.E	pol	Ref	Log k (predicted)
test 1	-22.81	12.25	35.74	0.5056
test 2	-10.84	12.91	34.07	0.8008
test 3	-17.92	14.75	40.39	0.6453
test 4	-8.03	8.12	23.22	0.8762
test 5	-10.21	15.92	43.74	0.9503
test 6	-14.46	14.75	40.39	0.7782
test 7	-12.72	16.04	48.11	1.027
test 8	-18.82	14.75	45	0.8003
test 9	-12.15	17.89	52.36	1.0613
test 10	-12.9	14.75	43.06	0.9313

Results & Discussion:

Find a relationship between structural features combined with the biological activity shown by its short little Quantitative Structure-Activity Relationship (QSAR) is called [2]. The results show that the proposed methods have suitable ability to predict indices of various compounds and addition, the proposed models have enough sustainability.

To establish this connection, the multiple linear regression (MLR) was used. By this method important describes to extract the final model are selected; that most of them by different computational software can be accounted [2]. Software used to calculate descriptors participating in the model presented in this study include: Hyperchem and Gaussian 98.

According to the tables and graphs presented in this study will be seen that a suitable QSAR model can predict up to a family of compounds used; also can use this equation, the activity of biological compounds as well as other programs computer and computational predictions, and with it the risks, costs and hardships of laboratory work can be avoided.

Conclusion:

After review and study on a group of cyclic nitrogen Compounds conclusion was that the best relationship QSAR for compounds that contain three descriptors Refractivity (Ref), Polarizability (Pol) and Hydration Energy (H.E) is.

References:

[1] J. R. Parsons and H. A. Govers, *Quantitative structure-activity relationship for biodegradation*, *Ecotoxicol. Environ. Safety*., **1990**, 19, 12.
[2] E. A. Castro, A. A. Toropov, et al, *Theochem*., **2003**, 19, 129.
[3] M. Curt, M. Rhem, *Journal of Computational Chemistry*. **1997**, 18, 2, 182.

High-level quantum chemical calculations of O_3–H_2O complexes

[a]Hossein Roohi, [b]Elham Ahamadepour

[a]*Department of Chemistry, Faculty of Science, University of Guilan, Rasht*

[b]*Islamic Azad University of Parsian branch, Bandarabbas*

(Email: elhamahmadipour@gmail.com)

Introduction

Reaction of ozone with other species is one of the best investigated chemical reactions as is reported in many research papers published in the recent years**.** It has been predicted that the O_3–H_2O complex is another source of OH radical in the troposphere according reaction:

O_3–H_2O + hν → 2OH + O_2

Microwave spectra of the O_3–H_2O complex in gas phase has been observed with a pulsed-beam Fabry-Perot cavity Fourier-transform microwave spectrometer**.** Recently, Shibuya et al. [1] has been applied matrix isolation infrared spectroscopy together with ab initio calculations to study of ozone-water complexes. They have demonstrated the existence of only one stable conformer (double-decker). They obtained the value of 2.8661 Å for distance between the center oxygen atom of ozone and the oxygen atom of water, which is smaller than experimental value (2.957 Å). This work aims to study the possible existence of O_3–H_2O complexes at high levels of computational chemistry in order to find most stable structure in which its structural parameters to be good agreement with the experimental values. We found two new complexes in this work which has not been reported previously. All interactions in O_3–H_2O complexes are characterized by quantum theory of atoms in molecules(QTAIM)analysis.

Computational details

The calculations were performed using the B3LYP, MP2, MP4(SDTQ), CCSD, CCSD(T), QCISD and QCISD(T) methods. The following Pople and Dunning type basis sets were used: 6-311++G(2d,2p), AUG-cc-pVDZ and AUG-cc-pVTZ. The counterpoise procedure (CP) [2] was used to correct basis set superposition error (BSSE) in the calculation of binding energies. The Bader theory was also applied to find critical points and to characterize them.

Topological properties have been calculated at MP2/6-311++G(2d,2p) level of theory by AIM2000 program package.

Results and discussion

We found six complexes in interaction between H_2O and O_3. To the best of our knowledge, **LM5** and **LM6** were not reported previously. At all levels of theory, **LM1** and **LM2** complexes have C_s symmetry. All calculations indicate the complex **LM2** is more stable than the complex **LM1**. Both complexes are non-hydrogen bond complex and exhibit the double O···O interactions**.** The calculated distance between the center of mass of O_3 and H_2O (O2···O4) is 2.932, 2.927, 3.093 and 3.111 Å at MP2/AUG-cc-pVTZ, QCISD(T)/AUG-cc-pVDZ, CCSD/AUG-cc-pVDZ and QCISD(T)/AUG-cc-pVDZ levels of theory, respectively. The values obtained at MP2/AUG-cc-pVTZ, QCISD(T)/AUG-cc-pVDZ levels are in close agreement with the experimental value of 2.957 Å. The calculated distance between the center of mass of O_3 and H_2O (O2···O4) is 2.932, 2.927, 3.093 and 3.111 Å at MP2/AUG-cc-pVTZ, QCISD(T)/AUG-cc-pVDZ, CCSD/AUG-cc-pVDZ and QCISD(T)/AUG-cc-pVDZ levels of theory, respectively. The values obtained at MP2/AUG-cc-pVTZ, QCISD(T)/AUG-cc-pVDZ levels are in close agreement with the experimental value of 2.957 Å**.** The AIM calculations predict the electrostatic characteristic of O···O and O···H interactions in O_3–H_2O complexes.

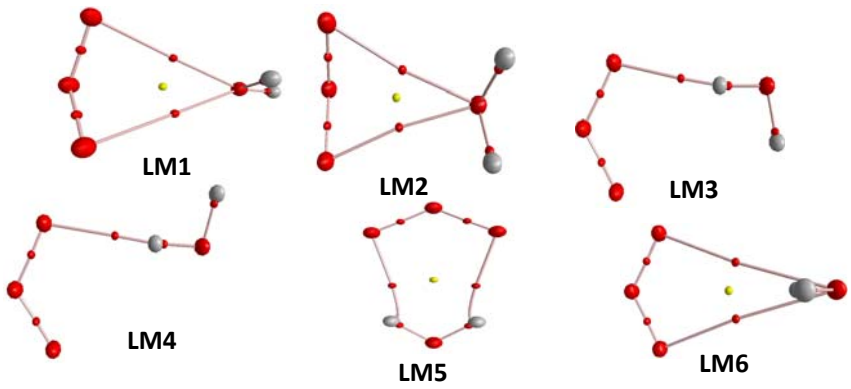

References

[1] M. Tsuge, K. Tsuji, A. Kawai, A. Kawai, K. Shibuya, J. Phys. Chem. A 111 (2007) 3540.

[2] R.F.W. Bader, H. Essen, J Chem. Phys. 80 (1994) 1943.

[3] S. F. Boys, F. Bernardi, Mol. Phys. 19 (1990) 553.

QSPR Study of Critical Temperature of Some Organic Compounds Using Multiple Linear Regression Method

A.R. Ahmadi Gandomani*[a], M. M. Papari[b], Z. Amini[a] and M. Lotfi[b]

[a]*Department of Chemistry, Islamic Azad University, Firouzabad Branch, Firouzabad, Iran*

(r.ahmadi90@yahoo.com)

[b]*Department of Chemistry, Shiraz University of Technology, Shiraz, Iran*

(papari@sutech.ac.ir)

Keywords: QSPR, MLR, Semiempirical AM1, DECHEMA database, Critical temperature.

Introduction

The objective of quantitative structure-property relationship (QSPR) models are to allow the prediction of physic-chemical properties of untested and sometimes yet unavailable compounds and to provide insight of which relevant and consistent chemical properties are determinant for the Thermodynamic property of compounds [1, 2]. The present work addresses the detailed procedure to predict critical temperature of several organic compounds.

Results and Discussion

A QSPR study was performed to develop models that relate the property of 132 organic compounds to their critical temperatures (T_c). QSPR models have a good ability to correlate and predict the critical temperature of organic compounds. A subset of 132 molecules was selected from the DECHEMA database [3]. The chemical structure of the molecules was drawn by the Hyperchem and CS Chem3D Ultra softwares. Semiempirical Austin Model 1 (AM1) calculations were used for geometry optimization of the studied molecules by these softwares. The Hyperchem, CS Chem 3D Ultra and Dragon softwares were employed for generating all descriptors. Eventually, 1172 descriptors were calculated for each molecule. A linear QSPR model for T_c was obtained using stepwise multiple linear regression (MLR) procedure. Prior to MLR procedure the detected co-linearity between some calculated descriptors were omitted. Among all models that developed by MLR method, a four parametric model was chosen as the best one:

T_c = 155.4 (± 24.55) + 14.98 (± 0.695) SDeg + 21.94 (± 3.357) H-050 + 490.3 (± 48.15) Mv - 22.75 (± 3.031) *P* (1)

In this equation, sum of degrees (SDeg) is among steric descriptors, H attached to hetero atom (H-050) is related to atom-centred fragments, mean atomic van der Waals volume (Mv) belongs to constitutional descriptors and partition coefficient (octanol / water) (*P*) is a thermodynamic descriptor. The statistical parameters of aforementioned correlation is:

N= 132 R^2*= 0.9214* *Se = 29.997* *F = 372.32*

Conclusions:

QSPR models are now well established and are used to correlate varied, and often complex, thermo-physical properties of molecules.

References:

[1] A.R. Katritzky, L. Mu, M. Karelson, A QSPR study of the solubility of gases and vapours in water, J. Chem. Inf. Comp. Sci. 36 (6) (1996)
1162–1168.

[2] S.S. Godavarthy, R.L. Robinson Jr., K.A.M. Gasem, SVRC-QSPR model for predicting saturated vapor pressures of pure fluids, Fluid Phase Equilib. 246 (2006) 39–51.

[3]. K.H. Simmrock, R. Janowsky, A. Ohnsorge, Critical Data of Pure Substances, Chemistry Data Series, vol. II, Part 2, DECHEMA, Frankfurt am Main, 1986.

Investigation of the Effect of Serin Side Chain Angle on the Stability of Gly-Ser-Gly Tripeptide Motif: An Ab initio Study

Behzad Chahkandi, Majid Mohammad Hosseini, Cobra Ahmady*
Chemistry Department, Islamic Azad University, Shahrood branch, Shahrood, Iran
(Corresponding author email:Shahrzad745@gmail.com)

Keywords: Protein Folding, Ttripeptide, Gly-Ser-Gly, Abinitio, HF

Introduction

During the second half of the 20th century, the scientists have started a new research on the structure of proteins. [1]

The folding or second structure of protein, is a multi-variable function from torsional angles. For studying on this subject, we must know peptide models of protein and we have to study peptide and protein conformations, in attention to the stereo interactions of R groups. (See Fig.1) [2]

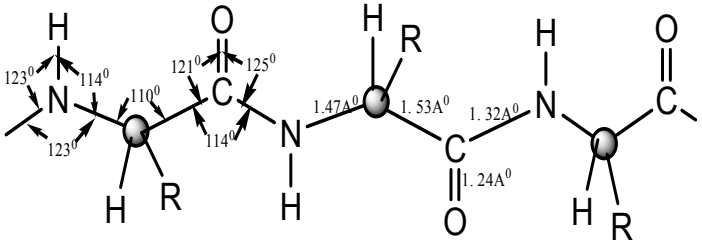

Fig 1. Stereochemical configuration of peptide bond; (C-N) bond has the double bond property. Carbon of carbonyl, N, and connected atoms whit them, are at the one page.

In this study, there are results of search about the most stable conformation of Gly-Ser-Gly. These conformers were defined by rotation of dihedral angles of side-chain (χ). This tripeptide (Gly-Ser-Gly) is in the structure of Fibrogen protein (curractly in structure of hexa-peptide of fibroin: Gly-Ser-Gly-Ala-Gly-Ala). [3]

Methods

In this work, we have studied the effect of side chain torsional angle (χ) on conformational stability of Gly-Ser-Gly tripeptide. For this purpose the side chain torsional angle (χ) was changed at 30^0 intervals, from 0^0 to 360^0. (See Fig 2) For determining the stable conformers of Gly-Ser-Gly tripeptide that obtained from varying χ , the Abinitio calculations were carried out at HF/6-31G* and HF/6-311G** levels of theory. All of calculations performed by using Gaussian03 program. [4]

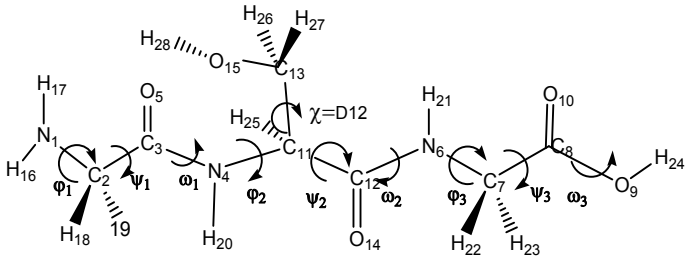

Fig, 2 Stereochemical configuration of GSG tripeptide; the side chain torsional angle (χ) is shown with D12.

Results and discussion

The obtained energies from optimized structures show that there are three minima at $\chi=60^0$, $\chi=180^0$ and $\chi= -90^0$. However among all states the conformer that $\chi= -90^0$ has the most stability. (See Fig. 3)

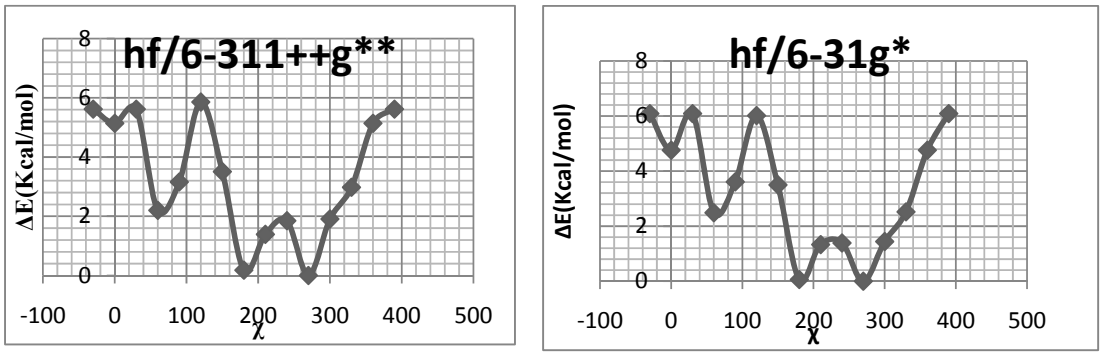

Fig. 3 Relative energies (ΔE) of various conformers obtained from changing side chain torsional angle (χ)

References:

[1] M.A. Berg et al. /Prospects in computational molecular medicin: a millennial mega-project on peptide folding, *Journal of Molecular Structure (Theochem),* 500(200)5-58

[2] R.T. Morrison, R.N. Boyd, *organic Chemistry,* Vol.3, 6th ed. 1992

[3]Norbert Sewald and Hans-Dieter Jakubke, *Peptide: Chemistry and Biology*, WILEY-VCH, Second, Revised and Update Edition

[4] Gaussian 03, Revision C.02, G. W. Trucks, H. B. Schlegel, , G. E. Scuseria, M. A. Robb, J. R. Cheeseman, J. A. Pople, et al. Gaussian, Inc., Wallingford CT, 2004.

Theoretical investigation of the feasibility of the formation of $C_{59}B$ and $C_{59}Al$ fullerenes /glycine complexes: DFT calculations

Nasim Ahmadian[a], Masoud Darvish Ganji*[,a] and Nasim Danesh[a]

[a] Department of Chemistry, Islamic Azad University, Ghaemshahr Branch, Iran

(Email: ganji_md@yahoo.com)

Keywords: $C_{59}Al/C_{59}B$ complex, Glycine, DFT, Adsorption

Introduction:

Recently much attention has been directed to fullerenes, the hollow carbon cages discovered in 1985 [1], as nanometer-scaled structures. Fullerene nanocages play a significant role in cellular uptake, protein binding, and translocation from portal of entry to the target site, etc. However, due to its small size, there are noteworthy theoretical investigations on the interaction between glycine (as a backbone of a protein) and surface of fullerene-nanocages motivating us to more comprehensive studies in sophisticated cases associated with biomolecules and fullerene nanocages [2,3]. In the present work, we have investigated the capability of $C_{59}Al$ and $C_{59}B$ fullerenes for the glycine adsorption by means of (DFT) based calculations.

Method:

All the configurations were drawn employing Hyper Chem software and all the computations were carried out using the ab initio DFT method using the standard Kohn–Sham equations and has been very efficient for large atomic systems [4].

Results and discussion:

we have considered the binding of the glycine on the exterior surface of the $C_{59}Al$ and $C_{59}B$ fullerene cages to study the adsorption behavior of glycine-$C_{59}Al/C_{59}B$ complexes. Several possible configurations were created for a glycine molecule approaching the top of Al and B atom of the cages via its three active sites. After full structural optimization of the considered systems, the obtained results reveal that the binding of glycine to the cages generates more

stable complexes with binding energies (with BSSE correction) of -1.64 eV (37.89 Kcal/mol) via carbonyl oxygen (O) for gly/$C_{59}B$ and amino nitrogen (N) for gly/$C_{59}Al$, respectively, see Fig. 1(a). Furthermore, Mulliken charge analysis has been performed to evaluate the amount of electron transfers between glycine /$C_{59}Al$-$C_{59}B$ complexes. The calculated results shows 0.486 e charge transferred from glycine to the $C_{59}Al$ complex and 0.31 e charge transferred from glycine to the $C_{59}B$ complex. The extension of the bond lengths of adsorbed glycine onto $C_{59}Al$ nanocage, specially the bond length of N-C (from 1.450 to 1.484) for the most stable configuration, are indications of the strong interaction of glycine with $C_{59}Al$ cage via its active sites.

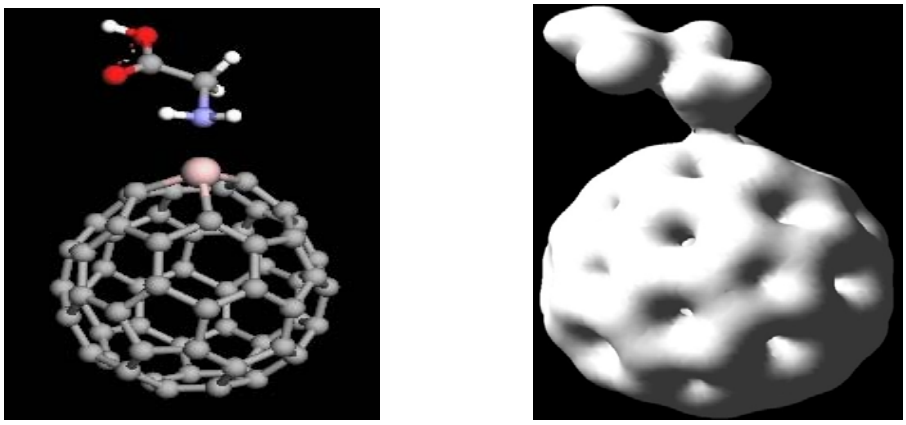

Fig. 1. (a) The most stable configuration of $C_{59}Al$/Gly complex via amino nitrogen (N) active site. (b) isosurface of the total electron density for $C_{59}Al$/Gly complex where 0.03 was used as an isovalue of total electron density, showing the binding between the $C_{59}Al$ and the glycine molecule.

In addition, the total electron density map of the electronic densities was analyzed for the most stable configuration of $C_{59}Al$ complex (represented Fig. 1(b)). it is clearly revealed that strong hybridization of the N and C atoms with nanocage states occurs, resulting in a significant charge
transfer in the system.

Conclusion:

The calculated results show that glycine is strongly bound to the outer surface of $C_{59}AL$ and $C_{59}B$ nanocages on the top site directly above the Al atom and the boron atom with a binding energy –1.64 eV. Mulliken population analysis suggests that significant hybridization

between the respective orbitals of the two entities takes place and charge transfers from glycine toward the$C_{59}Al$ and $C_{59}B$ nanocages.

References:

[1] H.W. Kroto, J.R. Heath, S.C.O. Brien, R.F. Curl, R.E. Smalley, Nature 318 (1985) 162.

[2] D.J. Zhou, L.B. Gan, L.B. Xu, C.P. Luo, C.H. Huang, Fullerene Sci. Technol. 3 (1995) 127.

[3] M.B. Messaouda, F. Moussa, B. Tangour, H. Szwarc, M. Abderrabba, J. Mol. Struct.: Theochem. 809 (2007) 153.

[4] D. Sa´nchez-Portal, P. Ordejo´ n, E. Artacho, J.M. Soler, Int. J. Quantum Chem. 65 (1997) 53.

Theoretical investigation of the feasibility of the formation of $C_{59}B$ and $C_{59}Al$ fullerenes /glycine complexes: DFT calculations

Nasim Ahmadian[a], Masoud Darvish Ganji*[,a] and Nasim Danesh[a]
[a] Department of Chemistry, Islamic Azad University, Ghaemshahr Branch, Iran
(Email: ganji_md@yahoo.com)

Keywords: $C_{59}Al/C_{59}B$ complex, Glycine, DFT, Adsorption

Introduction:

Recently much attention has been directed to fullerenes, the hollow carbon cages discovered in 1985 [1], as nanometer-scaled structures. Fullerene nanocages play a significant role in cellular uptake, protein binding, and translocation from portal of entry to the target site, etc. However, due to its small size, there are noteworthy theoretical investigations on the interaction between glycine (as a backbone of a protein) and surface of fullerene-nanocages motivating us to more comprehensive studies in sophisticated cases associated with biomolecules and fullerene nanocages [2,3]. In the present work, we have investigated the capability of $C_{59}Al$ and $C_{59}B$ fullerenes for the glycine adsorption by means of (DFT) based calculations.

Method:

All the configurations were drawn employing Hyper Chem software and all the computations were carried out using the ab initio DFT method using the standard Kohn–Sham equations and has been very efficient for large atomic systems [4].

Results and discussion:

we have considered the binding of the glycine on the exterior surface of the $C_{59}Al$ and $C_{59}B$ fullerene cages to study the adsorption behavior of glycine-$C_{59}Al/C_{59}B$ complexes. Several possible configurations were created for a glycine molecule approaching the top of Al and B atom of the cages via its three active sites. After full structural optimization of the considered systems, the obtained results reveal that the binding of glycine to the cages generates more stable complexes with binding energies (with BSSE correction) of -1.64 eV (37.89 Kcal/mol) via carbonyl oxygen (O) for gly/$C_{59}B$ and amino nitrogen (N) for gly/$C_{59}Al$, respectively, see Fig. 1(a). Furthermore, Mulliken charge analysis has been performed to evaluate the amount

of electron transfers between glycine /C_{59}Al-C_{59}B complexes. The calculated results shows 0.486 e charge transferred from glycine to the C_{59}Al complex and 0.31 e charge transferred from glycine to the C_{59}B complex. The extension of the bond lengths of adsorbed glycine onto C_{59}Al nanocage, specially the bond length of N-C (from 1.450 to 1.484) for the most stable configuration, are indications of the strong interaction of glycine with C_{59}Al cage via its active sites.

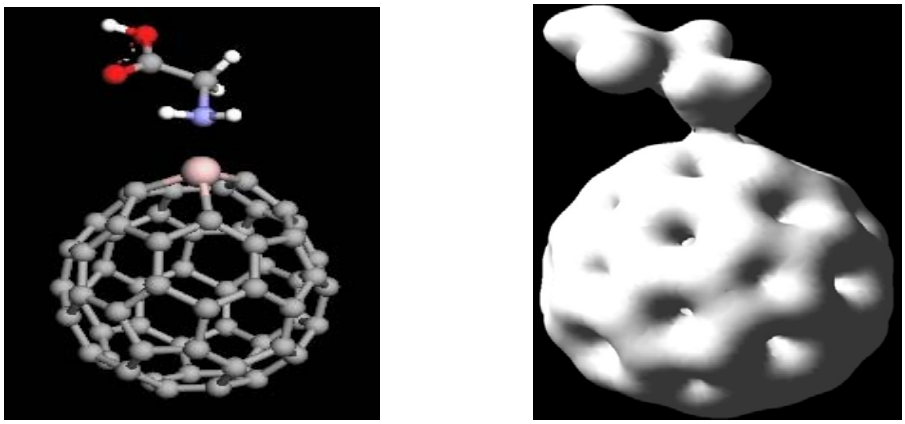

Fig. 1. (a) The most stable configuration of C_{59}Al/Gly complex via amino nitrogen (N) active site. (b) isosurface of the total electron density for C_{59}Al/Gly complex where 0.03 was used as an isovalue of total electron density, showing the binding between the C_{59}Al and the glycine molecule.

In addition, the total electron density map of the electronic densities was analyzed for the most stable configuration of C_{59}Al complex (represented Fig. 1(b)). it is clearly revealed that strong hybridization of the N and C atoms with nanocage states occurs, resulting in a significant charge

transfer in the system.

Conclusion:

The calculated results show that glycine is strongly bound to the outer surface of C_{59}AL and C_{59}B nanocages on the top site directly above the Al atom and the boron atom with a binding energy –1.64 eV. Mulliken population analysis suggests that significant hybridization between the respective orbitals of the two entities takes place and charge transfers from glycine toward theC_{59}Al and C_{59}B nanocages.

References:

[1] H.W. Kroto, J.R. Heath, S.C.O. Brien, R.F. Curl, R.E. Smalley, Nature 318 (1985) 162.

[2] D.J. Zhou, L.B. Gan, L.B. Xu, C.P. Luo, C.H. Huang, Fullerene Sci. Technol. 3 (1995) 127.

[3] M.B. Messaouda, F. Moussa, B. Tangour, H. Szwarc, M. Abderrabba, J. Mol. Struct.: Theochem. 809 (2007) 153.

[4] D. Sa´nchez-Portal, P. Ordejo´ n, E. Artacho, J.M. Soler, Int. J. Quantum Chem. 65 (1997) 53.

Hydrogen bonding patterns of 2-aminopyridinium nicotinic acetate; structural and vibrational theoretical analysis

*M.H. Akhbari shad[a], H.Hooshyar[b], B. Khezri[c]

[a,b,c] Department of Chemistry, Islamic Azad University Mahabad Branch, Islamic Azad University Mahabad, Iran

Email: muhammadakhbari@yahoo.com

Key Words: 2-Aminopyridine, nicotinic acetate, hydrogen bonding, ab initio

Introduction

para-Aminopyridine is a commonly used drug for the treatment of neurological ailments, such as multiple sclerosis, with tests showing that *para*-aminopyridine improves motor functions in multiple sclerosis patients[1]. In episodic ataxia type 2, it functions as a potassium channel blocker [2]. Nicotinic acid (vitamin B3), known as niacin, is a lipid-lowering agent widely used to treat hypertriglyceridemia by the inhibition of lipolysis in adipose tissue [3].The nicotinic acid complex 5-methylpyrazine-2-carboxylic acid 4-oxide is a commonly used drug for hypercholesterolemia [4]. The enzyme nicotinic acid mononucleotide adenylyltransferase is essential for the synthesis of nicotinamide adenine dinucleotide in all living cells and is a potential target for antibiotics [5].

Methods

Geometry optimizations were carried out with the Gaussian view 3.01, Gaussian 03. The geometries were fully optimized, without symmetry restrictions, using the 6-31G* and 6-311G** basis sets at the Hartree-Fock theory (RHF), and Becke's three-parameter exchange functional combined with the LYP correlation functional (B3LYP).

Results and Discussion

1. Geometric parameters: In this work, we performed full geometry optimization of the title compound. As follows from this comparison, the bond lengths and angles calculated for title compound show quite good agreement with experimental values.The optimized geometries with atomic labels are shown in Figure 1.

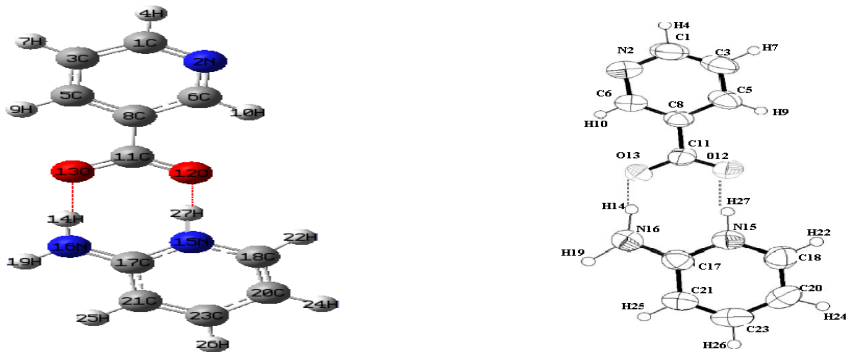

(a) (b)

Figure1. The optimized molecular structure (a) and ORTEP-3 view (b) of the title compound, with the atom numbering scheme.

The typical intramolecular hydrogen bond is observed between two carbonyl oxygen atom and amino group hydrogen atom with graph-set notation (Table 1).

Table 1. Hydrogen Bonding Geometry (A^0) calculated by HF/6-31+G*method and basis set

D–H· · ·A	complex				monomer
	D–H	H· · ·A	D· · ·A	D–H· · ·A	D–H
N16-H14…O13	1.0124	1.8634	2.8734	175.14	0.9967
N15-H27…O12	1.0307	1.7070	2.7361	175.96	

2. Vibrational Spectra: Vibrational analysis is performed by the density functional and *ab initio* correlated methods. The calculated fundamental vibrational modes and assignments of the vibrational frequencies (cm^{-1}) of the title compound were calculated on the HF and DFT methods.

3. Thermodynamic properties:

Table2. Calculated dipole moments (D),zero-point vibrational energy (kcal/mol),thermal energy(kcal/mol), thermal correction to enthalpy and Gibbs free energy(kcal/mol)

Parameter	HF/6-311g(d,p)			HF /6-31g(d)			
	a	b	c	a	b	c	*C
E_{th}	۶۵,۰۰۱ (+85.2)	۷۳,۹۰۳ (+76.3)	۱۵۰,۱۷۹	۶۵,۵۱۳ (+85.8)	۷۴,۵۳۴ (+76.8)	۱۵۱,۳۵۴	۱۴۰,۶۰
D. Mom	(۲,۸۸۶۸ (-0.02)	۱,۹۹۰۴ (+0.87)	۲,۸۵۹۹	۲,۹۱۵۶ (-0.03)	۲,۰۷۲۲ (+0.81)	۲,۸۸۲۸	۳,۴۹۱۰
Z.P.V	۶۰,۸۹۳۱ (+80.8)	۷۰,۶۲ (+71.1)	۱۴۱,۷۴۲	۶۱,۴۰۲۸ (+81.6)	۷۱,۲۶۸ (+71.7)	142.968	131.75
Hcorr	۶۵,۵۹۳ (+85.2)	۷۴,۴۹۸ (+76.3)	۱۵۰,۷۷۱	۶۶,۱۰۶ (+85.8)	۷۵,۱۲۷ (+76.8)	۱۵۱,۹۴۵	۱۴۱,۲۶۹
Gcorr	۰,۰۶۴۴۶۷ (+0.118)	0.08376 (+0.1)	۰,۱۸۲۴۹۷	۰,۰۶۵۲۲۸ (+0.12)	۰,۰۸۴۸۰۳ (+0.1)	0.18449	0.16634

*C calculated by B3LYP/6-311g (d,p) level and theory a:nicotinic acid b: 2-aminopyridine c:complex

Conclusions

Quantum mechanical ab initio calculations at the HF/6-31g(d) , 6-311g(d,p) and the DFT method at the B3LYP/6-31g(d) , 6-311g(d,p) level have been used to predict the geometries and intermolecular hydrogen bonding between the amino group of the 2-aminopyridine and the oxygen atoms of the nicotinic acetate. Both the six-member rings are planar. The cations and anions are linked together in chains along the [001] direction by N-H…O hydrogen bonds.

References

[1] Schwid, S.R.; Petrie, M.D.; Mc Dermott, M.P.; Tierney, D.S.; Mason, D.H.; Goodman, A.D. *Neurology*

1997, *48,* 817–821.

[2] Strupp, M.; Kalla, R.; Dichgans,M.; Freilinger, T.; Glasauer, S.; Brandt, T. *Neurology.* **2004**, *62,* 1623–1625.

[3] Athimoolam, S.; Rajaram, R.K. *Acta Cryst.* **2005**, *E61,* 2764–2767.

Small ligand binding to heme model compounds: A DFT and CASSCF study

Vahideh Alizadeh[a] , Mehdi D. Esrafili [*b]

[a] Department of Chemistry, Faculty of Basic Sciences, Islamic Azad University, Tabriz Branch, Tabriz, Iran

[b] Department of Chemistry, University of Maragheh, Maragheh, Iran (esrafili@maragheh.ac.ir)

Introduction

The binding and dissociation reactions of small ligands such as O_2, CO, and NO with heme group are crucial for the activity of these diatomic molecules in respiration and regulation processes. Transport and storage of dioxygen is possible in living organisms because of the reversible reaction of O_2 with hemoglobin and myoglobin, respectively [1].

The present study focuses on the quantum chemical description of heme-ligand interactions. This binding step has been extensively studied after flash photolysis of the CO, O_2, or NO ligand [2] and involves a small energy barrier, known as the recombination barrier, which varies between ligands. Moreover, for the reactions of these small ligands, with ferrous deoxy-myoglobin, the need to change the spin-state may contribute to the intrinsic additional barrier [3]. Ferrous deoxy-myoglobin has a high-spin quintet iron atom, while oxy- and carbonmonoxy-myoglobin have singlet ground states, and nitroxy-myoglobin is a doublet. This means that the so-called spin-forbidden reactions of singlet CO, doublet O_2, or triplet O_2 with the heme group require at least one spin state change.

Our calculations use three molecular systems, shown in Figure 1, to represent the heme group. The largest and most reasonable is FeP(Im), where P is a porphine ring and Im is an imidazole group. FeP(Im) has been used to investigate the reactions of CO and O_2 with deoxy-heme and to assess how well density functional theory (DFT) and complete active space self-consistence filed (CASSCF) predict heme-type geometries. The smaller models **1** and **2** are $[Fe(C_nH_{n+2}N_2)_2(NH_3)]$, where n = 1 or 3, respectively.

Computational Details

All calculations were performed by *Gaussian03* program. Geometries were optimized at DFT level by using the B3LYP method. The cc-pVDZ and cc-pVTZ basis sets were used for

Fe and other atoms, respectively. For CASSCF calculations, the active space was constructed by distributing 8 electrons in 12 orbitals: five orbitals with predominant iron 3d character, a second 3d′ shell describing the double-shell correlation effect within the 3d shell, and the bonding Fe-porphine nitrogen, σ(Fe-N_P), and anti-bonding σ*(Fe-N_P) combination. Our all CASSCF (8,12) binding energies were calculated using B3LYP geometries.

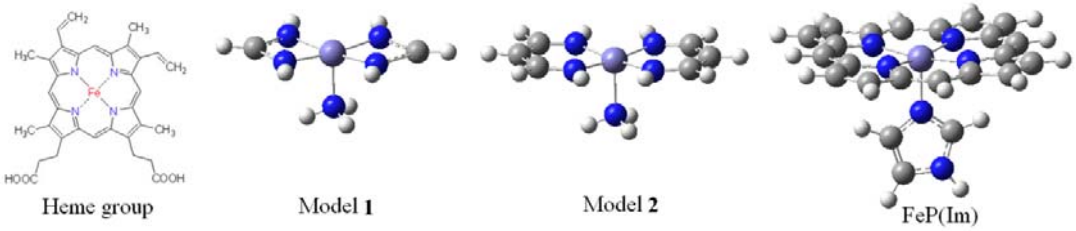

Figure 1- Molecular structure of Heme group, Model **1**, Model **2** and FeP(Im)

Results and Discussion:

Table 1 shows the relative energies of singlet, and triplet spin states of carbonmonoxy and oxy-heme models. For CO interactions, both DFT and CASSCF methods predict that high-spin state significantly more favored in model **1** and **2** than for the full porphyrin case, with the both methods predicting the singlet to lie about 17 kcal mol^{-1} below the quintet state. Binding of CO to deoxyheme is found to involve a significant barrier of ca. 3 kcal/mol, due to the need to cross from the quintet potential energy surface to the singlet state. In the case of O_2 interaction, our calculations indicate that for model **1** and **2**, the triplet spin state is the ground state and the stabilization energy follows as triplet> quintet> singlet. Since, the ground state of FeP(Im)-O_2 is known to be a singlet from electron spin resonance study [4], our calculations show a proper open shell singlet ground state for this system. The calculated -6.7 kcal/mol binding enthalpy is in good agreement with other theoretical works [5].

Table 1- DFT and CASSCF(8,12) energies (in kcal/mol) of singlet, triplet, and quintet spin states of carbonmonoxy and oxy-heme compounds

compound	^{1}Fe		^{3}Fe		^{5}Fe	
	B3LYP	CASSCF(8,12)	B3LYP	CASSCF(8,12)	B3LYP	CASSCF(8,12)
Model 1-CO	+9.1	+7.95	+19.32	+18.83	0.00	0.00
Model 2-CO	-5.01	-4.13	+2.17	+3.06	0.00	0.00
FeP(Im)-CO	-17.02	-15.44	+2.88	+2.45	0.00	0.00

Model 1-O_2	+4.55	+3.69	-12.03	-10.04	0.00	0.00
Model 2- O_2	+4.31	+3.88	-12.09	-10.09	0.00	0.00
FeP(Im)-O_2	-18.76	-16.22	-14.72	-14.53	0.00	0.00

References:

[1] Richter-Addo, G. B.; Legzdins, P.; Burstyn, J. *Chem. Rev.* 2002, 102, 857.

[2] Austin, R. H.; Beeson, K. W.; Eisenstein, L.; Frauenfelder, *Biochemistry* 1975, 14, 5355.

[3] Cornelius, P. A.; Hochstrasser, R. M.; Steele, A. W. *J. Mol. Biol.*1983, 163, 119.

[4] Momenteau, M.; Reed, C. A. *Chem. Rev.* 1994, 94, 659.

[5] Blomberg, L. M.; Blomberg, M. R. A. *J. Inorg. Biochem.* 2005, 99, 949.

Design of nanoscale molecular wire based on NO2- three phenylacetylen Effect of external electric field on electron transfer

R.Eskandar Filabi*[a], Z.Bayat[a], S. Nikooie[a.] Z. Chamani

[a]*Department of Chemistry, Islamic Azad University -Quchan Branch, Iran*

filabi63@yahoo.com

Abstract

Theoretical investigation has been performed on electron transport properties ofNO2 - Three phenyl acetylene based molecules sandwiched between two gold surfaces . The geometries and electronic structures of a thiol-terminated molecular diode interacting with metal clusters Au. The application of EF may increase the molecular conjugation and the induced dipole moment, while decrease the HOMO–LUMO gap.

Keywords: molecular wire, electric field, conjugation, gap

Introduction:

A molecular wire is an organic molecule that forms a conducting bridge between electronic contacts. A single organic molecule is likely to be the smallest entity to conduct electricity and thus molecular wires present many interesting challenges to fundamental chnological applications, such as organic. switching devices and nanoscale memories [1].

Computational details:

We have used one and three metal atoms as model systems to study the interactions between the molecule and metal atoms. The metal clusters used in this calculation are connected at either one end or both end the sulfur terminated molecule.

The calculations have been performed at the density functional theory level with the B3LYP functional. The basis set is split 6-31G*for C, H, N, O, N, S atoms and the Los Alamos National Laboratory effective core potentials with a double-zeta valence (LANL2DZ)for the gold atoms [2]. The molecule consists of three benzene rings to NO2 connected to each other by an acetylene group Fig1.

Fig1:

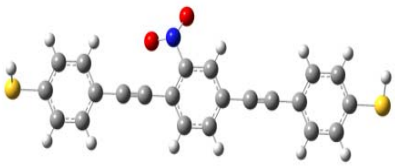

Results and discussion:

1. Electronic structure of the free molecular diode and molecular wire The optimized structure of the molecular diode has a planar geometry as the ground-state configuration. In order to further understand the interactions of the terminal sulfur atoms with the group metals we have optimized the geometries and electronic structures of theAu3SH, molecules.

Fig2:

a) b)

c) d)

The energy gaps for the free molecular diode decrease when an additional metal atom is added. This is due to the localization of the LUMO energy level on the metal atoms.

Table 1 summarizes the geometries and energeticsof these complexes. Table1:

	$Homo_{(ev)}$	$Lumo_{(ev)}$	$HLG_{(ev)}$	DS-M(A)	<C-S-M	DM-M
HSWSH	-5.587	-2.579	3.008		96	
AuSWSH	-5.507	-3.879	1.626	2.31	106	
AuSWSAu	-5.430	-3.856	1.573	2.31	106	
HSWSAu3	-5.266	-4.773	0.493	2.37	107.11	2(2.72),2.64
Au3SWSAu3	-5.117	-4.703	0.407	2.37	107.11	2(2.72),2.64

2. Effect of external field:

Fig.3 presents the Mulliken charge variation on each atom for complexes b under the ffect of the electric field. The figure clearly demonstrates the charge transfer from one to the other end of molecule. It is obvious that with the increase of EF the charge on the S26 decreases where as the charge on the sulfur of the opposite end (S25) increases.

Fig3:

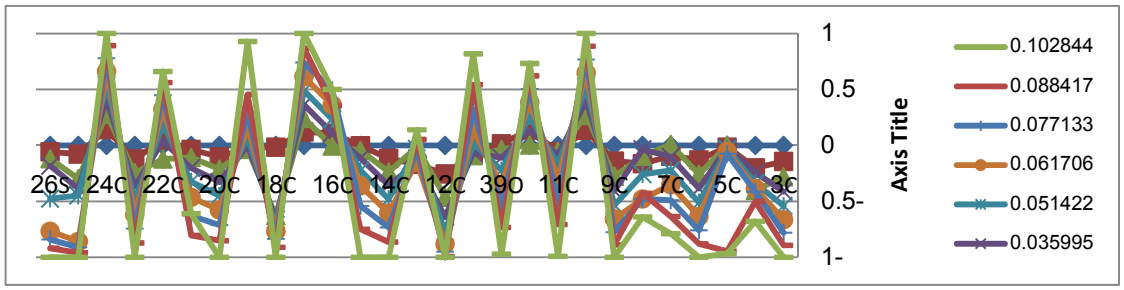

Conclusion:

Analysis of the electronic structure and molecular orbital's suggests that the inclusion of metal atoms shifts the energy levels of the free molecule upwards; however, the conduction MO's of the molecule are not significantly affected.

References:

[1] C.N. Lau, D.R. Stewart, R.S. Williams, M. Bockrath, Nano Lett. 4 (2004) 569.

[2] W.R. Wadt, P.J. Hay, J. Chem. Phys. 82 (1985) 284.

Bond critical point properties as descriptor of aromaticity

A. Ashrafi
Department of Chemistry, Shiraz University, Shiraz, Iran
(Email: abolfazlashrafi@gmail.com)

Keywords: Aromaticity indices, BCP properties, AIM, Aromatic ring

Introduction

Aromaticity is a widely used concept in physical organic chemistry. Because of the importance of aromaticity, there have been many attempts to rationalize and quantify this property. However, because of its multiple manifestations, there is not any generally accepted single quantative definition of aromaticity. According to the most definition of Schleyer and co-workers [1], aromaticity is a manifestation of electron delocalization in closed circuits, results in energy reduction. The present study is directed to show how the properties derived from the topological analysis of the electron density can be applied for description of different aromaticity indices.

Methods

The calculations carried out in this research have been done with Gaussian 98 program [2] using 6-311++G** basis set at the density functional method, with the Becke's three-parameter exchange functional with LYP correlation functional (B3LYP). The AIM2000 program [3] was used for topological analysis of electron density.

Results and Discussion

In the last work, we have derived properties from topological analysis of electron density at the ring critical point, RCP, in 43 aromatic rings. In this research, the characteristics of the electron density at the RCP and BCP are analyzed as descriptors describing the aromaticity in 41 aromatic rings. Molecules containing 1 to 4 six-membered rings have considered, some of them including heteroatom in their structures (Figure 1). We have calculated these properties and the values of HOMA, NICS (1), PDI, ATI, FLU, Δ_6^{π} and SA indices of given rings. The conclusions are consisted with previous investigations in which we founded that various

aromaticity indices correlated with BCP properties in different manner. The results obtained from the correlation between aromaticty indices and BCP properties for benzenoid aromatic hydrocarbons indicate that ATI and Δ_6^{π} show the best correlation with most of BCP properties whereas HOMA and SA indices are found to be the best correlation with most of RCP properties (Table 1). In the case where we have a set of different aromatic rings including heterocyclics, individual BCP properties may not reveal high correlation with aromaticity indices. Since the intercorrelation between BCP parameters themselves are quite good, the BCP properties can be used together in a vector serving as a descriptor for a ring. Indeed, $P=(\rho(r_c),\nabla^2\rho(r_c),\lambda_1,\lambda_2,\lambda_3,G(r_c),H(r_c),\varepsilon)$ is an eight-dimensional vector of properties evaluated at the bond critical point and the data matrix of BCP properties for 41 aromatic rings has a dimension of (41 x 8).

Conclusions

In this work, the characteristics of the electron density at the BCP are analyzed as descriptors describing the aromaticity in 41 aromatic rings. The results are similar to previous investigations in which we founded that inclusion of heterocyclic compounds in the set of aromatic rings under investigation may cause obvious discrepancy in the correlation between BCP properties and aromaticity indices. Principal component analysis has been used to compress the BCP data matrix of 41 aromatic rings into principal components and each aromaticity indices were modeled as a function of the first three PCs using multiple linear regressions.

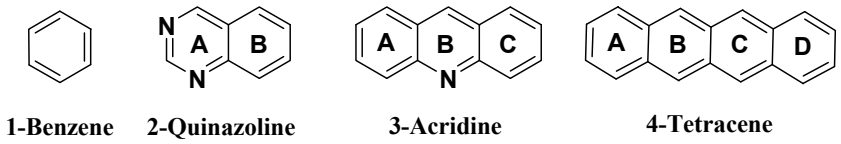

1-Benzene **2-Quinazoline** **3-Acridine** **4-Tetracene**

Figure 1. Some of studied aromatic molecules.

Table 1. Correlation between some of aromaticity indices and critical point properties for benzenoid aromatic hydrocarbons.

Index	[a] HOMA	[a]ATI	[a] Δ_6^{π}	[a] SA	[b] HOMA	[b]ATI	[b] Δ_6^{π}	[b] SA
$\rho(r_c)$	0.790	1.0	0.972	0.924	0.963	0.809	0.652	0.964

$\nabla^2\rho(r_c)$	0.637	0.972	1.0	0.812	0.954	0.826	0.675	0.976
G(r_C)	0.924	0.924	0.812	1.0	0.958	0.818	0.664	0.973
H(r_C)	0.756	0.998	0.982	0.907	0.902	0.853	0.726	0.967
λ_1	0.765	0.999	0.980	0.908	0.947	0.837	0.694	0.965
λ_2	0.629	0.965	0.996	0.795	0.799	0.847	0.757	0.912
λ_3	0.365	0.840	0.940	0.587	0.944	0.710	0.535	0.898
ε	0.930	0.874	0.745	0.982	0.234	0.061	0.152	0.050

[a] Correlation with BCP properties

[b] Correlation with RCP properties

References

[1] Schleyer, P. v. R. et al Chem. Rev. 105 (2005) 3842.

[2] Frisch, M. J. et al Gaussian 98, Revision A.7,Gaussian, Inc., Pittsburgh PA, 1998.

[3] Bader, R. F. W. AIM2000 Program, ver 2.0, Hamilton; McMaster University, (2000).

A Computational Study for the Decontamination of Reaction of DMMP by ZnO Nano-particles

Amir Aminifar[1] *,F. R. Nikmaram [2], Seyed Morteza Ashrafi shahri [1]

1: Iran, Tehran, Imam Hossein Comprehensive University, Department of Chemistry
2: Iran, Tehran, Islamic Azad University Rey, Department of Chemistry
**aaminifar@hotmail.com*

Key words: DMMP (dimethyl methyl phosphonat), Nano-computing, Removal of contamination, Reactions absorb energy Gibbs

Introduction:

Nerve agent are compounds used to disable and kill human being , less effective one are usually used as pesticides. Employing the first time these compounds goes back to the First World War. Today's these materials are usually used by terrorist groups and so on [1]. Knowledge eliminate nerve agent pollution can improve health of human society, because of hazardous and different mechanism of these materials, researchers prefer to use computational methods to investigate their decontamination reaction [2]. In this project we test the Quantum computational methods and compare the results with experimental one . In this paper we focus on absorbing DMMP on ZnO. The zinc oxide has a very high melting point and the surface of zinc oxide is a Lewis acid and Lewis base, these properties caused the absorption properties in a wide variety range of phosphonyl components[3].

Models , methods and computational calculation:

All calculations were done using the *Gaussian 98* programs . Both MP2 and B3LYP method and 6-31 G *, 6-31 G basis sets levels were used in our calculation. The rotational constant , IR spectrum , angles and length of the molecules' compared with Anderson values were reported [4]. In basis of all factors we use B3LYP/6-31G * theoretical level for calculations .

Results and Discussion:

DMMP easily adsorb in both ZnO and Zn_3O_3 species , the results were indicated that this compound absorb DMMP through oxygen atom (in phosphonyl group) that connected in Zn atoms ,IR data and chemical shifts of $89cm^{-1}$ to lower frequency and remaining constant

other frequencies may confirmed this idea. The absorption energy of DMMP on ZnO and Zn_3O_3 in B3LYP/6-31G * level were equal to -43.53 K cal/mol and – 46.45 K cal/mol , this result may indicated the effect of ZnO size had a low effect on absorption reaction (approximately 6 percent). Also, the change of Gibbs free energy in calculation &experimental method are 5.6 Kcal/mol, the difference between the experimental and computational ($\Delta G_{experimental}$ =3 Kcal/mol) [5] maybe depended to environmental parameter.
Also in this study, the role of temperature in reaction determined by IR spectrum. Varying the peak position and peak intensity shows that raising the temperature from 298 to 350 K is caused DMMP to hydrolysed. This subject comfirmed with experimental data. [5,6]

1-1): Optimized image DMMP at B3LYP/6-31G (a) the temperature of 298 K

b: DMMP image at 350 K

Conclusions :

we may concluded theoretical and experimental , the change of Gibbs free energy had less deviation . Size of nano zinc oxide had less effected for decontaminating DMMP .The most suitable theoretical level for decontaminating reaction studies is B3LYP/6-31G * .Rapture of DMMP molecules is occurred at 350K.

References:

[1] S. M. Kanan, C. P. Tripp; Langmuir; 2002, 18, 722-728.
[2] V. M .Bermudez; J. Phys. Chem. C; 2007, 111, 9314-9323.
[3] D. P. Norton, M. Inoue, M. Yano; Appl. Phys. Lett.; 2005,86, 105-203.
[4] M. P. Andersson, P. Uvdal; J. Phys. Chem. A; 2005, 109, 2937.
[5] A. Aminifar and M. Ezzati;MA thesis , Imam Hossein University, Department of Chemistry ; 2010.
[6] V. M. Bermudez; J. Phys. Chem. C; 2007, 111, 3719-3728.

Fisher Information and the Stability of Complexes

M. Solimannejad[a], S. Noorizadeh[*b] and M. Aarabi[b]

[a]Chem. Dept., College of Sciences, Arak Univ. Arak, Iran

[b]Chemistry Dept., College of Sciences, Shahid Chamran Univ., Ahwaz, Iran, (noorizadeh_s@scu.ac.ir)

Keywords: Information Theory, Fisher Information, Information Content, Binding Energy.

Introduction

One of the cornerstones of the Quantum Information Theory is the Fisher information [1], which measures the information-theoretic content of the density of a system. For the spreading of total electron density ρ(r) of an atomic or molecular system with a total number of N electrons, the Fisher information of ρ(r) is given by:

$$F(r) = \int \frac{|\nabla\rho(r)|^2}{\rho(r)} dr = -\int \nabla^2\sigma(r)\mathrm{Ln}\,\sigma(r)\, dr \qquad (1)$$

It is known that F is local measure of smoothness (disorder) of the electron localization.

Many attempts have been made to use this information measure in chemical systems [2-4]. In this contribution the connection between Fisher Information density and the stability of some complexes is investigated.

Result and Discussion

The Fisher information content of a complex can be constructed in two ways; which are as:

$$F_1 = \sum_{i=1} \nabla^2\rho_{ci} Ln\, \rho_{ci} \qquad (2)$$

$$F_2 = (\sum_{i=1} \nabla^2\rho_{ci})\ Ln\ (\sum_{i=1} \rho_{ci}) \qquad (3)$$

where ρ_{ci} and $\nabla^2\rho_{ci}$ are the electron density and the Laplacian of electron density of the ith bond critical point between two monomers, respectively. Four complexes with different local minima (s) are considered in this study; which are included Isocyanic dimer (s=13), glyoxal dimer (s=8), nitrosyl hydride with ozone (s=4) and Hydroperoxyl radical with dihydrogen trioxide (s=6). The topological parameters are gathered from previous work [5].The evaluated two Fisher contents for different local minima of the Hydroperoxyl radical with dihydrogen trioxide complex is given in Table 1 as an example. It is found that in all cases the evaluated Fisher contents from approach 1 (F_1) show a better correlation with the calculated binding

energies of the complexes. The correlation coefficients of F_1 with the binding energies for different complexes are collected in Table 2. In some cases one of the calculated binding energies from MP_2 is overestimated (for example S_6 in Table 2). By removing this point from correlation graph, the regression coefficient will have been improved. The improved regressions are also given in parenthesis (see Table 2). Therefore it seems that the evaluated Fisher contents are a better descriptor for the predicting the stability of different minima of a molecule than the obtained binding energies from MP_2 methods.

Table 1. Evaluated Fisher contents (F_1 and F_2) and calculated binding energies for different local minima of the Hydroperoxyl radical with dihydrogen trioxide complex.

Molecule	F_1	F_2	E_{MP2}	$E_{MP2+BSSE}$	E_{M05-2x}
S_1	0.691817	0.552140	-46.07	-26.43	-45.91
S_2	0.646763	0.522075	-40.14	-21.09	-40.48
S_3	0.618174	0.504505	-32.23	-17.59	-35.09
S_4	0.598541	0.489579	-30.31	-15.63	-32.04
S_5	0.468485	0.392734	-26.28	-12.35	-27.05
S_6	0.320932	0.320932	-25.35	-12.37	-

Table 2. Regression coefficients of the evaluated F_1 with different binding energies of the considered complexes. The obtained regressions by excluding the off points are given in parenthesis.

	Isosyanic Acid	HOO-HOOOH	Nytrosyl Hydride	Glyoxal
E_{MP2}	0.746 (0.951)	0.702 (0.983)	0.863 (0.969)	0.974 (0.981)
$E_{MP2+BSSE}$	0.645 (0.822)	0.686 (0.999)	0.003 (0.992)	0.938 (0.951)
E_{M05-2x}	-	0.862 (0.989)	0.998 (0.998)	0.953 (0.966)

Conclusion

The calculated Fisher information content, from topological parameters of bond critical points of a complex, has some relation with the binding energy of the complex. It is claimed that these contents can be used for predicting the global minima of a system among different local minima.

References

[1] R.A. Fisher Proc. Cambridge. Philol., Soc. **22**, 700 (1925).

[2] A. Nagy, E. Romera Chem. Phys. Lett. **490**, 242 (2010).

[3] A. Grassi, Int. J. Quantum Chem. **108**, 774 (2010).

[4] A. Nagy, S. Liu Phys. Lett. **A 372**, 1654 (2008).

[5] M. Solimannejad, S. Massahi, S. Scheiner J. Mol. Struct. (Theochem) **913**, 50 (2009).

Calculation of pK_b for some biologically important molecules

M. Afsharizadeh*[a], M. Namazian[a], M. R. Noorbala[a], A. Benvidi[a]

[a]Department of Chemistry, Yazd University, Yazd, Iran

Keywords: G3MP2, pK_b, CPCM, Solvation energies, Biological activities

Introduction

[1,2,4]triazolo[1,5-a]pyrimidine-7-amines are anti-cancer drugs and have been used against human liver cancer [1]. Their biological activities are reported as IC50. The increase of their activities for the substitutes (R^1) of Cl, F, OCF_3 and CF_3 suggested that their acid-base properties might be a factor. In this work, we have investigated the acid-base properties of some structurally similar compounds by calculation of pK_b.

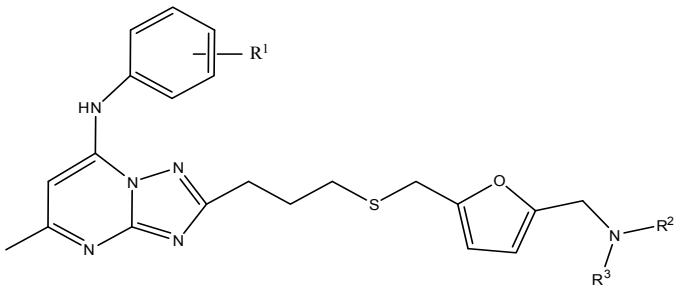

[1,2,4]triazolo[1,5-a]pyrimidine-7-amine

Computational Methods

Gas-phase Gibbs free energies of the studied molecules have been calculated using G3MP2 method which approximates QCISD(T) energies with a large triple zeta basis, in conjunction with MP2 level of theory [2]. The G3MP2 method employs the geometries which are optimized at MP2 (full)/6-31G (d) level of theory. To calculate solvation energies, a popular continuum model of solvation, the conductor-like polarizable continuum model (CPCM) have been used at HF/6-311+G (d,p) level of theory [3]. The radii of the united atom topological model, optimized for the Hartree-Fock method (UAHF) have been chosen for solvation energies and the rest of parameters of the models have been kept as default values [3]. All geometries of the studied species have been optimized fully in the presence of solvent.

Scheme 1 shows a thermodynamic cycle used to calculate the pK_b values. In this cycle, A and NH_3 indicates the studied molecule and reference molecule, respectively.

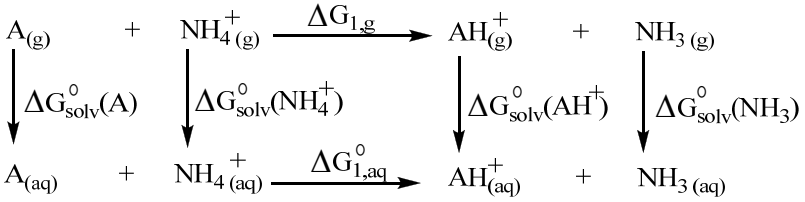

Scheme 1. The thermodynamic cycle used for calculation of pK_b.

We have calculated pK_b based on the Equation 1 [4]:

$$pK_b(A) = [\Delta G°_{1,eq}/(2.303\ RT)] + pK_b\ (NH_3) \qquad (1)$$

Results and conclusion

The theoretical values of pK_b for some simple similar molecules, have been found in good agreement with the experimental values as shown by Fig. 1. The comparison of theoretical and experimental values shows that the mean absolute deviations (MAD) are less than 0.5 pK_b unit.

Using the same methodology, we have calculated pK_b for the structurally similar compounds of studied drugs. These results show that the acid-base properties are in agreement with the available biological activities of the studied compounds.

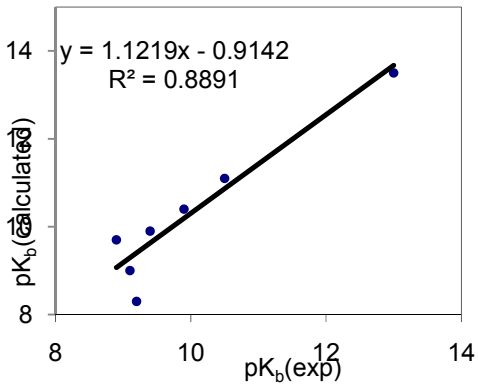

Fig. 1. Comparison of calculated pK_b with the experimental values.

References:

[1] Zhang, N.; Ayral-Kaloustian, S.; Nguyen, T.; Afragola, J.; Hernandez, R.; Lucas, J.; Gibbons. J.; Beyer, C. *J. Med. Chem.* **2007**, *50*, 319.

[2] Curtiss, L.A.; Redfern, P.C.; Raghavachari, K.; Rassolov, V. *J. Chem. Phys*. **1999**, *110*, 4703.

[3] Namazian, M.; Zakery, M.; Noorbala, M. R.; Coote, M. L. *Chem. Phys. Lett.* **2008***, 451,* 163.

[4] Ho, J.; Coote, M. L.; *J. Theor. Chem. Acc*. **2010**, *125* , 3.

A segmented principal component analysis–regression approach to quantitative structure–activity relationship modeling

Maryam Elyasi[a,*] , Bahram Hemmateenejad,[a,b] ,Ramin Miri,[a]

[a] Medicinal & Natural Products Chemistry Research Center, Shiraz University of Medical Sciences, Shiraz, Iran

[b] Department of Chemistry, Shiraz University, Shiraz, Iran

Keywords: Quantitative structure-activity relationship; Principal component regression; Segmented

Introduction:

The major problem associated with application of principal component regression (PCR) in QSAR studies is that this model extracts the eignvectors solely from the matrix of deccriptors, which might not have essentially good relationship with the biological activity.

Method:

This article describes a novel segmentation approach to PCR (SPCAR), in which the descriptors are firstly segmented to different blocks and then principal component analysis (PCA) is applied on each segment to extract significant principal components (PCs). In this way, the PCs having useful and redundant information are separated. Descriptor segmentation is achieved utilizing different unsupervised pattern recognition methods such as PCA, Kohonen networks and SIMCA. The number of segments should be optimized to give the best performances. A linear regression analysis based on stepwise selection of variables is then employed to connect a relationship between the informative extracted PCs and biological activity. The loading of these extracted PCs are then used to identify those descriptors represent the highest impact on the activity/property under study. The proposed method was applied to model different data sets including gas chromatography Kovats retention index of terpenoids, calcium channel antagonist activity of dihydropyridine derivatives and kinetic of the O-methylation of phenols.

Results and disussion:

A comparison between the conventional PCR algorithm and SPCAR shows that the cross-validation and prediction correlation coefficients for SPCAR and PCR are 0.822 and 0.766; 0.523 and 0.563 respectively .

Conclusion:

The models obtained by SPCAR method for all studied data set represented best performances with respect to conventional PCR. In addition, in almost all cases, SPCAR could discover models of higher prediction ability with respect to the previously reported

Refrences:

[1] J. Polanski, A. Bak, R. Gieleciak, T. Magdziarz, J. Chem. Inf. Model. 46 (2006) 2310–2318.

[2] M.P. Freitas, Curr. Comput.-Aided Drug Des. 3 (2007) 235–239.

[3] M.M.C. Ferreira, J. Braz, Chem. Soc. 13 (2002) 742–753.

[4] B. Hemmateenejad, J. Chemometr. 18 (2004) 475–485.

[5] C.W. Yap, H. Li, Z.L. Ji, Y.Z. Chen, Mini-Rev. Med. Chem. 7 (2007) 1097–1107.

Application of CDFS strategy and genetic algorithm-partial least square to quantitative structure-retention relationship study of analgesic drugs

Maryam Elyasi[a,*] ,Bahram Hemmateenejad,[a,b] ,Katayoun Javidnia,[a] Ramin Miri,[a]

[a] Medicinal & Natural Products Chemistry Research Center, Shiraz University of Medical Sciences, Shiraz, Iran

[b] Department of Chemistry, Shiraz University, Shiraz, Iran

Keywords: Combined data splitting-feature selection; Analgesic; Genetic algorithm; Partial least squares

Introduction:

An analgesic is any medicine intended to relieve pain. Aspirin, acetaminophen, ibuprofen, and naproxen sodium are examples of these drugs. These drugs present no danger for most people when taken in the recommended dosage. But some conditions make taking even these common painkillers dangerous for the kidneys. In this aspect, QSRR can be employed to find the retention behavior of the analgesic drugs and to find a suitable model for predicting the retention index of new or even non-synthesized analgesics. This simplifies the development of chromatographic methods for analysis of new compounds.

Method:

In the CDFS methodology, the data are first split into calibration and validation many times (here, 20 times). Each validation subset is composed of 20% of total data, which are randomly selected. In each splitting, the rest of the data are considered as calibration subset.

The combined data splitting feature selection (CDFS) is a new strategy in quantitative structure-property relation (QSPR) analysis, in which the sampling of training set from data set is performed repeatedly to find a subset of molecular descriptors producing a stable QSPR model insensitive to the presence or absence of one or more compounds. Here, we used genetic algorithm-partial least square (GA-PLS) as modeling method in CDFS methodology and applied it to QSPR study of the reversed-phase high performance chromatographic retention of the analgesic drugs.

Result and Discussion:

A set of 58 analgesic drugs with known Kovats retention index were selected and a large number of theoretical descriptors was calculated for each molecule. The random sampling of the training set (80% of data) was performed iteratively 20 times and the reminder molecules were used as validation set. Each time, the most appropriate QSPR model was produced by GA-PLS. The selected descriptors of each run were then analyzed for similarity and frequency distribution. The final QSPR model, which was created using the common descriptors between 50% of runs, has squared correlation coefficient of 0.924, 0.865 and 0.903 for training, validation and cross-validation, respectively. In addition, it is able to reproduce 85% of variances in the retention factor of external test set compounds.

Conclusion:

In comparison with conventional stepwise selection method, CDFS resulted in simpler models with higher prediction ability.

Refrences:

[1] P. Gramatica, QSAR Comb. Sci. 2007, 26, 694-701.
[2] P.X. Liu, W. Long, Int. J. Mol. Sci. 2009, 10, 1978-1998.
[3] B. Hemmateenejad, M. Yazdani, Anal. Chim. Acta, 2009, 634, 27-35.
[4] B. Hemmateenejad, K. Javidnia, M. Nematollahi, M. Elyasi, J. Iran. Chem. Soc., 2009, 6, 420-435.
[5] B. Hemmateenejad, K. Javidnia, M. Elyasi, Anal. Chim. Acta 2007, 592, 72–81.
[6] M. Jalali-Heravi, Z. Garkani-Nejad, A. Kyani, QSAR Comb. Sci. 2008, 27, 137-146.

Quantitative structure–retention relationship for the Kovats retention indices of a large set of Cardioactive drugs

Maryam Elyasi[a] ,Bahram Hemmateenejad,[a,b] ,Ramin Miri,[a] ,Maryam Parish,[a]

[a] Medicinal & Natural Products Chemistry Research Center, Shiraz University of Medical Sciences, Shiraz, Iran

[b] Department of Chemistry, Shiraz University, Shiraz, Iran

Keywords: QSAR, cardioactive, dendogram, y-ranking ,random

Introduction:

Quantitative structure–activity relationship (QSAR) research field has been widely developed because of its powerful ability to predict drug activity. Quantitative structure-retention relationship (QSRR) is a variant of QSPR, in which the effect of solute structure on the retention behavior in different chromatographic methods (e.g., thin layer chromatography, gas chromatography, liquid chromatography, electrophoresis and so on).QSRR studies have been widely used for modeling of drugs' retentions in different chromatographic methods. In this aspect, QSRR can be employed to find the retention behavior of the cardioactive drugs and to find a suitable model for predicting the retention index of new or even non-synthesized cardioactives. This simplifies the development of chromatographic methods for analysis of new compounds.

Methods:

In this article, a QSRR study was conducted on Kovats retention index of 43 cardioactive drugs employing the three different methods, including random, y-ranking and dendogram for ten different sets of descriptors, including chemical, topological, quantum chemical and constitutionals. In this work, a total of 159 descriptors were calculated. Firstly, the *y*-ranking method was used. The molecules were ranked based on retention index, then calibration and prediction set based on y-ranking was buliding, on the other hand we used dendrogram method for build calibration and prediction sets too. Also we product the calibration and prediction sets randomly.

Result and discussion:

For different methods we applied on our data set we deduced different models then we comparison their results with each other .In all models we can find the partner descriptors. In this article the common descriptors are J3D and nSK, which they are among the geometrical and constitutional descriptors respectively.

Conclusion:

We consider that for building a good model that have high ability to predict the best results, the type of building calibration and prediction sets are not important but the multiplicity of our work is important.

References:

[1] C. Hansch, D. Hoekman, H. Gao, Comparative QSAR: toward a deeper understanding of chemicobiological interactions, Chem. Rev. 96 (1996) 1045–1076.

[2] C. Hansch, A. Leo, Exploring QSAR: Fundamentals and Applications in Chemistry and Biology, ACS Publishers, Washington, DC, 1995.

[3] R. Todeschini, V. Consonni, Handbook of Molecular Descriptors, Wiley-VCH, Weinheim, 2000.

[4] M. Jalali-Heravi, Z. Garkani-Nejad, A. Kyani, QSAR Comb. Sci. 2008, 27, 137-146.

[5] J. Ghasemil, S. Saaidpour, J. Chromatogr. Sci. 2009, 47, 156-163.

Theoretical Study of Spin-Spin Coupling Constants in Hydrogen-Bonded Uracil-Nitrosamine Complexes

Hossein Roohi [a], Elham Anjomshoa[b]

[a]Department of Chemistry, Faculty of Science, University of Guilan, P.O. Box 41335-1914 , Rasht, Iran

[a]Department of Chemistry, Faculty of Science, University of Sistan & Baluchestan, Zahedan, Iran

Keywords: Spin–Spin**,** NMR**,** Uracil**,** Nitrosamine.

Introduction

The NMR criterions are more valuable than the structural ones, since they are applicable not only to crystals but to neat liquids and solutions as well. Conventionally, magnetic shielding constants (or chemical shifts) and especially spin–spin coupling constants ^{1}J have been used for the purpose [1]. In recent years, a new set of parameters –the intermolecular indirect nuclear spin–spin coupling constants – have been measured, providing a unique direct experimental evidence for hydrogen-bond formation and broadening the spectrum of properties characterizing such interactions [2,3,4]. In the present paper, we have investigated the intermolecular dihydrogen bonds formed from interaction between **NA** and **U**. The correlations between the NMR spectroscopic properties and binding energy, H-bond distance, electron density topography have been investigated.

Computational details

The geometry optimizations were performed using MP2, B3LYP and B3PW91 methods in conjunction with 6-311++G(2d,2p) basis set. Vibrational frequencies calculated using the B3LYP and B3PW91 methods were used to characterize stationary points as minima and to evaluate zero-point vibrational energies (ZPVE). Spin-spin coupling constants involving ^{13}C, ^{15}N, ^{17}O, and ^{1}H in all monomers and complexes were computed at B3LYP/6-311++G(2d,2p) level on the structures optimized at MP2/6-311++G(2d,2p) level of theory.

Results and discussions

One-Bond Spin-Spin Coupling Constants. Relationship between electronic BE and sum of $^{1h}J(H_{NA}\cdots Y)$ and $^{1h}J(H_{U}\cdots Y)$ SSCCs in **U-NA** complexes is depicted in Fig. 1a. **UN1** with greater BE has greater $^{1h}J(H_{NA}\cdots Y)$ + $^{1h}J(H_{U}\cdots Y)$. The linear correlation between sum of $^{1h}J(H_{NA}\cdots Y)$ and $^{1h}J(H_{U}\cdots Y)$ SSCCs and sum of electron densities at corresponding hydrogen-

bond critical points, HBCPs, are depicted in Fig. 1b with correlation coefficient of 0.980 and 0.991 for eight- and seven-membered ring complexes, respectively.

Two-Bond Spin-Spin Coupling Constants. The MP2/6-311++G(2d,2p) binding energies (BEs) of complexes in each series correlate with sum of $^{2h}J_{O\cdots N}$ and $^{2h}J_{N(C)\cdots N(O)}$ SSCCs. This relationship is displayed in Fig. 1c. The red-shifts of N(C)–H stretching frequencies (Δν) calculated at B3LYP/6-311++G(2d,2p) level are well correlated with the $^{2h}J_{N(C)\cdots N(O)}$ SSCCs upon H-bond formation in **U–NA** complexes (Fig. 2a). The correlation between sum of $^{2h}J_{O\cdots N}$ and $^{2h}J_{N(C)\cdots N(O)}$ SSCCs and corresponding H-bond distances are presented in Fig. 2b. As can be seen, increase in SSCCs in both types of complexes is connected with decrease in H-bond distances. ^{2h}J values correlate well with the electron densities ρ(r) at the HB critical points (HBCP). The relationship between sum $^{2h}J_{N(C)\cdots N(O)}$ and $^{2h}J_{O\cdots N}$ SSCCs and sum of electron density at $H_U\cdots N(O)_{NA}$ and $H_{NA}\cdots O_U$ HBCPs are depicted in Fig. 2c.

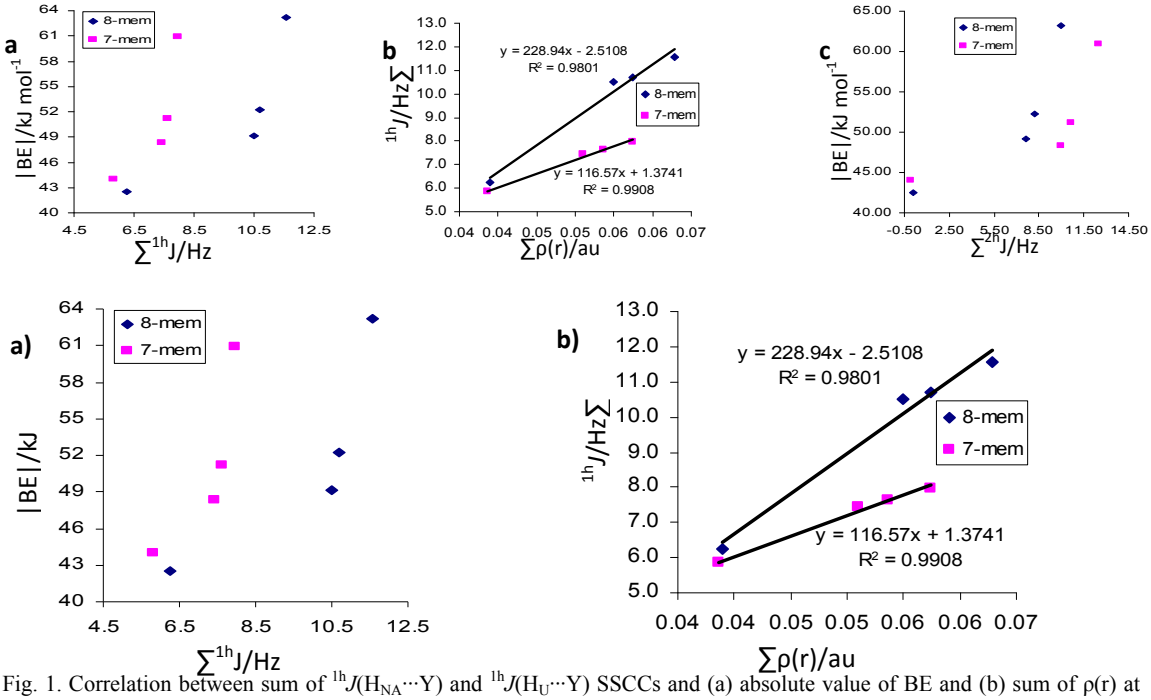

Fig. 1. Correlation between sum of $^{1h}J(H_{NA}\cdots Y)$ and $^{1h}J(H_U\cdots Y)$ SSCCs and (a) absolute value of BE and (b) sum of ρ(r) at the corresponding HBCPs in eight- and seven-membered ring complexes (c) Correlation between absolute BE and sum of $^{2h}J_{O\cdots N}$ and $^{2h}J_{N(C)\cdots N(O)}$ SSCCs in eight- and seven-membered ring complexes.

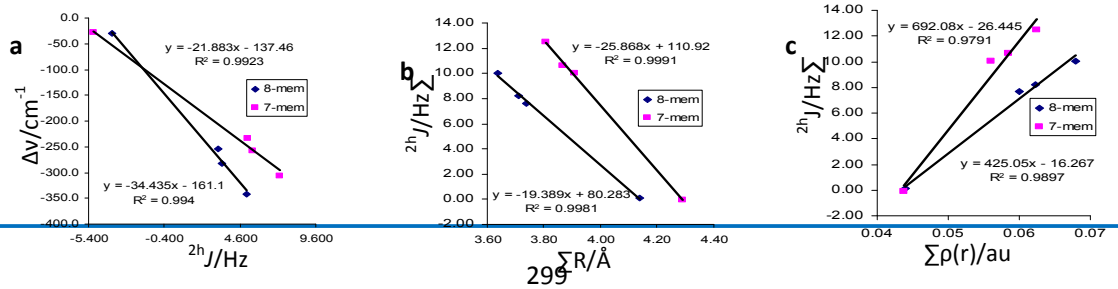

Fig. 2. (a) Red-shift of N–H_U stretching frequency ($\Delta\nu/cm^{-1}$) versus the $^{2h}J_{N(C)\cdots N(O)}$ SSCC Correlation between sum of $^{2h}J_{O\cdots N}$ and $^{2h}J_{N(C)\cdots N(O)}$ SSCCs and (b) sum of corresponding H-bond distances (R) and (c) sum of ρ(r) at the corresponding HBCPs in eight- and seven-membered ring complexes.

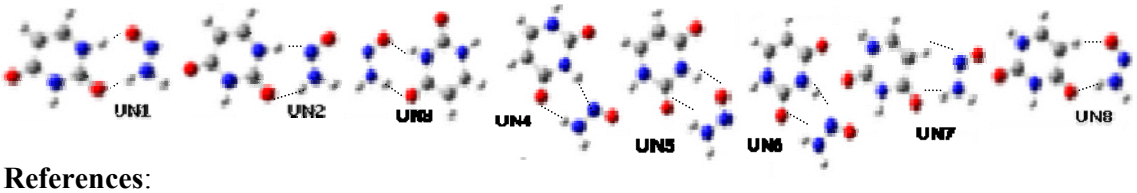

References:

[1] N. Juranic, S. Macura, J. Am. Chem. Soc. 123 (2001) 4099. (b) V. Sychrovsky, J. Vacek, P. Hobza, L. Zidek, V. Sklenar, D. Cremer, J. Phys. Chem. B 106 (2002) 10242.

[2] F. Cordier, S. Grzesiek, J. Am. Chem. Soc. 121 (1999) 1601.

[3] A.J. Dingley, S. Grzesiek, J. Am. Chem. Soc. 120 (1998) 8293.

[4] A.J. Dingley, F. Cordier, S. Grzesiek, Concept. Magn. Reson. 13 (2001) 103.

Ab initio study of the intramolecular proton transfer in guanidines

A. Enami[1] and Sabzyan[2*]

[1]Department of Chemistry, Khuzestan Science & Research Branch, Islamic Azad University, Ahwaz, I. R. Iran.

[2]Department of Chemistry, University of Isfahan, Isfahan 81746-73441, I. R. Iran.

Email: sabzyan@sci.ui.ac.ir

Abstract

Structure and bonding properties and proton transfer phenomenon in guanidine and its methyl-, fluoro- and trifluoromethyl- derivatives in the neutral, protonated (cation, +) and deprotonated (anion, –) states are studied computationally using B3LYP/6-311++G** method. First, geometries of these compounds are optimized and their electronic and bonding characteristics are calculated and studied. Then, energy surface and transition state (TS) structures over the corresponding intramolecular proton transfer path (between the amine and imine nitrogen atoms) are calculated and analyzed. Intrinsic reaction coordinate (IRC) diagrams obtained in this study all showing smooth paths between the stationary points of the reactants and products and the TS point.

Keywords: Guanidine, Proton Transfer, IRC, Transition State, B3LYP/6-311++G**

Introduction

Guanidine (**G**) with molecular formula $(NH_2)_2CNH$ is a strong base with a *p*Ka=12.5 which is solid in the room temperature with a melting point of 50 °C. In this molecule, there are one imino- and two amino- nitrogen atoms bonded to the only carbon atom. From acid-base point of view these two types of nitrogen atoms in **G** behave differently. Derivatives of **G** have the general formula of $(R^1R^2N)(R^3R^4N)CNR^5$ are obtained by substituting its protons with various functional groups R^1 to R^5. **G** and its derivatives are important materials in biochemistry due to their unique structures determined mainly by their interesting intramolecular proton transfer schemes, Fig. 1 (left), which is defined and controlled by substitutions. In this work, substitution (methyl-, fluoro- and trifluoromethyl-) effects on the properties of **G** and its protonation and deprotonation energies and proton transfer are studied using B3LYP/6-311++G** method.

Computational Method

First, Geometry optimization, vibrational and thermochemical analyses are carried out on the two imino- and amino- isomers of methylguanidine, fluoroguanidine, trifluoroguanidine in their netural, protonated and deprotonated states. Next, the TS structures of the intramolecular proton transfer motion are found based on QST2 approach and their corresponding intrinsic reaction coordinates (IRC) are calculated for a limited number of structural points with diagonal Hessian. The transfer path are characterized based on the NBO and Löwdin population (atomic and bond electron densities) analysis. A typical IRC curve obtained for the proton transfer in methylguanidine is shown in Fig. 1 (right).

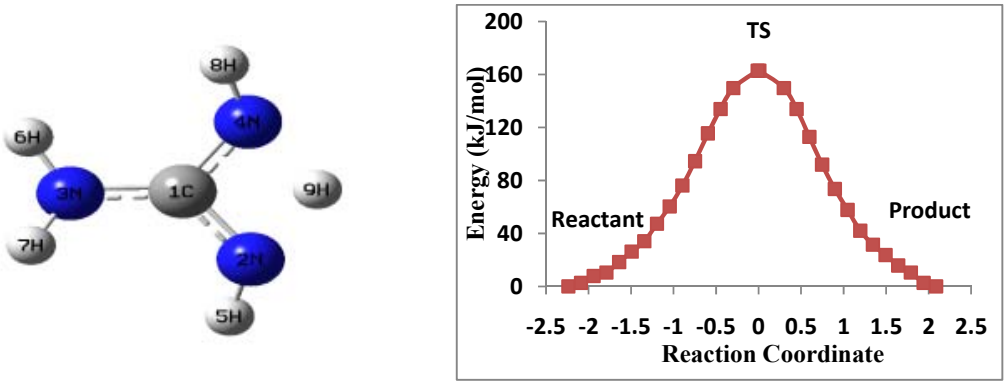

Fig. 1: Molecular structure of guanidine and its proton transfer scheme (left), and an example of the potential energy curve of the proton transfer along the IRC in methylguanidine in its neutral state.

Results and Discussion

Analyses of the energy barrier and the charge densities of the bonds over the proton transfer path (IRC) in the guanidine molecule and its derivatives in the neutral, protonated N3a-H^+ and N2i-H^+ (proton on the amine-N and imine-N atoms) and deprotonated N3a$^-$ states shows that in the neutral state, the N3a-CF_3 and N3a-F substitutions result in an increase in TS energy and the charge density of the N4a-H9 bond (H9 is the transferring proton). In the TS of the N3a-H^+ protonated **G** and its derivatives, the transferring proton has the largest positive charge. For example, in the N3a-H^+ protonated state, the N3a-F and N3a-CH_3 guanidines have the highest energy barrier, and the N3a-CH_3 substituted guanidine has the largest charge density of the N4a-H9 bond in the TS. In the N2i-H^+ protonated state, the proton transfer energy barriers for methylguanidine cation and trifluromethyleguanidine are

higher. In this protonated state, charge density of the N4a-H9 bond in the TS of the N3a-CF_3 and N3a-CH_3 guanidines is larger. In the deprotonated state ($N3a^-$), the proton transfer energy barrier and the charge density of the N4a-H8 bond in the N3a-CH_3, N3a-F and N3a-CF_3 ubstituted guanidine ions is larger than that of the unsubstituted guanidine ion.

Conclusion

In the neutral and deprotonated states, the N3a-CF_3 substituted guanidine, and in the N3a-H^+ protonated state, the N3a-F substituted guanidine has the highest proton transfer barrier (TS) energy and the largest charge density for the N4-H8/9 bond.

References

[1] I. Fernández et al., J. Phys. Org. Chem., 21 (2008) 713-717.

[2] E.D. Raczynska et al., J. Phys. Org. Chem., 16 (2003) 91-106.

[3] B. Amekraz et al. New J. of Appl. Chem., 20 (1996) 1011-1021.

Thermochemistry and Structure of Guanosine Analoge 2- Amino-6 Mercapto-7-Methylpurine Ribonucleoside (MESG) Phosphorolysis Reaction Substitution Mechanism

Afsaneh Amiri*, Mohadese Ohadi*, Parastoo Jamshidi
Department of Chemistry, Islamic Azad University, Central Tehran Branch, Tehran, Iran.
Email: afsaamiri@gmail.com
Department of Chemistry, Islamic Azad University, Central Tehran Branch, Tehran, Iran.

Keywords:2-Amino-6-mercapto-7-methylpurine Ribonucleoside, MESG, PNP enzyme, Ab-initio

Introduction

2-Amino-6-mercapto-7-methylpurine ribonucleoside (MESG) scheme (1) is a very important substrate for the continuous spectrophotometric assay of inorganic phosphate and for measuring phosphate release kinetics in biological systems.[1] In addition, MESG has been employed in the discovery of purine nucleoside phosphorylase (PNP) enzyme inhibitors.[2] It has been established that this molecule is an important substrate for PNP. PNP plays a role in clinical medicine,[3] especially because this enzyme is associated with profound immunodeficiency in T-cell function.[4,5] Human PNP is therefore a target for the development of drugs to treat immunological disorders, such as rheumatoid arthritis, psoriasis, inflammatory bowel disorders and multiple sclerosis, and T-cell proliferative disorders. The enzymatic promoted phosphorolysis reaction of (MESG) catalyzed by PNP may proceed through a transition state blueprint (Scheme 1). It is possible to initiate a discussion whether the mechanism may proceed through an SN1 or SN2 mechanism for PNP substrates. [6] A total inversion of the chiral centre in the ribose-1-phosphate product indicates an SN2 mechanism; however, many studies conducted by Schramm's group indicate an SN1 mechanism

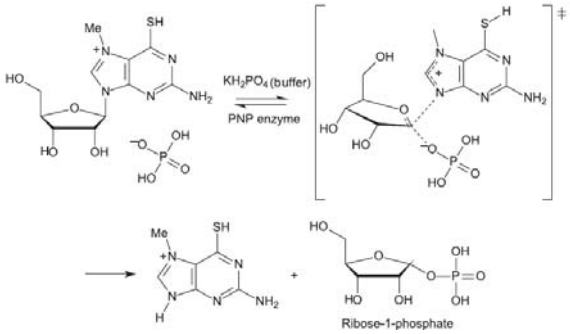

Scheme1. Proposed transition state blueprint for the phosphorolysis reaction of MESG

Computational Method

The method and basis set were chosen on the basis of the size and the number of orbitals in the molecule. The binding energy gradient was estimated to be 0.05 kcal using the conjugate gradient optimization method (Polad-Ribiere algorithm). In order to reach the Global Minimum, some structural parameters of the initially optimized molecules were changed manually and the molecular structures were re-optimized. This procedure was repeated until the most stable structure was obtained. HF/6-311G (d, p) optimizations of ingredients was done by Gaussian 98. The final structure was done to include the effect of electron correlation and adding the polarization function as well as to reduce the basis sets superposition error (BSSE).

Result and Discussion

It is possible to initiate a discussion whether the mechanism may proceed through an SN1 or SN2 mechanism for PNP substrates. A total inversion of the chiral centre in the ribose-1-phosphate product indicates an SN2 mechanism; however, many studies conducted by Schramm's group indicate an SN1 mechanism. According to the calculation results the basic pH tautomers are energetically more stable than the acidic pH tautomers. The effective activation energies would be approximately 120.02 kJ mol-1 in the 3-21G level, and larger than 64.8 kJ mol-1 in the highest calculation level (6-31G**), which indicate that the SN2 mechanism, under these conditions, would be highly improbable. Indeed, it can be energetically discarded.

Conclusion

The results clearly indicate that the SN1 pathway would be preferred. In fact, in the enzymatic environment, the idea of an SN1 mechanism is fairly acceptable.

References

[1] Webb, M. R.; *Proc. Natl. Acad. Sci. U. S. A*. **1992**, *89*, 4884.

[2] Cheng, J. M.; Farutin, V.; Wu, Z. J.; Jacob-Mosier, G.; Riley, B.; Hakimi, R.; Cordes, E. H.; *Bioorg. Chem.* **1999**, *27*, 307.

[3] Montgomery, J. A.; *Expert Opin. Invest. Drugs* **1994**, *3*, 1303.

[4] Markert, M. L.; *Immunodefic. Rev.* **1991**, *3*, 45.

[5] Giblett, E. R.; Ammann, A. J.; Sandman, R.; Wara, D. W.; Diamond, L. K.; *Lancet* **1975**, *1*, 1010.

[6] Kline, P. C.; Schramm, V. L.; *Biochemistry* **1995**, *34*, 1153.

The theoretical studies of ion-pairing phenomenon in NaF aqueous solution

A.Iraji[a], S B.Sohrabi[a b]

[a]Sience and Research, Branch, Islamic Azad University Tehran iran,,

[a] Department of chemistry, Surface Chemistry Research Laboratory, Iran University of Science and Technology, P.O. Box 16765-163, Tehran, Iran.

Abstract

The hydration of sodium fluoride ion-pair is investigated by the DFT method. The hydration number of sodium fluoride ion-pair is determined by comparing the experimental and theoretical results. The effect of number of water molecules on the properties of ion-pairs is investigated by determining NQR and NMR parameters. Also, the relation between the chemical shifts and the energy gap between the highest occupied molecular orbital (HOMO) and low-lying virtual molecular orbital (LUMO) is investigated.

Introduction

In the Debye–Hückel theory, it is assumed that strong electrolytes completely dissociate in aqueous solution [1]. Hydration of ion-pairs is an essential process in the solvation of ionic crystals into water, chemical reactions in aqueous solution, and stability and functionality of biological systems [2].The ion-association contribution, in turn, can be studied both theoretically and experimentally [3]. Also, we investigated the effect of the number of water molecules present on the ion-pair properties by determining the NQR and NMR parameters.

Methods

DFT calculations were carried out using the Gaussian 98 suite of programs. Geometry optimization was performed using then DFT calculations with B3LYP level and LANL2DZ basis set. The gauge-included atomic orbital (GIAO) approach was used in the chemical shielding tensor calculations.The principal eigenvalues of chemical shielding tensors σ_{11}, σ_{22}, and σ_{33}, were found to have the following relationship:

$\sigma_{33} > \sigma_{22} > \sigma_{11}$

Chemical shielding anisotropy ($\Delta\sigma$) was obtained by $\Delta\sigma = \sigma_{33} - (\sigma_{22} + \sigma_{11})/2$, and chemical shielding isotropy (σ_{iso}) was obtained by $\sigma_{iso} = (\sigma_{11} + \sigma_{22} + \sigma_{33})/3$. To convert σ_{iso} (^{19}F) to chemical shift isotropy, δ_{iso}, $CFCl_3$ (σ_{iso} (^{19}F) = 192.7 ppm) was chosen as the reference, $\delta_{iso} = \sigma_{iso,r} - \sigma_{iso,s}$, where the subscripts ''r'' and ''s'' refer to the reference and sample, respectively.The principal eigenvalues for EFG tensors q_{xx}, q_{yy} and q_{zz} have the following relationship: $|q_{zz}| \geq |q_{yy}| \geq |q_{xx}|$

Another important parameter which refers to the deviation of charge distribution from cylindrical symmetry is the asymmetry parameter (η) obtained by:

$$\eta = |q_{yy} - q_{xx}| / |q_{yy}|$$

Results and discussion

The subject of ion association was applied to specific case where electrostatic interactions are chemically more significant than structural considerations. The non-ideality of aqueous electrolyte solutions was viewed as having physical (activity coefficient) and chemical (ion pairing) components, whose contributions depend on the magnitudes of ionic charges, concentrations, and dielectric constants.

Conclusion

In this work, the effect of these factors on thermodynamic values of solubility product and stability constant of formation of ion-pair was investigated both theoretically. Also, the HOMO–LUMO energy gap shows that the ion-pair hydrated with six water molecules is the most stable hydrated ion-pair.

References

[1] J.o M. Bockris, A.K.N. Reddy, second ed., Modern Electrochemistry, vol. 1, Plenum Press, New York/London, 1998.

[2] C.W. Davies, J. Chem. Soc. (1938) 2093.

[3] H.S. Harned, B.B. Owen, Physical Chemistry of Electrolytic Solutions, Third edition, 1958, p. 697.

An analytical potential energy surface for BeH2-He dimer from ab initio calculations

S. M. Atashzar[a,b], A. Maghari[b], M. H. Karimi-Jafaria[a]*

[a]*Computational Chemistry Laboratory, NSTRI, Tehran, Iran*

[b]*Department of Physical Chemistry, College of Science, University of Tehran, Tehran, Iran*

(E-mail: mhkarimijafari@gmail.com)

Keywords: Van der Waals complex, Intermolecular forces, BeH2-He dimer ,CCSD(T).

Introduction

A new 3D potential energy surface (PES) for BeH2-He has been reported. The potential energies were calculated using the supermolecular method at the Coupled-Cluster with Single and Double and Perturbative Triple excitations [CCSD(T)] level, using a large basis set supplemented with midpoint bond functions. The rigid molecule approximation has been used for BeH2. Ab initio calculations of the PES of Van der Waals complexes initially reproduce the PES in the form of tables of numbers, which have to be interpolated or extrapolated for desired applications. It can commonly be described adequately when one applies a high level post Hartree-Fock method in conjunction with an extended basis set. To overcome these difficulties, application of bond functions located somewhere between monomers seems to be a wise solution. The complex has the lowest energy at the T-shaped configuration. The CCSD(T) PES is characterized by a global minimum of -18.75 cm^{-1} at R_e = 3.417Å and θ_e = 90.. There are no local minima in the linear configurations.

Computational Method

The geometry of the BeH2-He complex in which BeH2 is kept linear is described with the Jacobi coordinates (R, θ) where R denotes the distance from the carbon atom to the argon atom; θ denotes the enclosed angle between the vector ***R.*** The PES of BeH2-He was constructed at the CCSD (T) level[1]. The aug-cc-pVQZ basis set of Woon and Dunning for all atoms[2] were used plus bond function located at the center of the vdW

bond. The supermolecular approach was employed to produce the intermolecular potential and the full counterpoise procedure[3] was used to correct for basis set superposition error.

Results and discussion

The intermolecular interaction energy between two rigid linear molecules can be expanded as follows:

$$U(R,\theta)=\sum_{\lambda}V_{\lambda}(R)A_{\lambda}(\theta)$$

.The expansion coefficients can then be written as:

$$V_{\lambda}(R)=\int A_{\lambda}(\theta)U(R,\theta)d\theta$$

The actual calculation of these coefficients can be performed by calculating for a given value of R the potential $U(R,\theta)$ in a grid of points such that the integrations can be carried out by numerically quadrature. Thus the ab initio calculations were performed in a 300 points Gauss-Legendre grid for θ. This integration rule seems to be natural for our functional and coordinate system. Angular basis functions are:

$$A_{\lambda}(\theta)=P_{\lambda}(\cos\theta)$$

where $P_{\lambda}(\cos\theta)$ stands for the associated Legendre polynomials. The full potential is obtained by fitting the radial coefficients over the grid of R points with the following general form:

$$V_{\lambda}(R)=e^{a-br}(\sum_{m}g_{m}R^{m})-\sum_{n}\frac{C_{n}}{R^{n}}F_{n}$$

Before complete exploration of the PES the efficiency of different computational levels was investigated by some test calculations along an angular slice of PES. Accordingly the best compromise between accuracy and computational cost is achieved at the CCSD(T)/aug-cc-PVQZ+b level of theory. Our investigation shows that the global minimum of the PES is corresponded to *Re*= 3.479 Å and θ_e=90.Figure 1and 2 respectively are related to three-dimensional potential energy surface and its Contour plot:

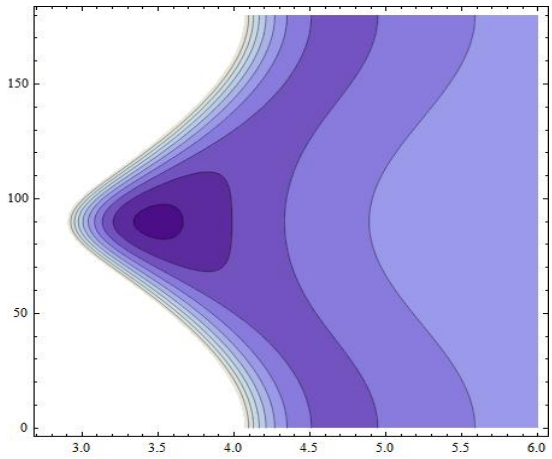

FIG. 2. Contour plots of the intermolecular potential energy surface for the ground state of BeH2-He

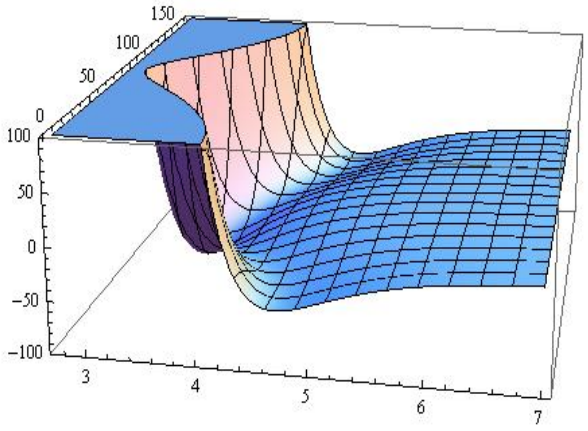

FIG. 1. Three-dimensional potential energy of the intermolecular potential energy surface for the ground state of BeH2-He

References

[1] K. Raghavachari, G. W. Trucks, J. A. Pople, and M. Head-Gordon, Chem. Phys. Lett. **157**, 479 _1989_.

[2] D. E. Woon and T. H. Dunning, J. Chem. Phys. **98**, 1358 _1993_.

[3] S. F. Boys and F. Bernardi, Mol. Phys. **19**, 553 _1970_.

Complete basis set, hybrid-DFT study and NBO interpretation of conformational behaviors of 2-substituted cyclohexanones

Azarakhshi[*a].F, Masnabadi[a].N, Yahyaei[b].H, Boggs[c].J.E, and Nori-Shargh[a].D

a) *Chemistry Department, Arak Branch, Islamic Azad University, Arak, Iran (fa_azarakhshi@yahoo.com)*

b) *Chemistry Department, Zanjan Branch, Islamic Azad University, Zanjan, Iran*

c) *Institute for Theoretical Chemistry, Chemistry and Biochemistry Department, the University of Texas at Austin, TX 78712-0165, United States.*

Keywords: generalized anomeric effects, ab initio, NBO, 2-substituted cyclohexanones

Introduction

In 2003, Tormena and co-workers determined the conformational equilibrium of 2-methoxy- (**1**), 2-methylthio- (**2**) 2-methylselenoclohexanone (**3**) in various solvents by measurement of the $^3J_{H\text{-}2\text{-}H3}$ couplings.[1] They reproduced the results obtained by Lambert and co-workers[2] and pointed out that the axial predominance for compounds **2** and **3** is attributed to hyperconjugation between the electron lone pair of the hetero-substituents and the π^*_{CO} orbital however, the gauche effect in the equatorial conformation of compound **1** should be more effective in stabilizing this conformation. It seems the proportions of the axial conformations of 2-methoxy- (**1**), 2-methylthio- (**2**), 2-methylseleno- (**3**), 2-fluoro- (**4**), 2-chloro- (**5**) and 2-bromocyclohexanone (**6**) can be the result of the competition of the steric repulsions, dipole-dipole interactions and electron delocalizations, therefore, the presented arguments by Tormena and co-workers for the axial predominance in compounds **2** and 3 and the equatorial conformation preference in compound **1** solely in terms of LPX→π^*_{CO} and gauche effect can be questioned.

Computational details

Composite complete basis set (CBS), hybrid DFT and ab initio molecular orbital calculations were carried out using the CBS-4, B3LYP/6-311+G** and HF/6-311+G** levels of theory with the GAUSSIAN 03 package of programs.[3] The most stable conformations of the axial and equatorial conformations of 2-methoxy- (**1**), 2-methylthio- (**2**) and 2-

methylselenocyclohexanone (**3**) were found by changing and scanning the dihedral angles C_1-C_2-X-CH_3. An NBO analysis was then performed using the HF/6-311+G** level for the axial and equatorial conformations by the NBO 5.G program *via* the PC-GAMESS interface.[4]

Results and Discussion

All methods used showed that the axial conformation stability increased from **1** to **3** and also from **4** to **6** which is in agreement with reported NMR data. The results obtained by CBS-4, B3LYP/6-311+G** and HF/6-311+G** levels for compounds **1**, **5** and **6** are very similar, but the CBS-4 results for compound **4** are not in agreement with the reported experimental data (vapor phase). The NBO analysis showed that the *GAE* increases from compound **1** to compound **3** and also from compound **4** to compound **6**. The low axial conformer populations of compound **1** and **4** can be reasonably explained by their small *GAE*. *GE* does not have significant impact on the conformational behaviors of compounds **1-6** and *GAE* succeeds in accounting qualitatively for the increase of the axial preferences in both series of compounds. The results showed that the calculated $\Delta(TSEE_{eq\text{-}ax})$ values decrease from compound **4** to compound **6** which contradicts the suggested arguments in the literature about these compounds. On the other hand, the calculated differences between the dipole moment values of the axial and equatorial conformations, $\Delta(\mu_{eq}\text{-}\mu_{ax})$, increase from compound **1** to compound **2** but decrease from compound **2** to compound **3** and also decrease from compound **4** to compound **6**. The calculated *GAE* values are more significant for the explanation of the conformational preferences of compounds **1-6** than the dipole-dipole repulsion effects.

Conclusion

NBO results revealed that the rationalization of the conformational preference solely in terms of the *GAE* succeeds in accounting qualitatively for the increase of the axial preferences from compound **1** to compound **3** and from compound **4** to compound **6**.

References

[1] M.P. Freitas, C.F. Tormena, J.C. Garcia, R. Rittner, R.J. Abraham, E.A. Basso, F.P. Santos, J.C. Cedran, *J. Phys. Org. Chem*. **2003**, *16*, 833-838 and references therein.

[2] E. A. Basso, C. Kaiser, R. Rittner, J. B. Lambert, *J. Org. Chem*. **1993**, *58*, 7865-7869.

[3] M.J. Frisch, et al, Gaussian 03, Revision B.03, Gaussian, Inc., Wallingford CT, **2004**.

[4] E. D. Glendening, J. K. Badenhoop, A. E. Reed, J. E. Carpenter, J. A. Bohmann, C. M. Morales, F. Weinhold, Theoretical Chemistry Institute, University of Wisconsin, Madison, WI, **2004**. NBO Version 5.G.

Molecular Dynamics Study on the Effect of Curcumin on Amyloid *β*-Peptide Aggregation

Afsaneh Azadi, Davood Ajloo
School of Chemistry, Damghan University, Damghan, Iran
(Email: Azadi.afsane@yahoo.com)
ajloo@du.ac.ir

Key word: Alzheimer, Curcimin, Inhibitation effect

Introduction:

Mechanism of Alzheimer's disease is related to gradual deposition of amyloid fibrils[1]. Recently, major research has involved the development of compounds capable of inhibiting or reversing the A*β* aggregation process, such as curcumin. Curcumin is extracted from plant *Curcuma longa* Linn[2]. Most computational investigations of the structure and dynamics of A*β*-peptides have focused on fragments from the full-length A*β*. A*β*16-22 is one of the shortest fibril-forming *β*-amyloid fragments yet reported and experimental evidence of amyloid formation is available[3].

Method:

In order to investigate the molecular mechanism of inhibition of amyloid β-peptide (Aβ) aggregation by Curcumin, molecular dynamics simulations of two monomers of A*β*16-22 in the absence and presence of 2, 4 and 6 molecules of curcumines were performed. Initial coordinates for the Aβ16-22 monomer were extracted from mode 2 of the Aβ42 peptide available in the Protein Data Bank (PDB code 1BA4). Force field parameters and the topology for curcumin molecules were generated using the PRODRG2 server. Four systems were simulated. We perform 20 ns MD simulation for each system. Aβ16-22 is one of the shortest fibril-forming β-amyloid fragments yet reported.

The simulation trajectories were analyzed using several auxiliary programs provided with the GROMACS 3.3 package. The programs include: 1-g_hbond for the H-bond interactions between hydrogen donors and acceptors. 2-The radial distribution function (RDF) is the density of probability of finding a particle at distance r from the reference particle.

Results and Discussion:

Comparison of analysis in 4 systems showed interpeptide HB decreased due to increasing the curcumin molecules. In order to better understanding, the average number of HB between two monomers was investigated. The average number of HBs between monomers was 1.28 in the absence, and 0.96, 0.65 and 0.19 in the presence of 2, 4 and 6 curcumin, respectively (Fig. a)

We can follow the aggregation of curcumin molecules from diminishing of HB between the curcumin and solvent molecules. Fig b. Fig c show radial distribution functions of the water molecules around peptides. The number of solvent molecules around the peptides decreases by increasing the curcumin molecules, so we can see accumulation of curcumine around peptides. Fig d shows curcumin molecules aggregate between two monomers so prevent from near monomers.

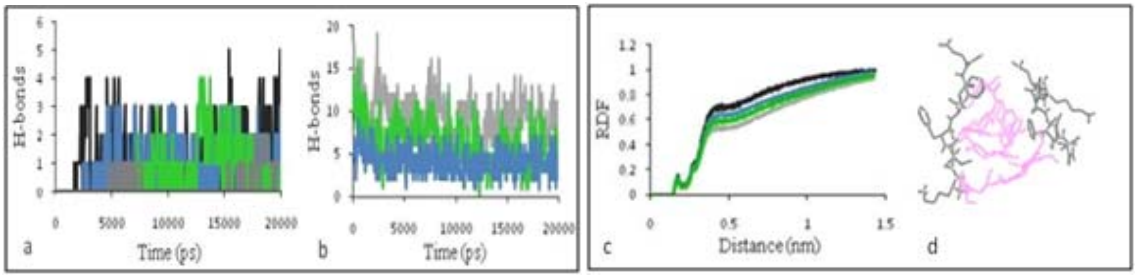

Fig. (a) Number of HB between two monomers versus time (b) Number of HB between curcumin and water molecules versus time. (c) RDF of the water molecule around peptides versus distance, in the absence (black line), and the presence of the 2 (blue line) 4 (green line) and 6 curcumin (grey line). (d) Molecular snapshot obtained by DS Visualizer program for a system including 6 curcumin (pink color represents curcumin molecules).

Conclusions:

The results confirmed that Aβ16-22 aggregation is prevented by increasing the number of curcumin molecules. Curcumin molecules inhibit the peptides aggregation by accumulation of curcumines between two monomers of Aβ16-22.

References :

[1] Yang. C, Li. J, Li. Y, Zhu. X., (2009). *J. Mol. Struct. Vol.* 895, PP. 1–8.

[2] Ringman. J.M, Frautschy. S.A, Cole. G.M, Masterman. D.L, Cummings.J.L., (2005). *Curr Alzheimer Res,* Vol. 2, PP. 131-136.

[3] Santini, S., Mousseau, N., Derreumaux, P., (2004).. *J. Am. Chem. Soc*. Vol.126, PP. 11509-11516.

QSAR analysis of curcumin derivatives as anticancer agents

Afsaneh Azadi, Davood Ajloo
School of Chemistry, Damghan University, Damghan, Iran
(Email: azadi.afsane@yahoo.com)

Key word: Curcumin, Cancers

Introduction:

Curcumin is a biphenolic compound with hydroxyl groups at the ortho-position on the two aromatic rings that are connected by a β-diketone bridge, containing two double bonds (dienone).[1] is the primary bioactive compound isolated from turmeric. One of the most important aspects of curcumin is its effectiveness against various types of cancer. The biological data used in this study are the inhibition of cancer (IC50) of a series of curcumin derivatives that obtained by Fuchs and worker[2]. Where, IC50 represents the molar concentration producing 50% inhibition of cell growth in 48h.

Method:

The resulting optimum geometry for curcumin derivative of Hyperchem was transferred into the Dragon v.5.0 program for generation of 1497 molecular descriptors. QSPR study for prediction of IC50 was done for these compounds. IC50 were predicted by multiple linear regressions. MLR were used to select descriptors which are responsible for IC50 of these compounds.

Results and Discussion:

The stepwise correlation coefficients for prediction of IC50 by MLR method were 0.96. Plot of the calculated values of IC50from MLR model versus the experimental values of them are represented in figure 1. The regression equation used here to predict IC50 is as follows:

IC50 Pred= -60.044+ 28.579(RDF115m)-52.844(Mor04v) +20.561(R8p) +161.571(Mor28m)

This equation shows inhibition effect is increased by increasing of weight and hydrophobic inhibitor and decreas volume those.

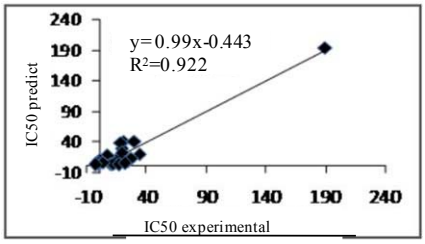

Fig1: Correlation between predicted and experimental

Table 1. Definition of R and the values of free energy of Gibbs and

Compound	R1	R2	R3	R4	R5	R6	IC50
Curcumin	OCH_3	OH	H	-	-	-	19.8±2.1
1	OCH_3	H	H	-	-	-	40±4.9
2	H	OH	H	-	-	-	27.3±6.6
3	OH	OCH_3	H	-	-	-	40
4	OCH_3	OH	OCH_3	-	-	-	37.2±4.1
5	OCH_3	OSO_2NH_2	H	-	-	-	7.5±1.8
6	OCH_3	OCH_3	H	-	-	-	5.9±1.3
7	OAC	OAC	H	-	-	-	12.9±2.3
8	OCH_3	OSO2NH2	OCH_3	-	-	-	13.1±2.1
9	OSO_2NH_2	OCH3	H	-	-	-	7.4±1.6
10	-	-		OCH_3	OH	-	20.9±4.8
11	-	-		OSO_2NH_2	OH	-	193±5.4
12	-	-		-	-	H	5.6±2
13	-	-		-	-	OCH_3	16.2±1.4
14	OCH_3	OH	H	-	-	-	3.9±1.1
15	OH	OCH_3	H	-	-	-	5.9±0.9
16	H	OH	H	-	-	-	9.5±0.9
17	OCH_3	OCH3	H	-	-	-	2.9±0.6
18	OCH_3	H	OCH_3	-	-	-	2.5±0.5
19	OCH_3	OH	OCH_3	-	-	-	3.6±1.3
20	OCH3	OSO2NH2	H	-	-	-	6.1±0.3
21	H	OSO2NH2	H	-	-	-	5.1±0.8
22	OCH3	OSO2NH2	OCH3	-	-	-	2.4±0.2
23	-	-	-	-	-	-	2.1±1.1

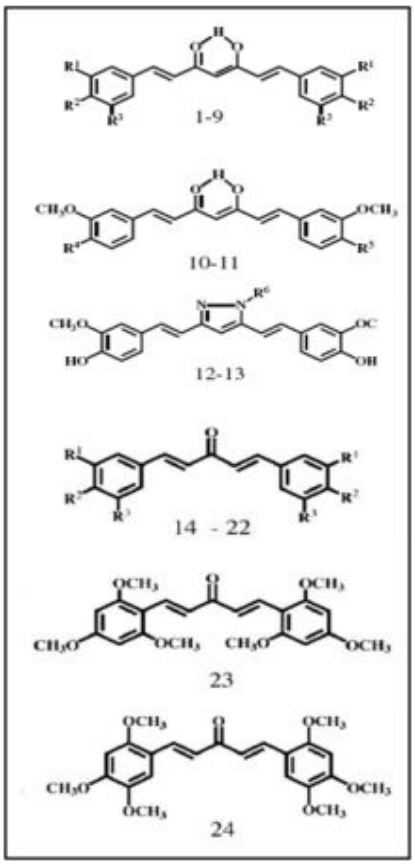

Fig. 2: Analogues of curcumin.

Reference:

[1] Begum. A. N, Jones. M. R, Lim. G. P, Morihara. T, Kim. P, Heath. D. D, Rock. C. L, Pruitt. M. A, Yang. F, Hudspeth. B, Hu. S, Faull. K. F, Teter. B, Cole. G. M, Frautschy. S. A., (2008). *JPET*. Vol. 326, PP. 196–208.

[2] Fuchs. J. R, Pandit. B, Bhasin.D , Etter. J. P, Regan. N, Abdelhamid. D, Li. C, Lin. J, Li. P. K., (2009). *Bioorg. Med. Chem. Lett*. Vol. 19. 2065–2069.

Computational analysis of Diphenyl quinoxaline and Bis-methyl quinoxaline Derivative by ab-initio calculation

Nafiseh Ghorbani, Bahareh Bastan, Afsaneh Amiri*, Asma Darvishzadeh, Saman Naghibi, Kamyar Daraei

Department of Chemistry, Islamic Azad University, Central Tehran Branch, Tehran, Iran.

afsaamiri@gmail.com

Keywords: Quinoxaline derivatives, Ab-initio**,** 3-benzylidene-7-alkoxychroman-4-one

Introduction

Quinoxaline derivatives are a very important class of nitrogen-containing compounds and have been widly used in dyes,pharmaceuticals,and electrical/photochemical materials[1]. In this research study, the formation potential and vibration analysis of 3 quinoxaline derivatives with the names of: 2,3-diphenyl quinoaline , 2,3-Bis (4-methoxy-phenyl) quinoxaline , 2,3-Bis(4-methoxy-phenyl)-6-methylquinoxaline[1] Fig. 1 have been investigated.

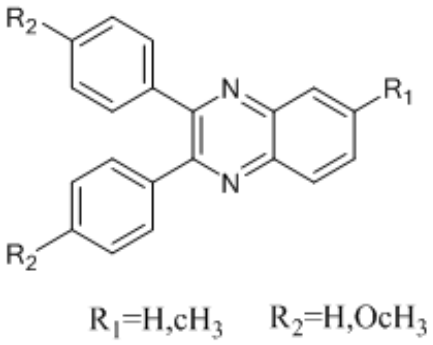

Fig. 1: Quinoxaline Derivatives

Material and Methods

The entire calculations were performed at hartree-fock(HF) method[2] with 6-311G (d,p) basis set on a Pentium IV (2.99GHZ) personal computer using the Gaussian 03w,program package ,utilizing gradient geometry optimization. The vibrational frequencies for this derivatives were calculated with this method and then scaled [3] by 0.8929 and 0.963, respectively.

Result and Discussion

The binding energy gradient was estimated to be 0.05 kcal using the conjugate gradient optimization method (Polad-Ribiere algorithm). In order to reach the Global Minimum, some structural parameters of the initially optimized molecules were changed manually and the molecular structures were re-optimized. This procedure was repeated until the most stable structure was obtained. B3LYP/6-311G (d, p) optimizations of three derivatives of 3-benzylidene-7-alkoxychroman-4-one [4] was done by Gaussian 98. The final structure was done to include the effect of electron correlation and adding the polarization function as well as to reduce the basis sets superposition error (BSSE).

Conclusion

Band frequencies and intensities in the IR spectra of quinoxaline derivatives have been calculated. The results have good correlation with the experimental IR spectra.

References

[1] Heravi, M.M, K.bakhtiari,M.H.Tehrani,N.M.Javadi,H.H.Oskooie;Arkivok (2006) 16.
[2] W.J.Hehre, L.Radom, P.V.R.Schleyer, J.A.pople, Ab initio Molecular Orbital Theory,Wiley, New York,1986
[3] P.L.Fast, J.Corchado, M.L.Sanches, D.G.Truhar, J.Phys.Chem. A103 (1999) 3139
[4] A.Foroumadi, A.Samdzadeh-Kermani, S.Emami, G.Dehghan, M.sorkhi, M.heidari, M.Abdollahi, A.Shafiee, Bio org.Med.Chem.Lett 17 (2007) 6764-6769

Host-Guest Inclusion Complex Formation between Cucurbit [n] urils with Anticancer Drug based on Gold (III)

S. Bagherifar[a], Z. B. Nojini*[b] , S. Samiee[b] , M. Riyahi[a]

[a]Department of Chemistry, Science & Research Branch

[b] Department of Chemistry, Faculty of Science, Shahid Chamran University, Ahwaz, Iran

E-mail: S. Bagherifar@yahoo.com

Keywords: Cucurbit[n] uril, N,N-dimethyldithiocarbamate, DFT, Gold compounds, Anti Cancer drug

Introduction

After the discovery of the anticancer activity of Cisplatin, a great deal of attention was to platinum compounds. The outstanding anticancer effects observed for platinum (II) compounds suggested that other metal-based compounds might be similarly useful as antitumor drugs. Gold (III) compounds looked pair wise very attractive for cancer treatment as the gold (III) centers are known to originate square planar complexes that are isoelectronic and isostructural to those of platinum (II) [1]. Cucurbit[n]uril is a family of homologues which are most favored cavitands for host-guest complex formation [2].

Computational Method

All the structures were optimized using the density functional theory (DFT) and B3PW91 with Lanl2dz basis set. The inclusion process was simulated by putting the guest in one end of CB[n] cavity and then letting it pass through the CB[n] cavity by steps.

Result and Discussion

Energies were computed at the level of B3PW91/LANL2DZ theory on the optimized geometry. To examine the binding properties of these complex formation, we calculated the total energy of the CB[n]-[DMDT(Au) Cl_2] n=5, 6 as well as the pristine CB[n] and[DMDT(Au) Cl_2] molecule. The complex formation energy, E, was calculated using the following expression:

$$\Delta E = E_{(complex)} - \left(E_{CB[n]} + E_{drug}\right) \qquad (1)$$

The electronic chemical potential (μ) was calculated as half of the energy of the highest occupied molecular orbital (HOMO) plus the lowest unoccupied molecular orbital (LUMO) as follows:

$$\mu = \frac{(E_{HOMO}+E_{LUMO})}{2} \quad (2)$$

The stability energy values for the complexes as well as each components, and HOMO, LUMO and energy gap for complex formation between CB[n] n=5 ,6 with [DMDT(Au) Cl_2] listed in Table 1. Results show that the complex formation with CB[6] with Drug is stable that of CB[5]/drug. Also, The results of potential energy surface show that the [DMDT(Au) Cl_2] drug is located out of the cavity of the CB[n] with 1:1 stoichiometry.

Table1. Electronic energies and HOMO, LUMO and Gap energy of the inclusion complexations of CB[n] n=5, 6[DMDT(Au) Cl_2] of the DFT/lanl2dz optimized structures.

Type	E(Kcal/mol)	Δ*E*(Kcal/mol)	HOMO(eV)	LUMO(eV)	Gap energy	μ
CB[5]	-1,886,973	-	-6.65	0.389	7.039	-3.130
CB[6]	-2,264,376	-	-6.714	0.469	7.183	-3.122
[DMDT(Au) Cl_2]	-224,861	-	-7.457	-4.65	2.807	-6.053
CB[5]/Drug	-2,111,854	-20	-6.277	-3.352	2.92	-4.814
CB[6]/Drug	-2,489,263	-26	-6.418	-3.488	2.93	-4.953

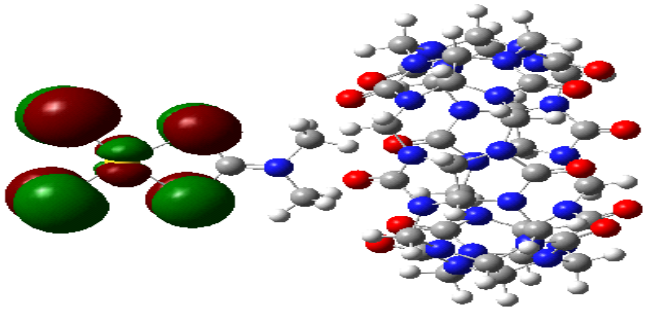

Fig.1: Typically contour plots of HOMO for CB[6]/ [DMDT(Au) Cl_2] complex.

Conclusions

The obtain result of energy indicate that complex CB[6]/Drug is more stable than CB[5]/Drug.

References

[1] A. Bindoli, M. Pia Rigobello, G. Scutari. Coordination chemistry Reviews 253(2009) 1692-1707

[2] A. Suvitha, H. Mizuseki, N. Ohuchi, J. Incl Phenom Macrocycl Chem 66 (2010) 213-218

Investigation of Gases Physisorption through Silicon Carbide Nanotubes: a Grand Canonical Monte Carlo simulation study

M. A. Begherinia[*,1], M. Shadman[2], Z. Ahadi[3], S. Yeganegi[2], M. Giahi[1]

[1]*Department Chemistry, Faculty of Basic science, Islamic Azad University, Lahijan branch, Lahijan, Iran.*

*(*Email: mabagherinia@yahoo.com)*

[2]*Department of Physical and Inorganic Chemistry, Faculty of Chemistry, University of Mazandaran, Babolsar, Iran.*

[3]*Department of Science and Engineering, Faculty of Basic science, Islamic Azad University, Abhar branch, Abhar, Iran.*

Keywords: Adsorption, Silicon Carbide, Nanotubes, Grand Canonical, Monte Carlo, Langmuir equation

Introduction

Nowadays, storage of fluids is a fundamental goal of molecular adsorption through micro/nano porous materials that has become an ever increasingly important topic in nano-scientific researches. Consequently the investigation of the physisorption of small molecules inside single wall nanotubes (SWNTs) from the experimental and theoretical studies such as computing modeling studies has been started to illustrate SWNTs might be a good candidate for a practical gas storage material or not [1-3].

Very recently, Sun et al. have reported the synthesis of silicon carbide (SiC) nanotubes produced via the reaction of Si with carbon nanotubes [4]. Menon et al, also investigated the structure and stability of various SiC nanotube structures using the generalized tight-binding molecular- dynamics (GTBMD) scheme of Menon and Subbaswamy and ab initio methods [4]. They found the bond lengths of SiC nanotube is about 1.87 Å that is larger than bond length of boron nitride (BNNT) nanotube (1.44 Å) and carbon nanotube (1.42 Å). Therefore, SiCNT is considered to has the faster rate gas penetration through the wall of BNNT and CNT.

As far as we concern, the experimental and theoretical results of hydrogen storage in SiCNTs have been reported [5], but SiCNTs have not being considered to be characterized by the

other gases. Therefore in the present work, we evaluate the storage properties of single-wall SiC nanotubes by GCMC computing for methane and nitrogen adsorption.

Computational methodology

We use GCMC simulations [1-2] to study methane and nitrogen loading separately in some of SWSiCNTs. The nanotubes have rigid structures, and no geometry variation of the adsorbent is considered, since the induced geometric variation of nanotubes can be neglected by gases at room temperature.

Results and discussion

We used the GCMC simulations to obtain the weight percentage of methane and nitrogen that can be stored in (6,6), (9,9) and (12,12) SiCNTs under different thermodynamic conditions. Figure 1 and 2 present the adsorptivity of methane and nitrogen inside SiCNTs at 175 K and under 1 to 100 bar pressure, respectively. It is should be noted that our simulations have not completed and would be continued.

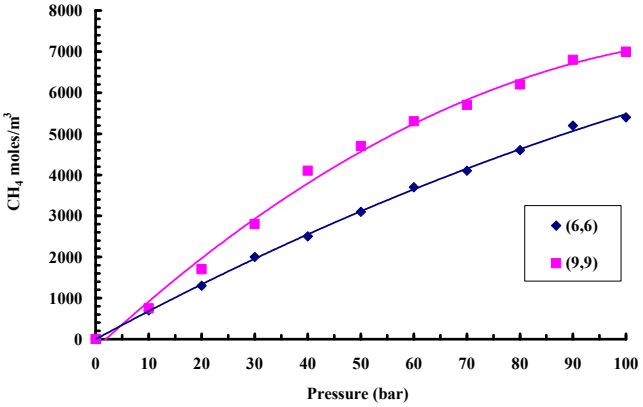

Figure1. CH_4 storage inside (6,6) and (9,9) SWSiCNTs

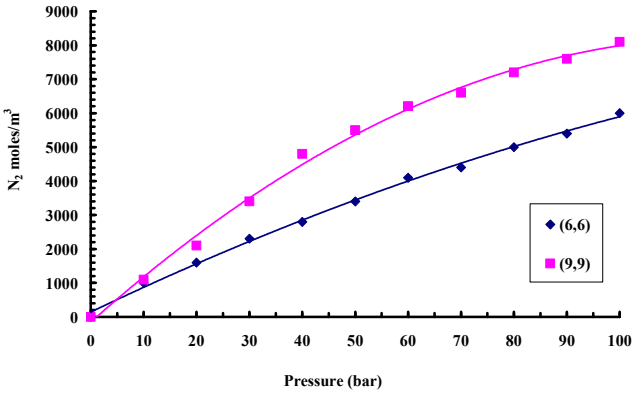

Figure2. N_2 storage inside (6,6) and (9,9) SWSiCNTs

References:

[1] Cheng, J., Zhang, L., Ding, R., Ding, Z., Wang, X., and Wang, Z. (2007) *International Journal of Hydrogen Energy,* 32: 3402-3405.

[2] Cheng, J., Ding, R., Liu, Y., Ding, Z., Wang, X., and Zhang, L. (2007) *Computational Materials Science,* 40: 341-344.

[3] Marmier, A., Spohr, H., Cooke, D.J., Kerisit, S., Brodholt, J.P., Wilson, PB, and Prker, S.C. (2005) *Molecular Simulation,* 31: 385-389.

[4] Menon, M., Richter, E., Andriotis, A. (2004) *Physical Review B,* 69:115322.

[5] Malek. K., Sahimi. M., (2010) *J. Chem. Phys.* 132: 014310

DFT Study of β- Elimination Various Mechanisms of Tricholoro[choloro(methyl)germyl] Silane

A.Bodaghi[1]*, S.Jameh-Bozorgi[1], H. Shirani[2], J. Hosseini[1] and H.Soleymanabadi[2]

(Email: alibodaghi@ymail.com)

[1] Chemistry Department, Faculty of Sciences, Islamic Azad University, Toyserkan Branch, Toyserkan, Iran

[2] Young Researchers Club, Islamic Azad University, Toyserkan Branch, Toyserkan ,Iran

Introduction:

The pyrolytic elimination is a model reaction, which probably dominates most pyrolytic processes. A simple reaction of this type can be written as follows (heating is symbolized by Δ):

Among pyrolytic eliminations, b-eliminations, with two groups lost from adjacent atoms, are probably the most common. These reactions take place typically by an Ei mechanism. Since pyrolytic elimination takes place with no other reagent present and often requires gas phase, the typical E2 mechanism where a proton is pulled by a base is not common. Two β - eliminations involving an Ei mechanism with different sizes of cyclic transition state are shown below[1-2].

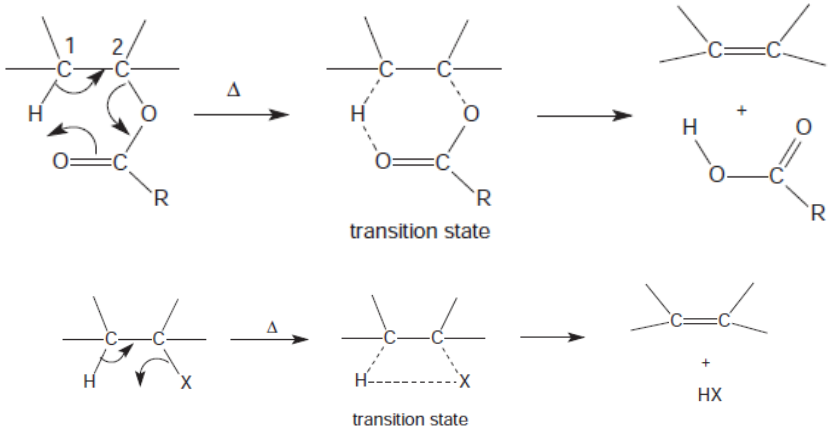

In this research work, β- Elimination Various Mechanisms of Tricholoro [choloro (methyl) germyl] Silane were studied by Density Functional Theory .

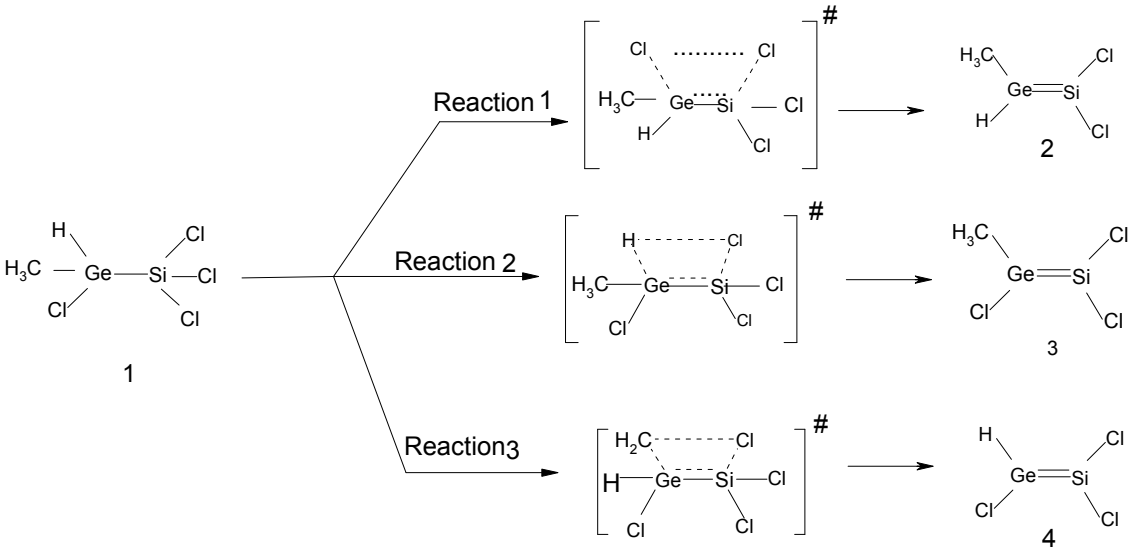

Method:

Ab initio calculations were carried out using B3LYP/3-21G* levels of theory with the GAUSSIAN 03 package of [4] implemented on a pentum-PC computer with Intel(R)Core(TM)2 Duo CPU T9600 @ 2.8GHz processor. Initial estimation of the structural geometry of Indole, Indolizine and Isoindole was obtained by program Chemoffice 2010 and for further optimization of geometry was used the MM2 method of the Chem3D program. Energy-minimum molecular geometries were located by minimizing energy, with respect to all geometrical coordinates without imposing any symmetrical constraints. The nature of the stationary points for compound **1** and transition state structures of reactions 1–3 has been fixed by means of the number of imaginary frequencies. The structures of the molecular transition state geometries were located using the optimized geometries of the equilibrium molecular structures according to the Dewar et al. procedure (keyword SADDLE).20. These geometry structures were reoptimized by the QST2 subroutine at B3LYP/3-21G* level.

Results and discussions:

The β- Elimination Various Mechanisms of Tricholoro[choloro(methyl)germyl] Silane were investigated using ab initio Molecular Orbital (MO) and Density Functional Theory. The results showed that the β- Elimination reaction is a unimolecular process and the occurred from four centered transition state. (See scheme). Sum of the Zero point energy (ZPE) and total electronic energy(E_{el}) (E_0=ZPE+E_{el}) for all of them calculated on the B3LYP/3-21G* level of theory(table) [3]. Studies on the B3LYP/3-21G* level of theory show that the barrier height of the decomposition of the compound 1 to 2-4 (reactions 1-3) is *126.43*, *62.31*, and *92.49* kcal. mol−1, respectively . It showes that the barrier height of the decomposion of the compound 1 to 3 is lower than another possible compounds.

System method	ZPE[b]	E_{ele}	E_0	ΔE^a_0
1	0.0483294483	-4228.2320058	-4228.179100	0.00000 (0.00000)
2	0.0453311586	-4228.0272256	-4227.977602	0.00000 (0.00000)
3	0.0457420509	-4228.1346544	-4228.084581	0.00000 (0.00000)
4	0.0472120551	-4228.1163006	-4228.064618	0.00000 (0.00000)
[1→2]#	0.045307773	-4228.027209	-4227.977611	0.201489 (126.4343475)
[1→3]#	0.04528520955	-4228.1293773	-4228.079804	0.099296 (62.30824)
[1→4]#	0.045494127	-4228.0815	-4228.031698	0.147402 (92.494755)

[a]Relative to the most stable geometry
[b]Corrected by multiplying by a scaling factor (0.9135)
[c]Numbers in parenthesis are the corresponding values in kcal mol^{-1}

Conclusion:

Ab initio B3LYP density functional-theory calculations provide a picture from structural and energetic of view for the various pathways of the decomposition of compound 1 to 2–4. B3LYP/3-21G* results reveal a higher barrier height for reaction 1 than that of reactions 2 and 3. These results are justified by Mulliken charge distribution values in the ground-state structure of compounbd 1 and transition state structures of reactions 1– 3.

Acknowledgment:

This reaserch was supported by the Islamic Azad University, Toyserkan Branch, Toyserkan, Iran.

References :

[1]. Pyrolysis of Organic Molecules with Applications to Health and Enviromental; *Serban C. Moldoveanu*; R.J. Reynolds Tobacco Co; (2010).

[2]. H.Heany ,Chem .Rev., 62,81(1962).

[3].Stewart JJP.Quantum Chemistry Program Exchange,Vol.13mNo.455,193.

[4]. Frisch Mj.et al.GAUSSIAN 98 (Revision A.3). Gaussian,Inc.:Pittsburgh,PA,USA,(1998).

DFT Study of the Aromatic Stabilization Energy (ASE) of Siline

A.Bodaghi[1], S.Jameh-Bozorgi[1], H. Soleymanabadi[1]*

(Email: alibodaghi@ymail.com)

[1] Chemistry Department, Faculty of Sciences, Islamic Azad University, Toyserkan Branch, Toyserkan, Iran

Keywords: *ASE, Siline, DFT Calculation, B3LYP, GAUSSIAN 03*

Introduction:

A silabenzene is a heteroaromatic compound containing one or more silicon atoms instead of carbon atom in Benzene. Silabenzenes have been the targets of many theoretical and synthetic studies by organic chemists interested in the question of whether heavy Benzenes exhibit aromaticity. Silicon, although a member of Group IV, does not form stable multiply-bonded compounds [l] and it has never been observed substituted for carbon in a stable heteroaromatic system, although methyl-Silabenzene has been postulated as an as yet nonisolated intermediate. In this research ASE of siline was calculated by using GAUSSIAN 03 package of programs [2].

Method:

Density functional theory (DFT) calculations were carried out with the Gaussian 03 program.The geometries of silabenzenes were fully optimized using the three parameter hybrid DFT of Becke (B3LYP) [3] with the 6-311++g(d,p)basis set[4] implemented on a pentum-PC computer with Intel(R)Core(TM)2 Duo CPU T9600 @ 2.8GHz processor.

Result and discussion:

In this work, the total energy (E_T) (in Hartree) of The all geometries of silabenzene were calculated by B3LYP method and with the 6-311++G(d,p) basis set (see table 2), and then the aromatic stabilization energy (ASE) (KJ/mol) of) Siline was obtained from these data The results of calculations show that of aromatic stabilization energy of siline by using B3LYP/ 6-311++G(d,p) are: 145.2376 KJ/mol. These results are listed in table(1)

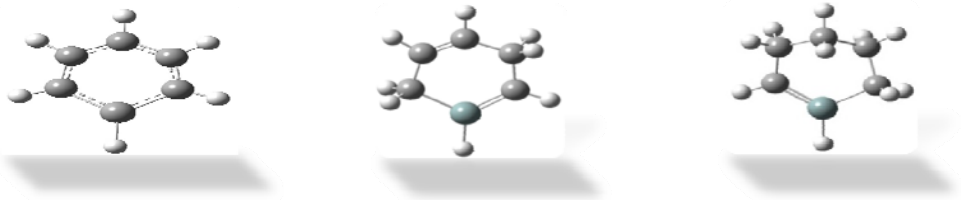

Method	siline	2,5-dihydrosiline	2,3,4,5-tetrahydrosiline
6-311+G**	-483.6733887[a]	-484.8492293[a]	-486.080388[a]
Aromatic Stabilization Energy (ASE)	0.0553181[a] (145.2376)[c]		

Table 1. The ASE (Kcal/mol)Calculated by B3LYP method
[a]E_T (in Hartree)
[c]Numbers in parenthesis are the corresponding values in KJ. mol^{-1}

Compound	DFT total energy	3D shape of molecules
Siline(Silabenzene)	-483.6733887	
2,3-dihydrosiline	-484.8552709	
1,4-dihydrosiline	-484.8865779	
1,2-dihydrosiline	-484.8888029	
2,3,4,5-tetrahydrosiline	-486.080388	
1,2,3,6-tetrahydrosiline	-486.1148444	
1,2,3,4-tetrahydrosiline	-486.1161506	

2,3-dihydrosiline	-484.8552712	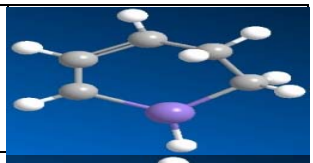
2,5-dihydrosiline	-484.8492293	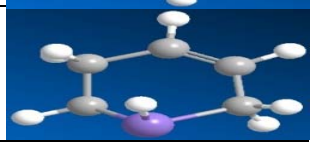

Table 1. The E_T (Hartree) Calculated by B3LYP method

Conclusion:

The quantum chemical calculations show that siline is an aromatic organic compound. The amount of calculated ASE of *Siline(*Silabenzene *)* in these basis set shows that average of this energy is about 145.24 $KJ.\ mol^{-1}$, According to the experimental results is acceptable.

References :

[1]L.E Gusel'nikov,N.S. Nametkin and V.M Vdovin,Accounts Chem. Res.8,**1975**,18.

[2] M. j. Frisch et al. *GAUSSIAN 03*, Revision C. 01, Gaussian Inc., Wallingford. CT.

[3] Becke, A. D. *J. Chem. Phys*. **1993**, *98*, 5648.

[4] Hariharan, P. S., Pople, J. A. *Theor. Chim. Acta* **1973**, *28*, 213.

Effect of alkyl groups substitution on the strength of intramolecular hydrogen bond and vibrational spectrum of Naphthazarin

F. Badalkhani-Khamseh and M. Zahedi-Tabrizi*
Department of Chemistry, Alzahra University, Tehran, Iran
Zahedi@ alzahra.ac.ir

Keywords: 5,8-Dihydroxy-1,4-naphthoquinone, Naphthazarin, Intramolecular Hydrogen Bond, Density Functional Theory.

Introduction

5,8-Dihydroxy-1,4naphthoquinone, commonly known as naphthazarin (NZ), is a biologically active pigment obtainable from natural sources. It shows antimicrobial, cytotoxic, antivirial, antifungal, anti-inflammatory, antioxidant and antitumor activity, wound healing and antithrombotic properties[1-3]. A structure with C_{2v} symmetry has been suggested for NZ in solution with fast proton rearrangement from one pair of oxygen atoms to the other by NMR, vibrational spectroscopic studies and ab initio calculations[4-6]. The ^{1}H NMR spectra show that for NZ and 2,6- and 2,7-dimethylnaphthazarin the structures of minimum energy correspond to two degenerate tautomers with two asymmetric hydrogen bonds in which the two hydroxyls are on the same ring[7]. The unsymmetric substitutions such as 2-methyl and 2,3-dimethyl, distorts the double minimum potential so that mainly one tautomer exists both in solution and in the solid state. According to X-ray diffraction investigations the major tautomer bears the methyl substituents in the quinonoid ring[8].

Methods of Analysis

The Gaussian 03 program was used for all quantum mechanical computations. The full geometry optimization, calculations of hydrogen bond strength (the energy difference between *cis*-enol and *trans*-enol conformers) and vibrational frequency calculations were performed by DFT method at B3LYP level with 6-31G** basis set. Proton chemical shift of

the hydroxyl groups in NZ and it's alkyl substituents was calculated at this theoretical level by GIAO method.

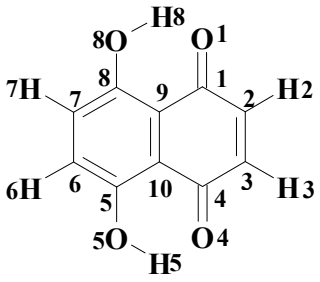

Fig. 1. Numbering system and the C_{2v} structure of NZ.

Results and discussion

The geometries and labeling of the atoms in NZ are given in Fig. 1. Several alkyl substituted derivatives of NZ have been theoretically investigated in order to study inductive or steric effects on the intramolecular hydrogen bond strength. Some geometrical parameters such as O…O , O—H and C=O distances and also OHO angles are compared in these compounds. Performed calculations on 15 derivatives of NZ show that in all of themγOH / γ OD is more than naphthazarin.

Conclusion

The calculated results such as OH/ OD stretching and in-plane bending and O…O stretching modes are consistent with stronger hydrogen bond in alkyl substituted NZ compared to that naphthazarin. Vibrational frequencies and structural parameters are in good agreement with ^{1}H NMR results.

References

[1] B. Park, H. Lee, S. Lee, X. Piao, G. R. Takeoka, R. Y. Wong, Y. Ahn, J. Kim, J. Ethnopharm. 105 (2006) 255.

[2] A. Arnone, L. Merlini, R. Mondelli, G. Nasini, E. Ragg, L. Scaglioni, U. Weiss, J. Chem. Soc. Perkin Trans. II (8) (1993), 1447.

[3] V. P. Papageorgiou, A. N. Assimopoulou, E. A. Couladouros, D. Hepworth, K. C. Nicolaou, Angew. Chem. Int. Ed. 38 (1999), 270.

[4] J. M. Dumas, A. Cohen, M. Gomez, Bull. Soc. Chim. Fr. (1972), 1340.

[5] C. J. H. Schutte, S. O. Paul, R. Smit, J. Mol. Struct. 297 (1993), 235.

[6] Y. H. Mariam, R. N. Musin, J. Mol. Struct. 549 (2001), 123.

[7] J. R. de la Vega, J. H. Busch, J. H. Schauble, K. L. Kunze, B. E. Haggert, J. Am. Chem. Soc. 104 (1982), 3295.

[8] A. Olivieri, I. C. Paul, D. Y. Curtin, Magn. Reson. Chem. 28 (1990), 119.

The effects of substituent position on hydrogen bonding and cooperativity of N···HF interactions in X-prydazine··· $(HF)_2$

Ali Ebrahimi, Mostafa Habibi-Khorassani and Farideh badichi Akher
Department of Chemistry, University of Sistan and Baluchestan, P.O. Box 98135-674, Zahedan, Iran
(E-mail:faridehbadichi@yahoo.com)

Keywords: Prydazine; Hydrogen bond; Cooperativity effect; AIM.

Introduction:

The diazine rings are building blocks of many important natural synthetic compounds, such as nucleotides [1]. The six membered nitrogenated aromatic rings such as diazines are the most studied molecules [2]. The hydrogen bonding between pyridine base (and other six-membered nitrogenated aromatic rings) and water (and some other proton donors) were periodically studied by theoretical and experimental methods [3]. In the present study, three complexes indicated in Figure 1 have been selected to study the effect of substituent position on hydrogen bonding and the cooperativity of N···HF interactions.

Methods:

All geometries have been optimized by Gaussian03 program package using the B3LYP methods in conjunction with the 6-311++G (d,p) basis set. The topological properties of electron charge density were calculated by AIM method at the B3LYP/6-311++G (d,p) level.

Results and discussion:

The complexation energies for complexes **1**-**3** are presented in Table 1. In all cases, the binding energy for complex **1** is lower than the sum of binding energies of complexes **2** and **3**. The N9···H and N8···H bond lengths in complex **1** are longer than complexes **2** and **3**, respectively (see Table 2). The ρ values calculated by AIM method at the intermolecular bond critical points (BCPs) are given in Table 3. The ρN9···H and ρN8···H values in complex **1** are lower than these in complexes **2** and **3**, respectively. A negative cooperativity is observed for the ρN8···H and ρN9···H values in trimolecular complex **1**. In addition, the stabilization

energies of complexes become more negative by electron-donating substituents, while the behavior is reversed by the electron-withdrawing substituents. Because of electronegativity of O atom, the induction is predominant over the resonance with OH functional group in complex **2**. This behavior is not observed by OCH_3 functional group because of electron-donatting of CH_3 group.

Conclusions:

The complexation energies and the results obtained from AIM analysis are in good agreement with the negative cooperativity of the N9···H and N8···H hydrogen bonds in complex **1,** and the binding energy becomes more negative with the electron-donating substituents (with the exception of complex **2** with the OH functional group), while the behavior is reversed by electron-withdrawing substituent.

Table 1. The binding energies calculated at the B3LYP/6-311++G(d,p) in kcal mol^{-1}

	1	**2**	**3**	**1+3**
OCH_3	-25.268	-13.514	-14.078	-27.592
OH	-24.411	-13.188	-13.610	-26.798
H	-24.069	-13.214	-13.214	-26.428
CN	-20.370	-11.077	-11.292	-22.369
NO_2	-20.265	-10.738	-10.738	-21.641

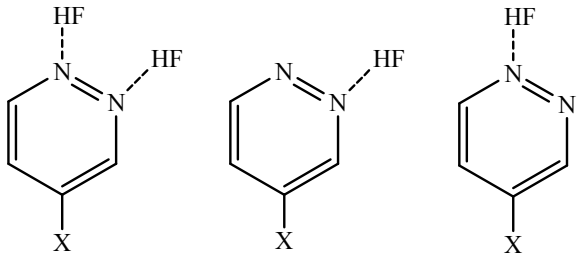

Figure1. The X-prydazine···$(HF)_n$ complexes considered in the present work. (X = OCH_3, OH, H, CN, NO_2 and n=1,2).

Table 2. The N···H bond lengths optimized at the B3LYP/6-311++G(d,p) level in (Å)

	1	2	3
OCH_3	1.716(1.702)	1.667	1.653
OH	1.726(1.707)	1.670	1.663
H	1.723(1.722)	1.672	1.672
CN	1.755(1.753)	1.708	1.704
NO_2	1.760(1.762)	1.716	1.714

The data in the parentheses correspond to the N9···H bond length.

Table 3. The ρ values calculated at the N···H BCPs

	1	2	3
OCH_3	0.0491 (0.0508)	0.0560	0.0579
OH	0.0479(0.0502)	0.0556	0.0565
H	0.0483(0.0483)	0.0554	0.0554
CN	0.0443(0.0445)	0.0501	0.0507
NO_2	0.0445(0.0442)	0.0490	0.0401

The data in the parentheses correspond to the N9···H BCP.

References:

[] Bread, S.; Reva, I. D.; Lapinski, L.; Nowak, M. J.; Fausto, R. Journal of Molecular Structure. 786 (2006) 193-206.

[2] Singh, D.; Ojha, A. K.; kiefer, W.; Singh, R. Vibrational Spectroscopy. 49 (2009) 242-250.

[3] Ebrahimi, A.; Habibi, M.; Masoodi, H. R. Chemical physics. 340 (2007) 85-92.

Calculation of diffusion constant of water in sodium dodecyl sulfate solution: molecular dynamics simulation approach

Mohammad Reza Bozorgmehr*[a], S. Ali Beyramabadi[a] and Ali Morsali[a]

[a] Department of Chemistry, Faculty of Science, Islamic Azad University, Mashad Branch, Mashhad, Iran

Email: bozorgmehr@mshiau.ac.ir

Introduction

Diffusion is the tendency of molecules to spread into an available space. This tendency is a result of the intrinsic thermal energy (heat) found in all molecules at temperatures above absolute zero. The translational mobility of molecules is best described by the diffusion constant. The effect of sodium dodecyl sulfate (SDS) on the water diffusion constant is the subject of this project.

Method

All calculations were carried out using gromacs3.3.1 package [1]. The molecular dynamics simulations were carried out using periodic boundary conditions. To do this, nine cubic simulation boxes were defined with the dimensions of $7\times7\times7nm^3$. 0, 4, 8, 12, 16, 20, 24, 28 and 32 SDS molecules were placed in the center of the each box; subsequently the boxes were filled with 10000 water molecules. To do this, the SDS molecules were overlaid by equilibrated simple point charge (SPC) water boxes. To neutralize the system appropriate number of Na^+ ions added to each box. 40 molecules of glycine and 5 molecules of Tris were added to each simulation box. The aim of adding of glycine and Tris molecules according to reference [2] is to prepare buffer solution with pH=8.3.

Results and disscussion

Effects of SDS on the dynamic behavior of water were studied with aid of diffusion coefficient parameter. Diffusion coefficient were computed using Einstein's expression,

$$D = \lim_{t\to\infty} \frac{1}{2dt}\frac{1}{n}\sum_{j}^{n}\left\langle\left[x_j(0)-x_j(t)\right]^2\right\rangle \qquad (1)$$

Where d is the space dimension, n the number of particles, $x(t)$ the position of the particle at time t. Diffusion coefficients of water were calculated in absence and presence of various concentration of SDS and were shown in Fig. 1.

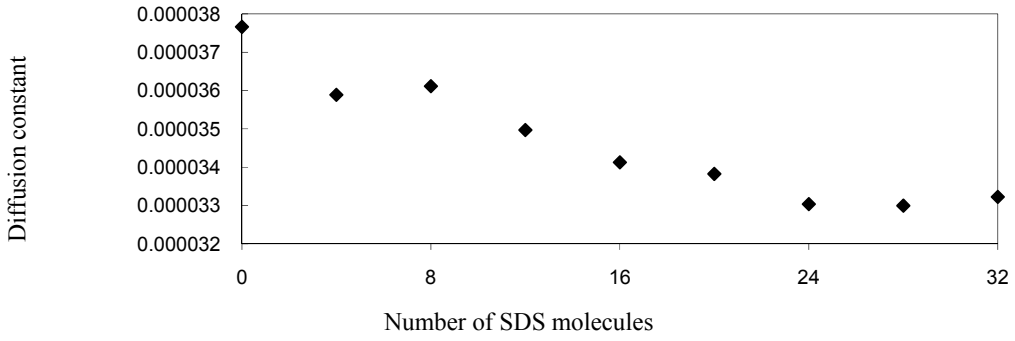

Fig.1: Diffusion constants (cm^2/s) of water versus number of SDS molecules.

The obtained values for diffusion coefficients in this work are comparable to that found previously for water molecule [3]. For pure water the self-diffusion constant is $2.3\times10^{-5}\,cm^2/s$, a value that is difficult to reproduce in simulations due to approximates applied in simple classical model and inadequate span time of simulation.

Conclusion

A conclusion central to our study is that the effects of SDS on the behavior of water are different in different concentrations.

Keywords: Sodium Dodecyl Sulfate, molecular dynamics simulation, Diffusion Constant, bovine carbonic anhydrase.

References

[1] E. Lindahl, B. Hess, D. van der Spoel, Comp. Phys. Comm. 91 (1995) 43-56.

[2] L. Katherine, I. G. Gudiksen, J. Yang, A. R. Urbach, D. T., Moustakas, G. M. Whitesides, JACS 127 (2005) 4707-4714.

[3] C. D. Bruce, S. Senapati, M. L. Berkowitz, L. Perera, M. D. E. Forbes, J. Phys. Chem. B. 106 (2002) 10902-10907

The dominant resonance structure of adenosine and adenosine like molecules

Ali Ebrahimi, Sophia Bazzi* and Mostafa Habibi-Khorassani
Department of Chemistry, University of Sistan and Baluchestan, P.O. Box 98135-674, Zahedan, Iran
(E-mail: sophia.bazzi@yahoo.com)

Introduction:

The real structure is a weighted average over all the probable resonance structures. The natural resonance theory (NRT) [1,2], which is based on natural bond orbital (NBO) analysis [3], calculates the weighting of a particular resonance structure that represents a particular bonding pattern. In the present study, a new method has been used to determine the dominant resonance structure of 3-methyl-2'–deoxyadenosine.

Methods:

All geometries have been optimized by the hybrid Hartree Fock density functional theory B3LYP in conjunction with the 6–311++G** basis set using Gaussian03 [4] program package.

Results and discussion:

The 3-methyl-2'–deoxyadenosine (3MDA) has been modeled by replacing the sugar phosphate backbone and 3'-hydroxyl group with hydrogen atoms. The model 3MDA has been deprotonated at N6 atom by deleting H1a; in this case the lone pair of N6 atom can participate in the new conjugation with the C2-N1 and C4-C5 bonds. The lengths of C4-N3, C2-N3, C6-N1, and C5-C6 bonds increase while the lengths of C2-N1 and C4-C5 bonds decrease upon deprotonation (see Figure 1).

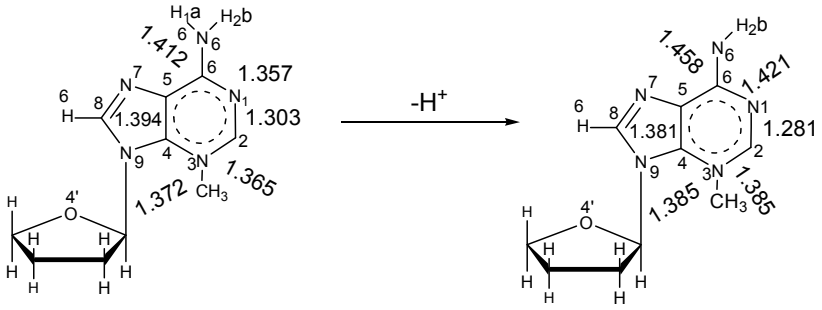

Figure 1. The normal and deprotanated forms of 3MDA and the most relevant bond lengths.

According to Figure 2, based on resonance structure **1**, an increase in the length of C2-N3 and C6-N1 and a decrease in the length of C2-N1 bond is expected upon deprotonation. On the other hand, based on the resonance structure **2**, an increase in the length of C5-C6 and C4-N3 and a decrease in the length of C4-C5 is expected upon deprotonation. (see Figure 2).

1 **2**

Figure 2. The two main resonance structures of adenosine.

According to Figure 1, the changes in the lengths of mentioned bonds are acceptable based on the resonance structures **1** and **2**. What structure is dominant resonance structure? To answer this question the changes in the lengths of C2-N3, C6-N1 and C2-N1 bonds are compared with the changes in length of C4-N3, C5-C6 and C4-C5 bonds, respectively, upon deprotonation of 3-methyl-2'–deoxyadenosine. As can be seen in Figure 1, the changes of the lengths of C2-N3, C6-N1 and C2-N1 bonds are higher than those of C4-N3, C5-C6 and C4-C5, respectively, which confirms the domination of structure **1**. According to eq. (1), the calculated weighting ratio (W.R) of **1** to **2** is equal to 1.01, in which r_d and r_n are the lengths of a bond in the deprotonated and normal forms.

$$W.R = \left[\frac{r_d}{r_n}(C6N1) + \frac{r_n}{r_d}(C2N1) + \frac{r_d}{r_n}(C2N3)\right] \Big/ \left[\frac{r_d}{r_n}(C6C5) + \frac{r_n}{r_d}(C4C5) + \frac{r_d}{r_n}(C4N3)\right] \qquad \text{eq. (1)}$$

Our results are in a very good agreement with the previous results calculated based on NRT method [**Error! Bookmark not defined.**] in which the dominant resonance structure was predicted to be **1** and the W.R was equal to 1.01 according to following equation:

W.R = [weighting of structure **1** / weighting of structure **2**] = (9.92/9.87) = 1.01

Conclusions:

The weighting ratio of resonance structures of adenosine and adenosine like molecules estimated through comparing the relevant bond lengths in the normal and deprotonated forms.

Refrences:

[1] Sun, G.; Nicklaus, M. C. Theor Chem Acc 2007, 117, 323.
[2] Glendening, E.D.; Weinhold, F. J Comput Chem 1998, 19,593.
[3] Reed, A. E.; Curtiss, L. A.; Weinhold, F. Chem. Rev., 1988, 88, 899.
[4] Frisch, M.J. et al., Gaussian 03 (Revision B.03) Gaussian, Inc, Pittsburgh, PA, 2003.

Probing ^{13}C chemical shielding tensors in cryptolepine and 2,7-dibromocryptolepine for antiplasmodial activity

Hadi Behzadi*[a], Mohamad Reza Talei Bavil Olyai[b]

[a]Department of Chemistry, Islamic Azad University South Tehran Branch, Tehran, Iran

(E-mail: behzadihadi@yahoo.com)

[b]Department of Chemistry, Islamic Azad University Karaj Branch, Karaj, Iran

Key words: Cryptolepine, Malaria, DFT, chemical shielding, Antiplasmodial activity

Introduction:

Cryptolepine **1**, an indoloquinoline alkaloide, is the most potent antiplasmodial compound known; it is derived from the West African plant *Cryptolepis Sanguinolenta* [1]. Four different *Plasmodium* species are responsible for malaria infection to humans: *P. vivax*, *P. ovale*, *P. malariae*, and the most severe one world, *P.falciparum* [2]. A dibromoanalogue cryptolepine **2**, was found to be 10 times more potent than cryptolepine [3]. One significant problem in the fight against malaria is the appearance of resistance to known treatment.

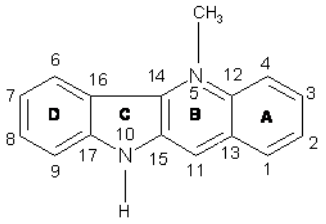

1

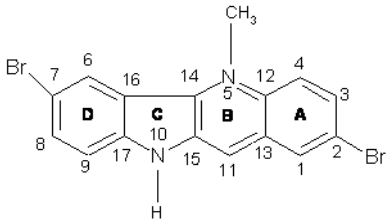

2

The aim of this paper is to determine if electronic properties around carbon nuclei may be used as marker to distinguishing different activity of compounds **1** and **2** (Figure 1). Thus, we were encouraged to calculate CS tensors at each carbon for indoloquinolines (compounds **1** and **2)** to determine how bromosubstitutions affects tensor elements and causes more activity for substituted cryptolepine.

Computational details:

The structure of indoloquinoline compounds **1** and **2** were optimized using the B3LYP/6-31G* [4]. Shielding calculations were performed using fully polarized 6-311++ G** basis

sets. This method and basis sets were previously tested on organic compounds and can produce reliable results for the CS tensor and their orientations. The calculations were performed using Gaussian 98 suite of programs [5].

Results and discussions:

In the present study, we calculated the carbon shielding tensors of cryptolepine **1** and 2,7-dibromocryptolepine **2** to investigate the relationship between electronic properties of these compounds and their difference in antimalarial activity. The bromo substitutions at the 2 and 7 positions of cryptolepine affect not only CS tensors of carbons in the substituted **A** and **D** rings, but CS tensors of carbons in **B** and **C** as well. Changes in isotropic chemical shielding $\Delta\sigma_{iso}$ are 0.11 – 17.70 ppm, where CS components σ_{ii} show a larger range of 0.11– 49.44 ppm from unsubstituted to bromosubstituted cryptolepine. The changes in shielding tensors of C1-C3 in **A** ring of quinoline and C6- C8 in **D** ring of indole are significant, where σ_{33} is the most affected tensor. The σ_{33} tensors decrease by an average 12.10 ppm from cryptolepine to bromosubstituted cryptolepine. C2 and C7 are deshielded about 49 ppm and ortho carbons change by 19-24 ppm. As a result, it seems that significant decreasing of σ_{33} component for all carbons in the **A** and **D** rings of bromosubstituted cryptolepine could be related to higher activity of this compound compared to bare cryptolepine. Decreasing in isotropic values for carbons in **A** and **D** rings of substituted relative to unsubstituted cryptolepine is mainly caused by the σ_{33} component of carbons.

Conclusion:

In the present study, we address some of the questions by an explanation of the electronic effect of bromosubstitutions on the cryptolepine structure through calculations of ^{13}C chemical shielding tensors and atomic charges. The substituted and ortho carbons are affected the most by the substitutions. Large decreases in the σ_{33} component and compensating increases in the σ_{11} tensors for carbons of the **A** and **D** rings of 2,7-dibromocryptolepine relative to bare cryptolepine were found. It is supposed that the enhanced activity of bromo-substituted cryptolepine is related to decreasing in σ electron density and increase in π-electron density for ortho and para positions. These changes in electronic structure and

properties may play a role in understanding the binding of cryptolepine molecules to DNA and hence aid in rational design of novel anti-malarial drugs.

References:

[1] Delvaux E, *J. Pharm. Belg*. 13 (1931) 973.

[2] Oliveria AB, Ânidolabela MF, Braga FC, Jacome R LRP, Varott FP, Povoa MM, *An Acad Bras Cienc* 81(2009) 715.

[3] Wrigth CW, *J. Pharm. Pharmacol*. 59 (2007) 899.

[4] A. D. Becke, *Phys. Rev. A* 38 (1988) 3098.

[5] M.J. Frisch et al., Gaussian 98 (Revision A. 11), Gaussian, Inc, Pittsburgh, PA (2001).

Direct calculation of Henry's law constants from Gibbs Free Energy Using the Computational Method

Z.Bayat

Department of Chemistry, Islamic Azad University Quchan Branch, Iran

Abstract

Delivery of anti-viral agents into the central nervous system (CNS) is clinically important. Nucleoside analogues are major clinically used anti-viral agents [1]. In this study Henry's law constants at T = 293.2 K are calculated for several Nucleoside Analogues in water by density functional theory (DFT) methods at B3LYP/6-31G* and Hartree Fock (HF/6-31G*) levels of theory using the Poisson-Boltzmann solvation model. Keyword: Nucleoside Analogues, DFT, Henry law, Free energy

Introduction

ΔG_{sol} is a key property to estimate the fate of a chemical once it is released in the environment. From an environmental point of view, an important partition coefficient is the Henry's law constant (K) which can be calculated straightforwardly from the free energies of solvation in water.[2]

$$K\ (\rho\ ,T\ ) = \ RT\ \ \rho\ \exp\ \left(\frac{\Delta\ G_{\ sol}}{RT}\right)$$

Where ρ is the density of the pure solvent, which is equal to that of the solvation in the limit of infinite dilution. According to the above discussion, the caculation of log P of Nucleoside analogouse is important.We have selected eleven Nucleoside analouges that have important clinically activity.

Computational Method

The geometry of the molecules used here was fully optimized by Hartree – Fock (HF) and DFT (B3LYP) calculations with the 6-31G* basis set (HF/6-31G*) in the Gaussian 03 package. The Gibbs solvation free energies of drugs in water were calculated based on HF and B3LYP methods for Nucleoside Analogues.

Results and Discussion

The results are presented in Table 1. HF/6-31g* estimated more negative solvation free energies than the B3LYP/6-31G* method in PCM model. Henry's law constant was calculated from equation (1) by using of free energy solvation.

Conclusions

In this study, we have applied ab initio method for calculation of some properties and the free energy solvation in two solvents. The first calculations began with the geometry optimization of drugs by using of Hartree Fock and DFT methods . Then, solvation free energy of drugs was calculated in the water based on HF and B3LYP method at three basis sets.

Table 1. the solvation Gibbs free energy in water and Henry's costant based on HF/6-31G* and B3lyp/6-31G*

compound	$\Delta G_{sol(water)/HF}$	K(ρ,T)/HF	$\Delta G_{sol(water)/B3lyp}$	K(ρ,T)/B3lyp
Zalcytabine	-22.20	568.93	-19.52	571.77
zidovudine	-27.61	572.70	-22.86	563.75
stavudine	-15.18	563.75	-13.84	579.13
didanosine	-21.68	569.43	-18.70	572.30
Theophelline	-19.63	571.40	-17.07	573.87
caffeine	-13.36	577.48	-12.92	577.908
Theobromine	-18.50	572.49	-16.43	574.50
Phenobarbital	-9.07	581.68	-8.87	581.87
cyclobarbital	-9.42	581.33	-7.10	583.61
Acilclovire	-29.26	562.19	-25.35	565.91
thiopental	-7.39	583.33	-4.96	585.73

References

[1] ***Hasegawa, T.*; *Kawaguchi, T.*** Delivery of anti-viral nucleoside analogs. *J. Curr. Med. Chem. Anti-Infective Agents.,* **2002**, 1, 55-63.

[2] Robert , W. ; William H. Green*. Ab Initio Aqueous Thermochemistry, *J. Phys. Chem. B* 2007, *111,* 11968-11983

Cu(II) Complex of the N,N′-Dipyridoxyl (1,3-propanediamine) Schiff-Base Ligand: A DFT Study

S. A. Beyramabadi*, M. R. Bozorgmehr and A. Morsali
Department of Chemistry, Faculty of Science, Islamic Azad University, Mashhad branch, Mashhad, Iran
(E-mail: beiramabadi@mshdiau.ac.ir)

Keywords: Schiff-base; Density Functional Theory; IR Assignment; Copper (II), Salen.

Introduction

Due to structural varieties and very unique characteristics, the Schiff bases are the most versatile studied ligands in coordination chemistry [١,٢]. Theoretical analysis of the IR and NMR spectra is an important tool to ensure suitability of the proposed structures for chemical compounds [3]. The x-ray structures of the N,N′-dipyridoxyl(1,3-propanediamine) [= H_2L] Schiff-base ligand and its Cu(II) salen complex, [Cu(L)(H_2O)], have not been determined. Here, their geometries optimization together with theoretical assignment of their IR and ^{1}H-NMR spectra have been performed by using density functional theory (DFT).

Methods

All the present calculations have been performed by using the Gaussian 98 program package [4], where the B3LYP functional [5] of the DFT method was employed. Geometries of the H_2L ligand and its Cu complex were optimized at 6-31G(d,p) basis sets expect for the Cu atom where LANL2DZ basis sets were used. The fully optimized geometries of the ligand and complex were used as input structures for calculation of their vibrational frequencies and the ^{1}H NMR chemical shifts of H_2L (GIAO method) at the same computational level.

Results and Discussion

The optimized geometries of the ligand and its Cu complex are shown in Fig. 1, where two pyridine rings of the H_2L ligand make a dihedral angle of approximately 70.0° with each other. The calculated O1H1…N1 and O2H2…N2 hydrogen bonds are 171.7 and 171.3 pm respectively. The engagement in the hydrogen bond interactions causes to longer phenolic O-H bonds than alcoholic O-H ones. During complex formation, two substituted pyridine rings

rotate around the C17-N1 and C18-N2 single bonds, which puts them roughly in the same plane. This provides structural requirements for the complex formation, so that the O1…O2 and N1…N2 distances decrease in the complex. The L^{2-} acts as a dianionic-tetradentate ligand in N,N,O^-,O^- manner via the deprotonated phenolic oxygens and the azomethine nitrogens. These coordinating atoms of L^{2-} occupy equatorial positions, where the axial position of the square-pyramidal Cu(II) complex has been occupied by H_2O ligand. The calculated structural parameters are in agreement with the experimental values reported for similar compounds.

In the IR spectrum of complex, the symmetrical stretching modes of C8=N1 and C16=N2 bonds appear at lower energy by 10 cm^{-1} in comparison with the free ligand. Also, the stretching vibrations of phenolic C-O bonds shift to the higher frequencies by 23 cm^{-1} in the spectrum of the complex. These confirm coordination of the ligand through the azomethine nitrogens and phenolic oxygens. Some new bands are appeared in the IR spectrum of Cu complex, which are assigned to the Cu-O vibrations and vibration modes of the H_2O ligand. The phenolic protons are engaged in the intramolecular hydrogen bond interaction (O-H…N), which shifts their ^1H NMR signals upfield.

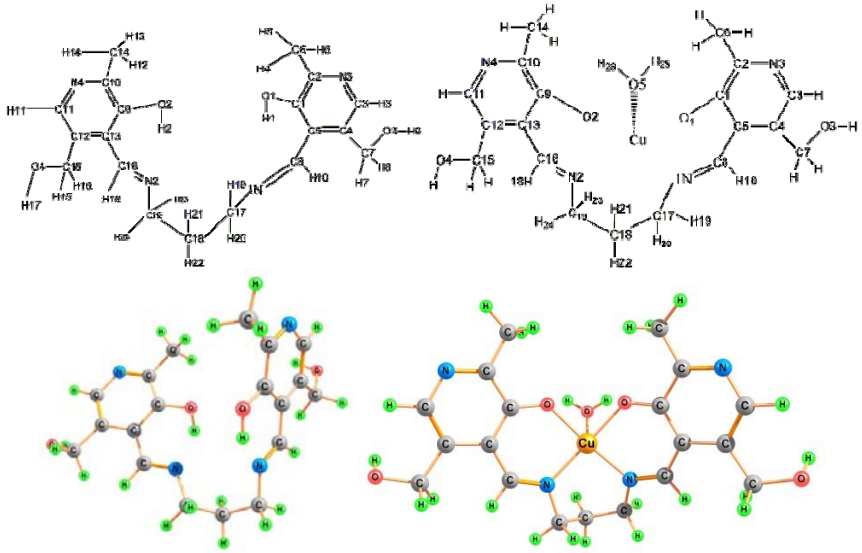

Figure 1. The B3LYP optimized geometries of the H_2L ligand and its Cu complex together with their labeling.

Conclusions

The V-shape molecule of the titled ligand isn't planar, which acts as a dianionic-tetradentate ligand via the deprotonated phenolic oxygens and the azomethine nitrogens. The H_2O ligand occupies the axial position of the square-planar Cu(II) complex. The DFT calculated IR

frequencies and ^{1}H NMR chemical shifts are well in agreement with the experimental results, confirming suitability of the optimized geometries for the ligand and its Cu complex.

References:

[1] D. Yu, H. Xiaoxia, S. Xiaoli, Z. Zhiling, Wuhan Univ. *J. Nat. Sci.* 15 (2010) 165-170.

[2] D. Kumar, P.K. Gupta, A. Syamal, *J. Chem. Sci.* 117 (2005) 247-253.

[3] D.C. Young, Computational Chemistry: A Practical Guide for Applying Techniques to Real-World Problems, John Wiley & Sons, Inc., 2001.

[4] M.J. Frisch, et al. *Gaussian 98*, Revision A.7; Gaussian, Inc.: Pittsburgh PA, 1998.

[5] C. Lee, W. Yang, R.G. Parr, *Phys. Rev. B* 37 (1988) 785-789.

Study Of The Rearrangement Mechanism [3,3] Of Structure 3-methylhexa-1,5-dien-3-ol Using Ab initio Calculation With NBO Analysis

R.Soleymani*[a,c] , M.biglari[b], O.Basiri[b] , F.Afshari[a,b], M.karimi[d]

[a]*Chemistry Department, Faculty of Sciences, Islamic Azad University, Touyserkan Branch, Young researchers Club, Touyserkan ,Iran*

(Email: nima_soleimany@yahoo.com)

[b]*Chemistry Department, Faculty of Sciences, Islamic Azad University Touyserkan Branch, Touyserkan, Iran*

[c] *Chemistry Department, Faculty of Sciences, Islamic Azad University Yadegare emam Branch, Tehran, Iran*

[d] *Chemistry Department, Faculty of Sciences, Islamic Azad University Omidie Branch, Omidie, Iran*

Abstract

Ab initio calculation of quantum mechanism on structure 3-methylhexa-1,5-dien-3-ol and its transformation to structure (Z)-hepta-2,6-dien-2-ol were done which its results showed that this type of rearrangement [3,3] needs 68.5499825 Kcal/mol energy and the process of this rearrangement is exothermic. Also NBO analysis showed that this mechanism is allowed from the aspect of synchronism and the reaction normally complies with the rules of cycloaddition reaction.

Keywords: Ab initio; Cycloaddition reaction; ;DFT; NBO; Rearrangement [3,3]

Introduction

Rearrangement [3,3] is a kind of sigmatropic reactions which such as electro cyclic reactions and cycloadditions are controlled by orbital synchronism aspects. Totally in this mechanism one atom or a substituted group with. Sigma bond immigrate from one position to the other , during pay electron system. This mechanism can be used in experimental reaction for reaching to a better result[1].

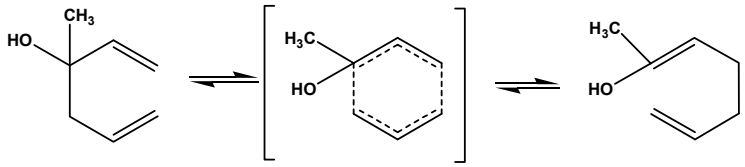

1 **2** **3**

Methods

For calculations Ab initio and DFT method used GAUSSIAN 03 software[1]. In this calculation firstly designed structure 3-methylhexa-1,5-dien-3-ol by Chemoffice 2010 software and optimization operated by using Gaussian software and B3LYP , HF method[3]. Too for initial transition state used Winmopac version 2 and SADDLE keyword. Also for calculation Natural Bond Orbital (NBO) used NBO-version 3 and for total calculation used pentum-PC computer with intel core 2 Due 2.66 GHZ processor.

Result and discussion

The obtained results of Ab initio quantum mechanic calculation at the theory of the level B3LYP and HF together with 6-311+G** and 3-21G basic set are reported in the following table. In this table calculated energies (in Hartree) for the important geometries of rearrangement reaction of structure 1- 3.

Method	Structure	ZPE	Eele	E_0	ΔE_0[a]
HF/ 6-311+G**	1	0.188729	-346.9587794	-346.770051	0.011023 (6.91693250)[a]
	2	0.188617	-346.9476452	-346.759028	
	3	0.188778	-346.9475370	-346.758759	
B3LYP 3-21G	1	0.176022	-347.2391515	-347.063129	0.109265 (68.5637875)[a]
	2	0.173111	-347.1269757	-346.953864	
	3	0.176008	-347.2391512	-347.063143	
B3LYP 6-311+G**	1	0.174013	-349.2592421	-349.085229	0.109243 (68.5499825)[a]
	2	0.172352	-349.1483381	-348.975986	
	3	0.174012	-349.2592422	-349.085230	

[a]Numbers in parenthesis are the corresponding values in kcal mol^{-1}

Method	Structure	Dipole moment (Debye)	Thermal capacity (Cal/Mol-Kelvin)	Entropy (Cal/Mol-Kelvin)	E (Thermal) KCal/Mol
HF/6-311+G**	1	1.6746	28.813	83.642	123.060
	[1→2][#]	1.8445	28.921	84.319	123.044
	2	1.8278	28.760	84.165	123.093
B3LYP/3-21G	1	0.9337	34.499	98.251	116.569
	[1→2][#]	2.1485	32.442	86.521	113.791
	2	0.9336	34.502	98.517	116.567
B3LYP/6-311+G**	1	1.0121	35.053	98.508	115.366
	[1→2][#]	2.1199	31.764	86.264	113.184
	2	1.0121	35.054	98.508	115.365

Conclusion

Ab initio quantum mechanic calculation and Density of Function Theory (DFT) method at theory of the level HF/6-311+G** , B3LYP/3-21G and B3LYP/6-311+G** showed that sigmatropic mechanism [3,3] of transformation structure 3-methylhexa-1,5-dien-3-ol to (Z)-hepta-2,6-dien-2-ol needs 68.5499825 Kcal/mol energy and the process of this reaction is exothermic. Also hence the number of atoms in the ring is an even number the group sigma bond can exist at two heads of or in the middle of pay system. The results of NBO analysis , confirmed it too and showed that during reaction. A pay bond is broken and a new sigma pay bond is formed and also pay bonds move.

References

[1] Martin O. Cloonan, *Application of the Cplex-isoelectronic theory* , International Journal of Hydrogen Energy Volume 32, Issue 14, Pages 3026-3039 , September **2007**

[2] M. j. Frisch et al. *GAUSSIAN 03*, Revision C. 01, Gaussian Inc.,Wallingford. CT, **2004**.

[3] www.CambridgeSoft.com,*CambridgeSoft Corporation*, All Rights Reserved. ©**1998-2010**

Theoretical Study for Reaction between Triethylphosphite and Activated Acetylenic Esters in the Presence of NH Heterocyclic Compound 1-phenyl pyrazolidin-3-one

S. M. Habibi Khorassani*[a], M. T. Maghsoodlou[a], A. Ebrahimi[a] and A.Paknahad[a]

e-mail: smhabibius@yahoo.com

[a]*Department of Chemistry, University of Sistan and Baluchestan, P.O. Box 98135-674, Zahedan, Iran*

Keywords: Stable phosphorus ylides; dialkyl acetylenedicarboxylates; ***Z*** and ***E*** isomer; AIM method

Introduction

In the current works, the stability of the Z and E isomers was undertaken for the two isomer of a phosphorus ylide by means of atoms in molecules (AIM) analysis. A facile synthesis of the reaction between triphenylphosphine **1**, dialkyl acetylendicarboxylates **2** and 1-phenyl pyrazolidin-3-one **3** (as a NH-acid)has been investigated obtaining significant date . The reaction is shown in Figure **1**. The Z and E isomers were optimized for all ylide structures at HF/6-31G(d,p) level of theory[1] by Gaussian03 package program[2]. The energy of both isomers have been calculated at B3LYP/6-311++G(d,p) level. Atoms in molecules (AIM) analysis at HF/6-31G(d,p) level of theory have been performed in order to gain a better understanding of most geometrical parameters in both *E*-**4(a, b)** and *Z*-**4(a, b)** of phosphorus ylides. The numbers of critical points and intramolecular hydrogen bonds as well as the charge of atoms that constructed on the Z and E isomers have been recognized. The results altogether reveal the effective factors on stability of *Z* and *E* ylide isomers.

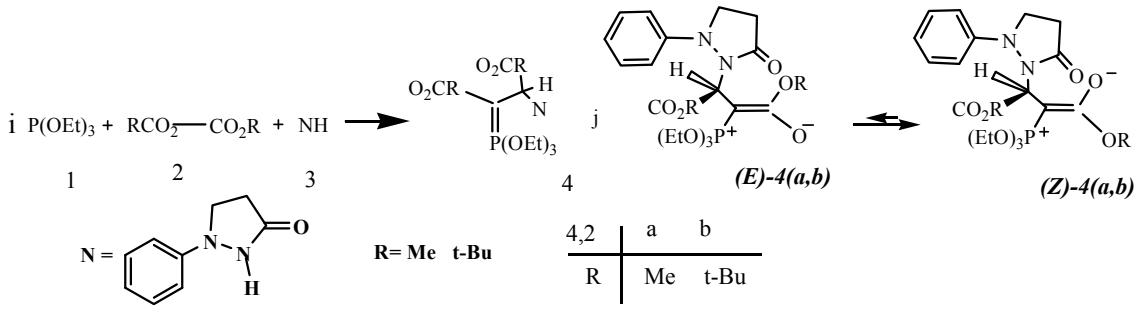

Figure 1: (i) The reaction between triphenylphosphine **1,** dialkyl acetylenedicarboxylate **2** (**2a** or **2b)** and 1-phenyl pyrazolidin-3-one for generation of stable phosphorus ylides **4** (**4a** or **4b**), **(j)** The two isomers (*Z)*-**4a** and (*E*) - **4a** (major and minor) of ylide **4a**

Results and Discussion

Theoretical study and Calculations

The relative stabilization energies for both [*Z*-**4(a, b)** and *E*-**4(a, b)**] isomers are reported in Table **1**, as can be seen, *Z*-**4a** and *Z*-**4b** isomers are more stable than *E*-**4a** and *E*-**4b** forms (0.22 and 2.48 kcal/mol respectively) at B3LYP level.

Table **1**: The relative energy (kcal/mol) for both Z and E isomers of ylides **4a** and **4b**, obtained as HF/6-31G(d,p) and B3LYP/6-311++G(d,p) levels**.**

Conformer	HF	B3LYP
Z-4**a**	0.00	0.00
E-4**a**	0.25	0.22
Z-4**b**	0.00	0.00
E-4**b**	3.06	2.48

Further investigation was undertaken in order to determine more effective factors on stability of both isomers, on the basis of AIM calculations [3] at HF/6-31G(d,p) level of theory by the AIM2000 program package [4]. The number of hydrogen bonds in both categories (*E*-**4a** and *Z*-**4a**) and (*E*-**4b** and *Z*-**4b**) are (6 and 8) and also (14 and 15), respectively (See Table **2** and **3**).

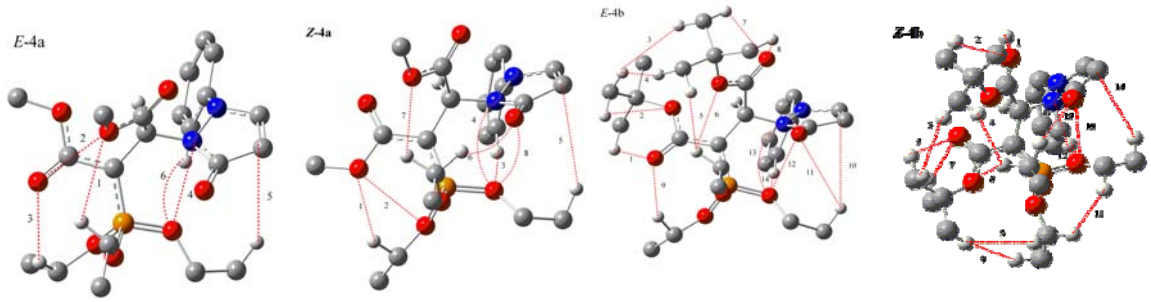

Figure 2: Intramolecular hydrogen bonds (dotted lines) in *E*-**4a,** *Z*-**4a,** *E*-**4b** and *Z*-**4b** isomers of stable ylide **4a** and **4b** recpectivly.

Table **2**: The values of $\rho \times 10^3$, $\nabla^2\rho \times 10^3$ and Hamiltonian $H(r) \times 10^4$ for both *Z*-**4a** and *E*-**4a** isomers of ylide **4a** calculated at the hydrogen bond critical points. All quantities are in atomic units

E	ρ	$\nabla^2\rho$	H(r)	Z	ρ	$\nabla^2\rho$	H(r)
1	5.10	21.99	-10.70	1	10.12	41.84	-12.36
2	8.41	34.69	-5.94	2	13.74	53.47	-4.87
3	12.18	48.52	-13.11	3	4.68	20.35	-9.44
4	12.96	42.79	-1.00	4	12.86	42.58	-1.07
5	2.22	6.98	-4.07	5	2.32	7.32	-4.24
6	5.06	21.53	-9.36	6	10.74	38.44	-6.32
				7	6.08	25.07	-10.67
				8	10.76	40.73	-3.60

Table 3: The values of $\rho \times 10^3$, $\nabla^2\rho \times 10^3$ and Hamiltonian $H(r) \times 10^4$ for both *Z*-**4b** and *E*-**4b** isomers of ylide **4b** calculated at the hydrogen bond critical points. All quantities are in atomic units

E	ρ	$\nabla^2\rho$	H(r)	Z	ρ	$\nabla^2\rho$	H(r)
1	12.7	48.7	-12.4	1	12.76	49.54	-13.46
2	13.0	49.0	-4.19	2	12.22	47.66	-13.65
3	1.99	6.92	-6.40	3	2.19	7.57	-4.96
4	2.71	9.63	-9.97	4	3.10	11.48	-7.38
5	4.12	15.6	-9.37	5	2.16	7.83	-4.61
6	3.89	17.3	-3.64	6	13.13	49.78	-7.38
7	12.6	48.5	-13.9	7	4.39	20.38	-9.83
8	13.0	50.5	-12.1	8	12.47	47.96	-12.92
9	12.7	49.8	-7.32	9	2.058	7.470	-4.81
10	2.38	7.40	7.32	10	2.86	8.88	-4.88
11	9.00	32.8	-5.05	11	9.05	36.97	-5.61
12	10.5	40.6	-1.02	12	3.61	14.22	-8.36
13	13.8	45.5	-9.23	13	4.84	20.65	-9.33
14	5.44	22.7	-9.22	14	12.65	41.35	-0.55
				15	5.23	20.91	-8.99

On the basis of theoretical calculations (Table **1**), the difference between the relative stability of the *E*-**4a** in gas phase is small (0.22 kcal/mol). Perhaps this negligible difference is not taken more considerably in solution media for **4a**, for this reason it is possible to see the two isomers of **4a** and **4b** (both *Z* and *E* isomers).In contrary,this diference for the two isomers of ylide (Z-4b) and (E-4b) is considerable large,for this reason,only a single isomer can be observed for ylide **4b**. Experimental results [5] obtained from the ^{1}H, ^{13}C, ^{31}P NMR for the two isomers in ylides **4a** and isomer alone of **4b** showed that those are consistent with the results of the theoretical calculations.

Conclusion

The assignment of the Z and E isomers as a major or minor form in both ylides **4a** and **4b** were undertaken by AIM method. Quantum mechanical calculation was used to clarify how ylides **4a** and **4b** exist in solution as a mixture of the two geometrical isomers.

References

[1] M. J. Frisch, et al. Gaussian 03, Revision C. 01, Gaussian, Inc., Wallingford CT, 2004

[2] A. E. Reed, R. B. Weinstock, F.J. J. Weinhold, Chem. Phys, 83 (1985) 735.

[3] R. F. W. Bader, Atoms in molecules A Quantum Theory, Oxford University, New York, (1990).

[4] F. W.Biegler König, J.Schönbohm, D. J. Bayles, Comput. Chem. 22(2001) 545.

[5] A. A. Esmaili, M. Ghereghloo, M.R. Islami, H.R. Bijanzadeh, *Tetrahedron*, 59 (2003) 4785.

Calculation of pKa values of phenolic acid and phenol derivatives in aqueous and non aqueous solution using density functional theory

Mohammd Alimoradi, Hadi Shafiei*, Ghazaleh Pashmchi

Department of chemistry,Faculty of Science,Islamic Azad University,Arak Branch, Iran

E-mail: M_ghobeyti@yahoo.com

Abstract

This work presents calculated values of the pKa for a series of phenolic acids in aqueous and nonaqueous solvents as water and MeCN. The pKa values have been calculated using density functional theory(DFT). The conductor polarizable continum model(CPCM) is used to describe th solvent. Using these models , we successfully predicted the pKa of phenolic acids in aqueous and nonaqueous solvents.

Keyword: Density functional theory, phenolic acid, aqueous and nonaquueous solvent, CPMC

Introduction

The pKa of a compound is an important property in both the life science and chemistry. Since the tendency of a compound to donate or accept a proton is fundamental to understanding many chemical and biochemical process[1-4]. The pKa value of a molecule determines the amount of protonated and nonprotonated forms of a specific pH. The Handeson-Hasselbach equation that shown below, allows such determinations:

$$pH = pKa + \log\frac{[unprotonated\ \ form]}{[protonated\ \ form]}$$

It is possible in principal to calculate pKa values using quantum mechanics. Gas phase free energy and solvation free energy values can be calculated and these results can then be used to determine pKa's. The following thermodynamic cycle illustrates the deprotonation of a phenolic acid.

$$\begin{array}{ccccc} AH_{gas} & \xrightarrow{\Delta G_{gas}} & A^-_{gas} & + & H^+_{gas} \\ \downarrow \Delta G_{sol} & & \downarrow \Delta G_{sol} & & \downarrow \Delta G_{sol} \\ AH_{sol} & \xrightarrow{\Delta G_{sols}} & A^-_{sol} & + & H^+_{sol} \end{array}$$

From this equation, values can be calculated in two ways: absolutely and relatively. We did chose relative pKa calculations, where we have tow phenolic acids(given by AH and BH). The following equation was used:

$$pKa_{(BH)} = pKa_{(AH)} + \Delta pKa$$

Since

$pKa = \Delta G_{aq} / 2.303RT$, *were* $\Delta\Delta G_{aq} = \Delta G_{(BH)} - \Delta G_{(BH)}$

$\Delta G_{aq}(AH) = G_{gas}(A^-) + G_{gas}(H^+) - G_{gas}(AH) + \Delta G_{sol}(A^-) + \Delta G_{sol}(H^-) - \Delta G_{sol}(AH)$ *and*

$\Delta G_{aq}(BH) = G_{gas}(B^-) + G_{gas}(H^+) - G_{gas}(BH) + \Delta G_{sol}(B^-) + \Delta G_{sol}(H^+) - \Delta G_{sol}(BH)$ *so that*

$\Delta\Delta G_{aq} = G_{gas}(B^-) - G_{gas}(A^-) - G_{gas}(BH) + G_{gas}(AH) + \Delta G_{(BH)} + \Delta G_{sol}(B^-) - \Delta G_{sol}(A^-)$
$- \Delta G_{sol}(BH) + \Delta G_{sol}(AH)$

thus, for relative pKa calculations, the following equation was used:

$$pKa_{(BH)} = pKa_{(AH)} + \left\{ \begin{array}{l} G_{gas}(B^-) - G_{gas}(A^-) - G_{gas}(BH) + G_{gas}(AH) + \Delta G_{(BH)} \\ + \Delta G_{sol}(B^-) - \Delta G_{sol}(A^-) - \Delta G_{sol}(BH) + \Delta G_{sol}(AH) \end{array} \Big/ 2.303RT \right\}$$

Results and discussion

We started nine phenolic acids and performed calculation on them. All calculation were performed with Gussian03 software. We started by building the acids and their corresponding ions and optimizing each species at the Hartree-Fock(HF) and density function theory(DFT) level with 6-31+g basis set.

Then its applied to calculate the pKa values for a variety of organic acid in several aqueous and nonaqueous solvents as water and MeCN.

compound		4-floro phenol	2-methyl phenol	3-methyl phenol	4-methy phenol	3-nitro phenol	2-nitro phenol	4-nitro phenol	phenol	3-bromo phenol
pKa in H_2O	Exp	9.95	10.28	10.08	10.19	8.39	7.24	7.16	9.95	9.11
	Theory	10.11	9.91	10.28	10.25	8.21	6.94	7.36	9.93	9.14
pKa in 10%(v/v) MeCN	Exp	9.79	9.98	10.15	9.44	9.38	8.23	8.45	9.92	10.22
	Theory	9.93	8.72	10.34	9.24	9.67	8.43	8.86	10.23	10.34

References

[1] A. M. Magill, B. F. Yates, Aust.J. Chem. 57 (2004) 1205.

[2] A. M. Magill, K. J. Cavell, B.F. Yates, J. Am. Chem. Soc. 126 (2004) 8717.

[3] Y. Fu, L. Liu, H.- Z. Yu, Y. Wang, Q. –X. Guo, J. Am. Chem. Soc. 127 (2005) 7227

[4] E.C. Shere, G. M. Turner, T. N. Lively,and G. C. Shields, J. Molecular Modeling, 62 (1996)

A DFT study on the adsorption of O_2, N_2, CO and CH_4 on Single Wall Aluminium Phosphide nanotubes

K. Azizi* and H. Poursadegh
Department of Chemistry, University of Kurdistan, Sanandaj, Iran
(Email:azizkhald822@yahoo.com)

Keywords: Density Functional Theory; Electronic structure; Aluminum Phosphide Nanotubes; Gas adsorption.

Introduction:

Aluminium phosphide nanotubes (AlPNTs) are new groups of inorganic nanotubes that have been synthesized empirically [1]. Previous studies have shown that, AlPNTs are semiconductive materials with a band gap of 2.1-3.73 ev and the band gap increases with the tube diameter. While several theoretical studies have been done on AlPNTs [2], the process of gas adsorption on these kinds of nanotubes has not been investigated. It is known that the conductivity of SWNTs can change due to the gas adsorption process [3]. Therefore, the band gap information may be used as a basis for application of SWNTs as gas sensor. In this research, adsorption of O_2, N_2, CO and CH_4, on the interior and exterior surface of zigzag and armchair AlPNTs was studied by using ab initio calculations [4].

Computational Methods:

The structures of isolated species and molecular complexes were optimized with DFT method at the hybrid functional B3LYP and the medium-size basis set 6-311++d,p level. No molecular symmetry constraint was applied; rather full optimization of all bond lengths and angles was carried out. The equilibrium geometries were confirmed by a subsequent calculation of force constants and vibration analysis. Each species was found to be a minima by having no negative values in the frequency calculation. Adsorption energies, E_{ad}, were obtained as the difference between the energy of the complex and the combined energies of the species in isolation. All calculations on the isolated species and molecular complexes were performed within GAUSSIAN 03 program package.

Results and Discussion:

Figure 1 shows the optimized structures of different gases adsorbed on exterior surface of zigzag (7,0) AlP nanotube.. It can be seen in Fig. 1 that this nanotubes consist of two cylindrical layers, in which the inner and outer cylinders are composed of aluminum and phosphorus atoms, respectively.

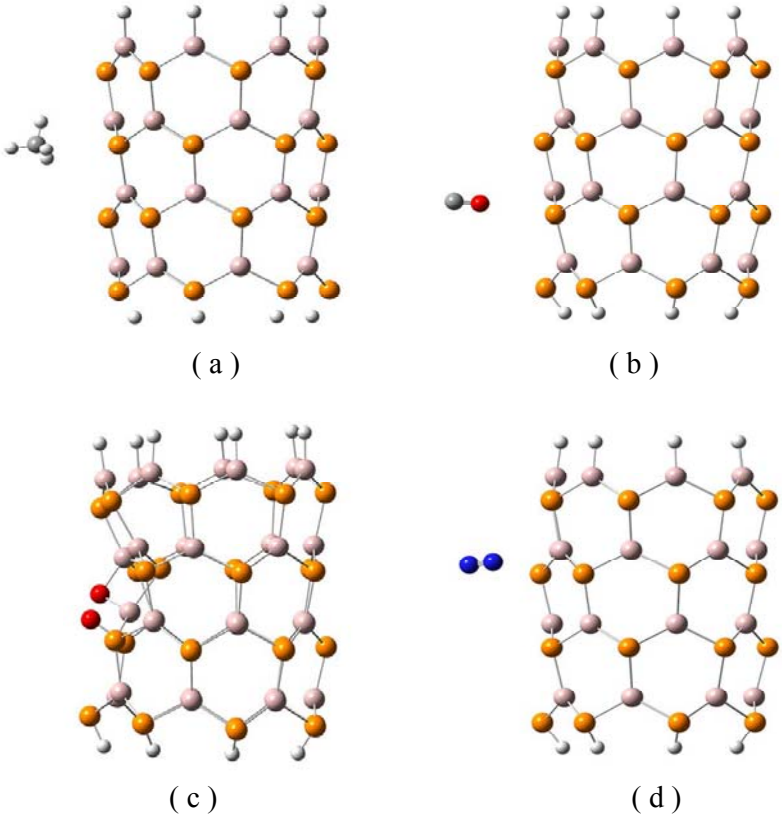

Figure 1. The optimized structures of zigzag (7,0) AlP nanotube in presence of different gases, (a)CH_4, (b) CO, (c) O_2 and (d) N_2.

In Table 1, the energies of adsorption of O_2, N_2, CO and CH_4 on both inner and outer surfaces of (7, 0) AlPNT are given in kcal.mol^{-1}. As shown in Table 1, the maximum value of E_{ad} is belong to the chemisorption of O_2 on the inner surface of nanotube and the other gases are physisorbed on both inside and outside of (7,0) AlP nanotube. Among the physisorbed gases, the maximum and minimum values of E_{ad} are belong to CO and CH_4 gases respectively. As

can be seen in Table 1, the adsorption energy of CO is considerably more than that of N_2, while, it is demonstrated that CO and N_2 molecules have similar behavior when they adsorbed on single wall carbon nanotubes. Therefore, one may expected that the electrostatic interactions have an essential role in adsorption of gases on surface of AlP nanotubes. This finding is confirmed by small E_{ad} of CH_4. Based on the values of HOMO-LUMO gap, given in Table 1, the conductivity of (7,0) AlP nanotube changes partially due to gas adsorption process. In the case of O_2 gas, the HOMO-LUMO gap considerably changed due to performing a chemisorption process. Among the physisorbed gases, the effects of N_2 and CO molecules are stronger than that of CH4. Therefore there is a direct relation between the energy of adsorption and HOMO –LUMO energy gap variation.

Table 1: The electronic properties of gas adsorption inside and outside of zigzag (7,0) AlP nanotube.

	CO (in)	CO (out)	N_2 (in)	N_2 (out)	O_2 (in)	O_2 (out)	CH_4 (in)	CH_4 (out)
R_{min}(Å)	3.35	3.90	4.61	3.75	--------	--------	4.54	3.51
E_{ad}(kcal.mol^{-1})	35.07	28.99	15.67	18.93	150.12	68.93	0.37	2.24
Δ(HOMO-LUMO gap)*	-4.20	0.82	0.19	0.13	-58.42	-16.07	-0.16	-5.61

* $\Delta(\text{HOMO-LUMO gap}) = (\text{HOMO-LUMO gap})_{\text{gas-NT}} - (\text{HOMO-LUMO gap})_{\text{pure}}$, (kcal.mol^{-1})

References:

[1] S Lisenkov, G Vinogradov and N Lebedev , *Jetp Letters*, 81(**2005**) 185 .

[2] M Mirzaei and M Mirzaei *Theochem* (**2010**).

[3] E Durgun and Ciraci,Turk.J.Phys 29(**2005**)307 .

[4] R Wang, D Zhang , K Zhou, X Liu, THEOCHEM 806(**2007**) 93 .

Host-Guest Inclusion Complex Formation of Mefenamic acid with CD_S

M. Taghavizade*[a], Z. B. Nojini[b]

[a] Department of Chemistry, Science and Research Branch, Islamic Azad University ,Khouzestan, Iran

[b] Department of Chemistry, Faculty of Science, Shahid Chamran University, Ahwaz, Iran

E-mail: marzie_taghavi_teach@yahoo.com

Key words: CD_S, Mefenamic acid, Ab-initio, inclusion complexes

Introduction

Cyclodextrins are cyclic oligosaccharides consisting of 6, 7, and 8 glucose units respectively. They have been widely used as host molecules. Mefenamic acid (2-[(2,3-dimethylphenyl) amino]benzoic acid) is a non-steroid drug with strong analgesic, anti-inflammatory and anti-pyretic properties, widely applied in therapeutics [1, 2]. Most computational studies of CD involve host-guest complexation, their structures, and energies, preferred bonding orientations, and so on are typically calculated

Computational method

The complexation processes of various CD_S with drug were studied by using HF/6-31G ab initio method. The initial structure of β-CD and drug were fully optimized with HF methods. The inclusion complexation was emulated by entering the guest molecule from one end of CD and then letting it pass through the host molecule in steps.

Results and discussion

The penetrations of mefnamic acid in cavity of CD_S were studied. The results are summarize in Table 1 The energy variation involved in the inclusion emulation indicates that the complexes prefer to adopt inclusion geometry with the guest inside the host cavity, in order to increase the Vander Waals attraction, dipole-dipole and hydrogen-bonding interaction between host and guest. We calculated the stabilization energy difference (ΔE) between the complexes and their original compounds as below:

$$(\Delta E)=E_{complex}-(E_{CD}+E_{Drug}) \qquad (1)$$

Table1. Electronic energies and HOMO, LUMO and Gap energy of the inclusion complexations of CD_S with Mefnamicacid of the HF/6-31G optimized structures.

Type	E Kj/mol))	ΔE kj/mol))	Homo (ev)	Lumo (ev)	μ	Gap energy
α-CD	944085-	-	304/8-	836/11	141/20	08/3
β-CD	11156932-	-	012/11-	533/4	545/15	187/3
mefnamic acid	2049640	-	932/7-	446/2	378/10	65/1
α-CD + mefnamic acid	11612803-	764/119078-	005/8-	340/2	346/10	53/3
β-CD +mefnamic acid	13206592-	6912/19-	926/7-	397/2	323/10	54/4

Figure 1. The energy variations of the β-CD/ Mefenamic acid

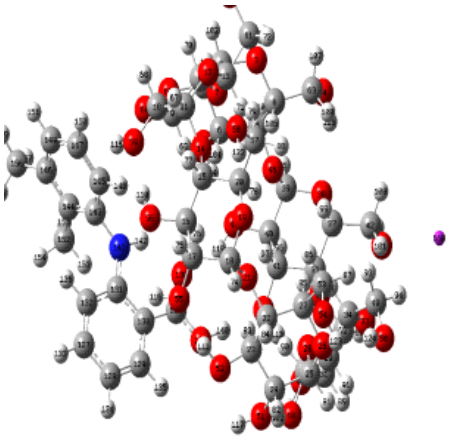

Figure2. The optimized structures of β-CD/ mefnamic acid with HF/6-31G level of theory

Conclusion

The energy variation involved in the inclusion emulation indicates that the complexes prefer to adopt inclusion geometry with the guest inside the host cavity. Also, the results of stabilization energies show the complex of β-CD/mefnamic acid is more stable than □-CD/ mefnamic acxid.

References

[1] T. Hladon, J. Pawlaczyk, B. Szafran, J. Inclusion. Phenomn. Macro. Chem. 35: 497(1999)
[2] J. Szjetly: Chem. Rev. 98, 11743. (2008)

Theoretical study of water interaction with graphene and carbon nanotubes

S. Javadian Farzaneh[a]*, F. Taghavi[a], S. M. Hashemianzadeh[b]

[a]*Department of Chemistry, Tarbiat Modares University, Tehran, 14155-4838, I. R. Iran.*

javadian_s@modares.ac.ir

[b] *Molecular Simulation Research Laboratory, Department of Chemistry, Iran University of Science and Technology, Tehran, I. R. Iran*

Keywords: Carbon Nanotube, DFT Calculation, Water, Morse Potential, Graphene Sheet

Introduction:

Water is indispensable to human beings and any phenomenon related with the water has a unique place. The ability of water to be adsorbed in the neighborhood of different surfaces has been the object of many computational works [1]. The confinement of the water molecules on the carbon nanotubes as an important storage device is of immense interest due to the strange behavior that water show when confined in a space having nanometer size [2]. On the contrary, the absorption of water molecule outside carbon nanotubes is crucial issue to find out how the nanotube surface is changed by this absorption. Simulating water molecules in interaction with carbon nanotubes have been performed with the Lenard-jones potential model in the past [3,4]. However, there are no good studies about the potential model of the absorption of water inside and outside carbon nanotubes.

The goal of this work is to realize the features of interactions between water molecules with carbon nanotube using ab initio methods. We want to use this potential model instead of Lenard-jones potential in our future simulation works. In this study, we first calculate the structure and energies of water molecule on graphene sheet (as a model of carbon nanotube network) to clarify the nature of interaction between water and carbon nanotube. We also calculated the interaction energies of water inside and outside of carbon nanotube to find the best model potential for these kinds of calculations.

Method:

Total-energy electronic-structure calculations have been performed based on the density-functional theory to examine interactions between the walls of CNTs and water molecules. All calculations were carried out using hybrid density functional theory B3LYP method with 6-31G basis set as suited in the G03W program.

Results and discussion:

We first carry out total energy calculation of water on a graphene to find out the best place on this sheet for the absorption of water molecules. We put the water molecule on three regular sites (on-top site, a hollow site, and a bridge site) as shown in Figure 1 (a). We consider four different positions for water on this sheet as you can see in Figure 1(b).

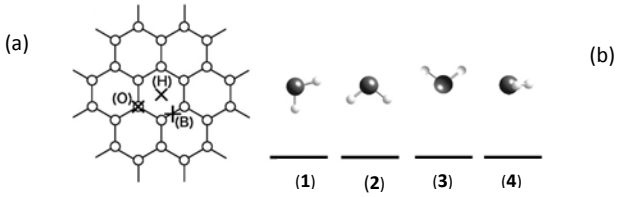

Figure 1: (a) on three regular adsorption sites on graphene sheet: on-top (O), a hollow (H), and a bridge (B) site. (b) Four different positions for water on this sheet.

The calculated adsorption energy of water molecule and the graphene sheet for each position is shown in Table 1. As shown in this table, the position (1) has the biggest absorption energy. We can conclude that the position (1) may be the best orientation for the adsorption of water on carbon networks. In this position, the direction of two hydrogen atoms is toward the sheet and the induction of dipole moment water on graphene sheet would be easier.

Table 1: The adsorption energies of a water molecule on a graphene sheet in the unit of (meV).

position	Site		
	On top	Hallow	Bridge
(1)	34.4	32.4	34.4
(2)	34.0	27.1	34.3
(3)	32.1	24.3	28.3
(4)	28.5	20.2	24.8

We also calculate the interaction energies of water outside carbon nanotube in different distances to find the best model potential for these kinds of calculations. We find out that the Morse potential is the best fitted model potential for water in interaction outside of carbon nanotube (figure 2). This is a very important result that can be used in future simulation of these kinds of systems.

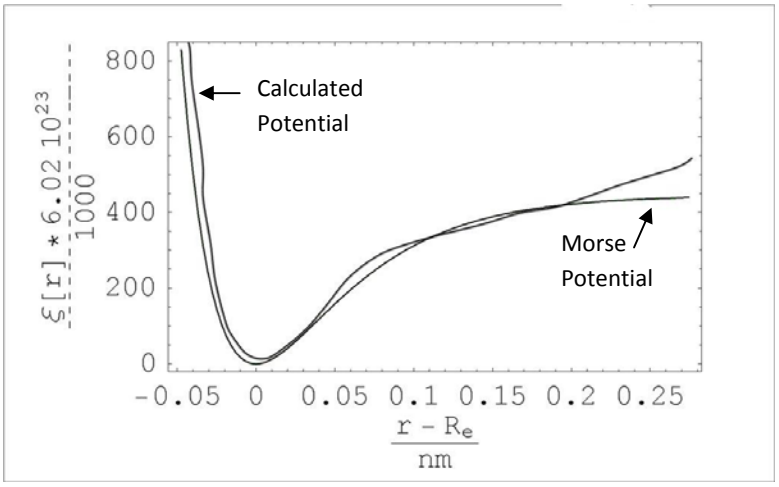

Figure 2: The fitted potential energy of water outside carbon nanotube to the Morse potential.

References:

[1].M. C. Gordillo and J. Martı´, J. Chem. Phys. **117**, 3425 (2002).

[2]. L. D. Gelb, K. E. Gubbins, R. Radhakrishnan, and M. Sliwinska-Bartkowaik, Rep. Prog. Phys. **62**, 1573 (1999).

[3]. F. Mikami, K. Matsuda, H. Kataura and Y. Maniwa. AcsNano. 3, 1279 (2009).

[4]. Q. Yuan and Y. P. Zhao. J. Am. Chem. Soc. 131, 6374 (2009).

Role of aromatic π-bridge on electron transport property in Nanowire

E. Taghizadeh*[a],b. Z.Bayat[b] ,.[b]s.Danesh nia[b,] S. Nikooie[b]

[a]Department of Chemistry,yonug researchers club, Islamic Azad University -Quchan Branch, Iran

[b] Department of Chemistry Islamic Azad University -Quchan Branch, Iran

Elnaz64_t@yahoo.com

Abstract

Theoretical investigation has been performed on electron transport properties of 4, 4'- diamino biphenyl based molecules that is sandwiched between two gold surfaces. Density functional calculations are performed to analyze the conduction process through various aromatic bridges in a donor–bridge–donor (NH2 B NH2) molecular wire through frontier molecular orbital analysis. According to Systematic study on the molecular orbital populations, five member hetero-aromatic rings (electron-rich) in the conduction path are inserted between the donor–donor complexes. Values of Potential barrier (PB) that have been determined experimentally and reached the conclusion is mentioned later in this paper.

Keywords: Potential barrier, molecular wire

Introduction

A molecular wire is an organic molecule that forms a conducting bridge between electronic contacts(table1). The PB values needed for the electron conduction process in a molecule are thus calculated as given equation [1]. PB = 1/2 HLG + q

Where q=0 for LUMO as conduction channel. $q=\Delta E_{LUMO}$ when the conduction channel is other than LUMO (if LUMO is not fully delocalized, the conduction channel will be still higher unoccupied orbital (LUMO + n) which is fully delocalized all over the molecule and the ΔE_{LUMO} will be equal to E_{LUMO+n}-E_{LUMO}) and 1/2 HLG is the measure of the Fermi level which according to assumption lies in the middle of HOMO–LUMO gap.(Table2)

Table 1

NH2B1NH2	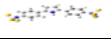
NH2B2NH2	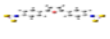
NH2B3NH2	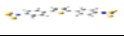

Computational details

The calculations have been performed at the density functional theory level with the B3LYP functional. The basis set is split 6-31G* for N atom and (LANL2DZ) for the gold atoms [2]. Each gold cluster consists of three gold atoms that were placed as an equilateral triangle with sides of 2.88 Å; the relative positions of the gold atoms were fixed in each triangle. The linker was positioned in the hollow site of the gold cluster and the distance between the two gold surfaces was fixed in space and all other geometric parameters were optimized.

Results and Discussion

HOMO–LUMO gap (HLG) is a key parameter for determining the conductance property. This parameter calculated for molecules and complexes. Natural bond orbital (NBO) (fig 1) analysis has been carried out in order to explore the nature of Au–L (L is the terminal atom of the linker) interface in greater details .The orbital character and the occupancy of the bond between Au and the linker (Au–L) are collected in (Table 3). To summarize, Au can covalently couple with NBN through nitrogen linkages. It is interesting to describe the change in molecular levels after interaction with gold clusters.

Conclusion

Though such decrease in PB values is not exceptionally high still when such molecules will be tailored into polymeric type, a largely reduced PB can be expected.

These observations give us an insight how to modulate tunable parameters such as the external field and the nature of interfacial contact in the operation of molecular wire.

Table 2 Frontier molecular orbital energies and PB values (ineV)

Molecule	LUMO	HOMO	PB
NB1N	-5.17	-8.41	1.61
NB2N	-5.08	-8.20	1.55
NB3N	-5.20	-8.45	1.62

Table 3 Orbital character of Au-L bonds

Complex	Bond	Occupancy	Au(%) N(%)	Contribution (%)		
				S	P	d
1	Au-N	1.87	Au(34.98) N(65.02)	90.66	0.53	8.82
2	Au-N	1.81	Au(50.74) N(49.74)	98.01	0.26	1.73
3	Au-N	1.94	Au(32.46) N(67.54)	90.78	0.41	8.81

Fig 1 NBO

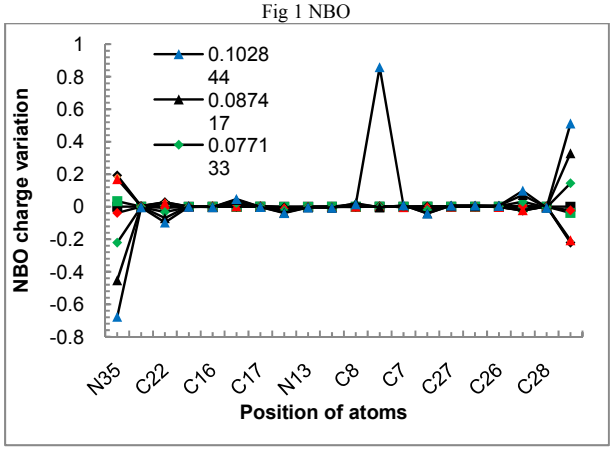

Reference:

[1] Y. Luo, C. -K. Wang, Y. Fu, Chem. Phys. Lett 2003, 369, 299

[2] W. R. Wadt, P. J. Hay, J. Chem. Phys 1985, 82, 284.

Quantum Chemical Study of Proton Transfer Reaction between $(HF)_{n = 1-4}$ Clusters and Anilide Anion

Hossein Roohi[a], Reza Taghizadeh[a]

[a]*Department of Chemistry, Faculty of Science, University of Guilan, Rasht, Iran*

Introduction

Proton transfer (PT) is a common phenomenon in the chemical and biological sciences [1-4]. Ionic hydrogen bond (IHB) interactions are implicated in ionic crystals and clusters, ion solvation, electrolytes, and acid–base chemistry. The importance of this interaction in proton solvation, surface phenomenon, self-assembly process in supramolecular chemistry, and biomolecular structure and function has also been recognized. The formation of IHB in simple H-bonded complexes involves partial proton transfer from the donor to the acceptor. To the best of our knowledge, influence of size of HF clusters on the proton transfer between HF and anilide anion (**An**) has been not reported. The aim of the present work is to characterize the IHB formed between anilide anion and $(HF)_n$ (n = 1-4).

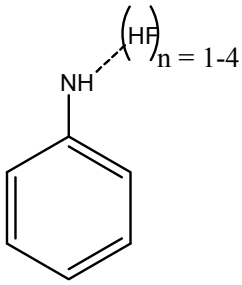

Scheme 1

Computational details

The geometries of all structures were optimized using B3LYP and MP2 methods in conjuction with the 6-31++G(d,p), 6-31++G(2d,2p) and 6-311++G(2d,2p) basis sets. The B3LYP calculated vibrational frequencies have been used to characterize stationary points and calculation of zero-point vibrational energy (ZPVE). Topological properties were calculated at MP2/6-311++G(2d,2p) level of theory by the AIM2000 program package. The NBO analysis was carried out on the MP2/6-311++G(2d,2p) wave functions using version 3.1 of NBO package included in Gaussian 03 program package.

Results and discussions

The effect of HF cluster size on the switch between $HN^-\cdots H–F$ and $N–H\cdots F^-$ proton transfer in **An**–$(HF)_{n = 1-4}$ complexes (Scheme 1) were investigated by means of quantum chemical methods. The change in H-bond strength due to variation of HF cluster size were well monitored by change in binding energy (BE), structural parameter, electron density topography, natural charge, charge transfer and percentage of p-character of N atom in C–N bond. The calculated BEs for formation of **An**–$(HF)_{n = 1-4}$ complexes correlate well with $HN^-\cdots HF$ distance (Fig. 1). The results show that the strength of $HN^-\cdots HF$ H-bonds increases by increase in size of HF cluster. Therefore, $HN^-\cdots H–F \rightarrow N–H\cdots F^-$ switching enhances by increase in extent of salvation. NBO analysis reveals that the occupancy of the LP of nitrogen atom increases with an increase in size of cluster. The topological properties of electron density at H-bond critical points demonstrate that the $HN^-\cdots H$ H-bonds in all complexes are partially covalent in nature.

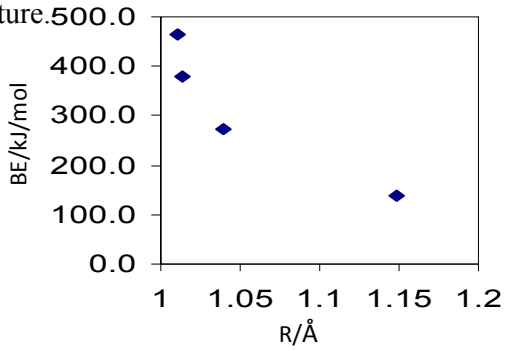

Fig. 1 Correlation between BEs and H-bond distances at MP2/6-311++G(2d,2p) level

Conclusions

Our results at all levels of theory show that the transfer of proton between anilide anion and HF enhances by increase in size of HF cluster. All H-bond interactions are characterized as partial covalent.

References:

[1] Cha, Y.; Murray, C. J.; Klinman, J. P. Science **1989**, 243, 1325.

[2] Hu, X.; Li, H.; Liang, W.; Han, S. J. Phys. Chem. B **2004**, 108, 12999.

[3] Kim, Y. J. Phys. Chem. A **1998**, 102, 3025.

[4] D. S. Ahn, S. Lee, B. Kim, *Chem. Phys. Lett.* **2004**, 390, 384.

The Effect of Water on the Equilibrium and Rate Constant of Tautomerism in Hydroxamic Acids

H. Tavakol* and T. Hadad
[a]Department of Chemistry, University of Zabol, Zabol, Iran
(Email:hosein_ta@yahoo.com)

Keywords: Tautomerism, DFT, Hydroxamic Acid, Solvent assisting

Introduction

Hydroxamic acids (HAs) are important class of compounds due to their significant role in biological reactions [1]. Because of their importance, HAs have been the subject of some computational investigations focused mainly on their structural, photochemical and acid-base properties [2-4]. Moreover, they are interesting compounds because of their versatility in tautomerism. Since tautomerism in the HAs affect their chemical and biological activities, especially their chelating properties, it is very important to know the complete scheme of tautomerism and the reaction pathways between different tautomers. In this line, effects of different substitutions and more importantly, effect of solvent on this tautomerism should also be worked out clearly.

Methods

Gaussian 98 program package was employed to calculate molecular parameters, frequencies, solvent effects and kinetic and thermodynamic properties of eight selected hydroxamic acids using B3LYP/6-311++G** level of theory. The absence of imaginary frequencies verified that all structures were true minima. In each pair of tautomers, stationary point geometry with one imaginary frequency has been found and identified as a transition state at the B3LYP/6-311++G** level of theory by applying Schlegel's synchronous-transit-guided quasi-Newton (QST3) method. Furthermore, intrinsic reaction coordinate (IRC) calculations proved that each reaction linked the correct products with reactants. Zero point vibrational energies (ZPVE) and other frequency results were corrected with appropriate scaling factor.

Results and discussion

Three tautomers were identified for each HAs, namely the keto form (N-hydroxy amide, **a**), iminol form (α-hydroxy oxime, **b**) and nitroso form (α-nitroso alcohol, **c**). In all cases, the order of stability of tautomers is found to be as tautomer **a** > tautomer **b** > tautomer **c**. Furthermore, two transition states are found between tautomers. **TS1** (between **a** and **b**) is more stable than **TS2** (between **b** and **c**). The energetic data confirm that because of high energy barriers between tautomers, their interconversions are very slow at room temperature.

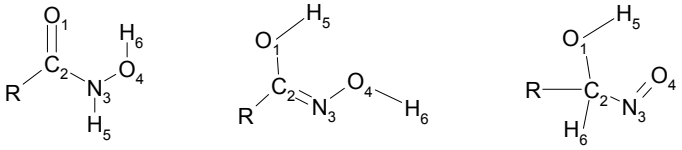

a (keto-form) **b** (oxime-form) **c** (nitroso-form)

Solvation data show no important difference between gas phase and solvent media. As an example, the maximum rate constant in acetone is 1.2×10^{-15} Sec^{-1}, very near to that in the gas phase (1.3×10^{-15} Sec^{-1}) and all energetic results in solvent (ΔG_{solv}) have a little difference with those in the gas phase.

To examine water-assisted tautomerism, geometry optimization of the tautomers and transition state species of molecule **1** and location of its reaction path have been carried out in the presence of 1-3 water molecules. Activation barriers in the presence of water molecules are in general lower than those in the gas phase. This difference increases with the increase of water molecules. Our results show that the presence of water molecules has more intensive effects on kinetic results (rate constants) versus thermodynamic results (equilibrium constants).

Conclusion

In this work, DFT calculation have applied to study of tautomerism in some hydroxamic acids in the gas phase, in solvent and in presence of 1-3 water molecules. In all cases, the order of stability of tautomers is found to be as tautomer **a** > tautomer **b** > tautomer **c**. Furthermore, two transition states are found between tautomers. **TS1** (between tautomers **a** and **b**) is more stable than **TS2** (between tautomers **b** and **c**). Our results confirm the available experimental data approving higher stability of the tautomer **a**. Because of high energy barriers between tautomers, their interconversions are very slow at room temperature. Moreover, geometry

optimization of the tautomers and transition state species of molecule **1** and location of its reaction path have been carried out at the same level of theory in the presence of 1-3 water molecules. Activation barriers in the presence of water molecules are in general lower than those in the gas phase. This difference increases with the increase of water molecules.

References:

[1] J. Telegdi, T. Rigo and E. K alm, J. Electroanal. Chem., 582 (2005) 191.
[2] R. Senthilnithy, S. Weerasinghe and D.P. Dissanayake, THEOCHEM, 851 (2008) 109.
[3] S.J. Yen, Ch.Y. Lin and J.J. Ho, J. Phys. Chem. A, 104 (2000) 11771.
[4] M. Sałdyka and Z. Mielke, Vib. Spectrosc., 45 (2007) 46.

Study of Isomery Scheme in Acetyl Hydrazides by DFT Calculations

H. Tavakol[a]*, Saeed Amiraslanzadeh Mamagani[b]

[a]Department of Chemistry,Faculty of Science,University of Zabol, Zabol, Iran

[b]Enghelab-Islami Techniqual College, Moalem Square, Yaftabad, Tehran, Iran

(Email:hosein_ta@yahoo.com)

Keywords: Hydrazide; DFT; Isomer; Solvent effect.

Introduction

Study of isomerism [1], especially by computational methods, is one of the most important topics in chemistry. Recently, theoretical study of isomerism [2-4] received renewed attention due to its importance on determination of compound applications. As well as, compounds containing different isomers have been the subject of interest by chemists. Hydrazides and acyl hydrazides [5] are also interesting because of their versatility in isomerism. Therefore, continuing our interest on theoretical study of isomerism in organic compounds and because isomerism in acyl hydrazides affects their chemical activities especially their ligand properties, it will be very important to learn about the complete scheme of isomerism in acyl hydrazides.

Methods

Gaussian 98 program package was employed to find the optimized structures of N'-acetyl formohydrazide isomers (9 tautomers and 18 isomers) using B3LYP/6-311++G** and B3LYP/AUG-CC-PVTZ levels of theory. The absence of imaginary frequencies verified that all structures were true minima. From outputs of these calculations, important molecular parameters, IR frequencies and energetic results were extracted. Zero point vibrational energies (ZPVE) and other frequency results were corrected with appropriate scaling factor. Free energies of solvation for all isomers were calculated using SCRF keyword with Tomasi's polarized continuum (PCM) model. Four different solvents (cyclohexane, chloroform, acetone and DMSO) with different dielectric constants have been used as solvent.

Results and discussion

The relative stabilities of isomers in the gas phase are found to be as 1, 2E, 2Z, 4Z, 4E, 6EE, 5, 6EZ, 6ZZ, 6ZE, 3E, 7E, 9E, 3Z, 7Z, 9Z, 8E, and 8Z. In addition, in all tautomers except tautomer 4, the *E* isomer is more stable than *Z* isomer. Viewing results, it can be observed that in isomer 4E, there is an unfavorable spatial interaction between methyl and formyl groups. This interaction can be responsible for the less stability of 4E versus 4Z. ΔG between *cis* and *trans* isomers is variable from 2.03 in tautomers 2 to 11.4 in tautomers 8. Observing optimized structure of 8Z shows that there is unfavorable interaction between methylene and hydroxyl groups. This interaction (between large groups) is responsible for large instability of 8Z versus 8E while in tautomers 2, only two hydrogens (small atoms) have spatial interaction in *Z* isomer. Therefore, it is not strange that ΔG between 2E and 2Z will be very small.

To examine solvent effect, the relative stabilities have been calculated in different solvents (acetone, chloroform, cyclohexane and DMSO). The relative stabilities in solvents are similar to those in the gas phase except in 6EZ and 9E because these isomers have respectively the minimum and maximum average ΔG solvations among all isomers.

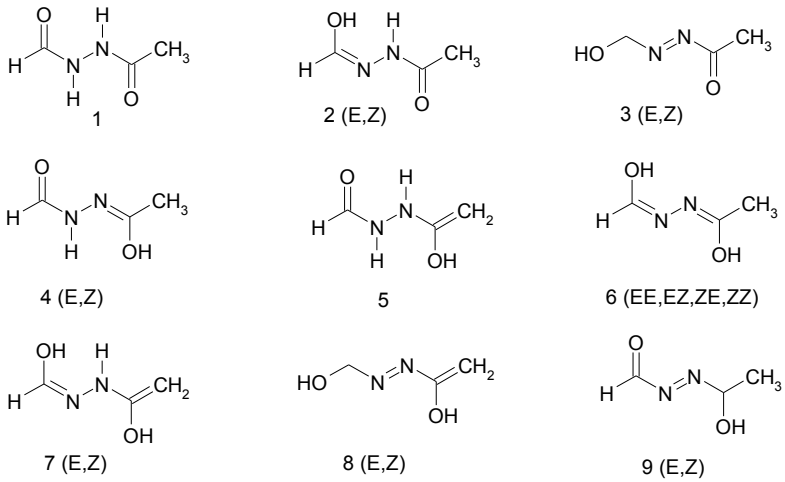

Conclusion

In this work, DFT calculations have been applied to study of structures, molecular parameters, vibrational frequencies and relative energies of 18 possible isomers of N'-acetyl formohydrazide using the B3LYP/6-311++G** and B3LYP/AUG-CC-PVTZ levels of theory. Moreover, the effects of solvent on the stability order of these isomers have been studied using four different solvents (acetone, Chloroform, DMSO and cyclohexane). The relative

stabilities in solvents are similar to those in the gas phase except in 6EZ and 9E because these isomers have respectively the minimum and maximum average ΔG solvations among all isomers.

References:

[1] N.V. Belova, H. Oberhammer, G.V. Girichev J. Phys. Chem. A, 112 (2008) 3209.

[2] B.I. Buzykin, E.V. Mronova, V.N. Nabiullin, N.M. Azancheev, L.V. Awakumova, I.K. Rizvanov, A.T. Gubaiduffin, I.A. Litvinov J. Gen. Chem., 78 (2008) 461.

[3] R. Dobosz, E. Kolehmainen, A. Valkonen, B. Osmiaowski, Tetrahedron, 63 (2007) 9172.

[4] A.D. Dubonosov, V.I. Minkin, V.A. Bren, E.N. Shepelenko, A.V. Tsukanov, A.G. Starikov, G.S. Borodkin, Tetrahedron, 64 (2008) 3160.

[5] B. Li, R. J. Bemish, D. R. Bill, S. Brenek, R. A. Buzon, Org. Synth., 81 (2005) 254.

Synthesis and DFT studies of 1-Amino-5-thiol tetrazole as corrosion inhibitors

Abbas Teimouri*[a], Nasrin. Soltani[b], Alireza Najafi Chermahini[c]

a. *Department of Chemistry, Payame Noor university (PNU), Isfahan, Iran.*
E-mail: a_teimouri@pnu.iut.ac.ir

b. *Payame Noor University (PNU), Shahin Shahr Branch, Isfahan, Iran.*

c. *Department of Chemistry, Yasouj University, Yasouj, Yasouj Iran.*

Key words: Corrosion inhibitors; mild steel; theoretical studies; DFT.

Introduction

Most of the well-known acid inhibitors are organic compounds containing nitrogen, sulphur and/or oxygen atoms. The influence of such organic compounds, on the corrosion of mild steel in acidic solution has been investigated by several authors. The inhibition property of these compounds is attributed to their molecular structure. The inhibiting effect is generally explained by the formation of a physical and/or chemical adsorption film on the metal surface. Organic compounds of acetone type have been reported to be excellent corrosion inhibitors for the corrosion of mild steel in acidic solutions [1-3]. As a part of our ongoing research program for synthesis and theoretical studies of organic compounds [4-6] in this paper we report the synthesis of 1-Amino-5-thiol tetrazole and to study the inhibition action of this compounds on the corrosion of mild steel in acid media and to compare their protection powers. In addition quantum mechanic calculation carry out for the compounds by performing HF and DFT levels of theory using the standard 6-31G* basis set. All measurements showed that inhibition efficiencies enhanced with increase of inhibitor concentration.

Results and discussion

Quantum Chemical Study

Complete geometrical optimization of molecules was carried out with Gaussian 98 program at HF and density functional theory (DFT) levels of theory using the standard 6-31G* basis set, starting without any geometry constraints for full geometry optimizations. The

optimized molecular structures of the inhibitors are given in figure. This basis set is known to provide accurate geometries and electronic properties for a wide range of organic compounds. E_{HOMO} often is associated with the electron donating ability of the molecule. High values of E_{HOMO} are likely to indicate a tendency of the molecule to donate electrons to appropriate acceptor molecules with low-energy, empty molecular orbitals. Therefore, the energy of the lowest unoccupied molecular orbitals indicates the ability of the molecule to accept electrons. The lower value of E_{LUMO}, the more probable it is that the molecule accepts electrons. The energy gap between LUMO and HOMO (ΔE=ELUMO-EHOMO) is a parameter with the smaller value causes higher inhibition efficiencies of the molecule.

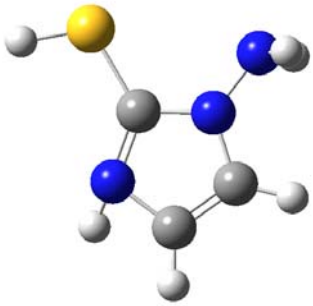

Figure. Optimized molecular structure of 1-Amino-5-thiol tetrazole (ball and stick model)

Conclusions

1-Amino-5-thiol tetrazole was synthesized, characterized and as new inhibitors for the corrosion of mild steel in acid media. The studied compound is excellent inhibitors and act as the mixed type inhibitors for mild steel corrosion in sulphuric acid solution. Density functional (DFT) calculations have been carried out for the title compounds by performing HF and DFT levels of theory using the standard 6-31G* basis set.

References

[1] Uhlig, H.H. Revie, R.W., *Corrosion and Corrosion Control*, Wiley, New York, 1985.

[2] Sastri, V.S., *Corrosion Inhibitors, Principles and Application*, John Wiley and Sons, New York, 1998.

[3] Elachouri, M. Hajji, M.S. Kertit, S. Essasi, E.M. Salem, M. Coudert, M., *Corros. Sci*. **37** (1995) 381.

[4] Teimouri, A. Najafi Chermahini, A. Shahraki, Dabbagh, H. A. M., *Spectrochimica*. *Acta*. *A*: **69**, (2008) 449.

[5] Teimouri, A. Najafi Chermahini, A. Emami, M., *Spectrochimica*. *Acta*. *A*: **71** (2008), 1516.

[6] Teimouri, A. Najafi Chermahini, A. Taban, K., *Spectrochimica*. *Acta*. *A*: **72** (2009), 369

DFT Study Of Isolobal Compounds, Metallotropic and Prototropic 1,2-Shifts Of Cyclopentadienyle derivatives

S. Jameh-Bozorghi[1,*], A. R. Namdari[2], Z. Javanshir[3],

1- *Chemistry Department, Faculty of science, Islamic Azad University, Toyserkan Branch,Ttoyserkan, Iran*

sjamehbozorgi@gmail.com

2- *Chemistry Department, Faculty of science, Islamic Azad University, Shahre Rey Branch, Shahre Rey, Iran*

3- *Chemistry Department, Faculty of science, Islamic Azad University, Arak Branch, Arak, Iran*

Keywords: DFT calculation, Isolobal, Sigma tropic, cyclopentadienyl

Introduction

Fluxional σ-cyclopentadienyl compounds such as (η^1-C_5H_5)2Hg and (η^5- C_5H_5) (η^1-C_5H_5)$Fe(CO)_2$ were first discovered by Piper and Wilkinson in 1965.[1] The authors discussed in an undetailed but essentially correct manner why fast intramolecular 1,2-migrations of the metal moiety around the cyclopentadienyl ring occur.

The isolobal principle in organometallic chemistry devised by Roald Hoffmann[2]. The methyl radical is isolobal with the metal carbonyl species manganese pentacarbonyl $Mn(CO)_5$ because both molecules have a single electron in a hybrid orbital pointing away from the plane of the molecule (though they are not isoelectronic). This resemblance is reflected in the chemistry of both molecules. As the methyl radical can dimerize to ethane, $Mn(CO)_5$ can dimerize to $(CO)_5$Mn-$Mn(CO)_5$ and both radicals can even form $Mn(CO)_5CH_3$.

In this work, we report the results of a theoretical investigation of the structural properties of compounds **1** and **2** and migration isolobal groups on cyclopentadienyl ring which was performed by ab initio molecular orbital (MO) and density functional methods (DFT), using the GAUSSIAN 2003 package programs.

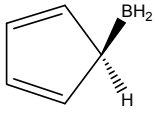

1

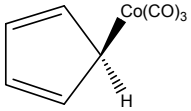

2

Calculation detail

DFT calculation were carried out using B3LYP/6-311+G** level of theory with the GAUSSIAN 2003 package of programs [3] on a personal computer. Energy-minimum molecular geometries were located by minimizing energy with respect to all geometrical coordinates without imposing any structure symmetrical constraints and transition state structures obtained by QST2 subroutine.

Results and discussion

The 1,2-shift mechanisms for the $Co(CO)_3$ and hydrogen migrations were investigated and reaction pathways are shown in Figure1. Also this reaction mechanism carried out for BH_2 migration. This results reviled that barrier energy for migration of BH_2 and $Co(CO)_3$ is 0.15 and 3 kcal.mol^{-1}. Bond lengths of C-B and C-Co are 1.562 and 2.095 Angstrom. Also, prototropic shifts for compound **1** have lower migration energy than compound **2**.

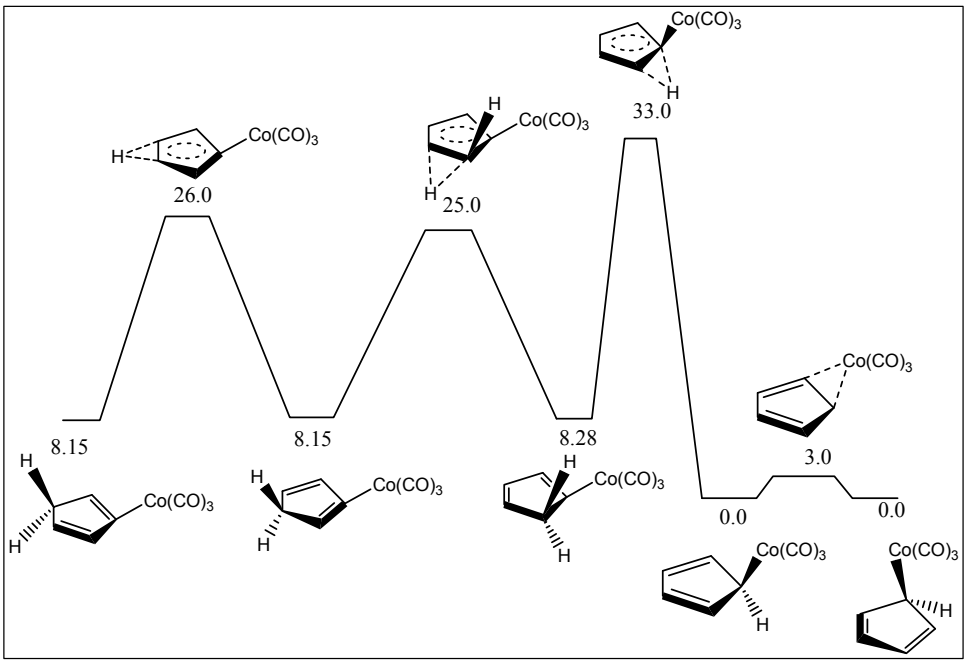

Conclusion

The calculated results by B3LYP/6-311+G** show that the most stable isomers of compounds **1** and **2** are the allylic isomers. Bond length of B-C is longer than Co-C but

sigmatropic barrier energy for BH_2 migration is higher than $Co(CO)_3$ migration because in Co-C bond π-back bonding is present and then this bond is stronger than B-C.

Reference

[1] G. Wilkinson and T. S. Piper, *Inorg. Nucl. Chem.*, **2,** 32 (1956); (b) T. S. Piper and G. Wilkinson, *Inorg. Nucl. Chem.*, **3,** 104 (1956).

[2] Roald Hoffmann; *Angewandte Chemie International Edition;* **21**, 10 (**1982)** 711-724

Neighboring group's effect in sigmatropic migration on indol rings. A theoretical study and NBO analysis.

S. Jameh-Bozorghi[1,*], F. Naseri[2] and Z. Javanshir[2],

4- *Chemistry Department, Faculty of science, Islamic Azad University, Toyserkan Branch,Ttoyserkan, Iran*

sjamehbozorgi@gmail.com

5- *Chemistry Department, Faculty of science, Islamic Azad University, Arak Branch, Arak, Iran*

Keywords: DFT calculation, Borotropic shift, prototropic shift, indol

Introduction

Sigmatropic Migration of many fragment on aromatic rings have been observed. These compounds are fluxional. Experimental [1] and theoretical [2] studies for barrier energies and rate of (σ)metallotropic and (σ)prototropic shift on Fluxional compounds carried out. Those researches showed that (σ)prototropic shift has higher activation energy than (σ)metallotropic shift and therefore metal groups migration is very fast on room temperature. In the chemical literatures is not exist the neighboring effect in these migrations, therefore in this work, we report the results of a theoretical investigation of the structural and energetic properties of (1H-inden-1-yl)borane(**1**), (4,5,6,7-tetrafluoro-1H-inden-1-yl)borane(**2**) and (4,5,6,7-tetramethyl-1H-inden-1-yl)borane(**3**). Effect of Methyl as an electron donor and flour as an electron acceptor groups in compounds **2** and **3** were investigated was by ab initio molecular orbital (MO) and density functional methods (DFT), using the GAUSSIAN 2003 package programs and NBO 3.1.

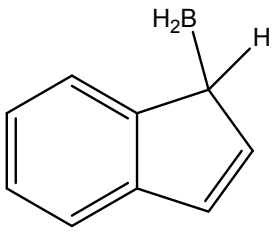

1

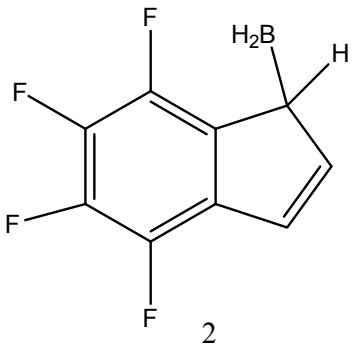

2

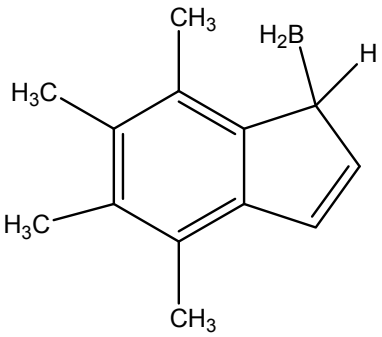

3

Calculation detail

DFT calculation were carried out using B3LYP/6-311+G** level of theory with the GAUSSIAN 2003 package of programs [3] on a personal computer. Energy-minimum molecular geometries were located by minimizing energy with respect to all geometrical coordinates without imposing any structure symmetrical constraints and transition state structures obtained by QST2 subroutine. Natural Bond Orbital (NBO) analysis was then performed at the B3LYP/6-311+G** level by the NBO 3.1 program included in the GAUSSIAN 03 package of programs.

Results and discussion

Structural properties, energies behavior and NBO analysis was performed for 1,2-shift mechanisms for the BH_2 and hydrogen migrations were investigated by using B3LYP/6-311+G** , HF/6-311+G** and MP2/6-311+G** levels of theory for compounds **1**, **2** and **3**. Reaction pathways are shown in Figure1. These results revealed that barrier energy for migration of H is higher than BH_2. calculation results showed that F(electronegative) and Me(electropositive) groups in compounds **2** and **3** growth the barrier heights in borotropic an prototropic shift.

Methyl group is electropositive and conduct electrons to indol rings and then electron density of B-C and H-C bonds increased and finally barrier height increase. Fluore is electronegative but this atom conduct nonbonding electrons to indol rings by resonance and then barrier height increase again. These results have a good agreement with structural and NBO results.

In these compounds 1,2-boroteopic shift is impossible. When BH_2 is in vinylic position these compounds are not in ground state. Infra Red (IR) vibrational frequencies (one imaginary frequency) and Aromatic Stabilization Energy (ASE = 16.62 $Kcal.mol^{-1}$) results showed that this structure is a transition state structure (fig.1). Therefore borotropic shift is a 1,3-sigmatropic shift.

Conclusion

1) The calculated results by B3LYP/6-311+G** , HF/6-311+G** and MP2/6-311+G** levels of theory for compounds **1**, **2** and **3** show that the most stable isomers of these

compounds are the allylic isomers and prototropic shift has higher barrier energy than borotropic shift.

2) IR and ASE calculation results and NBO analysis showed that prototropic sift is a 1,2-sigmatropic migration but borotropic shift is a 1,3-sigmatropic shift.

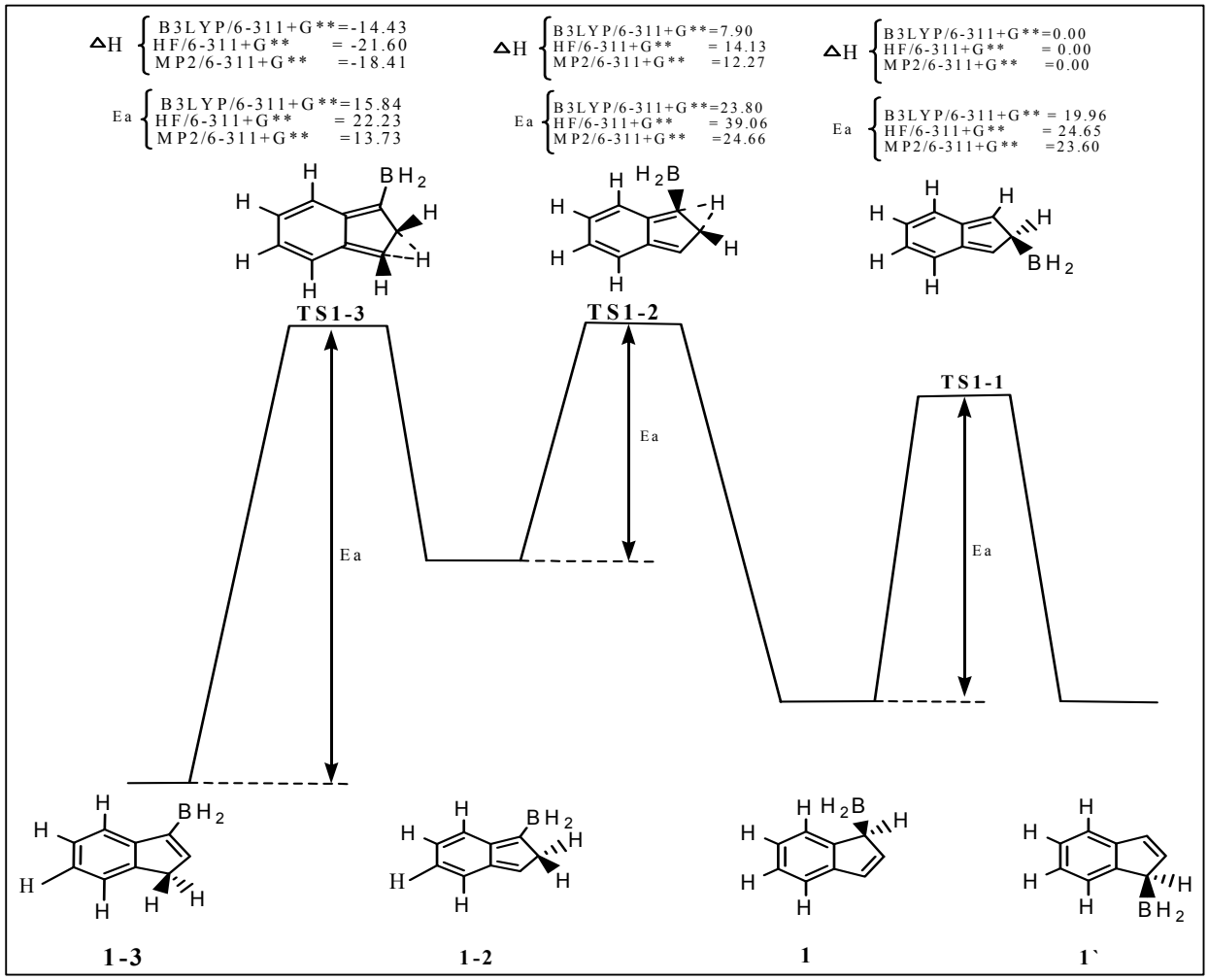

Figure 1: B3LYP, HF and MP2 energy diagram for various sigmatropic shifts in compound **1**

Reference:

[1] G. Wilkinson and T. S. Piper, *Inorg. Nucl. Chem.*, **2,** 32 (1956); (b) T. S. Piper and G. Wilkinson, *Inorg. Nucl. Chem.*, **3,** 104 (1956).

[2] D. Nori-Shargh, H. Aghabozorgh, K. Zare,M. R. Talei, Bavil Olyai, and S. Jameh-Bozorghi, *Phosphorus, Sulfur and Silicon*, **178,** 341 (2003)

Theoretical Study of Free Energies of Electrontransfer in the supramolecular complexes of Vitamin B_{12} with Fullerenes C_n Nanostructurs

Avat (Arman) Taherpour* and Ahmad Jafari

Chemistry Department, Facullty of science, Islamic Azad University Arak Branch

P.O.Box 38135-567,, Arak, Iran.

avatarman.taherpour@gmail.com & a.taherpour@iau-arak.ac.ir

ahmad.jafari28@yahoo.com

Abstract:

Vitamin B_{12} is the known essential biomolecule with a stable cobalt-carbon bond, that it is an coordinate compound. One of the main classes of carbon alotrops are fullerenes that the unusual structures and physiochemical properties of these molecules have been discovered. In any potential applications and physicochemical properties of fullerenes and their derivatives have been introduced. The first to fourth free energies of electron transfer and kinetic rate constants of the electrontransfer, $\Delta G_{et(1)}$ to $\Delta G_{et(4)}$ and $k_{et(1)}$ to $k_{et(4)}$, respectively were calculated for the supramolecular complexes of vitamin B_{12} with Fullerens C_n(n=60-300). These calculations were carried out in accordance with the Marcus and electron transfer theory.

Keywords: Fullerenes, Vitamin B_{12}, Electron transfer process, Rate constants, Free energy, Molecular modeling

Introduction:

With the primarily aim at a better understanding of enzymatic reactions, the biochemical and physical chemistry of Vitamin B_{12} and its derivatives have received considerable attention in the past decades. Up to now, various empty carbon fullerenes whit different numbers (n) such as C_{60}, C_{70}, C_{76}, C_{82} and C_{86}, have been obtained. Topological indices are digital values that are assigned based on chemical composition. These values are purported to correlate chemical structures with various chemical and physical properties.

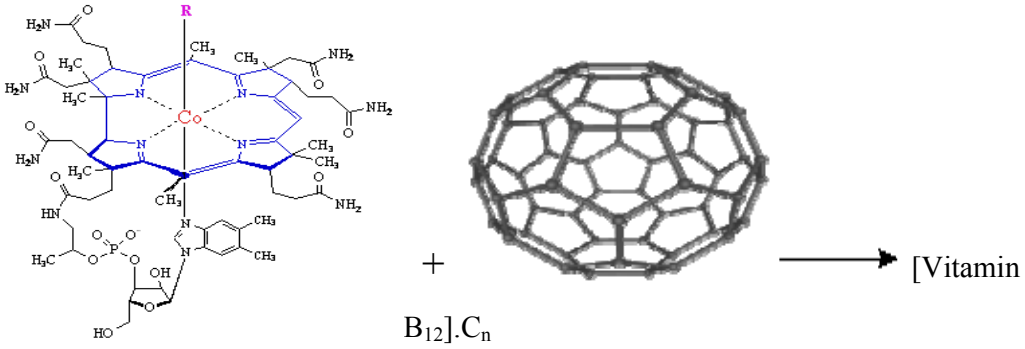

Mathematical method:

The number of carbon atoms of these fullerenes (C_n) was utilized as a structral index for the supramolecular complexe compounds. In this study, all graphs were generated using the Microsoft Office Exell 2003 program. Using the number of carbon atoms contained within the C_n fullerenes, several valuable properties of the fullerenes can be calculated. These calculations are based on the electrontransfer and marcus theory.

Results and discussion:

In the previous reports had been shown that all redox data for B_{12} determined by cyclic voltametry. the reported oxidation potential of Vitamin B_{12} is 1.21 V. By using the electron transfer equation which obtained in this modeling, it is possible to calculate the values of $\Delta G_{et(1)}$ to $\Delta G_{et(4)}$ of [Vitamin B_{12}].C_n supramolecular complexes. The $\Delta G_{et(1)}^{\#}$ to $\Delta G_{et(4)}^{\#}$ for [Vitamin B_{12}].C_n, (n=60-300) supramolecular complexes are predicted by using the appropriate equations. The calculated values of the free electron transfer energies of $\Delta G_{et(1)}$ to $\Delta G_{et(4)}$ for selected [Vitamin B_{12}].C_n supramolecular complexes (n = 60, 70, 76, 82 and 86) in the equations were interpreted. There was good agreement between the calculated and the predicted values. In lieu of increasing the number of carbons atoms in the fullerene structure, the values of $\Delta G_{et(1)}$ to $\Delta G_{et(4)}$ were decreased. The supramolecular complex structures which were discussed here and the calculated values of $\Delta G_{et(n)}$, $\Delta G_{et(n)}^{\#}$ and $k_{et(n)}$ corresponding to these supramolecular complexes were neither synthesized nor reported before.

References

[1] Taherpour, A.A ., *Phosphorus, Sulfur, and Silicon*, 185:422–432, 2010.

[2] Vilakazi, S.L ., et al (2000)electrochimica Acta, 46:453-461

[3] Taherpour, A.A ., and Maleki, M ., *Analytical Letters*, 43: 658–673, 2010.

[4] Taherpour, A.A ., *Chem Phys Lett,* 469: 135-139, 2009.

Pseudo Jahn-Teller effect analysis of hydrogen bonding in the enol forms of propandial, propandithial and propandiselenal

Jalali.E [a,*] , Mousavi.S.N[b] , Yahyaei.H[c] and Nori-Shargh.D[b]

a) *Chemistry Department, Science Faculty, Damghan branch, Islamic Azad University, Damghan, Iran*

**Corresponding author. E-mail: ala.jalali@gmail.com*

b) *Chemistry Department, Science Faculty, Arak branch, Islamic Azad University, Arak, Iran*

c) *Chemistry Department, Zanjan Branch, Islamic Azad University, P.O.Box: 49195-467, Zanjan, Iran*

Keywords: Pseudo Jahn-Teller Effect, Hybrid-DFT, Propandial, Propandithial, Propandiselenal

Introduction

The structure of the enol froms of the symmetric β-diketon compounds has C_s symmetry. The origin of these differences from their higher symmetric forms (i.e. C_{2v} structure) is of significant interest. It is well known that the only source of structural distortions of high-symmetry configurations of any molecular system is the Jahn-Teller (JT) effect (JTE), including the proper JTE for systems in electronically degenerate states, the Renner-Teller effect (RTE) for linear molecules, and pseudo JTE (PJTE) for any system.[1,2] Since the electronic ground states of propandial, propandithial and propandiselenal are nondegenerate, it is natural to assume that all the observed distortions from the highest-symmetry linear configuration are due to, and only to the PJTE. The present paper is devoted to the exploration of this possibility.

Computational details

The hybrid-DFT based method (B3LYP) was used with Def2-TZVPP basis set on all atoms with the GAUSSIAN 03 package of programs.[3] Time dependent density functional theory (TD-DFT), which is one of the most popular tools in the studies of excited states of molecular systems, was used to study the electronic configurations of the enol forms of propandial, propandithial and propandiselenal. Configuration interaction with single excitations (CIS) was performed on the optimized geometries.

Results and Discussion

The structural properties and hydrogen bonding in propandial, propandithial and propandiselenal have been investigated by means of hybrid-density functional theory (hybrid-DFT: B3LYP/Def2-TZVPP) level of theory. The distortions of high-symmetry (C_{2v}) configurations of propandial, propandithial and propandiselenal are as the contribution of the pseudo Jahn-Teller effect (PJTE) which is the only source of instability of high-symmetry configurations in degenerate and non-degenerate states.[1,2] The main contributions to the distortions of high-symmetry (C_{2v}) configurations to their plane symmetrical configurations (C_s symmetry) of propandial, propandithial and propandiselenal are due to the PJTE by mixing the ground A_1 states and second excited B_2 states [in propandial: HOMO(B_1)-LUMO(A_2); in propandithial: HOMO-1(B_1)-LUMO(A_2), HOMO(B_2)-LUMO+3(A_1), HOMO(B_2)-LUMO+9(A_1); in propandiselenal: HOMO-1(B_1)-LUMO(A_2), HOMO(B_2)-LUMO+1(A_1), HOMO(B_2)-LUMO+2(A_1)], resulting in a PJT (A_1 + B_2) $\otimes$ b_2 problem. The energy gaps between reference states (Δ) in the C_{2v} and C_s configurations decrease from propandial to propandiselenal (i.e. 4.92, 3.41 and 3.02 eV for propandial, propandithial and propandiselenal, respectively), therefore, the PJT stabilization energy for $C_{2v} \rightarrow C_s$ distortions increases from propandial to propandiselenal.

Conclusion

The B3LYP/Def2-TZVPP and TDDFT results revealed that the main contributions to the distortions of high-symmetry (C_{2v}) configurations to their plane symmetrical configurations (C_s symmetry) of propandial, propandithial and propandiselenal are due to the PJTE by mixing the ground A_1 states and second excited B_2 states resulting in a PJT (A_1 + B_2) $\otimes$ b_2 problem.

References

[1] Bersuker, I.B. *Chem. Rev*. **2001**, *101*, 1067.

[2] Bersuker, I. B. *The Jahn-Teller Effect*; Cambridge University Press: New York, **2006**.

[3] Frisch, M.J. et al, Gaussian 03, Revision B.03, Gaussian, Inc., Wallingford CT, **2004**.

Ab Initio Study of the Cooperativity in Ethanol-Water Heterotrimers

S. Jalili* and Z. Zargar
Department of Chemistry, K. N. Toosi University of Technology, Tehran, Iran
(Email: sjalili@kntu.ac.ir)

Keywords: Ethanol-water complex, Hydrogen bonding, Heterotrimers, Cooperative effects, Density functional theory, Atoms in molecules theory

Introduction

Molecular associations formed by hydrogen bonding have a crucial role in many physical, chemical and biological systems. It is possible to explain the formation of molecular clusters at the microscopic level. Examples of these clusters are the structures formed in the ethanol-water azeotrope. Understanding the molecular structure of these clusters may be useful for ethanol purification processes [1].

The potential energy surface of $(ethanol)_2$-water heterotrimers has recently been studied using density functional theory (DFT) calculations [2]. Using three different conformers for ethanol (g1, g2, t: gauche1, gauche2, trans) and various donor-acceptor combinations, 36 minimum-energy structures have been obtained and classified in six different groups. In this work, we have studied characteristic structures from these six groups in order to gain more insight to the important factors in their stability. The specific stability of cyclic structures have been explained using cooperative effects and atoms in molecules (AIM) analyses.

Methods

Quantum mechanical calculations have been performed using Gaussian 03 program. The geometry optimization and frequency calculations were performed using b3lyp/6-31+G* level of theory for six $(ethanol)_2$-water heterotrimers (Fig. 1). These complexes are named according to the donor or acceptor properties of water and ethanol.

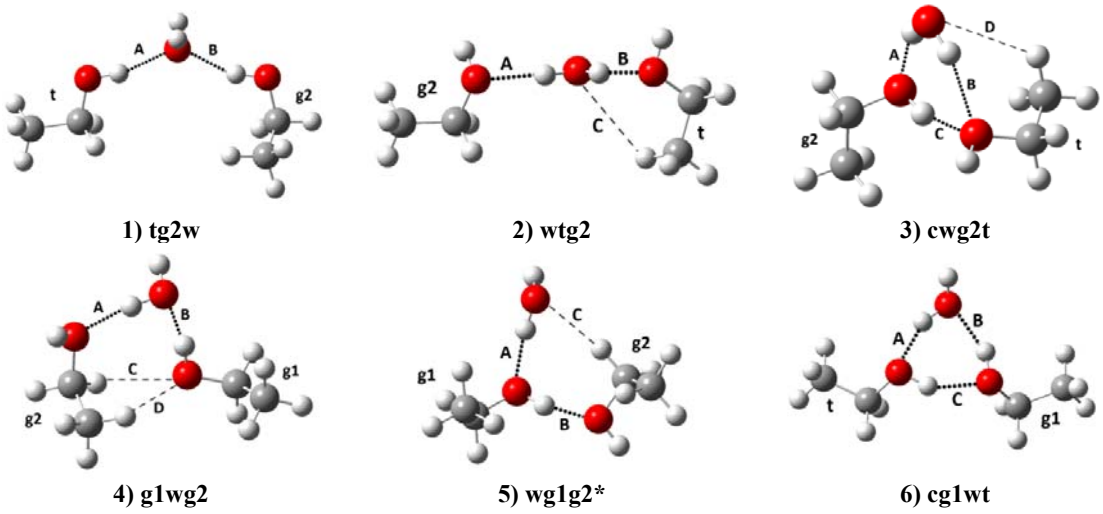

Fig. 1 The structure of six studied heterotrimers, with the predicted primary (dotted) and secondary (dashed) hydrogen bonds. The molecules are named according to the ethanol conformers (g1, g2, t).

The binding energy was calculated for each complex, including the corrections for zero-point energy (ZPE) and basis-set superposition error (BSSE) [3]. The Cooperativity effects were investigated using the additive interaction energy,

$$\Delta E_{\text{add}} = \Delta E_{\text{ABC}} - \Delta E_{\text{AB}} - \Delta E_{\text{AC}} - \Delta E_{\text{BC}} \quad (1)$$

in which the first term is the energy difference between the trimer and three monomers in the geometry of complex and using the complete basis set for the complex, and the subsequent terms are similar quantities for three dimers which can be distinguished in the trimer. AIM calculations were also used to confirm the existence of the hydrogen bonds.

Results and discussion

The thermodynamic properties of complexes are summarized in Table 1. Based on these data, the order of stability in the complexes is cg1wt > wg1g2* ≈ g1wg2 > cg2wt > wtg2 > tg2w. Analysis of trimerization energies shows that the most stable configuration is the cyclic geometric pattern formed by three primary hydrogen bonds (cg1wt), where all the molecules are proton acceptor and proton donor at the same time. This is a consequence of cooperative effects, which are reflected in a large and negative value of the additive interaction energy.

Table 1. Calculated thermodynamic properties of complexes. Values are in kcal/mol.

complex	E (a.u.)	E_{hb}	$E_{hb,ZPE}$	$E_{hb,ZPE,BSSE}$	ΔE_{add}
tg2w	−386.5303	−10.41	−7.38	−5.28	0.42
wtg2	−386.5322	−11.59	−8.10	−6.17	0.74
cg2wt	−386.5331	−12.19	−8.73	−6.58	0.36
g1wg2	−386.5375	−15.00	−11.32	−9.04	−1.82
wg1g2*	−386.5373	−14.90	−11.37	−9.25	−1.52
cg1wt	−386.5431	−18.44	−14.21	−11.83	−2.64

Conclusions

Even though the C−H···O interactions are weaker than the primary (O−H···O) hydrogen bonds, they seem to influence the stability of some clusters. Although these calculations have been performed in the gas phase, the results may be useful as a guide to the understanding of interactions in larger ethanol-water complexes formed in the azeotropes.

References

[1] A.E. Farrell, et al., Science 311 (2006) 506.

[2] S. M. Mejia, J. F. Espinal, A. Restrepo, F. Mondragón, J. Phys. Chem. A 111 (2007) 8250.

[3] S. Jalili, M. Akhavan, Theor. Chem. Acc. 118 (2007) 947.

Interaction of Glucose with Gold Clusters

Z. Jamshidi
Chemistry and Chemical Engineering Research Center of Iran,
P.O. Box 14335-186, Tehran, Iran
jamshidi@ccerci.ac.ir, na.jamshidi@gmail.com

Introduction

Biosensors are becoming essential in the fields of health care, chemical and biological analysis, environmental monitoring, and good processing industries.[1] Among them, glucose and carbohydrates sensors, as one of the most popular biosensors, have been extensively investigated and the development of sensing devices for the fast and reliable determination of them has been a subject of different studies.[2]

Detailed understanding of the nature of interaction between metal particles and conjugated biomolecular systems in nanoparticle complexes is of fundamental importance in the development and design of sensors and miniature devices and have been the subject of several experimental and theoretical investigations in recent years.[3-6] However, the understanding of the mechanism of the bonding between gold nanoparticles and glucose and the factors that control its efficiency is rather limited. Therefore, in this paper we investigate theoretically the interaction of *α-D*-glucose with cationic, anionic, and neutral Au_3 clusters which serve as simple catalytic models of Au nanoparticles. Natural bond orbital (NBO) analysis was applied to calculate the charge transfer and natural population analysis (NPA) of the complexes.

Method of Calculations

Geometries of the *α-D*-glucose complexes with neutral, anionic, and cationic forms of the gold trimers were fully optimized using the density functional theory (DFT) with B3LYP functional. The 6-31+G** basis set was used for the atoms in glucose, while for gold atom the Lanl2DZ basis set was applied. The harmonic vibrational frequencies and corresponding zero point vibrational energies (ZPVE) were calculated in all the optimized geometries, and real frequencies were obtained in all the cases. In the present calculations the Gaussian 03 suite of programs was employed. The NBO analysis was conducted for these complexes in order to obtain the natural charges and charge transfer.

Results and Discussion

Trimer gold clusters in cationic (Au_3^+), anionic (Au_3^-), and neutral (Au_3) forms were selected as simple catalytic models of Au nanoparticles during this work. The initial geometries of *α-D*-glucose complexes with Au_3^+, Au_3^-, and Au_3 metal clusters were generated by placing these metal clusters near the active sites of glucose (hydroxyl group). Electron rich oxygen atom in hydroxyl group donate electron density to the orbital of gold clusters through their lone pairs, and make highly stable Au–O bond. On the other hand, gold clusters can also play the role as a proton acceptor and form nonconventional H-bonds with hydroxyl groups (Au…H–O). Optimized structures of the *α-D*-glucose complexes with Au_3 metal clusters are shown in Figure 1. Vibrational analysis has been carried out on the optimized structures of the glucose, in order to examine the effect of gold complexation on the stretching frequencies of the certain functional group (O–H and C–O) in the glucose.

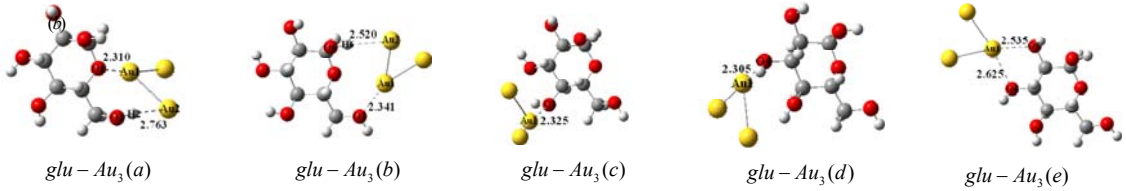

$glu - Au_3(a)$ $glu - Au_3(b)$ $glu - Au_3(c)$ $glu - Au_3(d)$ $glu - Au_3(e)$

Figure 1. Optimized geometries of neutral Au_3 cluster with α-D-glucose; the bond lengths are given in angstroms.

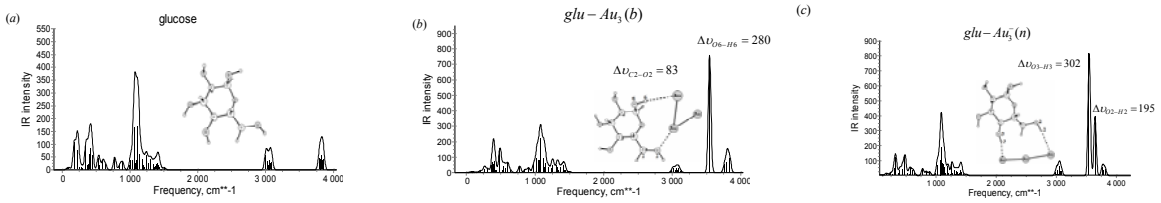

Figure 2. IR spectrum and intensity of glucose (a) , $glu - Au_3(b)$ (b) and $glu - Au_3^-(n)$ (c) complexes.

References

[1] Rakow, N. A.; Suslick, K. S. *Nature (London)* **2000**, *406*, 710.

[2] Reach, G.; Wilson, G. S. *Anal. Chem.* **1992**, *64*, 381A.

[3] Ratner, M.; Ratner, D. *Nanotechnology: A Gentle Introduction to the Next Big Idea*; Prentice Hall: Upper Saddle River, NJ, 2002. ((4) Slocik, J. M.; Moore, J. T.; Wright, D. W. *Nano Lett.* **2002**, *169*, 1151.

[5] Felice, R. D.; Selloni, A.; Molinari, E. *J. Phys. Chem. B* **2003**, *107*, 1151.

[6] Kryachko, E. S.; Remacle, F. *Nano Lett.* **2005**, *5*, 735.

The Influence of Para-substituents on the proton affinity of pyridine

A. Ebrahimi, S.M. Habibi, M. Jahantab*

Department of Chemistry, University of Sistan and Baluchestan, Zahedan, Iran

(E-mail: mahjoube.jahantab@yahoo.com)

Keywords: Proton affinity, Pyridine derivative, Electrostatic potential, Hammett constants

Introduction:

The proton affinity (PA) of a molecule is generally defined as the change in enthalpy associated with the addition of a proton to a molecule M in the reaction $M + H^+ \rightarrow MH^+$. PA reflects the intrinsic basicity of a chemical compound in absence of any solvent effects [1]. In this work, the effects of electron-donating (ED) and electron-withdrawing (EW) substituents on the PA of pyridine (see Fig. 1) have been estimated to investigate the relationships between PA and different properties including topological properties of electron density at the N-H bond critical points (BCP) calculated by the atoms in molecules (AIM) method [2], the molecular electrostatic potentials (MEP), the structural parameters, and the Hammett constants.

Methods:

The structures have been optimized at the B3LYP/6-311++G(d,p) level of theory using the Gaussian03 program package [3]. The vibrational frequencies have been calculated at the same level, when the harmonic frequencies were scaled by 0.962 [4,5]. The PA at 298.15 K is defined as the enthalpy change, during the protonation process.

$PA = \Delta H^0_g(M) + \Delta H^0_g(H^+) - \Delta H^0_g(MH^+)$, where $\Delta H^0_g(H^+) = 2.5RT = 1.48$ kcal/mol.

The topological properties of electron charge density were analyzed by the AIM method using AIM2000 package [6]. The freely available MOLEKEL program [7] has been used to visualize the MEP. The most negative-valued MEP point (V_{min}) can be obtained from the visual inspection of MEP data for the lone-pair region of the nitrogen atom in the pyridine.

Results and Discussion:

The calculated PA values for pyridine derivatives are reported in Table 1. The ED groups make the nitrogen lone pair more available for the proton and increase the PA values relative to pyridine. This value increases more with increasing the electron-donating ability of

substituents. This behavior is reversed by the EW substituents, which deactivates the pyridine ring. The increase in the proton affinity is accompanied by the increase in the ρ value calculated at the N-H BCP and the decrease in the MEP value for the lone pair region of the nitrogen. The PA values are in linear relationship with the ρ and MEP values with correlation coefficients higher than 0.96 (see Fig. 2).

PA = 1059.2 ρ – 3359.6 and PA = -709.87 MEP + 156.25.

On the other hand, the ρ and MEP values (and the PA values) are in linear relationship with Hammett constants.

Table 1. Proton affinity (kcal mol^{-1}), electron density ρ (e/au^3), Laplacian of electron density $\nabla^2\rho$ (e/au^5) and the results of MEP analysis

	PA	$\rho_{BCP}\times10$	$-\nabla^2\rho$	- MEP × 10^2
$N(CH_3)_2$	242.0	3.401	1.762	12.5
$NH(CH_3)$	239.9	3.399	1.765	11.3
NH2	236.9	3.396	1.769	11.0
CH_3	228.4	3.385	1.778	10.3
H	223.7	3.381	1.783	9.9
Br	220.9	3.381	1.783	8.9
Cl	220.3	3.380	1.784	9.0
F	219.1	3.378	1.789	9.1
CHO	216.8	3.378	1.790	8.5
CN	211.8	3.373	1.792	7.8
NO2	209.0	3.370	1.798	7.5

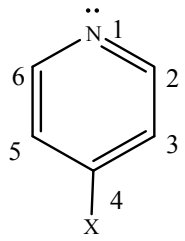

X ≡ $N(CH_3)_2$, $NH(CH_3)$, NH_2, CH_3, CHO, Br, Cl, F, CN, NO_2

Fig. 1 Numbering of the positions in the pyridine derivatives.

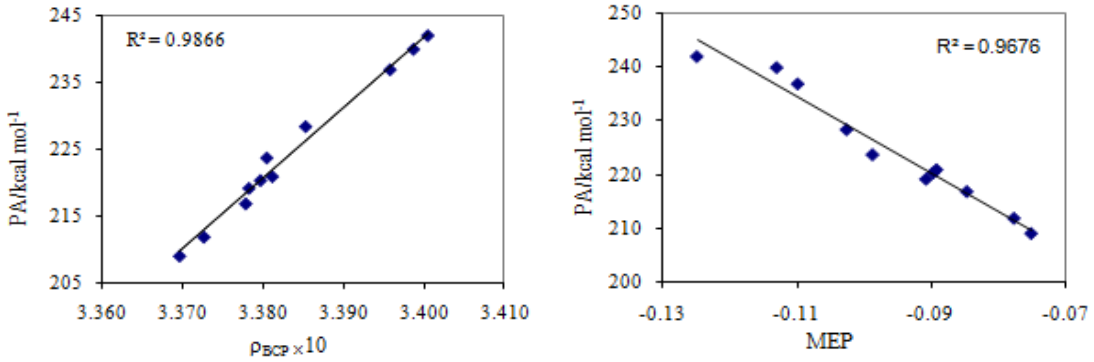

Fig. 2 Linear correlation between the PA and a) the electron density, and b) the MEP value around the nitrogen.

Conclusion:

The ED substituents increase PA, whereas the EW groups decrease it. From linear relations between the PA values and the ρ, MEP, and Hammett constants, the proton affinity could be estimated without energy calculation.

References

[] J.M.L. Martin, J.P. Frangois, R. Gijbels, J.Computational Chemistry, 10, 3, 346, 1989.

[2] R.F.W. Bader, Oxford University Press, Oxford, 1990.

[3] M.J. Frisch, et al, Gaussian 03 (Revision B.03), Gaussian, Inc, Pittsburgh, PA, 2003.

[4] M.P. Andersson, P. Uvdal, J.Phys.Chem.A, 109, 2937, 2005.

[5] A.P. Scott, L. Radom, J.Phys.Chem, 100, 16502, 1996.

[6] F.W. Biegler König, J. Schönbohm, D. Bayles, J.Comput.Chem, 22, 545, 2001.

[7] P. Flukiger, H.P. Luthi, S. Portmann, J.Weber, Molekel 4.0, Swiss Center for Scientific Computing, Manno, Switzerland, 2000.

The electronic structure studies and investigation of interaction embedded molecules in nano capsule by computational calculations

M. Kia[a] , M. Jahangiri Lahkani*[b]

[a] Department of Chemistry, Rasht Branch, Islamic Azad University, Rasht, Iran

[b]Islamic Azad University, Rasht Branch, Young Researchers Club, Rasht, Iran

(Email: Jahangiri86@yahoo.com)

Keywords: Fullerenes, Encapsulating energy, Ab initio calculation

Introduction

When fullerenes were first discovered [1], there was much excitement about practical applications. It was speculated that buckyballs would make great lubricants, rolling like little ball bearings between other molecules. Or perhaps drugs could be trapped inside the cages, and then released slowly by a triggering mechanism that could break open the cages inside the body. C60 is a molecule that consists of 60 carbon atoms, arranged as 12 pentagons and 20 hexagons [2].

Methods

The focus of this work was on the benzene, pyridine, pyrazine, pyrimidine, pyridazine, cyclopropane, cyclobutane, thiophene, methane, ammonia, thioure molecules trapped in C_{60}. All geometry optimizations have been performed using 3-21G and 6-31G basis sets and the Hartree-Fock and DFT methods, which is implemented in the Gaussian98, Gview, Hyper Chem and Chem3D programs. In this model study, bond lenghts between pentagonal-hexagonal rings and hexagonal-hexagonal rings, encapsulating energies and bond lengths were determined in the free state and in the custody of C_{60}.

Using energies obtained for them, encapsulating energies were calculated by the following equation [3]. encapsulating energy is defined into the energy consumed to enter a molecule into nanocapsule or nanotube. $DE=E[X@C_{60}]-E[C_{60}]-E[X]$

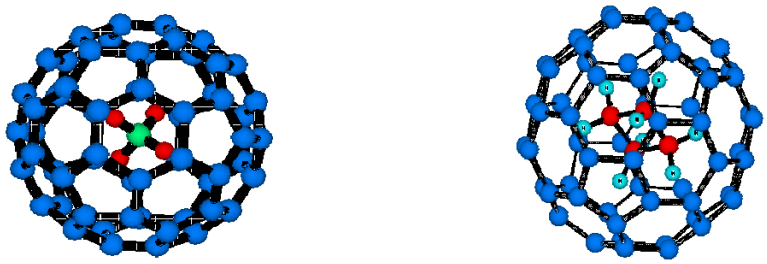

(a) (b)

Fig. 1: Optimized structure of (a) $CH_4@C_{60}$ and (b) CYCLOBUTANE@C_{60} as computed at the B3LYP/6-31G

Results and Discussion

The bond lengths obtained for the pentagonal-hexagonal rings and hexagonal-hexagonal rings using 3-21G and 6-31G basis sets and Hartree-Fock level of theory and the B3LYP density function method show that obtained results are in agreement with experimental data[4].

In this study encapsulating energy was calculated by HF(3-21G), HF(6-31G), B3LYP(3-21G) and B3LYP(6-31G) methods. It is found that the amount of encapsulating energy obtained through B3LYP(3-21G) method for most molecules more than the amount of encapsulating energy obtained through HF(3-21G) method, but the amount of encapsulating energy obtained through B3LYP(6-31G) method for most molecules is less than the amount of encapsulating energy HF(6-31G) method.

Besides, calculated bond lengths of benzene, pyridine, pyrazine, pyrimidine, pyridazine, cyclopropane, cyclobutane, thiophene, methane, ammonia, thioure molecules trapped in C_{60} being identified with put the above molecules in space of C_{60} all bond length are reduced. The reason of this can be, reducing the repulsive because decrease bond length.

Table 1. Optimized bond length of pentagonal[5,6] and hexagonal[6,6] rings in the C_{60}(Å)

Experimental			Theoretical		
Methode	[5,6]-bonds	[6,6]-bonds	Methode	[5,6]-bonds	[6,6]-bonds
NMR	1.448	1.370	HF(3-21G)	1.453	1.367
diffr. Neutron	1.444	1.391	HF(6-31G)	1.452	1.375

Table 2. Encapsulating energies of X@C_{60} molecules($Kcal.mol^{-1}$)

Molecule	HF/3-21G	HF/6-31G	B3LYP/3-21G	B3LYP/6-31G
$CH_4@C_{60}$	5.495	17.242	3.295	9.978
Cyclobutane@C_{60}	220.079	919.896	747.045	258.252

Conclusion

Thus this study gives the basic knowledge of structure of fullerenes and their applications.The fullerenes can be used as carrier molecules and drugs.

References

[1] Kroto, H. W., Heath, J. R., O'Brien, S. C., Curl, R. F. and Smalley, R. E.,1985, "C60: Buckminsterfullerene" Nature, 318, pp.162-163.

[2] Diwan, Parag, and Bharadwaj, Ashish, 2005, "The nanoscope, Encyclopedia of Nano science and Nanotecnology", Vol. 1, pp. 250-276.

[3] Sun, Q., Wang, Q., Kawazoe, Y., and Jena, P., "Physical Review" B 66,245425, 2002

[4] Stobinski, L., Peszke, J., and Hong-Ming Lin, "Rev.Adv.Mater.Sci." 363-370, 5, 2003

Design Of Nanoscale Molecular Wire Based On Cis and trans-butadiene : Role of linkage

Z. Chamani* [a], Z.Bayat [a],s.danesh nia [a],R.Ekandarfilabi [a]
[a] *Department of Chemistry, Islamic Azad University -Quchan Branch, Iran*
Chemist1782_63@yahoo.com

Abstract :
Theoretical investigation has been performed on electron transport properties of Cis-Butadiene and Trans-Butadiene molecules sandwiched between two gold surfaces. Different linkers such as sulfur, nitrogen, SH and NH2 have been considered to study the role of linkage in the conduction properties of the molecular wire. The electronic conduction has been analyzed from the change in the shape of molecular orbitals and the evolution of the HOMO– LUMO gap of the molecule-gold complexes under the influence of the electric filed.

Keywords:Cis- Butadiene , Trans-Butadiene ,molecular wire, HOMO, LUMO,HLG molecular wire,

Introduction:
A single organic molecule is likely to be the smallest entity to conduct electricity and thus molecular wires present many interesting challenges to fundamental science as well as enormous potential for technological applications, such as organic switching devices [1–4] and nanoscale memories [5,6].

Methods:
The calculations have been performed at the density functional theory level with the B3LYP functional. The basis set is split 6-31G* for C, H, N, S atoms and the Los Alamos National Laboratory effective core potentials with a double-zeta valence (LANL2DZ) for the gold atoms [7].

Results and discussion:

Table1(a:cis,b:trans) gives a comparison of the energy levels of HOMO and LUMO levels as well as their gap (HLG) for FOUR free molecules. The corresponding molecular orbital pictures for molecules obtained from their optimized geometries are visualized in Table 2 (a:cis,b:trans).

Table 1. (a,b): HOMO, LUMO and HLG levels (in eV) for the free molecule.

NO.	MOLECULE	HOMO	LUMO	HLG
1.	SH	7.51592	4.5498	2.9660
2.	NS	-6.0767	-4.55993	1.51680

NO.	MOLECULE	HOMO	LUMO	HLG
1.	**SH**	-5.31568	-0.965633	**4.349434**
2.	**NS**	-5.270408	-4.668317	**0.602091**

Table . 2(a,b) The shape of HOMI and LUMO orbitals for the free molecules.

Conclusions:

In the present study we focus on the geometric and electronic structure of Cis- Butadiene and Trans-Butadiene -based molecular wire, however the electron transport properties can be also studied based on the non-equilibrium Green's function formalism.

LINKER	HOMO	LUMO
SH		
CS	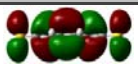	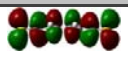

LINKER	HOMO	LUMO
SH		
CS		

Reference:

[1] C. Joachim, J.K. Gimzewski, R.R. Schlittler, C. Chavy, Phys. Rev. Lett. 74 (1995 2102.

[2] T. Oyamada, H. Tanaka, H. Sasabe, C. Adachi, Appl. Phys. Lett. 83 (2003) 1252.

[3] L. Ma, S. Pyo, J. Ouyang, Q. Xu, Y. Yang, Appl. Phys. Lett. 82 (2003) 1419

[4] D.R. Stewart, D.A.A. Ohlberg, P.A. Beck, Y. Chen, R.S. Williams, J.O. Jeppesen, K.A. Nielsen, J.F. Stoddart, Nano Lett. 4 (2004) 133.

[5] J. He, L. Ma, J. Wu, Y. Yang, J. Appl. Phys. 97 (2005) 064507.

[6] C.N. Lau, D.R. Stewart, R.S. Williams, M. Bockrath, Nano Lett. 4 (2004) 569.

[7] W.R. Wadt, P.J. Hay, J. Chem. Phys. 82 (1985) 284

Conformational Analysis of Sidechian in HCO-Gly-L-ILeu-Gly-NH_2 Tripeptide Model. A DFT Study

Behzad Chahkandi, Bentolhoda Ashrafi*
Department of Chemistry, Islamic Azad University ,Shahrood Branch, Shahrood, Iran.
Email:bchahkandi@gmail.com

Keywords: Protein Folding, Tripeptide, DFT, Side Chain, IsoLeucine.

Introduction

Proteins are polymers of the 21 naturally occurring amino acids can both in the L- and D-enantiomeric configuration [1].

One step towards better understanding of a disease is the conformational analysis of its component structures [2]. There are too many conformational space of the protein structure in a timely fashion. Thus, it may be that the conformational search must be restricted in some way as to direct folding to a native conformation which is both stable and kinetically acessible [3]. Except Gly with the smallest sidechain, H, other amino acid residues have bigger sidechain, as like as IsoLeucine, the sidechain interaction is characterized by the dihedral angle vector χ. Conformational analysis of all amino acids within a peptide sequence would allow for a better understanding of the behaviors of these molecules[4].

In this work, we investigated the effect of IsoLeucine side chain torsional angles on the stability of done HCO-Gly-L-ILeu-Gly-NH_2 tripeptide model and the most stable conformation of sidechain was determined.

Methods

The geometry optimization of HCO-Gly-L-ILeu-Gly-NH_2 tripeptide carried out by using Gaussian 98 program [5], with DFT calculations at the B3LYP/6-31G(d) level of theory. Our tripeptide sidechain has two dihedral angels : χ_1, χ_2 . The first SC dihedral angle (χ_1) rotated around N4-C6-C8-C12 atoms,(C6-C8 bond), in order to find more stable states and then the second sidechain dihedral angle (χ_2), rotated around C6-C8-C12-C13 atoms, (C8-C12 bond), and the most stable conformer was determined.

Results and discussion

a) *The first dihedral angle χ_1*

This study is contain 2 stages, in the first stage, χ_1 that is the lower side chain torsional angle (see Fig 1) was changed at 30° intervals from 0° to 360° and we determined three more stable structure among 12 computations.

We found three more stable states in the 300° or -60°, 60° and 180° that they known as these title: negative gauche (g^-), positive gauche (g^+) and anti states, respectively. Among three states, g- is the most stable conformation.

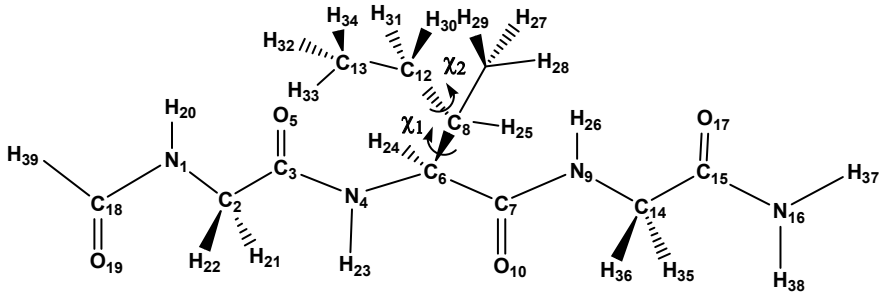

Fig.1. Schematic diagram with sidechain dihedral angles definitions for HCO-GLY-L-ILEU-GLY-NH_2 tripeptide

b) *The second dihedral angle*

In the second stage, we kept χ_1 in the g-, g+ and anti states and then χ_2 was changed same as the first stage for each states g-, g+ and anti. The most stable conformation with two stable angles appeared in -60 (g-), -60 (g-) state.

Conclusion

The importance aim in this research was finding the most stable structure of HCO-Gly-L-ILeu-Gly-NH_2 tripeptide model as a small part of one of oligopeptide chains in human body. We found the most stable conformers in the most stable sidechain dihedral angles of IsoLeucine residue in g-,g- state at B3LYP/6-31G(d) level of theory.

References:

[1] Chou P.Y.; Fasman G., *Biochemistry*. **1974**, *13*, 211.

[2] Perczel, A.; McAllister, M.A.; Csa´sza´r, P.; Csizmadia I.G., *Am J.Chem. Soc*. **1993**, *288*, 115.

[3] McAllister, M.A.; Perczel,A.; Csaszar, P.; Csizmadia,I.G.; Struct, J. Mol. *Theochem.* **1993**, 288, *161–180*.

[4] Perczel,A.; Angyan, J.G.; Kajtar,M.; Viviani,W.; Rivail,J.L.; Marcoccia,J.F.; Csizmadia, G.*Chem.Soc*. **1991**, 113, *6256–6265*

[5] Gaussian 98, Revision A.7, M. J. Frisch, G. W. Trucks, H. B. Schlegel, et al. Gaussian, Inc., Pittsburgh PA, 1998.

Investigation of the tautomerism in a derivative of oxadiazol in gas phase: A DFT study

Behzad Chahkandi*, Sayyed Faramarz Tayyari, Meysam kosary
Department of Chemistry, Islamic Azad University, Shahrood Branch, Shahrood, Iran

Keywords: DFT, Abinitio, Tautomerism, Oxadiazole

Introduction

Comparison between –CH=CH– of benzenoid hydrocarbons and either the divalent –S– or –O– in their sulfur and oxygen containing counterparts is a well-known subject within benzenoid hydrocarbon and heterocyclic chemistry. New analogues of pyrimidine bases are of interest as potential biologically activeagents. 1,3,4-Oxadiazoles[1] have attracted an interest in medicinal chemistry as ester and amide bioisoesters for a number of biological targets.[2]. In particular the 2-amino-1,3,4-oxadiazoles have recently been reported to exhibitpromising anti-tumour[3] , antiviral[4] and anti-inflammatory[5] activities.

A theoretical study and attempt to better characterize the geometric parameters of 5-Amino-2,3-dihydro-1,3,4-oxadiazol-2-one tautomers (see Fig1) in the gas phase, we report here the results of DFT calculations at the B3LYP level, using 6-311++G(d,p) basis set.

In this research we optimized the geometry of various tautomers of 5-Amino-2,3-dihydro-1,3,4-oxadiazol-2-one in gas phase. (see Fig 1)

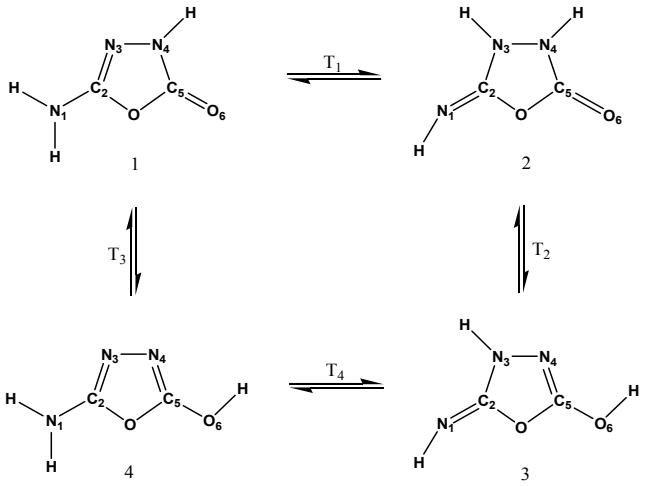

Fig1. 5-Amino-2,3-dihydro-1,3,4-oxadiazol-2-one tautomers

Methods

Standard ab initio molecular orbital calculations were carried out using the Gaussian-03 programs. The geometries of 5-Amino-2,3-dihydro-1,3,4-oxadiazol-2-one tautomers (Figure 1) have been optimized using the 6-311++G(d,p) basis set. The optimizations were initially done at the DFT calculations were done using B3LYP exchange-correlation functional, The geometry optimizations were performed with 6-311++G(d,p) basis set

Results and Discussion

The tautomers studied in the present work are 1, 2, 3 and 4; they are illustrated in Figure 1. result of DFT studied in this sector, The significant changes are in the C–O bond distance and C–N bond distance. The optimized C(5)–O(6) distance of 1.32626 Å at 6-311++G** in **3** and C(5)–O(6) distance of 1.32890 Å at 6-311++G** in **4** is shortened to 1.19689 Å in **1** and 1.19097 Å in **2** on account of the double bond. The optimized C(2)–N(3) distance of 1.40403 Å at in **2** and C(2)–N(3) distance of 1.37669 Å in **3** is shortened to 1.28891 Å in **1** and 1.28846 Å in **4** on account of the double bond.

The calculated total, Gibbs free energy at 298 K, and The absolute and relative (ΔE) energies, together at various levels are given Table 2 for the four tautomers. In the calculation of the relative energies the energy of **1** was taken as reference. At the DFT calculation it appears that **1** is the most stable tautomer. The energies stabilities of the various tautomers are also maintained at the DFT calculation (**1 > 2 > 4 > 3**).

Conclusion

1.The energies stabilities of the various tautomers are also maintained at the DFT calculation (**1 > 2 > 4 > 3**).

2.The optimized C(2)–N(3) distance of 1.40403 Å at in **2** and C(2)–N(3) distance of 1.37669 Å in **3** is shortened to 1.28891 Å in **1** and 1.28846 Å in **4** on account of the double bond.

3.At the DFT calculation it appears that **1** is the most stable tautomer.

References

[1] The chemistry of 1,3,4-oxadiazoles has been reviewed: (a) Hetzheim, A.; Moeckel,K. Adv. Heterocycl. Chem. 1966, 7, 183; (b) Hill, J. In Comprehensive Heterocyclic Chemistry; Potts, K. T., Ed.; Pergamon: Oxford, 1984; Vol. 6, pp 427–446.

[2] (a) Leung, D.; Du,W.; Hardouin, C.; Cheng, H.; Hwang, I.; Cravatt, B. F.; Boger, D.L. Bioorg. Med. Chem. Lett. 2005, 15, 1423; (b) Omar, F. A.; Mahfouz, N. M.;Rahman, M. A. Eur. J. Med. Chem. 1996, 31, 819

[3] (a) Liszkiewicz, H.; Kowalska, M. W.; Wietrzyk, J.; Opolski,A. Ind. J. Chem. Sec. B - Org. Chem. Inc. Med. Chem. 2003,42(11), 2846–2852. (b) Lokanatha Rai, K. M.; Linganna, N.Farmaco 2000, 55, 389–392.

[4] Tan, T. M.; Chen, Y.; Kong, K. H.; Bai, J.; Li, Y.; Lim, S.G.; Ang, T. H.; Lam, Y. Antivir. Res. 2006, 71, 7.

[5] M.D. Mullican, M.W. Wilson, D.T. Connor, C.R. Kostlan, D.J.Schrier, R.D. Dyer, Design of 5-(3,5-di-tert-butyl-4-hydroxyphenyl)-1,3,4-thiadiazoles, -1,3,4-oxadiazoles and -1,2,4-triazoles as orally-active, nonulcerogenic antiinflammatory agents, J.Med. Chem. 36 (1993) 1090–1099.

Structural study of cerebral human aquaporin-4(hAQP4) in hyperthermia conditions

Mohammad Haji Malek kheyli [*a], Majid Monajjemi [b], Babak Khalili [c], Marjan Alikahi [d]

[a] Department of Chemistry, science & Research Branch, Islamic Azad University, Tehran, Iran
(Email:mohammad.Haji@gmail.com)

[b,c] Department of Chemistry, science & Research Branch, Islamic Azad University, Tehran, Iran

[d] Young researchers club, Islamic Azad University-Varamin Branch, Iran

Keywords: Hyperthermia, Haqp-4, Cerebral Edema, The radius of gyration

Introduction

The aquaporin (AQP) family includes both AQPs that conduct water, but not glycerol, and aquaglyceroporins that mediate diffusion of water, glycerol, and certain other small molecules in their neutral form across biological membranes. In humans, 13 different AQPs (AQP0-12) provide for transport in different tissues, each of which has broad clinical importance [1, 2].

Aquaporin 4 is the predominant water channel in the mammalian brain, abundantly expressed in the blood-brain and brain cerebrospinal fluid interfaces of glial cells. Its function in cerebral water balance has implications in neuropathological disorders, including brain edema, stroke, and head injuries [3, 4].

Besides AQP4, AQP1 and AQP9 are also expressed in the brain [5]; AQP1 is expressed in the epithelial cells of the choroid plexus, and has a role in cerebrospinal fluid production, whereas AQP4 is localized to the endfeet of astrocytes in contact with the blood vessels of the blood-brain barrier and in astrocytic processes in contact with synapses [6].

Computation method

In this research all of computations have been done in the level of theory HF with STO-3G, 3-21G, 6-31G, 6-31G* and 6-31G** basis-sets and distances between His-201 and Arg-216 amino acids were studied. The radius of gyration was determined after nomination of the best distance by the use of survey resultant of basis-sets.

Results and discussion

After survey resultant of basis-sets and comparison of data was specified that His-201 and Arg-216 amino acids have constant distance in 2.8 Å and its clear in 6-31G** basis-set because of undermost level of energy(Fig.1).

By the use of measure of the radius of gyration resultant in this basis-set and various temperatures was determined that present conduit in aquapoin-4 protein is opened with increasing body temperature and passed water value from conduit will be uncontrollable, therefore causes brain edema(Fig.2).

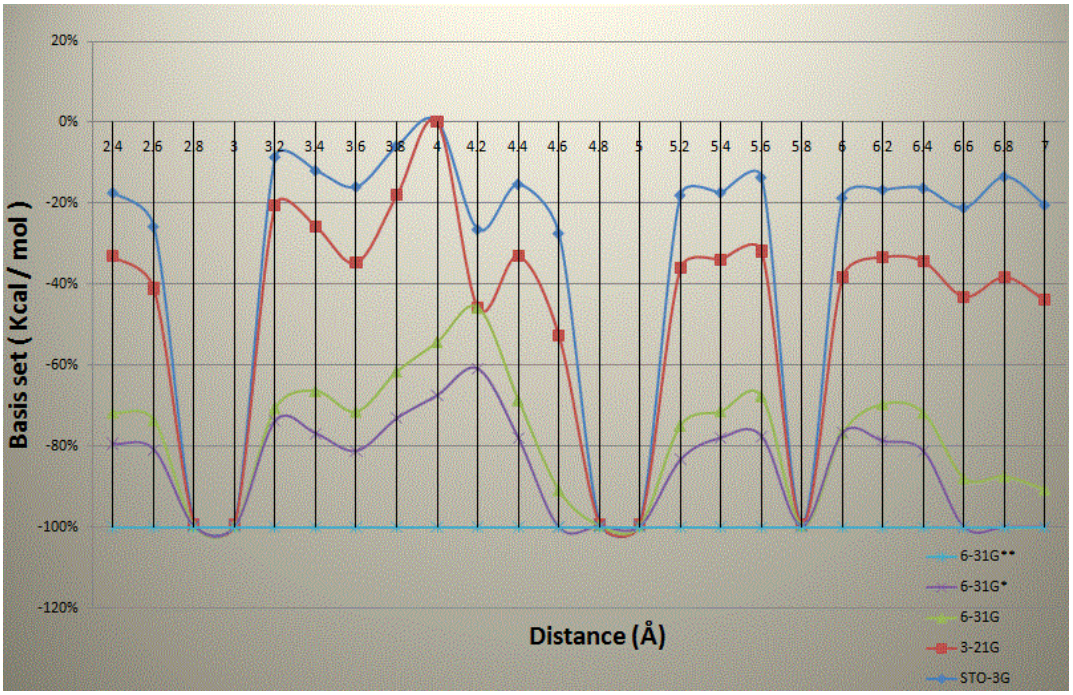

Fig.1. Distances between His-201 and Arg-216 amino acids based on basis sets.

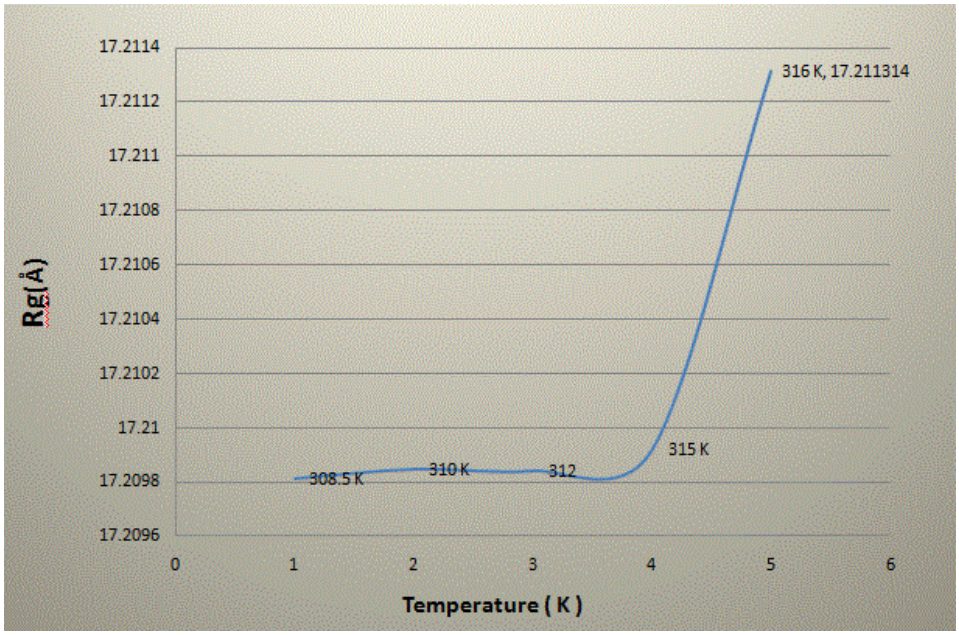

Fig.2. The radius of gyration based on body temperature.

References:

[1]. Rojek A, Praetorius J, Frokiaer J, Nielsen S, Fenton RA (2008) A current view of the mammalian aquaglyceroporins. *Annu Rev Physiol* 70:301–327.

[2]. King LS,KozonoD, Agre P (2004) From structure to disease: The evolving tale of aquaporin biology. *Nat Rev Mol Cell Biol* 5:687–698.

[3]. Badaut J, Brunet JF, Regli L (2007) Aquaporins in the brain:Fromaqueduct to ‘‘multi-duct.’’ *Metab Brain Dis* 22:251–263.

[4]. Manley GT, et al. (2000) Aquaporin-4 deletion in mice reduces brain edema after acute water intoxication and ischemic stroke. *Nat Med* 6:159–163.

[5]. Badaut J, Lasbennes F, Magistretti PJ, Regli L (2002) Aquaporins in Brain: Distribution, Physiology, and Pathophysiology. *J Cereb Blood Flow Metab* 22:367–378.

[6]. Detmers FJM, et al. (2006) Quaternary ammonium compounds as water channel blockers: Specificity, potency, and site of action. *J Biol Chem* 281:14207–14214.

Study mechanism of catalytic reaction of co_2 and H_2 in gas phase

Mohammad Haji Malek Kheyli*[a], Marjan Alikahi[b], Majid Monajjemi[a], Mohsen Shabani[c].

[a] *Chemistry Department, Islamic Azad University, science & Research Branch, Tehran, Iran*

(Email:Mohammad.Haji@gmail.com)

[b] *Young researchers club, Islamic Azad University-Varamin Branch, Iran*

[c] *Chemistry Department, Islamic Azad University-Varamin Branch, Iran*

Introduction

Emitted carbon dioxide has been implicated as one of the major sources of global warming. Therefore the conversion of carbon dioxide into alcohols in an environmentally desirable process, making use of an abundant, cheap resource. In this research synthesis of ethanol from co_2 and H_2 was studied on Tio_2 (001) surface by the use of DFT methods and its new proposition. Carbon dioxide adsorbed chemically on titanium atom and hydrogen atom adsorbed on oxygen on Tio_2 (001) surface. In this research, a ten step mechanism for ethanol synthesis has been suggested corresponding to reported methanol synthesis.

Computation method

In this research all of computations have been done in the level of theory B3LYP with basis-sets LanL2DZ for titanium atoms and 6-31G for the rest atoms (H, C, O…). All of seated components on the surface optimized and determined transition state structures by the use of SCAN method.

Results and discussion

Suggested Mechanism of ethanol synthesis has been brought in figure 1.

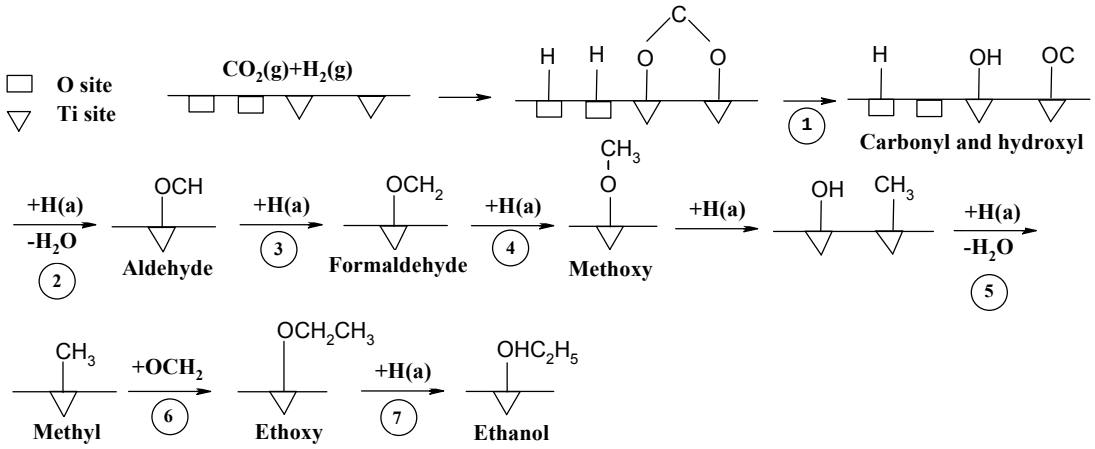

Fig.1.Suggested Mechanism of ethanol synthesis from CO_2 and H_2

Total energy of titanium oxide, carbon dioxide and hydrogen have been picked out as era in figure 2 and relative energy disparate steps of mechanism reaction have been reported. By attention to calculated energies for transition states, convert step of adsorbed OCH_3 to adsorbed CH_3 (TS_5) got highest level of energy and this value is 144.05 Kcal/mol. Thus it is rate-limiting step.

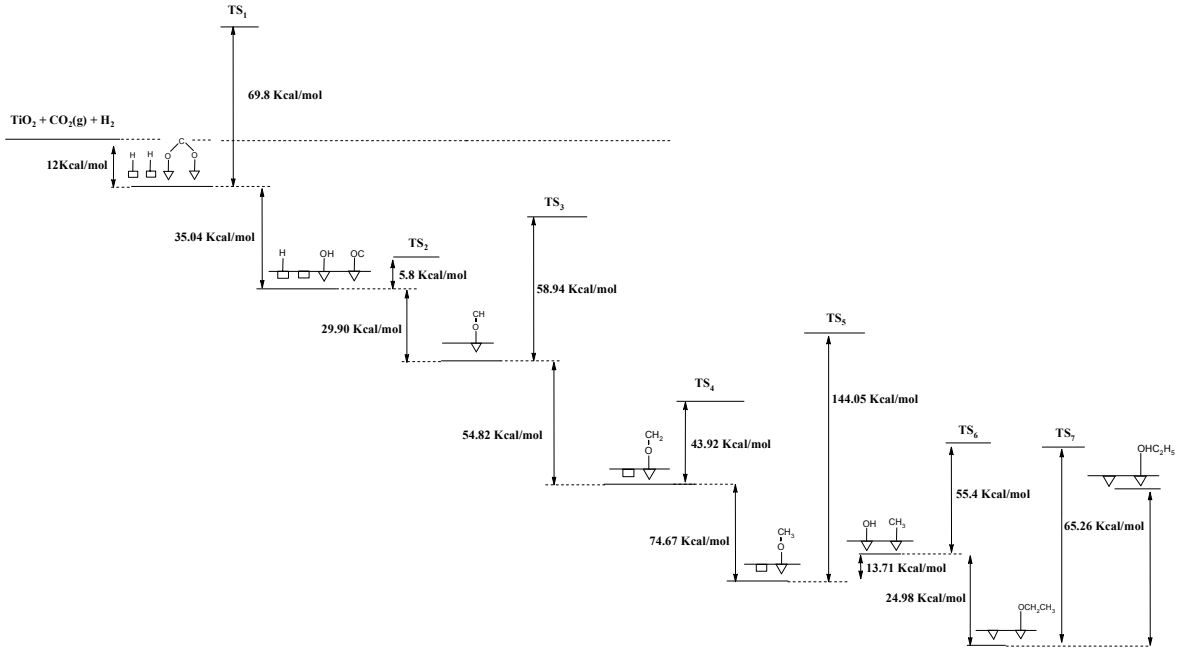

Fig.2. Comparison of relative energy disparate steps of mechanism reaction

References:

[1]. Izumi, Y., Kurakata, H., and Aika, k., *J. cata*, 175**,** 236–244 (1998).

[2]. Kurakata, H., Izumi, Y., and Aika, K., *Chem. Commun.*, 389–390 (1996).

[3]. Sachtler,W. M. H., *Faraday Discuss. Chem. Soc.* **72**, 7–31 (1981).

[4]. Sinfelt, J. H., Via, G. H., and Lytle, F. W., *Catal. Rev. Sci. Eng.* **26**, 81–140 (1984).

[5].Y ongMan Choi and Ping Liu (2009) Mechanism of Ethanol Synthesis from Syngas on Rh(111). *J. Am. Chem. Soc.*, Article ASAP doi

[6]. Kakumoto, T. and Watanabe, T., *catalysis Today,* 36, 39-44 (1997).

[7]. Kakumoto, T., *Energy Convers. Mgmt*., 36, 661 (1995).

[8].M. Bowker, H. Houghton, K.C. Waugh, J. Chem. Soc., Faraday Trans. 77 (1981) 3023.

[9].G.C. Chinchen, P.J. Denny, D.G. Parker, M.S. Spencer, K.C. Waugh, D.A. Whan, Appl. Catal. 30 (1987) 333.

Molecular structure and intramolecular hydrogen bonding of Heptane-3,5-dione. A DFT study

Z. Hajian [a], A-R. Nekoei [*,b], M. Vakili [c], A. Kanaani [d]

[a] Islamic Azad University, Marvdasht Branch. Department of Chemistry, Marvdasht, Iran

[b] Department of Chemistry, Shiraz University of Technology, Shiraz, 71555-313, Iran

[c] Department of Chemistry, Ferdowsi University of Mashhad, Mashhad 91774-1436, Iran

[d] School of Chemistry, Damghan University of Basic Sciences, Iran

Keywords: Heptane-3,5-dione; β-dicarbonyl; Intramolecular hydrogen bond; Density Functional Theory

Introduction

It is straightforward to show that a β-dicarbonyl, with at least one α-hydrogen, can transform bidirectionally into two enol forms by keto-enol tautomerism as illustrated in Fig. 1. Involved hydroxyl, carbonyl, and alkene functional groups of both enol forms contain six atoms that can contribute in a π-electronic resonance conjugation to induce a six-membered ring like structure referred to as a chelated ring. The noteworthy aim in ongoing research is to crosscheck the effects of different β-substitutions on the stabilities and IHB strengths of the two mentioned enol forms. Successive substitution of the CH_3 groups of acetylacetone (AA, R1=R3=CH_3, see Fig. 1) by $-C(CH_3)_3$ groups increase the enol content of β-dicarbonyl, that confirmed by ^{1}H-NMR spectroscopy studies [1]. These studies indicate that 2,2,6,6-tetramethyl-3,5-heptanedione (TMHD, R1=R3=$C(CH_3)_3$) in the liquid phase is completely in the enol form, whereas the enol contents for 5,5-dimethyl-2,4-hexanedione (DMHD, R_1=CH_3, R_3=$C(CH_3)_3$) and AA are 94% and 79% [2], respectively. The NMR chemical shifts of the enolated protons in these compounds have indicated that substitution of the CH_3 groups of AA by t-But groups increase the IHB strength.

Heptane-3,5-dione (hereafter HPD) has two ethyl groups substituted for methyl groups in the β-positions of AA. This paper predicts the conformational stabilities, geometrical parameters and IHB strength of HPD molecule. Then, the calculated stable conformations, geometrical parameters, the IHB energies and ^{1}H-NMR shifts for HPD will be compared with AA, DMHD and TMHD results [3]. These comparisons give a clear understanding for the effects

of the substitution of the methyl groups of AA, and the t-But groups of DMHD and TMHD, by the ethyl groups on the structure and hydrogen bond strength of HPD.

Method of Analysis

All possible keto and enol conformers of HPD were fully optimized at the B3LYP level of Density functional theory (DFT) with 6-31G** basis set, using Gaussian 03W software package. The properties of stable cis-enol conformations are also computed at B3LYP level with the basis sets of 6-311G** and 6-311++G**.

Results and Discussion

For HPD, among several cis-enol conformers that are engaged in a six-membered ring intramolecular hydrogen bonded system, there are only four E1-E4 stable forms (other forms turns to these stable forms). The structures of these conformers, atom numbering of the system and their relative stabilities (in kcal/mol) are shown in Fig 2. The relative energies clearly suggest that the chelated cis-enol E1 and E2 forms are so stable that the presence of other conformers in significant amounts is unlikely. The selected of fully optimized geometrical parameters of E1 and E2 conformers of HPD, besides the averaged geometrical parameters for HPD, AA, DMHD and TMHD, calculated at the B3LYP/6-311++G** level of theory, are given in Table 1. According to the summarized results, especially by comparisons of O···O and O···H bond distances, O−H band lengths and OHO bond angles, the following trend in hydrogen bond strength is concluded TMHD > DMHD > AA > HPD. These calculated data clearly suggest that ethyl substitutions for t-But and even for CH_3 groups at β-position of a β-dicarbonyl decrease the intramolecular hydrogen bond strength. This result is in excellent agreement with the experimental NMR chemical shifts of enolated proton summarized in Table 2. The averaged IHB energy (E_{HB}) for HPD calculated at B3LYP/6-311++G** level of theory is 15.73 kcal/mol, compared to 15.34, 15.58 and 16.27 kcal/mol for AA, DMHD and TMHD, respectively. This comparison, also confirm the mentioned theoretical and experimental results for the effect of ethyl substitution in β-position on IHB strength of β-dicarbonyls.

The enol contents in pure liquid of AA, DMHD and TMHD have been reported to be 79% and 94% and 100% respectively [2]. A comparison between these values and the

corresponding value for pure liquid of HPD (76%) gives a clear understanding for the decreasing effect of substitutions of the methyl groups by the ethyl groups in AA (and also substitutions of the t-But groups by the ethyl groups in TMHD) on the enol content of the compounds.

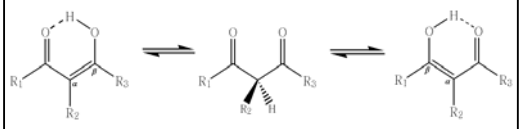

Fig. 1: The keto-enol tautomerism leads to two different chelated enol forms for *β*-dicarbonyls.

Table1: The geometrical parameters and IHB energies for *cis*-enol forms, all calculated at B3LYP/6-311++G** level, besides proton chemical shifts of HPD, AA, DMHD and TMHD.

	HPD			AA	DMHD	TMHD
distances(Å)	*E1*	*E2*	Avg.	Avg.	Avg.	Avg.
C2–O1	1.245	1.245	1.245	1.249	1.247	1.249
C2–C3	1.445	1.446	1.445	1.442	1.444	1.443
C3–C4	1.369	1.369	1.369	1.371	1.372	1.374
C4–O5	1.328	1.329	1.328	1.324	1.325	1.326
O5–H6	1.001	1.001	1.001	1.005	1.006	1.008
O1···H6	1.641	1.640	1.640	1.622	1.608	1.583
O1···O5	2.548	2.547	2.547	2.537	2.525	2.507
C2–C8	1.519	1.519	1.519	1.511	1.534	1.541
C4–C9	1.500	1.503	1.502	1.494	1.501	1.523
∠O1H6O5	148.4	148.4	148.4	148.8	149.2	150.3
E_{HB}(kcal/mol)	15.83	15.63	15.73	15.87	16.57	17.90
δOH(ppm)	15.04			15.34	15.58	16.27
Enol (%)	76			79	94	100

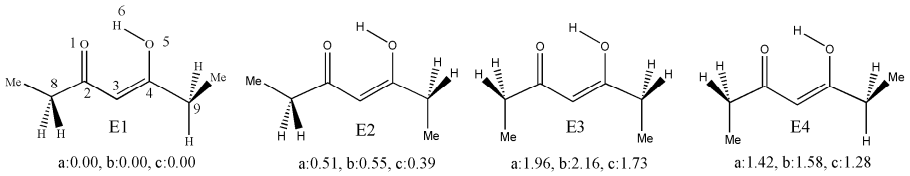

Fig 2: The atom numbering, relative stabilities and possible chelated *cis*-enol tautomers of HPD calculated at B3LYP level (a: 6-31g**, b: 6-311g** and c: 6-311++g** basis sets).

Conclusion

The comparisons of geometries, E_{HB} values, NMR proton chemical shifts and the enol contents of HPD with those of AA, DMHD and TMHD indicated a decreasing effect of substitutions of methyl and t-But groups by the ethyl groups on the enol content and hydrogen bond strength of β-dicarbonyls.

References

[1] N.N. Shapetko, *Org. Mag. Res.* 5 (1973) 215.

[2] G.K. Schweitzer, E.W. Benson, *J. Chem. Eng. Data* 13 (1968) 452.

[3] M.Vakili, S.F.Tayyari, A.-R.Nekoei, H.Miremad, S.Salemi, R.E.Sammelson, *J. Mol. Struct*. 970 (2010) 160.

Formation of Cobalt complexes with N_2O_2 donor Tetradentate Schiff Base Ligands. A DFT study

A. zare [*, a], Z. Hajian [a]

[a] Islamic Azad University, Marvdasht Branch. Department of Chemistry, Marvdasht, Iran

E-mail: ahad_zare@yahoo.com

Keywords:DFT study, Cobalt complexes, Schiff Base

Introduction

Coordination complexes of transition metals are topic subject of detailed investigation in various branches of chemistry [1–4]. An especial interest focuses on chelate complexes of such metals as iron, nickel and cobalt with different polydentate ligands. Particular attention for these complexes is due to their ability for reversal addition of oxygen. This phenomenon is cause to use complexes of the metals in modeling of a breathing process, in developing of methods of an industrial oxygen production and applying the complexes as oxygen transfer agents in high effective and selective catalysis of various organic substances oxidation. In this study structure of Co(II) complexes with various Schiff bases and reactions of their formation are researched by means of quantum chemistry.

Calculation methods

All calculations were performed at the UB3LYP/6-31G** level of theory which is accurate enough for the investigation of complexes of the first transition metal row. Vibrational frequencies were calculated for all optimized structures to confirm that they were true minimums. The entropy and the zero point energy during calculations of Gibbs free energies at the 298.15 K were computed with a corresponding scale factor.

Results and Discussion

Reaction of most stable conformations of the complexes forming by Schemes 1 was considered in order to determine their relative stability (Fig. 1). we study the reactions here by their modeling under gas-phase conditions. According to calculation data obtained, Co(II)

ions with the ligands produce chelate compounds with coordinate number 4 and have close to tetrahedral structure. Thus complexes with the central metal ions forming four intramolecular bonds were found. Structural parameters of the ligands fragment interacting with the metal are presented in Table 1.

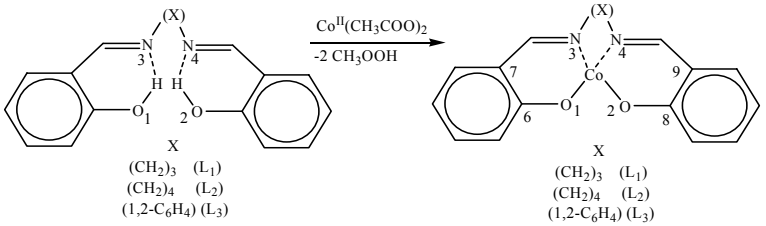

Fig. 1: Schemes of reaction considered of the complexes CoL_1–CoL_3 formation.

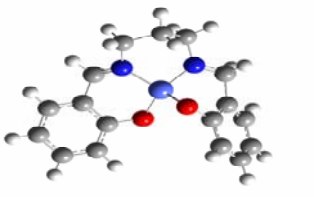

Fig. 2: spatial arrangement of $Co^{2+}(L_1)$

It has been found, the presence of geometrical strain in compounds CoL_1 and CoL_3 leads to distortion from an ideal tetrahedron (Fig.2). Therefore, the tetrahedral centers in the complexes of type CoL_2 are most regular in the case of both CoL_1 and CoL_3.

Table 1: Structural features of the complexes of cobalt obtained at the UB3LYP/6-31G** level of

Parameter complexes	N3–N4	O1–O2	∠ N3CoN4	∠ O1CoO2	∠ O1CoN3	∠ O2CoN4
CoL_1	2.89	2.87	106.15	106.40	100.35	102.73
CoL_2	3.16	2.91	116.68	108.69	100.05	103.93
CoL_3	2.61	2.78	92.50	101.71	100.10	103.08

Values of Gibbs free energies and enthalpies of the complex formation at 298.15 K via noticed reactions are reported in Table 2. According to calculated Gibbs free energies, the complexes formation will proceed spontaneously. Calculation data shows, that the formation of the complexes CoL_2 is most profitable in the cobalt (II). According to experimental data, definite sterical requirement to metal ion is one of the necessary conditions of reversal addition of simple gaseous molecule to the initial complexonates. The other important condition is high stability of transition-metal chelate complex, and it is known the more stable complex is, the more preference of its binding with O_2 will take place.

Table 2: Enthalpy (in kJ/mol), entropy (in kJ/mol K) and Gibbs free energy (in kJ/mol) of the reactions of cobalt complexes formation, at the UB3LYP/6-31G** level of theory

Ion of metal complexes	$\Delta H°_{298}$	$T * \Delta S°_{298}$	$\Delta G°_{298}$
CoL_1	-43	31	-74
CoL_2	-64	37	-101
CoL_3	-36	29	-65

Conclusion

By performing calculations at the UB3LYP/6- 31G** level, it has been demonstrated that the central fragment of the complexes between N_2O_2 donor Schiff bases and ions Co(II) has a pseudo tetrahedral structure. Results of research show that definite increase of the polymethylene chain binding nitrogens of the imine groups leads to growth of stability the complexes studied. The formation of seven membered rings seems to be most favorable.

References

[1] A.E. Martell, M. Calvin, Chemistry of Metal Chelate Compounds, Prentice Hall Inc., New York, 1992.

[2] P.V. Bernhardt, G.A. Lawrance, in: J.A. McCleverty, T.J. Meyer (Eds.), Comprehensive Coordination Chemistry II. From Biology to Nanotechnology, vol. 6, Elsevier, 2005.

[3] S.M. Roberts, G. Poignant, Catalysts for Fine Chemical Synthesis: Hydrolysis, Oxidation and Reduction, vol. 1, Springer, 2002.

[4] B.G. Davis, D.P.G. Emmerson, J.A.G. Williams, Oxidation and Reduction, in Organic Reaction Mechanisms, John Wiley & Sons, 1998.

Quantum mechanical study of interaction between 1-methyl-2-thioxoimidazolidin-4-one and I_2 in the gas phase.

T. Hadadi[a*], H. Tavakol[a], H. Roohi[b], Z.Razmara[a]

[a]*Department of Chemistry, Faculty of Science, University of Zabol, Zabol, Iran*

[a]*Department of Chemistry, Faculty of Science, University of Guilan, Rasht, Iran*

Keywords: Tautomer, Complex, Interaction, Hyperthyroidism, NBO and AIM analysis

Introduction:

Interaction of organic molecules with iodine has been widely observed in biological systems [1] especially in human's thyroid [2]. In this category, imidazoline [3], and related compounds like thioimidazoline derivatives [4] are known as iodine absorbent in human's body [5]. Methimazole, as a most important member of this group, make powerful complex with iodine. This complex can prevent the first step of biosynthesis of thyroid's hormones to prevent hyperthyroidism. As a result, each compound with powerful complex with iodine can be used as a new drug in this category. By study of structures of previous hyperthyroidism drugs, 1-methyl-2-thioxoimidazolidin-4-one(T_1) was suggested to study of its structure and complexation properties to iodine in this research.

Methods:

In our researches, geometry optimizations and frequency calculations were performed using B3LYP method and 6-31+G*, 6-31++G**, 6-31+G(2d,2p) and 6-31++G** basis sets and NBO analysis of all tautomers were calculated using B3LYP/6-31++G** level of theory. All optimizations, frequency calculations and NBO analyses were carried out using the Gaussian 03 program package. All results of frequency calculations have been corrected with appropriate scaling factor. AIM analyses were performed using AIM200 program. This method has been presented useful information about intermolecular interactions and characterization of bonds through the analysis of the electron density.

In this research, molecular parameters, relative energies and vibrational frequencies of DFT, AIM and NBO analysis of 1-methyl-2-thioxoimidazolidin-4-one and tautomers (T_1-T_5) in Interaction with Iodine and its tautomer and the properties of their complexes with iodine have been calculated to determine the capability of this molecules in interaction with iodine and treatment of hyperthyroidism.

Results and discution:

Calculated Gibbs free energy values showed that T_1 is the most stable tautomer in the gas phase. The NBO indicates that the sum of $E^{(2)}$ terms corresponding to the delocalization of N_2 and N_4 lone pairs to the NBO acceptors in the thione tautomer is greater than its value in the thione tautomer. As mentioned, the experimental results indicate that two T_1(thione)-I_2 stereoisomeric complexes can be formed. The S-I distance in the planar complex (3.057) is shorter the perpendicular complex (3.145), Thus, as the I-I bond length increases the S-I distance decreases.

In all methods show that the Gibbs free energy of the planar from is smaller than the perpendicular form of the thione tautomer. The result of the NBO analysis indicate that the occupation number of the δ*(I-I) antibonding in the planar complex is greater than the perpendicular complex. In addition, it is expected that the Lp(s) occupation number in the planar complex to be greater than the other complex. It seems that the second factor in the stabilizing of the planar complex with respect to the perpendicular is the interaction between S-bonded iodine lone pair with δ*(N-H) antibonding. At the first sight, the results presented and discussed above indicate that all levels of theory the thione form of T_1 are the preferred tautomer in the gas phase. The most stable form of T_1-I_2 (thione) complex is predicted to the planar form in agreement with the experimental results. The NBO analysis reveals that the two change transfer interaction, Lp(S)→ δ*(I-I) and Lp(I)→ δ*(N-H), cause that the planar complex of T_1-I_2 to be preferred complex. Aim analysis shows that the charge density and its application at the S-I bond critical point of the planar complex are greater than the other complex. In addition, a critical point is observed at the NH-bond in the planar complex close to the hydrogen atom.

Conclution:

The result presented and discussed above indicate that at all level of theory the thion from of T_1 is the preferred tautomer in the gas phase. The most stable from of T_1-I_2 (thione) complex in the gas phase is predicted to be planar from in agreement with the experimental results.

References:

[1]H. Kohn, B. A. Kohn, M. L. Steenberg, J. P. Buckley, J. Med. Chem. 20 (1977) 158.

[2] C. Laurence, M. J. El-Ghomari, M. Lucon, J. Chem. Soc., Perkin Trans. 2 (1998) 1159.

[3]A. Taurog. , J . Biochem. Biophys. 24 (1996) 330.

[4]C. Laurence, M.J. El-Ghomari, J-Y. Le Questel, M. Berthelot, R. Mokhisse, J. Chem. Soc. Perkin Trans. 2 (1998) 1545.

[5]B. Jemec, Acta Pathol. Microbiol. Scand. A 78 (1970) 151.

Ab initio study of earth alkaline metals interactions with some phthalocyaninato anion derivatives, structure and stability constant

Vahideh Hadigheh-Rezvan[a], Ali Shokri[b], Zaker eyvazzadeh[a], Farshid Firozi-Ajirlu[a]
v_h_rezvan@yahoo.com, ashokry1391@yahoo.com
[a]Department of Chemistry, Islamic Azad University Ardabil Branch, Ardabil, Iran.
[b]Department of Chemistry, Payameh Noor University, Ardabil Branch, Ardabil, Iran.

Keywords: metal Phthalocyanines, *ab initio*, stability constant, free Gibbs energy

Introduction:

Phthalocyanine compounds with the formula MPc (Pc.phthalocyaninato anion $C_{32}H_{16}A$, A=H2 or divalent metals) have been widely used as organic dye stuff because of their intense absorption of light in the visible and ultraviolet regions, their excellent stability to chemical or thermal treatments, and their relatively low cost[1-4]. The most stable structure of MPc has been shown to be square planar and to be classified into a D_{4h} point group [5-7]. In the case of MH_2, the molecular symmetry is reduced to D_{2h} due to two hydrogen atoms in the middle of the Pc ring. In a recent book on metal phthalocyanines (MPcs) these compounds were called "a gift to molecular physics" because of their unique properties which found so many different remarkable applications. More than 70 different elemental ions, can be incorporated into the central cavity of Pc and an enormous number of derivatives can be synthesized. In spite of all this abundance of data, there are,however, only two papers published so far where structures of three MPcs were established in *the gas phase*. So we have been studied the structures of some MPcs ($M=Ca^{2+}$, Mg^{2+})(1)by quantum mechanics theoretically methods.

Computational details:

All the calculations have been performed using the GAUSSIAN 03 quantum chemical package. Method of Hartree-Fock in combination with basis set, 6-31G has been employed in searching for the most stable structures. In all the cases, the steady-state nature (minimum on the potential energy surface) of the optimized ligands, complexes and cations has been confirmed by calculating the corresponding frequencies at the same computational level. All

calculations were carried out at gas phase and standard conditions(P=1 atm, T=298.15K). The free Gibss energy of complex formation reaction and stability constant have been determined as: pK= stability constant

$Pc + M^{2+} \leftrightarrow PcM$ $\Delta G°(298) = G°(298)(MPc) - [G°(298)(M^{2+}) + G°(298)(Pc)]$

$\Delta G\ (298) = \Delta G°(298) + RTLnK_P$ and $\Delta G\ (298)=0$ so $\Delta G°(298) = - RTLnK_P$

Results and discussion:

The free Gibbs energy of complexe formation for some phetalocyanine derivatives (pc) with Mg^{2+} and Ca^{2+} were calculated , then k_p was abtained .Table 1 and 2 show results for MgPc and CaPc complexes respectively. K_p for MgPc's are 10^{20} times larger than CaPc. In the two types complexes electron – with drawing Groups($COCH_3$, COH, CF_3 ,CN)on PC decrease k_p almost 10^{50} times.

Table-1 Thermochemical parameters for magnesium(Mg) complexes obtained from quantum mechanics calculations(HF/6-31G)

M^{2+}	Y	ΔG^0(Kcal/mol)	K_p
$^{2+}$ Mg	H	-683.98	$\times 10^{497}$ 9.5
	OH	-676.30	$\times 10^{492}$ 2.42
	$COCH_3$	-640.06	$\times 10^{466}$ 1
	COH	-627.51	$\times 10^{456}$ 7.34
	CF_3	-614.67	$\times 10^{447}$ 3.29
	CN	-611.98	$\times 10^{445}$ 3.6

Table-2 Thermochemical parameters for Calsium(Ca) complexes obtained from quantum mechanics calculations
(HF/6-31G)

M^{2+}	Y	ΔG^0(Kcal/mol)	K_p
Ca^{2+}	H	-533.84	$\times 10^{388}$ 4.56
	OH	-523.60	$\times 10^{381}$ 1.6
	$COCH_3$	-489.04	$\times 10^{356}$ 1.11
	COH	-488.16	$\times 10^{356}$ 4.95
	CF_3	-467.70	$\times 10^{340}$ 3.23
	CN	-464.55	$\times 10^{338}$ 1.67

Conclusions:

All of studied complexes are formed quantitatively and are very stable so we predicte size of cation affects equilibrium, small cation are formed very easily so Bepc complexes are the most stable with the largest K_p . The differency between K_p are so that we can separate these cations from a mixture.

References:

[1] Kroto, J. R. Heath, S. C. Brien, R. F. Curl, and R. E. Smalley, *Nature* (London) **18**, 2 (1985).

[2] Kra Tschmer, L. D. Lamb, K. Fostiropoulos, and D. R. Huffman, *Nature* (London) **347**, 354 (1990).

[3] R. Heath, S. C. Brien, Q. Zhang, Y. Liu, R. F. Curl, H. W.Kroto, F. K. Tittel, and R. E. Smalley, *J. Am. Chem. Soc*. **107**, 7779 (1985).

[4] Chai, T. Guo, C. Jin, R. E. Haufler, L. P. F. Chibante, J. Fune,L. Wang, J. M. Alford, and R. E. Smalley, *J. Phys. Chem*. **95**,7564 (1991).

[5] D. Johnson, M. S. de Vries, J. Salem, D. S. Bethune, and C.Yannoni, *Nature* (London) **355**, 239 (1992).

[6] H. Weaver, Y. Chai, G. H. Kroll, C. Jin, T. R. Ohno, R. E.Haufler, T. Guo, J. M. Alford, J. Conceicao, L. P. F. Chibante, A.Jain, G. Palmer, and R. E. Smalley, Chem. Phys. Lett. **190**, 460(1992).

[7] Shinohara, H. Sato, Y. Saito, M. Ohkohchi, and Y. Ando, Nature(London) **357**, 52 (1992).

DFT study of earth alkaline metal interaction with squarate and its derivatives dianions:structure and stability constant

Vahideh Hadigheh–Rezvan*, Rasol Baradari, Maryam Mohammadoghli, Zaker Eivazzadeh
Email: v_h_rezvan@yahoo.com, maryamm_4893@yahoo.com, z.eyvazzadeh@yahoo.com
Department of Chemistry, Izlamic Azad University, Ardabil Branch, Ardabil, Iran.

Introduction:

The cyclic oxocarbons represent an interesting class of compounds. The simplicity of the structures and the existence of the electroisomeres tempt one to conclude that there might be simple regularities and trends in the properties of these compounds that call for more attention to systematization. The structure and bonding of oxocarbons [1–13] have been investigated extensively. In the structure of this group of molecules the carbon atoms are attached to carbonyl or enolic oxygens or to their hyderated equivalents [14]. There exist two prototypal subgroups within the oxocarbon family the oxocarbon dianions $(CnOn)^{-2}$ and neutral cyclic compounds (CnOn) [15]. The main oxocarbon representatives are rhodizonate (n=6), croconate (n=5), squarate (n=4) and deltate (n=3). There are extensive literature and reviews [16-17] on oxocarbons center on experimental aspects. The complete or partial replacement of oxygen in the oxocarbons by analogues substituents, viz. sulfur and selenium or related ones leads to a series of compounds that are called 'pseudooxocarbons' [18]. We have been studied interactions between squarate and its derivatives dianions with metallic cations(group IIA) and for resulted complexes structural and thermodynamically properties were obtained. These complexes have industrial importance as a candidate of new catalysts and cation separators from mixtures. Needless to say, since it is essentially dynamic, only an *ab-initio* molecular dynamics simulation can offer the desirable information about the process of complex formation.

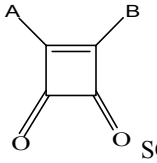

SQUARATE

Computational details:

All the calculations have been performed using the GAUSSIAN 03 quantum chemical package . Method of LSDA in combination with basis set, 6-311+G(d,p) has been employed in searching for the most stable structures. In all the cases, the steady-state nature (minimum on the potential energy surface) of the optimized complexes and cations and ligands has been confirmed by calculating the corresponding frequencies at the same level All calculations were carried out at gas phase and standard conditions(P=1 atm, T=298.15K). The standard free Gibss energy of complex formation has been determined as:

$L + M^{2+} \leftrightarrow ML$ reaction of complex formation

$\Delta G^0(298) = G°(ML) - [G°(L) + G°(M^{2+})]$

$\Delta G(298) = \Delta G^0(298) + RTLnK_p \qquad \Delta G(298) = 0 \qquad so \qquad \Delta G^0 = -RTLnK_P \qquad K_P = e^{-\Delta G0/RT}$

Results and discussion:

In point of view theory Kp value is in range of zero and infinity.Large value of Kp means more stability for complex. Table show all studied complexes are stable. Berelium cation have the most stable complexes.

A	M	B	ΔH° (Kcal/mol)	ΔG°(Kcal/mol)	K_p	charge
O		$CHNO_2$	-706.4	-687.6	8.8×10^{503}	0
〃	Be^{+2}	$C(CN)_2$	-655.25	-636.94	6.5×10^{466}	0
〃		$N(CH_3)_2$	-469.36	-450.6	2.5×10^{257}	1
〃		$CHNO_2$	-545.56	-517.8	3.1×10^{379}	0
〃	Mg^{+2}	$C(CN)_2$	-512.28	-494.75	3.9×10^{362}	0
〃		$N(CH_3)_2$	-341.12	-323.2	7.6×10^{236}	1
〃		$CHNO_2$	-489.14	-471.2	2.3×10^{345}	0
〃	Ca^{+2}	$C(CN)_2$	-458.97	-439.44	1.2×10^{322}	0

Conclusions:

As the smallest cation, Be^{2+} forms complex with squarates quantitatively. Electron withdrawing groups($CHNO_2$, $C(CN)_2$) make the complexes more stable and Electron donor group inversely becomes all the complexes produced less.

References.

[1] R. West, D.L. Powell, *J. Am. Chem. Soc*. 85 (1963) 2577.

[2] L. Farnell, L. Radom, M.A. Vincent, *J. Mol. Struct. (Theochem)* 76(1981) 76.

[3] A. Moyano, F. Serratosa, *J. Mol. Struct. (Theochem*) 90 (1982) 131.

[4] W.C.J. Herndon, *J. Mol. Struct. (Theochem)* 103 (1983) 219.

[5] F. Serratosa, *Acc. Chem. Res*. 16 (1983) 170.

[6] T.K. Ha, C. Puebla, *J. Mol. Struct. (Theochem)* 137 (1986) 183.

[7] M. Campos-Vallette, K.A. Puebla, C. Puebla, *Spectrosc. Lett*. 21 (1988)303.

[8] H. Torii, M. Tasumi, *J. Mol. Struct. (Theochem)* 334 (1995) 15.

[9] G. Cerioni, R. Janoschek, Z. Rappoport, T.T. Tidwell, *J. Org. Chem*. 1(1996) 6212.

[10] Z. Chen, L.R. Sutton, D. Moran, A. Hirsch, W. Thiel, P.v.R. Schleyer,*J. Org. Chem*. 68 (2003) 8808.

[11] G. Maier, J. Schrot, H.P. Reisenauer, G. Frenking, V. Jonas, *Chem. Ber*.125 (1992) 265.

[12] G.M.A. Junqueira, W.R. Rocha, W.B. De Almeida, H.F. Dos Santos,*J. Mol. Struct. (Theochem)* 684 (2004) 141.

[13] H. Sabzyzn, M. Noorbala, *J. Mol. Struct. (Theochem)* 626 (2003) 143.

[14] G.A. Olah, J. Bausch, G. Rasul, H. George, G.K. Surya Prakash, *J. Am.Chem. Soc.* 115 (1993) 8060.

[15] P.V.R. Schleyer, K. Najafian, B. Kiran, H. Jiao, *J. Org. Chem*. 65 (2000)426.

[16] G. Seitz, P. Imming, Chem. Rev. 92 (1992) 1227.

[17] B.A. Hess, L.J. Schaad, *J. Am. Chem. Soc*. 93 (1971) 305.

[18] L.J. Schaad, B.A. Hess, *J. Am. Chem. Soc*. 94 (1972) 3068.

Electronic Structural Studies of One Dimensional Fused Oligo-Selenophenes, Free Electron transfer, Activation Energies and Kinetic Properties in Nano Supramolecular Complexes of The Compounds with Fullerenes

Avat(Arman)Taherpour*, Hadi Shafie and Masoumeh Harizi

Chemistry Department, Faculty of Science, Islamic Azad University,P. O. Box 38135-567, Arak, Iran

E-mail: avatarman.taherpour@ gmail.com and E-mail: masoumeh.harizi@ gmail.com

Abstract:

In this study, hybrid of Time–dependent density functional theory (TD-DFT) calculations have been carried out for neutral species of the fused selenophene oligomers, denoted by Se(*x*), where *x* represents the number of selenophene rings in the oligomer, to elucidate the electronic structures at ground states. The number of carbon atoms in the fullerenes was used as an index to establish a relationship between the structures one dimensional fused oligo-selenophene derivatives, Se(n) **1-5** as the most well-known redox systems and fullerenes C_n (n=60,70,76,82 & 86) which create [Se(x)].C_n (x=1-5). The relationship between the number of carbon atoms and the free energies of electron transfer ($\Delta G_{et(1)}$ to $\Delta G_{et(4)}$) are assessed using the electron transfer equation for the nano supramolecular [Se(x)].C_n (x=1-5) **6-10** complexes. Calculations are presented for the four reduction potentials ($^{Red.}E_1$ to $^{Red.}E_4$) of fullerenes C_n. The results were used to calculate the four free-energies of electron transfer ($\Delta G_{et(1)}$ to $\Delta G_{et(4)}$) of the supramolecular complexes [Se(x)].C_n (x=1-5) for fullerenes C_{60} to C_{300}. The first to forth free activation energies of electron transfer and kinetic rate constants of the electron transfers, $\Delta G^{\#}_{et(n)}$ ($\Delta G_{et(1)}{}^{\#}$ to $\Delta G_{et(4)}{}^{\#}$) and k_{et} (n=1-4), respectively, were also calculated in this study for the nano supramolecular complexes in accordance with the *Marcus* theory.

Keywords: Fullerenes; One dimensional fused oligo-selenophenes; Free energy of electron transfer; Electron transfer properties; Activated free energies of electron transfer; Kinetic constant of electron transfer; Marcus Theory; Molecular modeling.

Introduction:

Polyselenophenes are one-dimensional π-conjugated polymers that are utilized as conducting materials and field effect transistors [1,2]. Also, oligo-five-membered ring compounds have a possibility for application to high-performance molecular devices such as photocurrent multipliers and organic semiconductors [3]. However, the problem of chemical stability still remains. In fact, only octamers are known to have large oligoselrnophenes with no side chains. To develop a stable compound composed of heterocyclic five membered rings, several modified oligomers have been synthesized and their electronic properties have been systematically investigated. This study elaborates upon the relationship between the number of carbon atoms and the four free energies of electron transfer ($\Delta G_{et(1)}$ to $\Delta G_{et(4)}$) of fullerenes C_n (n=60, 70, 76, 82 and 86) with Se(x), **1-5**, on the basis of the four reduction potentials ($^{Red.}E_1$ to $^{Red.}E_4$) of the fullerenes, as assessed by applying the electron transfer equation to create [Se(x)].C_n (x=1-5) **6-10**. The results were extended to calculate the four free energies of electron transfer ($\Delta G_{et(1)}$ to $\Delta G_{et(4)}$) of other supramolecular complexes of Se(x) **1-5** as a class of electron-transfer radicals, with fullerenes C_{60} to C_{300} ([Se(x)].C_n (n=1-5), supramlecular complexes.[4-6]

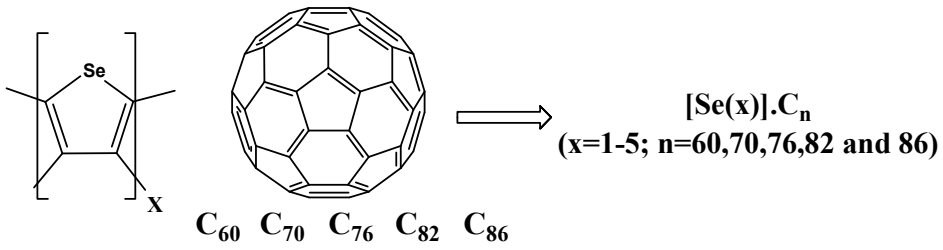

Calculations Methods and Discussion:

All of the calculations were carried out at the hybrid of Time–dependent density functional theory (TD-DFT) method at B3LYP/6-311G^{++}(p,d) level of theory. Fused selenophene oligomers [Se(*x*)] (*x*=1-5) were examined. First, the initial geometries of neutral fused selenophene oligomers [Se(*x*)] were determined. Using the optimized geometries of neutral molecules species of Se(*x*) were further optimized at the B3LYP/6-311G^{++}(p,d) levels of theory. All mathematical and graphing operations were performed using *MATLAB-7.4.0(R2007a)* and *Microsoft Office Excel-2003* programs. Using the number of carbon atoms contained within the C_n fullerenes, several valuable properties of the fullerenes can be calculated. The values were used to calculate the four free energies of electron transfer

($\Delta G_{et(1)}$ to $\Delta G_{et(4)}$), according to the electron transfer (ET) equation for [Se(x)].C_n (x=1-5; n=60,70,76,82 & 86) supramlecular nano complexes. In this study were calculated the four free energies of electron transfer ($\Delta G_{et(1)}$ to $\Delta G_{et(4)}$) of [Se(x)].C_n (x=1-5). The study also calculated the first to fourth activate free energies of electron transfer and kinetic rate constants of the electron transfers, $\Delta G^{\#}_{et(n)}$ and k_{et} (n=1-4), respectively, as assessed using the *Marcus* theory and the equations on the basis of the first to fourth reduction potentials ($^{Red.}E_1$ to $^{Red.}E_4$) of fullerenes C_n (n=60, 70, 76, 82 and 86) for the predicted supramolecular complexes [Se(x)].C_n (x=1-5) nano supramlecular complexes.

References:

[1] Yoshino K, *et al*., *Japan. J. Appl. Phys.* **28,** L138 (1989).

[2] Kim Y M, *et al*., *Macromolecules* **39,** 4081 (2006).

[3] Xu Z, Fivhou D, Horowitz G and Garnier F, *J. Electroanal. Chem.* **267,** 339 (1989).

[4] Taherpour A. A., *Fullerenes, Nanotubes and Carbon Nanostructures*, **17(1)**, 26 (2009).

[5] Taherpour A. A., *Chem. Phys. Lett*., **469**, 135 (2009).

[6] Taherpour A. A., *J. Phys. Chem. C*, 113(**14**), 5402 (2009).

Quantitative Structural Relationship Study on Octanol-Water Partitioning Coefficients, Total Biodegradation, LC_{50} and Water solubility of One Dimensional Fused Oligo-Thiophenes

Avat(Arman)Taherpour*, Hadi Shafie and Masoumeh Harizi

Chemistry Department, Graduate School, Islamic Azad University, Arak Branch, P. O. Box 38135-567, Arak, Iran

E-mail: avatarman.taherpour@gmail.com and E-mail:masoumeh.harizi @gmail.com*

Abstract:

The octanol-water partition coefficient (K_{ow}) is a measure of the equilibrium concentration of a compound between octanol and water that indicates the potential for partitioning in to soil organic matter (i.e., a high K_{ow} indicates a compound which will preferentially partition into soil organic matter rather than water). Biodegradation (TB_d) is another useful and important factors in chemical and biochemical studies. Graph theory is a sub discipline of mathematics that is closely related to both topology and combinatory concepts. Here, was used the number of sulfur atoms (S_x; x=1-10) of the one dimensional fused oligo-thiophenes **1-10** for molecular description of structure-property relationship studies for the logarithm of calculated Octanol-Water partitioning coefficients, total biodegradation, lethal concentration and water solubility in 25ºC ($logK_{ow}$, TB_d (mol/h and gr/h), LC_{50} and S_w, respectively) in one dimensional fused oligo-thiophenes **1-10**.

Keywords: Molecular topology; QSAR; Octanol-Water partitioning coefficient; Biodegradation; LC_{50}, Water solubility; One dimensional fused Oligo-Thiophenes.

Introduction:

One of the main one-dimensional π-conjugated polymers are polythiophenes that they have been utilized as conducting materials and field effect transistors [1,2]. Also, oligo-five-membered ring compounds have a possibility for application to high-performance molecular devices such as photocurrent multipliers and organic semiconductors [3]. However, the property of chemical stability is one of the important problems of this group of oligomers (**1-**

10). To develop a stable compound composed of heterocyclic five membered rings, several modified oligomers have been synthesized and their electronic properties have been systematically investigated. So, it is important to investigate some of the main environmentally factors of the one dimensional fused oligo-thiophenes **1-10**. This study elaborates upon the relationship between the number of sulfur atoms (S_x; x=1-10) and four selected biophysical and chemical data, i.e. $logK_{ow}$, TB_d (mol/h and gr/h), LC_{50} and S_w.[4]

Discussions:

The octanol-water partition coefficient (K_{ow}) is a measure of the equilibrium concentration of a compound between octanol and water that indicates the potential for partitioning in to soil organic matter. This coefficient is inversely related to the solubility of a compound in water. The $logK_{ow}$ is used in models to estimate plant and soil invertebrate bioaccumulation factors. The $logK_{ow}$ is commonly used in QSAR studies and drug design, since this property is related to drug absorption, bioavailability, metabolism, and toxicity. Biodegradation is usually quantified by incubating a chemical compound in presence of a degrader, and measuring some factors like oxygen or production of CO_2. An LC_{50} value is the concentration of a material in air that will kill 50% of the test subjects (animals, typically mice or rats) when administered as a single exposure (typically 1 or 4 hours). The water solubility (S_w, $mg.L^{-1}/25ºC$) factor were measured and calculated for compounds **1-10** as well. [4]

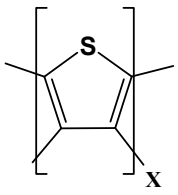

X=1-10

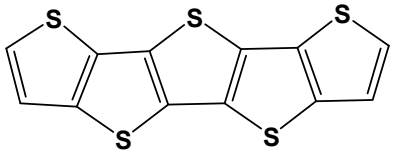

One dimensional fused oligo-thiophene-S_5

In this study, have been calculated and studied the relationships the number of sulfur atoms (S_x; x=1-10) of one dimensional fused oligo-thiophenes **1-10** as a molecular descriptor and the structureal-properties as: the logarithm of calculated Octanol-Water partitioning coefficients, total biodegradation, lethal concentration and water solubility in 25ºC ($logK_{ow}$, TB_d (mol/h and gr/h), LC_{50} and S_w, respectively) in one dimensional fused oligo-thiophenes **1-10**. There were good agreements between the above data. By using the Equations of this

model, it is possible to calculate the values of $logK_{ow,}$ TB_d (mol/h and gr/h), LC_{50} and S_w for this class of important compounds.

References:

[1] Yoshino K, *et al*., *Japan. J. Appl. Phys.* **28,** L138 (1989).

[2] Kim Y M, *et al*., *Macromolecules* **39,** 4081 (2006).

[3] Xu Z, Fivhou D, Horowitz G and Garnier F, *J. Electroanal. Chem.* **267,** 339 (1989).

[4] Taherpour A. A., Taherpour A., Taherpour Zh. And Taherpour O, *Physics and Chemistry of Liquids,* **47**(4) 349 (2009).

Theoretical and Experimental Study of the poly fused selenophene(n) Electronic Spectra

Avat(Arman) Taherpour, Hadi Shafiei*,Masoumeh Harizi and Behnoud Hormozi

Chemistry Derpartment, Faculty of Science, Islamic Azad University, Arak Branch

(hshafie2005@yahoo.com)(masoumeh.harizi @Gmail.com)

Abstract:

Using a combination of the Time-dependent(TD) density functional theory(DFT) and the polarizable continuum model,we have investigated the UV-Visible spectra of poly fused selenophene(n) oligomer,where (n=1-5) represented the number of selenophene rings in the oligomer.We have used the Gassian 03 package of programs to perform the geometry optimization,vibrational analysis and excited stat evaluation for the full set of fused selenophene(n) oligomer.The level theory and basis set have been applied in this work are B3LYP and 6-311++G(d,p).The topology of the frontier orbitals can be correlated to the evolution of the λ_{max}.Indeed,adding more fused rings mostly modifies the LUMO.Whereas changing the nature of the reactive rings implies stronger HOMO variations.

Keywords: poly Selenophene,λ_{max},Gaussian03,UV-Visible,Density-functional theory

Introduction:

Highly conjugated polymers, such as poly-diacetylene and poly(*p*-phenylene), have been widely used as semiconductor, electroluminescent (EL), and photoconductive materials. Thisoriginates from the π-electron system delocalized widely along a one-dimensional polymer chain.Polyselenophene and its related compounds have attracted considerable attention over the past decade in view of their potential applications in electronic and optoelectronic devices.

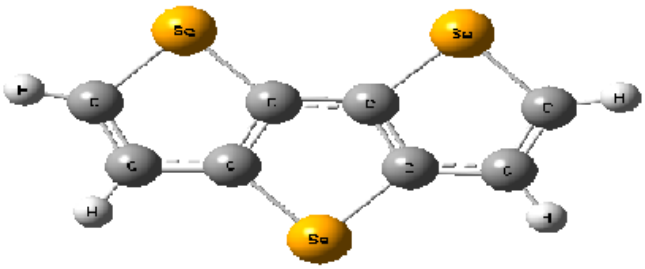

(Figure-1):poly-fused selenophene (n=3)

Polyselenophenes are one-dimensional π-conjugated polymers that are utilized as conducting materials and field effect transistors. Also, oligo-five-membered ring compounds have a possibility for application to high-performance molecular devices such as photocurrent multipliers and organic semiconductors. However, the problem of chemical stability still remains.

Results and Discussion:

We have used the Gaussian 03 package of programs,with level theory and basis set,B3LYP and 6-311++G(d,p) respectively, to calculate λ_{max} of poly oligomer selenophene(n),where n represented the number of selenophene rings.The experimental λ_{max} of selenophene ring has been reported 225 nm,whereas the λ_{max} has been calculated for this compound,is 255nm.

(Table -1) comparison the number of selenophene fused rings V.S $\lambda_{max.}$

n	1	2	3	4	5
$\lambda_{max(cal)}$	234.40	289.81	307.61	367.16	401.40
$\lambda_{max(exp)}$	255	-	-	-	-

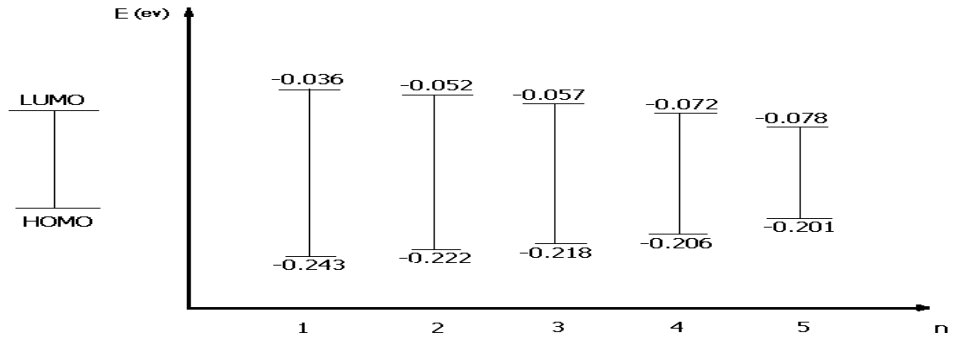

(Diagram-1) The energy of LUMO-HOMO gap V.S number of selenophene fused rings.

Conclusions:

From the present calculations, we have investigated some of the spectroscopic parameters, i.e. the longest wavelength of maximal absorption(λ_{max}) and the energy of LUMO-HOMO gap of selenophene fused rings by using level theory and basis set **B3LYP** and **6-311++G(d,p)** respectively**.**

References:

[1] Maurel,F.,et al.,Journal of Photochemistry and Photobiology A:Chemistry 199(2008)211-233.

[2] Kawabata,H.,et al.,Japanese Journal of Applied Physics.,Vol.47,No.1,2008,pp.420-424.

[3] Kawabata,H.,et al.,Sci.Technol.Adv.Mater.9(2008)024405(6pp).

Omission of Ecstacy - Like Drugs by Nanotubes: A DFT/NBO Approach

M. Hesabi [1,*] , N. Dalili Mansour[1]

[1]Department of Chemistry, Faculty of science, Islamic Azad University, Rasht Branch, Rasht, Iran.

[*] Marhesabi @gmail.com

Keywords: Nanotube, Ecstacy, Methamphetamine, Amphetamine, NBO, DFT.

Introduction:

These days Ecstacy is an Amphetamine derivative called MDMA (Methylene Dioxy Methamphetamine) , the use of Amphetamine –like drugs is spread by addicts. Frequent consumption of these drugs can disturb the normal function in the human body. The use of Amphetamine and Amphetamine-like drugs is contraindicated in patients with narrow-angle glaucoma or anatomically narrow angles. They elevate cardiac output and blood pressure making them dangerous for use by patients with a history of heart disease or hypertension.

Amphetamine and other Amphetamine-type overdoses are rarely fatal but can lead to a number of different symptoms, including psychosis, chest pain, hypertension, and produce losses in several markers of brain dopamine and serotonin neurons. [1]

In this work because of the importance of these drug's overdoses, the nanotube ability in omission of them is investigated.

Computational method:

All of the calculations are carried out by a pc computer which has Intel(R) Pentium(R) Dual CPU with 2 GB RAM. At first a nanotube including 60 C atoms (6,6) is formed by Nanotube Modeler Package. [2] Then this nanotube is optimized by GaussView [3] and Gaussian03 [4] softwares by DFT/B3LYP method and 6-31G basis set (fig. 1). The selected drugs are made by GaussView and optimized by Gaussian03 by B3LYP/6-31G method [5] (fig. 2- 4). Then the composites between nanotube and Amphetamine /Metamphetamine/ Ecstacy are formed and optimized by B3LYP/6-31G method (Fig. 5-7). For optimized molecules hybridations, Bond angles and bond lengths are calculated. After optimization of composites, the single point energies are obtained by B3LYP/6-311++G** method. Delocalization of electron density between the filled (bonding or lone pair) Lewis type NBOS and empty (antibonding

and Rydberg) non-Lewis NBOS are calculated by NBO (Natural Bond Orbital) analyzing by B3LYP/6-31G level. [6]

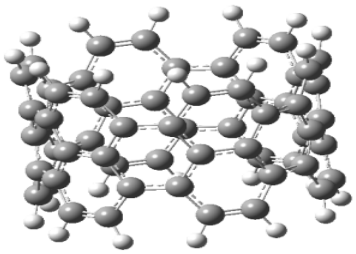

Fig. 1. Nanotube (6,6)

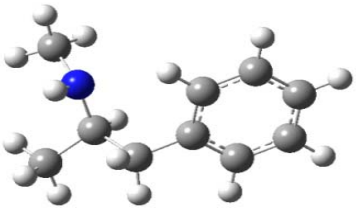

Fig. 2. Ecstacy

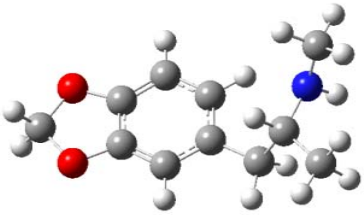

Fig. 3. Methamphetamine

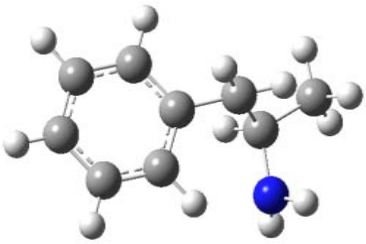

Fig. 3. Amphetamine

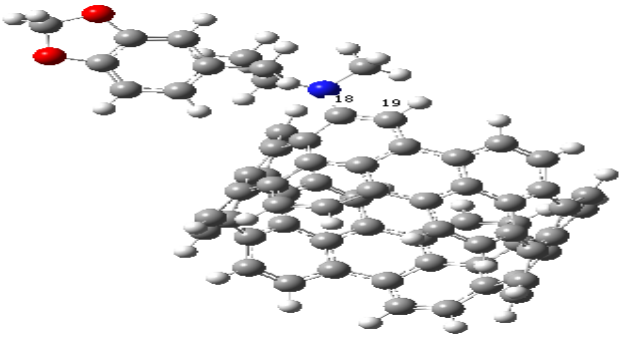

Fig. 4. Nanotube - Ecstacy (composite 1)

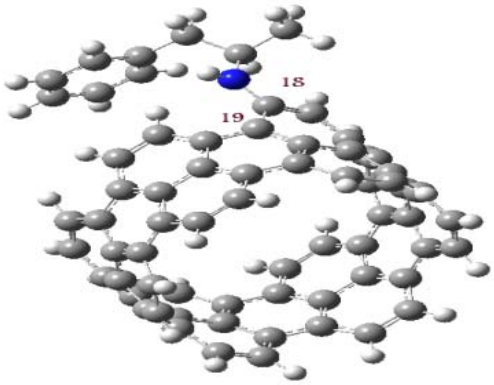

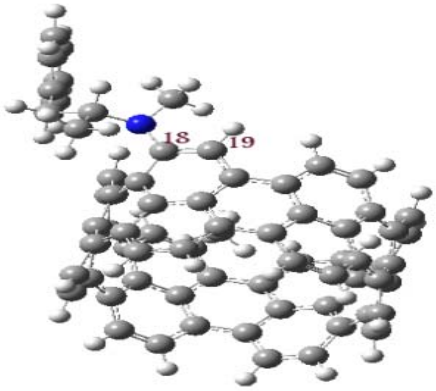

Fig. 6. Nanotube - Amphetamine (composite 2)

Fig. 7. Nanotube - Methamphetamine (composite 3)

Result and discussion:

The obtained relative energies and relative single point energies are shown in Table 1

Agent	Energy/kcalmol^{-1}	Single point energy/kcalmol^{-1}
Ecstacy	1442737.2615	1442534.7509
Nanotube	480788.891	480454.584
Nanotube - Ecstacy	0	-795.6238
Methamphetamine	1560993.0767	1560865.6548
Nanotube - MethAmphetamine	118261.2843	117528.2943
Amphetamine	1585651.5187	1585547.5876
Nanotube - Amphetamine	142910.2929	142189.6451

Table 1. Obtained relative energies and relative single point energies by B3LYP/6-31G and B3LYP/6-311++G**,respectively

As it can be seen the composites between drugs and nanotube are more stable than the single agents. By evaluating the energy of the reactions (1: Ecstacy + nanotube → composite 1, 2: Methamphetamine + nanotube → composite 2, 3: Amphetamine + nanotube → composite3), it is clear that these reactions are exothermic reactions (ΔE_1= -1839314.2283 kcalmol^{-1} , ΔE_2= - 1957570.0435 kcalmol^{-1} and ΔE_3= - 1982228.4855 kcalmol^{-1}).

The hybrid values, bond lengths and angles are shown in table 2.

Table 2. Obtained parameters calculated by DFT

Agent	C_{18} Hybrid	N Hybrid	C_{18}-N bond length/Å	C_{19}-C_{18}-N bond angle	C_{18} Mulliken Charge	N Mulliken Charge
Nanotube - Ecstacy	$SP^{2.48}$	$SP^{1.92}$	1.507	123.37	0.2778	-0.5700
Nanotube - Methamphetamine	$SP^{2.49}$	$SP^{1.69}$	1.417	122.56	0.2401	-0.5717
Nanotube - Amphetamine	$SP^{2.48}$	$SP^{1.69}$	1.387	123.23	0.3287	-0.7154

It is obvious that the C_{18} hybrid is almost the same in three composites but N hybrid for Nanotube-Ecstacy composite is different from the others. The results show that by increasing the p orbital share in hybridation, the bond length increases too. So this hybrid can affect on bond angle, too. As it can be seen the charges of N and C in Nanotube-Amphetamin is different from the others. It can be because of presence of methyl group in Methamphetamine and Ecstacy. In Nanotube- Amphetamin because of absence of methyl group, electron affinity of nitrogen causes some pressure on C of Nanotube and causes it to be more positive. So the N becomes more negative. But in Methamphetamine and Ecstacy presence of methyl group cause N pressure on C to become less.

The NBO parameters are shown in table 3.

Nanotube - Ecstacy		Nanotube - Amphetamine		Nanotube - Methamphetamine	
Donor →**Acceptor**	**E_2/ kcalmol^{-1}**	***Donor*** →**Acceptor**	**E_2/ kcalmol^{-1}**	***Donor*** →**Acceptor**	**E_2/ kcalmol^{-1}**
$\sigma_{C18-N} \rightarrow \sigma^*_{C18-C19}$	2.18	$\sigma_{C18-N} \rightarrow \sigma^*_{C18-C19}$	1.29	$\sigma_{C18-N} \rightarrow \sigma^*_{C18-C19}$	1.21
$\sigma_{C18-N} \rightarrow \sigma^*_{C18-C24}$	1.18	$\sigma_{C18-N} \rightarrow \sigma^*_{C18-C24}$	2.38	$\sigma_{C18-N} \rightarrow \sigma^*_{C18-C24}$	2.14
$\sigma_{C18-N} \rightarrow \sigma^*_{C19-C21}$	1.57	$\sigma_{C18-N} \rightarrow \sigma^*_{C19-C21}$	1.11	$\sigma_{C18-N} \rightarrow \sigma^*_{C19-C21}$	1.23
$\sigma_{C18-N} \rightarrow \sigma^*_{C24-C26}$	1.06	$\sigma_{C18-N} \rightarrow \sigma^*_{C24-C26}$	1.49	$\sigma_{C18-N} \rightarrow \sigma^*_{C24-C26}$	1.64
$LP(1)_N \rightarrow \pi^*_{C18-C24}$	23.89	$LP(1)_N \rightarrow \pi^*_{C18-C24}$	40.64	$LP(1)_N \rightarrow \pi^*_{C18-C24}$	15.42
$LP(1)_N \rightarrow \sigma^*_{C18-C24}$	3.21	$LP(1)_N \rightarrow \sigma^*_{C18-C24}$	1.72	$LP(1)_N \rightarrow \sigma^*_{C18-C24}$	5.00

Table 3. The second-order perturbation energy E_2 (Donor - Acceptor) calculated at B3LYP /6-31G level

Delocalization of electron density between the filled (bonding or lone- pair) Lewis type NBOS and empty (antibonding and Rydberg) non-Lewis NBOS are lead to loss of occupancy from the localized NBOS of the idealized Lewis structure into the empty non-Lewis orbitals. For each donor NBO and acceptor NBO the stabilization energy (E_2) is presented as the second-order perturbation interaction energy (E_2). [7-9]

These results show the hyperconjugation between the nitrogen lone pairs or orbitals as donors and some σ^* or π^* orbitals as acceptors can occure. The most important transfer in all three composites is $LP_N \rightarrow \pi^*_{C18-24}$, which has the highest energy and can make the structures more stable than single agents.

Conclusion:

The results show the composites between drugs and Nanotube are more stable than the single agents. The difference in hybridization of C and N atoms can cause to a difference between bond lengths, angles and charges. From NBO calculating some donor atoms (LP_N) can transfer electron to accepter atoms (σ^* or π^* in carbon of Nanotube) and so the composites become more stable. So because of the formation of stable composites between Nanotubes and Ecstacy-like drugs, Nanotubes can be used for omission of these drugs in overdose cases.

References:

[1] www.Wikipedia.org.

[2] www.jcrystal.com/products/wincnt/Nanotube.

[3] A. Frisch, A.B. Nielsen and A.J. Holder, *Gaussview Users Manual*, Gaussian Inc (2000).

[4] M. J. Frisch et al . Gaussian03, Revision D. 01 , Gaussian Inc. Walling ford CT (2004).

[5] A. D. Becke, *J.chem. phys*. 98 (1993) 785.

[6] L. Padmaja 1, M. Amalanathan, C. Ravikumar, I. Hubert Joe, *Spectrochimica Acta A* 74 (2009) 349–356.

[7] E.Zaedi, M. Aghaie, K.Zare, *J.Mol.struct*.(*THEOCHEM*),905 (2009)101-105.

[8] H. Roohi, A. Ebrahimi, S.M. Habibi, E. Jarahi, *J.Mol.struct*.(*THEOCHEM*),772(2006) 65-73.

[9]D.Nori-shargh,F.R.oohi, F. Deyhimi, R. Naeem-Abyaneh, *J.Mol.struct*.(*THEOCHEM*), 763(2006) 21-28.

Ab initio study and NBO analysis on the stability of the stereoisomers of 1,4,5,8-tetraoxadecalin, 1,4,5,8-tetrathiadecalin and 1,4,5,8-tetraselenadecalin

Hassanzadeh. N *[a], Bahrami. A[b], Kosari. M [c]

[a]*Department of Chemistry, Ahvaz Branch, Islamic Azad University, Ahvaz, Iran*

(E-mail: nhzadeh_212@yahoo.com)

[b] *Department of Physics ,Ahvaz Branch, Islamic Azad University, Ahvaz, Iran*

[c] *Department of Chemistry , Science Faculty, Arak Branch, Islamic Azad University, Arak, Iran*

Keywords: Anomeric Effects, Ab initio, NBO, 1,4,5,8-Tetraoxadecalin

Introduction

It is well known that the stereoelectronic interactions could play an important role on the conformational properties of hetero- cyclic compounds. The most dominant conformation-con- trolling factor in carbohydrate compounds is known as anomeric effect (AE). It should be noted that the AE is in favour of the axial conformation of a six-membered saturated ring in opposition to the steric effect which normally leads to a preference for the equatorial conformation. In this context, there is a stereoelectronic preference for conformations in which the best donor lone pair is antiperiplanar to the best acceptor bond. Praly and Lemieux have stressed that the AE must be considered as the difference be- tween the sum of the endo- and exo-Anomeric Effects (e.g. endo-AE and exo-AE) in the equatorial conformer and the same sum for theaxial conformer. Also, they have suggested that there is noendo-AE in the equatorial conformer, therefore, it is exclusivelystabilized by exo-AE interactions.

$$\text{Anomeric Effect}=(\text{exo - AE}_{eq}) - (\text{ exo - AE}_{ax} + \text{endo - AE}_{ax})$$

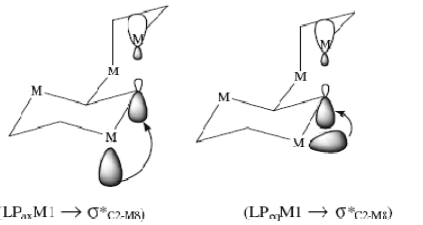

Fig. 1. Schematic representation of the electronic delocalization between non-bonding and anti-bonding orbitals ($LP_{ax}M1 \rightarrow \sigma^*_{C2\text{-}M8}$, $LP_{eq}M1 \rightarrow \sigma^*_{C2\text{-}M8}$) in compounds 1–3.

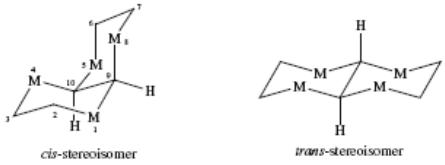

[Numbering used for compounds 1-3 (1: M=O; 2: M=S; 3: M=Se)

Scheme 1. Schematic representation of the stereoisomers of compounds 1-3.

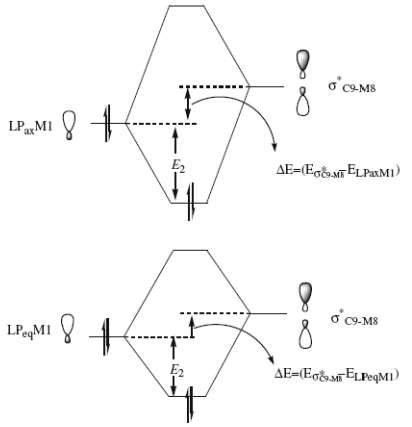

Fig. 2. Schematic representation of stabilization energy (resonance energy) (E_2) associated with donor (non-bonding)–acceptor (anti-bonding) interactions.

Methods:

NBO analysis, ab initio molecular orbital (MO: MP2/6-311+G**//HF/6-311+G**) and hybrid-density functional theory (hybrid-DFT: B3LYP/6-311+G**//HF/6-311+G**) based methods were used to study the anomeric effects (AE) on the stability of the cis- and trans-stereoisomers of 1,4,5,8-tetraoxadecalin (1), 1,4,5,8-tetrathiadecalin (2) and 1,4,5,8-tetraselenadecalin (3).

Results and discussion

The B3LYP/6-311+G**//HF/6-311+G** results revealed that the cis-stereoisomers of compounds 1–3 are more stable than their trans-stereoisomers by about 4.26, 1.03 and 0.70 kcal mol^{-1}, respectively. Also, the cis-stereoisomers of compounds 1–3 are more stable than their trans-stereoisomers by about 4.18, 2.11 and 01.18 kcal mol-1, respectively, as calculated at the MP2/6-311+G**//HF/6-311+G** level of theory. In addition, HF/6-311+G**//HF/6-311+G** results revealed that the Gibbs free energy difference (Gcis _ Gtrans) values (e.g. GFEDcis–trans) between the cis- and trans-stereoisomers decrease from compound 1 to compound 3. On the other hand, the NBO analysis of donor–acceptor (bond-antibond) interactions revealed that the anomeric effects (AE) for compounds 1–3 are -22.08, -17.84 and -13.22 kcal mol^{-1}, respectively. The decrease of the AE could fairly explain the decrease of the GFEDcis–trans from compound 1 to compound 3. On the other hand, the decrease of the donor–acceptor interactions associated with LPaxM1→ σ*C9–O8 electronic delocalizations could fairly explain the increase of occupancies of LPaxM1 non-bonding orbitals and the

decrease of occupancies of σ*C9–O8 anti-bonding orbitals from the cis-stereoisomers of compound 1 to compound 3.

References:

[1] P.L.A. Popelier, Comput. Phys. Commun. 93 (1996) 212–240.

[2] F. Freeman, A. Phornvoranunt, W.J. Hehre, J. Phys. Org. Chem. 11 (1998) 831.

[3] I. Arnason, G.K. Thorarinson, E. Matern, J. Mol. Struct. (THEOCHEM) 91 (1998) 454.

[4] V.M. Rayon, C. Barrientos, A. Largo, J. Mol. Struct. (Theochem) 432 (1998) 75.

[5] M. Remko, P.D. Lyne, W.G. Richards, Phys. Chem. Chem. Phys. 1 (1999) 5353.

[6] D. Nori-Shargh, F. Roohi, F. Deyhimi, R. Naeem-Abyaneh, J. Mol. Struct. (THEOCHEM) 763 (2006)21.

The relation of Temperature & Constant equilibria of CN model of Tautomeric Equilibria of 6-Hydroxy-5-Flourocytosine(OHFC)

Sorour Hasani [*a], Behzad Chahkandi[b]

[a]Department of Chemistry, University of Tehran, Tehran ,Iran

Email address:sorour.hasani@gmail.com

Email address:bchahkandi@gmail.com

[b]Department of Physics, University of Shahrood, Iran

Keywords: 6-Hydroxy-5-Flucytosine , Antifungal, Exothermic, Endothermic, Mutation, Nucleotid bases, Tautomerism.

Introduction

Nucleic acids are polymer molecules composed of two kinds of bases , purine , and pyrimidine [1]. Tautomerism as one of the possible mechanism of mutation in DNA , has extended area for studies[2]. Tautomerism of nitrogen heterocycles has long been associated in molecular biology with the natural purines and pyrimidines, and the presumed role of their rare tautomeric forms in spontaneous mutagenesis. 5-flucytosine [FC] that uses as antifungal agent is an antifungal agent used for the treatment of severe fungal. The ^{19}F NMR analysis of biofluids shows two compounds involving a direct metabolism of 5-FC were found that one of them is 6-Hydroxy-5- Flucytosine (OHFC) [3]. In the present work, optimized geometries of 17 possible tautomers of The (OHFC) will be studied with the DFT quantum calcutaions at the 6-31G** basis set level. According to The presence of 17 possible tautomers and 30 tautomeric equilibria we will investigate the effect of temperature on constant euilibria of tautomeric equilibria in CN model.

Computational methods

In this paper for determinating of optimized geometries and energy of different tautomers of OHFC, quantum calculations at B3LYP level were used with the 6-31G** basis set. The thermodynamic properties and the effect of changes of temperature (298°K-398°K) on

tautomeric equilibria of OHFC were obtained by using of the frequency calculations. All calculations were carried out by using Gussian 98.

Results and discussion

The 6-31G**optimized geometries and tautomeric equilibria process of OHFC are shown in fig.1.

According to that atom (H) is moving between which two atoms,we considered structural models of

CO,CN,NN,NO that order of these models is given in Table1. One of study that we performed, is

investigation of effect of temperature on equilibrium constant (K_{eq}) of equilibria. For this studying, we change temperature of reaction from 298° K to 398°. Here we only discusse about this effect

on CN (methyl imine- vinyl amine case) model.

The calculations were performed at B3LYP/6-31G** level. Through these changes of temperature on equilibria with assumption of that ΔH is constant we can apply $\text{Log k} = \frac{-\Delta H^\circ}{2/303R}\frac{1}{T} + c$ (Eq.1) and investigate changing of lnK with temperature for CN model (Fig.3) .

According to the data of K_{eq} that obtained with use of $\Delta G^\circ = -RTLn\,K$ (Eq.2) we can say that ,T3 and T25 are endothermic process ,as temperature increase, value of equilibrium constant increase .In the reminder reactions (T7,T17,T22) that are exothermic , as temperature increases, value of equilibrium constant of that reaction decreaces (Fig.3).

Table 1: Tautomeric equilibria based onStructura models (CO,CN,NO,NN)

CO	CN	NO		NN
T5	T3	T1	T16	T8
T12	T7	T2	T18	T9
T13	T17	T23	T19	T26
T14	T22	T4	T20	T28
T15	T25	T6	T21	T30
		T10	T24	
		T11	T27	
		T29		

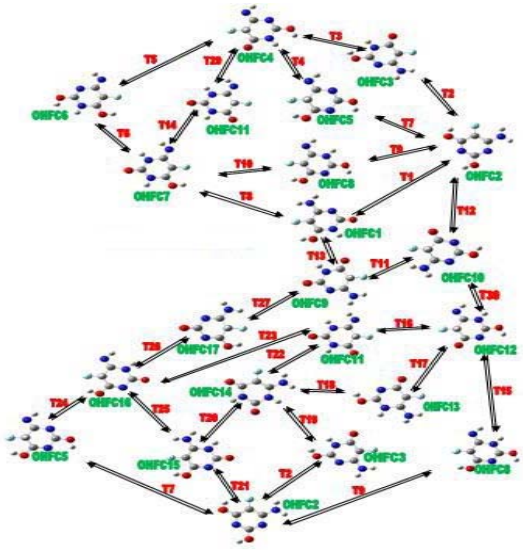

fig.1..Tautomeric equilibria

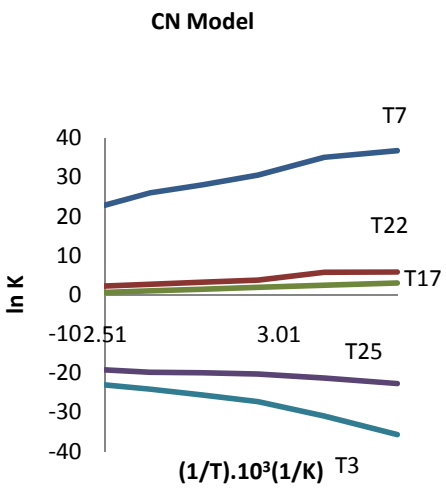

Fig.3.Effect of tempeeature on equilibria of CN model.

conclusion :

In this study we consider different structural models and focus on effect of temperature on CN structural model.For the considered reactions, temperature of considered reactions become decisive factor for thermodynamic conditions. For exothermic reactions(T17,T7,T22) with negative variation of enthalpy , condition that $\Delta G < 0$ will be satisfied at lower temperature.In endothermic is shown that increase of temperature causes increase of equilibrium constant of the reaction, as a result of equilibrium state proceeding in direction of products formation.For the exothermic reactions ,it is shown that increase in temperature corresponding in decrease of equilibrium constant values as result of proceeding of reactions in direction of the reactant formation.In endothermic reaction with positive variation in enthoropy, in case of $\Delta G > 0$ proceeding of reactions occurs in direction of the product formation.

References

[1] J. S. KwiatkowskriI., J. bartl and W. B. Person.J. Am.Chem. Soc. 110, 2353 (1988).

[2] J.D. Watson, F.H.C. Crick, Nature 171 (1953) 964–967.

[3]Organic Syntheses, Coll. Vol. 4, p.182 (1963); Vol. 35, p.34 (1955)

DFT Study on the Lithium Bond Interaction of Thiophene and Furan with $LiCH_3$

F. Hosseini[a] and H. Shirani IL Beigi[b,*]

[a]Department of Chemistry, Giulan University, Guilan, Iran

[b]Young Researchers Club, Islamic Azad University, Toyserkan Branch, Toyserkan, Iran

[*]Email: shiranihossein@gmail.com

Abstract

Three stable geometric configurations of C_4H_4Y (Y=O, S)---CH_3Li complexes were obtained by complete optimization at B3LYP/6-311++G** and MP2/6-311++G** levels. C_4H_4O---CH_3Li system has two stable configurations (complexes I and II), but C_4H_4S---CH_3Li system has only one stable configuration (complex III). The calculations showed that all the C10—Li14 bond lengths increased obviously but the blue-shift of C10—Li14 stretching frequency occurred after formed complexes. Zero-point vibrational energy corrections of complexes I—III is −45.757, −35.700 and −39.107 $kJ \cdot mol^{-1}$, respectively. The analyses on the combining interaction with the atom-in-molecules theory (AIM) also showed that a relatively strong lithium bond interaction presented in furan homologues C_4H_4Y---$LiCH_3$ systems. Natural bond orbital theory (NBO) analysis has been performed, and the results revealed that the complex I is formed with n-σ type lithium bond interaction between C_4H_4O and $LiCH_3$, complex II is formed with π-s type lithium bond interaction between C_4H_4O and $LiCH_3$, and complex III is formed with π-s and n-s type lithium bond interactions between C_4H_4S and $LiCH_3$, respectively.

Keywords: DFT-B3LYP, C_4H_4Y---$LiCH_3$ lithium bond complexes, NBO

Introduction

Intermolecular interaction plays an important role in the fields of physics, biology, chemistry and materials science. It has captured the interest of chemists for a long time and reports about its theory and experiment have been well represented [1]. It has been found that a lot of physical and chemical phenomena are closely related to the intermolecular weak interactions including hydrogen bond [2], π-cation, halogen bond, lithium Bond [3], etc. To date, lithium-bond has been identified in a variety of systems and the concept of lithium-bond has become

important in many fields. However, studies on lithium-bond interaction are relatively rare. So, we are interested in if there is any lithium bond interaction between furan homologues C_4H_4Y (Y=O, S), the lithium-bond acceptors, and CH_3-Li, the lithiumbond donors, and how the interaction takes place. Thus, given the absence of both experimental and theoretical studies on the lithium-bond interactions of furan homologues with CH3Li, the present study reports the results of a high-level theoretical study on the nature of the mentioned interactions. Herein, we optimized the geometries of C_4H_4Y (Y=O, S)---$LiCH_3$ system on the potential surface with B3LYP calculation.

Methods

Previous studies have proved that the theoretical calculation of hydrogen bond system must include electronic correlation energy. MP2 and B3LPY both include the calculation of correlation energy. MP2 could investigate all intermolecular interaction energy, including electrostatic energy, induced energy and dispersion energy. On the contrary, in B3LPY method, the calculation of interaction energy does not completely include dispersion energy and stabilization energy may also be underestimated. But B3LPY method has been proved reliable during the geometry optimization and transition state calculation [4]. Therefore, we adopt the 6-311++G** basis set for all atoms.

Results and Discussion

All possible geometric configurations on the potential surface of monomers and C_4H_4Y (Y=O, S)---LiCH3 complexes were optimized at the B3LYP/6-311++G** level. Two configurations of C_4H_4O---$LiCH_3$ were obtained, but only one configuration of C_4H_4S---$LiCH_3$ was obtained. According to the frequency analysis, no imaginary frequency occurs in all configurations and they are stable state points. The optimized geometries are shown in Figure 1. Configurations I—III all have C1 symmetry. The interaction strength between monomers could be clarified according to second-order stabilization energy (Eij (2)) obtained from the NBO analysis. As NBO theory indicates, the larger the stabilization energy Eij (2) is, the stronger the interaction of donor and acceptor orbits will be [5]. In other words, the donor electrons are easier to transfer to the acceptor orbits. In the 3 complexes, the CH_3Li moieties can be seen as the electron acceptor, and the C_4H_4Y (Y=O, S) moieties can be seen as the electron donors.

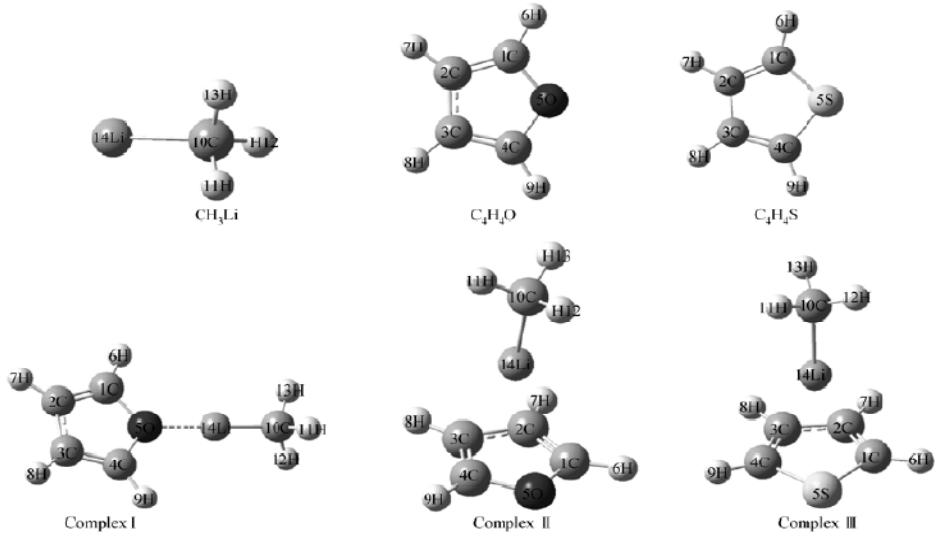

Figure 1. The optimized geometries of various species calculated at the B3LYP/6-311++G** level.

Conclusion

The accurate binding energy ΔECP+ZPE, which was corrected with CP correction method and zero-point vibrational energy correction at the MP2/6-311++G** level, of the three complexes was −45.757, −35.700 and −39.107 kJ·mol^{-1}, respectively. On the basis of the NBO analysis, we confirmed that complex I was formed with n-σ type lithium bond interaction between C_4H_4O and CH_3Li, in which the furan ring offers its lone-pair electron (LP1(O5)) to the σ*(C10—Li14) orbit, and the concomitances of charge transference from furan ring to CH_3Li occurred. For complex II, there was formed π-s type lithium bond interaction between C_4H_4O and $LiCH_3$, in which the furan ring offers its π electrons to the empty 2s orbit of lithium atom. For complex III (C_4H_4S---CH_3Li system), π-s and n-s type lithium bond interactions coexist, in which the thiophene ring offers its lone-pair electrons (LP1(S5) and LP2(S5)) and its π electrons to the empty 2s orbit of lithium atom, the concomitances of charge transference from thiophene ring to CH_3Li take place. AIM analysis showed that a relatively strong lithium bond interaction presented unquestionably in furan homologues C_4H_4Y (Y=O, S)---CH_3Li systems.

References

[1] Weber J M, Kelley J A, Robertson W H, et al. Hydration of a structured excess charge

distribution. *J Chem Phys*, 114, (2001), 2698-2706

[2] Yang Y, Zhang W J, Theoretical study of N–H…H–B blue-shifted dihydrogen bond. *J Mol Struct. (Themchem)*, 814, (2007), 113-117.

[3] Vila A, Vila E, Mosquera R , A. Topological characterisation of intermolecular lithium bonding. *Chem Phys*, 326, (2006), 401- 408.

[4] Su M D, Chu S Y. Density functional study of some germylene insertion reactions. *J Am Chem Soc*., 121, (1999), 4229-4237.

[5] H. Shirani; S. Jameh-Bozorghi, *J. Iran. Chem. Res*. 3, (2010), 17-30.

Experimental and computational study of Tautomerism in N,N' bis(2-thiazolyl) phenylphosphonic diamide

Kh. Gholivand*, S. Farshadian, and Z. Hosseini

Email: farshadian@modares.ac.ir

Department of Chemistry, Faculty of Science, Tarbiat Modares University, P. O. Box: 14115-175, Tehran, Iran.

Keywords: 2-Aminothiazole, Tautomerism, Phosphonic diamide, Computational study

Introduction

Heterocyclic tautomerism has been studied extensively for the past two decades due to its biological importance and highly solvent-dependent nature. 2-Aminothiazoles are able to tautomerize and can exist in either amino- or imino-form. Recently, molecular orbital calculations were performed on 2-, 4- and 5- aminothiazoles using different calculation levels in order to study the 1,3-hydrogen transfer between the amino group and the endocyclic nitrogen atom or carbon atom at position five [1]. In this work, the synthesis of a phosphonic diamide containing the 2-aminothiazole moiety is described and structural and conformational properties are analyzed.

Methods

N,N' bis(2-thiazolyl) phenylphosphonic diamide was prepared by treating chloroform solutions of 2-aminothiazole and phenylphosphonic dichloride using a 2:1 M ratio in the presence of triethylamine as a Lewis base catalyst. All quantum chemical calculations were performed with the GAUSSIAN 98 program package [2]. Structural and conformational properties are analyzed using a combined approach involving crystallographic data and theoretical calculations at the B3LYP and MP2 (with 6-311++G(3df,2p) and CBSB7 basis sets) level of approximations.

Results and Disscussion

The crystalline solid consist of the imine tautomer – with the tautomeric proton attached to the endocyclic nitrogen atom –, and the dihedral angles around the N_{exo}–C bonds amount 5.5(2) and 10.9(2)° – with the phosphorous on the same side of the endocyclic sulfur atoms. The B3LYP method computes a mixed structure with non-equivalent thiazole rings in which one

of endocyclic nitrogen atom in the thiazole ring is protonated, while the other thiazole group is deprotonated as the most stable form for the gas phase molecule. The two conformations (named as A and B in the molecular structures showed in Table 1) of the amine and imine tautomers are computed to be also stable forms, located at 1.09 (amine_A) and 2.44 kcal/mol (imine_A) higher in energy than the imine/amine form, respectively, at the B3LYP/CBSB7 level. The order of the computed stability exhibits little effect on the basis sets. However, a different description is obtained by applying the MP2 method: a drastic change is obtained in the relative stability values. In this case the most stable tautomer corresponds to the amine form. The structure with only one thiazole ring protonated has intermediate energy values, i.e. ca. 4.6 kcal/mol at the same level of calculation.

Table 1. Relative energies (kcal/mol) calculated at the B3LYP and MP2 methods for plausible tautomers of *N,N´* bis(2-thiazolyl) phenylphosphonic diamide in different conformations.

Form	Molecular structure	B3LYP			MP2	
		6-31+G*	6-311++G**	CBSB7	6-311++G**	CBSB7
Imine_A	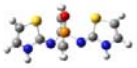	3.11	2.87	2.44	13.10	11.58
Imine_B		4.89	4.62	4.55	14.98	12.62
Imine/amine		0.00	0.00	0.00	5.11	4.57
Amine_A		0.58	0.68	1.09	0.00	0.00
Amine_B		1.12	0.92	1.49	2.00	1.42

Conclusions

The crystalline solid consist of the imine tautomer and the B3LYP method computes a mixed structure with non-equivalent thiazole rings as the most stable form for the gas phase molecule.

References:

[1] Papadopoulou C., Geronikaki A., Hadjipavlou-Litina D., *Farmaco 60* (2005) 969.

[2] Frisch MJ, Trucks GW, Schlegel HB, Scuseria GE, Robb MA, Cheeseman JR, Zakrzewski VG, Montgomery JA, et al. (1998) Gaussian 98, revision A.7. Gaussian, Inc. Pittsburgh, PA.

Effect of water molecules on zeolites stability : a molecular modeling study

R.Hakimelahi[a]

[a]Department of Chemistry, Islamic Azad university,Jahrom branch,Iran.

(Email: R.Hakimelahi2002@gmail.com)

Keywords: Zeolite, Stability, Water molecule, HF, B3LYP.

Introduction:

Zeolites are inorganic crystalline solids with small pores (1-20 Å diameter) running throughout the solid[1]. They are aluminosilicate framework structures made from corner sharing SiO_4 and AlO_4 tetrahedra. The general formula of zeolite is M_a^{n+} $[Si_xAl_yO_z]$. mH_2O where M_a^{n+} are extraframework cations; $[Si_xAl_yO_z]$ is the zeolite framework; and mH_2O are absorbed water molecules or $M_{m/z}.mAlO_2.nSiO_2$ .qH_2O which Z is metal charge. About 40 natural zeolites and more than 150 zeolites have been synthesized. Natural and synthetic zeolites are used commercially because of their unique useful characteristics, such as uniform intrinsic pore diameter, surface charge, ion exchange, adsorption and separation capability[2], opening the door to a wide range of applications in various industries as agricultural projects[3], forestry, livestock and marine, environmental conservation, civil engineering , public health, desert greening , urban development, brewing, pharmaceutical , cosmetic , paper, rubber and food. Zeolites act as magnets drawing toxins to them, capturing them in their cage and removing them from the body. They act to reduce health risks[4], as a potent antioxidant, balancing bodily pH levels, act to chelate and remove allergens, heavy metals and other carcinogens from the body, and stabilize and regulate immune system. Computational prediction of adsorption of some molecules in porous materials has great impact on the basic and applied research in chemical engineering and material sciences[5]. In this research , the role of water in stability of zeolites has been showed.

Methods:

In this work, we report an approach based on DFT and show that water molecules cause stability of zeolites. HF and B3LYP confirm tendency of zeolites to absorb more molecules

of water. we consider a part of cancrinit zeolite as a macromolecule, $Na_6[(AlO_2)_6(SiO_2)_6].nH_2O$.

Results and Discussion :

Because of studying a part of a large molecule as a symbolic representation, in order to perfect of oxygen capacity , they link to hydrogen and because of no access of suitable pore for cations in the small part of the macromolecule to neutralize negative charge, we use H^+ and join it to the certain bridge oxygen between Al and Si. When we set one or more molecules of water inside the zeolite, it is attached to system via hydrogen bond. We base the zeolite without any water(Z) and give it zero energy and express the energy of others(zeolites with one to four water molecules) compared to it. Stability energies have reported in table1.

Table1. Relative energy(kcal mol^{-1}) of zeolite with different numbers of water

Z with different numbers of water	HF $10^3 kcalmol^{-1}$	B3LYP $10^3 kcalmol^{-1}$
Z	0	0
$Z.H_2O$	-46.62	-47.10
$Z.2H_2O$	-82.71	-94.27
$Z.3H_2O$	-140.72	-141.54
$Z.4H_2O$	-187.85	-188.10

Conclusions:

Calculation show that there is an upright relationship between stability and the number of water molecules, so zeolite assists water infiltration and retention in the soil due to its very porous properties and the capillary suction it exerts. Acting as a natural wetting agent, it is an excellent amendment for non wetting sands and to assit water distribution through soils.

References:

[1] A. Martucci, A. Alberti, etc. Microporous and Mesoporous Materials, 63(2003), 33-42.
[2] N. Widiastuti, H. Wu, M. Ang, D. Zhang, Desalination, 218(2008), 271-280.

[3] N. Zwingmann, B. Singh, D.R. Mackinnon, R. Gilkes , Applied Clay Science, 46(2009), 7-12.

[4] G. Cerri, M. de' Gennaro, M.C. Bonferoni, C. Caramella, Applied Clay Science, 27(2004), 141-150.

[5] A. Miyamoto, Y. Kobayashi, M. Elanany, H. Tsuboi, M. Koyama, A. Endou,etc. Microporous and Mesoporous Materials, 101(2007), 324-333.

Effect of solvent on the H-bond strength in trifluoroacetylacetone

Azadeh Khaneh* [a], Sayyed Faramarz Tayyari [b], Mohammad Mehdi Riazi [a]

[a] Department of Chemistry, Shahroud Branch, Islamic Azad University, Shahroud

[b] Department of Chemistry, Neyshabur Branch, Islamic Azad University, Neyshabur

(*Email:*www.galia_1983@yahoo.com)

Introduction

The enol forms of -diketones are able to form strong intramolecular hydrogen bonds [1, 2]. In some of these systems, especially in fluorinated compounds, the strength of hydrogen bond is solvent dependent. The aim of this work is study of solvent effects on the hydrogen bond strength in these systems. Therefore, three compounds, acetylacetone (AA), trifluoro-acetylacetone (TFAA) and hexafluoro-acetylacetone (HFAA) are selected. HFAA and AA are symmetric compounds, i.e. by H transfer no change in the structure of the system occurs. However, there are two different structures for unsymmetrical compounds such as TFAA, in one of them the OH group is near the CH_3 group and in the other near the CF_3 group. These two structures are designated by 2-TFAA and 4-TFAA [1].

Calculations

All calculations were performed using Gaussian 03. The full geometry optimization of the cis-enol form and its corresponding open structure for all b-diketones under study were performed with the hybrid density functional B3LYP, using 6-31G*, 6-31G**, 6-311++G*, and 6-311++G** basis sets, which are believed to give relatively accurate results for these systems.

To test the influence of solvent on the molecular structure, the geometry was optimized with the help of the self-consistent reaction field (SCRF), the Onsager (SCRF = dipole) model with an in the 1-78 range. Some geometrical parameters, such as O…O distance, O-H bond length are plotted against dielectric constant.

Results and discussion

Variations of O-H, O···O, and O···H vs dielectric constant, □□ are studied for AA, TFAA, and HFAA. By considering the behavior of these parameters against □□ it is concluded that the hydrogen bond strength of AA and HFAA is not considerably changed by change of media, while the H-bond strength in 2-TFAA and 4-TFAA are considerably increased and decreased upon increasing the solvent polarity, respectively. These behaviors are interpreted by effect of solvent on the charge distribution on CF_3 group. When a polar solvent approaches a CF_3 group, some of the negative charge on the CF_3 group transfers to the solvent media, therefore, CF_3 group at6tract some of the electron charge on its nearest carbonyl or hydroxyl groups. In case of 2-TFAA the nearest group is the hydroxyl group which result of less negative charge on O atom and so more acidic character of the hydroxyl group, hence, forming stronger H-bond. But in the case of 4-TFAA, the nearest group to the CF_3 group is the carbonyl group. Charge transfer from CF_3 group to the solvent results in the less negative O atom therefore, forming weaker H-bond system.

Conclusion

Both 2-TFAA and 4-TFAA are affected by salvation and changing the dielectric constant of the solvent. However, on increasing the dielectric constant of solvent the hydrogen bond strength of these tautomers changes in different direction. The H-bond strength of 2-TFAA is increased by increasing the dielectric constant of the solvent and the H-bond strength of 4-TFAA is decreased.

References

[1] M. Zahedi-Tabrizi, F. Tayyari, Z. Moosavi-Tekyeh, A. Jalali, S.F. Tayyari, Spectrochim. Acta 65A (2006) 387–396.

[2] S.F. Tayyari, F. Milani-Nejad, Spectrochim. Acta 56A (2000) 2679.

Conformation analysis, tautomerism, and vibrational assignment of 1-amino-2-keto-6-cyclohexene

Shokooh Khavari [a], Sayyed Faramarz Tayyari [b] A.H.Pangh[c]
Chemistry Department, Islamic Azad University, Shahrood Branch, Shahrood
Chemistry Department, Ferdowsi University of Mashhad, Mashhad
Payame Noor University , branch of gorgan,gorgan,Iran

Introduction

Theoretically, 1-amino-2-keto, 6-cyclohexene (AKC) is capable to form 18 tautomers. This compound is prepared from amination of 1,2-hexanedione. The study of AKC is useful for understanding the nature of intramolecular hydrogen bond in the amino-ketones with 5-membered chelated ring.

The aim of this work is study of Tautomerism, conformational analysis, and predicting the vibrational spectra of AKC and comparing the strength of its intramolecular H-bond with that in 4-amino-pentane-2-one [1], which forms a 6-membered intramolecular H-bond.

Method of calculation

The calculations of geometrical parameters and frequencies were performed using the Gaussian 03 program package [2]. In this work, we applied the DFT method including the hybrid gradient-corrected exchange functional proposed by Becke [3] with the gradient corrected correlation functional of Lee, Yang, and Parr [4], B3LYP, using the basis set 6-31G**. The relative stability of 18 different tautomers of this compound is obtained.

Results and discussion

AKC, theoretically, can exist in three main forms, amino-ketone, imino-ketone, and imino-enol, which with considering all possible conformations one can consider 18 different tautomers.

According to our calculations the aminoketone tautomer engaged in an intramolecular H-bond is the most stable tautomer (AK-1) and theoretical thermodynamics calculations indicate that almost only this tautomer predominantly (about 100%) exists in the sample. There are three

more aminoketones (AK-2, AK-3, and AK-4) which have much higher energy than that of AK-1 (7.4-12.3 kcal/mol). The major difference between these tautomers is position of double bond which changes the □-electron conjugation in the system. AK-4 is about 4 cal/mol more stable than AK-2 and AK-3 tautomers. This energy difference is caused by conjugation between C=O and C=C bonds. Of course, this conjugation can not affect the □-electron delocalization in the H-bonded ring, suggested by Gilli et al. [5]. The imino-ketones are the next stable tautomers, with an energy difference of about 3 kcal/mol for one of this tautomers. However, imino-enols have the highest energy (with an energy difference of 13-26 kcal/mol) and any contribution of them in the sample is unlikely.

References

[1] S. F. Tayyari, M. Fazli, F. Milani-Nejad, J. Mol. Struct. (Theochem), 541 (2001) 11.
[2] Gaussian 03, Revision B.05, M.J. Frisch, et al. Gaussian Inc., Pittsburgh PA, 2003.
[3] A.D. Becke, J. Chem. Phys. 98 (1993) 5648.
[4] C. Lee, W. Yang, R.G. Parr, Phys. Rev. B37 (1988) 785.
[5] V. Bertolasi, P. Gilli, V. Ferretti, G. Gilli, J. Am. Chem. Soc. 113 (1991) 4617.

Surface calculation for Adsorption of Atomic Hydrogen on V(111)

B. Khezri[a,*] *,D. Setamdideh*[b] *, S. Khanahmadzadeh*[c]*, H. Zhiyan*[d]

[a, b, c, d]*Department of Chemistry, Islamic Azad University , Mahabad Brunch ,Mahabad, Iran*

[*]*(Email: khezry55@yahoo.com)*

Abstract

Our theoretical work tries to explain the experimental facts of, giving a study of H desorption from V(111). It can be shown that the surface quality (structure, chemical composition) plays an important role with respect to desorption energies. From several theoretical models we conclude that all surface H4 sites should be occupied, either by H or contaminants as C or O. Desorption from these sites will not take place as the adatoms are bound very strongly.

Keywords: VASP, V(111), Adsorption of Atomic Hydrogen, Surface calculation

Introduction

Both the clean surface as well as the C and O contaminated surface (i.e. C and O were coadsorbed to H) were considered in our models. In addition, we also studied the mechanism of absorption and diffusion of hydrogen into bulk V because of the well-known property of V of storing hydrogen.

Computational methods

All calculations presented in this paper were performed with the Vienna Abinitio Simulation Package (VASP). The surface calculations were done at the calculated bulk lattice parameter. Most calculations were done with a p(2×2) super cell with 7 layers within a repeated slab model relaxing the first and second layers of V(111). For modeling adsorption, the adatoms were placed on both surfaces of the slab.

Results and Discussion

Clean V (111)

The clean V(111) surface shows a strong contraction between first and second layer. The calculated value depends on the potential that was applied. In case of the ultra-soft

pseudopotential used in this study, the interlayer distance between first and second layer is reduced by 0.235 ˚A (about 15%) as compared to the experimental 0.13 ˚A. The reason for this apparent discrepancy is also described in [3].

Comparison of the different adsorption sites for c (2×2) coverage

In our study, we considered fourfold coordinated hollow (H4), twofold coordinated bridge (B2) and finally one-fold coordinated top (T1) sites. To get a feeling for the relative stability of the different sites, we first calculated a c(2x2) type coverage of 0.5.

In our study, we considered fourfold coordinated hollow (H4), twofold coordinated bridge (B2) and finally one-fold coordinated top (T1) sites. To get a feeling for the relative stability of the different sites, we first calculated a c(2x2) type coverage of 0.5.

The results for H4, B2, and T1 — as tabulated in Tab.1 — show clearly, that adsorption on T1 can be ruled out, for it is energetically less favorable by 0.85 eV than the most stable H4 site. In contrast to this great difference in stability, the B2 site and the H4 site with an adsorption energy of −0.61 and −0.71 eV per H atom respectively, are close to each other, and that's why we will consider these two sites in all further calculations.

Table1: Characteristics of the H surface adsorption: layer relaxation Δdij between layer i and j [%] (V bulk layer distance is 1.50 ˚A), height of H above the V surface hH [˚A], and adsorption energy E [eV] per average H atom are given. All calculations were done in a 2x2 cell with 7 V layers, In case of on top adsorption, hH gives the bond length of H to the V atom below.

Coverage	type and site	Δd12	Δd23	hH	E
clean V(111)		-15.1	+1.2		
0.25	p(2x2)H4	-14.6	+1.5	0.58	-0.67
0.25	p(2x2)B2	-12.0	+0.4	1.28	-0.65
0.5	c(2x2)H4	-16.1	+1.7	0.58	-0.70
0.5	c(2x2)B2	-8.1	-0.5	1.23	-0.57
0.5	c(2x2)T1	-9.2	+1.2	1.60	+0.14
0.5	p(2x1)H4	-15.6	+1.4	0.61	-0.67
1.0	p(1x1)H4	-15.5	+1.6	0.58	-0.70
1.0	p(1x1)B2	-0.6	-3.1	1.06	-0.46
1.25	p(1x1)H4p(2x2)B2	-8.5	0.0	1.40 (B2)	-0.70
1.5	p(1x1)H4c(2x2)B2	-3.1	-1.5	1.27 (B2)	-0.61
1.75	p(1x1)H4p(2x2)B2	+0.9	-1.8	1.23(B21)	-0.48
2.0	p(1x1)H4p(1x1)B2	+7.5	-3.4	1.13 (B2)	-0.45
2.0	c(1x1)B2	+8.6	-6.2	0.90	-0.34

For the most stable site H4 we find the somewhat surprising result that the strong contraction of −15.2% of Δ12 of clean V(111) remains even after H adsorption (Δ12 = -16.2%) in contrast to the usual experience that adsorption counteracts reconstruction of clean surfaces. This was derived for C and O adsorption (see [2], [3]) whereas for B2 adsorption the contraction was only partially released to Δ12 = -8.1%. The interlayer spacing of the second and third V layer was not significantly affected.

H diffusion into the V bulk

To get the exact results, we have to relax the atoms. For the minima, all coordinates of the hydrogens and the outermost 4 V layers were allowed to relax, whereas for the maxima we had to fix the z coordinates of hydrogen and the surrounding V atoms, otherwise H would fall into the minimum. The same was done with a V(111) surface, where all H4 sites were occupied by H (see Fig. 1 right panel). We relaxed again the outermost 4 V layers and of course the H atoms forming the p(1×1) coverage.

The MD simulation for B2 H on the clean surface shows a deep minimum for the surface adsorbed B2 H. After relaxation we get an adsorption energy of −0.61 eV, which is more than for the minima of the subsurface or bulk states. The barrier from site B2(1) above the surface

to the next lower stable position B2(2) which occurs 0.29 ˚A below the V surface layer (or 1.02 ˚A above the second V layer) is calculated to be 0.51 eV, the barrier for the opposite movement from B2(2) to B2(1) is very low, namely 0.04 eV. Most other barriers in both directions lie in the range of 0.3 to 0.4 eV, just the barrier from B2(3) to B2(4) is somewhat smaller (0.14 eV). This is the change from subsurface to bulk region, as B2(4) shows already bulk-like absorption energies.

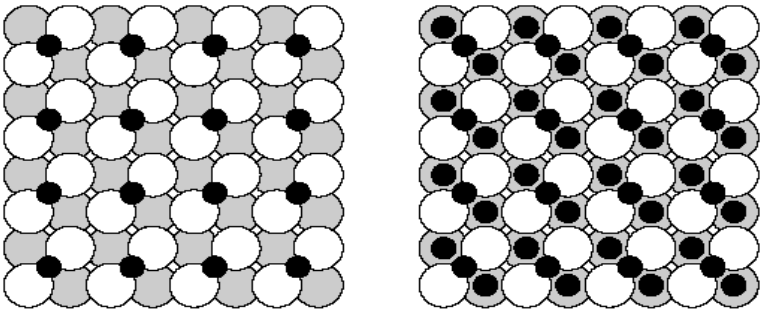

Figure 1: Start geometries used for studying the energetics of B2 H digging into V bulk. c(2×2)B2 H covered V(110) surface (left panel) and p(1×1)H4c(2×2)B2 H covered V(111) surface (right panel). H atoms black, V surface atoms white, V subsurface atoms grey.

Conclusion

Our theoretical work tries to explain the experimental facts of, giving a study of H desorption from V(111). It can be shown that the surface quality (structure, chemical composition) plays an important role with respect to desorption energies. From several theoretical models we conclude that all surface H4 sites should be occupied, either by H or contaminants as C or O. Desorption from these sites will not take place as the adatoms are bound very strongly.

Desorption will rather occur from surface B2 sites and the B2-corresponding sites of the subsurface region and bulk. For a coverage higher than 1.65 ML H, no more surface B2 sites will be occupied and subsurface and bulk H can desorb directly through the free B2 sites. Also, in case of C or O contaminations we have shown that the B2 surface sites close to C or O in H4 sites, are empty and therefore give way for H desorbing from below.

Because there are some uncertainties in the assignment of the experimental desorption peaks, it is not clear if the atoms adsorb on the surface or diffuse (are absorbed) into the vanadium material. We therefore use the nomenclature ”ad/bsorption” energy.

References:

[1] G. Krenn, C. Eibl, W. Mauritsch, E.L.D. Hebenstreit, P. Varga, and A. Winkler. Surf. Sci., 445:343, 2000.

[2] S. Crampin and P.J. Rous. Surf. Sci., 244:L137, 1991.

[3] M. Beutl, J. Lesnik, E. Lundgren, C. Konvicka, P. Varga, and K.D. Rendulic. Surf. Sci., 447:245, 2000.

[4] H.B. Nielsen V. Jensen, J.N. Andersen and D.L. Adams. Surf. Sci., 116:66, 1982.

[5] W. Bergermayer, R. Koller, C. Konvicka, M. Schmid, G. Kresse, J. Redinger, P. Varga, and R. Podloucky. Surf. Sci., 497:294, 2002.

Theoretical, NMR Study, Kinetics and a Mechanistic Investigation of the Reaction between Triphenylphosphine, Dialkyl acetylenedicarboxylates and Acetyl acetone

Mostafa Habibi-Khorassani*[a], Ali Ebrahimi[a], Malek Taher Maghsoodlou[a], Zohreh Khajehali[a]

[a] *Department of Chemistry, University of Sistan and Baluchestan, P.O.Box 98135-674, Zahedan, Iran*

(E-mail: smhabibi_usb@yahoo.com)

Keywords: stable phosphorus ylides, dialkyl acetylenedicarboxylates, Z and E isomers, AIM method, Acetyl acetone.

Introduction:

In continuation of our current interest in the development of new approaches to heterocyclic and carbocyclic systems, the kinetics and mechanistic study along with theoritical calculations of a facile, synthesis of the reaction between triphenylphosphine **1**, dialkyl acetylenedicarboxylates **2** and acetyl acetone **3** (as a protic/nucleophilic reagent) were investigated for generation of phosphorus ylides **4a-c** involving the two geometrical isomers such as *Z*- and *E*- isomersm. Synthesis of which was earlier reported. For assignment of the two Z and E isomers as a minor or major form in phosphorus ylides **4a-b** containing a acetyl acetone, first the Z- and the E- isomers were optimized for all ylide structures at HF/6-31G(d,p) level of theory by Gaussian03 package program. The relative stabilization energies of both the geometrical isomers have been calculated at B3LYP/6-311++G** level. Atoms in molecules (AIM) and natural population analysis (NPA) methods and CHelpG keyword at HF/6-31G(d,p) level of theory have been performed in order to gain a better understanding of the most geometrical parameters of both the E-**4(a,b)** and the Z-**4(a,b)** of phosphorus ylides. The numbers of critical points and intramolecular hydrogen bonds as well as the charge of atoms that constructed on the Z- and E- isomers have been recognized. The results altogether reveal the effective factors on stability of Z- and E- ylide isomers. In addition, $J_{x\text{-}y}$, the values of proton and carbon coupling constants and also chemical shifts (δ^{H}_{iso}, δ^{C}_{iso}) have been calculated at mentioned level using SPINSPIN keyword.

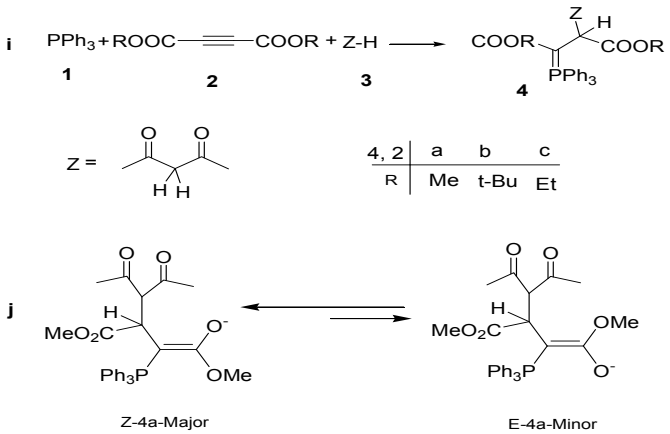

Fig. 1 (i) The reaction between triphenylphosphine **1**, dialkyl acetylenedicarboxylate **2** (**2a** or **2b**) and acetyl acetone **3** for generation of stable phosphorus ylides **4** (**4a** or **4b**). (**j**) The two isomers *E*-**4a** and *Z*-**4a** (major and minor, respectively) of ylide **4a**.

Results and discussion (Calculations):

In order to determine more stable form of both the geometrical isomers [*Z*-**4(a, b)** and *E*-**4(a, b)**] of ylides (**4a** or **4b**), which is shown in Fig.1, first their structures were optimized at HF/6-31G(d,p) level of theory by Gaussian03 package program. Also relative stabilization energy of the two isomers have been calculated at HF/6-31G(d,p) and B3LYP/6-311++G** levels. The relative stabilization energies for the two [*Z*-**4(a, b)** and *E*-**4(a, b)**] isomers are reported in Table 1, as can be seen, *E*-**4a** and *E*-**4b** isomers are more stable than *Z*-**4a** and *Z*-**4b** forms (0.53 and 0.22 kcal/mol, respectively) at B3LYP level.

Table 1: The relative energy (kcal/mol) for both the *Z*- and *E*- isomers of ylides **4a** and **4b**, obtained at HF/6-31G (d,p) and B3LYP/6-311++G(d,p) levels**.**

Geometrical isomer	HF	B3LYP
Z-**4a**	0.59	0.53
E-**4a**	0.00	0.00
Z-**4b**	0.26	0.22
E-**4b**	0.00	0.00

Also, the charge on different atoms which are calculated by atoms in molecules (AIM) and natural population analysis (NPA) methods and also CHelpG keyword at HF/6-31G(d,p) level are reported for the two *Z*- and *E*- isomers of ylides **4a** and **4b**. There is good agreement between the results in three methods.

Kinetics Studies:

To gain further insight into mechanism in reaction between triphenylphosphin **1**, dialkyl acetylene dicarboxylates **2** and acetyl acetone **3** (as a protic/nucleophilic reagent) for generation of phosphorus ylids 4a-b, a kinetics study of the reactions was undertaken by UV spectrophotometeric technique. The result have been accumulated in Table 2.

Table 2: values of overall second order rate constant for the reactions between (**1,2a** and **3**), (**1,2b** and **3**) and (**1,2c** and **3**) in the presence of solvents such as 1,2-dichloroethane and 1,4-dioxane, respectively, at all temperatures investigated.

Reactions	Solvent	ε	k_2. mol^{-1}.L.min^{-1}			
			15.0 °C	20.0 °C	25.0 °C	30.0 °C
1,2a and **3**	1,4-dioxane	2	518.2	536.2	615.1	692.3
1,2a and **3**	1,2-dichloroethane	10	599.5	633.1	667.2	800.8
1,2c and **3**	1,4-dioxane	2	413.6	449.8	501.5	577.9
1,2c and **3**	1,2-dichloroethane	10	459.1	498.7	572.6	649.9
1,2b and **3**	1,4-dioxane	2	54.5	64.7	75.6	91.3
1,2b and **3**	1,2-dichloroethane	10	63.2	78.4	95.1	122.6

Conclusion:

The assignment of the *Z*- and *E*- isomers as a minor or major form in both the ylides 4a and 4b was undertaken by atoms in molecules (AIM) and natural population analysis (NPA) methods and CHelpG keyword. Quantum mechanical calculation was clarified how the ylides 4a and 4b exist in solution as a mixture of the two geometrical isomers. This result was in good agreement with the experimental data. In addition, the NMR study on the basis of theoretical calculation were employed for determination of chemical shifts and coupling constants of the two major *Z*-4(a, b) and minor *E*-4(a, b) geometrical isomers and Kinetics investigation of the reactions was undertaken using UV spectrophotometry. The results can be summarized as follow: (1) the appropriate wavelengths and concentrations were determined to follow the reaction kinetics. (2) The overall reaction order followed second-order kinetics and the reaction orders with respect to triphenylphosphine, dialkyl acetylenedicarboxylate and acetyl acetone were one, one and zero respectively. (3) The values of the second-order rate constants of all reactions were calculated automatically with respect to the standard equation, using the software associated with the Cary-300 UV equipment. (4) The rates of all reactions were accelerated at higher temperatures. Under the same conditions, the activation energy for the reaction with di-*tert*-butyl acetylenedicarboxylate 2b (24.7 kJ/mol) was higher than that

for the both reactions which were followed by the diethyl acetylenedicarboxylate 2c (16.1 kJ/mol) and dimethyl acetylenedicarboxylate 2a (14.5 kJ/mol) in 1,2-dichloroethane (5) The rates of all reactions were increased in solvents of higher dielectric constant and this can be related to differences in stabilization by the solvent of the reactants and the activated complex in the transition state. (6) Increased steric bulk in the alkyl groups of the dialkyl acetylenedicarboxylates, accompanied by the correspondingly greater inductive effect, reduced the overall reaction rate. (7) With respect to the experimental data, the first step of proposed mechanism was recognized as a rate-determining step (k_2) and this was confirmed based upon the steady-state approximation. (8) Also, the third step was identified as a fast step (k_3). (9) The activation parameters involving $\Delta G^{\#}$, $\Delta S^{\#}$ and $\Delta H^{\#}$ were reported for the first step of three reactions.

References:

[1] S.M.Habibi, A.Ebrahimi, M.T.Maghsoodlou, *Phosphorus, Sulfur Silicon*. 559-566 (2010).

[2] S.M.Habibi, M.T.Maghsoodlou, A.Ebrahimi, H.Saravani, M.Zakarianezhad, Z.Khajehali, *Progress in reaction kinetics and mechanism*, 261-288 (2009)

[3] I.Yavari, F.Nasiri, H.Djahaniani, *Phosphorus, sulfur and silicon*, **178**, 2627-2638 (2003).

[4] M.T.Maghsoodlou, S.M Habibi-Khorassani, *J. Chem. Research,* **2**, 79-82 (2008).

The comparative study of transport properties of furan, thiophene and selenophen dithoils in Nano Electronics

E. Zahedi[1,*], A. Pangh[2], S. Jalili[3], A. Khajeh Mirzaie[1]

[1] Chemistry Department, Islamic Azad University, Damghan Branch, Damghan, Iran

e_zahedi1357@yahoo.com akbar_mirzaie1352@yahoo.com

[2] Shahid Beheshti Tarbiat Moallem Center of Gonbad Kavoos, Gonbad Kavoos, Iran

[3] Department of Chemistry, K. N. Toosi University of Technology, Tehran, Iran,

Keyword: Nano electronic, Green function, MPSH, Transmission

Introduction:

Molecular electronics or nano-electronics is the electronic transport by nano devices or organic molecules which is bridged between two electron reservoirs such as metallic electrodes that the result of miniaturization of silicon devices and Moor law's. Among the complicated inorganic complexes and long organic chains, aromatic rings that have delocalized electrons are better choice than other molecules.. Aromatic system such as benzene bithiol has been studied by many research groups using experimental and theoretical methods in molecular electronics [1-2].

In the previous studies, we investigated the thiophene molecule inserted between two gold electrodes as a molecular wire and highlighted the effect of end atom such as S, Se and Te and composition of electrodes such as alloying on the electronic transport properties and their application in molecular electronics[3-4]. In this paper, we consider the typical conjugated molecule such as furan, thiophene and selenophen dithoils sandwiched between two gold electrodes to inspect the effect of O, S and Se atoms in five member heterocyclic thiophen-like rings on the electronic transport properties.

Theory

One of the important factors in the molecular electronics is the current passing through the molecule. This factor is potential application of molecules in nanoscale devices. In this study

The Landauer-Buttiker theory is used to calculate the *I-V* characteristics of molecules inserted between two electrodes. This formalism relates the current *I* to bias voltage *V* and transmission probability *T(E,V)* of electron with energy *E*. The transmission function *T(E,V)* can be calculated using the Green function technique[5].

Results and discussion

The optimized geometric structure of a TBT molecule is presented in Figure 1. This molecule contains two S–H terminal groups which bond to the gold atoms by removing an H atom from each of the S–H groups. The energy level of HOMO and LUMO are -5.687, -5.744, -5.745 eV and -3.952, -3.898, -3.893 eV respectively and energy gap is 1.735, 1.846 and 1.852 eV respectively for furan dithiole (FDT), thiophen dithiole (TDT) and selenophen dithiole (SDT) and shows that the HOMO of three molecules are closer than LUMO to the Fermi energy then more contribution to the electron transport from molecules.

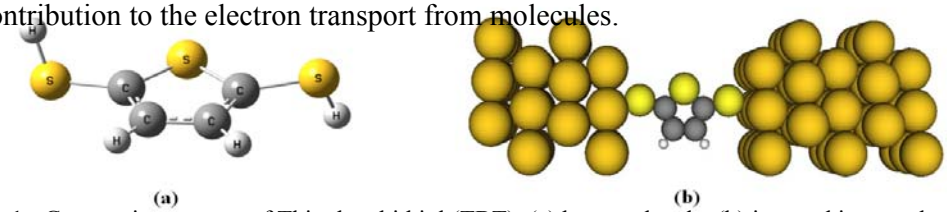

Fig. 1 : Geometric structure of Thiophen bithiol (TBT); (a) bare molecule, (b) inserted in two electrodes

Calculated transmission spectra at zero bias voltage are depicted in Figure 2 and the blue rhombic up to the spectrum is the position of Molecular Projected Self-consistent Hamiltonian (MPSH) of referred molecules when attached to the electrodes. In common sence, the transmission peaks height is mainly determined by orbital delocalization. Looking at the transmission spectra of all three systems, it is appear that very transmission peaks near the Fermi energy for selenophen dithoil than other two systems. This leads to high current pass through the molecule.

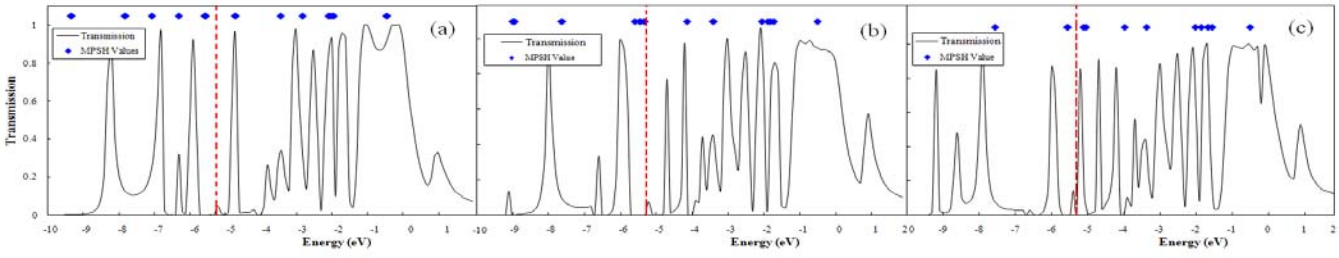

Fig. 2: Transmission spectra for (a)Furan dithiol, (b) Thiophen dithiol, (c) Selenophen dithiol at zero bias voltage.

The authors acknowledge the kind financial support provided by the research council of Islamic Azad University, Damghan Branch.

References:

[1] W. Tian, S. Datta, S. Hong, R.G. Reifenberger, J.I. Henderson, Physica E, 1 (1998) 304.

[2] A. Johansson, S. Stafström, Chem. Phys. Lett., 322 (2000) 301.

[3] S. Jalili, A. H. Pangh, Int. J. M. Phys. B, 2009, 23, 5657-5669.

[4] S. Jalili, A. H. Pangh, J. Comput. Theor. Nanosci. 2010, 7, 1-11.

[5] S. Datta, Nanotechnology, 15 (2004) S433

Theoretical study of of hydrogen storage in Li–ethylene complex via DFT

A. Khajeh-mirzaie, M.M. Riazi, S.R. Emamian, Ehsan Zahedi*
Chemistry Department, Islamic Azad University, Shahrood Branch, Shahrood, Iran.
akbar_mirzaie1352@yahoo.com e_zahedi@iau-shahrood.ac.ir

Keywords: DFT; Hydrogen storage; Li-ethylene complex; BSSE

Introduction:

Hydrogen storage using carbon nanotubes (CNTs) or other nanostructures have recently attracted a great deal of theoretical and experimental researches [1], because hydrogen is an ideal energy carrier in fuels, reversible batteries, etc. However, the crucial problem now is the discovery of new materials which can store a large amount of hydrogen in its molecular form at ambient conditions. Recently Zahedi et al. studied the hydrogen absorption in first row transition metals–ethylene complex via DFT methods and results submitted for publication in Molecular Simulation. In this Letter, we focus on the interaction of hydrogen with Li-ethylene complex. DFT methods not only have the cheap computational cost but also typically sufficient accuracy for both dense matter and isolated molecules [2].

Computational details:

All the geometry optimizations and energy calculations are performed using Gaussian 09 program package [3] at the level of density functional theory (DFT) with MPW1PW91/6-311++G** for adsorption of Li on ethylene and hydrogen molecules on Li atom.

Results and discussion:

The calculation of the binding energies for addition of Li atom to C_2H_4 and addition of hydrogen molecule to LiC_2H_4 complex were corrected for basis set superposition using the counterpoise (CP) method [4]. The optimized geometry of Li-C_2H_4-H_2 is shown below.

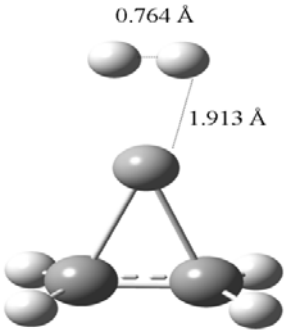

The binding energy of the Li to the ethylene molecule was calculated to be -14.624 kJ/mol. The Li–C and C–C distances for this configuration are 2.055 and 1.419 Å, respectively. This adsorption is so weak that it should belong to chemical adsorption. In another case, the hydrogen molecule was absorbed in molecular form with C_2v symmetry on the top of Li atom in complex form with a binding energy of -20.385 kJ/mol. The Li–H and H–H distances for this configuration are 1.913 and 0.764 Å, respectively. Obviously the adsorption of hydrogen molecule on Li complex is weak and the hydrogen desorption is not difficult.

References:

[1] Y.L. Zhao, R.Q. Zhang, R.S. Wang, Chemical Physics Letters 398 (2004) 62.

[2] S. Li, V.R. Cooper, T. Thonhauser, A. Puzder, D.C. Langreth, J. Phys. Chem. A 112 (2008) 9031.

[3] M.J. Frisch et al., Gaussian 09, Revision A.02-SMP, Gaussian Inc., Wallingford CT, 2009.

[4] S.F. Boys, F. Bernardi, Mol. Phys. 19 (1970) 553.

Molecular orbital analysis of frontier orbital's and Effect of external electric field on electron transfer in 3, 6-Diphenyltetrazine as a molecular wire

S. Danesh Nia[a], Z. Bayat [a,]*, E. Taghizadeh[b], Z. Chamani[a]

[a]*Department of Chemistry, Islamic Azad University-Quchan Branch, Iran*

(z.bayat@ymail.com)

[b]*Young Researchers Club, Islamic Azad University-Quchan Branch, Iran*

Abstract

The electron transport characteristics of a 3, 6-Diphenyltetrazine (DPT) single molecular conductors are investigated via the density functional theory (DFT) method. Different linkers such as sulfur, nitrogen, CN and NO have been considered. Bonding natures at the interfacial contact were performed by means of the natural bond orbital (NBO) analysis. The dependence of the molecular electronic structure of the gold–molecule complexes on the external electric field (EF) has been also studied.

Keywords: 3, 6-Diphenyltetrazine; Nano molecular wire; Effect of linkage; DFT

Introduction:

The nanowires generally are single crystalline and have diameters of in the range 1–200nm and the length is several microns or longer [1]. A theoretical analysis of the frontier molecular orbitals of these molecules will give a clear picture of the structure–property relationship.

computational details:

we have carried out all the calculations using DFT, i.e. the geometric structures of all the molecules are optimized using hybrid B3LYP method with 6-31G* basis set for nonmetal atoms (C, N, S) and LANL2DZ for the metal atoms (the gold atoms) implemented in the Gaussian03 program[2].

Results and discussion:

We compared the energies of HOMO, LUMO and the HLG levels for DPT with four different linkages (Table. 1). As representative examples, the spatial

Table. 1. HOMO, LUMO and HLG levels (in eV) for the free molecules.

NO.	Molecule	HOMO	HOMO -1	HOMO -3	LUMO	LUMO +1	HLG
1	HS-DPT-SH	-5.964			-2.659		3.697
2	H_2N-DPT-NH_2	-5.277			-2.138	-2.267	3.664
5	NC-DPT-CN	-6.903	-7.211		-3.342		4.001
8	ON-DPT-NO	-6.317		7.308	-3.627		3.681

distribution of the 1-4 molecules is illustrated in (Table 2). This distributions lead to the conduction delocalized LUMO shifts up and HOMO shifts down for facilitate electronic transportation. The atomic charges are calculated using the natural bond orbital (NBO)

Table. 2. The shape of HOMO and LUMO orbital's for the free molecules and the delocalization forms of some of the molecules that use institute localization forms

Molecule	HOMO	LUMO	HOMO –1	HOMO – 3	LUMO +1
1	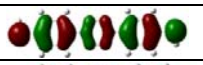	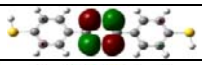			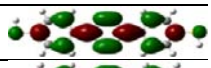
2		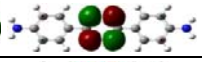			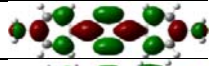
5		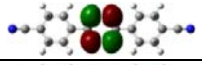			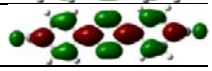
8	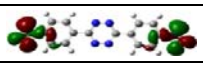	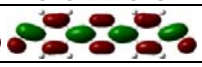			

approach. NBOs are obtained by the division of one-particle density matrix of the molecular orbital into the atomic or inter atomic blocks. Hence, NBO is a sort of the localized orbital and obtained with the occupation number. The orbital character and the occupancy of the bond between Au and the linker (Au–L) are collected in (Table. 3) for the stable contacts in complexes 1 and 2. We study changes of NBO charge under the various EF on each atom for complexes 1 in (Fig.1). The figure clearly demonstrates the NBO charge in the molecule it is obvious that with the increase of EF the charge on the S1 and S14 increases.

Table. 3. Orbital character of the Au–L bonds.

Complex	Bond	Occupancy		Contribution (%)		
				s	p	d
1	Au –S	1.86	Au(21.39)	98.53	0.77	0.70
			S(78.61)	0.11	99.89	0.01
2	Au - N	1.50	Au(7.49)	86.05	1.97	11.98
			N(92.51)	0.00	99.99	0.01

Fig. 1. NBO charge variation on each atom for complex 1 under various EF with respects to the zero EF case.

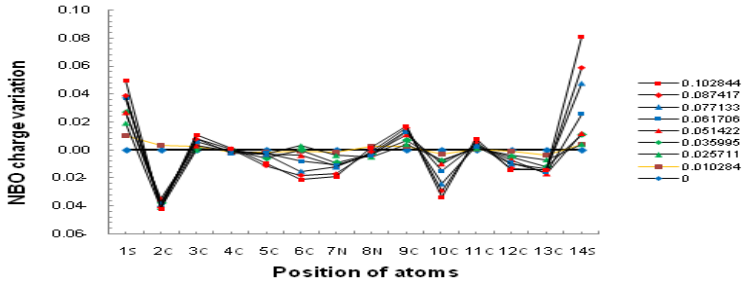

Conclusions:

We found that the metal-molecule interface acquires important role in the relation between the metallic Fermi energy and the adjacent molecular orbital but also in the practical realization of a real electrical stable contact.

References:

[1] W. Yiying, Y. Haoquan, Y. Peidong, Catalysis 19 (2002) 2

[2] A. Mohajeri, A. Zare; Com. Mat. Sci. 45 (2009) 935–940

Theoretical and experimental study of the vibrational spectra of *N*-benzoyl phosphoramidic dichloride, dichloro phosphinyl urea and dichloro phosphinyl carbamat

N. Dorosti*[a], K. Gholivand, F. Ghaziani, F. Abdevali
Department of Chemistry, Faculty of Science, Tarbiat Modares University, P.O. Box 14115-175, Tehran, Iran.
Email: ndorosti@modares.ac.ir

Keywords: Vibrational spectra; Theoretical calculations; Urea; Carbamate; NBO

Introduction

Carbacylamidophosphate which have -C(O)NHP(O)- in molecular core unit are phosphoro-aza analogues of β-diketones. These compounds have been applied as anticancer agents [1, 2], insecticides, pesticides and ureas inhibitor [3]. They also are potential bidentate O, O-donor chelating ligands for metal ions, particulary for lanthanides [4, 5]. Since importance of phosphoramides and measuring of orbital interactions and stabilization energies these compounds [6, 7], we study in this paper effect of phenyl group on these interactions (such as $lp_{(N)} \longrightarrow \sigma^*_{P\text{-}Cl}$, $lp_{(N)} \quad \pi^*_{C=O}$). Then we replace NH and its isoelectronic group (i.e, O) between phenyl and carbonyl groups and investigate the efficacy of these groups on donor-acceptor electronic properties in the [-C(O)NHP(O)Cl_2].

Methods

^1H, ^{13}C, and ^{31}P spectra were recorded on a Bruker (Avance DRS) 500 MHZ spectrometer. Infrared (IR) spectra were obtained using KBr pellets on a Shimadzu IR-60 model spectrometer. All quantum chemical calculations were performed with GAUSSIAN 98 system of programs, implemented in the Pentium 4 computer.

Result and Discussion

Due to the interest of this family of compounds, we report in this work calculated structural parameters and spectroscopic properties. The molecule **3** containing phenoxy group shows much changes for δ_P, δNH_{amide} and $\delta_{C=O}$ than other molecules. Also, NBO analysis (HF/6-

311+G**) for these molecules reveals that amidic groups have nearly the same electronic configuration around the planar amide moiety. The occurrence of a single lone pair orbital formally located at the nitrogen atom is clearly observed for these species. This orbital is a pure p-type [lp(N)] lone pair. Furthermore, a negative hyperconjugative interaction is observed, characterized by strong $lp_{(N)} \rightarrow \sigma^*_{(P\text{-}Cl)}$ electron donations. Worthy to be mentioned, electron donation from lp(N) to neither $\sigma^*_{(P=O)}$ nor $\sigma^*_{(C\text{-}C)}$ vacant orbitals are observed. Also, insertion of the NH group between phenyl ring and C=O group causes decreasing of interaction lp(O) of phosphoryl group with $\sigma^*_{(P\text{-}N)}$. Replacement of NH with O atom resulted in an increase in title interaction. Further, introduction of NH and O groups enhanced $LP_N \rightarrow \pi^*_{CO}$.

Conclusion

The donor-acceptor electronic properties in the [–C(O)NHPCl$_2$] group is characterized by the expected resonance interaction of the p-type nitrogen lone pair and the pi antibonding carbonyl orbital [$lp_{(N)} \rightarrow \pi^*_{(CO)}$], as well as by the hyperconjugative interactions involving the electron donation from the $lp_{(N)}$ orbital toward the $\sigma^*_{(P\text{-}Cl)}$vacant antibonding orbital [$lp_{(N)} \rightarrow \sigma^*_{(P\text{-}Cl)}$] and lp(N, O) of aniline and phenoxy groups toward the $\pi^*_{(CO)}$ [$lp_{(N, O)} \rightarrow \pi^*_{(CO)}$].

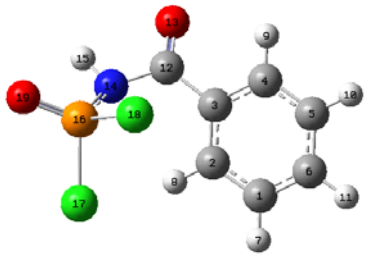

(1)

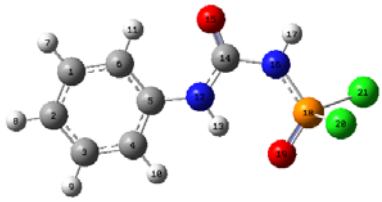

(2)

(3)

References:

[1] Z. Li, J. Han, Y. Jiang, P. Browne, R.J. Knox, L. Hu., *Bioinorg Med Chem*. **2003**, 11, 4171.

[2] O.N. Riebrova, V.N. Biyushkin, L.D. Protsenko *et. al*., Dokl. A. N.UCCR. **1984**, 274, 328.

[3] K. Jaroslav, F. Swetdloff, US Patent 4,517,003, **1985**.

[4] K.E. Gubina, J.A. Shatrava, V.A. Ovchynnikov, V.M. Amirkhanov, *Polyhedron*. **2000**, 19, 2203.

[5] K.E. Gubina, V.M. Amirkhanov, *Z. Naturforsch*. **2000**, 55b, 1015.

[8] A. G. Iriarte , E.H. Cutin , M.F. Erben , S.E. Ulic ,J. L. Jios, C.O. Della Ve´dova, *Vib. Spectrosc.* **2008**, 46, 107.

[9] A.G. Iriarte, M.F. Erben, K. Gholivand , J.L. Jios, S. E. Ulic, C. O. Della Ve´dova, *J. Mol. Struct.* **2008**, 886, 66.

Calculation of electron affinity of nitrogenated aromatic heterocycle compounds

M. Darijani*[a], M. Namazian[a], M. R. Noorbala[a], B. F. Mirjalili[a]
[a]Department of Chemistry, Yazd University, Yazd. P.O.Box 89195-741, Iran

Keywords: electron affinity, G3, nitrogenated aromatic heterocycles

Introduction

One important group of nitrogenated heterocycles are six-membered heterocyclic compounds with the general formula, $N_n(CH)_{6-n}$, with n =1-6. This series of compounds ranges from the very familiar pyridine to the heretofore unknown pentazine (N_5CH) [1]. Electron affinity play a key role in electron transfer processes occurring in the gas-phase such as atmospheric chemistry or in condensed phase such as electrochemistry and biochemistry [2]. Electron affinity is defined as the energy difference between the neutral and the negative ion in their most stable state [3]. In the present work, we have calculated the absolute electron affinity of nitrogenated heterocycles using high-level composite ab initio methods. The aim of this work is to assess the ability of recently developed computational methods for the calculation of electron affinities of nitrogenated heterocycles compounds. The theoretical values were compared with available experimental values. We also studied the effect of nitrogen on electron affinity.

Computational details

Standard ab initio molecular orbital theory calculations were carried out using Gaussian 03. Calculations were performed using a variety of high-level ab initio methods from the G3 family, including G3(MP2), G3(MP2)//B3-LYP, G3, G3//B3-LYP methods. The G3 methods approximate QCISD(T) calculations with a large triple zeta basis set via additivity approximations at the MP2 (also MP3 or MP4, depend on the method) levels of theory. The difference between the G3 and G3//B3-LYP methods as well as G3(MP2) and G3(MP2)//B3-LYP methods is that the B3-LYP/6-31G(d) level of theory is used for geometry optimization and frequency calculations in G3(MP2)//B3-LYP and G3//B3-LYP methods, whereas,

MP2(Full)/6-31G(d) level of theory is used for geometry optimization and HF/6-31G(d) for frequency calculations in the G3(MP2) and G3 methods [4].

Results and discussion

Table 1 shows electron affinity calculation of nitrogenated heterocycles at variety of levels of theory. By convention, a positive EA indicates that the resulting anion is stable and a negative value means that the anion is unstable with respect to electron detachment. The results show that with increasing the number of nitrogen atoms in ring, the electron affinity is increased. There are some available experimental values for the studied compounds. The deviations of the theoretical values of electron affinity for these compounds from the experimental values are not significant. These deviations are within the range of -2 to +2 kcal/mol except for the pyrimidine. The largest deviation occurs for 1,3-diazine. There is a possibility that the source of problem could be with the experimental value, in this case.

Table1 Electron affinity of nitrogenated heterocycle compounds calculated at different levels of theory at 0 °K

compound	G3	G3//B3LYP	G3(MP2)//B3LYP	G3(MP2)	exp [5]
Pyridine	-0.63	-0.61	-0.57	-0.59	-0.62
1,2-Diazine	-0.04	-0.04	-0.02	-0.03	0.0
1,3-Diazine	-0.22	-0.22	-0.21	-0.21	0.0
1,4-Diazine	-0.03	-0.02	0.02	-0.01	0.0
1,2,3-Triazine	0.35	0.37	0.39	0.35	-
1,2,4-Triazine	0.5۵	0.56	0.58	0.55	-
1,3,5-Triazine	-0.02	0.04	0.07	0.03	0.0
1,2,3,4-Tetrazine	0.97	0.97	0.99	0.97	-
1,2,3,5-Tetrazine	0.95	1.02	1.03	1.01	-
1,2,4,5-Tetrazine	1.36	1.34	1.34	1.34	-
Pentazine	1.77	1.66	1.67	1.59	-

Conclusions

The electron affinity of nitrogenated heterocycle compounds have been calculated and compared with experimental values. Good agreement between theory and experiment has been found. Among studied G3 methods, both G3(MP2) and G3(MP2)//B3-LYP have be

found to be good methods to calculate electron affinity for heterocyclic compounds considering the length of calculations.

References

[1] Mo, O.; Depaz, J. L. G.; Yanez, M. *J. Mol. Struct. Theochem.* **1987**, *150*, 135**.**

[2] Periquet, V.; Moreau, A.; Carles, S.; Schermann, J.P.; Desfrancois .C. *J. Electron. Spect. Relat. Phenom*. **2000**, *106*, 141.

[3] Namazian, M.; Coote, M. L. *J. Phys. Chem. A***. 2007**, *111*, 7227.

[4] Baboul, A. G.; Curtiss, L. A. P.; Redfern, C.; Raghavachari, K. *J. Chem. Phys*. **1999**, *110* , 7650.

[5] Nenner, I.; Schultz, G. J. *J. Chem. Phys*. **1975**, *62*, 1747.

Synthesis, characterization, crystal structure and ab initio calculation of a novel proton transfer compound of Zinc(II)

Zohreh Derikvand*[a], Beheshteh Sohrabi[b], Andia Nemati[c], Helen Stoeckli-Evans[d]

[a]*Department of Chemistry, Faculty of Science, Islamic Azad University, Khorramabad Branch, Khorramabad, Iran.*

zderik@yahoo.com

[b]*Faculty of Chemistry, Iran University of Science and Technology, P.O. Box 16765-163, Tehran, Iran.*

[c]*Iran Compiling Encyclopedia Foundation, Tajrish, Tehran, Iran.*

[d]*Institute of Physics, Institute of Physics, University of Neuchâtel, rue Emile-Argand 11, CH-2009 Neuchâtel, Switzerland*

Abstract

A novel compound with formula unit, $(C_{14}H_{13}N_2)[Zn(C_7H_3NO_5)(C_7H_4NO_4)].2.35H_2O$ or $(dmpH)[Zn(hypydc)(hypydcH)]\cdot 2.35H_2O$, was synthesized and characterized by IR, ^1H NMR and ^{13}C NMR spectroscopy, elemental analysis, single crystal X-ray diffractometry. Moreover, Optimized geometry and the corresponding electronic structure, vibrational frequencies, ^1H NMR and ^{13}C NMR spectroscopy of $(dmpH)[Zn(hypydc)(hypydcH)]\cdot 2.35H_2O$ have been calculated using ab initio methods DFT- B3LYP with 6-31G** basis set.

Keywords: Zinc complex, X-ray crystal structure, Ab initio calculations, Chelidamic acid.

Introduction

Various metal complexes containing monocarboxylic acids have been well known and the publications of many structurally characterized examples of these classes of compounds demonstrate the versatility of the carboxylate group as an inner sphere ligand [1]. Pyridinedicarboxylic (Dipicolinic) acid forms stable chelates with simple metal ions, and can display widely varying coordination demeanour, functioning as a bidentate [2], tridentate [3], meridian [4] or bridging ligand [5].4-Hydroxypyridine-2,6-dicarboxylic acid ($hypydcH_2$), or chelidamic acid, is widely used in biochemistry, organic chemistry, medical chemistry and even in HIV investigations [6].

Experimental and theoretical,

1. Materials and Methods

Chelidamic acid, 2,9-dimethyl-1,10-phenanthroline, zinc(II) nitrate hexahydrate, were purchased from Merck. Melting points were determined applying a Barnstead Electrothermal 9200 apparatus. ^{1}HNMR spectra were recorded on a Bruker ARX 300 and 500 MHz instrument. IR spectra were recorded in the range of 4000-400 cm^{-1} on a Perkin-Elmer Spectrum RXI FT-IR spectrophotometer using KBr pellet. Elemental analysis was performed with a Heraus CHN Pro apparatus. The X-ray data was obtained with a STOE IPDS Diffractometer.

The fully optimized geometries and the corresponding electronic structures, vibrational frequencies, ^{1}H NMR and ^{13}C NMR spectroscopy of (dmpH)[Zn(hypydc)(hypydcH)]·2.35H_2O have been calculated using ab initio density function theory (DFT) using Becke's three-parameter hybrid functional combined with the Lee-Yang-Parr correlation functional (B3LYP) level of theory with 6-31G** basis set. All ab initio calculations were performed using GAUSSIAN 98 package.

Results and discussion

The compound was synthesis by hypydcH_2, dmp and zinc(II) nitrate in 2:2:1 molar ratio as shown in Scheme 1. In the ^{1}HNMR of (dmpH)[Zn(hpydc)(hypydcH)]·2.35H_2O**,** it can be seen two characteristic peaks of $dmpH^{+}$,$(hypydc)^{2-}$ and $(hypydcH)^{-}$. Because of the symmetric structure of the compound, in the ^{13}CNMR spectrum, eleven peaks attributed to carboxylate, different aromatic ring carbon atoms and two methylen groups are observed.

1. Crystal structure

The crystallographic data of the title compound is set in Table 1 and the results are compared to theoretical data.This compound contains a $[Zn(hypydc)(hypydcH)]^{-}$ anion, a $(dmpH)^{+}$ cation and 2.35 uncoordinated water molecules (Fig. 1). In the anion, the Zn^{II} atom is six-coordinated by two N atoms (N1 and N2) that occupy the axial positions, and four O atoms (O1, O3, O6 and O8) from the carboxylate groups of the $(hypydc)^{2-}$ and $(hypydcH)^{-}$ fragments, in the equatorial plane. Also, we investigated O–H···O, N–H···O, N–H···N and C–H···O type interactions by experimental and theoretical data.

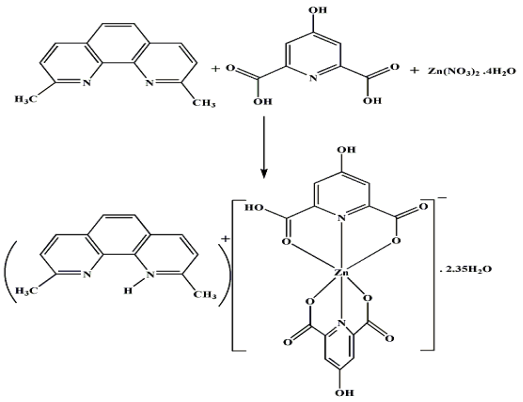

Scheme 1. The synthetic route of preparation.

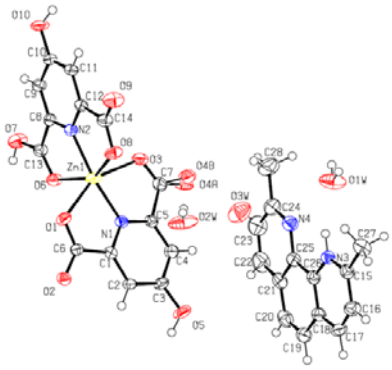

Fig.1 Molecular structure of the title compound.

Table 1
Selected bond lengths, bond angles and torsion angles.

	[a] Ex	[b] Cal		Ex	Cal
Zn1—O1	2.114 (2)	2.077	Zn1—O8	2.119 (2)	1.949
Zn1—O3	2.328 (2)	2.047	Zn1—N1	1.995 (2)	2.008
Zn1—O6	2.407 (2)	2.827	Zn1—N2	1.987 (2)	2.089
O1—Zn1—O3	152.13 (7)	155.26	O3—Zn1—N2	90.06 (8)	100.522
O1—Zn1—O6	92.06 (7)	85.93	O6—Zn1—O8	151.69 (7)	148.36
O1—Zn1—O8	96.69 (8)	98.22	O6—Zn1—N1	95.36 (8)	78.02
O1—Zn1—N1	79.48 (8)	77.13	O6—Zn1—N2	73.50 (8)	65.52
O1—Zn1—N2	116.98 (8)	97.73	O8—Zn1—N1	112.68 (8)	133.55
O3—Zn1—O6	89.23 (7)	86.58	O8—Zn1—N2	78.54 (8)	82.85
O3—Zn1—O8	95.24 (8)	100.49	N1—Zn1—N2	159.81 (9)	143.50
O3—Zn1—N1	72.69 (8)	78.25			
O6—Zn1—O1—C6	96.47 (18)	-78.70	O6—Zn1—O3—C7	−93.78 (2)	78.78

[a] The experimental bond lengths, bond angles and torsion angles.

[b] The computational bond lengths, bond angles and torsion angles.

Conclusion

In summary in this article synthesis and characterization of (dmpH)[Zn(hypydc) (hypydcH)] ·2. 35H_2O is reported. In this compound, chelidamate act as a tridentate ligand and neocuproine act as a counter ion for balancing the charge and good sites to form various hydrogen bonds, C–O···π, C—H···π and π–π stacking interactions.

References

[1] R. C. Mehrotra, R. Bohra, Metal Carboxylates, Academic Press, London, (1983).

[2] D. Ventur, K. Wieghardt, J. Weiss, Z. Anorg. Allg. Chem. 524 (1985) 40-50.

[3] M. Chatterjee, S. Ghosh, Bo-Mu Wu, T. C. W. Mak, Polyhedron 17 (1998)1369-1374.

[4] M. G. B. Drew, G. W. A. Fowles, R. W. Matthews, R.A. Walton, J. Am. Chem. Soc. 91 (1969) 7769-7771.

[5] G. Nardin, L. Randaccio, R.P. Bonomo, E. Rizzaretti, J. Chem. Soc., Dalton Trans. (1980) 369-375.

[6]V. Berl, I. Hue, R. G. Khoury, J. M. Lehn. Chem. Eur. J. 7 (2001) 2798 and references cited therein.

Ab initio and DFT study of Tautomerism of Pyrazolinones

Zeinab Dalirnasab,*[a,b] Alireza Najafi Chermahini,[c] Sudabeh Dalirnasab,[d] Javad Rok Rok.[e]

[a] *Department of Chemistry, Faculty of Chemistry, University of Jahrom Payam Noor*

[b] *University of Applied Science of Arak*

[c] *Department of Chemistry, Faculty of Chemistry, University of ,Yasouj.*

[d] *Department of Chemistry, Faculty of Chemistry, University of Shiraz*

[e] *. University of Applied Science of Arak*

Corresponding Author E-mail: dalirnasab@gmail.com

Keywords: Ab initio, DFT, Tautomerism, Pyrazolinones

Introduction

Pyrazolinones are oxo derivatives of pyrazoline. Pyrazolinones act as effective anti-oxidant [1] for rubber, oil and responsible for inhibition of odor formation in synthetic detergent [2]. They possess wide range of pharmacological activities as bactericidal [3], Anti-rheumatic [4], etc.

Method

In the present study tautomerism of pyrazolinone have been investigated using ab initio and density functional theory using 6-31++g (d,p) basis function. Four tautomers (**a-d**) were found for the titled compound. In the first stage the energies and relative stabilities of these forms have calculated in the gas and solution.

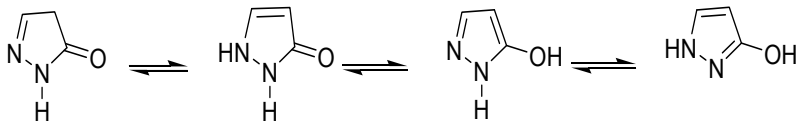

a b c d

Table:Calculated total energies at B3LYP- 6-31++G** and relative stability in the gas phase and solvents

Form	**A**	**B**	**C**	**D**
	E1-E4 (kcal/mol)	**E2-E4 (kcal/mol)**	**E3-E4 (kcal/mol)**	**E4 hartee**
Gas	0.586	5.073	3.93	-301.4467544
THF	1.41	0.416	2.81	-301.4656772
DMSO	2.52	0.264	2.46	-301.4702079
Water	2.79	0.418	2.32	-301.4709103
Methanol	2.42	0.264	2.48	-301.4698355

Conclusion

Based on our thoretical calculations the order of stability was found as **d**>**a**>**c**>**b** in the gas phase and.in the solution the order of stability was found as **d**>**b**>**c**, **a**.

References:

[1] Howland, U. S Pat. **1949**, *2*, 458.

[2] Flett, U. S Pat. **1949**, *2*, 469.

[3] Fujisowa, Pharmaceutical Col. Ltd. Japan. **1964**, *67*, 108

[4] H. G. Garg, N. Kaur. J. Med. Chem. **1972**, *15*, 554.

Solvent Effect on Albumin: a Theoretical Approach

N. Dalili. Mansour[1,*], A. Sojasi[2], M. Hesabi[1]

[*]dalili@iaurasht.ac.ir

[1] Department of Chemistry, Faculty of science , Rasht Branch, Islamic Azad University, Rasht, Iran.

[2] Department of Physics, Faculty of science, Rasht Branch, Islamic Azad University, Rasht, Iran.

Keywords: Albumin, Simulation, Heat Capacity, Ethanol, Methanol.

Introduction:

Serum Albumin is the most abundant protein in blood plasma. It plays two important roles in body [1]: a) Transports some hormones and drugs. The most important compounds transported by Albumin are L-Tryptophan, Naproxen, Ibuprofen, Diazepam and fatty acids with medium chains [2]. b) Regulates osmotic pressure in body.

Because of the importance of Albumin as a drug transporter, in this paper Albumin's simulation is carried out by three techniques including Monte Carlo, Molecular Dynamics and Langevin Dynamics and the effect of alcohol on its structure is investigated [3-6].

Computational Method

In this work, Albumin's active sites are downloaded from RCSB PROTEIN DATA BANK. The PDB ID applied in this paper is 1GAB in which the structure of Albumin-binding domain is investigated by NMR techniques. After finding this PDB, HyperChem 7 software is applied for investigation in Methanol, Ethanol and water solutions of protein separately.

At first these active sites are put in Water, Ethanol and Methanol solutions which have concentration about 10% (w-w), separately. Then by using molecular mechanics level, opls force field and Polak-Ribiere algorithm, the geometry of these systems are optimized and for the optimized structures potential energy are evaluated by 3 techniques of simulation (MC, MD and LD) in different time steps and temperature range from 273K to 303K every 5 degrees. Then the potential energy versus temperature diagrams and potential energy versus time step diagrams are described in different initial temperatures in these techniques. Finally the energy of Albumin-water system has been optimized and compared by Albumin-Methanol and Albumin-Ethanol systems.

Results and Discussions

By calculating the potential energy versus time step diagrams, it is understandable that there is a regular change in potential energy versus time step by increasing initial temperature in MD and LD simulation techniques, but it is irregular in diagrams obtained by MC method. This difference is because of the techniques used in simulations. In macromolecules, MC simulation is not suitable for calculating energy and since Albumin is a macromolecule, so this irregular trend is obtained. Also with analyzing the energy versus temperature diagrams, it is obvious that by increasing temperature, the potential energy decreases. Because in MD and LD methods, the system under studying is microcanonic and total energy in such systems is constant. So by increasing temperature, the kinetic energy increases and because total energy should be constant, consequently potential energy decreases. Another result obtained in this work is the optimized energy in Albumin-Water system (-11413.18945 kcal/mol) is more than optimized energy in Albumin-Methanol system (-11670 kcal/mol) and Albumin-Ethanol system (-11497.6 kcal/mol). So by changing solvent from Water to Alcohol, the system becomes more stable and its ability of transporting drugs and hormones becomes less. It is because of acidic pH of Albumin that causes it to be more stable in basic solvents. So Alcohol causes Albumin to be poisoned. Also by calculating $\Delta E_{kinetics}$ and its related ΔT, the values of heat capacity of Albumin in these solvents are calculated and are shown in table 1.

Table1. Calculated heat Capacities

Reagent	Albumin-Water	Albumin-Methanol	Albumin-Ethanol
C/ ($kcalmol^{-1}K^{-1}$)	6.58	7.02	7.15

By adding of molecular mass of solvent, the value of heat capacity becomes more.

Acknoeledgements:

The authors would like to thank Islamic Azad University-Rasht Branch because of supporting this research.

References:

[1] www.Sigma-aldrich.com

[2] T. Bo,J. Pawliszyn, J. Chromatography A, 1105 (2006) 25-32.

[3] B. Cao, S. Endsley, N. H. Andersen, J. Bioorganic & Medicinal Chemistry, 11 (2003) 69-75.

[4] T. Peters, '["All About Albumin", Academic Press, San Diego, CA, 1996.

[5] M. P. Allen, Lecture Notes, NIC Series, Vol. 23, ISBN 3-00-012642-4, 2004.

[6] M. A. Quevedo, S. R. Ribone, G. N. Moroni, M. C. Briñón, J. Bioorg. Med. Chem. Vol. 16, Issu6, 15 (2008) 2779-279.

Molecular dynamics simulation of the scattering of Ar from the SiC surface

Hassan Sabzyan*, Arezoo Dehbashi
Department of Chemistry, University of Isfahan, Isfahan 81746-73441, I. R. Iran.

Introduction

Silicon carbide is an important material in coating industry due to its higher chemical stability. One of the interesting usages of this compound is to coat external surfaces of aircrafts in aeronautics industries [1]. Instability of the silicon carbide surface in aeronautics industries is due to the collision and scattering of atmospheric species. Since, experimental studies on the stability of surface coatings such as SiC is very expensive and time-consuming, computational studies can be use to investigate the response of this coating to the collision of this species with much less efforts and expenses. Moreover, results of computational studies provide detailed information at the molecular level of the process of interest not accessible experimentally, which can be used to optimally design the material and processing of coatings. There are several theoretical and computational methods used for the study of scattering processes from exact quantum mechanical computational close-coupling method which is limited to small and simple systems only to purely classical mechanical methods which can be used for very large systems but qualitatively only. Among all methods, molecular dynamic simulation (MDS) is most effective.

The aim of this work is to study scattering pattern and the response of the SiC surface to the collisions of Ar species using MDS not studied specifically before in numerous experimental and theoretical studies [2-3].

Computational Method

The computational box setup used in this MDS is shown in Fig.1. The Ar reservoir contains 8 molecules which are first equilibrated and speeded up (with 20 and 40 Å/ps) in the scattering beam direction. Both C and Si surfaces are examined in these MDS. In the preparation step, an NVT MDS are carried out with 500000 and 5000-50000 steps at T=300K (for the lattice) and T=2000 K (for the beam) temperatures. The scattering MDS is carried out with NVE ensemble without any scaling of the velocity and energy for 40000 steps of δt=0.1

fs. A set of MDS is also run for the equilibrium velocities at 2000K without any speed-up procedure under the same condition but with 300000 time steps of δt=0.1 fs. To extract the scattering pattern, a set of five parallel/perpendicular planar detectors (located at appropriate distances perpendicular to the +x, –x, +y, –y and +z axes) is devised and the times and positions of the scattered species are probed. Each scattering pattern is formed by the analysis of the results of 10 independent MDS. The time-of-flight of the scattering atoms are also calculated and its correlation with the lost/acquired kinetic energy is investigated. Interactions of the SiC and Ar systems are modeled using Dreiding and Satake force fields. The Ar-Si and Ar-C force field are calculated using mixing rule.

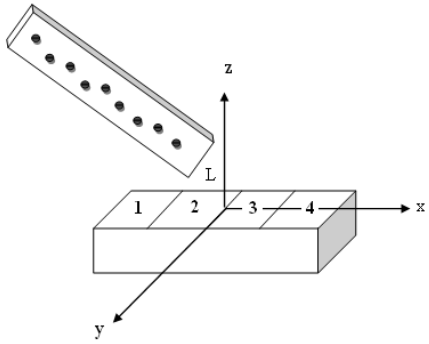

Fig. 1: The setup used in this work for the MDS of the scattering of Ar from the SiC surface.

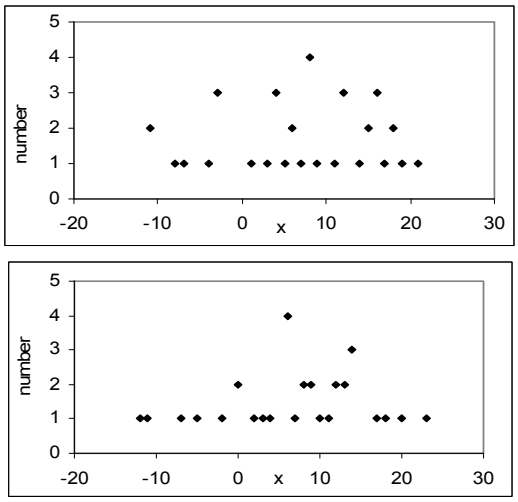

Fig. 2: The simulated pattern of the scattering of Ar from the C and Si surfaces of a 6×6×3 SiC nanocrystal.

Results and Conclusion

Typical results of the scattering patterns and correlation of the differential kinetic energy with time of flight are presented in Figs. 2 and 3. As can be seen from these figures, our simulation can differentiate between the two C and Si surfaces of the SiC crystal, and the speed of the Ar atomic beam has significant effects on the time of flight of scattered species. The inverse correlation between the differential kinetic energy and the time of flight is quite physical.

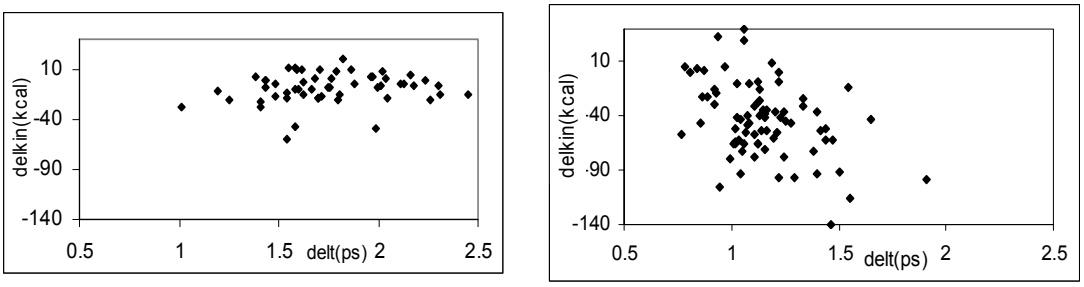

Fig. 3: Correlation of the differential kinetic energy and time of flight of the MDS of the scattering Ar atoms from the Si surface of a 6×6×3 SiC nanocrystal with two different jet beam speeds.

References

[1] G.W. Hunter et al, NASA TR-107444, 1997; R. A. Miller, J. Therm. Spray, 6 (1997) 35.

[2] N. Fukomoto, et al, Appl. Surf. Sci., 255 (2008) 1391.

[3] K. R. Krantzman et al., J. Phys. Chem., 113 (2009) 3239.

Investigation of the Effective Factors to the Formation Of Thiosemicarbazone Complexes with Fukui Function

M. Dehdab[a*] and M. Narimani[b]

[a]Dipartment of Chemistry, Faculty of Engineering, Islamic Azad University, Alishahr Branch , Bushehr, Iran
dehdab_37@yahoo.com

[b]Dipartment of Chemistry, Faculty of Engineering, Islamic Azad University, Omidieh Branch, Omidieh, Iran

Abstract

Some factors which contribute in formation of member chelating of thiosemcarbazon are studied in gas phase by functional framework density with B3LYP and 6-311++G** basis set. It is show that original factors for such coordination mode of thiosemicarbazone are the steric factor of the thiosemicarbazone ligands itself and It is found that reaction thiosemicarbazon with metals is controlled by frontier molecular orbital.

Keywords: Thiosemicarbazone; Fukui; Density Functional; Steric Factor

Introduction

Natarajan et al. [1]and Bhattacharya et al. [2-4] recently have reported that some factors effect for coordination mode of thiosemcarbazon such as:

1. formation of intramolecular hydrogen bonding
2. the steric bulk of the R_2 , R_1 group
3. stereochemistry thiosemicarbazone ligand itself
4. bulkiness of co-ligand
5. metal atom

Figure1.The considered steric structure in this study

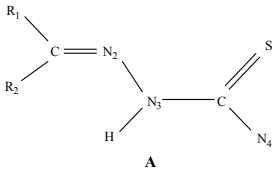

A

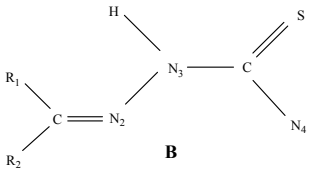

B

In this present work, we have investigated first, second and third factors with the electronic Fukui function. The electronic Fukui function $f(\boldsymbol{r})$ was introduced by Parr and Yang [5] as a

generalization of Fukui's frontier MO Concept [6] and plays a key role in linking frontier MO theory and the HSAB principle. To describe the site reactivity or site selectivity, Yang et al. [7] proposed an atom-condensed Fukui function based on the idea of electronic population around an atom in a molecule. The condensed Fukui function for an atom *k* undergoing nucleophilic, electrophilic, or radical attack can be defined respectively as:

$$f_k^+ \approx q_k^{N_0+1} - q_k^{N_0} \quad (7)$$

$$f_k^- \approx q_k^{N_0} - q_k^{N_0-1} \quad (8)$$

$$f_k^0 \approx \frac{1}{2}\left(q_k^{N_0+1} - q_k^{N_0-1} \right) \quad (9)$$

Where q_k's are electronic population of the *k*th atom of a particular species.

Computational details

The density functional theory implemented in the Gaussian 98 computational package was used to optimize the geometry of Thiosemicarbazones derivatives in the gas phase. All the optimizations have been performed using functional framework density with B3LYP and 6-311++G** basis set [8].

Results and discussion

Thiosemicarbazones usually bind to a metal ion giving complexes in which thiosemicarbazones (TSCs) behave as chelating ligands. They are well know chelating ligands coordinating to the metal ion through the sulphur and one of the hydrazinic nitrogen atoms (N_2 or N_3) Coordination through N_3 results in an unusual four member chelated ring while with N_2 hydrazinic nitrogen a more stable five member chelated ring results. Bhattacharya et al. have observed that formation of such a ring depends primarily on the size of R_1 only if R_1 is fairly small (e.g., R_1=CH_3) formation of a five-memberd ring possible, but if R_1 is relatively large(e.g., R_1=aryl), such a ring cannot be formed[9].To study first factor, groups have selected that by removing the hydroxyl group from the R_1 group prevent any intera molecular hydrogen bonding . Then to study second factor, groups have selected that R_1 group is small or R_1 , R_2 are similar. In general, thiosemicarbazon ligands can exist tow different steric structure as A or B that used in the present work is given in figure 1. The present work has

originated from our attempt to find out the actual driving force behind such coordination mode of the thiosemicarbazone ligand.to do that ligand A and B is kept unchanged while R_1 and R_2 groups is changed. If reaction is controlled by charge we have expected for complexes with a four member chelated ring for form A, B ,the most negative charge have belong to S, N_3 atoms and for complexes with a five members chelated ring for forms A, B, the most negative charge have belong to S, N_2 atoms. first, charge of S, N_2, N_3, N_4 atoms are calculated. in most cases negative charge is not belong to S, N_2, N_3 atoms for forms A, B .Therefore reaction of thiosemicarbazone with metal is not controlled by charge. It is mentioned that chemical reaction thiosemicarbazone with metal is electrophilic. Then negative Fukui of S, N_2, N_3, N_4 atoms are calculated. for form A the value of the negative fukui function for S, N_2 atoms is observed to be more than the of remainder and for form B the value of the negative fukui function for S, N_3 atoms is observed to be the most .

Conclusion

According to calculation demonstrated that even when R_1, R_2 is a bulky constituent, for form A, five member chelated complex can be formed and for form B four member chelated complex can be formed. Therefore it is expected that in the reaction of thiosemicarbazon with transition metals in formation thiosemicarbazon complexes The actual driving force for such coordination mode of thiosemicarbazone is the steric chemistry of thiosemicarbazone. From the obtained results it is found that reaction thiosemicarbazon with metals is controlled by frontier molecular orbital.

References

[1] R. Prabhakaran, S. V. Renukadevi, R. Karvembu, R. Huang, J. Mautz, G. Huttner, R. Subashkumar, K. Natarajan, Eur. J. Med. Chem. 43 (2008) 268.

[2] F. Basuli, S. M. Peng, S. Bhattacharya, Inorg. Chem. 39 (2000) 1120.

[3] R. Acharyya, S. Dutta, F. Basuli, S. M. Peng, G. H. Lee, L. R. Falvello, S. Bhattacharya, Inorg. Chem. 45 (2006) 1252.

[4] S. Halder, R. J. Butcher, S. Bhattacharya, Polyhedron, 26 (2007) 2741.

[5] R. G. Parr, W. Yang, J. Am. Chem. Soc. 106 (1984) 4049.

[6] S. Kato, Theor. Chem. Acc. 103 (2000) 219

[7] R. G. Parr; W. Yang, J. Am. Chem. Soc. 106 (1984) 1976.

[8] M. J. Frisch et al, Gassian 98, revision A. 7, Gaussian, Inc., Pittsburgh, PA, (1998).

[9] J. S. Casas, M.S. Garcia-Tasende, J. Sordo, Coord. Chem. Rev. 209 (2000) 197.

Theoretical studies on tautomerism of amino isoxazole derivatives in the gas phase

Alireza Salimi beni*, Alireza Najafi Chermahini*, Mahboobeh Dehghan

Faculty of Science, Department of Chemistry, Yasouj University, Yasouj, Iran

(E-mail: Salimibeni@mail.yu.ac.ir)

Keywords: Isoxazole, Calculations, Molecular orbital, DFT, Ab initio.

Introduction: Isoxazoles play interesting roles in medicinal and agricultural chemistry and serve as important synthetic building blocks. Synthesis of substituted isoxazole derivatives is particularly important because a lot of compounds containing the isoxazole ring system are known to have variety of biological activities in pharmaceutical and agriculturalareas. Their range of uses includes medicinal, herbicidal, fungicidal, pesticidal applications, dyes, insulating oils, and lubricant [1]. Isoxazoles have found continuing application in medicinal chemistry, several examples of which have advanced to general medical practice [2]. Isoxazole and its derivatives play an important role in the synthesis of potential medicines including anti-infective, antitumour, cardiovascular and nervous system agents. Isoxazole derivatives have also served as a versatile building block in organic synthesis [3].

Methods: Ab initio and DFT molecular orbital calculations have been performed on the intramolecular tautomerism of all five isomers of amino isoxazole in the gas phase. All stationary points' transition structures were optimized at the HF/6-311++G(d,p) and B3LYP/6-311++G(d,p) levels of theory and confirmed by frequency calculations. The intrinsic reaction coordinates (IRC) for the tautomeric processes were traced to connect the transition structures and the corresponding substituted tautomeric pairs. The energy barriers calculated at various levels of theory are reported for each tautomeric interconversion.

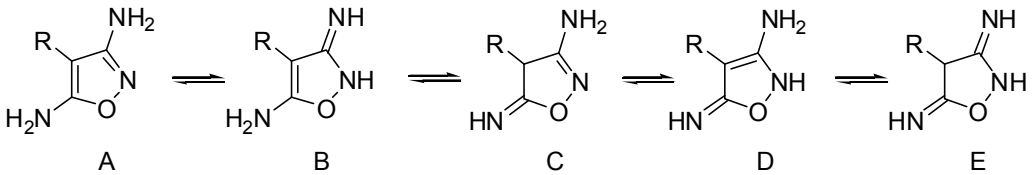

R=H, CH_3, F, CL, NO, NO_2, CN, C≡CH

Results and discussion: The results of HF and DFT calculations show that compound **A** is the most stable tautomer in the gas phase in order of **A>C>D>B>E**

References:

[1]Kim, H. J.; Hwang, K. J.;

[2] Lee, J. H. *Biosci Biotech Biochem* **1994**, *58,* 1191; (b) Hwang, K. J.; Kim, H. J.; Lee, J. H. *Korean J Med Chem* **1994**, *4,* 2.

[3] Pevarello, P.; Amici, R.; Brasca, M. G.; Villa, M.; Varasi, M. *Targets Heterocycl. Syst***. 1999**, *3*, 301.

[4] Cicchi, S.; Cordero, F. M.; Giomi, D. *Prog. Heterocycl. Chem*. **2003**, *15,* 261.

MD simulation of thermodynamic and structural properties of gold nano clusters.

R. Dehghanpoor[a], S. Jalili*[a]

[a]department of Chemistry, KN. Toosi University of Technology. P. O.15875-4416.Tehran, Iran.

Keywords: molecular dynamics simulations, nano clusters, cluster alloys, thermodynamic properties, structural properties

Introduction

Applications of clusters in innovative technology seem to be endless, for example Nanogolds have many perspective applications in various fields, such as bio electrocatalysis, sensors, and nanotechnology. Many experimental studies on nanocatalysts have focused on correlating catalytic activity with particle size. While particle size is an important consideration, many other factors such as geometry, composition, oxidation state, and chemical/physical environment can play a role in determining NP reactivity.

A detailed knowledge of the melting process of the clusters is essential to understand their special properties and applications. The purpose of study of pure gold clusters with various sizes is showing the size effect in the thermodynamic and structural properties of these clusters. Study of gold alloy clusters along the pure cluster is summarized in the following:

1- Effect of impurities as the core shell and multi layer in the thermodynamic and structural properties of pure clusters (Type of incoming element, the amount of incoming atoms, the impurity layer, construction Terms of alloy clusters)

2- Achieve the specific structure that shows unexpectedly behaviors. (Increasing the phase transition temperature range …)

Methods

In this work, structural and thermodynamic properties of pure and alloy gold Nano - clusters, with atomic numbers 55 to 561, is considered with the method of molecular dynamic simulation and using the DL-POLY software. Sutton Chen potential model has been used for the Calculation of interactions.

Results and discussion

With increasing cluster size, melting transition temperature rises and the phase transition temperature range "distance of premelting and melting temperature" extended. The extent of its range is one factor in high catalytic properties of small cluster.

Table1: Pre-melting and phase transition temperature for pure gold clusters with atomic numbers 55 to 561.

Melting transition	Premelting temperature	Cluster
500	200	Au_{55}
500	250	Au_{87}
550	300	Au_{147}
600	400	Au_{201}
550	400	Au_{249}
600	400	Au_{309}
600	450	Au_{321}
650	500	Au_{561}

in spite of it is said that metal clusters have unpredictable behavior in the nano size range, Comparison between results for the pure clusters with various size show similar behavior for clusters with the same number of layers.

Fig1: Heat capacity of gold pure and alloy cluster with 147 atom

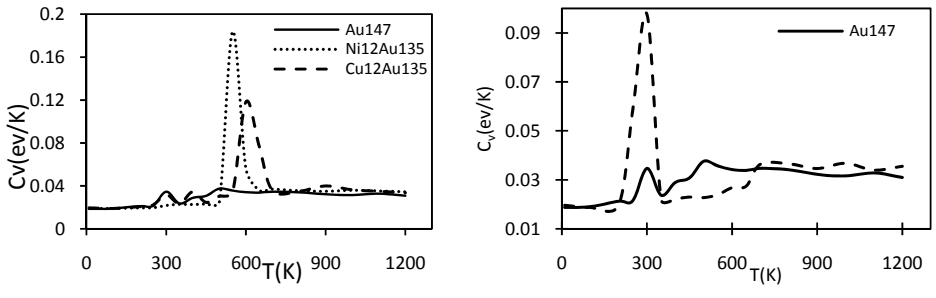

$Ni_{12}Cu_{43}$ Au_{92} cluster turns to I_h structure, and has higher thermal stability,Despite high thermal stability there is no sharp peak at the phase transition temperature.

Conclusion

Results for clusters alloy shows that if we provide conditions for clusters in which smaller metal with higher melting point laid in the inner layer, cluster takes Ih form. And this Ih cluster could have more thermal stability and this stability is correlated with this fact that the number of layers together with similar metal must be at least. In This study we observed that the heat capacity diagrams for three metal cluster alloys with Ih structure, have a lot of similarities with cluster Au_{55} and $Cu_{12}Au_{43}$ that their high catalytic properties is proven.

References

[1] Riccardo Ferrando, Julius Jellinek, and Roy L. Johnston, Chemical Reviews, **108**, (2008)

[2] Yanting. Wang, S.Teitel, j.Chemical Physics, **122**, 214722, (2005)

[3] Yi Gao, Nan Shao, Satya Bulusu, X. C. Zeng, J. Phys. Chem. C, **112**, 8234, (2008)

[4] Tuóba Davran-Candan, M. Erdem Günay, Ramazan, J.Chem.Phys, **132**, 174113, (2010)

Intramolecular H-Bonding and π-electron delocalization in 5- [N-hydro carboxamido] barbituric acid

A. Nowroozi*, S. Dahmardeh, F. Akbari, M. Poorsargol, F. Naroei

Department of Chemistry, Faculty of Science, University of Sistan and Baluchestan, P.O. Box 98135-674, Zahedan, Iran

(Email: dahmardeh_s@yahoo.com)

Keywords:

5- [N-hydro carboxamido] barbituric acid, HOMA, Intramolecular H-Bonding and π-electron delocalization

Introduction:

The compounds containing pyrimidine ring play an important role in many biological systems [1], where they exist in nucleic acids, several vitamins, coenzymes and antibiotics. Pyrimidines appear in all living cells and are vitally involved in many biological processes. Barbituric acid (2, 4, 6-pyrimidinetrione) has a pyrimidine nucleus. Barbituric acid derivatives are a well-known class of compounds with various pharmacological activities [2], Owing to this property, barbituric acid and their various substituted derivatives are very important compounds in biological chemistry and medicine. Hydrogen bonding is one of the most important concepts which play a key role in the chemistry of living systems. The information on intramolecular hydrogen bonding is, in particular, very useful to understand various molecular properties. The intramolecular H-bonding can be sometimes responsible for the molecular geometries as well as the stability of a certain predominant conformation. Resonance assisted H-bond (RAHB) is a particular subject of hydrogen bond as describing the π-electron delocalization within the ring created due to intramolecular H-bond formation. The purpose of this work was to analyze the interrelation between stabilization and π-electron delocalization for 5- [N-hydro carboxamido] barbituric acid (CBA). The stability of forms was measured by means of the energy of isomerization. The HOMA index was applied to describe π-electron distribution. 5- [N-hydro carboxamido] barbituric acid (CBA) could be postulated as assuming a tricyclic structure through hydrogen bond formation (fig. 1). As shown in fig.1 CBA can participate in the keto-enol tautomerism and lead to two

forms, external amide (EA) and internal amide (IA). Furthermore, the simultaneously existence of pyrimidine ring and two quasi rings is caused that the competition between the intramolecular hydrogen bond and amide resonance is occurred and interest this molecule for more considerations.

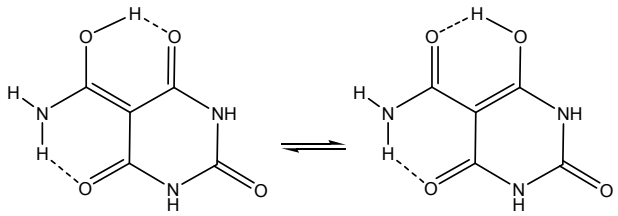

IA EA

Fig.1. Tautomeric equilibria and H-bonding in CBA

Computational methods:

The calculations in the present study were performed using Gaussian 03 series of programs. The geometry optimizations were carried out at B3LYP/6-311++G** levels of theory. Relative electronic energy (ΔE) was calculated to estimate relative stabilities.

The Harmonic Oscillator Model of Aromaticity (HOMA) was estimated from the theoretically derived bond lengths using the equation: $HOMA=1- \alpha /n \sum (R_{opt} - R_i)^2$

Where n is the number of bonds and R_{opt} and R_i are optimal bond lengths and bond lengths in a real system, respectively, and a is an empirical constant chosen to give HOMA=0 for the hypothetical Kekule structures and HOMA=1 for the system with all bonds equal to the optimal value.

Results and discussion:

Our theoretical results show that IA conformer has extra stability respect to other forms and it is global minimum. Evaluation of hydrogen bond energy by Schuster method for OH…O, clearly predicts that HB strength in IA is lower than the EA. Also, estimation of hydrogen bond energy by Espinosa method for NH…O, reveals that HB strength in EA is lower than the IA. The results of H(r) and LP (O) $\rightarrow \sigma^*_{OH}$ are given similar results. On the other hand, The IA form with more delocalized π-electrons in the both quasi rings is more stable than the EA form, however, pyrimidine ring in IA form has less delocalized π-electrons. Furthermore, In this case, H-bonding is an important but not the main factor that decides about tautomeric preference. π-electron

delocalization in the phenyl ring seems to be responsible for tautomeric stabilities. In summary, origin of tautomeric preference is mainly due to resonance assisted hydrogen bond in NCCCO ring.

References:

[] F. Hueso, N.A. Ill ´ an, M.N. Moreno, J.M. Mart´ınez, M.J. Ram´ırez, J. Inorg. Biochem. 94 (2003) 326.

[2] M. V. Jovanovic, E. R. Biehl, J. Org. Chem. 1987, 24, 191–204.

A Theoretical Investigation Structure of Two Ionic Liquids $(C_6H_5)_3PH^+[As_2S_3X]^-$, (X= Cl, I)

S.Zabihi[a], A.Fayyazi[a], G.Geimachy[a], M.Fada[a],Sh.Ghammamy[b,*], H. Tavakol[c]
shghamamy@yahoo.com
[a]Department of Chemistry, Faculty of Science, Islamic Azad University, Ardabil Branch, Iran
[b]Department of Chemistry, Faculty of Science, Imam Khomeini International University, Ghazvin,Iran.
[c] Department of Chemistry, Faculty of Science, Zabol University, Zabol, Iran

Keywords: Ab Initio calculations , ionic liquid, DFT, B3LYP/LANL2DZ

Introduction

Room temperature ionic liquids (RTILs) are non-flammable, non-volatile, thermally stable solvents and as much as very promising replacements for the traditional volatile organic solvent. Ionic liquids, as a class of novel environmental 'green solvents', have remarkable new properties and promising applications in many fields [1].

All synthesized ionic liquids were characterized by IR. Therefore, the theoretical investigations on ionic liquids are the area of interest for many researchers, in which the geometry was optimized at using ab initio level of theory. In addition, synthesized structures were optimized at the B3LYP/LANL2DZ level of theory and then the structures, molecular specifications, and infrared spectra of these were extracted using Gaussian03 program. Theoretical data show good agreement with the experimental results.[2-3]

Methods

The structures of two compounds $[P(C_6H_5)_3H]^+$ $[As_2S_3Cl]^-$and $[P(C_6H_5)_3H]^+$ $[As_2S_3I]^-$were drawn and optimized in Hyperchem 7.0 program suite. We applied the DFT method to optimize and calculate molecular properties of synthesized compounds. All calculations were done by using the Gaussian03 programs .For DFT, Becke's three-parameter exchange functional was used in combination with the Lee–Yang–Parr correlation functional (B3LYP) with LANL2DZ basis set. All ionic molecules were used without any symmetry restriction, and C1 symmetry was assumed for all molecules.[4] Calculations were done in the gas phase. After the optimization procedures, frequency calculations were done to extract vibrational

mode and test the correctness of true minima. The vibrational frequencies and intensities (spectra) and the eigenvectors for the normal modes were corrected with the appropriate factor and displayed on a computer screen to identify the dominatingmotions. The calculated and experimental vibrational spectra are in good agreement.

Results and Discussion

We continue to focus on the synthesis and characterization of various ionic liquids. In this paper, we report the synthesis of the some new ionic liquids containing $[P(C_6H_5)_3H]^+$ $[As_2S_3Cl]^-$ and $[P(C_6H_5)_3H]^+$ $[As_2S_3I]^-$. Ionic liquids were synthesized through a two-step reaction. After preparing ionic liquids, all of them were characterized by IR and other popular experimentalmethods, and these data have already been mentioned. Moreover, most important observed vibrational modes of ionic liquids in 300–4000 cm^{-1} range. All reported frequencies corresponding to vibrational mode and the quantity of these frequencies agree with other similar compounds. In most of cases, frequencies in all of the tow ionic liquids are nearly the same and the difference between their frequencies is very small.

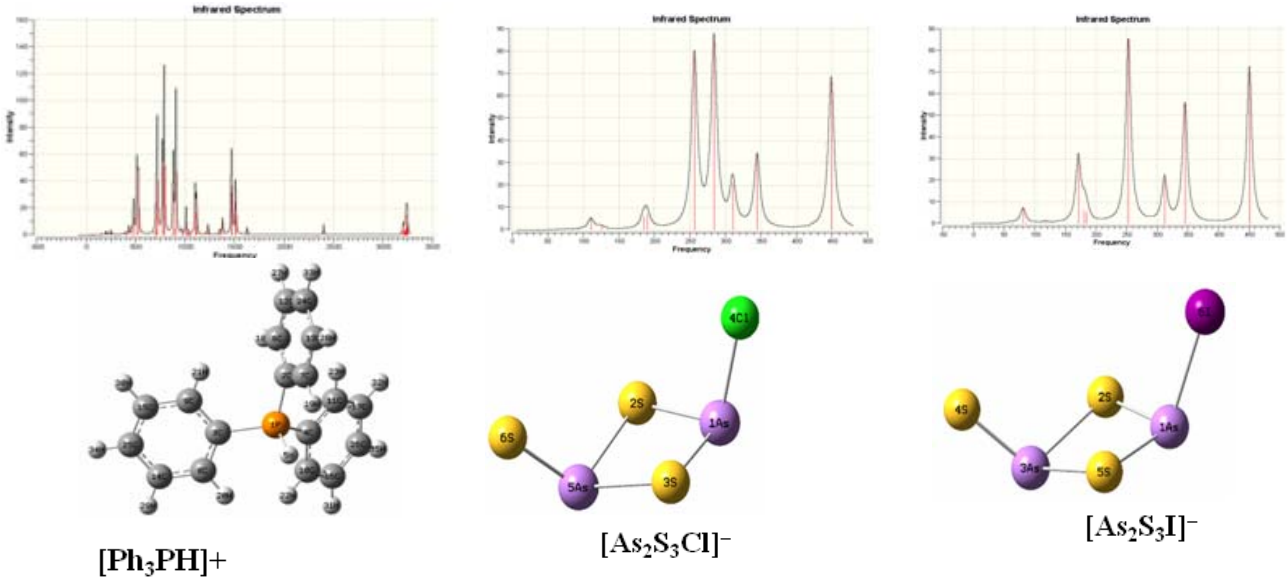

FIGURE 1 Graphical representation of calculated (uncorrected) infrared spectrum of ionic liquids.

Conclusions

In summary, preparation and experimental and theoretical characterization of some phosphorus-based ionic liquids are reported. Our reported technique is very simple and easy

to follow at low temperature and does not require any severe conditions. Moreover, synthesized ionic liquids are very stable (because of their simple structure) with very lowmelting points thatmay have more applications.

References :

[1] T. Walton, Room-temperature ionic liquids. Solvents for synthesis and catalysis. Chem.
[2] Becke, A. D. J Chem Phys 1993, 5648.
[3] Lee, C. T.; Yang, W. T.; Parr, R. G. Phys Rev B 1988, 37, 785.
[4] Lee, C.; Yang, W.; Parr, R. G. Phys Rev B 1988, 37, 785.

Ab Initio Study of Structure of Phosphorus-Based Ionic Liquids

S.Zabihi[a], A.Fayyazi[a], G.Geimachy[a], Sh.Ghammamy[b,*], R.Pooseh[a]
shghamamy@yahoo.com
[a]Department of Chemistry, Faculty of Science, Islamic Azad University, Ardabil Branch, Iran
[b]Department of Chemistry, Faculty of Science, Imam Khomeini International University, Ghazvin,Iran.

Keywords: Ab Initio calculations , ionic liquid, DFT, B3LYP/LANL2DZ

Introduction

Ionic Liquids (ILs) is the generic term for a class of materials, consisting entirely of ions and being liquid below 100°C.Room temperature ionic liquids (RTILs) are non-flammable, non-volatile, thermally stable solvents and as much as very promising replacements for the traditional volatile organic solvent. Ionic liquids, as a class of novel environmental 'green solvents', have remarkable new properties and promising applications in many fields [1].
All synthesized ionic liquids were characterized by IR. In addition, synthesized structures were optimized at the B3LYP/LANL2DZ level of theory and then the structures, molecular specifications, and infrared spectra of these were extracted using Gaussian03 program. Theoretical data show good agreement with the experimental results.[2-3]

Methods

We applied the DFT method to optimize and calculate molecular properties of synthesized compounds. All calculations were done by using the Gaussian03 programs .For DFT, Becke's three-parameter exchange functional was used in combination with the Lee–Yang–Parr correlation functional (B3LYP) with LANL2DZ basis set. All ionic molecules were used without any symmetry restriction, and C1 symmetry was assumed for all molecules. Calculations were done in the gas phase.[4-5] After the optimization procedures, frequency calculations were done to extract vibrational mode and test the correctness of true minima. The vibrational frequencies and intensities (spectra) and the eigenvectors for the normal modes were corrected with the appropriate factor and displayed on a computer screen to

identify the dominatingmotions. The calculated and experimental vibrational spectra are in good agreement.

Results and Discussion

We continue to focus on the synthesis and characterization of various ionic liquids. In this paper, we report the synthesis of the some new ionic liquids containing $[PCl_3CH_3COO]^-$ anion and $[PCl_3N_3]^-$. Ionic liquids were synthesized through a one-step reaction. After preparing ionic liquids, all of them were characterized by IR and other popular experimentalmethods, and these data have already been mentioned. Moreover, most important observed vibrational modes of ionic liquids in 300–4000 cm^{-1} range. All reported frequencies corresponding to vibrational mode and the quantity of these frequencies agree with other similar compounds. In most of cases, frequencies in all of the tow ionic liquids are nearly the same and the difference between their frequencies is very small.

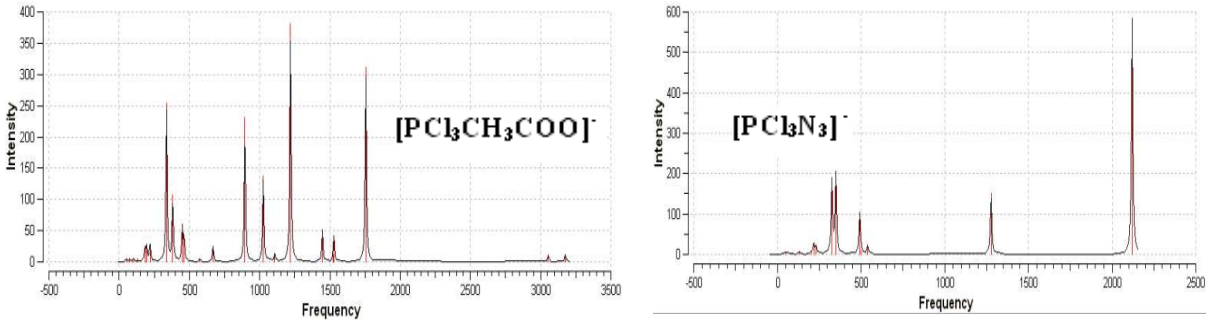

Graphical representation of calculated (uncorrected) infrared spectrum of ionic liquids.

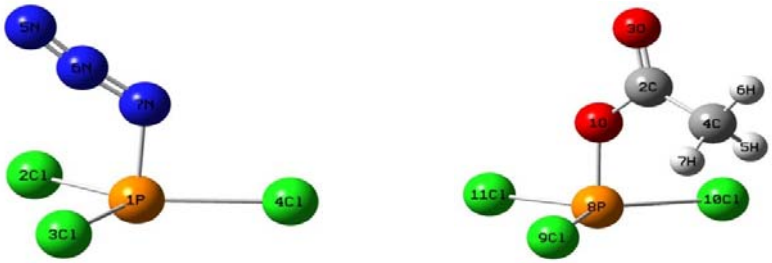

Conclusions

In summary, preparation and experimental and theoretical characterization of some phosphorus-based ionic liquids are reported. Our reported technique is very simple and easy

to follow at low temperature and does not require any severe conditions. Moreover, synthesized ionic liquids are very stable (because of their simple structure) with very lowmelting points thatmay have more applications.

References :

[1] Leadbeater, N. E., Torenius, H. M., Tye, H., *Tetrahedron* ***59***, 2253 (2003).

[2] Frisch, M. J.; Gaussian 03, Revision C02, Gaussian, Inc, Wallingford CT, 2004.

[3] Becke, A. D. J Chem Phys 1993, 5648.

[4] Lee, C. T.; Yang, W. T.; Parr, R. G. Phys Rev B 1988, 37, 785.

[5] Lee, C.; Yang, W.; Parr, R. G. Phys Rev B 1988, 37, 785.

Theoretical Investigation of Hydrogen Storages in SWSiCNTs

M. Rahimi Galugahi [a], S. Yeganegi [b], M. Shadman [b]

[a] Department of Chemistry, Faculty of Science, Islamic Azad University, Shahrood branch, Shahrood, Iran.

[b] Department of Physical and Inorganic Chemistry, Mazandaran University, Babulsar, Iran.

(e-mail: sdyeganegi@gmail.com)

Keywords: SWSiCNTs, GCMC, Langmuir-Freundlich isotherms, Hydrogen storage.

Introduction

The investigation of the physisorption of small molecules inside single-wall nanotubes (SWNTs) from the experimental and theoretical studies such as computing modeling studies has been started to illustrate SWNTs might be a good candidate for a practical gas storage material or not. One of the important small molecules that many researchers have been considered to is hydrogen and understanding hydrogen adsorption behavior in nanotubes, at the molecular level, will guide us to design new materials for H_2 storage enhancing industry. In this papper, we measure the storge of hydrogen inside single-wall silicon carbide nanotubes (SWSiCNTs) and investigate the Langmuir, Freundlich and Langmuir-Freundlich adsorption behavior of hydrogen to illustrate the mechanism of the hydrogen adsorptivity in SWSiCNT. Howevere our results show that the simulation data are correlated by the Langmuir-Freundlich equation.

Potential Models and Simulation Details

In this work, it is assumed that the nanotube has a rigid structure and no geometry variation of the adsorbent is considered, since the induced geometric variation of nanotubes by gases can be neglected at room temperature. The fluid molecules considered as sphere the fluid-fluid interaction was described using the typical 12-6 Lennard-Jones pair potential that parameters ε_{ij} and σ_{ij} between different particles are calculated by the Lorentz–Berthelot rules [1-2]. The moves are repeated until the number of hydrogen molecules in the simulation cell comes to the equilibrium and each simulation consists of 4×10^7 GCMC moves [3-4].

Results and Discussion

This section illustrates the effects of pressure, temperature and pore size on physisorption of pure hydrogen in SWSiCNTs by using GCMC simulations. The simulation were performed at a fixed length of 40 Å for four chiral nanotubes (8, 8), (9, 9), (15, 15) and (22, 22) with ranges of temperature (77.15, 133.15, 177.15 and 298.15 K) and pressure (0-15 MPa). Figure 1 shows that the hydrogen storage capacity of SWSiCNTs increases with increasing of pressure

and decreases with increasing of temperature. The variation of the adsorption of hydrogen with pressure is more pronounced for lower temperatures. Also the difference of the adsorption between different nanotubes is larger for the lowest temperature and the highest pressure. The isotherm equations that have used in this study are Langmuir ($q = \frac{q_m k P}{1+kP}$), Freundlich ($q = bP^n$), and Langmuir-Fruendlich ($q = \frac{q_m k P^n}{1+kP^n}$) [5]. In addition, the deviation parameter on the amount adsorbed, ($D = \frac{1}{n}\sum_i^n \left|\frac{N_i^{obs} - N_i^{cal}}{N_i^{obs}}\right|$) was utilized to compare the correlation results with simulation data [6]. For all systems, the adsorption isotherms are nonlinearity. The amount adsorbed of hydrogen increased significantly at low pressure, under 3 MPa. The Langmuir-Freundlich equation was used for all systems because this equation shows the minimum value of the average deviation parameter.

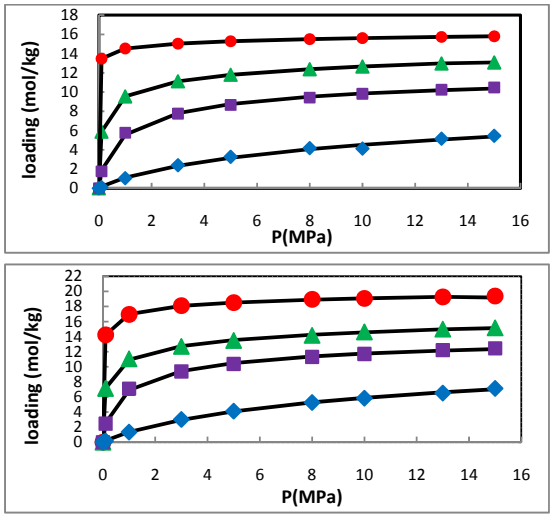

(a): (8, 8) SiCNT

(b): (9, 9) SiCNT

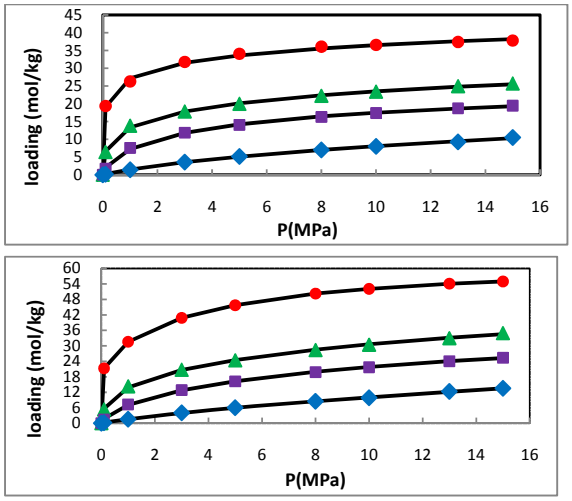

(c): (15, 15) SiCNT **(d): (22, 22) SiCNT**

Fig1. Simulation and fitted isotherms of H_2 onto Silicon-Carbon Nanotubes: ●, 77.15 K; ▲, 133.15 K; ■, 177.15 K; ◆, 298.15 K GCMC Simulations onto (a): (8, 8) SiCNT, (b): (9, 9) SiCNT, (c): (15, 15) SiCNT and (d): (22, 22) SiCNT ; ─ ,L-F model.

References

[1] J. Cheng, L. Zhang, R. Ding, *International Journal of Hydrogen Energy* **32**:3402–3405 (2007)

[2] X. Li, W. Yang, B. Liu, *NANO LETTERS.* Vol. **7**, No. 12, 3709-3715(2007).

[3] A. Gupta, S. Chempath, M.J. Sanborn, *Molecular Simulation* **29**:29-46 (2003).

[4] http://zeolites.cqe.northwestern.edu.

[5] Yang, R. T. *Gas Separation by Adsorption Processes*; Butterworth:Boston, MA, (1987).

[6] B-U. Choi, D-K. Choi, Y-W. Lee, *J. Chem. Eng. Data,* **48**, 603-607 (2003).

Tautomerism and vibrational assignment of methyl acetoacetate

M. Rastaghi chalki [1], S.F. Tayyari *[1,2],S. Ali-Asgari[1]

[1] Department of Chemistry, Islamic Azad University, Shahroud Branch, Shahroud

[2] Department of Chemistry, Science and Research Branch, Islamic Azad University, Khorasan Razavi, Iran

marziehrastaghi@yahoo.com & sftayyari@yahoo.com

Keywords: Methyl acetoacetate; Vibrational spectra; Tautomerism; Intramolecular hydrogen bonding.

Introduction

Methyl acetoacetate (MAA) is a □-ketoester which is engaged in keto-enol tautomerism equilibrium [1,2]. This compound, because of its simplicity, is a good candidate for studying, both theoretically and experimentally, of hydrogen bonding and tautomerism. MAA, at least theoretically, is capable to exist as a mixture of different tautomers and conformers. The aim of this project is study of the structure, tautomerism, hydrogen bonding, and vibrational assignment of MAA.

Calculations

The calculations of geometrical parameters were performed using the Gaussian 03 program package and B3LYP approach in conjunction with the 6-31G(d,p) and 6-311G(d,p) basis sets without any symmetry restrictions. The harmonic vibrational frequencies and IR and Raman intensities have been obtained at the B3LYP/6-311G(d,p) level of theory.

Results and discussion

After fully optimization, the relative energies (calculated at the 6-311G(d,p)) of the possible tautomers and conformers of MAA have been obtained. According to our calculations, the cis-enol form is the most stable tautomer and is considerably more stable than diketo form and all non chelated enol forms. However, vibrational spectra indicate that the keto form predominates in the sample. This discrepancy is interpreted as inadequacy of the basis sets for comparing the energy of keto and enol tautomers and also the effects of media. The

energy difference between keto and chelated enol tautomers is considerably decreased when we applied the zero point energy correction and doing the calculations in the solutions. However, if we use the free energy instead of zero point energy, which also considers entropy effect at the desired temperature, the results favor the presence of keto form in the sample. This is the result of higher entropy value of keto compared with that in the enol form and is in excellent agreement with the experimental data. Comparison of the relative energies of the cis-enol form and the trans-enol form indicates that the hydrogen bond strength (the energy difference between cis- and trans-enol forms) is about *14.5 kcal/mol.* The relative energies of other enol forms are considerably high; therefore, their presence in the sample is unlikely.

In this work we also discuss the vibrational spectra of this compound and compare those frequencies which are directly related to the H-bond strength with several □-diketones and relate the H-bond strength to the structural parameters.

Conclusion

The FT IR and FT Raman spectra of MAA have been investigated by means of DFT calculations. According to both calculations and experimental results, there is a keto-enol equilibrium in the neat and solution samples of MAA. The intramolecular H-bond is relatively strong in the chelated enol form of MAA.

References:

[1] M. M. Folkendt, B. E. Weiss-Lopez, J. P. Chauvel Jr., N. S. True, J. Phys. Chem., 89 (1985) 3347–3352.

[2] J. W. Bunting, J. P. Kanter, J. Am. Chem. Soc.,115 (1993) 11705–11715

Catalytic oxidation of CO on Pt(001) and Pd(001) surfaces. An Ab initio study

Roghieh Rasouli Mehrabani*[a]Mohsen shabani[b],Ali Akbar Salari[a], Sheida Sarmast[a]
[a]Department of chemistry,Islamic Azad University,Shahre Rey Branch
parvan502002@yahoo.com
[b]Department of chemistry,Islamic Azad University,Varamin Branch

Abstract:

Catalytic oxidation of carbon monoxide on transition metal surface is important .In this investigation.We study reaction between CO and O on Pt and Pd surfaces,and used an Ab initio Density Functional Theory (DFT).

We used B3lyp theoretical and 6-31G (d) basis set for carbon and oxygen . Also Lanl2DZ
basis set for Pt and Pd .The oxidation occurs Langmuir- Hinshelwood mechanism,where CO molecule adsorb on the surface and react with chemisorb oxygen atom.

Keywords:CO oxidation, DFT theory, Lanl2DZ basis set,Langmuir-Hinshelwood, Transition state.

Introduction:

Platinum together with palladium is used as industrial catalysts,especially in catalytic converters for combustion oxidation of CO.This is important to effort the understanding of the simple catalytic oxidation of CO on Pt (001) and Pd (001) [1] .The aim of this study is catalytic oxidation of CO to CO_2 in present of oxygen on surface Pt (001) and Pd (001) using Ab initio
calculation. Also we investigate reactions and transition state (TS).

Methods:

All calculations were made using Gaussian 03.Optimized geometric were detemind using Density Functional Theory with B3lyp.We used 6-31G(d) basis set for CO and O,that are top

site on metals surfaces ,and with Lanl2DZ basis set for Pt and Pd .At final we calculated the transition state (TS) using scan program in the structure offered.

Fig.1show that CO and O are top site on Pt and Pd surfaces .

Pt Pd

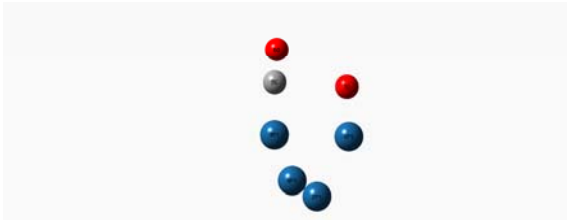

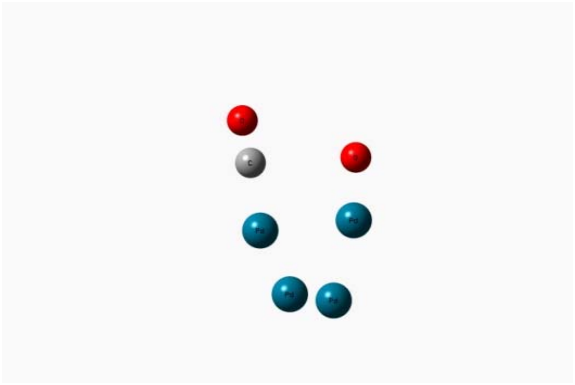

Table1. Energy and E_{TS} calculation for CO and O for Pt and Pd :

	E(au)	E_{TS}(au)
Pt-O	-589.9135549	-
Pt-CO	-551.7403036	-
Pt (CO+O)	-665.0692552	-662.89673
Pd-O	-۵۸۲,۱۰۳۲۶۲۱	-
Pd-CO	-۶۲۰,۲۹۰۶۵۵۱	-
Pd (CO+O)	-۶۹۵,۴۰۴۱۷۹۳	-۶۹۴,۷۴۳۶۵

Results:

We calculated the activation energy (E_a)for Pt and Pd:

Pt: E_a= ۱۳۵۱,۳۱۰۶۷ kcal/mol.

Pd: E_a= ۴۱۰,۸۴۹۲۲۴ kcal/mol.

We concluded the E_a for Pt is more than for Pd. It seem that Pt surface is better for CO oxidation.

Reference:

[1]T. Campbell, G. Ertl, H. Kuipers, and J. Segner, J. Chem. Phys. **73**, 5862 ,1980.

Are M_3^+ (M = H, Li, Na, K) Clusters Aromatic?

Zahra Badri[a], Cina Foroutan-Nejad[a], Parviz Rashidi-Ranjbar*[a]

[a] *School of Chemistry, College of Science, University of Tehran, Tehran, Iran.*

Fax: 0098 21 6649 5291 ; Tel: +98 21 6111 3301

Email :ranjbar@khayam.ut.ac.ir

M_3^+ (M = H, Li, Na, K) clusters have been considered as examples of *s*-atomic orbital, σ-aromaticity for years [1]. NICS computations are in line with this picture as large negative NICS values are obtained at the center of these clusters [2]. However, there are serious doubts about the nature of aromaticity of these clusters because electron concentrations, i.e. Non-Nuclear Attractors (NNA), are present at the center of these clusters [3], Figure 1.

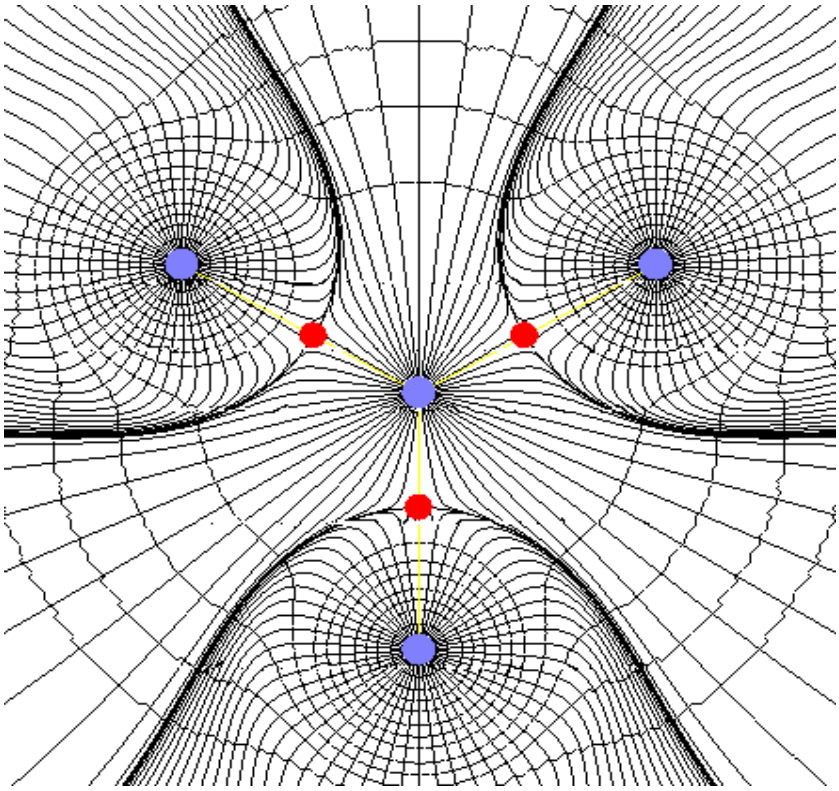

Figure 1. Topology of electron density of the Li_3^+; four blue circles (larger circles) are (3,-3) critical points corresponding to three lithium nuclei and the non-nuclear attractor (the central point). The red circles (smaller circles) represent (3,-1) critical points.

A recent study confirms that one-electron density indeed affects the NICS values [4]. A large electron density causes large negative NICS values although this does not necessarily mean aromaticity. In order to solve this discrepancy electronic structure and magnetic shielding of these species are studied precisely.

Geometries of all clusters are optimized to their local minima, i.e. no imaginary frequency, at the B3LYP/6-311+G(d) computational level; magnetic properties of local minima are studied while number of electrons in each cluster are varied. According to electron counting rule of aromaticity for metallic clusters [1], addition or elimination of electrons from these clusters should result in antiaromatic character. Magnetic properties of negatively charged species as well as triply positive charged ones suggest that addition/elimination of electrons does not change the magnetic properties into what is expected from an antiaromatic species. This confirms that large negative NICS values at the center of these clusters are not result of the magnetic aromaticity.

In summary, these species are not σ-aromatic and the high electron density, i.e. NNA, at the center of these molecules is the source of large negative NICS values.

Keywords: Metal Cluster, Non-Nuclear Attractor, Magnetic Aromaticity, Electron Density

References:

[1] D. Yu. Zubarev, B. B. Averkiev, H.–J. Zhai, L.–S. Wang, A. I. Boldyrev, *Phys. Chem. Chem. Phys.*, 2008, **10**, 257.

[2] Z. Chen, C. S. Wannere, C. Corminboeuf, R. Puchta, P. v. R. Schleyer, *Chem. Rev.*, 2005, **105**, 3842.

[3] C. Foroutan-Nejad, P. Rashidi-Ranjbar, *J. Mol. Struct. THEOCHEM*., 2009, **901**, 243.

[4] C. Foroutan-Nejad, S. Shahbazian, P. Rashidi-Ranjbar, *Phys. Chem. Chem. Phys.*, 2010, **12**, 12630.

Structure and Bonding in $M_3(CO)_3$ Complexes: A New Class of Metal Carbonyls

Cina Foroutan-Nejad[a], Shant Shahbazian[b], Parviz Rashidi-Ranjbar*[a]

[a] *School of Chemistry, College of Science, University of Tehran, Tehran, Iran.*

Fax: 0098 21 6649 5291 ; Tel: +98 21 6111 3301

Email: *ranjbar@khayam.ut.ac.ir*

[b] *Department of Chemistry, Faculty of Sciences, Shahid Beheshti University, G.C., Evin, Tehran, Iran. Tel: +98 21 2990 2883*

Keywords: Metal Clusters, Aromaticity, Chemical Bond, Metal Carbonyl, Inverted Donation

Recently, employing the matrix isolation and FT-IR spectroscopy, $Ti_3(CO)_3$ a novel titanium-carbonyl species with an interesting planar geometry and electronic structure has been characterized, Figure 1 [1]. The structure of $Ti_3(CO)_3$ was verified based on a detailed comparison of the experimental and computational IR spectrum where the isotope substitutions and concomitant ab initio computations strengthened the tentative assignment. Probably the unusual feature of the published work on $Ti_3(CO)_3$ rests on the claim that this species is "potentially antiaromatic" reflected in the title of published paper. However, this characterization is questionable due to using a wrong methodology for assessing aromaticity and the fact that this molecule is a global minimum.

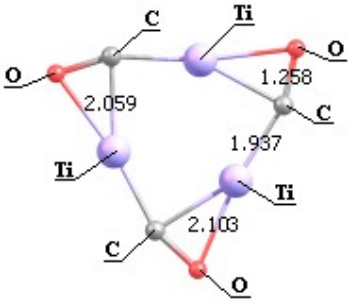

Figure 1. The structure of $Ti_3(CO)_3$ at B3LYP/6-311+G(2df) level of theory.

Nature of bonding and aromaticity of $Ti_3(CO)_3$, is studied at twelve computational levels (Four DFT levels including B3LYP, BP86, LSDA and MPWPW91 with three different basis sets 6-311+g(d), 6-311+G(2df) and 6-311+G(3d2f)) heedfully. Based on NICS methodology,[2] it is proven that not only $Ti_3(CO)_3$ is not an antiaromatic complex but also is the first synthesized example of d-block, $\sigma + \pi$ aromatic species.

A unique bonding pattern in $Ti_3(CO)_3$ based on electron donation from the *sd* metal orbitals to the antibonding orbitals of carbonyl was found without σ-donation from carbonyl to metal. Qualitative MO picture and quantitative QTAIM analysis both confirm this bonding pattern. Energy decomposition analysis at BP86/TZVP level completes the puzzle and confirms the presence of *inverted donation*. Atomization energies reveals the efficiency of this bonding mechanism as the bonding energy between metal and carbonyl is more than twice larger than usual metal-carbonyl bonds in titanium carbonyl complexes. A quick survey among first row transition metals showed that, other local minima with similar structures ($V_3(CO)_3^+$, $Ni_3(CO)_3$, $Cu_3(CO)_3^-$) are also conceivable and $Ti_3(CO)_3$ is the first synthesized species of an unknown family, Figure 2.

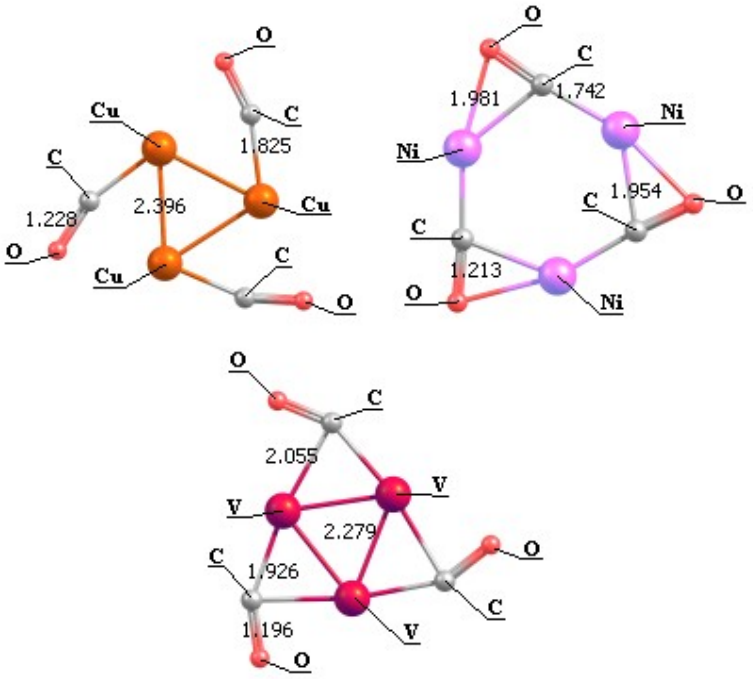

Figure 2. Structure of predicted species at B3LYP/6-311+G(d) level.

Based on the NICS methodology and orbital morphology $V_3(CO)_3^+$ is verified as a triple-aromatic species with σ-, π- and δ-aromaticity. However, $Ni_3(CO)_3$ and $Cu_3(CO)_3^-$ are characterized as non-aromatic. The full details have been reported elsewhere [3].

References:

[1] Q. Xu, L. Jiang, N. Tsumori, *Angew. Chem. Int. Ed.* **2005**, *44*, 4338.

[2] Z. Chen, C. S. Wannere, C. Corminboeuf, R. Puchta, P. v. R. Schleyer, *Chem. Rev.*, 2005, **105**, 3842.

[3] C. Foroutan-Nejad, Sh. Shahbazian, P. R. Ranjbar, *Phys. Chem. Chem. Phys.*, (accepted)

Aromaticity analysis of stable guanine tautomers in the gas phase via DFT

M. Reza gholi beiki, S. Mozaffari, A. Pangh, S.H. Mortazavi, Ehsan Zahedi*
Chemistry Department, Islamic Azad University, Shahrood Branch, Shahrood, Iran.
mehrakbeiki@yahoo.com e_zahedi@iau-shahrood.ac.ir

Keywords: NICS; Stability; DFT; Guanine

Introduction

The aromaticity is important parameter used frequently as a reactivity measure of many organic and even some inorganic molecules [1]. About 50% of all known organic compounds may be characterized by more or less pronounced aromatic character. This is especially important for heterocyclic compounds since this class comprises many species of great biological importance such as porphyrins and nucleic acid bases [2]. Guanine is one of the most important nucleic acid bases (NAB) occuring in both DNA and RNA. In addition to being the largest NAB, it has also the most complex tautomeric equilibria [3]. The concept of NICS was introduced by Schleyer et al. in 1996 [4] as a measure of aromaticity and antiaromaticity (or non-aromaticity). It is based on a probe with no basis functions (bq) which is placed at or above the geometrical center of a conjugated ring .

Computational Details and Results

All calculations has been carried out at the B3LYP/6-311++G(d,p) level of theory using Gaussian 03 software package [5]. Ball/stick structures and numbering system of the three stable tautomers of adenine is presented in below fig and the stability is in the order T3>T1>T2>T4.

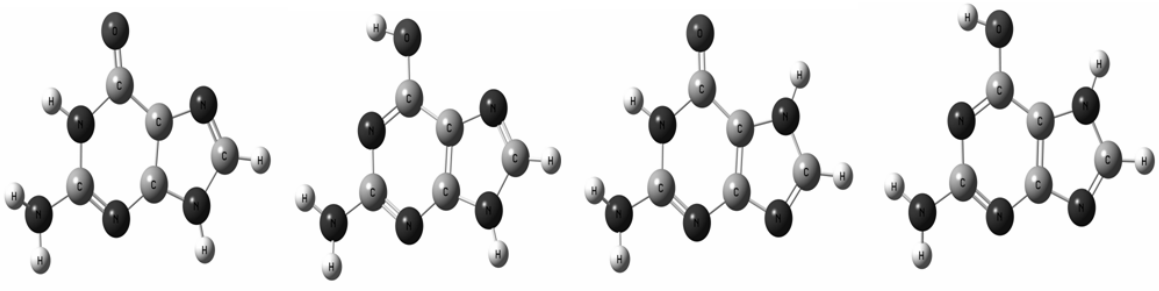

T1 T2 T3 T4

On the basis of NICS plots five and six membered rings in all stable tautomers of guanine show considerable aromaticity. Interesting, for all four stable tautomers of adenine NICS values at the minimum point of five membered rings are more negative (i.e. indicating more

aromaticity) than six membered rings. It should be noted that the overall aromaticity of tautomers is better indicated by its ΣNICS value. The strongest aromatic quality was found for the T4 tautomer. The other tautomers were also characterized by significant relative aromaticity, but less compared to the T4 tautomer. The T1 tautomer had the least aromaticity. It is clear that the order of relative aromaticity of the different tautomers is not similar to the relative energies.

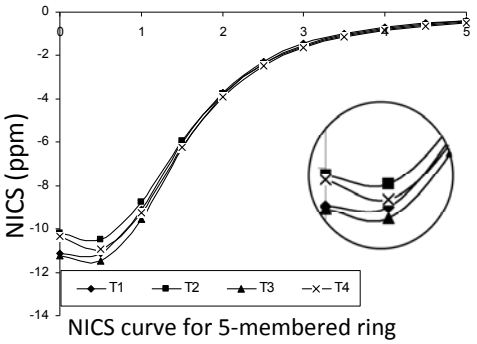

NICS curve for 5-membered ring

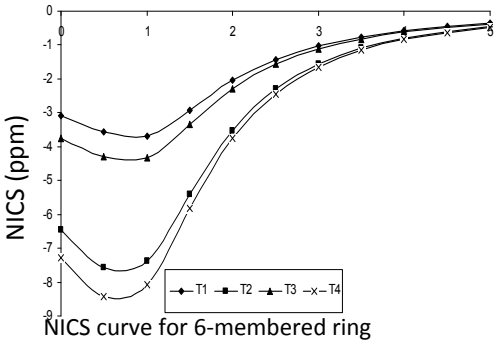

NICS curve for 6-membered ring

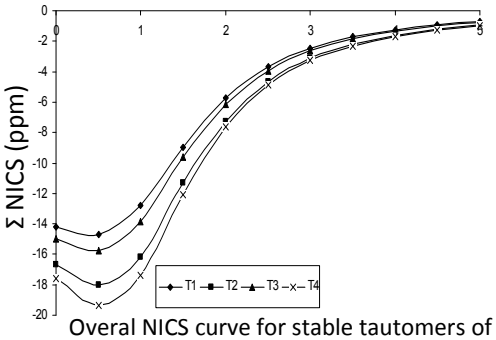

Overal NICS curve for stable tautomers of guanine

Reference:

[1] T.M. Krygowski, M.K. Cyran´ski, Z. Czarnocki, G. Hafelinger, A.R. Katritzky, Tetrahedron 56 (2000) 1783.

[2] Piotr Cysewski Journal of Molecular Structure: THEOCHEM 714 (2005) 29.

[3] A.K. Chandra, Minh Tho Nguyen, T. Uchimaru, Th. Zeegers-Huyskens, Journal of Molecular Structure 555 (2000) 61.

[4] P.V.R. Schleyer, C. Maerker, A. Dransfield, H. Jiao, N.J.R. van Eikema Hommes, J. Am. Chem. Soc. 118 (1996) 6317.

[5] M.J. Frisch et al., Gaussian 03, Revision E.01, Gaussian Inc., Wallingford CT, 2004.

Keto-Enol Tautomerism in Tetraketonate Ligands. A Density Functional Theory and Experimental study

Hamid Golchoubian*, Ehsan Rezaee, Davood Farmanzadeh
Department of Physical-Inorganic chemistry, the university of Mazandaran, Babolsar, Iran
(e-mail : h.golchobian@umz.ac.ir)

Keywords: tetraacetylethane, DFT study, tetraketone, tautomerism.

Introduction:

Beta-diketones and tetraketones represent two of the most important classes of chelating ligands [1]. These ligands lose their proton(s) in basic media to produce anions in which able to coordinate strongly to metal ions. Equilibrium exists between *enol* and *keto* forms of the tetraketonate ligands and its stability depends on the nature of solvent as well as substituent attached [2]. In this work the effect of some solvents with different dielectric constant on the tautomerism of four various tetraketonate ligands shown in scheme 1 were investigated by the DFT level of theory and compared the theoretical results with those of the experimental results taken form ^{1}HNMR spectroscopy.

Scheme 1

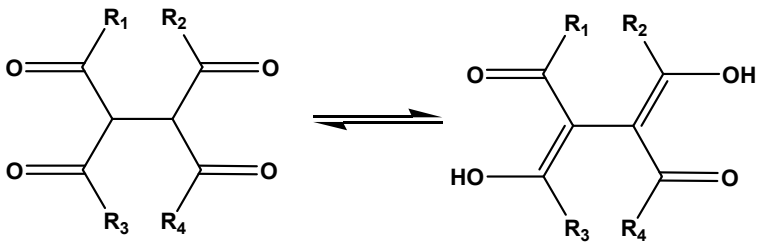

R_1, R_4 = CH_3, CH_2CH_3
R_2, R_3 = CH_3, CF_3

Experimental and method:

3,4-diacetyl -2,5-hexanedione was prepared and purified according to the method described in the literature [3]. ^{1}H NMR spectra were recorded on a Bruker 400 DRX Spectrometer in solvent of dmso (d6) and D_2O. All geometries of the four ligands were fully optimized at the DFT, Becke's three parameters hybrid functional (B3) [4] with non-local correlation functional of Lee-Yang-Parr (LYP) [5,6] level of theory and the 6-31++G** basis set using Gaussian 03 program. The calculations were performed in the presence of a solvent molecule using an Onsager model (SCRF). Frequency analysis is also performed to ensure that the resulted geometries are in the global minimum of the potential surface.

Results and discussion:

The dipole moments and stability energy of the tautomeric forms of the ligands were investigated in three solvents, chloroform, acetonitrile and dimethylsulfoxide, with dielectric constants of 4.9, 36.6 and 46.7, respectively. The obtained results show that the *enol* forms of the tautomeric species is generally predominate over the corresponding *keto* form in all solvents and ligands used. The results were supported by ^{1}HNMR and ^{13}CNMR studies. In cases of 3,4-bis(triflouroacetyl)-2,5-hexanedione and 4,5-bis(triflouroacetyl)-3,6-octanedione the presence of the electronegative substituents lead to existence of two *enol* forms with different energy levels. These constitutional isomers have also been investigated in various solvents.

Conclusion:

It could be concluded that the *enolic* tautomers are more stable than the *keto* counterparts in different solvents, even in solvent with a high dielectric constant as a consequence of intermolecular hydrogen bonds. Existence of an electronegative substituent like CF_3 stabilizes more *enolic* form due to the formation of the stronger hydrogen bonds.

References:

[1] J. B. Lambert, Z. Liu, J. Chem. Cryst. **2007**, 37, 629.

[2] J. N. Spencer, E. S. Holmbe, M. R. Kirshenbaum, D. W. Firth, P. B. Pinto, Can. J. Chem. **1982**, 60, 1178.

[3] R. G. Charles, Org. Syn., **1963,** Coll. Vol. 4, 869.

[4] A. D. Becke, J. Chem. Phys. **1993**, 98, 5648.

[5] B. Miehlich, A. Savin, H. Stoll, H. Preuss, Chem. Phys. Lett. **1989**, 157, 200.

[6] C. Lee, W. Yang, R. G. Parr, Phys. Rev. B **1988**, 37, 785.

Charge Density Analysis of Halogenated Boron Nitride Nanosheets; QTAIM for σ and π orbitals

S. Fakhraee [*,a], L. Rezaie [b]

[a] Department of Chemistry, College of Sciences, Payame Noor university, Shiraz, 71365-944, Iran.

(Email: Fakhraee@spnu.ac.ir)

[b] Department of Chemistry, College of Sciences, Azad university, Marvdasht, Iran.

Keywords: boron nitride nanosheet, QTAIM, σ and π charge density, AIM atomic charge

Introduction

It has been more than 10 years since the discovery of Boron Nitride (BN) nanostructures. Numerous investigations were carried out about BN nanostructures. Nowadays, BN nanostructures produced in large scale and chemistry of these structures have an important role in composites production. In general BN has a similar structure with graphite in which carbon atoms were replaced by equal atoms of both boron and nitrogen. The applications of BN nanostructures, that identify their importance, are including: improvement of thermal and mechanical properties of polymer composites, applications in electronic devices, and nano-drugs and attraction and storage of fuels like hydrogen molecules.[1]

The electronic density changes in the BN nanostructures would affect observable properties of these structures. These changes can be separated for σ and π contributions of electron density, when the molecule is planar.[2] It is proved that the theory of atoms in molecules (AIM), introduced by Bader, is successful in description of electronic density of molecules and its changes.[3] AIM theory is based on the electronic density ρ(r) graphs and all of the molecular specifications are expressed by these topology. In this theory, critical point (CP) in the electron density is defined as a point in space at which the first derivatives of the density vanish. In fact, there is a line with maximum density between two atoms that named bond path (BP). The point on the bond path which is maximum in the inter-atomic surface is called bond critical point (BCP). The main criterion for creation of a bond between two atoms is the existence of a BCP in the line of maximum density between two atoms or bond path.

Although most of the researches based on the AIM theory apply σ-framework of charge density, changing the π contribution of charge density has a strong influence on observable properties of π bond containing molecules, indirectly. In the present work, our effort is to analyze the π bond charge density changes in BN sheet molecules, individually. These changes would be studied in the presence of halogen substitutions on BN planar sheets.

Methodology:

In the present work, the BN sheet was applied to study in the presence and absence of R substitution (R: F, Cl, Br). Gaussian 03 package was used to molecular optimization, and computation of wave function at HF/6-31g* level of theory. Frequency test was applied to ensure that the structures are in minimum energy structure. Figure 1 represents typical optimized structure of BN sheets with halogen groups were halogens are connected to the nitrogen number 50 (N50).

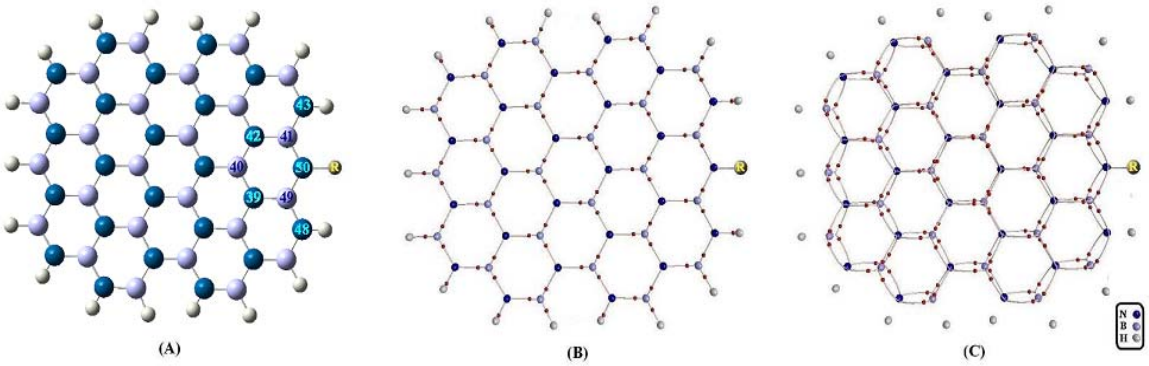

Figure 1: (A): Typical optimized structure of BN sheet substituted by R (R: H, F, Cl, Br). (B): The molecular graph of BN sheet showing the collection *of* σ-BPs and associated BCPs. (C): π -BPs and BCPs for BN sheet.

AIM2000 program [4] was applied to analyze the wave function of π and σ orbitals in the presence and absence of halogens. Figure 1(B) and 1(C) demonstrate σ and π separated graphs, obtained by AIM program, for typical BN sheet with R substitution. Figure 2 represents enlarged graphs in Fig. 1 for σ orbitals (a, b, c, d) and π orbitals (e, f, g, h), separately. The BCPs 1 to 7 presented in Fig. 2 show the most changes in ρ_{BCP} among the other BCPs of BN sheet after substitution. For other BCPs the change in ρ_{BCP} is negligible so they were omitted from tables and figures. Because of the perfect symmetry in BN sheet molecule, results associated with BCPs 2, 4, and 6 are the same as 3, 5 and 7.

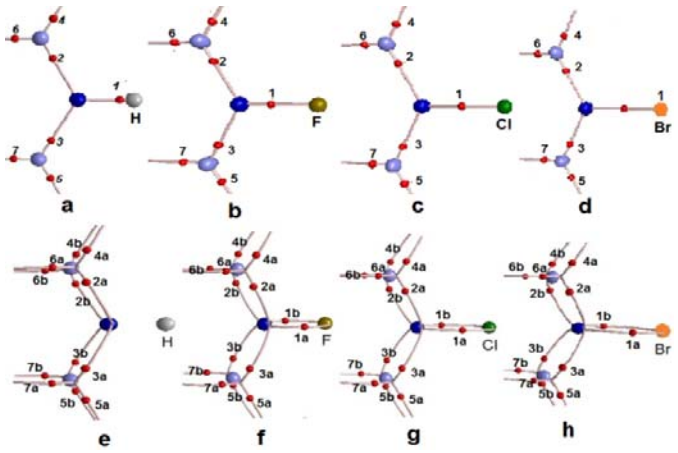

Figure 2: σ and π AIM diagrams zoomed in on the substituted site.

Charge density at BCPs number 1 to 6 in BN nanostructures was obtained and summarized in Table 1 for σ and π system, individually. The values of AIM atomic charges and bond lengths associated with BCPs number 1 to 6 was determined and reported in Table 2.

Table 1: Calculated charge density for BCPs 1-7 which have significant changes respect to other BCPs on BN sheet.

Structure	*Charge Density (ρ_{BCP})*									
	σ type BCPs				*π type BCPs*					
	1	**2**	**4**	**6**	**1**		**2**		**4**		**6**	
					a	**b**	**a**	**b**	**a**	**b**	**a**	**b**
BN Sheet	0.3422	0.2004	0.1984	0.1951	-		0.0213		0.0205		0.0194	
BN Sheet - F	0.2971	0.1978	0.2065	0.1986	0.0426		0.0211		0.0218		0.0203	
BN Sheet - Cl	0.2194	0.1891	0.2051	0.1972	0.0272		0.0206		0.0217		0.0200	
BN Sheet - Br	0.1673	0.1893	0.2047	0.1969	0.0223		0.0205		0.0216		0.0199	

Table 2: AIM atomic charge and bond length for atoms and bonds with significant changes respect to BN sheet.

Structure	*AIM atomic charges*					*Bond length (A°)*			
	$N_{۵۰}$	$B_{۴۱}$	N_{42}	$B_{۴۰}$	N_{43}	N_{50}-B_{41}	B_{41}-N_{42}	N_{42}-B_{40}	B_{41}-N_{43}
BN Sheet	-1.853	2.433	-2.33۱	2.419	-1.876	1.427	1.447	1.443	1.434
BN Sheet - F	-1.140	2.427	-2.325	2.426	-1.904	1.428	1.420	1.441	1.445
BN Sheet - Cl	-1.587	2.430	-2.423	2.423	-1.910	1.445	1.422	1.444	1.445
BN Sheet - Br	-1.728	2.429	-2.325	2.422	-2.615	1.444	1.423	1.445	1.445

Results and discussions

The obtaining results from AIM analysis for σ and π systems of BN sheet substituted by halogen atoms demonstrate double bonds formation between halogen and N50. The charge density for both σ and π systems would change in presence of halogens on BN sheet. For instance, ρ_{BCP} decreases for BCP 2 and increases for BCP 4 in halogenated BN sheets respect to BN sheet without substitution, while their corresponding bond length N_{50}-B_{41} and B_{41}-N_{43} increases and decreases, respectively. Comparing ρ_{BCP} 1-6 for π and σ systems in Table 1

shows that the trend in π system is completely similar to that of σ system. Table 2 also confirms the changes in AIM atomic charges for atoms on the ring connected to halogen atoms increases the polarity of B-N bonds.

Conclusion

The σ and π contribution of charge density were identified, individually, by AIM theory for BN sheets in presence and absence halogen atoms. The results show that the charge density behaves similarly in π and σ system. The halogenations in BN sheets cause to change in charge density, atomic charge and bond length of hexagonal BN ring connected to substitution and also the two vicinal N atoms of the ring. The other B and N atoms remain unchanged.

References

[] A. L. M. Reddy, A. E. Tanur, G. C. Walker, Synthesis and hydrogen storage properties of different types of boron nitride nanostructures , International Journal of Hydrogen Energy, 35(9), 2010,4138-4143.

[2] S. M. Azami, J. Phys. Chem. A., 114, 2010, 11794.

[3] R. F. W. Bader, Atoms *in Molecules: A Quantum Theory*, Oxford University Press Inc., New York, 1995.

[4] R. F. W. Bader*, AIM 2000 program package,* Version 2.0: McMaster University: Hamilton, Ontario, 2002.

Geometry optimization of some glycoluril-derived molecular clips

E. Rezaei-Seresht*[a], A. Morsali[b] and A. Beyramabadi[b]

[a]Department of Chemistry, Faculty of Sciences, Sabzevar Tarbiat Moallem University, Sabzevar, Iran

(Email: rezaei_seresht@yahoo.com)

[b]Department of Chemistry, Faculty of Sciences, Islamic Azad University, Mashhad, Iran

Keywords: Geometry Optimization, 6-31 G** Basis Set, Molecular Clip, Glycoluril.

Introduction

The design and synthesis of host molecules for neutral guests continues to be an area of the great interest in supramolecular chemistry [1]. In recent years a series of receptors derived from the concave molecule glycoluril have been developed by Nolte's group [2-4]. These receptors, which are known molecular clips, bind dihydroxybenzenes by hydrogen bonding interactions between the hydroxyl groups of the guest and the urea carbonyl groups of the host and by π-π stacking interactions between the guest and the host side-walls. In the next studies, molecular clips with large variety of side walls have been synthesized and the supramolecular chemistry of these clips has been extensively studied [5, 6].

Results and discussion

DFT geometry optimization

DFT calculations were employed in order to optimize the minimum energy geometry of the clips In this study, the effect of two factors on the geometry of the clips were examined. First, the rigidity of the glycoluril scaffold (the more rigid biphenyl-, and bipyridine glycoluril) and second, the extent of steric hindrance around the clip cavity (tetramethyl- and dimethylbenzene side-walls versus benzene side-wall) (Figure 1).

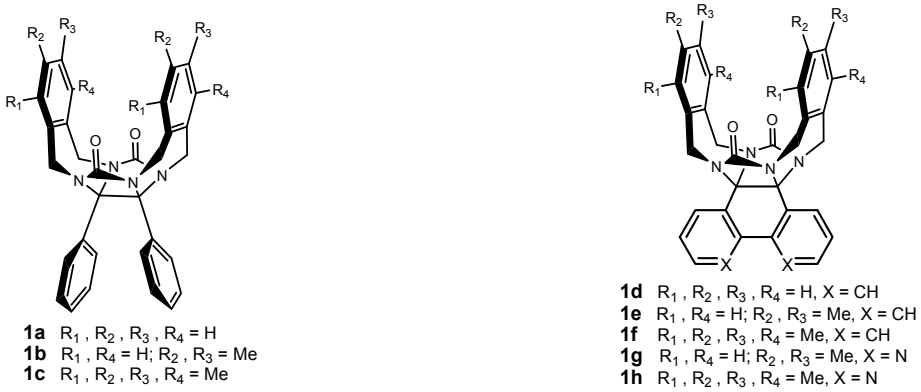

Figure 1

The optimization results showed that biphenyl-, and bipyridine-derived clips (**1d-h**) have more stability due to the longer conjugation of their aromatic π systems. Surprisingly, increasing of the extent of substitution on the aromatic side-walls imparts more stability to the clip molecules. We found that the spatial distance between two oxygens of the carbonyl groups, which is a criterion of folding of the fused imidazolone rings, depends only on the glycoluril framework and not to type of the side-walls. However, one of the best relationships in this study has appeared as 'center-to-center' distance. Indeed, it is the distance between two centers of the rings of the aromatic side-walls and it appropriately reflects the degree of tightness or looseness of the clip cavity (Figure 2).

Figure 2. Computer-optimized structure of the representative clip **1d** (left: front view; right: side view)

Also, it was found that in the case of the most substituted clips **1c**, **1f**, and **1h**, the clip cavity is tightest. Another interesting feature of the optimization results is dependence of the dihedral angles between the fused imidazolone rings as well as, the aromatic side walls to the extent of the cavity substitution and the rigidity of the structure. Because of the planarity of the biphenyl moiety, the molecular clips **1d-f** have more rigid structure than the clips **1a-c**.

Conclusion

The results of this study show that the larger steric interactions may be occurred between the glycoluril scaffolds of compounds **1d-f** and the methylene protons resulting in more squeezed cavities compared to the cavities of diphenylglycoluril-derived clips **1a-c**. Also, the substitution degree of the aromatic side-walls makes the clip cavity tighter.

References

[1] Lehn, J.M. *Comprehensive supramoleacular chemistry*; Elsevier science Ltd: Oxford, 1996, Vol.2.

[2] Sijbesma, R. P.; Nolte, R. J. M. *Top. Curr. Chem*. **1995**, *179*, 25.

[3] Rowan, A. E.; Elemans, J. A. A. W.; Nolte, R. J. M. *Acc. Chem. Res.* **1999**, *32*, 995.

[4] Elemans, J. A. A. W.; Rowan, A. E. Nolte, R. J. M. *Ind. Eng. Chem. Res*. **2000**, *39*, 3419.

[5] Reek, J. N. H.; Elemans, J. A. A. W.; Nolte, R. J. M. *J. Org. Chem.* **1997**, *62*, 2234.

Reek, J. N. H.; Priem, A. H.; Engelkamp, H.; Rowan, A. E.; Elemans, J. A. A. W.; Nolte, R.J.M. *J. Am. Chem. Soc.* **1997**, *119*, 9956.

QSAR studies on the 4-hydroxybenzaldehyde derivatives as tyrosinase inhibitors

Afasaneh Rezaie*[a], Davood Ajloo[b]

a-Deparment of Chemistry, Islamic Azad University Shahrood Brabch, Tehran Street, Shahrood, Iran

[b]-School of Chemistry, Damghan University, Damghan, Iran

Tyrosinase is a multifunctional copper-containing enzyme widely distributed in microorganisms, plants and animals [1]. It is well known that tyrosinase can catalyzes two distinct reactions of melanin synthesis, the hydroxylation of monophenols to o-diphephenols (monophenolase activity) and the oxidation of o-diphenols to o-quinones (diphenolase activity) [2]. On the other hand, QSAR methods are the powerful tools for investigation of correlation between structure and activity. In this work we selected different categories of tyrosinase inhibitors. The quantitative equation between experimental parameters ($logIC_{50}$) and structural descriptors such as volume, molecular weight, polarity, aromaticty and hydrophobicity was obtained. The QSAR studies were performed on chemically diverse molecules belonging to substituted 4-hydroxybenzaldehyde derivatives. The following results were obtained

LogIC50=1.439-1.183*var919-0.178*var693- 1.133*var826+20.106*var143+0.215*var835

Table 1 Definition of descriptors

Descriptors	Definition	Class
Mor29e	3D-MoRSE - signal 29 / weighted by atomic Sanderson electronegativities	3D-MoRSE descriptors
RDF100m	Radial Distribution Function - 10.0 / weighted by atomic masses	RDF descriptors
Mor32u	3D-MoRSE - signal 32 / unweighted	3D-MoRSE descriptors
PW5	path/walk 5 - Randic shape index	topological descriptors
Mor09m	3D-MoRSE - signal 09 / weighted by atomic masses	3D-MoRSE descriptors

Results of principal component analysis is as follow

Log Ic50=-0.152*Size-0.122*Hydrophobicity+0.106*Aromaticity+0.053*Shape

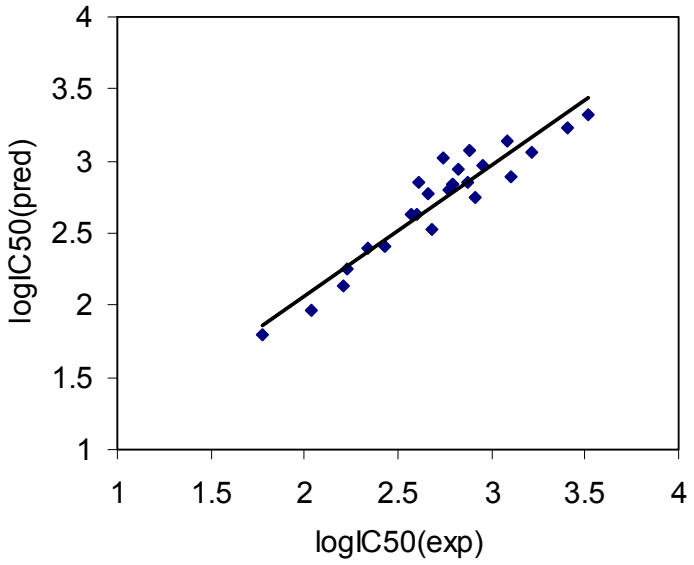

Fig. 1 Correlation between predicted and experimental $\log IC_{50}$ for tyrosinase inhibitors.

Key words: QSAR, Tyrosinase, Molecular descriptors,

References

[1] M. Jimenez, S. Chazarra, J. Escribano, J. Cabanes, F. Garcia-Carmona, J. Agric. Food Chem. 49 (2001) 4060–4063.

[2] N. Yokochi, T. Morita, T. Yagi, J. Agric. Food Chem. 51 (2003) 2733–2736.

Theoretical Investigation of Intermolecular forces in Ionic liquids

A .Maghari*[a] , Z .Jamshidi*[b] and Z .Rezaei*[a]

[a]Department of Chemistry, University of Tehran, Tehran, Iran

[b]Chemistry and Chemical Engineering Research Center of Iran, Tehran, Iran

maghari@khayam.ut.ac.ir, jamshidi@ccerci.ac.ir, zrezaei@ut.ac.ir

Keywords: Ionic liquids, Intermolecular forces, [Bmim][I], [Bmim][Br]

Introduction

The class of Ionic liquids (ILs) has been known due their unique properties as potential designer solvents for wide range of applications.[1] In order to design ionic liquids, it is necessary to make a link between the fundamental properties of the system such as electronic structure and inter-molecular force and specific macromolecular physical and chemical properties.[2] In room-temperature ILs there is a complex interplay of forces –Coulombic, dipole–dipole, dipole–induced dipole, dispersion and hydrogen bond– which has yet to be unraveled. Therefore to interplay the nature of bonds, in this work the QTAIM and EDA analyses were carried out on 1-butyl-3-methylimidazolium bromide [Bmim][Br] and iodide [Bmim][I] B3LYP optimized structures. Also natural bond orbital (NBO) analysis has been performed as useful reference point for an analysis of the charge distribution and charge transfer in selected ILs.

Methods

Geometries of the [Bmim][Br] and [Bmim][I] ILs were fully optimized using the density functional theory (DFT) with B3LYP functional. MP2 single point calculation has been run on optimized structure. The pseudopotential-based augmented correlation-consistent basis sets, aug-cc-pVDZ-PP, based on the small core relativistic pseudopotentials (PPs) of Figgen et al, was used for Br and I, and the Pople 6-31++G(d,p) basis set was used for 1-butyl-3-methylimidazolium [Bmim]. These calculations have been done using Gaussian 03 suite of programs. Structures have been fully optimized, under no symmetry constraints, and the B3LYP structures confirmed by frequency analysis. To reveal the nature of bonds, the NBO, QTAIM, and EDA analyses were carried out on the B3LYP optimized structures.

Results and Discussion

Geometry optimization started by placing anion near the active sites of cation, and obtained multiple stable structures[3] for homologous ion pair; however, we decided to work on four different optimized conformers which exhibited in Figure 1. The differences of anion charges (Δq) before and after complexation have been calculated by NPA charges.

Table 1 has been shown that for different conformers of [Bmim][I], this IL has less intermolecular interaction comparing to [Bmim][Br], that should be related to significant dispersion of iodide. The dipole moment of the resultant ion pair is large, and varies between 9.66 and 18.37 debye (Table 1). It shows that dipole–dipole forces play an important role in IL's intermolecular forces.

A correlation between the amount of Δq and the relative stability of each dimer pair has been obtained from Table 1. [Bmim][Br] conformers have more charge differences and are more stable comparing [Bmim][I] dimer pairs (considering interaction energies E_{int} shown in Table 1 as a standard value exposing stability).

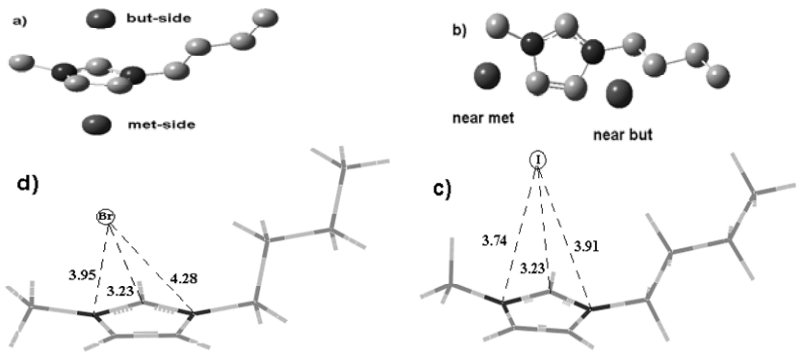

Figure 1. Location of primary cation–anion interaction sites for [Bmim]I, and Br : a) anion out-of-plane b) anion in-plane c) opt [Bmim][I] and d) opt [Bmim][Br]

Table 1. Charge difference (Δq in e), dipole moments (μ in debye) and interaction energies (E_{int} in kcal mol^{-1}) at the B3LYP level for [Bmim]I and Br conformers.

	Δq_{Br}	Δq_{I}	μ_{Br}	μ_{I}	$E_{int(Br)}$	$E_{int(I)}$
Opt	0.161	0.149	12.5610	11.1612	-80.683	-75.424
Buthyl side	0.160	0.151	12.5291	11.0420	-80.676	-75.418
Methyle side	0.173	0.170	9.6662	10.6943	-79.819	-75.368
Near buthyle	0.120	0.112	16.7018	17.8979	-73.512	-68.392

Near methyle	0.132	0.119	18.1290	18.3726	-72.699	-67.598

Reference

[1] M .J .Earle, K .R .Seddon. *Pure Appl. Chem*. **2000**, 72, 1391.

[2] B .L .Bhargava, S .Balasubramanian .*Chem .Phys. Lett* **2006**, *417*, 486.

[3] P .A .Hunt, B .Kirchner, T .Welton *Chem. Eur. J*. **2006**, *12*, 6762.

Silicon Nanotube as a Potential Candidate for Efficient H2 and He Storage: First Principle Calculations

S. Saleheh Razavi*[1], Fatemeh cigarchi [1],S. Majid Hashemianzadeh [1]

[1]Molecular Simulation Research Laboratory, Department of Chemistry, Iran University of Science and Technology, Tehran, Iran

srazavi @chem.iust.ac.ir

Keywords: DFT Calculatio, Hydrogen storage, Morse Potential, Gas Adsorption.

Introduction:

Hydrogen has been recognized as an ideal energy carrier with heating value three times higher than petroleum[1]. However, several studies have been performed to meet the goals of U.S. Department of Energy (DOE) Hydrogen plan, 6.5 wt%, most of them have failed to approach the proposed target. In addition, only a few researches have been reported on hydrogen adsorption behaviour of SiNTs [2] and shown SiNTs can perform more practically than CNTs, thus can be considered as a capable candidate for hydrogen storage. To our knowledge, there are no studies providing good data either for adsorption of other gases on SiNTs or gas mixtures. Therefore, we studied a theoretical method, combination of ab initio calculations and canonical Monte Carlo simulation, to investigate the interaction of hydrogen and helium on single-walled SiNTs.

Models and simulation methods:

Our research was carried out using three armchair SiNTs with different diameters which their cluster models were applied to avoid heavy computations: For both the (7, 7) with diameter of 15.0 Å and (9, 9) SiNTs with diameter of 19.3 Å, a small curved graphene-like sheet cluster model, and for (5, 5) SiNT with diameter of 10.8 Å, a cylindrical cluster model separating symmetrically from corresponding SiNTs.[2]All the energy calculations have been performed at the level of density functional theory (DFT) employing MP1PW91 along with the 6-311++g** basis set for highly interacting atoms using the GAUSSIAN 03 program.[22] By considering three different adsorption sites for interacting helium and hydrogen with SiNTs:

1) top of silicon atom, 2) middle of Si-Si bond, and 3) centre of hexagonal ring(hollow site), the binding energy for each site was computed as the following equation to explore the most appropriate site of adsorption:[2,4]

$E_{binding} = E_{gas\text{-}model\ cluster} - (E_{gas} + E_{model\text{-}cluster})$ (1)

Our results show that,the hollow adsorption site was considered as the most favorable one. Therefore, we limited our computations to the investigation of adsorption of H2 and He gas molecules with hexagon center of SiNT to investigate H2/SiNTs and He/SiNTs potential energy curves.Continuing our investigations, it should be mentioned that the proper choice potential equation as a link between ab initio calculation and Monte Carlo simulation is of vital importance, Therefore, three models of potential functions including (12-6), (9-6) lennard-Jones and Morse equation are selected. The (12-6), (9-6) lennard-Jones equations couldn't be fitted with the H2 and He potential curves , shown in figure 1, whereas we found that the Morse potential (eq 2) is the most favourable potential model, which has a very good coincidence with the results driven from the ab initio calculations for both hydrogen and helium due to slower slope in their repulsion branch.

Figure 1. Potential energy curves for a) interacting hydrogen and b) helium with hollow adsorption site for (5, 5), (7, 7), and (9, 9) SWSiNTs.

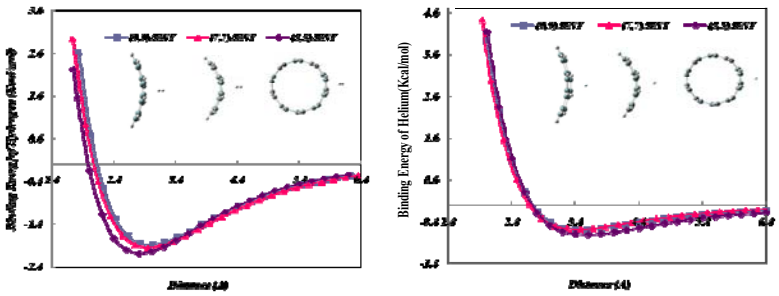

The Morse potential is represented as follows: [2]

$$U_i = 2D[X^2 - 2X], \qquad X = \exp\left(-\frac{g}{2}\left(\frac{r_i}{r_e} - 1\right)\right): \tag{2}$$

The amount of parameters of Morse potential for both H_2 and He are reported in table (1).

Table 1. Calculated Morse potential parameters for interaction of H_2 and He with hollow sites of three different SiNTs

Morse potential parameter	outside the tube wall for (5, 5) SiNT		outside the tube wall for (7, 7) SiNT		outside the tube wall for (9, 9) SiNT	
	H2	He	H2	He	H2	He
D(kcal/mol)	1. 1	0. 36	0.983	0. 297	0. 973	0. 304
g	4. 83	5. 745	4. 768	5. 719	4.98	5. 956
re(A)	2. 79	3. 586	2. 98	3. 637	2. 944	3. 575

Conclusion:

In summary, the binding energies for both hydrogen and helium with different SiNTs were determined via ab initio calculations and fitted by Morse potential equation. The binding energies for hydrogen adsorption on the surface of tubes are considerably stronger than helium. Since the interaction energies of H2 and He with SiNTs are in the region of physisorption through the van der waals interaction, and with the intention to the fact that helium is a noble gas with quite different physicochemical properties against hydrogen and lower polarizability than H2, binding energies for helium adsorption on the surface of tubes are noticeably lower than hydrogen.

References:

[1] Zhou, L. Renewable and Sustainable Energy Reviews **2005**, 9, 395-408.

[2] Lan, J.; Cheng, D.; Cao, D.; Wang, W. The Journal of Physical Chemistry C **2008**, 112, 5598-5604.

[3] Lee, C.; Yang, W.; Parr, R. G. Physical Review B **1988**, 37, 785-789

[4] Lithoxoos, G. P.; Samios, J.; Carissan, Y. The Journal of Physical Chemistry C **2008**, 112, 16725-16728

Hydrolysis Chemistry of the Molybdocene dichloride: a Theoretical study on the Reaction Mechanism

M. Zakarianezhad*[a] and B. Makiabadi

[a]Department of Chemistry, Faculty of Science, Payam Noor University, Sirjan Center, Sirjan, Iran

(E-mail: mzakarianejad@yahoo.com)

[b]Sirjan Engineering College, Shahid Bahonar University, P.O. Box 78185439, Sirjan, Iran

Keywords: Molybdocene dichloride, Hydrolysis, Concerted Mechanism, Rate Constant

Introduction

The interest in molybdocene dichloride and related metallocenes has dominated by their remarkable catalytic properties in organic synthesis and as polymerization catalysts [1,2]. Testing of a range of metallocene dichlorides identified Cp_2MCl_2 (M=Ti, V, Nb and Mo) as cytotoxic agents with potential as anticancer agents [3]. The hydrolysis chemistry of these compounds is complex, typically involving the formation of a number of dimeric and oligomeric species. The structure of the hydrolysis products is highly dependent on the pH and is often inferred only from titration studies.

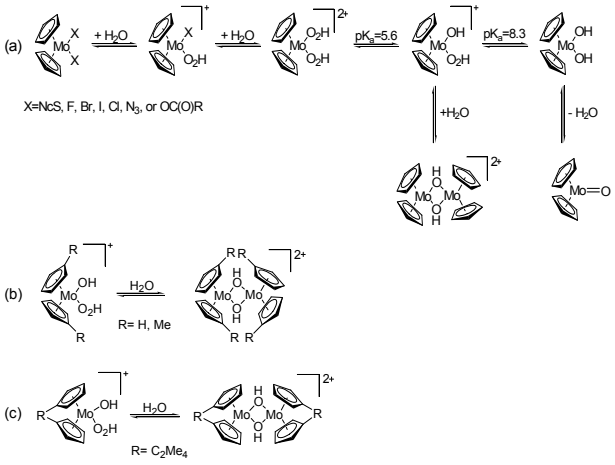

Scheme 1.

In most cases, hydrolysis of the coordinated halide or pseudo-halide ligands occurs first and affords aquated metallocene complexes, with OH or OH_2 ligands replacing X (Scheme 1). The dissociation rate of the second X^- is dependent of X in Cp_2MoX_2. Taking into account

the kinetic parameters and finding the most favorable reaction mechanism, has promoted us to investigate the hydrolysis chemistry of molybdocenes in a detailed theoretical study.

Methods

Quantum chemical computations were carried out with the Gaussian 03 series of programs. Full geometry optimizations of stable species and transition states (TS) were performed in the gas phase by employing the hybrid density functional B3LYP with the aug-cc-pVDZ (cc-pVDZ-pp for Mo) and aug-cc-pVTZ (cc-pVTZ-pp for Mo) basis sets. It has been demonstrated that B3LYP and MP2 levels of theory give similar results. Vibrational frequency calculations were carried out for all complexes at the B3LYP/aug-cc-pVDZ and the B3LYP/aug-cc-pVTZ levels to calculate the zero point energy (ZPE). To take into account condensed-phase effects, single-point calculations were also performed on the gas-phase-optimized geometries using the polarizable continuum model (PCM) of Tomasi et al. with the united atom Hartree-Fock (UAHF) parametrization. To check the reliability of our computational scheme, we also optimized at the B1B95/SDB-aug-cc-pVTZ level of theory, the key critical structures involved in the most favorable mechanisms previously found at the B3LYP level of theory.

Results and Discussion

Three paths are found in the first and the second hydrolysis step in which, the water molecule attacks to the Mo atom and the chloride atom goes out spontaneously. In summary, the first hydrolysis step exhibits similar geometric features to the second hydrolysis step. The rate constants (k) were calculated within the transition state theory, using Eyring equation. We also investigated another plausible mechanism in the first and the second hydrolysis steps. This mechanism includes the cleavage of the Mo-Cl bond in the first time and adding of the water molecule to the structure in the next time. This process will repeat for adding of the second water molecules in the second hydrolysis step. Results indicate that the recent proposed mechanism is in a good agreement with the experimental data. Also, interesting results obtained from the effect of the substituted groups on the hydrolysis steps and equilibrium constants.

Conclusions

The energetic properties, including the relevant thermodynamic quantities and the estimation of the rate constants, were obtained from the computations. Results indicate that S_N1 mechanism is the concerted mechanism of the hydrolysis processes. The computed values of free energy barriers $\Delta G^{\circ}(aq)$ and rate constants (k) in aqueous solution, for the first and second hydrolysis steps, are in excellent agreement with the experimental results under the same conditions.

References

[1] H.G. Alt, A. Koeppl, Chem. Rev. 100 (2000) 1205.

[2] P.C. Moehring, N.J. Coville, J. Organomet. Chem. 479 (1994) 1.

[3] P. Kopf-Maier, M. Leitner, H. Kopf, J. Inorg. Nucl. Chem. 42 (1980) 1789.

Calculation of the Partition Coefficient by the QSAR Method for Some of Adamantane Drug Derivatives

Z.Bayat*, M.Zanoozy, M.Fakoor.YazdanAbad
Department of chemistry, Islamic Azad University-Quchan Branch, Iran
z.bayat@ymail.com

Abstract
Diamondoids are classed with organic nanostructures; therefore, adamantane derivatives have become particularly popular with the development of nanotechnologies.The applications of adamantane derivatives are diverse: from antiviral drugs to nanorobots and molecular machines.

Keywords: partition coefficient,Mathematical modeling,QSAR, MLR,DFT

Introduction

In this report our goal was to study the partition coefficient (logP) of adamantane derivatives and also to examine the relationship between the physicochemical properties and logP of adamantane derivatives. Correlations between the logP and structural characteristics of adamantane derivatives were found based on the QSAR (Quantitative Structure_Activity Relationships) method.

Methods

Quantum-chemical calculations were performed with Gaussian 03 package and HyperChem program package, version 8.0, by Density Functional Theory (DFT) methods and at the 6-31+G** basis set.

Results and discussion

Also Multiple Linear Regressions (MLR) were employed to model the relationships between molecular descriptors and logP of molecules using stepwise method. The following modeles with the best statistic parameters were obtained. logP were calculated by the following models and compared with experimental values.(Table. 1)

$LogP = 1.289(\pm0.194)\ HE + 0.434(\pm0.116)\ \Delta G_w + 1.733(\pm0.808)$

(B3LYP/6-31+G**) (1) (R= 0.940 R^2= 0.884 $Q^2_{=\ 0.72}$ F= 61.21 N=19)

$LogP = 2.234\ (\pm0.347)\ HE + 0.433\ (\pm0.094)\ \Delta G_w + -0.009(\ 0.003\ )SAAP + 1.831(\pm0.656)$

(B3LYP/6-31+G**) (2) (R= 0.964 R^2=0 .929 $Q^2_{=}$ 0.77 F= 65.15 N = 19)

COMPOUND	$LogP_{EXP}$	$LogP_{Eq1}$	$LogP_{Eq2}$

adamantane	2.69	2.68	2.87
1 3 dimethyl adamantane	3.56	3.76	3.75
1-buthyl adamantane	4.31	4.40	4.57
1-ethyl adamantane	3.52	3.43	3.55
1-isopropyl adamantane	3.85	3.80	3.87
1-propyl adamantane	3.92	3.95	4.09
2-buthyl adamantane	4.21	4.26	4.47
2-ethyl adamantane	3.42	3.30	3.47
2-isopropyl adamantane	3.75	3.36	3.49
2-methyl adamantane	3.02	3.04	3.20
2-propyl adamantane	3.81	3.51	3.69
1-methyladamantane	3.13	3.22	3.31
1- sec buthyl adamantane	4.25	4.25	4.35
1-tert-buthyl adamantane	4.29	4.04	4.03
1-ethyl-3-methyl-adamantane	4.35	4.04	4.06
1.3.5.7.tetra methyl adamantane	4.42	4.87	4.68
1.3 diethyl adamantane	4.35	4.32	4.37
1-n-n dimethyl adamantane	1.88	2.38	2.04
2-isobuthyl adamantane	4.15	4.21	4.32

Commonly used descriptors in the QSAR analysis are presented in Table 2.

Descriptor	Symbol	Example
Quantum chemical descriptors	Molecular Polarizability	MP
	Electrostatic Potentialc	EP
	solvation Free Energy(in Octanol)	ΔG_{OCT}
	solvation Free Energy(in water)	ΔG_{WATER}
	Isotropic Parameterd	Σ
	Mulliken Charge	MC
	Molecular Dipole Moment	MDP
	Highest Occupied	HOMO
	Lowest Unoccupied	LUMO
	difference between	E_{Gap}
	Hardness	H
	Electro negativity	X
Chemical Properties	Softness (S=1/ η)	S
	Partition Coefficient	Log P
	Molecule surface area	SA
	Hydration Energy	HE
	Refractivity	REF
	Mass	M

Conclusions

The aim of this work is the development, using theoretical molecular descriptors, and the proposal of externally validated general QSAR models for the prediction of (logP) for a wide

compounds.The use of descriptors calculated only from molecular structure eliminates the need for experimental determination of activity for use in the correlation and allows for the estimation of (logP)for molecules not yet synthesized.

References

[1]. Miroshnichenko, E.A., Lebedev, V.P., and Matyushin, Yu.N., *Dokl. Ross. Akad. Nauk*, 2002, vol. 382,no. 4, pp. 497_ 499.

[2]. Mansoori, G.A., in *The Next Industrial Revolution:Proc. 1st Conf. on Nanotechnology*, 2002, vol. 2,pp. 53_59.

[3]. Takeushi, H., *Rev. Toyota CRDL*, 2001, vol. 36, no. 3,p. 9.

Thermodynamics , Solvents effects and Theoretical studies of Acenaphthylene

R.Zhiani*[a], M.Monajjemi[b], Sh.Salari[c] , A.Fallahnejad[d]

[a] Department of Chemistry, Islamic Azad University, neyshabur, Iran
(Email: R_Zhiani2006@yahoo.com)
[b] Department of Chemistry, Science and research Branch, Islamic Azad University, Tehran, Iran
[c] Department of Chemistry , Islamic Azad University,Yazd, Iran
[d] Islamic Azad University_Yazd Branch Young Researchers Club

Abstract

Some of the Acenaphthylene properties were calculated in this study. free energy of solvation, free energy of cavity formation, Henry's law constant, and other properties of Acenaphthylene in dry phase, three solvents have been calculated with Ab initio method base on density functional theory (DFT) at B31yp/6-3Ig, B3Iyp/6-31g*, B3Iyp/631 +g* and B3Iyp/6-31 ++g** three solvents were used in this study are polar and non-polar solvents with different dielectric constants. The results show that the free energy of solvation of Acenaphthylene in non-polar solvents such as n-heptane is more negative than the polar solvents like water**.**

Keywords : Acenaphthylene; Ab initio; DFT; Free energy solvation

Introduction

Polycyclic aromatic hydrocarbons (PAH) containing unsaturated five membered rings externally fused to six-membered ring perimeters (CP-PAHs) are important in several context[1]. CP-PAHs have been identified as ubiquitous combustion effluents, and several representatives have been shown to possess considerable genotoxic activities [2].

Geochemical processes yield PAHs when natural organic matter(NOM) is exposed to high pressure and temperature.This compounds can be source pollutants (e.g. oil spill) or non point source (e.g. atmospheric deposition) and are among the most widespread organic pollutants. Anthropogenic practices , such as industrial processing, petroleum spills, and in complete combustion of fuel , also contribute to high levels of PAHs in the enviroment [3-7].

(PAHs) with external cyclopenta - fused five membered rings, such as the cyclopenta – fused naphthalene (Acenaphthylen) derivatives , belong to the class of nonalternant polycyclic aromatic hydrocarbons and may exhibit unusual (Photo) physical properties. Several qualitative models, e.g.Plat's ring perimeter model[8] Clar's model[9] and Randics conjugated

circuits model [10,11] have either been or are frequently used for the rationalization of the properties and the reactivity of PAHs.

Solvent effects on thermochemical phenomena remain a challenging area of investigation for physicalal chemists. Many organic chemistry reactions take place in solution and, thus, it is important for realistic theoretical models to accurately describe

solvent effects. Furthermore, in processes involving biomolecules, such as enzyme catalysis, surrounding enzymatic structure can significantly influence chemical reactivity. However Ab initio molecular orbital theory at the SCF level and OFT method has been shown to be capable of the accurate prediction of geometry and thermochemisry for small hydrocarbons. Two highly productive approaches to solution of the electronic "Schrodinger " equation have arisen over the past 50 years.

Wave function-based approaches expand the electronic wave function as a sum of Slater determinants, the orbital and coefficients of which are optimized by various numerical procedures. Hartree-Fock theory is the simplest method of this type, involving optimization of a single determinant. However, its usefulness is limited because of complete neglect of electron correlation. The second class of theoretical approaches are based on the density functional theory (DFT), which follows the Hohenberg-Kohn theorem mandates expression of the total energy of the system as a functional of the electron density. Because the electron density depends on only three coordinates (as opposed to the 3N coordinates of N electrons), the computational effort required to solve the equations of DFT is comparable with that required for Hartree-Fock theory, thus rendering DFT highly attractive from the point of view of computational implementation. However, the correct functional of the energy is unknown and has to be constructed by heuristic approximation. Initial functionals, based principally on behavior of the electron gas were lacking in the accuracy required for chemical applications. Break through over the past two decades [12 -16] have led to the development of functional capable of remarkable accuracy and breadth of applicability across the periodic table.

Theoretical method

For small molecules in the gas phase and in solution, Ab initio quantum chemical calculations can provide results approaching benchmark accuracy and they are used routinely to complement experimental studies. A wide variety of properties, including structures [17], thermochemistry including activation barriers [17], spectroscopic quantities of various types

[18], and responses to external perturbations can be computed effectively. SCRF methods (or simply ignoring the solvent entirely, an approximation that is sometimes acceptable, particularly in non polar solvents or when a quantity that is insensitive to the dielectric of the environment is being computed) enable a relatively straight forward extension of gas phase quantum chemical methods to obtaining results for molecules in solution. Optimization of the accuracy of continuum solvation methods is far from a solved problem. furthermore, there is some evidence that the inclusion of a small number of explicit water molecules can improve results [19], but methods of this type must be formulated very carefully to avoid double counting. The Ab initio calculations were performed by GAUSSIAN 98 program. The basis sets were used are 6- 31 G, 6- 31 G*, 631 + G*, and 6-31 + + G** . This basis sets were selected for considering of effects of polar and diffusion Parameters on various properties. Structural parameters are optimized at the basis sets. The optimized geometry parameters are used to obtain total electronic energies. Long-range effects of the solvents (water, n-heptane and cyclohexane) are taken into account by means of a dielectric continuum represented by the polarizable continuum model (PCM). We have used the PCM model for geometry optimizations and energy calculations. In the polarizable continuous (PCM) model, the cavity was used of molecular shape and was built by interlocking spheres. The radii of the spheres were obtained by scaling the atomic Van der waals radii. The surface of each sphere was divided in 60 triangular tesserae (default value) for the calculation of the surface-charge distribution. In the present paper, we have employed the PCM model to determine the solvent effects on the geometric parameters of reaction processes.

Results and discussion

Result of free energy of solvation in water, cyclohexane and n-heptane at 298.15K for Acenaphthylene determined bas on DFT calculations at four basis sets are shown in the following tables.

Table1. Solvation free energy (kcal/mol) for the Acenaphthylene determined from B3Iyp/6-3IG, B31yp/6-31 G*, B31yp/6-31 +G*, B3Iyp/6- 31 ++G** calculations were performed in different solvents at 298.15 K.

	SOLVENT	ΔG_{sol}
B3lyp/6-31G	Water	-0.69
	Cyclohexane	-3.96
	n-Heptane	-4.29
B3lyp/6-31G*	Water	-0.83
	Cyclohexane	-4.04
	n-Heptane	-4.37

B3lyp/6-31+G*	Water	-0.95
	Cyclohexane	-4.05
	n-Heptane	-4.38
B3lyp/6-31++G*	Water	-0.94
	Cyclohexane	-4.03
	n-Heptane	-4.37

Acenaphthylene is a non-polar molecule, so its solvation in a polar solvent such as water is so less. The results from the theoretical computations in table1 confirm this subject. As we know the negative solvation energy shows the solvation has been done. As it is clear in table l all the solvation energy calculated with all the methods are negative and its values for n-heptane is more than cyclohexane and also more than water. There are energies of cavity formation (kcal/mol) in water, cyclohexane and n- heptane at 298.15 K for Acenaphthylene in table 2 these energies was determined from DFT calculations.

Table 2. Cavity formation of free energy (kcal/mol) for the Acenaphthylene was obtained from B3Iyp/6-31 G , B3Iyp/6-3IG*, B3Iyp/6-31+G*, B3Iyp/6-31++G** calculations in different solvents at 298.15 K.

	SOLVENT	$T = 298.15$
B3lyp/6-31G	Water	18.38
	Cyclohexane	13.93
	n-Heptane	12.02
B3lyp/6-31G*	Water	18.31
	Cyclohexane	13.58
	n-Heptane	11.97
B3lyp/6-31+G*	Water	18.33
	Cyclohexane	13.59
	n-Heptane	11.97
B3lyp/6-31++G*	Water	18.33
	Cyclohexane	13.59
	n-Heptane	11.37

We know formation of cavity in solvation process is a difficult step and consume energy. As the Table 2 Show free energies of cavity formation are positive. On the other hand the solubility of Acenaphthylene in water is lower than non-polar solvents and formation of cavity in water more difficult than the other solvents.

The Henry's law constant in water, cyclohexane and n-heptane at 298.15k for Acenaphthylene were calculated with Eq 6.

Table3. Henry's law constant determined from B3lyp/6-3IG , B3Iyp/6-3IG*, B31yp/6-31 +G*,B3Iyp/6-31 ++G**calculations were used Eq 6.

	SOLVENT	$T = 298.15$
B3lyp/6-31G	Water	581.8905
	Cyclohexane	458.7909
	n-Heptane	402.6221
B3lyp/6-31G*	Water	585.9577
	Cyclohexane	458.7166
	n-Heptane	402.5758
B3lyp/6-31+G*	Water	585.9578
	Cyclohexane	458.7089
	n-Heptane	402.5690
B3lyp/6-31++G*	Water	585.9677
	Cyclohexane	485.7244
	n-Heptane	402.9558

As it mentioned previously the Henry's law constant has a close relationship with solvation energy. Table 3, shows that the constant values of Henry's law constants for water are more than cyclcohexane and both of them are more than n-heptane and these are completely fit the last results.

The previous calculations shows that the solvation energy for n-heptane is more negative than cyclohexane and both of them are more negative that water.

Conclusion

The solubility results permit the validation of molecular force fields that attempt to describe the solute - solvent interactions in solution. Molecular simulation can be used to calculate the solvation properties starting from a specification of the molecular structure and interactions of the chemical species presenting the system. Predictive simulation tools can be used to complement experiments whenever these are too difficult, for example, when solubility is very low or when working conditions involve extreme temperatures or high pressure.

Calculation of solubility can be achieved for gaseous solutes and whit a slightly different procedure. Also for solutes that exist in the form of condensed phase at standard conditions [20].

The molecular mechanisms determining the dissolution process can be investigated by simulation by isolating the effect of different terms in the interactions. The structure of the solution, concerning the arrangement of the solvation shells around the solute, can be predicted by simulation, even in systems where the low concentration of solute precludes obtaining diffraction data.

PCM has proved useful in describing the effects of the solvent on some characteristics of the molecule in solution. All PCM calculations in this study have been performed in GAUSSIAN 98 package.

References

[1] Harvay.R.G.Polycyclic Aromatic Hydrocarbons: Wiley-VCH: NewYork , (1997).

[2] For a review, see : wiersum, U.E.; Jenneskens,L.W.In Gas -phase Reactions in Organic Synthesis; Vallec,Y.Ed; Gordon and Breach Science publishers; Amsterdam , (1997); chapter

[3] E.A.Guthire, F.K.Pfaender, Environ. Sci. Technol.32 (1998) 501.

[4] G.Cornelissen, H.Rigterink, M.M. Ferdinandy, P.C.Van Noort. Sci. Technol. 32(1998) 966.

[5] C.S.Ragle. R.R.Engebretson, R.Von Wandruszka. Soil Sci. 162(1997) 106.

[6] J.J.Pignatello, B.Xing. Environ. Sci. Technol.30(1996)1.

[7] J.R.Platt. J.Chem. Phys.22(1954) 1448-1455.

[8] E.Clar, Polycyclic Hydrocarbons; Academic Press Inc,: London, (1964).

[9] M.Randi'c. Chem Phys.Lett.38(1976) 68-70.

[10] M.Randi'c. Tetrahedron 33(1977) 1905-1920.

[11] M.Randi'c. J.Am. Chem. Soc.99 (1977) 444-450.

[12] Kohn, W., Becke, A. D. & Parr, R. G. J. Phys. Chern. 100 (1996) 12974-12980.

[13] Johnson, B. G., Gill, P. M. W. & Pople, J. A. J. Chern. Phys. 98 (1993) 5612-5626.

[14] Becke, A. D. Phys. Rev. A 38 (1998) 30983100.

[15] Becke, A. D. J. Chern. Phys. 98(1993) 5648-5652.

[16] Lee, C. T., Yang, W. T. & Parr, R. G. Phys. Rev. B 37(1988) 785-789.

[17] Guner, v., Khuong, K. S., Leach, A. G., Lee, P. S., Bartberger, M. D. & Houk, K. N. J. Phys. Chern. A 107(2003) 11445-11459.

[18] Gauss, J. & Stanton, J. F. J. Chern. Phys. 104(1996) 2574-2583.

[19] Rempe, S. B., Asthagiri, D. & Pratt, L. R. Chern. Phys. 6(2004) 1966-1969 .

[20] J.Deschamaps. M.F.Costa, A.A.H.Padua.J.Fluorine Chem. 125(2004) 409.

Density Functional Theory (DFT) Study for Enthalpy of Formation of Coronene

S.Jameh-Bozorgi[ab]*, H.Soleymanabadi[a] , A.Bodaghi[a], H.Zaheri[c] , and E.Sheikhi[d]

(Email:sjamehbozorgi@gmail.com)

[a] *Chemistry Department, Faculty of Sciences, Islamic Azad University, Touyserkan Branch, Touyserkan, Iran*

[b] *Chemistry Department, Faculty of science, Islamic Azad University, Arak Branch, Arak, Iran*

[c] *Chemistry Department, Faculty of Sciences, Islamic Azad University, Touyserkan Branch, Young researchers Club, Touyserkan ,Iran*

[d] *Chemistry Department, Faculty of science, Islamic Azad University, Rasht Branch, Rasht, Iran*

Keywords:DFT,coronene,optimized,B3LYP

Introduction:

Coronene is an aromatic polycyclic hydrocarbon generated by the incomplete combustion of fossil fuels and vegetable combustibles in vehicular traffic and industrial emissions.by contrast ,the physical chemistry of this compound and its derivatives is receiving increased attention due to its charge transport and light-emitting capabilities in ordered films, characteristics with potential technological applications in optical and organic electronics . Furthermore, coronene is a key compound for the estimation of resonance and bond energy of fullerenes . This feature is perhaps the most important motivation to measure its thermochemical properties with the greatest accuracy. Unfortunately, data for this polycyclic aromatic hydrocarbon are scarce and dispersed over a wide range . The present study involves the measurement of several thermochemical quantities and enthalpy of formation of coronene.

Methode:

The geometry of the systems has been fully optimized with the hybrid DFT /B3LYP [1-2] computational method and the 6-311+G(d,p) basis set[3],within the Gaussian 03 package[4].DFT calculations were performed on an DELL 1555 Computer ,Frequency calculations have been carried out to confirm that the structures obtained correspond to energetic minima.

Result and discussion:

The theoretical gas phase enthalpy of formation of coronene at T =298.15 K was derived from the calculated change of enthalpy, $\Delta_r H(298.15\ K)$, involved in the hypothetical homodesmic reaction proposed by Schulman [5]:

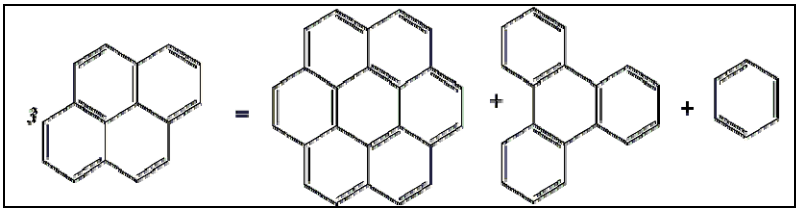

Equation (1)

The DFT total energy, zero-point energies (ZPE) and thermal corrections to enthalpy (ΔH_{corrr}) of coronene, pyrene, triphenylene,and benzene resulting from computational calculations of optimized structures and an analysis of vibrational frequencies are shown in table 1. From these values and equation (1), the $\Delta_r H°$ is computed as:

$$\Delta \mathbf{rH°(298K)} = \sum (\boldsymbol{E_{total}} + \mathbf{ZPE} + \Delta \mathbf{H_{corr}})\mathbf{product} - \sum (\mathbf{E}_{\boldsymbol{total}} + \mathbf{ZPE} + \Delta \mathbf{H_{corr}})\mathbf{reactant}$$

Molecule	*DFT total energy*	*ZPE*	H_{corr}	*E(thermal)*
Pyrene	*-615.9159999*	*0.206143*	*0.2171919*	*135.697*[a]
Coronene	*-922.1006833*	*0.2763043*	*0.2914193*	*182.276*[a]
Triphenylene	*-693.3445697*	*0.2403967*	*0.2536897*	*158.600*[a]
Benzene	***-232.3112711***	***0.1001791***	***0.1055211***	***65.623***[a]

Table 1.Total energies, zero-point energies, and thermal corrections to the enthalpy in hartrees
[a] contributions to the thermal energy correction in kcal mol^{-1}

The resulting homodesmic reaction enthalpy computed in this way is $\Delta_r H$ (298.15 K) =-28.93 $kj.mol^{-1}$,in good agreement with respect to the range of values obtained by Schulman[5]. Thus, the gas-phase enthalpy of formation for coronene is derived from equation (1) as:

$$\Delta_f \mathbf{H°(coronene, 298K)} = \Delta_f \mathbf{H(298K)} + \mathbf{3}\Delta_f \mathbf{H°(pyrene)} - \Delta_f \mathbf{H°(triphenylene)} - \Delta_f \mathbf{H°(benzene)}$$

Conclusion:

where the experimental enthalpies of formation for pyrene, triphenylene, and benzene are taken from the compilation of Pedley [6] and given as {(225.52 ± 1.25), (274.05 ± 4.18), and (82.42 ± 0.84)} $kj.mol^{-1}$, respectively. The final resulting value of the theoretical gas phase

enthalpy of formation of coronene is $\Delta_f H$ (298K) = 291.15 kj.mol^{-1} According to the experimental results is acceptable[6].

References :

[1] Bean, G. P. J. Org. Chem. 1998, 63, 2497e2506.

[2] Becke, A. D. J. Chem. Phys. 1993, 98, 5648e5652.

[3] Lee, C.; Yang, W.; Parr, R. G. Phys. Rev. B 1988, 37, 785e789.

[4] M. j. Frisch et al. GAUSSIAN 03, Revision C. 01, Gaussian Inc., Wallingford. CT, (2004).

[5] J.M. Schulman, R.L. Disch, J. Phys. Chem. A 101 (1997) 9176–9179.

[6] J. B. Pedley, Thermochemical Data and Structures of Organic Compounds, vol. I, Thermodynamic Research Center, College Station, Texas, USA, 1994.

The Study Amount Of ASE And NICS Structure 3H-[1,3]diborolo[4,5-d][1,3]diborinine By Theoretical Method

R.Soleymani*[a,b] and F.Afshari[a]

[a] *Chemistry Department, Faculty of Sciences, Islamic Azad University, Touyserkan Branch, Young researchers Club, Touyserkan ,Iran*
(Email: nima_soleimany@yahoo.com)
[b] *Chemistry Department, Faculty of Sciences, Islamic Azad University Shahre-rey Branch, Tehran, Iran*

Keywords: Ab initio; ASE ; DFT ; NICS ; NBO

Introduction

ASE (aromatic stabilization energy) is caused by ring aromatic properties which the rings aromatic is created by pay electron resonance which this factor cause the decreasement of energy level and structures stability. We use the following structures for calculation ASE [1].

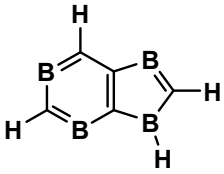

1

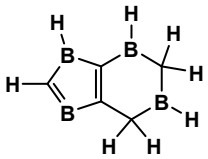

2

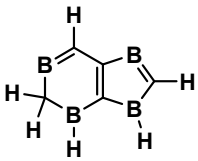

3

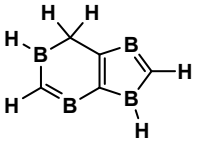

4

Calculation methods

Ab initio calculations were performed using levels of theory with the GAUSSIAN 03 package of programs [2] implemented on a Pentium IV computer with a Intel 730 MHz processor. Firstly, the considered models were allowed to fully relax during the geometrical optimization by the HF and DFT exchange-functional method. Secondly, the NBO and GIAO calculations were carried out on the three geometrically optimized compounds by UHF and DFT method and the above mentioned standard basis set.

Result and discussion

The obtained results of quantum mechanism are reported in table (1) which this table shows the amount of ASE for this structure. Also in table (2) the amount of NICS are reported in different distance.

Table1: Calculated zero point energy (ZPE) ,Electronic energy (Eele), Total energy(E_0) and aromatic stabilization energy ASE (in Hartree) of compounds 1- 4 by B3LYP,HF/6-311+G** method

method	HF/6-311+G**				B3LYP/6-311+G**			
Structure	ZPE	Eele	E_0	ASE	ZPE	Eele	E_0	ASE
1	0.085348	-290.301896	-290.216548	0.000193 (0.1211075)[a]	0.080071	-292.2662277	-292.186156	0.005066 (3.178915)[a]
2	0.127759	-292.7187339	-292.590975		0.120203	-294.7474315	-294.627228	
3	0.106681	-291.5064830	-291.399802		0.100687	-293.5075720	-293.406885	
4	0.107481	-291.5153947	-291.407914		0.101127	-293.5126917	-293.411565	

[a]Number in parentheses are corresponding ASE values in kcal.mol^{-1}

Table 2:Calculated nuclear independent chemical shifts values in ppm by GIAO-B3LYP/6-311+G** method

5 membered ring	No of dummy atom	Distance of hetrocycle center(A)	NICS values (ppm)	**6 membered ring**	No of dummy atom	Distance of hetrocycle center(A)	NICS values (ppm)
	1	2.00	-5.1675		1	2.00	-1.5131
	2	1.50	-7.9826		2	1.50	-3.3561
	3	1.00	-15.7645		3	1.00	-6.5961
	4	0.50	-13.6231		4	0.50	-13.4291
	5	0.00	-11.1060		5	0.00	-18.5725

Conclusion

Using initial Ab initio calculation , the amount of ASE was obtained for structure 3H-[1,3]diborolo[4,5-d][1,3]diborinine 3.178915 Kcal/mol .Also the results of calculation the amount of NICS showed that the maximum amount of isotropic magnetic for 5 member ring is at the distance of 1.00 angstrom above the ring and its amount is equal to -15.7645 ppm and the maximum amount of isotropic magnetic for 6 member ring is at the distance of 0.00 angstrom above the ring and its amount equal to -18.5725 ppm. Also NBO analysis showed

that the amount of aromatic properties of the structure increased by the effect of pay electrons resonance and the energy of the level decreased due to decreasing of electron density which this factor cause the stability of the structure.

References

[1] Andrew Pelter and Keith Smith, *Boron Stabilization*, Comprehensive Organic Synthesis Volume 2, Pages 487-503, **1991**

[2] M. j. Frisch et al. *GAUSSIAN 03*, Revision C. 01, Gaussian Inc.,Wallingford. CT, **2004**.

Investigation Two Step Mechanism Of Scheiner Aziridine Synthesis By Ab initio and DFT Studies

R.Soleymani*[a,b], F.Afshari[a]

[a]Chemistry Department, Faculty of Sciences, Islamic Azad University, Touyserkan Branch, Young researchers Club, Touyserkan ,Iran

(Email: nima_soleimany@yahoo.com)

[b]Chemistry Department, Faculty of Sciences, Islamic Azad University Shahre-rey Branch, Tehran, Iran

Keywords: Ab initio ; Banana bond ; DFT ;Scheiner Aziridine ; 1,2,3-triazoline

Introduction

Empirical results of aziridine synthesis showed that in conditions such as light , high temperature and atmosphere is necessary to perform this reaction[1,2]. Also for calculation density functional theory (DFT) used B3LYP method with 6-311++g** basis set. The B3LYP method combines Becke,s three-Parameter exchange (B3) function with the correlation function of Lee-Yong-Parr (LYP).[3,4]

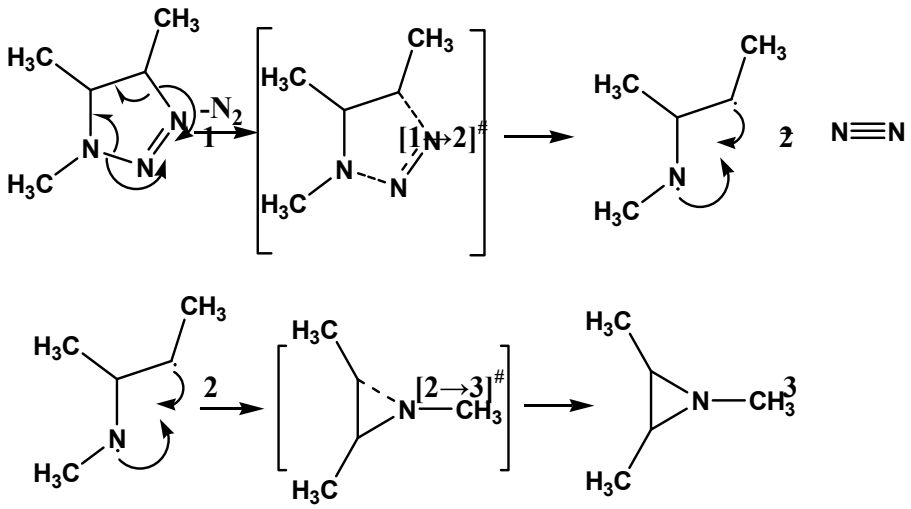

Calculation method

Quantum mechanical calculation at DFT method level of theory using to investigation mechanism of scheiner Aziridine synthesis. Initial optimization operated by using Winmopac version 2.0 software and AM1 method.Firstly the transition mode of structure simulate by using keyword SADDLE . Then transition state obtained GAUSSIAN 03W package program and keyword QST3 . For this purpose using pentum IV computer with a intel core i7 Ghz processor. Eventually, the final optimization and calculation of energy levels operated in theory of the level B3LYP/6-311++G**.

Result and discussion

Quantum mechanic calculation of shows the energetic amounts adjusted for this mechanism in following table.

Total energy (E_0) , Zero Point energy (ZPE) , Electronic energy (E_{ele}) , Activation energy(ΔE_0) in Hartree

Method	B3LYP/6-311++G**			
Geometry	ZPE[b]	Eele	E_0	ΔE_0[a]
1	0.157289	-361.4968910	-361.339601	
[1→2]#	0.151164	-361.3927251	-361.241561	0.0980400 (61.5201)[c]
2	0.158487	-361.4974002	-361.338913	
[2→3]#	0.156736	-361.4778923	-361.321532	
3	0.158540	-361.4972707	-361.338731	0.017381 (10.9065)[c]

[a]Relative to the most stable geometry
[b]Corrected by multiplying by a scaling factor (0.9135)
[c]Numbers in parenthesis are the corresponding values in kcal mol^{-1}

Conclusion

Process of Aziridine synthesis by optical demolition or quick thermal decomposition in atmosphere of 1,2,3-triazoline composition was investigated using Ab initio and DFT methods which the obtained results showed that Ea_1 of this structure is 61.5201 Kcal/mol and Ea_2 of this mechanism is 10.9065 Kcal/mol and mechanism process is totally endothermic. Also cis or trans state of product chain depends on primary molecules configuration. Also bond angle in aziridine is about 60 degrees which is far more than normal state (109.5 degrees). This state is documented according to banana bond model or bent bond.

References

[1] Scheiner Aziridine Synthesis , Wolff , *A. Ann* . **1912** , 394,30

[2] Scheiner , P .; Vaughan, W.R.*J.Org.Chem*.**1961**,26 1923

[3] C. Lee, W. Yang and R. G. Parr, *Phys. Rev*. B, 37, 785,**1988**.

[4] M. j. Frisch et al. *GAUSSIAN 03*, Revision C. 01, Gaussian Inc.,Wallingford. CT, **2004**.

Spectroscopic Investigations Structure Ethil-3-Amino Benzoat with Ab initio and DFT studies

R.Soleymani*[a,c] , F.Afshari[a]

[a] Chemistry Department, Faculty of Sciences, Islamic Azad University, Touyserkan Branch, Young researchers Club, Touyserkan ,Iran

(Email: nima_soleimany@yahoo.com)

[b] Chemistry Department, Faculty of Sciences, Islamic Azad University Shahre-rey Branch, Tehran, Iran

Keywords: Ab initio; Anisotropy ; Ethil-3-Amino Benzoat ; Long-range coupling

Introduction

A composition has C_1 point group , degree of freedom is equal to molecular mass is equal to 165.07898 amu and its index of hydrogen coficiency is equal to 5. This composition is synthesized empirically in the laboratory[1] .You can see structure in the following figure.

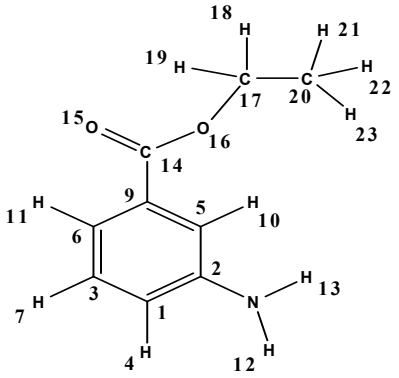

Calculation method

For calculation vibrational spectroscopic , chemical shift and NMR spectrum with theoretical method using computer Pentium IV-Intel i7 2.8 GHZ processor and Gaussian 03w software [1]. For this purpose used B3LYP/6-311+G** and HF/6-311+G** methods. Also empirical results ^{1}H-NMR spectrum is obtained with 300 MHZ devicied and ^{13}C-NMR spectrum is obtained with 75 MHZ device using $CDCl_3$ solvent. The FTIR spectrum wsa recorded by KBr pellet method on a Bruker IFS 66V spectrometer equipped with a Globar source , Ge/KBr beam splitter , and a TGS detector in the range of 4000-400 cm^{-1}. The spectral resolution was ±2 cm^{-1}

.

Result and discussion

The obtained results of ab initio and empirical methods a are reported in the following table.

Results Infrared Spectrum (IR)

Method	Experimental		B3LYP/6-311+G**		HF/6-311+G**		Assignment
Important mode nos	Intensity	Wave number (cm^{-1})	Intensity	Wave number (cm^{-1})	Intensity	Wave Number (cm^{-1})	
1	60.10	680.32	9.049	792.79	11.88	736.44	υ m-chain
2	81.01	760.34	66.95	769.58	13.51	752.02	υ m-chain
3	44.37	880.29	11.18	896.14	99.44	855.30	υ m-chain
4	66.20	1020.1	33.15	1038.3	17.40	1125.2	υ C-O
5	89.16	1213.2	80.57	1110.1	68.47	1200.5	υ C-C
6	77.23	1360.0	84.49	1317.2	84.92	1371.2	υ C=C
7	80.74	1460.7	20.60	1484.6	98.36	1440.3	υ C=C
8	90.65	1708.2	97.41	1762.3	54.48	1775.3	υ C=O
9	58.86	2986.3	18.32	3035.2	23.12	3171.0	υ C-H
10	72.08	3400.5	40.27	3211.9	56.00	3237.6	υ N-H
11	43.20	3408.0	21.60	3570.8	20.14	3883.6	υ N-H

[a] Value in Hartree - [b] Value in Cal/Mol.K - [c] Value in Debye - [d] Value in Kcal/mol

Method	B3LYP/6-311+G**							
Geometrical	ZPVE [d]	ZPE [a]	Total Energy [a]	Enthalpy [a]	Gibbs Free Energy [a]	Heat Capacity [b]	Total Entropy [b]	Dipole Moment [c]
Amount	117.62968	0.187455	-554.77635	-554.76375	-554.81469	43.592	107.219	3.4908
Method	HF/6-311+G**							
Amount	125.89511	0.200627	-551.36108	-551.34914	-551.39878	40.554	104.484	3.2689

Results NMR Spectrums

^{13}C-NMR Spectrum			^{1}H-NMR Spectrum		
Method	Experimental	B3lyp/6-311+g**	Method	Experimental	B3lyp/6-311+g**
Number atoms	Chemical Shifts(ppm)	Chemical Shifts(ppm)	Number atoms	Chemical Shifts(ppm)	Chemical Shifts(ppm)
C_1	116.2	115.003	H_4	7.41	7.21
C_2	131.2	132.237	H_7	7.23	6.98
C_3	119.5	118.446	H_{10}	7.36	7.12
C_5	129.4	117.981	H_{11}	6.83	6.05
C_6	120.8	121.260	H_{12}	3.88	3.43
C_9	147.3	142.927	H_{13}	3.85	3.17
C_{14}	167.1	168.117	H_{18}	4.37	3.84
C_{17}	17.89	13.6830	H_{19}	4.31	4.22
C_{20}	82.01	68.2443	H_{21}	1.40	1.10
			H_{22}	1.46	1.13
			H_{23}	1.45	1.12

Conclusion

Theoretical investigation together with the obtained experiences on structure Ethil-3-Amino Benzoat showed that C=O group is appeared in 1708 cm^{-1} which this amount is reasoble for an Ester. Also the existed doublet in 3400 cm^{-1} in infrared spectrum proves Amin kind 1 presence. ^{13}C-NMR spectrum proved the presence of nine peak which showed nine carbons. Carbon atom in C=O group appears in 167 ppm and aromatic carbons appear in 129,120,119,116 ppm respectively which shows a two chain ring. Undoubtedly in ^{1}H-NMR long-range coupling has been occurred , Anisotropy effect cause that the proton near to C=O moves to the low field. Also a flat NH_2 peak appears with 2 proton integral in 3.8 ppm. Which totally presence of Ethil-3-Amino Benzoat composition is proved.

References

[1] Donald L. Pavia et al , *Introduction to spectroscopy*, Saunders golden sunburst series, Department of chemistry Washington university **(1996)**.

[2] M. j. Frisch et al. *GAUSSIAN 03*, Revision C. 01, Gaussian Inc.,Wallingford. CT, **(2004)**.

Theoretical DFT investigation of the application of adsorbed silver on C_{60} as Anti-HIV drug

K.Azizi* and A.Sohrabinia

Department of Chemistry,University of Kurdistan, Sanandaj,Iran

(Email:azizkhald822@yahoo.com)

Introduction

Silver also silver-based compounds is highly antimicrobial due to its antiseptic properties to several species of bacteria. In fact Silver nanoparticles interact with the outer membrane of bacteria and it causes structural changes leading to degradation and at last death of the microbe . For example, silver nanoparticles sized 1-10nm attached to HIV-1 and prevented the virus from bonding to host cells[1,2]. The HIV envelope (Env) glycoprotein (gp) 120 is a highly disulfide-bonded molecule that attaches HIV to the lymphocyte surface receptors CD4 and CXCR4 [3]. The mechanism of the antibacterial action of silver nanoparticles is closely relevant to their interaction with the two disulfide bonds placed in the carboxyl half of the HIV-1 gp120 glycoprotein. This is an area that has been led in binding to the CD4 receptor [4]. It has been specified that the nano structures such as carbon nanotubes, Fullerene derivatives, can transport drug to the target cells. Since functionalised CNT and Fullerene derivatives display low toxicity and are not immunogenic, such systems hold great potential in the field of nanobiotechnology and nanomedicine[5] . In this work, in order to achieve this purpose, we studied the adsorbablity and stability of silver on the outer surface of C_{60} in gas phase and interaction betwen silver adsorbed on C_{60} with DMDS, because DMDS have disulfid bond and similar to area in HIV-1 gp120 that has been led in binding to the CD4 receptor.

Computational Methods

The structures of isolated species and molecular complexes were optimized with DFT method at the hybrid functional B3LYP and the small-size basis set 3-21G* level. The Raman spectra were also calculated in order to give further insight on the cleavage process of disulfide bond.

Among the readily available basis set defined for silver, the 3-21G* basis set is manageable in size and accuracy. Interaction energies were obtained as the difference between the energy of the complex and the combined energies of the species in isolation, using Eq. (1) Local charge, hybridization and orbital occupancies at each atom were calculated according to Mulliken population analysis.

$E_{ad} = E_{Ag\text{-}C60} - (E_{Ag} + E_{C60})$ Eq. (1)

All calculations on the isolated species and molecular complexes were performed within GAUSSIAN 03 program package.

Results and discussion

Figure 1 shows the optimized structure of adsorbed silver atom on the surface of C_{60} in the gas phase. In order to find the most stable configuration, silver atom has been located at different distances from outer surface of C_{60}. After full structural optimization, the Ag atom always, locates on C-C bond, regardless of the initial location. the energies of HOMO and LUMO of Ag, C60, Ag-C_{60} and DMDS systems are given in Table 1. It can be seen from Table 1 the energy gap $(Ag)_{HOMO}$ - $(C_{60})_{LUMO}$ considerably smaller than that of $(C_{60})_{HOMO}$ - $(Ag)_{LUMO}$. Hence based on the theory of frontier molecular orbitals (FMO) a significant overlaps and electron density transfer between the HOMO of Ag atom and the LUMO of C_{60} can be performed which in turn lead to a considerable amount of energy of adsorption. [6]

Table 1. The energies of frontier orbitals for C_{60} and silver atom.

Parameters	C60	Ag
E_{HOMO}(eV)	-0.2391	-0.16
E_{LUMO}(eV)	-0.1312	-0.0114

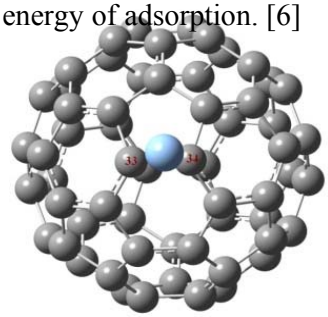

Fig . 1

A comparison between the desorption energy for atomic Ag on the C_{60} surface, 19.45 kcal/mol, and molar sublimation energy of silver atoms, 76.56 kcal/mol [7] show that it is energetically more favorable for disulfide bond to add to Ag-C_{60} than the silver nanoparticles. As shown in Figure 2, the charge distributions in $(Ag\text{-}C_{60})_{HOMO}$ and $Ag_{(HOMO)}$ are similar to each other, and there is a similarities between $(Ag\text{-}C60)_{LUMO}$ and $C60_{LUMO}$ as well. Therefore,

it is reasonable to expect that during electrophilic reactions including Ag-C_{60}, the Ag_{HOMO} plays the major role.

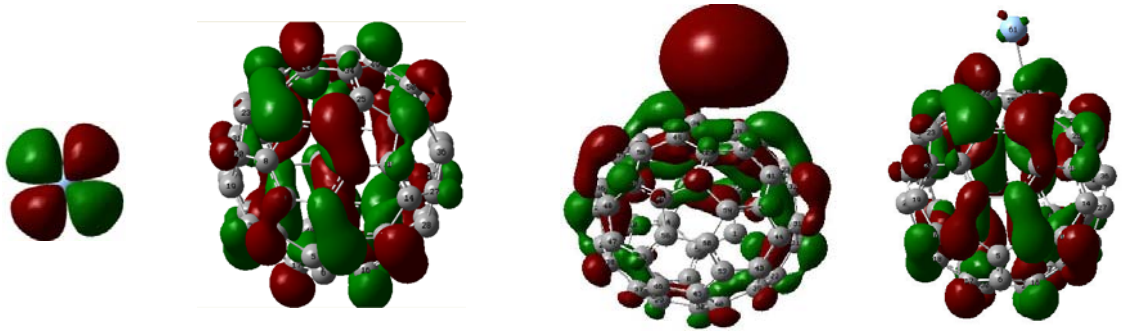

(a) (b) (c) (d)

Fig .2 shows the schematic diagrams of HOMO of Ag (a), LUMO of C60(b), HOMO(c) and LUMO(d) of Ag-C60.

The interaction between Adsorbed silver on C_{60} and disulfide bond

As shown in Figure 3, in both cases, Ag+DMDS and Ag-C_{60}+DMDS, the disulfide bond is broken into separated MeS units.

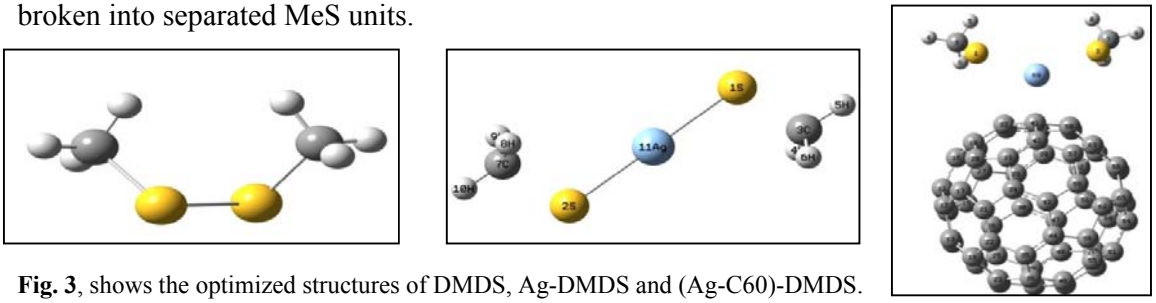

Fig. 3, shows the optimized structures of DMDS, Ag-DMDS and (Ag-C60)-DMDS.

The results of NBO calculation gives the S-S bond hybridization of DMDS as $sp^{17.5}$, while these calculations don't confirm the existence of S-S bond in Ag+DMDS or Ag-C60+DMDS.In addition figure (4a) show that the S-S vibration peak for DMDS, which located at 421 -627 cm^{-1}, will be omitted in spectra of Ag-C60+DMDS and in return a new peak, corresponding to S-Ag-S vibration, emerged at 297 cm^{-1} as depicted in figure(4b). This indicates that the S-S bond is broken due to the reaction of Ag or Ag-C60 with DMDS.

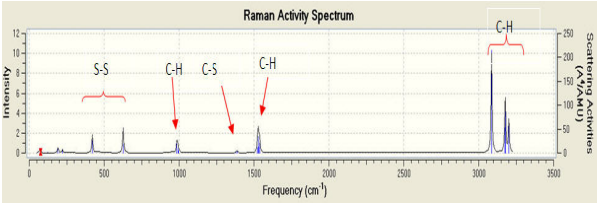

Fig.(4a) Raman activity Spectrum of DMDS

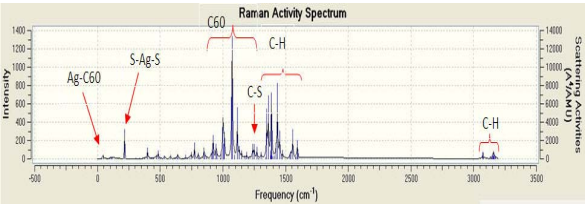

Fig.(4b) Raman activity Spectrum of Ag-C60-DMDS

Conclusion

The results of NBO calculation and vibrational spectrums indicate that the Ag atom effectively cleavages the S-S bond in both Ag+DMDS and Ag-C_{60}+DMDS systems. It is expected that Ag-C_{60} can show the same behavior in interaction with the disulfide bond of gp120 of HIV-1 and can result in stopping HIV-1 from activating by causing a perturbation in gp120-CD4 interaction.

References

[1] Luis J, Burt Ju, Mor*ones* J R, Bragado A, Gao X, Lara H and Yacam M, *Journal of Nanobiotechnology* (**2005**)

[2] Lu L, Sun RW, Chen R, Hui CK, Ho CM, Luk JM, Lau GK, Che CM,. *Antivir Ther*, 13(**2008**) 253.

[3] Barbouche R, Raymond M, Jones I M and Fenouillet, *Journal of biological chemistry,***(2003)** 3131–3136

[4] G.E. McDonnell, *Chemical Disinfection. Antisepsis, disinfection, andsterilization* **(2007)** 111-115

[5] Bosi S, Da Ros T, Spalluto G and Prato M, *European Journal of Medicinal Chemistry* 38 (**2003**) 913_ 923

[6] Wang LS, Han SK, *Chemical Engineering Industry Press*(**1997**) 60–8

[7] Nanda K, Maisels A, Kruis F, Fissan H and Stappert S, *Phys. Rev. Lett* (**2003**) 91, 106,102

Comparison of Oxygen-Metal bonding in crown ethers with Nitrogen-Metal in similar compounds in gas and solvent phase using Quantum Mechanical study

S.Seyedi*[a] , M.Shabani[b] , A.A.Salari[a] and F.Mokhles[a]

[a] Department of Chemistry, Azad University of Tehran.Shahr –e- Rey

[b]Islamic Azad University, Varamin-Pishva Branch, Tehran- Iran

Email: saras3245@yahoo.com

Abstract:

In this research the bond of Oxygen-Metal in 12-crown-4 is compared with the bond of Nitrogen-Metal in 12-azocrown-4. At first, both of them is optimized first in gas phase and then in solvent phase using DFT/B3LYP method and 6-31G(d) Basis set. Then we put in hole of each one of them Sodium, Potassium, Calcium cations and optimized them in the gas and solvent phase. Binding energy is calculated for all systems. In all cases azocrown ethers have more negative binding energy than crown ethers.

Keywords: Crown ether, Azocrown ether, Gas and Solvent phase, Density Functional Theory

Introduction:

Crown ethers belong to cyclic ethers that have cofactor ethers with high solvency. Heteroatoms cause the inside of crown ethers to be reach in electron. Therefore, crown ethers would behave as host in the presence of guest ion. In other words, cations can bind with heteroatoms in the ring.

Methods:

(A)In this study,12-crown-4 and 12-azocrown-4 are optimized using DFT/B3LYP method,6-31G(d) Basis set and by Gaussian 2003.The optimized structures are shown in figure1.

Figure1b:12-azocrown-4

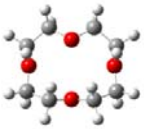

Figure 1a:12-crown-4

Optimized structures energies in gas phase are shown in Table 1.

Table 1: Calculated energies in gas phase

crown ether(gas)	energy(RB+HF-LYP)(a.u.)	Binding Energy(a.u.)	B.E.(kcal/mol)
12-crown-4	-615.3110185	—	—
12-crown-4/Na^+	-777.5072345	-0.11498721	-72.15550916
12-crown-4/K^+	-1215.114751	-0.07874284	-49.41184079
12-crown-4/Ca^{2+}	-1292.454244	-0.27636523	-173.4216691
12-azocrown-4	-535.8318387	—	—
12-azocrown-4/Na^+	-698.0555269	-0.14245938	-89.39454308
12-azocrown-4/K^+	-1135.652495	-0.09566665	-60.03168387
12-azocrown-4/Ca^{2+}	-1213.018363	-0.3196634	-200.5916605

In this table binding energy in kcal/mol is calculated by multiplying the binding energy in (a.u.) with the constant value of 627.509. Then energy of Sodium, Potassium andCalcium metallic ions are calculated with similar method and Basis set, in gas phase, as presented in table 2.

Table2: Calculated energy for metallic ions

Ion	Energy (a.u)
Na^+	-162.08122881
K^+	-599.72498924
Ca^{2+}	-676.86686073

In the next stage, in separate experiments, each of the selected cations are put in the holes of optimized crown ether and azocrown ethers. Then, the structures were optimized, using similar method and Basis set. The binding energies are calculated using equation 1.

$$E_{binding} = E_{crown\text{-}ion} - (E_{crown} + E_{metallic\ ion}) \qquad (1)$$

The calculated binding energies were shown in table 1.

(B) Now, at first 12-crown-4 and 12-azocrown-4 are optimized in solvent phase with CPCM model and the following solvents: Water, Acetonitrile, and Carbon Tetra Chloride. The optimized structures energies in solvent phase are listed in table 3.

Table3: Calculated energy in solvent phase

crown ether(sol)	energy(RB+HF-LYP)	Binding E(a.u.)	B.E.(kcal/mol)
12-crown-4/H_2O	-615.323612	—	—
12-crown-4/Na^+/H_2O	-777.597777	-0.0175681	-11.02414086
12-crown-4/K^+/H_2O	-1215.201318	-0.014957	-9.385652113
12-crown-4/Ca^{2+}/H_2O	-1292.8078	-0.0017803	-1.117154273
12-azocrown-4/H_2O	-535.8509024	—	—
12-azocrown-4/Na^+/H_2O	-698.1457508	-0.0382515	-24.00316051
12-azocrown-4/K^+/H_2O	-1135.740064	-0.0264138	16.57489722
12-azocrown-4/Ca^{2+}/H_2O	-1213.369602	-0.0362919	-22.77349388
12-crown-4/AN	-615.3227494	—	—
12-crown-4/Na^+/AN	-777.5958295	-0.0190655	-11.96377284
12-crown-4/K^+/AN	-1215.198874	-0.0154055	-9.6670899
12-crown-4/Ca^{2+}/AN	-1292.799396	-0.0033026	-2.072411223
12-azocrown-4/AN	-535.8489756	—	—
12-azocrown-4/Na^+/AN	-698.1434011	-0.0404109	-25.35820345
12-azocrown-4/K^+/AN	-1135.738211	-0.0285163	-17.8942349
12-azocrown-4/Ca^{2+}/AN	-1213.36109	-0.0387705	-24.32883768
12-crown-4/CCl_4	-615.3169989	—	—
12-crown-4/Na^+/CCl_4	-777.5562353	-0.0601041	-37.71586369
12-crown-4/K^+/CCl_4	-1215.161315	-0.042423	-26.62081431
12-crown-4/Ca^{2+}/CCl_4	-1292.644214	-0.1167101	-73.23663814
12-azocrown-4/CCl_4	-535.8405147	—	—
12-azocrown-4/Na^+/CCl_4	-698.1040448	-0.0843977	-52.96031633
12-azocrown-4/K^+/CCl_4	-1135.699771	-0.0573641	-35.99648903
12-azocrown-4/Ca^{2+}/CCl_4	-1213.204953	-0.1539332	-96.5944684

Now the energies of Sodium, Potassium, and Calcium metallic ions are calculated with similar method and Basis set and CPCM solvent model in the presence of three kinds of previously mentioned solvents. The results are presented in table 4.

Table4: Calculated energy for metallic ions in variant solvent

Ion	Energy(a.u.)/H_2O	Energy(a.u.)/AN	Energy(a.u.)/CCl_4

Na^+	- 162.25659685	- 162.25401463	- 162.17913243
K^+	- 599.86274783	- 599.86071914	- 599.80189225
Ca^{2+}	- 677.48240672	- 677.47334306	- 677.21050413

Afterwards, each of the selected cations are put in the holes of optimized 12-crown-4 and 12-azocrown-4. Then, the structures were optimized, using the previously mentioned solvents. The calculated binding energies were presented in table 3.

Results:

1-In all cases azocrown ethers have more negative binding energy than crown ethers in gas and solvent phases.

2-In solvent phase, the binding energy resulting from optimizing in the presence of Carbon Tetra Chloride solvent is more negative than Acetonitrile and Water in all cases with all cations.

3- In solvent phase, the binding energy resulting from optimizing in the presence of Acetonitrile solvent is more negative than Water in all cases.

4- In gas phase, the binding energy for crown ethers and azocrown ethers in the presence of Ca^{2+} is more negative than Na^+ and binding energy in the presence of Na^+ is more negative than K^+:

$Ca^{2+}>Na^+>K^+$

5- In solvent phase, the binding energy for crown ethers in different solvents is as the following:

H_2O: $Na^+>K^+>Ca^{2+}$

Acetonitrile: $Na^+>K^+>Ca^{2+}$

CCl_4: $Ca^{2+}>Na^+>K^+$

6- In solvent phase, the binding energy for azocrown ethers in different solvents is as the following:

H_2O: $Na^+>Ca^{2+}>K^+$

Aceto Nitryle: $Na^+>Ca^{2+}>K^+$

CCl_4: $Ca^{2+}>Na^+>K^+$

References:

[1] Crown Compounds:Toward Future Applications,in:S.R.Cooper(Ed.),VCH,1992.

[2] Hancock,R.D.;Martell,A.E.Chem. Rev. 98(1989) 1875.

[3] R.D. Hancock,A.E Martell,Chem. Rev. 98(1989) 1875.

Survey of solvent polarity effect on stability of Oxygen-Metal bond in 12-crown-4 and Nitrogen-Metal bond in 12-azocrown-4 using CPCM model by QM

S.Seyedi *[a], M.Shabani[b], A.A.Salari[a] and F.Mokhles[a]

[a] Department of chemistry ,Azad University of Tehran.Shahr –e- Rey

[b]Islamic Azad university, Varamin-Pishva Branch, Tehran- Iran

Email: saras3245@yahoo.com

Keywords: Crown ether, Azocrown ether, Solvent phase, QM

Introduction:

In this research we study solvent polarity effect on heteroatom-metal bond in 12-crown-4 and 12-azocrown-4 using DFT/B3LYP method, 6-31G(d) Basis set, CPCM model and Gaussian 2003. We use metallic ions: Na^+, K^+, Ca^{2+} in the presence of Water, Acetonitrile, Carbon Tetra Chloride solvents. Results of calculated binding energy show that azocrown ethers have more stable bond with metallic ions than crown ethers, because they have more negative binding energy than crown ethers. Comparing optimized structures in different solvents, it is concluded that if solvent has less polarity, binding energy would be more negative. Therefore, the binding energy resulting from Carbon Tetra Chloride is more negative than Acetonitrile and Water in all cases with all cations. Similarly, binding energy resulting from Acetonitrile is more negative than Water in all cases.

Methods:

We used two structures of 12-crown-4 and 12-azocrown-4 in solvent phase in the presence of three kinds of solvents: Water with maximum polarity, Acetonitrile with medium polarity and Carbon Tetra Chloride with low polarity.

At first, 12-crown-4 and 12-azocrown-4 are optimized alone and in the presence of one of selected solvents by DFT/B3LYP method, 6-31G(d) Basis set, CPCM model and Gaussian 2003. Then ions energies are calculated in the presence of each three kinds of solvents by similar method. Results are shown in table 1.

Table1: Calculated energies for metallic ions in different solvents

Ion	Energy(a.u.)/H_2O	Energy(a.u.)/AN	Energy(a.u.)/CCl_4
Na^+	- 162.25659685	- 162.25401463	- 162.17913243
K^+	- 599.86274783	- 599.86071914	- 599.80189225
Ca^{2+}	- 677.48240672	- 677.47334306	- 677.21050413

Eventually, each of the selected ions is put in 12-crown-4 and 12-azocrown-4 holes in the presence of one solvent and they are optimized with similar method. The optimized figures for some of structures are as follows:

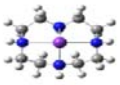

Figre4:12-Azocrown-4 with K^+ in CCl_4

Figre3: 12-crown-4 with Ca^{2+} in Acetonitrile

Figre2:12-crown-4with Na^+ in water

Figre1:12-crown-4 in water

Results of the optimization are shown in table 2.

Table2: Calculated energies in different solvents

crown ether	energy(RB+HF-LYP)	Binding Energy(a.u.)	B.E.(kcal/mol)
12-crown-4/H_2O	-615.323612	—	—
12-crown-4/Na^+/H_2O	-777.597777	-0.0175681	-11.02414086
12-crown-4/K^+/H_2O	-1215.201318	-0.014957	-9.385652113
12-crown-4/Ca^{2+}/H_2O	-1292.8078	-0.0017803	-1.117154273
12-azocrown-4/H_2O	-535.8509024	—	—
12-azocrown-4/Na^+/H_2O	-698.1457508	-0.0382515	-24.00316051
12-azocrown-4/K^+/H_2O	-1135.740064	-0.0264138	16.57489722
12-azocrown-4/Ca^{2+}/H_2O	-1213.369602	-0.0362919	-22.77349388
12-crown-4/AN	-615.3227494	—	—
12-crown-4/Na^+/AN	-777.5958295	-0.0190655	-11.96377284
12-crown-4/K^+/AN	-1215.198874	-0.0154055	-9.6670899
12-crown-4/Ca^{2+}/AN	-1292.799396	-0.0033026	-2.072411223
12-azocrown-4/AN	-535.8489756	—	—
12-azocrown-4/Na^+/AN	-698.1434011	-0.0404109	-25.35820345
12-azocrown-4/K^+/AN	-1135.738211	-0.0285163	-17.8942349
12-azocrown-4/Ca^{2+}/AN	-1213.36109	-0.0387705	-24.32883768
12-crown-4/CCl_4	-615.3169989	—	—
12-crown-4/Na^+/CCl_4	-777.5562353	-0.0601041	-37.71586369
12-crown-4/K^+/CCl_4	-1215.161315	-0.042423	-26.62081431
12-crown-4/Ca^{2+}/CCl_4	-1292.644214	-0.1167101	-73.23663814
12-azocrown-4/CCl_4	-535.8405147	—	—
12-azocrown-4/Na^+/CCl_4	-698.1040448	-0.0843977	-52.96031633
12-azocrown-4/K^+/CCl_4	-1135.699771	-0.0573641	-35.99648903
12-azocrown-4/Ca^{2+}/CCl_4	-1213.204953	-0.1539332	-96.5944684

In this table binding energy is calculated using equation 1.

$$E_{binding} = E_{crown\text{-}ion} - (E_{crown} + E_{metallic\ ion}) \quad (1)$$

Ion-heteroatom distances are shown in table 3. In this table A, B, C, D are the distances from first, second, third and fourth heteroatom to ion, respectively.

Table 3: Ion-heteroatom distances

crown ether(sol)	A	B	C	D	Average
12-crown-4/H_2O	—	—	—	—	—
12-crown-4/Na^+/H_2O	Na-O1=2.43386	Na-O2=2.38005	Na-O3=2.42784	Na-O4=2.56464	2.4515975
12-crown-4/K^+/H_2O	K-O1=2.82061	K-O2=2.80799	K-O3=2.81564	K-O4=3.18263	2.9067175
12-crown-4/Ca^{2+}/H_2O	Ca-O1=2.64914	Ca-O2=2.54064	Ca-O3=2.62844	Ca-O4=2.63543	2.6134125
12-azocrown-4/H_2O	—	—	—	—	—
12-azocrown-4/Na^+/H_2O	Na-N1=2.55229	Na-N2=2.48291	Na-N3=2.41346	Na-N4=2.48109	2.4824375
12-azocrown-4/K^+/H_2O	K-N1=3.06189	K-N2=2.86522	K-N3=2.82515	K-N4=2.86626	2.90463
12-azocrown-4/Ca^{2+}/H_2O	Ca-N1=2.66494	Ca-N2=2.67037	Ca-N3=2.58407	Ca-N4=2.67887	2.6495625
12-crown-4/AN	—	—	—	—	—
12-crown-4/Na^+/AN	Na-O1=2.44961	Na-O2=2.39584	Na-O3=2.45599	Na-O4=2.54418	2.461405
12-crown-4/K^+/AN	K-O1=2.80619	K-O2=2.7200366	K-O3=2.80952	K-O4=3.12889	2.885815
12-crown-4/Ca^{2+}/AN	Ca-O1=2.64024	Ca-O2=2.56482	Ca-O3=2.65649	Ca-O4=2.57781	2.6020034
12-azocrown-4/AN	—	—	—	—	—
12-azocrown-4/Na^+/AN	Na-N1=2.52820	Na-N2=2.46413	Na-N3=2.40517	Na-N4=2.46597	2.4658675
12-azocrown-4/K^+/AN	K-N1=3.04420	K-N2=2.86212	K-N3=2.83267	K-N4=2.86478	2.9009425
12-azocrown-4/Ca^{2+}/AN	Ca-N1=2.64954	Ca-N2=2.62211	Ca-N3=2.61325	Ca-N4=2.64246	2.63184
12-crown-4/CCl_4	—	—	—	—	—
12-crown-4/Na^+/CCl_4	Na-O1=2.37687	Na-O2=2.32319	Na-O3=2.38149	Na-O4=2.42454	2.3765225
12-crown-4/K^+/CCl_4	K-O1=2.74907	K-O2=2.75531	K-O3=2.74892	K-O4=2.94865	2.8004875
12-crown-4/Ca^{2+}/CCl_4	Ca-O1=2.46739	Ca-O2=2.49568	Ca-O3=2.45606	Ca-O4=2.42694	2.4615175
12-azocrown-4/CCl_4	—	—	—	—	—
12-azocrown-4/Na^+/CCl_4	Na-N1=2.47088	Na-N2=2.43687	Na-N3=2.37530	Na-N4=2.43773	2.430195
12-azocrown-4/K^+/CCl_4	K-N1=2.96247	K-N2=2.83762	K-N3=2.80251	K-N4=2.83715	2.8599375
12-azocrown-4/Ca^{2+}/CCl_4	Ca-N1=2.55627	Ca-N2=2.57789	Ca-N3=2.51062	Ca-N4=2.56800	2.553195

Based on the results of these tables,diagram of energy according to dielectric constant is obtained.For example,this diagram for12-crown-4 in the presence of $Ca^{2+}$is shown in diagram1,based on the results of table 4.

Table 4: Energy and dielectric constant for 12-crown-4 in different solvents and in the presence of Ca^{2+}

Solvent	Dielectric Cons.	Ea.u.	ΔE1(kcal/mol
CCl4	2.228	-1292.644214	0
Aceto Nitryle	36.64	-1292.799396	-97.37810164
H2O	78.39	-1292.8078	-102.6516873

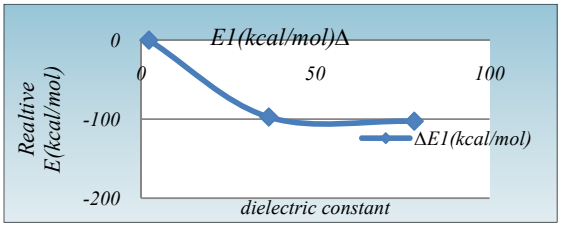

Diagram 1: Energy according to dielectric constant for 12-crown-4

Also diagram for 12-azocrown-4 in the presence of Ca^{2+} is shown in diagram 2, based on the results of table 5.

Table 5: Energy and dielectric constant for 12-azocrown-4 in different solvents and in the presence of Ca^{2+}

solvent	Dielectric Cons.	E(a.u.)	ΔE(kcal/mol)
CCl4	2.228	-1213.204953	0
Aceto Nitryle	36.64	-1213.36109	-97.97737273
H2O	78.39	-1213.369602	-103.3187293

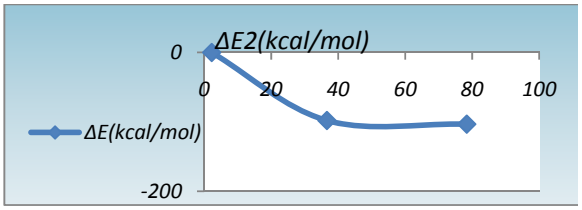

Diagram 2: Energy according to dielectric constant for 12-azocrown-4

Similar diagrams may be obtained for other cases.

Results and discussion:

1-Bond length of heteroatoms with metals in crown ethers and azocrown ethers in three kinds of solvents, is in the following order: $K^{+}>Ca^{2+}>Na^{+}$

2- As the dielectric constant increases, the energy become more negative. In other words, interaction of solvent with the solvate is increased.

3-As the polarity of solvent increases, stability of solvate is also increased.

4-Different solvent may be sorted as the following, based on the increasing order of negative energy: water< Acetonitrile< Carbon Tetra Chloride.

Conclusion:

In this paper solvent polarity effect on heteroatom-metal bond in 12-crown-4 and 12-azocrown-4 using DFT/B3LYP method, 6-31G(d) Basis set, CPCM model and Gaussian 2003, is studied. According to the results of this study, the binding energy resulting from Carbon Tetra Chloride is more negative than Acetonitrile and Water in all cases with all cations. Similarly, binding energy resulting from Acetonitrile is more negative than Water in all cases.

References:

[1] Hancock,R.D.;Martell,A.E.Chem. Rev. 98(1989) 1875.
[2] Saunders,M.;Am,J.Chem.Soc.109(1987)3150.

A Comparative Study of Hydrogen and Helium Physisorption on Carbon and Silicon Nanotubes Using Monte Carlo Simulation

Fatemeh cigarchi*[a] ,S. Saleheh Razavi[a], S. Majid Hashemianzadeh [a]

[a]Molecular Simulation Research Laboratory, Department of Chemistry, Iran University of Science and Technology, Tehran, Iran

cigarchi_f@chem.iust.ac.ir

Keywords: Monte Carlo simulation, Lennard-Jones Potential, Morse Potential, Gas Adsorption

Introduction:

In the past 10 years, many efforts have been focused on the hydrogen adsorption capacity of carbon nanotubes (CNTs) due to potential application of hydrogen for fuel cell vehicles[1,2]. However, most of these efforts failed to reach the gravimetric density (6.5 wt %) proposed by the U.S. Department of Energy (DOE) for the hydrogen plan of fuel cell vehicles. With the successful synthesis of silicon nanotubes (SiNTs) by the chemical vapour deposition (CVD) method in 2002[3], a lot of other methods were also developed to fabricate the SiNTs [4,5] and well-aligned SiNT arrays. Compared to carbon, silicon has more electrons in the outer shells, which leads to higher polarizability and a stronger dispersion force. Accordingly, the SiNT may exhibit a stronger van der Waals (VDW) attraction to gases than CNTs. Therefore, we have reported a multiscale theoretical method to investigate adsorption of hydrogen and helium in the SiNTs in our previous works, submitted in 14th physical chemistry conference [8,9], and in this paper we present the comparison of the gravimetric adsorption capacities of hydrogen and helium in the SiNT and CNT, at the same thermodynamic condition using Monte Carlo simulation method.

Models and simulation methods:

A standard MC simulation was carried out at a fixed volume, temperature, and sum of the species for the adsorption of pure H2 and He and H2/He mixtures on both SiNT and CNT. The cut off radius of 2.5 σ applied to the LJ potential interactions. For each isotherm point, $5*10^7$ configurations were generated. The system was achieved to equilibrate after $2*10^7$ steps, and the remaining $3*10^7$ configurations were used to obtain ensemble average values

for thermodynamic properties. One SWNT placed in the center of box with dimensions of (100.0 Å ×100.0 Å ×45.0 Å). The intermolecular interactions between H2 -H2 [6] and He-He [7] were calculated using the (12-6) Lennard-Jones (LJ) potential. The total interactions between adsorbate and SWSiNTs were represented using the Morse potential equation which has been investigated in our previous work [8,9]. It should be mentioned that for investigating the adsorption of hydrogen and helium on (8, 8) SWCNT, the (12-6) LJ potential with the values of 28.2 K and 2.98 Å for ε_{c-c} and σ_{c-c} parameters were used [10]. In addition, Lorentz-Berthelot combining rules were also applied for cross interactions .In this section with the intention of comparison the adsorption behaviour of hydrogen and helium in SiNT and CNT, all the Monte Carlo calculations are performed at the same thermodynamic states for both (5,5)SiNT and (8,8)CNT which is isodiameter to (5,5)SiNT, and equal heights of 37A. The adsorption capacities for both pure hydrogen and helium are represented in Figure **1**.

Figure 1. Comparison the adsorption capacity of a) hydrogen b) helium in (5, 5) SiNT and (8, 8) CNT at T=50K versus pressure.

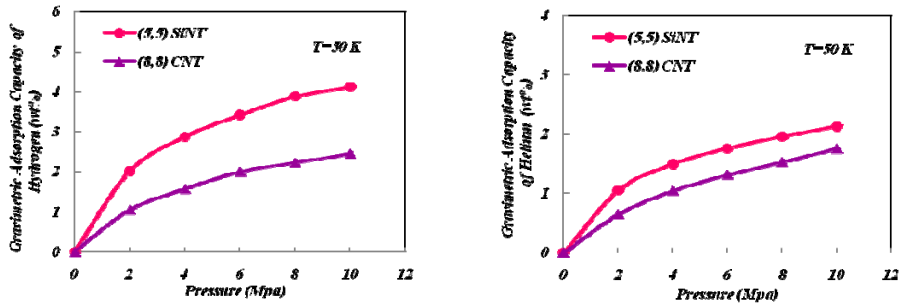

(a) (b)

All the adsorption isotherms are characterized by type1 (Langmuir shape). It is clear that the adsorption magnitude of both hydrogen and helium in (5, 5) SiNT is greater than that of (8,8) CNT. These results represent that, although silicon and carbon belong to group IV of periodic Table, further electrons in silicon outer shell make it more polarisable than CNT which results the stronger VDW interaction between gas and surface of SiNTs than that of CNT. Therefore, it stands to reason that the gravimetric adsorption capacities of gases show greater magnitude in SiNT compared to CNT. Our results indicate adsorption improvement of 83%, 74%, and 68% for hydrogen and 42%, 28%, and 21% for helium in (5, 5) SiNT at corresponding pressure of 4, 8 and 10 MPa compared to adsorption in (8, 8) CNT. For the purpose of comparison the adsorption magnitude of hydrogen in the presence of helium in (8, 8) CNT with isodiameter (5, 5) SiNT, all CMC calculations are performed for both of SiNT and CNT

in the same theoretical condition .Our results obtained from this part of study are presented in Figure 2 and Table 1 and 2. It should be noted that the adsorption increase of hydrogen in the presence of helium in SiNT is greater than isodiameter CNT.

Figure 2 : Comparison the gravimetric storage capacity of hydrogen in the mixture with helium and in the absence of helium in SiNT and CNT versus mole fraction at T=50 K and P=2 MPa.

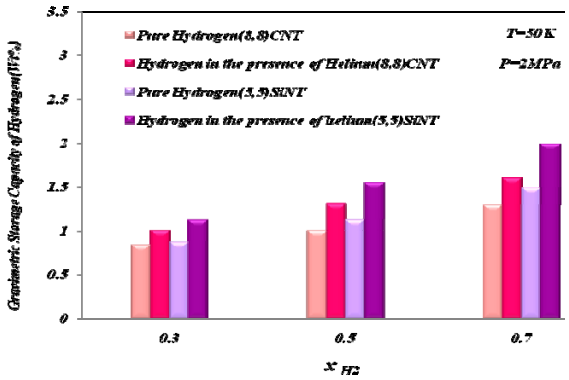

Table 1: Comparison the gravimetric storage capacity of hydrogen in the mixture with helium and in the absence of helium in SiNT and CNT

Kinds of Sint	0.3	0.5	0.7	Pure
(5,5)SiNT	2.172989	2.39497	2.549106	2.01594
(8,8)CNT	1.075541	1.175719	1.245633	1.042365

Table1 2. Improvement of Gravimetric adsorption capacity of hydrogen in the presence of helium in SiNT and CNT at different mole fraction.

Kinds of Sint	0.3	0.5	0.7
(5,5)SiNT	8%	19%	27%
(8,8)CNT	4%	13%	20%

Conclusion:

In summary, comparative studies of similar simulation calculation for (8, 8) CNT with equal diameter as (5, 5) SiNT, indicates that the SiNT represent greater adsorption capacity compared to CNT. This issue is based on the stronger VDW interaction between hydrogen and SiNT compared to CNT as a result of further electrons in silicon outer shell, which makes it more polarisable than CNT. Furthermore, we explore that, the adsorption increase of hydrogen in the presence of helium in SiNT is greater than isodiameter CNT. Therefore, we

can noticeably suggest silicon nanotube as a performable material for efficiently hydrogen adsorption not only in pure state but also in the presence of helium.

References:

[1] Zhou, L. Renewable and Sustainable Energy Reviews 2005, 9, 395-408.

[2] Schlapbach, L.; Zuttel, A. Nature 2001, 414, 353-358.

[3] Schmidt, O. G.; Eberl, K. Nature 2001, 410, 168-168.

[4] Sha, J.; Niu, J.; Ma, X.; Xu, J.; Zhang, X.; Yang, Q.; Yang, D. Advanced Materials 2002, 14, 1219-1221.

[5] Jeong, S. Y.; Kim, J. Y.; Yang, H. D.; Yoon, B. N.; Choi, S. H.; Kang, H. K.; Yang, C. W.; Lee, Y. H. Advanced Materials 2003 15 ,1172 -1176

[6] Lan, J.; Cheng, D.; Cao, D.; Wang, W. The J. of Phys. Chemistry C 2008, 112, 5598-5604

[7] Firlej, L.; Kuchta, B. Colloids and Surfaces A: Phys. & Eng. Aspects **2004**, 241, 149-154.

[8] Razavi, S.S.; Cigarchi, F.; Hashemianzadeh, S.M. ; Submitted in 14th conference of physical chemistry of Iran

[9] Yari, F.; Hashemianzadeh,S.M.; Razavi, S.S.; Cigarchi, F.; Submitted in 14th conference of physical chemistry of Iran

[10] Firlej, L.; Kuchta, B. Colloids and Surfaces A: Phys. & Eng. Aspects 2004, 241, 149-154.

[11] Huang, L.; Zhang, L.; Shao, Q.; Lu, L.; Lu, X.; Jiang, S.; Shen, W. The Journal of Physical Chemistry C 2007, 111, 11912-11920.

Aggregation behavior of gelatin in aqueous solution: A molecular dynamics simulation approach

M. Foroutan [a], N. Taheri Ghazvini[b] and A. Shamloo [a]

Email: A.shamloo@khayam.ut.ac.ir

a- Department of Physical Chemistry, School of Chemistry, College of Science, University of Tehran, Tehran, Iran.

b- Department of Polymer science, School of Chemistry, College of Science, University of Tehran, Tehran, Iran.

Keywords: Gelatin, Aggregation, Molecular dynamic simulation, Triple-helix.

Introduction

Gelatin, a protein obtained from denatured collagen, is a biopolymer that is extensively used in food industry, pharmaceutical and photography industries. Simulation is a good way to predicate the mechanism of aggregation gelatin chains in solution. When aggregation (association or cross linking) dominates over fragmentation (scission or breakage), gelation may occur, manifested by an unbounded increase in the weight-average mass or molecular weight due to initial network formation [1]. In the present work, we have performed molecular dynamic (MD) simulation to model reversible associating polymers in aqueous solution of gelatin.

Simulation details

Gelatin contains many glycine, proline and 4-hydroxyproline residues and so on. A typical structure is -Ala-Gly-Pro-Arg-Gly-Glu-4Hyp-Gly-Pro. Calculations were performed with the GROMACS package using the gromacs force field (gmx) for all-hydrogen amino acid parameters. Non-bonded van-der-Waals' interactions are modeled by a Lennard-Jones potential with a cut-off distance of 1.0 nm. Water molecules were modeled using the SPC/E model. An $11\times11\times11$ nm^3 cubic computational cell with periodic boundary conditions applied in all three principal directions and time step was 1 fs. All MD simulations were performed in the NPT ensemble, for three concentrations 1%, 2% and 2.8% at different temperatures including (275, 288, 293 and 313) K. The minimized complex structures were then subjected

first to an NVT simulation. The final structures from these simulations were then used to initiate isobar MD simulation for 1200 ps.

Results and Discussion

We used MD simulation to model reversible associating gelatin in aqueous solution, which mimic the triple-helix aggregation mechanism proposed to gelatin systems [2]. Also, in the present work, the several proposed models were examined to determine the mechanism of aggregation gelatin chains in solution with different concentrations. Figure 1 shows snapshots of gelatin system with concentration 2.8% at two temperatures (275 and 288) K.

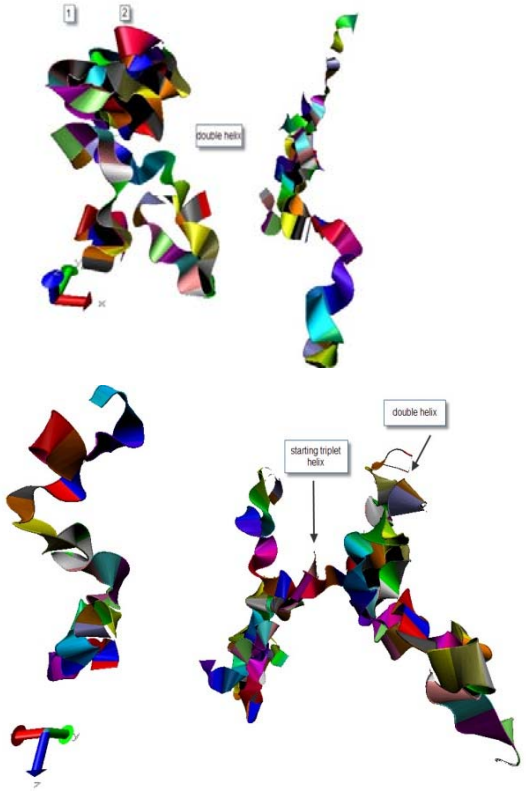

Figure 1- Front views of representative snapshots for 4 gelatin chains in 2.8% gelatin system at 275K (left side) and 288K (right side). Water molecules are not shown for clarity.

Our results show that at gelation point the intramolecular forces play more important role than intermolecular forces and also at high concentration (2.8%) and in gelation temperature, the opportunity for the formation of intramolecular forces is more than that in other temperatures. By increasing the concentration of gelatin system, the gelation point is delayed and gelation

temperature increases. The obtained radial distribution function and the time history of the number of hydrogen bonding during simulation were two useful methods for interpreting our results.

References

[1] R. Li, B. J. McCoy. Journal of Colloid and Interface Science 291(2005) 375.

[2] Y. Piñeiro et al. Physical Review E. 79 (2009) 041409.

Molecular Dynamic Simulation of the Influence of Charged Carbon Nanotubes on Gelation Behavior

M. Foroutan [a], N. Taheri Ghazvini[b] and A. Shamloo [a]

Email: A.shamloo@khayam.ut.ac.ir

a- Department of Physical Chemistry, School of Chemistry, College of Science, University of Tehran, Tehran, Iran.

b- Department of Polymer science, School of Chemistry, College of Science, University of Tehran, Tehran, Iran.

Keywords: Gelatin, Aggregation, Molecular dynamic simulation, Triple-helix, Nanotube

Introduction

The polymers that are composed of electrically charged monomers have a wide range of industrial applications. They are also important building blocks of live organisms such as DNA, RNA and GELTIN [1]. We can change the properties of reversible aggregation–fragmentation processes by additives, temperature changes, or other thermodynamic state conditions. Charged surface are important additives for altering and enhancing the properties of polymers. In this paper we investigate the influence of charged nanotube as charged surface on the possibility of gelation, gel point, and gelation temperature.

Simulation details

A charged (5,5) single walled carbon nanotube was used as a charged surface. Gelatin contains many glycine, proline and 4-hydroxyproline residues and so on. A typical structure is -Ala-Gly-Pro-Arg-Gly-Glu-4Hyp-Gly-Pro. Calculations were performed with the GROMACS package using the gromacs force field (gmx) for all-hydrogen amino acid parameters. Non-bonded van-der-Waals' interactions are modeled by a Lennard-Jones potential with a cut-off distance of 1.0 nm. Water molecules were modeled using the SPC/E model. An 16×16×16 nm^3 cubic computational cell with periodic boundary conditions applied in all three principal directions and time step was 1 fs. All MD simulations were performed in the NPT ensemble. The minimized complex structures were then subjected first to an NVT simulation. The final structures from these simulations were then used to initiate isobar MD simulation for 1200 ps.

Results and Discussion

Figure 1 shows snapshots for (5, 5) CNTs covered by gelatin chains at initial and the last time simulation in 288K. As shown in Figure 1, the gelatin chains located around the charged nanotube try to approach to it and by passing time they absorb on it. Figure shows well that in presence of nanotube, polymer chains are aggregated and there in no strong interaction between nanotube and polymer chains. In agreement with this result, recently, it has been shown that if interactions between polymer and charged nano surface, like nanotube and nanoparticles, are relatively weak, the polymer matrix promoted nano particle aggregation [2].

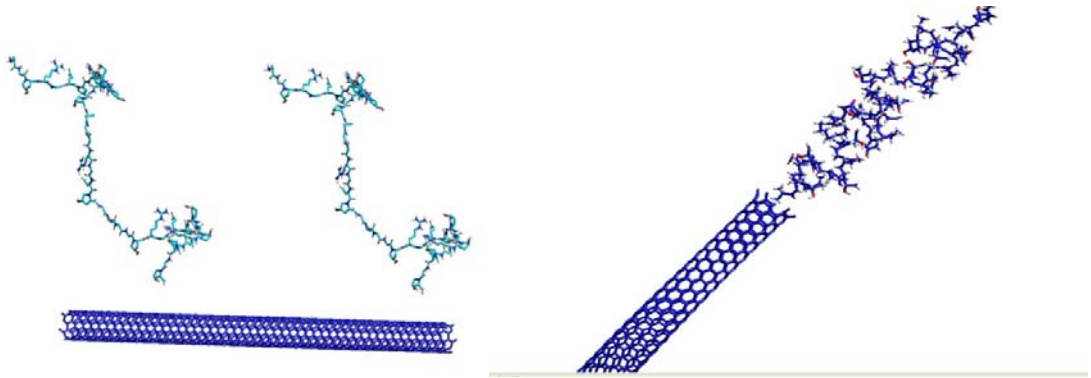

Figure 1- Views of representative snapshots for (5, 5) CNTs covered by gelatin chains at initial (left side) and the last time simulation (right side) in 288K.

Increasingly attractive nano surface–polymer interactions led to strong adsorption of the polymer chains on the surface of the charged surface. The electrostatic interaction induces adsorption of gelatin chains on nanotube. It takes place before the formation of hydrogen bonding that leads to triplet helix clusters. Above observations has been supported by radial distribution functions and the time history of the number of hydrogen bonding during simulation. Our results show that in the presence of charged nanotube the time and temperature of gelation of system is increased.

References

[1] A.V. Dobrynin et al. J. Polym. Sc.i, B, Polym. Phys. 42 (2004) 3513.

[2] N. Pawar and H. B. Bohidar. J. Chem. Phys. 131(2009) 045103.

Interaction of Sodium ion with Amino Acids as building block of Peptides

Hamid Reza Shamlouei[1*], Mohammad Javad Gohar, Tayebe Darakhsh, and Davoud Ashouri
[1]Islamic Azad University, Doroud Branch, Science Department
[*]shamluei@iau-doroud.ac.ir

Introduction

The metal ions have important rules in structure and function of proteins and other biomolecules [1]. The rule of metals as cofactor is greatly magnified in activation of enzyme [2,3,4,5]. Understanding the mechanism of activation, inhibition and other reactions, in which the metal ions have a critical rule, are achieved by clarifying the interaction of metal ions with protein sequence. The alkali metal cations and specially sodium are undoubtedly much abundant ions in biological systems. They act as which bind weakly to organic are ideally suited in generating ionic gradients across membranes by the sodium/potassium pump for the maintenance of osmotic balance [**Error! Bookmark not defined.**]. The nervous system function seriously depend on the activity of the Na^+/K^+ pump, the transporter responsible for maintaining steep Na^+ and K^+ gradients across the neuron plasma membrane.

The study of the interaction between sodium ion and biosystems may be unreachable because of the complexity of the biomolecules. it seems that the first estimation of these interactions can be obtained by studying the interaction of the metal ions with the simple molecule such as alcohol, amide, amine and other molecules containing functional group resemble to functional group exist in biomolecules. Therefore extended research was done to understand the nature of these interactions [6,7,8,9]. In this research interaction of sodium ion with amino acids were studied.

Computational details and selection of models

Optimum structures for several substituted Amino Acids, complex of sodium with these Amino Acids and sodium bond dimer of them were calculated by gaussian03 package and HF and B3LYP with the 6-311++g** basis set. In Fig.1 the general formula of Amino Acid in two ionic and neutral forms is shown. Chemical formula of groups where replaced instead of R1 and R2 is shown in Table 1.

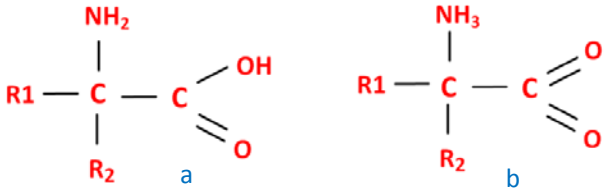

Fig.1 General formula of two neutral (a) and ionic forms (b) forms of Amino Acids

Table 1. the chemical formula for the selected substitution

R1	R2	R1	R2
H	H	H	SH
H	CH_3	SH	SH
CH_3	CH_3	H	SiH_3
H	F	SiH_3	SiH_3
F	F	H	NH_2
H	COOH	NH_2	NH_2

After obtaining the optimum structure for each molecule, the nonbonding orbital analysis of them was done. Finally the thermodynamic properties of each species were calculated.

Results and discussion

1. Structure and stability

The optimized structures for substituted Amino Acids were obtained. For instance the structure of Alanine which amino acid substituted with H and CH_3 is shown in Fig.2**Fig.5**.

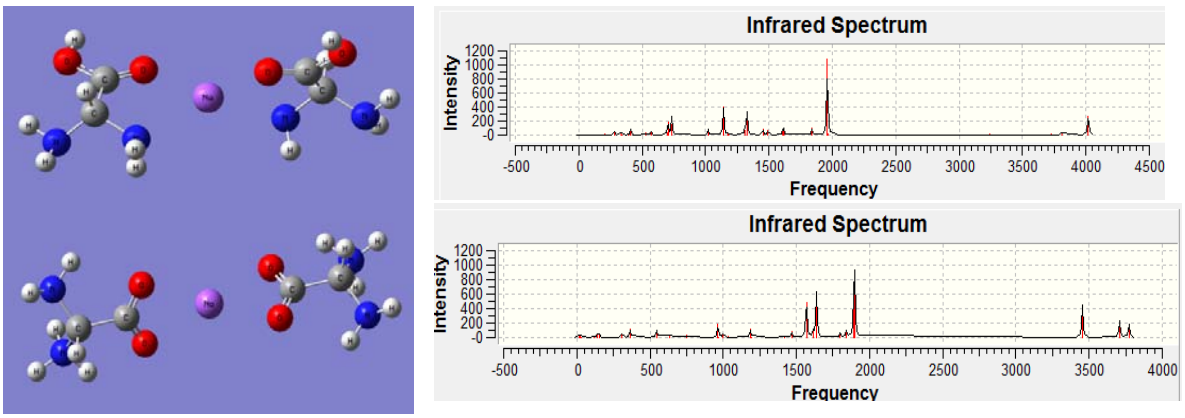

Fig.2 structure and IR spectrum of sodium ion bonded dimer of two forms of Amino Acid in which R1=H and R2=NH_2

2. Neutral versus ionic form of Amino Acids

The barrier for proton transferring from C-O-H group to NH2 gropu was calculated and the differences between them were studied in Fig.3. Fig.3 shows that in the situation R1=H and R2=H, the neutral form of amino acids are more stable. The difference in energy of two forms of amino acids were calculated and shows that this difference highly affected by substitutions.

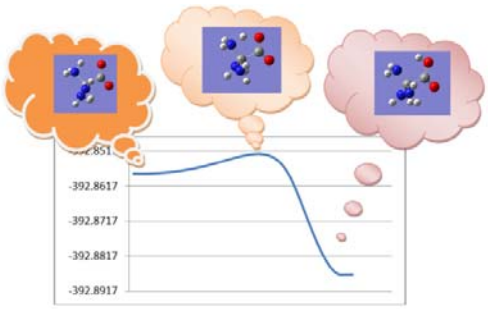

Fig.3 Transformation energy barrier for proton from NH_2 group to C=O group

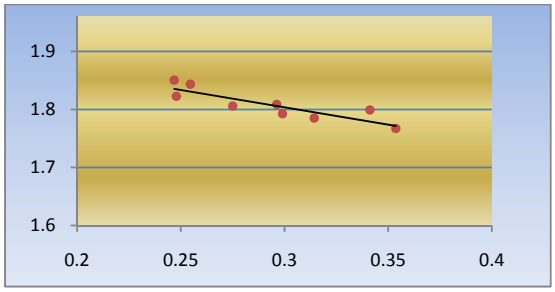

Fig.4 the results of sodium ion bond length versus □ factor

3. Bond length and enthalpy of formation

The bond lengths of sodium ion to oxygen in dimer were calculated by same method mentioned previously. In Fig.4, the bond length of sodium to oxygen is plotted versus □ factor. The □ factor which represents the decrease in charge on sodium ion is defined as;

Calculated enthalpy of formation also show same trend as demonstrated in Fig.4.

Conclusion

Different substituted amino acids were selected and difference in energy for neutral and ionic form of them was calculated. Results show that the energy difference between two structures significantly is affected by nature of substitutional group. In continuation, the structure of sodium ion bonded dimer of amino acids and its species were calculated. the bond length of sodium ion to oxygen in dimer, was calculated and it was shown that the strength of the bond increases as charge of sodium ion decreases. Finally the analysis of energy parameters of dimer formation process were done and observed trend was same as seen in analysis of bond length.

References

[] Robert R. Crichton, Biological Inorganic Chemistry an Introduction, Elsevier, 1st edition. 2008

[2] Z. Rappoport and I. Marek, The chemistry of organomagnesium compounds, 2008 John Wiley & Sons, Ltd

[3] R.B. Davies and E.P. Abraham, Biochem. J., (1974) 143, p.129

[4] J. A. Cowan, Chem. Rev. 1998, 98, p.1067

[5] Russ Hille, Chem. Rev., 1996, 96, p.2757

[6] M. T. Rodgers and P. B. Armentrout, J. Phys. Chem. A., 1997, 101, p.2614

[7] M. T. Rodgers, P. B. Armentrout, J. Phys. Chem. A., 1999, 103, p.4955.

[8] U. Senapati, D. De, B.R. De, Journal of Molecular Structure: THEOCHEM 894, (2009) p.71.

[9] Zahra Aliakbar Tehrani, Alireza Fattahi, Ali Pourjavadi, Carbohydrate Research, 344, (2009) p.771

Lithium Ion Bond Dimer of Substituted Ketones, Study the Substitutional Groups Effect on Structure, Stability and Enthalpy of Formation

Hamid Reza Shamlouei*[1] and Reza Karimi[2]

[1,2]*Islamic Azad University, Gachsaran Branch, Science Department*

**shamlouei@iaug.ac.ir*

Introduction

Rule of metal ions in biological systems structure and function not wearing to anyone. They have important rule in protein function and other biomolecules [1]. The rule of metals as cofactor is greatly magnified in activation of enzyme [2,3,4,5].

The alkali metal cations are undoubtedly much abundant ions in biological systems. They act as which bind weakly to organic are ideally suited in generating ionic gradients across membranes and for the maintenance of osmotic balance [**Error! Bookmark not defined.**]. on the other hand the lithium ion as an alkali metal ion have an important application as anti mania drug for the depression disease [6]. Understanding the mechanism of activation inhibition and other reaction, in which the metal ions have a critical rule, is achieved by clarifying the interaction of protein sequences and the metal ions.

Study of the interactions between lithium ion with biological molecule may be unreachable because of the complexity of the biomolecules. it seems that the first estimation of these interactions can be obtained by studying the interaction of the metal(lithium) ions with the simple molecule such as alcohol, amide, amine and other molecules containing functional group resemble to functional group exist in biomolecules. This research deals with the lithium ion bond dimer of some substituted ketones and study the effects of the group's nature on structure, stability and heat of formation of them. This could be considered as beginning to understanding the interaction of metal ion on small organic molecules as an estimation of biological systems.

Computational details

Optimum structures for several substituted molecules of ketones, ketones bind with lithium ion and lithium bond dimer of them were calculated. Dimers studied in this research are homo dimer and hetero dimers that refers to same or different ligands used in their structure. all of

the calculations were performed by gaussian03 package and HF, B3LYP and MP2 with the 6-311++g** basis set. in Table 1 the chemical formula of the selected substituted ketones has been shown.

Table 2 the chemical formula for the optimized molecules

	Name of monomer		Name of monomer		Name of monomer
1	$(CH_3)_2$-CO-$(CH_3)_2$	4	$(SiH_3)_2$-CO-$(SiH_3)_2$	7	F_2-CO-F_2
2	CH_3-H-CO-CH_3-H	5	H_2-CO-H_2	8	NH_2-H-CO-NH_2-H
3	SiH_3-H-CO-SiH_3-H	6	F-H-CO-F-H	9	$(NH_2)_2$-CO-$(NH_2)_2$

After obtaining the optimum structure for each molecule, the natural orbital analysis of them was done and then the partial charge for them extracted. Finally the thermodynamic properties of each species were calculated.

Results and discussion

1. Lithium ion homo dimers

Optimized structure for the monomer, monomer bind with lithium and lithium bond homo dimer of each substituted ketones molecules, in which two attached groups are the same, was obtained. For instance the structure of acetone, acetone bind with lithium ion and lithium ion bond dimer of acetone are shown in Fig.5.

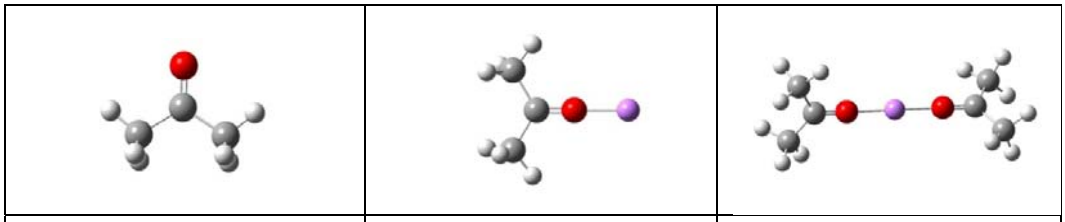

Fig.5: Optimized structure for (*a*) acetone, (*b*) acetone bonded with lithium ion and (*c*) lithium ion bond dimer of acetone

Stability of the dimers was estimated by noticing the infrared spectra for them. All homo and hetero dimers have no negative number in infrared spectrum so they are stable.

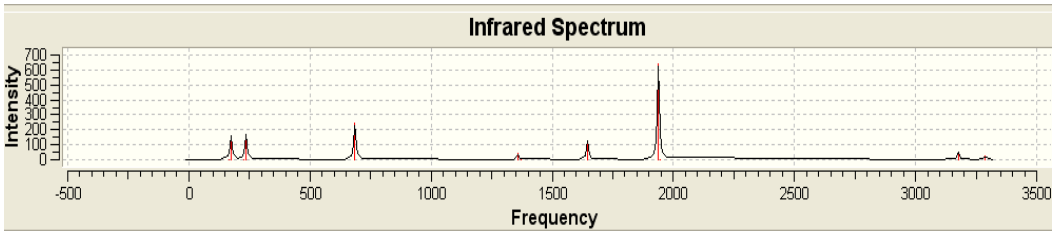

Fig.6: infrared Spectrum for lithium ion bond dimer of acetone

Two bonds of Li^+ to two carbonyl groups are almost the same. In this search, parameter ζ was defined as;

ζ=total charge-calculated charge on Li ion

the Li-O bond length which located between lithium ion and some substituted ketone were plotted versus ζ in Fig.7.

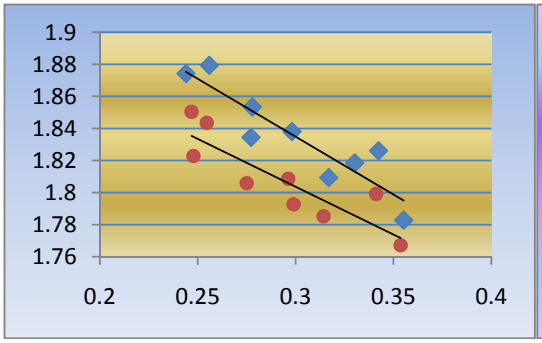

Fig.7 the Li-O bond length versus ζ

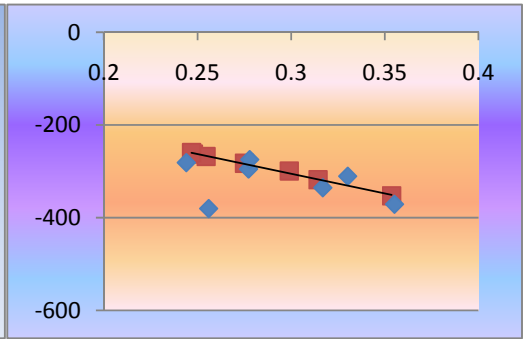

Fig.8 enthalpy of formation of lithium ion bonded dimer

In Fig.8 the enthalpy of formation for the lithium ion bonded dimer versus parameter ζ was plotted. Fig.7 shows that as the □ increase, the bond length of Li-O decreases. This means that if one factor stabilize the positive charge and reduce it, the bonding of Li-O to it will be strengthened. In Fig.8 the enthalpy of formation for different substituted dimer is shown.

Conclusion

In this research the stability of lithium bond dimer of substituted ketones were studied to estimate the nature of their interactions. After optimization of the structure of homodimer, charge, bond length and energy analysis were done. Stability of all dimers were measured by calculation of Infrared spectrum. in bond length analysis of dimer it was seen that the bond length of Li decreases as □ factor increases.

References

[] R.R. Crichton, Biological Inorganic Chemistry an Introduction, Elsevier, 1st edition. 2008

[2] Z. Rappoport and I. Marek, The chemistry of organomagnesium compounds, 2008 John Wiley & Sons, Ltd

[3] R.B. Davies and E.P. Abraham, Biochem. J., (1974) 143, p.129

[4] J. A. Cowan, Chem. Rev. 1998, 98, p.1067

[5] R. Hille, Chem. Rev., 1996, 96, p.2757
[6] R. Goldberg, Drugs Across the Spectrum, Sixth edition, 2009, WADSWORTH CENGAGE learning.

Ab initio and DFT Calculation of Conformational Properties and Thermodynamic Properties of Sterically Congested 1,1,1-Trifluoro-2-(5-aryl-1,3,4-oxadiazol-2-yl)-2-propanol Derivatives

Nahid Shajari* and Hooriye Yahyaei

Chemistry Department, Zanjan Branch, Islamic Azad University, P.O.Box: 49195-467, Zanjan, Iran

Corresponding Author E-mail: n_shajari120@yahoo.com

Keywords: DFT, Ab initio; NMR calculations

Introduction

In the past decade, IR spectroscopy have become important techniques for obtaining information on chemical structures and are applied in virtually all branches of chemistry. Vibrational spectroscopy is used extensively in organic chemistry for the identification of functional groups of organic compounds as well as for studies on molecular conformation, reaction kinetics, etc [1]. Density functional theory (DFT) has become a major tool in the methodological arsenal of computational organic chemists. DFTmethods are increasingly applied to representative pharmacological compounds aiming to elucidate their molecular structures, electronic properties and bonds, the establishment of electronic and structural factors of selected reactions and their mechanisms. Experimental measurements and theoretical calculations on vibrational frequencies become one of the key factors in the molecular structure correlations design. For a proper understanding of IR and Raman spectra, a reliable assignment of all vibrational bands is essential. For this purpose, the quantum chemical methods, ranging from semi-empirical to DFT approaches, are invaluable tools [2-4], each method having its own advantages. The semiempirical calculations provide very fast, and in certain circumstances fairly good theoretical results, being applicable to large molecular systems. HF methods are able to give good results provided a reasonable basis set and an appropriate correlation treatment is taken into account. On the other hand, DFT methods, particularly hybrid functional methods, have evolved to a powerful quantum chemical tool for the determination of the electronic structure of molecules. Among these, the B3LYP combination is the most used since it proved its ability in reproducing various molecular properties, including vibrational spectra. The combined use of B3LYP functional

and standard split valence basis set 6-31G* has been previously shown to provide an excellent compromise between accuracy and computational efficiency of vibrational spectra for large and medium-size molecules. In connection with our recent interest to multicomponent reactions, we report synthesis and FT-IR studies of 1,1,1-trifluoro-2-(5-aryl-1,3,4-oxadiazol-2-yl)-2-propanol derivatives (4a-f) from three-components reaction between, (*N*-isocyanimino)triphenylphosphorane, 1,1,1-trifluoroacetone and aromatic (or heteroaromatic) carboxylic acids (3-methylbenzoic acid, 1-naphthalenecarboxylic acid, 2-naphthalenecarboxylic acid, 2-furancarboxylic acid and 2-thiophenecarboxylic acid) . The B3LYP/HF calculations for computation of FT-IR spectra have been carried out for the title compounds at the 6-31G* and 6-311++G** basis set levels. Predicted vibrational frequencies have been assigned and compared with experimental FT-IR spectra and they are supported each other.

Computational details

The vibrational wavenumbers were calculated using the Gaussian 98 software package on a Pentium IV personal computer. Geometry optimizations were performed with B3LYP/6-31G* , B3LYP/6-311++G**, and HF/6-311++G** methods. The DFT technique employed the Becke3 (B3) (Becke 1992) exchange functional which supplement with Lee, Yang, Parr (LYP) (Lee et al., 1988) correlation functional. Molecular geometries were fully optimized by Berny's optimization algorithm.

Results and Discussion

The (*N*-isocyanimino)triphenylphosphorane, 1,1,1-trifluoroacetone and aromatic (or heteroaromatic) carboxylic acids in dichloromethane react together in a 1:1:1 ratio at room temperature to produce 1,1,1-trifluoro-2-(5-aryl-1,3,4-oxadiazol-2-yl)-2-propanol derivatives. The reaction proceeds smoothly and cleanly under mild conditions and no side reactions are observed. The structures of the products were deduced from their IR, 1H NMR, 13C NMR and elemental analyses. In the present study, we report the B3LYP/HF calculation results for sterically congested 2,5-disubstituted 1,3,4-oxadiazoles derivatives in order to give their optimal molecular geometry and vibrational modes. Here, we focus on the use of modern density functional theory to fully account for the experimental vibrational IR data for the

products. In the literature, any theoretical vibrational studies on the title compounds were not found. The schematic drawing with the theoretical geometric structure is shown in this paper. The observed FT-IR bands and calculated wavenumbers and assignments are given. On the basis of our calculations and experimental infrared spectra, we made a reliable one-to-one correspondence between our fundamentals and any of our wavenumbers calculated by B3LYP and HF methods. For the title compound the strong band at 3406 in the FT-IR spectrum is assignes as υNH mode. The calculated value for this mode are 3405, 3406, 3420, and 3410 cm−1 for HF/6-311++G**, B3LYP/6-31G*, and B3LYP/6-311++G** levels, respectively. The carbonyl stretching C=O vibration of ketone for compound appears at 1724. The calculated value for this mode are 1719, 1719, 1721, and 1720 cm−1 for HF/6-31G*, HF/6-311++G**, B3LYP/6-31G*, and B3LYP/6-311++G** levels, respectively.

The overall agreement between theory and experiment is quite reasonable for all methods that we have used. We further found a reliable one-to-one correspondence between our fundamentals and any of our calculated frequencies. There is an excellent agreement between experimental and theoretical results. In order to compare of this agreement, the correlation graphic based on the theoretical and experimental data has been investigated.

Experimental(general)

Starting materials and solvents were obtained from Merck (Germany) and Fluka (Switzerland) and were used without further purification. The methods used to follow the reactions were TLC and NMR. TLC and NMR indicated that there is no side product. Melting points were measured on an Electrothermal 9100 apparatus and are uncorrected. IR spectra were measured on a Jasco 6300 FTIR spectrometer. ^{1}H and ^{13}C NMR spectra were measured ($CDCl_3$ solution) with a BRUKER DRX-250 AVANCE spectrometer at 250.0 and 62.5 MHz, respectively. Elemental analyses were performed using a Heraeus CHN-O-Rapid analyzer. Mass spectra were recorded on a FINNIGAN-MATT 8430 mass spectrometer operating at an ionization potential of 20 eV. Flash chromatography columns were prepared from Merck silica gel powder.

Refrences:

[1] V. Krishnakumar, R. Mathammal, J. Raman Spectrosc., 40 (2009) 1599-1604.

[2] D. Avci, Y. Atalay, Int. J. Quantum Chem., 109 (2009) 328-341.

[3] B. Giese, D. McNaughton, Phys. Chem. Chem. Phys., 4, (2002) 5161-5170.

[4] W. Ma, Y. Fang, Journal of Nanoparticle Research 8 (2006) 761–767.

NMR spin–spin coupling constants in five pyridine aldehyde derivatives Experimental and DFT-B3LYP studies

Nahid Shajari*, Hooriye Yahyaei and Shahla Masoudian
Chemistry Department, Zanjan Branch, Islamic Azad University, P.O.Box: 49195-467, Zanjan, Iran
Corresponding Author E-mail: n_shajari120@yahoo.com

Introduction

During the last decade an important breakthrough in the calculation of NMR spin–spin coupling constants took place when the coupled-perturbed approach was implemented within the DFT framework [1–3]. At present with this methodology an interesting variety of spin–spin coupling constants can be calculatedwithgood accuracy inpolyatomic systems using reasonable computational resources. Inthis way, using a combination of experimental and computational chemistry, new stereospecific trends of coupling constants can be studied. This knowledge can help to understand how several intra-molecular interactions affect some spin–spin couplings, increasing the utility of these parameters for studying larger compounds. Many properties of J(13C,13C) couplings are already known and excellent review papers are found in the literature describing some of them. The main aim of this work is to study the potential of J(5J(HC) spin–spin couplings to determine the conformation of an aldehyde, CHO, group when it plays the role of a side-chain in an aromatic compound. The CHO group presents several interesting features, like, for instance the high stereospecificity of the,H) long-range coupling in benzaldehydes, 1, where Hff5J(His the formyl proton, and H is bonded to the aromatic ring. A similar stereospecificity was employed by several authors to determine the preferential conformation of monosubstituted pyridine aldehydes in solution through the measurement of such long-rangef,H) couplings. Such results are consistent with those obtained using other experimental techniques.

Computational details

All DFT calculations carried out in this work were performed using the hybrid B3LYP . This functional was chosen since it is known that for calculation of spin– spin coupling constants in hydrocarbons yield reliable results . It is important to note that lately, for

calculating spin–spin couplings Helgaker et al. studied the performance of three functionals However, the B3LYP functional was finally chosen since forJ(C,C) couplings in aromatic compounds a very good agreement was found between calculated and experimental couplings.

Results and discussion

In paper are compared the relative energies of rotamers cis, and trans ofcompounds calculated at the DFT-B3LYP/6-311G** level. These estimations of the energy difference between the two planar rotamers in both compounds were calculated without introducing any vibrational correction. For compound 2,thecis conformer correspondstothe C–HCf bondeclipsingtheringN–Cbond, while in compound the cis conformer corresponds to the C–HCfbondeclipsingtheringC–C2312bond.Inagreementwith results known from the literature, in compound the cis rotamer, is preferential in 4.8 kcal/mol with respect to 13the trans rotamer, for calculations corresponding to an isolated molecule, i.e. 3Z1 in the PCM model. When compound 2 in an infinitely diluted DMSO solution (3Z 46.7 in the PCM model) is considered, then the present calculations predict that cis is still preferential with respect to trance, but only in 2.2 kcal/mol. However, this difference in energy is still large enough to estimate that at room temperature J(C,13C) spin–spin coupling constants in solution are practically contributed only by 2a and not by 2b.In3, the present calculations predict that 3a is still the preferential rotamer but for 3Z46.7itisonly0.3kcal/molbelow3b.Thisisinlinewithresultsknownfromtheliterature,and it can be assumed that the observed NMR parameters in solution, like those studied in this work. J(13C,13C) spin–spin couplings were measured at natural abundance in five pyridine aldehyde derivatives. Such couplings were also calculated at the DFT-B3LYP-6-311++G** level of theory where special attention was paid to their possible stereospecific behaviors.Dielectric solvent effects were calculated on all four isotropic contributions to J(13C,13C) couplings using the polarization continuum model,PCM. It is observed that the inclusion of dielectric solvent effects in general leads to a better agreement between calculated and experimental couplings. 2J(13CC,13CA) couplings were observed to be sensitive to the aldehyde side-chain conformation (coupling pathway: CC–Ci–CA, where CC stands for the carbonyl-, Ci is the aromatic ipso- and CA is an adjacent aromatic-C atom). This is a positive coupling and becomes unusually large for a trans configuration between the carbonyl CaO and the CC–Ci bonds. In this conformation, there is an enhancement of conjugative interactions involving the p(CaO) and

p(CCaCi) bonding and antibonding orbitals.

Conclusions

Dielectric solvent effects on J(C,C) couplings in pyridine aldehyde derivatives seem to show a saturation effect for close to 10.It is observed that the general agreement between calculated and measured J(C,C) couplings is improved when taken into account dielectric solvent effects in calculated couplings. As noted previously in other aromatic compounds, calculated couplings at the DFT-B3LYP-6-311G**/EPR-III level of theory seem to perform very well in compounds studied in this work. According to results reported above, a is the preferential conformation as a consequence of a particular interplay between electrostatic and negative hyperconjugative interactions involving the oxygen lone-pair of p character. The attractive electrostatic N–H interactions inhibit both two other compound hyperconjugations ., and therefore it seems they counteract the destabilizing effect of those inhibitions. Probably, similar conclusions hold.

Refrences

[1] V. Sychrovsky ´ , J. Gra ¨ fenstein, D. Cremer, J. Chem. Phys. 113 (2000) 3530.

[2] T. Helgaker, M. Watson, N.C. Handy, J. Chem. Phys. 113 (2000) 9402.

[3] V. Barone, J.E. Peralta, R.H. Contreras, J.P. Snyder, J. Phys. Chem., A 106 (2002) 5607

NQR analysis of two phosphoramidates

Zahra Shariatinia, Vahid Tavasolinasab

Department of Chemistry, Amirkabir University of Technology, P. O. Box: 159163-4311, Tehran, Iran.
Tel: +982164543298. Fax: +982164543296. (E-mail: shariati@aut.ac.ir)

The structures of two phosphoric triamides with formula $C_6H_5NHP(O)[NHC_6H_4C(O)OCH_3]_2$ (**1**) and $C_6H_5NHP(O)[NHC_6H_4C(O)OCH_2CH_3]_2$ (**2**) were optimized using Gaussian 98 software at B3LYP and B3PW91 methods with standard 6-31G* basis sets. Nuclear quadrupole coupling constants (χ) were calculated for the quadrupole ^{14}N, ^{2}H and ^{17}O atoms. The χ values for the oxygen atoms of P=O and C=O bonds are about 5.0 and 10.0 MHz, respectively. For the ^{14}N atoms the χ values are about 4.0-5.0 MHz, and for the ^{2}H atoms they are near 200-300 kHz.

Keywords: phosphoric triamides; *ab initio* computations; DFT; NQR

Introduction

Phosphoramidates chemistry covers a wide area for applications in science and technology [1,2]. Many efforts have been made for the synthesis, characterization and structural investigations on these compounds [3]. *Ab initio* quantum chemical computations were applied on them both to predict the structural parameters [4]. It is noteworthy that as far as we know the nuclear quadrupole coupling constants of these molecules have not been reported so far. Calculation of nuclear quadrupole coupling constants (χs) of nuclei with spin ≥ 1 is a powerful tool to estimate the structural properties of the molecules [5]. In this work, the structures of two phosphoramidates were optimized at B3LYP/6-31G* and B3PW91/6-31G* methods using Gaussian 98 software [6]. Nuclear quadrupole coupling constants (χ) were calculated for the quadrupole ^{14}N, ^{2}H and ^{17}O atoms. The χ values of ^{17}O atoms in C=O bonds are nearly two times greater than those of P=O bonds.

Results and discussion

In this study, the geometry of two phosphoric triamides with formula $C_6H_5NHP(O)[NHC_6H_4C(O)OCH_3]_2$ (**1**) and $C_6H_5NHP(O)[NHC_6H_4C(O)OCH_2CH_3]_2$ (**2**) have been optimized using the Gaussian 98 software [6] at B3LYP/6-31G* and B3PW91/6-31G* levels of theory, Figure 1. In these molecules, the angles around the P atom indicate a distorted conformation. All P-N bonds are shorter than the typical P-N single bond (1.77 Å [7]) whereas the P=O bond lengths are longer than the P=O bond length (1.45 Å) [7]. In these molecules, the nitrogen environment is practically planar.

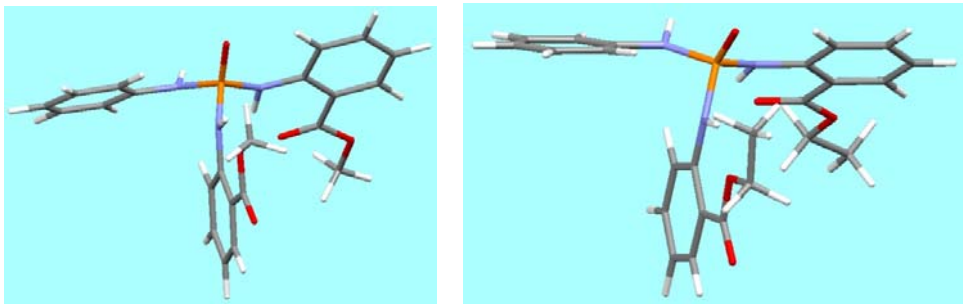

1 **2**

Figure 1. Optimized structures obtained for compounds **1, 2**.

The stabilization energies were calculated using the equation $\Delta E = E(molecule) - \Sigma_i E(i)$, i = atom (Table 1). The results show that compound **2** is more stable than **1** and also the B3LYP method presents higher negative stabilization energies than B3PW91. The calculated nuclear quadrupole coupling constants (χ) were obtained about 4.0-5.0 MHz for ^{14}N nuclei and near 200-300 kHz for the ^{2}H atoms. The χ values for the ^{17}O atoms of P=O and C=O bonds are about 5.0 and 10.0 MHz, respectively.

Table 1. The stabilization energies (ΔE, kcal mole^{-1}) of compounds **1**, **2**[*]

Compound	B3LYP/6-31G*	B3PW91/6-31G*
1	-6942.899	-6002.564
2	-7535.628	-6598.970

[*] $\Delta E = E(molecule) - \Sigma_i E(i)$, i = atom.

Acknowledgements

The financial support of this work by the Research Office of Amirkabir University of Technology is gratefully acknowledged.

References

[1] Zou X.J., Jin G.Y., Zhang Z.X., *J. Agricult. Food Chem*. **2002**, *50*, 1451.

[2] Akgür S.A., Öztürk P., Solak I., Moral A.R., Ege B., *Forensic Sci. Int*. **2003**, *133*, 136.

[3] Gholivand K., Mostaanzadeh H., Shariatinia Z., Oroujzadeh N. *Main Group Chem*. **2006**, *5*, 95.

[4] Gholivand K., Shariatinia Z., Pourayoubi M. *Polyhedron* **2006**, *25*, 711.

[5] Esrafili M.D., Behzadi H., Hadipour N.L. *Chem. Phys*. **2008**, *348*, 175.

[6] Frisch, M.J. *et al.*, Gaussian 98, Revision A9, Gaussian, Inc.; Pittsburgh, PA, **1998**.

[7] Corbridge D.E.C. *Phosphorus, an Outline of Its Chemistry, Biochemistry and Technology*, 5th Ed., Elsevier, the Netherlands, **1995**.

Structural study of two organically modified silica compounds (ormosils)

Zahra Shariatinia, Vahid Tavasolinasab

Department of Chemistry, Amirkabir University of Technology, P. O. Box: 159163-4311, Tehran, Iran.

Tel: +982164543298. Fax: +982164543296. (E-mail: shariati@aut.ac.ir)

The structures of two organosilicon compounds with formula $(OCH_3)_3Si(CH_2)_3NHC(O)NH(CH_2)_6NHC(O)NH(CH_2)_3Si(OCH_3)_3$ (**1**) and $(OCH_2CH_3)_3Si(CH_2)_3NHC(O)NH(CH_2)_6NHC(O)NH(CH_2)_3Si(OCH_2CH_3)_3$ (**2**), obtained from the reaction of TMSA and TESA with 1,6-diisocyanatohexane, were optimized using Gaussian 98 software at HF and B3LYP methods with standard 6-31G* basis set. Nuclear quadrupole coupling constants (χ) were calculated for the quadrupole ^{14}N, ^{2}H and ^{17}O atoms. The χ values for the oxygen atoms of C-O and C=O bonds are about 9.0-10.0 MHz, respectively. For the ^{14}N atoms the χ values are about 5.0 MHz, and for the ^{2}H atoms they are near 300 kHz.

Keywords: organosilicon; *ab initio* computations; DFT; NQR

Introduction

Hybrid inorganic-organic materials of organically modified silicas (ormosils) are one of the most significant classes of compounds owing to their various applications. Synthesis, characterization and complexation with Pd(II) of ormosils as well as applications of the complexes as catalysts in organic reactions were reported [1-3]. *Ab initio* calculations were done on mesostructured silica materials to predict the NMR chemical shifts as well as hypercojugative interactions [4]. In this work, the structures of two ormosils with formula $(OCH_3)_3Si(CH_2)_3NHC(O)NH(CH_2)_6NHC(O)NH(CH_2)_3Si(OCH_3)_3$ (**1**) and $(OCH_2CH_3)_3Si(CH_2)_3NHC(O)NH(CH_2)_6NHC(O)NH(CH_2)_3Si(OCH_2CH_3)_3$ (**2**) were optimized at HF/6-31G* and B3LYP/6-31G* methods using Gaussian 98 software [5]. Nuclear quadrupole coupling constants (χ) were calculated for the quadrupole ^{14}N, ^{2}H and ^{17}O atoms.

Results and discussion

In this study, the geometry of two organically modified silicas (ormosils) with formula $(OCH_3)_3Si(CH_2)_3NHC(O)NH(CH_2)_6NHC(O)NH(CH_2)_3Si(OCH_3)_3$ (**1**) and $(OCH_2CH_3)_3Si(CH_2)_3NHC(O)NH(CH_2)_6NHC(O)NH(CH_2)_3Si(OCH_2CH_3)_3$ (**2**) have been optimized using the Gaussian 98 software [5] at HF/6-31G* and B3LYP/6-31G* levels of theory, Figure 1. In these structures the two C=O bonds indicate *cis* conformations with C=O…C=O torsion angles equal to ~175°.

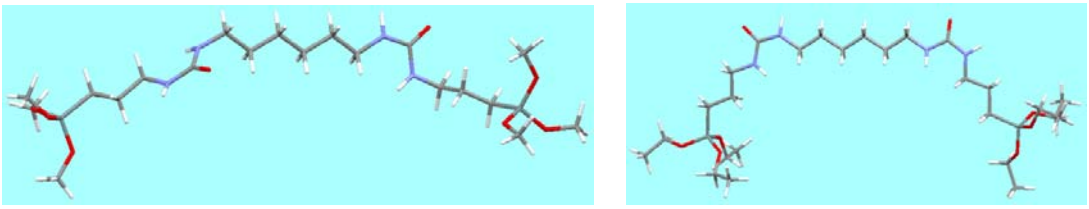

1 **2**

Figure 1. Optimized structures obtained for compounds **1, 2**.

The stabilization energies were calculated using the equation $\Delta E = E(molecule) - \Sigma_i E(i)$, i = atom (Table 1). In these molecules, the nitrogen environment is practically planar. The results show that compound **2** is more stable than **1** and also the B3LYP method presents higher negative stabilization energies than HF. The calculated nuclear quadrupole coupling constants (χ) were obtained about 5.0 MHz for ^{14}N nuclei and near 300 kHz for the ^{2}H atoms. The χ values for the ^{17}O atoms of C-O and C=O bonds are about 9.0-10.0 MHz.

Table 1. The stabilization energies (ΔE, kcal mole^{-1}) of compounds **1**, **2**[*]

Compound	HF/6-31G*	B3LYP/6-31G*
1	-6923.130	-9102.260
2	-8288.463	-10882.530

[*] $\Delta E = E(molecule) - \Sigma_i E(i)$, i = atom.

Acknowledgements

The financial support of this work by the Research Office of Amirkabir University of Technology is gratefully acknowledged.

References

[1] Polshettiwar V., Varma R. S. *Tetrahedron* **2008**, *64*, 4637.

[2] Bandini M., Luque R., Budarin V., Macquarrie D. J. *Tetrahedron* **2005**, *61*, 9860.

[3] Polshettiwar V., Molnár Á. *Tetrahedron* **2007**, *63*, 6949.

[4] Fernandez L., Viruela-Martin P., Latorre J., Guillem C., Beltrán A., Amorós P. *J. Mol. Struct.: Theochem* **2007**, *822*, 89.

[5] Frisch M.J. *et al.*, Gaussian 98, Revision A9, Gaussian, Inc.; Pittsburgh, PA, **1998**.

The O-H…O hydrogen bond interactions between aspirin and an ormosil compound

Zahra Shariatinia, Vahid Tavasolinasab

Department of Chemistry, Amirkabir University of Technology, P. O. Box: 159163-4311, Tehran, Iran.

Tel: +982164543298. Fax: +982164543296. (E-mail: shariati@aut.ac.ir)

The hydrogen bonding interactions between two aspirin molecules and an organosilicon compound with formula $(OCH_3)_3Si(CH_2)_3NHC(O)NH(CH_2)_6$ $NHC(O)NH(CH_2)_3Si(OCH_3)_3$ were evaluated using Gaussian 98 software at HF method with standard 6-31G* basis set. The binding energy ΔE_{bind} of the optimized system has been calculated taking into account the basis set superposition error (BSSE) correction. Also, the nuclear quadrupole coupling constants (χ) were calculated for the quadrupole ^{14}N, ^{2}H and ^{17}O atoms. The χ values for the oxygen atoms of C-O, Si-O and C=O bonds are about 8.0-10.0 MHz. For the ^{14}N atoms the χ values are ~5.0 MHz, for the ^{2}H atoms of NH and OH groups they are near 300 kHz but ~200 kHz for the ^{2}H atoms of CH groups.

Keywords: organosilicon; aspirin; hydrogen bond; NQR; BSSE; *ab initio* computations

Introduction

Organically modified silicates can be utilized to uptake inorganic metal cations for purification, extraction and separation purposes [1]. These types of compounds can also be used in fuel cells or carbon paste electrodes [2]. Luminescence and energy transfer of organically modified silica xerogels (OMSX) doped and undoped with Eu^{3+} and Tb^{3+} were studied [3]. *Ab initio* calculations were done on mesostructured silica materials to predict the NMR chemical shifts as well as hypercojugative interactions [4]. In this work, hydrogen bonding interactions between two aspirin molecules and an organosilicon compound with formula $(OCH_3)_3Si(CH_2)_3NHC(O)NH(CH_2)_6NHC(O)NH(CH_2)_3Si(OCH_3)_3$ were studied at HF/6-31G* level using Gaussian 98 software [5]. Furthermore, the nuclear quadrupole coupling constants (χ) were calculated for the quadrupole ^{14}N, ^{2}H and ^{17}O atoms.

Results and discussion

In this study, the hydrogen bonding interactions between two aspirin molecules and an organosilicon compound with formula $(OCH_3)_3Si(CH_2)_3NHC(O)NH(CH_2)_6$ NHC(O) $NH(CH_2)_3$ $Si(OCH_3)_3$ were studied using the Gaussian 98 software [5] at HF/6-31G* level of theory, Figure 1. In these structures the two C=O bonds indicate pseudo-*trans* conformations with C=O…C=O torsion angles equal to ~-100°.

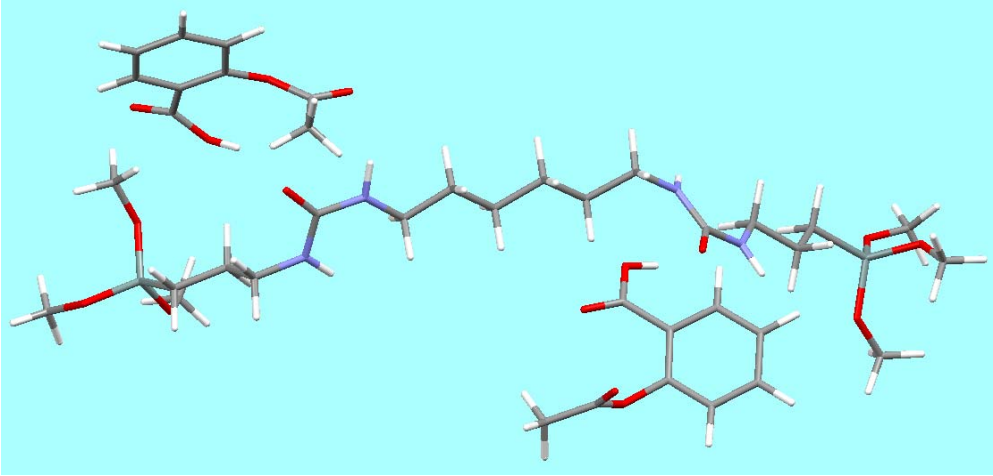

Figure 1. Optimized structure obtained for the title compound.

The binding energy, ΔE_{bind}, was obtained (-15.59 kcal/mol) from the equation [6] $\Delta E_{bind} = E_{(complex)} - [E_{(MAA)} + E_{(\alpha\text{-or }\beta\text{-glucose})}] + BSSE$. The basis set superposition error (BSSE) using counterpoise correction developed by Boys and Bernardi [7]. The calculated nuclear quadrupole coupling constants (χ) were obtained ~5.0 MHz for ^{14}N nuclei, near 300 kHz for the ^{2}H atoms of NH and OH groups but they are about 200 kHz for the ^{2}H atoms of CH groups. The χ values for the ^{17}O atoms of C-O, Si-O and C=O bonds are ~8.0-10.0 MHz.

Acknowledgements

The financial support of this work by the Research Office of Amirkabir University of Technology is gratefully acknowledged.

References

[1] Walcarius A., Etienne M., Delacote C. *Anal. Chim. Acta* **2004**, *508*, 87.

[2] Sayen S., Walcarius A. *J. Electroanal. Chem.* **2005**, *581*, 70.

[3] Y. Han, J. Lin, *J. Solid State Chem.* **2003**, *171*, 396.

[4] Fernandez L., Viruela-Martin P., Latorre J., Guillem C., Beltrán A., Amorós P. *J. Mol. Struct.: Theochem* **2007**, *822*, 89.

[5] Frisch M.J. *et al.*, Gaussian 98, Revision A9, Gaussian, Inc.; Pittsburgh, PA, **1998**.

[6] Kowalska A., Stobiecka A., Wysocki S. *J. Mol. Struct.: Theochem* **2009**, 901, 88.

[7] Boys S.B., Bernardi F. *Mol. Phys*. **1970**, *19*, 553.

Electron Density Analysis of σ and π Orbitals in Boron Nitride Nano-sheets Substituted by Cyanide, Thiocyanate and Isothiocyanate

S. Fakhraee [*,a], S. Sharifpour [b]

[a] Department of Chemistry, College of Sciences, Payame Noor university of Shiraz, Shiraz, 71365-944, Iran.
(Email: Fakhraee@spnu.ac.ir)

[b] Department of Chemistry, College of Sciences, Payame Noor university of Yazd, Ardakan,19٥, Iran.

Keywords: boron nitride nanosheet, QTAIM, σ and π charge density, AIM atomic charge

Introduction

The first discovery sparks of boron nitride (BN) nanostructure were appeared when Rubio anticipated it can be produced from substitution of C atoms in carbon nanostructures by B and N atoms [1]. Nowadays, it has been proved that the BN nanostructures are more favorable than carbon nanostructures to apply in many fields of science and technology. As a matter of fact, this distinction between BN structures and carbon nanostructures is owing to ionic character of BN bonds, which may induce an extra dipole moment and hence a stronger ability to absorb the atoms and molecules.

One of the most important aspects of computational studies of BN structures is the exact recognition of their electronic structures and their charge density. Electron density analysis of molecules can be performed by various methods in quantum chemistry. A useful tool for this purpose is quantum theory of atoms in molecules (QTAIM) introduced by Bader [2]. The theory of atoms in molecules offers a concise description of the electronic structure of molecules in terms of the topological properties of the charge density. The current QTAIM formulation is constructed so that only the σ-skeleton can be detected via the total charge density topology for bond paths (BPs) and bond critical points (BCPs). However, for planar molecules, the molecular π system can be detected as well by AIM theory, and similar concepts can be generalized to π bonds too. This generalization is based on the fact that σ and π components of charge density rigorously do not mix for linear and planar molecules [3].

In the present work, planar structure BN sheet are considered to investigate σ and π components of charge density, individually. To characterize the π system of BN sheet, the QTAIM concept of BCP is applied to the charge density topology, provided by both σ and π-

type canonical molecular orbital**.** Including the different substitutions on BN sheet leads to a change in charge density on the surface of this molecule. The charge density reorganization on the BN sheet affects the properties which are related to charge density. This motivated us to study the charge density changes in BN sheets substituted by π bond containing molecules such as cyanide, thiocyanate and isothiocyanate.

Theoretical Method

All the computational calculations including geometry and wave function optimization were carried out in HF/6-31g* level of theory by Gaussian 03W program. The frequency analysis was applied to confirm that the system possesses a minimum energy equilibrium structure. Figure 1(A) shows typical optimized structure of BN sheet where R refers to H, CN, SCN and NCS substitutions which are connected to nitrogen number 50 (N_{50}) of BN sheet. The wave function for each structure was analyzed by AIM 2000 package [4]. This program was applied to represent the topological graphs of charge density corresponding to molecular σ and π systems. The BCPs and BPs graph for typical BN sheet structure with R substitution is separately presented in σ and π systems in Figure 1(B) and 1(C), respectively. In order to obtain π-BCP and BP graphs individually, the σ contribution of charge density of each structure was excluded and the analysis was performed only on π contribution. Figure 2 represents the σ-AIM graphs (a, b, c, d) and their corresponding π graphs (e, f, g, h) for each substitution in large scale. The analyses demonstrate formation of double bond in connection between substitution and N_{50} of BN sheet for all structures which are presented by BCP 1 in σ bonds and 1a and 1b in π bonds. Table 1 summarizes the value of charge density ρ at BCPs number 1 to 7 represented in Fig.2 for both σ and π systems which are including most changes in charge density.

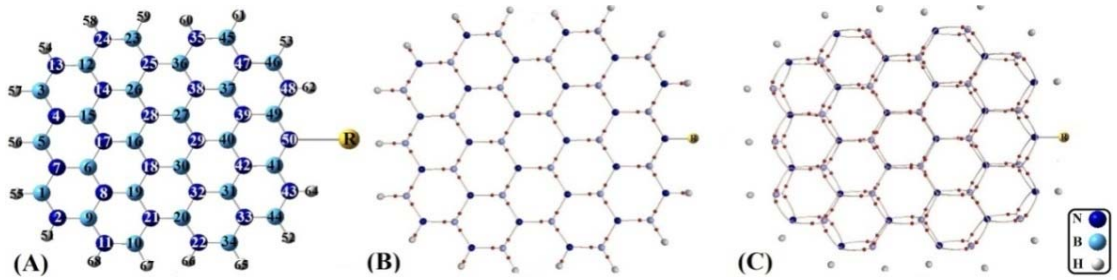

Figure 1: (A): Typical optimized structure of BN sheet substituted by R (R: H, CN, SCN and NCS). (B): The molecular graph of BN sheet showing the collection of σ-BPs and associated BCPs. (C): π-BPs and BCPs for BN sheet.

In order to investigate the effect of substitutions on reorganization of charge density of BN sheets, the AIM atomic charges of B and N atoms and also B-N bond lengths of BN sheet and was obtained and tabulated in Table 2.

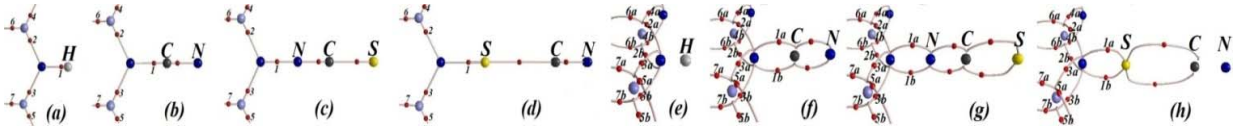

Figure 2. σ-BPs and their BCPs for BN, BN-CN, BN-NCS, and BN-SCN sheets in a, b, c, and d and the same for π in e, f, g, and h figures.

Results and discussions

The results in Table 1 and 2 show that the most significant changes occurs in atomic charges, bond lengths and ρ_{BCPs} related to B and N atoms of BN ring connected to substitution and its vicinal nitrogen atoms (N_{43} and N_{48}). The other BCPs don't show considerable changes in their properties respect to BN sheet without substitution. Because of symmetry in BN sheet molecule the atomic charge, bond length and ρ_{BCP} of the B_{49} and B_{41}, N_{39} and N_{42}, and also N43 and N48 are identical. Therefore, the results are expressed only for one of them in following tables.

Table 1: Calculated charge density for BCPs 1-7 with significant changes respect to other BCPs on BN sheet.

Structure	*Charge Density(ρ_{BCP})*								
	σ type BCPs				*π type BCPs*				
	1	*2*	*4*	*6*	*1*		*2*	*4*	*6*
					a	*b*	*a* *b*	*a* *b*	*a* *b*
BN Sheet	*0.3422*	*0.200٤*	*0.1984*	*0.195١*	-		*0.021٣*	*0.020٥*	*0.019٤*
BN Sheet - CN	*0.3481*	*0.1812*	*0.2075*	*0.2022*	*0.0395*		*0.0184*	*0.0222*	*0.0206*
BN Sheet - NCS	*0.3582*	*0.1850*	*0.2078*	*0.2020*	*0.0467*		*0.0197*	*0.022٤*	*0.0207*
BN Sheet - SCN	*0.2266*	*0.1594*	*0.2158*	*0.2087*	*0.040١*		*0.0124*	*0.024٤*	*0.0223*

Table 2: AIM atomic charge and bond length for atoms and bonds with significant changes respect to BN sheet.

Structure	AIM atomic charges					Bond length (A°)			
	$N_{۵۰}$	$B_{۴۹}$	$N_{۳۹}$	$B_{۴۰}$	N_{48}	N_{50}-B_{49}	B_{49}-N_{39}	N_{39}-B_{40}	B_{49}-N_{48}
BN Sheet	*-1.853*	*2.433*	*-2.33 ۱*	*2.419*	*-1.876*	*1.427*	*1.447*	*1.443*	*1.434*
BN Sheet – CN	*-1.748*	*2.430*	*-2.336*	*2.423*	*-1.932*	*1.462*	*1.434*	*1.445*	*1.419*
BN Sheet – NCS	*-1.225*	*2.428*	*-2.332*	*2.423*	*-1.891*	*1.454*	*1.435*	*1.446*	*1.417*
BN Sheet – SCN	*-1.906*	*2.419*	*-2.310*	*2.426*	*-1.908*	*1.526*	*1.422*	*1.452*	*1.404*

Comparing the value of bond lengths and charge densities in above tables demonstrates an increase in σ type ρ_{BCP} number 4 and decrease in its associated bond length, B_{49}-N_{48}. Also, one can see a large decrease in ρ_{BCP} number 2 after substitution which causes some increase in N_{50}-B_{49} bond length. It can be seen that, the same trend is exactly appeared in π bond systems. The conjugation of π bonds in BN sheet and its substitutions will affect atomic charges on BN sheet atoms near the substitution which is presented in Table 2. The substitutions change the polarity of BN bonds on BN sheet. This can help to attract other molecules.

Conclusion

The σ and π contribution of charge density were separated and studied separately by QTAIM for BN sheets with and without CN, SCN, and NCS substitutions. The results show that the π system obeys the same trend in σ system. The π bond containing systems conjugated with BN sheet cause to change in density, atomic charge and bond length of hexagonal BN ring connected to substitution and also the two vicinal N atoms of the ring.

References

[1] A. Rubio, J. L Corkill, M. L. Cohen, Theory of graphitic boron nitride nanotubes. *Phys. Rev. B*., 49, 1994, 5081.

[2] R. F. W. Bader, *Atoms in Molecules: A Quantum Theory*, Oxford University Press Inc., New York, 1995.

[3] S. M. Azami, *J. Phys. Chem. A*., 114, 2010, 11794.

[4] R. F. W. Bader, *AIM 2000 program package,* Version 2.0: McMaster University: Hamilton, Ontario, 2002.

Quantum chemical studies of some Schiff bases as corrosion inhibitors on mild steel

R. Shafiei[a], E. Jamalizadeh[b], S.M.A. Hosseini[b]*

[a]Department of Chemistry, Payame Noor University (PNU), Kerman, Iran

[b] Department of Chemistry, Faculty of Science, Shahid Bahonar University of Kerman, Kerman 76175, Iran.

(s.m.a.hosseini@mail.uk.ac.ir)

Keywords: Quantum Chemical Calculation; Corrosion Inhibition; Schiff Base; Mild Steel

Introduction

Mild steel is widely used in fabrication of reaction vessels, store tanks, petroleum refineries, and so on. The main problem of using mild steel is its acidic solutions [1,2]. The use of organic inhibitors is one of the most practical methods for protection against corrosion in acidic media. Recently, H. Ashassi et al. experimentally found that Schiff bases i.e. Benzylidene-pyridine-2-yl-amine(A) , (4-Methyl-Benzylidene)-pyridine-2-yl-amine(B) , (4-Chloro-Benzylidene)-pyridine-2-yl-amine(C) , Benzylidene-pyrimidine-2-yl-amine(D) , (4-Methyl-Benzylidene)-pyrimidine-2-yl-amine(E) , (4-Chloro-Benzylidene)-pyrimidine-2-yl-amine(F) show inhibitive properties for mild steel in 1M HCl solution [3]. The present research find apparent correlation between parameters resulted by quantum chemical calculations related to the structure of Schiff bases and their ability to inhibit the corrosion process.

Computational Details

Complete geometry optimization of molecule and all quantum chemical calculations were performed at the DFT B_3LYP level using 6-31G++(d,P) basis set. Furthermore, inhibitor/iron system optimization was performed by LANL2DZ basis sets. The calculations in water solvent and IEFPCM is used for this purpose. All calculations were performed with the help of Gaussian03 computer codes [4], working on 2.3 GHz dual processors.

Results and Discussion

Highest occupied molecular orbital energy level (E_H), the energy of the lowest unoccupied molecular orbital (E_L), E_L-E_H, the dipole momentum (μ), the electron charge on nitrogen atoms (q_{N1}) and (q_{N2}) were determined, Table 1. In addition, the best adjusted linear regression coefficient (R^2) for inhibition efficiency versus calculated quantum chemical parameters for inhibitors also represented. As results shows, the differences of inhibiting molecules efficiencies can be best expounded in terms of (μ) with correlation coefficients above 0.92. The calculated values of inhibition efficiency work out by regression analyses of IE% versus (μ) are given in Table 1. Comparison of calculated inhibition efficiencies with experimental results exhibits excellent agreement.

Table 1. Quantum chemical parameters and experimental data for substituted inhibitors.

Inhibitor Designation	E_H (au)	E_L (au)	E_L-E_H (au)	μ (D)	q_{N1} (ev)	q_{N2} (ev)	IE% (Exp)	IE% (Cald.)
A	-0.241	-0.077	0.164	5.166	-0.173	-0.272	99.16	98.53
B	-0.237	-0.075	0.162	5.265	-0.168	-0.276	99.39	98.88
C	-0.242	-0.081	0.161	5.620	-0.168	-0.276	99.59	100.00
D	-0.250	-0.085	0.165	3.200	-0.167	-0.262	90.00	91.56
E	-0.244	-0.083	0.161	3.105	-0.172	-0.270	92.80	91.23
F	-0.250	-0.088	0.162	4.568	-0.157	-0.265	95.80	96.41
R^2	0.557	0.440	0.142	0.922	0.129	0.695		

From the molecular orbital density distribution of the inhibitors, one can see that the electron density of the HOMO and LUMO orbitals is well proportioned. This kind of structure is difficult to form chemical bond active centres, which proved the probability of the physical adsorption between the interaction sites [5] which is consistent with experimental results ($\Delta G \cong 33 KJ.mol^{-1}$). To find favourite site for adsorption, inhibitor/iron system was optimized. The result of inhibitor molecule/iron atom optimization reveals adsorption position due to the lone pair electron of nitrogen atoms as the most stable state (Fig. 1).

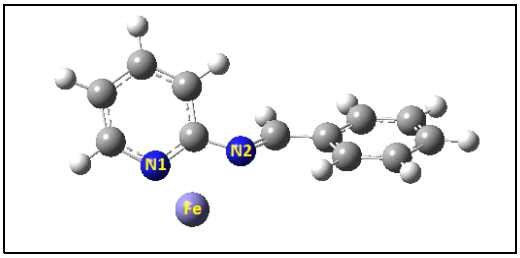

Fig. 1. The A molecule in interaction with iron atom.

Conclusion

The relationship between molecular structure of these compounds and their inhibition efficiency indicated that the inhibition efficiency has lucid correlation with the dipole moment. Frontier orbital theory results proved the probability of the physical adsorption between the interaction sites. The result of inhibitor/iron optimization revealed adsorption position due to the lone pair electron of oxygen atoms of nitro group as the most stable state.

Refrences

[1] Gulsen Avci, Aspects 317 (2008) 730.

[2] C. Kustu, C.K. Emregul, O. Atakol, 49 (2007) 2800.

[3] H. Ashassi-Sorkhabia, B. Shaabani, D. Seifzadeh , Electrochimica Acta, 50 (2005) 3446.

[4] M.J. Frisch et al., Gaussian 03, Revision B.03, Inc. Pittsburgh PA, 2003 .

[5] Y. Yan, W. Li, L. Cai, B. Hau, Electrochim. Acta 53 (2008) 5953.

Interaction of Calcium Ion with Amino Acids as the Proteins Building Blocks

F. Shafiei[a], H.R. Shamlouei[a*]
[a] Islamic Azad University, Gachsaran Branch, Science Department
shamluei@iaug.ac.ir

1. Introduction

The role of Calcium in biological systems not wearing to anyone. Calcium, together with sodium, potassium and magnesium, is one of the metals required by living systems in macro-amounts. indeed it represents 1.5–2% of an adult's total body weight. The biominerals that constitute teeth and bones contain the majority of the body's calcium (~99%). Yet the 1% that remains within the cells and tissues has enormous importance in the regulation of a whole series of cellular responses [i]. The processes in which Ca^{2+} play important roles, include muscle contractions, hormone secretion, glycolysis, gluconeogenesis**,** ion transport, cell division and cell growth[ii].

The intense researches were done previously to find the calcium binding to proteins [iii, iv, v].

As the result of importance of Ca^{2+} in biological systems, understanding the interaction of metal ion to protein chain is very important for knowing the mechanism of enzyme activation and other biological function of Calcium ion and the pharmaceutical function of it. This research deals with the calcium ion bond dimer of some substituted Amino Acids and study the effects of the group's nature on structure, stability and heat of formation of them. This could be considered as beginning to understanding the interaction of calcium ion on Amino Acids as an estimation of biological systems.

2. Selection of Compound and Computational Method

Amino Acids are building block of proteins in which have amine (NH_2) and carboxylic group acid attached to single carbon. There are two forms of Amino Acids; neutral and ionic forms. General formula of two neutral (a) and ionic forms (b) forms of Amino Acids are shown in **Fig.1**.

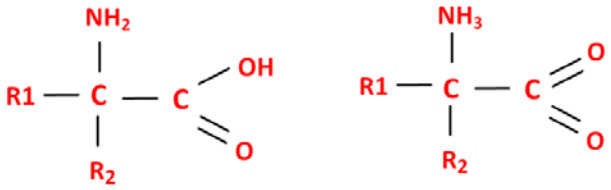

Fig.9 General formula of two neutral (a) and ionic forms (b) forms of Amino Acids

Table3 list of substitutions which located instead of R1 and R2 groups in **Fig.1**

R1	R2	R1	R2
H	H	H	SH
H	CH_3	SH	SH
CH_3	CH_3	H	SiH_3
H	F	SiH_3	SiH_3
F	F	H	NH_2
H	COOH	NH_2	NH_2
COOH	COOH		

The substitution R1 and R2 were chosen in manner that the properties of them are changed from electron withdrawing groups to electron releasing groups. In Table6list of substitution which selected to be locate in place of R1 and R2 is shown. Substituted Amino Acids, calcium ion bonded to Amino Acids and calcium ion bonded dimer of them was chosen to study the interaction of calcium ion with substituted Amino Acids.

The structure of each species in this research include; Amino Acids, calcium ion attached to Amino Acids and calcium ion bonded dimer of them were optimized by HF method, 6-311++G** basis set and gaussian03 package. Energy parameters, IR spectrum and NMR of each species were calculated by using same method and basis set described previously.

3. Results and discussion

3.1. Structure and stability of Amino Acids, calcium ion bonded to Amino Acids and calcium ion bonded dimer of them

Structure of all species such as Amino Acids, calcium ion bonded to Amino Acids and calcium ion bonded dimer of them was calculated. The structure and IR Spectrum of the calcium ion bonded dimer of Amino Acid which R1 and R2 are H is shown in Fig.10.

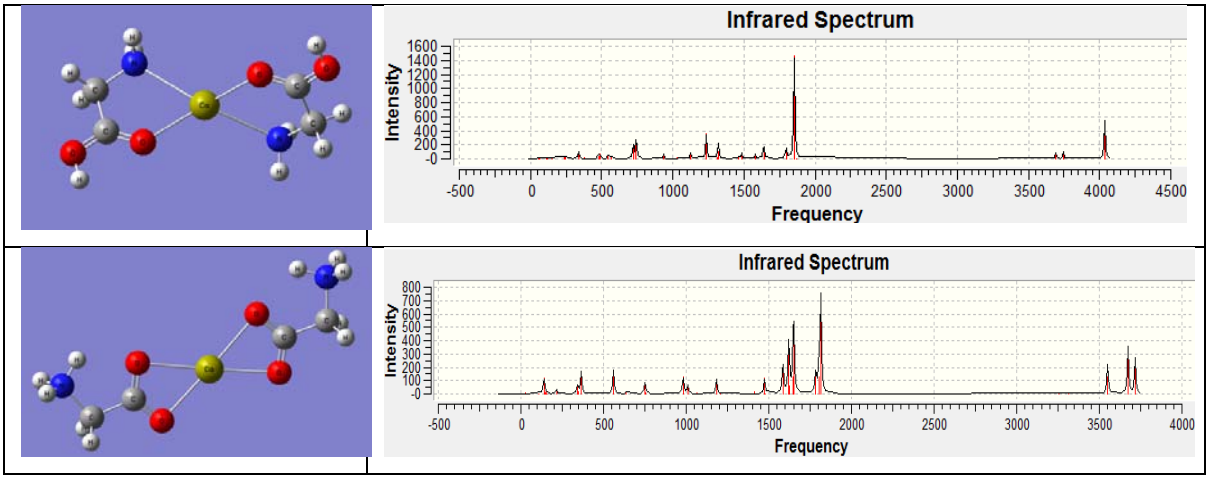

Fig.10 structure and IR spectrum of calcium ion bonded dimer of two forms of Amino Acid in which R1=H and R2=H

Since observing the IR spectrum of the dimers shows no negative vibrational mode in its spectrum, the dimers are stable.

3.2. Calcium ion bond strength and enthalpy of formation for calcium bonded dimer of Amino Acids

The calcium ion bond length to oxygen or nitrogen shows the strength of it. In **Error! Reference source not found.**, the Ca^{2+} bond length versus calcium charge in dimer is plotted. In Fig.4, plot of the enthalpy of formation for the different dimers versus calcium charge in them is shown.

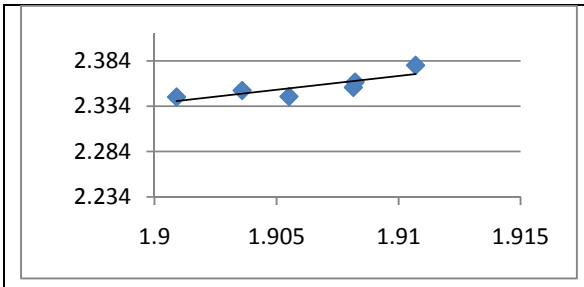

Fig.11 the results of calcium ion bond length versus calcium charge in dimer

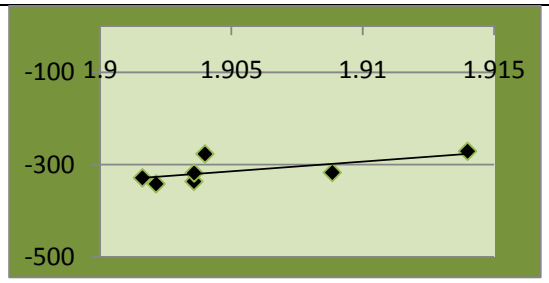

Fig.12 the enthalpy of formation for the different dimers versus calcium charge in dimer

As shown in Fig.3 and Fig.4, when the charge in central calcium ion in dimer decreases the strength of calcium bond to amino acids is strengthen and the enthalpy of formation of dimer increases.

4. Conclusion

The structure and stability of calcium ion bonded dimers of different substituted amino acids which resembled the interaction of calcium ion with proteins, were calculated by ab initio calculations. The energy parameters of them were analyzed by same method and show that each parameter such as electron releasing or withdrawing properties of substitutions makes the dimer more stable.

Refernces

[] Robert R. Crichton, Biological Inorganic Chemistry: An Introduction, 2008, 1st edition, Elsevier, Amsterdam, Netherlands.

[] Ivano Bertini, Harry B. Gray, Stephen J. Lippard, Joan Selverestone Valentine, Bioinorganic chemistry, 1994, University Science Books, Mill Valley, California.

[]Robert H. Kretsinger and Clive E. Nockolds, Journal of Biological Chemistry, 1973, 248, 3313

[ ]sohan S. Jande, L. Maler and D. Erik M. Lawson, Nature 294, 765 – 767.

[]M.R. Celio and C.W. Heizmann, Nature 293, 300 – 302.

Theoretical study of Sulfur Adsorption on Ni(111) Surface

Amir N. Shamkhali* and Kobra Gharaghanabadi
Department of Chemistry, University of Mohaghegh Ardabili, Ardabil 56199-11367, Iran. (Email: amir_n_shamkhali@yahoo.com)
Keywords: Adsorption, Vibrational frequency, DFT, Sulfur

Introduction

Nickel has been widely used as anode for solid oxide fuel cells (SOFCs) because of its excellent catalytic ability for hydrogen oxidation, good electronic conductivity and low cost. Sulfur adsorption on metal surface has been of considerable interest due to the poisoning activity of S with respect to the catalytic properties of surfaces. The adsorption of sulfur based species found within hydrocarbon fuels have been known to cause the degradation of the solid oxide fuel cell [1].

Computational method

In this work we investigated the adsorption of sulfur on Ni (111) surface corresponding to the coverage value of 0.25 ML, by DFT method using ABINIT package. The exchange–correlation functional is treated within the generalized gradient approximation (GGA) with Predew-Burke-Ernzerholf (PBE) functional is applied, for optimization and frequency calculations in this adsorption system [2]. A slab with 5 layers and 15 Å vacuum selected for these calculations as shown in Figure 1. Also the 4×4×1 and 6×6×1 k-point mesh are used for optimization and frequency calculations, respectively. The plane waves with 40 hartree cut off energy are used for all calculations. For Ni and S atoms, the Trouiller-Martins pseudopotentials are included in calculations [3].

Results and discussion:

After structural optimization, the S-Ni bond length and the distance of S from the surface are 2.17 and 1.60 Å, respectively. The stretching frequency of adsorptive bond is calculated from the fitting of three and five points within harmonic and Morse oscillator models, respectively. Each of these points is calculated statistically by moving S atom about the minimum location along the z direction. This method gives 240.4 and 341.3 cm^{-1}, respectively for harmonic and

Morse potential models, for stretching frequency of adsorptive bond which is comparable with experimental data [4].

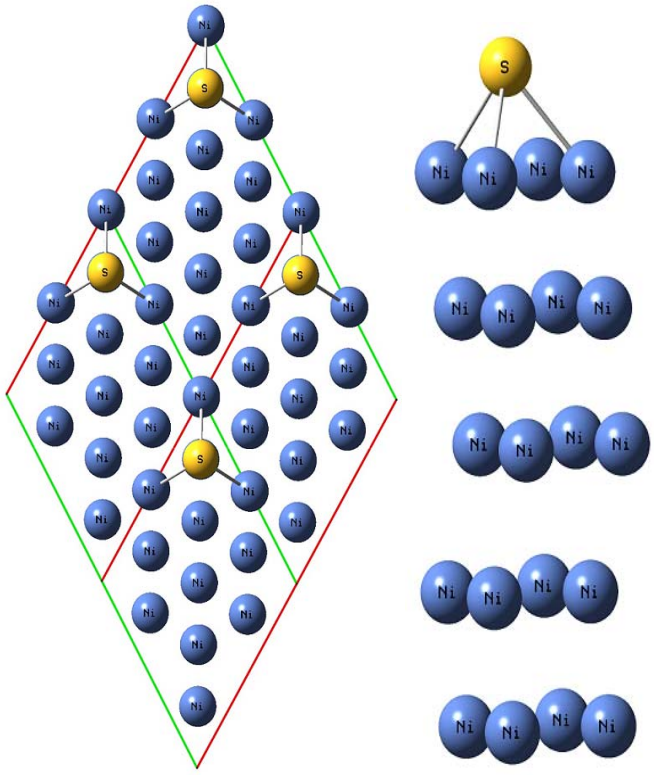

(a) (b)

Figure 1: P(2×2) adsorption structure of S on Ni(111) surface (a), and the selected slab model for it (b).

Conclusions

These results imply that for atomic adsorbates, the anharmonic effects are more important than molecular types. This phenomenon can be related to the mechanical and electrical anharmonicities.

Refrences

[1] M. Chen,P. G. Clark Jr., T. Mueller, C.M. Freind, *Phys. Rev. B* **60**,11783 (1999).

[2] J.P. Perdew K. Burke, M. Ernzerholf. *Phys. Rev.Lett.***77**,3805 (1996).

[3] See http://www.abinit.org/downloads/psp-link/psp-links/gga-fhi.

[4] J. H. Wang, Z. Cheng, J. L. Bredas, M. Liu, *J. Chem. Phys.* **127**, 214705 (2007).

Relative stability of thymine dimer conformers: a theoretical study

Ali Ebrahimi, Mostafa Habibi-Khorassani and Asiye Shahraki
Department of Chemistry, University of Sistan & Baluchestan, Zahedan, Iran
(E-mail: asiye.shahraki@gmail.com)

Keywords:Thymine dimer, Cyclobutane pyrimidine dimer, DNA photolyase, Spore photoproduct, Dewar valence isomer.

Introduction:

The ultraviolet light can leads to the formation of pyrimidine dimer in single and double strands of DNA [1] such as thymine dimer. There are eight potential isomers for pyrimidine dimer, including cyclobutane pyrimidine dimer (CPD) (cis-syn, trans-syn1, trans-syn2, trans-anti, cis-anti), Dewar valence isomer, Spore and (6-4) photoproduct [2]. CPD is repaired by DNA photolyase enzyme. The electron transfer from enzyme to dimer results in the repair of dimer [3]. In this work, the relative stability of thymine dimer conformers and the chemical potentials of electrons have been considered for CPD by means of density functional theory (DFT) methods.

Methods:

Thymine dimers have been modeled by replacing the sugar phosphate backbone with hydrogen atoms. All conformers have been optimized at the B3LYP/6-31G** level of theory by Gaussian03 program package [4]. All conformers are presented in Figure 1.

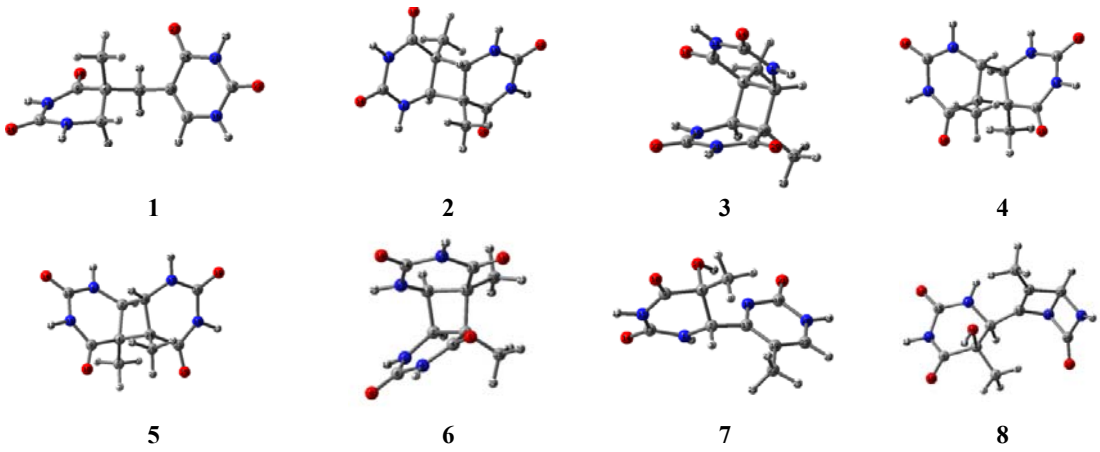

Figure1. structures **1-8** correspond to Spore photoproduct, trans-anti, cis-anti, trans-syn1, trans-syn2, cis-syn, (6-4) photoproduct, Dewar valence isomer, respectively.

Results and discussion:

As can be seen in Table 1, the trend in the relative energy is **1** > **2** > **3** > **4** > **5** > **6** > **7** > **8**. In conformer **1**, the thymine rings are identical in shape and one of CH_3 groups fixes between two rings; thus, the steric crowding is minimized, such that **1** becomes the most stable conformer. During the dimerization process, one of the thymine rings converts into two 4-membered rings in Dewar valence isomer (see Fig. 1). As a result, the Dewar valence isomer is the least stable conformer. The thymine rings do not change upon CPD formation.

Table 1. Relative energies (RE; in kcal/mol) and chemical potentials of electrons

	1	**2**	**3**	**4**	**5**	**6**	**7**	**8**
RE	0.00	11.96	12.28	13.31	13.31	15.87	26.04	80.29
μ		-0.1531	-0.1500	-0.1492	-0.1491	-0.1480		

CPDs are more stable than Dewar and (6-4) photoproduct. The steric crowding affects the stability of CPDs. The trend in the chemical potential of electron (μ) in CPDs is **2** > **3** > **4** > **5** > **6**. The value of μ calculated for **2** is more negative than the other conformers. As a result, the electron transfer to **2** is more difficult than the other conformers. Since the value of μ is less negative in **6**, the electron transfer to **6** is easier than the other conformers. The trend in the μ values of CPDs is in agreement with the relative stability of these conformers. The μ becomes more negative by the increase in the stability of conformer.

Conclusions:

The stability of thymine dimer conformers depends strongly to the stereochemistry. The cis-syn is less stable than the other CPDs. The values of μ clearly demonstrate that the repair of cis-syn conformer by electron transfer from enzyme to dimer is easier than the other CPDs.

References:

[1] F. Masson, T. Laino, I. Tavemelli, U. Rothlisberger ,J. Hutter, *J. Am. Chem. Soc*. 130 (2008) 3443-3450.

[2] D.G. T. Su, J.L.-F. Kao, M.L. Gross, J-S. A. Taylor, *J. Am. Chem. Soc*. 130 (2008) 11328-11337.

[3] C.B. Harrison, L.L. O'Neil,O. Wiest, *J. Phys. Chem. A* 109 (2005) 7001-7012.

[4] M.J. Frish et al. Gaussian 03 (Revision B.03), Gaussian, Inc, Pittsburgh, PA, 2003

Synthesis, Experimental and Theoretical Studies on the Crystal Structure and FTIR Spectra of N,N'-(2,2-dimetylpropane)-bis (dihydroxylacetophenone)

I. Sheikhshoaie*[a] and V. Saheb[a]

[a]*Department of Chemistry, Shahid-Bahonar University of Kerman, Iran*

(shoaie@mail.uk.ac.ir)

Introduction

Schiff base compounds are important from both theoretical and experimental standpoints. These compounds have been used in several areas such as homogenous catalysis, bioinorganic chemistry and dye lasers [1,2]. In this research, a novel Schiff base is prepared and the crystallographic data for its structure is reported. Electronic structure calculations are performed to obtain the geometrical parameters and also FTIR spectrum of the title compound. The calculated results are compared with the experimental data.

Method

A novel Schiff base ligand N,N'-(2,2-dimetylpropane)-bis(dihydroxylacetophenone) (NDHA) is prepared through the condensation of 2-hydroxylacetophenone and 2,2-dimethyl 1,3- amino propane in methanol at room temperature. The yellow crystalline precipitate is used for X-ray crystallography and measuring Fourier Transform Infrared (FTIR) spectrum. The B3LYP and PW91PW91 method along with 6-31+G(d,p) basis set, and MP2 method along with 4-31G(d) are used to optimize the geometry and calculate the FTIR spectrum of the compound. The bond lengths, bond angles and vibrational frequencies are determined experimentally and compared with those obtained theoretically. A vibrational assignment and analysis of the fundamental modes of the compound is performed.

Results and Discussions

The crystal structure analysis of the title compound confirmed the structure of the compound as N,N'-(2,2-dimetylpropane)-bis(dihydroxylacetophenone). Experimental and theoretical Fourier transform infrared (FTIR) spectra of the compound are depicted in Fig. 1. The

geometry of the molecule is optimized at the MP2, B3LYP and PW91PW91 levels of theory. Some experimental selected bond lengths and bond angles are provided in a table in comparison with theoretical results.

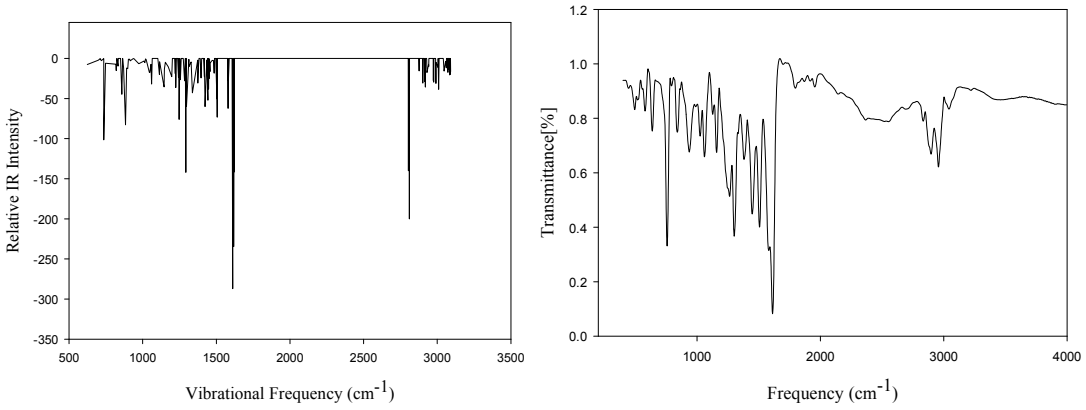

Conclusions

A number of important results emerge from this study. The computed bond lengths and bond angles at the MP2 level are in better agreement with experimental data in comparison with B3LYP and PW91PW91 density functional methods. However, the MP2 calculation, even with a small basis set 4-31G(d), is much more time–consuming than DFT methods. The vibrational frequencies computed at B3LYP are in good agreement with experimental data.

References

[1] H. Schiff, Ann. Chem. Pharm. Suppl. 3 (1864), 343.

[2] I. Sheikhshoaie and V. Saheb, Spectrochimica Acta Part A 77 (2010), 1069.

Computational Study of All Fluorothiophenes and Chlorothiophenes as Candidates for Nano-wires

H. Shirani IL Beigi[a,*] and S. Jameh-Bozorghi[b]

[a]*Young Researchers Club, Islamic Azad University, Toyserkan Branch, Toyserkan, Iran*

[*]*Email: shiranihossein@gmail.com*

[b]*Department of Chemistry, Islamic Azad University, Toyserkan Branch, Toyserkan, Iran*

Abstract

Electronic, structural, and spectroscopic properties of neutral and ionized singly mono-, di-, tri-, tetra-, fluorothiophenes and chlorothiophenes are studied using ab initio, density functional theory and B3LYP method with the 6-311++G** basis set. The effects of the number and position of the substituents on the electrochemical properties of the thiophene ring have been studied. Using the optimized structures obtained for these molecules and their cations, vibrational frequencies and NMR shielding constants of these compounds have also been calculated and analyzed. The results of this study, including NBO charge and spin-density distribution, size and direction of the dipole moment vector, ionization potential, electric polarizability, HOMO-LUMO gaps and NICS analyses, show that among all of these compounds 3-fluorothiophene have the most suitable conditions for electropolymerization, this means that, compared with other fluorothiophenes, this monomer have a higher capacity for electropolymerization as well as higher electric conductance.

Keywords: DFT-B3LYP; Fluorothiophenes; Chlorthiophenes

Introduction

Conducting polymers because of change in their optical and electrical properties in nanometeric dimension are most probable systems for nanoelectronical applications [1]. polyanilines can produce one-dimension morphologies, such as polymer nanostructures (nano-tube, -wire, -fiber, -filament -rod, -composite and -particle) the most researches is done about that [2]. Nanomaterials paid attentions more scientist to itself because of the high applications of nanotechnology in different sciences such as: medicine, petrochemical,

materials, electronic, quantumic computers and etc [3]. conductive polymers are typical of materials that play important roles in nanomatrial field [4].

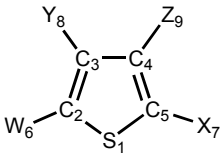

T: W=X=Y=Z=H	thiophene
A: W=F, X=Y=Z=H	2-fluorothiophene
B: Y=F, W=X=Z=H	3-fluorothiophene
C: W=Y=F, X=Z=H	2,3-difluorothiophene
D: W=Z=F, X=Y=H	2,4-difluorothiophene
E: W=X=F, Y=Z=H	2,5-difluorothiophene
F: Y=Z=F, W=X=H	3,4-difluorothiophene
G: W=Y=Z=F, X=H	2,3,4-trifluorothiophene
H: W=X=Y=F, Z=H	2,3,5-trifluorothiophene
I: W=X=Y=Z=F	2,3,4,5-tetrafluorothiophene
A*: W=Cl, X=Y=Z=H	2-chlorothiophene
B*: Y=Cl, W=X=Z=H	3-chlorothiophene
C*: W=Y=Cl, X=Z=H	2,3-dichlorothiophene
D*: W=Z=Cl, X=Y=H	2,4-dichlorothiophene
E*: W=X=Cl, Y=Z=H	2,5-dichlorothiophene
F*: Y=Z=Cl, W=X=H	3,4-dichlorothiophene
G*: W=Y=Z=Cl, X=H	2,3,4-trichlorothiophene
H*: W=X=Y=Cl, Z=H	2,3,5-trichlorothiophene
I*: W=X=Y=Z=Cl	2,3,4,5-tetrachlorothiophene

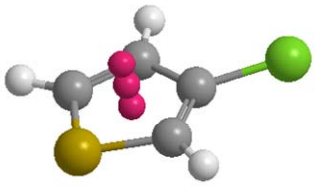

[Scheme]

Figure 1. All possible mono-, di-, tri-, tetra- of fluorothiophenes and chlorothiophenes.

Methods

As DFT-B3LYP method has proved usefull, appropriate and cost-efective method [5]. Calculation of the properties of over interesd it is used with 6-311+G** basise set throngent this study, as implemented in the G98W software. Structures of fluorothiophenes and chlorothiophenes are optimized using B3LYP/6-311+G** method. Atomic chaeges are calculated using NBO method [6].

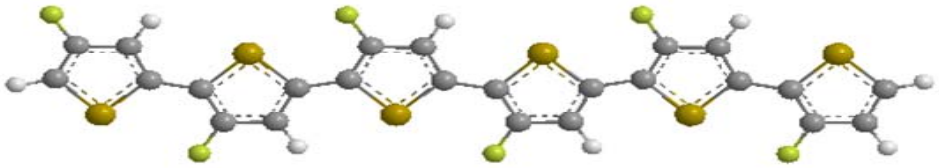

Figure 2. 3-fluorothiophene tetramer (B tetramer).

Results and Discussion

To predict the bonding-characteristic behavior of the fluorothiophenes and chlorothiophenes rings in their corresponding polymer chains and to determine the extent of the π-conjugation character of these polymers, we have used the ***Fn*** coefficient for each thiophene ring in the

isolated fluorothiophenes and chlorothiophenes. The calculated values of the ***Fn*** coefficient for all fluorothiophenes and chlorothiophenes shown that the molecule B have the smallest values of the ***Fn*** coefficient. In both series of molecules and their cation radicals, charge- and spin-density distributions have similar trends with the number and position of the substituted chlorine and fluorine atoms. Also HLG values for all of the fluorothiophenes and chlorothiophenes are very good for transit than valance band to conducting band. NICS results showed that compound B has the largest quantity of negative value therefore this compound has the largest electrical current and conductivity. For all fluoranilines and their cations, the positive charge (obtained of NBO charge) is distributed mainly on the C3 position in Figure1. The distribution charge on the C3 carbon atom for monomer G cation radicale shows that, possibly, the electropolymerization rate for monomer B is greater than thiophene and other copmounds. Consequently, it can be said that compared with other fluorothiophenes and chlorothiophenes the electric conductivity of polymer blends obtained from the B monomer is higher than other compounds. NICS results showed that compound B has the largest quantity of negative value (-15.85 for 0.5 angstrom upper than polymer rings), therefore this compound has the largest electrical current and conductivity at 0.5 angstrom upper than polymer rings.

Conclusion

Fluoroanilines have been designed as monomers for conductive polymers (as candidate monomer for nano-wires) in the hope of having modified chemical and electrical properties. Density functional theory DFT-B3LYP/6-311+G** calculations have been carried out successfully to study. It was shown that compound B is possible candidate to replace thiophene in the synthesis of corresponding conducting polymers with modified characteristics compared to polythiophene. Compared to thiophene, monomer B is more soluble in water.

References

[1] H. Shirani; S. Jameh-Bozorghi, *J. Iran. Chem. Res.* 3 (2010).

[2] M. S. Ram, Srinivasan Palaniappan, *Journal of Molecular Catalysis* 201, (2003), 289.

[3] Campbel, T. E.; Hodgson, A. *J.; Wallace, G. G. Electroanalysis*, 11, (1999) 215.

[4] Kincal, D.; Kamer, A.; Chield, A. D.; Reynold, R. *J. Synth. Met*., 92, (1998) 53.

[5] Z. Chan, C. S. Wannere, C. corminboeuf, R. Puchta, and P. V. R. Schlyere, *Chem. Rew*, 105 (2005) 3842.
[6] N. Sundaraganesan, H. Umamaheswari, B. Dominic Joshua, , *J. Molecular Struct.*, 850 (2008) 84.

Density Functional Theory of All Chlorothiophenes Radical Cations

H. Shirani IL Beigi[a,*] and S. Jameh-Bozorghi[b]

[a]Young Researchers Club, Islamic Azad University, Toyserkan Branch, Toyserkan, Iran

[*]Email: shiranihossein@gmail.com

[b]Department of Chemistry, Islamic Azad University, Toyserkan Branch, Toyserkan, Iran

Abstract

In this paper, electronic, structural, and properties of mono-, di-, tri-, and tetrachlorothiophenes radical cations are studied using the density functional theory and B3LYP method with 6-311++G** basis set. Also, the effects of the number and position of the substituent of chlorine atom on the properties of the thiophene radical cation ring have been studied using optimized structures obtained for these molecules; vibrational frequencies, nuclear chemical shielding constants, spin-density distribution, size and direction of the dipole moment vector, ionization potential, electric polarizabilities and NICS values of these compounds have been calculated and analyzed.

Keywords: DFT-B3LYP, Chlorthiophenes radical cations, Conducting polymers

Introduction

Electrically-conducting polymers such as advanced materials and the new class of 'synthetic metals' have drawn high attention in the last years [1,2]. There has been growing interest in research on conducting polymer nano since they incorporate the advantages of organic conductors with low-dimensional systems and so create interesting physicochemical properties and potentially useful applications [3-5]. Among intrinsic conducting polymers with conjugated double bonds, polythiophenes (PTHs) are suitable for commercial applications. The objective of the present research is to study electronic and structural properties of all chlorothiophene radical cations (shown in Figure 1) using DFT-UB3LYP method.

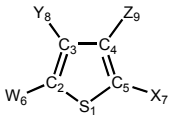

T: W=X=Y=Z=H thiophene
A: W=Cl, X=Y=Z=H 2-chlorothiophene
B: Y=Cl, W=X=Z=H 3-chlorothiophene
C: W=Y=Cl, X=Z=H 2,3-dichlorothiophene
D: W=Z=Cl, X=Y=H 2,4-dichlorothiophene
E: W=X=Cl, Y=Z=H 2,5-dichlorothiophene
F: Y=Z=Cl, W=X=H 3,4-dichlorothiophene
G: W=Y=Z=Cl, X=H 2,3,4-trichlorothiophene
H: W=X=Y=Cl, Z=H 2,3,5-trichlorothiophene
I: W=X=Y=Z=Cl 2,3,4,5-tetrachlorothiophene

Figure 1. All possible mono-, di-, tri-, and tetrachlorothiophene isomers studied in this research.

Methods

Initially, structures of representative mono-, di-, tri-, and tetrachlorothiophenes were optimized using UB3LYP/6-311++G** method [6]. The geometries are optimized using standard gradient techniques with default parameters set in G98W. Vibrational frequencies with their IR intensities are calculated with a scale factor of 0.8929.

Results and Discussion

To predict the bonding-characteristic behavior of the chlorothiophene radical cation rings in their corresponding polymer chains and to determine the extent of the π-conjugation character of these polymers, we have used the ***Fn*** coefficient for each thiophene ring in the isolated chlorothiophene radical cations [1]. The calculated values of the ***Fn*** coefficient for all chlorothiophene radiacal cations shown that the molecule B have the smallest values of the ***Fn*** coefficient. In both series of molecules and their cation radicals, charge- and spin-density distributions have similar trends with the number and position of the substituted chlorine atoms. Also HLG values for all of the chlorothiophene radical cations are very good for transit than valance band to conducting band. NICS results showed that compound B has the largest quantity of negative value therefore this compound has the largest electrical current and conductivity.

Conclusion

B3LYP method with 6-311++G** basis set calculations have been carried out successfully to study the structural, electronic and spectroscopic properties of all chlorothiophenes. Based on B3LYP/6-311++G** optimized structural parameters, especially the quinoid character, values of dipole moment vector, spin density distribution, ionization potential, vibrational frequencies and NICS have been calculated and analyzed. Accordingly, Compound **B** is possible candidate among all compounds in the synthesis of corresponding conducting polymers with modified characteristics.

References

[1] H. Shirani & S. Jameh-Bozorghi, *J. Iran. Chem. Res.* 3 (2010).

[2] M. S. Ram, Srinivasan Palaniappan, *Journal of Molecular Catalysis* 201, (2003), 289.

[3] Campbel, T. E.; Hodgson, A. *J.; Wallace, G. G. Electroanalysis*, 11, (1999) 215.

[4] Kincal, D.; Kamer, A.; Chield, A. D.; Reynold, R. *J. Synth. Met*., 92, (1998) 53.

[5] Z. Chan, C. S. Wannere, C. corminboeuf, R. Puchta, and P. V. R. Schlyere, *Chem. Rew*, 105 (2005) 3842.

[6] N. Sundaraganesan, H. Umamaheswari, B. Dominic Joshua, , *J. Molecular Struct.*, 850 (2008) 84.

Quantum Mechanical Study on All Fluoroanilines as Candidate Monomers for New Conductive Polymers (as Nano-wires)

H. Shirani IL Beigi[a,*] and S. Jameh-Bozorghi[b]

[a]*Young Researchers Club, Islamic Azad University, Toyserkan Branch, Toyserkan, Iran*

[*]*Email: shiranihossein@gmail.com*

[b]*Department of Chemistry, Islamic Azad University, Toyserkan Branch, Toyserkan, Iran*

Abstract

Structural and electronic characteristics of the neutral and ionized mono-, di-, tri-, tetra-, and penta-fluoroanilines are studied using DFT- B3LYP method with the 6-311+G** basis set. Effects of the number and position of the substituents on the electrochemical properties of the aniline ring have been studied. Vibrational frequencies, nuclear chemical shielding constants, charge and spin-density distribution, size and direction of the dipole moment vector, ionization potential, electric polarizability, HOMO-LUMO gaps and NICS have also been calculated and analyzed. Results of this study show that among all of these compounds *2,5-difluoroaniline* and *2-fluoroaniline* as candidate monomers for intelligent polymeric nano-wires have the most suitable conditions for electropolymerization.

Keywords: DFT-B3LYP, Conductive polymers, Nano-wires, Fluoroanilines

Introduction

Conducting polymers because of change in their optical and electrical properties in nanometeric dimension are most probable systems for nanoelectronical applications [1]. polyanilines can produce one-dimension morphologies, such as polymer nanostructures (nano-tube, -wire, -fiber, -filament -rod, -composite and -particle) the most researches is done about that [2]. Nanomaterials paid attentions more scientist to itself because of the high applications of nanotechnology in different sciences such as: medicine, petrochemical, materials, electronic, quantumic computers and etc [3]. Conductive polymers are typical of materials that play important roles in nanomatrial field [4]. It has been known from the early years of conducting polymer research that polyaniline fibrils of ~100 nm in diameter can form "naturally" during electrochemical polymerization on the surface of the electrodes [5].

Conducting filaments of polyaniline have been prepared in the 3-nanometer-wide hexagonal channel system of the aluminosilicate [6]. PANIs have been used as biosensors, gas sensors, microactuators, data storage, polymer batteries and electronic devices [7,8].

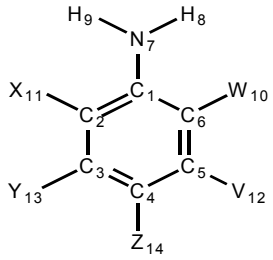

A: X=Y=W=V=H	aniline
B: X=F, Y=Z=V=W=H	2-fluorobenzenamine
C: Y=F, X=Z=V=W=H	3-fluorobenzenamine
D: Z=F, X=Y=V=W=H	4-fluorobenzenamine
E: X=Y=F, Z=V=W=H	2,3-difluorobenzenamine
F: X=Z=F, Y=V=W=H	2,4-difluorobenzenamine
G: X=V=F, Y=Z=W=H	2,5-difluorobenzenamine
H: X=W=F, Y=Z=V=H	2,6-difluorobenzenamine
I: Y=Z=F, X=V=W=H	3,4-difluorobenzenamine
J: Y=V=F, X=Z=W=H	3,5-difluorobenzenamine
K: X=Y=Z=F, V=W=H	2,3,4-trifluorobenzenamine
L: X=Y=V=F, Z=W=H	2,3,5-trifluorobenzenamine
M: X=Y=W=F, Z=V=H	2,3,6-trifluorobenzenamine
N: X=Z=W=F, V=Y=H	2,4,6-trifluorobenzenamine
O: Y=Z=V=F, X=W=H	3,4,5-trifluorobenzenamine
P: X=Z=V=F, Y=W=H	2,4,5-trifluorobenzenamine
Q: X=Y=Z=V=F, W=H	2,3,4,5-tetrafluorobenzenamine
R: X=Y=Z=W=F, V=H	2,3,4,6-tetrafluorobenzenamine
S: X=Y=V=W=F, Z=H	2,3,5,6-tetrafluorobenzenamine
T: X=Y=Z=V=W=F	2,3,4,5,6-Pentafluorobenzenamine

Figure 1. All possible mono-, di-, tri-, tetra-, and penta-fluoroaniline isomers.

Methods

As DFT-B3LYP method has proved usefull, appropriate and cost-efective method [9]. Calculation of the properties of over interesd it is used with 6-311+G** basise set throngent this study, as implemented in the G98W software [10]. Structures of fluoroanilines are optimized using B3LYP/6-311+G** method. Atomic chaeges are calculated using NBO method.

Results and Discussion

To predict the bonding-characteristic behavior of the fluoroaniline rings and to determine the extent of the π-conjugation character of these polymers, we have used the ***Fn*** coefficient for each aniline ring {***Fn= 2R23/(R12+R34)***.

In this equation, R23 is the length of the C2-C3 bond in the aniline ring at form cation radical, and [(R12 + R34)/2] is the average length of the C1-C2 and C3-C4 bonds. Molecules **G** and **B** and their cations have the smallest values of the ***Fn*** coefficient(0.984 and 0.986 for **B** and **G** respectively). Therefore, the quinoid character of monomers **G** and **B** is greater than

that of other fluoroanilines. This shows that double bonds in these molecules are more delocalized. This means that, compared with other fluoroanilines, these two monomers have a higher capacity for electropolymerization as well as higher electric conductance. Also spin density that is distributed mainly on the C4 and N7 positions in Figure1, is most for **G** monomer. Therefore the electropolymerization rate for monomer **G** is greater than aniline and 2-fluoroaniline. Orientations of the polymer chains in the condensed phase are the most important parameters affecting the electric charge transport properties of polymers. It is obvious that the HLG values for all of the fluoroanilines are very good for transit than valance band to conducting band. It should be noted here that HLG values are not the only parameters that determine electric conductance of a polymer film. Orientation and alignment of the monomers in the polymer chain are two other determining characteristics that play important roles in the electrical conductance. In terms of the zero-point energy (ZPE), it can be said that the ZPE for molecule **B** (67.55 $kcalmol^{-1}$) is greater than that for molecules C and D. The value of the ZPE for molecule **G** (62.39 $kcalmol^{-1}$) is greater than other isomers.

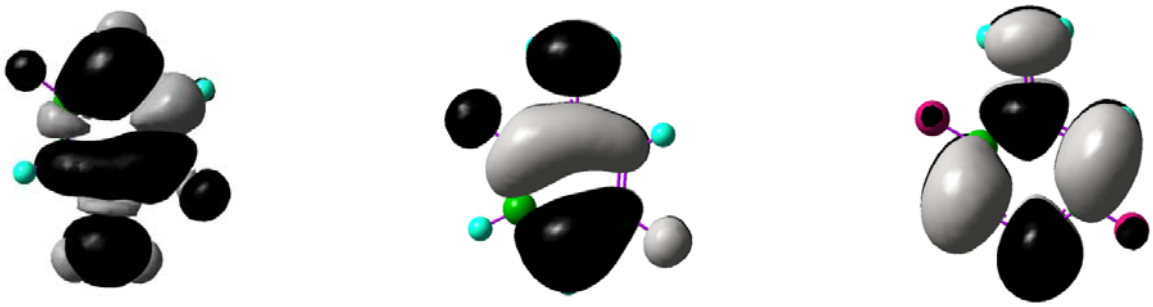

[Scheme] Spin density, HOMO and LUMO for 2,5-difluoroaniline.

Conclusion

Fluoroanilines have been designed as monomers for conductive polymers (as candidate monomer for nano-wires) in the hope of having modified chemical and electrical properties. Density functional theory DFT-B3LYP/6-311+G** calculations have been carried out successfully to study. it was shown that compounds B and G are possible candidates to replace aniline in the synthesis of corresponding conducting polymers with modified characteristics compared to polyaniline. Compared to aniline, B and G fluoroaniline monomers are more soluble in water. These characteristics increase the efficiency of the electrochemical polymerization processes on these two monomers for applications of

nanotechnology for produce nanofilaments and nanowires with these two monomers.

References

[1] H. Shirani.; S. Jameh-Bozorghi, *J. Iran. Chem. Res.* 3 (2010).

[2] M. S. Ram, Srinivasan Palaniappan, *J. Molecular Catalysis* 201, (2003) 289.

[3] In Encyclopedia of Nanoscience and Nanotechnology, Vol. 2, H. S. Nalwa (Ed.), pp. 105–131, American Scientific Publishers, Los Angeles (2004).

[4] X. Zhang, W. J. Goux, S. K. Manohar. *J. Am. Chem. Soc.,* 126, (2004) 4502.

[5] Gordon G. Wallace , Geoffrey M. Spinks, Leon A. P. Kane-Maguire, Peter R. Teasda, Conductive electroactive polymers: intelligent polymer systems., CRC Press, Queensland, (2009).

[6] Y. Wei, Y. Sun, G.-W. Jang, X. Tang. *J. Polym. Sci*., Part C: Polym 28,(1990) 81.

[7] Chun-Guey. Wu, Thomas. Bein*, j. Science*, 1757,(1994) 264

[8] Skothiem, T. A., Elsenbaumer, R., Reynolds, J.; Handbook of Conducting Polymers; Marcel Dekker: New York, (1998).

[9] Mo¨lder U, Burk P, Koppel IA. *J. Mol. Struct. (THEOCHEM)*, 81–89, (2004) 712.

[10] Alkorta I, Elguero *J. Struct. Chem*., 77–79, (2005) 16.

Characterization of Molecular Interactions in [Mim^+][BF_4^-] Ionic Liquid by NMR and IR Techniques: An ab Initio Study

Hossein Roohi [a], Roya Salehi[b]

[a]Department of Chemistry, Faculty of Science, University of Guilan, Box 41335-1914 ,Rasht, Iran

[a]Department of Chemistry, Faculty of Science, University of Sistan & Baluchestan, Zahedan, Iran

(Email:R.salehi88@ymail.com)

Keywords. Ionic liquid, Methyl imidazolium, Hydrogen bond, Ion pair

Introduction

Ionic liquid (IL), a kind of novel compound consisting of inorganic anion and organic cation,, known as ambient temperature molten salts, exhibit attractive properties including negligible vapor pressure, nonflammability, extraordinarily high chemical and thermal stability and controllable hydrophobicity [1,2,3]. To the best of our knowledge, interaction between MIM^+ and BF_4^- ions has not been characterized theoretically by IR and NMR techniques. In the present paper, all ion pairs formed from interaction between MIM^+ and BF_4^- ions have been characterized in terms of vibrational frequency of normal modes, isotropic chemical shift and spin-spin coupling constants.

Computational Details

All the structures studied in this work were optimized by using B3LYP in conjunction with 6-311++G(2d,2p) basis set The B3LYP calculated vibrational frequencies have been used to characterize stationary points and calculation of zero-point vibrational energy (ZPVE). The vibrational frequencies were calculated without scaling. Spin-spin coupling constants involving ^{13}C, ^{15}N, ^{19}F, ^{11}B and ^{1}H in all monomers and complexes were computed at B3LYP/6-311++G(2d,2p) level .

Results and Discussion

The ionic liquid modeled herein is the cation Mim^+ (methyl imidazolium) coupled with the anion BF_4^-. Molecular graphs (including the critical points and bond paths) of the all four complexes are shown in Fig. 1. As can be seen, all structures are cyclic with three hydrogen

bonds involved in the interaction. In **A** and **B** ion pairs, three F atoms of BF_4^- act as proton acceptors and N–H and C–H bonds of Mim^+ as proton donors. In **C** and **D** ion pairs, instead of N–H, two and three C–H bonds in Mim^+ acts as proton donors, respectively.

1. Vibrational frequencies. Owing to greater stability of **A** and **B** complexes with respect to the **C** and **D** ones, we discuss vibrational frequencies of **A** and **B** complexes. A substantial red-shift is observed in the fundamental N–H stretching vibrational frequency. The red-shifts of N–H stretching vibrational frequency of Mim^+ involved in F···H–N interaction upon formation of **A** and **B** complexes are greater for **A** than **B** indicating F···H–N interaction in **B** ion pair is stronger than that of **A** one. The red-shift in stretching vibrational frequency of C–H bond involved in interaction is 3.8 cm^{-1} for **A** and 18.3 cm^{-1} for **B** The analysis of normal modes of BF_4^- shows a blue-shift of 149.3 and 139.8 cm^{-1} for the B–F stretching with respect to the corresponding free anion value of 1042.6 cm^{-1}, which is accompanied by its bond contraction in the complex.

2. Isotropic Chemical Shifts. The changes of isotropic chemical shifts of the bridging hydrogens, $\Delta\sigma_{iso}(H)$, and change of electronic density ($\Delta\rho$) at bridged H atoms are reported in Table 1. As can be seen, changes in isotropic chemical shift of bridging hydrogens for both complexes are negative. The negative character of $\Delta\sigma_{iso}(H)$ is explained by the deshielding of the bridging hydrogen H that is induced by the formation of the hydrogen bond.

3. One-and Two Bond Spin-Spin Coupling Constants. The intermolecular spin-spin coupling constants (SSCCs) $^1J(X–H)$ and $^{2h}J(X–Y)$ across the X–H···Y hydrogen bonds in Mim^+BF4^- complexes are given in Table 2. The absolute value of ^1J of N-H involved in interaction decreases upon complex formation and that of C-H increases. Sum of absolute value of ^{2h}J for most stable complex **B** is greater than that of **A**.

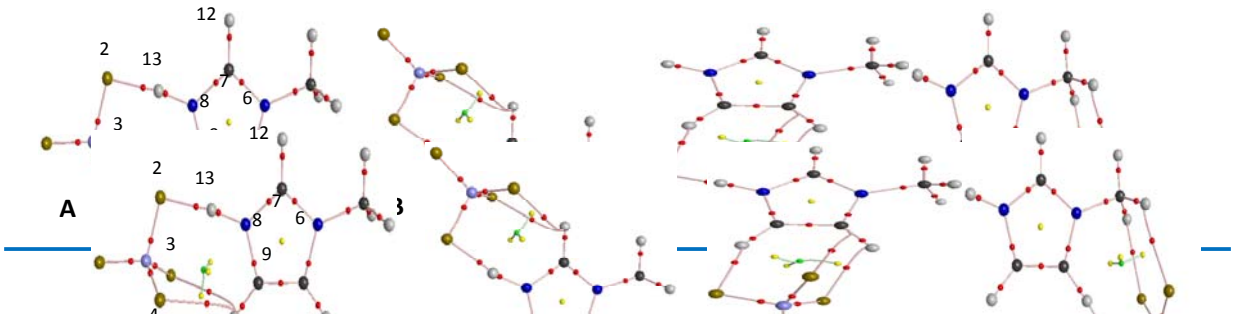

Fig. 1. Molecular graphs of the of **A–D** complexes.

Table 1. Changes in NMR chemical shifts and electron density of bridging H caused by complexation Mim^+ with BF_4^- at B3LYP/6-311++G(2d,2p) level.

	$\Delta\sigma_{iso}$(H)/ppm		Δρ(H)/au	
	A	**B**	**A**	**B**
H12		-1.6339		-0.0269
H13	-7.7810	-6.7034	-0.0289	-0.0299
H14	-1.1557		-0.0198	

Table 2. One- and two bond Spin Spin coupling constants (Hz) at B3LYP/6-311++G(2d,2p) level.

	J		
	Mim+	**A**	**B**
C7-H12	209.94		214.69
N8-H13	-95.46	-88.62	-91.20
C9-H14	194.93	197.16	
C7-F3			22.70
C7-F4			3.24
N8-F		-47.12	-41.07
C9-F3		17.05	
C9-F4		0.41	

References

[1] Shamsi, S. A.; Danielson, N. D. *J. Sep. Sci.* 2007, 30, 1729–1750.

[2] Earle, M. J.; Esperanca, J.; Gilea, M. A.; Lopes, J. N. C.; Rebelo, L. P. N.; Magee, J. W.; Seddon, K. R.; Widegren, J. A. Nature 2006, 439, 831–834.

[3] Wasserscheid, P. Nature 2006, 439, 797–797.

Molecular structure and intramolecular hydrogen bonding of 1,1,1-trifluoro-5,5-dimethyl-2,4-hexanedione. A DFT study (Part I)

N. Sanati [a], A-R. Nekoei [*,b], M. Vakili [c], A. Kanaani [d]

[a] *Islamic Azad University, Marvdasht Branch. Department of Chemistry, Marvdasht, Iran*

[b] *Department of Chemistry, Shiraz University of Technology, Shiraz, 71555-313, Iran*

[c] *Department of Chemistry, Ferdowsi University of Mashhad, Mashhad 91774-1436, Iran*

[d] *School of Chemistry, Damghan University of Basic Sciences, Iran*

Keywords:1,1,1-trifluoro-5,5-dimethyl-2,4-hexanedione; β-dicarbonyl; Intramolecular hydrogen bond; Density Functional Theory

Introduction

Tautomer equilibrium given in Fig. 1 shows that two keto-enol tautomerisms are possible for β-dicarbonyls. The position of the keto-enol equilibrium for this class of compounds differs according to electronic characteristics of the substitutions and the nature of the solvents. The *cis*-enol forms of *β*-dicarbonyls are stabilized by a strong intramolecular hydrogen bond [1-3]. Several experimental data suggest that electron-withdrawing group substitution at *β*-position, such as the trifluoromethyl group ($-CF_3$), decreases the strength of the intramolecular hydrogen bond (IHB), whilst substitution of alkyl group in this position increases the IHB strength. 1,1,1-trifluoro-5,5-dimethyl-2,4-hexanedione, TFMHD, has two different *β*-substituted groups with different electron-withdrawing, donating and steric effects. Therefore, it is interesting to cross-check these effects on conformational stabilities, molecular structure and IHB strength. The aim of the present paper is to predict IHB strength of TFMHD by means of density functional theory (DFT) levels.

Method of Analysis

All possible cis-enol conformers of TFMHD were fully optimized at the B3LYP level of theory with the 6-31G** and 6-311++G** basis sets, and at MP2, B3PW91 and G96LYP levels with 6-31G** basis set, using Gaussian 03W program.

Results and Discussion

From the theoretical point of view, by considering the conformations of t-butyl and trifluoromethyl (-CF_3) groups in TFMHD, with respect to the plane of the molecule and with respect to each other, 64 enol and 16 keto forms can be drawn for TFMHD molecule. The enol contents in pure liquid forms of trifluoroacetylacetone (TFAA, R1=CH_3 and R3=CF_3, in Fig. 1) and 5,5-dimethyl-2,4-hexanedione (DMHD, R1=CH_3, R3=$C(Me)_3$) have been reported to be 96% and 88%, while that of TFMHD is 100%. A comparison between these values gives a clear understanding for the enhancing effect of the substitution of the methyl groups by the t-butyl and trifluoromethyl groups on the enol content. Therefore we are getting focused on the enol conformers of TFMHD.

Among the enol forms, only eight of them (I-VIII) are engaged in a six-member ring intramolecular hydrogen bonded system. The structures of these conformers, atom numbering of the system and their relative stabilities (in kcal/mol) are shown in Fig 2. The selected of fully optimized geometrical parameters of I, II and III conformers of TFMHD besides the averaged geometrical parameters for TFMHD, DMHD and TFAA, calculated at the B3LYP/6-311++G** level of theory, are given in Table 1. Several experimental data suggest that substitution of electron-withdrawing group, such as trifluoromethyl, at β-position of a β-dicarbonyls decreases the strength of the intramolecular hydrogen bond, whilst substitution of an electron donor, such as t-butyl group, increases the IHB strength. TFMHD has two β-substituted groups with different electron-withdrawing, electron donating and steric effects. According to the results summarized in Table 1, especially by comparisons of O···O, O···H and O−H bond distances and OHO bond angles, the IHB strength of TFMHD is concluded to be stronger and weaker than those of TFAA and DMHD, respectively.

Table1: The geometrical parameters of the *cis*-enol forms of TFMHD, DMHD and TFAA, all calculated at B3LYP/6-311++G** level.

	TFMHD				DMHD	TFA
distances (Å)	*I*	*II*	*III*	Avg	Avg	Avg
C–C	1.425	1.455	1.460	1.447	1.444	1.526
C=C	1.380	1.360	1.357	1.366	1.372	1.378
C–O	1.322	1.316	1.320	1.319	1.325	1.320
C=O	1.238	1.244	1.241	1.241	1.247	1.237
O–H	0.999	1.008	1.003	1.003	1.006	0.997
O···H	1.649	1.607	1.640	1.632	1.608	1.672
O···O	2.552	2.516	2.538	2.535	2.525	2.566
C2–C7 (t-but)	1.519	1.522	1.521	1.521	1.534	1.492
C4–C8 (CF_3)	1.550	1.536	1.534	1.540	1.501	1.550
angles(°)						
O1H6O5	148.0	147.3	146.6	147.3	149.2	146.8

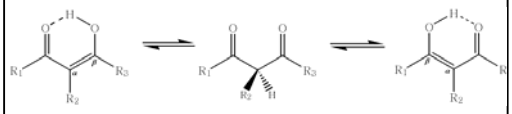

Fig. 1: The keto-enol tautomerism leads to two different chelated enol forms for *β*-dicarbonyls.

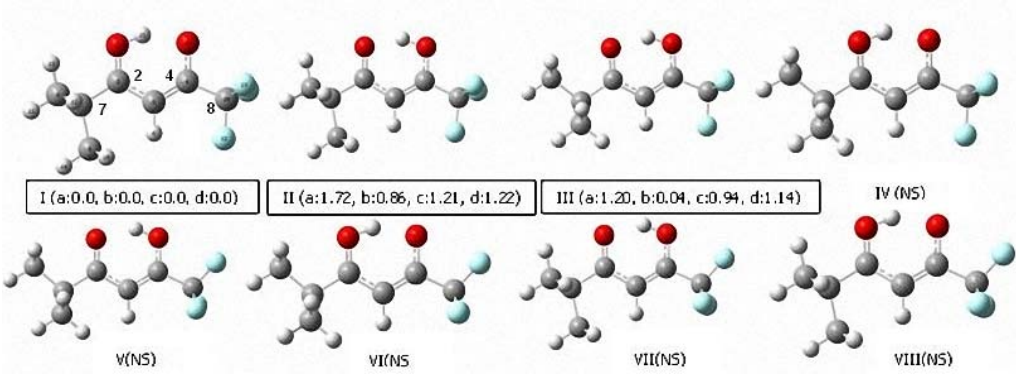

Fig 2: The atom numbering, relative stabilities and possible chelated *cis*-enol tautomers of TFMHD (a: B3LYP/6-311++g**, b: MP2, c: B3PW91 and d: G96LYP at 6-31G** basis set).

Conclusion

The geometries of three stable chelated enol forms of TFMHD are fully optimized at B3LYP (DFT) level of theory. Comparisons between the structural parameters show that the hydrogen bond strength of TFMHD lies between those of DMHD and TFAA.

References

[1] S.F. Tayyari, M. Vakili, A.-R. Nekoei, H. Rahemi, Y.A. Wang, Spectrochim. Acta A, 66 (2007) 626.

[2] M. Zahedi-Tabrizi, F. Tayyari, Z. Moosavi-Tekyeh, A. Jalali, S.F. Tayyari, Spectrochim. Acta A 65 (2006) 387.

[3] M. Vakili, S.F. Tayyari, A. Kanaani , A-R. Nekoei; submitted to 14th Iran Physical Chemistry Seminar.

The examination of thermodynamical of bicyclic, tricyclic and hetrocyclic Alkanes in affinity proton reaction

M.Keshavarz[a*] ,F. Nader shahbaz[b],F.Tavousi[a]

[a]*Chemistry Department, Islamic Azad University-, Shahreza Branch, P. O. Box 311- 86145, Shahreza, Isfahan, Iran*

Email:keshavarz@iaush.ac.ir

[b]*Chemistry Department, Islamic Azad University, Science and Research Branch Ahwaz, Ahwaz, Iran*

Abstract

TheSTudy of Thermodynamic some Polycyclic and heterocyclic compound in Proton affinity reactions with quantum mechanic methods. Using calculations of Abinitio (HF) method and Dencity Function Theory (DFT) with base sets of 6-311++G** and 6-31 G**.

Keywords: polycyclic-thermodynamical- quantum mechanic,heterocyclic,Proton affinity

Introduction

Protonation/deporotonation is the first step in many fundamental chemical rearrangements and in most enzymatic reactions.Two quantities are used to characterize the ability of a molecule in the gas phase to accept aproton.The gas phase basicity is the negative of the free energy change associated with the reaction.The more frequently used index ,the porotonaffinity,is the negative of the enthalpy change at standard conditions.The recent progress in the Density Functional Theory (DFT)approaches make this method another candidate for reliable calculation of proton affinities ,howere ,the performance of the method in this field is still mostly untested.

Method:

Density functional theory (DFT) is a quantum mechanical theory used in physics and chemistry to investigate the electronic structure (principally the ground state) of many-body systems, in particular atoms, molecules, and the condensed phases. With this theory, the properties of a many-electron system can be determined by using functionals, i.e. functions of another function, which in this case is the spatially dependent electron density. Hence the name density functional theory comes from the use of functionals of the electron density.

DFT is among the most popular and versatile methods available in condensed-matter physics, computational physics, and computational chemistry.

Results And Discussion

The Thermodynamic Parameters such as enthalpy Gibbs free energy , Thermal energy are calculated using quantum mechanicPrincipley such as maximum hardness Principle (MHP) , and minimum electrophilicity Principle (MHP) to compare the stability of reactants and products.

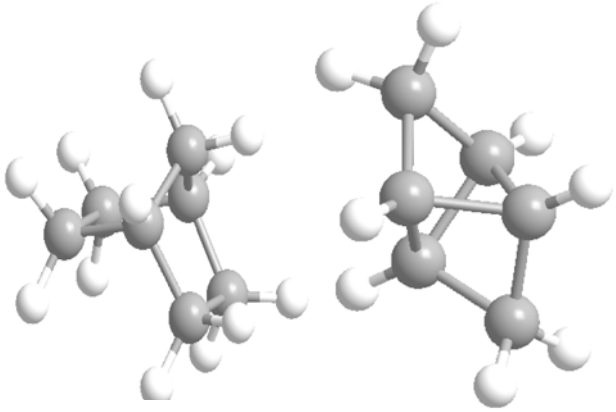

(C)
Bicyclo(2,2,1)Heptan

(G)
Tricyclo (1,1,1,1)Hegzan

ΔH,ΔG,ΔQB3lyp/6-311++G**method(HF)

Molecule	*ΔH*	*ΔG*	*ΔQ*
A	-۰/۲۲۹۴	-۱۹۵/۲۹۸۶	-۰/۶۵۸۵
B	۰/۰۱۲۹	-۰/۲۲۴	-۰/۶۶۶۵
C	-۰/۰۱۶۹	-۰/۰۰۶۴	-۰/۶۶۴۴
D	۰/۰۱۳۵	۰/۰۱۳۳	-۰/۶۵۴۹
E	۰/۰۱۳۲	-۰/۰۰۷۲	-۰/۶۵۷۷
F	-۰/۰۰۶۸	-۰/۰۰۴۷	-۰/۴۹۱۲
G	۰/۰۱۳۹	-۰/۰۱۱	-۰/۵۶۰۴
H	۰/۰۴۳۸	۰/۰۴۴۱	-۳۹/۹۷۲۷
I	۰/۴۳۸۴	-۰/۰۰۵۵	-۰/۶۷۳۳
J	۰/۰۱۳۴	-۰/۰۰۵۹	-۰/۶۶۱۱
K	۰/۰۱۴	۰/۰۱۵۳	-۰/۶۵۵۴
L	۰/۰۱۳۳	۰/۰۱۴	-۰/۶۴۴۹

Conclusion

The Obtained results show that calculation of thermal energy is more appropriate than other thermodynamic parameters, since in the calculation of enthalpy and Gibbs free energy gibbs with two methods of HF and B3LYP and two applied base sets, none of the products were more stable than reactanty materials., but in the calculation of thermal energy, all of the products were more stable than product , using any methods and base set.

References

[1] Aiz man. A, Contrera. R. (2005) *Tetrahedron*, Lett 61, 889-895.

[2] Becke. A. D. (1996) Phys, Rev

[3] Daudel. R, Lefevre. R. and mosar.C (1959) *Quantum chemistry*Newyork, Inter. Science Publishers.

[4] DeBroglic. L (1925) *Debroglic*, Ann 3, 220

[5] deGroot. A, Buda.H.J.M (1996),*Chem.Phys*.Lett.

[6] Domingo. L.R, Aurell.M.J (2002) *Tetrahedron*Lett 58, 4417, 44231.

[7] Feynman. R. PandHibbs. A.R (1965) *Quantum Mechanics and Path Integrals*, McGraw.Hill.

[8] Fuji. P, Tanaka. K, (1994) *Tetrahedron*.

[9] Hollas. M (1996) *Modern Spectroscopy*, 3th ed, John wiley and sons

[10] Young. D.V. (2002), *Computational chemistry*Jhonwiley and sons.

Theoretical Studies of Aromaticity Criterion and Ligand Fluxionality in [M*($\eta 1-cp$) (L')]

Alireza Ariafard[a],Elham S.Tabatabaie*[a],tahmineh mehrabi [a]

[a]*Department of Chemistry, Member of Young researchers club, Faculty of Science, Central Tehran Branch, Islamic Azad University, Shahrak Gharb, Tehran, Iran.*

Email: elh.tabatabaie@yahoo.com

Abstract:

In the present study, Density Function Theory (DFT) was used to investigate the mechanistic factors affecting cp ligand fluxionally in a series of complexes **[M* (η1-Cp) (L')]** including different metals and different ligands. Remarkable agreement was achieved with the experiment for the barrier heights of the 1,5-shift for complexes of transition metals such as [Fe(η1-Cp) (η5-Cp)$CO)_2$].

The barriers have been properly rationalized in terms of hyperconjugation metal- cp bond strength and steric effects. The results reveal that hyperconjugation depends on the metal element and its charge. A detailed theoretical explanation of the factors involved in all of these 1,5 -shifts are also provided.

Keywords:1,5 shift; Fluxionality; Hyperconjugation; Reaction energy; Aromaticity; Density Functional Theory (DFT).

Introduction:

With the purpose of confirming non-rigidity demeanor mechanism in several main metal complexes, theoretical studies have been used. In 1988, Mary Nick studied η1 and η5 ring shifts of **[Ti (η5-$Cp)_2$ (η1-Cp)]** complex. Her findings revealed that there exists an excellent correlation with experimental data obtained at room temperature [1]. Later on, Vieiros [2] theoretically analyzed the flexibility of **[Mo (η1-Cp) (η5-Cp)($Ntbu)_2$]** complex using Density Function Theory (DFT) method. Also, Catton and co-workers [3-10] for the first time confirmed that metal migration around (η1-Cp) in [Fe(η1-Cp) (η5-Cp)$CO)_2$] can occur via sequential 1-5 shifts. Subsequently, the interconversion (η1-Cp) bonding modes in transition and main metals complexes has been the subject of several experimental studies [3-11]. In this

paper, we aim to perform a theoretical study of the σ-π hyperconjugation , aromaticity, as well as the 1,5-shift process in a variety of (η1-Cp) main metals by (η1-Cp) in the complexes [M(η1-Cp)(CH_3)$_3$](M=C, Si, Ge`, Sn); [M(η1-Cp) (CH_3)$_2$](M=B, Ge, As, Sb) using DFT**.** Choice of the model complexes was made with the purpose to consider the effect of charge, metal center, and ancillary ligand. Furthermore, Nuclease Independent Chemical Shift (NICS) calculations were carried out so as to confirm aromatic character of the components.

Computational Details:

Gaussian 03 was used to fully optimize all the structures reported in this paper at B3LYP level of DFT. The effective core potentials of Hay and Wadt with double- ζ valence basis sets(LanL2DZ). The 6-31G(d) [33] basis set was utilized for H, B, and C. Polarization functions were also added for C (ζ f =0.6), Si (ζ f = 0.263), Ge (ζ f = 0.246), Sn (ζ f = 0.183), B (ζ f = 0.207), Sb (ζ f = 0.211), and As (ζ f =0.293) . Furthermore, NICS calculations were carried out at B3LYP level of DFT for structure optimization and by GIAO method in order to determine the aromatic character of (η1-Cp) ligand. Also, the natural bond orbital (NBO) calculations were performed at B3LYP level and 6-31G /LanL2DZ basis set. All the calculations were executed in Gaussian 03 software environment.

Results and Discussion

Density function theory (DFT) is considered fairly more reliable than Hartree Fock for NMR chemical shift calculations **.**Cheeseman *et al.* have carried out a systematic study of chemical shifts for a series of molecules and found that DFT results are better than SCF results of similar accuracy. In the beginning, aromaticity criterion of main metals in the groups III, IV, and V were investigated by NICS calculations. Fig. 1 demonstrates the profiles of these components. The results of NICS calculations listed in Table 1 are indicative of the fact that NICS values increase as we move down a main group. For instance, NICS value increase at [M (η1-Cp)(CH_3)$_3$](M=C, Si, Ge`, Sn) as we move down in the fourth group. An interesting correlation of ionization potentials with the fluxional behavior of 1 to 8 compounds indicates that the σ-π hyperconjugation of the relevant C cyclopentadienyl–M bonds with the ring diene systems, in the ground state structure of cyclopentadienyl compounds, appears to be an important factor in controlling the rate of sigmatropic rearrangement To estimate the reaction

energy resulted of [M(η1-Cp)(CH_3)$_3$](M=C, Si, Ge`, Sn) and [M($\eta 1-cp$) (CH_3)$_2$](M=B, Ge, As, Sb) components, we designed the isodesmic reactions shown in Fig. 2. In these isodesmic reactions, the (η1-Cp) ring is broken in such a way that the resultant small species does not contain conjugation. It should be noted that different Δ*E* can be obtained from different isodesmic reactions. In a study **,** certain isodesmic reactions were designed in such a way that the resulting smaller molecules also contain significant conjugation. Therefore, the Δ*E* reaction energy based on such isodesmic reactions is smaller than our results. The calculated Δ*E* reaction energies listed in Table 1 are in good accordance with results acquired from NICS calculations. Fig. 2 demonstrates isodesmic reactions. In addition, values of aromaticity criterion increase down a group, which causes δ_{M-C5} bond between (η1-Cp)ring and metal to become more flexible and delocalize easier around π-cp bond and causes an increase in migration of π- electrons and their effect on aromaticity criterion. δ bond between(η1-Cp)ring and metal is defined as an ionic bond. The more the electronegativity difference increases in a group, the lower electronegativity the metal atom has, according to Pauling principle [46] and that bond seems to be near to an ionic bond. Also, when the electronegativity difference between two atoms in a bond decreases due to reduction in electronegativity of metal (M), it is expected that the bond converts to a covalent bond. For instance, experimental results showed that according to Pauling principle, the electronegativity values of C, Si, Ge, and Sn in the fourth group for of [M(η1-Cp)(CH_3)$_3$](M=C, Si, Ge`, Sn) are 2.55, 1.90, 2.01, and 1.96, respectively. Also, electronegativity values of B, Ga, Sb, and As in the third and fifth groups for [M(η1-Cp)((CH_3)$_2$](M=B, Ge, As, Sb) are 2.04, 1.81, 2.05, and 1.8, respectively. These results show that electronegativity decreases down a group and as explained earlier, the bond exhibits ionic bond characteristics. When δ-bond between (η1-Cp) ring and metal (M) is non-rigid, it acts like an ionic bond; thus, π electron migration increases which causes an enhancement in aromaticity criterion.NBO Fock matrix based on B3LYP/ 6-31G and B3LYP /LanL2DZ optimized ground stable geometries. In the present work, the stabilization energies (E_2) associated with (δ→π*) delocalization in 1-8 compounds were systematically and quantitatively calculated using NBO analysis. The results achieved by NBO analysis of donor-acceptor interactions in compounds 1-8 are 1.10, 6.78, 7.54, 14.72, 0.054, 0.09, 6.68, and 10.95 kcal/mol, respectively. These results revealed an increase at δ_{M-C5}→ π* resonance energies. Also, calculated results of stabilization energy corresponding to delocalization of

$\delta_{M-C5} \rightarrow \pi^*$ bond at (η1-Cp)ring are in good agreement with hyperconjugation energy results.The calculated results of NBO method at B3LYP level and LanL2DZ basis set are listed in Table 2, which show that the metal decrease in a group leads to carbon increase; therefore, movement of π electrons increases which in turn causes aromatic characteristic to rise. Furthermore, Mulliken charge and Natural charge gained by NBO calculations of maintained components in Table 2 clarify that, negative charge of cyclopantadyenyl ring decreases as we move down a group; hence, charge of the metal atom gets positive and the bond between metal and the other atom will be similar to an ionic bond. Like other results illustrated in Fig. 2, highest values of E_2 for the discussed compound in this section show that E_2 values for heavy metals are higher in comparison with other metals. This pattern is opposite to results of Schleyer's calculation on cyclopentadienes, in which 5,5-disubstituted with electropositive groups [49] that shown the conjugation energy increases from M=C to M=Sn. Therefore, it is expected that charge decrease on metal atom causes more convenient delocalization of δ_{CM-C5} at $\pi^*\eta^1$–Cp bond.In comparison, hyperconjucation and stabilization energy (E_2) in complexes containing M- C(η^1–Cp) (M=main group elements) depend on the metal (M): these energies are higher in the case of heavier metals. It can be explained by electronegativity of M. In a main group, M- η^1-Cp bond for heavier metals has lower electronegativity and bond characteristics are similar to an ionic bond. Thus, conjugation takes place easier in heavier metals of a main group. As a result, all comparisons in NICS and reaction energy results illustrate that aromatic character increases down a group, which is in good agreement with Graph 1 showing the reaction energy differences toward NICS values (Graph 1). Due to the fact that, the bond between (η1-Cp) group and metal atom (M) is more non-rigid, the electronegativity difference thus increases and causes the bond to be more ionic, which could be a reason for easier delocalization of δ-bond at π-cp bond, as well as π electrons movement and increase in hyperconjugation. As a result, all these factors encourage a component to show more aromatic characteristic.

Conclusion:

Density functional theory calculations have been used to study the fluxionally of cp ligands and the ligand (CH_3) dissociation reactions in [M (η1-Cp) (cH_3)$_3$], M= C, Si, Ge, and Sn, and

[M (η1-Cp) (cH_3)$_2$], M=B, Ga, Sb, and As. In summery, the following conclusions can be made based upon the calculation findings:

1-In this study, we have considered 1,5-shift migration of some transition and main elements including different ligands. On this base, NICS and reaction energy results show that, the aromaticity character increases due to flexibility increase of M and C(η1 C_5H_5) bond and electronegativity difference enhances. Also, natural and Mulliken charge of these elements calculated by NBO show minus charge on cp ring increasing down a group. As a consequence, the central metal gains positive charge and the bond between them converts to ionic bond; afterwards, the δ bond between M and C(η1 C5H5) delocalizes easily at π-cp bond and hence the π- electrons' instability increases at cp ring which causes increment in hyperconjugation and aromaticity character.

2-Two different isomers were located for the (η1-Cp) complexes. These two isomers are connected to each other via the rotation of (η1-Cp) about the M-C (η1-Cp) bond. The barrier to the rotation was found to be independent of the identity of metal center, ancillary ligands, and charge balance on the metal.

3-The stabilization energies associated with 6-π hyperconjugation (delocalization of the M-C (η1-Cp) δ bond to adjacent π* orbitals on (η1-Cp) decreases while the net charge increases on the complexes of transition metals. Opposite of this phenomenon occurs for complexes of main metals.

4-Hyperconjugation and stabilization energy (E_2) in complexes containing M- η^1–CP (M=main group elements) fundamentally depend on the metal (M) and the charge on the metal. These energies are higher for heavier metals. Despite the result obtained from our calculation, it is quite clear that M electronegativity of the metal should be high in the main group and electronegativity M- C(η1 – CP) bonding for heavier metals increases. Also, bond characteristics are similar to that of an ionic bond. Therefore, conjugation is carried out easier in heavier metals in a main group and aromaticity criterion also increases in such metals.

Scheme 1.

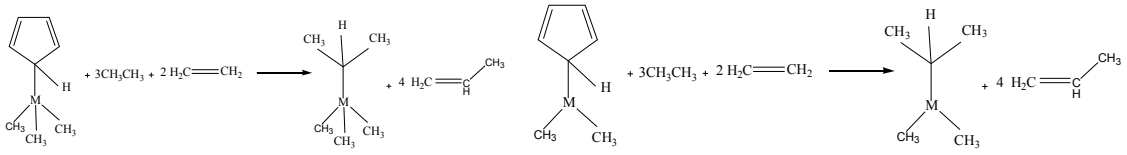

Table1: Reaction energies obtained from the isodesmic equation , NICS(0) and NICS(1) values were calculated for the species [M(η1-Cp)(CH_3)$_3$](M=C, Si, Ge`, Sn); [M(η1-Cp)(CH_3)$_2$](M=B, Ge, As, Sb) using the B3LYP/6-31G, B3LYP/LANL2DZ calculations.

[M(η1-Cp)(L)]L:(CH_3)$_3$,(CH_2)$_2$]		C	Si	Ge	Sn	B	Ga	As	Sb
ΔE(KCal/Mol)		-2.02	+3.41	+2.08	+7.7	+2.9	+13.6	+1.3	+3.8
NICS	Z=0	-3.10	-6.05	-5.70	-8.30	-6.1	-11.6	-5.3	-7.2
	Z=1	-4.20	-6.74	-6.50	-8.05	-6.6	-12.3	-5.7	-6.8

Table2:The calculated NBO partial and natural charges:($q_{(\eta1\text{-}Cp)}$) and (q_M) on these complexes and also contribution of C5 in the $\sigma_{M\text{-}C5}$ bond for species[M(η1-Cp) (CH_3)$_3$](M=C, Si, Ge`, Sn); [M (η1-Cp) (CH_3)$_2$](M=B, Ge, As, Sb).

[M(η1-Cp)(L)] ,L:(CH3)3,(CH_3)$_2$		C	Si	Ge	Sn	B	Ga	As	Sb
Contribution of C5 in the $\sigma_{M\text{-}C5}$ bond		51.24%	76.34%	75.72%	78.58%	71.78%	80.02%	67.95%	72.22%
Mulliken charge	q_M	-0.246	0.4403	0.554	0.9264	0.597	0.6482	0.2372	0.516
	$q_{(\eta1\text{-}C5H5)}$	0.007	-0.180	-0.220	-0.318	-0.240	-0.302	-0.135	-0.476
NBO (natural charge)	q_M	-0.002	1.904	1.887	2.091	1.014	1.775	1.034	1.295
	$q_{(\eta1\text{-}C5H5)}$	-0.043	-0.525	-0.521	-0.581	-0.359	-0.625	-0.387	-0.239

Chart1. The calculated ΔE (in kcal/mol) for compounds 1-8 plotted as a function of (NICS(1)).

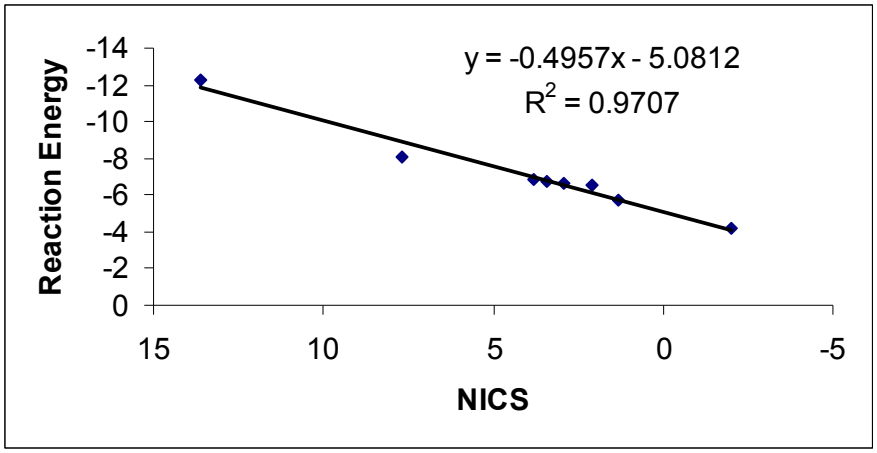

References and Notes:

[1]Hanse,M.L.; Mary nick, D.S.U.**J.*Am.Chem.Soc*.1988,*110*,**2358**.

[2] Romao,C.C.;Vieiros,L.F.***Organomatalics*.2007,***26***,1777**.

[3]Cotton,F.A.;Yogupski,G.***J.Am.Chem.Soc*.1976,***89***,6136**.

[4] Cotton,F.A.;Legzdins,P.***J.Am.Chem.Soc*.1968,***90***,6232**.

[5] Calderon,J.L.; Cotton,F.A.;Legzdins,P**. *J.Am.Chem.Soc*.1967,***89***,6136.

[6] Calderon,J.L.; Cotton,F.A.;Deboer,B.G.;F.A.Takats, ***J.Am.Chem.Soc*.1970,***92***,3801.

[7]Calderon,J.L.; Cotton, B.G.;F.A.Takats, ***J.Am.Chem.Soc*.1970,***92***,3801.

[8] Campbell,A.J.;Fyfe,C.A.;Goel,R.G.;Maslowsky,E.,Jr.;Senoff,G.V.***J.Am.Chem.Soc*.**
1972,*94*,8387.

[9]Cotton ,F.A.; ***J.Inorg.Chem*.2002,***41***,643**.

[10]Gridenv,I.D.Coord.***J.Chem.Rev*.2008,***252,***1798**.

[11] Jutzi,P**. *J.Chem.Rev*.1986,***86,***983**.

Theoretical study of mercapto acetic acid-capped Si_5 silicon quantum dot

D. Farmanzadeh[1]*; L. Tabari Shahandasht[2]

1,2 Faculty of Chemistry, University of Mazandaran, Babolsar, Islamic Republic of Iran;

(E-mail: d.farmanzad@umz.ac.ir)

Key Words: Quantum dot (QD), Mercapto acetic acid (MAA), DFT, CIS

Introduction

Quantum dots (QDs) have attracted great interests in recent years due to their particular electronic and optic properties. Among the various QDs, silicon quantum dots, SiQDs because of their good potential in biomedical applications and as candidates for new optoelectronics sensors and devices are special attractive [1]. SiQDs can be modified to achieve better properties by binding appropriate functional groups to their surfaces. Furthermore, thiol−alkyl acids have been one of the most commonly used surface chemistries for water solubility and bioconjugation. The thiol–alkyl acid surface chemistry is ultraviolet photo oxidation of ligands, and less efficient photoluminescence than other surface chemistries [2]. In this study, we investigate theoretically the small diameter SiQD (Si_5H_{12}) which was capped its surface with mercapto acetic acid.

Computation Methods

The Si_5 QD has been considered in both ground and excited state. The ground state calculations were performed using the DFT- B3LYP/6-31G* level of theory. The excited state calculations were performed using the configuration interaction using single-excitation (CIS), which express the wave function of given excited state as a linear combination of singly excited determinants, each obtained from a Hartree-Fock reference determinant by replacing an occupied spin-orbital with a virtual spin-orbital. All calculations were performer by Gaussian 03W suite program.

Results and Discussion

The difference between the highest occupied molecular orbital (HOMO) and the lowest unoccupied molecular orbital (LUMO) energy, known as the energy (band) gap or simply HLG, is an important factor in study of QDs. The calculated HOMO and LUMO energy levels, HLG, and absorption and emission energy for Si_5 in both ground and excited states are shown in Table1. It can be seen from this table that the HLG of MAA-Si_5 QDs are smaller than of corresponding H-Si_5 QD in both ground and excited states. The absorption and emission energies decrease with increasing number of absorbed MAA molecules. The absorption wave length shows a red shift when Si_5 capped with MAA molecules. It is found that the emission energy is less than the absorption energy and the emission peak exhibits a red-shift because of the relaxation under excitation.

Table1. The energies of HOMO and LUMO (eV), and energy gaps between HOMO and LUMO, HLG (eV), the absorption and emission energies (eV) of Si_5 in the ground and first singlet excited states.

	GROUND STATE					EXCITED STATE				
	E(HOMO)	E(LUMO)	HLG	E(abs)	λ(nm)	E(HOMO)	E(LUMO)	HLG	E(emi)	λ(nm)
Si_5H_{12}	-7.70	-0.16	7.54	7.559	164.22	-10.39	3.03	13.43	4.681	264.88
$Si_5H_{11}(MAA)_1$	-6.79	-1.02	5.78	4.454	278.34	-9.95	2.46	12.41	3.012	411.67
$Si_5H_{10}(MAA)_2$	-6.75	-1.23	5.52	4.453	278.40	-9.87	2.19	12.06	3.007	412.34
$Si_5H_9(MAA)_3$	-6.51	-1.13	5.38	4.447	278.80	-9.51	2.18	11.71	3.003	412.84

Conclusion

The surface of SiQDs can be capped by MAA molecules, which can be effective in preventing surface oxidation. The absorbed MAA molecules reduce the optical gap in ground state and significantly enhance absorbance and fluorescence of SiQDs. Finally, our study verifies that the mercapto acetic acid is a good protecting molecule for SiQDs, as it reduces the surface oxidation rate and maintains optical properties in the visible region.

References

[1] Nagesha, D; Whitehead, M. A.; Coffer, J. L. *Adv. Mater.* 2005, *17*, 921.

[2] Aldana, J.; Wang, Y. A.; Peng, X. *J. Am. Chem. Soc.* 2001, *123*, 8844.

Gas molecule adsorption in boron nitride nanotube and nanotube bundles

M.Keshavarz[a]; K.Toghraee[b*]

[a]Department of chemistry, University Azad of Shahreza, Shahreza, Iran

Email: Keshavarz@iaush.ac.ir

[b] Department of chemistry, University Azad of Shahreza, Shahreza, Iran

Email: ch.Toghraee87@iaush.ac.ir

Abstract:

We studied gases molecules H_2 and CO on single walled boron nitride nanotube and bundles using by Density Functional Method (DFT). Equilibrium position, adsorption energy and charge transfer are obtained for boron nitride nanotube armchair (4, 4). Both molecules adsorb weakly on nanotube single-walled and can be either charge donors to the nanotube. We find that the gas CO adsorption on the bundle interstitial is stronger than gas H_2. However the binding energy of hydrogen on boron nitride nanotubes is increased by as much as %40 compared to that on carbon nanotubes. [1]

Key words: DFT, B3LYP, 6-31G, Basis set

Introduction:

Gas adsorption in boron nitride nanotube and nanotube bundles is an important issue for both fundamental research and technical application of nanotubes. Considerable experimental and theoretical efforts have been devoted to hydrogen storage in nanotube based materials. The effect of gas environment on the electronic properties of boron nitride nanotubes have recently attracted certain attentions .The adsorption of carbon mono oxide (CO) gas on SWNT BN(4,4) at room temperature was study by DFT calculations . In this paper we report first principles calculations on individual SWNT and tube bundles with adsorption of variety of gas molecules including CO and H_2.

Computational methods:

The self-consistent field (SCF) electronic structure calculation are performed based on density functional theory (DFT) . The equilibrium geometry , adsorption energy and charge transfer are calculated by using the b3lyp method and 6-31g basis set . we find that both the equilibrium distance and the adsorption energy are well reproduced by our present DFT scheme . In order to investigate the binding of hydrogen or carbon mono oxide on BN nanotube we perform a series of total energy calculations using density functional methods .

Results and discussion:

We obtained the gas molecule on different sites of nanotube (Hc : hexagon center , Br: bridge bundle BN , TB : on top of the boron atom and TN : on top of the nitrogen atom). Q(e)Table [1] summarizes our results on the equilibrium tube-molecule distance , adsorption energy and charge transfer for H_2 and CO molecules on BN(4,4) SWNT . In general these gas molecules are weakly binded to the nanotube and the tube-molecule interaction can be identified as physisorption . H_2 molecule is charge donor or acceptor with small charge transfer ($\geq$-0.0063 , $\leq$ 0.002 electron per molecule) and weak binding (<0.24 ev) . For CO which is charge donor the charge transfer is not negligible. This is also reflected in their larger adsorption energies. Both the gasses have larger adsorption energies in the state vertical on the top of the boron atom (TB) . But no substantial electron density overlap is found in the region between the gas molecule and nanotube , indicating that no chemical bond is formed .The binding curve for CO and H_2 molecules adsorbed on BN(4,4) SWNT are shown in figure 1 and 2.

Site	**TB**		**TN**		**Hc**		**Br**	
State	H	V	H	V	H	V	H	V
CO								
D(Å)	3.5	2.5	3	3.5	3.5	2.5	3.5	4
E_a(mev)	12	274	69	53	96	123	177	201
Q(e)	+0.009	+0.019	+0.008	+0.004	+0.008	+0.014	+0.01	+0.002
H_2								
D(Å)	3.5	4	4	3	3.5	3	4.5	3.5
E_a(mev)	148	236	102	19	43	35	195	83
Q(e)	+0.002	-0.0001	+0.0004	-0.0063	+0.001	-0.004	0.002	-0.0015

Table 1: Equilibrium tube-molecule distance (D), adsorption energy (Ea) and charge transfer (Q) of molecules H_2 and CO on BN(4,4) individual SWNT . Results are given for the sites : TB (top of a boron atom) , TN (top of a nitrogen atom), Br(top of the center BN bond) , Hc (top of the center BN hexagon) and state gas molecule : H (horizontal) and V (vertical)

The given numbers for D is the distance between center of the site (TB, TN, Hc, and Br) and center of the bond gas molecule in the horizontal form or center of the nearest atom gas molecule to tube in the vertical form. The adsorption energy E_a is defined as the total energy gained by molecule adsorption at equilibrium distance: $E_a = E_{tot}$ (tube + molecule) – E (tube) – E (molecule)

Conclusions:

All molecules are weakly adsorbed on SWNT with small charge transfer, while they can be either a charge donor or an acceptor of the nanotube .The adsorption of some gas molecules on SWNT can cause a significant change in electronic and transport properties of the nanotube due to the charge transfer and charge fluctuation. The molecule adsorption on top of the boron atom and surface of the nanotube bundle is stronger that on the other sites.

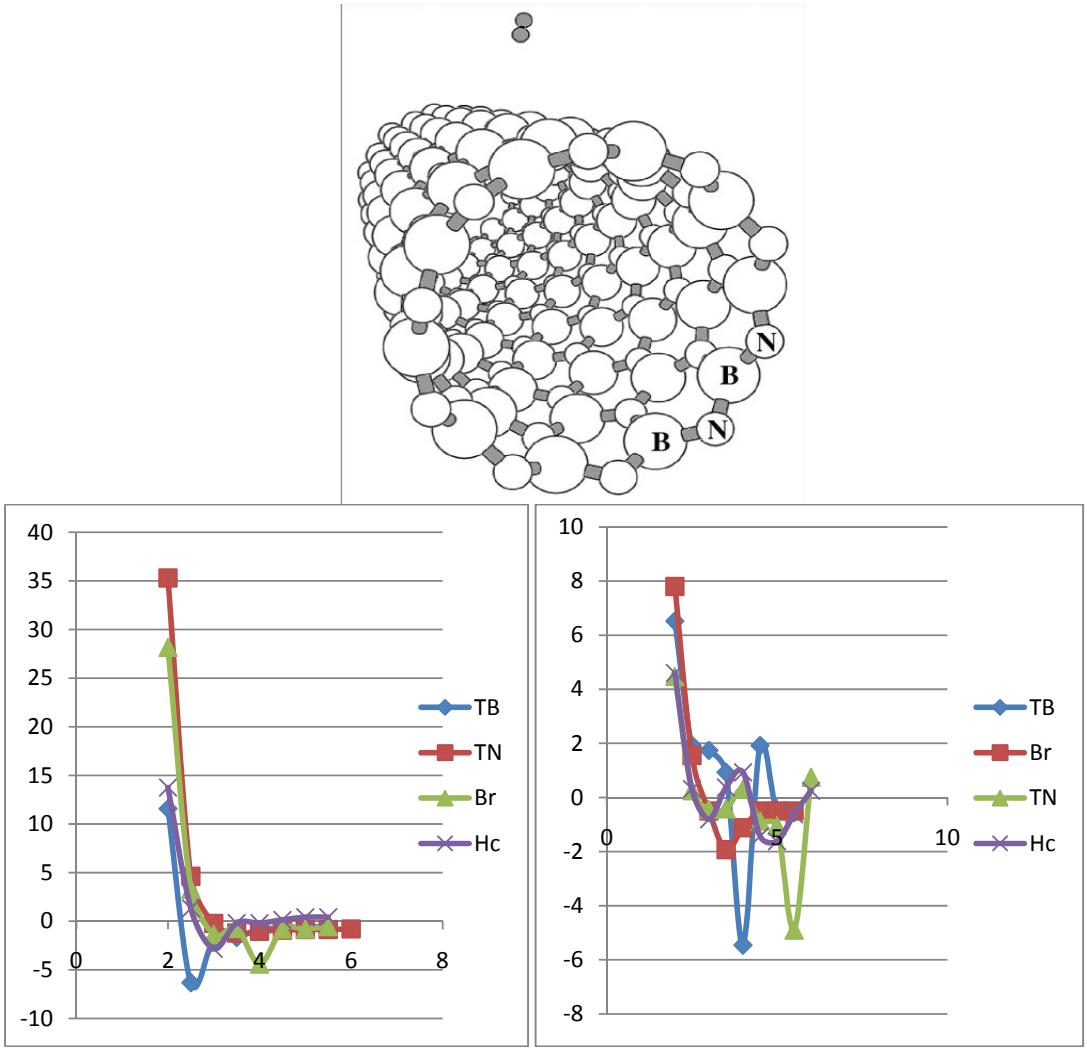

Figuer1: Adsorption energy (KCal/Mol) as function of tube-molecule distance (Å) for CO (left) and H_2 (right) on BN(4,4) for vertical state

Reference:

[1] Seung-Hoon Jhi and Young-Kyun Kwon PHYSICAL REVIEW B69, 245407(2004)

[2] Jijum Zaho, Alper Buldum, Jiehan and Jian Ping LU (2002) Nanotechnology 13 (2002) 195_200

NO2 and CO2 molecules adsorption in boron nitride nanotube

K.Toghraee*[a], M.Keshavarz[b]

[a] Department of chemistry, University Azad of Shahreza, Shahreza, Iran

Email: Ch.toghraee87@iaush.ac.ir

[b] Department of chemistry, University Azad of Shahreza, Shahreza, Iran

Email: Keshavarz@iaush.ac.ir

Abstract:

Studied gases molecules NO_2 and CO_2 on single walled boron nitride nanotube armchair using by Density Functional Method (DFT). Equilibrium position, adsorption energy dipole moment and charge transfer are obtained for both kinds of gases at state horizontal and state vertical. NO_2 molecules adsorb on boron nitride nanotube armchair (4, 4) and can be either charge donors to the nanotube. The electronic properties of tube are sensitive to the adsorption of certain gases such as NO_2 and CO. Our theoretical results show that adsorption polar molecules are stronger than none polar.

Key words: DFT, B3LYP, 6-31G, Basis set

Introduction:

Gas adsorption in boron nitride nanotube and nanotube bundles is an important issue for both fundamental research and technical application of nanotubes. The effects of gas environment on the electronic properties of boron- nitride nanotube have recently attracted certain attentions. [1] Adsorption of Carbon die oxide (CO_2) and nitrogen die oxide (NO_2) gases on boron – nitride nanotube (4, 4) at room temperature is study by density functional calculation. The equilibrium geometry, adsorption energy and charge transfer are calculated by using the 6-31G basis set and B3LYP method. The self consistent filed (SCF) electronic structure calculate are performed based on density functional theory (DFT).Different possible adsorption sites, TB (top of the boron atom), TN(top of the nitrogen atom), HC(top of the center of the boron-nitrogen hexagon) and Br(top of the center of the boron-nitride bond) have been considered. The effects of gas environment on the electronic properties of boron nitride nanotubes have recently attracted certain attentions. In this paper we report calculations on individual SWNT and tube bundles with adsorption of variety of gas molecules including CO_2 and NO_2.

Computational methods:

The self-consistent field (SCF) electronic structure calculation are performed based on density functional theory (DFT).We find that both the equilibrium distance and the adsorption energy are well reproduced by our present DFT scheme . In order to investigate the binding of NO_2 or CO_2 on BN nanotube we perform a series of total energy calculations using density functional methods .

Results and discussion:

Table 1 summarizes our results on the equilibrium tube-molecule distance, adsorption energy, charge transfer and dipole moment for NO_2 and CO_2 molecules on boron-nitride nanotube(4, 4).

Both these gases molecules are weakly bonded to the nanotube and the tube-molecule interaction can be identified as physisorption. Both molecules studied are charge donors with small charge transfer (electron per molecule). For NO_2 at near the tube (less than 2.5 angstroms), molecule is charge acceptor and adsorb is not seen. An adsorption gas NO_2 in the vertical state is seen larger than state horizontal. For CO_2 molecule in the horizontal state adsorption energy and charge transfer is positive and adsorb is seen only top of the nitrogen atom on tube.

For NO_2 molecule the adsorption energy and charge transfer is negative for distance over the 2.5 angstroms and molecule is donor charge.

Site	**TB**		**TN**		**HC**		**Br**	
State	H	V	H	V	H	V	H	V
CO2								
D(Å)	3.5	4	3.5	4.5	3.5	4.5	3.5	4.5
E_a(mev)	-7.54	-20.81	-72.85	-61.58	+11.27	- 26.45	-71.98	- 10.41
Q(e)	0.0084	0.0172	0.0045	0.0058	0.0085	0.0124	0.0084	0.0083
Dipole	0.0923	0.6086	0.0038	0.2989	0.0578	0.4297	0.0376	0.3774
NO_2								
D(Å)	3.5	2.5	3.25	3	3.25	3.5	3.5	4
E_a(mev)	+32.52	-45.96	-70.25	-142.67	-70.68	-45.97	-56.37	-228.96
Q(e)	0.007	-0.0242	0.0087	-0.0107	0.0101	0.0027	0.0088	0.0018
Dipole	0.2065	0.1033	0.2926	0.3765	0.2303	0.1328	0.1889	

Table 1: Equilibrium tube-molecule distance (D), adsorption energy (Ea) , charge transfer (Q) and dipole moment of molecules CO_2 and NO_2 on BN(4,4) individual SWNT . Results are given for the sites : TB (top of a boron atom) , TN (top of a nitrogen atom), Br(top of the center BN bond) , HC (top of the center BN hexagon) and state gas molecule : H (horizontal) and V (vertical)

The given numbers for D is the distance between center of the site (TB, TN, HC, and Br) and center of the bond gas molecule in the horizontal form or center of the nearest atom gas molecule to tube in the vertical form. The adsorption energy E_a is defined as the total energy gained by molecule adsorption at equilibrium distance: $E_a = E_{tot}$ (tube + molecule) – E (tube) – E (molecule)

E (BN) = -2868.11355

E (CO_2) = -188.5002697

E (NO_2) = -204.9874502

Conclusions:

The gas molecule adsorption on the nanotube boron-nitride armchair for polar molecules is stronger than non polar molecules. Polar molecules are donor charge and tube boron-nitride is acceptor charge. For adsorption gases molecules on boron nitride nanotubes, charge transfer must be from molecule to the tube and molecule must be able to charge transfer to the tube. CO_2 molecule is non polar.

Reference:

[1] Seung-Hoon Jhi and Young-Kyun Kwon PHYSICAL REVIEW B69, 245407(2004)

Quantum Chemical Study of Interaction between Methimazole and M^{z+} (Ca^{2+}, Mg^{2+}, Na^{+} and Li^{+})

Hossein Roohi[a] Elham Zahiri*[b]

[a]*Department of Chemistry* , Faculty of Science, *University of Gilan, rasht, Iran*

[b]*Department of Chemistry* , *University of Sirjan Payame Noor, Sirjan, Iran*

Email: zahiri.elham@Gmail.com

Keywords: Methimazole (MMI); MMI–M^{z+} complexes; NBO and AIM analysis

Introduction

Carbimazole, methimazole (MMI) and propyltiouracil are anti-thyroid drugs. All anti-thyroid agents contain the thiourea pharmacophore. This pharmacophore must possess significant electron donor properties at the sulfur atom. Therefore, it has been proposed that the donor properties of anti-thyroid agents are the origin of their anti-thyroid action [1-2]. These anti-thyroid drugs could interact with the cations. In the present paper, interaction between M^{z+} with MMI has been investigated at various levels of theory. Two stable planar and perpendicular complexes were found on the potential energy surface of interaction between MMI and mentioned cations, as shown in Scheme 1.

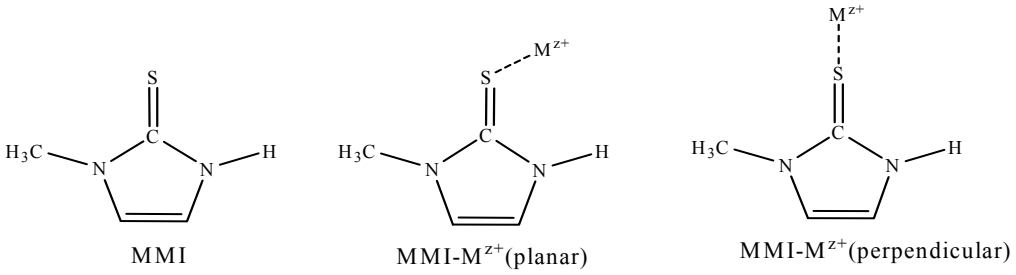

Scheme 1.

Methods

All geometries of MMI-M^{z+} complexes were optimized with the HF/6-311++G(d,p), B3LYP/6-311++G(d,p), B3LYP/6-311++G(2d,2p), B3LYP/6-311++G(2df,2pd), MP2/6-311++G(d,p) and MP2/6-311++G(2d,2p) levels as a part of the GAUSSIAN 03 computational package. In order to provide the frequencies needed in the computation of the thermodynamic functions, frequency calculations were also carried out for all these compounds. The NBO

analysis was carried out with the MP2/6-311++G(2d,2p) method for MMI–M^{z+} complexes. AIM analysis was also performed by AIM2000 package and AIM method within the GAUSSIAN program at the MP2/6-311++G(2d,2p) level.

Results and discussion

All levels of theory show that the Gibbs free energy of the perpendicular form is smaller than the planar form. Therefore, the perpendicular complex is more stable than the planar one in agreement with the experimental results. The analysis of energy of complexes shows that complex MMI-Li^+ is more stable than MMI-Na^+ and MMI-Mg^{2+} complexe is more stable than MMI-Ca^{2+}. In addition, results of HF, B3LYP and MP2 methods suggest that the MMI-Mg^{2+}(perp.) is more stable than the other complexes. NBO results also reveal that the lone pair of S, LP(S), participate as donor and the LP*(M^{z+}) anti bond as acceptor in a strong intermolecular charge transfer interaction. The charge transfer energy in most stable complexes is greater than weak stable ones. This interaction may be considered as a measure of the relative stability of these complexes. The bond critical point data showed that S…Li^+, S…Na^+, S…Ca^{2+} and S…Mg^{2+}(perp.) interactions have electrostatic character, whereas S…Mg^{2+}(plan.) one has partially covalent nature. The also results of AIM calculations show that the electronic density at BCP of S…M^{z+} interaction in most stable complex is greater than less stable ones.

Conclusions

Our results show that the perpendicular forms of complexes are more stable than planar one. The interaction energies of the complexes with bivalent ions are larger than those of monovalent ions. In each MMI-M^{z+} complex, binding energy increases as the size of cations decreases.

References

[1] C. Laurence, M.J. El Ghomari, M. Lucon, J. Chem. Soc., Perkin Trans. 2 1998; 1159.

[2] C. Laurence, M.J. El Ghomari, J.-Y. Le Questel, M. Berthelo, R. Mokhlisse, J. Chem. Soc., Perkin Trans. 2 1998; 1545.

The mutual relationship between H-bonding and π-stacking interactions in phenylalanine:(G···C) complexes

Ali Ebrahimi, Mostafa Habibi-Khorassani and Somaye Abedini
Department of Chemistry, University of Sistan and Baluchestan, Zahedan, Iran
(E-mail: abedini.1366@yahoo.com)

Keywords: Guanine, Cytosine, Phenylalanine, H-bonding, π –stacking.

Introduction:

H-bonding and π-stacking are two types of non-covalent interactions, which are the main interactions determining nucleic acid structure. H-bonding largely determines the stability of the double-helical structure of DNA [1]. The origins of stabilization are different for these interactions [2]; H-bonding originates mainly in electrostatic interaction while the stacking is mainly due to the dispersion energy [3]. In this work, the mutual relationship between π-stacking and H-bonding in phenylalanine:(G···C) complexes (see Fig. 1; ··· and : are used for the H-bonding and π-stacking, respectively) has been considered by a DFT method.

Methods:

Phenylalanine has been modeled by replacing the side chain with hydrogen atom. The complete optimization of structures have been performed by the MPWB1K [4] functional with the 6-311++G** basis set using Gaussian03 program package [5] (Fig. 1).

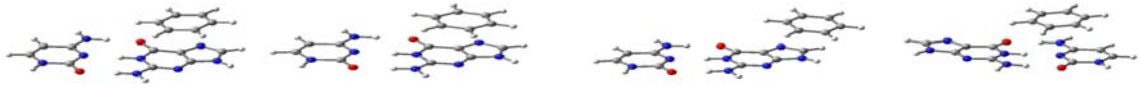

1 **2** **3** **4**

Figure 1. Stacking between Phenylalanine and six and five membered rings of guanine in G···C complex.

Results and discussion:

The binding energies calculated at the MPWB1K/6-311++G** level for trimolecular complexes are given in Table 1.

Table 1. H-bonding energy, π-Stacking and total binding energy calculated at the MPWB1K/6-311++G** level of theory

	T1	T2	T3	T4	D1	D2	D3	G···C
E_{Comp}	-30.06	-29.97	-30.45	-31.28				
E_{HB}	-26.81	-26.84	-26.78	-26.82				-26.94
E_S	-1.60	-1.66	-1.97		-3.65	-3.48	-3.71	

T and D refer to phenylalanine:(G···C) and phenylalanine:guanine, respectively

E_{HB} and E_S are the binding energies for bimolecular complexes with the structures optimized in trimolecular complexes (E_{HB} for hydrogen bonded and E_S for the π-stacked complexes).

The trend in the binding energies of complexes is **T4** > **T3** > **T1** > **T2**. The H-bonding and π-stacking energies are equal to -26.806 and -1.597 kcal/mol in complex **T1**. The H-bonding and π-stacking energies of optimized G···C and **D1** complexes are equal to -26.937 and -3.646 kcal/mol, respectively. Thus, the H-bonding weakens the π-stacking and vice versa, but the effect of H-bonding on π-stacking is stronger. The E_{HB} and E_S decrease by 0.131 and 2.049 kcal/mol, respectively, upon mutual influence of H-bonding and π-stacking. In complex **T2**, the trend in the changes of E_{HB} and E_S are similar to the complex **T1**; E_{HB} and E_S decrease by 0.100 and 1.818 kcal/mol, respectively. The highest change in E_{HB} and the lowest change in E_S correspond to complex **T3**. As a result, the most negative binding energy among complexes **T1-T3** corresponds to **T3**. In **T4** complex, the H-bonding energy is equal to -26.824 kcal/mol in the presence of π-stacking and the trend in the change is similar to complexes **T1-T3**; but, due to the interaction of phenylalanine with both guanine and cytosine bases, the effect of hydrogen bonding on stacking can not be calculated.

Conclusions:

The interplay of π-stacking and H-bonding results in the weakening of both interactions. Despite increasing the distance between phenylalanine ring and the groups involved in H-bond interactions in **T3**, when is compared with **T1** and **T2**, the highest change in H-bond energy corresponds to **T3**. On the other hand, the lowest change in π-stacking energy corresponds to **T3**.

References:

[] Saenger, W. *Principles of Nucleic Acid Structure*; Springer- Verlag: Berlin, Germany, 1984.

[2] Hobza, P.; Sponer, J. *J. Chem. Rev.* **1999**, *99*, 3247.

[3] Gil, A.; Branchadell, V.; Bertran, J. Oliva, A. *J. Chem. Phys. B* **2009,** *113,* 4907.

[4] Zhao, Y.; Truhlar, D. G. *J.* Phys. *Chem. A* **2004**, *108*, 6908.

[5] Frish M. J. et al. Gaussian 03 (Revision B.03), Gaussian, Inc, Pittsburgh, PA, **2003**.

Molecular dynamics simulation of fluid methane using two-body and three-body intermolecular potentials

Mohsen Abbaspour

Department of Chemistry, Sabzevar Tarbiat Moallem University, Sabzevar, Iran

(E-mail: abbaspour@sttu.ac.ir)

Keywords: Potential energy function, Three-body interactions, Molecular dynamics simulation, Equation of state, Radial distribution function, Self-diffusion coefficient.

Introduction

The interaction potential and the properties of fluid methane were the subject of numerous studies over the last two decades. The reason for this long-lasting interest is that methane is the major constituent of natural gas which is one of the most
promising alternative energy sources and one of its main advantages is that it is much cheaper and environmental friendly than petroleum-based fuels.

The purpose of the present paper is to perform the molecular dynamics (MD) simulation to obtain some thermodynamic (internal energy and pressure), structural (radial distribution function), and transport (self-diffusion coefficient) properties of fluid methane at different temperatures and densities using the one site OPLS [1], five sites OPLS-SITE [2], and two-body HFD-like [3] potentials. To take three-body forces into account, a mean-field term of Hauschild and Prausnitz [4] extended as a function of density and temperature and used with the two-body HFD-like potential which introduced as total potential. The MD simulation of methane has been also used to determine a new equation of state (EOS).

Results and discussion

The MD simulation has been performed to obtain reduced pressure and internal energy of methane using different potentials and compared with experiment [5] and previous MD and Monte Carlo (MC) simulations. It is shown that the simulated values of reduced pressure for methane were in good agreement with the experimental and literature values. It also shown that the three-body potential of Hauschild and Prausnitz has small but significant contribution

to the pressure values which decreases the simulated values to give better agreement with the experiment.

The simulated energy results of methane using the OPLS-SITE potential were in better agreement with the experiment than literature values and other potentials. In the other words, the energy results using the other potentials were smaller than those of the OPLS-SITE potential. It is also shown that the three-body potential of Hauschild and Prausnitz does not improve the energy results.

The MD simulation of the methane molecules has been used to determine methane EOS using the total potential for the reduced temperatures from 0.65 to 10 (105-1600 K) and reduced density from 0.1 to 1.0 (50-520 kg/m^3).

We have also determined the radial distribution function, g(r), of liquid methane using different potentials at T^*= 0.7 and ρ^*= 0.8 and the reduced self-diffusion values at T*=1.0. It is shown that the HFD-like and OPLS potentials give almost the same values of the simulated g(r) which were in better agreement with x-ray scattering experiment [6]. It is also shown that the simulated reduced self-diffusion values using the total potentials and those using the OPLS-SITE potential have better agreement with the experiment [7] than the OPLS potential at lower and higher densities, respectively.

Conclusions

The MD simulation has been performed to obtain pressure, internal energy, radial distribution function, and self-diffusion coefficient of fluid methane using one site OPLS, five sites OPLS-SITE, and two-body HFD-like potentials. The significance of this work is that the three-body potential of Hauschild and Prausnitz extended as a function of density and temperature and can be used with the HFD-like potential to improve the prediction of the pressures of fluid methane without requiring an expensive three-body calculation. The molecular dynamics simulation of methane has been also used to determine a new equation of state. The results are in a good agreement with experimental and theoretical values.

References

[1] W.L. Jorgensen, J.D. Madura, C.J. Swenson, J. Am. Chem. Soc. 106 (1984) 6638.

[2] G. Kaminski, E.M. Duffy, T. Matsui, W.L. Jorgensen, J. Phys. Chem. 98 (1994) 13077.

[3] E.K Goharshadi, M. Abbaspour, Fluid Phase Equilib. 212 (2003) 53.

[4] T. Hauschild, J.M. Prausnitz, Mol. Simul. 11 (1993) 177.

[5] NIST Chemistry Webbook. Available at http://webbook.nist.gov/chemistry/fluid.

[6] A. Habenschuss, E. Johnson, A.H. Narten, J. Chem. Phys. 74 (1981) 5234.

[7] K.R. Harris, N.J. Trappeniers, Physica A 104 (1980) 262.

Theoretical investigation on Hydrogen bonds in Base Pairs of DNA (C:G and A:T) by DFT and AIM

Narges Bagheri*[a], Pouria Abbasi[a]

[a] *Department of Physical Chemistry, Islamic Azad University of Firoozabad Branch, P. O. Box 74715-117 Fars, Iran*

(Email :Pouria_Abbasi64@yahoo.com)

Keywords: Hydrogen bond, DNA, Base Pairs, DFT, AIM, NBO

Introduction:

A hydrogen bond is the attractive interaction of a hydrogen atom with an electronegative atom such as nitrogen, oxygen or fluorine, that comes from another molecule or chemical group. The hydrogen must be covalently bonded to another electronegative atom to create the bond. A hydrogen atom attached to a relatively electronegative atom is a hydrogen bond donor. An electronegative atom is a hydrogen bond acceptor. These bonds can occur between molecules (intermolecularly), or within different parts of a single molecule (intramolecularly). The hydrogen bond (5 to 30 kJ/mole) is stronger than a van der Waals interaction, but weaker than covalent or ionic bonds. This type of bond occur in organic molecules such as DNA. Intermolecular interaction affects many biochemical processes, and it is important in the process of molecular recognition of DNA by small molecules. The interaction between nucleic acid bases is responsible for the structure of DNA [1]. In this article we study hydrogen bonds between guanine-cytosine (3 bonds) and adenine–thymine (2 bonds) by DFT (Density Functional Theory), AIM (Atoms In Molecule) and NBO (Natural Bond Orbital) computational methods [2].

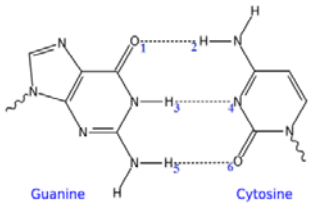

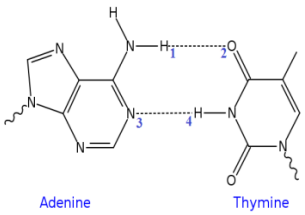

Computational Details:

Several types of A–T, C-G base pairs are optimized with 6-311++G** basis set using B3LYP method. The modified bonds are calculated at the mentioned level in A°. Electron density have been calculated at the B3LYP/6-311G** level by using atoms in molecules (AIM). AIM is a useful tool in analyzing hydrogen bonds. The charge distribution has also been investigated using natural bond orbital (NBO) analysis. All calculations were performed using Gaussian 03 and AIM 2000 programs [3].

Results and discussion:

The AIM methodology has been widely used to study of H-bonded systems and proved to be a useful and successful tool to the interpretation of the charge density. We have performed optimization of A:T and G:C pairs at B3LYP/6-311++G** and the obtained hydrogen bonds length, electron density and charge distributions, that are listed in this table.

H-Bond	Bond Length	Electron density	Charge
O_1–H_2	2.82	0.0387	0.937
H_3 –N_4	2.95	0.0337	0.952
H_5 –O_6	2.93	0.0292	0.833
H_1–O_2	2.95	0.0277	0.687
N_3–H_4	2.88	0.0406	0.578

hydrogen bonds length (A°), charge distributions of the derivatives removed one electron and electron density (e/au3) calculated at the B3LYP/6311++G**

Conclusions:

We have investigated the performance of popular computational method (B3LYP) for determination stability of the hydrogen bonds in DNA base pairs. We have calculated hydrogen bonds of N – H…..O, N – H……N, in G:C pair and O……H – N, N – H……N in A:T pair that saw O……H – N in G:C (2.82, 2.95A° and -31.644, -35.391 kcal/mol) pair are more stable than A:T (2.95A° and -17.431 kcal/mol) and N – H……O in A:T pair (2.88A° and -29.391 kcal/mol) is more stable than G:C pair (2.95A° and -17.162 kcal/mol). Also, the charge distribution analysis and electron density calculated prove to previous these stabilizations.

References:

[1] T.S. Moore, J. Chem. Soc., 101 (2000) 1635.

[2] R.W.F. Bader, Atoms in Molecules: A Quantum Theory, Oxford University Press, 1990.

[3] M.J. Frisch et al., GAUSSIAN 03, Revision E.01, Gaussian, Inc., Wallingford, CT, 2004.

Study on Synthesis of Acetyl salicylic acid (Aspirin) from Methylsalicylate by Computational Chemistry Methods

Narges Bagheri*[a], Pouria Abbasi[a]

[a]*Department of Physical Chemistry, Islamic Azad University, Firoozabad Branch, P. O. Box 74715-117 Fars, Iran*

(Email : Pouria_Abbasi64@yahoo.com)

Keywords: Aspirin, Methylsalicylate, DFT, QST2, Rate of reaction

Introduction:

A French chemist, Charles Frederic Gerhardt, was the first to prepare acetylsalicylic acid in 1853. In 1859, von Gilm obtained analytically pure acetylsalicylic acid (which he called "acetylierte Salicylsäure") by a reaction of salicylic acid and acetyl chloride. Aspirin is an acetyl derivative of salicylic acid that is a white, crystalline, weakly acidic substance, with a melting point of 135 °C (275 °F). The multi-step synthesis of aspirin that is shown below (These structures are written in shorthand. Every unlabeled vertex is a carbon, and hydrogen need to be added until each carbon has 4 bonds). In the first step, we will be performing a hydrolysis of methyl salicylate, otherwise known as, Oil of Wintergreen. In the second step, we will be performing a condensation reaction to produce us final product, acetylsalicylic acid. Methyl Salicylate is composed of an ester (RCOOR) (R indicates a carbon-containing group) and a phenol (C_6H_5OH). In the presence of sodium hydroxide the hydrolysis of the ester takes precedence over any chemical change in the phenol [1], [2]. In this article, we Study synthesis of 2-acetoxybenzoic acid from methyl 2-hydroxybenzoate by calculations of DFT (Density functional theory) and HF (Hartree fock) in solvent (water) phase. We have calculated $\Delta_f H^0$, $\Delta_f G^0$ and rate of reaction.

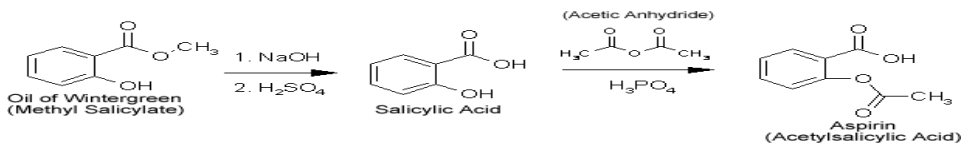

Computational details:

TS (QST2) and IRC methods have been used for finding energy maximum point and watching reaction route between reactants and products. All compounds have been fully optimized by density functional theory (B3LYP) with the 6-311++G** basis set. All calculations have been performed by using Gaussian 03 program [3].

Results and discussion:

Thermodynamic properties of this reaction have been calculated in Table 1.

Table1: Thermochemistry calculations (Hartree) at B3lyp/6-311++G**

Parameter	$C_8H_8O_3$	NaOH	$C_9H_8O_4$	$C_2H_4O_2$
E_0	-529.255582	-235.868879	-641.347907	-226.534237
E_{ZPE}	0.160439	0.011302	0.169079	0.065963
E_{tot}	0.169326	0.014581	0.180209	0.070322
H_{corr}	0.170270	0.015525	0.181153	0.071266
G_{corr}	0.125869	-0.001075	0.130299	0.039217
$E_0 + E_{ZPE}$	-529.095143	-235.857577	-539.178828	-226.468274
$E_0 + E_{tot}$	-529.086256	-235.854298	-539.167698	-226.463915
$E_0 + H_{corr}$	-529.085312	-235.853354	-539.209754	-226.462971
$E_0 + G_{corr}$	-529.129713	-235.869954	-539.217607	-226.495019

The benefit way for calculation of reaction enthalpies and free energies is calculation of heat of formation and gaining their sum and subtraction. We have calculated sum of electronic and thermal enthalpies and free energies ($E_0 + H_{corr}$) and ($E_0 + G_{corr}$) by Gaussian 03 that they are shortcut route. Finally, we have calculated $\Delta_f H^0$ and $\Delta_f G^0$ by using these parameters.

$$\Delta H^0 (298K) = \Sigma_{Products} {}^{\Delta}_{f}H(298k) - \Sigma_{Reactants} {}^{\Delta}_{f}H(298k)$$
$$= \Sigma_{Products} (E_0 + H_{corr}) - \Sigma_{Reactants} (E_0 + H_{corr})$$
$$= \{(-539.209754) + (-226.462971) - (-529.085312) + (-235.853354)\}$$
$$= -0.673058 * 627.5095 = -422.35 kcal/mol$$

$$\Delta G^0 (298K) = \Sigma_{Products} {}^{\Delta}_{f}G(298k) - \Sigma_{Reactants} {}^{\Delta}_{f}G(298k)$$
$$= \Sigma_{Products} (E_0 + G_{corr}) - \Sigma_{Reactants} (E_0 + G_{corr})$$
$$= \{(-539.217607) + (-226.495019) - (-529.129713) + (-235.869954)\}$$
$$= -0.712959 * 627.5095 = -447.388 kcal/mol$$

Table2: $E_{0+}G_{corr}$ for compounds

Compound	$E_{0+}G_{corr}$
$C_8H_8O_3 + NaOH$	-64.9996
$C_9H_8O_4 + C_2H_4O_2$	-65.7126
TS	-64.5821

$K(T) = \frac{k\,T}{h\,c}\, e^{-\Delta^{\pm}G/RT}$

$\Delta^{\pm}G^0$ = -764.5821 -(-764.9996) = 0.4175 Hartrees * 627.51 = 261.985 kcal/mol

K (298) = $1.38*10^{-23}(298) / 6.62*10^{-34}(1)$ exp (- 261.985*1000 / 1.98*298) = $3.77*10^{-55}$ s^{-1}

Conclusions:

We have investigated and calculated the rate and route of this reaction by density functional theory and hartree fock methods and show that rate of this reaction is fast. Also, we have calculated Δ_fH^0 and Δ_fG^0 (enthalphy of reaction and heat of formation) as a result of calculations $\Delta_fH^0 < 0$, $\Delta_fG^0 < 0$, that show us this reaction is a exothermic and spontaneous reaction.

References:

[1] C. Gerhardt, Annalen der Chemie und Pharmacie, 87 (1853) 149–179

[2] H. von Gilm, Annalen der Chemie und Pharmacie, 112 (1859) 180–185

[3] M.J. Frisch et al., GAUSSIAN 03, Revision E.01, Gaussian, Inc., Wallingford, CT, 2004.

Theoretical Study on the Aromaticity of BN-substituted Rings

S. Noorizadeh*, M. Abbasi
Chemistry Dept., College of Sciences, Shahid Chamran Univ. Ahwaz, Iran;
(e-mail:noorizadeh_s@scu.ac.ir)

Keywords: Aromaticity, NICS, NICS-Rate, Boron and Nitrogen Substitution

Introduction

The concept of Nucleus-Independent Chemical Shifts (NICS) was introduced by Schleyer [1] as a successful index for predicting the aromaticity of molecules. After that, some other NICS-based incides are defined [2]. Recently a new method for indication of aromaticity in cyclic compounds is proposed based on the variation of NICS index at different distances from the ring center [3]. It is shown that the presence of a solitary maximum/minimum in the NICS-Rate curve ($\frac{\Delta NICS}{\Delta r}$versus r) of a molecule indicates to aromaticity/antiaromaticity of the system; while if molecule shows both maximum and minimum in its curve, the absolute ratio of the maximum to the minimum NICS-Rates (NRR = $\left|\frac{NICS-Rate(max)}{NICS-Rate(min)}\right|$) is defined as a measure of aromaticity. NRR= 0.5 is found as the boundary between aromatic and nonaromatic systems.

In this work, the calculation of NICS and NICS-Rate indices have been performed to investigate the aromaticity of those n-membered rings (n=4, 5, 6, 7 and 8) in which different C-C bonds are substituted by isoelectronic B-N bonds.

Results and discussion

Sixty considered molecules are optimized at the Hartree-Fock (HF) level of theory with different basis sets included 3-21G**, 6-31G** and 6-311++G**. It should be mentioned that both neutral and ionic forms (cationic and anionic) of the 5-, 7- and 8-membered rings are considered in this study. The NICS values at different distances from the ring center of each molecule are calculated using the same level of theory and GIO approach. All the calculations are performed using the GAUSSIAN03W program.

The NICS-Rate curves of cyclobutadiene and its BN-substituted analogs are shown in Fig.1 for comparison as an example. Both of the NICS values and NICS-Rate curves of the BN-substituted compounds indicate to the less delocalization of π-electrons in these rings with respect to the cyclobutadiene molecule; which cases a decrease in the anti-aromaticity of these systems. This decrease might be due to large electronegativity difference between boron and nitrogen atoms in the B—N bond**.**

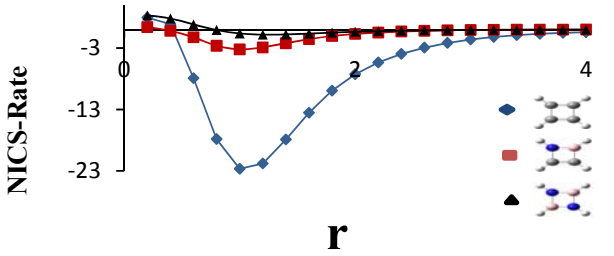

Fig. 1. NICS-Rate curves of the considered four-membered rings.

The same comparison is made between the other rings with the same size. The obtained results show that in all cases, replacing C—C double bonds with B—N bonds in a conjugated system decrease the aromatic character of the molecule, which is nicely reflected in its NICS and NICS-Rate curve. In some cases (35 molecules) the NICS-Rate curves show both maximum and minimum. The NICS-Rate curves of the 6-membered rings are given as an example in Fig.2. The evaluated NRR values for these molecules again successfully predict the aromaticity order of the system.

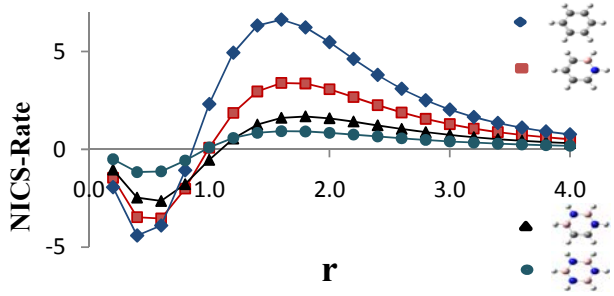

Fig. 2. NICS-Rate curves of the considered six-membered rings.

Conclusions

It is shown that BN-substituted conjugated rings significantly show less aromaticity/ antiaromaticity with respect to their hydrocarbon analogs. It may arise from the decrease in π-electron ring current, which is due to large electronegativity difference between boron and

nitrogen in B—N bonds. Both NICS values and NICS-Rate curves show successfully this decreasing in aromatic character of the considered molecules.

References

[1] P.v.R. Schleyer, H. Jiao, Pure Appl. Chem. 68 (1996) 209.

[2] H.F. Shaidaei, C.S. Wannere, C. Corminboenf, R. Puchta,P.v.R. Schleyer, Org. Lett. 8 (2006) 863.

[3] S. Noorizadeh, M. Dardab, Chem. Phys. Lett. 493 (2010) 376.

Theoretical Study of CO Adsorption on Armchair BN nanotube

Z. B. Nojini[a*], N. Abbasi[a], M. Haghbayan[a]
[a]Department of Chemistry, Faculty of Science, Shahid Chamran University, Ahvaz, Iran
E-mail:nasibe.abbasi@gmail.com

Abstract

Carbon monoxide adsorption on to (5, 5) single-wall boron nitride nanotube was studied using the density functional theory. Results show that when CO adsorption through C on the B atom of nanotube, has minimum adsorption energy and minimum distance between B-C atoms.

Keywords: BN nanotube, Adsorption energy, Carbon monoxide, DFT

Introduction

Since the discovery of boron nitride nanotubes (BNNTs) [1], much attention has been paid to this novel material, particularly to its suitability to gas storage [2].

Chemical gases such as CO is highly toxic to human beings and animals as it inhibit the consumption of oxygen by body tissues. It is colorless, odorless, and tasteless, and thus, human beings do not have timely alertness to it presence. Therefore, gas sensors with high sensitivity to this gas are highly desired.

Computational method

The adsorption of CO on (5,5) BNNT was studied DFT theory employing MPW1PW91/6-31g basis set with periodic boundary condition and using a CO molecule per unit cell in the tube axis direction. In this case the cell length is 2.51 Å.

Result and discussion

In this work, two configuration of CO molecule (-CO, and -OC) are considered relative to the possible sites of BNNT (top of the B and N atom). The adsorption energy of single molecular CO on tube is defined

$$E_{ads} = E\,(\text{NTs+CO}) - E\,(\text{NTs}) - E\,(\text{CO}), \qquad (1)$$

where E(NTs+CO) is the total energy of the system, E(NTs) is the energy of the substrate prior to CO adsorption, and. E(CO) is the total energy of a CO molecule in free space. The more negative E_{ads} is, the stronger the chemical binding, conversely, the less negative, the weaker the binding. If the adsorption energy is positive, it is thermodynamically unlikely for the CO to adsorb to the substrate. Table 1 summarize our results on the equilibrium distances and adsorption energies. Obtained data show that physical adsorption was occured when the CO is adsorb through C atom on the B atom (Figure 1). The equilibrium distance of C atom and B of BN nanotube is 3.12 Å and the adsorption energy is 0.399 (ev). Endothermic energies, $E_{ads} > 0$, mean that the adsorption is unstable energetically relative to the molecular CO and BN nanotube.

Table 1: Calculated Adsorption Energy (E_{ads}), equilibrium distance r_e(Å) for molecular CO Adsorption on the (5,5) BNNT

Configuration	site	r_e(Å)	E_{ads}(ev)
CO	B	3.12	0.399
	N	3.56	0.44
OC	B	3.31	0.43
	N	3.68	0.44

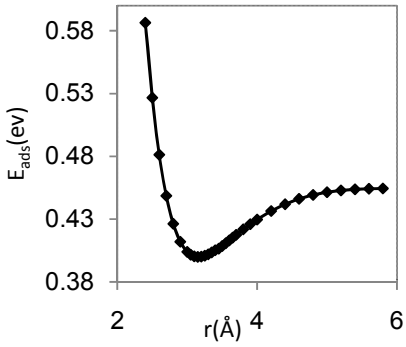

Figur1: Binding energy (ev) of molecular CO adsorbed on BNNTs for B-CO configuration

Conclusion

Results show that CO molecule was physical adsorption on BNNT effectively by physisorption.

References

[1] M D, Ganji, A, mirnejad, A, Najafi **2010** sci. Thechnol. Adv. Mater 11 545001

[2] W U X J, Yang J L, Hou J G and Zhu G S **2004** Phys. Rev. B 69 15 3411

The NO2 adsorption on the $C_{48}B_{12}$ heterofullerene: DFT study of B electric field gradient tensors

A. Abdollahian, Z. Halfinezhad, S. Ali-asgari, S.H. Mortazavi, Ehsan Zahedi*
Chemistry Department, Islamic Azad University, Shahrood Branch, Shahrood, Iran.
atiyeh.abdollahian@yahoo.com e_zahedi@iau-shahrood.ac.ir

Keywords: NQR; Heterofullerene; DFT; $C_{48}B_{12}$

Introduction:

Carbon exists in several forms in nature and one of carbon allotropes is fullerene. Fullerene was discovered as an unexpected surprise during vaporization of graphite by laser irradiation. The 1996 Nobel Prize for chemistry dedicated to H.W. Kroto, J.R. Heath, S.C. O'Brien, R.F. Curl, and R.E. Smalley in Rice Quantum Institute for their discovery in 1985. C_{60} is the most important member of the family of fullerenes [1]. The doping of carbon cages with boron and nitrogen atoms appears a promising way to modify the physical and chemical properties of fullerenes [2].

Results and discussion:

In the present work, adsorption behavior of an NO2 molecule on the two possible adsorption sites of $C_{48}B_{12}$ heterofullerene is taken into consideration and comparison. To demonstrate of the two possible adsorption sites on a $C_{48}B_{12}$ heterofullerene, we make used of the same labeling and numbering C_{60} Schlegel diagram in below Fig.

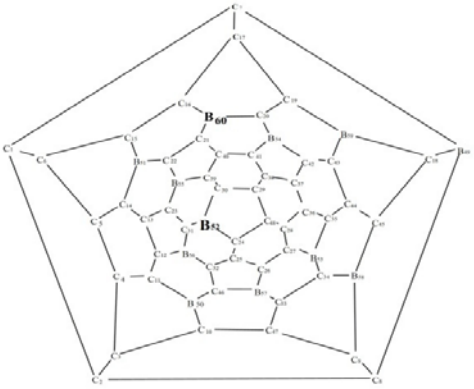

In this figure boron adsorption sites are defined with bold words and other boron sites don't studied, because they were similar in position and neighboring atoms with the three considered sites. Firstly, each of the three structures including perfect and NO2-attached $C_{48}B_{12}$ heterofullerenes at the two possible adsorption sites was allowed to fully relax during the geometrical optimization process performed at the B3LYP-DFT method and 6-31G* basis set using Gaussian 03 [3]. The optimization process reveals that dramatic influences observed for the geometrical structure of $C_{30}B_{15}N_{15}$ heterofullerene after the ammonia adsorption and B atom relaxes outwardly from spherical in the NO2-attached $C_{48}B_{12}$heterofullerene. At the next step, we calculated the nuclear quadrupole coupling constant [4] of B nuclei using B3LYP/6-311G** level of theory.

Table. The C_Q (MHz) parameters of B-11 in the z direction for $C_{48}B_{12}$ heterofullerene and NO2-attached $C_{48}B_{12}$heterofullerene in the two adsorption sites

Nuclei	perfect (before adsorption)	Site I (after adsorption)	Site II (after adsorption)
B 49	0.483732	0.477541	0.477625
B 50	0.483696	0.466416	0.481121
B 51	0.483638	0.475668	0.460572
B 52	0.483732	0.104303	0.456026
B 53	0.483638	0.482790	0.476459
B 54	0.483696	0.477756	0.479211
B 55	0.498291	0.476497	0.483062
B 56	0.498149	0.504947	0.498741
B 57	0.498124	0.491770	0.492583
B 58	0.498291	0.490821	0.495348
B 59	0.498149	0.493130	0.496385
B 60	0.498124	0.498765	0.137902

Conclusions:

Probing the results shows a heterogeneous electrostatic environment in the perfect model. Electrostatic environment of B.55-60 are stronger than the other ^{11}B. The C_Q parameters of B nuclei at the interaction sites decrease significantly after ammonia adsorption. Therefore, the C_Q parameters of B.52 and B.60 nuclei are significantly decreased in the NO2-attached forms which can be attributed to the rehybridization effect. This is consistent with the structural deformation induced by the NO2 adsorption. The other B nuclei do not show significant changes after the NO2 adsorption.

Reference:

[1] H.W. Kroto, J.R. Heath, S.C. O'Brien, R.F. Curl, and R.E. Smalley, Nature, 318 (1985)162.

[2] Ş. Erkoç, J. Mol. Struct. (Theochem) 684 (2004) 117.

[3] M.J. Frisch et al., Gaussian 03, Revision E.01, Gaussian Inc., Wallingford CT, 2004.

[4] J. Seliger, Nuclear Quadrupole Resonance, Theory - Encyclopedia of Spectroscopy and Spectrometry, Academic Press, 1672-1680 (2000).

Ab initio study on the stability and reactivity of DNA base pairs

K. Azizi* and B. Azizi

Department of Chemistry, University of Kurdistan, Sanandaj, Iran

(Email: azizkhald822@yahoo.com)

Introduction

Although deoxyribonucleic acid (DNA) is a relatively stable chemical substance, it's damage is often caused by various factors. While the stability of DNA investigated by both experimental and theoretical studies [1-3], there is not information to show how true coding in DNA replication is guarantied energetically. In this study the stabilization energy and reactivity of different possible base pairs including Adenine (A), Thymine (T), Cytosine (C) and guanine (G) estimated and compared to each other. The results show that AT and GC base pairs are considerably stable than the other possible outcomes. It is known that hydroxyl radical is on of the highly reactive species which can interact with DNA and induces DNA double strand-breaks [4]. The previous investigations show that the hydroxyl radical can stably exist near the hydrogen bond between adenine and thymine, or between guanine and cytosine. In this study the effect of hydroxyl radical on the stabilization and reactivity of different possible base pairs were also investigated.

Computational details

In all cases, we neglect the backbone of DNA and focus on the base pairs. The structures were optimized with DFT method at the hybrid functional B3LYP (Becke's three-parameter functional employing the Lee, Yang, and Parr correlation functional) and the energies calculated by using medium-size basis set 6-311++G(d,p) level. No molecular symmetry constraint was applied; rather full optimization of all bond lengths and angles was carried out. Local charge (LC) calculated according to Mulliken population analysis (MPA).

Results and discussion

The optimized structure of different possible base pairs, AC, AG, AT, GC, GT and TC are shown in Fig. 1. Table 1 includes the stabilization energy of base pairs either in presence and

absence of OH radical for both OH-UP and OH-LOW configurations. In the case of TC base pair the most stable configuration is OH-MIDDLE. As shown in Table 1, the stabilization energy of AT and GC pair bases are considerably superior to the other base pair configurations. Therefore, the formation of base pairs rather than AT and GC vanishes from energy point of view. Furthermore, the GC base pair more stable than AT due to the further number of hydrogen bonding. As can be seen in Table 1, while in presence of OH radical, the stabilization energy of AT and GC base pairs are decreased considerably, some base pairs become more stable due to interaction with OH radical. Therefore, one may expected that the formation of a few less stable base pairs (i.e. AG) established by OH radical.

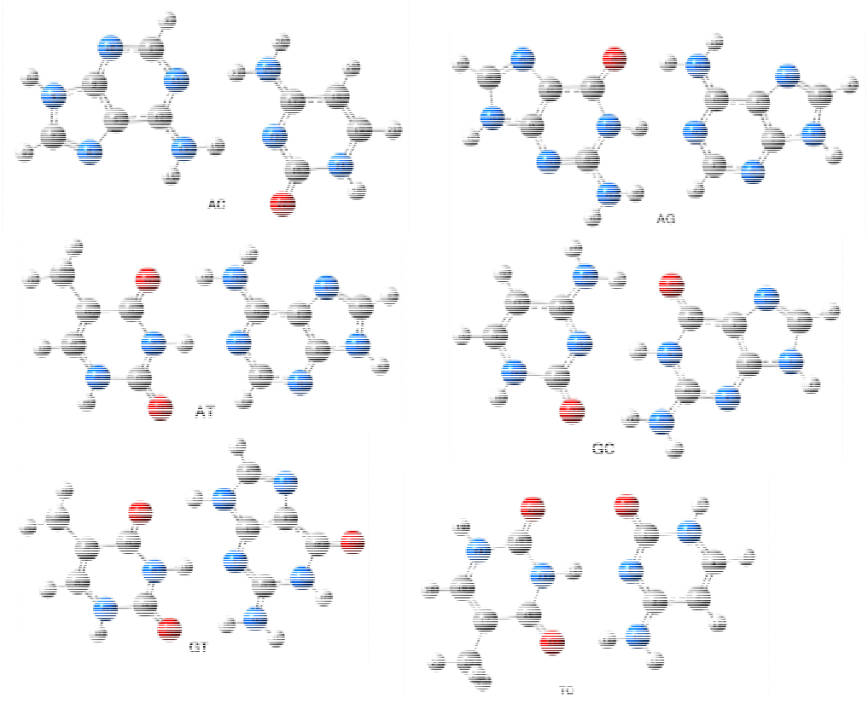

Fig. 1. The optimized structure of possible base pairs.

Table. 1. The stabilization and HOMO-LUMO gap energy of different possible base pairs in presence and absence of OH radical[#].

	Stabilization energy			HOMO-LUMO gap		
Base pair	Without OH	OH presence (UP)	OH presence (LOW)	Without OH	OH presence (UP)	OH presence (LOW)
AC	13.7	23.9	39.0	107.6	98.3	93.4
AG	14.1	-124.6	42.3	112.4	119.0	109.0
AT	239.9	108.0	107.3	109.2	110.5	110.5
GC	256.7	126.9	286.4	86.8	96.3	93.9
GT	16.8	22.3	*	90.7	87.2	*
TC	10.4	*	20.2**	121.2	*	116.6**

[#] Energy values are in $kcalmol^{-1}$. * Non Optimized structure. ** OH localized at middle point.

In order to estimate the effect of OH radical on reactivity of different base pairs, the HOMO-LUMO energy gaps were also calculated. As shown in Table 1, the reactivity of base pairs can be changed due to interaction with OH radical. However, the variation of HOMO-LUMO gap energy by OH radical does not considerable and one cannot expect base pairs undergo electrophilic attack in presence OH radical.

References

[1] Roger M. Wartell, Seyed H. Hosseini and Charles P.Moran Jr, *Nucleic Acids Research*, 18 (9) (**1990**) 2699.

[2] Kenneth. J. Breslauer, R. Fraks, H. Blocker and Luis A. Marky. *Proc. Natl. Acad. Sci. USA*
83 (**1986**) 3746.

[3] Mei. Qin et. all., *Indian Journal of Chemistry*, 49 (**2010**) 1332.

[4] Martin F. , Burrow P. D., Cloutier P., Hunting D. and Sanche L., *Phys.Rev.Lett.*, 93 (**2004**) 68101.

A DFT Study on the Interaction Between Hydroxyl and Phenyl radicals with DNA Base Pairs

K. Azizi* and M. Zarei

Department of Chemistry, University of Kurdistan, Sanandaj, Iran

(Email: azizkhald822@yahoo.com)

Introduction

Deoxyribonucleic acid, DNA, is very important molecule in biological systems and is comparatively stable chemical substance. DNA made by four nucleobases adenine (A), thymine (T) or, guanine (G), and cytosine (C) which are used by nature for storing the information of life. It is well known that the coupling of base pairs can affected by free radical intermediates which are produced in living systems under normal conditions [1]. On the other hand chemical species such as phenyl and phenoxy radicals can be generated by ionizing radiation, which can damage macromolecules, including DNA, proteins and lipids [2]. In the case of DNA, any change in structure can be treated as a mutation and some phenolic compounds have been shown to be cytotoxic and/or genotoxic in a variety of biological systems. Although, the phenoxy and phenyl radicals are very common materials in the environment, the role of these species in DNA damage process has not been investigated.

Computational details

The structures of isolated species and molecular complexes were optimized with the DFT/B3LYP/6-31g(d) level of ab initio calculation. In all cases, we neglect the backbone of DNA and focus on the base pairs. No molecular symmetry constraint was applied; rather full optimization of all bond lengths and angles was carried out. The energies and charges estimated by using medium-size basis set 6-311++G(d, p) and B3PW91 level of calculation. For any base pair two different initial positions for radicals, from upward and beneath of base pairs have been taken. The stabilization energy is calculated as the difference between the energy of base pair-radical complex with respect to the energy of constraint species at infinite separation.

Results and discussion

The optimized structure of base pair-radical complexes, AT-OH-Up, AT-Ph-Up, GC-OH-Up and GC-Ph-Up as samples are shown in Fig. 1. Table 1 includes the stabilization energy, SE, HOMO-LUMO energy gap,H-L gap, hydrogen bond lengths of base pairs either in presence and absence of two radicals.

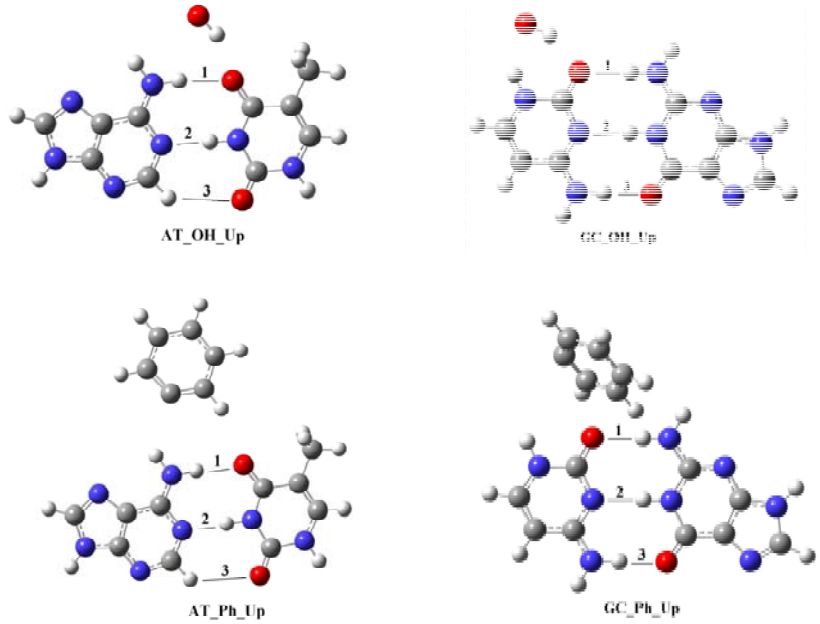

Figure 1.The optimized structures of some base pair-radical complexes

As can be see from table 1, the interaction of hydroxyl and phenyl radicals with base pairs can reduce stabilization energy. The reduction in stabilization energy correspond with increasing in hydrogen bond lengths and distance between base pairs.

Table 1. The structural and electronic properties of base pair-radical complexes.

Base pair	SE*	H-L gap**	B1#	B 2	B3
AT	239.9	109.2	2.95	2.88	3.67
AT_OH_Low	107.3	112.5	2.94	2.89	3.76
AT_OH_Up	108.0	110.5	3.02	2.87	3.62
GC	256.7	86.8	2.93	2.95	2.82
GC_OH_Low	286.4	93.9	2.91	2.96	2.84
GC_OH_Up	126.9	96.3	2.96	2.97	2.81
AT_Ph_Low	96.1	117.3	2.94	2.90	3.74
AT_Ph_Up	96.8	115.1	2.96	2.88	3.66
GC_Ph_Low	298.6	90.6	2.92	2.95	2.82
GC_Ph_Up	112.1	97.3	2.94	2.95	2.82

* Stabilization energy. ** The HOMO-LUMO energy gap. # Hydrogen bond length

In addition, the effect of both hydroxyl and Phenyl radicals on stabilization energy of AT base pair is more than that of GC. Furthermore, the effect of hydroxyl radical on stabilization energy of base pairs is more than phenyl radical, comparatively. There is a considerable stabilization energy for GC base pair when radicals are placed in low position inside base pairs. The effect of radicals on reactivity of AT and GC base pairs, can be evaluated by comparison HOMO-LUMO energy gaps of base pairs. As shown in Table 1, both radicals can change the reactivity of base pairs, although they show contrast effect. While both radicals decrease the reactivity of AT, the reactivity of GC has been increased due to interaction with hydroxyl and phenyl radicals.

References

[1] Clemens von Sonntag, Free-radical-induced DNA damage and its repair: a chemical perspective, Springer, 2006.

[2] Yunbo Li and Michael A. Trush, Cancer Research (Suppl.) 54 (1994) 1895.

A theoretical investigation on the adsorption of H_2, N_2 , CO and CH_4 gases on single wall silicon nanotubes

K. Azizi* and A. M. Rezvani
Department of Chemistry, University of Kurdistan, Sanandaj, Iran
(Email:azizkhald822@yahoo.com)

Keywords: Density Functional Theory; Electronic structure; Silicon Nanotubes; Gas adsorption.

Introduction:

Gas adsorption on inorganic nanotubes can be considered as a great issue for both essential research and applied application of this kind of nanotubes. The adsorptive characteristics of SWNTs in the gas phase caused their use as gas sensors of pollutant gases, storage of fuels, and removal of hazardous pollutants from gas streams [1]. With the successful synthesis of silicon nanotubes (SiNTs), [2] a few attentions has been paid to their application in hydrogen storage studies [3,4]. Compared to carbon, silicon has more electrons in the outer shells, therefore, SiNT may exhibit a stronger van der Waals attraction to nonpolar gases than CNTs. However, the interaction between SiNTs and other molecular gases than H_2 has not been investigated. Therefore, in this study the adsorption of carbon monoxide, oxygen, nitrogen and methane molecules with both inside and outside of armchair (5,5) SiNT, were investigated by using density functional theory method.

Computational Methods:

All structures were optimized with DFT method at the hybrid functional B3LYP and the medium-size basis set 6-31g(d) level of calculation. Despite previous works [3,4] no molecular symmetry constraint or nanotube size reduction was applied, rather full optimization of all bond lengths and angles was carried out. Adsorption energies, E_{ad}, were obtained as the difference between the energy of the SiNT-gas complex and the combined energies of the isolated SiNT and gas molecule. All calculations on the isolated species and molecular complexes were performed within GAUSSIAN 03 program package.

Results and Discussion:

Typical optimized structures of different gases adsorbed on armchair (5,5) SiNT are shown in Figure 1and Table 1 includes the energies of adsorption of different gases on both inner and outer surfaces of (5, 5) SiNT.

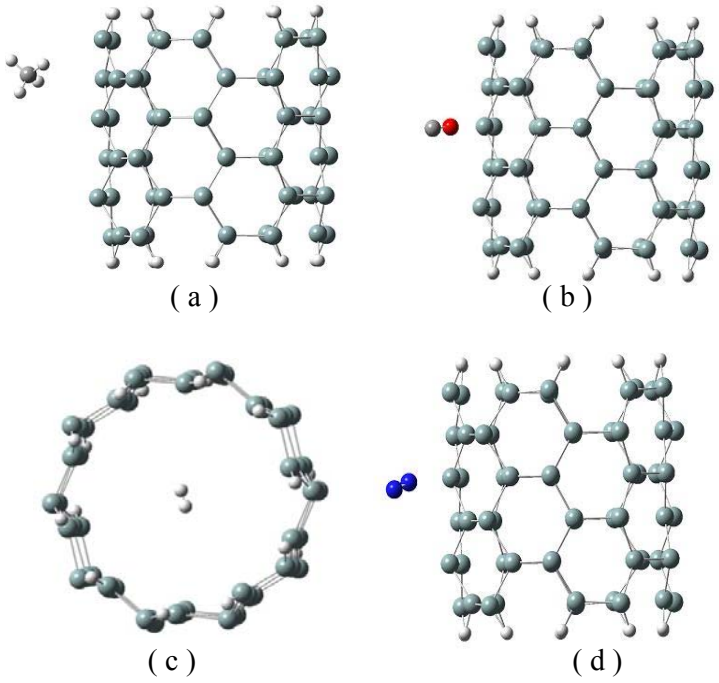

Figure 1. The optimized structures of adsorbed gases on armchair(5,5) SiNT, (a) CH_4, (b) CO, (c) H_2 and (d) N_2.

As can be seen from Table 1, the maximum values of E_{ad} were estimated for adsorption of CO and H_2 gases on the outer and inner surface of nanotube, respectively. Despite previous findings [3,4], the energy of adsorption of H_2 on the exterior surface of nanotube is negligible. The same behavior is shown by CH_4 and N_2 molecules. It is demonstrated that CO and N_2 molecules have similar behavior when they adsorbed on single wall carbon nanotubes. The considerable difference between energies of adsorption of N_2 and CO molecules may be attributed to the high polirizable electronic shells of nanotube. Table 1 is shown that for all gases, the charge transfer between gas and nanotube is negligible. Therefore, a considerable variation of electronic properties of nanotube does not expected due to gas adsorption proces.

Table 1: The electronic properties of gas adsorption inside and outside of zigzag (5,5) Si nanotube.

	CO (in)	CO (out)	N_2 (in)	N_2 (out)	H_2 (in)	H_2 (out)	CH_4 (in)	CH_4 (out)
E_{ad}(kcal.mol^{-1})	0.42	1799.49	3.80	3.04	1767.15	0.03	0.37	0.01
CT*(*e*)	0.007	0.002	0.001	0.000	0.00	0.000	-0.003	0.00

* Charge (NPA) transfer to nanotube.

References:

[1] R. Q. Long, R.T. Yang, J. Am. Chem. Soc. 123 (**2001**) 2058.

[2] J. Sha, J. J. Niu, X.Y. Ma, J. Xu, X. B. Zhang, Q. Yang and D. R. Yang,D. R. Adv. Mater. 14(**2002)**1219.

[3] G. P. Lithoxoos, J. Samios and Y. Carissan., J. Phys. Chem. C, 112 (**2008**)16725.

[4] L. Jianhui, C. Daojian, Dapeng Cao and W. Wenchuan., J. Phys. Chem. C, 112(**2008)** 5598.

Calculation the relationship between silicate species geometry and their ^{29}Si NMR chemical shifts

Seyed Naser Azizi[a] ,Salma Ehsani tilami*[a]
[a]Department of Chemistry, Mazandaran University, Babolsar, Iran
Email: salmaehsani@yahoo.com

Introduction:

Crystalline tectosilicates, such as zeolites, are among some of the most commercially important materials. Along with their traditional uses for catalysis, ion exchange, and separations, they have potential to synthesize 'designer' materials for specific applications [1]. Despite this effort, there have only been a few mechanisms proposed for the formation of such complex solids [2, 3]. Identification of the silicate species present in solution plays a key role and 29Si NMR spectroscopy proved to be a powerful technique for this purpose [3].However, extracting information about individual events using only experimental data is difficult, the chemistry of silica species has also been studied extensively using theoretical techniques [5]. In this study relation between chemical shift of twenty silicate species and their geometry was calculated and the equation between them was achieved that have a good agreement with experimental data.

Method:

Silicates optimization was performed by hyperchem and with semi empirical method and compared with their chemical shifts that calculated with standard Gaussian 03 program by RHF methods.

Results and discussion:

Figure (1) shows typical results for four silicate species in silicate solutions and table 1 gives calculated geometrical parameters. Correlation between ^{29}Si NMR chemical shifts of Q^4 situation and these geometrical parameters were explained by several schemes. Results from these schemes indicated that all of the relations between Y (chemical shift) and these geometrical parameters are linear. The correlation for X1, X2, X3 have linear negative slope,

while for X3 and X4 the positive slope has been found. These correlations could be explained with the following equation:

$$-\delta_{Q0}(Q^n) = a_1(4-n)R_{(Si-O)t} + a_2(4-n)R_{O-H} + a_3 nR_{(Si-O)b} + a_4 n<psi-o-si> + a_5(4-n)<psi-O-H> + B$$

Computation of a1-a5 and B constant was carried by multivariate linear regression method.

After the calculation final equation could be written by the following equation:

$$\delta_{TMS}(Q^n) = \mathbf{0.0007}\,(4-n)R_{(Si-O)t} - \mathbf{63.0754}\,(4-n)R_{O-H} - \mathbf{23.9662}\,nR_{(Si-O)b} - \mathbf{60.1886}\,n<psi-O-si> + \mathbf{0.0002}\,(4-n)<psi-O-H> + \mathbf{166.1191}$$

tables 1: gives typical calculated geometrical parameter

$(4-n)<psi-O-H>=X_5$	$n<psi-O-si>=X_4$	$nR_{(Si-O)b}=X_3$	$(4-n)R_{O-H}=X_2$	$(4-n)R_{(Si-O)t}=X_1$	Q^n	type of specie
0/950	0/500	1/690	2/846	0/189	Q^1	1
0/625	0/896	3/433	1/899	3/455	Q^2	2
0/623	0/894	3/433	1/898	3/456	Q^2	3
0/946	0/492	1/690	2/847	0/189	Q^1	3
0/303	1/383	5/132	0/950	1/725	Q^3	3

Figure (1) shows typical four silicate species in silicate solution

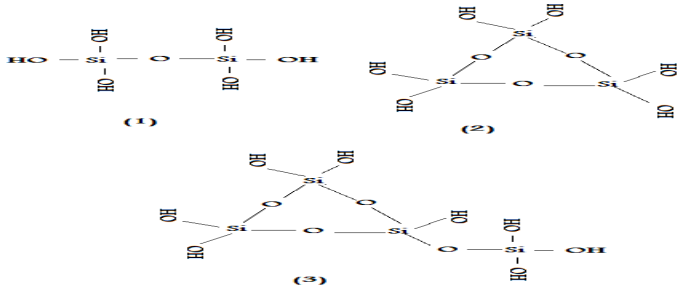

Conclusion:

In this study, correlation between angles and distance of atoms in silicates species were investigated. Chemical shift of Si atoms in silicates species were estimated by their geometrical parameters for twenty silicates species by multivariate linear regression. These results have a good agreement with experimental data.

Rrefrence:

[1] Davis, M. E. Ordered porous materials for emerging applications.*Nature* **2002**, *417* (6891), 813–821.

[2] Cundy, C. S.; Cox, P. A. The hydrothermal synthesis of zeolites:Precursors, intermediates and reaction mechanism. *Microporous Mesoporous Mater.* **2005**, *82, 1*–78.

[3] Cundy, C. S.; Cox, P. A. The hydrothermal synthesis of zeolites: History and development from the earliest days to the present time. *Chem. Re*V. **2003**, *103,* 663–701.

[5]. S.N.Azizi, A. Rostami and A. Godarzian, J. Phys. Soc. Jpn, **2005**, 74, 1609-1620.

DFT calculations of the anomeric effect of 5-(1,3-dithian-2-yl)-1H-tetrazol

Mahboobeh Azizi[a],Alireza Najafi Chermahini [a], Abbas Teimouri [b]

Assistant prof. of Organic Chemistry

[a] Department of Chemistry,Faculty of Science, Yasouj Uiniversity, Yasouj, Iran

(Email:mazizi@mail.yu.ac.ir or ma_azizi60@yahoo.com)

[b] Department of Chemistry, Payame Noor University, Isfahan, Iran

Introduction

The anomeric effect refers to the tendency of an electronegative substituent at C-1 of pyranosides, such as halogen atoms, to assume the axial rather than the equatorial conformation, contrary to the expectation from ordinary steric considerations. Since its discovery in 1955 [1] the anomeric effect has been a subject of numerous studies, and the origin of the effect seems now to be settled on a firm theoretical basis The phenomenon is not limited to carbohydrate chemistry but extends to stereochemistry of six-membered heterocyclic compounds such as 2-substituted thians (dithians) and 1,3-dithians. This effect extends also to acyclic molecules such as R–X–CH2– Z (X = O, S; Z = OCH3, halogen, etc.) [2,3]. This is called the ‘generalized anomeric effect. In the present study, the anomeric behavior of 5-(1,3-dithian-2-yl)-1H-tetrazol compound **A** has been investigated in the gas phase and solution.

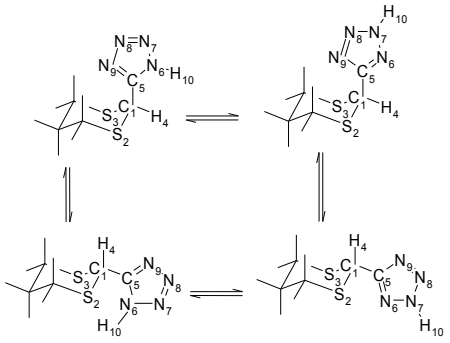

Scheme 1: the structure and numbering of isomers of titled compound

Computational method

All the structures studied in this work were fully optimized, without symmetry restrictions using density fanctional theory at B3LYP/6-31++G(d,p), and B3LYP /6-311++G(d,p) levels of theory using the GAUSSIAN 98 program package[4]. Since the main purpose of the present work was to estimate the energy difference between the axial and equatorial conformations of compound **A**, therefore, the energy minimization of compounds(scheme1) was carried out only for the axial and equatorial position of the tetrazol groups on a chair conformation of the heterocyclicrings.

Results and discussion

The structure and numbering of the examined molecules showed in Scheme1. The results obtained from theoretical calculations will be discussed in the light of the effect of the tetrazole ring on the geometry of the dithian ring, of the relative stability of axial/equatorial conformers and of the effects of hyperconjugative interactions derived from the DFT analysis on molecular properties. In the Table 1 results of relative stability of four isomers of compound **A** are presented. Based on these results it was found that the most stable isomer is **2Hax**. The stability of isomer **2Hax** over, **2Heq**, **1Hax**, **1Heq** was found 0.81, 2.86, 4.34, respectively, calculated by B3LYP/6-31++G(d,p) method. Table 2 shows the geometrical parameters of four isomers that investigated in the present study. It is expected that the anomeric effect influence the geometrical properties, i.e. bond lengths, and bond angles. The calculated C_1–S_2 bond length in the equatorial conformation of **1Heq** (1.8342 A °) is shorter than the axial (by 0.0228 A°) at the DFT B3LYP/6-311++G(d,p) level of theory. On the other hand, the calculated C_1-C_5 bond length in the axial conformation of **1Hax** (1.5030 A °) is greater than the equatorial by 0.0105 A°.

Table 1: relative stabilities of four isomers of titled compound (kcal/mol)

Basis set	1Hax	1Heq	2Hax	2Heq
6-31 ++G(d,p)	2.86	4.034	0	0.81
6-311 ++G(d,p)	3.13	4.37	0	0.96

Table2: bond lengths (Å) and bond angles (Degree) for the axial and equatorial isomers, calculated at B3LYP/6-311 ++G(d,p) basis function

	1Hax	1Heq	2Hax	2Heq
Bond lengths				
C_1-S_2	1.8507	1.8342	1.84314	1.8439
C_1-S_3	1.8279	1.8342	1.84316	1.8439
C_1-H_4	1.0925	1.0944	1.09272	1.0909
C_1-C_5	1.5030	1.4924	1.49563	1.4883
C_5-N_6	1.3518	1.3510	1.33396	1.3286
N_6-H_{10}	1.0099	1.0100	-	-
N_6-N_7	1.3481	1.3497	1.32988	1.3242
N_7-N_8	1.2875	1.2868	1.32578	1.3259
N_8-N_9	1.3619	1.3615	1.30885	1.3042
C_5-N_9	1.3168	1.3148	1.36393	1.3610
Bond Angle				
C_1-S_2-S_3	113.9524	114.4089	114.2936	113.8600
C_1-C_5-N_9	128.5998	127.5174	122.0507	122.6598
C_1-C_5-N_6	123.9865	124.7255	126.1732	125.3036
C_5-N_6-H_{10}	129.6262	130.1887	-	-
C_5-N_6-N_9	107.4080	107.7408	111.7761	112.0366
S_3-C_1-H_4	104.1076	106.7899	103.9713	108.0078
S_2-C_1-H_4	103.7265	107.7403	103.9718	108.0080

Refrences

[1] Edward, J. T. Chem. Ind. (London) 1955, 1102–1104.

[2] Lemieux, R. U. Pure Appl. Chem. 1971, 25, 527–548.

[3] Juaristi, E.; Cuevas, G. Tetrahedron 1992, 48, 5019–5087.

[4] M.J. Frisch, et all,. GAUSSIAN 98 (Revision A.3) Gaussian, Inc. Pittsburgh, PA, USA, 1998.

Correlation between structural propeties and bilogical activity of acetylcholinesterase in the presence of huperine and piperazine derivatives inhibitors

Hooman Asgarian*[a], Davood Ajloo[b]

[a]-Deparment of Chemistry, Islamic Azad University Shahrood Brabch, Tehran Street, Shahrood, Iran

[b]-School of Chemistry, Damghan University, Damghan, Iran

hooman_shimi_1382@yahoo.com, ajloo@du.ac.ir, ajloo2000@yahoo.com

One possible approach to treat Alzheimer's disease (AD) is to restore acetylcholine levels by inhibiting acetylcholinesterase (AChE) with reversible inhibitors [1]. Clinical trials have shown that AChE inhibitors such as physostigmine, donepezil, rivastigime, and galantamine effectively improve memory in some patients. Beside the synthesis of the AChE inhibitors, QSAR studies were done on the variety of inhibitors. These techniques are very powerful tools for prediction of enzyme activity. It is also applicable in all area of science such as chemistry and physics. So we used QSAR methods for prediction of $\log IC_{50}$. In this work, QSAR of some indanone hybrids [2] and benzophenone [3] derivatives was studied using with large number of descriptors. The structure of inhibitors was drown and optimized in Hyperchem. Then, some of descriptors calculated by Hyperchem, Gaussian and Dragon softwares. The multiple linear regression was performed by SPSS. Different equations were obtained between log IC50 and descriptors. The free energy of interaction (docking energy) was estimated by Autodock.

The following equation shows the correlation between $\log IC_{50}$ and of best selected descriptors. It has relatively good correlation.

The descriptors were classified by PCA. Correlation between $\log IC_{50}$ and principal components is as follow:

$$\log IC_{50} = 0.234 - 0.471\ Size - 0.149\ Aromaticity - 0.104\ Hydrophobicity - 0.065\ Shape$$

Table 1 listed the descriptors and their definitions Fig. 1 shows correlation between predicted and experimental $\log IC_{50}$

$$\log IC50 = -47.814 - 0.007(Mass) - 1.669(GGI4)$$
$$2.270(PJI3) + 12.928(BEHm2) + 0.43(RDF100u) + 4.937(HATS5u)$$

R= 0.889 S=0.376….. F= 21.408

Table 1 list of descriptors and their definition

Descriptor	definition	Class
MW	Molecular weight	Constitutional
GGI4	topological charge index of order 4	Galvez topol. charge indices
PJI3	3D Petijean shape index	geometrical descriptors
BEHm2	highest eigenvalue n. 2 of Burden matrix / weighted by atomic masses	BCUT descriptors
RDF100u	Radial Distribution Function - 10.0 / unweighted	RDF descriptors
HATS5u	leverage-weighted autocorrelation of lag 5 / unweighted	GETAWAY descriptors

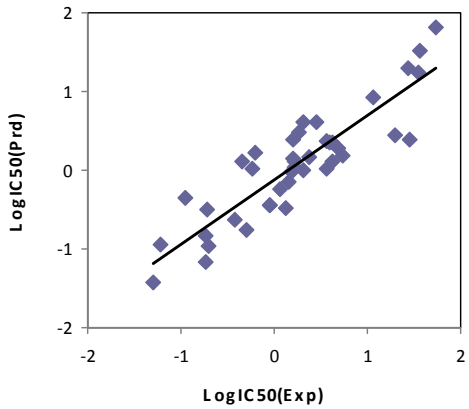

Fig. 1 Correlation between predicted and experimental $\log IC_{50}$

Key words: QSAR, Docking, PCA, Acetylcholinesterase, Huperines and piperazines.

References:

[1] Levy, R. Lancet 1978, 2, 944.

[2] Rizzo, S. Bartolini, M., Ceccarini, L. Piazzi, L. Gobbi, S. Cavalli, A. Recanatini M a, Andrisano, V. Rampa, A. Bioorganic & Medicinal Chemistry 2010, 18, 1749.

[3] Belluti, F. Piazzi, L, Bisi, A. Gobbi, S. Bartolini, M. Cavalli, A, Valenti, P. Rampa, A. European Journal of Medicinal Chemistry 2009, 44, 1341.

Temperature Dependency of Water Permeation through Carbon Nanotubes

A. Alizadeh, G. A. Parsafar*
Department of Chemistry, Sharif University of Technology, Tehran, Iran
alializadeh@mehr.sharif.edu

Key Word: Diffusion, Membrane Channels, Molecular Dynamic Simulation, Carbon Nanotube.

Introduction:

It is of interest to explore transfer of fluid through nanopores because of widespread applications for such systems [1]. While the mechanism of water permeation through channels is very complex, however, investigations such as effect of charge distributions as well as temperature on water permeation can shed light on the determinants of water and proton conduction in membrane water channels. We have investigated the effect of temperature on water permeation through some channels with different charge configurations, in the range of 280 K - 370 K.

Methods:

We consider a system composed of four ordered parallel structure of Carbon Nanotubes (CNTs)which are of (6,6) armchair type. At the initial time, the CNTs are empty and the water molecules get into them after a 200 ps interval for minimization and equilibration. All molecular dynamic calculations have been carried out using NAMD code [2] with CHARMM force field.

Results and discussion:

In order to investigate the mechanism of water permeation through modified CNTs, we applied charge distributions on CNTs wall which are in accordance with the proposed biological as well as channel membranes [3]. We have carried out two simulations for each

system, one without induced pressure difference to find out the diffusion permeation (p_d) and the other with induced pressure difference (p_f) to obtain the osmotic permeation.

We build tree kind of channels, one prototype CNT – denotes as model 0- and two modified ones. One is the modified CNTs with three positive and three negative charges on two sides of CNTs wall and positives on one side and negatives on the other side along *z*-direction, denoted as model 1. The other one, model 2, consists of modified CNTs with three charges on each side of CNT wall with two positive charges at two entrances and one negative charge between them with the opposite charge distribution on the other side.

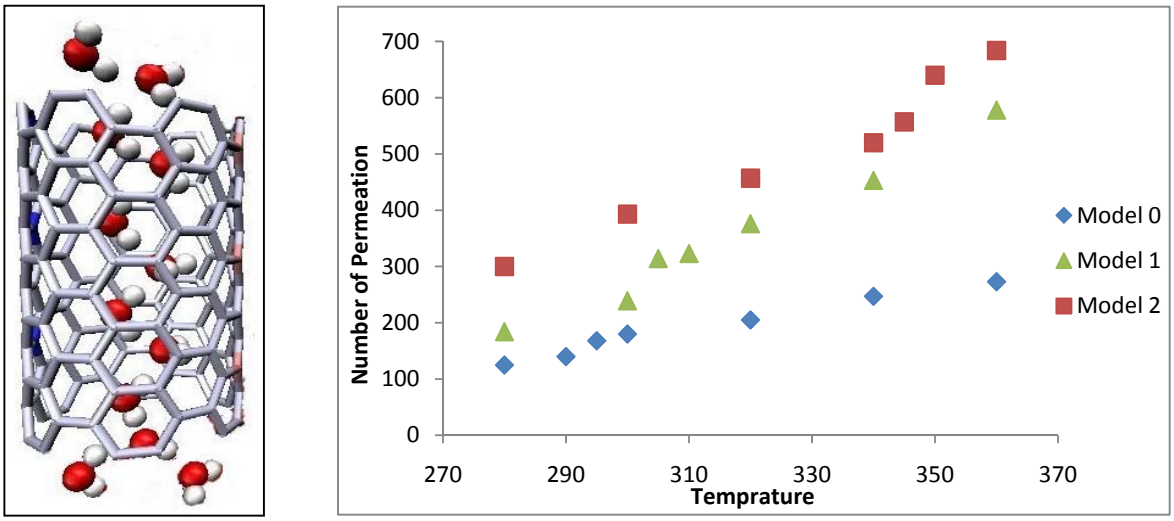

Figure 1: left: The side view of a channels; **Right:** the number of permeation event per channel for three model channels.

As one sees in figure 1, the number of permeation increases with temperature which is consistent with the Arrhenius relation. There is also, an abrupt jump in the number of permeation. But, as it can be seen, the jump temperature (*Tj*) which belongs to each system is different. As you see in figure1, The abrupt change in model 2, which is higher in number of permeation, has the highest *Tj*and The model 1, which has the less number of permeations, has the lowest *Tj*. It means that for each system, the more number of permeations,leads to a higher*Tj*.

Such phenomena can be explained on the basis of the Arrhenius relation and the energy profile in the channel. This result shows that the Tj is porportional to the decrease or increase in hopping energy barrier for such systems.

Conclusion:

Investigation of the dynamic properties though the nanopores could help finding the better applications as well as increasing the efficiency of such processes. The single file permeation through the nanochannels will be increased with temperature and there will be a jump in the permeation. This temperature jump is related to the number of permeations and for a higher temperature, the jumping temperature will be higher.

References:

[1] Turgut Bas-tug and SerdarKuyucak, **2006**,*Chemical Physics Letters,* 424, 82.

[2] L. Kale et al., **1999**,*J. Comp. Phys*., 151, 283.

[3] Mcree, D.E., et al., **1995**,*AngewandteChemie-International Edition*, 34, 93.

A systematic NMR and NQR investigation on the BN- substituted fullerenes - isoelectronic equivalents of C60 based on density functional theory

M. Anafcheh, R. Ghafouri, N. L. Hadipour*
Hadipour@modares.ac.ir
Department of Chemistry, Tarbiat Modares University, Tehran, Iran

Keywords: Heterofullerene, Schlegel diagrams, NMR, NQR, DFT

Introduction:

Heterofullerenes which have one or more carbon atoms substituted by other elements such as boron or nitrogen are expected to be used as semiconductors and building materials for nanometer electronics due to their potential novel properties,[1–3] such as superconductivity, hardness, photoinduced electron transfer and nonlinear optics. In 1991, Smalley and co-workers produced the first substituted fullerenes C60-2*x*B*x*(*x* =1–6) [4]. Later in the same year Rao et al [5] reported the preparation of a number of N-substituted fullerenes. Interestingly, Clusters of boron (B*x*) and nitrogen (N*x*) have also been reported by different groups. The isoelectron relationship between boron–nitrogen and dicarbon molecular fragment is well documented and is manifested in a variety of ways. Therefore it is reasonable to suppose that BN containing analogues of C60 will be stable. In this Letter, we report the results of a detailed density functional theoretical study (DFT) of the NMR and NQR parameters of a few BN-substituted C60 fullerenes.

Computational aspect:

All of the calculations reported in this Letter were carried out using the Gaussian suite of programs.. Geometries of all systems were fully optimized using B3LYP / 6-31+G* level of theory. Chemical shielding isotropy, σiso, is obtained by σiso =(σ_{11} + σ_{22} + σ_{33})/ 3. The principal EFG tensor eigenvalues, q_{zz}, q_{yy}, and q_{xx}, have the following relation: $|q_{zz}| > |q_{yy}| > |q_{xx}|$. The nuclear quadrupole coupling constant, C_Q, is obtained by $C_Q = e^2 q_{zz} Q/h$ (MHz). Another important parameter which refers to the deviation of charge distribution from cylindrical symmetry is the asymmetry parameter, $\eta_Q = |(qxx - qyy)/qzz|$. However, to the best

of our knowledge, there is no experimental NMR and NQR study on these clusters in the literature.

Result and discussion:

For the sake of clarity, the substitution patterns considered in the present study are illustrated by Schlegel diagrams, as shown in Figure 1. For example, the substitution of carbon atoms of one of the hexagon-hexagon bonds in the C60 fullerene by boron and nitrogen atoms will lead to the formation of C58BN with *Cs* symmetry. Substitution of carbon atoms continues in the same hexagonal ring until it is saturated with boron and nitrogen atoms. Complete BN substitution of one of the hexagonal rings will make a *C*3-symmetric heterofullerene (C*54*B*3*N*3*). Further BN substitutions are carried out by keeping the *C*3 symmetry in the system. Thus, three BN units are added in each step, and this substitution spreads in all directions of the previously substituted hexagonal ring. The carbon atoms connecting the pentagons that are in-plane with the *C*3 axis are left unsubstituted in each step. This eliminates the possibility of unstable BCN balls having homonuclear B-B and N-N bonds. This pattern of substitution continues until the formation of C*12* B*24*N*24* with *Ci* symmetry.

In a majority of cases, chemical shielding of carbon atoms adjacent to nitrogen because of the high electronegativity of nitrogen is very deshielded but those of boron atoms not change. However this affects show the regular pattern when at least one hexagonal ring is saturated with boron and nitrogen. It is worth pointing out that there is a good correlation between the dipole moment and component of EFG and CS tensors in most of the cases.

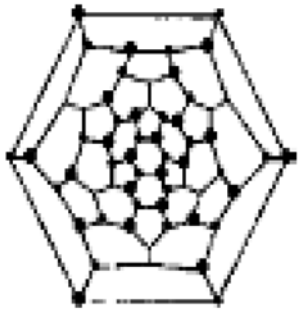

Fig1. Schlegel diagrams of BN- substituted fullerenes

Conclusion:

NMR and NQR parameters based on DFT calculations for a series of BN-substituted fullerenes suggest that properties of fullerenes can be fine-tuned by B, N substitution in the cage.

References:

[1] S. Nakano, M. Akaishi, T. Sasaki and S. Yamaoka, Chem. Mater., 1994, 6, 2246.

[2] H. W. Kroto, Science, 1988, 242, 1139.

[3] B. Yao, L. Liu and W. H. Su, J. Mater. Res., 1998, 13, 1753.

[4] T. Guo, C. Jin, R.E. Smalley, J. Chem. Phys. 95 (1991) 4948.

[5] T. Pradeep,V. Vijayakrishnan, A.K. Santra, C.N.R. Rao, J. Phys. Chem. 95 (1991) 10564.

[6] M.L. Jan, E-Y. Jamel, P.F. Jean, Chem. Phys. Lett 248 (1996) 95.

[7] I. Silaghi-Dumitrescu, F. Lara-Ochoa, I. Haiduc, J. Molec. Struc. (Theochem) 370 (1996)

Antioxidant activity and antioxidant mechanism of vitamin P in solution

Mina Ghiasi*
Department of Chemistry, Faculty of Science, Alzahra University, P.O.Box: 19835-389, Vanak, Tehran, Iran.
ghiasi@alzahra.ac.ir
Tel: +982188044051-9(2608), Fax: +982188041344

Abstract:

In this paper, we used a quantum mechanical approach to shed light on the antioxidant mechanism to scavenging hydroxyl radical ($^{\bullet}OH$) and superoxide radical ($O_2^{-\bullet}$) by vitamin p (rutin) in solution phase.

Keywords: Rutin, Antioxidant, DFT calculation, BDE, Spin density.

Introduction

In resent years, flavonoids have gained a tremendous interest as possible therapeutics against a wide variety of diseases, most of which involve radical damage. Until now, the mechanism of action and structural requirements has not been fully understood [1, 2]. In this study, DFT method appears to be the most relevant and appropriate for the description of phenolic compounds such as rutin, Figure 1. The $B_3LYP/6\text{-}311+G^{**}$ method appears as a good compromise between the quality of the results and the computational cost. The molecular properties which we used to investigate a possible antioxidant mechanism of rutin, was the spin density distribution of the radical formed after subtraction of a hydrogen atom.

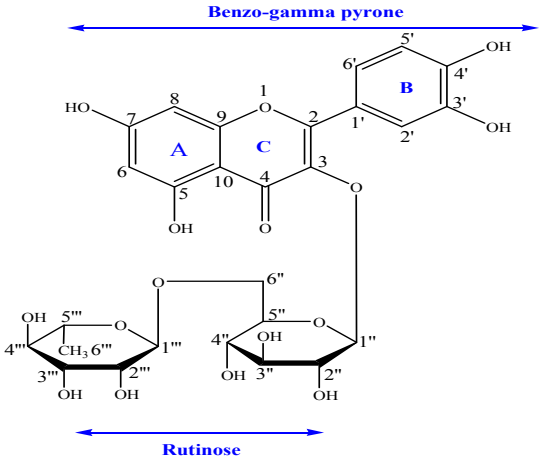

Figure1. Structure of vitamin p (rutin).

Computational details

Ab initio calculations were carried out with the Gaussian program series 98 using B_3LYP /6-311+G** level. Full optimizations were performed without any symmetry constrains. QST2 method was used to search for transition state. Transition state geometry was double checked by using IRC and FREQ calculations.

Results and discussion

Theoretical results confirm the important role of the B-ring and to shed light on the role of the 3'-OH and 4'-OH groups in the antioxidant properties of rutin. The calculated results show the following bond dissociation enthalpy (BDE) sequence for the OH groups: 3'-OH < 4'-OH< 7-OH<5-OH as expected. The reactivity of these two sites, 3'-OH and 4'-OH, of these results suggest that rutin has a potency to donate electron to reactive free radicals, converting them in to more stable non-reactive species and terminating the free radical chain reaction. Addition of hydroxyl radical to the rutin molecule lead to a stable intermediate which is converted directly to the stable products by releasing 10.8 Kcal/mol energy, Figure 2. In the nucleophilic attack of superoxide radical to the rutin an intermediate is initially formed and then the expected product is generated from second intermediate via a transition stat. The barrier energy for this reaction is about 6.5 Kcal/mol.

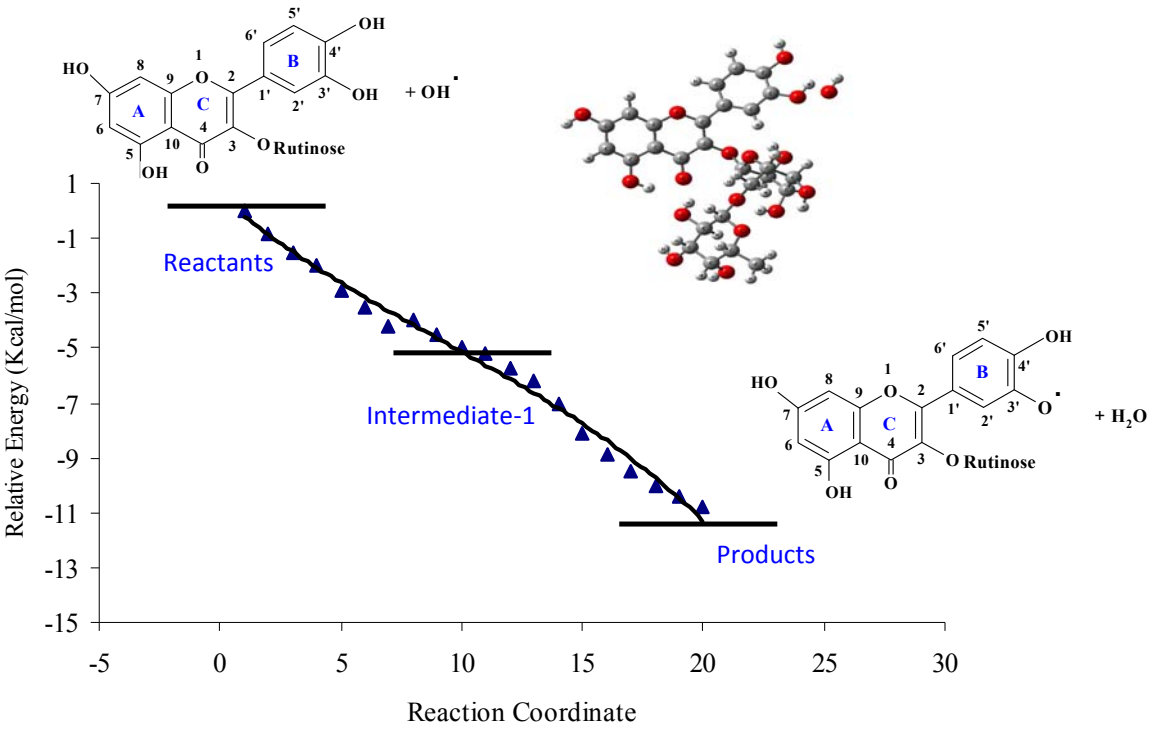

Figure 2. Energy diagram for the reaction of hydroxyl radical attack to the rutin.

References:

[1] P. M. Aron, J. A. Kennedy, Mol. Nutr. Food Res. 52 (2008) 79.

[2] B. Halliwell, Cardiovasc. Res. 73 (2007) 341.

DFT Study and NBO Analysis of Vanishing Nucleophilic Character for *N*-alkylation in Some Isatin Derivatives

F. Gheisi, A-R. Nekoei *, M.N. Soltani Rad

Department of Chemistry, Shiraz University of Technology, Shiraz, 71555-313, Iran

Keyword:NBO analysis, Isatin, *N*-alkylation, Conformational study, Nucleophilic power

Introduction

Isatin and its derivatives have been attracted considerable attention because they have various biological activities. The isatin exhibits two chemically dissimilar carbonyl groups [1], a lactam-carbonyl and a keto-carbonyl, as shown by position 2 and 3, respectively, in Fig. 1. A crystallographic data for isatin reveals that it is almost planar, with a bond length between the two carbonyls of 1.55 Å [2]. This large value was attributed to lone pair electron repulsion between the two oxygen atoms [2]. As shown in Fig. 1, isatin mainly reacts at three sites, including electrophilic aromatic substitution at C5, *N*-alkylation at *N*1, and carbonyl reaction at C3 [3].

The present study is focused on synthetic strategies of an important derivative of isatin in medicinal chemistry. Two synthetic procedures are shown in scheme (1).

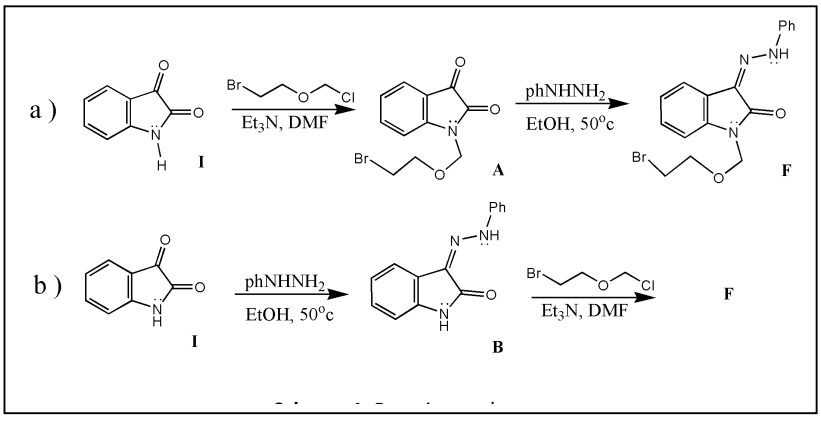

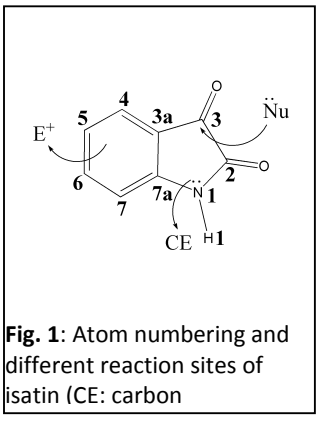

Fig. 1: Atom numbering and different reaction sites of isatin (CE: carbon

The first pathway (a) is the direct condensation of isatin in the presence of strong base Et_3N with 2-bromoethoxymethyl chloride (RX as electrophile for *N*-alkylation) that gave acyclic nucleoside A. Compound A subsequently converted to its hydrazone analogue **F**, using phenylhydrazine solution in EtOH. The second pathway (b) to obtain compound **F** may

assume to be direct condensation of **B** with 2-bromoethoxymethyl chloride, but it gave very poor yield of **F**. Since the RX used is very strong electrophile, the poor yield of this reaction should be because of vanishing nucleophilic character of *N*1 atom of intermediate **B**. Some previous studies suggest this could be attributed to the formation of intramolecular hydrogen bonding (IHB) in the enol form of compound **B**, in which there is no adjacent *H* atom to the atom *N*1, and so the nucleophilic power of *N*1 diminishes.

In this research, stable isomers and conformers for reactants and intermediates, and the reasons of their stability are investigated to illustrate the possible explanations of diminishing nucleophilic power of *N*1 in compound **B**. The best theoretical reason is discussed.

Method

All conformer optimizations were carried out using GAUSSIAN 03W software package applying DFT method. The level of B3LYP with 6-31G**, 6-311G** and 6-311++G** basis sets were used. NBO analyses were performed by GENNBO 5.0 for Windows, and NBO 3.1 module in G03W.

Results and Discussion

All altered possible isomers of isatin have been optimized at different levels and the results are shown in Fig. 2. As it is obvious, the keto form (**I**1) of isatin is such more stable that the existence of enol-forms is very unlikely, in agreement with the experimental crystallographic data [2]. Fig. 2 also shows the relative stabilities of possible isomers of intermediate **B**. Obviously, there is no enol form in which the *H*1 proton is engaged in IHB. Also, in comparison to **B**1, other forms with IHB (**B**3 and **B**4) are unexpectedly very instable. Therefore, according to the calculations at all mentioned level, the presence of other forms, but only **B**1 is improbable. Since the *H*1 in IHB as the reason for vanishing nucleophilic power of *N*1 was rejected, the NBO calculations were employed to find the reason. The reactants **I**1 and **B**1 showed no remarkable difference in nucleophilic property of *N*1 in NBO analyses. So, in the next step, assuming two-step reactions of **B**1 and **I**1 with RX in presence of base, the anions $\mathbf{B}^-$ and $\mathbf{I}^-$ were considered as nucleophiles. Performing optimizations and NBO analyses for these anions and comparing the results provided interesting results. In $\mathbf{B}^-$, the atom *N*1 has two σ-bonds and a π-bond (N1−C7a), while there are only two σ-bonds in $\mathbf{I}^-$, without any π-bond. Instead, $\mathbf{I}^-$ has two free lone pairs (one of $sp^{1.83}$ hybrid and occupancy of

1.93, other in pure p orbital with occupancy of 1.40) on *N*1, while there is just one lone pair in $\mathbf{B}^-$ (with $sp^{1.90}$ hybrid and occupancy of 1.93). So, turning a lone pair in $\mathbf{I}^-$ to a π-bond (having very strong interactions with some other orbitals) in $\mathbf{B}^-$ could be the main reason of diminishing nucleophilic power of *N*1 in $\mathbf{B}^-$. Detailed studies of NBO analyses (such as NRT, CMO and NLMO calculations), and comparing **B** with $\mathbf{B}^-$, and **I** with $\mathbf{I}^-$, result in more satisfactory findings.

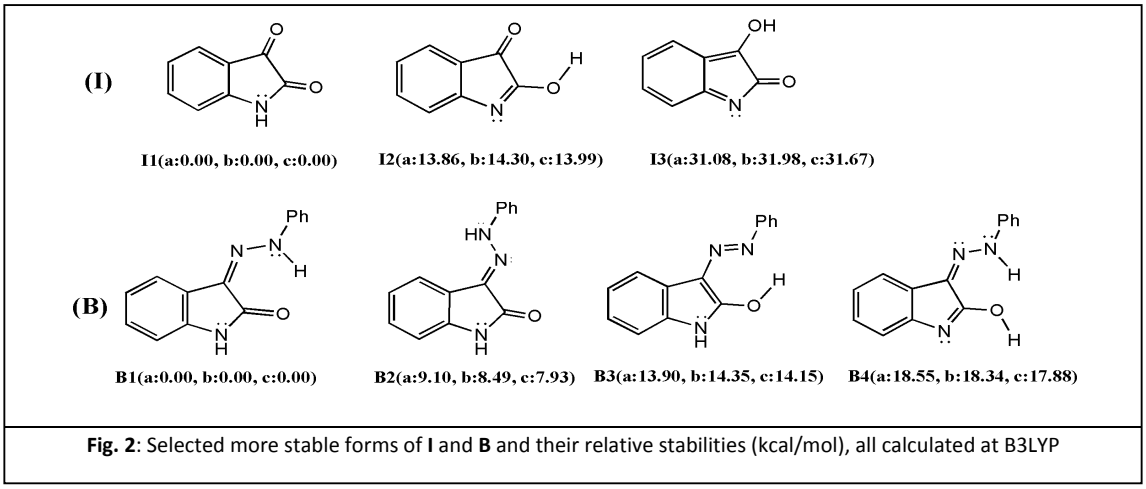

Fig. 2: Selected more stable forms of **I** and **B** and their relative stabilities (kcal/mol), all calculated at B3LYP

Conclusion

The *H*1 proton in IHB as the reason for vanishing nucleophilic power of *N*1 was rejected. The reactions of **B**1 and **I**1 with 2-bromoethoxymethyl chloride in presence of a base, are concluded to be two-step reactions, in which, in the first step the anions $\mathbf{B}^-$ and $\mathbf{I}^-$ form after base attack. Turning a lone pair in $\mathbf{I}^-$ to a π-bond in $\mathbf{B}^-$ could be the main reason of vanishing nucleophilic character of *N*1 in $\mathbf{B}^-$.

References

[1]W. C. Sumpter, *Chem. Rev*. 34 (1954) 407.

[2]Simon J. Garden; Angelo C. Pinto; James L. Wardell; B. John N. Lowc, *Acta. Cryst*. 62 (2006) 321.

[3]J. F. M. Da Silva, S. J. Garden, A. C. Pinto, *J. Braz. Chem. Soc.* 12 (2001) 273.

Prediction of retention of pesticides in reversed-phase high-performance liquid chromatography using classification and regression tree analysis and adaptive neuro-fuzzy inference systems

K. Zarei*, M. Atabati, L. Fatemi
School of Chemistry, Damghan University, Damghan, Iran
Email: *zarei@du.ac.ir*

Introduction

Pesticides are necessary and essential in agricultural production. However, the risk of residues in the food consumed is present, which are damaged to human. Therefore detection of pesticides residues in agricultural production is very important. Chromatography is the most suitable analytical tool for pesticide determination in water and foods [1-4]. Retention time is a very important parameter for qualitative analysis in chromatography. In this study a successful combination of feature selection and feature mapping tools, CART and ANFIS, is represented for prediction of retention of pesticides in reversed-phase high-performance liquid chromatography with different mobile phase composition. The results are promising and indicate the power of the CART-ANFIS techniques in developing methods with good prediction ability.

Experimental

Retention data (log K_{ex}) at different percents of water-acetonitrile mobile phase were obtained from the paper by D'Archivio et al. [5].

Molecular modeling and geometry optimization were performed by HyperChem. Dragon software was used for calculation of descriptors. SPSS software was used for running CART. MATLAB was used for running ANFIS (Fuzzy Logic Toolbox).

Results and discussion

Maximal tree was grown using the retention data. A total of 1497 descriptors obtained from Dragon software plus the amounts of %ACN were used as explanatory variables. The total dataset was randomly divided to three sets, as calibration, prediction and validation sets

with 119, 18 and 18 data, respectively. The regression tree was grown and then to select the optimal tree, ten fold cross-validation was used. The optimal tree was selected from the maximal tree, which was pruned back. For the optimal subtree with four terminal nodes, %ACN and two molecular descriptors were selected to describe the retention data. The selected molecular descriptors were logarithm of water/n-octanol partition coefficient (log $K_{ow)}$ and average molecular weight.

The three selected descriptors by CART were applied as input layer in construction of ANFIS. The number and type of the MFs needed for developing the ANFIS model were optimized using root mean square error (RMSE) for the prediction set (control set).

The architecture for optimized ANFIS model is shown in Fig. 1. Finally, to evaluate the predictive power of CART-ANFIS the optimized model was applied to all dataset (calibration, prediction and validation sets). The statistical results were shown in Tables 1.

Correlation and residual plot for CART-ANFIS model is shown in Figs. of 2 and 3, respectively. The high value of R^2=0.9940, for the total data set in Fig. 2 indicates that CART-ANFIS model can be considered as a powerful tool for the prediction of the retention time of pesticides. Propagation of the residuals on both sides of zero line in Fig. 3 indicates that the generated model has no systematic errors.

Keywords: Pesticides; Reversed-phase liquid chromatography; Retention model; Adaptive neuro-fuzzy inference system; Classification and regression tree

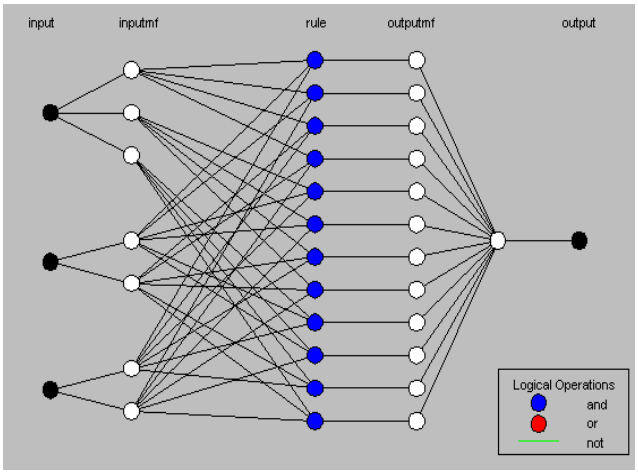

Fig. 1: optimized ANFIS model

Table 1: statistical results for CART-ANFIS

	MRE%	R^2	RMSE
Training	4.8124	0.9947	0.0267
Prediction	16.075	0.9889	0.0339
Validation	9.1204	0.9908	0.0358

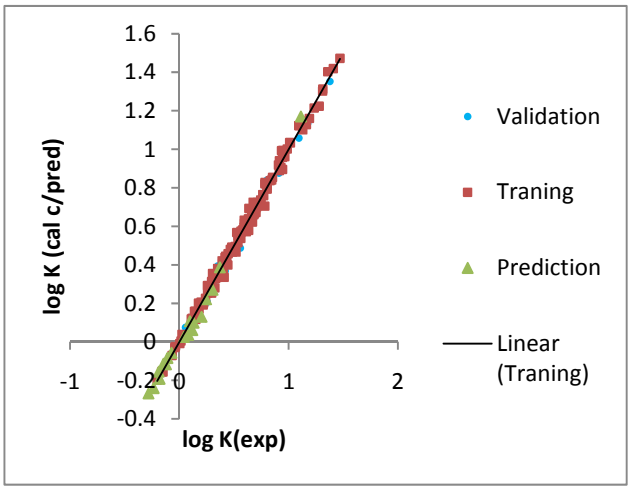

Fig. 2: plot of ANFIS calculated log K values against the experimental ones of the training, prediction and validation sets

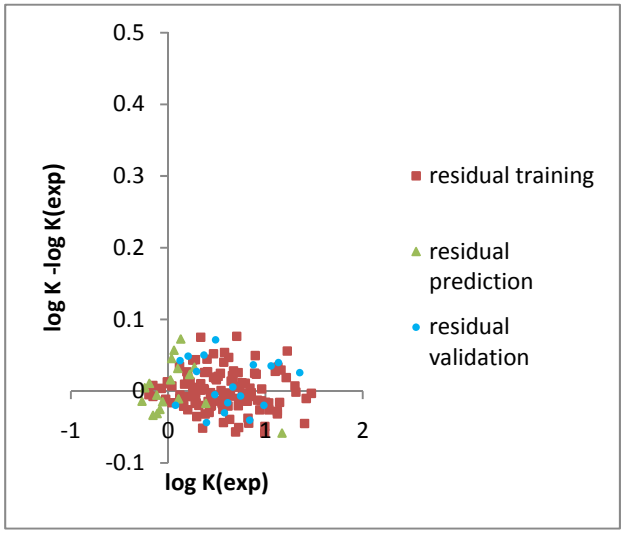

Fig. 3: plot residuals versus exprimental values of log K for the CART-ANFIS

References

[1] X. Li, F. Luan, H. Si, Z. Hu, M. Liu, Prediction of retention times for a large set of pesticides ortoxicants based on support vactor machine and the heuristic method, Toxicol. Lett. 175 (2007) 136-144

[2] A.A. D'Archivio, F. Ruggieri, P. Mazzeo, E. Tettamanti, Anal. Chim. Acta 593 (2007) 140–151.

[3] G.R. van der Hoft, P. van Zoonen, J. Chromatogr. A 843 (1999) 301.

[4] E. Hogendoorn, P. van Zoonen, J. Chromatogr. A 892 (2000) 435.

[5] A.A. D'Archivio, M.A. Maggi, P. Mazzeo, F. Ruggieri, Anal. Chim. Acta 646 (2009) 47-61.

Interaction of Coinage Metal Clusters with Noble Gases

A .Maghari*[a] ,Z .Jamshidi*[b] and M. Fakhraei Far [a]

[a]*Department of Chemistry, University of Tehran, Tehran, Iran*

[b]*Chemistry and Chemical Engineering Research Center of Iran, Tehran, Iran*

maghari@khayam.ut.ac.ir, jamshidi@ccerci.ac.ir

Keywords: Coinage Metals, noble gases, Interaction Energy

Introduction

In recent years, numerous studies have been carried out on the interaction between noble gases and coinage metals. Coinage metals show low tendency to the binding in contrast with the other elements, and these elements have unusual and different reactivity; Au has very high chemical activity due to relativistic effects (discrepancies between values calculated by models considering and not considering relativity). However in the case of noble gases, the more reactive noble gases are Kr, Xe, and Rn , due to their large polarizability and low ionization potential. Recently nanocluster coinage metals and compounds have attracted considerable attention due to their unique physical and chemical properties which depend strongly on cluster size. In the past few years, atomic and molecular chemisorptions on small coinage metal clusters, especially gold, have received considerable attention, both experimentally and theoretically. Therefore, in the present work, we focused on the interactions between coinage metal clusters and three noble gases including Kr, Xe, and Rn.

Method of Calculations

The interaction potential energy surface of the dimer and trimer of coinage metal clusters (CM = Cu, Ag and Au) complexes with noble gas (NG= Kr, Xe and Rn) are calculated by MP2 and DFT methods. The pseudopotential-based correlation-consistent polarized valence double and triple-ζ (cc-pVD(T)Z-PP) and augmented triple-ζ (aug-cc-pVTZ-PP) basis sets based on the small core relativistic pseudopotentials (PPs) of Figgen et al., were employed for RG and CM. These calculations have been done using Gaussian 03 suite of programs. The bond length, interaction energy and spectroscopic constants were obtained and to reveal the

nature of bonds, the NBO, QTAIM, and EDA analyses were carried out on the optimized structures.

Results and discussions

The potential energy curves (PECs), for the interaction between dimer metal clusters and noble gases have been calculated in two different orientations and the equilibrium bond lengths and binding energies have been obtained for these complexes. The expected trend of an increase in binding energy with increasing atomic number in NG is observed for each metal. Figure 1-(a) shows the interaction energy for Au_2…NG complexes. These binding energies (E_b) are in line with the trend of increasing polarizability of the NG atom and hence the increasing attractive dispersion forces. Figure 1-(b) also has shown interaction energy between CM_2…Xe. On first inspection the ternd of increasing E_b values for Cu_2…Xe, Ag_2…Xe, and Au_2…Xe complexes is unexpected, when the polarizibility of copper, silver, and gold are considered. Therefore, other effect beside dispersion forces should involve for interaction of these metal clusters with noble gases.

(a) (b)

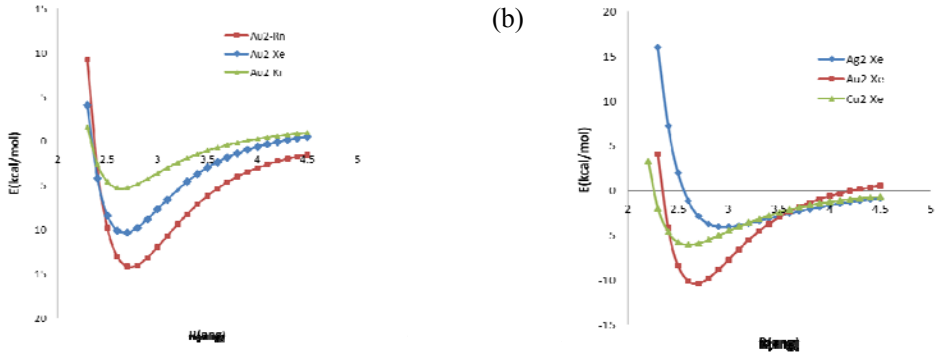

Figure 1: Potential-energy curves for the Au_2…NG(a) and CM_2…Xe(b) complexes at the MP2/aug-cc-pVTZ-pp level of theory.

Reference

[1] A. M. Gardner, R. J. Plowright, M. J. Watkins, T. G. Wright, and W. H. Breckenridge, *J. Chem. Phys*. **2010**, *132*, 184301.

[2]Y. Gao, W. Huang, J. Woodford, L.Wang, and C. zang , *J . Am. Chem. Soc*. **2009**, *131*, 9484.

[3]A. M. Gardner, C. D. Withers, J. B. Graneek, T. G. Wright, L. A. Viehland, and W. H. Breckenridge, *J. Phys.Chem. A* **2010**, *114*, 7631.

[4] T. Zeng and M. Klobukowski, *J. Phys.Chem. A* **2008**, *112*, 5236.

[5] W. H. Breckenridge, V.L. Ayles, and T. G. Wright, *J. Phys.Chem. A* **2008**, *112*, 4209.

[6] L. Belpassi, L. Infante, F. Tarantelli, and L. Visscher, *J. Am. Chem. Soc* **2008**, *130*, 1048.

Host- Guest Inclusion Complexes Formation of Local Benzocaine with Cyclodextrins; Computational Study

Kh. Farzadnia[a], Z. B. Nojini[*b]

[a]Department of Chemistry, Islamic Azad University, Sciences and Researches Branch, Khuzestan, Ahvaz, Iran

[b]Department of Chemistry, Faculty of Science, Shahid Chamran University, Ahvaz, Iran

Email: khalilfarzadnia@yahoo.com

Keywords Cyclodextrin, Inclusion complexation, Anesthetic drugs, Stabilization energy

Introduction

Cyclodextrins are macrocyclic oligomers of α-D-glucose.Three kind of CDs are mostly applied. They have 6-8 units of glucose; as follows: α-CD (6 units), β-CD(7-units) and δ-CD(8 units). CDs have a hydrophilic exterior and a hydrophobic cavity of appropriate dimension [1]. The purpose of this research is to obtain the most stable complex of α and β-CD/Benzocaine.

Computational Method

The complexes of α and β-CD/Benzo were optimized with HF and density functional theory (DFT) and B3LYP with 6-31G Basis set. The glycoside oxygen atoms of the α and β-CD were placed onto the XY-plane. The primary hydroxyl groups of α-CD were placed pointing toward the positive Z-axis [2].

Results and discussion

For the complex of β-CD With Benzocaine, energy of the inclusion Complex vs the z coordinate is shown in Fig.1 we calculated the total energy of the α and β-CD/Benzocaine. The complex formation energy, □E, was calculated using the following expression:

$$\square E = E_{(complex)} - (E_{CD} + E_{drug}) \quad (1)$$

The electronic chemical potential(μ) was calculated as half of the energy of the HOMO and LUMO as follows:

$$\mu=(E_{HOMO}+E_{LUMO})/2$$

(2)

The energies of HOMO and LUMO and Sabilization energy values of Host-guest complexes are summarized in Table 1.The results indicate that the energy gap between α – CD/Benzo is more than that of β-CD/Benzo with 1:1 stoichiometry

Table1. Electronic energies, HOMO, LUMO and Gap energy of the of the inclusion complexation of α and β-CDs with Benzocaine of the HF optimized structures

Species	ΔE(kj/mol)	E_{HOMO}(eV)	E_{LUMO}(eV)	EnergyGap	μ(eV)	η(eV)	ω
Benzocaine	-	- 8.08	3.04	11.12	-2.52	5.56	0.57
α-CD	-	-8.43	3.50	11.94	-2.46	5.97	0.50
β-CD	-	-8.53	3.71	12.25	-2.41	6.12	0.47
α-CD/Benzo	-4000	-8.33	2.65	10.99	-2.83	5.49	0.73
β-CD/Benzo	-3000	-8.16	2.58	10.75	-2.78	5.37	0.72

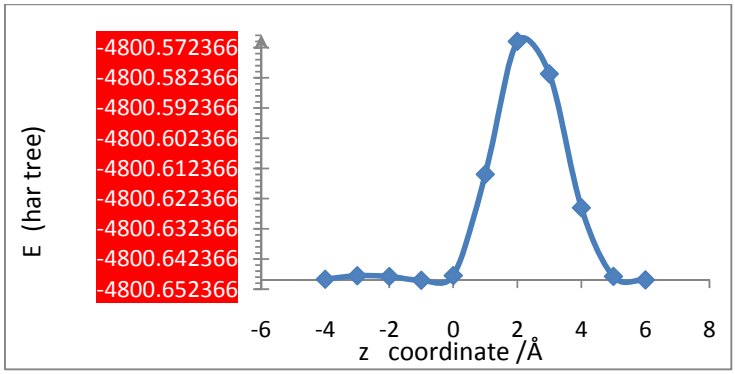

Fig.1 Graphic diagram for the emulation of the inclusion Complexation of Benzocaine into the β-CD

Conclusion

According to the results, in both of methods, HF and B3LYP with Basis set 6-31G,α-CD/Benzo is more stable than β-CD/Benzo.

References

[1] Lei L. and Qing-X Gj. Inclu. Phenom Macro. Chem. 50 (2004) 95

[2] Leil. Xia, S.kes Qing X J. Mol Struct. (Theochem) 531 (2000)128

Experimental and computational study of Tautomerism in N,N' bis(2-thiazolyl) phenylphosphonic diamide

Kh. Gholivand*, S. Farshadian, and Z. Hosseini

Email: farshadian@modares.ac.ir

Department of Chemistry, Faculty of Science, Tarbiat Modares University, P. O. Box: 14115-175, Tehran, Iran.

Keywords: 2-Aminothiazole, Tautomerism, Phosphonic diamide, Computational study

Introduction

Heterocyclic tautomerism has been studied extensively for the past two decades due to its biological importance and highly solvent-dependent nature. 2-Aminothiazoles are able to tautomerize and can exist in either amino- or imino-form. Recently, molecular orbital calculations were performed on 2-, 4- and 5- aminothiazoles using different calculation levels in order to study the 1,3-hydrogen transfer between the amino group and the endocyclic nitrogen atom or carbon atom at position five [1]. In this work, the synthesis of a phosphonic diamide containing the 2-aminothiazole moiety is described and structural and conformational properties are analyzed.

Methods

N,N' bis(2-thiazolyl) phenylphosphonic diamide was prepared by treating chloroform solutions of 2-aminothiazole and phenylphosphonic dichloride using a 2:1 M ratio in the presence of triethylamine as a Lewis base catalyst. All quantum chemical calculations were performed with the GAUSSIAN 98 program package [2]. Structural and conformational properties are analyzed using a combined approach involving crystallographic data and theoretical calculations at the B3LYP and MP2 (with 6-311++G(3df,2p) and CBSB7 basis sets) level of approximations.

Results and Disscussion

The crystalline solid consist of the imine tautomer – with the tautomeric proton attached to the endocyclic nitrogen atom –, and the dihedral angles around the N_{exo}–C bonds amount 5.5(2) and 10.9(2)° – with the phosphorous on the same side of the endocyclic sulfur atoms. The B3LYP method computes a mixed structure with non-equivalent thiazole rings in which one

of endocyclic nitrogen atom in the thiazole ring is protonated, while the other thiazole group is deprotonated as the most stable form for the gas phase molecule. The two conformations (named as A and B in the molecular structures showed in Table 1) of the amine and imine tautomers are computed to be also stable forms, located at 1.09 (amine_A) and 2.44 kcal/mol (imine_A) higher in energy than the imine/amine form, respectively, at the B3LYP/CBSB7 level. The order of the computed stability exhibits little effect on the basis sets. However, a different description is obtained by applying the MP2 method: a drastic change is obtained in the relative stability values. In this case the most stable tautomer corresponds to the amine form. The structure with only one thiazole ring protonated has intermediate energy values, i.e. ca. 4.6 kcal/mol at the same level of calculation.

Table 1. Relative energies (kcal/mol) calculated at the B3LYP and MP2 methods for plausible tautomers of *N,N´* bis(2-thiazolyl) phenylphosphonic diamide in different conformations.

Form	Molecular structure	B3LYP			MP2	
		6-31+G*	6-311++G**	CBSB7	6-311++G**	CBSB7
Imine_A		3.11	2.87	2.44	13.10	11.58
Imine_B		4.89	4.62	4.55	14.98	12.62
Imine/amine		0.00	0.00	0.00	5.11	4.57
Amine_A	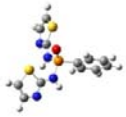	0.58	0.68	1.09	0.00	0.00
Amine_B	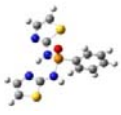	1.12	0.92	1.49	2.00	1.42

Conclusions

The crystalline solid consist of the imine tautomer and the B3LYP method computes a mixed structure with non-equivalent thiazole rings as the most stable form for the gas phase molecule.

References:

[1] Papadopoulou C., Geronikaki A., Hadjipavlou-Litina D., *Farmaco 60* (2005) 969.

[2] Frisch MJ, Trucks GW, Schlegel HB, Scuseria GE, Robb MA, Cheeseman JR, Zakrzewski VG, Montgomery JA, et al. (1998) Gaussian 98, revision A.7. Gaussian, Inc. Pittsburgh, PA.

Derivation of an equation for prediction of the thin layer depth of the extended–Langmuir model for binary liquids

Tahere Fereidoni Moghadam, Saeid Azizian*
Department of Physical Chemistry, Faculty of Chemistry, Bu-Ali Sina University, Hamedan, Iran
E-mail: t.Fereidoni@yahoo.com

Keywords: Extended Langmuir Model, Thin Layer Depth of Surface, Surface Tension

Introduction

Extended Langmuir model is a model which correlates the surface tension data with bulk composition. One of main objectives of this model is considering the surface as a thin layer of finite depth [1, 2]. In the present work we have combined the Gibbs equation with extended Langmuir model and derived a new equation for estimating the depth of surface thin layer for dilute binary liquid mixtures. All of the investigated systems were fitted to extended-Langmuir model and the parameters were estimated.

Methods

The beginning point to obtain the target equation is the Gibbs equation for binary mixtures[2]:

$$d\gamma = -(\frac{n_A^s}{\sigma} d\mu_A - \frac{n_B^s}{\sigma} d\mu_B) \qquad (1)$$

In this equation n_A^s and n_B^s are number of moles component A and B on surface, □□□is surface area, □□□is surface tension of solution, □□is chemical potential and:

$$d\mu_i = RTd\ln a_i = RT\frac{da_i}{a_i} \qquad (2)$$

where a_i is activity of component i.

By substitution this equation in equation (1), simplification and by using EL model has been obtained:

$$d\gamma = -RTh^s(1-\beta)(\frac{da_B}{v_A^m\gamma_B^a + (\beta v_B^m - v_A^m)a_B}) \qquad (3)$$

where v_A^m and v_B^m are volume fraction of component A and B, h^s is thin layer depth of surface, β is□ a constant and a measure of lyphobicity of solute and □$_B^a$ is activity coefficient component B.

we can assume that h^s decreases with x_B in a linear form:

$$h^s = h_0^s - fx_B \qquad (4)$$

where h_0^s is depth of surface thin layer in infinite dilute and f is constant and definition of:

$$\beta v_B^m - v_A^m = \Omega \qquad (5)$$

one arrive

$$d\gamma = -RT(\beta - 1)\left(\frac{h_0^s - fx_B}{v_A^m + \Omega x_B}\right)dx_B \qquad (6)$$

By integration at boundary conditions x_B=0 to x_B and γ_A to γ, we have

$$\pi = b'x_B + a'ln\left(1 + \frac{\Omega}{v_A^m}x_B\right) \qquad (7)$$

where

$$a' = RT(\beta - 1)\left[\frac{h_0^s}{\Omega} + \frac{fv_A^m}{\Omega^2}\right] \qquad (8)$$

and

$$b' = \frac{-RT(\beta - 1)f}{\Omega} \qquad (9)$$

Eq. (7) is a new equation which can be applied for the dilute region of binary liquid mixtures. Based on constants (a', b') of Eq. (7) one can obtain h_0^s and f and finally the depth of surface layer, h^s, as a function of bulk concentration, x_B.

Results and discussion

Based on present study it was found that the depth of surface layer in extended Langmuir model is not constant and decreases in a linear form with increase of solute bulk concentration figure (1). The depth of surface layer in the dilute region increases with increasing the size of solute and decreases with temperature.

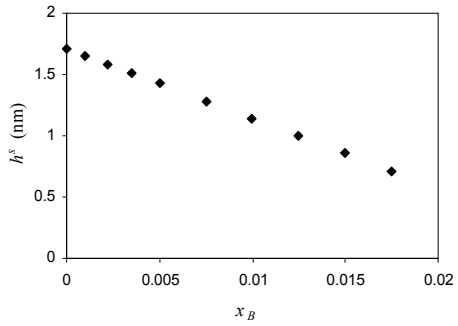

Fig.1 Variation of surface layer depth as a function of solute bulk mole fraction, for dilute aqueous solution of ethanol at 25ºC.

Conclusions

The present work shows that Eq. (7) is a suitable equation for analysis of surface behavior of dilute binary solutions.

References

[1] Piñeiro, Á.; Brocos, P.; Amigo, A.; Gracia-Fadrique, J.; Lemus, G. Langmuir, **2001,** 17, 4261.

[2] Brocos, P.; Gracia-Fadrique, J.; Amigo. A.; Piñeiro, Á. *Fluid Phase Equilib*. **2005**, 237, 140.

Quantitative structure–property relationship study of Kovats Retention Index of some of Adamantane derivatives using multiple linear regression

Z.Bayat*, M.Fakoor.YazdanAbad, M.Zanoozi
Department of chemistry, Islamic Azad University-Quchan Branch, Iran
z.bayat@ymail.com

Abstract
A quantitative structure–property relationship (QSPR) study was performed to develop models those relate the structures of 65 adamantane derivatives compounds to their Kovats Retention Index (RI). Modeling of RI of these compounds as a function of the theoretically derived descriptors was established by multiple linear regression (MLR).

Keywords: Retention Index,Mathematical modeling,QSPR, MLR,HF

Introduction

In this report Quantum-chemical calculations were performed with Gaussian 03 package and HyperChem program package, version 8.0, by HF methods and at the 6-31+G** basis set. Also Multiple Linear Regressions (MLR) were employed to model the relationships between molecular descriptors and retention index of molecules using stepwise method.

Methods

The descriptors are obtained directly from the chemical structure, e.g. constitutional, geometrical, and topological descriptors. In this work, we used Gaussian 03 for ab initio calculations. HF method at 6-31+G** were applied for optimization of adamantan derivatives and calculation of many of the descriptors .At first adamantan derivatives were built by Hyperchem software. A large number of descriptors were calculated by Gaussian package and Hyperchem software. One way to avoid data redundancy is to exclude descriptors that are highly intercorrelated with each other before performing statistical analysis. Those descriptors that were too strongly correlated with the others were rejected. MLR models were constructed in the present work using SPSS software.

results and discussion

The QSPR model were derived from using all descriptors and molecules followed by these equation:

RI = 109.020(±14.521) LogP + -44.556(±4.356) ΔG_{OCT} + -12.523 (±1.178) $\Sigma_{C\ 4}$+ 2.299(±.315) M+ 831.202(±46.526) (R^2 =0.919 F= 170.367 Q^2= 0.9048 R=0.959 N=65) (HF/6-31+G**)

Four descriptors for these compounds, molecular Mass (M), solvation Free Energyin Octanol (ΔG_{OCT}), Partition Coefficient (LogP), Isotropic Parameterd (Σ_{c4}) are taken as inputs for the Hartree-Fock calculation (abbreviated HF) model.

The experimental and calculated values of Retention Index listed in Table1

Compound	RI_{EXP}	RI_{Cal}	Compound	RI_{EXP}	RI_{Cal}
Adamantane	1118	1099.27	Adamantane-1-carboxylic acid	1556	1584.50
1, 2-dimethyl Adamantane	1236	1316.81	Adamantane-2-carboxylic acid	1529	1492.83
1, 3 dimethyl Adamantane	1151	1193.68	Adamantane-2-carboxylic acid	1467	1423.49
1,3,5 -Trimethyl adamantane	1163	1202.92	Methyl esters of- 2-methyl	1512	1546.76
1-Adamantanol	1268	1256.19	Methyl esters of- 3-ethyl	1579	1555.42
1-Bromomethyl adamantane	1488	1479.46	1-Bromo adamantane	1382	1413.28
1-Buthyl adamantane	1443	1408.63	1-Fluoro adamantane	1159	1201.5
1-Chloroadamantane	1298	1249.76	2-Chloro adamantane	1342	1377.65
1-Chloromethyladamantane	1404	1362.70	2-Fuoro adamantane	1182	1278.58
1-Ethyl adamantane	1260	1256.24	2-Propyl-2-adamantanol	1526	1472.48
1-Isopropyl adamantane	1358	1329.26	3,5,7-Trimethyl-1-	1304	1366.28
1-Propyl adamantane	1347	1331.91	3-Buthyy-1-adamantanol	1595	1541.09
2 ,2-Dimethyl adamantane	1269	1271.71	3-Ethyl-5,7-dimethyl -1-	1421	1506.98
2-Buthyl adamantane	1465	1430.19	3-Methyl-1-adamantanol	1283	1279.68
2-Ethyl-2-adamantanol	1446	1385.04	3-Propyl-1-adamantanol	1495	1454.24
2-Ethyl adamantane	1284	1276.72	Methyl-(1-adamanthyl) ketone	1443	1451.84
2-Isobuthyl-2-adamantanol	1570	1551.93	Propyl-(1-adamanthyl) ketone	1609	1620.27
2-Isobuthyl adamantane	1416	1438.35	2-Adamantanon	1320	1360.56
2-Isopropyl adamantane	1349	1355.90	Di methyl ester of 5,7-di	1769	1850.73
2-Methyl-2-adamantanol	1348	1327.72	1-Ethyl-3,5 di methyl	1279	1277.26
2-Methyl adamantane	1196	1231.26	Methyl-(2-adamanthyl)ketone	1445	1450.45
2-Propyl adamantane	1371	1353.87	3-(1-Adamanthyl)pentane	1559	1477.52
3-5 Dimethyl 1 hydroxy methyl	1425	1356.64	1-Hydroxy methyl adamantane	1402	1332.95
3 ,5-Dimethyl-1-adamantanol	1295	1255.58	Esters of adamantane1-	1449	1421.98
3, 5-dimethyl -1-bromo	1401	1422.96	Esters of adamantane 1-	1603	1586.14
3-Ethyl-1-adamantanol	1283	1379.15	Methyl ester of 3,5 di methyl	1467	1447.18
3-Isopropyl-1-adamantanol	1506	1515.69	2-Adamantanol	1329	1328.83
5,7-Dimethyl1-3 adamantandiol1.	1438	1415.51	Ehyl-(1-adamanthyl)ketone	1529	1546.53
Adamantane-1-carboxylic acid	1508	1502.96	2-Methylene adamantane	1160	1154.64
Adamantane-1-carboxylic acid iso	1658	1654.57	2-Methyl-1-hydroxy methyl	1490	1457.73
Adamantane-1-carboxylic acid iso	1532	1570.27	2-Buthyl-2-adamantanol	1620	1563.28
Adamantane-1-carboxylic acid sec-	1631	1650.78	2-Bromoadamantane	1426	1451.86

Commonly used descriptors in the QSPR analysis are presented in Table 2.

Descriptor	Symbol	Example
Quantum chemical descriptors	Molecular Polarizability	MP
	Electrostatic Potentialc	EP
	solvation Free Energy(in Octanol)	ΔG_{OCT}
	solvation Free Energy(in water)	ΔG_{WATER}
	Isotropic Parameterd	Σ
	Mulliken Charge	MC
	Molecular Dipole Moment	MDP
	Highest Occupied	HOMO
	Lowest Unoccupied	LUMO
	difference between	E_{Gap}
	Hardness	H
	Electro negativity	*X*
Chemical Properties	Softness (S=1/ η)	S
	Partition Coefficient	Log P
	Molecule surface area	SA
	Hydration Energy	HE
	Refractivity	REF
	Mass	M

Conclusions

The aim of this work is the development, using theoretical molecular descriptors, and the proposal of externally validated general QSPR models for the prediction of Kovats Retention index(RI) for a wide compounds.The use of descriptors calculated only from molecular structure eliminates the need for experimental determination of properties for use in the correlation and allows for the estimation of Kovats retention index(RI)for molecules not yet synthesized.

references

[1] J.A. Platts, S.P. Oldfield, M.M. Reif, A. Palmucci, E. Gabano, D. Osella, J. Inorg. Biochem. 100 (2006) 1199.

[2] R. Bosque, J. Sales, E. Bosch, M. Roses, M.C. Garcia-Alvarez-Coque, J.R. Torres-Lapasio, J. Chem. Inf. Comput. Sci. 43 (2003) 1240.

[3] M. Jalali-Heravi, M.H. Fatemi, J. Chromatogr. A 915 (2001) 177.

[4] Z. Garakani-Nejad, M. Karlovits, W. Demuth, T. Stimpfl, W. Vycudilik, M. Jalali-Heravi, K. Varmuza, J. Chromatogr. A 1028 (2004) 287.

A DFT-Based Study of the Room-Temperature Reactions of CH_3F with Main-Group Atomic Cations Ga^+, Ge^+, As^+ and Se^+

Marjan Firouzbakht,[a] Zahra Jamshidi,[b] and Alireza Shayesteh*,[a]

[a] *School of Chemistry, College of Science, University of Tehran, Tehran, Iran*

[b] *Chemistry and Chemical Engineering Research Center of Iran, P.O. Box 14335-186, Tehran, Iran*

Email:shayesteh@khayam.ut.ac.ir

Introduction

Gas-phase reactions of methylfluoride with the main-group atomic cations Ga^+, Ge^+, As^+ and Se^+ have been investigated experimentally by Zhao et al.[1].They observed the following reactions at room temperature:

$$Ga^+ + CH_3F \rightarrow Ga^+(FCH_3)$$

$$Ga^+ + CH_3F \rightarrow GeF^+ + CH_3$$

$$As^+ + CH_3F \rightarrow AsCH_2^+ + HF$$

$$Se^+ + CH_3F \rightarrow \text{No Reaction}$$

Recently, similar reactions with methane (CH_4) were studied at room temperature [2]. Zhang et al.[3] interpreted the experimental results using DFT calculations. We have performed similar DFT calculations to obtain the energies and structures of reaction products, intermediates and transition states.

Computational Details

The calculations were performed using Gaussian03. The geometries of all stationary points were optimized at the unrestricted UB3LYP level of theory; the 6-311++G** basis set without inclusion of relativistic effects was employed. Transition structures were found using the QST3 method. The ground and the first excited states of atomic cations were considered for the reactions. The ground electronic states are: $Ga^+(^1S)$, $Ge^+(^2P)$, $As^+(^3P)$, $Se^+(^4P)$, and the first excited states are : $Ga^+(^3P)$, $Ge^+(^4P)$, $As^+(^1D)$, $Se^+(^2D)$.

Results

The preliminary results of our DFT calculations are listed in Tables1 and 2.

Table 1. Relative energies (kcal mol^{-1}) of reaction products and intermediates for Se^+/CH_3F.

	$Se^+ + CH_3F$	$Se^+(FCH_3)$ **(1)**	$[FSeCH_3]^+$ **(2)**	TS[2,3]	$[FSeHCH_2]^+$ **(3)**	$HF + [SeCH_2]^+$ **(4)**
Doublet	46.72	-10.09	-44.57	13.40	-11.03	-40.50
Quartet	0	-18.63	24.47	-	-	-

Table 2. Relative energies (kcal mol^{-1}) of reaction products and intermediates for As^+/CH_3F.

	$As^+ + CH_3F$	$As^+(FCH_3)$ **(1)**	$[FAsCH_3]^+$ **(2)**	$[FAsHCH_2]^+$ **(3)**	$HF + [AsCH_2]^+$ **(4)**
Singlet	34.40	-43.70	-73.07	-4.65	-38.92
Triplet	0	-39.70	-34.85	21.01	-17.90

Work in progress

We are optimizing the structures of all intermediates and transition structures, and considering various reaction products for the As^+/CH_3F reaction. Our preliminary results for the Se^+/CH_3F reaction show that formation of $[FSeCH_3]^+$ is possible through a quartet-doublet crossing of the potential energy surfaces.

References

[1] X. Zhao, G. K. Koyanagi, and D. K. Bohme, J. Phys. Chem. A, 110, 10607 (2006).

[2] X. Zhang and H. Schwarz, Chem. Eur. J., 15, 11559 (2009).

[3] A. Shayesteh, V. V. Lavrov, G. K. Koyanagi, and D. K. Bohme, J. Phys. Chem. A, 113, 5602 (2009).

A Theoretical Study on the Heteropentalenes Aromaticity

S. Noorizadeh and Sh. Firoozi

Chemistry Dept., College of Sciences, Shahid ChamranUniversity, Ahwaz, Iran

(noorizadeh_s@scu.ac.ir)

Keywords: Aromaticity, Heteropentalenes, Hardness, Morse Electrophilicity.

Introduction

One of the criteria,which is frequently used in aromaticity indication, is the isomerization method [1]. This method is based on the difference between total energies computed for a *methyl* derivative of the aromatic system and its structurally closely related nonaromatic exocyclic *methylene* isomer. The difference between the electrophilicity values of these isomers is called relative electrophilicity and is recently used as a measure of aromaticity of molecular systems [2]. Also a *Morse-like function* is considered for the energy of a system and a new electrophilicity (Morse Electrophilicity) is introduced [3]. In this contribution, it is attempted to study the aromaticity of some heteropentalenes using the relative hardness and electrophilicity values of these compounds.

Methods

Using Janak's and quadratic approximations, the definitions of hardness (η) and electrophilicity (ω) as reactivity descriptors are:

$$\omega_J \cong \frac{(\varepsilon_L + \varepsilon_H)^2}{8(\varepsilon_L - \varepsilon_H)} \qquad \eta \cong (\varepsilon_L - \varepsilon_H) \qquad (1)$$

and

$$\omega_Q \cong \frac{(IP + EA)^2}{8(IP - EA)} \qquad \eta \cong (IP - EA) \qquad (2)$$

where ε_H, ε_L, IP and EA are the HOMO energy, LUMO energy, Ionization potential and electron affinity, respectively. Also according to the Morse model, the electrophilicityof a chemical species has the following form:

$$\omega_M = \alpha \left\{1 - e^{-\beta(N_0 - \delta)}\right\}^2 \qquad (3)$$

where α, β and δ are the adjustable parameters. The considered heteropentalenes are optimized by using Gaussisn 98W program with different methods and basis sets (HF and B3LYP with 6-31G** and 6-311++G** basis set). The obtained energies for the methyl and methylene isomers are used in calculations of the relative hardnesses ($\Delta\eta$) and relative electrophilicities ($\Delta\omega$) with both Janak and quadratic approximations.

Results and Discussion

The considered molecules are depicted in Fig. 1; and the calculated relative electrophilicities are gathered in Table 1. It should be noted that, according to the Maximum Hardness and Minimum Electrophilicity Principles (MHP and MEP), the relative hardness and relative elecctrophilicity values for aromatic systems should be positive and negative, respectively. The obtained results show that, in many cases relative hardness can not be a good descriptor for indicating the aromaticity; whereas the obtained relative electrophilicities from Morse model is reliable and correctly predict the order of aromaticities in these rings (see Table 1). Note that, a good correlation is observed between the obtained electrophilicities from Janak and quadratic approximations (R^2=0.943), and therefore they give the same results; whereas such correlation is not observed between the Morse and Janak electrophilicities (R^2=0.454).

Molecule	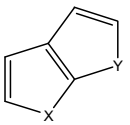		Molecule	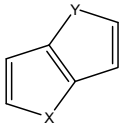	
	X	Y		X	Y
1NN	N	N	2NN	N	N
1SS	S	S	2SS	S	S
1OO	O	O	2OO	O	O
1NS	N	S	2NS	N	S
1NO	N	O	2NO	N	O
1SO	S	O	2SO	S	O
1SN	S	N	2SN	S	N
1ON	O	N	2ON	O	N
1OS	O	S	2OS	O	S

Fig. 1. Considered molecules in this study

Conclusion

It is shown that the relative electrophiicity index is more successfull in identification of aromaticity in heteropentalene molecules then the relative hardness. In addition, using Morse like electrophilicity give more reliable aromaticities than the other approximations.

Table 1. Calculated relative electrophilicities using both Janak's, quadratic approximations and Morse like function with different levels of theory. All values are in a.u.

Molecule	HF/6-31G**		HF/6-311++G**		B3LYP/6-31G**		
	ΔωJ	ΔωQ	ΔωJ	ΔωQ	ΔωJ	ΔωQ	ΔωM
1NN	-0.22528587	-0.20029536	0.178330021	0.482091727	-1.154648704	-0.510071971	-0.50816277
1SS	0.220816482	0.307796825	0.674015969	1.987430813	-0.561292302	-0.08784961	-0.07813823
1OO	-0.137200962	-0.265258876	-0.198681123	1.396526799	-0.746976863	-0.203901659	-0.040236501
1NS	-0.197062724	-0.197495747	0.3445836	-1.0661355	-0.859139363	-0.385657846	-0.707814178
1NO	-0.191888257	-0.324730151	0.298881066	1.222127148	-0.966467563	-0.390741712	-0.146914354
1SO	0.100086056	0.243100186	0.681198067	0.909099795	-0.630529932	0.004571411	-0.410218783
1SN	0.047601951	0.365642056	0.506175117	0.944359419	-0.476589527	-0.047930448	-0.246218537
1ON	-0.165972233	-0.202280132	0.35843153	1.58647337	-0.809669262	-0.289568585	-0.089002448
1OS	0.000863057	0.064893089	0.452238058	1.727872604	-0.398143461	-0.212904728	-0.347184781
2NN	-0.53641054	-0.57117341	-0.114430073	-0.256275991	-2.152098855	-1.039979987	-0.825050898
2SS	-0.135030547	0.042153735	0.47221042	-0.507531786	-1.807885978	-0.605395902	-0.741564582
2OO	-0.51350123	-0.568740399	0.195763947	0.159874859	-1.962808009	-0.873750859	-0.552375429
2NS	-0.672633594	-0.297698369	0.256648503	0.925707673	-2.645274617	-1.188840177	-0.882139289
2NO	-0.653318531	-0.72138747	3.39479058	0.281130719	-2.46850192	-1.125623144	-0.525829203
2SO	-0.090415814	0.274501392	0.47249134	1.891799209	-1.452849959	-0.474367579	-0.546163367
2SN	-3.620620038	0.139982708	0.399816159	-0.115216975	-1.392291268	-0.509655391	-0.405000129
2ON	-0.485755918	-0.509251076	0.129787733	1.671715073	-1.809691261	-0.838824867	-0.375364701
2OS	-0.50059139	0.181676545	0.267968896	1.122284478	-2.120805433	-0.912878608	-0.403788566

References

[1] P.v.R. Schleyer, F. Fuhlhofer, Org. Lett. 4 (2002) 2873.

[2] S. Noorizadeh, E. Shakerzadeh, Chem. Phys. Lett. 484 (2010) 363.

[3] S. Noorizadeh, E. Shakerzadeh, J. Phys. Chem A 112 (2008) 3486.

Calculation of Octanol/Water Partition Coefficients*(log P) for some Benzimidazole and derivatives drugs using Solvation Free Energies

Z.Bayat*,S.Qaneinasab
Department of chemistry, Islamic Azad University-Quchan Branch, Iran
z.bayat@ymail.com

Abstract:
The logP for some Benzimidazole and derivatives drugs were calculated using PCM model at B3LYP/6-31+G** level, following the thermodynamic integration approach. The results reported here indicate that the log P calculated in this approach is closer to the experimental values compared to other *Ab initio* methods.

Keywords: Free energy solvation, log P, *Ab Initio*, Benzimidazole , PCM, QSAR

Introduction

A different approach to all of the above is to use information of the free energy of solvation in water and in octanol to estimate the partition coefficient From Gibbs free energies of solvation in two different phases at temperature *T*, one can calculate the corresponding partition coefficient, according to the following expression:

$$\log P = -\left(\frac{\Delta G_{sol,oct} - \Delta G_{sol,w}}{2.30\ RT} \right)$$

Where R is gas constant and T is the temperature. The solvation free energy is used to compute the logP based on equation above and only solvation free energies in water and 1-octanol are needed to calculate log P.

Results and Discussion

In this study the geometry of the molecules used here was fully optimized in DFT calculations with the 6-31+G** basis set with the Gaussian 03 package. These values and the logP obtained from Hyperchem software and other methods (such as QSAR, using various software and algorithem) in different works are given in Table 1.

Drugs	Clogp(other metodes)	cLogp	Logpexp	Logp hyper
Albendazole	2.2–2.92(a)	3.351	3.83	2.13
Mebendazole	2.44–2.52(a)	3.1669	3.73	2.682

Fenbendazole	3.07–4.01(a)	3.0712	3.93	3.001
Benzimidazole	0.8–0.95(a)	0.5818	1.5	0.942T
Thiabendazole	1.58–1.76(a)	1.1931	2.55	1.855
flubendazole	1.98–2.41(a)	4.1685	3.32	1.699
compund1	1.7(b)	2.459907	1.97	1.97
compund2	2.02(b)	3.977095	2.37	2.413
compund3	2.19(b)	3.093296	1.85	2.3
I-CH3	3.96(c)	3.5131	4.85	4.367
I-F	3.65 (c)	3.638305	4.5	3.149
I-CL	4.27 (c)	3.527830		4.367
I-OCH3	3.55(c)	3.64567	4.28	3.647
II-CH3	3.14(c)	2.776601	3.6	3.734
II-F	3.08(c)	2.864981	3.25	2.591
II-CL	3.60(c)	1.244683	3.85	2.969
II-OCH3	2.83(c)	2.754506	3.04	3.014
III-CH3	3.85(c)	3.623575	4.55	4.668
III-F	3.55(c)	3.74878	4.2	3.525
III-CL	4.18(c)	4.183314	4.78	3.904
III-OCH3	3.46(c)	3.58675	3.97	3.948
5,6-dimethylbenzimidazole dimethylbenzimidazole	1.89(d)	1.060559	2.35	1.877
Oxibendazole	1.86–2.63(e)	2.9239	2.6	1.787
oxfendazole	1.88–2.13(a)	3.859255	2.03	2.022

Figure1. The values calculated at B3LYP/6-31+G**

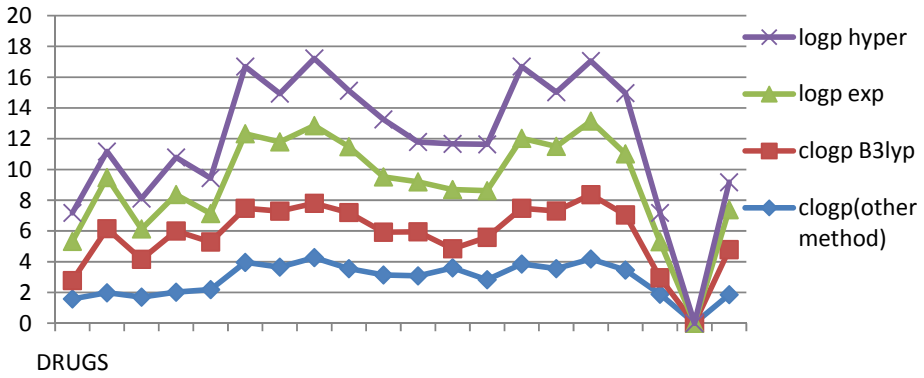

Conclusions

we have applied abinitio methods for the calculation of some properties and the free solvation energy in two solvents. The calculations began with the geometry optimization of drug

molecules using DFT method.The results showed that B3LYP /6-31+G** method provides results closer to experimental values compared to other methods.

Figure2. show the Chemical structures of the Benzimidazole.

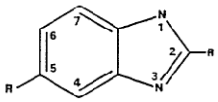

References:

[1] Leo, A.; Hansch, C.; Elkins, D. Partition Coefficients and Their Uses. *Chem. Re*V. **1971**, *71* (6), 525–616.

[2] Hansch, C.; Leo, A.; Hoekman, D. *Exploring QSAR: Hydrophobic, Electronic and Steric Constants*. American Chemical Society: Washington, DC, 1995.

[3] Sangster, J. *Octanol-Water Partitioning Coefficients: Fundamentals and Physical Chemistry*. John Willey & Sons: Chichester, U.K., 1997.

[4] Perlovich, G. L.; Kurkov, S. V.; Kinchin, A. N.; Bauer- Brandl, A. Solvation and Hydration Characteristics of Ibuprofen and Acetylsalicylic Acid. *AAPS PharmSciTech***2004**, *6* (1), 1–9.

Ab initio studies and NBO analysis of peri cyclic reaction mechanism between Pyridine and Furan

S. Jameh-Bozorghi[1] , A. Gaempanah[2],

1-Chemistry Department, Faculty of science, Islamic Azad University, Toyserkan Branch,Toyserkan, Iran

2-Chemistry Department, Faculty of science, Islamic Azad University, Arak Branch, Arak, Iran

Introduction

Reaction between 3-halopyridines and furan produce two different isomers (scheme 1) [1]. 2,3-pyridyne and 3,4-pyridyne are intermediates in these reactions. 3,4-pyridyne formations is faster than 2,3-pyridyne [2] because barrier energy of 2,3-elemination reaction of 3-halopyridine (except 3-fluoropyridine) is higher than 3,4-elimination. Reaction between pyridines and furan occurred through the Diels-Alder cycloaddition reaction. In this reaction percentage of products is difference. The main goal of this work is mechanistic study of this pericyclic reaction and suggested major and minor products, Also Natural Bond Orbital (NBO) analysis will use to investigate the nature of the bonds in reactant, transition states and products.

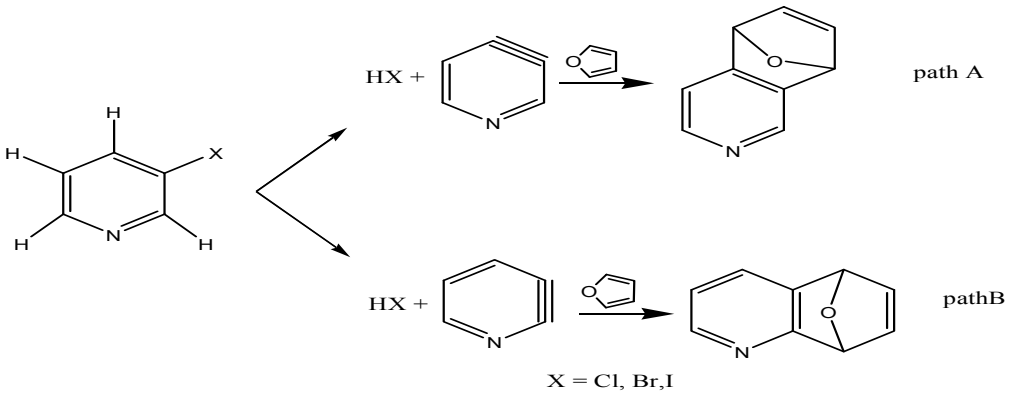

Scheme 1

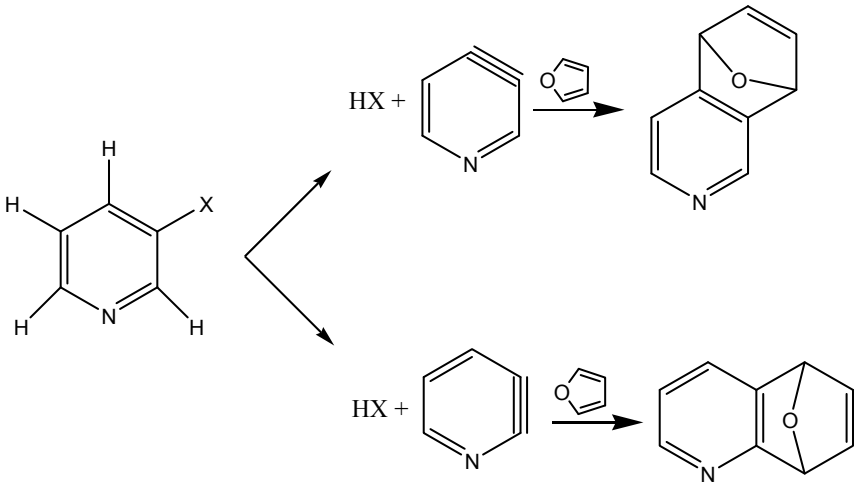

X = Cl, Br,I

Theoretical methods

DFT calculation were carried out using B3LYP/6-311+G** level of theory with the GAUSSIAN 2003 package of programs [3] on a personal computer. Energy-minimum molecular geometries were located by minimizing energy with respect to all geometrical coordinates without imposing any structure symmetrical constraints and transition state structures obtained by QST2 subroutine.

Results and discussions

DFT-B3LYP/6-311+G** calculation results showed that the activation energy for cycloaddition of furan to 3,4-Pyridyne and 2,3-Pyridyne are 15.028 and 35,2 kcal/mol respectively. Also these results revealed that $\Delta H_{reaction}$ is -37.65 and -19.58 kcal.mol^{-1} respectively. Therefore these reactions are exothermic and product of pathway B is major product.

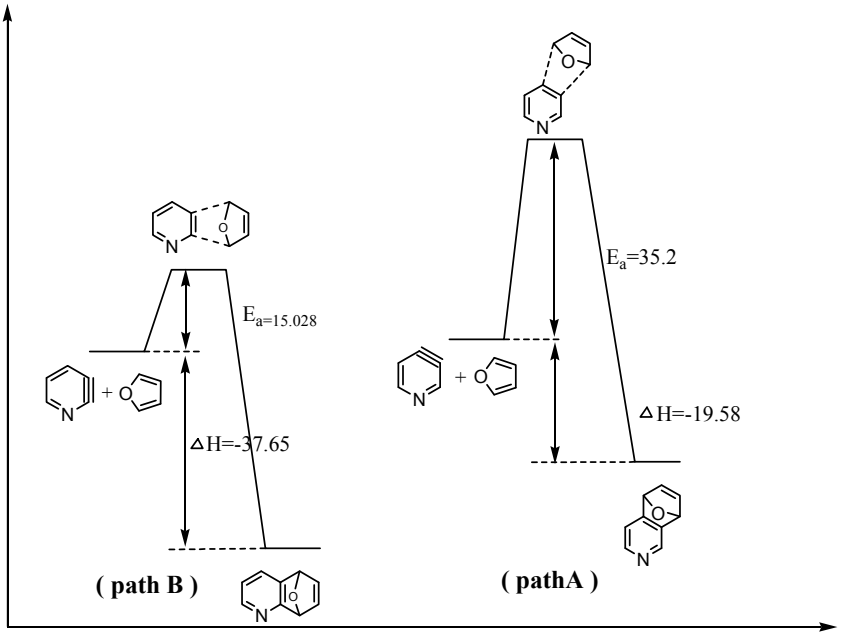

Fig 1: calculated b3lyp/6-311+g** profile of pericyclic reaction of pyridine isomers and furan

Conclusion

Calculation results showed that pericyclic reaction through pathway A has higher barrier energy therefore path B is major pathway of reaction. These results have a good agreement with experimental data [2].

Reference

[1] M. Winkler, B. Cakir and W. Sander**;** *J. Am. Chem. Soc*.**; 19** 126 (2004) 6135-49

[2**]** S. J. Connon and A. F. Hegarty**;***Tetrahedron Letters* **42**, 4 (2001), 735-737

Thermodynamic study of porphyrin derivatives aggregation, Molecular Dynamics (MD) Simulation study of aggregation, Calculation of Gibbs free energy and equilibrium constant and Prediction of equilibrium constant by QSPR and PCA model

Maryam Ghadamgahi*, Davood Ajloo
Department of chemistry, University of Damghan, Damghan, Iran
*E-mail: ghadamgahi63_2010@yahoo.com

Keywords: Porphyrin, Molecular Dynamics Simulation, Gibbs free energy, Aggregation.

1. Introduction:

We have extensively studied the aggregation of 85 porphyrins derivatives. Here we have report on a thermodynamic study of such aggregation behavior on varying the derivatives of porphyrins. Porphyrins are a class of compounds which play a relevant role in chemistry and biology [1,2]. The different kinetics of aggregation is revealed from the results of our MD simulations, which is helpful for understanding the different effect of derivatives on aggregation to design new drugs for photodynamic therapy with better efficiency in future [3].

2. Materials and Methods:

8 ns of MD simulation using the GROMACS program, thermodynamic study to predict the binding energy by Auto Dock tool, using $\Delta G_{bind} = -RT\ln K$ equation for calculation of equilibrium constant, generation of 1497 molecular descriptors by Dragon v.5.0 and QSPR study by MLR and PCA analyses with SPSS 16 were done for 85 porphyrin derivatives.

3. Result and discussion:

The outcomes of the simulations have shown that, the presence of various side groups causes different aggregation pattern. The correlation coefficient for prediction of equilibrium constant by MLR and PCA methods were 0.923 and 0.732 respectively. Variation of averaged distances between the mass centers of five porphyrins vs. time (Fig.1), Correlation between predicted and experimental K (Fig.2) and structure of studied porphyrin (Fig.3) are presented. Results of equilibrium constant and binding Gibbs energy are presented in following table.

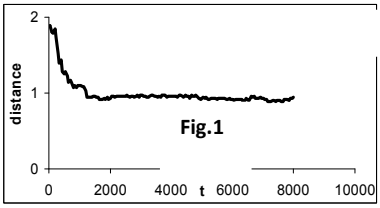

R=0.923

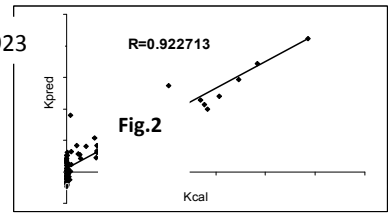

Fig.3

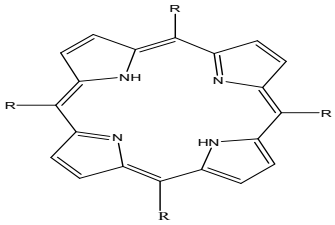

4. Conclusion:

Different aggregation of porphyrin in aqueous solution depend on derivatives were observed from descending distance diagrams of simulation. Investigation of different substitute effect on self aggregation and free energy were investigated and results are presented.

Table1. Definition of R and the values of free energy of Gibbs and binding constant

No	R	ΔG_{bind}	*K*	No	R	ΔG_{bind}	*K*
1	CH_2OH(1)	-5.68	14641.09	44	NH_3(1)	-5.47	10269.86
2	OCH_3(1)	-5.36	8528.906	45	$NHCH_3$(1)	-5.39	8972.11
3	CH_2OH(2,ortho)	-6.51	59466.9	46	NO(1)	-6.01	25561.57
4	CH_2OH(4)	-6.72	84778.2	47	OH(1)	-5.25	7083.078
5	OCH_3(3)	-5.13	5783.849	48	Ph(1)	-6.31	42422.88
6	Br(4)	-5.13	5783.849	49	C_2H_5(2)	-5.98	24298.88
7	CH_2OH(4)	-6.86	107388.2	50	CH_3(2)	-5.77	17044.23
8	CH_3(4)	-6.52	60479.62	51	COH(2)	-6.38	47745.94
9	Cl(4)	-5.64	13684.8	52	$CONH_3$(2)	-7.51	321848.1
10	C_2H_5(4)	-7.04	145534	53	NH_3(2)	-6.76	90702.49
11	NCH_3(4)	-9.07	4484529	54	$NHCH_3$(2)	-5.87	20179.71
12	OH(4)	-5.79	17629.7	55	NO(2)	-6.9	114892.5
13	OCH_3(4)	-5.05	5052.972	56	OH(2)	-5.37	8674.153
14	Ph(4)Br(1)	-9.29	6502188	57	Ph(2)	-7.78	507764.5
15	Ph(4)CH_3(1)	-9.49	9114538	58	CH_3(3)	-6.18	34061.31
16	Ph(4Cl(1)	-9.42	8098384	59	$COCH_3$(3)	-6.84	103822
17	Ph(4)Br(2,orto)	-9.43	8236299	60	$CONH_3$(3)	-8.5	271840
18	Ph(4)CH_3(2)	-9.56	10258195	61	NH_3(3)	-6.76	90702.49
19	Ph(4)Cl(2,ortho)	-9.47	8811851	62	NO(30	-7.78	507764.5
20	Ph(4)Cl(3)	-9.42	8098384	63	OH(3)	-5.53	11364.94
21	Ph(4)Br(4)	-9.46	8664298	64	Ph(3)	-8.8	2842533
22	Ph(4)CH_3(4)	-10.07	24271270	65	$CONH_3$(4)	-7.58	362232.3
23	Ph(4)Cl(4)	-9.41	7962778	66	NH_3(4)	-6.53	61509.59
24	Porphyrin	-5.07	5226.541	67	Ph(4)C_2H_5(1)	-9.52	9588174
25	Ph(4)Br(3)	-9.32	6840074	68	Ph(4)$COCH_3$(1)	-9.32	6840074
26	Ph(4)$COCH_3$(4)	-9.87	17314796	69	Ph(4)(COH(1)	-9.42	8098384
27	Ph(4)NO(4)	-8.37	1375162	70	Ph(4)$CONH_3$(1)	-9.3	6612920

28	Ph(4)	-9.37	7442684	71	$Ph(4)NH_3(1)$	-9.32	6840074
29	$Ph(4)C_2H_5(4)$	-9.72	13440364	72	$Ph(4)OCH_3(1)$	-9.12	4879616
30	$Ph(4)CH_2NH_2(4)$	-8.19	1014720	73	Ph(4)OH(10	-9.12	4879616
31	$Ph(4)CH_2OH(4)$	-8.85	3092960	74	Ph(4)C2H5(2)	-7.62	387545.1
32	$Ph(4)CH_3(3)$	-9.93	19161077	75	$Ph(4)COCH_3(2)$	-9.75	14138792
33	$Ph(4)CONH_3(4)$	-8.85	3092960	76	Ph(4)COH(2)	-9.35	7195518
34	Ph(4)COH(4)	-9.21	5680538	77	$Ph(4)CONH_3(2)$	-9.8	15384418
35	$Ph(4)NH_3(4)$	-9.09	4638573	78	$Ph(4)NH_3(2)$	-9.25	6077493
36	$Ph(4)OCH_3(4)$	-8.28	1181273	79	$Ph(4)OCH_3(2)$	-8.97	3787733
37	Ph(4)OH(4)	-8.34	1307232	80	Ph(4)OH(2)	-8.83	2990245
38	$C_2H_5(1)$	-5.52	11174.64	81	$Ph(4)COCH_3(3)$	-9.3	6612920
39	$CH_2NH_3(1)$	-6.42	51082.42	82	Ph(4)COH(3)	-8.84	3041169
40	$CH_3(1)$	-5.46	10097.9	83	$Ph(4)CONH_3(3)$	-9.33	6956560
41	$COCH_3(1)$	-5.84	19182.87	84	$Ph(4)NH_3(3)$	-8.59	1993869
42	COH(1)	-5.64	13684.8	85	Ph(4)OH(3)	-9.74	13902040
43	$CONH_3(1)$	-7.01	138344.9				

In conclusion, the porphyrins under investigation, exhibits different aggregation behavior with different rate and free energy depend on type of derivatives.

Refrences:

[1]. W. Zheng, N. Shan, L. Yu, X. Wang, J. *Dyes and Pigments.* (2008), 153-157.

[2]. M. Pompe, M. Veber**,** *Atmospheric Environment,* 35 (2001) 3781–3788.

[3]. A. Habibi, M. Nooshyar, *Korean Chem. Soc*, 26 (2005**)** 1.

Kinetic study of salt and concentration effect on the porphyrin derivatives aggregation and calculation of relaxation time and rate constant by Molecular Dynamics Simulation

Maryam Ghadamgahi*, Davood Ajloo
Department of chemistry, University of Damghan, Damghan, Iran
*E-mail: ghadamgahi63_2010@yahoo.com

Keywords: Porphyrin, Aggregation, Rate constant, Molecular Dynamics Simulation.

Introduction:

Porphyrin pigments are key ingredients in biological electron-transfer processes such as photosynthetic and mitochondrial membrane reactions [1].The simulations have been confirmed that porphyrin aggregation is increased in a dose-dependent manner and the kinetics of formation of one such very large assembly has been reported. In particular, this porphyrin, upon salt addition, is able to form micrometric sized clusters [2]. The aim of present work is the presentation of the kinetic parameters of the selected derivatives and investigation of different substitute effect on self aggregation and kinetic of aggregation.

Methods:

All MD simulations were carried out using the GROMACS 3.3 .1 in 8ns. Variation of distance between the mass centers of porphyrin were obtained and averaged. Data of averaged distance were transferred in to ORIGIN version 5 software and first order exponential decay was used in order to calculate the relaxation time and kinetic constant of compounds. Kinetic parameters were determined by fitting scatter curve of distance. $d = d_0 e^{-t/\tau}$

Result and discussion:

The kinetic of the porphyrin derivatives in aqueous solutions were investigated as a function of the concentration of compound and salt addition in to the system Relaxation times of compounds from fitted exponential first order diagrams were obtained. Distance diagrams are reported in following figures and from these diagrams increase in the aggregation of

porphyrin derivatives by increasing the number of porphyrin and salt in systems have been obtained. Relaxation times and kinetic Constant of different porphyrin derivatives are presented in the following table (1). Kinetic constants were calculated by the equation: $k=1/\tau$

Conclusion:

In conclusion, the porphyrins under investigation exhibit an aggregation behavior. Results of distance diagrams have shown different rate aggregation depend on derivatives. Kinetic constant of porphyrin aggregation were compared by increasing the number of porphyrins (concentration effect) and salt (NACL). It was shown that an increase in the kinetic constant are associated with increasing concentration and salt to the box of simulation. By increasing the number of porphyrin, rate of aggregation and the kinetic constant were increased and these effects have been proved to be important in kinetic of aggregation.

Table1: Definition of R, relaxation times, kinetic Constant and number of molecule and salt

Nom	R	No.mol	No.salt	τ	$k=1/\tau$	Nom	R	No. mol	No.salt	τ	$k=1/\tau$
1	H	2	0	1456.867	0.00069	16	4 CH_3	5	15	6900,901	0,00014
2	H	3	0	963.1325	0.00104	17	4 CH_3	5	45	1294,866	0,00077
3	H	5	0	290.6835	0.00344	18	4 CH_3	5	55	874,8689	0,00114
4	4Ph+1CH_3	2	0	953,0436	0,00105	19	4CH_2OH	5	15	2843,465	0,00035
5	4Ph+1CH_3	3	0	941,3569	0,00106	20	4CH_2OH	5	45	1177,141	0,00085
6	4Ph+1 CH_3	5	0	835,6869	0,00120	21	4CH_2OH	5	55	913,0813	0,00109
7	4Ph+2 CH_3	2	0	9105,764	0,00011	22	4OMe	5	15	6087,737	0,00016
8	4Ph+2 CH_3	3	0	3445,084	0,00029	23	4OMe	5	45	1424,428	0,00070
9	4Ph+2 CH_3	5	0	1586,311	0,00063	24	4OMe	5	55	598,1034	0,00167
10	4 CH_3	2	0	829590,2	0.000001	25	Ph+4 CH_3	5	15	4147,334	0,00024
11	4 CH_3	3	0	45230,88	0.00002	26	Ph+4 CH_3	5	45	1129,865	0,00088
12	4 CH_3	5	0	478,3542	0,00209	27	Ph+4 CH_3	5	55	1113,7	0,00090
13	H	5	15	3475.604	0,00029	28	Ph+4COH	5	15	2114,976	0,00047
14	H	5	45	2013.249	0,00050	29	Ph+4COH	5	45	1989,838	0,00050
15	H	5	55	564,2742	0,00177	30	Ph+4COH	5	55	738,0901	0,00135

Number in R list show the number of R.

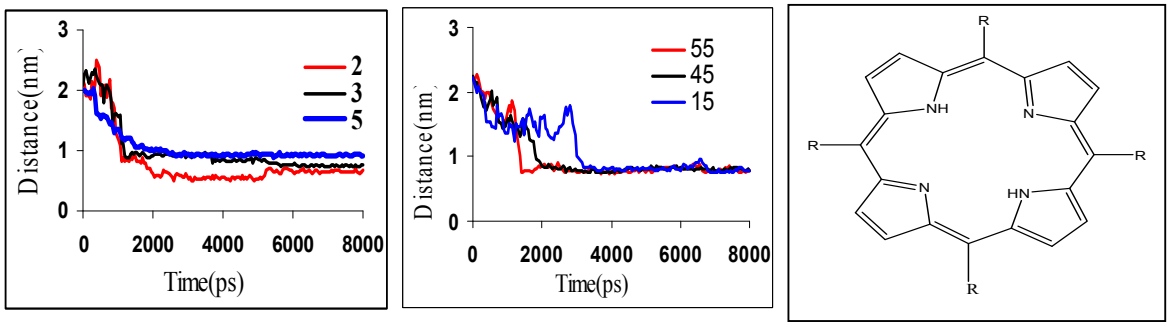

Figure1. Distance diagrams of concentration effect of system Nom.4, 5 and 6(left Fig), salt effect of system Nom 19, 20 and 21(middle Fig) and structure of studied porphyrin (right)

Aggregation rate of porphyrin derivatives were drastically increased by addition of salt or increasing concentration as we expected

References:

[1]. L.M. Scolaro, M. Castriciano, A. Romeo, A. Mazzaglia, F. Mallamace, N. Micali, *Physica A*., 2002, 304. 158- 169.

[2]. J. R.Darwent, I. McCubbin, D. Phillips, *Chem*.S*oc*., 1982, 18. 3347.

Interactions and chemisorption at different coverages studied by DFT :CO on Co surface

F.Ghorbani Naieni*[a],A. A. Salari[a].M. Shabani[b], L. Nassaji jahromi[a], Z. Ahoo[a]

[a]*Department of Chemistry, Islamic Azad University, Shahre-Rey Branch, Thran, Iran*

(E-mail: F_Ghorbani2010@yahoo.com)

[b] *Department of Chemistry, Islamic Azad University, Varamin-Pishva Branch, Tehran, Iran*

Abstract

We use density functional theory (DFT) method for accurate chemisorption energies to calculate the chemisorption energy for CO on Co surface for various adsorbate densities and patterns.We identify adsorbate through-space repulsion,bonding competition,and substrate-mediated electron delocalization as key factors determining the preferred chemisorption patterns for Co and adsorbate coverages.

Keywords: Density functional theory, Carbon monoxide ,Cobalt (001), Chemisorption,

Introduction

The prototypical CO/transition metal adsorption systems,though extensively studied, continue to be of significant contemporary research interest[1-2].There are many studies that address adsorbate-adsorbate interactions,and it is beyond the present scop to review these and other studies in full[3-4-5].

Computational Methods

In the present study ,we investigate the chemisorption of CO on Co,adsorption site,and CO overlayer pattern.DFT calculations are carried out using the B3LYP and norm –conserving optimized pseudopotentials with the designed nonlocal method for metals [6-7].CO chemisorption is modeled at coverages of Θ=0.25,0.5,0.75,and 1 ML(monolayer).In these calculations,the CO bond is held perpendicular to the surface.Values for E_{chem} are calculated as

$$E_{chem}=(-E_{surface-CO}+NE_{CO}+E_{surface})/N \qquad (1)$$

Where *N* is the number of CO molecules per unit cell.On the (001)surface of Co,we modeled. chemisorption at Θ=0.25,0.5,0.75,and 1 at top adsorption site,as shown in figure 1.

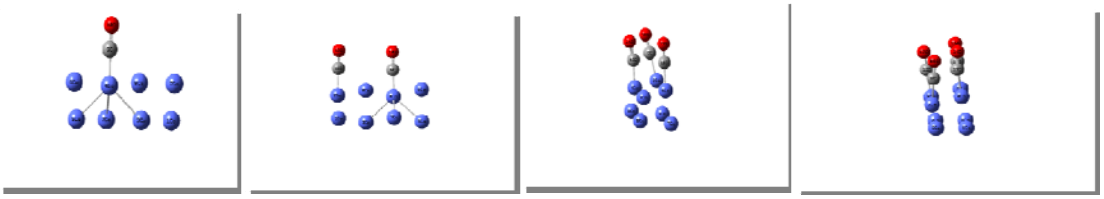

Θ=0.25 Θ=0.5 Θ=0.75 Θ=1

Figure1.Schematic of the (001) surface with CO at Θ=0.25,0.5,0.75,and 1 ML(monolayer).

TABLE1: Results for CO E_{chem} at Different Θ Values on the (001) surface of Co. All value $E_{chem}$for the top site is reported

site	Θ	E_{M-CO}	Ead(a.u)	E(eV)	E(kcal/mol)	E(kJ/mol)
top	0.25	-1273.46	-0.10567	-2.87545	-66.308427	-277.434
	0.5	-1386.84	-0.08986	-2.44528	-56.388835	-235.930
	0.75	-1500.22	-0.08089	-2.20134	-50.763514	-212.394
	1	-1613.58	-0.07546	-2.05337	-47.351192	-198.117

Figure2.Calculated chemisorption energies at different coverages

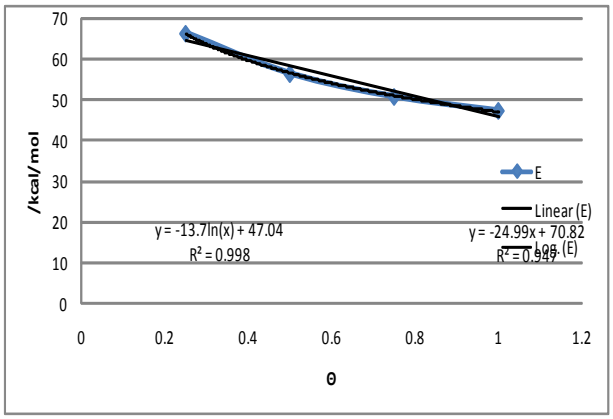

Results and discussion

We can estimate the energetic cost of placing adsorbates at nearest-neighbor distances from our top site chemisorption results.Our data set includes different coverages exclusively top site chemisorbed structures at Θ=0.25,0.5,0.75,and 1 ML(monolayer). We deduce that this increase in repulsion must be due to d electrons changing the adsorbed CO electronic structure.The increased number of CO on the surface appreciably affect the chemisorption energies.

Conclusion

We identify adsorbate through-space repulsion,bonding competition,and substrate-mediated electron delocalization as key factors determining the preferred chemisorption patterns for Co and adsorbate coverages.Results show that the back-donation from the metal *d*-bonds into the CO 2π* orbitals increase.Increased filling of the 2π* orbitals strengthens the repulsion between chemisorbed CO molecules,while increased interadsorbate separation weakens it.

References

[1] N. A. Besley, J. Chem. Phys. 122 (2005) 1847006.

[2] S. Yamagishi, T. Fujimoto, Y. Inada, H. Orita, J. Phys. Chem. B 109 (2005) 8899.

[3] B. N. J. Persson, M. Tüshaus, A. M. Bradshaw, J. Chem. Phys. 92(1990) 5034.

[4] R.. Brako, D. Šok ević, Surf. Sci. 469 (2000) 185.

[5] D. H. Wei, D. C. Skelton, S. D. Kevan, Surf. Sci. 381(1997) 49.

[6] N. J. Ramer, A. M. Rappe, Phys. Rev. B 59 (1999) 12471.

[7] I. Grinberg, N. J. Ramer, A. M. Rappe, Phys. Rev. B: Condens. Matter Mater. Phys. 63 (2001)201102(R).

Theory of CO adsorption on Co (001)by Density Functional Theory (DFT)

F.Ghorbani Naieni*[a],A. A. Salari[a].M. Shabani[b] L. Nassaji jahromi[a], Z. Ahoo[a]

[a]*Department of Chemistry, Islamic Azad University, Shahre-Rey Branch, Thran, Iran*

(E-mail: F_Ghorbani2010@yahoo.com)

[b] *Department of Chemistry, Islamic Azad University, Varamin-Pishva Branch, Tehran, Iran*

Abstract

Adsorption of CO on Co(001) surface has been investigated by density functionaltheory(DFT) method.Adsorption energies,structures,and vibrational frequencies of CO on this surface is studied. Adsorption in atop,bridge,and three-fold fcc position are considered.Particularly, we show that the atop site becomes most favorable for the c(2×1×1) structure at1/4 monolayer.

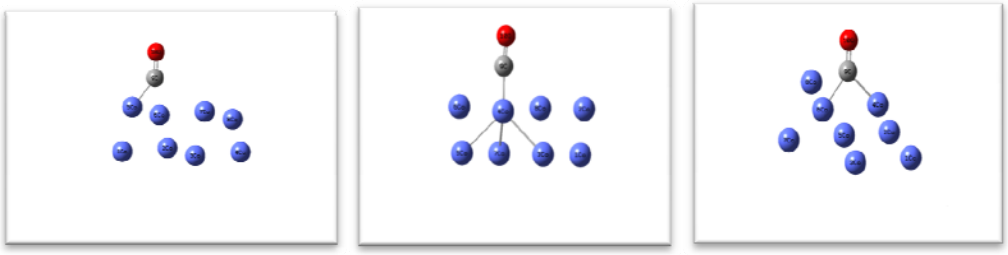

a)Hollow b)Atop c) Bridge

Figure1.Typical adsorption structures of CO on Co(001)

Keywords: Density functional theory, Carbon monoxide ,Cobalt (001,) Adsorption

Introduction

Carbon monoxide (CO) adsorption on transition metal surfaces has been the subject of many theoretical studies up to now[1-2].There are much discussion on CO site preference on transition metals[3-4].Extending the work on Co,we have been continuously undertaking an extensive investigation of CO adsorption on Co surfaces to study the structure sensitivity of CO adsorption.Some result on Co(0001),Co(111),($10\bar{1}0$) have been already published and the result on Co(001)surface is reported in the present paper.

Computational Methods

This work was carried out with the GAUSSIAN 03 program package[5]. The geometries of CO,Co(001) were respectively optimized using density functional theory (DFT) at the B3LYP level on different basis sets 6-31G*and LANL2DZ[6-7].For Co (001), an un-reconstructed c(2×1×1) surface unit cell(including 8 Co atoms) was chosen to model adsorption of CO for a low coverage of 1/4 monolayer. Adsorption energies were computed by subtracting the energies of the gas- phase CO molecule and surface from the energy of the adsorption system ,as shown in

$E_{ad}=E(CO/Surface)-E(CO)-E(Surface)$ (1)

With this definition a negative E_{ad} corresponds to stable adsorption on the surface .The experimentally determinded Co lattice constant of 3.5441A˚was used for the production of the surfaces.Under the present computational conditions the C-O bond length for free CO molecule was calculated as 1.13759A˚ in good agreement with the experimental value of 1.13 A˚[8].Frequency of free CO molecule (d(C-O)=1.13759 A˚) was calculated as2208.61019 cm^{-1}This value is close The experimental harmonic value (2143cm^{-1})[8].Three adsorption sites(atop,bridge,and hollow) were investigated by attaching the carbon atom of CO to the surface.

Table 1

Calculated properties of cobalt-CO overlayer with admolecules placed at various sites (a=atop,b=bridge,f=three-fold fcc) above Co(001)surface.

Site	Surface	d(CO)	d(Co-C)	E_{ad}	ν
a	Co(001)	1.1698	1.735	-2.8754504	1945.88
b		1.188	1.927	- 2.8710748	1777.52
c		1.1928	1.99	-1.7380329	1773.24

Molecule length d(CO),distance of C from the nearest Co atom d(Co-C). E_{ad}(in eV)is the adsorption energies per molecule. ν(in cm^{-1}) is the CO stretching-mode frequency.

Results and discussion

In Table 1, we present the calculated structure and energy data. ν is the calculated CO stretching frequency.The C-O stretching frequencies are calculated as1945.88, 1777.52,

and1773.24 cm^{-1} for the atop,bridge,and hollow sites respectively. The calculated frequencies for the atop,bridge,and hollow sites also agree well with the experimental data[9-10]. The Co-C and C-O distances for the atop,bridge,andhollow sites are in good agreement with the experimental LEED[11].The negative value of the adsorption energy indicates that the adsorption is an exothermic process.Furthermore adsorption energy on atop site is most favorable.

Conclusion

Adsorption of CO on Co(001) surface has been investigated by density functional theory(DFT) method.Adsorption energies,structures,and vibrational frequencies of CO on this surface is studied. Calculated C-O stretching frequencies agree experimental data.For Co(001),CO adsorbs at the bridge, hollow and atop sites at low coverage but the atop site becomes most favorable for the c(2×1×1) structure at1/4 monolayer.

References

[1] G. Kresse, A. Gil and P. Sautet, Phys. Rev. B 68 (2003) 073401.

[2] F. Abild-Pedersen and M.P. Andersson, Surf. Sci. 601 (2007) 1747.

[3] M. Gajdoš, A. Eichler and J. Hafner, J. Phys. Condens. Matter 16 (2004) 1141.

[4] D.E. Jiang and E.A. Carter, Surf. Sci. 570 (2004) 167.

[5] M.J.Frisch, G.W. Trucks, H.B. Schlegel, G.E. Scuseria, M.A. Robb, J.R. Cheeseman, J.A., Jr. Montgomery, T. Vreven, K.N. Kudin, J.C. Burant, et al. Gaussian 03, Revision E.01;Gaussian Inc.: Wallingford, CT, USA, 2004.

[6] R. Krishnan, J.S. Binkley, R. Seeger, J.A. Pople, Self-Consistent Molecular Orbital Methods. 20.Basis set for Correlated Wave-functions. J. Chem. Phys. 72 (1980) 650–654.

[7] M.J. Frisch, Gaussian 94, Revision E.2; Gaussian: Pittsburgh, PA, USA, 1995.

[8] CRC Handbook of Chemistry and Physics, 81st ed.; Lide, D. R., Ed.; CRC Press: Boca Raton, FL, 2000.

[9] S.E. Mason, I. Grinberg and A.M. Rappe, Phys. Rev. B 69 (2004) 161401(R).

[10] F. Abild-Pedersen and M.P. Andersson, Surf. Sci. 601 (2007) 1747.

[11] J. Lahtinen, J. Vaari, K. Kauraala, E.A. Soares and M.A. Van Hove, Surf. Sci. 448 (2000) 269.

The investigation of Hydrogen Bond Interactions in Fluoroacetic Acid Dimer Using DensityFunctional Theory

F.Ghorbani Naieni*[a], S.Rezaiee,[a]A. A. Salari[a].M. Shabani[b]

[a]*Department of Chemistry, Islamic Azad University, Shahre-Rey Branch, Thran, Iran*

(E-mail: F_Ghorbani2010@yahoo.com)

[b] *Department of Chemistry, Islamic Azad University, Varamin-Pishva Branch, Tehran, Iran*

Abstract

Density functional theory method have been employed to study all theoretically possible conformers of fluoroacetic acid. Molecular geometries and energetic monomers and dimers in gaseous phase have been obtained using B3LYP level of theory, implementing 6-311++G(d,p) basis set. In addition, it was found that in comparison with acetic acid the strength of hydrogen
bonding in fluoroacetic acid decreased.

KeyWords: Hydrogen bonding, Fluoroacetic acid, DFT calculation,Gaussian03

Introduction

Hydrogen bonding has been a very interesting issue for chemists for a long time since it can account for characteristics of many chemical and biological phenomena. A sound knowledge of hydrogen bond is fundamental to understand chemical structures,enzyme catalysis, material properties, self assembly phenomena,and functions of molecular and biological devices and machines[1-3]. It is well known that carboxylic acids form in the gas phase and solution cyclic structure with two very strong O-H…O=C hydrogen bonds.

Computational Methods

The ground-state properties of the monomers and the dimers of fluoroacetic acid have been calculated by using B3LYP method at 6-311++G(d,p) basis set level. All computations have been performed on a personal computer using the Gaussian 03 program package and Gaussview molecular visualization program [4-5]. The uncorrected interaction energies were obtained by
subtracting the energy of two fully optimized monomers from the energy of the dimers:

$E_{int} = E_{X-Y} - E_X - E_Y$ (1)

where E_X, E_Y and E_{X-Y} are the electronic energies of first fluoroacetic acid molecule, second one and dimer, respectively.

Table 1. Calculated total energies of fluoroacetic acid dimers and Calculated binding energies of the doubly hydrogen bonded fluoroacetic acid dimers using the 6-311++G(d,p) basis set at B3LYP method.

No. of F	E(X-Y)	Hydrogen bonding (a.u)	Hydrogen bonding (kcal/mol)	Hydrogen bonding (kJ/mol)
0-0	-458.354609	-0.02495317	-15.6693431	-65.52919285
1-1	-656.8656272	-0.0251349	-15.78346046	-66.00643162
2-2	-855.4010413	-0.02457528	-15.43204708	-64.53682087
3-3	-1053.953782	-0.02259182	-14.18653337	-59.32808255
1-2	-756.133311	-0.02483189	-15.59318533	-65.21070103
1-3	-855.4104052	-0.02456422	-15.42510195	-64.50777635
2-3	-954.6779054	-0.02407752	-15.11947868	-63.22965986
1-0	-557.6106417	-0.0255677	-16.05523722	-67.14300203
2-0	-656.8787328	-0.02567191	-16.12067588	-67.41666655
3-0	-756.1560983	-0.02567558	-16.12298046	-67.42630429

The values of Total energies and Calculated binding energies of the doubly hydrogen bonded are in Hartree, (kcal/mol), (kJ/mol).

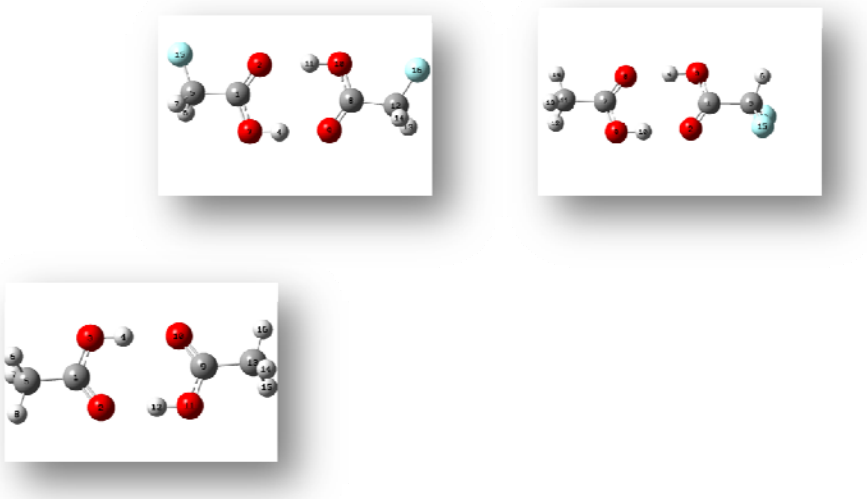

Figure 1. The optimized conformations of fluoroacetic acid dimers at B3LYP/6-311++G(d,p) level of theory.

Table 2. Some optimized geometric parameter of the ten lowest energy conformers of fluoroacetic acid dimers obtained at B3LYP level of theory with the 6-311++G(d,p) basis set.

No. of F	0-0	1-1	2-2	3-3	1-2	1-3	2-3	1-0	2-0	3-0
R(HO)	1.6847	1.68371	1.68847	1.68939	1.71086	1.73491	1.71586	1.64796	1.74102	1.76339

Bond lengths in Å.

Results and discussion

The properties of conformers of fluoroacetic acid, well reproduced at the DFT using 6-311++G(d,p) basis set are presented in Table 1. The effect of replace of a hydrogen atom with a fluorine atom on the geometrical parameters can be compared with the aceticacid geometries. For example in the acetic acid, the previously calculated C=O and C-C bond lengths using b3lyp/6-31+G(d) method were reported as 1.23158 Å and 1.50573 Å respectively.Comparison with our results shows that fluorination causes a decrease in the C=O and C-O bond lengths and increase in theC-C bond length. For instance, the C=O bond length calculated at b3lyp/6-311++G(d,p) level decreased to 1.21649, 1.21459, 1.21359, 1.21343 Å and 1.21327 for the(1-0),(2-0),(3-0),(3-1),(3-2)and(3-3) respectively.

Conclusion

The hydrogen bond interaction of complex between fluoroacetic acid has been analyzed by B3LYP method employing the 6-311++G(d,p)basis set. Four monomers and ten dimers were considered and suggests that these structures are localgeometrical parameters in monomer so that carbonyl and carboxylic acid hydrogen bond lengths increase. In comparison with acetic acid, it was found that replacement of hydrogen by an electron with drawing group leads to a decrease of strength of hydrogen bonding.

References

[1] S. Scheiner, Hydrogen Bonding; Oxford University Press: NewYork, 1997.

[2] G. A. Jeffery, In Introduction to Hydrogen Bonding; Oxford UniversityPress: New York, 1997.

[3] P. Hobza, Z. Havlas, Chem. Rev. 100(2000) 4253.

[4] M. J. Frisch, et al., Gaussian 03, Revision C.02, Gaussian Inc.,Pittsburg, PA, 2003.

[5] A.Frisch, A. B.Nielsen, J. Holder, Gauss View User Manual,Gaussian.

Hydrogen Bonding Effects on Relative Stability of Molybdate-Phosphonic Acid Complex by DFT Study

M. H .Ghorbani*, R. Fazaeli, A. Ghoorchian

Department of Applied Chemistry, Faculty of Technical & Engineering, Islamic Azad University, South Tehran Branch, Tehran, Iran

(Email: MH_Ghorbani@azad.ac.ir)

Keywords: Molybdate-Phosphonic Acid (MPA), Dielectric Constants, Solvent Effects, DFT, Hydrogen Bond.

Introduction

Hydrogen bonding will be discussed in terms of observable properties such as geometrical parameters and interaction energy. The researches [1] have shown the usefulness of the AIM models in interpreting the strength of some simple hydrogen-bonded systems such as methanol-water, phosphonic acid, and phosphinoxides and aminoxides. We studied the hydrogen bonding effect on structure and relative stability of Molybdate-Phosphonic Acid (MPA) Complex in different solvents [2] and their dielectric constants have been carried out by using computational study at the level of density functional theory (DFT) methods [3]. Characterization of the hydrogen bonding interaction between Molybdate and Phosphonic acid has been well studied by theoretical calculations. Phosphonic acid complexes provide suitable benchmark systems for studying much weaker interactions than typical chemical bonds and require, therefore, calculations with high accuracy. The influence of the environment has been discussed with respect to the solvent effect computations using PCM solvation models. The PCM cavity is defined by using Pauling [4] radius for each solute atom.

Methods

All calculations were carried out with the GAUSSIAN03W program [5]. Geometry optimizations in the solvent phase for all components and complex were performed at the DFT [6] level with B3LYP and B3PW91 functionals and with two series of basis sets:

A. Dunning basis set plus polarized functions (D95**) for hydrogen and oxygen atoms; LANL2DZ for Molybdenum and Phosphor [7]. The effective core potential of Wadt and Hay is also included for Mo and P.
B. Double-zeta valance basis set plus polarized and diffuse functions (6-31+G(d,p)) for hydrogen and oxygen atoms; LANL2DZ for Molybdenum and Phosphor. The effective core potential of Wadt and Hay is also included for Mo and P.

Results and Discussions

The equilibrium structure obtained respectively hydrogen-bond calculation in the B3LYP/(H,O):6-31+G**+(Mo,P):LANL2DZ. In this investigation are shown that the longest hydrogen bonds correspond to O…H bonds present in MPA complex, while small deviations of hydrogen-bond angles from 180° manifest themselves in the complex of MPA, with increase of polarity solvent. Interestingly, MPA complex, which according to the calculations are strongly bound species among the hydrogen-bonded systems have also the shortest hydrogen bonds and almost straight hydrogen-bond angles. The shorter hydrogen bonds and the straight hydrogen-bond angles do not necessarily reflect stronger binding. On the contrary, significantly high calculated interaction energies, display two O...H hydrogen bonds and the deviation from 180° in the corresponding O-H…O angles.

Conclusion

The hydrogen bond interaction of 1:1 complex between Molybdate and Phosphonic acid has been analyzed by DFT method employing different basis set levels. Our theoretical studies indicate that the stability information of a single complex in different polarity of solvents could not be directly used to obtain stability data for hydrogen-bonded assemblies in general. It is noteworthy that the geometrical analysis of the hydrogen bonds may present useful insights into their cooperative effects affecting the complex stabilities. The best results of energetic and geometry for this group of complexes were obtained by B3LYP/(H,O):6-31+G**+(Mo,P):LANL2DZ calculations. The calculated results showed the solvents with higher dielectric constants strengthen the intermolecular hydrogen bonding interaction between Molybdate and Phosphonic Acid. The best results for energetic and geometrical

ground state and solvent effect computations in used of different various polarities of solvents were obtained with Becke3LYP calculations.

References:

[1]Alkorta, I.; Barrios, L.; Rozas, I.; Elguero, J. J. Mol. Struct. (THEOCHEM) 496 (2000) 131.

[2]Hadjadj-Aoul, R.; Bouyacoub, A.; Krallafa, A.; Volatron, F.; J. Molecular Structure: THEOCHEM 849 (2008) 8-16.

[3] Maciej Witwicki , Julia Jezierska, Chemical Physics Letters 493 (2010) 364–370.

[4] Paulo J. Mendes, Tiago J.L. Silva, A.J. Palace Carvalho, J.P. Prates Ramalho, Journal of Molecular Structure: THEOCHEM 946 (2010) 33–42.

[5] Gaussian 03, Revision B.01, Gaussian, Inc., Wallingford CT, (2004).

[6]Yiying Zhou, William H. Nelson, Radiation Physics and Chemistry 79 (2010) 479–489.

[7] H. Tavakol, Journal of Molecular Structure: THEOCHEM 954 (2010) 16–21.

Calculation of pK_b values of Aniline and its derivatives in aqueous solution

B. Ghalami-Choobar*, A. Ghiami-Shomami

Department of Chemistry, Faculty of Science, University of Guilan, P.O. Box: 19141, Rasht, Iran

E-mail address: B-Ghalami@guilan.ac.ir *(B. Ghalami-Choobar)*

Keywords: Free energy solvation, pK_b . PCM. Aniline

Intruoduction

The equilibrium constant is an important physico-chemical parameter of a substance, and determination of the acidity/ basicity of chemical compounds are matter of general interest for chemists as well as a matter of practical interest for chemical and pharmaceutical industries [1]. There are several experimental methods for the determination of equilibrium constant. However; the correlation of theoretical and experimental data can allow the development of predictive models to determine the pK_b of compounds for which no experimental data are yet available [2-3]. In this work, calculations of the pK_b values were performed on aniline and its derivatives by using Gaussian 03 software. Gas-phase energies were calculated using common basis sets at Hartree-Fock (HF) and B3LYP levels. Free energies of solvation were computed using the polarized continuum model (PCM). Results were compared with the experimental pK_b data.

Method

The pK_b values of anilines in aqueous solution were calculated in according to the following reaction 1 by using of equation 2.

$$B_{aq} + H^+_{aq} \xrightarrow{\Delta G^\circ_{aq}} BH^+_{aq} \qquad (1)$$

$$\Delta G^\circ_{aq} = -2.303RT \log K_b \qquad (2)$$

Where ΔG°_{aq} indicates to the free energy of protonation in an aqueous solution. The general approach to calculating ΔG°_{aq} was used on the basis of the thermodynamic cycle A.

$$\begin{array}{ccc} B(g) + H^+(g) & \xrightarrow{\Delta G^\circ(gas)} & BH^+(g) \\ \downarrow \Delta G^\circ_s B \quad \downarrow \Delta G^\circ_s \mathrm{H}^+ & & \downarrow \Delta G^\circ_s \mathrm{BH}^+ \\ B(aq) + H^+(aq) & \xrightarrow{\Delta G^\circ(aq)} & BH^+(aq) \end{array}$$

Scheme1. Thermodynamic cycle A

Using the thermodynamic cycle A, the values were calculated using the equation 3.

$$\Delta G^{\circ}_{aq} = \left(G^{\circ}_{g}BH^{+} - G^{\circ}_{g}B\right) + \left(\Delta G^{\circ}_{s}\mathrm{BH}^{+} - \Delta G^{\circ}_{s}B\right) + 269 \qquad (3)$$

All of calculations in gas -phase and aqueous -phase were made on aniline and its derivatives by using Gaussian 03 software. The optimized basis set 6-31G** were used for all of computing levels.

Results and discussion

The HF and B3LYP methods were applied to derive the free-energy changes of the gas-phase reaction, and the PCM model was used for the solvation energy in aqueous solution. The results for all 12 bases were shown in Table 1. As shown in figure 1, there is a very good correlation between the experimental and the calculated values of pK_b with a correlation coefficient 0.920 and 0.953 for HF and B3LYP, respectively. It can be concluded which DFT calculations in comparison with HF calculations of basicity constants provide satisfactory results.

Table1: The pK_b values of compounds

No	Compound name	EXP[a]	HF	B3LYP
1	Aniline	9.13	9.13	8.97
2	4-Chloro aniline	10.02	10.91	10.62
3	4-Methyl aniline	8.92	7.05	8.12
4	4-Bromo aniline	10.11	10.66	10.66
5	4-Cyano aniline	12.26	13.99	14.01
6	4-Fluoro aniline	9.35	9.49	9.21
7	2-Fluoro aniline	10.80	11.73	11.94
8	2-Methyl aniline	9.55	8.67	8.90
9	2-Bromo aniline	11.47	13.16	13.36
10	3-Chloro aniline	10.48	11.41	11.44
11	3-Bromo aniline	10.47	11.36	11.31
12	3-Ethoxy aniline	9.82	9.60	9.07

a:The values taken from ref.[4]

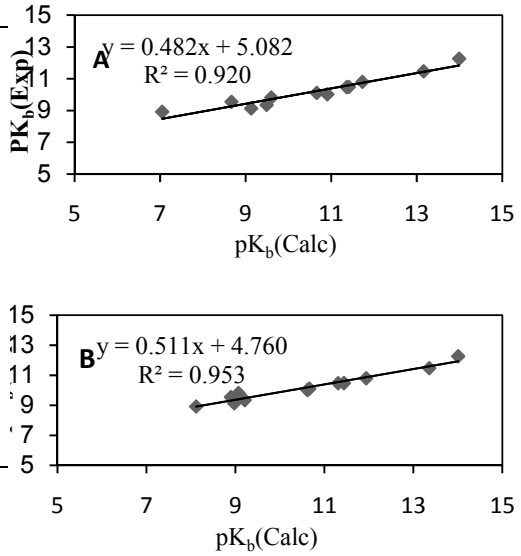

Figure 1.Correlation of the experimental and calculated values with HF (A) and B3LYP(B) methods

References:

[1] R. Flammang, N. Dechamps, L. Pascal, Y. Van Haverbeke, P. Gerbaux, P.-C. Nam and M.T. Nguyen, Lett. Org. Chem. 1 (2004) 23-30

[2] T. N. Brown , N. Mora-Diez J. Phys. Chem. B 110 (2006) 9270-9279

[3] F.Z. Erdemgil, S. S¸ Anli, N. S¸ Anli, G. O¨ zkan, J. Barbosa , J. Guiteras, J.L. Beltr´an, Talanta 72 (2007) 489–496

[4] R.David, CRC Handbook of Chemistry and Physics 90 thEdition (2010)

Theoretical study, an efficient synthesis rout to, and a kinetics and mechanistic investigation of reaction between triphenylphosphine and dimethyl acetylenedicarboxylate in the presence of NH dicarbonyl compounds

S. M. Habibi Khorassani[*a], M. T. Maghsoodlou[a], A. Ebrahimi[a], M. A. Kazemian[a], M, Zakarianejad[a]

[a]*Department of Chemistry, University of Sistan and Baluchestan, P.O. Box 98135-674, Zahedan, Iran*

Email:kazemean@yahoo.com

Keywords: Stable phosphorus ylides; dialkyl acetylenedicarboxylates; ***Z*** and ***E*** rotamer; AIM method; Intramolecular hydrogen bond; Theoretical calculations

Introduction

Phosphorus ylides are important reagents in synthetic organic chemistry, especially in the synthesis of naturally occurring products, compounds with biological and pharmacological activity [1-6]. Most of the phosphonium salts are usually made from the reaction of phosphine and an alkyl halide [4-6], though they can be obtained by Michael addition of phosphorus nucleophiles to activated olefins[2,3]. In the current work, we now describe the reaction between triphenylphosphine **1** and dimethyl acetylenedicarboxylate **2** in the presence of NH dicarbonyl compounds **3** (such as 1,2-dibenzoylhydrazine, ethyl 2-(3-nitrophenylamino)-2-oxoacetate and ethyl 2-(4-nitrophenylamino)-2-oxoacetate) which lead to the corresponding stable phosphorus ylides **4(a,c)** involving the two *Z*- and *E*- geometrical isomers in fairly high yield.(Figure 1). The structures of compounds **4a-c** were deduced from their IR, ^{1}H, ^{13}C and ^{31}P NMR spectra.

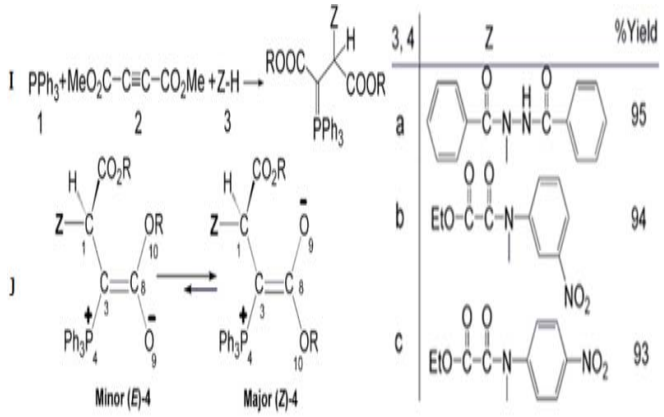

Figure **1: (I)** The reaction between triphenylphosphine **1,** dialkyl acetylenedicarboxylate **2** and 2-aminothiophenol **3** for generation of stable phosphorus ylides **4** (**4a** or **4b** and or **4c**), **(J)** Two isomers *Z* and *E* (major and minor) of ylide **4**

Results and Discussion

Theoretical study

Determination of the more stable isomer is possible by ^{31}P, ^{13}C and ^{1}H NMR techniques. For this reason, quantum mechanical calculations have been employed in order to gain a better understanding of the most important geometrical parameters and also relative energies of both isomers. In order to determine which is more stable form of both the *Z*-**4** or the *E*-**4** isomers in the synthesized ylides (**4a, 4b** and **4c**) in comparison with the *Z´*-**4** or the *E´*-**4** speculative ylides **4a´, 4b´** and **4c´** [hypothetical reaction between di-tert-buthyl acetylenedicarboxylate (instead of dimethyl acetylenedicarboxylate) and triphenylphosphine in the presence of NH dicarbonyl compound that presented in this work], first the structures were optimized at the HF/6-31G (gas phase) level of theory by using Gaussian03 program package.[4] Also relative stabilization energy and geometries have been calculated at the HF/6-31G (gas phase) and the B3LYP/6-311++G(d,p) (both gas and solution phases) levels of theory (for single point energy), respectively. Some bond lengths corresponding to the speculative and synthesized ylides are reported in Table **1;** and relative energies to the speculative and synthesized ylides are reported in Table **2**.

Table 1. Some bond lengths (in Å) and dihedral angles (in degree) corresponding to the hypothetical and synthesized ylide for the two geometrical isomers.

		C1-C3	C8-O9	C8-O10	C3-C8	P4C3	P4C3C8O9	C1C3C8O9
(1)	*E*-**4a**	1.498	1.244	1.372	1.399	1.799	3.121	-166.541
	Z-**4a**	1.497	1.242	1.375	1.400	1.801	-175.66	10.95
	E-**4a´**	1.498	1.244	1.372	1.398	1.799	3.121	-166.543
	Z-**4a´**	1.499	1.248	1.367	1.400	1.793	-178.567	9.372
(2)	*E*-**4b**	1.497	1.242	1.375	1.400	1.800	4.316	-164.759
	Z-**4b**	1.499	1.248	1.365	1.397	1.794	-177.381	10.488
	E-**4b´**	1.494	1.248	1.373	1.403	1.804	3.741	-167.652
	Z-**4b´**	1.499	1.251	1.363	1.400	1.795	-176.564	10.339
(3)	*E*-**4c**	1.498	1.242	1.375	1.400	1.800	4.962	-164.207
	Z-**4c**	1.499	1.249	1.363	1.400	1.796	-177.024	11.052
	E-**4c´**	1.495	1.247	1.365	1.403	1.804	4.534	-166.612
	Z-**4c´**	1.500	1.251	1.363	1.400	1.796	-176.012	10.836

Table 2. The relative energies (kJ.mol^{-1}) for the two geometrical isomers corresponding to the hypothetical and synthesized ylide in both gas and liquid phases.

phase	1, 2-Dichloroethane(ε=10)	Ethyl Acetate(ε=6)	1,4-Dioxan(ε=2)	Gas(ε=0)
E-**4a**	4.78[b]	5.19[b]	4.43[b]	10.7 [b](15.3)[a]
Z-**4a**	0.00	0.00	0.00	0.00
E-**4a´**	8.28	10.9	10.7	10.9 (19.9)
Z-**4a´**	0.00	0.00	0.00	0.00
E-**4b**	1.86	2.78	1.02	2.70 (3.73)
Z-**4b**	0.00	0.00	0.00	0.00
E-**4b´**	15.9	16.6	16.1	11.9 (23.0)
Z-**4b´**	0.00	0.00	0.00	0.00
E-**4c**	0.00	0.68	0.00	3.06 (5.13)
Z-**4c**	0.33	0.00	1.63	0.00
E-**4c´**	15.6	15.9	14.8	13.7 (25.5)
Z-**4c´**	0.00	0.00	0.00	0.00

[a] The data in the parentheses calculated at the HF/6-31G levels of theory.
[b] The data calculated at the B3LYP/6-311++G(d,p)

Kinetics Studies

To gain further insight into the reaction mechanism between triphenylphosphin **1,** dimethyl acetylenedicarboxylate **2** and ethyl 2-(4-nitrophenylamino)-2-oxoacetate **3c** (as an N-H dicarbonyl compound) for generation of phosphorus ylide **4c,** a kinetic study of the reactions was undertaken by UV spectrophotometeric technique. The results are accumulated in tables 3 and 4 respectively.

Table 3. Values of overall second order rate constant for the reactions between **(1, 2** and **3c)** and **(1, 2** and **3a)** in the presence of solvents such as 1, 2-dichloroethane and 1,4-dioxan, respectively, at all temperatures investigated.

reactions	Solvent	ε	k_2.M^{-1}.min^{-1}			
			12.0ºC	17.0ºC	22.0ºC	27.0ºC
1, 2 and 3c	1,2-dichloroethane	10	481.3	545.1	622.4	742.1
	1,4-dioxan	2	340.1	378.0	446.7	532.6
1, 2 and 3a	1,2-dichloroethane	10	696.2	741.5	826.2	948.1
	1,4-dioxan	2	505.2	564.0	654.7	761.5

Table 4 The activation parameters involving $\Delta G^{\#}$, $\Delta S^{\#}$ and $\Delta H^{\#}$ for the reactions between **(1, 2** and **3c)** and **(1, 2** and **3a**) at 12.0ºC in 1, 2-dicholoroethane.

reactions	$\Delta G^{\#}$(kJ.mol^{-1})	$\Delta H^{\#}$(kJ.mol^{-1})	$\Delta S^{\#}$(kJ.mol^{-1}.K^{-1})
1, 2 and **3c**	101.65	14.96	-0.32
1, 2 and **3a**	100.77	9.86	-0.32

Conclusions

We have prepared the novel dicarbonyl compounds stable phosphorus ylides using a one-pot reaction between triphenylphosphine and dimethyl acetylenedicarboxylate compounds in the presence of N-H dicarbonyl compounds such as 1,2-dibenzoylhydrazine, ethyl 2-(3-nitrophenylamino)-2oxoacetate and ethyl 2-(4-nitrophenylamino)-2-oxoacetate. The result of kinetics investigation of can be summarized as follow: (**1**) The overall reaction order followed second-order kinetics and the reaction orders with respect to triphenylphosphine, dimethyl acetylenedicarboxylate and 1,2-dibenzoylhydrazine, ethyl 2-(3-nitrophenylamino)-2-oxoacetate or ethyl 2-(4-nitrophenylamino)-2-oxoacetate were one, one and zero respectively. (**2**) The rates of all reactions were accelerated at higher temperatures. Under the same conditions, the activation energy for the reaction with **3c** (19.7 kJ/mol) was higher than that for the reaction which were followed by the **3a** (14.6 kJ/mol) in 1,2-dichloroethane (**3**) The rates of all reactions were increased in solvents with higher dielectric constant.(**4**) With respect to the experimental data, the first step of proposed mechanism was recognized as a rate-determining step (k_2) and, This was confirmed based upon the steady-state approximation. (**5**) Also, the third step was identified as a fast step (k_3). (**6**) The activation parameters involving $\Delta G^{\#}$, $\Delta S^{\#}$ and $\Delta H^{\#}$ were reported for the two reactions. Herein, the ^{1}H, ^{13}C and ^{31}P NMR data showed that the two *E*- and *Z*- isomers in a series of synthesized ylides **4a-c** containing dimethyl acetylendicarboxylate have the abundance percentage of 65% (*Z*-**4a**), 60% (*Z*-**4b**) and 60% (*Z*-**4c**) as the major forms. Herein, theoretical data, indicated that when di-tert-buthyl acetylenedicarboxylate is practically replaced instead of dimethyl acetylenedicarboxylate in reaction shown in Figure 1, due to the very high restricted barrier energy and the very large intramolecular hydrogen bond, a lone isomer can be generated as a product alone.

References

[1] Cadogan, J. I. G. Organophosphorus Reagents in Organic Synthesis, Academic Press, New York, 1979.

[2] M. T .Maghsoodlou, N. Hazeri, G. Afshari, U Niroumand. Phosphorus, Sulphur, and Silicon. 181 (2006) 681.

[3] S. M. Habibi-Khorassani, M. T. Maghsoodlou, H. Roohi, M. Zakarianejad, M. Moradian, Progress in Reaction Kinetics and Mechanism 30 (2005) 127-144.

[4] M. J. Frisch, et al. Gaussian 03, Revision A. 7, Gaussian, Inc., Pittsburg h, PC, 2003.

[5] A. E. Reed, R. B. Weinstock, F.J. J. Weinhold, Chem. Phys, 83 (1985) 735.

[6] R. F. W. Bader, Atoms in molecules A Quantum Theory, Oxford University, New York, (1990).

Ab initio study of the intramolecular hydrogen bonding

M. Kadkhodaei[1], and H.R. Shamlouei[*2]
[1,2] slamic Azad University, Doroud Branch
[*]shamlouei@iau-doroud.ac.ir

Introduction

A hydrogen bond is the attractive interaction of a hydrogen atom with an electronegative atom, such as nitrogen, oxygen or fluorine, that comes from another molecule or chemical group[1]. The hydrogen must be covalently bonded to another electronegative atom to create the bond. These bonds can occur between molecules (intermolecularly), or within different parts of a single molecule (intramolecularly) [2]. This type of bond occurs in both inorganic molecules such as water and organic molecules such as DNA. Intramolecular hydrogen bonds are the most important interactions, as these interactions provide the stability for secondary structures, such as helices or sheets and responsible for the secondary, tertiary, and quaternary structures of proteins and nucleic acids. [3, 4,5]. As the result of the effect of the intramolecular hydrogen-bonding interactionson the protein structure, it plays important roles in regulating the structure and the function of chemical and biological systems [6].
this research, deals with the existence of intramolecular hydrogen bonding and then the effect of this interaction on molecular rotation around an internal bond. Additionally, the strength of this bonding was studied in this research.

Compound Selection and Computational Details

Selected compound must have at least on internal hydrogen bonding for this reason a substituted butane molecule were chosen in manner that the molecule have intramolecular hydrogen bonding. In **Fig.13**, general formula of selected substituted butane molecules is shown. In Table 4, list of substitution which can be used in place of R1 and R2 is shown.

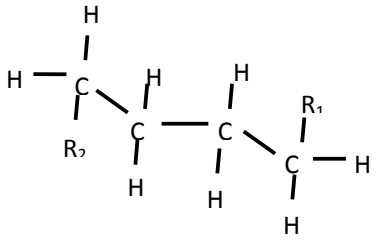

Fig.13 the general formula of substituted Butane molecule

Table 4 list of substitution which can be used in place of R1 and R2

R1	R2	R1	R2	R1	R2
OH	OH	OH	NH_2	OH	F
R1	R2	R1	R2	R1	R2
NH_2	NH_2	NH_2	F		

It is important to notice that there are two conformations of each molecule in which two conformations are the same in structure but one of them have a conformation which can form a hydrogen bonding and the other conformation cannot create intramolecular hydrogen bonding. For instance two conformations of molecule in which R1 and R2 are OH groups are shown in Fig.14.

Fig.14 two conformations of OH-CH_2-CH_2-CH_2-CH_2-OH

Results and Discussion

For calculation of intramolecular hydrogen bonding, rotation around C-C bond was done for two conformations of each molecule and rotational barrier of them were calculated. Difference of potential calculated for these two conformations may be due to intramolecular hydrogen bonding. In Fig.15, potential barrier of two conformations of OH-CH_2-CH_2-CH_2-CH_2-OH is shown.

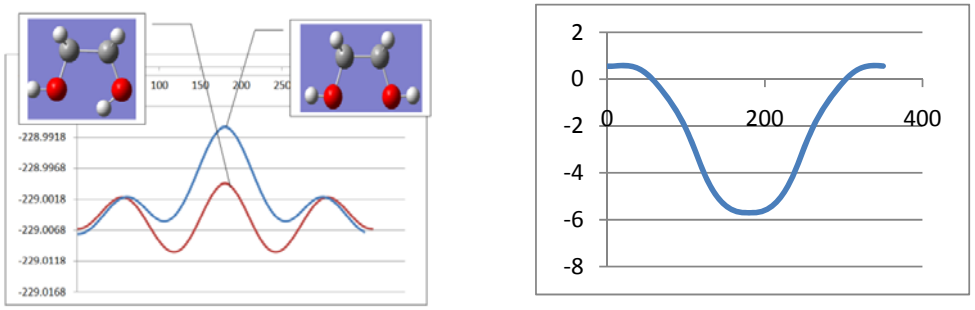

A b

Fig.15 (a) the potential barrier and (b) difference of energy for two conformations of OH-CH_2-CH_2-CH_2-CH_2-OH molecule.

The difference between the values in two conformations, relate to strength of hydrogen bonding. The maximum difference for each couple are calculated and then printed in Table5.

Table5 differences between energy in two conformations

R1	R2	□E (kcal/mol)	R1	R2	□E (kcal/mol)	R1	R2	□E (kcal/mol)
OH	OH	-5.706	OH	NH_2	-5.448	OH	F	-3.405
R1	R2	□E (kcal/mol)	R1	R2	□E (kcal/mol)			
NH_2	NH_2	-3.540	NH_2	F	-2.570			

Discussion

Rotational barrier for five substituted butane molecules were calculated in two conformations. Formation of intramolecular hydrogen bonding has intense effect on the potential barrirer. Additionally the difference of maximum in two potential barrier plots can be related to strength of hydrogen bonding. The values of DE which showed in Table5, demonstrate that the hydrogen bonding in molecules have two OH groups is more stronger than others and the molecule which has NH_2 and F groups display minimum strength in hydrogen bonding.

References

[]Campbell, Neil A.; Brad Williamson; Robin J. Heyden (2006). Biology: Exploring Life. Boston, Massachusetts: Pearson Prentice Hall.ISBN 0-13-250882-6.

[2] International Union of Pure and Applied Chemistry. "hydrogen bond". Compendium of Chemical Terminology Internet edition.

[3]G.A. Jeffrey, W. Saenger, Hydrogen Bonding in Biological Structures, Springer- Verlag, Berlin, 1991.

[4]G.A. Jeffrey, An Introduction to Hydrogen Bonding, Oxford University Press, New York, 1997.

[5]G.R. Desiraju, T. Steiner, The Weak Hydrogen Bond in Structural Chemistry and Biology, Oxford University Press, New York, 1999.

[6]Yosuke Hisamatsu , Yuki Fukumi, Naohiro Shirai, Shin-ichi Ikeda, Kazunori Odashima, Tetrahedron Letters, Vol.49, (2008) pp.2005–2009

Study of intermolecular contacts in the (proline-rich homeodomain) PRH – DNA complex using molecular dynamics simulations

L. Karami*, S. Jalili
Department of Chemistry, K. N. Toosi University of Technology, Tehran,Iran
*E-mail: karami.leila1@gmail.com

Keywords: MD simulation, PRH-DNA complex, Hydrogen bond, Interfacial waters.

Introduction

The PRH (proline-rich homeodomain) protein is a critical regulator of vertebrate development. PRH is able to regulate cell proliferation and differentiation and is a DNA binding protein that can repress and activate the transcription of its target genes using multiple mechanisms. The PRH protein contains a proline-rich N-terminal domain, a central homeodomain (H1-L-H2-T-H3) that mediates DNA binding, and an acidic C-terminal domain [1]. Based on biochemical data, Q50 homeodomains, like PRH, prefer DNA sequences such as TAATTA and TAATGG. Here we perform explicit water molecular dynamics simulations aimed at elucidating the intermolecular contacts in the PRH – DNA complex and the role of water molecules at atomic level of detail.

Methods

The starting coordinate of PRH–DNA complex was obtained from 3D alignment of the PRH (PDB: 2E1O) and the HD–DNA complexes (PDB: 1IG7) using 3D-superimpose in Strap. MD simulations of PRH-DNA complex were performed using the AMBER 03 force field and GROMACS 4.0.7 simulation package. The integration time step was 2 fs. Structures were collected every 4 ps for analysis. The following protocol was used for MD simulation: an energy minimization was performed using the steepest descent and conjugate gradient method. After that, 1000 ps of MD in NVT ensemble, was preformed for equilibration. Finally, Production run was performed for 5 ns in NPT ensemble. Two atoms are considered to form a stable direct H-bond (A···H–D) if the acceptor-hydrogen distance is less than 2.4 Å and the acceptor-hydrogen donor angle is greater than 130° [2]. Interfacial hydration water

molecules were identified by applying a cut-off of 2.6 Å for the distance of water to protein and DNA atoms simultaneously.

Results and discussion

Protein–DNA complexes are held together by hydrogen bonds, which can be either direct or mediated by water molecules. Table 1 presents the direct hydrogen bonds extracted from simulation. Only contacts populated > 40% in the last 1 ns of the trajectory are listed. As shown in Table 1, between secondary structure elements of the PRH, N-terminal (Gly 1, Lys 2, Arg 7 and Phe 8) and Helix-3 (Gln 44, Gln 50, Asn 51, Arg 53 and Arg 57) residues are involved in direct hydrogen bond between PRH and DNA more than the rest. These observed interactions are in a good agreement with experimental data [3]. For example, Asn 51 is conserved in nearly all of the known homeodomains. It has been found to form hydrogen bonds with a conserved adenine in the DNA binding site. In this simulation, Asn 51 forms a hydrogen bond to Ade 6. We determined a particular water molecule to be interfacial water if it appears in the interface for a total of at least 300 ps of the last 1ns. As can be seen from Figure 1, most these interfacial water molecules are placed around the Helix-3 (recognition helix) and N-terminal.

Table 1.

Direct hydrogen bonds in MD simulation

Residue	DNA	Population
Asn 51 (H3)	Ade 6 (b)	98
Arg 7 (N-ter)	Ade 5 (p)	97
Gln 44 (H3)	Ade 6 (p)	96
Asn 51 (H3)	Ade 6 (b)	94
Gly 1 (N-ter)	Ade 23 (b)	92
Phe 8 (N-ter)	Ade 5 (p)	88
Arg 53 (H3)	Ade 19 (p)	77
Gln 50 (H3)	Cyt 18 (b)	76
Arg 57 (H3)	Ade 20 (p)	43
Lys 2 (N-ter)	Ade 23 (p)	40

b: base atoms, p: phosphate oxygens

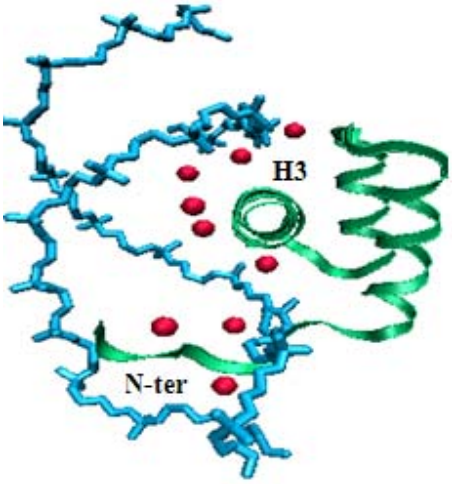

Fig. 1. Hydration at the PRH-DNA interface

Conclusion

All these interactions are maintained during the simulations, albeit with varying population. Between N-terminal and Helix-3 residues, Arg 7 (97%) and Asn 5 (98%) have most population, consequently, most effect in stabilization of the complex during simulation, respectively. Interfacial water molecules, forming water mediated HBs, result in stability of complex.

Reference:

[1] A. Soufi, P-S Jayaraman, Biochem. J. 412 (2008) 399.

[2] D. van der Spoel, P. J. van Maaren, J. Phys. Chem. B. 110 (2006) 4393.

[3] S. Neidle, G. H. Goodwin, FEBS Letters, 345 (1994) 93.

Electric field effects on the switching of molecular switch via DFT

F. Karimi, M. Rezaie, S.J. Hosseini, E. Zahedi*
Chemistry Department, Islamic Azad University, Shahrood Branch, Shahrood, Iran.
Fereshteh.karimi278@gmail.com e_zahedi@iau-shahrood.ac.ir

Keywords: Molecular switch; DFT; HLG; Fermi level

Introduction:

Molecular-scale electronics is developing rapidly because of advances in the synthesis of suitably tailored organic structures, bringing us closer to the ultimate miniaturization of nanoelectronic devices [1]. A dominant trend in the design of electronic and photonic devices in recent decades has been a decrease in their dimensions. According to Moore's rule [2], which predicts an exponential decrease in the average size of the constituent elements of these devices, one may expect them to reach the order of molecular dimensions within a short time. In this work, we studied the performance of 1,2-bis(5-methyl-2,2-bithiophen-4-yl)cyclopent-1-ene and close state of this molecule under external electric field with variable strengths in terms of a number of molecular response parameters.

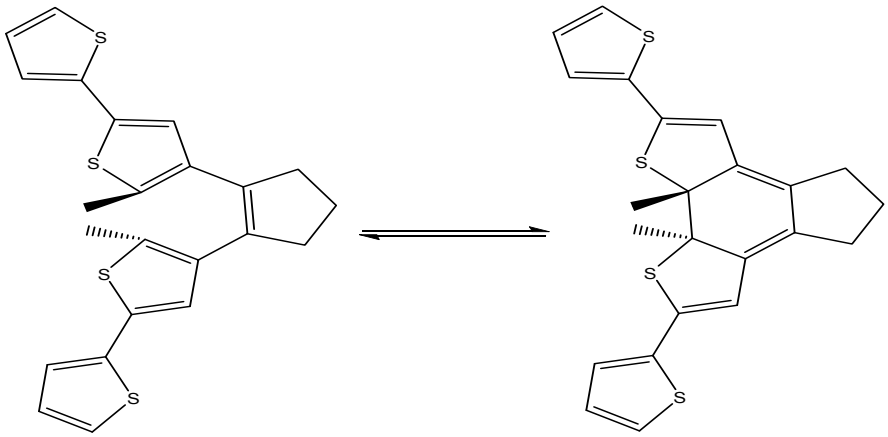

Results and discussion:

All calculations has been carried out at the B3LYP/6-31G* level of theory using GAUSSIAN 03 software package [3]. Values of the HLG, E_F and dipole moment (as an index measuring the response to external electric field), calculated for the nanoswitch at different electric field strengths are presented in below figures. The trend of the electric dipole moment clearly predicts that interaction of the proposed molecular switch with the poles (electrodes) of the nanoelectronic circuit increases considerably with increasing the external electric field strengths. This is due to the fact that at higher field strengths, the molecule undergoes structural changes that consequently change its electronic characteristics. The HLG values are consequently decreased by increasing the field strength. This trend shows that application of the external electric field results in more destabilization of both groups of occupied and virtual molecular orbitals, especially the frontier orbitals including HOMO and LUMO.

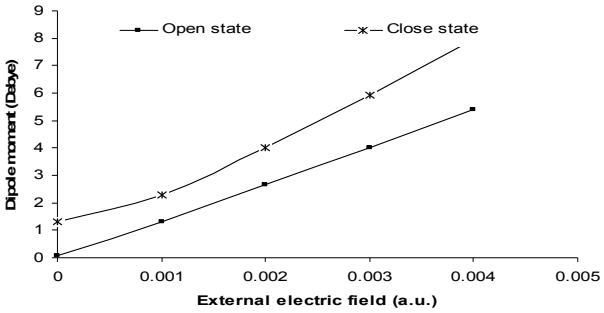

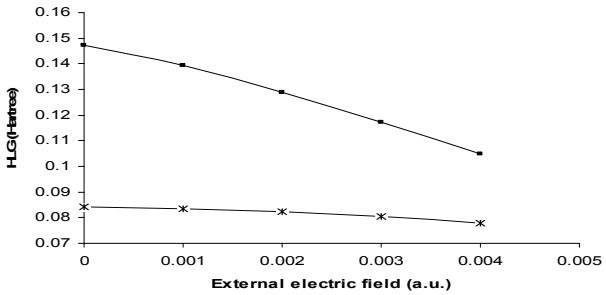

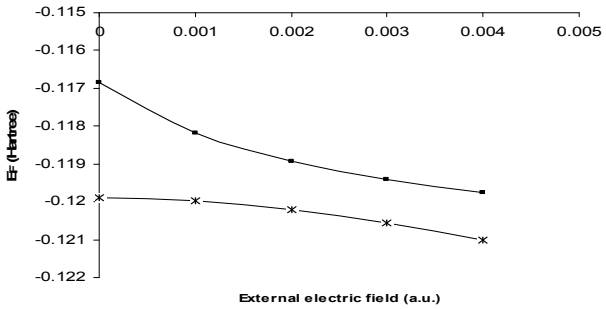

Conclusions:

It can thus be concluded that the conduction band gap of this molecular switch is decreased with increasing strength of the electric field. These trends are consistent with what observed for structural changes and the Fermi level energies of the molecular switch decrease with increasing electric field strength.

References:

[1] M.A. Safarpour, S.M. Hashemianzadeh, A. Kasaeian, J Mol Model (2008) 14, 315–323.

[2] G.E. Moore, Electronics (1965) 38, 114–117.

[3] M.J. Frisch et al., Gaussian 03, Revision E.01, Gaussian Inc., Wallingford CT, 2004.

Artificial neural network modeling for density prediction of 1-alkanols over a wide range of temperatures and pressures using group contribution method

Z. Kalantar*, and S. Sha'abani
Faculty of chemistry, Shahrood University of Technology, Shahrood, Iran
zkalantar@shahroodut.ac.ir , zahrakalantar@yahoo.com

Key Words: Artificial neural network, 1- Alkanols, Density, Group Contribution Method

Introduction

The liquid density is a very important parameter for both heat transfer and mass transfer calculations in the design of chemical processes. Although experimental data can be very accurate, it is difficult to provide all the data needed for every compound. Thus, new predictive technique for liquid density is not only welcomed but a necessity for the chemical industries. In the past decade, the topic of neural network (NN) has generated widespread interest and popularity. The popularity of this technique is due to their success in data analysis because they are indeed self learning mechanisms which don't require the traditional skills of a programmer. In recent years, combination of group contribution method (GCM) with neural networks resulted in a new type of neural networks called GCM based neural networks. In this work we modeled and optimized an artificial neural network for density prediction of 1-alkanols using group contribution method.

Methods

1-Data Set: The *pvT* data for different 1-alkanols [1-4] was randomly divided into 3 groups: training, validation and test sets consisting of 288, 87 and 65 data, respectively.

2- *Descriptor Selection*: The selection of relevant descriptors is an important step to construct a predictive model. The first selected descriptors were temperature and pressure because density is related to them. The other descriptors are selected based on group contribution method. After analyzing the chemical structure of all compounds in this work, 3 functionally groups namely; methyl, methylene and CH_2OH, were found useful. The number of occurrences of these functional groups for each compound as well as two experimental descriptors; temperature and pressure are used as input parameters for the model.

3- *Generation of Neural Network Based on Group Contribution*: A feed forward artificial neural network with a Lenenberg-Marquardt algorithm was used to process the non-linear relationship between the relevant descriptors and density. A three layer network with a Log-

sigmoidal transfer function was designed. The initial weights were randomly selected between 0 and 1. The optimization of the weights and biases was carried out according to the Levenberg-Marquardt algorithm.

Results and Discussion

An artificial neural network (ANN) was constructed using 5 neurons in input layer and 1 neuron in output layer that predicts density by network. The number of neuron in the hidden layer is unknown and need to be optimized. Plots of RMSET and RMSEV versus the number of node in the hidden layer show that 7 nodes in hidden layer is optimum value. Also the results demonstrate that overfitting does not exist for this artificial neural network model and training is stopped after 100 iterations. The capability of the model has been evaluated by predicting values of density by the optimized GCM-ANN model for the validation and test sets. The excellent prediction results, reveals the capability of this model. Also, the performance of the ANN model was evaluated by plotting the estimated values versus the experimental values of density for the validation and test sets, see Fig. 1. As a result, it was found that properly selected and train artificial neural network (ANN) could fairly represent dependents of the density for 1-alkanols to the molecular structures.

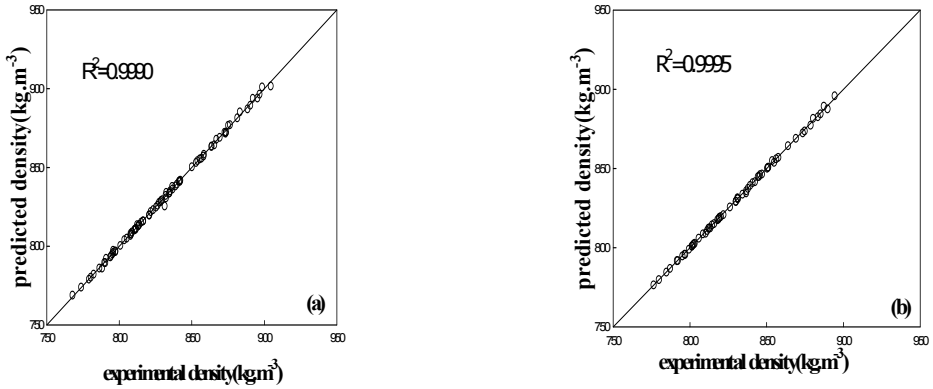

Fig. 1. Plot of predicted density versus experimental density for (a) validation set and (b) test set.

References

[1] Kubota, H., Tanaka, Y., Makita, T., *Int. J. Thermophys.*, **8**, (1987), 47.

[2] Wappmann, S., Karger, N., Lüdemann, H.-D., *J. Chem. Eng. Data*, **40** (1995), 233.

[3] Matsuo, S., Makita, T., *Int. J. Thermophys.*, **10** (1989), 885.

[4] Dzida, M., *J. Chem. Eng. Data*, **52** (2007), 521.

A new neural network group contribution model for density prediction of *n*-alkanes: A combined effect of pressure and temperature

Z. Kalantar* and S. Sha'abani
Faculty of chemistry, Shahrood University of Technology, Shahrood, Iran
zkalantar@shahroodut.ac.ir , zahrakalantar@yahoo.com

Key Words: Artificial neural network, *n*- Alkanes, Density, Group Contribution Method

Introduction

In the study of a chemical, biochemical and environmental system, knowledge of a variety of physical and chemical properties of pure compounds and mixtures under specified conditions is required. It is not always possible, however, to find reliable experimental values of these properties for the compounds of interest in the literature, nor it is practical to measure such properties as the need arises.

The method of group contribution has been a powerful tool for predicting physical and thermodynamic properties from the chemical structure and state of matters. This method is easy, quick, and reliable for prediction of different properties. In this work, a combination of group contribution method (GCM) and artificial neural network (ANN) were successfully developed for the modeling and predicting of density of *n*-alkanes over a wide range of temperature and pressure.

Methods

1-*Data Set*: The *pvT* data for different *n*-alkanes (C5, C8, C10 [1], C6 [2], C7 [3], C9 [4], C12 [5], C15, C17 [6], C18, C19 [7]) at different temperatures (298.15-398.15K) and pressures (0.1- 460MPa) was randomly divided into 3 groups: training set, validation set and test set consisting of 427, 122 and 109 data, respectively.

2- *Descriptor Selection*: The first selected descriptors were temperature and pressure because density is related to them. The other descriptors are selected based on group contribution method. After analyzing the chemical structure of all compounds in this work, 2 functionally groups namely; methyl and methylene, were found useful. The number of occurrences of these functional groups for each compound as well as two experimental descriptors; temperature and pressure are used as input parameters for the model.

3- *Generation of Neural Network Based on Group Contribution*: A feed forward artificial neural network with a Lenenberg-Marquardt algorithm was used to process the non-linear relationship between the relevant descriptors and density. A three layer network with a logarithm-sigmoidal transfer function was designed.

Results and Discussion

An artificial neural network (ANN) was constructed using 4 input including the number of methyl and methylene groups, temperature and pressure and 1 neuron in output layer that predicts density by network. The number of neuron in the hidden layer is unknown and need to be optimized. Plots of root mean square error of training (RMSET) and validation (RMSEV) sets versus the number of node in the hidden layer show that 6 nodes in hidden layer is optimum value. Also the results demonstrate that overfitting does not exist for this ANN model and training is stopped after 80 iterations. The capability of the model has been evaluated by predicting values of density by the optimized GCM-ANN model for the validation and test sets. The excellent prediction results, reveals the capability of this model. Also, the performance of the ANN model was evaluated by plotting the predicted values versus the experimental values of density for the validation and test sets, see Fig. 1. As a result, using group contribution descriptors along with optimized ANN model the density of *n*-alkanes may be calculated properly.

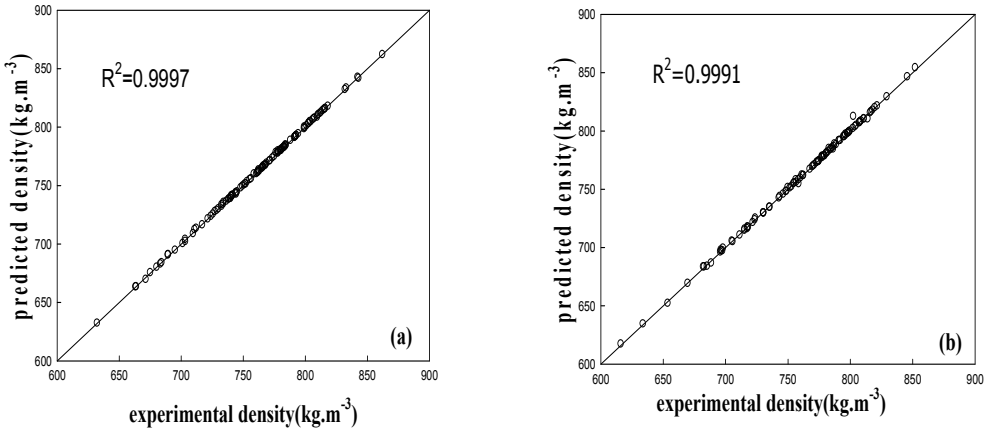

Fig. 1. Plot of predicted density versus experimental density for (a) validation set and (b) test set.

References

[1]. C. M. B. P. Oliveira, W. A. Wakeham, *Int. J. Thermophysics*, **13** (1992) 773.

[2]. J. H. Dymond, K. J. Young, J.D. Isdale, *J. Chem. Thermodynamics*, **11** (1979) 887.

[3]. L. Morávková, J. Linek, *J. Chem. Thermodynamics*, **34** (2002) 1397.

[4]. T. Grindley, J. E. Lind, *J. Chem. Phys*, **68** (1978) 5046.

[5]. T. S. Khasanshin, A. P. Shchamialiou, O. G. Poddubskij, *Int. J. Thermophysics*, **24** (2003) 1277

[6]. J. L. Daridon, H. Carrier, B. Lagourette, *Int. J. Thermophysics*, **23** (2002) 697.

[7]. S. Dutour, J. L. Daridon, B. Lagourette, *Int. J. Thermophysics*, **21** (2000) 173.

Theoretical Study of Super Cell Al-doped Single- Walled Carbon Nanotubes (Al-SWNT) as CO Sensor

Masood Hamadanian[1,2,1*], Forough Kalantari Fotooh[2]

[1]Institute of Nano Science and Nano Technology, University of Kashan, Kashan, I.R. Iran.

[2]Department of Physical Chemistry, Faculty of Chemistry, University of Kashan, I.R. Iran.

Keywords: Single walled Nanotube, Al-doped SWCNT, Adsorption , DFT calculations

Introduction

Carbon nanotubes (CNTs) are promising nanoscale molecular sensors for detecting toxic gases and other species, such as NH_3 and NO_2[1]. Theoretical [2] and experimental [3] reports suggest that CO does not engage in charge transfer with bare SWNTs. DFT calculations have been also shown that Al-doped (8,0) SWCNT presents good sensitivity to CO, compared with the intrinsic SWCNT [4]. In this paper DFT calculations were performed to elucidate the relationship between the electronic structures of Al-doped SWCNTs and the adsorption of CO molecules to different positions of (10,0) SWCNT, in order to reveal some clues for chemical sensor design**.**

Computational method

DFT calculations were performed by Quantum Espresso package using local density approximation (LDA) with ultrasoft pseudopotential. The energy cutoff for plane wave calculations was set to be 50 Ry for all structures. The positions of all the atoms in the super cell were fully relaxed during geometry optimizations. On the other hand, the optimized k-point was selected to be seven points.

Results and discussion

` Corresponding author. Tel.: +98 361 5912382; fax: +98 361 5552930.
E-mail address: hamadani@kashanu.ac.ir (M. Hamadanian).

Figure 1 represents the geometries of pristine and Al-doped (10,0) SWCNT. We find out that these doping of Al with larger diameter caused the deformation of the six-membered ring near the Al-atom protruding the SWCNT surface and significant changes in bond lengths.

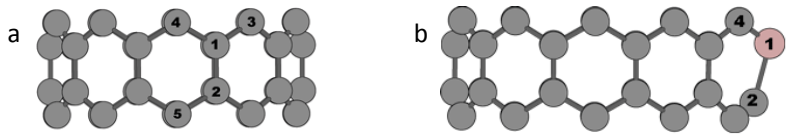

Figure 1. Optimized structures of (a) (10,0) SWCNT (b) 2.5% Al-doped (10,0)SWCNT

Band structures and density of states (DOSs) of these nanotubes near the Fermi levels are presented in figures 2a-2b. As shown in figure 2b after doping Al with 2.5% concentration, some new levels appear in the band region of the pristine CNTs, which are originated from acceptor nature of the doped Al impurities and therefore the tube is changed in to a p-type semiconductor.

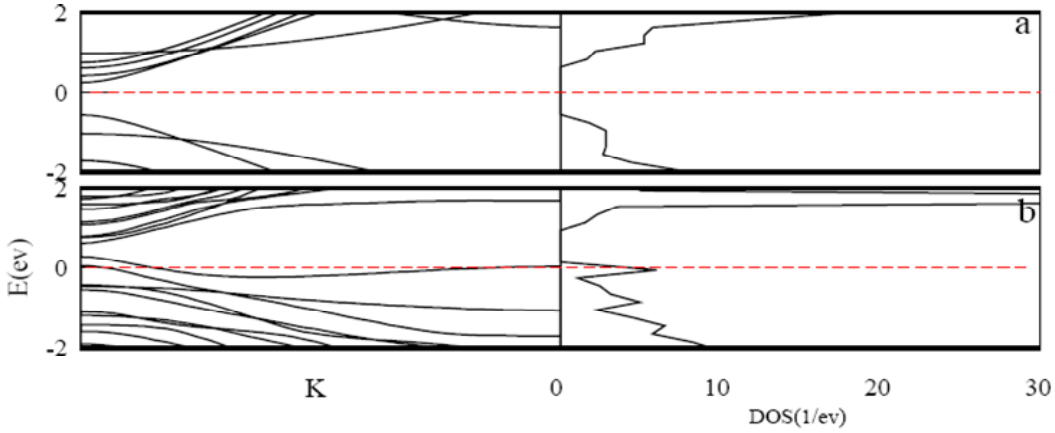

Figure 2. Band structures and DOSs of (a) pristine (10,0) SWCNT (b) 2.5% Al-doped (10,0)SWCNT

To study the effect of adsorption of CO on nanotubes, three configurations for the adsorbed CO have been considered and the CO molecule was adsorbed from C or O directions toward the nanotube. The electronic band structure and DOS of the CO adsorbed (10,0) SWCNT do not change significantly near the Fermi level which confirms that the CO can only be adsorbed weakly on pristine SWCNTs. On the other hand, after CO adsorption on 2.5% Al-doped SWCNT, some drastic changes of properties of the nanotube have been observed which make these modified nanotubes acceptable sensors for detecting the CO toxic gas (see figures 3a-3b)

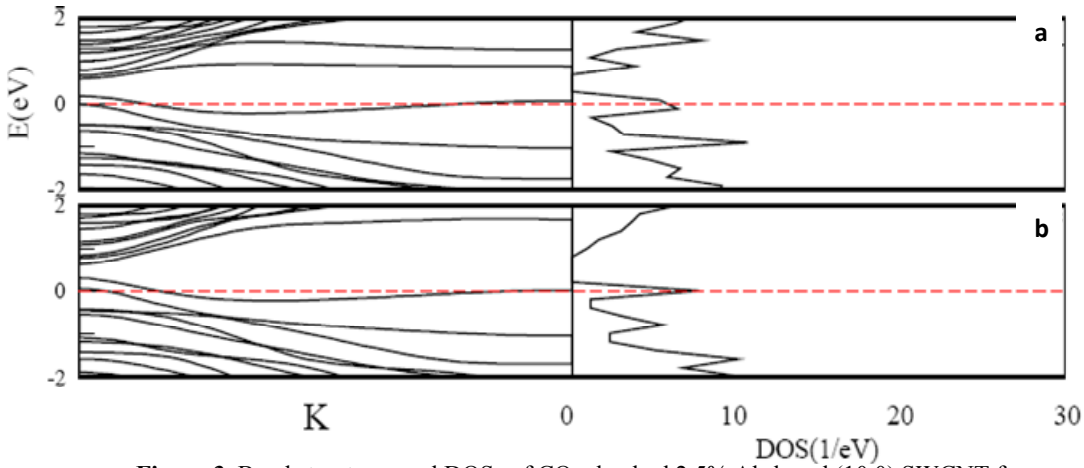

Figure 3. Band structures and DOSs of CO adsorbed 2.5% Al-doped (10,0) SWCNT from (a) C atom of CO (b) O atom of CO

Refrences:

[1] J. Kong, N. Franklin, C. Zhou, M. Chapline, S. Peng, K. Cho, H. Dai, Science 287 (2000) 622.

[2] S. Peng, K. Cho, Nanotechnology 11 (2000) 57.

[3] S. Santucci, S. Picozzi, F. Di. Gregorio, L. Lozzi, C. Cantalini, L. Valentini, J. M. Kenny, B. Delley, J. Chem. Phys. 119 (2003) 10904.

[4] R. Wang, D. Zhang, W. Sun, Z. Han, C. Liu, THEOCHEM 806 (2007) 93.

Determination of formation constants of methyl glyoxale in presence of urea and DDP by ab initio method

Farhoush Kiani*[a] , Abbas Ali Rostami[b] , Sasan Sharifi[c] , Mohammad Javad Chaichi[b], Azar Bahadori[c] and Anthony K. Campbell[e]

[a] *Chemistry Department, Islamic Azad University, Ayatollah Amoli Branch, Amol, Iran*

[b] *Physical and Inorganic Chemistry Department, Faculty of Chemistry, University of Mazandaran, Babolsar, Iran*

[c] *Chemistry Department, Islamic Azad University, Arak Branch, Arak, Iran*

[e] *Medical Biochemistry Department, Cardiff University, Cardiff, UK*

Keywords: Ab initio method, Methylglyoxal, Formation constant, DMQ, 4Mio

Introduction

Methylglyoxal (MG) is a metabolite of glucose [1]. It is a highly reactive α-oxaldehyde formed in many enzymatic and non-enzymatic reactions. It is found in trace amounts in the environment [2], food and beverages [2,3] and in the cell tissues. MG is produced from dihydroxy acetone phosphate (DHAP) by methylglyoxale synthase [1,4]. The combination of MG with amine groups of proteins and other metabolites are reported [2]. Methylglyoxal may be assayed in chemical and biological systems by fluorescent derivitization with 1,2-diamino-4,5-dimethoxybenzene (DDB) to form 6,7-dimethoxy-2-methylquinoxaline (DMQ) [4,6]. On the other hand, during the last two decades there has been much interest in developing a methodology enabling theoretical prediction of pK_f values, employing various quantum theoretical techniques [7]. In this study, the formation constants of MG with urea and DDP were determined by an ab initio method and at a temperature of 25 $^{\circ}$C.

Computational method

In this study, the optimized geometries of the initial molecules (MG, Urea, 4Mio and 67Dmq) and the practical numbering system adopted for performing the calculations by the semi empirical PM3 method were included in program CS Chem3D version 5.0. All the geometries of the initial molecules were optimized with the Gaussian 98 program packages using the

B3LYP/6-31+G(d) methods and the default convergence criteria. Then, polarized continuum models (PCM) have been applied to calculate free energy differences for mentioned species.

Results and Discussion

According to the Gaussian calculations based on the quantum mechanics principals, the stability of molecules and formation constants are investigated. As shown in equations of 1 and 2, MG in presence of urea and DDP can perform bellow reactions:

MG + Urea $\longrightarrow$ 4Mio + $2H_2O$ (1)

MG + DDB $\longrightarrow$ 67Dmq + $2H_2O$ (2)

The calculations shown that the formation constant (K_f) of Urea-MG adduct is very low (2.53×10^{-23}) and for the DDB-MG is high (1.19×10^{11}). These results confirm experimental tests by HPLC that Urea-MG adduct (4Mio) is not stable and after formation, decompose during the time and produce free MG, that can be react with DDB in the solution. Therefore, 4Mio

(4-methyl-imidazol-2-one) is a control kinetic production and DMQ is a control thermodynamic production. The optimized structures of MG, Urea, 4Mio, DDB and DMQ are shown in figures 1 and 2.

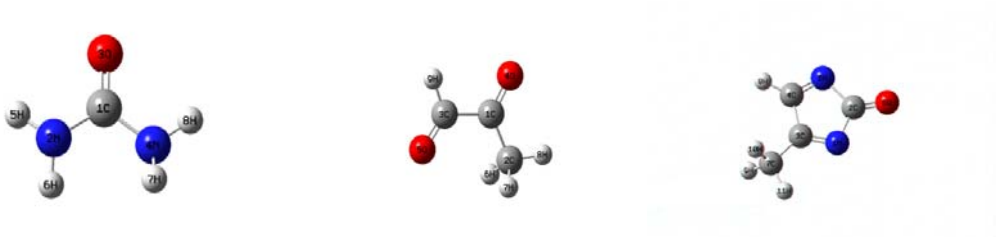

Fig. 1 The optimized structures of MG, Urea and 4Mio for carrying out the calculations.

Fig. 2 The optimized structures of DDB and DMQ for carrying out the calculations.

References

[1] M. Mukohada, H. Yamawaki, H. Nomura, M. Okada and Y. Hara, *J. Pharmacol. Sci*., 190, 305 (**2009**).

[2] I. Nemet, L. Vara-Defterdarovic, and Z. Turk, Mol. *Nutr. Food Res*., 50, 1105 (**2006**).

[3] T. Hayashi and T. Shibamoto, *J. Agric. Food Chem*., 33, 1090 (**1985**).

[4] P. J. Thornalley, A. LangBorg and H. Minhas, *Bio. Chem. J*., 344, 109 (**1999**).

[5] A. C. Mclellan and P. J. Thornalley, *Anal. Chim. Acta*, 263, 137 (**1992**).

[6] I. Nemet, L. Varge- Defterdarovic and Z. Turk, *Clin. Biochem*., 37, 875 (**2004**).

[7] C. P. Kelly, C. J. Cramer and D. G. Truhlar, *J. Phys. Chem. A*, 110, 2493 (**2006**).

Quantum Chemical Study on the Reaction Mechanism of 1H-benzo[d]imidazol-2-amine and 2-Benzyli denemalononitrile

M.Mousavi*, Z. Keivani
Department of Chemistry, Shahid Bahonar University of Kerman, P.O. Box 76169, Kerman, Iran.
(*Email: mmousavi@mail.uk.ac.ir)

Keywords: Semiempirical methods, DFT calculations**,** Benzoimidazole, Reaction Simulation, denemalononitrile, Activation Energy

Introduction

Usually, reaction mechanism is proposed according to the experimental evidences which are derived during the reaction. Although, experimental studies are straightforward, but detection of short lifetime and transitory compounds during a reaction is very difficult, expensive and time consuming process [1]. Alternatively, theoretical and computational chemistry are useful and powerful means in simulation of reaction mechanism and choosing the most favorable reaction pathway by understanding intermediates and transition states of the reaction mechanism. In this way, the reaction mechanisms could be theoretically confirmed completed or either proposed [2]. In the present work, the reaction mechanism of 1H-benzo[d]imidazol-2-amine and 2-benzyli denemalononitrile were studied to evaluate the proposed mechanism for the reaction.

Methods

Stereochemistry of the reaction of 1H-benzo[d]imidazol-2-amine and 2-benzyli denemalononitrile indicates that there are two possible pathways for the reaction which could either lead to the generation of 4-amino-2-phenyl-2,10-dihydropyrimido[1,2-a][1,3] benzimidazol-3-yl-cyanide (pathway 1) or 2-amino-4-phenyl-2,10-dihydropyrimido[1,2-a][1,2] benzimidazol-3-yl-cyanide (pathway 2) as reaction products. Here, efforts have been made to evaluate the proposed reaction mechanism by applying semi-empirical and DFT quantum mechanical calculations. Therefore, the theoretical methods were used to estimate the activation energy of each reaction step through construction of transition state and the

structure of the intermediate compounds. Comparison of the calculated activation energies of reaction steps can be used to find out the rate determining step in the mechanism, and consequently the more favorable pathway and major product.

Results and Discussions

The two possible reaction pathways were investigated carefully and all of the transition states and intermediates were derived and optimized using AM1 semiempirical and B3LYP/6-311G(d,p) methods implemented in Gaussian 03 software. Frequency calculations were carried out in order to confirm the structures which were suggested for ground states and transition states. Comparison of the activation energies for the two pathways (Figure 1) indicates that the larger activation energies for ring formation (i.e. TS2 and TS3) and hydrogen elimination (NH_2 formation) (i.e. TS3 and TS4) steps prevent the production of 2-amino-4-phenyl-2,10-dihydropyrimido[1,2-a][1,2]benzimidazol-3-yl-cyanide (pathway 2), so that 4-amino-2-phenyl-2,10-dihydropyrimido[1,2-a][1,3]benzimidazol-3-yl-cyanide is formed as the energetically favored product in pathway 1.

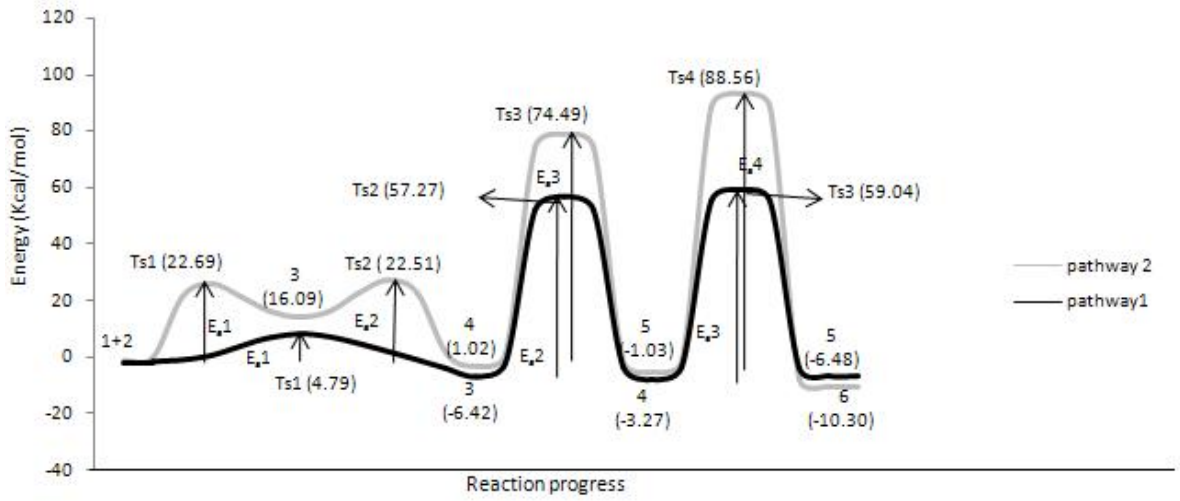

Figure 1: Comparison of energy profile and activation energies for reaction of 1H-benzo[d]imidazol-2-amine and 2-benzyli denemalononitrile in a) pathway1 and b) pathway 2.

Conclusions

The reaction mechanisms were successfully simulated using the quantum mechanical methods in reasonable time and cost. It is obtained that the smaller activation energies for ring

formation and hydrogen elimination in pathway 1 derive it to be more favorable. These results completely confirm the experimentally proposed mechanisms for the reaction.

References

[1]Antonio J. Mota, Luis lvarez de Cienfuegos , Rafael Robles, *Journal of Molecular Structure: THEOCHEM* 944 (2010) 43–52

[2]Bo Long, Jia-Rong Cheng, Xin-feng Tan, Wei-jun Zhang , *Journal of Molecular Structure: THEOCHEM* 916 (2009) 159–167.

Simulation of reaction mechanism of 2-aminobenzoimidazol and allenic nitriles using quantum mechanical calculations

M.Mousavi*, Z. Keivani
Department of Chemistry, Shahid Bahonar University of Kerman, P.O. Box 76169, Kerman, Iran.
(* E-mail: mmousavi@mail.uk.ac.ir)

Keywords: Semiempirical methods, Benzoimidazole, Allenic nitriles, Reaction Simulation.

Introduction

The benzimidazole compounds possess broad spectrum of biological properties and were investigated for their antiviral (anti-HIV), anticancer and antibacterial activities. Therefore, synthesis studies and reaction mechanism evaluations of benzoimidazole are of great importance to chemists and biochemists [1]. It is shown that, theoretical and computational chemistry are useful and powerful means in simulation of reaction mechanism and choosing the most favorable reaction pathway by understanding intermediates and transition states of the reaction mechanism. In this way, the reaction mechanisms could be theoretically confirmed, completed or even proposed [2]. Here the reaction mechanism of 2-aminobenzoimidazol and allenic nitriles was studied to evaluate the proposed mechanisms for the reaction.

Methods

Stereochemistry of the reaction of 2-aminobenzoimidazol and allenic nitriles indicates that there are two possible pathways for the reaction which could either lead to the generation of 2-amino-4-(1-methylpropyle) pyrimido[1,2-a]benzimidazolesas (A) in the first pathway or 4-amino-2-(1-methylpropyle) pyrimido [1,2-a]benzimidazoles (B) in the second pathway as the reaction products [3]. To accomplish simulation of a reaction mechanism, various steps including geometry optimization, reactants collisions, intermediate and transition state recognitions have to be carried out. Therefore, PM3 semi-empirical method was applied to estimate the activation energy of each reaction step through construction of transition state and the structure of the intermediate compounds. Comparison of the calculated activation

energies of reaction steps can be used to find out the rate determining step in the mechanism, and consequently the more favorable pathway and major product.

Results and Discussions

The two possible reaction pathways were examined carefully and all of the transition states and intermediates were derived and optimized using PM3 semiempirical method implemented in Gaussian 03 software. Frequency calculations were carried out in order to identify the structures which are assigned to ground states and transition states [1-2].

Comparison of the activation energies for the two pathways (Figure 1) are indicative that the larger activation energies for ring formation (i.e. Ts 3) and hydrogen elimination (NH_2 formation) (i.e. Ts 5) steps prevent the production of B in the second pathway and thus, A is formed as the energetically favored product in the first pathway.

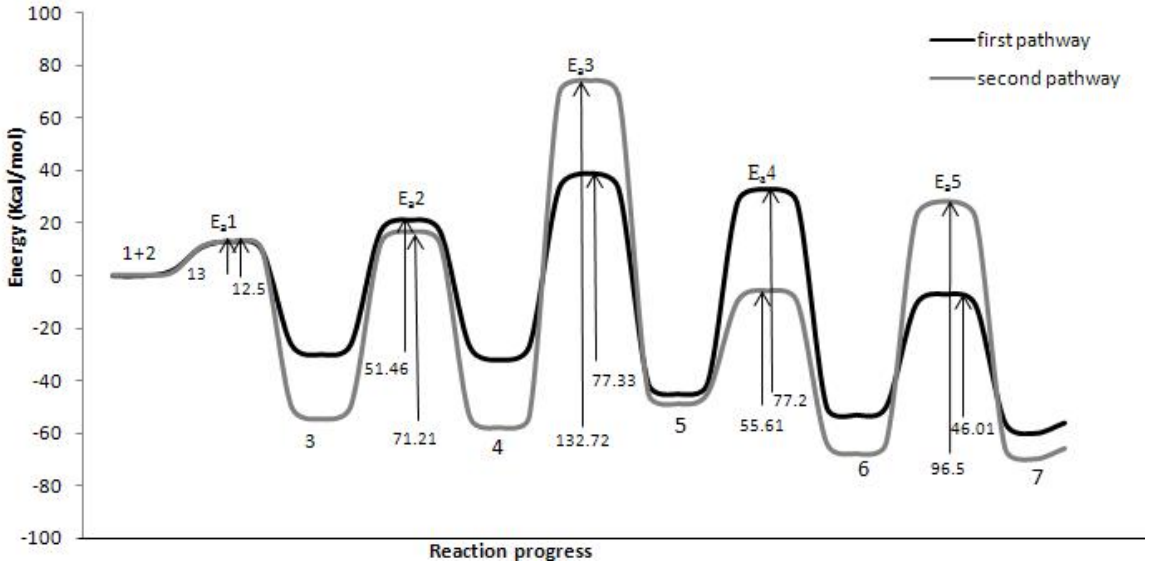

Figure 1: Energy profile and activation energies for reaction of 2-aminobenzoimidazol and allenic nitriles through

a) the first pathway and b) the second pathway.

Conclusions

The reaction mechanism was successfully simulated using semiempirical methods. The whole reaction mechanisms can be examined completely and easily using the calculations in a

reasonable time and cost and it is also possible to proposed new routes when it is necessary. These findings are consistent with the experimental results.

References

[1] Antonio J. Mota, Luis lvarez de Cienfuegos , Rafael Robles, *Journal of Molecular Structure: THEOCHEM* 944 (2010) 43–52

[2] Bo Long, Jia-Rong Cheng, Xin-feng Tan, Wei-jun Zhang , *Journal of Molecular Structure: THEOCHEM* 916 (2009) 159–167.

[3]Zacharias Tanee Fomum, Emmanuel Fondjo Sopbue, Dietrich Döpp, *J. Chem. Soc*., *Perkin Trans. 1*, 2001, 457–461

Prediction of Critical Pressure of Some Organic Compounds Using QSPR Method

M. M. Papari *, Z. Amini, M. Lotfi and A. R. Ahmadi Gandomani
Department of Chemistry, Shiraz University of Technology, Shiraz, P.O. Box: 71555-313, Iran
Email: papari@sutech.ac.ir
Fax: +98-711-726-1288

Keywords: QSPR, MLR, Semiempirical AM1, DECHEMA database, Critical pressure.

Introduction:

QSPR models are now well established and are used to correlate varied, and often complex, thermo-physical properties of molecules. The QSPR approach has been applied in many different areas [1,2]. The present study is devoted to applying a quantitative structure–property relationship (QSPR) study to 138 organic compounds to investigate the quantitative effect of structural properties of compounds on their critical pressure (P_c).

Results and Discussion:

A subset of 138 molecules was selected from the DECHEMA database [3] and then divided into a training set of 120 compounds to develop the models and a prediction set of 18 compounds to evaluate the model. The chemical structure of the molecules was drawn by the Hyperchem and CS Chem3D Ultra softwares. Semiempirical Austin Model 1 (AM1) calculations were used for geometry optimization of the studied molecules by these softwares. The Hyperchem, CS Chem 3D Ultra and Dragon softwares were employed for generating all descriptors. Eventually, 1172 descriptors were calculated for each molecule. After omitting the existing co-linearity between some calculated descriptors, the number of descriptors reduced to 620. A linear QSPR model for P_c was obtained using stepwise multiple linear regression (MLR) procedure. Among all achieved models developed by MLR method, a six parametric model was chosen as the best one:

$P_{c`}$ = 7.713 (± 0.562) - 1.090 (± 0.347) BELp2 - 1.190 (± 0.123) Mor13u - 3.614 (± 0.373) R5m + 2.594 (± 0.519) Mor21v - 8.639 (± 2.228) R2p+ - 0.4922 (± 0.168) MATS3v (1)

The statistical parameters of above-mentioned correlation are as follows:

$R^2_{training}$= 0.8199, $R^2_{prediction}$= 0.7394, SE $_{training}$ = 0.3802, SE $_{prediction}$ = 0.5173, and F = 372.32.

In equation (1), BELp2 corresponds to lowest eigenvalue n. 2 of Burden matrix / weighted by atomic polarizabilities, which is among BCUT descriptors. Mor13u is 3D-MoRSE-signal 13 / unweighted and Mor21v is 3D-MoRSE - signal 21 / weighted by atomic van der Waals volumes, which both are related to 3D-MoRSE descriptors. R5m is R autocorrelation of lag 5 / weighted by atomic masses and R2p+ is R maximal autocorrelation of lag 2 / weighted by atomic polarizabilities and both are among GETAWAY descriptors. MATS3v is Moran autocorrelation-lag 3 / weighted by atomic van der Waals volumes and belongs to 2D autocorrelation descriptors.

Conclusions

QSPR models have a good ability to correlate and predict the critical properties such as critical pressure of organic compounds.

References:

[1] A.R. Katritzky, L. Mu, M. Karelson, A QSPR study of the solubility of gases and vapours in water, J. Chem. Inf. Comp. Sci. 36 (6) (1996)1162–1168.

[2] S. S. Godavarthy, R.L. Robinson Jr., K.A.M. Gasem, SVRC-QSPR model for predicting saturated vapor pressures of pure fluids, Fluid Phase Equilib.246 (2006) 39–51.

[3] K. H. Simmrock, R. Janowsky, A. Ohnsorge, Critical Data of Pure Substances, Chemistry Data Series, vol. II, Part 2, DECHEMA, Frankfurt am Main, 1986.

Determination Of The Molecular Weight Of PAMAM Dendrimer Using LouMass Created Model

O. Louie*[a] , A.H. Massoudi[a] , H.Vahedi [a] and S. Sadjjadifar [a]

[a]Chemistry Department, Payame Noor University (PNU), Mashhad, Iran.

E-mail:O_louie2001 @yahoo.com

Keywords: Loumass Model, Dendrimer, Polyamidoamin(PAMAM), Molecular Weight

Extended Abstract

Introduction:

Plyamidoamine (PAMAM) dendrimers represent an exciting new class of macromolecular architecture called "dense star" polymers[1]. Unlike classical polymers, dendrimers have a high degree of molecular uniformity, narrow molecular weight distribution, specific size and shape characteristics, and a highly- functionalized end group surface. The manufacturing process is a series of repetitive steps starting with a central initiator core. Each subsequent growth step represents a new "generation" of polymer with a larger molecular diameter, twice the number of reactive surface sites, and approximately double the molecular weight of the preceding generation. The term "dendrimer" was derived from its tree-like branching structure. In 1985, Newkome et al. published the first molecular tree - an “arborol” (Latin: arbor: tree) based on the 1 → 3 branching pattern, simultaneously Tomalia published his 1 → 2 branched PAMAMs or “dendrimers”[1- 4].

Method:

The Molecular weight of any AB2 type dendrimers were calculated by suggested theoretical equation.The molecular weight determination of various generations of an AB2 dendrimer were calculated for PAMAM with ethylenediamine (EDA) core using the new suggested equation. The molecular weight of a dendrimer is the sum of the molecular weight of branches (M_r)and the molecular weight of core (M_{core}) [5,6].

$$Mw_n = M_{Core} + (LMNC\, z_0)\, M_r \quad \text{(LouMass Model)}$$

In this reaserch was synthesized the Polyamidoamine (PAMAM) dendrimer with core of diisopropanolamine. The core has one active sites (Z_o = 1), which can construct two branches for generation 1(G1), six branches for generation 2(G2) and fourteen branches for generation 3(G3) and 30 branches for generation 4(G4). Lou-Mass Number Collection (LMNC) can provide the number of branches in PAMAM dendrimer AB_2 for any generation where n is the number of each generation.

$$LMNC = 2\times2(2^n-1) \quad (1)$$

One can generalize the above equation (1) to any type of dendrimer AB2 by taking account of active positions (Z_0) of the core to the equation (1):

$$LMNC = 2Z_0(2^n-1) \quad (2)$$

So, the number of the branches for any generations and for any type of dendrimer AB_2 (*i.e.* with Z_o=1, 2, 3 and 4) can be obtained from the equation (2). And could be illustrated as a mathematical collection (LMNC).

$LMNCZ_o$ =1 = {2, 6, 14, 30, 62, 126, …}

$LMNCZ_o$ =2 = {4, 12, 28, 60, 124, 252, …}

$LMNCZ_o$ =3 = {6, 18, 42, 90, 186, 378, …}

$LMNCZ_o$ =4 = {8, 24, 56, 120, 248, 504, …}

The results for 3 generations of the AB2 dendrimer were outlined in Table 1. Calculation of molecular weight was carried out for Generation Number (G_n)of 1-3 PAMAM and the results were summarized in bellow Table.

Table1: $LMNCZ_o$, Molecular weight M_w

Generation Number(G_n)	LMNC $z_0 = 2$	M_w reported	ref	Calculate M_w $M_{core=}60, M_{r=}$ 15	ref	Error %
1	4	517	1,6	520	6	0.58
2	12	1435	1,6	1440	6	0.35
3	28	3256	1,6	3280	6	0.74

The molecular weight of any AB2 type dendrimers were calculated by suggested theoretical equation and compared to those reported. It was found that there are no remarkable differences between the calculated and reported data [6].

Amin

References

[1] Newkome, G. R.; Shreiner, C. D.; *Polymer* 2008, 49, 1-173.

[2] Massoudi, A.H.; Vahedi, H.; Louie, O.; Sajjadifar, S.*; The 5 th Chemistry Conference Payame Noor University* , Tehran, Iran,2008.34-36 .

[3] Massoudi, A.H.; Vahedi, H.; Louie, O.; Sajjadifar, S.*; The 14 th Chemistry Conference*Zabol, Iran,2008.71

[4] Xiangyang Shi, Wojciech Lesniak, Mohammad T. Islam, Maria C. MuN. iz, Lajos P. Balogh, James R. Baker Jr**.** *A: Physicochem. Eng.* 2006, 272, 139–150.

[5] Han, M, Chen P and Yang X, *Polymer,* 2005**,** 49, 3481-3488

[6] Massoudi, A.H.; Vahedi, H.; Louie, O.; Sajjadifar, S.*;E_J.Chem* 2009, 6(3), 681-684

[7] Louie,O. Massoudi, A.H.; Vahedi, H.; Sajjadifar, S.*;J. Polymer, 2009,50;5505-5607*

Ab initio and DFT studies of the CO-O_2 complex

M. Noorbala[a], M. Mobasheri[*a], M. Namazian[a]

[a] Department of Chemistry, Yazd University, Yazd, Iran

Keywords: Intermolecular Potential Energy Surfaces (IPES), CO-O_2 dimer, Ab initio, UMP2 DFT-B3LYP, BSSE

Introduction:

The general interest in the structure, spectroscopy and dynamics of van der Waals complexes has continued to increase during the last decade [1]. The interplay between experiment and theory has been crucial in the development of this area where often theory has been able to match the detailed and accurate experimental measurements [2-3]. The structures of van der Waals dimers of CO-O_2 are studied using ab initio and density functional calculations.

Methods:

The intermolecular potential energy surfaces (IPES) of the CO-O_2 system were investigated employing a series of basis set such as correlation-consistent basis sets, cc-pVXZ, and aug-cc-pVXZ (X=D,T) at UMP2 and DFT B3LYP levels of theory. In addition, IPS was examined with cc-pVDZ and aug-cc-pVDZ basis sets at QCISD method. A 0.1 Å step size has been used for the intermolecular R between the CO and O_2 of the monomers (from 2.5 to 10 Å). Six types of conformations of CO-O_2 have been studied: two linear, one parallel, and three T-shaped [4].

Results and discussion:

The uncorrected potential energy curves at UMP2 and QCISD theory levels show the typical form of an interaction potential consisting of attractive and repulsive parts that result in a potential well depth. It is shown that the basic features of the potential energy curves do not vary for any type of basis set, but the characteristics specially, potential well-depth is sensitive to the type of basis set. Counterpoise correction (CP) has been used to eliminate the

basis set superposition error (BSSE) on the potential energy curves obtained for CO-O_2 system. In different relative orientation of two CO and O_2 monomers with each other, the uncorrected and BSSE-corrected IPES's have been calculated and the characteristics of these potential energy curves such as well-depth, position minimum, well width and hard sphere collision parameter have been studied. The calculated potential energy curves are very sensitive to the basis set, theory levels, the intermolecular distance R, and the relative orientation of the two CO and O_2 monomers.

Fig. 1. shows the comparison of uncorrected and corrected results for T-shaped configuration using QCISD, UMP2, and B3LYP methods and aug-cc–pVDZ basis set.

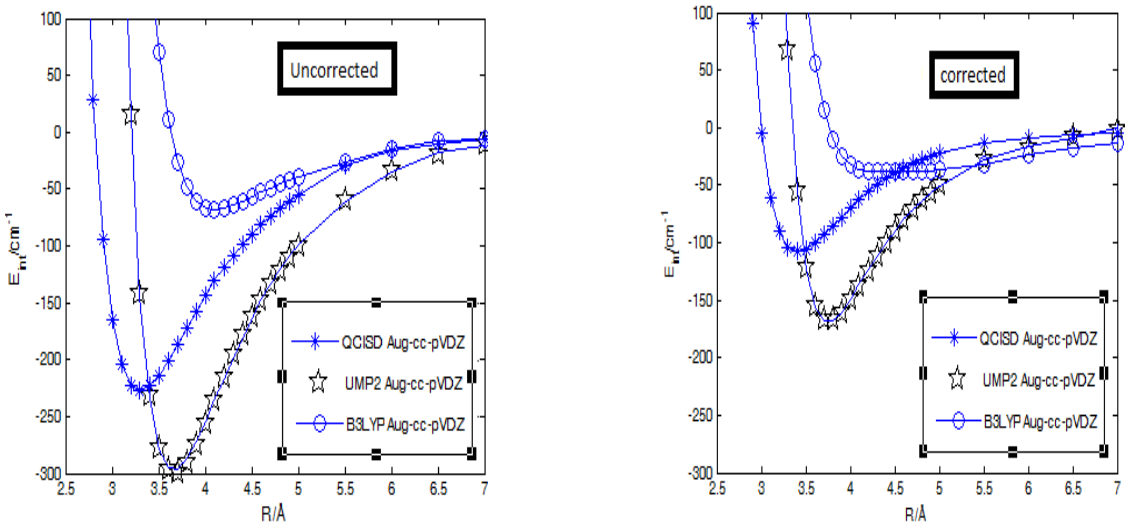

Fig 1. Uncorrected and corrected IPES's using three different QCISD, UMP2, and B3LYP theory levels and aug-cc–pVDZ basis set for T-shaped structure.

Conclusions:

The calculated potential energy curves are very sensitive to the basis set, theory levels and the relative orientation of the studied monomers. The best agreement with the experimental values of hard sphere, potential well, and vibration frequency is achieved by UMP2 theory level and aug-cc-pVTZ basis set [5].

References:

[1] Noorbala M. R.; Sabzyan H. *J. Mol. Struct*., (*Theochem*)., 678 **(2004)** 67.

[2] Sabzyan, H.; Noorbala M. R. *J. Mol. Struct*., (*Theochem*). 636 **(2003)** 185.

[3] W. Byers Brown, M.A. Vincent, K. Trollope, I.H. Hillier, *Chem. Phys. Lett.* 192 **(1992)** 213.

[4] van Lenthe, J. H.; van Duijneveldt-van de Rijdt, M J. G. C.; Van Duijneveldt F. B. *Adv. Chem. Phys*. 69 **(1987)** 521.

[5] Chndler, D. W.; Ewing, G. E.; *J. Phys. Chem*. 1994-1998 **(1981)** 85

Complexation of Trivalent Lanthanides by Isoelectronic Phosphoryl Donors: Insights from DFT Investigation

Khodayar Gholivand,*[a] Hamid R. Mahzouni,[a] Mehdi D. Esrafili[b]

[a]*Department of Chemistry, Tarbiat Modares University, Tehran, Iran*

[b]*Department of Chemistry, University of Maragheh, Maragheh, Iran*

Email: hrmahzouni@yahoo.com and gholi_kh@modares.ac.ir

Introduction

Phosphoryl containing ligands have potential to establish strong non-covalent interaction with lanthanides (Ln). Quantum mechanical calculations on the structural, electronic and energy aspects of non-covalent interactions of Ln^{3+} cations with phosphine oxides (**PO**s) and phosphate esters (**PE**s) have been extensively performed [1–3], but not with *phosphoramides*, **PA**s. Hence, we have decided to compare the small isoelectronic ligands R_3PO (group 1; R= CH_3, NH_2, OH and F, and group 2; R= CH_2Me, NHMe, OMe and Cl) as complexant agents for lanthanides. The effect of cation size on the ligand binding strength was also investigated.

Computational Methods

The geometries of free ligands **L** and complexes **L**–Ln^{3+} were fully optimized in vacuum at B3LYP level using the Gaussian 98 package [4]. The 46+4f^n electrons of Ln^{3+} ions were modeled by quasirelativistic effective core potentials (RECPs) of the Dolg et al. [5], with the affiliated (7s6p5d)/[5s4p3d] basis set for valence. The other small atoms were described by 6–31+G* standard basis set. Atoms in molecules (AIM) and Natural Population Analyses (NPA) were performed to investigate the charge distributions in free ligands **L** and complexes **L**–Ln^{3+}. The interaction energies (ΔEs) have been calculated and then corrected for basis set superposition error based on the counterpoise (CP) method [6].

Results and Discussion

The negative charge localized on phosphoryl oxygen atom, $q(O_P)$, and the *p* character of lone pair of O_P, $Lp(O_P)$, decrease from **PA**s to phosphoryl trihalides (**PH**s) in the order **PA>PO>PE>PH** (Table 1). Thus, **PA**s are expected to be more potent for cation binding.

The **PA**–Ln^{3+} distances are shorter than those of **PO** complexes. This difference is more sensible when the electron donation ability of ligands is increased. Table 2 shows that the $O_P\cdots Ln^{3+}$ distance decreases in the order **PH>PE>PO>PA**. The charge density (ρ) value at the bcp of $O_P\cdots Ln^{3+}$ increases slightly from **PO** to **PA** complexes.

Table 1. Electronic parameters of free ligands

R	Dipole Moment (Debye)	$q(O_P)^a$	Hybridization of Lp(O_P)
Me	4.650	–1.480	$sp^{0.48}$
NH_2	4.312	–1.492	$sp^{0.49}$
OH	3.355	–1.469	$sp^{0.44}$
F	1.583	–1.407	$sp^{0.36}$
CH_2Me	4.846	–1.485	$sp^{0.50}$
NHMe	4.216	–1.493	$sp^{0.52}$
OMe	3.832	–1.471	$sp^{0.47}$
Cl	2.271	–1.370	$sp^{0.45}$

[a]The AIM charges are represented

The $O_P\cdots Ln^{3+}$ distance decreases in series of La>Eu>Lu, due to the cation hardness effect. The charge transfer Lp(O_P)→5d(metal) is more intense in **PA** complexes and the electronic population in metal 5d orbital increases as **PH**<**PE**<**PO**<**PA**. CP-corrected attraction energies ($|\Delta E_{CP}|$) follow the sequence **PA>PO>PE>PH**. Complete CP-corrected interaction energies ($\Delta E_{C\text{-}CP}$) are obtained when deformation energies of subunits are considered [7] in Eq; $\Delta E_{C\text{-}CP} = \Delta E_{CP} + \Delta E_{def}(L) + \Delta E_{def}(M)$. The term of $\Delta E_{def}(M)$ is zero for M because it is an atomic species. The results show that **PA**s are more deformable that **PO**s. Hence, the trend in $|\Delta E_{C\text{-}CP}|$ values differs from that of $|\Delta E_{CP}|$ and it is in line with the trend in dipole moment of free ligands.

Table 2. Ln–O_P distance (Å), charge density (ρ, in au) at bcp of Ln…O_P, natural electron configuration (NEC) of metal 5d orbital, interaction energies (ΔEs, in kcal/mol)

Ln^{3+}	R	d(Ln–O_P) / ρ	NEC of 5d Orbital	$\Delta E_{deformation}$	$\Delta E_{CP\text{-}corrected}$	$\Delta E_{C\text{-}CP}$
La^{3+}	Me	2.053 / 0.120	$5d^{0.24}$	28.6	–256.5	–227.8
	NH_2	2.049 / 0.122	$5d^{0.25}$	49.7	–274.4	–224.7
	OH	2.082 / 0.111	$5d^{0.19}$	46.7	–238.0	–191.2
	F	2.161 / 0.091	$5d^{0.13}$	26.2	–152.4	–126.2
Eu^{3+}	Me	1.961 / 0.134	$5d^{0.29}$	31.7	–283.1	–251.4
	NH_2	1.957 / 0.136	$5d^{0.30}$	55.3	–304.0	–248.6
	OH	1.986 / 0.124	$5d^{0.24}$	51.7	–264.4	–212.7
	F	2.053 / 0.104	$5d^{0.17}$	30.1	–173.0	–142.9
Lu^{3+}	Me	1.880 / 0.141	$5d^{0.39}$	33.7	–307.6	–273.9
	NH_2	1.876 / 0.143	$5d^{0.40}$	58.8	–330.1	–271.3
	OH	1.900 / 0.132	$5d^{0.31}$	55.0	–288.9	–234.0
	F	1.957 / 0.113	$5d^{0.22}$	33.2	–194.7	–161.5
	CH_2Me	1.869 / 0.146	$5d^{0.43}$	34.9	–328.7	–293.8
	NHMe	1.857 / 0.153	$5d^{0.47}$	76.8	–370.2	–293.4
	OMe	1.871 / 0.144	$5d^{0.39}$	69.7	–340.8	–271.1
	Cl	1.905 / 0.131	$5d^{0.32}$	39.2	–250.4	–211.2

Conclusions

In summary, the strength of Ln-ligand bond in **PA** complexes is more than that in the other phosphoryl donors. The cation affinity of **PA**s is very close to that of **PO**s and drops markedly in the cases of **PE**s and **PH**s. Taking into account that the synthesis pathway of **PA**s

is relatively inexpensive, they can be considered as good alternatives for **PO**s in lanthanide complexation.

References

[1] Berny, F. et al. *Inorg. Chem.* **1999**, *38*, 1244–1252.

[2] Schurhammer, R. et al. *J Chem Soc Perkin Trans. 2* **1999**, 2423–2431.

[3] Troxler, L. et al. *J Mol Struct: (THEOCHEM*) **1998**, *431*, 151–163.

[4] Frisch, M. J. et al. Gaussian 98, revision A.7, Gaussian, Inc.; Pittsburgh, PA, 1998.

[5] (a) Dolg, M. et al. *Theor. Chim. Acta.* **1989**, *75*, 173–194. (b) Dolg, M. et al. *Theor. Chim. Acta.* **1993**, *85*, 441–450.

[6] Boys, S. F.; Bernardi, F. *Mol. Phys*. **1970**, *19*, 553–566.

[7] Kim, C. K. et al. *J. Phys. Chem. A* **2009**, *113*,513–519.

Indirect Effect of 4f-shell on the Lanthanide-Ligand Bond

Khodayar Gholivand,*[,a] Hamid R. Mahzouni,[a] Mehdi D. Esrafili[b]

[a]*Department of Chemistry, Tarbiat Modares University, Tehran, Iran*

[b] *Department of Chemistry, University of Maragheh, Maragheh, Iran*

Email: hrmahzouni@yahoo.com and gholi_kh@modares.ac.ir

Introduction

Phosphoramides are well known as good complexant agents for lanthanides (Ln) [1,2]. The treatment of the 4f orbital in lanthanide bonding is still a subject of challenge [3]. In this work, the Ce(III) complexes of known phosphoramides have been subjected to test the effective core potentials (ECPs) with 4f electrons included in both the main core and the valence shell during the geometry optimizations. Schematic illustration of the structure of complexes **1**–**3** are shown in Scheme 1.

Scheme 1

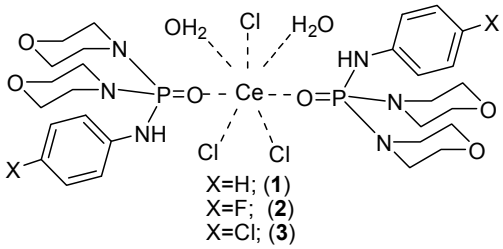

Computational Methods

QM calculations have been carried out using the Gaussian 98 package [4] at B3PW91 level. The quasi-relativistic effective core potential (RECP) of Dolg et al., and its affiliated (7s6p5d)/[5s4p3d] basis set [5] were used for Ce, and 6-31G* for other small atoms. In order to investigate the effect of f-shell electrons on the Ln–L bond, we have used both of $4f^{1}$-in-core (47MWB) and $4f^{1}$-in-valence (46MWB) ECPs for Ce complexes with multiplicity 1 and 2, respectively.

Results and discussion

The complexes **1**–**3** are marked as **1**(46)–**3**(46) and **1**(47)–**3**(47), where digits 46 and 47 in parentheses refer to the number of electron in ECP considered. It is found that the optimized

Ce–O_P distances in **n**(46) structures are smaller (by about 0.014–0.021 Å) than those in **n**(47) ones (Table 1), indicating that the Ce–L distance decreases noticeably when $4f^1$ electron is explicitly considered in the valence. It should be noted that the Ce–O_P distances in optimized **n**(46) complexes are closer to the X-ray data comparing to those of **n**(47) ones.

Taking into account the natural electron configuration [core]$4f^1$ for isolated Ce^{+3}(47) cation, the electron configuration [core]$5d^1$ can be considered as an evidence of 4f→5d electron transfer in Ce^{+3}(46) for which 46 electrons are located in the ECP. King et al. [6] have previously shown that the possible [$4f^n s^2$] → [$4f^{n-1}5d^1 6s^2$] promotion can be occurred in lanthanides, that affects the strength and stability of metal–ligand bond due to the 5d orbitals contribution to the Ln–L bonding [3]. The results of NPA in Table 1 show the natural electron configuration [core]$6s^{0.16}4f^{0.01}5d^{1.31}$, as an example, for Ce in complex **1**(46) with vacant 4f orbitals. It is noteworthy that the presence of electronic populations in 5d and 6s orbitals is not only due to the 4f→5d electronic promotion, but also is related somewhat to ligand to metal charge transfer (LMCT). We have recently shown that the Lp(O_P)→5d(metal) transition is relatively strong in Ln-phosphoramide complexes [1]. Moreover, 4f orbitals do not form any constructive interaction with the frontier orbitals of ligands. The molecular orbital coefficients of 4f orbital are zero for all of the Ce–L bonds that is representative for the formation of Ce–L bond without the sharing of 4f electrons. However, the electronic population of 4f shell is translocated to 5d orbitals when they are considered in the valence. The shortening of Ln–L distance has some effects on the LMCT. The ChelpG charges for metal ions are represented in Table 1. The ChelpG charges for Ce ions in **n**(46) complexes are smaller (by about 0.1–0.2 |e|) than those in **n**(47) analogues. Table 1 shows also that the negative charge of chloride counterions increases slightly from **n**(46) to **n**(47) complexes. This indicates that LMCT is more intense in the former group, agreeing with the shortening of Ce–L distance in **n**(46) complexes.

Table 1. Ce-L bond lengths and electronic features of complexes **1**–**3**

Compound	*d*(Ce…O_P)/Å		(ρ)[a]	*q*(Ce)	*q*(Cl)	NEC[b] of Ce^{3+}
	X-ray	Calculated		NBO / CHelpG		
1(46)	2.371(2)	2.393	0.050	2.518 / 1.639	–0.837	[core]$6s^{0.16}4f^{0.01}5d^{1.31}$
1(47)		2.407	0.048	------- / 1.765	–0.846	–
2(46)	2.373(4)	2.391	0.050	2.518 / 1.601	–0.837	[core]$6s^{0.17}4f^{0.01}5d^{1.31}$
2(47)		2.409	0.048	------- / 1.740	–0.845	–
3(46)	2.371(2)	2.389	0.053	2.558 / 1.474	–0.823	[core]$6s^{0.17}4f^{0.01}5d^{1.26}$
3(47)		2.410	0.049	------- / 1.674	–0.831	–

[a]Charge density (in au) at the bcp of Ce…O_P bond path, [b]NEC stands for natural electron configuration

Conclusions

In summary, although the NBO analysis revealed that f-electrons do not participate in Ln–L bonds, the decrease in Ce–L distances is related to some indirect effects of the f-electrons when they are considered in the valence.

References

[1] Gholivand, K. et al. *Theor. Chem. Acc.* **2010**, *127*, 539–550.

[2] Gholivand, K. et al. *Inorg. Chim. Acta.* **2010**, *363*, 2318–2324.

[3] Maron, L.; Eisenstein, O. J. *Phys. Chem. A* **2000**, *104*, 7140–7143.

[4] Frisch, M. J. et al. Gaussian 98, revision A.7, Gaussian, Inc.; Pittsburgh, PA, 1998.

[5] (a) Dolg, M. et al. *Theor. Chim. Acta.* **1989**, *75*, 173–194. (b) Dolg, M. et al. *Theor. Chim. Acta.* **1993**, *85*, 441–450.

[6] King, W. A. et al. *J. Am. Chem. Soc.* **1996**, *118*, 627–635.

The Effect of Cut-off length on the LC-LE Transition in DPPC Monolayers

Delara Mohammad-Aghaie
Department of Chemistry, College of Sciences, Shiraz University of Technology, Shiraz, 71555-313, IRAN
d_aghaie@sutech.ac.ir

KeyWords: DPPC, Molecular Dynamics Simulation, Surface Pressure isotherm, Cutoff.

Introduction

Monolayers are characterized experimentally by their surface pressure-area isotherms. The surface pressure $\Pi = \gamma_0 - \gamma_m$, where γ_0 and γ_m are the surface tensions of pure water and the monolayer respectively. In our previous work [1] we reported pressure-area isotherms of DPPC monolayers at four different temperatures, ranging from 273K to 310K (See Fig.6 in ref. 1). We could show obvious liquid condensed (LC) to liquid expanded (LE) phase transition on a time scale of almost 60 ns. A complementary structural analysis confirmed the existence of the phase transition. It has been shown in computer simulations of simple liquids that the cutoff used to truncate the dispersion interactions can have a significant impact on the phase diagram, obtained. [2]

Thus we selected two cut-off values (1.0 nm and 1.7 nm) to explore their effect on the shape and position of surface pressure-area isotherms. Also, we could see that how cut-off length affects the radial distribution functions and hydrocarbon lengths of the DPPC monolayer.

Computational Details

The initial configuration of DPPC monolayer was prepared by 64 times replicating a single DPPC molecule. The phospholipids were arranged in a square two dimensional lattice and the head groups were partially immersed in one of the water surfaces of a pre-equilibrated water film containing $4x10^3$ water molecules. The Berger et. al. forcefield [3] and the TIP4P/2005 water model, were selected to simulate the phospholipids and the water film respectively . All the interatomic bonds are rigid, and the angles and improper dihedrals are modelled through the GROMOS forcefield. Non bonded interactions were handled through a combination of Lennard-Jones and Coulombic terms and we employed full periodic boundary conditions in all the simulations. All the calculations and analysis were performed using GROMACS simulation software. [4]

Constant surface tension and temperature simulations on DPPC-TIP4P/2005 system were performed with the two cut-off values. In this way we can check the sensitivity of the pressure area isotherms and the structural properties of the monolayer to the cut-off value.

Results and Discussion

Fig. 1 shows the obtained surface pressure-area isotherms for the studied systems. Each point on the isotherms has been obtained from simulations, spanning, 60 ns. The isotherms clearly show that longer cutoff results in a shift of the surface pressure-area isotherm to lower areas per phospholipid with a concomitant decrease in the corresponding surface pressure. This observation is consistent with an increase in the dispersion interactions with the cut-off. The surface pressure isotherm of DPPC-TIP4P/2005 with cut-off value of 1.7 nm, shows the clear change of slope related to the LC-LE phase transition.

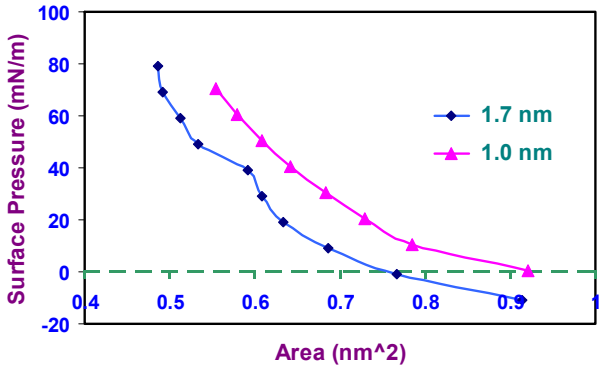

Fig. 1 Dependence of the surface pressure-area isotherms of DPPC monolayer with the cut-off

Figure. 2 shows the RDF plots for DPPC-TIP4P/2005 system with the two cutoff values. Again the effect of cut-off is evident here. In the case of short cutoff, we do not see evidence for phase transition, whereas for the longer cutoff there is a distinctive change in the long range behavior of the RDFs, which is connected to the nucleation of the LC phase.

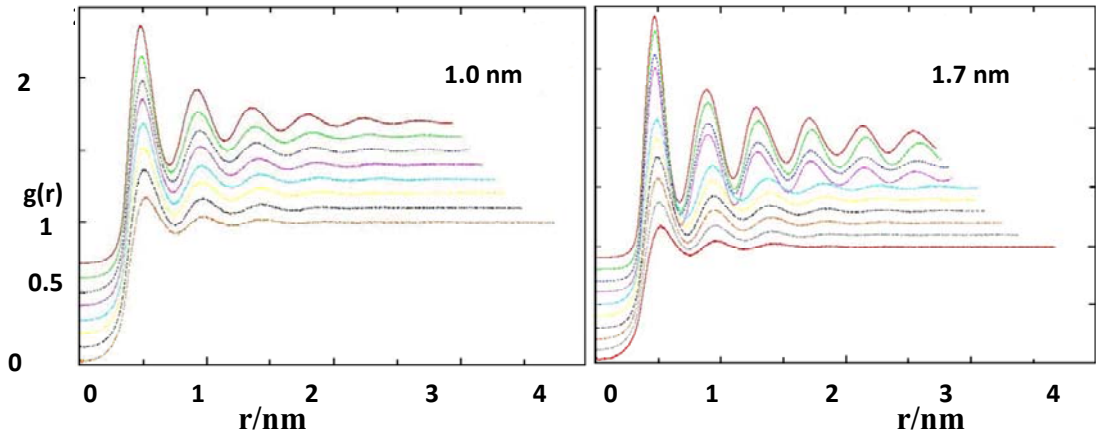

Fig. 2 Radial distribution functions (RDF) of the carbon atoms in the phospholipid chains. Successive RDF's have been shifted vertically by 0.2 units for greater clarity. Bottom RDF, smallest Π value; top RDF, largest Π value. Each graph corresponds to one point in the surface pressure-area isotherm Fig.1

References

[1] D. Mohammad-Aghaie, E. Macé, Ch. Sennoga, J. Seddon, and F. Bresme, *J. Phys. Chem. B,* **114**, No. 3, (2010), 1325.

[2] B. Smit, *J. Chem. Phys.,* **96**, (1992), 8639.

[3] O. Berger, O. Edholm, F. Jähnig, *Biophys. J.*, **72**, (1997), 2002.

[4] E. Lindahl, B. Hess, and D. van der Spoel. *J. Mol. Modeling* , **7**, (2001), 306.

Tautomeric equilibriums conformational intramolecular hydrogen bonding and π-electron delocalization in dinitrosomethane - a quantum chemical study

P. Mohammadzadeh Jahani*[a], A. Nowroozi, M.A.Rezayat

[a] Department of Chemistry, Faculty of Science, University of Sistan and Baluchestan, P.O. Box 98135-674, Zahedan, Iran

(mjpeyman@yahoo.com: E-mail)

Keywords: dinitrosomethane, Intramolecular hydrogen bond, AIM and NBO.

Introduction

Hydrogen bonding is a well-known phenomenon and a steering factor in many physical, chemical and biochemical processes [1, 2]. However, due to the variety of interactions classified as H-bonds, it is very difficult to indicate strictly their properties [3]. There is conventional X-H…Y H-bonds where X-H indicates the proton donating bond, Y is the proton acceptor, and both X and Y atoms are usually electronegative. Such meaning is in line with the definition of hydrogen bonding stated by Pauling [4].

Nitrosomethane (CH_3NO) is the simplest form of C-nitroso compounds. Therefore it can be a good model for investigation of properties and further researches about these compounds. It is obvious that medicinal properties and carcinogenic features of C-nitroso compounds can be investigated by studying this compound.

By substitution a nitroso group on the carbon atom of nitrosomethane compound, dinitrosomethane will be formed and can be participated in the dinitrosomethane ↔ Nitroso-oxim methane equilibrium (Fig. I). At this equilibrium, there are two type of tautomer, dinitrosomethane (DNM) and Nitroso-oxim methane (NOM) which interconverts to each other by tautomeric equilibriums. The appropriate arrangement of Nitroso-oxim functional groups in NOM-11 causes forming a symmetric and simple RAHB system with two heteroatom (N) is formed.

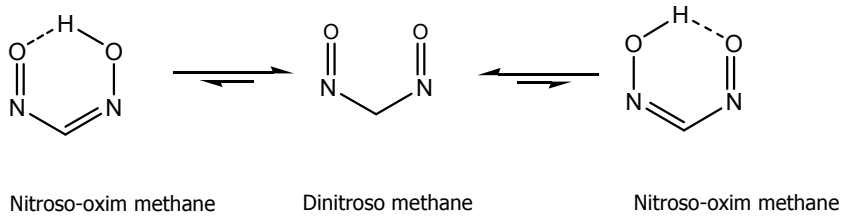

Fig 1. Nitroso-oxim methane↔Dinitroso methane tautomeric equilibriums in DNM.

Computational methods

All of the computations in the present study were performed by Gaussian 03 series of programs [5]. The geometry optimizations were carried out by HF, B3LYP, MP2 and MP4 methods with the most popular basis set, 6-311++G(d, p**)**. Harmonic vibrational frequencies were evaluated at same levels in order to confirm the nature of the stationary points found and to account for the zero point vibrational energy (ZPVE) correction. Furthermore, to have more precise energies for conformational equilibriums the high level ab-initio methods, G2MP2, G2, and G3, were employed. The natural bond orbital (NBO) [6] and quantum theory of atoms in molecules (QTAIM) [7] were applied as a powerful approach for evaluation of the hydrogen bond strength in the chelated conformer.

Results and discussion

Theoretically, DNM has about 11 different conformers, which systematically arranged in two tautomeric classes, DN and NO with 3 and 8 members, respectively (Fig.2). The computational results reveal that lone pair-lone pair repulsion between oxygen and nitrogen atoms and π-electron delocalization are two superior factors in determining the most stable conformation of dinitrosomethane and Nitroso-oxim methane tautomers, respectively. The relative energies all of the forms at different computational levels shows that the most stable form (NO-24) has relatively significant energy difference with other conformers due to lying N=O,C=N double bonds in trans state respect to each other, result in minimizing the lone pair repulsion between oxygen and nitrogen atoms (Fig.3).

The evaluation of hydrogen bond energy by Spinosa, isodesmic and empirical energy-geometry correlations methods at all of the computational levels in DNM and MA molecules clearly predict that, except the isodesmic method, in other methods energy of hydrogen bond

in DNM is higher than the corresponding value of MA[8]. In other word, it can be concluded that the presence of a heteroatom (N) significantly increased the IHB strength in DNM molecule. Also the results of quantum theory of atoms in molecules, the natural bond orbital analyses and geometrical parameters are consistent with the IHB energy conclusion. Our theoretical calculations reveal that the NO conformers are more stable than the DN ones. The population analyses of the possible conformations by NBO predict that the π-electron delocalization, especially LP (O)→ π $^*_{C=N}$ charge transfer, and repulsion energy are the origin of tautomeric preference.

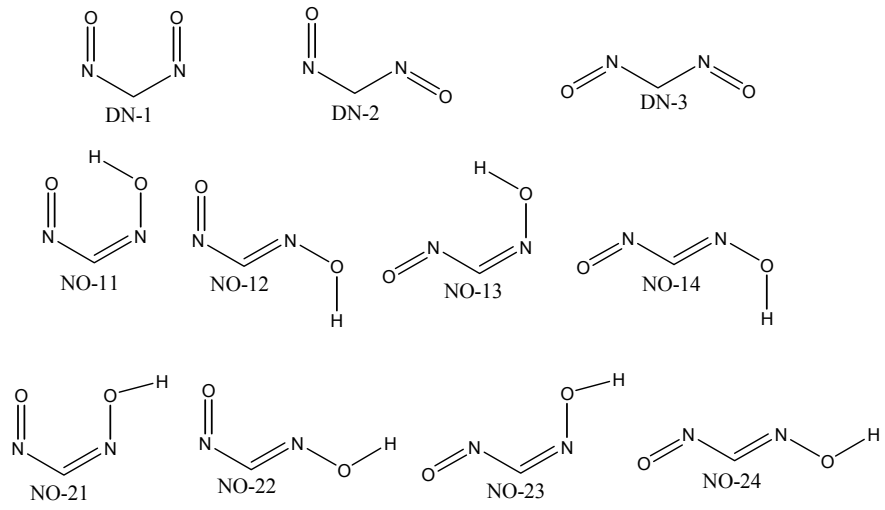

Fig 2. All of the plausible theoretical conformers of DNM.

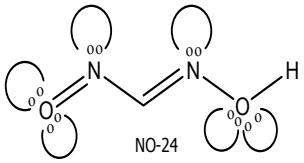

Fig3.Rearrangement of Trans state N=O, C=N double bonds and decline of lone pair-lone pair repulsion between oxygen and nitrogen atoms in most stable conformers.

References:

[1] G. A. Jeffrey, W. Saenger, Hydrogen Bonding in Biological Structures; Springer-Verlag: Berlin 1991.

[2] G. A. Jeffrey, an Introduction to Hydrogen Bonding; Oxford University Press: New York, 1997

[3] G. R Desiraju, T. Steiner, The weak hydrogen bond in structural chemistry and biology; Oxford University Press: New York, 1999.

[4] L. Pauling, the Nature of the Chemical Bond, 3rd ed.; Cornell.

Theoretical study of lone pair-lone pair repulsion in Dinitrosamine↔ Diazene, hydroxynitroso tautomeric equilibrium and determining the most stable conformer in gas phase

P. Mohammadzadeh Jahani*[a], A. Nowroozi, M.A.Rezayat

[a] Department of Chemistry, Faculty of Science, University of Sistan and Baluchestan, P.O. Box 98135-674, Zahedan, Iran

(mjpeyman@yahoo.com:E-mail)

Keywords: dinitrosoamine, Intramolecular hydrogen bond, repulsion energy, AIM, NBO.

Introduction

The nitrosamine compounds constitute a family of potent carcinogen, which are readily from a diverse set of nitrogen compounds and nitrite or its derivatives [1, 2]. By substitution a nitroso group on the nitrogen atom of nitrosamine compound, dinitrosamine (DNA) will be formed and can be participated in the Dinitrosamine (DNA) ↔ Diazene, hydroxynitroso (DHN) tautomeric equilibrium. Theoretically, DNA has about 11 different conformers, which systematically arrange in two tautomeric classes, DNA and DHN with 3 and 8 members, respectively. (Fig.1).

Computational methods

Computations were carried out at HF, B3LYP and MP2 levels with the most popular basis set, 6-311++G(d,p) and the equilibrium conformations were determined. Furthermore to have more reliable results, the total energies of all the equilibrium conformers were recomputed at the high level ab-initio methods such as G2MP2, G2, and G3 in gas phase .Quantum theory of atoms in molecules (QTAIM) [3] was applied as a powerful approach for evaluation of the hydrogen bond strength.

Results and discussion

In the present study Spinosa, isodesmic and empirical energy-geometry correlations methods are used in calculating IHB energy in DHN-11,DHN13 and MA molecules[4,5,6].It is evident from this calculation that, energy of hydrogen bond in DHN-11 is lowest than the

corresponding value of MA. Also. In other word, it can be concluded that the presence of tree heteroatom (N) significantly decreased the IHB strength in DHN-11 conformer. But DHN-13 have lowest IHB energy due to the formation of hydrogen bonding with five-member ring, therefore order of IHB energy is as follows: MA > DHN-11 >DHN-13

Conclusions

The computational results emphases that DNA-3 is the most stable form because there is the least lone pair-lone pair repulsion between oxygen and nitrogen atoms. Also, DHN-13 is the most unstable form due to the formation of hydrogen bonding with five-member ring and higher repulsion energy (Fig2).

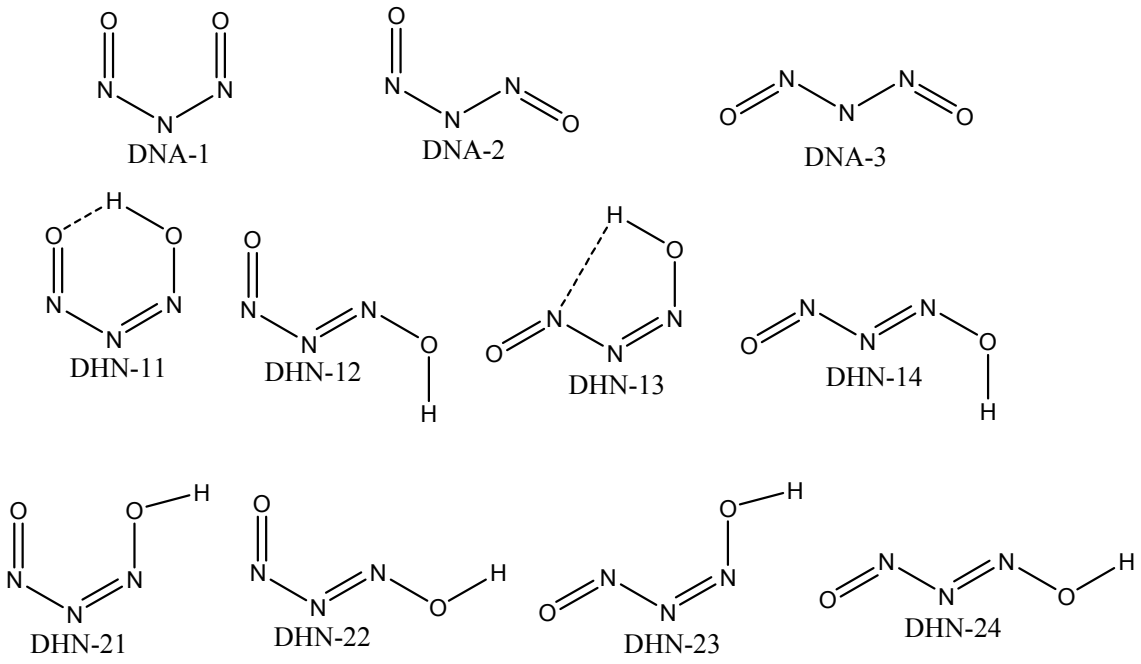

Fig1. All of the plausible theoretical conformers of DNA.

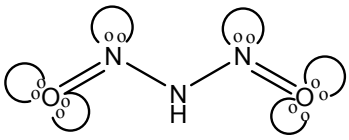

DNA-3

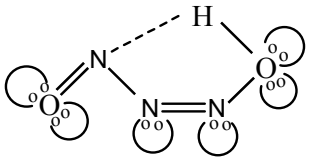

DHN-13

Fig2.lone pair-lone pair repulsion between oxygen and nitrogen atoms in DHN-13.

References:

[1] F.Murad, Angew Chem. Int. Ed. 38(1999**)**1856.

[2] P. Jiang, Q .Ximei, Q. Chunhui, W. Dianxun.Chem Phys Lett, 277(1997**)** 508

[3] R. F. W. Bader, Atoms in Molecules. A Quantum Theory, Clarendon, Oxford, U.K. 1990

[4] E.Spinosa, C.Lecomte, E.Molins, Chemical Physics Letters .300(1999)745-748

[5] I. Rozas, I. Alkorta, J. Elguero, Intramolecular Hydrogen Bonds in ortho-Substituted Hydroxybenzenes and in 8-Substituted 1-Hydroxynaphthalenes: Can a Methyl Group Be an Acceptor of Hydrogen Bonds? J.Phys. Chem. A.105 (2001)10462-10467.

[6] Jeffrey N. Woodford. J. Phys. Chem. A, 111(2007) 8519-8530.

Tel.: +983442214847, 09133464182

Quantitative structure - property relationship studies of density for primary alcohols using artificial neural network

Z.kalantar*, H.Nikoofard and L. Mohammadi
School of Chemistry, Shahrood University of Technology, Shahrood, Iran
Email: zahrakalantar@yahoo.com and zkalantar@shahroodut.ac.ir

Introduction

The liquid density is very important parameter for both heat transfer and mass transfer calculation in the design of chemical process. Although experimental data can be very accurate, it is difficult to provide all the data needed for the compounds of interest in the literature. Therefore, estimation methods are generally employed in these situations. The quantitative structure-property relationship (QSPR) method seems to be the most promising fields of the practical application of the thermodynamic models to describe the real systems. Using this approach, structural parameters such as geometric, electronic and physicochemical descriptors can be generated for molecules and a subset can be selected that best describes the density. Although, many different techniques have been used for constructing QSPR models, artificial neural network (ANN) has become popular for constructing these models in the past decade. The popularity of this technique is due to their success where complex nonlinear relationships exist among data. The main aim of the present work was to development of a quantitative structure– property relationship (QSPR) model using artificial neural network for density prediction of primary alcohols.

Method

The *pVT* data for different primary alcohols (C_2 [1],C_3 [2],C_4 [3],C_5 [4],C_6 [5],C_7 [6],C_8 [7],C_9 [8],C_{10} and C_{12} [7]) was randomly divided into 3groups:training set ,validation set and test set consisting 396, 86 and 86 data, respectively. In order to calculate the theoretical descriptors the molecular structures were constructed with the aid of Hyperchem 7.1and were optimized using AM1algoritm. The molecular geometries of compounds were further optimized by dragon package2.1. As a result, total of 1481 theoretical descriptor were calculated for each compound in the data set. The method of stepwise MLR was used to select the most important

descriptor relating the density to the descriptors. Then, three-layer network with a tangantsigmoid (*tansig*) transfer function was designed. The optimization of ANN parameters (weights and biases) and architecture was carried out using Levenberg-Marquardt algorithm for back-propagation of error.

Result and Discussion

An ANN model was constructed using 3 input including two experimental descriptors; pressure and temperature, and one theoretically derived descriptor, geometric mean on the leverage magnitude (HGM) that were chosen by the stepwise variables selection techniques and 1 neuron in output layer that predicts density by network. The number of neuron in the hidden layer is unknown and need to be optimized. The root mean square error of training (RMSET) and validation (RMSEV) sets were obtained at various iterations for different number of neurons at the hidden layer and the minimum value of RMSEV was selected as the optimum value. Plot of RMSET and RMSEV versus the number of node in the hidden layer showed that 10 nodes in hidden layer is optimum value. Also the results demonstrate that over fitting does not exist for this artificial neural network (ANN) model and training is stopped after 100 iterations. Then, generated ANN with architecture 3-10-1 was trained using the training set for the optimization of the weights and biases The capability of the optimized ANN model has been evaluated by predicting values of density for the validation and test sets. The excellent prediction results, reveals the capability of this model. Also, the performance of this model was evaluated by plotting the estimated values versus the experimental values of density for the validation and test sets, see fig.1. The MSE and mean percentage error were 0.1026 and 0.0268 for the validation set and 0.5831 and 0.0364 for the test set, respectively.

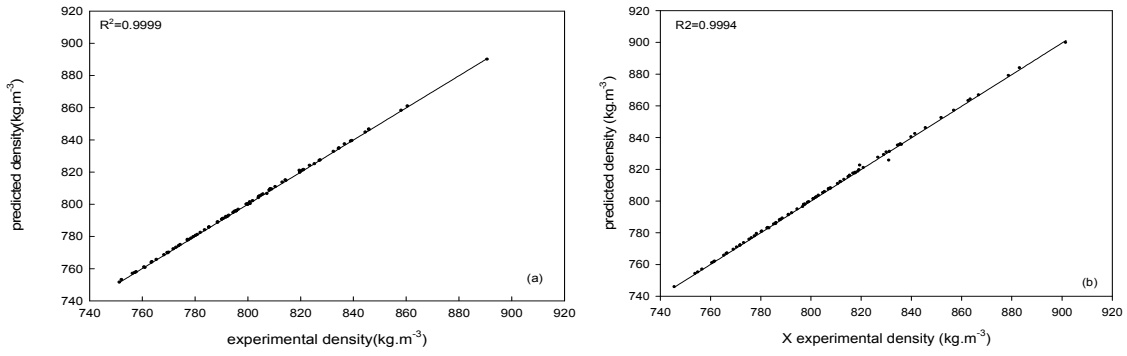

Fig.1.plot of predicted density versus experimental density for (a) prediction set and (b) test set.

Conclusion

The ANN model was developed for density prediction of 1-alcholes over a wide range of pressure and temperature. The performance of the ANN model was compared with MLR model. The results indicate the superiority of the ANN model over that of the MLR model.

References

[1] H. Kubata, Y.Tanaka, and T.Makita, *Int. J. Thermophys.*, **8** (1987) 47.

[2] A. Zuniga-Moreno and L. A. Galicia-Luna, *J. Chem. Eng. Data*, **47** (2002) 155.

[3] A. Zuniga-Moreno *et al.*, *J. Chem. Thermodynamics*, **39** (2007) 254.

[4] C. Boned, A. Baylaucq, J. P. Bazile, *Fluid Phase Equilibria*, **270** (2008) 69.

[5] F. Audonnet and A. A. H. Padua, *J. Chem. Eng. Data*, **23** (2002) 1537.

[6] A. Zuniga-Moreno *et al.*, *J.Chem. Thermodynamics*, **40** (2008) 98.

[7] S. Matsuo and T.Makita, *Int. J. Thermophys.*, **10** (1989) 885.

[8] M. Dzida, *J. Chem. Eng. Data*, **52** (2007) 52.

Multiple linear regression (MLR) modeling for density prediction of 1-alkanols over a wide range of temperatures and pressures using theoretically derived descriptors

Z. Kalantar*, H.Nikoofard, and L. Mohammadi

School of Chemistry, Shahrood University of Technology, Shahrood, Iran

Email: zahrakalantar@yahoo.com and zkalantar@shahroodut.ac.ir

Introduction

The base for design and simulation of many chemical processing units is a set of physical and thermodynamic properties of compounds in a process that undergoes some forms of transformation. It is not always possible, however, to find experimental values of the properties for the compounds of interest in the literature. Since, it is not practical to measure them as the need arises, estimation methods are generally employed in this and other similar situations. One of these methods is linear modeling such as multiple linear regressions (MLR) method and partial least square (PLS) method. In the present work, we developed a MLR model for density prediction of 1-alkanoles using theoretically derived descriptors.

Methods

The *pVT* data for different 1-alkanol from 2 to 12 carbon atom number (C_2 [1], C_3 [2], C_4 [3], C_5 [4], C_6 [5], C_7 [6], C_8 [7], C_9 [8], C_{10} and C_{12} [7]) was randomly divided into 3groups: training set, validation set and test set consisting 396, 86, 86 data, respectively. In order to calculate the theoretical descriptors the molecular structures were constructed with the aid of Hyperchem 7.1 and were optimized using AM1 algorithm. The molecular geometries of compounds were further optimized by dragon package2.1. As a result, total of 1481 theoretical descriptor were calculated for each compound in the data set. The method of stepwise MLR was used to select the most important descriptors and to calculate the coefficient relating the density to the descriptors. One calculated and two experimental descriptors, pressure and temperature, were selected as the most feasible descriptors. The calculated descriptor is geometric mean on the leverage magnitude (HGM).

Result and discussion

Multiple parameter linear correlation of density values for different 1-alkanols versus the selected descriptors gives the results in Table 1.

Table 1. The name of descriptors, their symbols and coefficients in multiple linear regression

Name of descriptor	Symbol	Coefficient
Pressure	*p*	0.516
Temperature	*T*	-0.705
Geometric mean on the leverage magnitude	HGM	-2.236
Constant		1053.898

Therefore, the MLR equation is ρ=1053.898 - 2.236HGM - 0.705T + 0.516p.

The capability of the model has been evaluated by predicting values of density by the constructed MLR model for the prediction and test sets. The excellent prediction results, reveals the capability of this model. Also, the performance of this model was evaluated by plotting the estimated values versus the experimental values of density for the validation and test sets, see fig.1. The MSE and mean percentage errors were 15.10 and 0.370 for the validation set and 16.92 and 0.383 for the test set.

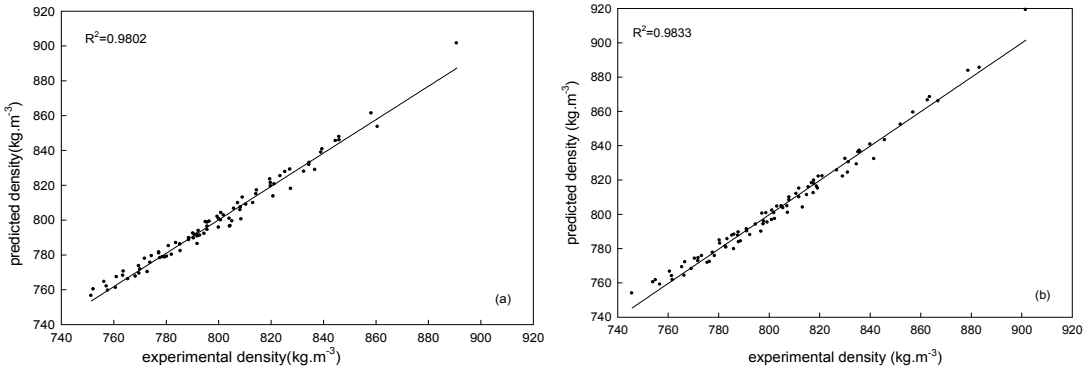

Fig.1.plot of predicted density versus experimental density for (a) validation set and (b) test set

Refrence

[1] H. Kubata, Y.Tanaka, and T.Makita, *Int. J. Thermophys.*, **8** (1987) 47.

[2] A. Zuniga-Moreno and L. A. Galicia-Luna, *J. Chem. Eng. Data*, **47** (2002) 155.

[3] A. Zuniga-Moreno *et al.*, *J. Chem. Thermodynamics*, **39** (2007) 254.

[4] C. Boned, A. Baylaucq, J. P. Bazile, *Fluid Phase Equilibria*, **270** (2008) 69.

[5] F. Audonnet and A. A. H. Padua, *J. Chem. Eng. Data*, **23** (2002) 1537.

[6] A. Zuniga-Moreno *et al.*, *J.Chem. Thermodynamics*, **40** (2008) 98.

[7] S. Matsuo and T.Makita, *Int. J. Thermophys.*, **10** (1989) 885.

[8] M. Dzida, *J. Chem. Eng. Data*, **52** (2007) 52.

Theoretical investigation of the S_N1 reaction of 1-bromo-2-3 dimethyl propane withOH^-

S.mahmoodi asl*
University of Payamnoorassaloyeh,bushehr,Iran
Email:Mahmoodi_sattar@yahoo.com

Abstract:
We have theoretically investigated the mechanism of nucleophilicsubstation reaction S_N1 by Gaussian software and HF, DFT, MP2(3-21g, 6-31g) basis set.In this paper the mechanism of reactionstudied with calculation energy of each step and determintion the structure transition state.The results show that the mechanism of reaction was doing with rarregment of molecules to stable carbocation and agreement to experimental result.

Keyword: Ab initio method, HF,Transitionstate,DFT, **S_N1** reaction

Introduction:
More than a hundred years after itwas recognized [1], the **S_N1** reaction continues to fascinate chemists. Despite a vast amount of information from synthetic and mechanistic studies of nucleophiles' substitution reactions in solution and despite the quite helpful rule-of-thumb explanations of **S_N1** reactivity given in textbooks [2–5], the molecular characteristics that steer the outcome and velocities of nucleophilic substitution reactions are still under investigation and debate, and the underlying electronic structure relationships are rather poorly understood. There exists a very valuable literature on quantum chemical modelling of **S_N1** reactions, which was recently critically reviewed. For this reason the consistency of early calculations of barriers [6-17] by simpler and more approximate methods like HF, DFT and MP2 with small and medium sized basis sets should be reconsidered.
For any nucleophilic substitution of this kind (only the anionic case is illustrated)

$$Y^- + RX \rightarrow RY + X^-$$

Method:
Quantum chemical calculations were carried out using the program system Gaussian 03 [18]. Relevant critical points (reactants, transition structures (TS), and products) of the potential energy surface were characterized by complete optimization of the molecular geometries using the hybrid density functional scheme B3LYP [18] with the 6-31G(d) basis set, which is

abbreviated by B3LYP/6-31G(d) as well as MøllerPlesset perturbation theory (MP2) [18] with the same basis set.

Results and discussion:

The reaction pathways between 1-bromo-2-3 dimethylpropane and anOH^-follow the same pattern. The reaction pathway is characterized by four distinct structures; separated reactants,a two carbocation a transition structure (TS), and the separated products (SP).

(I) (II)

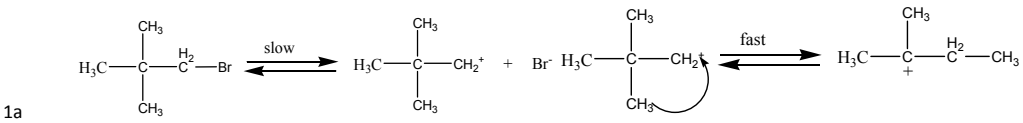

1a

(III)

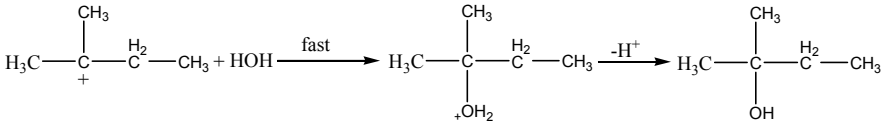

For initial step each molecules optimization with B3LYP/6-31g (d) and then calculation the energy of each structure with HF, MP2, B3LYP method(table1).The chart of shows in this apparent that the stability of structure for investigation of mechanistic with comparison energy of each structure(Figure2)

For determainationthe structure translation state it was each reactant and productoptimization with B3LYP/6-31G basis set.anduse the QST2 method. The structure of transition stateand the diagram ofstudied TS shown in Figure2

Table1.zero point energy (ZPE)(KJ mol^-) for compound

compound	Theoritical			
	HF(3-21G)	HF(6-31G)	MP2(6-31G)	B3LYP(6-31G)
1a	-1728.621	-1735.334	-1735.652	-1737.384
2b	-121.983	-122.615	-123.033	-123.546
3c	-122.129	-123.759	-123.035	-123.698
4d	-169.232	-170.099	-170.471	-171.250

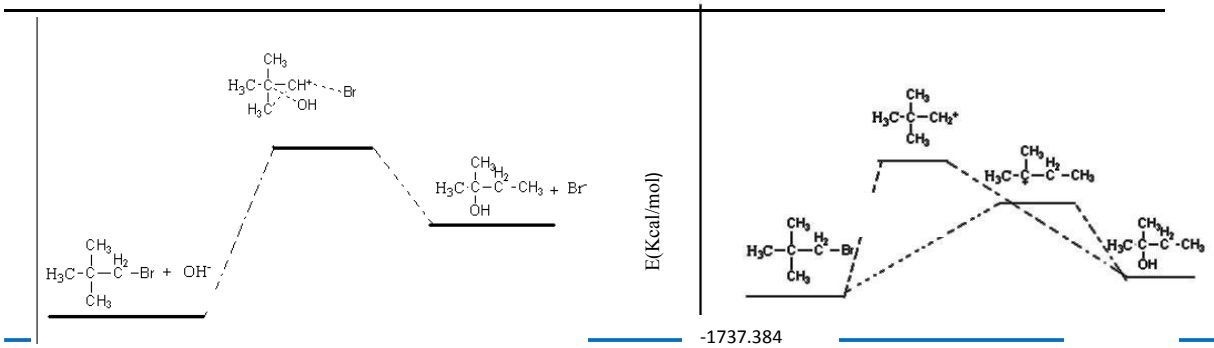

Fig1. Potential energy profileof theS_N1 reaction (B3LYP/6-31G)

Conclusion:

The present study provides adetailed insight into the reaction of in gas phase ,using electronic structure calculation.four stationary point have been located in the potential energy surface:reactant,twocarbocation,transition state structure and product.Geometries were optimized and vibrational frequencies were calculated at the DFT levels.intermediates and TSs of the reaction pathways in both single and triplet electronic state have been characterized by the vibration analysis and IRC calculation and possible mechanisms for the reaction were discussed in some detail.

References:

[1] P. Walden, Ber. 26 (1893) 210

[2] C.K. Ingold, Structure and Mechanism in Organic Chemistry, Cornell UniversityPress, Ithaca, NY, 1953.

[3] T.H. Lowry, K.S. Richardson, Mechanism and Theory in Organic Chemistry,second ed., Harper & Row, New York, 1981.

[4] J. March, Advanced Organic Chemistry, fourth ed., JohnWiley, New York, 1992.

[5] N. Isaacs, Physical Organic Chemistry, second ed., Longman Scientific &Technical, Burnt Mill, Harlow, Essex, UK, 1995.

[6] J. Chandrasekhar, S.F. Smith, W.L. Jorgensen, J. Am. Chem. Soc. 106,(1984) 3049.

[7] J. Chandrasekhar, S.F. Smith, W.L. Jorgensen, J. Am. Chem. Soc. 107,(1985) 154.

[8] J.A. Dodd, J.I. Brauman, J. Am. Chem. Soc. 106 (1984) 5356. [13] D. Kost, K. Aviram, JACS 108 (1986) 2006.

[9] S. Shaik, Nouv. J. Chim. 6 (1982) 159.

[10] S. Shaik, Prog. Phys. Org. Chem. 15 (1985) 197.

[11] Z. Shi, R.J. Boyd, J. Am. Chem. Soc. 111 (1989) 1575.

[12] Z. Shi, R.J. Boyd, J. Am. Chem. Soc. 112 (1990) 6789.

[13] Z. Shi, R.J. Boyd, J. Am. Chem. Soc. 113 (1991) 2434.

[14] B.D. Wladkowski, W.D. Allen, J.I. Brauman, J. Phys. Chem. 98 (1994)13532.

[15] B.D. Wladkowski, K.F. Lim,W.D. Allen, J.I. Brauman, J. Am. Chem. Soc.114 (1992) 9136.

[16] S.Wolfe, D.J. Mitchell, H.B. Schlegel, J. Am. Chem. Soc. 103 (1981) 7692.

[17] S.Wolfe, D.J. Mitchell, H.B. Schlegel, J. Am. Chem. Soc. 103 (1981) 7694.

[18] A.D. Becke, J. Chem. Phys. 98 (1993) 5648.

Ab Initio and DFT Studies, NBO and NICS Analysis of Dehalohydogenation Reaction of 2-halo-2,3-dihydropyridine

Z. Mahmoodi[a,*], H. Shirani IL Beigi[b] , S. Jameh-Bozorghi[b], M. Rad[b] and H. Irannezhad[a]

[a]*Department of Chemistry, Islamic Azad University, Arak Branch, Arak, Iran*

[b]*Department of Chemistry, Islamic Azad University, Toyserkan Branch, Toyserkan, Iran*

[*]*Email: Mahmoodi_zahra80@yahoo.com*

Abstract

Decomposition of 2-fluoro2,3-dihydropyridine(1), 2-chloro2,3-dihydropyridine(3), 2-bromo2,3-dihydropyridine(5) to pyridine was investigated using ab initio Molecular Orbital (MO) and Density Functional Theory (DFT). For all HX (X=F, Cl, Br) elimination reactions examined here, transition states have a four-centered transition structure. Study on the B3LYP/6-311+G** level of theory revealed that the required energy for the decomposition of compounds 1, 3 and 5 to pyridine is 32.483165 23.329822 and 19.987130 kcal mol^{-1}, respectively. HF/6-311+G**// B3LYP /6-311+G** calculated barrier height for the decomposition of compound 1, 3 and 5 to pyridine is 52.061165, 31.720752 and 25.866177 kcal mol^{-1}, respectively. Also, MP2/6-311+G**// B3LYP /6-311+G** results indicated that the barrier height for the decomposition of compound 1, 3 and 5 to pyridine is 41.448885, 41.768282 and 37.129175 kcal mol^{-1}, respectively. Natural Bond Orbital (NBO) population analysis and Nuclear Independent Chemical Shift (NICS) results showed that, reactants are non-aromatic but products of elimination reaction are aromatic, C-H and C-X bonds are broken and H-X bond is appear.

Keywords: Ab initio; NBO; 2-halo-2,3-dihydropyridine

Introduction

Decomposition mechanism of 2-halo-2,3-dihydropyridines to pyridine was investigated using ab initio Molecular Orbital (MO) and Density Functional Theory (DFT). The experimental study of the kinetic of dissociation process of 2-halo-2,3-dihydropyridinies, showed that the decomposition reaction of 2-halo-2,3-dihydropyridinie is a unimolecular process [1]. In this work, ab initio molecular orbital (MO), [2-5] DFT (B3LYP) methods [6] and NBO analysis

were performed for the investigation of the pyrolysis reactions of 2-fluoro2,3-dihydropyridine(1), 2-chloro2,3-dihydropyridine(3) and 2-bromo2,3-dihydropyridine(5) to pyridine.

Methods

Ab initio calculations were carried out using B3LYP/6-311+G**, HF/6-311+G**// B3LYP /6-311+G**, and MP2/6-311+G**// B3LYP /6-311+G** levels of theory with the GAUSSIAN 98 package of programs [7] implemented on a Pentium–PC computer with a 7300 MHz processor. Initial estimation of the structural geometry of the compound 1, 3 and 5 were obtained by a molecular mechanic program PCMODEL (88.0) and for further optimization of geometry, we used the PM3 method of the MOPAC 7.0 computer program [8,9]. The GAUSSIAN 98 package of programs were finally used to perform ab initio calculations at the B3LYP/6-311+G** level.

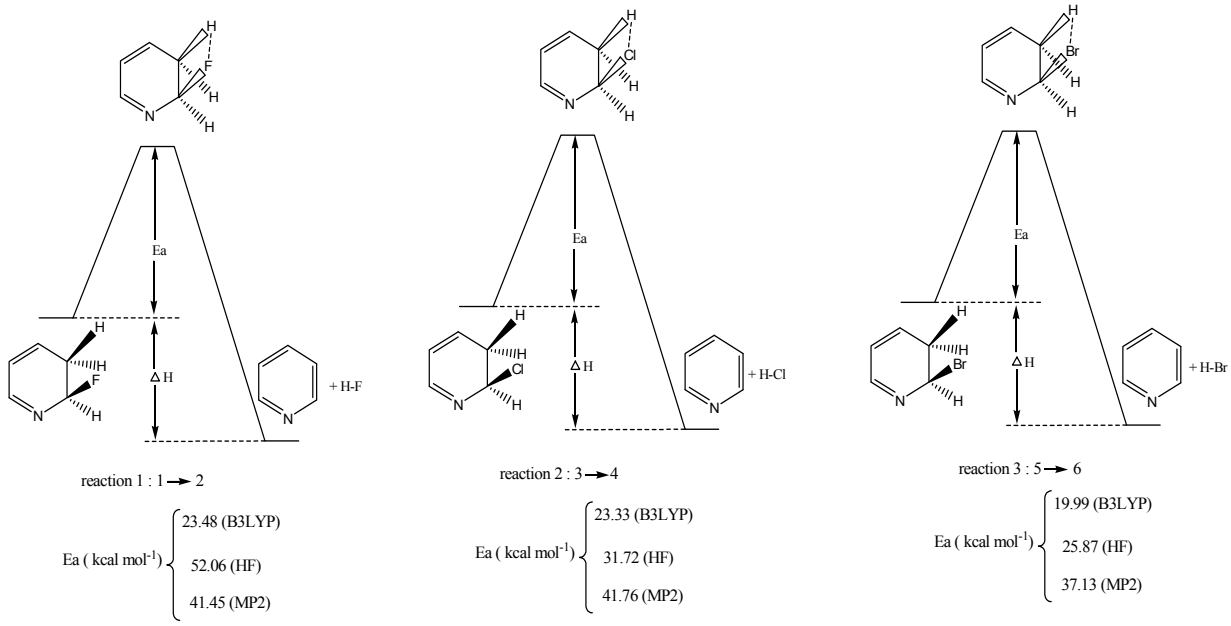

Figure 1:

B3LYP, HF and MP2 energy diagram of decomposition of compounds **1**,**3** and **5.**

Results and Discussion

Zero point (ZPE) and total electronic (Eel) energies (E0 = ZPE + Eel) for the energy minimum and energy maximum geometries of the decomposition of compound 1, 3 and 5 to pyridine were calculated on the B3LYP/6-311+G**// B3LYP/6-311+G** level of theory. For single-point energy calculations, both HF/6-311+G**// B3LYP /6-311+G**and MP2/6-311+G**// B3LYP /6-311+G** methods were used and are given in Table 1. Studies on the B3LYP/6-311+G**, HF/6-311+G**// B3LYP /6-311+G**, and MP2/6-311+G**// B3LYP /6-311+G** of theory show that the barrier height of the decomposition of the compound 1 to pyridine and HF (reaction 1) is 32.483165, 52.061165 and 41.448885 kcal mol^{-1}, respectively. These calculation results for compound 2 revealed that the barrier height of reaction 2 is 23.329822, 31.720752 and 41.768282 kcal mol^{-1}, respectively. Also, barrier height of reaction 3 is 19.987130, 25.866177 and 37.129175 kcal mol^{-1}, respectively (see Figure 1). It is well known that the strength of C-X bonds decreases, while the bond length increases with the size of halide atom. The lengths of C-F, C-Cl and C-Br bonds determined were found to be 1.41, 1.86 and 2.04 Å, respectively, in agreement with energetic behavior and other experimental data. C2-C3 bond lengths in reactants are greater than transition states and products in reactions 1-3 that showed that C=C double bond formed in products.

Conclusion

Ab initio HF, MP2, and B3LYP density functional-theory calculations provide a picture from structural, energetic, and natural charge distributions points of view for the decomposition mechanisem of compound 1, 3 and 5 to pyridine and HX (X=F, Cl, Br). B3LYP/6-311+G**// B3LYP/6-311+G**, HF/6-311+G**// B3LYP /6-311+G**, and MP2/6-311+G**// B3LYP /6-311+G** results reveal that a lower barrier height for reaction 3 than that of reactions 1 and 2. These results are justified by natural charge distribution values, calculated structural parameters and NBO results analysis in the ground-state structure of compounds 1,3 and 5 and transition state structures of reactions 1– 3. NBO analysis revealed that resonance energies in products are greater than reactants. Therefore, the number of conjugated π bond increased in products. Also, NICS results showed that reactants are non-aromatic but products are aromatic compounds. Consequently, the calculated data could be considered as fairly acceptable and useful information from the QSAR point of view in the corresponding organic

compounds, which are further confirmed by the corresponding energetic and structural results generated by the NBO analysis and NICS results.

References

[1] B. Liu, *J. Chem. Phys*. 80, (1984), 581.

[2] A.D. Becke, *J. Chem. Phys*. 98, (1993), 5648.

[3] C. Lee, W. Yang, R.G. Parr, *Phys. Rev*. 37, (1988), 785.

[4] W.J. Hehri, L. Radom, P.v.R. Schleyer, J.A. Pople, Ab Initio Molecular Orbital Theory, Wiley,New York,(1986).

[5] J.M. Seminario, P. Politzer (Eds.), Modern Density Functional Theory. A Tool for Chemistry,Elsevier, Amsterdam, (1995).

[6] Mo¨lder U, Burk P, Koppel IA. *J. Mol. Struct. (THEOCHEM)* ., 712 , (2004), 81–89.

[7] Alkorta I, Elguero *J. Struct. Chem*., 16 , (2005), 77–79.

[8] A. Rahaman, L.M. Raff, *J. Phys. Chem*. A 105, (2001) 2156.

[9] S. Kuns_agi-M_at_e, E. V_egh, G. Nagy, L. Koll_ar, *J. Phys. Chem. A* 106, (2002), 6319.

Density Functional Theory Study of the Rreaction Mechanism of the DNA Repairing Enzyme Alkylguanine

Z. Mahmoodi[a,*], H. Shirani IL Beigi[b], A. bodaghi[b], J. Hosseini[b], H. Soleymanabadi[b], M.Nouraliei[b] and H. Irannezhad[a]

[a]*Department of Chemistry, Islamic Azad University, Arak Branch, Arak, Iran*

[b]*Department of Chemistry, Islamic Azad University, Toyserkan Branch, Toyserkan, Iran*

[*]*Email: mahmoodi_zahra80@yahoo.com*

Abstract

The reaction mechanism of human O6-alkylguanine-DNA alkyltransferase (AGT) is studied using density functional theory. AGT repairs alkylated DNA by directly removing the alkyl group from the O6 position of the guanine. A quantum chemical model of the active site was devised based on the recent crystal structure of the AGT–DNA complex. The potential energy curve is calculated and the stationary points are characterized. It is concluded that the previously proposed reaction mechanism is energetically plausible.

Keywords: Density functional theory; AGT; DNA

Introduction

O6-Alkylguanine-DNA alkyltransferase (AGT), also known as O6-methylguanine-DNA methyltransferase (MGMT), repairs the alkylated DNA by directly removing the alkyl group from the O6 position of the guanine [1,2]. It works by transferring the alkyl lesion to an active site cysteine residue in an irreversible stoichiometric suicide reaction. After completing its task, the alkylated enzyme is degraded in the ubiquitin pathway. Human AGT is a target in cancer therapy because it repairs damage induced by anticancer chemotherapies [3]. The main features of the active site-base interaction for the human AGT are shown in Figure 1. In the present study, we use the hybrid density functional theory method to examine the energetic feasibility of this suggested mechanism.

Methods

All geometries and energies presented in the present study are computed using the B3LYP density functional theory method as implemented in the GAUSSIAN 03 program package [4]. Geometry optimizations were performed using the 6-31G(d,p) basis set.

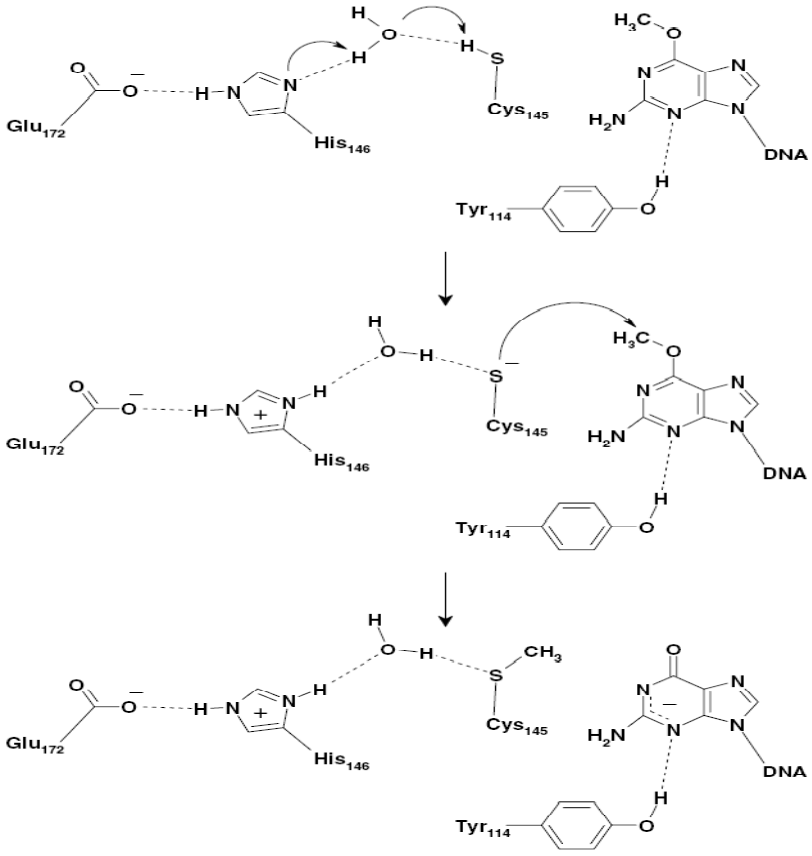

Figure 1: Proposed reaction mechanism of AGT.

Results and Discussion

Having established that the proton transfer resulting in the creation of the thiolate anion is energetically feasible, the next step is to transfer the methyl group from the O6 position of the guanine to the thiolate, thereby repairing the DNA. The transition state (TS2) for this SN2 methyl transfer was located and confirmed by a frequency calculation to have an imaginary frequency of - 475i cm^{-1}.

Conclusion

In this Letter, we have used a quantum chemical cluster model to examine the energetic feasibility of the chemical steps of the DNA repair mechanism of O6-alkylguanine-DNA alkyltransferase (AGT). The active site model is based on the recent X-ray structure of the AGT–DNA complex and consists of 74 atoms. The calculations confirm the suggested mechanism, in which Cys145 first is activated by a proton transfer to His146, mediated by a water molecule. The resulting thiolate is then able to perform a nucleophilic attack on the methyl group.

References

[1] S. Mitra, DNA Repair 6 (2007) 1064.
[2] J.L. Tubbs, A.E. Pegg, J.A. Tainer, DNA Repair 6 (2007) 1100.
[3] Q. Fang, S.L. Gerson, Clin. Cancer Res. 12 (2006) 328.
[4] M.J. Frisch et al., GAUSSIAN 03 (Revision C.02), Gaussian Inc., Wallingford, CT, 2004.

Quantum Mechanical Study of Aniline and its Radical Cation; Predicting Electronic, Structures, and Spectroscopic Properties

Z. Mahmoodi[a,*], H. Shirani IL Beigi[b], S. Jameh-Bozorghi[b], M. Yazdani[b] and H. Iran nezhad[a]

[a]*Department of Chemistry, Islamic Azad University, Arak Branch, Arak, Iran*

[b]*Department of Chemistry, Islamic Azad University, Toyserkan Branch, Toyserkan, Iran*

[*]*Email: mahmoodi_zahra80@yahoo.com*

Abstract

Comprehensive studies of the molecular and electronic structures, vibrational frequencies, and infrared and Raman intensities of the aniline radical cation, $C_6H_5NH_2$ 1 have been performed by using the unrestricted density functional (UB3LYP) and UMP2 methods with the extended 6-311++G** basis set. For comparison, analogous calculations were carried out for the closed-shell neutral aniline. The studies provided detailed insight into the bonding changes that take place in aniline upon ionization. The natural bond orbital (NBO) Analysis has revealed that the pp-radical conjugative interactions are of prime importance in stabilizing the planar, quinoid-type structure of the aniline radical cation. The theoretical vibrational frequencies of aniline, calculated by the B3LYP method, show excellent agreement with the available experimental data. In contrast, the MP2 method is deficient in predicting the frequencies of several modes in aniline, despite the use of the extended basis set in calculations. The frequencies of aniline radical cation, calculated at the UB3LYP/ 6-311++G** level, are in very good agreement with the recently reported experimental data from zero kinetic energy photoelectron and infrared depletion spectroscopic studies.

Keywords: DFT-B3LYP; NBO; Aniline

Introduction

Recent progress in the infrared spectroscopy of isolated molecular clusters in a supersonic jet has made it possible to provide detailed information on the nature of hydrogen bond interactions between molecules. Aniline, the simplest aromatic amine, is a very good model system for studying molecular complexes by infrared depletion spectroscopy [1].

Methods

The optimized equilibrium structure, harmonic frequencies, infrared intensities, and Raman scattering activities of aniline have been calculated by the density functional threeparameter hybrid model [2] and ab initio MP2 method [3]. For the radical cation, the corresponding unrestricted (UB3LYP and UMP2) methods have been used.

Results and Discussion

C–N bond is slightly bent and it makes an angle g of about 1.5°–2.3° with the horizontal axis . It should be noted that the bond lengths and angles of the neutral aniline calculated at the MP2/6-311++G level are in excellent agreement with the microwave data. For example, the experimental C–N bond length as well as C–C distances in the ring are almost reproduced at this level of theory. The B3LYP calculated geometry of aniline is also in very good agreement with experiment. The results of the NBO analysis performed for the closed-shell ground state of aniline indicate that the electronic interactions in the ring are dominated by strong conjugation allowing each localized π bond orbital to delocalize into two adjacent π* antibonding NBOs ($\pi_i \rightarrow \pi_j^*$). These interactions are similar to those calculated for benzene.46. Also, very important in the neutral aniline is the electron donation from the nitrogen lone pair orbital, LPN , to the antibonding acceptor π^*_{CC} orbitals in the ring. The LP_N orbital has 90.6% *p*-character and is occupied by 1.8508 electrons (this is consistent with a delocalization of electron density from the idealized occupancy of 2.0 e).

Conclusion

For the aniline radical cation, the calculations with the unrestricted B3LYP method indicates a planar, quinoidal-type structure of the molecule. The UMP2 method with the large basis set, 6-311++G** Overestimates the quinoid character of the ring. According to B3LYP results, ionization of aniline leads to a delocalization of the positive charge to the phenol fragment, and to an almost equal increase of a charge on the nitrogen atom in the ring. In contrast, the UMP2/6-311++G** Calculation predicts the biggest accommodation of the positive charge on the C_4 atom.

References

[1] T. Nakanaga, N. K. Piracha, and F. Ito, *J. Phys. Chem*. A 105, (2001), 4211.

[2] Frisch M J et al, Wallingford CT, Gaussian Inc., 2004.

[3] C. Lee, W. Yang, and R. G. Parr, *Phys. Rev*. B 37, (1988), 785.

Study of Mechanism Keto-Enol Tautomerism (isomeric reaction) structure "1,3,5,2,4,6-triazatrisilinan-2-one" by Using Quantum Mechanic

R.Moradi[a,*] ,S.Jameh-Bozorgi[b], M.Nouraliei[a], H.Shirani[a] and H.Soleymanabadi[a]

[a],young researchers club, Islamic Azad University, Touyserkan Branch, Touyserkan, Iran
(Email: reza.moradi_bi@yahoo.com)

[b] Chemistry Department , Faculty of sciences, Islamic Azad University, Touyserkan Branch, Touyserkan, Iran

Keywords: Quantum calculation, DFT- B3LYP, Keto-Enol, Tautomerism

Introduction:

Tautomerism is the movement of an atom or a group of atoms in a molecular structure and providing the new from that may this new from more stable or more unstable than initial form .One of the most important of available processes in containing carbonyl groups is their tautomerism that it operated in neutral environment with less intensity in comparison with acidic and alkaline environments[1].There are two forms in ketone and enol tautomerism . That usually ketone is less stable than enol. In such usually suitable catalyst in such mechanics , is acidic and alkaline catalysts.In this research we studied on the structure and rate of levels of energy of "1,3,5,2,4,6-triazatrisilinan-2-one" in tautomerism reaction by using initial quantum mechanic and DFT methods.

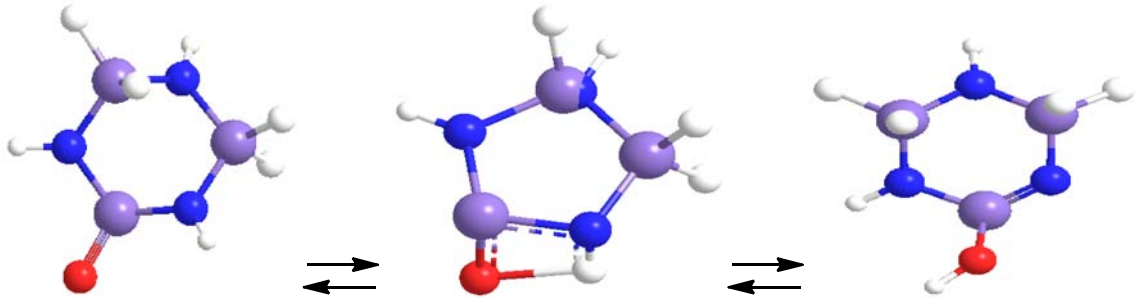

Figure 1 : Calculated B3LYP/6-311+ G** profile for Tautomerism structure "1,3,5,2,4,6-triazatrisilinan-2-one"

Method

The geometries of all compounds at gas phase were fully optimized at DFT(B3LYP)levels of

theory using the Gaussian 03 set of programs [2]. The standard 6-311+G** basis set was used for all atoms. Calculations were performed on a Pentium–PC with Intel(R)Core(TM)2 Duo CPU T9600, 2.8GHz processor. Initial estimation of the structural geometry of "1,3,5,2,4,6-triazatrisilinan-2-one"was obtained by program Chemoffice 2010 and for further optimization of geometry was used the MM2 method of the Chem3D program [3].

Table1: Calculated energies (in Hartree) for the important geometries of Tautomerism

[a]Relative to the most stable geometry

Method	**B3LYP/6-311+G****		
Geometry	Reactive	Transition State	Product
ZPE	0.089144	0.084393	0.096953
E_{ele}	-1112.5195103	-1112.4353734	-1112.5023668
E_0	-1112.430366	-1112.350987	-1112.405413
ΔE^a_0	0.079379(49.8103225)[b]		

[b]Numbers in parenthesis are the corresponding values in kcal mol^{-1}

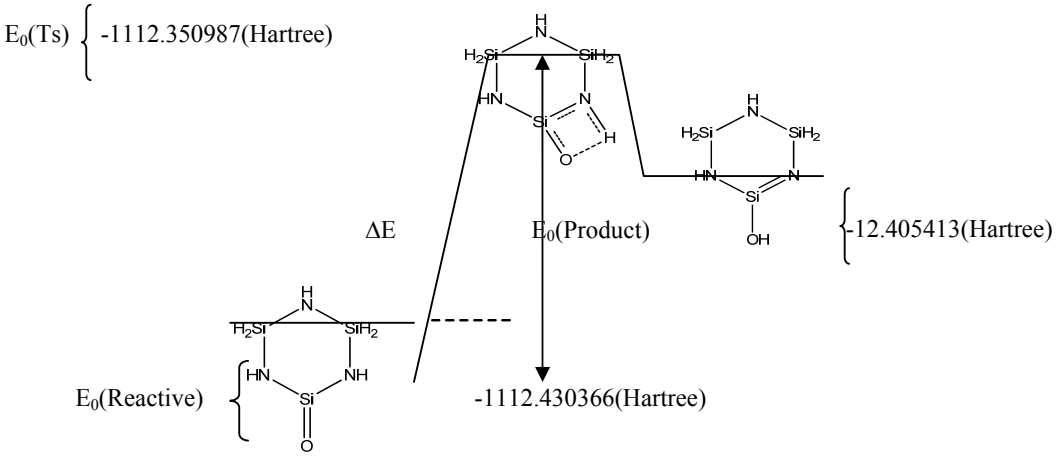

Figure2 : Calculated B3LYP/6-311+G** profile for tautomersim structure "1,3,5,2,4,6-triazatrisilinan-2-one"

Result and discussion

After calculation in the desired energy levels were predicted information that has been reported

in the table below.

Conclusion

Initial restructuring process of the energy levels of a product structure using quantum mechanic
researches and density of function theory at the theory of the level of B3LYP with 6-311+G** basics set showed that this process can be done with reagent of 49.8103225 Kcal/mol energy and
the mechanism of this reaction is Endothermic.

References

[1]John Mc Murry ,*Organic chemistry* ,5th ed ,**2000.**

[2] M. j. Frisch et al. *GAUSSIAN 03*, Revision C. 01, Gaussian Inc., Wallingford. CT, **2004.**

[3] www.CambridgeSoft.com,*CambridgeSoft Corporation*, All Rights Reserved. **©1998-2009.**

Study of Structure, Properties, Aromatic Stabilization Energy(ASE) of ((R)-5-(azetidin-2-ylmethoxy)-2-chloropyridine) by Using calculation DFT Method with NICS Analysis

R.Moradi*[a,b] ,S.Ebrahimi[d], M.Moradi[c], M.Nouraliei[a] , H.Shirani[a]

[a]*Department of Chemistry, Faculty of science, Islamic Azad University, Touyserkan Branch, young researchers club, Touyserkan, Iran*

[b]*Department of Applied Chemistry, Faculty of science, Islamic Azad University, North Tehran Branch, Tehran, Iran*

(Email: reza.moradi_bi@yahoo.com)

[c]*Department of Computer Engineering, Islamic Azad University, Malayer Branch, young researchers club, Malayer, Iran*

[d]*Department of Chemistry, Faculty of science, Islamic Azad University, malayer Branch, malayer, Iran*

Keywords : (R)-5-(azetidin-2-ylmethoxy)-2-chloropyridine, ASE, DFT, NICS

Introduction

Structure (2) obtained from chloropyridine derivatives. The chloropyridine structure is a heterocyclic ring, analogous to the six-membered benzene ring but with three carbons replaced by nitrogens. chloropyridine compounds are often used as the basis for various herbicides. Cyanuric chlorides obtained from react through a chlorine group with hydroxyl groups present in cellulose fibres in nucleophilic substitution [1].This combinations mostly are used as a catalyse in some of specific reaction . In many year ago ,studies such as this is done the level of theory in the case of ratio of aromatic stability of structure of (R)-5-(azetidin-2-ylmethoxy)-2-chloropyridine. But this studies are done in the level of semi empirical and empirical . That the result was near to empirical result[2]. However spectrum IR, Raman and NMR of combination are attained or obtained by DFT method and were attained or obtained spectrum empirical result that the results was useful and satisfactory.The aromatic stabilization energy (ASE) reveals higher stability of compoun Nuclear independent NMR Isotropic Chemical Shift (NICS), has become the most widely used aromaticity probe due to its simplicity and efficiency. In this research, ASE and NICS calculations were carried out for compounds with using GAUSSIAN 03 package of programs [3].

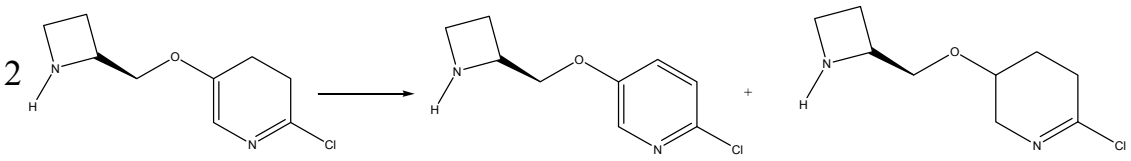

1 2 3

Figure1: Calculated B3LYP/6-311+ G** profile for (R)-5-(azetidin-2-ylmethoxy)-2-chloropyridine

Method

The geometry of the system has been fully optimized with the hybrid DFT-B3LYP. DFT calculations were performed with the GAUSSIAN 03 programs on a Pentium-PC computer with 3600 MHz processor. The vibrational frequency calculations of the molecule in the liquid phase, were carried by using the Onsager SCRF method at the B3LYP/6-311+G**.

Result and discussion

The ASE, NICS, calculations of (R)-5-(azetidin-2-ylmethoxy)-2-chloropyridine calculated by DFT level with the 6-311+G(d,p) basis sets. The results of calculations show that ASE of compound by using B3LYP/6-311+G** is 375.72 Kcal/mol, respectively (table 1). The aromatic character of compound is demonstrated by their NICS values. The table 2 summarize NICS (0), (0.5), (1.0) data at the uniform GIAO-B3LYP/6-311+G** levels of theory .

Table 1 : B3LYP/6-311+G** calculated zero point energies (ZPE) ,Electronic energy (Eele), Total energies(E_0) and aromatic stabilization energies ASE for (R)-5-(azetidin-2-ylmethoxy)-2-chloropyridine.

Structure	No.of dummy atom	Distance of hetrocycle center	NICS values(ppm)
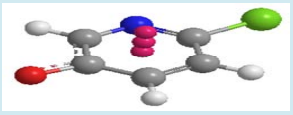	3	1.00	-9.6309
	2	0.50	-9.9161
	1	0.00	-8.5554

a: Energy according(kcal /mol)

Table 2: GIAO-B3LYP/6-311+G** Calculated nuclear independent chemical shifts (NICS) values in ppm for (R)-5-(azetidin-2-ylmethoxy)-2-chloropyridine.

Conclusion

in the level of theory B3LYP/6-311+G**, its determined that the extent of aromatic stabilization energy of structure (R)-5-(azetidin-2-ylmethoxy)-2-chloropyridine in Gas solution is more than aromatic stabilization energy in that amount of that equals 375.723783 ($kcal.mol^{-1}$). However the most amount of the magnetic isotropic is placed 0.50 angstrom on

Method	B3LYP/6-311+G**		
Geometry	1	2	3
ZPE	0.213654	0.191393	0.224070
E_{ele}	-995.8040831	-994.6232737	-996.3742848
E_0	-995.590429	-994.431881	-996.150214
ASE	0.598763(375.723783)[a]		

top of the ring that equals -9.9161 ppm. After the study of particulars structure combination of (R)-5-(azetidin-2-ylmethoxy)-2-chloropyridine , its found that bond order and density of electrons are the same in all the ring. However the structure of (R)-5-(azetidin-2-ylmethoxy)-

2-chloropyridine that include high electrostatic potential take Participation easily inside the electrophillic reaction.

References:

[1] V. Galasso, Chemical Physics Letters , Volume 472, Issues 4-6,Pages 237-242, 20 April **2009**

[2] G. Giacomellia and A. Porcheddua , chloropyridine,Comprehensive Heterocyclic Chemistry III ,University of Sassari, Sassari, Italy , Pages 197, Volume 9, 1 April **2008.**

[3] M. j. Frisch et al. *GAUSSIAN 03*, Revision C. 01, Gaussian Inc.,Wallingford. CT, **2004.**

Numerical simulation of silicon carbide polymers (6H-SiC & 3C-SiC) as the active area for 0.83 µm wavelength semiconductor Laser

A. Marjani[a*], S. Marjani[b] and S. Shirazian[a]

[a] *Department of Chemistry, Arak Branch, Islamic Azad University-Arak-Iran*

[*] *Corresponding author- Faculty Member of Islamic Azad University-Arak Branch:*

Email: a-marjani@iau-arak.ac.ir

[b] *Department of Electrical Engineering, Arak Branch, Islamic Azad University-Arak-Iran*

Abstract

Numerical simulation of a 6H-SiC/3C-SiC edge emitting laser employing the active region with 3C well embedded in 6H barriers show photoluminescence (PL) that can be interpreted in terms of a type-II heterostructure character and a built-in electric field due to the pyroelectricity of 6H using an industrial-based numerical simulator was studied in this work. The basic design goal was to use silicon carbide polymers and decrease the threshold current and stable optical wavelength of the lasers with silicon carbide polymers reported in earlier similar devices.

Keywords: Numerical simulation, Silicon carbide, 6H-SiC, 3C-SiC, Semiconductor laser

Introduction

Silicon carbide has many stable polytypes, including cubic zinc-blended, hexagonal and rhombohedral polytypes. In the cubic zinc-blended structure, labeled as 3C-SiC or β-SiC, Si and C occupy ordered sites in a diamond framework. In hexagonal polytypes nH-SiC and rhombohedral polytypes n R-SiC, generally referred to as αη-SiC, n Si-C bilayers consisting of C and Si layers stack in the primitive unit cell. The aim of this work is to simulate a 6H-SiC/3C-SiC edge emitting laser [1].

Theory

The basis of the simulation is to solve two-dimensional Poisson's equation and the continuity equations for electrons and holes [2].

$$\nabla.(\varepsilon\nabla\Psi) = \rho \qquad (1)$$

$$\frac{dn}{dt} = G_n - R_n + \frac{1}{q}\nabla.j_n \qquad (2)$$

$$\frac{dp}{dt} = G_p - R_p + \frac{1}{q}\nabla.j_p \qquad (3)$$

To simulate semiconductor lasers, the basic semiconductor equations (1)-(3) are solved self-consistently together with the Helmholtz, lattice heat flow and the photon rate equations.

Simulation results

Figure 1 shows the light-current (L-I) curve where the current increased from 0 to 3.4 A. If the laser is to be used in any kind of an optical system, it is important to consider the characteristics of the output beam. The maximum output power is limited by heating. Recent device modeling shows that spatial holebuming and leakage over the carrier confinement barriers are limiting the output power as the device heats up. As the temperature rises due to resistive heating, leakage over the 6H-SiC barriers starts to dominate over other recombination mechanisms and eventually causes the laser to stop emitting.

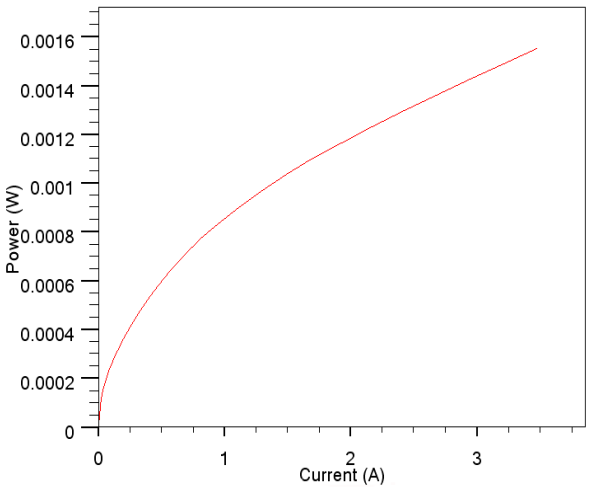

Figure 1: light-current (L-I) curve.

Conclusion

In this paper, we have developed a numerical laser model operating in the 830-nm wavelength regime. The basic design goal was to use silicon carbide polymers and decrease the threshold current and stable optical wavelength of the lasers with silicon carbide polymers.

References

[1] R. F. Kazarinov and M. R. Pinto, "Canier transport in laser heterostructures", IEEE J. Quantum Electron., vol. 30, no. 1, pp. 49-53, 1994.

[2]SILVACO International, ATLAS User's Manual, USA, SILVACO International Incorporated (2007).

Ab initio study and NBO interpretation of conformational behaviors of 2-(diphenylphosphinoyl)-1,3-dioxane and its analogues containing S and Se atoms

N. Masnabadi*[a], H. Yahyaei[b], F. Azarakhshi[c], A. Madhi Tazekand[d], D. Nori-Shargh[d]

[a]*Department of Chemistry, Roudehen, Branch, Islamic Azad University, Roudehen, Iran*
(Email:masnabadi2009@gmail.com)

[b]*Department of Chemistry, Zanjan Branch, Islamic Azad University, Zanjan, Iran*

[c]*Department of Chemistry, Varamin Branch, Islamic Azad University, Varamin, Iran*

[d]*Department of Chemistry, Arak Branch, Islamic Azad University, Arak, Iran*

Keywords: Anomeric Effects, ab initio, NBO, 2-(diphenylphosphinoyl)-1,3-dioxane, 2-(diphenylphosphinoyl)-1,3-dithiane, 2-(diphenylphosphinoyl)-1,3-diselenane

Introduction

In 1987, Mokolajczyk and co-workers have indicated *AEs* in the Carbon-Sulfur-Cacrbon-Phosphorus, CSCP, systems.[1,2] The same year the magnitude of the anomeric effect involving the Ph2P-S group in 1,3-dithiane (ca. 3.8 kcal mol^{-1}) has estimated by Juaristi *et a*l.[3] The *AE* in the CSCP system has been found in 2-(diphenylphosphinoyl)-1,3,5-trithiane and for some other phosphorus-containing substituents at the C-2 atom of 1,3-dithiane and oxathiane rings. Also, the *AE* involving sulfur has been found in various C-2-substituted thianes, 1,3-oxathianes, 1,3-dithianes. In these compounds, the *AE* has interpreted in terms of $n_S \rightarrow \sigma^*_{C\text{-}Substitution}$ negative hyperconjugation by Pinto et al., Tschierske et al., and Juaristi et al. Such an interpretation has been based on the dependence of axial preference on electron-withdrawing properties of the C2-Substitution, however, the problem of the nature of the *AE* in the MCP (M = O, S and Se) systems is still a matter of controversy.

Computational details

Ab initio calculations were carried out using density functional theory (DFT: B3LYP/6-31G*//HF/6-31G*) and molecular orbital (MO: MP2/6-31G*//HF/6-31G*) based methods with the GAUSSIAN 98 package of programs.[4]

Results and Discussion

The NBO analysis, hybrid-density functional theory (hybrid-DFT) and ab initio molecular orbital based methods were used to study the impact of the *anomeric effect* (*AE*) on the conformational behaviors of 2-(diphenylphosphinoyl)-1,3-dioxane(**1**), [2-(diphenylthiophosphinoyl)-1,3-dioxane (**2**), 2-(diphenylselenophosphinoyl)-1,3-dioxane (**3**)], 2-(diphenylphosphinoyl)-1,3-dithiane (**4**), 2-(diphenylthiophosphinoyl)-1,3-dithiane (**5**), 2-(diphenylselenophosphinoyl)-1,3-dithiane (**6**), 2-(diphenylphosphinoyl)-1,3-diselenane (**7**), 2-(diphenylthiophosphinoyl)-1,3-diselenane (**8**) and 2-(diphenylselenophosphinoyl)-1,3-diselenane (**9**).[1,2] In this work, the stereoelectronic interactions associated with the *AE* and also conformational and structural properties of compounds **1-9** were investigated computationally using both ab initio MO and DFT methods.

MP2/6-311+G**//HF/6-31G* and B3LYP/6-311+G**//HF/6-31G* results revealed that the chair conformation with the equatorial diphenylphosphinoyl group of compound **1** is more stable than its axial conformation, while the strong axial preference is observed in compounds **2** and **3**. On the other hand, the NBO analysis of donor-acceptor (bond-antibond) interactions revealed that the *Anomeric Effect* (*AE*) for compounds **1-3** are -9.82, -6.55 and -5.26 kcal mol^{-1}, respectively. Contrary to the decrease of the *AE* values from compound **1** to compound **3**, the precise structural parameters (which could influence the srteric repulsions) could fairly explain the strong axial preference in compounds **2** and **3**. Further, the correlation between the *AE*, structural parameters and conformational behavior of compounds **4-9** has investigated.

Conclusion

It can be concluded that the conformational behavior of compounds **1-9** are not controlled only by *AE* associated with LP→σ* delocalizations, therefore, it seems that other

factors (such as: steric interactions, orbital overlap (S) and dipole moment) could influence the conformational preference in compounds **1-9**.

References:

[1] Mikolajczyk, M., Graczyk, P., and Blaczewski, P. *Tetrahedron Lett.* **1987**, 28, 573-576.

[2] Mikolajczyk, M. *Pure Appl. Chem*. **1987**, 57, 983-988.

[3] Juaristi, E., Lopez-Nunez, N. A., Valenzuela, B. A., Valle, L., Toscano, R. A., and Soriano-Garcia, M. *J. Org. Chem*. **1987**, 52, 5185-5189.

[4] Frisch, M. J., et al., GAUSSIAN 98 (Revision A.3), Gaussian Inc. Pittsburgh, PA, USA, 1998.

Interfacial binding between single-walled carbon nanotubes and hydrophobic and hydrophilic polymers

M. Foroutan, M. Moshari
Department of Physical Chemistry, School of Chemistry, College of Science, University of Tehran, Tehran, Iran,
Mahshad.Moshari@khayam.ut.ac.ir

Key word: Carbon nanotubes, Vinyl pyrrolidone, Vinyl acetate, Interaction Energy, Gyration radius.

Introduction

Significant efforts have been made to design and fabricate nanotube-based composites (nanocomposites) since the pioneering report on carbon nanotube (CNT)–polymer composites by Ajayan et al.[1] Now, It is well-known that the structure and properties of the interface between CNTs and polymer matrix play a major role in determining the mechanical performance and structural integrity of such nanocomposites. The recent research works emphasize that the interaction between the CNT and the polymer is strongly influenced by the specific monomer structure of polymer. [2] In this work the molecular dynamic (MD) simulation method is used to study the interfacial binding between the single-walled CNTs and two polymers, poly vinyl pyrrolidone (polymer A) as a hydrophilic polymer and poly vinyl acetate (polymer B) as a hydrophobic polymer.

Computational Procedure

We used a canonical ensemble (constant NVT) with undefined boundary conditions for considering the simulated volume were equals to infinite. The velocity form of Verlet algorithm method and the Nose-Hoover thermostat algorithm were used to integrate the equations of motion with a time step of 1.0 fs and temperature control of 300 K, respectively. All MD simulations have performed using the AMBER force field. Non-bonded van-der-Waals interactions were modeled by a Lennard-Jones potential with a cut-off distance of 0.9 nm.

Results and Discussion

The intermolecular interaction energies between CNTs and copolymer molecules, the plots of radial distribution function and the gyration radios are three methods which were used to describe the behavior of simulated systems.

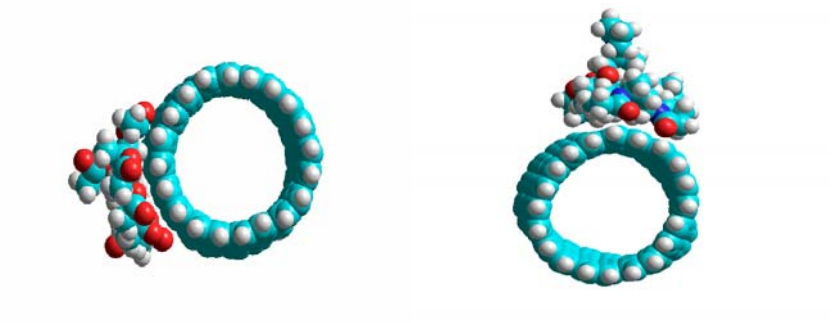

Figure 1- MD simulation snapshots (cross-sectional view) of the wrapping of a CNT (10,10) by poly vinyl pyrrolidone (Left side) and poly vinyl acetate (Right side).

To characterize the overall size of polymer chains on the CNT surface, we calculated their R_g. Figure 2 shows the radius of gyration evolution for polymers A and B. As this figure shows, the radius of gyration of hydrophobic polymer B is more than that of hydrophilic polymer A, since the interaction energy of hydrophobic polymer B is more than that of hydrophilic polymer A. It is reminded that carbon nanotubes have hydrophobic nature and have proper interaction energies with hydrophobic materials.

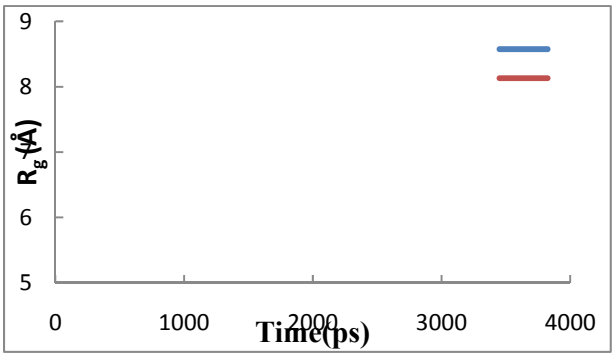

Figure 2- The radius of gyration (R_g) evolution for polymers A and B after interaction with CNT.

References

[1] Ajayan, P. M.; Stephan, O.; Colliex, C.; Trauth, D. *Science* 1994, *265*, 1212.

[2] Foroutan, M.; Taghavi N., A. *J. Phys. Chem. B* 2010, *114,* 5320.

First-principle study of carbon monoxide adsorption on silicon nanotube arrays.

E. Masumian*, S.M. Hashemianzadeh, O. Mostajabi Srahangi and
M. Moghimi Waskasi
Department of Chemistry, Iran University of Science and Technology, Tehran, Iran (Email: masumiyan@gmail.com)

Keywords: Silicon Nanotube, Carbon Monoxide, Binding Energy, Density Functional Theory (DFT), Density of States (DOS)

Introduction

Carbon monoxide (CO), is a colorless, odorless and tasteless gas which is highly toxic to humans and animals in higher quantities. Many studies have been performed for adsorption and sensing of carbon monoxide in order to eliminate this gas. Since their discovery by ijima,[1] carbon nanotubes (CNTs), due to their structural features, such as high aspect ratios, large surface area, as well as unique thermal and electronic properties, have been a candidate for gas sensing[2], but it has been recognized that pure CNTs could not adsorb and also sense CO effectively[3]. With the synthesis of silicon nanotubes (SiNTs) in 2002[4], a lot of methods were also developed to fabricate the SiNTs and well-aligned SiNT arrays. Compared to carbon, silicon has more electrons in the outer shells, which leads to higher polarizability and a stronger dispersion force[5]. In this paper, we report a theoretical method to investigate adsorption of CO in the SiNT arrays.

Methods

We considered an armchair (5, 5) silicon nanotube. The dangling bonds were saturated by hydrogen atoms at the two end. Our structures optimizations and the total energy calculations are based on density functional theory (DFT). To achieve more accurate data, the CO molecule and its nearest six silicon atom were treated with the 6-311++G(d,p) basis set, whereas the other atoms were treated with the 3-21G basis set. All the calculations were

carried out by the MPW1PW91 exchange-correlation function, which can supply a more accurate dispersion force than B3LYP[5].

Results and Discussion

There are three typical adsorption sites: on-top, bridge, and hollow. All these cases have been considered for adsorption of CO on the SiNT surface. Our results show that, among different adsorption orientations, CO adsorbing on the hollow sites with the C-O bond vertical to the tube surface is the most favorable adsorption mode for both inside and outside the SiNT wall. the CO molecules can be adsorbed on the hollow sites with the binding energy of about −0.40 eV. To investigate the effect of the CO adsorption on the electronic structure, we plot the partial density of states (DOS) of the system with and without the CO molecule. DOS plots show that the electronic properties have changed upon the CO gases.

Conclusion

In summary, the ab-initio studies indicate that the SiNT array gives a higher CO adsorption energy than the CNT array. Excellent performance of the SiNT array in CO adsorption is attributed to the denser electron cloud of the SiNT surface compared to the CNT surface, which produces much stronger van der Waals attraction to carbon monoxide. SiNT due to its sensitive electronic structure shows the great respond against the molecules adsorption and it is very suitable to sense the gas molecules such as carbon monoxide.

References

[1] Iijima, S. Helical microtubules of graphitic carbon. Nature 1991,354, 56.

[2] Zhao, J.-x.; Ding, Y.-h., Can Silicon Carbide Nanotubes Sense Carbon Dioxide? Journal of Chemical Theory and Computation 2009, 5, (4), 1099-1105.

[3] Zhao, J.-X.; Ding, Y.-H., Theoretical study of the interactions of carbon monoxide with Rh-decorated (8,0) single-walled carbon nanotubes. Materials Chemistry and Physics 2008, 110, (2-3), 411-416.

[4] Sha, J.; Niu, J.; Ma, X.; Xu, J.; Zhang, X.; Yang, Q.; Yang, D., Silicon Nanotubes. Advanced Materials 2002, 14, (17), 1219-1221.

[5] Lan, J.; Cheng, D.; Cao, D.; Wang, W., Silicon Nanotube as a Promising Candidate for Hydrogen Storage: From the First Principle Calculations to Grand Canonical Monte Carlo Simulations. The Journal of Physical Chemistry C 2008, 112, (14), 5598-5604.

Computational Studies of the water splitting using Ruthenium organometalic and Influence of Electric Fields on Absorption

M. Moghimi Waskasi *, S. M Hashemianzadeh, O. Mostajabi Sarhangi and E. Masumian

Department of Chemistry, Iran University of Science and Technology, Tehran, Iran (Email: m.moghimi.w@gmail.com)

Keywords: DFT; TD-DFT; Heteroleptic Ruthenium dye; Water splitting.

Introduction

Hydrogen and oxygen evolution from water using semiconductors and light is an important issue in the exploitation of solar radiation as a sustainable energy. Hydrogen generation from clean and environmentally friendly sources such as solar energy is required. Photoelectrochemical (PEC) water splitting, also known as solar-driven water splitting, is one of the most promising means of producing hydrogen from a renewable source. In 1972, Fujishima and Honda first reported the photo-assisted splitting water into H_2 and O_2 on TiO_2. In this process, water molecules are broken into hydrogen and oxygen, using sunlight. There are several advantages to this approach, such as abundance of solar energy, inexpensive raw materials, and ease of mass production [١].

Methods

Geometry optimizations of the heteroleptic ruthenium dye sensitizers in the ground state and in water solution have been performed with DFT using the Gaussian 98W program. The geometries were fully optimized in gas at hybrid DFT levels by B3LYP functions. For Ru we use a LanL2DZ basis set. All geometry optimizations were computed in water solution using the CPCM solvation model and with the 3-21G basis set. The vertical excitation energies were calculated for all geometries by the B3LYP functional within the TD-DFT methodology. Natural bond orbital (NBO) analysis was also conducted on optimized geometries with the NBO program.

Results and Discussion

The Results shows that all of the spectra in the range of 350-600 nm are contributed by MLCT transitions, that is, excitation from the highest occupied Ru 4d orbitals to the lowest unoccupied bipyridine ligand π^* orbitals. In this region, the simulated spectrum of the gas-phase heteroleptic ruthenium dye shows one peak at 446.17 nm with the oscillator strength of 0.1325 and in present electric fields peaks at 717.35nm with the oscillator strength of 0.0021. Our results strongly indicate that the field effect on metal organic-dye could be red-shifed. Such electric fields could lead to a change in the absorption spectrum due to the Stark effect. This peak corresponds to the lowest-energy excitation, which shows strong HOMO→LUMO character. An analysis of the HOMO and LUMO clearly shows that this excitation corresponds to an electron transfer from the metal center to the bipyridine ligands. For the heteroleptic ruthenium dye in water solution calculated using the C-PCM model, the peak of the spectrum appears at 464.23 nm, a 18.05-nm red shift from the gas-phase spectrum. The oscillator strength of the lowest-energy excitation increases from 0.132 to 0.135.

Conclusion

The molecular geometries, electronic structures, and optical absorption spectra of heteroleptic ruthenium dye both in the gas phase and in water solution have been investigated by mean of combined DFT/TD-DFT calculations. A frontier orbital analysis shows that the five HOMOs have predominantly Ru 4d character whereas the four LUMOs are composed of the antibonding combination of the C 2p orbitals of bipyridines. The spectra in the range of 350-600 nm originate from metal-to-ligand charge-transfer (MLCT) transitions, whereas the spectra in the range of 350-400 nm are excitations mainly from the metal Ru 4d orbitals to the carboxyl group π^* orbitals. The solvent effect strengthens the short-range interaction by dispersing the repulsive interaction and weakens the long-range interaction by coupling the respective dipole moments of different moieties. Inclusion of field effects decreases the oscillator strength and results in red shifts of the spectra of heteroleptic ruthenium dye.

References

[1] C. A. G. O. K. V. S. Ranjan, *Light, Water, Hydrogen The Solar Generation of Hydrogen by Water Photoelectrolysis*: springer 2008.

[2] M. C.-S. R.M.Navarro, M.C.Alvarez-Galvan,F.delValle and J.L.G.Fierro, "Hydrogen production from renewable sources: biomass and photocatalytic opportunities," *Energy & Environmental Science,* vol. ۲, pp. ۵۴-۳۵,2008.

[3] K. S. Ryu Abe, Kohjiro Hara and Bunsho Ohtani, "Robust dye-sensitized overall water splitting system with two-step photoexcitation of coumarin dyes and metal oxide semiconductors," *The Royal Society of Chemistry,* pp. ۳۵۷۷–۳۵۷۹, 2009.

[4] W. J. Youngblood, S.-H. A. Lee, Y. Kobayashi, E. A. Hernandez-Pagan, P. G. Hoertz, T. A. Moore, A. L. Moore, D. Gust, and T. E. Mallouk, "Photoassisted Overall Water Splitting in a Visible Light-Absorbing Dye-Sensitized Photoelectrochemical Cell," *Journal of the American Chemical Society,* vol. ۱۳۱, pp. ۹۲۷-۹۲۶, 2009.

[5] W. J. Youngblood, S.-H. A. Lee, K. Maeda, and T. E. Mallouk, "Visible Light Water Splitting Using Dye-Sensitized Oxide Semiconductors," *Accounts of Chemical Research,* vol. ۴۲, pp. ۱۹۷۳-۱۹۶۶, 2009.

Study of Coumarin NKX-2807 Dye sensitizer solar cell by Computational Method

O. Mostajabi Srahangi *, S. M. Hashemianzadeh,
M. Moghimi Waskasi and E. Masumian
Department of Chemistry, Iran University of Science and Technology, Tehran, Iran
(Email: mostajabi.s83@gmail.com)

Keywords: DFT; TD-DFT; Coumarin NKX-2807; Dye Sensitizer Solar Cell

Introduction

The conversion of sunlight to electricity using dye-sensitized solar cells (DSCs) represents one of the most promising methods for future large-scale power production from renewable energy sources[1-3] . Up to now, two kinds of dye sensitizers, which are generally known as metal-organic complexes and metal-free organic dyes, were studied extensively. In metal-organic complexes, especially the noble metal ruthenium polypyridyl complexes, including N3 and black dye etc. that were presented by Gratzel et al., have proved to be the best dye sensitizers with overall energy conversion efficiency greater than 10% under air mass (AM) 1.5 irradiation [4-5]. Organic dyes, because of their many advantages, such as high molar extinction coefficients, convenience of customized molecular design for desired photophysical and photochemical properties, inexpensiveness with no transition metals contained, and environment-friendliness,10 are suitable as photosensitizers for DSC. Among the organic dyes employed for DSSCs so far, coumarin dyes are one kind of promising dye stuff and have been studied systematically [6-7].

Methods

Geometry optimizations of the NKX-2807 coumarin dye in the ground state and in ethanol solution. Calculations were performed with DFT using the Gaussian 98W program. The geometries were fully optimized in vacuo at hybrid DFT levels by B3LYP functions. All geometry optimizations were computed in water solution using the CPCM solvation model

and with the 6-311G(d) basis set. The vertical excitation energies were calculated for all geometries by the B3LYP functional within the TD-DFT methodology.

Results and Discussion

This Results shows that all of the spectra in the range of 200-700 nm are contributed by transitions from the highest occupied orbitals to the lowest unoccupied orbitals. In this region, the simulated spectrum of the gas-phase NKX-2807 dye shows one peak at 525.08 nm with the oscillator strength of 1.31. This peak corresponds to the lowest-energy excitation, which shows strong HOMO → LUMO character. For the NKX-2697 dye in ethanol solution calculated using the C-PCM model, the peak of the spectrum appears at 590.2 nm, a 65nm red shift from the gas-phase spectrum. The oscillator strength of the lowest-energy excitation increases from 1.31 to 1.56.

Conclusion

In this study, we have theoretically investigated the excited-state energies and properties in a NKX-2807 coumarin dye molecule for use dye sensitizer solar cell applications. For this dye, excited-state energies and properties were obtained using the TD-DFT formalism both in gas and ethanol. TD-DFT calculation has provided valuable information on the nature of the electronic transitions that are involved in the light absorption and electron transfer process. The solvent effects are taken into account by the CPCM. The ethanol solution is found to induce a red shift in the vertical excitation energy due to the stabilization of the HOMO. we conclude that the red shift in solution is mainly caused by the polarization of the solvent .Organic dyes with a coumarin derivative as the electron donor, connected with methine and thiophene as the π-conjugation linkage and two-CN groups as the electron acceptor, have been studied as sensitizers for DSSCs. In the light of the concept of the D-Π-A structure, increasing the electron-withdrawing ability of acceptors would red shift the absorption peak. Our preliminary results indicate that linking two-CN groups to the π-conjugation bridge was successful in extending the photoresponse to longer wavelength.

References

[1] O'Regan, B.; Gratzel, M. *Nature* , 353,(**1991**), 737.

[2] Hagfeldt, A.; Gratzel, M. *Acc. Chem. Res*., 33,**(2000)**, 269..

[3] Hara, K.; Sugihara, H.; Tachibana, Y.; Islam, A.; Yanagida, M.;Sayama, K.; Arakawa, H.; Fujihashi, G.; Horiguchi, T.; Kinoshita, T.*Langmuir* 17, **(2001**), 5992–5999.

[4] E. Muller, P. Liska, N. Vlachopoulos, M. Gratzel, *J. Am. Chem. Soc*. 115 (**1993**) 6382.

[5] M.K. Nazeeruddin, P. Pechy, T. Renouard, S.M. Zakeeruddin, R. Humphry-Baker,P. Comte, P. Liska, L. Cevey, E. Costa, V. Shklover, L. Spiccia, G.B. Deacon, C.A.Bignozzi, M. Gratzel, *J. Am. Chem. Soc*. 123 (**2001**) 1613.

[6] Hara, K.; Wang, Z.-S.; Sato, T.; Furube, A.; Katoh, R.; Sugihara,H.; Dan-oh, Y.; Kasada, C.; Shinpo, A.; Suga, S. *J. Phys. Chem. B* 109, (**2005**),15476.

[7] Zhong-Sheng Wang, Yan Cui, Yasufumi Dan-oh, Chiaki Kasada, Akira Shinpo, and Kohjiro Hara,*J. Phys. Chem. C* 112, **(2008**), 17011–17017.

To acquire computational IR spectra and computational Energy of Kaempferol molecule and Comparing with Kaempferol experimental spectrum and experimental energy

E.Mofarrah* andA.Salari, A. Taghva manesh, El. Mofarrah

Azad university of Shahre rey , , Azad university of central Tehran , Department of chemical Engineering Amirkabir university ,Iran

(e_ Mofarrah@yahoo.com)

Keywords : Kaempferol- Antioxidant-Flavonoid- IR-FTIR-RHF,6-31++G - B3LYP6,311+G

Introduction

To obtain the exact structure of molecule of kaempferol study of its molecular energy and IR.Spectra in order to obtain the physicochemical characteristics of Kaempferol and study of the biological and biochemical characteristics of this substance .

Kaempferol is a natural flavonoid . Kaempferol is has been isolated from tea, broccoli, Delphinium, Witch-hazel, grapefruit, brussels sprouts, apples and other plant sources[1].

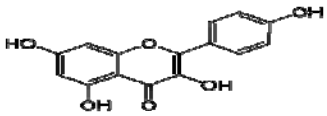

Chemical name3,5,7-trihydroxy-2-(4-hydroxyphenlyl)-4H-1-benzonpyran-4-one[2]

Kaempferol is well-known as one of anti oxidants biologically and thus can be used as an effective medicine for defeating a number of cancers[3].

Method

In this research shape and energy molecule in gas phase was limited using Ab initio quantum and Restriced Hartree-Fock (RHF)was examind through series of 6-31G to 6-311++G(d,p).

Method	Energy(au)
RHF/6-31G	-1022.46140114
RHF/6-31+G	-1022.49157297
RHF/6-31++G	-1022.49212840
RHF/6-311G	-1022.69700718
RHF/6-311++G**	-1023.15121223

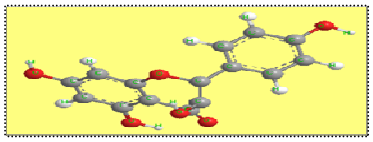

Keampferol Structure by Gaussian View software

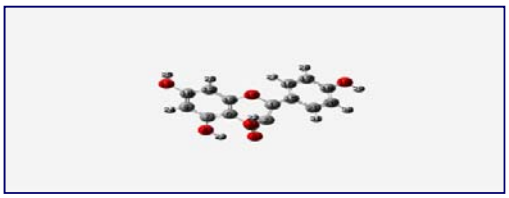

Keampferol optimize Structures in RHFmethod is used with 6-31++G serie

After energy calculating by Gaussian 2003 software ,we Compared them with Kaempferol energy experimental (1022.58au) [4].

In this research, we obtained Kaempferol FTIR spectrum in order to better analyze the spectra and comparing the spectrum of Kaempferol molecule with IR computational spectra[5] of Kaempferolmolecule, Kaempferol FTIR spectrum was obtained from Fourier transfrormation [6]of experimental IR spectrum that carried out by using Digitizer program and MATLAB 7.4 software.

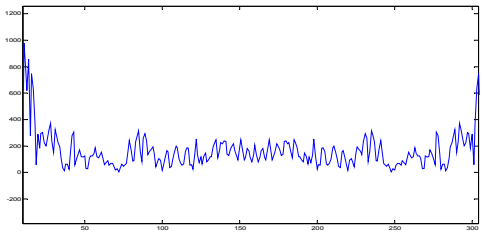

Kaempferol molecule's FTIR spectrum

Method	Standard deviation
B3LYP 6-31G	4.476342
B3LYP 6-31G(d)	4.778566
B3LYP 6-311+G	3.899832
B3LYP 6- 311+G(d,p)	4.0280852
B3LYP 6-311++G	3.967397
B 3LYP 6-311++G(d,p)	4.132597

We obtained IR spectra calculating by Gaussian 2003 software, then we compared them with Kaempferol molecule's FTIR spectrum.

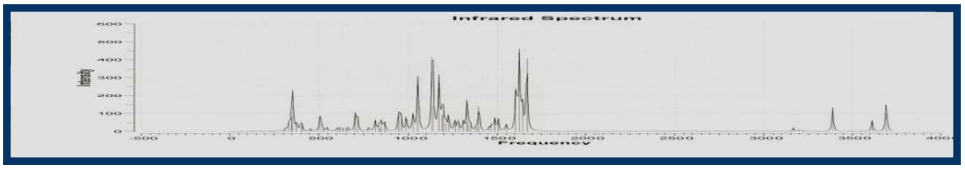

Kaempferol IR spectra B3LYP method is used with 6-311+G series

Result and discussion

Comparing measuared Energy with Energy experimental [1022.58au] of Kaempferol molecul ,RHFmethod is used with 6-31++G series the most similarity with experimental

Comparing measured frequencies of IR spectra with experimental spectrum and Comparing standard deviations of Kaempferol molecule, B3LYP method is used with 6-311+G series has minimum standard deviation and the most similarity with experimental results

conclusion

Kaempfero is well- known as one of anti oxidants biologically and thus can be used as an effective medicine for defeating a number of cancers . This molecule is also effective on prevention of oxidation disadvantages in cells,fats and DNA.prevents from arteries blocks and also prevents from oxidation and formation of low-density of lipoprotein in blood.

Therefore with this research can be carried out for optimization of particulars and molecule function through investigation of the said parameters.

Refrence

[1] kaempferol From Wikipedia, the free encyclopedia

[2] Kaempferol-Wikipedia,the free encyclopedia.9/12/2

[3] Phytochemicals/Kaempferol.10/14/2006

[4] Monica Leopoldini, Nino Russo*, and Marirosa Toscano Gas and Liquid phase Acidity of Natural Antioxidants,J.Agric.Food Chem .2006,54,3078-3085

[5] 1967Sadtler Research Laboratories,Inc.Philadelphia,Pa,19104,U.S.A

[6] en.wikipedia.org/wiki/Fourier_transform_infrared_spectroscopy

Theoretical calculation of phenylalanine protonation constants in gas phase and comparison with the experimental values in aqueous solution

Faezeh mofidi* and Farrokh Gharib

Department of Chemistry, Shahid Beheshti University, Evin, Tehran, Iran

(*E-mail : fa.mofidi@gmail.com*)

Keywords: Phenylalanine, Protonation constants, Theoretical calculation, Density functional theory

Introduction:

The importance and vital role of amino acids and their peptides in living systems is well known. The protonation and proton transfer processes of amino acids are among the most important factors in determining structure، property and function of these biological molecules، such as energy transfer، charge distribution، acid-base reactions، and catalysis[1]. Based on the proton affinities of the various possible sites، the protonation of amino acids is generally presumed to occur at the amine nitrogen of the n-terminus or a nitrogen of a basic side chain. The protonated form of gas-phase amino acids has been the subject of extended theoretical studies for several years[2].

Phenylalanine is one of the three aromatic amino acids in which the aromatic residues are the side chains. The aromatic residues have been recognized as very important groups in biological systems because of their structural and functional roles[3].

This work deals with the calculation of phenylalanine protonation constants in the gas phase using a computational method and compare with the values obtained in aqueous solution.

Theoretical Section

The geometry optimization and calculation of the properties of the neutral and protonated phenylalanine were carried out at the DFT level of theory with B3LYP functional using 6-311++G(d،p) basis set.

The protonation constant, pK_a, of an acid HA is given by:

$$pK_a = \frac{1}{2.303RT}\Delta G^0_{deprot,aq}$$

In above equation, ΔG^0_{deprot} is defined as

$$\Delta G^0_{deprot} = \Delta G^0_{(A^-)} + \Delta G^0_{(H^+)} - \Delta G^0_{(HA)}$$

The standard Gibbs free energy of each species in the gas phase and at its standard state (ideal gas at 1atm and 298K), $\Delta G^0_{[HA(g)]}$, $\Delta G^0_{[A^-(g)]}$, is obtained by

$$\Delta G^0_g = E_{0K} + ZPE + \Delta\Delta G_{0\to298}$$

where E_{0K} is the total energy of the molecule at 0K, ZPE is the ziro-point energy and $\Delta\Delta G_{0\to298}$ represents the Gibbs free energy change from 0 to 298K at 1atm. E_{0K}, is calculated at the optimum geometry, ZPE and $\Delta\Delta G_{0\to298}$ are calculated from the vibrational frequencies. Translational and rotational free energy contribution is also calculated in the ideal gas approximation[4].

We use $\Delta G^0_{[H^+(g)]} = 2.5RT - T\Delta S = 1.48 - 7.76 = -6.28\ kcal/mol$ at 298K and 1atm.

Result and discussion:

The protonation constants of phenylalanine were calculated in gas phase using density functional theory and also in aqueous solution by a potentiometric method for comparison and are listed in following table.

protonation constants	aqueous solution	gas phase
pK_{a1}	1.83	150.7
pK_{a2}	9.13	234.7

As shown in above, K_a values increase and therefore pK_a values decrease in gas phase rather than aqueous solution. The difference between pK_{a1} and pK_{a2} in gas phase in comparison with solution appeared that solvent molecules have the important role in stability of species. This can be due to the effect of the strong intramolecular hydrogen bonds or the solvent-solute electrostatic and nonelectrostatic interactions in solution. These reasons are caused to decrease protonation constants in aqueous solution in comparison with gas phase.

References

[1] F. Gharib, A. Farajtabar, A.M. Farahani, F. Bahmani, Journal of Chemical and Engineering Data 55 (2010) 327.

[2] G. Bouchoux, S. Bourcier, V. Blank, S. Desaphy, Journal of J. Phys. Chem. B 113 (2009) 5549.

[3] R.Wu, T. B. McMahon, Journal of ChemPhysChem 9 (2008) 2826.

[4] Y. H. Jang, W. A. Goddard, K. T. Noyes, L. C. Sowers, Journal of J. Phys. Chem. B 107 (2003) 344.

The quantum-chemical calculation of NMR one- and two bond spin–spin coupling constants in the $N^-\cdots H–OH \rightarrow N–H\cdots OH^-$ Switching

Hossein Roohi [a, b], Behnaz Moghadam [a]*

[a]*Department of Chemistry, Faculty of Science, University of Sistan & Baluchestan, P.O. Box 98135-674, Zahedan, Iran*

[b]*Department of Chemistry, Faculty of Science, University of Guilan, Namjoh Street, P.O. Box 41335-1914 , Rasht, Iran*

Email: b.moghadam87@yahoo.com

Keywords: NMR, Aniline, Proton transfer

Introductions

Nuclear magnetic resonance spectroscopy is a widespread and well-established method of structural analysis. In particular, NMR spectroscopy plays an important role in detection and characterization of hydrogen bonds. Ab initio calculations of effect of size of clusters on the nuclear spin-spin coupling constants in H-bonded systems have lately attracted a lot of attention. The modeling of the nuclear spin-spin coupling constants in molecules interacting with the environment is still a new field, but the interest in this subject is growing [1,2]. Aniline and its derivatives are convenient systems to study intermolecular H-bonding [3]. To the best of our knowledge, influence of size of H_2O cluster and substituents in para position on the spin-spin coupling constants (SSCC) correspond to the transfer of proton between H_2O and p-substituted anilide anion has not been reported. The aim of the present study is to investigate the correlation between SSCC and binding energy, structural parameters, electron density topography and shift of vibrational frequency in $X–C_6H_5NH^-\cdots(H_2O)n \rightarrow X\text{-}C_6H_5NH_2\cdots(OH^-)H_2O_{n-1}$ switching process. (X= H, CH_3, OCH_3, NO, NO_2, CHO)

Computational details

The geometries of all complexes were optimized at B3LYP/6-311++G(2d,2p) level of theory. The B3LYP calculated vibrational frequencies have been used to characterize stationary points and calculation of zero-point vibrational energy (ZPVE). Spin-spin coupling

constants involving ^{13}C, ^{15}N, ^{17}O, and ^{1}H in all monomers and complexes were computed at B3LYP/6-311++G(2d,2p) level.

Results and discussions

There is a relationship between electronic BE and sum of $^{2h}J(N\cdots O)$ SSCCs in X-A-$(W)_{1,2}$ and X-Ph-$NH_2(OH^-)(W)_{2,3}$ complexes (Fig. 1a). Complex with greater BE has greater $^{2h}J_{N\cdots O}$. The linear correlation between Red-shift of O–H stretching frequencies ($\Delta\nu/cm^{-1}$) versus the $^{2h}J_{N\cdots O}$ SSCCs in X-A-$W_{1,2}$ are depicted in (Fig. 1b). Relationship between sum of $^{2h}J_{N\cdots O}$ and $^{2h}J_{O\cdots O}$ SSCCs and sum of corresponding H-bond distances (R) in X-A-W_n complexes are given in Fig. 2a. Correlation between sum of $^{2h}J_{N\cdots O}$ and $^{2h}J_{O\cdots O}$ SSCCs and sum of ρ(r) at the corresponding HBCPs in X-A-W_n complexes are shown in Fig. 2b. As can be seen correlation between mentioned properties and two-bond SSCC is linear in our interested complexes.

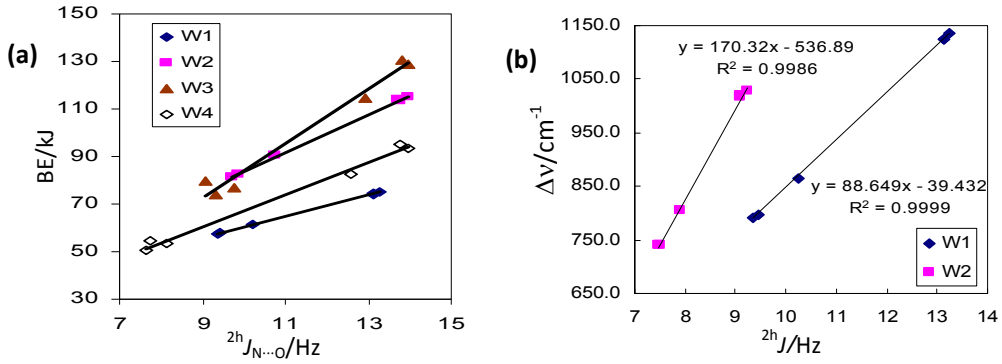

Fig. 1. Correlation between absolute value of BE and $^{2h}J(N\cdots O)$ SSCCs in X-A-$(W)_{1,2}$ (symbolized as W1 and W2) and X-Ph-$NH_2(OH^-)(W)_{2,3}$ (symbolized as W3 and W4). (b) Red-shift of O–H stretching frequency ($\Delta\nu/cm^{-1}$) versus the $^{2h}J_{N7\cdots O14}$ SSCC in X-A-$W_{1,2}$.

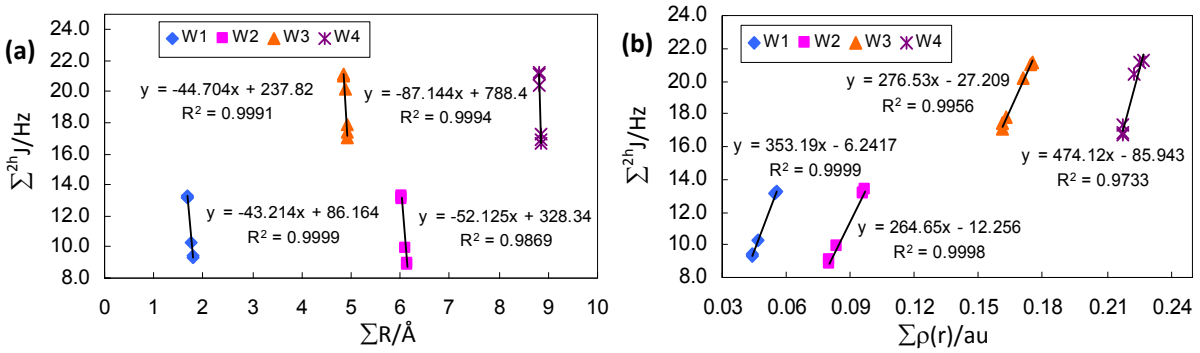

Fig. 2. (a) Correlation between sum of $^{2h}J_{N\cdots O}$ and $^{2h}J_{O\cdots O}$ SSCCs and sum of corresponding H-bond distances (R) in X-A-W_n complexes. (b) Correlation between sum of $^{2h}J_{N\cdots O}$ and $^{2h}J_{O\cdots O}$ SSCCs and sum of ρ(r) at the corresponding HBCPs in X-A-W_n complexes.

References:

[] J. E. Del Bene, J. Elguero, *J. Phys. Chem. A* 2007, *111,* 6443-6448.

[2] H. Cybulski, M. Pecul, J. Sadlej, *Chemical Physics* 2006, 326, 431–444.

[3] H. Szatyłowicz, T. M. Krygowski, J. E. Zachara-Horeglad, *J. Chem. Inf. Model.* 2007, 875-886.

DFT study H_2O_2 trapped inside Boron nitride nanotubes

M. Moghimi[a,*], Mohammad T. Baei[b]

[a]Islamic Azad University, Gonbad Branch, Department of Chemistry, Gonbad, Golestan, Iran

moghimi_m52@yahoo.com

[b]Islamic Azad University, Azadshahr Branch, Department of Chemistry, Azadshahr, Iran

Keywords: Boron nitride nanotubes (BNNTs), Adsorption, Binding energy, DFT

Introduction

Boron nitride nanotubes (BNNTs) are inorganic analogues of carbon nanotubes (CNTs) and possess physical properties suitable for broad variety of applications [1]. BNNTs are wide gap semiconductors with almost same band gaps of 5.5 eV, independent of the tube diameter, helicity, and the number of tube walls, and they are chemically and thermally more stable. In the present communication, we present a case study of torsional motion of H_2O_2 inside a carbon nanotube. Several studies have been done in the past about the torsional dynamics of H_2O_2 and its variants [2]. However, the effect of confinement has not been discussed so far. The chirality changing torsional motion of H_2O_2 is suitably selected so that it can give additional information on the nature of the interaction by scanning through the surface of the cage during its internal motion.

Computational Methods

The density functional theoretical method with the B3LYP functional and the 6-31G* basis set was used for all the calculations. As a first step, (5, 5) armchair BNNTs ($B_{25}N_{25}H_{20}$) with length of 10 Å have been selected. The terminal boron and nitrogen atoms are hydrogenated to saturate the valency of the atoms and have diameter of 7.16 Å. While keeping the bond lengths and bond angles of H_2O_2 at their optimized equilibrium geometry values, the dihedral angle is varied from 0° to 180° at 10° intervals. Single point energy calculations have been carried out for each of these geometries. Similar calculations have been done for H_2O_2 encapsulated inside nanotubes, keeping the geometries of BNNT as in their optimized structures. Various orientations of H_2O_2 inside the BNNT are considered. The binding energy

(E_{bind}) of H_2O_2@BNNT for all the geometries is calculated as follows: $E_{bind} = E_{complex} - (E_{BNNT} + E_{H2O2})$

Results and discussion

The relative orientation of the guest species inside a carbon nanotube affects significantly the interaction between the guest species and the host cage. Considering the size of the nanotube under investigation, H_2O_2 can orient inside the tube in different ways. However, we limited our study to some selected orientations. This includes mainly two categories: (I) orientation of the O–O bond along the tube (AT) axis and (II) orientation of the O–O bond perpendicular to the tube (PT) axis and pointing towards the centre of the two diametrically opposite B-N bonds. For the second case, we considered two sub categories: (II.a) O–H bonds pointing towards the open end of the tube when H_2O_2 is in its cis geometry and (II b) O–H bonds pointing towards the surface of the cage (orientation of H_2O_2 perpendicular to that in (II.a)). Hereafter these orientations are referred to as AT, PTA and PTP type geometries, respectively. In all the above cases, the centre of mass of the O–O bond is coincident with the centre of the tube. Snapshots of the torsional motion of H_2O_2 in the various geometries discussed above are given in Fig. 1 and the variation of the binding energy with respect to the dihedral angle as shown in Fig. 2

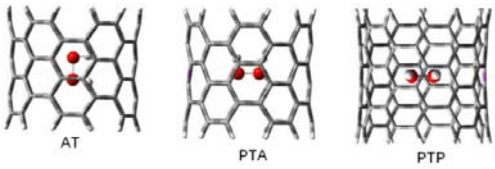

Fig. 1. Snapshots of the torsional motion of H2O2 inside the carbon nanotube for various types of geometries considered in the present study

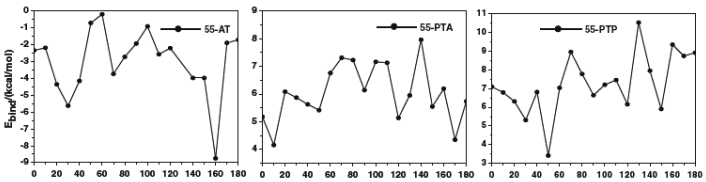

Fig. 2. Variation of the binding energy as a function of the dihedral angle of H2O2 for different types of orientations inside (5,5)

Conclusion

Among the three types of orientations AT, PTA and PTP for the (5,5) nanotubes, the AT-type geometry shows stabilization of the guest species inside the cage. The PT-type geometries of H_2O_2 are unstable inside the tube. When the O–O bond is oriented perpendicular to the cage, the shortest distance between the oxygen atom and the B-N atoms (2.8 Å) is less than the sum of their corresponding vander Waals radii (3.2 Å). When compared to the dipole moment of free H_2O_2 for different dihedral angles, the dipole moments of the complexes is significantly reduced.

References

[1] D. Golberg, Y. Bando, C.C. Tang, C.Y. Zhi, Adv. Mater. 19 (2007) 2413.

[2] S.A. Shevlin, Z.X. Guo, Phys. Rev. B 76 (2007) 024104.

Ab initio and DFT study of the interaction between glycine and nitrosamine

B. Makiabadi*[a] and M. Zakarianezhad [b]

[a]Sirjan Engineering College, Shahid Bahonar University, P.O. Box 78185439, Sirjan, Iran

(E-mail:bmakiabadi@yahoo.com)

[b]Department of Chemistry, Faculty of Science, Payam Noor University, Sirjan Center, Sirjan, Iran

Keywords: Glycine, Nitrosamine, Binding energy, Hydrogen bond interaction

Introduction

Amino acids are building blocks of proteins (polypeptides), which are the most important class of biological macromolecules. The primary attention has, however, been paid to glycine (Gly) which is the simplest amino acid. Since it represents a small and highly polar organic molecule containing several functional groups, its studies are of fundamental importance for understanding chemical bonding and evaluating links between modern theories and experimental observations [1–2]. Most of nitrosamines are carcinogenic compound and play an important role in the development of tumors and cancer in animals. N-nitrosamines are believed to require metabolic activation to exert their carcinogenic effect [3].

Methods

For the study of interactions between glycine and nitrosamine, DFT computations were carried out using B3LYP hybrid density functional method and the 6-311++G (2d,2p) basis set on a Pentium 4 computer. The counterpoise procedure (CP) was used to correct for basis set superposition error (BSSE) in the calculation of binding energy.

Result and discussion

First of all, we considered all sites for interaction between glycine and nitrosamine. We found seven minima structures. As shown in Fig. 1, all optimized complexes have cyclic structures with two H-bonds involved in the interaction. The GN5 structure is nine membered cyclic complex, GN2,GN3 and GN6 structures are seven membered cyclic complexes and GN1, GN4 and GN7 structures are eight one. From Fig. 1, GN1,GN5 and GN7 structures contain two H…O hydrogen bond interactions, while GN2, GN3, GN4 and GN6 structures contains

two H-bonds type interactions (O…H and N...H). The calculated interaction energies for GN complexes are listed in Table 1. The electronic binding energies (D_e) range from -50.99 to -12.76 kJ/mol. From the values presented in table 1, it can be seen that the relative stability order of the seven complexes is GN1> GN2> GN3> GN4> GN5> GN6> GN7. The structure GN1 is the most stable and cyclic structure GN7 is the less stable.

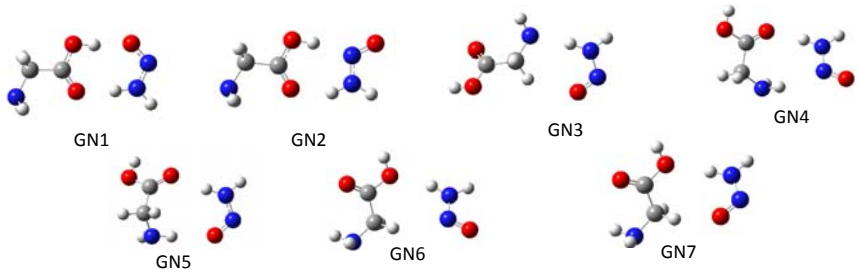

Fig. 1. Optimized structural for GN complexes

Table 1. Binding energies (kJ/mol) obtained at B3LYP/6-311++G (2d, 2p) levelof theory.

	Bsse	De	De^{Bsse}
GN 1	1.76	-50.99	-49.23
GN 2	1.73	-46.18	-44.45
GN 3	1.32	-29.26	-27.94
GN 4	1.26	-28.30	27.04
GN 5	1.35	-21.89	-20.54
GN 6	1.22	-12.85	-11.63
GN 7	1.26	-12.67	-11.41

D_e = Electronic binding energy, D_e^{Bsse}= D_e+ Bsse

Conclusions

All the structures studied in this work were optimized by using B3LYP method with 6-311++G(2d,2p) basis set. Seven minima structures were found for glycine–nitrosamine interactions. All optimized complexes have cyclic structures with two H-bonds involved in the interaction. The structure GN1 is the most stable and cyclic structure GN7 is the least stable.

References

[1] K. Kaznacheyev, A. Osanna, C. Jacobsen, O. Plashkevych, O. Vahtras, H. Ågren, V. Carravetta, A.P. Hitchcock, J. Phys. Chem. A. 106 (2002) 3153.

[2] M. Nyberg, J. Hasselstrom, O. Karis, N. Wassdahl, M. Weinelt, A. Nilsson, L.G.M. Pettersson, J. Chem. Phys. 112 (2000) 5420.

[3] M. Sulc, B. Kubickova, V. Maslova, P. Hodek, gen. Physiol. Biophys. 23 (2004) 424.

Structural and Thermodynamic Study of $M(bp)Cl_2$ complex by DFT Methods

T.Molaaghaee*[1],Kh.Kalateh[2]

Faculty of science, azad university, Branch of shahr-e-rey

tiyam60_27@yahoo.com

Keywords: 2, 2' –bipyridine,Gaussian98, BSSE Calculations, E_{corr}

Introduction:

Bipyridine is a chemical compound with $C_5H_4N_2$ formula, and Bpy, names It is a chelat ligand and forms complexes with most of transition metals .many of these complexes have optical properties For the first time the pure 2,2'-bipyridine was synthesized by copper picolinate distillation. At last of 19th centry. more facile methods developed by Ni catalyst.

Computational method:

Optimization calculation of ligands and complexes were performed by Gaussian 98 software; chem Office, chem draw , chem craft and Gaussian 98 softwares were used too. Initially 2, 2'-bipyridine was optimized at HF/6-31g, B_3LYP/6-31g**, B_3LYP/6-311g levels and B_3LYP/6-31g** method/basis set was selected for later calculation. Then -COOH, $-CH_3$ and $-NH_2$ groups at 4, 4' position and one $-CH_3$ group at 3 positions added to ligand and optimization, for calculation of thermodynamic parmeters and prediction of these compounds properties such as bond angles were performed.

Then Zn, Cd and Hg transition metals for creation of complexes were investigated, optimization computations of complexes were performed and influence of different metals on electronic properties of complexes was studied by BSSE method.

Result and discussion:

In aspect of experimental results was considered tetrahedral geometry for complexes.

Structural parameters such bond lengths, bond angles and dihedral angles were determined. It is considered Cl-M-N-N dihedral angles is 105.47466°, 102.32392°, 99.1878° for Zn, Cd and Hg complexes respectively which shows Zn complex is closer to tetrahedral structure.

TABLE 1: Calculated dihedral angles for complexes by B3LYP/6-31g** Method

ANGEL	NMN(2-21-7)	ClMCl(22-21-23)	ClMNN(22-21-2-7)	ClMNCl(22-21-7-23)
Znbp(Cl)2	75.54664	131.34747	105.47466	149.04413
Cdbp(Cl)2	68.60739	137.60143	102.32392	155.33931
Hgbp(Cl)2	64.56449	146.2502	99.1878	161.59557

Thermodynamic parameters including logK, ΔG, ΔE, ΔH and ΔS were calculated. Zn complex with 1139.5443 for logK has the most stability.

TABLE 2: Calculated Thermodynamic parameters

LOGK	Znbp(CH3)	Cdbp(CH3)	Hgbp(CH3)
B3LYP/6-31g**	461.661886	448.18399	444.112888

Basis set super position energy calculation was performed to correction energy results. E_{corr} was -1479.7333, -1463.163 and -1417.8135 for Zn, Cd, Hg respectively which indicate more stability for Zn complex. In general, results show that zinc complex structure is closer to tetrahedral geometry and is the most stable complex.

TABLE3: Calculated BSSE

	Etot	EMopt	ELopt	EMNUC	EM	ELNUC	EL	ΔEBSSE	EBSSE	Eint	Ecorr
Zn	-1481.527	-65.5958	-495.39	-1415.74	-65.5958	-986.065	-495.39	-1479.696	2218.4392	-0.0373	-1479.7333
Cd	-1463.978	-48.07965	-495.39	-1415.751	-48.07965	-968.53	-495.39	-1463.156	-1463.163	-0.00638	-1463.163
Hg	-1458.618	-42.7845	-495.39	-1415.755	-42.7845	-963.1904	-495.39	-1417.874	-2218.549	0.0605	-1417.8135

References:

[1]H. B. A, G. Day, M. Lewis. j, chem. Soc. perkin trans,2,2713(1998)

[2] Y. Wang, & et.al., Inorganica Chemimica Acta (2008), inedited

[3] L. Y. Kong, Z. H. Zhang, T. Okamura, M. J. Fei, W. Y. Sun, N. Ueyama, Chem. Lett. 33(2004) 1572

[4] John Mc Murry ,*Organic chemistry* ,5th ed ,2000

The Ab initio Study and NBO Analysis on the Structural Sof the fMet-tRNA

Ali Akbar Salari [a] ,Somaye Mollababaei [b*] ,Maziar Noei [c]

[a,b]*Chemistry Department, Islamic Azad University-Shahre Rey Branch, Tehran , Iran*

[c]*Chemistry Department, Islamic Azad University- Mahshahr Branch, Mahshahr, Iran*

Corresponding Author E-mail:somaye.molababaei@gmail.com

Abstract:

Formylmethionine is always the first amino acid in polypeptide chain , although frequently it is removed after translation .In this case we studied about amino acid linkage to the proper tRNA which this process is controlled by the amino-acyl-tRNA synthesize .Theoretical study of binding the amino acid (formylmethionine) to tRNA has been performed using quantum computational ab initio HF and density functional B3LYP method using 3-21G(d,p) basis set in the different solvents to calculate structural optimization and the major stabilizing orbital for the bond (fMet-tRNA) were calculated by natural bond orbital(NBO) methodology.

Keyword: Natural bond orbital(NBO), fMet-tRNA ,Hartree-fock(HF),Density functional theory(DFT)

Introduction

It is generally accepted that initiation of protein synthesis in Escherichia coli starts with formyl-methionine, directed by the codons AUG or GUG. Protein synthesis proceeds by transfer of the growing polypeptide chain from the tRNA bound to the ribosomal P site to the incoming aminoacyl-tRNA in the adjacent A site. After translocation of the ribosome in the 30 direction of the mRNA, by the action of elongation factor G, the A site again becomes empty and the next codon exposed so that a new aminoacyl-tRNA ternary complex can be selected [1].Synthetic polynucleotide containing AUG And/or GUG codons as well as natural mRNA have been used extensively in order to elucidate the mechanism of initiation of

protein synthesis [2].we selected adenine of tRNA structure(first nucleotide in acceptor arm of tRNA structure) and then perform modeling of fMet-tRNA. (Fig 1)

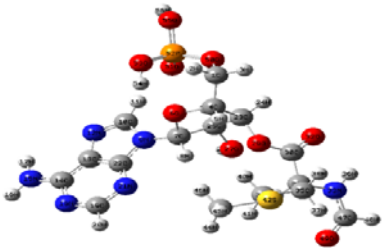

Fig .1: structure of Adenine + fMet of fMet-tRNA

Results and discussion

In this paper HF and DFT/B3LYP methods with 3-21G* basis set were Employed for investigating the structure optimization and energy minimization of fMet-tRNA (Fig1) have been summarized in Table 1.The HF and DFT energies are of particular interest because they provide results for interactions appearing in solvent medium considered in this letter, which are in accord with biological behavior of Adenine + fMet of fMet-tRNA. Furthermore, recent papers often tend to ask about the role of water solvent effect on the stability of Adenine + fMet of fMet-tRNA structure. The detailed results of relative energy values for Adenine + fMet of fMet-tRNA structure in gas , DMSO , CHCL3 and water solvents optimized at the HF and B3LYP levels of theory with 3-21G* basis set are summarized in Table (1)

Table1:optimization Energy for each Method

	E(kcal/mol)			
3-21G*	**Gas**	**$CHCL_3$**	**DMSO**	**H2O**
HF	**-3738.1213366**	**-3738.1244432**	**-3738.1213031**	**-3738.1213011**
B3LYP	**-3755.0439622**	**-3755.0463986**	**-3755.0438037**	**-3755.0438020**

The most important interaction between “filled” (donor) Lewis-type NBO and “empty” (acceptor) non-Lewis is reported in Table (2) , the level of B3LYP/ 3-21G* basis set at the DFT theory. we observed interaction between Donor NBO , the LP(1,2) of O29 , O32 and Acceptor NBO, the σ*(C30-O32) , π*(C30 - O32) , σ * (O29 - C30) of fMet-tRNA structure.

Table2: Second Order Perturbation Theory Analysis of Fock Matrix in NBO Basis Threshold for printing:0.50 (kcal/mol)

B3LYP/3-21G* method

Phase	Donor NBO (i)	Acceptor NBO (j)	E(2) (kcal/mol)
Gas	LP (1) O29	σ* C30 - O32	7.25
	LP (2) O29	π* C30 - O32	55.35
	LP (1) O32	σ* O29 - C30	0.72
	LP (2) O32	σ* O29 - C30	37.09
CHCL3	LP (1) O29	σ* C30 - O32	7.28
	LP (2) O29	π* C30 - O32	55.66
	LP (1) O32	σ* O29 - C 30	0.71
	LP (2) O32	σ* O29 - C 30	36.98
DMSO	LP (1) O29	σ* C30 - O 32	8.34
	LP (2) O29	π* C30 - O32	50.45
	LP (1) O32	σ* O29 - C30	1.55
	LP (2) O32	σ* O29 - C30	37.09
H2O	LP (1) O29	σ* C30 - O 32	7.25
	LP (2) O29	π* C30 - O32	55.35
	LP (1) O32	σ* O29 - C 30	0.72
	LP (2) O32	σ* O29 - C 30	37.09

Conclusion

1-we observed a decrease in the bond lengths of the O29-C30 of the structure by the increase of solvent dielectric constant.

2-The results obtained through theoretical calculations revealed that there is an effective interaction between the O_{32} lone pair(Lp)and sigma antibonding orbital (σ*)of O_{29}-C_{30}.This interaction can reflact the electron transference(hyperconjugative effect) between the orbital localized in these atoms.

3-there was an increase in the relative stability of the interested structure through the improvement of basis set and including electron correlations , Hence, the most stable structure is perceived in the CHCL3 solution at the B3LYP/3-21G* level of theory.

References

[1] Ogle, J.M., and Ramakrishnan, V.(2005). Structural insights into translational fidelity.Annu. Rev. *Biochem.* 74, 129-177.

[2] Grunberg-Manago, M.(1977).Initiation mechanisms of protein syntehesis.*Prog. Nuel.Acid Res. Mol.Biol.* 20,209-284.

Quantitative Structure-Property Relationship(QSPR) Study for Prediction of Gibbs Free Energy of Formation of Alkenes

F. Mollaie Poli*[a], R. Behjatmanesh Ardakani [b]

[a]Department of Chemistry, Payame Noor University of Sirjan, Kerman, Iran

(Emai: f.mollaie@yahoo.com)

[b]Department of Chemistry, Payame Noor University of Ardakan, Yazd, Iran

Keywords: Alkenes, Gibbs free energy of formation, MLR, QSPR

Introduction

The study of the quantitative relationship between property/activity and molecular structure (QSPR/QSAR) is an important research area in computational chemistry and has been widely used in the predication of physico-chemical properties and biological activities of organic compounds [1]. In this work, a QSPR study is performed to develop an accurate model for the prediction of Gibbs free energy of formation (ΔG_f^o) for a set of 36 alkenes. For this purpose, multivariate linear regression (MLR) is applied to establish quantitative linear relationship between ΔG_f^o and molecular descriptors.

Methods

The experimental standard ΔGf° values (in kJ mol^{-1}) at 298 K of 36 alkenes were taken from the Chemical Properties Handbook [2]. The data set was randomly split into a training set of 27compounds and a test set of 9 compounds for the MLR model. HyperChem, Gaussian 98 and Dragon packages were used for calculation of 49 molecular descriptors. dipole moment, HOMO and LUMO energies, minimum and maximum partial charges, Polarizabilty, hardness, etc were calculated by the ab initio b3lyp/6-311G(d) using GUASSIAN 98 software. The stepwise regression and cross-validation were performed respectively using the statistical software SPSS and MATLAB software.

Result and Discussion

The result was the following three-variable equation:

$$\Delta G_f^o = -34.78 - 23.979Ss + 3.735P + 1784.341\omega \quad (1)$$

In Equation (1), Ss is the Sum of kier–Hall electrotopological states, P is Polarizabilty and ω is electrophilicity. Without standardization of above equation, it is not possible to discuss about importance of variables in the prediction model. Following equation is obtained after standardization:

$$\Delta G_f^o = -0.863Ss - .406P + 1.147\omega \quad (2)$$

The goodness-of-fit of the resulted QSPR models were judged using statistical parameters such as correlation coefficient (R), Squared correlation coefficient (R^2), Adjusted R^2 (R^2_{Adj}), standard error of regression (S.E), and variance ratio (F) at specified degrees of freedom. The generated QSPR equations were also validated by leave-one-out cross – validation correlation coefficient (R^2_{cv}). The predictive ability of a QSPR model should be tested on an external set of data that has not been taken into account during the process of developing the model. In particular, to assess the predictive power of QSPR models the correlation coefficient between the predicted and observed property of compounds from an external test (r^2), the correlation coefficients for regressions through the origin (predicted versus observed activities, or observed versus predicted activities, i.e., r_0^2 or $r'_0{}^2$ respectively), and the slope of the regression lines through the origin (k and k', respectively) were calculated [3]. Considered a QSPR model to be predictive, if all of the following conditions are satisfied: (i) $R^2_{cv} > 0.5$, (ii) $r^2 > 0.6$, (iii) r_0^2 or $r'_0{}^2$ is close to r^2 and (iv) $0.85 \le k \le 1.15$ or $0.85 \le k' \le 1.15$. the statistical parameters and the multi-collinearity among variables respectively are shown in Table 1. The plot of predicted versus experimental $\Delta G_f°$ for the training shown in Figures 1 suggest that the alkenes follow a straight line.

TABLE 1. Statistical parameters

R	R^2	R^2_{Adj}	S.E	F	R^2_{cv}	r^2	r^2	$r'_0{}^2$	k	K'
0.998	**0.995**	**0.994**	**4.11**	**1547.34**	**0.990**	**0.9985**	**0.9891**	**0.9894**	**0.91**	**1.0**

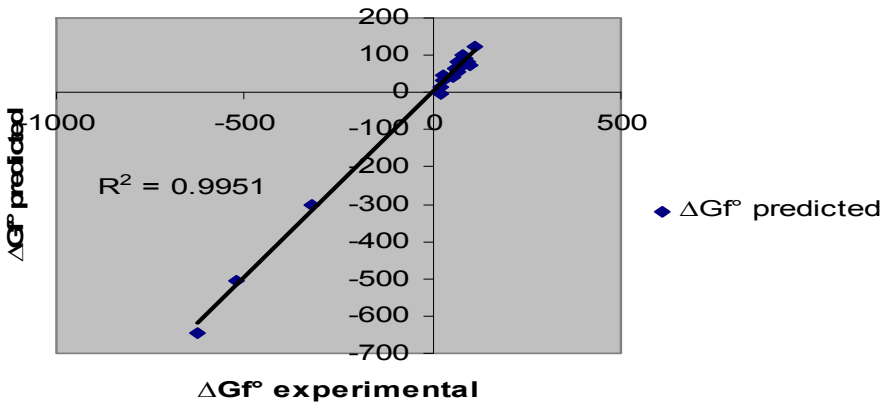

Fig. 1: Predicted versus experimental values of ΔGf° for training set by MLR

Conclusions

The results show close agreement between Predicted values and experimental ones, which demonstrates the reliability of the QSPR model.

References

[1] M. Karelson, V. Lobanov, A. Katritzky, Chem. Rev, 96 (1996) 1027.

[2] J.A. Dean, LANGE'S HANDBOOK OF CHEMISTRY,.1999.

[3] A. Golbraikh, A. Tropsha, J. Molecular Graphics and Modeling. 20 (2002) 269.

Conformational behaviors of trans-2,3- and trans-2,5-dihalo-1,4-dioxanes. A complete basis set, hybrid-DFT study and NBO interpretation

Mousavi[a,*].S.N , Yahyayi[b].H , Nori-Shargh[a].D

d) *Chemistry Department, Science Faculty, Arak branch, Islamic Azad University, Arak, Iran*

**Corresponding author. E-mail: Negar_mousavi@ymail.com*

e) *Chemistry Department, Zanjan Branch, Islamic Azad University, P.O.Box: 49195-467, Zanjan, Iran*

Keywords: Anomeric Effects, Stereoelectronic Interactions, Molecular Modeling, Ab initio, NBO, Dihalo-1,4-dithiane

Introduction

In 1992, Matias and co-workers analyzed the structure of compound 5 by neutron diffraction technique.[1] The bond lengths not involving hydrogen atoms are in agreement with reported X-ray analysis[2] to within 0.004 Å. There is insufficient published experimental information about the stereoelctronic interactions in 2,3-dichloro-, 2,3-dibromo- and 2,5-dibromo-1,4-dioxanes and also there is no published experimental or quantitative theoretical data about the donor-acceptor delocalization effects on the conformational properties of trans-2,3-dihalo-1,4-dioxane [halo = F (**1**), Cl (**2**), Br (**3**)] and trans-2,5-dihalo-1,4-dioxane [halo = F (**4**), Cl (**5**), Br (6)]. In this work, the stereoelectronic interactions associated with the *AE* and also the conformational and structural properties of compounds 1-6 were investigated computationally using complete basis set composite method CBS-4, hybrid-DFT based methods and natural bond orbital (NBO) analysis.[3,4]

Computational details

Composite complete basis set (CBS) and hybrid DFT calculations were carried out using the CBS-4 and B3LYP/6-311+G** levels of theory with the GAUSSIAN 03 package of programs.[3] The main purpose of the present work was to study the impacts of the stereoelectronic interaction effects, dipole-dipole interactions and the total of the pairwise steric exchange energies (*PSEE*) for disjoint interactions between i and j natural localized molecular orbitals ($NLMO_{i,j}$) (*PSEE*) on the conformational preferences (i.e. axial and equatorial conformations) in compounds **1-6**. An NBO analysis was then performed for the

axial and equatorial conformations of compounds 1-6 by the NBO 5.G program contained in the PC-GAMESS interface.4

Results and Discussion

Complete basis set CBS-4, hybrid-density functional theory (B3LYP/6-311+G**//B3LYP/6-311+G**) based methods and NBO interpretation were used to study the conformational behaviors of trans-2,3-dihalo-1,4-dioxane [halo = F (**1**), Cl (**2**), Br (**3**)] and trans-2,5-dihalo-1,4-dioxane [halo = F (**4**), Cl (**5**), Br (**6**)]. Both methods showed that the axial conformations of compounds **1-5** are more stable than their equatorial conformation*s* but CBS-4 resulted in an equatorial preference for compound **6**. The Gibbs free energy difference (G_{eq}–G_{ax}) values (i.e. $\Delta G_{eq\text{-}ax}$) at 298.15 K and 1 atm between the axial and equatorial conformations decrease from compound **1** to compound **2** but increase from compound **2** to compound **3**. Also, the calculated $\Delta G_{eq\text{-}ax}$ values decrease from compound **4** to compound **6**. The NBO analysis of donor-acceptor (LP→σ*) interactions showed that the *anomeric effects* (*AE*) increase from compound **1** to compound **3** and also from compound **4** to compound **6**. On the other hand, the calculated dipole moment values between the axial and equatorial conformations [$\Delta(\mu_{eq} - \mu_{ax})$] decrease from compound **1** to compound **3**. The conflict between the increase of *AE* and the decrease of $\Delta(\mu_{eq} - \mu_{ax})$ values could explain the variation of the calculated $\Delta G_{eq\text{-}ax}$ for compounds **1-3**. The Gibbs free energy difference values between the axial and equatorial conformations (i.e. $\Delta G_{ax\text{-}ax}$ and $\Delta G_{eq\text{-}eq}$) of compounds **1** and **4**, **2** and **5** and also **3** and **6** have been calculated.

Conclusion

The *AE* increase from compound **1** to compound **3** and also from compound **4** to compound **6**. the rationalization of the conformation preference solely in terms of the *AE* fails to account quantitatively for the conformation preferences in compounds **1-6**. The decrease of the calculated $\Delta G_{ax\text{-}eq}$ from compound **1** to compound **2** and its increase from compound **2** to compound **3** could be a result of conflicting effect of the *AE* and $\Delta(\mu_{eq}\text{-}\mu_{ax})$.

References

[1]G.A. Jeffrey, J.R. Ruble, P. Matias, P.K. McMullan, P. Luger, J. Buschmann, Acta Cryst., C49, 707-709 (**1992**).

[2]C. Altona, C. Knobler, C. Romers, *Acta Cryst*., 16, 1217 (**1963**).

[3]M.J. Frisch, et al, Gaussian 03, Revision B.03, Gaussian, Inc., Wallingford CT, (**2004)**.

E.D. Glendening, J.K. Badenhoop, A.E. Reed, J.E. Carpenter, J.A. Bohmann, C.M. Morales, F. Weinhold, Theoretical Chemistry Institute, University of Wisconsin, Madison, WI, (**2004)**. NBO Version 5.G.

Theoretical Investigation of Corrosion Inhibition Effect of Imidazole and its Derivatives on Mild Steel Using Cluster Model

M. Mousavi*[a], M. Mohammadalizadeh[a], A. Khosravan[b]

[a] Department of Chemistry, Faculty of Sciences, Shahid Bahonar University of Kerman, P.O. Box 76175-133 , Kerman, Iran

(*Email:mmousavi@mail.uk.ac.ir)

[b] Department of Material Sciences and Engineering, International Center of Science, High Technology & Environmental Sciences, P.O. Box 76315-117, Mahan, Kerman, Iran

Keywords: Mild steel corrosion, Imidazole derivatives Cluster model, DFT calculation

Introduction

Corrosion is an electrochemical destructive process of a metal or alloy with its environment which leads to loss of useful properties of materials. Imidazoles, benzoimidazols and their derivatives are organic inhibitors which can form feedback coordinate covalent bonds with metal surface. Theoretical and computational chemistry are useful and powerful means in choosing the most appropriate and effective inhibitor by understanding the inhibition mechanism prior to any experiment. In the present work, efforts have been made to develop a method which enables us to directly predict the inhibition behavior of imidazole and a series of its derivatives on mild steel surface.

Methods

According to cluster model, the interaction of the corrosion inhibitor molecule with the metal surface is considered, locally. The cluster model has been applied to hcp crystal lattice of cementite, which involve features of (001). Four different adsorption modes could be visualized in the (001) plane and are described as modes A to D. Thus, the quantum chemical study is restricted to the calculation of interaction energy between the inhibitor molecule and the unit cell atoms upon which the adsorption is directly tacking place. The interaction energy between the inhibitor molecule and the metal surface, $E_{int.}$, can be calculated according to Eq. 1:

$$E_{int.} = E_{inhibitor\text{-}cluster} - (E_{cluster} + E_{inhibitor}) \quad (1)$$

where, $E_{inhibitor}$, $E_{cluster}$ and $E_{inhibitor\text{-}cluster}$ are electronic energies of the inhibitor molecule, the mild steel cluster and of the inhibitor-mild steel system, respectively [2].

Results and discussion

The interaction energies of imidazole and its seven derivatives on the (001) surface of mild steel were determined by using DFT quantum chemical calculations and the cluster model. Here, the structures of inhibitor molecules and mild steel unit cell were optimized via B_3LYP/6-31++G (d,p) and B_3LYP/LANL1MB methods, respectively. Subsequently, the calculation of interaction energies begin by placing the inhibitor molecule in front of the mild steel unit cell at a non-interactive distance (2.5 Å) based on one of the adsorption modes (A to D). It is then followed by gradually decreasing the distance in stepwise manner (0.05 Å) until the system reaches an equilibrium state with the most favorable interaction energy. At each step, the geometry optimization and the energy calculation of the inhibitor-mild steel unit cell system were carried out using B_3LYP/LANL1MB method, so that the equilibrium distance (r_{min}) and the minimum energy ($E_{min.}$ or $E_{inhibitor\text{-}cluster}$) for the system could be extracted. Finally, interaction energy for the inhibitor-mild steel system was calculated by using electronic energies in the Eq. 1. It is necessary to mention that after calculating the energies, zero point energy (ZPE) and basis set superposition error (BSSE) corrections were also imposed.

To find out which mode of adsorption is mostly in favor of corrosion inhibition, a comparison between the interactions energies of each adsorption mode (A to D) had to be made. Correlation coefficient between the calculated interaction energies of A and C modes and the experimental corrosion inhibition were found to be 0.94 and 0.95, respectively. This means that, nearly 90% of inhibition variation of the imidazole derivatives can be described by considering perpendicular interaction of the inhibitors and iron atoms in the mild steel unit cell.

Conclusions

It was found that the interaction energies of inhibitor molecules only with iron atoms can lead to a good agreement with the experimental corrosion efficiencies. The adsorption of imidazole and its derivatives on mild steel surface takes place mostly through perpendicular

adsorption of the nitrogen atom of imidazole ring on iron and carbon atoms of the mild steel unit cell. It seems that the corrosion inhibition ability of any compound which may be used as an inhibitor can be estimated by applying the regression equation which relates the calculated interaction energies with corrosion inhibition efficiencies, and in this way the number of experimental runs and the cost of investigation will decrease considerably in any corrosion inhibition study.

References

[1] R. M. Issa, M. K. Awad, F. M. Atlam, Appl. Surf. Sci. 255 (2008) 2433-2441.

[2] M.R. Arshadi, M. Lashgari, Gh. A. Parsafar, Materials Chemistry and Physics 86 (2004) 311–314.

[3] S. G. Zhang, W. Lei, M. Z. Xia, F. Y. Wang, J. Mol. Struct. (Theochem) 732 (2005) 173-182.

Selectivity Coefficient and Extraction Power Modeling of 1, 1-Dimethylsila-17-crown-6 and 18-Crown-6 for Some Alkali Metal Cations

M. Mousavi*, M. Zohrabi
Department of chemistry, Shahid Bahonar University of Kerman, P.O.Box 76169, Kerman, Iran
(* Email: mmousavi@mail.uk.ac.ir)

Keywords: Selectivity coefficient modeling, DFT calculations, DMS17C6, 18C6

Introduction

Selectivity of any chemical sensor is clearly one of its most important characteristics as this property often determines whether the sensor can be used reliably for the target sample or not. In electrochemistry, selectivity of a sensor is shown by selectivity coefficient ($K_{A,B}$), a constant which is directly related to distribution coefficient and is mostly determined experimentally. Recently, theoretical calculations have become a powerful tool for understanding the mechanism of selective capture and transportation of metal ions by ionophores [1]. In the present work, efforts have been made to develop a method which enables us to evaluate selectivity and extraction power of 1,1-dimethylsila-17-crown-6 (DMS17C6) and 18-crown-6 (18C6) for some alkali metal ions.

Methods

In order to study the relative stability of "host–guest" complexes, the free "host" (ionophore) and its corresponding complexes with Li^+, Na^+, K^+ were studied. The following coordination reaction model was used to calculate the relative binding energy of the complexes with cations: $M^+ + L \leftrightarrow ML^+$ (1)

In this study, the selectivity and extraction power is determined by distribution coefficient (K_e) which is defined as the ratio of formation constants of the complexes (K_{fc}) to formation constant of hydrated cation (K_{fw}), as follow: $K_e = K_{fc}/K_{fw}$ (2)

in which K_f is given by $\Delta G_f = -RT \ln K_f$ [1]. The selectivity coefficient is considered as an equilibrium constant for ion exchange reaction between ions A and B and can be defined as $K_{A,B} = K_{fcA}/K_{fcB}$ [2].

All calculations for the system were conducted using B3LYP/6–31G(d,p) density functional theory (DFT) method. The binding energies were corrected by zero point energy (ZPE) and basis set superposition error (BSSE). The solvent effects were studied by polarized continuum dielectric model (PCM).

Results and discussion

The calculated parameters for the complexes and hydrated cations are listed in the following table. The calculated results indicate that, the affinity order between the cations under consideration and both ionophores is $K^+ > Na^+ > Li^+$. The vibration frequencies calculated for these complexes are all positive which indicates that these complexes are located at the minimal points of the potential energy surfaces.

	[M(DMS17C6)]				**[M(18C6)]**			
	$\Delta G_{int.}$*	K_{fc}	K_e	$K_{A,B}$	$\Delta G_{int.}$*	K_{fc}	K_e	$K_{A,B}$
K^+	-256.19	7.67E+44	7.16E-18	1	-283.74	5.16E+49	4.82E-13	1
Na^+	-341.12	5.81E+59	6.57E-20	1.32E-15	-356.10	2.45E+62	2.77E-17	2.11E-13
Li^+	-414.93	4.97E+72	5.95E-24	1.54E-28	-426.19	4.67E+74	5.58E-22	1.10E-25

*Gibbs free energy of interactions (kJ/mol) in gas phase at 298 K.

Conclusions

It is concluded that the metal extraction efficiency for the complexes of DMS17C6 and 18C6 fall in the order of $K^+ > Na^+ > Li^+$, so that they extract K^+ more selectively. The DMS17C6 shows higher selectivity towards K^+ than does 18C6. The higher selectivity of DMS17C6 for metal ions is the result of synergism between the ionic size effect and the electron-withdrawing ability of the metal ion. The results obtained are in complete agreement with the experimental results reported elsewhere [3]. This method of calculation could be used to design or choose a suitable ionophore for a specific cation and in this way the number of experimental runs and the cost of investigation should decrease considerably.

References

[1] K.-S. Diao, H.-J.Wang, Z.-M.Qiu, *J. solution chem*. 38 (2009) 713-724.

[2] V. Ruangpornvisuti, B. Wanno, *J. Mol. Model* 13 (2007) 65-77.

[3] M.Colilla , P.Aranda, M.Darder, E.Ruiz-Hitzky, *C. R. Chimie* 13 (2010) 227-236.

Prediction of high-pressure vapor-liquid equilibria in binary mixtures of carbon dioxide and benzene compounds by artificial neural networks and genetic algorithm

S.S.Mousavian* , D.Ashouri , S.F.Mousavian

Department of chemistry, Islamic Azad University, Gachsaran Branch, Gachsaran, Iran

Abstract

High-pressure vapor-liquid equilibria (HP-VLE) are of increasing interest in physical chemistry, mainly owing to the growing field of supercritical extraction. Here the results of an experimental study of HP-VLE of binary systems of a supercritical fluid (carbon dioxide) and a benzene compound (ethylbenzene, isopropylbenzene (cumene), 1,2,4- trimethylbenzene (pseudocumene), 1,3,5_trimethylbenzene (mesitylene), ethenylbenzene (styrene) and isopropenylbenzene (methylstyrene)) at temperatures between about 313 and 393 K and at pressures between about 6 and 18 MPa are reported. The results are simulated by artificial neural networks. For increasing the efficiency of neural networks, genetic algorithm was used to optimize parameters of the neural network such as the number of neurons in the hidden layer, the momentum rate and the learning rate. Finally, the model of neural network optimized by genetic algorithm was selected as the best model due to its agreement with experimental data and greater flexibility compared to equation of state.

Keywords : Neural networks, Carbon dioxide, VLE, Genetic algorithm, Aromatics

Introduction

For all binary systems the vapor-liquid equilibrium was measured at 313, 353 and 393 K. For the mixture with isopropylbenzene the temperatures 333 and 373 K were investigated additionally. The experimental data for carbon dioxide- isopropylbenzene are given in Tablel. Literature data are available for the systems with ethylbenzene [1,2], 1,3,5-trimethylbenzene[3] and ethenylbenzene [2], which will be compared with the results of the present work in the result section.

Artificial neural networks

Artificial neural networks that are mathematical techniques to deal with different types of problems are the networks of interconnected processing elements or neurons. ANNs can be trained to learn the relationship between two sets of input and output data. Multilayer perceptrons (MLPs), the best known type of neural networks, consist of input, hidden and output layers. The number of independent parameters affecting the outputs specifies the number of neurons in the input layer. The number of neurons in the hidden layer has been determined by minimizing MSE (mean square error). For this purpose 80% of data were used for training and cross-validation, and the remainders were used for testing the networks. Input variable of this network contain molecular weight, acentric factor, critical pressure, temperature and density. K value is the output of this network.

Table 1 : Vapour-liquid equilibria for the system carbon dioxide (1) + isopropylbenzene (2)

T (K)	P (MPa)	X_1 (mol/mol)	Y_2 (mol/mol)	T (K)	P (MPa)	X_1 (mol/mol)	Y_2 (mol/mol)
313.2 (Training)	6.10	0.5704	0.0018	373.2 (Testing)	5.69	0.2805	0.0106
	6.60	0.6362	0.0022		8.18	0.4005	0.0127
	7.10	0.7071	0.0023		9.59	0.4680	0.0144
	7.61	0.8066	0.0028		12.24	0.5899	0.0178
	8.11	0.9040	0.0045		13.54	0.6361	0.0287
					14.26	0.6700	0.0299
333.2 (Testing)	6.15	0.4333	0.0031		15.49	0.7642	0.0559
	7.17	0.5127	0.0041		16.28	0.7716	0.0613
	8.18	0.5882	0.0054				
	9.20	0.6866	0.0062	393.1 (Training)	6.15	0.2734	0.0195
	10.21	0.7857	0.0099		8.18	0.3508	0.0203
	10.72	0.8392	0.0130		10.21	0.4350	0.0231
					12.24	0.5105	0.0260
353.2 (Training)	6.15	0.3591	0.0067		12.26	0.5961	0.0363
	8.18	0.4691	0.0062		16.28	0.6743	0.501
	10.21	0.5838	0.0085		18.31	0.7800	0.0921
	12.25	0.7041	0.0188				
	12.24	0.7079	0.0184				
	13.84	0.8086	0.0307				

Results and discussions

In this study, four different experimental data sets have been used to design the networks. The numbers of neurons for the hidden layers have been achieved by GA–ANNs. Table 2 gives the optimal mean square error and number of neurons in the hidden layer by the GA method.

Table 2 : Result of neural networks with different neurons in hidden layer According to table 2, the network with 9 neurons in hidden layer is selected and trained. The result of network for training data and testing data are shown in Figure 1 and 2 respectively.

Number of neurons in hidden layer	1	2	3	4	5	6	7	8	9	10
MSE	1.7×10^{-3}	1.3×10^{-3}	2.2×10^{-4}	4.6×10^{-4}	8.0×10^{-4}	1.7×10^{-4}	2.7×10^{-4}	2.1×10^{-4}	1.6×10^{-4}	2.8×10^{-4}
R^2	0.970	0.981	0.9910	0.989	0.983	0.9923	0.9904	0.9908	0.9973	0.9903

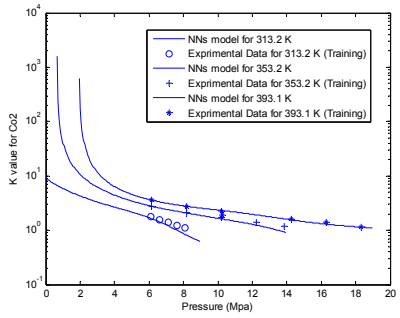

Fig 1 : Simulating results for training data

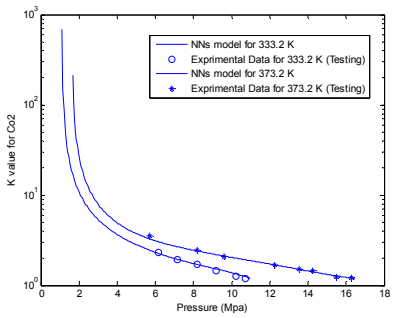

Fig 2 : Simulating results for testing data

These figures show that artificial neural network simulation agree with experimental data.

References

[1] Mohamed, R.S. and Holder, G.D., 1987. High pressure phase behavior in systems containing CO2 and heavier compounds with similar vapor pressures. Fluid Phase Equilibria, 32: 295-317.

[2] Tan, C.-S., Yarn, S.-J. and Hsu, J.-H., 1991. Vapor-liquid equilibria for the systems carbon dioxide-ethylbenzene and carbon dioxide-styrene. J. Chem. Eng. Data, 36: 23-25

[3]Huang,S.S.-S.andRobinson,D.B.,1985.The Equilibrium phase properties of selected mesitylene binary systems: Mesitylene-methane and mesitylene-carbon dioxide. Can. J. Chem. Eng., 63: 126-130.

[4] Ambrose, D., 1980. Vapour-liquid critical properties. NPL Report 107

[5] Yaws, C. A., 1977. Physical Properties. McGraw-Hill, New York.

Estimation of liquefied natural gas (LNG) densities from its composition, temperature and pressure without dielectric constant data by artificial neural network

S.S.Mousavian* , D.Ashouri , S.F.Mousavian

Department of chemistry, Islamic Azad University, Gachsaran Branch, Gachsaran, Iran

*Email: S.Mousavian@iaug.ac.ir

Abstract

In this study a new approach based on artificial neural networks (ANNs) has been used to estimate liquefied natural gas (LNG) densities. The main parameters affecting the density of LNG are mainly composition, temperature and pressure.

In order to develop, train and test such models, a comprehensive, accurate and consistent set of density data has been obtained for the major components [6] of LNG and for mixtures of these components. Most of these data were obtained with a magnetic suspension densimeter. [6] Comparing the results of this ANNs and the calculated results from dielectric constant [5] shows that the results of ANNs have a better agreement with experimental data.

Keywords: Density, Artificial neural networks, LNG, Experimental data

Introduction

A large-scale project has been carried out to provide one or more mathematical models to predict the density of a liquefied natural gas (LNG) mixture to within an uncertainty of 0.1%, given the temperature, composition and pressure of the liquid mixture. Such models will serve as a basis for custody transfer. The mathematical models developed for this purpose have ranged from simple empirical models [1-4] to those that are theoretically based [2-4] and, consequently, much more complex. For example there is a model based on dielectric constant data to estimate density of LNG but the dielectric constant of a fluid is closely related to its density through the Clausius-Mossotti (CM) function. This work try to estimate the density of LNG based on artificial neural networks without any parameter of container.

Artificial neural networks

In general neural networks are simply mathematical techniques designed to accomplish a variety of tasks. Neural networks can be configured in various arrangements to perform a range of tasks including pattern recognition, data mining, classification, and process modeling. ANNs are networks of interconnected simple units (nodes) that are based on a greatly simplified model of the human brain.

The architecture of an ANN consists of input, hidden, and output layers. The number of neurons (nodes) in the input and output layers is the same as the number of the known independent parameters. The number of hidden neurons has been determined during the training process by trial and error method. Input variable of this network contain molecular pressure, temperature and mole percent of N_2, CH_4, n- C_4H_{10}, i- C_4H_{10}, C_2H_6, C_3H_8, n- C_5H_{12}, i- C_5H_{12}. Density of LNG is the output of this network.

Results and discussions

For this purpose 71 different data were used. Sixty nine percent of data were used for training and cross-validation, and the remainders were used for testing the networks. The numbers of neurons for the hidden layers have been achieved by trial and error method. At first a network with one hidden layer were used. The result of this network with different neurons in hidden layer is shown in table 1.

Table 1 : Result of neural networks with different neurons in hidden layer for network with one hidden layer

Number of neurons in hidden layer	1	2	3	4	5	6	7	8	9	10
MSE	0.05296	0.03701	0.1418	0.0508	0.07792	0.03934	0.07792	0.06085	0.1297	0.1111
R^2	0.989	0.9904	0.9904	0.9908	0.991	0.991	0.991	0.9924	0.9924	0.9924

The amounts of MSE show that the network with one hidden layer isn't suitable for estimation of density. Then a network with two hidden layer were used. The numbers of neurons in hidden layers obtain 4 and 3 respectively by trial and error. The result of this network is shown in figure 1 and figure 2 for training data and all data respectively.

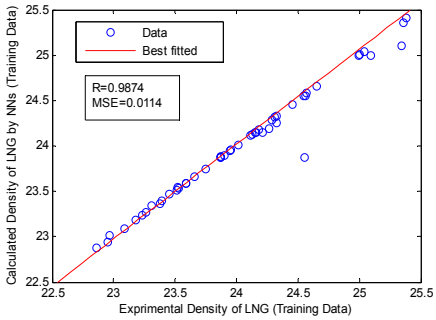

Fig 1 : Simulating result for training data

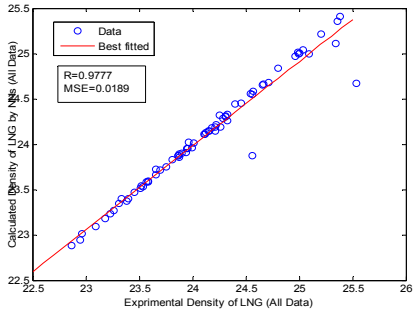

Fig 2 : Simulating result for all data

These figures show that the NNs model have good agreement with experimental data.

References :

[1] Hiza, MJ. *Fluid Phase Equilibria 2* (1978) 27

[2] McCarty, R.D. Nat Bur Stand (US), Interagency Report NBSIR 77-867 (1977)

[3] McCarty, R.D. Nat Bur Stand (US), Technical Note 1030 (1980)

[4] McCarty, *R.D.JChem Thermodynamics* 14 (1982) 837

[5] Haynes, W.M. Cryogenics . aug 1983

[6] Haynes, W.M./dem *Thermodynamics* 14 (1982)603

[7] Hiza, MJ., Haynes, W.M., Parrish, W.R. / *Chem Thermodynamics* 9 (1977) 873

[8] Hiza, M.J., Haynes, W.M. j *Chem Thermodynamics* 12 (1980) 1

[9] Haynes, W.M.j.chem *Thermodynamics* 14 (1982)603

A new approach for estimation of PVT properties of Trifluoroiodomethane (CF_3I) in gaseous phasebased on artificial neural networks model

S.S.Mousavian* , M.Omidi, D.Ashouri, R.AlizadehN.Ghizinia,
Department of chemistry, Islamic Azad University, Gachsaran Branch, Gachsaran, Iran
*Email: S.Mousavian@iaug.ac.ir

Abstract

Equations of state are useful for description of fluid properties such as pressure-volume-temperature (PVT). However, the success estimation of such correlations depends mainly on the range of data which have originated. Therefore new models are highly required. In this work a new method is proposed based on Artificial Neural Network (ANN) for estimation of PVT properties of compounds.Some 143 pressure-volume-temperature data points in gaseous phase for trifluoroiodomethane (CF_3I) havebeen measured using Burnett/isochoric methods.Different training schemes for the back propagation learning algorithm, such as; Scaled Conjugate Gradient (SCG), Levenberg-Marquardt (LM) and Resilient back Propagation (RP) methods were used. The accuracy and trend stability of the trained networks were tested against unseen data. The LM algorithm with eight neurons in the hidden layer has proved to be the best suitable algorithm with the minimum Mean Square Error (MSE) of 0.0018. The ANN's capability to estimate the PVT properties is one of the best estimating method with high performance.

Keywords: PVT, Artificial neural network, CF_3I, property

Introduction

According to the Nov. 25, 1992 Copenhagen revision of the Montreal Protocol, CFCs have already been phased out in developed countries. As a traditional and effective refrigerant, CFC-12 is widely used in numerous applications. Alternatives to CFC-12 must be developed that are environmentally acceptable and can be used in high capacity, high efficiency applications. So far many achievements have been made in developing alternatives to CFCs. HFC-134a has been widely used as a replacement for CFC-12, especially in the USA, Japan,

UK and France. However, it requires physical retrofitting of equipment and does not mix with conventional lubricants. It also has a higher global warming potential (GWP) value. Even though they are flammable, hydrocarbons are considered to be another promising alternative, especially in Germany. CF_3I has been found to be non-ozone depleting, miscible with mineral oil and compatible with refrigeration system materials. It also has an extremely low GWP value and very low acute toxicity. Therefore, it is also been considered as a promising alternative, especially as a component in mixtures, to replace CFC-12 [2,3]. However there has been no reliable data published in recent years. Therefore, the thermophysical properties of CF_3I are of great interest, especially the pressure volume-temperature (PVT) properties.

Artificial neural networks

The architecture of an ANN consists of input, hidden, and output layers. The number of neurons (nodes) in the input and output layers is the same as the number of the known independent parameters. The number of hidden neurons has been determined during the training process by trial and error method. Input variable of this network contain pressure and temperature. Density of CF_3I is the output of this network.

Results and discussions

Sixty nine percent of data were used for training and cross-validation, and the remainders were used for testing the networks.A network with one hidden layer was used. The result of this network with different neurons in hidden layer is shown in table 1.

Table 1 : Result of neural networks with different neurons in hidden layer

Number of neurons in hidden layer	1	2	3	4	5	6	7	8	9	10
MSE	10.4694	0.5483	0.1176	0.0207	0.0131	0.1136	0.0545	0.0013	0.0073	0.0303
R^2	0.9956	0.9998	0.9999	1.0000	1.0000	1.0000	1.0000	1.0000	1.0000	1.0000

According to table 1, the network with 8 neurons in hidden layer is selected and trained. The result of network for all data and testing data are shown in Figure 1 and 2 respectively.

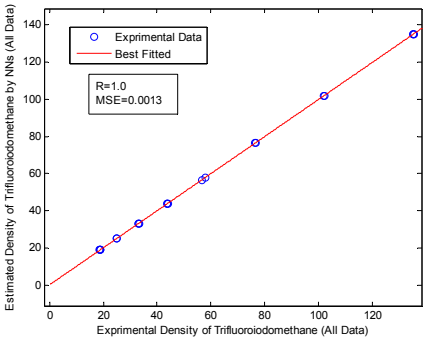

Fig 1 : Simulating results for all data

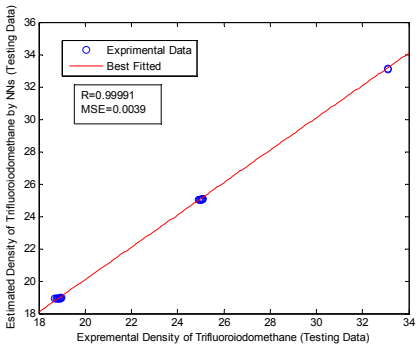

Fiq2 : Simulating results for testing data

These figures show that artificial neural network simulation agree with experimental data.

Reference :

[1] Y.Y. Duan, M,S. Zhu and L.Z. Han, Experimental vapor pressure data and a vapor pressure equation for trifluoroiodomethane(CF3I), Fluid Phase Equil., 121 (1996) 227-234.

[2] L. Lankford and J. Nimitz, A new class of high-performance, environmentally sound refrigerants, The Int. CFC and Halon Alternatives Conf., Washington, DC, USA. 1993.

[3] X.Y. Zhao, L. Shi, M.S. Zhu and L.Z. Han, L.Z., A new generation of long-term refrigerants as CFC-12 alternatives,Proceedings of The Int. CFC and Halon Alternatives Conf., Washington, DC, USA, 1995, pp. 286-293.

[4] Y.Y Duan, M.S Zhu, L. Shi, L. Z. Han, Experimental pressure-volume-temperature data and an equation ofstate for trifluoroiodomethane (CF3I) in gaseous phase, Fluid Phase Equilibria 131 (1997) 233-241

Investigation on the structure and aromaticity of dipeptides including histidine

N. Bagheri*[a], Z. Momeni[b]

[a, b]Department of Chemistry, Islamic Azad University, Firoozabad Branch, Firoozabad, Fars, Iran

(Email: nrgs.bagheri@gmail.com)

Introduction

Proteins are at the center of action in biological processes. Nearly all the molecular transformations that define cellular metabolism are mediated by protein catalysis. Virtually every property that characterizes a living organism is affected by proteins [1]. Proteins differ only in the sequence in which amino acids are assembled into polymeric chains. The secret to their functional diversity lies partly in the chemical diversity of the amino acid but primarily in the diversity of the three-dimensional structures that these building blocks can form, simply by being linked in different sequences. The unique functional properties of proteins can be understood only in terms of their relationship to the 3D structure of proteins [2]. It is therefore of interest to determine the factors, that resolve the 3D structure of protein from primary structure. The prediction of 3D structure of a protein from the knowledge of linear sequence of amino acids has been described as the determination of the second half of the genetic code [3].

Computational Methods

All molecules properties, including geometry, electric field gradient and electronic structure parameters have been obtained at B3LYP/6-311++G** level of theory, as this method and basis set has been used successfully in literature for amino acids. Such calculations have been performed using GAUSSIAN 03 package . AIM theory by Bader and AIM2000 software have been applied in this research as well.

Results and Discussion

The sevene dipeptides were constructed with different combinations in which histidine is fixed at the N-terminus position. The C-terminus position is named as X-position. In these dipeptides, the X-position is varied with different amino acids, which are connected to the

fixed histidine end at N-terminus position. Seven different amino acids are chosen for X-position and they are asparagines (Asn), alanine (Ala), glycine (Gly), serine (Ser), arginine (Arg), tyrosine (Tyr) and valine (Val). All these are taken as neutral species. In order to distinguish stability of amino acids under investigation, we use an index based on electric field gradient. Electric field gradient based on ethan and ethylene references has been applied for first time by Pakiari and Bagheri in 2010. The electric field gradient tensor is a symmetric second rank tensor with zero off diagonal elements which can be expressed in an axis system. Furthermore, it can be shown that the field gradient tensor is traceless. Thus, the quantity of $q = \partial^2 V / \partial z^2$ is a component which can be assigned to "EFG" in this research. After structures optimization of amino acids and frequency test has been done for all structure, electric field gradient tensor calculation has been calculated for all histidine ring as delocalized form of aromatic ring. $\sum EFG^{(0)}$ for delocalized and localized forms has been calculated and $\Delta EFG^{(0)}$ is obtained for histidine rings of all seven dipeptide in which histidine is fixed at the N-terminus position. These studies show that His-val is the most aromatic compounds among these molecules under study.

X-amino acid	$\sum EFG^{(0)}$	$\Delta EFG^{(0)}$
His- Asn	۱۷,۱۰۳5	1.4606
His- Ala	۱۷,۱۱۶۱	1.4732
His- Val	۱۷,۱۴۱۰	1.4981
His- Gly	۱۷,۱۱۴۸	1.4719
His- Ser	۱۷,۱۰۹9	1.4670
His- Arg	۱۷,۰۷۰۶	1.4277
His- Tyr	17.1153	1.4724

Conclusion

The structural parameters investigated in this work through some light on the conformational stability of small amino acid sequences. Optimizations of the structures of the dipeptides applying DFT-B3LYP [6-31g*] level of theory gives pretty well energy values. The bond length and bond angle data of the amide plane obtained after rigorous calculations do not vary much. So, we can say that the amide plane is more or less fixed. Aromaticity indices of histidine rings show that the stability of the ring is sensitive to kind of amino acid residues. So , we can say that the histidine ring has more aromaticity in presence of valine while is less aromatic in presence of arginine.

References

[1] D. Voet, J.G. Voet, C.W. Prat, Fundamentals of Biochemistry, John Wiley and Sons Inc., 1998.

[2] T.E. Cerighton, Proteins, second ed., W.H. Freeman and Company, New York, 1993.

[3] D.E. Metzler, Biochemistry, second ed., vol. 1, Harcourt Academic Press, 2001.

Effects of salt on interactions between components of aqueous solution containing surfactant and carbon nanotube: A molecular dynamics simulation approach

M. Foroutan, F. Mirzaie Milani
Department of Physical Chemistry, School of Chemistry, College of Science, University of Tehran, Tehran, Iran.
f.mirzaie.milani@khayam.ut.ac.ir

Key word: Carbon nanotube, Surfactant, Salt, Aggregation, Simulation

Introduction

Single-walled carbon nanotubes (SWCNTs) can be dispersed as individuals in water using surfactants. Any change in the surface charge density of the surfactant, or its solubility, that eliminates the electrostatic repulsion between the nanotubes will cause SWNTs to aggregate. By controlling the intermolecular and surface forces of surfactant in water, it is possible to engineer the resultant VdW attraction between SWNTs [1]. On the other hand, one technique has been improved by Arnold *et al*. [2], who, using bile salts such as sodium cholate in addition to surfactants, demonstrated that it is possible to separate SWNTs on the basis of their diameter and electronic structure. However, it is still not clear how surfactants self-assemble on carbon nanotubes in the presence of salt. A detailed understanding of the structure of surfactant aggregates adsorbed on SWNTs in the presence of salt is the goal of this work.

Simulation details

We used a canonical ensemble (constant NVT) with undefined boundary conditions for considering the simulated volume were equals to infinite. The velocity form of Verlet algorithm method and the Nose-Hoover thermostat algorithm were used to integrate the equations of motion with a time step of 1.0 fs and temperature control of 300 K, respectively. Non-bonded van-der-Waals' interactions are modeled by a Lennard-Jones potential with a cut-off distance of 1.0 nm. Water molecules were modeled using the SPC/E model. In our simulation the time step was 1 fs. Simulations were conducted for 3ns., for system containing 1153 water molecules, 25 surfactant CTAB molecules and (3, 12, 25, 50) salt NaCl

molecules and a (5,5) CNT.

Result and discussion

In the present study, we performed a MD simulation in a four-component system, including water, surfactant (CTAB), SWNTs and salt, to address the unresolved issue regarding the self-assembly structure of adsorbed CTAB surfactants onto SWNT surface in the presence of salt. Efforts have also been made to calculate the radial distribution function (RDF) and potential of mean force between two nanoscopic components, in order to shed new light on the dispersion and stability mechanism of SWCNT in aqueous CTAB solution in the presence of salt.

To the best of our knowledge, this is the first simulation of complex interaction behavior on the atomic level in a four-component system. Figure 1 shows simulated system containing SWCNT, salt, surfactant and water.

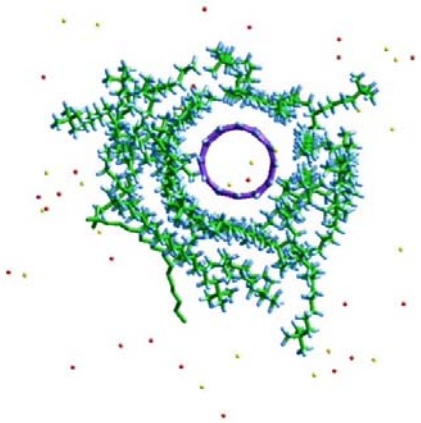

Figure 1- Front view of representative snapshot for (5,5) CNT covered by surfactants in the presence of salt molecules. Water molecules are not shown for clarity.

We calculated the radial distribution functions (RDFs) for all components of system including cation and anion of salt, carbon atoms of nanotube and different atoms of surfactant. Our results indicates that salt addition have a significant effect on the distribution of surfactant molecules around the carbon nanotube. Also the RDF between N of surfactant head groups and Cl^- atom of NaCl show that when more Cl^- ions located around polar head group of surfactant, tendency of surfactants for aggregating around CNT, increases**.**

References

[1] Tan, Y.; Resasco, D. E. *J. Phys. Chem. B* **2005**, *109*, 14454.

[2] Arnold, M. S.; Green, A. A.; Hulvat, J. F.; Stupp, S. I.; Hersam, M. C. *Nat. Nanotechnol.* **2006**, *1*, 60.

Temperature effect on the aggregation behavior of CTAB surfactant around the carbon nanotubes

M. Foroutan, F. Mirzaie Milani
Department of Physical Chemistry, School of Chemistry, College of Science, University of Tehran, Tehran, Iran.
f.mirzaie.milani@khayam.ut.ac.ir

Keywords: Carbon Nanotubes, CTAB Surfactants, Aggregation, MD Simulation

Introduction

Carbon nanotubes (CNT) have attracted widespread interest in research and increasing industrial attentions [1]. However due to strong van der Waals forces, carbon nanotubes tend to form aggregated CNTs in solutions. Surfactant adsorption has an important role in the standard procedure for the preparation of high weight fraction individually dispersed single-walled carbon nanotubes [2]. In the present work the aqueous solutions containing cetyl trimethylammonium bromide (CTAB) surfactants and (5, 5) single-walled CNTs are studied at six temperatures, (300, 310, 320, 330, 340 and 350) K using molecular dynamics simulation approach.

Simulation details

Molecular dynamics (MD) simulations of our system were carried out using a 3.6 nm by 4.0 nm by 4.0 nm^3 cubic computational cell with periodic boundary conditions applied in all three principal directions. Non-bonded van-der-Waals' interactions were modeled by a Lennard-Jones potential with a cut-off distance of 1.0 nm. Water molecules were modeled using the SPC/E model. In our simulation the time step was 1 fs. and the simulation were conducted for 3ns. 1153 water molecules and 25 CTAB molecules were placed in the cell.

Result and discussion

The two-layer adsorption of CTAB surfactant molecules around the nanotube at 300 K can be seen in figure 1a. As figure 1a shows by increasing the temperature from 300 K to 350 K, the second shell of surfactants is destroyed and monolayer adsorbed around nanotube and micelle

structures of surfactant are appeared. Figure 2 shows the potential of mean force between carbon nanotube and surfactants. This figure shows that by approaching the surfactants to nanotube, the potential is reduced totally. It can be assigned to association of surfactant molecules around the CNT. At the temperature associated with the maximum value for energy barrier, surfactants can pass the energy barrier and could reach to the first layer, thus the number of surfactants of the first layer is decreased.

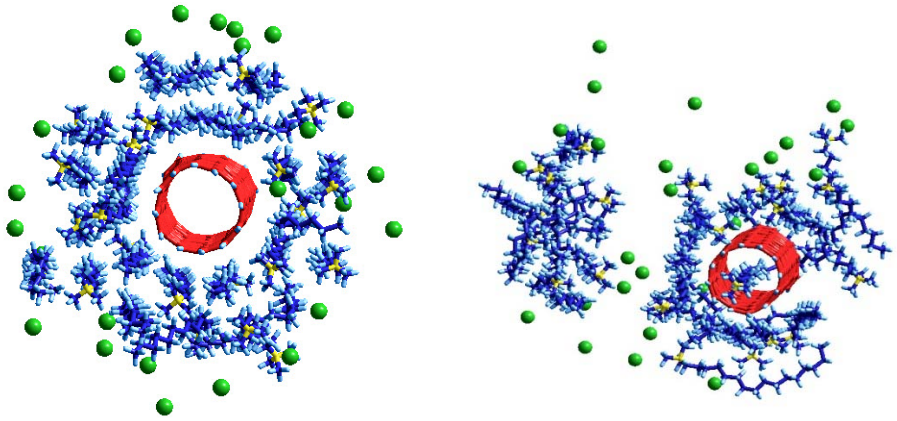

Figure 1- Front views of representative snapshots for (5,5) CNTs covered by surfactants at 300 K (Left) and 350 K (Right). Water molecules are not shown for clarity.

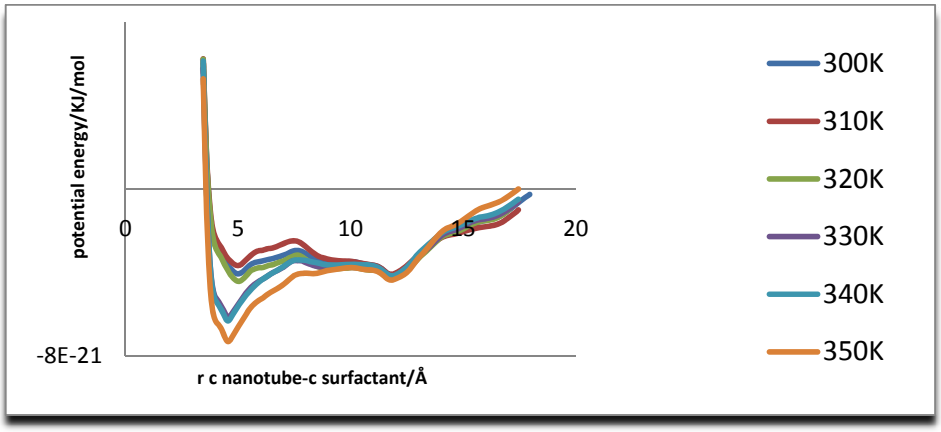

Figure 2- Potential of mean force between carbon nanotube and surfactants.

Also, we investigated the radial distribution functions for surfactant-surfactant interaction in the presence of nanotube and water at all six temperatures. The obtained results show as temperature increases the interaction between the surfactant tail groups decreases.

References

[1] P. Angelikopoulos, H. Bock. Langmuir 26 (2010) 899–907.

[2] Z. Xu, X. Yang, Z. Yang. Nano Lett. 10 (2010) 985–991.

Conformational Effects of the Leucine Side Chain on the Stability of HCO-GLY-L-LEU-GLY-NH_2 Tripeptide Motif: An Abinitio Study

Behzad Chahkandi, Majid Mohammad Hosseini, Sahar Naderi*

Department of Chemistry, Islamic Azad University, Shahrood Branch, Shahrood, Iran.

Email: naderi.sahar09@gmail.com

Keywords: Protein Folding, Tripeptide, Abinitio, Side Chain, Leucine.

Introduction

Finding solution to the protein folding problem has been steadily pursued for decades [1]. During the last several decades very studies were carried out on peptides to find the rules that govern protein folding [2].Tripeptide models are ongoing models in peptide folding studies.In a tripeptide, three amino acid residues are bound together at their amid groups, forming a short oligopeptide chain [3]. All residues except glycine amino acid, exist as pairs of enantiomers (L and D stereoisomers), since they have stereo center at their α-carbons [3]. Protein folding can be defined as a function of backbone torsional angles (Φ,ψ,ω) [4].

Methods

In this research we determined the stability of various conformers of HCO-GLY-L-LEU-GLY-NH_2 tripeptide that obtained from varying of side chain torsional angles χ_1 and χ_2 (see Fig 1). For this purpose the abinitio molecular calculations were carried out at HF/6-31G (d) level of theory. All of calculations performed by using Gaussian03 program. [5]

This research contains two steps:

In the first step , the side chain torsional angle (N_9, C_{11}, C_{13}, C_{15}) (χ_1), was changed at 30° intervals from 0° to 360° and by using optimization calculations at HF/6-31G(d) level the stable conformers were obtained.

In the second step, torsional angle (C_{11}, C_{13}, C_{15}, C_{16}) (χ_2), was rotated at 30° intervals from 0° to 360° when the χ_1 was fixed in three minima that found from the first step (see Fig.1).

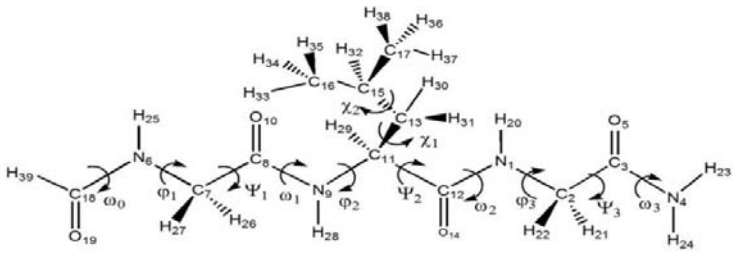

Fig.1. Schematic diagram with torsional angle definitions for HCO-GLY-L-LEU-GLY-NH_2

Results and discussion

The results that obtained contain:

1. First step

Three minima for χ_1 are gauche (-)(g^-),(χ_1=-60°), gauche (+)(g^+),(χ_1=60°), and anti(a) (χ_1=180°) conformers, that among of them (g^-) conformer has the lowest energy (see Fig.2).

2. Second step:
   - 2.1. Three minima for χ_2 are in: 300°(-60°), 210°, 60° angles respectively when the χ_1 was fixed in (g^-) conformer (see Fig.3).
   - 2.2. Three minima for χ_2 are in: 210°, 270°, 60° angles respectively when the χ_1 was fixed in (g^+) conformer.
   - 2.3. Three minima for χ_2 are in: 180°, 270°, 60° angles respectively when the χ_1 was fixed in anti (a) conformer.

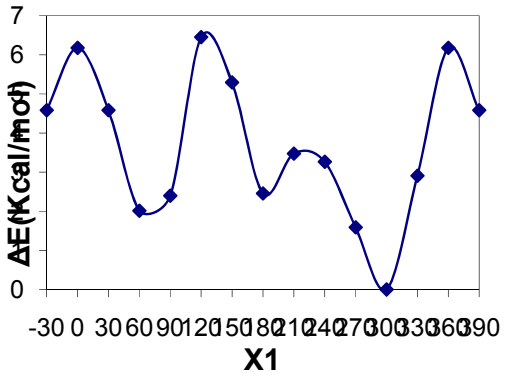

Fig.2. Relative energy curve as a function of dihedral angle (χ_1)

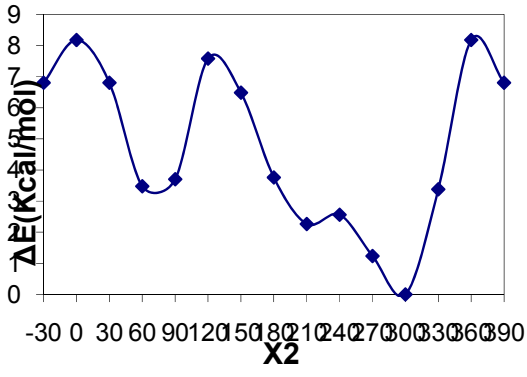

Fig.3. Relative energy curve as a function of dihedral angle (χ_2) when the χ_1 was fixed in the most stable state (g^-)

Conclusions

The results obtained from two steps show when χ_1 and χ_2 are -60° (g^-g^-) the structure has the most stability. And also the angles of optimized backbone are in state of extended conformation or β_L β_L β_L (in β_L conformer, backbone torsional angles in ideal state are Φ=-180°, ψ=180°)

References

[1] C.Dale Keefe, Jason K.Pearson, J.Mol.Struct. (THEOCHEM) 679 (2004) 65-72.

[2] M.A.Berg, G.A.Chasse, E.Derety, et al. J.Mol.Struct. (THEOCHEM) 500 (2000)5-58.

[3] Azar Mehdizadeh, Gregory A.Chass, Odon Farkas, Andras Perczel, et al. J.Mol.Struct. (THEOCHEM) 588(2002) 187-200.

[4] Szilard N.Fejer, Zsuzsanna A.Jenei, Gabor Paragi, J.Mol.Struct.(THEOCHEM)666-667(2003) 303-310.

[5] Gaussian 03, Revision C.02, J. Frisc, G. W. Trucks, H. B. Schlegel, G. E. Scuseria, M. A. Robb, J. R. Cheeseman, and J. A. Pople, et al. Gaussian, Inc., Wallingford CT, 2004.

A DFT study on the electronic and structural properties of C34 fullerene and X substituted fullerene (X=Si, N)

F.Naderi*

Shahr e Qods branch, Islamic Azad University, Iran.

*Corresponding author: F.naderi@shahryariau.ac.ir

Abstract

Our DFT calculations lead to some C_{34} heterofullerenes (C_{34}, $C_{33}Si$ and $C_{33}N$) .The relative stability is predicted based on the theoretical data. In addition, vibrational spectra of proposed stable neutral species, as well as the infrared intensities are calculated.

Key word: fullerene, doped, B3LYP, Bindng Energy

Introduction

Carbon can be in several forms. Amorphous, graphite and diamond. Fullerenes are accepted as the fourth form of solid carbon. They are basically, large carbon cage molecules. By far the most common one is C60. Since the discovery of fullerenes in mid eighties and nanotubes in nineties,a whole range of studies have been conducted on these particles[1-6].

Since the discovery of carbon fullerene there have been intense efforts towards finding or designing fullerene structures of other materials to have a better control over material properties in general.

Computational methods

Full geometry optimizations are accomplished without any symmetry constraints by means of DFT hybrid functional B3LYP [7-10] as implemented in GAUSSIAN 98 [11]. Vibrational frequency computations confirm that the fully optimized structures are indeed minima (NIMAG = 0).Binding energies per atom are calculated.

Results and Discussion

C_{34} and $C_{33}X$, (X=Si and N) is given in Fig.1.

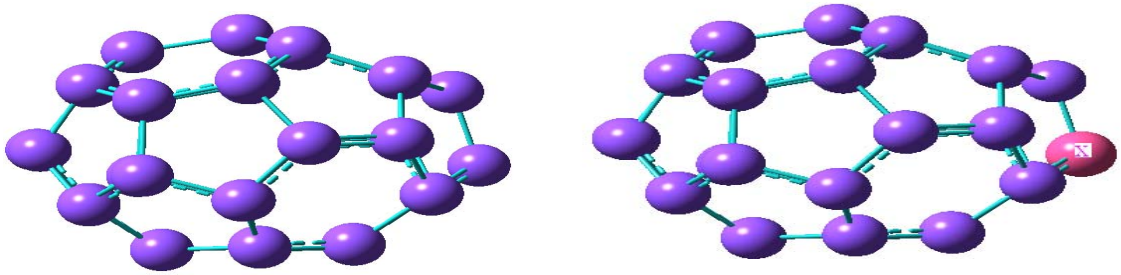

a) b)

Fig.1. Optimized geometry of a) C34 and b) C33X (X=Si , N).

Binding energy per atom, a criterion of stability, is calculated to be 6.072 eV/atom for C34 at the B3LYP/cc-pVDZ level (table 2). Substituting C atoms with X reduces this value which is the result of the weakness of X–C bond vs. C–C bond. Their calculated binding energy are 4.384, 4.875eV/atom, respectively for X= N and Si, less than that of C_{34} with 33 equivalent C–C bonds. Normal harmonic vibrational frequencies and their related information are calculated. Finally, the very strong IR bands are predicted at 1673.10 and 1845.11 cm^{-1}, with intensities of 430.37 and 572.08 km/mol for C34, at 1659.86 and 1814.95 cm^{-1}, with intensities of 973.837and 1018.847 km/mol for C33N, at 1660.57 and 1812.327 cm^{-1}, with intensities of 977.847and 1058.547 km/mol for C33Si.

Conclusion

We compute the structural and IR properties of C_{34} and $C_{33}X$ heterofullerenes at the B3LYP/cc-pVDZ level. Some interesting results are found. From the data obtained from calculation, we found that there is strong correlation between the stability of pure C_{34} fullerene molecule and the numbers of different C–C bonds.

References

[l] H.W. Rroto, A.W. Allaf and S.P. Balm, Chem. Rev. 91 (1991) 1213.

[2] R.F. Curl and R.E. Smalley, Sci. Am. (October 1991) 54.

[3] R.E. Haufler, J. Conccicao, L.P.F. Chibante, Y. Chai, N.E.Byrne, S. Flangan, M.M. Haley, S.C. O'Brien, C. Pan, W.E.Billups, M.A. Ciufolini, R.H. Hauge, J.L. Mat-grave, L.J.Wilson, R.F. Curl and R.E. Smalley, J. Phys. Chem. 94 (1990) 8634.

[4] W. Kr%chmer, K Fostiropoulos and D.R. Huffman, Chem.Phys. Letters 170 (1990) 167.

[5] T. Guo, M.D. Pemer, Y. Chai, M.J. Alford, R.E. Haufler,SM. McClure, T. Ohno, J.H. Weaver, G.E. Scuseria and R.E. Smalley, Science, in press.

[6]P.R. Birkett, P.B. Hitchcock, H.W. Rroto, R. Taylor and D.R.M. Walton, Nature 357 (1992) 479.

[7]Adina K. Ott, Gregory A. Rechtsteiner, Christian Felix, Oliver Hampe, Martin F. Jarrold, and Richard P. Van Duyne, J. Chem. Phys. 109, 9652 ,1998.

[8] A.D. Becke, Phys. Rev. A 38 (1988) 3098.

[9] C. Lee, W. Yang, R.G. Parr, Phys. Rev. B 37 (1988) 785.

[10] A.D. Becke, J. Chem. Phys. 98 (1993) 5648.

[11] M.J. Frisch et al., GAUSSIAN 98, Gaussian Inc., Pittsburgh, PA, 1998 .

Chemisorption of Hydrogen on Graphene by using Density Functional Theory

S.Shojaee[1], F.Naderi*'[2], M.Monajjemi [3]

1. Ph.D Student ,Science and Research Branch, Islamic Azad University,Tehran ,Iran

2. Department of basic science ,Shahr e Qods Branch, Islamic Azad University, Iran

3. Department of Chemistry ,Science and Research Branch, Islamic Azad University,Tehran ,Iran

Introduction

The synthesis of monolayer graphite (i.e. graphene) is under study both experimentally and computationally. In recent years, hydrogen-based fuel systems have been considered to be a highly important topic of research for future energy schemes as hydrogen is a more efficient fuel in comparison to the existing carbonaceous fossil fuels . Despite many recent technological developments in the hydrogen-based fuel systems, it is still an enormous challenge to have a safe and efficient reversible hydrogen storage system at ambient conditions . One of the possible ways for such storage is the efficient hydrogen adsorption/desorption in a controllable system. Now a day a large amount of experimental and theoretical work were reported on the characterization of the interaction between the graphene surface and the adsorbate molecules. The unusual properties of carriers in graphene are a result of the gapless and roughly linear electron dispersion at the vicinity of the Fermi level at two inequivalent points of the Brilouin zone. In this work, we perform main calculations for the H atom adsorbated on graphen.For studies and calculation of adsorption we used Density Functional Theory (DFT) approaches method.

Computational method

In this work we optimized the geometries of the graphene and graphene with hydrogen using PW91VWN,PW91PL,MPWLYP,G96LYP,G96PL/3-21G,6-31G,6-31G*/3-21G,6-31G,6-31G* levels of theory, All calculations were performed by Gaussian 98 program package.

Results and Discussions

In recent years, hydrogen-based fuel systems have been considered to be a highly

important topic of research for future energy schemes. Carbon, being a small atom with a half-filled shell, is able to mix its valence s and p orbital to various degrees, thereby forming the building block for extended structures of incredibly different electronic, magnetic and mechanical properties. We present the most important structural parameters determined for the addition of a hydrogen atom to graphene . The structures determined for the graphene with a hydrogen atom is presented in Figure 1. The outward movement of the carbon atom that is bonded to hydrogen is 0.48 Å. This result is determined by Casolo et al. , using the plane wave code VASP.

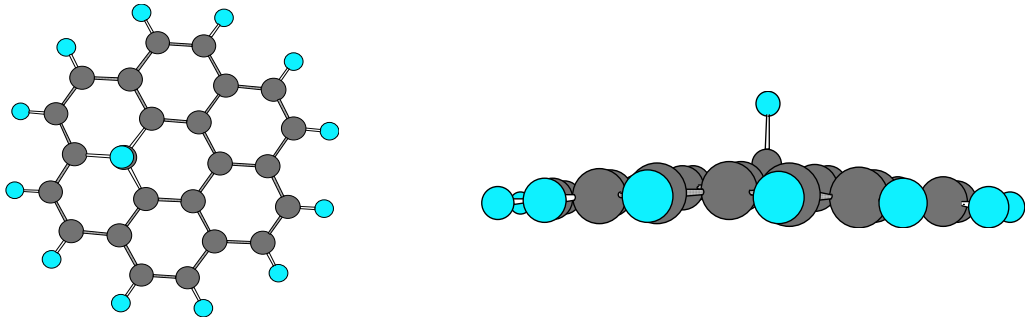

Figure1. Graphene with a hydrogen atom optimized by PW91VWN/6-31G* level of theory.

We studied the chemisorptions of hydrogen on geraphen containing 24 carbon atoms. The geometric parameters in PW91VWN are 1.119A° for C-H bond, 1.532A°, 1.525A°, and 1.525A° for the C-C bond which are near the C-H chemisorptions. The smallest value in all basis sets is related to PW91VWN and the largest one is related to MPWLYP. As expected, we have found that the energy of geraphene with H using PW91VWN method is smaller than the one experienced by the MPWLYP; the computed values are -580172.0675 and -575371.6925 kcalmol^{-1}, respectively.Entropy has been evaluated by standard statistical thermodynamic methods. Finally, Gibbs free energy of the reaction has been evaluated by using expression (1):

$$\Delta G\,(T) = \Delta H\,(T) - T\,\Delta S\,(T) \qquad (1)$$

The entropies, enthalpies and Gibbs free energies are important thermo chemical parameters for below reaction:

Geraphene + H----- Geraphene-H

Conclusions

In this paper, we have presented results of theoretical investigations when the addition of hydrogen to graphene. Structural parameters determined were in excellent agreement with our 5 methods and 3 basis sets. The free energy change for the single H addition to graphene at 298 K and enthalpy and entropy changes was determined.

References

[1] k.S.Novoselov,A.k.Geim,S.V.Morozov,D.Jiang,M.I.Katsnelson,I.V.Grigorieva,S.V.Dubonos, and A.A.Firsov,Nature(London)438,197(2005).

[2] R. Coontz and B. Hanson, Science **305**, 957 (2004).

[3] L. Schlapbach and A. Züttel, Nature **414**, 353 (2001).

[4] E. Klontzas, A. Mavrandonakis, E. Tylianakis, and G. E. Froudakis, Nano Lett. **8**, 1572 (2008).

[5] A. Nikitin, X. Li, Z. Zhang, H. Ogasawara, H. Dai, and A. Nilsson, Nano Lett. **8**, 162(2008).

[6] A.D. Becke, Phys. Rev. A 38 (1988) 3089.

[7] J.P. Perdew, Phys. Rev. B 33 (1986) 8822.

[8] S. Casolo, O.L. Lovnik, R. Martinazzo, G.F. Tantardini, J. Chem. Phys. 130 (2008).

Interaction Of Molecular Hydrogen with $C_{20(Ih)}$, $C_{24(D6d)}$ and $C_{26(D3h)}$ Fullerene Nano Structure Surfaces, A Computational Study

F.R,Nikmaram*, M.Nami Saie, M.Shahsovan, M.Zamani, J.Najafpour

Department of Chemistry, Faculty of science, Islamic Azad University Shahr-e-Rey Branch, Tehran,IRAN

NIKMARAM88@IAUSR.AC.IR

Key Words: Fullerene , Nano structure , Surfaces, Molecular Hydrogen

Introduction:

Fullerenes are begining to find a diverse range of applications including biomedical [1], antioxidants, bio-and chemical sensors, encapsulation noble gases inside the Fullerene cages, and gas adsorption on Fullerene [1-3].

In the H_2 molecule, the valence electrons are all involved in the H-H σ-bond and there are no additional electrons which may interact with the substrate atoms. Consequently, chemisorption of hydrogen on Fullerenes is almost invariably a dissociative process in which the H-H bond is broken [4], thereby permitting the hydrogen molecule interact with the surface of Fullerenes at vertical position on pentagon carbon.

Methods:

We investigated the adsorption behavior of H_2 on Fullerene Nano structure surfaces, including stabilities, Binding Energies, adsorption Enthalpies (ΔH_{ads}), and change of charge on the adsorbent carbon based on a density-functional theory method, PW91, with 6-31G basis set by Gaussian 98 package [5]. Harmonic vibrational frequencies were calculated to confirm that the optimized structures were local minima on the potential energy surface, therefore we considered that C-H and H-H distances to be variable and other distances are fixed (fig1). Also atom in molecules (AIM) quantum theory were carried out to study the interaction forces. QTAIM calculations have been done using AIM2000 package [6]. The AIM analysis for the optimized structures has been performed to obtain the topological properties of the bonds, such as the bond critical points (BCP), Laplacian of ρ_b ($\nabla^2\rho_b$) at bond critical points , and density of total energy (H_b) (fig2).

Results and Discussion:

The ΔH_{ads} , ΔG_{ads} , ΔS_{ads} Binding Energy and change of Charge values show that the ($C_{24(D6d)}$,H_2) structure may be more chemically stable than the $C_{20(Ih)}$ and $C_{26(D3h)}$ structures (table1).

As is known, the ($\nabla^2\rho_b$)identifies whether the charge of the region is locally depleted ($\nabla^2\rho_b$ >0) or concentrated ($\nabla^2\rho_b$ <0). All of the interactions between H_2 and Fullerenes are van der walls,

because of values of $\nabla^2\rho_b$ >0, ρ_b order of 10^{-3} and H_b>0 . (Table2)

Tablel: Thermodynamic functions at 25 °C

Structure	$\Delta H_{(ads)}$ kcal.mol^{-1}	$\Delta G_{(ads)}$ kcal.mol^{-1}	$\Delta S_{(ads)}$ cal.mol^{-1}	Δcharge (ads)	$E_{Binding}$ kcal.mol^{-1}
C_{20},H_2	-0.353	2.532	-11.197	-0.004	1.255
C_{24},H_2	-0.374	2.478	-9.566	-0.032	1.883
C_{26},H_2	-0.242	4.747	-16.729	-0.004	0.756

Table2: QTAIM Results

Fullerens (fopt)	ρ_b (a.u)	$\frac{1}{4}\nabla^2\rho_b$ a.u	V_b a.u	G_b a.u	H_b a.u
C_{20},H_2	0.0036	+0.0025	-0.0012	+0.0019	+0.0007
C_{24},H_2	0.0030	+0.0022	-0.0012	+0.0016	+0.0004
C_{26},H_2	0.0036	+0.0025	-0.0013	+0.0019	+0.0006

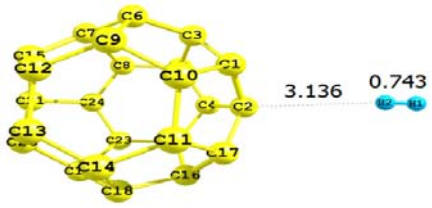

Fig1: Optimized geometry of C_{24} , H_2 at PW91/6-31G

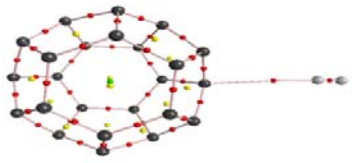

fig2: Critical points of bonds of C_{24},H_2

Conclusions:

Based on results it can be concluded that ($C_{24(D6d)}$,H_2) structure may be more chemically stable than the ($C_{20(Ih)}$, H_2) and ($C_{26(D3h)}$, H2) structures .

References:

[1] Bosi,S. Eur.J.Med.Chem. 38, 913-923 (2003)

[2] Gharbi,N. Nano Lett 5,2578-2585 (2005)

[3] Tim S.Jakubov, Adsorption 14,727-732 (2008)

[4] Morris Sylvin, Surface Chemistry (Adsorption), Sarup & Sons,New Dehli (2005)

[5] FRISCH M.J., Trucks G. W., Schlegel H. B., Scuseria G. E., Robb M. A., Cheeseman J. R.,
and Pople J. A. 1998. *Gaussian 98, Revision A.7* Gaussian, Inc., Pittsburgh PA.

[6] F. Biegler-K◌nig, J. Sch◌nbohm, D. Bayles, AIM2000 - A Program to Analyze and Visualize Atoms in Molecules, J. Comp. Chem., 22, 545 (2001)

Closed Shell Species containing Hypercoordinate Planar Si in $Cu_6H_6Si^q$: Theoretical Investigation of Structure and Bonding

Jamshid Najafpour*[,1], Gholam Hossein Shafiee[2], Maryam Nasirianpour[2]

1. Department of Chemistry, Faculty of science, Islamic Azad University Shahr-e-Rey Branch, Tehran, P.O. Box: 18155-144, Iran

j.najafpour@gmail.com

2. Department of Chemistry, Islamic Azad University Gachsaran Branch, Gachsaran, Kohghiloye-Boyerahmad, Iran

Keywords: Silicon planar, Structure, QTAIM

Introduction

Considerable progress has been achieved in the past thirty years on planar coordinate carbons, including tetra-, penta- and hexa-coordinate planar carbons [1].

It is recently proposed a general pattern for planar tetra-, penta-, hexa-, hepta-, and octa-coordiante silicon [2,3]. It is also designed planar hexa-coordinate silicon (phSi) in the perfect hexaagons of Cu_6H_6Si [1].

In the present study, we report new quantum chemical calculations for hexa-coordinate silicon in $Cu_6H_6Si^q$ complexes that contain Si centers in a perfect hexagonal hydrocopper (Cu_6H_6) with D_{6h}, C_{2v} and C_{6v} symmetries that q is as neutral, negative and positive in these complexes (Figure 1).

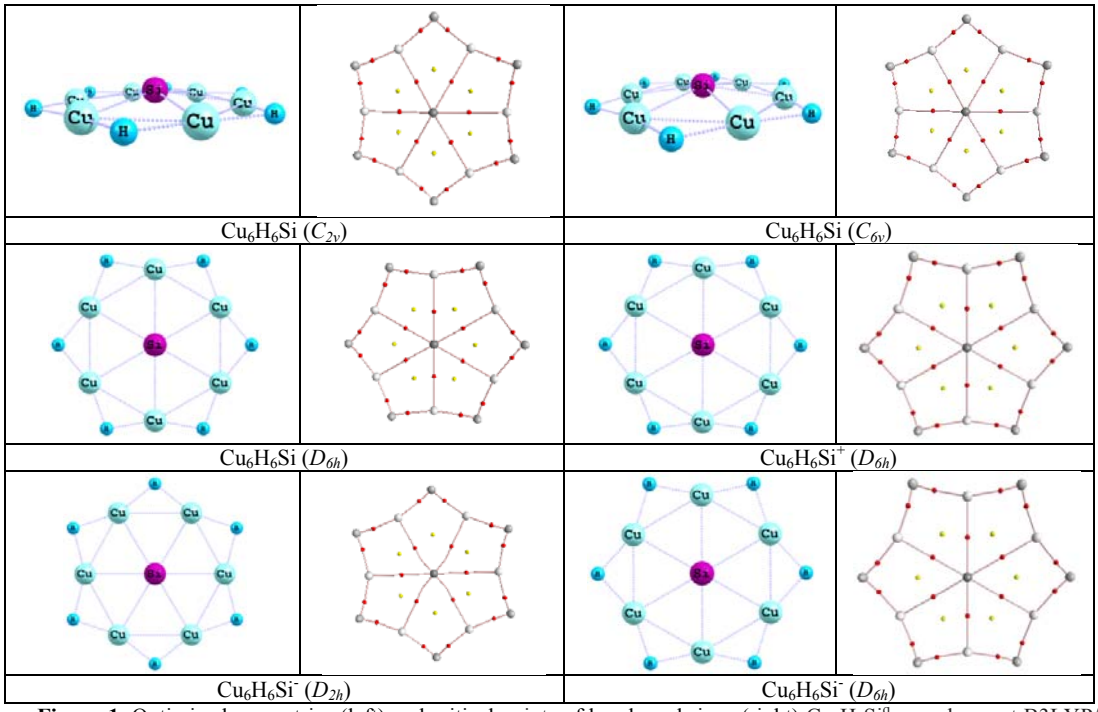

Figure 1. Optimized geometries (left) and critical points of bonds and rings (right) $Cu_6H_6Si^q$ complexes at B3LYP/6-311+G(d,p).
(Red points are Bond Critical Points: BCPs; Yellow points are Ring Critical Points: RCPs;The lines are Bond Paths: BPs.)

Computational Methodology

Here, we use the density functional theory (DFT) with B3LYP. These calculations were performed within 6-311+G(d,p) basis set and imaginary frequencies checked at the same theoretical level. All *ab initio* calculations have been performed using Spartan '08, Version 1.2.0 [4] and PC GAMESS, Version 7.1.G [5] and QTAIM calculations have been done using AIM2000 package [6].

The optimized bond lengths R (Å), lowest vibrational frequencies υ_{min} (cm^{-1}), total energy and Zero-Point Correction of $Cu_6H_6Si^q$ complexes are obtained as Table 1.

Also quantum theory of atoms in molecules (QTAIM) was carried out to gain the electron densities of $Cu_5H_5Si^q$ complexes at equilibrium geometries (Figure 1 and Table 2).

Results and Discussions

According to Table 1, these results show that Cu_6H_6Si complexes with C_{2v} and C_{6v} symmetries are local minimum species and with D_{6h} symmetry is transition state species. The

$Cu_6H_6Si^+$ complex with D_{6h} symmetry is local minimum species. The $Cu_6H_6Si^-$ complexes with D_{2h} and D_{6h} symmetries are transition state species.

Table 1. Optimized bond lengths R (Å), lowest vibrational frequencies υ_{min} (cm^{-1}), total energy and Zero-Point Correction of $Cu_6H_6Si^q$ complexes at B3LYP/6-311+G(d,p)

	Cu_6H_6Si (C_{2v})	Cu_6H_6Si (C_{6v})	Cu_6H_6Si (D_{6h})	$Cu_6H_6Si^+$ (D_{6h})	$Cu_6H_6Si^-$ (D_{2h})	$Cu_6H_6Si^-$ (D_{6h})
R_{Cu-Cu} (Å)	2.452	2.454	2.462	2.523	2.515 2.411	2.465
R_{Cu-H} (Å)	1.601 1.602	1.601	1.600	1.595	1.649 1.643	1.662
R_{Cu-Si} (Å)	2.475 2.476	2.475	2.462	2.523	2.410 2.463	2.465
υ_{min} (cm^{-1})	39.10	41.19	-21.59	43.49	-38.65	-39.59
Total energy (a.u.)	-10136.27447	-10136.27468	-10136.27440	-10136.04205	-10136.35357	-10136.34764
ZPE (kcal/mol)	32.888	32.111	32.011	33.081	29.339	28.495
	LM	LM	TS	LM	TS	TS
LM: Local Minimum, TS: Transition condition						

The AIM analysis [7] for the optimized structures has been performed to obtain the topological properties of the bonds, such as the Laplacian of ρ_b ($\nabla^2\rho_b$) at bond critical points, the bond critical points (BCP) and the ring critical points (RCP) and also the bond paths (BP). As is known, the $\nabla^2\rho_b$ identifies whether the charge of the region is locally depleted ($\nabla^2\rho_b > 0$) or concentrated ($\nabla^2\rho_b < 0$). The former is typically associated with interactions between closed-shell systems (ionic bonds, hydrogen bonds, and van der Waals molecules), whereas the latter characterizes shared interactions (covalent bonds), where the electron density concentrates in the internuclear region [8]. The latter is required for bond formation.

Table 2. Bond lnghts (Å), ρ_b and $\nabla^2\rho_b$ of the bonds in $Cu_6H_6Si^q$ complexes at B3LYP/6-311+G(d,p)

complex	BCP's number	Connected Atoms	Bond lenghts	ρ_b	$\nabla^2\rho_b$
Cu_6H_6Si (C_{2v})	1	Cu-Si	2.475, 2.476	0.046	0.006
	2	Cu-H	1.601, 1.602	0.097	0.049
Cu_6H_6Si (C_{6v})	1	Cu-Si	2.475	0.046	0.006
	2	Cu-H	1.601	0.097	0.049
Cu_6H_6Si (D_{6h})	1	Cu-Si	2.462	0.047	0.006
	2	Cu-H	1.600	0.097	0.049
$Cu_6H_6Si^+$ (D_{6h})	1	Cu-Si	2.523	0.044	0.006
	2	Cu-H	1.595	0.098	0.048
$Cu_6H_6Si^-$ (D_{2h})	1	Cu-Si	2.410, 2.463	0.057, 0.048	0.007, 0.006
	2	Cu-H	1.649, 1.643	0.093, 0.088	0.048, 0.043
$Cu_6H_6Si^-$ (D_{6h})	1	Cu-Si	2.465	0.053	0.007
	2	Cu-H	1.662	0.085	0.043

The complete list of bond critical points of electron density and their mathematical characters have been gathered in Table 2 for $Cu_6H_6Si^q$ complexes. According to Table 2, in all cases closed-shell interactions exist between Cu-Si and Cu-H connected atoms. In attention to Gillespie-Popelier discussion [9] and Table 2, Cu-Si and Cu-H bonded interactions in $Cu_6H_6Si^q$ complexes are ionic. No bond path between Cu-Cu atoms has been observed in all species.

Reference

[1] S.-D. Li, G.-M. Ren, C.-Q. Miao, *Inorg. Chem*., 2004, **43**, 6331.

[2] S.-D. Li, C.-Q. Miao, J.-C. Guo, G.-M. Ren, *J. Am. Chem. Soc*., 2004, **126**, 16227.

[3] S.-D. Li, J.-C. Guo, C.-Q. Miao, G.-M. Ren, *J. Phys. Chem. A*, 2005, **109**, 4133.

[4] Spartan '08, Version 1.2.0, B.J. Deppmeier, A.J. Driessen, T.S. Hehre, W.J. Hehre, J.A. Johnson, P.E. Klunzinger, J.M. Leonard, I.N. Pham, W.J. Pietro, Jianguo Yu, Wavefunction, Inc., Irvine, CA, 2008.

[5] A.A. Granovsky, http://classic.chem.msu.su/gran/gamess/index.html, M.W. Schmidt, K.K. Baldridge, J.A. Boatz, S.T. Elbert, M.S. Gordon, J.H. Jensen, S. Koseki, N. Matsunaga, K.A. Nguyen, S.J. Su, T.L. Windus together with M. Dupuis, J.A. Montgomery, *J. Comp. Chem*., 1993, **14**, 1347.

Crystal Density Prediction based on QTAIM.
I. Acyclic and Monocyclic Nitramines

Jamshid Najafpour*, Ali Akbar Salari, Najme Ghorbani

Department of Chemistry, Faculty of science, Islamic Azad University Shahr-e-Rey Branch, Tehran, P.O. Box: 18155-144, Iran

j.najafpour@gmail.com

Keywords: Density prediction, Nitramines, QTAIM

Introduction

In this paper, we report on a simple and convenient methodology for rapidly predicting the crystalline densities of energetic nitramines based on the quantum chemical computations. This group of compounds is a source of explosives or propellants that possess predominantly high energy content, and they have numerous important applications in both civilian and military fields for a long time.

Computational details

In comparison with other methods, B3LYP/6-31G(d,p) is most accurate and economical to predict the solid-state densities of energetic nitramines [1]. So the density functional theory (DFT) with B3LYP method and 6-31G(d,p) basis set have been employed to predict the molecular volumes and densities of a series of energetic nitramines including acyclic and monocyclic molecules (Figure 1 and 2).

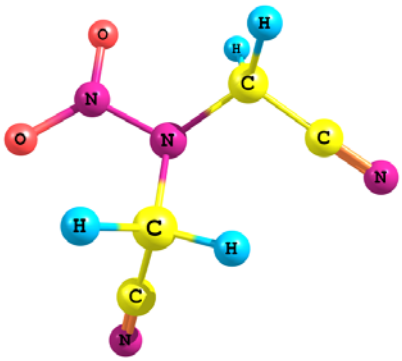

BCMN

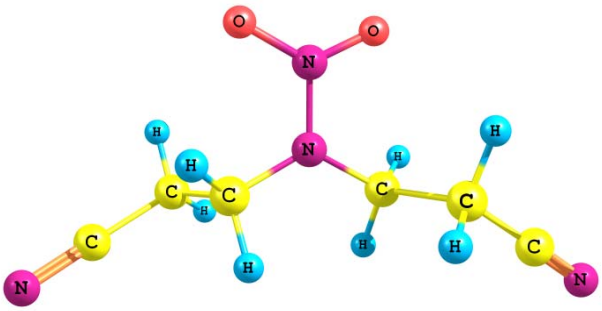

BCEN

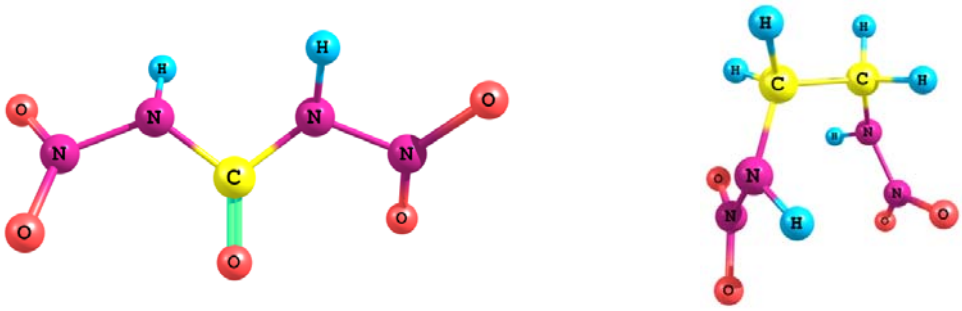

DNU EDNA

Figure 1. Optimized geometries of acyclic nitramines at B3LYP/6-31G(d,p).

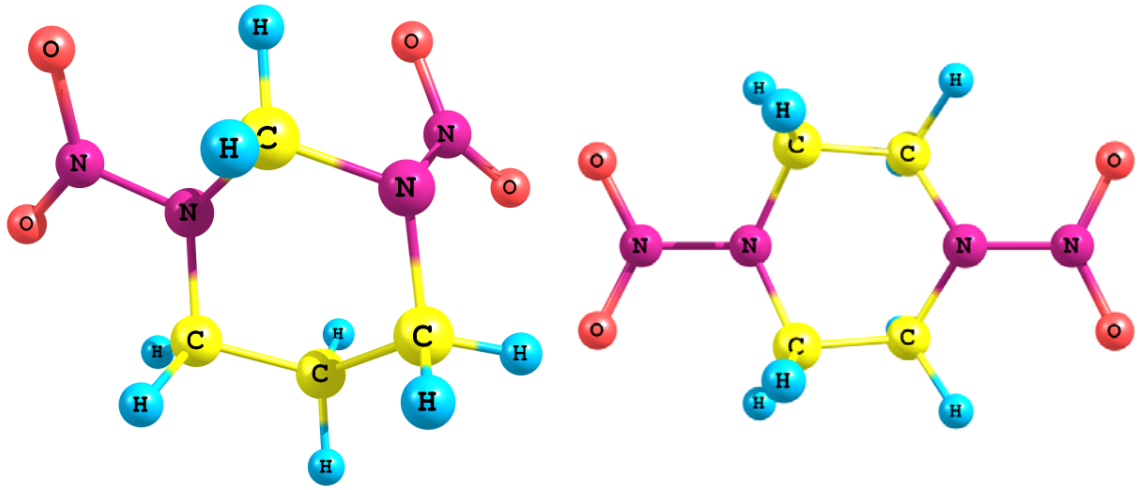

m-DNDC P-DNDC

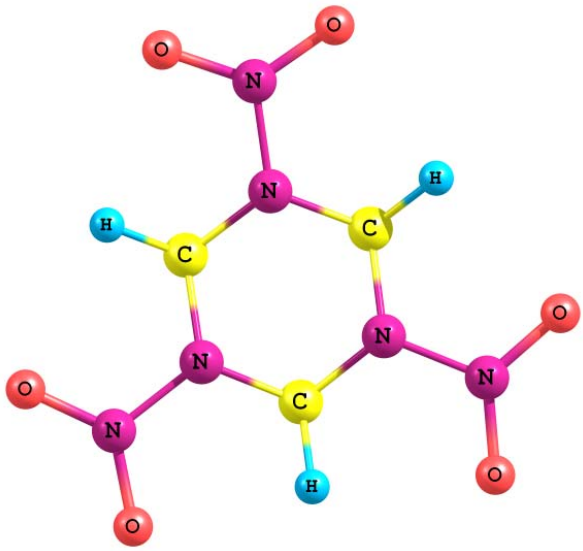

RDX

Figure 2. Optimized geometries of monocyclic nitramines at B3LYP/6-31G(d,p).

All DFT calculations were performed by Spartan '08, Version 1.2.0 [2] and PC GAMESS7.1.G package [3]. The QTAIM computations were done on the appropriate wave function derived from DFT computation in molecules. All these computations were performed using AIM2000 program [4].

Results and discussion

The molecular volume is summation of atomic volume of atoms in a molecule that can be obtained by Quantum Theory of Atoms in Molecules (QTAIM). The atomic volume is defined as the space bounded by the intersection of the zero-flux surface(s) bounding the atom from the molecular interior and a chosen outer isodensity envelope (if a side of this atom's basin extends to infinity). While a molecule extends in principle to infinity, an outer isodensity of ρ=0.001 a.u. is usually chosen as its outer bounding surface [5,6].

The result show that the calculated ρ in Table 1 is in good agreement with the experimental crystalline densities [1].

Table 1. Calculated molecular volumes and crystalline densities of acyclic and monocyclic nitramines at B3LYP/6-31G(d,p) in comparison with experimental densities

Material	M (g/mol)	vol [0.001]*	ρ (cal) gr/cm^3	ρ (exp) [1] gr/cm^3

Bis(cyanomethyl)nitramine (BCMN)	140.11	1051.10	1.49	1.50
Bis(cyanoethyl)nitramine (BCEN)	168.16	1359.86	1.38	1.36
N,N´-dinitrourea (DNU)	150.07	909.94	1.85	1.98
Ethylene dinitroamine (EDNA)	150.11	1050.29	1.60	1.71
1,3-Dinitro-1,3-diazacyclohexane (m-DNDC)	176.14	1237.06	1.59	1.57
1,4-Dinitro-1,4-diazacyclohexane (p-DNDC)	176.14	1231.13	1.60	1.63
1,3,5-Trinitro-1,3,5-triazacyclohexane (RDX)	222.14	1391.78	1.79	1.81

*The atomic volume is integrated over atomic basin (Ω) to the contour surface of 0.001 a.u.

Reference

[1] L. Qiu, H. Xiao, X. Gong, X. Ju,W. Zhu, *Journal of Hazardous Materials*, 2007, **141**, 280.

[2]Spartan '08, Version 1.2.0, B.J. Deppmeier, A.J. Driessen, T.S. Hehre, W.J. Hehre, J.A. Johnson, P.E. Klunzinger, J.M. Leonard, I.N. Pham, W.J. Pietro, Jianguo Yu, Wavefunction, Inc., Irvine, CA, 2008.

[3]A.A. Granovsky, http://classic.chem.msu.su/gran/gamess/index.html, M.W. Schmidt, K.K. Baldridge, J.A. Boatz, S.T. Elbert, M.S. Gordon, J.H. Jensen, S. Koseki, N. Matsunaga, K.A. Nguyen, S.J. Su, T.L. Windus together with M. Dupuis, J.A. Montgomery, *J. Comp. Chem*., 1993, **14**, 1347.

[4]F. Biegler-König, J. Schönbohm, D. Bayles, AIM2000 - A Program to Analyze and Visualize Atoms in Molecules, *J. Comp. Chem*., 2001, **22**, 545.

[5]R.F.W. Bader, Atoms in Molecules: A Quantum Theory, Oxford University Press: Oxford, U.K., 1990.

[6]C.F. Matta, R.J. Boyd, The Quantum Theory of Atoms in Molecules, Wiley-VCH, 2007.

Computational Assessment of ADME Properties of antiplasmodial drugs

A. Najafi*

Islamic Azad University, Young Researchers Club, Hamedan Branch, Hamedan, Iran

(*Email:* najafi@iauh.ac.ir, am.najafi@yahoo.com).

Malaria kills 1–2 million people each year and 300–500 million new clinical cases of malaria are reported annually [1]. We used a series of 4-aminoquinoline antimalarial compounds with experimentally determined ADME properties were taken from the literature [2]. In silico predictive models for antimalarial activity (IC_{50}), Blood-to-plasma concentration ratio (R_b), and Inhibition of cytochrome P450 (CYPs) were developed for new 4-Aminoquinoline Antimalarial Compounds using multiple linear regression (MLR) analysis. Genetic algorithms (GA) were used as a variable selection method [3].

Antimalarial activities against Chloroquine-sensitive (3D7) and Chloroquine-resistant (W2) strains of *P. falciparum* were constructed with up to five descriptors. The plots of validation models are shown in Figure 1.

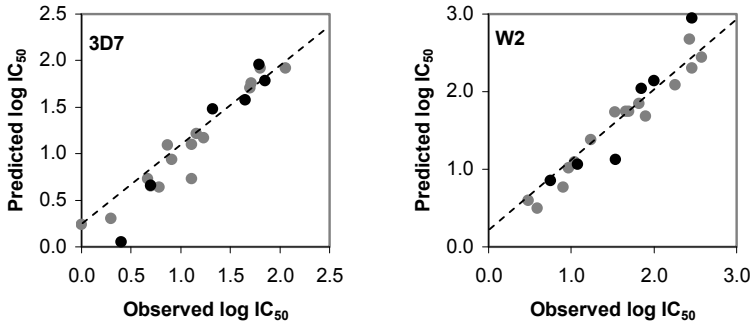

Figure 1. Plot of the predicted vs. observed of growth inhibition of 3D7 and W2 strains of *P. falciparum*. The LOO cross-validation compounds are represented as grey dots and six derivatives used as test set as black dots

Drug distribution in blood, defined as drug blood-to-plasma concentration ratio (R_b), is a fundamental pharmacokinetic parameter. The MLR models have good statistical quality with low prediction error. The correlations between the predicted and experimental values of R_b are shown in Figure 2.

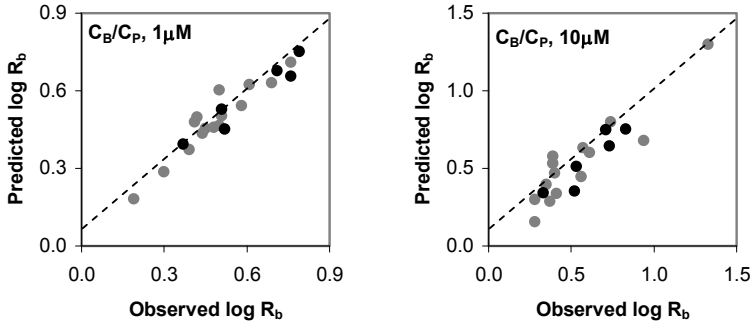

Figure 2. Plot of the predicted vs. observed log Rb that was measured for each of the compounds at 1 and 10 μM. The LOO cross-validation of compounds are represented as grey dots and test set as black dots

Inhibition of CYPs can lead to drug-drug interactions and therefore it is considered important to evaluate potential drug candidates for CYP-inhibitory activities.

Computational models were generated to predict the cytochrome P450 1A2, 2C9, 2C19, 2D6, and 3A4 inhibitions using GA based MLR methods. External validation yielded statistically significant and accurate predictions. The training and test sets and statistical parameters for each CYP model are also presented in Table 1.

Table1. Prediction ability of the MLR models in the external validation set for Different P450 Inhibitors

	Training set				Test set	
CYP	R^2	R^2_{adj}	RMSE	F	R^2_{pred}	RMSE
2B6 (1□M)	0.98	0.96	0.03	19.51	0.74	0.01
2B6 (10□M)	0.96	0.94	0.01	43.13	0.39	0.02
2C9 (1□M)	0.95	0.92	0.01	34.90	0.61	0.02
2C9 (10□M)	0.97	0.95	0.02	58.67	0.91	0.04
2C19 (1□M)	0.95	0.93	0.01	36.67	0.84	0.02
2C19 (10□M)	0.96	0.94	0.01	55.82	0.78	0.01
2D6 (1□M)	0.93	0.89	0.04	24.37	0.82	0.03
2D6 (10□M)	0.95	0.93	0.08	50.51	0.92	0.13
3A4 (1□M)	0.90	0.85	0.01	16.39	0.96	0.01
3A4 (10□M)	0.92	0.89	0.03	28.60	0.97	0.07
3A4 (1□M)	0.94	0.91	0.01	29.12	0.92	0.02
3A4 (10□M)	0.87	0.81	0.05	16.32	0.89	0.07

Keywords: Plasmodium, Blood-to-plasma ratio, Cytochrome P450, QSAR

References:

[1] F.J. Gamo, L.M. Sanz, J. Vidal, C. de Cozar, E. Alvarez, *nature*, **2010**, 465, 305.

[2] S. Ray, P. B. Madrid, P. Catz, S.E. LeValley, M.J. Furniss, L.L. Rausch, R.K. Guy, J.L. DeRisi, L.V. Iyer, C.E. Green and J.C. Mirsalis, *J. Med. Chem.* **2010**, 53, 3685.

[3] R. Ghavami, A. Najafi, M. Sajadi, F. Djanati, *J. Mol. Graphics. Model.* **2008**, 27, 105.

Conformational behaviors of methanediol, methanedithiol and methanediselenol. A hybrid-DFT study and NBO interpretation

Nejad Rezaei[a],*.L, Mousavi[b].S.N, Yahyayi[c].H, Hassanzadeh[d].N, and Nori-Shargh[b].D

a)Chemistry Department, Science Faculty, Saveh Branch, Islamic Azad University, Saveh, Iran

Rezaee-l@hotmail.com

b)Chemistry Department, Science Faculty, Arak Branch, Islamic Azad University, Arak, Iran

c)Chemistry Department, Zanjan Branch, Islamic Azad University, P.O.Box: 49195-467, Zanjan, Iran

d)Chemistry Department, Science Faculty, Ahwaz Branch, Islamic Azad University, Ahwaz, Iran

Keywords: Generalized Anomeric EDffect, Ab initio, NBO, Methanediol, Methanedithiol, Methanediselenol

Introdauction

Since the preferred geometry of many molecules can be viewed as the result of the maximization of an interaction between the best donor lone pair and the best acceptor bond,[1] the stereoelectronic interactions are expected to play an important role in the conformational properties of heterocyclic compounds.[2,3] The most dominant conformation-controlling factor in carbohydrate compounds is known as the *anomeric effect* (*AE*).[4] Although the importance of the hyperconjugative interactions in some acyclic compounds has investigated, there is insufficient published experimental information about the stereoelctronic interactions in methanediol (**1**), methanedithiol (**2**) and methanediselenol (**3**).

Computational details

Hybrid DFT calculations were carried out using the CBS-4 and B3LYP/6-311+G** levels of theory with the GAUSSIAN 03 package of programs.[5] The main purpose of the present work was to study the impacts of the stereoelectronic interaction effects, dipole-dipole interactions on the conformational preferences (i.e. axial and equatorial conformations) in compounds **1-3**. An NBO analysis was then performed for the axial and equatorial conformations of compounds **1-3** by the NBO 5.G program contained in the PC-GAMESS interface.[6]

Results and Discussion

Hybrid-density functional theory (B3LYP/6-311++G**) based methods and NBO interpretation were used to study the conformational behaviors of of methanediol (**1**), methanedithiol (**2**) and methanediselenol (**3**). The most stable conformations of compounds **1-3** were found by changing and scanning the dihedral angles H_1-C_2-O_3-C_3. The results obtained showed that the axial symmetrical (C_2) conformations of compounds **1-3** are more stable than their plane symmetrical (C_s) and unsymmetrical (C_1) conformations. The Gibbs free energy difference at 298.15 K and 1 atm values between the axial symmetrical (C_2) and plane symmetrical (C_s) conformations (i.e. $\Delta G_{Cs\text{-}C2}$) decrease from compound **1** to compound **3** but the Gibbs free energy difference values between the axial symmetrical (C_2) and unsymmetrical (C_1) conformations conformations (i.e. $\Delta G_{C1\text{-}C2}$) increase from compound **1** to compound **3**. The NBO analysis of donor-acceptor (LP→σ*) interactions showed that the *generalized anomeric effects* (*GAE*) decrease from compound **1** to compound **3**. In addition, the calculated dipole moment values between the axial symmetrical (C_2) and plane symmetrical (C_s) conformations [$\Delta(\mu_{Cs} - \mu_{C2})$] decrease from compound **1** to compound **3**. There is no conflict between the decrease of *GAE* and $\Delta(\mu_{Cs} - \mu_{C2})$ values. The correlations between the *GAE*, bond orders, pairwise steric exchange energies (*PSEE*), $\Delta G_{Cs\text{-}C2}$, $\Delta G_{C1\text{-}C2}$, dipole-dipole interactions, structural parameters and conformational behaviors of compounds **1-3** have been investigated.

Conclusion

The *AE* decrease from compound **1** to compound **3,** the rationalization of the conformation preference solely in terms of the *AE* succeeds to account quantitatively for the conformation preferences in compounds **1-3**.

Refrences:

[1]J.-M. Lehn, G. Wipff; H-B. Burgi, *Helv. Chim. Acta* **1974**, *57*, 493.
[2]D. Nori-Shargh, H. Yahyaei, J .E. Boggs, *J. Mol. Graph. Model.* **2010**, *28*, 807.
[3]D. Nori-Shargh, J.E Boggs, *J. Phys. Org. Chem*. **2010**, doi:10.1002/poc.1728.
[4]E. Juaristi, G. Cuevas, A. Vela, *J. Am. Chem. Soc*. **1994**, *116*, 5796 -5804.
[5]M.J. Frisch, et al, Gaussian 03, Revision B.03, Gaussian, Inc., Wallingford CT, **2004**.

[6]E.D. Glendening, J.K. Badenhoop, A.E. Reed, J.E. Carpenter, J.A. Bohmann, C.M. Morales, F. Weinhold, Theoretical Chemistry Institute, University of Wisconsin, Madison, WI, **2004**. NBO Version 5.G.

A theoretical study of H and D adsorption on Ni(111) surface : A DFT calculation.

L. Nassaji jahromi*[a],A. A. Salari[a],M. Shabani[b], F.Ghorbani Naieni[a], Z. Ahoo[a]

[a]*Department of Chemistry, Islamic Azad University, Shahre-Rey Branch, Thran, Iran*

[b] *Department of Chemistry, Islamic Azad University, Varamin-Pishva Branch, Tehran, Iran*

Corresponding Author E-mail: leila32nasaj@yahoo.com

Abstract

In the investigation we measured H (D) thermal Energies for hydrogen(H) and deuterium (D) adsorption on Ni(111) at coverage θ=0.25 0n A top site. Finite temperature quantum behavior of hydrogen adsorbates on Ni(111) surface is simulated using DFT calculations. This allows consideration of substrate atom dynamics.We showed that D thermal Energie is more than H in whole of the temperatures and thermal Energies increased with decreasing of temperatures from 1000 K to 15 K. From 200K down to 15K,the quantum delocalization of the adsorbate is considerable, and therefore, temperature dependence of distributions is weak. In this case, the isotope effect is larger[1-2-3].

Keywords: Density- functional calculation; Nickel (111) surface; DFT study; Hydrogen ; Deuterium; Isotope effect; Chemisorptions.

Introduction

To better understand the mechanism of adsorption of selection, is very important knowing the nature Insights species participating in the reaction, the main goal of this study calculated the heat of adsorption at the different temperatures by methods of density-functional theory (DFT) of quantum chemistry calculations with GAUSSIAN03 program package. In this study used deuterium (hydrogen), Deuterium is isotope of hydrogen.

Computational Methods

For the calculation at first we start of Ni surface. Unit cell of the nickel has a fcc crystal ,Miller index in this calculation is (111).The was used for the production of the

experimentally determinded Ni lattice constant of 3.5228 A˚ surfaces. The geometries of H(D),Ni(111) were respectively optimized using density functional theory (DFT) at the B3LYP level on different basis sets 6-31G*and LANL2DZ. Top site is considered in this calculation. Adsorption energies were computed by subtracting the energies of the gas- phase H(D) atom and surface from the energy of the adsorption system,as show in

$E_{ad}=E(\text{H/Surface})-E(1/2H_2)-E(\text{Surface})$

For simplification of calculation, we optimize two parameters, that is, the distance between hydrogen atoms (R_{H-H}) and the distance between cluster surface and hydrogen atoms ($R^{\perp}$), while the metal cluster was fixed with the lattice constant. We also fixed the direction to hydrogen atom as top site.

Results and discussion

Ni_4 (111) surface monolayer are three sites; top,bridge and Hallow(threefold).We considered top site in this calculation. Calculation results is visible in Table (1).

Table 1 - Energy of chemical adsorption of hydrogen atom on Ni_4 (111) surface

site	θ	EM-H2	E_{ads}(a.u)	E_{ad}(ev)	E_{ads}(kJ/mol)	$d_{(A°)}$(Ni-H)	$d^{\perp}_{(A°)}$
top	0.25	-677.76	-0.231345	-6.29	-607.4	1.48974	1.48974

Isotope effects on chemical adsorption of heat

Hydrogen has three isotopes. We want to compare the heat of chemical adsorption of two isotopes, D and H together. Isotopes have equal number of electrons then optimize their structure is identical and the difference is in the number of neutrons and the atomic mass. We can calculate heat of adsorption D If mass of deuterium replacs hydrogen in the range of optimized structure in terms. We rise temperature of 15 K 1000. In Table 2, we present the calculated energy data. By decrease the temperature; decreases chemical adsorbtion H and D on Ni4 (111) single-layer, free energy and increase thermal enthalpy and thermal energy and zero point does not change (all energies in terms of Hartry have been reported). Can be concluded to reduce the temperature by reducing the movement of gas molecules on the surface, time of contact gas adsorbed are increaseing with surface, physical adsorption is increased and possibility will increase chemical adsorption.

Table 2 - Effect change of temperature on chemical adsorption in the D and H on Ni_4 (111) monolayer.

K دما		thermal Energies	zero-point Energies	thermal Enthalpies	thermal Free Energies
1000	H	-677.723564	-677.754115	-677.723564	-677.907321
	D	-677.727392	-677.755214	-677.724225	-677.908858
400	H	-677.74445	-677.754115	-677.743183	-677.804761
	D	-677.745489	-677.755214	-677.744222	-677.805917
298.15	H	-677.745705	-677.752446	-677.744761	-677.78754
	D	-677.748387	-677.755214	-677.747443	-677.79066
130	H	-677.751808	-677.754115	-677.751397	-677.767007
	D	-677.752904	-677.755214	-677.752493	-677.768118
100	H	-677.752527	-677.754115	-677.75221	-677.763508
	D	-677.753624	-677.755214	-677.753307	-677.764615
70	H	-677.753169	-677.754115	-677.752948	-677.760245
	D	-677.754267	-677.755214	-677.754045	-677.761349
15	H	-677.753972	-677.754115	-677.753924	-677.755107
	D	-677.75507	-677.755214	-677.755023	-677.756207

Relationship Temperature with heat of chemical adsorption H and D on Ni_4 (111) monolayer, is visible respectively in tables (3) and (4). For adsorbed best results -677.723564 heat of adsorption H in 1000 K that is released the lowest heat of adsorption we have considered as a baseline we have and calculated based on changes thermal Energies.

Table 3 -The relationship Temperature with heat of chemical adsorption in H on Ni4 (111) monolayer.

T (K)	adsorption energies (kcal/mol)	Change of thermal energies	thermal energies (Hartry)
1000	0	0	-677.723564
400	13.105965	-0.020886	-677.74445
298.15	13.8934775	-0.022141	-677.745705
130	17.72311	-0.028244	-677.751808
100	18.1742825	-0.028963	-677.752527
70	18.5771375	-0.029605	-677.753169
15	19.08102	-0.030408	-677.753972

Table 4 - The relationship Temperature with heat of chemical adsorption in D on Ni4 (111) monolayer.

T (K)	adsorption energies (kcal/mol)	Change of thermal energies	thermal energies (Hartry)
1000	2.40207	-0.003828	-677.727392
400	13.7579375	-0.021925	-677.745489
298.15	15.5764325	-0.024823	-677.748387
130	18.41085	-0.02934	-677.752904
100	18.86265	-0.03006	-677.753624
70	19.2661325	-0.030703	-677.754267
15	19.770015	-0.031506	-677.75507

All the temperatures chemical adsorption Deuterium more than Hydrogen If we compare the results of the tables (3)and (4) .

Figure 1 - Comparison the strength of the adsorption hydrogen and deuterium at various temperatures.

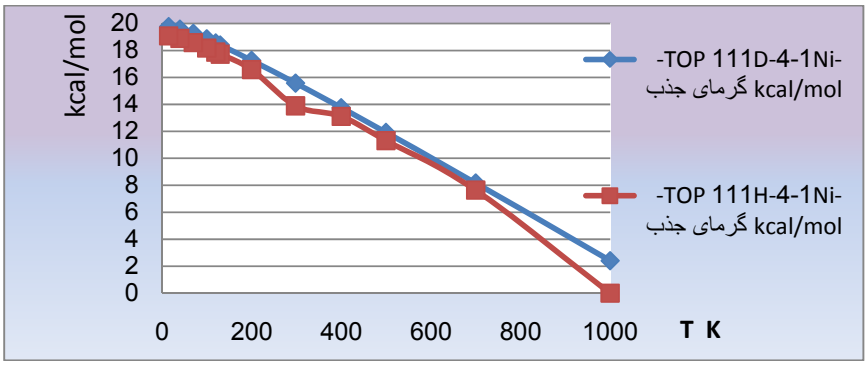

These can be justified due to the Entropy and Enthalpy of deuterium are more than hydrogen at all temperatures. So based on $G^0=H^0-TS^0$ deuterium adsorb stronger than hydrogen on Ni_4 (111) surface. The Gibbs free energy will be more negative. On the other hand based on $-(G-E_0)=Rlnq$ and is equal the zero point energy(E_0) in hydrogen and deuterium then Gibbs free energy is a direct relationship with "q" function (function sharing), on the other hand We know that the "q" function is divided into direct relationship with mass, so can be concluded that the "q" function of the deuterium more and Gibbs free energy will be more negative because the mass of deuterium is more than hydrogen.

Conclusion

1. Thermal Energies increased with decreasing of temperatures from 1000 K to 15 K. Reduce temperature to reduce movement of gas molecules on the surface by self adsorption, increase physical adsorption and the subsequent increases in chemical adsorption.
2. D thermal Energie is more than H in whole of the temperatures

Reference

[1]Lee,A. ; Zhu,X.D.; Deng,L. Phys. Rev,1992,B 46, (23), 15472.
[2] Leino.M. ;Nieminen.J.et al.Surface Science,2006,600,1860.
[3]Guvenc.Z.B; Guvenc.D. Surface Science,2003,529,11.
[4]Ishiwatari,R.; Tachikawa,M. 2004, 736, 383.
[5] Kresse,G. ; Hafner,J. Surf. Sci, 2000, 459, 287.

[6]Shiga,M. ; Yamaguchi,M.; Kaburaki,H. Phys. Rev, 2003, B 68 , 245402.

Density-functional study of the chemisorption of atomic H on Ni (111) and (100) surfaces.

L. Nassaji jahromi*[a],A. A. Salari[a],M. Shabani[b], F.Ghorbani Naieni[a], Z. Ahoo[a]

[a]Department of Chemistry, Islamic Azad University, Shahre-Rey Branch, Thran, Iran

[b] Department of Chemistry, Islamic Azad University, Varamin-Pishva Branch, Tehran, Iran

Corresponding Author E-mail: leila32nasaj@yahoo.com

Abstract

The adsorption of atomic H on all three low-index of Ni (111) and (100) surfaces has been studied using gradient-corrected density-functional calculations. Our technique is based on ultrasoft pseudopotential. Ni4 and Ni8 clusters are used as a small single and second layer models, Full H-coverage and 0.25, 0.5, 0.75 H-coverage in atop, bridge, and hollow position are considered[1]. Trends in the adsorption energy, repulsion between adsorbed hydrogen atoms, and diffusion barriers are discussed in detail. The results are compared with experiments, showing a good agreement with the structural models derived from experimental data. the (DFT) studies indicate the Ni(001)and Ni(111) surfaces as a strongly correlated energetically heterogeneous surface that the hydrogen atoms may adsorb either on bridge sites (energetically more favorable) or hollow sites and by increasing the surface coverage, the heat of adsorption decreases. [2-3]

Keywords: Chemisorption; Density functional calculations; Hydrogen atom;; Nickel; Surface.

Introduction

Hydrogen energy has attracted a great deal of attention from the viewpoint of energy saving and environmental problem [4–5]. In recent years, hydrogen-absorbing alloys are utilized for the transportation of hydrogen and as catalyst, since they have ability for quick occlusion and release of hydrogen, without great change of the structure and the composition of the crystal [1,3]. On the other hand, it has long been known that transition metals become brittle when small concentration of hydrogen impurity exists, called ‘hydrogen embrittlement’. Although most character of hydrogen has been known, this phenomenon is still unsolved. In order to treat hydrogen occlusion and hydrogen embrittlement microscopically, it is necessary to elucidate the mechanism of hydrogen adsorption on metal surface as the first step. In the

present work we focus on the nickel metal. There are many experimental data for low-index surface of nickel for more than 40 years [6–7]. Consequently, a wealth of experimental data has accumulated, and a clear picture of the features induced by adsorption has emerged. It is interesting however, that only a few accurate density-functional calculations have been reported to date. The major motivation of the present work is to fill this gap.

Computational method

We have employed the B3LYP/LANL2DZ level for Ni and B3LYP/ 6-31G** for H of calculation with GAUSSIAN03 program package. In the LANL2DZ basis set, the core electrons of nickel atom are incorporated into Hay–Wadt effective core potential, while the 3s, 3p, 3d, and 4s electrons are explicitly treated as split valence basis set [8,9].The (001)and (111)surfaces are adopted the adsorption surface. We picke up Ni_4,Ni_8small clusters as nickel surfaces, shown in Figs. 1-3, respectively ,where the distances between nickel atoms are fixed with the lattice constant. The results of calculation on cluster models strongly depend on the cluster size, and one should make comparison between the results for the different model sizes for more precise estimation. Though we actually calculated the models with much larger sizes,the SCF calculations did not converge due to the quasi-degeneration of molecular orbitals for Ni clusters,unfortunately. The experimentally determinded Ni lattice constant of 3.5228A˚was used for the production of the surfaces. For simplification of calculation, we optimize two parameters, that is, the distance between hydrogen atoms ($R_{H–H}$) and the distance between cluster surface and hydrogen atoms ($R^{\perp}$), while the metal cluster was fixed with the lattice constant. We also fixed the direction to hydrogen molecule as the threefold, bridge, and top sites. Adsorption energies were computed by subtracting the energies of the gas- phase H atom and surface from the energy of the adsorption system,as show in

$E_{ad}=E(\mathrm{H/Surface})-E(1/2\mathrm{H_2})-E(\mathrm{Surface})$

Results and discussion

1.Ni_4(111)surface

a.TOp b.Bridge C.Hollow

Fig. 1. Schematic illustration of H adsorption on Ni4(111) cluster for three sites.

Table 1 : Summary of reaction energies and geometries for hydrogen on Ni (111) surfaces.

site	θ	EM-H2	E_{ads} (a.u)	E_{ads}(ev)	E_{ads} (kJ/mol)	d (A°) (Ni-H)	$d^{\perp}$(A°)
bridge	0.25	-677.77	-0.24209	-6.6	-635.6	1.61218	1.20066
Hollow	0.25	-677.76	-0.232963	-6.34	-611.64	1.79203	1.22351
top	0.25	-677.76	-0.231345	-6.29	-607.4	1.48974	1.48974
H adsorption on Ni4(111) cluster for bridge and top sites.							
bridge	0.5	-678.25	-0.113241	-3.1	-297.31	1.5969	1.00015
top	1	-679.41	-0.009095	-0.25	-23.9	1.4337875	

2 .Ni_4(001) surface

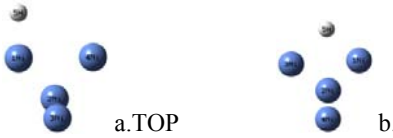

a.TOP b.Bridge

Fig.2. Schematic illustration of H adsorption on Ni4(001) cluster for three sites.

Table 2 : Summary of reaction energies and geometries for hydrogen on Ni (001) surfaces.

site	θ	EM-H2	E_{ads} (a.u)	E_{ads}(ev)	E_{ads} (kJ/mol)	d (A°) (Ni-H)	$d^{\perp}$(A°)
bridge	0.25	-677.7748	-0.1191527	-3.24231	-312.8	1.7	1.29
top	0.25	-677.7607	-0.1050887	-2.85961	-275.9	1.57	1.57

3 .Ni_8(001) surface

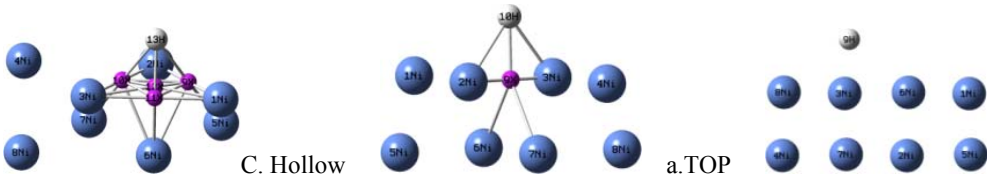

b.Bridge C. Hollow a.TOP

Fig.3. Schematic illustration of H adsorption on Ni8(001) cluster for three sites.

Table 3: Summary of reaction energies and geometries for hydrogen on Ni_8 (001) surfaces.

site	θ	EM-H2	E_{ads} (a.u)	E_{ads}(ev)	E_{ads} (kJ/mol)	$d^{\perp}$(A°)
Hollow	0.25	-1355.0492	-0.306	-8.331	-803.8	1.12
bridge	0.25	-1355.0548	-0.312	-8.5	-818.45	1.3
top	0.25	-1355.0245	-0.281	-7.66	-738.88	1.55
	0.5	-1355.4262	-0.0914	-2.5	-240.0	1.48
	0.75	-1356.1555	-0.1373	-3.7	-360.5	1.52
	1.0	-1356.5742	-0.0825	-2.5	-216.8	1.466

The tests for the Ni_8 (001) surfaces are summarizd in Table 3. By increasing surface coverage the heat of adsorption is decreased Because There are interactions between adsorbed hydrogen atoms.and the relationship is approximately logarithmic and follows Frndlysh isotherms. Perpendicular distance of hydrogen from the surface also decreases because the occupied orbitals of the hydrogen molecule interacts with $3dz^2$ orbital ,while virtual orbitals with 3dxy and $3dx^2$-y^2. When the contribution of orbital $3dx^2$-y^2 and 3dxy lower than $3dz^2$ increases lines of the anti-bonding hydrogen molecules. As a result increases distance R H-H and decreases d ⊥.The hydrogen atoms can be absorbed in bridge and Hollow sites that chemical adsorption in bridge sites is more favorable.

Conclusion

In this work we proposed the model of adsorption H on Ni(001) and Ni(111) surfaces has been investigated by density functional theory(DFT) method. Adsorption energies ,structures Perpendicular distance,of H on this surface is studied. H adsorbs at the bridge, hollow and atop sites the bridge site becomes most favorable and by increasing surface coverage the heat of adsorption is decreases.

References

[1] R.Ishiwatari,M.Tachikawa,736(2004) 383.

[2] T.R. Mattsson, G. Wahnstro¨m, Phys. Rev. B 31 (3) (1995) 1885

[3] G.Kresse,J. Hafner. Surf. Sci. 459,(2000) 287.

[4] Y. Fukai, K. Tanaka, H. Uchida, Hydorgen and Metals, Uchidaroukakuho,1998.

[5] J. O'M Bockris, Energy: the Solar-Hydrogen Alternative, Architectura Press, London, 1976.

[6] K. Christmann, R.J. Behm, G. Ertl, M.A. Van Hove, W.H. Weinberg,
J. Chem. Phys. 70 (1979) 4168.

[7] I. Stensgaard, F. Jakobsen, Phys. Rev. Lett. 54 (1985) 711.

[8] T.H. Dunning Jr., P.J. Hay, in: H.F. Schaefer III (Ed.), Modern Theoretical Chemistry, vol. 3, Plenum, New York, 1976, pp. 1–28.

[9] P.J. Hay, W.R. Wadt, J. Chem. Phys. 82 (1985) 270.

First principles study of the adsorption and dissociation of hydrogen molecules on nickel(001) surface.Using Quantum Mechanics.

L. Nassaji jahromi*[a],A. A. Salari[a],M. Shabani[b], F.Ghorbani Naieni[a], Z. Ahoo[a]

[a]*Department of Chemistry, Islamic Azad University, Shahre-Rey Branch, Thran, Iran*

[b] *Department of Chemistry, Islamic Azad University, Varamin-Pishva Branch, Tehran, Iran*

Corresponding Author E-mail: leila32nasaj@yahoo.com

Abstract

The adsorption and dissociation of gasses on the metal surfaces has been large interest in the past years by quantm mechanics studies for catalizers[1-2] .We consider there different adsorption sites,Top,Bridge and Hollow (threefold) sites for H_2 adsorption on Ni(001) in the present work intraction and adsorption properties of hydrogen with a Ni(001) single crystal surface are examinad using Hartree-Fock study and density function theory calculations based on pseudo-potential treatment[3-4].This study predicts that H_2 prefer to dissociation and adsorb at Ni(001)single crystal surface and show H_2 in bridge and hollow sites,more dissociate than the top sites[5-6].

Keywords: Nickel (001); DFT study; Hydrogent; Chemisorptions.

Introduction

Adsorption of hydrogen is commonly used for selective measurement of metal surface area of supported nickel catalysts[7-8]. The method is based on a simple assumption that the stoichiometry of hydrogen adsorption on supported nickel attains the same value as for unsupported nickel. However, now it is evident that various supports influence the interaction of hydrogen with nickel considerably [9-10] and the effect depends on number of factors such as type of support, way of preparation and pretreatment conditions [11]. Although the importance of this fact in relation to characterization of supported catalysts is well recognized, there are no current studies of that problem.To better understand the mechanism of adsorption of selection, is very important knowing the nature Insights species participating in the reaction, the main goal of this study Chemical proof of hydrogen adsorption on the Ni(001) surface by methods of DFT calculations with GAUSSIAN03 program package.

Computational Methods

For this purpose hydrogen molecule on the surface Ni4 (001) monolayer, are three sites adsorbed . Unit cell of the nickel has a fcc crystal .The was used for the production of the experimentally determinded Ni lattice constant of 3.5228 A˚ surfaces. The geometries of H,Ni(001) were respectively optimized using density functional theory (DFT) at the B3LYP level on different basis sets 6-31G*and LANL2DZ. Top,brigde and hollow(threefold) sites are considered in this calculation. Adsorption energies were computed by subtracting the energies of the gas- phase H atom and surface from the energy of the adsorption system,as show in

E_{ad}=E(H/Surface)-E(1/2H_2)-E(Surface)

For single-point calculations in this way we act in the molecules near the surface and calculate single-point energy. In the other stages Hydrogen molecules put at varying distances from the surface and sited single-point calculation in each of the points. After determining the most appropriate distance from the surface increases length bond of hydrogen- hydrogen,and we observe heat of absorption. If heat of adsorbtion more negative with the length of bond hydrogen- hydrogen, so type of adsorption is dissociative chemical absorption otherwise physical adsorption.

Results and discussion

1.Top site

Allow hydrogen molecules attraction 1.0 to 1.7 Å distance from the surface to top site locations with a scan command and calculated adsorb energy. the distance 1.58 had the most negative energy and is stable. The distances and energy values in Table (1) has been recorded.

Figure 1 -Schematic illustration of changing distance H_2 from the surface Ni_4 (001) monolayer in top site .

Table 1 – Values of single Point Energy Adsorbed (in terms of Hartry) by changing the distance H_2 from the surface Ni_4 (001) monolayer on top site.

d□ Å	HartryEM-H2	d□ Å	EM-H2 Hartry
1.0	-678.00347	1.5	-678.18258
1.1	-678.08685	1.54	-678.18336
1.12	-678.13574	1.58	-678.18353
1.25	-678.18258	1.62	-678.18322
1.4	-678.17689	1.7	-678.18165

In the next stage put hydrogen (6x-1Ni) d 1.58 Å of surface and increased length of bond hydrogen- hydrogen (7H-6H) of 0.74279 (length of bond hydrogen optimazatiom)to 0.8428 Å energy absorption the terms of kJ / mol according to the crystal energy Ni4 (001) (-676.9866401 Hartry) and mentioned relations obtains. In this case decreases the adsorption energy from - 13.4 to -15.7 (kcal / mol) which indicates that hydrogen molecules are segregated to some extent.

2.Hollow site

hydrogen molecules put 0.6 to 1.6 Å distance from the surface on nickel in hollow site and change 5x- 6x distance . Results and shape of structure has been recorded on Figures (2) and(3) .

Figure 2 - Schematic illustration of H_2 adsorption on Ni4(001) cluster for threefold site. As can be seen, 1.2 Å distance of surface had the most negative energy and is more stable.

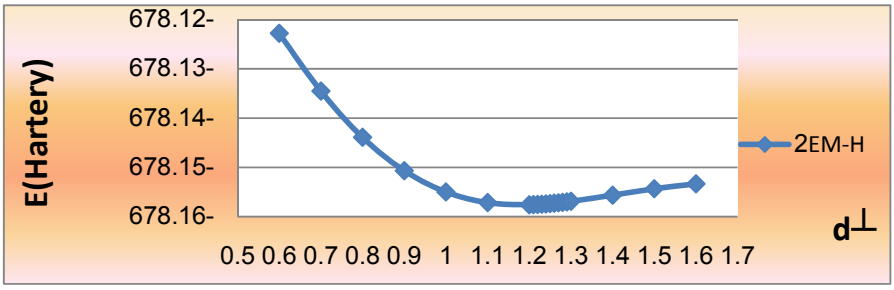

Figure 3 - Schematic illustration of heat of absorption by chenges distance H_2 on Ni4 (001) surface in Hollow site.

In the next stage put hydrogen (6x-1Ni) d1.2 Å of surface and increased length of bond

hydrogen- hydrogen (7H-8H) of 0.74279 (length of bond hydrogen optimazatiom)to 1.06 Å energy absorption the terms of kJ / mol according to the crystal energy Ni4 (001) (-676.9866401 Hartry) and mentioned relations obtains. In this case decreases the adsorption energy from 2.8 to -7.44 (kcal / mol) which indicates that hydrogen molecules are segregated to some extent. Figure (4) reflect this. Hydrogen molecule partial resolution will be better adsorbedative.

Table 3 - Effect of increasing length of bond hydrogen- hydrogen on energy absorption in hollow site.

d (H-H) Å	d (H-X) Å	EM-H2	E_{ads}(a.u)	E(kcal/mol)
0.7428	0.3714	-678.1576	0.004532	2.843516
0.8028	0.4014	-678.16397	-0.00184	-1.15366
0.8428	0.4214	-678.1668	-0.00467	-2.92948
0.9228	0.4614	-678.16975	-0.00762	-4.78061
1.0428	0.5214	-678.17399	-0.01186	-7.44121

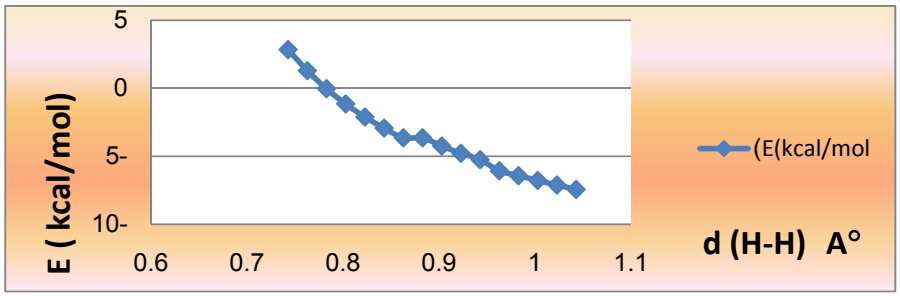

Figure 4 - Schematic illustration of - Effect of increasing length of bond hydrogen- hydrogen on energy absorption in hollow site.

3. bridge site.

Allow hydrogen molecules attraction 1.0 to 1.57 Å distance from the surface to bridge site (change 6x-5x)1.352 Å distance of surface had the most negative energy and is more stable. Results are shown in Table (3) and Figure (5)and (6) .

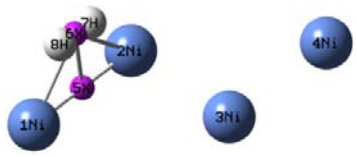

Figure 5 - Schematic illustration of the structure for changing the distance from the surface H2 Ni4 (001) single-layer absorption in bridge site.

Table 3. Values of single Point Energy Adsorbed (in terms of Hartry) by changing the distance H_2 from the surface Ni_4 (001) monolayer on bridge site.

d□ Å	EM-H2	d□ Å	EM-H2
1.084	-678.15909	1.232	-678.17121
1.152	-678.16621	1.332	-678.17362
1.162	-678.16702	1.352	-678.17371
1.172	-678.16777	1.372	-678.17368
1.212	-678.17026	1.572	-678.16953

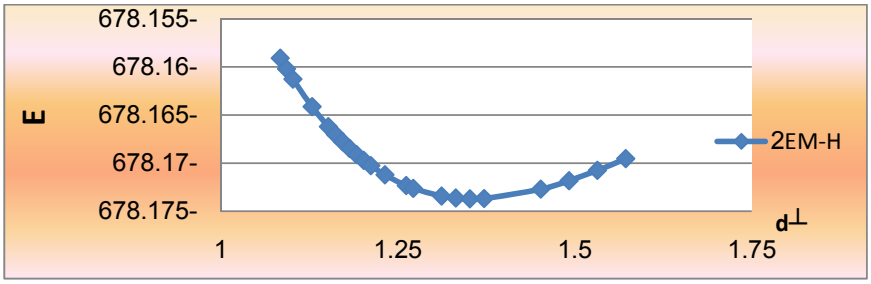

Figure 6. Schematic illustration of heat of absorption by chenges distance H_2 on Ni4 (001) surface in bridge site.

In the next stage put hydrogen (6x-1Ni) 1.352 Å of surface and increased length of bond hydrogen- hydrogen (7H-8H) of 0.74279 (length of bond hydrogen optimazatiom)to 0.86 Å energy absorption the terms of kJ / mol according to the crystal energy Ni4 (001) (-676.9866401 Hartry) and mentioned relations obtains. In this case decreases the adsorption energy from -7.26 to -13.0 (kcal / mol) which indicates that hydrogen molecules are segregated to some extent in bridge site ,too.The value of energy in this site is more than negative two other sites.

Conclusion

The adsorption of hydrogen on the nickel surface in all three sites is and dissociative chemisorption. if compare the energy of adsorption in three sites together , we find the top site more favorable for physical adsorption then separation of molecules and chemical absorption will occur in bridge site.

Reference

[1] W. Rudzinski, T. Panczyk, Adsorption 8 (2002) 23.

[2] H.J. Kreuzer, S.H. Payne, in: W. Rudzinski, W.A. Steele, G.Zgrablich (Eds.), Equilibria and Dynamics of Gas Adsorption on Heterogeneous Solid Surfaces, Elsevier, New York, 1997.

[3] J. Shan, J.F.M. Aarts, A.W. Kleyn, L.B.F. Juurlink, Phys. Chem. Chem. Phys. 10(2008) 2227.

[4] J.W.C. Liberatori, R.U. Ribeiro, D. Zanchet, F.B. Noronha, J.M.C. Bueno, Applied Catalysis A General 327 (2007) 197.

[5] D.R. Killelea, V.L. Campbell, N.S. Shumann, A.L. Utz, Science 319 (2008) 790

[6] B. Bhatia, D.S. Sholl, J. Chem. Phys. 122 (2005) 204707.

[7] Buffoni.N, Pompeo.F, Santori. G, Nichio. N. Catalysis Communications 10 (2009) 1656–1660

[8] S. Badescu, S.C. Ying, T. Ala-Nissila¨, Phys. Rev. Lett. 86 (22) (2001)

[9] S.J. Tauster, S.C. Fung, R.T.K. Baker, J.A. Horsley, Science 211 (1981) 1121.

[10] I. Swart, P. Gruene, A. Fielicke, G. Meijer, B.M. Weckhuysen, F.M. de Groot,Phys. Chem. Chem. Phys. 10 (2008) 5743.

[11] R. Burch, in: Z. Paal, P.G. Menon (Eds.), Hydrogen Effect in Catalysis,
Marcel Dekker, 1988, p. 347.

Investigated the possibility of formation of stable complex between C60 fullerene and oxazepam by using Density Functional Theory (DFT) calculations

M.Nashtahosseini[a], S.Yeganegi[a], M.D.Ganji*[b]

[a]*Department of Physical Chemistry, Faculty of Chemistry, University of Mazandaran, Babolsar, 47415 ,Iran.*
(Email:mn216hosseini@yahoo.com)

[b]*Department of Chemistry, Islamic Azad University, Qaemshahr Branch, Mazandaran, Iran.*

Keyword: fullerene, oxazepam, DFT, BSSE.

Introduction:

Among the various types of nanomaterials, fullerenes are of great interest due to their unique properties, which make them very attractive for a wide range of applications specially in bio-area [1]. Oxazepam, one of the major benzodiazepines derivatives, are used for its sedative, anxiety-relieving and muscle-relaxing effects. Oxazepam works by acting on receptors in the brain called GABA receptors [2]. It's well recognized that the transport and bioavailability of drugs are significant factors in improving their distribution, therapeutics, and selectivity, and in ameliorating their toxic effects. Carbon based nano structures have been proposed as effective nanovectors for the drug delivery of therapeutic compounds [3]. In this work, we have investigated the possibility of formation of stable complex between C60 fullerene and oxazepam by using Density Functional Theory (DFT) calculations.

Method:

We have employed the first-principles approaches (ab initio) using numerical atomic orbitals as basis set. We make use of the generalized gradient approximation (GGA) with the Perdew–Burke–Ernzerhof (PBE) functional in density functional theory and the standard norm-conserving Troullier–Martins pseudo-potentials. We have used the SIESTA code, which solves the standard Kohn–Sham equations and has been demonstrated to be very efficient for large atomic systems. The calculations are done using a double-ζ basis composed of numerical atomic orbitals of finite range augmented by polarization functions (DZP) for all simulated atoms [4].

Results and discussion:

Several configurations were selected for oxazepam molecule approaching the five and six-member rings of the cage, the bridge sites above the C-C bonds and the top site directly above the (C-top) via its Cl, hydroxyl oxygen (OH) and carbonyl oxygen (CO) active sites. The calculated binding energies show that the adsorption of oxazepam via carbonyl oxygen active site upon the C atom of the C60 is the most stable configuration (Fig1). The binding energy was obtained by using the basis set super position error (BSSE) correction via the formula:

$$E_b = E\ (C60\text{-}Oxaz.) - [E\ (C60_{ghost} - Oxaz.) + E\ (C60 - Oxaz._{.ghost})\ ]$$

where the E(C60/ Oxazepam) is the total energy of the C60 interacting with the Oxazepam. The 'ghost' molecule/C60 corresponds to additional basis wave functions centered at the position of the Oxazepam or the C60, but without any atomic potential.

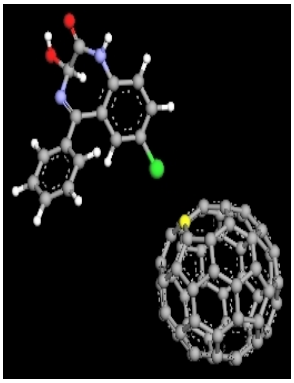

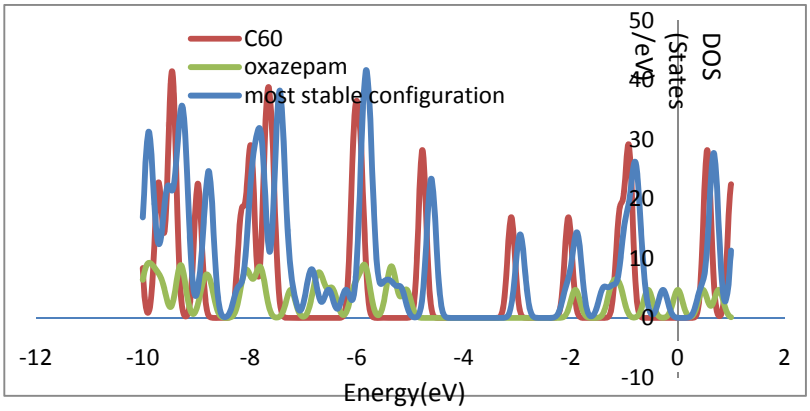

Fig.1 The most stable configuration

Fig.2 Plot Dos

The results obtained for the most stable configuration show that the binding energy and the amount of electron transfer between Oxazepam and C60 nanocage are -0.138 Kcal/mol and 0.01e, respectively. The density of state (DOS) for the combined system of Oxazepam–C60 as shown in Fig. 2. It can be seen from the figure that the DOS of the combined system of the Oxazepam–C60 complex is almost exactly the superposition of the DOS of the individual parts. This finding indicates that the Oxazepam is interacting weakly and that no significant hybridization between the respective orbitals of the two entities takes place.

Conclusoin:

A weak interaction can be seen from the low amount of charge transfer and the weak adsorption energy of Oxazepam-C60 complex even for the most stable configuration.

References:

[1] E. Nakamura, H. Isobe, Acc. Chem. Res. 36 (2003) 807.

[2] Whiting, P. J. Drug Discov. 8 (2003), 445

[3] K. Kostarelos et al., Nature 2 (2007) 108.

[4] Ganji, MD; Yazdani, H; Mirnejad**,** A, Physica E 42 (2010) 2184–2189.

Resonance assisted intramolecular hydrogen bonding of 6-hydroxy-6-(2-thienyl)-2-thenoylfulvene

A-R. Nekoei [*,a], M. Vakili [b], S. F. Tayyari [b], S. Salemi [c],

[a] Department of Chemistry, Shiraz University of Technology, Shiraz, 71555-313, Iran

[b] Department of Chemistry, Ferdowsi University of Mashhad, Mashhad 91774-1436, Iran

[c] Department of Chemistry, Sabzevar Tarbiat Moallem University, Iran

Keywords: Diacylcyclopentadiene, Dithenoylcyclopentadien, Intramolecular hydrogen bond, Resonance assisted hydrogen bond.

Introduction

1,2-diacylcyclopentadiene (1,2-DACP) compounds (also known as fulvene compounds) belong to a category of γ-dicarbonyl compounds with the capability of forming intramolecular hydrogen bond (IHB) (see Fig.1). In the enol form of these compounds, as a result of IHB, and because of a long π-electronic conjugation between carbonyl and cyclopentadiene double bands, a 7-membered ring-like structure (see Fig.1) is formed which is referred to as chelated or enolone ring (like 6-membered chelated ring in β-dicarbonyls). Since the chelated ring is heptagonal [1], the spatial orientations (distances and angles) for O and H−O segments of molecule are more proper to form much stronger O···H−O hydrogen bond in 1,2-DACPs, in comparison to that of β-dicarbonyls. Also the longer resonance structure of delocalized π-electrons makes the resonance assisted intramolecular hydrogen band, RAHB [2], in this type of γ-dicarbonyls to be stronger than that of β-dicarbonyls.

In the present work, 1,2-dithenoylcyclopentadien (DTCP) has been investigated with special attention to its IHB, in order to obtain detailed information on the conformational relative stabilities, structures and electron conjugation in its resonance assisted hydrogen bond (RAHB). It is also important to estimate the barrier height for proton transfer and the strength of the IHB, which is the main factor governing the conformational stability.

Method of Analysis

All quantum calculations were carried out with the GAUSSIAN 03 software package, applying the modern density functional theory, DFT, at B3LYP level using variety of basis sets.

Results and Discussion

There are 74 different keto and enol conformers for DTCP. Among 16 more stable cis-enol forms, there are only 4 chelated enol forms, i.e. the CE1, CE2, CE3, and CE4 conformers in Fig. 2, which have the seven-membered chelated ring of the IHB. These are so stable that the presence of other conformers in significant amounts in the sample is unlikely. This is predicted from all levels of calculation that the conformations CE4 and CE1 are the most stable and the most unstable chelated forms, respectively.

The barrier heights for proton transfers in the mentioned four chelated conformers of DTCP are given in Table 1. The barrier height energies, E_{BH}, for these conformers, calculated at B3LYP/6-31G** level using HC forms in Fig. 2 as transition state, are in the range of 0.31-0.39 kcal/mol. For α-cyanoacetylacetone (CNAA) and dibenzoylmethane (DBM) molecules with the strongest IHBs that have been reported for β-dicarbonyls, the proton transfer barrier heights were calculated to be 1.33 and 1.61 kcal/mol, respectively. Thus, the barriers for proton transfer in all DTCP conformers are significantly much lower than those in all mentioned β-dicarbonyls. These results also confirm that the IHB in DTCP conformers is stronger even than those in the strongest IHBs reported in β-dicarbonyls. This is confirmed by theoretical IHB energies (E_{HB}) reported in Table 1.

Comparing C=C, C−C and S−C bond lengths of each thienyl group in DTCP with the corresponding bonds of heterocyclic aromatic thiophene molecule with C_2v symmetry, suggest a well-oriented π-electron conjugations between the thienyl rings and the enol ring of DTCP.

It has been shown in the enol forms of β-dicarbonyl compounds that the Gilli's symmetry coordinates, q_1 (d_{C-C} - $d_{C=C}$), q_2 (d_{C-O} - $d_{C=O}$), and Q (q_1+ q_2) [3], offer a criterion for the bond equalization in their chelated ring due to their resonance assisted hydrogen bonding (RAHB). The values of q_1=0.15 and q_2=0.17 for the standard bond distances in the absence of π delocalization [3] lead to Q=0.32 for the completely π-localized enol forms, while Q=0.0 corresponds to the fully π-delocalized structures [2, 3]. For comparison, the calculated values for Q parameters of DTCP and several compounds with RAHD are also given in Table 1. The trend of these values is as: DTCP < DBM < BA (benzoylacetone) < TTFA (thenoyltrifluoroacetone) < CNAA < TMHD (2,2,6,6-tetramethyl-3,5-heptanedione) < AA,

from which three points can be clearly indicated. First, the resonance conjugation of phenyl, thienyl, cyclopentadiene and cyano groups assist the delocalization of π-electrons in chelated ring of IHB. Secondly, the IHB strengths (according to NMR proton chemical shift studies), which don't follow the mentioned trend of Q values, should depend on some other parameters besides the resonance assisting of functional groups in IHB. Third, the delocalization in 7-membered chelated ring of DTCP γ-dicarbonyl compound is very much more assisted compared to that in 6-membered chelated ring of β-dicarbonyl molecules.

Conclusion

The IHB in DTCP conformers is stronger even than those in the strongest IHBs reported in β-dicarbonyls. Well-oriented π-electron conjugations between the thienyl rings and the enol ring of DTCP are confirmed. Also, the delocalization in 7-membered chelated ring of DTCP γ-dicarbonyl compound has been shown to be very much more assisted compared to that in 6-membered chelated ring of β-dicarbonyl molecules.

Table 1: Gilli's symmetry parameter (Q), IHB energy (E_{HB}) and barrier height energy (E_{BH}) of DTCP and some selected β-dicarbonyls (energies in kcal/mol).

	DTCP	DBM	BA	TTFA	CNAA	TMHD	AA
E_{BH} [a]	0.39	1.61	NC	1.89	1.33	1.28	1.71
E_{HB} [b]	19.34	16.15	16.07	13.89	16.26	17.09	15.87
Q [b]	0.082	0.133	0.140	0.142	0.144	0.147	0.150

a:calculated at B3LYP/6-31G**; NC: not calculated .
b: calculated at B3LYP/6-311++G**.

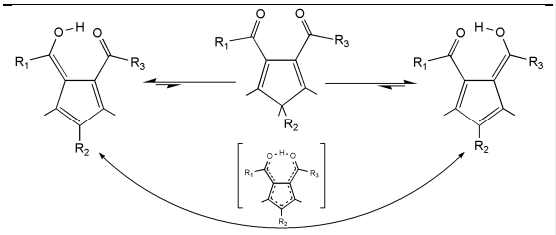

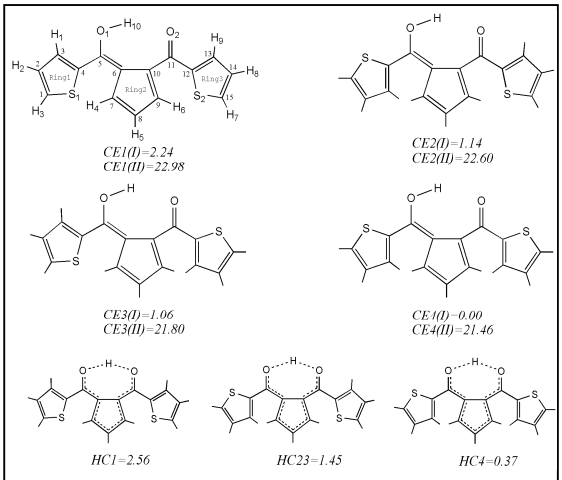

Fig 2: Cis-enol and H-centered forms of DTCP, and their relative stability, calculated at B3LYP/6-31G** level.

References

[1] R.S. Brown, A. Tse, T. Nakashima, R.C. Haddon, *J. Am. Chem. Soc*.101 (1979) 3157.

[2] V. Bertolasi, P. Gilli, V. Ferretti, G. Gilli, *G. J. Chem. Soc. Perkin Trans*. 2 (1997) 945.

V. Bertolasi, P. Gilli, V. Ferretti, G. Gilli, *J. Am. Chem. Soc.* 113 (1991) 4617.

Theoretical studies of some new synthesized four coordinated cadmium complexes

M. Montazerozohori[1] , H. Tavakol[2] ,A. Hojjati[1] and K. Nozarian

[1]*Department of Chemistry, Yasouj University, Yasouj 75918-74831, P. O. Box353, Iran.*

[2]*Department of Chemistry, Faculty of Science, University of Zabol, Zabol, Iran.*

(E- mail: mmzohori@mail.yu.ac.ir)

Abstract

Some new cadmium complexes of a symmetric bidentate Schiff base(L) were synthesized and characterized by IR, ^{1}H and ^{13}C NMR spectroscopies. Moreover, optimized structures, molecular parameters and vibrational frequencies were calculated at the B3LYP/LANL2DZ level of theory. Some important parameters such as bond lengthes, bond angles, dihedral angles, ΔH, ΔG, total energy and etc were extracted for optimized structures.

Keywords: Schiff base, Complex, Cadmium, Optimization.

Introduction

Several Schiff base have been studied in the past because of their wide applicability. The derivatives of such compounds and their metal complexes, and also after suitable structural modifications, may be used as bioactive materials for medicines, biological, pharmacological, clinical and analytical applications[1-4].

Experimental

Preparation of* N,N′-bis((E)-3(2-nitrophenylallylidene)benzenediamine *and its complexes.

To a solution of 3-(2-nitrophenylpropenal (4 mmol) in absolute methanol (10 mL) was added a solution of ethylenediamine (2 mmol) in absolute methanol (10 mL) and severely stirred for 3-4 hours to obtain the ligand with good purity with yield of 75%. The cadmium(II) complexes were prepared by stepwise addition and stirring of the ligand (0.5 mmol) to the respective 0.5 mmol of cadmium(II) halides in methanol (15 mL) for 1-3 hours.

Computational method

All DFT calculations were done by using the Gaussian 98 program [5] with B3LYP [6] method and LANL2DZ basis set. All molecules have been used without any symmetry restriction and C1 symmetry was assumed for all molecules. Calculations have been done in the gas phase. Some important parameters were extracted.

Results and discussion

The results of optimization show that the geometry of complexes is pseudo-tetrahedral as it would expect for d^{10} group metal ions in four coordinated complexes. The optimized structure of $CdLI_2$ is seen in scheme 1. Some important bond lengths, bond angles and totional angles are summarized in Table 1, 2 and 3.

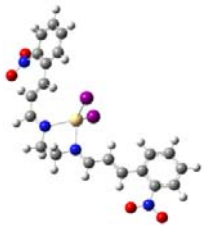

Figure 1

Table 1- Some important bond lengths.

molecule	$CdLCl_2$	$CdLBr_2$	$CdLI_2$	Ligand
M-N	2.25	2.24	2.27	-
M-N'	2.27	2.26	2.26	-
M-X	2.56	2.75	2.94	-
M-X'	2.56	2.75	2.98	-
C_2=N	1.34	1.34	1.33	1.33
$C_{2'}$=N'	1.33	1.33	1.33	1.33

Table 2- Some important bond angles.

molecule	$CdLCl_2$	$CdLBr_2$	$CdLI_2$
N'-M-N	77.39	78.73	78.22
N'-M-X	111.75	112.70	112.43
N'-M-X'	108.76	108.28	102.78
N-M-X	111.78	110.18	111.99
N-M-X'	111.38	114.23	112.66
X-M-X'	125.52	123.80	127.32

Table 3- Some important tortion angles.

molecule	$CdLCl_2$	$CdLBr_2$	$CdLI_2$	Ligand
N'-$C_{1'}$-C_1-N	-48.16	-50.38	-50.87	-61.98
N-C_2-C_3-C_4	-29.90	-22.71	-31.12	-0.13
C_3-C_4-C_5-C_6	117.15	118.76	-10.51	17.30
N'-$C_{2'}$-$C_{3'}$-$C_{4'}$	178.92	179.34	179.29	179.98
$C_{3'}$-$C_{4'}$-$C_{5'}$-$C_{6'}$	178.23	178.63	179.01	-179.70

Various energies of complexes after optimization at the mentioned level of theoretical method are summarized in Table 4. The results show the values HF-energy, ΔH, ΔG and total energy of complexes are being more positive from cadmium chloride complexes to cadmium iodide one.

Table 4- HF-energy, ΔH, ΔG and total energy of ligand and itscomplexes

Molecule	$CdLCl_2$	$CdLBr_2$	$CdLI_2$	L(ligand)
HF energy	-1354.2112	-1350.6574	-1347.0991	-1276.0508
Corrected ZPE	0.35744395	0.357097029	0.356954801	0.353874796

Corrected total energy	-1353.853784	-1350.300298	-1346.742126	-1275.69695
Corrected Gibs Free energy	-1353.925169	-1350.374257	-1346.816731	-1275.760272
Total elect. En	-1353.808259	-1350.254453	-1346.696197	-1275.657169
Corrected Enthalpy	-1353.821821	-1350.268001	-1346.709739	-1275.670586

Finally, optimized structures, molecular parameters were calculated at the B3LYP/LANL2DZ level of theory. Theoretical data results pseudo –tetrahedral geometry for complexes.

References

[1] R. D. Jones , R. D . Summerville , F. Basolo, Chem . Rev. 79 (1979) 139.

[2] G. Henrici-Olive and S. Olive, The Chem. Catal . Hydrogenation of Carbon Monoxide, Springer, Berlin,
(1984), p . 152.

[3] J. Costamagna, J. Vargas, R. Lattore, A. Alvarado , G. Mena, Coord. Chem , Rev. 119 (1992) 67.

[4] Z. Popovic, V. Roje, Gordana, G. Pavlovic, D. Matkovic, M. Rajic, I. Leban, Polyhedron 23 (2004) 1293.

[5] M.J. Frisch, Gaussian 03, Revision C02, Gaussian, Inc, Wallingford CT,(2004).

[6] A.D. Becke, J. Chem. Phys. 5648(1993).

Study of Diels-Alder reactions Between of structures bicyclo[2.2.2]oct-2-ene And pyrrole by using Ab initio molecular orbital and DFT Method

M.Nouraliei[a],R.Soleymani*[a,b]and F.Sarabi[c]

[a]*Department of Chemistry, Islamic Azad University of Touyserkan, Young researchers Club, Touyserkan , Iran*

(Email: nima_soleymani@yahoo.com)

[b]*Department of Chemistry, Islamic Azad University of Shahre-rey Tehran, Tehran ,Iran*

[c]*Department of Chemistry, Islamic Azad University of Rasht, Rasht,Iran*

Keywords: Ab initio, Cycloaddition , DFT , Diels-alder reaction , NBO

Introduction

S)-1-acetylcyclohex-3-enecarbonitrile is one ofcompositions that produce during cycloadditionreaction of Diels-Alder ,that the mechanism of itsproduction operate experimentally based on belowreaction[1]:

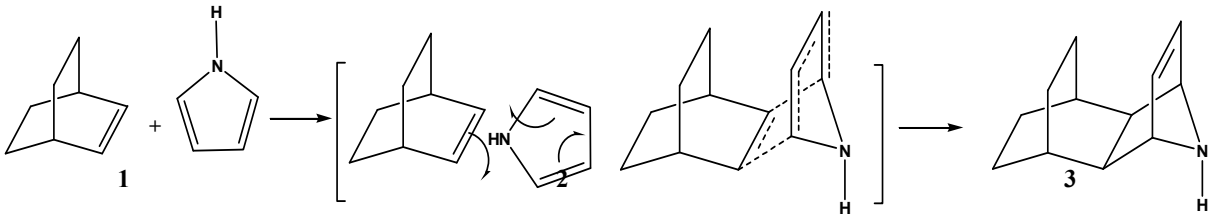

Calculation methods

The calculations of quantum mechanics in theory levelby using UHF and DFT theory method operated on thestructure of 1 structure . Inorder to this, firstly the structure of initial matter andproduct matter designed by using ChemOffice 2008software[2], and initial optimization operated by usingWinmopac version 2.0 software and PM3 method .Thetransition mode of structure simulate by using keywordSADDLE and then transition state GAUSSIAN 03Wpackage program and keyword QST3 implemented on apentum-PC computer with a 530 MHz processor , usedfor finalization[3]. Eventually, the final optimization andcalculation of energy levels operated in theory of thelevels HF/6-311+G** and B3LYP/6-311+G**.

Result and discussion

The results (E_0) total energy , (E_{ele}) electronic energy ,(ZPE)zero point energy and (E_a)activation energy reported infolowingtable.

Method	B3LYP/6-311+G**				HF/6-311+G**			
Geometry	ZPE	E_{ele}	E_0	ΔE_0	ZPE	E_{ele}	E_0	ΔE_0
Reactive	0.270743	- 522.351594	-522.080851	0.063819 (40.04642)[a]	0.289866	-518.8389858	-518.549120	0.081736 (51.28934)[a]
Transition State	0.265329	-522 .282361	-522.017032		0.284637	-518.7520217	-518.467384	
Product	0.266714	-522.3023188	-522.035605		0.289865	-518.8389857	-518.549120	

[a] value energyin kcal mol^{-1}

Conclusion

The process of production of (1R,4S,4aS,5S,8R)-1,4,4a,5,6,7,8,8a-octahydro-1,4-epimino-5,8-ethanonaphthalene structure during cycloaddition Diels-alder reaction studied during quantum mechanics calculation and density functional theory (DFT) in level of the HF/6-311+G** and B3LYP/6-311+G** that results show a kind of σ head to head overlap between two p orbital of alkene with tow orbitals that belong to dyene carbon that lead to production of two new C-C (σ bond) and as a result production of pericyclic ring transition state.This reaction is endothermic and the rate of activation energy for this reaction is equivalent with 40.04642(kcal.mol^{-1}) and transition state has high energy level ,almost equal -327565.68(kcal.mol^{-1}) .

References

[1] J. McMurry., *Organic Chemistry*, 7th Ed., (**2008**).

[2]www.CambridgeSoft.com,*CambridgeSoft Corporation*, All Rights Reserved. ©**1998-2010**

[3] M. j. Frisch et al. *GAUSSIAN 03*, Revision C. 01, Gaussian Inc., Wallingford. CT, **(2004)**.

The Study Transformation Of Vinyl Cyclopropane To Cyclopentane Via Transition State Of De Radical Using Quantum Mechanic Calculation

M. nouraliei[a] , R.Soleymani*[a,b] and M.Karimi[c]

[a]*Department of Chemistry, Islamic Azad University of Touyserkan, Young researchers Club, Touyserkan , Iran*

(Email: nima_soleymani@yahoo.com)

[b]*Department of Chemistry, Islamic Azad University of Shahre-rey Tehran, Tehran ,Iran*

[c]*Department of Chemistry, Islamic Azad University of Omidieh, Omidieh,Iran*

Keywords: Cyclopentane ; DFT ; Vinyl cyclopropane ; Wood ward – Hoffman rules

Introduction

The process of this reaction has been done empirical in the laboratory and totally space position of R_1 and R_2 to each other follows Wood ward – Hoffman rules [1,2].

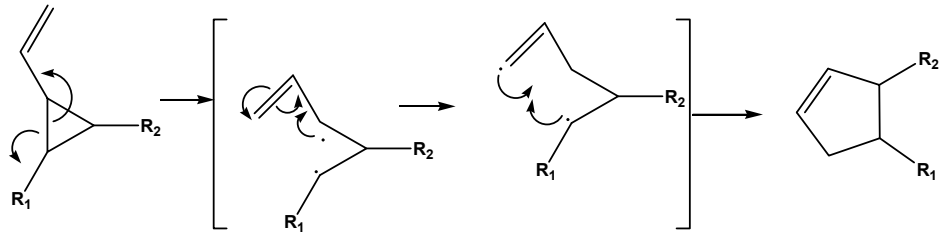

Reactive TS Product

R_1 , R_2 = CH_3

Method

For calculation density functional theory (DFT) and Ab initio methods in theory of the level B3LYP/6-311+G** and HF/6-311+G** used Gaussian 03w package program[2]. Also for this purpose used computer Pentium 4 with intel 2.13 GHZ processor.

Result and discussion

Total calculation for rearrangement mechanism of structure vinyl cyclopropane To cyclopentane by theoretical methods reported in following table.

TABLE1: The results calculated energetic (in Hartree)

Methods	**B3LYP/6-311+G****			**HF/6-311+G****		
Structure	**Reactive**	**TS**	**Product**	**Reactive**	**TS**	**Product**
ZPE	0.116334	0.109885	0.116334	0.123689	0.114676	0.123693
E_{ele}	-195.3452652	-195.218966	-195.3452649	-194.024097	-193.819665	-194.024096
E^0	-195.228939	-195.109081	-195.228931	-193.900408	-193.704989	-193.900404
ΔE_0	0.1262992 (79.252748)[a]			0.204432 (128.28108)[a]		

[a]Numbers in kcal mol^{-1}

Conclusion

Results showed that this reaction is a rearrangement which follows Wood ward – Hoffman rules. Transforming structure vinyl cyclopropane To cyclopentane will be accompanied by transition state of 2-(Z)-pentene-1,5-diradical. This transition state exist in Z form and E form. But finally only Z form turns to cyclopentane which is accompanied by 79.252748 Kcal/mol energy reagent.

References

[1] Vinylcyclopropane – Cyclopentene Rearrangement , Neureiter , *N.P.J.Org.Chem*.**1959**,2,4 204.4

[2] Baldwin, *J . E . Chem Rev*. **2003**, 103,1179

[3] M. j. Frisch et al. *GAUSSIAN 03*, Revision C. 01, Gaussian Inc.,Wallingford. CT, **2004**.

A reliable relation for analysis mole fraction of Carbone monoxide in a typical liquid propellant engine

M. Norouzi Bakhsh*, M.R. Nayeb Hosseini
Department of chemistry, Malek-ashtar University of Technology, Esfahan, Iran
(Email: m_norouzi@mut-es.ac.ir)

Keyword: Mole fraction, Carbone monoxide, Liquid propellant, Analysis, Combustion products

Introduction

Analysis of combustion products and combustion condition such as oxidizer to fuel ratio, combustion chamber pressure and environmentally consideration ,thrust profile are one of the important section off accept or reject of the fuel. One of the pollutant gases are Carbone monoxide, so we want to find a reliable relation for analysis mole fraction of Carbone monoxide in combustion of liquid butane and liquid oxygen by special software in high pressure.

Result and discussion

In general reaction between butane and oxygen are in this form:

$$C_4H_{10} + 6.5\ O_2 \rightarrow 4\ CO_2 + 5\ H_2O$$

Oxygen to fuel mass ratio is:$\frac{208}{58}$. We use CEC[2] software [1] for analysis mole fraction of Carbone monoxide in combustion products. By considering that we use stoichiometry mass balance between oxidizer and fuel. Because of high pressure and temperature combustion products are reacted together and formed other species like Carbone monoxide The relation which concluded is:

$$X = ZY^{-0.22} \qquad (1.1)$$

X is mole fraction of Carbone monoxide in combustion products and Y is ratio of nozzle exit area to nozzle throat area (A_E/A_t), and Z is a function of pressure:

[۲] -Chemical Equilibrium composition Calculation

$$Z = -0.0002P + 0.198 \qquad (1.2)$$

Pressure is entered in relation (1.2) at atmosphere unite. In Table1 You see the calculation results and software results and error percent between calculations and software.

Table 1. Comparison between theoretical calculation and software results in mole fraction of Carbone monoxide

A_E/A_T	P(atm)	Calculated result	Software result	%error
13	25	0.1115	0.1127	-1.07
9	40	0.1172	0.1186	-0.91
8	30	0.1215	0.1221	-0.46
2	20	0.1666	0.1639	-1.64
5	50	0.1319	0.1324	-0.38
16	35	0.1038	0.1020	+1.77

Conclusion:

Carbone monoxide is an important pollutant gas which causes destroying Ozone layer. By achieving a reliable relation for analysis mole fraction of Carbone monoxide in a typical liquid propellant engine we can analysis mole fraction of Carbone monoxide and by adjusting condition such as pressure and temperature you can obtain good performance.

Reference

[1] Gordon, S., and McBridge, B. J., Computer Program for Calculation of Complex Chemical Equilibrium Compositions, Rocket Performance, Incident and Reflected Shocks, and Chapman− Jouguet Detonations, NASA SP-273, 1971.

Relations between combustion chamber pressure and CO-CO_2 equilibrium in C_2-C_8 hydrocarbons combustion products using CEA code

M. Norouzi Bakhsh*, M.R. Nayeb Hosseini
Department of chemistry, Malek-ashtar University of Technology, Esfahan, Iran
(Email: m_norouzi@mut-es.ac.ir)

Introduction:

The CO-CO_2 equilibrium depends on two important factors, temperature and pressure. In high temperature, the equilibrium will shift to CO formation because direction of the reaction toward CO_2 is exothermic. According to Le Chatelier law, the formation of CO_2 in high pressure is favorable [1,2]. In this paper, the effect of high pressure and temperature on CO-CO_2 equilibrium in C2-C8 hydrocarbons combustion products is investigated by CEA code.

Methods:

Most gas-phase thermodynamic functions were calculated from molecular constant data using ideal gas partition functions. All result accomplished by CEAgui, a graphical-user-interface for CEA2, version 2 of NASA Glenn's computer program Chemical Equilibrium with Applications. The analysis, definitions, and examples are the same as those given in the CEA manuals [3]. Pure oxygen was selected as oxidant in a stoichiometric mixture.

Results and Discussion:

Results of computation are shown in Tables 1 and 2. As shown, the mole fraction of CO is increased in higher pressures. Also with increasing in combustion chamber pressure we see that the temperature will increase. There is very important result that the pressure of combustion chamber is more effective than temperature in CO-CO_2 equilibrium. Thus, for higher combustion chamber pressures, we can obtain a better combustion rate and more energy and efficiency.

Conclusions:

Increasing combustion chamber pressure will increase CO_2 mole fraction and decrease CO mole fraction in combustion products of C_2-C_8 hydrocarbons. Thus, the higher combustion chamber pressures lead to a better combustion rate and more energy and efficiency.

Table 1. Mole fractions of CO & CO_2 in combustion products

Combustion chamber pressure (bar)	39.477		49.346		59.215		69.085	
	Mole fraction CO	Mole fraction CO_2	Mole fraction CO	Mole fraction CO_2	Mole fraction CO	Mole fraction CO_2	Mole fraction CO	Mole fraction CO_2
C_2H_6	0.17549	0.15556	0.17421	0.15791	0.17311	0.15989	0.17214	0.16162
C_3H_8	0.18777	0.16451	0.18643	0.16700	0.18527	0.16910	0.18425	0.17093
C_4H_{10}	0.19457	0.16938	0.19319	0.17195	0.19201	0.17412	0.19097	0.17600
C_5H_{12}	0.19891	0.17243	0.19751	0.17505	0.19631	0.17726	0.19527	0.17913
C_6H_{14}	0.23832	0.15715	0.23733	0.15945	0.23646	0.16139	0.23569	0.17957
C_7H_{16}	0.20415	0.17597	0.20275	0.17860	0.20150	0.18090	0.20042	0.18287
C_8H_{18}	0.20582	0.17714	0.20439	0.17983	0.20316	0.18210	0.20208	0.18408

Table 2. Combustion chamber Temperatures (K)

Combustion chamber pressure (bar)	39.477	49.346	59.215	69.085
C_2H_6	3598.13	3631.99	3659.83	3683.48
C_3H_8	3612.39	3646.70	3674.91	3698.90
C_4H_{10}	3620.13	3654.67	3683.09	3707.26
C_5H_{12}	3625.08	3659.78	3688.33	3712.79
C_6H_{14}	3641.77	3676.75	3705.52	3729.96
C_7H_{16}	3631.27	3666.33	3694.87	3719.29
C_8H_{18}	3633.15	3668.10	3696.86	3721.32

References:

[1] TOYOTA Motor Sales USA. Inc. Emission # 1, combustion chemistry

[2] G. A. Olah, "chemistry of energetic materials", Defense Sciences Office DARPA Arlington, Virginia

[3] NASA RP-1311 Part I, 1994 and Part II, 1996.

N-Derivatives of Tsallis Entropy Density

S. Noorizadeh

Chemistry Dept., College of Sciences, Shahid Chamran Univ., Ahwaz, Iran; (noorizadeh_s@scu.ac.ir)

Keywords: Information Theory, Shannon Entropy, Tsallis Entropy, Fukui Function.

Introduction

The Shannon entropy [1], which is a measure of delocalization of electron density, is one of the cornerstones of the Quantum Information theory. Tsallis [2] proposed a generalization of the Boltzmann-Gibbs entropic measure. The new entropy functional, which is called Tsallis entropy, has the form:

$$T(r) = \frac{1-\int p(r)^q \, dr}{q-1} \qquad (1)$$

in which p(r) is the normalized probability distribution function and q is a positive number, which describes the degree of non-additivity. For $q \to 1$, the Tsallis entropy reduces to the Shannon entropy.

In recent years some attempts have been made to use the Information theory concepts in the chemical systems [3]. In this contribution, it is attempted to derive first and second N-derivatives of the Tsallis entropy density. The obtained relations, which show the variation of the information content of a system during the change of electrons, are evaluated for some atomic systems.

Result and Discussion

Since in density functional theory, the electron density is considered as the carrier of information, for a homogenous of N electrons which are constrained in a volume V, the density per particle or *shape function* ($\sigma(r) = \rho(r)/N$) can be considered as the probability distribution function. Therefore the Tsallis entropy could be written in the following form:

$$T_N(r) = \int \frac{\sigma(r)-\sigma(r)^q}{q-1} dr = \int t_N(r) \, dr \qquad (2)$$

where $t_N(r)$ is considered as the Tsallis entropy density. The first derivative of this density with respect to the number of electrons is given by:

$$\left(\frac{\partial t_N(r)}{\partial N}\right)_v = \frac{f(r)-\sigma(r)}{N(q-1)}\{1 - q\,\sigma(r)^{q-1}\} \quad (3)$$

where f(r) is the Fukui function. The difference $f(r) - \sigma(r)$, carries information about the inhomogeneity in the electron density of system. Therefore it seems that the change in the Tsallis entropy density of a chemical system during the course of a reaction is due to the inhomogeneity of electron density. For a one-electron system this derivative changes to:

$$\left(\frac{\partial t_1(r)}{\partial N}\right)_v = \frac{f(r)-\rho(r)}{(q-1)}\{1 - q\,\rho(r)^{q-1}\} \quad (4)$$

The difference between these two derivatives (eqs. (3) and (4)) may consider as the electronic correlations entropy. These derivatives are evaluated for the first two raw elements of the periodic table. The obtained electron densities using MP2/6-311++G** method from the AIM2000 software are used for the calculation of Fukuies. Taking the Li atom as an example, the radial distribution of the first derivative of the Tsallis entropy density (with different q) are shown in Fig. 1.

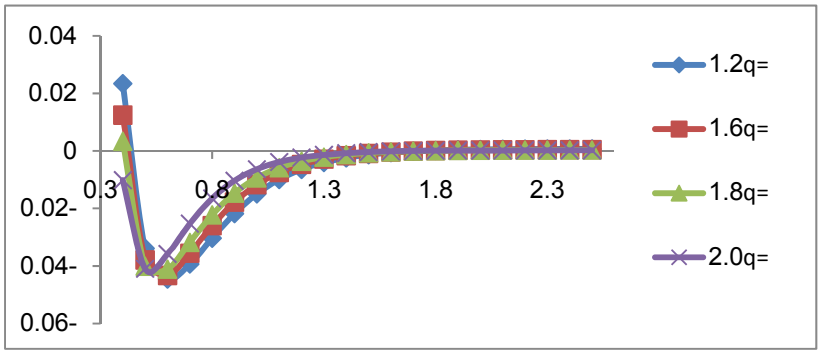

Fig. 1. Radial distribution of Tsallis entropy derivative for Li atom.

The obtained second derivative of the Tsallis entropy density has the following form:

$$\left(\frac{\partial^2 t(r)}{\partial N^2}\right)_v = \frac{[1-q\,\sigma^{q-1}(r)]}{q-1}\left\{\frac{f^{(2)}(r)}{N} - \frac{2[f(r)-\sigma(r)]}{N^2}\right\} - \frac{[f(r)-\sigma(r)]^2}{N^2} q\,\sigma^{q-2}(r) \quad (5)$$

where $f^{(2)}(r)$ is dual descriptor, which could be considered as an indicator for both the nucleophilic and electrophilic regions . Therefore this derivative can be used as an orientation/selectivity descriptor in a chemical reaction.

Conclusion

It is shown that the first and second derivatives of the Tsallis entropy density, which is the generalized form of the Shannon entropy density, have something to do with the

inhomogeneity of the electron density. This inhomogeneity causes the changes in statistical entropies during the course of a reaction.

References

[1] C.E. Shannon, Bell Syst. Tech. J. **27**, 379 (1948).

[2] C. Tsallis, J. Stat. Phys. **52**, 479 (1988).

[3] S. Noorizadeh and E. Shakerzadeh, Phys. Chem. Chem. Phys. **413**, 347 (2010).

The influence of the substituents on the structural properties of the pyridines complexes of OsO_4 and methyltrioxorhenium

Fatemeh Niroomand Hosseini*
niroomand55@hotmail.com
Department of Chemistry, Islamic Azad University, Shiraz Branch, Shiraz, Iran

Keywords: rhenium; osmium; equilibrium; pyridines

Introduction

Osmium tetroxide has been widely employed for the *cis*-dihydroxylation of olefins under mild conditions. This reaction is of fundamental importance in nature and many oxidation systems have been developed for this transformation [1]. On the other hand, methyltrioxorhenium CH_3ReO_3 or MTO, containing a metal-methyl bond, is a reactant stable to hydrolysis, and can act in the presence of H_2O_2 or O_2 as a highly efficient and selective catalyst for a number of reactions, among them epoxidation of alkenes [2]. In both cases, N-donor ligands like pyridine and its derivatives (i.e OsO_4.L and MTO.L) can accelerate the rate of the reactions.

Method

Density functional calculations were performed with the program suite Gaussian03 [3]. The LANL2DZ basis set was used with B3LYP method. All geometries were optimized. To evaluate and ensure the optimized structures of the molecules, frequency calculations were carried out using analytical second derivatives. In all cases only real frequencies were obtained for the optimized structures.

Result and discussion

To consider the influence of the remote substituents on the structural properties of the OsO_4.L and MTO.L complexes, where L = pyridine and its derivatives, density functional theory (DFT) were performed with the program suite Gaussian03 [3] for 6 different pyridine complexes. The bond distances from DFT-optimized structures (B3LYP/LANL2DZ) for the

compounds OsO_4.L and MTO.L along with DFT-optimized structures for these complexes are calculated. In each case the geometry at the metal is distorted trigonal bipyramidal, but the bond length of the N-Os(VIII) and N-Re(VII) is influenced significantly by the substituent on the pyridine ring. The M-N (M=Os or Re) bond lengths of the OsO_4.L and MTO.L complexes apparently depend on the basicity of the pyridine ligands. For example the Re-N bond length of the 4-methylpyridine complex is more than 0.043 Å shorter than the corresponding bond length for the 3-chloropyridine complex (2.445 Å vs 2.488 Å, respectively).

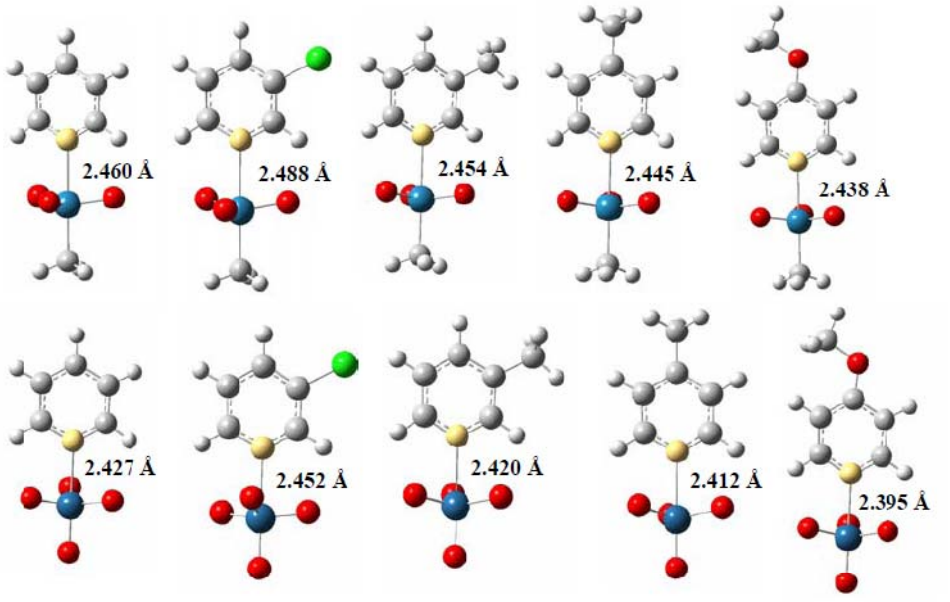

Figure. The DFT-optimized structures and calculated bond distances for the compounds OsO_4.L and MTO.L.

Conclusion

On the basis of density functional theory (DFT) calculations, the M-N (M=Os or Re) bond lengths of the OsO_4.L and MTO.L complexes apparently depend on the basicity of the pyridine ligands.

References

[1] (a) H.C. Kolb, M.S. Van Nieuwenhze, K.B. Sharpless, Chem. Rev. 94 (1994) 2483; (b) U. Sundermeier, C. Döbler, M. Beller, in: J.E. Bäckvall (Ed.),Modern Oxidation Methods, Wiley-VCH, Weinheim, 2004; (c) M. Schroder, Chem. Rev. 80 (1980) 187.

[2] (a) D. Sica, D. Musumeci, F. Zollo, S. De Marino, Eur. J. Org. Chem., (2001) 3731; (b) W.A. Herrmann, R.W. Fischer, D.W. Marz, Angew. Chem., Int. Ed. Engl., 30 (1991) 1638; (c) A.M. Al-Ajlouni, J.H. Espenson, J. Am. Chem. Soc., 117 (1995) 9243.

[3] M. J. Frisch, et. al., *GAUSSIAN 03 (Revision A.1)*, Gaussian, Inc., Wallingford, CT, 2004.

Prediction of aqueous pK_a values of drugs: A theoretical study

H. Dezhampanah, B. Ghalami-Choobar*, P.Nikparsa

Department of Chemistry, Faculty of Science, University of Guilan, P.O.Box:19141, Rasht, Iran

E-mail address: B-Ghalami@guilan.ac.ir (B.Ghalami-Choobar)

Keywords: pKa, PCM, B3LYP, dissociation

Introduction

The pK_a value plays a very significant role in many aspects of drug absorption, metabolism, and excretion [1]. Pharmaceutical companies now days need to evaluate the pK_a of any potential lead before proceeding to its optimization. However, the experimental evaluation of the pK_a of the potential drugs is not always possible and can be tedious. Therefore, an accurate computational approach is needed [2]. In this work, calculations of pK_a values were performed on the enoxacin and norfloxacin drugs by using Gaussian 98 software. Gas-phase energies were calculated using common basis set at B3LYP level. Free energies of solvation were computed using the polarized continuum model (PCM). Results were compared with experimental pK_a data.

Method

The pK_a values of the compounds in aqueous solution were calculated in according to the following dissociation reaction 1 by using of equation 2.

$$\longrightarrow \quad AH(aq) \qquad A^-(aq) + H^+(aq) \tag{1}$$

$$\Delta G^0(aq) = -2.303\ RT\ \log K_a \tag{2}$$

Where ΔG°_{aq} indicates to the free energy change of the dissociation reaction in aqueous solution. The general approach to calculating ΔG°_{aq} was used on the basis of the thermodynamic cycle A (see figure1).

Using the thermodynamic cycle A, the values were calculated using the equation 3.

$$\Delta G^0(aq) = [G^0(g)\ A^- - G^0(g)\ AH] + [\Delta G^0(solv)\ A^- - \Delta G^0(solv)\ AH] - 270.88 \tag{3}$$

All of calculations in gas -phase and aqueous -phase were made by using Gaussian 98 software. The optimized basis set 6-31G** were used for all of computing.

Results and discussion

The B3LYP method was applied to derive the free-energy changes of the gas-phase reaction and the PCM model was used for the solvation energy in aqueous solution. Firstly, the calculations of the pK_a values were determined for 7 acids and results were shown in Table 1**.** As shown in figure 2, there is a very good correlation of between the experimental and the calculated values of pK_a with a correlation coefficient 0.884 for B3LYP method according to follow equation:

pKa(exp)= A pKa(Calc)+ B (4)

Where A and B are the constant parameters. Finally, the pK_a values of the enoxacin and norfloxacin drugs contain to extended aromatic rings were predicted by using the equation 4 and the results were given in table 2. As been observed, the experimental and predicted values have a difference of less than 0.2 pK_a unit.

Table 1. The pK_b values of compounds

Compound	pKa(calc)	pKa(exp)
Benzoic acid	3.51	4.2
4,fluoro-Benzoic acid	4.11	4.15
4,cyano-Benzoic acid	3.18	3.55
4,phenyl-Benzoic acid	4.54	4.49
3,chloro-Benzoic acid	3.54	3.84
3,bromo-Benzoic acid	3.67	3.81
4,methylamino Benzoic acid	5.96	5.03

Table 2. Comparison of experimental and predicted values of compounds

Compound	pKa(Predicted)	pKa(exp)
Enoxacin	6.12	6.31[a]
Norfloxain	6.26	6.40[b]

a: The value taken from ref.[3]

b: The value taken from ref.[4]

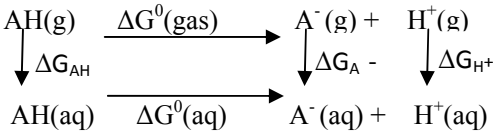

Figure1. Thermodynamic cycle A

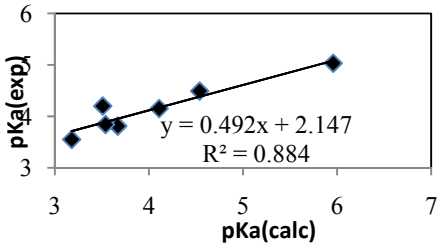

Figure2. Correlation of the experimental and the calculated values of pK_a

References

[1] S. Zhang, J. Baker, Peter Pulay, J. Phys. Chem. A, 114 (2010) 425

[2] G. K. Kinsella, F. Fordringuez, Bioorg. Med. Chem 15(2007) 2880

[3] F. Ja-You, L. Hung-Hong, J. Control. Release, 54 (1998) 293

[4] P. H.Lee, S. A. Ayyampalayam, Mol. pharmaceutics, *4* (2007)498

Hammett Constant on Benzoic acid substituted & Phenylacetic acid substituted in aqueous phases, a DFT study

F.R.Nikmaram*[a], F.Moradi[a], A.Abrari[a]

a)Department of Chemistry, Faculty of science, Islamic Azad University Shahr-e-Rey Branch, Tehran,IRAN

Abstract

Hammett constants (σ) can be important factor to understanding substitution and position effects on Benzoic acid. This report describes a computational study of ΔG° and **σ** for six substituted Benzoic acid (x= F,Cl,OH,NH_2,CN,NO_2) and Phenylacetic acid substituted (X= OH,NH_2) at para and meta positions in gas and aqueous phases by DFT method and compare to avilable experimental and theoretical results.

Key words*:* Hammett Constant, Benzoic acid, Phenylacetic acid substituted, Aqueous phases

Introduction

Hammett quantified the effect of substituent on any reaction by defining an empirical electronic substituent parameter (σ) which is derived from the acidity constants, K_aó s of substituted benzoic acids.The Hammett Equation relates the relative magnitude of the equilibrium constants to a reaction constant ρ and a substituent constant σ.For the ionization of benzoic acid and Phenylacetic acid in pure water at 25 ºC, the constant ρ is defined as 1.00 and 0.56, separately.

Methods

In this work , we employed DFT method with Lee-yang-Parr ó s correlation Functional (B3LYP) and 6-31 G** basis set. All calculation were carried out with the Gaussian 98 program[1] by a CPU corei7(2G RAM) computer with the windows XP operating system.The solvent effect is taken into account using the self-consistent reaction field (SCRF) method [2]-this method is based on the onsager reaction field theory of electrostatic salvation [3]-by using either the Integration Equation Formalism Polarizable Continuum Model (IEF-PCM)[4].The harmonic vibrational frequencis of the fully optimized structures were calculated to confirm the stationary point as a local minima with all positive frequencies,and to provide the

thermodynamic quantitative properties.

Results

We study the linear free energy relationship and valuse of σ for six substituted benzoic acid (X = F,Cl,OH,NH_2,CN,NO_2) at para and meta positions in gas phase and in aqueous phase.The calculated free energies by B3LYP/6-31G** of molecular and ionic forms of benzoiec acid and six substituted benzoic acid (X= F,Cl,OH,NH_2,CN,NO_2) at para and meta positions in gas phase are in agreement with the Ref[5],calculated by MP2/6-31+G(d,p)(Table1). The linear free energy relationship and values of calculated and experimental for σ are given in Table2.[6,7].

Conculsion

The Hammett plot for calculated results show Fairly good linear correlations at gas phase(r= 0.97 (para),r=0.85(meta))and at aqueous phase(r=0.95(para),r=0.89(meta))in compare to experimental linear correlation. The electron donating substituent NH_2 at meta and para and OH at para positions have negative value for σ. The other substituents have positive value for σ, due to electron withdrawing effect.

The results have shown that substituent resonance effects are dominated by the greater σ_P for NO_2 and CN, and inductiv effects for NH_2,OH, F and Cl substituents to be important (Table2).We use this strategy for σ calculations at phenylacetic acid substituted (X= OH, NH_2) in gas and aqueous phases. ΔG° in aqueous phase are given by the expression:

$C_6H_5COOH_{(aq)} + H_2O \rightarrow C_6H_5COO^-_{(aq)} + H_3O^+_{(aq)}$

$\Delta G_1^\circ = -2.3RT \log \{([A^-]_{aq}[H_3O^+]_{aq})/([HA]_{aq}[H_2O])\} = -2.3RT \log\{K_a/H_2O\}$

$\Delta G_1^\circ = 1.36\, Pk_a + 2.36$

That $\Delta G^\circ_f H_3O^+_{(aq)}$ and $\Delta G^\circ H_2O_{(l)}$ are -237.19 kJ/mol.

$PK_H - PK_x = \rho\sigma$

From the frequency calculations with all positive frequencies , we obtained the G° value for structures (molecular and ionic form) in gas and aquoeus phases. It is predicted that on benzoic acid the electron donating substituents (NH_2 at meta and para and OH at para positions) with negative value of σ may decrease the acidity constant of the reaction.The electron withdrawing substituent (F,Cl,CN,NO_2,$(OH)_{meta}$) with $\sigma_m > 0$ and $\sigma_p > 0$ can

increase the acidity constant of the reaction.We found that substituents of OH at para and NH_2 at para and meta positions on phenyl acetic acid decrease the acidity constant due to electron donating properties. Substituent of OH at meta on phenyl acetic acid with electron withdrawing role is leading to increase of acidity constant.

Table1: calculated G° values

	B3lyp/6-31G**		Ref[a]	
type	molecule	ion	molecule	ion
Benzoic acid	-420.8642	-420.3435	-419.6321	-419.0812
p-Cl	-880.4609	-879.9484	-878.6576	-878.1136
p-NO_2	-625.3670	-624.8774	-623.6466	-623.1135

a.Ref[5,6,7]

Table2: Calculated σ in gas & aqueous phases and Experimental values

	B3lyp/6-31G** (gas)		B3lyp/6-31G** (in water)		Exp[a] In water	
substitute	σ_m	σ_p	σ_m	σ_p	σ_m	σ_p
NO2	9.07	10.58	0.98	1.01	0.74	0.78
CN	8.60	9.30	1.60	1.50	0.61	0.65
NH2	-1.30	-3.20	-0.47	-0.87	-0.21	-0.63
OH	0.55	-0.99	0.26	-0.40	0.13	-0.38
F	-2.20	2.28	0.56	0.30	0.34	0.06
Cl	4.99	4.50	1.03	0.76	0.37	0.22

a.Ref[5]: calculated by MP2/6-31 + G (d,p)

References:

[1] M . J . Frisch , G . w . Trucks , H . B .Schlegel , G . E . Scuserial , etal . , Gaussian 98 , Revision A . 7 (Gaussian , Inc . , Pittsburgh PA , 1998) .

[2] Y . L . eang , J . Bao . Y . Sun , and J . Yang , J . The or Biol . 238 , 85 (2006)

[3] Z . G . Kudritskaya and V.I.Danilov , J . Theor . Biol . 59 , 303 (1976)

[4]M.T.Cances,V.Mennucci, J.Tomasi, J.Chem. Physic. 107 (1997) 3032.

[5] M . Namazian , Journal of the Iranian chemical society , vol2 , No . 1 . (2005) , PR 65-70

[6] C . Hansch , A . Leo , chem . Rev . ; 1991 ; 91 ; pp . ; 165-195

[7] P.Butvin , J . A . Jaafreh , J . svetlik and E . Havranek , chem . papers , 53 , 315 (1999)

Calculation of wax appearance temperature in the crude oil storage tanks in Khark Island based on a numerical method

M. Farzaneh-gord[a], H. Nikoofard[b], M. Saadat-targhi, A. Nabati, A. Rasekh
a) The Faculty of Mechanical Engineering, Shahrood University of Technology, Shahrood, Iran
b) The Faculty of Chemistry, Shahrood University of Technology, Shahrood, Iran

Keywords: Numerical method, Solar radiation, Wax, Angstrom model, Khark Island

Introduction

One of the major difficulties related to crude oil storage tank is accumulated sludge at the bottom of the storage tank. Sludge which is mostly composed of asphaltene and wax particles decreases the tank storage capacity and causes corrosion [1]. The temperature is the importance parameter which has an effect on wax precipitation. During the different seasons of the year as solar radiation increases or decreases, the temperature of the oil tank goes up or down. In the present work, we evaluate the crude oil temperature in order to determine wax precipitation conditions. A numerical method and Angstrom model have been developed for solving the energy equation and estimating the solar radiation respectively, to predict the average crude oil temperature.

The Experimental procedure

In the experimental investigation, a crude oil storage tank (28th storage tank) in the Khark Island is selected as the case study. Average crude oil temperature have been measured and compared by the numerical result and those values calculated from API. The numerical procedure for predicting crude oil temperature and wax precipitation could be divided into the following steps: predicting the solar radiation, developing a numerical method for solving the energy equation and calculating the average crude oil temperature.

Results & Discussion

For estimating solar radiation several engineering models have been proposed [2]. In all of the models the weather condition and geographic location are important factors. By Angstrom model, solar radiation can be calculated using the following equation

$$\frac{H}{H_\circ} = a + \mathrm{b}\frac{\mathrm{S}}{\mathrm{S}_\circ} \qquad (1)$$

Where H_0 is cloudless hourly global irradiation received, *a* and *b* are coefficients that must be chosen according to the location and weather conditions , S and S_0 are average sunshine duration and cloudless sunshine duration, respectively. The results of numerical method and experimental data for tank temperature are shown in table 1. As the surface is imposing to ambient condition (and solar radiation), the surface temperature is expected to be higher than average tank temperature especially at later of the day. This could be seen in results of table 1. But generally, the numerical results are in good agreement with measured values.

Table 1: Comparison between numerical and experimental values of tank temperature

Date	Time	Experimental	Numerical Analysis
2 June 2009	10:30 A.M.	41.8 ^{o}C	40.13 ^{o}C
25 February 2009	8:30 A.M.	19.8 ^{o}C	20.49 ^{o}C
25 February 2009	2:30 P.M.	22.7 ^{o}C	21.49 ^{o}C

Conclusions

Based on the numerical method, a program has been developed which is capable of predicting transient (or averaged) the crude oil tank temperature. The numerical results of tank temperature have been compared with available experimental values and show a good agreement. It could be seen that the numerical method predicts slightly higher and lower temperature during first and last 6 months of the year comparing to API proposed equation respectively. This is probably due to simplicity of the API (AP-42 standard) which did not consider the effects of other parameters such as wind speed in this equation. It should be noted that knowing the precise crud oil temperature is mandatory for predicting of wax precipitation in storage tanks.

Reference

[1] Venkatesan and J. L. Creek, OTC 18798, Texas, USA (2007).

[2] Zekai¸ Sen. *Solar Energy Fundamentals and Modeling Techniques*. Londen: Springer Veriag. p. 47-140 (2008).

Using a thermodynamic model to predict the wax precipitation magnitude in crude oil storage tanks

M. Farzaneh-gord[a], H. Nikoofard[b] , M. Saadat-targhu, A. Nabati, A. Rasekh
a) The Faculty of Mechanical Engineering, Shahrood University of Technology, Shahrood, Iran
b) The Faculty of Chemistry, Shahrood University of Technology, Shahrood, Iran

Keywords: Storage tank; Wax precipitation; Thermodynamic model, Khark Island

Introduction

There are several major difficulties related to crude oil storage tank. One of the major difficulties is accumulated sludge at the bottom of the storage tank. Sludge which is mostly composed of asphaltene and wax particles decreases the tank storage capacity and causes corrosion. Although the temperature and pressure affects asphaltene and wax precipitation, but for crude oil storage tank, the temperature is the only parameters (pressure is nearly constant) which has an effect on wax precipitation and consequently on the accumulated sludge in the tank [1]. During the different seasons of the year as solar radiation increases or decreases, the temperature of the oil tank goes up or down. We evaluated the crude oil temperature in parallel study and here, amount of wax precipitation has been predicted. A thermodynamic model has been developed to determine the wax precipitation based on average crude oil temperature that calculated from energy equation.

The Experimental procedure

In the experimental investigation, a crude oil storage tank (28th storage tank) in the Khark Island is selected as the case study and average crude oil temperature have been measured for two days and compared by the numerical result and the values calculated from API standard for a crude oil storage tank in the Khark. The tank is an external pontoon floating roof type with 114 meter in diameter and 17 meter in height. The tank could store up to 1 million barrel of crude oil with API=33.36. During the current study, the tank has been filled with light crude oil.

Results & Discussion

The modeling of wax precipitation in crude oil is based on the thermodynamic description of the equilibrium between the solid wax and the oil liquid phases. The thermodynamic equilibrium relates to the solid and liquid fugacities. The relation between pure solid and liquid component fugacity can be obtained using the following equation that discussed by Firoozabadi [2].

$$f^{s}_{pure\ i}(P,T)=f^{l}_{pure\ i}(P,T)*\exp\left(\left[\frac{\Delta H^{f}_{i}}{RT^{f}_{i}}\left(1-\frac{T^{f}_{i}}{T}\right)\right]-\left(\frac{P\Delta v_{i}}{RT}\right)\right)$$

In this way, the effects of tank temperature on amount of wax precipitation were determined and shown in Fig. 1.

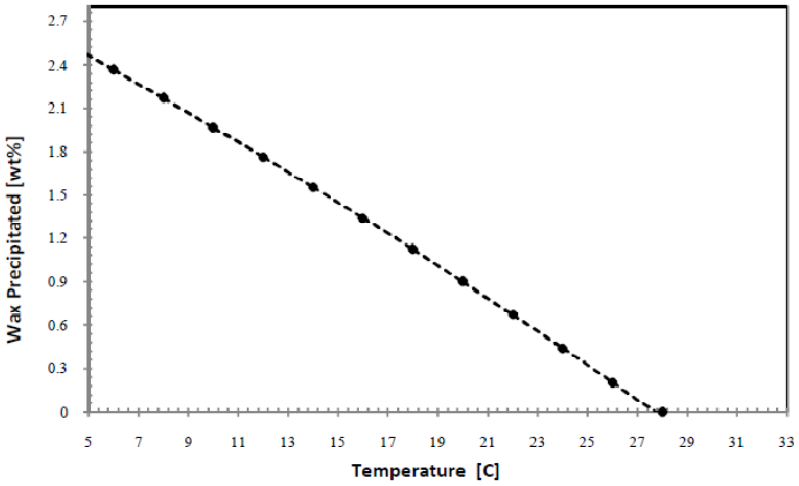

Fig. 1. The effect of temperature on wax precipitations (weight %)

Conclusions

In the present work, the results shown that the wax appearance temperature (WAT) is approximately 28°C and the wax precipitation will be occurred when the crude oil temperature is below the wax appearance temperature. Also, it is known that wax precipitation disappears for more than 3 months when the absorptivity of the exterior surface paint increases from 0.1 to 0.9. This is probably resulted in considerable drop in sludge formation in bottom of the tank.

Reference

[1] Erickson, V.G. Niesen, T.S. Brown, SPE 26548, (1993).

[2] Firoozabadi, *Thermodynamics of Hydrocarbon Reservoirs*, 1st ed. , McGraw-Hill, New York, P. 295-311 (1999).

Interactions of Diphenylacetylene Molecular Diode with Small Metal Cluster of Au: First-Principles Calculations On Nanowire

S. Nikooie*[a], Z.Bayat[a], R.EskandarFilabi[a], E. Taghizadeh[b]

[a]Department of Chemistry, Islamic Azad University -Quchan Branch, Iran

[b]Department of Chemistry,yonug researchers club, Islamic Azad University -Quchan Branch, Iran

nikoie63@yahoo.com

Abstract

Theoretical investigation has been performed on electron transport properties of diphenylacetylene based molecules sandwiched between four Geometry metal Au clusters. Linker such CN have been considered to study the role of linkage in the conduction proper ties of the molecular wire. The electronic conduction has been analyzed from the change in the shape of molecular orbitals and the evolution of the HOMO– LUMO gap of the molecule-gold complexes under the influence of the electric filed.

Keywords: conjugated molecular, Au clusters, Nanowire, Molecularwire.

Introduction

It is well recognized that the energy difference between highest occupied molecular orbital(HOMO) and the lowest unoccupied molecular orbital (LUMO) known as HOMO–LUMO gap (HLG) is a key parameter determining the conductance property .In our investigated systems, the para hydrogens of two phenyl rings have been replaced by linker CN classified into atomic.

Computational details

The calculations have been performed at the density functional theory level with the B3LYP functional. The basis set is split 6-31G* for CN atom and the Los Alamos National Laboratory effective core potentials with a double-zeta valence (LANL2DZ) for the gold atoms. All of the calculations described in this work were per performed with the GAUSSIAN 03 software package. The calculations are preceded in three steps. In the first

step a geometry optimization of diphenylacetylene joint to linker CN (Scheme 1) was carried out. Then the interaction between molecules with four state Au cluster's were studied.

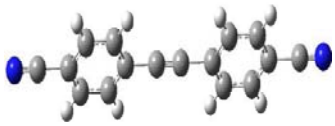

Scheme 1

Results and discussion

Comparison of the energy levelsTable 1 gives a comparison of the energy levels of HOMO and LUMO levels as well as their gap HLG) for Electronic structure of free molecules. The shape of HOMO and LUMO orbitals for the free molecules the higher the delocalization, the faster the electron tr ansfer [1].

Table 1 summarizes the geometries and energeticsof these complexes.

	HOMO	LUMO	HLG	D_{L-m}	<c-L-m	D_{m-m}
NC DPA CN	**-6.659**	**-2.618**	**3.951**	**2.12**	----------	----------
AU NC DPA CN	**-5.451**	**-2.839**	**2.611**	**2.12**	**102.26**	----------
AU NC DPA CN AU	**-4.356**	**-4.178**	**0.178**	**2.12**	**102.26**	----------
AU3 NC DPA CN AU3	**-4.014**	**-3.824**	**0.19**	**2.12**	**104.94**	**2×2.72** **2.64**
AU3 NC DPA CN	**-4.420**	**-3.164**	**1.255**	**2.12**	**104.94**	**2×2.72** **2.64**

Interaction with gold cluster

a) 

b) 

c) 

d) 

We compared just the bond distance between terminal atom and Au because the geometries for other atoms of the phenyl rings are barely affected. The energy gaps for the free molecular diode decrease when an additional metal atom is added. This is due to the localization of the LUMO energy level on the metal atoms. The addition of Au atoms stabilizes the HOMO energy levels of the molecule The result of Au atom addition is consistent with an earlier calculation.

Effect of external field:

In fig 1 At zero field DPAs have longer single bonds and shorter double bond. When EF increases the carbon–carbon single bonds are shortened and the double bonds tend to be elongated resulting in a decreased bond length alternation. This variation of bond lengths corresponds to the balance of the conjugation within the whole molecule under the interaction with electric field. The pelectron density changes all over the molecule due to the polarization of the bonds.

Fig1:

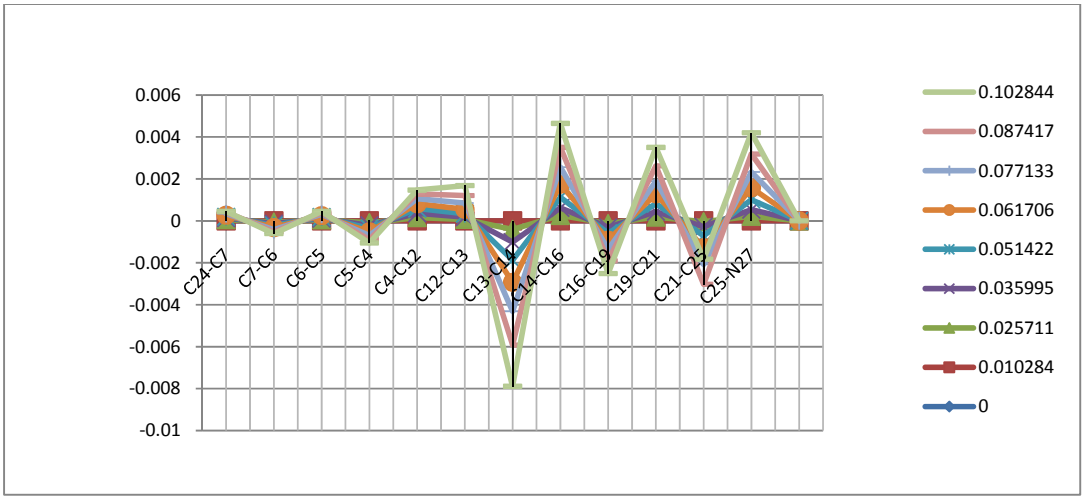

Refrence:

[1] J.M. Seminario, A.G. Zacarias, J.M. Tour, J. AM. Chem. Soc. 122 (2003) 3015.

Theoretical Study of Structural Relationships and Electrochemical Properties of NanoSupramolecular [Cytochromes]@C_n Complexes

Behnoud Hormozi and Avat (Arman) Taherpour*

Chemistry Derpartment, Faculty of Science, Islamic Azad University, Arak Branch

(a.taherpour@iau- arak.ac.ir &avatarman.taherpour@Gmail.com)

(behnoudhormozi_chem@Gmail.com)

Abstract:

Cytochromes are,in general,membrane-bound hemoproteins that contain heme groups and carry out electron transport.Fullerenes are family of carbon allotropes,molecules composed entirely of carbon,that take the forms of spheres,ellipsolids and cylinders. Topological have been successfully used to construct effective and useful mathematical methods to establish clear relationships between structural data and the physical propertiesof these materials. In this study,the number of carbon atoms in the fullerenes was used as an index to establish a relationship between the structure of Cytochroms c , b , a_3, p-450 as the most well-know redox systems and fullerenes C_n(n=60, 70, 76, 82 and 86),which create [Cytochrom c]@C_n,**A**-1 to **A**-5,[Cytochrom b]@C_n,**B**-1 to **B**-5 ,[Cytochrom a_3]@C_n,**C**1-**C**5, [Cytochrom p-450]@C_n, **D**1-**D**5. The relationship between the number of carbon atoms and the free energies of electron transfer ($\Delta G_{et(1)}$ to $\Delta G_{et(4)}$) are assessed using the ET equation for **A**-1 to **A**-5, **B**-1 to **B**-5, **C**-1 to **C**-5 and **D**-1to **D**-5 supramolecular [Y].C_n(Y=Cytochrom c, Cytochrom b,Cytochrom a_3,Cytochrom p-450) complexes.calculations are presented for the four oxidation potentials ($^{ox}E_1$ to $^{ox}E_4$) of fullerenes Cn. The results were used to calculate the four free energies of electron transfer ($\Delta G_{et(1)}$ to $\Delta G_{et(4)}$) of supramolecular complexes **A**-1 to **A**-5 , **B**-1 to **B**-5 , **C**-1 to **C**-5 and **D**-1 to **D**-5 for fullerenes C_n(n=60-300) .

Keywords: Fullerenes,Cytochroms,Free energy,Electron transfer,Oxidation potential

Introduction:

Cytochroms are found in the mitochondrial inner membrane and endoplasmic reticulum of eukaryotes, in the chloroplasts of plauts, in photosynthetic micro organisms , and in bacteria. Since the discovery of the fullerenes (C_n) one of the main class of carbon compounds,the

unusual structure and properties of these molecules have been discovered and many potential applications and physicochemical properties have been introduced .

Mathematical Methods:

Using the number of carbon atoms contained within the C_n fullerenes, several valuable properties of the fullerenes can be calculated.The values were used to calculate the four free energy of electron transfer($\Delta G_{(1)}$ to $\Delta G_{(4)}$),according to the Rehm-Weller equation for [Cytochroms]@C_n.Both linear (MLR:Multiple Linear Regressions) and nonlinear (ANN:Artificial Neural Network) models were used in study.All graphs were generated using the Microsoft Office Excel 2003 program.The Rehm-Weller equation estimates the free energy change between an electron donor(D) and an acceptor(A) as

$$\Delta G^0 = e\,[E_D{}^0 - E_A{}^0] - \Delta E^* + \omega_1 \qquad \text{(Equation-1)}$$

Where e is the unit electrical charge, $E_D{}^0$ and $E_A{}^0$ are the reduction potentials of the electron donor and acceptor,respectively,$\Delta E^*$is the energy of the singlet or triplet excited state and ω_1 is the work required to bring the donor and acceptor within the electron transfer(ET)distance.

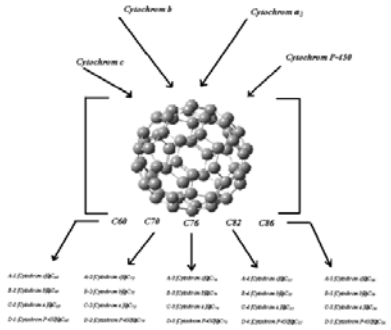

Results and Discussion:

In the reports has shown that all redox data for Cytochroms c, b, a_3, P-450 were determined by cyclic voltammetry. The reported readuction potentials of them are(-0.39V),(-0.36V),(-0.34V),(-0.165V).Here,we calculated four free energies of electron transfer ($\Delta G_{et(1)}$ to $\Delta G_{et(4)}$) of other supramolecular complexes of Cytochroms (c,b,a_3,P-450) with fullerenes C_{60} to C_{300}([Cytochroms]@C_n).

Conclusions:

By using the equations of this model,a good approximation for $\Delta G_{et(1)}$ to $\Delta G_{et(4)}$ for[Cytochroms] @C_n supramolecular complexes of the fullerenes C_n(n=60-300) was calculated.The novel supramolecular complexes discussed have neither been synthesized nor reported previously.

References:

[1] Taherpour, A.A.(2009)Fullerenes,Nanotubes and Carbon Nanostructures,17(1)26-37.

[2] Raphael,A.L.,et al(1991)J.Am.Chem.soc,113,1038-1040.

[3] Reid,L.S.,et al(1982)J.Am.Chem.Soc.104,7516-7519.

[4] Rivera,M.,et al(1998)Biochemistry,37(6),1485-1494.

[5] Taherpour,A.A.,et al(2010)Analytical Letters,43:658-673

The NO2 attached $C_{30}B_{15}N_{15}$ heterofullerene: A Computational Nuclear Magnetic resonance study

Z. Halfinezhad, A. Abdollahian, S.J. Hosseini, S.H. Mortazavi, Ehsan Zahedi*
Chemistry Department, Islamic Azad University, Shahrood Branch, Shahrood, Iran.
Zahra.halfinezhad@gmail.com e_zahedi@iau-shahrood.ac.ir

Keywords: NMR; Heterofullerene; DFT; CSI

Introduction:

Heterofullerenes are fullerene molecules in which one or more carbon atoms are replaced by heteroatoms via on-ball doping [1]. The doping of carbon cages with boron and nitrogen atoms appears a promising way to modify the physical and chemical properties of fullerenes [2]. $(BN)_n$ clusters are currently much interest for their great stability [3], therefore the inclusion of both nitrogen and boron dopants is the best candidate for the formation of heterofullerenes with general formula $C_{60-2n}B_nN_n$. BN doped C_{60} contain the same number of π electrons as C_{60} and therefore both compounds are isoelectronic. The calculation of nuclear magnetic resonance (NMR) using density functional theory (DFT) techniques has become a major and powerful technique in the investigation of molecular structure [4].

Results and discussion :

In the present work, adsorption behavior of an NO2 molecule on the three possible adsorption sites of $C_{30}B_{15}N_{15}$ heterofullerene is taken into consideration and comparison. To demonstrate of the three possible adsorption sites on a $C_{30}B_{15}N_{15}$ heterofullerene, we make used of the same labeling and numbering C_{60} Schlegel diagram in below Fig. In this figure boron adsorption sites are defined with bold words and other boron sites don't studied, because they were similar in position and neighboring atoms with the three considered sites.

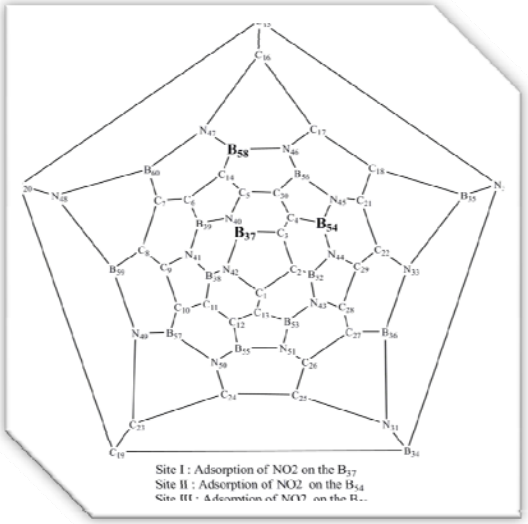

Firstly, each of the four structures including perfect and NO2-attached $C_{30}B_{15}N_{15}$ heterofullerenes at the three possible adsorption sites was allowed to fully relax during the geometrical optimization process performed at the B3LYP-DFT method and 6-31G* basis set using Gaussian 03 [5]. The optimization process reveals that dramatic influences observed for the geometrical structure of $C_{30}B_{15}N_{15}$ heterofullerene after the ammonia adsorption and B atom relaxes outwardly from spherical in the NO2-attached $C_{30}B_{15}N_{15}$ heterofullerene. At the next step, the chemical shielding (CS) tensors of B and N nuclei were calculated using B3LYP/6-311G** level of theory and converted to experimentally measurable nuclear magnetic resonance (NMR) parameters, i.e. chemical-shielding isotropic (CSI) and chemical shielding anisotropic (CSA).

Conclusions:

In the perfect model, the NMR parameters (CSI and CSA) show that the B.37 and B.38 have the smallest CSI, and B.57 has the largest CSI, furthermore, N.40 has the smallest and N.32 has the largest CSI. Our calculations revealed that in the NO2-attached form the B atom chemically bonded to NO2 molecule has the largest chemical-shielding isotropic (CSI) value among the other boron nuclei. The CSA of B.37, B.54, B.58 and N.61 nuclei are decreased after the adsorption and indicated that the electronic charge distribution around these nuclei becomes more symmetric as a result of the adsorption.

Reference:

[1] M. Ghorbani, M. Jalali, Dig. J. Nanomater. Bios. 3 (2008) 269.

[2] E. Emanuele, F. Negri, G. Orlandi, Inorg. Chim. Acta. 360 (2007) 1052.

[3] S.H. Xu, M.Y. Zhang, Y.Y. Zhao, B.G. Chen, J. Zhang, C.C. Sun, Chem. Phys. Lett. 423 (2006) 212.

[4] A. Seif , A. Boshra, J. Mol. Struct. (THEOCHEM) 895 (2009) 96.

[5] M.J. Frisch et al., Gaussian 03, Revision E.01, Gaussian Inc., Wallingford CT, 2004.

A Theoretical Study of the Interaction Between dacarbazine and BX3 (X=F, Cl) Systems

†H.Hooshyar[a], R. Sadeghi[b], S. Khanahmadzadeh[c]

[a,c] Department of Chemistry, Islamic Azad University Mahabad Branch, Islamic Azad University Mahabad, Iran

[b]Department of Chemistry, Faculty of Science, University of Kurdistan, Sanandaj, Iran

Email: h_hshyr@yahoo.com

KEY WORDS: dacarbazine, BX3, ab initio, enthalpy, Gibbs energy

Introduction

Boron contained compounds are electron deficient compounds and have been extensively used as catalysts in chemical reactions. There have been many experimental and theoretical reports [1–3] about the donor–accepter complexes involving BH3, BF3, BCl3 and etc. Still, boron is an essential trace element, and excess or scarcity of boron will cause adverse effect on them [4–6]. In this paper, we chose the B3LYP method of density functional theory (DFT) and the Hartree-Fock method (HF) theory of ab initio calculations to study intermolecular interaction as the electron correlation is evident in these systems, to study the dacarbazine – BX3 (X=F, Cl) systems.

Computational details

In this work, full geometry optimizations have been performed with the GAUSSIAN03 Package at the Becke3-parameter hybrid exchange functions and Lee-Young-Parr correlation functional (B3LYP) level using the 6-31G** basis set. The Hartree-Fock method (HF) theory of ab initio calculations has been used as well for comparison.

Results and discussion

Eight energy minimum conformers, four conformers (a)–(d) for dacarbazine-BF_3 and four Conformers (e)–(h) for dacarbazine-BCl_3, were obtained without imaginary frequencies by

calculations at the B3LYP/6-31G** levels from the various initial configurations for dacarbazine-BX3. For (a)–(c) and (e)–(g), BX3 is placed near the N atom and for (d) and (h),BX3 is located over the O atom. All the optimized geometries at the B3LYP/6-31G** level with atomic labels are shown in Fig. 1. Surface potential energy calculations are carried out with scanning B-O and B-N bond participating in the donor-acceptor complexes.

Thermodynamic properties of dacarbazine-BX3 systems

The changes of enthalpy, $\Delta_r H^0$, and Gibbs energy, $\Delta_r G^0$, for the formation reaction of the complexes can be obtained (Table 1). From Table 1 it can be seen that the most stable conformers, a and e, in the two systems have the highest.

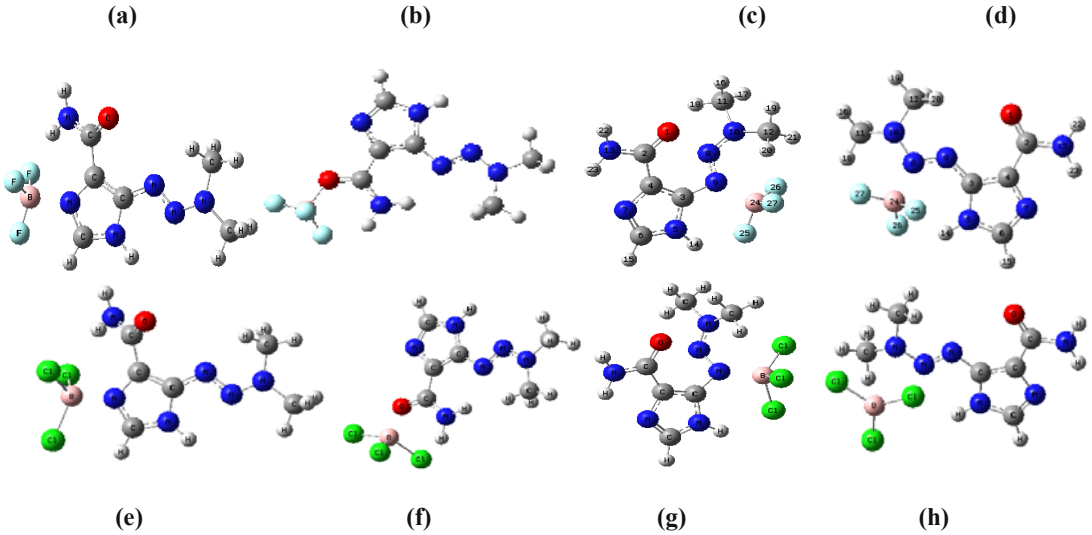

Fig. 1 Optimized structures (B3LYP/6-31G**) and atomic labels of conformers for dacarbazine-BX3 complexes

Table 1 Thermodynamic data for the formation of dacarbazine-BX3 (X=F, Cl) complexes at 298.15K and 101.325 kPa calculations at the B3LYP/6-31G** level

conformer	$H^{o}_{298.15}$/Hartree	$G^{o}_{298.15}$/Hartree	ΔH_r °/ kJ·mol^{-1}	ΔG_r °/ kJ·mol^{-1}	μ(D)
dacarbazine	-۶۳۸,۱۷۶۴۲۵	-۶۳۸,۲۳۱۸۶۰			
BF3	-۳۲۴,۵۳۶۲۴۳	-۳۲۴,۵۶۶۸۴۲			
BCl3	-۱۴۰۵,۵۴۹۶۹۹	-۱۴۰۵,۵۸۴۲۲۶			
a	-۹۶۲,۷۴۷۸۴۶	-۹۶۲,۸۱۱۹۵۸	-92.359	-34.803	۱۰,۳۶۸۳
b	-۹۶۲,۷۴۲۷۸۳	-۹۶۲,۸۰۷۴۶۳	-79.067	-23.00	۱۶,۶۵۱۱
c	-۹۶۲,۷۳۳۲۹۴	-۹۶۲,۷۹۵۳۲۹	-54.153	8.856	۳,۳۳۲۶
d	-۹۶۲,۷۲۵۵۹۹	-۹۶۲,۷۸۷۵۳۳	-33.950	29.324	۲,۹۷۹۴
e	-۲۰۴۳,۷۵۷۸۴۵	-۲۰۴۳,۸۲۷۶۴۲	-83.283	-30.340	۱۹,۱۵۷۲
f	-۲۰۴۳,۷۵۶۱۸۰	-۲۰۴۳,۸۲۳۶۹۴	-78.912	-19.975	۱۲,۴۳۹۰
g	-۲۰۴۳,۷۳۲۲۵۱	-۲۰۴۳,۷۹۷۹۴۳	-16.086	47.634	۶,۳۲۱۴
h	-۲۰۴۳,۷۲۵۴۶۴	-۲۰۴۳,۸۰۱۶۴۹	1.7328	37.904	۵,۰۱۵۱

Conclusions

Four different conformers corresponding to the minimum points on the molecular energy hyper surface were found for each of the dacarbazine-BF3 and dacarbazine-BCl3 systems. In conformers of (a) and (e), the oxygen atom of cytosine donated its lone-pair electron to the empty p orbital of the boron atom and it exhibited the most structural stability.

References

[1] P. Tarakeshwar, S.J. Lee, J.Y. Lee, K.S. Kim, J. Phys. Chem. B 103 (1999) 184.

[2] P. Tarakeshwar, J.Y. Lee, K.S. Kim, J. Phys. Chem. A 102 (1998) 2253.

[3] L.M. Nxumalo, T.A. Ford, J. Mol. Struct. (Theochem) 369 (1996).

[4] C.D. Hunt, J. Trace, Elem. Exp. Med. (1996) 9185.

[5] F.H. Nielsen, S.K. Gallagher, L.K. Johnson, J. Trace, Elem. Exp. Med. (1992) 5237.

[6] D. Whorton, J. Haas, L. Trent, Environ. Health Perspect. (1994) 102129.

Prediction of LD50for some of the anti-cancer drugs from QSAR methods

S. Vahdani[a]*, Z.Bayat[a],M.sarem[b]

z.bayat@ymail.com

[a]*Department of Chemistry, Islamic Azad University Quchan Branch, Iran*

[b]*Department of Chemistry,payamnour university mashhad,iran*

Introduction

Anthracycline antibiotics are among the most effective chemotherapy agents currently in use for cancer treatment; however irreversible cardiac damage is a major dose-limiting toxicity, restricting life-time cumulative dose. It is important to determine whether a candidate molecule is capable of penetrating the toxicity in drug discovery and development [1]. The aim of this paper is to establish a predictive model for LD50 penetration using simple descriptors. The usefulness of the quantum chemical descriptors, calculated at the level of the DFT theories using 6-31G* basis set for QSAR study of anti-cancer drugs was examined. Multiple Linear Regressions (MLR) was employed to model the relationships between molecular descriptors and biological activities of molecules using stepwise method as variable selection tools.

Keywords: QSAR, anti-cancer drugs, LD50, DFT

Methodology

The biological data used in this study are the drug concentration required to inhibit 50% of sensitive cell growth (LD50) of the set of 13 anti-cancer drugs derivatives [2, 3]. For this purpose, descriptors of the structure are commonly used. All of the molecules were drawn into the Hyper Chem. In this work, we used Gaussian 03 for abinitio calculations. DFT method at 6-31G* were applied for optimization of anti-cancer drugs and calculation of many of the descriptors. A large number of descriptors were calculated by Gaussian package and Hyperchem software.

Results

In a QSAR study, generally, the quality of a model is expressed by its fitting ability and prediction ability, and of these the prediction ability is the more important. With the selected descriptors, we have built a linear model using the training set data, and the following equation was obtained:

$$pLD50=18.79(\pm1.399)+41.62MC_1\ (\pm3.66)+\ 34.12MC_{24}\ (\pm8.36)$$

$$N=13\quad R^2=0.933\ F=69.224\qquad R^2_{adj}=0.919\quad Q^2_{LOO}=0.899\quad Q^2_{LGO}=0.893$$

In this equation, N is the number of compounds, R^2 is the squared correlation coefficient, Q^2_{LOO}, Q^2_{LGO} are the squared cross-validation coefficients for leave one out, bootstrapping and external test set respectively, F is the Fisher F statistic. The figures in parentheses are the standard deviations. The built model was used to predict the test set data and the prediction results are given in Table 1. As can be seen from Table 1, the calculated values for the LD50are in good agreement with those of the experimental values. The predicted values for LD50 for the compounds in the training and test sets using equation were plotted against the experimental LD50 values in Figure 1.

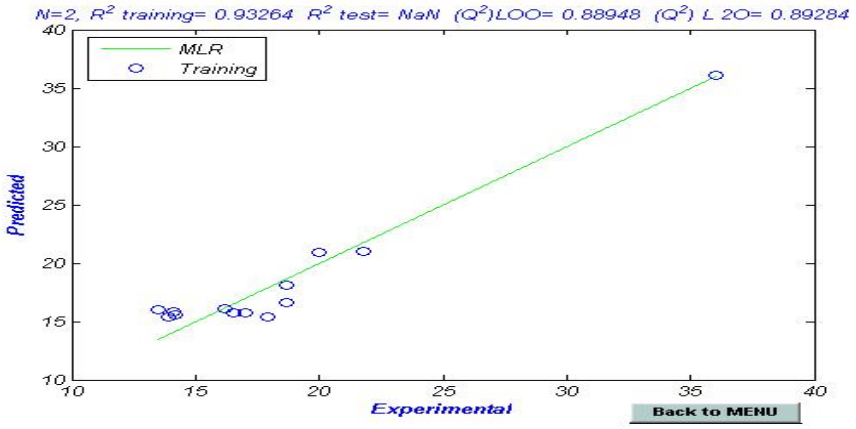

Figure1. The predicted versus the experimental LD50by MLR.

Table 1. Chemical structures and the corresponding observed and predicted LD50values by the MLR method.

Compounds	Exp.	Pred.	Ref.	Compounds	Exp.	Pred.	Ref.
Carminomycin	13.5[a]	16.01	2	Hydroxy doxorubicin	17.9	15.39	3
Valrubicin	13.9	15.38	2	esodaunorubicin	18.7	16.60	2
Esorubicin	14.1	15.79	3	aclacinomycin	18.7	18.11	3
Epirubicin	14.2	15.58	3	Danorubicin	20	20.93	3
Idarubicin	16.2	16.10	3	Doxorubicin	21.8	20.98	3
Alkavin	16.5	15.71	2	Pyrromycin	36	36.08	2
Morpholino doxorubicin	17	15.78	2				

a= mg/kg

Conclusion:

In this article, a QSAR study of 13 anti-cancer drugs was performed based on the theoretical molecular descriptors calculated by the GAUSSIAN software and selected. The built model was assessed comprehensively (internal and external validation) and all the validations indicated that the QSAR model built was robust and satisfactory, and that the selected descriptors could account for the structural features responsible for the anti-cancer drugs activity of the compounds. The QSAR model developed in this study can provide a useful tool to predict the activity of new compounds and also to design new compounds with high activity.

References

[1] Kohji TAKARA,Toshiyuki SAKAEDA, *Biol. Pharm. Bull.* **25**(6) 771—778 (2002).

[2] Monneret C. Eur. J. Med. Chem. **36**, 483-493(2001)

[3] http://www.chemidplus.com

Maximizing the solar energy storage for water-soluble four-substituted Norbornadiene-Quadricyclane system: DFT calculations

E. Vessally*, S. aryana
Payame Noor University (PNU), Zanjan, Iran
E-mail: vessally@yahoo.com

Introduction

nowadays find the reply to energy problems through the employment of the environmentally secure "solar energy" has received much attention [1]. The alteration of quadricyclane, **2**, to norbornadiene, **1**, leads to create heat energies. The **1** / **2** system is used for solar energy storage [2], in molecular switching [3], in isoelectronic devices , as a data storage compound [3], as photodynamic chemosensor for metal cations, as a potential photoresponsive organic magnet [4] and as an energetic binder for solid rocket propellants .

Computational Methods

The molecular structures of four-substituted norbornadienes (**1_X**) and quadricyclanes (**2_X**), were studied using *ab initio* methods. Geometry optimizations were carried out by B3LYB/6-311++G** in the *Gaussian* 03 program.

Results and Discussion

As a continuation of our works, in this research we studied the photochemical energy storage in the ground states of **1_X** / **2_X** system (**X** attached at both carbon atoms of C_2=C_3 and C_5=C_6) with substitution of four electron donating groups (pull-pull), four electron withdrawing groups (push-push) and electron donating-electron withdrawing groups (pull-push). It has been found that extent of solar energy storage at carbon C_2, C_3, C_5 or C_6 is generally more than at either carbons (C_1 and C_7) [5]. Thus, we select carbon C_2, C_3, C_5 and C_6 to investigation of solar energy storage. Another words C_2, C_3, C_5 and C_6 is more sensetive to substitutent effect than C_1 and/or C_7.

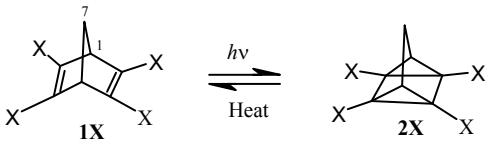

Extend of the solar energy stored in this system is measured simply by calculating the energy gaps between the ground states of $\mathbf{1_X}$ and $\mathbf{2_X}$. Apparently, there was no practical need to consider the excited states and/or the type(s) of the mechanism involved. Thermal energy gaps, $\Delta E_{(1x)-(2x)}$, enthalpy gaps, $\Delta H_{(1x)-(2x)}$ and free energy gaps, $\Delta G_{(1x)-(2x)}$, in kcalmol^{-1}, between norbornadienes ($\mathbf{1_X}$) and their corresponding quadricyclanes ($\mathbf{2_X}$) were calculated at B3LYP/6-311++G** level of theory.

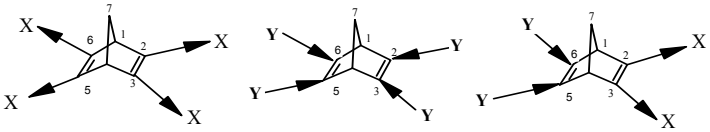

Gibbs free energy gaps between $\mathbf{1_X}$ and $\mathbf{2_X}$, $\Delta G_{(1x)-(2x)}$, is the least when two electron withdrawing substituents (pull-pull) were attached at double bond C_2=C_3 and two electron donating substituents (push-push) were attached at double bond C_5=C_6 (Table 1). The $\Delta G_{(1x)-(2x)}$, is the most when four electron donating substituents (push-push) were attached at double bond C_2=C_3 and C_5=C_6. However, the $\Delta G_{(1x)-(2x)}$, is increased when electron donating and electron withdrawing substituents (push-pull) were attached at two sides of double bonds C_2=C_3 and C_5=C_6, respectively. Hence, extend of solar energy storage is the least for $\mathbf{1_{CONH2,OH}}$ (-22.45) and the most for $\mathbf{1_{OH}}$ (-32.76) (in kcal/mol) (Table 3). The solar energy storage changes for compounds $\mathbf{1_X}$ are in the order: $\mathbf{1_{OH}}$ (-32.13) > $\mathbf{1_{NH2}}$ (-30.25) > $\mathbf{1_{CN}}$ (30.13) > >$\mathbf{1_{CONH2}}$(-29.67) >$\mathbf{1_{CN-NH2}}$ (-28.13) > $\mathbf{1_{CO2H-OH}}$ (-22.89) > $\mathbf{1_{CONH2-0H}}$ (-22.45).

The other discussions and sunlight absorption spectra would be presented.

Conclusion

Gibbs free energy gaps between $\mathbf{1_X}$ and $\mathbf{2_X}$, $\Delta G_{(1x)-(2x)}$, or solar energy storage is increased when two electron donating and two electron withdrawing substituents (push-pull) were attached at both sides of double bonds C_2=C_3 and C_5=C_6. However, The $\Delta G_{(1x)-(2x)}$, is the most when four electron donating substituents (push-push) were attached at two sides of double

bonds C_2=C_3 and C_5=C_6. Extend of solar energy storage is the least for $\mathbf{1}_{\mathbf{CONH2,OH}}$ and the most for $\mathbf{1}_{\mathbf{OH}}$.

Reference

[1] W. Fub, K.K. Pushpa, W.E. Schmid, Photochem. Photobiol. Sci. **1,** 60 (2002).

[2] Y. Inadomi, K. Morihashi, O. Kikuchi, J. Mol. Struct. **434,** 59 (1998).

[3] H. Nishino, Y. Inoue, Jpn. Kokai Tokkyo Koho IP2000086588, (2000).

[4] S. Nakatsuji, Y. Ogawa, S. Takeuchi, H. Akutsu, J. Yamada, A. Naito, K. Sudo, N. Yasuoka, J. Chem. Soc. Perkin Trans. **2,** 1969 (2000).

[5] M.Z. Kassaee, E. Vessally, J. Mol. Struct. (Theochem) **716,** 159 (2005).

Energy surface studies of divalent five-membered ring derivative XC_4H_3C: DFT calculations

E. Vessally*
Payame Noor University (PNU), Zanjan, Iran
E-mail: vessally@yahoo.com

Introduction

Since 1991, when the first stable carbene has been prepared and described [1], the chemistry of carbenes has greatly been developed. Carbenes are important intermediates in a variety of the chemical reactions. They have been extensively studied both experimentally and theoretically [2–3]. Moreover, there has been significant synthetic interest in the production of the silylene and germylene analogues of the carbine. In this work, DFT calculations were carried out to study the substitution effects on the singlet–triplet splitting of Arduengo-type carbenes XC_4H_3C (Scheme).

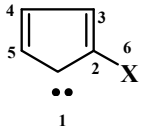

Computational Methods

The molecular structures of XC_4H_3C were studied using *ab initio* methods. Geometry optimizations were carried out by B3LYB/6-311++G** in the *Gaussian* 03 program.

Results and Discussion

The $\Delta G_{s\text{-}t}$ between the singlet and triplet states of XC_4H_3C were increased at B3LYP/6-311++G** level in the order (in kcal/mol): X = -F (-11.44) > -Cl (-10.99) > -Br (-10.79) > -NO_2 (-10.70) > -CF_3 (-10.32) > -H (-9.59) > -CH_3 (-9.56) > -OH (-9.21) > -NH_2 (-6.13). The calculated $\Delta G_{s\text{-}t}$ for XC_4H_3C indicated that the singlet states of XC_4H_3C were generally stabilized when the electron donating groups were used at α-position. However, the stability of the singlet state is the most when halogen substituents were used at α-position of XC_4H_3C. The influence of the substituents on the carbene ground-state multiplicity has been discussed in the introduction section.

The bond length C_1:-C_2 in contrast to C_1:-C_5, increased when the electron donating substituents were used. Electron donating substituents push the nonbonding electrons toward carbenic center at the direction of C_5-C_1. We found that the lone pair electrons at carbenic center achieve a σ^2 configuration for the singlet state of C_4H_4C. Therefore, a vacant *p* orbital remains at carbenic center which could accommodate to electron current. However, the bond length C_1:-C_2 in contrast to C_1:-C_5, slightly increased when the electron withdrawing substituents were used. The electrons in σ^2 orbital could not overlap with *p* orbital of carbon-carbon double bond as well as with electron withdrawing substituents.

Except for X = NH_2 and –OH, a larger bond angle C_2-C:$_1$-C_5 was found for the singlet states of XC_4H_3C respect to corresponding to triplet states. Larger bond angle C_2-C:$_1$-C_5 for the singlet states of XC_4H_3C led to *p* character of nonbonding electron; destabilizing the singlet states. However, bond angle C_2-C:$_1$-C_5 for the triplet states of XC_4H_3C have a slight changes when the electron donating and withdrawing substituents were used.

The lowest chemical hardness (η=0.071 a.u.), chemical potential (μ=-0.151 a.u.) as well as electronegativity (χ=0.151 a.u.) were reasonably belong to the singlet state of -$NH_2C_4H_3C$. The highest electrophilicity value (ω) for the triplet states of -XC_4H_3C is higher respect to the related singlet states. However, the highest electrophilicity value (ω=0.204 and ω =0.259 a.u.) were reasonably obtained for the singlet and triplet states of -$NO_2C_4H_3C$, respectively. The highest maximum charge transfer (ΔN_{max} = 2.120) was obtained for the singlet state of -$NH_2C_4H_3C$.

Conclusion

Calculated $\Delta G_{s\text{-}t}$ at B3LYP/6-311++G** level for α-substitued divalent five-membered rings XC_4H_3C indicated that the singlet states of XC_4H_3C were generally stabilized when the electron donating substituents were used at α-position. The higher η, μ, χ, **D** and ΔN_{max} were obtained to the singlet state of -$NH_2C_4H_3C$ while the higher ω was obtained for the singlet and triplet states of -$NO_2C_4H_3C$.

Reference

[1] A. J. Arduengo, R. L. Harlow and M. Kline, *J. Am. Chem. Soc.* 113 (1991) 361-363.

[2] P. S. Skell and R. C. Woodworth, *J. Am. Chem. Soc.* 78 (1956) 4496-4497.

[3] D. Bourissou, O. Guerret, F. P. Gabbai, and G. Bertrand, *Chem. Rev.,* 100 (2000) 39-92.

DFT Calculations on aromatic character of triafluavenes and their heavier analogues, XC_5H_4 (X = C, Si, Ge, N, P, and As)

E. Vessally*, S. Fateh Basharzad
Islamic Azad University, Miyaneh Branch, Miyaneh, Iran
E-mail: **vessally@yahoo.com**

Introduction

The simplest but most highly strained fulvalene, C_6H_4, is named triafulvalene, $\mathbf{1_C}$. Triafulvalene remains unknown until last with comparatively few reports directed to the synthesis of $\mathbf{1_C}$ and its derivatives [1-4]. This molecule has never been synthesized but the synthesis of the substituted species which restricted to three accounts of ring-fused derivatives have been reported [1-2]. Later, the steric substituents have been used due to increase the stability of the substituted benzotriafulvalenes [3]. In this paper, the aromatic character and other properties of triafluavenes and their heavier analogues, XC_5H_4, $\mathbf{1_X}$ and $\mathbf{2_X}$ (X = C, Si, Ge, N, P, and As) was calculated.

Computational *Methods*

The molecular structures of $\mathbf{1_X}$ and $\mathbf{2_X}$ were studied using ab initio methods. Geometry optimizations were carried out by B3LYB/6-311++G** in the Gaussian 03 program (Scheme).

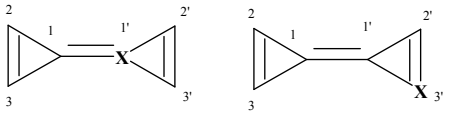

X = C, $\mathbf{1_C}$; Si, $\mathbf{1_{Si}}$; Ge, $\mathbf{1_{Ge}}$ N, $\mathbf{1_N}$; P, $\mathbf{1_P}$; As, $\mathbf{1_{As}}$

X = N, $\mathbf{2_N}$; P, $\mathbf{2_P}$; As, $\mathbf{2_{As}}$

Results and Discussion

The stability of $\mathbf{1_X}$ and $\mathbf{2_X}$ may be related to the aromatic character of each ring. Therefore, the aromatic character for two rings of $\mathbf{1_X}$ and $\mathbf{2_X}$ determined through magnetic criterion. Nuclear independent chemical shifts (NICS) calculation procedure is the most important magnetic criterion for the determination of the aromatic character. The NICS calculations were separately carried out for both rings of $\mathbf{1_X}$ as well as $\mathbf{2_X}$. All NICS calculations were done at B3LYP/6-311+G** level of theory. The aromatic character is not a directly measurable or computable

quantity. Aromatic character is generally evaluated on the basis of magnetic, energetic and geometric criteria. Magnetic criterion is measured through nuclear independent chemical shifts (NICS) calculations. NICS(1.0) calculations for $\mathbf{1_X}$ as well as $\mathbf{2_X}$ indicated that $\mathbf{1_C}$ has a non-aromatic character. DFT calculations revealed the highest aromatic character for $\mathbf{1_{Ge}}$ respect to $\mathbf{1_{Si}}$ and $\mathbf{1_C}$ in the heteroatom-ring. However, the highest aromatic character was obtained for $\mathbf{1_N}$ and $\mathbf{2_{As}}$ in the heteroatom-ring. Moreover, the highest aromatic character was obtained for $\mathbf{1_{Si}}$, $\mathbf{1_{As}}$ and $\mathbf{2_{As}}$ in the non-heteroatom ring. It may be concluded that the replacement of heavy atoms at three-member ring was generally raised the aromatic character since the three-membered ring achieve a more positive charge at atoms (1') as well as aromatic character respect to negative charge at atoms (1). Therefore, the three membered rings tend to have two electrons (according to Huckel 4n + 2 rule) in the ring when a heavy atom or a electropositive atom was used in the ring. The obtained aromatic character for $\mathbf{1_X}$ and $\mathbf{2_X}$ via magnetic criterion by NICS (1.0) procedure confirmed the aromatic character which obtained through geometric parameters.

Conclusion

Full geometry optimizations were indicated that global minimum structures for $\mathbf{1_C}$, $\mathbf{1_{Ge}}$ and $\mathbf{2_{Si}}$ have planar conformation while for $\mathbf{1_{Si}}$, $\mathbf{1_{Ge}}$ and $\mathbf{1_{Sn}}$ have nonplanar conformation. DFT calculations indicated an aromatic character in a ring of $\mathbf{1_X}$ and $\mathbf{2_X}$, which was exchanged with a heavier atom.

Reference

[1] R. Neidlein, V. Poignee, W. Kramer, C. Glueck, Angew. Chem. Int. Ed. Engl. **1986**, 25, 731–734.

[2] M. J. Cooney, B. Halton, unpublished observations, **1994**.

[3] B. Halton, M. J. Cooney, C. S. Jones, R. Boese, D. Bläser, *Org. Lett.* **2004**, *6*, 4017–4020.

[4] B. Halton, *Eur. J. Org. Chem.* **2005**, 3391–3414.

Interaction of potassium ion with Amino Acid as Model of Peptide Chain

K.Yarijou[a], and H.R. Shamlouei[a*]
[a] Islamic Azad University, Gachsaran Branch, Gachsaran, I.R. Iran
*shamluei@iaug.ac.ir

Introduction

The metal ions have important rules in structure and function of proteins and other biomolecules [1]. The rule of metals as cofactor is greatly magnified in activation of enzyme [2,3]. Understanding the mechanism of activation, inhibition and other reactions, in which the metal ions have a critical rule, are achieved by clarifying the interaction of metal ions with protein sequence. The alkali metal cations, specially sodium and potassium are undoubtedly much abundant ions in biological systems. They act as which bind weakly to organic are ideally suited in generating ionic gradients across membranes by the sodium/potassium pump for the maintenance of osmotic balance [**Error! Bookmark not defined.**]. The nervous system function seriously depend on the activity of the Na^+/K^+ pump, the transporter responsible for maintaining steep Na^+ and K^+ gradients across the neuron plasma membrane. Study of the interaction between potassium ion and biosystems may be unreachable because of the complexity of the biomolecules. it seems that the first estimation of these interactions can be obtained by studying the interaction of the metal ions with the simple molecule such as alcohol, amide, amine and other molecules containing functional group resemble to functional group exist in biomolecules. In this manner, extended research was done to understand the nature of the interactions [4,5]. In this research the interaction of potassium ion with amino acids as building blocks of proteins studied. This research can be considered as starting point in finding the interaction of potassium ion interaction with proteins.

Selection of Compound and Computational Method

Amino Acids are building block of proteins in which have amine (NH_2) and carboxylic group acid attached to single carbon. There are two forms of Amino Acids; neutral and ionic forms. General formula of two neutral (a) and ionic forms (b) forms of Amino Acids are shown in Fig.1.

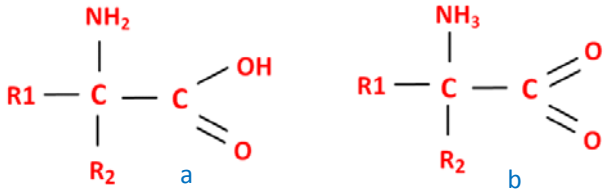

Fig.16 General formula of two neutral (a) and ionic forms (b) forms of Amino Acids

Table6 list of substitutions which located instead of R1 and R2 groups in Fig.1

R1	R2	R1	R2
H	H	H	SH
H	CH_3	SH	SH
CH_3	CH_3	H	SiH_3
H	F	SiH_3	SiH_3
F	F	H	NH_2
H	COOH	NH_2	NH_2
COOH	COOH		

The substitution R1 and R2 were chosen in manner that the properties of them are changed from electron withdrawing groups to electron releasing groups. In Table6 list of substitutions which selected to be locate in place of R1 and R2 is shown. Substituted Amino Acids, potassium ion bonded to Amino Acids and potassium ion bonded dimer of them was chosen to study the interaction of potassium ion with substituted Amino Acids.

The structure of each species in this research include; Amino Acids, potassium ion attached to Amino Acids and potassium ion bonded dimer of them were optimized by HF method, 6-311++G** basis set and gaussian03 package. Energy parameters, IR spectrum and NMR of each species were calculated by using same method and basis set described previously.

Results and discussion

1. Structure and stability of Amino Acids, potassium ion bonded to Amino Acids and potassium ion bonded dimer of them

Structure of all species such as Amino Acids, potassium ion bonded to Amino Acids and potassium ion bonded dimer of them was calculated. The structure and IR spectrum of the potassium ion bonded dimer of Amino Acid which R1 and R2 are H is shown in Fig.17.

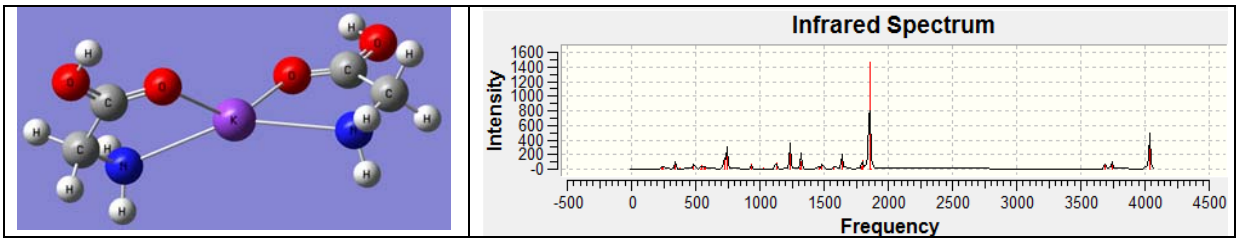

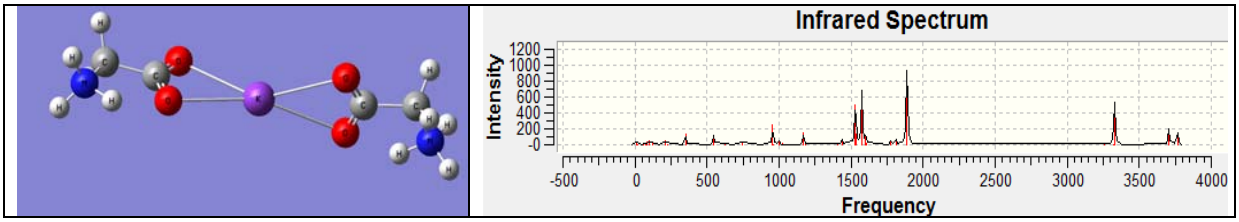

Fig.17 structure and IR spectrum of potassium ion bonded dimer of two forms of Amino Acid in which R1=H and R2=H

Since observing the IR spectrum of the dimers shows no negative vibrational mode in its spectrum, the dimers are stable.

2. potassium ion bond strength and enthalpy of formation for potassium bonded dimer of Amino Acids

The potassium ion bond length to oxygen or nitrogen shows the strength of it. Decrease in potassium positive charge or □ factor can be defined as Eq.1

$$\sigma = charge\ of\ isolated\ K^{+} - charge\ of\ K^{+}\ in\ dimer$$

In **Error! Reference source not found.**, the bond length of K^{+} to Oxygen or Nitrogen versus decrease in potassium charge or □ factor is plotted. In Fig.4, plot of the enthalpy of formation for the different dimers versus □ factor is shown.

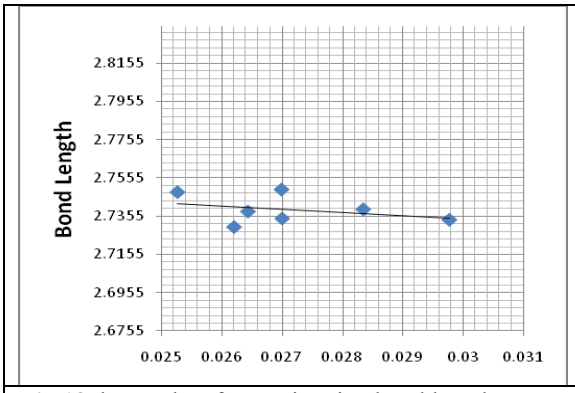

Fig.18 the results of potassium ion bond length versus □ factor

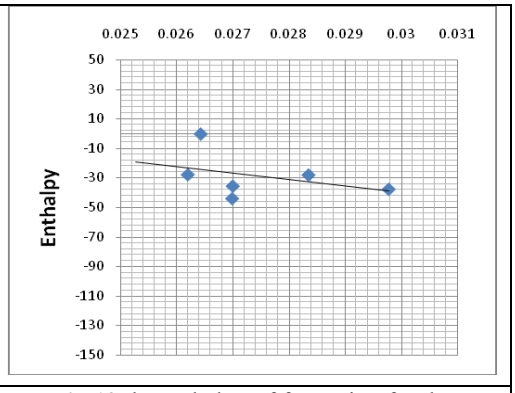

Fig.19 the enthalpy of formation for the different dimers versus □ factor

As shown in Fig.3 and Fig.4, when the charge in central potassium ion in dimer decreases (higher □ factor) the strength of potassium bond to amino acids is strengthen and the enthalpy of formation of dimer increases.

Conclusion

The structure and stability of potassium ion bonded dimers of different substituted amino acids which resembled the interaction of potassium ion with proteins, were calculated by ab initio calculations. The energy parameters of them were analyzed by same method and show that each parameter such as electron releasing or withdrawing properties of substitutions reduced positive charge on potassium ion, makes the dimer more stable.

Refernces

[] Robert R. Crichton, Biological Inorganic Chemistry an Introduction, Elsevier, 1st edition. 2008

3[2] J. A. Cowan, Chem. Rev. 1998, 98, p.1067

[3] Russ Hille, Chem. Rev., 1996, 96, p.2757

[4] Toshihiro Fujii, Hiroaki Tokiwa, Hiroshi Ichikawa, Journal of Molecular Structure (Theochem) 339, (1995) p.209.

[5] M. T. Rodgers and P. B. Armentrout, J. Phys. Chem. A., 1997, 101, p.2614

[3] .forouzandehdel@mehr.sharif.ir

Investigation of the adsorptive behavior of Hydrogen in the presence of Helium on Silicon Nanotubes: Canonical Monte Carlo Simulation

Faramarz yari*[1] ,S. Majid Hashemianzadeh[1], S.Saleheh Razavi[1], Fatemeh cigarchi[1]
Molecular Simulation Research Labratory, Department of Chemistry, Iran University of Science and Technology, Tehran, Iran
faramarzyari@yahoo.com

Keywords: Monte Carlo simulation, lennard-JonePotential, Morse Potential, Gas Adsorption

Introduction:

One of the major drawbacks in the way of transition to Hydrogen economy is difficulty of achieving materials that can store Hydrogen with high gravimetric and volumetric density, fast kinetics, and favourable thermodynamics that the reversible Hydrogen adsorption and desorption at near-ambient conditions can occur [1-3]. Regarding difficulties of storage via gas compression, liquefaction or metal hydride, studying new perception of Hydrogen storage such as physical adsorption on nano-materials has been considered to meet the goals of U.S. Department of Energy (DOE)[2,4,5]. With the successful synthesis of silicon nanotubes (SiNTs) by the chemical vapour deposition (CVD) method in 2002[6], a lot of other methods were also developed to fabricate the SiNTs [7]. Compared to carbon, silicon has more electrons in the outer shells, which leads to higher polarizability, stronger dispersion force and accordingly stronger van der Waals (VDW) attraction to gases than CNTs. Since few studies have been done on hydrogen adsorption area in SiNT [8,9], a more potential candidate for hydrogen storage compared to CNT, We reported a multiscale theoretical method to investigate adsorption behaviour of Hydrogen in the presence of Helium in SiNTs. The multiscale theoretical method combines the first-principle calculations to obtain the binding energy between Hydrogen and Helium with SiNTs, shown in our previous study [10], and a canonical Monte Carlo (CMC) simulation, presented in this paper, to evaluate the Hydrogen adsorption capacity in the mixture of H2 /He in SiNTs, where the calculated binding energy is provided as an input in the CMC simulation.

Models and simulation methods:

In view of the fact that Helium is a small inert gas atom with no strong VDW interaction either among its molecules or with others, we inject this gas to Hydrogen in order to develop our understanding on the effect of Helium to Hydrogen system. A standard MC simulation was carried out at a fixed volume, temperature, and sum of the species for the adsorption of pure H2 and H2/He mixtures on SiNTs. The cut-off radius of 2.5 σ applied to the LJ potential interactions. For each isotherm point, $5*10^7$ configurations were generated. The system was achieved to equilibrate after $2*10^7$ steps, and the remaining $3*10^7$ configurations were used to

Table 1. Calculated Morse potential parameters for interaction of H_2 and He with hollow sites of three different SiNTs

Morse potential parameter	outside the tube wall for (5, 5) SiNT		outside the tube wall for (7, 7) SiNT		outside the tube wall for (9, 9) SiNT	
	H2	He	H2	He	H2	He
D(kcal/mol)	1. 1	0. 36	0.983	0. 297	0. 973	0. 304
g	4. 83	5. 745	4. 768	5. 719	4.98	5. 956
re(A)	2. 79	3. 586	2. 98	3. 637	2. 944	3. 575

obtain ensemble average values for thermodynamic properties. One SWSiNT placed in the center of box with dimensions of (100 Å ×100.Å ×45Å). The intermolecular interactions between H2 -H2 [8] and He-He [11] were calculated using the (12-6) Lennard-Jones (LJ) potential. The total interactions between adsorbate and SWSiNTs were represented using the Morse potential equation, which is investigated in our
Previous work [10] and reported in Table 1.

Figure1 reveals the effect of helium on the adsorption capacity of Hydrogen in three different pore width and constant temperature and pressure of 50 K and 2 MPa, respectively. Results show remarkable enhancement in the gravimetric storage capacities of H2 in the presence of He as compared to pure H2. This improvement of hydrogen adsorption capacity is attributed to the potential interaction between hydrogen and helium which is two times weaker than that for pure hydrogen ($\varepsilon_{H2\text{-}He}$=20.89 K), therefore, hydrogen in the presence of helium can adsorb more easily than pure system. The amount of Hydrogen adsorption and the percentage of

improvement in adsorption capacity of H2 for (5, 5), (7,7) and (9, 9) SiNTs at T=50 K and P=2 MPa in X_{H2}= 0.3, 0.5 and 0.7 are reported in Table 2 and 3.

Figure 1: Gravimetric storage capacity of hydrogen in the mixture with He and in the pure system versus mole fraction in SiNTs of different pore sizes, T=50 K and P=2 MPa.

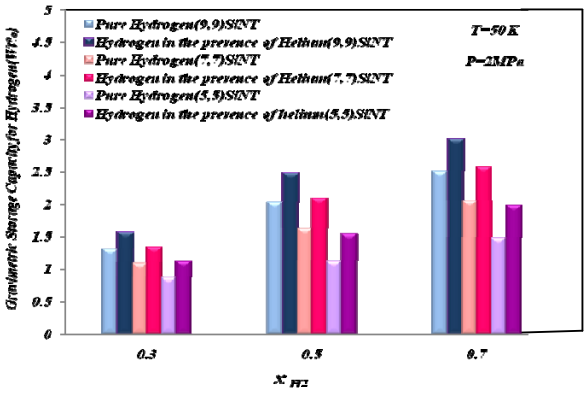

Table 2: Gravimetric adsorption capacity of H2 in different SiNTs and mole fractions						
	H2 Wt% in (5, 5)SiNT		**H2 Wt% in (7, 7) SiNT**		**H2 Wt% in (9, 9) SiNT**	
	H2 in H2 /He mixture	**Pure H2**	**H2 in H2 /He mixture**	**Pure H2**	**H2 in H2 /He mixture**	**Pure H2**
0.3	1.1244	0.8735	1.3445	1.0876	1.3247	1.1144
0.5	1.5457	1.1235	2.0985	1.6267	2.4724	2.0345
0.7	1.9876	1.4856	2.58	2.0563	2.9989	2.5067

Table 3: % Improvement of Gravimetric adsorption capacity of hydrogen in the presence of helium at different SiNTs and mole fraction			
	%Improvement of gravimetric adsorption capacity in (5, 5) SiNT	**%Improvement of gravimetric adsorptioncapacity in (7, 7) SiNT**	**%Improvement of gravimetric adsorption capacity in (9, 9) SiNT**
0.3	٢٨,٦٣٨٩	٢٣,٣٠٣١	١٨,٨٧٣
0.5	٣٧,٥٧٢٨	٢٩,٠٠٤٦	٢١,٥٢٣١
0.7	٣٣,٧٩١٠٦	٢٥,٤٦٥٥١	١٩,٦٣٢٥١

Conclusion:

In summary, Injection of helium to system leads to hydrogen dilution and must be carefully considered from two aspects. From one side, dilution of hydrogen during addition of helium increases the safety of system which is undoubtedly more opportune for fuel cell applications.

on the other hand, considering this fact that helium cannot be a strong competitor in adsorption for hydrogen and it only perform as a diluter factor, addition of helium to the system decrease the interactions between molecules, increase the possibility of hydrogen approach to the surface of tube and consequently enhance the magnitude of hydrogen adsorption. It is meant that comparison the identical number of hydrogen molecules in pure and mixture systems under the same theoretical conditions indicate the enhancement in hydrogen adsorption in the presence of helium compared to pure state. Moreover, It should be mentioned that the maximum hydrogen adsorption improvement is attributed to (5, 5) SiNT and X_{H2} =0.5 at the constant temperature and pressure of 50 K and 2MPa, respectively.

Reference:

[1]. Sun, Q.; Wang, Q.; Jena, P. Nano Letters **2005**, 5, 1273-1277.

[2]. Liu, Z. International Journal of Hydrogen Energy **2007**, 32, 3987-3989

[3]. Cho, J. H.; Park, C. R. Catalysis Today **2007**, 120, 407-412.

[4]. Schlapbach, L.; Zuttel, A. *Nature* **2001**, *414*, 353-358.

[5]. Jord-Beneyto, M.; Suɔrez-Garcيa, F.; Lozano-Castelló, D.; Cazorla-Amorós, D.; Linares-Solano, A. Carbon **2007**, 45, 293-303

[6] .Schmidt, O. G.; Eberl, K. Nature 2001, 410, 168-168.

[7]. Sha, J.; Niu, J.; Ma, X.; Xu, J.; Zhang, X.; Yang, Q.; Yang, D. Advanced Materials 2002, 14, 1219-1221

[8]. Lan, J.; Cheng, D.; Cao, D.; Wang, W. The J. of Phys. Chemistry C **2008**, 112, 5598-5604

[9]. Lithoxoos, G. P.; Samios, J.; Carissan, Y. The J. Phys. Chemistry C **2008**, 112, 16725-16728

[10]. Razavi, S.S.; Cigarchi, F.; Hashemianzadeh, S.M.; Submitted in 14th conference of physical chemistry of Iran

[11]. Firlej, L.; Kuchta, B. Colloids and Surfaces A: Phys. & Eng. Aspects **2004**, 241, 149-154.

Host-Guest Inclusion Complex Formation between Cucurbit [n]urils with Anticancer Drug

F. Yavari[a], Z. B. Nojini[*b], S.Samiee[b]

[a] Department of Chemistry, Science and Research Branch, Islamic Azad University ,Khouzestan , Iran

[b] Department of Chemistry, Faculty of Science, Shahid Chamran University, Ahwaz, Iran

E-mail:Chemist_project2009@yahoo.com

Keywords: Cucurbit[n]uril, Nedaplatin, DFT, Inclusion Complex

Introduction

Cucurbit[n]uril is a family of homologues which are most favored cavitands for host-guest complex formation [1]. Encapsulation of drugs inside a Cucurbit[n]urils provides two benefits. First, it protects the drugs from degradation. Secondly, encapsulation can increase the specificity of the drugs, and uptake into cancerous cells [2].

Computational Method

All the structures were optimized using the density functional theory (DFT) and B3PW91 with LANL2DZ basis set. The inclusion process was simulated by putting the guest in one end of CB[n] n=5, 6 and 7 cavity and then letting it pass through the CB[n] n=5, 6 and 7 cavity by steps.

Result and Discussion

Energies were computed at the level of DFT/LANL2DZ, on the optimized geometry. The electronic chemical potential (μ) was calculated as half of the energy of the highest occupied molecular orbital (HOMO) plus the lowest unoccupied molecular orbital (LUMO) as follows:

$$\mu = \frac{(E_{HOMO}+E_{LUMO})}{2} \qquad (1)$$

The operational definition of hardness (η) was obtained as follow:

$$\eta = \frac{(E_{LUMO}-E_{HOMO})}{2} \qquad (2)$$

hard molecules thus have a large HOMO-LUMO gap and soft molecule have a small one. To examine the binding properties of these complex formation, we calculated the total energy of the CB[n]/Nedaplatin n=5, 6 and 7 as well as the pristine CB[n] and nedaplatin molecule. The complex formation energy, *E*, was calculated using the following expression:

$$E = E_{(complex)} - \left(E_{CB[n]} + E_{drug}\right) \quad (3)$$

The stability energy values for the complexes as well as each components, and HOMO, LUMO and energy gap for complex formation between CB[n] n=5 ,6 and 7 with Nedaplatin are listed in Table 1. Chemical potential (μ) values show the transfer of charge from the metal center to the CB[n] unit and NBO analysis shows the existence of hydrogen bonding between the oxygen portal and amine hydrogen. The results of potential energy surface show that the Nedaplatin is located out of the cavity of the CB[n] with 1:1 stoichiometry. High values of Gap energy for CB[n]'s show that they are rigid molecules and resist with change of electron density.

Table1. Electronic energies and HOMO, LUMO, Gap energy and chemical potential of the inclusion complexations of CB[n] n=5, 6 and 7 with Nedaplatin

Type	E(Kcal/mol)	ΔE(Kcal/mol)	HOMO(eV)	LUMO(eV)	Gap energy	μ(eV)
CB[5]	-1,886,973	-	-6.64	0.381	7.021	-3.126
CB[6]	-2,264,376	-	-6.694	0.462	7.156	-3.116
CB[7]	-2,641,773	-	-6.748	0.462	7.21	-3.143
Nedaplatin	-335,894	-	-5.388	-0.517	4.871	-2.939
CB[5]/Drug	-2,222,898	-31	-3.537	-0.354	3.183	-1.946
CB[6]/Drug	-2,600,284	-14	-3.755	-0.082	3.673	-1.919
CB[7]/Drug	-2,977,692	-25	-3.839	-0.027	3.812	-1.932

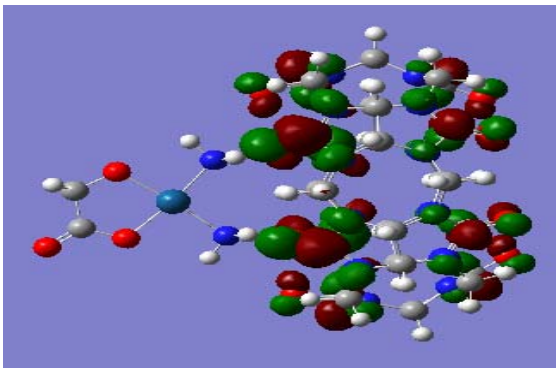

Fig.1: Typically contour plots of LUMO for CB[6]/Nedaplatin complex.

Conclusions

Results show that the Complex formation of Nedaplatin with CB[5] is more stable than other complexes.

References

[1] A. Suvitha, H. Mizuseki, N. Ohuchi,J. Incl Phenom Macrocycl Chem 66 (2010) 213-218

[2] N. J. Wheate, J. Inorg. Biochem.102 (2008) 2060-2066.

Theoretical Study of inclusion Complex Formation between Cucurbit [n]urils n=5, 6 and 7 with anticancer Cisplatin Drug

F. Yavari[a], Z. B. Nojini*[b],S.Samiee[b]

[a] Department of Chemistry, Science and Research Branch, Islamic Azad University ,Khouzestan, Ahwaz, Iran

[b] Department of Chemistry, Faculty of Science, Shahid Chamran University, Ahwaz, Iran

E-mail:Chemist_project2009@yahoo.com

Keywords: Cucurbit[n]uril, Cisplatin, DFT, Inclusion Complex, Electrophilicity, Hardness

Introduction

The successful development of metal-containing anticancer drug clearly starts with cis-DIAMINEDICHLORO-PLATINUM (II), cis-$[PtCl_2(NH_3)_2]$, often referred to as Cisplatin. Cisplatin, as one of the leading metal-based drugs, is widely used in the treatment of cancer. Significant side effects and drug resistance, however, have limited its clinical applications[1].

A hydrophobic cavity and many polar carbonyl groups surrounding the opening portals are the common features of a relatively new receptor family, the cucurbit[n]uril compounds (Q[n]s) [2].

Computational Method

All calculation on host-guest inclusion complex formation of the CB[n] n=5, 6 and 7 with anticancer Cisplatin drug were made with GAUSSIAN G03 package.

Result and discussion

To understand the formation and stability of the inclusion complex we have calculated the formation energy and ΔE for the CB[5], CB[6] and CB[7] with Cisplatin as the host at the DFT/LANL2DZ and the results are provided in Table 1. The electronic chemical potential (μ) and electrophilicity (ω) were calculated as follow:

$$\mu = \frac{(E_{HOMO}+E_{LUMO})}{2} \qquad (1)$$

$$\omega = \frac{\mu^2}{2\eta} \qquad (2)$$

The operational definition of hardness (η) and Gap energy were obtained as follow:

$$\eta = \frac{(E_{LUMO}-E_{HOMO})}{2} \qquad (3)$$

$$Gap = LUMO - HOMO \quad (4)$$

The complex formation energy, E, was calculated using the following expression:

$$\Delta E = E_{(complex)} - \left(E_{CB[n]} + E_{drug}\right) \quad (5)$$

Table1. Electronic energies and HOMO, LUMO, Gap energy, μ, η and ω of the inclusion complexations of CB[n] n=5, 6 and 7 with Cisplatin

Type	E(Kcal/mol)	ΔE(Kcal/mol)	HOMO(eV)	LUMO(eV)	Gap energy	μ(eV)	η(eV)	ω(eV)
CB[5]	-1,886,973	-	-6.64	0.381	7.021	-3.129	3.51	1.395
CB[6]	-2,264,376	-	-6.694	0.462	7.156	-3.116	3.565	1.362
CB[7]	-2,641,773	-	-6.748	0.462	7.21	-3.143	3.592	1.375
Cisplatin	-164,621	-	-6.313	-1.796	4.517	-4.054	2.258	3.639
CB[5]/Drug	-2,051,568	26	-5.113	-0.435	4.678	-2.774	2.339	1.644
CB[6]/Drug	-2,429,003	-6	-5.116	-0.218	4.898	-2.667	2.45	1.452
CB[7]/Drug	-2,806,368	26	-4.707	-0.008	4.715	-2.357	2.349	1.182

Results show that the complex formation is stable than isolated molecules. Positive ΔE for CB[5,6]/ Cisplatin shows that complex formation of the Cisplatin is endothermic for CB[5,6].

The results of potential energy surface show that the Cisplatin penetrate into the cavity of the CB[n] and the formed complexes have minimum energy. NBO analysis shows the existence of hydrogen bonding between the oxygen portal cucurbit and amine hydrogen drug.

The results of electrophilicity show that the Cisplatin is as lewis acid.

The structures of all complexes at the minimum energy of complexation optimized at the level of DFT/LANL2DZ.

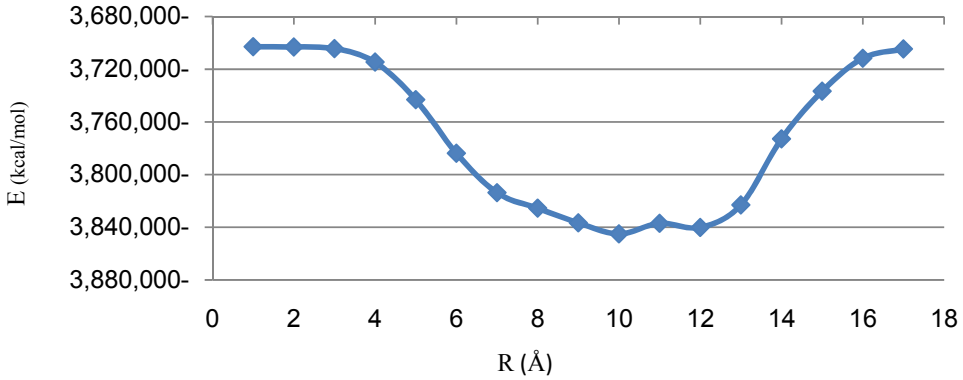

Fig.1: Graphic diagram for emulation of the inclusion complexation of Cisplatin into CB[6].

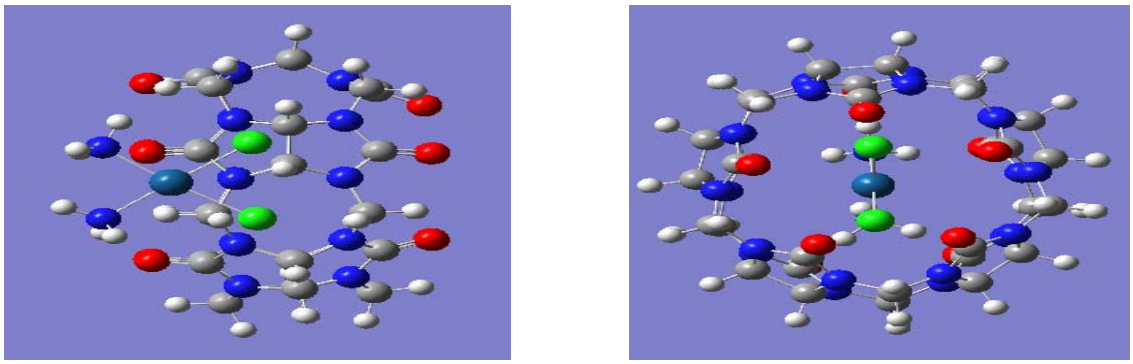

(a) (b)

Fig.2: Optimized structure of **a)** side view of CB[5]/Cisplatin **b)** birds eye-view of CB[5]/Cisplatin

Conclusion

. Results show that the Complex formation of Cisplatin with CB[6] is more stable than other complexes.

References

[1] Kostova, Recent Patents on Anti-Cancer Drug Discovery. 1 (2006) 1-22.

[2] I. W.A. Freeman, W.L. Mock, J. Am. Chem. Soc. 103 (1981) 7367.

Investigation of tautomerism and intramolecular hydrogen bond of monohydroxynaphthazarin

M.Yousofizadeh and M. Zahedi-Tabrizi*
Department of Chemistry, Alzahra University, Tehran, Iran
Zahedi@ alzahra.ac.ir

Keywords: Naphthazarin, Intramolecular hydrogen bond,Vibrational assignment, Density functional theory

Introduction:

There is considerable interest in the study on hydroxylated naphthazarins because of their use in development of cardioprotective preparations [1] and other applications [2-3]. Some substituted monohydroxylated naphthazarins were synthesized and studied by IR spectroscopy in aprotic organic solvents at ambient temperature. ^{1}H NMR studies have shown that naphthazarins undergo rapid proton exchange between α-hydroxyl and carbonyl groups for time –averaged spectra [4] . FTIR and Raman spectra, vibrational assignment, and density functional theory calculations of naphthzarin showed two weak intramolecular hydrogen bond [5].

Method of Analysis:

Geometrical calculation was performed using Gaussian 03 program. Geometries of hydroxynaphthazarins are fully optimized with hybrid density functional B3LYP using 6-311++G** and 6-31G ** basis sets. The vibrational frequencies and ^{1}H chemical shifts of these compounds were computed at the levels and basis sets.

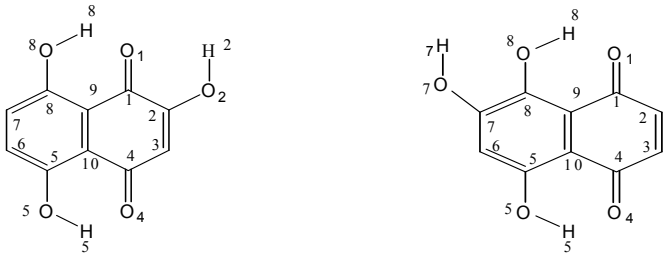

FIG . 1. Numbering system and the structure of 2-hydroxynaphthazarin and 7-hydroxynaphthazarin

Results and discussion:

The geometry of 2-hydroxynaphthazarin and 7-hydroxynaphthazarin and the atom numbering system are given in Fig. 1. Some geometrical parameters and also ^{1}H chemical shifts are compared in Table 1. According to Table 1, substitution of one of the hydrogen atoms in naphthazarin (NZ) by a hydroxyl group in C2 reduces the O5... O4 distance about 0.01 A°.
This result is in agreement with the ^{1}H NMR chemical shift which indicates a downfield by about 0.23 ppm.

Table 1. Some structural parameters and proton chemical shifts of hydroxynaphthazarins and naphthazarin .

Parameter	2-hydroxynaphthazarin	7-hydroxynaphthazarin	Naphthazarin [d]
δH5-O5 [a]	12.96	12.79	12.73
O5…O4 [b]	2.58	1.71	2.59
O5-H5…O4 [c]	146.77	147.06	146.31
H5-O 5	1.02	0.96	0.99
δH8-O8 [a]	11.69	13.09	12.73
O1…O8 [b]	2.63	2.58	2.59
O8-H8…O1 [c]	144.77	145.41	146.31
H8-O8 [b]	1.02	0.96	0.99

a) Hydrogen chemical shift (ppm), b) distance (A°), c) angle (degree) d) data from [5].

Conclusion:

Comparison of the vibrational frequency and structural parameters and also ^{1}H chemical shifts of 2-hydroxynaphthazarin with NZ reveals a weaker H-bond in O8...H8 and stronger hydrogen bond in O5...H5 than that in NZ. The calculated O…O distances are in good agreement with NMR results.
The hydrogen bond in 7-hydroxynaphthazarin is stronger than NZ, which is in good agreement with O…O distances and ^{1}H NMR chemical shift.

References

[1] V. P. Glazunov, A.Ya. Tchizhova, N. D. Pokhilo, V. Ph. Anufrievand G. B. Elyakov, Tetrahedron, 58 (2002)1751-1757.
[2] M. Service and A. C. Wardlaw, Comp. Biochem. Physiol. 79 (1984)161-163.
[3] D. Chen, Z. Hao, X. Zhao, Z. Mang, J. Mol. Struct. (THEOCHEM) 803 (2007) 73-77.
[4] W. I. Shiau, E. N. Duessler, E. C. Paul, D. Y. Curtin, J. Am. Chem. Soc.

102(1980)4546-4548.

[5] M. Zahedi-Tabrizi, S. F. Tayyari, F. Tayyari, M. Behforouz, Spectrochim. Acta. 60A (2004) 111-120.

Classical Thermodynamics

Investigation of solvatocromic parameters of Kamlet and Taft on protonation constants of Glycine in different aqueous solutions of methanol

Gh. Ebrahimzadeh Rajaei*[a] , F. Gharib[b], A. Shamel[a], N. Mohammadian[a], H. Hasrat[a]

[a] *Department of Chemistry, Islamic Azad University, Ardabil Branch, Ardabil, Iran*

E-mail: Farzad_rajaei@yahoo.com

[b]*Department of Chemistry, Shahid Beheshti University, Tehran, Evin, Iran*

Abstract

The protonation constants of Glycine have been determined in different aqueous solutions of methanol at 25 °C and constant ionic strength 0.1 mol dm^{-3} sodium perchlorate, using potentiometric technique. The present work is concerned with the study of protonation equilibria of Glycine in water-methanol mixture solution over a wide pH range. Macroscopic and microscopic properties of water-methanol mixtures have been employed to analyze the solvent effect on protonation constants. Macroscopic parameters of media such as dielectric constant (D) and microscopic solvatocromic parameters of Kamlet and Taft (α, β and π^*) have been used for this purpose. Potentiometric method has been used to analyze the diprotonated (H_2L^+) and monoprotonated (HL) forms of glycine in different aqueous solutions of methanol, simultaneously. pH dependence of absorbance of H_2L^+ and HL have also been analyzed. The protonation constants of Glycine in aqueous –methanol solution were obtained at 25˚C over the composition range of 0 to 40 vol.% methanol at constant ionic strength. The solvent effect and variation of solvent composition on LogK values were discussed.

Keywords: Protonation constant, Slvent effect, Kamlet and Taft's parameters, Glycine

Introduction

Chemists are usually interested to understand solvent effects on the overall solution capabilities that depend on all possible intermolecular interactions between solute and solvent molecules. The search for finding a correlating factor goes back to the work of Thomson and Nernst who suggested a connection between the dielectric constant of a solvent and its dissociating power [1,2]. The interactions between solvent and solute molecules are separated in literature into specific and nonspecific. As a result, linear functions with few parameters for description of the

solvent effect are proposed. One of the most interesting is that proposed by Kamlet and Taft [3]. Moreover, the solvent–solvent interactions produced in solvent mixtures can affect the solute–solvent interactions and therefore they can also affect preferential salvations. In the present work, The protonation constants of Glycine in aqueous –methanol solution were obtained at (25±0.1)˚C over the composition range of 0 to 40 vol.% methanol at constant ionic strength 0.1 mol dm^{-3} sodium perchlorate, using potentiometric technique.

Experimental

Methanol was obtained from Merck as analytical reagent grade material and was used without further purifications. The chloridric acid (Fluka or Aldrich) was used without further purification. The purity of chloridric acid checked by titration with standard base, was found to be better than 99%. The NaoH solution was prepared from titrisol solution (Merck) and its concentration was determined by several titrations with standard HCl. Titration of Glycine solution in acidic form at the same ionic strength as the sample under study, carried out to determine pH. The solutions were protected from atmospheric CO_2. All dilute solutions were prepared from double-distilled water with a specific conductance equal to 1.3±0.1 $\mu\Omega^{-1}cm^{-1}$. Precisa pH 960 101 Stirrer potentiometer and a balance mod. Sartorius CP124S (With 0.1 mg accuracy) were used in this work.The potentiometry measurements were made in a thermostatted cell compartment at the desired temperature (25±0.1)°C on THERMOMIX MM thermostat.

Results and Discussion

If we consider the dissociation of Glycine

(1) $H_2L^+ \leftrightarrow HL + H^+$

(2) $HL \leftrightarrow L^- + H^+$

The dissociation constants K_{1d} and K_{2d} are given by $K_{1d} = \frac{[HL][H^+]}{[H_2L^+]}$ and $K_{2d} = \frac{[L^-][H^+]}{[HL]}$

The protonation constants K_1 and K_2 are versus of dissociation constants K_{d1} and K_{d2} respectively. Using the solvatochromic solvent parameters, the multi-parameter Eq. (3) has been proposed

(3) $\log K = A + a\alpha + b\beta + S\pi^*$

where A represents the regression value and π^* is the index of the solvent dipolarity/polarizability, which is a measure of the ability of a solvent to stabilize a

charge or a dipole by its own dielectric effects. The π* scale was selected to run from 0.0 for cyclohexanone to 1.0 for dimethylsulfoxide. The α coefficient represents the solvent hydrogen-bond donor (HBD) acidity; in other words, it describes the ability of a solvent to donate a proton in a solvent to a solute hydrogen-bond. The α scale extends from 0.0 for non-HBD solvents to about 1.0 for methanol. The β coefficient is a measure of a solvent hydrogen-bond acceptor (HBA) basicity and describes the ability of a solvent to accept a proton in a solute to a solvent hydrogen-bond. The β scale was selected to extend from 0.0 for non-(HBA) solvents to about 1.0 for hexamethylphosphoric acid triamide [4]. The protonation constant values and Kamlet and Taft's solvatochromic parameters are collected in Table 1.

Table 1
The protonation constants of Glycine in different solutions of methanol+water at 25 ˚C and Kamlet and Taft's solvatochromic parameters

%Methanol	$LogK_1$	$LogK_2$	D				a	b
0	2.40	9.84	78.74	1.13	0.18	1.14	1.24	0.18
10	2.50	9.62	72.99	1.18	0.23	1.12	1.18	0.23
20	2.58	9.55	67.11	1.11	0.29	1.10	1.12	0.29
30	2.66	9.49	60.98	1.06	0.30	1.07	1.06	0.35
40	2.74	9.34	52.15	1.02	0.41	1.03	1.00	0.41

We used the Gauss–Newton linear least-squares method in the computer program to refine the log K by minimizing the error squares sum from Eq. (4):

(4) $S=\sum(a_i-b_i)^2$

Where a_i is a quasi-experimental formation constant and b_i is the calculated one. The solvent polarity parameter of media, π*, increases with increasing the mole fraction of water in aqueous solutions of methanol. If the π* of media was the only factor for the solvent effect, it may be expected that log K_1 in water should be greater than those of all the other aqueous solutions of methanol. However, the protonation constant ($logK_1$) increases with increasing the solvent hydrogen-bond acceptor basicity parameter, β, and decreases with increasing the solvent polarity π*, as well as increases with decreasing the hydrogenbond donor acidity parameter of the solvents, α. For $LogK_2$ this results is vice versa. The coefficients of π*, α and β in Eq. (3) are

very different to each other and are in the order of $\beta > \pi^* > \alpha$, and indicate that the hydrogen-bond acceptor basicity parameter is the most important one in determining of $\log K_1$ and $\alpha > \beta > \pi^*$ indicate that the hydrogen-bond donor acidity parameter is the most important one in determining of $\log K_2$.

References:

[1] J.J. Thomson, Philos. Mag. 36 (1893) 313.

[2] W. Nernst, Z. Phys. Chem. 13 (1894) 535.

[3] M.J. Kamlet, J.M. Abboud, M.H. Abraham, R.W. Taft, J. Org. Chem. 48 (1983) 2877.

[4] F. Gharib, K. Zare, B. Mohammadi, Journal of Molecular Liquids 124 (2006) 63 – 67.

Spectrophotometric Studies of Alkali and Alkali Earth Metal Ions Complexes of Mono Amino Derivative of Calix[4]arene

N. Osouleddini [a]*

[a]*Department of Chemistry, Islamic Azad University, Ardabil Branch,Ardabil , Iran*

(Email: osouleddini.n@gmail.com)

Keywords: Formation constant, Alkali metal cation, Alkali earth metal cation, Amino Calix[4]arene

Introduction

Calix[*n*]arenes are cyclic oligomers obtained by condensation of formaldehyde with *p*-alkyl-phenols in the basic environments[1].Calix[*n*]arenes are basket-shaped compounds with potential interest for host-guest complexation[2].Fine control of the size of calix[*n*]arenes,by changing the value of *n* and introduction of various functional groups on the lower or upper rims, makes it possible to prepare a variety of molecules with various applications[3].In this work the four functionality ligating groups in the lower rim(Fig.1)as well as in the upper rim of the ligand are independently modified to increase their binding abilities and make them more specific for chelating by the metal ions.The selectivity of the alkali and alkali earth cations towards the ligands is specified and discussed.

Spectrophotometric Measurements

All measurements were carried out at 25° C using a spectrophotometer scanning (UV-Vis 2101 Shimadzu) with a computer. 2 mL solution of the ligand (2.0×10^{-4} – 2.5×10^{-4} mol dm^{-3}) were titrated with stepwise addition of an alkali or alkali earth cation solution (1.0×10^{-3} mol dm^{-3}), all in the same solvent (methanol-chloroform 30:70 by volume). The UV-Vis spectra of the mixtures undergo small changes at 270-310 nm, but the measured absorbances were sufficient to allow the treatment of the data with the computer program.

Results and discussion

The complex M_pL_q formed is characterized by its stoichiometry, p and q, where M and L represent each metal ion and each ligand, respectively.To determine the formation constant of complexation, K, Eq. 1 is defined, $pM^+ + qSC4 \rightleftharpoons M^+_pSC_{4\,q}$ $K = [M^+_pSC_{4\,q}] / [M^+]^p[SC_4]^q$ (1)

Absorbance, A, was measured by successive addition of an alkali and alkali earth metal cation solution to the ligand solution, see experimental section. Treatment of the spectrophotometric data obtained during the titrations were conducted with the computer program Squad [2]. All proposed species existed in significant concentration were checked over a reasonable range of data. As expected, polynuclear complexes were systematically rejected by the computer program. The model finally chosen, formed by ML, resulted in a satisfactory numerical and graphical fitting for all systems. The average formation constant values of the 1:1 complex species of the ligand with cations in the specified wavelengths are listed in Table 1.

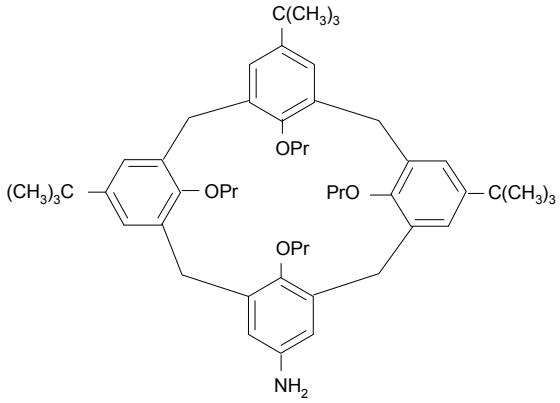

Fig. 1. The structure of 5,11 , 17-tris(tert-butyl)-23 amino-25, 26, 27, 28- tetrapropoxy calix[4]arene(L)

Table 1.Average values of log *K* at different wavelengths for the alkali and alkali earth cations at 25 °C

metal ion	log *K*
Li^+	3.95 ± 0.04
Na^+	3.54 ± 0.05
K^+	3.52 ± 0.02
Rb^+	3.49 ± 0.03
Cs^+	3.46 ± 0.05

metal ion	log *K*
Mg^{2+}	4.96 ± 0.04
Ca^{2+}	4.49 ± 0.03
Sr^{2+}	3.71 ± 0.05
Ba^{2+}	3.19 ± 0.04

Figure 2 shows a break point when the concentration of metal ion to the ligand ratios reaches unity,indicating the formation of 1:1 complexes of the ligand with all cations. This behavior indicates a relatively stable complex for Li^+ and Mg^{2+} and less stable species for the other cations specially for Cs^+ and Ba^{2+}. Figure 3 shows that the formation constant values of the complexes increase with decreasing the ionic radius of the cations.The binding selectivity of the ligands towards the alkali cations based on the formation constant values of the complexes is in the order of $Li^+ > Na^+ > K^+ > Rb^+ > Cs^+$ and for the alkali earth cations is in the order of $Mg^{2+} > Ca^{2+} > Sr^{2+} > Ba^{2+}$. Also, alkali earth cations form more stable complexes than the other cations because of high electrostatic interactions by ligand.

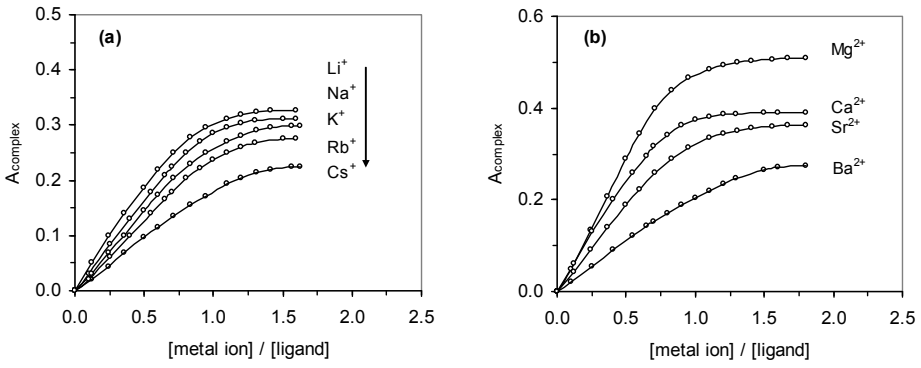

Fig. 2. Spectrophotometric titration plots of the ligands L, (a) by the alkali metal, and (b)alkali earth metal ions, at 25 °C and 270 nm.

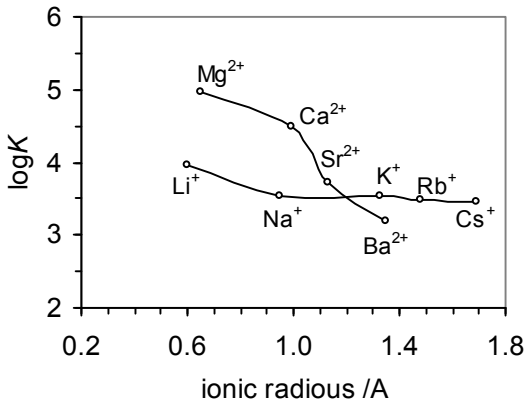

Fig. 3. The plots of log *K* versus the ionic radii of the alkali and alkali earth cations at 25 °C.

References

[1] C. D. Gutsche, *Calixarenes* (The Royal Society of Chemistry, Cambridge, 1989).

[2] I. Mohammed-Ziegler, B. Poor,M. Kubinyi,A. Grun, and I. Bitter, J.Mol.Struct.**39**,650 (2003).

[3] M. Chiba, H. Kim, and N. Kitamura, J. Photo. Chem. Biolog., **151**, 67 (2002).

Investigation Sigmatropic Rearrangements of Structure 1-(cyclopenta-2,4-dienyl)-1H-phosphole Using Primary Mechanic Quantum and Density Function Theory (DFT) With NBO Analysis

R.Soleymani*[a,b] and F.Afshari[a]

[a] *Chemistry Department, Faculty of Sciences, Islamic Azad University, Touyserkan Branch, Young researchers Club, Touyserkan ,Iran*

(Email: nima_soleimany@yahoo.com)

[b] *Chemistry Department, Faculty of Sciences, Islamic Azad University Shahre-rey Branch, Tehran, Iran*

Keywords: Ab initio; DFT ; NBO ; Sigmatropic Rearrangements

Introduction

After passing several experimental stages , similar and like structure 1-(cyclopenta-2,4-dienyl)-1H-phosphole is synthesized in the laboratory .This structure has the different properties : Chemical Formula C_9H_9P , Exact Mass 148.04 , Molecular Weight 148.14 , m/z 148.04 (100.0%), 149.05 (9.8%) , Elemental Analysis C, 72.97; H, 6.12; P, 20.91 - Boiling Point 476.45 (K) - MR 53.17 (cm3/mol) Henry's Law 0.38 .[1]

(B3LYP)

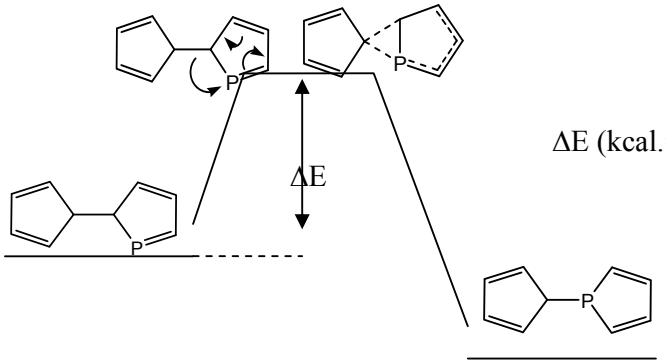

$$\Delta E\ (kcal.mol^{-1}) = \begin{cases} 2.867675 \\ 3.535962\ (HF) \end{cases}$$

Calculation method

Initial optimization operated by using Winmopac version 2.0 software and AM1 method .The transition mode of structure simulate by using keyword SADDLE and then transition state GAUSSIAN 03W package program and keyword QST2 implemented on a pentum-PC computer with a 430 MHz processor , used for finalization[2]. Eventually, the final

optimization and calculation of energy levels operated in theory of the levels HF/6-311+G** and B3LYP/6-311+G**. Also NBO-version 03 program used for calculations of natural bond orbital

Result and discussion

Researches on quantum mechanic and DFT at the theory of the level B3LYP and HF for sigmatropic rearrangement mechanism of structure 2-(cyclopenta-2,4-dienyl)-2H-phosphole and changing it to structure 1-(cyclopenta-2,4-dienyl)-1H-phosphole were reported in the table below. In this table reported energies (in Hartree) for the important geometries of sigmatropic rearrangement reaction.

Method	**B3LYP/6-311+G****			**HF/6-311+G****		
Geometry	Reactive	Transition State	Product	Reactive	Transition State	Product
ZPE	0.149296	0.149139	0.149295	0.160112	0.159973	0.160109
E_{ele}	-689.7683617	-689.7636356	-689.7683616	-686.8007301	-686.7949561	-686.8007266
E_0	-689.619066	-689.614496	-689.619067	-686.640618	-686.634983	-686.640617
ΔE_0	0.00457(2.867675)[a]			0.00563(3.535962)[a]		

[a]Numbers in parenthesis are the corresponding values in kcal mol^{-1}

Conclusion

Investigations have been done the mechanism of sigmatropic rearrangements of changing the structure1-(cyclopenta-2,4-dienyl)-1H-phosphole to the 2-(cyclopenta-2,4-dienyl)-2H-phosphole using the quantum mechanic and DFT method and the results show that this process can be done with reagent of 2.867675 Kcal/mol (B3LYP method) and 3.535962 Kcal/mol (HF method) energy . The mechanism of this reaction is exothermic .The results of NBO also show that this reaction is accompanied by the transfer of pay electrons and breaking of sigma bond between two rings and constructing a new sigma bond between phosphorus and ring that of donor - acceptor interaction shows the resonance energy л→л* delocalization. Too in this structure bond order not same and similar.

References

[1]. R.M.G. Roberts and A.S. Wells, *A new synthetic route to monophosphaferrocenes*, Inorganica Chimica Acta, Volume 112, Issue 2, 17 February **1986**, Pages 171-175.

[2]. M. j. Frisch et al. *GAUSSIAN 03*, Revision C. 01, Gaussian Inc.,Wallingford. CT, **2004**.

Modification of Tao-Mason Equation of State: Application to Ionic Liquids

S. Amighi[a], M. M. Papari*[a], J. Moghadasi[b]

[a] Department of Chemistry, Shiraz University of Technology, Shiraz, 71555-313, Iran

[b]Department of Chemistry, ShirazUniversity, Shiraz, 71454, Iran

Email: papari@sutech.ac.ir, Fax: +98-711-726-1288

Key words: Equation of state, Ionic Liquids, Volumetric Properties

Introduction

Ionic liquids (ILs) came into focus recently as new materials offering several highly promising applications. Their physico-chemical properties allows one to use them as solvents in chemical synthesis and in newly designed batteries, fuel cells or super capacitors. The modification of the Tao-Mason equation of state to predict volumetric properties of several classes of ILs is the subject of the present work.

Theory

The general frame of the Tao-Mason EOS is [1]:

$$\frac{P}{\rho kT}=1+(B(T)-\bar{\alpha}(T))\rho+\frac{\bar{\alpha}(T)\rho}{1-\rho b(T)\lambda}+A_1(\bar{\alpha}(T)-B(T))b(T)\rho^2\frac{(e^{kTc/T}-A_2)}{1+1.8(\rho b(T))^4} \quad (1)$$

Where

$$A_1 = 0.143\ ; \quad (2)$$

$$A_2 = 1.64+2.65[e^{(\kappa-1.093)}-1]; \quad (3)$$

$$\kappa = 1.093+0.26[(\omega+0.002)^{1/2}+4.50(\omega+0.002)] \quad (4)$$

the second virial coefficient from the following expression [2]:

$$B(T)\rho_{nb}=0.1-0.054\left(\frac{\Delta H_{vap}}{RT}\right)^2-0.00028\left(\frac{\Delta H_{vap}}{RT}\right)^4 \quad (5)$$

The following equation was employed to predict the enthalpy of vaporization:

$$\Delta H_{vap}(IL)=\sum n_i\Delta H_i+\sum n_j\Delta H_j \quad (6)$$

In this equation, n_i i the number of elements of the ith type in the ionic liquid and ΔH_j the contribution of the jth structural correction [3].

Results and discussion

In the present study, we followed the modification of the above-mentioned EOS cited in ref. 4 and applied to 30 ionic liquids. Our results showed that the proposed EOS can accurately predict the density of studied ILs. From 3330 experimental points examined in this work, the overall average absolute deviation (AAD) was found to be 1.34%.

Typically, Fig. 1 shows the deviation of calculated densities of ionic liquid [Bmim][BF4] from experimental ones [5].

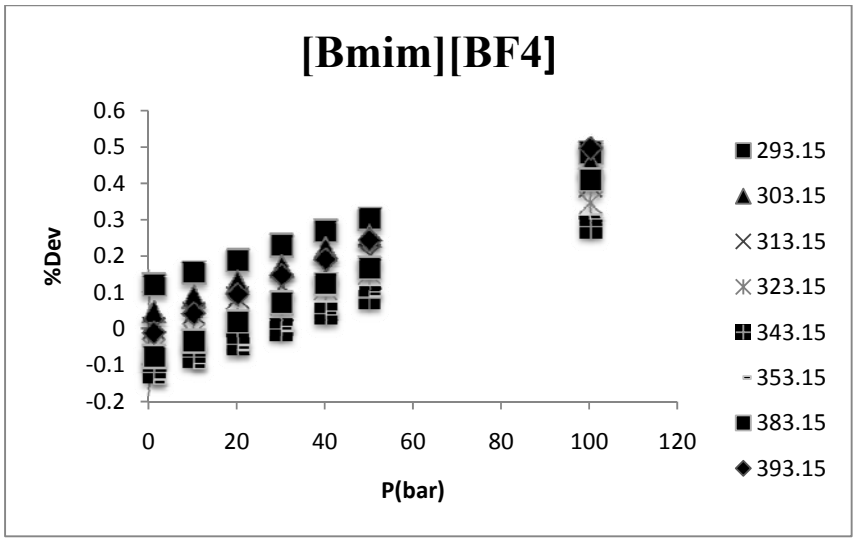

References:

[1] Tao, F. M., and Mason, E. A. *J. Chem. Phys*. **1994**, 100, 9075.

[2] Sheikh S., Papari M. M. and Boushehri, A. *Ind. Eng. Chem. Res.* **2002,** *41, 3274.*

[3] Verevkin, P. S. *AngewandteChemie*. **2008**, 47, 5071.

[4] PapariM. M., NejabatR,Moghadasi J, Campo A*, Int. J. Refrig. (In Press).*

[5] Ramesh L. Gardas, Mara G. Freire,Pedro J. Carvalho, Isabel M. Marrucho, Isabel M. A. Fonseca,Abel G. M. Ferreira, and Joa˜o A. P. Coutinho*,J. Chem. Eng. Data.***200**752, 80-88.

LLE Data of Ternary Aqueous Mixtures of (Acetic Acid + Cyholexane or Cyclohexanol or Cyclohexanone)

Kh. Bahrpaima[a], M. Kiyani[a], I. Naddaf[b]

[a]*Department of Chemistry, Islamic Azad University, Firoozabad Btanch, Iran*

Kh.bahrpaima@gmail.com

[a]*Department of Chemical Engineering, Islamic Azad University, Omidiyeh Btanch, Iran*

Keywords: Liquid- liquid Equilibrium, Extraction, UNIQUAC model, Acetic acid

Introduction:

Technique of liquid – liquid extraction is one of the most important separation processes in the chemical industries. The accurate interpretation of phase equilibria for multi-component mixtures is a fundamental key to improve this technique [1, 2]. In this work, the liquid-liquid phase behavior of aqueous acetic acid in three other organic solvents (cyholexane or cyclohexanol + cyclohexanone) at 298.2 K at normal pressure is presented. The experimental tie–lines data were correlated by the UNIQUAC equations [4].

Methods:

The experimental points that identify tie-lines in the phase diagram were measured by using a glass cell. The prepared mixtures with known compositions were located inside the cell and were vigorously agitated with a magnetic stirrer for 4 h, in order to allow a close contact between the phases. The mixtures were then settled for 4 h to completely separate in two liquid phases and to get the equilibrium. After separation, samples of both phases collected from each phase and analyzed to determine their compositions. The concentrations of acetic acid in both of the phases were indicated by potentiomeric NaOH titration in presence of phenolphthalein as an indicator.

Results and Discussion:

The experimental tie lines data for the ternary mixtures of (water + acetic acid + cyholexane or cyclohexanol or cyclohexanone) at 298.2 K are presented.

The effectiveness of extraction of the acetic acid by organic solvents is given by the separation factor, S. The separation factor is defined as the ratio of distribution coefficients of acetic acid, D_2, to water, D_1, $S = D_2 / D_1$. The experimental results are shown the separation factor for cyholexane (56.2) > cyclohexanol (13.3) > cyclohexanone (6.5) solutions, therefore can be concluded that cyholexane is better for extraction of acetic acid from aqueous solutions.

The UNIQUAC model was used to correlate the experimental data. The experimental ternary LLE data of (water + acetic acid + cyholexane), (water + acetic acid + cyclohexanol) and (water + acetic acid + cyclohexanone) were correlated using the UNIQUAC model. Fig 1 is shown phase diagram for the ternary system of (water + acetic acid + cyholexane) at 298.2 K.

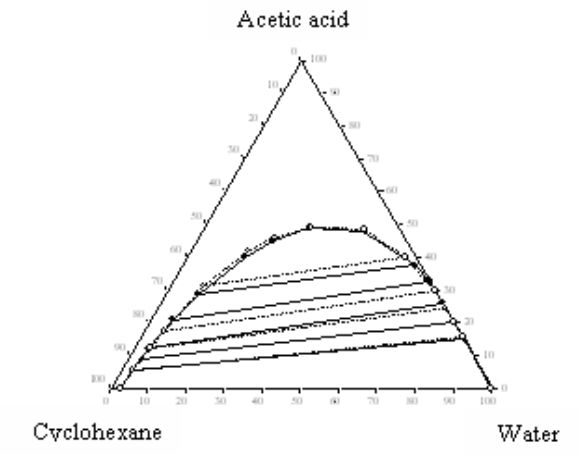

Figure 1. LLE phase diagram for (water + acetic acid + cyholexane) at 298.2 K. (●) Experimental points, (○) Correlated data

The root-mean-square deviation (RMSD) can be taken as a measure of precision of the correlations. The RMSD value was calculated from the difference between the experimental and calculated mole fractions according to the following equation:

$$\mathrm{RMSD} = 100\sqrt{\frac{\sum_{k=1}^{n}\sum_{j=1}^{2}\sum_{i=1}^{3}\left(x_{ijk} - \hat{x}_{ijk}\right)^2}{6n}} \qquad (2)$$

Values of RMSD for (water + acetic acid + cyholexane), (water + acetic acid + cyclohexanol) and (water + acetic acid + cyclohexanone) at 298.2 K are 0.56, 0.63 and 0.91, respectively.

Conclusions:

The LLE data for the ternary systems of (water + acetic acid + cyholexane), (water + acetic acid + cyclohexanol) and (water + acetic acid + cyclohexanone) were studied at 298.2 K. It can be concluded that cyholexane is better for extraction of acetic acid from aqueous solutions than cyclohexanol and cyclohexanone. The UNIQUAC solution model was satisfactorily used to correlate the experimental LLE results for acetic acid studied mixtures.

References:

[1] C. Wu, B. Chu, G. Stell, Makromol. Chem., Macromol. Symp. 45,(1991) ,75-79.
[2] R. Satta, N. Dimitrijevic, H. Manev, Eur. J. Pharmacol. 473(2-3), (2003), 149-52
[3] D. S. Abrams, J. M. Prausnitz, AIChE J. 21, (1975), 116–128.

Crossover parametric equation of sate using complete scaling

Amin Bakhshandeh, Hassan Behnejad*
Department of Physical Chemistry, School of Chemistry, University College of Science, University of Tehran, Tehran 14155, Iran
behnejad@khayam.ut.ac.ir,

Introduction:

Nowadays critical phenomena in fluids and fluids mixture are one of the paid intentioned topics in physics and chemistry. Studying physical and thermo physical properties of fluids and fluids mixture near their critical points are very difficult which is arised as a result of fluids sudden behavior change near critical point [1]. As an example, fluids obey Mean-field equation of state far away from critical point, while near the critical point we can't study them with the classical equations of state [2].

Fluids exhibit large fluctuation in order parameter near critical point and it has been shown that critical fluctuation causes non-analytical singularity in thermodynamic surface near critical point [3]. Indeed, close to critical point, the range of fluctuation becomes much larger than any microscopic length so that molecular interactions aren't important anymore and this results universality.

Although the scaling hypothesis is very powerful but the range of its validity is very short, and most of the researchers who study the fluids behavior need an equation of state that cover much more wider range. Therefore, a crossover function is inserted to equation of state which changes the shape of the equation near and far away from critical point. It means that near the critical point equation of state predicts correct critical exponents and amplitudes along with the prediction of classical exponents and amplitudes far away from the critical point (Mean-Field) that results in a wider range for the equation of state[4].

In this work susceptibility critical amplitude of water system was evaluated using complete scaling theory to obtain corresponding critical amplitude both above and below the critical point. Then, by employing the complete scaling diameter density, two system dependent parameters a_3 and b_2 were calculated followed by the calculation of the complete scaling critical and mean field amplitudes, and the corresponding parameters of crossover parametric

equation of state for this system. Finally the parametric crossover equation of state with applying complete scaling model has been introduced.

Fisher proposed that to consider all asymmetric nature of the critical phase transition it is needed to relate scaling fields to all physical fields. So he defined scaling filed as :

$h_1 = \Delta\tilde{\mu} + a_1\Delta\tilde{T} + a_2\Delta\tilde{P}$, $h_2 = \Delta\tilde{T} + b_2\Delta\tilde{\mu} + b_3\Delta\tilde{P}$, $h_3 = \Delta\tilde{P} + c_2\Delta\tilde{\mu} + c_3\Delta\tilde{T}$

(1)

All above coefficients aren't independent and related to each other, for example Anisimov showed that $a_2 = a_3c_3 = -a_3\left(\frac{\partial\tilde{P}}{\partial\tilde{T}}\right)_c$, $c_3 = \left(\frac{\partial\tilde{P}}{\partial\tilde{T}}\right)_{cxc,c}$. By using above equations the thermodynamic relations may be obtained as follow:

$\tilde{\rho} = \frac{1+\varphi_1+b_2\varphi_2}{1-a_3\varphi_1-b_3\varphi_2}$

(2)

Method:

Power low equations aren't useful far away from critical point because they show real critical exponent but fluids far from critical point obey mean filed theory and show mean filed critical exponent .

To make these equations applicable far away from critical point a function Y (crossover function) is added to some equations . This function obeys a coupled equation as :

$1-(1-\overline{u})Y = \overline{u}(1+\Lambda^2/\kappa^2)^{1/2}\,Y^{\nu/\Delta_s}$

(3)

where $\kappa^2 = rY^{(2\nu-1)/\Delta_s}$ which is plotted in fig.1

The asymptotic crossover parametric model can be applied to a fluid such as water to find all thermodynamic data at a specific point in the phase diagram. As an example one can find heat capacity amplitude with the aforementioned parameters equal to 31.7 ($A_0^+ = 1.6821 m_0 l_0$) which is in agreement with the value reported in Ref. [5]. Finally, we evaluated the gas and liquid phase density by using crossover parametric equation of state and complete scaling with the aid of the evaluated set of parameters. Applying eqs. (3), and fixing $\left(\frac{\Lambda}{c_t{}^{1/2}}\right) = 3.14$ we obtained $\overline{u}$=0.379 for water system.

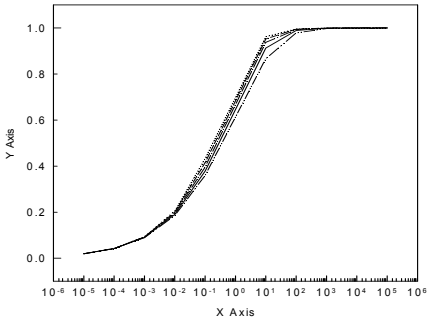

Fig1

Conclusion:

The effect of complete scaling on asymptotic crossover parametric equation of states was studied and the corresponding critical amplitudes formulations were derived. The theory has been applied to water vapor - liquid coexistence and susceptibility data as a one component fluid. As complete scaling predicts, to evaluate Γ_0^-, parameters a_3 and b_2 were needed. Here, by fitting the available density diameter data the mixing parameters, a_3 and b_2 were obtained and consequently, $\Gamma_0^{\pm}$ above and below the critical point was calculated. Employing Γ_0^- and B_0 as the susceptibility and density difference amplitudes two system dependent parameters m_0 and l_0 were calculated.

Reference:

[1] M.Kardar, Statistical Physics of Fields , Cambridge University Press(2000).

[2] K. Huang,Statistical Mechanics, John Wiley, Singapore(1967).

[3]A.K. Wyczalkowska, M.A. Anisimov and J.V. Sengers, Physica A 334(2004)482-512 .

[4] A.K. Wyczalkowska, M.A. Anisimov and J.V. Sengers, Fluid Phase Equilibria, 158 (1999) 5

[5] A. Kostrowicka Wyczalkowska, Kh. S. Abdulkadirova, M. A. Anisiomv, and J. V. Sengers, J. Chem. Phys., 133(2000)12.

Equilibrium Study of Complexes of Thallium(I) ion with L-phenylalanylglycine and glycyl-L-phenylalanine

A. Bahadori*[a], S. Sharifi [a], F. Kiani [b] and E. Hetiatian [a]

[a]*Department of Chemistry, University of Islamic Azad, Arak, Iran*

(Email: bahadori.az@gmail.com)

[b]*Department of Physical and Inorganic Chemistry, University of Mazandaran, Mazandaran, Iran*

Keywords: Thallium (I) complexes, L-phenylalanylglycine, Glycyl-L-phenylalanine, Stability Constants

Introduction

The accurate determination of acidity and stability constants values are fundamental to understanding the behavior of ligands and their interaction with metal ions in aqueous solution [1]. Thallium has been recognized as a toxic element for many years. This element acts on the central nervous system and induces inflammatory response. Thallium (I) shows marked similarities to that of potassium cation. On the other hand, the recent increased use of peptides in biomedical therapy is a result of their large range of activity and specificity, usually with low toxicity and rapid metabolization [2]. Thus, the interaction between metal ions with amino acids, peptides and proteins plays an important role in biochemistry and biology. Spectrophotometry is one of the most powerful methods for the investigation of solution equilibria [3-5]. In view of the above, the present work reports a study of thallium (I) complexes with dipeptides of glycyl-L-phenylalanine (gly-L-phe) and L-phenylalanylglycine (L-phe gly) at 25 ^{o}C and constant ionic strength using a combination of potentiometric and spectrophotometric techniques.

Method

All the chemicals used were of analytical reagent grade. Thallium (I) nitrate, gly-L-phe and L-phe gly (Merck) were employed without further purification. All the standard solutions were prepared using deionized and twice-distilled water with specific conductance equal to (1.8 ± 0.1) □□$^{-1}$cm^{-1}. A Horiba pH-meter, M-12 was used for pH measurements. The hydrogen ion concentration was measured with an Ingold UO 3234 glass electrode and

Ingold UO 3236 calomel electrod. Spectrophotometric titrations were performed on a UV-Vis Lambada 25 double beam spectrophotometer from 200 to 350 nm and optical path 1.000 cm. All measurements were carried out at temperature (25.0 ± 0.1) °C and ionic strength 0.1 mol dm^{-3} $NaClO_4$. The pH-meter was calibrated for the relevant H^+ concentration [3]. Volumes of 25 cm^3 acidic solution of Tl^+ in the concentration range 5×10^{-6} mol dm^{-3} was titrated with an

Table 1. Average values of the protonation and formation constants of Tl (I) with L-phe gly and Gly-L-phe at 25 °C and ionic strengths, I, 0.1 mol dm^{-3} $NaClO_4$

Species	log □$_{011}$	log □$_{021}$	log□$_{□□□}$	log□$_{101}$
L-phenylalanyl glycine	3.7037 ± 0.0029	7.5236 ± 0.0032	12.15 ± 0.20	3.39 ± 0.20
glycyl-L-phenyalanine	3.2314 ± 0.0020	8.1106 ± 0.0047	11.36 ± 0.11	2.13 ± 0.06

alkali solution of each ligand (the ratios of metal ion to ligand 1:100). Ionic strength was maintained at 0.1 mol dm^{-3} $NaClO_4$. The –log $[H^+]$ and absorbance were measured after addition of a few drops of titrant, and this procedure extended up to required –log $[H^+]$.

Results and Discussion

The complex $M_xH_yL_z^{(nx+y-z)+}$ formed is characterized by its stoichiometry (x:y:z), where M and L represent the metal ion and a fully dissociated ligand, respectively. To determine the formation constant of the complexation, eq 2 is defined by □$_{xyz}$ [2]

$$xM^+ + yH^+ + zL^- \rightleftharpoons M_xH_yL_z^{(x+y-z)+} \qquad \beta_{xyz} = [M_xH_yL_z^{(x+y-z)+}] / ([M^+]^x[H^+]^y[L^-]^z) \quad (1)$$

Different models including ML_2, MH_2L and M_2L … were tested and the formation constants for the species were calculated by the program. The models finally chosen, formed by $Tl(HL)^+$ and TlL, for L-phe gly and gly-L-phe in the pH range of study 1.5 to 10.5 (figure 1).

Conclusion

In this work, the study of Tl (I) with L-phe gly and gly-L-phe interaction was attempted in order to better understand the influence the presence of a benzyl group in the stability of

dipeptides to bind thallium (I). Table 1 shows the formation constant values of MHL and ML species formed by L-phe gly are much higher than the corresponding values of gly-L-phe.

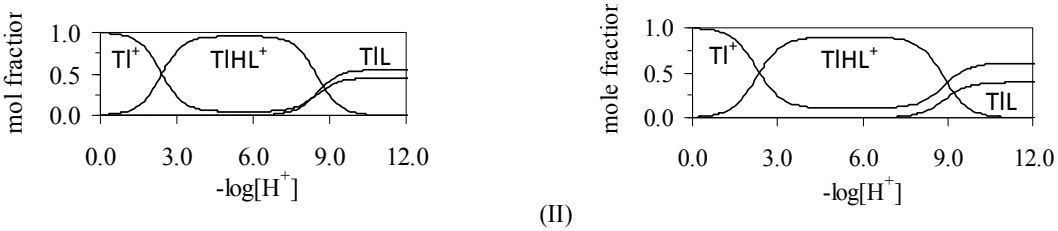

Fig. 1. Distribution curves for (I) Tl (I)-phe gly and (II) Tl (I)- gly-L-phe

References

[1] J. Ghasemi, A. Niazi, M. Maeder, J. Braz. Chem. Soc. 18 (2007) 267.

[2] S. Sharifi, D. Nori-shagh, A. Bahadory, J. Braz. Chem. Soc. 18 (2007) 1011.

[3] F. Gharib, M. Monajjemi, S. Ketabi, Main Group Met. Chem. 27 (2004) 71.

[4] Li, W. B. Wahl, W. Oeh, U. Hollriegl, V. Roth, P. Radiat. Prot. Dosim. 125 (2007) 500.

[5] F. Kiani, A. A. Rostami, S. Sharifi, F. Gharib, J. Chem. Eng. Data 54 (2009) 3261.

Complex formation of thallium (I) ion with adenine and adenosine at different temperatures

E. Heiatian[a], S. Sharifi [a], A. Niazi [a] and A. Bahadori*[a]

[a]*Department of Chemistry, University of Islamic Azad, Arak, Iran*

(Email: bahadori.az@gmail.com)

Keywords: Thallium (I) complexes, Adenine, Adenosine, Equispec program.

Introduction

Research results have clearly demonstrated that certain metal ions play a basic role in directing a number of biochemical processes. Thallium has been recognized as a toxic element for many years. Since thallium (I) shows marked similarities to that of potassium cation, its interaction with nucleotides, the monomeric units of DNA and RNA, in aqueous would be of a major biochemical interest [1]. In the living cell, there are found nucleoproteins. These compounds control heredity on the molecular level [2]. This revealed the need for comprehensive studies of metal ion-bioligand interactions, as model systems. Spectroscopic methods are in general highly sensitive and are frequently used to analyze chemical equilibria in solution [1-5]. In 1971 Lawton and Sylvestre introduced chemometric methods for spectral analysis. In the present work, the formation constants of thallium (I) ion with the heterocyclic bases of adenine and adenosine in aqueous solution were studied using a combination of potentiometric and spectrophotometric methods at different temperatures and constant ionic strength by means of computer fitting of the pH-absorbance data with appropriate mass balance equations. A sophisticated method based on chemometrical concepts was applied in order to determine formation constants. For this purpose, the computer program equispec was used to extract the desired information from the spectral data. The affect of temperature on the formation constants were studied and thermodynamic functions have been obtained for the complexes of thallium (I) with heterocyclic bases.

Methods

Adenine, adenosine and thallium (I) nitrate were of analytical reagent grade (Merck). These chemicals were used without further purification. All solutions were prepared in

deionized water with specific conductance equal to (1.8±0.1) □□$^{-1}$ cm^{-1}. A HORIBA M-12 pH-meter furnished with a combined glass-saturated calomel electrode was calibrated at pH 3.00 and 9.00 [2]. A HP-8453 spectrophotometer controlled by a computer was used for UV-Vis spectra acquisition. The data were transferred to a computer for subsequent analysis using MATLAB software, version 6.5 and for processing by using equispec program, version 3.1. All measurements were carried out at six different temperatures and ionic strength 0.1 mol dm^{-3} $NaClO_4$. Volumes of 10 cm^3 acidic solution of Tl^+ (3.85×10^{-5} to 2.8×10^{-4} mol dm^{-3}) were titrated with an alkali solution of the heterocyclic bases (5.6×10^{-5} to 2.8×10^{-4} mol dm^{-3}).

Results and Discussion

The formation constants thallium (I) ion with the heterocyclic bases of adenine and adenosine were determined using a potentiometric and spectrophotometric technique. Different models including ML, MHL and several polynuclear and protonated species were tested by the program. The models finally chosen, formed by ML and MHL for the studied systems, resulted in a satisfactory fitting. The calculated values of the formation constants for different experiments are showed in Figure 1. The results show apparent formation constants are corresponding to thermodynamic constants.

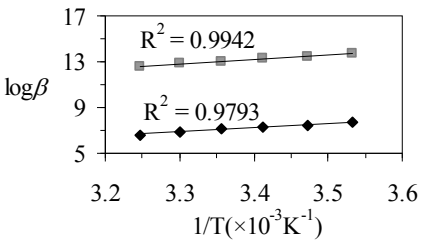

(I)

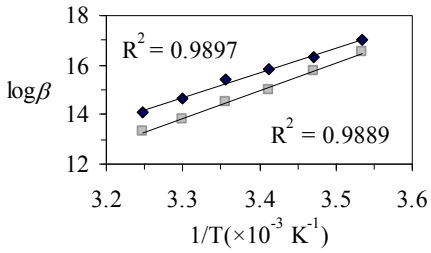

(II)

Figure 1. Curve log□□ vs. 1/T for (I) Tl(I)-Adenine, (II) Tl(I)-Adenosine systems

Conclusion

The formation constants of Tl (I) with adenine and adenosine at different temperature were evaluated with equispec program. Equispec is a computer program using the matrix based MATLAB environment for second order global analysis of spectrophotometric equilibrium data. The enthalpy and entropy of the reactions were determined from the dependence of the equilibrium constants on the temperature, Van't Hoff equation (Table 1).

Table 1. Values of thermodynamic parameters for the Tl (I) with heterocyclic bases at 25 ºC

	$p\ M^+ + q\ H^+ + r\ L^- \rightleftarrows M_p H_q L_r^{(p+q-r)}$				$\beta_{pqr}=[M_p H_q L_r^{(p+q-r)}]/([M^+]^p [H^+]^q [L^-]^r)$			
	ΔH (KJ/mol)	ΔS (J/mol)	ΔG (KJ/mol)	$\log \beta_{111}$	ΔH (KJ/mol)	ΔS (J/mol)	ΔG (KJ/mol)	$\log \beta_{101}$
Adenine	-30.92	-45.18	-44.17	13.07 ± 0.11	-32.15	0.62	-31.96	7.10 ± 0.13
Adenosine	17.58	42.27	4.98	14.45 ± 0.17	82.81	151.16	37.74	15.44 ± 0.19

References

[1] S. Sharifi, D. Nori-shagh, A. Bahadory, J. Braz. Chem. Soc. 18 (2007) 1011.

[2] A. Niazi, M. Ghalie, A. Yazdanipour, J. Ghasemi, Spectrochim. Acta, Part A 64 (2006) 660.

[3] F. Kiani, A. A. Rostami, S. Sharifi, F. Gharib, J. Chem. Eng. Data 54 (2009) 3261.

[4] E. Fernández, L. García-Río, J. C. Mejuto, M. Parajó, Spectrochim. Acta, Part A 66 (2007) 1102.

[5] A. Niazi., A. A. Rezaei, F. Shahhosseini, Ann. Chim. (Rome) 97 (2007) 199.

Investigation on Volumetric Properties for Binary Systems at Temperature range *T*= (293.15 to 333.15) K

Mahboobe Behroozi*[a], Hossein Ali Zarei[a]

[a]*Department of Physical Chemistry, Faculty of Chemistry, Bu-Ali Sina University, Hamedan 65174, Iran*

E-mail: m.behroozi@basu.ac.ir

***Keywords*:** Density, Excess molar volume, Isoamyl acetate, Alkanol

Introduction

Recently, investigation on the thermophysical properties of esters, due to their widespread use in industrial processes has increased [1-3]. Despite of the investigation on esters, few studies have been reported on thermodynamic properties of isoamyl acetate binary mixtures .The studied mixtures were isoamyl acetate + alcohols (C_1-C_4). Excess molar volume was obtained from density data.

Experimental

Density measurements for pure components and binary mixtures were carried out with an Anton Paar digital vibrating U-tube densimeter (DMA-4500) with an uncertainty of $5\cdot10^{-5}$ g$\cdot$cm^{-3}. The mixtures were prepared in dark airtight stopper bottles by mass, using a Mettler AB 204-N balance accurate to ±0.1 mg, with entire range of composition. The uncertainty of the mole fraction was less than $\pm1\cdot10^{-4}$**.**

Results and discussions

The measured densities of six binary mixtures containing isoamyl acetate + (methanol, ethanol, 1-propanol, 2-propanol, 1-butanol and 2-butanol) at different temperatures were used to calculate V_m^E. The V_m^E values were calculated by the following equation.

$$V_m^E = \sum_{i=1}^{2} x_i M_i (\rho^{-1} - \rho_i^{-1}),$$

where M_i is molecular mass, ρ_i and ρ are density of the pure component and mixture respectively. The binary mixtures values were fitted to a Redlich–Kister equation [4] and graphically were represented in Figure 1. The values of V_m^E for all the binary mixtures (except for isoamyl acetate + methanol mixture) are positive over the whole range of composition and from T = (293.15 to 333.15) K. The V_m^E values increase with increasing carbon chain length of alkanol as well as temperature. The positive V_m^E is related to interactions with structure disrupting effect and negative V_m^E is due to interactions with structure making effect as well as packing effect.

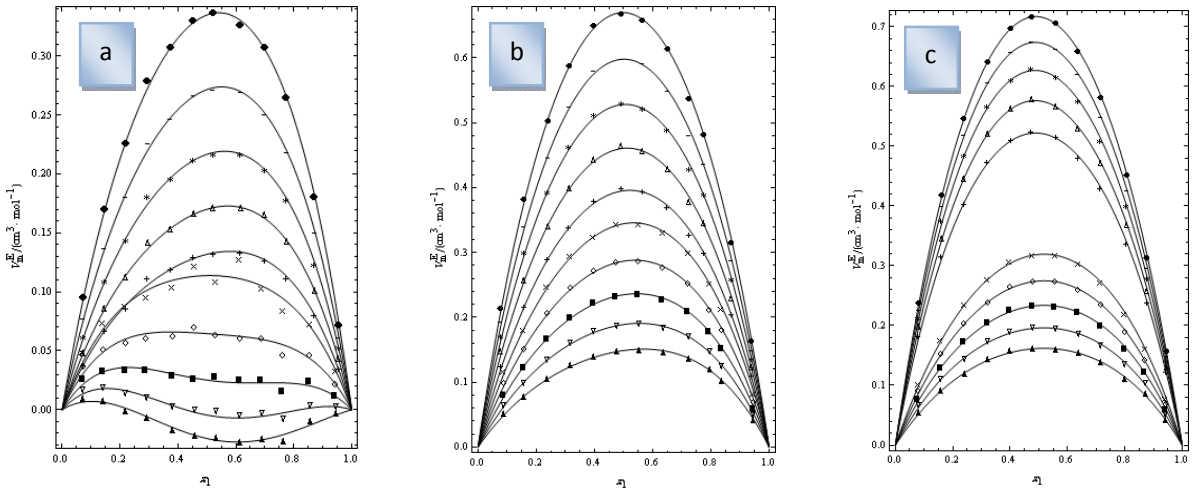

FIGURE 1. Excess molar volumes of two binary mixtures at different temperatures:(a),{Isoamyl acetate (1) + methanol };▲, 293.15 K;□ , 303.15 K; , 313.15 K; , 323.15 K; ×, 333.15 K. {Isoamyl acetate (1) + ethanol };+ , 293.15 K; Δ,303.15 K; ⁎,313.15 K; □, 323.15 K; ●,333.15 K. (b),{Isoamyl acetate (1) + 1-propanol };▲, 293.15 K;□ , 303.15 K; , 313.15 K; , 323.15 K; ×, 333.15 K. {Isoamyl acetate (1) + 2-propanol };+ , 293.15 K; Δ,303.15 K; ⁎,313.15 K; □, 323.15 K; ●,333.15 K. (c) ,{Isoamyl acetate (1) + 1-butanol };▲, 293.15 K;□ , 303.15 K; , 313.15 K; , 323.15 K; ×, 333.15 K.),{Isoamyl acetate (1) + 2-banol };+ , 293.15 K; Δ,303.15 K; ⁎,313.15 K; □, 323.15 K; ●,333.15 K.

Conclusion

Density of six binary mixtures containing isoamyl acetate and primary and secondary alcohols (C_1-C_4) were measured over a wide range of temperatures. Excess molar volume, was calculated by density data and fitted to Readlich–Kister equation. The V_m^E values are positive (except for isoamyl acetate + methanol mixture) in the entire range of composition and temperatures and become more positive with increasing temperature.

References

[1] Y.W. Sheu, C.H. Tu, J. Chem. Eng. Data 50 (2005) 1706-1710.

[2] M.V. Rathnam, S. Mohite, M.S. Kumar, J. Chem. Eng. Data 54 (2009) 305-309.

[3] S.L. Oswal, S.S.R. Putta, Thermochim. Acta 373 (2001) 141-152.

[4] O. Redlich, A.T. Kister, Ind. Eng. Chem. 40 (1948) 345-348.

Modification of Tao - Mason Equation of State for Low Temperatures

Farideh Pahlavan[2], Mohammad Mehdi Papari[1,*], and Jalil Moghadasi[2]

[1] Department of Chemistry, Shiraz Universityof thechnology,

Email: papari @ sutech.ac.ir

[2] Department of Chemistry, Shiraz University, Shiraz, 71454, Iran

Keywords: Equation of State; Enthalpy; Entropy; Refrigerants

Introduction

Refrigerants are the working fluids in refrigeration, air conditioning and heat pumping systems. Therefore, it is needless to state that the thermodynamic properties of this class of fluids play an essential role in various kind of design for equipment and the selection of refrigerants. The thermodynamic properties of refrigerants and their harmful effects on the environment should be known before they can be considered for large scale applications. Hence, there is a strong and current need of an equation of state (EOS) suitable to represent both volumetric and equilibrium properties of refrigerant to be used as working fluids in existing and future refrigeration. one of the equation of states that is based on statistical mechanics and are be used for predicting properties of refrigerants is Tao-Mason equation of state (TM EOS)[1].

Method

In the present study, we modify TM EOS and then use Sheikh-Papari-Boushehri (SPB) [2] and Tsonopoulos [3] correlation equations.

Results and Discussion

The objective of the present work is to simplify the TM equation of state in order that this EOS can be used in low temperature with few parameters. We have successfully modified this EOS for pure fluids, selecting pure refrigerant fluids as the test systems and calculated densities, enthalpies and entropies as thermodynamic properties. The considered refrigerants are: R11, R12, R13, R14, R21, R22, R23, R32, R41, R113, R114, R115 R116, R123, R124,

R125, R134a, R141b, R142b, R143a, R152a. R218, R227eaR236fa, R245fa, R245ca, RC318 وR236ea.

Conclusion

The new equation of state is capable of predicting vapor and liquid densities, enthalpies and entropies of considered fluids with average absolute deviations (AAD) of 0.58%, 1.41% ,3.90% and 3.92% in the temperature interval 100K≤T≤600K and pressure range 0 bar≤P≤70 bar (table1).

Table 1: Vapor densities, enthalpies and entropies of Refrigerants

Refrigerant	Range of temperate (K)	Range of pressure	Density of vapor	Density of liquid	Range of temperate (K)	Range of pressure (bar)	Enthalpy	Entropy
R11	*200-500*	0-70	0.7	0.47	300-600	0-30	4.14	4.37
R12	150-450	0-70	0.38	0.54	200-400	0-30	4.21	4.24
R13	100-300	0-70	0.78	0.9	200-400	0-35	3.36	3.54
R14	100-300	0-40	0.4	1.4	200-400	0-40	2.25	2.14
R22	200-550	0-50	0.28	1.29	200-500	0-30	3.74	3.83
R114	300-500	0-40	0.71	0.70	300-500	0-20	3.40	3.16
R115	180-380	0-60	1.36	0.84	300-500	0-25	3.22	3.13
R116	180-380	0-45	0.78	0.8	200-400	0-25	2.45	2.11
R124	230-330	0-60	0.24	0.93	250-450	0-13	4.53	4.50
R125	175-375	0-60	0.74	0.57	300-500	0-25	3.00	2.85
R134a	170-370	0-60	0.59	0.52	250-450	0-20	4.09	4.22
R236ea	250-500	0-60	0.66	1.24	300-500	0-20	4.17	4.34
R236fa	200-500	0-60	0.34	0.59	300-500	0-20	4.37	4.39
R245ca	200-500	0-60	0.43	0.72	300-500	0-10	4.96	5.02

Reference

[1] F. M. Tao, and E. A. Mason, *J. Chem. Phys*, ***100***, 9075-9084 (1994).

[2] S. Sheikh, M.M. Papari, and A.Boushehri; *Ind. Eng. Chem. Res*., **41**, 3274-3281 (2002).

[3] C. Tsonopoulos. AlChE J., **20**, 263-272 (1974).

Application of the extended solvation model for Thermodynamics of binding copper ion to *Jack Bean Urease*

E. Poorakbar Esfahani [a,c,*] G. Rezaei Behbehani [b], A. A. Saboury [c], L. Barzegar [b]

[a] *Biology Department, Payam Noor University, Tehran, Iran*

(E-mail:epoor2000@yahoo.com)

[b] *Department of Chemistry, Imam Khomeini InternationalUniversity, Qazvin, Iran*

[c] *Institute of Biochemistry and Biophysics, University of Tehran,Tehran, Iran*

Keywords: Urease, Copper ion, Isothermal titration Calorimetry, Solvation model.

Introduction:

Jack bean urease (JBU) possesses nickel ions in the active site, whose task is to activate the substrate and water for the reaction. Ureases play an important role in the overall nitrogen metabolism in nature. Their key function is to provide organisms with nitrogen in the form of ammonia for growth [1,2]. The rapidly increasing importance of urea fertilizer in world agriculture has stimulated research to find methods of reducing the problems associated with the use of this fertilizer. One approach to overcome the problems is to find compounds that would inhibit the Urease activity. Heavy metal ions inhibit ureases .Hg^{2+}, Ag^{+}, and Cu^{2+} ions practically known as the strongest inhibitors [3]. In this study, we have attempted to find the binding parameters and conformational changes of JBU due to its binding with Cu^{2+} ion.

Methods:

Jack bean urease and $Cu(NO_3)_2$ obtained from sigma chemical Co. The buffer solution used in the experiments was 30 mM Tris, pH 7.0, which was obtained from Merck. Experiments were carried out at two temperatures of 27 and 37 °C. The experiments were performed with the 4-channel commercial microcalorimetric system, Thermal Activity Monitor 2277 (Thermometric, Sweden).

Results and Discussion:

We have shown previously [4] that the heats of the macromolecules + ligand interactions, q, can be reproduced by Eq. 1 in the aqueous solvent systems:

$$q=q_{max}x'_B-\delta^{\theta}_A(x'_AL_A+x'_BL_B)-(\delta^{\theta}_B-\delta^{\theta}_A)(x'_AL_A+x'_BL_B)x'_B \qquad (1)$$

The parameters δ^{θ}_A and δ^{θ}_B are the indexes of JBU structural changes in the low and high Cu^{2+} concentrations, respectively. The positive values for δ^{θ}_A or δ^{θ}_B indicate that Cu^{2+} stabilized the JBU structure and vice versa. If the ligand binds at each site independently, the binding is non-cooperative. $p>1$ or $p<1$ indicate positive or negative cooperatives of macromolecule for binding with ligand respectively; p = 1 indicates that the binding is non-cooperative. For a set of identical and independent binding sites; also, we have previously [5] introduced the following equation:

$$(\Delta q/q_{max})M_0= ((\Delta q/q)L_0)(1/g)-K_d/g \qquad (2)$$

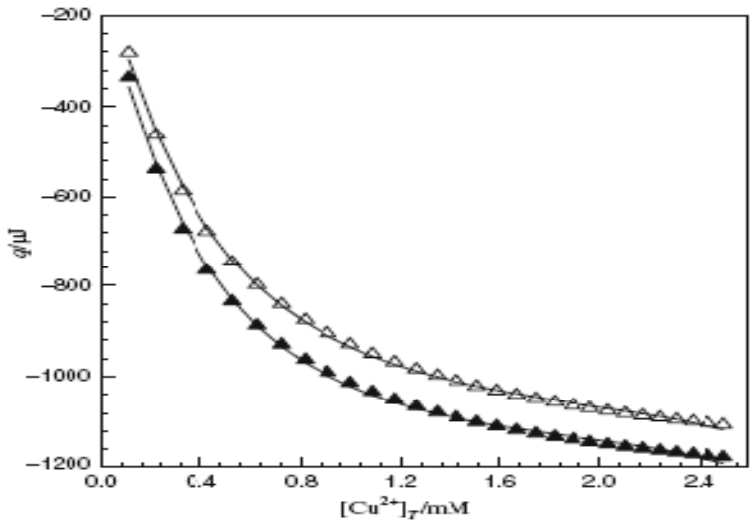

Fig 1: Comparison between the experimental heats T=300K (fitted triangle), T=310K (open triangle) for JBU + Cu^{2+} interactions and calculated data via Eq. 1.

The Positive δ^{θ}_B values for JBU + Cu^{2+} interaction indicate that Cu^{2+} presumably promote JBU aggregation or inhibit the ureolytic activity by inducing protein polymerization along with blockage of sulfydryl groups. The negative δ^{θ}_A values indicate that JBU + Cu^{2+} complexes are unstable and Cu^{2+} ions are weakly bound to JBU in the low Cu^{2+} concentration domain. P=1 indicates that the binding is non-cooperative.

Table 1: Binding parameters for JBU + Cu^{2+} interactions recovered from Eqs. 1 and 8.

Parameters(K)	*P*	δ_A^θ	δ_B^θ	$\Delta H / kJ\ mol^{-1}$	$K_d / \mu M$	*g*
T=300	1	-0.078 ± 0.031	1.604 ± 0.013	-15.198 ± 0.013	284.883 ± 0.081	12
T=310	1	-0.138 ± 0.021	1.282 ± 0.011	-14.597 ± 0.011	345.855 ± 0.023	12

Conclusions:

It was found that the linear range of JBU inhibition by Cu^{2+} ions for this mixture was from 0.11 to 2.5 mM [Fig.1]. It was indicated that there are a set of 12 identical and non-cooperative sites for Cu^{2+} ion. The binding of Cu^{2+} ion with JBU is exothermic with dissociation equilibrium constants of 284.883 and 345.855 μM at 300 and 310 K, respectively [Table 1].

References:

[1] Krajewska B. J Enzyme Inhibit Med Chem2008; 23:535–542.

[2]Krajewska B, Zaborska W, Chudy MJ. J InorgBiochem.2004; 98:1160–1168.

[3] Font M, Dominguez MJ, Sanmartin C, Palop JA, San-Francisco S, Urrutia O, Houdusse F, Garcia-Mina JM. J Agric Food Chem. 2008; 56:8451–8460.

[4] Rezaei Behbehani G. J Therm Anal Calorim.2009; 96:631–635.

[5] Saboury, A. A. J. Iran. Chem. Soc., 3 (2006) 1.

Thermodynamic Study Of Ni(II)-G lycinamide Complex By Spectrophotometric Method In Various Temperatures And pH=4.0 , I=0.4

Nilofar.Tajdini[a]*
nilofar_tajdini@yahoo.com
[a]*Department of Chemistry, Islamic Azad University, Vramin Pishva, Iran*

Keywords: Glycinamide, SQUAD, Optical absorption, Formation constants

Introduction

Nickel is an essential element for many archea, bacteria and plants and may yet be found to play a role in the metabolism of higher organisms [1]. Ni(II) crosses cell membranes via calcium channel and probably competes with Ca^{2+} for specific intracellular receptors [2].

Methods

All experiments were carried out in double distillated water at pH=4.0 potassium hydrogen phthalate ,hydrochloric acid buffer and 0.4M $NaClO_4$. In all experiments, the complex solutions were freshly prepared before spectral analysis. In typical experiment, 2ml of $Ni(NO_3)_2$ solution 0.034M in 0.4M $NaClO_4$ (ionic strength) was titrated by glycinamide 0.272M solution.UV-Vis spectra of combinations were recorded in range of 200-800nm in 10 minutes after adding 50µl glycinamide solution.about 15 adds were taken place.about 50 wavelengths showing suitable variations by adding glycinamide solution were chosen and their absorbance rate was recorded.

Results and discussion

The figure1 show typical titration spectras of $Ni(NO_3)_2$ upon increasing addition of glycinamide at 25.0°C. The observed spectral changes were used for determining the combining constants due to by using SQUAD program which was developed to empower the evaluation of the best combining constants due to absorbance measurements by using a non-linear least-square method. The input data consist of (a) the absorbance values(b) the total glycinamide and $Ni(NO_3)_2$ concentrations.

$$U = \sum_{i=1}^{I} \sum_{k=1}^{NW} \left(A_{i,k}^{cal} - A_{i,k}^{obs} \right)^2$$

(1)

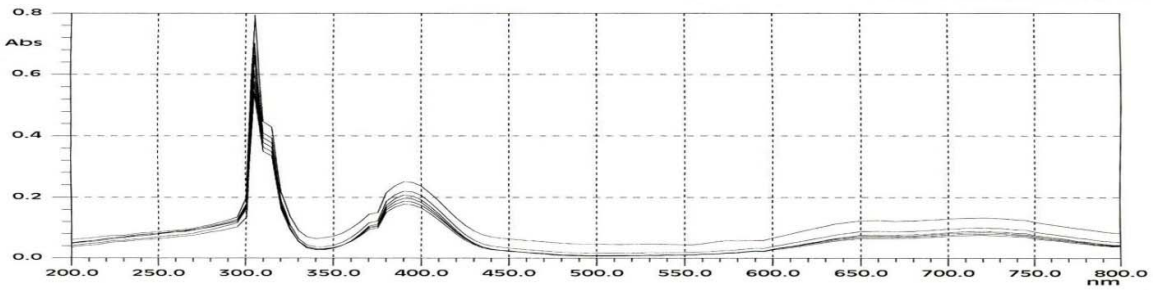

Fig. 1.The titration absorption spectra of $Ni(NO_3)_2$ (0.034M) by Ga (0.272M) in $NaClO_4$ 0.4M at 298K

Table1:Thermodynamic parameters and binding constants for binding of $Ni(NO_3)_2$ to Glycinamide

T (K)	log β (M^{-1})	ΔG^0_T (kJ mol^{-1})	ΔH^0_T (kJ mol^{-1})	ΔS^0_T (J mol^{-1} K^{-1})
283	5.51±0.85	-29.9	293.8	1143.8
288	6.72±0.67	-37.1	293.8	1149.0
293	7.42	-41.6	293.8	1144.7
298	8.33±0.00	-47.5	293.8	1145.3
303	9.15	-53.1	293.8	1144.9

$$\Delta G^o = -RT \ln K$$

$$d \ln K' = -\left(\Delta H^{o'} / R \right) d(1/T)$$

$$\Delta S^{o'} = \left(\Delta H^{o'} - \Delta G^{o'} \right) / T$$

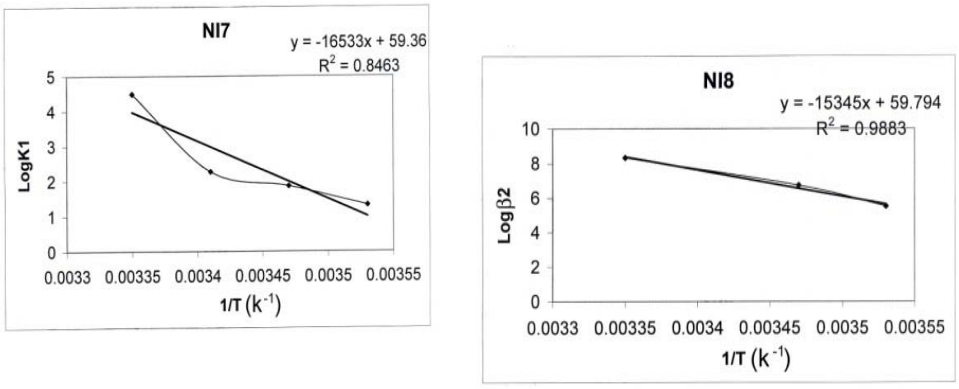

Fig2,3. The vant't Hoff plot of Ga to $Ni(NO_3)_2$

Conclusion

in respect to our results,the stoichiometry of glycinamide-$Ni(NO_3)_2$ combining are as 1:1 and 2:1. shaping these combinations in our results is increased entropy ($\Delta S^o>0$). shaping constants are as magnitude in a satisfactory way concluding relative stability of studied complexes ($\Delta G^o<0$).

References

[1] R.P. Hausinger, in:Biochemistry Of Nickel, Vol 12**,** Plenum Press, New York, p.40 (1993).

[2] M.A. Zoroddu, M. Peana, T. Kowalik-Jankowska, J. Inorg. Biochem.,98,931 (2004).

Application of a simple calorimetric data analysis on the binding study of some metal ions by human growth hormone

E.Tazikeh-Lemeski [*a] , A. A. Saboury [b]
[a],* Islamic Azad University, Gorgan Branch, Department of Chemistry , Gorgan, Iran
*Corresponding Author: elham_tazike@yahoo.com
[b] Institute of Biochemistry and Biophysics, University of Tehran, Tehran, Iran

Abstract

The interaction of human growth hormone (hGH) with some divalent metal ions was studied by isothermal titration calorimetry at two temperatures of 27 °C and 37 °C in aqueous solution. It was found that there are a set of, three, three and two identical and non-interacting binding sites for Cu^{2+}, Zn^{2+} and Hg^{2+} ions,respectively. We found the intrinsic dissociation equilibrium constant (K) and the molar enthalpy of binding (ΔH). The results obtained indicate that the stability of the protein increases due to the binding of metal ions using ITC.

Keywords: Human Growth Hormone (hGH), Isothermal Titration Calorimetry (ITC), Metal Ion, Metal Binding.

Introduction

There are some reports on the binding properties and structural changes of hGH due to its interaction with metal ions [1-10]. The metal-binding site in hGH is located in the hydrophobic core. A well-resolved crystal structure of hGH has been obtained, showing that metal-binding site is likely composed of ^{18}His and ^{21}His on helix I and ^{174}Glu on helix IV [4]. Some metal ions like Zn^{2+}, Cd^{2+}, Hg^{2+} and $Co^{2+}$are known to promote hGH reversible dimerization. But in the presence of some other ions like Ca^{2+}, Ba^{2+}, Mg^{2+}, Pb^{2+}, Al^{2+}, Fe^{2+} and Fe^{3+}, there is no significant dimerization of hGH in solutions [2]. In this paper, the interaction between some metal ions and hGH has been investigated in neutral aqueous solution to clarify thermodynamics of Cu^{2+}, Zn^{2+} and Hg^{2+} binding properties. One of the unique aspects of this report is using a simple calorimetric data analysis to attempt clarify the stability of this protein.

Material and Method

hGH were provided by the National Research Center of Genetic Engineering and

Biotechnology (NRCGEB), Tehran, Iran. The isothermal titration microcalorimetric experiments were performed with Thermal Activity Monitor (TAM) 2277, Thermometric, Sweden. Metal ions solution (100 mM) was injected by use of a Hamilton syringe into the calorimetric titration vessel, which contained 1.8 mL hGH (60 □M). Injection of metal ion solution into the perfusion vessel was repeated 30 times, with 20□ □L per injection.

Result and Discussion

According to the recently data analysis method, using:

$$\frac{\Delta q}{q_{\max}} M_0 = (\frac{\Delta q}{q}) L_0 \frac{1}{g} - \frac{K}{g} \qquad (1)$$

The number of site bindings are 3, 3 and 2 for Cu^{2+}, Zn^{2+} and Hg^{2+},respectively, obtained from the slope and value of K, obtained from the vertical-intercept plot for a set of identical and independent binding sites are 1.32 mM, 1.64 mM for Cu^{2+} and 1.54 mM, 1.93 mM for Zn^{2+} and 4.2 mM, 5.1 mM for Hg^{2+} at 27 °C and 37 °C, respectively. Dividing the q_{max} amounts by g values, give ΔH=16.40 kJ/mol for Cu^{2+} and ΔH=17.1 kJ/mol for Zn^{2+} and ΔH= 14.2 kJ/mol for Hg^{2+} at 27 °C and 37 °C, respectively.

For a set of identical and independent binding sites, we have before shown [11-14].

$$\Delta H = 1/A_i \left\{ (B_i + K) - \left[(B_i + K)^2 - C_i \right]^{1/2} \right\} \qquad (2)$$

A series of reasonable values for K is inserted into equation (2) and corresponding amounts for ΔH are calculated and the graph ΔH versus K is constructed. Curves of all titration steps will intersect in one point, which represents true amounts for ΔH and K.

In conclusion, there is a set of three , three and two identical and non-interacting binding sites for Cu^{2+}, Zn^{2+} and Hg^{2+} ,respectively, on the surface of hGH. In the current study, it can be concluded that the this metal ions bonding process increases the protein stability of hGH.

References

[1]. G. Dienys, J. Sereikaite, V. Luksa, O. Jarutiene, E. Mistiniene, V. A. Bumelis. Bioconjugate. Chem. **11,** 646-651 (2000)

[2]. T. H. Yang, J. L. Cleland, X. J. Lam, D. Meyer, L. S. Jones, T. W. Randolph, M. C. Manning, J. F. Carpenter. J. Pharm. Sci. **89,** 1480-1485 (2000)

[3]. S. W. Hovorka, T. D. Williams, C. Schöneich. Anal. Biochem. **300,** 206-211 (2002)

[4]. A. A. Saboury, M. S. Atri, M. H. Sanati, A. A. Moosavi-Movahedi, K. Haghbeen. Int. J. Biol. Macromol. **36,** 305-309 (2005)

[5]. A. A. Saboury, M. S. Atri, M. H. Sanati, M. Sadeghi. J. Thermal. Anal. Cal. **83**, 175-179 (2006)

[6]. A. A. Saboury, M. S. Atri, M. H. Sanati, A. A. Moosavi-Movahedi, G. H. Hakimelahi, M. Sadeghi. Biopolymers. **81**, 120-126 (2006)

[7]. G. Rezaei Behbehani, A. A. Saboury. J. Therm. Anal. Cal. **89,** 852-861 (2007)

[8]. M. S. Atri, A. A. Saboury, M. Rezaei-Tavirani, M. H. Sanati, A. A. Moosavi-Movahedi, M. Sadeghi, H. Mansuri-Torshizi, N. Khodabandeh. Thermochimica Acta. **438,** 178-183 (2005)

[9]. A. A. Saboury, H. Ghourchaei, M. H. Sanati, M. S. Atri, M. Rezaei-Tawirani, G. H. Hakimelahi. J. Therm. Anal. Cal. **89,** 921-927 (2007)

[10]. K. M. Duda, C. L. Brooks. Protein Eng. **16,** 531-534 (2003)

[11]. A. A. Saboury. J. Iran. Chem. Soc. **3,** 1-21 (2006)

[12]. M. Ghadermarzi, A. A. Saboury, A. A. Moosavi-Movahedi. Polish J. Chem. **72,** 2024-2029 (1998)

[13]. A. A. Saboury, A. Divsalar, G. Ataie, A. A. Moosavi-Movahedi, M. R. Housaindokht, G. H. Hakimelahi. J. Biochem. Mol. Biol. **35,** 302-305 (2002)

[14]. A. A. Saboury. J. Thermal. Anal. Cal. **72,** 93-103 (2003)

Volumetric and transport properties of ternary poly ethylene glycol di-methyl ether 2000 + poly ethylene glycol 400 + water and the corresponding binary aqueous solutions: measurement and correlation

Mohammed Taghi Zafarani-Moattar and Nastaran Tohidifar*
Physical Chemistry Department, University of Tabriz, Tabriz, Iran
(Email: n_tohidifar@yahoo.com)

Keywords: Density; Apparent specific volume; Viscosity; Polymer solutions; Eyring-Wilson model; Eyring-NRTL model

Introduction

A knowledge of thermodynamic and transport properties of binary aqueous solutions is important in engineering, designing new technological processes and also in developing theoretical models. In this work, densities, speed of sounds, and viscosities of binary aqueous solutions of PEG400, PEGDME2000 and ternary solution of {PEGDME2000 + PEG400 + water} were determined experimentally at T = (293.15, 298.15, 303.15, 308.15, and 313.15) K.

Methods

PEGDME2000 and PEG400 were obtained from Merck. All solutions were prepared afresh by mass with precision 10^{-7} kg. Density and sound velocity of mixtures were measured using a densimeter with uncertainty of $\pm 3.0\times10^{-6}$ g·cm^{-3} and ±0.1 m·s^{-1}, respectively. Viscosity measurements were carried out with a viscometer with accuracy of ±0.001 mPa·s and uncertainty was estimated to be ± 0.5 %.

Results and discussion

The obtained density (d) data at T = (293.15 K to 313.15) K for binary aqueous solutions of PEGDME2000 and PEG400 were used to calculate the apparent specific volume of the polymer, $\phi_{app,p}$, and were correlated with Redlich-Mayer equation [1] and another equation suggested by Laliberté and Cooper [2] for binary solutions. At five temperatures the

performance of Redlich-Mayer equation with six parameters is better than the Laliberté and Cooper [2] equation with five parameters for representing apparent specific volume of both binary polymer solutions.

In this work, we examined the reliability of Laliberté and Cooper [2] equation for prediction of density of investigated ternary system.

$$\rho = \frac{1}{w_1 \bar{v}_1 + w_{p1} \bar{v}_{app,p1} + w_{p2} \bar{v}_{app,p2}} \quad (1)$$

The average relative deviation (ARD (d) = 0.32) show that there is a good agreement between experimental and predicted density values by the equation (1) over a wide range of temperature and concentration for the studied {PEGDME2000 + PEG400 + water} system.

Based on the speed of sound and density values, the isentropic compressibility values, κ_s (Pa^{-1}), were calculated for the investigated binary polymer solutions through Laplace–Newton's equation.

The measured viscosity (η) values of (PEGDME2000 + water) and (PEG400 + water) systems at different temperatures have been correlated with the Eyring-Wilson [3] and Eyring-NRTL [4] models. In both the Eyring-Wilson [3] and Eyring-NRTL [4] models we added the temperature dependency proposed by Wu [5] for polymer solutions. Comparison between experimental and calculated viscosity data are shown in figure 1 for (PEG400 + water) system. We can conclude that while the performance of Eyring-NRTL model [4] is better than Eyring-Wilson model [3] for (PEGDME2000 + water) system, for (PEG400 + water) system the Eyring-Wilson model [3] works better than the Eyring- NRTL model [4].

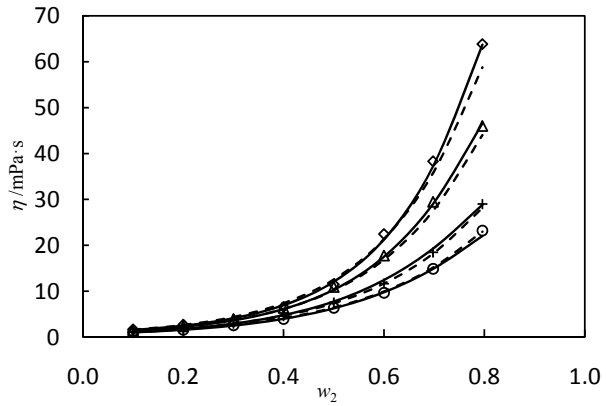

FIGURE 1. Plot of experimental and calculated viscosity values as a function of polymer mass fraction (□□) at different temperatures for (PEG400 + water) system: ◊, T = 293.15 K; Δ, T = 298.15 K; +, T = 308.15 K; ○, T = 313.15 K; ____, Eyring-Wilson model; - - - -, Eyring-NRTL model.

A Grunberg-like equation was used by Gunduz [6] has been used to correlate the viscosity data of {PEGDME2000 + PEG400 + water} at T = (293.15, 298.15, 308.15, and 313.15) K. The proposed equation has the following form for the {PEGDME2000 (p1) + PEG400 (p2) + water} system:

□□□$_{mix}$ = □$_1$□□□$_{p1}$ + □$_2$□□□$_{p2}$ + □$_1$□$_2$□

(2)

On the basis of the obtained ARD values, we conclude that this equation is fairly good in representing the viscosity of the investigated ternary system. This equation is fairly good in predicting the viscosity for the investigated ternary system at temperatures at which no experimental data are available.

Conclusion

Apparent specific volume values for the binary polymer solutions were calculated based on the density and were successfully fitted to the Redlich-Mayer with temperature dependency and to an empirical equation proposed by Laliberté and Cooper for binary electrolyte solutions. The viscosity data for aqueous binary polymer solutions were correlated with Eyring-Wilson and Eyring-NRTL models satisfactorily. Finally, the applicability of correlation and prediction method used by Gunduz was tested for the investigated ternary system at different temperatures.

References:

[1] S. Kirinčič, C. Klofutar, Fluid Phase Equilib. 149 (1998) 233–247.
[2] M. Laliberté, E. Cooper, J. Chem. Eng. Data 49 (2004) 1141–1151.
[3] R. Sadeghi, J. Chem. Thermodyn. 37 (2005) 445-448.
[4] L.T. Novak, C.C. Chen, Y. Song, Ind. Eng. Chem. Res. 43 (2004) 6231-6237.
[5] Y.T. Wu, Z.Q. Zhu, D.Q. Lin, L.H. Mei, Fluid Phase Equilib. 121 (1996) 125-139.
[6] U. Gunduz, J. Chromatogr. B 681 (1996) 263-269.

Thermodynamic investigation of L-methionine partitioning in aqueous two-phase systems of PPG + sodium phosphate salts + H_2O at different temperatures

[1]Alireza Salabat, [1,2]Somayeh Tiani Moghadam*, [3]Rahmat Sadeghi

1. *Chemistry Department, Arak University, P. O. Box 38156-879, Arak, Iran*
2. *Sama technical and vocational training school, Islamic Azad University, Arak Branch, Arak, Iran*
3. *Department of Chemistry, University of Kurdistan, Sanandaj, Kurdistan 66135, Iran*

Abstract

The partitioning behavior of L-methionine has been studied in aqueous two-phase systems of poly (propylene glycol) + sodium phosphate salts + H_2O at different temperatures. The effects of tie line length, salt type, and temperature on the partition coefficient of this amino acid have been studied. In addition, thermodynamic parameters ($\Delta H°$, $\Delta S°$and $\Delta G°$) as a function of temperature were calculated. The results showed that increasing tie line length led to decreasing of the partition coefficient. We also showed that the partition coefficients of the amino acid in the systems containing Na_3PO_4 are greater than the other two salts. Moreover, it is verified that increasing temperature led to decreasing the partition coefficient.

Keywords: ATPS; PPG; Sodium phosphate salts; Partition coefficient; Methionine

Introduction

Liquid-liquid extraction using aqueous two-phase systems (ATPS) is a powerful technique for the separation and purification of biological materials [1]. In our previous work partitioning behavior of three amino acids, in aqueous two-phase systems formed by PPG and some inorganic salts have been studied [2]. The partitioning behavior of three other amino acids, have been Investigated in two different types of polymer-based and surfactant-based aqueous two phase systems [3,4]. In continuation of our research works on application of ATP systems, the partitioning behavior of the amino acid L-methionine, in aqueous two-phase systems of PPG+ sodium phosphate salts + H_2O at different temperatures has been studied.

Experiments

1. Materials. PPG 400, Sodium di-hydrogen phosphate, di-sodium hydrogen phosphate, tri-sodium phosphate, L-methionine and double distilled and deionized water.

2. Preparation of two-phase systems. Aqueous two-phase systems were prepared from solid PPG 400 and one of the salts and L-methionine in pure water. The mixtures were shaken for about 60 min and then placed in a thermostatic water bath at different temperatures for at least 48 h, as indicated by the absence of turbidity in each phase. After equilibration of the systems, samples of approximately 3 mL from the upper and lower phases were removed for analysis. ***3. Analysis of the samples.*** The liquid-liquid equilibrium data for ternary systems PPG + sodium phosphate salts + H_2O taken from Sadeghi et al. [5]. The amino acid concentrations were determined by electrochemical method.

Results and Discussion

1. Effect of TLL on the amino acid partitioning. Figures 1 to 3 show the dependence of partition coefficients on the TLL at different temperatures for various salts. As can be seen, in all systems with increasing TLL the partition coefficient of the amino acid is decreased.

2. Effect of salt type on the amino acid partitioning. As a sample for 298.15 K this effect has been presented in Fig. 4. As a result the partition coefficients of methionine in the systems containing Na_3PO_4 are greater than the other two systems.

3. Effect of temperature on the amino acid partitioning. The effect of temperature can be seen from Figures 1 to 3. These figures show that increasing temperature lead to decrease of the partition coefficients.

4. Thermodynamics of the amino acid partitioning

The standard enthalpy, entropy and Gibbs free energy changes ($\Delta H°$, $\Delta S°$ and $\Delta G°$) were calculated for the first tie-line of the ATP systems. For system Na_3PO_4 at 298.15 K, methionine transfer to the top phase is enthalpically driven may be due to a strong interaction between PPG and salt.

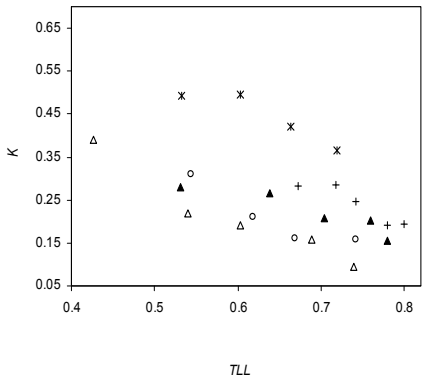

Fig. 1. Effect of temperature and tie-line length on the partition coefficient of L- methionine in ATPS of PPG 400 + NaH_2PO_4 + H_2O at * 298.15 K, Δ 303.15 K, □ 308.15, □ 313.15 K, + 318.15 K

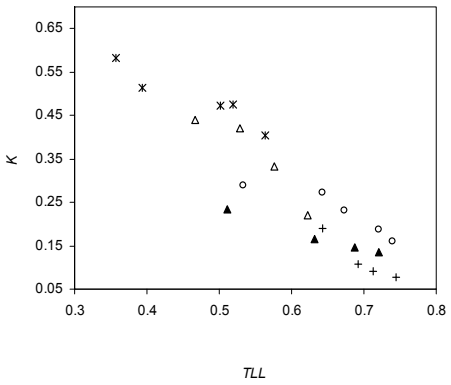

Fig. 2. Effect of temperature and tie-line length on the partition coefficient of L- methionine in ATPS of PPG 400 + Na2HPO4 + H2O at * 298.15 K, Δ 303.15 K, □ 308.15, □ 313.15 K, + 318.15 K

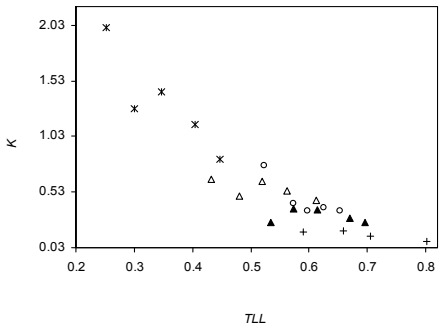

Fig. 3. Effect of temperature and tie line length on the partition coefficient of L- methionine in ATPS of PPG 400 + Na3PO4 + H2O at * 298.15 K, Δ 303.15 K, □ 308.15, □ 313.15 K, + 318.15 K

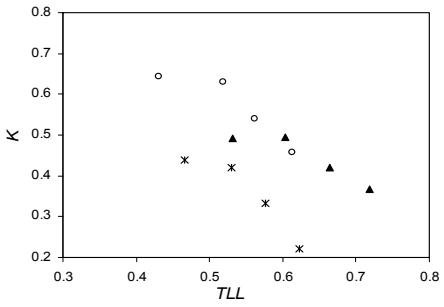

Fig. 4. Effect of salt type on the partition coefficient of L- methionine in ATPS of PPG 400 + Salts + H2O at 298.15 K; □ NaH2PO4, * Na2HPO4, □ Na3PO4

Conclusion

In this research partition coefficients of amino acid L-methionine were obtained in aqueous two phase systems of PPG400 + phosphate salts + H_2O at different temperatures. The effects of the salt type, tie-line length and temperature on amino acid partitioning were also determined. The results showed that in all systems increasing tie-line length lead to decrease of the partition coefficient. Moreover, it is verified that the partition coefficient of the amino acid in the system containing Na_3PO_4 is greater than the other two salts.

Thermodynamic parameters associated with the transfer of methionine from the salt-enriched phase to the polymer-enriched phase also were calculated. The obtained results sowed that, for all systems (except for Na_3PO_4 at 298.15 K), free energy changes adopt positive values and then entropic changes overcome enthalpic changes and for system Na_3PO_4 at 298.15 K, the enthalpic changes overcome entropic changes. It is also verified that transfer of methionine from bottom phase to top phase is an exothermic process and the decrease in temperature should be favorable to this process.

References

[1] P.A. Albertsson, Partition of Cell Particles and Macromolecules, 3rd ed., Wiley-Interscience, New York, 1986.

[2] A. Salabat, M.H. Abnosi, A.R. Bahar, J. Chromatogr. B 858 (2007) 234–238.

[3] A. Salabat, M.H. Abnosi, A. Motahari, J. Chem. Eng. Data 53 (2008) 2018-2021.

[4] A. Salabat, S. Tiani Moghadam, M. Rahmati Far, J Solution Chem. In press.

[5] R. Sadeghi, B. Jamehbozorg, Fluid Phase Equilibria, 280 (2009) 68–75.

Excess Molar Volumes for the Binary and Ternary Mixtures of 2-Methyltetrahydrofuran + Chlorobenzene + Cyclopentanone at 298.15 K for the Liquid Region and at Ambient Pressure

M. Jafari*, H. Iloukhani

Department of Physical Chemistry, Faculty of Chemistry, University of Bu-Ali Sina, Hamedan , Iran

E-mail: mm_jjafari@yahoo.com

Keywords • Density • Excess molar volumes • Chlorobenzene • Cibulka equation

Introduction

Densities ρ of the ternary mixtures consist of 2-methyltetrahydrofuran + chlorobenzene + cyclopentanone at 298.15 K and constituted binary mixtures 2-methyltetrahydrofuran + cyclopentanone, chlorobenzene + 2-methyltetrahydrofuran, and chlorobenzene + cyclopentanone was measured for the liquid region and at ambient pressure for the whole composition range. Excess molar volumes, V_m^E from the mole fraction average for the mixtures were derived from the experimental data. The binary and ternary data of V_m^E, was correlated as a function of the mole fraction by using the Redlich–Kister and the Cibulka equations, respectively. The experimental results are analyzed to discuss the nature and strength of intermolecular interactions in these mixtures.

Methods

Binary and ternary mixtures were prepared by mixing of components and each mixture was immediately used after it was well-mixed by shaking. The densities of mixtures were measured with an Anton Paar digital densimeter.

Results and Discussion

Excess molar volumes, V_m^E, from mole fraction average, for three binary mixtures at 298.15 K was calculated from:

$$V_m^E = \sum_{i=1}^{N} x_i M_i \left(\frac{1}{\rho} - \frac{1}{\rho_i} \right) \quad (1)$$

The excess molar volume V_m^E (x = 0.5) decreases in the sequence: 2-methyltetrahydrofuran + cyclopentanone > chlorobenzene + cyclopentanone > chlorobenzene + 2-methyltetrahydrofuran. Figure 1 shows the excess molar volumes for the three binary mixtures at 298.15 K. For the mixture 2-methyltetrahydrofuran + cyclopentanone the negative values for V_m^E is due to dipole-dipole interactions between carbonyl group of cyclopentanone and oxygen atom of 2-methyltetrahydrofuran ring. The interactions between chlorobenzene + cyclopentanone give a negative contribution to V_m^E [1]. The negative value of V_m^E for this mixture suggest a specific interaction between components due to the existence of London and dipolar forces between ketone and chlorobenzene. For the mixture chlorobenzene + 2-methyltetrahydrofuran the negative values of V_m^E may be due to dipolar forces between chlorine atom of chlorobenzene and oxygen atom of 2-methyltetrahydrofuran ring.

The excess molar volumes V_m^E, represented mathematically by the Redlich–Kister equation for correlating the experimental data. [2] $V_m^E = x(1-x)\sum A_i (2x-1)^i$ (2)

The derived data, V_m^E, for the ternary mixture were correlated respectively using the equation

$$V^E{}_{123} = V^E{}_{bin} + x_1 x_2 x_3 \Delta_{123} \quad (3)$$

and

$$V^E{}_{bin} = \sum_{i=1}^{3} \sum_{j>i}^{3} V^E{}_{ij} \quad (4)$$

The ternary contribution term Δ_{123} was correlated using the expression suggested by Cibulka [3]

$$\Delta_{123} = B_0 + B_1 x_1 + B_2 x_2 \quad (5)$$

The ternary parameters, B_0, B_1, and B_2, were determined with the optimization algorithm similar to that for the binary parameters. The fitting parameters and the corresponding

standard deviations are given in Table 1. As can be expected, the ternary mixture shows negative values of V_m^E values of at all compositions.

Conclusions

Densities, for binary and ternary mixtures consist of 2-methyltetrahydrofuran, chlorobenzene, and cyclopentanone have been measured at 298.15 K for binary and ternary mixtures, respectively, and the corresponding excess volumes have been calculated. The derived values have been discussed, and we conclude that the main property responsible for negative excess molar volumes is the dipolar force between unlike molecules.

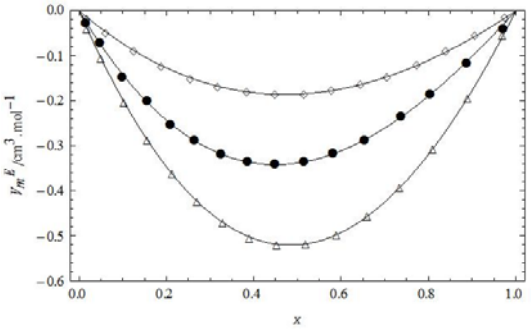

Figure 1. Excess molar volumes V_m^E of binary mixtures: ◇, 2-methyltetrahydrofuran + cyclopentanone; △, chlorobenzene + 2-methyltetrahydrofuran; ● chlorobenzene + cyclopentanone.

Table 1. Parameters and Standard Deviations of ternary Mixtures at 298.15 K

V_m^E / cm^3·mol^{-1}	B_0	B_1	B_2	σ
	0.61093	–0.85117	–0.47422	9.8×10^{-3}

References

[1] Brocos, A. Pineiro, R. Bravo, A. Amigo, Phys. Chem. Chem. Phys. 5 (2003) 550.

[2] Iloukhani, H.; Samiey, B. Chem. Thermodyn. 2007, 39, 206–217.

[3] Cibulka, I. Collect. Czech, Chem. Commun. 1982, 47, 1414–1419.

PHYSICO CHEMICAL STUDY OF THE URMIA LAKE WATERS. Variations of Activity Coefficients of Major Ions and Density of Water Caused by Evaporation

E. Jannatdoust*[a], S. Rezvantalab[a], F. Kheiri[b]

[a] *Urmia University of Technology, P.O. Box 57155/419, Urmia, I.R. Iran*

[*] *E-mail: jannatdost.e@gmail.com*

[b] *Department of Chemistry, Faculty of Science, Urmia University, Urmia, I.R. Iran*

Keywords: Uemia Lake, Pitzer model, Activity Coefficients, Density

Introduction

Urmia Lake - salt lake in northwestern Iran - has been facing a grave crisis over the past 10 years. Reduction of water depth by 6 meters and the salinity ranges from 330 to 400 gr/lit, increasing water salinity to saturation level is alarming indications of gradual total desiccation of the beautiful and unique ecosystem, the Lake Urmia [1]. Urmia Lake is classified as oceanic; being of the sodium- chloride- sulfate type. Na, K, Ca, Li and Mg are the main cations with Cl, SO_4, and HCO_3 as the main anions [2]. In this paper, study of some physico-chemical properties of Urmia lake water, variation of the ion activity coefficients of major ions and density of lake water due to water evaporation is simulated.

Methods

The system of equations developed by Pitzer was used in calculating the ionic activity coefficients in solutions of moderate and high concentrations. These equations give a good account of the properties of the major seawater components [3]. Therefore, we decided to use the Pitzer model for the estimation of conventional single-ion activity coefficients of major ions in Urmia lake water [4]. For study of the changes in the density of Urmia lake water, salinity is best suited to characterize a conservative constituent. The evaporation salinities were determined by the chlorinity variation on the evaporation time and compared with experimental data [5].

Results and discussion

We used information published by Heydari et al. about evaporation of lake water at 25 °C [6]. The measured compositions are shown in figure 1. Increasing of ion activity coefficient depend of ion concentration on evaporation time (fig.2).

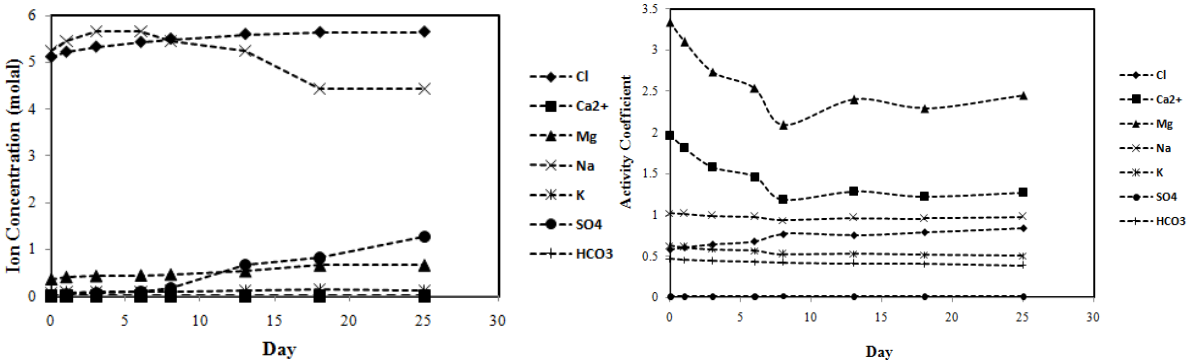

Fig1. change in ion concentrations during the evaporation time

Fig2. change in ion activity coefficient during the evaporation time

Increasing of Cl concentration led to increase in density. There is good agreement between experimental [6] and measured density (fig.3).

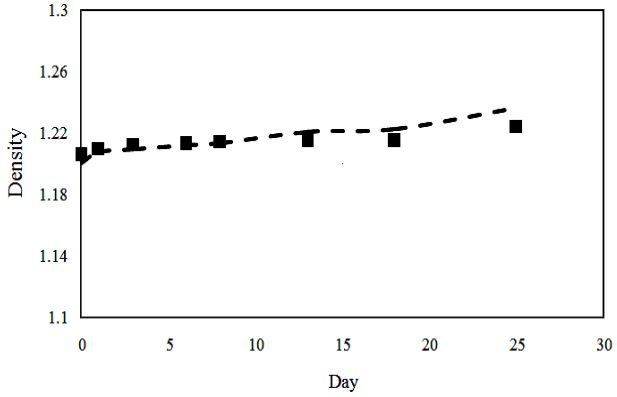

Fig. 4 variation of lake water density in the isothermal evaporation: experimental [9] (■) and measured (- -)

Conclusions

Due to recent years of progressive dry climate in the area the water level of Urmia lakehas decreased significantly. The excess of evaporation has led to a significant increase in salt concentration in the Urmia Lake water body. Cl ion is at slightly higher concentration in the lake water. In this work, single-ion activity coefficients of major ions in Urmia lake water and

density, have been estimated using thermodynamic equations of mixed electrolyte in 25℃ temperature. There was good agreement between experimental and measured density.

Reference

[1] www.urmiana.com

[2] A. Eimanifar, and F. Mohebbi, Saline Systems, 3:5 (2007) 1-8.

[3] F. J. Millero, Marine Chemistry, 11, (1982) 209-222.

[4] E. Jannatdoust, S. Rezvantalab, F. kheiri, ICHEC13, 25-28 October, 2010

[5] E. Jannatdoust, S. Rezvantalab, CELCO2010, Tehran, Iran.

[6] M. Mokhtarpour, N. Heydari, A. S. Sakeni, A.A. Soltan, MIC 2009, Kish, Iran.

Application of ERAS-model and Prigogine–Flory–Patterson theory to excess molar volume of ternary mixtures of 2-chlorobutane + butylacetate + isobutanol at 298.15K

K. Khanlarzadeh*, H. Iloukhani

Department of Physical Chemistry, Faculty of Chemistry, University of Bu-Ali Sina, Hamedan , Iran

E-mail: kh.khanlarzadeh@basu.ac.ir

Keywords: 2-Chlorobutane; Butylacetate; Isobutanol; PFP theory; ERAS-model.

ABSTRACT

Excess molar volumes V_m^E, for ternary and constituted binaries of 2-chlorobutane, butylacetate and isobutanol were derived from density measurements and correlated as a function of mole fraction by using the Redlich–Kister and the Cibulka equations for binary and ternary mixtures, respectively. Partial molar volumes, $\bar{V}_{m,i}$, partial molar volumes at infinite dilution $\bar{V}_{m,i}^0$, and apparent molar volumes $V_{\varphi,i}$, were also calculated. For all binary mixtures, V_m^E, is positive. The experimental results of the constituted binary mixtures have been used to test the applicability of the extended real associated solution (ERAS-model) and Prigogine–Flory–Paterson (PFP) theory.

Introduction

The thermodynamic properties of room temperature polar liquids (RTPLs) as solvent with other polar compounds in some extent, especially volumetric properties have been received an increasing attention in the last years from fundamental and applied points of view [1]. Much effort of RTPLs has been devoted to the study of RTPLs + alcohol binary systems, mainly motivated by their solubility. In this work excess molar volumes of ternary and constituted binary mixtures of 2-chlorobutane, butylacetate and isobutanol by means of the ERAS-model [2] and PFP theory [3] are investigated.

Methods

2-chlorobutane (w > 0.99), butylacetate (w > 0.99), isobutanol (w > 0.99), were purchased from Merck and used without further purifications. The density of the compounds and their binary and ternary mixtures were measured with an Anton Paar digital densimeter. Binary

and ternary mixtures were prepared by mixing of components and each mixture was immediately used after it was well-mixed by shaking.

Results and Discussion

Excess molar volumes for all mixtures were calculated from density results as follow:

$$V_m^E = \sum_{i=1}^{N} x_i M_i(\rho^{-1} - \rho_i{}^{-1})$$

where ρ, is the density of the mixture, and ρ_i, is the density of pure component. The corresponding V_m^E, values of ternary mixtures at 298.15 K are plotted Figure 1. The experimental results for all binary and ternary mixtures were fitted by Redlich–Kister [4] and Cibulka [5] equations. Excess molar volumes for binary mixtures are described qualitatively by the PFP and ERAS-models. The standard deviations between experiment and models are satisfactory for systems under study. Table 1 presents the coefficient of Redlich–Kister, PFP and ERAS-models.

Conclusion

Excess molar volumes V_m^E, of binary and ternary mixtures of 2-chlorobutan + butylacetate + isobutanol were calculated by using measured densities at 298.15 K. V_m^E, for all binary mixtures are positive over the whole range of mole fractions. Positive values would indicate that molecular interactions between different molecules are weaker than interactions between molecules in the same pure liquid and that repulsive forces dominate the behavior of the solutions. PFP and ERAS-models were applied to V_m^E, and results showed that the ERAS-model was better to reproduce the experimental data rather than PFP theory.

Table 1. Coefficients of Redlich–Kister equation, PFP theory and Eras-model.

component	A_0	A_1	A_2	$\chi_{1,2}$	P^*	Free olume	Interactional	K_{AB}	Δv^*
2-Chlorobutane	0.236	–0.03	–0.092	8.5	502.895	–0.0733	0.1689	0	0
Butylacetate	1.276	–0.189	0.193	14.5	464.819	–0.1192	0.2523	0.88	–3.55
Isobutanol	3.827	0.019	0.106	52.5	472.134	–0.0105	0.9115	4.35	–0.514

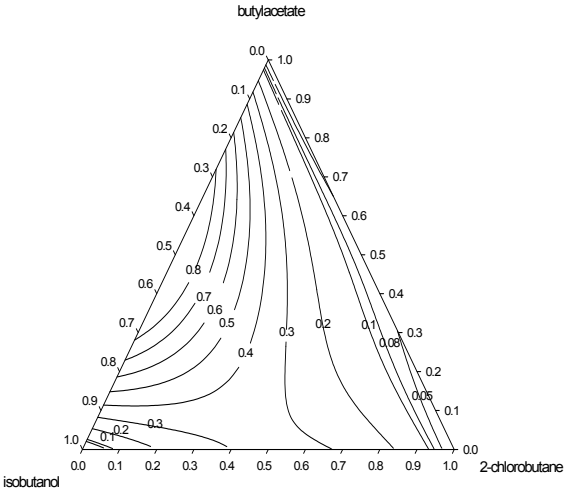

References

[1] H. Iloukhani, K. Khanlarzadeh, Thermochim. Acta 38 (2010) 190 – 200.

[2] A. Heintz, Ber. Bunsenges. Phys. Chem. 89 (1985) 172 – 182.

[3] P. J. Flory, J. Am. Chem. Soc. 87 (1965) 1833–1838.

[4]O.J.Redlich,A.T.Kister,Ind.Eng.Chem.40(1948) 345 – 348.

[5] Y. Cibulka, Collect. Czech. Commun. 47 (1982) 1414 – 1419.

Transport and Electromagnetic Properties of Butylacetate with 1-Chloroalkanes

K. Khanlarzadeh*, H. Iloukhani

Department of Physical Chemistry, Faculty of Chemistry, University of Bu-Ali Sina, Hamedan , Iran

E-mail: kh.khanlarzadeh@basu.ac.ir

Keywords : Viscosity Deviations • Refractive Index Deviations • Butylacetate • 1-Chloroalkanes

Introduction

In this project, we have reported densities ρ, viscosities η, and refractive indices n_D, for the binary mixtures formed by butyl acetate + 1-chlorobutane + 1-chloropentane + 1-chlorohexane + 1-chloroheptane and + 1-chlorooctane at 298.15 K. The derived viscosity deviations $\Delta\eta$, and the refractive index deviations Δn_D, were calculated and were fitted to the Redlich–Kister equation to determine the fitting parameters and the standard deviations. The viscosity data for the binary mixtures were correlated to the semi-empirical McAllister's three-body interaction [2].

methods

Binary and ternary mixtures were prepared by mixing of components and each mixture was immediately used after it was well-mixed by shaking. The densities of mixtures were measured with an Anton Paar digital densimeter and viscosities were measured with an Ubbelohde viscometer. Refractive indices were measured using a digital Abbe-type refractometer.

Results and Discussion

Viscosity deviations $\Delta\eta$, and refractive index deviations, Δn_D , were calculated for binaries of butyl acetate + 1-chlorobutane, + 1-chloropentane, + 1-chlorohexane, + 1-chloroheptane and + 1-chlorooctane at 298.15 K. The deviation of the viscosity from the mole fraction average $\Delta\eta$, is given by:

$$\Delta\eta = \eta - \sum x_i \eta_i \qquad (1)$$

where η is the absolute viscosity of the mixtures and η_i is the absolute viscosity of pure component i. The values are graphically represented as a function of mole fraction at 298.15

K (Fig. 1). It is observed that the $\Delta\eta$ values are negative for all the studied systems over the whole composition ranges. This reveals that the strength of specific interaction is not the only factor influencing the viscosity deviation of liquid mixtures. The molecular size and shape of the components also play an equally important role. The deviation in the refractive index Δn_D, was calculated from the mole fraction average as: $\Delta n_D = n_D - \sum x_i n_{Di}$ (2)

For the whole composition range, the Δn_D, values are positive for butyl acetate + 1-chlorooctane, + 1-chloroheptane, + 1-chlorohexane, and negative for butyl acetate + 1-chloropentane and + 1-chlorobutane (Fig. 2). The negative values are explained in terms of vacant spaces between unlike molecules. The mixing functions $\Delta\eta$, and Δn_D were represented mathematically by the Redlich–Kister equation for correlating the experimental data.

$$\Delta Q_{1,2} = x_1 x_2 \sum A_k (2x_1 - 1)^k \qquad (3)$$

where $\Delta Q_{1,2}$ refers to $\Delta\eta$, or Δn_D for each binary pair, x_1 and x_2 is the mole fraction of each component, and A_k values are the coefficients. The values of coefficients A_k are summarized along with the standard deviations between the experimental and the fitted values of the respective functions in Table 1. The standard deviation is defined by:

$$\sigma = \left[\sum_{i=1}^{n} \frac{\left(\Delta Q_i^{exptl} - \Delta Q_i^{calcd} \right)^2}{n - p} \right]^{1/2}$$

where n is the number of experimental points and p is the number of adjustable parameters. McAllister's [3] multibody interaction model is widely used for correlating the kinematic viscosity of binary mixtures with mole fraction.

Conclusion

Densities, viscosities, and refractive indices for binary mixtures consist of butylacetate + 1-choloroalkanes were measured at 298.15 K and the corresponding viscosity and refractive index deviations have been calculated. The results showed that the main property responsible for thermodynamic behavior is the repulsive force in studied systems. The negative viscosity deviations indicates that the forces between pairs of unlike molecules is less than the forces between like molecules due to repulsive forces and difference in shape and size of component molecules. Refractive index deviations proved that empty spaces and vacancy play an important role in electromagnetic behavior.

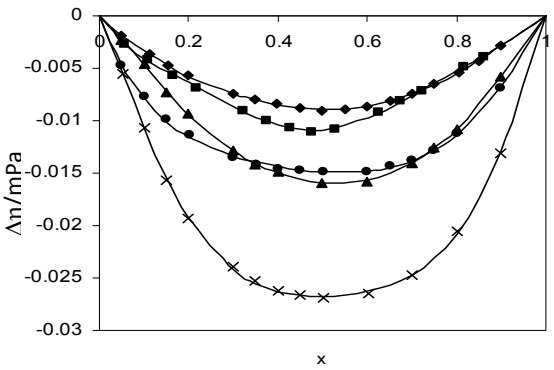

Fig.1. Viscosity deviations vs. mole fraction.

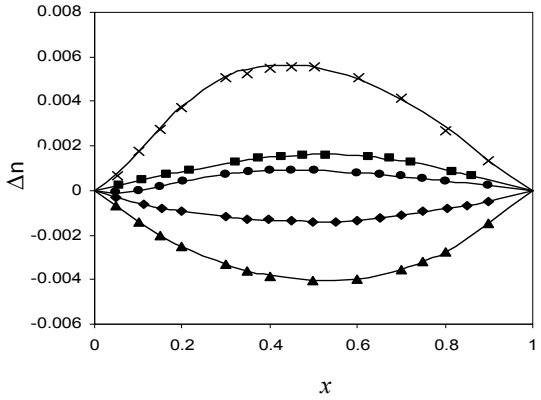

Fig. 2. Refractive index deviations vs. mole fraction.

Table 1 Values of , A_k , and standard deviations, σ, viscosity and refractive index deviations for binary mixtures

system	A_0	A_1	A_2	A_3	A_4	σ
x -butyl acetate + $(1-x)$ 1-chlorobutane						
$\Delta\eta$ /mPa s	–0.035	–0.2				0.0001
Δn_D	–0.005					0.0001
x butyl acetate (**1**) + $(1-x)$ 1-chloropentane (**2**)						
$\Delta\eta$ /mPa s	–0.065	–0.007	0.01			0.0002
Δn_D	–0.016	–0.001				0.00007
x butyl acetate (**1**) + $(1-x)$ 1-chlorohexane (**2**)						
$\Delta\eta$ /mPa s	0.041	0.0064	0.07	0.014		0.0004
Δn_D	0.006	0	–0.002			0.0001
x butyl acetate (**1**) + $(1-x)$ 1-chloroheptane (**2**)						
$\Delta\eta$ /mPa s	–0.0003	–0.003	0.037			0.0003
Δn_D	0.004	0	–0.004	0.004		0.00006
x butyl acetate (**1**) + $(1-x)$ 1-chlorooctane (**2**)						
$\Delta\eta$ /mPa s	–0.110	–0.014	–0.029			0.0005
Δn_D	0.023	–0.003	–0.01			0.0001

Table 2 Adjustable parameters of viscosity correlating McAllister equation and standard deviations

Equation	butyl acetate +				
	1-chlorobutane	1-chloropentane	1-chlorohexane	1-hloroheptane	1-chlorooctane
$\ln A_{12}$	–0.4417	–0.3856	–0.2295	–0.3002	0.0376
$\ln A_{21}$	–0.5964	–0.4495	–0.1412	–0.3079	–0.1442
σ	0.0002	0.0013	0.0016	0.0002	0.0003

References

[1] H. Iloukhani, K. Khanlarzadeh, Thermochim. Acta 38 (2010) 190.

[2] R. A. McAllister, AIChE J 6 (1960) 42.

[3] Brocos, A. Pineiro, R. Bravo, A. Amigo, Phys. Chem. Chem. Phys. 5 (2003) 550.

Molecular Interactions in Solutions of 1, 3-Propanediol + 1-Alkanols

M. Almasi [a], L. Khosravi[*a]

[a] Department of Chemistry, Science and Research Branch, Islamic Azad University, Khouzestan, Iran

Email: m.almasi@srbiau.ac.ir

Key words: Density, Excess molar volume, 1-Alkanols, 1,3-propanediol

Introduction:

Excess properties of mixtures provide information about the molecular interactions between the various components and can be used for the development of molecular models describing the thermodynamic behavior of mixtures [1]. This paper is a part of an ongoing research effort to measure and characterize the properties of mixtures containing alkanols [2]. It reports the densities and excess molar volumes of Alkanols at various Temperatures (293.15, 298.15,303.15,318.15) K.

Methods:

1,3-propanediol, methanol, ethanol, 1-propanol, 1-butanol, 1-pentanol were purchased from Merck with purity higher than 99 %, (All) and used without further purifications. The density of the pure compounds and mixtures was measured by pycnometer. The temperature in the cell was regulated to ± 0.01 K.

Results and Discussion:

The excess molar volumes of the solutions of molar composition x were calculated at various temperatures (293.15,298.15,303.15,313.15) K from the densities of the pure liquids and their mixtures according to the following equation

$$V_m^E = \sum_{i=1}^{N} x_i M_i (\rho^{-1} - \rho_i^{-1}) \qquad (1)$$

where ρ is the density of the mixture, ρ_i is the density of pure component i, x_i is the mole fraction, M_i is the molar mass of component i, and N stands for the number of components in the mixture. The corresponding V_m^E values of binary mixtures of 1,3-propanediol (1) + 1-

alkanols (2) measured and plotted against mole fraction of 1,3-propanediol at T = 298.15 K in Figure 1. Each set of results were fitted using a Redlich–Kister polynomial [3] , which for binary mixtures is

$$Y^E = x_1(1-x_1)\sum_{k=0}^{N} A_k(1-2x_1)^k \qquad (2)$$

Where x_1 is the mole fraction of 1,3-propanediol. A_k is adjustable parameter obtained by least-squares method, and k is the degree of the polynomials. Excess molar volume of 1,3-propanediol with 1-alkanols is negative in the region of enrichment of 1- Alkanols and become positive when the mole fraction of 1,3-propanediol increased. The negative range of V_m^E values indicate strong specific interactions through dipolar association between 1-alkanols and 1,3-propanediol molecules. Positive one is due to strike hindrance between 1,3-propanediol and 1-alkanol molecules.

Conclusions:

Excess molar volumes of1,3-propanediol and 1-alkanols were obtained from experimental results and fitted by Redlich–Kister type equation. Excess molar volume is both negative and positive at the mole fraction range.

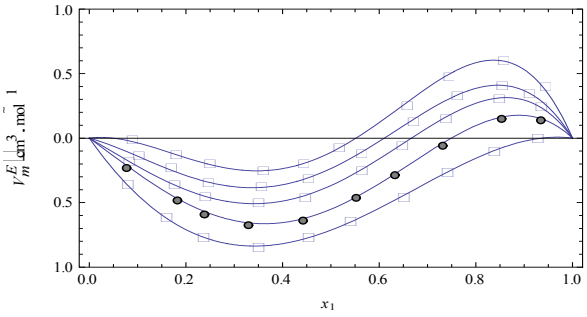

FIGURE 1. Excess molar volumes V_m^E vs. mole fraction of 1,3-propanediol for binary mixtures of 1,3-propanediol with (⬚) methanol, (●) ethanol, (■) 1- propanol, (◊) 1-butanol, (▲) 1-pentanol, at T = 298.15 K. The solid curves were calculated from coefficients of equation (2).

References

[1] Kim, E. S.; Marsh, K. N. Excess volumes for 2-methyl-2-propanol + water at 5 K intervals from 303.15 to 323.15 K. *J. Chem. Eng. Data* **1988**, *33*, 288 – 292.

[2] 6. Almasi, M.; Iloukhani, H. Densities, Viscosities, and Refractive Indices of Binary Mixtures of Acetophenone and 2-Alkanols. J. Chem. Eng.Data **2010**, 55, 1416–1420.

[3] Redlich, O. J.; Kister, A.T. Thermodynamic of non electrolyte solutions: algebraic representation of thermodynamic properties and the classification of solutions. *Ind. Eng. Chem.* **1948**, *40*, 345 – 348.

Excess Molar Volumes of Binary Liquid Organic Mixtures Containing (2-Methyl-1-buthanol + N,N-Dimethyl aniline + Benzyl alcohol) at Different Temperatures and Ambient Pressure.

M. Khosravian*, H. Iloukhani
(Email: mahnaz_khosravian_000@yahoo.com)
Department of Physical Chemistry, Faculty of Chemistry, University of Bu Ali Sina, Hamedan, Iran

Keywords: Binary mixture, Excess volume, Temperature dependence, Redlich–Kister equation

Introduction

The Thermodynamics of organic mixtures project [1] is a project in which systems of organic liquids are investigated in order of increasing complexity of molecular structure and interactions. Attention is paid to the electronic structure and configuration of the organic molecules. In this study, we present excess molar volume for binary mixtures of (2-Methyl-1-buthanol (MB) + N,N-Dimethyl aniline (DMA) + Benzyl alcohol (BA)) at atmospheric pressure and T = (298.15, 308.15 and 318.15) K over the entire range of composition. The aim of this work is to provide a set of data in order to assess the influence of the temperature on the molecular interactions between organic mixtures.

Methods

The pure components were high purity grade reagents from Merck. The densities at T=298.15K agreed closely with the literature values. Binary mixtures were prepared just before use by mass using a Mettler AB-204 balance with a precision of ± 10^{-4} g. The densities of the pure components and mixtures were measured using an Anton Paar DMA 4500 digital vibrating U-tube densimeter, with automatic viscosity correction. The densities of the samples were observed with a reproducibility of ±10^{-5} g/cm^3.

Results and Discussion

The V_m^E values were calculated from the mixtures densities, ρ, and the densities, ρ_i, and molar masses, M_i, of pure components i (i = 1,2) by using the relation [2]:

$$V_m^E = [xM_1 + (1-x)M_2]/\rho - [xM_1/\rho_1 + (1-x)M_2/\rho_2] \quad \text{(Eq. 1)}$$

The experimental V_m^E of the binary mixture at different temperatures are graphically represented in Figure 1. This Figure indicates that binary mixtures of DMA+MB and BA+MB showed positive and negative values of V_m^E in all mole fractions respectively. Binary mixture of DMA+BA shows an inversion sign in the behavior of the values of V_m^E.

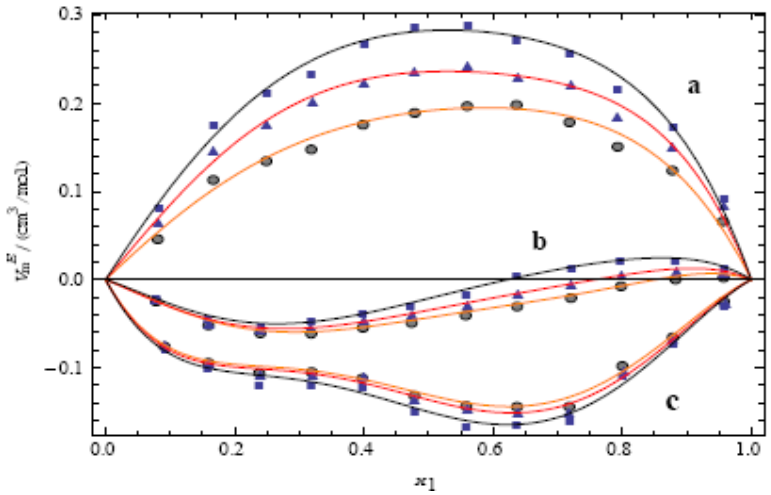

Excess molar volume V_m^E (cm^3/mol) for the binary mixtures of DMA (x_1) + [(a) MB, (b) BA)], BA (x_1) +[(c) MB] at: (●) 298.15 K; (▲) 308.15 K; (■) 318.15 K.

The experimental results for all systems were fitted by the method of least squares with all points weighted equally to the Redlich–Kister polynomial equation [3]:

$$V_m^E /(cm^3.mol^{-1}) = x(1-x)\sum_{i=0}^{j} A_i (1-2x)^i \quad \text{(Eq. 2)}$$

where x denotes the mole fraction of component(1), A_i is the polynomial coefficients, j is the polynomial degree, respectively.

The standard deviation of fit (σ_{st}) is defined by:

$$\sigma_{st} /cm^3.mol^{-1} = [(\sum_i (V_{cal}^E - V_{\exp}^E)_i^2)/N - n]^{1/2} \quad \text{(Eq. 3.)}$$

where N is the number of experimental data and n s the number of the fitted parameters. In each case, the optimum number of coefficients is ascertained from the examination of the variation in standard deviation (σ_{st}) [2].

Conclusions

It can be observed from the experimental results that V_m^E curves are shifted in a regular way with increasing temperature. Due to the steric effect, the molecular packing or contraction is stronger for (BA)+ (MB) compared to (BA)+ (DMA).and weak interactions in (DMA)+(MB) mixture and this interaction decreases with the increase in temperature.

References:

[1] H. Iloukhani, M. Almasi, Thermochim. Acta, 495 (2009) 139.
[2] M. Almasi, H. Iloukhani, J. Chem. Eng. Data, 55 (2010) 3918.
[3] O. J. Redlich, A. T. Kister, Ind. Eng. Chem., 40 (1948) 345.

DensitieS, Viscosities and Excess Molar Properties of binary mixtures of N,N-Dimethylformamide with Ethanol and Water from (293.15 to 313.15) K

Zainab khatibi[1,2]*, Abbas A. Rostami[1], Abdollah Omrani[1] and Freidoon Ashrafi[2]

[1]Faculty of chemistry, University of Mazandaran, Babolsar, Iran

[2]Department of Chemistry of Payam Noor University of Sari, Iran

(Email: rostami@umz.ac.ir)

Keyword : density , Viscosity and excess molar properties Dimethylformamide

Introduction

Density (ρ) and viscosity (η) of liquid mixtures are required in the most engineering calculations where fluid flow or mixing is an important factor. Moreover, knowledge of the dependence of densities and viscosities of liquid mixtures on composition is of great interest from a theoretical stand point since it may lead to better recognition of the fundamental behavior of liquid systems. The studies of excess thermodynamic properties are of considerable interest in understanding the intermolecular interaction in binary liquid mixtures [1].

Materials and Methods

N,N-dimethylformamid, Ethanol and water all of high purity x > 0.99 on a mole basis were purchased from Merck. The mass measurements were made on a single pan Mettler balance with an accuracy of 0.0001g. Density (ρ) measurements of pure components and the binary mixtures over the complet composition rang were carried out Anton Paar oscillating U-tube densimeter (DA 500) with $\pm 10^{-4}$ g.cm^{-3} accuracy.

It was calibrated with double - distilled water and air. The kinematic viscosity was measured with Ubbelohde viscometers with a Schott-Geräte automatic measuring unit model AVS 400 having a transparent thermostat which allows temperature stabilization at tolerance of 0.01 K.

Results and discussion

Excess molar volumes can be explained in terms of positive contributions from due to breaking of like interactions of the pure liquids and negative contributions from the formation of unlike interactions. Positive excess viscosities and excess Gibbs energies of activation for viscous flow indicate that there are interaction between unlike molecules [2]. The excess molar volume (V^E), viscosity deviation ($\Delta\eta$), and excess Gibbs energy of activation for viscous flow (G^{*E}) were calculated through the following equation [3]:

$$\mathbf{V}^{\mathrm{E}} = = \frac{M1\,X1+M2X2}{\rho m} - \left[\frac{\mathrm{M1X1}}{\rho 1} + \frac{\mathrm{M2X2}}{\rho 2}\right] \qquad (\mathbf{1})$$

Where for each equation, x, M and ρ are the mole fraction, the molar mass, the density, respectively.

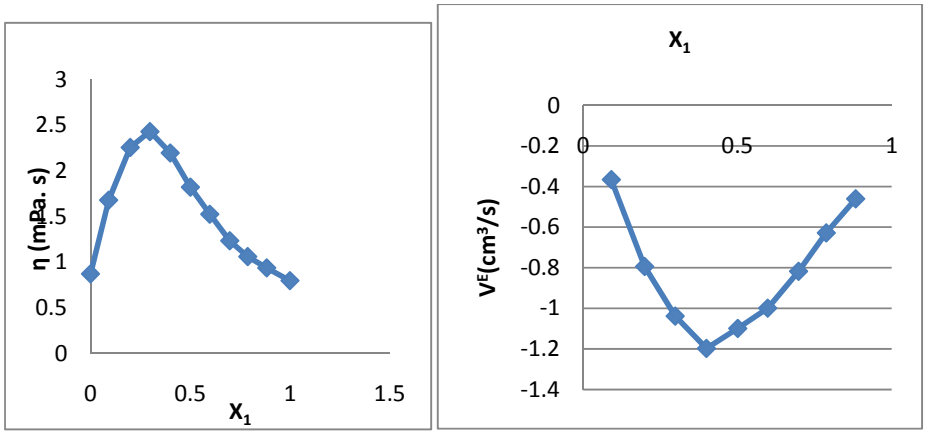

Fig. 1. Experimental viscosity (η_m) and experimental excess molar volume (V^E) of the binary mixtures (DMF + Water) as a function of mole fraction

Conclusions

The densities and viscosities of aqueous (N,N-Dimethylformamide + Water) and (N,N-Dimethylformamide + ethanol) solutions have been measured over the entire concentration range at temperatures from 293.15 to 313.15 K. Viscosity values decrease with temperature for N,N Dimethylformamid + Water aqueous solutions. The viscosity and density data have been fitted by a suitable polynomial relation to estimate the interaction parameters.

References

[1]. F. Giro, M.F. Goncalves, A.G.M. Ferreira, I.M.A. Fonseca, Fluid Phase Equilib. 204 (2003) 217

[2]. Zoreb˛ski, E.; Lubowiecka, B. *J.* Chem. Thermodyn **2009**, *41*, 197–204.

[3]. Yang, C,; Lai, H.;Liu Z. J. Chem. Eng. Data 2006, 51 584-589.

Effect of N_4-type-Schiff base on the solute-solvent interactions of ionic liquid, 1-pentyl-3-methylimidazolium bromide of in acetonitrile solutions

M.khoshalhan[a]*, H. Shekaari[b], A. Bezaatpour[a]

[a] Department of Chemistry,University of Mohaghegh Ardabili, Ardabil, Iran
[b] Department of Physical Chemistry,University of Tabriz, Tabriz Iran
[a]Email:maryamkhoshalhan@yahoo.com

Introduction

In recent years, there has been an increasing interest in exploiting the potential of ionic liquids as reaction media aimed to develop green chemistry, avoiding the use of volatile organic solvents [1]. It seems that the investigation of solute-solvent interactions between the ionic liquid, organic solvent and Schiff base [2] can be interested. Volumetric properties are regarded sensitive tools for understanding of molecular interactions in solutions.

Therefore, In this work, we present our results on density measurements of 1-pentyl-3- methylimidazolium bromide [PMIm]Br + N_4-Type-Schiff base + acetonitrile ternary mixtures (MeCN) at the range of temperatures at atmospheric pressure. The standard partial molar volumes the studied mixtures have been calculated using these experimental data and used to interpretation of various solute-solvent interactions occurring between components of solution.

Experimental

1-Pentyl-3-methylimidazolium bromide, [PMIm]Br was synthesized by direct alkylation of N-methylimidazole with an excess of 1-bromoheptane in a round bottom flask at 353.15K for 48 h under a nitrogen atmosphere. Density data were continuously measured using a vibrating tube densimeter apparatus (Anton Paar, DMA 4500M).

Results and discussion

The experimental density, d, values as function of ionic liquid concentration, m, for mixtures, [PMIm]Br + N_4-Type-Schiff base + acetonitrile ternary mixtures at T = (298.15–328.15)K. The apparent molar volumes, V_ϕ of [PMIm]Br were calculated from the densities of the solutions using the following equation:

$$V_\phi = \frac{M}{d} - \frac{d - d_0}{m d d_0} \quad (2)$$

where m is molality of [PMIm]Br in N_4-Type-Schiff base+ acetonitrile solutions, d and d_0 are densities of the solutions and pure solvent, respectively, M is molar mass of [PMIm]Br. The calculated V_ϕ values are given in Table 1. The standard partial molar volumes of the [PMIm]Br, V_φ^0 were calculated by the least-squares method through the fitting of the following equation [3]

$$V_\phi = V_\phi^0 + S_v m \quad (3)$$

The standard partial molar volumes, V_φ^0 along with the S_v values are given in Table 1.

Table 1

The Values of Standard Partial Molar Volume of [PMIm]Br in N_4-Type-Schiff base+ acetonitrile solutions, V_ϕ^0 / $m^3 \cdot mol^{-1}$, Slope, S_v / $m^3 \cdot mol^{-3/2} \cdot kg^{1/2}$ Various Experimental Temperatures

T(K)	288.15		298.15		308.15		318.15	
m	$10^6 \cdot V_\phi^0$ □	$10^6 \cdot S_v$	$10^6 \cdot V_\phi^0$	$10^6 \cdot S_v$	$10^6 \cdot V_\phi^0$ □□□□□□0$^6 \cdot S_v$□□		$10^6 \cdot V_\phi^0$	$10^6 \cdot S_v$
0.00	167.97	13.561	164.23	17.71	163.59	19.95	162.92	21.11
0.02	167.54	14.783	163.90	19.15	162.73	20.34	162.10	22.15
0.04	167.17	15.202	163.71	20.68	162.51	21.45	161.83	24.12
0.06	166.97	16.869	163.40	22.79	162.42	22.80	161.63	25.96
0.08	166.01	17.680	162.98	23.79	161.08	24.33	161.40	27.34

It can be concluded that the addition of N_4-Type-Schiff base to this ionic liquid in MeCN solutions release the MeCN molecules from the first solvation shell of solvated ionic liquid and thus probably strong solute-solvent interactions is formed between MeCM and N_4-Type-Schiff.

Conclusions

The results show that the values of V_φ^0 for [PMIm]Br decrease with increasing concentration of N_4-Type-Schiff base. These results suggest that addition of N_4-Type-Schiff

base to this ionic liquid in MeCN solutions leads to weakening the solute-solvent interactions between MeCN and [PMIm]Br ionic liquid due to the hydrogen bonding between the *H(2)-C* position of imidazolium ring of the ionic liquid cation and Schiff base.

References

[1] P. Wasserscheid, W. Keim, Angew. Chem., Int. Ed., 39 (2000) 3772-3789.

[2] D.M. Boghaei, E. Askarizadeh, A. Bezaatpour, Spectrochim. Acta A 69 (2008) 624-628.

[3] A. N. Manin, L. E. Shmukler, L. P. Safonova, G.L. Perlovich, J. Chem. Thermodyn. 42 (2010) 429-435.

Association constants of ionic liquid, 1-pentyl-3-methylimidazolium bromide in acetonitrile + N_4-type -Schiff base binary mixtures at *T*=298.15 K

M.khoshalhan[a]*, H. Shekaari[b], A. Bezaatpour[a]
[a] Department of Chemistry,University of Mohaghegh Ardabili, Ardabil, Iran
[b] Department of Physical Chemistry,University of Tabriz, Tabriz Iran
[a]Email:maryamkhoshalhan@yahoo.com

Keywords: N_4-Type -Schiff base, ion association constants, limiting molar conductivities, Electrical conductance

Introduction

Recently, tetradentate Schiff base compounds have been prepared and extensively studied in many areas such as optical data storage devices [1]. Therefore, there is necessary to study of solute-solvent interactions occurring in the mixtures of Schiff base compounds with other compounds such as ionic liquids as neoretic solvents with unique thermophysical properties [2]. In this work, electrical conductances of ionic liquid, 1-pentyl-3-methylimidazolium bromide, [PMIm]Br in the presence of acetonitrile + N_4-type-Schiff base binary mixtures have been measured. The experimental conductivity data have been analyzed by means of the low concentration Chemical Model (lcCM) conductivity equation [3] and the ion association constant, K_A, limiting molar conductivity, □□ and distance parameter, *R* have been obtained, and the results was used to interpretation of solute–solvent interactions and the effect of ionic liquids on the studied tetradentate Schiff base.

Experimental

1-Pentyl-3-methylimidazolium bromide, [PMIm]Br was synthesized by direct alkylation of N-methylimidazole with an excess of 1-bromoheptane in a round bottom flask at 353.15K for 48 h under a nitrogen atmosphere. Electrical conductance measurements were carried out on a digital conductivity meter (Metrohm, 712) with a sensitivity of 0.1%.

Results and discussion

The measured molar conductivities, □ of ionic liquid in N_4-Type-Schiff base (L_1) + MeCN binary mixtures at *T* = 298.15K show that the molar conductivity of ionic liquid decreases with an increase in Schiff base concentration.

The low concentration Chemical Model of conductivity equation is applied for the correlation of conductance data.

$$\Lambda := \alpha\left[\Lambda_0 - S(c\alpha)^{\frac{1}{2}} + Ec\alpha\cdot\ln(c\alpha) + J_1\, c\alpha + J_2\cdot(c\alpha)^{\frac{3}{2}}\right] \quad (1)$$

where α is the fraction of oppositely charged ions acting as ion pairs, and γ are the ion association constant of ionic liquids, distance parameter, and the corresponding mean activity coefficient of the free ions, respectively. The values of *KA,* Λ_0 and *R* obtained by this procedure are summarized in Table1

Table1 *KA*, Λ_0, *R*, and $\sigma(\Lambda)$ of ([PMIm]Br +L_1 + MeCN in low concentrations at

Molality(L1)	K_A	Λ_0	$10^{10} \times R$(m)	$\sigma(\Lambda)$
0.0000	49.2	22.06	28.4	0.25
0.0452	53.9	16.26	22.6	0.17
0.0991	64.9	17.10	17.2	0.10
0.1211	65.5	16.62	9.61	0.23
0.1550	94.7	16.30	5.4	0.14

This table shows that that the values of Λ_0 for ionic liquid decrease with increasing Schiff base concentration. It can be explained in terms of increase in viscosity of the medium with an increase in Schiff base concentration which causes retarding the mobility of the ions in solution and strong ion association with an increase Schiff base content of the mixtures.

The K_a values also increase with increasing of Schiff base content in MeCN. This trend is also an indication of the strong interaction between cation and anion of ionic liquid in the presence of Schiff base. This conclusion can be interpreted in terms of structural changes of the studied ternary mixtures.

Conclusions

These results suggest that addition of ionic liquid to MeCN solutions of Schiff base leads to strengthening the solute-solvent interactions between MeCN and Schiff base due to the strong dipolar interactions between them.

References

[1] Gakias, S.; Rix, C.; Fowlessa, A.; Wills-Johnson, G.; Latham, K.; White, J. A *J. Mol. Struct*. **2005**, *737*, 69 – 74.

[2] J. Dupont, R.F. Souza, P.A.Z. Suarez, Chem. Rev. 102 (2002) 3667–3692.

[3 J.M.G. Barthel, H. Krienke, W. Kunz, Physical Chemistry of Electrolyte Solutions—Modern Aspects, Steinkopff, Darmstadt, Springer, New York, 1998.

A modified Mean spherical Approximation model for prediction of mean ionic activity coefficient in mixed electrolyte solution

Mahin Memarnejad [a], M.R. Dehghani [a,*]

[a] School of Chemical Engineering, Iran University of Science and Technology, Tehran, Iran
Thermodynamic Research libratory
Email address: m_dehghani@iust.ac.ir

Aqueous electrolyte solutions have many applications in many industrial and natural processes. In this field many thermodynamic models have been presented for prediction and correlation of thermodynamic properties in electrolyte solutions. In the primitive version of MSA model, the cation diameter usually has been considered as a function of electrolyte concentration or ionic strength while the anion diameter has been kept constant and equal to its Pauling size. In this work the Dehghani-Modarress Mean Spherical Approximation model has been used and extended for prediction of mean ionic activity coefficients in single and mixed aqueous electrolyte solutions at different temperatures. In order to predict the mean ionic activity coefficient, a concentration dependency has been considered for both cationic size parameter and dielectric constant of solvent. To calculate the mean ionic activity coefficient at different temperatures using the DM-MSA model, a temperature dependency has been considered for model parameters. This model has been evaluated through calculation of average absolute relative deviation (AARD%) for mean ionic activity coefficient obtained and results have been compared with extended UNIQUAC model.

Keywords: Electrolyte solutions, Mean spherical approximation, Mixed electrolyte solutions; Activity coefficient

Theory

In this work, cation diameter and dielectric constant have been selected as model parameters. Experimental data on mean ionic activity coefficients have been utilized for determination of model parameters. Using these parameters, the values of the mean ionic activity coefficient have been calculated for the single and mixed electrolyte solutions. The values of AARD % have been compared with those obtained by the previous version of MSA models as well as Extended UNIQUAC model. Parameters of Extended UNIQUAC model are surface area and

volume parameters as well as energy parameters. These parameters are those obtained by Thomsen et al. A linear temperature dependency has been considered for three parameters of DM-MSA model. The values of parameters of MSA model for several single electrolyte solutions and AARD% are tabulated here. In addition, temperature dependency of parameters in a range of temperature and mean AARD% are presented in a table. These values have been compared with Extended UNIQUAC model. As it is shown, the DM-MSA model can calculate the mean ionic activity coefficient efficiently and better than previous versions of this model and Extended UNIQUAC model.

Table 1

Electrolyte	Parameters of the DM-MSA			m_{max}	AARD(%)		
	□□□(Å)	□+1(Å mol^{-1}l)	□(mol^{-1}l)		DM-MSA	GV-MSA	BMCSL-MSA
KNO_3	-0.3992	0.0441	0.127	3.5	0.1397	3.5625	1.3524
$NaClO_3$	1.4966	-0.1384	0.2822	3.5	0.1767	1.4753	1.2933
$NaClO_4$	1.6526	-0.2431	0.2264	6	0.1621	3.5412	3.0523
HBr	5.4516	-0.143	0.2412	3	0.0508	0.0671	0.0464
HCl	5.1569	-0.1285	0.1726	6	0.0733	0.2524	0.0676
$BaCl_2$	5.6901	-0.2584	0.1736	1.8	0.5463	0.7926	0.5549
$SrCl_2$	6.0484	-0.177	0.2027	4	0.4405	1.1084	0.3904
$MgCl_2$	6.5118	-0.2725	0.1529	5	0.3363	1.988	0.3162
LiCl	4.9957	-0.1016	0.1935	5	0.1677	0.246	0.1739
$CaCl_2$	6.602	-0.2846	0.256	6	0.8306	1.2102	1.3068
CsCl	1.7531	-0.0075	0.0143	10	0.125	0.3218	0.2896
NH_4Cl	3.7253	-0.0018	0.2056	3	0.2352	0.3182	0.2406
RbI	2.1392	-0.0164	0.1012	5	0.0936	0.1055	0.1021
Total AARD%					0.26	1.153	0.706

Table 2-Temperature dependence parameters

Electrolyte	□0(Å K^{-1})	□1(Å mol^{-1}L K^{-1})	a_0(K^{-1})	T/ K	MAARD%		C (mol kg^{-1})
					Extended UNIQUAC	DM-MSA1	
NaCl	0.0279	-0.0027	-0.5015	273.15-373.15	2.091	0.778	4
KCl	0.0194	-0.0016	-0.3669	273.15-373.15	1.496	0.4436	4
HCl	0.0024	-0.0001	-0.4226	273.15-323.15	0.663	0.4419	4
$BaCl_2$	0.0808	-0.0229	-0.966	273.15-318.15	6.5454	0.8108	1.5
$SrCl_2$	-0.0117	0.0035	-0.3419	283.15-343.15	5.938	1.084	0.3
NH_4Cl	-0.0068	0.0016	-0.1617	323.15-373.15	3.563	3.4916	6

References

[1] J.P. Simonin, L. Blum, P. Turq, J. Phys. Chem. 100 (1996) 7704-7709.

[2] C. Ghotbi, G. Azimi, V. Taghikhani, J.H. Vera, Ind. Eng. Chem. 42 (2003) 1279-1284.

[3] G.A. Mansoori, N.F. Carnahan, K.E. Starling, T.W. Leland, J. Chem. Phys. 54 (1971) 1523-1525.

[4] M.R. Dehghani, H. Modarress, J. Mol. Liquids 142 (2008) 45-52.

[5] K. Thomsen, P. Rasmussen, Chem. Eng. Sci. 54 (1999) 1787-1802.

Study of complexation of DL-Penicillamine with Molybdenum (VI)

R. Rahimi [a*], F. Salimi [a], A. Shamel [a], R. Mahmudi[a], E. Mosaddegh Ardebili [a], S.Babashpour [b]

[a] Department of Chemistry, Faculty of Science, Islamic Azad University, Ardabil Branch, Ardabil, Iran

[b] Department of Chemistry, Islamic Azad University, Young Researchers club, ArdabilBranch, Ardabil, Iran

(E-mail:Aylar.rahimi2010@yahoo.com)

Key words: DL_Penicillamine, stability constant, complexation, spectrophotometry, molybdenum.

Introduction

The implication of molybdenum(VI) and (V) in the function of several metaloenzymse and particularly in enzymatic redox reactions prompted us to study the coordination chemistry of molybdenum with α-amino acid ligands in aqueous solution [1,2]. The redox enzyme xanthine oxidase is a thiolo enzyme which is thought to involve molybdenum-sulfur bonding [2]. The molybdoprotein constituent of nitrogenase is olso a sulfur-containing enzyme, and it is tentatively presumed to contain molybdenum-sulfur linkages, although with much less compelling evidence than in the xanthine oxidase case [2]. The equilibria of Mo(VI)in aqueous solution are complex, and various polynuclear species are formed in acidic solution (pH<4)[3]. in basic solution, little or no complex is formed [4] due to the exceedingly high stability of MoO_4[2]. In this study the stability constants and molar ratio of the complexes of Mo(VI) with DL-Penicillamine in aqueous solution were calculated by continuous variation method.

Experimental

DL-Penicillamine (E. Merck, analytical reagent grade) was recrystallized from hot water washed with ethanol, and dried over P_2O_5, and the concentration of its solution was checked by several titrations against standard alkalis. The NaOH solution was prepared from titrisol solution (E. Merck), and its concentration was determined by titration with standard HCl. Perchloric acid, sodium per chlorate, and sodium molybdate were supplied from E. Merck and were used without further purification. All dilute solution were prepared from double distilled water. All measurements were performed at (25±0.1) ℃ and pH=5.85. The constant

ionic strength was maintained to 0.1 mol.dm^{-3} with sodium per chlorate. Spectrophotometric measurements were performed on a UV_vis Shimadzu 2100 spectrophotometer with a GDU-20 computer and thermo stated matched 10 mm quartz cells.

Results and Discussion

Spectrophotometric Studies (UV-IR) . Using the continuous variations method, we determined the absorbances of solutions of Mo (VI) and Penicillamin of total concentration 8.0 $\times 10^{-3}$ mol.dm^{-3} in the UV range (260- 275 nm) at a constant –log [H^+] of 5.8. The observed absorbances were corrected for unreacted Mo from eq 1 and plotted in Figure 1.

$$A_C = A_{obs} \_ \varepsilon_0[\text{Mo (VI)}] \qquad (1)$$

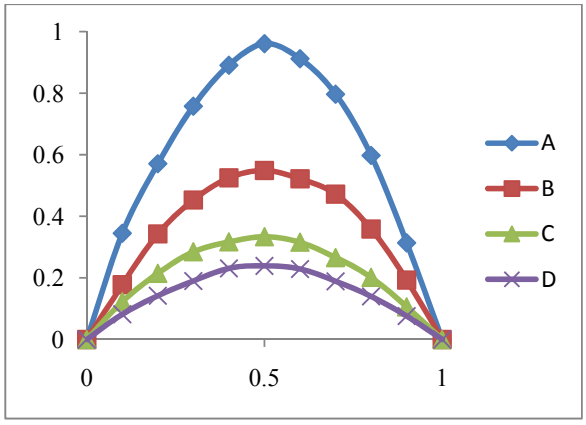

Figure 1. Continuous variation plots corrected absosbances of MoO_3L^{-2} versus mole Fraction of Mo (VI) at 25 ℃ , an ionic strength 0.1 mol.dm^{-3} $NaClO_4$, and different Wavelength: (A) 260, (B) 265, (C) 270, (D) 275 nm.

In Figure 1, a rather sharp maximum at a mole fraction of Mo (VI) equal to 0.5 was obtained, indicating a 1:1 complex formation. At the maximum point of the plot, the concentration of the complex is:

$$[C]=A_C/\varepsilon_C \qquad (2)$$

At –log [H^+] =5.8, the composition of the complex indicated by spectrophotometric measurements is MoO_3L^{-2}.The formation of a 1;1 complex with tridentate penicillamine, thus, has Mo/ligand/proton equal to 1:1:2 stoichiometry as:

$$MoO_4^{-2} + L^{2-} + 2H^+ \rightleftarrows MoO_3L^{2-} + H_2O \qquad (3)$$

With the stability constant, K_S, as

$$K_S = [MoO_3L^{2-}]/[MoO_4^{2-}][L^{2-}][H^+]^2 \qquad (4)$$

The IR spectrum of this complex that were crystallized at –log [H^+] =6 shows that the tridentate ligands coordinated to a cis-trioxo molybdenum core according to Figure 2.

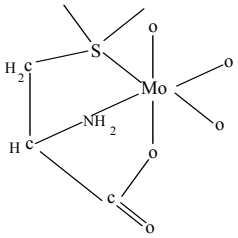

Figure 2.

Conclusion

DL_Penicillamine, an α - amino acid, forms reasonably stable complex with Mo (VI) . The complexation of the complex was determined by the continuous variations method. It was shown that Mo (VI) forms a mononuclear 1:1 complex with DL_Penicillamine of type MoO_3L^{-2} at –log [H^+] = 5.8.The higher log K_S values obtained for the Mo (VI) + penicillamine system shows that this complex is more than stable complex of cysteine because inductive effects of the two CH_3 groups in the penicillamine.

References

[1] Kendrick, M. J.; May, M. T.; Plishka, M. J.; Robinson, K. D. Metals in Biological Systems; Ellis Horwood: New York, 1992

[2] Gharib, F.; Afrazeh Dogaheh, L. Ionic Strength Dependence of Formation Constants, Complexation of Mo (VI) with Cysteine. J. Chem. Eng. Data 2003,48 , 999_1003.

[3] Johanson, E. S.; Jones, O. Complexation between Molybdenum (VI) and Histidine. Least Squares Treatment of Potentiometric Titration Data. Acta Chem. Scand.1981, 35, 233_237.

[4] Greenwood, N. N.; Earnshaw, A. Chemistry of Elements; Pergamon Press: Oxford, 1985.

Determination of thermodynamic properties of ternary mixtures of {1-butanol (1) + hexylamine (2) + *n*-heptane (3)} at different temperatures: Experimental results and application of the Flory theory.

Mahdi Rakhshi *[a], Saleh Bagheri[b]

Faculty of Chemistry, University of Bu Ali Sina, Hamadan, Iran

(Emil:rakhshi_chem@yahoo.com)

[b]*Theoritical and Physical Chemistry Department , Faculty of Chemistry, Islamic Azad University ,Tehran 19936-53171,Iran*

Keywords*:* Thermal expansion coefficients, Flory theory**.**

Introduction

Thermal expansion coefficients α , and their excess values α^E , and isothermal coefficient of pressure excess molar enthalpy $(\partial H_m^E/\partial P)_{T,x}$ ، of the binary and ternary mixtures formed by 1-butanol + hexylamine + *n*-heptane were measured at (288.15 to 323.15) K for the liquid region and at ambient pressure . The thermal expansion coefficients α , and their excess values α^E , and isothermal coefficient of pressure excess molar enthalpy $(\partial H_m^E/\partial P)_{T,x}$ ، were calculated from experimental densities.

Methods

The excess thermal expansion coefficients and isothermal coefficient of pressure excess molar enthalpy were correlated as a function of the mole fraction by using the Redlich–Kister [1-3] equation for binary and , Cibulka[1-3], Jasinski and Malanowski[1-4] , Singe *et al*[1-4], Pintos *et al* [1-4], Calvo *et al*[1-4], Kohler[1], and Jacob - Fitzner [1-4] for ternary mixture ,respectively. in this work for predicted the experimental and other thermodynamic parameters we used the flory model [5].

Results and discussion

The Flory model has been commonly employed to analyse the molar volume of the mixture and the excess molar volume parting from the equation of the state in function of the reduced variables:

$$\frac{\tilde{P}\,\tilde{v}}{\tilde{T}} = \left[\frac{\tilde{v}^{\frac{1}{3}}}{\tilde{v}^{\frac{1}{3}} - 1}\right] - \left[\frac{1}{\tilde{v}\,\tilde{T}}\right] \tag{1}$$

Where

$$\tilde{v} = \frac{V}{V^{*}} = \left[\frac{1 + (\frac{4}{3})\alpha T}{(1 + \alpha T)}\right]^{3} \tag{2}$$

$$\tilde{T} = \frac{T}{T^{*}} = \left[\frac{\tilde{v}^{\frac{1}{3}} - 1}{(\tilde{v}^{\frac{4}{3}})}\right] \tag{3}$$

Theoretical values of $\left[\frac{\partial V_m^E}{\partial T}\right]$ were calculated from the Flory theory using :

$$T\left[\frac{\partial V_m^E}{\partial T}\right] = \left[\sum_{i=1}^{2} x_i V_i^{*}[\tilde{T}(\frac{\partial \tilde{v}}{\partial T})] - [\sum_{i=1}^{2} x_i V_i^{*}(\tilde{T}(\frac{\partial \tilde{v}}{\partial T}))]_i\right] \tag{4}$$

where

$$\tilde{T}\left[\frac{\partial \tilde{v}}{\partial \tilde{T}}\right] = \left[\frac{\tilde{v}(1 - \tilde{v}^{\frac{-1}{3}})}{[(\frac{4}{3})\tilde{v}^{\frac{-1}{3}} - 1]}\right] \tag{5}$$

In the present study the value of the reduced volume for the liquids and their mixtures $\tilde{v}$ was determined for α values of the mixtures usig the eq (5) . The excess function $\left[\frac{\partial V_m^E}{\partial T}\right]$ was computed by analytical differentiation of eq (2) at (288.15 K to 323.15 K) and V_m^E of this work we have also obtained isothermal coefficient of pressure excess molar enthalpy , $(\partial H_m^E / \partial P)_{T,x}$, and excess thermal expansions coefficient α^E .

Conclusions

The comparison between experimental and theoretical values are graphically represented in Fig1 (A_1 and A_2). The obtained results show a good agreement between theory and experimental data. The flory parameters for pure components at different temperates are given in Table1.

Table 1. Flory and related parameters of pure components at different temperature

	T/K	$10^4\alpha/K^{-1}$	ρ/g ·cm^{-3}	V^* /(cm^3· mol^{-1})	T^* / K^{-1}	$\tilde{v}$	$\tilde{T}$
1-Butanol	288.15	9.298	0.813373	74.2960	5423.6663	1.2265	0.0531
	323.15	10.201	0.786238	74.2902	5424.4009	1.2690	0.0596
hexylamine	288.15	11.055	0.768637	104.3629	4924.9229	1.2616	0.0585
	323.15	11.732	0.738636	105.3227	5056.3912	1.3009	0.0639
n-Heptane	288.15	12.249	0.687954	113.4265	4670.3564	1.2842	0.0617
	323.15	13.349	0.657896	114.2979	4763.0440	1.3326	0.0678

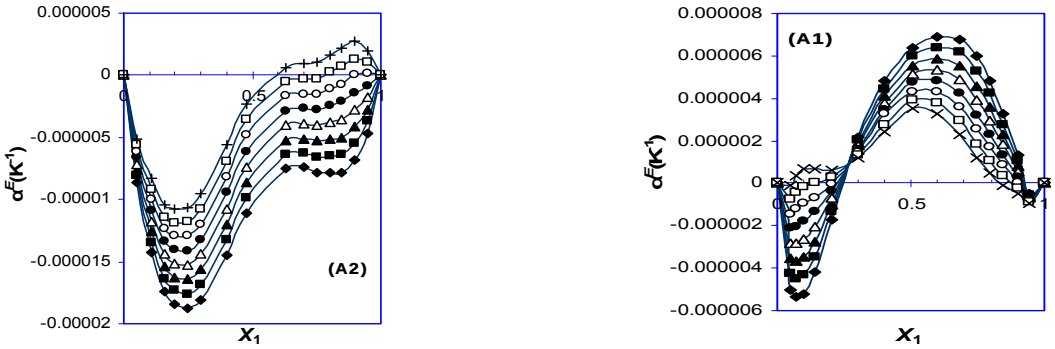

Fig. 1 . Plot of excess thermal expansion coefficients αE, against mole fraction for {(A1); hexylamine+ *n*-heptane , (A2); 1-butanol + hexylamine }at[(◆)288.15 K, (■)293.15K, (▲)298.15K,(Δ)303.15K,(•)308.15K, (○)313.15K,(□)318.15K, (+)323.15 K). Solid lines represent the corresponding correlations by the Flory theory equation.

Refrences

[1] M.Rezaei-Sameti, H.Iloukhani, M. Rakhshi, *J. Mol. Liq.* 149 , (2009) 96**.**

[2]H. Iloukhani, M. Rakhshi, *J. Mol. Liq.* 149, (2009) 86.

[3] M.Rezaei-Sameti, H.Iloukhani, M. Rakhshi, *Russ.J. Phy .Chem A.* 149 , (2010) 2023**.**

[3] I. R. Radovic, M.N. Kijevcanin,S.B. Serbanovic,B.D. Djordjevic . Fluid Phase Equilib. 298,(2010)117 .

[4] P.J. Flory, J. Am. Chem. Soc. 87 (1965) 1833.

Volumetric properties of {*n*-butyl acetate + 1-butanol, 2-butanol,+ 1,2-butanediol and 1,3-butanediol } at temperature between [298.15 to 308.15] K. theoretical and experimental study.

Hossein Iloukhani[a] , Mahdi Rakhshi *[a] ,Mahdi Rezaei-Sameti[b] and Saleh Bagheri[c]

[a] *Faculty of Chemistry, University of Bu Ali Sina, Hamadan, Iran*

(Emil:rakhshi_chem@yahoo.com)

[b] *Department of Chemistry, Faculty of Science, Malayer University , Malayer, Iran*

[c] *Theoritical and Physical Chemistry Department , Faculty of Chemistry, Islamic Azad University ,Tehran 19936-53171,Iran*

Keywords: *n*-butylacetate, 1-butanol , 1,2-butanediol .

Introduction

This paper, as part of a continuing study in our laboratory [1–3], presents experimental densities for the binary systems formed by *n*-butylacetate + 1-butanol, 2-butanol,+ 1,2-butanediol and 1,3-butanediol. Experimental data for these properties allow us to test various .fitting and predictive equations appearing in the literature. As computer design of chemical properties requires mathematical models to predict or describe transport properties of pure liquids and their mixtures over the entire range of composition engineering. The excess properties are analyzed because of their importance for inferring which type of interactions predominates in liquid mixtures.

Methods

The density of the compounds and their binary mixtures were measured with Anton Paar DMA 4500 oscillating U-tube densitometer, operated in the static mode and the uncertainties were estimated to be within $\pm 1 \cdot 10^{-5} g \cdot cm^{-3}$. The temperature in the cell was regulated to ± 0.01 K with solid-state thermostat. The apparatus was calibrated once a day with dry air and double-distilled freshly degassed water.

Results and discussion

Densities, and excess molar volume of the binary mixtures formed by *n*-butylacetate + 1-butanol,2-butanol,+ 1,2-butanediol and 1,3-butanediol were measured at (298.15 to 308.15) K for the liquid region and at ambient pressure (81.5) k Pa , for the whole composition range. the excess molar volumes, $V_{\mathrm{m}}^{\mathrm{E}}$, of the binary mixtures were calculated from the densities using the following equation:

$$V_m^E(\mathrm{cm}^3.\mathrm{mol}^{-1}) = \sum_{i=1}^{n} \frac{x_i M_i}{\rho} - \sum_{i=1}^{n} \frac{x_i M_i}{\rho_i} \qquad (1)$$

where n is the number of components, x_i is the mole fraction of component i in the mixture, M_i its molecular weight, and ρ and ρ_i are the measured densities of the mixture, and the pure component, respectively the experimental data of constitute were correlated as a function of the mole fraction by using the Redlich–Kister[3] equation for binary . The values of $V_{\mathrm{m}}^{\mathrm{E}}$ as well as the Redlich–Kister fits are plotted in Fig.1 for the concentration dependence of the excess molar volumes.

Table1 .. Parameters of Redlich-Kister [3] and the standard deviations for binary mixtures { *n*-butylacetate + 1-butanol, and *n*-butylacetate +1,2-butanediol)}at *T*=(298.15,303.15, and 308.15)K.

	p					$\sigma(V_{\mathrm{m}}^{\mathrm{E}}/\mathrm{cm}^3\mathrm{mol}^{-1})$
q	0	1	2	3	4	
			{*n*-butylacetate (1) + 1-butanol(2) }			
0	-130.056	0.84082	-0.0013	29.6942	-0.2009	0.001
1	0.00034	426.867	-2.8349	0.0047	21.4267	
2	-0.13791	0.0002	598.642	-3.9195	0.0064	
			{*n*-butylacetate (1) + 1,2-butanediol (2) }			
0	-288.696	1.8665	-0.003	-265.684	1.7313	0.004
1	-0.0028	333.913	-2.195	0.00361101	902.753	
2	-5.9821	0.00991	972.418	-6.4119	0.0106	

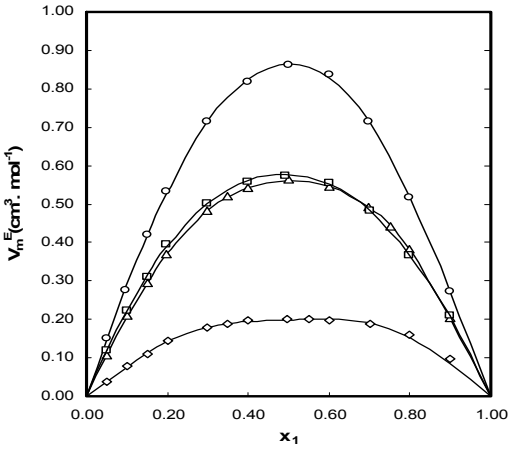

Excess molar volumes (V_m^E) for {(◇) *n* -butylacetate (1) + 1-butanol (2)},{ (△) *N* -butylacetate (1) + 2-butanol (2) }, {(□) *N* -butylacetate (1) + 1,2-butanediol (2)}, {(○) *N* -butylacetate (1) + 1,3 -butanediol (2)}at 303.15 K The solid curves were calculated from parameters of equation (2) given in table 1.

Refrences

[1] M.Rezaei-Sameti, H.Iloukhani, M. Rakhshi, *Russ.J. Phy .Chem A.* 149 , (2010) **2023**.

[2] M.Rezaei-Sameti, H.Iloukhani, M. Rakhshi, *J. Mol. Liq.* **149** , (2009) **96.**

[3] H. Iloukhani, M. Rakhshi, *J. Mol. Liq.* **149**, (2009) **86**.

Density of Refrigerants from Cubic Equations of State

Seyed Ahmad Razavizadeh
Department of Chemistry, Islamic Azad University, Darab, Fars, Iran

Keyword: Equation of state, Refrigerants, Density, Thermo physical properties

Introduction

Before van der Waals some attempts were made to represent the real behavior of gases, but none of these attempts were general, until van der Waals presented simple and generalized equation of state.

Accurate knowledge and prediction of the thermo-physical properties of refrigerants, is of great importance to evaluate the performance of refrigeration cycles and to determine the optimum composition of new working fluids in pure and mixture states. The development of models for representation and prediction of physical properties and phase equilibria as well as the improvement of current equations of state (EOSs) is of particular interest for the refrigeration industry. In addition to experimental measurements, the common way to determine the thermodynamic properties of pure fluids and fluid mixtures is by means of equation of state. There are a large number of cubic EOSs in literature, but we investigated the EOSs that don't need any compound dependent data except T_c, P_c, Z_c and acentric factor, ω and so their usage is simple[1-6].

Results

The deviations of the equations of state for compressed liquid, saturated liquid, and near critical region densities are shown in Table 1.

Conclusion

Cubic equations of state are useful in prediction of density of refrigerants in good precision, and depend on refrigerant type, temperature and pressure range; the best equation can be used. We recommended ALS, PTV, Kubic and PR equations for gaseous, PTV and

ALS for compressed liquid and PTV for saturated liquid densities because of their precision and simplicity, although ST has a good result for compressed and saturated liquid densities.

Table 1. Deviation of equations of state from experimental data

Author	Compressed liquid density	Saturated liquid density	Gaseous density	Near critical region
Adachi, Lu and Sugie (ALS)	4.82	6.74	1.15	11.24
Harmens-Knapp (HK)	7.64	8.25	1.38	10.88
Kubic	8.29	8.21	1.11	12.20
Kim, Lin and Chao (KLC)	7.21	6.69	4.87	28.16
Soave (SRK)	9.53	13.03	2.56	19.42
Schmidt and Wenzel (SW)	5.02	6.83	1.25	12.84
Yu and Lu (YL)	5.16	7.01	1.25	12.58
Nasrifar and Moshfeghian (NM)	5.23	7.21	1.80	12.08
Peng-Robinson(PR)	5.69	7.18	1.16	13.44
Patel-Teja (PT)	5.49	7.14	1.17	10.56
Iwai, Margerum and Lu (IML)	17.70	20.58	2.41	29.22
Trebble and Bishnoi (TB)	5.96	6.81	2.31	7.96
Salim and Trebble (ST)	4.70	4.92	3.03	8.03
Twu, Coon and Cunninghum(TCC)	6.04	8.09	1.17	12.18
Valderrama (PTV[2]	4.78	4.62	1.17	8.50
Translated Peng-Robinson (TPR)	5.13	7.18	1.23	12.68
Twu-Sim-Tasson (TST)	9.65	9.56	1.28	9.15
Mohsen-nia Modarress and Mansoori (MMM)	7.33	7.47	1.63	12.46

References

[1] J. O. Valderrama, Ind. Eng. Chem. Res. **42**, 1603 (2003).1618

[2] O. Redlich, J. N. S. Kwong, *Chem. Rev.* **44**, 233 (1949).244

[3] G. Soave, *Chem, Eng. Sci.* **27**, 1197 (1972)1203.

[4] M. A. Trebble, P. R. Bishnoi, *Fluid Phase Equilib.* **35**, 1 (1987).18

[5] Kh. Nasrifar, M. A. Moshfeghian, *Fluid Phase Equilib*. **190**, 73 (2001).88

[6] N. C. Patel, A. S. Teja, *Chem. Eng. Sci.* **37**, 463 (1982).473

Kinetics and thermodynamic parameters for aromatic compounds adsorption by molecular sieve 13X

Hossein Faghihian[a],Leila Riazi[a,b*],Mahmood Beigi[b]

[a]*Department of chemistry, Islamic Azad University. Shahreza Branch*

[b]*R&D Department,Iran Chemical Industries Investment Company(I.C.I.I.C.),Isfahan,Iran*

Corresponding author:riazi_leila@yahoo.com

Key words: Aromatics,Adsorption.Molecular sieve 13X,Thermodynamic,Kinetic

Introduction

The development of refining process of liquid paraffins related to problem of improving their quality by removing aromatic compounds is essential. Aromatic hydrocarbons as the priority pollutants to deal with,are environmental hazardous and carcinogens[1]. Most of these compounds are hydrophobic with high boiling and melting points and possess low water solubility and electrochemical stability. Therefore they can exist and be accumulated in the environment for long times. Adsorption has been an effective separation process for a wide variety of applications, especially for removal of unwanted pollutants[2]. Molecular sieves have been applied industrially for many years for the separation of impurities from n-alkanes by selective adsorption[3].

In this research measurment of equilibrium extent, kinetic of adsorption of aromatic hydrocarbon includes alkylbenzenes,alkylnaphtalene and biphenyls from C_{10}-C_{13} n-parraffin mixture on zeolitic molecular sieve 13X was carried out in batch mode[4]. The kinetic model of pseudo-second order equation has been successfully applied to predict the adsorption (R^2=99.97). Various thermodynamic parameters, ΔH°, $\Delta S^\circ$and ΔG° ,were computed from equilibrium constant values. Finally we find that the aromatics adsorption on molecular sieve 13X is a spontaneous and exothermic nature process.

Methods

1. Materials:

Molecular sieve 13X was prepared by Zeochem company by Z10-3 code with unit cell formula : $Na_{86}\,[(AlO_2)_{86}(SiO_2)_{106}]\cdot xH_2O$

Some physical properties of molecular sieve 13X are presented in table 1.

Pore Diameter (nm)	Bulk density (kg/m^3)	Crushing strength (N)	Commercial bead size (mm)	Moisture capacity (mg/g)	Loss on ignition (575c/3h, %Wt)	Carbondioxide capacity (mg/g)
1	610-640	25-80	1.5-2.5	255	1.5	175

Table 1. physical properties of Molecular Sieve 13X**.**

The C_{10}-C_{13} n-paraffin mixture with 3.5% aromatic content from Iran Chemical Industries Investment Company(I.C.I.I.C.) was used as dearomatization feed [5].

2.Procedure:

The adsorption process for equilibrium studies was performed in a batch mode by a rotary evaporator using 50mL of liquid normal paraffin and 10 g of molecular sieve 13X different temperature upto 145°C. The molecular sieve 13X was activated at 350°C for 1 hour prior to the adsorption process. Kinetic studies were made by a batch technique at room temperature (25±1°C). known amount of 13X were placed in teflon flasks of 250 ml capacity containing 50 ml paraffin mixture with 3.4%w aromatic content.

Results and discussion

1. Thermodynamic parameters

The effect of temperature on aromatics removal by molecular sieve 13X was studied(Fig.1).Removal efficiency decreases with the increase of temperature.This could be attributed to this fact ,that higher temperature is unfavorable to exothermic reaction once equilibrium is attained.The equilibrium experimental data was used to calculate various thermodynamic parameters, ΔH°,$\Delta S^\circ$and ΔG°using following equation:

$K_C=C_{Ae}/C_{Se}$

$\Delta G^\circ=-RT \ln K_C$

$\ln K_C= \Delta S^\circ/R- \Delta H^\circ/RT$

where K_C is the equilibrium constant, C_{Ae} is the amount of adsorbate on the adsorbent per L of solution at equilibrium(mg/L),C_{Se} is the equilibrium concentration of adsorbate in the solution(mg/L).T is the solution temperature(K) and R is the gas constant and is equal to 8.314 J/mol K.

ΔH°, ΔS°were calculated from the slope and intercept of linear plot of 1/T versus ln K_C (Fig.2).The values of ΔH°=-3.027 kJ/mol , ΔS°=1.886 J/mol K and ΔG° varies from -3.58 to -3.8 kJ/mol at different temperatures.

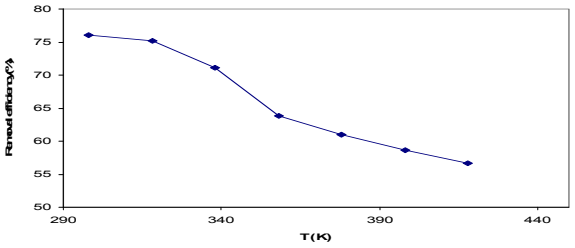

Fig 1.Effect of temperature on aromatics adsorption

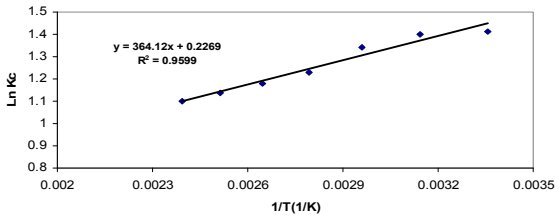

Fig 2.Equilibrium constant as a function of tempreature

2. Kinetic parameters

The effect of contact time on aromatics removal on molecular sieve 13X was obtained(Fig.3). It was observed that the aromatics adsorption rate increase dramatically in the initial times of experiment and reach equilibrium after 195 min. Pseudo second-order model was used for analysis of aromatics adsorption kinetics. This model is representes as:

$t/q_t = 1/k_2 q_e^2 + 1/q_e\ t$

where q_t is the amount of adsorbate (mg/gr) at time t, k_2 is the rate constant(g/mg min). Pseudo second-order kinetic plot for aromatics adsorption on 13X at 25°C was shown in Fig.4.Values of q_e =85.47(mg/gr) and k_2 =0.0011(g/mg min) calculated from the slope and intercept of linear plot of t versus t/q_t.

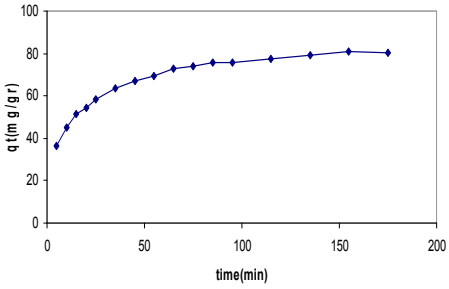

Fig 3. Effect of contact time on qt adsorption

(initial aromatic solution 50 ml 3.4% on 12 gr 13x)

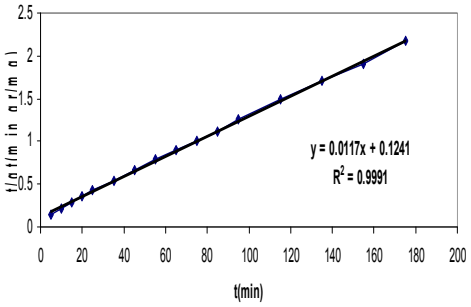

Fig 4.Pseudo second order kinetic plot for aromatics

(intial aromatic solution 50 ml 3.4%w on 12 gr 13x)

Conclusion

The results indicates that aromatics adsorption by 13X is spontaneous and exothermic process. The positive value of the standard entropy change ΔS° indicates that randomless increasewith the removal of aromatics. The higher correlation coefficient value (R^2=99.97)indicates that the aromatics adsorption by 13X follows pseudo second-ordermodel.

References

[1] Roy J.Irwin,national park service,Environmental contaminants encyclopedia,July 1,1997

[2] Kocal JosePh, 1994, U.S. Pat. 5276,231

[3] Wang Ching-Me ,Chang Kuei-Sen, and -Wang Chung Tsair, Adsorption Equilibria of Aromatic Compounds on Activated Carbon,Silica Gel, and 13X Zeolite, J. Chem. Eng. Data 2004, 49, 527-531

[4] Al-Zaid, K.,Owaysi, F., & Eltekov,Y. (1989). Sorption of aromatic compounds from solutions by zeolite 13x. Science Publishers , 945-952

[5]UOP method 495-00,Aromatics in Molex n-paraffin productd by ultraviolet spectrophotometry.

Calculation of *PVTx* properties for (propane + n-butane) in the temperature range from 280 to 440 K and pressures up 200MPa using by critical point parameters

Sajjad Zare[a] and Zahra Sharafi[a,*]
[a]Islamic Azad University, Marvdasht branch, Chemistry Department, Marvdasht, Iran
Email: zahra_sharafi@yahoo.com

Key words: *hard-sphere-chain theory, extension to mixtures*

Introduction

A modified perturbed hard sphere chain equation of state has been developed for fluid mixtures. Knowing the critical constants of fluids as well as one adjustable substance-dependent parameter *r* as input data [1] is sufficient for this purpose. We have tested the predicted equation of state against the experimental data [2] for several mixtures of propane and n-butane. The agreement with experiment is quite good.

Method

The present equation of state can be generalized to mixtures of any number of components as:

$$\frac{P}{\rho kT} = 1 + \rho \sum_i \sum_j F_{ij}^2 b_{ij} g_{ij}(d^+) - \frac{\eta(5-2\eta)}{(2-\eta)(1-\eta)} \sum_i x_i (r_i - 1) - \frac{\rho}{kT}(q_{1a} + q_{1b}\eta) \sum_i F_i a_i$$
$$- \frac{\rho}{kT} \sum_i \sum_j F_{ij}^2 a_{ij} \left[q_{2a} + q_{2b}\eta + (q_{3a} + q_{3b}\eta) F_{ij} \right] \qquad (1)$$

where x_i and x_j are mole fractions of components *i* and *j*, respectively, r_i is the number of segments for the *i*-th component [1], $g_{ij}(d^+)$ is the pair radial distribution function of hard-sphere mixtures at contact proposed by Song. et al. [3]. $F_i = x_i r_i$, $F_{ij} = (F_i F_j)^{1/2}$, and the summations run over all the components. For each unlike pair of components ($i \neq j$), additional parameters, a_{ij} and b_{ij} are calculated by extending eqs.(8) and (9) from ref. [4] to mixtures as:

$$a_{ij} r_{ij}^2 \rho_{Cij} / T_{Cij} = a_1 \exp(-a_2 \frac{r_{ij} T}{T_{Cij}}) + a_3 \exp\left[- a_4 \left(\frac{r_{ij} T}{T_{Cij}} \right)^{3/2} \right] \qquad (2)$$

and

$$b_{ij} r_{ij} \rho_{Cij} = b_1 \exp(-b_2 \frac{r_{ij} T}{T_{Cij}}) + b_3 \exp\left[- b_4 \left(\frac{r_{ij} T}{T_{Cij}} \right)^{3/2} \right] \quad (3)$$

Finally, a simple geometric mean for $(T_C)_{ij}/r_{ij}$ and an arithmetic mean for $(\rho_C)_{ij} r_{ij}$ as follow

$$(T_C)_{ij} / r_{ij} = [(T_C)_i / r_i (T_C)_j / r_j]^{1/2} \quad (4)$$

and

$$\frac{1}{(\rho_C)_{ij} r_{ij}} = \frac{1}{8} [\frac{1}{(\rho_C)_i^{1/3} r_i^{1/3}} + \frac{1}{(\rho_C)_j^{1/3} r_j^{1/3}}]^3 \quad (5)$$

can be employed to calculate a_{ij} and b_{ij} in the right hand side of eqs. (2) and (3). These extended formulae, are shown to give accurate results for fluid mixtures in the following section.

Results and Discussions

Actually the purpose of this work is to show how the proposed equation of state can predict *PVTx* properties of fluid mixtures without knowing the detailed shape of the potential enegy curve. Just it is sufficient to know the critical constants of pure fluids to determine the temperature–dependent parameters of the EoS. Comparisons with experimental data [2] in the Table I. show that the agreement is quit well over a wide range of temperatures and pressures.

Table I. predicted results for the compressed liquid densities of mixtures (propane + n- butane)

X_1	T (K)	P (MPa)	ρ_{exp}(kg·m^{-3})	NP[a]	*AAD*%[b]
0.2729	280	1-200	578.8-701.5	19	-1.7654
	360	2-200	467.0-663.1	18	-1.554
	440	10-200	365.4-628.5	15	-1.020
0.7308	320	2-200	489.9-659.1	18	-2.714
	360	3-200	409.7-639.8	17	-3.012
	400	10-200	383.2-620.6	15	-3.073
	440	20-200	389.8-604.1	14	-2.973

[a] NP: number of data points [b] $AAD\% = 1/N \sum_{i=1}^{N} 100 \left| \frac{\rho_{i,\exp} - \rho_{i,cal}}{\rho_{i,\exp}} \right|$

Reference

[1] Eslami H., Fluid Phase Equilib. **216** (2004) 21-26.

[2] Miyamoto H., and Uematsu M., J. Chem. Thermodynamics. ۴۰(2) (2008) 240-247.

[3] Song Y., Mason E.A. J Chem. Phys. **91** (1989) 7840-7853.

[4] Eslami H., Farrokhnia. Int J. Refrigeration. **28** (2005) 1057-1063.

Study on Thermal Sability of DNA against of a water-soluble c porphyrin, meso-tetrakis (tetrafluoro trimethyl ammonium) phenyl porphinato Nickel(II) acetate

Authors:, N. Sohrabi,F. Fateminasab

Addresses: Laboratory of Physical Chemistry, Department of Chemistry, Shahinshahr Payamenoor University, Isfahan, Iran, email:nasrinsohrabi@yahoo.com.

Key words: Metalloporphyrin, Calf thymus DNA, Porphyrin-DNA interaction, UV/Vis spectra, Thermodynamic parameters.

Introduction

The interaction of water-soluble cationic porphyrins with DNA has been intensely studied due to its potential applications, which include probing for the structure and dynamics of nucleic acids, photodynamic therapy, cancer detection, virus inhibition, and artificial nucleases via their interaction with DNA[1]. In this work the binding of meso-tetrakis (tetrafluoro trimethyl ammonium)phenyl porphinato Nickel (II) acetate, [Ni(II)(TF_4TMAPP)] to calf thymus DNA has been studied in view of thermodynamic using UV/Vis spectroscopy. The physicochemical properties of [Ni(II)(TF_4TMAPP)] were investigated in 5mM phosphate buffer, pH 7.0 at varios environmental conditions.The melting curves of DNA at 260 nm was studied and analyzed at various mole ratios of above mentioned porphyrin to DNA.

Results and discussion:

The results represents no appreciable changes in the position of the spectra bands due to increasing of ionic strength. The interaction of[Ni(II)(TF_4TMAPP)] with calf thymus DNA at various conditions such as ionic strength, concentration and temperature was also investigated using UV/Vis technique. UV/Vis spectra of [Ni(II)(TF_4TMAPP)] in the various DNA concentration were analyzed in order to obtain the affinity and stoichiometries of binding using SQUAD software. The thermodynamic parameters of binding were estimated by running the measurements at various temperatures using Vant Hoff equation(Table 1 and Table 2). To determine binding mode of [Ni(II)(TF_4TMAPP)] to DNA of thermodynamic

stability of DNA in 5mM phosphate buffer, pH 7.0 at various mole ratio's complex [Ni(II)(TF_4TMAPP)] to DNA was studied. Analysis of curves of thermal denaturation was done using Santro and Bolen equation[2], non-linear least-squares analysis was used to fit all the data points of a transition curve according to the relation :

$$-\Delta\varepsilon_{260}(T)=\frac{(a_N+b_NT)+(a_D+b_DT)\exp[-\frac{\Delta H_m}{R}(\frac{1}{T}-\frac{1}{T_m})]}{1+\exp[-\frac{\Delta H_m}{R}(\frac{1}{T}-\frac{1}{T_m})]}$$

Table 1. Thermodynamic parameters and affinity constants for binding of [Ni(II)(TF_4TMAPP)] to DNA at 5mM phosphate buffer, pH 7.0 and various temperatures

T(K)	$\log K_1(M^{-1})$	$\Delta G_1°$(KJ/mol)	$\Delta H_1°$(KJ/mol)	$\Delta S_1°$(J.mol^{-1}.K^{-1})
298	5.20±0.27	-29.67±0.97	61.31±16.23	305.31±57.71
303	5.33±0.25	-30.92±1.51	61.31±16.23	301.41±58.54
308	5.58±0.18	-32.91±1.00	61.31±16.23	305.91±55.94
313	5.66±0.28	-33.92±1.86	61.31±16.23	304.26±58.12
318	5.88±0.37	-35.8±2.25	61.31±16.23	305.39±58.12

Table 2. Thermodynamic parameters and affinity constants for binding of [Ni(II)(TF_4TMAPP)] to DNA at 5mM phosphate buffer, pH 7.0 and various temperatures

T(K)	$\log K_2(M^{-1})$	$\Delta G_2°$(KJ/mol)	$\Delta H_2°$(KJ/mol)	$\Delta S_2°$(J.mol^{-1}.K^{-1})
298	4.15±0.09	-23.68±0.51	54.15±8.14	181.80±29.05
303	4.20±0.11	-24.37±0.64	54.15±8.14	178.80±28.98
308	4.28±0.12	-25.24±0.71	54.15±8.14	175.90±28.74
313	4.45±0.00	-27.21±0.00	54.15±8.14	173.10±26.02
318	4.73±0.26	-28.8±1.58	54.15±8.14	170.38±30.59

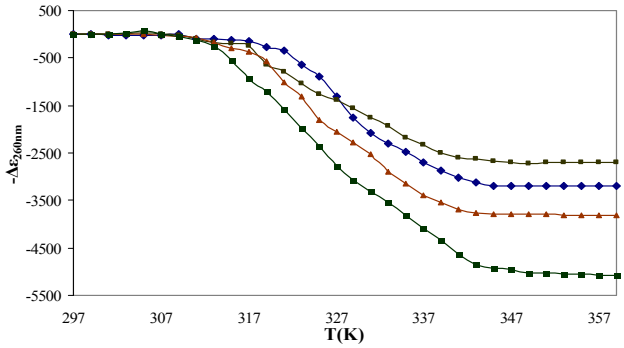

Fig.1:Melting profiles in the different molar ratios [Ni(II)(TF_4TMAPP)] /[DNA]

Conclusions

The results represents the existence of two heterogen binding modes for [Ni(II)(TF_4TMAPP)] with ct-DNA and The driving force in binding is entropy.

Refrences

[1] Luksiene Z. *Med. Tomas* **2003** , *39* , 1137-1150.

[2] Jia, T.; Jiang, Z. X.; Wang, K.; Li, Z. Y. *Biophys. Chem.* **2006,** *119,* 295-302.

Thermal stability of DNA against meso-tetrakis (tetrafluoro trimethyl ammonium) phenyl porphinato manganese(III) acetate A thermodynamic approach

Authors: Nasrin Sohrabi* , Mohammad Hadi Ghafaee

Addresses: Laboratory of Physical Chemistry, Department of Chemistry, Shahinshahr Payamenoor University, Isfahan, Iran, email:nasrinsohrabi@yahoo.com.

Key words: Metalloporphyrin, Calf thymus DNA, Porphyrin-DNA interaction, UV/Vis spectra, Thermodynamic parameters.

Introduction

The interaction of water-soluble cationic porphyrins with DNA has been intensely Studied due to its potential applications which include probing for the structure and dynamics of nucleic acids , detection of cancer, virus therapy, photodynamic therapy via their interaction with DNA[1].

Results and discussion

In this work the binding of meso-tetrakis (tetrafluoro trimethyl ammonium)phenyl porphinato manganese (III) acetate, Mn(TF_4TMAP) to calf thymus DNA has been studied in view of thermodynamic using UV/Vis spectroscopy.The interaction of Mn(TF_4TMAP) with calf thymus DNA at various conditions such as ionic strength, concentration and temperature was also investigated using UV/Vis technique. UV/Vis spectra of Mn(TF_4TMAP) in the various DNA concentration were analyzed in order to obtain the affinity and stoichiometries of binding using SQUAD software. The denaturation curves of ct-DNA was investigated. Using this curves the melting temperatures(the first derivative of curves) was calculated. Melting temperature of DNA decreased upon addition of Mn(TF_4TMAP) that also confirms the groove and outside binding modes.

Table 1. Thermodynamic parameters and affinity constants for binding of Mn(TF4TMAP)to DNA at 5mM phosphate buffer, pH 7.0 and various temperature

T(K)	$\log K_1(M^{-1})$	$\Delta G_1°$(KJ/mol)	$\Delta H_1°$(KJ/mol)	$\Delta S_1°$(J.mol^{-1}.K^{-1})
298	4.26±0.27	-24.30±1.54	12.36±1.07	123.02±8.76
308	4.34±0.25	-25.59±1.47	12.36±1.07	123.20±8.25
328	4.46±0.18	-28.00±1.13	12.36±1.07	123.05±6.71
338	4.52±0.28	-29.25±1.81	12.36±1.07	123.09±8.52

Table 2. Thermodynamic parameters and affinity constants for binding of Mn(TF4TMAP)to DNA at 5mM phosphate buffer, pH 7.0 and various temperatures

T(K)	$\log K_2(M^{-1})$	$\Delta G_2°$(KJ/mol)	$\Delta H_2°$(KJ/mol)	$\Delta S_2°$(J.mol^{-1}.K^{-1})
298	2.88±0.08	-16.43±0.45	67.62±1.86	282.04±7.75
308	3.45±0.08	-20.34±0.47	67.62±1.86	285.58±7.56
328	3.93±0.10	-25.74±0.63	67.62±1.86	284.64±7.59
338	4.30±0.02	-27.82±0.13	67.62±1.86	282.37±5.89

Table 3. DNA melting temperature changes up on increasing the molar ratio of Mn(TF4TMAP)to DNA

$\frac{[MnTF_4TMAPP]}{[DNA]}$	0	0.026	0.0523	0.1012
T_m(K)	341.66	336.34	335.74	334.65

Conclusion:

Mn(TF4TMAP) does not show concentration dependent aggregation over an extended concentration range. Addition of NaCl shows no significance electrolyte effect, no new band appears even in high concentration of salt. This result means that Mn(TF_4TMAP)does not form well defined aggregates (i.e. H or J type) even in high concentration of salt. Mn(TF_4TMAP) binds to external region of ct-DNA. The DNA-binding process was endothermic for Mn(TF_4TMAP)and has the large positive entropy value. These can be represent the predominate role of hydrophobic interactions and outside binding mode. The decreasing of melting temperature (T_m) of DNA upon addition of porphyrin represents the

existence of outside and groove binding mode[2]**.** The results represents the existence of two distinct binding sites for Mn(TF_4TMAP) on ct-DNA.The trend of spectral changes represents groove and outside binding modes.The thermodynamic parameters of binding were estimated by running the measurements at various temperatures using Vant Hoff equation. The results show that the driving force in binding is entropy. That is also is consistant with outside and groove binding modes

Refrences

[1] Luksiene Z. Med. Tomas 2003 , 39 , 1137-1150.

[2] Guo L, Dong W, Tong X, Dong C, Shuang Sh. Talanta. 2006;70:630–636.

Separation of aromatic hydrocarbons (toluene) from aliphatic hydrocarbon (n-Octane) by extraction with ethylene glycol

M. Mohsen-Nia *, F.S. Mohammad Doulabi, M.Massah Bidgoli

Thermodynamic Research Laboratory, Kashan University, Kashan, Iran

* Corresponding author. Tel. /fax: +98 361 5552935.

E-mail address: m.mohsennia@kashanu.ac.ir (M. Mohsen-Nia).

Keywords: Extraction, Activity coefficient, NRTL, UNIQUAC, Ethylene glycol

Introduction

From practical and economical aspects, the (liquid + liquid) extraction is a popular process for separation of aromatic hydrocarbons from alkanes [1]. The basic aim of these investigations was focused on the finding a non-toxic, inexpensive, and easily recoverable solvent for extraction processes in the industrial units [2]. The design and operations of (liquid + liquid) extraction processes require reliable LLE data of the different systems involved in a given process. In this work, we report the LLE results for the system {ethylene glycol (1) + toluene (2) + n-octane (3)} at T = (295.15, 301.15, and 307.15) K. The obtained results were correlated by the NRTL [3] and UNIQUAC [4] activity coefficient models and the parameters of the models, were evaluated and reported.

Experimental

The measured LLE data were determined by using a glass cell with a water jacket to maintain a constant temperature. The mixtures were prepared inside the glass cell and were vigorously agitated with a magnetic stirrer for 1 h and then left to settle for at least 20 h. The samples of both phases were analyzed by using a Perkin–Elmer model 8500 gas.

Table 1. Experimental LLE data for ternary mixtures {Ethylene glycol (1) + toluene (2) + n-Octane (3)}

x_1^o	x_2^o	x_3^o	x_1^e	x_2^e	x_3^e	S	K
{Ethylene glycol (1) + toluene (2) + n-Octane (3)} at T = 298.15 K							
0.0025	0.2790	0.7185	0.9333	0.0620	0.0047	33.93	0.222
0.0046	0.3618	0.6336	0.9048	0.0901	0.0051	30.93	0.249
0.0076	0.4752	0.5172	0.8683	0.1261	0.0056	24.47	0.265
0.0077	0.5308	0.4615	0.8532	0.1412	0.0056	21.92	0.266
0.0084	0.7736	0.2180	0.8146	0.1798	0.0057	15.11	0.267
{Ethylene glycol (1) + toluene (2) + n-Octane (3)} at T = 301.15 K							
0.0068	0.2853	0.7079	0.9167	0.0762	0.0071	26.62	0.267
0.0078	0.3655	0.6267	0.8925	0.1002	0.0073	23.60	0.247
0.0082	0.4901	0.5017	0.8497	0.1422	0.0081	17.96	0.290
0.0088	0.5129	0.4783	0.8405	0.1512	0.0083	16.94	0.294
0.0089	0.6812	0.3099	0.7863	0.2051	0.0086	10.84	0.301
{Ethylene glycol (1) + toluene (2) + n-Octane (3)} at T = 307.15 K							
0.0067	0.2294	0.7639	0.9298	0.0622	0.0083	24.94	0.271
0.0069	0.3278	0.6653	0.8914	0.0992	0.0094	21.37	0.302
0.0074	0.4387	0.5539	0.8580	0.1317	0.0103	16.14	0.300
0.0081	0.5006	0.4913	0.8270	0.1611	0.0119	13.28	0.321
0.0085	0.6103	0.3812	0.7907	0.1966	0.0127	9.670	0.332

Result and discussion

The mole fractions of each component and selectivity and distribution coefficient in the two equilibrium phases are presented in table 1. In the phase diagram (figure 1) the experimental and calculated mole fractions of two phases at equilibrium are presented. The obtained experimental selectivity and distribution coefficients show that toluene can be extracted from (toluene + n-octane) mixtures by using ethylene glycol as a suitable solvent. The experimental selectivity factors at three temperatures (295.15, 301.15, and 307.15) K are presented in figure 2, according to these figure, increasing the temperature decreases the selectivity.

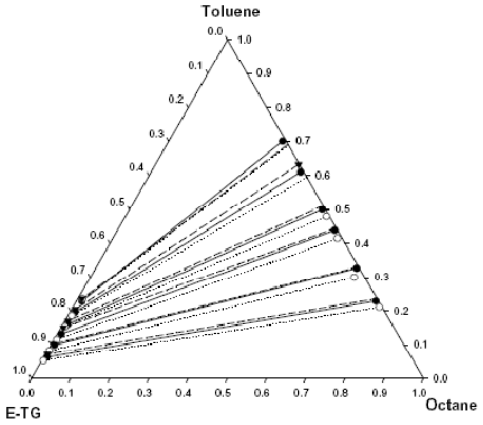

Figure ۱. LLE data at T = 295.15 K: •, experimental; ○, NRTL; ▼,UNIQUAC

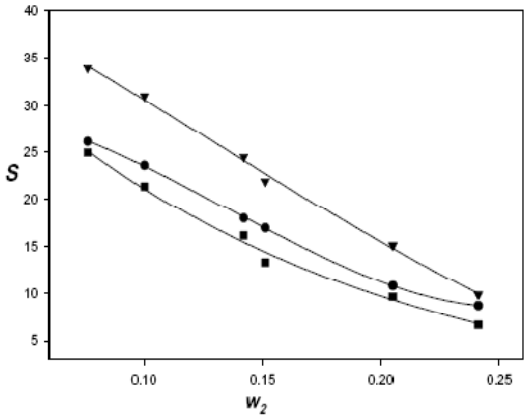

Figure 2. Plot of experimental selectivity T =.▼, 295.15 K □; • 301.15 K; ■ 307.15 K.

References:

[1] M. Mohsen-Nia, F.S. Mohammad Doulabi, J chem. thermodyn, **42**, 2010, 1281-1285.

[2] M. Mohsen-Nia, F.S. Mohammad Doulabi, Thermochim. Acta ,**445**, 2006, 82– 85.

[3] D.S. Abrams, J.M. Prausnitz, AICHE J. **21**, 1975, 116–128.

[4] H. Renon, J.M. Prausnitz, AICHE J. **14**, 1968, 135–144.

Interaction of dioxouranium(VI) ion with leucine

S. Seifi Arpatapeh [a*], M. Moazzami [a], F. Kamaly[a], E. Avarand [a], Y. Javadi [a], and E. Hazbeh [a], A. Shamel [a], F. Gharib [b]

[a] *Department of Chemistry, Islamic Azad University, Ardabil Branch, Iran*

(E-mail: so_seifi@yahoo.com)

[b] *Department of Chemistry, Shahid Beheshti University, Tehran, Evin, Iran*

Abstract

In this work, the formation of complex species of dioxouranium(VI) ion with leucine were studied in aqueous solution in the pH range of 1.0-3.5 at 25°C and constant ionic strength 0.1 mol dm^{-3} $NaClO_4$ using a combination of potentiometric and spectrophotometric techniques. Results showed evidence for formation of the following species: UO_2HL^{2+} and $UO_2(HL)_2^{2+}$.

Keywords: Dioxouranium(VI), Leucine, Spectrophotometry, Stability constant

Introduction

Uranium is a trace constituent in rock phosphate, which is extensively used as a source of phosphorous for fertilizers and livestock feed supplements. Calcium phosphate, for example, a source of calcium used as an animal feeding supplement, can present concentrations of uranium as high as 200 ppm. Thus, the investigation of the pathway, uranium (from feeding) → animal → human, is particularly important, as far as the radiological protection of the general population in concerned. Interaction between amino acids, peptides, and proteins with transition metal ions plays an important role in biochemistry and biology. Great attention has been paid to elucidating and interpreting the thermodynamic and structural characteristics of these biological ligands complexes.

Experimental

The present work deals with the study of dioxouranium(VI), UO_2^+, complexes by leucine. The method of determination of the stability constant based on the relation $A = f([H^+])$ [1-2]. Using a combination of spectrophotometric and potentiometric methods,

absorbance and pH were measured for a solution containing UO_2^+ with a large excess of ligand. Treatments of the spectrophotometric data in the range 250-285 nm (in the interval of 5 nm) obtained during the titrations as a function of the H^+ concentration was conducted with the computer program (Microsoft Excel Solver). The program allows calculation of stability constants for different stoichiometric models.

Results and Discussion

The complex $M_xH_yL_z^{(nx+y-z)+}$ formed, is characterized by its stoichiometry (x:y:z), where M and L represent the metal ion and ligand, respectively. To determine the stability constant of the complexation or protonation of the ligand, equation (1) is defined by β_{xyz} [1].

$$xM^{+n} + yH^+ + zL^- \leftrightarrows M_xH_yL_z^{(nx+y-z)+} \quad (1)$$

$$\beta_{xyz} = [M_xH_yL_z^{(nx+y-z)+}] / ([M^{+n}]^x[H^+]^y[L^-]^z) \quad (2)$$

The method of determining ε_M was previously described [1] and its values at different wavelengths are used in this work. Using a suitable computer program (Microsoft Excel Solver), the data were fitted for estimating the formation constant of equation (2). We used the Gauss - Newton nonlinear least - squares method in computer program to refine the absorbance by minimizing the error squares sum from the following equation.

$$U = \sum(a_i - b_i)^2$$

where a_i is a quasi-experimental and b_i is a calculated one.

The protonation constant of the ligand has been used for computation of the stability constants, β_{xyz}, of the metal-ligand. In aqueous solution the ligands exist in its anionic form (L^-), zwitterionic species (HL), and cationic form (H_2L^+). In acidic pH, in this case, the predominant species for complexation is HL. The spectrophotometric titration data were analyzed as before [2]. For finding the proposed species, the spectrophotometric titration data were analyzed by offering the following species to the computer program: UO_2L, UO_2HL^+, UO_2HL_2, $UO_2H_3L_2^{+2}$, $UO_2H_3L_3^+$, $UO_2H_4L_4^+$. As expected, all the proposed species were systematically rejected by the computer program except UO_2HL^+ and $UO_2(HL)_2^+$. A value for the formation constant of $UO_2H_2L^{+2}$ was calculated by the program, but the species was not considered further because the estimated error in its formation constant is unacceptable, and its inclusion does not improve the goodness of the fit. The model finally chosen, formed by UO_2HL^+ and $UO_2(HL)_2^+$, resulted in a satisfactory numerical and graphical fitting. The

equilibrium distribution of the species of UO_2^{2+}+ leucine system as a function of – log[H^+] is shown in Fig. 1 at 25 °C and ionic strength 0.1 mol dm^{-3} $NaClO_4$, as a typical example.

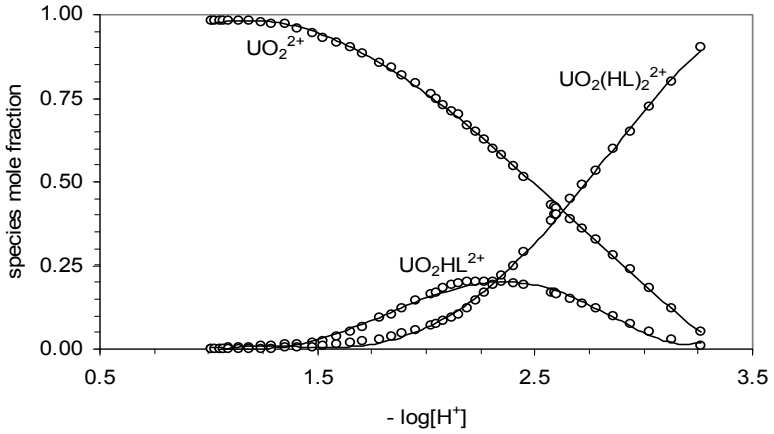

Fig. 1. The equilibrium distribution of the species in UO_2^{2+} + leucine system as a function of – log[H^+] at 25 °C and ionic strength 0.1 mol dm^{-3} $NaClO_4$.

References

[1] F. Gharib, Phys. Chem. Liq. 45 (2007) 105.

[2] F. Gharib, M. Sayadian, A. Shamel, M. M. Moghaddam, J. Mol. Liq. 138 (2008) 9.

Vapor-Liquid Equilibria of Non-Aqueous Polymer Solutions from the Experimental Vapor-Pressure Osmometery and Molecular Thermodynamics Modelling

R. Sadeghi[a], Y. Shahebrahimi[b]

[a]Department of Chemistry, University of Kurdistan, Sanandaj, Iran

(Email: rsadeghi@uok.ac.ir)

[b]Department of Chemical Engineering, University of Kurdistan, Sanandaj, Iran

Keywords: Polymer solution, Vapor pressure osmometry, Thermodynamics,Vapor-liquid equilibria.

Introduction:

The availability of solvent and polymer activity coefficient is of great importance in the design and operation of polymer processes and separation processes such as polymer devolatilization, per-evaporation, the selection of the optimum membrane for a given separation process. The removal of solvents or nonpolymerized monomers from the produced polymer requires the knowledge of vapor-liquid equilibrium (VLE), i.e., the solvent activity coefficients [1,2]. In the first part of this work, vapor-liquid equilibria behavior of the solutions of wide range of polymers including poly(ethylene glycol) 400 (PEG400), poly(ethylene glycol dimethylether) (PEGDME) 250, 500 and 2000, and poly(propylene glycol) 400 (PPG400) in methanol, ethanol and 2-propanol were determined at $T = 318.15$ K by the vapor pressure osmometery method. In the second part of this work, the obtained solvent activity data were correlated by a thermodynamic model which is a combination of the modified Flory-Huggins model based on the salvation theory and a segment based local composition model (for physical interactions).

Methods

In this work, solvent activities of investigated polymer solutions were obtained from the vapor pressure osmometery. The vapor pressure osmometery was performed with the help of an osmomat K-7000 (Knauer). With this method, the vapor pressure is measured indirectly

by using thermistrors to measure voltage changes caused by changes in temperature. First the osmometer was calibraied using different solutions of LiBr for each solvent, yielding a function which correaltes the panel reading to the corresponding concentrations of the LioBr solution. Then the measurements for the different polymer solutions were carried out. The water activity for the standard LiBr solutions at different concentrations and alcohol solvents at T = 318.15 K has been calculated from the correlation of Pitzer ion-interaction model [3-5].

Results, Discusion and Conclusions

In the first part of this work, the experimental solvent activity of solutions of PEG400, PEGDME250, 500 and 2000 and PPG400 in methanol, ethanol and 2-propanol were obtained at 318.15 K. The effect of solvent, molecular weight and structure of polymer on the vapor-liquid equilibrium behavior of the studied solutions were investigated. It was found that for a certain polymer mass fraction, solvent actvities of aqueous and nonaqueous polymer solution increase by increasing molecular weight of polymer. Also for particular polymer in different solvent, with adding carbon to molecule of solvent, the solvent activity decrease. A new molecular thermodynamics model has been used for the correlation of the vapor-liquid equilibrium data of the investigated polymer solutions. The model gives a good representation of solvent activities over measured concentration range. In this model, the excess Gibbs free energy G^E of polymer solutions is considered as consisting of two additive parts, chemical contribution, G^E_{chem} and physical contribution, G^E_{phys}.

$$G^E = G^E_{chem} + G^E_{phys}$$

The chemical contribution incorporates the chemical association theory to account for the hydrogen bonds between solvent and polymer. The physical contribution is represented by a segemnt based local composition model.

References

[1]G. D. Pappa, E. C. Voutsas, Ind. Eng. Chem, 38 (1999) 4975.

[2]L. S. Wang, J. Ahlers, Ind. Eng. Chem,42 (2003) 6205.

[3] K. Nasirzadeh, R. Neueder,W. Kunz, Chem. Thermodynamics, 36 (2004) 511.

[4]J.T. Safarov, Fluid Phase Equilibria, 236 (2005) 87.

[5] Javid T. Safarov . Fluid Phase Equilibria, 243 (2006) 38.

Densities and excess molar volumes of DiisoPropylamine and 1-Alkanols

M. Almasi [a], M. Shojaa Bakhtiar[*a]

[a] Department of Chemistry, Science and Research Branch, Islamic Azad University, Khouzestan, Iran

Email: m.almasi@srbiau.ac.ir

Key words: Density, Excess molar volume, 1-Alkanols, Diisopropylamine

Introduction:

The thermodynamic and transport properties of liquids and liquid mixtures have been used to understand the molecular interactions between the components of the mixture and also for engineering applications concerning heat transfer, mass transfer and fluid flow[1]. This paper is a part of an ongoing research effort to measure and characterize the properties of mixtures containing alkanols[2]. It reports the densities and excess molar volumes at temperatures(293.15,298.15,303.15 and 313.15)K.

Methods:

Diisopropylamine, methanol, ethanol, 1-propanol, 1-butanol, 1-pentanol were purchased from Merck with purity higher than 99 %, (All) and used without further purifications. The density of the pure compounds and mixtures was measured by pycnometer. The temperature in the cell was regulated to ± 0.01 K.

Results and Discussion:

The excess molar volumes of the solutions of molar composition x were calculated at various temperatures from the densities of the pure liquids and their mixtures according to the following equation

$$V_m^E = \sum_{i=1}^{N} x_i M_i (\rho^{-1} - \rho_i^{-1}) \qquad (1)$$

where ρ is the density of the mixture, ρ_i is the density of pure component i, x_i is the mole fraction, M_i is the molar mass of component i, and N stands for the number of components in the mixture. The corresponding V_m^E values of binary mixtures of Diisopropylamine (1) + 1-

alkanols (2) measured and plotted against mole fraction of Diisopropylamine at T = 298.15 K in Figure 1. Each set of results were fitted using a Redlich–Kister polynomial [3] , which for binary mixtures is

$$Y^E = x_1(1-x_1)\sum_{k=0}^{N} A_k(1-2x_1)^k \qquad (2)$$

Where x_1 is the mole fraction of Diisopropylamine. A_k is adjustable parameter obtained by least-squares method, and k is the degree of the polynomials. Excess molar volume of Diisopropylamine with 1-alkanols is negative over the whole range of mole fractions. The negative V_m^E values mentioned systems indicate strong specific interactions through dipolar association between 1-alkanols and Diisopropylamine molecules over the entire composition range, revealing that the chemical forces between the dissimilar molecules are dominant in these investigated mixtures.

Conclusions:

Excess molar volumes, Diisopropylamine and 1-alkanols were obtained from experimental results and fitted by Redlich–Kister type equation. negative values of excess molar volume suggested that the main factor in the interactional forces is chemical interactions

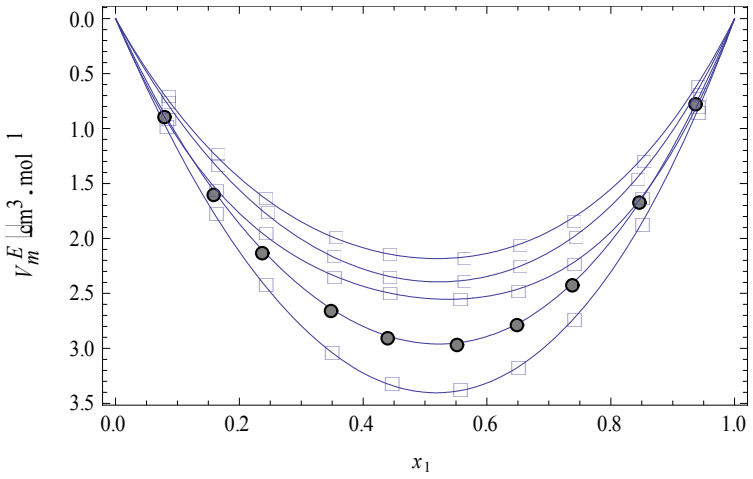

FIGURE 1. Excess molar volumes V_m^E vs. mole fraction of Diisopropylamine for binary mixtures of Diisopropylamine with (▫) methanol, (●) ethanol, (■) 1- propanol, (◊) 1-butanol, (▲) 1-pentanol, at T = 298.15 K. The solid curves were calculated from coefficients of equation (2).

References

[1] Kim, E. S.; Marsh, K. N. Excess volumes for 2-methyl-2-propanol + water at 5 K intervals from 303.15 to 323.15 K. *J. Chem. Eng. Data* **1988**, *33*, 288 – 292.

[2] Iloukhani, H.; Parsa, J. B.; Saboury, A. A. Excess molar enthalpies of binary mixtures of N,N-dimethylformamide plus six 2-alkanols. *J. Chem. Eng. Data* **2000**, *45*, 1016 – 1018 ([3] Redlich, O. J.; Kister, A.T. Thermodynamic of non electrolyte solutions: algebraic representation of thermodynamic properties and the classification of solutions. *Ind. Eng. Chem.* **1948**, *40*, 345 – 348.

Magnesium Ion Interaction with Amino Acids as simple model of the Proteins

Z. Shekari[a], H.R. Shamlouei[a*]

[a] Islamic Azad University, Gachsaran Branch, Science Department
shamluei@iaug.ac.ir

Introduction

Magnesium is an essential element in biological systems. It occurs typically as the Mg^{2+} ion. It is an essential mineral nutrient for life [1,2]and is present in every cell type in every organism. For example, ATP (adenosine triphosphate), the main source of energy in cells, must be bound to a magnesium ion in order to be biologically active. What is called ATP is often actually Mg-ATP.[4].Similarly,magnesium plays a role in the stability of all polyphosphate compounds in the cells, including those associated with DNA and RNA synthesis [1].The presence of Mg^{2+} can affect the break down reaction of DNA it is required for a number of steps during nucleic acid (DNA and RNA) [2,3]. For the understanding the mechanism of magnesium ion activity in biological system functions, it is necessary to study the interaction of magnesium ion with protein chain. But the protein sequence has complicated structure and number of atoms exceeds from limits that the computational instrument could be calculate the interactions. Interaction of magnesium ion with simple system such as amino acids may be considered as estimation of interaction of metal ion with protein. In this research the structure and properties of magnesium ion bonded to the different substituted amino acids were calculate by ab initio methods.

Selection of Compound and Computational Method

Amino Acids are building block of proteins in which have amine (NH_2) and carboxylic group acid attached to single carbon. There are two forms of Amino Acids; neutral and ionic forms. General formula of two neutral (a) and ionic forms (b) forms of Amino Acids are shown in **Error! Reference source not found.**.

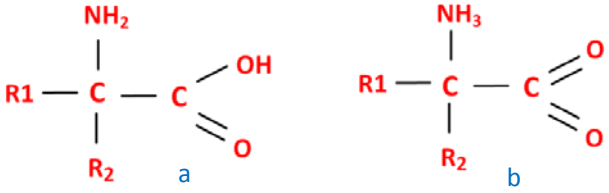

Fig.1 General formula of two neutral (a) and ionic forms (b) forms of Amino Acids

Table1 list of substitutions which located instead of R1 and R2 groups in **Error! Reference source not found.**

R1	R2	R1	R2
H	H	H	SH
H	CH_3	SH	SH
CH_3	CH_3	H	SiH_3
H	F	SiH_3	SiH_3
F	F	H	NH_2
H	COOH	NH_2	NH_2
COOH	COOH		

The substitution R1 and R2 were chosen in manner that the properties of them are changed from electron withdrawing groups to electron releasing groups. In **Error! Reference source not found.**list of substitution which selected to be locate in place of R1 and R2 is shown. Substituted Amino Acids, magnesium ion bonded to Amino Acids and magnesium ion bonded dimer of them was chosen to study the interaction of magnesium ion with substituted Amino Acids.

The structure of each species in this research include; Amino Acids, magnesium ion attached to Amino Acids and magnesium ion bonded dimer of them were optimized by HF method, 6-311++G** basis set and gaussian03 package. Energy parameters, IR spectrum and NMR of each species were calculated by using same method and basis set described previously.

Results and discussion

1. Structure and stability of Amino Acids, complex of Magnesium ion with Amino Acids and magnesium ion bonded dimer of them

Structure of species involve in formation of dimers of different Amino Acids include; substituted amino acids, magnesium ion bonded to Amino Acids and magnesium ion bonded dimer of them was calculated by methods as mentioned previously. The structure of the magnesium ion bonded dimer of Amino Acid which R1 and R2 are H and NH_2 respectively are shown in **Error! Reference source not found.**.

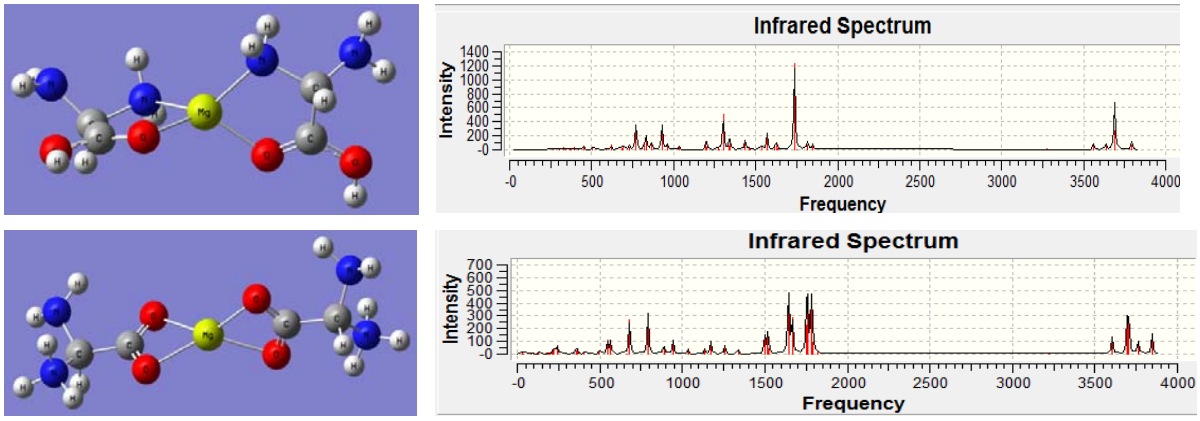

Fig.2 structure and IR spectrum of magnesium ion bonded dimer of two forms of Amino Acid in which R1=H and R2=NH_2

Since observing the IR spectrum of the dimers shows no negative vibrational mode in its spectrum, the dimers are stable.

2. strength of magnesium ion bond and enthalpy of formation for magnesium bonded dimer of Amino Acids

The bond length of oxygen or nitrogen with magnesium ion shows the strength of it. Decrease in magnesium positive charge or □ factor can be defined as Eq.1

$$\sigma = charge\ of\ isolated\ Mg^{2+} - charge\ of\ Mg^{2+}\ in\ dimer$$

The Mg^{2+} bond length versus decrease in magnesium positive charge or □ factor is shown In **Error! Reference source not found.**. In **Error! Reference source not found.**, the plot of the enthalpy of formation for the different dimers versus □ factor of them is shown.

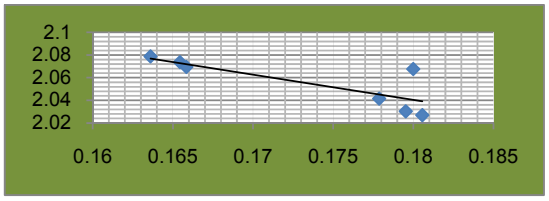

Fig.3 the results of magnesium ion bond length versus □ factor

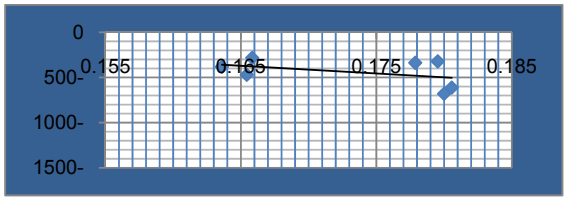

Fig.4 the enthalpy of formation for the different dimers versus □ factor

As shown in **Error! Reference source not found.** and **Error! Reference source not found.**, when the charge in central magnesium ion in dimer decreases, the strength of magnesium bond to amino acids is strengthen and the enthalpy of formation of dimer increases.

Conclusion

The structure and stability of magnesium ion bonded dimers of different substituted amino acids which resembled the interaction of magnesium ion with proteins, were calculated by ab initio calculations. The energy parameters of them were analyzed by same method and show that each parameter such as electron releasing or withdrawing properties of substitutions makes the dimer more stable.

Refernces

[1] Lusk, J.E., Williams, R.J.P., and Kennedy, E.P. (1968). "Magnesium and the growth of Escherichia coli". Journal of Biological Chemistry 243 (10): 2618–2624

[2]Crichton, R.R. Biological Inorganic Chemistry: An Introduction, 2008, 1st edition, Elsevier, Amsterdam, Netherlands.

[3] Bertini,I., Gray H.B., Lippard, S.J., Valentine, J.S., Bioinorganic chemistry, 1994, University Science Books, Mill Valley, California.

[4] Kohwi, Y., and Shigematsu, T.K., PNAS June 1, 1988 , vol. 85 no. 11 3781-3785

[5]Murk Rose, D., Polnaszek, C. F., Bryant, R. G., Biopolymers, Volume 21, Issue 3, pages 653–664, March 1982

Thermodynamic determination of protonation constants of gallic acid using the SIT method

Kh. Shamsazar * [a], P.farzaneh [a] , A. Shamel [a] and F. Gharib [b]

[a] *Chemistry Department, Islamic Azad University, Ardabil Branch, Ardabil, Iran*

(E-mail: khadijeh.shamsazar@gmil.com)

[b] *Chemistry Department, Shahid Beheshti University, Tehran, Evin, Iran*

Keywords: Gallic acid, Protonation constant, SIT model, Spectrophotometric and potentiometric methods

Introduction

The protonation constant values of gallic acid were studied at 25 °C and different ionic strengths, 0.1-1.0 mol dm^{-3} $NaClO_4$, using a combination of spectrophotometric and potentiometric techniques. The dependence of protonation constants on ionic strength was taken into accounts using a Debye-Huckel type equation (molar concentration scale) and the SIT (specific ion interaction theory) approach (molal concentration scale).

As is well known, thermodynamic data always refer to a selected standard state. The definition given by IUPAC is well adopted and states that at the standard state the activity coefficient of a solute in a solution should be unity. However, this is a strict condition and usually not accessible for many (or maybe all) reactions and so any measurements (or all) cannot be made accurately in this state. Precise thermodynamic information for these systems can apparently be obtained in the presence of an inert electrolyte of sufficiently high concentration, ensuring that the activity factors are reasonably constant throughout the measurements.

Experimental

All measurements were carried out at 25 °C. The ionic strength was maintained from 0.1 to1.0 mol dm^{-3} with sodium perchlorate. A Jenway research pH-meter, model 3520 (with a precision of 0.001 units), was used for $-\log[H^+]$ measurements. The pH-meter was calibrated for the relevant H^+ concentration with a solution of 1.00×10^{-2} mol dm^{-3} perchloric solutions containing 0.09 mol dm^{-3} sodium perchlorate, for adjusting the ionic strength to 0.1

mol dm^{-3}. The same procedure was performed for the other ionic strengths. The junction potential corrections were calculated from Eq (1)

$$-\log[H^+]_{real} = -\log[H^+]_{measured} + a + b[H^+]_{measured} \quad (1)$$

where a and b were determined by measuring the hydrogen ion concentration for two different solutions of $HClO_4$ or NaOH with sufficient $NaClO_4$ to adjust the ionic strength. Spectrophotometric measurements were performed on a UV-Vis Shimadzu 2100 spectrophotometer with a Pentium 4 computer and using thermostated matched 10 mm quartz cells.

Results and Discussion

The dependence on ionic strength of protonation constant was taken into account by using the SIT model [1]. The protonation constants were determined experimentally and the values are then converted to the molality scale according to the conversion factors determined by Baes and Mesmer. Finally, the thermodynamic protonation constant, $K°_m$, is determined from the experimental constant, K_m, using a weighted linear extrapolation to the zero ionic strength. The logarithm of the thermodynamic protonation constant may be written as:

$$\log K° = \log K^m + \log \gamma_{HnL^{(1-n)-}} - \log \gamma_{L^-} - n\log \gamma_{H^+} \quad (2)$$

Substituting the activity coefficients of each species into Eq (2) and rearranging gives

$$\log K°_1 = \log K^m_1 + Z^*D - \Delta\varepsilon_1 I_m \quad (3)$$

$$\log K°_2 = \log K^m_2 + Z^*D - \Delta\varepsilon_2 I_m \quad (4)$$

where $Z^* = \Sigma[(\text{charges})^2_{reactants} - (\text{charges})^2_{products}]$, K^m is the apparent protonation constant in molal scale, and $\Delta\varepsilon$ represents the summation of the specific ion interaction terms as $\Delta\varepsilon_1 = \varepsilon(L^-, Na^+) + 2\varepsilon(H^+, \text{supporting electrolyte anion}) - \varepsilon(H_2L^+, \text{supporting electrolyte anion})$ and $\Delta\varepsilon_2 = \varepsilon(L^-, Na^+) + \varepsilon(H^+, \text{supporting electrolyte anion})$ for various supporting electrolytes. Considering Eq (3), the values of $\Delta\varepsilon_1$ and $\log K^o_1$ are obtained using a weighted linear regression of the $\log K^m_1 + Z^*D$ as a function of the ionic strength (in molal scale). The procedure has been applied for the determination of $\log K^o_2$ and $\Delta\varepsilon_2$, using Eq (4).

References

[1] F. Gharib, A. Farajtabar, J. Mol. Chem. 135 (2007) 27.

Calculation the Surface Tension of Isomers of Pure Hydrocarbons

Setareh Sheikh*,[1] , Saeid Liaghatmadar[1]

[1] *Department of Chemistry, Islamic Azad University- Shiraz Branch, Shiraz, Iran*

Sheikh_set@yahoo.com

Abstract

In this work a new method has been proposed to calculate surface tension for isomers of pure hydrocarbons. The relative molar mass, critical temperature and acentric factor are three parameters which are applied. This method was used to calculate surface tension values for 54 isomers of *n*-alkane and 5 isomers of the 1-alkene homologous series in a relatively large range of temperatures. Average relative errors for 488 points of these 59 isomers are less than 2.30 %.

Keywords: Surface tension, Pure hydrocarbon isomers, Calculation method, Homologous series

Introduction

Surface tension is one of the most significant thermophysical properties. It is important for most separation processes involving mass transfer operations like extraction, distillation, absorption and adsorption and for the coating and adhesives industries such as paints, detergents, and agrochemicals. The petroleum industry requires the surface tension data of pure hydrocarbons. Some scientists have tried to develop experimental methods of measuring this thermophysical property [1-7] and on the other hand; some investigators have interested in developing theoretical models to predict this phenomenological behavior [8-15].

Calculation method

The method proposed in this work is:

$$\gamma = \mathbf{50}\,\tau^{1.2} + \frac{\omega}{M} \qquad (1)$$

In this equation, γ is the surface tension; τ is a reverse reduced temperature scale

(τ = 1-T/T_c), T and T_c are temperature and vapour-liquid critical temperature in kelvin, respectively; ω is acentric factor and *M* is the relative molar mass. The experimental data and acentric factor are taken from two references [16-17].

Results and discussions

Eq.(1) was applied for calculating surface tension values for six pure hydrocarbons at several temperatures and table 1 gives a summary of the results. 54 isomers of *n*-alkane and 5 isomers of the 1-alkene homologous series are considered in a relatively large range of temperatures. As it can be seen in table 1, the correspondence between calculated values and experimental ones is satisfactory and acceptable.

Table1

Results of the estimation of surface tension values for hydrocarbon isomers

Average Relative Error in percent (ARE%) , the temperature range (ΔT)

Hydrocarbon	ΔT (K)	Number of isomers	ARE (%)
n-hexane	283-333	4	1.48
n-heptane	253-363	8	2.23
n-octane	283-373	14	1.83
n-nonane	283-333	28	2.29
1-hexene	283-303	3	1.66
1-heptene	283-303	2	1.99

Conclusion

This method was applied for calculating the surface tension of 488 points of 59 different pure isomers of the *n*-alkanes and 1-alkenes homologous series in a relatively large range of temperatures. Only three simple parameters, *M*, T_c , ω ; which are the relative molar mass, the critical temperature and acentric factor respectively; are used for calculating surface tension and comparison between experimental values and calculated ones, supports this calculation method. Average relative errors for 488 points of these 59 isomers are less than 2.30 %.

References

[1] R.F.Brooks, K.C. Mills, *High Temp.-High Press*., **25**, 657(1993).

[2] H. Lin, Y.Y. Duan, Int. J. Thermophys., **24**, 1495 (2003).

[3] A.J. Queimada, F.A.E. Silva, A.I. Caco, I.M. Marrucho, J.A.P. Coutinho, Fluid Phase Equilib., **214**, 211 (2003).

[4] Y.Y. Yang, J.H. Deng, H.L. Yang, X.H. Zheng, G.Q. Che, Zh.Q. Huang, J. Chem. Thermodyn., **39,** 438 (2007).

[5] Y.Y. Zuo, Ch. Do , A. W. Neumann, Colloids and Surfaces A: Physicochem. Eng. Aspects, **299**,109 (2007).

[6] U. Alakoç, C. M. Megaridis, M. McNallan , D. B. Wallace, J. Colloid Interface Sci., **276**, 379 (2004).

[7] S. E. Bechtel, K. W. Koelling, W. Nguyen , G. Tan, J. Colloid Interface Sci., **245**,142 (2002).

[8] J.R. Brock, R.B. Bird, AIChE J., **1**, 174 (1955).

[9] J. Lielmezs, L.H. Merriman, Thermochim. Acta, **105**,383 (1986).

[10] J. Lielmezs, T.A. Herrick, Chem. Eng. J., **32**, 165 (1986).

[11] P.Li, P.Sh. Ma, J.G. Dai , W. Cao, Fluid Phase Equilib., **118**,13 (1996).

[12] S. Sheikh, A. Boushehri, High Temp.-High Press., **32**,233 (2000).

[13] A.J. Queimada, I.M. Marrucho, J.A.P. Coutinho, Fluid Phase Equilib., **183**, 229 (2001).

[14] C. Miqueu, B. Mendiboure, C. Graciaa , J. Lachaise, Fluid Phase Equilib., **218**, 189 (2004).

[15] L. F. Ramírez-Verduzco, A. Romero-Martínez, A. Trejo, Fluid Phase Equilib., **246**, 119 (2006).

[16] C.L.Yaws. *Chemical Properties Handbook,* McGraw-Hill, New York (1999).

[17]B.E. Poling, J.M. Prausnitz, J.P. O'Connell, *The Properties of Gases and Liquids*, McGraw-Hill, New York (2001).

The Influence of Quantum Effect on Deviation from the Linear Isotherm Regularity

F. Safdari[a] , G. A. Parsafar[b]

[a,b] Department of Chemistry, Sharif University of Technology, Tehran, Iran

(Email: fa.safdari@gmail.com)

Keywords: LIR EoS, Lennard-Jones (12, 6), Quantum Effects of Light Molecules and Hard Sphere Model.

Introduction:

A general regularity has been found based on an effective pair potential of Lennard-Jones (12, 6) for both dense nonmetallic and nonionic fluids and solids; namely, $(Z\text{-}1)V^2$ linearly varies with respect to ρ^2, this equation of state (EoS I) is known as LIR [1]. Unexpectedly, solid and liquid Ne indicate a significant deviations from EoS I [2]. The purpose of this research is to investigate the accuracy of the EoS I for the other systems including quantum light molecules such as He, H_2, and D_2 in both fluid and solid states, at different temperatures. Like neon, we have noticed that these systems, don't well obey EoS I. It is also shown in this work that, at higher temperatures and for the heavier species, EoS I becomes valid, due to decreasing the quantum effect.

Methods and Results:

We have used experimental *pvT* data for dense systems of light molecules in fluid state, for densities greater than the Boyle density and temperatures lower than twice of the Boyle temperature and also in the solid state to check the accuracy of the EoS I. As an example, results for H_2 at different temperatures are shown in Table 1.

Table1. Fitting EoS I in experimental data for H_2 at given temperatures [3, 4].

T(K)	Δp (MPa)	$\Delta\rho$ (mol/L)	R^2
4	0 - 1961	44 - 99	0.9560
50	10 - 220	28 - 57	0.9944
100	40 - 300	28 - 57	0.9978
150	30 - 57	30 - 57	0.9999

As shown in Table 1, it is obvious that H_2 at 4 K shows a significant deviation from EoS I. But, it behaves more according to EoS I when temperature increases.

Considering the fits to EoS I for monoatomic and diatomic molecules, it is interesting to check the predictive power of EoS I for some other molecules, the results are shown in Table 2. As we see, EoS I is more appropriate for the heavier molecules.

Table 2. Fitting EoS I in experimental data for given molecules [3].

Diatomic molecules	T(K)	Δp (kg/cm^2)	$\Delta \rho$ (mol/L)	R^2	**Monoatomic molecules**	T(K)	Δp (kg/cm^2)	$\Delta \rho$ (mol/L)	R^2
H_2	4	0 - 20000	44 - 99	0.9569	**He**	4	0 - 20000	58 - 156	0.9339
D_2	4	0 - 20000	51 - 105	0.9516	**Ne**	4	0 - 20000	71 - 106	0.9974
N_2	65	0 - 19000	34 - 51	0.9841	**Ar**	77	0 - 19000	41 - 57	0.9992

Discussion:

dense systems of light molecules don't well obey the EoS I because of the unbalance interactions of repulsion and attraction, due to the quantum effect. To verify such a conclusion, we have shown that the hard-sphere fluid remarkably deviates from EoS I, for wich only the repulsive forces exist among molecules (see Figure 1).

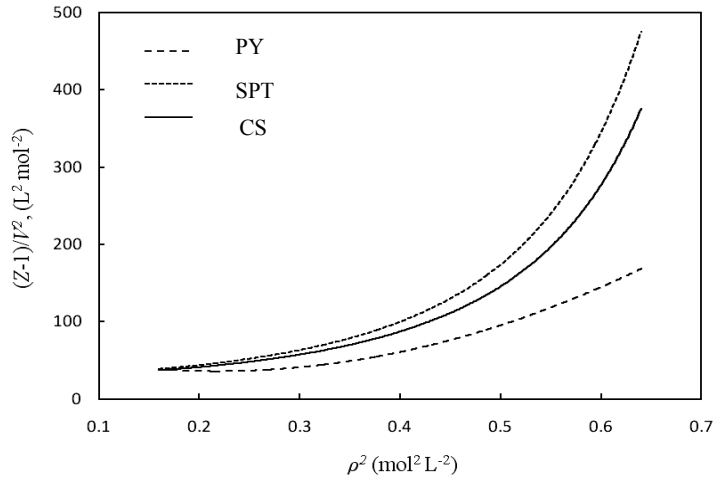

Figure 1. *(Z-1) V^2 vs ρ^2* for (PY), (SPT) and (CS) EoSs [5]

As shown in Figure 1, Percus-Yevick (PY), Scaled Particle Theory (SPT) and Carnahan Starling (CS) EoSs baed on the hard sphere model indicate significant deviation from EoS I.

Conclusion:

the dense systems of light molecules deviate from EoS I both in fluid and solid states because of unbalance interactions of repulsion and attraction. Also, since the quantum effect for light molecules of dense systems decreases with temperature, they behave more according to EoS I at higher temperatures. Furthermore, EoS I becomes more suitable for heavier molecules because of insignificant quantum effect.

References:

[1] G. A. Parsafar; E. A. Mason, J. Phys. Chem 97 (1993) 9048.

[2] G. A. Parsafar; H. V. Spohr; G. N. Patey, J. Phys. Chem B. 113 (2009) 11977.

[3] J.W. Stewart, J. Phys. Chem. Solids Pergamon Press. 1 (1956) 146 .

[4] J.W. Leachman; R.T. Jacobsen; E.W. Lemmon, J. Phys. Chem. Ref. Data, 38 (2009) 721.

[5] M. Khanpour; G.A. Parsafar, Chemical Physics. 333 (2007) 208.

MULTIWAVELENGTH SPECTROPHOTOMETRIC DETERMINATION OF STABILITY CONSTANTS OF COMPLEXES BETWEEN IRON(III) WITH 1-(2-tenoil)-4-treeFloro-2-[2-Hydroxi-3,5-Disolfophenilazo] -1,3 butadion.

Reza Solhnejad[*a], AfshinTagvamanesh[b]

a. Islamic azad university-Ardebil branch, Ardebil, Iran (Email:Solhnejad@gmail.com)

b. Islamic azad university-Ardebil branch

Keywords: MULTIWAVELENGTH, IRON(III), SPECTROPHOTOMETRIC, 1-(2-tenoil)-4-treeFloro-2-[2-Hydroxi-3,5-Disolfophenilazo] -1,3 butadion.

Introduction:

Determination of physicochemical properties of iron and its stability constants with a variety of ligands is done[1-2]. The goal of this research is to determine the forms of composed complexes between the IRON(III) and 1-(2-tenoil)-4-treeFloro-2-[2-Hydroxi-3,5-Disolfophenilazo] -1,3 butadion.The multiple linear regression (MLR) is used as calculation method and the calculation algorithm is implemented in the Mathematica 7 environment.

Metods and Discussion:

According to Beer's law , the absorbance of a solution is linear with respect to containing species concentrations

$$A = C\varepsilon$$

Where, A is a $r \times c$ dimensional matrix containing absorbances of r solutions in c different wavelength, and C is the $r \times k$ dimensional matrix containing the concentration of each species in the r different solutions, k is the number of species existing in the solution. The ε is a $k \times c$ dimensional matrix containing the absorbance coefficients of each species. The ε can be calculated from the following formula[3,4].

$$\varepsilon = \left(C^T C\right)^{-1} C^T A^{Exp}$$

The error is defined as following formula

$$Error = Trace\left[\left(A^{Cal} - A^{Exp}\right)^T \left(A^{Cal} - A^{Exp}\right)\right]$$

To calculate of the stability constants, β_{pqr}, we have minimized the above mentioned Error function until the convergence criteria is reached.

Conclusions.

The equilibrium equation in the systems which were investigated can be represented by the generic expression (charges omitted for simplification)

$$pM + qL + rH \square M_pL_qH_r \qquad \beta_{pqr} = \frac{[M_pL_qH_r]}{[M]^p[L]^q[H]^r}$$

Where, M, L and H stand for Fe(III), Ligand (fully deprotonated) and proton concentrations, p, q and r denote the stoichiometric coefficients. Formation constants were calculated using the computer program that has been programmed in *Mathematica 5.2* environment. Our study have showed that four complexes MLH, ML, ML_2, $MLOH$ were formed in the solution. Considering the ML_2H, M_2L_2 and similar complexes cause the increase of the error and negative absorbance coefficients that were not acceptable.

References

[1] Bulatov M.N ., Kalenkin N.P .L. Chemistry, 1986. 432 c.

[2] M.F.MEMEDOV., bako chemistry, 2007,852

[3] Krisztina Taka´cs-Nova´k a, Kin Y. Tam b,*, Journal of Pharmaceutical and Biomedical Analysis21 (2000) 1171–1182

[4] Marcelo M. Sena, Julio Cesar B. Fernandes, Laércio Rover Jr., Ronei J. Poppi, Lauro T. Kubota , Analytica Chimica Acta 409 (2000) 159–170

[5] Milan Melouna,∗, Tom´aˇs Syrov´ya, Aleˇs Vr´anab, Analytica Chimica Acta 533 (2005) 97–110

Thermodynamic Studies of Solutions of Poly(Vinylpyrrolidone) in Water, Methanol, Ethanol, Acetonitrile, 1-Propanol, 2-Propanol, and 1-Butanol at Different Temperatures

R. Sadeghi*[a] , S. Azizpour[b] and A. A. Salari[b]

[a]Department of Chemistry, University of Kurdistan, Sanandaj, Iran

[b]Department of Chemistry ,Islamic Azad University of shahr reyand

(rsadeghi@uok.ac.ir), (Azizpoors@yahoo.com)

Keywords: Poly(vinylpyrrolidone), Volumetric, Acostic, Viscometric.

Thermodynamic and transport properties such as volumetric, acoustical and viscometric of polymer solutions has been proven to be a very useful tool for understanding solute-solvent and solute-solute interactions in these solutions [1]. Although poly(vinylpyrrolidone) (PVP) is a very important polymer in respect to its uses [2], however information on the thermodynamics properties of aqueous or non-aqueous solutions of PVP is scarce in the literature [3]. In present study, precise density, ultrasonic velocity and viscosity measurements have been carried out on PVP in water, methanol, ethanol, acetonitrile, 1-propanol, 2-propanol and 1-butanol at T = (288.15, 293.15, 298.15, 303.15, 308.15 and 313.15) K at atmospheric pressure. The density and sound velocity of the mixtures were measured at different temperatures with a digital vibrating-tube analyzer (Anton Paar DSA 5000, Austria) with proportional temperature control that kept the samples at working temperature within $\pm 10^{-3}$ K. The uncertainties of density and ultrasonic velocity measurements were better than $\pm 5\times10^{-6}$ g·cm^{-3} and $\pm 2\times10^{-1}$ m·s^{-1}, respectively. Viscosities were measured with an Ostwald-type viscometer. The flow time of investigated solutions was measured with accuracy better than 0.05 s. For each solution the flow time was measured at least three times. The viscosity measurement was reproducible to within $\pm$ 0.1%. From these experimental data, the infinite dilution apparent specific volume and isentropic compressibility values of PVP in the investigated solvents have been obtained and their variations with temperature and type of solvents have also been obtained. The results have been interpreted in terms of the interactions between different solvents and the polymer. The variations of viscosity with the concentration of polymer, temperature and type of solvent

have been determined and correlated successfully with the segment-based Eyring-Wilson and NRTL viscosity models. It was found that the Wilson model produces better results than the NRTL model.

The values of the standard partial specific volumes, ϕ_V^0, for PVP in the investigated solvents increased along with an increase in temperature and at each temperature follow the order methanol < ethanol < 2-propanol < 1-propanol < butanol < water < acetonitrile. The values of the standard partial specific expansibilities, ϕ_E^0, for PVP in water, methanol, 2-propanol and acetonitrile decrease by increasing temperature, however, those in ethanol, 1-propanol and 1-butanol increase by increasing temperature. For the temperature range $T \leq 298.15$ K, the values of ϕ_E^0 follow the sequence water > 1-butanol > 2-propanol > 1-propanol > acetonitrile > ethanol > methanol but for temperature range $T > 298.15$ K follow the order water > 1-butanol > 1-propanol > 2-propanol > ethanol > acetonitrile > methanol. The infinite dilution apparent specific isentropic compressibilities, ϕ_K^0, of PVP in water and acetonitrile have positive values and in other investigated solvents have negative values. The results show that the values of ϕ_K^0 for PVP in non-aqueous solutions decrease as temperature increases, however these values in aqueous solutions increase by increasing temperature. At each temperature, the values of ϕ_K^0 of PVP in the investigated solvents follow the order acetonitrile > water > 1-butanol > 1-propanol > ethanol≈2-propanol > methanol. It may be expected that the PVP-solvent interaction follows the sequence water, acetonitrile, 1-butanol < 1-propanol < ethanol, 2-propanol < methanol. From the temperature dependence of ϕ_K^0 and $\kappa_s - \kappa_{s0}$, we can conclude that the PVP-water and PVP-non-aqueous solvents interactions respectively become weaker and stronger as temperature increases. The polymer concentration dependence of viscosity of the investigated PVP solutions becomes greater as temperature decrease and at the same condition, the magnitudes of both of η and η-η_0 follow the order acetonitrile < methanol < water < ethanol < 2-propanol < 1-propanol < 1-butanol.

References

[1]. W. Well, R. A. Pethrick, Polymer 23 (1982) 369-373.

[2]. F. Haaf, A. Sanner, F. Straub, Polymer J. 17 (1985) 143–152.

[3]. R. Sadeghi, M. T. Zafarani-Moattar, J. Chem. Thermodynamics 36 (2004) 665-670.

Determination of Protonation Constants of Guanosine in different Ionic Strength Using Spectroscopy

N.Azizi*,a, G.Geimachy[a], A.Shamel[a], F.Gharib[b], M.alipoor[a]

[a]Chemistry Department, Islamic Azad University, Ardabil Branch, Iran

E-mail: Azizin69@yahoo.com

[b] Chemistry Department, Shahid Beheshti University, Tehran, Evin, Iran

Keywords: Guanosine, ionic strengths, protonation constant, Daniel coefficients

Introduction

Guanosine is a purine nucleoside comprising guanine attached to a ribose (ribofuranose) ring via a β-N_9-glycosidic bond. The structure of guanosine bears similarities to that of the antiviral drug aciclovir, often used in herpes treatment.Guanosine is required for an RNA splicing reaction in mRNA, when a "self-splicing" intron removes itself from the mRNA message by cutting at both ends, re-ligating, and leaving just the exons on either side to be translated into protein.[1]

Moreover, a Daniel type equation was established for the dependence of formation constant on ionic strength. The main purpose of this work is investigating the effect of different ionic strengths, 0.1 to 1.0 mol dm^{-3} on the protonation constant of guanosine using spectrophotometry and potentiometry titration method.[2]

Methods

guanosine($C_{10}H_{13}N_5O_5$), were obtained from Merck as analytical reagent grade materials and used without further purification. Sodium chloride was from Merck and was dried under vacuum at room temperature for at least 72 hours before use. NaOH solution was prepared from a titrisol solution (Merck). HCl was from Merck and was used as supplied. In the current work, protonation constant of an Guanosine determined using spectrophotometry method in UV region of temperature 25+ 0.1°C in ionic power of 1 molar of NaCl (0.1, 0.3 , 0.5 , 0.7, 1.0). During the experiment, titration of pH range between 1 to 12, frequently measured and absorption rate in warelength of 280 to 340 recorded per 5 Nanometer.[3]

Results and Discussion

The method is principally based on A=f(pH) So, different reactions written, Considering experimental result and proper modeling of the species and then it is simulated using mathematica software. Required calculations performed on various models in Excell software and the best model obtained with minimization of errors. Finally, the model parameters calculated using kitting method Excell and the protonation constant of different values obtained in different warelength and ionic powers.[4]

1) $H_2L \leftrightarrow HL^- + H^+$ $\qquad K_1 = \frac{[HL^-][H^+]}{[H_2L]}$ $\qquad K_2 = \frac{[L^{-2}][H^+]}{[HL^-]}$

2) $HL^- \leftrightarrow L^{-2} + H^+$

However, we would $C_L = [L^{-2}] + [HL^-] + [H_2L]$ obtain the protonation constant, with calculating of Daniel coefficients in any favored ionic strength. where C and D are empirical coefficients whose values are considered. C(I- I*) and D($I^{1.5}$– $I^{*1.5}$)

$$Log\ K(I) = Log\ (I^*) - Z^*\left(\frac{\sqrt{I}}{2+3\sqrt{I}} - \frac{\sqrt{I^*}}{2+3\sqrt{I^*}}\right) + C(I - I^*) + D(I^{1.5} - I^{*1.5}) \quad \text{Eq. (1)}$$

The parameters C and D were determined by a regression method with a suitable computer program and reported in Table 1.

Table 1. Parameters for the dependence on ionic strength of the species stability constants at 25 °C

species	C	D
$[H_2L]$	0.35	0.26
$[L]^{2-}$	-0.3	0.92

Results of a series of investigations done by Daniele et al. showed that, when all the interactions occurring in the solution are considered, in the range 0≤I≤1 mol dm^{-3}, the empirical parameters are dependent on the stoichiometry of the formation reaction. It is noticeable that the introduction of the term D($I^{1.5}$– $I^{*1.5}$) very often improves the goodness of the fit.

Conclusions

At low ionic strength (less than about 0.1 mol dm^{-3}) these interactions are of primary importance. However, as the ionic strength increases, the ionic atmosphere becomes more compressed and screens the ionic charges more effectively, so that intermolecular interactions

(dipole–dipole or multipole– multipole) become more important. These forces at higher ionic strength possibly play a primary role between the ions and contribute to the C and D terms in Eq. (1).

References

[1] R.C. Tewari, M.N. Srivastava, Talanta (1973) 20.
[2] B.S. Sekhon, P.P. Singh, S. Chopra, Ind. J. Chem. 9 (1971) 485.
[3] V.V. Ramanujam, K. Rangaraj, Ind. J. Chem. 19 (1980) 382.
[4] A. Raghavan, M. Santappa, J. Inorg. Nucl. Chem. 35 (1973) 3363.

Investigating the Effect of Temperature on Protonation Constant of Guanosine

N.Azizi*,a, G.Geimachy[a], A.Shamel[a], F.Gharib[b], R.poorabass[a]

[a]Chemistry Department, Islamic Azad University, Ardabil Branch, Iran

E-mail: Azizin69@yahoo.com

[b]Chemistry Department, Shahid Beheshti University, Tehran, Evin, Iran

Keywords: Guanosine, protonation constants, temperature, spectrophotometry,

Introduction

Guanosine is a purine nucleoside comprising guanine attached to a ribose (ribofuranose) ring via a β-N_9-glycosidic bond. The structure of guanosine bears similarities to that of the antiviral drug aciclovir, often used in herpes treatment.Guanosine is required for an RNA splicing reaction in mRNA, when a "self-splicing" intron removes itself from the mRNA message by cutting at both ends, re-ligating, and leaving just the exons on either side to be translated into protein.[1-2]

The protonation constants are important for environmental scientists, chemical engineers, chemists, and specialists in related fields as these alter the reactivity, spectral properties, physical behavior, and solubility.[3] The main purpose of this paper is investigating the effect of temperature on the protonation constant of guanosine using spectrophotometry and potentiometry titration method.

Methods

guanosine($C_{10}H_{13}N_5O_5$), were obtained from Merck as analytical reagent grade materials and used without further purification. Sodium chloride was from Merck and was dried under vacuum at room temperature for at least 72 hours before use. NaOH solution was prepared from a titrisol solution (Merck). HCl was from Merck and was used as supplied.

The ionic strength was maintained to 0.1 mol dm^{-3} with sodium chloride. The pH-meter was calibrated for the relevant H^+ concentration with a solution of 0.01 mol dm^{-3} chloridric acid solution containing 0.09 mol dm^{-3} sodium chloride (for adjusting the ionic strength to 0.1 mol

dm^{-3}). For this standard solution, we set $-\log[H^+] = 2.0$. Junction potential corrections have been calculated from eq 1

$$-\log[H^+]_{real} = -\log[H^+]_{measured} + a + b[H^+]_{measured} \quad (1)$$

where a and b were determined by measuring of hydrogen ion concentration for two different solutions of HCl or NaOH with sufficient NaCl to adjust the ionic media.[4]

The protonation constants of uracil have been determined spectrophotometrically based on the relation A = f(pH). The measured absorbance, A, (270- 300 nm in the interval of 0.5 nm) and $-\log[H^+]$ from the spectrophotometric titration were conducted with the computer program. The program allows calculation of the protonation constants with different stoichiometry. The number of experimental points (absorbances versus $-\log[H^+]$) was more than 40 (maximum 50) for each titration run. During the experiments, the solutions were stable and the absorbance values did not change with time.

$$1)\ H_2L \leftrightarrow HL^- + H^+ \qquad K_1 = \frac{[HL^-][H^+]}{[H_2L]} \qquad K_2 = \frac{[L^{-2}][H^+]}{[HL^-]}$$
$$2)\ HL^- \leftrightarrow L^{-2} + H^+$$

$$C_L = [L^{-2}] + [HL^-] + [H_2L]$$

K_1 ,K_2 is equilibrium constants and C_L is total concentration of guanosine.

$$A = \varepsilon Cb \qquad b = 1$$
$$A_{cal} = \varepsilon_{H_2L}[H_2L] + \varepsilon_{HL}[HL^-] + \varepsilon_L[L^{2-}]$$

K_H is protonation constant and K_d is dissociation constant and is reverse of K_H. The protonation constants of guanosine were calculated at 20, 25, 30, 35 and 40°C using potentiometry titration method. Amounts of calculated log K_1 and log K_2 are listed in Table 1.

TABLE 1: Amounts of calculated log K in different temperatures

Temperature/°C	20	25	30	35	40
log K_1	2.43	2.34	2.25	2.2	2.15
log K_2	9.3	9.25	9.17	9.09	8.84

Conformation of theoretical and experimental curves is a main criterion for the positive amounts of protonation constants and also the proper amounts of molar absorption coefficients.

Conclusion

According to guanosine usages in medicine and pharmacology, the effect of temperature changes on the protonation constant of guanosine has been investigated in this research. Results indicate that when temperature increases the log K_1 and log K_2 decreases gradually and pK_1 and pK_2 increases. With temperature increase intense of protonation increases.

References:

[1].ALWORTH, W.L: Stereo chemistry and Its Application Biochemistry, Wiley- Inter Sclence, New York 1972.

[2]. F. Gharib, F. Jaberi, M. Zandvakili, Appl. Organometal Chem., 22, 215, 2006.

[3]. F. Gharib, E. Farzad, M. M. Amini, Can. J. Chem., 84, 1534, 2006.

[4]. Harper,H.,Rod well,V.W ,Mays,A. 16th ed.Lenge Medical Publication, 1977/A Review of physiological chemistry.

Modeling of the surface tension of liquid metals with density gradient theory

E. Faramarzi[a], M. H. Mousazadeh[*,b]

[a]Department of Physical Chemistry, School of Chemistry, University of Tehran, Tehran, Iran

faramarzi_ehsan@yahoo.com

[b]Department of Chemistry, Nuclear Science Research School, Nuclear Science & Technology Research Institute (NSTRI), 11365-3486, Tehran, Iran

Keywords: Density Gradient Theory, Metals, Equation of State, Surface Tension

Introduction

The interest of researchers to metals melts is significant in connection with their use as coolants in nuclear reactors. The surface tension has an important effect on the heat and mass transfer from interfaces. The main purpose of this work is to develop an approach that can accurately describe both the phase equilibrium and surface tensions for metals (Li, Na, K, Rb, Cs, Mg, Ca, Sr, Ba, Fe, Zn, Cd, In, Sn, Pb, Bi). To this end, the PC-SAFT [1] and density gradient theory (DGT) are used.

Method

The DGT was combined with PC-SAFT equation of state (EOS), in order to describe both the phase behaviors and the surface tension of different types of metals. In the DGT, the interface is a region in which the density changes from that of the high-density phase to that of the low density phase. Based on The Cahn–Hilliard theory the relationship between the energy in the interface and surface tension can be driven [2]

$$\gamma = 2\int_{\rho_V}^{\rho_L} \sqrt{\Delta f\left[\rho(z)\right]\kappa}\, d\rho(z) \qquad (1)$$

$$\Delta f\left[\rho(z)\right] = f_0\left[\rho(z)\right] - \rho(z)\,\mu + p \qquad (2)$$

Where γ *is surface tension,* $\rho(z)$ is the local number density of molecules at position Z, κ is the influence parameter and $f_0[\rho(z)]$ is the free energy density, μ and p are the chemical potential and pressure for bulk phases, respectively. The only two inputs of the theory are the

Helmholtz free-energy density and the influence parameter. The PC-SAFT equation of state was applied to determine Helmholtz free-energy density and bulk properties. The influence parameter is obtained by fitting to the experimental data of surface tension.

Results and discusion

The PC-SAFT equation of state is applied to metals in a wide range of pressure and temperature. The parameters of PC-SAFT were identified by correlating saturated liquid density. Fig. 1 presents the surface tensions for 8 metals calculated by DGT. From these figure, one can find that, by regressing the influence parameter with experimental data, PC-SAFT and DGT give satisfactory results for surface tensions.

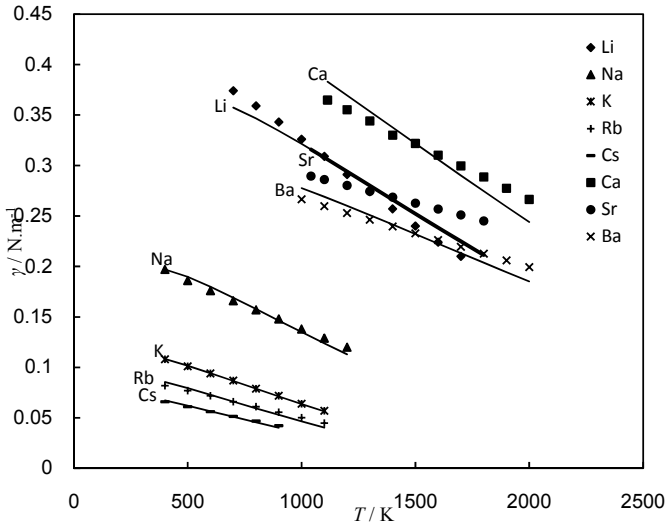

Fig. 4. Comparison between calculated (line) and experimental[3] results for surface tension metals.

References

[1] J. Gross, G. Sadowski, Ind. Eng. Chem. Res. 40 (2001) 1244-1260.

[2] J.W. Cahn, J.E. Hilliard, J. Chem. Phys. 28 (1958) 258-266.

[3] N.B. Vargaftik , Y.K. Vinogradov, V.S. Yargin, Handbook of Physical Properties of Liquids and Gases: Pure Substances and Mixtures, third ed., Begell House, New York, 1996.

Surface tension correlation for ionic liquids

E. Faramarzi[a], M. H. Mousazadeh[*,b]

[a]Department of Physical Chemistry, School of Chemistry, University of Tehran, Tehran, Iran

faramarzi_ehsan@yahoo.com

[b]Department of Chemistry, Nuclear Science Research School, Nuclear Science & Technology Research Institute (NSTRI), 11365-3486, Tehran, Iran

Keywords: Correlation, Corresponding states, Ionic liquids, Surface tension

Introduction

Ionic liquids (ILs) have received increasing attention due to their promising practice applications in chemistry and engineering [1]. They have a wide variety of unique thermophysical properties which include negligible vapor pressure, good thermal and chemical stability, high ionic conductivity, wide liquid region and so on. Liquid surface tension is also important in design of industrial applications. In this work, we propose simple regularities for surface tension of ILs, which has been applied for alkali metals, and alkali halids [2].

Method

The surface tension of ionic liquids is studied according to phenomenological scaling and the law of corresponding states. The reduced coordinates σ^*-T^*, where σ^* represents the reduced surface tension and T^* is the reduced temperature, are introduced for the prediction of the values of the surface tension from the melting point up to boiling point. It has been shown that the correlation can be expressed as a unique straight-line plot that requires only the melting and boiling point parameters, and can predict the surface tension accurately.

Results and discusion

It has been shown that the relationship between reduced surface tension, as well as with the reduced temperature, can be expressed as a unique straight-line plot with a linear correlation coefficient of 0.984. In this work we employ kT_b as the characteristic energy and no molecular parameters are involved. The proposed correlation has a simple form for easy

calculation, requiring only the melting and boiling point parameters, which are usually easy to acquire, and can predict the surface tension accurately. For a database of 385 data points for 30 ILs, the mean percent deviation observed was only **2.98**%.

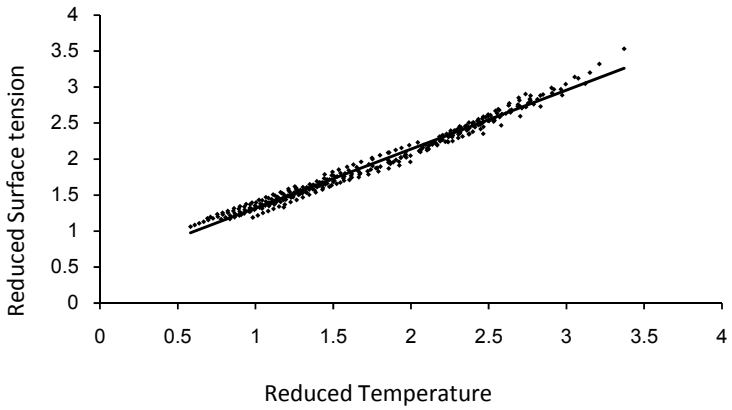

Fig 1. Correlation results of reduced surface tension, γ^*, *vs.* reduced temperature, T^*, for ionic liquids.

We illustrate the procedure by specific examples, that not to be used in correlation and results show the agreement with experimental data. A comparison between the predicted surface tension values and the QSPR correlation [3] for the some ionic liquids is reported. It is apparent that our correlation results are in good overall agreement with the experimental data over the entire temperature range.

Conclusions

The surface tension of 30 ionic liquids is studied according to law of corresponding states. It has been shown that the correlation can be expressed as a unique straight-line plot. The correlation uses more readily available input data than that of the critical point data or potential parameters. As far as our results show, the present correlation could be applicable to other ionic liquids.

References

[1] Chu X, Hu Y, Li J, Liang Q, Liu Y, Zhang X, Peng X, Yue W (2008) Chin J Chem Eng 16:881-884

[2] Ghatee MH, Mousazadeh MH, Boushehri A (1997) High Temp-High Press 29:717-722
[3] Gardas RL, Coutinho JAP (2008) Fluid Phase Equilibria 265:57–65

Complexation of dimethyltin(IV) dichloride with tyrosine

P. Farzaneh * [a], Kh. Shamsazar [a], A. Shamel [a] and F. Gharib[b]

[a] Department of Chemistry, Islamic Azad University, Ardabil, Iran

(E-mail: parissafarzaneh@yahoo.com)

[b] Department of Chemistry, Shahid Beheshti University, G. C., Evin, Tehran, Iran

Keywords: Dimethyltin(IV) dichloride, tyrosine, Spectroscopy, Stability constant,

Introduction

Organotin(IV) compounds have been shown to have high antitumour activity in vitro in a wide variety of human tumors. The increasing interest in the chemistry and biochemistry of organotin complexes has led to extend studies on their interactions with different naturally occurring ligands e.g. carbohydrates, nucleic acid derivatives, amino acids and peptides [1]. Therefore understanding of the interaction of organotin compounds with possible biological targets is highly desirable. In spite of these effects, the mechanism of action of these drugs in the living cell is not well understood. The activity of these compounds led to the hypothesis that these drugs hydrolyze easily in aqueous media and transport the active part (R_2Sn) inside the cells where it possibly reacts with DNA. The present work deals with the study of dimethyltin(IV) dichloride complexes by tyrosine. ^{1}H NMR investigation in aqueous solution confirmed the species formation.

Experimental

All measurements were carried out at 25 °C. Spectrophotometric measurements were performed on a UV-Vis Shimadzu 2100 spectrophotometer. ^{1}H NMR spectra of the ligand and the complexes were recorded on a Bruker DRX-300 MHz spectrometer in H_2O-D_2O (1:1 by volume) using TMS as an external reference. The solutions were prepared by mixing Me_2Sn(IV) with tyrosine in H_2O-D_2O solution to give a 1:1 mole ratio. The concentrations of the NMR samples were 1 mM.

Determination of the stability constant based on the relation A = f(pH) was performed using the computer program Squad. Absorbance, A, and pH were measured for a solution

containing dimethyltin(IV) and tyrosine. Treatments of the spectrophotometric data obtained during the titrations as a function of the [H^+], were conducted with the computer program. The program allows calculation of the stability constants for different stoichiometry models.

Results and Discussion

Using a combination of spectrophotometric and potentiometric methods different models including ML and MHL and several polynuclear and protonated species were tested by the computer program. As expected, polynuclear complexes were systematically rejected by the program (the charges are omitted for simplicity). The models finally chosen, formed by MHL and ML for the ligand, besides the hydrolysis products of $Me_2Sn(IV)^{2+}$ resulted in a satisfactory of numerical and graphical fitting.

^1H NMR of methyl signals both for tyrosine and the formed complex were recorded at different pH values. It was observed that the $^2J(Sn\text{-}^1H)$ values increase with decreasing the pH in NMR titration, which indicate a complex species besides the metal ion exists in solution [2]. Another reaction is occurred due to deprotonation of coordinated H_2O molecule and results the formation of a mixed hydroxo complexes. Evaluation of the titration curves, shows that the hydrolyzed species, are M(OH) and $M(OH)_2$. $^2J(Sn\text{-}^1H)$ values provide useful information on the C-Sn-C bond angle of the compounds in a sample and indirectly on the possible coordination numbers and geometry around the Sn atom. Two bond coupling, $^2J(Sn\text{-}^1H)$, of the $Me_2Sn(IV)^{2+}$ alone and its complex species with tyrosine were determined via the ^1H NMR spectra at different pH. It was observed the signal of the methyl protons in $Me_2Sn(IV)^{2+}$ are sharp and has almost the same chemical shift as in the solution of $Me_2Sn(IV)^{2+}$ alone. Using the quadratic equation of Lockhart, the average C-Sn-C bond angle at low pH and higher pH values for the species calculated from the coupling constants, are 175° and 135°, respectively. On this basis the structures of $Me_2Sn(IV)^{2+}$ and its complexes with tyrosine are proposed as an octahedral at low pH and distorted trigonal bipyramidal arrangement at higher pH.

References

[1] F. Gharib, F. Jaberi, Zandevakili, Appl. Organomet. Chem. 22 (2008) 751.

[2] F. Gharib, E. Farzad, M. M. Amini, Can. J. Chem. 849 (2006) 1534.

On the meaning of entropy

Shayan Forouzandehdel[1] and Afshin Shafiee[2]
Research Group On Foundations of Physics And Information,
Department of Chemistry, Sharif University of Technology,
P.O.Box, 11365-9516, Tehran, Iran

Abstract

After mentioning the origin of the most common metaphor for entropy ("disorder" metaphor) in the late 1800s by Boltzmann and listing some errors and confusing in its use in texts, we urge the abandonment of order-disorder in introducing entropy. Then, we discuss about the validity of the descriptor spreading, which involves the notions of space, time, and energy in a fundamental way.

Introduction

As is well-known, in 1865 Clausius gave the name entropy to a unique quotient for the process of a reversible change in thermal energy divided by the absolute temperature (dq_{rev}/T) [1]. Helmholtz in 1882 called entropy "Unordnung" (disorder) [2], and Gibbs wrote "entropy as mixed-up-ness" [3] and subsequently used by many authors. In the nineteenth century the greater "disorder" was chosen by Boltzmann to describe its higher entropy. Then the movement of macroscopic objects was also added to this idea. That is, a chemist may discuss entropy in his textbook with "things move spontaneously [toward] chaos or disorder". Or, may express, "Desktops illustrate the principle of a spontaneous tendency toward disorder in the universe…"

The most egregious errors in the past century of associating entropy with disorder have occurred simply and over the years, popular authors have learned that scientists talked about entropy in terms of disorder, and thereby entropy has become a code word for the "scientific" interpretation of everything disorderly from drunken parties to dysfunctional personal relationships, and even the decline of society.

[1] .forouzandehdel@mehr.sharif.ir
[2] . shafiee@sharif.edu

Claude E. Shannon's 1948 paper began the era of quantification of information and in it he adopted the word "entropy" to name the quantity that his equation defined [4]. This occurred because a friend, the brilliant mathematician John von Neumann, told him "call it entropy no one knows what entropy really is, so in a debate you will always have the advantage"[5].

So, they increase the complications of entropy definitions, some of these misunderstandings and definitions are listed below: Entropy of: 'Boltzmann' or 'Statistical', 'Boltzmann-Gibbs', 'Configurational' or 'positional', 'multiplicity' or 'optiony', 'Shannon' or 'information', ' Teachman-Shannon', 'Shannon-Weaver', 'Boltzmann-Shannon', 'Gibbs-Shannon', 'Boltzmann-Gibbs-Shannon (BGS)', 'Hartley', 'missing information', 'Fuzzy', 'human', 'freedom', 'unavailability of energy', 'flow' or 'Prigogine', 'production', 'low', 'material', 'mental', 'psychic', 'reduction', 'islands', 'Political', 'social', 'mixing', 'External', 'Psychological', 'Teleonomic', 'consumption', etc. (for example see [6-9].) These contain a broad range including physics, mathematics, chemistry, psychology, politics, economics, art, architect, etc. that these are only small parts of confusing aspects of entropy. All these definitions and names (which are sometimes the same conceptually) are for just a word like entropy which has been introduced by Clausius for dq_{rev}/T.

Discussion

Do all of these definitions characterize entropy? Here we discuss about one of the most common interpretations of entropy, i.e., the notion of disorder. Defining entropy increase as a change from order to disorder is misleading at best and incorrect at worst. Although Boltzmann described it this way in 1898, he did so innocently in the sense that he had never calculated the numerical values of W in $\Delta S = k_B \ln (W/W_0)$ (because the equation as well as k_B were not known, and W_0 was indeterminable before 1900–1912). In fact, $k_B = R/N_A$ was first stated and calculated by Planck in 1900 [10].

In addition, Boltzmann could not have had a valid quantitative way to evaluate his "complexions" (equivalent to modern microstates) because the distribution of energy among discrete levels via quantum mechanics was not developed until long after his death. Finally, Boltzmann's “probabilities” (W) had no reference value, no W_0, prior to the third law, whose basis ($W_0 = 1$) was established between 1906 and 1912. Therefore, Boltzmann's error in

stating “entropy is disorder” was innocent. Pitzer’s calculation of a mole of any substance at near 0 K shows that *none* can be more ordered than having the possibility of $10^{26,000,000,000,000,000,000}$ different accessible microstates! [11] If liquid water at 273 K with its $10^{1,991,000,000,000,000,000,000,000}$ accessible microstates (quantized molecular arrangements) is considered "disorderly", how can ice at 273 K that has $10^{1,299,000,000,000,000,000,000,000}$ accessible microstates be considered "orderly"?

On the other side, there is no general definition of disorder in the context of thermodynamics. Burgers observed that disorder “leads to anthropomorphic forms of reasoning which are often misleading.” [12]. Many people usually think that they can recognize disorder whenever they see it. Styer found that their confidence was misplaced when he tested their evaluation of "lattice gas models", patterns used in a wide variety of studies of physical phenomena [13]. His results showed that five diagrams that were checked were invalid; they had probably been selected to appear disorderly but were statistically not truly random.

Lambert critically assessed usage of the disorder metaphor in chemistry text books, and has successfully convinced the authors of 25 textbooks to remove statements relating entropy with disorder from new editions of their books [14]. Some other physicists support his statements in extended discussions with various examples.

Setting aside the “disorder” interpretation, one may state that entropy can measure the spontaneous dispersal of energy: how much energy is spread out in a process, or how widely spread out it becomes at a specific temperature. The metaphor of spreading is based explicitly upon space, time, and energy [15]. Space is intimately involved because energy tends to spread spatially as much as possible. This includes spreading of energy spatially during processes and temporal spreading over accessible microstates states in thermodynamic equilibrium. The spreading metaphor is powerful and offers a physically motivated, transparent alternative to the metaphors mentioned above. So, one may conclude that it is appropriate to view entropy’s symbol S as shorthand for spreading.

Conclusions

Although, scientifically, it seems that spreading is more appropriate than disorder, it is not free of deficiencies. The main problem is that exclusively its emphasis is on the energy aspect which arises some difficulties until the systems remains isolated. In this case the total energy

changes become zero. Therefore, there is neither heat transfer for changing the distribution of molecules nor work exchange. So no changes occur in energy states (i.e., "free expansion"). In some cases like the "crystallization of supercooled solution" and even "the crystallization of supersaturated solution(i.e., supersaturated solution of sodium sulfate)" not only does the energy spreading but also it concentrates A naive approach to justify the increase of spreading amount of energy in free expansion is the quantum particle in a box model. At room temperature since particles only occupy the ground rotational and vibrational states, only transitional states can be changed and these energy states influence the quantification of the microstates. In the cases of "free expansion" or "doubling the amount of a gas or liquid" or generally in other cases of volume increasing, certainly, the time of consequent collisions and main free path are increased due to volume increase. Consequently, the number of collisions in specified intervals will be decreased. In effect, the velocity distribution is changed and therefore the rate of occupied microstates is deduced.

References

[1] Clausius, R. (Poggendorff's) Ann. der Phys. und Chem. 1865, 125 (2), 353-399.

[2] Helmholtz, H. Wissenschaftliche Abhandlungen, Vol. 2; Johann Barth: Leipzig, 1883; p. 972.

[3] Gibbs, J. W. Collected Works, Vol. 1; Yale University Press: New Haven, CT, 1928; p. 418.

[4] Shannon, C. E. Bell System Tech. J. 1948, 27, 329-423, 623-656.

[5] Tribus, M., McIrvine, E. C. Sci. Am. 1971, 225, 180.

[6] Kurzynski, Michal. (2006). The Thermodynamic Machinery of Life (pg. 40). New York: Springer

[7] Baierlein, R.: Teaching the approach to thermodynamic equilibrium: some pictures that help. Am. J. Phys. 46, 1042–1045 (1978)

[8] Swanson, R.M.: Entropy measures amount of choice. J. Chem. Ed. 67, 206–208 (1990)

[9] Lindsay, Robert B. (1963). The Role of Science in Civilization, (section: "Information Theory andThermodynamics: Entropy", pgs. 153-65; section: "A Scientific Analogy: The Thermodynamic Imperative", pgs. 290-98). Westport: Greenwood Press. Dowden, Hutchinson & Ross.

[10] Laidler, K. J. The World of Physical Chemistry; Oxford University Press: Oxford, 1995; pp 318–319.
[11] Pitzer, Thermodynamics, 3rd edition, 1995, p. 67.
[12] Burgers, J.M.: Entropy and disorder. Br. J. Philos. Sci. 5, 70–71 (1954)
[13] Styer, D. F. Am. J. Phys. 2000, 68, 1090-1096.
[14] News for April 2004. http://www.entropysite.com/#news (accessed Jan 2005).
[15] Leff, H. S. Found Phys (2007) 37: 1744–1766.

VLE Calculations for Binary Mixtures Containing Surfactants Using the SAFT-VR equation of state

Elahe Maghami , Bahman Behzadi* , Farzaneh Feyzi
Thermodynamic Research Laboratory, School of Chemical Engineering , Iran University of Science and Technology, Narmak, Tehran 16846-13114, Iran
Behzadi@iust.ac.ir

Keywords: vapor–liquid equilibria, SAFT VR equation of state,Water, Alkane, Surfactant

Introduction:

Accurate models that can be reliably used for phase equilibrium calculations for systems containing surfactants are relatively scarce; a few investigations have used SAFT type equations of state (EOS's) for such mixtures. The CPA EOS has also been applied to phase equilibria for mixtures of glycolethers by Garrido et al. [1], and they have shown that this EOS can correlate experimental results for these systems accurately. Garcia Lisbona et al. [2] used the SAFT HS EOS for modeling three aqueous solutions of polyoxyethylene mixtures. Despite these preliminary results, the use of a more sophisticated version of the SAFT EOS is expected to improve the agreement with experiment of data. In this work the SAFT-VR equation of state has been applied for glycol-water, glycol-alkane and glycol-alcohol systems. The effect of different assumptions regarding model parameters and the number of associating sites has also been investigated.

Theory:

In the SAFT-VR approach [3], for a system of N molecules at temperature T, the Helmholtz free energy (A) is expressed as: $\frac{A}{NKT} = \frac{A^{ig}}{NKT} + \frac{A^{mono}}{NKT} + \frac{A^{chain}}{NKT} + \frac{A^{assoc}}{NKT}$ (1)

The superscripts refer to contributions accounting for an ideal gas (*ig*), dispersion interactions between the monomeric segments of the molecules (*mono*), formation of molecular chains from the segments (*chain*), and possible molecular association (hydrogen-bonding, etc.) (*assoc*) . Each associating molecule features a number of associating sites to mediate hydrogen bonding. The general equations that are used for the chain and association terms are common among most SAFT models, and the only differences are the correlations used for an exact representation of the radial distribution function (rdf) at contact distance, and dispersion energy terms corresponding to the studied fluid. In this work the square-well fluid model is

used for the dispersion term as developed in the original SAFT-VR model [3]. All necessary thermodynamic properties are derived from eq. (1) using standard relations.

Results and Discussion:

Vapor-liquid equilibrium for binary systems containing a surfactant has been studied in this work. Initially, pure component parameters have been obtained using available experimental data for vapor pressure decrease and/or phase composition. The parameters obtained for the pure components are used for the mixed systems, by applying binary interaction coefficients. The results are summarized in Table1. In binary systems composed of water with 1, 2-ethandiol, methanol with C1E1 and C2E1 and iC3E1, both components can form associating bonds, whereas in the other systems only one component is associating. Experimental data for a range of temperatures have been used to fit the dispersion and association energy binary interaction coefficients (k_{ij} and k_{ij}^{HB}, respectively). Elliott combining rules and a van der Waals 1-fluid mixing rule has been applied. A comparison of results with different number of sites in the associating component shows that for these systems two sites produce the best results.

Table 1: Optimized binary interaction parameters of the SAFT VR model for binary surfactant mixtures

Binary System	k_{ij}	K_{ij}^{HB}	%ΔP	Δy
methanol+2methoxyethanol	0	0	2.73	0.020
methanol+2ethoxyethanol	-0.078	-0.151	1.40	0.030
water+1,2ethandiol	0	-0.183	2.72	0.015
water+2methoxyethanol	-0.0584	-0.1662	8.34	0.055
water+2ethoxyethanol	-.0150	0.1930	11.2	0.075
water+ C4E0	-.0343	-0.0039	3.97	0.030
water+C4E1	-0.1143	0.0311	2.72	0.015
hexan+2ethoxyethanol	-0.250	0	12.6	0.049
cyclohexan+2ethoxyethanol	-0.250	0	12.6	0.049
heptane+2isopropoxyethanol	-0.075	0	5.90	0.033
hexan+ 2isopropoxyethanol	0.0812	0	6.80	0.011
Octane+C4E1	-0.300	0	6.49	0.020

Conclusion:

The SAFT-VR equation of state has been extended in this work to binary surfactant- water and surfactant-alkane systems. It has been successfully applied to model VLE in surfactant mixtures, including azeotropic binary systems, and an assessment of different assumptions regarding the molecular model has also been presented.

References

[1] Nuno M. Garrido, Georgios K. Folas, Georgios M. Kontogeorgis Fluid Phase Equilibria 273 (2008) 11–20

[2] M. Nieves Garcia-Lisbona,Amparo Galindo,George Jackson,, and Andrew N. Burgess , J. Am. Chem. Soc. 1998, 120, 4191-4199

[3] Alejandro Gil-Villegas, Amparo Galindo, Paul J. Whitehead, Stuart J. Mills, and George Jackson , J. Chem. Phys. 106 (10), 8 March 1997

Evaluation of thermodynamic properties of long chain organic compounds using GMA equation of state

A. Morsali*[a], M. M. Heravi[a], Z. Alavi[a] and M. Ghorbani[a]

[a] Faculty of Science, Department of Chemistry, Islamic Azad University–Mashhad Branch, Iran

* (Email: morsali@mshdiau.ac.ir)

Keywords: GMA Equation of state, Alkanes, Alcohols, Ketones, 1-carboxylic acids

Introduction

Concerning the scientific and industrial importance of long chain organic compounds, endeavors have been made in this research to use a simple and accurate equation of state for prediction of thermodynamic properties of these compounds. Using GMA equation of state, different groups of long chain organic compounds, including alkanes, alcohols, ketones and 1-carboxylic acids have been studied.

Theory

The GMA equation of state [1-3] is based on the average potential energy and is given as:

$$(2Z-1)V_m^3 = A(T) + B(T)\rho \quad (1)$$

where Z, V_m, and ρ are compressibility factor, molar volume, and molar density, respectively. The intercept and slope of this equation depend on temperature via the equations:

$$A(T) = A_0 - 2A_1/RT + 2A_2 \ln T/R \quad (2) \quad , B(T) = B_0 - 2B_1/RT + 2B_2 \ln T/R \quad (3)$$

where A_0–A_2 and B_0–B_2 are constants.

Results and discussion

We have used the experimental PVT data for C6H12 to C28H58, 1-Propanol, 2-Propanol, 1-Butanol, 2-Butanol, 1-Pentanol, 2-Pentanol, 3-Pentanol, 1-Hexanol, 1-Octanol, 1-Decanol, 1-Hexadecanol, 1,2-Butandiol, 2-Propanone, 2-Butanone, 3-Pentanone, 2-Hexanone, 1-Butanoic Acid, 1-Pentanoic Acid, 1-Hexanoic Acid, 1-Heptanoic Acid, 1-Octanoic Acid, 1-Decanoic Acid, 1-Dodecanoic Acid, 1-Tetradecanoic Acid and 1-Hexadecanoic Acid to plot $(2Z-1)V_m^3$ against ρ for each isotherm. As the table 1 shows the linearity holds very well for

all isotherms (some results). A more sensible test for the GMA equation of state is to calculate the differential thermodynamic properties, such as internal pressure (P_i), isothermal compressibility (κ) and thermal expansion coefficient (α) at different temperatures and pressures (Table 2 - 4).

Conclusion

It has been concluded and ascertained that GMA Eos is capable of predicting the density of these compounds with a high degree of accuracy. A more sensitive test for any state equation is the prediction of differential thermodynamic properties. For such a test, GMA Eos predicted these properties with an acceptable degree of accuracy.

Table1: The minimum and maximum square of correlation coefficient (R^2) of Eq. (1)

fluid	*T(K)*	$P_{min} - P_{max}$ (atm)	$\rho_{min} - \rho_{max}$ $(mol \cdot L^{-1})$	R^2 for GMA
C28H58	353.15-403.15	0.9869-1475.9439	1.900-2.102	0.9994
1-Decanol	298.15-348.15	0.9869-396.7432	5.009-5.368	0.9999
2-Hexanone	288.15-338.16	25.1369-3755.835	7.732-9.615	0.9997
1-Hexadecanoic Acid	353.15-373.15	0.9869-88.8231	3.230-3.313	0.9996

Table2: The average of absolute percent deviations of the calculated isothermal compressibility

Fluid	$T_{min} - T_{max}$ (K)	$P_{min} - P_{max}$ (atm)	$\rho_{min} - \rho_{max}$ $(mol \cdot L^{-1})$	$(100 \times \lvert \kappa_{exp} - \kappa_{cal} \rvert / \kappa_{exp})$, Average (min – max)
C15H32	310.8-408	344.6-3445.5	3.4971-4.0120	2.96(0.0450-5.39)
2-Hexanone	288.15-338.16	25.1369-3755.835	7.7323-9.6155	2.97(0.0731-5.451)

Table 3: Absolute percent deviations of the calculated thermal expansion coefficient

fluid	*T(K)*	ρ (mol·L^{-1})	α_{exp} (K^{-1})	α_{cal} (K^{-1})	$\lvert(\alpha_{exp} - \alpha_{cal})/\alpha_{exp}\rvert \times 100$
C8H18	298.03	6.1289	0.001164	0.001163	0.154
	348.14	5.764	0.001303	0.00128	1.758
3-Pentanone	313.15	9.2609	0.00123	0.001177	4.325
	338.15	8.996	0.00127	0.001139	10.285

Table 4: Absolute percent deviations of the calculated pressure

fluid	*T(K)*	ρ (mol L^{-1})	$P_{i,exp}$ (atm)	$P_{i,cal}$ (atm)	$\lvert(P_{i,exp} - P_{i,cal})/P_{i,exp}\rvert \times 100$
C16H34	323.15	3.33196	2884.136	3010.349	4.37608
	373.15	3.1796	2565.63	2556.572	0.353046
2-Butanone	288.15	11.267	3394.618	3850.865	13.44028
	338.15	10.56	2982.402	3378.232	13.27216

References:

[1] Goharshadi EK, Morsali A, Abbaspour M. Fluid Phase Equilibr.,230 (2005)170–5.

[2] Goharshadi EK, Berenji AR. J. Nucl. Mater., 348 (2006) 40–4.

[3] Goharshadi EK, Moosavi M. Thermo,chim. Acta, 447(2006) 64–8.

Thermodynamic study of reaction of tautomerization of 1-methyl-1H-pyrrol-3-ol

Fatemeh Ghassamipoor*[a]

[a]Department of Chemistry, University of Kohgiluyeh & Boyerahmad, Gachsaran , Iran
Email:f.qassami@gmail.com

Keywords: Thermodynamic , Tautomer , Pyrrole , Ab initio

Introduction

Pyrroles are heterocycles of great importance because of their presence in numerous products such as antioxidants[1], antibacterial, antitumor, anti-inflammatory[2],and antifungal agents. Moreover, they are a highly versatile class of intermediates in the synthesis of natural products as well as in heterocyclic chemistry[3]. Many methods have been developed for their synthesis, which include Knorr, Paal-Knorr, and Hantzsch syntheses and 1,3-dipolar. cycloaddition reactions[4].

Methods

Theoretical methods have used to study all of the channels of this reaction. Ab initio calculations were carried out using the Gaussian 03 program. The geometries of all the stationary points were optimized at the MPWB1K [5], methods with 6-311++G** basis set.

Results and Discussion

In this study thermodynamics of the following reaction have investigated .

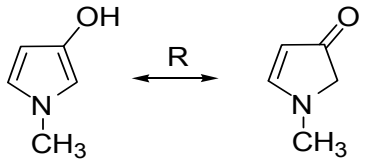

Molecule1 Molecule2

In this study we have reported one dimensional PES for some trajectories of the reactions of studied. (see diagram 1). As shown in this diagram, hydrogen atom is separated from oxigen atom of molecule 1, to produce molecule 2 via transition state.

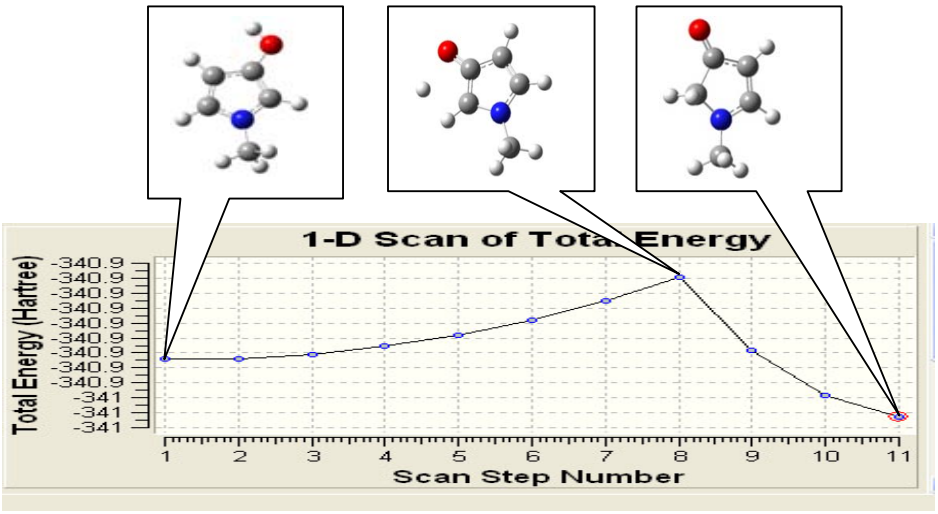

Diagram1.Potential energy surface for reaction of molecule 1 to produce molecule 2, with X=H

Harmonic vibrational frequencies were obtained at the MPWB1K/6-31++G(d,p) level in order to characterize stationary points as local minima or first-order saddle points and to obtain zero-point vibration energy corrections. The number of imaginary frequencies (0 or 1) indicates whether a minimum or a transition state has been located.Table 1.

Table 1. Harmonic Vibrational Frequency (cm^{-1}) for Various Species at MPWB1K/6-311++G(d,p) level.

Hf/6-311++G**	
Moleculen	Frequencies(cm^{-1})
Molecule1	3302.1,3314.9,3952.7,3143.1,3183.8,3275.6,1587.4,1673.3,1489.4,1495.1,1539.4,1418.4, 1452.8,1462.3,1174.3,1228.7,1306.1,1084.3,1108.2,1149.9,1084.3,1108.2,1149.9,811.9,1 011.9,1032.9,668.9,742.01,754.08,613.4,618.8,622.9,297.8,329.1,452.5,59.5,128.1,172.5
Molecule2	3167.6,3240.9,3305.9,3080.1,3122.4,3140.3,1640.3,1816.2,3036.6,1490.7,1495,1540.4,13 51.7,1453.5,1464.3,1208.1,1252.6,1343.2,1113.8,1146,1197.1, 966.5,982.2,1070.9,760,866.3,942.3,576.9,610.5,751,305,405.3,496.5,99.4, 147.2,208.1

Conclusion

Generalized free energy of activation for reaction have investigated to calculated equilibrium constant.rate constants, negative and positive of gibbes energy are important to comparison of stability of different reactions.

$\Delta G = G_2 - G_1$
$\Delta G = -RTLnK$
$LnK = -\Delta G/RT$
$K = e^{-\Delta G/RT}$

R is the gas constant(8.314 J/mol.k)
T is 298 K
K is equilibrium constant.

R	
ΔG(kj/mol)	23.77
K	6.813

References

[1] Lehuede, J.; Fauconneau, B.; Barrier, L.; Ourakow, M.; Piriou, A.; Vierfond, J. M. *Eur. J. Med. Chem.* **1999**,*34*, 991.

[2] Toja, E.; Selva, D.; Schiatti, P. *J. Med. Chem.* **1984**, *27*, 610

[3] Boger, D. L.; Boyce, C. W.; Labrili, M. A.; Sehon, C. A.; Lin, Q. *J. Am. Chem. Soc.* **1999**, *121*, 54.

[4] Berree, F.; Marchand, E.; Morel, G. *Tetrahedron Lett.* **1992**, *33*, 615 .

[5] Zhao, Y.; Truhlar, D. G. *J. Phys. Chem. A*. **2004**, *108*, 6908

Thermodynamic study of reaction of tautomerization 3-methyl-3,5-dihydro-imidazol-4-one

Narges Ghassamipoor*[a]

[a]Department of Chemistry, University of Kohgiluyeh & Boyerahmad, Gachsaran , Iran

Email:n.qassami@yahoo.com

Keywords : Thermodynamic ,Tautomerization ,Imidazol ,Gaussian

Introduction

Compounds with an imidazole ring system have many pharmacological properties and can play important roles in biochemical processes[1] .Several methods of imidazole synthesis can be found in the literature, including hetero-Cope rearrangement[2].four-component condensation of arylglyoxals; the combination of primary amines, carboxylic acids, and isocyanides on Wang resin[3] .

Methods

Theoretical methods have used to study all of the channels of this reaction. Ab initio calculations were carried out using the Gaussian 03 program. The geometries of all the stationary points were optimized at the MPWB1K [4], methods with 6-311++G** basis set.

Results and Discussion

In this study thermodynamics of the following reaction have investigated

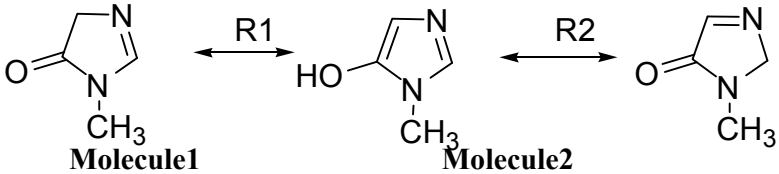

Molecule1 **Molecule2** **Molecule3**

In this study we have reported one dimensional PES for some trajectories of the reactions of studied. (see diagram 1). As shown in this diagram, hydrogen atom is separated from oxijen atom of molecule 1, to produce molecule 2 via transition state.

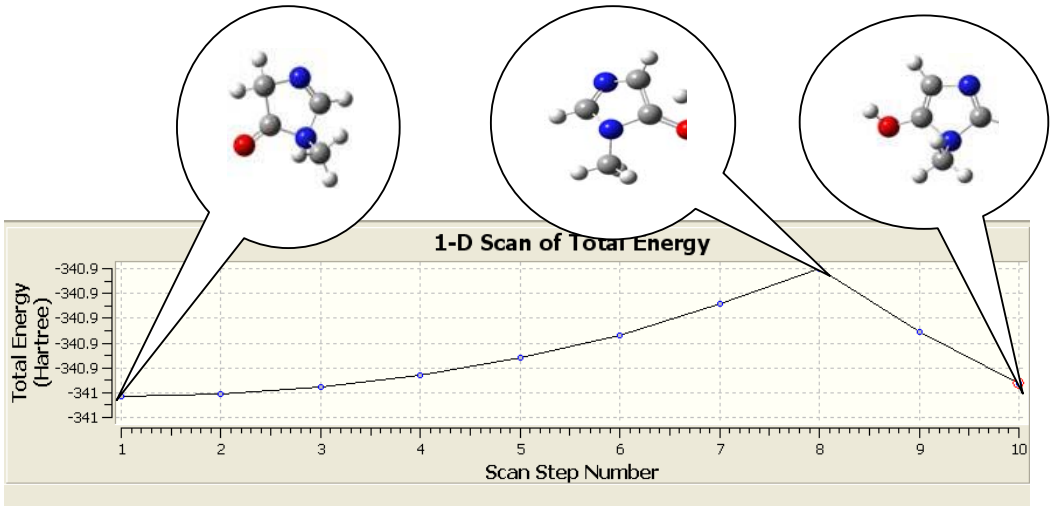

Diagram1.Potential energy surface for reaction of molecule 1 to produce molecule 2, with X=H

Harmonic vibrational frequencies were obtained at the MPWB1K/6-31++G(d,p) level in order to characterize stationary points as local minima or first-order saddle points and to obtain zero-point vibration energy corrections. The number of imaginary frequencies (0 or 1) indicates whether a minimum or a transition state has been located.Table 1.

Table 1. Harmonic Vibrational Frequency (cm^{-1}) for Various Species at MPWB1K/6-311++G(d,p) level.

Hf/6-311++G**	
Moleculen	**Frequencies(cm^{-1})**
Molecule1	3152.6, 3188.02, 3229.4, 3081.6, 3106.1, 3145.6, 1519.5, 1724.8, 1860.6, 1442.5, 1472.5, 1508.1, 1323.7, 1349.06, 1427.8, 1156.4, 1197.2, 1270.8, 1027.6 , 1058.9
Molecule2	3206.2, 3300.1, 3940.8, 1660.1, 3096.5, 3168.1, 1525.2, 1532.3, 1655.5, 1402.4, 1458.3, 1494.7, 1169.4, 1269.2, 1291.07, 1078.89, 1132.5, 1158.5, 736.1, 752.1, 879.1, 514.6, 662.6, 668.8, 261.3, 309.7, 474.4, 63.35, 88.63, 192.1
Molecule3	3130.7, 3180.30, 3239.06, 3064.02, 3069.3, 3098.23, 1536.51, 1720.6, 1844.90, 1469.57, 1496.19, 1503.15, 1328.51, 1338.96, 1448.96, 1166.96, 1222.37, 1288.28, 1047.0806, 1059. 2531, 1151.81, 888.92, 938.57, 1021.93, 683.32, 718.11, 738.63, 274.90, 403.96, 475.22, 124.26, 149.51, 207.65

Conclusions

Generalized free energy of activation for reactions have investigated to calculated equilibrium constant. rate constants, negative and positive of gibes energy are important to comparison of stability of different reactions.

$\Delta G = G_2 - G_1$
$\Delta G = -RT\ln K$
$\ln K = -\Delta G/RT$
$K = e^{-\Delta G/RT}$

R is the gas constant(8.314 J/mol.k)
T is 298 K
K is equilibrium constant.

R1	
ΔG(kj/mol)	-38.8
K	4.787

R2	
ΔG(kj/mol)	39.9
K	0.1997

References

[1] Lambardino, J. G.; Wiseman, E. H. *J. Med. Chem.* **1974**, *17*, 1182. 58890, 1982.

[2]) Lantos, I.; Zhang, W. Y.; Shiu, X.; Eggleston, D. S. *J. Org. Chem.* **1993**, *58*, 7092.

[3] Zhang, C.; Moran, E. J.; Woiwade, T. F.; Short, K. M.; Mjalli,A. M. M. *Tetrahedron Lett.*

1996, *37*, 751.

[4] Zhao, Y.; Truhlar, D. G. *J. Phys. Chem. A*. **2004**, *108*, 6908

Extraction of the butyric and propionic acid from aqueous solution by the iso-butyl acetate and cyclohexane at T=298.2K

Hossein Ghanadzadeh [a,b] *, Ali Ghanadzadeh [b] and Nastaran Dastmoozeh [b]

[a] *Department of Chemical Engineering , University of Guilan, Rasht , Iran*

(*Email: hggilani@guilan.ac.ir*)

[b] *Department of Chemistry, University of Guilan,41335 Rasht, Iran*

(Email: aggilani@guilan.ac.ir ; ndastmoozeh@yahoo.com)

Abstract

Liquid-phase equilibrium data of aqueous mixtures with organic solvents play an important role in the design and development of separation processes. In particular, liquid-liquid equilibria (LLE) investigations for ternary mixtures are important in the evaluation of industrial units for solvent extraction processes [1,2].

Experimental tie-line results and phase diagrams were obtained for the ternary systems of [water + butyric acid and propionic acid + isobutyl acetate and cyclohexane] at T=298.2K and atmospheric pressure. The experimental tie-line data were also compared with those correlated by the UNIQUAC and NRTL models. The consistency of the values of the experimental tie-lines was determined through the Bachman correlation equation. Distribution coefficients and separation factors were evaluated over the immiscibility regions and a comparison of the extracting capabilities of the solvents were made with respect to distribution coefficients and separation factors. The separation factor is defined as the ratio of distribution coefficients of the acid (2) to water (1), $S = D_2 / D_1$ .Where D_1 and D_2 are the distribution coefficients of water and the acid, respectively (Table1).Our purpose of this work is finding the best solvent for extraction of the butyric acid and propionic acid from aqueous solution. We determined the equilibrium values preparing the ternary mixtures of known compositions. For this process and measuring the LLE values was used a 250 cm^3 glass cell connected to a thermostat at T=298.2K. A water jacket was used to control the temperature of the cell to within ±0.1%. The prepared mixtures were placed in the extraction cell and were vigorously agitated by a magnetic stirrer for 4h.The mixtures were then settled for 4h at constant system temperature to separate completely into two liquid phases. After separation, samples of both phases were transparent and were carefully collected from each phase and

analyzed to determine their compositions. The concentrations of acids in both phases were determined by potentiometric NaOH titration in the presence of phenol phthale in as an indicator. The water content of the organic phase was measured by the Karl-Fisher method using Mettler Toledo DL 38 Karl–Fisher titrator.

Table1. Separation factors (S) and distribution coefficients of acids (D_2) and water (D_1).

D_2	D_1	S	D_2	D_1	S
water(1)+ propionic acid (2)+ isobutyl acetate (3)			*water(1)+butyric acid (2)+isobutyl acetate (3)*		
8.54	0.27	31.44	46.42	0.29	161.65
7.10	0.34	20.74	26.67	0.32	83.78
6.43	0.41	15.72	20.00	0.35	56.93
4.64	0.48	9.58	13.08	0.42	30.94
3.88	0.56	6.96	9.30	0.53	17.47
water(1)+ propionic acid (2)+ cyclohexane(3)			*water(1)+butyric acid (2)+ cyclohexane (3)*		
1.30	0.002	585.52	16.66	0.02	939.14
1.11	0.001	963.28	13.15	0.02	514.44
1.06	0.005	218.60	12.77	0.04	329.24
1.08	0.007	163.19	11.36	0.07	162.60
1.09	0.013	82.61	9.45	0.12	77.78

Tie-line data for these ternary systems were obtained at T=298.2K. Each ternary system exhibits Type-1 behaviour of the LLE. The experimental results indicate the superiority of the cyclohexane as the preferred solvent for the extraction of the two acids from its aqueous solutions. The immiscibility region was found to be large when the cyclohexane was used as an organic solvent for extraction of the two acid**s.** The cyclohexane for extraction of butyric acid is better than the propionic acid.

Keywords: LLE data; Ternary mixture; NRTL model; UNIQUAC model

References

[1]. H.Ghanadzadeh; A.Ghanadzadeh; R.Sariri. J.Chem.Thermodyn. 36 (2004) 1001–1006.

[2]. H.Ghanadzadeh; A.Ghanadzadeh; Kh.Bahrpaima; S.L.Seyed Saadat.J.Chem.Thermodyn. 40 (2008) 879–884.

Dynamic ^{1}H NMR Study of Carbon-Carbon Single Bond Rotational Energy Barriers in Highly Functionalized Thiohydantoins

M. M. Ghanbari*[a] and A. Shameli[b]

[a]Islamic Azad University, Sarvestan Branch, Department of Chemistry, Sarvestan, Iran (Email:@ m.mehdi.ghanbari@gmail.com)

[b]Islamic Azad University, Omidiyeh Branch, Department of Chemistry, Omidiyeh, Iran

Keywords: Restricted rotation; Intramolecular Wittig reaction; 2,5-dihydro-5,5-diaryl-2-thioxo-1H-imidazols.

introduction

Stable crystalline phosphorus ylides are obtained in excellent yields from the 1:1:1 addition reaction between 5,5-diarylthiohydantoins and dialkyl acetylenedicarboxylates in the presence of triphenylphosphine. These phosphoranes undergo smooth intramolecular Wittig reaction followed by an electrocyclic ring opening to produce dialkyl (E)-2-(2,5-dihydro-5,5-diaryl-2-thioxo-1H-imidazol-4-yl)fumarates in good yields. Dynamic effects were observed in the ^{1}H NMR spectra of these compounds and were attributed to restricted rotation around the Carbon-Carbon single bonds.

Results and Discussion

The ^{1}H and ^{13}C NMR spectra of compounds **4** show two different aryl groups, and the ^{1}H NMR spectra of compounds **4b** and **4d** exhibit characteristic $(AB)X_3$ patterns for the diastereotopic methylene protons (Scheme 1). The Ar-CH_3 region of the ^{1}H NMR spectrum of **4d** in $CDCl_3$ at ambient temperature (25°C) exhibits two sharp singlets for the Ar-CH_3 groups. The ^{1}H NMR of **4c** in 1,2-dichlorobenzene at 25°C is similar to that measured in $CDCl_3$. Increasing the temperature results in coalescence of the Ar-CH_3 resonances. At 90°C, a relatively broad singlet was observed for the Ar-CH3 groups. This dynamic NMR effect is attributed to restricted rotation around the single bond attaching the vinyl substituent to the 2-thioxo-1H-imidazole ring.

Although an extensive line shape analysis in relation to the dynamic NMR effect observed for **4c** was not undertaken in the present work, the variable temperature spectra are sufficient to calculate the free energy barrier as well as enthalpy and entropy of activation for

the restricted C–C bond rotation. From the coalescence of the methine protons and using the expression $k = \pi\Delta\nu/1.42$, the first-order rate constants (k) were calculated. Application of the absolute rate theory with a transmission coefficient of **4c** gives a free energy of activation ($\Delta G^{\neq}$) of 17x4.218 ± 2 kJ mol^{-1} for **4c**, where all known sources of errors are estimated and included [1-5].

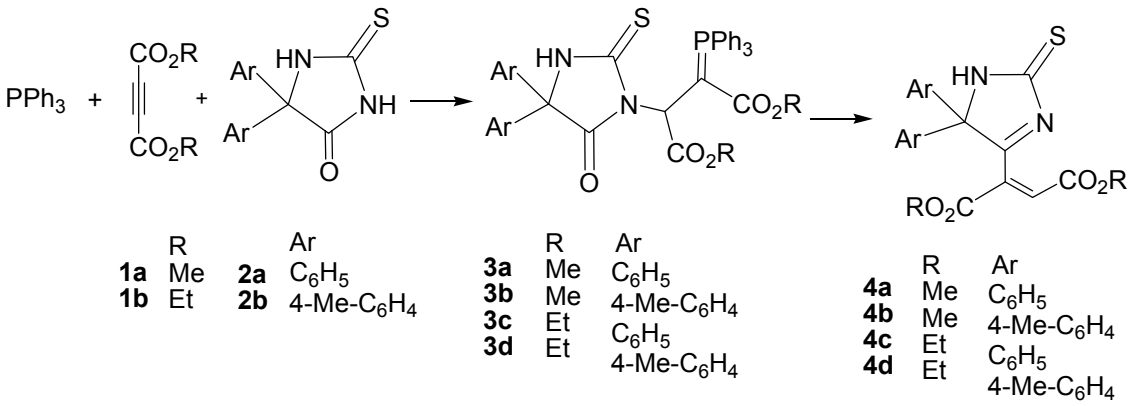

	R		Ar
1a	Me	**2a**	C_6H_5
1b	Et	**2b**	4-Me-C_6H_4

	R	Ar
3a	Me	C_6H_5
3b	Me	4-Me-C_6H_4
3c	Et	C_6H_5
3d	Et	4-Me-C_6H_4

	R	Ar
4a	Me	C_6H_5
4b	Me	4-Me-C_6H_4
4c	Et	C_6H_5
4d	Et	4-Me-C_6H_4

SCHEME 1. Synthesis of compounds **3** and **4**.

References:

[1] R. Engel, Synthesis of Carbon-Phosphorus Bonds., CRC Press, Boca Raton, FL (1998).

[2] HR. Hudson, In: Hartley FR (ed) The Chemistry of Organophosphorus Compounds., Vol. 1, Primary, Secondary and Tertiary Phosphines and Heterocyclic Organophosphorus (III) Compounds, Wiley, New York, pp 382–472 (1990).

[3] DEC. Corbridge, Phosphorus, An Outline of Chemistry, Biochemistry and Technology, 5th edn, Elsevier, Amsterdam (1995).

[4] K. B Becker, Tetrahedron, 36, 1717 (1980); E Zbiral, Synthesis., 775 (1974).

[5] E. L Eliel and S. H Wilen, Stereochemistry of Organic Compounds., Wiley, New York, pp 569–573 (1994).

Thermodynamic study of reaction of tautomerization of 5- methyl – 2,4-dihydro- pyrazol-3-one

Leila Kiyani*[a]

[a]Department of Chemistry, University of Kohgiluyeh & Boyerahmad, Gachsaran , Iran

Email:Leila.kiyani1@gmail.com

Keywords : Thermodynamic , Tautomer **,** pyrazol , Abinitio

Introduction

keto-enol tautomerism refers to a chemical-equilibrium between a keto form (a ketone or an aldehyde) and an enol (An alcohol). The enol and keto forms are said to be tautomers of each other. The interconversion of the two forms involves the movement of a proton and the shifting of bonding electrons; hence, the isomerism qualifies as tautomerism.

The keto-enol reaction is very important in structure of peptide and proteins[1] and proton transfer reaction the tautomerization is important in DNA reactions [2]. In this research the structure and thermodynamics of substituted ketones were calculated and the effect of substitutions on the proportion of energy in two structures was studied.

Methods

Theoretical methods have used to study all of the channels of this reaction. Ab initio calculations were carried out using the Gaussian 03 program. The geometries of all the stationary points were optimized at the MPWB1K [3], methods with 6-311++G** basis set.

Results and Discussion

In this study thermodynamics of the following reaction have investigated The calculated relative energies at MPWB1K/6-311++G** levels of theory are reported in diagrams 2.

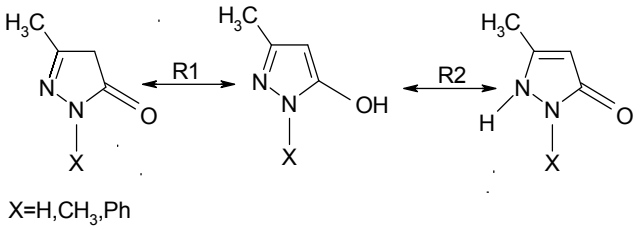

X=H,CH_3,Ph

Molecule1 Molecule2 Molecule3

In this study we have reported one dimensional PES for some trajectories of the reactions of studied. (see diagram 1). As shown in this diagram, hydrogen atom is separated from carbon atom of molecule 1, to produce molecule 2 via transition state.

Reaction path (bohr)

Diagram1.Potential energy surface for reaction of molecule 1 to produce molecule 2, with X=H

Relative energies of different species which corrected for zero point energies are plotted in diagram 2. as shown in these figure molecule 1 is more stable than molecule 2 and 3 (for x=H, CH_3 and Ph) . For X=Ph energy of molecule 2 and 3 are comparable.

Diagram2. Relative energies of different species for reaction in kJ mol^{-1} at the MPWB1K/6-31++G(d,p) level. All values are corrected for zero point energies.

Conclusions

Generalized free energy of activation for all reactions have investigated to calculated equilibrium constant.

Rate constants, negative and positive of gibes energy are important to comparison of stability of different reactions.

$\Delta G = G_2 - G_1$
$\Delta G = -RTLnK$
$LnK = -\Delta G/RT$
$K = e^{-\Delta G/RT}$

R is the gas constant(8.314 J/mol.k)
T is 298 K
K is equilibrium constant.

R1	X=H	X=CH3	X=Ph
G(kj/mol)	1.581	-2.37	2.9
K	0.531	0.95	0.313

R2	X=H	X=CH3	X=Ph
ΔG(kj/mol)	2.37	4.48	0.79
K	0.38	0.17	0.73

References

[1] Qiang-gen Li, Ying Xue, Guo-sen Yan, *Journal of Molecular Structure: Theochem.868* (**2008**|) 55–64.

[2] Michel Mons, Iliana Dimicoli, François Piuzzi, Benjamin Tardivel, and Mohamed Elhanine, *J. Phys. Chem. A*, **2002**, *106* (20), pp 5088–5094

[3] Zhao, Y.; Truhlar, D. G. *J. Phys. Chem. A*. **2004**, *108*, 6908

Thermodynamic study of reaction of tautomerization of 1H-indol-2,3-dione

Leila Kiyani*[a]

[a]Department of Chemistry, University of Kohgiluyeh & Boyerahmad, Gachsaran , Iran

Email:Leila.kiyani1@gmail.com

Keywords: Thermodynamic , Tautomer ,Indol, Ab initio

Introduction

Heterocycles play a major part in biochemical processes and are also side groups of the most typical and essential constituents of living cells [1].

The indole ring system is probably the most ubiquitous heterocycle in nature. Owing to the great structural diversity of biologically active indoles, it is not surprising that the indole ring system has become an important structural component in many pharmaceutical agents [2],[3] .

Methods

Theoretical methods have used to study all of the channels of this reaction. Ab initio calculations were carried out using the Gaussian 03 program. The geometries of all the stationary points were optimized at the MPWB1K [4], methods with 6-311++G** basis set.

Results and Discussion

In this study thermodynamics of the following reaction have investigated .

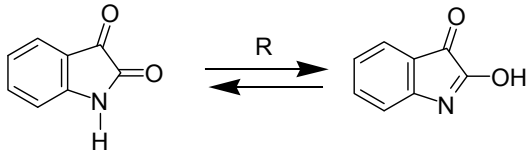

Molecule1 Molecule2

In this study we have reported one dimensional PES for some trajectories of the reactions of studied. (see diagram 1). As shown in this diagram, hydrogen atom is separated from Nitrogen atom of molecule 1, to produce molecule 2 via transition state.

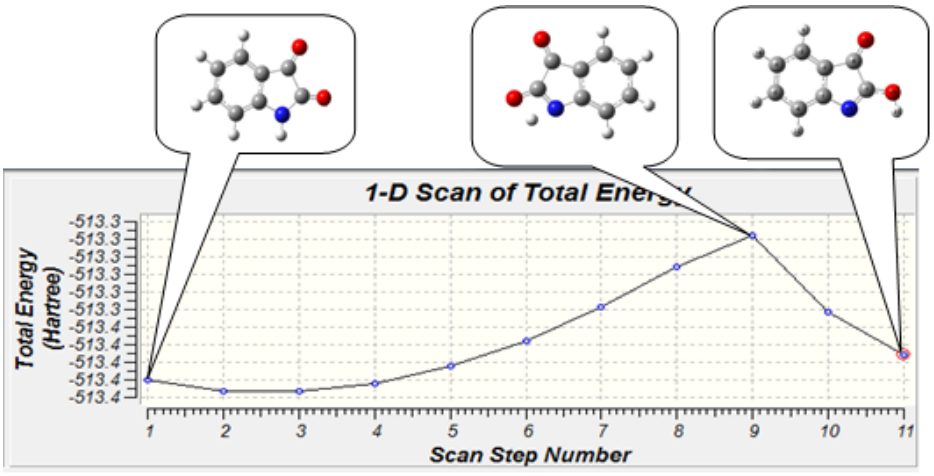

Diagram1.Potential energy surface for reaction of molecule 1 to produce molecule 2, with X=H

Harmonic vibrational frequencies were obtained at the MPWB1K/6-31++G(d,p) level in order to characterize stationary points as local minima or first-order saddle points and to obtain zero-point vibration energy corrections. The number of imaginary frequencies (0 or 1) indicates whether a minimum or a transition state has been located.Table 1.

Table 1. Harmonic Vibrational Frequency (cm^{-1}) for Various Species at MPWB1K/6-311++G(d,p) level.

Hf/6-311++G**	
Moleculen	Frequencies(cm^{-1})
Molecule1	3242.3,3251.7,3701.8,1894.4,3223.8,3235.8,1686.5,1708.7,1877.8,1435.5,1528.3,1543,1281.5,1333.7,1378.7,1182.2,1220.2,1230.9,1012.1,1061.3,1131,900.6,970.6,984.8,774.7,835.6,886.2,667.06,739.3,750.5,553.4,553.8,651.7,431.1,492.1,522.6,277.2,321.04,392.7,96,137.9,255
Molecule2	3145.6,3251.4,3841.6,1880.1,3222.1,3232.7,1686.5,1698.5,1742.6,1482.1,1506.8,1527.1,1259.7,1325,1397.8,1182.5,1194,1227.5,1006.2,1052,1177.8,901.06,977.9,983.07,773.5,818.5,888.3,649.5,734.5,746,566.7,604.4,643.7,422.9,488.2,547.7,291.7,294.3,374.2,116,138.4,275.2

Conclusion

Generalized free energy of activation for reaction have investigated to calculated equilibrium constant.

Rate constants, negative and positive of gibbes energy are important to comparison of stability of different reactions.

$\Delta G = G_2 - G_1$
$\Delta G = -RTLnK$
$LnK = -\Delta G/RT$
$K = e^{-\Delta G/RT}$

R is the gas constant(8.314 J/mol.k)
T is 298 K
K is equilibrium constant.

R	
ΔG(kj/mol)	0.1765
K	-0.0712

References

[1] Balaban, A. T.; Oniciu, D. C.; Katritzky, A. R. *Chem. Re*V. **2004**,*104*, 2777.

[2] Sundberg, R. J. *The Chemistry of Indoles*; Academic Press: New York, 1970.Oxford, 1996; Vol. 2, p 119.

[3] Sundberg, R. J. In *Comprehensi*V*e Heterocyclic Chemistry II*; Katritzky, A. R., Ress, C. W., Scriven, E. F. V., Bird, C. W., Eds.; Pergamon Press.

[4] Zhao, Y.; Truhlar, D. G. *J. Phys. Chem. A*. **2004**, *108*, 6908.

Compressed liquid densities for binary mixtures at temperatures from 280K to 440K at pressures up to 200 MPa

Maryam Mojahed Taghi[a] and Zahra Sharafi[a,*]
[a]Islamic Azad University, Marvdasht branch, Chemistry Department, Marvdasht, Iran
Email: Zahra_sharafi@yahoo.com

Keywords: equation of state, liquid densities of binary mixtures, boiling point.

Introduction

In this work, we apply an equation of state based on statistical-mechanical perturbation theory to liquid mixtures. Three temperature-dependent quantities are needed to use the equation of state (EOS): the second virial coefficient, $B(T)$, effective van der Waals covolume, $b(T)$, and a scaling factor, $\alpha(T)$. Based on the theory, all the three temperature-dependent parameters depend only on the repulsive branch of the potential function, and therefore, by our procedure, can be found from ΔH_{vap} and ρ_{nb}. It has considerable predictive power.

Method

In this section, we summarized the results of derivation of the statistical mechanical equation of state, which was derived by Ihm et al. [1], from statiscal-mechanical perturbation theory. This equation of state is:

$$\frac{P}{\rho kT} = 1 + \rho \sum_{ij} x_i x_j (B_{ij} - \alpha_{ij} F_{ij}) + \rho \sum_{ij} x_i x_j G_{ij} \alpha_{ij} \qquad (1)$$

where x_i and x_j are mole fractions, and the summations run over all components of mixture. The quantities α_{ij} and B_{ij} are related to the pair potential u_{ij} (r). G_{ij} and F_{ij} are defined [2] as follow

$$F_{ij} = \frac{1}{1-\xi_3} - \left(\frac{d_i d_j}{d_{ij}}\right) \frac{\frac{1}{6}\pi\rho\sum_k x_k {d_k}^2 (4\delta_k + 1)}{(1-\xi_3)(1+\frac{2}{3}\pi\rho\sum_k x_k {d_k}^3 \delta_k)} \qquad (2)$$

$$G_{ij} = \frac{1}{1-\xi_3} + \left(\frac{d_i d_j}{d_{ij}}\right) \frac{\frac{1}{6}\pi\rho\sum_k x_k {d_k}^2 (4\lambda_k - 1)}{(1-\xi_3)(1-\frac{2}{3}\pi\rho\sum_k x_k {d_k}^3 \lambda_k)} \qquad (3)$$

where

$$\xi_3 = \tfrac{1}{6}\pi\rho\sum_k x_k d_k^{\,3} \qquad (4)$$

with $\delta_k = 0.22\lambda_k$.

The equation for calculating d_k is :

$$b_k = \tfrac{2}{3}\pi d_k^{\,3} \qquad (5)$$

The simplest combining rules for predicting unlike-molecule interactions from like-molecule interactions are an arithmetic mean for $\rho_{nb}^{-1/3}$ and a geometric mean for ΔH_{vap} .

$$(\rho_{nb})_{ij}^{-1/3} = (1/2)[(\rho_{nb})_i^{-1/3} + (\rho_{nb})_j^{-1/3}] \qquad (6)$$

$$(\Delta H_{vap})_{i\,j} = [(\Delta H_{vap})_i\,(\Delta H_{vap})_j]^{1/2} \qquad (7)$$

Once $(\rho_{nb})_{ij}$ and $(\Delta H_{vap})_{ij}$ are known, the values of α_{ij}, b_{ij} and $(B_2)_{ij}$ follow according to Ref [3].

Result and Discussions

This work proves that the ISM equation of state can be applied to predict the *PVT* behavior for fluid mixtures. The most important advantage of this EOS than other equations is simplicity and also needs less input information for fluids. In practical, knowledge of only two constants, heat of vaporization and liquid density at the normal boiling point that are almost available for fluids is sufficient to determine the *PVT* surface of the fluids.The results in **Table I**. Show that agreement between our calculated data and experimental data is very good.

Table I. Comparisons between Calculated and Experimental Values [4] of Compressed Liquid Densities for Mixtures of (x_1 n-butane + x_2 isobutane)

X_1	T (K)	P (MPa)	ρ_{exp}(kg·m^{-3})	NP[a]	AAD%[b]
0.2625	280	1-200	580.7-706.1	19	2.378
	320	1-200	530.1-685.5	19	3.153
	440	20-200	485.3-648.3	16	3.634
0.4913	320	1-200	541.4-689.5	19	2.837
	440	30-200	483.2-637.8	13	3.691
0.7508	360	2-200	478.2-669.8	18	4.237
	440	10-200	384.5-635.7	15	4.824

[a] NP: number of data points

[b] $AAD\% = 1/N\sum_{i=1}^{N} 100\left|\dfrac{\rho_{i,\text{exp}} - \rho_{i,cal}}{\rho_{i,\text{exp}}}\right|$

References

[1] Ihm G., Song Y., Mason E.A., J. Chem. phys. **94** (1991) 3839.

[2] Ihm G., Song Y., Mason E.A., Mol. Phys. **75** (1992) 897.

[3] Sharafi Z., Boushehri A., Int. J. Thermophysics. **26(3)** (2005) 785.

[4] Miyamoto H., Koshi T., Uematsu M., J. Chem. Thermodynamics. **40(4)** 2008 567.

New Excess Gibbs Energy Equation for Modeling the Transport Properties of Polymer Solutions and Nanofluids at Different Temperatures

Mohammed Taghi Zafarani-Moattar and Roghayeh Majdan-Cegincara*
Email: majdan_26@yahoo.com
Physical Chemistry Department, University of Tabriz, Tabriz, Iran

Keywords: Excess Gibbs energy model; Polymer solutions; Nanofluid; New local composition model.

Introduction:

Knowledge of the dependence of viscosities of polymer solutions on composition is of great interest from a theoretical standpoint. Close examination of performance of Eyring-local composition models [1-3] in the modeling of viscosity values of polymer solutions indicates that for some systems satisfactory results are not obtained using these models. Here, we proposed a new local composition model (modified-NRF) for excess Gibbs energy of polymer solutions using local cell theory and considering different reference state assumptions and correction terms. The model has been used along with Eyring's absolute rate theory in the correlation of viscosity values of binary polymer solutions and nanofluids.

Theoretical framework:

Following Chen's approach we assume the existence of two types of cells, depending on the central species. One of the cells has a solvent central molecule and the other cell has a polymer segment as central species. Considering different reference state assumptions and correction terms we obtained the mNRF equation for polymer solutions as:

$$\frac{g^{ex,mNRF}}{RT} = \sum_{w''} x_{w''} \sum_{s} \sum_{w'} \sum_{w} \frac{X_w \lambda_{sw,w'w} (-X_w \Gamma_{w'w} - X_s \Gamma_{w'w} + 1)}{X_S + X_W} + \sum_{w''} \sum_{p} r_{p,w''} x_p \sum_{w} \sum_{s'} \sum_{s} \frac{X_s \lambda_{s's,ws} (X_s \Gamma_{s's} + X_w \Gamma_{s's} - 1)}{X_s + X_w}$$

$$\Gamma_{is} = \frac{\beta_{is,ws}}{\sum_{w'} X_{w'} \beta_{w'i,ws} + \sum_{s'} X_{s'} \beta_{is',ws}}, \quad \Gamma_{iw} = \frac{1}{\sum_{w'} X_{w'} \beta_{iw',iw} + \sum_{s} X_s \beta_{si,iw}}, \quad X_s = \frac{x_p}{\sum_i r_i x_i}, \quad X_w = \frac{x_w}{\sum_i r_i x_i},$$

$$\lambda_{ij,kl} = \lambda_{ij,lk} = \lambda_{ji,kl} = \lambda_{ji,lk} = -\lambda_{kl,ij} = -\lambda_{lk,ij} = -\lambda_{kl,ji} = -\lambda_{lk,ji}, \beta_{ji,li} = \exp\left(-\frac{g_{ji} - g_{li}}{ZRT} + \frac{\omega_{ij}}{RT}\right) \quad (1)$$

where x_w and x_p are the mole fraction of solvent and polymer. T is temperature and R is the universal constant of gases. Z is the nonrandom factor which was set to 8 in this work. Subscripts s and s′ represent the segments of polymer chain; w, w′ and w″ show the solvent molecules. $r_{p,w''}$ approximates the ratio of the molar volume of the polymer and corresponding solvent molecule, w″.

Results and discussion:

Proposed model on the basis of Eyring's absolute rate theory has been utilized in the correlation of viscosity values of nanofluids and polymer solutions with following equation:

$$\ln(\eta V) = \sum_{i=1}^{2} \ln(\eta_i V_i) + \left(\frac{g^{ex,mNRF}}{RT}\right) \quad (2)$$

where η and V are the viscosity and molar volume of mixture, respectively. Subscript i represent the pure component i. In the correlation of viscosity values of polymer solution temperature dependency for Eyring-mNRF model is considered as:

$$\lambda_w = \frac{a_w^0 (\frac{T}{T_0}) + a_w^1 (\frac{T}{T_0})^2}{RT}, \lambda_s = \frac{a_s^0 (\frac{T}{T_0}) + a_s^1 (\frac{T}{T_0})^2}{RT}, \omega_w = \frac{b_w^0 (\frac{T}{T_0}) + b_w^1 (\frac{T}{T_0})^2}{RT}, \omega_s = \frac{b_s^0 (\frac{T}{T_0}) + b_s^1 (\frac{T}{T_0})^2}{RT} \quad (3)$$

In Table 1 and 2 the obtained absolute average relative deviations, AARD, of the aforementioned model in the correlation of the viscosity values of binary polymer solutions and nanofluid are given along with the AARD values determined from other local composition models.

Table 1. Absolute average relative deviation, 100.AARD, of different viscosity models for the polymer + solvent Systems

system	M_n (g.mol^{-1})	T (°C)	number of data point	Eyring-polymer-NRTL	Eyring-segment-based-liquid-NRTL	Eyring-polymer-Wilson	Eyring-polymer-NRF	Eyring-polymer-NRF-Wilson	Eyring-mNRF
PEG +ethylacetate	400	25-35	33	12.77	1.77	2.15	1.42	1.75	1.35
PPG + ethanol	۴۰۰	25-55	۸۸	6.89	1.50	1.50	1.76	1.51	1.46
PPG +2-propanol	۴۰۰	25-55	۱۰۹	1.81	1.44	1.19	1.27	1.19	1.18
PVP + H2O	4088	25-55	108	1.70	1.68	1.86	1.36	1.29	1.29
PS + styrene	166000	20-60	81	9.37	11.66	16.86	76.83	76.83	8.31

Table 2. Absolute average relative deviation, 100.AARD, of Eyring-mNRF and Eyring-NRTL models obtained from viscosity fitting of nanofluids

system	number of data point	range of volume fraction	Eyring-mNRF-	Eyring-NRTL
CuO-H_2O	33	0.01-0.09	3.32	5.22
Al_2O_3-H_2O	۸۸	0.01-0.094	9.02	9.80

Conclusion:

New excess Gibbs energy model, mNRF, has been developed based on the local cells theory. The performance of the proposed model in the correlation of viscosity values of the binary polymer solutions and nanofluids has been tested. It was found that the performance of mNRF model in the correlation of transport properties of the binary polymer solutions and nanofluids is better than other local composition models.

References

[1]. L. T. Novak, C. C. Chen, Y. Song, Ind. Eng. Chem. Res. 43 (2004) 6231-6237.

[2]. R. Sadeghi, J. Chem. Thermodyn. 37 (2005) 445-448.

[3]. R. Sadeghi, Fluid Phase Equilib. 232 (2005) 70-73.

Simple Synthesis of Stable phosphorous Ylides Derived From Triethyl Phosphite Along With Dynamic ^{1}H NMR Study Around the Carbon-Carbon and Partial Carbon-Carbon Double Bonds in the Two Classes of Ylides Involving Triethyl Phosphite and Triphenylphosphine

S. M. Habibi-Khorassani*[a], A. Ebrahimi[a], M. T. Maghsoodlou[a], M. Mohammadi[a], and E.Aghdaei[a]

[a] *Department of Chemistry, The University of Sistan and Baluchestan, P.O. Box 98135-674, Zahedan, Iran.*

E-mail address: smhabibius@yahoo.com (S.M. Habibi-Khorassani).

Keywords: Dynamic 1H NMR,2-Mercaptobenzoxazole,Stable phosphorous ylide, Triethyl phosphite, NH heterocyclic compound, 2-Mercaptobenzimidazole

Introduction

In continuation of our research works on dynamic ^{1}H NMR phenomenon, we now describe this effect in reaction between dimethyl acetylenedicarboxylate and 2-mercaptobenzoxazole in the presence of triethyl phosphate**.**Synthesize of which has been reported previously[1].

Results and Discussion

1. Dynamic ^{1}H NMR for Ylide 4d Involving Triethyle Phosphite

The ^{1}H, ^{13}C and ^{31}P NMR spectra of ylide **4d** (synthesis of which has been reported previously[1]) are consistent with the presence of two isomers (see Figure 1-I). The ylide moiety of these compounds is strongly conjugated with the adjacent carbonyl group and rotation around the heteroaryl-carbon, carbon-carbon single bonds and also the partial carbon-carbon double bond in the *Z*-**4d** and *E*-**4d** rotational isomers are slow on the NMR time scale at ambient temperature. Herein, the ^{1}H NMR spectra of **4d** exhibits two doublets for methine proton (H-C-C=P, $^3J_{PH}$) at δ= 7.48 and 7.44 ppm, for the major and minor geometrical isomers, respectively. Effects of dynamic ^{1}H NMR around the each bond will be discussed next.

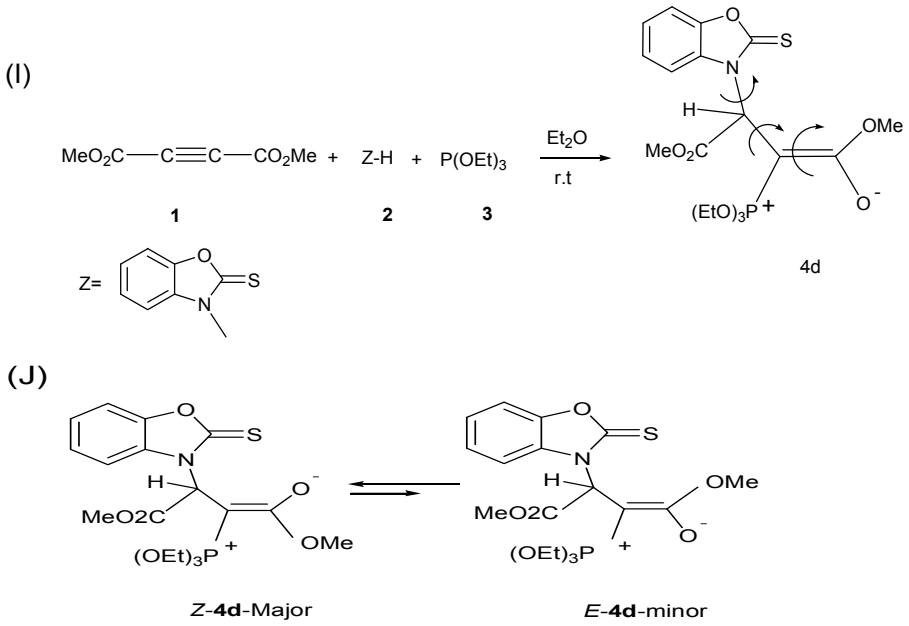

Figure 1. (**I**) Synthesis of ylide **4d** involving three possible dynamic ^{1}H NMR effects around heteroaryl-carbon , carbon-carbon single bonds and also carbon-carbon double bond.

2. Dynamic effect for the *E*-4d isomer ,as a result of restricted rotational process around the heteroaryl-carbon and carbon-carbon single bonds at 242 K and 236 K, respectively

The ^{1}H NMR spectrum for the *E*-**4d** showed a resonance arising from methine proton **(**H-C-C=P, $^{3}J_{PH}$) that is appreciably broadened in comparison with a corresponding doublet that measured at ambient temperature. This resonance coalescence at approximately -31 ºC (242 K) which is relevant to restricted rotational process around heteroaryl-carbon single bond. Moreover, when temperature was considerably reduced under zero, other coalescence occurred at -37ºC (236 K) that is related to the rotational process around the carbon-carbon single bond. Investigation of ^{1}H NMR spectra for *E*-**4d** at variable temperature allowed us to calculate the rotational energy barrier ($\Delta G^{\#}$) for the both restricted rotational processes around the heteroaryl-carbon (see Table 2) and also carbon-carbon single bonds (see Table 3). Using the expression $k_C = \pi\Delta\upsilon/\sqrt{2}$, first order rate constants calculated for both bond rotational processes. Application of the absolute rate theory with a transmission coefficient (k) of one gave free Gibss rotational energy barrier. With respect to the experimental data involving Tc and Kc, values of $\Delta H^{\#}$ and $\Delta S^{\#}$ [2,3] calculated for each process. Those are reported in Tables 2 and 3. Effect of temperature on the rate constant was investigated on the basis of measurement of different chemical shift in a series of other separate experiments.

The results were too small so that the changes in first order rate constant and Gibss free energy barrier are negligible in comparison with the results obtained at -31° C (242K).

Table 2. Selected ^{1}H chemical shifts (at 500.1 MHz, in ppm, Me_4Si) along with activation parameters of phosphorus ylide **4d** involving a 2-mercaptobenzoxazole, in acetone, for rotation around the heteroaryl-carbon single bond in the *E*-**4d** isomer.

T_c K	δ ppm	Δν Hz	$\Delta G^{\#\ 22\text{-}24}$ kJ/mol	$k_c^{\ 22\text{-}24}$ s^{-1}	$\Delta H^{\#\ 23}$ kJ/mol	$\Delta S^{\#\ 23}$ kJ/mol K	Ea kJ/mol
242	6.52, 6.45	31.9	12±1	70.8	70	0.24	72

Table 3. Selected ^{1}H chemical shifts (at 500.1 MHz, in ppm, Me_4Si) along with activation parameters of phosphorus ylide **4d** involving a 2-mercaptobenzoxazole, in acetone, for rotation around the carbon-carbon single bond in the *E*-**4d** isomer.

T_c K	δ ppm	Δν Hz	$\Delta G^{\#}$ kJ/mol	k_c s^{-1}
236	3.63, 3.51	58.00	11±1	182

Conclusions

In briefly,three possible dynamic ^{1}H NMR effects were investigated in a 2-mercaptobenzoxazole phosphorus ylide **4d** using a one-pot reaction between triethyl phosphite **3** and dimethyl acetylenedicarboxylate **1** in the presence of NH heterocyclic compound such as 2-mercaptobenzoxazole **2** Activation parameters around the carbon-carbon single bond and partial carbon-carbon double bond for the *Z*-**4d** and *E*-**4d** isomers were successfully calculated separately.

Notes and references

[1]. M. Rostamizadeh, M. T. Maghsoodlou, S. M. Habibi-Khorassani, N. Hazeri, F. Rostami Charati, M. A. Kazemian, B. Skelton and M. Makha, *Canadian. J. Chem,* Submit.

[2]. M. T. Maghsoodlou, R. Heydari, S. M. Habibi-khorassani, M. K. Rofouel, M Nassiri, E. Mosaddegh and A. Hassankhani, *J. Sulfur .Chem*. 2006, **27**, 341-346

[3]. F. A. Carey and R. J. Sundberg, *Advanced Organic*.1990.

Temperature Dependence on protonation constants of thymidine

N. Mohammadian[a] *,A.Shamel[a],J .Kalami [a], S.Asefi [a], S.Ebadi [a]
Gh. Ebrahimzadeh Rajaei [a]
[a] Department of Chemistry, Islamic Azad University, Ardabil Branch, Ardabil, Iran
E-mail:Nmohamadiant@yahoo.com

Abstract

The formation constant of the species formed in the systems to thymidine have been determined in different temperature and constant ionic strength(0.1 mol .dm^{-3} sodium perchlorate) using a combination of spectrophotometric and potentiometric techniques. The protonation and formation constants in various media were determined and thermodynamic parameters in software versus of vant-hoof and clark-Glew equation are calculated.

Keyword: thymidine , protonation constant,spectrophotometer , tempereature effect

Introduction

Thymidine and its nucleotides and nucleosides are very important compounds due to its vital roles within the living cells and in regulation of various in biological systems.[1,2]

The acid-base behavior of nucleotides, bases and poly-nucleotides is essential to deduce the speciation and the possible conformation changes with pH or the amount of organic solvent in solution acid dissociation constants are among the most useful physic-chemical measurements describing the extent of ionization of functional groups with respect to pH. This parameter is important in research areas such as pharmaceutical drug discovering and development,where it often has a vital role in order to understand the pharmacodynamic properties of new drug substances.[3,4]

Experimental

Thymidine ($C_{10}H_{14}N_2O_5$) obtained from fluka as analytical reagent grade materials and used without further purification. Sodium perchlorate was from Merck and was dried under vacuum at room temperature for at least 72 hours before use.NaOH solution was prepared

from a titrisol solution (Merck). Perchloric acid was from Merck and was used as supplied. All dilute solutions were prepared from double-distilled water with a conductivity equal to $1.3\pm0.1\mu Scm^{-1}$.

All measurements were performed between 25 to 50 °C.The ionic strength was maintained to 0.1 mol dm^{-3} With sodium perchlorate. The pH-meter was calibrated for the relevant H^+ concentration with a solution of 0.01 mol dm^{-3} Perchloric acid solution containing 0.09 mol dm^{-3} Sodium chloride .The protonation constants of thymidine have been determind spectrophotometrically based on the relation A= f(pH). The measured absorbance,A,(250-280nm in the interval of 5nm) and $-\log[H^+]$ from the spectrophotometric titration were conducted with the Computer program. The program allows calculation of the protonation constants with different stoichiometry. The number of experimental points (absorbances versus $-\log[H^+]$) was more than 40 (maximum 50) for each titration run. During the experiments , the solution were stable and the absorbance values did not change with time.

Results and Discussion

If we consider the dissociation of thymidine

(1) $H_2L^+ \leftrightarrow HL + H^+$

(2) $HL \leftrightarrow L^- + H^+$

The dissociation constants K_{1d} and K_{2d} are given by $K_{1d} = \frac{[HL][H^+]}{[H_2L^+]}$ and $K_{2d} = \frac{[L^-][H^+]}{[HL]}$

The protonation constants K_1 and K_2 are versus of dissociation constants K_{d1} and K_{d2} respectively.

The values of –logK in different temperatures are shown in below table.

Temperature/°C	298.15	303.15	308.15	313.15	318.15	323.15
-logK	9.91	9.765	9.66	9.512	9.453	9.352

According to the obtaind results , -logK decreases as the temperature increases , indicating a negative ΔH^0 .The thermodynamic parameters were calculated from the slope and intercept of logK versus 1/T using the Van't Hoff equation , which are ΔH^0= -27.864 $KJmol^{-1}$ and ΔS^0 = 96.124 $Jmol^{-1}K^{-1}$. However , the thermodynamic parameters considering the extended isobar lequation are as: ΔH^0=-27.853 $KJmol^{-1}$and ΔS^0=96.160 $Jmol^{-1}K^{-1}$.

References:

[1] .ALWORTH, W.L : Stereo chemistry and Its Application Biochemistry, Wiley- Inter Sclence, New York 1972.

[2] .F . Ghrib , F . Jaberi, M. Zandvakili, Appl. Organometal Chem., 22,215,2006.

[3] .F . Ghrib , M . Jaberi, A. Shamel, J. Chem.Eng. Data, 2008,53,1772-1778.

[4]. F . Ghrib , A. Shamel, J. Chem.Eng. Data, 2009,53(3),933-939.

Study of physical chemistry parameters serum and human blood plasma

M. Mohsen-Nia *, M.Massah Bidgoli, F.S. Mohammad Doulabi
Thermodynamic Research Laboratory, Kashan University, Kashan, Iran
* Corresponding author. Tel. /fax: +98 361 5552935.
E-mail address: m.mohsennia@kashanu.ac.ir (M. Mohsen-Nia).

Keywords: Plasma, Blood serum, Density, Viscosity.

Introduction:

Blood is a very complex mixture and is often referred to as liquid organ [1]. Blood can be separated by sedimentation into two main parts, the blood cells and blood plasma. After blood is withdrawn from a vein and allowed to clot, the clot slowly shrinks. As it does so, a clear fluid called serum is squeezed out. Thus, Serum is blood plasma without fibrinogen and other clotting factors [2]. Blood is an important fluid and the measurement of its viscosity and density can be used for distinguish diseases. The viscosity of blood depends on the viscosity of the plasma, in combination with the hematocrit [3].

Experimental:

Human blood serum and plasma from 10 healthy blood donors (male/female) were provided by blood transfusion service in Kashan. A 25 cm^3 calibrated glass pycnometer was used for density measurements. Viscosities of the samples were measured using a calibrated modified Ostwald viscometer (Cannon-Fenske glass capillary viscometers, CFRU, 9721-A50). A thermostatted water bath was used to attain thermal equilibrium. The temperature of the water bath was measured to a precision of (± 0.1 K).

Results and discussion:

The obtained density measurement results are reported in table 1. Fig. 1 shows the serum density variations versus temperature. Table 2 presents the results of viscosity measurements of serum and plasma samples. The viscosity variations of plasma as a function of temperature are showed in Fig 2. Fibrinogen is one of the plasma's proteins and in despite of only 5.5 percent volume of the whole proteins is the largest protein and acts as a macromolecule.

Fibrinogen has the most influence on plasma viscosity due to the dumbbell-shape and symmetrical molecular construction. Therefore, it can be expected that the viscosity of plasma at same temperature is higher than that for serum. The obtained data contradict the expected trend. This can be concluded that using chemicals such as citrates which is used as anticoagulation in the transfusion service may cause the contradiction. The obtained results showed that the measured densities and viscosities increase with an increase in temperature.

Table 1. The measured density of plasma and serum.

T(K)	Plasma density ($g.ml^{-1}$)					Serum density ($g.ml^{-1}$)				
	Sample 1	Sample 2	Sample 3	Sample 4	Sample 5	Sample 1	Sample 2	Sample 3	Sample 4	Sample 5
298	1.0238	۱.۰۲۵۲	۱.۰۲۴۶	۱.۰۲۵۶	۱.۰۲۴۳	۱.۰۲۵۷	۱.۰۲۵۹	۱.۰۲۵۴	۱.۰۲۶۲	۱.۰۲۵۵
303	۱.۰۲۲۲	۱.۰۲۳۷	۱.۰۲۳۱	۱.۰۲۴۰	۱.۰۲۲۸	۱.۰۲۳۸	۱.۰۲۴۲	۱.۰۲۳۷	۱.۰۲۴۸	۱.۰۲۳۹
308	۱.۰۲۰۵	۱.۰۲۲۳	۱.۰۲۱۷	۱.۰۲۲۶	۱.۰۲۱۳	۱.۰۲۲۳	۱.۰۲۲۷	۱.۰۲۱۸	۱.۰۲۳۲	۱.۰۲۱۹
310	۱.۰۱۹۶	۱.۰۲۱۵	۱.۰۲۱۲	۱.۰۲۲۰	۱.۰۲۰۶	۱.۰۲۱۵	۱.۰۲۲۷	۱.۰۲۱۱	۱.۰۲۲۵	۱.۰۲۱۲
313	۱.۰۱۸۷	۱.۰۲۰۶	۱.۰۲۰۴	۱.۰۲۱۲	۱.۰۱۹۷	۱.۰۲۰۸	۱.۰۲۱۳	۱.۰۱۹۸	۱.۰۲۱۳	۱.۰۲۰۴

Table 2. The measured viscosity of plasma and serum.

T(K)	Plasma viscosity (mpa.s)					Serum viscosity (mpa.s)				
	Sample 1	Sample 2	Sample 3	Sample 4	Sample 5	Sample 1	Sample 2	Sample 3	Sample 4	Sample 5
298	۱.۴۰۶۷	۱.۴۹۳۹	۱,۴۶۰۳	۱,۵۰۶۵	۱.۴۱۹۴	۱.۶۴۱۸	۱.۶۱۰۰	۱.۶۰۴۷	۱.۶۵۱۳	۱.۶۱۵۳
303	۱.۲۷۸۳	۱.۳۵۲۱	۱.۳۲۸۴	۱.۳۷۲۲	۱.۲۸۶۷	۱.۴۶۹۶	۱.۴۶۱۲	۱.۴۵۴۶	۱.۴۹۷۸	۱.۴۶۸۳
308	۱.۱۴۸۵	۱.۲۴۴۴	۱.۲۱۴۲	۱.۲۵۴۱	۱.۱۹۱۹	۱.۳۲۸۹	۱.۳۳۸۶	۱.۳۲۲۲	۱.۳۵۴۴	۱.۳۲۴۰
310	۱.۱۰۴۸	۱.۱۷۳۳	۱.۱۶۳۵	۱.۱۸۹۶	۱.۱۲۹۷	۱.۲۸۳۶	۱.۳۰۱۲	۱.۲۷۹۹	۱.۳۱۳۹	۱.۲۹۴۰
313	۱.۰۳۳۳	۱.۱۰۹۰	۱.۰۹۷۷	۱.۱۱۴۵	۱.۰۶۰۱	۱.۲۲۲۴	۱.۲۲۰۰	۱.۲۰۵۷	۱.۲۵۲۶	۱.۲۱۱۱

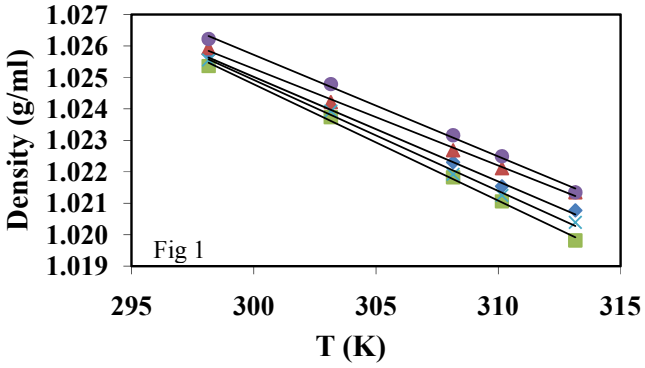

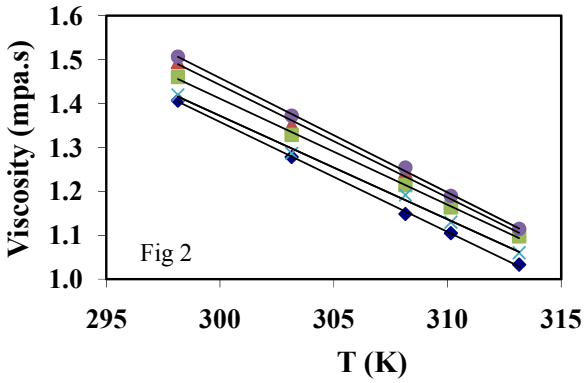

References:

[1] R.G. Owens, *J. Non-Newtonian Fluid Mech*, 140, 57, (2006).

[2] J. Schaller, S. Gerber, U. Kampfer, S. Lejon, Ch. Trachsel, *"Human Blood Plasma Proteins: Structure and Function*", John Wiley & Sons Ltd, England, (2008).

[3] E. Charm, S. Kurland, *"Blood Flow and Microcirculation*", John Wiley & Sons, New York Inc, (1974).

The Effect of Different Organic and Inorganic Electrolytes on the Thermodynamic Properties of Ionic Liquid 1-Butyl-3-methylimidazolium Iodide in Aqueous solutions

R. Sadeghi and B. Mostafa
Department of Chemistry, University of Kurdistan, Sanandaj, Iran
(Email: rsadeghi@uok.ac.ir), (Email:m_bahar155@yahoo.com)

Keywords: Ionic Liquid, 1-Buthyl-3-methylimidazolium iodide, Volumetric, Isentropic compressibility, Liquid-liquid equilibria.

Introduction

Aqueous two-phase systems (ATPS) are generated by mixing two mutually incompatible polymers [e.g. dextran and poly(ethylene glycol), PEG], one polymer and one salt (e.g. PEG and sodium citrate), or one ionic liquid (IL) and one salt in an aqueous solution above a certain critical concentration. Each phase contains mainly one of the compounds and a small amount of the other, with water as solvent in both phases with mass fraction (80 to 90) % in equilibrium phases. In recent years, ATPSs based on ILs (i.e., hydrophobic IL-water or hydrophilic IL-salt-water) have been investigated since Rogers et al. [1] demonstrated that the addition of potassium phosphate to an aqueous solution of a hydrophilic IL produces ATPS. These new ATPSs have been successfully used to separate testosterone, epitestosterone, opium alkaloids, and bovine serum albumin. The ILATPSs also have been demonstrated for extraction of antibiotics such as penicillin G, amoxicillin, and ampicillin [1]. In this work, the effects of the addition of $(NH_4)_3Cit$, K_3Cit, Na_3Cit, $(NH_4)_2HPO_4$, and $(NH_4)_3PO_4$ on the liquid-liquid phase diagram, apparent molar volume, and isentropic compressibility of aqueous solutions containing the model ionic liquid 1-butyl-3-methylimidazolium iodide, $[C_4mim][I]$, are investigated at different temperature.

Methods

The density and sound velocity of the mixtures were measured at different temperatures with a digital vibrating-tube analyzer (Anton Paar DSA 5000, Austria) with proportional temperature control that kept the samples at working temperature within $\pm 10^{-3}$ K. The experimental apparatus employed for determination of liquid-liquid equilibrium data is essentially similar to the one used previously [2]. A glass vessel was used to carry out the phase equilibrium determinations. The glass vessel was provided with an external jacket in which water at constant temperature was circulated using a thermostat. The temperature was controlled to within ±0.05 K. The binodal curves were determined by a cloud point titration method. A salt solution of known concentration was titrated with the IL solution or vice versa, until the solution turned turbid. The composition of the mixture was determined by mass on a Sartorius CP124S analytical balance.

Results, Discusion and Conclusions

In the resent work, in order to the study of the effects of electrolytes as well as temperature on the phase fluid behavior, apparent molar volume, and isentropic compressibility properties of aqueous solutions of [C_4mim][I], the liquid-liquid phase diagram, density, and speed of sound of aqueous solutions containing the ionic liquid [C_4mim][I] and inorganic and organic salts, $(NH_4)_3Cit$, K_3Cit, Na_3Cit, $(NH_4)_2HPO_4$, and $(NH_4)_3PO_4$ were measured at different temperature. The strength of salting-out effect for the investigated anions and cations respectively decreases in the order $PO_4^{3-} >> Cit^{3-}$ (high salt concentration) > HPO_4^{2-} > Cit^{3-} (low salt concentration) and $Na^+ > K^+ >> (NH4)^+$. The mutually liquid-liquid demixing in the studied aqueous IL-electrolyte systems is promoted by decreasing temperature and increasing charge on the anion of electrolyte. It was found that there is a relation between the relative concentration of various salts to form two-phase systems with [C_4mim][I] and apparent molar volume or isentropic compressibility of transfer of [C_4mim][I] from water to aqueous solutions of these salts. The effectiveness of the anions and cations of the investigated salts in the increasing the volume of [C_4mim][I] follows the sequence $PO_4^{3-} > HPO_4^{2-} > Cit^{3-}$ and $Na^+ > K^+ > (NH_4)^+$, respectively. The effectiveness of the anions and cations of the investigated salts in the increasing the apparent molar isentropic compressibility of [C_4mim][I] follows the sequence $PO_4^{3-} > Cit^{3-} > HPO_4^{2-}$ and $Na^+ > K^+ > (NH_4)^+$, respectively. Furthermore, the

effectiveness of the investigated electrolytes in the increasing the apparent molar volume or isentropic compressibility of [C_4mim][I] increases by decreasing temperature which is in consistent with our observation that by decreasing temperature the mutually liquid-liquid demixing in the studied aqueous IL-electrolyte systems is promoted.

References

[1] . K. E. Gutowski, G. A. Broker, J. Am. Chem. Soc. 125 (2003) 663.

[2]. R. Sadeghi, R. Golabiazar, H. Shekaari, J. Chem. Thermodyn.298 (2010), 231.

Temperature dependence on protonation constant of adenosine

M. Moazzami [a*], S. Seifi [a], S. Jozani [a], N. Azizi [a], A. Shamel [a], F.Gharib [b]

[a] Department of Chemistry, Islamic Azad University, Ardabil Branch, Iran

(E-mail: argavan_m_1385@yahoo.com)

[b] Department of Chemistry, Shahid Beheshti University, Tehran, Evin, Iran

Abstract

The temperature dependence on protonation constants of adenosine is studied using a combination of spectrophotometric and potentiometric methods at different temperature (25-50 °C) and various wavelengths (250 to 280 nm). The protonation constants were determined using a least squares regression analysis method with a suitable computer program. The Van't Hoff and Clark Glew equations have been employed to estimate the values of thermodynamic parameters of the protonation. The results show that the protonation constants decrease with increasing the temperature.

Keywords: Adenosine, Spectrophotometry, Protonation constant, Temperature effect

Introduction

Adenosine ($C_{10}H_{13}N_5O_4$) and its nucleotides and nucleosides are very important compounds due to their vital roles within the living cells and in regulation of various functions in biological systems. This compound is the building blocks in both DNA and is involved in a wide variety processes like cellular metabolism, cell bioenergetics, human cancer and immunodeficiency virus (HIV) markers. The acid-base behavior of nucleotides, nucleosides, bases and poly-nucleotides is essential to deduce the speciation and the possible conformational changes with pH or the amount of organic solvent in solution [1-2]. Acid dissociation constants are among the most useful physico-chemical measurements describing the extent of ionization of functional groups with respect to pH. These parameters are important in research areas such as pharmaceutical drug discovering and development, where it often has a vital role in order to understand the pharmacodynamic properties of new drug substances. Despite its recognized importance, there are only a few experimental contributions on the acid-base behavior and thermodynamic properties of adenosine.

Knowledge of the thermodynamic properties of adenosine is of great interest for decoding of the mechanism of multi-dentate ligand dissociation and for revealing the influence of the nature of the solvent and hydrophobicity. The protonation constants are important for environmental scientists, chemical engineers, chemists, and specialists in related fields as these alter the reactivity, spectral properties, physical behavior, and solubility.

Experimental

Adenosine obtained from Fluka as an analytical reagent grade material and used without further purification. Sodium perchlorate was from Merck and was dried under vacuum at room temperature for at least 72 hours before use. NaOH solution was prepared from a titrisol solution (Merck). Perchloric acid was from Merck and was used as supplied. All dilute solutions were prepared from double distilled water with a conductivity equal to 1.3 ± 0.1 μS cm^{-1}. All measurements were performed at 25 °C. The ionic strength was maintained to 0.1 mol dm^{-3} with sodium perchlorate. The pH-meter was calibrated for the relevant H^+ concentration with a solution of 0.01 mol dm^{-3} perchloric acid solution containing 0.09 mol dm^{-3} sodium chloride (for adjusting the ionic strength to 0.1 mol dm^{-3}). For this standard solution, we set $-\log[H^+] = 2.0$ Junction potential corrections have been calculated from eq 1

$$-\log[H^+]_{real} = -\log[H^+]_{measured} + a + b[H^+]_{measured} \quad (1)$$

where a and b were determined by measuring of hydrogen ion concentration for two different solutions of $HClO_4$ or NaOH with sufficient $NaClO_4$ to adjust the ionic media.

Results and Discussion

The protonation constants of adenosine have been determined spectrophotometrically based on the relation A = f(pH). The measured absorbance, A, (250- 280 nm in the interval of 5 nm) and $-\log[H^+]$ from the spectrophotometric titration were conducted with the computer program. During the experiments, the solutions were stable and the absorbance values did not change with time.

Table 1. The values of log K in different temperatures

Temperature/ °C	25	30	35	40	45	50
log K	3.889	3.731	3.620	3.522	3.402	3.297

$$HL \leftrightarrows H^+ + L^- \qquad K = \frac{[H^+]\,[L^-]}{[HL]}$$

According to the obtained results, logK decreases as the temperature increases, indicating a negative ΔH°. The thermodynamic parameters were calculated from the slope and intercept of log K versus 1/T using the Van't Hoff equation.

Acknowledgements

The authors could express their sincere thanks to Islamic Azad University that has supported this work.

References

[1]. F. Gharib, F. Jaberi, M. Zandvakili, Appl. Organometal Chem., 22, 215, 2006.

[2]. F. Gharib, E. Farzad, M. M. Amini, Can. J. Chem., 84, 1534, 2006.

Water Activity Measurements for Ternary 1-Hexyl-3-Methylimidazolium Chloride + Monomethyl Malonate Potassium Salt + Water and the Corresponding Binary Aqueous Solutions

R. Sadeghi*, A. Mahdavi
Department of Chemistry, University of Kurdistan, Sanandaj, Iran
(rsadeghi@uok.ac.ir)

Keywords: Water activity, Isopiestic, Ionic liquids, 1-Hexyl-3-methylimidazolium chloride, Monomethyl malonate potassium salt.

One of the most important thermodynamic properties of aqueous solutions is water activity which is an important and key thermodynamic property, because, it is closely related with the other thermodynamic properties such as vapor pressure, osmotic coefficient, activity coefficient, excess enthalpy, excess entropy, excess Gibbs energy and excess volume. It should, therefore, be useful to have information about vapor-liquid equilibria of the aqueous solutions in order to understand better and possibly predict the solution behavior. Vapor-liquid equilibria of electrolyte in water has been studied extensively [1], while the corresponding information on ionic liquids in water and in aqueous electrolyte solutions is more scarce. Therefore, in this study, the improved isopiestic method [2] has been used to obtain activities of water for ternary 1-hexyl-3-methylimidazolium chloride + monomethyl malonate potassium salt + water and the corresponding binary aqueous solutions at 298.15 K.

The isopiestic apparatus was similar to the one used by Ochs et al. [2]. The apparatus used for determination of water activity in the binary solutions consisted of five-leg manifold attached to round-bottom flasks. Two flasks contained the standard pure NaCl solutions, two flasks contained the pure sample (1-hexyl-3-methylimidazolium chloride or monomethyl malonate potassium salt) solutions and the central flask was used as a water reservoir. The apparatus used for determination of water activity in the ternary solutions consisted of seven-leg manifold attached to round-bottom flasks. Two flasks contained the standard pure NaCl solutions, one flask contained the pure 1-hexyl-3-methylimidazolium chloride solution, one flask contained the pure monomethyl malonate potassium salt solution, two flasks contained

the 1-hexyl-3-methylimidazolium chloride + monomethyl malonate potassium salt solutions and the central flask was used as a water reservoir. The apparatus was held in a constant-temperature bath at least 120 h for equilibrium. The osmotic coefficients for the standard aqueous NaCl solutions at different concentrations have been calculated from the correlation of Colin et al. [3].

In the present work, activities of water for 1-hexyl-3-methylimidazolium chloride + H_2O, monomethyl malonate potassium salt + H_2O and 1-hexyl-3-methylimidazolium chloride + monoethyl malonate potassium salt + H_2O systems at 298.15 K were measured at 298.15 K. From these measurements, values of the vapor pressure and osmotic coefficient of solutions and activity coefficient of solute and solvent were determined. Molar excess Gibbs free energy and molar Gibbs free energy change due to mixing of studied systems were calculated from the Pitzer model. The linear isopiestic relation (Zdanovskii-Stokes-Robinson rule) derived using the semi-ideal hydration model was applied for the constant water activity lines of the ternary system. Furthermore, comparisons between the vapor pressure depression of ternary solutions and the sum of those for the corresponding binary solutions with same molality of the ternary solution were made. The results have been interpreted in terms of the solute-water and solute-solute interactions.

References

[1] R. A. Robinson, R. H. Stokes, Electrolyte Solutions, 2nd ed.; Butterworths: London, 1965.

[2] L. R. Ochs, M. Kabiri Badr, H. Cabezas, AIChE J. 1990, 36, 2908-1912.

[3] E. Colin, W. Clarke, D. N. Glew, J. Phys. Chem. Ref. Data 1985, 14, 489-610.

Effects of Temperatures on the Interaction between Mushroom Tyrosinase and Phenyl Dithiocarbamate

G. Rezaei Behbehani*[a], A. A. Saboury[b] and M. Mehreshtiagh[a]

[a]Department of Chemistry, Imam Khomeini International University, Qazvin, Iran

(E-mail: grb402003@yahoo.com)

[b]Institute of Biochemistry and Biophysics, University of Tehran, Tehran, Iran

Keywords: Mushroom Tyrosinase, Phenyl Dithiocarbamate, Isothermal Titration Calorimetry, Solvation

Introduction

Tyrosinase is a copper-containing enzyme involved in melanin biosynthesis of various organisms. It is a monooxygenase catalysing the *o*-hydroxylation of monophenols to the corresponding catechols and the oxidation of catechols to the corresponding *o*-quinons. In mushroom as well as in fruits and vegetables, the enzyme is responsible for browning of wounded tissue exposed to air, a commercially undesirable phenomenon. Tyrosinase inhibitors have attracted interest recently due to undesired browning in vegetables and fruits in post-harvest handling [1]. Among the inhibitors, a distinction could be made between copper chelators, such as dithiocarbamate derivatives. One of the most powerful techniques useful to obtain additional information about the structure of biomacromolecule in biophysical chemistry field is isothermal titration calorimetry (ITC). In the present investigation, thermodynamic analysis is presented of the interaction between mushroom tyrosinase (MT) and phenyl dithiocarbamate at two temperatures of 27 and 37°C in phosphate buffer (10 mM; pH=6.8) by ITC. The extended solvation model provides more insights into this interaction for further understanding of the effect of phenyl dithiocarbamate on the stability and the strucrural changes of MT.

Model.

Methods

Mushroom tyrosinase was purchased from Sigma and phenyl dithiocarbamate was synthesized.

The isothermal titration microcalorimetric experiments were performed with the four channel commercial microcalorimetric system, Thermal Activity Monitor 2277, Thermometric, Sweden. Injection of phenyl dithiocarbamate solution (2.5 mM) into the calorimetric titration vessel, contained 1.8 mL MT (8.3 μM) was repeated 20 times, with 20 μL per injection.

Results and Discussion

The heats of the ligand+biomacromolecule interaction in the aqueous solvent systems, can be accounted for quantitatively in terms of Eq. 1 [2]:

$$q = q_{max} x'_B - \delta^{\theta}_A (x'_A L_A + x'_B L_B) - (\delta^{\theta}_B - \delta^{\theta}_A)(x'_A L_A + x'_B L_B) x'_B \quad (1)$$

$$x'_B = \frac{p x_B}{x_A + p x_B} \qquad x'_A = 1 - x'_B \qquad x_B = \frac{[Ligand]_T}{[Ligand]_{max}} \quad (2)$$

The obtained p=1 shows that the binding is non-cooperative.

$$L_A = \Delta H_{dilut} + x_B \left(\frac{\partial \Delta H_{dilut}}{\partial x_B}\right) \qquad L_B = \Delta H_{dilut} - x_A \left(\frac{\partial \Delta H_{dilut}}{\partial x_B}\right) \quad (3)$$

The positive values of δ^{θ}_A and δ^{θ}_B indicate that MT is substantially stabilized by phenyl dithiocarbamate at both of two temperatures. Derived heats of this solvation model is in principle compatible with experimental heats of ITC as shown in Fig. 1.

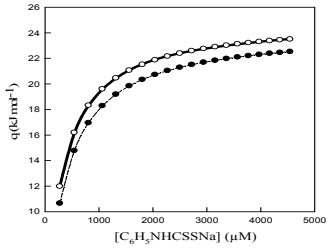

Fig. 1. Comparison between the experimental heats, q, for the interaction between Phenyl Dithiocarbamate and Mushroom Tyrosinase at 27°C (●), 37°C (O) and calculated datas (lines) at both temperatures via Eq. 1.

Using Eq. 2, the number of binding sites (g) and dissociation equilibrium constant (K_d) can be calculated and Finally, ΔG° and ΔS° can be calculated [3]:

$$\frac{\Delta q}{q_{max}} M_0 = \left(\frac{\Delta q}{q}\right) L_0 \frac{1}{g} - \frac{K_d}{g} \quad , \quad \Delta H^\circ = \frac{q_{max}}{g} \quad , \quad \Delta G^\circ = -RT \ln K_a \quad , \quad \Delta S^\circ = \frac{(\Delta H^\circ - \Delta G^\circ)}{T} \quad (4)$$

Conclusions

It was found that phenyl dithiocarbamate acted as a non-cooperative inhibitor of MT and there is a set of two identical and independent binding sites for phenyl dithiocarbamate on MT. All thermodynamic parameters are summarized in table 1.

p	δ^{θ}_{A}	δ^{θ}_{B}	K_d (μM)	K_a (μM^{-1})	g	ΔH° (kJ mol^{-1})	(kJ ΔG mol^{-1})	TΔS (kJ mol^{-1})	T (K)
1	3.9	3	341.4	0.0029	2	12.1	-19.9	32	300
1	4.7	5.3	288.7	0.0035	2	12.5	-21	33.5	310

References

[1]. S. Seo, V. K. Sharma, N. Sharma, J. Agric. Food Chem., 51 (2003) 2837.

[2]. G. Rezaei Behbehani, J. Chinese Chemical Letters, 20 (2009) 751.

[3]. A. A. Saboury, M. S. Atri. M. H. Sanati, M. Sadeghi, J. Thermal Analysis and Calorimetry, 83 (2006) 175.

Temperature-Dependent Viscosity of the Ionic Liquid 1-hexyl-3-methylimidazolium hexafluorophosphate Using New Potential Function

F. Niroomand Hosseini*[a], S. Mosavi[b]

[a]*Department of Chemistry, Islamic Azad University, Shiraz Branch, Shiraz, Iran*

(*Email: niroomand55@hotmail.com*)

[b]*Department of Chemistry, Islamic Azad University, Marvdasht Branch, Marvdasht, Iran*

Keywords: Ionic Liquid, Equation of State, Potential Function, Viscosity.

Introduction

Ionic liquids (ILs) are typically composed of organic cations and organic/inorganic anions. At ambient room temperature, they exist as liquids and have a wide variety of unique properties (for instance, negligible vapor pressure, favorable solvation behavior, low viscosity, and high reactivity and selectivity [1]). These features ensure that ILs are good candidates for "green chemistry" applications. ILs have been suggested to replace the environmentally unfriendly volatile organic solvents. In the past decade, there has been considerable interest in the applications of ILs (e.g., chemical reactions, separation processes, and renewable batteries [2,3]). Particularly, by varying the cation, anion, and/or substituent groups, the properties of ILs could be readily tuned to fit into a specific requirement. The increasing utilization of ILs in chemical and industrial processes requires reliable and systematic thermophysical properties such as activity coefficients, heats of mixing, densities, solubilities, vapor-liquid equilibria (VLE), and liquid-liquid equilibria (LLE). In addition, the transport properties are also needed (viscosity, electric conductivity, mutual diffusion coefficients, etc.). However, experimental measurements are time consuming and usually are difficult to control; thus, it is highly desirable to have predictive methods.

Results and discussion

The transport properties of a fluid are due to interparticle collisions, and therefore they must depend on the details of interaction potential at the short range. Most theoretical

investigations for thermophysical properties have shown that transport properties are sensitive to the steepness of the repulsion wall of the potential function. From this view, therefore, Lennard-Jones (12-6-3) type needs to be more justified for application in the calculation of transports [4]. By applying thermodynamic equation of state, it has been predicted that the isotherms $(Z-1)V$ for dense ion liquid are linear functions of (ρ) in the range of 312 K to 470 K. The interaction potential of this ion liquid is modeled by (12-6-3)-potential function so much the isotherms persist linear in the whole regions. The molecular parameters of the potential function $r_{\min}$ and ε have been calculated from *PVT* data of liquid state. The values of reduced collision integrals $\Omega^{(2,2)*}$ and $\Omega^{(2,3)*}$ are calculated from Chapman-Enskog solution [5] of the Boltzmann equation by using the LJ(12-6-3) potential function. For the calculate of the collision integrals, the algorithm of O'Hara and Smith is used. According to the kinetic theory of gases, the viscosity of a fluid can be predicted. Although the Enskog's theory can not be directly employed for the calculation of viscosities at liquid densities, but Alder *et. al*. [6,7] were able to describe the deviation from Enskog's theory by a correction factor as a function of the molar volume to predict viscosity at liquid state [8].

Conclusion

The comparison of our results for viscosity based on calculation of the modified Enskog's theory with experimental data shows that effective pair potential yields reasonable predictions of the viscosity of ion liquid over a wide range of temperature.

References:

[1] J. Heintz, *Chem. Thermodyn.*, **37**, 525, (2005).

[2] J. G. Huddleston, H. D. Willauer, R. P. Swatloski, A. E. Visser, R. D. Rogers, *Chem. Commun.* **16**, 1765, (1998).

[3] P. Y. Zhang, S. Lou, L. Y. Jin,W. B. Li, *Fine Chem.*, **22**, 324, (2005).

[4] G. A. Parsafar, H. V. Spohr, G. N. Patey, *J. Phys. Chem. B*, **113**, 11977, (2009).

[5] J. O. Hirschfelder, C. F. Curtiss, R. B. Bird, *Molecular Theory of Gases and Liquids,* Wiley, New York, (1965).

[6] J. H. Dymond, B. J. Alder, *J. Chem. Phys*. **45**, 2061, (1966).

[7] B. J. Alder, D. M. Gass, T. E. Wainwright, *J. Chem. Phys*. **53**, 3813, (1970).

[8] G. Raabe, B. D. Todd, R. J. Sadus, *J. Chem. Phys.* **123**, 034511, (2005).

Density, viscosity, refractive index and excess molar volume of poly(ethylene glycol) in water at various temperatures

Mehrdad Musavi*, Abbas A. Rostami and Abdollah Omrani
Faculty of Chemistry, University of Mazandaran, Babolsar, Iran
*Corresponding author e-mail address: Mehrdad.5824@yahoo.com

Keyword: Poly(ethylene glycol), Density, Viscosity, Excess molar volume, Refractive index

Introduction

In recent years, aqueous polymer solutions, especially poly(ethylene glycol) + water systems, have found wide-spread applications, mostly because of their use in two-phase aqueous systems for separation of biomolecular mixtures [1]. poly(ethylene glycol)s or PEGs are a linear or branched, with a wide variety of applications in the pharmaceutical, chemical, cosmetic, and food industries[2]. Despite the success of the aqueous two phase separation technique, data on the properties of phase systems that are necessary for the design of extraction processes and for the development of models that predict phase partitioning are few. previously published data showed the physical property of water and PEG solution [3-5]. In this work, we report the thermodynamic property of (PEG + water) prepared using PEG average molar mass 200 g/mol^{-1} over the entire composition range within the temperature range (298.15 , 303.15, 308.15) K.

Experimental

Materials. Analytical grade PEG with the number average molecular weight of 200 was purchased from Merck. Double-distilled water was used in making the solutions.

Apparatus and procedure. The mass measurements were made on a single pan Mettler balance with an accuracy of ± 0.01 mg. Density (ρ) measurements of pure components and binary mixtures over the complete composition range were carried out using Anton Paar oscillating u-tube densitometer (DA 500) with ± 10^{-4} g·cm-3 accuracy. The kinematic viscosity was measured with Ubbelohde viscometer with a Schott-Geräte automatic measuring unit model AVS 400 .

Results and discussion

The density and refractive index followed a linear behavior with temperature and solute concentration, but viscosity and excess molar volume followed a nonlinear relationship (figure1,2). The refractive index, as well as density and viscosity, increases with an increase in the concentration of PEG-200 and increases with decrease in temperature. This behavior is observed at each of the three temperatures utilized in this study. In order to afford the extent of molecular-level interactions within (PEG + water) we estimated excess molar volume (V^E) from experimental

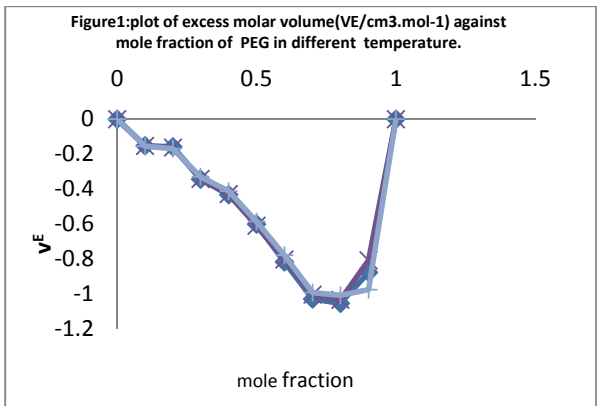

Figure1:plot of excess molar volume(VE/cm3.mol-1) against mole fraction of PEG in different temperature.

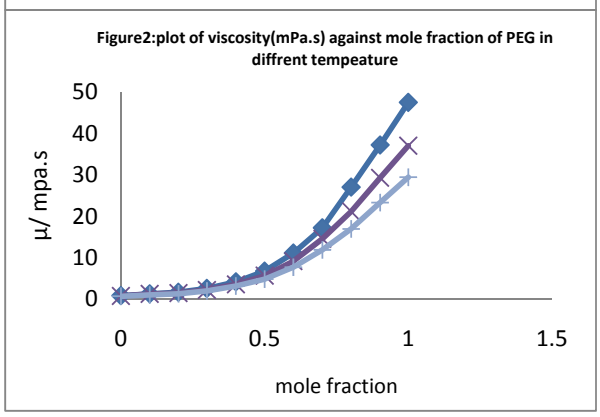

Figure2:plot of viscosity(mPa.s) against mole fraction of PEG in diffrent tempeature

density data using the relationship

$$V^E = \frac{(x_1M_1 + x_2M_2)}{\rho_m} - \left(\frac{x_1M_1}{\rho_1} + \frac{x_2M_2}{\rho_2}\right).$$

Here, x_1, x_2, and ρ_1, ρ_2 refer to the mole fractions and densities, respectively, of components1 and 2 in the mixture at a given temperature, and ρ_m is the density of the mixture. M_1 and M_2 are molar masses of components 1 and 2, respectively. The excess molar volumes at each temperature for (PEG + water) are presented as a function of X1, the mole fraction of PEG calculated using PEG average molar mass, in figure 1,2. It is clear that the values of the excess

molar volume are negative and are significant at each temperature throughout the entire composition range for all four (PEG + water). Interestingly, the maximum absolute excess molar volume for a (PEG + water) is observed in the water-rich region irrespective of the PEG average molar mass in the mixture, and it appears to shift to even more water-rich region as the average molar mass of PEG becomes higher in the mixture. Importantly, the absolute values of excess molar volumes for (PEG + water) appear to decrease with increasing temperature. The negative excess molar volumes usually indicate contraction in volumes upon mixing.

References

[1] Zaslavsky, B. Y. Aqueous two-phase partitioning. Physical chemistry and bioanalytical applications; Marcel Dekker Inc.: New York, 1995.

[2] Harris, J. M. Poly (ethylene glycol) Chemistry, Biothechnical and Biomedical applications; Plenum Press: New York, 1992.

[3] R.K. Singh, M.P. Singh, S.K. Chaurasia, Fluid Phase Equilib. 284 (2009) 10–13.

[4] M. Perumalsamy, T. Murugesan, J. Chem. Eng. Data 54 (2009) 1359–1366.

[5] H. Fang, Z. Jianbin, C. Guohua, W. Xionghui, J. Chem. Eng. Data 53 (2008) 2598–2601.

Excess Molar Volume of Nitromethane and 1-Alkanols

M. Almasi [a], L. Mousavi*[a]

[a] Department of Chemistry, Science and Research Branch, Islamic Azad University, Khouzestan, Iran

Email: m.almasi@srbiau.ac.ir

Key words: Density, Excess molar volume, 1-Alkanols, Nitromethane

Introduction:

Excess properties of mixtures provide information about the molecular interactions between the various components and can be used for the development of molecular models describing the thermodynamic behavior of mixtures [1]. Density, viscosity and refractive index data of binary liquid mixtures are very important from theoretical points of view, to understand liquid theory [2]. This paper reports the densities and excess molar volumes of Nitromethane and Alkanols at Temperatures(293.15-298.15-303.15-308.15) K.

Methods:

nitromethane, methanol, ethanol, 1-propanol, 1-butanol, 1-pentanol were purchased from Merck with purity higher than 99 %, (All) and used without further purifications. The density of the pure compounds and mixtures was measured by pycnometer. The temperature in the cell was regulated to ± 0.1 K.

Results and Discussion:

The excess molar volumes of the solutions of molar composition x were calculated at various temperatures from the densities of the pure liquids and their mixtures according to the following equation

$$V_m^E = \sum_{i=1}^{N} x_i M_i (\rho^{-1} - \rho_i^{-1}) \qquad (1)$$

where ρ is the density of the mixture, ρ_i is the density of pure component i, x_i is the mole fraction, M_i is the molar mass of component i, and N stands for the number of components in the mixture. The corresponding V_m^E values of binary mixtures of nitromethane (1) + 1-alkanols (2) measured and plotted against mole fraction of nitromethane at T = 308.15 K in

Figure 1. Each set of results were fitted using a Redlich–Kister polynomial [3] , which for binary mixtures is

$$Y^E = x_1(1-x_1)\sum_{k=0}^{N} A_k(1-2x_1)^k \qquad (2)$$

Where x_1 is the mole fraction of Nitromethane . A_k is adjustable parameter obtained by least-squares method, and k is the degree of the polynomials. Excess molar volume of Nitromethane with methanol and ethanol is negative in the region of enrichment of 1-Alkanols and for 1-propanol, 1-butanol and 1-pentanol is positive .The negative range of V_m^E values indicate strong specific interactions through dipolar association between 1-alkanols and nitromethane molecules. Positive one is due to strike hindrance between Nitromethane and 1-alkanol molecules.

Conclusions:

Excess molar volumes of nitromethane and 1-alkanols were obtained from experimental results and fitted by Redlich–Kister type equation. Excess molar volume is negative for (Nitromethane + methanol and ethanol) and positive at for other binary solutions.

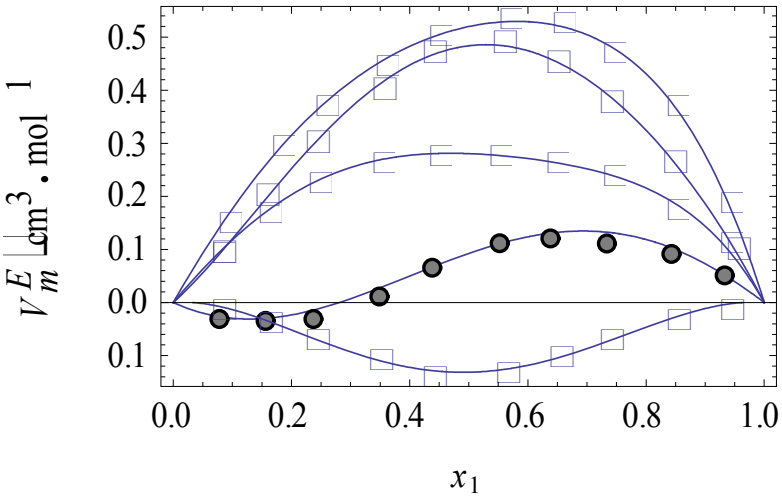

FIGURE 1. Excess molar volumes V_m^E vs. mole fraction of nitromethane for binary mixtures of Nitromethane with (■)methanol, (●) ethanol, (▲) 1- propanol,(⬚) 1-butanol, (◊)1-pentanol, at T = 303.15 K. The solid curves were calculated from coefficients of equation (2).

References

[1] Kim, E. S.; Marsh, K. N. Excess volumes for 2-methyl-2-propanol + water at 5 K intervals from 303.15 to 323.15 K. *J. Chem. Eng. Data* **1988**, *33*, 288 – 292.
[2] 6. Almasi, M.; Iloukhani, H. Densities, Viscosities, and Refractive Indices of Binary Mixtures of Acetophenone and 2-Alkanols. J. Chem. Eng.Data **2010**, 55, 1416–1420.
[3] Redlich, O. J.; Kister, A.T. Thermodynamic of non electrolyte solutions: algebraic representation of thermodynamic properties and the classification of solutions. *Ind. Eng. Chem.* **1948**, *40*, 345 – 348.

Thermodynamic study of poly(ethylene glycol) in water/1-propanol solutions by viscometry

Abbas Mehrdad*, Roghieh Moladoust

Department of Physical Chemistry, Faculty of Chemistry, University of Tabriz, Tabriz, Iran

(E-mail: a_mehrdad@tabrizu.ac.ir)

Abstract

In this work, the intrinsic viscosities of PEG with molar mass of 20 $kg \cdot mol^{-1}$ were measured in water/1-propanol solutions from (283.1 to 313.1) K. The expansion factors of the polymer chains were calculated from the intrinsic viscosity data. The thermodynamic parameters (entropy of dilution parameter, the heat of dilution parameter, theta temperature, polymer-solvent interaction parameter and second osmotic virial coefficient) were derived by the temperature dependence of the polymer chain expansion factor. The thermodynamic parameters indicate that mixtures of water/1-propanol are changed to the poorer solvents for PEG by increasing temperature and the quality of mixed water/1-propanol for poly(ethylene glycol) is less than pure water.

Keywords: Polymer solution, Poly(ethylene glycol), Intrinsic viscosity, Expansion factor

Introductionn

One of the most important transport properties in polymerization processes is the viscosity of polymer solutions. The viscosity of mixtures that contain polymers is much more difficult to predict than the viscosity of mixtures with low molecular weight components. Polymer-solvent and polymer-polymer mixture viscosity is an important physical property in polymer research and engineering [1]. When high molecular weight nonionic polymer molecules dissolve in a fluid, they typically expand to form spherical coils. In dilute solutions, the volume associated with each polymer coil contains one polymer molecule surrounded by a much larger mass of solvent. A polymer coil's hydrodynamic volume depends upon the polymer molecular weight and its thermodynamic interaction with the solvent [2]. The aim of this study was to determine the effect of temperature on the intrinsic viscosities of PEG in

mixtures of water/1-propanol and calculate some of the thermodynamic parameters by temperature dependence of expansion factor of the polymer chain.

Methods

PEG solutions were prepared gravimetrically by an analytical balance. The pol were prepared by dispersing the polymer powder into prepared 1-propanol aqueous solutions with volume fractions of 1-propanol = 0.10, 0.15 and 0.20. The polymer solutions were filtered before use by a filter with aperture 75 micrometer and their viscosities were measured using a jacketed Ubbelohde viscometer with 0.4 mm capillary. The temperature of solutions was kept constant by a temperature controller. Densities were measured with a U-tube vibrating densimeter.

Results and Discussion

ymer solutionsThe flow times of solutions of PEG in acetone aqueous solutions with volume fractions of

The flow times of solutions of PEG in mixed water/1-propanol with volume fractions of 1-propanol = 0.10, 0.15 and 0.20 were measured at various temperatures and concentrations of polymer and from these data, relative viscosities, are calculated. According to the Huggins equation the intrinsic viscosity of the polymer is obtained by extrapolation of reduced viscosity to zero polymer concentration. $\eta_{red} = [\eta] + k_H [\eta]^2 C$ Huggins equation

Flory and Fox further suggested that the temperature dependence of the expansion factor as follows [3]:

$$\alpha^5 - \alpha^3 = \left(\frac{27}{2^{1.5}\pi^{1.5}}\right)\left(\frac{\bar{v}^2}{N_A V_s}\right)\left(\frac{\langle R^2 \rangle_0}{M}\right)^{-1.5} \Psi M^{0.5}\left(1 - \frac{\theta}{T}\right)$$

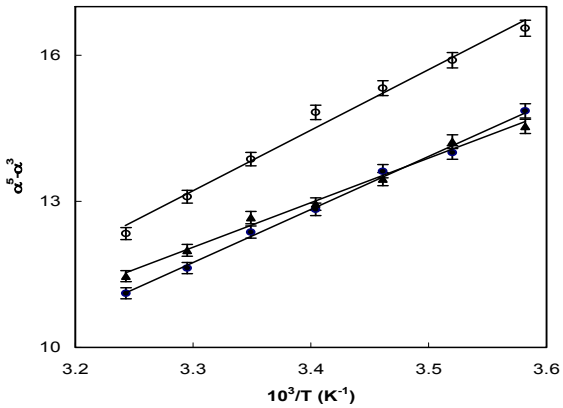

Figure 1. The plots of $(\alpha^5 - \alpha^3)$ versus $1/T$ for PEG in water/1-propanol with various volume fractions; ●, φ_P =0.10; ○, φ_P =0.15; ▲, φ_P =0.20.

From the intercept and slope of these plots the values of theta temperature (θ) and entropy of dilution parameter (Ψ) were calculated.

The obtained values of entropy of dilution parameter indicate that entropy of dilution parameter is negative for PEG in all volume fractions of 1-propanol that is, solvent molecules are ordered by PEG. However, the absolute value of entropy of dilution parameter for PEG in mixed water/1-propanol is less than of that in pure water. This behavior is maybe due to the interaction of PEG-water stronger than interaction of PEG-1-propanol; therefore the water molecules rather than 1-propanol are ordered by PEG. The values of polymer-solvent interaction parameter were calculated by:

$\chi = 0.5 + \kappa - \Psi$, $\kappa = \frac{\theta\Psi}{T}$ κ: The heat of dilution parameter

The obtained results indicate that polymer-solvent interaction parameter for PEG in all volume fractions of 1-propanol are increased by increasing temperature and the quality of mixed water/1-propanol for PEG were decreased by increasing temperature.

The obtained results indicate that of heat of dilution parameter is negative for PEG in all volume fractions of 1-propanol that is, interactions of segment-solvent is favored toward segment-segment in PEG.

The second osmotic virial coefficient in terms of the entropy of dilution parameter and the heat of dilution parameter can be expressed [4]:

$$A = \frac{\bar{V}^2}{V_s}(\Psi - \kappa)F(\alpha) \quad \text{where} \quad F(\alpha) = \sum_{n=0}^{\infty} \frac{(-2(\alpha^2 - 1))^n}{(n+1)!(n+1)^{1.5}}$$

The second osmotic virial coefficient is related to the quality of solvent in polymer solutions. The obtained results indicate that the quality of mixed water/1-propanol for PEG were decreased by increasing temperature.

Conclusion

In this work, the effect of temperature and solvent composition on the intrinsic viscosity of poly(ethylene glycol) was investigated. The polymer solution thermodynamic parameters were evaluated by temperature dependence of polymer chain expansion factor. The obtained thermodynamic parameters indicate that mixtures of water and 1-propanol becomes an increasingly poor solvent for poly(ethylene glycol) with increasing temperature.

References

[1] L.T. Novak, C. Chen, Y. Song, *Ind. Eng. Chem. Res.* 43 (2004) 6231-6237.

[2] T.S. Rushing, R.D Hester, *J. Appl. Polym. Sci.* 89 (2003) 2831-2835.

[3] P.J. Flory, T.G.Jr. Fox, *J. Am. Chem. Soc.* 73 (1951) 1904-1908.

[4] S. F. Sun, Physical Chemistry of Macromolecules: Basic Principles and Issues, John Wiley &Sons Inc, New York, 1994.

Design and Construction of Ion-Selective Electrode of CPC and Study on the CPC Micellization in Environmental Conditions

A.Nasirian*[a],M. Keshavarz[b]

[a,b]*Department of Chemistry, Islamic Azad University, Shahreza Branch, 311-86145, Shahreza, Isfahan, Iran*

E-mail: Afagh_nasirian@yahoo.com

Keywords: Ion selective electrode, Cetyl pridinium chloride (CPC), Silver wire- coated, Critical micelle concentration (CMC).

Introduction

special electrodes that are used to analyze a lot of compounds like shampoos, soaps and tooth A lot of ion selective electrodes (ISE) have been reported as sensor of cationic, anionic and neutral surfactants [1]. Most of these sensors act based on an ion exchanger that doesn't have any special reaction with analyte and are based on formation a charged complex with an inorganic cation about neutral analytes. In order to design a suitable membranous system, attempts started in early twentieth century based on biochemical and electrochemical researches [2, 3]. In this research at first we prepare the membranous ion selective electrode of surfactant. Surfactants as amphipathic materials aggregate in a specified concentration and produce micelle. Critical micelle concentration (CMC) depends on different structural and environmental parameters. Our purpose in this research is investigation of the effect of various concentration of alcohol on the cetyl pridinium chloride (CPC) micellization at 25 and 37°C in order to obtain comprehensive information about CMC of CPC in various conditions.

Methods

In this research project, micellization process of cationic surfactant of CPC in methanol, ethanol and propanol in various concentrations of 10%, 20% and 30% at 25°C was investigated and CMC was determined and related plots were constructed using Excel software.

Results and Discussion

Designed electrochemical cell for determining the surfactant concentration contains reference electrode of sodium and an ion selective electrode of surfactant. A specified volume of buffer solution consist of NaBr is used. After turning the potentiometer on, absolute volumes of surfactant are added gradually and potential difference is recorded. Analysis of CMC changes with kind and percentage of and trend of Emf changes versus [CPC] before and after the CMC are shown in Figur1.Increasing the alcohol percentage causes to decrease the amount of polarity and dielectric coefficient, this issue increase the attraction forces between opposite ions and causes to create ionic aggregations around the micelle. Figure 2, shows CMC changes of CPC versus different percentages of alcohol at 25°c.

Conclusion

CMC of CPC is 0.951mM at 25°c and I= 0.1mM NaBr in distilled water. With replacing the alcoholic solvents instead of distilled water, the CMC increases. Results are shown in Figures 2.

Fig1. *Emf variations versus log [CPC] in propanol (30%)*

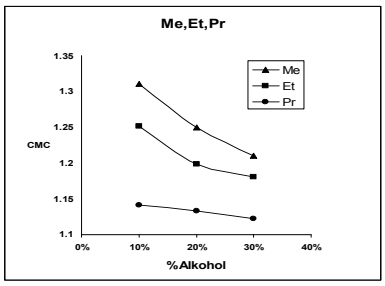

Fig. 2. *The curve of CMC and CPC*

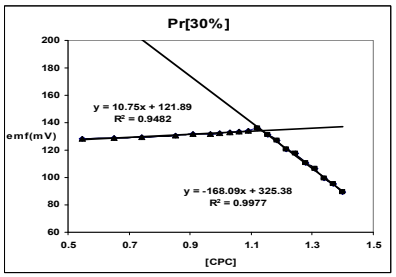

variations versus alcohol percentage

Emf amounts are presented in Table 1. Concentration of free surfactant in solution is calculated using equation mentioned as above. Increasing of CMC can be due to the hydrogen bond of alcohols with water that causes to destroy the water structure and decrease hydrophobicity of

Table 2: Emf data for prepared electrode of CPC in I= 0.1mM sodium bromide.

CpC mM	1.15	1.16	1.17	1.21	1.27	1.29	1.31	1.33	1.35	1.36	1.37
Emf $[Na^+](mV)$	31	51	60	68	77	84	92	109	115	124	130
Emf $[Br^-](mV)$	22	35	47	55	73	89	105	122	131	145	150

surfactants, so surfactant monomers become more stable in alcoholic environment and micelle is formed in higher concentrations.

References:

[1] E. Bakker, P. Buhlmann, E. Pretsch, Chem. Rev. , 98, 1593-1687,1998**.**

[2] A. G. Fogg, A. S. Pathan, D. T. Burns, Anal. Chim. Acta. **1974**, 69,238-242.

[3] *S. G. Cutler, D. G.* Hall*, P.* J. Meares*, Electroanal. Chem. ,* 85*, 145-161,* 1997.

Spectrophotometric and Thermodynamic Study of Praseodymium with Alizarin Red S Complex using EQUISPEC

B.Yasar[a,b], A.Niazi[a,b*] and Z.Hamedi[a]

a- Department of Chemistry, Faculty of Sciences, Islamic Azad University, Arak Branch, Arak, Iran

b- Young Researchers Club, Islamic Azad University, Arak Branch, Arak, Iran

**E-mail: ali.niazi@gmail.com*

Keywords: ARS; Praseodymium; Equilibrium; Stability constants, EQUISPEC

Introduction

The protonation and Pr(III) complexation of Alizarin Red S (ARS) in ionic strength 0.1 M KNO_3 at different temperature has been studied by EQUISPEC program [1-3]. In spectrophotometric titrations, linear or near-linear dependence of concentration profiles and the existence of minor species can cause difficulties in the evaluation of the data. Both calculated absorption spectra and the corresponding equilibrium constants are not or only poorly defined. The result is the inability to reliably fit a reasonable model to the data. In second order global analysis, a number of spectrophotometric titrations with different initial concentrations are simultaneously analyzed. In this way, conditions for the significant formation of all species can be obtained and consequently the concentration matrix is augmented to full rank. EQUISPEC is a computer program using the matrix based MATLAB environment for second order global analysis of spectrophotometric equilibrium data. The spectrophotometric titrations were carried out at least in four different metal to ligand ratios.

Materials.

Alizarin Red S, hydrochloric acid, sodium hydroxid, potassium nitrate and stock solution of praseodymium were analytical grade commercial products from Merck. These reagents were used without further purification. Standard stock solution of ARS and all the solution were prepared by dissolving in triply distilled water at acidified pH< 2.

Spectrophotometric Titrations

For the Pr/ARS titrations, absorption spectra were measured with an automatic titration set-up consisting of a computer interfaced to a HP8453 spectrophotometer, automatic stirrer, Metrohm 665 Dosimat automatic burette with 5 dispenser unit, a second syringe-burette, and a pH electrode. After each pH adjustment, solution is transferred into the cuvette and the absorption spectrum is recorded. The pH-meter was calibrated with at least three buffer solutions at pH 4.00, 7.00 and 11.00 (Reagecon Product labels). The uncertainty associated with these pH values are ±0.01 pH unit. Ionic strength was maintained at 0.1 mol L-1 by adding appropriate amounts of NaNO3.

Protonation constants of ARS and stability constants of Pr-ARS

The protonation were easily obtained in pH range 2-13 by the automatic titration apparatus at 25±0.5°C and I=0.1 mol L-1 (KNO3). The complexation of Pr3+ by ARS has been studied by titrating mixtures of Pr3+ and ARS at different temperature and I=0.1 mol L-1 (NaNO3) with standard solution of NaOH. The spectral measurements were carried out between 380 and 600 nm with 10 nm intervals. The concentrations of [ARS] and [Pr3+ to ARS] ratios in final solutions are 7.0×10-4 mol L-1 and 2:1, 1:1, 1:2, 1:3, 1:4, respectively. Then pH is adjusted in the range of 2-13 by adding hydrochloric acid and sodium hydroxide in titration vessel.

Computer hardware and software

All absorption spectra where digitized and transferred in ASCII format to an Athlon 2000 XP computer for analysis. Data treatment was done with MATLAB for windows (Mathworks, Version 6.5). The computer program EQUISPEC is written in MATLAB by M. Maeder et al.

Results and Discussion

The absorption spectra of ARS at various pH values in 350-600 nm intervals were recorded. Singular value decomposition analysis performed on all absorption data matrices obtained at various pH values for ARS gives the number of components that best represent the system. Protonation and complexation constants of ARS in several temperatures (10, 15, 20, 25, 30, 35 °C) were evaluated with EQUISPEC program using the corresponding spectra absorption-pH data. By inspection of the experimental spectra, it is hard to guess even the

number of protolytic species involved. The output of the program are pK_a, logβ values and their standard deviations, the number of principal component, projection vectors (loadings), concentration distribution diagrams, and the spectrum of each assumed species. The enthalpy and entropy of the different reactions were determined from the dependence of the equilibrium constants on the temperature (Van't Hoff equation). From the thermodynamic results the $T\Delta S^{\circ}$–ΔH° plot was sketched. Despite the above-mentioned variations which have deterministic effect on the thermodynamics parameters of complexation, the $T\Delta S$ versus ΔH° plot shows a fairly good linear correlation indicating the existence of enthalpy–entropy compensation in the complexation reactions [4, 5].

Table 1 . Values of log *K* and thermodynamic parameters for the protonation of ARS.

	10 °C	15 °C	20 °C	25 °C	30 °C	35 °C	ΔH (KJmol^{-1})	ΔS (J mol^{-1}K^{-1})	ΔG (KJmol^{-1})
pK_{a1}	6.02	5.72	5.51	5.32	5.16	4.92	70.377	58.259	53.015
pK_{a2}	10.98	10.84	10.66	10.50	10.34	10.14	55.75	5.8	54.16

Table 2. Logarithms of overall formation constants at 25°C and I=0.1 mol L-1 (KNO3).

	10 °C	15 °C	20 °C	25 °C	30 °C	35 °C	ΔH (KJ mol^{-1})	ΔS (J mol^{-1}K^{-1})	ΔG (KJ mol^{-1})
log K_1 (ML)	12.92	12.76	12.63	12.58	12.32	12.21	-103.45	-35.33	-93.80
log K_2 (ML2)	9.19	9.07	8.96	8.76	8.62	8.53	-46.18	-4.98	-44.82
log K_3 (MHL)	23.43	23.02	22.76	22.34	22.11	21.89	-46.65	-35.58	-36.93

References

[1] P. Bugnon, J.C. Chottard, J.L. Jestin, B. Bung, G. Laurenczy, M. Maeder, A.E. Merbach, A.D. Zuberbuhler, Anal. Chim. Acta 298 (1994) 193.

[2] J. Ghasemi, A. Niazi, M. Maeder, J. Braz. Chem. Soc. 18 (2007) 267.

[3] J. Ghasemi, A. Niazi, M. Kubista, A. Elbergali, Anal. Chim. Acta 455 (2002) 335.

[4] Y. Inoue, T. Hakushi, J. Chem. Soc. Perkin Trans. II (1985) 935.

[5] J. Ghasemi, M. Shamsipur, J. Coord. Chem. 36 (1995) 183.

[6] P. Bugnon, J.C. Chottard, J.L. Jestin, B. Bung, G. Laurenczy, M. Maeder, A.E. Merbach, A.D. Zuberbuhler, Anal. Chim. Acta 298 (1994) 193.

P-V-T Properties of non-Branches Heavy Alkanes

Fakhri Yousefi
Department of Chemistry, Yasouj University, Yasouj, 75914-353, Iran
(fyousefi@mail.yu.ac.ir)

Keywords: TM EOS, ISM EOS, Density, Second virial coefficient

Introduction

Actually the most fundamental tool in providing a basis to predict the thermophysical properties of matter is the equation of state. An accurate analytical equation of state for fluids is a very useful quantity, especially if it has a firm basis in statistical-mechanical theory.

In an earlier work, Tao and Mason [1] developed the present statistical-mechanical equations of state [2] to obtain an accurate description of the phase boundaries (vapor pressures). As expected, the correction turns out to affect mainly the metastable and unstable portions of the p-v loops, and has only a minor effect on the stable regions (where in fact it produces a small improvement in accuracy). The correction arises from the region of attraction forces, which is from distances greater than r_m, the position of the potential energy minimum. However, the overall structure of the final equation is quite similar to the previous ones, and gives accurate vapor pressures and improved orthobaric densities of the liquid and vapor from the triple point to near the critical point.

Theory

The final form of the TM EOS for single substances is given by

$$\frac{P}{\rho KT} = 1 + (B_2 - \alpha)\rho + \frac{\alpha\rho}{1-\lambda b\rho} + A_1(\alpha - B_2)b\rho^2 \frac{(e^{\frac{kT_c}{T}} - A_2)}{1+1.8(b\rho)^4} \quad (1)$$

For achieve to higher accuracy, we employed the correlation scheme of Ghatee and Boushehri [3] to predict the equation of state for the heavier members of n-alkanes. The correlation reads as:

$$B_2\rho_f = 0.0804 - 2.1288T^{*-1} + 8.5598T^{*-2} + 7.4294T^{*-3} - 3.3494T^{*-4} \quad (2)$$

$$T^* = \left[\frac{T^{3/2}}{T_{ref}T_f^{1/2}}\right]^{3/4} \quad (3)$$

$$T_{ref} = \frac{\gamma_f \rho_f^{-2/3} N^{1/3}}{R} \quad (4)$$

Where γ_f and ρ_f are the surface tension and the liquid density at the freezing point, respectively, and N is Avogadro's number. Knowing the temperature-dependent parameters, the equation of state can be applied to predict the liquid density of fluids over a wide range of temperatures and pressures.

Result and Discussion

We have taken the surface tension and the freezing point data from the tabulations of Vargaftik [4]. Knowing the temperature-dependent parameters, it takes only one experimental *P-V–T* datum point to calculate the free parameter of the equation of state, λ. we adjusted the parameter of λ for these systems by nonlinear regression method. The orthobaric liquid densities of C_{10} and C_{16} are calculated and compared with experiment [4], ISM EOS [5] and corresponding- states liquid densities (COSTALD) [6] in Fig 1 and 2. Comparison of our calculated results in Fig 1 and 2 with those obtained by the previous methods [5, 6] reveals that the absolute average deviation percent (AAD) corresponding to TM EOS, ISM EOS and COSTALD are 0.38%, 2.02% and 0.44% respectively. So the proposed model (TM) has more accurate prediction ability over non-branches heavy alkanes compared with other models.

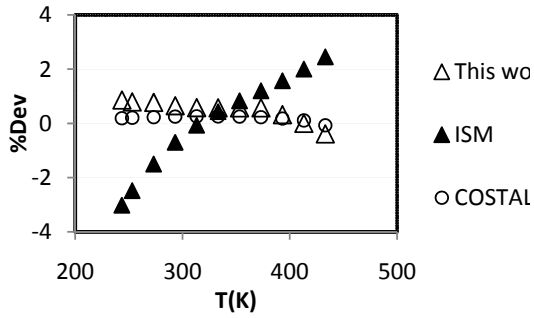

Figure1. Comparison of calculated density of $C_{10}H_{22}$ by TM EOS with experiment [4], ISM EOS [5] and COSTALD [6]

Figure2. Comparison of calculated density of $C_{16}H_{32}$ by TM EOS with experiment [4], ISM EOS [5] and COSTALD [6]

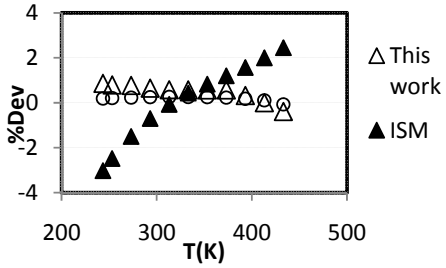

References

[1] Tao, F. M.; Mason, E. A. Statistical-Mechanical Equation of State for Nonpolar Fluids: Prediction of Phase Boundaries. *J. Chem. Phys.* **1994**, *100*, 9075.

[2] Ihm, G.; Song, Y.; Mason, E. A. Strong principle of corresponding states: Reduction of a p-v-T surface to a line, *Fluid Phase Equilibria*, **1992**, *75*, 117.

[3] Ghatee, M. H., and A. Boushehri, ‘ Equation of state for Compressed Liquids from Surface Tension.’ *Int. J. Thermophys*. **1996**, 17, 945.

[4] Vargaftik, N.B., 1983. Handbook of Physical Properties of Liquids and Gases, Hemisphere, New York.

[5] Eslami, H., ‘Equation of state for Nonpolat Fluids: Prediction from boiling Point Constants.’ *Int. J. Thermophys*.,**2000**, 21, 1123.

[6] Hankinson, R.W and G.H. Thomson., New correlation for saturated densities of liquids and their mixtures. *AIChE J*.,**1979**, 25, 653

Electrochemistry

Electrochemical fabrication and application of poly ortho aminophenol/TiO_2 nanocomposite films

A. Ehsani, M.G. Mahjani, M. Jafarian

Department of Chemistry, Faculty of science, K. N. Toosi University of Technology

E-mail address: a_ehsani@dena.kntu.ac.ir

Keywords: nanocomposite, POAP, TiO_2, impedance

Introduction

Inorganic nanoparticles of different nature and size can be combined with the conducting polymer, giving rise to a host of nanocomposite with interesting physical properties and important application potential**.** Extensive research has been reported involving various inorganic particles, such as, calcium carbonate, silica, titanium dioxide, carbon black and magnetite with either micrometer or nanometer sizes. Among these materials, TiO_2 is biocompatible, stable, and environmentally friendly and its electronic, optical, and dielectric properties can be enhanced by surface Modifications. They have widely been used as fillers for polymers for improvement of the dielectric properties. Various metal oxides have been employed to modify electrodes for investigating the electrochemical behavior of biomolecules [1–3].

Experimental

To inspect the influence of TiO_2 nanoparticles on the electropolymerization of OAP, this process was monitored on a conventional substrate electrode but in dispersed TiO_2 presence in the solution and then sonicated to obtain a uniform dispersion. Poly ortho aminophenol (POAP) nanocomposite with different particle size was deposited on a glassy carbon electrode in a solution of 0.01M OAP in 0.1M sulfuric acid by means of normal pulse voltammetry (NPV). The surface morphology of POAP films were studied by using the scanning electron microscopy (SEM).

Results and discussion

Cyclic voltammetry (CV) and electrochemical impedance spectroscopy (EIS), galvanostatic charge-discharge study show that the films of nanocomposite exhibiting highest capacitance.

Here it is important to mention that addition of TiO_2 into electrolyte solution affects the electropolymerization process. Higher coverage from the larger specific surface in SEM, high specific capacitance and a novel modified electrode with semiconducting properties are obtained. The high specific capacitance indicates this nanocomposite electrode suitable for supercapacitor application. To illustrate the performance of the resulting electrodes in supercapacitors, constant current discharge was performed to measure the capacitance in a 0.5 M $HClO_4$ solution. Galvanostatic discharge curves at a current of 0.1 mA between 0 and 0.8 V show that the TiO_2/PANI electrode cell presents higher capacitance than the pure POAP and this has been considered as the contribution of faradic pseudo capacitance of MWNT/POAP supercapacitor.

Conclusion

In summary, we have demonstrated a simple and general strategy, namely in situ electropolymerization by using the ionic surfactant as electrolyte. Surfactant SDS has played a key role in the synthesis of conducting polymer/TiO_2 nanocomposite films. We have introduced the TiO_2/POAP composite electrode to improve the specific capacitance and power characteristic of electrochemical capacitance. The TiO_2 has an obvious improvement effect, which makes the composites have more active sites for faradic reaction and larger specific capacitance than pure POAP.

References

[1] R. Gangopadhyay, A. De, Chem. Mater 12 (2000) 608.
[2] G.L. Teoh, K.Y. Liew, W.A.K. Mahmood, Material. Letters 61 (2007) 4947.
[3] G. L. Jadav, P. S. Singh, Membrane Science 328 (2009) 257.

Corrosion protection effect of poly ortho aminophenol nanocomposites

A. Ehsani, M.G. Mahjani, M. Jafarian

Department of Chemistry, Faculty of science, K. N. Toosi University of Technology

E-mail address: a_ehsani@dena.kntu.ac.ir

Keywords: corrosion, nanocomposite, POAP, Al_2O_3

Introduction

Conducting polymers, e.g., polyaniline and its derivatives, have been found to display interesting corrosion protection properties. In the past decade, the use of polyanilines as anticorrosion coatings had been explored as the potential candidates to replace the chromium-containing materials, which have adverse health and environmental concerns. Corrosion protection of polyaniline on steel is attributed to an increase in the corrosion potential and to the redox catalytic property of polyaniline in the formation of passive layer of metal oxide. Incorporation of nano-scale inorganic materials to organic coatings has become one of the most prevalent approaches leading to nanocomposite coating products. Nanocomposite made out of two different materials would have a very high interfacial contact. Dispersing nano-particles, instead of larger particles allows a coating formulator to increase the "interfacial material" content significantly [1-3].

Experimental

To inspect the influence of Al_2O_3 nanoparticles on the electropolymerization of ortho aminophenol and corrosion inhibitor effect, this process was monitored on a conventional substrate electrode but in dispersed Al_2O_3 presence in the solution and then sonicated to obtain a uniform dispersion. Poly ortho aminophenol (POAP) nanocomposite with different particle size was deposited on a steel electrode in a solution of 0.01M OAP in 0.1M sulfuric acid by means of normal pulse voltammetry (NPV). The surface morphology of POAP/ Al_2O_3 films were studied by using the scanning electron microscopy (SEM).

Results & discussion

Coatings prepared from poly orthoaminophenol (POAP)–nano-Al_2O_3 particles synthesized by in situ electropolymerisation were found to exhibit excellent corrosion resistance much superior to POAP in aggressive environments. The corrosion studies were carried out on steel plates coated with different concentrations of nano- Al_2O_3. The electrochemical impedance spectroscopy was studied at periodic intervals during exposure to hot saline conditions for prolonged durations over a period of 48 h. The open circuit potential (OCP) was found to shift with time to more anodic side much above that of bare steel. The presence of nano- Al_2O_3 was found to be vital in the prevention of corrosion and the shift of OCP to anodic side. From these data, one could envisage more than 100 times improvement in the corrosion resistance especially for POAP prepared with 8 wt% nano- Al_2O_3. The exceptional improvement of performance of these coatings has been associated with the increase in barrier to diffusion, prevention of charge transport by the nanosize Al_2O_3, redox properties of POAP as well as very large surface area available for the liberation of dopant due to nano-size additive.

Conclusion

In this study, we report successful attempt of making nanocomposite comprised of alumina nanoparticles modified by POAP for the purpose of corrosion protection of steel. Modified nanoparticles were used as coating filler. Coating was designated to perform as an active barrier to electrolyte diffusion. Properties of the coating were examined by electrochemical impedance spectroscopy.

References

[1] P. Ocon, A.B. Cristobal, P. Herrasti, E. Fatas, Corrosion Science 47 (2005) 649.

[2] A. Mirmohsemi, A. Oladegaragoze, Synth. Met. 114 (2000) 105.

[3] D.J. Chako, A.A. Leyva, Chem. Mater. 17 (2005) 13.

Investigation of Voltammetric Behavior of Co(II)-A Zeolite Modified Carbon Paste Electrode in the presence of Acetaminophen

A. Nezamzadeh and L. Ahmadpour*

[a]Dpartment of Chemistry, Islamic Azad University, Shahreza Branch

arnezamzadeh@iaush.ac.ir

l_ahmadpour3223@yahoo.com

Abstract

The modified carbon paste electrode was prepared by incorporation of Co(II)-zeoliteinthecarbonpaste matrix. Theelectrochemicaloxidation of acetaminophen was investigated at the surface of this modified electrode in KCl solution using cyclic voltammetry.

Key words: acetaminophen, modified electrode, cyclic voltammetry

Introduction

Acetaminophen (AC) or paracetamol, a widely used antipyretic and analgesic drug, is an effective and safe agent used worldwidefor the relief of mild to moderate pain associated with headaches,backaches, arthritis and postoperative pain [1].Many methods have been described for the determination of AC, such as titrimetry [2], spectrophotometry [3] and liquid-chromatography. But titrimetric and spectrophotometric methods involve a tedious extraction process prior tothe determination, and liquid chromatography methods are often time consuming. Electrochemical methods are being extensively used for their elegant and sensitive properties, including for analysis of AC [4].

Reagents,Chemicals and Apparatus

The graphite fine powder, paraffin oil,lithium, potassium, and sodium nitrates and all other chemicals were from Merck. AC obtained Raha Pharmaceutical Company and. Doubly distilled deionized water was used for preparing all solutions a. The electrochemical measurements were performed with an EG&G potentiostat/galvanostat and the powersuite software was used. An Ag/AgCl (3.0M KCl) electrode (+0.197V vs. NHE) andPt wire were

used as the reference and counter electrode respectively. A JENWAY 3505 pH meter was used for pH measurements.

Experimental

An appropriate amount of the Co(II)-exchanged zeolite was mixed with 100 mg graphite powder and then Nujol was added. After through hand mixing in a mortar to obtain a fine paste, a portion of the composite mixture was packed into the end of a polyethylene tube. Unmodified zeolite (NaA) Electrode was prepared in a similar way, using a carbon-paste with unmodified zeolite (NaA). The supporting electrolyte, 25 mL KCl (0.4 M), was placed in the cell and an appropriate amount of Acetaminophen was added. The solution was degassed with pure argon for at least 5 min [4].

Result and Discussions

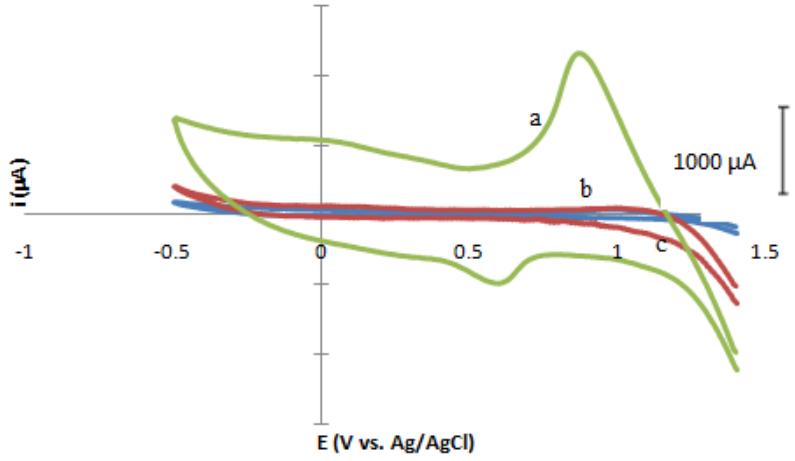

Figure 1. Cyclic voltammograms in 0.4 KCl, pH 5.5, at the scan rate of 50 mVs^{-1} for (a) the reaction on the modified carbon paste electrode Co(II)-A, (b) the same voltammogram run at the unmodified electrode and (c) the voltammogram at carbon-paste electrode.

Fig 1 shows voltammetric behavior of CP (c), unmodified carbon paste (b) and Co(II)A-CP (a) electrodes in a 0.4 M KCl solution. Due to ion exchange between the K^+ (in the solution) and Co^{2+} (in the zeolite), Co^{2+} undergoes a redox reaction at the surface of the electrode.

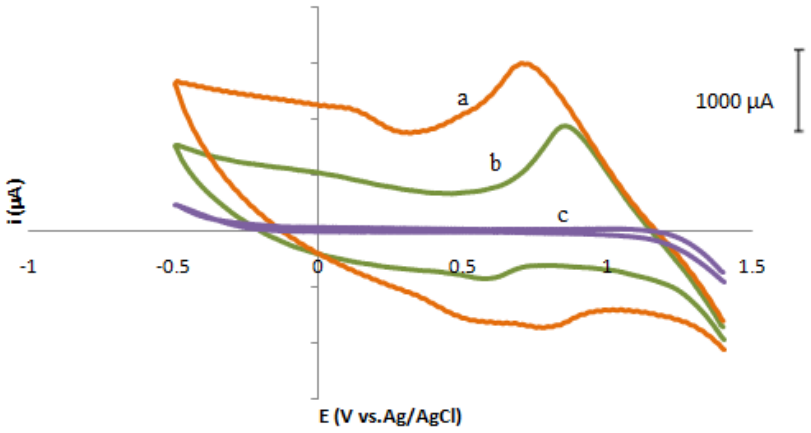

Figure 2. cyclic voltammograms in 0.4 KCl, pH 5.5, at the scan rate of 50 mVs^{-1}(a) for oxidation of 0.001 M AC at Co(II)-A zeolite (b) reaction at Co(II)-A zeolite absence of AC and (c) voltammograms at unmodified electerodein present of AC.

As Fig. 2 shows, addition of AC in the solution, causes an increase in peak current Hence the modified electrode uses for determination of AC in the aqueous solution. In the next experiments, effect of some experimental parameters such as, electrolyte type, scan rate, pH,… studied and good results obtained.

References

[1] J.Wang, R.P. Deo, P. Poulin, M. Mangey, J. Am. Chem. Soc. 125 (2003) 14706.

[2] G. Burgot, F. Auffret, J.L. Burgot, Anal. Chim.Acta 343 (1997) 125.

[3] M.R. Khoshayand, H. Abdollahi, M. Shariatpanahi, A. Saadatfard, A. Moham-madi, Spectrochim.Acta 70 (2008) 491.

[4] A. Nezamzadeh, M.K. Amini, H. Faghihian, Int. J. Electrochem. Sic. 2 (2007) 583-594

Development of a cloud point extraction and preconcentration method for Mg^{2+} and Cd^{2+} and Zn^{2+} prior to flame atomic absorption spectrometric determination

Ardeshir Shokrollahi[1]*, Sara Eslami[2], Ali Hossein Kianfar[1],

1 Chemistry Department, Yasouj University, Yasouj, Iran

2 Chemistry Department, Islamic Azad University of Firouzabad, Firouzabad 74715-117, Iran

E-mail: ashokrollahi@mail.yu.ac.ir

Abstract

A simple, sensitive and selective cloud point extraction method is described for the preconcentration and atomic absorption spectrometric determination of Mg^{2+} and Cd^{2+} and Zn^{2+}

in tea samples. After complexation with (E)-2-(2-hydroxybenzylideneamino) benzoic acid in basic medium, analyte ions are quantitatively extracted to the phase rich in Triton X-114 following centrifugation. The chemical variables affecting the preconcentration process were optimized.

Key words: Mg^{2+} and Cd^{2+} and Zn^{2+}, Cloud point, flame atomic absorption

Introduction

Mg^{2+} and Cd^{2+} and Zn^{2+} may be harmful if eaten in excessive amounts [1]. So, the determination and monitoring of these analytes is becoming increasingly importance in environmental samples. FAAS technique has not enough sensitivity therefore, preconcentration and separation of analyte are needed before measuring [2]. The use of preconcentration steps based on CPE offers a way that are simple, cheap, selective, sensitive [3,4].

Experimental and amount of materials

A typical cloud point experiment required the following steps: an aliquot of 15 ml of a solution containing 133.3 μg L^{-1} Mg^{2+} and 133.3 μg L^{-1} Zn^{2+} and 133/3 μg L^{-1} Cd^{2+} ions, 0.17% (w/v) Triton X-114 and acid (E)-2-(2-hydroxybenzylideneamino) benzoic acid (0.13

mM) was adjusted to pH 9 by addition of NaOH. The mixture was shaken for 1 min and left to stand in a thermo-stated bath at 65 °C, for 20 min. Separation of the phases was achieved by centrifugation at 3500 rpm for 15 min. The whole system was cooled in an icebath for 5 min that the surfactant rich phase would regain its viscosity. In this way, the bulk aqueous phase was easily decanted. The remaining micellar phase was dissolved to 0.5 mL in 1.0 M HNO_3 in methanol and the Mg^{2+} and Cd^{2+} and Zn^{2+} ions content was readily evaluated by FAAS.

Results and discussion

The aim of this paper is using a new Schiff base as a power complexing agent for the preconcentration and determination of trace amounts of Mg^{2+} and Cd^{2+} and Zn^{2+}ions in various real samples. In this regard, the influence of various effective parameters including pH, surfactant and ligand concentrations, heating time and temperature, centrifuge time and rate and the effect of electrolyte on absorbance were optimized.

Effect of pH

The formation of the metal–chelate and its chemical stability are two important factors influence on CPE. The pH plays a unique role on metal–chelate formation and subsequent extraction and proved to be the main parameter for CPE. Extraction yield depends on the pH at which complex formation is carried out. In this view, a set of similar experiments in the pH range of 2.0-11.0 was conducted according to the described procedure in experimental section and respective results are illustrated in Fig.1. The maximum sensitivity was obtained at pH 9.

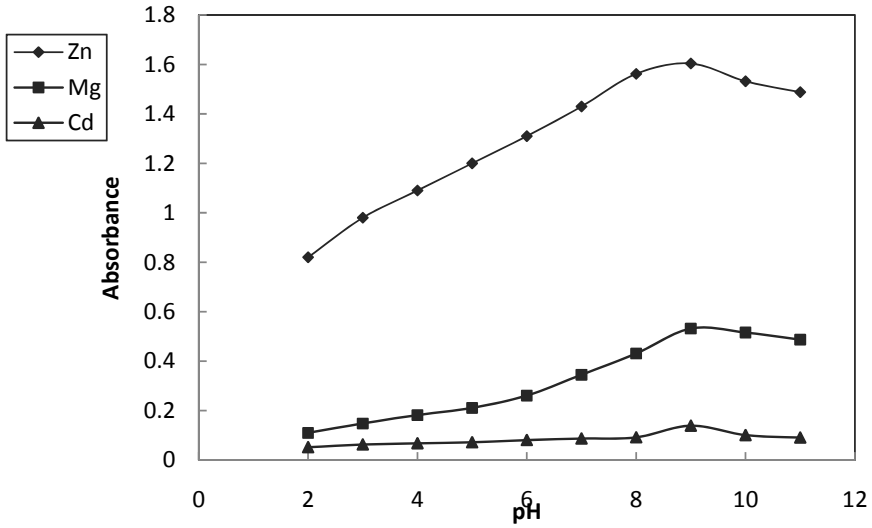

Effect of ligand concentration

The absorbance of extracted metal ions as a function of the concentration of ligand increasing of ligand concentration up to a 0.13 mM cause increases absorbance. Thus, a ligand concentration of 0.13 mM was chosen for optimization of other variables.

Effects of other experimental factors

The incubation time and equilibration temperature above the cloud point were thoroughly optimized. It is desirable to employ the shortest equilibration time and the lowest possible equilibration temperature, which compromise completion of the reaction and efficient separation of the phases. The dependence of extraction efficiency on equilibration temperature and time were studied within a range of 30–70 $^{\circ}$C and 5–30 min, respectively. The results showed that an equilibration temperature of 65°C and an equilibration time of 20 min are adequate to obtain quantitative extraction of two ions. The effect of the centrifugation time on the extraction efficiency was also studied within a range of 5–25 min. A centrifugation time of 15 min at 3500 rpm was selected for the entire procedure, since analyte extraction in this time is almost quantitative

Effect of Triton X-114 concentration

Type and concentration of surfactant are important factor, in cloud point extraction Triton X-114 was chosen as a proper surfactant due to it's physicochemical characteristics, low cloud

point temperature, commercial availability, relatively low price, low toxicity, it's high density in the surfactant-rich phase and facilitates phase separation. The variation in absorbance of extracted Mg^{2+} and Cd^{2+} and Zn^{2+} ions within the Triton X-114 concentration range of 6.6×10^{-3}- 0.2 % (w/v) was examined and the results are shown in Fig. 2. It can be seen that quantitative extraction was obtained with an optimum Triton X-114 concentration of 0.17% (w/v), where the highest absorbance for extracted Mg^{2+} and $Cd^{2+}$and Zn^{2+} ions was obtained.

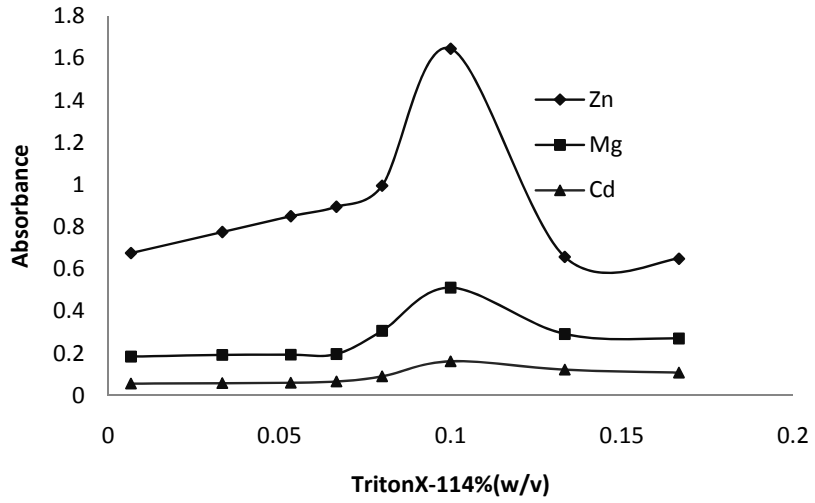

Interferences

In the view of high selectivity provided by FAAS, the only interferences studied were those related to preconcentration step*, i.e.,* those cations that may react with ligand and anions that may form complexes with Mg^{2+} and Cd^{2+} and Zn^{2+} and decrease extraction efficiency. Study of the possible interferences caused by cationic species was conducted with zinc(II), lead (II), cadmium (II), cobalt (II), aluminum (III), nickel (II) (for Mg^{2+}) and copper (II) (for Cd^{2+} and Zn^{2+}) ions under the experimental conditions used in the presence of a fixed concentration of 133.3 µg $L^{-1}$and 133.3 µg L^{-1} of Mg^{2+} and Cd^{2+} and Zn^{2+} respectively . There was no significant interference at a 1:100 ratio of Mg^{2+} and Cd^{2+} and Zn^{2+} to the cations.

Reference

[1] V. A. Lemos, M. S. Santos, G. T. David, M. V. Maciel, M. de Almeida Bezerra, *Journalof Hazardous Materials,* **2008**, *159,* 245–251.

[2] J. L. Manzoori, A. Bavili-Tabrizi, *Microchim. Acta*, **2003**, *141*, 201–207.

[3] A. Shokrollahi, M. Ghaedi, O. Hossaini, N. Khanjari, M. Soylak, *Journal of Hazardous Materials*, **2008**, *160*, 435-440.

[4] A. Sanz-Medel, M. R. Fernandez de la Campa, E. B. Gonzalez, M. L. Fernandez-Sanchez, *Spectrochim. Acta*, **1999,** *54*, 251.

Investigation on electrochemical behavior of poly (o-amino phenol) films synthesized by cyclic voltametry

Fatemeh . B . Hashemi*, Abbas. A. Rostamia and Abdollah. Omrani

Department of Chemistry,University of Mazandaran,Babolsar,Iran

(Email:fatemebagheralhashemi@yahoo.com)

Keywords: Poly(o-aminophenol) , Cyclic voltametry, Potentiostatic, Potentiodynamic.

Introduction

Conducting polymers synthesized electrochemically from compounds with conjucated π-bonds are of great interest in electrochemistry because of possible applications including rechargeable batteries [1], electrochromic display devices [2], corrosion protection materials [3] and electrochemical sensors [4]. In this article the films of POAP were synthesized electrochemically under potentiostatic and potentiodynamic conditions. The doping/dedoping behavior of the films at various PH were compared by CV technique.

Experimental

The monomer, o-amino phenol (OAP) was purchased from Merck. Sulfuric acid (Merck) 0.5M was used as the supporting electrolyte. Di hydrogen phosphate and di sodium hydrogen phosphate (Fluka) were also used as electrolyte solutions. All the experiments were performed using a Potentiostat/Galvanostat (SOLARTON SI 1287).

A three-electrode cell system was employed with glassy carbon as working, platinum as counter and Ag/AgCl(KCl : 3M) as refrence electrod. Electrods were rinsed with distilled water. Glassy- carbon was polished with alumina slurry on emery paper. Phosphate buffer solution (PBS) was prepared by 0.1M NaH_2PO_4-Na_2HPO_4. POAP films were potentiostatically grown at E=0.9V and potentiodynamically produced in a conventional three-electrode cell system, at a sweep rate (υ) of 50 mV s^{-1}, in a solution of OAP+sulfuric acid 0.1 M. The polymer disposited by CV from -0.2 to 0.6 v.

Results and discussion

Figure.1 show cyclic voltammograms of POAP films in pH=3 of sodium phosphate solution those formed by potentiostatic and potentiodynamic methods. This figure shows that the CV of potentiodynamic generated polymer film obtained at higher current. We observed that the film formed at potentiodynamic mods was less compact.The polymeric film deposited using potentiodynamic mode showed better conductivity. The work has been done at various pHs and the results showed that PH=3 is the best deposition condition.

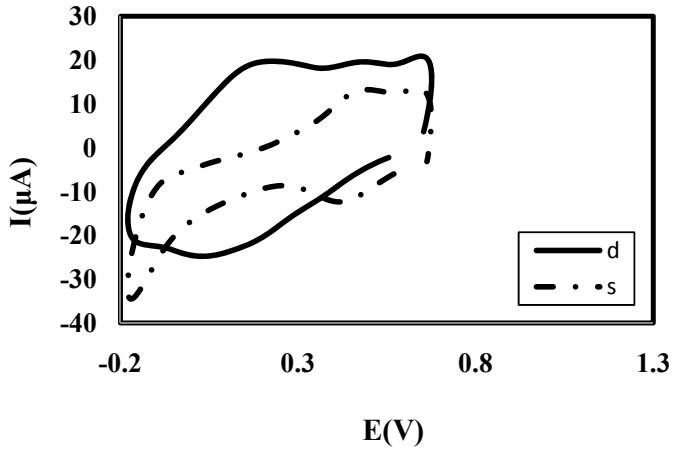

Fig.1 (s) cyclic voltammogram of potentiostatic formed polymer in the 0.1 M bafer phosphate in pH=3 (POAP film prepared at E= 0.9 v. in solution containing 0.1 M sulfuric acid). (d) potentiodynamic formed polymer in pH=3 of sodium phosphate solution.that formed in E=-0.2-0.6 V at 50 mV/s.

References

[1] M.S. Rahmanifar, M.F. Mousavi, M. Shamsipur, H. Heli, Synth. Met. 155 (2005) 480.

[2] A.A. Argun, J.R. Reynolds, J. Mater. Chem. 15 (2005) 1793.

[3] R.J. Holness, G. Williams, D.A. Worsley, H.N. McMurray, J. Electrochem. Soc 152 (2005) B73.

[4] M. Heitzmann, L. Basaez, F. Brovelli, C. Bucher, D. Limosin, E. Pereira, B.L. Rivas, G. Royal, E. Saint-Aman, J.-C. Moutet, Electroanalysis 17 (2005) 1970.

Comparison study between electroless and electrolysis Nickel coated graphite

A.Raufi kian*, F.Bohlooli, S.A.Seyed Sajadi,

Department of chemistry, Iran university of science and technology, Tehran, Iran

(abbas.kian@yahoo.com)

Abstract

Nickel-coated graphite have been prepared by electroless and electrolysis deposition process [1]. The characteristics and size of particles have been investigated. Also the effects of some electroless nickel bath stabilizers; potassium sodium tartarat tetrahydrate (PSTT) and sodiumdodecyl sulfate (SDS) in deposition which created by electroless, were investigated[2]. Scanning electron microscopy (SEM) images, XRD pattern of the composites used to describe the coating formed on graphite.

Keyword: Electrolysis, Electroless, Nickel-coated, Graphite

Introduction

electrolysis use to coat a surface with a thin layer of metal for protection against corrosion and wear. electroless deposit has the advantages of simplicity and feasibility over others in changing the characteristic of the graphite surface. Major advantages over the electro deposition process include the formation of a uniform deposit on irregular surface such as graphite[3, 4]. In present study we have compared tow deposition characteristics produced by electrolysis and electroless coating.

Experimental and Methods

Nickel sulfate ($NiSO_4.6H_2O$, 98.2%), sodium Hydroxyl(NaOH) , potassium sodium tartarat tetrahydrate(PSTT) , formaldehyde (HCHO 37%) , and sodium dodecyl sulfate (SDS) were purchased from Merck. The SEM and XRD used to describe the properties of depositions.

Result and discussion

By comparing the image (c) with images (a),(b) (fig 1), we see that in image (c) coating is more uniform and particles are more compact. As well as large particles (micrometer scale), created in electrolysis the empty space between the particles cannot be seen

Whereas in the image ((a),(b)) coating is more non-uniform And open spaces between the particles well observed.

On the other hand, if the (a) and (b) images compare; the image (b) shows particles are more fine and nono-scale with separate and specific granules. Whereas the size of particles in image (a) are large and also less distinct grains is seen.

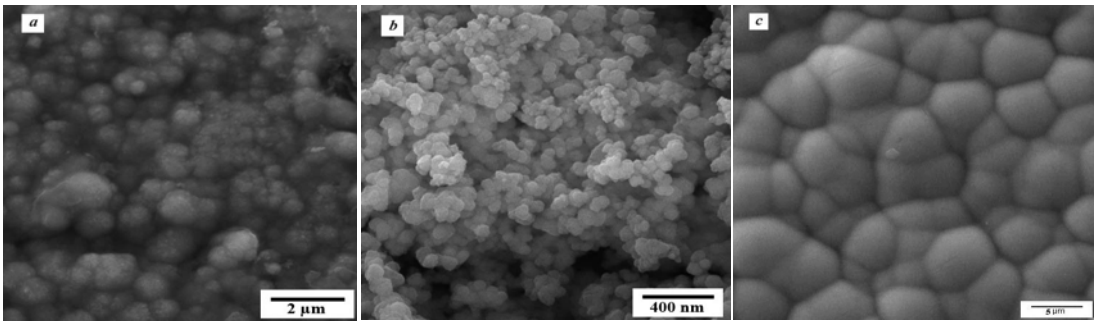

Figure 1. SEM microscopy images of nickel-coated graphite (a)electroless with PSTT as stabilizer (b) electroless with SDS as stabilizer (c) electrolysis.

Conclusion

The results show that the nickel coating on the surface of graphite created by electrolysis are uniform and have larger particles. While the coating created by electroless is non-uniform and particles size are smaller than electrolysis coating. Due to their applications one of two methods used for coating on graphite. Also with changing the type of stabilizers in electroless method, structure and type of coverage can be controlled.

References

[1] Arai S, Endo M, Hashizume S, Shimojima Y. Nickel-coated carbon nanofibers prepared by electroless deposition. Electrochemistry Communications. 2004;6(10):1029-31.

[2] Cheong WJ, Luan BL, Shoesmith DW. The effects of stabilizers on the bath stability of electroless Ni deposition and the deposit. Applied Surface Science. 2004;229(1-4):282-300.

[3] Li Q, Zeng G-Z, Zhao W-F, Chen G-H. Preparation and characterization of nickel-coated graphite nanosheets. Synthetic Metals. 2010;160(1-2):200-2.

[4] Shi Z, Wang X, Ding Z. The study of electroless deposition of nickel on graphite fibers. Applied Surface Science. 1999;140(1-2):106-10.

Corrosion behavior of electroless Zn-W-B deposits in the variety of metallic ratio

F. Bohlooli* , SH . Hashemi, S. A . Seyed sadjadi

Department of chemistry, Iran University of Science and Technology, Tehran, Iran

Email: fatemehbohlooli@gmail.com

Abstract

The formation of electroless Zn-W-B ternary alloy deposits was studied using varying metallic ratio. Variation in metallic ratio of the bath enables the formation of electroless Zn-W-B deposits with varying contents of zinc, tungsten. Morphology and chemical analysis deposits were investigated by SEM and EDAX. The results of corrosion test showed that in the metallic ratio of (Zn /Zn +w) =0.3 highest corrosion resistance observed.

Keywords: Electroless deposition, Zn-W-B alloy,SEM, Corrosion behavior

Introduction

Iron and steel, the most commonly used metal, corrode in many media including most outdoor atmospheres [1]. Zinc alloy are widely employed as sacrificial protective coatings to prevent corrosion of steel [2]. Tungsten has unique properties such as high hardness, tensile strength and higher melting point, etc. tungsten have created a lot of interest to add in zinc electroless bath that improves the corrosion resistance of zinc coating [3]. In this perspective, the aim of present work is to prepare electroless Zn-W-B ternary alloy deposits using plating baths with varying zinc to tungsten ratio and to evaluate their corrosion behavior.

Experimental

$ZnSO_4.7H_2O$ and $Na_2WO_4.2H_2O$ were used as the source of zinc and tungsten, respectively. Dimethylamine Borane (DMAB) was used as the reducing agent, which also forms the source of boron. Tri-sodium citrate was used as the complexing agent. The total concentration of $ZnSO_4.7H_2O$ and $Na_2WO_4.2H_2O$ were kept at 0.1M.Similarly, the concentrations of tri-sodium citrate and DMAB were kept constant at 0.1 M and 0.024M respectively. Metallic

ratio ($ZnSO_4$/ $ZnSO_4$ + Na_2WO_4) (0.1 – 0.9) were varied to study of corrosion behavior of deposits. Structure characteristics of surfaces were studied with scanning electron microscopy (SEM). Chemical analysis was carried out with energy-dispersive X-ray analysis (EDAX). For polarization tests, samples were protected with an adhesive film to leave a 1cm^2 surface in contact with the NaCl 3.5% solution.

Results and discussion

At least three polarization tests were carried out for each concentration. Fig 1 shows the polarization curve of the coatings in the variety of metallic ratio. The good corrosion resistance observed at the metallic ratio of (Zn /Zn +w) =0.3, attributed to the high amount of tungsten and compact structure which these results were found from analysis of EDAX and SEM, respectively.

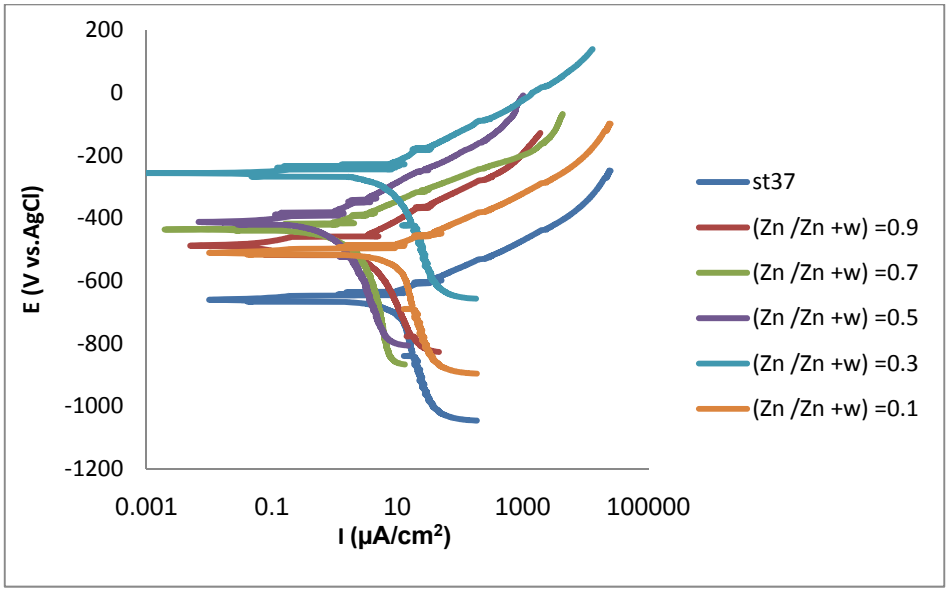

Fig. 1. Polarization curve of variety of metallic ratio of Zn-W-B coatings

Conclusion

Ternary Zn-W-B coatings were deposited in the variety of metallic ratio. It was found from the SEM observations that with increasing the amount of tungsten, compact structure were obtained. Polarization tests indicated that good corrosion resistance obtains in the high concentration of tungsten.

References

[1]. D.D.N. Singh, Rita Ghosh, Surface & Coatings Technology 201 (2006) 90–101

[2] Y. Hamlaoui, L. Tifouti, F. Pedraza, Corrosion Science 52 (2010) 1883–1888

[3]J.N. Balaraju, S. Millath Jahan, C. Anandan, K.S. Rajam, Surface & Coating Technology 200 (2006) 4885-4890

Electroless deposition of Zn-W-B coating on steel alloy

F. Bohlooli*, A. Raufi kian, S. A . Seyed sadjadi
Department of chemistry, Iran University of Science and Technology, Tehran, Iran
Email: fatemehbohlooli@gmail.com

Abstract

Ternary Zn-W-B alloy coating was deposited on st37 by electroless plating technique. Zinc sulfate and sodium tungstate were used as metal ion sources, and Dimethylamine Borane (DMAB) was used as a reducing agent. The effect of surfactant cetyltrimethyl ammonium bromide (CTAB) on the surface morphology and corrosion behavior was investigated. The Zn-W-B deposits were characterized by scanning electron microscopy (SEM) and energy-dispersive X-ray analysis (EDAX). SEM observation showed that in the presence of CTAB, the grain size was reduced and compact coating was obtained. Polarization curve indicate that coating composed of surfactant have high corrosion resistance than ones without surfactant.

Keywords: Electroless, Zn-W-B coating, Corrosion resistance, Steel alloy

Introduction

Electroless of zinc coatings alloyed with other metals is one of methods to improve their service characteristics [1]. The uniqe property of tungsten have created a lot of interest in the scientific community in developing ternary Zn-W-B alloys as a replacement for hexavalent chromium[2]. The aim of this work is to prepare electroless Zn-W-B ternary alloy deposits also the study of characteristics of the coatings in presence and absence of CTAB.

Experimental and method

St37 alloy was used as the substrate material for preparation of electroless Zn-W-B deposits. Electroless bath containing: $ZnSO_4.7H_2O$ (20g/l), $Na_2WO_4.2H_2O$ (10g/l), DMAB (1.6g/l), $Na_3C_6H_5O_7$ (35g/l), $C_{19}H_{42}BrN$ (0, 0.35g/l) was performed for 1 hour at 75^0C. During plating, the bath solution was agitated using a magnetic stirrer at 600 rpm,

and PH was adjusted with buffering agent. morphology of surface and chemical analysis of the coatings were studied by SEM with EDAX. corrosion tests carried out in the 3.5% NaCl solution.

Results and discussion

The scanning electron micrograph of the surface deposit Zn-W-B in absence and presence of CTAB, shown in Fig. 1(a,b).

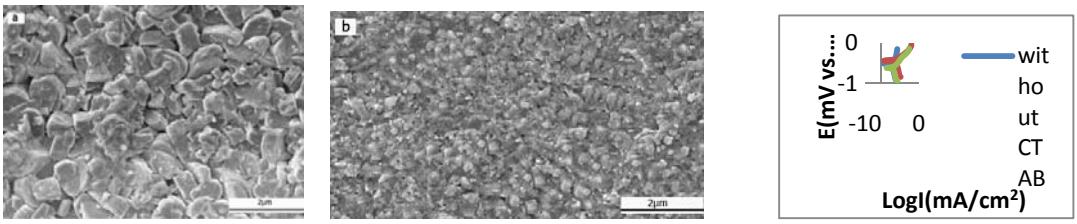

Fig. 1. Scanning electron micrographs of a) Zn-W-B without CTAB b) with CTAB c) Polarization curves of the coatings in the presence of CTAB and without it.

SEM observation shows that in the presence of CTAB grain size extremely reduced and compact coating was obtained. EDAX analysis showed that the content of tungsten in the both of Zn-W-B coatings were 9.18%. Fig.1(c) illustrate polarization curves for the both coatings. Indicating the deposit consist of CTAB has higher corrosion resistance than ones without one.

Conclusion

The electroless Zn-W-B on the steel was deposited from a citrate-base bath. SEM observation showed fine grain in the presence of CTAB surfactant and EDAX analysis showed that the contents of the coatings were kept constant. Due to the fine and compact structure of deposit the corrosion resistance improved in presence of CTAB.

References

[1] L. S. Tsybul'skaya, T. V. Gaevskaya, T. V. Byk, and G. N. Klavsut, Russion Jounal of Applied Chemistry 74 (2001) 1628-1632

[2] J.N. Balaraju, S. Millath Jahan, C. Anandan, K.S. Rajam, Surface & Coating

Technology 200 (2006) 4885-4890

[3] Z. Abdel Hamid, Surf. Interface Anal. 35 (2003) 496-501.

Amperometric Determination of Ascorbic Acid Based on Electrocatalytic Oxidation Using a Poly(Aniline-*co*-*ortho*-Phenylenediamine) Modified Electrode

A. Parsa*[a], Z. Doroudi[a], R. M. A. Tehrani[a] and M. Abdous[b]

[a]*Department of Chemistry, Islamic Azad University, Shahre Rey Branch, Tehran, Iran*

(Email: iausr.parsa@yahoo.com)

[b]*Department of Chemistry, Amirkabir University of Technology, Tehran, Iran*

Abstract

In this work the poly(aniline-*co*-*ortho*-phenylenediamine) (Ani–*co*–*o*PDA) modified composite graphite (CG) show excellent electrocatalytic response towards the oxidation of AA. The anodic peak potential of AA is shifted from +0.52 V at bare CG to +0.12 V at poly(Ani–*co*–*o*PDA) coated CG. A linear regression relationship between current and the AA concentration range, 5 to 40 mM, is obtained.

Keywords: Amperometric; Ascorbic Acid**;** Electrocatalytic; Modified Electrode; polyaniline

Introduction

The determination of ascorbic acid (AA) has become very important since AA is known to be present in human brain and also involves in several biological processes [1].

Several voltammetric studies of AA on the bare electrode have not been very successful [2, 3]. The main reason is being the high overpotential of AA besides the fouling effect of the oxidation products, poor reproducibility, low selectivity and poor sensitivity. Mediators [4, 5] and polymer modified [6, 7] electrodes have instead been used to improve the situation.

The electrochemical copolymerization of aniline (Ani) with its derivatives has been reported [8-10]. These have significantly improved the electrochemical activity of polyaniline by leap and bound. Recently, poly(aniline-*co*-*ortho*-phenylenediamine) (Ani–*co*–*o*PDA) modified composite graphite (CG) electrode has been prepared [11].

Methods

The electro copolymerization of Ani and *o*PDA was performed using 25 ml solution containing 50 mM monomers, 1 M H_3PO_4 and 0.06 M $Ca_3(PO_4)_2$ by sweeping the potential

between −0.7 and +0.8 V (vs. Ag/AgCl), at scan rate of 100 mVs^{-1} and under Oxygen-free nitrogen (OFN) atmosphere at 25 ± 2 ºC.

The voltammetric determinations of AA was performed using 25 ml solution containing 30 mM of AA and 1 M H_3PO_4 by sweeping the potential between −0.6 V to +1.0 V at scan rate of 100 mVs^{-1}, under OFN atmosphere and at 25 ± 2 ºC.

Results and discussion

Electrocatalytic oxidation of AA

The anodic peak potential (E_{pa}) of AA appears at +0.52 V on CG with the anodic peak current (I_{pa}) about 0.4 mA. It is an irreversible process. In contrast, the I_{pa} has increased to 1.7 mA and the E_{pa} shifted negatively to +0.12 V on the poly(Ani–*co*–*o*PDA) modified CG. Since the electro-oxidation of AA is convenient, this indicates the strong electrocatalytic property of poly(Ani–*co*–*o*PDA) modified CG to AA. The shifting of the E_{pa} is due to the kinetic effect in which a substantial increase in the rate of electron transfer from AA is observed.

Effect of AA concentration

In chronoamperometric experiments (Fig. 1), the current flowing through the poly(Ani–*co*–*o*PDA)/CG electrode at +0.12 V was measured as a function of concentration of AA in 1 M H_3PO_4. Fig. 1b shows a response by the modified electrode upon addition of AA. On the contrary, the bare CG electrode does not respond (Fig. 1a).

Effect of pH

The cyclic voltammograms (CVs) of 25 mM AA in supporting electrolytes at different pH values at poly(Ani–*co*–*o*PDA) modified CG electrode were made. It appears that there is a decrease in anodic peak current, I_{pa}, when pH is raised from 1 to 9. This is due to a decrease in the electrochemical activity of poly(Ani–*co*–*o*PDA). The copolymer has a higher electronic conductivity in acid medium and this conductivity decreases with an increase in pH. There is also positive shifting of anodic peak potential, E_{pa}. Thus, the electrocatalytic effect of poly(Ani–*co*–*o*PDA) modified CG electrode on the oxidation of AA decreases with an increase in pH.

Conclusion

The poly(Ani-*co*-*o*PDA) modified CG electrode is shown to possess catalytic activity towards the oxidation reaction of AA. As a result, the electro oxidation of AA on the modified

electrode is more feasible in acidic than in neutral and alkaline medium. This is shown by negative shift of E_{pa} of AA. The extension of catalytic reaction depends on charge transfer. The electrode process is diffusion-controlled. The study indicates the poly(Ani–*co*–*o*PDA)/CG electrode is useful for oxidation of AA over a wide range of pH. The peak currents are linearly dependent on AA at concentration below 40 mM.

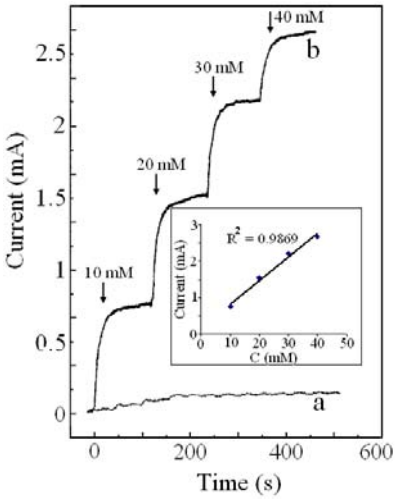

Figure 1. Chronoamperometric response of (a) bare CG electrode and (b) poly(Ani–*co*–*o*PDA)/CG electrode to changes in concentration of AA in 1 M H_3PO_4. Inset is the plot of I_{pa} *vs.* concentration of AA.

References:

[1]P.T. Mannisto, S. Kaakkola, Pharmacological Reviews 51/4 (1999) 593.

[2]R.P. Kalakodimi, M. Nookala, Analytical Chemistry 74/21 (2002) 5531.

[3]S.B. Khoo, F. Chen, Analytical Chemistry 74/22 (2002) 5734.

[4]C. Ueda, D.C.-S. Tse, T. Kuwana, Analytical Chemistry 54/6 (1982) 850.

[5]A.S.N. Murthy, Anita, Biosensors and Bioelectronics 9/6 (1994) 439.

[6]C. Mousty, B. Galland, S. Cosnier, Electroanalysis 13/3 (2001) 186.

[7]R.W. Murray, A.G. Ewing, R.A. Durst, Analytical Chemistry 59/5 (1987) 379A.

[8]S. Mu, Synthetic Metals 143/3 (2004) 259.

[9]S.H. Si, Y.J. Xu, L.H. Nie, S.Z. Yao, Electrochimica Acta 40/17 (1995) 2715.

[10]Y. Wei, R. Hariharan, S.A. Patel, Macromolecules 23/3 (1990) 758.

[11]A. Parsa, S. Ab Ghani, Polymer 49 (2008) 3702.

Inhibitive effect of organic compounds on the corrosion of copper and brass alloy in water cooling systems

A.A. Hamzeh[a], M. Parsa[b], S.M.A. Hosseini*[b]

[a]Department of Chemistry, Payam noor University of Kerman, Kerman, Iran

[b]Department of Chemistry, Shahid Bahonar University of Kerman, Kerman, Iran

E-mail address: s.m.a.hosseini@mail.uk.ac.ir

Keyword: Corrosion, Inhibitor, Copper, Brass alloy

Introduction

Copper is one of the most important materials in industry owing to its high electrical and thermal conductivities, mechanical workability, and its relatively noble properties, thus corrosion of copper and its inhibition have attracted the attention of many investigators [1-3]. In addition the surface of brass which contains copper is chemically, physically and energetically heterogeneous for several reasons which facilitate the corrosion process to operate on the surface. In this research the inhibition effects of two organic compounds: dimethyl2-[(5phenyl-4H-1,2,4-triazole-3-yl,sulphan- yl]-3-1,1,1-triphenyl-λ^5-phosphanilidine) soctinate (DMAD) and dimethyl 2[1-methyl-2-oxohyd razinocarbonyl]amino-3-1,1,1-triphenyl-λ^5phosphanilidine) soctinate (DMHD) on reducing the corrosion of copper and brass in water cooling system has been investigated.

Methods

In order to evaluate the inhibition efficiency of the metal and alloy, potentiostatic polarization technique was used and parameters affecting the inhibition efficiency such as concentration of inhibitors and temperature were also investigated. To check the morphology of the surface and to study the adsorption of inhibitor on the surface Scanning Electron Microscopy (SEM) and infrared spectra methods were employed.

Results and discussion

Potentiodynamic polarization curves for copper and brass in aqueous media in the presence of different concentrations of compounds DMAD and DMHD are plotted (not shown).Addition

of inhibitors did not change the corrosion potential appreciably but resulted in decrease of cathodic and anodic current densities remarkably, thus the inhibitors under investigations almost act as mixed-type inhibitors[4-5]. They reveal that the inhibition efficiency obtained, increased by increasing their concentration and increased by increasing temperature.

The values of surface coverage(θ) were plotted verses $\log C$ for different concentration of inhibitors the straight line (not shown) obtained, indicates that the adsorption of the inhibitors on the metal and alloy obey Temkin adsorption isotherm [6]. The values of ΔG revealed chemical adsorption of inhibitors on the surface. The SEM and IR spectra results indicated that a good protective film is formed on the copper and Brass surfaces.

Conclusion

The investigated organic compounds are good inhibitors which almost act as mixed inhibitors for copper and brass in cooling water system. Among the two organic compounds DMAD has higher inhibition efficiency and with increasing temperature its performance increased.

References:

[1] L. Nu´n´ez, E. Reguera, F. Corvo, E. Gonzalez, C. Vazquez, Corros. Sci. 47 (2005) 461.

[2] A. El Warraky, H.A. El Shayeb, E.M. Sherif, Anti-Corros. Methods Mater. 51 (2004) 52.

[3] A.T. Hoepner, S. Lattemann, Desalination, 152 (2002) 133

[4] M. Scendo, Corros. Sci. 49 (2007) 373.

[5] M. Behpour, S. M. Ghoreishi, M. Salavati-Niasari, B. Ebrahimi, Mater. Chem. Phys.107 (2008) 153.

[6] M.A.Quraishi, Rana Sardar, Danish Jamal, Mater. Chem. Phys.71 (2001) 309.

Optimization potentiometry method for determination of fluoride

E.M .hamidi , H .Akhlaghin nasab, M . Amiri*, M. Parsa
Department of pharmaceutical chemistry , Kerman university of medical science, Kerman, Iran
Occupational health ,Kerman health school ,Kerman,Iran
Department of pharmaceutical , Kerman university of medical science, Kerman, Iran
Department of Chemistry, Shahid Bahonar University of Kerman, Kerman, Iran
Amirimahnaz2008@yahoo.com

Keyword: Potentiometry, TISAB , Fluoride, ISE

Introduction:

The use of Ion Selective Electrodes in environmental analysis offer several advantages over other methods of analysis especially expense. The concentration of the analyte can then be calculated from the Nernst Equation. An ion-selective electrode (ISE), also known as a specific ion electrode (SIE), is a transducer that converts the activity of a specific ion dissolved in a solution into an electrical potential. Fluoride selective electrode based on LaF_3 crystals have good selectivity. It is selective to fluoride over other common anions by several orders of magnitude; only hydroxide ion causes serious interference. The pH of the solution analyzed is adjusted to approximately 5 to eliminate interference [1]. A total ionic strength adjustment buffer (TISAB) is a buffer solution to add for increasing the ionic strength of the solution helps to "fix" the ionic strength at a stable level, making a linear correlation between the logarithm of the concentration of analyte and the measured voltage. TISAB essentially masks most chemical interferences in the analyte solution and hence increases the accuracy of the reading. In previous works for determination of fluoride ratio of TISAB to water sample was ½ [2,3] , it was more than it need . Small amounts of fluoride are vital for the human organism, but it's toxic in larger amounts. The aim of this work is to determine fluoride in water by significant TISAB for controlling fluoride in water

Method:

A solid-state fluoride ion-selective electrode (Metrohm Model 6.0502.150) was used in conjunction with a double junction Ag/AgCl reference electrode (Metrohm Model

6.0726.100), with the outer compartment filled by a 10% (w/v) KNO_3 solution. The Metrohm Model 780 potentiometer was connected to a computer for recording the kinetic potentiometric data. All of the measurements were carried out at 25±0.2 °C in a double walled reaction cell with continuous magnetic stirring. Both the stirring speed and the electrode distance were kept constant throughout the experiment. The solutions, were mixed with a magnetic stirrer for 3 min. The electrode potentials of the sample solutions were directly compared with those of fluoride standard solutions. The salts of fluoride (NaF) and TISAB were purchased from Merck company(Germany)[3].Water samples were collected from Zerand city in Teflon bottles. The samples and fluoride standard solutions (0.10, 0.25, 0.75, 1.00 ppm) and sample were diluted with the TISAB. The first TISAB was 2 mL in 100 mL to sample and fluoride standard solutions and then we assey ionic strength of the solution if they were different then more TISAB must be added until we accept the same strength of the solution for all solutions. After that detection percentage was calculated if that wasn't sufficient the addition of TISAB must be continued until getting acceptable detection percentage.

Results:

detection percentage was not acceptable for ratio TISAB to water (1/100 ,1/60,1/30). Therefore we continue the ratio TISAB to water (1/20).Sensitive of electrode was sufficient and linear correlation was acceptable.The equation obtained from the calibration curve was E=0.388-52.66 log C

Concentration of fluoride that determined by potentiometric method was 0.25 ppm.

Conclusion:

The necessary amount of TISAB for determining fluoride ion in water was much lower than previous reports. Therefore this method was suggested for further determination. The concentration of fluoride (0.25 ppm) In Zarand city was less than allowed concentration since according to the World Health Organization (WHO) the maximal allowed concentration of fluoride in drinking water is from 0.5 to 1.0 mg/L.

Reference:

[1]Karimi M.A, Mashhadizadeh M.H, Mazloum-Ardakani M,Zand Monfared M.R. Anal. Bioanal. Electrochem., Vol. 2, No. 2,(2010) 52 – 66.

[2]Abdullah M. Aldrees a, Saad M. Al-Manea. The Saudi Dental Journal (2010) 22, 189–193

[3]Bazrafshan E, Ownegh K.A, Biglari H, Soori M.M, Motedaiien A.Study of water resource management in rural areas of Zahedan city during 1387-88 (Case Study: Evaluation of fluoride trend),4th international conference of Islamic world , 2010.

Syntheses and Investigation of Electrochemical Properties of Copper, Nickel, and Iron Complexes With Schiff Base Ligands.

N. jodat[*,1] , Z. Rezvani[2], K.Nejati[3], Z.Heidari[4].

[1] Departmant of chemistry, Faculty of Science, Payam Noor University-Tabriz center, Emamieh ,Hakim nezami street , Tabriz, Iran. (Email: nasrin.jodat@yahoo.com)

[2] Department of Chemistry, Faculty of Science, Azarbaijan University of Tarbiat Moallem, Tabriz, Iran(Email:z_rezvani@yahoo.com, Telefax:+984124327526)

Keywords: Schiff – base,2-hydroxy acetophenon, Azo, Cyclic voltammetry.

Introduction:

Schiff base Ligands and their transition metal complexes have been attracted more attentions in last century, because their anti- tomour and antiviral properties, liquid crystalline character and oxygen carrier catalyst properties.

In this research work , we have prepared a new bidentate azo ligand. Azo compound were prepared by coupling of benzene diazonium cholorid ion with 2-hydroxy acetophenon and under alkalin condition, and Schiff base ligand were then obtaind by the condensation of 5-phenilazo 2-hydroxy acetophenon with p-anizidin .

Copper (II), Iron (II), and Nickel (II) complexes of the Schiff base ligands were also prepared. The synthesized azo-linked Schiff base Ligand has been characterized by ^{1}HNMR ,IR and UV-vis spectroscopy.

Elemental analyses, IR spectra ,UV-vis spectroscopy were also used for the characterization of the complexes.

Result and discussion:

Azo-linked Schiff base Ligand interact with metal ions to form mononuclear, tetra coordinated metal complexes with a suggested structure, shown in figure1.

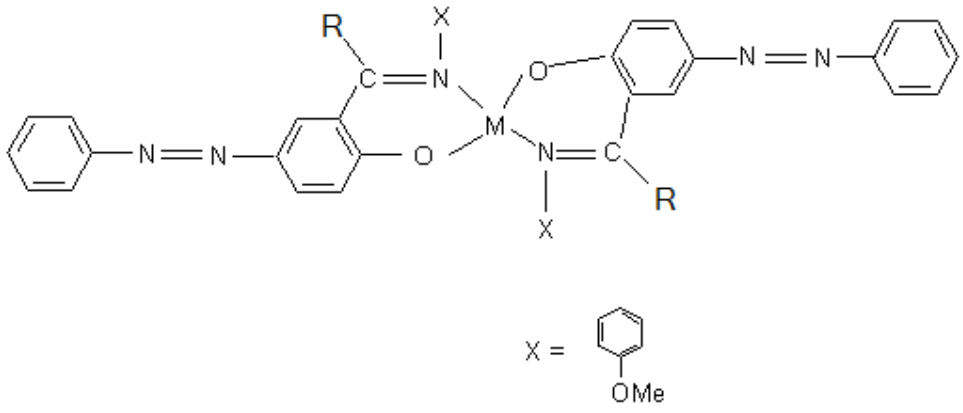

R= CH_3

M= Fe^{2+},Cu^{2+},Ni^{2+}

Figure 1.

A general formula of the complexes was $ML_2.nH_2O$ (n=2) where M is copper(II),Nickel(II) ,and Iron(II).

Cyclic voltammetric behaviour of Cu, Ni and Fe complexes have been investigated in DMF solution and by using glassy carbon as working electrode. In all cases, the redox potentials are correlated with the degree of tetrahedral distortion of the metal coordination environment.

References:

[1] Holm, R. H.; Everett, G. W.; Haravotr, Chakravorty. A. Prog. Inorg. Chem. 1996, 7, 83-214.

[2] Pyrz, J. W., Roe, A. I., Stern, L.J., Que, J. R., J. Am. Chem. Soc. 1985, 107: 614.

[3] M. Tumer, B. Erdogan, H. Koksal, S. Serin, M. Y. Nutku, synth, React. Inorg. Met. Org. Chem. 1998. 28, 529.

[4] Wen Tau Gao, Zheng, Z. Molecules, 2002. 7: 511-516.

[5] Zhang, J. X.; Zhau, Y.; Cai, G. J. Mol. Catal (China), 1997, 11, 41-44

Investigational Polymer Poly (m-Aminobenzoic Acid) on Glassy-Carbon Electrode Modified by Using Cyclic Voltametry Technique

N.Hamedian* [a], A.A.Rostami and A.Omrani [a].
Departman of Chemistry, University of Mazandaran, Babolsar, Iran
(Email:n_hamedian@yahoomail.com)

Key word: Electropolymerization, Chemical modified electrodes, Cyclic voltammetry, m-Aminobenzoic Acid, Glassy-Carbon.

Introduction

Chemical modified electrodes (CMEs) become a field of exiting research due to their unique electrode surfaces properties [1]. Many techniques were developed for preparation of modified electrodes, such as covalent bonding and polymer film [2]. Deposit a film of conducting polymer is essential to work in a medium with an electrolyte that can protect the electrode surface from dissolution without impeding the electropolymerization process [3]. Electropolymerization is a good approach to immobilized polymer as adjusting the electrochemical parameters can control film thickness characteristics [4,5].

Experimental

Apparatus and chemicals:

Cyclic voltammetry tests were perform with a (SOLARTON SI 1287) instrument. A conventional three-electrode system was employed with a bare or poly (m-ABA) modified electrode (1.0mm diameter) as the working electrode, a Ag/AgCl (KCl : 3 M) electrode as the reference electrode, and a platinum electrode as the countrer electrode. Phosphate buffer solutions (PBS) were prepared by 0.1M NaH_2PO_4 – Na_2HPO_4 and adjusting the pH with 0.1M HCl and 0.1M NaOH. The bare glassy-carbon electrode (GCE) was first polished with alumina slurry on emery paper. Then it was rinsed with distilled water. Finally, the electrode was disposed by cyclic sweeping from -1.5 to 2.5 V at 50 , 100, 150 and 200 mV/s for 20, 30 and 50 circles in pH 7.0 PBS containing 1.0×10^{-3} M (m-ABA) solution. All the measurements were carried out at room temperature.

Result and discussion

Cyclic voltammograms of 1.0×10^{-3} M (m-ABA) in pH 7.0 PBS at the GCE are shown in Fig.1. In the first scan, anodic peak 1 and cathodic peak 2 were observed with potential value at 1.6 and -0.7 V. From the second cycle, anodic peak 3 appeared with potential at 0.15 V .Then larger peaks were observed upon continuous scanning, reflecting the continuous growth of the film. It can also be observed that film growth was faster for the first cycles than for the other cycles. It showed polymerization-reached saturation.

This work carried out in various scan rate 50,100,150 and 200 mV/s and also formation of polymer poly(m-ABA) studied in various pH 5, 6, 7, 8, 9 and 10 that this result shown Fig.2

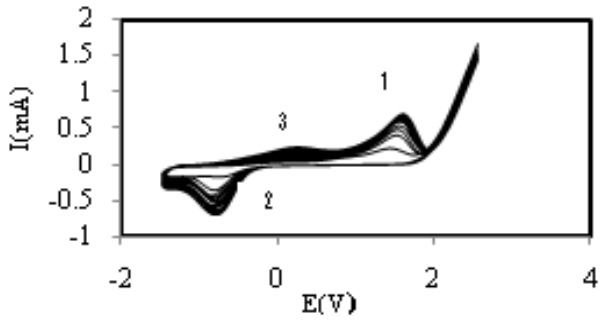

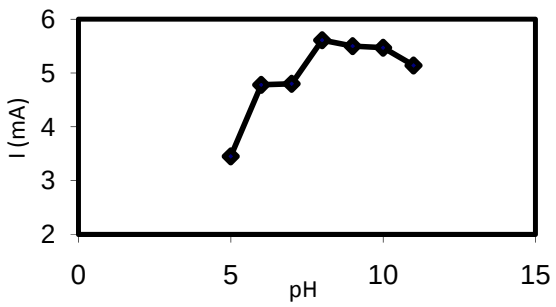

Fig.1. Cyclice voltammograms of 1.0×10^{-3} M m-ABA in pH 7.0 PBS at the GCE

Fig.2.Study of formation polymer in Ph 5.0 – 10.0

Finally these results indicated that maximum of current is in electropolymerization (m-ABA), in pH 8.0 and scan rate 200 mV/s.

References

1. W.Cheng, G.Jin, Y.Zhang, Russion of Electrochemistry, 41 (2005) 1059-1065.

2. P.Daum, R.W.Murry, Journal of Physicals Chemistry Society, 100 (1981) 389.

3. M.Sharifirad, A.Omrani, A.A.Rostami, M.Khoshroo,Journal of Electroanalitical Chemistry, 645 (2010) 541.

4. I.Kaya, A.Bilici, Polymers of Advanced Technologies, 21 (2010) 337-347.

5. P.Daum, R.W.Murray, Journal of Physical Chemistry, 85 (1981) 389.

A study on corrosion inhibitors for concrete application

[a]M.Amiri, J.Khajooie, EM.Hamidi,[b]S.M.A.Hosseini*

[a]Dept. of pharmaceutics, Faculty of pharmacy, Kerman University of Medical Science, Kerman, Iran
Amirimahnaz2008@yahoo.com
[b]Dept. of Chemistry, Faculty of Science, Shahid Bahonar University of Kerman, 76169, Kerman, Iran
hosseini1957@yahoo.com

Keywords: Corrosion inhibitor; Reinforcement Concrete; Chloride

Introduction

Corrosion of reinforcing steel is a widespread problem in concrete bridges. Corrosion inhibitors are considered as one of the most cost-effective solutions. During the last 15 years, they have been used more and more in both new and existing reinforced concrete bridges. Earlier studies of corrosion inhibitors focused on sodium benzoate [1,2], various nitrites (sodium, potassium and barium) and chromates/dichromate [3,4] as concrete admixtures to inhibit corrosion in reinforced concrete. In this paper, the effectiveness and performance of four corrosion-inhibiting systems were evaluated.

Experimental details:

The specimens (st37) were prepared by surface grinding with emery papers, from nos. 120 to 600, washed with double distilled water and degreased with acetone. Cylinders with exposed area about 4.5 cm^2, for electrochemical tests in simulated concrete pore Solutions were used. Electrochemical experiments were carried out in a Pyrex cell with three necks. A saturated calomel electrode (SCE) was used as reference electrode and a platinum plate was used as the counter electrode, all potentials were reported versus SCE. Preliminary tests were carried out in a saturated calcium hydroxide solution containing a chloride concentration of 0.5 M. The concentrations of all inhibitors were chosen as 5×10^{-2} and 5×10^{-1} M. The potential scan rate was 1 $mVs^{-1}$and it was scanned in the negative direction to corrosion potential (E_{corr}) and subsequently in the positive direction. Results were obtained at least three times.

Results and discussion:

It is generally believed that the alkaline nature of reinforced concrete is responsible for the initially protective environment that concrete provides for steel. This is usually reflected in passive or more noble corrosion potentials (or Ecorr values) for steel in concrete. Once aggressive ions such as chlorides migrate into concrete, conditions can become favorable for steel corrosion[5].

In the absence of additives, chloride reduces the width of the passive range to less than one-half. Some inhibitors presented in saturated $Ca(OH)_2$ solution (pH12.6) with 0.5 M chloride can delay the corrosion process on carbon steel, among the promising substances, only 0. 5 M calcium nitrite, 0.05 M BTA, 0. 5 M sodium nitrite are able to keep the inhibiting action throughout the exposure. The possibility to increase the inhibiting efficiencies (IE) by increasing the additive concentration was precluded also in the case of saturated calcium nitrite solution, which were close to the saturated conditions. Inhibitor Na_2PO_3F is less effective compared with the results obtained in the same solution in the absence of an inhibitor. Based on the evidence of the present investigations, Na_2PO_3F did not appear to be effectively transported into the concrete under the conditions studied and so did not provide substantial corrosion inhibition to the steel. As emphasized [6], no short-term laboratory investigation can fully simulate the performance of concrete repair systems that are used and exposed under different circumstances on real structures.

Conclusion:

In the absence of additives the width of the passive range reduces less than one-half due to chloride ion. The presence of inhibitors in saturated $Ca(OH)_2$ solution (pH12.6) with 0.5 M chloride delayed the corrosion process on carbon steel, among the promising substances, only 0. 5 M calcium nitrite, 0.05 M BTA, 0. 5 M sodium nitrite are able to keep the inhibiting action throughout the exposure.

References:

[1] Lewis JM, Mason CE, Brereton D.Civil Eng Public Works Rev 1956;51(602):881–2.

[2] Treadaway KW, Russel AD. Highways Public Works (1968);36:40–1.

[3] Griffin DF. ACI SP-49. American Concrete Institute; (1975) 95.

[4] Berke, NS. Corrosion 89, Paper 445, NACE, Houston, TX, 1989.

[5] H.G. Wheat Cement & Concrete Composites 24 (2002) 119.

[6] V.T. Ngala, C.L. Page, M.M. Page, Corros. Sci. 44 (2002) 2073.

Synthesis and investigation of spectroscopic and electrochemical propertiese of Mn,Ni and Cu complexes

Z.heidari[b],Z.rezvani [a], K.nejati[b],N.jodat[b]

[a] Department of Chemistry , Azarbaijan University of Tarbiat Moallem , Tabriz , Iran

[b] Department of Chemistry , Payame Noor University , Tabriz , Iran

Email: zeinabheidari@yahoo.com

Abstract:

New azo complexes of Mn,Ni,Cu with blue-violet light wavelength were synthesised

This article focuses on the ageing of Compact Disc- Recordable (CD-R),digital versatile disc-recordable(DVD-R) and Blue ray disc- Recordable(BD) using an organic dye layer for information writing.

Keywords: electrochemical**,**CD-R,DVD-R, BD-R,azo,Schiff base

Introduction:

R disces are generally composed of different superposed layers (polycarbonate (PC), organic dye, reflective layer, protective layer and a label) [1]

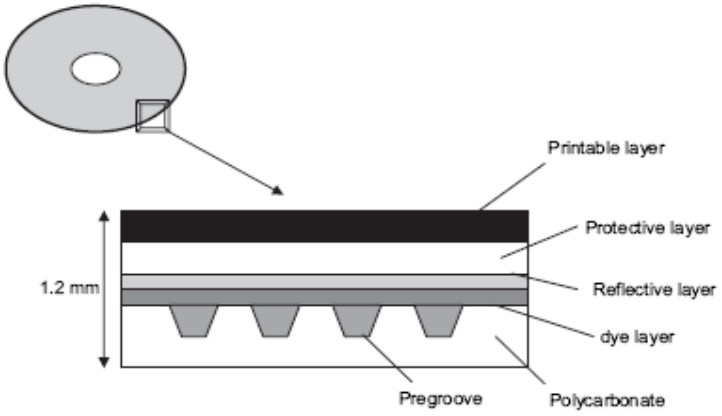

Scheme 1. Scheme of the structure of a CD-R (not at the real scale).

The choice of the recording material for use in CD-R, DVD_R and BD-R is between an organic dye and an inorganic material (alloy, oxide, nitride, etc.) [2] BD technology

employes a 405 nm laser, requires a new optical recording medium with high performance matching the 405 nm [3].however , most of the organic dye compounds now used in optical recording media do not suit to laser beams with a wavelength of 405 nm[4].

methods:

FTIR-^{1}HNMR-UV-Vis spectra and CV as well as solubility in organic solvents , melting points and elemental analyses.

results and discussion:

In this investigation new azo dyes of Ni, Cu and Mn complexes synthesized this tetradenated schiff base complexes with two o and two N donor atomes , have high density that is usefule for their applications in CD,DVD and BD.they are soluble in common organic solvents that is nessesery to making of thin layer filmes as dye layer in disces .they show high melting points(280-330),the FTIR spectra show the carbonyl group in preligand and C═N bands in ligands and shift of them in complexes to higher λ . in UV-Vis spectru new metal azo complexes have maximum absorption bands that were very near to ideal absorption bands in blue violet light and blue ray region(387-403.5) .

the^{1}HNMR show good resultes of preligand and ligand structure,elemental analyses were obtained and electrochemical propertiese investigated by cyclic voltametry in DMF solution and by using glassy carbon as working electrode at different rates (25-50-100-125-200-300-400-500 mv/s)and reduction and oxidations peakes were obtained.

conclusions:

New metal azo complexes were synthesized . Based on FTIR-^{1}HNMR-UV-Vis spectra and CV as well as solubility in organic solvents and high melting points this complexes are suitable for optical recording layers.

References:

[1]Florence Rollet, Sandrine Morlat-The´rias, Jean-Luc Gardette, Jean-Marc Fontaine,Jacques Perdereau, Jean-Dominique Polack Journal of Cultural Heritage 9 (2008) 234e243

[2] Hongu K, Miyakoshi T, Miyaoka Y, Hiroki T, Koyama O. Journal of Applied Physics Part 1 2007;46(6B):3936e8

[3]Zhimin chen,Yiqun wu,Fuxin Huang,Donghong Gu,Fuxi Gan Solid state communication 141(2007) 1-5

[4]Fuxin Huang,Yiqun Wu,Donghong Gu,Fuxi Gun. Spectrochimica Acta part a 61(2005)2856-2860

Experimental and theoretical investigation of the adsorption behaviour of synthesized organic compounds as inhibitors for mild steel corrosion in acid media

M. Salari, A. Khajouei, S. M. A. Hosseini*
Department of Chemistry, Shahid Bahonar University of Kerman, Kerman 76169, Iran
s.m.a.hosseini@mail.uk.ac.ir

Keywords: Mild Steel; Polarization; Inhibitor; Acid inhibition

Introduction:

There are various organic inhibitors which tend to decrease the corrosion rate of steel and iron in acidic solutions [1–4]. The choice of these compounds was based on the consideration that these compounds contain ∏- electrons and heteroatoms such as N and O, which induce greater adsorption of the inhibitor molecules onto the surface of mild steel. The aim of this work is to investigate the corrosion inhibition of mild steel in 0.5 M H_2SO_4 solution by aromatic amines derivatives namely: 4, 5-dinitrobenzene-1, 2-diamine (DDA), 4- nitrobenzene-1, 2-diamine (NDA) and 5-nitrobenzene-1, 2, 4-triamine (NTA) as corrosion inhibitors using weight loss and potentiodynamic polarization techniques. Quantum chemical studies are used for investigation of inhibitor adsorption position on metal surface.

Experimental:

The electrodes used were machined from steel sheets and were polished with emery papers 800-2500 grade for fine polishing. They were washed thoroughly with doubly distilled water then ultrasonically degreased with acetone. The new organic compounds were synthesized in our laboratory. For potentiodynamic polarization measurements, the cell was a conventional three electrode Pyrex glass vessel converter with Pt wire as counter electrode, saturated calomel electrode (SCE) as reference electrode and the mild steel sheet as working electrode. The surface area of each working electrode was 1 cm^2. The potentiodynamic current potential curves were recorded by changing the electrode potential automatically from -700 mV to -400

mV with scan rate of 1 mV s^{-1}. Experiments were performed on a BHP-206X Electrochemical Analysis System.

Results and Discussion:

It is observed that the addition of either compound induces a decrease in both anodic and cathodic current, the anodic decrease being more significant. The corrosion potential (E_{corr}) was observed to shift towards more noble potentials with increasing additive concentration. The parallel adsorption is owing to the presence of one or more active center for adsorption. The difference in the inhibition efficiencies of the two compounds lie in their structure. The effect of temperature indicates that the temperature increases the values of E_{corr}, shift in the negative direction and the values of I_{corr} increase. The activation energy is higher in the presence of inhibitor than their absence. This type of inhibitor retards the corrosion process at ordinary temperature [5]. Whereas the inhibition is considerably decreased at elevated temperature. The lower values of Ea are possibly good evidence for the physical adsorption mechanism of inhibitors on metal surface. The low and negative values of ΔG_{ads} indicate the spontaneous adsorption of inhibitor on the surface of steel. Distribution of LUMO and HOMO location on the nitro groups follow the progression DDA<NDA<NTA, which indicated that with decreasing nitro groups and increasing amine groups electron density of the HOMO and LUMO orbitals on remained nitro group increases.

Conclusion:

The investigated aromatic amines derivatives are efficient inhibitors for the corrosion of mild steel in 0.5 M sulfuric acid solution. The efficiency increases with increasing concentration of inhibitors. The corrosion inhibition efficiencies are in the order DDA<NDA<NTA. The adsorption of these inhibitors obeys the Langmuir adsorption isotherm. The relationship between molecular structure of these compounds and their inhibition efficiency indicated that it has lucid correlation with the lowest unoccupied molecular orbital energy levels and electron charge of oxygen atoms. Distribution of LUMO and HOMO location on the nitro groups, to follow the progression DDA<NDA<NTA, revealing that with decreasing nitro groups and increasing amine groups electron density of the HOMO and LUMO orbitals on remained nitro group increases. The result of inhibitor/iron optimization depicted adsorption

position which is due to the lone pair electron of oxygen atoms of nitro group as the most stable state.

References:

[1] F. Bentiss, M. Traisnel, M. Lagrenee, Corros. Sci. 42 (2000) 127-146.

[2] X. Li, L. Tang, L. Li, G. Mu, G. Liu, Corros. Sci. 48 (2006) 308-321.

[3] M. Benabdellah, A. Aouniti, A. Dafali, B. Hammouti, M. Benkaddour, A. Yahyi, A. Ettouhami, Appl. Surf. Sci. 252 (2006) 8341-8347.

[4] K.C. Emregul, M. Hayval, Mater. Chem. Phys. 83 (2004) 209-216.

[5] M.H.Wahdan, A.A. Hermas, M.S. Morad, Mater. Chem. Phys. 76 (2002) 111-118.

A new ion-selective electrode for potentiometric determination of Cr(III) ions and its computational studies

M. H. Fekri[a], H. Khanmohammadi[b], M. Darvishpour[c*], M,pass[d]

[a,d]Department of Chemistry, Islamic Azad University, Khorramabad Branch, Khorramabad, Iran.

[b]Department of Chemistry, Arak University, Arak, Iran.

[c]Department of Chemistry, Islamic Azad University, Arak Branch, Arak, Iran.

E-mail address:maryam_59d@yahoo.com

Abstract

A new macrocyclic ligand as a neutral carrier in the construction of a new PVC membrane electrode selective to Cr(III) ion was prepared. The electrode exhibits a good potentiometric response for Cr(III) over a wide concentration range 1.0×10^{-4} to 1.0×10^{-1} M with a slope 20.4 ± 0.5 mV/decade and low detection limit of 8.9×10^{-5} M. It has a fast response time ≤ 15 s. The best performance was observed with the membrance having the PVC-ligand-acetophenone-oleic acid composition 6:1:7:1. The structure of the ligand was also studied by HF calculations using a standard 6-31G* basis set.

Keywords: Ion selective electrode, PVC membrane, Cr(II) determination, Macrocycle, HF.

Introduction

A significant number of macrocyclic compounds including crown ethers, cryptands, aza-crowns and thiacrowns, which have been synthesized in various cavity sizes and shapes have already been exploited for the fabrication of poly(vinyl chloride) membrane electrodes for transition and heavy metal ions [1]. Ion selective electrodes (ISE_s) are membrane electrodes that respond selectively to ions in the presence of others[2]. In this paper, we report the use of new ligand(fig.1) as a neutral carrier in the construction of a new PVC membrane electrode selective to Cr(III) ion.

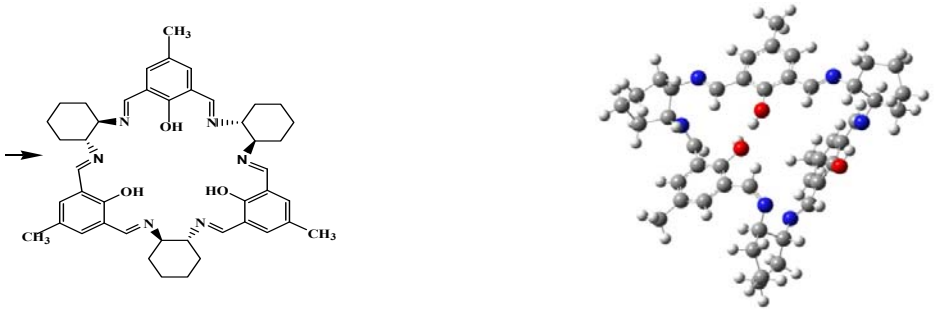

Fig. 1. structure of optimized ligand

Methods

A mixture of PVC, oleic acid, acetophenone and ionophore to give a total mass of 100 mg, was dissolved in about 2 mL of THF and the solution was mixed well. The resulting clear mixture was transferred into a glass dish of 2 cm diameter. The solvent was evaporated slowly until an oily concentrated mixture was obtained. A full optimization of the structure of ligand and its complexe are performed at the HF level of theory using gradient techniques with the Gaussian 03 set of programs.

Results and discussion

Among the different composition studied,membrane 8 incorporating 40.0 % PVC, 47.4 % AP, 5.8 % OA and 6.8 % ionophor shows the best sensitivity. The calibration plot is shown in Fig. 2, which indicates a linear range from 1.0×10^{-4} to 1.0×10^{-1} M Cr(III) with a Nernstian slope of 20.4 ± 0.5 mV/decade of Cr(III) concentration.and low detection limit of 8.9 × 10-5 M. It has a fast response time ≤ 15 s. The best performance was observed with the membrance having the PVC-ligand-acetophenone-oleic acid composition 6:1:7:1. The calculation methods showed stabilisation energy for ligand and its complexe are 2258.70 Hartree mol^{-1} and -3500.17 Hartree mol^{-1} respectively. The calculations predicted nonplanar structer for ligand.

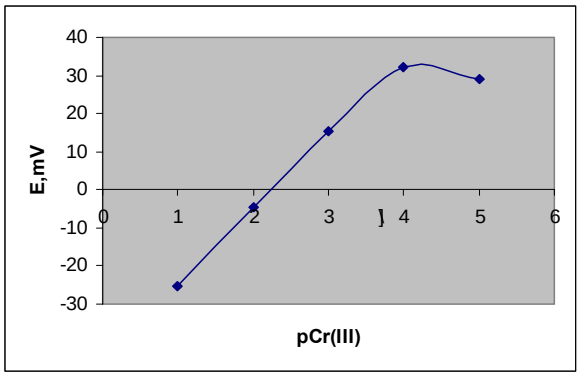

Fig. 2. Calibration plot of the Cr(III)-ISE based on ligan

Conclusions

Fabrication of a new ion specific ISE with high selectivity and sensitivity, wide linear concentration range, long lifetime, good reproducibility and low cost is always in need[3]. In this paper a new ion selective electrode is prepared that incloding special properties.

Refrences

[1] Moody, G.J., Saad, B.B., Thomas, J.D.R., sel. Electrode Rev., 1998, vol. 10, p. 71.

[2] BaKKer, E., Buhlmann, P., Pretsch, E., Electroanalysis, 1999, vol. 11, p. 915.

[3] Gholivand, M.B., Sharifpour, F., Talanta, 2003, vol. 60, p. 707.

Inhibition of mild steel corrosion in acid solution containing organic compounds

[a]F.Rezai ,[b]A.Dolatabadi, [a]E.Sedghamiz, [a]S.M.A.Hosseini*

[a]Department of Chemistry, Shahid Bahonar University of Kerman, Kerman 76169, Iran

[b]Department of Chemistry, Payame noor University of Kerman, Iran

E-mail:s.m.a.hosseini@uk.ac.ir

Keywords: Polarization, Organic compounds, Inhibition, SEM (scanning electron microscopy)

Introduction:

Several studies on corrosion inhibition of metallic materials using organic compounds have been reported [1-3]. Inhibitors are usually being used to protect metal from corrosive media. The present investigation was undertaken to compare the inhibitory effects of three compounds namely3-methyl-1H-pyrazol-5(4H)-one:A,Diethyl2-(2-pyridylsulfanyl)-3-(1,1,1-triphenyl-λ^5 -phosphanylidene) succinate:B and diethyl2[(2-amino-2-thioxoethanthioy)amino]-3-(1,1,1-triphenyl-λ^5 -phodphanylidene) succinate:C on the mild steel in 0.5 M H_2SO_4 solution at different temperatures (30-60 °C). Theoretical studies based on the chemical calculations have been done to support the experimental findings. In addition SEM micrographs were taken from the surface of the polarized samples to check the kind of the film formed on the surface in acid solution containing inhibitors.

Method:

Steel samples were mechanically polished using different grades of emery papers before inserting them in 0.5 M H_2SO_4 containing various concentrations of inhibitors. SCE and Pt were used as a reference and counter electrodes respectively. All of the polarization experiments were carried out potentiodynamicaly in a cell containing 100 mL of aerated solution. The range of potential was -700 to-300 mV with scanning rate of 2 mV/s and all the potential were recorded with respect to SCE.

Results and discussion:

Fig 1 illustrates the polarization curves for mild steel in 0.5 M H_2 SO_4 and solution containing various concentrations of Diethyl2-(2-pyridylsulfanyl)-3-(1,1,1-triphenyl-λ^5 -phosphanylidene) succinate at 30 °C. The overall results reveal that addition of inhibitors cause a decrease in anodic and cathodic current densities and also shift in corrosion potentials slightly towards noble direction. Therefore it may be concluded that the above mentioned compounds are acting as mixed-type inhibitors. It is observed that the corrosion inhibition efficiencies increase as the concentration of inhibitors increase. **Table 1** shows different corrosion parameters (E_{corr} ,$i_{corr,}$ θ and IE%) derived from polarization curves of mild steel in the absence and presence of 100 ppm of efficient inhibitor at different temperatures. These compounds contain heteroatom (O, S and N) that has been reported to cause inhibition of metal and alloys in acidic medium [4-5]. A considerable decrease in number of pits has been absorbed on the surface of mild steel exposed to the acid solution containing inhibitor. Thermodynamic values (ΔG, $E_{a,}$ ΔH and ΔS) show that the presence of inhibitors increase the activation energy whereas reduces the value of ΔG.

Fig1:

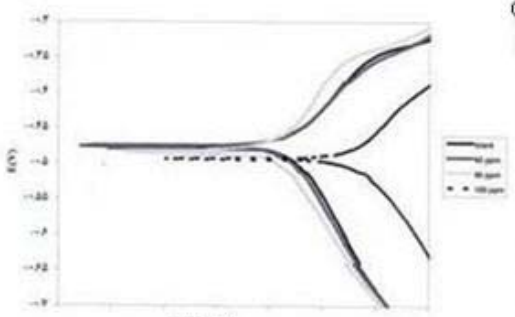

Polarization curves for mild steel in the absence and presence of efficient inhibitor at 30 C

Table1:

Corrosion parametres derived from polarization curves for mild steel in 0.5 H_2SO_4 at 30-60 C containing 100 ppm of efficient inhibitor

(° C)	$-E_{corr}$ (mV)	I_{corr} (μA/cm²)	$-E_{corr}$ (mV)	I_{corr} (μA/cm²)	θ	IE%
۳۰	۲۹۶	۷۰	۲۸۴	۱/۷	۰/۹۷۵	۹۷/۵
۴۰	۲۶۱	۹۲	۲۵۰	۲/۲	۰/۹۵۴	۹۵/۴
۵۰	۲۶۲	۱۲۲	۲۵۰	۹	۰/۹۴۲	۹۴/۲
۶۰	۲۲۸	۱۶۲	۲۲۶	۲۷	۰/۸۷۲	۷۷/۲

Conclusion:

Corrosion current density decreases and inhibition efficiency increases with increasing concentration of the investigated compounds while they are decreased with increasing temperature. The adsorption of the inhibitors on the surface of mild steel obeys Temkin adsorption isotherm. The negative values of ΔG indicate the spontaneous adsorption of the

inhibitors on the surface of mild steel. The SEM micrographs show that the protective film on the metal surface.

References:

[1] Proceedings of the 1st to 8th European Symposium on Corrosion Inhibitors, every 5 years held in Ferrara.

[2] M.El Achouri,
M.R.Infant,F.Izquiredp,S.Kertit,H.M.Gouttoya,B.Nciri,Corros.Sci.43(2001)19.

[3] D.Chebabe, Z.Ait Chikh,N.Hajjaji,A.Srhiri,F.Zucchi,Corros.Sci,45(2003) 309.

[4] E.E.Ebenso, Mater.Chem.Phys71(2002)62.

[5] H.Ashassi-Sorkhabi and S.A.Nabavi-Amir,ActaChim.Slov.47(2000)587.

The Removal Acid Red 88 (AR88) From Aquous Solution By Electrocoagulation

H. Zhian[*a] ,S. Khanahmazada[b] , H.Khandani[c]

[a]*Department of chemistry, University Azad branch Mohabad, Mohabad , Iran*

(Email:Hassan.zhian@yahoo.com)

[b]*Department of chemistry, University Azad branch Mohabad, Mohabad , Iran*

[c]*Department of chemistry, University Azad branch Mohabad, Mohabad , Iran*

Abstract:

One convenient method to removing colors is electro coagulation method, but every color has different properties that by determining the efficient factories the best conditions of color removing can be satisfied. In this study the electro coagulation method with red acid 88 will be investigated. Applying the DC electricity, the optimal conditions of the process with different types of electrodes (such as Fe, Al, graphite and …) in color removing from aqua solvate will be determined. Variables such as density of electric current, time, distance between two electrodes PH are very important. The results shows that a cell EC consists of singular electros in series connections with Alominium sacrifice electrode and Iron Anod and Catod are the best among the others [1].

Key word: Electro coagulation, Remove A.R 88, Color removing, Waste water colors.

Introduction:

Some type of water polluters are consists of solvates cleaners, colors pesticides and drugs. Since using these chemical syntax are increasingly developed, so thier effects on the environment and their dangers and effective method to destroying them must be studied[2].

In textile industry that a great amount of water is needed, filtration of west water is an important problem .It is worth mention that in Azo colors the colorize factor is (-N = N-) and by removing this factor the color will be removed. Red acid 88 is of type of mono Azo class that is solvable in water with the following structure:

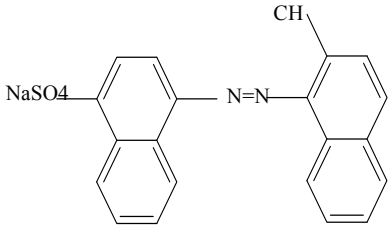

During the coagulation process colloid practical loose their electrics chares and change into large particles coagulation method is the best way to remove colloid practical of the waste water that is done by some specific chemical substance. Because decrease of dual layer defining potential the layer charge of colloid practical is decreased and would cause the coagulation process. In Anod the Iron and Aluminium and in Catod hydrogen gas is introduced. Hydrogen gas would cause the float particles on the surface of water. Basically coagulation is a process in which by adding a coagulant substance the waste substance are removed. Essentially the coagulant process is done because of electro static interaction and forming of colorful complex and physical surface absorption by adding coagulant substances [3].

Results and conclusion:

1. The rate of color motion is depended to some factors such as electrical density, time duration, primery concentration of colorful solvate [4].
2. This method is convenient to remove waste waters that contain red acid 88. In this process by electro chemical cell with Iron Anod and Aluminium Catode,Ph=6/7 , precipitation time = 5 min, density electric current = 100 Am^{-2} , temperature =298 K^0,

distance of the two electrodes is about 1.5 cm, electrolysis time = 4 min, we are able to clean 100% of waste waters[5].

Acknowledgements:

The authors could express their sincere thanks to Islamic Azad University –Mahabad Branch mohabadpersons and company that has supported this work.

References:

[1] Holt PH, Barton GW, Wark M., Mitchell AA. A quantitative comparison between chemical
dosing and electrocoagulations, Colloids Surf. A: [32] Letterman RD, Amirtharajah A, O'Melia CR. in: R.D. Letterman (Ed.), A Handbook of Water Supplies, fifth ed., AWWA, Mc Graw-Hill, New York, 1999.

[2] Chen X, Chen G, Yue PL. Separation of pollutants from restaurant wastewater by electrocoagulations. Sep Purif Technol 2000;19:65-76

[3] Daneshvar N, Ashassi -Sorkhabi H, Tizpar A. Decolorization of orange II by electrocoagulation method Sep Purif Technol 2003;31:153-16

[4] Gao P, Chen X, Shen F, Chen G. Removal of chromium(VI) from wastewater by ombined electrocoagulation-electroflotation without a filter, Sep Purif Technol 2005;43:117-123. Physicochem Eng Aspects 2002;211:233-24

[5] Nasser Modirshahla**,** Investigation of the removal of Tartrazine from aqueous solutions by electrocoagulation **,** Tabriz Branch
Science – Department of Chemistry Applied .(2005)

Electrochemical and quantum chemical calculations of two new Schiff bases as inhibitor for mild steel corrosion in hydrochloric acid

N. Soltani*[a], N. Rasouli[b]
a. Payame Noor University (PNU), Shahin Shahr Branch, Isfahan, Iran
(Email:soltani@kashanu.ac.ir)
b. Payame Noor University (PNU), Koohpayeh Branch, Isfahan, Iran

Keywords: Corrosion inhibition; mild steel; Schiff base; Quantum chemical calculations

Introduction

The use of inhibitors is one of the most practical methods for protection metal against corrosion, especially in acidic media [1]. Most of the well known acid inhibitors are organic compounds containing nitrogen, sulphur and/or oxygen atoms. These compounds can adsorb on the steel surface and block the active sites decreasing the corrosion rate. Moreover, many Schiff base compounds have been proved to be effective inhibitors for the corrosion of metals and alloys in acidic media [2–4]. In the present paper, in order to obtain as effective inhibitors, two Schiff base compounds (Fig. 1) have been studied by electrochemical techniques to investigate electrochemical behaviour of mild steel in 2 M HCl solution. The nature of inhibitor adsorption process and the effect of temperature are also studied and discussed.

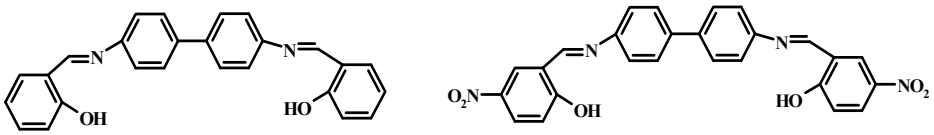

N, N'-bis (salisylaldehyde) benzidine **N, N'-bis (2-hydroxy-6-nitrobenzaldehyde) benzidine**

Fig. 1 Structure of studied Schiff bases

Methods

Polarizations measurements were carried out using AUTOLAB model PGSTAT 35. Electrochemical experiments were performed in a conventional three electrodes electrochemical cell at 25°C with the mild steel as a working electrode, a platinum counter electrode and silver–silver chloride (Ag/AgCl) electrode as reference electrode. All the quantum calculations were performed with complete geometry optimization by using standard Gaussian03 software package. The study of the relationship between inhibition efficiency of

the molecules and their electronic properties was carried out at the level of B3LYP with 6-311G** basis set.

Results and discussion

Table 1 represents all corrosion parameters obtained from Tafel polarization studies. These results show that by increasing inhibitor concentration, the corrosion current decreased. Moreover, these inhibitors cause no change in the anodic and cathodic Tafel slopes, indicating that the inhibitors are first adsorbed onto steel surface and therefore impedes by merely blocking the reaction sites of steel surface without affecting the anodic and cathodic reaction mechanism corrosion inhibition increases when the inhibitor concentration increases.

Table 1. Electrochemical polarization parameters for the mild steel in ٢ M HCl containing different concentrations of Schiff base I and Schiff base II

inhibitor	Concentration (mM)	$-E_{corr}$ (mV)	I_{corr} ($\mu A\ cm^{-2}$)	$-b_c$ ($mV\ dec^{-1}$)	b_a ($mV\ dec^{-1}$)	IE (%)
2 M HCl	-	414	419.9	83	75	-
Schiff base I	0.01	413	162.9	86	71	61.2
	0.05	408	175. 6	81	74	83.1
	0.10	404	293.7	88	73	96.3
Schiff base II	0.01	416	394.1	84	69	47.8
	0.05	418	130.7	85	71	73.4
	0.10	420	294.9	87	73	86.2

The inhibition efficiency values of two Schiff bases at a common concentration of 0.10 mM follow the order: Schiff base I > Schiff baseII. The quantum results were used to explain different inhibition effectiveness of the two molecules.

Conclusions

The results show that the IE increases with increase in inhibitor concentration. The inhibition efficiency data showed that compound Schiff base I has greater interaction with mild steel compared to compound Schiff base II. The thermodynamic parameters (K_{ads}, ΔG_{ads}) of adsorption for the studied compounds are calculated from their adsorption isotherms. The negative values of ΔG_{ads} (-39.02 $kJmol^{-1}$ for Schiff base I and -38.42 $kJmol^{-1}$for Schiff base II) show the spontaneity of the adsorption.

References

[1] B.V. Appa Raoa, Md. Yakub Iqbala, B. Sreedhar, Electrochim. Acta 55 (2010) 620.

[2] N. Soltani, M. Behpour, S.M. Ghoreishi, H. Naeimi, Corros. Sci. 52 (2010) 1351.

[3] M.A. Hegazy, Corros. Sci. 51 (2009) 2610.

[4] A. B. da Silva, E. D'Elia, J.A.C.P.Gomes, Corros. Sci. 52 (2010) 788.

Corrosion inhibitive properties of mono and bis morpholinomethyl-thiourea in acidic solution

N. Soltani*[a], A. Teimouri[b]

[a]Payame Noor University (PNU), Shahin Shahr Branch, Isfahan, Iran

[b]Payame Noor University (PNU), Isfahan, Iran

Keywords: Carbon steel; Corrosion inhibition; thiourea compounds; Quantum chemical calculations

Introduction

Industrial acids of various concentrations are extensively employed in various industrial processes, including acid pickling and acid descaling as well as in oil well acidification, and cause damage of corrosion [1]. Organic inhibitors generally protect the metal from corrosion by forming a film on the metal surface. Their effectiveness is related to the chemical composition, their molecular structure, and their affinities for the metal surface [2, 3]. The aim of this study is to investigate the inhibition effects of two thiourea compounds (Fig. 1) on the corrosion of carbon steel in HCl solution. The nature of inhibitor adsorption process and the effect of temperature were also studied and discussed.

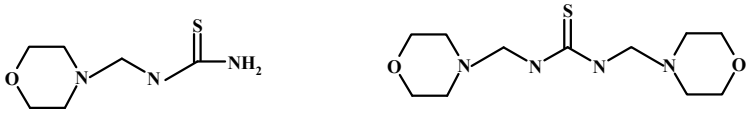

(I) N- morpholinomethylthiourea (II) N, N-bis morpholinomethylthiourea

Fig. 1. The names and structures of the investigated inhibitors.

Methods

Polarizations measurements were carried out using AUTOLAB model PGSTAT 35. Electrochemical experiments were performed in a conventional three electrodes electrochemical cell at 25°C with the carbon steel as a working electrode, a platinum counter electrode and silver–silver chloride (Ag/AgCl) electrode as reference electrode. Polarization data was analyzed using GPES electrochemical software. Electrochemical corrosion parameters obtained by extrapolation of the Tafel lines. Density functional (DFT) calculations

have been carried out for thiourea compounds by performing HF and DFT levels of theory using the standard 6-31G* basis set.

Results and Discussions

Anodic and cathodic polarization curves for carbon steel in 1M HCl with and without various concentrations of used inhibitors are shown in Fig 2. From Fig. 2, it is clear that both anodic metal dissolution and cathodic reduction reactions were inhibited when the thiourea compounds were added to the acid solution and this inhibition was more pronounced with increasing inhibitor concentration. The presence of inhibitors in HCl solution resulted in shift of corrosion potential towards positive direction in comparison with that obtained in the absence of inhibitor. These results indicate that two investigated inhibitors act as mixed type inhibitor with predominant control of anodic reaction.

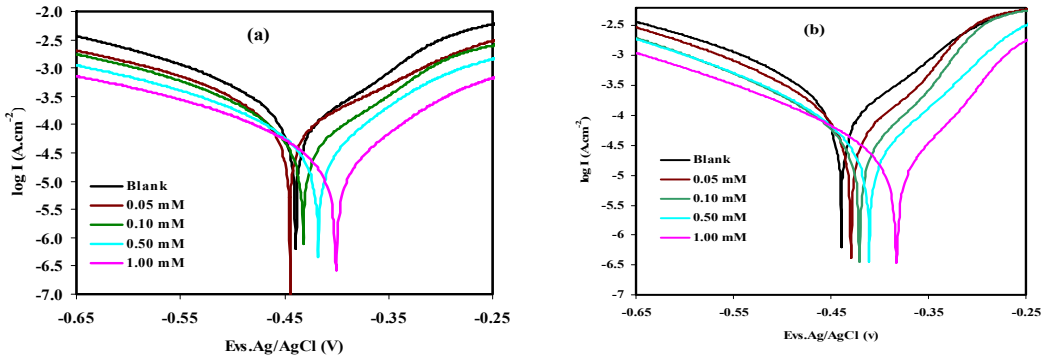

Fig. 2. Polarization curves for carbon steel in 1 M HCl in the absence and presence of different concentrations of (a) mono and (b) bis-morpholinomethylthiourea at 25 °C.

Conclusions

The inhibition efficiency data showed that compound mono has greater interaction with carbon steel compared to compound bis. However the difference between efficiencies was small and indicated that both compounds exhibit good effectiveness. The maximum inhibition efficiency (98.3%) was obtained with compound mono at a concentration of 1.0 mM. The value of K_{ads} is 5.31×10^5 and 4.12×10^5 M^{-1} and the value of ΔG^0_{ads} is found as 42.58 and 41.90 $kJmol^{-1}$ for inhibitor mono and bis- morpholinomethyl-urea, respectively. The value of

E_a is found as 56.8, 43.1 and 47.2 $kJmol^{-1}$ for 1.0 M HCl, mono and bis- morpholinomethyl thiourea respectively.

References

[1] B.V. Appa Rao, Md. Yakub Iqbal, B. Sreedhar, Electrochim. Acta, 55 (2010) 620.

[2]M. Behpour, S.M. Ghoreishi, N. Mohammadi, N. Soltan, M. Salavati-Niasari, Corros.Sci.52 (2010) 4046.

[3] K. Stanly Jacob, G. Parameswaran, Corros. Sci. 52 (2010) 224.

Formation of Lanthanum-Permanganate composite conversion coating on AZ61 magnesium alloy and investigation of its anti-corrosive properties

D. Seifzadeh*, A. Ghari-Haghighat
Email: dseyfzadeh@yahoo.com
Department of Applied Chemistry, University of Mohaghegh Ardabili, Ardabil, Iran

Keywords: Magnesium, Conversion Coating, Lanthanum, Permanganate, Corrosion

Introduction

Magnesium alloys are of great importance at present and future fields of engineering for their attractive combination of low density and high strength/weight ratio. However, since magnesium is intrinsically active in the environment, the corrosion resistance of magnesium alloys is generally inadequate, which limits their application [1, 2]. The aim of this work is to investigate the protection effect of Lanthanum-Permanganate (La-Per) conversion coating application on the corrosion of AZ61 magnesium alloy by electrochemical methods.

Experimental details

The AZ61 plates with a size of 1×1×0.3 cm were mounted in polyester in such a way that only 1cm^2 of samples was in contact with plating and corrosive solutions. The samples were polished from 220 down to 1200 grit using emery papers and then rinsed with double distilled water, ultrasonically cleaned in ethanol bath for 2-3 minutes and finally rinsed with double distilled water. The plating bath containing 0.4 g/lit $KMnO_4$ and 0.8 g/lit $La(NO_3)_2$ was used for conversion coating treatment. The operating temperature was 25ºC.

Results and discussions

A scanning electron microscope was used to observe the morphology of 30 min treated and untreated AZ61 sample after 10 min immersion in 3.5% NaCl corrosive solution. As it clear from images, there are no pits on the treated sample after immersion in NaCl solution.

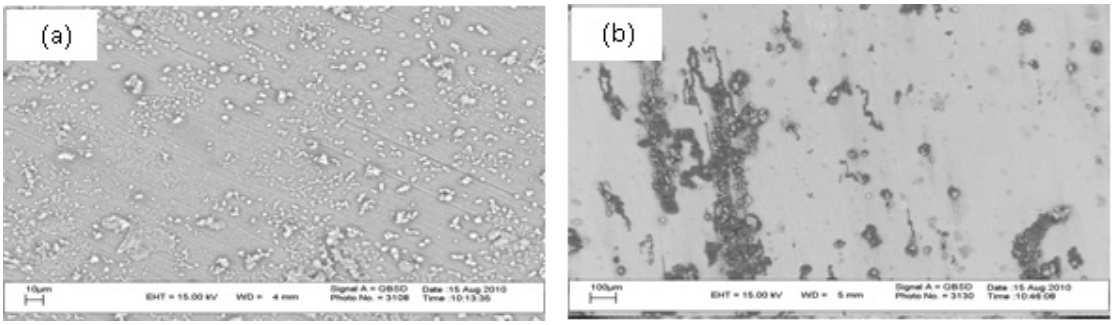

Fig. 1. SEM images of AZ61 samples after 10 min immersion in 3.5%NaCl solution. 30 min treated sample (a), untreated sample (b).

To determine the optimum plating time(with maximum corrosion protection), the polarization curves of coated AZ61 sample after different treatment times are obtained in 0.05 M sodium sulfate solution (Fig.1a). Also the polarization curve of untreated sample is shown in Fig1.b. The corresponding corrosion parameters are collected in Table 1.

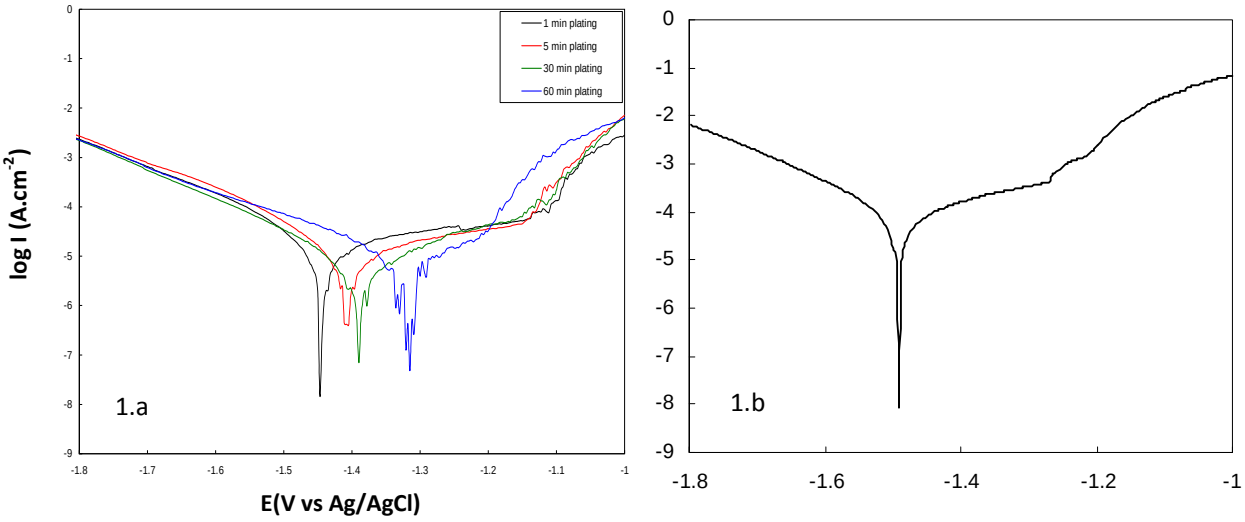

Fig.1 polarization curves of the treated samples for different times (1.a) and untreated sample (1.b) after 5 min immersion in the 0.05 M Na_2SO_4 solution

Table1. Corrosion parameters of treated an untreated samples in the 0.05 M Na_2SO_4 after 5 min immersion

Plating Time(min)	Immersion Time(min)	R_p ($\Omega.cm^2$)	B_a (V/dec)	B_c (V/dec)	I_{corr} (A/cm^2)	E_{corr} (V)
Blank	5	405.9	0.110	0.172	7.18×10^{-5}	-1.492
1		2365	0.169	0.097	1.13×10^{-5}	-1.447
5		3796.9	0.219	0.098	7.74×10^{-6}	-1.405
30		4304.9	0.135	0.100	5.79×10^{-6}	-1.417
60		3507.4	0.103	0.097	6.18×10^{-6}	-1.318

As it clear, the corrosion potentials of AZ61 samples are shifted to more noble values after the La-Per treatments. The corrosion currents (I_{corr}) of the used samples are significantly decreased after the conversion coating treatment. The best corrosion protection characteristic is observed for the sample treated for 30 min (optimum plating time). This results show that the lanthanum – permanganate treatment is an appropriate method to increase the corrosion resistance of AZ61 alloy. The same results are obtained by EIS studies (not shown).

References

[1]. R. F. Zheng, C.H. Liang; Materials and Corrosion, 58 (2007)193

[2]. M. F. Montemor, A. M. Simoes, M. J. Carmezim; Applied Surface Science 253 (2007) 6922–6931

The corrosion inhibition effect of 8-hydroxyquinoline on the AZ61 magnesium alloy in acidic media

D. Seifzadeh*, S. Hamzedoust Hasan Kiadeh
Email: seyfzadeh@yahoo.com
Applied Chemistry Department, Mohaghegh Ardabili University, Aradbil-Iran

Keywords: Magnesium, Corrosion, Inhibition, Electrochemical

Introduction

Magnesium alloys have potential wide application in automobiles, electronic and aerospace industries because of their optimal weight-to-strength ratios [1]. Wide application of magnesium alloys is limited due to their low corrosion resistance. The aim of this study is to investigate the inhibition effect of 8-hydroxyquinoline (8HQ) on the corrosion of AZ61 magnesium using two different electrochemical methods.

Experimental

AZ61 magnesium alloy samples with an exposure area of 0.5 cm^2 were tested. Prior to all measurement, magnesium alloy samples were polished successively with a sequence of emery papers of different grades (400,800 and 1500 grits). Before the corrosion testes, the samples were carefully degreased with ethanol, rinsed with double distilled water and finally dried with cool air. All experiments were performed in the lab condition.

Results and discussion

The potentiondynamic polarization curves (obtained by BHP2063 potentiostat) for magnesium alloy in 0.1 M HCl solution in the absence and presence of various concentrations of 8HQ are shown in Fig1.a. Also the corresponding Nyquist plots (obtained by μAUTOLAB2) are shown in Fig. 1b. Polarization method parameters are given in Table 1.

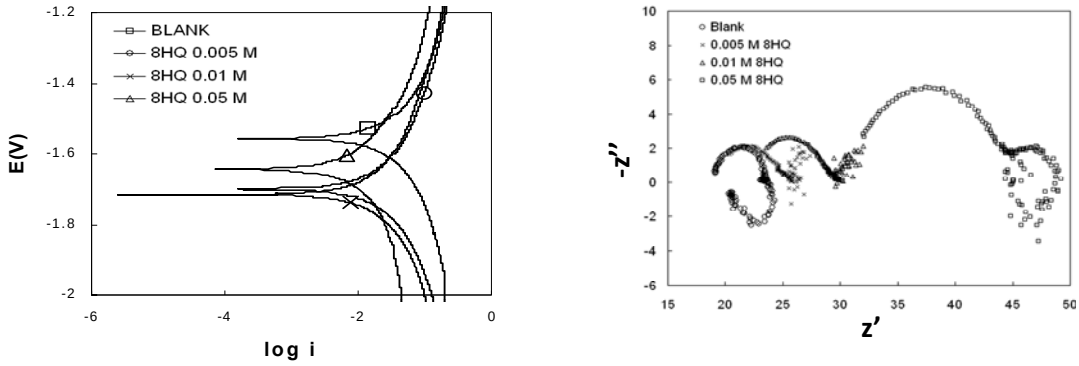

Fig.1. Polarization curves and Nyquist plots of AZ61 in 0.1 M HCl in the absence and presence of 8HQ after 60 min immersion

The results show that the corrosion rate of AZ61 samples in the 0.1 M HCl solution significantly decrease after the addition of 8HQ. This result indicates that the 8HQ compound can acts as a suitable inhibitor for AZ61 in the acidic media. Also the corrosion protection characteristics of 8HQ compound promotes when its concentration increases. The same results can be concluded from Nyquist plots. The diameters of both semicircles in the high and low frequencies have been increased after the addition of the inhibitor.

Table1. Corrosion parameters of AZ61 in the absence and presence of different concentrations of 8HQ

Polarization results							
C(M)	Time (min)	E_{corr}(v)	I_{corr}(A)	B_a(v/dec)	B_c(v/dec)	R_p(Ω)	η_p%
Blank	60	-1.557	0.014808	0.1182	0.1384	1.8694	
0.005	60	-1.702	†	†	0.1744	2.7525	32.1
0.01	60	-1.715	0.009531	0.1568	0.131	3.2515	42.5
0.05	60	-1.643	0.00555	0.1413	0.1454	5.606	66.7

Corrosion protection effect of 8HQ may be explained by formation of a non-soluble complex. Fig. 2 presents the FT-IR spectra of films prepared by 8HQ on the alloy surface (Fig. 2a) and the original 8HQ powder (Fig. 2b).

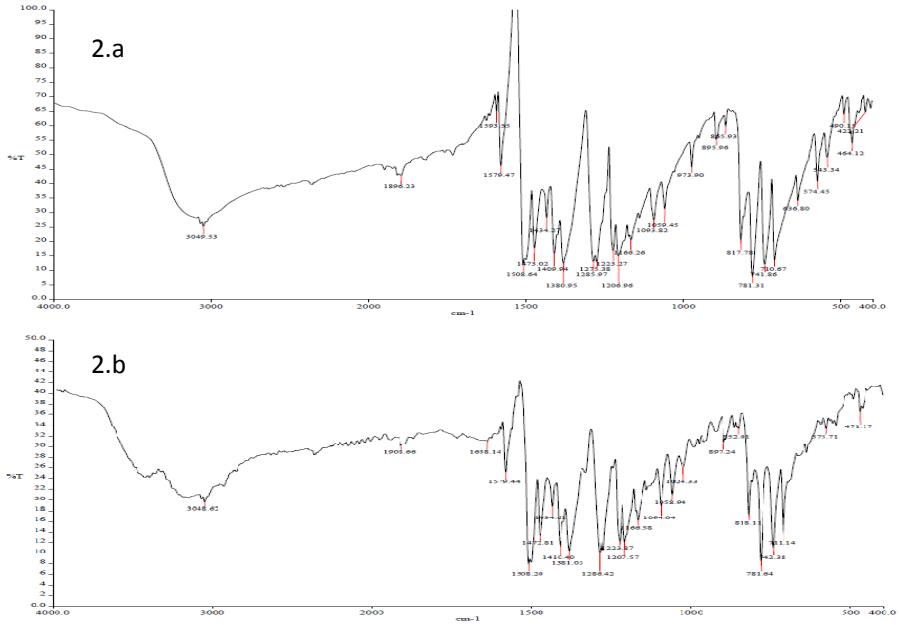

Fig 2. FTIR spectra of 8HQ powder (2.a) and its film on the AZ61 (2.b).

The increase in the energy of the intermolecular hydrogen bonds from about 3100 to 3200 cm^{-1} [1] (in Fig. 2a) is indicating a polymeric association between 8HQ molecules. In addition, intensity changes and energy shifts in some bands indicate the direct bonding between Mg atoms and 8HQ molecules via O and N atoms, and the formation of the $Mg(8HQ)_2$ film[3].

References

[1]. H. Wang, R. Akid, M. Gobara; Corrosion Science 52 (2010) 2565

[2]. H. Allachi, F. Chaouket, K. Draoui, Journal of Alloys and compounds 475(2009)300

[3]. H. Gao, Y. Dai, F. Luo, H. X. Zhang, Corrosion Science 52(2010)1

Sol-gel hybrid nanocomposites and its anticorrosive properties

E. Gholmoghani, D. Seifzadeh*,
Email:dseyfzadeh@yahoo.com
Applied Chemistry Department, Mohaghegh Ardabili University, Aradbil-Iran

Keywords: Sol – Gel Coating, Steel, MMT, Electrochemical Methods.

Introduction

Several methods have been employed to corrosion protection of mild steel. Sol gel process is one of the most appropriate technologies to protection of metals [1, 2]. In this work, the effect of montmorillonite (MMT) nanoparticles addition on the corrosion protection performance of hybrid sol gel coatings on mild steel has been studied using polarization and electrochemical impedance spectroscopy (EIS).

Experimental details

After mountinh in polyester, the mild steel samples(1.69cm^2 surface area) were polished using emery papers (220, 400 and 800) and then cleaned with distilled water, degreased with ethanol and finally dried using compressed air. The silane sol was synthesized by mixing 3-glycidoxypropyltrimethoxysilane (GPTMS), tetraethylorthosilicate (TEOS), and 2-propanol in 1:2:1.5 volume ratios. MMT nanoparticles were added to the mixture in the different concentrations. For acidic catalyze, aqueous solution of nitric acid (pH=1.5) was used [2]. The sol was stirred continuously for about 2 h and the obtained gel was dip coated on the steel by controlled withdrawal speed of 25cm /min. the obtained coating cured at 120 °C for 2 h digital furnace. Fig.1 shows the FTIR spectra of coatings prepared by sol gel method. The peak at 1056.54 cm^{-1} can be related to formation of Si−O−Si bond.

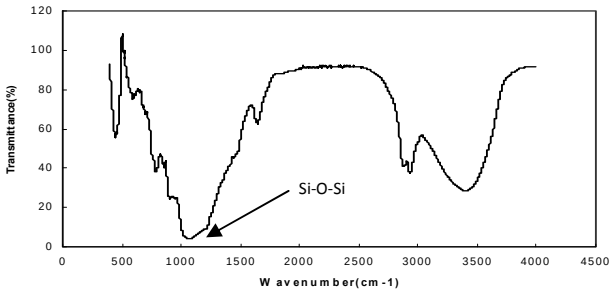

Fig.1. FT-IR spectra of coatings.

Results and discussion

Potentiodynamic polarization curves of sol gel coated samples with different contents of MMT nanoparticles in % 3.5 NaCl solution after 96 h immersion are shown in Fig2a. Also the Nyquist plots after 24 h immersion in the same media are shown Fig.2b.

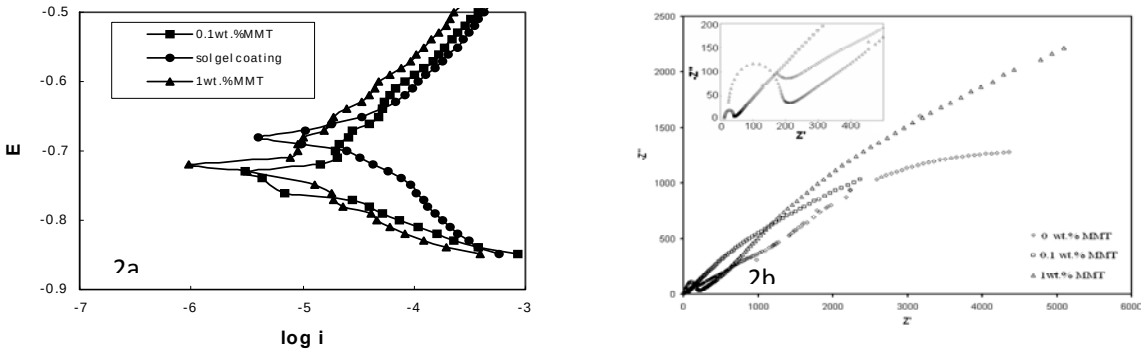

Fig. 2. Electrochemical behavior of sol gel coated mild steel samples in %3.5 NaCl. Polarization curves after 96h (Fig. 2a), Nyquist plots after 24 h (Fig.2b)

Polarization parameters and EIS results (obtained using two time constant equivalent circuit) are collected in Table 1. The results indicate the corrosion rate of sol gel coated mild steel samples decrease after the addition of MMT nanoparticles. The best result is obtained in the case of nanocomposite with 1% nanoparticle content. The results obtained from EIS and polarization studies are in good trend agreement.

Table 1. Electrochemical characteristics for sol-gel coated samples with different contents of MMT nanoparticle

Polarization results

MMT content (wt. %)	E_{corr} (V)	I_{corr} (Acm^{-2})	R_p (Ωcm^2)	b_c ($Vdec^{-1}$)	b_a ($Vdec^{-1}$)
0	-0.690	1.893×10^{-5}	1566.96	0.154	0.139
0.1	-0.740	8.403×10^{-6}	2107.76	0.066	0.0837
1	-0.720	4.93×10^{-6}	3821.09	0.066	0.127

EIS results

MMT content (wt. %)	$R_1(\Omega)$	$CPE_1(F)$	$R_2(\Omega)$	$CPE_2(F)$	$R_{tatal}(\Omega)$
0	†	†	7328	1.12×10^{-9}	≈7400
0.1	26	4.21×10^{-8}	8190	3.65×10^{-9}	8216
1	145	1.28×10^{-8}	19714	3.41×10^{-10}	19859

References

[1] N. P. Tavandashti, S. Sanjabi, T. Shahrabi; Progress in Organic Coatings 65 (2009) 182

[2] G. Ruhi, O. P. Modi, A. S. K. Sinha, I. B. Singh; Corrosion Science 50 (2008) 639

[3] H. Shi, F. Liu, E. Han; Progress in Organic Coatings 66 (2009) 183

Effect of different condition on anomalous diffusion in polypyrrole film

M.G. Mahjani*,A. Sharifi, A. Ehsani, M. Jafarian
Department of Chemistry K. N. Toosi University of Technology, Tehran, Iran
Corresponding author (E- mail: mahjani@kntu.ac.ir)

Keywords: Anomalous diffusion, Impedance spectroscopy, Polypyrrole, Porosity

Introduction

Anomalous diffusion is present in a variety of physical, chemical and biological systems and it is therefore a subject of active current research. This phenomenon can be observed in the diffusion in porous materials, in the charge carrier transport in amorphous semiconductors, and in the transfer of lipid granules in the biological membranes[1].

We present experimental results on the anomalous diffusion in conducting polymer film which are obtained by means of the electrochemical impedance spectroscopy technique. Different condition in synthesis of polymer film such as temperature, monomer concentration and film thickness can effect on the morphology and porosity of the film[2]. Difference in the porosity of the film can effect on the diffusion method of the particles through the polymer film and cause to anomalous to diffusion. Polypyrrole(PPy) film electrochemicaly deposited on glassy carbon electrode using the cyclic voltammetry method and the electrochemical impedance spectroscopy used to obtain the anomalous diffusion parameters.

Experimental

Polypyrrole(PPY) film on glassy carbon working electrode were prepared by cycling the potential from -0.5 to 0.9V vs SCE in solution of KClO4,and 0.1M, 0.2M, 0.3M, 0.4M, 0.5M of pyrrole monomer, different temperatures. thickness of the film changed by changing the number of cycled. electrochemical properties of PPy film investigated by impedance spectroscopy in frequency range of 100KHz to 5mHz in different dc offset potential and 5mv alternating potential.

Result and discussion

In the case of normal diffusion the straight line in low frequencies is 90° and decreasing in this angle is because of anomalous diffusion[3].

Investigation of electrochemical impedance spectrum in different conditions demonstrates that Increasing synthesis temperature and monomer concentration causes to enhance value of anomalous diffusion. Also increasing in polymer film thickness up to specific thickness causes to lower deviation of normal diffusion but after that anomalous diffusion increases again.(Fig1)

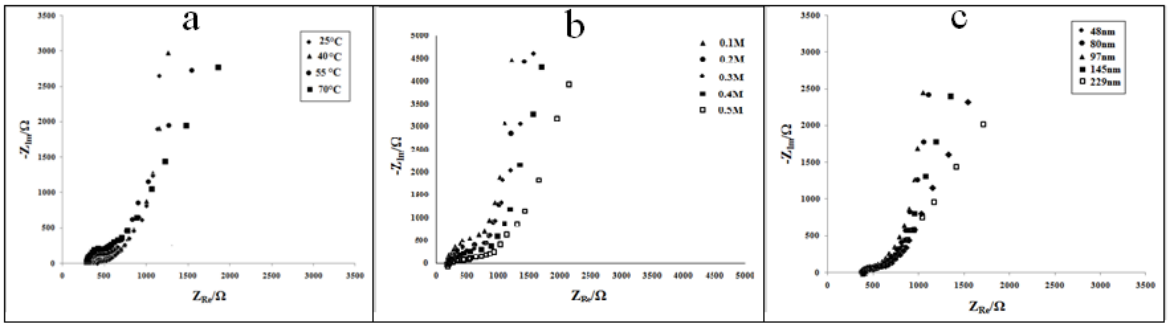

Fig1 Nyquest diagrams of poypyrrole film deposited on glassy carbon electrode in different a) synthesis temperature b) different monomer concentration and c) different film thicknesses.

References

[1] K. Dworecki, Physica A, 359(2006)24-32.

[2] A. kassim, Z. B. Basar, H. N. M. E. Mahmud, J. Chem. Sci, 114(2002)155-162.

[3] J. Bisquert, A. Compte, J. Electroanal. Chem. 499(2001)112.

Kinetic Study of Electrochemically Induced C-P Bond Formation of Catechols with Trialkylphosphites

M. Rafiee*[a], S. M. Shoaei[b], L. Khalafi[c]

[a]Department of Chemistry, Institute for Advanced Studies in Basic Sciences, Zanjan Iran

[b]Department of Chemistry, Islamic Azad University, Zanjan Branch, Zanjan, Iran

[c] Department of Chemistry, Islamic Azad University, Shahr-e-Qods Branch, Tehran, Iran

* rafiee@iasbs.ac.ir

Voltammetric behavior of catechol derivatives are well-known and were investigated in some papers [1]. In acidic and neutral media cyclic voltammograms of catechols show one anodic and corresponding cathodic peak with peak current ratio nearly unity for transformation of catechol to o-quinone and vice-versa [2]. Produced o-quinone is highly reactive species and undergoes some chemical reactions in the presence of nuclephiles. The height of catodic peak decreases due to removing o-quinone from the electrode surface. Decrease in cathodic peak is proportional to the rate of chemical reaction. In this work electrochemical oxidation of catechols in the presence of trimethylphosphite, triethylphosphite and triisopropylphosphite as nucleophiles have been studied using cyclic voltammetry and digital simulation. In the presence of triethylphosphite the cathodic peak current decrease at the pHs lower than 7.0 which enhanced by increase in pH.

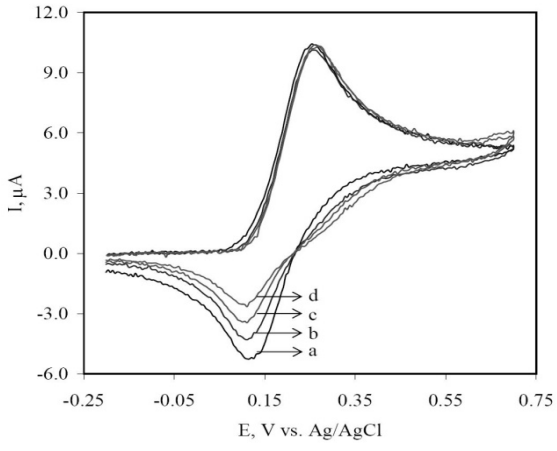

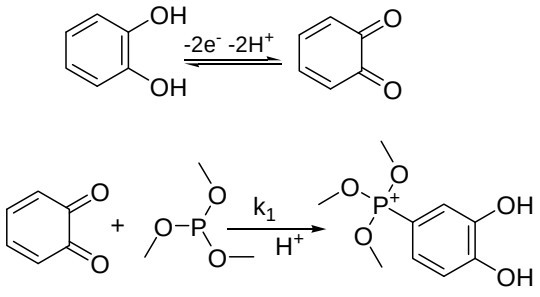

Figure 1. Cyclic voltamograms of 1.0 mM catechol in aqueous phosphate solution; (a) in the absence and (b) to (d) in the presence of 1.0, 2.0 and 3.0 mM triethylphosphite. Scan rate: 20 mV s^{-1},

aqueous phosphate solution, pH 6.0, and proposed mechanism.

Aqueous solution containing phosphate buffer (pH 6.0, 0.2M) was selected as optimum pH due to undesirable reactions at the pHs more than 7.0. Cathodic peak currents decrease with increase in trimethylphosphite concentration which confirms the reaction between o-quinone and triethylphosphite. EC mechanism has been deduced from voltammetric and diagnostic criteria. The o-quinones derived from electrochemical oxidation (E) of catechols, participate in a Michael addition reaction (C) with trimethylphosphite. The rate constants of chemical reaction were estimated by digital simulation of cyclic voltammograms using CVSIM, commercially available simulation software [3]. The results for the investigation of the electrochemical behavior of 3-methylcatechol, 4-methylcatechol, 3-methoxycatechol and 2,3-dihydroxybenzoic acid, in the presence of triethylphosphite and triisopropylphosphiteare studied same as catechol andtrimethylphosphite. The effect of substituation on catechols and trialkylphosphite were examined in this work.

Keywords: Cyclic Voltammetry, Digital Simulation, Catechol, Electrochemical Oxidation,

References

[1] M. Rafiee, D. Nematollahi, *Electroanalysis,*19 (**2007**) 1382

[2] D. Nematollahi, M. Rafiee, L. Fotouhi, *J. Iran. Chem. Soc.,* 6 (**2009**) 448.

[3] A. Afkhami, D. Nematollahi, L. Khalafi, M. Rafiee, *Int. J. Chem. Kinet.*, 37 (**2005**) 17.

Ionic liquid-based dispersive liquid-liquid microextraction and enhanced spectrophotometric determination of molybdenum (VI) in water and plant leaves samples by FO-LADS

Maysam Gharehbaghi, Farzaneh Shemirani *
Department of Analytical Chemistry, University College of Science, University of Tehran, Tehran, Iran P.O. Box 14155-6455, Tehran, Iran E-mail: shemiran@khayam.ut.ac.ir

Abstract

A new simple and rapid ionic liquid-based dispersive liquid-liquid microextraction (IL-DLLME) has been applied to preconcentrate trace levels of molybdenum (VI) as a prior step to its enhanced determination by fiber optic-linear array detection spectrophotometry (FO-LADS). In this method, a small amount of [Hmim][Tf_2N] (1-hexyl-3-methylimmidazolium bis (trifluormethylsulfonyl) imid) as an extraction solvent was applied to extract molybdenum - pyrogaloll red complex, which was formed in an aqueous solution in the presence of N-cetyl-N-N-N-trimethyl ammonium chloride as a sensitizing agent.

Introduction

There are many analytical techniques available for the determination of molybdenum, such as neutron activation analysis (NAA), inductively coupled plasma-mass spectrometry (ICP-MS) [1-2], inductively coupled plasma-atomic emission spectrometry (ICP-AES), flame atomic absorption spectrometry (FAAS), etc. Giving the fact that most of these methods require rather sophisticated and relatively high cost instruments and being aware of the essentiality of molybdenum monitoring, its determination by extractive spectrophotometry as a simple and low cost method has been considered of importance.

However, due to the presence of molybdenum in environmental and biological samples at low levels, not only its separation from associated elements is necessary but also the use of a preconcentration method is usually inevitable.

The preconcentration and determination of molybdenum has been studied when using liquid–liquid extraction (LLE), cloud point extraction (CPE), solid phase extraction (SPE) and homogeneous liquid-liquid microextraction (HLLME).

Most of LLE methods present some disadvantages like large volumes of solvents, which are expensive and toxic, high operation costs, possible formation of emulsions, large equipments and high residence time. Despite many benefits when using CPE, in rather high content of salt, the background is increased since the enrichment phase is composed of a little aqueous sample. Also in the presence of more than 3 % of water-miscible organic solvents, such as acetone phase, separation does not occur and the extraction system is destroyed [3]. SPE is a solventless, simple and convenient method, which combines extraction, preconcentration and sample introduction in one step. Unfortunately, large amounts of eluents are used in these methods. Other shortcomings are usually long extraction time, poor repeatability and neediness of an enormous volume of sample. Also preconcentration by HLLME method is simple and rapid, but the addition of one acid, base or salt for the conversion to biphasic system and preconcentration is inevitable. It is not a desirable subject because some analytes may be affected or decomposed by changing conditions.

Room-temperature ionic liquids (RTILs) have attracted increasing interest in analytical chemistry and are applied more and more as the extraction solvent, replacing the volatile solvent in the sample preparation [4], due to their unique chemical and physical properties, such as negligible vapour pressure, non-flammability, good extractability for various organic compounds and metal ions as neutral or charged complexes, as well as tunable viscosity and miscibility with water and organic solvents. Use of ILs in dispersive liquid-liquid microextraction (DLLME) has been suggested for the first time by our group in 2008 and it resulted into development of a new, simple and rapid method for preconcentration of trace levels of mercury as a prior step to its determination by spectrophotometric detection [5]. Along with the other mentioned methods, advantages of ionic liquid-based dispersive liquid-liquid microextraction (IL-DLLME) are simplicity of operation, rapidity, high recovery, high enrichment factor and environmental benignity, with wide application prospects in trace analysis. Besides, it seems to be a more low-priced method.

In this work the performance of IL-DLLME was investigated with an enhanced spectrophotometric determination of molybdenum in water and plant leaves samples using fiber optic linear array detection spectrophotometry (FO-LADS). It is noticeable that at λ_{max} = 612.0 nm an improvement of the absorbance signal of molybdenum complex in the presence of an appropriate sensitizing agent N-cetyl-N-N-N-trimethyl ammonium chloride (CTAC) is accessible (about twice the value). Moreover, the absorbance of the extracted ternary complex is stable and time independent. (Fig. 1)

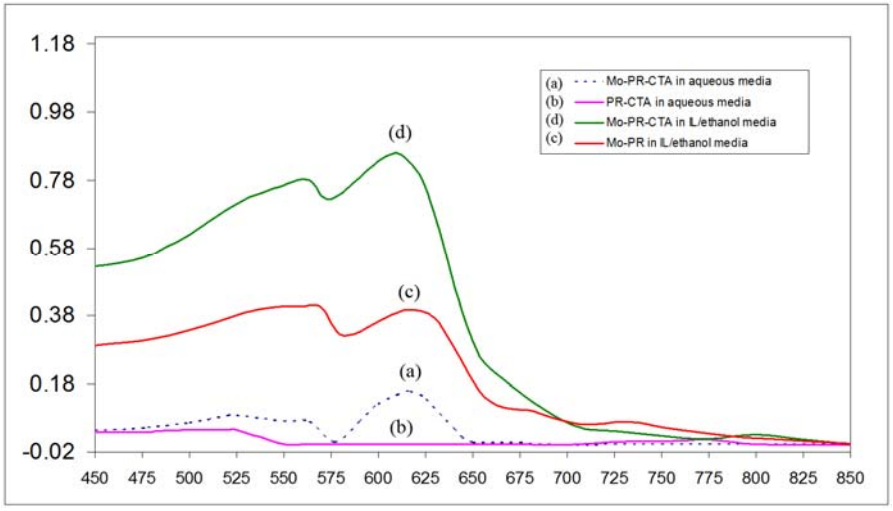

Fig. 1. Absorbance spectra of (a) Mo-PR-CTA and (b) PR-CTA in aqueous media, (c) Mo-PR and (d) Mo-PR-CTA in IL/ethanol media.

Figures of merit

Under optimum conditions, enhancement factor, detection limit and relative standard deviation (n = 5, for 30 μg L^{-1} of molybdenum (VI)) in 10 mL water sample were 72.6, 1.43 μg L^{-1} and 2.8 %, respectively. The calibration curve was investigated up to 100 ng mL^{-1}, which was linear and a good correlation coefficient (r = 0.9992) was obtained.

Conclusion

This method is simple, rapid for the extraction and preconcentration of Mo(VI) from various samples and is superior against a rather high content of salt (up to 20 %) and water-miscible organic solvents, such as acetone, compared with CPE. Further, in comparison with organic solvent extraction, it is much safer since only small amounts of IL are used, which is considered to be a 'green solvent' for various separation processes.

References

1. W. A. Simpkins, H. Louie, M. Wu, M. Harrison and D. Goldberg, *Food Chem.*, 2000, **71**, 423-433.
2. R. Koplik, M. Borkova, B. Bicanova, J. Polak, O. Mestek and J. Kominkova, *Food Chem.*, 2006, **99**, 158-167.
3. J. L. Manzoori and G. Karim-Nezhad, *Anal. Chim. Acta*, 2003, **484**, 155-161.
4. J. G. Huddleston, H. D. Willauer, R. P. Swatloski, A. E. Visser and R. D. Rogers, *Chemical Communications*, 1998, 1765-1766.
5. M. Gharehbaghi, F. Shemirani and M. Baghdadi, *International Journal of Environmental Analytical Chemistry*, 2009, **89**, 21-33.

Identifying purity of the synthesized 1,1,1-trichloro-3-methyl-3-phospholene by four methods including the conductance titration, potentiometric titration, differential potentiometric and UV spectrophotometer under non-aqueous and completely air-free conditions

M. Shahraki [a, *], S. M. Habibi Khorassani [b], A. Ebrahimi [b], M. T. Maghsoodlou [b], S. MR. Hosseini Tabatabei [a],S. Kiyani [a]

[a] Department of Chemistry, Islamic Azad University, Zahedan Branch, Zahedan, Iran

[b] Department of Chemistry, University of Sistan and Baluchestan, Zahedan, Iran

Email: meh_shahraki@yahoo.com

Keywords: Flame Retardant, Conductance Titration, Potentiometric Titration, Kinetic

Introduction

The purity of 1,1,1-trichloro-3-methyl-3-phospholene (TCMP) is considered important in its reaction with methanol under non-aqueous and completely air-free conditions for the preparation of 1-methoxy-3-methyl-2-phospholene oxide (MMPO) as a flame retardant (Fig. 1).[1,2] Additionally, in the kinetics studies of this reaction was highly necessary to identify the purity of the prepared TCMP for obtaining meaningful kinetic parameters. For the first time, this work surveys the electrochemical methods used for identifying purity of the synthesized TCMP which is sensitive to moisture and react with water based upon the approach detailed in Coleman's work.[3] These procedures involve the conductance titration, potentiometric, differential potentiometric and UV spectrophotometer under inert condition All equipments were especially designed and setup under inert condition and then calibrated. The obtained results from the potentiometric titration will be discussed in next section.

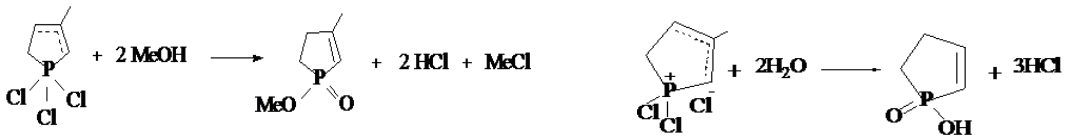

(i) (j) TCMP

Fig. 1. (i) Reaction between TCMP and methanol, (j) Reaction between TCMP and water

Results and discussion

To calibrate the system, the apparatus setup as shown in Fig. 2. The solution of KCl was titrated with the 0.100 M silver nitrate solution. After each addition of a known volume of $AgNO_3$, the cell potential was measured by the digital potentiometer. There was a good agreement between both the end and equivalence points. To perform a potentiometric titration experiment for the reaction between TCMP and water, about 0.2 g of TCMP was weighed and dissolved in 100 mL deionised water using the specially designed conical flask described for conductance titration. Using the apparatus shown in Fig. 2, 35 mL of the HCl solution obtained from the reaction of a known quantity of TCMP (0.1894 g) with water (each mole TCMP generates 3 mole of HCl) was titrated with 0.100 M $AgNO_3$ solution. After each addition of a known volume of $AgNO_3$ solution, the cell potential was measured using the digital potentiometer. Potentiometric titration data are reported in Table 1 and a titration curve is illustrated in Fig. 3.

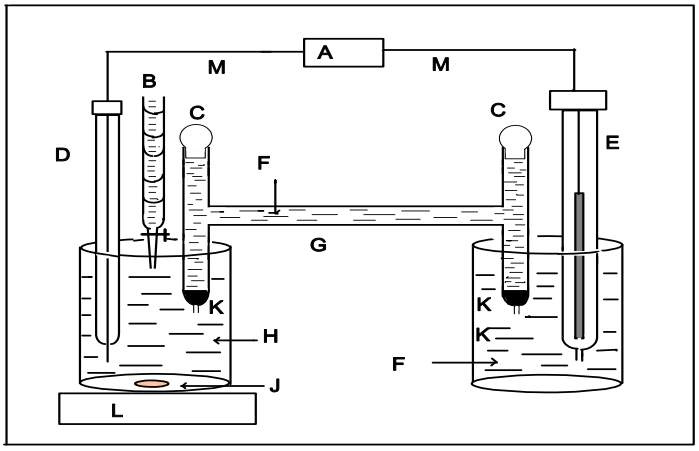

Fig. 2. Apparatus for potentiometric titration. A, Digital potentiometer recorder. B, Burette containing reagent, in these experiments 0.100 M standard silver nitrate. C, Glass stopper. D, Silver electrode as an indicator electrode. E, saturated calomel electrode as a reference electrode. F, Saturated KNO_3. G, Salt bridge. H, Sample solution. J, Teflon stirrer bar. K, Wad of cotton wood. L, Magnetic stirrer. M, connecting leads.

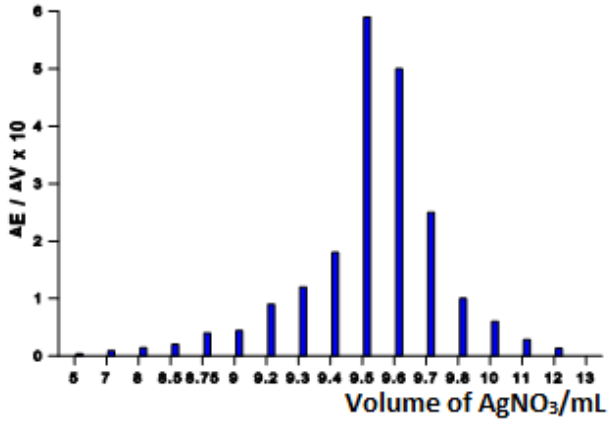

Fig. 3. Potentiometric titration curve of chloride generated ion in the reaction between TCMP (0.1894 g) and deionised water with 0.100 M $AgNO_3$.

These results confirm the generation of HCl solution, in practical, from the reaction of a known quantity of TCMP and water (each mole of TCMP generate 3 moles of HCL, Fig. 1) in comparison with theoretically predicted HCL solution, they are nearly same; this agreement shows that the purity of synthesized TCMP is extremely high.

Table 1. Potentiometric titration data for the titration of Cl^- (arising from the reaction between 0.1894 g of TCMP and water) with 0.100 M $AgNO_3$.

V_{AgNO3}[a]/mL	E/Volt	ΔE[b]/ΔV	V_{AgNO3}[c]/mL
0	0.155	-	0
5	0.175	4.0×10^{-3}	5
2	0.193	9.0×10^{-3}	7
1	0.207	1.4×10^{-2}	8
0.5	0.217	2.0×10^{-2}	8.5
0.25	0.227	4.0×10^{-2}	8.75
0.25	0.238	4.4×10^{-2}	9
0.1	0.242	4.0×10^{-2}	9.1
0.1	0.251	9.0×10^{-2}	9.2
o.1	0.263	1.2×10^{-1}	9.3
0.1	0.281	1.8×10^{-1}	9.4
0.1	0.340	5.9×10^{-1}	9.5
0.1	0.390	5.0×10^{-1}	9.6
0.1	0.415	2.5×10^{-1}	9.7
0.1	0.425	1.0×10^{-1}	9.8
0.1	0.436	1.1×10^{-1}	9.9
0.1	0.442	6.0×10^{-2}	10
1	0.470	2.8×10^{-2}	11
1	0.483	1.3×10^{-2}	12

[a] Volume of silver nitrate which is added in each step.
[b] As a typical example, $\Delta E/\Delta V$ is calculated for the first two step of Table 1: $\Delta E/\Delta V = 0.175 - 0.155/(5 - 0.0)=4\times10^{-3}$.
[c] Total volume of silver nitrate in each step.

Conclusions

Investigation of the UV spectral of the prepared TCMP indicated a demonstration of the high purity of the TCMP used. The conductance titration experiments for the measurement of HCl generated in the reaction between TCMP and water showed that the end point was overestimated due to interference. The results obtained from the potentiometric and differential titration experiments were much more reliable. These data showed that the volume of silver nitrate needed to reach the end point was exactly equivalent to the chlorine content predicted on the assumption that the TCMP sample was pure. Thus, the data are consistent with the synthesized TCMP being of high purity.

References

[1] W. B. McCormak, U.S. Patent Office., 2 663 736 & 3 663 737, 1953.

[3] G. V. Coleman, Development of novel flame retardants for polyurethane foams Ph.D. thesis, University of Salford. 1994.

[3] K. Bourikas, C. Kordulis, A. Lycourghiotis, Environ. Sci. Technol. 39 (2005) 4100.

The effect of surface area of working electrode on the electrochemical noise from pitting corrosion of Al2024

M. Shahidi[a], S. M. A. Hosseini[*b], A. H. Jafari[c]
[a]Department of Chemistry, Islamic Azad university, Kerman Branch, Kerman, Iran
[b]Department of Chemistry, Shahid Bahonar University, Kerman, Iran
s.m.a.hosseini@mail.uk.ac.ir
[c]Department of Material Science & Engineering, Shahid Bahonar University, Kerman, Iran

Keywords: Electrochemical noise, Pitting corrosion, Surface area, Standard deviation

Introduction

The measurement of electrochemical noise (EN) requires two nominally identical working electrodes (WE) connected through a zero resistance ammeter (ZRA) [1].

The effect of specimen area (A) on EN measurements has not been fully established. In general, the amplitude of current noise (measured as the standard deviation) is proportional to A^n. If current noise is considered to be produced by a large number of independent (and hence uncorrelated) current sources, then n=0.5 and if the current noise from different areas of a given electrode is expected to be correlated, then n=1. Hence n is expected to range from 0.5 (for uncorrelated noise) to 1 (for correlated noise) [2].

The goal of the present work is to study the effect of surface area of Al2024 on the standard deviation of current noise.

Methods

The disk specimens of Al2024 aluminum alloy, whose chemical composition is given in Table 1, with different areas: 2, 4, 20, 100 and 200 mm^2 were used to be embedded with resin. The working suface was polished by abrasive papers through 600-2500 grade, washed by distilled water, degreased by ethanol, finally dried in air.

Table 1 Chemical composition of Al2024

Cu	Mg	Mn	Ti	Zn	Fe	Si	Ni	Al

3.9	1.4	0.3	<0.15	<0.3	<0.5	<0.5	<0.1	Balance

All the experiments were carried out in a solution of NaCl 3.5% and $NaNO_2$ 1%. The time record were obtained after 10min from immersion, using a sampling rate of 2Hz for 1000s. EN measurements were carried out with an Autolab potentiostat 302N.

Results and discussion

The results are listed in Table 2. Plot of log(SD) vs. log(A) is shown in Fig 1. This figure demonstrated that SD of current is proportional to $A^{0.73}$, that is n=0.73.

Table 2

A (mm^2)	4	8	40	200	400
SD (amp)	2.28E-8	2.78E-8	1.56E-7	3.11E-7	5.77E-7

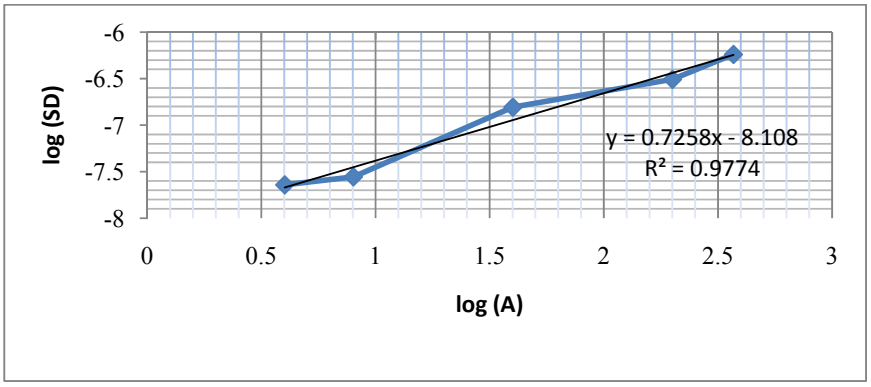

Figure 2

Conclutions

The results is shown that the pitting events are correlated. This means the occurrence of a pit will cause the potential of the WE's to fall, which will presumably reduce the probability of another pit initiating. As the potential rises again, so the probability of pit initiation will increase.

References

[1] U. Bertocci, C. Gabrielli, F. Huet, M. Keddam, J. Electrochem. Soc. 144 (1997), p.31.

[2] R. A. Cottis, Corrosion, 57, 3 (2001), p.265.

Electrocatalytic oxidation of aspirin at Multiwalled carbon nanotube-nickel phosphate nanoparticle modified carbon paste electrode

A. Samadi-Maybodi*[a], M.R. Ganjali[b], S.M. Pourali[a]

[a]*Department of Chemistry, Mazandaran University, Babolsar, Iran*

(E-mail: samadi@umz.ac.ir)

[b]*Center of Excellence in Electrochemistry, Faculty of Chemistry, University of Tehran, Tehran, Iran*

Keywords Aspirin, Multiwalled carbon nanotubes, Nickel phosphate, Modified CPE

Introduction

The determination of acetylsalicylic acid (ASA), known as aspirin, with electrochemical methods has caught much attention because of its sensitivity and simplicity [1]. Also, carbon nanotubes (CNTs) have received enormous attention in electroanalysis due to their unique properties such as high electrical conductivity, high chemical stability, and extremely mechanical strength. However, MWCNTs are regarded as metallic conductor with many active sites which enhance the sensitivity of electrochemical analysis. To our knowledge, however, no work on the determination of ASA has been reported using MWCNT and nickel phosphate nanoparticle simultaneously. In this research, electrocatalytic oxidation of aspirin (acetylsalicylic acid) has been investigated on a carbon paste electrode modified with nickel phoaphate nanoparticle and multiwalled carbon nanotubes (MWCNTs) using cyclic voltammetry and differential pulse voltammetry techniques at alkaline solution. The effect of some parameters such as potential scan rate, aspirin and NaOH concentraction, the amount of the modifiers were investigated on the aspirin oxidation at this electrode.

Methods

The optimized electrode was prepared using 26.6% of nickel phosphate nanoparticle, 4.4% of MWCNT, 46.6% of graphite and 22.2% wt of paraffin.

Results and Discussion

The typical voltammogram of the modified CPE in 0.1M NaOH solution in the potential range of 0-0.9 mV with potential scan rate of 10 mVs^{-1} represented a pair of redox peaks appears at 352 and 456 mV that are assigned to the Ni(II)/Ni(III) redox couples according to:

$$NiOOH + H_2O + e \Leftrightarrow Ni(OH)_2 + OH^- \qquad (1)$$

CVs of the modified electrode in the absence and presence of 5 mM ASA were obtained in different potential scan rates (2-350 mVs^{-1}). In the presence of aspirin, the anodic current and the associated anodic charge increased drastically [2]. Plotting the current function against the square root of the potential scan rate reveals negative slope, which confirms the electrocatalytic nature of the process. Figure 1 shows CVs (20 NS) of the 5mM ASA as the surface of the modified electrode in 0.4 M NaOH solution. Obvious negative shift and sharp rising of current responses was observed [3].

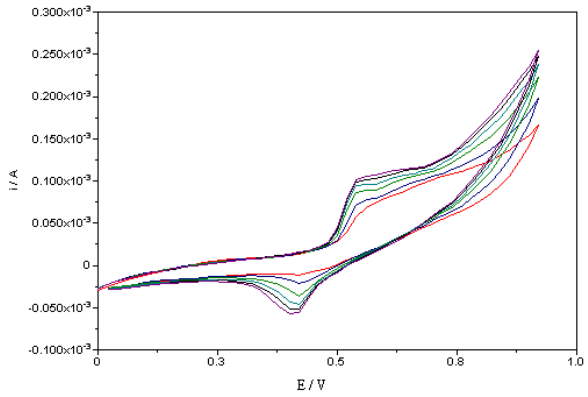

Fig. 1

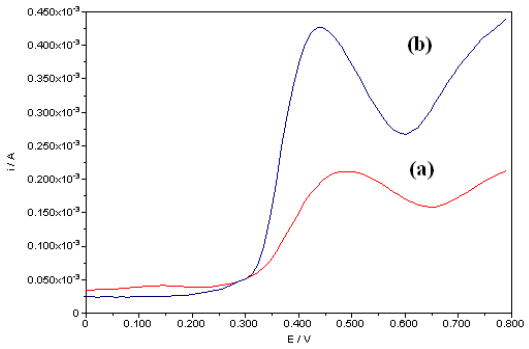

Fig. 2

By increasing NaOH concenteration up to 0.4M, I_a increases gradually because the anodic form of ASA would be increased. Then, it reaches to a plato. The E_a behaves reversely, it decreased up to 0.4 M NaOH, then became independent of the NaOH concenteration. Figure 2 shows the DPV in the absence and presence of 5 mM ASA.

Conclusion

In this work, we demonstrated the measurement of aspirin using MWCNT-nickel phosphate nanoparticle modified CPE. Our results indicated that this electrode provide a stable, high response and sensetive voltammetric detection of ASA.

References

[1] T. Lu, and Y. Tsai, *Sensors and Actuators B* 148 (2010) 590-594.

[2] S. Majidi, A. Jabbari, and H. Heli, *J Solid State Electrochem* 11 (2007) 601-607.

[3] W. Zhang, B. Xu, Y. Hong, Y. Yu, J. Ye, and J. Zhang, *J Solid State Electrochem* 14 (2010) 1713-1718.

Preconcentration of trace of copper (II) ions using Bis (3-nitrobenzylidene)-1,2-ethanediimine(BCBEN) on multiwalled carbon nanotubes and subsequent determination by AAS

M. Ghaedi*[a], M. Montazerzohori[a], J. Tashkhourian[b], M. Tabatabaei[c], H. Noormohamadi[c], M. Borhan[c]

a) Chemistry Department Yasouj University Yasouj Iran 75914-353.

b) Chemistry Department, Shiraz University, Shiraz, Iran

c)Chemistry Department, Firouzabad Azad University, Firouzabad, Iran

Corresponding author: .mail: m_ghaedi@mail.yu.ac.ir Telfax: +98-741-2223048.

Abstract

The determination of metal ions at trace level is very important in the content of environmental protection, food and agricultural chemistry as well as high purity materials. However, the direct determination of metal ions in complex matrices is limited due to their usually low concentrations and matrix interferences. In trace analysis, therefore, a preconcentration and/ or separation is necessary to improve sensitivity and selectivity of determination. Several procedures have been proposed and applied for enrichment and separation with atomic spectrometry detection according to the nature of the samples, the content of analytes and the measurement techniques [1–4]. Among them, the methods which are based on sorbent extraction have proven to be the most attractive ones due to their specificity and high preconcentration efficiency. The broad range of choice for sorbent materials along with various chelating reagents and eluents make this technique very attractive for sample pretreatment [5–9]. In the current study, a new sensitive and simple method for separation and peconcentration of Cu^{2+} ions from various real samples prior to its measurements by flame atomic absorption spectrometry (FAAS) is based on utilization of multiwalled carbon nanotube modifed with bis(3-nitrobenzylidene)-1,2-ethanediimine(BCBEN) as a solid phase extractant has been proposed. The influence of effective parametrs including pH, amount of ligand and solid phase, sample and eluent flow rate, and common coexisting ions on the Cu^{+2} ion recovery were examined. The optimum pH value for the separation and preconcentration of trace amount of Cu^{2+} ions on the new

sorbent was 6.0, and its maximum static adsorption capacity onto the MWCNT-**NBNBAEED** was higher than 60.57 mgg^{-1} at this pH and after 1 h contact time. At optimum value of all variables, the response is linear over the range of 0.01-0.4 μg ml^{-1} and detection limit ($3SD_b/m$, n=15) was 1.5 while respective preconcentration factor and enrichment factor was 200 and 36 and RSD was 3.1 %. The proposed procedure was applied to the analysis of various real samples.

Introduction

Solid phase extraction is an attractive separation preconcentration technique for heavy metal ions with some important advantages (simplicity, flexibility, economic, rapid, higher enrichment factors, absence of emulsion, low cost because of lower consumption of reagents, more importantly environment friendly). Various solid phase extraction materials have been successfully used for the preconcentration and separation of heavy metal ions at trace levels [8–12].

Moreover, they can be easily implemented and controlled in the flow systems. Carbon nanotubes (CNTs), a member in the carbon family, are relatively new materials that have attracted great attention in recent years also in analytical chemistry [10,11]. The hexagonal arrays of carbon atoms in graphite sheets of CNTs surface having strong interactions with other molecules as well as the large surface area make them promising solid sorbent for preconcentration procedures [12–14]. The studies concerning the application of carbon nanotubes for preconcentration are mostly limited to a single metallic species [15–19].

Experimental

Instruments

The measurements were performed with a Shimadzu 680 AA atomic absorption spectrometer equipped with a hollow cathode lamp and a deuterium background corrector at respective wavelengths using an air-acetylene flame. The set instrument parameters were those recommended by the manufacturer. A Metrohm 691 pH/Ion meter with a combined glass–calomel electrode was used for the adjustment of the pH of the test solution.

References

[20] A. Stafiej, K. Pyrzynska, Sep. Purif. Technol. 58 (2007) 49.

[21] H.P. Boehm, Carbon 40 (2002) 145.

[22] S.A. Dastgheib, D.A. Rockstraw, Carbon 40 (2002) 1843

[1] M.B. Arain, T.G. Kazi, M.K. Jamali, H.I. Afridi, N. Jalbani, J.A. Baig, Speciation of heavy metals in sediment by conventional, ultrasound and microwave assisted single extraction: a comparison with modified sequential extraction procedure, J. Hazard. Mater. 154 (2008) 998–1006.

[2] M.K. Jamali, T.G. Kazi, M.B. Arain, H.I. Afridi, N. Jalbani, A.R. Memon, Heavymetal contents of vegetables grown in soil, irrigated with mixtures ofwastewater and sewage sludge in Pakistan, using ultrasonic assisted pseudo-digestion, J. Agron. Crop Sci. 193 (2007) 218–228.

[3] M. Karve, R.V. Rajgor, Solid phase extraction of lead on octadecyl bonded silica membrane disk modified with Cyanex302 and determination by flame atomic absorption spectrometry, J. Hazard. Mater. 141 (2007) 607–613.

[13] R.S. Amais, C.R.T. Tarley, Experimental design approach in the diethyldithiocarbamatenickel chelate preconcentration using cloud point method and determination by GFAAS, Can. J. Anal. Sci. Spect. 53 (2008) 130–140.

Electrosynthesis of Benzoic acid from Toluene Using PbO_2 Electrode

H. Zaheri[1],S. Jameh-Bozorgi[*, 2], A. Bodaghi[2] and H. Soleymanabadi[1]

[1] *Young researchers Club, Islamic Azad University, Toyserkan Branch, Toyserkan, Iran*

[2]*Chemistry Department, Faculty of Sciences, Islamic Azad University, Toyserkan Branch,Toyserkan, Iran*

(Email: Sjamehbozorgi@gmail.com)

Key words: Electrosynthesis, PbO_2 Electrode, Benzoic acid, Toluene

Introduction:

Electrosynthesis in organic chemistry is the synthesis of chemical compounds in a electrochemical cell [1]-[2]. The main advantage of electrosynthesis over an ordinary redox reaction is avoidance of the potential wasteful other half-reaction and the ability to precisely tune the required potential. Electrosynthesis is actively studied as a science and also has many industrial applications. PbO_2 is an important electrode material due to its stability under aggressive conditions (i.e. high electrolyte acidity and high anode potentials), high electronic conductivity and low cost of material. Two major areas of applications of PbO_2 are as an electrode material for lead acid batteries and as a catalyst for electrosynthesis. PbO_2 exhibits different morphological forms that include the orthorhombic (α) and tetragonal (β) forms [3]. Our goal in this research is electrosynthesis of benzoic acid from toluene by using Lead dioxide electrode.

Methods:

In this study for the oxidation of toluene, PbO_2 electrode used as the anode electrode. For making this electrode, placed two clean sheets of lead in the H_2SO_4 (1M) solution and then set up electrolysis system. After 5 hours at current density10mA/cm^2 a brown layer of β-PbO_2 is formed on the anode electrode. After making the electrode, electrolysis mixture was prepared. In this mixture H_2SO_4 (electrolyte) and Acetonitrile (solvent) mixed in 2:1 ratio. PbO_2 electrode was placed in anodic part and steel cathode electrode was placed in the cathodic part of electrolysis cell. Then 16mmol toluene added to anolite and then plug anode while the slow round magnet in the solution and necessary amount of flow applies.

To determine the reaction progress and synthesis of benzoic acid the thin layer chromatography (TLC) was used. Combination of three solvents: ethylacetate, cyclohexan and dichloromethane were found suitable for TLC. For separation and purification of product we used distillation, extraction and finally recrystallization methods.

Results and discussion:

To ensure that the purified crystals are benzoic acid, the melting point was measured (121˚ C). IR spectroscopy techniques, was used to identify the product, the results are in Table 1.

Table1:The results of IR spectrum Benzoic acid of synthesis

Functional groups	*C=O*	*C-O*	*O-H*	*O-Hoop*
Wavenumbers(cm^{-1})	**1697**	**1320**	**2500-3400**	**930**
%Transmittance	**23**	**30**	**expand**	**58**

Ensure the synthesis of benzoic acid, density currents in different tests were performed until we reached the highest efficiency, the results are in Table 2.

Table2: The results of toluene oxidation in different conditions

Test of number	Surface of Pbo2 electrode	Current density (mA/cm^2)	Intensity flow (mA)	Potential (V)	Weight of Toluene (gr)	Weight of product (gr)	Time (hours)	Efficiency
1	$7cm^2$	8	56	2.8	1.5	0.5	4	33.3%
2	$7cm^2$	9	63	3	1.5	0.6	5	40%
3	$7cm^2$	10	70	3.1	1.5	0.75	5	50%
4	$7cm^2$	12	84	3.3	1.5	0.85	5.5	56.6%
5	$7cm^2$	14	98	3.4	1.5	0.93	6	62%
6	$7cm^2$	15	105	3.5	1.5	1.11	7	74%
7	$7cm^2$	16	112	3.6	1.5	0.96	8	64%

Conclusions:

According to the results of IR spectrum and melting point determination, electrosynthesis of Benzoic acid from Toluene with 74% efficiency and good economic sense was prepared. Consequently the best conditions of production is: stainless steel cathode electrode, PbO2 anode electrode, current density 15mA/cm^2 , intensity flow 105mA and finally time is seven hours.

Refrences:

[1] J. B. Sperry and D. L. Wright; *Chem. Soc. Rev.*, **35** (2006) 605.

[2] E. Steckhan; *Topics in Current Chemistry, Electrochemistr*y, Vol. 3, Springer, NY **1988**.

[3] N. Munichandraiah and S. Sathyanarayana, *J. Appl. Electrochem*., **18** (1988) 314.

Thiomorpholine-functionalized nanoporous mesopore as a sensing material for Cd^{2+}carbon paste electrode

Mehdi Asgari*, Mohammad Reza Ganjali

Center of Excellence in Electrochemistry, Faculty of Chemistry, University of Tehran, Tehran, Iran
Mehdi.asgari13@gmail.com

Introduction

The family of ordered mesoporous solids has found wide applications in electrochemistry, catalysis, separations, adsorption, coatings, or microelectronics [1, 2]. Due to their great porosity and uniform structure, access to the organofunctional groups attached to the mesopore walls is easy [3–5] and cause fast transport of the target analyte to the binding sites [6, 7].In this work, the construction of a selective sensor, a carbon paste electrode, modified with silica-based organic– inorganic hybrid materials containing thiol groups covalently attached to the solid framework via a propyl chain.

Experimental part

Preparation of substrate

To Prepare substrate (TM-MCM) MCM-41 Clear gel containing fumed silica and sodium silicate is slowly added to a clear CTMAB solution with stirring at room temperature. The resulting gel is transferred into a Teflon-lined autoclave and maintained for 24 h at 130°C. The resulting powder is filtered, washed with distilled water, and dried in air. As-synthesized MCM-41 (4.0 g) was stirred in 100 mL dry toluene solution containing 13 mL 3-(triethoxysilyl)-1-iodopropane under argon atmosphere. After 24 h reflux, the solid was filtered and washed with dry toluene. The filtered sample was dried and added to 80 mL dry toluene; then, 2.8 mL thiomorpholine was added to this solution under argon atmosphere. The mixture was refluxed for 24 h. After filtering, the solid was received, and the residual reagents were removed through washing with dry toluene

Preparation of the chemically modified carbon paste electrodes

The chemically modified carbon paste electrodes were prepared by thoroughly mixing graphite powder, 25%wt. paraffin oil and TMMCM-41 in proportions of 10.4, 14.9, 20.1, and

24.9 %wt., respectively. The electrode body was fabricated from a glass tube of i.d. 5 mm and a height of 3 cm.

EMF measurements

electrochemical cell can be represented as follows:

Ag,AgCl(s), KCl (3 mol L^{-1}) || sample solution |carbon paste electrode

Calibration graph was drawn by plotting the potential, E, versus the logarithm of the cadmium ion concentration.

Results and discussion:

The effect of the TMMCM-41 composition on the potentiometric response of the electrodes is shown in Table 1. As it can be seen from Table 1, CPE4 has the optimal electrode ingredient composition. To assess the applicability of proposed electrode in real samples, an attempt was made to determine cadmium in industrial cadmium electroplating wastewater samples. The obtained results are shown in Table 2. As it can be seen, there is a satisfactory agreement between the results of this sensor and those with inductively coupled plasma atomic emission spectroscopy (ICP-AES) analysis.

Table 1 Composition of carbon paste electrodes and their potentiometric response characteristics of chemically modified electrodes

Electrode	Composition (%)			Slope (mV $decade^{-1}$)	Linear range ($molL^{-1}$)	LOD ($molL^{-1}$)
	TMMCM-41	Graphite powder	Paraffin oil			
CPE1	0	75.0	25.0	9.1(±1.8)	-	-
CPE2	10.4	63.5	26.1	24.9(±1.8)	10^{-4}-10^{-2}	6.1×10^{-5}
CPE3	14.9	60.2	24.9	28.2(±1.6)	10^{-5}-10^{-2}	7.5×10^{-6}
CPE4	20.1	54.0	25.9	28.6(±1.2)	10^{-6}-10^{-2}	6.0×10^{-7}
CPE5	24.9	50.0	25.1	26.6(±1.4)	3.0×10^{-6}-10^{-2}	8.7×10^{-7}

Table 2 cadmium electroplating waste water sample analysis by using proposed cadmium sensor (CPE 4) and ICP-AES

samples	The proposed sensor (μgmL^{-1})	ICP-AES (μgmL^{-1})	Relative error (%)
Sample 1	4.73±0.34	4.56±0.23	3.72
Sample 2	5.10±0.42	4.90±0.33	4.08
Sample 3	4.0±0.27	3.87±0.30	3.35

References:

1. Beck JA, Vartuli JC (1996) Curr Opin Solid State Mater Sci 1:76–87

2. Feng X, Fryxell GE, Wang LQ, Kim AY, Liu J, Kemner KM (1997) Science 27:923–926

3. Mercier L, Pinnavaia TJ (1997) Adv Mater 9:500–503

4. Brown J, Richer R, Mercier L (2000) Micropor Mesopor Mater37:41–48

5. Yantasee W, Lin Y, Fryxell GE, Busche BJ, Birnbaum JC (2003) Separ Sci Technol 38:3809 3825

6. Bibby A, Mercier L (2002) Chem Mater 14:1591–1597

7. Walcarius A, Etienne M, Bessiere J (2002) Chem Mater 14:2757–2766

The Study Of Electrochemical Behavior of N_2O_2 Schiff-Base Co(III) Complexes

Rahman Alizadeh*, Mohamad Hadian, Nader Ghazinya, Marziyeh Eslamiyan, Zeinab Alizadeh

Department of Chemistry, Islamic Azad University, Gachsaran Branch 75816-48556, Iran

Corresponding Author E-mail: chem_hadian@yahoo.com

Keywords: Cobalt(III) complexes, Schiff base, Electrochemistry.

Introduction:

Schiff bases are useful constructing supra molecular structures [1-3]. Schiff base complexes are also known for their significant biological activities such as photosynthesis and transport of oxygen in mammalian and other respiratory systems [4,5]. A wide variety of cobalt(II) complexes are known to bind dioxygen, more or less reversibly, and therefore frequently studied as model compounds for natural oxygen carriers and for their use in O_2 storage, as well as in organic synthesis due to their catalytic properties under mild conditions [6]. Metal Schiff base complexes are well known catalysts, both in heterogeneous and homogeneous systems [7]. The electrochemical methods also provide highly valuable information regarding catalytic processes since catalytic conversions are frequently accompanied by the change in the structure of the complex and the oxidation state of the metal; however, the electrochemical approaches for these purposes have not been fully explored [8]. Knowledge of the electronic and steric effects that control the redox chemistry of these metal complexes may prove to be critical in the design of new catalysts. In this study, a series of complexes of the type $[Co(Chel)(PBu)_3]ClO_4.H_2O$ (Fig. 1) where the (Chel) are Naphen, Naphpen, and Naphophen has been synthesized and characterized by elemental analysis, UV–vis, IR, and ^1H NMR spectroscopy. The electrochemical properties of these complexes at a glassy-carbon electrode, in the potential range of 0.5 to –2.0 V (vs. Ag/AgCl), in DMF solution were investigated.

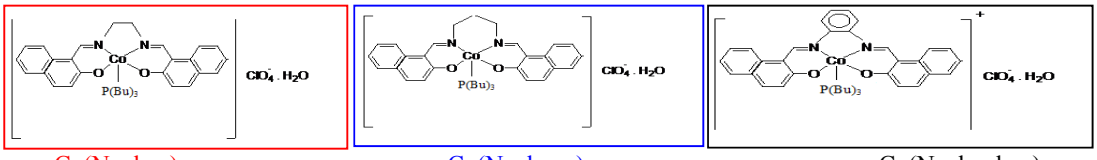

Fig. 1. The structure of $[Co(Chel)(PBu)_3]ClO_4.H_2O$, complexes.

Experimental

Materials and Apparatus

The materials and solvents used in this study were obtained from Merck, Fluka and Aldrich. All of the scanning UV-Vis spectra were recorded by Jasco V-530 spectrophotometer. The NMR spectra were recorded by Bruker Avance DPX 250 MHz spectrometer; IR spectra were recorded by Perkin Elmer Infrared spectrophotometer. Elemental microanalysis (C.H.N), was performed using a Heraeus CHN-O-RAPID elemental analysis. Cyclic voltammograms (CVs) were obtained using an Autolab modular electrochemical system (Eco Chemie, Ultrecht, The Netherlands) equipped with a PSTA 20 module and driven by GPES (Eco Chemie) in conjunction with a three-electrode system and a personal computer for data storage and processing. An Ag/AgCl (saturated KCl)/3 M KCl reference electrode, a Pt wire (counter electrode) and a glassy carbon working electrode, (Metrohm 0.0314 cm2) were employed for the electrochemical studies. Voltammetric measurements were performed at room temperature in DMF solution with 0.1 M tetrabutylammonium perchlorate as the supporting electrolyte.

Synthesis of the Ligands and Complexes

The ligands H_2Naphen, H_2Naphpen, and H_2Naphophen were prepared according to the literature [9,10]. The [Co Naphen (PBu_3)]$ClO_4.H_2O$, [Co Naphpen (PBu_3)]$ClO_4.H_2O$, [Co Naphpen (PBu_3)]$ClO_4.H_2O$ were prepared by methods described previously [9,11].

Results and Discussion:

All the newly synthesized complexes were colored solids and soluble in DMSO, DMF and methanol. Structure of the ligands and complexes (**Fig. 1**) were characterized on the basis of their micro analytical data, elemental analysis, melting points, IR, ^{1}H NMR and UV–Vis spectra. The IR and UV–Vis spectra of the complexes are compared with that of the free ligand to determine the changes that might have taken place during the complexation. The analytical data were in good agreement with the proposed stoichiometry of the complexes.

Electrochemical Studies

In order to investigate the effects of the Schiff base substitutions on the oxidation potential of type $[Co(Chel)(PBu)_3]ClO_4$. H_2O, voltammetric experiments were carried out in DMF solution at room temperature, taking into consideration the electrochemical behavior of the ligands to obtain more details of the electron transfer processes of these complexes. A typical cyclic voltammogram of the type $[Co(Naphen)(PBu_3)]^+$ complex in the potential range of 0.5 to -1.8 V (*vs*. Ag/AgCl) is shown in Fig. 2(red cycle). These peaks are according to equations 1, 2 and 3:

1)$[CoIII(Naphen)(\ PBu_3)]^+ + e^- \rightarrow [CoII(Naphen)] + PBu_3$; Electron added to the antibonding orbital (dz^2) and CoII complex is formed.

2)$[CoII(Naphen)] + e^- \rightarrow [CoI(Naphen)]$; quasi-reversible at lower potentials and CoI complex is formed.

3)$[Co^{II}(Naphen)] + PBu_3 \rightarrow [Co^{III}(Naphen)(\ PBu_3)]^+ + e^-$; fully-reversible and CoIII complex is formed.

Multiple scans resulted in nearly superposable cyclic voltammograms, thereby showing that the five coordinate geometry is stable in three oxidation states. The oxidation potentials for the different complexes are set out in Table 1.

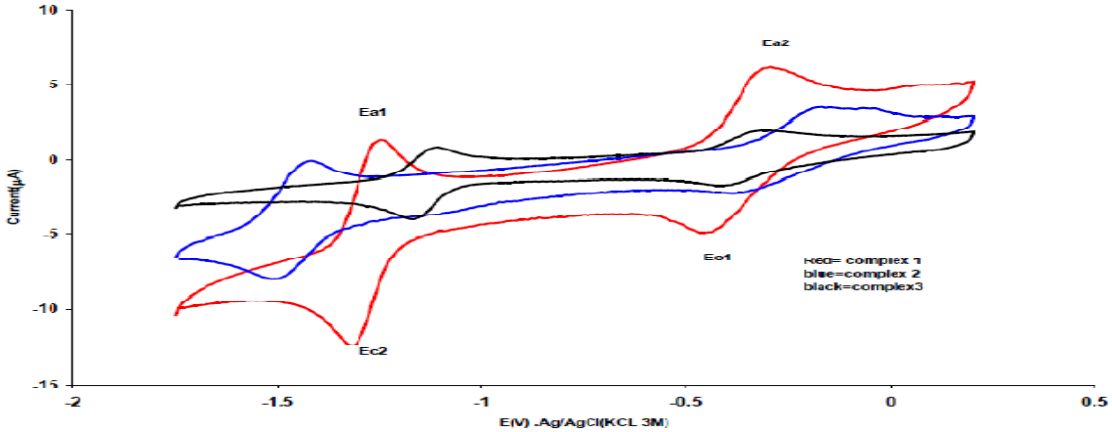

Fig. 2. Cyclic voltamograms of $[Co(Chel)(PBu)_3]$ complexes in 0.1 M, tetrabutylammonium perchlorate DMF solution at room temperature and scan rate of 100 mVs-1.

The Electronic And Steric Effects of Schiff Base Ligands

The influence of different substituents on the electronic structure of a series of the cobalt Schiff base complexes was determined by cyclic voltammetry (Table 1). The results show that in each series of ligands (all Schiff bases with aliphatic and aromatic imine bridges), the

anodic peak potential (Epa) corresponding to the intramolecular reductive coupling of the imine groups varies, as would be expected from the electronic effects of the substituents at positions 5,5' [12]. Similar results have been reported previously for analogous copper(II), nickel(II), and cobalt(III) systems, and have been interpreted under the assumption that the strong electron-withdrawing effects (with the best π −acceptor quality) stabilize the lower oxidation state while the electron-donating groups (with the least π −acceptor quality) have a reverse effect [13-14]. On the other hand, the range of potentials is varied by changing the steric and electronic parameters. Apparently, by increasing the steric effects of the Schiff base, the planarity of the complex is decreased. The donor power of salpn is less than that of salen and the salpn complexes are therefore oxidized at higher potentials[12]. Therefore, redox potentials of cobalt complexes concerning the electronic and steric effect is: naphophen > naphen > naphpn.

Table 1. Oxidation Potentials (in V) for $[Co(Chel)(PBu)_3]$ $ClO_4.H_2O$, in DMF (0.1 M, Tetrabutylammonium Perchlorate)

Complex	Chel	Ec_1(III→II)	Ea_1(I→II)	E_1(1/2)	Ea_2(II→III)	Ec_2(II→I)	E_2(1/2)
1	Naphen	-0.436	-1.25	-0.843	-0.31	-1.309	-0.809
2	Naphpn	-0.382	-1.426	-0.814	-0.175	-1.489	-0.832
3	Naphophen	-0.409	-1.111	-0.76	-0.299	-1.165	-0.732

Conclusion:

Tetradentate N_2O_2 type complexes of $[Co(Chel)(PBu)_3]ClO_4$. H_2O synthesized and characterized by elemental analysis, UV–vis, IR, and ^1H NMR spectroscopy. The redox properties of the complexes were extensively investigated by electrochemical method using cyclic voltammetry (CV). The range of potentials is varied by changing the steric and electronic parameters. Apparently, by increasing the steric effects of the Schiff base, the planarity of the complex is decreased. The donor power of salpn is less than that of salen and the salpn complexes are therefore oxidized at higher potentials. Therefore, redox potentials of cobalt complexes concerning the electronic and steric effect is: naphophen > naphen > naphpn.

Reference:

[1] P.G. Cozzi, Chem. Soc. Rev. 33 (2004) 410.

[2] R. Ziessel, Coord, Chem. Rev. 216 (2001) 195.

[3] P.H. Aubert, P. Aubert, M. Roche, P. Capdevielle, M. Maumy, Chem. Mater. 13 (2001) 2223.

[4] M. Ramesh, K.B. Chandrasekar, K.H. Redy, Indian J. Chem. 39A (2001)1337.

[5] P.K. Coughlin, S.J. Lippard, J. Am. Chem. Soc. 106 (1984) 2328.

[6] E.C. Niederhoffer, J.H. Timmons, A.E. Martell, Chem. Rev. 84 (1984) 137.

[7] S. Zhao, J. Zhao, D. Zhao, Carbohaydrate Res. 342 (2007) 254.

[8] A.S. Amarasekara, I. Mc Neal, J. Murillo, D. Green, A. Jennings, Catalysis Commun. 9 (2008) 2437.

[9] P.J. MacCarthy, R.J. Hovey, K. Ueno, A.E. Martel, J. Am. Chem. Soc. 77 (1955) 5820.

[10] N.S. Biradar, G.V. Karajagi, T.M. Aminabhavi, W.E. Rudzinski, Inorg. Chim. Acta 82 (1984) 211.

[11] M. Asadi, A.H. Sarvestani, Z. Asadi, M. Setoodeh Khah, Synth. React. Inorg. Met. -Org. Chem. 35 (2005) 639.

[12] A.H. Kianfar, S. Mohebbib. J. Iran. Chem. Soc.4 (2007) 215.

[13] A.H. Sarvestani, A. Salimi, S. Mohebbi, R. Hallaj, J. Chem. Res. (2005) 190.

[14] A.H. Sarvestani, S. Mohebbi, J. Chem. Res. (2006) 257.

Electrochemical study of acetaminophen in the presence of adrenaline

M. Alimoradi*,Q. Kamarei, V. Mahboobi,

Department of chemistry,Faculty of Science,Islamic Azad University,Arak Branch, Iran
(Alimoradi599@yahoo.com :Email)

Abstract

Electrochemical oxidation of acetaminophen (N–acetyl–p–aminophenol) has been studied in the presence of adrenaline as nucleophile in aqueous solution, by means of cyclic voltammetry and controlled-potential coulometry. The results indicate the participation of electrochemically generated N-acetyl-p-quinoneimine in Michael reaction with adrenaline to form the corresponding aminoquinone derivative. Based on EC mechanism, the observed homogeneous rate constant (k_0) of the above mentioned reaction is estimated by comparing the experimental cyclic voltammograms with the digital simulated results.

Keyword: Cyclic voltammetry, Acetaminophen, Coulometry, homogeneous rate constant, Michael addition.

Introduction

The electro-oxidation of APAP in aqueous media is intrest because that produced quinoneimine is an acceptor Michael addition reaction and attacked by various nucleophils such as amines. Scince medicine property of APAP is changed by substituted groups on aromatic ring of APAP we decide to investigate about it. Also, electrochemical methods, especially the voltammetric and amperometric ones give the opportunity to study the oxidation mechanisms, the redox metabolites and their detection from pharmaceuticals and body fluids [1-3]. Therefore in this work cyclic voltammetric study of acetaminophen in presence of adrenaline was performed.

Method

The cyclic voltammetric study was performed with glassy carbon disc electrode, platinium wire and SCE as working, counter and reference electrode respectivity. The working electrode used in controlled-potential coulometry and was an assembly of eight graphite rods (8mm

diameter and 6 cm length) and a large platinum gauze constituted the counter electrode. Since the mechanism is dependent on such parameters as, nature of nucleophile, electrolysis medium (solvent, acidity or pH...) and catechol type then initially these parameter wase optimated. After optimisig of parameters cyclic voltammetry, controlled-potential coulometry were performed using a Behpajoh model BHP-2062 potentiostat/galvanostat. All cyclic voltammetric experiments were performed in pH=6.0 in aqeous phosphate buffer(0.2 M) in 0.6-(-0.8) potential renge and various scan rate.

Results and Discussion

The electrochemical study of 2 mM solution of acetaminophen in an aqueous solution containing 0.2 M phosphate buffer (pH 6.0), at a bare glassy carbon electrode has been performed using cyclic voltammetry. The voltammogram shows one anodic (A_1) and corresponding cathodic peak (C_1), at 0.15 V and 0.22 V versus (SCE), respectively, which correspond to the transformation of acetaminophen (1) to N-acetyl-p-quinoneimine (1a) and vice-versa within a quasi-reversible two-electron process . The oxidation of acetaminophen in the presence of adrenaline as a nucleophile was studied in some details. In this case, the cathodic counterpart of the anodic peak A1 decreases.

With the aim of investigating of reactivity of intermediate *N*-acetyl-*p*-quinoneimine toward adrenaline, as well as estimation of observed chemical rate constant of this reaction, we investigated the electrochemical oxidation of acetaminophen in aqueous solutions in the presence of adrenaline. The results indicate the participation of electrochemically generated *N*-acetyl-*p*-quinoneimine in Michael reaction with adrenaline. Based on *EC* mechanism, the observed homogeneous rate constant (k_0) of the above mentioned reaction is estimated by comparing the experimental cyclic voltammograms with the digital simulated results.

References

[1] Y. Masubuchi, C. Suda, T. Horie, Journal of Hepatology, 42(2005) 110-116.

[2] D.W. Potter, D.W. Miller, J.A. Hinson, Mol. Pharmacol. 29(2), 1986,p 155-162

[3] E.Valero, P. Carrión, R. Varón, F. Garcĺa-Carmon,Analytical Biochemistry 318 (2003) 187–195

Determination of Phenol Redox Potential with a Ni-Al Layered Double Hydroxide Film Modified Glassy Carbon Electrode

K.Nejati[a] , O. gheibi[*] [a],Z.rezvani [b]and R . zabihi[a]

[a] Department of Chemistry , Payame Noor University , Tabriz , Iran

Email: ozragheibi@gmail.com

[b] Department of Chemistry , Azarbaijan University of Tarbiat Moallem , Tabriz , Iran

Abstract

Phenolic compounds are widely used chemicals and released into the environment. They are a class of polluting chemicals, easily absorbed by animals and human through the skin and mucous membranes. Therefore, the determination of phenolic compounds is of great importance due to their toxicity and persistency in environment. A stable phenol sensor was fabricated by electrochemical deposition of Ni/Al layered double hydroxide film on glassy carbon electrode (LDH/GCE).This non-enzymatic phenol sensor has been applied to determine Phenol redox potential with cyclic voltametery.

Keywords: sensor,Phenol , LDH, $Ni(NO_3)_2$, $Al(NO_3)_3$

Introduction

In recent years, layered double hydroxides (LDH), also known as anionic or hydrotalcite-like clays, have growing interest for using in the wide fields owing to their attracted desirable properties, which include good biocompatibility[1], intense adsorbability [2], high catalytic activity [3], low cost [4], and high chemical stability [5]. The general formula for these compounds is $[M_{1-x}^{2+} M_x^{3+} (OH)_2]^{b+}[A^{n-}]_{b/n} . m H_2O$, (Fig.1)where M^{2+} and M^{3+} are the divalent and trivalent cations. A^{n-} is an interlayer anion with a negative charge n , and b is the charge of the layer and m is the number of water molecules[6].

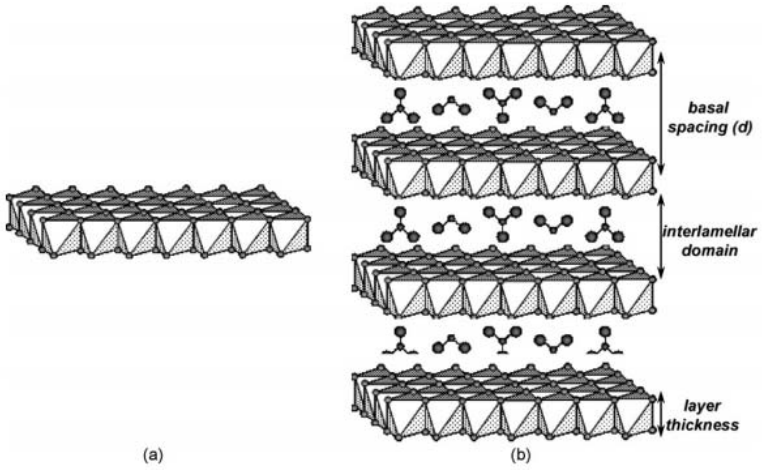

Fig. 1. Schematic structural representation: (a) brucite; (b) hydrotalcite.

A stable phenol sensor was fabricated by electrochemical deposition of Ni/Al layered double hydroxide film on glassy carbon electrode (LDH/GCE).This non-enzymatic phenol sensor has been applied to determine phenol redox potential with cyclic voltametery.

Experimental

The Ni-Al LDH modified GC (LDH/ GCE) electrode was prepared according to the reference [7]. After a pretreated GC electrode of 2 mm diameter was rinsed with carbondioxide- free water, and dried at room temperature. A film of Ni-Al LDHs was deposited on the electrode surface by cathodic reduction of a pH 3.3 solution containing0.12 M $Ni(NO_3)_2.6H_2O$, 0.04 M $Al(NO_3)_3.9H_2O$ and 0.15 M KNO_3. The electrochemical reaction was carried out in a singlecompartment, three-electrode cell by applying a potential (Eapp) of -0.9 V vs. SCE . The LDH/GC electrode obtained for a deposition time of 60 s was chosen as working electrode for performing the electrochemical measurements.

Results and discussion

Oxidation and reduction peak was obtained.electro-oxidation mechanism can be represented by the following reaction:

$$LDH–Ni(II) + OH_{sol}^- \rightleftharpoons LDH(OH^-)–Ni(III) + e- \quad (1)$$

$$LDH(OH^-)–Ni(III) + Phenol \rightarrow LDH–Ni(II) \quad (2)$$

Figure 2 gives the typical CVs of LDH/GC electrode in0.1 M NaOH with scan rates of 50–240 mV s-1.

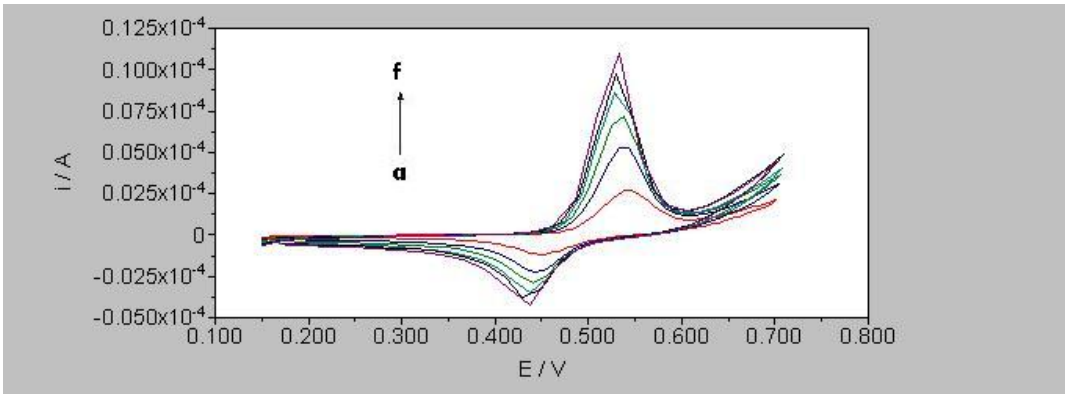

Fig. 2 Cyclic voltammograms of LDH/GC electrode in 0.1 mol L-1 NaOH at different scan rates. The selected scan rates are a 50, b 100, c140, d 180, e 200, f 240mV s-1

As shown in Fig. 3, when Phenol was added to 0.1 M NaOH, an increase in the I_a and I_c.

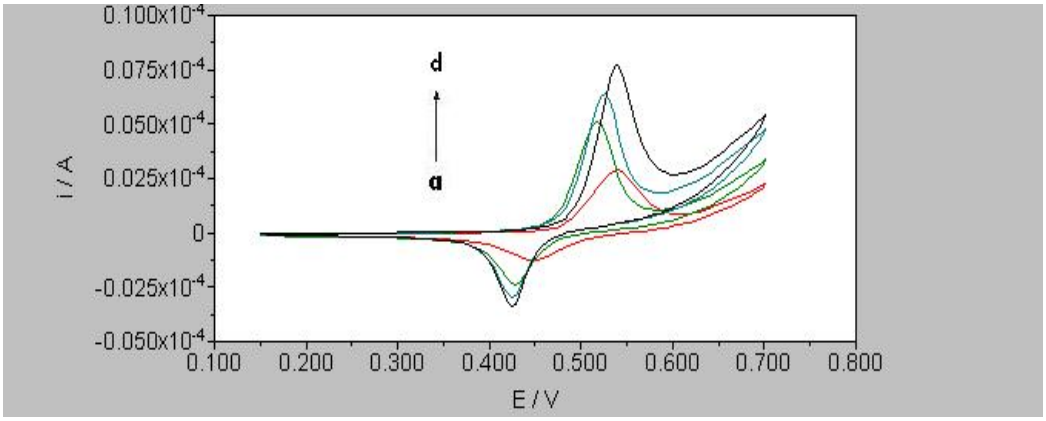

Fig. 3 Cyclic voltammograms of LDH/GC electrode in 0.1 M NaOH containing a 0 mM, b 0.05 mM ,c 0.1 and d 0.15 mM phenol. Scan rate, 50 mV s-1

Conclusions

Combining the advantageous features of inorganic lamellar materials (LDHs), electroactive Ni centers, and the electrosynthesis method, a stable Ni-Al LDH film was constructed on the surface of GC electrode without further immobilization. The prepared film was characterized by means of CV, and the results indicated that the Ni centers in the LDHs had high

electroactivity in 0.1 M NaOH., the LDH/GC electrode could be used for electrochemical nonenzymatic phenol concentration determination and exhibited many desirable properties such as high sensitivity, low detection limit, good reproducibility, long-term stability, fast current response, and low interference.

References:

[1] J. H. Choy, S. Y. Kwak, Y. J. Jeong, J. S. Park, Angew. Chem. Int. Ed. 2000, 39, 4041.

[2] F. Li, Y. Wang, Q. Yang, D. G. Evans, C. Forano, X. Duan, J. Hazard Mater. 2005, 125, 89.

[3] F. A. He, L. M. Zhang, J. Colloid. Interf. Sci. 2007, 315, 439.

[4] D. Shan, S. Cosnier, C. Mousty, Anal. Chem. 2003, 75, 3872.

[5] P. S. Braterman, Z. P. Xu, F. Yarberry, in Handbook of Layered Materials (Eds: S. M. Auerbach, K. A. Carrada, P. K. Dutta), Marcel Dekker, New York 2004, p. 373.

[6] F .Leroux , J .p .Besse, Chem Mater . 13 (2001)3507

[7]Scavetta E, Mignani A, Prandstraller D, Tonelli D (2007) Electrosynthesis of thin films of Ni, Al hydrotalcite like compounds. Chem Mater 19:4523

Thermodynamic study of the ternary mixed electrolyte ($NaCl+NiCl_2+H_2O$) system: Application of Pitzer model with higher-order electrostatic effects

Bahram Ghalami-Choobar*, Mohsen Mohammadian

Department of Chemistry, Faculty of Science, University of Guilan, P.O. Box: 19141, Rasht, Iran

E-mail address: B-Ghalami@guilan.ac.ir (B. Ghalami-Choobar)

Keywords: Pitzer model; NaCl; $NiCl_2$; emf method

Introduction

In recent years, there has been a growing interest in the measurement or prediction of the activity coefficients of electrolytes solution because of their importance in areas such as chemistry, biology and process engineering [1]. In the previous work, we have reported the results relating to the thermodynamic properties of binary and ternary electrolyte solutions [2-3]. As a continuation of our studies on the ternary systems, the thermodynamic properties of (NaCl + $NiCl_2$ + water) system using the potentiometric method are reported at T = 298.2 K.

Experimental and method

All of the potentiometric measurements were made by using a digital multimeter whose resolution was 0.1 mV. The output of the multimeter was connected to a personal computer for data acquisition. The potentiometric measurements were carried out on the galvanic cell without liquid junction of the type: Na–ISE | NaCl (m_1), $NiCl_2$ (m_2), H_2O | Ag-AgCl over total ionic strengths from 0.001 to 4.000 mol. kg^{-1} . Different series of the salt molal ratios r (r = m_{NaCl}/m_{NiCl2} = 2.5, 5.0, 7.5, 10.0) and pure NaCl were used for the measurement. The PVC based sodium ion selective electrode (Na-ISE) and Ag–AgCl electrode used in this work were prepared in our laboratory and had a reasonably good Nernst response. The Pitzer ion interaction model was used for the experimental data correlation and calculation of thermodynamic properties for mixed electrolyte solutions.

Results and discussion

The galvanic cell was used to determine the emf values of the mixed salts in the mixture at different ionic strengths I and mole fraction *y*. The experimental mean activity coefficients of NaCl in the mixture were derived from the Nernst equation 1.

$$E = E^{'} + k \lg[(m_1 + 2m_2)m_1 .\gamma_{\pm NaCl}^2 + k^{pot}(m_1 + 2m_2)^{1/2}.m_2^{1/2}.\gamma_{NiCl_2}] \quad (1)$$

The results relating to the mean activity coefficients of NaCl for r=5 were listed in Table 1. The mean activity coefficients of different series were also presented in Figure 1. The mixed ionic interaction parameters ($^{S}\theta_{NaNi}$ and ψ_{NaNiCl}) were evaluated (see table 2) for the studied ternary system with and without considering of higher-order electrostatic terms in according to the Pitzer model based on the equation2. Then, these obtained parameters were used for predicting the thermodynamic properties.

$$\ln \gamma_{\pm Nacl} = \ln \gamma_{\pm NaCl}^{0} + \frac{1}{3} yI[B_{NiCl_2} - 2B_{NaCl}] + \frac{1}{9} yI^2(y-6)C_{NaCl}^{\varphi} - \frac{\sqrt{2}}{36} yI^2(3-y)C_{NiCl_2}^{\varphi}$$
$$+ \frac{1}{6}(1-y)(3-y)I^2\left(2B_{NiaCl}^{'} + C_{NaCl}^{\varphi}\right) + \frac{\sqrt{21}}{24}(1-y)(3-y)I^2(2\sqrt{2}B_{NiaCl}^{'} + C_{NiCl_2}^{\varphi})$$
$$+ \frac{1}{3} yI[{}^{S}\theta_{NaNi} + {}^{E}\theta_{NaNi} + I(1-y)\,{}^{E}\theta_{NaNi}^{'} + I(1-\frac{2}{3}y)\psi_{NaNiCl}] \quad (2)$$

Table1. The results related to r=5

I (mol . kg^{-1})	m_{NaCl} (mol . kg^{-1})	E (mV)	$\gamma_{\pm NaCl}$
0.0010	0.0006	-208.9	0.9910
0.0100	0.0063	-109.9	0.8366
0.0495	0.0309	-37.8	0.7991
0.1001	0.0626	-5.9	0.7858
0.2500	0.1563	33.4	0.7338
0.5003	0.3127	63.8	0.7060
0.7503	0.4689	82.0	0.6968
1.0004	0.6253	95.5	0.6990
1.5002	0.9376	115.5	0.7172
2.0004	1.2503	130.6	0.7447
2.5001	1.5626	143.6	0.7885
3.0003	1.8752	154.2	0.8257
3.5002	2.1876	164.4	0.8817
4.0000	2.5000	172.8	0.9246

Table2. The obtained values for mixed ionic interaction parameters

$^{S}\theta$	Ψ	higher-order electrostatic terms
0.2159	-0.0534	without
0.3123	-0.0705	with

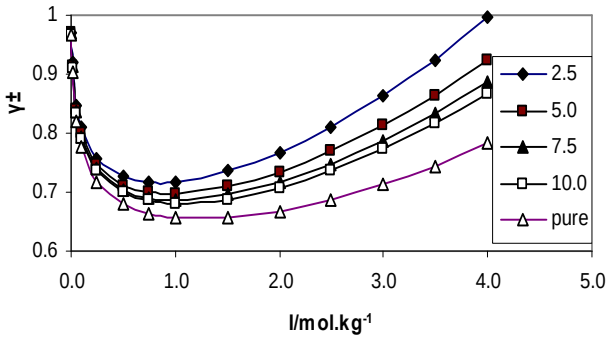

Figure1. The mean activity coefficients of NaCl for different series of the salt molal ratios r

References

[1] D.A. Palmer, J.A. Rard, S.L. Clegg, J. Chem. Thermodyn. 34 (2002) 63.

[2] B. Ghalami-Choobar, et al, J. Chem. Thermodyn. 42 (2010) 454.

[3] B. Ghalami-Choobar , M. Mohammadian J. Mol. Liq 154 (2010) 26

Surfactant Assisted Synthesis of MnO_2 Nanowires as New Electrochemical Supercapacitor Materials

Sayed Habib Kazemi [a,*]

[a] *Department of Chemistry, Institute for Advanced Studies in Basic Sciences (IASBS), Zanjan 45137-66731, Iran*

(*Corresponding autor: habibkazemi@iasbs.ac.ir)

Nanoscaled materials with controllable composition and morphology played important roles in nanotechnology research and applications [1-3]. Manganese oxide nanostructures are becoming electrode materials exhibiting ideal capacitance behavior also shows wide electrochemical potential window [4].

Keywords: Nanowire, Supercapacitor, Hydrothermal

Experimental:

All chemicals were purchased from Aldrich Company. In a typical synthesis $Mn(NO_3)_2$ and sodium dodecyl sulfate (SDS) dissolved in deionized water and sonicated, then transferred into an autoclave and heated up to 170 ^oC overnight. The solid product was then used in electrode texture. All electrochemical tests were run using Zennium-Zahner potentiostat/galvanostat. TEM imaging was performed using a Philips CM10 transmission electron microscope.

Result and discussions:

XRD results are in good agreement with the previously reported works [5]. TEM image shows the formation of MnO_2 nanowires under present conditions. It can be concluded that in the presence of low concentrations of the surfactant, MnO_2 crystal growth can be done up to formation of nanowires which capped by surfactant molecules (Figure 1, diameter is about 10 nm). The electrochemical behavior was examined by using cyclic voltammetry (CV). The representative CVs for the nanowired MnO2 based electrode is presented as Figure 2 and good correspondence of i *vs.* scan rate can be observed even at high scan rate up to 500 mVs^{-1} as an evidence of good electrochemical reversibility of the nanostructures. Galvanostatic charge and discharge tests, CD, were run at a 5 Ag^{-1} current density (Figure 3). Insignificant

loss in specific capacitance can be observed by successive charge and discharge cycles even up to more than 1000 cycles.

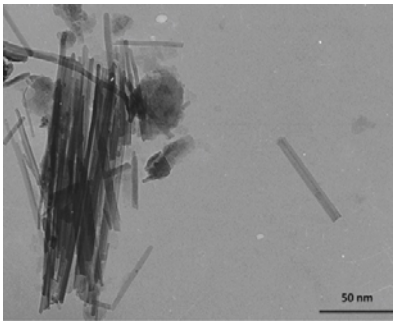

Figure 1: TEM image

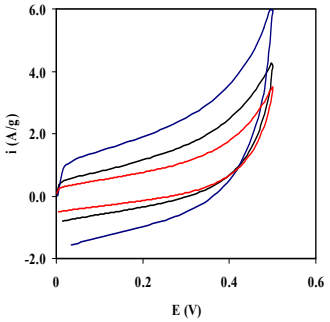

Figure 2: CVs at various scan rates

A Specific capacitance of 610 Fg^{-1} could be calculated based on the discharge plots. Figure4 represents the Nyquist plot obtained at the open circuit voltage, OCP. It is clear that the ohmic resistance is very low, less than 1 ohm, which is in good agreement with the CD results. Our results show that the better performance in comparison to previously reported cases are due to more effective diffusion of cations because of more effective surface area provided by carbon nanopowders and MnO_2 nanowires [6].

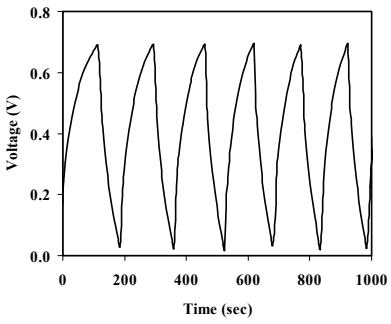

Figure 3: Charge and discharge plots

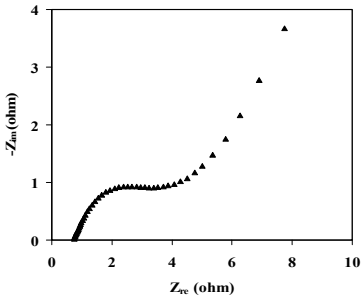

Figure 4: Nyquist plot at OCP

References:

[1] B.E. Conway, Electrochemical Supercapacitors, Scientific Fundamentals and Technological Applications (Kluwer Academic/Plenum Press, New York 1999)

[2] B.L. Cushing, V.L. Kolesnichenko, C.J. O'Connor: Chem. Rev. 104, 3893 (2004).

[3] V. Ruiz, C. Blanco, M. Granda, et al: J. Appl. Electrochem. 37, 717 (2007).

[4] T. Cottineau, M. Toupin, T. Delahaye, T. Brousse, D. Belanger: Appl. Phys. A 82, 599 (2006).
[5] F. Cheng, J. Shen, W. Ji, Z. Tao, J. Chen: ACS Appl. Mater. Interfaces 1, 460 (2009).
[6] C. Xu, H. Du, B. Li, F. Kang, Y.Zeng: J. Electrochem. Soc. 156, A435 (2009).

Cyclic voltammetric study of the 5-amino-2-hydroxybenzoic acid in the presence of 2-acetylcyclopentanone

M. Alimoradi*,M. karimi

Department of chemistry,Faculty of Science,Islamic Azad University,Arak Branch, Iran

Mohsen7198@yahoo.com

Abstract

Electrochemical oxidation of 5-amino-2-hydroxybenzoic acid has been studied in the presence of 2-acetylcyclopentanone as nucleophile in aqueous solution, by means of cyclic voltammetry and controlled-potential coulometry. The results indicate the participation of electrochemically generated quinoneimine in Michael reaction with 2-acetylcyclopentanone to form the corresponding aminoquinone derivative. In addition, according to the EC mechanism, the observed homogeneous rate constant (k_{obs}) for the reaction of aminoquinone derived from 5-amino-2-hydroxybenzoic acid with 2-acetylcyclopentanone has been estimated by digital simulation of cyclic voltammograms.

Keyword: Cyclic voltammetry, 5-amino-2-hydroxybenzoic acid, Coulometry, homogeneous rate constant, Michael addition.

Introduction

Aminohydroxybenzoic acid or their derivatives have been shown to exhibit biological activity in a number of different assays. 5-amino-2-hydroxybenzoic acid is a biosynthetic intermediate of antibiotics of the ansamycin, maytansinoid and mitomycin groups. Derivatives of 5-amino-2-hydroxybenzoic acid have been shown to be potent antisickling agent, leutriene anagonists, and carbapenem-cotaining antibiotics. In this work electrochemical behavior of 5-amino-2-hydroxybenzoic acid in presence of 2-acetylcyclopentanone was investigated and new derivatives of its was synthesized.

Method

The cyclic voltammetric study was performed with glassy carbon disc electrode, platinium wire and SCE as working, counter and reference electrode respectivity. The working electrode used in controlled-potential coulometry and was an assembly of eight graphite rods (8mm

diameter and 6 cm length) and a large platinum gauze constituted the counter electrode. Since the mechanism is dependent on such parameters as, nature of nucleophile, electrolysis medium (solvent, acidity or pH...) and catechol type then initially these parameter wase optimated. After optimisig of parameters cyclic voltammetry, controlled-potential coulometry were performed using a Behpajoh model BHP-2062 potentiostat/galvanostat. All cyclic voltammetric experiments were performed in pH=7.0 in aqeous phosphate buffer(0.2 M) in 0.6-(-0.8) potential renge and various scan rate.

Results and Discussion

The electrochemical study of 2 mM solution of 5-amino-2-hydroxybenzoic acid in an aqueous solution containing 0.2 M phosphate buffer (pH 7.0), at a bare glassy carbon electrode has been performed using cyclic voltammetry. The voltammogram shows one anodic (A_1) and corresponding cathodic peak (C_1), at 0.18 V and 0.25 V versus (SCE), respectively, which correspond to the transformation of 5-amino-2-hydroxybenzoic acid to quinoneimine and vice-versa within a quasi-reversible two-electron process . The oxidation of 5-amino-2-hydroxybenzoic acid in the presence of 2-acetylcyclopentanone as a nucleophile was studied in some details. In this case, the cathodic counterpart of the anodic peak A_1 decreases.

With the aim of investigating of reactivity of intermediate quinoneimine toward 2-acetylcyclopentanone, as well as estimation of observed chemical rate constant of this reaction, we investigated the electrochemical oxidation of 5-amino-2-hydroxybenzoic acid in aqueous solutions in the presence of 2-acetylcyclopentanone. The results indicate the participation of electrochemically generated *N*-acetyl-*p*-quinoneimine in Michael reaction with 2-acetylcyclopentanone. Based on *EC* mechanism, the observed homogeneous rate constant (k_0) of the above mentioned reaction is estimated by comparing the experimental cyclic voltammograms with the digital simulated results.

References

[1] D.Nematollahi, M. Alimoradi, M. Rafiee, J. Phys. Org. Chem. 20 (2007) 49–54

[2] D.Aematollahi, M. Alimoradi, S. waqifhusain, Electrochim. Acta, 51 (2006) 2620–2624

[3] D. Nematollahia, H. Shayani-Jama, M. Alimoradi, S. Niroomand, Electrochim. Acta, 54 (2009) 7407–7415

Investigation of Inhibition Effect of an Organic Compound on Corrosion Behavior of Stainless Steel Type 316 in Acidic Environment

N.Goudarzi[a], M.Peikari*[a], R.Motefakerfard[b]

[a]Technical Inspection Engineering Department, Petroleum University of Technology, Abadan

Email: peikari@put.ac.ir , narges.goudarzi@gmail.com

[b]Exploration Engineering Department, Petroleum University of Technology, Abadan

Keywords: Stainless Steel, Inhibitor, MBT,Potentiodynamic Polarization, EIS

Introduction

Stainless steel type 316 is one of the most popular steels used in corrosion resistant and high strength application. Acid solutions are generally used for the removal of undesirable scales and rust from the surface of stainless steel parts prior to and after use of industrial vessels [1]. Because of the general aggressivenessof acid solutions, inhibitors are commonly used to reduce the corrosion attack on steel parts. Organic adsorption compounds are effective as corrosion inhibitors because of the functional group containing heteroatoms such as nitrogen, sulfur, and oxygen [2]. The present work is devoted to investigate the corrosion behaviour of S.S.316 in acidic solution containing Citric acid 3% and Ammonium bifluoride 1%. The effect of addition of 2-MercaptoBenzoThiazole (MBT) as corrosion inhibitor was examined. MBT is sulfur based organic compound which can chemically adsorbed on the metal surface and retard the rate of both anodic and cathodic reactions [3, 4].

Experimental

Samples were produced from austenitic stainless steel AISI 316 with the bellow chemical composition (wt %): 1.33% Si, 1.2 Mn, 19.11 Cr, 11.00 Ni, 2.37 Mo and balance Fe.To prove effectiveness of MBT on reducing corrosion rate, weight loss method, potentiodynamic polarization method, and Electrochemical Impedance Spectroscopy were used. After analyzing the results and calculating inhibition efficiency by three methods, the best concentration of inhibitor was determined.

Concentration (ppm)	Corrosion rate (mpy)	Inhibition efficiency
Blank	35	-
50	13	62
60	10	71
70	6	83
80	2	94

Corrosion rate & inhibition efficiency of S.S.316 immersed in acid solution containing inhibitor

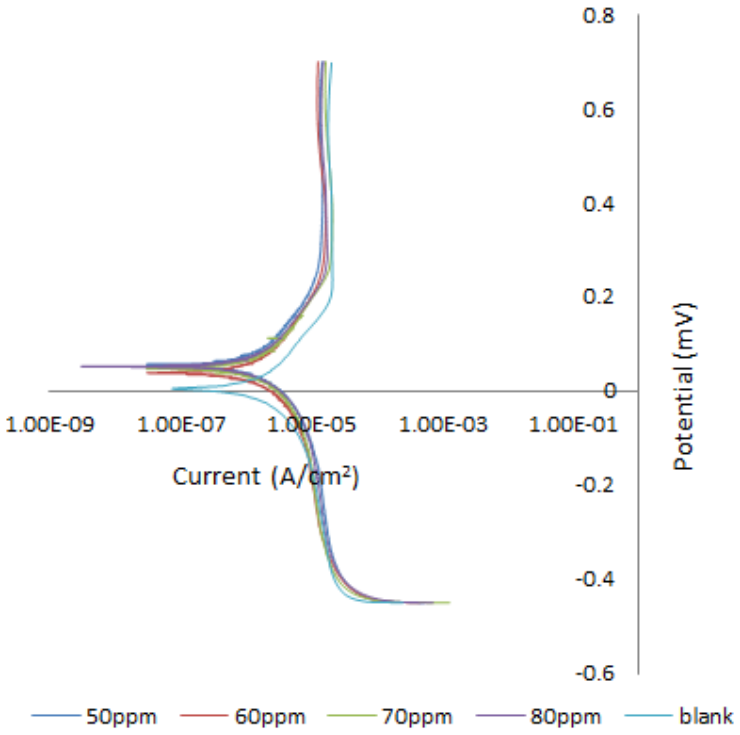

Polarization curves for S.S.316 in acid solution containing different concentrations of inhibitor

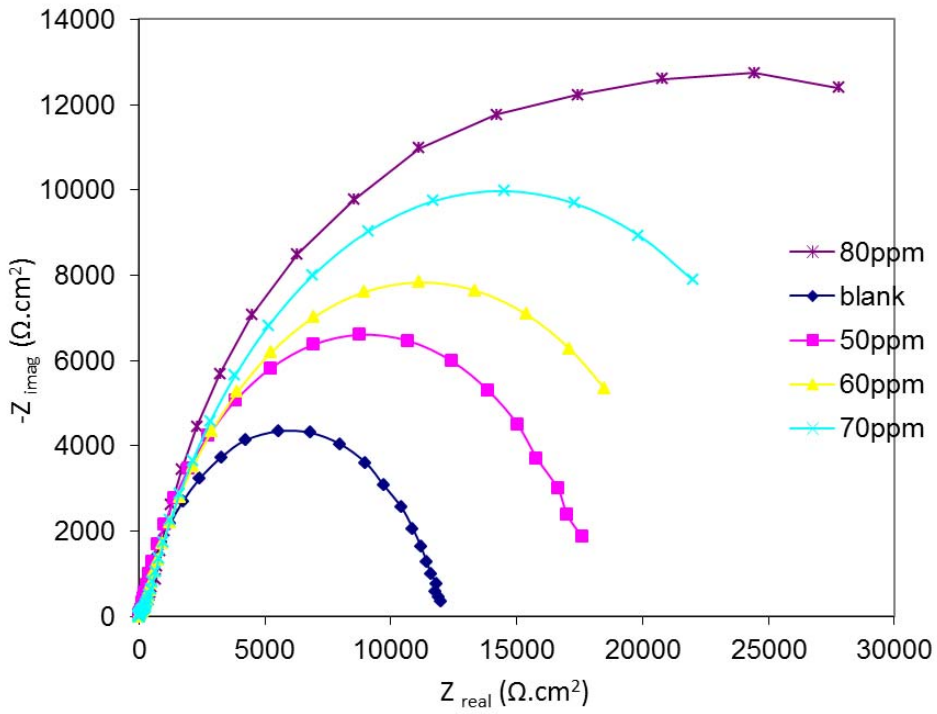

Nyquist plot for S.S.316 in acid solution containing different concentrations of inhibitor

Conclusion

The results proved that 2-MercaptoBenzoThiazoledisplayed good corrosioninhibition for S.S. 316 in acid solution of interest. High inhibition efficiency of 85% was obtained for the inhibitor concentration of 80 ppm at room temperature. MBT retards the rates of both catodic and anodic reaction, so it is a mixed type inhibitor which chemically adsorbed on steel surface.

References

[1] A.S.Fouda, M.Abdallah, S.M.Al-Ashrey, A.A.Abdel-Fattah, Desalination, 250, 2009

[2] M.Abdallah, Material Chemistry and Physics 82, 2003

[3] H.Amar, A.Tounsi, A.Makayssi, A.Derja, J.Benzakour, Corrosion Science, 49, 2007

[4] M.A. Migahed, Material Chemistry and Physics, 97, 2005

Ethanol electro-oxidation on Ni-Rh/Cu electrode and its application as anode in ethanol consuming fuel cells

F. Gobal, L. Majari Kasmaee*

Department of Chemistry, Sharif University of Technology, P.O. Box 11365-9516, Tehran, Iran
(*Email: kasmaee@mehr.sharif.ir*)

Keywords: Nickel–Rhodium alloy, Ethanol electro-oxidation, Alloy electrodeposition, Inhibitor, Fuel cell

Introduction:

Ethanol is known as a favorable fuel in fuel cells due to its ease of availability from renewable sources, low toxicity and having higher energy density compared to methanol. However its lower electro-oxidation kinetic is a hindrance and highly active electro-catalysts are sought to make Direct Ethanol Fuel Cell (DEFC) viable [1]. The purpose of the present study is detailed investigation of ethanol oxidation on Ni-Rh alloy in alkaline solutions aiming at comparing the electro-catalytic characteristics of Ni-Rh alloy with Ni electrode as well as a brief study of the detrimental anion effect.

Methods:

Ni-Rh alloy, Nickel and Rhodium films with geometric area of 0.05 cm^{-2} for the first two and 0.09 cm^{-2} for the last one, were deposited on copper foils using controlled cathode potential technique. In order to study the electro-catalytic properties of these electrodes, cyclic voltammetry and chronoamperometry were employed. The electrochemical studies were performed in a conventional three electrode cell powered by Behpajooh potentiostat / galvanostat (models PHP 2063+ and 2061-c). A Pt wire was used as the counter electrode. All potentials were measured against a Saturated Calomel Electrode (SCE).

Results and discussion:

Typical cyclic voltammogram of Ni-Rh/Cu in the potential range of -200 to 800 mV in 1 M NaOH solution in presence of 0.17 M ethanol is shown in figure 1-a. A cross over appearing

at around 450 mV / SCE leading to the formation of a hysteresis is a characteristic of electro-oxidation process via intermediates [2].

The cyclic voltammogram of Ni/Cu in the same solution and at the same range of potential is shown in figure 1-b. Comparing with figure 1-a, one can conclude that the ethanol's oxidation peak potential has shifted to less positive values for the alloy electrode and therefore Rhodium has increased the electro-catalytic efficiency. Also considering the increase in the current at alloy electrode, the electro-catalytic activities of Ni-Rh/Cu are over twice that of Ni/Cu electrode in different ethanol concentrations.

Kinetic properties of ethanol electro-oxidation process such as anodic transfer coefficient and exchange current density as well as diffusion coefficient of ethanol have been derived from the cyclic voltammograms and chronoamperograms and are 0.3, 1.3×10^{-4} A cm^{-2} and 1.2×10^{-6} cm^2 s^{-1} respectively.

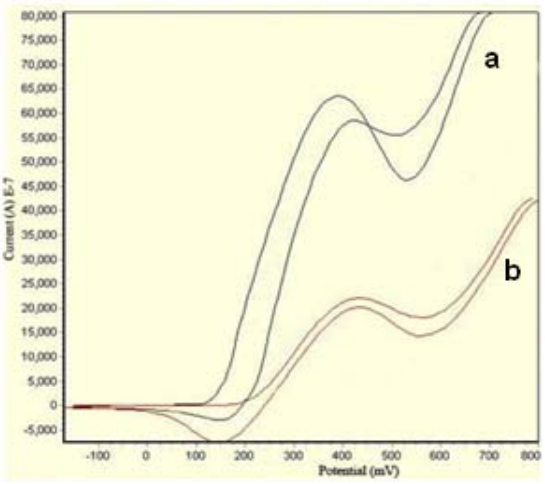

Figure 1: Cyclic Voltammograms in potentials between -200 and 800 mV in 1 M NaOH solutions containing 0.17 M ethanol on a: Ni/Cu b: Ni-Rh/Cu electrode (potential scan rate 100mV/s)

In order to study the poisoning effects of anions on Ni-Rh electrode in the ethanol electro-oxidation process, chloride, sulfate and phosphate anions have been added in different concentrations to the alkaline ethanol solutions and electro-oxidation processes were followed by cyclic voltammetry. Cyclic voltammograms show that there is a reverse relation between concentration of anions and the ethanol's oxidation current peaks meaning that there is a competition between anion and ethanol towards absorption on N-Rh alloy surface active sites.

It was found that Langmuir adsorption isotherm is roughly obeyed and equilibrium adsorption coefficient found to be 0.251, 0.373 and 1.660 for chloride, sulfate and phosphate anions respectively.

Conclusions:

This study presents the electro-oxidation of ethanol on Ni-Rh/Cu electrode in alkaline solutions. During this process, considerable increase in activity of about 200% has been witnessed on Ni-Rh/Cu alloy compared to Ni-electrode. Also, the kinetic parameters of ethanol electro-oxidation reaction on alloy electrode such as diffusion coefficient, anodic transfer coefficient and exchange current density have been calculated.

The poisoning effects of chloride, sulfate and phosphate anions have been studied which shows fair obey from Langmuir isotherm and these anions equilibrium adsorption coefficient were also derived.

References:

[1] A. J. Appleby, F. R. Foulkess, 'In Fuel Cell Hand Book', Van Nostrand Reinhold, New York, 1989, Chapter 11.

[2] R. Parsons, T. Van Der Noot, J. Electroanal. Chem., 257, (1988) 1.

Cr(III) Selective PVC Membrane Electrodes Based on Schiff base 1- (2- Pyridyl Azo)2-Naphtol Complex as an Ionophore

Ali MOGHIMI[1*] - Fatemeh AMOUZAD KHALILI[2]

[1]*Department of Chemistry, Varamin (Pishva) Branch Islamic Azad University, Varamin, Iran*

[2]*Department of Chemistry, Member of young researchers club, East Tehran Branch (Ghiam Dasht),Islamic Azad University ,Tehran, Iran*

* Corresponding author. e- mail: alimoghimi@iauvaramin.ac.ir

A novel and selective method for determination of trace amounts of Cr(III) ions using with Schiff base 1- (2- Pyridyl Azo)2-Naphtol has been explored as ionophore for preparing PVC-based membrane sensors selective to the Cr^{3+} ion. Potentiometric investigations indicate high affinity of these receptors for Cr(III) ion. The best performance was shown by the membrane of composition (w/w) of ionophore: 1 mg, PVC: 30 mg, DOP: 69 mg and KT*p*ClPB as additive were added 50 mol % relative to the ionophore in 2 ml THF. The proposed sensor's detection limit is 6.0×10^{-7} M over pH 4 at room temperature (Nernstian slope 33.06 mV/dec.) with a response time of 15 seconds and showed good selectivity to Cr(III) ion over a number of interfering cations.

Key Words*:* Schiff base, Cr(III)-ion selective electrode, Potentiometry, Ionophore, 1- (2-Pyridyl Azo)2-Naphtol

Introduction

Toxicological studies have proved that the degree of toxicity of an element directly depends on the species in which it is present. Cr(III) is considered as an essential micronutrient for humans and mammals in order to maintain glucose metabolism, where as Cr(VI) is a potentially carcinogenic agent.[1] The significant drawbacks of Cr(VI) are breathing disturbances, liver and digestion malfunctions, dermal corrosion and skin allergies.[2] Therefore, It is necessary to control the level of chromium in industrial effluent, natural and drinking waters. Speciation of chromium in environmental samples is of prime importance.

In this study, we prepare PVC membrane electrodes based on Schiff base 1- (2- Pyridyl Azo)2-Naphtol as an ionophore and were used for the determination of Cr(III) ion. The

proposed sensor revealed good selectivity and response for Cr^{3+} over a wide variety of other interfering metal ions.

Experimental

Preparation of polymeric ion-selective electrodes. The compositions of PVC-based Cr(III)-selective electrodes were summarized in Table 1, and the typical one (m-8) was 30 mg PVC, 69 mg plasticizer, 1 mg ionophore and KT*p*ClPB (50 mol % of ionophore). The ionophore, plasticizer and PVC were dissolved in the appropriate volume of THF and mechanically stirred. All membrane cocktails were cast in glass rings placed on glass plates for conventional ionselective electrodes. Solvent from PVC membrane was allowed to evaporate for at least 24 hours at room temperature. The thickness of the resulting membrane measured by micrometer was about 0.3 mm.

Results and Discussion

Schiff bases as ligands seem to be a potential ionophore for soft heavy metal ions in the PVC membrane electrodes, because of its excellent metal-binding properties, rapid exchange kinetics,

and water insolublilty.[3-5] 1- (2- Pyridyl Azo)2-Naphtol was used as an ionophore for preparing PVC membrane ion-selective electrodes for a wide variety of metal ions. We said in our previous study16 that the Cr^{3+} ISE membrane compositions were optimized to produce the best sensitivity and selectivity towards Cr(III) ion, because the sensitivity of the ion-selective electrodes depend on the nature of ionophore used as well as significantly on the membrane compositions and selectivity of the electrodes depends on the nature of ionophore. The optimization was carried out with varying of the ratio in PVC membrane components such as plasticizer and additive (KT*p*ClPB).

The Schiff base 1- (2- Pyridyl Azo)2-Naphtol was employed as Cr(III) selective ionophore in the preparation of Cr(III) ion selective electrode. The responses of the four electrodes (with different plasticizer) are shown in Figure 1.

Conclusion

As a final point, the membrane electrode incorporating 1- (2- Pyridyl Azo)2-Naphtol as an ion carrier can be used for the development of a Cr(III) ionselective electrode. Among membranes tested, polymeric membrane m-8 based on 1- (2- Pyridyl Azo)2-Naphtol with DOP and liphophilic additive of 50 mol % displays a good Nernstian response (33.06 mV/decade) over pH 4 at room temperature to Cr^{3+} ion and the limit of detection of 5×10^{-7} M within short time 15s. Most of metal ions could not hamper the selectivity to the Cr(III) ion. It can be concluded that the membrane electrode has a rapid potential response and excellent selectivity towards Cr(III) ion over other interfering metal ions. It could be used successfully for the determination of Cr(III) ion content in environmental and waste water samples.

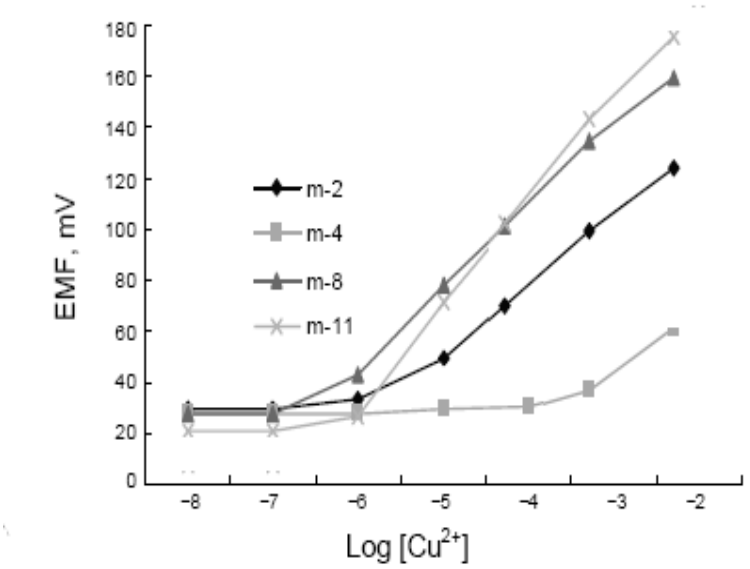

Figure 1. Potentiometric responses of the membrane prepared from different plasticizers with ionophore towards Cr^{3+}.

References

[1] Nriagu, J. O.; Nicboer, E. *Chromium in the Natural and Human Environment* , New York 1988.

[2]Camel, V. *Spectrochim. Acta Part B*, 2003, 58, 1177.

[3]Shamsipur, M.; Avanes, A.; Raoufi, M. K.; Sharghi, H.; Aghapour, G. *Talanta*, 2001,54, 863.

[4]27. Shamsipur, M.; Javanbakht, M.; Ghasemi, Z.; Ganjali, M. R., Lippolis, V.; Garau, A. *Sep. Purif. Technol.*, 2002 ,28, 141.

[5] Ganjali, M. R.; Pourjavid, M.R.; Hajiagha Babaei, L.; Niasari, M. S. *Quim. Nova*, 2004,27, 213.

Determination of trace amounts of copper(II) with a Cu^{2+}-PVC membrane sensor based on 2-amino-cyclopentene-1-dithiocarboxylic acid

Ali MOGHIMI[1*]- Fatemeh AMOUZAD KHALILI[2]

[1]*Department of Chemistry, Varamin (Pishva) Branch Islamic Azad University, Varamin, Iran*

[2]*Department of Chemistry, Member of young researchers club, East Tehran Branch (Ghiam Dasht),Islamic Azad University ,Tehran, Iran*

* Corresponding author. e- mail: alimoghimi@iauvaramin.ac.ir

Abstract

A simple and reproducible method for the rapid determination of trace amounts of copper(II) ions using poly(vinyl chloride) membrane electrode that is highly selective to Cu^{2+} ions was prepared by 2-amino-cyclopentene-1-dithiocarboxylic acid (ACDA) as a suitable neutral carrier. Membrane incorporating 2-amino-cyclopentene-1-dithiocarboxylic acid, as ionophore with composition ACDA:NaTPB:NB:PVC in the ratio 2:2:50:100s (w/w) exhibits the best result for potentiometric sensing of Cu^{2+} ions. The electrode exhibited a near-Nernstian response to Cu^{2+} in the concentration range of 5.0×10^{-6} to 5.0×10^{-2} M with a slope of 24.8 ± 0.5 mV per decade. The proposed sensor can be used over a period of 1 months. The lower limit of detection was 2.5×10^{-7} M. This electrode showed high selectivity with respect to alkaline, alkaline earth, and heavy metal ions and could be used over a pH range of 2.0–4.0. The method was applied to the determination of copper in different water samples.

Keywords: PVC Membrane; copper(II); Sensor; Potentiometry; Ion-selective electrode; 2-amino-cyclopentene-1-dithiocarboxylic acid.

Introduction

Copper is both vital and toxic for many biological systems[1,2] . Thus, the determination of trace amounts of Cu is becoming increasingly important because of the increased interest in environmental pollution [3].The Atlanta based Agency for Toxic Substances and Disease Registry (ATSDR) says their website that the copper is essential for good health. Moreover they provide accurate, reproducible and often selective determination of various ionic species.

Not only this, the ion-selective electrodes (ISEs) allow nondestructive, on line monitoring of particular ion in small volume of sample without any pretreatment.

Experimental Section

Reagents and equipments. Dibutyl(butyl)phosphonate (DBBP) from (Mobil, USA), 1-chloronaphthalene (CN), tris(2-ethylhexyl)phosphate (TEHP), dibutyl phthalate (DBP), tri-n-butylphosphate (TBP), 2-amino-cyclopentene-1-dithiocarboxylic acid and dioctyl phthalate (DOP) from (Merck, Germany), high molecular weight poly(vinyl chloride) (PVC) (Fluka, Switzerland) and sodium tetraphenyl borate (NaTPB) from (BDH, UK) were used as obtained. All the reagents used for this study were of analytical grade. Metal salt solutions were prepared in doubly distilled water. The potential measurements were performed with a multichannel potentiometer (Kosentech, Korea, Model AS MP8). A Varian atomic absorption spectrophotometer (AAS) with a graphite furnace was used to determine the concentration of metal ion in the standard solutions.

Electrode preparation and cell setup. Electrode membranes were prepared as suggested by Craggs et al.[4] Varying amounts of the ionophore along with appropriate amount of PVC were dissolved in tetrahydrofuran (THF) solvent. The obtained solution was poured into polyacrylate rings, placed on a smooth glass plate and allowed to evaporate at room temperature in a dust free closet. Transparent membrane was obtained after 48 hours. Its circular part having the 5 mm diameter was cut out and attached to one end of a hollow Pyrex glass tube. The effect of different plasticizers e.g. DBBP, CN, TBP, TEP, DBP and DOP as well as the anion excluder i.e. sodium tetraphenylborate was also studied. These additives affected the performance of membrane almost in each case. Varying amounts of these compounds were added to the ionophore, PVC, and THF solution prior to pouring it into the acrylic rings. The ratio of membrane ingredients was optimized after a good deal of experimentation.

Best efforts were made to prepare a membrane that generates reproducible and stable potentials. Further, the dummy membranes having only PVC as membrane ingredient were also tested to observe whether any background potential is produced due to binding material. Conditioning of all the membranes was done with 0.1 M Cu^{2+} solution.

The minimum time required for conditioning was 48 hours otherwise the membranes produced unstable potentials. The potential measurements were carried out using the following cell setup at 25 ± 0.1°C. Internal reference electrode (SCE)/ Internal solution 0.01 M $Cu(NO_3)_2$/PVC Membrane/Test solution/ External reference electrode (SCE). The saturated calomel electrodes (SCE) were used as internal and external reference electrodes. The concentration of the metal ion in the test solutions varied from 5.0×10^{-6} to 5.0×10^{-2} M. All the standard metal ion solutions were prepared by serial dilution with 2.0×10^{-1} M as stock solution. pH values of diluted solutions were checked and maintained between3-4. Each solution was stirred and potential readings were recorded. These potential values were plotted against negative logarithmic values of Cu ion activity to obtain the standard calibration curve.

Results and Discussion

Selection of the membrane. In preliminary experiments, the synthesized ionophore was used as a neutral carrier to prepare PVC based membranes and was tried to detect various metal ions. A number of membrane electrodes were prepared and conditioned in 0.1 M solution of different metal ion solutions namely Li^+, Na^+, K^+, Co^{2+}, Zn^{2+}, Hg^{2+}, Cd^{2+}, Ag^+, Ni^{2+}, La^{3+}, Ca^{2+}, and Mg^{2+} solutions for 2-3 days. The best potential response of the electrode was recorded for Cu^{2+} ions while all other ions exhibited lower potential response or no response at all. It suggested that Cu(II) ions could interact with the ionophore to form a better complex with the electron rich cavity in the comparison of the bivalent cations. This may be due to its higher charge and suitability which facilitated its attachment to the ionophore in a better way. Further, the rapid exchange kinetics of the resulting ligand-metal ion complex is responsible for the selective behavior of the ionophore towards Cu^{2+} in comparison to the other trivalent metal ions. Therefore, this membrane was used to develop a Cu(II) ions selective electrode. It is well known that some additives like anion excluders are useful as these compounds enhance the sensitivity and selectivity of cation selective membrane by reducing its resistance.[5] Also, in case of PVC based neutral carrier membranes, plasticizers if compatible with the ionophore, can provide a smooth surface to the membrane and thus enhance the response characteristics. Although the role of plasticizers is not very firmly established till date but it is assumed that these additives enhance the homogeneity of the PVC based membranes and provide liquid channels within the membrane which facilitates the

movement of charge carriers, which ultimately improves the response time and the sensitivity of the membranes. It can also improve the dielectric constant of the polymeric membrane and also the movement of ionophore and its metal complex.[5] Therefore, the effect on the performance of the membrane after the addition of anion excluder, sodium tetraphenyl borate (NaTPB) and plasticizers like DBP, DOP, TEP, TBP, CN, and DBBP was also studied. The ratio of membrane ingredients, time of contact and concentration of equilibrating solution were optimized so that the membrane could develop reproducible, noiseless, and stable potentials. Membrane to membrane reproducibility was assured by carefully following the optimum conditions of fabrication.

Effect of membrane composition on the working

Concentration range and the slope. The compositions of each best performing membrane and the results obtained for these are presented in Table 1. As expected dummy membranes, containing PVC only produced no potential. It revealed that there was no contribution or interference due to the binding material. It is clear from the data that the membrane containing PVC and ionophore only, in the ratio 5:100 shows a linear response in a narrow concentration range i.e. 4.0×10^{-5} - 1.0×10^{-1} M and its slope was recorded as 23 mV/decade of activity (Figure 1). The addition of anion excluder i.e. sodium tetraphenyl borate and plasticizers DBP, DOP, TEP, TBP, CN, and DBBP changed the response characteristics of all the membranes. The best working concentration range obtained for DBBP i.e. 5.0×10^{-6} - 5.0×10^{-2} M with a slope of 24.8 mV/decade of activity. This is due to the best homogeneity provided by DBBP and its compatibility to the membrane ingredients which resulted in the best obtained working concentration range and the Nernstian slope. Also, the response time for DBBP was the lowest, among all other studied membrane compositions, containing different plasticizers. Further, as the response characteristics of any membrane depend on the amount of ionophore, the effect of changing quantity of ionophore was also studied. The optimum ratio of best performing membrane is 2:2:50:100 for I:NaTPB:DBBP: PVC. If the amount of ionophore is less than this ratio, it affects the working concentration range adversely, although the effect on slope is not considerable. If the amount is increased further, it shows no improvement in any of the characteristics of the electrode. Therefore, membrane no. 5 was the best performing membrane and this composition was selected for further studies.

Table 1. Compositions and response characteristics of PVC based membranes having 2-amino-cyclopentene-1-dithiocarboxylic acid as electroactive material

S. No	(I)	DBP	DO P	CN	DBBP	NaTPB	PVC	Slope ± 0.2 mV / decade of activity	Response time (s)	Working concentration range (M)
1	10					1.0	100	23.4	~95	6.5×10^{-1}-1.0×10^{-1}
2	10	80				1.0	100	22.5	43	8.0×10^{-1} -1.1×10^{-1}
3	10		120			1.5	50	20.6	24	5.6×10^{-1}-1.2×10^{-1}
4	8			150		1 .0	50	20.8	26 -35	3.8×10^{-5} -1.0×10^{-2}
5	2				50	2.0	100	25.9	12	5.0×10^{-6}-5.0×10^{-2}

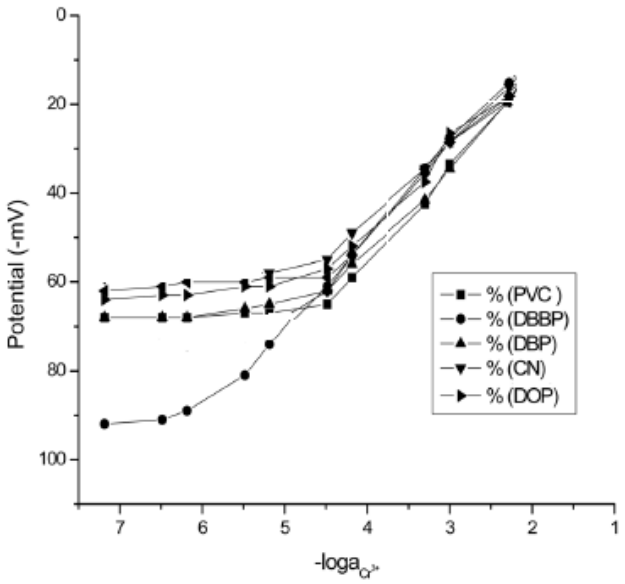

Figure 1. Potentiometric response of the PVC membrane sensor based on 2-amino-cyclopentene-1-dithiocarboxylic acid (ACDA) in the presence of different plasticizers.

Conclusion

An upper rim modified calixarene compound, has been used as a neutral carrier in PVC matrix, for the fabrication of a highly selective potentiometric electrode for Cu (II) ions. The response time of this ion selective electrode is low and it can successfully be used for 1 months. It works well in the pH range 2.0-4.0 and shows good selectivity for Cu(II) in the presence of other foreign cations which are generally present along with Cu(II) in real samples. A comparative study reveals that proposed electrode is better than some of the

existing electrodes in the characteristics namely response time,[6] and selectivity,[6,7] while it shows comparable results for the pH range, and working concentration range[5,7].

References

[1] I.H. Scheinberg, A.G. Morell, Ceruloplasmin, in: G.L.Eichhorn Ed. , *Inorganic Biochemistr*y, vol. 1, Elsevier,New York, **1973**, pp. 306.

[2] N.N. Greenwood, A. Earnshow, *Chemistry of Elements, Pergamon*, New York, **1984**.

[3] Y. Yamini, A. Tamaddon, *Talanta* **1999,**49 , 119.

[4] Craggs, A.; Moody, G. J.; Thomas, J. D. R. *J. Chem. Educ.* **1974**, 51, 541.

[5] Ammanmm, D.; Pretsch, E.; Simon, W.; Lindler, E.; Bezegh, A.; Pungor, E. *Anal. Chim. Acta* **1985,** 171, 119.

[6]Singh, A. K.; Gupta, V. K.; Gupta, B. *Anal. Chim. Acta* **2007**, 585, 171.

[7]Hyun, M. H.; Piao, M.-H.; Cho, Y. J.; Shim, Y.-B. *Electroanal.* **2004**, 16, 1785.

Pb^{2+}-DAAB Membrane sensor Based on Schiff base Isopropyl 2-[(isopropoxy carbothioyl)disulfanyl]ethanethioate(IIDE)

Ali MOGHIMI[1*]- Fatemeh AMOUZAD KHALILI[2]- Majid ABDOUSS[3]

[1]*Department of Chemistry, Varamin (Pishva) Branch Islamic Azad University, Varamin, Iran*

[2]*Department of Chemistry, Member of young researchers club, East Tehran Branch (Ghiam Dasht),Islamic Azad University ,Tehran, Iran*

[3]*Department of Chemistry, Amirkabir University of Technology, ,Tehran. Iran*

[*]Corresponding author. e- mail:alimoghimi@iauvaramin.ac.ir ;Kamran9537@yahoo.com

Abstract

A novel approach has been developed for the rapid determination of trace amounts of lead(II) ions using diazoaminobenzene (DAAB) and vinylpyridine (VP) membrane electrode that is highly selective to Pb^{2+} ions was prepared by Isopropyl 2-[(isopropoxy carbothioyl)disulfanyl]ethanethioate(IIDE) as a suitable neutral carrier. Membrane incorporating Isopropyl 2-[(isopropoxy carbothioyl) disulfanyl]ethanethioate(IIDE) , as ionophore with composition IIDE:VP:NaTPB: DAAB in the ratio 2:2:60:30 (w/w) exhibits the best result for potentiometric sensing of Pb^{2+} ions. The electrode exhibited a near-Nernstian response to Pb^{2+} in the concentration range of 2.0×10^{-6} to 2.0×10^{-2} M with a slope of 17.9 ± 0.3 mV per decade. The proposed sensor can be used over a period of 2 months. The lower limit of detection was 9.0×10^{-7} M. This electrode showed high selectivity with respect to alkaline, alkaline earth, and heavy metal ions and could be used over a pH range of 1.5–3.7. The method was applied to the determination of lead in different water samples.

Keywords: diazoaminobenzene (DAAB) and vinylpyridine (VP) membrane; lead(II); Sensor; Potentiometry; Ion-selective electrode; Isopropyl 2-[(isopropoxy carbothioyl)disulfanyl] ethanethioate (IIDE).

Introduction

Lead is one of the most ubiquitous elements in the environment and recognized as a major health risk to humans and animals [1,2]. Flame atomic absorption spectrometry (FAAS) is a simple technique, commonly used for determination of lead in water [3], soil [4,5] and plant

samples [6]. However, the determination of traces of lead by FAAS in such complex matrices is difficult due to its low sensitivity (0.01 μ g cm^{-3}) and the interfering effects of matrix components. Hence, separation step is frequently necessary to improve the detection limit and sensitivity [7] which is nowadays preferably done by solid phase extraction due to the several advantages it offers [8].

Experimental Section

Reagents and equipments vinylpyridine (VP) from (Merck), 1-chloronaphthalene (CN), tris(2-ethylhexyl)phosphate (TEHP), dibutyl phthalate (DBP), tri-n-butylphosphate (TBP) and dioctyl phthalate (DOP) from (Merck, Germany), high molecular weight diazoaminobenzene (DAAB) (Fluka, Switzerland) and sodium tetraphenyl borate (NaTPB) from (BDH, UK) were used as obtained. All the reagents used for this study were of analytical grade. Metal salt solutions were prepared in doubly distilled water. The potential measurements were performed with a multichannel potentiometer (Kosentech, Korea, Model AS MP8). A Varian atomic absorption spectrophotometer (AAS) with a graphite furnace was used to determine the concentration of metal ion in the standard solutions.

Electrode preparation and cell setup. Electrode membranes were prepared as suggested by Craggs et al.[9] Varying amounts of the ionophore along with appropriate amount of diazoaminobenzene (DAAB)were dissolved in tetrahydrofuran (THF) solvent. The obtained solution was poured into polyacrylate rings, placed on a smooth glass plate and allowed to evaporate at room temperature in a dust free closet. Transparent membrane was obtained after 48 hours. Its circular part having the 5 mm diameter was cut out and attached to one end of a hollow Pyrex glass tube. The effect of different plasticizers e.g. vinylpyridine (VP) , CN, TBP, TEP, DBP and DOP as well as the anion excluder i.e. sodium tetraphenylborate was also studied. These additives affected the performance of membrane almost in each case. Varying amounts of these compounds were added to the ionophore, diazoaminobenzene (DAAB) and THF solution prior to pouring it into the acrylic rings. The ratio of membrane ingredients was optimized after a good deal of experimentation.

Best efforts were made to prepare a membrane that generates reproducible and stable potentials. Further, the dummy membranes having only diazoaminobenzene (DAAB) as

membrane ingredient were also tested to observe whether any background potential is produced due to binding material. Conditioning of all the membranes was done with 0.1 M Pb^{2+} solution.

The minimum time required for conditioning was 48 hours otherwise the membranes produced unstable potentials. The potential measurements were carried out using the following cell setup at 25 ± 0.1°C. Internal reference electrode (SCE)/ Internal solution 0.01 M $Pb(NO_3)_2$/ diazoaminobenzene (DAAB) Membrane/Test solution/ External reference electrode (SCE). The saturated calomel electrodes (SCE) were used as internal and external reference electrodes. The concentration of the metal ion in the test solutions varied from 2.0×10^{-6} to 2.0×10^{-2} M. All the standard metal ion solutions were prepared by serial dilution with 2.0×10^{-1} M as stock solution. pH values of diluted solutions were checked and maintained between3-4. Each solution was stirred and potential readings were recorded. These potential values were plotted against negative logarithmic values of Pb ion activity to obtain the standard calibration curve.

Results and Discussion

Selection of the membrane. In preliminary experiments, the synthesized ionophore was used as a neutral carrier to prepare diazoaminobenzene (DAAB) based membranes and was tried to detect various metal ions. A number of membrane electrodes were prepared and conditioned in 0.1 M solution of different metal ion solutions namely Li^+, Na^+, K^+, Co^{2+}, Zn^{2+}, Cu^{2+}, Hg^{2+}, Cd^{2+}, Pb^{2+}, Ag^+, Ni^{2+}, La^{3+}, Ca^{2+}, and Mg^{2+} solutions for 2-3 days. The best potential response of the electrode was recorded for Pb^{2+} ions while all other ions exhibited lower potential response or no response at all. It suggested that Pb(II) ions could interact with the ionophore to form a better complex with the electron rich cavity in the comparison of the bivalent cations. This may be due to its higher charge and suitability which facilitated its attachment to the ionophore in a better way. Further, the rapid exchange kinetics of the resulting ligand-metal ion complex is responsible for the selective behavior of the ionophore towards Pb^{2+} in comparison to the other trivalent metal ions. Therefore, this membrane was used to develop a Pb(II) ions selective electrode. It is well known that some additives like anion excluders are useful as these compounds enhance the sensitivity and selectivity of cation selective membrane by reducing its resistance.[10] Also, in case of diazoaminobenzene

(DAAB) based neutral carrier membranes, plasticizers if compatible with the ionophore, can provide a smooth surface to the membrane and thus enhance the response characteristics. Although the role of plasticizers is not very firmly established till date but it is assumed that these additives enhance the homogeneity of the diazoaminobenzene (DAAB) based membranes and provide liquid channels within the membrane which facilitates the movement of charge carriers, which ultimately improves the response time and the sensitivity of the membranes. It can also improve the dielectric constant of the polymeric membrane and also the movement of ionophore and its metal complex. .[10] Therefore, the effect on the performance of the membrane after the addition of anion excluder, sodium tetraphenyl borate (NaTPB) and plasticizers like DBP, DOP, TEP, TBP, CN, and vinylpyridine (VP) was also studied. The ratio of membrane ingredients, time of contact and concentration of equilibrating solution were optimized so that the membrane could develop reproducible, noiseless, and stable potentials. Membrane to membrane reproducibility was assured by carefully following the optimum conditions of fabrication.

Effect of membrane composition on the working

Concentration range and the slope. The compositions of each best performing membrane and the results obtained for these are presented in Table 1. As expected dummy membranes, containing diazoaminobenzene (DAAB) only produced no potential. It revealed that there was no contribution or interference due to the binding material. It is clear from the data that the membrane containing diazoaminobenzene (DAAB) and ionophore only, in the ratio 5:100 shows a linear response in a narrow concentration range i.e. 4.0×10^{-5} - 1.0×10^{-1} M and its slope was recorded as 23 mV/decade of activity (Figure 1). The addition of anion excluder i.e. sodium tetraphenyl borate and plasticizers DBP, DOP, TEP, TBP, CN, and vinylpyridine (VP) changed the response characteristics of all the membranes. The best working concentration range obtained for vinylpyridine (VP) i.e. 2.0×10^{-6} to 2.0×10^{-2} M with a slope of 17.9 mV/decade of activity. This is due to the best homogeneity provided by vinylpyridine (VP) and its compatibility to the membrane ingredients which resulted in the best obtained working concentration range and the Nernstian slope. Also, the response time for vinylpyridine (VP) was the lowest, among all other studied membrane compositions, containing different plasticizers. Further, as the response characteristics of any membrane

depend on the amount of ionophore, the effect of changing quantity of ionophore was also studied. The optimum ratio of best performing membrane is 2:2:60:30 for I:NaTPB: vinylpyridine (VP) : diazoaminobenzene (DAAB). If the amount of ionophore is less than this ratio, it affects the working concentration range adversely, although the effect on slope is not considerable. If the amount is increased further, it shows no improvement in any of the characteristics of the electrode. Therefore, membrane no. 5 was the best performing membrane and this composition was selected for further studies.

Table 1. Compositions and response characteristics of diazoaminobenzene (DAAB) based membranes having Isopropyl 2-[(isopropoxy carbothioyl)disulfanyl]ethanethioate(IIDE) as electroactive material

S. No	(I)	DBP	DO P	TBP	V P	NaTPB	DAAB	Slope ± 0.2 mV / decad e of activity	Response time (s)	Working co ncentratio n range (M)
1	10					1.0	100	23.4	~80	7.5 × 10^{-1}-1 .0 × 10^{-1}
2	10	80				1.0	100	23.0	48	8.0 × 10^{-1} -1 .0 × 10^{-1}
3	10		110			1.0	100	24.0	25	5.6 × 10^{-1}-1 .0 × 10^{-1}
4	10			170		1.0	50	21.2	23	9.0 × 10^{-5}-1 .0 × 10^{-1}
5	2				2	60	30	17.9	10	2.0 × 10^{-6}-2 .0 × 10^{-2}

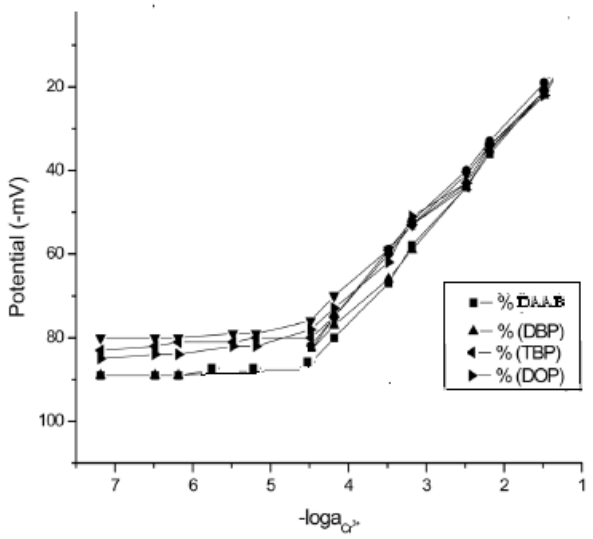

Figure 1. Potentiometric response of the DAAB membrane sensor based on Isopropyl 2-[(isopropoxy carbothioyl)disulfanyl]ethanethioate(IIDE) in the presence of different plasticizers.

Conclusion

An upper rim modified calixarene compound, has been used as a neutral carrier in DAAB matrix, for the fabrication of a highly selective potentiometric electrode for Pb (II) ions. The response time of this ion selective electrode is low and it can successfully be used for 2 months. It works well in the pH range 1.5–3.7and shows good selectivity for Pb(II) in the presence of other foreign cations which are generally present along with Pb(II) in real samples. A comparative study reveals that proposed electrode is better than some of the existing electrodes in the characteristics namely response time,[11] and selectivity,[11,12] while it shows comparable results for the pH range, and working concentration range[1,12].

References

[1] Sharma, R. K.; Goel, A. *Anal. Chim. Acta* **2005**, 534, 137.

[2]Current Status of Lead in India*, Released on World Environment Day* **2001**

[3] K. Suvardhan, K. Suresh Kumar, D. Rekha, B. Jayaraj, G. Krishnamurthy Naidu, P. Chiranjeevi, *Talanta* 68 ,**2006,** 735– 740.

[4]S. Tokalioglu, S. Kartal, *J. Trace Microprobe Tech*. 20 ,**2002**, 127.

[5]M. Shamsipur, F. Raoufi, H. Sharghi, *Talanta* 52 ,**2000**, 637.

[6] A.Moghimi*, Materials Science Research India* Volume 3(2a), ,**2006**, 195.

[7] K. Prasad, P. Gopikrishna, R. Kala, T. Prasada Rao, G.R.K. Naidu, *Talanta* 69 ,**2006**, 938.

[8]M. das Gracas, A.Korn, J.B. Andrade, D.S. de Jesus,V.A. Lemos, M.L.S.F. Bandeira, W.N.L. Santos, M.A. Bezerra, F.A.C. Amorim, A.S. Souza, S.L.C. Ferreira, *Talanta* 69 ,**2006**, 16.

[9]Craggs, A.; Moody, G. J.; Thomas, J. D. R. *J. Chem. Educ.* **1974**, 51, 541.

[10] Ammanmm, D.; Pretsch, E.; Simon, W.; Lindler, E.; Bezegh, A.; Pungor, E. *Anal. Chim. Acta* **1985,** 171, 119.

[11]Gholivand, M. B.; Sharifpour, F. *Talanta* **2003**, 60, 707.

[12] Singh, A. K.; Gupta, V. K.; Gupta, B. *Anal. Chim. Acta* **2007**, 585, 171.

Thermodynamic modeling of the KCl + proline + water system based on potentiometric measurements at 298.2 K

Bahram Ghalami-Choobar*, Samaneh Mirzaie

Department of Chemistry, Faculty of Science, University of Guilan, P.O. Box: 19141, Rasht, Iran

E-mail address: B-Ghalami@guilan.ac.ir (B. Ghalami-Choobar)

Keywords: Pitzer model; KCl; Proline; emf method

Introduction

The thermodynamic study of multi component electrolytic systems is of much importance, particularly for those which, due to their composition, are important in biological and industrial processes. Amino acids are important compounds within biological systems and they are directly involved in these processes. However, a more profound understanding of the electrolyte effect on amino acid solutions are still needed [1]. In the previous work, we have reported the results relating to the thermodynamic properties some of biological systems [2-3]. As a continuation of our studies, the thermodynamic properties of (KCl + proline + water) system containing 0, 2.5, 5.0, 7.5, 10, 12.5 and 15.0 % mass fraction of proline over ionic strength range from 0.001 to 3.000 mol kg^{-1} using the potentiometric method are reported at T = 298.2 K.

Experimental and method

All of the potentiometric measurements were made by using a digital multimeter whose resolution was 0.1 mV. The output of the multimeter was connected to a personal computer for data acquisition. The potentiometric experimewnts were carried out on the galvanic cell of the type Ag | AgCl | KCl (m) , proline (w %), H_2O (1-w) % |K-ISE. The PVC based potassium ion selective electrode (K-ISE) and Ag–AgCl electrode used in this work were prepared in our laboratory and had a reasonably good Nernst response. As usual, all measurements were performed under stirring conditions and the temperature was kept constant at 298.2K (±0.1 K), employing a double-wall container enabling the circulation of thermostat water from a Model GFL circulation. The Pitzer ion interaction model was used for the experimental data correlation and calculation of thermodynamic properties for mixed electrolyte solutions.

Results and discussion

The galvanic cell was used to determine the emf values for each series of the proline- water mixed solvent systems. The experimental mean activity coefficients of KCl in various proline- water mixed solvent systems were derived from the Nernst equation 1.

$$E = E^{\circ} + s\log(\gamma_{\pm,KCl} m) \quad (1)$$

Where E^0 and s indicate the cell constant potential and the Nernstian slope, respectively. The results relating to the mean activity coefficients of KCl for one of series were listed in Table 1. Natural logarithm of the mean activity coefficients of different series were also presented in Figure 1. The ionic interaction parameters ($\beta^{(0)}$, $\beta^{(1)}$ and C^{Φ}) were evaluated (see table 2) in according to the Pitzer model based on the equations 2-4. Then, these obtained parameters were used for predicting the thermodynamic properties.

$$\ln \gamma_{\pm,KCl} = f^{\gamma} + B^{\gamma}_{KCl} m + C^{\phi}_{KCl} m^2 \quad (2)$$

$$f^{\gamma} = -2A_{\phi}\left[\frac{\sqrt{I}}{(1+b\sqrt{I})} + \left(\frac{2}{b}\right)\ln(1+b\sqrt{I})\right] \quad (3)$$

$$B^{\gamma}_{KCl} = 2\beta^{(0)}_{KCl} + \left(\frac{2\beta^{(1)}_{KCl}}{\alpha^2 I}\right)\left[1-\left(1+\alpha\sqrt{I}-\frac{\alpha^2 I}{2}\right)e^{-\alpha\sqrt{I}}\right]$$

Table 1. The values of molality, emf and activity coefficients of KCl for w%=5

m	E	$\gamma_{\pm}$
0.0009	-87.0	0.9714
0.0100	1.8	0.9154
0.0502	75.2	0.8411
0.0982	111.6	0.8014
0.2459	151.9	0.7423
0.4921	182.5	0.6980
0.7398	201.6	0.6740
0.9866	215.1	0.6591
1.2339	224.8	0.6492
1.4809	233.2	0.6428
1.7278	240.6	0.6388
1.9738	246.6	0.6367
2.4685	257.7	0.6369
2.9555	268.0	0.6414

Table 2. The Pitzer ion interaction parameters

W%	A_{Φ}	$\beta^{(0)}$	$\beta^{(1)}$	C^{Φ}
0.0	0.3915	0.04835	0.2122	0.00121
5.0	0.3332	0.04194	0.1993	0.00093
7.5	0.3093	0.03917	0.1937	-0.00191

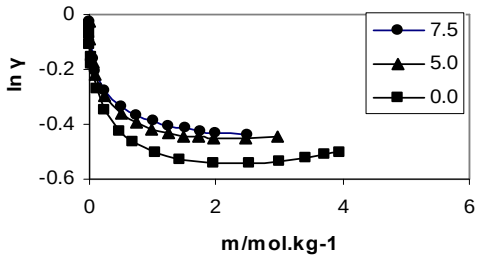

Figure1. The plot of ln $\gamma_{\pm}$ vs. m for different series of mass fraction of proline

References

[1] P. Venkatesu, M.J. Lee, H.M. Lin, J. Chem. Thermodyn. 39 (2007) 1206–1216.

[2] B. Ghalami-Choobar , M. Mohammadian, J. Mol. Liq 154 (2010) 26.

[3] B. Ghalami-Choobar, N. Mahmoodi,T. Nasiri-Louhesara. Phys. Chem. Liq , in press (2010).

Conductometric study of $NiCl_2$ in glucose -water mixtures at 298.2, 303.2, 308.2 and313.2 K

Bahram Ghalami-Choobar*, Toba Nasiri-Louhesara

Department of Chemistry, Faculty of Science, University of Guilan, P.O. Box: 19141, Rasht, Iran

E-mail address: B-Ghalami@guilan.ac.ir (B. Ghalami-Choobar)

Keywords: Conductivity, $NiCl_2$, glucose, Fuos-Edelson

Introduction

The temperature and concentration dependence of the electrolyte conductance has been proved as one of the most appropriate methods for studying ion-ion, ion-solvent and solvent-solvent interactions in solutions. Beside, the calculation of the electrical conductivity of aqueous electrolyte solutions is useful for many industrial processes such as batteries, plating, material transport, solid deposition, and corrosion [1-2]. In the present work, the results relating to the conductometric investigation of $NiCl_2$ in (0, 10, 20, 30 and 40% w) glucose - water mixtures at different temperatures 298.2, 303.2, 308.2 and313.2 K are reported. The experimental data were correlated by the Fuoss-Edelson equation, and its parameters, the limiting equivalent conductivity Λ_0, and the primary association constants, K_A, were evaluated.

Experimental and method

All of the conductivity experiments were made by using a digital conductivity meter whose resolution was 0.1 $\mu S \cdot cm^{-1}$. The output of the conductivity meter was connected to a personal computer for data acquisition. The cell used for conductivity measurements was calibrated using standard KCl solutions. The solutions were continuously stirred using a magnetic stirrer at a slow constant rate to avoid concentration gradients and were allowed to equilibrate for 4 min before the specific conductivity. A model GFL circulation water bath was used to maintain the temperature constant at the desired temperature (±0.1 K).

Results and discussion

The experimental equivalent conductivities, Λ, of the $NiCl_2$ as functions of equivalent concentration c in glucose + water mixture with mass fracrion of 10% at T = 298.2-313.2 K are given in Table 1. Figure 1 represents the plots of equivalent conductance Λ versus square

root of salt concentration *c* for $NiCl_2$ in (0, 10, 20, 30 and 40% w) glucose -water mixtures at 298.2 K. The conductance data were correlated with the Fuoss - Edelson equation 1

$$\Lambda F = \Lambda_{\circ} - XK_{1A} / \Lambda_{\circ} \quad (1)$$

$$X = c\gamma\Lambda F(\Lambda F - \Lambda_{\circ} / 2) \quad (2)$$

$$F = \left\{1 / (1 - \delta c^{0.5}) + (\Lambda_{\circ} - \lambda_{\circ}) / 2\Lambda\right\} / \left\{1 + (\Lambda_{\circ} - \lambda_{\circ}) / 2\Lambda_{\circ}\right\} \quad (3)$$

Where λ_0 is the limiting conductance of the anion (Cl^-), δ Onsager's slope, C is the normal concentration and γ is the ion activity coefficient which can be calculated by the Pitzer - Debye–Hückel equation . The derived conductivity parameters (Λ_0 and Ea) for the $NiCl_2$ in glucose -water mixtures at *T*= 298.2-313.2 K were presented in Tables 2-3.

Table 1. The values of Λ for w%=10

10^4C /M	298.2 /K	303.2 /K	308.2 /K	313.2 /K
		Λ(S.cm^2)		
2.0	125.0	135.4	157.1	150.7
6.0	113.5	126.6	139.4	140.9
12.3	107.9	119.7	131.7	134.0
20.6	104.7	114.1	127.1	129.4
30.9	103	110.2	123.1	125.0
43.1	100.4	108.9	120.9	123.3
57.6	98.7	105.6	118.8	121.2
74.1	97.8	103.7	116.6	119.4
92.4	96.6	102.2	114.9	118.3
113.0	95.1	100.7	113.1	115.9
137.7	93.7	99.3	112.2	114.0
631.4	83.7	87.1	97.6	100.6

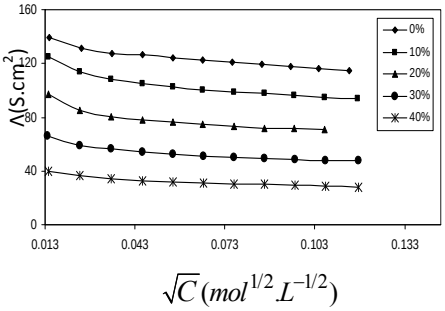

Figure 1. The plot of Λ vs. molar concentration of $NiCl_2$ at 298.2K

Table 2. The obtained values of Λ_0

T(K)	$\Lambda_{\circ}$ (S.cm^2) w (%)=0	10	20	30	40
298.2	135.9	115.4	84.2	58.6	34.5
303.2	147.3	125.6	105.7	64.6	38.4
308.2	166.5	142.4	113.6	76.8	46.4
313.2	169.4	147.9	116.2	80.5	51.0

Table 3. The obtained values of activation energy

w (%)	E_a(kJ.mol^{-1})
0	12.1
10	13.4
20	15.9
30	17.4
40	21.1

References

[1] G. M. Roger, S. Durand-Vidal, O. Bernard, P. Turq, J. Phys. Chem. B**,** *113 (*2009**)** 8670

[2] Y. F. Hu, X. M. Zhang, J. G Li, Q. Q. Liang, J. Phys. Chem. B*, 112 (* 2008) 15376

Fabrication and Analysis of Electrochemical Properties of LSM Cathode of Solid Oxide Fuel Cell

A.A. Naemi [*a], S. Razavi [b] and A.Nazari [a]

[a] Department of Physics, Islamic Azad University-Khorramabad Branch, Lorestan, Iran
(Email: aa.naimi@gmail.com)

[b] Department of Electrical Engineering, Islamic Azad University-Khorramabad Branch, Lorestan, Iran

Keyword: SOFC, Orthorhombic, calcinations, sinter, Sherer equation.

Introduction

Solid oxide fuel cell is one of the fuel cell types which transform chemical energy to electrical energy at the temperature range of 650˚C-1000˚C [1]. Cathode is one of the components of SOFC and for fabrication of LSM cathode there are lots of methods [2].

Experimental Procedures

In this paper LSM cathode is produced with slurry coating method using $La_2O_3, MnCO_3$ Sr_2CO_3 powders according to the following reaction

$$La_2O_3 + \frac{8}{1-x}MnCO_3 + \frac{x}{1-x}SrCO_3 \rightarrow \frac{2}{1-x}La_{1-x}Sr_xMnO_3 + \frac{x+1}{1-x}CO_2 + \frac{8-x}{1-x}O_2$$

In this method for preparing the conditions for interaction, the citric acid, nitric acid and glycol ethylene have been used [3]. Then, the samples are calcinated at 1400˚C and after that they are sintered at 1500˚C on the YSZ electrolyte [4].

Discussion and Conclusion

Fig. 1 shows the spectrum of the XRD of samples. In Fig. 1-c there is some unwanted peaks that is because of existence of Lanthanum which causes the production of $La_2Zr_2O_7$ and $SrZrO_3$ insulating phase in the interface cathode/electrolyte [6][8]. With XRD size of the grain using equation of Sherer is calculated, and also with XRD table the structure type and unit cell length and samples of $La_{0.8}Sr_{0.2}MnO_3$, $La_{0.85}Sr_{0.15}MnO_3$ and $La_{0.9}Sr_{0.1}MnO_3$ are calculated. Which the first two samples have monoclinic structure with unit cell length of $a = 5.52, b = 5.51, c = 7.75$ and $\beta = 90.75$ with grain size of 85.9nm and 83.25nm

respectively. The last sample has the rhombohedra structure with unit cell length of $a = 5.54$ and $b = 13.56$ and grain size of 91.03nm.

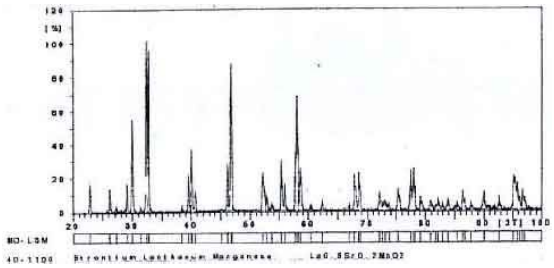

Fig. 1-a: XRD of $La_{0.8}Sr_{0.2}MnO_3$

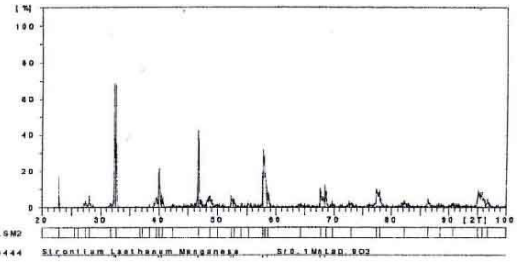

Fig. 1-b: XRD of $La_{0.85}Sr_{0.15}MnO_3$

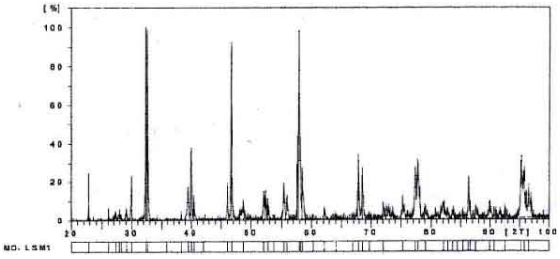

Fig. 1-c: XRD of $La_{0.9}Sr_{0.1}MnO_3$

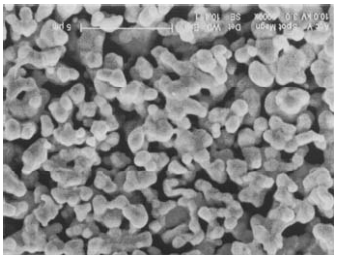

Fig. 2: SEM of samples

Then with comparing the results with the report presented by Kammer, our results are the same as his. Finally, with SEM, the amount of porosity of the all three samples became %35, which is the same as Kammer results [6].

Conclusion

The structure type and unit cell length depends on the amount of *Sr* doping, also the method we used here, results the same outcome as thin film method which has been used by Kammer.

References:

[1] B.Gharbage, M.Henult, T.Panier, Mater.Res, Bull, 105(1991)1001.

[2] L.W. Tai , R.A. Lessing, Mater.res,**7** (1992)183.

[3] L.J.de haart,R.A.Kuipers,k.j. de vries, Solide State Iinics Vol 123 p345-356.

[4] F.W.poulsen, N. Van der puil, Solid State Ionics 53-56 (1992) 1971.

[5] G. Stochniol, E. Syskakis, A. Naoumidis, J, amer. Ceram. Soc. 78 (1995) 1971.

[6] K. Kammer, Solid State Ionics 177 (2006) 1047–1051.

[7] S. Kakac, A. Pramuanjaroenkij, X.Y. Zhou International Journal of Hydrogen Energy 32 (2007) 761 – 786.

Modeling of Oxygen Electrochemical Reduction in Composite Cathode of Solid Oxide Fuel Cell

A.A. Naemi [*a], S. Razavi [b] and A.Nazari [a]

[a] Department of Physics, Islamic Azad University-Khorramabad Branch, Lorestan, Iran
(Email: aa.naimi@gmail.com)

[b] Department of Electrical Engineering, Islamic Azad University-Khorramabad Branch, Lorestan, Iran

Keywords: Cathode Model; Electrode Microstructure; Knudsen Diffusion; Electrochemical Active Area

Introduction

The performance of electrochemical fuel cell is depended on the activity electro catalysts and micro-structure of composite cathode (LSM/YSZ) and scientists believe that electrochemical reduction of oxygen most have a given constant step rates [1].

Methods

Electrochemical reduction of oxygen in the common interface contain diffusion, absorption, breakup of oxygen molecule on surface, electric load transfer and transfer of oxygen ion from triplet phase to lattice YSZ [2][3] that using impedance spectrum has confirmed the above steps [4][5]. So, with some calculation, LSM electrode current is

$$i = \frac{1}{1/(i_{0,3}(p_{O_2}/p^0_{O_2})^{1/2}\exp(f\eta))} + \frac{1}{1/(i_{0,5}(p_{O_2}/p^0_{O_2})^{1/2}\exp(-2f\eta))} - \frac{1}{1/(i_{0,3}\exp(f\eta)+1/(i_{0,5})}$$

With using Ohm law for electrical and ionic current and the equation of Stephan Maxwell for oxygen reduction, we have

$$\frac{d^2Y}{d\xi^2} = \frac{F(\rho^{eff}_{el}+\rho^{eff}_{io})\lambda_{TPBL}}{RTL^2} f(Y,\psi) \quad and \quad \frac{d^2\psi}{d\xi^2} = \frac{RT\lambda_{TPBL}}{4L^2FD^{eff}_{O_2-N_2}} f(Y,\psi)$$

Which

$$i = f(Y,\psi) = \frac{1}{1/(i_{0,3}(1-\exp(\psi)/x^0_{O_2})^{1/2}\exp(-Y))}$$

$$+ \frac{1}{1/(i_{0,5}(1-\exp(\psi)/x^0_{O_2})^{1/2}\exp(-2Y))} - \frac{1}{1/(i_{0,3}\exp(Y))+1/(i_{0,5})}$$

We have solved the above equation using Runge-Kutta numerical method with the initial value and model parameters [6][7][8][9][10][11].

Conclusion

In solving of the above equation, parameters like cathode thickness, particles size, particle size ratio and volume fraction have been used. i.e. the efficiency of cathode depends on the size of particles, YSM particles to LSM particles ratio, thickness of cathode and the length of the triplet phase. So, with bigger size of the particles the cathode has more efficiency; the lowest over potential is located in a specified radius and in thick cathode a small part of that is involved in current production. At the end, more partial oxygen pressure will result in less over potential.

All the above results were nearly as the same as the data experimental and paper reports presented by Kim [12].

References:

[1]C.W .Tanner, K.Z .Fung, A.V .Virkar, J .Electrochem .Soc .144 (1997) 21.

[2]P .Costamagna, P .Costa, V .Antonucci, Electrochim .Acta 43 (1998)375.

[3]X.J .Chen, K.A .Khor, S.H .Chan, J .Power Sources 123 (2003)17.

[4]P .Costamagna, P .Costa, E .Arato, Electrochim .Acta 43 (1998) 967.

[5]A.M .Svensson, S .Sunde, K .Nisoncioglu, J .Electrochem .Soc .145(1998) 1390.

[6]C.H .Kuo, P.K .Gupta, Acta Metall .Mater .43 (1995) 397.

[7]M .Suzuki, T .Oshima, Powder Technol .35 (1983) 159.

[8]S.P .Jiang, J.P .Zhang, K .Foger, J .Electrochem .Soc .147 (2000) 3195.

[9]C.J .Geankoplis, Mass Transport Phenomena, Holt, Rinehart, Winston,New York, (1972).

[10] D .Bouvard, F.F .Lange, Acta Metall .Mater .39 (1991)3083.

[11] S.B .Adler, j.a .Lane, B.C.H Steele, J.Electrochem.Soc .143 (1996) 3554.

[12] J. D .Kim, G.D .kim, J-.W .Moon, Y.I .Park, W-.H .Lee, K.Kobayashi, M .Nagai, C.E. Kim, Solid State Ionics 143 (2000) 379.

Theoretical and Experimental studies of the Electrochemistry of ortho – Hydroquinone and ortho – Benzoquinone

Hadi Shafie*, Masoomeh Nilchi, Behnoud Hormozi
Chemistry Department, Faculty of Science, Islamic Azad University, Arak Branch
(hshafie2005@yahoo.com),(mitranilchi@yahoo.com)

Abstract:
The geometric parameters, vibrational frequencies, and thermochemical values of ortho-hydroquinone (o-HQ) and ortho – Benzoquinone (o-BQ) were computed ab initio and by the density functional theory (DFT) method with the 6-31 G (d, p) basis set. the standard electrode potentials of half reaction for o-HQ and o-BQ were calculated using the free energies and solvation energies of O-HQ, o-BQ, p-Benzoquinone (P-BQ), and hydroquinone (p-HQ). The standard electrode potentials computed at the B3lyp / 6-31 G (d, p) levels were close to their experimental values.

Keyword: ortho Hydroquinone; ortho – Benzoquinone; Gaussian 03; Cyclic voltammetry.

Introduction:

The standard electrode potential is a very important Parameter in biochemistry, analytical chemistry, etc. In our previous work, we reported calculations of the standard electrode potential for a carbonyl compound [1].

Results and Discussion:

The electrochemical behavior of o-HQ. The voltammetric data on the oxidation of 5.0 mM o-HQ in 0.1 M phosphate buffer at pH 7.0 with a glass carbon electrode are shown in Fig.1.These data describe a chemically reversible oxidation process, as follows from similarly sized peaks of the forward and reverse scans, with an oxidation peak potential (E^{ox}) of 0.111V and a reduction peak potential (E^{red}) of 0.169 V versus saturated calomel electrode.

The conditional potential $E^{of} = (E^{ox} + E^{red})/2$ [2] were calculated as follows:

pH=7.0, $E^{of}= (0.111 + 0.0169)/2=0.14$ V.

pH 7. 0, $E_1^0 = 0.553$ V (25 ^oC).

$E_2^0 = E_1^0 + E_{SCE}$,

pH=7.0, $E_2^0 = 0.794$ V (25^OC)

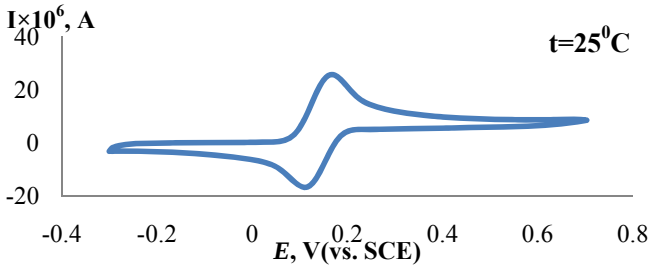

Fig.1.

Theoretical calculation of the standard electrode potential (E^0) of half reaction for o-HQ and o-BQ. A redox reaction can be divided into two half reactions as

$$\text{o-HQ (g)} + 2H^+(g) + 2e^-(g) = \text{o-BQ(g)}, \quad (1)$$

$$\text{p-BQ (g)} + 2H^+(g) + 2e^-(g) = \text{p-HQ(g)} \quad (2)$$

$$\text{o-HQ (g)} + \text{p-HQ(g)} = \text{o-BQ(g)} + \text{p-BQ(g)} \quad (3)$$

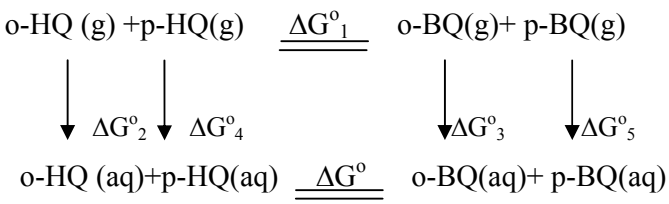

Fig. 2.

Conclusion:

The predicted standard potentials for the half reactions of o-HQ and P-BQ are in agreement with the experimental data. The reduced Gibbs energy of reaction (3) in the gas phase is written as

$\Delta G^o_1(298.15K) = G^o_{\text{o-BQ(g)}} + G^o_{\text{p-BQ(g)}} - G^o_{\text{o-HQ(g)}} - G^o_{\text{p-HQ(g)}}$, $\Delta_r G_2^0, \Delta_r G_3^0, \Delta_r G_4^0$ *and* $\Delta_r G_5^0$

The redox reaction in solution proceeds as shown in Fig. 2, where are the solvation energies of o-HQ, o-BQ, p-HQ, and p-BQ in water at 298.15 K and 1 atm, respectively.

G^o (298.15K, 1atm) $= G^o_{\text{o-BQ (aq)}} + G^o_{\text{p-BQ (aq)}} - G^o_{\text{o-HQ (aq)}} - G^o_{\text{p-HQ(aq)}} = (G^o_{\text{o-BQ (g)}} + \Delta_r G^o_3) + (G^o_{\text{p-BQ (g)}} + \Delta_r G^o_5) - (G^o_{\text{o-HQ (g)}} + \Delta_r G^o_2) - (G^o_{\text{p-HQ (g)}} + \Delta_r G^o_4) = \Delta_r G^o_1 + \Delta_r G^o_3 + \Delta_r G^0_5 - \Delta_r G^o_2 - \Delta_r G^o_4$.

The standard electrode potential (E^o) of half reaction for o-HQ and o-BQ is calculated as

ΔG^o (298.15K) $= -nf\,(E^o_{\text{o-HQ/ o-BQ}} - E^o_{\text{p-BQ/p-HQ}})$ $\quad E^o_{\text{o-HQ/ o-BQ}} = 0.694$ V

The theoretical values are in good agreement with the experimental standard electrode

potential (0.794V).

Reference:

[1] Y. Song, Y.Song, W. Xie, and D. Shi, Russ. J. Phys.Chem. 80, 1467 (2006).

[2] J. Wang, Analytical Electrochemistry, 2nd ed . (Wiley, New York, 2000).

Chemical Kinetics

Kinetic and thermochemistry study of the reaction $Cl_2 + Br \rightarrow ClBr + Cl$ by density functional theory calculations

Gh. Ebrahimzadeh Rajaei[*,a], H. Aghaie[b], M. Monajjemi[b], K. Zare[b,c]

[a] *Department of Chemistry, Islamic Azad University, Ardabil Branch, Ardabil, Iran*

E-mail: Farzad_rajaei@yahoo.com

[b] *Department of Chemistry, Science and Research Branch, Islamic Azad University, Tehran, Iran*

[c] *Department of Chemistry, Shahid Beheshti University, Tehran, Evin, Iran*

Abstract

The reaction between molecular chlorine and Br radical was investigated by density functional theory. Kinetics and thermochemistry functions of this reaction were studied using the DFT method B3LYP at 6-31G(d) level. The enthalpy and Gibbs free energy of reaction were predicted to be -3.33 kcal $mol^{-1}$and -3.79 kcal mol^{-1} respectively at 298.15 K in gas phase. The pre-exponential factor and activated energy values of the reaction were found to be 2.28×10^{10} L mol^{-1} s^{-1} and 460 cal mol^{-1} respectively.

Keywords: Density Functional Theory (DFT), Transition State Theory (TST), Rate constant, Chlorine

Introduction

Recently, theoretical studies based on the transition state theory (TST) have been carried out by many chemists for many reactions. In this work, we have used DFT–TST calculations to evaluate the rate constant $k_{TST}(T)$ for reaction (1).

(1) $Cl_{2(g)} + Br_{(g)} \rightarrow ClBr_{(g)} + Cl_{(g)}$

We performed DFT calculations of the electronic structures of reactants, products and activated complex involved in reaction (1). We used the electronic structure results with along the transition state theory to evaluate the rate constant $k_{TST}(T)$.

Computational method

All the DFT calculations reported in this paper were performed with the Gaussian program using the 6-31G(d) basis set. Each species is taken in the ground state. The structures of the

various stationary points were fully optimized and using a gradient convergence tolerance of less than 10^{-4}. The stationary structures, harmonic vibrational frequencies and zero point energy (ZPE) corrections for reactants, products and transition state Br-Cl-Cl complex are determined [1,2,3]. The rate coefficient for reaction becomes

(2) $$k_{TST}(\mathrm{T}) = \frac{k_B \mathrm{T}}{\mathrm{hc}^{\circ}} \mathrm{e}^{-\Delta^{\ddagger}\mathrm{G}^{\circ}/\mathrm{RT}} = \frac{k_B \mathrm{T}}{\mathrm{h}} \mathrm{e}^{\left(\mathrm{n}+\frac{\Delta^{\ddagger}\mathrm{S}^{\circ}}{\mathrm{R}}\right)} \mathrm{e}^{\frac{-E_a}{\mathrm{RT}}} = \mathrm{A}\mathrm{e}^{\frac{-E_a}{\mathrm{RT}}}$$

c° represent standard concentration. The activation energy of the reaction can be calculated by using only the energies of the transition state and of the reactants, and the energy barrier is obtained according to the following equation:

(3) $$E_a = E_{TS} - E_R + ZPE_{TS} - ZPE_R$$

For reaction energies at 298 K, thermal corrections (TCE) are applied [4,5,6]. Using the information in table 1, the enthalpy changes and Gibbs free energy changes of reaction can be calculated by

(4) $$\Delta H^{\circ}(298.15K) = \sum_{products}(\varepsilon_o + H_{corr}) - \sum_{reactants}(\varepsilon_o + H_{corr})$$

(5) $$\Delta G^{\circ}(298.15K) = \sum_{products}(\varepsilon_o + G_{corr}) - \sum_{reactants}(\varepsilon_o + G_{corr})$$

Also, entropy changes of reaction at 298.15 K can be calculated from $\Delta H^{\circ}(298.15K)$ and $\Delta G^{\circ}(298.15K)$.

Results and Discussion

The thermochemistry outputs from Gaussian are summarized in table 1.

Table 1: Calculated thermochemistry values from Gaussian for the reaction $Cl_2 + Br \rightarrow ClBr + Cl$

All values are in Hartree/particle.

	Br-Cl-Cl	Br	Cl-Cl	Br-Cl	Cl
ε_o	-3492.0175	-2571.6569	-920.3499	-3031.8757	-460.1362
ε_{ZPE}	0.001160	0.000000	0.001179	0.000991	0.000000
E_{tot}	0.005919	0.001416	0.003751	0.003628	0.001416
H_{corr}	0.006863	0.002360	0.004695	0.004572	0.002360
G_{corr}	-0.030516	-0.016830	-0.020672	-0.022684	-0.015677
$\varepsilon_o + \varepsilon_{ZPE}$	-3492.0163	-2571.6569	-920.3487	-3031.8747	-460.1362
$\varepsilon_o + E_{tot}$	-3492.0116	-2571.6555	-920.3461	-3031.8721	-460.1348
$\varepsilon_o + H_{corr}$	-3492.0106	-2571.6545	-920.3452	-3031.8712	-460.1339
$\varepsilon_o + G_{corr}$	-3492.0480	-2571.6737	-920.3705	-3031.8984	-460.1519

The pre-exponential factor and activated energy values of the reaction were found to be 2.28×10^{10} L mol^{-1} s^{-1} and 460 cal mol^{-1} using equation 2 and 3 respectively. The enthalpy and Gibbs free energy of reaction (1) was predicted to be -3.33 kcal $mol^{-1}$and -3.79 kcal mol^{-1} using equation 4 and 5 respectively at 298.15 K in gas phase. Finally the rate constant is calculated using Eq.(2). The rate constant of $Cl_{2(g)} + Br_{(g)} \rightarrow ClBr_{(g)} + Cl_{(g)}$ reaction is predicted to be 1.04×10^{10} L mol^{-1} s^{-1} at 298 K.

Acknowledgements

The author thanks Jamshid Najafpour for helpful discussions.

References:

[1] M. Francisco-Ma´ rquez et al. Chemical Physics 344 (2008) 273–280.

[2] H. Koussa et al. Journal of Molecular Structure: THEOCHEM 770 (2006) 149–156.

[3] E. Drougas et al. Journal of Molecular Structure: THEOCHEM 623 (2003) 211–219.

[4] P.R.P. Barreto et al. Journal of Molecular Structure: THEOCHEM 769 (2006) 201–205.

[5] A.C. Olleta, R.A. Taccone. Journal of Molecular Structure :THEOCHEM 507(2000)25–38.

[6] Kh.J. Devi et al. Chemical Physics Letters 480 (2009) 161–167.

Removal of malachite green from aqueous solution by use of alumina coated Fe_3O_4 magnetic nanoparticles

D. Farmanzadeh[a,*], F. Abgoon[a], P. Biparva[a]

[a]*Faculty of Chemistry, University of Mazandaran, Babolsar, Islamic Republic of Iran*

(Email: d. farmanzad@umz.ac.ir)

Keywords: Magnetic nanoparticles, Dye removal, Adsorption, Malachite green

Introduction

In recent years, extensive efforts have been focused on iron oxide nanoparticles due to their potential applications in different area. One of the important uses of magnetic nanoparticles (MNPs) is magnetic separation, especially in biological species separation. In this case, modified MNPs with affinity to purpose species are mixed, in mixing process the particle tag to the species. Then an external magnetic field applied to separate the tagged particles from the system [1]. Furthermore, in many industrials, removal of toxic dyes from wastewater is great interest. Little work has been reported on the use of MNPs to remove toxic dye from wastewater [2]. In current study, the Fe_3O_4/Al_2O_3 MNPs are synthesized and then this particles are used for removal of a cationic dye; malachite green, MG, from aqueous solution.

Methods

$FeCl_2$, $FeCl_3$ and HCl were mixed in degassed water. NaOH was added to this solution at 80 °C with continuous stirring. The wet particles were dried in oven. Al_2O_3 was dissolved in ethanol while Fe_3O_4 was added to this solution, under ultrasonic irradiation and the mixture of double distilled water with ethanol was added to this solution. MNPs were washed repeatedly with ethanol and dried in oven.

Results and discussion

The X-ray diffraction pattern was obtained for adsorbent to determine its properties and size (GBC X-ray diffractogram). Fig. 1 shows the wide angle X-ray diffractogram for the

synthesized Fe2O3/Al2O3 MNPs. The average crystallite size was 14 nm which calculated from X-ray diffraction peak using the Scherrer's formula [3].

Dye removal experiments were carried out by adding the dry weight of Fe_3O_4/Al_2O_3 MNPs in a range of 0.05- 0.4 by keeping the dye concentration constant 50 ppm. Followed by shaking at 200 rpm and centrifuged, the equilibrium concentrations of dye were measured with a UV-VIS spectrophotometer. The obtained results are shown in Fig. 2. From this figure it can be observed that the dye adsorption increases with increasing of adsorbent weight. The amount of adsorption at equilibrium, q_e (mg/g) was calculated by:

$$q_e=(C_0-C_e)\,V/M \qquad (1)$$

where C_0 and C_e (mg/l) are concentration of dye at initial and equilibrium, V is the volume of the solution (L) and M is the mass of dry used MNPs (g). The maximum dye removal was 52 mg/g. Several affecting factors and the adsorption kinetics of MG into the Fe_3O_4/Al_2O_3 MNPs are investigated.

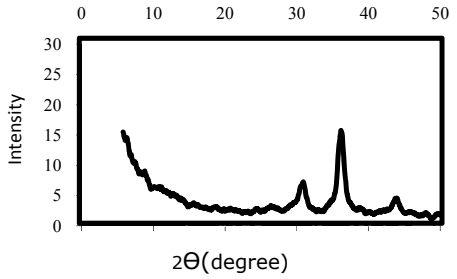

Fig 1. The XRD pattern of Fe_3O_4/Al_2O_3 MNPs.

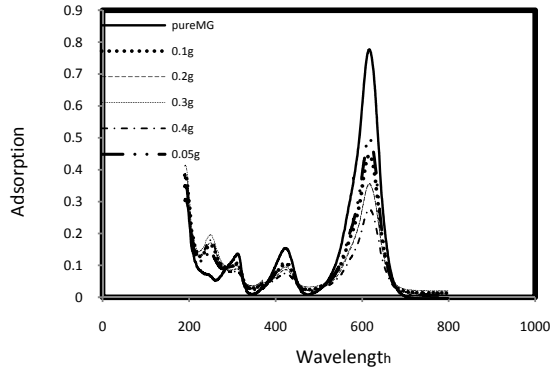

Fig. 2. Effect of different amount of Fe_3O_4/Al_2O_3 MNPs on the adsorption of MG.

Conclusion

A fast, simple and new magnetic removal of dye from aqueous solution has been successfully developed with Fe_3O_4/Al_2O_3 MNPs as adsorbent. MNPs with average size distribution of 14 nm have been utilized for malachite green dye removal. The maximum dye removal was 52 mg/g.

References

[1]. J. Sun et al. J Biomed. Mater. Res., DOI 80 A 333 (2007)

[2]. C.H. Yu, K.Y. Tam, C.C.H. Lo, S.C. Tsang, IEEE Trans. Magn. 43 (2007). 2436

[3]. H.P. Klug, L.E. Alexander, X-ray Diffraction Procedures, New York, Wiley, (1954) 512

Electrochemical study in self assembled monolayers modified electrode

A. Ehsani, M.G. Mahjani, M. Jafarian, A. Sharifi
Department of Chemistry, Faculty of science, K. N. Toosi University of Technology
E-mail address: a_ehsani@dena.kntu.ac.ir

Keywords: Self assembly, electrochemical, impedance, electron transfer

Introduction

Electron transfer has been extensively studied in the context of biological processes, sensors, artificial photosynthesis, and molecular electronics. Marcus theory predicts that the rate of electron transfer between a donor and an acceptor is dependent on the Gibbs free energy (G), reorganization energy (λ), temperature (T) and the electronic coupling between an electron donor and acceptor (H_{AB}). Recent interest in surface (electrode) modification has led to the study of electron transfer using electrodes modified with self-assembled monolayer's (SAMs) [1-3].

Results & discussion

SAMs provide an excellent platform for exploiting electrochemistry to study electron transfer processes because each variable (ΔG, H_{AB}, λ, T) can be controlled experimentally. For example, SAMs allow double layer effects to be controlled and eliminate problems associated with diffusive mass transport. Redox-modified SAMs have been designed to systematically study the correlation of ΔG, and H_{AB} to SAM components. A variety of electrochemical techniques are used to probe each of these electron transfer variables. The bridge controls the distance and coupling between the redox center and the electrode. Reorganization energy can be probed by changing the molecular environment of the redox center by using a variety of solvents or by changing the SAM composition. The effects of changing each of these variables can be quantified using electrochemical techniques.

SAMs are ideal systems for using electrochemistry to study long-range electron transfer events on electrodes. However, the multitude of electrochemical techniques available (and subsequent data analysis) can be daunting to novices of the field. In this work, we describe the most commonly used electrochemical methods to measure k and H_{AB} using redox-modified SAM systems in different substrates. These analytical methods include cyclic voltammetry,

AC voltammetry, chronoamperometry, and electrochemical impedance spectroscopy. Each of these methods has advantages and limitations. Further, a detailed description of data analysis for each of these techniques will be described.

Conclusion:

The composition and integrity of the monolayer and the electrode material influence the electron transfer kinetics and can be investigated using electrochemical methods such as cyclic voltammetry, AC voltammetry, chronoamperometry, and electrochemical impedance spectroscopy.

References

[1] M. Collison, E.F. Bowden, M.J. Tarlov, Langmuir 8 (1992) 1247.
[2] C.M.A. Brett, S. Kresak, T. Hianik, A.M.O. Bretta, Electroanalysis 15 (2003) 557.
[3] N.K. Chaki, K. Vijayamohanan, Biosens. Bioelectron. 17 (2002) 1.

Synthesis of new various ionic liquids and determination of their solvatochromic parameters

Seyed Saied Ahmadvand, Hadi Salari, Mohammad Reza Gholami

Department of Chemistry, Sharif University of Technology, Azadi Ave., P.O. Box 11365-9516, Tehran, Iran.
Sahmadvand63@ymail.com

Abstract

Room-temperature ionic liquids (RTILs) have recently gained increased interest as potential "green" replacements for volatile organic solvents due to their unique properties.[1-2] These compounds are typically composed of organic cations with organic or inorganic anions and have negligible vapor pressure and a wide liquid range (i.e., over 300 K).7 An ideal solvent should have a very low volatility and should be chemically and physically stable, recyclable, reusable, and eventually easy to handle. Moreover, solvents that allow more selective and rapid chemical transformations will have a significant impact. Ionic liquids were recognized as a novel class of solvents.8 Initially developed by electrochemists, they are increasingly implied in many applications such as electrolytes for electrochemical devices and processes and solvents for organic and catalytic reactions as well as for separation-extraction processes and production of new materials.[3-4] Solvatochromic parameters have been demonstrated to be successful in correlating a wide range of chemical and physical properties, involving solute-solvent interactions as well as biological activities of compounds. In this work, four solvatochromic parameters (i.e., ET N, normalized solvent polarity parameter; δ^*, dipolarity/polarizability; $\hat{a}$, hydrogen-bond acceptor basicity; R, hydrogen-bond donor acidity) have been determined for new synthesized ionic liquids at 25 °C. The solvatochromic indicators used are Reichardt's betaine dye for solvent polarity (ET(30) scale) as well as 4-nitroanisole and 4-nitroaniline for measuring the Kamlet-Taft parameters.[5]

Experimental

Ionic liquids were synthesized as described in following. 0.1 mol of given amine was placed in a three necked flask equipped with a dropping funnel, a reflux condenser and a thermometer. 0.1 mol of given acid was added dropwise to the flask while the solution was stirring vigorously. Stirring was continued for 24 h at room temperature to obtain a colorless

viscous clear liquid. The prepared IL was identified by FT-IR and H-NMR spectroscopy. Using Karl Fisher titration, no water
was found in freshly prepared IL. Solvatochromic parameters of ionic liquids were obtained as described in literature.

Results and discussion

Obtained solvatochromic parameters have been reported in table 1.

Conclusion

The E_T^N parameters will be reported subsequently.

ionic liquid	α	β	$^*\pi$
2-hydroxy ethyl ammonium format	1.01	0.59	**1.15**
2-hydroxy ethyl ammonium acetate	0.99	0.92	**1.21**
2-hydroxy ethyl ammonium dicholoro acetate	0.97	0.51	**1.25**
Triethyl ammonium acetate	0.73	0.94	**1.23**
Ethyl ammonium acetate	0.79	0.90	**1.18**
Dimethyl ammonium acetate	0.68	0.92	**1.16**

Conclusion

With changing of functional groups in ionic liquid's anion, β parameter showed the most sensitivity among other parameters. But with changing of functional group in cation, α and π^* showed the most sensitivity. Also, obtained resultys demonstrated that solvatochromic parameters don't alter remarkably by increasing length of carbonic chain.

References

[1] Wilkes, J. S.; Levisky, J. A.; Wilson, R. A.; Hussey, C. L. *Inorg.Chem.* 1982, *21*, 1263.

[2] Gordon, C. M. *Appl. Catal., A* 2001, *222*, 101.

[3] Dai, S.; Ju, Y. H.; Barnes, C. E. *J. Chem. Soc., Dalton Trans.* 1999 1201.

4. Adams, C. J., Earle, M. J.; Roberts, G.; Seddon, K. R. *J. Chem Soc., Chem. Commun.* 1998, 2097.

5. Kamlet M. J.; Taft, R. W. *J. Am. Chem. Soc.* 1976, *98*, 377.

Kinetic study of DPPH scavenging in the presence of mixture of zinc and vitamin C as an antioxidant

M. M. Heravi[*a], B. Haghi[a], P. Ardalan[b] and T. Ardalan[b]

[a]*Department of Chemistry, University of Islamic Azad, Mashhad Branch, Mashhad, Iran*

(Email: drmh@mshdiau.ac.ir)

[b]*Department of Chemistry, Islamic Azad University, Mashhad Branch, Mashhad, Iran*

young research club

Key Word: Antioxidant, DPPH, Kinetic, Free radical, UV-Vis spectrometry

Introduction

Reactions of free radicals and reactive oxygen species (ROS) with biological molecules in vivo play an important physiological role in many diseases [1-2]. 2,2-diphenyl l,1-picrylhydrazyl (DPPH) is a stable free radical and often used as substrate to evaluate the antioxidant capacity of an antioxidant [3]. This study was undertaken to investigate the free radical-scavenging and antioxidant activities of zinc, vitamin C and mixture of them. UV-Vis spectrometry method was used to evaluate the ability of zinc, vitamin C and mixture of them to scavenge DPPH radical. The kinetic parameters such as rate constant and activation energy in experimental conditions were calculated.

Methods

UV-Vis assay for DPPH

The H-transfer reactions from an antioxidant to DPPH were monitored using UV-Vis spectrophotometer (Perkin-Elmer Lambda 25). The temperature in the cell was kept at 25^{o}C by using a circulator. In a typical procedure, to 3mL of a freshly prepared 2×10^{-5} M solution of DPPH in acetonitrile, placed in the spectrometer cell, was added 30-80 µL of a freshly prepared 2×10^{-2} M solution of the antioxidant in the same solvent. Spectra were recorded every 1 min for the determination of rate constants.

Results and discussion

We have studied the ability of the antioxidants of zinc, vitamin C and mixture of them to

neutralize the free radicals such as DPPH radicals [4]. The decrease in DPPH absorption in the presence of zinc, vitamin C and mixture of them was monitored by measuring absorption spectra in the range of 400-900 nm at 25°C (Fig. 1A, B and C). The rate constants of the H atom abstraction by DPPH (k_1), in the presence of zinc, vitamin C and mixture of them were obtained (0.4209, 2.092 and 1.82 min^{-1}) respectively, under pseudo-first-order conditions at 25°C.

Conclusions

The free radical-scavenging activities and rate constants values discriminate well between zinc, vitamin C and mixture of them, showing that the vitamin C have better antioxidant properties at 25°C. The activation energies were obtained (43.14, -59 and -45.56 $kJ.mol^{-1}$) for zinc, vitamin C and mixture of them, respectively at (25 °C-40°C) temperature range.

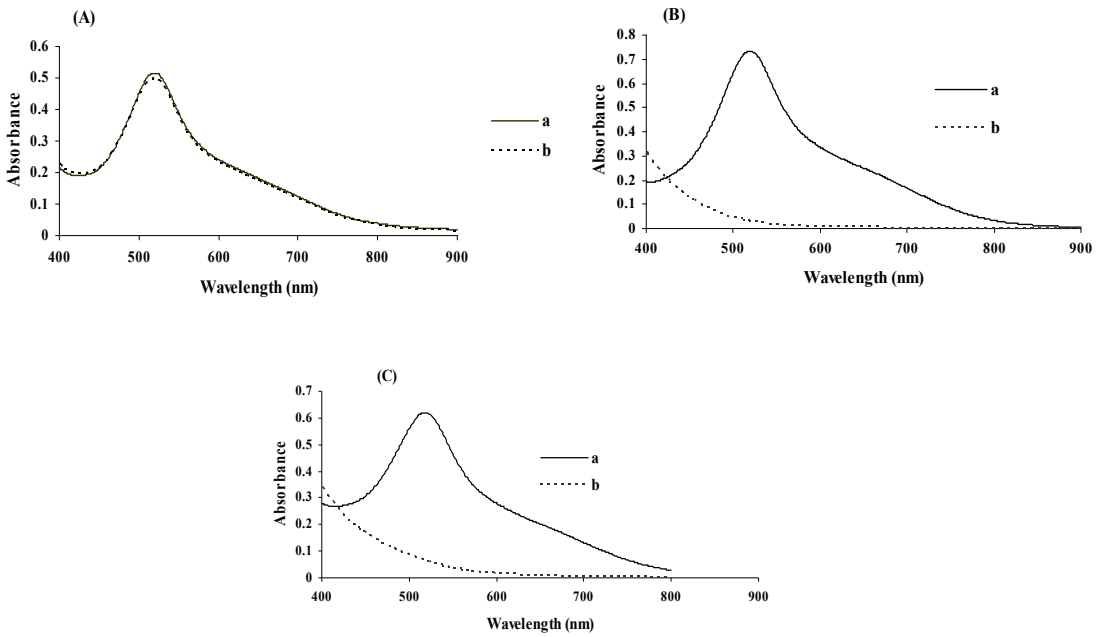

Figure 1- The spectra of DPPH in the presence of (A) zinc a) at time zero b) t = 16 min (B) vitamin C a) at time zero b) t = 4 min (C) zinc and vitamin C a) at time zero b) t = 3 min.

References

[1] Aruoma, O.I. (2003), Methodological considerations for characterizing potential antioxidant actions of bioactive components in plant foods. *Mutation Research*., **523-524**, 9-20.

[2] Jacobi, R.A.; Burri, B.J. (1996), Oxidative damage and defense. *Am J Clin Nutr*., **63**, 985-990.

[3] Kumar, S.S.; Priyadarsini, K.I.; Sainis, K.B. (2002), Free radical scavenging activity of vanillin and O-vanillin using 1,1-diphenyl-2-picrylhydrazyl (DPPH) radical. *Redox Report*., **7**, 35-40.

[4] Molyneux, P. (2004), The use of the stable free radical diphenylpicryl-hydrazyl (DPPH) for estimating antioxidant activity. *Songklanakarin J Sci Technol*., **26**, 211-219

Kinetic study of DPPH scavenging in the presence of saffron calycle extract as an antioxidant

P. Ardalan*[a], T. Ardalan[a], M. M. Heravi[b]

[a]Department of Chemistry, Islamic Azad University, Mashhad Branch, Mashhad, Iran
young research club

[b]Department of Chemistry, Islamic Azad University, Mashhad Branch, Mashhad, Iran
(Email:pooran_ardalan@yahoo.com)

Key Word: Kinetic study, Antioxidant, DPPH, Saffron, UV-Vis spectrometry.

Introduction

There has been an increasing concern for free-radical clearance. Human body contains various biomacromolecules such as proteins, lipids, vitamins, and carbohydrates, which are vulnerable to be attacked by reactive oxygen species (ROS). ROS include superoxide radical anion (O^{2-}), hydrogen peroxide (H_2O_2), hydroxyl radical (•OH) and singlet oxygen ($^1O^2$), which are normally generated during physiological metabolic activities [1,2]. ROS have been linked with aging and many degenerative diseases such as cancer, inflammation, immune system decline, cardiovascular diseases, neurological diseases, and atherosclerosis [3,4]. While synthetic antioxidants have potential health hazards, the search for natural radical scavengers (antioxidants) is of great interest among scientists [5,6].

Antioxidants are defined as substances that, when present at low concentrations compared with those of an oxidizable substrate, significantly delay or prevent oxidation of that substrate.6 Small-molecule antioxidants can be present extra- and intracellularly. Antioxidants work by preventing the formation of new free radical species, by converting existing free radicals into less harmful molecules, and by preventing chain reactions. DPPH is a stable free radical having maximum absorption at 517 nm [7] that accepts an electron or hydrogen radical to become stable diamagnetic molecule. In addition, DPPH is often used as substrate to evaluate the antioxidant capacity of an antioxidant (the unpaired electron is delocalized over N atoms and over O atoms, respectively).

In this study antioxidant effect of saffron calycle extract on DPPH scavenging has been studied.

Methods

UV-Vis assay for DPPH

The H-transfer reactions from an antioxidant to DPPH were monitored using UV-Vis spectrophotometer (Perkin-Elmer Lambda 25). The temperature in the cell was kept at 25°C by using a circulator. In a typical procedure, 3mL of DPPH solution (2×10^{-4} M) in acetonitrile, placed in the spectrometer cell, then 0.01 ml extract of saffron was added as an antioxidant. UV-Vis Spectra were recorded every 2 minute for the determination of rate constants.

Results and discussion

We have studied antioxidant effect of saffron calycle extract to neutralize the free radicals such as DPPH. The decrease in DPPH absorption in the presence of saffron calycle extract was monitored by measuring absorption spectra in the range of 400-900 nm at 25°C (Fig.1) The rate constants of the H atom abstraction by DPPH (k_1), in the presence of different amount of antioxidant (0.01, 0.02, 0.03 and 0.05 ml) were obtained 8.51×10^{-2}, 1.37×10^{-1}, 2.21×10^{-1}, 3.71×10^{-1} min^{-1} respectively, under pseudo-first-order conditions at 25°C.

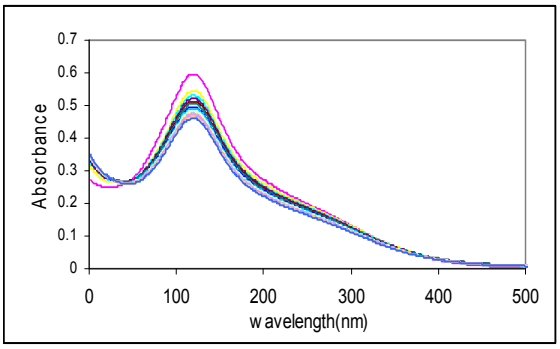

Figure 1- The spectra of DPPH (2×10^{-4} mol/L) in the presence of 0.01 ml extract of saffron calycle (T=25°C)

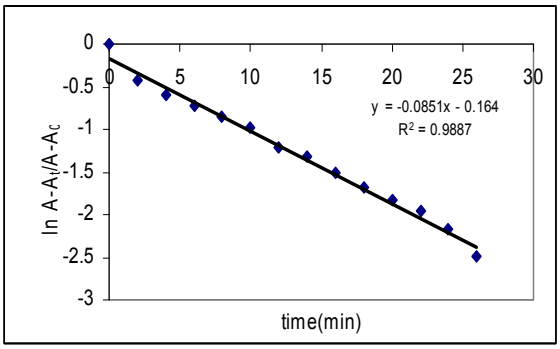

Figure 2- Plot of $Ln(A_t-A_\infty)/(A_0-A_\infty)$ versus time in the presence of 0.01 ml extract of saffron calycle (T=25°C)

Conclusions

The result of this study shown saffron calycle extract has a dramatic antioxidant effect. The rate constant of DPPH scavenging in the presence of saffron calycle extract has been increased by increasing of antioxidant. Saffron calycle extract, representing a complex system containing a variety of organic compounds with antioxidant and radical - scavenging activity,

has the potential to serve as a significant source of natural antioxidants in human nutrition.

References

[1] D.O. Kim, O.K. Chun, Y.J. Kim, H.Y. Moon, C.Y. Lee, J. Agric. Food Chem. 51 (2003) 6509-6515.

[2] K.D. Croft, Ann. NY Acad. Sci. 854 (1998) 435–442.

[3] B.N. Ames, M.K. Shigenaga, T.M. Hagen, Proc. Natl. Acad. Sci. U.S.A. 90 (1993) 7915–7922.

[4] F. Visioli, C. Galli, J. Agric. Food Chem. 46 (1998) 4292–4296.

[5] S. Bastinaetto, R. Quirion, Neurobiol. Aging 23 (2002) 891–897.

[6] M.G.L. Hetog, P.C.H. Hollman, D.P. Venema, J. Agric. Food Chem. 40(1992) 1591–1598.

[7] Kumar, S.S.; Priyadarsini, K.I.; Sainis, K.B. (2002), Free radical scavenging activity of vanillin and O-vanillin using 1,1-diphenyl-2-picrylhydrazyl (DPPH) radical. *Redox Report*., **7**, 35-40.

Singlet–triplet energy separations in divalent four-membered cyclic $C_2B_2X_2$ and CB_2SiX_2 (X = H, F, Cl, Br and I)

Sattar Arshadi*[a], Fatemeh Alipour[b], Mina Reyhani[b]

[a]*payame noor university, Behshahr unit*

Corresponding Author E-mail: chemistry_arshadi@yahoo.com

[b]*payame noor university, Sari unit*

Key word: Singlet, Triplet, Organoboron, silylenes, $\Delta G_{(T-S)}$

The 1,3-dibora-cyclobot-2-ylidene [1] is one of the most intriguing organo-boron compounds, and its unique bonding situation has stimulated much activity[2], and theoretical chemistry[3]. Singlet and triplet states of 1,3-dibora-cyclobot-2-ylidenes appear planar. In contrast, triplet states of sila-1,3-dibora-cyclobot-2-ylidenes appear planar while their corresponding singlet states are non-planar[4].

Singlet–triplet energy separations ($\Delta G_{(T-S)}$) for 1,3-dibora-cyclobot-2-ylidene are calculated and compared with their sila, analogues; at UB3LYP/ 6-311++G(3df,2p) levels of theory. Our calculation show 1,3-dibora-cyclobot-2-ylidene species have higher $\Delta G_{(T-S)}$ than their corresponding sila analogues.

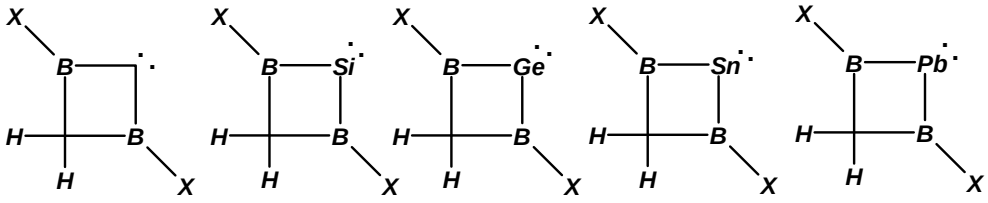

S-X-C And T-X-C	S-X-Si And T-X-Si	S-X-Ge And T-X-Ge	S-X-Sn And T-X-Sn	S-X-Pb And T-X-Pb

Fig. 1 Homologues divalent species of group 14 in the periodic table:
Series of halogenated cyclic carbenes, silylenes, germylenes, stanylenes and plumbylen

Table 5. Energy difference between X-singlet and the corresponding X-triplet: $\Delta E\ B_{(Triplet-\ Singlet)B}$, $\Delta H\ B_{(Triplet-\ Singlet)B}$ and $\Delta G\ B_{(Triplet-\ Singlet)B}$, for studied compounds.

	$\Delta E_{(T-S)}$	$\Delta H_{(T-S)}$	$\Delta G_{(T-S)}$
H-C	45.35	45.35	44.58
F-C	27.94	27.94	27.05
Cl-C	32.67	32.67	31.49
Br-C	33.18	33.18	31.60
I-C	34.36	34.36	33.26
H-Si	12.79	12.79	11.65
F-Si	2.57	2.57	1.69
Cl-Si	4.33	4.33	3.31
Br-Si	5.61	5.61	4.97
I-Si	4.44	4.44	2.88

References:

[1]Klusik H., Berndt A. angew.chem. 1983; 95:895; Angew. Chem., Int. Ed. Engl. 22 (1983)877.

[2]Berndt A. angew.chem. 1993; 105:1034; Angew. Chem., Int. Ed. Engl. 32 (1993)985.

[3]McKee ML. In*org. Chem*. 38 (**1999**)321.

[4]Kassaee M.Z. , Arshadi S., Acedy M., Vessally E. J. of Organometallic Chemistry 690 (2005) 3427.

Kinetics and thermodynamics of copper ions removal from aqueous solutions by use of Cu(II)-imprinted silica gel sorbent

H.Faghihian[a*] and K.Asghari[a]

[a]Dpartment of Chemistry,Islamic Azad University, Shahreza Branch

Email: Faghihian@iaush.ac.ir

Keywords: Cu(II)-imprinted sorbent, Kinetics, Thermodynamics, Silica gel

Introduction

Nowadayes solid-phase extraction is being widely used for separation of cations[1,2]. Ion-imprinted sorbents have outstanding advantages such as predetermined selectivity and can be useful to solid-phase extraction of transition metal ions in complex matrix [3].But the kinetics and thermodynamic parameters and mechanism of adsorption process has not been studied. In this research the kinetic and thermodynamic parameters for Cu^{2+} removal by Cu(II)-imprinted silica gel was investigated.

Experimental

N,N'-bis(4-hydroxy salicylidene)ethylene-1,2-diamine, $H_2[((OH)_2$-salen)]ligang was synthesized and characterized by FT-IR and UV-vis spectroscopy. This ligand then employed to synthesis of Cu(II)-$H_2[((OH)_2$-salen)] complex. The product was also characterized by FT-IR and UV-vis spectroscopy, and then was covalently anchored on silica gel surface. This anchorage was confirmed by thermal gravimetric analysis. The Cu content of the solid product was removed and leaved the Cu-imprinted silica gel sorbent. This sorbent was applied as a new sorbent for solid-phase extraction of Cu^{2+}under different experimental conditions which were optimized.

Result and discussion

1-Adsorption isotherms

Tow isotherms were tested for their ability to describe the experimental results, namely theLangmuire isotherm and the Freundlichisotherm.As can be seen in Table 1, Langmuire isotherm has good regression coefficient that shows the adsorption obeys this model[4]. According to this observation the results were interpreted.

Isotherms	parameters	R^2
Langmuire	q_o=27.78 (mg/g) b =0.0202 (L/mg)	0.992
Freundlich	K_f = 3.264 n = 3.195	0.883

Table1: Compersion of Langmuire and Freundlich parameters

2-Thermodynamic parameters

The effect of temperature on the removal of Cu^{2+} was also studied. It was found that the adsorption capacity increases as temperature increasing. To calculate values of the thermodynamic parameters describing the Cu^{2+} adsorption by Cu(II)-imprinted sorbent the Van ' t Hoff equation (also known as the Vukancic-Vukovic equation) was used.The values of ΔH^o and ΔS^o are 47.60 and 40.34 J/mol that shows that the adsorption process is endothermic ($\Delta H^o>0$). $\Delta S^o>0$ indicates that the entropy of Cu^{2+} ions adsorbing on ion-imprinted sorbent is higher than the hydrated lattice in solution phase.The calculated Gibbs free energy was calculated at 298°, 318° and 328° k were respectively-11.97, -12.78 and-13.18which indicates that the adsorption process is spontaneous.

3-Adsorption kinetics

The modeling of the kinetics of adsorption of Cu^{2+} on Cu(II)-imprinted sorbent was investigated by two common models, namely the Lagergren pseudo-first-order model and pseudo-second-order model.None of these models could not describe the adsorption kinetics withgood agreements with experimental results. The results were interpreted.

4-Adsorption mechanism

In order to gain insight into the mechanisms and rate controlling steps affecting the kinetics of adsorption, the kinetic experimental results were fitted to the Weber ' s intraparticle diffusion. This model is expressed as: $q_t = k_{id}\, t^{1/2} + C$ .The intercept of the linear plot of $q_t$aganst $t^{1/2}$ reflects the boundary layer effect.It found that the intraparticle diffusion was not only rate-controlling step.

Conclusion

Kinetics and thermodynamic parameters calculated in this study show that adsorption of Cu^{2+} on the Cu(II)-imprinted silica gel sorbent is mono layer adsorption with $\Delta H^o>0, \Delta S^o>0$ and $\Delta G^o<0$.

Refrences

[1] Zhang, N.; Suleiman, J.S.; He, M. and Hu, B.;*Talanta*, **2008**, *75*, 536-543.

[2] Jiang, N.; Chang, X.; Zheng, H.; He, Q. and Hu, Z.; *Anal. Chim.Acta*, **2006**, *577*, 225-231.

[3]Wang, Z.; Wu, G.and He, C.; *MicrochimActa*, **2009**, *165*, 151-157.

[4]Hameed, B. H.; Salman, J. M.; and Ahmad, A. L.; *J.Hazard. Mater.,***2009**, *163*, 121-126.

Kinetic Investigation of Decontaminating DMMP By ZnO-CaO Nanocomposite

A.Aminifar [a*], F.Khosravi [b]&M.Soltaninezhand[a]

Department of chemistry, Faculty of sciences, Imam hossein university, Tehran, Iran [a]

Department of civil engineering, Faculty of engineering, Imam hossein university, Tehran,Iran [b]

Email: aaminifar@hotmail.com

Key word: Kinetic of decontaminating, DMMP**,** Nano composite ZnO-CaO.

Introduction

Unfortunately, some of countries are not obey any international decisions, still Chemical Warfare Agents (CWAs), agricultural toxics and etc. are damaged environmental and human being life [1, 2]. Limited use of CWAs and uncontrolled agricultural toxics can produce massive injury and death in those who are unaware and unprepared [3] this is the main reason of our research ,the other word we can also consider ZnO nanoparticles have relieved great attention because of the unique catalytic, gas sensing, optical proprieties and cape energy equal to 3.4 ev.

Their non-toxcity, good electrical, optical and piezoelectric behavior make a unique application in solar cells ultraviolet lasers, transparent conductive oxides and etc. Our previous research has made nanocomposite of ZnO-CdO and have done a comprehensive kinetic studies over it , due to cape energy of CaO(6.9 ev) and economical view of it , we decided to synthesisZnO-CaO nano composite and determine rate of reaction at different temperatures and effect of solvent have also been studied.By reviewing literature we consider any one has not been done investigated kinetic verification of ZnO-CaO nano composite so far. It may consider our information may useful infield of decontamination Warfare agents ,solar structure, laser science and so on.

Experimental

All of used chemicals in our experiments were of AR grade. Zinc nitrate hexahydrates ($Zn(NO_3)_2.6H_2O$), calcium nitrate tetrahydrates ($Cd(NO_3)_2.4H_2O$) and polyvinyl alcohol (PVA) purchased from Loba Chimie (India). Sodium hydroxide (NaOH solvent purchased from Merck. Dimethyl methylphosphonate (DMMP) of more than 98% purity was purchased from Aldrich. PNMR spectroscopy was 250 MHz perkins.

Results and discussion

ZnO-CaO nano composite was synthesized by sol-gel pyrrolysis method based on the polyvinyl alcohol (PVA) polymeric network. The prepared nanocomposite was carefully characterized using scanning electron microscopy, X-ray dispersive energy analysis and x-ray diffraction. This average diameter was calculated by using Scherrer formula [4]:

$$d = \frac{0.94\,\lambda}{\beta\cos\theta}$$

Where d, λ, θ and β are the mean average diameter, the X-ray wavelength (λ = 1.5406 Å), Bragg diffraction angle, and full width at half maximum (FWHM). The average diameter of prepared ZnO-CaO nanocomposite was found to be about 45nm , then kinetic studies of the composite has been investigate intemperature15,25,35&45^{o}C it has observe the rate of the reaction has been obey first order (viz:figures1&2). The effect of solvents have also been investigated. It can concluded (Table 1) the slowest reaction has been run in methanol solvent .

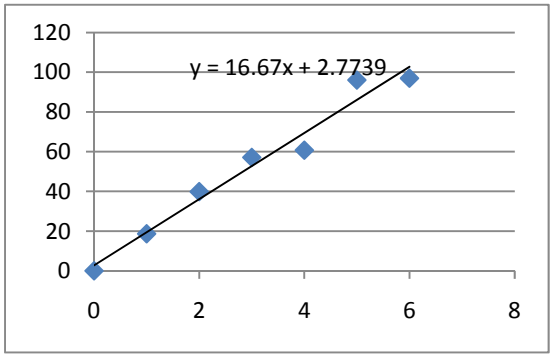

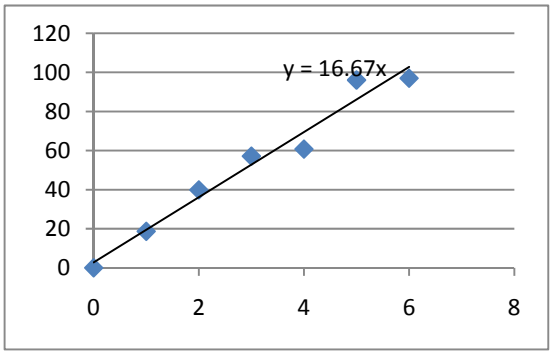

Figure-1:lna/(a-x);y-axis VS time x-axis in temperature 45^{0}C

Figure-2:lna/(a-x);y-axis VS time x-axis ; in temperature 15^{0}C

Solvent Pentanol		Ethanol solvent		Methanol solvent		Time (h)
Percentage of decreasing concentration of DMMP	Molar concentration of DMMP in time (M)	Percentage of decreasing concentration of DMMP	Molar concentration of DMMP in time (M)	Percentage of decreasing concentration of DMMP	Molar concentration of DMMP in time (M)	
0	0.03	0	0.03	0	0.03	0
34.51	0.0196	14.10	0.0257	9.34	0.0273	2
52.16	0.0143	28.43	0.0215	18.22	0.0245	3
62.08	0.0114	37.65	0.0187	23.32	0.0230	4
77.04	0.0069	45.17	0.0164	26.57	0.0211	5

Table-1: Compare the deceasing concentration of DMMP with Nano Zno-CaO composite in different solvents.

Conclusion

Order of the reaction between DMMP and nano composite ZnO-CaO with respective to DMMP is equal to one. Along methanol, ethanol and pentanol solvents , the suitable solvent for the adsorption of DMMP on nanocomposite is pentanol.

References:

[1] B. Singh, A. Saxena, A. K. Nigam, K. Ganesan, P. Pandey;" Impregnated silica nanoparticles for the reactive removal of sulphur mustard from solutions"; J. Hazar. Mater. ;161 (2009) 933–940.

[2] D. Waysbort, D. J. M. Garvey, W. R. Creasy, K. M. Morrissey, D. M. Hendrickson, H. D. Durst, ; "A decontamination system for chemical weapons agents using a liquid solution on a solid sorbent "; J. Hazard. Mater. ;161 (2009) 1114–1121.

[3] V. A. Utgoff;" The chalange of chemical weapons: An American perspective"; Macmillan, London;(1990) pp. 154 ibid 132-134.

[4] H. Karami, A. Aminifar, H. Tavallai, Z.A. Namdar, "PVA-based sol-gel synthesis and chaeacterization of CdO-ZnO nanocomposite" ;J. Clust. Sci.; 21 (2010) 1-9.

[5] A. Moballegh, H.R. Shahverdi, R. Aghababazadeh, A.R. Mirhabibi; " ZnO nanoparticles obtained by mechanochemical technique and the optical properties ";Surf. Sci.; 601 (2007) 2850–2854.

Kinetic study of substituent effect on the 1,3-dipolar cycloaddition of nitrones with acetylene: a Hammett study via DFT

Mahsa. Ilka, Saeed Reza Emamian*, Jafar. Aboli, Mahdiyeh.Ilka
Chemistry Department, Islamic Azad University, Shahrood Branch, Shahrood, Iran.
Corresponding Author E-mail: saeedreza_em@yahoo.com

Keyword: Hammett Equation; DFT; Substituent Effect; Nitrones

1,3-Dipolar cycloadditions offer suitable one-step routes for the production of a variety of five-membered heterocycles [1]. High stereospecificity/stereoselectivity associated with these reactions makes them synthetically significant [2]. Since the hetero-atoms such as nitrogen and oxygen are pharmacologically important, 1,3-dipolar cycloaddition reactions of nitrones with alkynes are one of the most valuable reactions in organic synthesis [3]. In this research, we extended our studies to discover the effect of substituent on the 1,3- dipolar cycloaddition reactions of substituted nitrones with acetylene (Fig. 1) by applying the Hammett equation (Eq. 1) [4]:

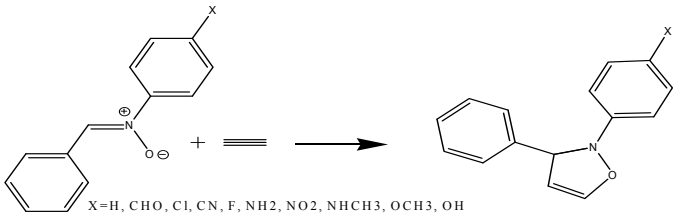

Fig. 1. The 1,3- dipolar cycloaddition reaction of nitrones with acethylene

$$\log \frac{k_x}{k_H} = \rho\sigma \qquad \text{(Eq. 1)}$$

where k_x is the rate constant for a substituent in para or meta position with respect to the side chain of a benzene derivative and k_H is the corresponding quantity for the unsubstituted compound; σ is the Hammett substituent constant which depends on the nature of substituent and ρ is a constant for a given reaction under a given set of conditions. The Hammett equation is an important example of linear free energy relationships (LFERs) which is widely used in studies of the chemical reactivity of substituted benzenes [5].

The structures corresponding to the reactants, TSs and products were optimized using the Gaussian 03 computational package [6] and with DFT method. The optimized geometries of the stationary points on the potential energy surfaces (PES) were performed using the Becke's three-parameter hybrid exchange functional with the correlation functional of Lee, Yang and Parr (B3LYP) with the 6-31+G* basis set.

The theoretical activation parameters and n_T (position of the transition structure along the reaction coordinate) were calculated at 298.15K (Table 1).

The Hammett ρ value of 1.0371 is obtained in the reaction of nitrones with acetylene and the correlation coefficient between $\log(k_x/k_H)$ and σ_p is 0.9771 (Fig. 2). This Hammett ρ value indicates that the electron withdrawing groups moderately increase the rate of reaction.

Table 1. Activation parameters and positions of the transition structures for the studied reactions

X	$\Delta G^{\circ\neq}$ (Kcal mol^{-1})	$\Delta H^{\circ\neq}$ (Kcal mol^{-1})	$\Delta S^{\circ\neq}$ (cal mol^{-1} K^{-1})	E_a (Kcal mol^{-1})	$k\times10^{-8}$ (mol/L)$^{-1}$S^{-1}	$\log k_x / k_H$	n_T
H	30.048	18.958	-37.199	20.143	1.421	0	0.355
Cl	29.807	18.698	-37.262	19.181	2.135	0.176	0.351
CN	29.037	17.907	-37.332	19.092	7.839	0.741	0.339
F	30.011	18.899	-37.274	20.084	1.513	0.027	0.354
CHO	29.144	17.996	-37.571	19.181	6.547	0.663	0.341
NH2	30.818	19.787	-36.996	20.972	0.387	-0.564	0.366
$NHCH_3$	31.051	19.890	-37.437	21.075	0.261	-0.735	0.370
NO2	28.764	17.602	-37.440	18.787	12.420	0.941	0.335
OCH3	30.454	19.414	-37.031	20.599	0.716	-0.297	0.361
OH	30.399	19.348	-37.071	20.532	0.786	-0.257	0.360

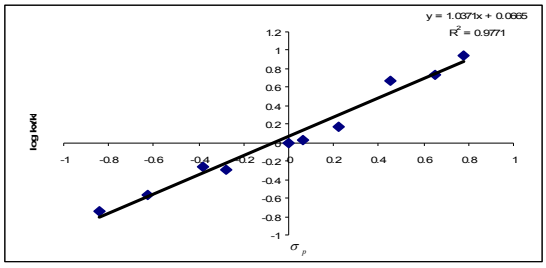

Fig. 2. Regression plot between $\log(k_X / k_H)$ and Hammett substituent constant at the para position (σ_P) for the studied reactions

Our results show that:

1. The reaction rate is increased by the electron-withdrawing groups (CN, NO_2, CHO) and is decreased by the electron-releasing groups (NH_2, OH, $NHCH_3$).

2. The NO_2-substituted product is the most stable kinetic product.

3. The values of n_T for various substituents are less than 0.5 which means the structures of transition states have less resemblance to the products.

References

[1] I. Namboothiri, N. Rastogi, B. Ganguly, S. Mobin, M. Cojocaru, *Tetrahedron*, 60 (2004) 1453.

[2] V. Sridharan, S. Muthusubramanian, S. Sivasubramanian, K. Polborn. *Tetrahedron*, 60 (2004) 8881.

[3] K. Phomkeona, T. Takemoto, Y. Ishima, K. Shibatomi, S. Iwasa, H. Nishiyama, *Tetrahedron*, 64 (2008) 1813.

[4] C. Ogretir, E. Acikkalp, T. Guray, *J. Mol. Struct*. (THEOCHEM), 538 (2001) 107.

[5] M. Segala, Y. Takahata, D.P. Chong, *J. Mol. Struct*. (THEOCHEM), 758 (2006) 61.

[6] M.J. Frisch et al.., Gaussian 03, Revision B.03, Gaussian Inc, Pittsburgh PA, 2003.

Molecular geometries of the anti-cancer drugs such as adriamycin and daunomycin based on theoretical study

S.Bagheri[a*],Z.Bayat[a],E.Taghizadeh[b]

[a] Department of Chemistry Islamic Azad University -Quchan Branch, Iran
[b]Department of Chemistry,yonug researchers club, Islamic Azad University -Quchan Branch, Iran
s_bagheri1316@yahoo.com

Abstract

Daunomycin (or daunorubicin) and adriamycin (or doxorubicin or 14-hydroxydaunomycin) are well known anti-cancer agents. They are commonly used in the treatment of a wide range of cancers, including hematological malignancies, many types of carcinoma, and soft tissue sarcomas. Molecular geometries of the anti-cancer drug molecules adriamycin and daunomycin were optimized using the B3LYP and HF levels at 6-31G* basis set ,then this results were compared with experimental values.

Keywords: Anti-cancer drugs; Molecular geometry; Ab initio calculation;

Introduction:

Adriamycin and Daunomycin are drugs used in cancer chemotherapy. They are anthracycline antibiotics and they are commonlyused in the treatment of a wide range of cancers. Biochemical evidencesuggests that these drugs make omplexes with DNAand thus block the processes of replication andtranscription [1–2]. Adriamycin has a wide spectrumof anti-cancer activity and has been used to treat acutelymphoblastic and myeloblastic leukaemias, malignant ymphomas of both Hodgkins and non-Hodgkins types, carcinoma of different parts of thehuman body, e.g. breast, lung, bladder, thyroid andovary, etc. [3–4]. Daunomycin is particularly usefulto treat leukemia in human beings. The structures ofadriamycin and daunomycin are only slightly different,but their activities are appreciably different (Fig. 1).

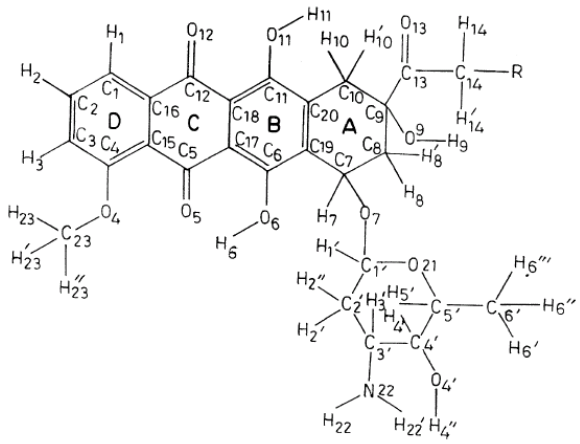

Fig. 1. Structures of adriamycin (R = OH) and daunomycin (R = H).

Method:

Molecular geometries of adriamycin and daunomycin (Fig. 1) were optimized using the restricted Hartree–Fock (RHF) procedure employing the 6-31G and 6-31G* basis sets. It was not possible to employ a more sophisticated basis set due to large sizes of the molecules.

Results and discussion

Molecular geometries of adriamycin and daunomycin(Fig. 1) were optimized using the Hartree–Fock (RHF) and B3LYP procedure employing the 6-31Gand 6-31G* basis sets. It was not possible to employ a more sophisticated basis set due to large sizes of the molecules. The molecular structures of adriamycin anddaunomycin are shown in Fig. 1. The geometries of these molecules optimized using the 6-31G and 6-31G* basis sets at the RHF level are presented in Table 1. Experimental X-ray crystallographic values of bond lengths, bond angles and dihedral angles of daunomycin [5] are included in Table 1 for the sake comparison with the calculated results.**Table 1:**Optimized bond lengths and bond angles of adriamycin and daunomycin using the 6-31G and 6-31G* basis sets.Values given in parentheses were obtained using the 6-31G* basis set

Geometrical parameters(Bond lengths and Bond angles)	Adriamycin(HF)	Adriamycin(B3LYP)	Daunomycin(HF)	Daunomycin(B3LYP)	Exptb
C2C3	1.381(1.381)	(1.383)	1.381 (1.381)	(1.392)	1.32
C2C1	1.383(1.380)	(1.382)	1.383 (1.380)	(1.389)	1.39
C1C16	1.385(1.385)	(1.385)	1.385 (1.385)	(1.395)	1.40
C15C16	1.403(1.399)	(1.396)	1.402 (1.399)	(1.411)	1.36
C4C15	1.406(1.411)	(1.404)	1.407 (1.411)	(1.426)	1.43
C4C3	1.393(1.392)	(1.390)	1.393 (1.392)	(1.403)	1.41
C3H3	1.069(1.071)	(1.069)	1.069 (1.071)	(1.082)	0.98
C2H2	1.072(1.075)	(1.072)	1.072 (1.075)	(1.086)	1.01
C4O4	1.354(1.332)	(1.345)	1.354 (1.332)	(1.349)	1.34
O4C23	1.432(1.401)	(1.432)	1.432 (1.401)	(1.421)	1.46
C23H23	1.082(1.084)	(1.081)	1.082 (1.084)	(1.097)	1.16
C5C15	1.482(1.493)	(1.476)	1.482 (1.493)	(1.477)	1.50
C5C17	1.477(1.483)	(1.485)	1.476 (1.482)	(1.480)	1.46
C17C18	1.420(1.425)	(1.408)	1.420 (1.426)	(1.423)	1.37
C18C12	1.460(1.469)	(1.485)	1.459 (1.468)	(1.484)	1.46
C12C16	1.484(1.496)	(1.491)	1.484 (1.496)	(1.502)	1.50
C12O12	1.236(1.209)	(1.217)	1.237 (1.209)	(1.225)	1.25
C5O5	1.235(1.208)	(1.230)	1.235 (1.208)	(1.246)	1.24
C6C17	1.381(1.379)	(1.392)	1.381 (1.379)	(1.414)	1.41
C19C20	1.369(1.365)	(1.383)	1.369 (1.365)	(1.392)	1.36
C9O9	1.438(1.412)	(1.427)	1.428 (1.403)	(1.339)	1.44
O9H9	0.958(0.951)	(0.954)	0.956 (0.950)	(0.979)	1.09
C10H10	1.081(1.082)	(1.085)	1.081 (1.082)	(1.099)	1.01
C13O13	1.218(1.192)	(1.214)	1.221 (1.194)	(1.221)	1.20
C14H14	1.084(1.088)	(1.084)	1.082 (1.084)	(1.095)	0.99
C13C14	1.511(1.525)	(1.506)	1.497 (1.510)	(1.510)	1.50
N22H22	0.995(1.002)	(0.994)	0.995 (1.002)	(1.017)	1.00
Bond angles					
C3C2C1	120.2(120.7)	(120.541)	120.2 (120.7)	(120.591)	124.4
C2C1C16	119.4(119.1)	(119.285)	119.4 (119.1)	(119.635)	115.8
C1C16C15	121.7(121.8)	(121.352)	121.7 (121.8)	(121.275)	123.1
C16C15C4	117.9 (118.3)	(118.574)	117.9 (118.3)	(118.374)	118.2
C15C4C3	120.0 (119.3)	(119.801)	120.0 (119.3)	(119.498)	119.2
C4C3C2	120.7 (120.8)	(120.411)	120.7 (120.8)	(120.624)	119.3
C15C5C17	119.0 (118.6)	(118.043)	119.0 (118.6)	(119.153)	116.6
C5C17C18	121.1 (121.2)	(120.805)	121.1 (121.2)	(121.836)	123.2
C17C18C12	119.6 (119.8)	(118.232)	119.6 (119.8)	(119.530)	119.9
C18C12C16	119.4 (118.8)	(117.421)	119.3 (118.8)	(117.890)	118.0
C17C6C19	120.9 (120.4)	(120.829)	121.0 (120.4)	(120.488)	120.0
C6C19C20	120.4 (120.5)	(119.087)	120.3 (120.4)	(119.411)	120.6
C19C20C11	119.5 (119.5)	(119.938)	119.1 (119.5)	(120.213)	119.3
C20C11C18	120.9 (120.3)	(121.095)	120.9 (120.3)	(120.727)	119.3
C7C8C9	111.7 (112.2)	(115.844)	111.9 (112.3)	(116.686)	113.7
C8C9C10	111.5 (110.7)	(109.209)	111.0 (110.4)	(108.782)	110.8
C9C10C20	115.5 (115.7)	(114.329)	115.3 (115.6)	(115.408)	111.8
C4O4C23	123.1 (121.0)	(122.950)	123.0 (121.0)	(119.393)	119.5
C6O6H6	112.6 (108.8)	(113.844)	112.6 (108.8)	(105.794)	11.4
C11O11H11	113.8 (109.6)	(115.288)	113.7 (109.6)	(109.249)	120.4
O4C23H23	111.1 (111.5)	(110.959)	111.1 (111.5)	(111.579)	108.4
C9O9H9	110.8 (108.6)	(112.204)	111.5 (109.0)	(105.119)	109.6
C9C13O13	120.0 (120.6)	(117.255)	118.8 (119.4)	(117.060)	117.3
C9C13C14	119.9 (119.1)	(120.808)	119.3 (119.0)	(122.296)	120.0
C13C14O14	113.3 (114.1)	(108.913)			
C19C7O7	111.3 (112.7)	(112.223)	111.5 (112.7)	(112.474)	107.5
C19C7H7	109.8 (109.3)	(108.047)	109.6 (109.2)	(107.215)	111.3

Conclusion:

We arrive at the following conclusions from the present study. There is agreement between experimental studies and theoretical study in this paper.

References

[1] A. diMarco, F. Arcamone, F. Zunino, Antibiotics, Springer,Berlin, 1974.

[2] M.W. Viswamitra, O. Kennard, P.G. Jones, G.M. Sheldrick, S.Salisbury, L. Falvello, Z. Shakked, Nature (London) 273 (1978) 687.

[3] M. Manfait, A.J.P. Alix, P. Jeannesson, J.-C. Jardillier, T.Theophanides, Nucleic Acids Res. 10 (1982) 3803.

[4] A. DiMarco, F. Arcamone, F. Zunino, in: J.W. Corcoran, E.F.Hahn (Eds.), Antiobiotics, Springer, Berlin, 1974, p. 101.

[5] C. Courseille, B. Busetta, S. Geoffre, Acta Cryst. B35 (1979)764.

Hydrohalogenation and hydration of asymmetric olefins: a DFT study

S. Ali-Asgari*[1], , E. Zahedi[1], M. Bakooi[1], S. Shabani[2]

[1]*Department of Chemistry, Islamic Azad University, Shahrood Branch, Shahrood, Iran.*

E-mail: safa1308@yahoo.com

[2]*Department of Chemistry, Payame Noor University, Zanjan Branch, Zanjan, Iran.*

Keywords: Electrophilic Addition; Hydrohalogenation; Hydration; Regioselectivity; DFT

The hydrohalogenation and hydration of the asymmetric olefins (CH_2=CHR) usually occur regio-specifically leading to the predominant formation of CH_3-CHRX [1]. Electrophilic addition to alkenes is one of the most widely studied reactions and characterized by two important properties, reactivity and regioselectivity. Regioselectivity has been proposed to follow the empirical Markovnikov's rule [2,3]. If the two carbon atoms at the double bond are linked to a different number of hydrogen atoms, the electrophilic species is preferentially went to the carbon atom with fewer hydrogen substituents (Markovnikov's rule) [4]. In this research, we extended the last studies on the effects of electron-donating and electron-withdrawing substituent groups in the electrophilic additions of HF, HBr and H_2O to asymmetric olefins by the quantum chemical calculations (Fig.1).

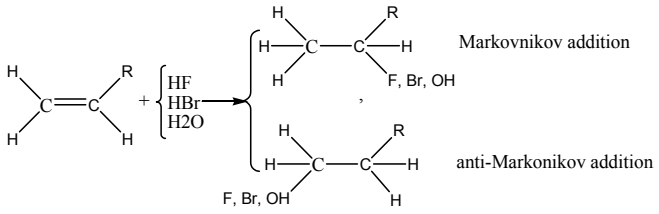

Fig. 1: The electrophilic additions of HF, HBr and H_2O to asymmetric olefins

All calculations were performed at the B3LYP/6-311G** level of theory using GAUSSIAN 03 package of programs. The activation energies and reaction rate constants are shown in Tables 1, 2 and 3.

Table 1: Activation energy and rate constant values for the addition reactions of hydrogen fluoride to asymmetric alkenes

R	Markovnikov addition		Anti-Markovnikov addition	
	k(mol/L)$^{-1}$ S^{-1}	E_a (kcal/mol)	k (mol/L)$^{-1}$ S^{-1}	E_a (kcal/mol)
NO_2	5.980×10^{-28}	74.920	9.114×10^{-24}	41.931
CH_3CH_2	5.011×10^{-10}	47.962	1.387×10^{-15}	56.005
OCN	3.548×10^{-13}	31.276	1.649×10^{-19}	61.157
OH	1.122×10^{-15}	31.154	3.844×10^{-30}	51.317

Table 2: Activation energy and rate constant values for the addition reactions of hydrogen bromide to asymmetric alkenes

R	Markovnikov addition		Anti-Markovnikov addition	
	K(mol/L)$^{-1}$ S^{-1}	E_a (kcal/mol)	k (mol/L)$^{-1}$ S^{-1}	E_a (kcal/mol)
NO_2	9.988×10^{-24}	42.529	2.057×10^{-21}	39.106
CH_3CH_2	3.781×10^{-12}	26.676	3.227×10^{-18}	35.227
OCN	1.921×10^{-16}	32.161	9.314×10^{-25}	43.892
OH	3.978×10^{-6}	18.657	2.247×10^{-23}	42.632

Table 3: Activation energy and rate constant values for the addition reactions of water to asymmetric alkenes

R	Markovnikov addition		Anti-Markovnikov addition	
	k(mol/L)$^{-1}$ S^{-1}	E_a (kcal/mol)	k (mol/L)$^{-1}$ S^{-1}	E_a (kcal/mol)
NO_2	1.161×10^{-33}	55.424	2.912×10^{-26}	44.787
CH_3CH_2	2.056×10^{-29}	49.543	1.631×10^{-33}	55.712
OCN	1.023×10^{-29}	49.754	1.423×10^{-23}	55.367
OH	2.821×10^{-28}	45.563	1.635×10^{-38}	62.465

The activation energies in the two possible channels indicated that the alkenes with electron donating substituent groups (CH_3CH_2, OH and OCN) prefer to give Markovnikov products while the alkene with electron withdrwing substituent group (NO_2) prefers to give anti-Markovnikov product. This can be understood because the electron withdrawing group distorts the π electron cloud toward itself and then leads to anti-Markovnikov addition [5,6].

References

[1] Z. Z. Yang, Y. L. Ding, D. X. Zhao, Chem. Phys., 9 (2008) 2379.

[2] V. Markovnikov, Liebigs Ann. Chem., 153 (1870) 228.

[3] A. Aizman, R. Contreras, M. Galvن, A. Cedillo, J.C. Santos, E. Chamorro, J. Phys. Chem., A 106 (2002) 7844.

[4] D. J. Cram, F. D.Greene, C. H. Depuy, J. Am. Chem. Soc., 78 (1956) 790.

[5] P. Hughe, J. Chem. Educ., 83 (2006)1152.

[6] Y. L. Ding, Z. Z. Yang . J. Mol. Struc.(THEOCHEM), 944 (2010) 105.

A New, Fast and Selective Kinetic Flow Injection Method for Determination of Morphine

Mohsen Keyvanfard*[a] and Nooshin Barzmehri[b]

[a]Islamic Azad University, Majlesi Branch, Faculty of Science, Isfahan, Iran

(E-mail: keyvan45638@yahoo.com)

[b]Islamic Azad University, Shahreza Branch, Departments of Chemistry, Isfahan, Iran

Keywords: Morphine, Flow Injection Analysis, Spectrophotometry, Spadns.

Introduction:

Morphine is a therapeutic drug that is used commonly for the control of pain and also abused as an illicit drug. It is known as a highly addictive and potent narcotic but drug users prefer heroin because of its more intense immediate effect. As heroin is hydrolysed in the organism to morphine the knowledge of the morphine content of biological fluids and tissues is indispensable for forensic and therapeutic purposes [1]. Different methods have been developed for the determination of morphine such as gas chromatography [2], chemiluminescence [3] and Spectrophotometry [4].

Methods:

In this work, a simple, selective and rapid flow injection method has been developed for determination of morphine. The method is based on its inhibition effect on the reaction of spadns and bromate in sulfuric acid medium. The reaction was monitored spectrophotometrically by measuring spadns absorbance at λ_{max} = 508 nm. Fig.1 shows the schematic diagram of the flow system.

Results and discussion:

The reagents and manifold variables, which have influences on the sensitivity, were investigated and the optimum conditions were established. The optimized conditions made it possible to determine morphine in the ranges of 5.0– 70.0 ng mL^{-1} with a detection limit of 3.3 ng mL^{-1} (s/n = 3). To study the selectivity of the proposed method, the effect of various species on the determination of 10.0 ng mL^{-1} of morphine was investigated. The tolerance

limit was defined as the concentration of added species causing a relative error less than 5%. The most of tested species did not interfere even when present in 100-fold excess over morphine. This shows that the proposed method is suitable for the determination of morphine in real samples. The proposed method has been successfully applied for analysis of ultra trace amounts of morphine in urine and morphine ampoules as real samples. The relative standard deviation (R.S.D.%) for 6 replicate measurements of 10, 40 and 55 ng mL^{-1} of morphine were 0.38%, 0.41% and 0.25 %, respectively.

Conclusions:

This method can be used for the determination of nanogram amounts of morphine with a sample rate of 25±5 samples/h. The main advantages of the method are its simplicity and its large dynamic range which make it possible to determine morphine in the real samples with satisfactory results.

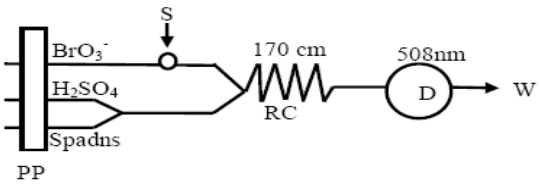

Fig.1 Schematic diagram of the flow system. (flow rate of 0.3 mL/min for each channel, sample loop volume of 200 µL, reaction coil length of 170 cm, absorbance wavelengths: λ_{max} = 508 nm); S, injection valve; RC, reaction coil; temperature, 60 ˚C; D, spectrophotometer; PP, peristaltic pump.

References:

[1] G. A. Milovanovic, M. A. Sekheta, *Mikrochim. Acta III*, (1984) 477–483

[2] U. Hofmann, S. Seefried, E. Schweizer, T. Ebner, G. Mikus, M. Eichelbaum, *J. Chromatogr. B*, 727 (1999) 81–88.

[3] P.S. Francisa, J.L. Adcock, J. Costin, S.D. Purcell, F.M. Pfeffer, N. Barnett, *J. Pharm. Biomed. Anal.*, 48 (2008) 508–518.

[4] M. Sarwar, T. Aman, *Microchem. J.*, 30 (1984) 304–309.

Removal of methylene blue dye by nano conducting polymer, Kinetic and Thermodynamic studies

M. Banimahd keivani* [a], A. Kiani Sarkaleh [b], H. Banimahd Keivani [c]

[*a] Department of Sea & River, Iranian Academic Center for Education Culture & Research (ACECR) Guilan Branch, Rasht, Iran

Email: keivani@acecr.ac.ir

[b] Department of Electrical Eng., Science & Research Branch, Islamic Azad University(IAU), Tehran, Iran

[c] Department of Chemistry, Ghaemshar branch, Islamic Azad University(IAU), Ghaemshahr, Iran

Abstract

In this paper we study kinetic and thermodynamic parameters for removal of methylene blue (MB) dye from aqueous solution by application nanoconducting polymer based on polyaniline (PAn) with coated on wood sawdust. It was found that second-order kinetics model (r^2 = 1) is more better than first-order kinetics model (r^2 = 0.586). The change in Gibb's free energy (ΔG°) , the change in entropy (ΔS°) and the change in enthalpy (ΔH°) were also investigated and calculated for this removal.

Keywords: Nanoconducting polymer, Polyaniline, Methylenblue, Kinetic, Thermodynamic

Introduction

Some of the physicochemical methods that have been employed to remove dye from wastewater include chemical precipitation, coagulation, membrane filtration, electrolysis and oxidation. [1-3]. Polyaniline (PAn) is a poly aromatic amine that can be easily synthesized chemically from bronsted acidic aqueous solutions [4]. Study of removal kinetic is important to evaluate an adsorption dynamics. In order to determining mechanism of adsorption processes such as chemical reaction and removal, the pseudo-first-order adsorption and the pseudo-second-order were used to examine the experimental data [5]. To study the effect of thermodynamic parameters, such as, the change in Gibb's free energy (ΔG°) , the change in entropy (ΔS°) and the change in enthalpy (ΔH°) were also investigated and calculated for adsorbent using following relations [6].

Methods

All chemicals used were analytical reagents grade and prepared in distilled water**.** Polyaniline was obtained from Merck and distilled before use. Absorbance measurements were carried out on a single beam Perkin-Elmer UV–Vis spectrophotometer with a 1 cm cell was used for measuring all of absorption data.

Results and Discussion

For the further investigation of kinetics data, the pseudo-second-order model was used. The linear forms of the both kinetic models are shown below:

$$Ln(q_e - q_t) = Ln\, q_e - k_1\, t \qquad \frac{t}{q_t} = \frac{1}{k_2 q_e^2} + \frac{t}{q_e}$$

Table 1 Adsorption kinetic parameters of MB onto PAn/SD

T(K)	Pseudo-first order				Pseudo-second order			
	q_e[a]	K_1	q_e[b]	r_1^2	q_e[a]	K_2	q_e[b]	r_2^2
298	4.91×10^{-3}	-0.013	4.974	0.586	4.950	-1.074	4.974	1

[a] Calculated [b] Experimental

The change in Gibb's free energy (ΔG°) , the change in entropy (ΔS°) and the change in enthalpy (ΔH°) were also investigated and calculated for adsorbent using following relations.

$$\Delta G^\circ = -RT\, Ln\, K_C \quad , \quad K_c = \frac{C_{Ad}}{C_e} \quad , \quad LnK_c = \frac{\Delta S^0}{R} - \frac{\Delta H^0}{R}(\frac{1}{T})$$

Table 2. Thermodynamic parameters for adsorption of MB onto PAn/SD

ΔG°(KJ mol^{-1})					ΔH° (J mol^{-1})	ΔS° (J mol^{-1})
298 K	308 K	318 K	328 K	338 K		
-4.410	-7.810	-9.444	-12.701	-21.985	112.65	389.17

Conclusion

Different between experimental and calculated q_e shows no applicability of the pseudo-first order model in predicting the kinetics of the MB adsorption onto the PAn/SD. For this removal the pseudo-second order model is better than the pseudo-first order model.

Thermodynamic calculation carried out the sorption of MB by PAn/SD was an endothermic process and this process had negative changes in Gibb's free energy.

References

[1] V. K. Garg, R. Gupta. A. Yadav, *Bioresource Technology,*(2000), 89, 121-124.

[2] N. Kannan, M. Meenakshisundaram, *Water, Air and Soil Pollution.* (2001), 138, 289-305.

[3] K. Kadirvelu, M. Palanival, R. Kalpana, *Bioresource Technology,* (2000), 74, 263-265.

[4] X. R. Zeng, T. Man Ko, *J. Polymer,* (1998), 39, 1187-1195.

[5] M. Zhao, Z. Tang, P. Liu, *J. Hazard. Mat.* (2008),158, 43-51.

[6] V. Vadivelan, K.V. Kumar, *J. Colloid Interface Sci.* (2005), 286, 90–100.

Kinetics and thermodynamic parameters for Pb^{2+} adsorption by polymeric iron and aluminum modifiedbentonie

H.Faghihian* and E.Bahramian

Dpartment of chemistry,Islamic Azad University,Shahrezal Branch

Email:elham_bahramian@yahoo.com

Introduction:

Growing pollution of surface underground water with simultaneously increasing demand for water of high quality parameters requires finding efficient and ecologically safe methods of water and sewage treatment[1,2].modified bentonite as low-cost adsorbents/ion exchangers for the removal of trace level heavy metal from potable water is being widely used[3]. But the kinetics and thermodynamic parameters and mechanism of adsorption process has not been studied. In this research the kinetic and thermodynamic parameters for Pb^{2+}removal by polymeric iron and aluminum modified bentonite wasinvestigated.

Experimental:

The polymeric Al/Fe modifiers were prepared following an established procedure[4]. Modification involved mixing of given amount of bentonite with the polymeric metal species for 4 h at 55^0C.The solid phase was applied as a new sorbent for Pb^{2+}adsorption under different experimental conditions.

Result and discution:

1-Adsorption isotherms:

Tow isotherms were tested for their ability to describe the experimental result , namely the Langmuire and the Freundlich isotherms. As can be seen in table1,theLangmuire isotherm has good regression coefficient that shows the adsorptin obeys the model [5].

"Isotherms	parameters	R2	sample
Langmuire	Q_0=149.253mg/g b=.0154L/mg	.9726	Sodium-bentonite
Freundlich	$K_{f=9.881}$ n=2.3490	.5707	
Langmuire	Q_0=60.60mg/g b=.0324L/mg	.9973	Polymeric Aluminum modified bentonite
Freundlich	$K_{f=6.317}$ n=2.729	.7587	
Langmuire	Q_0=21.83 mg/g b=.0142L/mg	.9991	Polymeric iron modified bentonite
Freundlich	$K_{f=1.9827}$ n=2.9231	.8392	

Table1: Compersion of Langmuire and Freundlich isotherm.

2-Thermodynamic parameters:

The effect of temperature on the adsorption of $Pb^{2+}$by polymeric Al modified bentonite and unmodified bentonite was carried out in the temperature range from 25 to 55^0C.The results showed that the adsorption capacity increased with increasing temperature which indicates that the adsorption process is endothermic in nature. For polymeric –Fe-modified-bentonite,adsorption process is exothermic which indicates that the entropy of Pb^{2+}ions adsorbing by sorbent is higher than the hydrated lattice in solution phase.The calculate Gibbs free energy at 298^0,308^0 and 328^0Kwas negative which indicate that the adsorption process is spontaneous.

3-Adsorption Kinetics:

The modeling of the kinetics of adsorption of $Pb^{2+}$by modified bentonite was investigated by two common models,namely the Lagergren pseudo-first-order model and pseudo-second-order model. Adsorption kinetics $Pb^{2+}$by polymeric-Al-modified bentonite can be described by pseudo-first-order.but for polymeric –Fe-modified bentonite, pseudo-second-order could describe the kinetics.

Refrences:

[1]Mulligan,C.; Yong,R.;Gibbs,B.; Engineering Geology,**2001**, 60, 193-207.

[2]Jiang,J.; Zeng,Z.;Pearce,P.;Water,Air and soil pollution,**2004**,158,53-65.

[3]Bobel,S.;Association,K.;Hazard.Mater,**2003,**97,219-243.

[4]Gray,K.;Yao,C.; Omelia,C.; American Water Association,**2002**,84,136-146.

[5]Hameed,B.; Salaman,J.; and ahmad,A.; J.Hazard.Mater.;**2009**,163, 121-126.

Investigation of Kinetic and Thermodynamic parameters for Adsorption of malachite green dye (MG) by nano electroactive polymer

M. Banimahd keivani* [a], R. Ansari [b], H. Pourmohammad [c]

[*a] Department of Sea & River, Iranian Academic Center for Education Culture & Research (ACECR) Guilan Branch, Rasht, Iran

Email: keivani@acecr.ac.ir

[b] Department of Chemistry, Guilan University, Rasht, Iran.

[c] Department of Chemistry, Ardabil branch, Islamic Azad University(IAU), Ardabil, Iran

Abstract

In this research, a nano composite of polyaniline sawdust (termed as Pan/SD) was prepared via chemical polymerization of aniline on the surface of sawdust for adsorption MG from aqueous solution. The effects of some important parameters such as kinetic and thermodynamic parameters were studied. In this paper obtained the pseudo-second order model kinetic is better than pseudo-first order model and this adsorption was an endothermic and spontaneous process

Keywords: Malachite Green, Nano polyaniline, Kinetic, Thermodynamic,

Introduction

The Textile industry is in the forefront in the use of dyes in its operations with more than 9000 types of dyes incorporated in the color index [1]. The discharge of colored waste is not only damaging the aesthetic nature of receiving streams, but also is toxic to the aquatic life [2]. Polyaniline (PAn) is a nano conducting polymer that can be easily synthesized chemically from bronsted acidic aqueous solutions [3]. Investigation of kinetic and thermodynamic parameters is important variable therefore MG as a typical basic textile dye was selected as a test probe.

Methods

Polymerization was carried out in aqueous solution. Polyaniline was obtained from Merck and Sawdust samples (SD) from walnut obtained from a local carpentry workshop.

Absorbance studies were carried out on a single beam Perkin-Elmer UV–Vis spectrophotometer with a 1 cm cell (λ_{max}= 620 nm) was used for measuring all of absorption data.

Results and Discussion

In order to monitor the kinetics of the adsorption of the MG dye over adsorbent, pseudo-first order and pseudo-second order rate equations were applied. The specific rate constants and other parameters were calculated using following mathematical forms:

$$Ln(q_e - q_t) = Ln\, q_e - k_1\, t \qquad \frac{t}{q_t} = \frac{1}{k_2 q_e^2} + \frac{t}{q_e}$$

Where k_1 and k_2 are the rate constants , q_e and q_t denote the amount adsorbed in mg g^{-1} at equilibrium and any time t, respectively.

Table 1 Adsorption kinetic parameters of MG onto PAn/SD

T(K)	Pseudo-first order				Pseudo-second order			
	q_e [a]	K_1	q_e [b]	r_1^2	q_e [a]	K_2	q_e [b]	r_2^2
298	11.19	-0.046	2.46	0.711	2.48	0.968	2.46	0.999

[a] Calculated [b] Experimental

To study the thermodynamic parameters , (ΔG°) , (ΔS°) and (ΔH°) were investigated and calculated for adsorbent using following relations.

$$\Delta G^\circ = -RT\, Ln\, K_C \quad , \quad K_c = \frac{C_{Ad}}{C_e} \quad , \quad LnK_c = \frac{\Delta S^0}{R} - \frac{\Delta H^0}{R}(\frac{1}{T})$$

Table 2 Thermodynamic parameters for adsorption of MG onto PAn/SD

T (K)	ΔG° (KJ mol^{-1})	ΔH° (KJ mol^{-1})	ΔS° (J mol^{-1})
298	- 9.63		
318	- 11.47	18.049	92.90

Conclusion

The amount of experimental and calculated q_e , shows that pseudo-second order model is useful for predicting the kinetics of the MG adsorption onto the PAn/SD. Therefore the pseudo-second order model is better. The ΔH° >0 as shown in Table 2 indicates endothermic

nature of adsorption. The $\Delta S^{\circ}>0$ shows increased randomness The negative values of ΔG° for the adsorption on PAni/SD due to from feasibility of the process and spontaneous nature of adsorption, whereby no energy input from outside of the system required.

References

[1] N. Kannan , M. Meenakshisundaram, *Water,Air and Soil Pollution,* (2001), 138, 289-305

[2] K. Kadirvelu, M. Palanival, , S. Rajeswari, *Bioresource Technology,* (2000),74, 263- 265

[3] R. Ansari , A. H. Alikhani, *J. Coat. Technol. Res.,* (2009), 6 (2), 221-227

Variational Transition State Theory Calculation of Thermal Rate Constant for Decomposition of Hydrazine to NH_2 Radicals

Afshin Taghva Manesh[*a], Reza Solhnejad[a]

a. *Department of Science. University of Islamic Azad University, Ardebil branch. Ardebil. Iran. (Email: taaf_2005@yahoo.com)*

Key words: Hydrazine , Unimolecular Decomposition, Varitional TST, Variational RRKM.

Introduction:

The chemistry of hydrazine is an interesting field of chemical investigations. The direct nitridation of metal surfaces with hydrazine is as possible passivation process[1,2]. During this process, a nitride film was grown by consuming the native semiconductor through reaction with hydrazine at high temperatures , T> 400K. Recently, the decomposition of bulk hydrazine on catalytic surface Pt[100] and Pt[111] under various conditions have been studied and different channels was observed[3]. The objective of this study is to investigate thermal dissociation channel of hydrazine to NH_2 radicals.

Methods and Discussion:

The energy specific microcanonical rate constant, k(J,E) , for the thermal dissociation of hydrazine were evaluated using RRKM theory. Since N-N dissociation pathway is barrier less reaction and has no classical well defined transition state, we have to obtain its generalized transition state on the potential energy surface using microcanonical variational transition state theory. According to the variational theory, the bottleneck of a reaction occurs at the point along the minimum energy path where the minimum number of states of transition state available, and the microcanonical rate constant is at the minimum. Therefore, the optimized geometries and frequencies of reactant and transition states have been calculated at the ump2/aug-cc-pvdz level of theory along the several points of the minimum energy path. The number of vibrational states and density of states was calculated according to the method of Whitten and Rabinnovitch[4].

Results:

The calculations have been carried out in the range of energy from E_0 to 100000cm^{-1} and J=50. In the Figure 1, we have curved the k(E,J) for three different rotational quantum numbers. The canonical rate constant, k(T), is calculated using numerical integration of microcanonical rate constant, k(E). And also, by means of plotting lnk(T) against 1/T, we have obtained the needed activation energy and the frequency factor for the N-N bond fission of the hydrazine. For state J=0, the obtained value for the activation energy and frequency factor are 327.97 kj/mol and $2.6\times10^{9}s^{-1}$ respectively. However, we have observed that an increase in J raises the activation energy. The increasing activation energy with J is a general phenomenon for bond fissions which have loose transition states[5,6], such as N-N bond fission in the hydrazine.

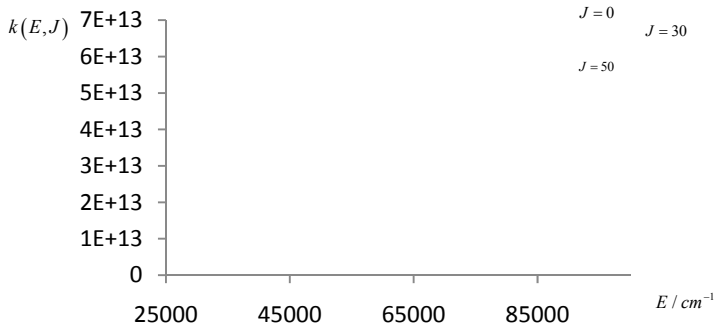

Figure 1. The calculated microcanonical rate constants are curved versus energy for three different rotational quantum numbers.

References:

[1] Luiza M. F. Dantas, Alaécio P. dos Reis, Sônia Maria C. N. Tanaka, José H. Zagal, Yo-Ying Chen and Auro A. Tanaka. *J. Braz. Chem. Soc.*, Vol. 19, No. 4, P. 720, 2008.

[2]Kirkland W Vogt., Paul A. Kohl., Joseph A. Abys. AIChE Journal, Vol. 41, No.10, P. 2282, 1995.

[3]Luzheng Zhang, Adri C. T. van Duin, Sergey V. Zybin and William A. Goddard III, *J. Phys. Chem. B*, *113,* 10770, 2009.

[4]Stephen E. Steint and B. S. Rabinovitch, THE JOURNAL OF CHEMICAL PHYSICS, Vol. 58, No. 6, MARCH 1973.

[5]Harrald V. Linnert and Jose M. Riveros, J. Braz. Chem. Soc., Vol. 2, No. 1, P. 42, 1991.

[6]WANG Yan, QIAN Ying, FENG Wenlin, LIU Ruozhuang, SCIENCE IN CHINA, Vol. 46 No. 3, P. 225, 2003.

Study the Effect of Type of Stirrer on the Mechanisms and the Chemical Kinetics of Vinylacetate Emulsion Polymerization

Navid Tavakkoli Rizi*[a], Abolfath Akbarzadeh[a], Javad Mokhtari[b], Abolfazl Habibi [a]

[a]Faculty of science, Islamic Azad Shahrerey Branch (Yadegar-e-Emam) University, Tehran, Iran,

tavakkoli.navid@yahoo.com

[b] Faculty of Engineering, Gilan University, Rasht, Iran,

Abstarct

Among many polymeric adhesives used in wood processing industry polyvinyl acetate has a rather wide application. It is used to glue tenon joints, doors, windows and other wooden articles. Bond strength is much higher than that of the wood itself. However, polyvinyl acetate is nonresistant to moisture polymer and if such adhesive joints are exploited in moist environment its strength substantially decreases [1].

Emulsion polymerization is a unique chemical process widely used to produce waterborne resins with various colloidal and physiochemical properties. Emulsion polymerization involves the propagation reaction of free radicals with monomer molecules in a very large number of discrete polymer particles (10^{16}–$10^{18} dm^{-3}$) dispersed in the continuous aqueous phase. The nucleation and growth of latex particles control the colloidal and physical properties of latex products. A typical emulsion polymerization formulation comprises monomer, water, surfactant and a water-soluble initiator [2].

Many mechanistic aspects of emulsion polymerization remain unclear despite a large number of studies. This is because there are several mechanistic processes that play a significant role in the formation and growth of latex particles. Classical emulsion polymerization can be divided into two primary stages: particle nucleation and growth. Several particle-nucleation mechanisms have been proposed: (1) nucleation in the monomer-swollen micelles, (2) nucleation in the aqueous phase via the precipitation of the oligomeric radicals generated in water, and (3) nucleation in the monomer droplets [3, 4].

In this research work, emulsion polymerization reaction of vinylacetate initiated by Ammonium Persulfate in the presence of Polyvinylalcohol as a protective colloid and nonylphenol-20 as an emulsifier during two series of reactions was performed.

The first experiment was accomplished by half-moon stirrer and the second experiment by anchor stirrer.

The results showed that the mechanism of the polymerization process was "nucleation in the aqueous phase via the precipitation of the oligomeric radicals generated in water " and by use of different tests such as rate of the conversion of monomer to polymer, total solid and etc, it was concluded that the chemical kinetics of the second experiment was improved and also qualitatively and quantitatively impressive on the type and the time of achievement to the final latex.

Key Words: Emulsion Polymerization, Chemical Kinetics, Mechanisms, Latex

References:

[1] The Structure and Adhesive Properties of Poly (vinyl acetate) Dispersion Modified with Organosilicon Compounds. D.Minelga.28 February 2003.

[2] Emulsion polymerization mechanisms and kinetics C.S.Chern, 15 February 2006, 443-486.

[3] Capek I, Lin S.Y., Hsu T.J., Chern C.S " Effect of Temperature on Styrene Emulsion Polymerization in the presence of Sodium Dodecyl Sulfate.II."J Polym Sci: part A, Vol.38, 2000, PP 1477-1486.

[4] Inferential closed-loop control of particle size distribution of styrene emulsion polymerization, H.Abedini, M.Shahrokhi, 24 January 2008,2378-2390.

Study the Effect of Feeding of the Initiator on the Mechanisms and the Chemical Kinetics of Vinyl acetate Emulsion Polymerization

Navid Tavakkoli Rizi*[a], Abolfath Akbarzadeh[a], Javad Mokhtari[b], Abolfazl Habibi [a]

[a]Faculty of science, Islamic Azad Shahrerey Branch (Yadegar-e-Emam) University, Tehran, Iran,

tavakkoli.navid@yahoo.com

[b] Faculty of Engineering, Gilan University, Rasht, Iran,

Abstarct

Among many polymeric adhesives used in wood processing industry polyvinyl acetate has a rather wide application. It is used to glue tenon joints, doors, windows and other wooden articles. Bond strength is much higher than that of the wood itself. However, polyvinyl acetate is nonresistant to moisture polymer and if such adhesive joints are exploited in moist environment its strength substantially decreases [1].

Emulsion polymerization is a unique chemical process widely used to produce waterborne resins with various colloidal and physiochemical properties. Emulsion polymerization involves the propagation reaction of free radicals with monomer molecules in a very large number of discrete polymer particles (10^{16}–$10^{18} dm^{-3}$) dispersed in the continuous aqueous phase. The nucleation and growth of latex particles control the colloidal and physical properties of latex products. A typical emulsion polymerization formulation comprises monomer, water, surfactant and a water-soluble initiator [2].

Many mechanistic aspects of emulsion polymerization remain unclear despite a large number of studies. This is because there are several mechanistic processes that play a significant role in the formation and growth of latex particles. Classical emulsion polymerization can be divided into two primary stages: particle nucleation and growth. Several particle-nucleation mechanisms have been proposed: (1) nucleation in the monomer-swollen micelles, (2) nucleation in the aqueous phase via the precipitation of the oligomeric radicals generated in water, and (3) nucleation in the monomer droplets [3, 4].

In this research work, emulsion polymerization reaction of vinylacetate initiated by Ammonium Persulfate in the presence of Polyvinylalcohol as a protective colloid and nonylphenol-20 as an emulsifier during two series of reactions was performed.

The first experiment was accomplished by gradual injection of initiator and the second experiment by immediate injection of initiator. By use of different tests such as rate of the conversion of monomer to polymer, total solid and etc, it was concluded that the second experiment was qualitatively and quantitatively impressive on the type and the time of achievement to the final latex.

The results showed that the mechanism of the polymerization process was "nucleation in the aqueous phase via the precipitation of the oligomeric radicals generated in water ".

Key Words: emulsion polymerization, emulsifier, radical initiator, latex

References:

[1] The Structure and Adhesive Properties of Poly (vinyl acetate) Dispersion Modified with Organosilicon Compounds. D.Minelga.28 February 2003.

[2] Emulsion polymerization mechanisms and kinetics C.S.Chern, 15 February 2006, 443-486.

[3] Capek I, Lin S.Y., Hsu T.J., Chern C.S " Effect of Temperature on Styrene Emulsion Polymerization in the presence of Sodium Dodecyl Sulfate.II."J Polym Sci: part A, Vol.38, 2000, PP 1477-1486.

[4] Inferential closed-loop control of particle size distribution of styrene emulsion polymerization, H.Abedini, M.Shahrokhi, 24 January 2008,2378-2390.

Ultrasound initiated emulsion polymerization of methyl methacrylate

F. Tavakkoli*, M.H. Entezari, G.H. Zohuri
(fatemeh.tavakkoli@yahoo.com)
Department of Chemistry, Ferdowsi University of Mashhad, 91775 Mashhad, Iran

Keywords: Methyl methacrylate; Emulsion polymerization; Ultrasonic irradiation; Radicals; addition.

Introduction

The synthesis of polymer latex particles by the classical emulsion polymerization method using chemical initiators has been extensively studied [1-2]. In recent years, application of ultrasound to promote free-radical emulsion polymerizations without of chemical initiators or hydrophobe has emerged as a novel technique to synthesize ultraclean polymer nanoparticles [3-5]. Emulsion polymerization which induced by ultrasonic irradiation has several advantages such as lower reaction temperature, faster polymerization rate, and no chemical initiators [6]. The aim objective of this study was to investigation the kinetics and mechanism of ultrasonically initiated polymerization methyl mathacylate in the presence of high intensity ultrasound.

Methods

MMA was washed with 10% aqueous solution of sodium hydroxide and distilled water to remove the inhibitor (hydroquinone) and then dried with anhydrous sodium sulphate**.** In all experiments, a mixture of monomer (7.5 g) and water (69 g) containing SDS (0.55 g) were placed into the sonochemical reaction vessel and the reaction system was deoxygenated by bubbling with argon for 15 min at room temperature. Then the ultrasound generator was switched on and the emulsion was subjected to ultrasonic irradiation. During the polymerization process, the argon gas stream was allowed to pass over the liquid mixture. The cooling water was circulated to maintain at a temperature of 30 ^{o}C.

Results and discussion

In this study, effect of different variables such as intensity of ultrasound, temperature, and concentration of surfactant on the polymerization were investigated. The results indicated that the conversion of monomer MA increased with increasing of intensity from 9.1 to 25.4 W/cm^2 after 1h of ultrasonic irradiation. It is suggested that in the higher intensity, there are more bubbles and also more violently bubbles collapse. Monomer conversion increased with increasing of temperature. Also, higher rates of polymerization were observed with increasing of surfactant`s concentration due to more stabilized monomer droplets capable of radical scavenging. The results confirmed that the mechanism involved sonochemical formation of the latex particles is similar to that of conventional miniemulsion polymerization. This means that polymerization was carried out in monomer droplets. Kinetic study shows that the polymerization was in agreement with pseudo-first-order model. The diameter of latex particles in the presence of ultrasound was in the range of 40-75 nm and the viscosity average molecular weights were 5.6×10^6 gr/mol.

Conclusion

In present study, ultrasonically initiated emulsion polymerization was done without any added initiator and factors affecting the polymerization have been investigated. The experimental results are consistent with a conventional miniemulsion polymerization mechanism. The kinetics of polymerization was obeyed the pseudo-first-order model. The particle size of PMMA latex was in the range 40- 75 nm because of the multiple influences of dispersion, emulsifying and disrupting effects of ultrasound.

References

[1] D.R. Bassett, A.E. Hamielec, Emulsion polymers and emulsion polymerization, American Chemical Society, Washington, D.C.,1980.

[2] K.Landfester, N. Bechthold , F.Tiorks, M.Antonietti, Macromoleculs 32 (1999) 679.

[3] R.V. Eldik, C.D. Hubbard, Chemistry Under Extreme and Non-Classical Conditions, John Wiley, New York, 1996.

[4] G.J. Price, Ultrasonics.Sonochem. 3 (1996) 229.

[5] S.K.Ooi, S.Biggs, Ultrason.sonochem 7 (2000) 125.

[6] H.Xia,Q.Wang, Y. Liao, X.Xu, S.M. Baxter, R.V. Slone, S.Wu, G.Swift, D.G. Westmoreland, Ultrasonics.Sonochem. 9 (2002) 151.

Kinetic Method for the Determination of Rutin by Its Catalytic Effect on the Reaction between Fast Yellow and Periodate in Acidic and Micellar Medium

Mohsen Keyvanfard[a*] and Zeynab Jalilian[b]

[a]*Faculty of Science, Islamic Azad University, Majlesi Branch, Isfahan, Iran*

(E-mail: keyvan45638@yahoo.com)

[b]*Departments of Chemistry, Islamic Azad University, Shahreza Branch, Isfahan, Iran*

Keywords: Kinetic Spectrophotometric, Rutin, Central Composite Design, Micellar media.

Introduction:

Rutin is found in fruit juices, vegetables, teas, tobaccos, coffees, traditional Chinese medicines and some soft drinks. It not only functions as antioxidation, antimutagenicity and improves the taste of some drinks, but also has been known to have some therapeutic and pharmacological effects, such as anticarcinohesis, prevention and cure of cardiac blood vessel disease, treatment of blood capillary and hypertension disease [1]. Therefore, it is important to develop simple and sensitive methods for the determination of this drug. Different methods have been developed for the determination of rutin such as Spectrophotometry [2, 3], chemiluminescence [4] amperometric biosensor [5] capillary electrophoresis with UV detection [6] voltammetry [7].

Methods:

The method is based on the catalytic effect of rutin on the reaction of fast yellow and periodate in acidic and micellar medium is reported. The reaction was monitored spectrophotometrically by measuring the decrease in absorbance of fast yellow at 427 nm with a fixed-time 0.5-7.0 min from initiation of the reaction. In the method described, the chemical variables were optimized using a chemometric approach. In this way central composite design (CCD) was used for the experimental design and response surface methodology (RSM) was used for the modeling.

Results and discussion:

In this work, a new, sensitive, simple, inexpensive and fast kinetic spectrophotometric method was developed for the determination of trace amounts of rutin over the range of 40-200 ng mL^{-1} and the detection limit is 15 ng mL^{-1}. To study the selectivity of the proposed method, the effect of various species on the determination of 70 ng mL^{-1} of rutin was investigated. The tolerance limit was defined as the concentration of added species causing a relative error less than 3%. The most of species did not interfere even when present in 1000-fold excess over rutin. This shows that the proposed method is suitable for the determination of rutin in real samples. The present method is simple, relatively sensitive, has a wide linear dynamic range and it has been applied to the determination of rutin in green tea and black tea samples. The relative standard deviation of 80, 120 and 160 ng mL^{-1} rutin for 5 replicate measurements was 0.81%, 0.63% and 1.04%, respectively.

Conclusions:

A simple, rapid and selective kinetic spectrophotometric catalytic procedure is developed for the determination of rutin. The main advantages of the method are its simplicity and its large dynamic range which make it possible to determine rutin in the real samples with satisfactory results.

References:

[1] S. WANG, L. DU, X. YAO, X. NIU, H. ZHUANG, *Annali di Chim.*, (2005), 95, 202.

[2] J.W. Costin, N. W. Barnett, S. W. Lewis, D. J. McGillivery, *Anal. Chim. Acta*, (2003), 47, 499.

[3] H.L. Jiang, Y.Z. He, H.Z. Zhao, Y.Y. Hu, *Anal. Chim. Acta*, (2004), 111, 512.

[4] Song Z.; Hou S. *Talanta* (2002), 57, 59.

[5] S. A.S. S. Gomes, J. M.F. Nogueira, M. J.F. Rebelo, *Biosens. Bioelectron.* (2004), 20, 1211.

[6] C.Li, A.Chen, X.Chen, X.Chen and Z.Hu, *J. Pharm. Biomed. Anal.* (2005), 39, 125.

[7] M.-E. Ghica, A. M.O. Brett, *Electroanalysis*, (2005), 17, 313.

Kinetic Studies of Photocatalytic Decomposition of Eriochrome Black T in Aquatic Suspension of Anatase Titanium Dioxide

M. Montazerozohori[1], S. Joohari[2]*, S. Nezami[1]

[1] *Chemistry Department, Yasouj University, Yasouj, 75918-74831, Post Box 353, Iran*

[2] *Basic Sciences Department, Islamic Azad University, Yasouj Branch, Yasouj, Iran*

(E-mail: shjoohari@yahoo.com; mmzohori@yahoo.com)

Keywords: Photocatalyst, Degradation, Irradiation, Eriochrome Black T.

Introduction

Heterogeneous photocatalysis has become an intensively considered technology for the purification, decontamination and deodorization of waste water and indoor air. Photocatalytic oxidation of organic compounds deserves special attention because of their toxicity and biodegradation resistance [1-8]. Eriochrome Black T is harmful if swallowed and may be harmful by inhalation or through skin contact. Also it is Eye irritant. Therefore degradation study and kinetic parameters seems to be a need for environmentally friendly chemists. In this work, photocatalytic degradation and kinetic studies of Eriochrome Black T in aqueous solution was carried out using anatase TiO_2 in a photocatalytic reactor under irradiation with 400W high pressure mercury lamp. Some physico-chemical parameters such as photocatalyst amount, pH and time were investigated. Finally some kinetic parameters of photodegradation were evaluated.

Methods

General procedure for photodegradation experiments

The photodegradation were carried out by irradiation of 20 ml continuous aerated, stirred aqueous solution of Eriochrome Black T in different pH as well as considered amounts of photocatalysts in photoreactor cell under 400W high pressure mercury lamp at constant temperature. After optimum time for degradation, photocatalyst was separated by centrifugation and photolyte was analyzed by UV-VIS spectrophotometric method.

Results and discussion

The effect of various factors

Different factors such as pH of solutions, amount of photocatalyst and irradiation time were evaluated. At first the effect of various parameters on degradation was investigated. The results are summarized in table 1. The results show that all three factor including photocatalyst, air and Ultraviolet irradiation are necessary for effective degradation.

The effect of pH

As shown in figure 1, among the various pHs in the range of 8-12, the optimum amount is related to pH= 12.

Table1- The effect of various factors on photodegradation.

Uv, Photocatalyst, O_2	Uv- Photocatalyst, Ar	UV, O_2	UV, Ar	Amount of photocatalyst(mg)	Time(min.)	pH
29.63	67.22	67.37	75.57	٢٠	١٨٠	pH=7(80 ppm)
24.58	55.00	55.20	63.80	١٠	١٥٠	pH=8(80 ppm)
38.39	62.50	62.78	70.11	٣٠	١٥٠	pH=10(80 ppm)
28.36	70.30	70.45	76.93	٢٠	١٩٥	pH=12(100 ppm)

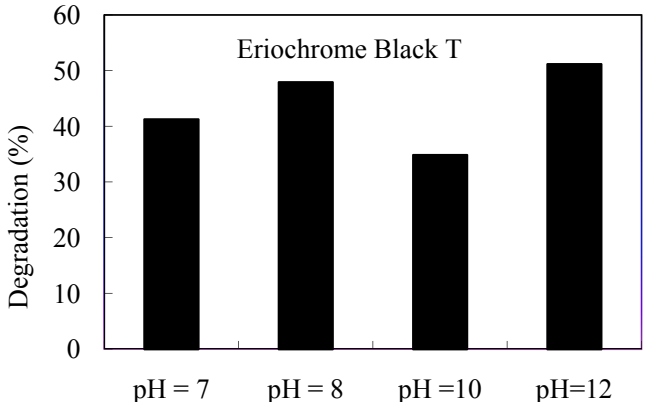

Figure 1- The effect of pH on photodegradation

Kinetic model

The degradation of titled compounds obeys the pseudo-first order kinetics (Eq. 1).

$$(-dc/dt)= kc \quad (Eq.1)$$

Where c is the concentration of Eriochrome black T and k is the experimental first-order rate constant. A plot of $\ln(C_0/C_t)$ versus time reveals a straight line, the slope of which upon linear regression equals the apparent first-order rate constant k (Fig. 2-1 to 2-4). The rate constant, k and K_A and K are summarized in Table 2.

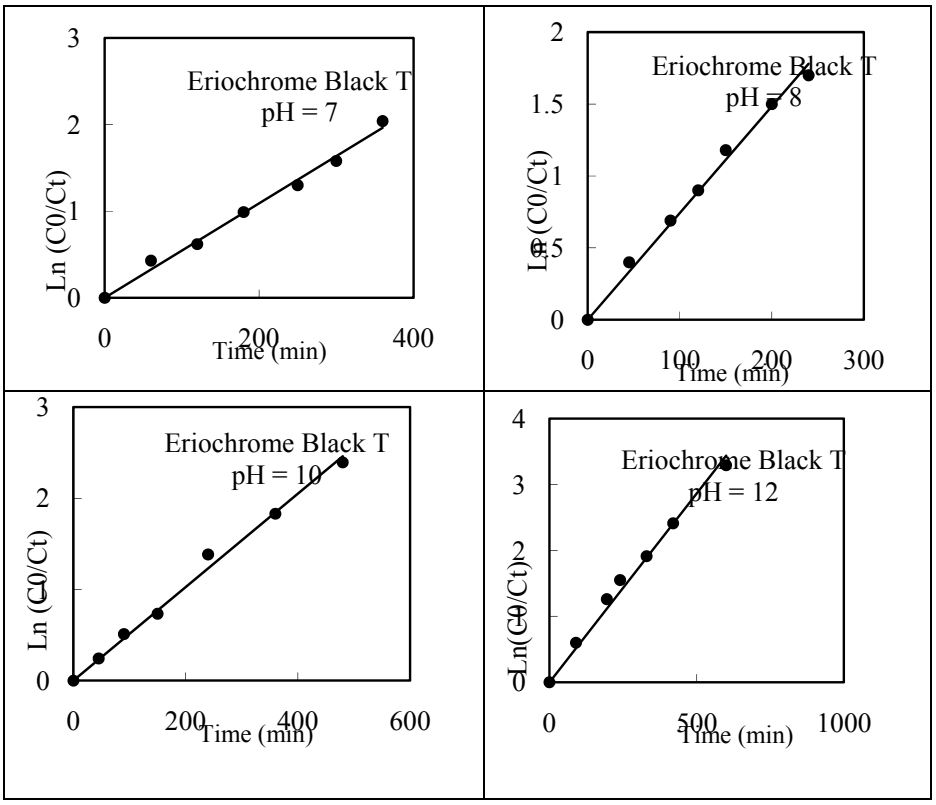

Figure 2- Kinetics of the degradation of Eriochrome black T at optimum amount of photocatalyst(2-1 to 2-4 respectively).

The results of linear plots of $1/R_{L\text{-}H}$ *versus* $1/C_0$ for Eriochrome black T on photocatalysts are also summarized in table 2, which tests the validity of the L-H model.

Table 2- Kinetic parameters of the degradation with initial concentration of Eriochrome black T in optimum conditions.

pH	k_{obs} (min^{-1})	K_A($mg.L^{-1}$)	k_r ($mg\ min^{-1}\ L^{-1}$)
pH=7(80 ppm)	5.5×10^{-3}	2.15×10^{-2}	0.7178
pH=8(80 ppm)	7.4×10^{-3}	8.60×10^{-3}	6.1500
pH=10(80 ppm)	5.1×10^{-3}	7.27×10^{-4}	70.4225
pH=12(100 ppm)	5.7×10^{-3}	4.70×10^{-1}	0.1810

Reference

[1] J. Peral, X. Domenech, D.F. Ollis, *J. Chem. Technol. Biotechnol.* **1997**, 70 117.

[2] R.M. Alberici, W.F. Jardim, *Appl. Catal. B: Environ.* **1997**, 14, 55.

[3] R. G. Zika, and W. J. Cooper, (1987) Photochemistry of environmental aquatic systems. ACS Sym. Ser., Am. Chem. Soc., Washington, **1987**, 327, 106-115.

[4] O. C.Zafiriou, J. Joussot-Dubien, R. G. Zika, *Environ. Sci. Technol.,* **1984**, 18(12), 358.

[5] O. Hutzinger, (Ed.), The Handbook of Environmental Chemistry, Springer-Verlage, Berlin(**1993**).

[6] D. Duline, H.Drossman, T. Mill, *Environ. Sci. Technol.,* **1986**, 20, 72.

[7] M. Montazerozohori, B. Karami, M. H. Habibi, *Ann. Chim.,* **2006**, 5-6, 285.

[8] M. Montazerozohori, M. H. Habibi, S. Joohari, V. Khodadostan, *Ann. Chim.* 2007, 97, 1015.

The Mechanisms and Chemical Kinetics of Styrene Emulsion Polymerization by Taguchi Method

Abolfazl Habibi*[a], Abolfath Akbarzadeh[a], Javad Mokhtari[b], Navid Tavakkoli Rizi [a]

[a] *Faculty of science, Islamic Azad Shahrerey Branch (Yadegar-e-Emam) University, Tehran, Iran,*

abolfazlhabibi63@yahoo.com

[b] *Faculty of Engineering, Gilan University, Rasht, Iran,*

Abstarct

In recent years the popularity of polystyrene has increased tremendously, particularly in view of more frequent use of this material in containers, in the automobile industry, in the toy industry, and in many other areas of commerce [1].

Many mechanistic aspects of emulsion polymerization remain unclear despite a large number of studies. This is because there are several mechanistic processes that play a significant role in the formation and growth of latex particles. Classical emulsion polymerization can be divided into two primary stages: particle nucleation and growth. Several particle-nucleation mechanisms have been proposed: (1) nucleation in the monomer-swollen micelles, (2) nucleation in the aqueous phase via the precipitation of the oligomeric radicals generated in water, and (3) nucleation in the monomer droplets [2].

Emulsion polymerization of styrene initiated by the radical initiator of potassium persulfate in the presence of sodium dodecyl sulfate (SDS) as an emulsifier was performed in which the conversion of styrene to polystyrene was improved and measured [3,4].

In this research work, emulsion polymerization reaction of styrene initiated by the radical initiator potassium persulfate in the presence of sodium dodecyl sulfate (SDS) as an emulsifier was performed in which the rate conversion of styrene to polystyrene was optimized and measured. Also, the effect of different parameters such as temperature, the concentration of the emulsifier, the concentration of the initiator, the proportion of the monomer to water and the effect of agitation on the chemical kinetics of the emulsion polymerization of styrene by Taguchi method (Qualitek 4 software) was investigated [5].

The accuracy of the outcoming results was evaluated by performing an experiment on the optimum conditions.

The results showed that the mechanism of the reaction was "nucleation in the monomer-swollen micelles". Moreover, in 400 rpm the chemical kinetics of the polymerization process was improved and the concentration of the emulsifier and the temperature had the most proportion in the mechanisms and chemical kinetics of this reaction. In the continuation of the research work the outcoming results of FT-IR and the outcoming thermogram of DSC was used to approve the optimum offering experiment.

Key Words: Emulsion Polymerization, Chemical Kinetics, Mechanisms, Taguchi Method

References:

[1] Polymerization of styrene, James M. Watson, Big Spring, Tex, June 22, 1993, 636,718.

[2] Capek I, Lin S.Y., Hsu T.J., Chern C.S " Effect of Temperature on Styrene Emulsion Polymerization in the presence of Sodium Dodecyl Sulfate.II."J Polym Sci: part A, Vol.38, 2000, PP 1477-1486.

[3] Emulsion polymerization mechanisms and kinetics C.S.Chern, 15 February 2006, 443-486.

[4] Inferential closed-loop control of particle size distribution of styrene emulsion polymerization, H.Abedini, M.Shahrokhi, 24 January 2008,2378-2390.

[5] Optimized synthesis of Carrageenan – graft – poly(sodium acrylate) superabsorbent hydrogel using the Taguchi method and investigation of its metal ion absorption, Ali Pourjavadi and Mohammad Sadegh Amini-Fazl. Polymer Research Laboratory, Department of Chemistry, Sharif University of Technology, Azadi Ave,2006. PO Box 11365-9516, Tehran, Iran.

Effect of three different surfactants, Triton X-100, cetyltrimethylammonium bromide (CTAB) and Sodium dodecylesolphate (SDS) on the spectrophotometric determination of sulfide based on phenothiazine dye production

S.F.Riazi[a] , M.Bahram[a],B. Hassanpour[b], S.Azimi[c]

[a]*Faculty of Chemistry urmia university, urmia, Iran*

(fardad.riazi@yahoo.com)

[b]*Faculty of Agricultural Engineering and Technology, University of Tehran, Karaj, Iran*

[c]*Faculty of Chemistry, Tarbiat Moallem University, Tehran, Iran*

Key words: central composite design, S^{2-}, liquid- liquid extraction, surfactants

Introduction

Sulfur is one of the most important components in waste water and can affect on human health [1].Thus, the determination of trace amounts of it is becoming increasingly important because of the increased interest in environmental pollution. In this study, preconcentration of s^{-2} by LLE was optimized using central composite design (CCD) [2]. The important aims of this article are, studying the effects of different surfactants on sulfide determination, figuring out the most important influential factor on desired interaction, selecting optimized conditions and finally illustrating possible interaction between variables.

Method

1.Reagents and apparatus

All analytical reagent grade chemicals and distilled water were used for preparing all aqueous Solutions. Three different surfactants were used; UV–vis absorption spectra were recorded using the spectrophotometer (PG mode T80) with 10mm quartz cell.

2. sulfide determination

In order to illustrate the surfactant effects on analyst signal (sulfide), absorbance spectra of different samples were analyzed. The sulfide content of different samples was determined by

the colorful product (phenothazine) of the reaction between sulfide and para phenyl di amine (PPD).

3. Statistical Software

Essential Regression and Experimental Design for Chemists and Engineers, EREGRESS, a Microsoft Excel and Matlab7a for analyzing the results and chemometrics method were used.

Results and discussion

1.Response Surface and Selection of Optimum Conditions

The obtained regression models were used to calculate the surface for each response variable separately. Figure 1 show the interaction between the interacted factors when the remaining factors have been kept on the fixed amount using the constructed model by EREGRESS software.

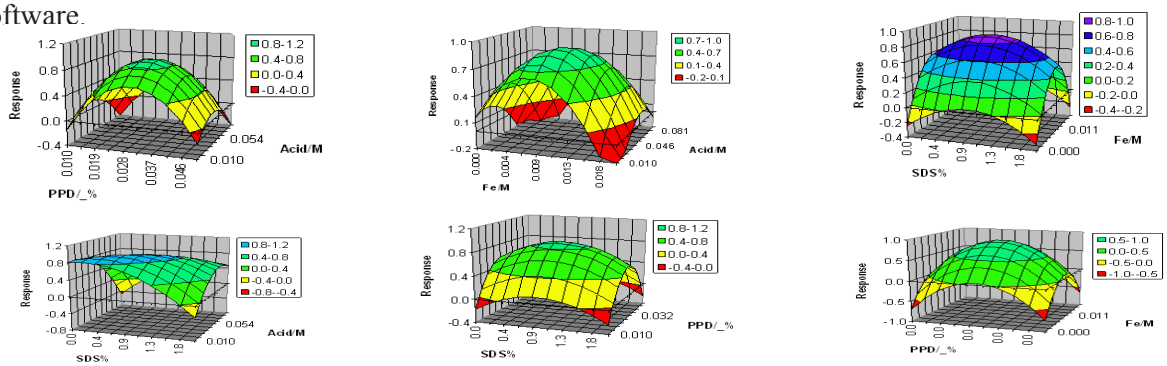

Figure1. Response surface of reaction between different factors

Finally the optimized conditions were obtained by the response surface (table1).

Table1. Optimum conditions obtained by response surface modeling.

parameter	optimum
PPD/ %	0.020-0.037
Fe^{+3}/ M	0.009-0.013
Acid/ M	0.030-0.040
SDS%	0.90-1.00

Table2. Sulfide determination in presence of surfactant

	Calibration linear range	^{2}
CTAB	0.2-2PPM	0.9818
SDS	0.2-2 PPM	0.9888
Tx-100	0.2-2PPM	0.994

Conclusion

Light glossy, high stability and easy applicable and inexpensive surfactants make them to suitable materials for spectrophotometeric analysis.

Our results show that there's a good correlation between application of surfactants and CCD method through traditional methods obtained results.

References

[1] Esmaieli sari, A. (2001) pollutants, Health and standards in Environment. Tarbiat moddaress press.

[2] myung known, C.(2004) Application of central composite design to simulate experiments. Third Asian simulation conference, Korea

Investigation of Kinetic, Mechanism and Solvent Effect of Aniline Addition to Acetylacetone

Hasanzadeh[a].N , Nori-Shargh [b].D, Norouzi[b] .V, Saroogh Farahani[b] .N, Yahyaei[c].H and Mousavi[b].S.N

a) *Chemistry Department, Science Faculty, Ahvaz Branch, Islamic Azad University,Ahvaz, Iran*
Email:nhzadeh_212@ yahoo.com

b) *Chemistry Department, Science Faculty, Arak Branch, Islamic Azad University, Arak, IranChemistry*

c) *Department, Zanjan Branch, Islamic Azad University, P.O.Box: 49195-467, Zanjan, Iran*

Keyword: Reiaction mecanism, Activation parameters, Rate equation, Ethyl propiolate, Aniline

Introduction

There is no published experimental data on the kinetics and mechanism[1,2] of the addition reaction of aniline to acetylacetone (see scheme 1), however, it is known that the reaction between aniline and acetylacetone produce the 2,4-dimethylquinoline. It seemed interesting to investigate the kinetic of the addition reaction of aniline to acetylacetone.

Material and Instrumentation:

Analytical grade aniline, acetylacetone, dichloromethane (DCM), acetonitryl (ACN), dimethylsulfoxide (DMSO) and tetrahydrofuran (THF) (Merck, Germany) compounds were used without additional purification. UV-Vis spectra were recorded on a Shimadzu 160A (Japan) spectrophotometer, and a quartz cell (l=1cm) was used for the spectrophotometric measurements. Initial aniline and acetylacetone concentrated stock solutions were, each time freshly prepared (volumetrically) before the use, in DCM, CAN, DMSO and THF used as solvents. The initial concentration of the stock solutions were calculated based on the declared manufacturer densities. The working solutions were each time prepared by dilution of the stock solution in DCM, CAN, DMSO and THF.

Results and Discussion

The kinetics and mechanism of the addition reaction between aniline and acetylacetone in dichloromethane (DCM), tetrahydrofuran (THF), acetonitryl (CAN) asnd dimethylsulfoxide (DMSO) and as solvents were investigsted by means of UV-Vis spectrophotometry technique. The reaction was monitored at 350, 495, 373 and 377 nm in THF, DMSO, ACN and DCM, respectively. The following Arrhenius equations were obtained:

In DCM: $\ln k = 11.25 - \frac{12.30}{RT}$; In THF: $\ln k = 11.09 - \frac{11.92}{RT}$;

In ACN: $\ln k = 8.42 - \frac{10.68}{RT}$; In DMSO: $\ln k = 7.04 - \frac{9.59}{RT}$

The resulted activation parameters E_a, $\Delta H^{\ddagger}$, $\Delta G^{\ddagger}$ and $\Delta S^{\ddagger}$ at 323 K were:

12.30, 11.71, 22.93 kcal mol^{-1} and –37.42 cal mol^{-1} K^{-1} in DCM;

11.92, 11.28, 23.72 kcal mol^{-1} and –38.51 cal mol^{-1} K^{-1} in THF;

10.68, 10.04, 24.19 kcal mol^{-1} and –43.81 cal mol^{-1} K^{-1} in ACN and

12.30, 11.71, 22.93 kcal mol^{-1} and –37.42 cal mol^{-1} K^{-1} in DMSO.

On the basis of the resulting experimental data, the following 3 steps mechanism could be proposed (see scheme 2). In the first step, aniline attacks the β-C of propiolate ester and a zwitterion is produced following a Cα-CC=O bond rotation producing a convenient conformation for H-caption. In the second and third steps, H-capture and H-transfer processes by aniline and the resulting aniliniom cation could take places, respectively. The above mechanism is confirmed by the following experimental and computational arguments.

Conclusion

The results suggest that the reaction is first order with respect to both aniline and acethylacetone. Baesd on the results obtained, the activation energy of the addition reaction of a aniline to acetylacetone decrease from DCM to DMSO (by increasing the dipole moment values of the solvents used).

References:

[1] Nori-Shargh, D.; Saroogh Farahani, N. Int J Chem Kinet **2004**, 472-479.

[2] Nori-Shargh, D.; Soofi, A.; Saroogh Farahani, N.; Deyhimi, F. Int J Chem Kinet **2005**, 37, 427-433.

Kinetic Studies of Photocatalytic Decomposition of Meyhyl Violet 6B in Aquatic Suspension of Anatase Titanium Dioxide

Morteza Montazerozohori*, Javad Hasanalian,
Department of Chemistry, Yasouj University, Yasouj,7591874831 Iran.
(E-Mail: mmzohory@yahoo.com)

Abstract

In this work, photocatalytic degradation and kinetic studies of methyl violet 6B in aqueous solution was carried out using anatase TiO_2 in a photocatalytic reactor under irradiation with 400W high pressure mercury lamp. Some physico-chemical parameters such as solvent, photocatalyst amount, pH and time were investigated. Rate constants span are reported at different pH. Also the Langmuir-Hinshelwood (L-H) rate constant, (k_r) and adsorption constant, (K_A) at various pH are reported.

Keywords: Photocatalytic Decomposition, Meyhyl violet 6B, Kinetic studies

Introduction

The development of photocatalysis processes offers a significant number of perspectives especially in gaseous phase depollution . It is proved that the photo-oxidizing properties of photocatalyst TiO_2 activated by UV plays an important role in the degradation of volatile organic compound (VOC). Heterogeneous photocatalysis is based on the absorption of UV radiations by TiO_2. This phenomenon leads to the degradation and oxidation of the compounds, according to a mechanism associates the pollutant's adsorption on the photocatalyst and radical degradation reactions[1-8].

Exprimental

Reagent: TiO_2 Powder, The pH of solution was adjusted using diluted aqueous buffers that were prepared by the following compounds: KH_2PO_4, Na_2HPO_4, NaOAc, HOAc, $Na_2B_4O_7$, HCl, H_2SO_4 and NaOH. In all experiments doubly distilled water was used , Methyl Violet 6B (an organic dye).

Apparatus: *Photochemical set containing 400W high pressure mercury lamp as shown in FIG.1* was used for photodegradation experiments. UV- VIS spectrophotometer, jasco 570, was used .

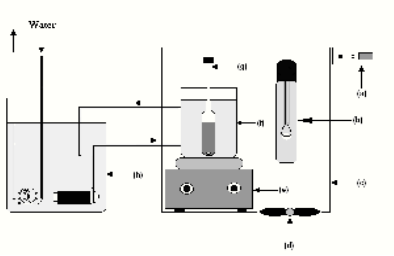

FIG.1- Photocatalytic setup for photodegradation experiments; a) Power supply; b) 400-W high-pressure Hg lamp; c) Photoreactor with aluminium foil as reflector for a full irradiation of catalyst; d) Fan; e) Magnetic stirrer; f) 2L Pyrex beaker; g) Photolytic cell; h) Water thermostat.

Results and Discussion

In this research, We investigated photocatalytic degradation of the title compound under various conditions including various times, pH, amount of catalyst.

The effect of various agents

Photocatalytic degradation was performed under various conditions as in Table 1. The results show the existance of air, UV and photocatalyst together is necessary for effective photodegradation of methyl violet 6B

Table1-The various conditions on photocatalytic degradation.

%Degredation	**Uv-Vis, Argon and photocatalyst**	**UV-Vis and oxygen**	**UV-Vis and Argon**	**Amount of photocatalyst (mg)**	**Time (min)**	pH (Conc.)
92.59	56.75	94.13	180.12	15	360	**pH=5 (200ppm)**
97.44	0.7	15.10	16.16	15	240	**pH=7 (20ppm)**
89.98	0.24	16.98	22.20	10	360	**pH=9 (40ppm)**

Reaction order and observed photodegradation rate constants at various pHs

The observed photodegradation rate constants, K at various pH were obtained from drawing the ln(C0/Ct) vs. t (in which C0= initiated concentration and t= reaction time) based on the below equation with some approximations(FIG.2).

$$Ln(\frac{C_0}{C}) = Kt$$

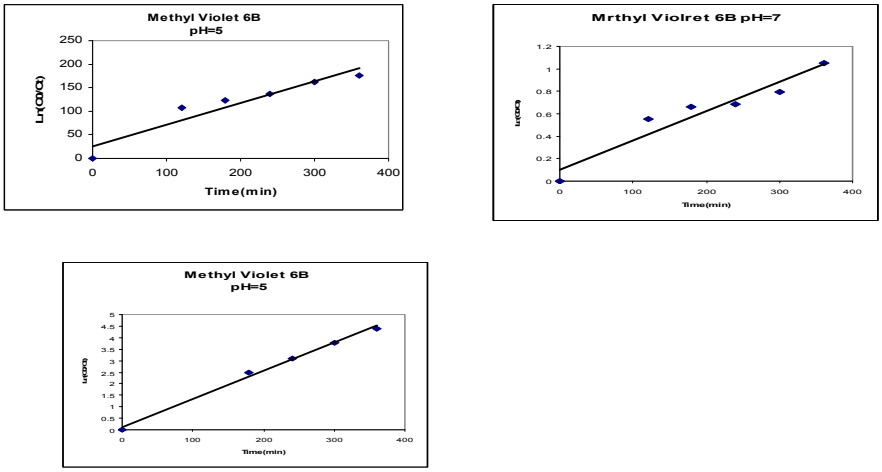

FIG.2

Kinetic model for methyl violet 6B at various pHs

Kinetic parameters of photodegradation of titled compound were obtained based on langmuir-Hinshelwood model from the diagram of 1/R vs. 1/C0 at various pHs(R= reaction rate and C0 = initiated concentration). The slope and intercept of this diagram results the absorption constants K_A, and photocatalytic degradation rate constants, k_r (FIG.3).

$$\frac{1}{R} = \frac{1}{k_r K_A C_0} + \frac{1}{k_r}$$

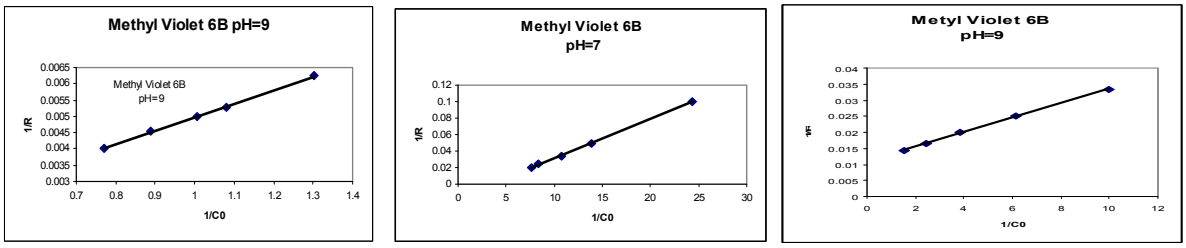

FIG. 3

The effect of pH on photodegradation kinetic parameters of methyl violet 6B:

The results in table 2 indicates that absoption costant at pH=7 is higher than acidic and basic medium. Photodegration rate constant at basic medium is higher than neutral and acidic medium. The equilibrium constant at pH=7 is the highest amount.

Table2- Kinetic parameters in various pH

pH=9	pH=7	pH=5	Methyl violet 6B
2.2×10^{-4}	8.4×10^{-3}	2.4×10^{-3}	K_A
54.4	39.3	25.5	k_r
2.1×10^{-2}	4.1×10^{-2}	1.1×10^{-2}	K

Reference

[1] Peral, J. Domenech, X. Ollis, D.F. J. Chem. Technol. Biotechnol. 1997, 70 117.

[2] Alberici, R.M. Jardim, W.F. Appl. Catal. B: Environ. 1997, 14, 55.

[3] Zika, R. G. and Cooper, W. J. (1987) Photochemistry of environmental aquatic systems. ACS Sym. Ser.,

Am. Chem. Soc., Washington, 1987, 327, 106-115.

[4] Zafiriou, O. C., Joussot-Dubien, J. and Zika,R. G. Environ. Sci. Technol., 1984, 18(12), 358.

[5] Hutzinger, O. (Ed.), The Handbook of Environmental Chemistry, Springer-Verlage, Berlin(1993).

[6] Duline, D., Drossman, H. and T. Mill, Environ. Sci. Technol., 1986, 20, 72.

[7] Montazerozohori, M. Karami, B. Habibi, M. H. Ann. Chim., 2006, 5-6, 285.

[8] Montazerozohori, M. Habibi, M. H. Joohari, S. Khodadostan,V. Ann. Chim. (2007), 97, 1015.

Effect of Counterion on the Thermokinetic and Thermodynamic of Solid State Linkage Isomerization Reactions of *trans*-$[Co(en)_2(ONO)_2]X$ ($X=ClO_4^-$, PF_6^-).

Nahid Hasani, Abbas Eslami*
Department of Physical-Inorganic Chemistry, University of Mazandaran, Babolsar, Iran
(Email: Eslami@umz.ac.ir)

Keywords: Linkage isomers, DSC, Interconversion, Counterion, Nitro and Nitrito

Introduction

Fascination and great attention to the ambient ligands, particularly nitrite ion (NO_2^-), back to early age of coordination chemistry in view of important participation of linkage isomerism in establishment of Werner coordination theory. Interconversion of linkage isomers studied both in solid and solution states by means of different spectral methods [1]. However, in spite of low heat exchange of isomerization reaction, thermal methods can provide reliable thermodynamic and kinetic data for the solid state investigation. In the present study, differential scanning calorimetry (DSC) was satisfactory exploited for investigation of solid state isomerization of two different salts of *trans*-$[Co(en)_2(NO_2)_2]X$ and *trans*-$[Co(en)_2(ONO)_2]X$ ($X=ClO_4^-$, PF_6^-). The isomerization may think to proceed successively through a two stage reaction (1):

Stage 1: *trans*$[Co(en)_2(ONO)_2]X \rightleftharpoons$ *trans*$[Co(en)_2(ONO)(NO_2)]X$

Stage 2: *trans*$[Co(en)_2(ONO)(NO_2)]X \rightleftharpoons$ *trans*$[Co(en)_2(NO_2)_2]X$

The results of this study may lead us to gain insight into the effect of nature of counterion on the kinetic and thermodynamic parameters of the reaction.

Experimental and method

Trans-$[Co(en)_2(ONO)_2]X$ [2] and trans-$[Co(en)_2(NO_2)_2]X$ [3] complexes were prepared and purified. DSC experiments were carried out using a Perkin-Elmer DSC calorimeter and conducted non-isothermally at linear heating rate of 10 $^0CMin^{-1}$.

Results and discussion

The results of present study showed that solid samples of pure *trans*$[Co(en)_2(ONO)_2]PF_6$ and *trans*$[Co(en)_2(NO_2)_2]PF_6$ are in metastable states and convert to an equilibrium stable state through two-stage processes at elevated temperature. Conversion of pure dinitrito isomer to equilibrium stable state is an exothermic process whereas a pure dinitro isomerization occurs via an endothermic process (The fig 1). Upon replacement of PF_6^- by ClO_4^- in solid samples a total conversion of dinitrito isomer to dinitro isomer has been observed. The thermodynamic and thermokinetic of linkage isomerization of both processes (conversion of dinitrito to dinitro and its reverse reaction) have been studied and the results were compared regarding to replacement of complex counter ion.

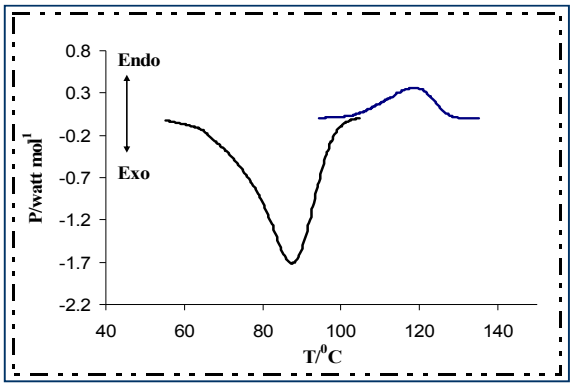

Fig 1.DSC curve of isomerization of *trans*$[Co(en)_2(ONO)_2]PF_6$ (exo) and *trans*$[Co(en)_2(NO_2)_2]PF_6$ (endo) in solid state.

Conclusion

The present research showed that the counterion has a considerable influence to interconversion and reversibility of these linkage isomers.

References:

[1] Tigran S. Kurtikyan,. **Inorg. Chem**, 2007, 46, 7024

[2] F. Seel and D.Meyer,. **Z.Anorg.All. Chem.**, 1974, 408, 275

[3] H. F. Holzclaw, Jr., D. P. Sheets and B. D. McCarty,. **Inorg. Synth**., 1953, 4, 176

Influence of Organic Coating on the Morphology and Thermal Decomposition kinetic of Octahydro-1, 3, 5, 7-tetranitro-1, 3, 5, 7-tetrazocine (HMX)

Abbas Eslami and Seyed Ghorban Hosseini*
Faculty of Chemistry, University of Mazandaran, P.O.Box 47416-95447, Babolsar, Iran
hoseinitol@yahoo.com (S. G. Hosseini)

Abstract:

Octahydro-1,3,5,7-tetranitro-1,3,5,7-tetrazocine (HMX) is a high explosive used in many plastic bonded explosives (PBX), double base propellants and propellant composite because of its high calorific potential, high density and smokeless combustion products. HMX exists in four solid phase polymorphs, labeled α-, β-, δ-, and γ-HMX. The β-phase of HMX has the highest density and is stable at room temperature; it is the form in which HMX is normally produced and used.

The microencapsulation of particulate energetic materials is aimed at the improvement of the product quality regarding processing, handling and storage. The basic aim of coating of an energetic compound with a binder is to reduce its sensitivity to some thermal, mechanical, and electrical stimuli. PBX is a composite energetic material (CEM), which contains an energetic compound as filler in a binder matrix.

In this work, fibrous nitrocellulose and stearic acid, as two common coating agents were used for microencapsulation of HMX crystalline particles through solvent/non-solvent and solvent evaporation, techniques.

Fourier transform-infrared spectroscopy (FT-IR) and scanning electron microscopy (SEM) have been used for the characterization of coating morphology. The effect of coating on HMX particles decomposition has been studied by means of differential thermal analysis (DTA), thermogravimetric (TG) and differential scanning calorimetry (DSC).

Our findings revealed that stearic acid, with solvent evaporation procedure, can provide effective coating shell around HMX microparticle. Also the effects of some parameters, such as coating agent to HMX weight ratio, stirring speed of the mixture and solvent distillation time on coating quality and thermal properties of coated particles have been investigated and the optimum condition has been proposed.

Also, the kinetic parameters such as activation energy and frequency factor of the decomposition processes of pure and microencapsulated HMX particles at optimum condition were obtained from the DSC data by non-isothermal methods proposed by ASTM E696. Our finding showed that the microencapsulated HMX particles at optimum condition with stearic acid has activation energy at least 20 ($KJ.mol^{-1}$) higher than compared to the pure one.

Pure HMX *Most stabilized HMX*

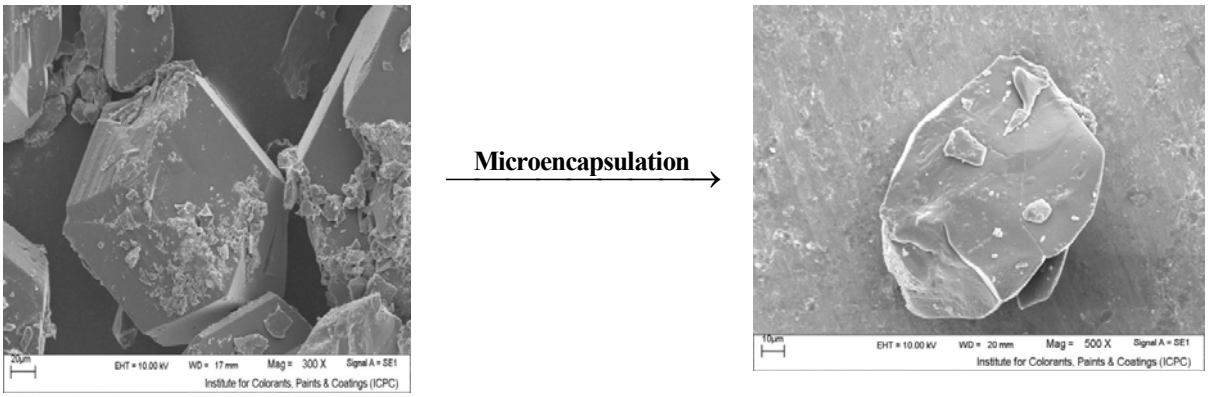

Decomposition at 285.7°C *Decomposition at 304.8°C*

Key words: HMX, Microencapsulation, Stearic acid, Nitrocellulose, Solvent evaporation, kinetic parameters.

References:

[1] Eslami A. Hosseini SG. Asadi V, Prog. Org. Coat. 65(2009) 269.

[2] Hosseini SG. Eslami A, Prog. Org. Coat. 68 (2010) 313.

[3] Mattos E.C, Propell Explos Pyrot 33 (2008) 44.

[4] Tompa A.S, W.F. Bryant Jr. Thermochim Acta 367-368 (2001) 433.

Thermoanalytical investigation of pyrotechnic reaction containing some carbohydrates with either potassium chlorate or potassium perchlorate

Seyed Ghorban Hosseini*, Abbas Eslami
Faculty of Chemistry, University of Mazandaran, P.O.Box 47416-95447, Babolsar, Iran
hoseinitol@yahoo.com (S.G.Hosseini)

Abstract:

The expression "pyrotechnics" comes from the Greek words pyros (Fire, heat) and techne (Art). Pyrotechnics compositions are based typically on finely divided mixtures of metallic or non-metallic elements as reducing agent with inorganic oxidizing agents. Pyrotechnic compositions may be used to produce heat, light, gas or smoke and these products lead to numerous applications. Closely related to the field of pyrotechnic reactions is the self-propagating synthesis of high temperature materials where the main interest lies in the properties of the solid product of combustion.

Thermal techniques provide powerful methods for these following reactions in solid state pyrotechnic compositions. In this study, thermal ignition of several binary pyrotechnic systems using sucrose, lactose or starch as fuel and one of the following oxidants: $KClO_3$, and $KClO_4$, were investigated. Differential thermal analysis (DTA) and thermogravimetry (TG) techniques have been employed to elucidate the reaction mechanism of these pyrotechnic systems in solid state. The apparent activation energy (E_a), $\Delta G^{\#}$, $\Delta H^{\#}$ and $\Delta S^{\#}$ of the redox reaction were obtained from the DSC experiments.

Based on these kinetic data and ignition reaction temperatures, relative reactivity of these mixtures was found to obey in following order: Fuel +$KClO_3$ > fuel +$KClO_4$. This trend can be related to the relative thermal stability of $KClO_x$ compounds (x = 1, 2, 3, 4): $KClO_4$ > $KClO_3$ > ($KClO_2$, KClO). Significantly, this order correlates with the stability of the oxyanions of chlorine and the stability of these oxyanions is due to the order of π-bonding extension for these compounds : ClO_4 > ClO_3 > ClO_2 > ClO.

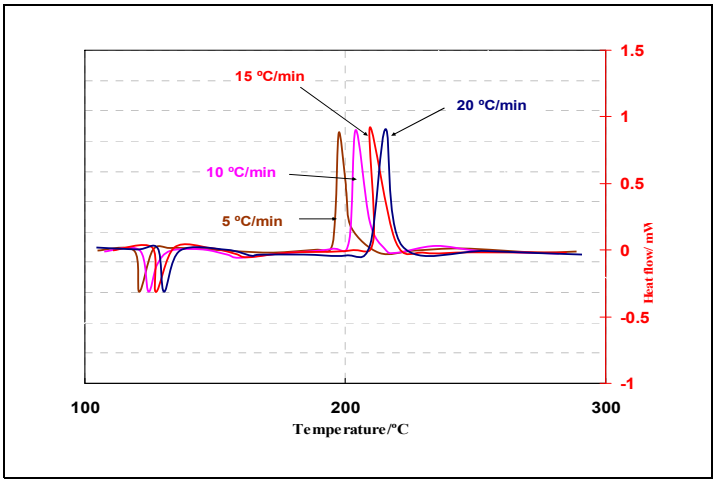

The effect of heating rate on the DSC curves of thermal ignition of lactose + $KClO_3$ mixture.

Kinetic Parameters of Thermal Ignition of Pyrotechnic Mixtures

Mixture	E (kJ.mol^{-1})	Frequency Factor Log A (s^{-1})	r*	$\Delta G^{\#}$ (kJ.mol^{-1})	$\Delta H^{\#}$ (kJ.mol^{-1})	$\Delta S^{\#}$ (J.mol^{-1}.K^{-1})
Sucrose+$KClO_3$	105	12.0	0.9925	113.4	101.25	-26.9
Lactose+$KClO_3$	135.7	14.5	0.9995	122.5	132.0	21.0
Starch+ $KClO_3$	211.7	17.9	0.9951	169.2	208.0	86.0
Sucrose+$KClO_4$	284.1	21.8	0.9968	207.8	280.3	160.7
Lactose+$KClO_4$	325.6	23.0	0.9929	239.0	322.0	184.0
Starch+ $KClO_4$	418	27.8	0.9968	290.0	414.3	275.5

r* linear regression coefficient

Key Words: Thermal Analysis, Pyrotechnic, Ignition Temperature, Kinetic parameters, Safety, Critical ignition temperature (T_b).

References:

[1] Eslami A. Hosseini SG. Asadi V, Prog. Org. Coat. 65(2009) 269.

[2] Brown, ME. J. Therm. Anal. Calorim. 65(2001) 323.

[3] Eslami, A. Hosseini, SG. Pourmortazavi, SM. Fuel 87(2008) 3339.

Kinetics of photochemical degradation process of Acid Yellow 199 on PZ- M^{n+}/TiO_2 , M^{n+}= Ce^{+3}, Fe^{+3}, Ag^{+} nanocomposites

M. Heidari[a], R. Fazaeli[b], M. Yousefi[a] , B. Amirpour[c] , S. Jalilehvand[c]

[a] *Department of Chemistry, Islamic Azad University, Shahre-rey Branch, Tehran, Iran*

[b] *Modeling and Optimization Research Center in Science and Engineering, Islamic Azad University, south Tehran Branch, Tehran, Iran*

(E-mail: r_fazaeli@azad.ac.ir)

[c]*Department of Marine Chemistry, Islamic Azad University, Science and Research Branch, Tehran, Iran*

With the advancement of experimental techniques, various semiconductors have been tested for their efficiencies towards dye degradation. The photocatalysed degradation of Acid Yellow 199 were investigated in aqueous suspensions of (PZ- M^{n+}/TiO_2) and M^{n+} (Ce^{+3}, Fe^{+3}, Ag^{+}) under a variety of conditions. The degradation was studied by monitoring the change in substrate concentration employing UV spectroscopic analysis technique. Finally kinetics of photocatalytic processes were studied. Organic dyes came up as one of the many new chemicals which could be used in many industrial activities. An ideal photocatalyst should exhibit the following features: (i) high reaction rate under band gap (or higher) irradiation; (ii) photostability; (iii) chemical and biological inactivity; and (iv) ready availability and low cost. Titanium dioxide mediated photocatalytic oxidation have been examined and used as photocatalysts for the degradation of environmental pollutants in water. In this work, the $PbZrO_3$ as a matrix was prepared by the sol–gel process.[1-5]

Doping $PbZrO_3$ with different oxidative agents (TiO_2, Ce^{+3}, Fe^{+3}, Ag^{+}) -Using Acid yellow 199 as a pollutant and a radical generator agent (H_2O_2) in the photoreactor: The photocatalytic activity was evaluated by photocatalytic oxidation of H_2O_2, TiO_2 and M^{n+} (Ce^{+3}, Fe^{+3}, Ag^{+})-doped $PbZrO_3$ (PZ- M^{n+}/TiO_2) with different ratios M^{n+}/TiO_2 (0.9, 0.1). The degradation was studied with using different parameters such as different ratios M^{n+}/TiO_2 and different radical generators such as hydrogen peroxide (H_2O_2). Finally variation of pH on degradation efficiency was studied. Table 1 shows the experimental results.[6-7]

Degradation efficiency = [(initial absorption – absorption in time t)/ initial absorption]×100

Result of 3 kinetic models (Lagergern, Elovich, Blanchard)for Ce^{+3}, Fe^{+3}, Ag^{+} are shown in table 2 with different doping ratios. Based on the values of correlation coefficient for each model, the researchers predict that in all cases Ce^{+3}- Ag^{+} Photocatalysts obey from pseudo-second order and Fe^{+3}-doped Photocatalyst obeys from pseudo- first order kinetics.

Lagergern: $\ln(q_e-q_t)=\ln q_e-kt$ Elovich: $q_t=1/\beta \ln(\alpha\beta)+1/\beta \ln t$ Blanchard:$t/q_t=1/k_2q_e^2+t/q_e$

Table -1 Exprimental results

Ce^{3+}/TiO_2 =0.1 Inatial pH = 7.72	Inatial hour	Second hour	Third hour	Ce^{3+}/TiO_2 =0.9 Inatial pH = 7.49	Inatial hour	Second hour	Third hour
Degradation %	43.79	53.21	60.07	Degradation %	75.19	76.15	77.31
Final pH	7.93	7.94	8.37	Final pH	8.06	8.15	8.12
Fe^{3+}/TiO_2=0.1 Inatial pH = 7.64	Inatial hour	Second hour	Third hour	Fe^{3+}/TiO_2 =0.9 Inatial pH = 7.68	Inatial hour	Second hour	Third hour
Degradation %	14.15	32.79	43.65	Degradation %	19.42	33.49	53.29
Final pH	8.05	8.01	7.88	Final pH	10.38	19.28	10.47
Ag^{+1}/TiO_2 =0.1 Inatial pH = 7.63	Inatial hour	Second hour	Third hour	Ag^{+1}/TiO_2=0.9 Inatial pH = 7.94	Inatial hour	Second hour	Third hour
Degradation %	3.39	26.82	40.45	Degradation %	13.76	1.7	21.52
Final pH	8.13	8.05	7.68	Final pH	10.17	10.23	10.30

Table -2 kinetic models for each Photocatalyst

Model	Ce^{3+}/TiO_2 =0.1	Fe^{3+}/TiO_2=0.1	Ag^{+1}/TiO_2 =0.1	Ce^{3+}/TiO_2 =0.9	Fe^{3+}/TiO_2=0.9	Ag^{+1}/TiO_2=0.9
1.lagergern	y = -0.015x - 11.42 R^2 = 0.966	y = -0.014x - 10.90 R^2 = 0.951	y = -0.015x - 10.68 R^2 = 0.955	y = -0.025x - 11.75 R^2 = 0.881	y = -0.014x - 10.65 R^2 = 0.860	y = -0.010x - 12.07 R^2 = 0.929
2.Elovich	y = 3E-06x - 2E-07 R^2 = 0.954	y = 6E-06x - 2E-05 R^2 = 0.916	y = 7E-06x - 3E-05 R^2 = 0.924	y = 3E-06x + 1E-05 R^2 = 0.830	y = 7E-06x - 2E-05 R^2 = 0.916	y = 2E-06x - 6E-06 R^2 = 0.921
3.Blanchard	y = 49166x + 1E+06 R^2 = 0.991	y = 13603x + 1E+07 R^2 = 0.193	y = -20144x + 5E+07 R^2 = 0.386	y = 39823x + 30993 R^2 = 0.999	y = 8707.x + 1E+07 R^2 = 0.384	y = 83333x + 3E+07 R^2 = 0.705

Keywords: Photocatalysis, Titanium dioxide; Acid Yellow 199; Degradation efficiency

References

[1]Journal of the European Ceramic Society 19 (1999) 1191 Hiromu Ohuchi, Sintarou Tsukamoto, Mitsuru Ishii and Hiromitsu Hayakawa1195

[2] Ceramics International 29 (2003) 35–39 S. Zahi, R. Bouaziz, N. Abdessalem, A. Boutarfaia

[3] Journal of the European Ceramic Society 19 (1999) 1255±1258 O. Sugiyama,a S. Saito,a K. Kato,b S. Osumi,b K. Murakamic and S. Kanekoc

[4]Solid State Communications 116 (2000) 507–511 X.G. Tanga, H.R. Zenga, A.L. Dinga, P.S. Qiua, W.G. Luoa, H.Q. Lib, D. Mob

[5] Thin Solid Films 423 (2003) 88–96 S.S.N. Bharadwaja, S.B. Krupanidhi

[6]Materials Chemistry and Physics 117 (2009) 338–342 B. Praveenkumara, G. Sreenivasalub, H.H. Kumara, D.K. Kharat a, M. Balasubramanianb, B.S. Murtyb,
[7]Chemical Engineering Journal 151 (2009) 10–18 M.A. Rauf, S. Salman Ashraf Chemistry Department, PO Box 17551, UAE University, Al-Ain, United Arab Emirates

The Study of Kinetic and Mechanism of Photocatalytic Reduction of CO_2 With H_2O

B. Khezri[*a] ,S. Khanahmazada[b] , D. Setamdideh[c]

[a, b, c]*Department of chemistry,Islamin Azad University, Mohabad branch, Mohabad , Iran*

[*]*(Email:khezry55@yahoo.com)*

Abstract

The goals of the present work are: (1) A theoretical analysis of possible reaction pathways to the synthesis of methanol and methane from CO2 and H2O and the selection of the best path from the view point of energy. (2) Investigation of the kinetic of assumed reactions.

For determination of mechanism, BOC-MP method is used. By using of this theory, it is possible to calculate the thermodynamic and kinetic parameters and therefore predict the intermediates and the mechanism of heterogeneous catalytic reaction. With attention to these results, in photocatalytic reduction of CO2, with decrease in the d-character of the supported metal on TiO2, production of methanol will increase. Upon the investigation of kinetics of the proposed mechanism, we deduced that when the Fermi level of the catalyst is raised, the rate of methanol formation will increase.

Keywords: Reduction of CO_2, Photocatalyst, Fermi level, TiO_2, methanol synthesis

Introduction

The large-scale emission of carbon dioxide in to the atmosphere has wrought of the most serious and dangerous problems upon the earth, especially with regard to the devastating consequences of the greenhouse effect. The reduction and/or fixation of carbon dioxide can be said to be one of the most important areas of research in chemistry today, not only for solving the many urgent problems resulting from the pollution of the global environment but also for finding ways to maintain vital carbon resources[1,2].

Furthermore, such research will make sense only if the reactions can be effectively and efficiently achieved using a natural energy source the most safe, clean, and ideal being solar energy . The utilization of solar energy for the reduction and/or fixation of carbon dioxide can be made possible by considering the following two reaction systems: (i) the photocatalytic

reduction and/or fixation of CO2 with H2O into CO, HCOOH, CH3OH, and CH4, etc. using reactive photocatalysts such as small particle powdered TiO2 semiconductors and, (ii) the photoelectrochemical reduction and/or fixation et CO2 in aqueous systems using semiconducting electrodes[3,4,5].

Conclusion and Discussion

To form methanol or when we use Cu and Cr on TiO_2 photocatalyst, below reaction mechanism is suggested:

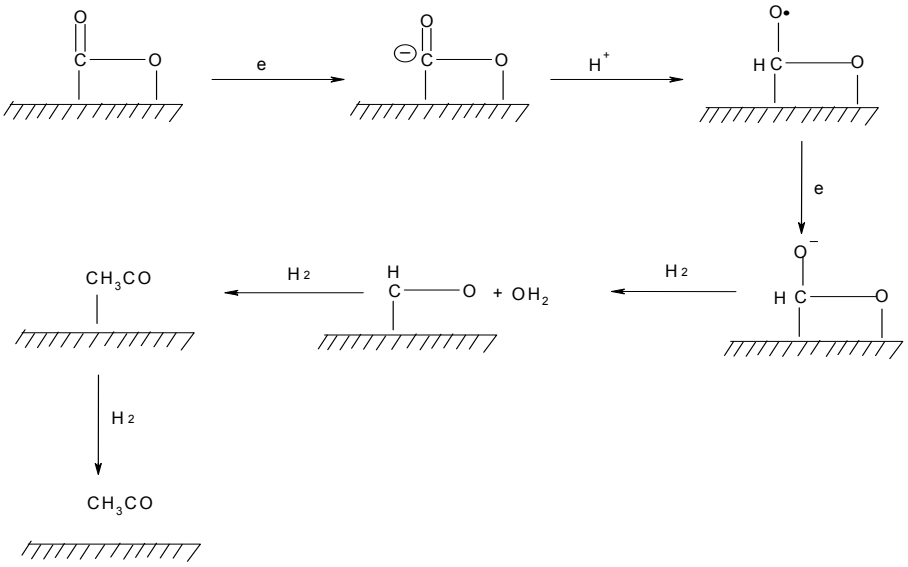

But methane formation mechanism by using Rh, Ru and Pt on TiO_2 is suggested like this:

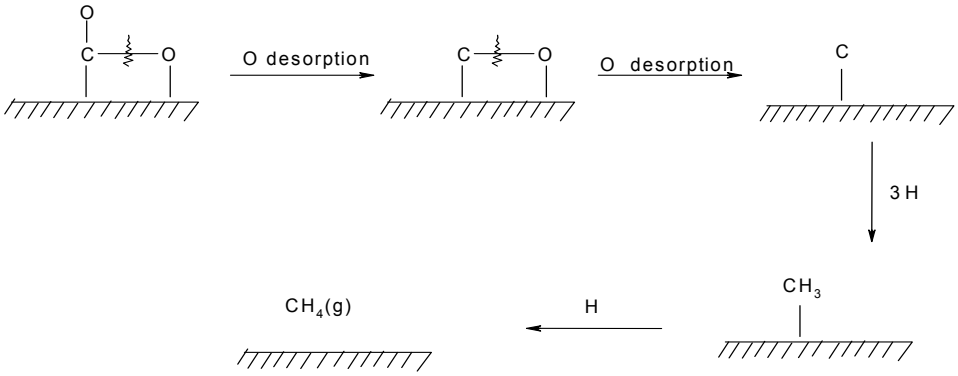

If we want to investigate the kinetic of suggested mechanism, we should first study the probability of trapping electron or hole by the formed species on the surface. There are obvious documents that show the adsorption of CO_2 is along with electron trapping.

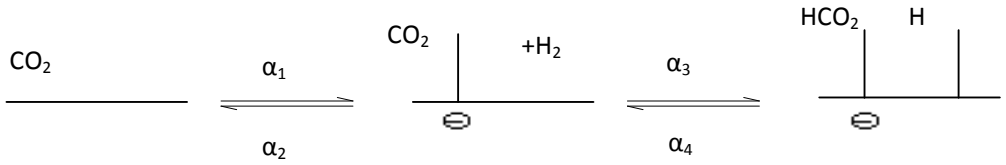

In next step, after dissociation adsorption:

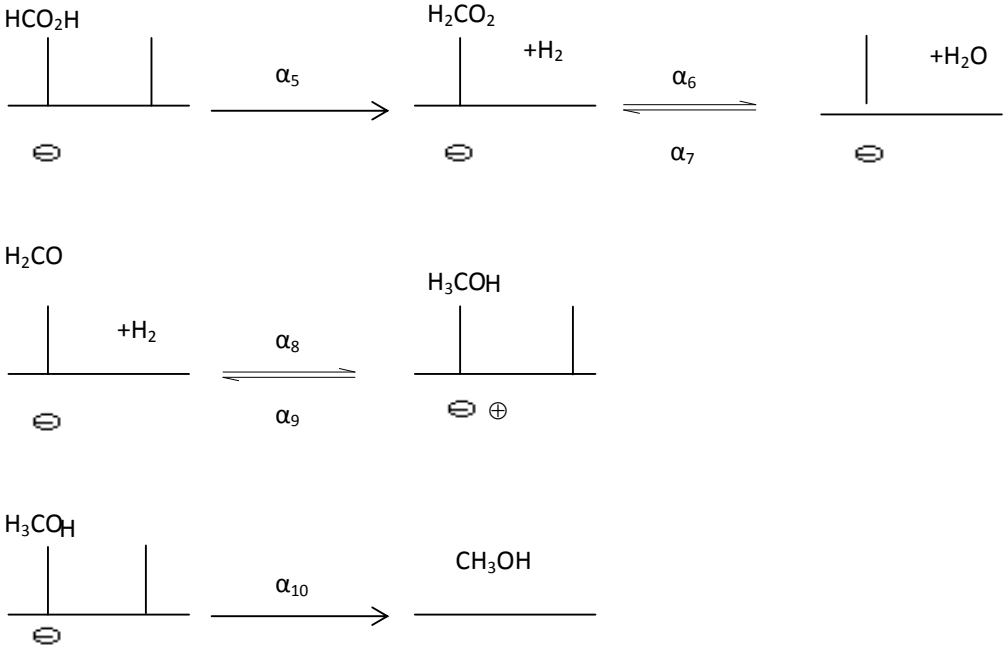

Now, it is possible to investigate the kinetic of above reaction and relate the rate and electronic properties of the photocatalyst. In the above mechanism the forward & reverse constants is shown by α1 to α10.

After all the necessary calculation done, the final formula for rate equation is:

$$\text{rate} = \alpha_{10}\ N^{-}_{H_3CO}\ N^{0}_{H} = \alpha_{10} * \frac{\alpha_5}{\alpha_{10}} * \frac{\alpha_3}{\alpha_4} * \frac{\alpha_1}{\alpha_2}\ \exp(-\frac{\omega_s^+}{KT}) \exp(+\frac{\varepsilon_s^+}{KT})\ P_{H_2}\ P_{CO_2}$$

Refereces

[1] Lo C.C., Hung C.H., Yuan C.S., Wu J.F., Photoreduction of carbon dioxide with H_2 and H_2O over TiO_2 and ZrO_2 in a circulated photocatalytic reactor, Sol Energy Mater Sol Cells, Netherlands, vol 91, pp1765, 2007.

[2] Dey G.R., Belapurkar A.D., Kishore K., Photo-catalytic reduction of carbon dioxide to methane using TiO2 as suspension in water, J Photochem Photobiol A: Chem, Netherlands, vol 163, pp503, 2004.

[3] Yahaya A.H., Gondal M.A., Hameed A., Selective laser enhanced photocatalytic conversion of CO2 into methanol, Chem Phys Lett, Netherlands, vol 400, pp206, 2004.

[4] Nguyen T-V., Wu J.C.S., Chiou C-H., Photoreduction of CO2 over Ruthenium dye-sensitized TiO2-based catalysts under concentrated natural sunlight, Catal Commun, Netherlands, vol 9, pp2073, 2008.

[5] Ozcan O., Yukruk F., Akkaya E.U., Uner D., Dye sensitized artificial photosynthesis in the gas phase over thin and thick TiO2 films under UV and visible light irradiation, Appl Catal B: Environm, Netherlands, vol 71, pp291, 2007.

Ab Initio Direct Dynamics Studies on the Reaction of CH3Cl with OH radical

Maryam Dehestani ,Fahimeh Shojaie
Department of Chemistry, Shahid Bahonar University of Kerman, Kerman, Iran
dehestani2002@yahoo.com

Abstract

Chlorinated alkanes are potential sources of chlorine in the stratosphere, where they can catalytically destroy ozone [1]. Methyl chloride, the most abundant halocarbon in the atmosphere, has received much attention as a natural source of chlorine atoms in the stratosphere [2]. Hydroxyl radical breaks down and removes many of the gases that pollute the air, including methyl chlorine. The reaction of CH_3Cl with OH has been studied; there are two possible pathways for this reaction [3, 4].

$$CH_3Cl + OH \xrightarrow{k_1} CH_2Cl + H_2O \quad (1)$$

$$CH_3Cl + OH \xrightarrow{k_2} CH_3 + HOCl \quad (2)$$

Up to now, no experimental and theoretical information has been available on the branching fraction $k_1/ (k_1 + K_2)$; therefore, theoretical investigations are very desirable to gain an understanding of the multiple channel reaction mechanisms of the reaction CH_3Cl+OH. The theoretical study of this reaction was performed by Theodora and co workers [4], who have reported ab initio calculations for the reaction (1) in the forward reaction and no calculations were performed for the reaction (2) and branching fraction. Furthermore, in this study, we will use the vibrational mode analysis to elucidate the relationships of the reactant region($s=-\infty$), the saddle point (s=0) and the product region($s=+\infty$). The extensive investigation shows that reaction mechanism is reliable. Comparison of modes shows that transition state has a reactant-like character in the reaction (1); it means this reaction is exothermic and for the reaction (2) transition state has a product-like character, it means this reaction is endothermic. These results are in excellent agreement with ref [3]. All ab initio calculations are carried out using the GAUSSIAN 03 program. The equilibrium geometries and frequencies of the stationary points (reactants, intermediates, products, and transition states) for the two reaction channels are calculated at the MP2/6-311+G (d, p) level of theory. At the same level, the

minimum energy path (MEP) for each reaction are obtained by intrinsic reaction coordinate (IRC) theory to confirm the number of imaginary frequencies (0 or 1) a local minimum or a transition state. For the two-channel reaction CH_3Cl+OH, the individual channel rate constants, $k_1$and k_2 calculated using the conventional transition state theory incorporating the Winger tunneling correction and the hindered rotor approximation at the G2MP2 method [5] in the temperature range 200–2000 K . (TST) incorporating the Winger tunneling correction (W) and the hindered rotor approximation (HR). Figures show the logarithm of calculated rate constants as a function of $10^3 / T$ for the reaction (1) and (2) [a] Ref .4 and [b] Ref .6.

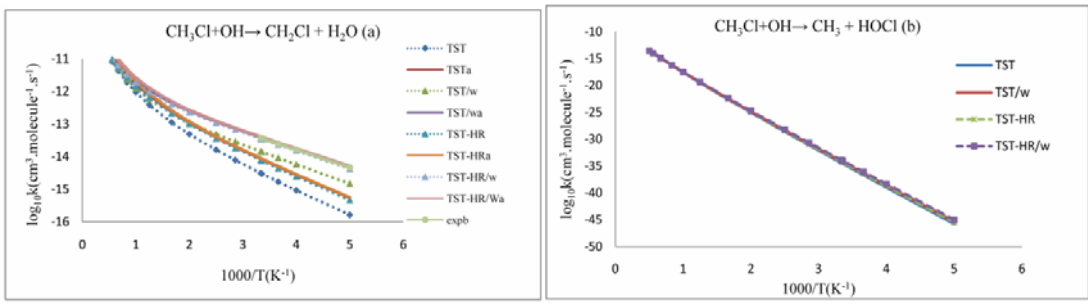

Results also indicate that, the H-abstraction is the major channel in the whole temperature range 200-2000K. The calculated rate constants for the major channel can be expressed, in $cm^3molecul^{-1}s^{-1}$, by the following fits:

$k = 6.91 \times 10^{-11} T^{-0.61} e^{\frac{-1290.05}{T}}$ for temperature range 200-400K and

$k = 9.11 \times 10^{-11} T^{-0.01} e^{\frac{-3576.25}{T}}$ for temperature range 400-2000K.

References

[1]Hsu, K. J.; DeMore, W. B. Geophys Res Lett 1994, 21, 805.

[2]Yokouchi, Y.; Noijiri, Y.; Barrie, L. A.; Toom-Sauntry, D.; Machida, T. ; Inuzuka, Y. ; Akimoto, H. ; Fujinuma, Li, H. J.; Y. ; Aoki, S. Nature, 2000, 403 , 295.

[3]Louis, F.; Gonzalez, C. A.; Huie, R. E.; Kurylo, M. J. J Phys Chem A, 2000, 104, 8773.

[4]Tzima, T. D.; Papayannis, D. K.; Melissas, V. S. J Chem Phys, 2005, 312, 169.

[5]Curtiss, L. A.; Raghavachari, K.; Pople, J. A. J Chem Phys, 1993, 98, 1293.

[6]Sander, S. P.; Finlayson-Pitts, B. J.; Friedl, R. R.; Golden, D. M.; Huie, R. E.; Kolb, C. E.; Kurylo, M. J.; Molina, M.J.; Moortgat, G. K.; Orkin, V. L.; Ravishankara, A. R. Chemical Kinetics and Photochemical Data for Use in Atmospheric Studies, Evaluation Number 14, JPL Publication 02-25, Jet Propulsion Laboratory, Pasadena, 2002.

Removal of vanadium anions from aqueous solutions by polyaniline modified Clinoptilolite

[1]H.Faghihian, [2]M.Rasekh
Department of Chemistry, Islamic Azad University, Shahreza, Iran
faghihian@iaush.ac.ir

Introduction

Unmodified zeolites show no affinity for anions due to the fact that their surfaces are negatively charged. However modified zeolites show high capacity toward anions and therefore have drawn much attention in recent years for removal of anionic pollutants. In this work clinoptilolite was modified with polyaniline by polymerization of anilinium cations in the zeolite channels and a composite of polyaniline/ clinoptilolite was obtained. Encapsulation of polyaniline in the clinoptilolite channels was confirmed by XRD and FTIR spectroscopy. The effect of a number of parameter such as initial concentration of the anions ,amount of the composite and contact time were determined and optimized.

Preparation of polyaniline/ clinoptilolite composite

A given amount of clinoptilolite was first dispersed in the 50 ml of 0.5 M sulfuric acid containing 0.2 M aniline. The mixture was then stirred for 48 hours at room temperature. The mixture was filtered and washed with excess of deionized water in order to remove free anilinium ions. The resulting wet solid was dispersed in 50 ml of 0.3 M sulfuric acid solution, containing 0.16g ammonium persulfate as oxidizing agent. Polymerization of anilinium cation inside clinoptilolite channels was carried out at room temperature for a period of 24 hours under magnetic stirring. The resulting composite was filtered, washed with excess deionized water and dried in vacuum for 24 hours.

Vanadium anion removal

NH_4VO_3 solutions were prepared in different concentrations ranged . 0.2 g of the composite was put into a beaker containing 50 ml of NH_4VO_3 solutions at different concentrations. The mixture was then stirred for 120 min at room temperature .The mixture was filtered and

washed with excess deionized of water. Measurement of unremoved vanadat ions was carried out by atomic adsorption spectroscopy [1,2] .

Results and discussion

The polyaniline/clinoptilolite nanocomposite was characterized by XRD and FT-IR technique. Adsorption of vanadat species was measured spectrophotometrically. Different experimental condition were investigated and optimized. The optimized adsorption conditions are as follows:equilibration time:120 min, initial concentration:1000 ppm, adsorbent dose 1.5 mg, initial pH=7 and optimized temperature=45^{0}C.The values are interpreted accordingly.

Equilibrium modeling

Tow isotherms were tested for their ability to describe the experimental results, namely the Langmuir isotherm, the Freundlich isotherm .

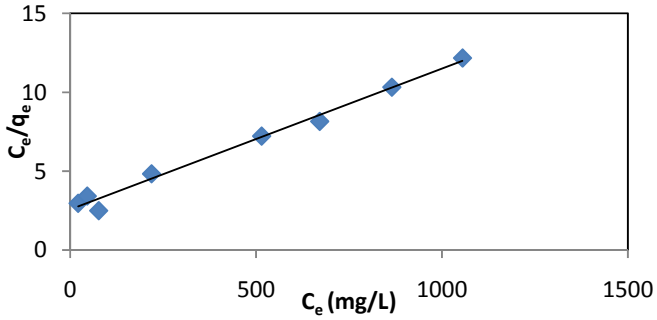

Fig1.Langmuir adsorption isotherm

The Langmuir isotherm fits the experimental data very well. It may be due to homogeneous distribution of active sites onto modification zeolite surface.

Thermodynamic parameters:

The effect of temperature on the adsorption of vanadium anions by polianilin modified clinoptilolite was carried out in the temperature range from 25 to 550C.The results showed that the adsorption capacity increased with increasing temperature which indicates that the adsorption process is endothermic in nature.The calculate Gibbs free energy at 2980,3080 and 3280Kwas negative which indicate that the adsorption process is spontaneous.

Refrence

[1] Jian Hu;Xuewen Wang;Liansheng Xiao;Songru Song;Baoqing Zhang;" Removal of vanadium from molybdate solution by ion exchange"J. Hydrometallurgy 95,(2009),203-206.

[2] Qinggang Li;Li Zeng;Liansheng Xiao;Yanan Yang;Qixiu Zhang;" Completely removing vanadium from ammonium molybdate solution using chelating ion exchange resins"J.Hydrometallurgy 98, (2009), 287-290.

Kinetic study on the,characterization and photocatalytic efficiency of ZnO/Bentonit for decolorization of Dye pollutant Acid Red 52 in a completely mixed batch reactor

Kazem Mahanpoor [a],Fattah_rabiee*[b]

[a]Department of Chemistry, Faculty of Science, Islamic Azad University, Arak Branch, Arak, Iran

E-mail: k_Mahanpoor@iau-Arak.ac.ir

[b]Department of Chemistry, Faculty of Science, Islamic Azad University, Arak Branch, Iran

Corresponding Author E-mail: Fattah_rabiee@yahoo.com

Abstract

In this research kinetic study on the Decolourization of Acid red 52 dye, was conducted using Zno catalyst supported on bentonite Zeolite as a catalyst in the presence of UV-C light and H_2O_2.The effects of different parameters such as amounts of catalyst, temperature of reaction ,initial concentration of the dye and H_2O_2 and initial pH of the dye solution on the degradation efficiency of the process were assessed. The results indicated that by using 38ppm of H_2O_2 and 100ppm of the catalyst at pH 5, about 97% total Acid Red 52 could be removed after 100 min in a batch photo-reactor. The structure, surface and morphology properties of the nanostrucred Zno on Bentonite have been investigated by XRD, SEM techniques. From kinetic view the reaction was first order and study of reaction rate was carried out with the use of first order kinetic equation. Acceptable results were gained in this examinations. According to this results, a method was obtained for photocatalytic analysis with the use of ZnO/BT catalyst, which by its development in an industrial form, it can be used for analyzing the waste water in loom or other industries.

Introduction

Industrial and Synthetic dyes are the major industrial pollutants and water contaminants [1,2]. Textile water introduced intensive colour and toxicity to aquatic system. Reactive dyes are widely used in the textile industries and chemistry because of its simple dyeing procedure and good stability during washing process [3]. But these processes have only limited success Homogeneous advanced oxidation process(AOP) employing hydrogen

peroxide with UV-light has been found to be very effective in the degradation of dye pollutants [4–8].

Experimental works

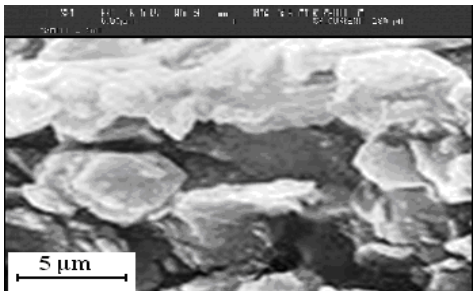

fig١: ZnO/Bentonite SEM

Results and discussion

The concentration of the residual dye in solution was calculated by cruve observed at (λmax =562 nm).

1. Chemical degradability of AR52

To evaluate the efficiency and the benefit of each condition on the dye degradation experiments were carried out under the following conditions: (1) dye/H_2O_2, (2) dye/UV, (3) dye/UV/H_2O_2, (4) dye/UV/ZnO/BT/H_2O_2

2. Kinetic analysis

In all the experiments the disappearance of dye during the first 80 min of oxidation could be described as a first order reaction kinetics with regard to dye concentration as it may be seen from the data. Initial decolorization rate constants were determined from the slope of _ln (C/C0) vs t (min) plots, where C0 and C are dye concentration at zero and t time, respectively.

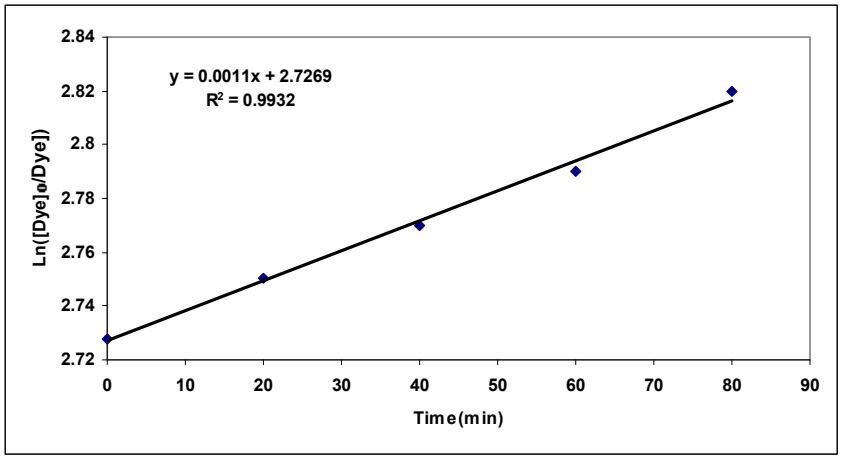

Fig2: Kinitic in removal of the dye AR52

Conclusions

H_2O_2 concentration 38ppm appear as optimum dosages decolorization,. The optimal parameters, for both processes, under the same operational conditions. decolorization rate could be described as a first order reaction kinetics .The removal rate of AR52can reach 98% when the illumination time is 80 mins. It is increased with the augment of illumination time. The highest removal rate can be got when the pH value of the solution is within 5

Reference

[1] Hofstandler, K., Kikkawa, K., Bauer, R., Novalic, C., and Heisier. *Environ. Sci. Technol.*, 1994, 28, 670.

[2]Kang SF, Liao CH, Chen MC. Chemosphere 2002, 46,923.

[3]Arslan I, Balcioglu IA, Bahnemann DW. Dyes and

Pigments 2000,47,207.

[4] Feng J, Hu X, Yue PL, Zhu HY, Lu GQ. Water Research 2003,37,3776.

[5] Neamtu M, Yediler A, Siminiceanu I, Kettrup A. Journal of Photochemistry and Photobiology

Chemistry 2001,141,247.

[6] Park H, Choi W. Journal of Photochemistry and Photobiology A: Chemistry 2003,159,241.

[7] Meric¸ S, Kaptan D, O¨ lmez T. Chemosphere 2004,54,43.

Kinetic study on the photodecolorization in the Optimal Photocatalytic Process of Dye pollutant Acid Red 52 in a completely mixed batch reactor by using Fenton Reagent +Zno/Bentonite+UVprocesses

Kazem Mahanpoor [a],Fattah_rabiee*[b]

[a]Department of Chemistry, Faculty of Science, Islamic Azad University, Arak Branch, Arak, Iran

E-mail: k_Mahanpoor@iau-Arak.ac.ir

[b]Department of Chemistry, Faculty of Science, Islamic Azad University, Arak Branch, Iran

Corresponding Author E-mail: Fattah_rabiee@yahoo.com

Abstract

In this paper kinetic study on the mineralization and decolourization of colored textile wastewater was investigated using Photo-Fenton process. Acid red 52 (AR52) was used as an acid dye model. The effect of decolourization parameters such as kinetic reaction ,ferric ion concentration, Zno/Bentonite concentration, dye concentration and PH and catalyst were investigated. The maximum iron (III) concentration was set to maximum allowable discharge level to environment. The rate of decolourization reaction decreased by increasing dye concentration and in the presence of the hydrogen peroxide. At concentrations employed in the study, the photocatalytic degradation of Acid Red 52 obeyed first order kinetics. The linear plot of log(C0/C) versus irradiation time t is shown For a comparative study, decolourization of AR52 was also performed by photocatalysis that is comprised with the hydrogen peroxide and combined Photo-Fenton – photocatalysis processes. The Photo-Fenton process had the greatest decolourization rate in comparison to photocatalysis and combined Photo-Fenton - photocatalysis processes

Keywords: Photo-Fenton process. Decolourization. Concentration.

Introduction

Industrial and Synthetic dyes are the major industrial pollutants and water contaminants. Textile water introduced intensive colour and toxicity to aquatic system[1]. Some physical and chemical techniques are currently available for the treatment of dye effluent[2-3]. But these processes have only limited success Homogeneous advanced oxidation process employing hydrogen peroxide with UV-light has been found to be very effective in the degradation of dye pollutants[4-6].

Experimental works

1. Analysis

A desired quantity of dye/Fe^{3+}/ H_2O_2/Catalyst solution was freshly prepared from $Fecl_3$, H_2O_2 and the dye stock solution. The color of the dye solution in the reaction mixture at different times, was obtained by the measure of the absorbance at maximum wavelength (λmax=562 nm) and by computing the concentration from calibration curve.

2. Effect of added ferric ion (Fe^{3+}) on the photodegradation of an Acid Red 52

The photodegradation of an acid red 52 was performed in the presence of 100 ppm ZnO/BT, 38 ppm H_2O_2/l and the UV radiation with a peak wavelength of 562 nm to investigate the effect of added Fe^{3+} concentration (Fig1).

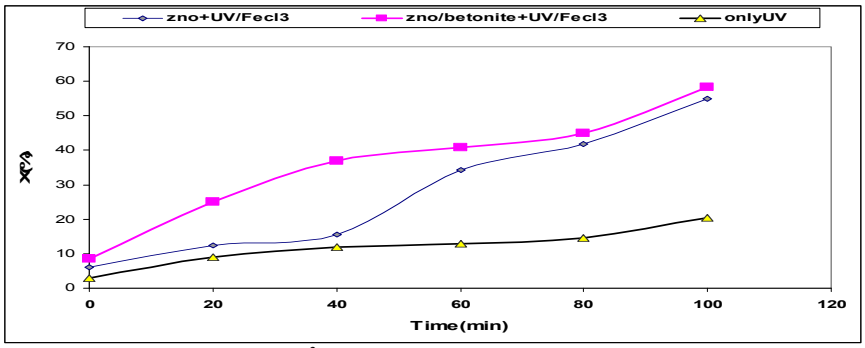

Fig. 1. Effect of add Fe^{3+} on the photodecolorization of the acid Red 52

Results and discussion

Fig. 2. Kinitic and relationship of the concentration catalyst vs the removal rate of the acid red 52 dye, in the presence of 100 mg Zno/BT, 38 mg H_2O_2/l, and the UV radiation (at the initial dye concentration of 100 mg /l, pH 5, and 25 _C).

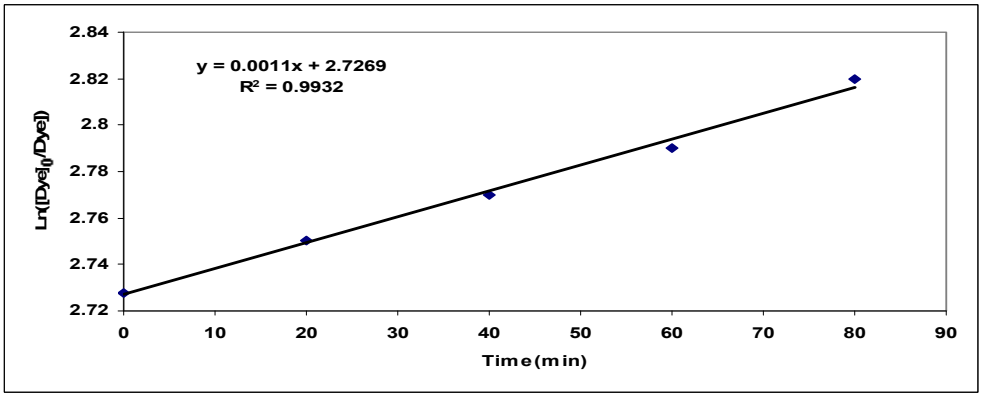

Fig. 2. Kinitic and relationship of the concentration catalyst

Conclusion

In all the experiments the disappearance of dye during the first 80 min of oxidation could be described as a first order reaction kinetics with regard to dye concentration as it may be seen from the data. Initial decolorization rate constants were determined from the slope of (C/C0) vs t (min) plots, where C0 and C are dye concentration at zero and t time, respectively.

Reference

[1]Meric¸ S, Kaptan D, O¨ lmez T. *Chemosphere* 2004,54,435

[2] Kang SF, Liao CH, Chen MC. *Chemosphere* 2002, 46,923

[3]Arslan I, Balcioglu IA, Bahnemann DW. *Dyes and Pigments* 2000,47,207

[4] Feng J, Hu X, Yue PL, Zhu HY, Lu GQ. *Water Research* 2003,37,3776

[5]Neamtu M, Yediler A, Siminiceanu I, Kettrup A. *Journal of Photochemistry and Photobiology :A Chemistry* 2001,141,247.

[6] Park H, Choi W. *Journal of Photochemistry and Photobiology A: Chemistry* 2003,159,241

Synthesis, characterization modified CdS/TiO_2 and Investigation of its photocatalytic activity on environmental Pollutants

A. Rahmani[1]*, S. Rahimnejad[2], M. R. Gholami[1]

E mail:Rahmani_a@mehr.sharif.ir

[1]*Department of chemistry, Sharif University of Technology, Tehran, Iran*

[2]*Department of Chemistry, Islamic Azad University Shahre-rey branch,Tehran,Iran*

Abstract

Nanosized CdS coupled TiO_2 nanocrystals were prepared by a microemulsion-mediated solvothermal method at relatively low temperatures. The prepared samples were characterized by diffuse reflactance spectroscopy (DRS), Scanning electron microscopy, (SEM) and X-Ray diffraction(XRD) , it was found that the CdS coupled TiO_2 consisted of uniform anatase and rutile TiO_2 of nanoparticles coated with highly dispersed cubic phase CdS nanocrystal. This photocatalyst was used to oxidize pollutants. Some compounds are resisting to oxidative degradation, research has swayed towards the reduction of them. The result indicates that modification of CdS-TiO_2 with electron-donating groups (EDG) such as amino acids is an effective way to enhance photodegradation of compounds.

Introduction

Nanosized particles of titanium dioxide (TiO_2) have excellent photocatalytic properties and have found applications in environmental remediation[1,2]. Lots of efforts have been made to modify titania in order to develop multifunctional materials and enhancing the photocatalytic performance. It has been reported that the composite structure can enhance the photocatalytic activity of the semiconductor catalysts. CdS–TiO_2 is an excellent candidate for Photo decomposition of pollutants due to its intrinsic energy band gap[3,4]. In CdS-nanocomposite CdS which is a narrow band gap semiconductor was added to TiO_2 to improve the response of TiO_2 to visible light and also TiO_2 prevents the photocorrision of CdS .

Experimental

Titanium tetraisopropoxide (TTIP) was used as a titanium precursors purchased from Merck. $Cd(NO_3)_2$ and $(NH_4)_2S$ were used as precursors of CdS obtained from Merck. A typical

synthesis of sample involved the use of cyclohexane as oil phase, Triton X-100 as surfactant and 1-hexanol as cosurfactant. The yellow slurry obtained was centrifuged and washed with ethanol and water. Finally modified CdS- TiO_2 catalyst was achieved by soaking the prepared TiO_2 for 24 h in ethanol solution of amino acids at room temperature. Photocatalytic activities of the samples were evaluated by investigation of methylene blue (MB) degradation in aqueous solution under visible light irradiation.

Results and Discussions

XRD analysis shows distinctive TiO_2 peaks that are corresponded to the anatase and rutile has not been changed by the modification using amino acids as (EDG) . The additional peaks are related to the CdS cubic phase. SEM images reveal that nanoparticles in the prepared powder are uniform with average size 45nm. In the presence of pure TiO_2, degradation of MB was not observed. Similarly, the degradation of MB with pure CdS was not significant. However, in the presence of the CdS/TiO_2 samples, the degradation of MB obviously increased and it would be expected that this activity will increase by coating (EDG) to photocatalyst. On the basis of these results obtained with infrared spectroscopy, we suggest that amino acids bind to the TiO_2 surface via the carboxyl group.

Conclusion

The effects of surface modification of CdS- TiO_2 with specific (EDG) on photocatalytic degradation of azo dyes were investigated. Due to the strong electron-donatin properties, they act as a hole trap to prevent electron/hole recombination and provide stable surface layer with reduction degradation pathway. In addition, (EDG) enhance both CdS-TiO_2 redox properties and adsorption of compounds .

References

[1] N. Serpone, E. Pelizzetti (Eds.), Photocatalysis: Fundamentals and Applications, John Wiley & Sons, New York, 1989.

[2] D.F. Ollis, H. Al-Ekabi (Eds.), Photocatalytic Purification and Treatment of Water and Air, Elsevier, Amsterdam, 1993.

[3] C.L. Jung, M.S. Yun, G.K. Tae, et al., Appl. Phys. Lett. 91 (2007) 113104-1.

[4] L. Hong, L.Z. Bao, F.F. Yun, et al., React. Kinet. Catal. Lett. 2 (2007) 239

Kinetics inhibition of angiotensin converting enzyme by Quail egg white protein hydrolysates fractions

Elham Rashidi Nasab[1], *Ahmad Asoodeh* [2,*], JamshidKhan Chamani[1]

[1] *Depart. of Biology, Faculty of Sciences, Islamic Azad University - Mashhad Branch, Mashhad, Iran*

[2]*Depart. of Chemistry, Faculty of Sciences, Ferdowsi University of Mashhad, Mashhad, Iran*

Author Corresponding: Asoodeh@um.ac.ir (A. Asoodeh)

Keywords: Quail egg white, HPLC, ACE, Lineweaver-Burk plots, Competitive inhibitor

Introduction:

Hypertension is a major chronic disease [1] and a common disease among adults; that often leads to serious health problems, thus research on medical treatments and preventive measures have been of increasing interest [2]. Angiotensin converting enzyme (ACE) plays an important role in blood pressure regulation [3, 4]. This study describes the kinetics of the inhibition of angiotensin converting enzyme by Quail egg white(QEW) protein hydrolysates fractions obtained from trypsin-papain hydrolysis to assess the angiotensin converting enzyme inhibitor activity of derived peptides.

Methods:

QEW hydrolyzed by trypsin-papain and hydrolysates at ratio of 20:1 respectively. The hydrolysis reaction was done at 37 ºC for 1-12 hours and 24 hour. The digestion reaction stopped using heating at 95 ºC for 15 minutes. After the centrifuging sample, the supernatant was filtered from10 and 1 kDa cutoff membranes respectively. The utterance of 1kD membrane was purified using C_{18} -HPLC and the inhibitor activity of different fractions was evaluated using N-[3-(2-Furyl)acryloyl]-L-phenylalanyl-glycyl-glycine(FAPGG) substrate.

Results:

The results showed that QEW proteins are a benefit source from bioactive peptides after hydrolyzed by trypsin-papain. Base upon our results, Maximum degree hydrolysis was observed at 2 hour.

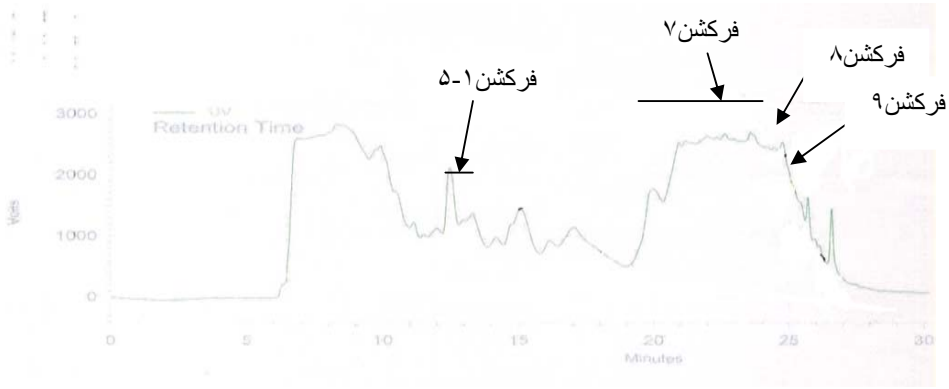

Fig 1. Reverse-phase HPLC profile of trypsin-papain fractions on c18 column.

The purified fractions of 5-1, 7, 8 and 9 have inhibitor activity 91.7%, 91.7 %, 62.4% and 90.8% respectively when they were compared with control. The IC_{50} of these fractions were shown 0.0136 mg/ml, 0.0136 mg/ml, 0.020 mg/ml and 0.0137 mg/ml respectively. Base on these enzyme inhibitory activities, fraction 7 was selected for kinetics studies to elucidate their mode of inhibition of ACE activity. The K_i for 0.0931 and 0.1552 mg/ml of peptide were 0.3097 and 0.7625 mg/ml, respectively.

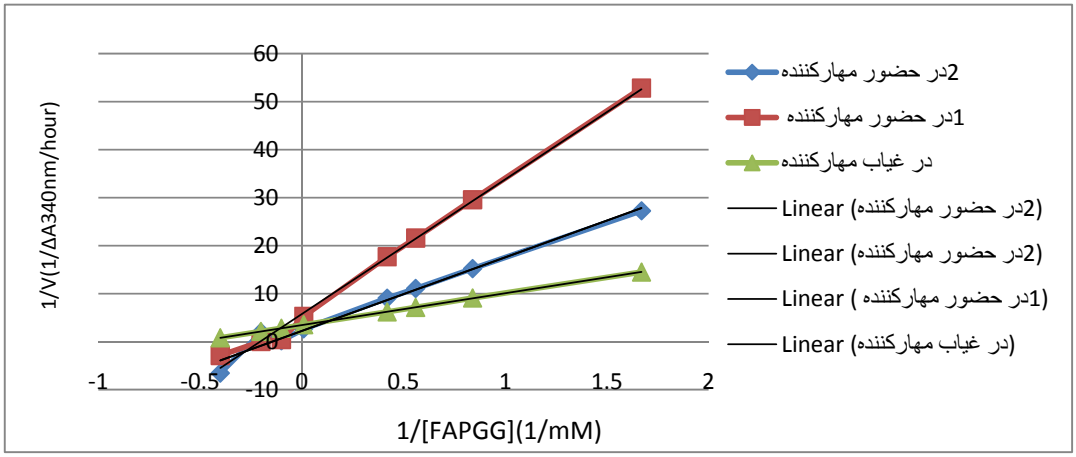

Fig 2. Lineweaver-Burk plots of ACE inhibition by the purified peptides: The ACE activities were measured in the presence or absence of the purified peptide. 1/V and 1/S represent the reciprocal velocity and substrate, respectively.

Kinetic parameters	control	F7(0.0931mg/ml)	F7 (0.1552 mg/ml)
K_m(mM)	0.1922	0.444	0.813
V_{max}(A.houre^{-1})	0.290	0.290	0.290
K_i(mg/ml)		0.3097	0.7625

Table 1. Kinetic constant of ACE inhibitor in the absence and presence of different concentration of trypsin-papain peptide fraction7.

Discussion:

In this study we used the enzymatic hydrolysate of QEW to investigate their inhibition potential of ACE. The Lineweaver-Burk plot indicates that the fraction 7 is competitive inhibitor. This means that peptide fraction 7 competes for the same active site as the substrate molecule. The peptide can combine with ACE molecule to produce a complex, regard of weather a substrate molecule is bound or not.

Conclusions:

The inhibition of the activities of ACE observed in this study is dependent on the ability of proteases used for hydrolysis to release bioactive peptide sequences from QEW proteins rather than the protein yield of low-molecular-weight peptides. Among different fractions, the fraction of 5-1 and 7 has maximum inhibitory percent and minimum value of IC_{50} and therefore, results showed that the inhibitor is stuck on the enzyme and prevents any substrate molecules from reacting with the enzyme. The QEW protein hydrolysates are benefit source of bioactive anti-hypertension peptides.

References

[1] Rafik Balti, Naima Nedjar-Arroume, Ali Bougatef, Didier Guillochon, Moncef Nasri., Food Research International 43(2010) 1136-1143.

[2] A. Fahmi, S. Morimura, H. C. Guo, T. Shigematsu, K. Kida, Y. Uemura. Process Biochemistry 39(2004) 1195-1200.

[3] H. J. Suh, J. H. Whang & H. Lee. Biotechnology Letters 21(1999) 1055-1058.

[4] Chibuike C. Udenigwe, Yin-Shiou Lin, Wen-Chi Hou, Rotimi E. Aluko. Journal of Functional Foods I (2009) 199-207.

Pyrolysis Kinetics Study of Coordination Polymer by Thermal Analysis

Sh. Rafiei[a], Kamran Akhbari[b], M. Oftadeh[c]

a. Emam Khomeini International University ,Ghazvin, Iran(shahnaz22rafiei@yahoo.com)

b. Tarbiat Modares University, Tehran, Iran

c. b. Payam- Noor University, Esfahan, Iran

Abstract:

In this paper, the thermal behavior of coordination polymer in a nitrogen atmosphere were studied by thermogravimetry technique . Coordination polymer in such as a 2D polymer with unique Ag–C bonds and 3D polymer built with the assistance of η^2 Ag–C bonds, [Ag2(l8-SB)] (1) [H2SB = 4-[(4-hydroxyphenyl)sulfonyl]-1-benzenol], [Tl4(l8-SB)2] (2), [Ag(l4-DPOAc)]n (3) [DPOAc = diphenylacetate] , [Tl(l3-DPOAc)]n (4), has been synthesized and characterized and its structure was determined by X-ray crystallography. The thermal stabilities of 1 and of its thallium(I) analogue, [Tl4(l8-SB)2] (2), also 3 and of its thallium(I) analogue(4), were studied by thermogravimetry (TG) and differential thermal analyses (DTA).The kinetic study was accomplished using TG curves based on weight loss as a function of temperature. The activation energy calculated as well as from the Arrhenius equations.

Keywords: Coordination polymer, Thermogravimetry study, Arrhenius equation, Activation energy.

Introduction

The use of bridging ligands for the controlled self-assembly of one-, two- or thee-dimensional metallo supramolecular species has been the subject of enormous study in recent years [1]. These supramolecular architectures are esthetically appealing and exhibit potential applications as molecular wires [2], electrical conductors and in host–guest chemistry [3]. The design of polymeric coinage d10 metal complexes with fascinating structures has received much attention [4], among these metals, silver has received much attention because silver (I) shows a tendency to form coordination polymers and unique Ag–C bonds [5].

Crystallographic data and details of the data collection and structure refinements of compound 1 are listed in Table 1.

Table 1 Crystal data and structure refinement for [Ag2(l8-SB)] (1)

Identification code	1
Empirical formula	C12H8Ag2O4S
Formula weight	463.98
Temperature	100(2) K
Wavelength 0.71073A °	
Crystal system Orthorhombic	
Space group Fmm2	
Unit cell dimensions	
a (A°) 17.9958(18)	
b (A°) 7.0921(7)	
c (A°) 9.2580(9)	
Volume (A ° 3) 1181.6(2)	
Z 4	
Density (calculated) (Mg/m3) 2.608	
Absorption coefficient (mm_1) 3.495	
F(000) 888	
Crystal size (mm) 0.36 _ 0.36 _ 0.22	
h Range for data collection (_) 2.26–28.25	
Index ranges _23 6 h 6 23, _9 6 k 6 9, _12 6 l 6 12	
Reflections collected 2893	
Independent reflections [R(int)] 821 [0.0157]	
Completeness to h (_) 28.28: 100.0%	
Absorption correction Multi-scan	
Maximum and minimum Transmission	
0.464 and 0.374	
Refinement method Full-matrix least-squares on F2	
Data/restraints/parameters 821/74/64	
Goodness-of-fit on F2 1.207	
Final R [I > 2r(I)] R1 = 0.0346, wR2 = 0.1005	
R indices (all data) R1 = 0.0349, wR2 = 0.1026	
Largest difference in peak and hole (eA ° _3)	
4.110 and _0.842	

Thermogravimetry analysis is a simple analytical technique that measures the weight loss (or weight gain) of a material as a function of temperature. As materials are heated, they can lose weight from a simple process such as drying, or from chemical reactions that liberate gasses. Thermo-analytical methods such as thermogravimetry(TG), differential thermal analysis (DTA) and differential scanning calorimetric (DSC) have proved to play important role in the study of thermal decomposition of solid fuels and coordination polymer [6,7].

Kinetic studies have become a crucial point in thermal analysis, in which the main purpose is to calculate the parameters of the Arrhenius equation. The knowledge of such parameters for energetic material and coordination polymer is also meaningful in order to elucidate miscibility/ compatibility and its efforts on thermal stability [8].The purpose of this was to study the thermal behavior coordination polymer by thermo gravimetric (TG) method. The influence of heating rate on the this compound was investigated.

Experimental Methods:

All chemicals were of reagent grade and were used as commercially obtained without further purification. The thermal behavior was measured with a Perkin-Elmer apparatus.

For experimental Parameters, 12 mg samples, a nitrogen atmosphere (100 ml min^{-1}), and a linear heating rate of 20 C min^{-1} were used. All experiments were performed over a temperature range of 25 to 800 C using platinum crucibles. Prior to the experiments, the TG apparatus was calibrated via the melting points of indium (156.6 ^{o}C), tin (231.9 ^{o}C) and aluminum (660.2 ^{o}C) standards under the same conditions as for the samples. Alumina was used as reference material in all experiments. The weight loss (TG signal) and the rate of weight loss (DTA signal) as a function of time or temperature were recorded, while the coordination polymer were subjected to a computer-controlled temperature program. The TG and DTA curves were obtained by a Perkin Elmer model instrument.

Compound 1 is very stable and does not decompose up to 419 _C, at which temperature decomposition starts. In this stage, exothermic removal of SB2_ occurs between 419 and 502 _C with a mass loss of 53.0% (calcd 53.5%). Mass loss calculations show that the final decomposition product is metallic silver, (Fig. 1). Compound 2 is much less stable at starts to decompose at 249 _C. The TG curve exhibits a distinct decomposition stage between 249 and 560 _C with a mass loss of 37.9%, (calcd 36.6% for the formation of thallium (I)oxide). The DTA curve displays a distinct endothermic peak at 240 _C and three exothermic peaks at 362, 398 and 532 _C, (Fig. 2).

Compound 3 is stable up to 235 _C. The TG curve exhibits a distinct decomposition stage between 235 and 480 _C with a mass loss of 63.0% (calcd. 63.6% for the formation of Ag2O). DTA curve displays three distinct exothermic peaks at 240, 300 and 450 _C and a endothermic peak at 600 _C. Compound 4 is stable up to 181 _C. TG curve exhibits a distinct decomposition stage between 193 and 550 _C with a mass loss of 48.5% (calcd. 48.9% for the

formation of Tl2O). The DTA curve displays a distinct endothermic peak at 181 _C and two exothermic peaks at 227 and 339 _C (see Figs. 3 and 4). Ea and A are listed in Table 2.

Results and discussion:

There are a number of approaches for modeling the complex pyrolysis process. The simplest is the empirical model, which employs global kinetics, where the Arrhenius expression is used to correlate the rates of mass loss with temperature [9].

The pyrolysis process of coordination polymer can be represented by the following reaction:

coordination polymer $\rightarrow$Volatile + Coke (1)

For analyzing the kinetics of TG/DTA data, the model assumes that the rate of weight loss of the total sample is dependent only on the rate constant, the remaining weight of the sample and its temperature with a reaction order of unity. The shift in the DTA peak is a measure of reactivity value.

The kinetic parameters of the thermal decomposition reactions were calculated by using an Arrhenius-type kinetic model assuming that there is rst-order reaction [10].The kinetic analysis of non-isothermal pyrolysis, in general, is based on the following equations:

$dW/dt = k.W^n$ (2)

$k = A \exp -E/RT$ (3)

$\text{Log}[(dW/dt).(1/w)] = \text{Log}A - E/2.303RT$ (4)

Where dW/dt is the rate of weight change of the reacting material in min^{-1}, A is the Arrhenius constant or pre-exponential factor in 1 min^{-1}, E is the activation energy in kJ mol^{-1}, T is the temperature in K, n is the reaction order and R is the gas constant in 8.314 J $mol^{-1}K^{-1}$.

In the model, the plot of Log[(dW/dt).(1/W)] against 1/T is a straight line with a slope of E/2.303R. The magnitude of the slope can be used to calculate the activation energy (E_a). The pre exponential factor (A) can be calculated from the intercept. The TG and DTG curves for coordination polymer recorded from temperature room to 850 ^oC are shown in Figure 4. Activation energy (E_a) by applying the Arrhenius equation (4). Arrhenius plot is shown in Figure 5, that the activation energy(E_a) value for coordination polymers were calculated

Conclusions

The rates pyrolysis of coordination polymer was calculated from the Arrhenius equation. This method seems to be very simple because the kinetic data can be obtained from TG and DTA

curves. Activation energy (E_a) and exponential factor (A) and details of the data collection are listed in Table 2.

Table 2

The activation energy (E_a) and exponential factor (A) for compounds 1 and 2

	E_a	A
compound 1	42.068	7.7492
compound 2	32.676	9.0866
compound 3	147.482	35.394
compound4	65.054	16.825

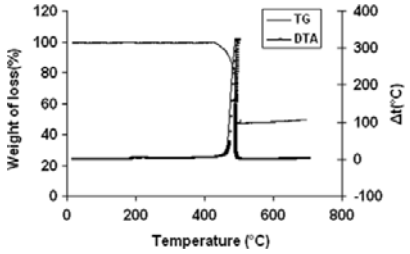

Fig. 1. Thermogram of compound [Ag2(l8-SB)] (1).

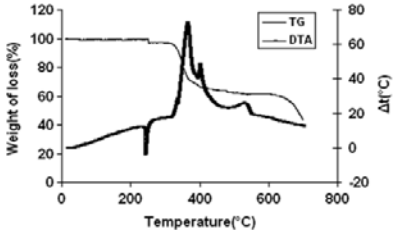

Fig. 2. Thermogram of compound [Tl4(l8-SB)2] (2).

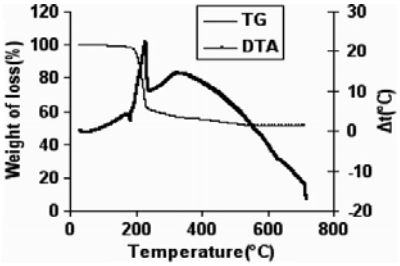

Fig. 3. Thermal behaviour of compound [Tl(l3-DPOAc)] (3).

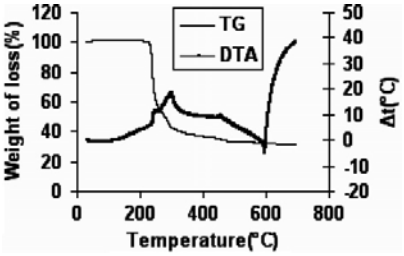

Fig. 4. Thermal behaviour of compound [Ag(l4-DPOAc)]n (4).

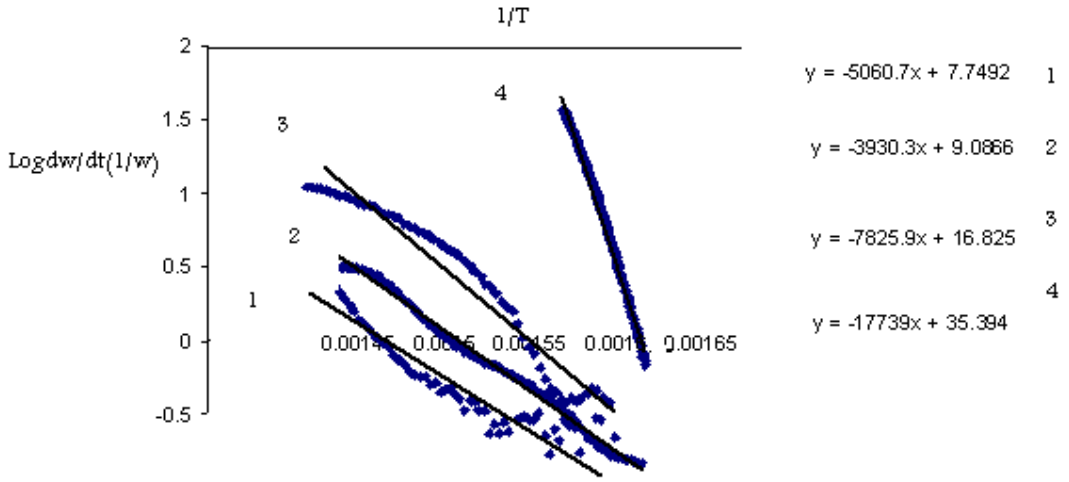

Fig.2 : Log[(dW/dt).(1/W)] against 1/T

References:

[1] S. Leininger, B. Olenyuk, P.J. Stang, Chem. Rev. 100 (2000) 853;

[2] K.-T. Wong, J.-M. Lehn, S.-M. Peng, G.-H. Lee, Chem.Commun. (2000) 2259;

[3] M. Aoyagi, K. Biradha, M. Fujita, J. Am. Chem. Soc. 121 (1999)7457;

[4] M.L. Tong, X.M. Chen, B.H. Ye, L.N. Ji, Angew. Chem. 111(1999) 2376;

[5] M. Munakata, L.P. Wu, G.L. Ning, T. Kuroda-Sowa, M.Maekawa, Y. Suenaga, N. Maeno, J. Am. Chem. Soc. 121 (1999),4968;

[6] O. O. Sonibare, O. A. Ehinola, L.Kea Giap and R. Egashira, J. *Appl. Sciences* 5(1) 104-107(**2005**).

[7] P Gabbott, *Principles and application of thermal analysis* (**2008**) Blackwell publishing LTD .

[8]S .M. Pourmortazavi, J. Kohsari, M.B. Teimori, S. S. Hajimirsadeghi, *Materials Letters* , 61(**2007**) 4670-4773.

[9] W. A. Kneller, *Thermochimica Acta*, **(1986)**108, 357-388.

[10] S.Wang, V. Sloval, B. S. Haynes, *Fuel Processing Technology***(2005)**86,651-660.

Effects of β-cyclodextrin on thermal stability of lysozyme at different pH

G. Rezaei Behbehani [a], A. Taherkhani [a], A. A. Saboury [b], A. A. Divsalar [b, c]Sh. Rafiei[a]

[a] Chemistry Department, faculty of science, Islamic Azad University, Takestan branch, Takestan, Iran. E-mail:grb402003@yahoo.com

[b] Institute of Biochemistry and Biophysics, University of Tehran, Tehran, Iran

[c] Department of Biological Sciences, Tarbiat Moallem University, Tehran, Iran

Abstract

Effects of β-cyclodextrin, βCD, on unfolding and aggregation of lysozyme was investigated at pH12 employing isothermal titration calorimetry (ITC) at 300 in 30mM Tris buffer solution. βCD was employed as an anti-aggregation agent and the heats obtained for lysozyme+βCD interactions are reported and analyzed in terms of the extended solvation theory. It was indicated that there are two sets of identical and non-cooperative sites for βCD.

Keywords: Lysozyme**;** Isothermal Titration Calorimetry; β-cyclodextrin; Binding parameters.

Introduction

Cyclodextrins (CDs) have been reported to suppress aggregate formation during the refolding of a wide range of proteins. Their potency is often ascribed to their affinity for aromatic amino acids, whose surface exposure would otherwise lead to protein association. However, no detailed structural studies are available. CDs inhibited the chemically induced aggregation and its inhibition was generally in the order of γ-CDs < α-CDs < β-CDs. Hydrophilic CDs reduced the thermally induced unfolding of lysozyme as shown by a decrease in the thermal unfolding temperature (T_m) value of lysozyme, suggesting that CDs destabilize native lysozyme or stabilize the unfolded state of lysozyme [1-3]. Electrophoresis data indicate that CDs, which promoted lysozyme refolding, arrested aggregation at the stage of smaller soluble aggregates [3].

In this work, we have attempted to find the binding parameters and conformational changes of lysozyme due to its binding with βCD at PHs 7 and 12. A structure-activity relationship study between βCD and refolding of lysozyme was performed, in order to better understand the

mechanism of βCD-assisted protein refolding and to identify βCD that could function as good protein folding agents.

Experimental

The isothermal titration calorimetric experiments were carried out on a VP-ITC ultra sensitive titration calorimeter (MicroCal, LLC, Northampton, MA). The microcalorimeter consists of a reference cell and a sample cell of 1.8mL in volume, with both cells insulated by an adiabatic shield. All solutions were thoroughly degassed before use by stirring under vacuum. The sample cell was loaded with lysozyme solution (1.26mM) and the reference cell contained buffer solution. The solution in the cell was stirred at 307 rpm by the syringe (equipped with micro propeller) filled with βCD solution (30mM) to ensure rapid mixing. Injections were started after baseline stability had been achieved. The titration of lysozyme with βCD solution involved 30 consecutive injections, the first injection was 5 μL and the remaining ones were 10 μL. In all cases, each injection was done in 6s at 3-min intervals. To correct the thermal effects due to βCD dilution, control experiments were done in which identical aliquots were injected into the buffer solution with the exception of lysozye. . The determined heats for lysozyme+βCD interaction were reported.

Results and discussion

We have shown previously [3-7] that the heats of the macromolecules + ligands interactions in the aqueous solvent systems can be reproduced by the following equation:

$$q = q_{\max} x'_{\mathrm{B}} - \delta^{\theta}_{\mathrm{A}}(x'_{\mathrm{A}} L_{\mathrm{A}} + x'_{\mathrm{B}} L_{\mathrm{B}}) - (\delta^{\theta}_{\mathrm{B}} - \delta^{\theta}_{\mathrm{A}})(x'_{\mathrm{A}} L_{\mathrm{A}} + x'_{\mathrm{B}} L_{\mathrm{B}}) x'_{\mathrm{B}} \qquad (1)$$

The parameters $\delta^{\theta}_{\mathrm{A}}$ and $\delta^{\theta}_{\mathrm{B}}$ reflect to the net effect of CD on the lysozyme stability in the low and high dextrin concentrations respectively. The positive values for $\delta^{\theta}_{\mathrm{A}}$ or $\delta^{\theta}_{\mathrm{B}}$ indicate that CD stabilizes the lysozyme structure and vice versa. x'_{B} can be expressed as follows:

$$x'_{\mathrm{B}} = \frac{p x_{\mathrm{B}}}{x_{\mathrm{A}} + p x_{\mathrm{B}}} \qquad (2)$$

$p > 1$ or $p<1$ indicate positive or negative cooperativity of macromolecule for binding with ligand respectively; $p=1$ indicates that the binding is non-cooperative. x'_{B} is the fraction of bound cyclodextrin and $x'_{\mathrm{A}} = 1 - x'_{\mathrm{B}}$ is the fraction of unbound cyclodextrin. We can express x_{B} as follows:

$$x_B = \frac{[CD]_T}{[CD]_{max}} \qquad x_A = 1 - x_B \qquad (3)$$

$[CD]_T$ is the total concentration of cyclodextrin and $[CD]_{max}$ is the maximum consternation of cyclodextrin. L_A and L_B are the relative contributions due to the fractions of unboundedand bounded ligand in the heats of dilution

The heats of lysozyme+CD interactions were fitted to Eq. 1 over the entire Theophylline concentrations. In the procedure, the only adjustable parameter (p) was changed until the best agreement between the experimental and calculated data was approached. δ_A^θ and δ_B^θ parameters have been also optimized to fit the data. The small relative standard coefficient errors and the high r^2 values (0.9999) support the method.

The clear breaks in the curve of heats, q, for lysozyme+βCD interaction indicate that there are two sets of binding sites on lysozyme. The dissociation equilibrium constant *(K_d)* and the number of binding sites "g" can be determined by the following equation [4-8]:

$$\frac{\Delta q}{q_{max}} M_0 = (\frac{\Delta q}{q}) L_0 \frac{1}{g} - \frac{K_d}{g} \qquad (5)$$

Where $\Delta q = q_{max} - q$ and q represents the heat value at a certain βCD *(L_0)* and lysozyme (M_0) concentrations and q_{max} represents the heat value upon saturation of all lysozyme molecule. Therefore, the plot of $(\frac{\Delta q}{q_{max}})M_0$ *vs.* $(\frac{\Delta q}{q})L_0$ should be a linear plot with slope of "$\frac{1}{g}$" and the vertical-intercept of $\frac{K_d}{g}$, which "g" and K_d can be obtained (table 1). If q and q_{max} are calculated per mole of lysozyme, then the standard molar enthalpy of binding for each binding site, ΔH^0, will be $\Delta H^0 = \frac{q_{max}}{g}$. The binding parameters for lysozyme + cyclodextrin interactions recovered from Eq. 1 were listed in Tables 1. δ_A^θ and δ_B^θ values for lysozyme+CD interaction are positive, indicating that in the low and high concentrations of β-cyclodextrin, lysozyme structure was stabilized.

Also these results suggest that the effects of βCD on lysozyme refolding are attributed to its ability to suppress aggregation of lysozyme. βCD reduced the unfolding of lysozyme as evidenced by large values of association equilibrium constants at pH 12, suggesting that βCD stabilize native or unfolded state of lysozyme.

Table 1 Binding parameters for lysozyme+βCD interaction recovered from Eqs.1 and 2 at pH 12. p=1 indicates that the binding is non-cooperative in two sets of binding sites. The positive values of δ_A^θ or δ_B^θ indicate that βCD stabilizes the lysozyme native structure The interaction is strong and both enthalpy and entropy driven.

parameters	First binding sites	Second binding sites
p	1	1
g_i	2.00±0.01	5.03±0.08
K_a/ M	110689.30±21.15	34903.13±13.06
ΔH/ kJ mol^{-1}site^{-1}	-115.76±0.45	-23.08±0.13
ΔG/ kJ mol^{-1} site^{-1}	-26.77±0.15	-25.92±0.25
ΔS/ kJ mol^{-1} site^{-1}	-0.29±0.02	0.01±0.01
δ_A^θ	-1.87±0.03	
δ_B^θ		-0.33±0.02

Reference

[1] Pirzadeh, P.; Moosavi-Movahedi, A.A.; Hemmateenejad, B.; Ahmad, F.; Shamsipur, M.; Saboury, A.A.: Chemometric studies of lysozyme upon interaction with sodium dodecyl sulfate and β-cyclodextrin. Colloids and Surfaces B: Biointerfaces **52** 31–38 (2006)

[2] Tavornvipas, S.; Hirayama' F.; Takeda, S.; Arima, H.; Uekama**,** K.: Effects of cyclodextrins on chemically and thermally induced unfolding and aggregation of lysozyme and basic fibroblast growth factor. J. Pharm. Sci. **95** 2722 – 2729 (2006)

[3] Desai, A.; Lee, C.; Sharma, L.; Sharma, A.: Biochimie **88** 1435-453 (2006)

[4] Rezaei Behbehani, G.; Saboury, A. A.; Fallah baghery, A.: A Thermodynamic Study on the Binding of Calcium Ion with Myelin Basic Protein. J. Solution Chem. **36**, 1311-1320 (2007)

[5] Rezaei Behbehani, G.; Divsalar, A.; Saboury, A.A.; Hajiand, R.; Rezaeid, Z.; Yahaghi, E.: A thermodynamic study on the binding of Cobalt and iron ions with bovine carbonic anhydrase II molecule at different temperatures. J Solution Chem **39** 1142–1152 (2010)

[6] Rezaei Behbehani, G.; Saboury, A.A.; Takeshi, E.: Determination of partial unfolding enthalpy for lysozyme upon interaction with dodecy ltrimethylammonium bromide using an extended solvation model. J. Mol. Recognit. **21**, 132-135 (2008)

[7] Rezaei Behbehani, G.; Saboury, A.A.: A directcalorimetric determination of denaturation enthalpy for lysozyme in sodiumdodecylsulfate, J. Coll. Surf. B: Biointerfaces. **61**, 224-228 (2007)

[8] Rezaei Behbehani, G.; Divsalar, A.; Bagheri, M. J.; Saboury, A. A.: A Thermodynamic Study on the Binding of human Serum Albumin with New synthesized Anti cancer Pd (II) complex. J. Solution Chem. (2008).

Kinetic modeling of Fischer-Tropsch Synthesis on supported Fe/Ni catalyst

Majid Sarkari[a]; F.Fazlollahi[a]; M.M Zarei[a]; H. Rezaei[a]; H. Atashi[*a], A.A. mirzaei[b], H.Ajamein[a]

Department of Chemical Engineering, University of Sistan & Baluchestan, Zahedan, Iran

Department of Chemistry, University of Sistan & Baluchestan, Zahedan, Iran

**Corresponding Author E-mail: h.ateshy@hamoon.ac.ir*

Abstract

A bimetallic Fe/Ni catalyst was prepared using the sol/gel technique in order to kinetic study in fixed-bed micro-reactor under the operation condition as follows: temperature of 220-260℃; H2/CO feed ratio of 1-2; pressure 1-12 bar and at constant space velocity of 4500 h^{-1}. All experiments were carried out in the absence film-mass-transfer resistance. The experiment data of this study were fitted fairly well by a semi empirical kinetic rate expression based on Langmuir-Hinshelwood-Hougen-Watson (LHHW) to form $-R_{CO} = kP_{CO}^{-1.33}P_{H2}^{0.83}/(1 + cPCO{-}1.33PH20.83)4$. Kinetic parameters were determined by means of Levenberg-Marquardt algorithm and the apparent activation energy and reaction enthalpy were obtained 67.38 kJ/mol and -36.47 kJ/mol, respectively.

Keywords: bimetallic catalyst; Fischer-Tropsch synthesis, sol/gel technique, Kinetic modeling,

Introduction

An approach to improve the selectivity of the classical Fischer–Tropsch (FT) process for conversion of synthesis gas to hydrocarbons involves the use of a bifunctional catalyst system containing a metal catalyst (FT catalyst) combined with a support [1]. The kinetic description of the FT reaction is very important task for the industrial practice, being a prerequisite for the industrial process design, optimization and simulation. In this probe the kinetics of FT reaction based on LHHW approach was studied and based on the statistical criteria appropriate model was obtained and the kinetics parameters were determined.

Experimental section

1. Preparation of Catalyst

Preparation of 40% Fe/60%Ni/10 wt.%La_2O_3 catalyst using sol/gel technique. $Fe(NO_3)_2 \cdot 9H_2O$ (5.89 g) and $Ni(NO_3)_2.6H_2O$ (6.07 g) was dissolved in 40 ml Tetra etoxicilan and 40 ml ethanol mixture at 80 °C. After stirring for 10 min, La_2O_3 (0.2 g) were added to a homogeneous transparent solution. in order to hydrate water of the nitrates, nitric acid (HNO_3) were added in the prepared solution. Then the sample was stirred at 30 °C for 1 h to give transparent monolithic gel. The gel was dried at 120 °C in vacuum, powdered and calcined at 650 °C for 6 h in air.

2. Catalytic performance

The reactor setup was exactly the same as during the preceding study that was published previously. To summarize briefly, the experiments were performed in a fixed-bed micro-reactor made of stainless steel with an inner diameter of 12mm.Three mass flow controllers (Brooks,Model,5850E) were used to adjust automatically flow rate of the inlet gases comprising CO, H2 and N2 (purity of 99.99%).). More details about the reactor system, as well as a schematic diagram, are presented elsewhere [2].

Result and discussion

1. Development and testing of the kinetic models

Totally, 24 experimental values were collected for kinetic study by table 1.

Table 1. **Values of CO Consumption Rate Using 40%Fe/60%Ni/10wt%La_2O_3 Catalyst**

No of exp	T (K)	P (bar)	H_2/CO	X_{CO}%	$-r_{CO} \times 10^{+5}$ (mol CO/gr_{cat}.min)
1	493	6.5	2	7.33	23.25
2	503	12	2	10.59	61.27
3	513	9.4	1.5	18.48	81.45
4	523	12.4	1.5	17.58	100.27
5	523	3.4	1.75	16.87	26.38
6	534	9.4	1.75	18.87	109.1

The models regarded during this research have been arranged into four classes and are presented in Tables 2.

Table 2. **Kinetic models**

Class	Kinetic expression	Parametric equation	model
I	$-r_{CO}=A\frac{P_{CO}P_{H_2}^2}{(1+b_{CO}P_{CO}P_{H_2})}$	$-r_{CO}=A\frac{P_{CO}^m P_{H_2}^n}{(1+b_{CO}P_{CO}^m P_{H_2}^n)}$	FT-I
II	$-r_{CO}=A\frac{P_{CO}P_{H_2}}{(1+b_{CO}P_{CO})^2}$	$-r_{CO}=A\frac{P_{CO}^m P_{H_2}^n}{(1+b_{CO}P_{CO}^m)^2}$	FT-II
III	$-r_{CO}=A\frac{P_{CO}P_{H_2}}{(1+b_{CO}P_{CO})^3}$	$-r_{CO}=A\frac{P_{CO}^m P_{H_2}^n}{(1+b_{CO}P_{CO}^m)^3}$	FT-III
IV	$-r_{CO}=A\frac{P_{CO}P_{H_2}^2}{\left(1+b_{CO}P_{CO}P_{H_2}^{0.5}\right)^4}$	$-r_{CO}=A\frac{P_{CO}^m P_{H_2}^n}{(1+b_{CO}P_{CO}^m P_{H_2}^n)^d}$	FT-VI

Where both of these parameters (A and b_{CO}) are temperature dependent and described according to the Arrhenius form equations, $A= A_0 \exp(-E/RT)$; $b_{CO}=b_0 \exp(-\Delta H/RT)$.

2. Statistical analysis

The rival rate expression of table (1) was also fitted to set of experimental data in order to estimation of the values of the kinetic parameters by minimizing the relative using the Levenberg-Marquardt algorithm. The results of the best kinetic rate expression show in Table (2)

Table 4.**Estimated values of the best parametric kinetic models and statistical criteria.**

Model	Kinetic parameter							Statistical indicator	
	A_0	b_0	E (k j/mol)	ΔH (kjlmol)	m	n	d	R^2_{adj}	Rmsd
FT-IV	3.760×10^{-5}	0.0095	67.38	-36.47	-1.33	0.83	4	0.972	8.72×10^{-7}

Units of k_0 and c_0 in FT-IV are, bar $^{-0.5}$ mol g^{-1} min^{-1} and bar $^{-0.5}$, respectively.

Conclusion

Experiments for the kinetics of CO consumption in the FTS reaction were conducted over bimetallic iron catalyst in fixed-bed micro-reactor over a range of reaction condition. Four classes of kinetic rate expression based on Langmuir-Hinshelwood-Hougen-Watson approach on the basis of a detailed set of possible reaction mechanism were developed.

The kinetic parameters were estimated from experimental data using non linear regression (Levenberg- Marquardt algorithm). The data of this study are fairly well fitted by the semi-empirical model FT-IV rate expression. The apparent activation energy and reaction enthalpy were obtained 67.38 kJ/mol and -36.47 kJ/mol, respectively.

References

[1] Ali. A Mirzaei, A. Beigbabaei, M. Galavy, A.Youssefi, **Fuel Processing Technology** 91(2010)335–347.

[2] H.Atashi, F.Siami, A.A.Mirzaei, M.Sarkari, **Journal of Industrial and Engineering Chemistry**16 (2010) 952–961

[3]Ali A. Mirzaei, M.Faizi, R. Habibpour, **Applied Catalysis A:General** 306 (2006) 98–107.

Intrinsic kinetic of catalized Fischer-Tropsch Synthesis over $Fe/Co/Al_2O_3$

Seyyed Mahmoud Musavi; Majid Sarkari[a]; F. Fazlollahi[a]; H. Atashi[*a], A.A. Mirzaei[b]
Department of Chemical Engineering, University of Sistan & Baluchistan, Zahedan, Iran
Department of Chemistry, University of Sistan & Baluchistan, Zahedan, Iran
*Corresponding Author E-mail: h.ateshy@hamoon.ac.ir

Abstract

In this paper, an experimental study was performed with impregnation $Fe/Co/Al_2O_3$ catalyst in a laboratory fixed bed micro-reactor to develop a macro kinetic expression for the Fischer-Tropsc synthesis (FTS) far as internal and external mass transfer diffusion. A kinetic model was found to be the preferred two-parameter rate equation of the reaction. It was shown that this model is assumes the following kinetically relevant steps in the cobalt-FT synthesis: CO dissociation occurs without hydrogen interaction and is not limiting step; the first hydrogen addition to surface carbon and the second hydrogen addition to surface oxygen are the rate-determining steps.

Keywords: *hydrogen interaction, mass transfer, rate-determine.*

Introduction

Fischer-Tropsch synthesis (FTS) is the conversion of synthesis gas, which refine to ultra-clean high cetane diesel fuels and chemical feed stocks [1]. Only the four group VIII metals, Fe, Co, Ni and Ru have sufficiently high activities for the hydrogenation of carbon monoxide to warrant possible application in the FT synthesis [2]. The product distribution has been influenced by process variable such as temperature, pressure, gas flow rate and H_2/CO ratio in feed. Kinetic of Fischer –Tropsch synthesis have been studied by many researcher and many mechanistic schemes have been proposed but among proposed mechanism the surface Carbide mechanism have been noted more than other mechanisms. But due to complexity and varied parallel steps with many species that affect the reaction path, the actual kinetic model has not been known completely [3]. The goal of this paper is represent kinetic model for CO consumption rate for FT synthesis.

Experimental Section

Catalyst Preparation.

The catalyst was (50%Fe/50%Co/90%wt.%Al_2O_3) prepared using impregnation procedure from mixed of Fe_2 $(NO_3)_3$. $9H_2O$ (98%, Merck, Germany) and Co $(NO_3)_2$ $4H_2O$ (97% , Merck, Germany). For preparation of the supported catalysts, amount (90wt %) Al_2O_3 (98%, Merck), has been added to the mixture of iron and cobalt nitrates with nominal ratio of resulting mixture heated to 120 °C for 16 hours and the calcinations have been occur in static air at 600°C for 6 hours. The catalyst used in this work was pressed, crushed and sieved to 5 mesh size.

Result and discussion

Removed of limitation of internal and external catalyst mass transfer diffusion

The kinetic measurements were performed in a fixed bed micro reactor. Prior to analysis, the effects of the pore and film mass-transfer resistances were tested and eliminated using appropriate operating conditions. To check the external transport resistances, the feed flow rate was changed with a corresponding change in catalyst loading, so that a constant space velocity was achieved. Because the points that correspond to the same GHSV but different flow rates are close together, as shown in Fig.2, it can be seen that over the range of interest, film resistance is not significant. To examine the internal diffusion resistance, 1.0 gram catalyst with different sizes, 125, 290, 365, 420 505 μm and were loaded under same conditions. As shown in Fig.3 no pore diffusion was evident for particle size lower than 0.3 mm. Therefore, under the test Conditions used, the internal and external mass-transfer limitations were not significant.

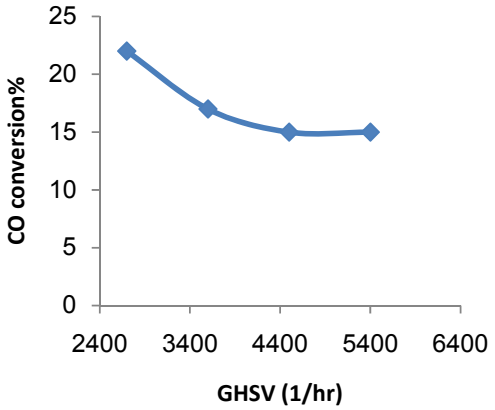

Fig1. Variation of the CO conversion as a function of the GHSV value. Conditions: 1atm, T: 590 K

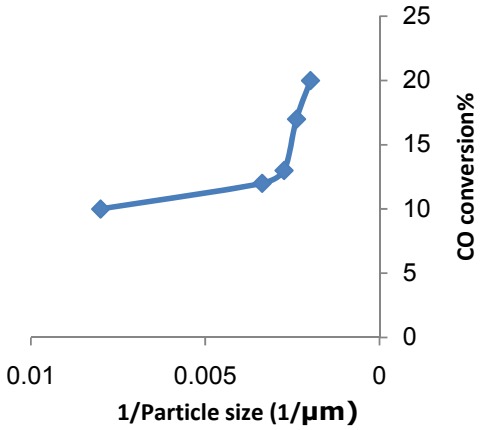

Fig 2. Variation of the CO conversion as a function particle size. Conditions: 1atm, T:623 K

Kinetic Model.

The kinetic tests were carried out over Fe-Co in fixed bed micro-reactor under the operation condition as follows: temperature of 230-280°C; H2/CO feed ratio of 1-2; pressure 4-16 bar and at constant space velocity of 4500 h^{-1}.

Overview of mechanism

The kinetic of Fischer –Tropsch synthesis have been studied by many researcher and many mechanistic schemes have been proposed but among proposed mechanism the surface Carbide mechanism have been noted more than other mechanisms. The bases of carbide mechanism was the dissociation of adsorbed CO and H2 to form dissociated adsorbed Carbon and Hydrogen followed by hydrogenation of adsorbed carbon with adsorbed dissociated hydrogen, hydrocarbon will be produce. The schem of this mechanism was illustrated in Figure 3.

α-Olefins

n-Paraffin

Fig 3. Reaction steps for the Carbide mechanism use in FTS

Conclusion

The intrinsic of the Fe-Co impregnation catalyst far as limitation of internal and external mass diffusion was investigated. The results illustrated that with increasing of particles size the selectivity of light olefin was increased. Therefore, the mechanistic aspects of Fischer-Tropsch synthesis reaction over catalyst proceed via carbide mechanism.

References

[1]. F.Gideon Botes, Braam van Dyk, and Craig McGregor., The Development of a Macro Kinetic Model for a Commercial Co/Pt/Al_2O_3 Fischer-Tropsch Catalyst, Ind. Eng. Chem. Res. 2009, 48, 10439–10447.

[2]. Ander Steinberg, M. dry, Fischer-Tropsch Technology, (Eds) Vol. 152, 2004.

[3]. Jung Hoon Yang et al., Mass transfer limitations on fixed-bed reactor for Fischer–Tropsch synthesis, Fuel Processing Technology 91 (2010) 285–289

Effect of catalyst preparation method in the product distribution in Fischer- Tropsch synthesis

Majid Sarkari[a] ; H. Ajamein[a]; F. Fazlollahi[a] ;M.M. Zarei[a];H. Rezaei[a];H. Atashi[*a], A.A. mirzaei[b]

Department of Chemical Engineering, University of Sistan & Baluchestan, Zahedan, Iran

Department of Chemistry, University of Sistan & Baluchestan, Zahedan, Iran

Corresponding Author E-mail: h.ateshy@hamoon.ac.ir

Abstract

In this investigation Fe/Mn/Al_2O_3 using Fischer-Tropsch Synthesis (FTS) was prepared in three different methods co-precipitation ,impregnation and sol-gel techniques to examine the operative parameters such as temperature , pressure and H_2/CO ratio to optimize the light olefins selectivity . The results illustrated that the catalyst which is prepared by the impregnation method had the less methane selectivity and obviously the more selectivity for light olefins than the other techniques.

Keywords: FTS; Fe/Mn/Al_2O_3; co-precipitation; light olefins

Introduction

Fischer–Tropsch synthesis (FTS) has attracted great interest due to the large variety of products that can be obtained, such as α-olefins, paraffin and oxygenate compounds or narrow distributions of certain families (i. e. C_2–C_4 alkenes, gasoline, and diesel). The combination of Fe–Mn [3–5], Co–Mn [6,7] and Fe–Co catalyst [1] with or without promoters favors the formation of C_2–C_4 alkenes. The aim of this research is investigation of the effect of catalyst preparation method of Fe/Mn catalyst in the product distribution in Fischer- Tropsch synthesis.

Experimental

Preparation of typical catalyst samples

Three kinds of Fe/Mn/Al_2O_3 catalyst were prepared with different methods. Typically, 50%Fe/50% Mn/10wt% Al_2O_3 by co-precipitated, 50%Fe/50%Mn/90%Al_2O_3 with

impregnation method and 50%Fe/50%Mn/5wt% Al_2O_3 with sol-gel technique were prepared. all of catalyst were optimized to light olefins (C_2-C_3 used to petrochemical feed stocks).

Results and discussion

The operative conditions such as temperature, pressure and H_2/CO ratio effects on selectivity of light olefins were investigated on three different catalyst preparation technique in fixed-bed micro-reactor. The effect of temperature on distribution of products was shown by figure (1).

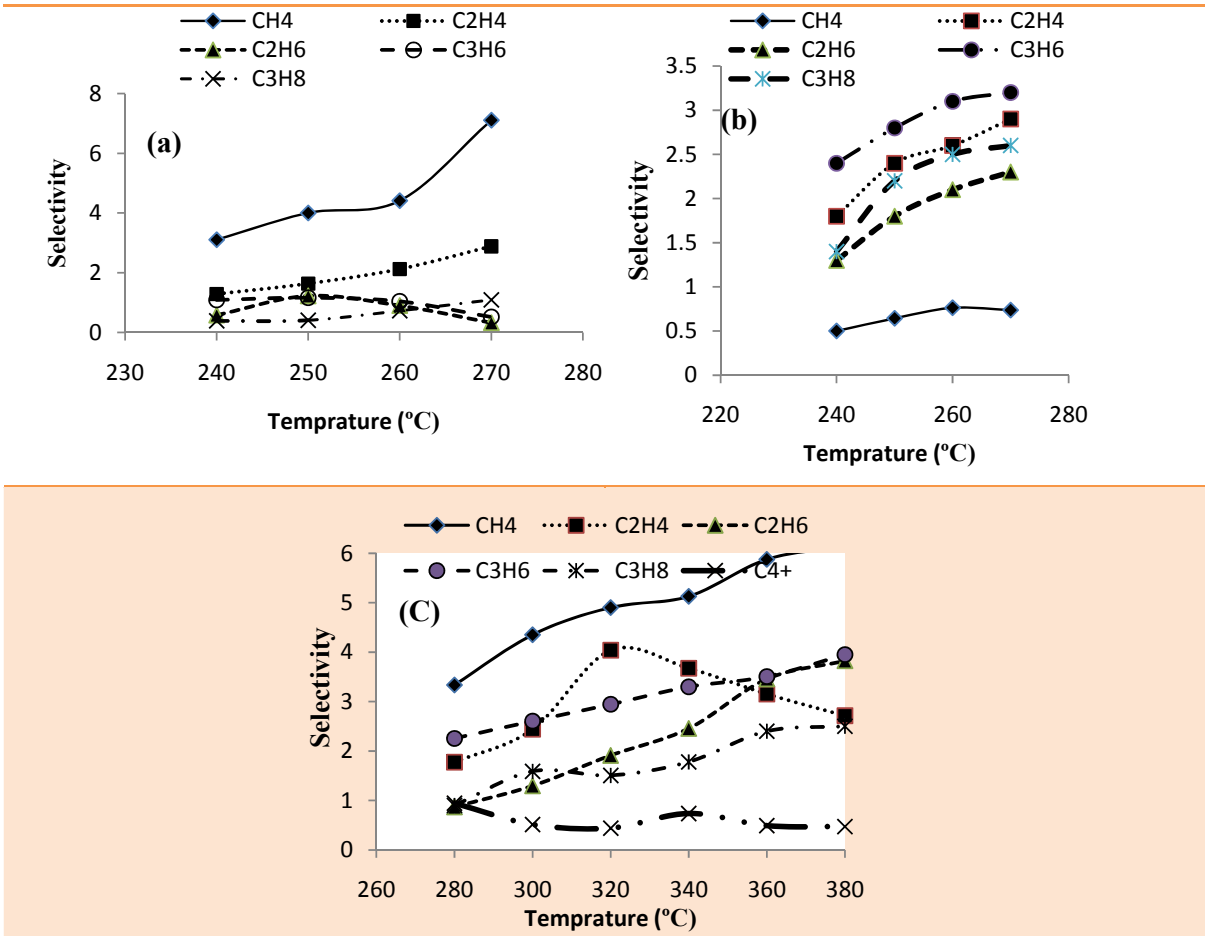

Figure 1. **Effect of temperature on Selectivity at P=5 bar; H_2/CO=3/2: a) co-precipitate Fe/Mn; b) impregnation Fe/Mn; c) sol-gel Fe/Mn**

Conclusion

The formulation and catalyst preparation method can effect on products distribution and kinetics of FTS. In this study the operative conditions such as temperature ,pressure and

H_2/CO ratio were investigated on catalysts sample. The results demonstrated that the catalyst which is prepared by the impregnation method had the less methane selectivity and obviously the more selectivity for light olefins than the other techniques.

References

[1] A.A. Mirzaei, R. Habibpour, E. Kashi, Appl. Catal. A: Gen. 296 (2005) 222.

Kinetic Study of Nitrous Acid Reaction with Flavonoids in the Absence and Presence of β-Cyclodextrin

L. Khalafi*[a], M. Rafiee[b], S. M. Shoaei[c]

[a] Department of Chemistry, Islamic Azad University, Shahr-e-Qods Branch, Tehran, Iran

* l_khalafi@yahoo.com

[b] Department of Chemistry, Institute for Advanced Studies in Basic Sciences, Zanjan, Iran

[c]Department of Chemistry, , Islamic Azad University, Zanjan Branch, Zanjan, Iran

Keywords: Catechin, Quercetin, Nitrous acid, β-Cyclodextrin.

Cyclodextrins are well known in host guest chemistry due to their unique ability to form inclusion complexes with numerous compounds. The interaction of guest molecules with cyclodextrin leads to apparent changes in their chemical properties, such as kinetic and thermodynamic parameters [1]. This work focuses on kinetic study of reaction of nitrous acid, as important compound in environmental chemistry, with quercetin and catechin as biologically important antioxidants in the absence and presence of β-cyclodextrin [2]. Kinetic studies have been performed using UV-Vis spectrophotometry in aqueous solutions and mild acidic conditions.

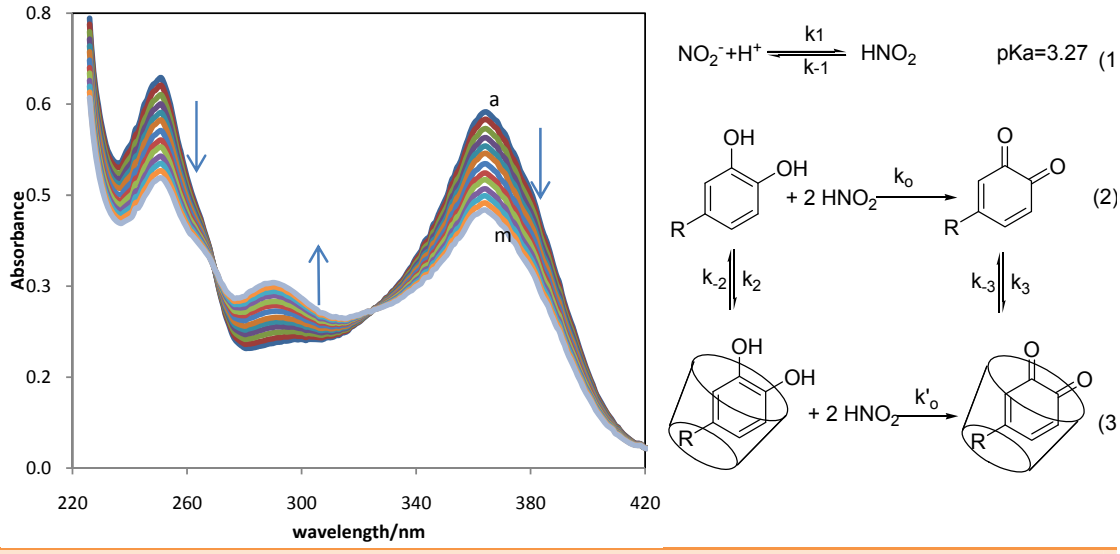

Fig. 1. Absorption spectra of 0.5 mM quercetin in the presence of 3.0 mM $NaNO_3$ with time; interval times 30 sec., pH 3.40 and solvent 85/15 water/ethanol. Proposed mechanism for the reaction in the presence of β–cyclodextrin.

Base on proposed mechanism these antioxidants participate in oxidation reaction with nitrous acid which derived from protonation of nitrite ion in mild acidic conditions. Corresponding quinones are proposed as relatively stable products were detected by spectrophotometric techniques. The effect of pH, nitrite ion and cylodextrin concentration have been studied on the reaction. The values of rate constants and equilibrium constants have been calculated by fitting through the data of the concentration profiles using Newton–Gauss algorithm. Presence of equilibrium between the reactant of these parallel reactions follows a complicated reaction pathway; then the kinetic profiles have been obtained by numerical integration using Matlab's solver, ode45, which is the standard Runge-Kutta algorithm [3]. The results indicate that these antioxidants can form relatively stable complexes with β-CD. The formation constants of the oxidized forms are lower than related parent molecules. The rate constant of complex forms are considerably lower than the free forms. Also the effect of pH on the reaction have been studied and the results show that the dependence of reaction to pH is related to the variation of nitrous acid percentage as oxidant in the reaction and the rate constants of the reactions are independent of pH.

References

[1] L. Khalafi, *Res. J. Chem. Environ*., 12 (**2008**) 102.

[2] A. Afkhami, L. Khalafi, *B. Chem. Soc. Jpn.,* 80 (**2007**) 1542.

[3] L. Khalafi, M. Rafiee, *J. Haz. Mater*., 174 (**2010**) 801.

Kinetic Analysis of the Removal of a Model Contaminant with Immobilized Titanium Dioxide Nanoparticles on Glass Beads in a Packed Bed Reactor

M.A. Behnajady, N. Modirshahla and B. Sheidaei*
Department of Chemistry, Faculty of Science, Islamic Azad University, Tabriz Branch, Tabriz, Iran
(Email: behnaz.sheidaei@gmail.com)

Keywords: Titanium Dioxide Nanoparticles, Immobilization, Packed Bed Reactor, Kinetic Analysis, C.I. Acid Orange 7

Introduction

Heterogeneous photocatalysis is a promising method among advanced oxidation processes (AOPs) which is able to breakdown many organic pollutants. This domain is particularly oriented towards application and has a strong impact on design and construction of new photochemical reactors [1]. Since photocatalysts are often applied as suspension [2], hence, the separation of photocatalyst particles from its aqueous suspensions represents a serious problem for practical engineering. Unfortunately little attention has been diverted to design photoreactors with immobilized TiO_2 on a solid surface [3]. In the present work we described kinetic analysis of the removal of Acid Orange 7 as a model pollutant in a packed bed photoreactor with immobilized catalyst on glass beads.

Experimental details

TiO_2-P25 (Degussa) was immobilized on glass beads by heat attachment method [3]. Then glass beads were packed into an annular reactor. For photocatalytic degradation of C.I. Acid Orange 7 (AO7) as a model contaminant from textile industry, a solution containing known concentration of AO7 was prepared and then known value of the prepared solution was transferred into a Pyrex beaker and agitated with a magnetic stirrer during experiment. The solution was recirculated with a peristaltic pump (Heidolph, PD 5001) with a known flow rate into the reactor and regularly, the AO7 concentration was analyzed at the outlet with a UV-vis spectrophotometer (Ultrospec 2000, Biotech pharmacia, England) at 485 nm.

Experiments were carried out in different AO7 concentrations, solution volumes, volumetric flow rates and light intensities.

Results

Kinetic analysis of AO7 removal in PBR photoreactor

The photocatalytic oxidation kinetics of many organic compounds has often been modeled with the modified Langmuir-Hinshelwood equation as Equation 1:

$$R = -\frac{d[\,AO7\,]}{dt} = \frac{k_{L-H}K_{ads}[\,AO7\,]}{1+K_{ads}[\,AO7\,]_0} = k_{ap}[\,AO7\,] \quad (1)$$

which

$$k_{ap} = \frac{k_{L-H}K_{ads}}{1+K_{ads}[\,AO7\,]_0} \quad (2)$$

where R is the reaction rate (mg L^{-1} min^{-1}), k_{L-H} the reaction rate constant (mg L^{-1} min^{-1}), K_{ads} the adsorption coefficient of AO7 on the TiO_2 particles (mg^{-1} L), [AO7] the concentration of AO7 (mg L^{-1}), and $[AO7]_0$ is the initial concentration of AO7 (mg L^{-1}). Equation 1 shows a pseudo-first order reaction with respect to the AO7 concentration. The semi-logarithmic graphs of the concentration of versus irradiation time yield straight lines indicating pseudo-first order reaction. The apparent reaction rate constants (k_{ap}) for photocatalytic degradation of AO7 were evaluated from experimental data using linear regression method. In all cases R^2 (correlation coefficient) values are higher than 0.98, which confirm the proposed kinetics for decolorization of AO7 in this process. The constants k_{L-H} and K_{ads} in L-H model were obtained with fitting k_{ap} to $[AO7]_0$ using the software Polymath (Version 6.0) as 0.74 mg L^{-1} min^{-1} and 0.081 mg^{-1} L, respectively.

Results show that the UV-light intensity plays an important role on the decolorization of AO7 in the UV/TiO_2 process. Figure 1a shows k_{ap} increases with increasing the UV-light intensity linearly. Because the UV irradiation generates the photons required for the electron transfer from the valence band to the conduction band of a semiconductor photocatalyst. As can be seen from Figure 1a, k_{ap} can be fitted to UV light intensity by Equation 3. With nonlinear regression analysis model parameters were calculated as following:

$$k_{ap} = 0.05[\,I_0\,]^{0.96} \quad , \quad R^2 = 0.99 \quad (3)$$

Two other important factors for removal of pollutant in PBR photoreactor are volumetric flow rate and volume of solution. Figure 1b and 1c shows k_{ap} increases with increasing the volumetric flow rate and decreasing of solution volume. With nonlinear regression analysis model parameters were calculated for volumetric flow rate (ν_0) and volume of solution (V) as following:

$$k_{ap} = 2.8 \times 10^{-3} [\nu_0]^{0.42} \quad , \quad R^2 = 0.99 \quad (4)$$

$$k_{ap} = 27.97 [V]^{-1.15} \quad , \quad R^2 = 0.98 \quad (5)$$

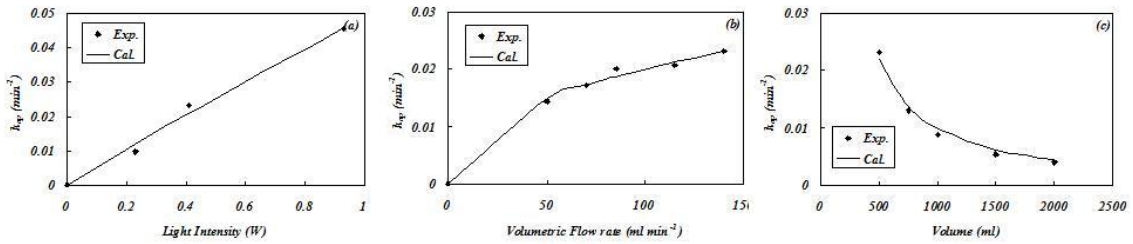

Figure 1. Plot of k_{ap} vs. light intensity (a), volumetric flow rate (b) and solution volume (c).

Development of rate equation

Results show that k_{ap} is a function of initial concentration of AO7 (mg L^{-1}), UV light intensity (W), volumetric flow rate (mL min^{-1}) and volume of solution (mL) as following:

$$k_{ap} = \frac{k_{\circ} I_0^m \nu_0^n V^O}{1 + K_{ads}[AO7]_0} \qquad (6)$$

From previous sections m, n, o, and K_{ads} values were estimated from experimental data. With substituting these values into Equation (6), we obtain reaction rate for removal of AO7 in PBR reactor as following:

$$\mathrm{R} = \frac{20.65\, I_0^{0.96}\, \nu_0^{0.42}\, V^{-1.15}}{1 + 0.081[AO7]_0} [\mathrm{AO7}] \quad (7)$$

Although the rate expression is empirical in nature, it provides information about the effect of operational parameters on the reaction rate in PBR reactor which is useful for the design.

Conclusion

UV/TiO_2 process with immobilized photocatalyst on glass beads can be used for efficient degradation of AO7 as a model contaminant from textile dyes. Nonlinear regression analysis

shows that the pseudo-first order rate constant is proportional with volumetric flow rate and light intensity, but it is inversely proportional to initial concentration of AO7 and solution volume. The k_{ap} values predicted from developed rate equation are in good agreement with the experimental data with correlation coefficient equal to 0.97.

References

[1] O. Legrini, E. Oliveros & A.M. Braun, Chem. Rev. 93 (1993) 671.

[2] M.A. Behnajady, N. Modirshahla, & R. Hamzavi, J. Hazard. Mater. 133 (2006) 226.

[3] M.A. Behnajady, N. Modirshahla, N. Daneshvar & M. Rabbani, Chem. Eng. J. 127 (2007) 167.

Theoretical Study on the Kinetics and Mechanism of the $O(^3P) + C_2H_3Cl$ Reaction

V. Saheb*[a] and S. Yazdani[b]

[a]Department of Chemistry, Shahid-Bahonar University of Kerman, Iran
(vahidsaheb@mail.uk.ac.ir)

[b]Department of Chemistry, Payame Noor University (PNU), Kerman, Iran

Keywords: kinetics, mechanism, vinyl chloride, RRKM.

Introduction

The $O(^3P) + C_2H_3Cl$ reaction is of great importance in atmospheric chemistry and in many combustion and plasma systems. Although there have been many studies of O atom reactions with a variety of unsaturated hydrocarbons, only limited information is available for halogenated alkenes [1]. In this research, the kinetic and mechanism of the electrophilic addition reaction of oxygen atom to vinyl chloride is studied by employing various quantum chemical methods. The computed rate constants are compared with the available experimental data.

Method

The triplet potential energy surface of the title reaction is initially explored at the BB1K/6-31+G(d,p) level of theory. Analytical harmonic vibrational frequencies are calculated at this level to verify the character of stationary points located (one imaginary frequency for a TS and all real frequencies for a minimum). The energies of stationary points are improved by using BB1K/MG3S, CCSD(T), and G3B3 levels of theory. Transition state and RRKM theories were used to calculate the rate constant for the disappearance of the reactants and branching ratios for different reaction channels.

Results and Discussions

The reaction occurs by addition of oxygen atom to both carbon atoms of vinyl chloride through a low barrier energy saddle point (1-20 kJ mol^{-1} depending on the level of theory employed), leading to an energy-rich intermediate. The chemically activated molecule formed

may dissociate to different products or isomerise to other activated molecules which in turn react to form other products as depicted in Fig 1. RRKM theory was used to calculate the energy-specific rate constants for decomposition of different activated intermediates to reactants, products or other activated intermediates. A RRKM-TST model from Berman and Lin is modified and used to calculate the rate of disappearance of the reactants and branching ratios for different reaction channels according to the mechanism shown in Fig1[2,3]. The results are in good accordance with the experimental data.

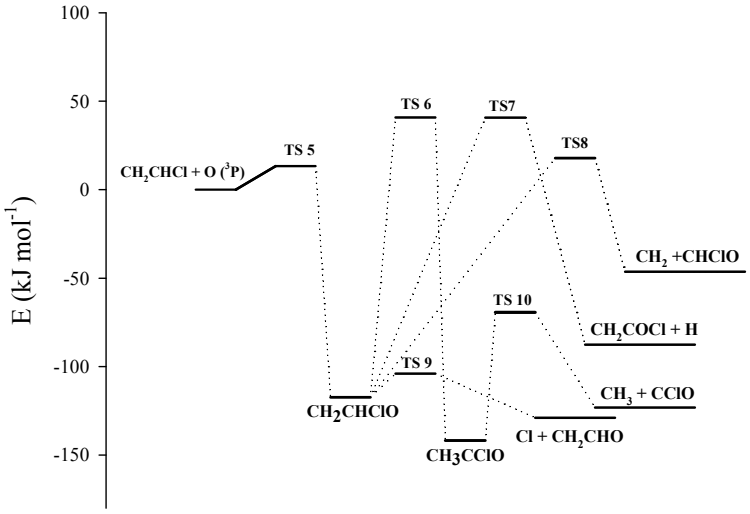

Conclusions

A number of important results emerge from this study. The $O(^3P)$ + C_2H_3Cl reaction is confirmed to occur via an electrophilic addition mechanism as the first reaction step. Different products could be formed through a complicated mechanism including several chemically-activated intermediates and transition states. Overall thermal rate coefficients computed at temperatures in the range of 200-2000 K are in good agreement with experimental data and can be fitted to a modified Arrhenius expression as

$k_{tot} = 1.99 \times 10^{8} \times (T/298)^{4.01} \times \exp(155.20/T)$ L mol^{-1} s^{-1}.

References

[1] R. J. Cvetanovic, *J. Phys. Chem. Ref. Data,* **16**, 261 (1987).

[2] K. A. Holbrook, M. J. Pilling, S. H. Robertson, *Unimolecular Reactions*, 2nd ed. John Wiley & Sons Ltd. Chichester, England, 1996.

[3] M. R. Berman, and M. C. Lin, *J. Phys. Chem*., **87**, 3933 (1983).

Theoretical Investigation of the Thermal Unimolecular Decomposition of Tertiary Butyl Bromide

V. Saheb*[a] and M. Paivar[b]

[a]Department of Chemistry, Shahid-Bahonar University of Kerman, Iran

(vahidsaheb@mail.uk.ac.ir)

[b]Department of Chemistry, Payame Noor University (PNU), Kerman, Iran

Keywords: kinetics, unimolecular, ab initio, butyl bromide.

Introduction

The gas phase unimolecular decomposition of bromoalkanes is very important for their role in atmospheric processes [1]. In this research, the kinetic and mechanism of the thermal unimolecular reaction of tert-butyl bromide reaction is studied by employing ab initio quantum chemical methods. The computed rate constants are compared with the available experimental data.

Method

The ab initio calculations are performed using Gaussian 03 program. The geometries of all the stationary points, i.e., minimum energy structures and the saddle points, are fully optimized at the MP2 level of theory with the 6-311+G(2d,p) basis set. Harmonic vibrational frequencies and zero-point energies of all species are calculated at the same level of theory. To improve the energy description of the stationary points, single-point calculations are made using MP2/6-311+G(2d,p) optimized geometries at the CCSD(T)/6-311+G(2df,2p) level of theory. Based on the information obtained from the potential energy surface, the high-pressure limiting rate constants for the unimolecular decomposition of tertiary butyl bromide is computed. The rate constants are calculated by means of transition state theory (TST) in the temperature range of 500 to 2500 K. The calculated rate constants are corrected for tunnelling effect by Wigner tunnelling formula.

Results and Discussions

It is revealed by many experimental measurements that the only important pathway for gas-phase unimolecular decomposition of tert-butyl bromide is HBr elimination reaction. Nonetheless, three possible reaction channels are supposed for unimolecular reaction of tert-butyl bromide.

$$\text{Tert-}C_4H_9Br \rightarrow \text{iso-}C_4H_8 \qquad \text{R1}$$
$$\rightarrow C_4H_9 + Br \qquad \text{R2}$$
$$\rightarrow C_3H_6Br + CH_3 \qquad \text{R3}$$

The calculated barrier heights for the reaction channels R1, R2 and R3 at the CCSD(T)/6-311+G(2df,2p) level of theory are 189.5, 324.6 and 405.8 kJ mol^{-1} respectively. The much higher barrier heights of the reaction channels R2 and R3 show that these reaction channels do have much smaller rate constant in comparison with the reaction channel R1. The calculated rate constant for the unimolecular HBr-elimination reaction of tert-butyl bromide is shown in Fig. 1 in comparison with the available experimental data.

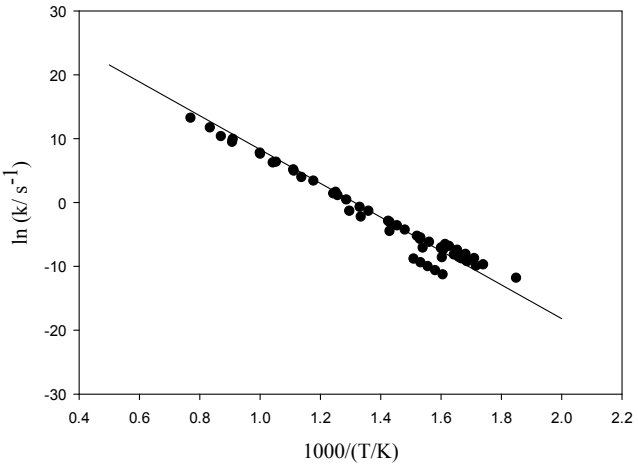

Conclusions

The thermal rate coefficients computed at temperatures in the range of 500-2500 K are in good agreement with experimental data and can be fitted to a Arrhenius expression as $k_{uni} = 1.27\times10^{15}\times\exp(220.15\text{kJ mol}^{-1}/RT)\ s^{-1}$.

References

[1] R. P. Wayne, *Chemistry of Atmospheres*, Oxford, UK, 2000.

[2] K. A. Holbrook, M. J. Pilling, S. H. Robertson, *Unimolecular Reactions*, 2nd ed. John Wiley & Sons Ltd. Chichester, England, 1996.

Potential of Fe(III) Protoporphyrin IX For Heterogenous Nanobiocatalysis at Mild Conditions

E. Salehi Siavashani [a], K. Nazari [a,*], F. Adhami [a], A. Mahmoudi [b], F. Safa Shams [a]

[a] Chemistry Dept., Shahr-Rey Branch, Islamic Azad University, Tehran/Iran, 18155-144

[b] Chemistry Department, Karaj Islamic Azad University, Karaj, Iran

E-mail: nazarikh@ripi.ir, Fadhami@gmail.com

Keywords: Iron(III)protoporphyrin, Hydrogen peroxide, MCM41, Oxidation, Metalloporphyrin

Modification of mesoporous MCM-41 by chemical and physical methods extends its application in biotechnology. Having large pores and huge number of silanol groups makes MCM-41 as a good candidate for immobilizing macromolecules, such as metalloporphyrins [1].

Porphyrins are well-known for their biological, catalytic, conductive, and photoactive properties [2]. They have also been investigated extensively in an effort to mimic enzymatic systems, especially those of the peroxidase family. Fe(III) protoporphyrin IX (Fe^{III}PPIX) has been interested as effective guest component for immobilization and creating new porous nanobiocatalysts. Among systems containing supported macromolecules, metalloporphyrin complexes present an important role in the field of oxidation reactions due to their inherent properties, and their suitable, compatible and effective functional groups [3].

Present work reports, catalytic activities of nanobiocatalysts of Fe(III) PPIX immobilized in modified MCM41. 3-aminopropyltriethoxy silane (APTS) was used for modification of MCM41 pore walls [4]. In order to enhance the catalytic activity of Fe^{III}PPIX, first the fifth coordination position of Fe atom was reacted with imidazol. Then, the immobilization reaction of Im-Fe^{III}PPIX with NH_2-MCM41 was carried out through amide bond formation between NH_2 group of NH_2-MCM41 and carboxyl groups of Im-Fe^{III}PPIX.

Oxidative catalytic activities of the prepared nanobiocatalysts were examined by ABTS (2,2-azino-di-3-ethyl-benzothizoline-(6)-Sulphonic acid) and phenolic derivatives in the presence of hydrogen peroxide and/or tert-butyl peroxide as oxidant [5,6]. Various oxidation reactions

were investigated by UV-Vis spectrophotometry to determine enzymatic parameters of the nanobiocatalysts.

Initial rates, rate constants $k_1$and k_3, K_m, V_{max}, k_{cat} and catalytic efficiency of nanobiocatalysts obtained from Michaelis–Menten, lineweaver-Burk and Eadie-Hofstee plots. Regression and fitting of experimental data into the kinetic equations was done by Excel-Solver software.

Results showed that these nanobiocatalysts can potentially mimics peroxidase enzyme in oxidation reactions of aromatic compounds in aqueous media at mild conditions of ambient temperature and atmospheric pressure.

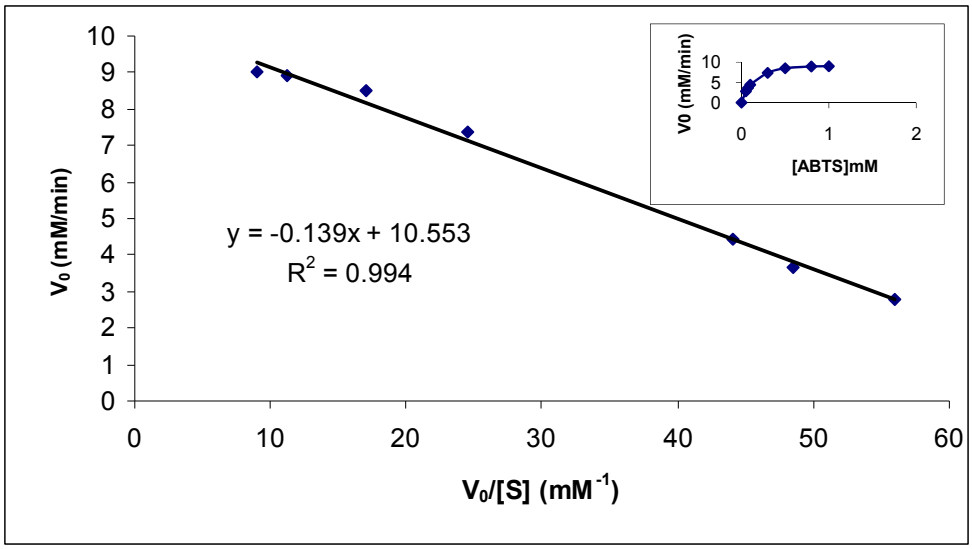

Eadie-Hofstee plot for oxidation of ABTS by Im-Fe^{III}PPIX/MCM41 catalyst at room temperature $[H_2O_2]$=0.5 mM and Im-Fe^{III}PPIX/MCM41=0.010 g.

References

[1] M. Trejda et al., Cat. Lett., **2006**, 108, 3-4.

[2] B.T. Holland et al., J. Phys. Chem. B, **1998**, 102, 4301-4309.

[3] A.A. Costa et al., J. Mol. Cat. A: Chem., **2008**, 282, 149-157

[4] K. Nazari et al., J. Mol.. Cat. A: Chem., **2005**, 239, 1-9.

[5] D.Q. Khieu et al., J. Incl. Phenom. Macrocycl. Chem., **2009**, 65, 73-81.

[6] B. Mohajerani et al., J. Mol. Cat. A: Chem., **2008**, 296, 28-35

Kinetic studies of peroxyoxalte chemiluminescence system in the presence of chlrophniramine maleate

Abdolraouf Samadi-Maybodi* and Reza Akhoondi

(E-mail: samadi@umz.ac.ir)

Analytical division, Faculty of Chemistry, University of Mazandaran, Babolsar, 47416 ۹۵۴۴۷, Iran.

Keywords: peroxyoxalte, chemiluminescence, kinetic, fluorophore, Chlorpheniramine maleate

Introduction

The brilliant emissions resulting from oxidation of certain oxalic acid derivatives, especially in the presence of a variety of fluorophores, are the bases of the most active area of current interest in chemiluminescence. The peroxyoxalate-chemiluminescence (PO-CL) system is based on the reaction of H_2O_2 with peroxyoxalate which result an intermediate [1]. The excited intermediate transfers its energy to an efficient fluorophore [2,3] through the chemically initiated electron exchange luminescence (CIEEL) mechanism. Also kinetic parameters for the (PO-CL) system with and without Chlorpheniramine maleate were calculated from the computer fitting of the corresponding chemiluminescence intensity/time profiles.

Methods

All chemical compounds were reagent-grade and purchased from Fluka chemical company (CH-9470, Buchs, Switzerland) and used as received without further purification. Quinoxaline derivative was prepared as described in the previous report [4]. Chemiluminescence detection was performed with a homemade apparatus equipped with a Model BPY47 photocell. In order to evaluate the kinetic data for the PO-CL system, a pooled-intermediate model was used.

Results and discussion

In order to evaluate the kinetic data for the PO-CL system, a pooled-intermediate model was used. The integrated rate equation for the CL intensity versus time is as follow:

$$I_t = [\frac{Mk_r}{k_f - k_r}][\exp(-k_r t) - \exp(-k_f t)]$$

Where, I_t is the CL intensity at time t, M is a theoretical maximum level of intensity if the reactants were entirely converted to a CL-generating material, k_r and k_f are, respectively, the first order rate constants for the rise and fall of the burst of CL. This model not only allows the determination of parameters of M, K_r and K_f but also it permits an estimation of the intensity at maximum level (J), the time of maximum intensity (T_{max}) and the total light yield (Y)

Results indicated that the integrated light emitted (Y) of the CL system is reduced in the presence of CPM but the fall rate constants (K_f) increased (fig 1).

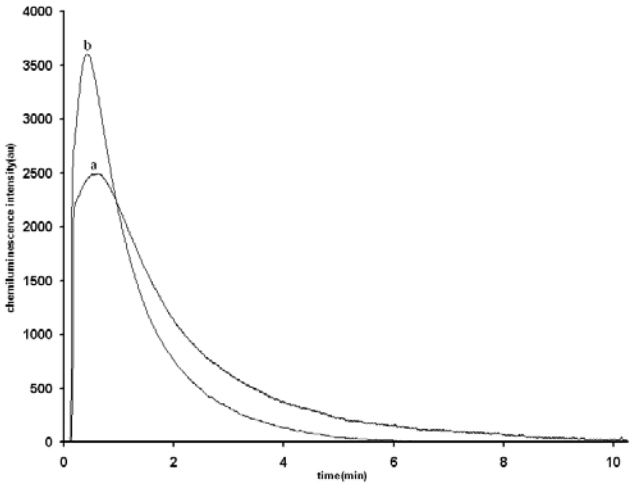

Figure 1. Chemiluminescence emission intensity as a function of time after mixing of H_2O_2, sodium salicylate, TCPO and 2,3-diphenylquinoxaline. a) In the absence of CPM b) in the presence of CPM.

Conclusion

The present study convincingly shows the enhancement of chemiluminescnce intensity of peroxyoxalte chemiluminescence system (TCPO- H_2O_2- sodium salicylate- fluorescer) in the presence of chlorpheniramine maleate.

A non-linear least-squares curve fitting program KINFIT was used to the first order rate constants for the rise k_r and fall k_f of the burst of chemiluminescence in the presence and absence of chlorpheniramine.

Reference

[1] A.Garcia, F.J. Ruperez, A. Marin, A. dela Maza, C. Barbas, *J. Chromatogr. B.*785 (2003) 237.

[2] C. Martínez-Algaba, J.M. Bermúdez-Saldaña, R.M.Villanueva-Camañas, S. Sagrado, M.J. Medina-Hernández, *J. Pharmaceut. Biomed. Anal*.40(2006) 312.

[4] A.R. Samadi-Maybodi, R. Akhoondi, M. J. Chaichi, *J Fluoresc*. 20 (2010) 671.

[5] T. Jonsson, K. Irgum, *Anal. Chem.* 72 (2000) 1373.

Physisorption studies of nickel nanoparticles loaded in MCM-41

Abdolraouf Samadi-Maybodi[a]*, Mohammad Teymouri[b] and Amir Vahid[a]

[a]*Analytical division, Faculty of Chemistry, University of Mazandaran, Babolsar, Iran.*

[b]*Research institute of petroleum industry, Tehran, Iran.*

(E-mail: samadi@umz.ac.ir)

Introduction

MCM-41 is a mesoporous molecular sieve which formed from the close packed silica-coated micelles of a surfactant template [1]. Because of its unique structural and physical properties; notably large surface area, tunable and large pore size, narrow pore size distribution and high thermal stability MCM-41 has attracted large attention in many fields such as catalysis [2] and optic [3]. Loading of nickel precursor inside the nanochennels of MCM-41, results in controlled growth of nanoparticles.

Methods

The molar composition of the synthesized samples were (1+5*x*) TEOS, 0.3 Cetyltrimethylammonium bromide (CTAB), 1.5 Sodium acetate, 2 Ethanol, 14 NH_3, 20 H_2O, *x* Ni, 3*x* toluene. *x* is the molar ratio of Ni/Si in the corresponding sample. Physisorption of Nitrogen was measured at 77 K using a BELSORP-max porosimeter. Prior to analysis the samples were outgassed in-vacuo for 4 hours at 573 K until a stable vacuum of 0.1 Pa was reached.

Results and Discussion

Figure 1 represents nitrogen physisorption isotherms of parent MCM-41, Ni3/MCM, Ni6/MCM and Ni7/MCM. Parent MCM-41, Ni3/MCM and Ni6/MCM (figure *a*-*c*) exhibit type IV isotherm, which is the typical characteristic of mesoporous materials. However, Ni7/MCM represents an isotherm which is more or less similar to type IV, but its shape extremely distorted and broadened. This phenomenon caused by high loading of nickel. The specific surface area was calculated from the linear part of the BET (Brunauer-Emmett-Teller) equation (P/P_0 = 0.05-0.25). Results indicated that BET surface area of Ni3/MCM and Ni6/MCM are comparable to that of parent MCM-41. In case of parent MCM-41, Ni3/MCM

and Ni6/MCM, filling of the mesopores takes place over a fairly narrow range of relative pressure.

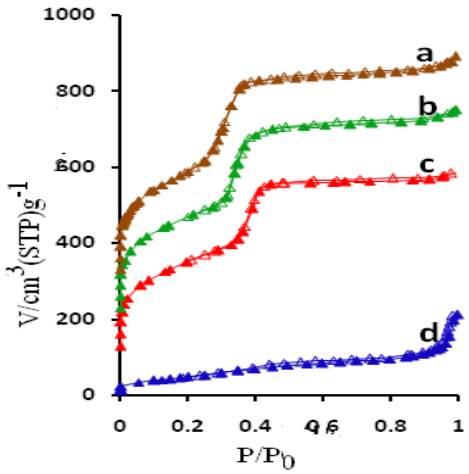

Figure 1. Nitrogen physisorption isotherms of *a*: parent MCM-41, *b*: Ni3/MCM, *c*: Ni6/MCM, *d*: Ni7/MCM.

A further indication for this statement is the fact that desorption branch of the isotherm around capillary condensation step nearly coincides with the adsorption branch which reveals the reversible nitrogen adsorption inside the mesopores. Furthermore, this reversible behavior implies that the most pores within the samples are open pores, connected directly to the surface of the MCM-41.

Conclusion

Results indicated that incorporation of nickel nanoparticles into mesopores of MCM-41 did not cause pore blocking. Results also specified that the most pores within the samples are open pores, connected directly to the surface of the MCM-41 and so are accessible for the guest molecules such as nitrogen.

References

[1] C.T. Kresge, M.E. Leonowicz, W.J. Roth, J.C. Vartuli, J.S. Beck, Nature 359 (1992) 710-712.

[2] A. Taguchi, F. Schuth, Microp. Mesop. Mater. 77 (2005) 1-45.

[3] K. Nakanishi, N. Tanaka, Acc. Chem. Res. 40 (2007) 863–873.

Kinetic study of photocatalytic degradation of azo dye disperse yellow 23 in water with ZnO supported on Clinoptilolite zeolite as a catalyst

Aboalfazl Soufi [*1], Kazem Mahanpoor [2], Hossean Malekhosseani [3]
1,2, 3) Department of Chemistry, Faculty of Science, Islamic Azad University, Arak Branch,
E-mail: kazem_mahanpoor@yahoo.com

Keywords: ZnO / CP, disperse yellow 23, solid-state dispersion, photocatalyst

Abstract

In this investigation photocatalytic degradation of azo dye disperse yellow 23 in water was studied. Zinc oxide was supported on CP using solid-state dispersion (SSD) method. The results show that the ZnO / CP (SSD) is an active photocatalyst. The maximum effect of photo degradation was observed at 10 wt.% ZnO, 90 wt% CP. A first order reaction with K = 0.0057 min^{-1} was observed the photocatalytic degradation reaction. The effects of some parameters such as pH, amount of photocatalyst, initial concentration of dye were also examined.

Introduction:

From the viewpoint of green chemistry, the photocatalytic decomposition of organic compounds in wastewater has attracted a great deal of attention [1]. ZnO is one of the most effective photocatalysts because it is biologically and chemically inert and photostable with near-UV band gap energy. Many researchers have examined some methods for fixing ZnO on supporting materials including glass beads [2], fiber glass [3], silica [4].

Experimental:

Degussa P-25 titanium dioxide and CP Zeolite powder The CP zeolite were purchased from Afrand tuska Co(Iran). Another materials were purchased from Merck (Germany). Double distilled water were used for preparation of requisite Solutions. The molecular structure of DY23 is shown in Fig.1.

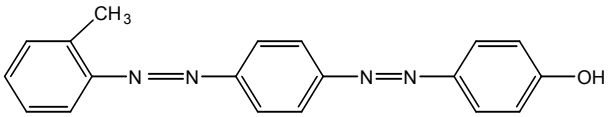

Fig. 1: Molecular Structure of Disperseyellow23

The solid state dispersion (SSD) method was used for preparing the Zeolite-based photocatalyst. In this method, ZnO was mixed with zeolite using ethanol as a solvent using agate pestle and mortar; the solvent was then removed by evaporation. Samples prepared by this method were dried at 110 ^{o}C and calcined in air at 450 ^{o}C for 5 h to obtain ZnO-supported zeolite catalysts.

Results and discussion: The effective decomposition of DY23 was observed when photocatalyst contained 10% ZnO and 90% CP, prepared by using solid state dispersion (SSD) method. The photodegradation efficiency increases with an increase in the amount of photocatalyst, up to a value of 40 ppm and then decreases when the catalyst concentration is increased. The photodegradation conversion of DY23 decreases with an increase in the initial concentration of DY23. Experimental data shows that the best results were obtained in acidic solution, (pH =6, X =100%)after 120 min. The kinetic of photo oxidation reaction is pseudo-ferst order with respect to dye concentration[5] . Fig. 2. shows the plot of Ln [DY23]/[DY23] versus irradiation time for DY23. The linearity of plot suggests that the photodegradation reaction approximately follows the pseudo-first order kinetics with K=0.0057min^{-1}.

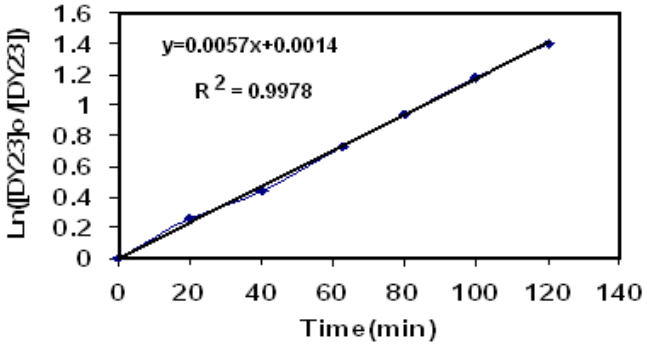

Fig. 2. Relationship between log[DY23] and irradiation time on photocatalytic degradation of DY23. $[DY23]_0$ = 100 ppm, , photocatalyst(10% ZnO+90% CP) = 50 ppm, pH=6.

References

[1] R. Pelegrini, P. Peralta-Zamora, A.R. de Andrade, J. Reyes, N. Duran, Appl. Catal. B 22 (1999) 83.

[2] A.A. Khodja, T. Sehili, J.F. Pilichowski, P. Boule, J. Photochem. Photobiol. A 141 (2001) 231.

[3] C. Galinado, P. Jacques, A. Kalt, Chemosphere 45 (2001) 997.

[4] M. Anpo, H. Nakaya, S. Kodama, Y. Kubokawal, K. Domen, T. Onishi, J. Phys. Chem. 90 (1986) 1633.

[5] A. Maurino, C. Guillard, J. M. Marinas, A. Fernandez, A. Aguera, J. M. Herrmann, Appl. Catal. B : Environ. 34(2001)241.

^{1}H NMR Technique for Kinetic Investigation of Equilibrium Between the two Z- and E-isomers in Stable Phosphorous Ylides.

S. M. Habibi-Khorassani*[a], A. Ebrahimi[a], M. T.Maghsoodlou[a], E. Aghdaei[a] and M.Mohammadi[a]

[a]*Department of Chemistry, University of Sistan and Baluchestan, P.O. Box 98135-674, Zahedan, Iran*

Email: *smhabibius@yahoo.com*

Keywords: ^{1}H NMR technique, Phosphorous ylide, Kinetic investigation,2-Indolinon, Triphenylphosphine

Introduction

Recently, different reports have been published on the synthesis of stable phosphorous ylides[1-2]from the reaction between triphenylphosphine and reactive acetylenic esters in the presence of N-H, C-H, O-H or S-H heterocyclic compounds. These ylides usually exist as a mixture of the two geometrical isomers (Z and E), although some of these exhibit only one geometrical[3-4]. Kinetic investigation of interchangeable process in equilibrium between the two Z- and E-isomers has not been yet studied. Herein, we now describe a full find out such as kinetics, thermodynamic and activation parameters for this conversion.

Results and Discussion

Synthesis of reaction between dimethyl acetylendicarboxylate **1** and 2-indolinon **2** in the presence of triphenylphosphine for generation of phosphorous ylides **3** has been reported earlier[5] involving the two Z- and E-geometrical isomers (Figure **1**).

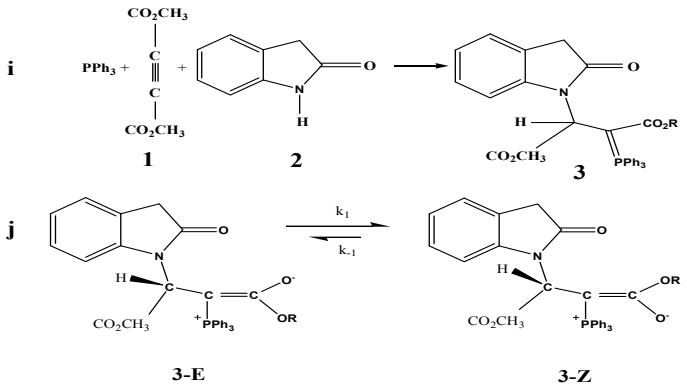

Figure 1. i) Synthesis of reaction between dimethyl acetylendicarboxylate **1** and 2- indolinon **2** in the presence of triphenylphosphine for generation of phosphorous ylide **3. j**) Interchangeable process between the two rotational isomers such a 3-E and 3-Z.

To determine the kinetics parameters for interchangeable process in opposing reaction between the two Z and E rotational isomers, consisting of one elementary reaction and its reverse (Figure **1**, **j**) , a kinetic study of the reaction was undertaken by the ^{1}H NMR technique. For each kinetic experiment, first a aliquot from freshly made solution of compound **3** was pipetted into a capillary ^{1}H NMR tube, keeping the temperature at -40˚C (233K) for a few minutes. Herein, ^{1}H NMR spectrum of compound **3** gave corresponding equilibrium concentration of each rotational isomers (Z and E) for first equilibrium state at -40˚C .They are in proportion with their integration surfaces. Then temperature was suddenly jumped to -30˚C and then the ^{1}H NMR spectrum of opposing reaction was recorded every 12 seconds until the completion of reaction (second equilibrium state). In this case, before the completion of reaction, concentration of each geometrical isomer as reaction proceed in $CDCl_3$, can be obtained from its corresponding integrating surface at each interval, herein , all the concentrations are relevant to the nonequilibrium state of the opposing reaction (before second equilibrium state). When the measurement of the corresponding integrating surface is being constant, opposing reaction is now in a second equilibrium state. Changes in the concentration value of E isomer (for example) can be calculated from the difference between the integrating surface of first equilibrium state (-40˚C) and the integrating surface of nonequilibrium state at each interval. They are reported in Table **1** at all times investigated during temperature jumped from -20˚C (253K) to -10˚C (263K).

Table 1: The concentration value of E isomer at all times investigated at **-10˚C (263K)**

t/s	۱۳۲	144	156	168
$X_E$mol / lit	0.033	0.035	0.044	0.045
Ln (m-x)	-4.32	-4.53	-6.20	-7.42

In the temperature range studied , the dependence of the first-order rate constant of the forward (k_1), reverse (k_{-1}) and overall reaction on reciprocal temperature are consistent with the Arrhenius equation, giving an activation energy of forward (E_{a1}), reverse (E_{a-1}) and overall reaction ($E_{a\ total}$), 16.9, 10.1 and 12.3 kJ.mol^{-1}, respectively.

Conclusions

For the first time, kinetic investigation of interchangeable process in equilibrium between the two Z -and E-isomers of stable phosphorous ylides was undertaken by the ^{1}H NMR technique. Activation parameters such as k_{-1}, k_1, k_{total}, E_{a1}, E_{a-1}, $E_{a\ total}$, $\Delta S^{\#}$, $\Delta H^{\#}$ and $\Delta G^{\#}$ along with thermodynamic parameters involving K_e, ΔH°, ΔG° and ΔS° were obtained on the basis of experimental data.

References

[1] Maghsoodlou, M.T.; Hazeri, N.; Habibi-Khorassani, S.M.; Ghulame Shahzadeh, A.; Nassiri, M. Phosphorus, Sulfur Silicon. **2006**, 181, 913.

[2] Treglon, P.A.; Laurence, G.S. J. Scient. Instrum. **1965**, 42, 869.

[3] Habibi-Khorassani, S.M.; Maghsoodlou, M.T.; Ebrahimi, A.; Kazemian, M. A.; Zakarianejad, M. Phosphorus, Sulfur Silicon Relat. Elem. **2009**, 11, 2959-2979.

[4] Habibi-Khorassani, S. M.; Maghsoodlou, M. T.; Ebrahimi, A.; Saravani, H.; Zakarianejad, M.; Ghahramaninezhat, M.; Kazemian, M. A.; Nassiri, M.; Khajehali, Z. Prog. React. Kinet. Mech. **2009**, 34, 301-328.

[5] Hazeri, N.; Habibi-Khorassani, S.M.; Maghsoodlou, M. T. Marandi, G.; Ghulame Shahzadeh, A.; Nassiri, M. Chem. Res.**2006**,215–217.

Reaction Dynamics of Sulfur with Ethylene on an Interpolated Potential Energy Surface

Leila Emad
Department of Chemistry, College of Sciences, Shiraz University, Shiraz, Iran
Email: Emad@susc.ac.ir

Introduction

Nowadays, investigation on the dynamics of the reactive species is one of the major aspects of the kinetics that has attracted the interest of many scientists who work in this field. Different methods have been proposed to study the dynamics of the reactions and the central issue in all of them is construction of potential energy surface.[1] Construction of the potential energy surfaces are normally based on the data obtained from quantum mechanical or semi-empirical calculations. One of the most effect methods in construction of the potential energy surfaces is the interpolation techniques.[2] Although, interpolating techniques in dynamics studies proved to be useful in some tetratomic systems, the cost of computational time prevents the use of expensive state-of-the-art ab initio correlated electronic structure calculations. In these methods, the classical dynamics simulations will be study on an interpolated potential energy surface constructed from ab initio or semi-empirical calculations.

In this study the dynamics of the reaction of ethylene with sulfur atoms has been investigated. This reaction is proceeds via the formation of an energized intermediate according to reaction R1.

$S + C_2H_4 \rightarrow C_2H_4S^*$ R1

From classical trajectory studies, the formation of possible end products, the corresponding reactive cross sections, and probabilities of formation of each product are investigated (N_r / N_T). These data are used to calculate the branching ratio and individual and total rate constants.

Computational method

To construct the potential energy surface the Gaussian 03 program was used. The structure of the stationary points and IRC calculations were performed at the CCD/6-

31+G(d,p) level of theory[3]. The initial potential energy surface (PES) was used to build a global PES by using GROW program.[4] The Constructed PES was used to run 1000 to 2000 trajectories to investigate the possible products. By means of initial determined conditions (the initial separation of the reactants, internal energies, and relative energies) it was possible to calculate the effect of each initial condition on the calculated cross section and probabilities. Once having reactive cross sections it was possible to have an expression for the rate constant based on the collision theory.

$$k(T) = g_e(T)\left(\frac{2}{k_B T}\right)^{3/2}\left(\frac{1}{\pi\mu}\right)^{1/2}\int_0^{\infty} E_{tr}\sigma^r \exp\left(-\frac{E_{tr}}{k_B T}\right)dE_{tr}$$

Results and Discussion

It was found the reactive cross section for reaction R1 decreases by increasing the relative translational energy. This kind of behavior is expected for those reactions producing energized intermediates. For those paths having saddle points the behavior was found to be vice versa. Some of the trajectories was found to go back to form the reactants, especially, at higher translational energies.

References

[1] Steinfeld, J. I.; Francisco, J. S.; Hase, W. L. Chemical Kinetics and Dynamics; Prentice Hall: Englewood Cliffs, NJ, 1989.

[2] Guo, Y.: Kawano, A.; Thompson, D. L. *J. Chem. Phys.* **2004**, *121*, 5091.

[3] Frisch , M.J. ; Trucks ,G.W. ;Schlegel ,H.B. *et al.* , GAUSSIAN03 , Revision E.01 , Gaussian , Inc. , Walling Ford CT , **2004** .

[4] Collins, M. A. *Adv. Chem. Phys*. **1996**, *93*, 389.

Photodegradation Kinetic Studies on Acid Yellow 36 in Aqueous solution

R.Fazaeli*[a], Z. Emadian Razavi[b], M.Yousefi[b], S. Ghasemi[b]
[a] Modeling and Optimization Research Center in Science and Engineering, Islamic Azad University-South Tehran Branch, Tehran, Iran
E-mail: r_fazaeli@azad.ac.ir
[b]Department of Chemistry, Islamic Azad University-Shahr-e- rey Branch, Tehran, Iran

Keywords: Photodegradation, Kinetic, Azo dye, Pseudo first and second-order.

Abstract

Photodegradation, as a cost-effective technology for the removal of soluble azo dyes pollutants and organics from aqueous solutions, has been extensively studied and most research mainly focused on the reaction kinetics. Thus, we attempted to offer a better understating of representative photodegradation kinetics with special focuses on theoretical approaches for derivation of some models such as the pseudo-first and second-order kinetic equations and general rate law equation.

The photodegradation of pollutants from aqueous solution plays an important role in wastewater treatment. The study of photodegradation kinetics in wastewater treatment is significant as it provides valuable insights into the mechanism of photodegradation reactions. Numerous systems have been investigated particularly during the past years. Most of these have been reported as first order kinetic processes. Bhattacharya and Venkobachar[1] presented a simple first order reversible kinetic model. The pseudo-first order rate equation of Lagergren has long been widely applied [2]. A second order rate equation and kinetic should correspond to a reversible second order reaction at low photocatalyst ratios.

The experimental data was analyzed by photodegradation of Acid Yellow 36 into the photochemical reactor at the presence of TiO_2 (rotile) and $K_2S_2O_8$. Aqueous AY36 solution was prepared at the concentration of 10^{-4}M. The sample was enclosed in cylindrical, quartz cell and exposed to the UV irradiation. Fig.1 shows the changes in UV spectra solution of AY36 after different time of photodegradation. Several models can be used to express the mechanism of photodegradation model for pseudo-first order rate expression has the Lagergrern[2] form: $\frac{dq_e}{dt} = k_1(q_e - q_t)$, Fig. (2), Where qt is the degradation capacity at time

t (mol.g-1) and k1 (min-1) is the rate constant of the pseudo first-order degradation. The kinetic data were further analyzed using Blanchard's pseudo second-order kinetic model [3]. This model is based one the assumption the degradation follows second order reaction. It can be expressed as $\frac{t}{q_t}=\frac{1}{k_2 q_e^2}+\frac{t}{q_e}$, Fig. (3), Where k2 (mol.gr-1 min-1) is the rate constant of the pseudo second –order reaction. The kinetic data can also be analyzed by intraparticle diffusion kinetics model, formulated as: $q_t = k_i t^{\frac{1}{2}} + C$, Fig.(4), Where ki (mol g-1 min-1/2) is the intraparticle diffusion rate constant and C (mol g-1) is a constant. Another kinetic data can be analyzed using Elovich kinetic model, formulated as: $q_t = \frac{1}{\beta}\ln(\alpha\beta)+\frac{1}{\beta}\ln(t)$, Fig. (5), Based on the obtained data from various kinetic models, the best correlation belongs to Blanchard's equation. The calculation results of pseudo first-order, pseudo second-order and intraparticle diffusion reaction rates are shown in Figs 2 to 5 respectively.

The optimum conditions for photodegradation of AY36 in aqueous solution followed at Pseudo-second order kinetic. The best degradation efficiency of 73% was achieved.

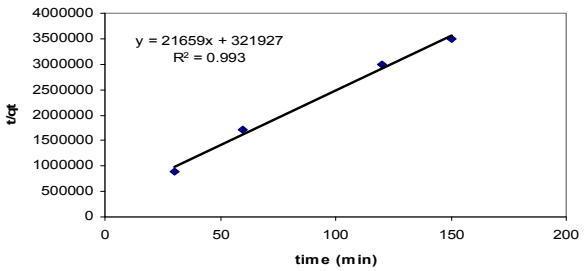

Fig.3. Blanchard plot for AY36

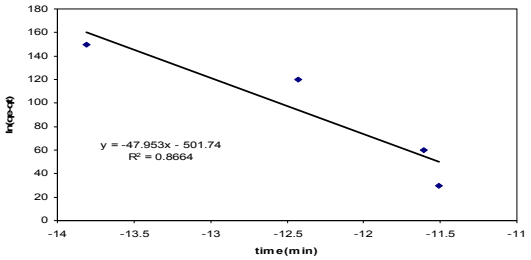

Fig.2. Lagergren plot for AY36

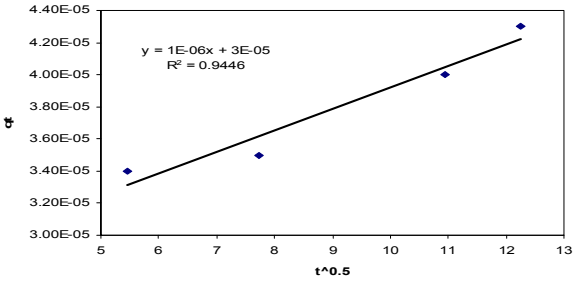

Fig.4. Weber plot for AY36

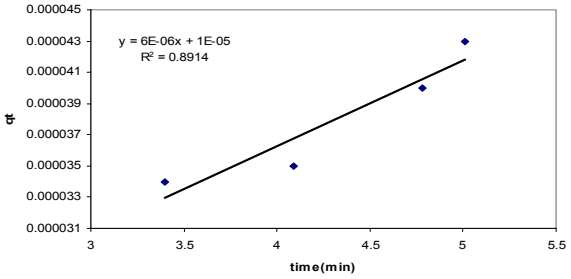

Fig5. Elovich plot for AY36

References

[1] Bhattacharya AK,Vekobachar C., "Removal of cadmium(II) by low cost adsorption.," JEnv Eng ASCE,1984,pp110-122.

[2] Dong, Y., He, L., & Yang, M., "Solar degradation of two azo dyes by photocatalysis using Fe (III)-oxalate complexes H2O2 under different weather conditions.," Dyes and Pigments,2008,pp343-350.

[3] Mielcarek J., Kula M., "kinetic Studies on Fluvastatin photodegradation in solution," React.Kinet.Catal.Lett,2005, 86(1),pp119-126.

Kinetics and mechanism of color removal of Direct Blue 71

R.Fazaeli[*a], Z. Emadian Razavi[b],M.Yousefi[b],S. Ghasemi[b]

[a] Modeling and Optimization Research Center in Science and Engineering, Islamic Azad University-South Tehran Branch, Tehran, Iran

E-mail: r_fazaeli@azad.ac.ir

[b]Department of Chemistry, Islamic Azad University Shahr-E- Rey Branch, Tehran, Iran

Introduction:

The photodegradation of pollutants from aqueous solution plays an important role in wastewater treatment. The study of photodegradation kinetics in wastewater treatment is significant as it provides valuable insights into the mechanism of photodegradation reactions. Photodegradation, as a cost-effective technology for the removal of soluble azo dyes pollutants and organics from aqueous solutions, has been extensively studied and most research mainly focused on the reaction kinetics. The removal of color from textile dye baths is one of the challenging problems in the field of environmental chemistry. Different techniques were applied, e.g. adsorption, oxidation, reduction, electrochemical, and membrane filtration [1]. A photodegradation of organic dyes, especially cationic dyes, by various adsorbents was the subject of several investigations.

Method:

Batch kinetic experiments were carried out for the degradation of Direct Blue 71 at the presence of TiO_2 catalyst and $K_2S_2O_8$ oxidant under UV irradiation. The experimental kinetics were fitted to the pseudo first and second order kinetics by liner method. Present investigation showed that it is appropriate to use a pseudo second-order expression as proposed by Ho and Blanchard. Thesestudies expressed the degradation kinetic of Direct Blue 71 in aqueous suspension. The stock solution of Direct Blue 71 was prepared by dissolving 0.1 g of Direct Blue 71 in one liter of distilled water. The experimental data was analyzed by photodegradation of Direct Blue 71 into the photochemical reactor at the presence of TiO_2 (rutile) and $K_2S_2O_8$. The samples were enclosed in cylindrical, quartz cell and exposed to the UV irradiation. Maximum efficiency was about 98.5% for 90 min.

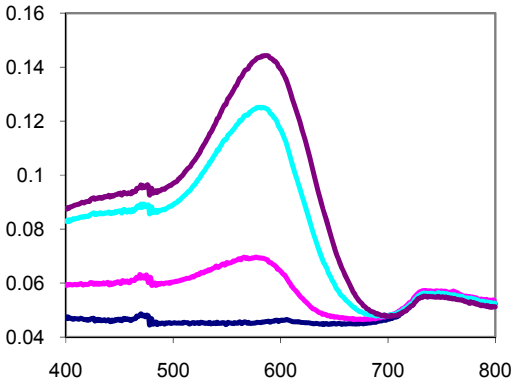

Mechanism of photodegradation, were included the several models such as Logergern[2], Blanchard[3], and Elovich[4], explain the pseudo first order and pseudo second order kinetic. A high degree of purification can be achieved by using the degradation method.

This table shows the kinetic of Direct Blue 71

Kinetic Model	General Formula	Regression equation	R^2
Logergern	$\frac{dq_e}{dt} = k_1(q_e - q_t)$	y = -0.052x – 12.74	0.977
Blanchard	$\frac{t}{q_t} = \frac{1}{k_2 q_e^2} + \frac{t}{q_e}$	y = 16713x	0.989
Elovich	$q_t = \frac{1}{\beta}\ln(\alpha\beta) + \frac{1}{\beta}\ln(t)$	y = 1E-06x + 3E-06	0.959
Intraparticle	$q_t = k_i t^{\frac{1}{2}} + C$	y = 4E-07x + 3E-06	0.980

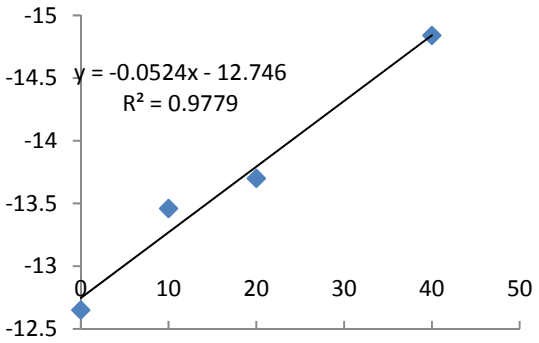

Logergern

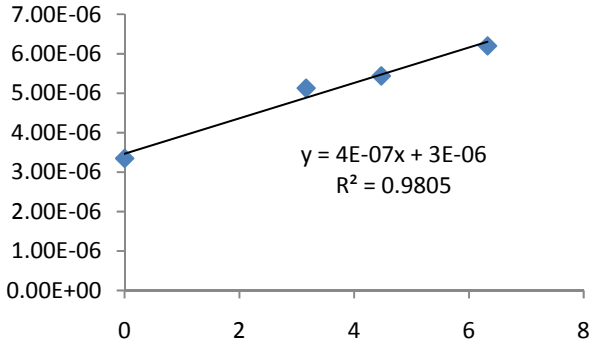

Intraparticle

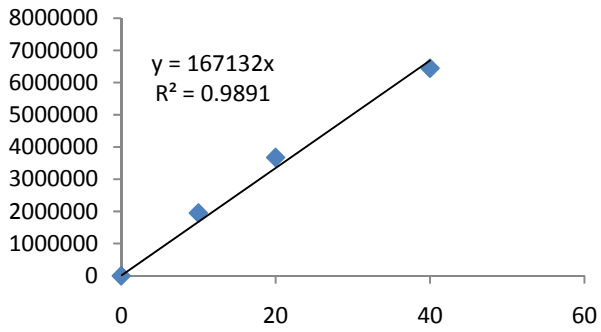

Blanchard

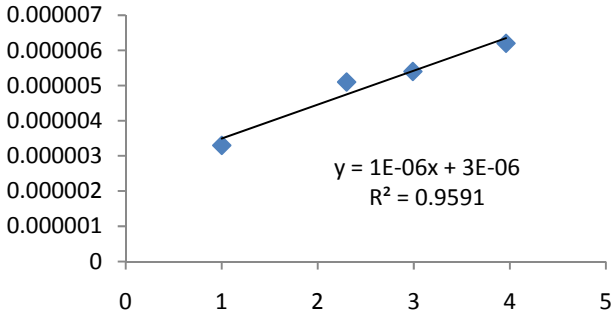

Elovich

Conclusion:

The photodegradation of azo dyes catalyzed by TiO_2 were carried out in reasonable efficiency by UV irradiation. Different parameters such as dose of catalysts and irradiation time were examined. The optimum conditions for photodegradation of DB71 in aqueous solution were determined. The best degradation efficiency of 98.5% was achieved. In this research we apply the accepted kinetic equations of photocatalyst degradation instead of adsorption. The highest correlation coefficients were obtained for the pseudo-second order kinetic model. This method is more cost-effective in comparison of previous reported methods with the same performancy.

Reference

[1] Ya- Li. Song, Ji-Tai. Li, and Bo. Bai, "TiO_2 - Assisted photodegradation of Direct Blue 78 in Aqueous Solution in sunlight" Water Air Soil Pollut, pp. 529–551, March 2010.

[2] Baskaralingam, P., Pulikesi, M., Elango, D., Ramamurthi,V., Sivanesan, "Adsorption of acid dye onto organobentonite"..,J. Hazard Mater.2006,138-144.

[3]Ho, Y.S., McKay, G., ",Pseudo-second order model for sorption processes", Process Biochem,1999 pp. 451-465.

[4]Weber, W.J. Jr., Morriss, J.C., "Kinetics of adsorption on carbon from solution", . J. Sanit. Eng. Div. Am. Soc. Civ. Eng. ,1963, pp31-60.

[5]Dong, Y., He, L., & Yang, M., "Solar degradation of two azo dyes by photocatalysis using Fe (III)-oxalate complexes H2O2 under different weather conditions.," Dyes and Pigments,2008,pp343-350.

[6] Huang, J.H., Liu, Y.F., Jin, Q.Z., "Adsorption studies of a Water soluble dye, Reactive Red MF-3B, using sonication -surfactant modified attapulgite clay". J. Hazard. Mater. 2007, 541-548.

Kinetic modelling of Fischer–Tropsch synthesis over Co/Ni/Al_2O_3 catalyst

Ali A. Mirzaei[a], M. Fatemi*[a], H. Atashi[b], S. Rezazade[a] and A. Zare[a]

[a]Department of Chemistry, Sistan & Baluchestan University, Zahedan, Iran

[b]Department of chemical Engineering, University of Sistan & Baluchestan, Zahedan, Iran

(E-Mail: mfatemi1985@yahoo.com)

Keywords: Fischer-Tropsch synthesis, Kinetic model, Cobalt-nickel catalysts.

Abstract

The catalyst was prepared by wet impregnation procedure (50-60ºC, in vacuum condition). The fresh catalyst was crushed and sieved to particles with diameters of under 70 µm, which has been proved to be a compromising particle size safe for neglect able intraparticle transfer limitations and promisingly easy operations to the reactor during the experiment. A 1.00 g catalyst was used for the kinetic experiments. The FT reactions was carried out at 493–523 K (P = 1–12 bar, H_2/CO = 1-3, GHSV = 4500 h^{-1}). The rate constants for the FTS reaction over the Co/Ni/Al_2O_3 catalyst were found and the obtained activation energy was 116.5 kj/mol.

Introduction

Fischer–Tropsch synthesis (FTS) is a catalytic process for the conversion of synthesis gas (CO and H_2) into mixture of linear liquid, solid hydrocarbons and oxygenates[1]. Cobalt-based catalysts greater stability facilitated our obtaining reproducible kinetic data[2]. The kinetic description of the FT reaction is a very important task for the industrial practice, being a prerequisite for the industrial FT process design, optimization and simulation. The complexity of the reaction products, however, makes the kinetics of the process quite hard to be accurately described [3].

Method

The catalyst tests were carried out in a fixed bed stainless steel microreactor. In a typical reduction procedure, operation conditions were adjusted to H_2=N_2=30 ml/min, 1 atm and 3600h^{-1} at 623K for 3hours. product streams were analyzed online using a gas chromatograph (Varian, Model 3400 Series) equipped with a 10-port sampling valve (Supelco company, USA, Visi Model), a sample loop, thermal conductivity detector (TCD), and flame ionization detector (FID). The FT reactions was carried out at 493–523 K (P=1–12bar, H_2/CO=1-3, GHSV= 4500 h^{-1}).

Results and Discussion

On the basis of proposed reaction mechanisms, the kinetics expression for the rate of CO was derived. Both the calculated CO consumption rate by PolyMath software and the experimental rate are satisfactorily adaptable. The final rate expression is obtained:

$$-R_{CO} = \frac{kP_{CO}P_{H_2}}{1+aP_{CO}}$$

The mechanism of FTS over aforesaid catalyst is in flowing**:**

$$C* + H* \xrightarrow{k_P} CH* + H* \xrightarrow{k_{P1}} CH_2*$$

Conclusions

A kinetic investigation was performed on an alumina supported cobalt-nickel-FT catalyst in a fixed bed reactor. CO dissociates via interaction with H. The first hydrogenation step is reversible and fast, while the second is slow and rate determining.

References:

[1] H. Atashi, F. Siami, A.A. Mirzaei, M. Sarkari; *Journal of Industrial and Engineering Chemistry* 16 (2010) 952–961

[2] A. Outi I. RAUTAVUOWand Hessel S. van der BAAN; *Applied Catalysis,* 1 (1981) 247-272

[3] C. G. Visconti, E. Tronconi, L. Lietti, R. Zennaro, P. Forzatti; *Chemical Engineering Science* 62 (2007) 5338 – 5343

Study of benzothiophene disulfurization by TiO_2 nanoparticles supported on clinptilolite

H.Faghihian[a*] and sh.Naeimib
Department of Chemistry, Islamic Azad University, Shahreza Branch
Email:naeimi_sh@yahoo.com

Introduction

Due to increasing environmental concern, special interest has been paid to the reduction of organosulfur compounds in transportation fuels [1]. Hydrodesulfurization (HDS), can remove most sulfur compounds, but some refractory sulfur compounds such as benzothiophene (BT) still stay in diesel oil. As a result, severe conditions such as higher temperature and more active catalysts are required to achieve ultra-low sulfur level of diesel oil [2].One idea that has drawn wide attention, as referred oxidative desulfurization (ODS), involves oxidizing the sulfur compounds [3]. TiO_2 nanoparticles as an photocatalyst can be fixed on an inert supports such as zeolite [4]. In this research, we examined oxidation of model sulfur compound (benzothiophene) in the presence of the photocatalyst synthesized by TiO_2 and clinoptilolite.

Experimental

1.preparation of TiO_2 nanoparticle

Titanium tetraisopropoxide (TTIP, 97%, Merck) was first mixed with isopropanol. A 250 ml solution of distilled water at various pH was used as the hydrolysis catalyst. Solutions were mixed together under vigorous stirring. The prepared precipitates were washed and dried at 100°C. Then yellow white powder was annealed at temperature from 200 to 800°C .The synthesized TiO_2 was deposited on the surface of clinoptilolite[5].

2.Desulfurization

N-hexan solution of BT with known amount of photocatalyst were placed in dark room undr UV irradiation for 0-10 h with magnetic stirring. Reactant samples were collected and analysed by HPLC.The effect of different parameters including amount of photocatalyst, TiO_2 content, irradiation time and initial concentration who studied and optimized.

Result and discussion

1.characterization materials

FTIR spectra and TEM image of the catalyst are shown in fig 1. It is clear that TiO_2 nanoparticle are immobilized on the surface of the zeolite and the structure of zeolite remaind intact after synthesis.

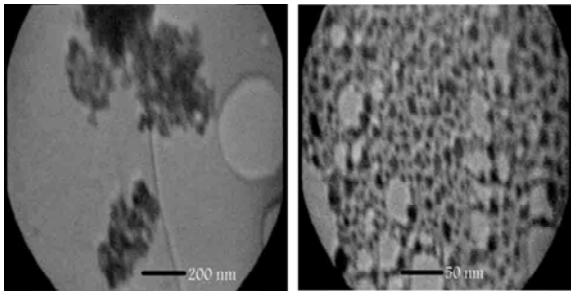

Figure1 (a). TEM image of photocatalyst

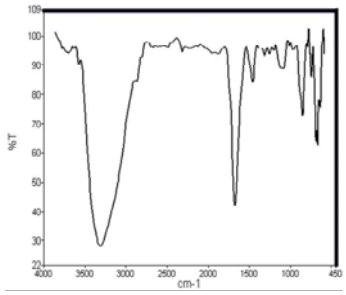

Figure1(b).FTIR spectra of photocatalyst

2. Optimization of Desulfurization

Degradation of BT at different experimental conditions were studied. Optimized reaction conditions are as follows: reaction time 300 min, amount of photocatalyst 0.4 g, initial concentration 200mg/L and percent of photocatalyst 20%. The degradation percentage of BT % 92 was obtained.

3.Kinetics of the reaction

The rate constant for the reaction was obtained from the pseudo first order equation :

$$-\ln(Ct/C\circ) = k_p t$$

Where C◦ and Ct are respectively the concentrations of substrate at time zero and time t(s) and k_p the first-order rate constant (s^{-1}). Application of the equation to the results showed that the photocatalytic oxidation follows first-order kinetics..

Conclusion

Photocatalytic oxidation of BT in n-hexan by TiO_2-supported clinoptilolite showed that this photocatalyst is the most highly active catalyst for oxidation desulfurization of BT at UV light irradiation.

Refrences

[1] Lai J; Luo G; J. Petroleum Science and Technology. 27 **(2009)** 781-787

[2] Chao Y; Li H; Zhu W; Zhu G; Yan Y; J. Petroleum Science and Technology. 28 **(2010)** 1242-1249.

[3] Salari D; Rostamizadeh K; J. Petroleum Science and Technology. 26 **(2008)** 382-397.

[4] Li F; Jiang Y; Yu L; Yang Z; Hou T; Sun Sh; J. 252 **(2005)** 1410-1416.

[5] Mahshed S; Askari M; Sasani Ghamsari M; J. Materials Processing Technology. 189 **(2007)** 296-300

Removal of vanadium anions from aqueous solutions by polyaniline modified Clinoptilolite

[1]H.Faghihian, [2]M.Rasekh
Department of Chemistry, Islamic Azad University, Shahreza, Iran
faghihian@iaush.ac.ir

Keyword: modified zeolite, polyaniline, clinoptilolite, vanadium anions.

Introduction

Unmodified zeolites show no affinity for anions due to the fact that their surfaces are negatively charged. However modified zeolites show high capacity toward anions and therefore have drawn much attention in recent years for removal of anionic pollutants. In this work clinoptilolite was modified with polyaniline by polymerization of anilinium cations in the zeolite channels and a composite of polyaniline/ clinoptilolite was obtained. Encapsulation of polyaniline in the clinoptilolite channels was confirmed by XRD and FTIR spectroscopy. The effect of a number of parameter such as initial concentration of the anions ,amount of the composite and contact time were determined and optimized.

Preparation of polyaniline/ clinoptilolite composite

A given amount of clinoptilolite was first dispersed in the 50 ml of 0.5 M sulfuric acid containing 0.2 M aniline. The mixture was then stirred for 48 hours at room temperature. The mixture was filtered and washed with excess of deionized water in order to remove free anilinium ions. The resulting wet solid was dispersed in 50 ml of 0.3 M sulfuric acid solution, containing 0.16g ammonium persulfate as oxidizing agent. Polymerization of anilinium cation inside clinoptilolite channels was carried out at room temperature for a period of 24 hours under magnetic stirring. The resulting composite was filtered, washed with excess deionized water and dried in vacuum for 24 hours.

Vanadium anion removal

NH_4VO_3 solutions were prepared in different concentrations ranged . 0.2 g of the composite was put into a beaker containing 50 ml of NH_4VO_3 solutions at different concentrations. The mixture was then stirred for 120 min at room temperature .The mixture was filtered and washed with excess deionized of water. Measurement of unremoved vanadat ions was carried out by atomic adsorption spectroscopy [1,2] .

Results and discussion

The polyaniline/clinoptilolite nanocomposite was characterized by XRD and FT-IR technique. Adsorption of vanadat species was measured spectrophotometrically. Different experimental condition were investigated and optimized. The optimized adsorption conditions are as follows:equilibration time:120 min, initial concentration:1000 ppm, adsorbent dose 1.5 mg, initial pH=7 and optimized temperature=45^0C.The values are interpreted accordingly.

Equilibrium modeling

Tow isotherms were tested for their ability to describe the experimental results, namely the Langmuir isotherm, the Freundlich isotherm [3].

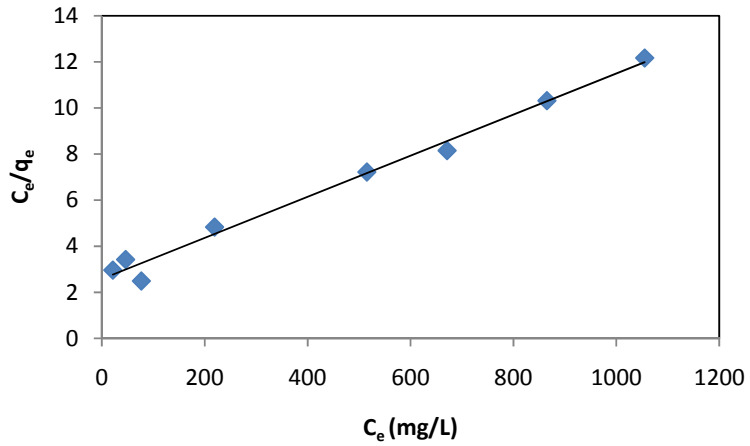

Fig1. Langmuir adsorption isotherm

The Langmuir isotherm fits the experimental data very well. It may be due to homogeneous distribution of active sites onto modification zeolite surface.

Refrence

[1] Jian Hu;Xuewen Wang;Liansheng Xiao;Songru Song;Baoqing Zhang;" Removal of vanadium from molybdate solution by ion exchange"J. Hydrometallurgy 95,(2009),203-206.

[2] Qinggang Li;Li Zeng;Liansheng Xiao;Yanan Yang;Qixiu Zhang;" Completely removing vanadium from ammonium molybdate solution using chelating ion exchange resins"J.Hydrometallurgy 98, (2009), 287-290.

[3] Langmuir l; "The adsorption of gases on plane surfaces of glass,mica and platinum" J.Am.chem.Soc.40,(1918),1361-1403.

Kinetics and thermodynamics parameters of Cu^{2+} removal by Cu(II)-imprinted silica gel sorbent

H.Faghihian[a*] and K.Asghari[a]

[a] *Department of Chemistry, Islamic Azad University, Shahreza Branch, young researchers club*

Email: Faghihian@iaush.ac.ir

Keywords: Cu(II)-imprinted sorbent, Kinetics, Thermodynamics, Silica gel

Introduction

Nowadays solid-phase extraction is being widely used for separation of cations [1, 2]. Ion-imprinted sorbents have outstanding advantages such as predetermined selectivity and they are excellent material for solid-phase extraction of some transition metal ions from complex matrix [3]. In this research the kinetic and thermodynamic parameters of Cu^{2+} adsorption by Cu(II)-imprinted silica gel was investigated. The results indicated that the adsorption process is spontaneous.

Experimental

N, N'-bis(4-hydroxy salicylidene)ethylene-1,2-diamine, H_2[$(OH)_2$-salen)] ligand was synthesized and characterized by FT-IR and UV-vis spectroscopy. This ligand was then employed for synthesis of Cu(II)-H_2[$(OH)_2$-salen)] complex. The product was also characterized by FT-IR and UV-vis spectroscopy, and then was covalently anchored on silica gel surface. This anchorage was confirmed by thermal gravimetric analysis. The Cu content of the product was removed by acid leaching and the Cu-imprinted silica gel sorbent was applied as a new sorbent for solid-phase extraction of Cu^{2+}. The effect of different experimental parameters was studied and optimized.

Result and discussion

1.Adsorption isotherms

Two different isotherms were examined to describe the experimental results, namely the Langmuir isotherm and the Freundlich isotherm. As shown in Table 1, the Langmuir isotherm

has good regression coefficient showing the fitness of the results to this model [4]. According to this observations the results were interpreted.

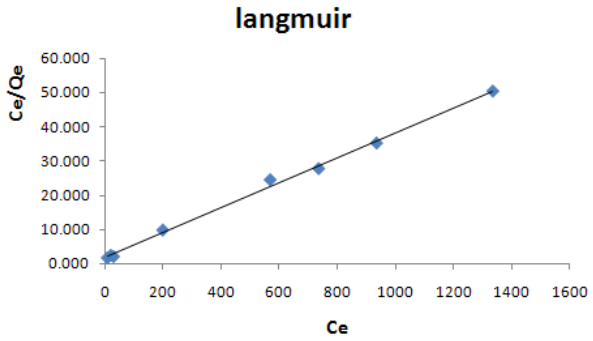

Figure 1: Langmuir isotherm

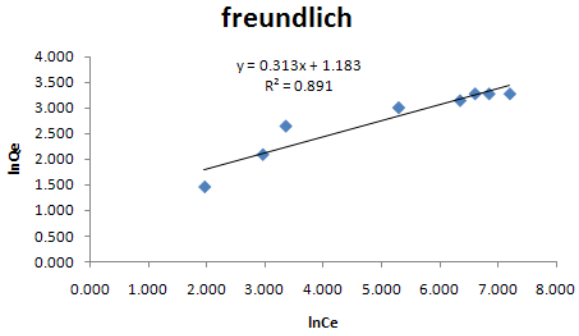

Figure 2: Langmuir isotherm

Isotherms	parameters	R^2
Langmuir	q_o =27.78 (mg/g) b =0.0202 (L/mg)	0.992
Freundlich	K_f = 3.264 n = 3.195	0.883

Table1: Comparison of Langmuir and Freundlich parameters

2.Thermodynamic parameters

The effect of temperature on the removal of Cu^{2+} was also studied. It was found that the adsorption capacity of the sorbent increases as temperature increases. To calculate the thermodynamic parameters of the process d, the Van't Hoff equation (also known as the Vukancic-Vukovic equation) was applied. The calculated values of ΔH^o and ΔS^o are

respectively 47.60 and 40.34 J/mol that shows that the adsorption process is endothermic process ($\Delta H^o>0$). Positive ΔS^0 indicates that the entropy of the adsorption of Cu^{2+} by ion-imprinted sorbent is higher than the hydrated lattice in solution phase. The Gibbs free energies calculated at 298°, 318° and 328° K were respectively -11.97, -12.78 and-13.18 which indicates that the adsorption process is spontaneous.

3-Adsorption kinetics

The modeling of the kinetics of adsorption of Cu^{2+} on Cu(II)-imprinted sorbent was investigated by two common models, namely the Lagergren pseudo-first-order model and pseudo-second-order model. None of these models could describe the adsorption kinetics perfectly. The results were interpreted.

4-Adsorption mechanism

In order to gain insight into the mechanisms and rate controlling steps affecting the kinetics of adsorption, the experimental results of the kinetic studies were fitted to the Weber's intra particle diffusion. This model is expressed as: $q_t = k_{id}\, t^{1/2} + C$ .The intercept of the linear plot of q_t against $t^{1/2}$ reflects the boundary layer effect. It was found that the intra particle diffusion was not only rate-controlling step.

Conclusion

Kinetics and thermodynamic parameters obtained in this study, showed that the adsorption of Cu^{2+} by Cu(II)-imprinted silica gel is mono layer adsorption with $\Delta H^o>0$,$\Delta S^o>0$ and $\Delta G^o<0$, which indicates that the adsorption process is endothermic and spontaneous.

Refrences

[1] Zhang, N.; Suleiman, J.S.; He, M. and Hu, B.;*Talanta*, **2008**, *75*, 536-543.

[2] Jiang, N.; Chang, X.; Zheng, H.; He, Q. and Hu, Z.; *Anal. Chim.Acta*, **2006**, *577*, 225-231.

[3]Wang, Z.; Wu, G.and He, C.; *MicrochimActa*, **2009**, *165*, 151-157.

[4]Hameed, B. H.; Salman, J. M.; and Ahmad, A. L.; *J.Hazard. Mater.,***2009**, *163*, 121-126.

Kinetic study and photocatalytic efficiency of Cu^{2+}-Nd^{3+}-doped TiO_2 and Nd^{3+}-doped TiO_2 nano particles for the degradation of Acid Red 151

Mohammad Yousefi[a*], Sakineh Ghasemi[a], Reza Fazaeli[b], Zeinab Emadian[a]

[a]*Department of chemistry, Islamic Azad University Shahr-rey Branch, Tehran, Iran*

Email: m.yousefi50@yahoo.com

[b]*Department of chemistry, Islamic Azad University south-Tehran Branch, Tehran, Iran*

Abstract

The photo degradation of Acid red 151(AR151) in aqueous solution employing a H_2O_2/ultraviolet system in a photochemical reactor was investigated. The kinetics of decolorization was studied by application of a kinetic model investigated. The results show that the reaction of decolorization followed pseudo-second order kinetics. Irradiation at 409.5 nm of the dye solution in the presence of H_2O_2 results in complete discoloration after 30 minutes of treatment.

Keywords: Photo degradation, Acid Red 151, UV/H_2O_2, Kinetic

Introduction:

Dye pollutants from the textile industry are a major source of environmental contamination. Color removal from textile wastewater has been a matter of considerable interest during the last two decades, not only because of the potential toxicity of certain dyes but also because of their coloring effect on natural waters [1]. Long-range transport of pollutants is dominated by a number of factors, which include: 1) physico-chemical characteristics of the compounds, 2) meteorological and climatic parameters of the atmosphere, and 3) storage capacity of the compartment (soil, water, etc.)[2]. In this process, a semiconductor inorganic material in nanometric scale is used as catalyst to promote the degradation/oxidation of these organic dyes [3].

Methods:

A uv/catalyst system was performed with four lamp 8W emitting wavelengths in the UV range and between 400-800 nm. The photocatalytic activity of samples was tested using AR 151 solution. The degradation was carried out in a quartz photocatalytic reactor. The photocatalytic degradation was carried out with 150ml aqueous AR151 solution containing 50cc H_2O_2 and 0.5 gr of catalyst. The characteristics of the dyes are as follows: Mw=280 g mol^{-1},λ max=409.5 nm (Scheme 1).

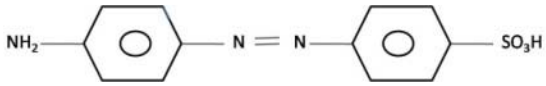

Scheme1. Molecular structure of the dye Acid Red 151

Result and discussion:

When the kinetics of the photocatalytic decolorization reactions were studied, it was found that the correlation between ln q_e/q_t and the irradiation time was linear. This is a typical first-order reaction plot. The slopes of the lines give the apparent rate constant (k). The Cu^{2+}-Nd^{3+}-doped TiO_2 nano particles kinetic expression can be presented as follows percentage photo degradation and equation legergren (fig 1.a): $\ln (q_e - q_t) = \ln q_e - k_1 t$, (fig1.b)%degradation $= \frac{C_0 - C_e}{C_0} \times 100$, The Ellovich model is given by the following (fig2.c): $q_t = \frac{1}{\beta}\ln(\alpha\beta) + \frac{1}{\beta}\ln(t)$ Pseudo-second–order equation (Blanchard) (fig2.d): $\frac{t}{qt} = \frac{1}{k_2 q_2^2} + \frac{t}{q_2}$

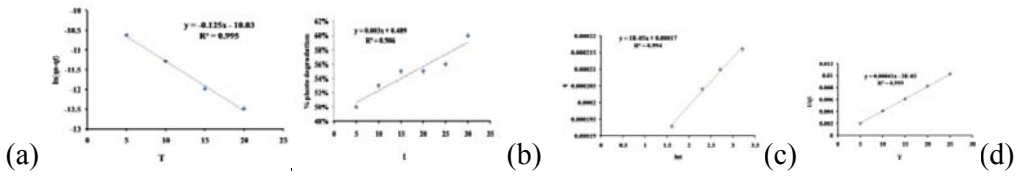

Fig1. (a) Equation legergren, (b) percentage photo degradation c) Ellovich, d) Blanchard

Reaction rate constants and Correlation coefficient and Intercept of various uv/catalyst systems (Table 1)

photo catalysts	Equation kinetics	Kinetics constants(h^{-1})	Correlation coefficient,R^2	Intercept
Nd^{3+}/TiO_2	Blanchard	3×10^{-5}	0.998	2.5×10^{-4}
	Ellovich	3×10^{-5}	0.867	1.8×10^{-4}
$Cu^{2+}/Nd^{3+}/TiO_2$	Blanchard	4.1×10^{-4}	0.999	-3×10^{-5}
	Ellovich	1×10^{-5}	0.994	1.7×10^{-4}

Conclusion:

The results show that the of Nd^{3+}/TiO_2 and$Cu^{2+}/Nd^{3+}/TiO_2$ nanoparticles decolorization followed pseudo-second order kinetics.

Reference:

[1]. A. Aleboyeh, et al, Environ Chem Lett, 1,161–164, (2003)

[2] Martí Nadal & Jason J. Wargent et al, J Atoms Chem, 55,241–252, (2006)

[3] Rafael Libanori. Tania R. Giraldi et al, J Sol-Gel Sci Technol, 49, 95–100, (2009)

Kinetic and Photo degradation study of azo dye in aqueous solutions catalyzed by $TiO_2/Nd^{+3}/ce^{+3}$ and chitosan masked TiO_2/Nd^{+3} nano particles

Sakineh Ghasemi[a*], Mohammad Yousefi[a], Reza Fazaeli[b], Zeinab Emadian[a]

[a]*Department of chemistry, Islamic Azad University Shahr-rey Branch, Tehran, Iran*

Email: s.ghasemy20@yahoo.com

[b]*Department of chemistry, Islamic Azad University south-Tehran Branch, Tehran, Iran*

Keywords: Doped TiO_2, Acid Red 151, Chitosan, Kinetic.

Abstract

This paper reports the photochemical degradation of Acid Red151 (AR) by using $TiO_2/Nd^{+3}/Ce^{+3}$ nano particle. The photo degradation reaction conformed to the pseudo-second order reaction kinetics. The maximum effect of photo degradation was observed after 120 minute. The photo- degradation of AR was studied in a batch reactor system illuminated with a four lamp 8W emitting wavelengths in the UV range and between 400-800 nm. The UV/H_2O_2 process appeared to be effective in removal of the AR decomposition was primarily ascribed to production of strong and nonselective oxidant-hydroxyl radicals within the system.

Introduction:

Titanium dioxide is one of the most effective photo catalysts because it is biologically and chemically inert and photo stable with near-UV band gap energy [1]. Typically, a combined UV/H_2O_2 process is more practical owning to involving a single-step dissociation of hydrogen peroxide to form two hydroxyl radicals ($^{\cdot}OH$). The hydroxyl radicals generated can non-selectively oxidize a broad variety of aqueous organic pollutants. Over the past decades, the process has been ascribed to successful decomposition of dyes and pharmaceutical intermediates appropriate conditions, the organic species can be mineralized without any secondary pollution [2].

Methods:

The photocatalytic activity of samples was tested using AR 151 solution. The degradation was carried out in a quartz photocatalytic reactor. The photocatalytic degradation was carried out with 150ml aqueous AR151 solution containing 50cc H_2O_2 and 0.5 gr of catalyst. The characteristics of the dyes are as follows: Mw=280 g mol^{-1},λ max=409.5 nm.

Results and discussion:

In order to determine the reaction rate and influencing factors, kinetic studies of the photo-degradation of AR151 by $TiO_2/Nd^{+3}/ce^{+3}$ nano particle were conducted under different experimental conditions. The kinetic expression can be presented as follows percentage photo degradation and equation legergren (fig 1.a): $\ln(q_e - q_t) = \ln q_e - k_1 t$, (fig1.b)%degradation $= \frac{C_0 - C_e}{C_0} \times 100$, The Ellovich model is given by the following (fig2.c) $q_t = \frac{1}{\beta}\ln(\alpha\beta) + \frac{1}{\beta}\ln(t)$, Pseudo-second–order equation (Blanchard) (fig2.d): $\frac{t}{qt} = \frac{1}{k_2 q_2^2} + \frac{t}{q_2}$

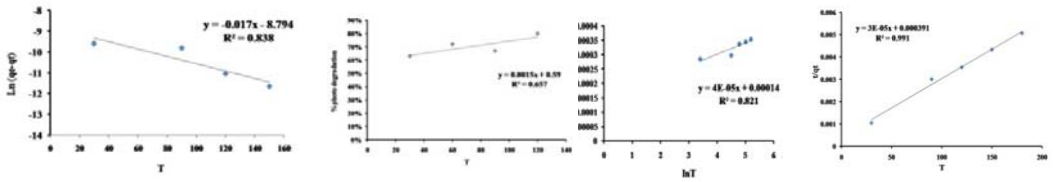

(a) (b) (c) (d)

Fig1. (a) Equation legergren, (b) percentage photo degradation c) Ellovich, d) Blanchard

Reaction rate constants and Correlation coefficient and Intercept of various uv/catalyst systems (Table 1)

photo catalysts	Equation kinetics	Kinetics constants(h^{-1})	Correlation cofficent,R^2	Intercept
chitosan/Nd^{3+}/TiO_2	Blanchard	3×10^{-5}	0.980	-2.1×10^{-4}
	Ellovich	3×10^{-6}	0.967	3.6×10^{-4}
$Ce^{3+}/Nd^{3+}/TiO_2$	Blanchard	3×10^{-5}	0.991	3.91×10^{-4}
	Ellovich	4×10^{-5}	0.821	1.4×10^{-4}

Conclusion:

The results show that the /chitosanNd^{3+}/TiO_2 andCe^{+3}/Nd^{3+}/TiO_2 nanoparticles decolorization followed pseudo-second order kinetics.

Reference:

[1] M. Nikazara, K. Gholivand, et al, Kinetics and Catalysis, 48, 2, 2007

[2] Li et al. J Zhejiang Univ Sci A, 10(11), 1660-1669, 2009

NMR study, AIM analysis, synthesis of rout to, kinetics and mechanistic investigation in the reaction between triphenylphosphine and dialkyl acetylenedicarboxylate in the presence of methylcarbamate

S. M. Habibi-Khorassani[a], A. Ebrahimi[a], M. T. Maghsoodlou[a], M. A. Kazemian[*a], M. Zakarianejad[a]

[a]*Department of Chemistry, The University of Sistan and Baluchestan, P. O. Box 98135-674, Zahedan, Iran*
E-mail: kazemean@yahoo.com

Keywords: Activated acetylenic esters; Methylcarbamate; Triphenylphosphine; Stable phosphorus ylides; Geometrical isomers

Introduction

Phosphorus ylides are important reagents in synthetic organic chemistry, especially in the synthesis of naturally occurring products, compounds with biological and pharmacological activity [1-4]. Most of the phosphonium salts are usually made from the reaction of phosphine and an alkyl halide [1-2], though they can be obtained by Michael addition of phosphorus nucleophiles to activated olefins[2,3]. In the current work, Triphenylphosphine reacts with dialkyl acetylenedicarboxylates in the presence of methylcarbamate to generate stable phosphorus ylides. These stable ylides exist in solution as a mixture of two geometrical isomers as a result of restricted rotation around the carbon-carbon partical double bond resulting from conjugation of the ylide moiety with the adjacent carbonyl group (Figure 1). The structures of compounds **4(a, b)** were deduced from their IR, ^{1}H, ^{13}C and ^{31}P NMR spectra.

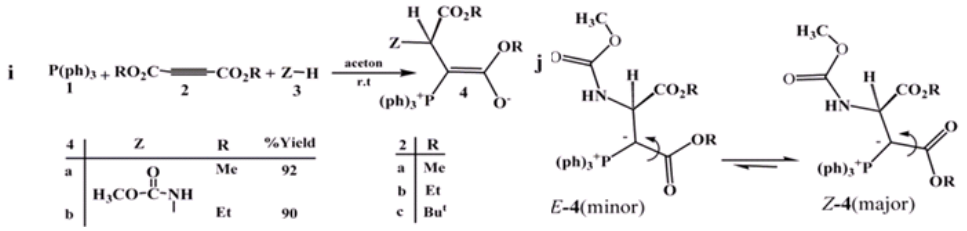

Figure 1. i) The reaction between triphenylphosphine **1**, dialkyl acetylenedicarboxylate **2** (**2a**, **2b** or **2c**) and methylcarbamate **3** for generation of stable phosphorus ylides **4** (**4a** or **4b**). **j)** The two *Z*-**4** and *E*-**4** rotational isomers (major and minor, respectively) of ylide **4a** or **4b**

Results and Discussion

Theoretical study

For assignment of the two *E*- and *Z*- isomers as a minor or major form in phosphorus ylides **4(a, b)** containing a methylcarbamate, first the *Z*- and *E*- isomers were optimized for all ylide structures at HF/6-31G(d,p) level of theory [5] by Gaussian98 package program [6]. The relative stabilization energies for both the geometrical isomers have been calculated at HF/6-31G(d,p) and B3LYP/6-311++G(d,p) levels. Atoms in molecules (AIM) and natural population analysis (NPA) methods and also CHelpG keyword at HF/6-31G(d,p) level of theory have been employed in order to gain a better understanding of the most geometrical parameters in both the *E*-**4(a, b)** and the *Z*-**4(a, b)** of phosphorus ylides. The numbers of critical points and intramolecular hydrogen bonds have been recognized as well as the charge of atoms that constructed on the two *Z*- and *E*- isomers. The results altogether reveal the effective factors on stability of the two *Z*- and *E*- ylide isomers. The relative stabilization energies for the two *Z*-**4(a, b)** and *E*-**4(a, b)** geometrical isomers (See Figures 2 and 3) are reported in Table 1, as can be seen, the *Z*-**4a** and the *Z*-**4b** isomers are more stable than the *E*-**4a** and the *E*-**4b** forms (1.54 and 1.82 kcal/mol, respectively) at B3LYP level.

Table 1. The relative energy (kcal/mol) for both the *Z*- and *E*- isomer of ylides, obtained at HF/6-31G(d,p) and B3LYP/6-311++G(d,p) levels.

Conformer	HF	B3LYP
Z-**4a**	0.00	0.00
E-**4a**	1.54	1.66
Z-**4b**	0.00	0.00
E-**4b**	1.82	1.96

Kinetic Studies

To gain further insight into the reaction mechanism between triphenylphosphin **1,** dialkyl acetylenedicarboxylates **(2a**, **2b** and **2c)** and methylcarbamate **3** (as a NH- heterocyclic compound) for generation of phosphorus ylids 4**a-c,** a kinetic study of the reactions was undertaken by UV spectrophotometeric technique. The results are accumulated in Tables **2** and **3** respectively.

Table 2: Values of overall second order rate constant for the reactions between (**1, 2c** and **3**), (**1, 2b** and **3**) and (**1, 2c** and **3**) in the presence of solvents such as 1, 2-dichloroethane and ethyl acetate, respectively, at all temperatures investigated.

reaction	Solvent	ε	k_2.M^{-1}.min^{-1}			
			12.0ºC	17.0ºC	12.0ºC	27.0ºC
1, **2c** and **3**	1,2-dichloroethane	10	59.6	86.3	112.5	144.4
	ethyl acetate	6	51.1	79.5	122.2	169.8
1, **2b** and **3**	1,2-dichloroethane	10	242.3	276.0	302.4	347.2
	ethyl acetate	6	158.0	195.1	228.5	256.6
1, **2a** and **3**	1,2-dichloroethane	10	341.0	371.1	413.2	458.3
	ethyl acetate	6	271.1	596.6	365.3	420.9

Table 3: The activation parameters involving $\Delta G^{\#}$, $\Delta S^{\#}$ and $\Delta H^{\#}$ for the reactions between **1, 2a** and **3**, **1, 2b** and **3** and also **1, 2c** and **3** at 12.0ºC in 1, 2-dicholoroethane.

reactions	$\Delta G^{\#}$(kJ.mol^{-1})	$\Delta H^{\#}$(kJ.mol^{-1})	$\Delta S^{\#}$(J.mol^{-1}.K^{-1})
1, 2a and **3**	102.46	9.26	-326.87
1, 2b and **3**	103.27	11.86	-320.58
1, 2c and **3**	106.60	36.76	-244.95

Conclusion

In conclusion, we have prepared novel phosphorus ylides **4a-b** using a one-pot reaction between triphenylphosphine and dialkyl acetylenedicarboxylates in the presence of methylcarbamate. The present method, carries the advantage that, not only the reaction is performed under neutral conditions, but also the substances can be mixed without any activation or modifications. The assignment of the *E*- and *Z*- isomers as a major or minor form in both the ylides **4a** and **4b** were undertaken by AIM and NPA methods and also CHelpG keyword. Quantum mechanical calculations were clarified how the ylides **4a** and **4b** exist in solution as a mixture of the two major (*Z*-**4a,** *Z*-**4b**) and minor (*E*-**4a,** *E*-**4b**) geometrical isomers, respectively. In addition, NMR study on the basis of theoretical calculations were just employed for determination of chemical shifts and coupling constants of the two major *Z*-**4a** and minor *E*-**4a** geometrical isomers. The results are compatible with the experimental data from the ^{1}H, ^{13}C and ^{13}P NMR spectroscopy. The results of kinetic investigation can be summarized as follow: (**1**) The overall reaction order followed second-order kinetics and the reaction orders with respect to triphenylphosphine, dialkyl acetylenedicarboxylate and methylcarbamate were one, one and zero respectively. (**2**) The values of the second-order rate constants of all reactions were calculated automatically with respect to the standard equation, using the software associated with the Cary-300 UV equipment. (**3**) The rates of all reactions were accelerated at higher temperatures. Under the same conditions, the activation energy for the reaction with di-*tert*-butyl

acetylenedicarboxylate **2c** (41.5 kJ/mol) was higher than that for the both reactions which were followed by the diethyl acetylenedicarboxylate **2b** (16.6 kJ/mol) and dimethyl acetylenedicarboxylate **2a** (14 kJ/mol) in 1,2-dichloroethane (**4**) The rates of all reactions were increased in solvents with higher dielectric constant.(**5**) With respect to the experimental data, the first step of proposed mechanism was recognized as a rate-determining step (k_2) and this was confirmed based upon the steady-state approximation. **(6**) Also, the third step was identified as a fast step (k_3). (**7**) The activation parameters involving $\Delta G^{\#}$, $\Delta S^{\#}$ and $\Delta H^{\#}$ were reported for three reactions.

References

[1] M. T. Maghsoodlou, S.M. Habibi-Khorasani, N. Hazeri, M. Nassiri, R. Kakaei, G. Marandi, *Phosphorus, Sulfur and Silicon*., 2006, 181, 553.

[2] A. Aminkhani, R. Kabiri, S. M. Habibi-Khorasani, R. Heydari, M. T. Maghsoodlou, G. Marandi, M. Lashkari, M. Rostamizadeh, *journal of sulfur chemistry*. 2009, 30, 500-506.

[3] M. T. Maghsoodlou, N. Hazeri, S. M. Habibi-Khorasani, R. Heydari, G. Marandi, M. Lashkari, Kh. Bagherpour, Z. Gharechaei, *Monash Chem,* 2010, 141, 351-356.

[4] N. Khir-el-Din, A. A. Nada, M. Ramla, M. F. Zayed, *Synthetic Communication*. 2002, 32, 591-603.

[5] Reed, A.E., Weinstock, R.B. and Weinhold, F.J*.*, *Chem. Phys*. 1985, 83, 735-746.

[6] Frisch, M.J., *et* al. Gaussian 98, Revision A. 7, Gaussian, Inc., Pittsburg h, PA, 1998.

[7] Bader, R.F.W., *Atoms in molecules A Quantum Theory*, Oxford University: New York, 1990.

[8] Biegler König, F.W., Schönbohm, J.and Bayles, D., *J. Comput. Chem*. 2001*,* 22, 545-559.

[9] Grabowski, S.J., *J. Mol. Struct*. 2001, 562, 137-143.

[10] Arnold, W.D., Oldfield, E., *J. Am. Chem. Soc*. 2000, 122, 12835-12841.

[11] Rozas, I, Alkorta, I and Elguero, J., *J. Am. Chem. Soc.* 2000, 122, 11154-11161.

[12] Schwartz, L. M.; Gelb, R. I. Alternative method of analyzing first-order kinetic data. *Anal. Chem*. 1978, 50, 1592-1594.

[13] Okubo, Maeda, T. Y.; Kitano, H. Inclusion Processes of Ionic Detergents by Cyclodextrins as Studied by Conductance Stopped-Flow Method. *J. Phys. Chem.* 1989, 93, 3721-3723

Comparing of sol-gel and solvothermal preparation of nano –structured zinc oxid thin films for photocatalytic Applications:solvevt effect

Najmieh Maleki* , Nasrin Talebian
Department of Chemistry, Faculty of Science, Islamic Azad University, Shahreza branch, I.R. Iran
Email : najmeh67@yahoo.com

Introdution

ZnO,as apotetial semiconductor with direct wide band gap(3.37 eV),has received enormous scientific attention because of its promising applications of optoelectronic nano –devices(1) Piezoelectric nano-generators(2),dye-sensitized solar cells(3),biodevices(4)and photocatalysts for degradation and elimination of environmental pollutanta(5).Recently,much effort has been devoted to study ZnO as a very promising photocatalyst for photocatalytic degradation of water

Pollutants.however,previous studies on the photocatalytic activity of ZnO nanomaterialswere carried out taking little account of its morphology.The morphologies of inorganic materials are confessed to have great effect on their widely varying properties and corresponding potential application(6).It is well known that ZnO exhibits the richest range of morphologies among the wide band gap semiconductors.As we have known,most methods for the synthesis of nano-scale ZnO demand high temperatures,special conditions,or tedious procedures,and the microstructure tailing of ZnO is difficult.Here in ,we report a simple low-temperature route to synthesize nano-structured ZnO thin film in the absence of surfactants under mild conditions.The photocatalytic degradation of solamin limit brown was compared favorably to study the morphology-dependent photocatalytic activity of as-prepared ZnO sample.

Methods

1-ZnO synthesis by two method,(A)sol-gel and (B)solvothermal,with different solvent (methanol,ethanol,isopropanol and 1,4-butandiol).In a sol-gel ,15/36g zinc zcetate dehydrate was dissolved in 100 ml used solvent under vigorous stirring at 60 o_C tempererature.Then ,required amount of MEA and CTAB was added drop by drop into the solution as a stabilizer.The molar of MEA to zinc acetate dehydrate to CTAB was maintained at 2:1:0.25.The solution was stirred at 60 oC for 2h to yield a clear and homogeneous solution

and then it was aged for 48h.The obtained sols were deposited on glass substrates using dip coating method.

In a solvothermal,ZnO prepared was two step.The first 30ml zinc nitrate 0/5mol/l and 6ml NH_3

was added in a another 30mlsolvent and CTAB was prepared andadd to first solvent,under vigorous stirring at 60oC and 30min.it was homougenous and in otoclave on 12h under 140oC

tempereature.This powdr loss is water by 300oC thermal,the second step it was added to acetyl-aceton (ACAC)and DD at 1:1:1.The solution was stirred for 12h to yield a clear and homogeneous solution and then it was aged for 24h.The obtained sols were deposited on glass substrates using dip coating method.

Results and discussions

The effect of differen method were on size nano-particle and different of morphology by using scanning electron microscopy(SEM),X-ray diffraction(XRD),and UV-vis spectroscopy, respectively. Photodegradation of solamin limit brown ,an azo dye used in Iran textile industries was tested as a model reaction to compare the photocatalytic activity(PCA)of the ZnO samples.

Morphology and structure

XRD patterns of the ZnO nanostructures are summarized in fig.1.All of the diffraction peaks in the patterns can be exactly indexed as the wurtzite ZnO with lattice constants a=0.3249nm and c=0.5206nm,which are agreed well with the values in the standard card (JCPDS 36-1451).

ZnO films synthesized in all solvent the preferred orientation along(002)and direction.

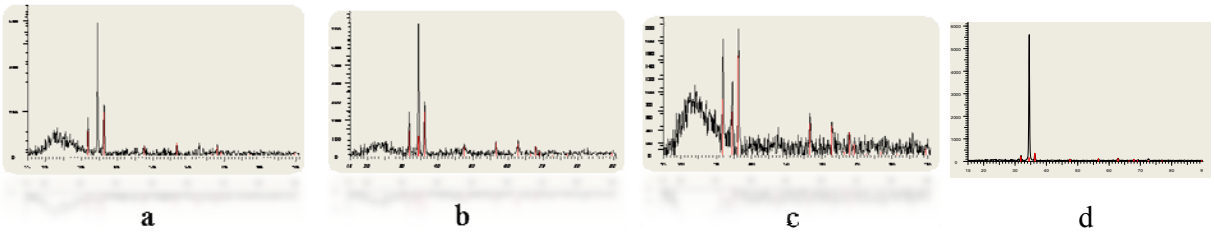

Fig.1.XRD patterns of ZnO thin films prepared in different solvents by solvothermal (a)methanol (b)etanol (isopropanol(d)1,4butandiol

XRD patterns of ZnO thin films by sol-gel method are same the patterns of solvothermal. SEM micrographs of samples with different morphology are shown in Fig.2.

a b c d

Fig2.SEM photographs of Zno with solvothermal (a)methanol(b)etanol(c)isopropanol (d)1,4butandiol

Conclusion

ZnO nanostructures were synthesized in solvents with different viscosities,and polarities Using sol-gel and solvothermal method in order to evaluence of solvent on structural,optical and photocatalytic properties.

References:

[1] X.D. Wang, C.J. Summers, Z.L. Wang, Nano Lett. 4 (2004) 423.

[2] Z.L.Wang, J.H. Song, Science **312** (2006) 242.

[3] M. Law, L.E. Greene, J.C. Johnson, R. Saykally, P.D. Yang, Nat. Mater. **4** (2005) 455.

[4] R. Yakimova, G. Steinhoff, R.M. Petoral Jr., C. Vahlberg, V. **22** (2007) 2780.

[5] C. Hariharan, Appl. Catal. A: Gen. **304** (2006) 55.

[6] A.P. Alivisatos, Science **271** (1996) 933.

Kinetics investigation of photocatalytic degredation of environmental organic pollutants using ZnO-Zeolite nano composites

N. Mohaghegh, Sh. Ghasemi, M. R. Gholami
Department of Chemistry, Sharif University of Technology, Azadi Ave., Tehran, Iran
Email: mohaghegh@mehr.sharif.ir

Introduction

ZnO nano particles and mordnite zeolite nano particles were prepared by precipitation method and hydrothermal method, respectively. The influence of solvent and surfactant in ZnO nano particles synthesis were studied to reform the structure of nano particles.These nano particles were based on different supports, in order to achieve efficient combinate mesoporous photocatalysts for the treatment and mineralization of Azo dyes. Synthesized catalysts characterized by X-ray diffraction (XRD), Scanning electron microscopy (SEM), Fourier transform-infrared spectra (FTIR), UV-Vis spectroscopy and BET techniques.[1] To investigated photocatalytic activity of the synthesized catalysts under UV irradiation, they were used to degradation bio-environmental pollutants such as acid blue 92 (AB92) textile dye. A detailed study on the photocatalytic degradation of AB92 under UV light in aqueous suspensions is presented. Effect of different parameters such as calcination temperature, amount of catalyst, pH and initial concentration of dye, temperature, ZnO loading have been examined on the yield and the speed of photocatalytic degradation process of AB92.The optimized amount of each of the mentioned parameters were determined and activity of the synthesized photocatalysis were compared. The best catalyst for the AB92 destruction process was nano composite of ZnO and Zeolite. [2]

Experimental

ZnO nanoparticles were prepared using the precipitation method. For the synthesis of ZnO nanostructures, the following procedure was used. 100 ml of 1 M NaOH solution and 100 ml of 1 mmol zinc acetate ($ZnAc_2$ _ $2H_2O$, Chameleon Reagent99%) solution, prepared using isopropanol, were mixed slowly with vigorous magnetic stirring at 40ºC. The reaction mixture was kept at 40ºC for 1 h. Mordenit zeolite nanocrystals with a uniform particle size were synthesized by a hydrothermal method. The incorporation of ZnO nanoclusters was

performed by impregnation of 0.3g zeolite into 100ml of a 5mol% $ZnAc_2$ solution over 14h. The powder was separated by centrifugation and dried at 80 ºC for 3h.

Result and discussion

1. X-ray diffraction analysis

X-ray diffraction (XRD) patterns of ZnO and ZnO/Mor with %5 and %25 catalysts are depicted in Fig. 1.

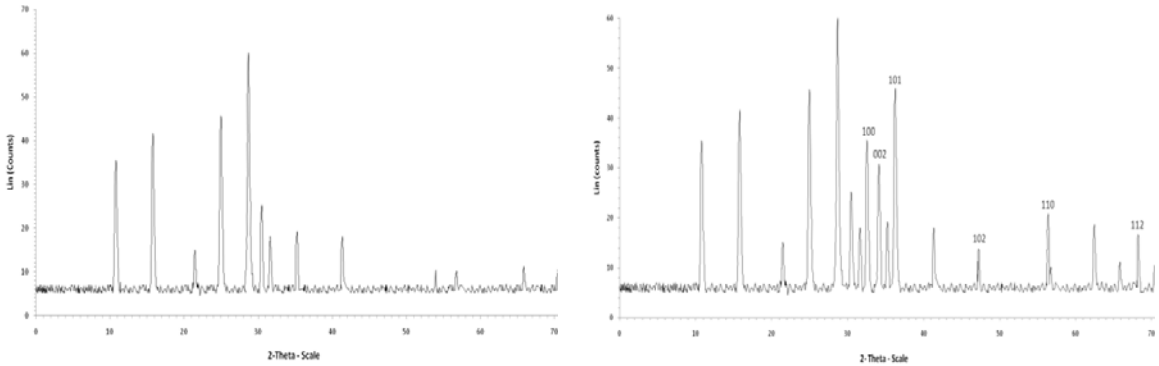

(a) (b)

Fig 1. XRD pattern of (a) ZnO/Zeolit 5% (b) ZnO/Zeolit 25%

2. SEM image analysis

Fig.2.(a) shows the ZnO nanoparticles synthesized without using any surfactant and ZnO nanoparticles aggregates with a wide range of size distribution. The average sizes of ZnO nanoparticles ranged from 300 to 350 nm and were irregularly shaped as aggregates. Effects of surfactant on the shape and size of ZnO nanoparticles are shown in Fig. 2.(b) Well shaped ZnO nanorods of 80 nm in diameter were formed when surfactant was used.

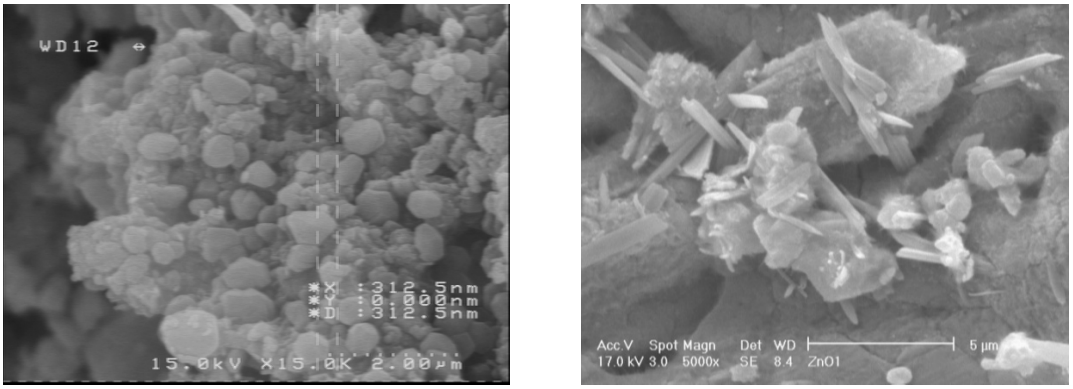

(a) (b)

Fig 2. SEM image of ZnO nanoparticels (a) without using any surfactant (b) with using surfactant

conclusion

SEM images show that the shape and size of the ZnO nanoparticles depend on the use of surfactant & solvent optimal temperature for calcination was 450°C. Photocatalytic degradation of AB92 over ZnO/Ac, ZnO/Al2O3 & ZnO/Mor supported catalysts revealed that mordenit selected as best support. photodegradation of AB92 decreases with an increasing in the initial concentration of AB92. Addition of ZnO concentration causes a decrease in the percentage of degradation. The photocatalytic decomposition of AB92 was most efficient in neutral and acidic solution photodegradation of AB92 increases with an increasing in the temperature, Photocatalytic degradation of AB92 was negligible when ZnO nanopowder and UV light were used on their own. The complete removal of AB92, after selection of optimal operational parameters, could be achieved in a relatively short time of about 1 h for ZnO catalyst about 45 min for ZnO/Mor-%25. photocatalytic degradation of AB92 with ZnO and zeolite based photocatalysts obeys apparently pseudo-first order kinetics.

References

[1] Chang SungLim a, JeongHoRyu., Journal of Crystal Growth 311 (2009) 486–489.

[2] A. Abdel Aal, Sawsan A. Mahmoud, Ahmed K. Aboul-Gheit., Materials Science and Engineering C 29 (2009) 831–835.

The Quantum study of the acetamide derivatives (TTA) as novel drugs Anti-HIV

N. Madadi Mahani [1] and M. Oftade [2]

[1] Department of chemistry, Payame Noor University (PNU), Sirjan, Iran

[2] Department of chemistry, Payame Noor University (PNU), Isfahan, Iran

Email:nmmadady@gmail.com

Keywords: Quantum Study, Anti –HIV Drug, Energy Gap, B3LYP.

Introduction

A major challenge facing medicinal chemistry over the last few years has been (and still remains) the development of antiretroviral drugs endowed with significantly improved cross-resistance profiles, high barrier to resistance and/or new modes of action for chronic use in combination therapies [1].

Human immunodeficiency virus type-1 reversetranscriptase (HIV-1 RT) is an important target for designing RT inhibitors to block the virus's replication and prevent AIDS-related disease. Two kinds of RT inhibitors, nucleoside reverse transcriptase inhibitors (NRTIs) and non-nucleoside reverse transcriptase inhibitors (NNRTIs), have been developed over the past twenty years. Despite NNRTIs such as three FDA-approved drugs, nevirapine, delavirdine and efavirenz, being highly specific and less toxic than nucleoside inhibitors, the rapid emergence of resistant HIV viral strains carrying mutation at residuesthat surround the NNRTI binding pocket limits the usefulness of NNRTI to treat HIV infection [2,3]. Among the representatives of the NNRTIs, sulfanyltriazoles (I) and sulfanyltetrazoles (II) (Fig. 1) have interesting structures and offer various opportunities on the skeleton of sulfanylazoles as lead compounds. Initially, a series of 2-(4- (2,4-dichlorophenyl)-1,2,3-thiadiazol-5-ylthio)-N-acetamide (TTA) analogues, which exhibited significant anti-HIV-1 activities [4].

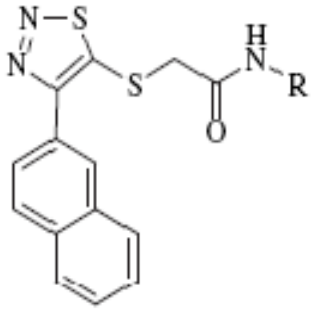

Fig.1. 2-(4-(naphthalen-2-yl)-1,2,3-thiadiazol-5-ylthio)acetamide derivatives

In order to understand the basis for the resilience of acetamide derivatives against mutation at molecular level and to help the design of further improved anti-AIDS agents therefore, quantum chemical calculations were applied. Theoretical investigation has been an alternative method for studies of the enzyme–inhibitor interaction in detail. However, such investigation of larger molecular system is limited by the computational effort required and the accuracy of the method used. Recently, accurate molecular modeling for larger molecules, such as those in molecular biology, became more feasible due to new developments in computational chemistry [5].

Methods

All geometries are optimized at the Becke's three- parameter hybrid functional (B3)with the nonlocal correlation of Lee-Yang-Parr (LYP) hybrid method by using Gaussian 03 suit of program. The 6-31G** basis set was used for acetamide derivatives and geometry optimization was carried out.

Results and Discussion

In this paper , we optimized of TTA_s with R= H, Ph, Ph-F , Ph –OH and Ph- Cl and calculated Total energy, HOMOs, LUMOs, Gap Energy, dipole moment and hardness of the compound based on B3LYP/6-31G**.

Table 1. Total energy, Gap Energy, dipole moment and hardness for molecules at B3LYP/6-31G**.

R	E(Hartree)	μ (Debye)	Gap Energy(Hartree)	Hardness(η)
H	-1575.974834	4.2955	0.26110	0.13055
Ph	-1807.022200	4.1750	0.22618	0.11309
Ph F	-1906.100929	3.2509	0.19301	0.09650
Ph OH	-1882.251142	3.6236	0.20611	0.10305
Ph Cl	-2266.368004	5.1668	0.12380	0.06190

It is observed that the substitution of deactivating groups causes decreasing energy and more stability compared with (R=H).also molecule with (R=Ph-Cl) has the highest dipole moment and the lowest gap energy and hardness because of more stability resonance , electronegativity of halides for example, F and Cl effects on the hardness and stability.

References

[1]A. Carta , S. Pricl , S. Piras , M. Fermeglia , P. La Colla and R. Loddo, Eur. J. Med. Chem. 44 (2009) 5117–5122.

[2] Y. H. Liang and F.E. Chen, Drug Discov Ther 1(2007)57-60.

[3] M. Kuno, S. Hannongbua and K. Morokuma, Chem. Phys. Lett. 380 (2003) 456–463.

[4] P. Zhan , X. Liu , Z. Fang, Zh.Li , Ch. Pannecouque and E. De Clercq , Eur. J. Med. Chem. , 44 (2009) 4648-4653.

[5] P. Nunrium , M. Kuno , S. Saen-oon and S. Hannongbua, Chem. Phys. Lett. 405 (2005) 198–202 .

ACE kinetic inhibition study of derived peptides from hydrolysis of HEWL by papain and trypsin

Mina Memarpoor-Yazdi[1], Ahmad Asoodeh[2,*], JamshidKhan Chamani[1]

[1]Department of Biology, Faculty of Sciences, Islamic Azad University-Mashhad Branch, Mashhad, Iran
[2]Department of Chemistry, Faculty of Sciences, Ferdowsi University of Mashhad, Iran
* Corresponding Author: Asoodeh@um.ac.ir

Key words: HEWL, Angiotensin converting enzyme, HPLC, Bioactive peptide

Introduction:

Many studies were centered on antihypertensive peptides derived from food proteins [1]. HEWL (Hen Egg White Lysozyme) is one of the major egg white proteins that showed antimicrobial [2] and antioxidant [3] activities. Angiotensin converting enzyme (ACE) plays a major role in the regulation of blood pressure [4,5]. The aim of this research is to determine the inhibitory pattern of purified peptides from tryptic-papainic hydrolysate of HEWL on ACE activity and also obtaining the kinetic parameters.

Methods:

The HEWL protein (0.25 gram) was hydrolyzed using treatment with trypsin and papain for 2hrs in 37 ºC. The enzymatic hydrolysis stopped by boiling for 15 min. The resulted solution centrifuged at 10000 RPM for 10 min and the supernatant solution was ulterafiltered and utterance of 10 kDa peptides were lyophilized and sub-fractionated using HPLC. A linear gradient of 5-25% acetonitrile in 0.1% TFA at flow rate of 2 ml/min was applied over 30 min and monitored the absorbance of 220 nm using UV detector. Finally ACE inhibitory effects of major peaks were studied.

Results:

Our research showed that in presence resulted hydrolysate from hydrolysis of HEWL by trypsin and papain the absorbance of 340 nm reduced less than from the control that shows those have ACE inhibitory activity. The kinetic parameters were showed in table1.

Table.1. The kinetic parameters of ACE inhibitory activity of F8 fraction.

	Control	F7 fraction (0.155mg/ml)	F7 fraction (0.310mg/ml)
K_m(mg/ml)	**2.369**	**0.483**	**0.328**
V_{max}(mM/min)	**0.366**	**0.148**	**0.115**
α	**1**	**1.236**	**1.523**
α/	**1**	**2.459**	**3.170**
K_I (mg/ml)	**-**	**1.081**	**1.213**
K_I /(mg/ml)	**-**	**2.304**	**2.860**

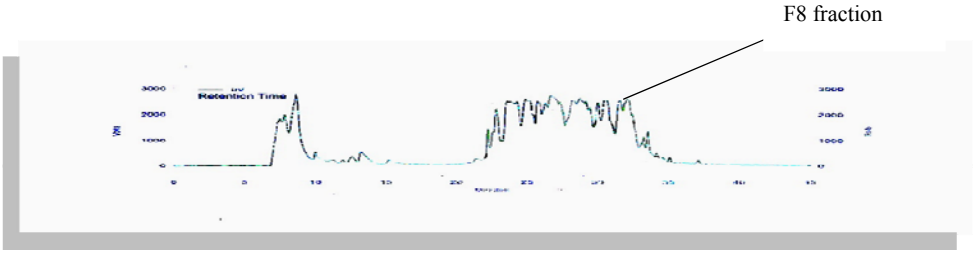

Fig.1. Reversed-phase gradient HPLC chromatogram. Separation was performed at room temperature on C_{18} clumn. A linear acetonitrile gradient 5-25% in 0. 1% TFA was applied. The flow rate was 2 ml/min and the absorbance was monitored at 220nm.

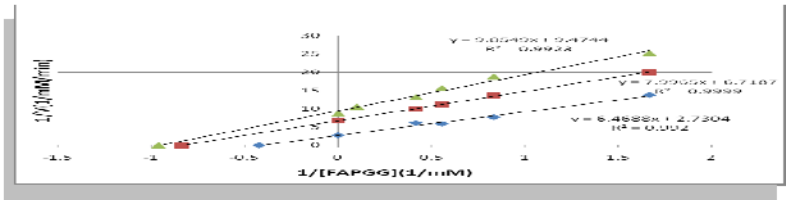

Fig.2. Line weaver-Burk plots of inhibition of ACE by the F8 fraction of purified peptide from tryptic-papainic hydrolysate of HEWL on ACE. ACE activities were measured in the absence ( ) or in the presence of F8 fraction of purified peptide from tryptic- papainic hydrolysate of HEWL (;0.155 mg/ml, ;0.310 mg/ml)

Discussion:

To obtain the active ACE inhibitor from HEWL, trypsin and papain was used to hydrolyze HEWL. Among purified peptides, F8 Fraction showed the highest ACE inhibition. The kinetic results showed that the mechanism of inhibitory activity was mix competitive which means that the F8 fraction can not bind to active site of ACE, but it may bind to ACE enzyme or substrate-enzyme complex.

Conclusion:

Purification of peptides from HEWL by HPLC method lead to release antihypertensive peptides. It was evaluated as a mix competitive inhibitor on ACE activity the assay for inhibitory pattern by Lineweaver–Burk plotting. HEWL trypsin-papainic hydrolysate may serve as useful source in the formulation of antihypertensive drugs and functional foods.

References:

[1] Miguel M and Aleixandre A: *J. Nutr* 2006, 136:1457-1460.

[2] Mine Y, Kovacs-Nolan J: World Poult Sci J 2006, 62:87-95.

[3] You S-J, Udenigwe C.C, Aluko R.E, Wu J: Food Research International 2010, 43:848-855.

[4] Jia J, Ma H, Zhao W, Wang Z, Tian W, Luo L, He R: Food Chemistry 2010, 119: 336-342.

[5] Hasan F, Kitagawa M, Kumada Y, Hashimoto N, Shiiba M, Katoh S, Tershima M: Process

Biochemistry 2006, 41:505-511.

Kinetic and equilibrium study of adsorption of Acid Red 14 with Bentonite

Hossean Malekhosseani [*1], *Kazem Mahanpoor* [2], *Aboalfazl Soufi* [3]

1,2, 3) Department of Chemistry, Faculty of Science, Islamic Azad University, Arak Branch

Abstract: Bentonite used adsorbent for this purpose because of its extended surface area, microporous structure, high adsorption capacity and high degree of surface reactivity.We investigated the equilibrium and kinetics of adsorption. The Langmuir and Freundlich equations were used to fit the equilibrium isotherm. The batch contact time method was used to measure the adsorption rate. Kinetic parameters were then evaluated.

Key word: Adsorption, Acid Red 14, Bentonite

Introduction: Since many organic dyes are harmful to human beings, the removal of colour from process or waste effluents becomes environmentally important. Due to the large degree of organics present in these molecules and the stability of modern dyes, conventional physicochemical and biological treatment methods are ineffective for their removal [1,2]. The adsorption process is one of the efficient methods to remove dyes from effluent [3].

Method: . Acid Red 14 was obtained from Aldrich Co. All other chemicals were purchased from Merck (Germany). Double distilled water was used for solution preparation. The solution pH was adjusted by adding a small amount of 0.1 M HCl or NaOH. A UV-VIS Spectrophotometer, Perkin-Elmer lambda25 was employed for absorbance measurements using silica cells of path length 1 cm. Adsorption experiments were carried out by shaking adsorbents with 50 ml dye solution of required concentration and pH at in a thermostated shaker operated at 150 rpm. The samples were withdrawn from the shaker and the dye solution was separated from the adsorbent by centrifugation. Dye concentration in the supernatant solution was estimated by measuring absorbance at maximum wavelength (λ max= 515 nm) and computing concentration from the calibration curve. Kinetics of adsorption was determined by analysing adsorptive uptake of the dye colour from aqueous solution at different time intervals. Isothermal studies were conducted by adding various doses of adsorbent and shaking the reaction mixture for the equilibrium time. Influence of the pH was studied by adjusting the reaction mixture to different initial pH value and analyzing

the residual colour for equilibrium contact time. The amount of dye adsorbed onto the carbons, qe (mg/g), was calculated by mass balance relationship [Eq. (1)].

$$q_e = (C_0 - C_e)\frac{V}{W} \qquad (1)$$

where C_0 and Ce are the initial and equilibrium liquid-phase concentrations of dye, respectively
(mg/l), V the volume of the solution (l), and W the weight of the carbon used (g).

Results and discussion: The kinetic of adsorption was studied for its possible importance in the treatment of dye containing industrial effluents. The influence of contact time on removal of AR14 by Bentonite is shown in Fig. 1. To attain equilibrium, it take 45 min for Bentonite respectively.

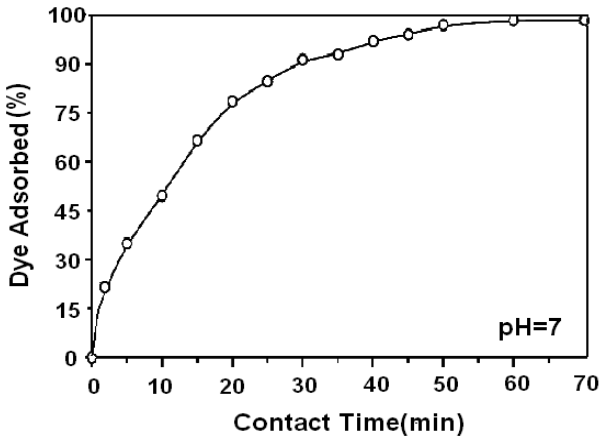

Fig. 1. Effect of contact time for the adsorption of Acid Red 14 on Bentonite.

Kinetic data were treated with the following Langergren's pseudo-first-order rate equation [4]:

$$\log(q_e - q_t) = \log q_e - K_{ad}t/2.033 \qquad (2)$$

where qe and qt refer to the amount of adsorption at the equilibrium and at any time t. The plot of log (q_e-q_t) versus t shows a straight line correlation coefficient >99), indicating the applicability of pseudofirst-order kinetics. The pseudo-first-order rate constants are calculated to be 0.062 min^{-1} at 25 ^{0}C.

References:

[1] McKay G., J Chem Technol Biotechnol 32(1982)759–72.

[2] [5] S. Rio, A. Delebarre, V. Hequet, P. Le, J. Blondin, J Chem Technol Biotechnol 77(2002) 382–388.

[3] P. Galiatsatou, M. Metaxas, V. Kasseloui-Rigopoulou, Mikrochimica Acta 136(2001)147–152.

[4] H.P. Boehm, Carbon 40 (2002) 145–149.

Photocatalytic Degradation Kinetics of Bromothymole blue in Aquatic System

M. Montazerozohori*, S. Nezami

[1] Chemistry Department, Yasouj University, Yasouj, 75918-74831, Post Box 353, Iran

(E-mail: mmzohory@yahoo.com)

Keywords: Photocatalyst, Degradation, Irradiation, Bromothymole blue.

Introduction

Heterogeneous photocatalysis offers an attractive alternative for wastewater treatment especially refractory aromatic compounds. Despite the great potential of photocatalytic process, it has not widely used industrially. The problems which haverestricted widespread commercialization of this attractive technology to date are the material handling problems presented by the fine particulate nature of TiO_2 and the fact that the polar surface of TiO_2 is not favorable for adsorption of organics in competition with water. As a result, no commercial application of TiO_2 photocatalysis to aqueous waste streams has yet emerged [1-8]. In this work, photocatalytic degradation of aqueous solution of Bromothymole blue was carried out in a photocatalytic reactor. The effect of some physical and chemical parameters such as amount of photocatalyst, pH, time of irradiation and solvent were studied.

Methods

General procedure for photocatalytic degradation experiments

The photodecomposition experiments were performed by irradiation of 20 ml continuous aerated, stirred aqueous solution of Bromothymole blue in various pH as well as considered amounts of photocatalysts in photoreactor cell under 400W high pressure mercury lamp at constant temperature. After effective degradation, photocatalyst was separated by centrifugation and title compound concentration was measured by spectrophotometric method.

Results and discussion

The effect of various factors

Different parameters such as pH of solutions, amount of photocatalyst and irradiation time were examined. The results are summarized in table 1. The results show that all three parameters of photocatalyst amount, air and irradiation are need for effective decomposition of compound.

The effect of pH

As shown in figure 1, increasing of pH lead to higher degradation percent(%). This phenomenon can be ascribed to higher hydroxyl radical generation during the phodegradation process in more basic conditions.

Table1- The effect of various parameters on photodegradation experiments.

UV, TiO_2, O_2	UV, TiO_2, Ar	UV, O_2	UV, Ar	TiO_2 (mg)	Time (min)	pHs
72.45	93.30	93.45	95.80	20	150	pH=2 (100ppm)
54.78	94.20	94.38	96.63	30	180	pH=5 (100ppm)
45.84	74.10	74.23	77.00	30	180	pH=7 (100ppm)
23.36	50.35	50.47	53.00	40	150	pH=9 (80ppm)
17.90	49.00	49.20	51.45	20	165	pH=12 (80ppm)

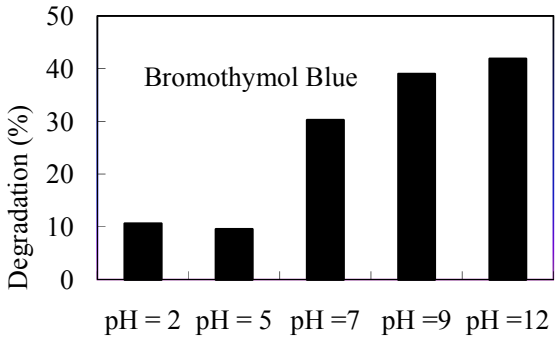

Figure 1- The effect of various pHs on degradation percent%

Kinetic study

The degradation of Bromothymole blue obeys the pseudo-first order kinetics (Eq. 1).

$$(-dc/dt)= kc \quad (Eq.1)$$

Where c is the concentration of Bromothymole blue and k is the experimental first-order rate constant. A plot of $ln(C_0/C_t)$ *versus* time reveals a straight line, the slope of which

upon linear regression equals the apparent first-order rate constant *k* (Fig. 2-1 to 2-4). The rate constant, *k* and K_A and K are summarized in Table 2.

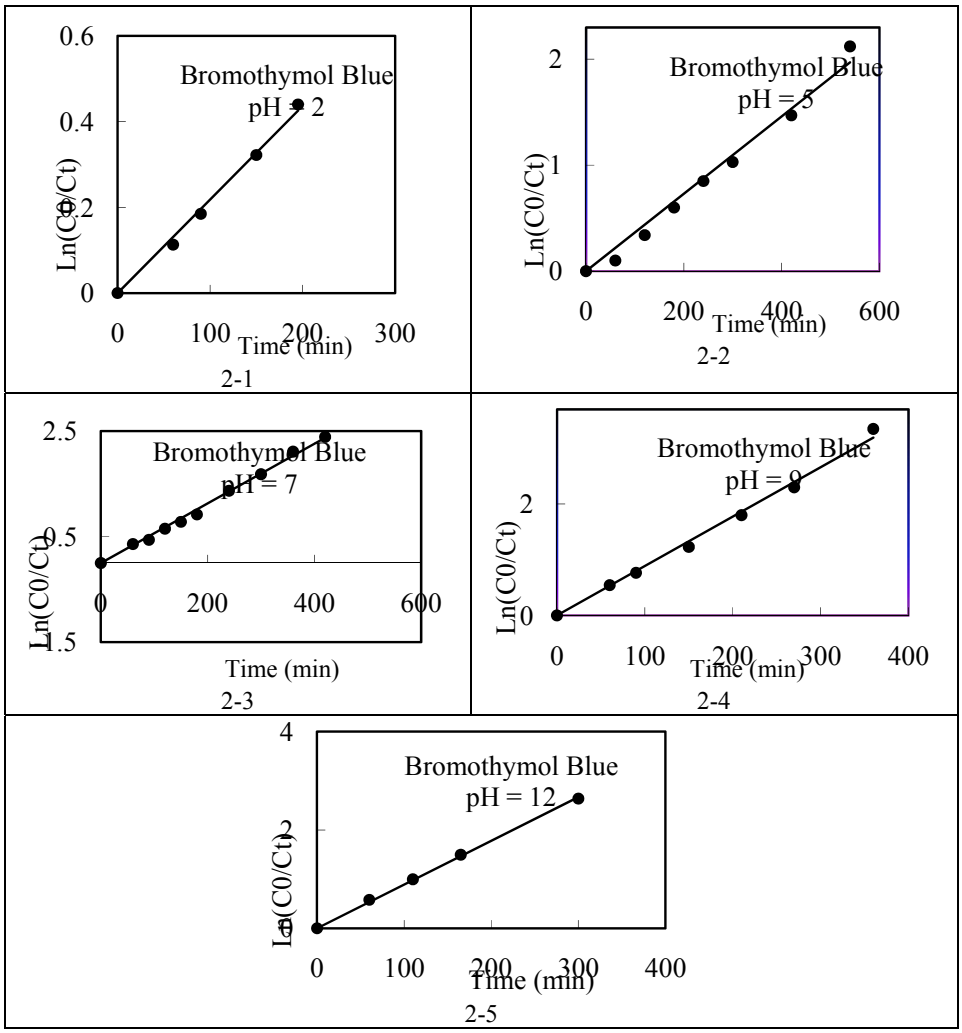

Figure 2- Kinetics of the degradation of Bromothymole blue at optimum amount of photocatalyst(2-1 to 2-5 respectively).

The results of linear plots of $1/R_{L-H}$ *versus* $1/C_0$ for Bromothymole blue on photocatalysts are also summarized in table 2, which tests the validity of the L-H model.

Table 2- Kinetic parameters of the degradation with initial concentration of Bromothymole blue in optimum conditions.

pH	k_{obs} (min^{-1})	K_A($mg.L^{-1}$)	k_r ($mg\ min^{-1}\ L^{-1}$)
pH=2 (100ppm)	2.2×10^{-3}	4.70×10^{-1}	0.1810
pH=5 (100ppm)	3.6×10^{-3}	4.48×10^{-1}	0.1610
pH=7 (100ppm)	5.6×10^{-3}	2.06×10^{-2}	0.7164
pH=9 (80ppm)	8.9×10^{-3}	4.86×10^{-2}	0.7021
pH=12 (80ppm)	8.9×10^{-3}	7.60×10^{-4}	10.3950

Reference

[1] M. Gratzel, F.H. Russel, *J. Phys. Chem.* (1990) 94.

[2] L. Palmisano, M. Schiavello, A. Sclafani, C. Martin, I. Martin, V. Rives, *Catal. Lett.* 24 (1994) 303–315.

[3] A. Milis, J. Peral, J. Domenech, *J. Mol. Catal.* 87 (1994) 67–74.

[4] W. Choi, A. Termin, M.R. Hoffmann, *J. Phys. Chem.* 98 (1994) 13669–13679.

[5] M.I. Litter, J.A. Navio, *J. Photochem. Photobiol.* A 98 (1996) 171– 181.

[6] J. Peral, X. Domenech, D.F. Ollis, *J. Chem. Technol. Biotechnol.* 70(1997) 117.

[2] R.M. Alberici, W.F. Jardim, *Appl. Catal. B: Environ.* 14(1997) 55.

[7] M. Montazerozohori, B. Karami, M. H. Habibi, *Ann. Chim.,* 5-6(2006) 285.

[8] M. Montazerozohori, M. H. Habibi, S. Joohari, V.Khodadostan, *Ann. Chim.* 97 (2007)1015.

Optimization and kinetic study of photocatalytic degradation of azo dye acid red 114 in water with ZnO/HZSM-5 zeolite as a catalyst

Kazem Mahanpoor [*1], Hossean Malekhosseani [2], Aboalfazl Soufi [3]

1,2, 3) Department of Chemistry, Faculty of Science, Islamic Azad University, Arak Branch,

kazem_mahanpoor@yahoo.com E-mail:

Abstract:

Zinc oxide with different amount was supported on HZSM-5 zeolite using solid state dispersion (SSD) method. The photocatalytic activity of these systems in the degradation of acid red 114 indicates that ZnO/HZSM-5 (SSD) is an active photocatalyst; the optimum photodegradation activity is seen at 10–15 wt.% ZnO/HZSM-5.The photocatalytic degradation rate follows pseudo-first order kinetic with respect to the AR114 concentration. Rate constant ($K = 8.2 \times 10^{-2}$ min-1) was estimated from the slope of the Ln[dye] versus time plot in the optimized conditions.

Keywords: Photodegradation; Photocatalysts; ZnO/zeolites; Azo dye wastewaters

Introduction

The fine ZnO powder or crystals can be dispersed in the water to be clarified by irradiation, but they should be removed by filtering after reaction, which is troublesome and costly. Thus, in order to solve this problem, many researchers have examined some methods for fixing ZnO on other supporting materials including glass beads [1], fiber glass [2], silica [3].

Experimental

The HZSM-5 zeolite ($SiO_2/Al_2O_3 = 50$) were purchased from Catalysis Society of Japan. Another materials were purchased from Merck (Germany). Zeolite-based photocatalysts were prepared by solid state dispersion (SSD) of ZnO. SSD initially involves mixing of ZnO and zeolite thoroughly using ethanol in agate pestle and mortar; the solvent was then removed by evaporation while mixing. Samples prepared by this method were dried at 110 °C and calcined in air at 450 °C for 6 h to obtain ZnO-supported zeolite catalysts. ZnO weight was maintained to obtain 2, 5, 10, and 15 wt.% in the finished forms of the catalyst. For UV/photocatalyst process, irradiation was

performed in a batch photoreactor of 2 liter in volume with a mercury lamp 48W (UV-C manufactured by Philips, Holland). UV-VIS Spectrophotometer, Perkin-Elmer lambda25 was employed for absorbance measurements using silica cells of path length 1 cm.

Results and discussion

Kinetics of photcatalytic degradation of AR114: When the Kinetics of the photocatalytic degradation reaction were studied it was found that the correlation between $\mathrm{Ln}\frac{c}{c_\circ}$ and the irradiation time was linear as shown Fig. 1. Shows the plot of Ln[AR114] versus irradiation time. The linearity of plot suggests that the photodegradation reaction approximately follows the pseudo-first order kinetics with K=0.0138min^{-1}.

The plot Ln[dye] versus irradiation time for AR114 was linear suggesting that the photodegradation reaction approximately follows the first order kinetics (Fig. 1). Rate constant (K = 8.2 × 10^{-3} min^{-1}) was estimated from the slope of the Ln[dye] versus time plot in the optimized conditions.

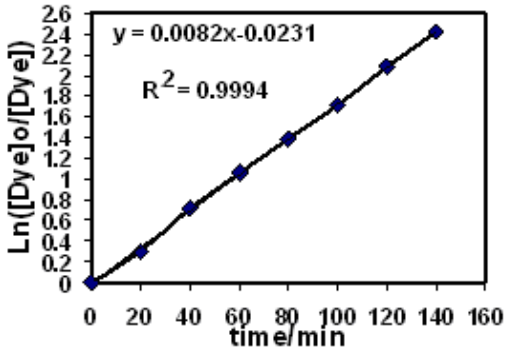

Fig. 1. Relationship between log[AR114] and irradiation time on photocatalytic degradation of AR114. $[AR114]_0$ = 50 ppm, , photocatalyst(15% ZnO+85% HZSM-5) = 40 ppm, pH=4.

References

[1] M.A. Fox, K.E. Doan, M.T. Dulay, Res. Chem. Intermed. 20 (1994) 711.

[2] J. Sabate, M.A. Anderson, M.A. Agumdo, J. Gimeniz, S. Cerveramarch, C.G. Hill Jr., J. Mol. Catal. 71 (1992) 57.

[3] V. Augugliaro, C. Baiocchi, A. Bianco-Prevot, E. Garcia-Lopez, V.Loddo, S. Malato, G. Marci, L. Palmisano, M. Pazzi, E. Pramauro, Chemosphere 49 (2002) 1223

[4] M. Anpo, H. Nakaya, S. Kodama, Y. Kubokawal, K. Domen, T. Onishi, J. Phys. Chem. 90 (1986) 1633.

[5] A. Maurino, C. Guillard, J. M. Marinas, A. Fernandez, A. Aguera, J. M. Herrmann, Appl. Catal. B : Environ. 34(2001)241.

An Investigation on the Key Intermediates in Fabrication of SiC Nanostructures

S. Hosein Mousavipour* and Vahid Saheb

Department of Chemistry, College of Sciences, Shiraz University, Shiraz, Iran

Email: mousavi@susc.ac.ir

Introduction

Silicon carbide (SiC) nanomaterials have found many structural and electronic applications.[1-3] SiC is one of the most important material for high temperature and high-power electronic applications due to its excellent properties, such as high mechanical strength, high thermal stability, high thermal conductivity, and large band gap. Because of their small dimensions, SiC nanomaterials might hold novel chemical and physical properties and act as highly functionalized material.

Although many efforts have been made to distinguish the mechanism of formation of SiC, still there are some uncertainties in this regards.[4] It would be interesting to know the gas phase mechanism for the formation of SiC nano-particles.

Conventionally, high-temperature physical thermal evaporation method is used to synthesize SiC nanostructures, which increases the industrial cost. Therefore, using a low-temperature synthetic method is an effective way to reduce the industrial cost. In this study, an autoclave Mg-catalyzed chemical co-reduction route is used for the synthesis of aligned SiC nanorods at relative lower temperature (600 ^{o}C).[2] Also, results of the pyrolysis of Methyltriclorosilane (MTS) in a flow system will be discussed.

Experimental Methods

In a typical experiment to synthesis SiC nanostructures, 1.0 mL MTS was added into a 5-mL stainless steel autoclave along with two pieces of Mg ribbon. The autoclave was tightly sealed and heated in an electric stove with an increasing speed of 20 ^{o}C/min and maintained at 600 ^{o}C for 1 h and then cooled to room temperature naturally. The ribbons were then collected from the autoclave, rinsed with distilled 1,2-Dichloroethane and washed with diluted hydrochloric and hydrofluoric acid and vacuum-dried at 50 ^{o}C for 1 h to be prepared for SEM, TEM, FTIR, and PL spectroscopy. To investigate the kinetics and mechanism of gas phase

thermal decomposition of MTS, a flow reactor as illustrated in reference 4 was used. The reaction was studied in the temperature range of 552 to 704 ^{o}C at 10 to 120 Torr pressure.

Results and Discussion

Fig. 1 shows the structures of SiC formed on the surface of Mg ribbons. It seems during the formation process of the SiC 1D nanostructures, metal Mg acted not only as catalyst but also as reducing agent. At 600°C the surface of Mg ribbons should melt and nanoscale Mg drops is formed due to the generation of heat of reaction. When the CH_3SiCl_3 molecules contact the Mg drops (acting as reducing agent and liquid catalyst), they will be reduced to Si and C atoms and SiC nanorods grow on this drops.

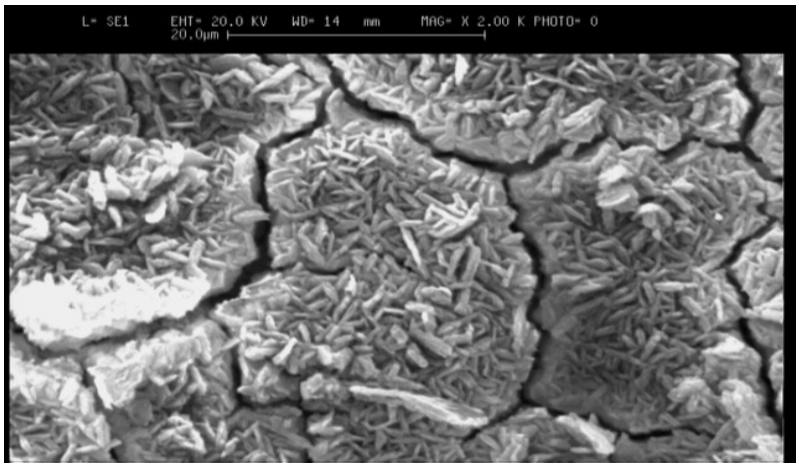

Conclusion

In summary, we will present the results of two types of experiments: Mg-catalyzed synthesis of SiC nanostructures and kinetics study on the unimolecular dissociation of MTS in gas phase to produce the reactive species for the formation of SiC. Silicon Carbide nanorods are formed by catalytic chemical co-reduction of MTS on the Mg surface. Our kinetics study reveals that $SiCl_3$ and CH_3 which are directly formed by MTS decomposition and adsorb on surfaces site cannot fulfill our experimental results of the deposition of SiC.

References

[1] F. De Jong and M. Meyyappan, *Diamond and Related Material* 5, (1996), 141.

[2] G. Y. Xi; X. Liu; X. Wang and Y. Qian, *J. Phys. Chem.* B 110, (2006), 14172.

[3] L. S. Liao; X. M. Bao; Z. F. Yang and N. B. Min, *Applied Phys. Lett.* 66, (1995), 2382.

[4] S. H. Mousavipour; V. Saheb and S. Ramazani, *J. Phys. Chem. A* 108, (2004), 1946.

Kinetic study of electron detachment reactions using ion mobility spectrometry

A. Abedi*[1]. F. Mirseadi[2]

[1] Department of science, Islamic Azad University, Shahreza Branch, abedi@iaush.ac.ir

[2] Department of science, Islamic Azad Universities, Shareza Branch,.fmirsaedi@yahoo.com

Keyword: Ion Mobility, Electron Detachment, Kinetic Study, Rate Constant

Introduction:

Ion mobility spectrometry (IMS) is basically an ion separation technique at atmospheric pressure. In this technique, ions are separated according to their individual velocities as they drift through an inert gas, driven by an electric field. It is a simple, inexpensive, and sensitive analytical method for the detection of organic trace compounds. Recently researchers are interested to investigate the kinetic of electron attachment reaction, dissociation reaction and proton transfer reaction by this method [1-5]. In the present study, we describe the use of ion mobility spectrometry for determination of thermal electron detachment (TED) reaction for the bromide ions Br^- over atmospheric pressure and a temperature range of 50–200 °C.

Experimental Section

The IMS apparatus with the continuous corona discharge as ionization source has been used in this study. Corona discharge source is constructed from a stainless steel needle and an aluminum ring in front of it. The IMS cell has been made from 16 aluminum rings that were separated from each other by non-conductive Teflon sheets. The aluminum rings are connected to each other by a series of resistors in order to form a uniform electric field. The system has an oven with ability to elevate temperature to 220^{o}C. The system works at atmospheric pressure. Carrier gas and drift gas in this experiment were argon. The electric field in drift region was about 250 $V.cm^{-1}$. We used syringe pump for introducing the sample vapor to the IMS cell. 1,4diboromo benzene was used in this study as sample without further purification. The follow rates of carrier and drift gas were 300 and 600 ml/min respectively.

Result and Discussion

Rate constants, k_{TED}, and their temperature dependence for the thermal electron detachment reaction of the Br^- anion ($Br^- \rightarrow Br + e$) have been determined by ion mobility spectrometry. By this method, Br^- ions that are produced in ionization region are periodically introduced to a drift tube containing argon gas. The drift tube contains a counter flowing current of drift gas that prevents the penetration of sample vapor into the drift region. In the drift tube, all ions and electrons are transported to a Faraday detection plate at rates determined by their respective mobilities and the applied electric field. Some of the Br^- ions are expected to undergo TED during the Br^- drift period, and this is expected to cause the apparent baseline between t = 0 and 3 ms as a tail of electron signal. This tail should be due to the thermally detached electrons that are produced as the Br^- packet passes through the drift tube. This is a first-order reaction. Because the mobility of electrons is several orders of magnitude greater than that of all negative ions, the occurrence of a thermal detachment event by Br^- anywhere along the drift tube is expected to result in the near-instantaneous arrival of that detached electron at the Faraday plate. Figure 1 shows the Br – peak and electron peak with tail that is related to the electrons produced from electron detachment reaction of Br^-. At all temperatures, the decay of the elevated baseline observed for electron signal is expected to be given by equation $\ln I = -k_{TED}\, t + C$, where I is the intensity of electron tail signal, t is the drift time of them, and C is constant. As it was shown in figure 2 a plot of ln I versus t is thereby expected to provide a straight line of slope equal to $-k_{TED}$. This is expected to provide a means of determining k_{TED} under different temperature conditions. The activation energy of electron detachment reaction was obtained from rate constant data at different temperatures based on Arrhenius equation.

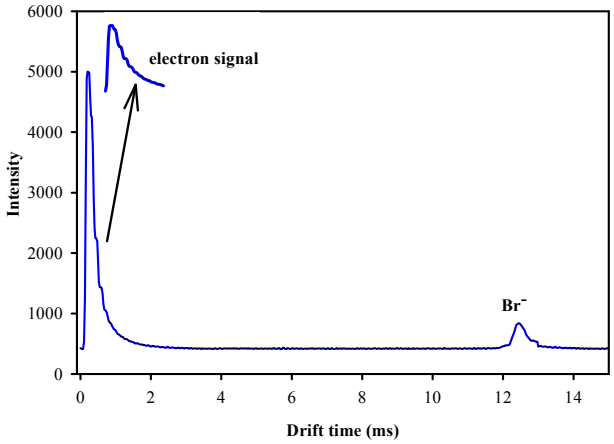

Figure 1: The ion mobility spectrum of Br^- and the tail of electron signal produced from thermal electron detachment reaction

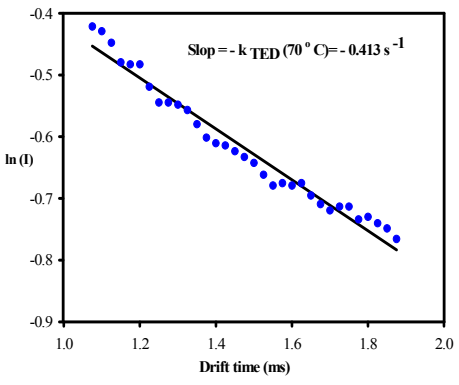

Figure 2: The logarithm of the signal intensity for electron tail versus t

Conclusions

We have shown here that the IMS method for studying gas phase ionic reactions at atmospheric pressures can be successfully applied to TED reactions. Rate constants were determined here for TED of the Br^- anion at different temperatures. We can also obtain the activation energy from rate constant data at different temperatures. It would seem likely that the results identified here for the TED reaction of Br^- might also be operative for other ion–molecule reaction systems.

References

[1] A. Bagno, A. Dono, S. Martinucci, C. Paradisi, G. Scorrano, Int. J. Mas. Spec., 1998, **179/180**, 349–357.

[2] K.E. Sahlstrom, W.B. Knighton, E.P. Grimsrud, Int. J. Mas. Spec., 1998, **179/180**, 117–127.

[3] D.H. Williamson, W.B. Knighton, E.P. Grimsrud, Int. J. Mas. Spec., 2000, **195/196**, 481–489.

[4] M. Tabrizchi and A. Abedi, J. Phys. Chem. A, 2004, **108**, 6319-6324.

[5] X. An, G. A. Eiceman and J. A. Stone, Int. J. Ion Mobil. Spec. 2010, **13**, 25–36.

Kinetics Investigation Reaction Between Thiourea AndDiethylethyl(1-methylbuthyl)malonate

K. Naimifar[a]*,A. Bazzaz[a], A. Aminifar[a], B. Ghorbani[a]
[a]Department of Chemistry,ImamHosseinUniversity,Tehran,Iran
E-mail:kazem_naimifar@yahoo.com

Keyword: Thiourea, Diethylethyl(1-methylbuthyl) malonate, Kinetics study, ΔG, Activation energy

Introduction

Thiourea is one of important hypnotic, antipyretic[1] and anticancer activitiesmedicine [2-3]. Kinetics studies on thiourea by several researchers have been investigated. They have usually studied derivative of thioureaviz phenyl thiourea, p-methyl phenyl thiourea, p-ethoxy phenyl thiourea and p-chlorophenylthiourea [4].Kinetics study of thioureawith benzylbromidoxidising agents and some other compound have also been reported [5]. But sofar they havenot reported any kinetics study onthioureawith diethylethyl(1-methylbuthyl)malonate.

Methods

Materials:

Thioureawas manufacturedby Merck company and diethylethyl(1-methylbuthyl)malonate had been synthsised in our labratury and it's structur had been characterised by H-NMR spectroscopy. All reagent we have used tobe AR-grade.

Experimental procedure

The temperatures of the kinetic study were 90, 100, 110 and 120˚C. The kinetic studies have been verified every two hours. The initial concentration of thiourea and diethylethyl(1-methylbuthyl) malonate were 0.78M and 0.05M respectivly. The variation of thiourea concentration has been done by potentiometry titration [6], and theconcentration variation of diethylethyl(1-methylbuthyl) malonatehas been done by titration [7]. The reaction has been stop by cooling effect.

Result and discution

The curve of rate constant of thioureaand diethylethyl(1-methylbuthyl) malonate have been drawn individually. As we can observed by figure (1-a) we concludedfromthiourea that the rate of reaction is first order at temperature 120˚C. The same result is obtaind by diethylethyl(1-mthylbuthyl) malonat figure (1-b). The same result is obtained at the other temperaturs.

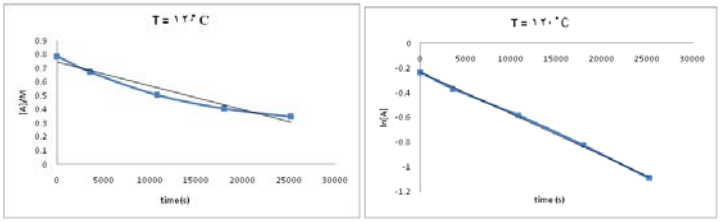

Figure (1-a) concentration and ln(con.) diagram thiourea by the time at temperature 120 ˚C

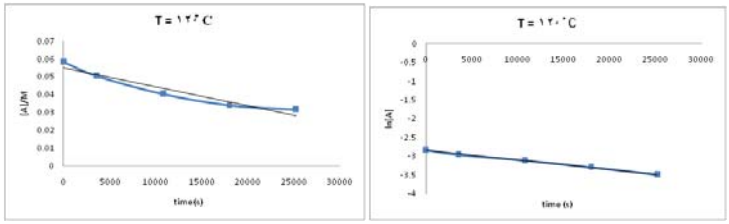

Figure (1-b) concentration and ln(con.) diagram diethylethyl(1 - methylbutyl)malonat by the time attemperature 120˚C

Fractional changmethod have also been used for determing the order of each compound, this method is also confirmed the result of previous kinetic study.

$$n = 1 + \frac{\log t2 - \log t1}{\log a1 - \log a2} (1)$$

Equation (1) is used to determine the order of reaction. n is indicated order of the reaction, a_1 and a_2 areconcentration of reactant at time t_1 and t_2.Activation energy ofthiourea and diethylethyl(1-methylbuthyl) malonate have been calculated tobe 35kJ and 48.5kJ respectivlly. The ΔG in temperetur 120˚C and atmospheric pressurewas equal to 33.66 kJmol[1].

Conclusions

Rate of reactionthiourea and diethylethyl(1-methylbuthyl) malonate are first order for any compound, overall rate of the reaction is equal to 2. Activation energy has been reported, the

ΔGhas been proved the reaction ofthiourea and diethylethyl(1-methylbuthyl) malonate is a slow reaction. Fractional chang(Half-life) and integral method have been confirmed the reaction have the same order.

References

[1]K. Kargosha,M. Khanmohammadi;AnalyticaChimicaActa; 2001, 437, 139–143.[2] W. Aumulkar; Chem. Ber; 1952, 85, 760.[3] M. Kajimoto; J. Pharm and Chem; 1952, 24, 443.[4] S.Z. Yao, F.J. He, L.H. Nie; Anal.Chim.Acta; 1992, 268,311.

[5] B. H. Zaware; Chemical and Pharmaceutical Research; 2009, 1(1): 276-281

[6] Soo Dong Yoh, Dae Soo Lee; Korean Chemical Society;1969, 13, 3.[7] H.J. Bowley, E.A.Crathorne, D.L. Gerrard; Analyst;1986,111, 539.

Kinetic of adsorption of methylen blue (MB) onto waste tea and waste tea/$CuFe_2O_4$ composite

Saeedeh Hashemian, Majeed Karimi
Islamic Azad University, Yazd branch, Chemistry department, Iran, Yazd

Abstract

The adsorption of MB from aqueous solution onto waste tea and waste tea/$CuFe_2O_4$ composite has been studied. The effects of several variables on the removal of MB were studied at 25 °C, including pH value, contact time and initial concentration of MB. Present experimental study shows that pH 9 favors enhanced adsorption. The results showed that from the contact time 75 min for waste tea desorption was done, but the waste tea/$CuFe_2O_4$ composite can adsorbed 99% MB 60 mg L^{-1} to 120 min. The pseudo-second order kinetic model was used to analyze. The adsorption process was similar for waste tea and waste tea/$CuFe_2O_4$ composite.

Keywords: Adsorption; kinetic; Methlen blue; Nanocomposite

Introduction

Dyes are widely used in the textile industry to color products. One of the major problems concerning textile wastewaters is colored effluent. This wastewater contains a variety of organic compounds and toxic substances, which are harmful to fish and other aquatic organisms [1]. The dye Methylen blue is widely used in analytical chemistry laboratories as a pH indicator to test pH ranges from 0 to 1.6 [2]. From the chemical structure of the dye it is observed that there are three aromatic rings attached to a central carbon atom.

The toxic nature of the dye can be explained by considering the fact that on decomposition it gives out hazardous products. These products are toxic and may cause several health problems to mankind as well as animals, thus MB attracts noteworthy attention to innovate effective techniques for its removal. Adsorption has gained favor in recent years due to proven efficiency in the removal of pollutants from effluents to stable forms for the above conventional method [3, 4].

Materials and Method

Waste tea was used as starting materials. The waste tea was preheated in an oven at 100 °C for about 48 h to reduce the moisture content. They were then crushed with a high speed mill and sieved on a sieve mechanical shaker, and the size fraction of lower than 180 μm that has been passed through US standard sieve number 80, was used in this study. Analytical grade copper (II) chloride dehydrates and ferric chlorides were obtained from Merck. $CuFe_2O_4$ was prepared using a co-precipitation method. $CuFe_2O_4$/waste tea composites were prepared using a co precipitation method. The waste tea was added into a 400 ml solution containing copper (II) chloride (0.02mol) and ferric chloride (0.04mol) at room temperature. The amount of waste tea was adjust to obtain $CuFe_2O_4$/waste tea mass ratio of 1:10 under vigorous magnetic-stirring, slowly raised the pH by adding NaOH (5mol l^{-}) solution to around 10 and stirring was continued for 30 min, and the stopped stirring. The suspension was heated to 95-100 ºC for 2h. After cooling, the prepared composite was repeatedly washed with distilled water. By a simple magnetic procedure, the obtained materials was separated from water and dried in an oven at 105 ºC. MV was purchased from Merck and used without further purification. The stock solution of MV was prepared with distilled water (100 mg l^{-1}). MV was analyzed by shimadzu 160A UV-Vis spectrophotometer. The crystalline structure of $CuFe_2O_4$ was determined using the X-ray powder diffraction method with a Philips PW1840 diffractometer using Ni-filtered Cu k_α radiation and wavelength 1.54˚A.

Results and discussion

1. Catalytic effect of $CuFe_2O_4$

The experiments were carried out with 50 ml of MV dye solutions on 0.1 g of waste tea, $CuFe_2O_4$ and $CuFe_2O_4$/waste tea composite. Fig. 1 shows the effects of agitation time. The plots show that the adsorption of MV increases with an increase in agitation time and attains equilibrium earlier of adsorption (30 min) for $CuFe_2O_4$/waste tea composite and more than 90%. In the equilibrium time of 60 min was needed for $CuFe_2O_4$/waste tea and $CuFe_2O_4$. The higher adsorption capacity of $CuFe_2O_4$/waste tea composite than that waste tea attributed to the presence of $CuFe_2O_4$ catalyst.

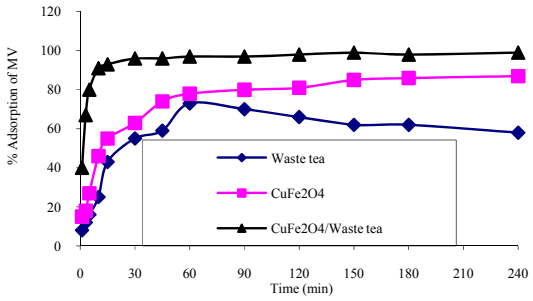

Fig. 1. Effect of time for adsorption of MV onto waste tea, $CuFe_2O_4$ and $CuFe_2O_4$/waste tea composite.

2. Effect of pH

Fig. 2 shows the effect of pH on the adsorption of MV onto $CuFe_2O_4$/waste tea. The adsorption capacity increased with increasing pH of the solution. The maximum adsorption capacity of MB on $CuFe_2O_4$/waste tea was observed at pH 10. The effect of pH on MV removal from $CuFe_2O_4$ and waste tea were similar. This could be explained by the fact that at low pH, more protons will be available to protonate hydroxyl groups, reducing the number of binding sites for the adsorption of MV. The adsorption behavior showed that adsorption of MV onto nanoparticle composite is governed by electrostatic interactions. The influence of pH on the adsorption capacity showed decreasing affinity with increasing electrostatic repulsion between MV and the adsorbent with a maximum value at pH 9.

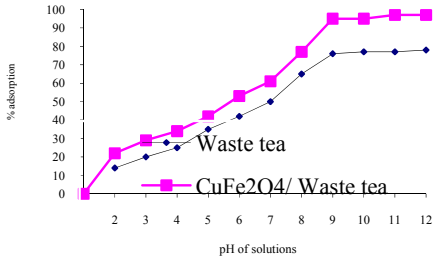

Fig. 2. Effect of pH for adsorption of MV onto waste tea, $CuFe_2O_4$ and $CuFe_2O_4$/waste tea composite for 50 ml MV 100 ppm and 0.1 g sorbent

3. Adsorption kinetics

The two adsorption kinetic modes used in this study are pseudo-first order and pseudo-second order equations.

The pseudo-second order model is based on adsorption equilibrium capacity. (Fig.3.)

$t/q=t/q_e+1/k_2q_e^2$

Conclusions

$CuFe_2O_4$/waste tea can be used as a cost effective adsorbent for removal of MV from water and wastewater. Alkaline pH is found to be better than acidic pH. The adsorption follows pseudo-second order kinetics.

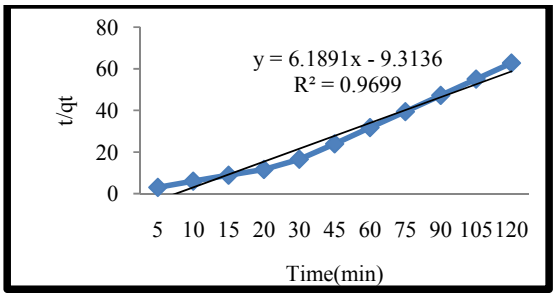

Fig. 3. Kinetics of MV adsorption onto $CuFe_2O_4$/waste tea composite for 50 ml of an initial concentration of 100 mg/l MB , pH 9, 0.1 g adsorbent for pseudo-second-order model

References

[1] Ramakrishna K. R., Viraraghavan T., Dye removal using low cost adsorbents, water Sci. Technol. 36 (2-3) (1997) 189-196.

[3] Wu R, Qu J, He H, YU Y, Removal of azo-dye acid red B (ARB) by adsorption and catalytic combustion using magnetic $CuFe_2O_4$ powder, Applied Catalysis B: Environmental 48 (2004) 49-56.

[4] Zhang G, Qu J, Liu H, Cooper A. T, W R, $CuFe_2O_4$/activated carbon composite: A novel magnetic adsorbent for the removal of acid orange II and catalytic regeneration ,Chemosphere 68 (2007)1058-1066.

Kinetics and thermodynamic of adsorption of methyl violet blue onto Fe_3O_4/bentonite nano magnetic composite

Saeedeh Hashemian
Islamic Azad University, Yazd Brunch, Chemistry Department, Yazd, Iran
Sa_hashemian@yahoo.com

Abstract

In this study Fe_3O_4 was used for adsorption of methyl violet as catalyst/adsorbent material. This magnetic composite was prepared using a simple chemical co-precipitation procedure. The magnetic composite mixed with bentonite as adsorbent and used for methyl violet (MV) dye removal from water. This magnetic powder adsorbent showed excellent catalytic properties. Powder XRD was used to characterize the prepared adsorbents. Powder XRD analysis of Fe_3O_4 indicated that the metal oxides mainly occurred in the form of spinel structure. The ferrite embedded in the matrix has nanoparticles 10 nm. The adsorption kinetics of MG on bentonite and magnetic powder composite is similar. The adsorption kinetics of MV onto Fe_3O_4/bentonite composites was pseudo-second order. The adsorption is strongly dependent on pH of the medium where the removal efficiency increases as the pH turns to alkaline range (pH 9). The results suggest of the higher adsorption capacity of the composites than that of natural bentonite attributed to the presence of Fe_3O_4 catalyst. The thermodynamic parameters of adsorption such as free energy of Gib s and enthalpy of adsorption were determined.

Keywords: Adsorption; composite; Fe_3O_4; methyl violet

Introduction

One of the major problems concerning textile wastewaters is colored effluent. This wastewater contains a variety of organic compounds and toxic substances, which are harmful to fish and other aquatic organisms [1]. There are several methods used to treat wastewaters which contain organic pollutants and dyes. These methods include physical and chemical processes such chemical coagulation [2], ozonation [3, 4] and adsorption [5, 6]. Activated

carbon is widely used as an adsorbent due to its high surface area and high adsorption capacity; however, it is relatively expensive which limits its usage [7-10]. For this reason, many researchers have investigated low-cost, locally available, biodegradable substitutes from natural sources to remove dyes from wastewater [11-16]. Adsorption process is one of the effective methods with the advantages of high treatment efficiency and no harmful by-product to treat water [17]. The focus of this study is investigating of adsorption capacity and catalytic activity of Fe_3O_4 ferrite spinel on the bentonite for adsorption of methyl methyl violet.

Experimental

Ferro (II) chloride dehydrates and ferric chlorides were obtained from Merck, and were both analytical grade. Fe_3O_4 and Fe_3O_4/bentonite were prepared using a co-precipitation method. The bentonite used in this study was obtained from Tavan silicate Co. of Iran. The bentonite was purified in the laboratory to remove carbonates, iron, hydroxide and organic matter. It was crushed, ground, sieved through 100 - 150 mesh and dried at 110°C in an oven for 2 h before use. Methyl violet was purchased from Merck and used without further purification. The stock solution of MV was prepared with distilled water (100 mg l^{-1}).

Fe_3O_4/bentonite magnetic composites were prepared using a chemical co-precipitation method. The bentonite was added into a 400 ml solution containing ferro(II) chloride (0.02mol) and ferric chloride (0.04mol) at room temperature. The amount of bentonite was adjust to obtain Fe_3O_4/bentonite mass ratio of 1:10 under vigorous magnetic-stirring, slowly raised the pH by adding NaOH (5mol l^{-1}) solution to around 10 and stirring was continued for 30 min, and the stopped stirring. The suspension was heated to 95-100 ºC for 2h. After cooling, the prepared magnetic composite was repeatedly washed with distilled water. By a simple magnetic procedure, the obtained materials was separated from water and dried in an oven at 105 ºC.

The crystalline structures of synthesized materials were determined using the X-ray powder diffraction method with a Philips PW1840 diffractometer using Ni-filtered Cu k_α radiation and wavelength 1.54˚A. Transition electron microscopy was carried out by means of a Hitachi S-3500.

Dye absorbance was measured with spectrophotometer (Shimadzo, model 16 A Japan). pH measurement was done with a Horiba pH meter (M13, Japan). Infrared spectrum is recorded

using FTIR instrument (Shimadzo-8700) for all samples in KBr medium between 400-4000cm^{-1}).

Results and discussion

1. Characterization of adsorbent (composites)

The XRD analysis of Fe_3O_4 indicated that the metal oxides mainly occurred in the form of spinel structure of Fe_3O_4. Fig 1a-c shows the XRD of bentonite, the prepared ferrite Fe_3O_4 and Fe_3O_4/bentonite composite. From result of XRD the binding process of bentonite did not result in the phase change of Fe_3O_4.

The X-ray diffraction patterns show well developed diffraction lines assigned to pure spinel phase, with all major peaks matching the standard pattern of Fe_3O_4, JCPDS 8-0234. The average crystallite size of the spinel phase has been estimated from the broadening of the (d=2.513) X-ray diffraction peak using the Scherrer equation [14] at about 45 nm for Fe_3O_4 and 12 nm for Fe_3O_4/bentonite composite.

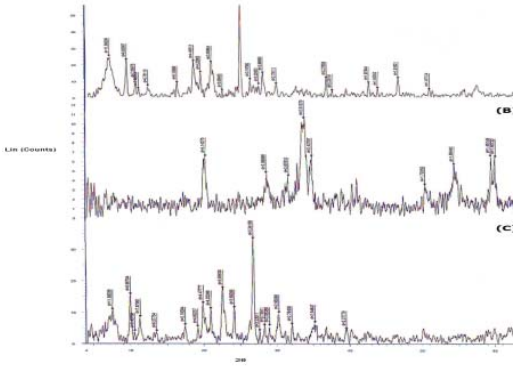

Fig. 1. Powder XRD for the (a) natural bentonite, (b) Fe_3O_4 and (c) Fe_3O_4 / bentonite composite.

The typical TEM micrograph of the Fe_3O_4/bentonite nanoparticles is shown the nanoparticles had a mean diameter of 10 nm. This reveals that the binding process did not significantly result in the agglomeration. This could be attributed to the reaction occurring only on the particle surface.

2. Effect of contact time

The experiments were carried out with 50 ml of MV dye solutions on 0.1 g of bentonite, Fe_3O_4 and Fe_3O_4/bentonite composite. Fig. 3 shows the effects of agitation time. The plots show that the adsorption of MV increases with an increase in agitation time and attains equilibrium earlier of adsorption (10 min) for composite more than 95%. As a result, higher adsorption efficiency was realized in a shorter adsorption time. The equilibrium time of 60 min was needed for bentonite and Fe_3O_4. The results also show that the % of MV removal for bentonite and Fe_3O_4 were about 70 and 80 % respectively. These results which show Fe_3O_4 composite, exhibit an excellent catalytic activity. This increase in adsorption capacity is related to changes in the surface properties of the adsorbent.

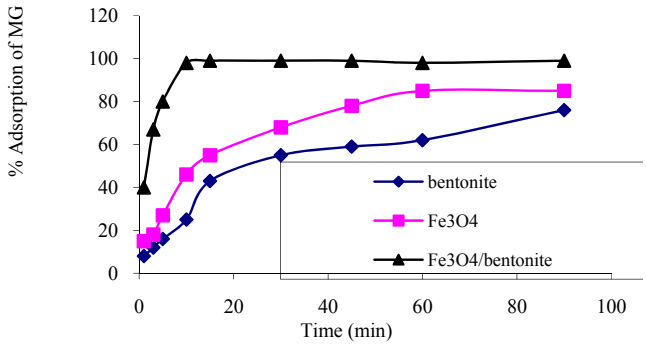

Fig. 3. Effect of contact time for adsorption of MV onto bentonite, Fe_3O_4 and Fe_3O_4/bentonite composite.

3. Adsorption kinetics and thermodynamics

The adsorption kinetics of MV on bentonite and Fe_3O_4/bentonite composite was iestigated The adsorption kinetics of MV on the composite was similar to bentonite. The adsorption process could be divided into two steps, a quick step and a slow one. In the first step, the adsorption rate was fast, and 99% of the equilibrium adsorption capacity was achieved within 10 min. In the subsequent step, the adsorption was slow and reached equilibrium at 2 h. The two adsorption kinetic modes used in this study are pseudo-first order and pseudo-second order equations. The adsorption kinetics of MV was pseudo-second order. The results of thermodynamics referred the negative value of $\Delta G°$.

References

[1] Ramakrishna K. R., Viraraghavan T., Dye removal using low cost adsorbents, water Sci. Technol. 36 (2-3) (1997) 189-196.

[2] Choi J H, Shin W. S, Lee S. H, Joo D. J, Lee J. D, Choi S. J. Application of synthetic poly(DADM) flocculants for dye wastewater treatment. Environ. Technol. 22 (2001)1025–1033.

[3] Benszedits V. Ozonation to decolor textile effluents. Am. Dye St. Rep. 69 (1980) 37–40.

[4] Wu J, Wang V, Ozonation of aqueous azo dye in a semi-batch reactor. Water Res. 35 (2001)1093–1099.

[5] McKay G, Color removal by adsorption. Am. Dyes St. Rep, 69 (3) (1980) 66–67.

[6] Tamura T, Miyoshi T, Boki K, Tanada S, Treatment of indigo carmine wastes with granular activated carbon and its adsorption process into micro pores. Jpn. J. Hyg. 42 (1987)858–864.

[7] A.S. Özcan A. S, Özcan A, Adsorption of acid dyes from aqueous solutions onto acid-activated bentonite, J. Colloid Interface Sci. 276 (2004) 39–46.

[8] Gupta V.K. and Ali I, Adsorbents for water treatment: low cost alternatives to carbon. In: A.T. Hubbard, Editor, Encyclopaedia of Surface and Colloid Science, Marcel Dekker, New York (2003) 1–34.

[9] Gupta V.K, Suhas I. Ali. I, Saini V.K, Removal of rhodamine B, fast green, and methylene blue from wastewater using red mud, an aluminum industry waste, Ind. Eng. Chem. Res. 43 (2004) 1740–1747.

[10] Gupta V.K, Suhas., Mohan D, Equilibrium uptake and sorption dynamics for the removal of a basic dye (basic red) using low-cost adsorbents, J. Colloid Interface Sci. 265 (2003) 257–264.

[11] Gupta V. K, Mittal A, Krishnan L, Gajbe V, Adsorption kinetics and column operations for the removal and recovery of malachite green from wastewater using bottom ash, Sep. Purif. Technol. 40 (2004) 87–96.

[12] Mittal A, Krishnan L.K, Gupta V.K, Use of waste materials-bottom ash and de-oiled soya, as potential adsorbents for the removal of Amaranth from aqueous solutions, J. Hazard. Mater. 117 (2005) 171–178.

[13] Srivastava S. k, Pant N, Pal N, Studies on the efficacy of local fertilizer waste as a low cost adsorbent. Water Res. 21 (1987)1389–1394.

[14] Özer D, Dursum G, Özer A, methylene blue adsorption from aqueous solutions by dehydrated peanut hull, J of Hazardous Materials 144 (2007) 171-179.

[15] Hameed B. H, Din A. T. M, Ahmad A. L, Adsorption of methylene blue onto bamboo-based activated carbon: Kinetic and equilibrium studies, J of Hazardous Materials 141 (2007) 819-825.

[16] Gong R, Ding Y, Li M, Yang C, Liu H, Sun Y, Utilization of powdered peanut hall as biosorbent for removal of anionic dyes from aqueous solution, Dyes and Pigment 64 (2005) 187-192.

[17] Hashemian. S, Study of adsorption of acid dye from aqueous solutions using bentonite , Main Group Chemistry, 6 97-107 (2007).

Investigation of Solvent Effect on the kinetics, Mechanism of para-choloroanil addition to triphenilphosphine

Yahyayi[a,*].H , Mousavi[b].S.N , Nori-Shargh[b].D

a) *Chemistry Department, Zanjan Branch, Islamic Azad University, P.O.Box: 49195-467, Zanjan, Iran*
**Corresponding author. E-mail: Hooriye_yahyaei@yahoo.com*
b) *Chemistry Department, Science Faculty, Arak branch, Islamic Azad University, Arak, Iran*

Keywords: Reaction Mechanism, Activation Parameters, Rate Equation, Parachloranil, Triphenylphosphine, Solvent Effect

Introduction

Based on the reported results, simple quinine such as para-benzoquinone yielded an adduct in which the structure of the addition compound is such that there is substitution in the quinone ring and there is a subsequent quaternization of the phosphorus atom. The structure of the compound formed may be either zwitterionic or of the ylide type.[1-3] Recently, we have reported the kinetics of the addition reaction of triphenylphosphine to *para*-benzoquinone[4] and also to *para*-naphtoquinone.[5] It seemed interesting to investigate the kinetic of the similar addition reaction of triphenylphosphine but using para-chloranil as a joint reactant (sse scheme).

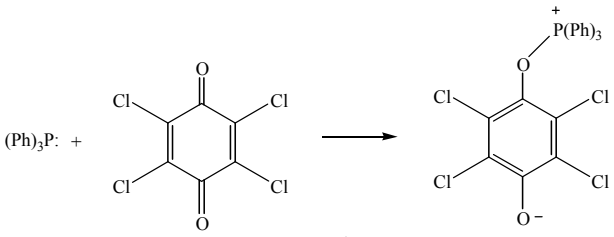

Scheme

Material and Instrumentation

Analytical grade para choloro anil, triphenilphosphine, chloroform, dicholoromethane, 1-cholorobutane and dichloroethane (Merk, Germany) compounds were used without addition purification. UV-Vis spectra were recorded on Agilent HP- 8453 spectrophotometer diode array, and a quartz cell (l=1cm) was used for the spectrophotometric measurements. Initial triphenylphosphine and parachloranil concentrated stock solutions

were, each time freshly prepared (volumetrically) before use, in chloroform, dicholoromethane, 1-cholorobutane and dichloroethane used as solvents. The initial concentration of the stock solutions was calculated based on the declared manufacturer densities. The working solutions were each time prepared by dilution of the stock solution in the above solvents.

Results and Discussion

The rate constants and the order of the reaction with respect to the reactants were determined using pseudo-first-order method was used also to calculate. The reaction was monitored by UV-Vis spectrophotometer at 320, 325, 320 and 320 nm by variable time method in choloroform, dicholoro methan,1-cholorobutan and dicholoro ethan, respectively. On the basis of the obtained results, the Arhenius equations of this reaction were obtained:

Solvent choloroform: $\log k = 5.36344 - (\frac{5.979}{2.303\,RT})$

Solvent dicholoromethan: $\log k = 4.13155 - (\frac{5.214}{2.303\,RT})$

Solvent 1-cholorobutan: $\log k = 3.25402 - (\frac{3.857}{2.303\,RT})$

Solvent dicholoro ethan: $\log k = 3.13155 - (\frac{3.214}{2.303RT})$

The obtained results show that the activation energy of this reaction decrease by the increase of the solvent polarity. Other activation parameters E_a, $\Delta H^{\ddagger}$, $\Delta G^{\ddagger}$ and $\Delta S^{\ddagger}$ at 298 K in the above Solvents are obtained.

Conclusion

The obtained reaction rate equation was found to be of first order both with respect to para-choloroanil and triphenilphosphine in the used Solvents. Also, the results obtained show that the activation energy of the addition reaction of triphenilphosphine to para-choloroanil decreases by increasing of the dipole moments of the solvents used.

References

[1]Ramirez, F.; Dershowitz, S. J Am Chem Soc **1956**, 78, 5614-5622.

[2]Hoffman, H.; Horner, L.; Hassel, G. Chem Ber **1958**, 91, 58-60.

[3]Ramirez, F.; Dermshowits, S. Chem Ind **1956**, 665-666.

[4]Nori-Shargh, D.; Saroogh Farahani, N. Int J Chem Kinet **2004**, 472-479.

[5]Nori-Shargh, D.; Soofi, A.; Saroogh Farahani, N.; Deyhimi, F. Int J Chem Kinet **2005**, 37, 427-433.

Selective removal of Ofloxacin compound by molecularly imprinted polymer (MIP)

Fariba Ahmadpour, Hayideh Sadeghi bagheri, Afsaneh Amiri*
Department of Chemistry, Islamic Azad University, Central Tehran Branch, Tehran, Iran
afsaamiri@gmail.com

Introduction

The Fluoroquinolones have emerged as one of the most important class of antibiotics which show excellent activity against both pathogenic Gram-negative and Gram-positive bacteria, as well as anaerobes. [1,2]However, their widespread application in human and food-producing animals has increased human health concerns because of their inducing pathogen resistance and possible allergic persensitivities in humans.[3-9] Molecular imprinting is a rapidly developing technique for the preparation of polymers having specific molecular recognition properties [13-16].Using molecularly imprinted polymers as selective sorbents of SPE procedures allow not only preconcentration cleaning of the sample but also selective isolation of the target analyte, which is important, particularly when the sample is complex and impurities can interfere with quantification.

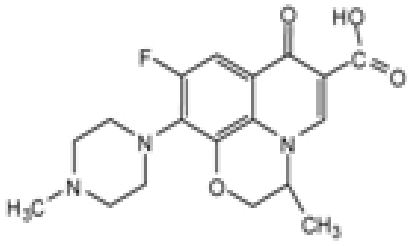

Fig-1 Ofloxacine molecular structure

Material and Methods

The water-compatible MIPs were improved and reformative from our previous results of 1.0mmol ofloxacin, 5mmol MAA, 30mmol EDMA, and .0.25mmol AIBN was dissolved in 15mL porogenic solvents (methanol:water = 9:1, v/v). Polymerization was performed under 60ºc in water bath for 17h. The obtained polymers were grinding and sieving and washing with Tetrahydrofuran and

Methanol,acetic acid, Trifluoracetic acid (TFA) to remove the templates.A non-imprinted blank polymer (NIP, in the absence of template) identical manner.

Result and discussion

Water- compatible molecularly imprinted polymers (MIPs) were prepared in water–methanol systems for selective extraction and separation ofloxacin from analyzing the residues of fluoroquinolones in biological samples. By using ethylene glycol dimethacrylate as crosslinker and reformative methanol‑water system as reaction medium, the improved water-compatible imprinted polymers were synthesized which show higher affinity to template and its analogues in aqueous environment. The MIP was synthesized by using methacrylic acid as the functional monomer, ethylene glycol dimethacrylate as a cross-linker and methanol‑water (9:1, v/v) as the porogenic solvent. Among the MIPs prepared, MAA-CO-EGDMA polymer showed excellent selectivity toward OFL the adsorption equilibrium was achieved within 4h and maximum partition coefficient of the molecularly non imprinted and molecularly imprinted polymer were investigated using adsorption test and were found to be 260 and 945.5 ml.g $^{-1}$ respectively. Its molecular recognition mechanisms were investigated by the molecular simulation and the experimental validation with uv-vis. The characteristics of the MIP were characterized by Fourier transform infrared spectroscopy. This method is simple and sensitive, and can be used as an alternative tool to the existing HPLC methods for analyzing the residues of Fluoroquinolones in biological samples.

Conclusions

Novel water-compatible MIPs were prepared in water–methanol system, which show high affinity and selectivity to the ofloxacin in aqueous environment.

References

[1] M. Martinez, P. McDermott, R. Walker, Vet. J. 172 (2006) 10.

[2] J.M. Blandeau, Clin. Ther. 21 (1999) 3.

[3] Z. Zeng, A. Dong, G. Yang, Z. Chen, X. Huang, J. Chromatogr. B 821 (2005) 202.

[4] G. Carlucci, J. Chromatogr. A 812 (1998) 343.

[5] L. Johnston, L. Mackay, M. Croft, J. Chromatogr. A 982 (2002) 97.

[6] J.Y. Shen, M.R. Kim, C.J. Lee, I.S. Kim, K.B. Lee, J.H. Shim, Anal. Chim. Acta 513 (2004) 451.

[7] H.A. Nguyen, J. Grellet, B.B. Ba, C. Quentin, M.C. Saux, J. Chromatogr. B 810 (2004) 77.

[8] A. Espinosa-Mansilla, A.M. Pena, D.G. Gomez, F.S. Lopez, Talanta 68 (2006) 1215.

[9] C. Maraschiello, E. Cusido, M. Abellan, J. Vilageliu, J. Chromatogr. B 754 (2001) 311.

[10] F. Belal, A.A. Al-Majed, A.M. Al-Obaid, Talanta 50 (1999) 765.

[11] J.A. Hernandez-Arteseros, J. Barbosa, R. Compano, M.D. Prat, J. Chromatogr. A 945 (2002) 1.

[12] V. Andreu, C. Blasco, Y. Pico, Trends Anal. Chem. 26 (2007) 534.

[13] E. Caro, R.M. Marce, P.A.G. Cormack, D.C. Sherrington, F. Borrull, Anal. Chim. Acta 562 (2006) 145.

[14] E. Caro, R.M. Marce, P.A.G. Cormack, D.C. Sherrington, F. Borrull, J. Sep. Sci. 29 (2006) 1230.

[15] S.A. Barker, J. Chromatogr. A 885 (2000) 115.

[16] S.A. Barker, J. Biochem. Biophys. Methods 70 (2007) 151.

Calixarenes as nano adsorbent of heavy metal Ions (Co^{2+}, Cr^{3+}, Ni^{2+}, Pb^{2+}, Zn^{2+})

Afsaneh Amiri*, Amir H. M. Sarafi , Fatemeh Pirouzi, Simin Tadayon, Fariba Ahmadpour

Department of Chemistry, Centeral Tehran Branch, Azad University, Tehran, Iran

afsaamiri@gmail.com

Introduction

Numerous attempts have been made to design new host systems which can selectively interact with the target guest and perform intriguing molecular recognition processes [1].

Calixarenes are synthetic macrocycles obtained by the condensation of p-substituted phenol and formaldehyde in alkaline medium [2]. Lower and upper rim fictionalizations of parent calixarenes had led to a large variety of derivatives. Fine control of the size of calix[n]arenes, by changing the value of n and the introduction of various functional groups makes. Cation-ligand interaction play an important role in the complexation of metal cations with benzene and with an extensive series of aromatic structures [3] In this research study, stability constants of metal cations and calix[4]arene and calix[6]arene in chloroform-methanol (50%-50% v/v) were determined at 25°C using spectrophotometric technique.

Material and Methods

1.5 cm^3 of Calixarene was titrated with stepwise addition of a cation solution in chloroform-methanol solution. The UV-Vis spectrum of the mixture undergoes small changes at 260–300 nm. Principle component analysis (PCA) was used for determination of the number of components in the absorbance data matrix and the formation constant of complex was obtained by using DATAN software on the spectrophotometric data.

Result and Discussion

The complex formation between the para-tert-butyl-calix[4] arene and some transition metal ions in organic solvent. Principle component analysis (PCA) was used for determination of the number of components in the absorbance data matrix and the formation constant of complex was obtained

using by DATAN on the spectrophotometric data and compared with other methods. All ligands have been shown to form exclusively 1: 1 (metal ion to ligand ratio) complexes with cations in our experimental conditions. $LogK_f$ of metal-ligand complexes are 5.03±0.10, 4.68±0.11, 5.32±0.11, 5.41±0.10 and 4.70±0.11 for Co^{2+}, Cr^{3+}, Ni^{2+}, Pb^{2+} and Zn^{2+} respectively.

Conclusion

This research study has been clearly shown that Calixarene complaxation have proper selectability factor for releasing heavy metals from the aqueous solution and although the Calixarene present two potential complexation sites, the complex stoichiometry was found to be 1: 1. This behavior may be explained by a negative allosteric effect, which has been found in complexing systems containing two conformationally subunit.

References

[1] C.D. Gutsche. Calixarenes Revisited, The Royal Society of Chemistry, Cambridge (1998).
[2] A.F. Danil de Namor, A.F. Casal, A. Pugliese, M.T. Goitia, M. Montero. J. Chem. Soc. Faraday Trans., 93, 3955 (1997).
[3] S. Mecozzi, A.P. West Jr., D.A. Dougherty. Proc. Natl. Acad. Sci. USA, 93, 10566 (1996).
[4] Z. Asfari, C. Bressot, J. Vicens, C. Hill, J.F. Dozol. Anal. Chem., 15, 3133 (1995).

Study Of Detoxification Reaction Of Organophosphors Compound By Nanomagnesium Oxide

A. Aminifar[a]*, B. Madah[a], S. Mohammadi[a]
[a] Department of Chemistry,Imam Hossein Comperhencive University,Tehran,Iran
E-mail:AAminifar@Hotmail.com

Introduction

A large number of pesticides, insecticides and chemical warfare agent such as sarin, soman and vx are based on phosphorus compounds. Decontamination and disposal of such compounds since many years ago, was on of the priorities and academic research centers around the world [1,2]. According to the results obtained from nanoparticles of metal oxides with the results of tests performed and factor such as crystal size, BET and activity of elements , have been approached that nano MgO and nano Al_2O_3 have unique properties [3,4]. In this research, Magnesium reaction of organophosphorus N,N dimethyl ,o,o dimethylphospho amido thioate[5] with MgO and nano MgO have been studied, In view of kinetic and applied physical chemistry adsorption parameter such as size of particle, solvents and etc. have been investigated.

PNMR and FT-IR techniques have been used for identifying the variation concentration, controlling of adsorption reaction and so on.

Method

Magnesium oxide (CM-MgO) was made by merck company with BET=31.5m^2/g. NanoMgO and N,N dimethyl ,o,o dimethylphospho amido thioate (op)are made by Imam Hossein University researcher's groups with BET 366.9m^2/g(15nm) and %98 purity respectively. Phosphoric acid is made by keto company with %85 purity the other compound are made by Merck company in AR-Grade.

PNMR spectroscopy was 250 MHz perkins and FT-IR and oven were shimatzu model and yamoto model respectively.

Result and discution

Phosphoric acid (3×10^{-2} M) solution as blank for organophosphorus compound was prepared, and N,N dimethyl ,o,o dimethylphosphoramidothioate in same range of molarity was also prepared,Rate of decrease organophosphorus concentration with CM-MgO and AP-MgO in different interval of time are reported in table 1 and table 2

Table-1-Decrease of concentration of op over CM-MgO in molar ratio (1:40) in different time

Adsorption % of OP with AP-MgO	Area of under peak(AP-MgO)	Molar concentration of op in time (M)	Blank Sample	Initial Molar concentration of op in time (M)	Time (min)	row
0	211.55	0.03	Phosphoric acid0.03M	0.03	0	1
2.74	205.76	0.0292	pbosphoric acid0.03M	0.03	5	2
9.26	191.96	0.0272	phosphoric acid0.03M	0.03	15	3
19.30	170.72	0.0242	pbosphoric acid0.03M	0.03	45	4
23.25	162.37	0.0230	pbosphoric acid0.03M	0.03	135	5
28.16	151.97	0.0215	pbosphoric acid0.03M	0.03	405	6

Table-2-Decrease of concentration of op over AP-MgO in molar ratio (1:40) in different time

Adsorption % of OP with AP-MgO	Area of under peak(AP- MgO)	Molar concentration of op in time (M)	Blank Sample	Initial Molar concentration of op in time (M)	Time (min)	row
0	199.4	0.03	Phosphoric acid0.03M	0.03	0	1
17.98	163.34	0.0246	pbosphoric acid0.03M	0.03	5	2
23.71	151.93	0.0229	phosphoric acid0.03M	0.03	15	3
37.37	124.73	0.0188	pbosphoric acid0.03M	0.03	45	4
46.48	106.58	0.0161	pbosphoric acid0.03M	0.03	135	5
59.70	80.25	0.0121	pbosphoric acid0.03M	0.03	405	6

Table-3 : Different Molar ratio of op and nano-Ap-MgO

Molar ratio(op/nanoAP-MgO)	The amount of op(Concentration 0.03 Molar)	The amount of nano MgO (g) -AP	Row
1:10	10	0.12	1
1:20	10	0.24	2
1:40	10	0.48	3

By verification the data, it is observed that adsorption of organophosphorus with AP-MgO in molar ratio 1:40 is more suitable for decontamination studied, this idea can also be confirmed by table 3. Effect of solvent in our research have been investigated, pentane will be most suitable solvent(table-4).

Table-4: compare the deceasing concentration of op adsorption of op with Nano-Ap-Mgo in different solvents

Solvent Pentane		**Cholorform solvent**		**Methanol solvent**		Time (MIN)
Percentage of decreasing concentration of op	Molar concentration of op in time (M)	Percentage of decreasing concentration of op	Molar concentration of op in time (M)(	Percentage of decreasing concentration of op	Molar concentration of op in time (M)	
0	0.03	0	0.03	0	0.03	0
34.51	0.0196	27.20	0.0218	13.22	0.0268	5
52.16	0.143	35.59	0.0193	27.78	0.0216	15
62.08	0.114	47.41	0.0158	38.61	0.0184	45
77.04	0.069	62.98	0.0111	46.89	0.0159	135
81.74	0.055	69.97	0.009	56.04	0.0132	405

In our researches reaction of DMMP (simulante Nerve agent) with nano AP-MgO has also studied..

Conclusions

Decontamination and adsorption of organophosphorus compound are maximized with nanoAP-MgO, the most suitable molar ratio between organophosphorus compound and nanoAP-MgO is equal to 1:40.Finally the nonpolar solvents maybe more suitable for this reaction.

References

[1] A.Aminifar and S. Ghadimi; "Decontamination of chemical and biological warfare agent";Imam Hossein University Publication ;2005.

[2]D.Jones, O. Kopper and etal;" Decontamination safety applications and product based on nano materials"; commercialization of Nano technology; 2, 1-7, 2006.

[3]S.Utamapanya, K.J.Klabunde ; " Nano scale metal oxide particles/ clusters as chemical reagent…";Chem .Mater.;175-181-1991.

[4]P.N.Kapoor, K.J.Klabunde." synthesis characterization and adsorption studies …" Chem.Mater; I4, 2922-29, 2002.

[5]S.Ggadimi and Asad . k ; MSC. Thesis ; Imam Hossein University ;2007.

Adsorption of phenanthroline from aquaes solution onto CMK-1 nanoporous sorbent by SPE method

M.B. Ghasemian[a], M. Anbia[a*], S. Shariati[b], S. Mandegarzad[a], S. Salehi[a]

[a] *Research Laboratory of Nanoporous Materials, Faculty of Chemistry, Iran University of Science and Technology, Farjam Street, Narmak, Tehran 16846, Iran*

(Email: anbia@iust.ac.ir)

[b] *Islamic azad university of Rasht, Department of Chemistry, Rasht, Iran*

Keyword: Phenanthroline , SPE , Nanoporous sorbent ,CMK-1/SDS

Introduction:

The selection of the appropriate extraction system is an important stage in the elaboration of analytical procedure.Solid-phase extraction is one of the most popular sample preparation methods. In this case, the knowledge of the interactions between isolated compounds, sorbent and elution solvents seems to be important. The selection of the appropriate sorbent is an important stage in the elaboration of the analytical method.

Methods:

In this study, a solid phase extraction (SPE) preconcentration system was developed for determination of phenanthroline at ppb level. The method is based on retention of phenanthroline on a column of nanoporous sorbent CMK-1 modified with dodecyl sulfate sodium salt (SDS) and subsequent elution with dimethyl sulfoxide (DMSO) and determination by UV-Vis at λ_{max}= 264 . The effect of sorbent mass, eluant volume and elution speed that could affect the performance of the system was investigated and optimized. At first, MCM-48 was synthesised as a sillica nanopprous sorbent according to the synthesis procedure described by Shao et al [1]. Then CMK-1 mesoporous carbon was prepared by using MCM-48 material as template and sucrose as the carbon source [2]. The obtained composite was then pyrolyzed in a nitrogen flow at 1173 K and kept under these conditions for 6 h to carbonize the polymer [3]. The carbon–silica composite thus obtained was washed with 1 M NaOH solution of 50% ethanol–50% H_2O twice at 363 K, in order to dissolve the

silica template completely. The carbon samples obtained after the silica removal were filtered, washed with ethanol and dried at 393 K [4]. Modification with SDS aionic surfactant was carried out by treating of CMK-1 sorbent in 100mL solution of SDS surfactant at respective critical micelle concentration. The modified sample was filtered without rinsing and dried at 110 ◦C [5]. Next, this obtained modified nanoporous sorbent packed between two frits into a SPE glass column. Afterward, a solution included specific concentration of phenanthroline passed throughout the sorbent in the SPE column [6]. A particular amount of Fe^{+2} was added to phenanthroline solution to make ferroin complex ($[Fe(phen)_3]^{2+}$) before suction the solution through the column. Ferrion complex attached to the negative tail of SDS and thus phenanthroline separeted from aqua solution. Percentage of phenanthroline adsorption was determined by measuring of phenanthroline concentration difference between primary solution and exited solution under the column [7]. Finally,different volumes of dimethyl sulfoxide (DMSO) used as eluent for recovery and desorption of phenanthroline into the CMK-1/SDS sorbent and desorped phenanthroline measured by UV-Vis[8].

Results and discussion:

The effect of sorbent mass, eluant volume and elution speed that could affect the performance of the system was optimized. The best recovery yield obtained for 0.02mgr of sorbent mass, 3ml of eluent solvent volume and 0.5ml/min of elution speed. The limit of detection (based on 3σ) was 11μgL^{-1}. Recovery and relative standard deviation (n=6) at 50μgL^{-1} level for phenanthroline were 89.5 and 3.3% respectively.

Conclusion:

The method and CMK-1/SDS sorbent was successfully, effectualy and selectively applied to adsorption and determination of phenanthroline in real water sample.

References:

[1] Mansoor Anbia, Seyyed Ershad Moradi - Applied Surface Science, Volume 255, Issue 9, 15 February 2009, Pages 5041-5047.

[2] Mansoor Anbia, Arezoo Ghaffari - Applied Surface Science, Volume 255, Issue 23, 15 September 2009, Pages 9487-9492.

[3] Mansoor Anbia, Nour Ali Mohammadi, Kaveh Mohammadi. 2010 Journal of Hazardous Materials 176 (1-3), pp. 965-972.

[4] Mansoor Anbia, Maryam Lashgari. 2009 Chemical Engineering Journal 150 (2-3), pp. 555-560.

[5]Mansoor Anbia, Seyyed Ershad Moradi, Chemical Engineering Journal, Volume 148, Issues 2-3, 15 May 2009, Pages 452-458.

[6]Mansoor Anbia, Saba Asl Hariri, Desalination, Volume 261, Issues 1-2, 15 October 2010, Pages 61-66.

[7]Mansoor Anbia, Nourali Mohammadi Desalination, Volume 249, Issue 1,30November 2009, Pages 150-153.

[8]Shabani, A.M.H., Dadfarnia, S., Dehghani, Z. - Talanta 2009, 79 (4), pp.1066-1070.

Nano-sono degradation and kinetic study of an azo dye using core-shell nanocrystals of CdS-TiO_2 fabricated by ultrasound

*Mohammad H. Entezari and Narjes Ghows
Department of Chemistry, Ferdowsi University of Mashhad, 91775, Mashhad, Iran
*Corresponding author: moh_entezari@yahoo.com

Abstract

A novel composite with a core-shell structure was prepared through the combination of microemulsion and ultrasound. The composite with a proper ratio has shown exceptional sonocatalytic activity in comparison to the pure nano-sized TiO_2 and CdS. This method was simultaneously able to decolorize and oxidize the dye with a complete mineralization due to the enhancement of mass transfer, cleaning the catalyst surface, and preventing the aggregation of particles. In this paper, two kinetic models of Langmuir–Hinshelwood and consecutive first-order reaction were investigated. The rate constants of sonocatalytic were higher than what obtained in the absence of the catalysts, solar and UV irradiation.

Keywords: Core-shell, Kinetic, Reactive black 5, Mineralization, Sonocatalytic degradation

Introduction

TiO_2 has some drawbacks [1]: (a) not applicable in visible light (b) fast recombination of the hole and electron pairs (c) low efficiency of UV light. Due to these limitations, significant efforts have been made over the last two decades for handling these problems [2]. Ultrasound is an easy and effective method under the mild conditions for preparing nonmaterials [3, 4]. It can improve the contact of the two components, crystallinity, and the formation of uniform coating [5, 6]. In this study, CdS/TiO_2 couples have been prepared by a combination of ultrasound and microemulsion in order to: (i) exploit the maximum optical absorption in the visible range, (ii) increase the surface contact between the two components (iii) facilitate the crystallization. Then the degradation of RB5 as a model pollutant is investigated under different conditions.

Experimental

A microemulsion with weight ratio between oil, CTAB, water, and co-surfactant was devided in two separate parts (A= contained sulfur in oil phase and B= cadmium chloride and ethylenediamine in aqueous phase) for preparing CdS. The synthesis of core-shell nanoparticles has carried out with combination of ultrasound and microemulsion by adding TTIP to the mixture. The precipitate was separated, washed and then dried. Then 50 mL of RB5 solution containing catalyst was sonicated for removal of dye. The other experiments were carried out under the same conditions by UV lamp and sunlight.

Results and discussion

The XRD peaks and the HRTEM for the composite confirm a core-shell structure. The results show that the sonocatalytic removal is more effective than UV light or sunlight in the presence of catalyst. This is due to the synergetic effect of ultrasound and semiconductor that may promote the formation of reactive oxygen species on the surface of catalyst and fast charge separation and transportation throughout the particles [1, 2]. In addition, the light and high temperature caused by cavitation effect can activate the electronic excitation. The TOC was fast, and then decreased slowly due to a detrimental effect of the adsorbed SO_4^{2-} ions on the catalyst surface [7]. The ultrasonic degradation follows L-H rate kinetics, but this model may not be valid at longer periods. Then, we examine a kinetic model of consecutive first-order reaction.

Conclusion

Ultrasound has a key role in the synthesis of the core-shell nanocomposites. The contact between the two nanoparticles is very important for electron transfer through the crystal interphase between TiO_2 and CdS. It results in separation of electron–hole pairs. In addition, for the removal of RB5, ultrasound has a pronounce effect on the de-aggregation of the nanocomposite particles, cleaning and sweeping the catalyst surface by acoustic micro-streaming. The sonocatalytic rate with the TiO_2/CdS is very fast compared to “only ultrasound” state, solar and UV.

Acknowledgment

This work has been supported by the "Iranian National Science Foundation: INSF" (No. 85103/31).

References

[1] J. Wang, et al., Ultrason. Sonochem. 16 (2009) 225–231.

[2] A. Kongkanand, et al., J. Am. Chem. Soc. 130 (2008) 4007–4015.

[3] M. H. Entezari, N. Ghows Ultrason. Sonochem. 18 (2011) 127–134.

[4] N. Ghows, M.H. Entezari, Ultrason. Sonochem 18 (2011) 629–634.

[5] S. Anandan, F. Grieser, M. Ashokkumar, J. Phys. Chem. C 112 (2008) 15102–15105.

[6] A.L. Morel, et al., acs nano 2 (2008) 847.

[7] C. Gomes da Silva, J. L. Faria, J. Photochem. Photobiol. A: Chem.155 (2003) 133.

Preparation of highly field polymers

H. Asiyanei, S. Moradi*, E. Joudaki and V. Jahansouz

Department of chemical engineering, faculty of Engineering , Arak University, Arak 38156-8-8849, Iran

(Email: s-morady@araku.ac.ir)

Abstract

MWCNT/PMMA composites were prepared by in situ ,ex situ and microemulsion methods. SEM microphotographs reveal that the MWCNT/PMMA composites that are prepared microemulsion adhere better than those prepared other method. MWCNT/PMMA composites wasprepared byMicroemulsion method exhibit a lower electrical resistivity and a lower percolation threshold than those prepared other method. The effects of the method of processingthe MWCNT/PMMA on the shielding effectiveness (SE) of the electromagnetic interference (EMI) of the MWCNT/PMMA composites was examined. The SE of EMI of MWCNT/PMMA increased with MWCNT content. The composites prepared bymicroemulsionmethos have higher SE values.

Introduction

Highly field polymers use for several purposes such as lubricants, anti radars and etc. We focused on anti radar purpose.

Radar is a detector which can find distances by radio waves. This system which works based on the electromagnetic waves provides some information about an object location by sending specific form of waves to the target and receiving the returned waves. The frequencies of radar waves or generally electromagnetic waves are in the range of 2-18 GHz. Anti radar coatings are applied to avoid the electromagnetic waves penetration. This research investigate some of the composites which are used as coating. In this research Multi Wall Carbon Nano tubes (MWCNT)/Poly Methyl Methacrylate (PMMA) composites was synthesized, and we measured their wave's absorption. A good absorption was the significant goal of this research and each coating has a good absorption. Important points in design and construction of the absorbents are: low thickness, low weight and volume, wide band, flexibility, low cost and having enough strength in every climate and environment.

Experimental procedure

1.Materials

Multiwalled carbon nanotubes (MWCNT) that hadbeen fabricated by CVD method were obtained from theCNT Company, Incheon, Korea. The purity of the MWCNTs was 93%. The diameter of the carbon nanotubes was 10–50 nm; the length was 1–25 lm. Methyl methacrylate (MMA) was obtained from Merck Co,Germany.sodium dodecyl solfanate(SDS), was obtained from Acros Organics Co., NJ,USA,(KPS) was obtained from Merck Co., Germany.

2.Sample preparation

1.5g SDS and MWCNTwere dissolved in 7.5 g of water and MMA was then addedto the SDS/water/mwcnt solution. 0.55 g of KPS was addedto the MWCNT/MMA/water/SDS solution. The mixturewas then refluxed at 60˚C for 24 h and the MMA monomerwas polymerized to form PMMA polymer. After the reaction, MWCNT/PMMA/water was poured on a plasticplate or were coated on a 0.1-mm-thick PE film.

3.Measurments properties

The morphological properties were elucidated using a Hitachi FESEM S-4200 scanning electron microscope(SEM).Surface electrical resistivities were measured using a four-point probe resistivity measurement system, C4S-54/5S from Cascade Microtech, NY, USA. The shielding effectiveness (SE) of electromagnetic interferenceof MWCNT/PMMA composites was analyzed using a HP 8722ES Vector Network Analyzer, Damaskos,Inc. Concordville, PA, USA. The SE test of the bulk material(200 mm · 200 mm · 1 mm). The frequencies used in the SE testingwere between 2 and 18 GHz.

Results and discussion

In Schelkunoff's theory[2],the shielding effectiveness(SE) against EMI is determined by the sum of the internal reflection loss at the exiting interface (loss of energy by multi-reflection, M), the absorption or penetration loss within the barrier itself (loss of the energy by absorption,A) and the initial reflection loss from both surfaces of the shield (loss of energy by first reflection, R) Table1show the shielding effectiveness against EMI of MWCNT/PMMA

composites.Table1show the shielding effectivenessagainst the EMI of the 4.76-wt%-coated MWCNT/PMMAcomposites prepared Micro emulsion and other method[1].

Table1: Effect MWCNT/PMMA PET film on the EMI shielding effectiveness.

Frequency, GHz	**2**	**4**	**6**	**8**	**10**	**12**	**14**	**16**	**18**
Prepared by other method - **dB**	-9	-22	-18	-23	-20	-58	-35	-28	-42
Prepared by micro emulsion - **dB**	-11	-26	-20	-23	-20	-68	-42	-35	-44

Conclusion

MWCNT/PMMA composites that are prepared microemulsion adhere better than those prepared other method. MWCNT/PMMA composites prepared Microemulsion exhibit a lower electrical resistivity and a lower percolation threshold than those prepared other method.

References

[1] S-M.Yuen, Ch-Ch.M.Ma, Ch-Ya.Chaung, K-Ch.Yu, Sh-Y.Wu, Ch-Ch.Yang,M-H.We i, effect of processing method on the shielding effectiveness of electromagnetic interference of MWCNT/ PMMA composites, Composites Science and Technology 2007.

[2] Lu Guanghong, Li Xiaotian, Jiang Hancheng. Electrical and shielding properties of ABS resin filled with nickel-coated carbon fibers.ComposSciTechnol 1996;56:193–200.

[3]Ch.Xiang , Y. Pan , J. Guo , Electromagnetic interference shieldineffectiveness of multi walled Carbon nanotube reinforced fused silica composites ,Ceramics International 33 (2007) 1293–1297.

[4]Zh . Fan, G. Luo., Z . Zhang, L. Zhou, F. Wei , Electromagnetic andmicrowave absorbing properties of multi-walled carbon nanotubes/polymer composites , Materials Science and Engineering B 132 (2006) 85–89 .

[5] H.Xu , S-M.Anlage , Microwave shielding of transparent and conducting single-walled carbon nanotube films , APPLIED PHYSICS LETTERS 90, 183119 _2007 .

Nickel nanoparticle-Poly(vinyl amine)/SBA-15 composite as a novel catalyst for swift and green reduction of nitro compounds to amines

Roozbeh Javad Kalbasi*, Amir Abbas Nourbakhsh, Farzaneh Babaknezhad
Department of Chemistry, Islamic Azad University, Shahreza Branch, 311-86145, Shahreza, Isfahan, Iran
Corresponding Author E-mail: rkalbasi@iaush.ac.ir

Keywords: Hybrid polymer; SBA-15; Nickel nanoparticle; Nitro reduction.

Introduction

Aromatic amines are of significant industrial importance, because they are widely used as the intermediates for synthesis of dyes, pharmaceuticals and agrochemicals. The reduction of aromatic nitro compounds is one of the most common methods for preparing the corresponding aromatic amines [1]. Numerous new reagents have been developed for the reduction of aromatic nitro compounds. Though some of these are widely used, still they have limitations based on safety and handling considerations. The catalytic hydrogenation is a clean and convenient method for producing amine in high yield. Therefore, the design of a catalyst, which can work under mild reaction conditions and give high catalytic performances, should be very interesting.

Recently, supported nanoparticles (NPs) of Pt, Pd, etc., with high surface-to-volume ratio compared to bulk catalytic materials, have been recognized as one of the most relevant catalysts for hydrogenation of nitrobenzene [2]. Due to the very active surface atoms, the naked NPs frequently aggregate to yield bulk like materials, which greatly reduce the catalytic activity and selectivity. To avoid the aggregation, catalytic NPs are usually stabilized by stabilizers or immobilized on various supports such as polymeric materials. The particles dispersed on the supports often gave rise to high catalytic activity and selectivity for a wide variety of nitrobenzenes. In the case of the supported MNPs, the surface properties of the supports are very important to the size and dispersion of metal particles, as well as the catalytic performances. The organic–inorganic hybrid mesoporous silicas, with controllable architecture, exceptionally high surface area and uniform pore size, together with the flexibility and reactivity of tailored organically functional groups, have attained increasing

attention in the recent years. The use of terminal organic groups (–SH, –NH_2, etc.) grafted in the channel of organic–inorganic hybrid mesoporous silicas has proven to be an efficient way to stabilize MNPs [3].

Experimental

In this work, nickel nanoparticles were prepared from $NiCl_2.6H_2O$ in the presence of poly vinyl amine grafted to mesoporous silica with $NaBH_4$ as reducing agent, after mixing the metal solution with the organic-inorganic hybrid composite.

Result and Discussion

The catalyst was characterized by FT-IR, XRD, TEM and BET techniques. The comparison between FT-IR spectra of PVAM/SBA-15 and Ni-PVAm/SBA-15 shows that nickel NPs are placed on the polymer. XRD patterns show fcc structure of nickel NPs, TEM images show that nickel NPs are in size of 3 nanometer and The BET specific surface areas and the pore size of mesoporous silica SBA-15, PVAm/SBA-15 and Ni-PVAm/SBA-15 had been calculated and shows that Ni entrance changes the mesoporous system to microporous one.

Conclusion

In the presence of this catalyst, the aromatic nitro compounds are quantitatively reduced by $NaBH_4$ to form the corresponding amines under atmospheric pressure in aqueous medium. Catalysis was due to the efficient nanoparticle mediated electron transfer from BH_4^- ion to the nitro compounds [4]. The effect of $NiCl_2$ concentration, $NaBH_4$ concentration, mesoporous silica content and reducing agent contents for nitro compounds reduction are also investigated. The catalyst showed excellent yield (100 %) in a short time (2 min), with excellent recycling capability.

References:

[1] J. F. Quinn , C. E. Bryant, K. C. Golden, B. T. Gregg; Tetrahedron Lett, 51, **2010**, 786.
[2] Q. Wang, H. Liu, H. Wang, J; Colloid Interface Sci, 190, **1997**, 380.
[3] Y. Jiang, Q. Gao; J. Am. Chem. Soc, 128, 2006, 716.

[4] N. Pradhan, A. Pal, T. Pal; Coll. Surf. A: Physicochem. Eng. Asp, 196, **2002**, 247.

Molecular Dynamic Simulation of Nanoconfined Decane

Hossein Eslami[a,b] and Saideh.Bagheri[b*]

[a]Department of Chemistry, College of Sciences, Shiraz University, Shiraz 71454, Iran.

[b]Department of Chemistry, College of Sciences, Persian Gulf University, Boushehr 75168, Iran.

E-mail: (S_bagheri2010@yahoo.com)

Keywords: Molecular dynamics, Solvation forces; Nanoconfined fluids, Decane.

Introduction

An understanding of the atomic processes occurring at the interfaces plays a central role in many technologically important phenomena such as adhesion, lubrication, coating, friction, wear, wetting, spreading, chromatography, and membrane separation [1]. In fact, confining a fluid between two solid surfaces, whose separations are just a few molecular diameters affects significantly both equilibrium and nonequilibrium properties of fluids. Recently, we have reported a simulation method [1] in which only the confined region is simulated at a constant number of confined particles, N, constant surface area, A, constant temperature, T, and constant parallel component of the pressure, $P_{||}$, which we call it NAPT ensemble simulation hereafter. In this method, the MD simulation method of Berendsen with coupling to an external bath is extended to keep the parallel component of pressure fixed by changing the distance between the confining surfaces [1]. In this work we have employed this simulation method to study the structure and dynamics of nanocofined decane between graphite surfaces.

Simulation Method and Results

The new NAPT ensemble simulation method [1,2] is applied to simulate decane molecules confined between graphite surfaces. A large number of systems in which the number of decane molecules varies between 100 and 150 were chosen for this purpose. In this simulation, the temperature was fixed at 400 K and $P_{||}$ was kept constant at 101.3 kPa, employing the method described in Refs. [1,2]. Shown in Figure 1 are the local density profile of decane molecules, calculated based on the position of all atoms in the simulation box, for two different systems as typical examples. As it is seen, the decane molecules form layered

structures in the vicinity of the confining surfaces. The number of well-formed layers changes with the surface separation.

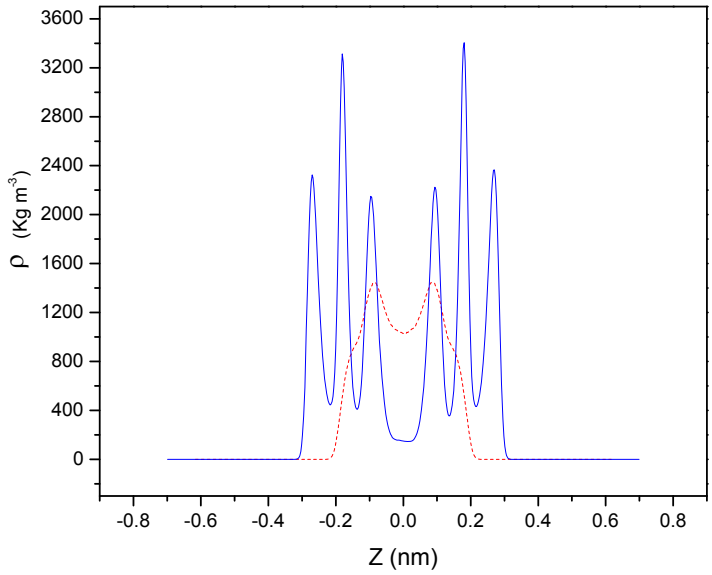

Figure (1) Local density profiles for systems consisting 115 (full curve) and 150 (dashed curve) decane molecules confined between graphene surfaces at T= 300 K and P=101.3 kPa.

Other results including the solvation force, step-wise variation of number of confined molecules with respect to the surface separation, orientation of end-to-end vectors (not shown here), indicate that decane molecules adopt a flattened conformation near the surfaces and the organization of layers depend on the solvation force oscillations. We have also calculated the diffusion coefficient of the chains in confinement. The results indicate that chains near the surfaces have a higher mobility than those of locating in the center of pore. The local dynamics of the confined chains has also been analyzed based on the autocorrelation of end-to-end vectors. In this case, the relaxation times show oscillatory behavior with out of phase oscillations with respect to the solvation force oscillations.

References

[1] Eslami, H.; F. Mozaffari, J. Moghadasi, F. Müller-Plathe, J. Chem. Phys. 2008, 129, 194702.

[2] Eslami, H.; Müller-Plathe, F. J. Phys. Chem. B 2009, 113, 5568.

Photocatalytic antibacterial avtivities of ZnO and SnO_2 thin films

Nasrin Talebian*, Elahe Badri
Department of Chemistry, Faculty of Science, Islamic Azad University, Shahreza branch, I.R. Iran
E-mail: talebian@iaush.ac.ir

Keywords: Zinc oxide; Nanofilms; Photocatalyst; Sol–gel method; Antibacterial.

Introduction

In recent years, the development of antimicrobial agents that have little or no negative impact on the natural environment has become important. Wastewater is expected to contain high levels of microorganisms and organic compounds; therefore, water disinfection has been an important and essential technology in biological and biochemical industries[1,2]. The aim of this study is to prepare the nano-sized single ZnO and SnO_2 films were prepared using sol-gel dip coating method and characterized with X-ray diffraction (XRD), scanning electron microscopy (SEM). Escherichia coli (E. coli, ATCC 25922) was selected as a model for evaluation of antibacterial property of samples.The antibacterial activity has been studied applying the so-called antibacterial-drop test. The bactericidal activity was estimated by relative number of bacteria survived calculated on the nutrient agar plates. It is found that ZnO coating exhibited a higher antibacterial activity. Furthermore, nano-structured films were active even in the absence of irradiation.

Experimental details

1- Film preparation

A precursor solutions was prepared from zinc acetate and $SnCl_4.5H_2O$. The solution was stirred and then refluxed for 3 h and after cooling to room temperature was dip-coated onto glass substrates at 20 $mm.s^{-1}$. Finally, the coated substrates were heated at 150 ^oC for 20 min after each coating. By repeating the above procedure three times, four layers of coatings were obtained. A final annealing was proceeded in air for 30 min at 500 ^oC.

2. Anti-bacterial performance

The antibacterial activity of coatings obtained against the bacteria E. coli was studied using the so-called antibacterial drop-test. Two samples of thin films were studied and one uncoated microscope glass was used as a blank. E. coli at a concentration of 10^6 CFU/ml were added drop wise using a dispenser onto the surface of each film. The samples were illuminated without and with four mercury lamps 8 W (Philips UV-A), at room temperature for 0.5, 1, 2, 3, 4, and 5 h, respectively. After each time period the bacteria containing drops were washed from the glass surfaces and the numbers of surviving bacteria on the Petri dishes were counted after incubation for 24 h at 37 °C.

Results and discussion

1. Structure properties

Fig.1. shows XRD patterns for ZnO and SnO2 thin films with patterns the tetragonal rutile structure of SnO2 film (S) and diffraction peaks for hexagonal wurtzite structure ZnO film (Z). SEM results also showed nano-scaled average diameters of particles (Fig.2).

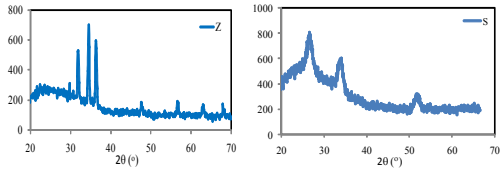

Fig. 1. XRD patterns of ZnO and SnO_2 films.

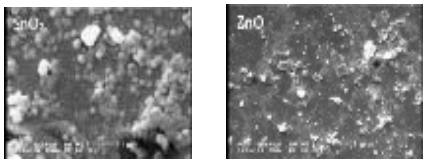

Fig. 2. SEM images of samples ZnO and SnO

2. Antibacterial activity

E. coli cells were exposed to different samples for up to 5 h to assess any bactericidal effect of the two catalysts under UV light and dark conditions. It is worthy to note that in the absence of UV light, two samples showed bactericidal activity. The photocatalytic reactivity order was SnO_2 as shown in Fig. 3.

Fig. 3. Photograph demonstrating the efficiency of SnO_2 on the number of CFU

dark	UV exposed	

3 h	5 h	3h	0.5h	
				SnO_2

Conclusion

The thin-film photocatalysts based on single ZnO and SnO_2 thin films prepared at glass substrates by sol-gel dip coating. The antimicrobial susceptibility was tested using bacteria E. coli. The highest photobiocide activity was found for ZnO.

References

[1] M. Koelsch, S. Cassaignon, J.F. Guillemoles, J.P. Jolivet,Thin Solid Films403 (2002) 312.
[2] R.S. Sonawane, B.B. Kale, M.K. Dongare, Mater. Chem. Phys. 85 (2004)52.

Quantum Chemical Predicting of Novel Organometallic Fullerene Complexs

Z. B. Nojini[a*] S. Samiee [a]

[a]Department of Chemistry, Faculty of Science, Shahid Chamran University, Ahwaz, Iran

E-mail: zb_nojini@scu.ac.ir and zb.nojini@gmail.com

Abstract

Predictions for Organometallic Fullerene structures and properties using theoretical study that could help in their possible experimental characterization, such as equilibrium geometries, electronic structures, are reported.

Keywords: Fullerene, Scandium, binding energy

Introduction

The advent of fullerene chemistry, discovery of C_{60} by Smalley and co-workers has opened new research in the field of molecular chemistry, material and condensed matter physics. In this respect, the metal- C_{60} interaction is interest both from a fundamental point of view and for the applications of C_{60} fullerenes as bulk interaction compounds with unique properties including suitable for hydrogen storage in the case of alkali metals [1].

Computational Method

The DFT calculations were carried out using G03 program package. The modified Perdew–Wang91 exchange plus the Perdew–Wang91 correlation (MPW1PW91) was used.

Results and discussion

To examine the binding properties of fullerene, we calculated the binding energy of the C_{60}-Sc as well as the pristine C_{60} molecule and Sc atom. The adsorption energy, E_{bind}, was calculated using the expression

$$E_{bind} = E_{(C_{60}-Sc)} - (E_{C_{60}} + E_{Sc}) \quad (1)$$

There are two adsorption sites for Sc on C_{60} were considered, (a) the center of the hexagonal ring H site, (b) the edge between two hexagonal rings D site. Results show that the complex formation is stable than isolated molecules. Secondly, all the calculated formation energies are negative. As defined by Eq. (1), this means that the complex formation of the scandium atom is exothermic for C_{60} (Table 1).

Table1. Binding energy, HOMO, LUMO and Gap (Δ) energy of Sc_nC_{60} system calculated by MPW1PW91/6-31G

Type	E_{bind}	HOMO	LUMO	Gap energy
C_{60}-Sc (D)	-1.632	-5.422	-3.035	2.388
C_{60}-Sc (H)	-2.131	-4.496	-3.086	1.410
C_{60}-Sc_2 (D)	-1.5121	-4.983	-2.781	2.203
C_{60}-Sc_2 (H)	-2.350	-3.874	-2.674	1.201

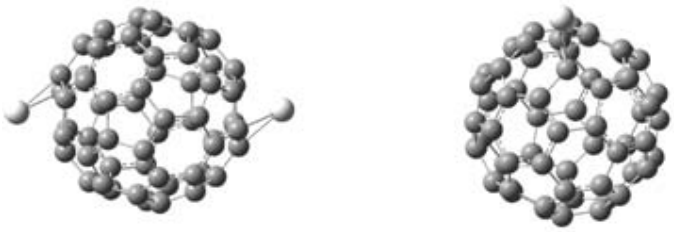

(a) (b)

Fig.1. Typically structures at each energy minimum obtained from MPW1PW91/6-31G for the C_{60}-Sc complexes: (a) H site, (b) D site

Conclusion

In conclusion, we have used first principal calculation to show that transition metal decorated C_{60} molecules exhibits remarkable stability than that pristine C_{60}.

References:

[1]F. Rabilloud, R. Antoine, M. Broyer, I. Compagnon, P. Dugourd, D. Rayane, and F. Calvo, J. Phys. Chem. C 111(2007) 17795

[2]M. Yamada, T. Akasaka, S. Nagase, Account. Chem. Res. 43(2010) 92-102

Investigation of Kinetic and Thermodynamic parameters for Adsorption of malachite green dye (MG) by nano electroactive polymer

M. Banimahd keivani* [a], R. Ansari [b], H. Pourmohammad [c]

[*a] Department of Sea & River, Iranian Academic Center for Education Culture & Research (ACECR) Guilan Branch, Rasht, Iran

Email: keivani@acecr.ac.ir

[b] Department of Chemistry, Guilan University, Rasht, Iran.

[c] Department of Chemistry, Ardabil branch, Islamic Azad University(IAU), Ardabil, Iran

Abstract

In this research, a nano composite of polyaniline sawdust (termed as Pan/SD) was prepared via chemical polymerization of aniline on the surface of sawdust for adsorption MG from aqueous solution. The effects of some important parameters such as kinetic and thermodynamic parameters were studied. In this paper obtained the pseudo-second order model kinetic is better than pseudo-first order model and this adsorption was an endothermic and spontaneous process

Keywords: Malachite Green, Nano polyaniline, Kinetic, Thermodynamic,

Introduction

The Textile industry is in the forefront in the use of dyes in its operations with more than 9000 types of dyes incorporated in the color index [1]. The discharge of colored waste is not only damaging the aesthetic nature of receiving streams, but also is toxic to the aquatic life [2]. Polyaniline (PAn) is a nano conducting polymer that can be easily synthesized chemically from bronsted acidic aqueous solutions [3]. Investigation of kinetic and thermodynamic parameters is important variable therefore MG as a typical basic textile dye was selected as a test probe.

Methods

Polymerization was carried out in aqueous solution. Polyaniline was obtained from Merck and Sawdust samples (SD) from walnut obtained from a local carpentry workshop. Absorbance studies were carried out on a single beam Perkin-Elmer UV–Vis spectrophotometer with a 1 cm cell (λ_{max}= 620 nm) was used for measuring all of absorption data.

Results and Discussion

In order to monitor the kinetics of the adsorption of the MG dye over adsorbent, pseudo-first order and pseudo-second order rate equations were applied. The specific rate constants and other parameters were calculated using following mathematical forms:

$$Ln(q_e - q_t) = Ln\, q_e - k_1\, t \qquad \frac{t}{q_t} = \frac{1}{k_2 q_e^2} + \frac{t}{q_e}$$

Where k_1 and k_2 are the rate constants , q_e and q_t denote the amount adsorbed in mg g^{-1} at equilibrium and any time t, respectively.

Table 1 Adsorption kinetic parameters of MG onto PAn/SD

T(K)	Pseudo-first order				Pseudo-second order			
	q_e[a]	K_1	q_e[b]	r_1^2	q_e[a]	K_2	q_e[b]	r_2^2
298	11.19	-0.046	2.46	0.711	2.48	0.968	2.46	0.999

[a] Calculated [b] Experimental

To study the thermodynamic parameters , (ΔG°) , (ΔS°) and (ΔH°) were investigated and calculated for adsorbent using following relations.

$$\Delta G^\circ = -RT\, Ln\, K_C \quad , \quad K_c = \frac{C_{Ad}}{C_e} \quad , \quad LnK_c = \frac{\Delta S^0}{R} - \frac{\Delta H^0}{R}\left(\frac{1}{T}\right)$$

Table 2 Thermodynamic parameters for adsorption of MG onto PAn/SD

T (K)	ΔG°(KJ mol^{-1})	ΔH°(KJ mol^{-1})	ΔS° (J mol^{-1})
298	- 9.63		
318	- 11.47	18.049	92.90

Conclusion

The amount of experimental and calculated q_e , shows that pseudo-second order model is useful for predicting the kinetics of the MG adsorption onto the PAn/SD. Therefore the pseudo-second order model is better. The $\Delta H^\circ > 0$ as shown in Table 2 indicates endothermic nature of adsorption. The $\Delta S^\circ > 0$ shows increased randomness The negative values of ΔG° for the adsorption on PAni/SD due to from feasibility of the process and spontaneous nature of adsorption, whereby no energy input from outside of the system required.

References

[1] N. Kannan , M. Meenakshisundaram, *Water,Air and Soil Pollution,* (2001), 138, 289-305

[2] K. Kadirvelu, M. Palanival, , S. Rajeswari, *Bioresource Technology,* (2000),74, 263- 265

[3] R. Ansari , A. H. Alikhani, *J. Coat. Technol. Res.,* (2009), 6 (2), 221-227

A novel adsorbent for removal of organic dye from aqueous solutions By application of polyaniline nano layer

M. Banimahd keivani* [a], R. Ansari [b], H. Banimahd Keivani [c]

[*a] Department of Sea & River, Iranian Academic Center for Education Culture & Research (ACECR) Guilan Branch, Rasht, Iran

Email: keivani@acecr.ac.ir

[b] Department of Chemistry, Guilan University, Rasht, Iran.

[c] Department of Chemistry, Ghaemshar branch, Islamic Azad University(IAU), Ghaemshahr, Iran

Abstract

In this current research, nano layer of polyaniline was synthesized chemically onto the surface of sawdust as a thin layer (termed as PAni/SD) and then was used for removal of organic dye (such as tartrazine) from aqueous solutions. The effects of some important parameters such as pH, initial concentration, sorbent dosage, contact time on organic dye were investigated.The treatments of the data were carried out using both Freundlich and Langmuir adsorption isotherms.

Keywords: Organic dye, Tartrazine, Polyaniline Nano Layer, Adsorption, Freundlich,Langmuir

Introduction

Synthetic dyes used for doing different cases in many commercial and industrial techniques. Tartrazine is extensively used in many fields of technology in soaps, cosmetics, shampoos and other hair products, textiles industry [1-2]. Tartrazine is a synthetic lemon yellow azo dye and water soluble [1]. Removal of hazardous dyes from wastewaters using economic means has become a real challenge to global scientists [3]. There has been great excitement about the technological applications conducting polymers owing to their unique possibility of combining properties from polymers (processability, chemical stability, and flexibility) metals (electrical conductivity, optical, and magnetic properties) [4].

Methods

A Solution of tartrazine with the concentration of 200 mg L^{-1} was prepared in deionized water, used as stock solution. Absorbance measurements were carried out on a single beam Perkin-Elmer UV–Vis spectrophotometer. The surface morphologies of polymer samples were studied using scanning electron microscopy (SEM) technique (Model VEGA).

Results and Discussion

For the effects of pH, initial tartrazine concentration, sorbent dosage and contact time were treated separately with different conditions. According to the results, the sorption of tartrazine by PAni/SD in pH range of 2-5 is very high. with increasing the initial concentration of tartrazine, sorption percentage decreased. With increasing amount of sorbent, sorption percentage of the dye is also increased gradually. dye removal was occurred with 40 minutes. We cannot explain more because 2 pages are not enough. The model of Freundlich and Langmuir isotherm are shown below.

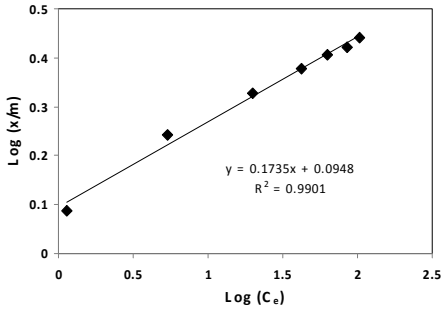

Figure 1 Freundlich Plot for the Sorption of Tartrazine onto PAni/SD

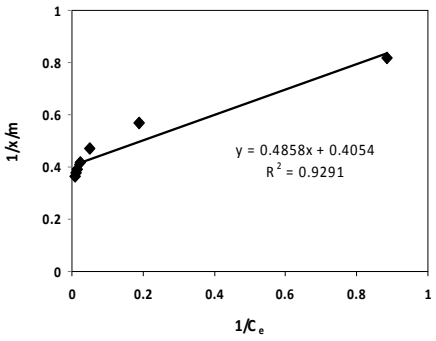

Figure 2 Langmuir Plot for the Sorption of Tartrazine onto PAni/SD

Conclusion

Sawdust as a very cheap and locally available biomaterial was found a suitable substrate for coating of polyaniline in order to be used as a new adsorbent for dye removal in this article. The highest uptake of tartrazine dye by PAni/SD was occurred in acidic conditions. High sorption capacity of PAni/SD for removal of tartrazine is supposed to be occurred via anion exchange process. However, due to the polar structure of both adsorbent and dye molecules, electrostatic or coulombic interactions between the anionic dye and the polymer, hydrogen

bonding or weak van der Waals forces and ion exchange processes are proposed mechanism for removal of dye by the used adsorbent.

References

[1] O. Tunay, I. Kabdasli, D. Ohron and G. Cansever, Water Sci. Technol., (1999),40 (1) ,237

[2] Wikipedia (http://wapedia.mobi/en/Tartrazine)

[3] V. K. Gupta, A. Mittal, A. Malviya and J. Mittal, J. Colloid & Interface Sci., (2009), 24,335

[4] Y. S. Negi and P. V. Adhyapak, J. Macromol. Sci., (2002), C42 (1), 35

Platinum Nanosheets at Liquid-Liquid Interface

Mehrangiz Bahrami*[a], S. Jafar Hoseini[a], Mehdi Rashidi[b]

[a]Department of Chemistry, Faculty of Sciences, Yasouj University, Yasouj, 74831, Iran

[b]Department of Chemistry, Faculty of Sciences, Shiraz University, Shiraz, 71454, Iran

email: mehrangiz.bahrami87@gmail.com

Keywords: Platinum, Nanosheet, Liquid Interface, Polyvinylpyrrolidone

Introduction

Over the past decade, research on design of novel platinum and platinum based nanomaterials with unique properties has been greatly intensified due to the potential for new applications and improving current applications. Since platinum is a precious metal, most of the recent efforts have focused on decreasing platinum utilization via increasing the catalytic efficiency of Pt-based catalysts by tailoring high-performance Pt-based nanostructured materials revealing that the shape of Pt nanoparticles plays a critical role in catalysis [1]. Interestingly, it has been established that the catalytic reactivity of platinum nanostructures depends highly on their morphology, and therefore the design and synthesis of well controlled shapes and sizes of platinum nanostructures is crucial for their applications, especially in the field of catalysis and electrocatalysis [2].

The liquid-liquid (organic-aqueous) interface has been used for preparation of metals, semiconductors and oxides nanocrystals . The method used to prepare thin film at the organic-aqueous interface involves dissolving relevant precursor in organic layer and injecting appropriate reagent in the aqueous layer. The reaction occurs at the interface giving rise to a film at the interface. A reduction in interfacial energy between the oil and water phase is responsible for assembling of particles at the interface [3].

Herein, we describe a new methodology for fabricating platinum (Pt) nanosheets with a thickness of 1 nm by the chemical reduction of $PtCl_2(SMe_2)_2$ complex at a toluene-water interface.

Methods:

$PtCl_2(SMe_2)_2$ was synthesized using a reported procedure [4]. In a typical experiment, the platinum nanosheets were prepared by allowing a solution of $PtCl_2(SMe_2)_2$ in toluene to stand in contact with double distilled water containing polyvinylpyrrolidone (PVP) as capping agent. Once the two layers were stabilized, appropriate volume of aqueous $NaBH_4$ was injected into the aqueous layer using a syringe with minimal disturbance to the toluene layer. With the passage of time, the color became more vivid, finally resulting in a film at the liquid-liquid interface.

Results and Discussion

X-ray diffraction (XRD) pattern (Fig. 1) of the platinum thin film deposited on a glass shows a number of prominent bragg reflections by their indices [(111), (200), (220), (311)], clearly revealing that the resultant thin film is Pt(0).

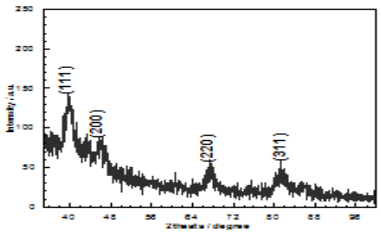

Fig. 1 XRD pattern of platinum thin film deposited on a glass

The thin film of platinum was sonicated in ethanol before drop casting on a carbon-coated copper grid. Transmission electron microscope (TEM) image (Fig. 2) confirmed the formation of platinum nanosheets with a thickness of 1 nm.

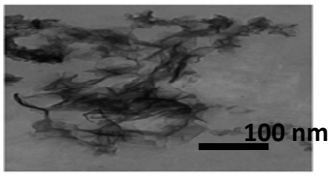

Fig. 2 TEM image of the platinum nanosheets

Conclusion:

Pt nanosheets have been prepared via a methodology based on a liquid-liquid interface, using PVP as capping agent. The resulting Pt nanosheets are less than 1 nm thick. In the absence of PVP, the resulting thin film contained only platinum nanoparticles and no nanosheets were

obtained. The results indicate that PVP plays an important role not only as a substrate for the adsorbing of Pt complex but also as a template for the formation of Pt nanosheets.

References:

[1] Aicheng Chen and Peter Holt-Hindle, *Chemical Reviews*, 2010, **110**, 3767.

[2] M. Subhramannia, & V. K. Pillai, *J. Mater. Chem.*2008, **18,** 5858.

[3] C.N. R. Rao and K. P. Kalyanikutty, *Acc. Chem. Res*., 2008, **41,** 489.

[4] M. Rashidi, A. R. Esmaeilbeig, N. Shahabadi and S. Tangestaninejad, *Journal of Organometallic Chemistry* 1998, **568,** 53.

Investigation and study of solvent effects on adsorption Bi atomic Gas (CO) on the carbon Nanotube surface using DFT calculation

M. keshavarz*[a], M. Beheshti[b]

[a] Department of Chemistry, Islamic Azad University, Shahreza Branch, P.O.Box 311-86145 Shahreza, Isfahan, Iran,Email keshavarz@iaush.ac.ir

[b] Department of Chemistry, Islamic Azad University, Shahreza Branch, P.O.Box 311-86145 Shahreza, Isfahan, Iran,tm_beheshti@yahoo.com

Abstract

In this study the gas molecule was approached nanotube surface both from carbon side and oxygen side in three positions top, bridge and center and in two directions vertically and horizontally and was calculated by B3LYP/3-21G** for nanotube and gas molecules in order to obtain the most stable adsorption state. Then we have investigated the solvent effects on the adsorption energy.

Keyword: Solvent effect, Quantum, DFT, SWCNT, Adsorption

Introduction

Single-wall nanotubes (Fig.1) are an important variety of carbon nanotube because they exhibit electric properties that are not shared by the multi-wall carbon nanotube (MWNT) variants [1,2]. Very high chemical stability and mechanical strength made the carbon nanotube a very important material in nanotechnology. The most active research area using carbon nanotubes includes applications to nanodivices, field emitters, gas sensors, hydrogen storage in fuel cells, and DNA recognition technology [3, 4].

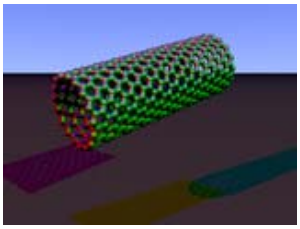

Fig .1: carbon nanotube shape (zigzag)

Methods

In this research adsorption of carbon monoxide (CO) molecule on Single-wall carbon nanotube SWNT) and zigzag (6, 0) CNT was investigated using quantum chemical calculations and Density Functional Method (DFT/3-21G**). In this study we have comparison between gas phase and solvent calculations the considered solvents (Nitromethane, Benzene, DMSO, acetone, Etc). Therefore in this study we investigate polar and non-polar solvents and adsorption gas molecules effect on the stability of SWNT in various solvent. (Table.1)

Table.1.adsorption energy in different solvents

Medium	Dielectric constant	E_{ads}
Water	78.39	-2393.21
DMSO	46.7	-2393.2
Nitromethane	38.2	-2393.199
Acetonitrile	36.64	-2393.198
Methanol	32.63	-2393.197
Ethanol	24.55	-2393.196
Acetone	20.7	-2393.195
DichloroEthane	10.36	-2393.194
DichloroMethane	8.93	-2393.193
THF	7.58	-2393.192
Aniline	6.89	-2393.191
ChloroBenzene	5.621	-2393.19
Chloroform	4.9	-2393.189
DiEthylEther	4.335	-2393.188
Toluene	2.379	-2393.187
Benzene	2.247	-2393.186
CarbonTetrachloride	2.228	-2393.185
CycloHexan	2.023	-2393.184
Heptane	1.92	-2393.183
Gas phase	1	-2393.178

Result and Discussion

In this research CO adsorption on outer side of CNT wall in different polar and non-polar solvents has been studied. it was determined that the most stable state for B3LYP/3-21G**

was TOP-H at a distance of 3.75Å from oxygen side. Based on this study CO adsorption in polar solvents on SWNT wall decreases, while it shows an increase in non-polar solvents due to CO molecule polarity.

References

[1] Iijima S., (**1991**), Helical microtubules of graphitic carbon, Nature 354, 56.

[2] Daniel S., TRao P., Rao K. S., Rani S. U., Naidu G. R. H., Lee H. Y. and Kawai T., (**2007**), Sensors and Actuators B,122,672.

[3] Kim, P.; Lieber, C. M. Science **1999**, 286, 2148.

[4] Williams, K. A.; Veenhuizen, P. T. M.; Torre, B. G.; Eritja, R.; Dekker, C. Nature **2002**, 420, 761.

Nanotechnology

Influence of solvent type on crystallite size, structure and photocatalytic activity of TiO_2 nanoparticles synthesized by sol-gel method

M.A. Behnajady*, H. Eskandarloo, N. Modirshahla and M. Shokri

Department of Chemistry, Faculty of Science, Islamic Azad University, Tabriz Branch, Tabriz, Iran

(Email: behnajady@iaut.ac.ir, behnajady@gmail.com)

Keywords: Titanium Dioxide Nanoparticles, Sol-Gel Method, Solvent Type, Photocatalytic Activity

Introduction

The use of semiconductor oxide nanoparticles as photocatalysts is well established and has shown great ability in the complete mineralization of organic pollutants [1-3]. Among these semiconductors, nanosized TiO_2 has been proved to be an excellent catalyst in the photocatalytic degradation of organic pollutants, because it is an effective, photostable, reusable, inexpensive, non-toxic and easily available catalyst [4,5].

There are many variables that affect the photoactivity of TiO_2 nanoparticles such as particle size, crystal structure and preparation method. Crystal structure and particle size are considered as important factors that determines photoactivity.

In this work, TiO_2 nanoparticles were prepared by sol-gel method in the presence of various solvents with different crystallite size and crystal structure. Photocatalytic activity of prepared TiO_2 nanoparticles tested in the removal of C.I. Acid Red 27 (AR27) as a model compound from monoazo anionic textile dyes.

Experimental details

Titanium dioxide nanoparticles were prepared from Titanium isopropoxide (TTIP) in different organic solvents (methanol (MeOH), ethanol (EtOH), and isopropyl alcohol (IsoprOH)) and distilled water. TTIP, solvent and water were maintained in a molar ratio 1:1:65. Water was added drop wise into the titanium solution during 3 h under vigorous stirring. Then the obtained sol was dried in an air oven at 80°C for 12 h. Calcination was carried out in air at 450°C during 3 h.

Decolorization of the AR27 was used as a model reaction to evaluate the photocatalytic activity of prepared nanoparticles.

Results

XRD pattern was used to investigate the crystallite size and crystal structure of the prepared TiO_2 nanoparticles. Figure 1 (a-c) depicts the X-ray diffraction patterns of TiO_2 nanoparticles prepared by the sol-gel method in the presence of different solvents.

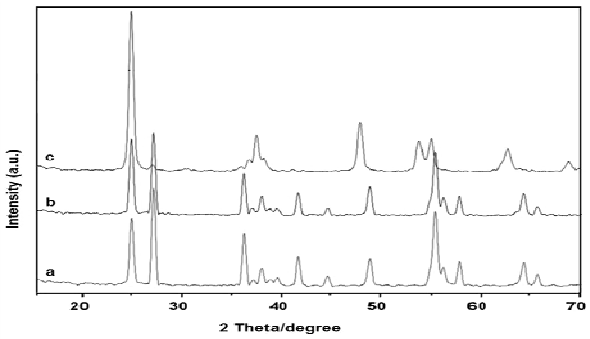

Figure 1. XRD patterns of TiO_2 catalysts synthesized in the presence of different solvents: (a) MeOH, (b) EtOH, (c) IsoprOH.

Structural properties and photocatalytic activity of TiO_2 nanoparticles are a function of solvent type. Average crystallite size, amount of each phase and photocatalytic activity of synthesized samples in the presence of MeOH, EtOH and IsoprOH solvents are reported in Table 1. The obtained nanopowders are a mixture of anatase and rutile phases with mean crystallite size between 12-29 nm.

Table 1. Crystalline phase, average particle size and photocatalytic activity of TiO_2 nanoparticles prepared in different solvents.

Solvent	Amount of each phase %	Crystallite size (nm)	k_{ap} (min^{-1})**
MeOH	A*: 95, R*: 5	D_A: 15, D_R: 12	0.36
EtOH	A: 44, R: 56	D_A: 20, D_R: 21	0.15
IsoprOH	A: 35, R: 65	D_A: 29, D_R: 22	0.1

*A=Anatase phase, R=Rutile phase, ** k_{ap} = Apparent first-order reaction rate constant

Results in Table 1 indicate that the type of solvent is very efficient in photocatalytic activity of TiO_2 nanoparticles. The maximum photocatalytic activity obtained for synthesized sample in MeOH. This can be in the result of more percent of anatase phase and also smaller crystallite size of TiO_2 nanoparticles [2].

The TEM image of the TiO_2 sample synthesized in the presence of MeOH as an organic solvent has been shown in Figure 2. The average particle size of the TiO_2 nanoparticles are less than 15 nm which is in agreement with the average crystallite size calculated from the XRD pattern.

To investigate the optical absorption properties of TiO_2 sample with high photocatalytic activity, Ultraviolet/visible diffuse reflectance spectra (DRS) was analyzed (Figure 2). The reflectance spectrum of TiO_2 sample shows an absorption threshold at 378 nm. The band gap energy estimated from the DRS plot for TiO_2 sample synthesized in the presence of MeOH as an organic solvent is 3.28 eV.

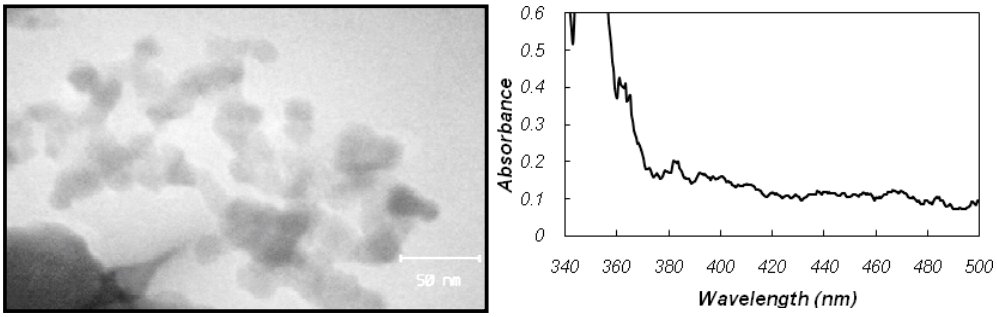

Figure 2. TEM image (left) and UV–vis DRS spectra (right) of the TiO_2 sample synthesized in the presence of MeOH.

Conclusion

The TiO_2 nanoparticles were obtained from titanium precursor through sol-gel method using different organic solvents. The particle size observed was in the range 15 nm, which also was confirmed by TEM. The photocatalytic removal of AR27 over nanosize TiO_2 synthesized in different organic solvents reveals higher activity for synthesized sample in the presence of methanol.

References

[1] M.A. Behnajady, N. Modirshahla, & R. Hamzavi, J. Hazard. Mater. 133 (2006) 226.

[2] M.A. Behnajady, N. Modirshahla, M. Shokri, H. Elham & A. Zeininezhad, J. Environ. Sci. Health: A 43 (2008) 460.

[3] L. Znaidi & R. S´eraphimova, Mater. Res. Bull. 36 (2001) 811.

[4] Q. Zhang, L. Gao & J. Guo, Appl. Catal. B 26 (2000) 207.

[5] Z. Wang, U. Helmersson & P.-O. Kall, Thin Solid Films. 405 (2002) 412.

Experimental investigation of thermal conductivity and viscosity of a new nanofluid containing MWCNTs and copper oxide nanoparticles

A.Salabat[a], P. Bourbour[a]*, H. Saydi[a]
[a]Department of Chemistry, University of Arak, Arak, Iran
p.nanochemist@gmail.com

Abstract

This paper presents an experimental investigation of thermal conductivity and viscosity of a new nanofluid composed of MWCNTs and CuO nanoparticles suspended in basefluid. The experiments were carried over temperature in 25, 30 and 35˚C. The obtained results verified that thermal conductivity of the nanofluid for 0.001 volume fraction of nanoparticles enhanced up to 11.8%, 26.5% and 52.9%, at 25, 30 and 35˚C, respectively.

Keywords: Nanoparticles, Nanofluid, Thermal conductivity, Viscosity**.**

Introduction

Nanofluids are new kinds of fluids engineered by dispersing nanoparticles in base fluids. In the last decade, nanofluids have gained significant attention due to their enhanced thermal properties. A fluid mixture of 60% ethylene glycol and 40% water by weight is most commonly used in many researches [1]. Determining the viscosity of the nanofluid is essential to establishing adequate pumping power as well as the convective heat transfer coefficient. Until now, only a few studies have addressed the viscous properties of nanoparticles suspensions at cold temperatures. Earlier research includes investigation of viscosity and thermal conductivity of copper oxide nanoparticles [2] and carbon nanotubes separately in ethylene glycol and water [3] have been presented, but no data is available for mixture of nanoparticles.

Experimental procedure

In our experiments, we used copper oxide nanoparticles with an average diameter of less than 60 nm. MWCNTs average length and diameter are 1-10 μm and 30 nm. Nanoparticles with different

volume concentrations were dispersed in a 60:40 (by weight) ethylene glycol and water mixture. Sample preparation was carried out using a very sensitive mass balance with an accuracy of 0.1 mg. An ultrasonic agitator similar to the preparation of nanofluids by Hwang et al. [3] was used. Sodium dodecyl sulphate (SDS) is used as surfactant when producing MWCNTs nanofluids. The KD2-probe portable analyzer used for thermal conductivity measurement and an LV DV-II+ Brookfield programmable viscometer was used for viscosity measurement.

Results and discussion

Portion of the experimental results for thermal conductivity and viscosity of nanofluids are shown in Figures 1 and 2, respectively.

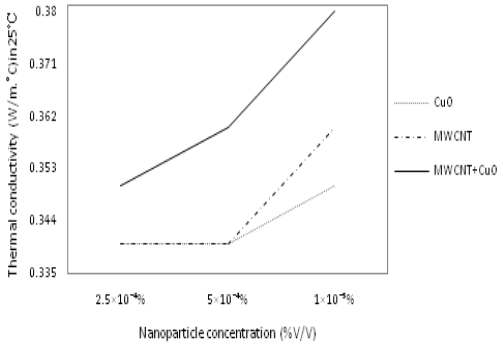

Fig. 1. Thermal conductivity and concentration relationship for CuO, MWCNT and CuO/MWCNT mixtures.

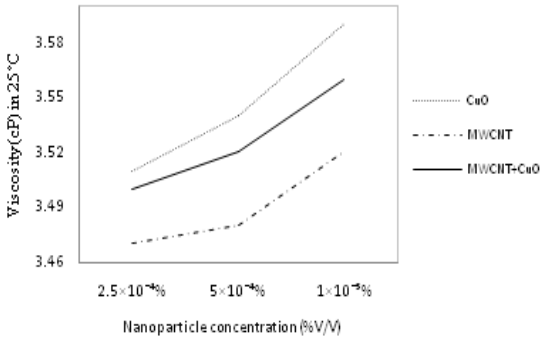

Fig. 2. Viscosity and concentration relationship for CuO, MWCNT and CuO/MWCNT mixtures.

As can be seen, thermal conductivity and viscosity of all systems increased with increasing nanoparticles volume fraction. According to Eastman et al [2], when 0.3 vol% of copper nanoparticles are suspended in ethylene glycol, thermal conductivity of the fluid increases by 40%. Hwang et al [3] report that the thermal conductivity of nanofluid was enhanced up to 11.3% at a MWCNT volume fraction of 0.01%. The results obtained in this research show that a better enhancement for thermal conductivity with mixture of nanoparticles.

Conclusions

As a new result it is verified that thermal conductivity for mixture of MWCNTs and CuO nanoparticles is greated than thermal conductivity of MWCNTs and CuO separately at the same concentration. Also viscosity of this nanofluid containing mixture of these nanoparticles is applicable.

References

[1] P.K. Namburu, D.P. Kulkarni, D. Misra, D. K. Das, Viscosity of copper oxide nanoparticles dispersed in ethylene glycol and water mixture, Experimental Thermal and Fluid Science 32 (2007) 397–402.

[2] J.A. Eastman, S.U.S. Choi, S. Li,W. Yu, L.J. Thompson, Appl. Phys. Lett. 78 (2001) 718.

[3] Y.J. Hwang,Y.C. Ahn, H.S. Shin, C.G. Lee, G.T. Kim, H.S. Park, J.K.Lee, Investigation on characteristics of thermal conductivity enhancement of nanofluids, Current Applied Physics 6 (2002) 1068-1071.

A study on the cloud thermodynamic and the impact of some micro powders it for the purpose of cloud seeding

Roya Pahlavan Hosseini

Islamic Azad University,Sciences and Researches Unit Tehran, Iran, Tehran

(rphosseini@yahoo.com:Email)

Keyword: , Thermodynamics,Micro,Cloud ,Cloud Seeding

Introduction

As time passes, advance in technology, requirements and problems of humans according to new circumstance are changing successively. Also, the human race attempts to overcome the new problems by more research and investigation and makes the better life by new tools.

15th international congress of weather (2007 Geneva) recommended supporting of weather modification activities by research and modeling in order to obtain deeper concepts about effects of weather modification on cloud production, precipitation, scientific assessment of weather actions.

Method

The most practical method for weather modification is applying of microphysical sensitivities. Because of by this way, a little artificial chaos can lead to considerable natural turbulence.

In this treatise, thermodynamics of cloud and the resulting events until attainment of precipitation will be discussed.

The principle of wffectiveness measurement of the iceforming reagent consists of the determination of the number of the ice crystals , whiche are formed during the introduction of a known quanity of investigated substance in the form of aerosol into the superercooled aqueous fog. Fog is created in the cooled cloud chamber with the aid of the intrudation of hot water vapor or mechanical dispersion of water . The reagent being investigated preliminarily is transferred into the aerosol in the separate reservoir – aerosol chamber. Crystal , which settle on the botten of cloud chamber ,fall on the film of the fixing agent , which after hardening preserves their imprints , or into the microthermostat,where the crystals remain in the period , sufficient for their calculation with the aid of the optical microscope.

The minimum and maximum measured values of the output of active particles depend on the method of registering of particles , volume of the utilized aerosol chamber and permissible quantity of reagent transferred into the aerosol . In this procedure they are respectively 10^7 and 10^{19} g^{-1}.

Equipment and the measurement instrumentation incloud:

The cloud chamber with volume 100 to 1000 L.

The aerosol chamber with volume 0.5 to 2 m^3.

Temperature minus 25 to 25$^{\circ C}$, hygrometer, psychrometer, syring , stop-watch, measurement of the mass, microscope.

Into the operational booklet necessary to write down: the designation of the reagent begin investigated , the name of the used generator of aerosol and characteristic of the utilized mode of its operation , date , the number of experiment , the temperature of fog, the volume of the sample of aerosol , the visual estimation of the approximate quantity of ice crystals in the beam of light. After processing of results into the booklet necessary to write down the average number of ice crystals in the field of sight of microscope , the total calculated number of crystals in the working volume of chamber , the mass of the reagent introduced into the chamber and the output of active particles calculated for the unit of mass of the investigated reagent.

Date	Number of the experiment	Temperature of fog T, °C	Mass of the piece of reagent m.mg	Number of the object plate	Volume of the sample of aerosol V, cm^3

Visual estimation of crystal number	Average number of ice crystals in the field of the sight $\bar{n}$	Total number of crystals in the volume of chamber n_π= nS/s	Mass Of introduced into the chamber reagent $m_\beta = \frac{m.v}{V}$, mg	Output of active particles $N = \frac{n_n}{m_\beta}$, g^{-1}

Result and Discussion

The obtained results of assessment shows injection of micro scale silver iodide particles into cloud can be effective.

We know longevity of cloud is not much. Therefore, the injection of suitable and effective nuclei or seed for precipitation into cloud can help to extraction of water and precipitation of cloud as rainfall on the earth and the sea.

Base on the research, since resemblance and similarity of silver iodide particles to natural nuclei and insolubility in water and thus a few environmental effectiveness, silver iodide particles are suitable for applying.

Investigation of potential precipitation and threshold of cloud seeding for cost reduction and prevention of over seeding and thus fall of potential in the target area and employing of thermodynamics method to determine threshold of seeding are important.

Conclusions

Also, the effects of silver iodide on weather modification and precipitation augment in micro scale will be investigated.

References

[1] Hans R.Pruppacher, James D.Klett, Microphysics of clouds and precipitation,2004

[2] John H. Robert A.Houze,Cloud Dynamics, 2003,page247-273

[3] Seinfeld, Spyros N. Pandis, Atmospheric Chemistry and Physics, 2006

[4] Plaude N.O. Study of the ice – forming properties of the aerosols of iodide silver and iodide -- lead // " Trudy CAO". – 2008. – Vyp.80.- pp. 24-40. (in Russian)

[5] SIMEONOV,P,konstantinov.p,2009,rangel researchand operational cloud modification a ctivities in Bulgaria

[6] C. Donald Ahrens, Essential of Meteorology (Section 5) 2010

Synthesis of nickel oxide nanoparticles from a triton X-100/cyclohexane/water reverse microemulsion system

H. Heli [1,*], F. Pourbahman [2]

1. Laboratory of Analytical and Physical Electrochemistry, Department of Chemistry, Islamic Azad University, Fars Science and Research Branch, P. O. Box: 73715-181, Marvdasht, Iran.

2. Department of Chemistry, Islamic Azad University, Firoozabad Branch, Firoozabad, Iran.

Abstract

Nanoparticles of nickel oxide were synthesized via a reverse microemulsion media. The microemulsion composed of triton X-100/cyclohexane/water ternary system. The reagents of the chemical reaction (nickel salt and …) were dissolved in the water part of the microemulsion separately, and two microemulsions were added. Nickel oxide was precipitated as nanoparticles. The nanoparticles were characterized by scanning electron microscopy (SEM).

Keywords: Triton X-100, Water in-oil-microemulsion, Nickel oxide, Nanoparticle.

Introduction

Nanoparticles have many applications due to their unique physical and chemical properties. Nickel oxide has been considered to be an ideal semiconductor of hole-type conductivity, which has been used in catalysis, electrocatalysis, gas sensor, batteries and magnetic devices. Therefore, great efforts have been devoted to synthesis of the nickel oxide nanoparticles.

Microemulsion is a simple media with suitable reaction environment for controlling shape and size of the nanoparticles and crystals with small size are produced. Water in-oil microemulsions, itself, are colloidal nanodispersions of water in oil which use to synthesis many metal oxide particles [1-3]. Reverse microemulsion is a thermodynamically stable system, which is used to carry out chemical reactions. These reverse micelle systems are heterogeneous with narrow size distribution. The dispersion water in microemulsion is a suitable reaction medium for synthesis of nanoparticles.

In this work, nickel oxide nanoparticles were synthesized in a triton X-100/cyclohexane /water reverse microemulsion system.

Experimental

The chemicals used were purchased from Merck. Two microemulsion media were prepared named as I and II. Microemulsion I was composed of 2 mmol triton X-100+25 ml cyclohexane+1.0 mmol Ni(NO3).6H2O dissolved in 5ml water. Microemulsion II was composed of 2 mmol triton X-100+25 ml cyclohexane+3.0 mmol NaOH dissolved in 5ml water. Microemulsion I was added into microemulsion II. Then the mixture was stirred for one hour. A solid bright green product was precipitated. The product was washed with redistilled water and ethanol, respectively. Surface morphological studies, structure and size of nickel oxides nanoparticles were studied using electron microscopy and x-ray diffraction patterns.

Results and discussion

Figure 1 shows a scanning electron microscopy image of the as-synthesized nickel oxide particles. Small particles with nanometer dimension are observed.

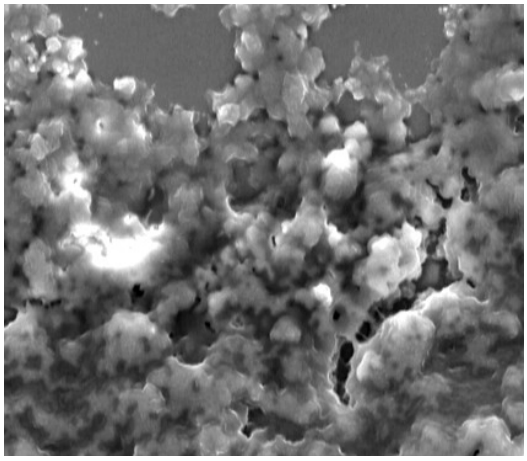

Fig. 1: SEM micrograph of the nickel oxide particles.

Figure 2 shows an XRD pattern of as synthesized nickel oxide particles. In the pattern, slightly broadened peaks are appeared. It is due to the nanometer-size effect of the samples [4]. Main diffraction peaks at 38°, 43°, 63° and 75° are indexed to (1 1 1), (2 0 0), (2 2 0) and (3 1 1) reflections, respectively. The peak positions are in good agreement with the standard diffraction data of powder cubic nickel oxide, indicating that there is no preferred orientation and the nanoparticles are polycrystalline with face center cubic structure.

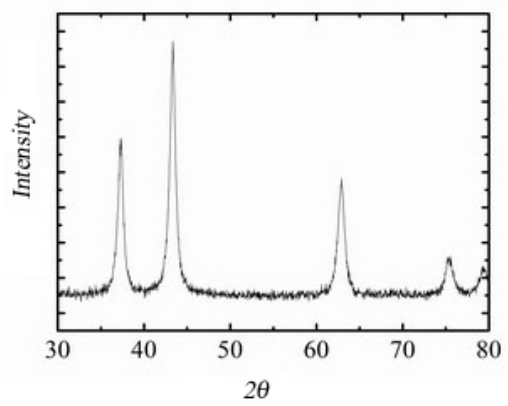

Fig. 2: An XRD pattern of the nickel oxide particles.

Conclusion

Microemulsions have received a lot of attention in the recent year.The main application for W/O microemulsions is preparation of nanoparticles. NiO nanoparticles were synthesized through water in-oil microemulsion.W/O microemulsion composed of triton X-100/cyclohexane/Nickel salt/water.which is a useful method to synthesisof metal oxides with different size and shape. The morphological of nanoparticles of NiO investigated by SEM.

Acknowledgements

The financial support of the Research Council of Islamic Azad University is acknowledged.

References

[1] I. Capek, Adv. Colloid Interface Sci. 110 (2004) 49.

[2] D. Chen, S. Liu, J. Li, N. Zhao, C. Shi, X. Du, J. Sheng, J. Alloys Compd. 475 (2009) 494.

[3] P.S. Khiew, S. Radiman, N.M. Huang, Md. Soot Ahamd, J. Cryst. Growth 268 (2004) 227.

[4] B.D. Cullity, Elements of X-Ray Diffraction, Addison-Wesley, Reading, 1978.

Ab initio Calculations Carbonic Nanotubes and Investigation of Interaction Atoms of Oxygen with that by Computational Calculations

M. Kia *[a], V. Pourghasem[a] and F. Niksolat[a]

[a] *Department of Chemistry, Rasht Branch, Islamic Azad University, Rasht, Iran*

(Email: kia@iau.ac.ir)

Keywords: Nanotube, Ab initio, Gaussian 98, Oxygen, Reaction energy

Introduction

It has been shown that the electronic properties of SWNTs are extremely sensitive to oxygen exposure [1]. Collins and co-workers found an increase in conductance of SWNTs exposed to oxygen at room temperature and that oxygen-saturated SWNT's have a higher conductance than SWNTs with less adsorbed oxygen. This trend has been attributed to an increase in the local density of states (LDOS) available for electron transport subsequent to oxygen adsorption. In a separate theoretical study [2], Rochefort and Avouris examined the effects of conductance on oxygen atom substitutionally doped SWNTs where doping was modeled by substituting a carbon atom with an oxygen atom. Using the metallic (6, 6) armchair nanotube as their model, they found a 30% decrease in conductance of a single oxygen atom doped nanotube. Similar effects may also exist for SWNTs with oxygen atoms confined inside the nanotube wall [3].

Methods

The method used in this work is quantum mechanics study. At First nanotube (10,0), oxygen atom and oxygen-nanotube are optimized by HF, DFT(B3LYP) methods and 3-21G, 6-31G basis sets, separately. Finally the reaction energies of oxygen atoms with nanotube were determined. Calculations were carried out using Nanotube modeler, Gview, Hyperchem, Chem3D and Gaussian 98 programs. These calculations, also were carrying out with addition 1 to 10 Oxygen atoms to nanotube.

Fig. 1: Optimized structure of oxygen-nanotube (10, 0) as computed at the B3LYP/6-31G

Results and Discussion

Calculations clearly show the reaction energy increases linearly as the number of oxygen atoms increase. In this research the effect of methods and basis sets on amount of reaction energy are studied. Results show the amount of reaction energy which is calculated in DFT (B3LYP) method is more than the amount of reaction energy which is calculated in HF method.

Also the calculation of reaction energy using of HF and DFT (B3LYP) methods are done in 3-21G and 6-31G basis sets. The results of reaction energy HF/3-21G and HF/6-31G and also are so near to each other.

Table 1. Reaction energies of four oxygen atoms with nanotube ($Kcal.mol^{-1}$)

Nanotube	Method	Reaction energy
$C_{80}H_{40}$	HF/3-21G	-
$C_{80}H_{40}O_4$	HF/3-21G	326.395
$C_{80}H_{40}O_4$	B3LYP/3-21G	513.739
$C_{80}H_{40}O_4$	HF/6-31G	300.428
$C_{80}H_{40}O_4$	B3LYP/6-31G	481.762

Conclusion

In this study the electrical and mechanical properties and also storage property of carbon nanotube have been studied. Nanotube with their different properties can be used in many research in different fields as their synthesis, carrier molecules and drugs, …

References

[1]. P. G. Collins, K. Bradley, M. Ishigami, and A. Zettl, Science 287, 1801(2000).

[2]. A. Rochefort and P. Avouris, J. Phys. Chem. A 104, 9807 (2000).

[3]. David J. Mann and Mathew D. Halls, JOURNAL OF CHEMICAL PHYSICS, VOLUME 116, NUMBER 20, 22 MAY 2002

Molecular dynamics simulations of polymer chains wrapping single-walled carbon nanotubes

M. Foroutan and A. Taghavi Nasrabadi*

Department of Physical Chemistry, School of Chemistry, College of Science, University of Tehran, Tehran, Iran.

Email: amirtaghavi@khayam.ut.ac.ir

Keywords: Carbon nanotube, Polymer, Simulation, Interface Energy

Introduction

One of the most significant applications of carbon nanotubes (CNTs) in composites materials is their usage as fiberlike reinforcers. The background of experimental works has introduced them as ultrastrong lightweight material reinforcements. It is well-established that the structure and properties of the interface between CNTs and polymer matrix plays a major role in determining the mechanical performance and structural integrity of nanocomposites. Molecular dynamics (MD) simulations can be used effectively in the study of reinforcement mechanisms in CNT–polymer composites because they can present a clear and vivid view of the interface between the polymer and the CNT. In this research, MD simulations were conducted to explore the interaction between CNTs and polythiophene (PT) and poly (2,6-pyridinylenevinylene-*co*-2,5-dioctyloxy-*p*-phenylenevinylene) (PPyPV). Fig.1 shows the chemical structures of polymers.

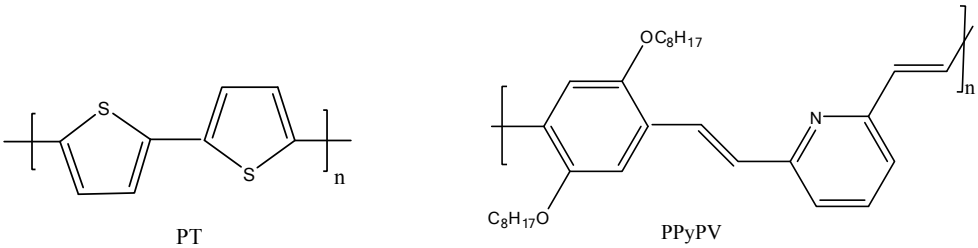

PT PPyPV

Fig. 1. Chemical structure of the polymers.

Methods

MD simulations were performed in Tinker molecular modeling package [1] using the MM3 force field. We considered a single-walled (10,10) CNT with fixed length of 110 Å. PT and PPyPV polymers were constructed with 20 and 2 monomer units, respectively. The velocity form of Verlet algorithm and the Nose-Hoover thermostat were used to integrate the equations of motion with a time step of 1.0 fs and temperature control of 300 K, respectively. A cutoff distance of 10 Å was

used for the van der Waals potentials. We used a canonical (constant NVT) ensemble with undefined boundary conditions.

Results and Discussion

The wrapping process is denoted as the enveloping of the surface of CNTs by polymers. The dynamic wrapping behavior of the polymer chains can be illustrated by tracking the intermolecular interaction energy between the CNT and polymers within the simulation time of wrapping process. The intermolecular interaction energy is defined as the sum of all the van der Waals energy terms that is computed only between the atoms of two opposite molecules (not among the atoms within single molecules). Fig. 2 represents the intermolecular interaction energy evolution for (10,10) CNT when interacts with individual molecules of PT and PPyPV at temperature of 300 K.

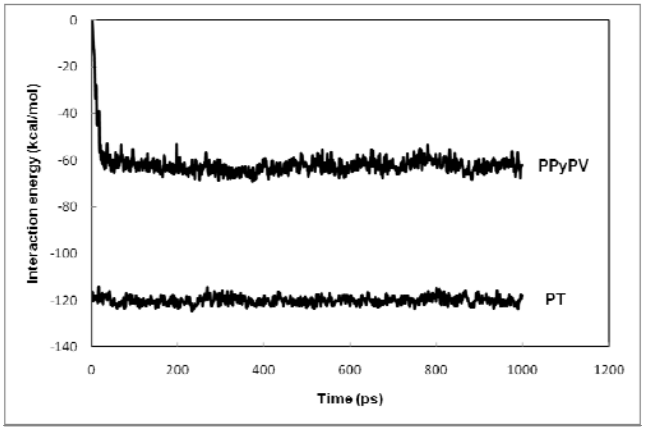

Fig. 2. Intermolecular interaction energy evolution for (10,10) CNT-polymer composites.

The simulated polymers have comparable numbers of atoms, i.e., 142 and 156 atoms for PT and PPyPV, respectively; hence the magnitude of the intermolecular interaction energy gives us a direct measure of the strength of their binding to the CNT. It is seen that PT exhibits the strongest interaction with the CNT. A logical explanation for the difference in their interaction energies is the difference in their specific monomer structures which has been reported recently by us [2].

Conclusions

The results show that the intermolecular interaction in our systems is strongly influenced by the specific monomer structure of polymer. Our simulation results suggest that the PT adheres to nanotubes better than PPyPV molecules.

References

[1] P. Ren, J.W. Ponder, J. Phys. Chem. B 107 (2003) 5933.

[2] M. Foroutan, A. Taghavi Nasrabadi, J. Phys. Chem. B 114 (2010) 5320.

The role of thermostat in the simulation of carbon nanotubes

Z. Tavangar*[a], B. Khoshnevisan[b], M. Yazdani[b], M. Rahimi[b]

[a]Faculty of Chemistry, University of Kashan, Kashan, Iran

[b]Department of Physics, University of Kashan, Kashan, Iran

Keywords: Carbon nanotube, MD simulation, Thermostat, Relaxation time, Integrated algorithm

Introduction

Carbon nanotubes (CNT) have generated increasing interest during the recent decade due to their unique properties. Numerous researches about CNTs are carried out by computational methods, such as molecular dynamics (MD) or Monte Carlo simulations. In this work, the effects of the thermostat type, the relaxation time and the integrated algorithm type have investigated for the MD simulation of the CNTs.

Methods

In this study, several zigzag and armchair CNTs with 30 Å length were considered as the total number of carbon atom includes in the simulation is 360 to 780. The periodic boundary condition was employed along the CNTs' axes and used NVT ensemble in all of the simulations.

The short range interaction of C-C bonds in carbon nanotubes are described by the Tersoff potential [1-2] and the H-H bond is modeled by Morse potential [3]. The intermolecular interactions are calculated using Lennard-Jones potentials [4].

Results and discussion

The effect of thermostat type in the simulation of the CNTs was studied by the MD simulation on the (**11**, **11**) CNT. Two types of thermostat, Berendsen or Nose-Hoover, were used and the other simulation conditions (such as initial geometry, time step (δt), simulation time and relaxation time of thermostat (τ)) were chosen the same in the both simulation. The results show that the temperature fluctuation when using the Berendsen thermostat is less than the Nose-Hoover thermostat but the shorter equilibration time and the lower equilibration energy is obtained by the Nose-Hoover thermostat (Fig. 1).

The simulations with the Nose-Hoover thermostat and different relaxation times from 0.04 to 0.4 ps with δt=0.0001 ps, shows that the system is equilibrated during the simulation time (200 ps) but the more stable energy is achieved in τ=0.4 ps. Whereas, the simulations by the Berendsen

thermostat is equilibrated (in the simulation time) just for τ =0.4 ps.

The Berendsen thermostat is extremely efficient for relaxing a system to the target temperature, but once the system has reached equilibrium, it might be more important to probe a correct canonical ensemble. So after equilibrium the Nose-Hoover thermostat works better.

The results of the MD simulation of a double walled carbon nanotube (DWCNT) clearly showed the effect of thermostat and relaxation time. The DWCNT (**11**, **11**)-(**26**, **0**) was simulated in the room temperature with time step δt=0.001 ps, the Nose-Hoover and the Berendsen thermostat and τ =0.1, 0.2, 0.3, 0.4 ps. For all of them as expected (because of the strong repulsive interaction due to close diameter values of two CNTs), after passing time the inner nanotube completely go out (Fig. 2), except for the Berendsen thermostat with τ =0.4 ps that show vibration movement.

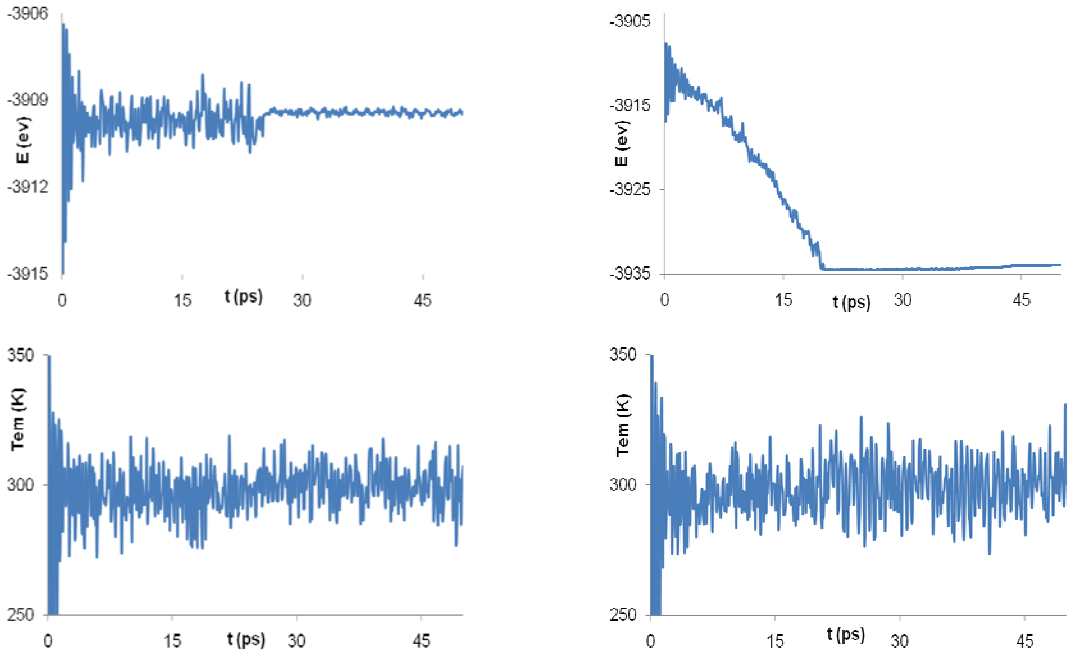

Fig 1: Time variation of energy (top row) and temperature (bottom row) in the simulation of (**11**, **11**) CNT using the Berendsen (left) and Nose-Hoover thermostat (right)

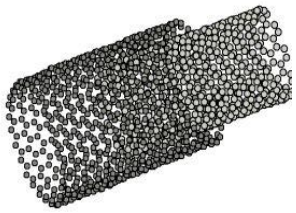

Fig: 2: Vibration movement of the (**11**, **11**)-(**26**, **0**) CNT in the simulation using the Berendsen thermostat and τ =0.4 ps

The role of integrated algorithm type was studied by the simulation of a (**12, 0**) CNT in a box containing 100 hydrogen molecules. In the initial geometry, the 4 Å distance between the molecules are considered and simulation was carried out in 82 K with the Nose-Hoover thermostat and δt=0.001 ps. When we used the Leap-Frog algorithm, the energy graph shows a shift after 60 ps due to separation of a carbon atom from the CNT wall. This problem is not observed using the velocity verlet algorithm that show how the integrated algorithm type affects the simulation results.

References

[1] Tersoff. J. Phys Rev Lett 1986;56:632.

[2] Tersoff J. Phys Rev B 1989;39:5566.

[3] Morse. P.M, Phys Rev. 1929;34:57

[4] Darkrim.F, Levesque. D, J. Chem. Phys. 1998;109:4981 .

Quantitative structure- activity relationship (QSAR) study of novel fullerene - nano analogues as potential HIV-1 PR inhibitor by mechanic quantum descriptors and chemometrics methods

Mahdie Tootooni and Ali Niazi*

Department of Chemistry, Islamic Azad University, Arak Branch, Arak, Iran

E-mail: ali.niazi@gmail.com

Abstract

A quantitative structure-activity relationships (QSAR) study is suggested for the prediction of binding energy of some fullerene - nano analogues as a function of molecular structures and using chemometrics methods such as PLS and GA-PLS and LS-SVM. The subset of descriptors, which resulted in the low prediction error, was selected by LS-SVM. This model was applied for the prediction of the binding energy of some fullerene - nano analogues, which were not in the modeling procedure. The resulted model showed high prediction ability with RMSEP of 0.51 and 0.26 and 0.05 for PLS and GA-PLS and LS-SVM models, respectively.

Keywords: Fullerene, HIV-1 PR, Mechanic quantum descriptor, Chemometrics

Introduction

A major step in constructing QSAR models is finding one or more molecular descriptors that represent variation in the structural property of the molecules by a number. Quantum chemical calculations are thus an attractive source of new molecular descriptors, which can, in principle, highest occupied molecular orbital (HOMO) and lowest unoccupied molecular orbital (LUMO) energies, molecular polarizability, dipole moments, and energies of molecule are examples of quantum chemical descriptors used in QSAR studies. In the present study, the PLS, GA-PLS and LS-SVM methods were applied in QSAR for modeling the relationship between the binding energies fullerene (Scheme: Structure of fullerene for example) as potential HIV inhibitors [1].

Methods

The PLS evaluations were carried out by using the PLS program from PLS-Toolbox Version 2.0 for use with Matlab from Eigenvector Research Inc. The LS-SVM optimization and model

results were obtained using the LS-SVM lab toolbox. Hyperchem, Version 6.03 and Gaussian 98 software were used for geometric optimization of the molecules and calculation of the quantum chemical descriptor [2].

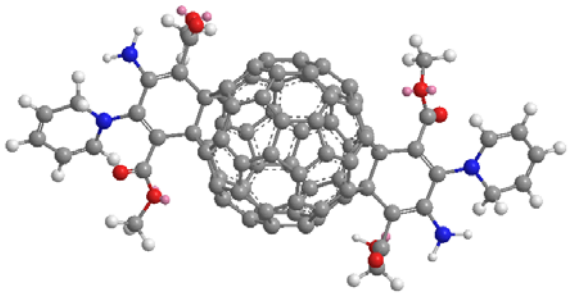

Scheme One of the numbers of structures of fulleren - nano analogues [2].

Results and discussion

According to the results, quantum chemical descriptors are suitable descriptors for describing the binding energies of fullerene derivatives. PLS, GA-PLS and LS-SVM [3] methods were used for modeling these descriptors as binding energies. Table 1 shows the results of predictions of binding energies by different methods and also, statistical parameters.

Table 1

	Predicted of Binding E		
Binding E	PLS	GA-PLS	LSSVM
-23.7	-23.12	-23.51	-23.75
-34.7	-34.93	-34.82	-34.63
-26.8	-26.11	-26.42	-26.82
-23.8	-23.36	-23.49	-23.85
RMSEP	**0.51**	**0.26**	**0.05**

RMSEP: Root mean squares of error of prediction

Conclusion

PLS, GA-PLS and LS-SVM were established to predict the binding energy of some fulleren-nano analogues. A suitable model with high statistical quality and low prediction errors was obtained. The model can accurately predict binding energy of some fulleren-nano analogues that do not exist in the modeling procedure.

References

[1] S. Durdagi, T. Mavromoustakos, N. Chonakis, M.G. Papadopoulos, Bioorg. Med. Chem. 16 (2008) 9957.

[2] A. Niazi, S. Jamehbozorghi, D. Norishargh, J. Hazard. Mat. 151 (2008) 603.

[3] A. Niazi, J. Ghasemi, A. Yazdanipour, Spectrochim. Acta Part A 68 (2007) 523.

Investigation and study of solvent effects physecochemistry adsorption Biatomic Gases on thecarbon Nanotube(8,0) surface :by study DFT

M.Keshavarz,[a] *Kh.Tavakoli[a],A.Kazemi[b]

[a]Chemistry Department, Islamic Azad University, Shahreza Branch, P. O. Box 311-86145, Shahreza, Isfahan, Iran

[b] Chemistry Department, Islamic Azad University, Shahrekord Branch, Shahrekord, Iran

Keywords:SWCNT,solvent,DFT,adsorption,SCRF

Introduction

Recent studies have shown that the physical properties of single-wall carbon nanotubes (SWCNT)could be modified by adsorption of foreign atoms or molecules.[14-16]Gas adsorption on carbon nanotubes is an important issue for both the fundamental research and technical applications of nanotubes.Selective reduction of nitrogen monoxide(NO)in oxidizing atmosphere has recently received much attention because it has a potential as a practical measure to remove NO_xemitted from diesel lean burn engines[17]. Recently,CO_2adsorption on SWCNTs has received attention[18-22]because the understanding of the adsorption of CO_2on SWCNTs is relevant to the potential use of SWCNTs in the separation of CO_2.which is both a respiratory gas and the most important green house gas.Zhao et al.studied the adsorption energies of $CO_2$and other small gas molecules on SWCNTs using the local density approximation-density functional theory(LDA-DFT)[18].

Calculation method

The method of DFT was proposed by Kohn and Hohenberg in 1964 as a complex method that different functions should be used in its calculations. Mer-Min in 1965 extended theory of Kohn and Hohenberg about main sets and final temperature and defined all properties and specifications in basis state of $n_i(r)$ means that function depends on r position so all information in wave functions are related to basis and exited states. All results of obtained theory in this research are based on quantum chemistry calculation of clusters. . In this regard the electronic structure of gases and Nano tube CNT was described using the method of density function theory (DFT) and it was realized that the B3LYP method should be used for exact describing of energy and also the function of 6-31G was applied for calculating the energy. Molecules of gases approach

horizontally and vertically in three states of 1- gases atom with Nano tube atoms in direct state (Top site) 2- gases atoms to bond of Nano tube with carbon of Nano tube (Bridge site) 3- gases atoms to center of Nano tube (Center site).

Result and discussion

In this research the oxygen molecule was approached to Nano tube surface and according to three structural position of Nano tube (Top, Bridge and center) in two horizontal and vertical form, the energy of each stage was calculated by Gaussian program. There are three states in clustery structure of Nano tube to which the oxygen molecule can approach and absorbed.The best adsorption sites for CO_2-SWCNT are the parallel approach of the CO_2 molecules to the nanotube wall on the Top-horizontal sites position oxygen.insince,the influence between a molecule in solution and its medium can describe most simply using Onsager model.in this model we have assumed that the solute is placed in a spherical cavity inside the solvent.the latter is described as a homogeneous,polarizable medium of dielectric constant.We started our studies at B3lyp/6-31G gas phase geometry and nitro methane,DMSO,Acetone and Benzene surrounding single-wall carbon nanotube (SWCNT)and mixed of them either. The results obtained from Onsager model calculations illustrated using the energy difference between these conformers which quite sensitive to the polarity of the surrounding solvent.The solvent effect has been calculation using SCRF model. According to this method ,the total energy of solute and solvent,which depends on the dielectric constant ε_v,has been listed in Table (3) for translate gas molecules in inside nanotube these various distance point .

Conclusion

In this work,we investigation solvents effects and Energy adsorption on the stability of SWCNT in various solvent.Abinatio calculations were carried out with GAUSSIAN 03W program using density functional theory (DFT) at the B3lyp/6-31G level of theory.Because of the geraphene sheet of single-wall carbon nanotube it is logical and satisfactory finding that the water can be suggested as the most improper solvent for structural properties of SWCNT due to its strongly hydrophobic characteristic.

References :

[1]C.Matranga,L.Chen,M.Smith,E.Bittner,J.K.Johnson,B.Bockrath,J.Phys.Chem.B107**(2003)**1290

[2]W.L.Yim,O.Byl,J.T.Yates Jr.,J.K.Johnson,J.Chem.120(**2004**)5377.

[3]L.Chen,J.K.Johnson,Phys.Rev.Lett.94**(2005)**125701.

[4]P.Wayne .Richard. Chemistry Of Atmospheres.Third Edition Oxford University.(2000)

[5]M.A.Gomez-Garcia,V.Pitchon.A,Kiennemann.Environmemt International. **(2005).**31.445-467

[6]. M.D .Ganji,Phys Letters A.,**(2008)** ,372,3277-3282.

[7] An,W.,Wu,X.,Zeng,X.C.,**(2008)**,J.Phys.chem.c,112,5744-5755.

[8] Wu,R.Q.,Yang,M.,Lu,Y.H.,Feng,Y.p.,**(2008)**,J.phys.chem.c,112,15985-15988.

[9]Ashrafi,A.,Ghasemi,A.S.,Babanejed,S.A,Rahim,M.,**(2010)**,Res.J.Appl.Sci.Eng.Technol.,2(6),547-551.

[10] Rafati, A.A., Hashemianzadeh ,S.M., Nojini ,Z.B., ,**(2008)**,J.phys.chem.c112,3597-3604.

Synthesis of A Novel Carbon Nanotube Reinforced Solid Sorbent Based on Sol-gel Technology for Extraction And Determination of Aflatoxins(B1,B2)

Zarrin Es'haghi[3,*], Hoda Sorayaei[1], Fateme Samadi[2], Ali Khazaeefar[3], Mahboobeh Masroornia[1], Amirhosein Zamanzade[1], farida Zohuorian[1], Mahdi Moghadam poor[4], Ali Samadi[5]

[1]*Department of Chemistry , Faculty of Sciences, Islamic Azad University, Mashhad Branch, P.O. Box 91735-413, Mashhad , Iran*

[2]*Islamic Azad University , Young Researchers Club, Mashhad Branch, Mashhad , Iran,*

[3] *Department of Chemistry , Faculty of Sciences, Payame Noor University, Mashhad, Iran*

[4]*Department of Power Engineering, Islamic Azad University, Gonabad Branch.*

[5]*Department of Power Engineering,Birjand University.*

Keywords: Aflatoxin B1,B2,Sol-Gel,Solid Phase Microextraction,HPLC

Introduction

Aflatoxins B1, B2, like the other aflatoxins are two of the most frequent mycotoxins occurring on agricultural commodities in the field and during storage under a wide range of climatic conditions and/or during technical transformation and preparation of food [1]. Aflatoxins B1,B2 could also very easily contaminate food and feed products .It is potent toxin with severe effects on animal and human health, e.g. cyto-, nephro- or neurotoxic, carcinogenic, mutagenic, immunosuppressive and estrogenic effects .Therefore, special attention has been accorded to aflatoxins B1,B2 especially in feed. The maximum level of aflatoxins B1,B2 was set at 2µg/kg (max.) especially in groundnuts, nuts, dried fruits and cereals .The requirement to apply this regulatory limit has prompted the development of some analytical methods for the qualitative and quantitative determination of aflatoxins B1,B2 in different samples, such as food, feed, and other biological materials. The extraction and purification of aflatoxins from cereals and their derivatives is usually performed by a methanol–water liquid-liquid extraction followed by a clean-up step that is applied via an immune-affinity (IA) column or solid-phase extraction (SPE) . The IA procedure is time and solvent consuming and requires a high expertise level and the use of expensive disposable cartridges. Therefore, the development of new, fast and less costly extraction and purification methods could be considered a very important task for the analysis of aflatoxins in foodstuffs. A new possible approach that could eliminate disadvantages of the conventional methods could be the use of solid-phase microextraction (SPME) coupled with HPLC–DAD.

Preparation of Solid-phase microextraction device

In this work, the sols were prepared by the basic based catalyzed method from a solution containing PTMS, alkalize water and ethanol. Equal volumes of PTMS and EtOH were added into a vial and stirred for 10 min. Then the alkalize water was added into the vial and the mixture was stirred continually to promote the hydrolysis and condensation reactions .The functionalized MWCNTs (F-MWCNTs) were added to the sol. The polypropylene hollow-fiber was cut into small segments with a length of 2.0 Cm Liquid sol containing F-MWCNTs was injected into the fibers by a syringe.

Results and discussion

The optimization of the SPME parameters should allow to reach the highest value of the extraction ratio, a low desorption time, a high repeatability and reliability (even with real sample). For liquid samples and/or extracts the SPME extraction efficiency can be influenced by different parameters, such as pH, extraction time, temperature, desorption time. Among the tested sol-gels based on PTMS has showed the greatest extraction capability .This result could be explained considering that PTMS possesses a medium polarity, very similar to the aflatoxins B1,B2 that do not contain any strong acid or basic group .

Conclusions

A simple SPME–HPLC–DAD method for AFB1, AFB2 determination in cereal-based foods has been developed for the first time .The HPLC optimized procedure consisted of a simple isocratic elution .The use of the SPME allowed the simplification of the extraction/clean-up step respect to other techniques such as IA[2] .Compared to the most accredited clean-up step by IA, SPME has led to higher LOD and LOQ, but still well below the legal limits. Furthermore, this technique is fast, if compared with the complete analytical process using IA columns, simple to use and not expensive, considering that under most conditions SPME fibers can be used from 50 to 100 times. Work is currently in progress to extend the application of the proposed approach to other real matrixes and mycotoxins, and to perform an extensive method validation.

References

[1] P.M .Scott, J .Assoc .Off .Anal .Chem .70 (1987)276.

[2] B. Sarımehmetoglu, O. Kuplulu, T.H. Celik, Food Control 15 (2004) 45.

Sonocatalytic degradation of azo dye with ZnO nanoparticle prepared by solvotermal method

* N. Talebian ,M.R. Nilforoushan,F. Jazaeri Mogaddas

*Department of Chemistry, Faculty of Science, Islamic Azad University, Shahreza branch, I.R.

talebian@iaush.ac.ir

Keywords: zinc oxide; solvothermal method;photocatalytic activity; X-ray diffraction; nanorod

Introduction

Ultrasound has been attracting attention as an advanced degradation process for the elimination of the hazardouschemical substances in water [1–3]. The phenomenon ofcavitation, i.e., the nucleation, growth, and collapse ofsmall gas bubbles in liquids, is the basis of a varietyof mechanical and chemical processes induced in liquidsby ultrasounds [4–6].Chemical reactions with $^{\cdot}OH$ from cavitationbubbles are referred to as sonochemical reactions which are promising for novel method of environmental processingsuch as waste water treatment. In this paper sonocatalytic degradation ofChrome Intra Orange G, an azo dye used in Iran textile industries, with ZnO nanorodswas used as sonocatalyst because of itsbiological and chemical properties such as high catalytic activity, high chemical stability, inexpensive and low toxicity. The obtained results may be a more advisable choice for the treatments of non- or low-transparent industrial wastewaters in future.

Methods

In a typical synthesis, 0.01 mol of $Zn(Ac)_2{\cdot}2H_2O$ powders were placed into a Teflon-lined stainless steel autoclave of 50 mL capacity to which 30 ml of 80 wt.% hydrazine hydrate aqueous solutions were added respectively with stirring. The autoclave was maintained at 90 °C for 12 h, then air cooled to room temperature. The as-formed white precipitate was filtered, washed with distilled water, and annealed in the air at 500 °C. For sonocatalitic test, catalyst (0.1, 0.25 and 0.5 g) was suspended in 100 mL of dye solution (5, 10 and 15 ppm) and the mixture was then stirred for 20 min to in the absence of UV light. Afterwards, this suspension was placed in an ultrasound apparatus with low power. After certain time intervals, the absorption decay of UV–vis spectra of dye was followedat λ_{max}.

Result and discussion

1. Characterization

XRDpattern and SEMmicrograph of ZnO nanopowder shown in Fig. 1 and Fig. 2, respectively. The characteristic XRD peaks correspond to the hexagonal phase of hydroxyl-free nanocrystalline ZnO. The average particle size of ZnO was estimated about 73nm.

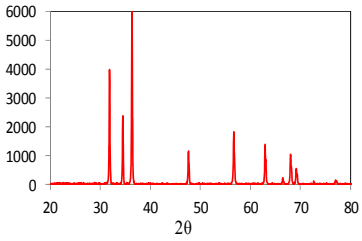

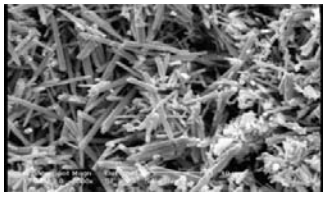

Fig. 1. XRD patterns of ZnOFig. 2. SEM of ZnO nanorod

2. Sonocatalytic degradation

The sonocatalytic activity of ZnO is shown as a function pH solution in Fig. 3. As observed the highest degradation was obtained at pH 4.

Conclusion

In this study, the sonocatalytic activity of nano-sized ZnO powders wasexamined through the degradation of Chrome Intra Orange G under ultrasonic irradiation. Since the semiconductor photocatalysis is not suitable for the treatments of non- or low-transparent organicwastewaters, the heightening of catalytic activity and shortening of degradation time are achieved using sonocatalytic process in present work.

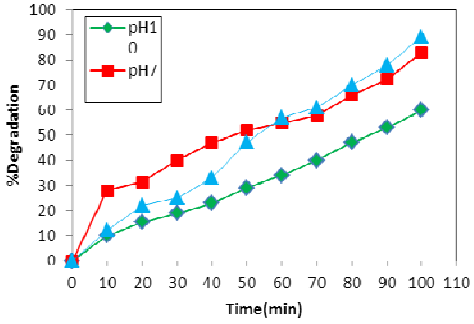

Fig. 3. Sonocatalytic activity of ZnO as a function pH solution.

References

[1] H. Destaillats, H.-M. Hung, M.R. Hoffmann, Environ. Sci. Technol.34 (2000) 311.

[2] Y. Nagata, M. Nakagawa, H. Okuno, Y. Mizukoshi, B. Yim, Y.Maeda, Ultrason. Sonochem. 7 (2000) 115.

[3] C. Stavarache, B. Yim, M. Vinatoru, Y.Maeda, Ultrason. Sonochem.9 (2002) 291.

[4] C.M. Sehgal, S.Y. Wang, J. Am. Chem. Soc. 103 (1981) 6606.

[5] K.S. Suslick, in: K.S. Suslick (Ed.), Ultrasound: Its Chemical,Physical and Biological Effects, VCH, New York, 1988, p. 123.

[6] K.S. Suslick, Science 247 (1990) 1439.

Measurement of 2-nitrobenzaldehyde, 3-nitrobenzaldehyde Adsorption on Nano –tube carbon

Mahdi vadi [1],* bita jafari yazdi [2]
[1]Islamic azad university-fasa [2]Islamic azad university-Firozabad
*bitajafariyazdi@yahoo.com

Abstract:
In this article the aim is to examine 2-nitrobenzaldehyde,3-nitrobenzaldehyde adsorption degree on multi-rim nano-tube Carbon. Adsorption on multi –rim Nano- tube surfaces has been examined by using spectroscopy and has been compared through "Langmouir" and "Frundlich" models. In comparison to other models "Langmouir" equation has th
e best. Correspondence with empirical results.

Keyword: adsorption, 2-nitrobenzaldehyde,3-nitrobenzaldehyde , nano-tube carbon, Langmouir" equation.

Introduction:

After finding of nano-tube carbon by "lijma" in 1991, this combinations found vast development in physical and chemical aspects(1). Synthesis combination ways, extended soon(2). There has been used various definition in defining the nano-particles, however specifically, nano- particles are microscopic particles with less than 100 nano-meter sides, witch can be organic or non-organic(as powder or contribution in liquid). Nano-particles are so much small that can bee said there is not much disorder ness in them. And therefore hard metals can be produced by them ,metal elements such as lithium(Li), potassium(k),

Experiment section:

First weight 4 samples of 0.022 gr. Of nano-tube carbon and then prepare 4 solutions with 150000, 250000, 40000 , 50000 mg/lit concentration, closed their doors, and put it on the magnetic mixer for 10' (min),In order to mix it consistently and after filtrating it through spectroscopy, measure solution absorption . we also measure the adsorption of

2-nitrobenzaldehyde,3-nitrobenzaldehyde solution in non-existence of (lack of) nano – tube carbon, which has been stated in table 1 .all experiments carried out in laboratory temperature(22∓2).

results and discussion

Table (1) is shown aldehyds adsorption degree in lack of nano – tube carbon on solvent (ethanol), figure (1) has been displayed 2-nitrobenzaldehyde,3-nitrobenzaldehyde adsorption degree with different concentration after passing by multi- rim nano –tube carbon. As you see with surge in all the solution concentration adsorption degree is increased. Present research indicated the nano – tube carbon in concentration of 0/022 gr. has higher practicability for absorbing 2-nitrobenzaldehyde,3-nitrobenzaldehyde parameters including

2-nitrobenzaldehyde,3-nitrobenzaldehyde concentration absorbing type, has more effect in adsorption efficiency. And in Concentration of 50000 Mg/Lit has obtained its maximum degree. And it has mentioned in table (1) both related constants with this isotherm and also consistency coefficient R_2 in linear form of double isotherm.

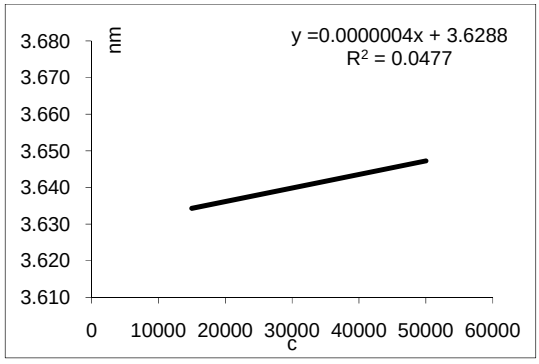

Fig1:2-nitrobenzaldehyde adsorption on carbon nano-tube

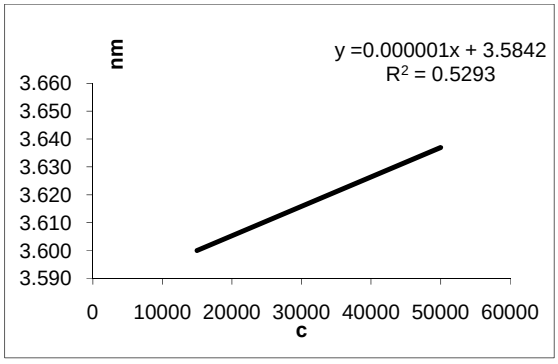

Fig1:3-nitrobenzaldehyde adsorption on carbon nano- tube

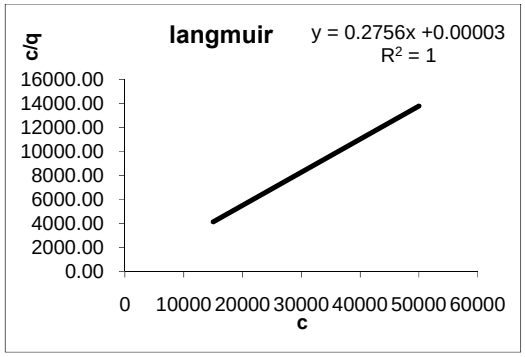

Fig2: isotherm Langmuir of 2-nitro benzaldehyde

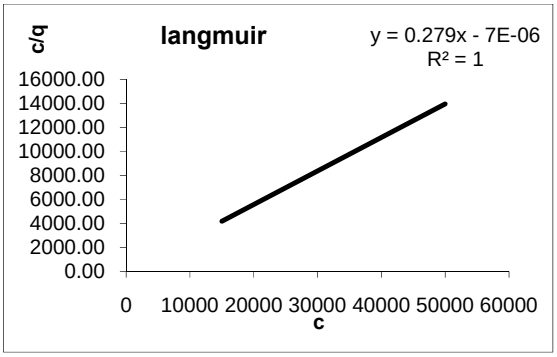

Fig2: isotherm Langmuir of 3-nitrobenzaldehyde

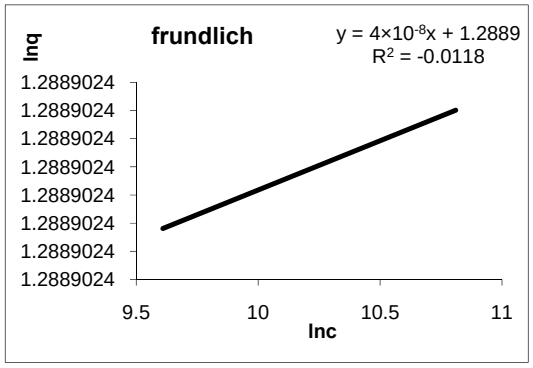

Fig3: isotherm frundlich of 2-nitrobenzaldehyde

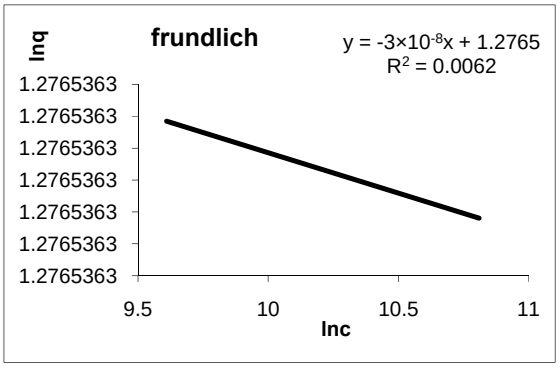

Fig3: isotherm frundlich of 3- nitrobenzaldehyde

2-nitrobenaldehyde

c	q	nm
1	3.60	3.53
2	3.61	3.56
3	3.62	3.57
4	3.63	3.58

	Langmuir			frundlich	
R^2	Q_m	K_d	R^2	n	K_f
1	3.6	0.0001	0.0118	25×10^7	3.60

3-nitrobenzaldehyde

c	q	nm
1	3.580	3.56
2	3.581	3.57
3	3.581	3.57
4	3.582	3.58

	Langmuir			frundlich	
R^2	Q_m	K_d	R^2	n	K_f
1	3.5	0.00002	0.0062	33×10^7	3.58

References:

[1]. S.Lijima, Nature 354 (1991), P.56

[2]. C; N; R; Rao B.C.Satishkumar, A.Govindaraj and M.Nath,chem. Phys, chem. 2 (2201), P.78

[3]. N.Bendiab, E.Anglaret, j-l.bantignies, A.Zahab, J.L.Sauvajol, P.Petit, C.Mathis and S.Lefrant, Phy,Rev.B64(2001),P.245424

[4]. A.S.Claye,N.M.Nemes, A.Janossy and J.E.Fischer,Phy.Rev.B62(2002),P.R4845

[5]. Bahr,J.L.;Tour,J.MJ.Mater.Chem.2002,12,1952

[6]. Basiuk,E.V.;Monroy-Pelaez,M,Puente-Lee,I;Basiuk,V.A.Nano Lett,2004,4,863

[7]. Chen,R.J;Zhang,Y;Wang;D;Dai,H,J.Am.Chem.Soc.2001,123,3838

[8]. Mathias Lehmann.Melanie Dettling.Herwig Brunner.Gunter E.M .Tovar.Journal of chromatography .

B.808(2004)43-50

[9]. Nanoworld and diamoids.m,monjajemi ISBN978-964-8407-62-4.P,55-56

[10]. Oraganic chemistry,sth.ed,2000.mcmurry,john.ISBN964-6724-77-9.P,331-332

Theoretical Study of Free Electrontransfer Energy Properties of $C_n@[(C_{60}R')_6\text{-}C_{30}H_{54}O_{18}Sn_6]$ Supramolecular Comlexes

Rouhollah Jalajerdi [a] and Avat (Arman) Taherpour*[b]

[a]Young Researchers Club, Islamic Azad University, Arak Branch, Iran

[b]Chemistry Department, Faculty of Science, Islamic Azad University, P. O. Box 38135-567, Arak,Iran

E-mail: avatarman.taherpour@ gmail.com and a.taherpour@iau-arak.ac.ir

Abstract

In this study, to establish a good relationship between the structures of fullerenes C_n (n=60, 70, 76, 82 and 86) and hexafullerene -organostannoxane, which create $C_n@[(C_{60}R')_6\text{-}C_{30}H_{54}O_{18}Sn_6]$ was utilized the number of carbon atoms within the fullerenes as an index. The relationship between the number of carbon atoms and the free-energies of electron transfer ($\Delta G_{et(1)}$ and $\Delta G_{et(2)}$) for $C_n@[(C_{60}R')_6\text{-}C_{30}H_{54}O_{18}Sn_6]$ supramolecular complexes have investigated. The calculations have presented on the basis of the two reduction potentials ($^{Red.}E_1$ and $^{Red.}E_2$) of hexafullerene-organostannoxane $[(C_{60}R')_6\text{-}C_{30}H_{54}O_{18}Sn_6]$. The results used to calculate the two free-energies of electron transfer ($\Delta G_{et(1)}$ and $\Delta G_{et(2)}$) of $C_n@[(C_{60}R')_6\text{-}C_{30}H_{54}O_{18}Sn_6]$ supramolecular complexes as well as the first and second free activation energies of electron transfer and kinetic rate constants of the electron transfers $\Delta G_{et(1)}^{\#}$, $\Delta G_{et(2)}^{\#}$ and $k_{et(n)}$ (n=1,2), in accordance with the *Marcus* theorem for fullerenes C_{60} to C_{300}.

Keywords: Fullerenes; Free energy of electron transfer; Hexafullerene-organostannoxane.

Introduction:

Dendrimer chemistry and fullerenes have crossed each other to give rise to a new interdisciplinary field in which the imagination of chemists has allowed the design and construction of unprecedented fullerene-based nanoarchitectures. Indeed, C_{60} itself is a convenient core for dendrimer chemistry and specific advantages are brought about by the encapsulation of a fullerene moiety in the middle of a dendritic structure. Organotin chemistry is an attractive tool for the preparation of multi-functional nanostructures. The organostannoxane cages can be self-assembled in almost quantitative yields under very mild reaction conditions. Up to now, various empty carbon fullerenes with a different number "n," such as C_{60}, C_{70}, C_{76}, C_{82} and C_{86} and so on, have been

obtained. Topological indices are digital values which are assigned based on chemical composition. These values are purported to correlate chemical structures with various chemical and physical properties such as the free-energies of electron transfer ($\Delta G_{et(1)}$ and $\Delta G_{et(2)}$). They have been successfully used to construct effective and useful mathematical methods for establishing good relationships between structural data and the physcochemical properties of these materials.

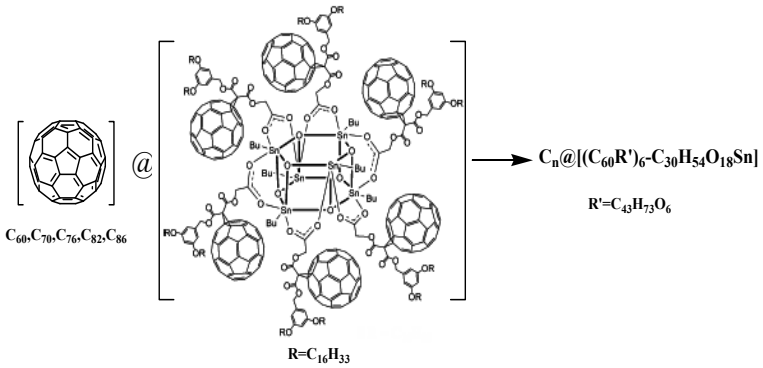

Mathematical method:

The number of carbon atoms of these the fullerenes (C_n) was utilized as a structural index for compounds. The number of carbon atoms in these the fullerenes (C_n) seems to be a useful numerical and structural value for characterizing the empty fullerenes. For modeling, both linear (MLR:Multiple Linear Regressions) and nonlinear (ANN:Artificial Neural Network) models were examined in this study. Other indices were examined and the best results and equations for extending the physicochemical and electrochemical data were chosen.

Results and Discussion:

The known hexafullerene-organostannoxane and fullerenes (C_n) have important pharmaceutical and physicochemical properties. The theoretical thermodynamics, kinetics and electrochemical data of $C_n@[(C_{60}R')_6\text{-}C_{30}H_{54}O_{18}Sn_6]$ were reported here. These include the two free-energies of electron transfer ($\Delta G_{et(1)}$ and $\Delta G_{et(2)}$) Using the number of carbon atoms (n), along with the equations of the model, one can derive sound structural relationships between the aforementioned physicochemical data. By using the equations of this model, was calculated a good approximation for $\Delta G_{et(1)}$ and $\Delta G_{et(2)}$ for $C_n@[(C_{60}R')_6\text{-}C_{30}H_{54}O_{18}Sn_6]$ of the fullerenes C_{60} to C_{300}. The first and second free activation energies of electron transfer and kinetic rate constants of the electron transfers $\Delta G_{et(n)}^{\#}$ and $k_{et(n)}$ (n=1,2) for fullerenes C_{60} to C_{300} were achived in accordance

with the *Marcus* theorem. The novel supramolecular complexes discussed here, have neither been synthesized nor reported previously.

References:

[1] J. F. Nierengarten., *J. Mater. Chem*., 2008, 18, 1547–1554.

[2] K. L. Wooley, C. J. Hawker, J. M. J. Frechet., *J. Am. Chem. Soc*., 1993, 115, 9836.

[3] A. A.Taherpour., *Chem. Phys. Lett*., 469 (2009) 135-139.

[4] A. A.Taherpour., *J. Phys. Chem. C* 113 (2009) 5402.

Free activation energies and Kinetic rate constants of the Electron Transfers properties studies of Biferrocene derivatives with Fullerenes

Rouhollah Jalajerdi [a] and Avat (Arman) Taherpour*[b]

[a]Young Researchers Club, Islamic Azad University, Arak Branch, Iran

[b]Chemistry Department, Faculty of Science, Islamic Azad University, P. O. Box 38135-567, Arak,Iran

E-mail: avatarman.taherpour@ gmail.com and a.taherpour@iau-arak.ac.ir

Abstract

The study of electron transfer in organic compounds is very important from the point of them as organic conductors. The electrochemical oxidation some of the Biferrocene derivatives were studied at various carbon electrodes. Fullerenes C_n , are a class of spherical carbon allotrope group with unique properties. Electron transfer between fullerenes and other molecules is thought to involve the transfer of electrons between molecules surrounding the fullerene cage. In this study, the number of carbon atoms in the fullerenes was used as an index to establish a relationship between the structures of Biferrocene derivatives and fullerenes C_n (n=60, 70, 76, 82 and 86), which create [Fc-R-Fc]@C_n. The relationship between the number of carbon atoms and the free energies of electron transfer ($\Delta G_{et(1)}$ to $\Delta G_{et(4)}$) are assessed using the electron transfer equation for [Fc-R-Fc]@C_n supramolecular complexes as well as the four free activation energies and kinetic rate constants of the electron transfers $\Delta G_{et(n)}^{\#}$ and $k_{et(n)}$ (n=1-4), in accordance with the *Marcus* theorem for fullerenes C_{60} to C_{300}. Calculations are presented for the four reduction potentials ($^{Red.}E_1$ to $^{Red.}E_4$) of fullerenes C_n.

Keywords: Fullerenes; free activation energies; Biferrocene derivetives; kinetic rate constant

Introduction:

Biferrocene derivetives has been extensively used to demonstrate potential application in electroanalysis, biomedicine, materials science , electronics, semiconductors, among others. The chemical, physical and mechanical properties of empty and endohedral fullerenes have been the subject of many studies. In particular, bridging two ferrocenes subunit generates redox systems which have been the subject of recent studies due to their great potential as partially oxidized species exhibiting mixed-valence behavior or electronic delocalization and as models for poly (ferrocenyl) silane materials. Up to now, various empty carbon fullerenes with a different number

"n," such as C_{60}, C_{70}, C_{76}, C_{82} and C_{86} and so on, have been obtained. Topological indices are digital values which are assigned based on chemical composition. These values are purported to correlate chemical structures with various chemical and physical properties such as the free-energies of electron transfer ($\Delta G_{et(1)}$ and $\Delta G_{et(4)}$).

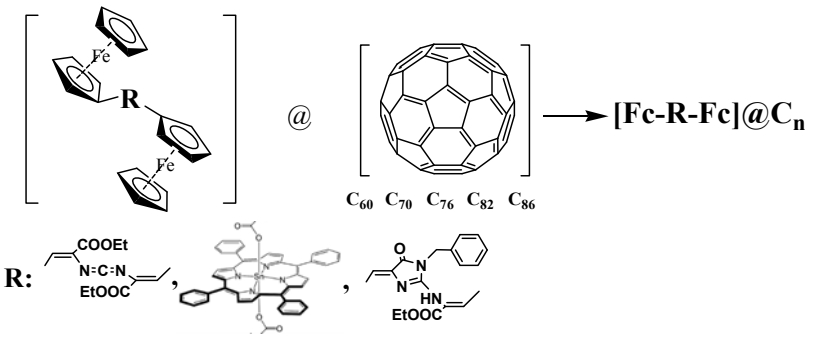

Fig.1. The conjectured structures of [Fc-R-Fc] and fullerenes C_n which create [Fc-R-Fc]@C_n .

Mathematical method:

The number of carbon atoms of these the fullerenes (C_n) was utilized as a structural index for compounds. The number of carbon atoms in these the fullerenes (C_n) seems to be a useful numerical and structural value for characterizing the empty fullerenes. For modeling, both linear (MLR:Multiple Linear Regressions) and nonlinear (ANN:Artificial Neural Network) models were examined in this study. Other indices were examined and the best results and equations for extending the physicochemical and electrochemical data were chosen.

Results and Discussion:

Biferrocene derivetives and fullerenes have important pharmaceutical and physicochemical properties. The electrochemical data of [Fc-R-Fc]@C_n were reported here. These include the four free activation energies and kinetic rate constants of electron transfer $\Delta G_{et(n)}^{\#}$ and $k_{et(n)}$ (n=1-4) Using the number of carbon atoms (n), along with the equations of the model, one can derive sound structural relationships between the aforementioned physicochemical data. By using the equations of this model, was calculated a good approximation for $\Delta G_{et(1)}$ to $\Delta G_{et(4)}$ for [Fc-R-Fc]@C_n of the fullerenes C_{60} to C_{300}. The four free activation energies of electron transfer and kinetic rate constants of the electron transfers $\Delta G_{et(n)}^{\#}$ and $k_{et(n)}$ (n=1-4) for fullerenes C_{60} to C_{300}

were achived in accordance with the *Marcus* theorem. The novel supramolecular complexes discussed here, have neither been synthesized nor reported previously.

Table 1: The data values on the $\Delta G_{et(n)}^{\#}$ and $k_{et(n)}$ (n=1-4) for $[Sn(Tpp)(Fc\text{-}COO)_2]@C_n$.

No	Formula of C_n	$\Delta G_{et(n)}^{\#}$ and $k_{et(n)}$ of $[Sn(Tpp)(Fc\text{-}COO)_2]@C_n$							
		$\Delta G_{et(1)}^{\#}$	$k_{et(1)}$	$\Delta G_{et(2)}^{\#}$	$k_{et(2)}$	$\Delta G_{et(3)}^{\#}$	$k_{et(3)}$	$\Delta G_{et(4)}^{\#}$	$k_{et(4)}$
1	C_{60}	27.67	5.07e-15	36.43	2.14e-29	46.81	2.23e-50	57.42	2.97e-76
2	C_{70}	26.98	5.10e-14	35.97	1.45e-28	44.97	2.40e-46	54.88	1.19e-69
3	C_{76}	23.52	2.82e-9	30.90	5.75e-20	44.51	2.32e-45	50.96	5.75e-60
4	C_{82}	17.76	0.02	25.83	2.17e-12	38.28	8.02e-33	46.58	7.23e-50
5	C_{86}	15.22	7.68	21.45	1.15e-6	38.74	1.07e-33	47.04	6.83e-51

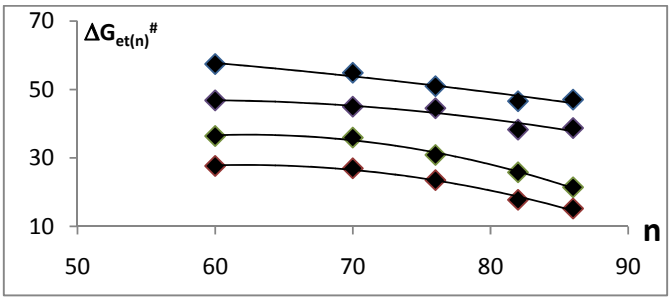

Figure 1. relationship between the n of C_n(n=60,70,76,82,86) and free activation energies of electron transfer ($\Delta G_{et(n)}^{\#}$ in kcal mol^{-1}) of $[Sn(Tpp)(Fc\text{-}COO)_2]@C_n$.

References:

[1] (a) H. W. Kroto, J. R. Heath, S. C. O'Brien, R. F. Curl and R. E. Smalley, *Nature*, 318 (1985) 162. (b) H. W. Kroto, *Nature*, 329 (1987) 529.

[2] H. Shen, *Molecular Physics*, 105(17-18) (2007) 2405–2409.

[3] A. A.Taherpour., *Chem. Phys. Lett*., 469 (2009) 135-139.

[4] A. A.Taherpour., *J. Phys. Chem. C* 113 (2009) 5402.

Quantitative Structural Relationships Studies of Free Activated Energies and Kinetics of Electron Transfer of Metal Nitride Cluster Fullerenes $Y_3N@C_{80}$ Methano Cluster Fullerenes $Y_3N@C_{80}$ Methano Mono Adduct Derivatives in[X-UT-V][$Y_3N@C_{80}$-[6,6] (R: DEM, ex-TTF and OCH_2-AQ) Supramolecular Complexes.

Avat (Arman) Taherpour*[a], Amir Mohammad Hashemi[a] and Rouhollah Jalajerdi[b]

[a]Chemistry Department, Faculty of Science, Islamic Azad University, P. O. Box 38135-567, Arak, Iran

[b]Young Researchers Club, Islamic Azad University, Arak Branch, Iran

Email:avatarman.taherpour@gmail.com

Keywords: Fullerenes; Organo-metallofullerenes; Nitride metal clusters;

Abstract:

Since the discovery of fullerenes as a class of nanostructure compounds, many potential applications have been suggested for their unusual structures and properties. Electron transfer between fullerenes and other molecules is thought to involve the transfer of electrons between molecules surrounding the fullerene cage. One class of interesting molecules is the mono adduct methanofullerene derivatives ($Y_3N@C_{80}$-[6,6]-Methanofullerene-R). Electron transfer between C_{80} derivatives such as nitride Yttrium cluster $Y_3N@C_{80}$-[6,6]-Methanofullerene-R (R=DEM, exTTF and OCH_2-AQ) and other molecules is thought to involve the transfer of electrons between molecules surrounding the fullerene cage. In this study, the relationships between this index and oxidation potential ($^{ox}E_1$) of, as well as the first and second free energies of electron transfer ($\Delta G_{et(n)}$, for n=1, 2, which is given by the *electron transfer (ET)* equation) between thiocrown ethers and the nitride Yttrium cluster derivatives as [X-UT-V][$Y_3N@C_{80}$-[6,6]-Methanofullerene-R] (R=DEM, exTTF and OCH_2-AQ) supramolecular complexes are presented and investigated. The first and second free energies of electron transfer and kinetic rate constants of the electron transfers, $\Delta G^{\#}_{et(n)}$ and k_{et} (n=1,2), respectively, were also calculated in this study for [X-UT-Y][$Y_3N@C_{80}$-[6,6]-Methanofullerene-R] (R=DEM, exTTF and OCH_2-AQ) .

Introduction:

The unique properties of molecular allotropic forms of carbon led to the discovery of a whole new set of carbon-based substances known as fullerenes and the derivatives. Fullerenes are more

reactive than planar aromatics because an important driving force for addition reactions is the reduction of strain, which results from pyramidalization in the sp^2-carbon network. Since then of 1985, metal-containing endohedral fullerenes (EMFs) have attracted special attention as a new class of technologically relevant materials due to their combined fullerene-like and metallic properties The unsaturated, *cis*-geometry thiocrown ethers (thiocrown ether), comprise a group with interesting physiochemical properties, in light of their conformational restrictions compared to corresponding saturated systems and the sizes of their cavities. The presence of sulfur atoms gives rise to the unique properties of thiocrown ethers. The *cis*-unsaturated

Considered.The wide variety of useful applications of graph theory shows that this branch of discrete mathematics can benefit various fields of sciences. Graph theory has been found to be an effective tool in *QSAR* and *QSPR*. A graph is a topological concept rather than a geometrical concept, and hence Euclidean metric lengths, angles and three-dimensional spatial configurations have no meaning. Numerous studies have related these fields using topological indices (*TI*). Numerous applications have shown that one can utilize the topological index as a very useful tool for molecular structural studies, which can be used to describe and predict reactivity and structural properties, in addition to biological and toxicological characters of compounds. One group of *TI* was founded by Randić, who introduced the molecular branching index

The ratio of the sum of the number of carbon atoms (n_c) to the number of sulfur atoms (n_s) to the product of these two numbers (μ_{cs}) was a useful numerical and structural value in the studies reported here on the unsaturated thiocrown ethers.

Quantitative structural relationships studies of the μ_{cs} index with respect to the oxidation potentials ($^{ox}E_1$) of thiocrown ethers .

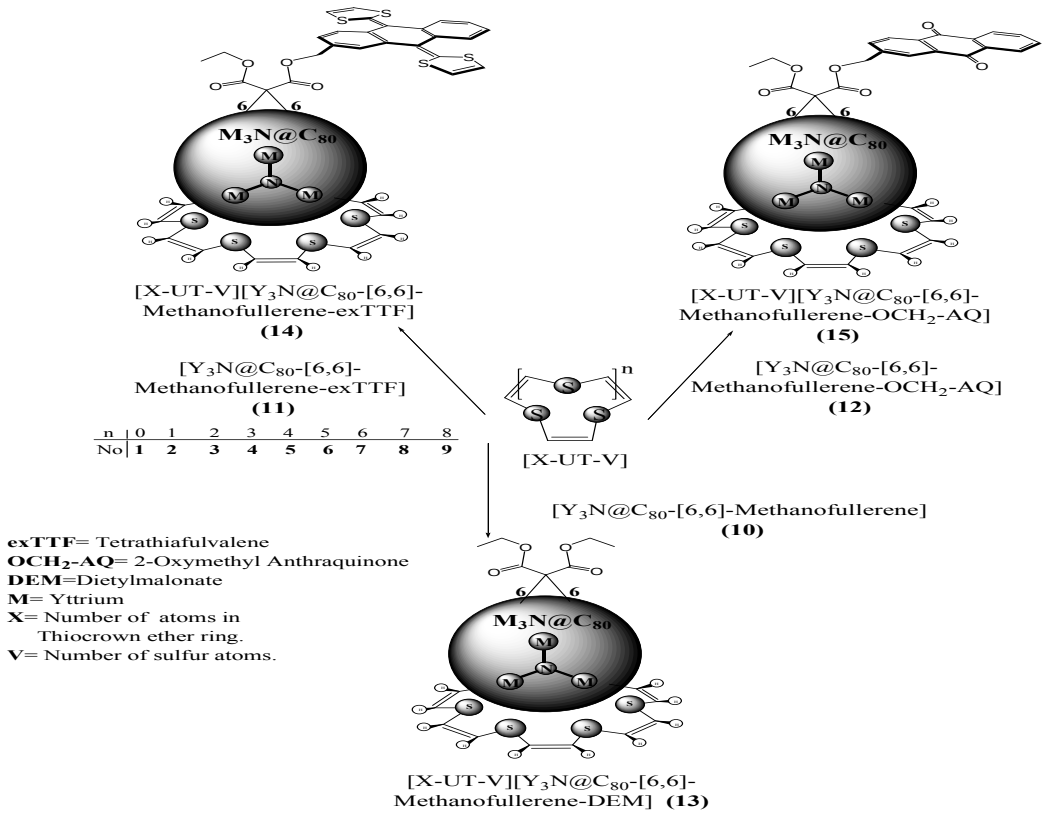

Figure-1: The structures of unsaturated thiocrown ethers **1-9** with [$Y_3N@C_{80}$-[6,6]-Methanofullerene-R] (R=DEM, exTTF and OCH_2-AQ) **10-12**, to produce supramolecular complexes [X-UT-Y][$Y_3N@C_{80}$-[6,6]-Methanofullerene-R] **13-15**.

Graphing and Mathematical Method:

All mathematical and graphing operations were performed using *Microsoft Office Excel-2003* program. The number of carbon atoms in these the fullerenes (C_n) seems to be a useful numerical and structural value for characterizing the empty fullerenes. For modeling, both linear (MLR:Multiple Linear Regressions) and nonlinear (ANN:Artificial Neural Network) models were examined in this study. Other indices were examined and the best results and equations for extending the physicochemical and electrochemical data were chosen.

Result and Discussion:

Using Equations 2 and 3, it is possible to calculate the first and second activate free energies of electron transfer and kinetic rate constants of the electron transfers, $\Delta G^{\#}_{et(n)}$ and $k_{et(n)}$ (n=1-2), respectively, for compounds referred above in accordance with Marcus theory. Figure 3 shows the surfaces of the free energies of electron transfer $\Delta G_{et(n)}$ and $\Delta G_{et(n)}{}^{\#}$ (n=1-2) between [X-UT-Y]

and [$Y_3N@C_{80}$-[6,6]-Methanofullerene-R] (R=DEM, exTTF and OCH_2-AQ) as [X-UT-Y][$Y_3N@C_{80}$-[6,6]-Methanofullerene-R] (R=DEM, exTTF and OCH_2-AQ) complexes. The values of the first and second activation free energies of electron transfer, $\Delta G^{\#}_{et(n)}$ (n=1-2) for, decrease with $\Delta G_{et(n)}$ and μ_{cs} descriptor, while the kinetic rate constants of the electron transfers $k_{et(n)}$ (n=1-2), increase with decreasing $\Delta G_{et(n)}$ and $\Delta G_{et(n)}{}^{\#}$ (n=1-3) . For [$Y_3N@C_{80}$-[6,6]-Methanofullerene-R] (R=DEM, exTTF and OCH_2-AQ), there have been reported two reduction potentials ($^{red}E_1$ and $^{red}E_2$) states. The *cis*-unsaturated thiocrown ethers have important physicochemical properties.

These equations allow one to calculate $\Delta G_{et(n)}$ (n=1-2), $\Delta G^{\#}_{et(n)}$ and $k_{et(n)}$ (n=1-2) on the basis of the first and second reduction potential ($^{red}E_1$ and $^{red}E_2$) of for the supramolecular complex groups were calculated using the *Rehm-Weller* equation concern *Marcus* theory.

References:

[1] A. A.Taherpour., *Chem. Phys. Lett.*, 469 (2009) 135-139.

[2] A. A.Taherpour., *J. Phys. Chem. C* 113 (2009) 5402.

Antibacterial activity of quaternary imidazolium salts

Jalal, Razieh*, Goharshadi, Elaheh, Sajadi, S.Hashem, Eshkil, Fatemeh
Department of Chemistry, Faculty of Sciences, Ferdowsi University of Mashhad, Mashhad 91779, Iran. razieh@ferdowsi.um.ac.ir

1. Introduction

Quaternary ammonium compounds are generally known to be bioactive substances and are used mainly for environmental disinfection, disinfection of medical equipment, and disinfection in hospitals. The mode of antimicrobial action of quaternary ammonium compounds consists of their interaction with cytoplasmic membrane of bacteria and the subsequent loss of permeability properties of the membrane. Ionic liquids, a class of neoteric solvent, can be used as media for a wide range of chemical reactions due to the ease with which they can be recycled and reused [1-3].

In the present research, we evaluated the antibacterial properties of 1-alkyl-3-methylimidazolium compounds: 1-buthyl-3-methylimidazolium bis {(trifluoromethyl) sulfonyl} amide, [C_4mim] [NTf_2] & 1-hexyl-3- methylimidazolium bis {(trifluoromethyl) sulfonyl} amide [C_6mim][NTf2].

2. Methods

The antibacterial activity was measured by bacterial growth inhibition expressed as minimal inhibitory concentration (MIC) and minimum bactericidal concentration (MBC) values. The minimum inhibitory concentration and minimum bactericidal concentration were established by the tube dilution method. Following one day exposure of bacterial cells to each compound, the MIC values (μM) were determined (Fig. 1A). Then, 25μl of each solutions were cultured on a solid agar medium (3 plates for each solutions) and after 48 hours the colonies on each plate were counted (Fig. 1B).

3. Results and discussion

The MIC (μM) and MBC (μM) values for DH-5α *E.coli* of these ionic liquids are compared in Table 1. As shown by the results, the salts studied are active against bacteria. Their activities are greatly affected by the alkyl chain length in the alkyl substituent.

Imidazolium salts had very good antibacterial activity against the examined gram-negative bacteria. The antibacterial active properties of the salts depend upon the alkyl chain length in the imidazolium ring. Among the used imidazolium salts, the imidazolium salts containing a long

alkyl chain into the imidazolium ring structure leads to broad spectrum active antibacterial agents which not only have bacteriostatic properties but could be powerful bactericides.

Keywords: Ionic Liquids, Quaternary imidazolium salts, Antibacterial Activity, Escherichia coli.

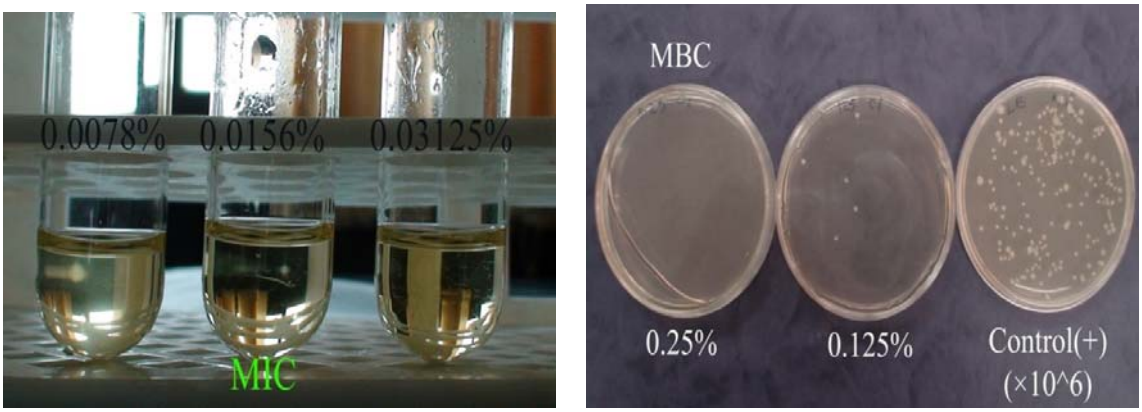

Fig. 1. A) MIC and MBC of [C_6mim][NTf2].

Table 1. MIC & MBC values of [C_4mim][NTf2] and [C_6mim][NTf2].

	Compound	**MIC (µM)**	**MBC (µM)**
***E. coli* DH5-α**	[C_4mim][NTf2]	16.83 x 10^3	44.87 x 10^3
	[C_6mim][NTf2]	350	5590

4. References

1. Crosthwaite, J.M. *J. Chem. Thermodyn.* **2005**, 37, 559-568.
2. Raabe, G. *J. Chem. Phys.* **2008**, 128, 154509.
3. Li, X. *Science in China B.* **2006**, 49, 385-401.

Molecular Dynamics Simulation Study of the Melting of a Graphite-Supported Copper Nanocluster

S. Jalili* and K. Mochani

Department of Chemistry, K. N. Toosi University of Technology, Tehran, Iran

(Email: sjalili@kntu.ac.ir)

Keywords: Molecular dynamics simulation, Cluster melting, Graphite-supported nanoclusters, Copper clusters

Introduction

In recent years, metal clusters have been paid much attention due to their importance in heterogeneous catalysis [1]. The thermodynamics properties and the catalytic behavior of nanoclusters is strongly dependent on their size. Therefore, a large number of studies have been focused on the size-dependent behavior of gas-phase clusters to produce nanostructured materials with tailored properties by depositing clusters on solid surfaces.

Molecular dynamics (MD) is a useful tool for a detailed understanding of the properties of supported nanoclusters, such as their melting phenomena [2-3]. In this work, we have studied the melting behavior of a graphite-supported copper cluster, using molecular dynamics simulations.

Methods

Classical molecular dynamics simulations were performed on a 256-atom cubic copper cluster adsorbed on a model graphite surface. The graphite was modeled as two carbon layers in ABAB arrangement with dimensions of 49.2 × 42.6 × 6.8 $(Å)^3$ and 1600 carbon atoms. The cluster was placed 3 Å above the graphite surface (Fig. 1a). The graphite model was kept rigid and constant during the simulations and the periodic boundary conditions were applied in *x* and *y* directions.

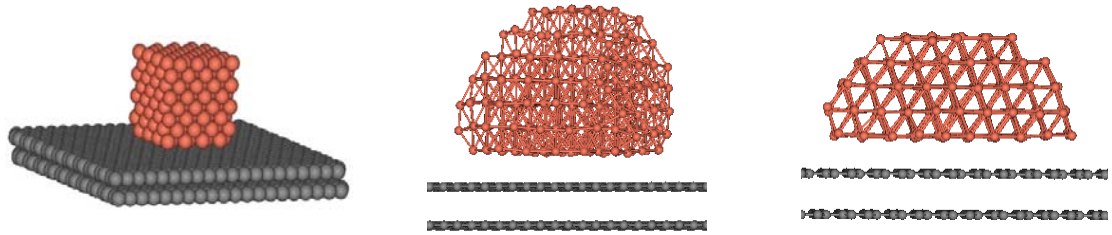

(a) **(b)** **(c)**

Fig. 1 The initial supported copper cluster (a), along with the structures obtained at 300 K during the heating (b) and cooling (c) processes.

The Cu-Cu interactions were modeled using the Sutten-Chen potential with parameters taken from the literature [3]. Lennard-Jones potential with ε = 0.019996 eV and σ = 3.225 Å was used for Cu-C interactions. Simulations were performed at different temperatures in the range of 200-1800 K to heat and from 1800 K back to 300 K to cool the cluster. Equation of motion were integrated using the leap-frog algorithm with a time step of 1 fs. Each system was first equilibrated for 400 ps and then the production run was conducted for 200 ps. The trajectories were analyzed to extract the caloric curves and radial density profiles.

Results and discussion

Fig. 2 shows the caloric curve for the supported copper cluster. Simulations in the range of 700-900 K with 20 K intervals showed that the melting point is 770 K, which is much lower than the melting point of bulk copper (the experimental value is 1356.15 K [3]). At large temperatures, the heating and cooling curves are similar, but below the melting temperature, a hysteresis is observed in the potential energy, which shows that the melting process is not completely reversible and is attributed to the surface melting [2]. The cooling curve lies below the heating curve, which means that the final structure is more stable than the initial.

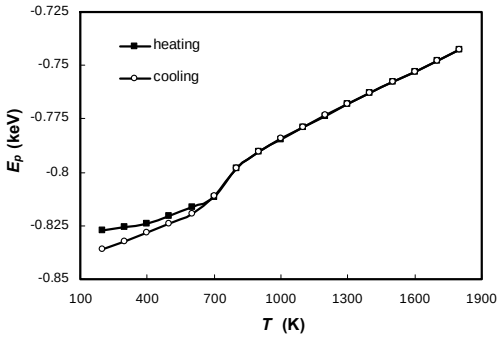

Fig. 2 The caloric curves.

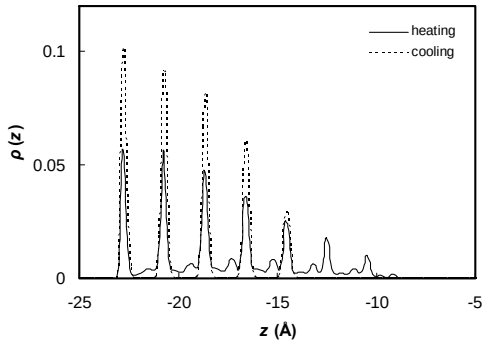

Fig. 3 Density profiles.

The irreversibility of the meting process is reflected in the cluster shape as determined from the z-density profiles at 300 K, during the heating and cooling process, Fig. 3. There is a difference in number and spacing of layers in these states, which is also obvious from Fig. 1.

Conclusions

The melting behavior of the studied cluster has the characteristic properties of nanoclusters, such as the irreversibility and surface melting. The fcc structure of the solid copper changes to a hcp type structure, before transformation to a liquid phase.

References

[1] U. Heiz, E. L. Bullock, J. Mater. Chem. 14 (2004) 564.

[2] S.-P. Huang, P. B. Balbuena, Mol. Phys. 100 (2002) 2165.

[3] S.-P. Huang, D. S. Mainardi, P. B. Balbuena, Surf. Sci. 545 (2003) 163.

Study of Electronic Properties of Functionalized Double-Walled CNT

M. Jamali*, S. Jalili
Department of Chemistry, K. N. Toosi University of Technology, Tehran, Iran
*E-mail: jamali@dena.kntu.ac.ir

Keywords: Double-walled nanotube, Electronic properties, Band structure, Density of state.

Introduction

Numerous theoretical works have shown the metallic or semiconducting properties of individual, single wall tubes (SWTs) as a function of diameter and helicity, but treating the electronic properties of multiwall nanotubes (MWNT) has been dealt with in far less detail [1], the difficulty lying in determining the extent of the interaction. The double-wall carbon nanotube (DWCNT) with metallic layers can be used as a coaxial cable or a capacitor. Although DWCNTs are constructed from two SWCNTs with the same, or different, chiralities, the electronic properties of each nanotube within a DWCNT can be different from those of an isolated SWCNT. In this study, the electronic properties of (6,0)@(13,0) and NH_2-functionalized (6,0)@(13,0) are studied. The effect of functionalization on DWCNT has been elucidated from band structures, DOS and LDOS.

Methods

All caculations were carried out using the Quantum-Espresso package in which the DFT methodology is implemented using plane wave expansions and pseudopotentials [2]. The structures considered here are (6,0) ,(13,0) nanotubes and (6,0)@(13,0) and NH_2-functionalized (6,0)@(13,0) double-walled nanotubes. The cutoff energies for plane waves were chosen to be 540 eV. Calculations were performed in the supercell approximation, the supercell was large enough to ensure that the vacuum space was at least 12 Å for all nanotubes. The lattice parameter along the axial direction of the nanotube is twice the unit length of the pristine nanotube and DWNT. The Brillouin zones for the (6,0),(13,0),(6,0)@(13,0) and NH2-functionalized (6,0)@(13,0) supercells were sampled with 1×1×9, 1×1×7, 1×1×6 and 1×1×5 Monkhorst-Pack meshes [3], respectively, which were determined after appropriate convergence tests.

Results and Discussion

The purpose of this study is effect of covalently functionalized (6,0)@(13,0) nanotube with NH_2 group, on the electronic properties and structure of double-walled carbon nantotube. As shown in Figure 1, the NH_2 functional group induces local distortion along the radial direction on the tube sidewall. This distortion can be understood by the local sp^3 rehybridization of the C–N bonding.

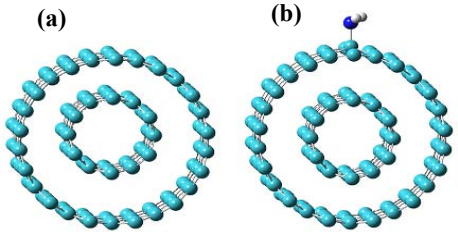

Fig 1. Optimized structure of DWCNT (a) and NH2- functionalized DWCNT (b).

Energy band structures for (6,0), (13,0), (6,0)@(13,0) and NH_2-functionalized (6,0)@(13,0) were calculated in our work and are given in Figure 2. (6,0) carbon nanotube is metal and (13,0) is semiconductor with 0.88eV gap. The result shows that in this case the DWCN become metallic. The behavior of the (6,0)@(13,0) DWCNT is explained in terms of two factors which influence its electronic conduction properties. First, the interaction between the walls of the inner and outer SWCNTs due to $2p_z$ orbitals which are perpendicular to the cylindrical walls surface, and second, the states of the inner wall fill the energy gap of outer wall. In NH_2-functionalized DWCNT the Fermi level is shifted into the valence band and new states are appeared in the top of valance band in comparison with (6,0)@(13,0) , so this functional group cause a p-type semiconductor.

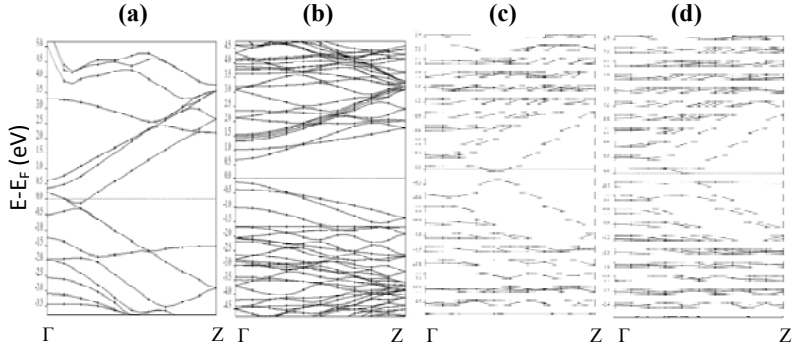

Fig 2. Electronic band structures for: (a) (6,0) SWNT; (b) (13,0) SWNT; (c) (6,0)@(13,0) DWNT and (d) (6,0)@(13,0)/NH2 DWNT. The dotted lines correspond to the Fermi energy.

Conclusion

In this essay, we elucidated electronic band structures of DWCT and DWCNT/NH2. Our calculations indicate that in DWCNT/NH2 a small gap is opened between the valence band and the conduction band and the Fermi level moves to the valance band (p-type).

References

[1] A. Charlier, E. McRae, R. Heyd, M.F. Charlier, *Carbon*, **37**, 1779 (1999).

[2] P. Giannozzi, S. Baroni, *J.Phys.:Condens.Matter*, **21**, 395502 (2009).

[3] H. J. Monkhorst. J. D. Pack. *Phys. Rev*. **B 13**, 5188 (1976).

Free Activated Energies and Kinetic Properites of Electron Transfer Studies of [R].C_n (R=Cytochrome-c peroxidase, Cytochrome-c oxidase, Tyrosinase and Ascorbate oxidase) Nanostructur Complexes

Nazanin Jahangiri and Avat(Arman)Taherpour*

Chemistry Department, Faculty of Science, Islamic Azad University,Arak Branch,P. O. Box 38135-567, Arak, Iran

E-mail: avatarman.taherpour@ gmail.com and ataherpour@ iau.-arak.ac.ir

Abstract:

This study elaborates upon the relationship between the number of carbon atoms and the four free energies of electron transfer ($\Delta G_{et(1)}$ to $\Delta G_{et(4)}$) of Cytochrome-c peroxidase, Cytochrome-c oxidase, Tyrosinase and Ascorbate oxidase, **1-4** as the most well-known enzyme molecular systems and fullerenes C_n (n=60, 70, 76, 82 and 86), on the basis of the four reduction potentials ($^{Red.}E_1$ to $^{Red.}E_4$) of the fullerenes, as assessed by applying the electron transfer(ET) equation to create [Cytochrome-c peroxidase].C_n, **A-1** to **A-5**, [Cytochrome-c oxidase].C_n, **B-1** to **B-5**, [Tyrosinase].C_n, **C-1** to **C-5** and [Ascorbate oxidase].C_n, **D-1** to **D-5**. The results were extended to calculate the four free energies of electron transfer ($\Delta G_{et(1)}$ to $\Delta G_{et(4)}$) of other supramolecular complexes of **1-4** as a class of electron-transfer species, with fullerenes C_{60} to C_{300} ([(R)].C_n, supramlecular complexes. The study also calculated the first to fourth activate free energies of electron transfer and kinetic rate constants of the electron transfers, $\Delta G^{\#}_{et(n)}$ and k_{et} (n=1-4), respectively, as assessed using the *Marcus* theory and the equations on the basis of the first to fourth reduction potentials ($^{Red.}E_1$ to $^{Red.}E_4$) of fullerenes C_n (n=60, 70, 76, 82 and 86) for the predicted supramolecular complexes [Cytochrome-c peroxidase].C_n, [Cytochrome-c oxidase].C_n, [Tyrosinase].C_n and [Ascorbate oxidase].C_n.

Keywords: Fullerenes; Cytochrome-c peroxidase; Cytochrome-c oxidase; Tyrosinase; Ascorbate oxidase; Free activation energies of electron transfer; Molecular modeling.

Introduction:

The reduction of electron transfer distance leads to an electronic communication between the electrode and redox proteins. Adsorbed proteins are available to further enzymes and thus

bioelectronic redox chains can be created. However, covalent fixation of redox proteins in an oriented arrangement on alkane thiols self-assembled on gold electrodes are only accessible to small signal molecules. This restriction is a result of the reduction of the mobility. A solution to this problem is expected from designed redox proteins and enzymes with engineered electron pathways. In this study, the number of carbon atoms in the fullerenes was used as an descriptor to establish a relationship between the structures of Cytochrome-c peroxidase, Cytochrome-c oxidase, Tyrosinase and Ascorbate oxidase, **1-4** as the most well-known enzyme molecular systems and fullerenes C_n (n=60, 70, 76, 82 and 86), which create [Cytochrome-c peroxidase].C_n, **A-1** to **A-5**, [Cytochrome-c oxidase].C_n, **B-1** to **B-5**, [Tyrosinase].C_n, **C-1** to **C-5** and [Ascorbate oxidase].C_n, **D-1** to **D-5**. The relationship between the number of carbon atoms and the free energies of electron transfer ($\Delta G_{et(n)}$, n=1-4) are assessed using the *electron transfer* (ET) equation for **A-1** to **A-5**, **B1** to **B-5**, **C-1** to **C-5** and **D-1** to **D-5** supramolecular [R].C_n (R= Cytochrome-c peroxidase, Cytochrome-c oxidase, Tyrosinase and Ascorbate oxidase) complexes in different electrochemical properties.[1-3]

Graphing and Mathematical Method:

All mathematical and graphing operations were performed using *MATLAB-7.4.0(R2007a)* and *Microsoft Office Excel-2003* programs. Using the number of carbon atoms contained within the C_n fullerenes, several valuable properties of the fullerenes can be calculated. The values were used to calculate the four free energies of electron transfer ($\Delta G_{et(1)}$ to $\Delta G_{et(4)}$), according to the ET equation for create [Cytochrome-c peroxidase].C_n, **A-1** to **A-5**, [Cytochrome-c oxidase].C_n, **B-1** to **B-5**, [Tyrosinase].C_n, **C-1** to **C-5** and [Ascorbate oxidase].C_n, **D-1** to **D-5** supramlecular nano complexes. Some of the other indices were examined, and the best results and equations for extending the physicochemical data were chosen.[4]

Discussion:

Electron transfer (ET) is one of the most important chemical processes in nature, plays a central role in many biological, physical and chemical (both organic and inorganic) systems. Solid state electronics depends on the control of the ET in semiconductors, and the new area of molecular electronics depends critically on the understanding and the control of the transfer of

electrons in and between molecules and nanostructures. The results include the four free-energies of electron transfer ($\Delta G_{et(1)}$ to $\Delta G_{et(4)}$), calculated using the electron transfer equation and $\Delta G^{\#}_{et(n)}$ as well as $k_{et(n)}$ (n=1-4) using equations of the *Marcus* theory for the supramolecular complexes. Using the number of carbon atoms (n), along with the equations of the model, one can derive sound structural relationships between the aforementioned physicochemical data. These equations allow one to calculate $\Delta G_{et(n)}$ (n=1-4), $\Delta G^{\#}_{et(n)}$ and $k_{et(n)}$ (n=1-4) for cephalosporin antibiotics, of the fullerenes (C_{60}, C_{70}, C_{76}, C_{82}, C_{86}, C_{78}, C_{84}, C_{120}, C_{132}, C_{140}, C_{146}, C_{150}, C_{160}, C_{162}, C_{240}, C_{276}, C_{288} and C_{300}). Marcus theory of electron transfer implies rather weak (<0.05eV) electronic coupling between the initial and final states and presumes that the transition state is close to the crossing point of the LE and CT terms.[1-3]

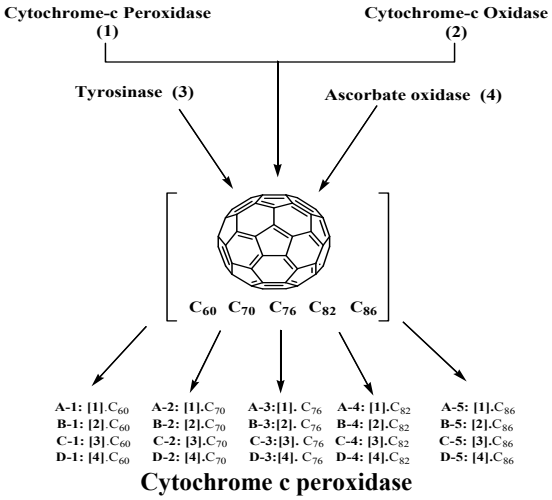

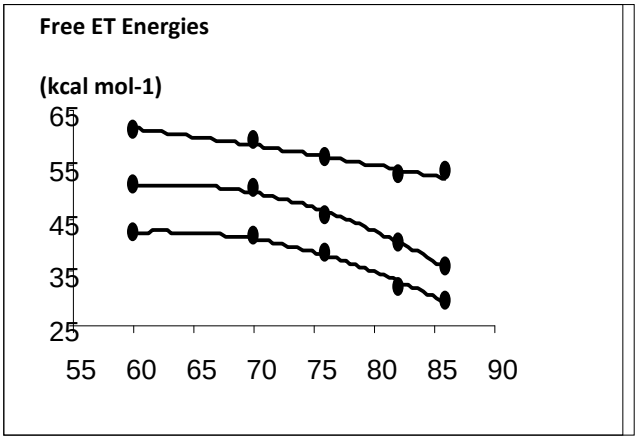

The model allows one to calculate $\Delta G_{et(n)}$ (n=1-4), $\Delta G^{\#}_{et(n)}$ and $k_{et(n)}$ (n=1-4) for the [Cytochrome-c peroxidase], [Cytochrome-c oxidase], [Tyrosinase] and [Ascorbate oxidase] of the fullerenes C_{60}, C_{70}, C_{76}, C_{82}, C_{86}, C_{78}, C_{84}, C_{120}, C_{132}, C_{140}, C_{146}, C_{150}, C_{160}, C_{162}, C_{240}, C_{276}, C_{288} and C_{300}. Using the number of carbon atoms (n), along with the equations of the model, one can derive sound structural relationships between the aforementioned physicochemical data. The novel nano supramolecular complexes discussed have neither been synthesized nor reported previously.

References:

[1] Scheller F. W., et al., Reviews in Molecular Biotechnology, 82, 411-424 (2002).

[2] Bianco, P., Taye, A., Haladjian, J., 1994. Incorporation of cytochrome c and cytochrome c3 within poly Žester-sulfonic acid. films cast on pyrolytic graphite electrodes. J. Electroanal. Chem. 377, 299.

[3] Brunori, M., Wilson, M.T., 1982. Cytochrome oxidase. Trends Biochem. Soc. 7, 295.

[4] Taherpour A. A., *Fullerenes, Nanotubes and Carbon Nanostructures*, 17(1), 26 (2009).

Preparation of NiO-CaO Nanoparticles and Its Photocatalysis Effect on Photodegradition on Acid Blue 92

Ali Reza Harifi-Mood and Helaleh Javadi Matin
Department of Chemistry, Tarbiat Moallem University, Tehran , Iran
(Email: helale_73@yahoo.com)

Keywords: Nickel oxide- Calcium oxide, Photocatalysis, Acid blue

Introduction

Semiconductor-based photo catalysis has attracted much attention due to its application in degrading organic contaminants from wastewater with solar energy in recent years [1]. Photo catalytic degradation has proven to be a promising technology for the removal of various organic pollutants in wastewater for its many attractive advantages, including the environmental friendly feature, relatively low cost and little energy consumption [2]. In this work, we contribute a new NiO–CaO photocatalyst, which is active in the photo catalytic oxidative decomposition of organic contaminants under visible-light irradiation. These NiO–CaO photocatalysts showed high catalytic activity in the oxidative decomposition of Acid Blue 92 as an organic molecule under visible-light irradiation.

Experimental Section

Synthesis and characterization of NiO–CaO photocatalysts

Aqueous solutions of Ca $(NO_3)_2$. $4H_2O$ and Ni $(NO_3)_2$. $6H_2O$ were mixed together in 1:1 molar ratio under stirring. The precipitates formed after a stoichiometric amount of NaOH was added into the above aqueous solution. The mixtures were stirred for 30 min at room temperature. Afterward, the precipitates were centrifuged, washed with de-ionized water, and dried at 100˚C in air for 2 h. The obtained powder was then calcined at 700˚C for 6 h to produce crystalline materials. The SEM image of synthesized catalyst shows an excellent morphology in nano-scale particles (Figure 1).

Photo catalytic decomposition of acid blue 92

The photo catalytic activity under visible-light irradiation of the NiO–CaO samples was evaluated by using acid blue 92(AB92) as the model substrate. 100 mL AB92 (100 mg/L)

aqueous solution buffered in different pHs and 1.0 g of photocatalyst powder were mixed in a glass photo reactor. The above solution was photo irradiated by using a 160W Xe lamp as light source under continuous stirring. At a defined time interval, the concentration of AB92 in the photocatalytic reaction was analyzed by using an UV–vis spectrophotometer.

Results and Discussion

Figure 2 shows the decrease in concentration of an aqueous AB92 solution over a 4 hours period in the presence of NiO–CaO photocatalyst. In the presence of the NiO–CaO sample, 96.5% of AB92 was photo catalytically degraded under visible-light irradiation.

One possible reason for the higher photo catalytic activity of the NiO–CaO samples is suggested by the data. Since NiO is a p-type semiconductor and CaO is an n-type semiconductor, many micro p–n junction CaO/NiO photo catalysts will be engendered at the interface of the NiO and CaO nanoparticles when CaO is doped into NiO nanoparticles. At equilibrium, an inner electric field forms that makes the NiO p-type semiconductor regions assume negative charges while the CaO regions have positive charges. Under visible-light irradiation, electron–hole pairs may be generated on the surface of the CaO n-type semiconductor.

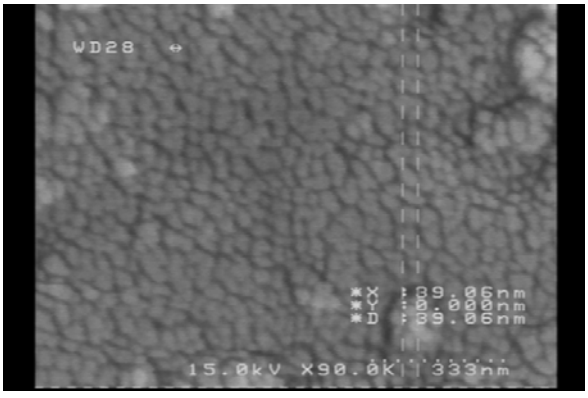

Figure 1: The SEM image of NiO–CaO particles calcined at 700˚C for 6 h.

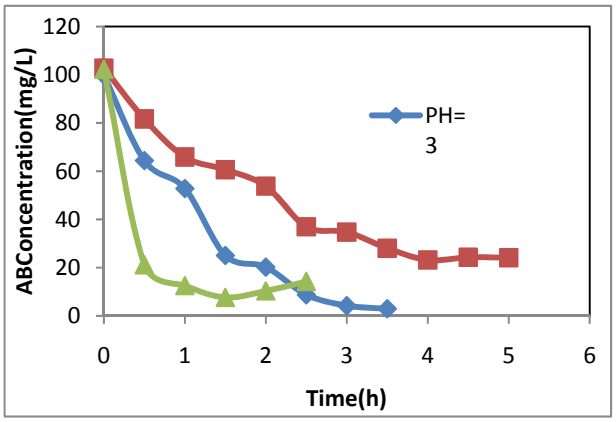

Figure 2: Degradation of AB92 under visible-light irradiation in presence of the NiO–CaO at different pHs.

References

[1] R. Asahi, T. Morikawa, T. Ohwaki, K. Aoki, Y. Taga, Science 293 (2001) 269–271.

[2] O.C. Compton, E.C. Carroll, J. Phys. Chem. C 111 (2007) 14589–14592.

Synthesis and characterization of a silicone containing vinylic monomers and its uses in the nanocomposite emulsion

Hamid Javaherian Naghash , Bahman johari, Monireh Mohammad Salehi Darani

Department of Chemistry, Islamic Azad University, Shahreza, Shahreza, Iran

E-mail: Javaherian @ iaush.ac.ir

E-mail:Bahmanjohari2010@yahoo.com

Introduction:

Silicone-acrylate emulsion have been widely used as adhesives, architectural coatings, textile coatings, and hide finishes because of its various advantages, such as good film forming property; high adhesive strength; resistance to high and low temperature, chemicals, water, weather, ultraviolet; and anticontamination [1–8]. However, the application of silicone–acrylate emulsion was limited because the price of silicone was high. The Polymer/Layered Silicate (PLS) nanocomposite have drawn much research attention because they effectuate in improving material properties by the presence of a small amount of layered silicate, and promise superior or unique properties in comparison with those of the conventional polymer composites, including increased modulus, decreased thermal expansion coefficient, increased heat distortion temperature, reduced gas permeability , better fire-retardant properties, enhanced ionic conductivity, low flammability, increased solvent resistance, lower material cost, and the ease of preparation and processing. PLS nanocomposite can be prepared in four main ways: solution intercalation, in situ intercalative polymerization, melts interaction, and template synthesis. montmorillonite (MMT) was a kind of layered silicate, which was used usually. It has been particularly important in forming effective polymer nanocomposite. It belongs to a smectite group of clay minerals that has 2:1 type of layer structure, in which a central alumina octahedral sheet is sandwiched between two silica tetrahedral sheets. Polyacrylate/OMMT nanocomposites being made by the in situ polymerization route have been reported, and the properties have been substantially enhanced. PLS nanocomposite was actively studied. However, there has been few studies on the PLS nanocomposite emulsion. In this article, we prepared the poly (silicone-co-crylate)/montmorillonite nanocomposite emulsion with different OMMT contents (0, 0.5, 1.0, 1.5 and 2 wt %) and organosilicone (1.50, 3.0 and 5.0 wt %) via in situ intercalative

polymerization, and investigated the properties of nanocomposite emulsion and the influence of different contents of OMMT and organosilicone on the nanocomposite emulsion.

Experimental:

1- Preparation of OMMT

The required weights of MMT and distilled water were put into a three-necked flask. Sodium silicate was added to adjust pH to 11. The mixture was allowed stand for 1 day after stirring for 4 h, at room temperature. The supernatant of the mixture was subsequently poured into another flask, and followed by addition of the required weights of CTAB. The blend was heated up to 90 °C and stirred at the same temperature for 2 h. After that, the blend was washed using distilled water to make it free from bromide ions and filtrated with pump down. Finally, the resultant was dried in a vacuum oven and ground to 300 meshes.

2- Preparation of emulsion

The given weights of BA, MMA, MAA, and OMMT were premixed for 1 day to get mixture I. Initiator was dissolved in distilled water to make 10 % of solution. Two-thirds of the required weights of distilled water, emulsifier, and total protective colloid and buffer agent were put into a dried three-necked flask equipped with a stirrer, a thermometer, and a condenser. The mixture was heated to 52 °C, then, the mixture I was added into the flask. The blend was stirred vigorously at 52–55 °C for 10 min to obtain preemulsion. 1/8 of the preemulsion were taken into another flask and heated to 75 °C. Then, 1/3 of given amounts of initiator solution, emulsifier and distilled water were added to the flask. The blend was reacted for 30 min and a seed emulsion was obtained. Two-thirds of initiator solution was added to remaining 7/8 of the preemulsion. The preemulsion with initiator and MEPMHSE were, respectively, dropped into the seed emulsion at the same time in about 2 h, and kept at 75 °C for another 2 h. Then, the system was heated up to (81±1) °C and maintained at this temperature for 1.5 h. Finally, a kind of white fluid poly (silicone-co-acrylate)/ montmorillonite nanocomposite emulsion was obtained.

3-Synthesis of silicone containing acrylic monomer (MEPMHSE)

In a 50 ml three–necked round bottom flask which was dried, purged with nitrogen, equipped with a reflux condenser, a dropping funnel and nitrogen inlet, 10 g (4.42 mmol)

polymethylhydrosiloxane (PMHS), 10 ml benzene and 2 ml triethylamine (TEA) were taken. To this, 0.60 g (4.42 mmol) 2-hydroxyethyl methacrylate (HEMA) was added drop-wise maintaining temperature at 70 °C under nitrogen atmosphere. After complete addition, the reaction mixture was maintained at 70 °C for 3 h and then 1 h under stirring at room temperature. Use of TEA promotes the desirable condensation between polymethylhydrosiloxane -H and 2-hydroxyethyl methacrylate-OH and avoids the self-condensation of silicone intermediates. The viscous crude product was recovered after removing the solvent using an evaporator and the residue was finally dried in a vacuum at 25 °C. The final product was viscous white oil. Yield = 7 g, 66 %. The reaction path is given in Scheme 1.

Result and discution:

A new silicone containing acrylic monomer, methacryloxyethyl polymethylhydrosiloxane ether (MEPMHSE), based on polymethylhydrosiloxane (PMHS) and 2-hydroxyethyl methacrylate (HEMA) has been synthesized for formulation of nanocomposite emulsion. Then Poly (silicone-co-acrylate)/montmorillonite (PSAM) /nanocomposite emulsion were prepared by in situ intercalative emulsion polymerization of methyl methacrylate (MMA), butyl acrylate (BA), methacrylic acid (MAA) and MEPMHSE, in the presence of organic modified montmorillonite (OMMT) with different OMMT contents (0, 0.5, 1.0, 1.5 and 2 wt %). It is evident that the properties of silicone–acrylate emulsion were improved by the intercalative polymerization of acrylate and silicone in the presence of OMMT. The property of nanocomposite emulsion containing 1 wt % OMMT was the best one, and the following advantages were obtained: smaller particle size, faster drying speed, smaller surface tension, and improved resistance to water by the incorporation of OMMT.

References

[1] S.Q. Huang, H. Peng, H. Huang, S.B. Li, New Chem. Materials 9 (1997) 22.
[2] W.S. Ma, J.H. He, Z.Y. Ou, H.M. Pan, Paint Coat. Ind. 4 (2003) 1.
[3] J. Wang, F.X. Chu, China Adhesives 5 (2003) 52.
[4] H.J. Naghash, A. Karimzadeh, A.R. Massah, J. Appl. Polym. Sci. 112 (2009) 1037.
[5] H.J. Naghash, S. Mallakpour, P.Y. Forushani, N. Uyanik, Polymer (Korea), 32 (2008) 95.

[6] H.J. Naghash, A. Karimzadeh, A.R. Momeni, A.R. Massah, H. Aliyan, Turk. J. Chem. 31 (2007) 257.

[7] H.J. Naghash, S. Mallakpour, N. Mokhtarian, Prog. Org. Coat. 55 (2006) 375.

[8] H.J. Naghash, S. Mallakpour, N. Kayhan, Iran. Polym. J. 14 (2005) 211.

Influence of the Gas Flow and Growth Time on Multi-Walled Carbon Nanotube Synthesis by HFCVD

Ramin Cheraghali[a], Mahmood Ghoranneviss[b], Shahram Moradi[c]

[a]*Faculty of Science, Islamic Azad University-Saveh Branch*

Ramincheraghali@yahoo.com

[b] *Plasma Physics Research Centre, Science and Research Branch, Islamic Azad University, Tehran*

[a] *Department of Chemistry, Tehran North Branch, Islamic Azad University, Tehran*

Abstract:

The effect of gas flow and time of growth on different stages in the deposition process occurring during carbon nanotube deposition on steel substrates in the HFCVD technique has been investigated. For characterization of the deposit, Raman spectroscopy has been used to explore the composition of the MWCNT films grown under different mixtures of C2H2 and H2.

In addition, the morphology and microstructure of the MWCNTs were examined by scanning electron microscopy (SEM). The results showed that the optimum relative flow rate of hydrocarbon to Hydrogen is 0.01 *(*C_2H_2/H_2 = 1/100). We observed the best time for growth of multiwalled carbon nanotubes with a better structure is 10 min, but at longer time, the amount of impurities increased.

Keywords: Gas flow, Growth time, Carbon nanotube, HFCVD

References:

[1] Ijima. S., "Helical microtubules of graphite carbon", Nature, 354,56-8(1991).

[2] Peng. X. H., Chang. L., Hui. M. C., "Purification of carbon nanotubes", Carbon 46, 2003 –2025, (2008).

[3] Chen. M. L., Hong. B. C., Yu. P. L., Hong. B. X., Yi. Z., "The effect of electrolytic oxidation on the electrochemical properties of multi-walled carbon nanotubes", *Carbon*, 44, 2919–2924(2006).

Nano bio-glass as an antibacterial compound against multi drug resistant Pseudomonas aeruginosa

Forough Hafezi[3], Abbas ali Imani Fooladi[2], Afsaneh Amiri[3], Fatemeh Hosseinnejad[3], Farideh Rahmani[4] and Mohammad Reza Nourani[1*]

1. *Chemical injury Research Center, Baqiyatallah medical Sciences University Tehran, Iran.*
2. *Molecular Biology Research Center, Baqiyatallah medical Sciences University Tehran, Iran*
3. *Department of Chemistry, Islamic Azad University, Central Tehran Branch, Tehran, Iran*
4. *Department of Microbiology, Islamic Azad University, Zanjan, Iran*

** Corresponding author: Mohammad reza Nourani Email: r.nourani@yahoo.com*

Key words: Antibacterial activity, Pseudomonas aeruginosa,Bioactive glass,Nanopowder

Introduction

Bioactive materials are defined as materials eliciting a specific biological response at the interface of the material and tissue, resulting in the formation of a bond between them [1].Over the past decades, bioactive glass has played a central role in the bone regeneration field, due to its excellent bioactivity, osteoconductivity, and even osteoinductivity and the biomaterial component is a critical determinant of the ultimate success of the tissue engineered graft[2]. Biocompatible, tissue-bonding bioactive glasses (BAGs) were first introduced in the early 1970s [*3*]. The aim of this work was to evaluate the antibacterial effect of bioactive glass nanopowders. The antibacterial activity was studied using multi drug Pseudomonas aeruginosa[4].

Materials and methods

In this study nanopowders of bioactive glass (BG) were synthesized and Bioglass/Gelatin nanocomposite scaffold was made through Sol-Gel.[5,6] The chemical compositions of the prepared samples were as predicted, and the particle size of the samples with an amorphous structure mainly ranged over 20–90 nm. Then antibacterial effects of bioactive glass nanoparticles on Pseudomonas aeruginosa were determined by Minimum Inhibitory Concentration (MIC) and Minimum Bacterial Concentration (MBC) method[7].MIC is the

smallest concentration of an antimicrobial agent that inhibits the growth of bacteria. MBC The is the lowest concentration of antibiotic required to kill the germ.

Results and discussion

The resulting bioactive glass nano powder was analyzed by X-ray diffraction (XRD) with Siemens-Brucker D5000 diffractometer (Germany). The XRD analysis showed that the synthesized nano powder had an amorphous structure.The result of MIC and MBC showed that

The bioactive glass nano powder was inhibited growth of multi drug resistant Pseudomonas aeruginosa.

Conclusions

The bioactive glass Nano-powder revealed the high antibacterial activity. Therefore it is a convenience candidate for fabrication of bio-implant scaffolds and prevents super infection after implantation

References

[1] L. L. Hench And Ö. Andersson, in "An Introduction to Bioceramics" (World Scientific Publishing Co, Singapore, 1993) p. 41

[2] Sachlos E. and Caernuszka JT. (2003) European Cells and Materials 5: 29-40.

[3] L. L. Hench , H. A. Paschall, J. Biomed. Mater. Res. **7** (1973) 25

[4]V. Mortazavi, M. Mehdikhani Nahrkhalaji, M. H. Fathi, S. B. Mousavi, B. Nasr Esfahani,(2010)journal of Biomedical Materials Research Part A94,pages160-168.

[5] H. Lu, Saadiq F. El-Amin,1 Kimberli D. Scott,1 Cato T, 2003 Wiley Periodicals, Inc. J Biomed Mater Res 64A: 465–474, 2003

[6] Hae-Won Kim, Hyoun-Ee Kim, and Jonathan C. Knowles. Adv. Funct. Mater. 2006, 16, 1529–1535

[7] J. Biosci., Vol. 10, Number 1, March 1986, pp. 137-144.

Preparation and characterization of cupper sulfide nanoparticles in presence of [EMIM][$EtSO_4$] by a simple refluxing method

A. Habibi-Yangjeh[1*], V. Taghvaei[1], M. Behboudnia[2]

[1]*Department of Chemistry, University of Mohaghegh Ardabili, P.O. Box 179, Ardabil, Iran. (Email: ahabibi@uma.ac.ir)*

[2]*Department of Physics, Urmia University of Technology, P.O. Box 57155-419, Urmia, Iran.*

Key words: Nanoparticles, Room-temperature ionic liquid, Cupper sulfide, Adsorption.

Introduction

Semiconductor particles with nano-scales have drawn considerable interest in recent years, because of their special properties, such as large surface-to-volume ratio, increased activity, special electronic properties and unique optical properties as compared to those of the bulk materials. As an important p-type semiconductor, copper sulfide (CuS), as an important member of the semiconductor family, exhibits many interesting properties and has great potential in a versatile range of applications such as cathode material of lithium batteries, nanometer-scale switches solar controller and solar radiation absorber, nonlinear optical material, and catalyst [1]. From a combination of organic cations and various anions, room-temperature ionic liquids (RTILs) are obtained. RTILs with various interesting properties have received much attention in preparation of various nanomaterials [2-4].

1-Ethyl-3-methylimidazolium ethyl sulfate ([EMIM][$EtSO_4$]) is a novel RTIL with potential industrial applications. For this reason, in continuing our investigations about nanomaterials [2-5], refluxing method as a simple and low temperature technique was applied for preparation of CuS nanoparticles in presence of [EMIM][$EtSO_4$] and their properties was investigated.

Experimental

The X-ray diffraction (XRD) patterns were recorded on Philips Xpert X-ray diffractometer with Cu Kα radiation (λ= 0.15406 nm). Surface morphology and distribution of particles were studied *via* LEO 1430VP scanning electron microscope (SEM). The purity and elemental analysis of the products were obtained by energy dispersive analysis of X-rays (EDX) on the same LEO 1430VP instrument. In typical synthesis procedures, cupper acetate monohydrate

(5.16 g) was dissolved in 50 ml of aqueous solution of the RTIL (1:1 in volume) under stirring at room temperature. Also, 1.95 g of TAA was dissolved slowly in the solution under magnetic stirring. The solution was refluxed at approximately 95 °C for 60 min. The formed suspension was centrifuged and washed three times with double distilled water and ethanol and dried in an oven at 50 °C for 24 h.

Results and discussion

To investigate the effect of solvent on properties of the nanoparticles, parallel experiments were carried out. The preparation procedures were similar to each other, except for changes in the solvent. The diffraction peaks are corresponding to (101), (102), (103), (110), (108), and (116) planes of hexagonal type CuS crystal system (JCPDS reference code: 6-465). The XRD patterns demonstrate that mean particles size of the nanoparticles prepared in presence of the RTIL is smaller than the prepared sample in water. The purity and composition of the products were studied by energy dispersive X-ray spectroscopy (EDX). The average atomic percentage ratio of Cu:S is 47.2:52.8 and 45.5:54.5 for the particles prepared in water and aqueous solution of the RTIL, respectively. Morphology of the nanoparticles was investigated by scanning electron microscope (SEM). The results demonstrate that grain size of the samples produced in water is larger than the prepared sample in water. Although the nanoparticles are agglomerating, however the boundaries between single crystallites are clearly observable. In order to compare ability of the prepared nanoparticles for adsorption of MB molecules, adsorption capacity (Q_e) of the prepared samples was calculated by 60 minutes adsorption in dark [6]. The values of Q_e for the nanoparticles prepared in water and aqueous solution of the RTIL are 3.40×10^{-6} and 6.11×10^{-6} mol/g, respectively. Increasing adsorption capacity for the prepared nanoparticles in presence of the RTIL can be attributed to higher surface area of the nanoparticles due to lower aggregation and smaller grain sizes. When aqueous solutions of the RTIL are used as a reaction medium, the solutes are solvated by ions; thus, the reactions proceeds in an environmentally different from that water or ordinary organic solvents are used. Hydrogen-bonding and electrostatic interactions between imidazolum ring of the RTIL and sulfide moiety of CuS can greatly inhibit growth of the nanoparticles. Then, these interactions playing a crucial role in formation of small sized and low aggregated nanomaterials.

References:

[1] K. J. Wang, G. D. Li, J. X. Li, Q. Wang, J. S. Chen, Cryst. Growth Des. 7, 2265 (2007).

[2] M. Esmaili, A. Habibi-Yangjeh, J. Alloys Compd. 496, 650 (2010).

[3] V. Taghvaei, A. Habibi-Yangjeh, M. Behboudnia, J. Iran. Chem. Soc. 7, S175 (2010).

[4] M. Barzegar, A. Habibi-Yangjeh, M. Behboudnia, J. Phys. Chem. Solids 70, 1353 (2009).

[5] F. Jafari-Zare, A. Habibi-Yangjeh, Chin. J. Chem. 28, 349 (2010).

Theoretical Study on the Influence of Carbon Nanotubes in Cp_2ZrCl_2-Based Ethylene Polymerization

H. Hajiabadi*[a], A. Nowroozi[a], M. Hassani[a]

[a]*Department of Chemistry, Faculty of Science, University of Sistan and Baluchestan*

Haji309@gmail.com :*Email*

Ethylene polymerizationis one of the most important large-scale industryprocesses, where a variety of different transition metalcomplexes is used to produce high-quality commercialproducts [1-3].Group 4-based, homogeneous single-site catalysts showhighly catalytic activity for olefin polymerization [4,5]. Due to the unique mechanical, electrical, thermal, andoptical properties, carbon nanotubes (CNTs) have beeninvestigated for CNT/polymer composites, nanoelectronics,electron field emitters, chemical sensors, and other applications[6,7].In addition, because CNTs show a good electronmobility and have a very large steric bulkiness, they can be agood candidate as a ligand that tunes the reactivity of metalcatalyzedreactions electronically and sterically. It has been reported that catalyticbehavior of Cp_2ZrCl_2 in ethylene polymerization, where Cp is cyclopentadiene, can be modified by using multiwall carbon nanotubes (MWCNTs) [8]. In this case, Cp rings intimately interacted with the sidewalls ofMWCNTs. In this work, we investigatedsingle wall carbon nanotubes (SWCNTs) interaction withCp_2ZrCl_2catalyst and influence of such interaction in ethylene polymerizationby quantum chemistry methods.Structures of solo zirconocene based catalyst and CNT aided ones in different steps of ethylene polymerization reaction were optimized by Density Function Theory (DFT) [9,10] computations and their catalytic behavior were compared in term of energetic, steric and electronic properties. Our results reveal that interaction between CNT and catalyst results in improve catalyst activity and also led to larger polyethylene molecular weight (MW).

Keywords: Ethylene Polymerization, Cp_2ZrCl_2, Single Wall Carbon Nanotubes (SWCNTs), Density Function Theory (DFT).

References:

[1] Brintzinger, H. H.; Fischer, D.; Mu¨ llhaupt, R.; Rieger, B.; Waymouth, R. M. Angew. Chem., Int. Ed. Engl. 1995, 34, 1143.

[2] Allen, G. Comprehensive Polymer Science, 1st ed.; PergamonPress: Oxford, 1989; Vol. 4.

[3] McKnight, A. L.; Waymouth, R. M. Chem. Rev. 1998, 98, 2587-2598.

[4] L. Resconi, L.Cavallo, A. Fait, F. Piemontesi, Chem. Rev. 2000, 100, 1253.

[5] H. G. Alt, A. Ko¨ppl, Chem. Rev. 2000, 100, 1205.

[6] P. M. Ajayan, Chem. Rev. 1999, 99, 1787.

[7] M. Quyang, J.-L. Huang, C. M. Lieber, Acc. Chem. Res.2002, 35, 1018.

[8] Sungjin Park, SeungWoong Yoon, Kyung-Bok Lee, Dong Jin Kim, Young Hwan Jung, YoungkyuDo,Hyun-jong Paik,Insung S. Choi.,Macromol. Rapid Commun. 2006, 27, 47–50.

[9] Hohenberg, P.; Kohn, W. Phys. ReV. 1964, 136, B864.

[10] Kohn, W.; Sham, L. J. Phys. ReV. 1965, 140, A1133.

Carbon Nanotubes as a ligand in Titanium based Ethylene Polymerization; anAb initio Study

H. Hajiabadi[a], A. Nowroozi[a], S. H. M.Moghaddam[b]

[a]*Department of Chemistry, Faculty of Science, University of Sistan and Baluchestan*

Haji309@gmail.com :*Email*

[b]*Iran Polymer and Petrochemical Institute, P.O. Box: 14965/115, Tehran, Iran*

Single-site polyolefin catalysts, i.e., titanium based catalyst, combined with methylaluminoxane (MAO) as a cocatalyst have been the subject of intense research [1-3]. These systems efficiently catalyze α-olefin polymerization and the ligands at the transition metal center provide the possibility to tailor polymer properties such as molecular weight, molecular weight distribution, and stereoregularity [4, 5].Due to the unique mechanical, electrical, thermal, andoptical properties, carbon nanotubes (CNTs) have beeninvestigated for CNT/polymer composites, nanoelectronics,electron field emitters, chemical sensors, and other applications [6,7].In addition, because CNTs show a good electronmobility and have a very large steric bulkiness, they can be agood candidate as a ligand that tunes the reactivity of metalcatalyzedreactions electronically and sterically. It has been reported that catalytic behavior of Group 4-based catalyst in ethylene polymerization can be modified by using multiwall carbon nanotubes (MWCNTs) [8]. In this case, Cp rings intimately interacted with the sidewalls ofMWCNTs. In this work, we investigated single wall carbon nanotubes (SWCNTs) interaction with Cp_2TiCl_2catalyst, where Cp is cyclopentadiene. Influence of such interaction in ethylene polymerization has been analyzed by quantum chemistry methods. Structures of solo titanium based catalyst and CNT aided ones in different steps of ethylene polymerization reaction were optimized by Density Function Theory (DFT) [9,10] computations and their catalytic behavior were compared in term of energetic, steric and electronic properties. Our results reveal that interaction between CNT and catalyst results in improve catalyst activity and also led to polyethylene with larger molecular weight (MW).

Keywords: Ethylene Polymerization, Cp_2TiCl_2, Single Wall Carbon Nanotubes (MWCNTs), Density Function Theory (DFT).

References:

[1]Chien, J. C.; Dawei, H. J. Polym. Sci., Part A: Polym. Chem.1991, 29, 1609.

[2] Kaminsky, W.; Miri, M.; Sinn, H.; Woldt, R. Makromol. Chem. Rapid Commun. 1983, 4, 417.

[3] Ewen, J. A. J. Am. Chem. Soc. 1984, 106, 6355.

[4] Chien, J. C.; Dawei, H. J. Polym. Sci., Part A: Polym. Chem.1991, 29, 1585.

[5] Uozumi, T.; Soga, K. Makromol. Chem. 1992, 193, 823.

[6] P. M. Ajayan, Chem. Rev. 1999, 99, 1787.

[7] M. Quyang, J.-L. Huang, C. M. Lieber, Acc. Chem. Res.2002, 35, 1018.

[8] Sungjin Park, SeungWoong Yoon, Kyung-Bok Lee, Dong Jin Kim, Young Hwan Jung, YoungkyuDo,Hyun-jong Paik,Insung S. Choi.,Macromol. Rapid Commun. 2006, 27, 47–50.

[9] Hohenberg, P.; Kohn, W. Phys. ReV. 1964, 136, B864.

[10] Kohn, W.; Sham, L. J. Phys. ReV. 1965, 140, A1133.

Fabrication, Characterization, and Measurement of Optical Properties of Zirconia Nanoparticles

M. Hadadian and E. K. Goharshadi
Dept. of Chemistry, Ferdowsi University of Mashhad, Mashhad 91779, Iran
Email: m.hadadian@ymail.com

Introduction

Zirconia , ZrO_2, is a widely used ceramic material exhibiting excellent properties such as low thermal conductivity, high coefficient of thermal expansion, high thermal stability, high oxygen ion conductivity, high strength, high fracture toughness and high thermal shock resistance enabling it to be used as thermal barrier coating, cutting tools, refractory material, as catalyst/catalyst support [1]. The crystal phases of zirconia can be classified as three kinds: monoclinic, tetragonal and cubic. It has been proved that toughness of zirconia will increase if phase transformation from tetragonal to monoclinic zirconia occurs [2]. Many properties of nanocrystalline zirconia are fundamentally different from those of conventional micrometer-sized zirconia because of the small crystallite dimension. They exhibit increased strength and ductility, enhanced diffusivity, and increased edges and corners, all beneficial for applications in catalysis, electronics, and ceramics [3].

Nano-sized zirconia have been prepared using various methods including sol-gel, precipitation, hydrothermal methods, gas phase synthesis, microwave, sonochemical, and microemulsion methods.

The purpose of the present study is to fabricate zirconia nanopowders via a versatile, clean, and non-toxic method based on microwave irradiation process. The nanoparticles have been characterized by X-ray diffraction (XRD), Fourier transform infrared spectroscopy and ultraviolet-visible spectroscopy (UV). The optical properties of prepared nanoparticles have been studied as well.

Results and Discussion

The XRD pattern of the synthesized zirconia nanoparticles is shown in figure 1. The diffractogram reveals the formation of highly crystalline product with high phase purity. The diffraction pattern confirms that monoclinic zirconia was purely formed. The average grain

particle size of zirconia calculated from the full width at half-maximum of the peak using well-known Debye Scherrer's equation is about 20 nm.

The optical responses of the zirconia nanoparticles dispersed in ethanol have been investigated via UV-vis absorption spectroscopy. The band gap energy of 4.83 eV was calculated using the UV-vis spectrum.

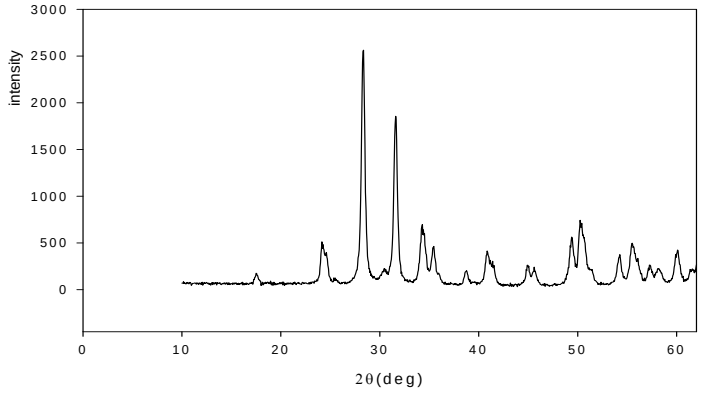

Figure 1. The XRD of zirconia nanoparticles

Conclusion

Ziconia nanoparticles were fabricated via a simple but efficient route and its optical band gap was measured as well.

References

[1] N. Chandra, D. K. Singh, M. Sharma, R. K. Upadhyay, S.S. Amritphale, S.K. Sanghi; *J. Colloid & Interface Sci.* **342** (2010) 327–332.

[2] J. Zhang, B. Song,W. Peng,Y. Feng, B. Xu; *Mater. Chem. Phys.***123** (2010) 606–609.

[3] Y. Cong, B. Li, S. Yue, D.Fan; *J. Phys. Chem. C* **113**(2009) 13974–13978

SiC nanotubes: a novel materials for oxygen adsorption

M. D. Ganji *, M. Hesami and B. Ahaz
Department of Chemistry, Islamic Azad University, Ghaemshahr Branch, Mazandaran, Iran
* Corresponding author: E-mail: ganji_md@yahoo.com Tel: 911 113 7150.

Keywords: Adsorption; Oxygen molecule; DFT; SiCNTs; CNTs; Sensors

Introduction

There is a strong interest in gas adsorption by carbon nanotubes [1]. Sensitivity of their electronic properties to oxygen exposure can be used as the basis for a chemical sensor. Recent experimental data [2] have shown that the transport properties of single-wall nanotubes (SWNT) change dramatically upon exposure to gas molecules such as O_2, NO_2, NH_3, and many other gases, at ambient temperature. Practical applications to the production of better gas sensors (‘‘thermoelectric nano-nose’’) have been envisioned [2]. A recent quantum chemistry calculation at the MP2 level [3] founds very weak binding, due to physisorption, and minimal charge transfer. SiCNTs are considered to have the advantages over CNTs because they may possess high reactivity of exterior surface facilitating to sidewall decoration and stability against oxidation in air at high temperature [4] which may have potential applications in nanoelectronic devices. In this work, we investigate the interaction of a single O_2 molecule with SWSiCNTs using first-principles simulations.

Computational method

We have performed *ab initio* calculations based on the generalized gradient approximation (GGA) with the Perdew–Burke–Ernzerhof (PBE) functional [5] in density functional theory and the standard norm-conserving Troullier–Martins pseudo-potentials [6]. The calculations are done using a split-valence double-zeta plus polarization function (DZP) as basis set.

Results and discussions

We have considered a zigzag (5, 0) SiCNT which consists of alternating C and Si atoms, as depicted in figure 1. The calculated average Si–C bond length of these tubes is about 1.819 Å in agreement with the theoretical results [7]. Several possible configurations were selected for

the approaching molecule to the wall of the tube as represented in figure 1. To find the approximate stable adsorption configuration, the structure of the tube and the O–O bond lengths (1.228 Å) of the O_2 molecule were fixed, while the distance between the tube and the molecule was varied, to obtain the system energy as a function of the separation. Figure 2 shows the calculated adsorption energy (binding energy) of the considered systems. The binding energy is calculated from: $E_b = E_{NT\text{-}O2} - E_{NT} - E_{O2}$ where $E_{NT\text{-}O2}$, E_{NT} and E_{O2} are the total energies of the tube with an adsorbed O_2 molecule, the pure nanotube and the O_2 molecule, respectively.

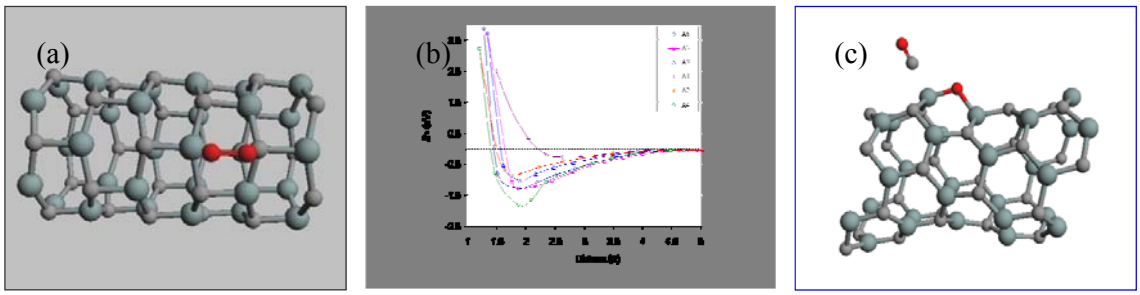

Figure 1. (a) Atomistic configuration of adsorbed O_2 molecule on the SiCNT. (b) Binding energy of an oxygen molecule as a function of the separation distance of the closest oxygen atom to the outer side-wall of the (5, 0) SiCNT. (c) The optimized geometric structure of most stable state of SiCNT/O_2 system

The most stable configuration of O_2 is the parallel approach of the O_2 molecule to the (5, 0) SiC nanotube wall on the center of a hexagon of Si and C atoms. After full structural optimization of the most stable systems we found that the adsorption of O_2 on the SiC nanotubes, results in a distortion of the tube structure (Fig. 1 (c)). The calculated binding energy E_b and average Si–O equilibrium distance, after optimization, are about -38.22 eV (-881.57 kcal/mol) and 1.698 Å**,** respectively.

Conclusion

First-principles calculations predicted that the O_2 adsorptive capability of silicon carbide nanotube is much stronger than that of carbon nanotubes. This might have potential for gas detection and energy storage.

References

[1] H.J. Liu, J.P. Zhai, C.T. Chan and Z.K. Tang, Nanotechnology18 (2007) 065704.

[2] P.G. Collins, K. Bradley, M. Ishigami and A. Zettl, Science 287 (2000) 1801.

[3] J. Zhao, A. Buldum, J. Han, and J. P. Lu, Nanotechnology 13 (2002) 195.

[4] X.H. Sun, C.P. Li, W.K. Wong, N.B. Wong, C.S. Lee, S.T. Lee, B.K. Teo, J. Am. Chem. Soc. 124 (2002) 14464.

[5] J.P. Perdew, K. Burke, M. Ernzerhof, Phys. Rev. Lett. 77 (1996) 3865.

[6] N. Troullier, J.L. Martins, Phys. Rev. B 43 (1991) 1993.

[7] M. Zhao, Y. Xia, F. Li, R.Q. Zhang, S.-T. Lee, Phys. Rev. B 71 (2005) 085312.

Multi drug resistant Staphylococcus aureus inhibited by nano bio-glass powder

Fatemeh Hosseinnejad[3], Mohammad Reza Nourani[1] , Afsaneh Amiri[3], Forough Hafezi[3], ,Farideh Rahmani[4], and Abbas ali Imani Fooladi[2*]

1.Chemical injury Research Center, Baqiyatallah medical Sciences University Tehran, Iran

2.Molecular Biology Research Center, Baqiyatallah medical Sciences University Tehran, Iran

3.Department of Chemistry, Islamic Azad University, Central Tehran Branch, Tehran, Iran

4.Department of Microbiology, Islamic Azad University, Zanjan, Iran

** Corresponding author: Abbas ali Imani Fooladi Email: imanifouladi.a@gmail.com*

Key words: Antibacterial activity, Staphylococcus aureus, Nano Bio-glass

Introduction

Biodegradable polymer/bioactive glass (BG) composites in the form of scaffolds and membranes have been intensively studied because of their good biocompatibility and bioactivity as hard tissue regeneration materials[1].Bioactive silicate glasses (e.g. 45S5 BioglassR) with compositions in the system SiO2- Na2O-CaO-P2O5, having <55% SiO2 were discovered [2]. The chemical compositions of the prepared samples were as predicted, and the particle size of the samples with an amorphous structure mainly ranged over 20–90 nm.

recently studied offer remarkable advantages as the inorganic components of composite scaffolds due to their high bioactivity index (Class A), and their ability to bond to both soft and hard connective tissues. Class A bioactive materials are osteogenetic and osteoconductive materials while Class B bioactive materials (such as hydroxyapatite) exhibit only osteoconductivity.[2]

Certain bioactive glasses have been shown to exhibit antibacterial activity. The aim of this work was to evaluate the antibacterial effect of against the one of the most resistant bacteria Staphylococcus aureus by bioactive glass nanopowders. [3]

Materials and methods

The composition of the studied bioactive glass belongs to the system SiO2-CaO-P2O5, Bioactive glass nano-powders were prepared using the sol-gel method. The prepared

nanopowders mainly ranged between 20 and 90 nm in size. Antibacterial effects of sol-gel-derived bioactive glass nanoparticle on standard and clinical multi drug resistant Staphylococcus aureus determined by MIC and MBC methods.

Result and discussion

We found the antibacterial activity of bioactive glass in this study and This may result from one of the surface reactions. Particulate Bioglass is one example to exert a considerable antibacterial effect on standard and clinical multi drug resistant Staphylococcus aureus bacteria.

Conclusion

The bioactive glass nano-powders showed the high antibacterial activity; therefore bioactive glass should be a suitable candidate for bio-implant scaffolds and prevent secondary infection after implantation.

References

[1] M. Saleh Dadash1, M. Nasr Esfahany, R. Ebrahimi, S. Karbasi , H. Vali, A Comparative Study on Mechanical and Adhesion Properties of Calcinated and Non Calcinated Nanobioglass-Titania Nano Composite Coatings on Stainless Steel Substrates, Sharif University of Technology, June 2010,scientia iranica

[2] Q. Chen, J. A. Roether and A. R. Boccaccini*, Tissue Engineering Scaffolds from Bioactive Glass and Composite Materials, Topics in Tissue Engineering, Vol. 4. Eds. N Ashammakhi, R Reis, F Chiellini © 2008.

[3] V. Mortazavi, M. Mehdikhani Nahrkhalaji, M. H. Fathi, S. B. Mousavi, B. Nasr Esfahani, Antibacterial effects of sol-gel-derived bioactive glass nanoparticle on aerobic bacteria, Published online, February 2010 in Wiley InterScience.

Adsorption of Methane on Single-walled Silicon Carbide Nanotube

Z. B. Nojini[a*], M. Haghbayan[a], N. Abbasi[a]
[a]Department of Chemistry, Faculty of Science, Shahid Chamran University, Ahvaz, Iran
E-mail:maryam.haghbayan@gmail.com

Abstract

The adsorption of CH_4 molecule on the (4, 4) single wall silicon carbide nanotube, was investigated. Several possible adsorption sites in the tube have been considered. Results show that when CH_4 adsorb through $-CH_3$ groups on the T_1 site, has minimum adsorption energy.

Keywords: SiCNT, Adsorption energy, DFT, Methane.

Introduction

Many researches are interested in the adsorption of methane, which is a major component of natural gas. In addition, due to the very high pressure used in compressed natural gas (CNG) storage, adsorption storage of natural gas is an attractive subject [1]. The recently synthesized silicon carbide nanotube (SiCNT) has been found to be a semiconducting material of great technological interest for devices designed to operate at high temperatures, high power, and harsh environment. SiCNTs have also proven useful for hydrogen storage, since the binding energy of the tubes with hydrogen molecules are 20% larger than that of CNTs [2].

Methodology

The adsorption of methane on (4, 4) SiCNT was studied using density functional theory employing MPW1PW91/6-31G basis set with periodic boundary condition**.** CH_4 molecule per unit cell in the tube axis direction was used. In this case the cell length is 3.1 Å. The molecular binding energy; E_b was obtained using the following expression:

$$E_b=E_{NT+Methane}-(E_{NT}+E_{Methane}) \quad (1)$$

where E_{NT}, $E_{NT+Methane}$ and $E_{Methane}$ are the total energies of a free nanotube, nanotube with methane and a single methane molecule respectively.

Results and discussion

To examine the adsorption behavior of CH_4 molecules on SiCNTs, we considered two orientation of the CH_4 molecule (-CH and CH_3 groups) relative to the several possible adsorption sites of SiCNT, T_1 (top of the C atom), T_2 (top of the Si atom), T_3 (top of the Si-C bond), and H (top of the center of hexagon). The equilibrium distances and binding energies for these sites are listed in Table 1. We found that the CH_4 is preferentially adsorbed, through its $-CH_3$ groups on the T_1 site (Figure 1). The equilibrium distance between the C atom of CH_4 and Si atom of nanotube is 4.4Å and the calculated binding energy for this site is 5.4658 $kcalmol^{-1}$. E_b >0 corresponds to the endothermic physical adsorption.

Table1: Equilibrium tube-molecule distance (r_e) of CH_4 adsorption on (4, 4) SiCNT.

SiCNT site	r_e (Å)	E_b ($kcalmol^{-1}$)
	-CH	
T1	4.3859	15.3982
T2	4.8778	10.7525
T3	4.1887	12.9217
H	4.7235	17.9490
	-CH3	
T1	4.4000	5.4658
T2	4.0000	11.7951
T3	4.3000	9.8757
H	4.5000	6.4250

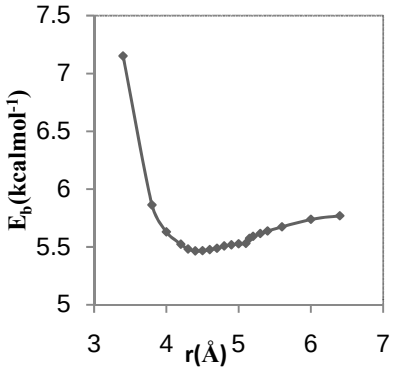

Figur1: Adsorption energy as function of tube-molecule distance (Å) for $–CH_3$ groups on the T_1 site.

Conclusion

All binding energies obtained are positive. Results show that T_1 site is favorable than the others.

References

[1] D. Cao.; W. Wang. Phys. Chem. Chem. Phys. 2001, 3, 3150-3155.

[2] J. X. Zhao.; Y. H. Ding. J. Chem. Theory Compute. 2009, 5, 1099-1105.

Adsorption isotherms of alkali metal and alkaline earth metal ions on multiwall carbon nanotube

S. Haghshenas[a]*, M. Abbasi[a], M. Vadi[b]

[a] Department of Chemistry, Islamic Azad university, Firoozabad branch, Firoozabad, Fars, Iran

[b] Department of Chemistry, Islamic Azad university, Fasa branch, Fasa, Fars, Iran

E-mail: salma.haghshenas@yahoo.com

Keyword: adsorption isotherm, alkali metal, alkaline earth metal, multiwall carbon nanotube

Introduction

The removal of metal ions from effluents is of importance to many countries of the world both environmentally and for water re-use. The application of low-cost sorbents including carbonaceous materials, agricultural products and waste by-products has been investigated [1]. Most of this work has shown that natural products can be good sorbents for heavy metals**.** CNTs have been proven to possess great potential as superior adsorbents for removing many kinds of organic and inorganic pollutants such as dioxin, 1,2-dichlorobenzene, trihalomethanes, soil organic matters and various divalent metal ions from aqueous solution [2]. In each system, the isotherm constants for the Langmuir, Freundlich and Temkin isotherms have been determined. The utilization of CNTs for the treatment of water and wastewater containing divalent metal ions is gaining more attention as a simple and effective means of pollution control.

Materials and methods

The metal solutions were prepared from 1000 mg/L stock solutions containing nitrate salts (Merck). The concentrations of metals were performed by atomic absorption spectrometry using a Perkin-Elmer 3110 apparatus. After shaking for 4 h, the metal concentration in the aqueous solutions was determined by atomic absorption spectrophotometer.

Result and discussion

The equilibrium sorption isotherm is fundamentally important in the design of sorption systems. Equilibrium studies in sorption give the capacity of the sorbents. It is described by

sorption isotherm characterized by certain constants whose values express the surface properties and affinity of the sorbents. Equilibrium relationships between sorbent and sorbate are described by sorption isotherms, usually the ratio between the quantity sorbed and that remaining in the solution at a fixed temperature at equilibrium. (fig.1) the metal ion sorption equilibrium data are commonly correlated with the Langmuir or the Freundlich equations. The Langmuir equation is valid for dynamic equilibrium sorption process on completely homogenous surfaces while the Freundlich equation is applicable to heterogeneous surface. Several researchers reported that the metal ion sorption onto CNTs can be described by both Langmuir and Freundlich equations [3, 4] In order to investigate the sorption isotherm, three equilibrium models were analyzed. These included the Langmuir, the Freundlich and the Temkin isotherms.

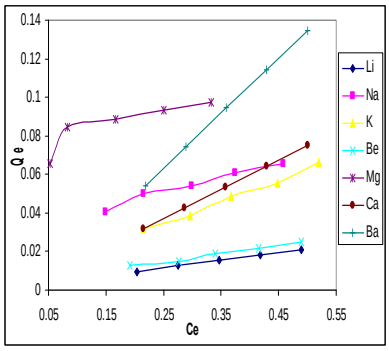

Fig1: Adsorption capacity of CNT for the initial concentration metal ions

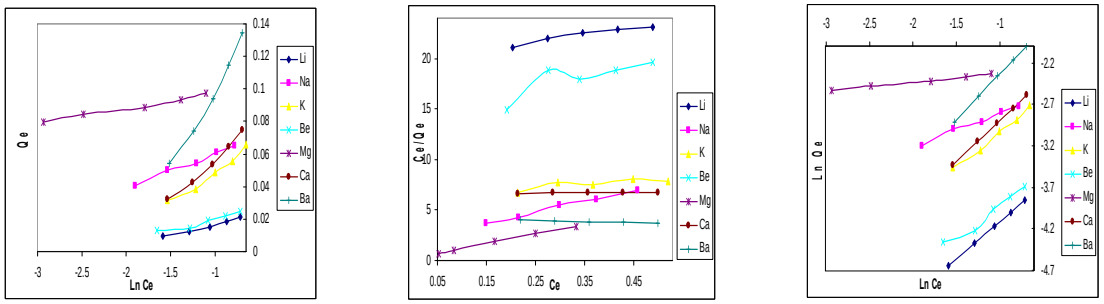

a b c

Fig1. a: Langmuir isotherms, b: Freundlich isotherm and c: Temkin isotherm of metal ions sorbed on MWCNTs.

Table 1.

Isotherm constants for metal ions sorption onto CNTs

	Li	Na	K	Be	Mg	Ca	Ba
Langmuir							
q_m, (mg/g)	0.14482	0.091651	0.298481	0.075712	0.101377	0.84305	0.912409
Ka, (dm^3/mg)	0.346591	5.320103	0.527797	0.976851	5.69848	0.003344	0.258631
r^2	0.9444	0.9932	0.669	0.6767	0.9983	0.4859	0.932
Freundlich							
Kf, (mg/g)(dm^3/mg)$^{1/n}$	25.03062	10.96491	9.007882	24.08044	9.247932	6.684557	3.458379
1/n	0.8957	0.4141	0.8335	0.7387	0.1032	0.9988	1.0989
r^2	0.9998	0.9842	0.9869	0.9612	0.9852	1	0.9999
Temkin							
Kt, (Lmg^{-1})	9.897752	44.74259	9.943062	12.50734	47.79834	8.497063	7.701775
B1	0.013	0.0216	0.0384	0.0133	0.0091	0.0501	0.0965
r^2	0.9833	0.9882	0.9609	0.9406	0.9799	0.9845	0.9854

These values of the correlation coefficients indicate that there is not a strong positive relationship for the data and that the metal/CNTs sorption data follows the Langmuir sorption isotherm. However, data are found in good agreement of the Freundlich sorption isotherm. We observe that there is an accessible competition between Temkin model and Freundlich model. (Table 1)

Conclusion:

In summary, the experimental results were fitted to the Langmuir, Freundlich and Temkin isotherms to obtain the characteristic parameters of each model. The Langmuir isotherm was found to well represent the measured sorption data for alkalis earth metal and Both the Freundlich and Temkin isotherms were found to well represent the measured sorption data for alkalis metal. According to the evaluation using the Langmuir equation, the maximum sorption capacities of metal ions onto multiwall carbon nanotube.

References

[1] Nguyen C, Do DD. Carbon 2001; 39:1327_ 36.

[2] G. P. Rao, C. Lu, F. Su, Separation and Purification Technology 58 (2007) 224–231

[3] Longmuir I. Journal of the American Chemical Society 1916; 38:2221_ 95.

[4] u¨ ber die adsorption in lo¨sungen. Zeitschrift fu¨ r Physikalische Chemie 1906;57:385_ 470.

Efficient Removal of sunset yellow by Cadmium telluride nanoparticle loaded on activated carbon

Hekmati[a], M. Ghaedi*[b], Reza sahraei[c], Ali daneshfar[c], Nahid Shokri[c]

Chemistry Department, Gachsaran Azad University, Gachsaran, Iran

Corresponding author:\

Tel&fax. (0098)-741-2223048,

E-mail: m_ghaedi@mail.yu.ac.ir (M. Ghaedi)

Keywords: *Adsorption;* sunset yellow*; activated carbon; kinetic;* Cadmium telluride*;* nanoparticle

Abstract

Dyes are considered to be highly toxic and can cause permanent injury to the eyes and skin of humans and animals. Sunset yellow(SY)is used in different processes such as dying silk, wool, leather, jute, cotton, biological stain, dermatological agent, veterinary medicine, green ink manufacture, intestinal parasites, fungus textile dying, paper printing, as staining constituent of bacteriological media and as a antiseptic selective bacteriostatic agent. Effluent coming out from these industries is highly colored and cause water pollution and need be treated before its disposal. Adsorption is one of the efficient techniques for the treatment of dye containing waste water in comparison with other techniques like flocculation, biodegradation, membrane separation and different oxidation processes in terms of initial cost, simplicity of design, ease of operation and non toxicity of adsorbent. Although, activated carbon, with large surface area, micro-porous character is an efficient adsorbent for dye removal, but commercially available activated carbons are still considered as expensive materials due to the relatively expensive starting material such as coal. Hence, the process of dye removal by adsorption is being diverted to the use of lower cost adsorbents so that the process becomes economically feasible. This has prompted many researchers to study the feasibility of using low cost substances as alternate adsorbents including agro-waste. In general, many agro-wastes are either arbitrarily discarded or set on fire. Utilization of these materials should bring economic and social benefits to mankind. These low cost adsorbents are being considered as alternative to commercial activated carbon that can be used for

reducing the pollution of wastewaters at a reasonable cost. Hence, there is a scope for the identification and preparation of more economical and effective sorbents from agro-waste.

In the present study experiments were carried out to remove sunset yellow dye by adsorption technique using a novel adsorbent prepared from Cadmium telluride nanoparticle loaded on activated carbon.

Characterization of Prepared adsorbent was characterized by using BET surface area measurement, FTIR, SEM and elemental analysis. Various parameters such as initial dye concentration, adsorbent dose, pH and temperature were studied to observe their effect on the dye adsorption process. Thermodynamic parameters were calculated to know the nature of adsorption. Three different kinetic models for the adsorption of dye were presented. The equilibrium data were tested with Langmuir, Freundlich and Tempkin isotherm models. This fundamental study will be helpful for further application in designing an adsorber for the treatment of dye containing effluent coming out from dying industries

More than 90% removal efficiency was obtained within 30 min at adsorbent dose of 0.02 g/L for initial dye concentration of 25 mg/L. The percentage of dye removal remains almost constant within the pH range of around 1 – 5. The adsorption of dye was found to follow a pseudo-second-order rate equation. Intra particle diffusion model was studied in order to determine the rate limiting step of the adsorption process. Langmuir isotherm model was fitted the best for the adsorption system with an adsorption capacity of 2.09 mg/g of adsorbent.

The present adsorbent may be considered as an alternative for the better performance of the sunset yellow dye removal from its aqueous medium.

The percentage adsorption is maximal at pH value of around 1 and decreases with basic strength of the dye solution. The percentage adsorption decreases from about 100% to 70% for the initial dye concentrations of 25 mg/L at the end of the experiment when the pH is gradually increse from 1 to 5. Adsorption kinetic follows pseudo-second-order kinetics. Adsorption capacity increases with temperature. The temperature effect is used to calculate the change in activation enthalpy (ΔH^0), free energy of adsorption (ΔG^0) and entropy (ΔS^0). The equilibrium data are analyzed using Langmuir, Freundlich and Tempkin isotherm equations. The result shows that the experimental data are best correlated by Langmuir isotherm.

References

[1] Inbaraj, B.S., Sulochana, N., 2002. Basic dye adsorption on a low cost carbonaceous sorbent: kinetic and equilibrium studies. Indian J Chem Technol. 9, 8–20.

[2] Fatma, C., Dursun, O., Ahmet, O., Ayla, O., 2007. Low cost removal of reactive dyes using wheat bran. J. Hazard. Mater. 146 (1–2), 408–416.

[3] Armagan, B., Turan, M., Celik, M.S., 2004. Equilibrium studies on the adsorption of reactive azo dyes into zeolite. Desalination 170, 33–39.

[4] Aydin, H., Baysal, G., 2006. Adsorption of acid dyes in aqueous solutions by shells of bittim (Pistacia khinjuk Stocks). Desalination 196, 248-259.

The Effect of TGA as a Coating for Zinc Cadmium Sulfid Ouantum Dots

F. Khodarahmi, E.Saievar-Iranizad*
Department of Physics, Tarbiat Modares University, Tehran,I.R. Iran
)* (saievare@modares.ac.ir

Introduction

Aqueous semiconductor quantum dots (QDs) are a great interest because of their unique properties, including strong luminescence, long luminescence life time,size-dependent luminescence color,broad absorption, and narrow emission profile[1-2].. In order to tune the size of the semiconductor crystal and prevent surface defects, capping molecules, mostly thioacids,are used during the synthesis[3-4].Here, we report the influence of TGA/ (Zn+Cd) ratio on the absorbance edge,excitonic peak, and Pl peak maximum.

Methods

Synthesis of $Zn_{0.5}Cd_{0.5}$S

A typical synthesis is described as follows: enough amounts of cadmium sulfate and zinc acetate were dissolved in water and appropriate amount of thioglycolic acid (TGA) was added to the solution. The pH of the solution was adjusted to 7 with 1M NaOH. 25 milliliters of $Na_2\,S$ solution was added to this solution.

Results and Disscution

Figure 1, 2 shows the UV-vis absorption and PL spectra of $Zn_{0.5}Cd_{0.5}$S nanoparticles prepared at room temperature and pH 7. All nanoparticles absorb at lower wavelengths than the bulk $Zn_{0.5}Cd_{0.5}$S, indicating quantum confinement. The PL peak maximum and absorbance edge show a red shift at TGA/ (Zn+Cd) 7.5 with a more intense excitonic peak.

Coclusions

Within the range of 1.8-10.5 TGA/ (Zn+Cd) ratio, there was a noticeably stronger luminescence intensity at 7.5 and significantly weaker luminescence intensity at 1.8. it is possible that at low loading of TGA not enough surface coverage was achieved to prevent surface defects.

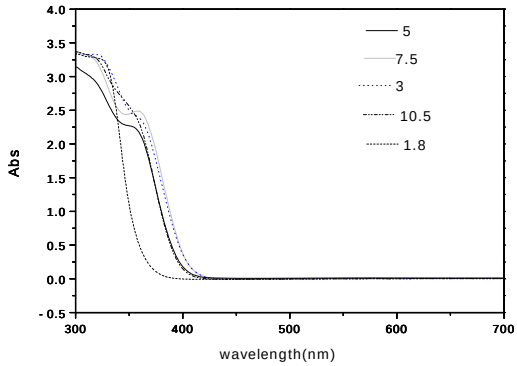

Figure1. Absorption spectra of $Zn_{0.5}Cd_{0.5}S$ – TGA nanoparticles prepared with various TGA/ (Zn+Cd).

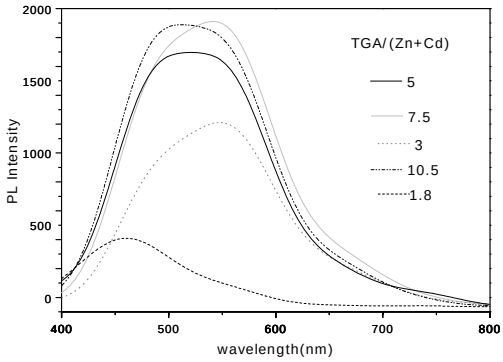

Figure2. PL spectra of $Zn_{0.5}Cd_{0.5}S$ – TGA nanoparticles prepared with various TGA/ (Zn+Cd).

References

[1] H.Kobayashi, Y.Hama, T.Barrett,C.A.S.Regino,Y.Urano.Nano Lett.2007,7,1711

[2]A.M.Derfus, A.A.Chen, D.H.Min, E.Ruoslahti, S.N.bhatia, Bioconjugate Chem. 2007, 18,1391

[3] J.Aldana, Y.A.Wang, X.G.Peng, J.Am.Chem.Soc.2001, 123, 8844

[4] H.Zhang, Z.Zhou, B.Yang, M.Y.Gao.J.Phys.Chem.B2003, 107, 8

Effects of MWCNT on polymerization kinetics of epoxy resin and 1,4-Bis(3-aminopropoxy) butane

S.khostavan*[a], A. Omrani[a] and A. A. Rostami[a]

[a]*Department of Chemistry, University of Mazandaran, Babolsar, Iran*

(Email:s.khostavan@gmail.com)

Keywords: Cure kinetics, Nanocomposite, Carbon nanotube, Differential Scanning Calorimetry.

Introduction

During the last decade, due to the emergence of a new generation of high-technology materials, the number of research groups involved in nano structured materials has increased exponentially [1-3]. The aim of present study is to clarify the effect of multi-wall carbon nanotube (MWCNT) on curing behavior of DGEBA using dynamic and isothermal calorimetry.

Experimental

The epoxy system used in this work was D.E.R 332 DGEBA from Sigma Aldrich with an epoxy equivalent weight of 175 equiv. g^{-1}. 1,4-Bis (3-aminopropoxy) butane was purchased from Fluka and used as hardner. MWCNT was also prepared from Sigma Aldrich and used without further purification. The stoichiometric ratio of epoxy resin and diamine were mixed and the mixture was stirred by ultrasonic stirrer for 30 min. Then, the optimum weight of carbon nanotube was added to the mixture and ultrasonated for additional 10 min. A NETZSCH DSC 200 F3 unit was employed for calorimetriy measurements. To measure the heat of reaction and T_g of the fully cured samples, non-isothermal DSC experiments were conducted in the range of 25–300 ℃ in nitrogen atmosphere at $20℃.min^{-1}$. Kinetic studies were also performed using DSC working isothermally at temperature interval from 70 to 100℃.

Results and discussion

The general kinetic description of a cured system is based on the following rate equation:

$$\frac{d\alpha}{dt} = kf(\alpha) = Aexp\left(-\frac{Ea}{RT}\right)f(\alpha) \quad (1)$$

Where, α is the degree of cure, t is the time, $d\alpha/dt$ is the curing rate, k is the rate constant as a function of temperature, Ea is the apparent activation energy, A is the pre-exponential factor; and $f(\alpha)$ is the reaction model, which is related to the reaction mechanism. Kinetic analysis was done by Šesták-Berggren (SB) model which is a two-parameter autocatalytic model that can be expressed as [4]:

$$f(\alpha) = \alpha^m(1-\alpha)^n \quad (2)$$

Where, m and n are the reaction orders. The reaction order n and the logarithm of the pre-exponential factor ($\ln A$)can be calculated from the logarithmic form of Eq. (1):

$$\ln\left[\left(\frac{d\alpha}{dt}\right)\exp\left(\frac{Ea}{RT}\right)\right] = \ln A + n\ln[\alpha^P(1-\alpha)] \quad (2)$$

Where, the kinetic parameter ratio P is: $P = \frac{m}{n} = \frac{\alpha_m}{1-\alpha_m}$ (3)

Here, α_m is maximum point of $(d\alpha/dt)$ against conversion curves at different temperatures. From the slope and intercept of the linear relationship $ln\,[(d\alpha/dt)\ exp\,(Ea/RT)\,]$ versus $\ln A + n\ln[\alpha^P(1-\alpha)]$, we obtained the reaction order n and $\ln A$, respectively. The reaction order m can be obtained from $m = p \times n$. We used an average value of the reaction energy from differential isoconversional methods in our calculations.

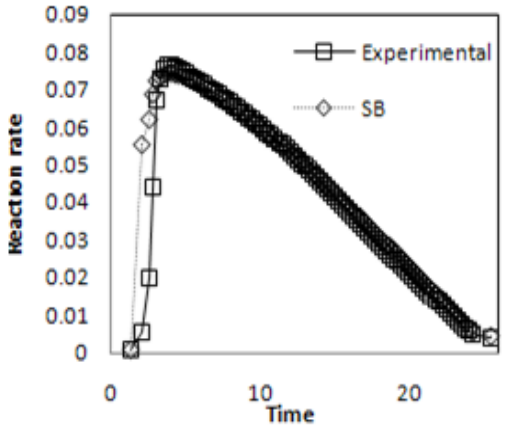

Fig.1. Comparison of experimental and theoretical reaction rate in 70°C

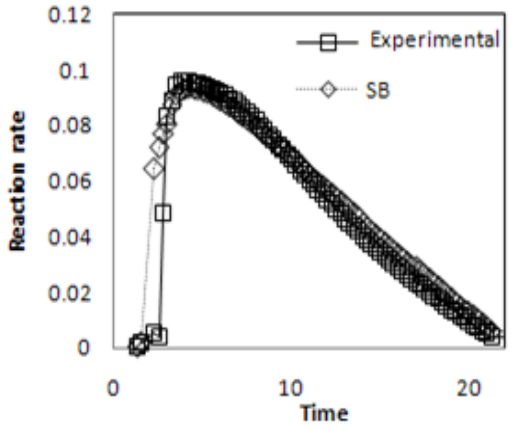

Fig.2. Comparison of experimental and theoretical reaction rate in 80°C

Conclusion

The effect of different concentrations of MWCNT on thermal curing of epoxy/1,4-Bis(3-aminopropoxy) butane system was studied using isothermal and nonisothermal DSC. The concentration of 5% MWCNT was considered to be the optimum level of loading as the result

of maximum reaction heat. Šesták-Berggren (SB) model was used to estimate the kinetic parameters. The overall reaction orders lies approximately between 0.5 and 0.65. As it is appear from Fig.s 1 and 2 the model showed a good fitting of the experimental data.

References:

[1] A. Omrani, A. A. Rostami, E. Sedaghat, Thermochimica Acta, 497 (2010) 21–26.
[2] C. H. Chen, F. S. Yen, Composites: Part A, 40 (2009) 463-468.
[3] T. Zhou, X. Wang, X. Liu, D. Xiong, Carbon, 47 (2009) 1112-1118.
[4] J. Šesták, G. Berggren, Thermochimica Acta, 3 (1971) 1–12.

Study on cure kinetics of epoxy / 1,4-Bis(3-aminopropoxy) butane / MWCNT system by nonisothermal differential scanning calorimetry

S. Khostavan[a], A. Omrani*[a], A. A. Rostami[a] and Y. Vazifeshenas[b]

[a]*Department of Chemistry, University of Mazandaran, Babolsar, Iran*

[b]*Department of Mechanical Engineering, Babol University of Technology, Babol, Iran*

(Email:Omrani@umz.ac.ir)

Keywords: Activation energy, Nanocomposite, MWCNT, Differential Scanning Calorimetry.

Introduction

Epoxy resins are polymer-forming systems which produce highly cross-linked structures, traditionally filled with micro size fillers with exceptional toughness, adhesion, and chemical resistance. Recent researches show that nanofillers are more efficient than the traditional since better adhesion between the resin and nanoparticles is observed due to high surface area of nanoparticles [1, 2].

Experimental

The used epoxy resin was (DGEBA) D.E.R 332 from Sigma Aldrich with an epoxy equivalent weight of 175 equiv. g^{-1}. The curing agent was 1,4-Bis (3-aminopropoxy) butane from Fluka and multi-wall carbon nanotube (MWCNT) was also purchased from Sigma Aldrich with a purity more than 90%. The stoichiometric ratio of epoxy resin and diamine were mixed and the mixture was stirred by ultrasonic stirrer for 30 min. Then, the optimum weight of carbon nanotube was added to the mixture and ultrasonated for additional 10 min. A NETZSCH DSC 200 F3 unit using nitrogen atmosphere was employed for calorimetriy measurements. The samples were heated from 25 to 250 ℃ at five different heating rates (2.5, 5, 10, 15 and 20 $℃.min^{-1}$) to follow the heat evolution due to the chemical reaction occurring at this temperature range.

Results and discussion

Kinetic analysis of nonisothermal resin-cured system is based on the rate equation as follow:

$$\frac{d\alpha}{dt} = \beta \frac{d\alpha}{dt} = k(T)f(\alpha) \quad (1)$$

Where, $k(T)$ is a temperature dependent reaction rate constant, $f(\alpha)$ is the differential conversion function depending on the reaction mechanism, β is a constant heating rate; and $k(T)$ is the rate constant which is temperature dependent according to the Arrhenius law.

Flynn-Wall-Ozawa (FWO) method: The isoconversional integral method of FWO was utilized to determine the activation energy at various conversions using following equation**:**

$$\ln\beta = \ln\left(\frac{AE_\alpha}{R}\right) - \ln g(\alpha) \quad -5.331 - 1.052\left(\frac{E_\alpha}{RT}\right) \quad , \quad g(\alpha) = \int_0^\alpha \frac{d\alpha}{f\alpha} \quad (2)$$

Advanced isoconversional method: An advanced isoconversional method developed by Vyazovkin [3] was employed to interpret the curing behavior of the selected system. It is based on the minimization of the following equation:

$$\Omega = \sum_{i=1}^{n} \sum_{j\neq i}^{n} I(E_{a\alpha}, T_{\alpha,i})\beta_j / I(E_{a\alpha}, T_{\alpha,j})\beta_i \quad , \quad I(E_{a\alpha}, T_{\alpha,i}) = \int_0^{T_{\alpha i}} e^{-E_{a\alpha}/RT} dT \quad (3)$$

Where, the $I(E_{a\alpha}, T_{\alpha,i})$ values in Eq.(3) may be found by numerical integration as well with the help of the Senum–Yang approximation in which $x = E_a/RT$:

$$I = (E_a/RT)p(x) \quad , \quad p(x) = \exp(-x)/x(x^2 + 10x + 18)/(x^3 + 12x^2 + 36x + 24) \quad (4)$$

In this study, the experimented data was analyzed by mathematical software, Maple 12. Calculated activation energies using the FWO and advanced isoconversional methods are 54.58 and 42.13 (kJ/mol) respectively. Less accurate result was obtained by the FWO method because of the error induced by the use of a less accurate approximation.

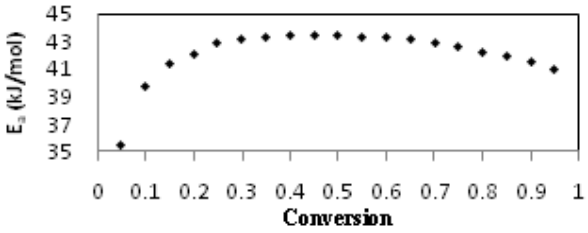

Fig.1 plot of activation energy dependance on the conversion

The dependence of activation energy upon conversion is shown in Fig. 1.

Conclusion

To produce a reinforced epoxy-based nanocomposite, MWCNTs were added into epoxy resin in the presence of 1,4-Bis (3-aminopropoxy) butane as curing agent at the optimum loading

level of 5 wt%. Flynn-Wall-Ozawa and advanced isoconversional kinetic models were used to calculate the activation energy using DSC data. The experimental dependence of E_a on α determined from isoconversional methods of dynamic DSC data can be used to describe the reaction mechanism. The experimentally evaluated values of activation energies are reasonable and consistent to the literature data for similar systems.

References:

[1] J. Njuguna, K. Pielichowski, S. Desai, Polym. Adv. Technol. 19 (2008) 947–959.

[2] A. L. Gerson, H. A. Bruck, A. R. Hopkins, K. Segal, Composites: Part A 41 (2010) 729–736.

[3] S. Vyazovkin, N. Sbirazzuoli, I. Dranca, Macromol. Chem. Phys. 207 (2006) 1126.

Immobilization of cellulase enzyme onto magnetic nanoparticles and determination of its activity and stability

Kamyar Khoshnevisan*[a,c], Abdol-Khalegh Bordbar[b], Dariush Davoodi[c], Mohammad Barkhi[c] and Masumeh Noruzi[c]

[a]Biotechnology Engineering Department, Modern science and Technology Faculty, University of Isfahan

[b]Department of Chemistry, University of Isfahan, Isfahan, 81746-73441, Iran

[c]Nano Technology Department, Agricultural Biotechnology Research Institute of Iran (ABRII), Karaj, Iran

Key words: Immobilization of enzyme, Cellulase enzyme, Magnetic nanoparticles, Activity of Enzyme

Introduction

The immobilization of bioactive substances such as proteins, anti bodies and enzymes onto inorganic supports is a significant device for the fabrication of a varied range of functional materials or tools. The immobilization of enzyme for example, is one of the important issues for providing many advantages such as improved stability, simple separation from reaction mixture, and possible modulation of the catalytic properties [1,2]. Nanotechnology is of interest for enzyme immobilization but, for industrial biotechnology, immobilized enzyme nanoparticles could be difficult to handle and recover by centrifugation or filtration. Among these nanoparticles, magnetic nanoparticles (MNPs) are much admired when used in conjunction with bioactive materials consisting proteins, peptides, enzymes, antibodies and nucleic acids, due to their unique properties. MNPs are biocompatible superparamagnetic materials that have low toxicity and can be attracted by a magnetic field and are simply separable in solution [4-7]. In the present work, the direct binding of cellulase enzyme onto magnetic nanoparticles was investigated. The structure of the magnetic nanoparticles was characterized using FTIR spectroscopy. The stability and activity of bound cellulase were also examined.

Method

2 ml of magnetic nanoparticles without organic stabilizer containing 60 mg nanoparticles was added to 8 ml of cellulase (0.25 mg/ml) soluble in acetate buffer (pH 5) and the reaction

mixture was carried out in shaker incubator for 7 hr at room temperature. The amount of protein in the supernatant was determined by a colorimetric method at 595 nm with the Bio-Rad Protein Assay.

The enzyme activity was measured by the CMC activity method.

Result and discussion

It was found that the percentage of celluase bound was about 99%. These results show that in all the binding operations, there were sufficiently available amount of particles to bind the enzymes till complete saturation. It was found that reducing the weight ratio of cellulase to Fe_3O_4 below 0.033 caused an increase in lipase binding up to 100% [5]. The binding of cellulase onto magnetic nanoparticles was investigated by FT-IR.

Analyzing the size of prepared nanoparticles carried out according to dynamic light scattering (DLS) technique. The average size of the MNPs was 30 nm. The size of MNPs was shown by the TEM microscopy. The effect of temperature on the activity of the free and immobilized cellulase was examined. Loss of storage stability is a main subject in enzyme preservation. The storage stability of the cellulase enzyme was calculated for 5 hr. The effect of pH on the activity of the free and immobilized cellulase was examined. The immobilized enzyme has been showed a remarkable increasing due to influence of pH on enzyme.

References

[1] H. Jia, Z. Guangyu and Wang P, Catalytic behaviors of enzymes attached to nanoparticles: the effect of particle mobility, Biotech Bioeng. **84 (**2003), pp. 407-413.

[2] U. T Bornscheuer, Immobilized enzymes: how to create more suitable biocatalyst, Angew. Chem. Int Ed. **42 (**2003), pp. 3336-3337

[3] C.E. Wyman, Handbook on Bioethanol Production and Utilization. (1996) Taylor and Francis.

[4] M.H. Liao and D.H. Chen: Immobilization of yeast alcohol deshydrogenase on magnetic nanoparticles, Biotechnol Lett. **23 (**2001), pp. 1723-1727.

[5] S.H. Huang, M.H. Liao and D.H Chen, Direct binding and characterization of lipase onto magnetic nanoparticles, Biotechnol Prog. **19 (**2003), pp. 1095-1100.

[6] M. Koneracka', P. Kopcansky', M. Antalik, M. Timko, C.N. Ramchand, D. Lobo, R. Mehta and R.V. Upadhyay: Immobilization of proteins and enzymes to fine magnetic particles, J Magn Magn Mater. **201** (1999), pp. 427-430.

[7] A. Kondo and H. Fukuda, Preparation of thermo-sensitive magnetic hydrogen microspheres and application to enzyme immobilization, J Fermen Bioeng. **84 (**1997), pp. 337-341.

Encapsulation of azafullerenes inside the single-walled carbon nanotubes: density-functional theory based treatments

M. D. Ganji [*, a], M. Rezvani [b] Gh. Valizadeh [a] and M. Mousavy [a]

[a] Department of chemistry, Islamic Azad University, Ghaemshahr Branch, Mazandaran, Iran

[b] Young researchers club, Islamic Azad University, Tehran central Branch, Tehran, Iran

Keywords: Azafullerene; Peapods; SWCNTs; Encapsulation; DFT

* Corresponding author. E-mail: ganji_md@yahoo.com, Tel: 98 911 113 7150.

Introduction

The discovery of C_{60} fullerenes encapsulated inside SWCNTs, the peapods [1], has opened the road for the study of a unique class of nanoscopic hybrid materials with unusual properties [2]. Filling nanotubes with molecules which transfer charge may be an efficient means for altering the tube's band structure, giving rise to molecular device components and as building elements of ultra-fast computer memories. The nitrogen doped fullerene, $C_{59}N$ (azafullerene), that has been successfully synthesized [3] posses a rich chemistry due to its enhanced reactivity in comparison with pristine fullerenes. It was previously shown that tube–azafullerene interaction is similar to the tube–C_{60} interaction. As a starting point in understanding interactions with much more complex peapod systems, we carried out calculations within density functional theory on the interaction between $C_{59}N$ fullerene and SWCNTs.

Computational methods

We employed self-consistent charge-density-functional-based tight-binding (SCC-DFTB) method [4] to determine the most stable geometries. Total energy calculations are performed by using the *ab initio* DFT code method [5]. The exchange–correlation energy is in the form of a Perdew-Burke-Ernzerhof (PBE) generalized gradient approximation (GGA) functional. Norm-conserving pseudopotentials generated by using the Troullier-Martins scheme are adopted to describe the electron-ion interaction. From the well known expression for calculating the molecular binding energies, E_b are obtained for various cases of our study. $E_b = E_{C59N\,@\,CNT} - E_{C59N} - E_{CNT}$

Results and discussion

To simulate the binding of an encapsulated azafullerene ($C_{59}N$) to the inner side-wall of the SWCNTs, zig zag (16, 0) and armchair (9, 9) structures are considered as typical semi conducting

and metallic nanotubes with similar diameters (12.438 Å and 12.112 Å, respectively). $C_{59}N$@SWNT system is optimized starting from five different initial geometrical configurations.

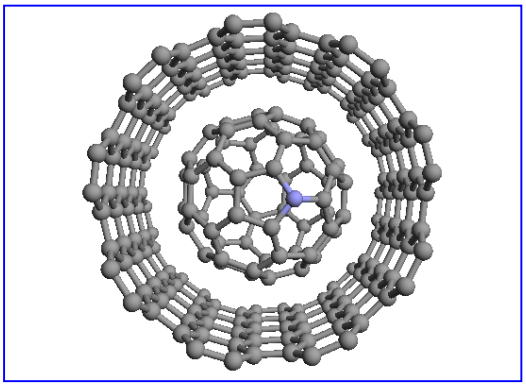

Figure 1. Model for an azafullerene ($C_{59}N$) molecule encapsulated inside the (9, 9) SWCNT (a) front and (b) side view.

After full structural optimization of the considered systems we find that azafullerene prefers to be encapsulated inside the semi conducting nanotubes in comparison with the metallic one. For both examined SWNTs the most stable configurations of $C_{59}N$@nanotube system are achieved when the nitrogen atom of $C_{59}N$ is situated approximately over the center of a six-member ring of the nanotube. Our finding shows that the C_{60}/SWCNT interaction is similar to the azafullerene/SWCNT interaction, in good agreement with the observed experimental result [6].

Conclusions

The azafullerene affinity for the metallic nanotube is stronger than for semiconducting one. The energy values and N–C distances obtained from the *ab initio* calculations are typical for the physisorption. Azafullerene cages might be able to form stable bindings to SWCNTs via their nitrogen active sites.

References

[1] B.W. Smith, M. Monthioux and D.E. Luzzi, Nature 396 (1998) 323.

[2] M. Hodak, L.A. Girifalco, Chem. Phys. Lett. 350 (2001) 405.

[3] A. Hirsch and B. Nuber, Acc. Chem. Res. 32 (1999) 795.

[4] B. Aradi, B. Hourahine, Th. Frauenheim, J. Phys. Chem. A 111 (2007) 5678.

[5] J.M. Soler, E. Artacho, J.D. Gale, A. García, J. Junquera, P. Ordejón, D. Sánchez-Portal, J. Phys.: Condens Matter 14 (2002) 2745.

[6] F. Simon, H. Kuzmany, F. Fülöp, A. Jánossy, J. Bernardi, F. Hauke, and A. Hirsch, Phys. Stat. Sol. (b) 243 (13) (2006) 3263.

Molecular Dynamic Simulation of Adsorption of CO_2 on Carbon Nanotubes

S.S. Delbaz*,a, J. Jahanbin[b] , H.R. Shamlouei[a]and A.Taghvamanesh[a]

a. Department of Chemistry, Islamic Azad University of Gachsaran, Gachsaran, Iran

saeid.delbaz@gmail.com

b. Molecular Simulations Lab., Azarbaijan University of TarbiatMoalleem, Tabriz, Iran

Introduction

Carbon nanotube is special form of carbon which has high capacity for absorbing the gases. Single-walled nanotubes SWNTs are the simplest of the carbon nanaotubes, being but a single graphite plane rolled into a thin tube [1,2]. In this research the SWCNTs as gas adsorbent for CO_2 gas was investigated theoretically.

Computational Details

The nanotube which selected in this research, was 3,3 with 10 unit cells. The simulations were performed in canonical ensemble (NVT) and temperature was set to 200, 300 and 400K. The dimensions of the simulation box were set to 25 Angstrom and the periodic boundary condition in three dimensions were used. All simulations is done by the DL_POLY_2.20 package and Drieding force field implemented in this package.

Results and discussion

The weight percent of CO_2 was set to 40%, 60% and 80% that correspond to 18, 27 and 36 molecule of CO_2. After receiving the equilibrium, the average energy was calculated. Table1 has been contained the absorption energy.

	Temperature	Adsorbing Energy		
		18 molecules	27 molecules	36 molecules
1	200K	-1.4388	-1.3626	-1.2787
2	300K	-1.0537	-1.3760	-0.8877
3	400K	-0.7137	-0.6827	-0.6427

Table1. Calculated absorbing energy in various temperatures

The effect of temperature and CO_2 weight percent have been treated on by the calculation of the RDF's of the CO_2 around the SWCT. Some of the results have been presented in the

figures 1 and 2. The Figure 1 has been contained the effect of temperature on the RDF of CO_2 over SWCT for weight percent of 40% CO_2. Figure 2 has been contained the variations of the maximum points of the RDF's for studied weight percents of CO_2 vs. the temperature.

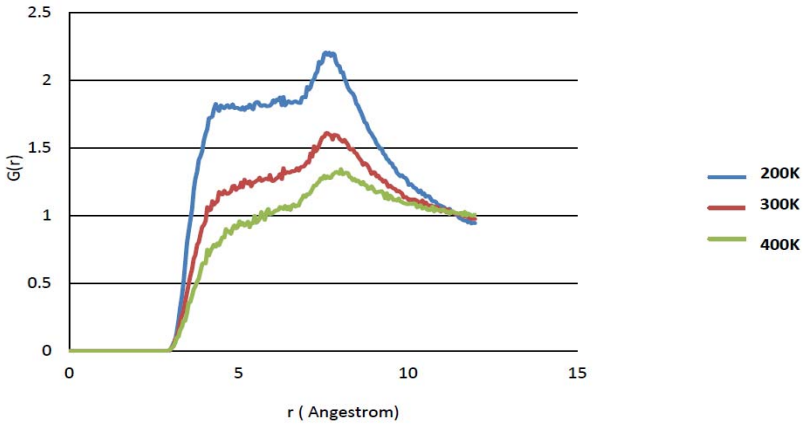

Figure 1. RDF for 40% of CO_2 around SWCT at various temperatures

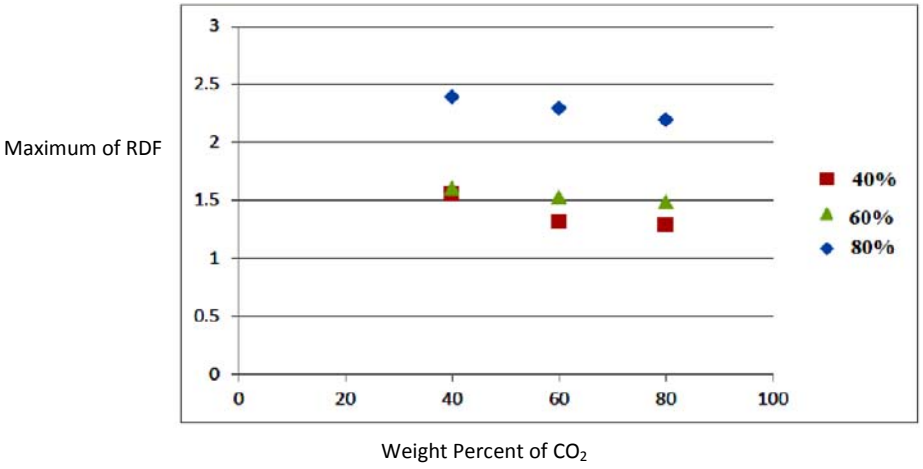

Figure 2. RDF for CO_2 around SWCT for various CO_2 weight percents at 200 K .

A close examination of the results show that the maximum peak in RDF of CO_2 around nanotube decreases as temperature increases. Also, the maximum of RDF's decreases as the weight percent of CO_2 are increased.

References

[1] S. Iijima and T. Ichihashi, Nature, London, 363, 603, 1993

[2] D. S. Bethune, C. H. Kiang, M. S. Devries, G. Gorman, R. Savoy, J. Vazquez, and R. Beyers, Nature, London, 363, 605, 1993.

DFT Study and NBO Analysis of Nanotubes Containing NSAID Drugs

N. Dalili Mansour[1], Sh. Rahmdel[1], B. Pakdel[1]

[1]Department of Chemistry, Faculty of science, Islamic Azad University, Rasht Branch, Rasht, Iran.

Keywords: Nanotube, Naproxen, Ibuprofen, DFT, NBO.

Introduction:

Ibuprofen, Naproxen and Aspirin are all NSAIDs (non-steroidal anti inflammatory drugs.) Among other actions their main mechanism of action is to block a group of enzymes called COX (cyclo-oxygenase) enzymes. They reduce pain (analgesic), reduce high temperatures (antipyrexial), reduce swelling (anti-inflammatory) and make the blood less likely to clot (antithrombolic). As they're all in the same group, they all have similar side effects and risks, however the severity of each side effect varies across the drugs, for instance naproxen is less likely to cause heart problems than ibuprofen. Common side effects include gastric irritation (the reason they should be taken with food) and bleeding. Other drugs in this group include diclofenac and the coxibs (however these have more specific action). [1]

By carrying out fundamental projects scientists have expressed their hope to develop the use of carbon Nanotubes to release vaccines. It is important to release drugs in cells without damaging healthy cells of tissue under studying. Researchers have shown Nanotubes can do this duty perfectly.[2,3] Applying different functional groups with their particular properties in various body cells is a concept that is issued in the field of biomedicine. However, identification of these functional groups and covalent or noncovalent bonds between Nanotubes and these functional groups are noticeable subjects in chemistry.[3]

In this work the interactions between nonstroidal anti inflamation drugs called Naproxen and Ibuprofen with a Nanotube (6,6) containing 60 carbon atoms are investigated.

Computational method:

All of the calculations are carried out by a pc computer which has Intel(R) Pentium(R) Dual CPU with 2 GB RAM. A Nanotube including 60 C atoms (6,6) is formed by Nanotube Modeler package. [4] Geometry Optimization is performed by GaussView [5] and Gaussian 03 [6] softwares by DFT/B3LYP method [7] and 6-31G basis set (Fig. 1). The selected drugs are made by GaussView and optimized by Gaussian 03 by B3LYP/6-31G method (Fig. 2,3).

Then the composites between Nanotube and Naproxen/Ibuprofen are formed and optimized by B3LYP/6-31G method (Fig. 4,5). For optimized molecules hybridations, Bond angles and bond lengths are calculated. After optimization of composites, the single point energies are obtained by B3LYP/6-311++G** method. Natural bond orbital (NBO) [8] calculations have been also performed for all structures using the standard 6-31G basis set.

Agent	Energy/kcalmol^{-1}	Single point energy/kcalmol^{-1}
Naproxen	1442729.2802	1442598.6277
Nanotube	480788.8910	480454.5840
Nanotube-Naproxen	0	-467.2640

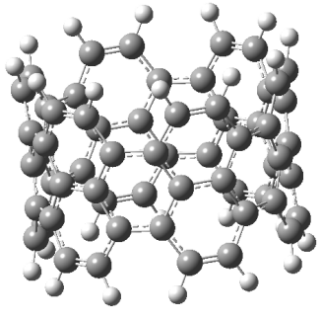

Fig 1. Nanotub

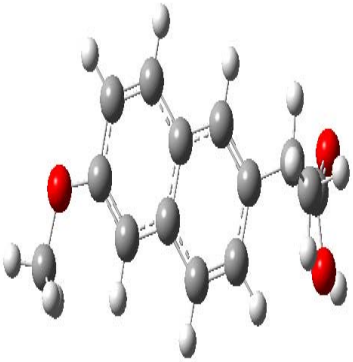

Fig. 2. Naproxen

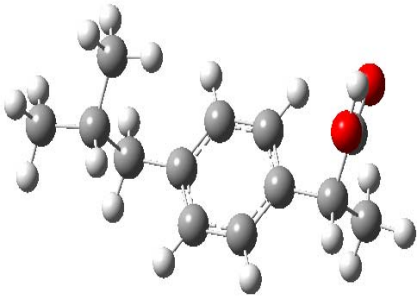

Fig. 3. Ibuprofen

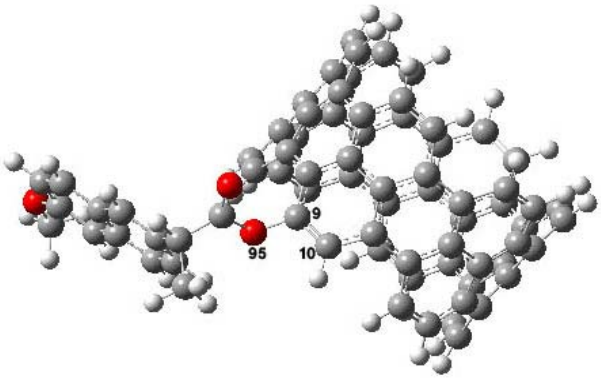

Fig. 4. Nanotube-Naproxen (composite 1)

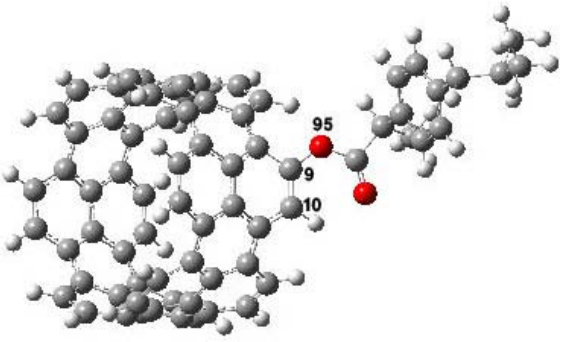

Fig. 5. Nanotube-Ibuprofen (composite 2)

Result and discussion:

The obtained relative energies and relative single point energies are shown in Table 1.

Ibuprofen	1514557.0829	1512194.7930
Nanotube-Ibuprofen	69571.3270	69123.2230

Table.1 Obtained relative energies and single point energies calculated by B3LYP/6-31G and B3LYP/6-311++G** method, respectively .

The results show that the composites between drugs and Nanotube are more stable than the single agents. By evaluating the energy of the reactions (1: Naproxen + Nanotube → composite 1 , 2: Ibuprofen + Nanotube → composite 2), it is clear that these reactions are exothermic reactions (ΔE_1= -1923518.1712 kcalmol^{-1} and ΔE_2= - 1925774.6469 kcalmol^{-1}). Table 2 shows the type of hybridations, bond lengths, bond angles and Mulliken charges. It is obvious that the carbon hybrids are the same in two copmposites. But by increasing p share in oxygen atom of Nanotube - Naproxen composite , the C_9 - O_{95} bond length becomes more , and the obtained bond angles can be described because of this reason , too. It is also clear that because of the similarity of the drug's structures, the Mulliken charges of C_9 and O_{95} are the same in two composites.

Table 2. Obtained parameters calculating by B3LYP/6-31G level

Agent	**C_9 Hybridation**	**O_{95} Hybridation**	**C_9-O_{95} bond length/Å**	**C_{10}-C_9-O_{95} bond angle**	**C_9 Mulliken Charge**	**O_{95} Mulliken Charge**
Nanotube-Naproxen	$SP^{3.42}$	$SP^{2.19}$	1.427	121.68	0.217763	-0.566756
Nanotube-Ibuprofen	$SP^{3.42}$	SP^{2}	1.388	124.22	0.224885	-0.580167

Also NBO calculation results are shown in table 3. In this context, a study of hyperconjugative interactions has been completed . Hyperconjugation may be given as a stabilizing effect that arises from an overlap between an occupied orbital when these orbitals are properly oriented. This noncovalent bonding-antibonding interaction can be quantitatively described in terms of the NBO approach that is experessed by means of the second-order perturbation interaction energy (E_2) [9-11]. This energy represents the estimate of the off – diagonal NBO Fock matrix elements. Here we are interested in the interactions between the Oxygen Lone Pairs Orbitals as donors and some acceptor orbitals that the most important of them are as follow: In Nanotube – Ibuprofen composite hyperconjugation in $LP(1)_{O95}$ →

б*$_{C9-C10}$ and LP(2) $_{O95}$ → π* $_{C9\ -C10}$ have maximum energy . In Nanotube - Naproxen composite the most important transfers are LP (1)$_{O95}$ → π* $_{C9-C10}$ and LP(2)$_{O95}$ → б*$_{C9-O95}$ also б $_{C8-C10}$ → б*$_{C9-\ O95}$ and б$_{C14C16}$ → б*$_{C9-O95}$ transfers are so important in this composite.

Nanotube - Naproxen		Nanotube - Iboprofen	
Donor→Acceptor	**E_2 /kcalmol^{-1}**	**Donor→Acceptor**	**E_2 /kcalmol^{-1}**
$\sigma_{C8-C10} \rightarrow \sigma^*_{C9-O95}$	4.84	$\sigma_{C9-O95} \rightarrow \sigma^*_{C8-C10}$	1.49
$\sigma_{C14-C16} \rightarrow \sigma^*_{C9-O95}$	4.33	$\sigma_{C9-O95} \rightarrow \sigma^*_{C14-C16}$	1.26
$LP(1)_{O95} \rightarrow \pi^*_{C9-C10}$	3.80	$\sigma_{C8-C10} \rightarrow \sigma^*_{C9-O95}$	5.97
$\sigma_{C86-C90} \rightarrow \sigma^*_{C9-O95}$	3.40	$\sigma_{C85-C88} \rightarrow \sigma^*_{C9-O95}$	3.81
$LP(2)_{O95} \rightarrow \sigma^*_{C9-C10}$	4.07	$\sigma_{C8-C10} \rightarrow \sigma^*_{C9-O95}$	5.97
$LP(2)_{O95} \rightarrow \pi^*_{C9-C10}$	3.40	$LP(1)_{O95} \rightarrow \sigma^*_{C9-C10}$	5.53
$LP(2)_{O95} \rightarrow \sigma^*_{C9-C16}$	3.90	$LP(2)_{O95} \rightarrow \pi^*_{C9-C10}$	22.48

Table 3. The second- order perturbation energy $E_{(2)}$ (donor→acceptor) calculated at B3LYP/6-31G level

Table 4 and Fig. 6 and 7 display HOMO and LUMO orbitals energies in these composites.

Agent	Energy of HOMO/kcalmol^{-1}	Energy of LUMO/kcalmol^{-1}
Nanotube – Naproxen	-4.4623	-2.0850
Nanotube – Ibuprofen	-5.3091	-1.6227

Table 4. HOMO and LUMO Orbital energies /Kcalmol^{-1}

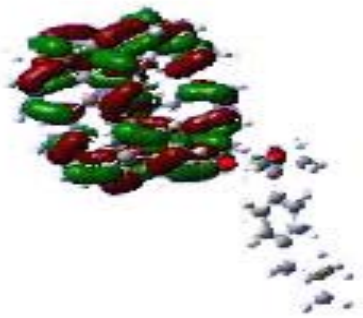

Fig.6. HOMO and LUMO orbitals in Nanotube – Ibuprofen

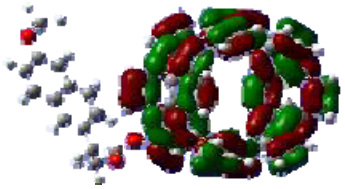

Fig. 7. HOMO and LUMO orbitals in Nanotube - Naproxen

Conclusion:

In this work the results show the composites between Nanotube and drugs are more stable than the single agents. Hybridation of C and O can change in two composites and so have some effects on bond lengths and bond angles. In two composites Mulliken charges are the same.

NBO analysis displays that some donor – acceptor interactions between LP of oxygen atom and π* or б* orbital of carbon of Nanotube can make the structures more stable.

References:

[1] www.Wikipedia.org.

[2] Mylvaganam,K., Zhang, L. C. , *J. Phys. Chem., B* 108, 2004, 5217.

[3] Stobinski, L., Peszke, J., Lin, H. M., *Rev. Adv. Mater. Sci.,* 5, 2003, 363.

[4] www.jcrystal.com/products/wincnt/Nanotube.

[5] A. Frisch, A.B. Nielsen and A.J. Holder, *Gaussview Users Manual*, Gaussian Inc (2000).

[6] M. J. Frisch et al . Gaussian03, Revision D. 01 , Gaussian Inc. Walling ford CT (2004).

[7] A. D. Becke, *J.chem. phys*. 98 (1993) 785.

[8] A. E. Reed, L. A. Curtiss, F. Weinhold, Chem. Rev. 88 (1988) 899.

[9] L. Padmaja 1, M. Amalanathan, C. Ravikumar, I. Hubert Joe, *Spectrochimica Acta A* 74 (2009) 349.

[10] E. Zaedi, M. Aghaie, K.Zare*, J.Mol.struct*.(*THEOCHEM*),905 (2009)101.

[11] S. Sebastian, N. Sundaraganesan, J. Spectrochimica Acta A, 75 (2010) 941.

Curing kinetics and thermodynamics of epoxy/anhydride/nanoalumina system

Abdollah Omrani*[1], Abbas Ali Rostami[1], Fatemeh Ravari[1]

[1] Faculty of chemistry, University of Mazandaran, P.O. Box 453, Babolsar, Iran

(Email:Omrani@umz.ac.ir)

Keywords: kinetics, thermodynamics, Horie method, DSC, nanoparticles

Introduction

Epoxy resins are the most important classes of thermosetting resins and find application in surface coating, composite matrices, adhesive, and encapsulation of electronic components. An epoxy resin becomes an insoluble thermosetting polymer when it reacts with a cross-linking agent [1]. Differential scanning calorimetry (DSC), which measures the heat flow of the sample as a function of temperature and time, has extensively used to study the cure kinetics of various thermosetting polymers.

Experimntal

Glycerol diglycidyl ether (GDE) and 3,3-dimethylglutaric anhydride (DGA) were mixed in stoichiometric ratio ($X_{ep} = 0.33$) and then nanoalumina (10 parts per hundred (phr)) is added as reinforcing agent. All the samples were prepared by mixing the three reactants, GDE, DGA, and nanoalunina, with continuous stirring for about 15 min. Ultrasonic dispersion treatment was then used for 20 min to produce homogenous blends. In the last stage, the initiator was added at $X_{TEA} = 0.0188$.

Results and discusion

1.Horie's method [2]

The curing reaction of GDE/DGA/nanoalumina system was studied at four different isothermal temperatures of 110, 120, 130, and 140°C. To determine the kinetic parameters, we utilized the kinetic model proposed by Horie. According to this model, the reaction rate can be described:

$$\frac{d\alpha}{dt} = (k_1 + k_2\alpha)(1-\alpha)^n \qquad (1)$$

Various selection of n allows to obtain a good fitting of the experimental data. We found that the best linear fitting of the experimental results is correspound to $n = 1$ at all the isothermal temperatures. The calculated conversion plot is shown in Figure 1. Clearly, up to 95% degree of cure, the calculated results has a good agreement with the experimental data.

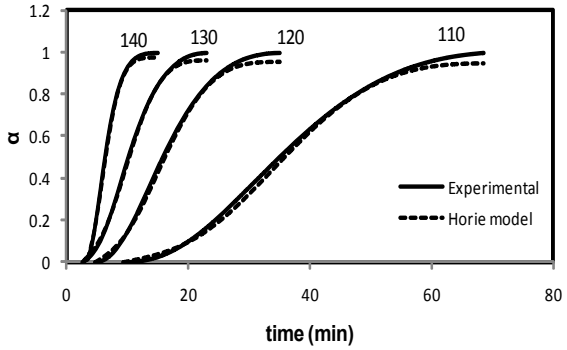

Figure 1

2. Thermodynamic study

Changes in thermodynamic functions of $\Delta S^{\neq}$, $\Delta H^{\neq}$, and $\Delta G^{\neq}$ were estimated using the data obtained by kinetic analysis section according to the TS theory [3]. This can be represented by the following scheme:

$$A + B \xleftrightarrow{k^{\neq}} (AB)^{\neq} \xrightarrow{k} P \qquad (2)$$

According to the TS theory, the following equation can be used

$$\ln(\frac{k}{T}) = \ln[(\frac{k_B}{h})e^{\frac{\Delta S^{\neq}}{R}}] - \frac{\Delta H^{\neq}}{RT} \qquad (3)$$

Linear plots of $\ln(k_i / T)$ against 1/T permit us to compute the values of $\Delta S^{\neq}$ and $\Delta H^{\neq}$ for the cured nanocomposite.

Conclusions

The curing kinetics and thermodynamics of GDE/ DGA/ nanoalumina system was examined by DSC technique. Isothermal kinetic parameters are estimated using the Horie model. This model worked very well in the whole rang of chemically controlled reaction. Thermodynamic

parameters such as enthalpy, entropy and Gibbs free energy changes (ΔG) were also calculated using the rate constants from the kinetic analysis and transition state (TS) theory.

Reference

[1] D. Rosu, C.N. Cascaval, F. Mustata, C. Ciobanu, Thermochim. Acta. 383 (2002) 119-127.

[2] A. Omrani, A.A. Rostami, M. Ghaemy, J. Appl. Polym. Sci. 101 (2006) 1257-1265.

[3] M. Ghaemy, A.A. Rostami, A. Omrani, Polym. Int. 55 (2006) 279-284.

Cure characteristics of a low viscosus epoxy based on nanocomposite

Abdollah omrani [1*], Abbas Ali Rostami [1], Fatemeh Ravari [1], Arezu Mashak [2]

[1] Faculty of chemistry, University of Mazandaran, P.O. Box 453, Babolsar, Iran
(E-mail:Omrani@umz.ac.ir)

[2] Iran Polymer and Petrochemical Institute, P.O. Box, 14965-115, Tehran, Iran

Keywords: Sestak-Berggren, DSC, epoxy, curing kinetics, nanoalumina

Introduction

Epoxy resins are widely used as coatings, electronic materials, matrix of composites and structural applications. The curing process of thermosetting polymers involves the change from low molecular weight liquids to high molecular weight amorphous polymers or three dimensional networks as the result of exothermic chemical reaction [1]. Curing kinetic of epoxy resins have been studied with various techniques such as infrared spectroscopy and thermal analysis using isothermal or dynamic differential scanning calorimetry (DSC) technique [2].

Experimntal

Glycerol diglycidyl ether (GDE) and 3,3-dimethylglutaric anhydride (DGA) were mixed in stoichiometric ratio ($X_{ep} = 0.33$) and then nanoalumina (at 10 W%) added to the above mixture. The three component were mixed mechanically for 30 min to produce homogenous blends and then keep in a refrigerator prior to calorimetry tests. Dynamic DSC scans were performed at five different heating rates: 2.5, 5, 7.5, 10 and 15 ^{0}C/mim on a Perkin Elmer DSC-7 under nitrogen.

Results and discusion

Malek's method [3,4]

The values of E_a measured from advanced isoconversional method, can be then used to find the appropriate kinetic model that best describes the curing reaction. For this purpose, we need appealing specific functions of $Y(\alpha)$ and $Z(\alpha)$ as follows:

$$Y(\alpha) = (\frac{d\alpha}{dt})e^{x} \quad (1)$$

$$Z(\alpha) = \pi(x)(\frac{d\alpha}{dt})\frac{T}{\beta} \quad (2)$$

The $Y(\alpha)$ function is proportional to $f(\alpha)$ function, being characteristic for a given model. The characteristics of both $Y(\alpha)$ and $Z(\alpha)$ functions permit to find the most suitable kinetic model as well. These functions give a maximum value at α_M and α_P^{∞}, corresponding to the functions of $Y(\alpha)$ and $Z(\alpha)$. These data indicated that the two-parameter Sestak–Berggren autocatalytic model can describe the curing process.

$$\frac{d\alpha}{dt} = K(T)f(\alpha) = \exp\left(\frac{-E_a}{RT}\right)\alpha^m(1-\alpha)^n \quad (3)$$

The kinetic parameter n is calculated by the slope of the linear dependence of $\ln[(d\alpha/dt)\exp(E_a/RT)]$ against $\ln[\alpha^P(1-\alpha)]$. The value of m was estimated using the equation $m = p \times n$, where $P = \alpha_M/(1-\alpha_M)$. The correctness of the kinetic model proposed by the Sestak-Berggren was verified by plotting the experimental and theoretical $d\alpha/dt$ versus temperature.

Conclusions

Our results showed that the curing reaction of the selected system obeys an autocatalytic mechanism. For dynamic condition, it was established that the two-parameter autocatalytic model is the best choice to explain curing kinetics. The agreement between the theoretical prediction and experimental reaction rate was reliable.

References

[1] A.J. Cedeno, H. Vazquez-Torres, Polym. Int. 54 (2005) 1141-1152.

[2] W. Chen, P. Li, Y. Yu, X. Yang, J. Appl. Polym. Sci. 107 (2008) 1493-1499.

[3]D. Rosu, C.N. Cascaval, F. Mustata, C. Ciobanu, Thermochim. Acta. 383 (2002) 119-127.

[4]M.J. Yoo, S.H. Kim, S.D. Park, W.S. Lee, J.W. Sun, J.H. Choi, S. Nahm, Eur. Polym. J. 46 (2010) 1158-1162.

Influence of the Acidity on the Combustion Synthesis of Nanocrystalline Al_2O_3 Powders

Jalal Shakhs Emampour[a], Sayyed Mojtaba Zabarjad[b], Mostafa Rajabzadeh[*a]

[a]Departmnt of Chemistry, Ferdowsi University of Mashhad, Mashhad, Iran
(mo_ra826@stu-mail.um.ac.ir)
[b]Department of Engineer, Ferdowsi University of Mashhad, Mashhad, Iran

Keywords: Combustion synthesis, Alumina, Glycin, Urea

Introduction

Combustion synthesis is a particularly simple, safe and rapid fabrication process wherein the main advantages are energy and time savings [1]. The main parameters influencing the reaction include type of the main fuel, fuel to oxidizer ratio, the amount of oxidizer in excess, ratio of fuels, pH of the solution and rate of calcination [2, 3]. In general,a good fuel should not react violently nor produce toxic gases, and must act as a complexing agent for metal cations [4].

Method

Nanocrystalline alumina powders were synthesized by the combustion method using urea and glycin as fuels. For this purpose Aluminum nitrate nonahydrate $Al(NO_3)_3.9H_2O$ and urea and glycin were used as initial materials. The single-phase α-Al2O3 powder has resulted after heat treatment at 1150°C .

Results and discussion

Powders have been characterized by X-ray diffractometry (XRD), scanning electron microscopy SEM, and transmission electron microscopy TEM and EDS. Adjustment of pH was done by addition of nitric acid. Addition of these materials would change the concentration of nitrate ions, and it can change the amount The increase of nitrate ions in the low pHs is expected to decrease the enthalpy of exothermic reaction by decreasing the fuel to oxidizer ratio. Thus the rate of combustion reaction would decrease and in this condition alumina particles come closer to foam structure and agglomeration will increase [5].

Conclusions

The best results were obtained when the synthesis was carried out in acidic environments quite and used urea as main fuel .

Refrences:

[1] M. EDRISSI., R. NOROUZBEIGI., Materials Science-Poland, Vol. 25, No. 4, 2007

[2] ARUNA S.T., RAJAM K.S., Mater. Res. Bull., 39 (2004), 157.

[3] PENG T., LIU X., DAI K., XIAO J., SONG H., Mater. Res. Bull., 41 (2006), 1638.

[4] KINGSLEY J.J., PEDERSON L.R., J. Mater. Res. Soc. Symp. Proc., 296 (1993), 361.

[5] PATHAK L.C., SINGH T.B., DAS S., VERMA A.K., RAMACHANDRARAO P., Mater. Lett., 57 (2002), 380.

Chemical shielding (CS) tensors of Nitrogen and Boron doped in nano-scale C60: A Computational study

Mahdi Rezaei-Sameti[b], Mahdi Rakhshi *[a]

[a] Faculty of Chemistry, University of Bu Ali Sina, Hamadan, Iran

(Emil:rakhshi_chem@yahoo.com)

[b] Department of Applied Chemistry, Faculty of Science, Malayer University, Malayer, 65174, Iran

Key word: nano-Fullerene , NMR, DFT, Nitrogen and Born doped

Introduction

The electrochemical properties of the Fullerene C60 have been studied since the early 1990s, when these materials became available in macroscopic quantities [1]. Recently, significant efforts have been dedicated, both experimentally and theoretically [2-3], to study of structure and electronic properties of Fullerene and effort on how to employ them in nano materials applications [4].

Methods

In this computational research, the properties of the electronic structure and chemical shielding parameters of the Fullerene (C60) and influence of Nitrogen and Boron doped (N and B-doped) on this component (Figs. 1) have been investigated by performing density functional theory (DFT) calculations of the NMR parameters. The structures of three models of C60 were firstly optimized by hybrid density functional theory and B3LYP functional based method and 6-31G** standard basis set, using Gaussian 03package of program , and then the chemical shielding (CS) tensors at the sites of ^{13}C nuclei are calculated based on the gauge included atomic orbital (GIAO) approach. The pristine and the N, B-doped structures have been allowed to relax by all atomic geometrical optimization. Subsequently, the isotropic and anisotropic chemical shielding (CS^{I} and CS^{A}) parameters have been calculated for the ^{13}C atoms present in both of the pristine and the B, N-doped structures (See fig. 1).

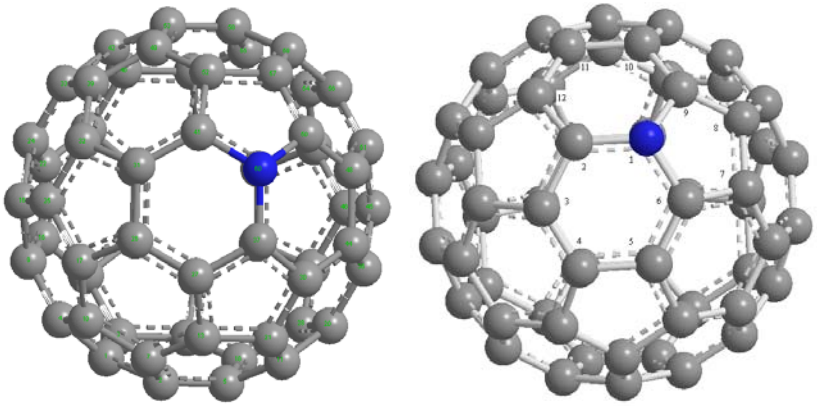

Fig. 1 2D views of N and B doped C60,

Results and discussion

The results show that the CSI values of ^{13}C sites in the N and B-doped model of fullerene have different trend. The results show that the value of the bond angles (6–7–8 and 6–7–8) placed at sides of N and B-doped are decreased largely from 120^{o} to 108^{o} and the bond angle (11–12–2) in two models increased from 108^{o} to 120^{o}.

Conclusions

The comparison between N-doped and B-doped models shows that, the values of CSI and CSA for N-doped model undergo more remarkable changes than B-doped model because of the lone pair of electrons in the nitrogen valence shell.

References

[1] H.W. Kroto, J.R. Heath, S.C.O ´ Brien, R.F. Curl, R.E. Smalley, Nature., **318**,(1985**)** 162.

[2] V.I. Sokolov: Russian chemical bulletin **42**, (1992) 1.

[3] M.S. Dresselhaus, G. Dresselhaus and Ph. Avouris: *Carbon Nanotubes,* 2001**.**

[4] R. Tenne, L. Margulis, M. Genut and G. Hodes: Nature **360**, (1992)444.

Lead(II) Removal From Water by Nanosphere Adsorbent: Equilibrium Study and Error Analysis

R. Rostamian*, A. A. Rafati

Department of Physical Chemistry, Faculty of Chemistry, Bu-Ali Sina University, Hamedan, Iran

(Email: r.rostamian@gmail.com)

Keywords: Adsorption, Heavy metal, Nanosphere adsorbent, Isotherm, Non-linear regression

Introduction

Heavy metals such as lead often be found in industrial wastewater. The stricter environment regulation on the discharge of heavy metals makes it necessary to develop various technologies for the removal. Adsorption is one of the few promising alternatives for this purpose. For environmental applications, the development of functionalized nanoporous materials is necessary, especially for the preparation of heavy metal adsorbents. The present work is aimed at evaluating the isotherm for the adsorption of Pb^{2+} onto thiol functionalized silica nano hollow sphere (thiol-SNHS).

Methods

1. Materials: Thiol-SNHS with the specific surface area of 834 (m^2g^{-1}) were synthesized in our laboratory and reported in our previous work [1], lead nitrate ($Pb(NO_3)_2$, ≥ 99. 5%, Merck) as a lead source and was used without further purification. The Pb^{+2} concentrations were determined by using an atomic absorption spectrometer (SpectrAA-220 Varian).

2. 2. Experimental: These isotherms were obtained by employing the initial concentration of Pb^{+2} in the range of 1 to 90 with adding 0.01 g of thiol-SNHS and shake them for 24 hours. The amount of Pb^{2+} adsorbed by 1 g of thiol-SNHS at equilibrium is called the Pb^{+2} adsorption capacity, q_e. The q_e value can be calculated with formula as described below [2]:

$$q_e = \frac{C_0 - C_e}{m} \times V \qquad (1)$$

where, q_e is the Pb^{+2} adsorption capacity (mg g^{-1} adsorbent), C_0 is the initial concentration of Pb^{+2} (mg L^{-1}), C_e is the Pb^{+2} concentration at the equilibrium found in the solution (mg L^{-1}), m is the mass of thiol-SNHS (g), and V is total volume of solution (L). The relationship between q_e and C_e is called the adsorption isotherm. The Langmuir, Freundlich, Temkin, Redlich-Peterson and Sips isotherms are the equations most frequently used to represent data on adsorption from solution [2]. In order to confirm the fit model for the adsorption system, it is necessary to analyze the data using five analysis. The seven error functions employed in this study are as follows: R^2, X^2, ARE, S_{RE} and $MPSD$ [2].

Results and Discussion

The experimental data were fitted to the isotherm models using Wolfram Mathematica software and the graphical representations of these models is presented in Figure 1.

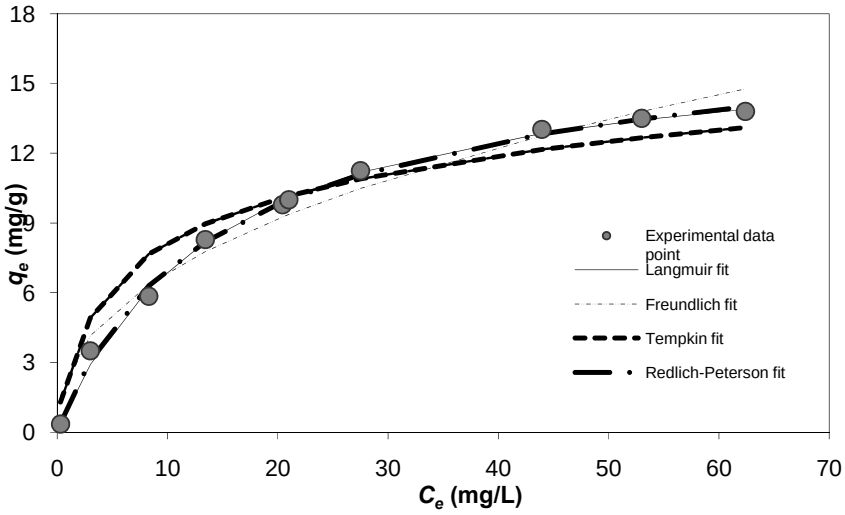

Figure 1. The nonlinear fitted curve with different isotherms applied to Pb^{2+} adsorption by thiol-SNHS.

The values of error function (R^2, X^2, ARE, S_{RE} and $MPSD$) showed isotherm data fit very well with the Sips isotherm.

Conclusions

The adsorption isotherm to removal Pb^{2+} using thiol-SNHS was carried out in batch experimental system. The Sips isotherm was found to be applicable for the adsorption

equilibrium data. The adsorption studies showed that thiol-SNHS can be employed for the selectively removal of Pb(II).

References:

1. R. Rostamian, A. A. Rafati, *13th Iranian physical chemistry seminar proceeding*, **2010**, Vol.2, 497-498, Shiraz, Iran.

2. K.Y. Foo, B.H. Hameed, *Chemical Engineering Journal*, **2010**, Vol.156, 2–10

Preparation of Zinc(II) Oxide Nanoparticles by Decompositin of A New Initial Nano-coordination polymer

Z. Rashidi. Ranjbar, A. Morsali*

Department of Chemistry, Faculty of Sciences, Tarbiat Modares University, P.O. Box 14115-4838, Tehran, Islamic Republic of Iran Tel: +98-21-8011001, Fax: +98-21-8009730

Keywords: Nanoparticle, Zinc(II) Oxide, Surfactant, Sonochemical, Nano Coordination Polymer (NCP)

Introduction:

Coordination polymers or "inorganic and organic hybrid polymers" are infinite structures with specific applications such as; NLO, catalysis, gas storage, conductivity, magnetic and so on [1-3]. It is notable that both size and shape of solid materials influence on the Chemical and physical properties. By decreasing the size of structures; the ratio of surface area to volume would be increased. Therefore some chemical and physical properties of them would be altered [4].

Methods:

a)Nano-size Compound 1: An alcoholic(10 ml methanol) 1:1 solution of 0.156g (1 mmol) 4,4'-bipy and 0.238g (1 mmol) 3-bpdh was poured dropwise into to a 10 ml 1:1 solution of 0.057 g (1mmol) Zinc(II) acetate dihydrate and 0.122g (1mmol) sodium perchlorate, under the ultrasonic irradiation. So, a large amount of compound **1** in nano-scale obtained. d.p. = 250 °C.

b)Zinc(II) oxide nanoparticles: To prepare zinc(II) oxide nanostructures by surfactant, nano-size compound **1** (583 mg, 0.5 mmol) was dispersed in 8 mL (25 mmol) oleic acid (OA). This solution was heated to 473 K for 1 hours under air atmosphere in an electric furnace. At the end of the reaction, a black precipitate was formed. A small amount of toluene and a large excess of EtOH were added to the reaction solution, and ZnO precipitate was separated by centrifugation. The solid was washed with EtOH and dried. Also, ZnO nanoparticles were prepared by heating compound **1** in nano-scale in an electrical furnace at 673 K, separately.

Result and discussion:

The crystalline material as bulk form of $[Zn(\mu\text{-}4,4'\text{-bipy})(\mu\text{-}3\text{-bpdh})(H_2O)_2].(4,4'\text{-bipy})_{0.5}.(ClO_4)_2$ (**1**) was provided from slow evaporation. The compound **1** has been synthesized in nano-size by addition reagents in ultrasonic bath (60 Hz). The IR spectra of compound **1** in bulk form and nano size are the same. Figure 1a shows the simulated XRD pattern from single crystal X-ray data of the compound **1** and Figure 1b shows the XRD pattern of compound **1** in nano-size. Acceptable matches were observed between them. These results indicate this compound obtained as a mono-phase in bulk crystalline form and the structure of crystalline bulk form and nano-scale are completely the same. The morphology, structure and size of the nanostructure of compound **1** were investigated by Scanning Electron Microscopy (Figure 2). Some gray powder of hexagonal zinc(II) oxide obtained from direct calcination at 500 °C and decomposition in presence of oleic acid at 200 °C of compound **1** nanorods. X-ray Powder Diffraction of these products shows in Figure 3. Figure 4 a,b shows two different size of zinc(II) oxide that obtained from calcination and decomposition of compound **1** nanorods.

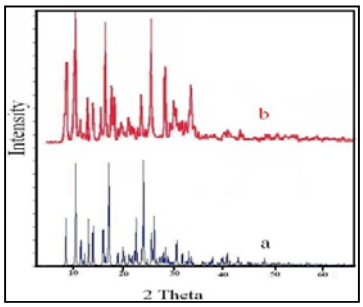

Figure 1. XRD patterns of a) simulated based on single crystal data of compound **1** b) nano-size of compound **1**

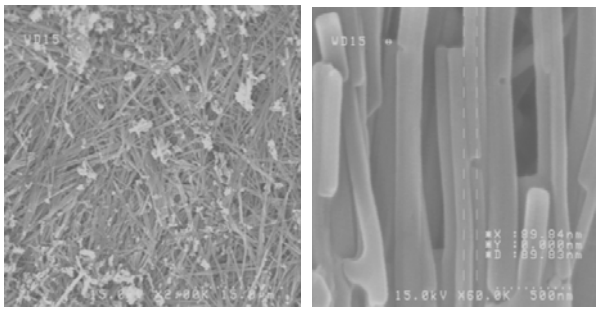

Figure 2. The SEM images of compound (**1**) in nanorods morphology

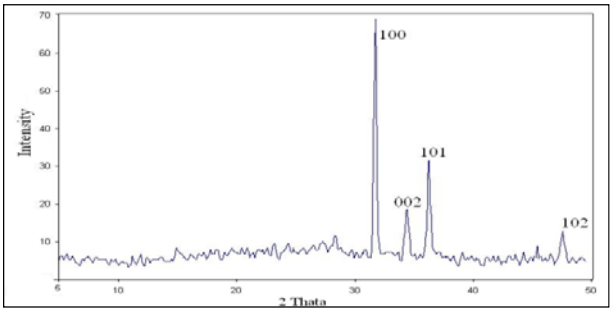

Figure 3. XRD pattern of ZnO nanoparticles prepared by calcinations at 673 k and decomposition at 473 K.

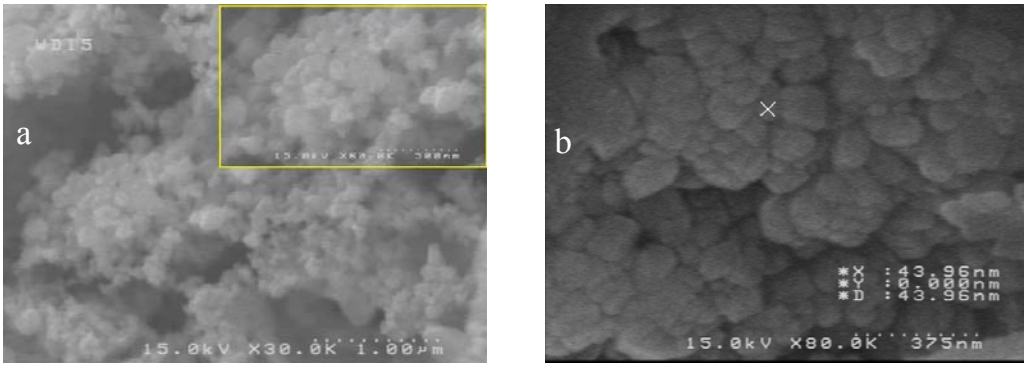

Figure 4. The SEM image of zinc (II) oxide nanoparticles prepared by a) thermal treatment with oleic acid (Decomposition)

Refrences:

[1] H. Liang, Q. Tang, K. Yu, S. Li, J. Ke, Materials Letters., **61** (2007) 1020.

[2] G. I. N. Waterhouse, G. A. Bowmaker , J. B. Metson, Phys. Chem. Chem. Phys., **3** (2001) 3838.

[3] M. Yang, J. G. Zhao, J. J. Li, Colloids and Surfaces A: Physicochem. Eng. Aspects., **295** (2007) 81.

[4] A. N. Goldstein, C. M. Echer, A. P. Alivisatos, science., **256** (1996) 1425.

Interaction between defective carbon nanotubes and amino acids from first-principles

M. D. Ganji [a,] *, M. Rezvani [b] and S. Mahmoudi [a]

Department of Chemistry, Islamic Azad University, Ghaemshahr Branch, Mazandaran, Iran

Young researchers club, Islamic Azad University, Tehran Central Branch, Tehran, Iran

* Corresponding author. E-mail: ganji_md@yahoo.com, Tel: 98 911 113 7150.

Keywords: Amino acids; SWCNTs; Defects; Adsorption; Density functional theory

Introduction

One of the recent researches on carbon nanotubes (CNT) focuses on the combination of CNTs with many different biological substances including proteins, to form hybrid materials that, provides potential for developing immobilization of biological substances, sensors and drug delivery systems [1]. Therefore, a fundamental theoretical and systematic understanding on bridging carbon nanotubes with biological substances should be essential. Recently, we investigated the interaction of amino acids with a perfect (10, 0) semiconducting CNT [2]. In the present effort we have carried out geometric optimization calculations using the DFT method on the adsorption of amino acids Gly, His, Phe and Cys on the zig-zag (10, 0) SWCNT with structural defects.

Computational methods

The structural optimizations of carbon nanotubes and amino acids are carried out using the density functional based tight binding (DFTB) method [3]. The total energy calculations are carried out using the GGA with the Perdew-Burke-Ernzerhof (PBE) functional to treat electron exchange correlation [4] with a double-ζ plus polarization (DZP) basis set. The molecular adsorption energies, E_{ads}, are obtained for various cases of our study: $E_{ads} = E_{CNT-AA} - E_{CNT} - E_{AA}$.

Results and discussion

Various possible configurations were considered for a molecule approaching the center of a heptagon/hexagon/pentagon of carbon atoms via its various active sites (Fig. 1). After full structural optimization of the considered systems, we find that His bound rather strongly to the pentagon of carbon atoms of defected tube, while the binding for Cys with the CNT surface (pentagon ring) is the weakest. The binding energy for the energetically favorable complex is determined to be -0.87 eV. It can be understood from the comparison of the obtained binding energies with the previous study [2], that except for the Gly amino acid the binding energy of all type of considered amino acids is increased (~ 15%) for adsorption on the defected CNTs. The obtained results reveal also that amino acids are weakly bound to the outer surface of the defected nanotubes, having adsorption energies comparable to the adsorbed nucleic acid bases and gas molecules on carbon nanotubes [5].

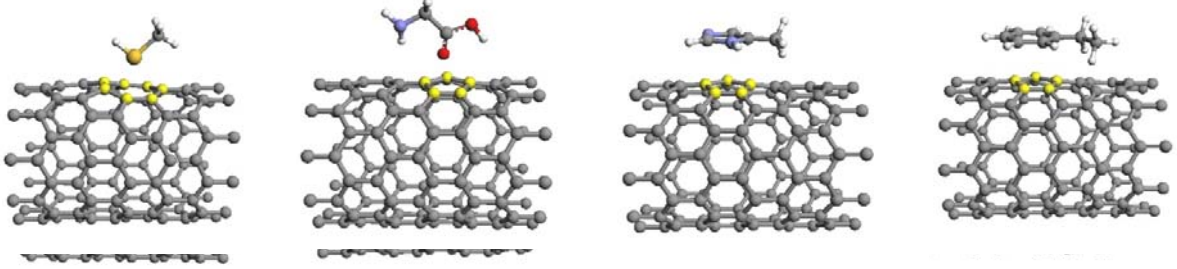

Figure 1. Model for different adsorption states for selected amino acids (a) Cys, (b) Gly, (c) His and (d) Phen on the defected sidewall of the (10, 0) CNT. Atom colors: grey—carbon, white—hydrogen, blue—nitrogen and red—oxygen.

Conclusion

We found that if for specific applications amino acids or even entire proteins are to be adsorbed on the defected nanotubes through the amino acids molecules discussed in this paper, then doing so through His amino acid may give the most favorable results and defects have an important contribution to the adsorption mechanism of SWCNTs.

References

[1] X. Zhao, and J.K. Johnson, J. Am. Chem. Soc. 129(34) (2007) 10438.

[2] M.D. Ganji, Diamond Related Mater. 18 (2009) 662.

[3] B. Aradi, B. Hourahine, and Th. Frauenheim, J. Phys. Chem. A 111 (2007) 5678.

[4] J.P. Perdew, K. Burke, and M. Ernzerhof, Phys. Rev. Lett. 77 (1996) 3865.

[5] M.D. Ganji, Phys. Lett. A 372 (2008) 3277.

Sono-synthesis of Mn_3O_4 nanoparticles in different media without additives

T. Rohani Bastami[b*], M.H. Entezari[a]
Department of Chemistry, Ferdowsi University of Mashhad, 91775 Mashhad, Iran
(tahereh.rohani@gmail.com)

Keywords: Nanoparticle, Ultrasound, Aqueous medium, Olive oil, Almond oil, Paraffin

Introduction

The properties of transition metal oxide nanoparticles are different from those of the bulk materials in many areas such as optical, magnetic, and electrical properties [1]. Mn_3O_4 has different applications in industry such as applying as a catalyst for oxidation of CH4, reduction of nitrobenzene, and decomposition of waste NOx [2]. Several methods were used for the synthesis of Mn_3O_4 nanoparticles with different sizes and shapes. Sonochemistry as an effective and powerful technique is used for the synthesis of nanomaterial under normal conditions (ambient pressure and temperature)[3]. The aim of the current research is the synthesis of manganese oxide nanoparticle (hausmannite) under normal conditions in different media with ultrasonic waves. Aqueous solutions of manganese acetate (II) and dispersion of aqueous phase containing manganese salt in different oils were used for this synthesis.

Methods

4mL of saturated solution of $Mn(OAc)_2$ and 30mL of oil were added in a 100mL beaker. The two immiscible phases were uniformed and the emulsion was established by sonication of solution at initial temperature of 20 ˚C. The temperature of immersed vessel in an ice bath was increased to about 73 ˚C during the initial 5min and then by removing the ice bath, the temperature was raised to about 95 ˚C. The position of probe was fixed by its immersion to 1 cm in the initial oil phase. The sonication was continued to 35, 20, and 17 min for paraffin, almond oil and olive oil, respectively. The reaction products were centrifuged at 15000rpm for 20 min and then washed with n-hexane and boiled water many times to remove the oil phase from the solid particles. Finally, the solid particles were dried at 100 ˚C.

Result and discussion

According to the X-ray diffraction patterns of the samples prepared in different media under ultrasound, it is found that all the products are in agreement with the XRD pattern of hausmannite. The TEM results show that the type of oil has an effect on the size and shape of nanoparticles. The sample prepared in vegetable oils as an oil phase shows spherical shape with maximum size of ~7 nm, but in mineral oil as an oil phase, the nanoparticle exhibits diamond shape with maximum size of 50 nm.

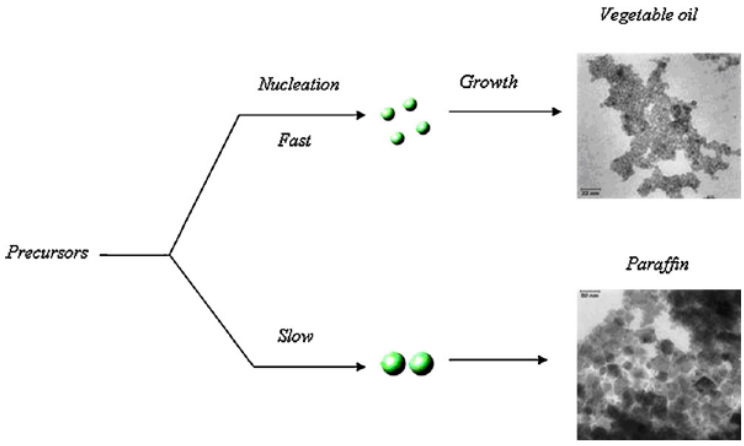

Schematic representation of nanocrystal synthesis.

Conclusion

This study has demonstrated that manganese acetate is a proper precursor for the formation of Mn_3O_4 nanoparticles. The synthesis was carried out under normal condition and without any additives by applying ultrasonic waves in different media. The results show that the size and shape of the nanoparticles depends on the type of medium and the same product was formed in different media. The XRD patterns confirm that the ultrasound can crystallize the product without calcinations. The higher crystallinity was found when the continuous phase was mineral oil. Ultrasound itself generates strong forces for proper dispersion of oil phases in water.

The droplets act as a reactor for the formation of the product and affected the shape and size of the nanoparticles.

References

[1] W. Wang, L. Ao, Synthesis and optical properties of Mn3O4 nanowires by decomposing MnCO3 nanoparticles in flux, Cryst. Growth Des. 8 (2008) 358–362.

[2] E.R. Stobble, B.A. Boer, J.W. Geus, The reduction and oxidation behaviour of manganese oxides, Catal. Today 47 (1999) 161–167.

[3] M. Sivakumar, A. Towata, K. Yasui, T. Tuziuti, Y. Iida, A new ultrasonic cavitation approach for the synthesis of zinc ferrite nanocrystals, Curr. Appl. Phys. 6 (2006) 591–593.

Hydrothermal synthesis of nanosized TiO_2 and Au/TiO_2 catalysts prepared by microwave-assisted deposition

M.M.Heravi*[a], N.Reihani[a], E.Maleki[a]

[a]*Faculty of science, Departmant of chemistry, Islamic Azad University-Mashhad Branch ,Iran*

(Email:drmh@mshdiau.ac,ir)*

Keyword: TiO_2, Hydrothermal , Au/TiO_2 , Microwave-assisted deposition

Introduction

TiO_2 has three crystal phases,i.e,anatase,rutile and brookite.nano-size TiO_2 photocatalysts has recently gained attention for their unique feartures which are different from macromoleculesin their quanta effect regional confinement of matter ,and high surface are as,etc.interestingly a series of recent reports suggested that hydrothermal methods under acidic conditions were applicable to the synthesis of rutile nanocrystallites.Gold catalysts were prepared by several methods.our study focused on synthesis of nanosized TiO_2 and then Au/TiO_2 catalyst prepared by microwave-assisted deposition method.

Experimental

Tio_2 synthesis

Nano TiO_2 was prepared by the fallowing route $TiCl_4$(100 ml,Ti 16.5 wt%) was diluted with ice-water under vigorous stirring.A 3M Na_2CO_3 aqueous solution (326 ml) was added dropwise into the transparent $TiCl_4$ aqueous to obtain a white precipitate , giving a suspension of PH =10.Hydrofluoric acid(50%) and nitric acid(60%) and ion exchanged water were added into suspension was peptized at 70 $^\circ$ C for 3h and then autoclaved(300 ml,designe by our group) at 220° C for 4h.

Catalyst preparation

Gold catalyst was prepared by microwave-assisted deposition method using $HAuCl_4$ solution as gold precursor.$HAuCl_4$ and TiO_2 were adjusted at PH=9 using 0.1M NH_4OH before illumination.The light source used was(MILESTONE MICROSYNTH MA020/A).The

irradiation time was 1 min with a stirring speed of 1500 rpm.After irradiation the solution was filtered and washed with deionized water until no Cl^- was detected with $AgNO_3$ solution.

Characterization

The nano Tio_2 particles were characterized by XRD patterns(Fig.1),and the Au/TiO_2 catalyst with a transmission electron microscopy(TEM), (Philips CM 120 KV) and a scanning electron microscopy(SEM),(VEGATS-513M M)Fig.2

Result and Discussion

Rutile phase of TiO_2 had been considered to be active and had more surface area for microwave-assisted deposition method,than another phases.when PH value increased during preparation,the amount of gold deposited on the support decreased and the best PH value was PH=9.

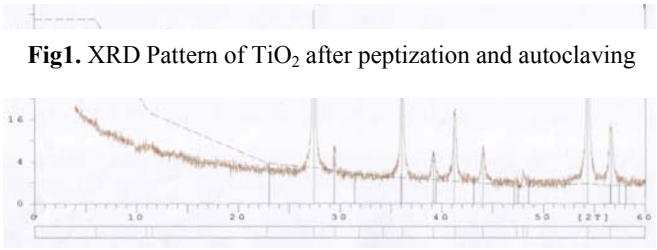

Fig1. XRD Pattern of TiO_2 after peptization and autoclaving

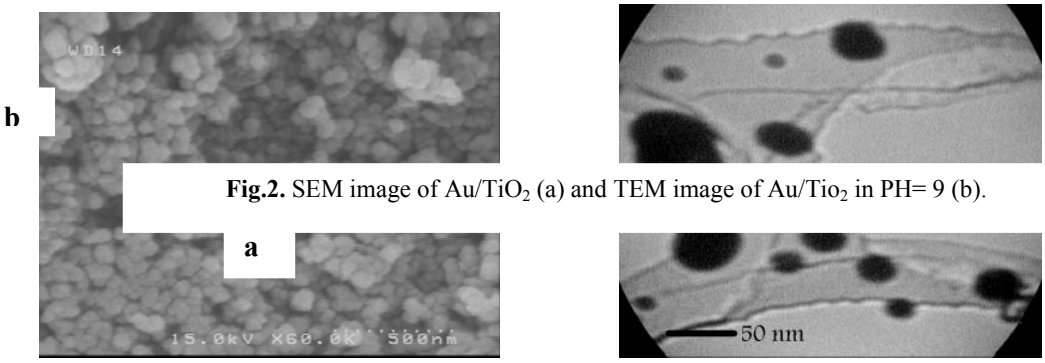

Fig.2. SEM image of Au/TiO_2 (a) and TEM image of Au/Tio_2 in PH= 9 (b).

Refrences:

[1]T. Kasuga, M.Hiramatsu, A Hoson, T.Sekino and K.Niihara, Langmuir 14 (1998) 3160.

[2] K.Yanagisawa andJ. Ovenstone, J. Phys.Chem. B, 1999 , 103, 7781.

[3] J. Yu, L.Yue, Sh Liu , B Huang , X Zhang, Elsevier 2009.03.034.

Theoritical Electrochemical Study and Free Energies of Electrontransfer of Dopamin (DA) with Fullerenes C_{60} Nanostructurs Complexes

Avat (Arman) Taherpour* and Mohammad Rizehbandi
Chemistry Department, Facullty of science, Islamic Azad University Arak Branch
P.O.Box 38135-567,, Arak, Iran.
avatarman.taherpour@gmail.com & ataherpour@iau-arak.ac.ir

Abstract: In this study, the number of carbon atoms in fullerenes was used as discriptors to establish a good relationship between the structure of Serotonin and Fullerenes C_n (n= 60, 70, 76, 82 and 86). The first to fourth free activation energies of electron transfer and kinetic rate constant of the electrontransfer, $\Delta G_{et}^{\#}{}_{(n)}$ and $k_{et}^{\#}{}_{(n)}$, n=1-4 , respectively were calculated,for Serotonin with Fulleren C_n complexes. This calculation were carried out with the Marcus in accordance theory.[1-4]

Keywords: Fulerenes, Dopamin, Rate constants, Free energies of electron transfer

Introduction:

Since its discovery in the 1950s, dopamine (DA) is one of the most significant catecholamine, belongs to the family of excitatory chemical neurotransmitter and plays a very important role in the function of central nervous, renal, hormonal and cardiovascular system, which is related with several diseases such as schizophrenia and Parkinsonism and to HIV infection

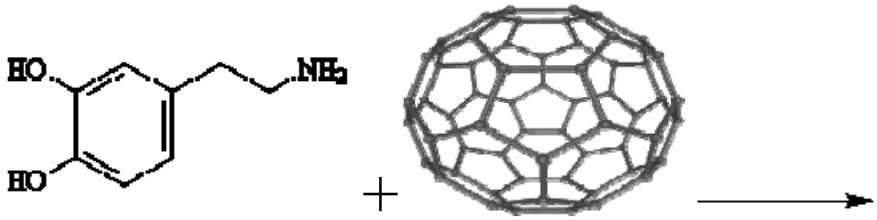

[Dopamin]@[c_n] Fig 1: Dopamin and fulleren [C_n=C_{60}, C_{70}, C_{76}, C_{82}, C_{86}]

Mathematical method:

The number of carbon atoms of these fullerenes (C_n) was utilized as a structral index for compounds. Of this study all graphs were generated using the Microsoft Office Exell 2003 program. Using the number of carbon atoms contained within the C_n fullerenes, several valuable properties of the fullerenes can be calculated. This calculation are based on theelectrontransfer theory.

Results and discussion:

By using the equations which obtained in this modeling, it is possible to calculate the values of $\Delta G_{et(1)}^{\#}$ to $\Delta G_{et(4)}^{\#}$ of [Dopamin]@[c_n] supramolecular complexes. The $\Delta G_{et(n)}$ (n=1-4) for [Dopamin]@[c_n] supramolecular complexes (C_n=C_{60}, C_{70}, C_{76}, C_{82}, C_{86}, C_{78}, C_{84}, C_{120}, C_{132}, C_{140}, C_{146}, C_{150}, C_{160}, C_{162}, C_{240}, C_{276}, C_{288} and C_{300}) are predicted by using the appropriate equations. By utilizing these results, the electron transfer energies of $\Delta G_{et(n)}$ (n=1-4) of the complexes between serotonin derivatives with fullerenes (C_{60}, C_{70}, C_{76}, C_{82}, C_{86}, C_{78}, C_{84}, C_{120}, C_{132}, C_{140}, C_{146}, C_{150}, C_{160}, C_{162}, C_{240}, C_{276}, C_{288} and C_{300}) were approximated. The calculated values of the free electron transfer energies of $\Delta G_{et(n)}^{\#}$ (n=1-4) for selected [Dopamin]@[c_n] supramolecular complexes (n = 60, 70, 76, 82 and 86) in the equations were interpreted. There was good agreement between the calculated and the predicted values. In lieu of increasing the number of carbons atoms in the fullerene structure, the values of $\Delta G_{et(n)}^{\#}$ (n=1-4) were decreased. The supramolecular complex structures which were discussed here and the calculated values of $\Delta G_{et(n)}^{\#}$ (n=1-4) corresponding to these supramolecular complexes were neither synthesized nor reported before.

References

1- A.A.Taherpour,and Maryam Maleki, *Analytical Letters*, 43: 658–673, 2010.

2- A.A.Taherpour,and Esmat Mohammadinasab, *Fullerenes*, *Nanotubes and Carbon Nanostructures*, 18: 72–86, 2010.

3- A.A.Taherpour, *Phosphorus, Sulfur, and Silicon*, 185:422–432, 2010.

4- A.A.Taherpour, *Chem Phys Lett,* 469: 135-139, 2009.

5- M. Grossman,G. Glosser, J. Kalmanson, J. Morris, M.B. Stern, H.I. Hurtig, *J. Neurol. Sci*. 184 (2001).

6- N. Rein, R.C. Rocha, H.E. Toma, *J. Inorg. Biochem*. 85 (2001) 155.

Theoritical Electrochemical Study and Free Energies of Electrontransfer of Serotonin with Fullerenes C_{60} Nanostructurs Complexes

Avat (Arman) Taherpour* and Mohammad Rizehbandi
Chemistry Department, Facullty of science, Islamic Azad University Arak Branch
P.O.Box 38135-567,, Arak, Iran.
avatarman.taherpour@gmail.com & ataherpour@iau-arak.ac.ir

Abstract: In this study, the number of carbon atoms in fullerenes was used as discriptors to establish a good relationship between the structure of Serotonin and Fullerenes C_n (n= 60, 70, 76, 82 and 86). The first to fourth free activation energies of electron transfer and kinetic rate constant of the electrontransfer, $\Delta G_{et(n)}$ and $k_{et(n)}$, n=1-4 , respectively were calculated,for Serotonin with Fulleren C_n complexes. This calculation were carried out with the Marcus in accordance theory.[1-4]

Keywords: Fullerenes, Serotonin, Free energies of electron transfer, Rate constants

Introduction:

Serotonin (5-Hydroxytryptamine) (Fig:1) is a monoamine neurotransmitter. Biochemically derived from tryptophan, serotonin is primarily found in the gastrointestinal (GI) tract, platelets, and in the central nervous system (CNS) of humans and animals. Serotonin is mainly metabolized to 5-HIAA, chiefly by the liver. Metabolism involves first oxidation by monoamine oxidase (MAO) to the corresponding aldehyde. This is followed by oxidation by aldehyde dehydrogenase to 5-HIAA, the indole acetic acid derivative.[4-6]

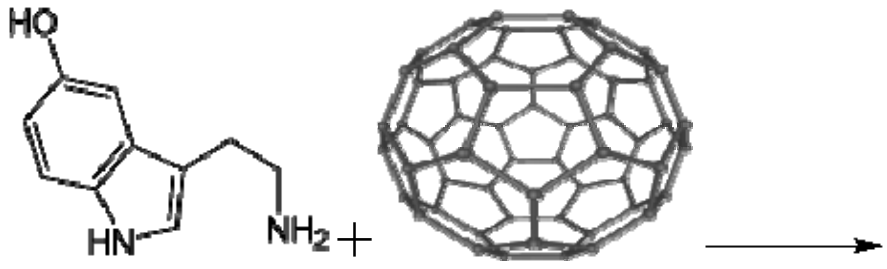

[Serotonin]@[c_n]

Fig 1: Serotonin and fulleren [C_n=C_{60}, C_{70}, C_{76}, C_{82}, C_{86}]

Mathematical method:

The number of carbon atoms of these fullerenes (C_n) was utilized as a structral index for the compounds.Of this study all graphs were generated using the Microsoft Office Exell 2003 program. Using the number of carbon atoms contained within the C_n fullerenes, several valuable properties of the fullerenes can be calculated. This calculation are based on the electrontransfer theory.

Results and discussion:

By using the equations which obtained in this modeling, it is possible to calculate the values of $\Delta G_{et(1)}$ to $\Delta G_{et(4)}$ of [Serotonin]@[c_n] supramolecular complexes. The $\Delta G_{et(n)}^{\#}$ (n=1-4) for [Serotonin]@[c_n] supramolecular complexes (C_n=C_{60}, C_{70}, C_{76}, C_{82}, C_{86}, C_{78}, C_{84}, C_{120}, C_{132}, C_{140}, C_{146}, C_{150}, C_{160}, C_{162}, C_{240}, C_{276}, C_{288} and C_{300}) are predicted by using the appropriate equations. By utilizing these results, the electron transfer energies of $\Delta G_{et(n)}$ (n=1-4) of the complexes between Serotonin derivatives with fullerenes (C_{60}, C_{70}, C_{76}, C_{82}, C_{86}, C_{78}, C_{84}, C_{120}, C_{132}, C_{140}, C_{146}, C_{150}, C_{160}, C_{162}, C_{240}, C_{276}, C_{288} and C_{300}) were approximated. The calculated values of the free electron transfer energies of $\Delta G_{et(n)}$ (n=1-4) for selected [Serotonin]@[C_n] supramolecular complexes (n = 60, 70, 76, 82 and 86) in the equations were interpreted. There was good agreement between the calculated and the predicted values. In lieu of increasing the number of carbons atoms in the fullerene structure, the values of $\Delta G_{et(n)}$ (n=1-4) were decreased. The supramolecular complex structures which were discussed here and the calculated values of $\Delta G_{et(n)}$ (n=1-4) corresponding to these supramolecular complexes were neither synthesized nor reported before.

References

1- A.A.Taherpour, *Phosphorus, Sulfur, and Silicon*, 185:422–432, 2010.

2- A.A.Taherpour and Esmat Mohammadinasab, *Fullerenes*, *Nanotubes and Carbon Nanostructures*, 18: 72–86, 2010.

3- A.A.Taherpour and Maryam Maleki, *Analytical Letters*, 43: 658–673, 2010.

4- A.A.Taherpour, *Chem Phys Lett,* 469: 135-139, 2009.
5- M Berger, *JA Gray*, BL Roth (2009)."The expanded biology of serotonin". *Annu. Rev Med.*60:355-66.

6- MM Rapport, *AA Green*, IH Page ."Serum vasoconstrictor, serotonin; isolation and characterization". *J. Biol. Chem*. 176 (3): 1243–51,1948.

Enhancement of the photocatalytic activity of doped and co-doped TiO_2 nanoparticles by metal and non-metal atoms and phase transformation

A. Reisi-Vanani* and M. hamadanian
Department of physical chemistry, Faculty of chemistry, University of Kashan, Kashan, Iran
(E-mail: areisi@kashanu.ac.ir)

Keywords: Codoped TiO_2, Sol-Gel growth, Photocatalytic activity, Nanoparticle, Degradation.

Introduction

Heterogeneous photocatalysis by TiO_2 semiconductors is promising for elimination of hazard environmental pollutants. Many techniques have been examined to achieve the extend of the absorption wavelength range of TiO_2 in visible region, such as, dye sensitized, transition metals doping [1] and noble metal deposition. Recently, C, N, S, F, B anion-doped TiO_2 photocatalysts which show a relatively high level of activity under visible-light irradiation have been reported [2]. Some studies demonstrated that the co-doping with transition metal and nonmetallic element could effectively modify the electronic structures of TiO_2 and shift its absorption edge to a lower energy [3, 4]. The sol–gel technique has been adopted as one of the versatile methods for the preparation of metal and nonmetal doped nanocrystalline TiO_2. Since this method is a solution process, it allows flexibility in parameter control with its relatively slow reaction process. This permits tailoring of certain desired structural characteristics such as compositional homogeneity, grain size, particle morphology and porosity.

Methods

The typical synthesis procedure for TiO_2 and doped TiO_2 nanoparticles has been described in our previous work [5]. Preparation of metal, nonmetal and metal-nonmetal-codoped TiO_2 nanoparticles was the same as that of TiO_2, except that the water used for the synthesis, 98.8 mL, contained the required amount of thiourea (as source of S) and $CuCl_2.2H_2O$, $Fe(NO_3)_3.9H_2O$ and $CoNO_3.6H_2O$ (as source of metals). The samples were characterized with XRD, SEM-EDX, TEM, DRS and FT-IR analysis.

Results and discussion

The XRD patterns were shown that in all samples only anatase phase structure was detected when calcination temperature was 500 °C (Fig. 1). The average size of nanoparticles was estimated from the Scherrer equation on the anatase diffraction peak (10-16 nm). Thermodynamic stability of anatase phase compared to rutile in smaller crystallites is a well known phenomenon and hence the increased stability of the anatase phase observed here is due to the restriction in crystallite growth imposed by dopant. SEM micrographs show that nanoparticles are uniform, global and slightly agglomerated. Images also reveal that the doping of metal and nonmetal does not leave any change in morphology of the catalyst surface. TEM images of samples from which the particle sizes of the samples were found to be around 8-13 nm, which confirm XRD results. It can be concluded that the addition of dopants to titania hinders the growth of nanoparticles. The DRS results show a red shift in the absorption onset value in the case of metal and nonmetal added titania that indicate dopant decreases band gap of the catalyst (Fig. 2).

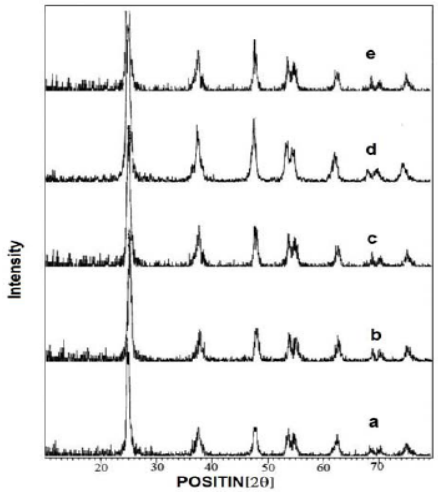

Fig. 1. XRD patterns of: (a) pure TiO_2, (b) 0.1%, (c) 0.5%, (d) 1.0% and (e) 5.0% Co/TiO_2

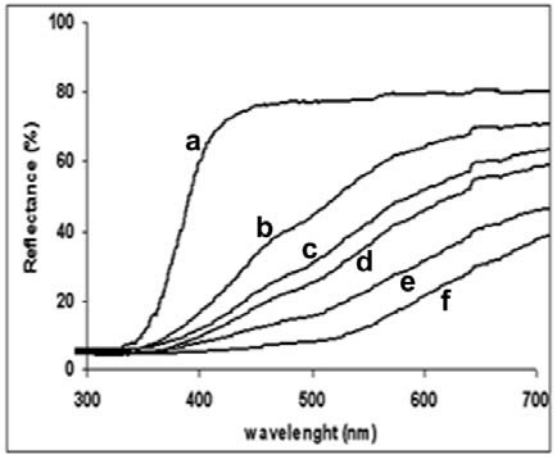

Fig. 2. DRS of (a) pure TiO_2, (b) 0.25, (c) 0.5, (d) 1.0, (e) 2.0 and (f) 5.0% Fe,0.05%S-codoped TiO_2

FT-IR spectra of samples show peaks corresponding to stretching vibrations of the O–H and bending vibrations of the adsorbed water molecules about 3350–3450 cm^{-1} and 1620–1635

cm^{-1}, respectively. In the region below 1000 cm^{-1}, several peaks were ascribed to absorption bands of Ti-O (653-550 cm^{-1}) and O-Ti-O flexion vibration (495-436cm^{-1}). Degradation of MO in the presence of samples under UV and visible irradiation was followed by UV-Vis spectroscopy. The significantly higher photocatalytic activity of metal and nonmetal codoped TiO_2 may be due to the synergetic effect of metal and nanmetal in the co-doped TiO_2. This is favorable to separate the electron-hole pairs and improve the photocatalytic activity. On the other hand, the presence of electron occupied intra band-gap levels in S-doped TiO_2 photocatalysts may be responsible for visible light absorption, which is another critical factor to improve the photocatalytic activity of the codoped TiO_2 catalyst.

Conclusions

Effect of the entrance of metal and nonmetal atom to TiO_2 nanoparticles showed that morphology and shape does not leave any change but the size decreases and photocatalytic activity increases under visible irradiation. Also results show a red shift in the absorption onset value in the case of metal and nonmetal added to titania that indicate dopant decreases band gap of the catalysts. XRD results showed only anatase phase was detected in 500 °C. Effect of calcination temperature showed the dopants have a significant role on the phase transformation and delay anatase to rutile phase transformation. Because of synergetic effects of metal and nonmetal, codoped TiO_2 catalyst has higher photocatalytic activity than undoped and doped TiO_2.

References

[1]W. Zhao, C.C. Chen, X.Z. Li, J.C. Zhao, J. Phys. Chem. B 106 (2002) 5022.
[2]R. Asahi, T. Morikawa, T. Ohwaki, K. Aoki, Y. Taga, Science 293 (2001) 269.
[3] M. Hamadanian, A. Reisi-Vanani, A. Majedi, Mater. Chem. Phys. 116 (2009) 376.
[4]X. Yang, C. Cao, K. Hohn, L. Erickson, R. Maghrang, D. Hamal, J. Catal. 252 (2007) 296.
[5]M. Hamadanian, A. Reisi-Vanani, A. Majedi, Appl. Surf. Sci. 256 (2010) 1837.

A novel multicomponent synthesis of 1,4-dihydropyrimidine Derivatives Using silver nanocrystals

Salehe Zavar, Bahareh Sadeghi*,Fereshteh Karimi,Zahra Nasirian

Department of Chemistry, Islamic Azad University, Yazd Branch, Yazd, Iran

Corresponding author E-Mail: bsadeghia@gmail.com

Keywords: Nanocrystals**,** 1,3-Diketone, Aldehydes**,** Amine

Introduction:

Over the past decade, metallic nanoparticles have drawn intense interest due to their potential applications in microelectronics , catalysis , and optics . Silver nanoparticles are mostly synthesized through various colloidal processes involving surfactant-stabilized silver nanoparticles in liquid phases through chemical reduction of silver salts in aqueous solutions.With some exceptions, most ofthe chemical synthetic approaches are based on the reduction of water-soluble silver salt precursors, $AgNO_3$ and its derivatives, by boron hydrides, alcohols, citrates, and alkyl sulfates. Heterogeneous catalysts can be recovered and reused, whereas homogeneous catalysts are less stable and contaminate reaction mixtures [1]. systems are of great interest and importance due to their applications in industry and developing technologies [2]. The use of solid acids has many advantages over liquid acids such as ease of handling, decreasing reactor and plant corrosion problems, and environmentally safe disposal [3]. Azaheterocycles constitute a very important class of compounds. In particular, pyrimidines are of chemical and pharmacological interest. Compounds containing a pyrimidine ring system have been shown to possess antitumor, antibacterial, antifungal,anticonvulsant activities [4].

Methods:

Preparation of silver nanoparticles:

Silver nitrate (3 mol) and DDA (0.3 mol) were dissolved into n-butylamine (2 mol)/toluene (300 ml) completely, which resulted in a molar concentration [Ag] above 2 M. After addition of equimolarreductant, the solution became dark brown and then was refluxed for 1 h. After

completion of the reaction, products were precipitated by addition of an acetone/methanol mixture. The precipitates were collected through a glass funnel filter and then washed several times with methanol and acetone.

General procedure for the synthesis of dihydropyrimidines:

A mixture of the aldehyde, the 1,3-diketone,amine, ammonium acetate and silver nanocrystals in ethanol was refluxed. The progress of the reaction was followed by TLC.After the completion of the reaction, the mixture was filtered to remove the catalyst. By evaporation of the solvent, the crude product was recrystallized from ethanol to obtain the pure compound.

Results and discussion:

In this paper, we attempted to synthesize organicsolublesilver nanocrystalsin the organic phase using silver nitrate as a precursor. Also, these silver nanocrystals have to satisfy low cost and stable dispersability. The former may be achieved through synthesis of narrowly dispersed silver nanocrystals in the highly concentrated organic phase using only cheap generic chemicals. In continution of our investigation about application of solid acids in organic synthesis [5] we investigated the synthesis of 1,4-dihydropyrimidinein the presence of silver nanocrystals as a inorganic solid acid. To optimize the reaction conditions, the reaction of 3-nitro benzaldehyde,acetylacetone and *O*-Anisidinewas used as a model reaction. According to the obtained data, using the silver nanocrystals(0.002 g) under solvent (EtOH) in reflux is the best condition for the 1,4-dihydropyrimidin formation. Therefore, some benzaldehyde,amine and 1,3-diketonewere subjected to 1,4-dihydropyrimidin(Scheme 1).

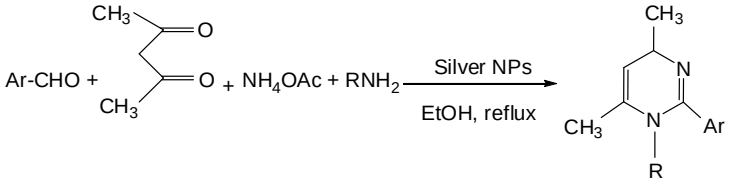

Scheme1.silvernanocrystalscatalyzed synthesis of dihydropyrimidine.

Conclusion:

In this work we report a mild procedure for the synthesis of different 1,4-dihydropyrimidin by solid phase acidic catalyst with improved yields.

References

[1] Minakata, S.; Komatsu, M.*Chem. Rev.* 711-724.

[2] Sheldon,R.A.;Downing,R.S. *Appl. Catal. A Gen.***1999,**189, 163.

[3]Mirjalili, B. F.; Hashemi, M. M.; Sadeghi, B.;Emtiazi,H.*J Chin ChemSoc*,**2009**, *56*,38.

[4] Agarwal, A.; Srivastava, K.; Puri, S.K.; Chauhan, P.M.S. *Bioorg. Med. Chem.* **2005**, *13*, 4645.

[5] Sadeghi, B.; Mirjalili, B. F.; Hashemi, M. M. *Tetrahedron Lett.* **2008**, *49*, 2575.

Controlling the nucleation and growth process in the synthesis of copper Nanopowder Via disproportionation method

Y.Zeraatkish*[a],E.Keshavarzy[b],Y.Ghayb[c]

[a]*Department of Chemistry, Isfahan University of* Technology

EMAIL:YOSEFKISH2@GMAIL.COM

[b]*Department of Chemistry, Isfahan University of* Technology

[c]*Department of Chemistry, Isfahan University of* Technology

Keywords: disproportionation, nucleation, Plasmonic spectra, inorganic polymer, effective collision

Introduction

There are diverse approaches to the preparation of the copper nanopowder. Some of them are controlled chemical reduction [1], electrochemical reduction [2], γ-Irradiation [3] and Sonochemical [4] techniques. In this project copper Nanopowder were synthesized via disproportionation reaction in aqueous solution. The effects of temperature and the kinetics of nucleation as physical factors were investigated on the size of particles. Temperature and nucleation rate controlling was performed by gradually replacing of HCl with NaCl during the reactions. The kind, size and shape of Copper Nanopowder were characterized by X-ray diffraction (XRD), scanning electron microscopy (SEM) respectively. The Plasmonic spectra of some samples were obtained.

Expriments:

10 gr $CuCl_2.2H_2O$ dissolved in 25 ml distilled water. The specific value of HCl / NaCl or both added to this solution (table 1). After that 1gr Cu^0 dissolved in the solution with heating above 60 $C^0$and stirring spontaneously. After disappearing of Cu^0 from the reaction dish, a solution of ethylene diamine (6.3 mL) in distilled water (40 mL) that was prepared in another beaker was added to the reaction dish. Copper powder precipitated in the bottom of the reaction dish. The powder obtained, was washed with distilled water and was dried at room condition.

Result and discussion:

XRD pattern of sample demonstrates the formation of pure copper particles (figure: 1).As can be seen in table (1) reducing the amount of acid from experiments (1-5) decreases the maximum wavelength (λ_m) of Plasmonic spectra, this indicates that the particles size are reduced [5].reducing the particles size is caused by decreasing the amount of reaction heat from experiments. In the experiments (1-5) used HCL that is a strong acid and en ligand as strong base. High heat that is produced via acid – base reaction between en and HCl in the end stage of experiments caused growth in the particles size. High temperature increases collision between the nucleuses during nucleus generation. These effective collisions increase the growth of particles. Experiment (5) yielded particles size is smaller than the particle size produced in experiment (1) because of reducing the HCl value from reaction and replacing it with NaCl that caused reducing in the heat of acid –bas reaction. The SEM images show that the particles of sample No.5 (figure: 2) is smaller than sample No. 1 particles (figure: 3). This result is conformed to alterations of maximum wavelengths (table1). One important note is that the spectrum of sample No. 6 has no any pick in its Plasmonic spectrum (table: 1). The SEM image shows that the particles size of sample No. 6 has a micrometer scale (4). Comparing the SEM images of samples No. 6 and No. 5 Shows that the completely eliminating of acid from synthesis process has caused much growth (nano to micro dimension) in the particles size. This growth is resulted by formation of an inorganic polymer [6] in the solution that this polymer decreased the reaction kinetics and nucleation process rate. Therefore decreasing the nucleation process rate caused the growing in the particles size.

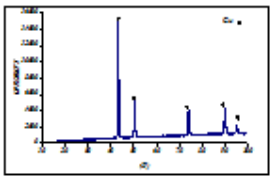

Figure1:XRD pattern

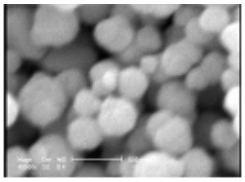

Figure2:SEM image of sample 1

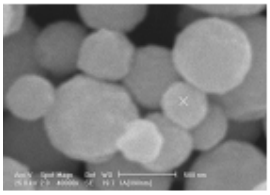

Figure3: SEM image of sample 1

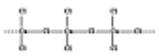

Figure 5:Inorganic polymer

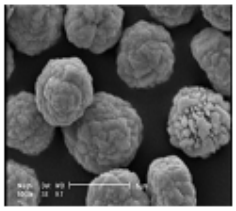

Figure4:SEM image of sample 6

Table: 1

Ex.No	HCl (ml)	NaCl (gr)	$CuCl_2$ (gr)	Cu^0 (gr)	En (ml)	λ_{max}
1	5	0	10	1	75	617
2	4	1	10	1	75	612
3	3	2	10	1	75	605
4	2	3	10	1	75	604
5	1	4	10	1	75	596
6	0	5	10	1	75	-

Conclusion:

Results show that HCl replacing with NaCl without complete elimination of HCl decreased copper particles size in the disproportionation reaction. Complete elimination of HCl caused the great growth in the copper particles size and producing the micrometer particles.

References:

[1] Cheng, X. Zhang, X. Yin, H. Wang, A, 2006, Applied Surface Science, 253, 2727.

[2] Zhang, J. Liu, W. Sun, J. Sun, H. Guo, J. 2006, Materials Science and Engineering ,433,257.

[3] Joshi, S.S., Patil, S. F. Iyer, V. and Mahumuni, S. 1998, NanoStructured Materials. 107, 1135.

[4] Dhas, A.N, 1998, Chemical Matterial. 10, 1446.

[5] Chan, G.H., Zhao, ., Hicks, E.M and Schatz, G.C., *Nano Letters*, Vol. 7, No. 7, 1947, 2007.

[6] Shriver, D.F., Atkins, P.W., Inorganic Chemistry, Oxford University Press, 1999.

The effect of normal extractors on copper nanopowder Size and morphology

Y. Zeraatkish*[a], E. Keshavarzy[b], Y. Ghayeb [c]
[a,b,c]Department of Chemistry, Isfahan University of Technology
EMAIL:YOSEFKISH2@GMAIL.COM

Keywords: normal extractor**,** disproportionation**,** aqueous medium**,**

Introduction

There is significant interest and ongoing research in the preparation and synthesis of nanomaterials [1]. The shape and size of a nanoparticle influences its properties and they are two important parameters to application of nanoparticles [1, 2]. Copper nanoparticles have many applications in science and technology therefore synthesis and controlling the size and morphology of copper nanoparticles is earned much attention in the last decade [3-11].

In this project in order to understand the effects of normal extractors on size and morphology of Cu nanopowder synthesized by disproportionation reaction in aqueous medium three organic liquids chloroform(CH_3Cl), n-hexane(C_6H_8) and dichloromethane(CH_2Cl_2) used as extractors .The particles size and morphology were investigated using scanning electron microscopy (SEM).The results show that using n-hexane and chloroform as extractor deceased the copper particles size while dichloromethane extractor caused interesting change in morphology of the particles.

Method

Copper nanopowder was synthesized via disproportionation method in aqueous medium [12]. In reported method after preparation of Cu^+ (aq) to performance of disproportionation reaction and appearing of copper precipitation ethylene diamine (en) is added into solution as a strong ligand [12].But in current project before initiation of the disproportionation reaction (before adding the ligand) an extractor (n-hexane, chloroform or dichloromethane) is added into solution dish. After mixing two phases (extractor and aqueous solution) with intense stirring the reaction would be initiated by adding the ligand (en).The copper particles appeared in extractor phase and then were collected for analysis.

Results and discussion

Figure 1 is the SEM image of copper nanopowder that synthesized via disproportionation reaction without the presence of any extractor. Figures 2 and 3 show a great decreasing in particles size that synthesized at presence of 180 ml n-hexane as extractor. These images brightly show that copper particles size are less than 100 nanometer figure 3. The SEM images of synthesized copper particles at presence of 180 ml chloroform show the aggregations of tiny particles figure 4, 5. But the SEM images of the particles that synthesized at presence of dichloromethane show different morphology and no great decreasing in the particles size figure 6, 7. In these images (figure 6, 7) is observed nanometeric particles that form huge spherical microparticles.

In these experiments organic liquids extract metal nucleus in the growth stage of particle production that this action prohibited growth of particles.

In absence of coating agents all particles flocculated after preparation figure 3,5,7. Also the results indicate that the particles size and morphology depend on properties of extractors. N-hexane and chloroform that have lower dielectric constant (1.9, 4.8 respectively) and polarity than dichloromethane (9.1) caused more decreasing in particles size.

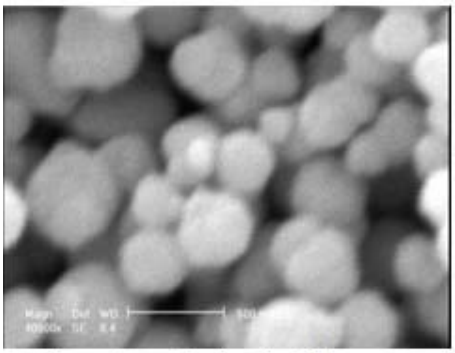

Figure1:scale bar is 500 nm

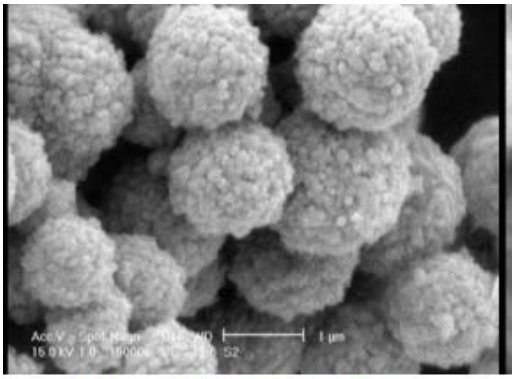

Figure 2: scale bar is 1 µm

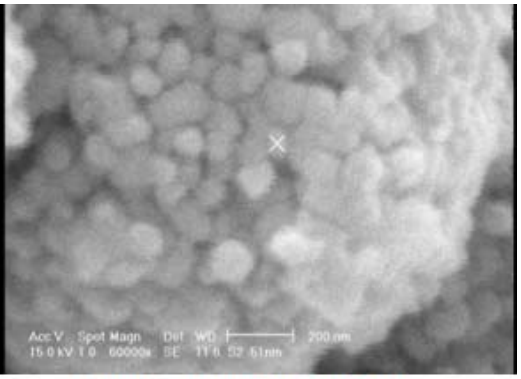

Figure 3:scale bar is 200nm

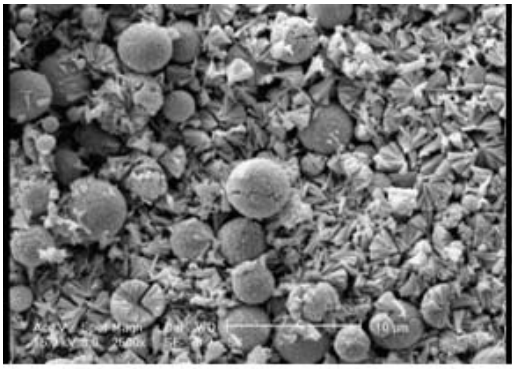

Figure 4: scale bar is 10 µm

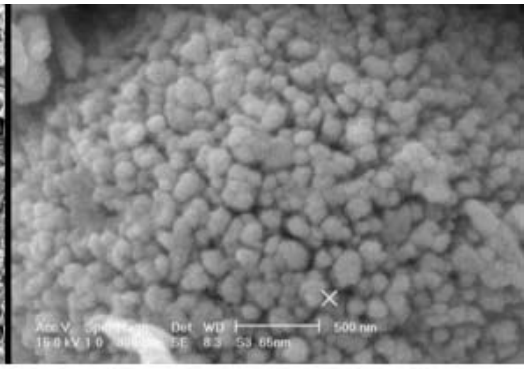

Figure 5: scale bar is 500nm

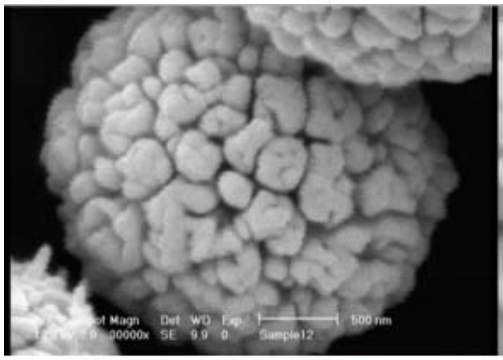

Figure6: scale bar 500nm

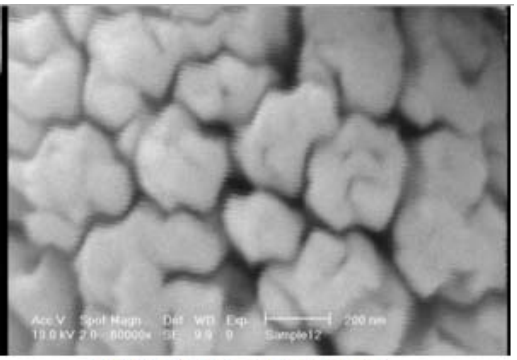

Figure7:scale bar 200nm

Conclusion

In this project the effect of three organic extractors examined on size and shape of the copper particles that synthesized via disproportionation method in aqueous solution. The results show all obtained particles are spherical and size of particles decreased with decreasing polarity and dielectric constant of extractors.

References

[1] Jason B. Thompson, and Christopher B. Roberts *J. Phys. Chem. B* **2001,** *105,* 2297-2302.

[2] Tapan K. Sau, Andrey L. Rogach, Frank Ja¨ckel, Thomas A. Klar, and Jochen Feldmann, Adv. Mater. 2010, 22, 1805–1825

[3].Ren, X. Chen, D. and Tang, F., 2005, Chemical Physics, 109, 15803.

[4].Khanna, P.K. Gaikwad, S. Adhyapak, P.V. Singh, N. Marimuthu, R. 2007, Materials Letters, 61,4711.

[5].Joshi, S.S., Patil, S. F. Iyer, V. and Mahumuni, S. 1998, NanoStructured Materials. 107, 1135.

[6] Dhas, A.N, 1998, Chemical Matterial. 10, 1446.

[7]. Haas, I. Shanmugum, S. and Gedanken, A., 2006, Chemical Physics, 110, 16947.

[8].Salkar, R.A. Jeevandam, P. Kataby, G. et al,2000, Chemical Physics,104,893.

[9].Zhang, J. et all. 2006, Materials Science and Engineering ,433,257.

[10]. H Zhu, H. Zhang, C. Yin, Y. 2004, *Journal of Crystal Growth*, 270,722.

[11]Zhang, X. Cheng, X. Yin, H. Yuan, J. C. Xu, C. 2008, Applied surface science, 254, 5757.

[12] Zeraatkish, Y. Modification copper nanopowder synthesis and synthesis copper and copper oxide nanopowder via disproportionation method, M.S Thesis, Isfahan University of technology.2009

Study of Absorption Hydrogen in Different Places of C_{24} by Density Functional Theory (DFT) Computational Chemistry Method

Narges Bagheri [1]*, Mohammad Erfan Zand[2]

Department of Chemistry, Islamic Azad University, Firoozabad Branch, P. O. Box 74715-117 Firoozabad, Fars, Iran

[1](nrgs.bagheri@gmail.com)

[2](Erfanzand@gmail.com)

Keywords: Fullerene, Hydrogen, Adsorption, DFT, Energy Gap

Introduction

One of the most interesting discoveries of the last two decades by a new form of carbon other has been Fullerene name compound that have the shape of carbon [1]. Computational chemistry methods can be used to analysis of nano materials [2]. Developments in electronic structure methods, in particular in density functional theory (DFT), with the continuous increase of available computing capacities to deliver unprecedented power to computational experiments on atomistic level . Robustness of DFT makes this technique the method of choice in assisting the design and development of the next generation of devices for nanoscale applications. The underlying principle of DFT is that the total energy of the system is a unique functional of the electron density, hence it is natural that there exist a large number of computer programs that are designed for calculations of the total energy [3].

Computational method

All calculations have been performed in gas phase using Density Functional Theory (DFT) method of B3LYP at 6-31G* standard basis set is used Gaussian 03w package of program.

Results and details

In this work, we have studied adsorption of hydrogen in different 21 places of C_{24} and three point of coordinated axis by Density Functional Theory (DFT) computational method.

After doing the calculation, we have obtained the total energy of system, HLG (HOMO – LUMO Gap).

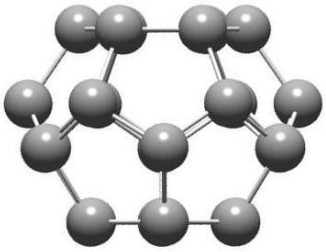

Fig 1 – structure of C_{24} (Up and Down C_{24} is absorption site)

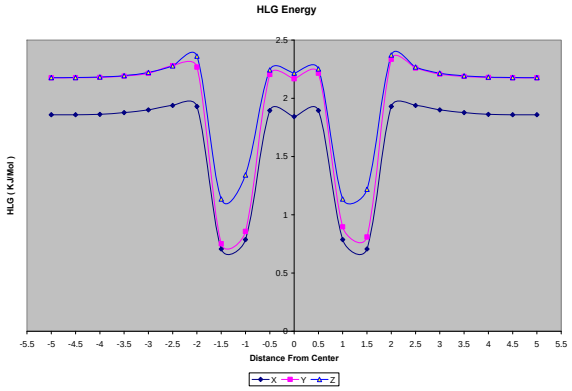

Chart 1 – HOMO – LUMO - GAP energy (KJ/Mol)

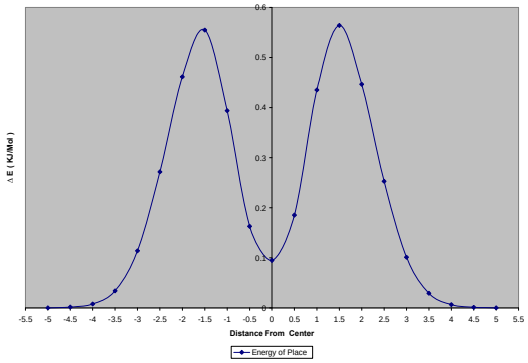

Chart 2 – Total energy of C_{24} and H_2 system (KJ/Mol)

Conclusion

In this paper, it has been investigated the most stable structure of hydrogen with C_{24} in different places of the molecule. To gain this purpose, the total energy of system has been calculated in different places from 5 A^0 of molecule to carbon center and then in different points to 5 A^0 from carbon center of C_{24}. Based on theoretical observation and reviewing the HLG energy, we found the stable place in center of C_{24}.Diagram of energy is plotted in Chart 1 and 2. HLG parameter has been calculated. The results show that the most stable structure has the greatest value of Homo-Lumo energy.

Reference

[1] H.W. Kroto, J.R. Heath, S.C. OflBrien, R.F. Curl, R.E. Smalley, Nature 318 (1985) 162.

[2] B. Sitharaman, R.D. Bolskar, I. Rusakova, L.J. Wilson, Nano Lett. 4 (2004) 2373.

[3] A.D. Becke, Phys. Rev. A 38 (1998) 3098.

Synthesis and theoretical modeling of Platinum nano-particle on Al2O3 in presence of various ionic liquids for kinetic investigation of hydrogenation reactions

Leila Ziedabadinejad [a], Mahbubeh Tasviri [a], Reza Vatan Meidanshahi [b], Mohammad Reza Golami[a]

[a] Department of Chemistry, Sharif University of Technology, Tehran, Iran

[b] Department of Chemistry and Biochemistry, Georgia Institute of Technology, Georgia, USA

lzeidabadi@yahoo.com

Introduction

Room temperature ionic liquids (ILs), which are generally composed of a bulky organic cation and a weakly coordinating anion, have attracted significant attention in many fields of chemistry and industry as environmentally benign solvents. ILs have many advantages, such as a low interface intension and high chemical and thermal stability[1]. They can create an electrostatic protection layer for the transition- metal nanoparticles[2]. Dupont et al. and other researchers 27-29 have recently reported that imidazoliumbased ionic liquids are an interesting medium for the formation and stabilization of catalytically active transitionmetal nanoparticles such as Pt, Pd, Ir, Rh, Co, Au, and Ag. However, up to now, no studies have been reported for the creation of Pt(0) in ionic liquids, and the role of ILs played in the formation of nanoparticles is not clear.[3]

However, the wide spread use of ILs have been limited due to their high cost and lack of knowledge of their physico-chemical properties and their biodegradability concerns. Economical catalysts can be introduced by coating the surface of heterogeneous catalyst with ILs, which even have small amounts of ILs, provide the same catalytic properties as the bulk sample.

There are several different techniques and approaches that can be used to immobilize and support ILs, such as simple impregnation, grafting, polymerization, sol-gel method, encapsulation, or pore trapping[4]. A novel, straightforward preparation method involves impregnation of the support material with an IL, diluted with a molecular solvent that is easily evaporated, such as acetone. The dilution followed by evaporation of the co-solvent results in a uniform and thin ionic liquid layer on the support material. The IL can be assumed to remain liquid when immobilized on a solid support, because if the IL formed a solid surface

on palladium particles, the catalyst would not be as active as it is. As SILCA catalysts prepared in such a way are applied in a liquid-phase process, a bulk solvent that is not miscible with the IL should be selected. In parallel to the ionic liquid immobilization, transition-metal ions or complexes can be dissolved into the IL layer. These organometallic species can then further be reduced to metallic nanoparticles. In this work, Pt nanoparticle was synthesis by uniform and thin various ionic liquid layer on the support material and mixture of ILs have been used to elucidate the influence of IL on catalyst selectivity in hydrogenation of C=C and C=O double bond. The catalysts have been prepared by simple impregnation method, and then synchronized hydrogenation cyclohexene and acetone has been investigated as a reaction model.

Experimental

Several different SILCAs were prepared according to the following method. IL (~150 mg) and hexacholoro palatinate acid ($Pt(Cl)_6$) (50 mg; Aldrich, 99%) were both dissolved into dry metanol (15 mL). The solution was poured over a Al_2O_3. Wetted catalyst was kept in an oven, at 80 °C, for 2 h until all metanol was evaporated, thus leaving only a layer of IL on Al_2O_3 into which $Pt(Cl)_6$ was dissolved. Catalysts were reduced at 120 °C under hydrogen flow, leaving platinum nanoparticles in an IL layer on Al_2O_3. As a result in all cases, a catalyst that contained platinum nanoparticles residing in an IL layer which, in turn, was immobilized on Al_2O_3 was achieved.

Result and disscution

The XRD pattern of Pt/Al_2O_3 shows four peaks at 2θ=40, 46.7, 67.7 and 81.7 which are attributed to (111), (200), (220) and (311) plans respectively and match well with those expected for FCC platinum crystals. Mean size of Pt nano particle supported on alumina was calculated from XRD line broadening using Scherrer's equation, $L = 0.94\lambda/b\cos\theta$; in which λ is the wavelength of X-ray and b is the relative peak broadening. The crystalline size of 5.3 nm was obtained for Pt particles.. SEM images reveal that nanoparticles in the in presence of ionic liquid are uniform with average size 25nm. In the presence of pure HEAF, hydrogenation of C=O bond toward to C=C bond shows the most selectivities and rates.

Conclution

A kinetic model based on surface reactions as rate-determining steps was derived for the hydrogenation of cyclohexene with supported ionic liquid catalysts (SILCAs). The model was successfully applied to the hydrogenation of cyclohexene over two catalysts that contained different ionic liquids and palladium particles on γ-alummina.

As demonstrated by this hydrogenation process, it is evident that an ionic liquid layer residing on a heterogeneous support can enhance the reaction rate and affect the selectivity of the reaction, even though only small amounts of ionic liquids and active metals were used in the catalysts. Thus, an enhanced catalyst performance can be reached in an economic and elegant way. Rahmani.atefeh@yahoo.com

references

[1].Pasi V, Tapio S, and Jyri-Pekka Mikkola, Kinetics of Cinnamaldehyde Hydrogenation by Supported Ionic Liquid Catalysts (SILCA). Ind. Eng. Chem. Res. 2009, 48, 10335—10342.

[2].Bonho te, P.; Dias, A.-P.; Papageorgiou, N.; Kalyanasundaram, K.; Gra‹tzel, M. Hydrophobic, Highly Conductive Ambient Temperature Molten Salts. Inorg. Chem. 1996, 35, 1168.

[3]. Rogers, R. D.; Seddon, K. R. Ionic LiquidssSolvents of the Future. Science 2003, 302, 792.

[4]. Seddon, K. R. Ionic Liquids a Taste of the Future. Nature Mater. 2003, 2, 363.

FABRICATION, CHARACTERIZATION,AND MEASUREMENT OF SOME TRANSPORT PROPERTIES OF α-Fe_2O_3 AND Fe_3O_4 MAGNETIC NANOFLUIDS

Elaheh K. Goharshadi[a,b], Sayyed Hashem Sajjadi[c], Maryam Abareshi,[a] and, Seyed Mojtaba Zebarjadd[d]

Email: gohari@ferdowsi.um.ac.ir

[a] Department of Chemistry, Ferdowsi University of Mashhad, Mashhad 91779, Iran

[b]Center of Nano Research, Ferdowsi University of Mashhad, Mashhad 91775-1436, Iran

[c] Department of Chemistry, Sharif University of Technology, Tehran, Iran

[d]Department of Materials Science and Engineering, Engineering Faculty, Ferdowsi University of Mashhad, Mashhad, 91775-1111, Iran

Keywords: Magnetic nanoparticles, Nanofluid,Viscosity, Thermal conductivity.

Introduction

Nanosized iron oxide particles have multiple practical applications, for example, in drug delivery, magnetic hyperthermia, magnetic resonance imaging, pigments, and photocatalysis [1]. The magnetic nanofluid, ferrofluid, behaves as a smart fluid due to some of its unique features. They have some applications in a variety of fields such as electronic packing, mechanical engineering, aerospace, and bioengineering [2,3].

Although the magnetic properties of the magnetic nanofluids are the subject of intensive studies, there are few data in the literature concerning their thermal and rheolegical properties. The first goal of the present study is to investigate the effect of both temperature and volume fraction on the thermal conductivity of Fe_3O_4-water nanofluids. For this purpose, we were synthesized Fe_3O_4 nanoparticles by co-precipitation method. The second aim of this work is to measure the viscosity of □□Fe_2O_3-glycerol nanofluids as a function of temperature, volume fraction, and shear rate. For this purpose, we were synthesized □□Fe_2O_3 nanoparticles with solvothermal route.

Results and discussion

Superparamagnetic Fe_3O_4 nanoparticles were successfully synthesized by a simple and cost-effective co-precipitation method in different conditions. The XRD, TEM,FTIR, and VSM techniques were used to characterize the structure, size, purity, and magnetic properties of the nanoparticles. The best crystallinity was observed for pH initial=1.5 and pH final = 9.5. Fe_3O_4 nanofluids were prepared by dispersing Fe_3O_4 nanoparticles in distilled water as the base fluid. Tetramethyl ammonium hydroxide was used to improve the dispersion of Fe_3O_4 in distilled water. Measurement of zeta potential of nanofluids shows that Fe_3O_4 nanofluids have good stability.

The effective thermal conductivity of Fe_3O_4 nanofluids with different volume fractions was investigated experimentally at 10, 20, 30, and 40 ^oC. The experimental results were also compared with some different theoretical models. Among the models, the Murshed model gives better predictions of the thermal conductivity of these nanofluids compared with the classical models.

□□□□□Fe_2O_3 nanoparticles were prepared by solvothermal method. The nanoparticles were characterized by XRD and TEM. The □□Fe_2O_3 nanoparticles were dispersed in a glycerol as the base fluid. Both experimental and theoretical work was performed on the rheological behavior of α-Fe_2O_3-glycerol nanofluids. The experiments were done at different temperatures, shear rates, and volume fractions.

Conclusions

The measurement of thermal conductivity and viscosity of Fe_3O_4 and nanofluids contains the following conclusions:

1. The relative thermal conductivity of nanofluids increases with increasing volume fraction and temperature.
2. Thermal conductivity of Fe_3O_4 nanofluids increases up to 11.5% as the volume fraction of nanoparticles increase up to 3 vol % at 40 ^oC.
3. α-Fe_2O_3-glycerol nanofluids are non-Newtonian fluids with shear-thinning. The viscosity of nanofluids significantly decreases with increasing temperature and increases with increasing particle volumeconcentration.
4. The rheological behavior of □□Fe_2O_3-glycerol nanofluids can not be predicted by Einstein, Brinkman, and Batchelor models.

References

[1] S. W. Cao and Y. J. Phys. Chem. C 112 (2008) 6253.

[2] J. Li, Y. Huang, X. Liu, Y. Lin, L. Bai, and Q. Li, Sci. Tech. Adv. Mater. 8 (2007) 448.

[3] R. Tackett, C. Sudakar, R. Naik, G. Lawes, C. Rablau, and P. P. Vaishnava, J. Magn. Magn. Mater. 320 (2008) 2755.

Vibrational Spectroscopic Investigations , Ab Initio and DFT Studies of Structure Nano Fullerene ($C_{20}MnH$) and Nano Fullerene ($N_{10}B_{10}MnH$)

H.Soleymanabadi[a] and R.Soleymani*[a,b]

[a] *Chemistry Department, Faculty of Sciences, Islamic Azad University, Touyserkan Branch, Young researchers Club, Touyserkan ,Iran*

(Email: nima_soleimany@yahoo.com)

[b] *Chemistry Department, Faculty of Sciences, Islamic Azad University Shahre-rey Branch, Tehran, Iran*

Keywords: Ab initio; DFT ; Nano fullerene ; Vibrational spectroscopic

Introduction

This structures is not synthesized empirically in laboratory. But mechanic quantum calculation showed this two structure has higher stability. This compositions characteristics are as follows : or structure Nano fullerene (1) Molecular mass 295.94587 amu , empirical formula $C_{20}MnH$, number of atoms 22 , number of bonds 36 , bond length B-C (1.30 to 1.42 A) and point group C_1, m/z: 304.08 (100.0%), 305.07 (90.9%), 303.08 (65.7%), 306.07 (38.4%), 302.08 (28.4%), 301.09 (8.4%), 300.09 (1.7%), 307.07 (1.4%) , Elemental Analysis: B, 35.55; H, 0.33; Mn, 18.06; N, 46.06 Also for structure Nano fullerene(2) molecular mass 306.06966 amu , empirical formula $N_{10}B_{10}MnH$,number of atoms 22 ,number of bond 36 and bond length C-C (1.1 to 1.5 A) and point group C_1, m/z: 295.95 (100.0%), 296.95 (21.6%), 297.95 (2.2%) , Elemental Analysis: C, 81.11; H, 0.34; Mn, 18.55 [1].

1

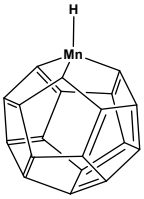

2

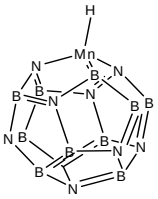

Calculation method

For calculation ab initio and DFT method used computer pentum 4 PC (intel core i7 2.66 GHZ

processor with 4 GB of RAM) . Firstly designed nano fullerene by nano tube software and for final optimization used Gaussian 98 Package of programs with B3LYP method by 3-21G and 6-31G basic set. Also for calculation Natural Bond Orbital used NBO-version 3 soft ware.

Result and discussion

Infrared spectrum 1 and 2 structure compared and its description is reported in table 1. Also different amount of energy level are reported in table 2.

TABLE 1: Results Infrared Spectrum (IR) and important mode nos for structure 1 and 2.

Structure	1		2	
Method	B3LYP/6-31G		B3LYP/6-31G	
Important mode nos	Intensity	Wave number (cm^{-1})	Intensity	Wave number (cm^{-1})
1	9.0821	705.260	50.751	721.111
2	13.176	773.700	36.369	759.288
3	28.740	1040.41	35.546	1101.81
4	20.350	1204.63	42.216	1120.61
5	39.562	1279.64	108.59	1155.84
6	54.749	1316.62	386.22	1202.92
7	10.057	1379.96	398.86	1289.33
8	153.03	1410.73	186.41	1395.79
9	194.69	1965.56	276.89	1935.58

TABLE 2: The results total energy(E_0) , Zero point energy (ZPE) , Entropy (S) in temperatures 298.15 K , Total energy thermal (E thermal)

Structure	**1**							
Method	B3LYP/3-21G				B3LYP/6-31G			
Geometry	ZPE[a]	E_0[a]	Entropy[b]	E (Thermal)[a]	ZPE[a]	E_0[a]	Entropy[b]	E (Thermal)[a]
Amount	75.769	-1194245.433	93.223	81.475	75.524	-1200091.274	94.405	81.419
Structure	**2**							
Method	B3LYP/3-21G				B3LYP/6-31G			
Geometry	ZPE[a]	E_0[a]	Entropy[b]	E (Thermal)[a]	ZPE[a]	E_0[a]	Entropy[b]	E (Thermal)[a]
Amount	68.164	-1216064.192	99.932	75.038	67.867	-1221998.312	100.57	74.835

[a]: in Kcal/mol
[b]: in Cal/mol.Kelvin

Conclusion

Calculation Ab initio and DFT method showed amount total energy for structure 1 equal -1200091.274 Kcal/mol and for structure 2 equal -1221998.312 Kcal/mol which shows high stability of structure 2. Also NBO analysis showed that amount of pay electron movement are high and this caused a change in bond order amount.

References :

[1] An Yong Li and Qian Shu Li, A new method for electronic structure of the fullerene C_{20} *Journal of molecular structure THEOCHEM* ,volume 432, 25 May **1998**, Pages 115-120

[2]M. J. Frisch et al, *GAUSSIAN 98* (Revision A.3) Gaussian, Inc.: Pittsburgh, PA, USA, **1998**.

Photoluminescence emission and UV-vis absorption investigation of ZnO nanostructures: effect of size and morphology

Moeen Sohrabi, Mehdi Rezapour*
Department of chemistry, Faculty of science, Islamic azad university, Shareza branch, Shahraza, Isfahan, Iran
Corresponding author's E-mail: rezapoor.mehdi@yahoo.com

Abstract

ZnO nanostructures (NSs) with different size and morphologies have been synthesized by solvothermal synthesis method and Photoluminescence emission, UV-vis absorption have been studied. The obtained products have been characterized by means of XRD, SEM and BET.

Results showed that size and morphology can effectively influence the Photoluminescence emission and UV-vis absorption of ZnO NSs.

Keywords: Photoluminescence emission, UV-vis absorption, ZnO nanostructure, Morphology.

Introduction:

The formation of nanostructures with controlled size and morphologies has been the focus of intensive research recently [1]. ZnO is a semiconductor with wide bandgap of 3.37 eV and a large exciton binding energy of 60 meV. ZnO has received much research attention due to its low toxicity and low price, high chemical and thermal stability, high transparency in the visible wavelength range, unique optical properties. In this study we investigated that how the morphology and size of ZnO NSs can influence the Photoluminescence emission and UV-vis absorption properties.

Experimental:

Appropriate amount of Zinc acetate dihydtate and solvent mixed under vigorous stirring. Then transferred into stainless steel autoclave and kept for 20 hours at 150 Cº. Obtained powders washed with ethanol and DDI water and dried at 80 Cº. For synthesis of ZnO nanorod, 1-hexanol was used as solvent and for synthesis of ZnO nanoparticles, ethanol was used as solvent.

Results and discussions:

Figure 1 shows the XRD pattern of ZnO NSs. As you can see all peaks are sharp and intense that reveals well crystalline ZnO have been synthesized. The calculated size shows that ZnO nanoparticles are larger than nanorods (nanoparticles: 55 nm, nano rods: 38 nm).

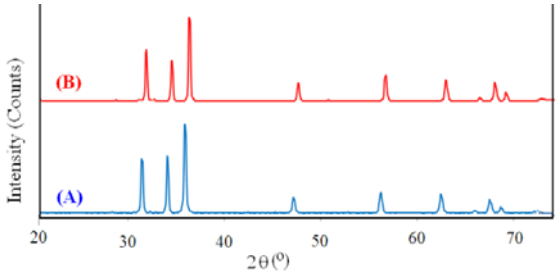

Fig. 1. XRD pattern of A: ZnO nanoparticles and B: ZnO nanorods.

Figure 2 shows SEM images of ZnO NSs. Results shows that ZnO nanoparticles and nanorods have been synthesized. And also the size results of XRD confirms by SEM.

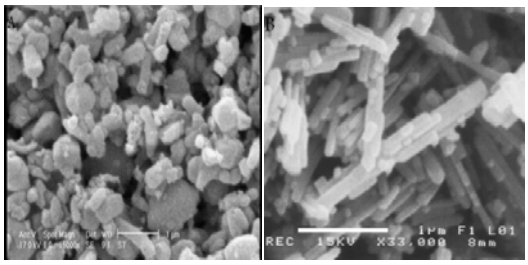

Fig. 2. SEM images of left: ZnO nanoparticles and right: ZnO nanorods.

Figure 3 shows the Photoluminescence emission of ZnO nanostructures. As you can see the Photoluminescence emission intensity increases when our nanostructures are rod shape and also smaller. We have emissions in UV region and visible region due to defects.

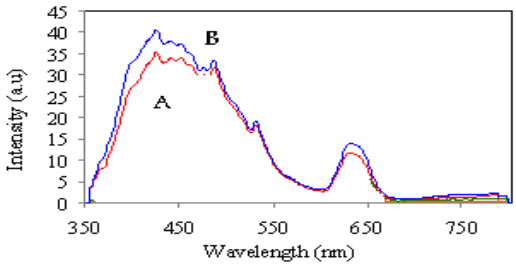

Fig. 3. Photoluminescence emission spectrum of A: ZnO nanoparticles and B: ZnO nanorods

Figure 4 shows the UV-vis absorption spectra of ZnO nanostructures. A shift in absorption edge to a higher wavelength is observed about ZnO nanoparticles with larger particles.

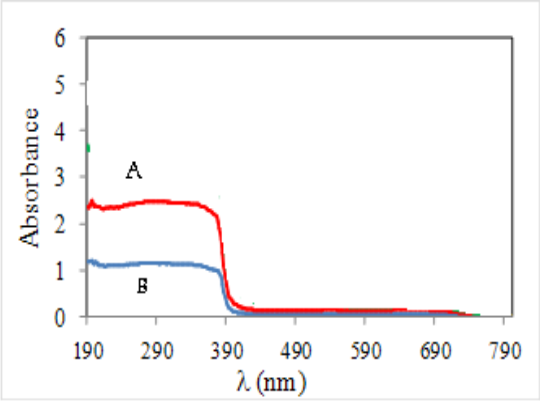

Fig. 4. UV-vis absorption spectra of A: ZnO nanoparticles and B: ZnO nanorods.

BET analysis also showed ZnO NSs with rod shape and smaller size have larger surface area.

Conclusion:

In summery ZnO NSs with rod shape and small size shows optimum properties of Photoluminescence emission and UV-vis absorption.

References:

[1] D. Lo, Mater. Sci. Eng. B 80 (2001) 383.

First-Principles Calculation of CO Adsorption on Most Stable Boron Nitride Cage $(BN)_{36}$

Fatemeh Cigarchi*[a], S.Salehe Razavi[a], S.Majid Hashemianzadeh[a]

[a] Molecular Simulation Research Laboratory, Department of Chemistry, Iran University of Science and Technology, Tehran, Iran

cigarchi_f@chem.iust.ac.ir

Keywords: Carbon monoxide, Greenhouse gas, Boron nitride, Inorganic fullerenes, First Principles calculation.

Introduction:

Carbon monoxide is a colorless, odorless, tasteless and seriously toxic gas which is only a very weak direct greenhouse gas, but has important indirect effects on global warming. Some research has been done on CO interaction with nanostructure materials like functionalized singlewall carbon nanotubes with Rh, Al, Pt, B, N and boron nitride nanotubes to investigate their sensing or capturing ability [1-4]. Oku et al synthesized boron nitride (BN) nanocage clusters (B_nN_n: n=12–60) by an arc-melting method, and characterized them by mass spectrometry and high-resolution electron microscopy [5]. In agreement with Oku, Wu et al investigated the structure and stability of the $(BN)_{36}$ monomer cages. They found that the most stable isomer has T_d symmetry with 32 hexagons (F6) and six squares (F4), and the six F4 have their maximal separations, following the isolated square rule [6]. However, despite the large amount of research devoted to $(BN)_{36}$ since its discovery and preparation [7-11], no adsorption studies of CO on this material has been reported to date.

Methods:

All the molecular geometries, NBO analysis, HOMO and LUMO energy and energy calculations in the ground state have been calculated by using density functional theory at the level of mpw1pw91/3-21G* using the GAUSSIAN 03 program. The natural bonding orbital (NBO) calculations were performed using NBO 5 program. It has been shown previously that the adsorption of CO through the C atom is more energetically favorable than through the O atom [1,4]. Hence we considered 3 nonequivalent sites for CO adsorption on the most stable isomer of $(BN)_{36}$: A) on top of a hexagon surrounded with 5 hexagons and 1 tetragon, B) on

top of a tetragon, C) on top of a hexagon surrounded with 6 hexagons (Figure 1). Using this procedure the binding energies were calculated according to the equation (1):

$$E_b(BN + CO) = E_T(BN + CO) - [E_T(BN) + E_T(CO)] \quad (1)$$

Where E_b is the binding energy between the $(BN)_{36}$ and the adsorbed CO molecule, E_T [BN + CO] is the nanocage total energy with an adsorbed molecule, E_T [BN] and E_T [CO] are the total energies of the isolated systems. The corresponding results have been tabulated in Table1.

Figure 2: Different possible adsorption sites: (A) top of a of a hexagon surrounded with 5 hexagons and 1 tetragon , (B) top of a tetragon , C top of a hexagon surrounded with 6 hexagons.

Results and Discussion:

The binding energies for CO on BN cage are of the order of hundreds of meV. These results indicate that only a physisorption occurs for CO molecules on the BN-cage surface. However, it is of interest to note that the most stable configuration after structural optimization occurs for adsorption on the boron atom of site B(top of a tetragon) with the binding energy of -0.615 eV. This can be attributed to the fact that the electronegativity of N (e_N =3.04) is considerably larger than that of B (e_B=2.04), which leads a charge transfer from B to N so that the electronic charge density distribution along the BN bond is strongly asymmetric. Therefore, B atoms act as cations while N atoms act as anions in BN nanocage. Furthermore, borane requires two further electrons to obey the effective atomic number (EAN) rule, and this can be achieved by interacting with a CO molecule through a σ donation. 3D plots of highest occupied molecular orbitals (HOMOs) and lowest unoccupied molecular orbitals (LUMOs) (not shown in this paper) indicate that The HOMO is mostly located over the C atom of the CO and the LUMO orbital is situated on B atoms of the tetragonal ring. The HOMO→LUMO transition implies an electron density transfer to B from
C of carbon monoxide.

Natural atomic hybrids of which the NBO is composed for the C-B bond and antibond are given below:

$\sigma_{BC} = 0.539\ B\ (sp^{6.22}d^{0.01}) + 0.842\ C\ (sp^{0.54})$ $\sigma_{BC}^{*} = 0.842\ B\ (sp^{6.22}d^{0.01}) - 0.539\ C\ (sp^{0.54})$

As it is evident, boron hybrid orbitals have more P characteristics than carbon orbitals.These results validate the EAN rule explanation for this case.

In addition,the second order Fock matrix was carried out to evaluate the donor–acceptor interactions in the NBO analysis. Some possible interactions between "filled"(donor) Lewis-type NBOs and "empty" (acceptor) non-Lewis NBOs, and estimating their energetic importance by 2nd-order perturbation theory for the optimized structure of CO adsorption on site B are presented in Table 2. For each donor (i) and acceptor (j), the stabilization energy E(2) associated with the delocalization i→j is estimated as equation (2) where q_i is the donor orbital occupancy, are ε_i and ε_j diagonal elements and F(i, j) is the off diagonal NBO Fock matrix element.

$$E(2) = \Delta E_{ij} = q_i \frac{F(i,j)^2}{\varepsilon_j - \varepsilon_i} \qquad (2)$$

Table 1. binding energies in eV for CO adsorption on various sites of a $(BN)_{36}$.

Adsorption Site	*Binding Energy(eV)*	*Position of CO after optimization*
A	-0.163355	On top of hexagon
B	-0.615384	On top of a B atom of the ring
C	0.489137	On top of a B atom of the ring

The results of natural atomic charges for atoms of a tetragon and CO adsorbed on it after structural optimization calculated by NBO 5 are tabulated in Table 3. In this case the $C\text{-}B_{37}$ distance is 1.75 A^0 after geometrical optimization.

Table 2. Second order perturbation theory analysis of Fock matrix in NBO basis for CO adsorption on site B.

Donor NBO(i)	Acceptor NBO(j)	E(2) (Kcal/mol)
BD (2) N 9- B10	BD*(2) B21- N22	51.35
BD (2) N39- B40	BD*(2) N12- B15	62.6
BD (2) B 5- N13	LP*(1) B14	50.65
BD (2) N 9- B10	BD*(2) B21- N22	51.35
BD (2) B47- N63	BD*(2) B60- N61	51.53
BD (2) N43- B44	BD*(2) N24- B32	62.44
BD (2) B51- N57	BD*(2) B66- N67	52.34
BD (2) B58- N59	BD*(2) N56- B62	52.06
BD (2) B66- N67	LP*(1) B72	54.94
BD (2) B69- N71	LP*(1) B72	86.91
LP (1) N 4	BD*(2) B 5- N13	64.18
LP (1) N 7	BD*(2) B49- N50	59.21

Table 3. Natural charges for atoms of a tetragon and CO adsorbed on it.

Atom	Natural Charge
N_{38}	-1.13230
B_{19}	1.05811
N_{18}	-1.13231
B_{37}	0.68910
C	0.81129
O	-0.35262

Conclusion:

In summary, on the whole $(BN)_{36}$ nanocages are not sensitive to the presence of CO molecules on the cage surface, only a physical adsorption occurs. We show that the most stable configuration ocuurs for adsorption of CO on top of a B atom of a tetragon ring,since B is a good Lewis acid with unoccupied P orbital, thus interacts with CO,which is known as a well ligand in inorganic chemistry, to follow the EAN rule. 3D surface of frontier HOMO and LUMO orbitals, NBO calculations and atomic charges confirm these outcomes and commentaries.

References:

[1] Baierle, R. J.; Schmidt, T. M.; Fazzio, A. Solid State Communications **2007**, 142, 49-53.

[2] Zhao, J.-X.; Ding, Y.-H. Materials Chemistry and Physics **2008**, 110, 411-416.

[3] Wang, R.; Zhang, D.; Sun, W.; Han, Z.; Liu, C. Journal of Molecular Structure: THEOCHEM **2007**, 806, 93-97.

[4] Yeung, C. S.; Liu, L. V.; Wang, Y. A. Journal of Physical Chemistry C **2008**, 112, 7401-7411.

[5]Oku, T.; Narita, I.; Nishiwaki, A. Materials and Manufacturing Processes **2004**, 19, 1215-1239.

[6] Wu, H. S.; Xu, X. H.; Strout, D. L.; Jiao, H. Journal of Molecular Modeling **2005**, 12, 1-8.

[7] Oku, T.; Hirano, T.; Kuno, M.; Kusunose, T.; Niihara, K.; Suganuma, K. Materials Science and Engineering B: Solid-State Materials for Advanced Technology **2000**, 74, 206-217.

[8] Oku, T.; Narita, I.; Nishiwaki, A. Journal of Physics and Chemistry of Solids **2004**, 65, 369-372.

[9] Alexandre, S. S.; Mazzoni, M. S. C.; Chacham, H. Applied Physics Letters **1999**, 75, 61-63.

[10] Oku, T.; Suganuma, K. Diamond and Related Materials **2001**, 10, 1205-1209.

[11] Silaghi-Dumitrescu, I.; Haiduc, I.; Sowerby, D. B. Inorganic Chemistry **1993**, 32, 3755-3758.

Cleavage of epoxides into halohydrins with elemental iodine in the presence of nano catalyst ZrO_2

Authors: A.Shameli[*a], M.M.Ghanbari[b]

[a] Department of Chemistry, *Islamic azad university Omidyeh branch, Iran, Omidyeh*

[b] Department of Chemistry ,*Islamic azad university Sarvestan branch, Iran, Sarvestan*

*corresponding letter: shameli678@gmail.com

Abstract:

The ring opening of epoxides with elemental iodine nano catalyst ZrO_2 affords vicinal iodo alcohols in high yields. This new procedure occurs regioselectivety under neutral and mild conditions in various aprotic solvents even when sensitive functional groups are present

Keywords: halohydrin, nanocatalyst, regioselectivety, epoxid

There is a continued interest in the regioselective ring opening of oxiranes to the corresponding vicinal halohydrins. Although a variety of new and mild procedures to effect this transformation have been reported, most of them have some limitations.[1]The reaction is typically performed with hydrogen halides, but the harsh reaction conditions and the low observed regioselectivity in the opening of unsymmetrical epoxides have prompted a search for more selective and milder procedures. Recently, it has been found that epoxides can be converted into halohydrins by means of elemental halogen,[2] but this method has limitations such as low yield, long reaction times, low regioselectivity and formation of acetonide byproducts in addition to the expected iodo adduct. Furthermore, iodination does not occur in aprotic solvents other than acetone.

In conjunction with ongoing work in our laboratory on the synthesis and formation of complex heterocyclic compounds containing donor nitrogen atoms, with neutral molecules such as iodine,[3-5] we found out that ZrO_2 with frame nano efficiently catalyzed the addition of elemental iodine to epoxides under mild reaction conditions with high regioselectivity. In this study, we wish to report the results of the reactions of some epoxides with elemental iodine in the presence of a sub-stoichiometric amount of ZrO_2 (Scheme 1, Table 1).

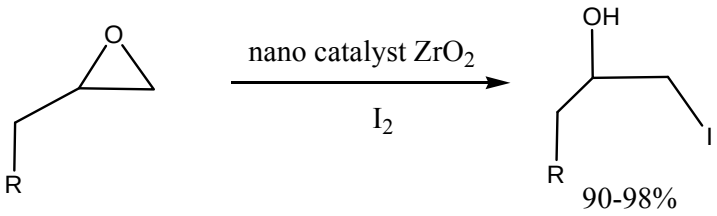

R= CH_2Ph, Ph, CH_2Ph(paraCl), CH_2Ph(para NO_2)

Scheme 1

Table 1

ENTRY	SOLVENT	catalyst(%mol)	Time(h)	Isolate yield (%)
1	-	10	6	50
2	THF	10	8	50
3	MeOH	10	8	30
4	EtOH	10	8	25
5	CCl_4	10	8	30
6	CH_3CN	10	5	50
7	H_2O	10	24	trace
8	CH_2Cl_2	10	10min	80
9	CH_2Cl_2	15	5min	95
10	CH_2Cl_2	20	5min	95

Epoxide (1 mmol) in CH2Cl2 (5 mL) was added to a stirred ZrO_2 catalyst (0.1 mmol) in at room temperature. Next, a solution of elemental Iodin (1 mmol) in CH2Cl2 (5 mL) was added portion-wise (15 min) to the above mixture. The progress of the reaction was monitored by TLC. After complete disappearance of the starting material, the reaction mixture was washed with 10% aqueous Na2S2O3 (2×10 mL) and water (2×10 mL). The aqueous layer was extracted with CH2Cl2 (2×10 mL).The combined organic layer was dried over anhydrous MgSO4 and evaporated to give crude alcohol–catalyst. The crude products were purified on a column of silica gel. The solvent was evaporated and pure halohydrin was obtained. The halohydrins obtained throughout this procedure were identified by comparison, where possible, with authentic samples prepared in accordance with literature procedures.

In conclusion, this new method appears to be highly competitive with the other methods reported in the literature. The reaction occurs in neutral and mild conditions on the acid-sensitive substrates and vicinal halohydrins were obtained in high yields and region-selectivity. In addition, in comparison with our previous methods, ZrO_2 is cheaper, less step need for preparation, and overall yield is higher.

The calculations are being done profiles for reaction ring opening epoxid will have been studied and the structure of all transition states were located at Gaussian level.

References

[1] Fiesers' Reagents for Organic Synthesis, Smith, J. G., Fieser, M., Eds.; New York, **1990**; looking for: halohydrins and derivatives. (b) Bonini, C.; Righi, G. Synthesis **1994**, 225. (c) Larock, R. C. Comprehensive Organic Transformations. VCH: New York, 1989; pp 508–509.

[2] Konaklieva, M. I.; Dahi, M. L.; Turos, E. Tetrahedron Lett. **1992**, 33, 7093.

[3](a) Sharghi, H.; Massah, A. R.; Eshghi, H.; Niknam, K. J. Org. Chem. **1998**, 63, 1455. (b) Sharghi, H.; Niknam, K.; Pooyan, M. Tetrahedron **2001**, 57, 6057. (c) Gangali, M. R.; Eshghi, H.; Sharghi, H.; Shamsipur, M. J. Electroanal. Chem. **1996**, 405, 177. (d) Sharghi, H.; Massah, A. R.; Abedi, M. Talanta 1999, 49, 531.

[4] Sharghi, H.; Nasseri, M. A.; Niknam, K. J. Org. Chem. **2001**, 66, 7287.

[5] K. Niknam, T. Nasehi / Tetrahedron 58 (**2002**) 10259–10261

Study of the effect of the various metal contacts on the electronic properties of a molecular wire metal/Thymine/metal

F. Shariati Ashrafi*[a] , H. Milani Moghadam[a]

[a]Department of physics, University of Mazandaran, Babolsar , Iran

(Email:fatemeh.shariati64@gmail.com)

Keyword: Molecular wires, Thymine, metal, Density of state

Introduction

The trend in solid-state electronics is towards smaller and smaller devices, from microelectronics to nanoelectronics and further, and logically the process must end with molecular electronics [1]. Recently, there have been significant advances in the fabrication and demonstration of molecular electronic wire [2-3]. In this study, the modeling of the metal/Sulfur-Thymine-Sulfur/metal, molecular wire that Thymine (one of the bases of DNA, Figure 1) used as a molecular bridge and Au, Ag, Cu used as an electrode. Most the time in electrode/molecule contact use Sulfur atom for better stick metal/Sulfur [4]. We consider the various Metal (Au, Ag, Cu) contacts effect on the electronic properties of the molecular wires metal/Sulfur-Thymine-Sulfur/metal. We investigate how the energy gap, Density of States and Electrical Dipole Moment in three structures change by the metal contacts**.** Where the TAu stands for 1Au/Sulfur-Thymine-Sulfur/1Au molecular wire, TAg stands for 1Ag/Sulfur-Thymine-Sulfur/1Ag molecular wire and TCu stands for 1Cu/Sulfur-Thymine-Sulfur/1Cu molecular wire.

Methods

All calculations are performed using Gaussian03 program. The metal/Thymine/metal structure is optimized at Density Functional Theory (B3LYP) method. It is used the basis set 6-31G* for C, N, H, O and S atoms and LanL2DZ for Au, Ag, Cu atoms.

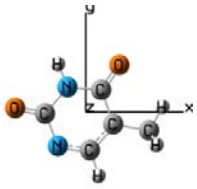

Figure 1:

The Thymine molecule

Figure 2 : The TAu molecular wire

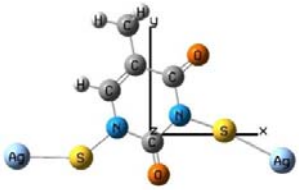

Figure 3: The TAg molecular wire.

Figure 4:The TCu molecular wire.

Results and discussion

The HOMO-LUMO gap (HLG), in Thymine structure is 5.5 eV. So the thymine molecule has a insulator-like behavior in molecular junction. HLG extremely decreases by attaching metal atoms (Au, Ag, Cu) to the Sulfur-Thymine-Sulfur structure (see Fig. 5). Greatest dipole moment direction to the TAu, TAg, TCu structures i.e. along the +X axis. Figure 6 show Total electrical dipole moment P_T in the structures and Figure 7 show the density of electronic states (DOS) of the TAu, TAg, TCu molecular wires.

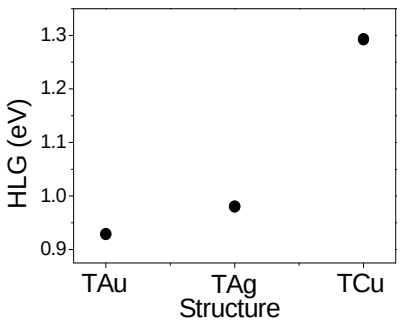

Fig. 5: The HLG vs. structures.

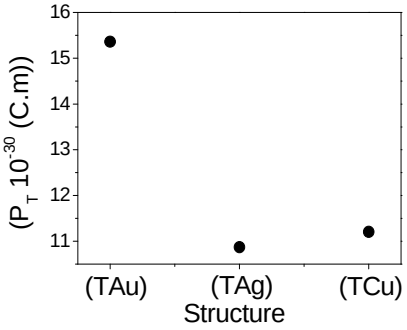

Fig. 6: Total electrical dipole moment, P_T vs. structures.

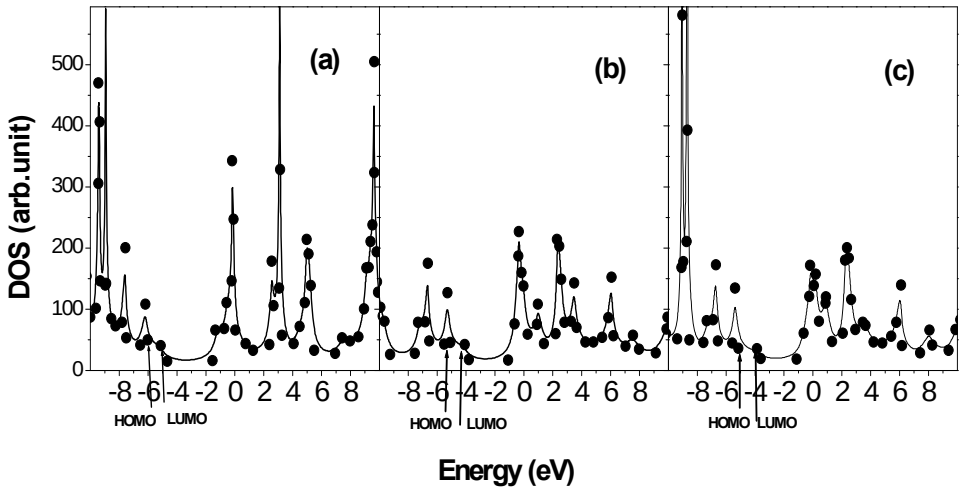

Fig 7: The DOS vs. energy in the structures: (a) The TAu molecular wire (b) The TAg molecular wire (c) The TCu molecular wire

Conclusions

In this study we consider the electronic properties of the TAu, TAg, TCu molecular wires. The TAu, TAg, TCu molecular wires have a semiconductor-like behavior in molecular junction. Total electrical dipole moment P_T and DOS increases in the TAu molecular wire.

Reference

[1] M.A. Reed, C. Zhou, C.J. Muller, T.P. Burgin, J.M. Tour, Science **279** (1997) 252.

[2] S.Liu *et al,* Nano Lett. **5** (2005) 1071.

[3]. N.Ranjan *et al,* Mol. Phys. **40** (2004) 125.

[4] D.Millar, L.Venkataraman, H.Doerrer, Phys.Chem., **111** (2007) 1763.

Synthesis and characterization of Multilayer nanocore-shell latex via surface cross-linking emulsion polymerization

F. Shafie

Department of Chemistry, Islamic Azad University of Shahreza, Shahreza, Iran

(Email:feizalah61@gmail.com)

Keywords: Multilayer, Nanocore-shell, Raspberry-like, Emulsion

Introduction

The preparation of core-shell latex with a defined morphology has been a topic of great interest with many major developments within the past few decades. these emulsions have unique properties and many industrial applications, such as impact modifiers, adhesives,and coatings. However, a well-defined core-shell structure is not easy to achieve it has been demonstrated that both thermodynamic and kinetic factors dictate particle morphology.Various alternative structures, such as confetti-like, raspberry-like, and sandwich-like have been described as the intermediates of the phase separation process in literature.

We describe a method for the synthesis of phase-separated polymer latex with a monodisperse and multilayer core–shell (MMLCS) morphology by surface cross-linking emulsion polymerization. poly(butyl-acrylate)(PBA) was used for the seed and the core of the latex, the inner shell was poly(butyl acrylate-styrene) cross-linked with divinylbenzene (DVB) to avoid phase inversion, and the poly(methyl methacrylate-butyl acrylate-glycidyl methacrylate) was the outer shell. TEM, DSC, were used to characterize this Monodisperse and multilayer core–shell (MMLCS) emulsion. the multilayer core–shell structure was clearly shown in TEM micrographs, and the three-phase separation was confirmed by DSC analysis the average diameters of MMLCS latex were 126 nm, 14 nm, and 14 nm. In this work, one MMLCS latex system was obtained by surface cross-linking emulsion polymerization.the poly(butyl acrylate)(PBA) was used for the core of the latex, the poly(butyl acrylate-styrene) (P(BA-St)) as the inner shell, and poly (methyl methacrylate-butyl acrylate-glycidyl methacrylate) (P(MMA-PBA-GMA)) as the outer shell. by repeating this method, different functional or hydrophilic polymers, such as GMA, methacrylic acid (MAA), acrylic acid(AA), can be

successfully polymerized in the hydrophilic core or the hydrophobic shells of MMLCS emulsions.

method

A monodisperse and multilayer core–shell (MMLCS) emulsionwas prepared by emulsion polymerization, which used 1-nonylphenyloxy-2-deca(oxyethylene)-3-allyloxypropane ammonium sulfate(SE-10N) as the polymerizable surfactant and sodium alkylated diphenyl ether disulfonate(DSB) as the anionic surfactant.

The PBA core was synthesized by seed polymerization using the PBA seed at 75±2 °C for 3.5 h. After the reaction temperature was reached, 20 g BA monomer and the aqueous solutions of initiators (0.055 g APS dissolved in 10 g distilled water and the 0.025 g SBS dissolved in 10 g distilled water) were added to the stirred reactor respectively at 10 ml/h in order to favor the formation of seed particles with a narrow size distribution. the stirring rate was controlled at 250 rpm.the inner shell was obtained during the second stage of polymerization. the emulsion polymerization was carried out at 75±2 °C for 3 h in a nitrogen atmosphere after all of themonomers were added completely.the outer shell was formed during the third stage of polymerization.Aqueous solutions of initiator, 10 g MMA monomer, 5 g GMA monomer, 5 g BA monomer, aqueous solutions of surfactants(SE-10N)and DSB aqueous solution were added into another flask with 72 g PBA/P(BA-St) core–shell emulsion at 10ml/h for 1 h. after 4 h of polymerization at 75±2 °C in a nitrogen atmosphere, the MMLCS emulsion preparation was completed.

Results and discussion

TEM micrograph show the PBA/P (BA-St) core–shell emulsion and the PBA core emulsion. the light inner region is the PBA seed core and the dark outer region is the P (BA-St) shell. PS chain is more hydrophobic, but in this emulsion system no phase inversion took place. this is due to the addition of DVB solution, the key step to obtain the PBA/P (BA-St) core-shell emulsion in this process. Compared with the core–shell emulsion and the core emulsion, it was found that the two layers (the lighter PBA core and the darker P (BA-St) shell) were obvious in the PBA/P (BA-St) core–shell emulsion. the darker PS domain structure can be clearly seen near the outer layer of the particles. as mentioned above, the shell layer was cross-linked using DVB. there is evidence of the formation of the core–shell structure. the

continuous shell is darker than the core due to the staining of the PS. the TEM micrograph shows the three continuous layers (the PBA core, the P (BA-St) inner shell and the P (MMA-PBA-GMA) outer shell) in the MMLCS core–shell emulsion. the darker region is the P (BA-St) shell, the lighter innerregion is the PBA core and the lighter outer region is the P (MMA-PBA-GMA) shell. stained PS can be seen in the middle continuous layer of the particles. these show the synthesized emulsion formed a MMLCS structure. the TEM micrograph of nanostructured polymer film without staining shows an almost ideal hexagonal pattern of deformed particles.and shows how close contact packing of the particles leads to the position of particles at different depths of the sample. TEM micrographs showed that the nanoparticles maintained their structure during film formation and these structured emulsions formed nanostructured polymer films after drying at ambient temperature.

Conclusion

MMLCS latex was prepared by a method via surface cross-linking emulsion polymerization for the synthesis of phase-separated polymer latex, which used the DVB as cross-linking agent. the multilayer core-shell structure was clearly shown in the TEM micrographs, and the three-phase separation of the MMLCS emulsion was confirmed by DSC analysis. the TEM micrograph showed that the average diameters of MMLCS emulsion were about of 126 nm, 14 nm, and 14- nm,

References

[1] Sherman Jr, Robert L, Ford Warren T. Small core/thick shell polystyrene/poly(methyl methacrylate) latexes. Ind Eng Chem Res 2005;44:8538–41.

[2] Aguiar A, Gonzalez-Villegas S, Rabelero M, Mendizabal E, Puig JE. Core–shell polymers with improved mechanical properties prepared by microemulsion polymerization. Macromolecules 1999;32:6767–71.

[3] Mahdavian Ali Reza, Ashjari Mohsen, Mobarakeh Hamid Salehi. Nanocomposite particles with core–shell morphology. I. Preparation and characterization of Fe3O4- poly(butyl acrylate-styrene) particles viaminiemulsion polymerization. J Appl Polym

Synthesis of Siloxane/Poly (styrene-co-butyl acrylate)Nanocomposite via Miniemulsion Polymerization

F. Shafie

Department of Chemistry, Islamic Azad University of Shahreza, Shahreza, Iran

(Email:feizalah61@gmail.com)

Keywords: Siloxane,Styrene-co-butyl acrylate, Nanocomposite, Miniemulsion

Introduction

In recent years, the strategy for designing and fabricating organic–inorganic nanocomposite particles has attracted burgeoning interest because these composite particles can display novel and enhanced properties (e.g., mechanical, chemical, electrical, rheological, magnetic, and optical) bythe independent alteration of the compositions, dimensions, and structures of the cores and shells. a series of Siloxne/poly (styrene-co-butyl acrylate) nanocomposite microspheres with various morphologies (e.g., multicore–shell, normal core–shell, and raspberry-like) were synthesized via miniemulsion polymerization. the results showed that the morphology of the composite latex particles was strongly influenced by the presence or absence of the soft monomer (butyl acrylate), the particle sizes of the silica, and the emulsifier concentrations. the incorporation of the soft monomer helped in forming the multicore-shell structure.

number of methods have been successfully demonstrated for generating nanocomposite microspheres with different interesting morphologies, such as raspberry-like,coreshell, currant-bun-like, dumb-bell-like, snowman-like, daisy-shaped, and multipod-lik structures. a mong the different morphologies, raspberry-like and core–shell particles are the most frequently acquired. raspberry-like microspheres with a polymer as the core or shell and nanosilica as the corresponding shell or core could also be obtained via aqueous dispersion polymerization23 and surfactant-free polymerization. in fact,the core–shell morphology with the polymer as the core and nanosilica as the shell or with the nanosilica as the core and polymer as the shell can also be obtained via dispersion polymerization,conventional emulsion polymerization, and surfactant-free emulsion polymerization.until now, however, whether the polymer was used as the core or shell for raspberry-like and core–shell structures,

the polymer was always synthesized by a hard monomer such as styrene (St) or methyl methacrylate, probably because researchers hoped to observe the morphology of the composite particles clearly or to synthesize composite particles as templates. In this study, we synthesized a series of nanocomposite particles with nanosilica as the core and the copolymer poly(styrene-co-butyl acrylate) [P(St–BA)] of a hard monomer (St) and a soft monomer [butyl acrylate (BA)] as the shell via miniemulsion polymerization, which is a particularly attractive technique for obtaining nanocomposite particles.33–36 The objective of this research was understanding whether the incorporation of a soft monomer influenced the morphology of the composite particles or not because soft monomers are always employed for polymerization for a lot of practical applications.[1,2]

method

Nanosilica particles were prepared according to the well-known Stober procedure.[3]the composite particles were prepared by miniemulsion polymerization MPS-modified silica powder was first dispersed in a mixture of 10 g of the monomers (6 g of St and 4gofBA) and 0.4g of hexadecane withtheaid of ultrasound.the miniemulsions Surface Tension were determined. each sample was measured 10 times to obtain the average surface tension.the sizes and morphologies of the composite particles and the pure PSt latex were characterized with a transmission electron.

Result and discussion

A series of nanocomposite microspheres were synthesized via miniemulsion polymerization with various St/BA weight ratios, SDS contents, and particle sizes of nanosilica illustrates the TEM micrographs of the composite latex articles obtained with different St/BA weight ratios (10/0, 6/4, and 4/6) in the presence of 90 nm silica beads. obviously, the ratios of St to BA had a drastic impact on the morphology of the composite particles. when only the hard monomer was used for the polymer (St/BA ¼ 10/0), the composite particles presented a core–shell structure, but when the soft monomer was incorporated into the polymer (St/BA ¼ 6/4 or 4/6), more than two silica beads were embedded inside each latex particle, forming a multi-core–shell structure however; too much soft monomer content probably caused some adhesion between the composite particles. BA and its polymer have much lower surface free energies, incorporating the BA monomer should decrease the surface energy of the

miniemulsion,increasing the droplet size of the miniemulsion. we determined the sizes of the droplets and the surface tensions of composite particles with different compositions. as more BA was incorporated the surface tension decreased and the droplet size indeed increased; obviously, these increasing droplets could accommodate more than two silica beads then polymerized to form composite particles. in addition, the MPS-modified silica par-ticles had a surface structure similar to that of the BA molecules, which also helped in lodging more silica particles in each droplet, which was then polymerized to form composite particles.

Conclusions

On the basis of this study, a series of SiO2/P (St–BA) nanocomposite particles with various morphologies (e.g., multicore-shell, normal core-shell, and raspberry-like) were prepared via miniemulsion polymerization. the incorporation of BA into the polymer was propitious for causing a multicore–shell morphology in comparison with only a hard monomer in the polymer, other parameters being equal. Increasing the particle size of silica or decreasing the emulsifier content tended to form a normal core-shell or even rasp-berry-like structure. these nanocomposite particles could possibl find potential applications for high-hardness, abrasion-resistant coatings or other novel functional materials.

References

1. Yu, Y. J.; Yang, C. Q.; Gao, Y.; Si, Z. H.; Chen, W.;Wang, Z. Q.; Xue, G. J Polym Sci Part A: PolymChem 2005, 43, 6105.

2. Grubbs, R. B. J Polym Sci Part A: Polym Chem2005, 43, 4323.

3. Wu, C. S. J Polym Sci Part A: Polym Chem 2005,43, 1690.

Synthesis of water-soluble, core–shell organo-silica nanoparticle with controllable size via sol-gel process

F. Shafie

Department of Chemistry, Islamic Azad University of Shahreza, Shahreza, Iran

(Email:feizalah61@gmail.com)

Keywords:Water-soluble, Core–shell, Organo-silica, Nanoparticle, Controllable size, Sol-gel

Introduction

Organo-silica nanoparticles have recently attracted consider-able interest due to their potential applications in optics, functional materials and biosciences Compared with inorganic silica nanoparticles, typically prepared by the Stöber method these new organo-silica nanoparticles differin several aspects from silica particles made from tetraethyloxysilane(TEOS) alone . the negative surface charge is smaller, the density is and the siloxane structure is less condensed and possesses a larger surface area than the inorganic silica nanoparticles. More importantly, by properly choosing starting materials at the synthetic stage, these organo-silica nanoparticles can be readily modified to render them both biologically compatible and chemically functional through a single step synthesis.Currently, organo-silica nanoparticles are usually synthesized by hydrolysis and polycondensation of substituted alkoxysilanes, R-Si(OR0)3 which contain a nonhydrolyzable Si–C bond instead of the pure alkoxysilanes such as TEOS.[1] as the substituent R can be functionalized, biological and chemical functionalization of nanostructures can be achieved in a one-pot synthesis procedure to fine-tune and modify or further engineer properties of the nanoparticles. poly(ethylene glycol) (PEG) is an important water-soluble ligand that is known to be biocompatible and is currently being used for drug delivery.[2]

,We report a facile and effective approach to synthesize water-soluble core–shell organo-silica nanoparticles by cohydrolysis and copolycondensation reactions of mixtures of PEG and hydroxyl-containing starting materials at room temperature. it was found that the nanoparticle size could be controlled by varying the molar ratios of starting materials. the resulting nanoparticles were characterized by FTIR,TEM and TGA.This work demonstrates that water-

soluble and size-controllable organo-silica nanoparticles can be simply prepared via sol-gel process by properly choosing the starting materials.

methods

The organo-silica nanoparticles were synthesized by hydrolysis and condensation of the precursormixture of organotriethoxysilane and organotrimethoxysilane containing hydroxyl and poly(ethlenglycol) groups respectively in the presence of H2O, surfactant BTC,and NaOH at room temperature.the following typical procedure was used to synthesize the nanoparticles. HMTEOS and PEG6-9 were mixed with a series of different molar ratios

Results and discussion

In this experiment, we chose to use a base catalyzed sol-gelprocess in the presence of surfactant, which provides a number of advantages for the preparation of organo-silica nanoparticles. PEG6-9 contains a long water-soluble and biocompatible ligand which is expected to endow the particles with aqueous solvent affinity and biocompatibility if this ligand presents on the surface of the particles. in addition, the long chain of the PEG can effectively separate the particles as it is not involved in the hydrolysis and condensation reactions. additionally, the PEG6-9 could not form large particles alone in the sol–gel process due to the steric effect of the long PEG chain. thus, it is an ideal surface coupling agent in the preparation of water-soluble silica particles with compatibility. HMTEOS contains a non hydrolyzed substituent that can contribute to the low density of the resultant nanoparticles by reducing the possible condensing sites between various intermediate species after hydrolysis. this results in a final product that has a more open or loose structure than conventional silica nanoparticles obtained using the Stöber method with TEOS alone .

Conclusions

Highly water-soluble organo-silica nanoparticles with controllable size were synthesized in a facile one pot reaction via the sol-gel process by using PEG and hydroxyl group substituted organoalkoxylsilanes in the present of a surfactant. Size control of nanoparticles with diameters ranging from 12 to 20 nm was achieved by varying the molar ratio of PEG6-9 to HMTEOS. FTIR,TEM,and TGA studies showed that the particle has a core-shell structure. the particle core consists of a denser organo-silica network, resulting from the HMTEOS and the shell consists of a monolayer of PEG from PEG6-9. due to the high water-solubility,

biocompatibility, and smaller size, these organo-silica particles are expected to be useful in applications involving bioscience, biomaterials, and drug delivery. research is underway using these particles for the synthesis of prosthetic materials.

References

[1] A.M. Jakob, T.M. Schmedake, Chem. Mater. 18 (2006) 3173.

[2] L. Wang, M.C. Estévez, M. O'Donoghue, W.H. Tan, Langmuir 24 (2008) 1635.

The preparation of silver doped ZnO nanoparticles via microemulsion, and their application in photocatalytic degradation of C.I. Acid Yellow 23

M. Shokri [a]*, M. G. Hosseini[b], R. Najjar[c], M. Khosravi[d], Q. Zarbpoor[a]

[a] *Department of Applied Chemistry, Faculty of Science, Islamic Azad University, Tabriz Branch, Tabriz, Iran*
E-mail: shokri_m@yahoo.com ; shokri@iaut.ac.ir

[b] *Electrochemical Research Laboratory, Faculty of Chemistry, University of Tabriz, Tabriz, Iran*

[c] *Polymer Research Laboratory, Faculty of Chemistry, University of Tabriz, Tabriz, Iran*

[d] *Department of Applied Chemistry, Faculty of Chemistry, Islamic Azad University, Tehran-North Branch, Tehran, Iran*

Keywords: Heterogeneous photocatalysis, UV/ ZnO, Ag doped ZnO, Microemulsion, Acid Yellow 23

Introduction

In modern purification techniques employing semiconductor mediated photooxidation of toxic substances, zinc oxide (ZnO) and titanium dioxide (TiO_2) are the most widely used metal oxides due to their unique blend of properties. It has been found that the photocatalytic performance of ZnO (a suitable alternative semiconductor to TiO_2) can be improved by constructing a silver–ZnO composite because of the increase in the rate of electron-transfer process by metal silver [1,2]. In this contribution, the photocatalytic decolorization of Acid Yellow 23 (AY23) as a representative mono azo dye, on Ag loaded ZnO nanoparticles (Ag/ZnO) prepared in microemulsion, was studied.

Methods

Zinc acetate, diethylene glycol 99%, $AgNO_3$ 99.9%, hydrazine 80%. *n*-heptane 99%-(Merck); Sodium bis(2-ethylhexyl)sulphosuccinate (AOT, 96%), AY23 (λ_{max} 429 nm)-(Acros).

1. Preparation of Ag/ZnO photocatalyst

Rod-like ZnO nanoparticles were synthesized by the hydrolysis of zinc acetate under heating in diethylene glycol with referring to a procedure described in the literature [3]. The Ag/ZnO catalysts were prepared by two microemulsion technique (*n*-heptane/AOT/water/$N_2H_4.H_2O$ or $AgNO_3$; $[H_2O]/[AOT]=5$; [*n*-heptane/water] =250; aqueous phase $[N_2H_4.H_2O]=0.6$ M and

[Ag^+] = 0.2 M). The reducing agent containing microemulsion was added to the metal precursor microemulsion containing proper amount of ZnO, and the mixture was kept stirring vigorously for 30 minutes. The nanoparticles were obtained by adding acetone, centrifuging the precipitate, dried at 85ºC for 12h, and finally calcined at 450ºC for 3 h.

2. Photocatalytic Study

A solution containing desired amounts of AY23 (20 mgL^{-1}) and photocatalyst were prepared and agitated for 30 min in the darkness. Afterwards, 100ml of the above suspension was transferred into a borosilicate petri dish as photoreactor. The reaction mixture was UV irradiated by using 15 W UV lamp and then at certain reaction intervals the concentration of AY23 was determined using a UV-Vis spectrophotometer.

Results and Discussion

1. The characterization of Ag/ZnO nanoparticles

The SEM and EDX analysis of prepared Ag/ZnO nanoparticles results confirmed the loading of Ag on ZnO rod-like nanoparticles (Fig.1.a,b).

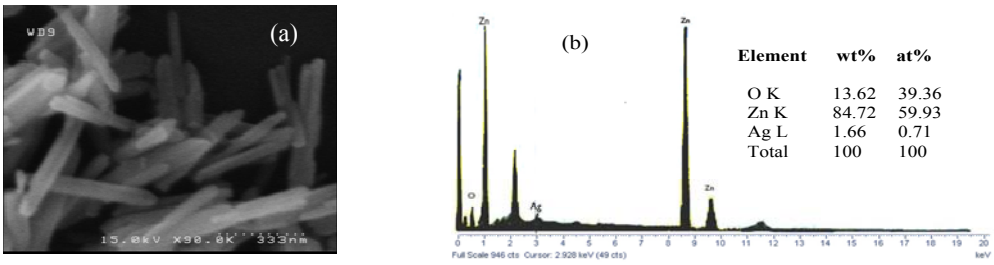

Fig.1. a) SEM micrograph and b) EDX analysis of 2wt% Ag/ZnO nanoparticles

2. The effect of Ag loading on the Photocatalytic activity

According to the results (Fig.2), by increasing of the Ag loading until 2wt%, the photocatalytic activity of the catalyst increases. Excessive coverage of ZnO catalyst with Ag nanoparticles limits the amount of light reaching to the ZnO surface, reducing the number of photogenerated e^--h^+ pairs and consequently, lowering the ZnO photoactivity [4].

3. The effect of catalyst dosage on the Photocatalytic activity

The results (Fig.3) showed that increasing the catalyst dosage causes increasing the reaction rate. However, a large increase higher than 400 mgL^{-1} of Ag/ZnO, can cause the limits the intensity of the light penetration that decreases the photocatalytic activity [5].

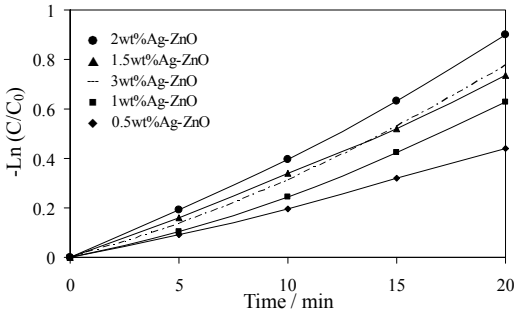

Fig.2. Effect of Ag loading on the photocatalytic degradation ([Catalyst] = 400 mg l^{-1}).

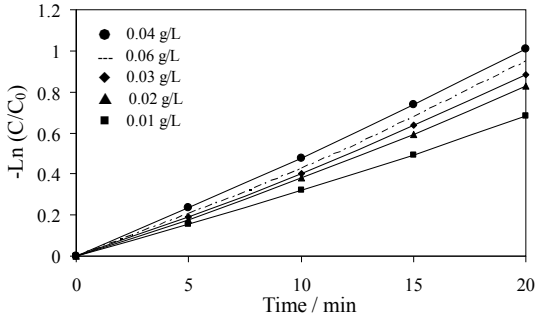

Fig.3. Effect of 2 wt% Ag/ZnO catalyst dosage on the photocatalytic degradation.

4.Kinetic analysis

The good linearity of the $-\ln(C/C_0)$ versus irradiation time plot, with high R^2 values (Fig.2 and Fig.3), suggests that the photocatalytic reaction approximately followed the pseudo-first order kinetic. The rate constant calculated for the reaction carried out at the optimum condition (2wt% Ag loading at 400 mgL^{-1} of Ag/ZnO) was 0.0505 min^{-1} (R^2 = 0.999). Similar values of correlation coefficients (R^2 > 0.99) for the $-\ln(C/C_0)$ versus irradiation time plots have been calculated for the experiments carried out at the conditions other than optimum condition.

Conclusion

The characterization of Ag/ZnO synthesized via microemulsion method and ZnO, using SEM and EDX techniques revealed the dispersion of silver metal on the surface of ZnO. It was found that the 2wt% Ag loading at 400 mgL^{-1} of Ag/ZnO has been optimum conditions to achieve the highest efficiency of the AY23 photodegradation**.** It was found that the photo-degradation obeyed the pseudo-first order kinetic reaction in the presence of synthesized Ag/ZnO photocatalysts. The apparent reaction rate constants (k_{app}) were evaluated from experimental data using a linear regression. In all cases, R^2 (correlation coefficient) values are higher than 0.99, which confirm the proposed kinetics for degradation of AY23 in this process.

References

[1] M. J. Height, S. E. Pratsinis , O. Mekasuwandumrong, Appl.Catal., 63 (2006) 305.

[2] C. Song, Y. Lin, D. Wang, Z. Hu., Mater. Lett., 64 (2010) 1595.

[3] Yi Hu, Hung-Jiun Chen, J. Nanopart. Res., 10 (2008) 401.

[4] R. Georgekutty, M. Seery, S. Pillai, Phys. Chem., 112 (2008) 13563.

[5] B. Sun, A.V. Vorontsov & P.G. Smirniotis: Langmuir, 19 (2003), 3151.

Photocatalytic degradation of Cefazolin in aqueous solution using TiO_2 nanoparticles under UV light - A kinetic approach

M.G. Hosseini [a], M. Shokri*[b], R. Najjar[c] and M.A.A. Yavari [b]

[a] *Electrochemical Research Laboratory, Faculty of Chemistry, University of Tabriz, Tabriz, Iran*

[b] *Department of Applied Chemistry, Faculty of Science, Islamic Azad University, Tabriz Branch, Tabriz, Iran*

* *(Email: shokri_m@yahoo.com ; shokri@iaut.ac.ir)*

[c] *Polymer Research Laboratory, Faculty of Chemistry, University of Tabriz, Tabriz, Iran*

Keywords: Antibiotic; Cefazolin; UV/TiO_2; Photocatalysis

Introduction

Pharmaceutical compounds including antibiotics have been observed in surface water, ground water, sewage effluent and even in drinking water. A problem that may be created by the presence of antibiotics in low concentration in the environment is the development of antibiotic resistant bacteria [1]. Heterogeneous photocatalysis is an economical and harmless technology for removal of organic pollutants, among them, TiO_2 mediated semiconductor photocatalysis is gaining more importance due to its high production of hydroxyl radicals [2]. The aim of this study was to determine the effects of catalyst concentration and pH, on the photocatalytic degradation of Cefazolin, and the kinetics of reaction under UV light.

Methods

TiO_2-P25 Degussa, 80% anatase, 20% rutile were used as a supporting material. Cefazolin (Fig.1) as a model antibiotic pollutant purchased from ACROS organics (USA).

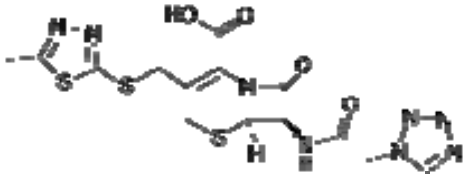

Fig. 1. Molecular Structure of cefazolin

For the investigation of the photocatalytic activity of UV/TiO_2 nanoparticles towards degradation of Cefazolin, a solution containing desired amounts of Cefazolin and photocatalyst were prepared and agitated for 30 min in the darkness. Then, 100 ml of the

above suspension was transferred into the photoreactor. Afterwards, while stirring of the solution by the magnetic stirrer, the UV lamp (15 W, λ_{max}=254 nm, light intensity = 35 W/m^2) was switched on to start the reaction. At certain reaction intervals, 5 ml of sample was withdrawn, and the catalyst was removed by centrifugation. The concentration of remaining Cefazolin was determined by means of a UV-Vis spectrophotometer at λ_{max} = 271 nm.

Results and discussion

1. Effect of TiO_2 concentration

To observe the effect of TiO_2 concentration, initial TiO_2 concentration was varied in the range of 0.02–0.06 gL^{-1} at a fixed Cefazolin concentration (20 mgL^{-1}) in aqueous solution (at natural pH ≈ 3.5). Based on the results (Fig. 2), the optimum TiO_2 concentration for degradation of Cefazolin antibiotic in aqueous solution is 0.04 g/L. Further increase of TiO_2 concentration did not produce significant improvement in antibiotic degradation. This may be due to the decreasing light penetration that affects inversely the photocatalytic reaction [2].

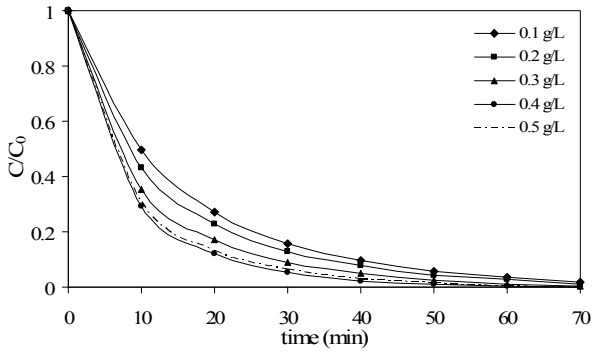

Fig. 2. Effect of TiO_2 concentration on Cefazolin degradation.

2. Effect of pH

To study the effect of initial pH on degradation of Cefazolin, experiments were conducted by varying the pH in the range 3–11. According to the results, pH had a great effect on the antibiotic degradation, and the highest degradation was achieved at pH = 5 (Fig. 3).

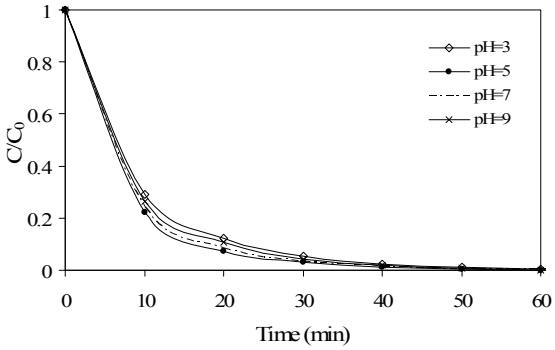

Fig. 3. Effect of pH on degradation of Cefazolin

3. Kinetics of photocatalytic degradation of Cefazolin

To study the kinetics of photocatalytic degradation of Cefazolin, experiments were conducted under optimum operating conditions ($[TiO_2]$ = 0.04 gL^{-1}, initial Cefazolin concentration = 20 mgL^{-1} and solution pH = 5). Fig. 4 shows the plots of -Ln([antibiotic]/[antibiotic]$_0$) vs. irradiation time for the photodegradation of Cefazolin. The good linearity of the $-\ln(C/C_0)$ versus irradiation time plot, with R^2 values of 0.9925, suggests that the photocatalytic reaction approximately followed the pseudo-first order kinetic. The rate constant calculated for the reaction carried out at the optimum condition was 0.1122 min^{-1}. Similar values of correlation coefficients ($R^2 > 0.99$) for the $-\ln(C/C_0)$ versus irradiation time plots have been calculated for the experiments carried out at the conditions other than optimum condition [3].

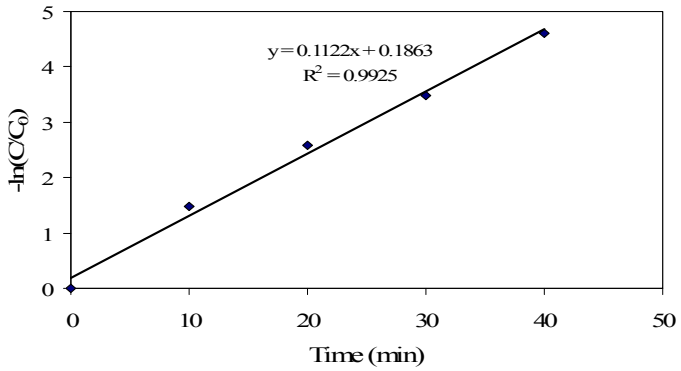

Fig. 4. Kinetics of Cefazolin photodegradation under optimum conditions

Conclusions

Degradation of Cefazolin antibiotics in aqueous solution by TiO_2 photocatalysis under UV (254 nm) irradiation was studied. The amount of TiO_2 has an important influence on the reaction rate. The optimum conditions for the photocatalytic degradation of Cefazolin were found to be pH = 5 and catalyst dosage of 0.04 gL^{-1}. The semi-logarithmic graphs of the concentration of Cefazolin in the presence of different concentrations of TiO_2 versus irradiation time yield straight lines indicating pseudo-first order reaction.

References

[1] E. S. Elmolla., M. Chaudhuri, (2010), Desalination,Vol. 252, pp. 46–52.

[2] M.N. Abellan, B. Bayarri, J. Gimenez, J. Costa, (2007), Appl. Catal. B, Vol. 74, pp 233–241.

[3] M.N. Abellan, J. Gimenez, S. Esplugas, (2009), Catal.Today, Vol. 144, pp.131–136.

Photodegradation of Chloramphenicol in aqueous solution using Ag-doped TiO_2 as catalyst

M. Shokri*, N. Modirshahla, M.A. Behnajady, A. Jodat

Department of Applied Chemistry, Faculty of Science, Islamic Azad University, Tabriz Branch, Tabriz, Iran

** Email: shokri_m@yahoo.com ; shokri@iaut.ac.ir*

Keywords: photodegradation; Photodeposition; Ag-TiO_2; Chloramphenicol

Introduction

Chloramphenicol is a broad-spectrum antibiotic exhibiting activity against both Gram-positive and Gram-negative bacteria, as well as other groups of microorganisms. However, Chloramphenicol is, in certain susceptible individuals, associated with serious toxic effects in humans including bone marrow depression, particularly severe in the form of fatal aplastic anemia [1]. It has been demonstrated that heterogeneous photocatalysis using TiO_2 as catalyst can be an alternative to conventional methods for the removal of organic pollutants from water and air. The current study provides results describing the heterogeneous photocatalytic oxidation of the antibiotic Chloramphenicol, over TiO_2 and Ag-TiO_2 nanoparticles under the illumination of UV light, in various experimental conditions.

Methods

$AgNO_3$ (99.9%) obtained from Merck. TiO_2-P25 Degussa, 80% anatase, 20% rutile; BET area 50 m^2/g; primary size 21 nm, were used as a supporting material. Chloramphenicol (Fig. 1) as a model antibiotic pollutant purchased from ACROS organics (USA).

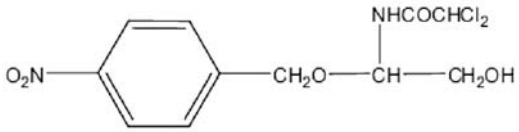

Fig.1. Molecular Structure of Chloramphenicol

1. Preparation of Ag/TiO_2 photocatalyst

First 2.72 g of TiO_2 was added to 100 ml of deionised water. Then the required amount of $AgNO_3$ for doping was added into the suspension of TiO_2. The pH of TiO_2 suspension was

adjusted to 3. Then the mixture was irradiated with UV light (30 W, λ_{max}=254 nm) for 3 h and then dried at 100 ºC for 12 h. The dried solids calcined at 300ºC for 3 h in a furnace.

2. Investigation of photocatalytic activities

A solution containing desired amounts of Chloramphenicol (20mgL^{-1}) and photocatalyst were prepared and agitated for 30 min in the darkness. Afterwards, 100 ml of the above suspension was transferred into a borosilicate petri dish as photoreactor. The reaction mixture was UV irradiated by using UV lamp (15 W) and then at certain reaction intervals the concentration of Chloramphenicol was determined using a UV-Vis spectrophotometer at λ_{max} = 275 nm.

Results and discussion

1. The characterization of Ag/TiO_2 nanoparticles

As can be seen in Fig.2a, the spherical shape of TiO_2 weren't changed by Ag loading. The EDX analysis (Fig.2b) also confirmed the loading of Ag on TiO_2 nanoparticles.

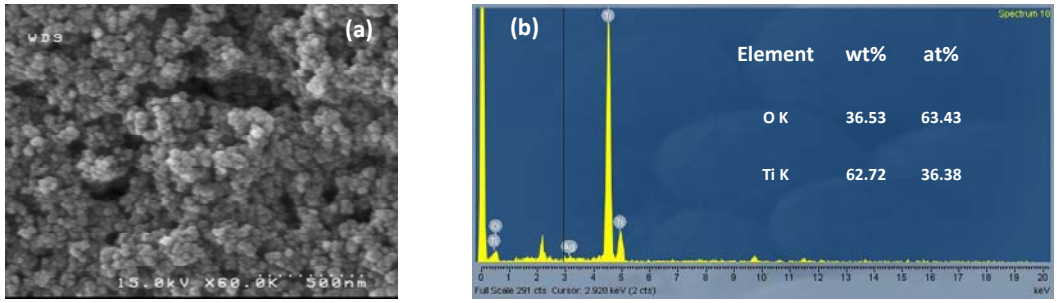

Fig.2. a) SEM micrograph and b) EDX analysis of 0.96wt% Ag/TiO_2 nanoparticles

2. The effect of Ag loading on the Photocatalytic activity

The results in Fig.3 showed that the photocatalytic activity of Ag doped TiO_2 increased with an increase in the Ag-doping up to optimum value (0.96wt %) and then decreased. The higher activity of Ag/TiO_2 is due to the enhancement of electron-hole separation by the electron trapping of silver particles [2]. Excessive coverage of TiO_2 catalyst with Ag nanoparticles limits the amount of light reaching to the TiO_2 surface, reducing the number of photogenerated e^--h^+ pairs and consequently, lowering the TiO_2 photoactivity [3].

3. The effect of catalyst dosage on the Photocatalytic activity

When the initial pollutant concentration (C_o) is a millimolar (C_o is small) the rate equation simply can be written as an apparent first order equation:

$$-\ln (C/C_o) = k_{app}\, t$$

A plot of $-\ln (C/C_o)$ versus time represents a straight line, the slope of the best line fitted to the data points equals to the apparent first-order rate constant k_{app}.

The good linearity of the $-\ln(C/C_0)$ versus irradiation time plot, with $R^2 > 0.99$, suggests that the photocatalytic reaction approximately followed the pseudo-first order kinetic. The rate constant calculated for the degradation of Chloramphenicol carried out at the different dosages of catalyst are presented in Fig.4. The catalyst dosage for maximum degradation of 20 mgL^{-1} of Chloramphenicol was 900 mgL^{-1} under the experimental conditions. The increase in the amount of catalyst increased the number of active sites on the photocatalyst surface, which in turn increased the number of hydroxyl, and superoxide radicals. When the concentration of catalyst was increased above the optimum value, the degradation rate decreased due to an increase in the turbidity of the suspension and a decrease in UV light penetration as a result of increased scattering effect [4, 5].

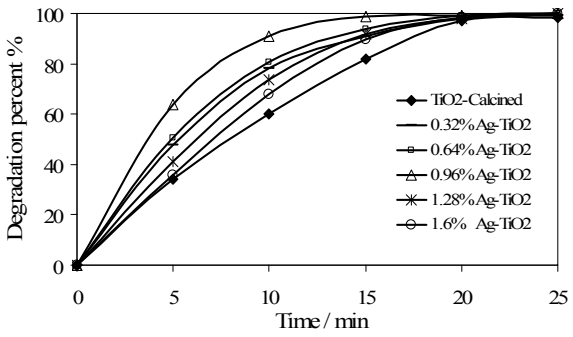

Fig.3. Effect of Ag loading on the photocatalytic degradation ([Catalyst] = 300 mg L^{-1}).

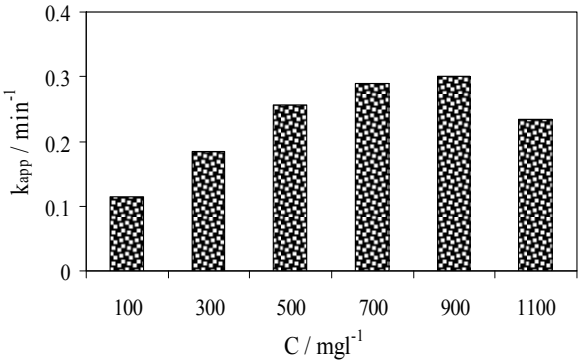

Fig.4. Effect of 0.96 wt% Ag/TiO_2 catalyst dosage on the photocatalytic degradation.

Conclusion

The present investigation showed that the photocatalytic efficiency of TiO_2 nanoparticles for the degradation of Chloramphenicol, can be significantly improved by depositing an optimum amount of Ag metals. The characterization of Ag-TiO_2 nanoparticles synthesized via photodeposition method using SEM and EDX techniques revealed the dispersion of silver metal on the surface of TiO_2. It was found that the 0.96wt% Ag loading at 900 mgL^{-1} of Ag-TiO_2 has been optimum conditions to achieve the highest efficiency of the Chloramphenicol

photodegradation**.** The semi-logarithmic graphs of the concentration of Chloramphenicol in the presence of different concentrations of photocatalyst versus irradiation time yield straight lines indicating pseudo-first order reaction.

References

[1] A. Chatzitakis, C. Berberidou, I. Paspaltsis, G. Kyriakou, T. Sklaviadis, I. Poulios, Water Res., 42 (2008) 386.

[2] N. Sobana, M. Muruganadham, M. Swaminathan, J. Mol. Catal. A., 258 (2006) 124.

[3] B. Sun, A.V. Vorontsov, P.G. Smirniotis, Langmuir, 19 (2003), 3151.

[4] I.K. Konstantinou, T.A. Albanis, Appl. Catal. B., 49 (2004) 1.

[5] M. Pera-Titus, V.G. Molina, M.A. Banos, J. Gimenez, S. Esplugas, Appl. Catal. B., 47 (2004) 219.

Effects of Complexing Agent on Structural, Morphological and Optical Properties of Chemical Deposited CdS Thin Films

R. Sahraei[a,*], N. Shokri[a,b], A. Karimi[a,b], A. Daneshfar[a], S. Shahriyar[c], and N. Niasadegh[d]

[a]*Department of Chemistry, University of Ilam, Ilam ,Iran*

[b]*Department of Chemistry, Payam-e Nour University, Urmia, Iran*

[c]*Department of Chemistry, Science and Research Branch, Islamic Azad - Khozestan-Iran*

[d]*Department of Physics, Islamic Azad University of Qom, Qom*

[*] *(Email: reza_sahrai@yahoo.com)*

Keywords:Semiconductors, Nanostructures, CdS thin films, Chemical deposition

Introduction

In recent years, the application of cadmium sulfide (CdS) films for window layers in CdS/CdTe, CdS/$CuInSe_2$ and CdS/$Cu(InGa)Se_2$. High efficiency solar cells have increased the studies on this technologically relevant semiconductor material [1]. Cadmium sulfide (CdS) in a nanocrystalline thin films form can be prepared by a variety of methods (both physical and chemical) like sol–gel, electrostatic deposition, sputtering, vacuum evaporation, and chemical bath deposition (CBD) [2,3]. CBD has the advantages of being a simple, low temperature, and inexpensive large-area deposition technique. In fact, compared to all other techniques mentioned earlier, CBD is known to greatly enhance the performance of CdS windows used in the above mentioned solar cells [4].

Experimental

The chemical bath was an aqueous solution of 6 ml cadmium acetate dehydrate 1 M, 30 ml thioacetamide 0.4 M, 20 ml ammonia acetate 2 M, and different complexing agents: 20 ml ethylenediamine 0.5 M or 15 ml ethylenediamine tetra acetic acide 0.2 M (EDTA) as a complexing agent for cadmium ions . The temperature of the chemical bath was 50 ˚C and the pH was adjusted to 7. A deposition time of 8 h was chosen for all experiments.

Results and discussion

The effects of complexing agents on the phases of CdS films were investigated by means of XRD. The crystal quality of the samples was studied by recording the XRD patterns in the

range of 20–60˚. Both films are cubic with a strong (111) reflection at 2θ=26.5°, and two weaker (220) and (311) peaks that confirmed the cubic phase of both films.

The optical properties of CdS thin films were measured by UV spectrometer. Figure 2 show the transmittance (T) spectra of the (CBD) CdS thin films grown at 50 ˚C by different complexing agents in the wavelength range 300-800 nm. As it can be seen, the transparencies of the CdS films in the visible region strongly depend on the complexing agent used in the CBD. When the complexing agent is EDTA, the CdS film displays high transmission in the visible region; on the other hand, when the complexing agent is ethylenediamine, the transmission of the CdS film in the visible region is low.

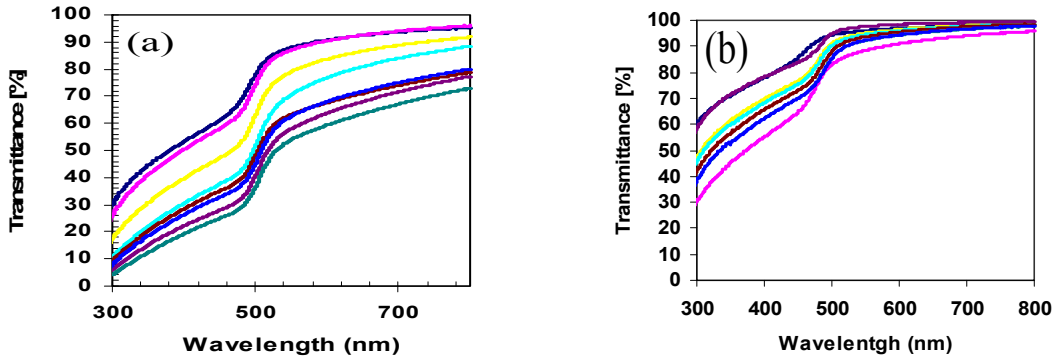

Fig.1. Optical transmittance spectra of CdS thin films deposited at 50˚ C by different complexing agents. (a) ethylenediamine (b) ethylenediamine tetra acetic acid.

Conclusions

The Nanocrystalline thin films of CdS were successfully deposited by chemical bath deposition method. A blue shift is observed in the spectra comparing to that of the bulk CdS. The band gap measured for ethylenediamine was found to be in the range of 2.7-3.2 eV and for ethylenediamine tetra acetic acid was in the range of 3.4-3.8 eV.

References

[1] D. A. Mazon-Montijo, M. S. Lerma, M. Q. Lopez, M. El-Bouanani H. N. Alshareef, F.J. Espinoza Beltran, R. Ramirez-Bon, Applied Surface Science 254 (2007) 499–505.

[2] Meysam Karimi, Mohammad Rabiee, Fathollah Moztarzadeh, Mohammadreza Tahriri, Masoud Bodaghi, Current Applied Physics 9 (2009) 1263–1268.

[3] Jae-Hyeong Lee, Jun-SinYi, Kea-Joon Yang, Joon-Hoon Park, Ryum-Duk Oh, Thin Solid Films 431–432 (2003) 344–348.

[4] H. Khallaf, Isaiah O. Oladeji, Lee Chow, Thin Solid Films 516 (2008) 5967–5973.

Investigation of the Effects of Temperature on Properties of Nanocrystalline CdS Thin Films

R. Sahraei[a,*], N. Shokri[a,b], S. Shahriyar[c], A. Daneshfar[a], and A. Karimi[a,b]

[a]*Department of Chemistry, University of Ilam, Ilam ,Iran*

[b]*Department of Chemistry, Payam-e Nour University, Urmia, Iran*

[c]*Department of Chemistry, Science and Research Branch, Islamic Azad - Khozestan-Iran*

[*] *(Email: reza_sahrai@yahoo.com)*

Keywords:Nanostructures, CdS thin films, Chemical deposition

Introduction

Nanocrystalline semiconductor structures have been an area of great research interest over the last decade [1]. Due to the direct and wide band gap of CdS semiconductor, CdS thin films have attracted much interest as a potential candidate for optoelectronic devices [2]. Chemical bath deposition (CBD) has been proven to be the most suitable method to produce CdS thin films for photovoltaic applications because it is an efficient, cost-effective, and large-scale method [2]. In the CBD process, the influence of the deposition parameters on film formation, particularly the role of deposition temperature on the film structure and properties, is extremely critical [3].

Experimental

Cadmium sulfide (CdS) thin films have been deposited on the glass substrates using CBD method. Stock solutions of 10 ml cadmium acetate dehydrate (0.5 M), 20 ml ethylenediamine (0.5 M) such as complexing agent, 20 ml ammonia acetate (2 M) and 30 ml thioacetamide (0.5 M) were prepared. PH was adjusted to 5 by adding a 1 M HCl solution. The deposition was carried out at 25, 50 and 75 ˚C for 30, 4, and 1 h, respectively.

Results and discussion

The optical transmittance spectra of CdS films deposited at three temperatures of 25, 50 and 75˚C, in the wavelength range of 300–800nm are shown in Fig.1 (left). It can be seen that the absorption edge of the spectra shifted towards shorter wavelengths in the lower absorption

temperatures. The energy gaps of the films at various temperatures have been determined by extrapolating the linear portion of the plots of $(\alpha h\nu)^2$ against hν to the energy axis [4]. Increasing in E_g of deposited films at low temperature can be assigned to the quantum size effect as expected from a nanocrystalline nature of the CdS thin films.

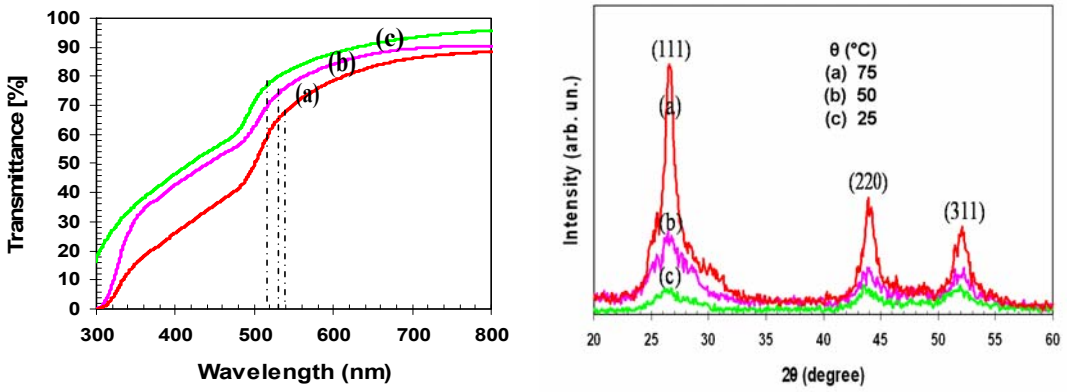

Fig.1. Optical transmittance spectra (left) and XRD patern (right) of CdS thin films deposited at various temperatures: (a) 25, (b) 50, and (c) 75 ˚C.

X-ray diffraction patterns in Fig. 1 (right) show the crystallinity of the CdS thin films deposited at various temperatures of 25, 50 and 75 ˚C, respectively. The diffraction patterns show a three broad peaks observed in the diffractogram at around 26.5, 43.8 and 52.3 reveal a cubic lattice structure of CdS (β-CdS phase). With the increase of temperature of reaction, there is an increase in intensity and sharpening of the peaks, which is caused by improving crystallinity of the crystals and increasing of the crystallite size.

Conclusions

Nanocrystalline CdS thin films were deposited by the simple CBD method from an acidic solution (pH=5.0) with varied solution temperatures from 25 to 75 ◦C. The obtained films were homogeneous, strongly adherent, and present high optical transmission with an energy gap value of about 3.90 eV. Transmittance measurements of CdS thin films clearly show a shifting of the band gap energy with bath temperature.

References

[1] H. Moualkia, S. Hariech, M. SAida, N. Attaf and E. L. Laifa, J. Phys. D: Appl. Phys. 42 (2009) 135404 (7pp).

[2] Hui Zhang, Xiangyang Ma, Deren Yang, Materials Letters 58 (2003) 5–9.

[3] H. Moualkia, S. Hariech, M.S. Aida, Thin Solid Films 518 (2009)1259–1262.

Synthesis of keggin-type phosphomolybdate nanoparticles by microemulsion method

Saeed Shahbazi, Majid Masteri-Farahani*
Chemistry Department, Faculty of Science, Tarbiat Moallem University, Tehran, Iran
E-mail address: mfarahany@yahoo.com

Abstract

$Q_3[PMo_{12}O_{40}]$ nanoparticles were synthesized by microemulsion method and thoroughly characterized by chemical analysis, FT-IR spectroscopy, CHN Analysis, X-ray powder diffraction (XRD) and scanning electron microscopy (SEM). The resulted nanoparticles are keggin-type of phosphomolybdate.

Keywords: polyoxometalate; nanoparticle; phosphomolybdate; microemulsion

Introduction

Heteropolyacids (HPAs) are early transition metal oxygen anion cluster that exhibit a wide range of molecular sizes, compositions, and architectures. Among various HPA structural classes, the keggin-type HPAs have been widely employed as catalysts in homogeneous and heterogeneous systems for acid-base and oxidation reactions. One of the great advantages of HPA catalysts is their great thermal stability. The (α) $[PMo_{12}O_{40}]^{3-}$ ion has a central tetrahedrally coordinated phosphorus atom, surrounded by four groups of three edge-share octahedral (Mo_3O_{13} subunits). These are linked in turn to each other through shared oxygen atoms and to the central PO_4 unit, giving a species with overall T_d symmetry. In the present paper, HPAs were synthesized by microemulsion method.

Experimental

The microemulsion system used in this study consisted of CTAB as a surfactant, butanol as a co-surfactant, isooctan as the continuous oil phase, and the sodium molybdate, disodium hydrogen phosphate aqueous solution as aqueous phase.

Firstly, in flask 1, Na_2MoO_4 and Na_2HPO_4 were dissolved in water, and then in another flask, microemulsion system was prepared by dissolving CTAB in co-surfactant. Secondly, the content

of flask 1 was added to flask 2 with stirring. Finally, HCl was added to microemulsion system and yellow precipitation was formed.

Results and discussion

Characteristic IR bands of the phosphomolybdate (PMo) appeared at 1061 (P- O bond), 955 (Mo=O bond), 881, and 798 cm^{-1} (Mo-O-Mo). The SEM images showed that PMo nanoparticles were spherical. The XRD patterns showed fine structures that indicated the formation of PMo nanoparticles in nanoscale. Elemental analysis for PMo was found: C(28.14%); H(5.0%); N(1.72 %). FT-IR spectroscopy, XRD and SEM analyses showed that the nanoparticles of keggin-typ phosphomolybdate were successfully prepared by microemulsion method.

References

[1] Enny Silviani, Robert Burns, J. Mol. Catal. A: 219 (2004) 327–342.

[2] In K. Song, Mark A. Barteau, J. Mol. Catal. A: 212 (2004) 229–236.

[3] Heesoo Kim, Ji Chul Jung , Pil Kim, Sung Ho Yeom, Kwan-Young Lee, In Kyu Song , J. Mol. Catal. A: 259 (2006) 150–155.

[4]Heesoo Kim, Ji Chul Jung , Sung Ho Yeom, Kwan-Young Lee , In Kyu Song, J. Mol. Catal. A: 248 (2006) 21–25.

[5] Xin Zhang, Kwong-Yu Chan, J. Mater. Chem. 12(2002) 1203–1206.

Investigations on the physical properties of the nanocrystalline CdSe thin films deposited by chemical bath deposition method

S. Shahriyar [a], R. Sahraei[b,*], A. Daneshfar[b], N. shokri[b,c], A. karime[b,c]

[a]Department of Chemistry, Science and Research Branch, Islamic Azad University - Khozestan-Iran

[b]Department of Chemistry, University of Ilam, Ilam ,Iran

[c]Department of Chemistry, Payam-e Nour University, Urmia, Iran

(*E-mail:reza_sahrai@yahoo.com)

Keywords: Nanocrystallins CdSe, Optical properties, Thin film

Introduction

Chemical bath deposition (CBD) method has been used for many years to prepare thin films of chalcogenide semiconductors. In this method, semiconductors thin films are deposited on substrate immersed in dilute solution containing metal ions and a source of complexing agent and selenide ions [1, 2]. The properties of materials prepared by the CBD method critically depend on various preparative parameters such as the sources and concentration of metal and chalgonide ions, the pH of the resultant solution, deposition time, temperature, etc [3]. in this work, CdSe thin films were prepared by CBD at temperature 80 °C. The X-ray diffraction (XRD), the energy dispersive X-ray analysis (EDAX) analysis, Scanning electron microscopy (SEM) and optical absorption techniques are used to characterize the CdSe thin films.

Experimental

CdSe thin film was prepared by first mixing 10 ml of 1 M $Cd(SO_4)_28H_2O$, 10 ml of 0.2 M EDTA, and 30 ml of freshly prepared Na_2SeSo_3 solution and the rest was completed with deionized water to make the total volume of the solution 50 ml. The pH of the solution was adjusted to 3.48 by addition of HCl solution. The mixture was poured into a beaker and heated to 80 °C. When the temperature reached the deposition temperature, four pre-cleaned glass slides were introduced into the solution and then waited for different deposition times 3.0, 3.5, 4.0 and 4.5 h in order to study the growth rate of the process.

Results and discussion

Fig. 1 (left) shows X-ray spectra made for CdSe films with different deposition times such as 3.0, 3.5, 4.0 and 4.5 h. The XRD patterns of the CdSe film exhibit three distinguished peaks at the angles of 25.6º, 42.7º and 50.8º corresponding to diffraction of the (111), (220) and (311) planes of the cubic phase, respectively. In Fig. 1, as the deposition time increases the intensity of CdSe (111) peak increases and this peak becomes narrower indicating an improvement of the crystallinity. The SEM micrograph of the CdSe thin film is shown in Fig. 1 (right). It is observed that film is nanocrystalline, homogeneous, relatively without cracks or holes and well covered to the substrate. The CdSe films showed optical transmission 75–93% in the visible range. These results are much better than previous reports that show optical transmittance 70% in the visible region. The band-gap value was calculated in the range of 2.8–3.4 eV. The band-gap values are higher than bulk value of cubic CdSe because of quantum confinement of CdSe nanocrystals. The average atomic ratio of Se/Cd, calculated from the quantification of the peaks, gives the value of 0.58, 0.59, 0.60 and 0.62 for different deposition times 3.0, 3.5, 4.0 and 4.5 h, respectively. These results indicate that the average atomic ratio of Se/Cd increases with increasing deposition time, ratios of the films are lower than the stoichiometric ratio (Se/Cd = 1) and the surface of the samples is rich in metal.

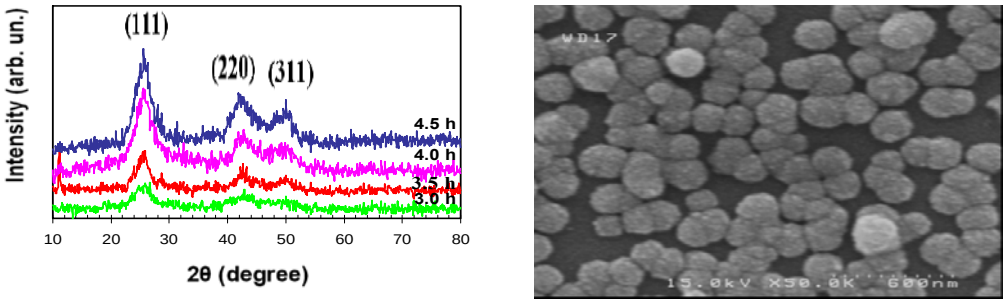

Fig. 1. X-ray diffraction patterns and for CdSe films deposited at 80 °C with different deposition times (left) and SEM image of the CdSe deposited at 80 °C (right).

Conclusion

nanocrystalline CdSe films can be deposited on glass substrates by the CBD method. It is particularly observed that the best crystallinity of the CdSe thin films is obtained at 80 °C with 4.5 h. The films are in good quality, adherent and uniform. The CdSe thin films have cubic phase and preferred orientation in the (111) plane. The grain sizes are estimated to be in the range of 2–10 nm. Optical measurements show that the films possess 75–93%

transmittance in the visible region. Energy band gaps of the nanocrystalline CdSe films are in the range of 2.8–3.4 eV.

Refererces

[1] A. Goudarzi, G. Motedayen Aval, R. sahraei, Thin Solid Films 516 (2008) 4953–4957.

[2] P. Nemec, M. Simurda, at all, Journal of Crystal Growth 292 (2006) 78–86.

[3] S. Erat, H. Metin, M. Arı, Materials Chemistry and Physics 111 (2008) 114–120

The effect of the pH value on the growth and properties of the chemical deposited CdSe thin films

R. Sahraei[a,*], S. Shahriyar[b], A. Daneshfar[a], N. shokri[a,c], A. karimi[a,c]

[a]*Department of Chemistry, University of Ilam, Ilam ,Iran*

[b]*Department of Chemistry, Science and Research Branch, Islamic Azad University - Khozestan-Iran*

[c]*Department of Chemistry, Payam-e Nour University, Urmia, Iran*

*(*E-mail:reza_sahrai@yahoo.com)*

Keywords: Thin film, Chemical bath deposition, Optical properties, Nanostructures

Introduction

Cadmium selenide is widely used A^{II}–B^{VI} group semiconductor whose band gap (E_g=1.7 eV) lies in the solar energy spectrum [1, 2]. CdSe thin films can be deposited by various techniques such as electro-deposition, spray pyrolysis, and chemical bath deposition (CBD) [3]. Among these methods chemical bath deposition (CBD) has greater advantages than others. Chemical bath deposition is quiet simple, does not require sophisticated instruments and large area deposition is possible [4]. In this work, we report the preparation and characterization of CdSe thin films by chemical bath deposition. The effect of pH parameter on the structural and optical properties of CdSe thin films has been studied.

Experimental

For deposition of CdSe thin films, 6ml of 1M $Cd(CH_3COO)_2$, and5 ml of 0.2 M trimethylamine solution were mixed in beaker. Then 30 ml of freshly prepared Na_2SeSo_3 solution was added slowly with constant stirring and finally 60 ml diluted deionized water was added to the beaker. The glass substrates were kept in reaction mixture for 1h at the desired temperature (60 °C) and the pH of the bath was varied from 3.18 to 10.2. The CdSe thin films were characterized by X-ray diffraction (XRD), energy dispersive X-ray analysis (EDAX) techniques and UV–Vis spectrophotometer. The thin film thicknesses were measured by a Dektak profilometer.

Results and discussion

The plot of $(\alpha h\nu)^2$ vs $(h\nu)$ is shown in Fig. 1a which is linear at the absorption edge, indicating a direct transition. The straight line portion is extrapolated to the energy axis and when $(\alpha h\nu)^2$

= 0, the intercept gives the band gap energy of CdSe. The band gap energy is found to be in the range 2.6 to 3.3 eV depending on the pH of the deposition solution and the variation is depicted in Fig. 1b. The blue shift in the band gap value as compared to the bulk value as well as higher band gap value at pH other than 7.1 may be due to the difference in the composition of the CdSe compound and smaller grain size. In order to study growth kinetics, CdSe thin films were deposited from deposition baths maintained at different pH values for different time intervals. Fig. 1c shows the plot of variation of the CdSe film thickness deposited at different pH of the bath. It is observed that as pH of the bath increases, film thickness increases, attains maximum thickness (320 nm at pH 7.1) and thereafter decreases with further increase in pH. At pH 7.1, the deposition solution becomes transparent and there is formation of uniform and adherent film on the substrate. The diffraction peaks at $2\theta = 29.2^0$, 48.1^0 and 57.1^0 are attributed to (111), (220) and (311) planes, respectively of cubic CdSe phase. Quantitative analysis of the film was carried out using the EDAX technique for CdSe thin films deposited at pH 3.18, 7.2 and 10.2 to study the composition in the film. It shows that the film deposited at pH 3.18 and 10.2 is cadmium and selenium rich, respectively, whereas the film deposited at pH 7.1 is nearly stoichiometric.

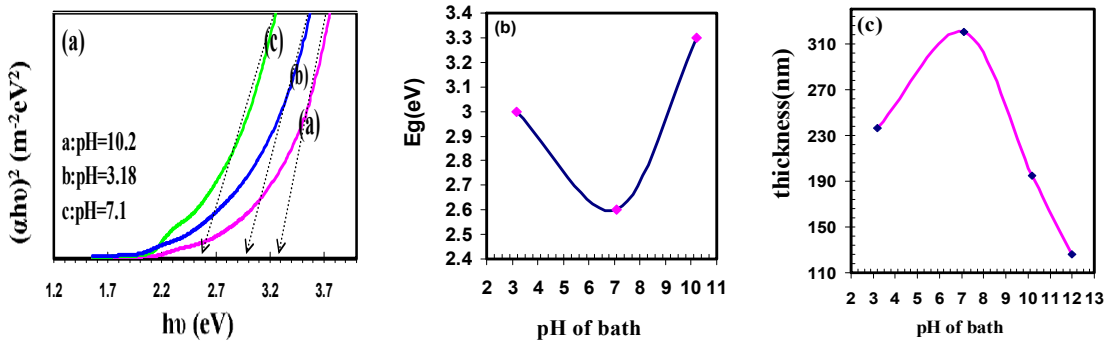

Fig.1 Variation of (a) $(\alpha h\nu)^2$ vs ($h\nu$) and (b) band gap energy and (c) Plot of film thickness of CdSe thin films deposited at different pH values of bath.

Conclusions

In conclusion, CdSe thin films have been successfully chemical deposition and the effect of pH of deposition solution on structural and optical properties is studied. Nearly stoichiometric films with better structural and optical properties were obtained at pH 7.2. XRD study revealed nanocrystalline nature of the films with cubic phase. Optical absorption study

revealed direct band gap nature with band gap energy in the range 2.6 to 3.3 eV depending on the pH of bath.

References

[1]. R B Kale and C D Lokhande, Semicond. Sci. Technol. 20 (2005) 1–9.

[2]. S. Erat, H. Metina, M. Arıb, Materials Chemistry and Physics 111 (2008) 114–120

[3]. O. Millo, D. katz, Phys. Rev. Lett., 86 (2001) 5751.

Effect of external electric field in a GaAs/AlAs quantum dot

E. Sadeghi, S. Alirezaie
Department of Physics,Yasouj University, Yasouj, Iran 75914-353
sadeghi@mail.yu.ac.ir

Keywords: Effective mass approximation, Modified Bessel function, Polarization

Introduction

With the great progress of semiconductor nanostructure technology, it has been possible to fabricate various kinds of low-dimensional quantum systems. Among these systems, the quantum dot (QD) system is of great interest because its strong geometrical confinement makes its physical properties, such as optical and electron-transport characteristics, greatly different from those of the bulk material. One of the major concerns in such systems is the effect of spatial electric field on the energy levels of charge carriers [1]. The application of an electric field is equivalent to introducing an additional confining potential, so it gives rise to a polarization of the carrier distribution and to an energy shift of the quantum states.

Method

The Schrödinger equation describing the interaction of an electron in the external electric field in the tetragonal quantum dot is given as:

$$[-\nabla^2 + V(r) + \vec{F}.\vec{r}\,]\Psi(r) = E\Psi(r) \quad (1)$$

Where the quantum confining potential energy of an electron in a tetragonal QD is:

$$V(x,y,z) = \begin{cases} 0, & inside\ the\ dot\ a \times a \times c \\ \infty, & else\ where \end{cases} \quad (2)$$

Using the separation of variable method the wave function can be written as $\Psi(r) = \psi_1(x)\,\psi_2(y)\,\psi_3(z)$, and the Schrödinger equations are separated into 3 similar equations:

$$\frac{-1}{\psi_1(x)}\frac{d^2\psi_1(x)}{dx^2} + \eta \sin\theta\ \cos\varphi\ x + V(r) = E_x \quad (3)$$

Where $\eta = eFa^*/R^*$ is the dimensionless measure of the electric field. With appropriate change of variable Eq.(3) transformed to:

$$t^2R'' + tR' - \left(\frac{1}{9} + \frac{4t^2}{9}\right)R = 0 \quad (4)$$

The equation is the modified Bessel equation, thus, the solution of Schrödinger equation in terms of the combination of modified Bessel functions (I) could be written as:

$$\psi_1(u) = A_1\sqrt{u}\, I_{\frac{1}{3}}\left(\frac{2}{3}\, u^{\frac{3}{2}}\right) + A_2\sqrt{u}\, I_{-\frac{1}{3}}\left(\frac{2}{3}\, u^{\frac{3}{2}}\right) \quad (5)$$

The polarization of charge carrier and flux due to the external electric field are written as:

$$\frac{p}{e} = \langle \Psi(r)|\vec{F}.\vec{r}/\eta|\Psi(r)\rangle_{F\neq 0} + \langle \Psi_0(r)|\vec{F}.\vec{r}/\eta|\Psi_0(r)\rangle_{F=0} \quad (6)$$

$$\Phi = aF[c\ \sin\theta\ (\cos\varphi + \sin\varphi) + a\ \cos\theta) \quad (7)$$

Results and discussion

The variation of the energy with the electric field flux for $0.35 < c/a < 8.0$ is presented in Fig.1. According to this figure, the energies have a minimum at $\frac{c}{a} = 1$, and shift to higher values as the electric field flux increases. The energy for a fixed value of the electric flux decreases with electric field increases. The calculated energies are in good agreement with Akbas's results [2]. The polarization versus θ for different values of the electric field, and for two choices of c/a ratio are shown in Fig.2. It can be seen that the polarization depend on both θ and $x(=\frac{c}{a})$, such that for a given values of x_2 (or x_1) and F, the polarization decreases (or increases) as θ increase. The results are in good agreement with Akbas' calculations. The polarizations for different value of electric field are coincident for x_1. This is because, there is a competition between the strength of electric field and c/a ratio, so that in the case of $\frac{c}{a} = x_1$, polarization has higher dependence on c/a relative to the field strength.

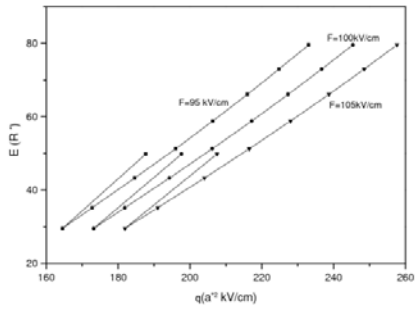

Figure 1

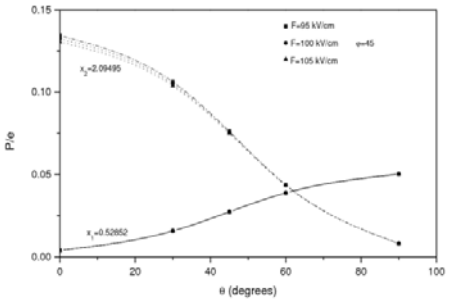

Figure 2

References:

[1] S. S. Li, J. B. Xia, J. Appl. Phys.**100**, 083714 (2006)

[2] H. Akbas, C. Dane, K. Kasapoglu, N. Talip, Physica E **40**, 627 (20

Undoped and doped SnO_2 thin films: influence of doping on the photocatalytic degradation of 2-clorophenol

Azam Salehi*, Nasrin Talebian

Department of Chemistry, Faculty of Science, Islamic Azad University, Shahreza branch, I.R. Iran
E-mail: talebian@iaush.ac.ir

Introduction

The photocatalytic degradation of organic compounds is investigated as a means of purifying water [1]. In particular, phenols constitute an important class of water pollutants. Human activities, such as water disinfection, waste incineration and uncontrolled use of herbicides, [2]. The degradation of organic pollutants using ZnO photocatalysis has been previously investigated [3, 4]. However, no significant effort has been made in evaluating the photocatalytic efficiency of SnO_2 on2-coloro phenol oxidation and the factors affecting it in particular, as doped system with metals such as Ag and Al. The present work focuses on the photocatalytic properties of SnO_2, Ag-doped and Al-doped SnO_2 nanostructured thin films prepared by SGDC technique toward phenol degradation. The influence of the dopant molar ratio, , 2-clorophenol initial concentration and structure characteristics of the photocatalysts has been investigated on their photocatalytic activity.

Results and discussions

1. Preparation of sols

SnO_2: The sol precursor was prepared by dissolving aliquots of 13.5 g of $SnCl_2$ $2H_2O$ in 100 ml of absolute ethanol and then refluxing during 2.5 h.

A range of SnO_2 films were made using aluminum and silver dopants with Sn/dopant molar ratio 1:2, 1:4 and 1:10.

Ag: SnO_2 and Al: SnO_2 : The procedure was identical to that for the SnO_2 sol except required amount of $AgNO_3$ and $Al(NO_3)_3.9H_2O$ dissolved in the same mixed solvent and stirred for ~1 h which was then added drop wise to the solution obtained in the first step and it was stirred again for 1 h.

2. Characterization of the films

Fig. 1c shows the characteristic XRD spectra of the sample

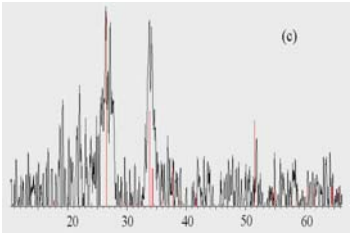

respectively. The pattern of SnO_2 films display the (110), (101), (200) and (211) diffraction peaks of the cassiterite SnO_2 crystalline phase.for example: C Al- SnO_2) films

Surfaces of M–doped SnO_2 films are quiet smooth, as observed by SEM. The average particle size of SnO_2 decreases from about 87 to 40 nm with metal doping (Fig. 2a).

Fig. 2.sem of Al– SnO_2 films

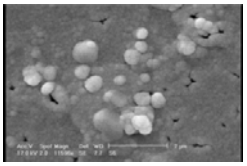

3. Photocatalytic studies

Typical absorption spectra of 2-coloro phenol solution, initial concentration ranging 5 ppm, in which Ag- SnO_2 film were settled and exposed to UV radiations for different time durations up to 8 ,. These studies are performed on undoped and M-doped SnO_2 films up to Sn/Ag

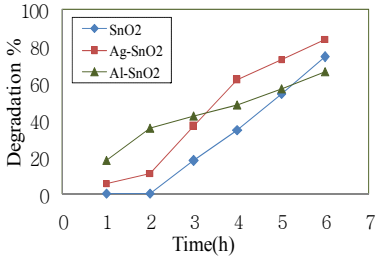

Fig. 3. Photocatalytic degradation of2-coloro phenol as a function of time

molar ratio 2:1. Ag– and Al–doped SnO_2 thin film showed the highest and lowest photocatalytic efficiency, respectively (Fig. 3)

To enhance the degradation rate or photocatalytic activity in the sample, it is necessary that more charge carriers (electrons and holes) should be available for the reactions. The results showed that the photocatalytic activities of the Ag-doped SnO_2 films were promoted

compared with SnO_2. Such promotion can be attributed to reduction of band gap after Ag doping which allow the exit of electron from doped SnO_2 catalyst at low UV-light energy.

Conclusions

1. Ag nanoparticles substantially enhance the of photocatalytic performance of SnO_2 for the degradation of phenol. At the optimum Ag loading, which corresponded to an average Au particle size of ~32 nm, the kinetic rate constant for phenol degradation was higher than that for $USnO_2$.

3. The surface of Al–doped SnO_2 has the defect structure due to smaller particle size and

2. This rate enhancement may be due to injection of photoexcited electrons from semiconducting Ag into the SnO_2 conduction band.

low crystallinity, then e^- may be trapped by Sn ions at the surface. This results to photoactivity reduction for Al-SnO_2 films.

References:

[1] M. Schiavello (Ed.), Photocatalysis and Environment, Kluwer Academic Publishers, Dordrecht, 1988.

[2] K.R. Krijgsheld, A. van der Gen, Chemosphere **15** (1986) 825.

[3] J. Nishio, M. Tokumura, H.T. Znad, Y. Kawase, J. Hazard. Mater. **B138** (2006) 106.

[4] E. Evgenidou, I. Konstantinou, K. Fytianos, I. Poulios, Catalysis Today **124** (2007) 156.

Low temperature preparation and characterization of ZnO nanoparticles supported on activated carbon and their photocatalytic activity

M. Sabri*[a] and A. Habibi-Yangjeh[b]

[a] *Department of Chemistry, Comprehensive Scientific Applicable University, Kangan, Iran*
(email: mina20sabri@yahoo.com)

[b] *Department of Chemistry, Faculty of Science, University of Mohaghegh Ardabili, Ardabil, Iran*

Keywords: Zinc oxide, Photocatalysis, Activated carbon, Methyl orange, Nanoparticle.

Introduction

In recent years, heterogeneous photocatalysis has emerged as an efficient technology to purify air and water [1]. Despite the positive attributes of photocatalysts, poor adsorption properties of semiconductors lead to great limitation. To circumvent this limitation, several attempts have been made to improve the efficiency of photocatalysts by using suitable supports [2]. Although, there are extensive studies on photocatalytic activity of TiO_2 supported on activated carbon [3], however studies about supported ZnO on activated carbon are very rare [4]. Then, we have employed a refluxing method as a mild and environmentally benign technique for preparation of nano-sized ZnO supported on activated carbon and its photocatalytic activity towards photodegradation of methyl orange (MO) was carried out.

Experimental

The X-ray diffraction (XRD) patterns were recorded on Philips Xpert X-ray diffractometer with Cu Kα radiation (λ= 0.15406 nm). Surface morphology and distribution of particles were studied *via* LEO 1430VP scanning electron microscope (SEM). Diffuse reflectance spectra (DRS) were recorded by a Scinco 4100 apparatus. Nanoparticles of ZnO were supported with different loading on activated carbon (80, 82.5, 85, 89 and 91.9 wt. % ZnO) with refluxing method. The photocatalytic activity of the catalysts was studied by degradation of MO as a target pollutant. A UV Osram lamp of 125 W with the major fraction of irradiation occurring at 365 nm was used.

Results and discussion

Powder XRD patterns for the samples manifest that the bare and supported ZnO have high crystallinity. The XRD patterns of the supported ZnO indicate that ZnO loading on the adsorbent did not change structure of ZnO. The particle sizes supported (85 wt. % ZnO) and bare ZnO are 20 and 25 nm, respectively.

The results obtained by SEM images demonstrate that ZnO nanoparticles are irregular nanoplates with different sizes. DRS for the activated carbon, bare ZnO and the supported photocatalysts were obtained. An absorption peak about at 350 nm was observed for the nanoparticles of bare and supported ZnO. This absorption wavelength is lower than the bulk ZnO with absorption at 384 nm. Similar to our previous works, this can be attributed to quantum confinement effect of the ZnO nanoparticles [5, 6]. It is clear that there is not remarkable change in absorption wavelength for the supported ZnO. Then, it can be concluded that ZnO nanoparticles have been loaded on surface of the activated carbon, instead onto the pores and cavities. Photocatalytic degradation of MO was carried out in a batch reactor and the reaction variables were optimized in order to obtaining maximum degradation efficiency. The essential reaction parameters of (i) composition of the photocatalyst, (ii) calcination temperature, (iii) catalyst weight, (iv) initial MO concentration, and (v) pH of solution were varied and the results were described. To compare influence of the activated carbon on photocatalytic activity of ZnO nanoparticles, the photodegradation experiments were carried out by supported and unsupported ZnO in optimized conditions (calcination temperature=300°C, catalyst weight=0.10g, [MO]=4.9×10^{-5}M and pH=7). The results revealed that bare ZnO requires approximately 220 minutes for complete degradation of MO whereas the supported ZnO requires only 150 min. The higher efficiency of the supported ZnO can be attributed to the greater adsorption of MO on the photocatalyst. The reaction rate constant for degradation of MO using the supported ZnO is approximately 1.45 times higher than bare ZnO. The adsorption capacity of activated carbon enhances the chance of OH radicals attack on the adsorbed MO resulting faster degradation rate.

References:

[1] T. Sano, E. Puzenat, C. Guillard, C. Geantet, S. Matsuzawa, J. Mol. Catal. A: Chem. 284, 127 (2008).

[2] M. Huang, C. Xu, Z. Wu, Y. Huang, J. Lin, J. Wu, Dyes Pigments 77, 327 (2008).

[3] S. X. Lin, X. Y. Chen, X. Chen, J. Hazard. Mater. 143, 257 (2007).

[4] N. Sobana, M. Muruganandam, M. Swaminathan, Catal. Commun. 9, 262 (2008).

[5] V. Taghvaei, A. Habibi-Yangjeh, M. Behboudnia, Physica E 42, 1973 (2010).

[6] M. Esmaili, A. Habibi-Yangjeh, J. Alloys Compd. 496, 650 (2010).

Free Activation Energies and kinetic Properties Study of Tetraazachlorine-Fullerene C_{60} as [TAC-C_{60}-R].C_n (n= 60, 70, 76, 82, 86); R=OBu, Supramolecular Complexes

Avat (Arman) Taherpour* and Soudeh Safari
Chemistry Department, Facullty of science, Islamic Azad University Arak Branch
P.O.Box 38135-567,, Arak, Iran.
avatarman.taherpour@gmail.com & ataherpour@iau-arak.ac.ir

Abstract: In this study, the number of carbon atoms in fullerenes was used as discriptors to establish a good relationship between the structure of Tetraazachlorine and Fullerenes C_n (n= 60, 70, 76, 82 and 86). The first to forth free activation energies of electron transfer and kinetic rate constant of the electrontransfer, ($\Delta G^{\neq}_{et(n)}$ and $k_{et(n)}$, n=1-4 , respectively were calculated in this study for tetraazachlorine–Fullerene C_n complexes with used calculated of four free energies of electrontransfer $\Delta G_{et(n)}$ ($\Delta G_{et(1)}$ *to* $\Delta G_{et(4)}$), of this supramolecular complexes. This calculation are agree with the Marcus theory.

Keywords: Fulerenes, Tetraazachlorine-Fulleren C_{60}, Rate constants, Free activation energies.

Introduction:

Metal phthalocyanine (**1** and **2**) class of compounds attractd world-wide interest because of their interesting properties like chemical inertness, excellent thermal stability. Vary high clouring properties, catalytic activity, semiconductivity, photoconductivity and the like electrical conductivity are the important properties of the phthalocyanine compounds which attracted great deal of interest since 1948.

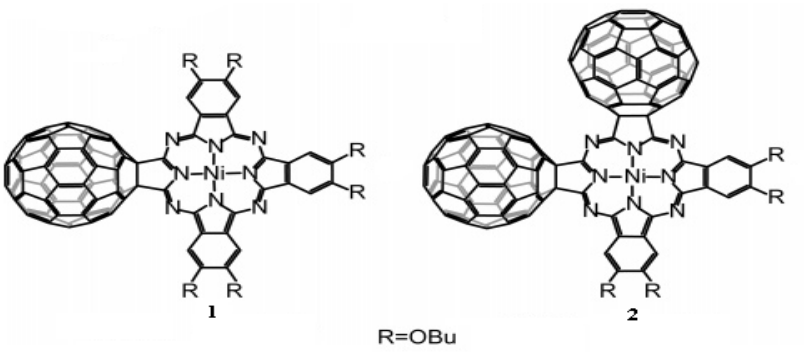

Mathematical method:

The number of carbon atoms of these fullerenes (C_n) was utilized as a structral index for compounds. All graghs were generated using the Microsoft Office Exell 2003 program. Using the number of carbon atoms contained within the C_n fullerenes, several valuable properties of the fullerenes can be calculated. This calculation are agree with the Marcus theory.

Results and discussion:

By using the equations which obtained in this modeling, it is possible to calculate the values of $\Delta G_{et(1)}^{\#}$ to $\Delta G_{et(4)}^{\#}$ of [TAC-C_{60}-R] supramolecular complexes. The $\Delta G_{et(n)}$ (n=1-4) for [TAC-C_{60}-R] supramolecular complexes (C_n=C_{60}, C_{70}, C_{76}, C_{82}, C_{86}, C_{78}, C_{84}, C_{120}, C_{132}, C_{140}, C_{146}, C_{150}, C_{160}, C_{162}, C_{240}, C_{276}, C_{288} and C_{300}) are predicted by using the appropriate equations. By utilizing these results, the electron transfer energies of $\Delta G_{et(n)}$ (n=1-4) of the complexes between selectedTetraazachlorin derivatives with fullerenes (C_{60}, C_{70}, C_{76}, C_{82}, C_{86}, C_{78}, C_{84}, C_{120}, C_{132}, C_{140}, C_{146}, C_{150}, C_{160}, C_{162}, C_{240}, C_{276}, C_{288} and C_{300}) were approximated. The calculated values of the free electron transfer energies of $\Delta G_{et(n)}^{\#}$ (n=1-4) for selected [TAC-C_{60}-R] supramolecular complexes (n = 60, 70, 76, 82 and 86) in the equations were interpreted. There was good agreement between the calculated and the predicted values. In lieu of increasing the number of carbons atoms in the fullerene structure, the values of $\Delta G_{et(n)}^{\#}$ (n=1-4) decreased. The supramolecular complex structures which were discussed here and the calculated values of $\Delta G_{et(n)}^{\#}$ (n=1-4) corresponding to these supramolecular complexes were neither synthesized nor reported before.

References

1-Avat(Arman)Taherpour and Esmat Mohammadinasab, *Fullerenes*, *Nanotubes and Carbon Nanostructures*, 18: 72–86, 2010.

2-Avat(Arman)Taherpour and Maryam Maleki, *Analytical Letters*, 43: 658–673, 2010.

3-Avat(Arman)Taherpour, *Phosphorus, Sulfur, and Silicon*, 185:422–432, 2010.

4- Avat(Arman)Taherpour, *Chem Phys Lett,* 469: 135-139, 2009.

5-C.C,Leznoff.,A.B.P,Lever.,Eds. *Phthalocyanines:Properties and Applications;VCH:New York., 1989- 1996;Vols. 1-4*

Preparation and Catalytic Performance of $Fe^{III}PPIX/NH_2$-MCM-41 Nanobiocatalysts through Oxidation Reactions

F. Safa Shams[a], F. Adhami [a], K. Nazari [a,*], A.Mahoudi [b], E. Salehi Siavashani [a]

[a] Chemistry Dept., Shahr Rey Branch, Islamic Azad University, Tehran/Iran, 18155-144

[b] Chemistry Department, Karaj Islamic Azad University, Karaj, Iran

E-mail: nazarikh@ripi.ir, fadhami@gmail.com

Keywords: Nano-porous , Modification , MCM-41, Heme , Nanobiocatalyst

Introduction

Discovery of silica based mesoporous compounds of M41S family has extended new applications and contributions in the chemistry and biosciences. One of the important applications is their usage as catalysts in chemical industry [1]. Chemical modification of such nano-porous compounds with various functional groups and molecules will improve the catalyst activity and properties [2]. Fe (III) protoporphyrin IX or Heme ($Fe^{III}PPIX$) -as a heterocyclic macrocyclic compound consisting four pyrrol rings- is the prosthetic group and active site of hemoenzymes. Connection of this complex to the modified the mesoporous compound makes the nanobiocatalysts [3, 4].

Experimental section

In the present work heme was separated from human blood cells [5] and covalent bonding of heme to MCM-41 was carried out by two procedures:

1. Amine modified MCM-41 mesoporous compound was prepared by the condensation reaction of 3-amino propyl trimethoxysilane (APTS) with silanol groups of MCM-41[6]. Then, heme was solved in alkaline solution, after setting the pH; it was covalently immobilized on the amine modified MCM-41 mesoporous compound (amide bond formation between the propionates of heme and amine group of APTS). 2. It is also possible to react heme with APTS first (amide bond formation) and then the immobilization reaction will be done between the heme/APTS and MCM-41 (condensation reaction). Furthermore, presence of the specific functional groups in the pyrrol ring or addition of amine electron donors on the fifth coordination position of iron atom in the heme will enhance the biocatalyst activity

[7].Modified heme samples using imidazole as the enhancer, were prepared at different ratios of imidazole/heme and the ratios with the maximum catalytic activity in the oxidation reaction were identified.

Results and Discussion

The obtained heterogeneous nanobiocatalysts were characterized by FTIR, Atomic Absorption spectroscopy (AA) and diffuse reflectance UV-Vis spectrophotometry techniques. XRD and BET techniques were also used to characterize the structure, pore size and specific surface area the porous catalysts.The prepared nanobiocatalysts were used for various oxidation reactions, for instance oxidative radical formation by ABTS in the presence of hydrogen peroxide. The reactions were examined by the changes of absorbance vs time in various conditions.

Conclusions

Different reactions showed high activity, selectivity and stability in various oxidation reactions. The kinetic parameters such as Initial rates, rate constants k_1 and k_3, K_m, V_{max}, k_{cat} and catalytic efficiency for each catalyst can be determined by various kinds of plots and diagrams such as Michaelis–Menten, lineweaver-Burk and Eadie-Hofstee plots.Results showed that procedure and the ratio of principal materials are important on application of the catalyst.

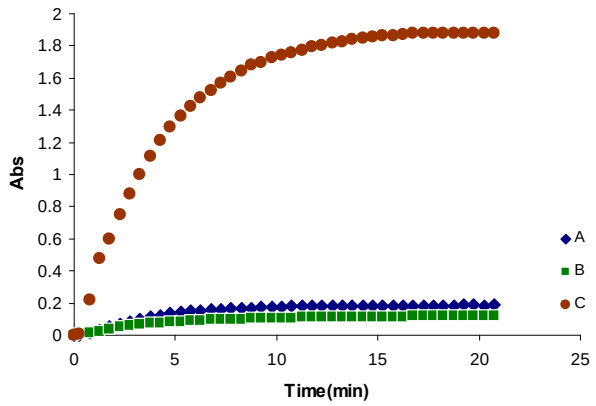

Comparison the operation of three nanobiocatalysts in the same conditions
A) MNT+FePo (pH=8), 1mg B) MNT+FePo (DMSO), 1mg
C) NH_2-FePO+ MCM-41, 0.25 mg

References:

[1] A.P. Wight, et al. Chem. Rev. **2002**, 102, 3589-3614.

[2] M. Trejda et al. Cat. Lett., **2006**, 108, 3-4.

[3] B.T. Holland et al., J. Phys. Chem. B, **1998**, 102, 4301-4309.

[4] A.A. Costa et al. J. Mol. Cat. A: Chem., **2008**, 282, 149-157

[5] European Patent, "Process for the preparation of heme/hemin".1990, 0427690A1

[6] K. Nazari, et al., J. Mol. Cat. A: Chemical **2005**, 239, 1-9.

[7] J. Long, et al., Chinese Org. Letters. **2002**, 4, 1911-1914.

Photocatalytic enhancement of Ag-doped ZnO nanotubes

Parvin Samadi, Alireza Zolfaghari*, Hamid Reza Mortaheb, Hani Sayahi
Chemistry and Chemical Engineering Research Center of Iran, E-mail: zolfaghari@ccerci.ac.ir

Keywords: Znic oxide, Nanotube, Ag-doped, Photocatalytic activity

Introduction

Wurtzite ZnO has attracted much interest for its fundamental research and potential device applications including electrical, optoelectronic, photovoltaic device and sensor[1]. Recently, intensive research has been focused on fabricating one-dimensional (1D) ZnO nanostructures such as nanotubes, nanowires (rod) and nanobelts (ring) owing to their shape induced novel properties and potential applications [2]. Doping is an effective and facile method to modify the physical properties of the base materials [3]. Doping impurities into 1D ZnO nanostructures to improve the band gap structure and PL properties is worthy to be explored and thereafter their photocatalytic activity [4]. In this study, for the first time, we have synthesized the silver doped wurtzite ZnO nanotubes to investigate the improvement of photocatalytic activity of the nanotubes.

Exprimental

All the chemicals used in our experiments are analytical grade reagents without further purification. $Zn(NO_3)_2.6H_2O$ (3 g) and PEG 2000 (0.9 g) was dissolved in the 375 ml distilled water under the magnetic stirring. Then, $NH_3.H_2O$ (1M) and $AgNO_3$ dispersed in the solution. Finally, the obtained mixture (pH=10) was heated to 70° C and continued with this constant temperature until the reaction was complete (after 24h). The precipitation was filtered out, washed several times with alcohol and water and then dried at 60° C under the atmosphere.

The photocatalytic activity measurements of the ZnO samples were carried out based on photodegradation monitoring of organic dyes of acid blue (200 ppm) under UV light (at radiation of 254 nm) using visible spectroscopy.

Result and discussion

The morphology of the synthesized nanotubes was examined using scanning electron microscope (SEM). Figure 1 displays the SEM images of undoped and Ag-doped ZnO nanotubes growth by hydrothermal process at 70°C for 24 h. The morphology of doped and undoped nanotubes are different in a way that average diameter and length of undoped nanotubes are 470 nm and 4 □m, respectively, whereas these value for doped nanotubes are 280 nm and 2.6□□m.

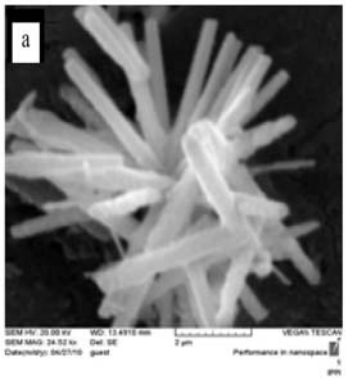

Fig 1. SEM images of (a) undoped nanotubes and (b) Ag doped nanotube

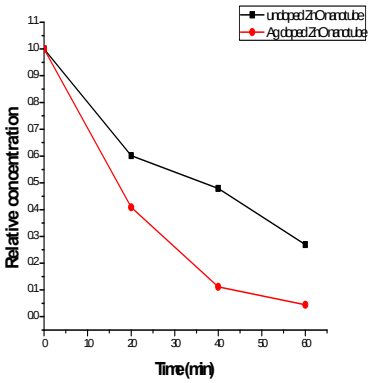

Fig 2. Photodegradation of acid blue versus time

The doped and the undoped ZnO nanotubes were tested for the applicability in photodegrading organic dyes of acid blue, in presence UV irradiation. The comparative results are shown in Figure 2. The plots shows that the acid blue was degraded up to 95% of initial concentration in presence of doped ZnO nanotube in 60 min, however undoped ZnO nanotube in the same condition degraded 73% of initial concentration of dye. These results demonstrate that degradation rate of Ag doped ZnO nanotube is much higher than undoped ZnO nanotube.

References

[1] X. H. Jinxia Duan, Enke Wang, *Materials Letters* **2006**, *60*, 4.
[2] J. Z. Mashkoor Ahmad, Caofeng Pan, Wang Yan, Materials Science and Engineering B **2010**, 4.
[3] P. X. Y. J.T. Chen, J. Wang, R.F. Zhuo, D. Yan, J.J. Feng, F. Zhang, Applied Surface Science **2009**, 255, 6.
[4] C. Y. Chao Cheng, Zhong-Jie Jiang, Journal of Photochemistry and Photobiology A **2008,** 195, 5.

A Novel Polypropylen Fiber Supported Nano Preyssler Solid Phase Microextraction Based on Sol-gel Technique in Determination of Aflatoxins (G1,G2)

Mahboobe Masroornia[1],fateme Samadi[2,*], Zarrin Eshaghi[3],Farida Zohuorian[1],Hoda Sorayae[1],Ali Khazaefar[3],Mahdi Moghadam poor[4],Ali Samadi[5],Amirhosein zamanzade[1]

[1]*Department of Chemistry , Faculty of Sciences, Islamic Azad University, Mashhad Branch, P.O. Box 91735-413, Mashhad , Iran*

[2]*Islamic Azad University , Young Researchers Club, Mashhad Branch, Mashhad , Iran,*

[3] *Department of Chemistry , Faculty of Sciences, Payame Noor University, Mashhad, Iran*

[4]*Department of Power Engineering, Islamic Azad University, Gonabad Branch.*

[5]*Department of Power Engineering ,Birjand University.*

Keywords: Aflatoxin G1,G2, Nano Preyssler,Soloid Phase Microextraction,Sol-Gel

Introduction

A silica-based organic-inorganic polymer hybrid sol-gel sorbent which was protected by polypropylene hollow fiber was used in this research for extraction, pre-concentration and determination of aflatoxins (G1,G2) combining High Performance Liquid Chromatography and UV detection. In this new technique the sol containing nano preyssler was prepared by the sol-gel method via the reaction of tetra methoxysilane (TMOS) with an alkaline catalyst. Afterward this sol was injected into a polypropylene hollow fiber for insitu gelation process. The sol – gel process involves evolution of inorganic networks through the formation of a colloidal suspension (sol) and gelation of the sol to form a network in continuous liquid phase (gel). The main objective of the present study was to apply extraction field in order to concentrate aflatoxins alongside sol–gel surface in order to increase the interaction capability with external molecules. This research is on the current state of the art and future trends in the developments of solid phase microextraction (SPME) device using hollow fiber protected sol–gel method. The method validation was included and satisfying results with high pre-concentration factors were obtained.

Preparation of Solid-phase microextraction device

In this work, the sols were prepared by the alkaline based catalyzed method from a solution containing TMOS, alkaline water and ethanol. Equal volumes of TMOS and EtOH were added into a vial and stirred for 10 min. Then the alkaline water was added into the vial and the mixture was stirred continually to promote the hydrolysis and condensation reactions.The nano preyssler was added to the sol. The polypropylene hollow-fiber, was cut into small segments with a length of 2.0 cm. Liquid sol containing nano preyssler was injected into the fibers by a syringe.

Results and discussion

For liquid samples and/or extracts the SPME extraction efficiency can be influenced by different parameters, such as pH, extraction time, temperature, desorption time. Among the tested sol-gels based on TMOS has showed the greatest extraction capability .This result could be explained considering that TMOS possesses a medium polarity, very similar to the of aflatoxins G1,G2 that do not contain any strong acid or basic group . in the case of aflatoxins G1,G2 being the pKa equal to 10.09±0.20, the dependence of the extraction yield in the pH range 3.5–8.6[1], can be ascribed only to the differences in the sorbent polarity, indicates that the best pH value to obtain the higher SPME extraction yield is around 7.5.

Conclusions

A simple SPME–HPLC–DAD method for AFG1, AFG2 determination in cereal-based foods has been developed for the first time .The HPLC optimized procedure consisted of a simple isocratic elution .The use of the SPME allowed the simplification of the extraction/clean-up step respect to other techniques such as IA[2] .Compared to the most accredited clean-up step by IA[3], SPME has led to higher LOD and LOQ, but still well below the legal limits. Furthermore, this technique is fast, if compared with the complete analytical process using IA columns, simple to use and not expensive, considering that under most conditions SPME fibers can be used from 50 to 100 times.Work is currently in progress to extend the application of the proposed approach to other real matrixes and mycotoxins, and to perform an extensive method validation.

References

[1] P.M .Scott, J .Assoc .Off .Anal .Chem .70 (1987)276.

[2] B. Sarımehmetoglu, O. Kuplulu, T.H. Celik, Food Control 15 (2004) 45.

[3] R. Porter, P. van der Logt, S. Howell, M. Kyrolainen-Reay, A. Badley, Biosens. Bioelectron. 16 (2001) 875.

Malathion Determination in Environmental Samples using a Sol gel based on HF-SPME Supported Functionalized Multi Walled Carbon Nanotube by High Performance Liquid Chromatography, UV Detector (HPLC-DAD)

Zarrin Eshaghi[3,*],fateme Samadi[2] , Mahmoud Ebrahimi[1] ,Farida Zohuorian[1],Hoda Sorayae[1],Ali Khazaefar[3],Mahdi Moghadam poor[4],Ali Samadi[5],Amirhosein zamanzade[1],Armin Oskuian[6]

[1]*Department of Chemistry , Faculty of Sciences, Islamic Azad University, Mashhad Branch, P.O. Box 91735-413, Mashhad , Iran*

[2]*Islamic Azad University , Young Researchers Club, Mashhad Branch, Mashhad , Iran,*

[3] *Department of Chemistry , Faculty of Sciences, Payame Noor University, Mashhad, Iran*

[4]*Department of Power Engineering, Islamic Azad University, Gonabad Branch.*

[5]*Department of Power Engineering,Birjand University.*

[6]*Department of Agricultural ,Islamic Azad University , mashhad Branch*

Keywords: malathion,Sol-Gel,Solid Phase Microextraction,Carbon Nanotube

Introduction

Organophosphorus (OP) compounds are one of the most common causes of poisonings in human [1]. These compounds are known mainly for their neurotoxic effects in mammals acting through inhibition of acetylcholinesterase (AChE) . Several researches have done that OPs induce oxidative stress in rats and humans leading to excessive generation of reactive oxygen species (ROS), and alterations in antioxidant and radical scavenging system independent of AChE effects. Malathion as one of the most commonly used OPs in house and agriculture is the most common cause of poisoning and deaths, mainly in developing countries. A silica-based organic-inorganic polymer hybrid sol-gel sorbent which was protected by polypropylene hollow fiber was used in this research for extraction, pre-concentration and determination of malathion combining High Performance Liquid Chromatography and UV detection. In this new technique the sol containing carbon nanotube was prepared by the sol-gel method via the reaction of MTMOS with PMHS. The method validation was included and satisfying results with high pre-concentration factors were obtained.

Experimental

1.Preparation of the sol solution

To improve the solubility of CNTs in organic solution, the functionalized CNTs (CNTs-OH and CNTs-COOH) were used[2] . A 2-mg amount of functionalized CNTs was dissolved in 400µL MTMOS, and then 50µL distilled water and 50mg PMHS were added . Then 50µL TFA was added to the resulting solution with ultrasonic agitation for 10min and stable sol solution was formed. Here the functionalized CNTs contribute at two levels during sol–gel fabrication. Firstly, it improved the solubility of CNTs. Using non-functionalized CNTs, no stable homogenous solution was obtained. In addition, in the gelification step, SiOR chains formed in polymerization process and contribute to the formation of the matrix structure [3]

Results and discussion

For liquid samples and/or extracts the SPME extraction efficiency can be influenced by different parameters, such as pH, extraction time, temperature, desorption time. Among the tested sol-gels based on MTMOS has showed the greatest extraction capability .This result could be explained considering that MTMOS possesses a medium polarity, very similar to the Malathion that do not contain any strong acid or basic group.

Conclusion

This extraction technique requires very little sample solution and little expensive and toxic organic solvents. It is a promising pre-treatment method for the fast, trace analysis in many complicated matrixes such as environmental and biological samples .The method has a high pre-concentration factor and excellent selective cleanup of Malathion samples as the very complicated analytes. Good linearity and reasonable relative recovery were also obtained. We used the method to isolate Malathion from real samples and found it to have many advantages over conventional methods.

Refrences

[1] M. Abdollahi, N. Jalali, O. Sabzevari, R. Hosseini, T. Ghanea, A retrospective study of poisoning in Tehran, J. Toxicol. Clin. Toxicol. 35 (1997) 387–393.

[2] N. Zhang, J. Xie, M. Guers, V.K. Varadan, Smart Mater. Struct. 13 (2004) N1.

[3] L. Berguiga, J. Bellessa, F. Vocanson, E. Bernstein, J.C. Plenet,Opt.Mater. 28 (2006)167.

High Surface Area of Copper nanoparticles-polyacryl amide/SBA-15 composite: A New Class of Heterogeneous Nanocomposite Catalyst

Roozbeh Javad Kalbasi[*,1], Amir Abbas Nourbakhsh[2], Maniya Zia[1]

[1] *Department of Chemistry, Islamic Azad University, Shahreza Branch, 311-86145, Shahreza, Isfahan, Iran*

Corresponding Author E-mail: rkalbasi@iaush.ac.ir

[2] *Department of Ceramic, Islamic Azad University, Shahreza Branch, 311-86145, Shahreza, Isfahan, Iran*

Keywords: Cu-PAM/SBA-15 nanocomposite, Surface chemistry, Heterogeneous catalysts

Introduction

Heterogeneous catalysts possess obvious advantages in product isolation and catalyst recycling use [1]. With the advent of new surface-sensitive analytical techniques, however, amore basic understanding of the surface chemistry underlying heterogeneous catalytic processes developed [2]. There are many polymer/nanoparticle composite materials could be achieved by preassembling the inorganic nanoparticles with the organic polymer [3]. However, the process usually suffers from some disadvantages such as absence of complete heterogeneity, the limited activity due to the extremely low surface area of the polymer beadsand also high temperature annealing generally causes the thermal degradation of organic polymers. In order to dissolve these disadvantages, we report, the synthesis and characterization of a novel heterogeneous nanocomposites catalyst in which small (5 nm diameter) copper nanoparticles are highly dispersed and grafted on the polyacryl amide (PAM)/SBA-15 by an in-situ polymerization route.

Method

The PAM/SBA-15 was used as a support. Cu nanoparticles were assembled to above polymer composite by an aqueous solution of Copper (II) chloride dihydrate ($CuCl_2.2H_2O$) as a source of Copper ions and Sodium borohydrate ($NaBH_4$) as a reducing agent. The Reaction mixture, stirring rapidly and was further stirred at 85°C for about an hour to afford a brown suspension. The Reaction was filtered, and washed with several portions of distilled water and finally with methanol.

Results and discussion

The physical and chemical properties of Cu-PAM/SBA-15 nanocomposite were investigated using FT-IR, XRD, BET, SEM, TGA and TEM techniques. The specific surface area and the pore size of mesoporous silica SBA-15, PAM/SBA-15 and Cu-PAM/SBA-15 had been calculated using Brunauer–Emmett–Teller (BET) and Barrett–Joyner–Halenda (BJH) methodsrespectively (Table 1). It is clear that calcined SBA-15 has a high BET surface area (1430 m^2/g), a large pore volume (1.9 cm^3/g) and a pore size (9.9 nm), indicative of its potential application as host inorganic materials. Cu-PAM/SBA-15 exhibits a smaller specific area 89 $m^2\ g^{-1}$ in comparison with it's of pure SBA-15. Although these textural properties were smaller than those found for mesoporous silica SBA-15, Cu-PAM/SBA-15 had still mesoporous form (according to isotherm NO. IV of IUPAC) and did not block the pores of the SBA-15. Also Cu-PAM/SBA-15 showed almost four times higher surface area in comparison with that Cu-PAM nanocomposite. Therefore, it was suitable to act as a heterogeneous catalyst for oxidation of benzyl alcohol by tert-butyl hydroperoxide as an oxidant and n-hexane as solvent in reflux temperature (Scheme 1). The Fig. 1 displays the transmission electron micrograph (TEM) of Cu-PAM/SBA-15. The mean diameter of Cu nanoparticles was 5 nm.

Conclusion

In this article, the focus is on synthesis of novel Copper nanoparticle-PAM/SBA-15 composite. This catalyst possesses obvious advantages in high surface area, complete heterogeneity and high thermal stability due to use of SBA-15. The catalyst was very stable and could be reusable for more than six times without losing activity.

Table 1. Surface data of Cu-PAM/SBA-15

Sample	BET surface area ($m^2\ g^{-1}$)	Pore volume ($cm^3\ g^{-1}$)	Pore diameter (nm)
Mesoporous silica SBA-15	1430	1.90	9.9
PAM/SBA-15	409	0.61	5.9
Cu-PAM/SBA-15	89	0.18	7.9

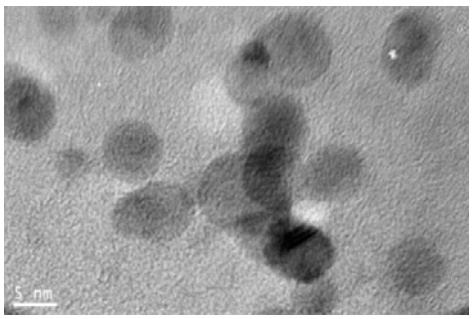

Fig 1. TEM of Cu-PAM/SBA-15

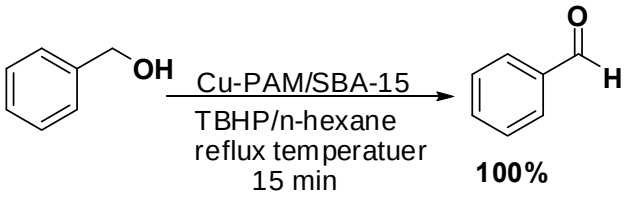

Scheme 1.

References:

[1] Ali, S.R.; Bansal, V.K.; Khanb, A.A.; Jainc, S.K.; Ansarid, M.A. *J. Mol. Catal. A. Chem*. **2009**, *303*, 60.

[2] Francisco, Z. *Surface Science*. **2002**, *947, 500.*

[3]Wei, Qing-Bo.; Luo, Yan-Ling.; Zhang, Chang-Hu.; Fan, Li-Hua.; Chen, Ya-Shao. *Sen. Act. B*. **2008**, *134*, 49.

Free Energies and Kinetic Properties Studies of Nanostructure Complexes of 1,3,5-Trisubstituted Oligoaryleneethynylene Benzene Star-shaped Molecules and Fullerenes

Avat Arman Taherpour*

Chemistry Department, Faculty of Science, Islamic Azad University-Arak Branch,P.O. Box 38135-567, Arak, Iran E-mail: ataherpour@iau-arak.ac.ir & avatarman.taherpour@gmail.com

Abstract: The 1,3,5-benzene core acts as an effective π-electron center to conjugate with the oligoaryleneethynylene groups of the 1,3,5-trisubstituted oligoaryleneethynylene benzene star-shaped molecules. These interesting molecules are currently considered because of their wide potential applications. Some of them can act as discotic liquid crystals (DLCs). Fullerenes C_n, are a class of spherical carbon allotrope group with unique properties. Electron transfer between fullerenes and other molecules is thought to involve the transfer of electrons between molecules surrounding the fullerene cage. The half-wave potential, $E_{1/2}$, was correlated with the calculated energies of lowest unoccupied molecular orbital (E_{LUMO}) and highest occupied molecular orbital (E_{HOMO}) of the compounds studies. In this study, the relationships between the photophysical data indices and oxidation potential ($^{ox}E_1$) of the star shapes molecules **1-19**, as well as the first and second free energies of electron transfer ($\Delta G_{et(n)}$, for n=1, 2, which is given by the *Rehm-Weller* equation) between **1-19** and the fullerenes (C_n=C_{60}, C_{70}, C_{76}, C_{82} and C_{86}) **20-24** as [Star-shapes][C_n] (C_n=C_{60}, C_{70}, C_{76}, C_{82} and C_{86}) supramolecular complexes are presented and investigated. The first and second free energies of electron transfer and kinetic rate constants of the electron transfers, $\Delta G^{\#}_{et(n)}$ and k_{et} (n=1,2), respectively, were also calculated in this study for [Star-shapes][C_n] (C_n=C_{60}, C_{70}, C_{76}, C_{82} and C_{86}) and in accordance with the *Marcus* theory. The complexes were not synthesized nor reported before.

Keywords: Fullerenes; Electron transfer reaction; Star-shaped molecule; Photophysical data; Marcus theory; Molecular Modeling.

Introduction: Star-shaped macromolecules, which contain benzene as a core for the star-shape, have been investigated as branched macromolecules, and have received significant attention in the elucidation of structure-property relationships.[1-3] Some types of the molecules, with a trivalent core and three poly π-structures, have attracted much attention and been utilized in different areas of science because of their interesting potential, especially for electronic studies. Because of the properties of 1,3,5-trisubstituted oligoaryleneethynylene benzene star-shaped molecules, they can act as: *discotic liquid crystals* (DLCs), *light-emitting diodes* (LEDs), *field effect transistors* (FETs), and *non linear optics* (NLO).[1] Study of the electronic properties of these materials with respect to their photophysical properties can be useful and interesting. Especially with respect to their LED character and quantum yield (Φ_f), only a few reports have been reported in the literature.[4]

Fullerenes are more reactive than planar aromatics because an important driving force for addition reactions is the reduction of strain, which results from pyramidalization in the sp^2-carbon network [4]. Since then of 1985, metal-containing endohedral fullerenes (EMFs) have attracted special attention as a new class of technologically relevant materials due to their combined fullerene-like and metallic properties. In most EMFs, introduction of metal atoms into carbon cages leads to an increase in the electron affinity relative to the corresponding empty-cages.

Discussion: Although star polymers constitute a gate group of branched macromolecular structures, the synthesis and study of the properties of star-shaped polymers remains challenging, and well defined star polymers are often difficult to prepare in a controlled manner.[2] The photophysical data (such as: quantum yield (Φ_f), fluorescence emission maximum (λ_{em}), and absorbance maximum wavelength (λ_{abs}) of **1-19**) seems to be the useful numerical and structural values for the star-shapes **1-19** that were utilized here.[4] The equation-1 estimates the free energy change between a donor and an acceptor as:

$$k_{et} = \frac{k_{el}}{1 + \frac{k_{el}}{k_{et}\sqrt{z}}\left[\exp\left(\frac{\Delta G^{\dagger}}{RT}\right) - \exp\left(\frac{\Delta G^{\dagger}_{min}}{RT}\right)\right]} \qquad \text{(Eq. 1)}$$

Marcus theory is currently the dominant theory of electron transfer in chemistry. Marcus theory is so widely accepted because it makes surprising predictions about electron transfer rates that have been nonetheless supported experimentally over the last several decades. Electron transfer (ET) is one of the most important chemical processes in nature, playing plays

a central role in many biological, physical and chemical (both organic and inorganic) systems. The relationships between $E_{1/2}$ and E_{HOMO} (or E_{LUMO}) for a series of compounds, demonstrates that they have a similar mechanism of the electron transfer reaction during electron transfer reaction.[5] The structures of complexes which are shown in figure-1 were not synthesized nor reported before.

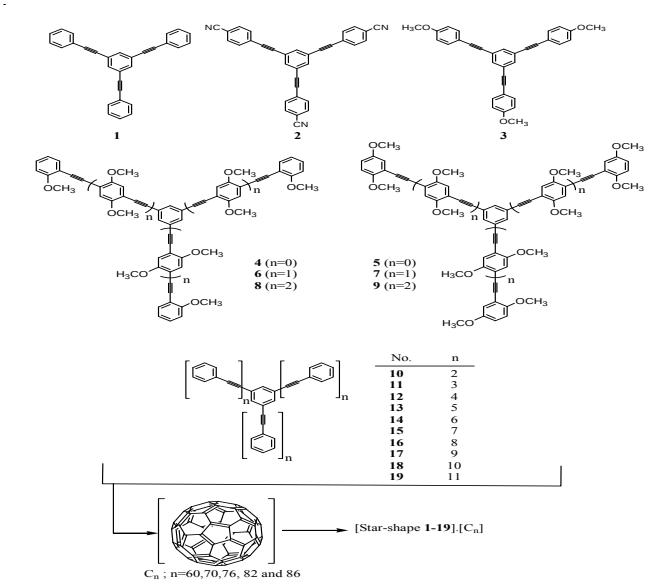

References:

[1] Y. Yamaguchi, T. Ochi, S. Miyamura, T. Tanaka, S. Kobayashi, T. Wakamiya, Y. Matsubara and Z.-i. Yoshida, *J. Am. Chem. Soc.,* **2006**, 128, 4504-4505.

[2] L. E. Casey, V. Kalpana, and E. L.Timothy, *Macromolecules,* **2006**, 39, 3132-3139.

[3] N. Hadjichristidis, *J. Polym. Sci., Part A: Polym. Chem.* **1999**, 37,857.

[4] A.A. Taherpour, *Physics and Chemistry of Liquids,* 48(3), **2010**, 289–297.

[5] D. Nematollahi, A. A. Taherpour, S. Jameh-Bozorghi2, A. Mansouri, B. Dadpou, *Int. J. Electrochem. Sci.,* 5, **2010**, 867–879.

Theoretical and QSR Studies of Free Energies of Electron Transfer of *Cis*-Unsaturated Thiocrown Ethers and Their Nanostructures Complexes [X-UT-Y][M@C_{82}](M=Ce & Gd)

Avat (Arman) Taherpour

Chemistry Department, Faculty of Science, Islamic Azad University, P. O. Box 38135-567, Arak, Iran

ataherpour@iau-arak.ac.ir *and* avatarman.taherpour@gmail.com

Abstract: Unsaturated thiocrown ethers with *cis*-geometry are a group of crown ethers that, in light of the size of their cavities and their conformational restriction compared to a corresponding saturated system (**1-9**), demonstrate interesting properties for physicochemical studies. Endohedral lanthanidofullerenes M@C_x (x = 82 and M = Ce & Gd) were introduced as a new class of the spherical fullerene group with unique properties. Two of these molecules are the Ce@C_{82} **(10)** and Gd@C_{82} **(11)**. The supramolecular complexes of **1-9** with Ce@C_{82} **(10)** and Gd@C_{82} **(11)** have been shown to possess a host-guest interaction for electron transfer processes, and these behaviors have previously been reported. In this study, the relationship between this index and oxidation potential ($^{ox}E_1$) of **1-9**, as well as the free energy of electron transfer (ΔG_{et}, by the electron transfer (ET) equation) between **1-9** and **10** and **11** as [X-UT-Y][Ce@C_{82}] **(12)** and [X-UT-Y][Gd@C_{82}] **(13)** complexes, are presented.

Keywords: Endohedral metallofullerenes; Oxidation potential; Unsaturated thiocrown ethers; Molecular topology.

Introduction: Since the discovery of fullerenes (C_n), one of the main classes of carbon compounds, and the unusual structures and properties of these molecules, many potential applications and physicochemical properties have been discovered and introduced.[1-3] Endohedral metallofullerenes (EMF) were first introduced as a new spherical fullerene group with unique properties.[3,4] One of the common structural molecules is the M@C_{82} complex. Formation of EMF(s) is thought to involve the transfer of electrons from the encapsulated metal atoms to the surrounding fullerene cage. In 1991, Smalley and his collaborators demonstrated that fullerenolanthanides can be produced by laser vaporization of graphite and lanthanum oxide and extracted by toluene. The physical measurements, such as EPR, mass spectrometry, extended X-ray absorption fine structure (EXAFS) and X-ray photoelectron spectroscopy (XPS), were performed on the extracts containing the mixture of

fullerenolanthanides and empty fullerenes. The presence of sulfur atoms in the structure of crown ethers accounts for the different properties of thiocrown ethers. The compounds **1-9** were synthesized and their structures were confirmed.[4-8]

n	0	1	2	3	4	5	6	7	8
No	**1**	**2**	**3**	**4**	**5**	**6**	**7**	**8**	**9**

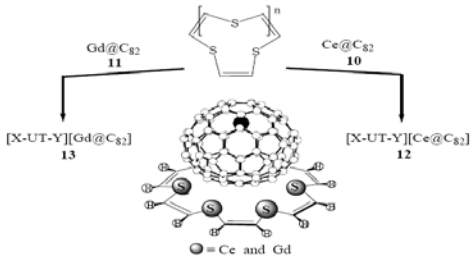

Figure-1: The total structures of unsaturated thiocrown ethers **1-9**, their supramolecular complexes of [X-UT-Y][Ce@C_{82}] **(12)** & [X-UT-Y][Gd@C_{82}] **(13)**.

The ratio of μ_{cs} was a useful numerical and structural value of the unsaturated thiocrown ethers **1-9** that were utilized here. In this work, the electrochemical behaviors of a series of M@C_{82} (where M = Ce or Gd) by studying the relationship between the index μ_{cs} and oxidation potential ($^{ox}E_1$) of **1-9**, as well as the free energy of electron transfer (ΔG_{et}) between **1-9** and **10** and **11** as [X-UT-Y][Ce@C_{82}] **(12)** and [X-UT-Y][Gd@C_{82}] **(13)** complexes were investigated.[4-8]

Graphs and Method: The ratio of summation of the number of carbon atoms (n_c) and the number of sulfur atoms (n_s) to the product of these two numbers (μ_{cs}) seems to be a useful numerical and structural value for the unsaturated thiocrown ethers **1-9** that were utilized here.[5-7] The equation-1 estimates the free energy change between a donor and an acceptor as:

$$k_q = \frac{k_c}{1 + \frac{k_c}{K_d Z}\left[\exp\left(\frac{\Delta G^{*}}{RT}\right) + \exp\left(\frac{\Delta_{r,T}G^{m}}{RT}\right)\right]} \qquad \text{(Eq. 1)}$$

Discussion: The achived values demonstrated that μ_{cs} decreases with increasing molecular size of the compounds **1-9**. In the related values for the complexes of [X-UT-Y] **1-9** with Ce@C_{84} **(10)** and Gd@C_{82} **(11)** are also shown. The results show the calculated values of oxidation potential ($^{ox}E_1$), as well as the free energy of electron transfer (ΔG_{et}) between some of the [X-UT-Y] and their complexes with **10** and **11**. Figure 2 shows the relationship between the values of μ_{cs} and the free energies of electron transfer (ΔG_{et}) between **1-9** and the first reduction potential ($^{red}E_1$) of Ce@C_{82} **(10)** for [X-UT-Y][Ce@C_{82}] complexes **(12)**. Equation 4 describes Fig. 2 and shows the *Nieperian* logarithmic behavior of the relationship between ΔG_{et} and μ_{cs}. The R-squared value (R^2) for this graph is 0.9847.

$$\Delta G_{et} = (7.1)\mathrm{Ln}(\mu_{cs})]+34.0 \qquad \text{(Eq. 2)}$$

In light of this high correlation between μ_{cs} and the free energy of electron transfer (ΔG_{et}) between **1-9** and the first reduction potential ($^{red}E_1$) of Ce@C_{82} **(10)**, it is possible to use μ_{cs} to calculate the (ΔG_{et}) of [X-UT-Y][Ce@C_{82}] complexes. With increasing ring size of these compounds, the values of μ_{cs} decrease.

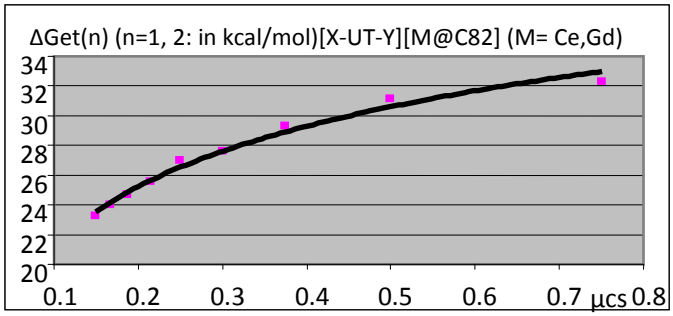

The ratio of μ_{cs} shows a high correlation with the physicochemical and structural values of the unsaturated thiocrown ethers **1-9**. The results show the calculated values of free energy of electron transfer (ΔG_{et}) of the [X-UT-Y][Ce@C_{82}] **(12)** and [X-UT-Y][Gd@C_{82}] **(13)** supramolecular complexes on the basis of the first and second reduction potentials ($^{red}E_1$ and $^{red}E_2$) of Ce@C_{82} **(10)** and Gd@C_{82} **(11)**. The data for the compounds and their complexes were not previously reported. The compounds [X-UT-Y][Ce@C_{82}] **(12)** and [X-UT-Y][Gd@C_{82}] **(13)** supramolecular complexes were neither synthesized nor reported previously.

Conclusion: The electrochemical data of **1-9** were reported here, including oxidation potential ($^{ox}E_1$) and the free energy of electron transfer (ΔG_{et}) on the basis of the first and second reduction potentials ($^{red}E_1$ and $^{red}E_2$) of **10** and **11** for the predicted complexes of [X-UT-Y][Ce@C_{82}] **(12)** and [X-UT-Y][Gd@C_{82}] **(13)**. The predicted values of ΔG_{et} for **12** and **13** were calculated by using the ET equation. By utilizing the equations of this model, one can calculate the values for the **1-9** with Ce@C_{82} **(10)** and Gd@C_{82} **(11)**.

References:

[1] P. A. Psaras and H. D. Langford, eds., *Advancing Materials Research, U.S. National Academy of Engineering and National Academy of Sciences,* National Academy Press, Washington, DC, 1987.

[2] H. Singh Nalwa, *Nanostructured Materials and Nanotechnology-Concise Edition,* Edited by H. Singh Nalwa, Hitachi Research Laboratory, Hitachi Ltd., Ibaraki, Japan, 2nd Ed.-2002.

[3] Eiji Ōsawa, *Perspectives of Fullerene Nanotechnology,* Edited by: Eiji Ōsawa, *Nanocarbon Research Institute, Chiba,* MOSCOW-1th Ed., 2002.

[4] A.A. Taherpour, *Chem Phys Lett ,* 469 (2009) 135-139.

[5] A.A. Taherpour, *J. Phys. Chem. C*, 113 (2009) 5402–5408.

[6] A.A. Taherpour, *Phosphorus, Sulfur, and Silicon*, 185 (2010) 422–432.

[7] A.A. Taherpour, *Chem Phys Lett ,* 483 (2009) 233-240.

[8] A.A. Taherpour and M. Maleki, *Analy. Lett.,* 43(4) (2010) 658.

Synthesis of SnO_2 nanoparticles by solid state-reaction

Ali Taherkhani[1,2]*,Atefeh Taheri Asghari[1] ,A.Novinrooz[1] ,Hafezeh Nabipour[1,2] ,M.Mirzaie[1]

[1]*Islamic Azad University, Takestan Branch, ◌Department of Science, Takestan, Iran.*

[2]*Member of Young Researchers Club, Islamic Azad University, Takestan, Iran.*

Corresponding Author E-mail: ali_taherkhany@yahoo.com

Keywords: nanoparticles, SnO_2, $SnCl_4.5H_2O$

The synthesis of nanoparticles has become a highly developed field owing to the scientific and technological interest due to the structural peculiarities and unusual physical and chemical properties they may lead to [1] and [2]. Nano-scaled particles are of great importance if the conformation of ceramics is considered; they have been found to enhance the mechanical, electrical, thermal, catalytic and optical properties of diverse ceramic materials [3] and [4]. SnO_2 nanoparticles have been synthesized by soli state-reaction method. (0.01 mol) powder of $SnCl_4.5H_2O$ and (0.01 mol) $SrCl_2$ were used as starting solid materials. The powders were weighed with ratio 2:1 from Sn:Sr in preparation of SnO_2. Each of this was ball-milled at room temperature for 30 minutes using zirconia's balls as a milling medium.The mixing process accompanied by emission of water vapor from surface. The product was washed, treated in an ultrasonic bath for ten minutes and then centrifuged (8000 rpm) for about 15 minutes. The yield was calcined at different temperature between 200-1000 °C. This is a convenient route to large-scale synthesis of SnO_2 nanoparticles with average diameters to about 70 nm. X-ray powder diffraction, scanning electron microscopy, Fourier transform infrared spectrum were used to characterize the as-prepared SnO_2 nanoparticles.

References

[1] K.J. Klanbunde, Nanoscale Materials in Chemistry, John Wiley & Sons, Inc., New York (2001).

[2] In: A.S. Edelstein and R.C. Cammarata, Editors, *Nanomaterials: Synthesis, Properties and Applications. Series in Micro and Nanoscience and Technology*, Institute of Physics Publishing Ltd., Bristol (2002).

[3] F.F. Lange, *J. Am. Ceram. Soc.* **72** (1989), p. 3.

[4] W. Luan, L. Gao and J. Guo, *Nanostruct. Mater.* **10** (1998), p. 1119.

Synthesis and characterization of zinc oxide nanoparticle

M .Abedi[a] , A.R.Salehirad[b] , H.Najafgholi[c] , A.R.Rezvani[*d]
Department of Chemistry, University of Sistan & Baluchestan , Zahedan , Iran
(Rezvani2001ir@yahoo.ca)

Keywords: Nano ZnO, Nano particle, Characterization , Calcination, Synthesis

Introduction:

Zinc oxide has various properties such as: catalyst properties, antidote ,quale semiconductor, magnetic property and wide band gap about 3.37 ev. Because of this properties , zinc oxide has a wide range of applications in industry and laboratory, catalyst, pigments, optical materials, biomedical and spintronics. Zinc oxide nano structures exist in various shape like one-dimentional (nanowires, nanoroads, nanobelts), two-dimensional (nanonails, nanobridges) and three-dimentional like nanoparticles [1,2]. ZnO nanoparticle synthesized with several methods such as, Solochemical processing, Microwave, Emulsion and sol-gel methods [3- 5]. In this study we synthesized nano ZnO by using $(NH_4)_2[Zn(dipic)_2]$ such as precursor.

Methods:

Nano zinc oxide was prepared in two- step, at first, preparation of $(NH_4)_2[Zn(dipic)_2]$ using $Zn(NO_3)_2.6H2O$ and ammonium 2,6-Pyridinedicarboxylate with molar ratio 1/2 of Zn^{+2}/dipic and then calcination of precursor in 450,550,650 degrees of centigrade for 2 hour.

Result and discussion:

1.X-raydiffraction

Using XRD spectrum and Sherrer's equation, the size of nanoparticles obtained about 27, 29 and 31 nanometer in various temperature of calcination and show the size of nanoparticles grows with increasing of temperature.

2. Thermal behaviors of precursor powders

TGA shows the precursor loses its weight in three -step and fixed after 470°C and 19.26% of precursor remained in 600°C.

3. FT-IR

In the present study FT-IR reports that precursor has absorption bands in 3069, 2630 and 1705 cm^{-1}, the C=O vibration stretching modes occur at 1705 cm^{-1} corresponding to two carboxylic groups of dipic and it,s nanoparticles have bands in 480, 1061 and 3437 cm^{-1}. Absorption in 480 cm^{-1} is because of Zn=O stretching.

4. TEM

TEM image shows the morphology of products and the nanoparticles are spherical.

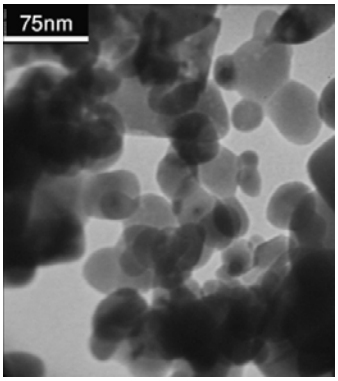

Conclusion:

This investigation was confirmed that the dipic ligand can be used for synthesis of nano ZnO and the size of particles increases with increasing the temperature.

References

[1] Y.W. Heo, D.P. Norton, L.C. Tien, Y. Kwon, B.S. Kang, F. Ren, S.J. Pearton, J. R. LaRoche, Mater. Sci. Eng. R47(2004)1.

[2] Nano Lett., Vol. 3, No. 2, 2003.

[3] M. R. Vaezi, S. K. Sadrnezhaad. Materials and Design 28 (2007) 515–519.

[4] Yu-Ling Wei, Pei-Chi Chang. Physics and Chemistry of Solids 69 (2008) 688–692.

[5] Yongjun He. Powder Technology 147 (2004) 59– 63.

Use of equilibrium concentrations in determining Langmuir,Freundlich and Temkin isotherms for adsorption of Complexation of aminoacids with Fe(II)ion by carbon nanotube

M.Vadi[a],_M.abbasi *[b],S.haghshenas[b],A.maleki[b]
a.Department of Chemistry, Islamic Azad university, Fasa branch, Fars, Iran
b.Department of Chemistry, Islamic Azad university, Firoozabad branch Fars, Iran
(Email:abbasimarjan_63@yahoo.com)

Key word: Adsorption, Isotherm, Complex, Fe(II)ion, Carbon nanotube

Introduction:

Basic nitrogen-containing compounds, biogenic aminoacids are formed in plant microbial, and animal cells under the action of microorganisms. These are biologically important compounds, and ther formation of many of them precedes the synthesis of alkaloids and hormones, neuromediators, phospholipids and vitamin components, and initiators of numerous enzynatie reactions. solute or contaminant uptake by an adsorbent is most often measured with batch equilibrium test.[1] The adsorption isotherm is the most important information wich indicates how adsorbate molecules are distributed between the liquid and solid phase when the adsorption process reaches equilibrium.[2] Evaluation of parameters in the isotherm is a complished by obtaining a linear from of the isotherm and the best fitting line for data is obtained by maximizing the coefficient of determination r^2. This study adopted the Langmuire, Freundlich and Temkin isotherms[3-5] to describe equilibrium adsorption.

methods:

We used the UV-VIS spectroscopy for studied physicochemical properties of some aminoaside, at various environmental conditions, such as concentration, temperature and ionic strength. Then the interaction of aminoacids with MWCNT was investigated.

results and discussion:

The Langmuire isotherm represents the equilibrium distribution of aminoacieds between the solid and liquid phasas and often expressed as:

$Qe=Q_{max}KC_e/1+KC_e$ (1)

From these equations and their linear plots, the values of the Langmuir constants were determined and the results are shown in Fig1. where Q_{max} is the maximum adsorption capacity corresponding to the site saturation and K is the Langmuir

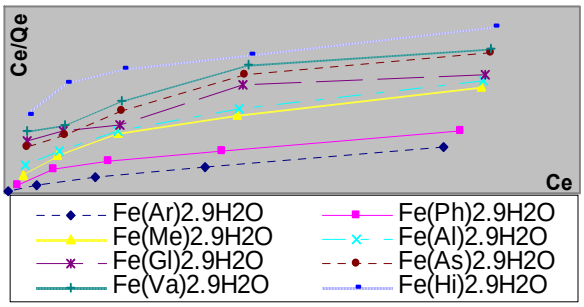

Fig1. Langmuir adsorption isotherm for complexation of aminoacides

constant related to the adsorption-desorption energy and to the affinity of the binding sites for the complexations of aminoacids that the Q_{max} values exhibited by the [Fe(L.Arginine)$_2$.9H$_2$O]and [Fe(L.Phenylalanine)$_2$.9H$_2$O are higher than those corresponding to other sorbent complexations. From the linear of Freundlich isotherm, equation can be written as follows:

$\ln Q_e=1/n\ln C_e+\ln K_F$ (2)

where K_F and n are Freundlich constants related to adsorption capacity and intensity, respectively. It can be seen from Fig2 that Freundlich model agrees well with our experimental data, with the correlation coefficient values being close to one. A more homogeneous system has and n valueunity, while a more heterogeneous system will have n value approaching zero. The constant K_F related to adsorption capacity is higher for adsorption of [Fe(L.Arginine)$_2$.9H$_2$O]and [Fe(L.Phenylalanine)$_2$.9H$_2$O onto CNT wich is consistent with the experimental observations.

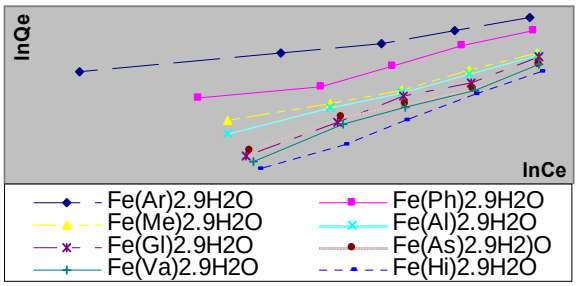

Fig2. Freundlich adsorption isotherm for complexation of aminoacides

Fig3 shows the temkin isotherm that the adsorption is characterized by K_T that is a uniform distribution of the binding energy, upto some maximum binding energy and often expressed as: $\ln Q_e = B \ln K_T + \ln C_e$ (3)

In this study the maximum temkin equilibrium constant (KT) related to [Fe(L.Arginine)$_2$.9H$_2$O]and [Fe(L.Phenylalanine)$_2$.9H$_2$O.

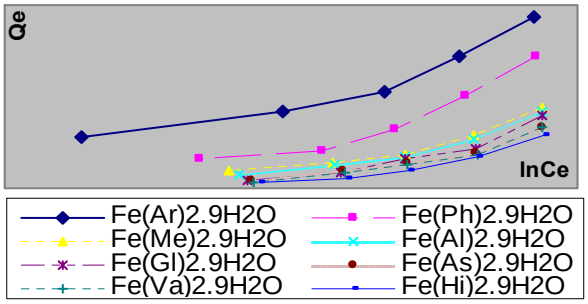

Fig3. Temkin adsorption isotherm for complexation of aminoacides

Conclusions:

In conclusion, the adsorption capacity of MWCNT for [Fe(L.Arginine)$_2$.9H$_2$O]and [Fe(L.Phenylalanine)$_2$.9H$_2$O is much higher than of the aminoacids. The results showed that adsorption equilibrium data fitted well to the Freundlich isotherm that is proved a suitable method for characterizing the heterogeneity of surface energy. The heterogeneity of surface energy of MWCNT gradually decline while the adsorption a mount of aminoacids increases.

References:

[1] Venkatesan, N., Yoshimitsu, J., Ito, Y., Shibata, N., Takada, K., 2005. Biomaterials26 (34), 7154 -7163.

[2] Juang, R., Wu, F., Tseng, R., 1996.Adsorpton isotherms of phenolic compounds from aqueous solutions onto activated carbon fibers. J. Chem. Eng. Data 41,487- 492.

[3] Lnngmuir.I., J. Amer. Chem. Soc. 40, 1361(1918)

[4] Chen, ZS., Xing, B., McGill, W.B., 1999. Aunified sorption Variable for environmental applications of the Freundlich isotherm. J. Environ. Qual. 28, 1422 -1428.

[5] Temkin, M. J., Jphys. Chem(Moscow)14, 1153(1940).

Study of adsorption capacity of multiwalled carbon nanotubes after the adsorption of complexation of aminoacids with Cu(II) ion with adsorption isotherms

M.Vadi[a], M.Abbasi *[b],S.Haghshenas[b].A,Maleki[b]
a.Department of Chemistry, Islamic Azad university, Fasa branch, Fars, Iran
b.Department of Chemistry, Islamic Azad university, Firoozabad branch, Fars, Iran
(Email:abbasimarjan_63@yahoo.com)

Key word: Adsorption, Isotherm, Aminoacids, Cu(II)ion, Carbon nanotube

Introduction:

In the past thirty years, the explosive growth of nanotechnology has developed challenging innovation in pharmacology which could revolutionize the delivery of biologically active cmpounds.[1]Note that when the equilibrium concentration is used it is more difficult to compare different adsorbents or contaminants since the rang of equilibrium concentrations, may not correspond. Evaluation of the parameters is a complished by obtaining a linear from of the isotherm and the best fitting line for the data is obtained by maximizing the coefficient of determination r^2.[2]

Method:

Multiwalled carbon nanotubes were purchased from Aldrich, with 5-10 nm in outer diameter, surface area of 40-600m^2/g and purity above 95%. The aminoacids solutions were prepared. from 1000mg/L and complexation of those with stock solutions containing nitrat salts(Merck) The concentration of this complexation were performed by UV-Vis -2550 spectrophotometer, from 200 to 300nm.

Results and discussion:

Equilibrium studies that give the capacity of the adsorbentand adsorbate are described by adsorption isotherms which is usually the ratio between the quantity adsorbed and that remained in solution at equilibrium at fixed temperature.[3-6]The experimental data were correlated by Langmuire[4], Freundlich[5], Temkin[6] models.(Fig.1-3)

The Langmuir equation (Eq.1)is used to estimate the maximum adsorption capacity corresponding to complete monolayer coverage on the adsorbent surface that parameters of this model are shown in Table1. $Ce/Qe=1/bQ_m+Ce/Q_m$ (Eq.1)

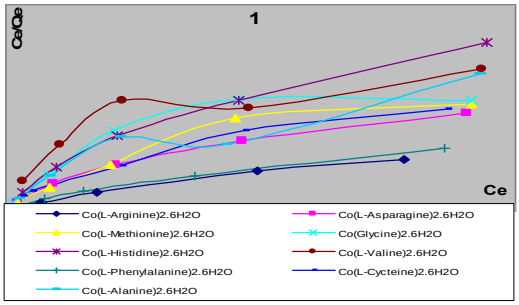

Fig1. Langmuir isotherm for complexation of amino acids with Cu(II) ion

The Freundlich equation (Eq.2) used to estimate the adsorption intensity of sorbent towards the adsorbate. The constants 1/n and K_F were determined in Table1. $Qe=K_FCe^{1/n}$ (Eq.2)

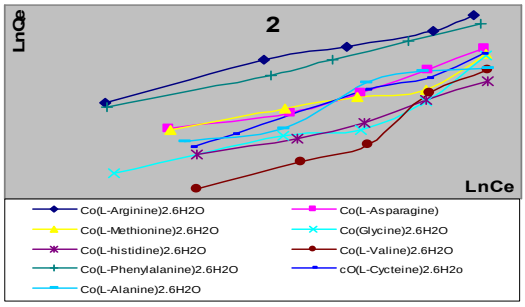

Fig2. Freundlich isotherm for complexation of amino acids with Cu(II) ion

The Temkin isotherm equation(Eq.3) assumes that the heatat adsorption of all the molecules in the layer decreases linearly with coverage due to adsorbent-adsorbate interactions and that the adsorption is characterized by a uniform distribution of the binding energies and the

Temkin equilibrium constant are shown in Table3. $Q_e=B_1\ln K_T+B_1\ln C_e$ (Eq.3)

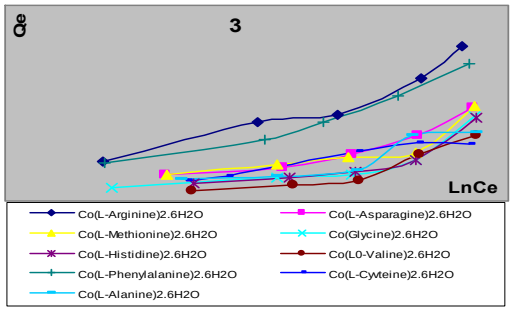

Fig3. Temkin isotherm for complexation of amino acids with Cu(II) ion

The adsorption capacity of complexation of aminoacids with Cu(II) ion on MWCNT increased with increase of concentration (Fig.4).

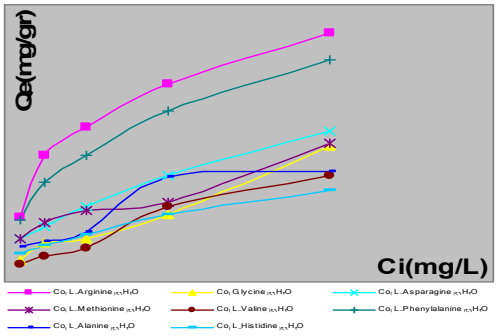

Fig4. Adsorption capacity of CNT for the initial concentratiom of complexation of aminoacides with Cu(II) ion

Complexion of Copper(II) with aminoacids	Temkin	Langmuir	Freundlich
Valine	R^2=.83 B=0.66 KT=0.88	R^2=0.75 Qm= 4.03 KL=0.047	R^2=0.94 1/n=0.55 KF=0.32
Arginine	R^2=0.95 B=1.01 KT=9.37	R^2=0.97 Qm= 6.57 KL=0.30	R^2=0.98 1/n=0.30 KF=2.16
Alanine	R^2=0.79 B=0.60 KT=2.37	R^2=.90 Qm=3.35 KL=0.13	R^2=0.92 1/n=0.36 KF=0.83
Asparagine	R^2=0.85 B=0.70 KT=3.09	R^2=0.93 Qm= 4.3 KL=0.13	R^2=0.94 1/n=0.33 KF=1.01
Cystein	R^2=0.94 B=0.73 KT=2.07	R^2=.94 Qm=3.90 KL=0.14	R^2=0.99 1/n=0.42 KF=0.75
Glycine	R^2=0.67 B=0.55 KT=2.61	R^2=0.68 Qm= 3.98 KL=0.074	R^2=0.88 1/n=0.38 KF=0.95
Histidin	R^2=0.90 B=0.46	R^2=0.95 Qm= 2.63	R^2=0.97 1/n=0.34

	B=0.91 KT=8.10	Qm= 6.06 KL=0.25	1/n=0.29 KF=1.90
Methionine	R^2=0.77 B=0.56 KT=4.68	R^2=0.87 Qm= 3.73 KL=0.14	R^2=0.90 1/n=0.28 KF=1.04

Table1. Calculated Langmuir.Freundlich and Temkin isotherm parameters for complexations of aminoacids with Cu(II) ion

Conclutions:

The competitive adsorption capacity of some complexation of aminoacids with Cu(II) ion by MWCNT was studied, and showed that the adsorption affinity of complexation by CNT followed the $Cu(Ar)_2.3H_2O$> $Cu(Ph)_2.3H_2O$ > $Cu(As)_2.3H_2O$ > $Cu(Gl)_2.3H_2O$ >$Cu(Al)_2.3H_2O$ > $Cu(Me)_2.3H_2O$ > $Cu(Va)_2.3H_2O$ > $Cu(Hi)_2.3H_2O$.The experimental data for complexation adsorption onto CNT were analyzed using the Freundlich adsorption isotherm model, which is applicable to highly heterogeneous surfaces.

References:

[1] Jain, K., 2004. Drug Discovery Today: Technoligies 1(2), 7578.

[2] Ho, Y.s., Porter, J.F., Mekay, G., 2002. Equilibrium isotherm Studies for the sorption of divalent metal ions onto Peat: Copper, nickel and lead single component systems. Water Air sil pollut.141, 1-33.

[3] C.J.M. Chain, L.C.Shih, H.J. Tsai, T.K.Liu, Cabon 45(2007)1254.

[4]Langmuir.L, J. Amer. Chem. Soc. 40, 1361(1918)

[5]Chen, ZS., Xing, B., McGill, W.B., 1999. Aunified sorption Variable for environmental applications of the Freundlich isotherm. J. Environ. Qual. 28, 1422 -1428.

[6]Temkin, M. J., Jphys. Chem(Moscow)14, 1153(1940).

Molecular modeling investigation of the role of negatively charged amino acid residues in acidophilicity and thermostability of glucose isomerase

O. Azimi[1], H. Vahedian-Movahed[1], M.R. Saberi[2]*

1. Department of Biology, Faculty of Sciences, Islamic Azad University-Mashhad Branch, Mashhad, Iran

2. Medicinal Chemistry Department, School of Pharmacy, Mashhad University of Medical Sciences, Mashhad, Iran

Keywords: *glucose Isomerase, rational protein design, molecular modeling, low pH*

Introduction :

Streptomyces is the largest genus of Actinobacteria and the type genus of the family Streptomycetaceae .Over 500 species of Streptomyces bacteria have been described .As with the other Actinobacteria,streptomycetes are gram-positive,and have genomes with high GC-content.In enzymology, a xylose isomerase (EC 5.3.1.5) is an enzyme that catalyzes the chemical reaction D-xylose ⇌D-xylulose .This enzyme belongs to the family of isomerases.The enzyme is used industrially to convert glucose to fructose in the manufacture of high-fructose corn syrup. It is sometimes referred to as "glucose isomerase. Characterizing the role of amino acid residue involved in low pH activity of enzyme is very important task in protein engineering. Glucose Isomerase (GI) is an example of such enzyme needs to be optimally active at low pH. Also, thermostability is another important property for commercialization of any enzymes since it facilitates their purification. Therefore, this study was conducted in order to characterize those responsible amino acid residues in order to be used in further steps in rational design of such target enzyme.

Methods:

site-directed mutagenesis by SpdbV®, energy minimization by MM^+ force filed, tests of ERRAT and Ramachndran plot in order to evaluate the residues stereochemistry, quantitative analysis of protein secondary structure by Vega ZZ® program.

Results and Discussion:

analyzing the amino acid sequences by multiple alignments against the available sequences with low pH activity and of 3D-structures suggest E8A, E68A and E210D substitution as candidate mutants with low pH profile. Also, the potential substitutions leading to thermostability were determined as E165M, D296E and D363E. Then, the proposed mutants were all prepared and energy minimized to further characterize their role in conformational stability of the protein.

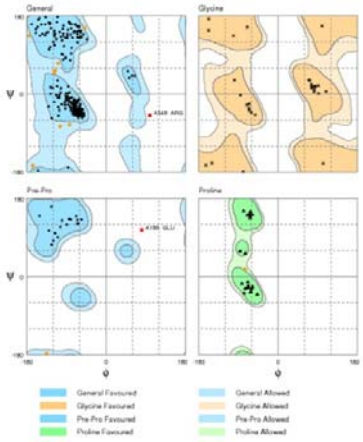

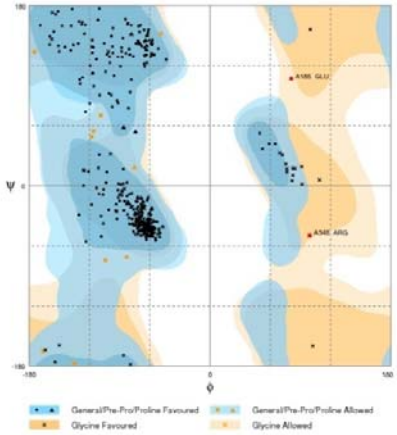

Structure	Primary pdb	Mutant 1	Mutant 2	Mutant 3
Number of residues in favoured region [no. (Percentage)]	**373(96.9%)**	**Befor: 96.9% After: 96.4%**	**Befor: 96.9% After: 96.4%**	**Befor: 96.9% After: 96.4%**
Number of residues in allowed region	**10 (2.6%)**	**B: 2.6% A: 3.1%**	**B: 2.6% A: 3.1%**	**B: 2.6% A: 3.1%**
Number of residues in outlier region	**2 (0.5%)**	**B: 0.5% A: 0.5%**	**B: 0.5% A: 0.5%**	**B: 0.5% A: 0.5%**

Structure	Primary pdb	Mutant 1	Mutant 2	Mutant 3
Pre-ERRAT	**94.444**	**93.915**	**94.444**	**93.915**
Post-ERRAT	**94.709**	**94.444**	**94.709**	**94.444**

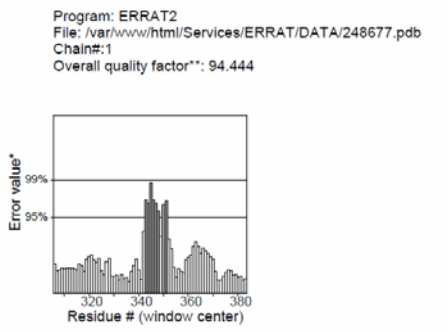

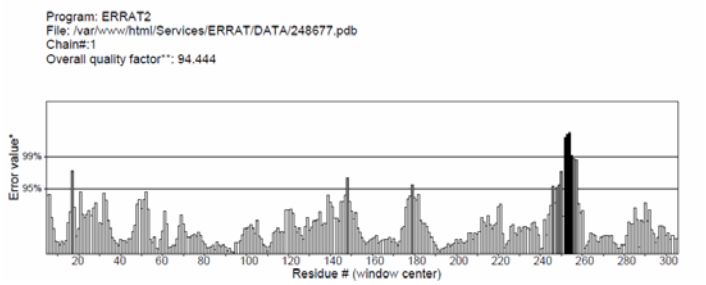

Conclusion:

This work provides useful information pertaining to rational design of an acidophil and thermostable GI. Probably, the negatively charged residues E8, 68, 10, locating at the surface of the enzyme, replacement with A8, 68 and D10 (possessing lower pK_a than of E) reduces the number of ionizable groups and the pK_a. This led to lower protein-protein interactions in which reduce the aggregation of enzyme. The detailed discussion will be presented. In conclusion, these results could be promising in the design of GI being optimally active at low pH and with facilitated purification.

Reference

- H. Jun, Y. Bing, Z. Keying and Ch. Daiwen "Functional characterization of a recombinant thermostable xylanase from Pichiapastoris: A hybrid enzyme being suitable for xylooligosaccharides production",**48** (2009) 87–92

- B. Al Balaa, K. Brijs, K. Gebruers, J. Vandenhaute, J. Wouters and I. Housen "Xylanase XYL1p from Scytalidium acidophilum: Site-directed mutagenesis and acidophilic adaptation", **100** (2009) 6465–6471

- M.A Borgi , K. Srih-Belguith , M. Ben Ali, M. Mezghani, S. Tranier, R. Haser and S. Bejar "Glucose isomerase of the *Streptomyces* sp. SK strain: purification,sequence analysis and implication of alanine 103 residue
in the enzyme thermostability and acidotolerance", **86** (2004) 561–568

- U.T Bornscheuer and M. Pohl "Improved biocatalysts by directed evolution and rational protein design"**, 5** (2001)137–143

-M. Fathi Najafi, D. Deobagkar and D. Deobagkar "PuriWcation and characterization of an extracellular _-amylase from *Bacillus subtilis* AX20"**, 41** (2005) 349–354

Visible light-induced degradation of Acid Yellow 23 over titanium dioxide modified with platinum: A Kinetic approach

M. Shokri*, N. Modirshahla, M.A. Behnajady, M. Alizad
Department of Applied Chemistry, Faculty of Science, Islamic Azad University, Tabriz Branch, Tabriz, Iran
** E-mail: shokri@iaut.ac.ir ; shokri_m@yahoo.com*

INTRODUCTION

Recently TiO_2 photocatalysts have been utilized successfully in various fields such as removal of organic pollutants. However, a major problem encountered is that TiO_2 does not work as a photocatalyst with visible light [1]. In this contribution, platinum doped TiO_2 (Pt/TiO_2) nanoparticles were synthesized by photodeposition (PD) method. The influences of the platinum loading and catalyst dosage on the photocatalytic oxidation of azo dye (AY23), under the illumination of visible light were investigated.

METHODS

Hexachloroplatinic acid (H_2PtCl_6, 98%) obtained from Merck. TiO_2-P25 Degussa, 80% anatase, 20% rutile; BET area 50 m^2/g; primary size 21 nm, were used as a supporting material. AY23 as a model pollutant from textile industry purchased from ACROS organics (USA).

The preparation of platinum doped TiO_2 nanoparticles

First 2 g of TiO_2 was added to 100 ml of deionised water. Then the required amount of H_2PtCl_6 for doping was added into the suspension of TiO_2. The pH of TiO_2 suspension was adjusted to 3. Then the mixture was irradiated with UV light (30 W, λ_{max}=254 nm) for 3 h and then dried at 100 °C for 12 h. The dried solids calcined at 300 °C for 3 h in a furnace.

Investigation of photocatalytic activities

For the investigation of the photocatalytic activity of Pt/TiO_2 nanoparticles, a solution (100 ml) containing desired amounts of AY23 (20 mgL^{-1}) and photocatalyst were prepared and transferred into a borosilicate petri dish as photoreactor. Afterwards, the visible lamp (OSRAM, 500 W; 125 kLx) was switched on to start the reaction. Then at certain reaction

intervals, the concentration of remaining AY23 was determined by means of a UV-Vis spectrophotometer at λ_{max} = 428 nm.

RESULTS AND DISCUSSION

Characterization

The XRD patterns of TiO_2 nanoparticles before and after Pt modification (1 wt%) are presented in Fig. 1. It is worth noting that no peaks of Pt were observed in the case of Pt/TiO_2, suggesting that the Platinum dopants are merely placed on the surface of the crystals [2].

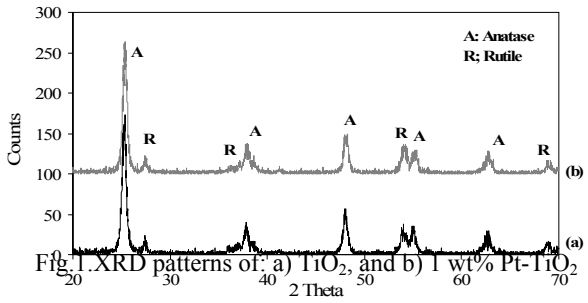

Fig.1.XRD patterns of: a) TiO_2, and b) 1 wt% Pt-TiO_2

The effect of doping content of platinum

The results in Fig. 2 showed that the photocatalytic activity of Pt doped TiO_2 increased with an increase in the Pt doping up to optimum value (1wt%) and then decreased. Excessive coverage of TiO_2 catalyst surface limits the amount of light reaching to the TiO_2 surface, reducing the number of photogenerated e^--h^+ pairs, and consequently, lowering the TiO_2 photoactivity [3].

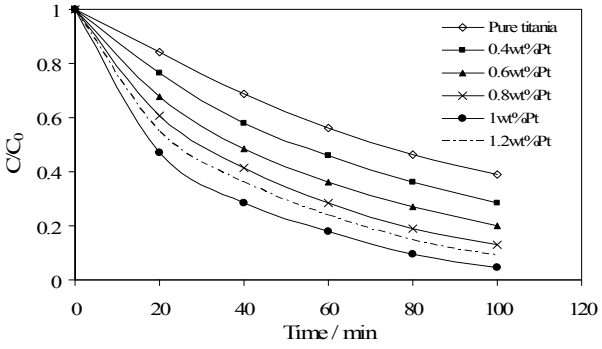

Fig.2. AY 23 concentration ratio as a function of exposure time under different Pt- loadings of Pt/TiO_2 (C_0: initial AY 23 concentration, 20 mgL^{-1}; [Catalyst] = 500 mg l^{-1}, initial solution pH ≈ 5.5) under Vis irradiation

The effect of catalyst dosage

As can be seen in Fig. 3, increasing the catalyst dosage results in increasing the generation of active species to react with organic molecules, consequently increasing the reaction rate. However, a large increase in catalyst dosage can cause the limitation of the light penetration that affects inversely the photocatalytic reaction [4].

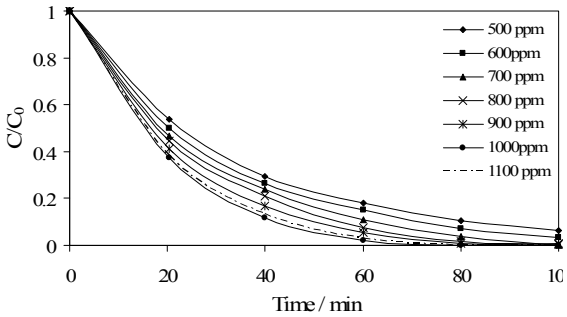

Fig.3. AY 23 concentration ratio as a function of exposure time under different dosages of Pt/TiO_2 (initial AY 23 concentration, 20 ppm; initial solution pH ≈ 5.5) under visible irradiation.

Kinetic analysis

To study the kinetic of photocatalytic degradation of AY23, experiments was conducted in the optimum operating conditions (1000 mgL^{-1} of 1wt% Pt/TiO_2 and pure TiO_2). The good linearity of the $-\ln(C/C_0)$ versus irradiation time plot, with high R^2 values (Fig. 4), suggests that the photocatalytic reaction approximately followed the pseudo-first order kinetic. The rate constant calculated for the reaction carried out at the optimum condition was 0.0672 min^{-1}. Similar values of correlation coefficients ($R^2 > 0.996$) for the $-\ln(C/C_0)$ versus irradiation time plots have been calculated for the experiments carried out at the conditions other than optimum condition.

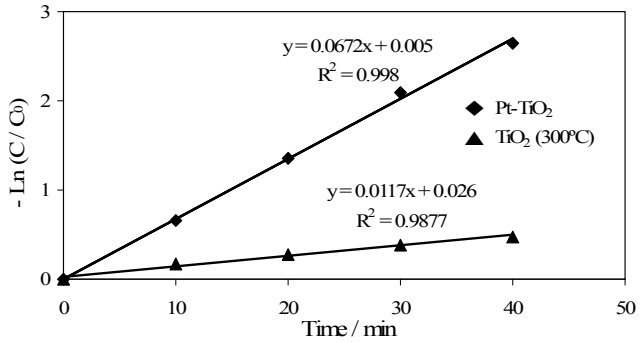

Fig.4. Kinetic plot of AY23 photodegradation for:

CONCLUSIONS

The present investigation showed that the photocatalytic efficiency of TiO_2 nanoparticles for the degradation of Acid Yellow 23 can be significantly improved by depositing of Pt. The effects of the influencing factors, showing the optimum values of 1% Pt and 1000 mgL^{-1} Pt-TiO_2. The semi-logarithmic graphs of the concentration of AY23 in the presence of different concentrations of Pt/TiO_2 versus irradiation time yield straight lines ($R^2 \geq 0.985$) indicating pseudo-first order reaction.

REFERENCES

[1] Y. Ishibai, J. Sato, T. Nishikawa, S. Miyagishi, (2008), Appl. Catal. B, 79, 117–121.

[2] S. Chavadej, P. Phuaphromyod, E. Gulari, P. Rangsunvigit, T. Sreethawong, 2008, Chem. Eng. J.,137, 489-495.

[3] C.H. Wu, 2004**, Che**mosphere, 57, 601-608.

[4] A. Sclafani, J.M. Herrmann, 1998, J.Photochem. Photobiol. A: Chem. 113, 181-188.

14th Iranian Physical Chemistry Conference
University of Tehran, Kish, February 25-28, 2011

Surface Modification of Detonation Nanodiamond

M. Mohammad Taheri[a], S.A. Sajjadi[a],* S.M. Zebarjad[a], M. H. Avazkonandeh[a], and M. Abbasi[a]

[a]*Department of Materials science and Engineering, Ferdowsi University of Mashhad, Mashhad, 91775-1111, Iran (Email: sajjadi@ferdowsi.um.ac.ir)*

One of the major members of nanocarbon family is detonation nanodiamond (DND) that finds more applications in industry. For confirmation we refer to recent reviews [1-3] and a book [4] on nanodiamond materials. One of the primary fields of application is as reinforcement phase in polymer nanocomposites [5]. To insure good dispersion in any media it needs proper surface modification or functionalization [6-10]. The aim of this paper is to study surface modification of DNDs by oxidation in air and concentrated acid treating to generate carboxylic groups.

The DNDs were supplied from NaBond Technologies co. Ltd, China. The as-received (AR) material was studied by TEM, FTIR, and TGA. Two routes were selected for modifying DNDs surface, one way heat treatment (oxidation) in air, and the other way oxidation in air followed by concentrated acids treating (carboxylation). In the first route, some DNDs were placed in crucible in a furnace with air atmosphere in 450°C for 2 hours. Then the heat treated (HT) DNDs were studied by FTIR and TGA. In the second route, 1g HT-DNDs were sonicated in 50 mL, 3:1 mixture of concentrated sulfuric (98%) and nitric (70%) acids in a Branson 3510 sonication bath for 3 hours. Then the mixture was poured in 800 mL, 85°C deionized water and stirred for 10h. Washing of the acid treated (AT) DNDs was done by repeatedly centrifugation and sonication. The resultant slurry was dried in 80°C for 4h in a vacuum oven. The resultant powder was then studied by FTIR. To examine the effects of each modification treatment on dispersion capability of nanoparticles, the AR, HT, and AT powders were dispersed in Isopropanol by 30min sonication. The particle size distribution was determined by a Malvern-MAL1015189 instrument. To investigate the colloidal stability of nanoparticles, they were dispersed in DI water by 30min sonication and then colloidal stability after 2 weeks, 1 month, and 2 months were examined.

The TEM analysis showed that the DNDs are spherical in shape with the average size less than 10nm. The TGA curve showed only one peak around 560°C that corresponds to oxidation of DND itself and also reveals the high purity of the AR material. The FTIR results showed surface functional groups of AR-DNDs are OH, CN, C=O (from CO_2), and COOH. But after oxidation in air the C=O peak was appeared in FTIR spectrum around 1750 cm^{-1}. The other major effect is the oxidation of non-diamond carbon from the surface shell of particles. It is believed that both C=O bonds and non-diamond carbon encourage the agglomeration of particles [6]. The TGA curves before and after heat treatment are both the same. After carboxylation, FTIR spectrum shows only peaks for OH, C-O, and C=O. Such a spectrum corresponds to carboxylic group [11]. Results of particle size analysis are shown in figure 1. It is apparent that the surface modifications strongly influence the dispersion capability of nanoparticles. Among them the AT-DND shows the finest distribution that implies more effectiveness of carboxylation process.

The stability of the nanoparticles in DI water is also investigated. The AR-DNDs are precipitated after 2 weeks that reveals low stability of the sample. The HT and AT-DNDs are almost identical.

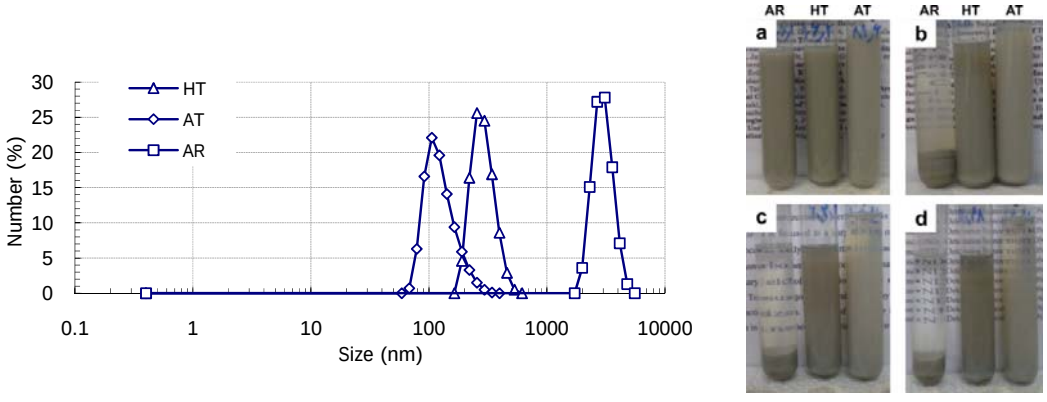

(A) (B)

Figure 1 (A) Particle size distribution of AR, HT, and AT-DNDs after 30min sonication in isopropanol and (B) stability of AR-, HT-, and AT-DNDs in DI water after (a) sonication, (b) 2 weeks, (c) 1 month, and (d) 2 months.

Keywords: Detonation nanodiamond, Functionalization, Air oxidation, Carboxylation.

References

[1] A. M. Schrand, S. A. Ciftan Hens, O. A. Shenderova, *Critical Reviews in Solid State and Materials Sciences* **34** (2009) 18.

[2] O. A. Shenderova, V. V. Zhirnov, D. W. Brenner, *Critical Reviews in Solid State and Materials Sciences* **27** (2002) 227.

[3] Y. Hu, O. Shenderova, Z. Hu, C. W. Padgett, D.W. Brenner, *Reports on Progress in Physics* **69** (2006) 1847.

[4] O. A. Shenderova, D. M. Gruen, Ultrananocrystalline Diamond, William Andrew Publishing, NW, 2006.

[5] V. Yu. Dolmatov, *Journal of Superhard Materials* 29 (1) (2007) 1.

[6] O. Shenderova, I. Petrov, J. Walsh *et al.*, *Diamond & Related Materials* **15** (2006) 1799.

[7] B. V. Spitsyn, J. L. Davidson, M. N. Gradoboev *et al.*, *Diamond & Related Materials* **15** (2006) 296.

[8] K. D. Behler, A. Stravato, V. Mochalin, G. Korneva, G. Yushin, Y. Gogotsi, *acsnano* **3** (2009) 363.

[9] S. Ida, T. Tsubota, S. Tanii, M. Nagata, Y. Matsumoto, *Langmuir* **19** (2003) 9693.

[10] A. Y. Jee, M. Lee, *Current Applied Physics* **9** (2009) e144.

[11] D. L. Pavia, G. M. Lampman, G. S. Kriz, J. R. Vyvyan, Introduction to Spectroscopy, Brooks/Cole, Cengage Learning, CA, 2009.

Kinetic degradation of 4-chloro-2-nitrophenol by nanocatalyzed ozonation

Ali Mehrizad[1], Samad M. Tabatabaei[2] and Parvin Gharbani[2]*

[1]Department of Chemistry, Science and Research Branch, Islamic Azad University, East Azarbayjan, Tabriz, Iran

[2]Department of Chemistry, Islamic Azad University, Ahar Branch, Ahar, Iran

e-mail: parvingharbani @yahoo.com

Keywords: Heterogeneous catalytic, Total organic carbon, Nano ZnO catalys, Ozone,Kinetic

Introduction

4-Chloro-2-nitrophenol (4C2NP), selected as a model compound in the present study, is widely available in bulk drugs and pesticide wastes [1]. Heterogeneous catalytic ozonation is a novel type of advanced oxidation, which combines ozone with the adsorptive and oxidative properties of solid-phase metal oxides to achieve mineralization of organic pollutants [2]. Therefore, the objectives of this study was to determine the kinetic degradation of 4C2NP by nano-ZnO catalyzed ozonation.

methods

Catalytic activity measurements in degradation of 4C2NP were carried out in a semi-batch stirred reactor, where ozone gas was continuously poured through a fine-bubble ceramic diffuser into a glass reactor (2000 ml) with 1L of aqueous solution containing 12 mgL^{-1} of 4C2NP and 0.3 g of nano-ZnO that was completely mixed with a magnetic stirring bar. Gas flow was kept constant at 1L min^{-1}, having an ozone concentration of 5.64 mgL^{-1}. Nano-ZnO particles were dispersed in the solution as soon as the ozone gas contacted the 4C2NP solution. The contact time was 30 min and samples were withdrawn at different intervals (1, 2, 5, 10, 15, 20, 30 minutes) to determine the residual concentration of 4C2NP by both the photometric and the HPLC methods. During the reaction, the reactor was sealed to avoid the evaporation of aqueous ozone.

results and discussion

It was found, the degradation efficiency of 4C2NP changed with the variation of pH in the solution. From the results, it can found that in ZnO heterogeneous catalytic ozonation, the surface property of metal oxides rather than OH^- ions in the solution was the main factor determining the catalytic activity. During the catalytic ozonation, the degradation of 4C2NP at pH 3 was higher than that of pH 7 and 9. After 2 min., under acidic condition (pH = 3) the degradation efficiency of 4C2NP was as high as 85.26%, while in the solutions with pH 7–9, was about 31-49%. It is clear that pH affects the aggregation of ZnO particles. It is already well known that nanosized particles tend to form aggregates when they are suspended in water [3], and it depends on the concentration of particles and the pH of solution. The size of ZnO gets to 350 nm at pH = 7.5 and the decomposition rate was decreased with an increase in the pH levels [4]. This was due to increase size of the ZnO particles and the subsequently decreased surface area. A kinetic study of 4C2NP removal in the presence of nano ZnO at different pHs (3, 7 and 9) was carried out. The reaction form of 4C2NP with Nano-ZnO/O_3 can be written as: $\frac{d[4C2NP]}{dt} = -k_{O_3}.[4C2NP][O_3][ZnO] + k_{OH^0}[4C2NP][OH^\bullet][ZnO]$ (1)

Here, [4C2NP], [O_3], [$OH^\bullet$] and [ZnO] are the concentration of 4C2NP, ozone, hydroxyl radicals and zinc oxide, respectively. k_{O_3} and k_{OH}. are the rate constants of 4C2NP with ozone and hydroxyl radicals, respectively. According to [5] direct reaction of molecular ozone with phenolic compounds was predominant during the ozonation at pH values lower than 12. Therefore, the rate equation can be written in the form:

$$\frac{d[4C2NP]}{dt} = -k_{O_3}.[4C2NP][O_3][ZnO] \quad (2)$$

If a reactor system is desired where compound A, is to be removed by reaction with B and C and the concentration of B and C can be regarded constant, only the concentration of compound A changes and the reaction can be regarded as pseudo first order[6]. So, the disappearance rate can be expressed in the form: $\frac{d[4C2NP]}{dt} = -k'_{O_3}[4C2NP]$ (3)

k'_{O_3} is a pseudo first-order constant rate reaction of 4C2NP with nano-ZnO/O_3 .

The integration of (3) Leads to: $$Ln\frac{[4C2NP]_0}{[4C2NP]}=k'_{O_3}.t \quad (4)$$

The decomposition rate of 4C2NP was found to decrease with increasing pH values. The measured rate constants of 4C2NP with O_3/ZnO are 4.47×10^{-3} s^{-1} (pH =3), 3.10×10^{-3} s^{-1} (pH=7) and 1.885×10^{-3} s^{-1} (pH =9). It can be concluded that much degradation rate of 4C2NP with O_3/ZnO is occurred at acidic pH. This result show adsorption trend of 4C2NP on the nano ZnO surface, which was pH-dependent and occurred at pH<4.

Measurments TOC for O_3/nano ZnO and O_3 systems was 54.99 and 7.46%, respectively. This result indicates 4C2NP in water was rapidly mineralized by the O_3/nano ZnO than O_3 alone. So, it can be concluded that 4C2NP cannot be totally mineralized from catalyzed ozonation, even by the O_3/nano ZnO methods. It is clear that only part of 4C2NP was mineralized and some degradation intermediates were formed during the ozonation of 4C2NP.

conclusions

The results showed that the rate of 4C2NP decomposition on the surface of ZnO was strongly pH dependent due to decreased active sites on the surface of ZnO and in the ZnO catalyzed ozonation, the oxidation efficiency of 4C2NP was higher at low pH (pH =3) than high pH (pH =9).

References

[1] P. Saritha, C.Aparana, V.Himabindu, Y.Anjaneyulu, J. Hazard. Mater.149(2007)609-614.

[2] W.J. Huang, G.C. Fang, C.C. Wang, Colloids and Surf. A: Physicochem. Eng. Aspects. 260 (2005) 45–51.

[3] J. Hoigne, H. Bader, Water Research, 17(1985)173.

[4] H. Jung, H. Choi, Applied Catalysis B: Environmental, 66(2006) 288.

[5] A. Goi, M. Trapido, T. Tuhkanen, Advances in Environmental Research 8(2004) 303.

[6] C.Gottschalk, J.A.Libra, A.Saupe, Ozonation of Water and Wastewater, New york, 2000.

14th Iranian Physical Chemistry Conference
University of Tehran, Kish, February 25-28, 2011

Synthesis temperature effect on optical properties of water-soluble luminescent CdZnTe nanocrystals

S. Gholami Kaliji*, E. Saievar Iranizad

Faculty of Science, Department of Physics, Tarbiat Modares University, Tehran, Iran

Keywords: CdZnTe nanocrystals, Synthesis temperature, PL spectra, UV-vis, XRD.

Introduction:

Synthesis of ternary alloyed nanocrystals is a new approach to produce II-VI luminescent semiconductor nanocrystals; and only a limited number of studies have been reported for preparation of alloyed nanocrystals via chemical routs [1]. In this research, CdZnTe nanocrystals were synthesized in aqueous media. Our method is of particular interest due to low temperature, simple facilities, low cost and bio compatible. Also, influence of synthesis temperature on optical properties of nanocrystals is evaluated.

Experimental:

Colloidal $Cd_{1-x}Zn_xTe$ nanocrystals were prepared by the reaction between Cd^{2+} and Zn^{2+} with sodium hydrogen tellurium (NaHTe) solution, using $NabH_4$(>98.0%), tellurium powder (99%), thioglycolic acid (TGA) (97%), $3CdSO_4.8H_2O$ (99%), $Zn(CH_3COO)_2.2H_2O$, NaOH in D.I.water and then refluxing the result mixture solution. In this work, synthesis temperature verified from 80 to 125^oC. X-ray diffraction pattern was carried out by Philips MRD X'pert Pro system with Co Ka radiation (λ=1.78897 nm). The photoluminescence (PL) measurements were performed by an Avante spectrometer (Ava Spec-2048 TEC) and the UV-vis absorption spectra were measured by a UNICO spectrophotometer (UV-4802). All the measurements were performed at room temperature.

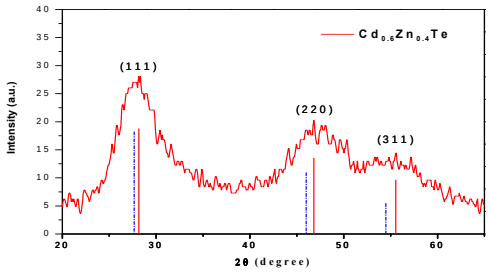

Fig. 1. XRD spectra of $Cd_{0.6}Zn_{0.4}Te$; CZT peacks(solid line) shift to the bigger angles as compared to CdTe's(dash line).

Result and discussion:

In this work, $Cd_{1-x}Zn_xTe$ nanocrystals were synthesized using the colloidal chemistry method. XRD was performed on the centrifuged and extracted particles. Fig.1 shows X-ray diffraction pattern of alloyed $Cd_{1-x}Zn_xTe$ nanocrystals for x=0.4. The XRD peaks are broadened due to the nanosized crystalline phases. The peaks corresponded to the reflection from (111), (220) and (311) crystalline planes (JCPDS No.50-1439). This pattern reveals that they possess a FCC type of crystallographic structure. The diffraction peaks of $Cd_{0.6}Zn_{0.4}Te$ in compare to CdTe, shift to larger angels, which may be attributed to the change in cell parameter produced by the difference of atomic radii between Zn and Cd. Furthermore, the mean diameter of the nanocrystals was also estimated about 2.6 nm, according to the Scherer's equation. We have studied the influence of Synthesis temperature in determining the optical properties of the alloyed nanocrystals. The concentration of precursor and the growth time were kept constant, and only the synthesis temperature was changed from 80 to 125^{o}C. It was observed in our experiments that the reaction solutions are easy to deposit with increasing refluxing time when synthesis temperature was higher than 110^{o}C. It may be due to the quick growth and easier conglomeration of nanocrystals at a high temperature. The normalized PL and absorption spectra of $Cd_{1-x}Zn_xTe$ alloyed nanocrystals for x=0.4 that formed at the various temperature are given in fig.2(a) and fig.2(b), respectively. The red-shift of the absorption and emission spectra of $Cd_{0.6}Zn_{0.4}Te$ nanocrystals with increasing synthesis temperature were observed. Meanwhile, the sharp absorption and narrow PL spectra reveals highly monodisperse distribution. Generally, heating causes slow growth, which is in agreement with "Ostwald ripening" [2]. This result, suggests that the size of $Cd_{1-x}Zn_xTe$ nanocrystals increases gradually with synthesis temperature from 80 to 125^{o}C, and in order to avoid the

conglomeration of nanocrystals and obtain small nanocrystals, synthesis temperature is supposed to be lower than 110°C.

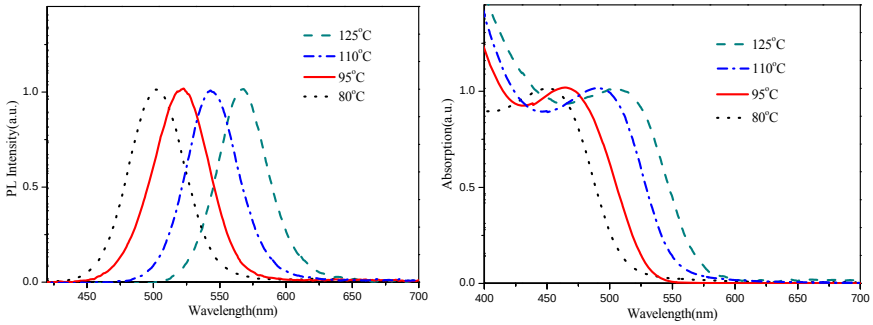

Fig.2. PL spectra (a) and Absorption spectra (b) of CZT Nanocrystals synthesized at different temperature.

Conclusions:

In this paper, $Cd_{1-x}Zn_xTe$ nanocrystals were synthesized for x=0.4 in aqueous phase with TGA as stabilizer. The samples have been characterized by XRD, which confirm that the nanocrystals are formed and crystal structure is FCC. The optical properties of the nanoparticles can be affected by synthesis temperature and it can be observed a red shift in PL and absorption peaks by increasing the synthesis temperature. All obtained samples display a narrow PL and sharp absorption spectra.

References:

[1] Piven N., Susha A.S.,Doblinger M.; J.Phys. Chem. C, 112, 15253, (2008)

[2] Zhou Y., Antonietti M.; J.Am. Chem. Soc. 125, 14960, (2003)

14th Iranian Physical Chemistry Conference
University of Tehran, Kish, February 25-28, 2011

A novel method for the synthesis of core-shell nanocrystal (CdS-TiO_2) without surfactant

Narjes Ghows and *Mohammad H. Entezari
Department of Chemistry, Ferdowsi University of Mashhad, 91775, Mashhad, Iran
*Corresponding author: moh_entezari@yahoo.com

Abstract

The core-shell of nanocomposites was prepared at a relatively low temperature by using ultrasonic waves, sol-gel and microemulsion under mild conditions without any post thermal treatment. Ultrasonic irradiation can control the hydrolysis and condensation of TTIP and formation of a gradient TiO_2 shell around the CdS core. This technique avoids some problems that normally exist in conventional synthesis such as the presence of different additives and calcinations. Increasing the amount of TiO_2 led to a red-shift of the optical absorption band in composite. Characterization of nanocomposites has been studied by HRTEM, TEM, XRD, BET and UV-vis spectroscopy.

Keywords: Nanoparticle, Ultrasound, Microemulsion, Core-shell, TTIP, TiO_2, CdS

Introduction

In recent years, core/shell-structured composite materials have attracted increasing interest of materials scientists due to their unique optical and electronic properties [1, 2]. The uniform deposition of inorganic material on small core particles is often problematic due to the lack of coating methods and poor surface interactions under the usual experimental conditions [3]. Ultrasound is an easy and effective method under the mild conditions for preparing nonmaterials [3, 4]. It can improve the contact of the two components, crystallinity, and formation of uniform coating [5, 6]. It seems that the combination of ultrasound with sol-gel and micro-emulsion is a suitable method for the synthesis of coupled semiconductors. In this paper, a new method has been developed to produce CdS/TiO_2 nanocomposite (core/shell) by using ultrasonic waves under mild conditions.

Experimental

A microemulsion with weight ratio between oil, ethylendiamine, water, and CS_2 was produced by ultrasound for preparing CdS. The synthesis of core-shell nanoparticles has been carried out with combination of ultrasound and microemulsion by adding TTIP to the mixture. Also, nanocrystalline TiO_2 was synthesized by hydrolysis of titanium tetra-isopropoxide (TTIP) in the presence of de-ionized water and TTIP under ultrasonic irradiation. The obtained precipitates were separated, washed and then dried.

Results and discussion

In the present study, it is confirmed that ultrasonic irradiation would favor the formation of nanocomposite (core/shell) at relatively low temperature. The results of XRD and HRTEM show that nano-particles have uniform spherical morphology and confirm that TiO_2 is uniformly coated on the surface of CdS. Also, the preparation method has an important role on the structure and properties of the composites. Increasing the TiO_2 led to an optical absorption band red-shift of composite. Rapid synthesis with uniform deposition might be attributed to the physical and chemical effects of cavitation. Cavitation removes surface contamination which helps to adhere the inorganic clusters more uniformly [3, 4]. On the other hand, shock waves and turbulent flows drive nanoparticles together, increasing adsorption and fuse under ultrasonic cavitation [7] to form core-shells.

Conclusion

In summary, CdS-TiO_2 core–shell nano-composites have been synthesized by low-temperature, short reaction time accompanied with uniform shape under microemulsion without surfactant and ultrasound. This is due to the cavitation process which produces strong shock waves and intense local heating that results in an increase in mass transfer and diffusion of species and enhances the crystallinity of the nano-particles. In addition, optical analysis revealed that increasing the amount of TiO_2 leads to an absorption band red-shift in composite.

Acknowledgment

This work has been supported by the "Iranian National Science Foundation: INSF" (No. 85103/31).

References

[1] P.V. Kamat, J. Phys. Chem. C 111 (2007) 2834-2860.

[2] P.V. Kamat, J. Phys. Chem. C 112 (2008) 18737.

[3]J. H. Bang, K. S. Suslick, J. Am. Chem. Soc. 129(2007) 2242-2243.

[4] S. Anandan, F. Grieser, M. Ashokkumar, J. Phys. Chem. C 112 (2008) 15102–15105.

[5] M. H. Entezari, N. Ghows Ultrason. Sonochem. 18 (2011) 127–134.

[6] N. Ghows, M.H. Entezari, Ultrason. Sonochem 18 (2011) 629–634.

[7] D. Radziuk, et al., J. Phys. Chem. C 114 (2010) 1835–1843.

14th Iranian Physical Chemistry Conference
University of Tehran, Kish, February 25-28, 2011

Study of the aggregation behavior of surfactants in aqueous solution containing carbon nanotube via molecular dynamics simulations

M. Foroutan, M. fatemi
Department of Physical Chemistry, School of Chemistry, College of Science, University of Tehran, Tehran, Iran,
m.fatemi@khayam.ut.ac.ir

Key word: Carbon nanotube (CNT), Molecular Dynamics (MD) Simulation, Triton surfactant

Introduction

A large amount of research is available concerning the dispersion of aggregated carbon nonotubes by surfactants and also mechanisms for the interaction between aggregated surfactants and carbon nanotubes [1, 2]. It is reminded that CNTs have hydrophobic nature and have proper interaction energies with hydrophobic materials. In this project the behavior of surfactant triton in aqueous solution containing one CNT has been examined.

Computational Procedure

In this study, an armchair CNT with length of 25 Å was interacted with triton surfactants, using a canonical ensemble (constant NVT). The velocity form of Verlet algorithm method and the Nose-Hoover thermostat algorithm were used to integrate the equations of motion with a time step of 1.0 fs and temperature control of 300 K, respectively. All MD simulations have performed using the AMBER99 force field. Non-bonded van-der-Waals interactions were modeled by a Lennard-Jones potential with a cut-off distance of 1.2 nm.

Results and Discussion

Representative simulation snapshot for (10, 10) single-walled nanotubes covered by 6 triton surfactant molecules at 300 K are shown in figure 1. The intermolecular interaction energies

between CNT and triton surfactant molecules used to describe the behavior of simulated systems.

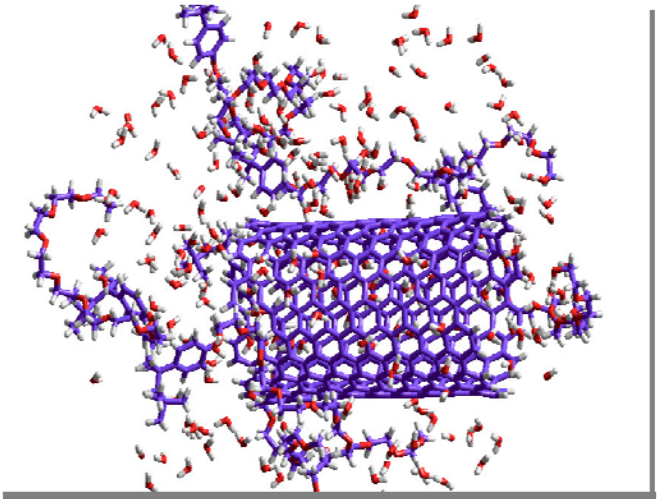

Figure 1. Front view snapshot for a (10, 10) signal wall nanotube covered by 6 triton surfactant molecules in water solution.

The obtained results show that how surfactant molecules aggregate around the nanotube. Radial distribution functions for different atoms of surfactant respect to carbon atom of carbon nanotube have been used for describing the aggregation of surfactant molecules.

References

[1] M.F. Islam, D. M. Bergey, A. T. Johnson, and A. G. Yodh, Nano letters, 2003, 269-273.

[2] E. J. F. Carvalho and M. C. Santos, The European Physical Journal, 2010, 147-150.

14th Iranian Physical Chemistry Conference
University of Tehran, Kish, February 25-28, 2011

Thermal Decomposition Behavior of Nano-Cyclotrimethylenetrinitramine(RDX)

M. Fathollahi[a]*, S. Tavangar[a], S. H. Moatamed′oshariati[a]

mfathollahy@yahoo.com

[a]Faculty of Material and Manufacturing Technologies, Malek Ashtar University of Technology,

Abstract:

RDX, named hexahydro-1, 3, 5-trinitro-1, 3, 5-triazine or cyclotrimethylenetrinitramine, a high explosive energetic material, plays an important role in defence industry in many countries [1]. Size, shape, and internal defects are very important properties of explosives crystals. Particle size of energetic materials can influence the initiation process through changes in pore size and particle size distribution which should affect hotspot formation, through changes in the specific energy density, and through changes in the shock Hugoniot. It is useful to discern which effects are strongest. A lot of studies have been devoted to investigate the effects of explosive crystal characteristics on the shock-detonation transition of explosives. The explosive crystal properties studied were the size, the shape and the surface, and the defects at different scales inside the explosive crystals. Unfortunately, the particle size and size distribution of energetic materials produced in industrial processes are frequently not those desired for subsequent use of this materials, and as a result, special comminution and recrystallization operation are carried out in order achieve the decreased characteristics [2].

Very fine energetic materials and nanocomposites, characterized by an ultra fine grain size, have created a high interest in recent years by virtue of their unusual energetic properties [3]. Studies have shown that the thermal behavior of very fine-scaled materials is quite different from usual energetic powders. Ultra fine explosive powders have been used as a solid propellant and explosive mixture components to increase efficiency [4].

Techniques of thermal analysis such as DTA, TG and DSC have been largely used in the study of explosive decomposition kinetics in isothermal and non-isothermal conditions [5]. Thermo-analytical study of high energy materials is important not only for understanding the kinetics of their thermal decomposition but also for assessing the effect of their exothermic

decomposition on the potential hazards in their handling, processing and storage [6]. Kinetic studies also provide useful information on thermal stability and life expectancy of the energetic materials under different thermal environment at storage [7].

This work refers to study of the thermal decomposition of hexahydro-1,3,5-trinitro-1,3,5-triazine or cyclotrimethylenetrinitramine (RDX) nanoparticles by simultaneous thermogravimetery - differential thermal analysis (TG/DTA) and differential scanning calorimetry (DSC) under non-isothermal conditions, at various heating rates from 5 to 20°C min-1. The influence of the particle size on the thermal decomposition of RDX samples with various particle sizes was verified. The activation energy for the decomposition of each sample was calculated using the peak temperature shift methods, proposed by Kissinger. A significant variation in the results was observed according to the range of the used particle size. The results showed that, as the particle size of RDX increased, the thermal decomposition temperature of RDX and the decomposition activation energies ranges enhanced. However, at a constant heating rate, the decomposition temperatures of the smaller particles were lower than those of larger ones. The values of activation energy obtained by Kissinger method show that activation energy for micron sized RDX 1.5 times is higher that nano-RDX. The critical temperature for thermal explosion of each sample was calculated. Also, the values of ΔS#, ΔH# and ΔG# of decomposition reaction for each particle size were computed.

The effect of DSC heating rate on the thermal decomposition of RDX with different particle size (micron and nano-sized samples) was studied. It was observed that the heating rate is an important factor in the thermal decomposition of RDX. The results show that as the heating rate increase, the decomposition peak shift to higher temperature. However, at a constant heating rate, this temperature was decrease as the particle size was reduced. The activation energy and the pre-exponential factor were obtained by Kissinger method for all samples. The present study shows that the values of activation energy and pre-exponential factor decrease by reducing the particle size of RDX samples. The critical temperature of thermal explosion of the compound with various particle size was calculated. On the other hand, the values of ΔS#, ΔH# and ΔG# of the reaction at Tp0 were computed for all samples.

Kinetic and Thermodynamic Parameters of Thermal Decomposition for RDX

Mean average particle size (nm)	E_a (KJ.mol^{-1})	Frequency Factor Log A (S^{-1})	r*	$\Delta G^{\#}$ (KJ.mol^{-1})	$\Delta H^{\#}$ (KJ.mol^{-1})	$\Delta S^{\#}$ (J.mol^{-1}.K^{-1})
50000	272.3	27.8	0.9983	460.4	266.0	-391
300	236.3	24.5	0.9953	424.4	230.0	-391
250	181.0	18.9	0.9965	369.2	174.8	-391
180	161.1	16.9	0.9956	349.2	154.9	-391

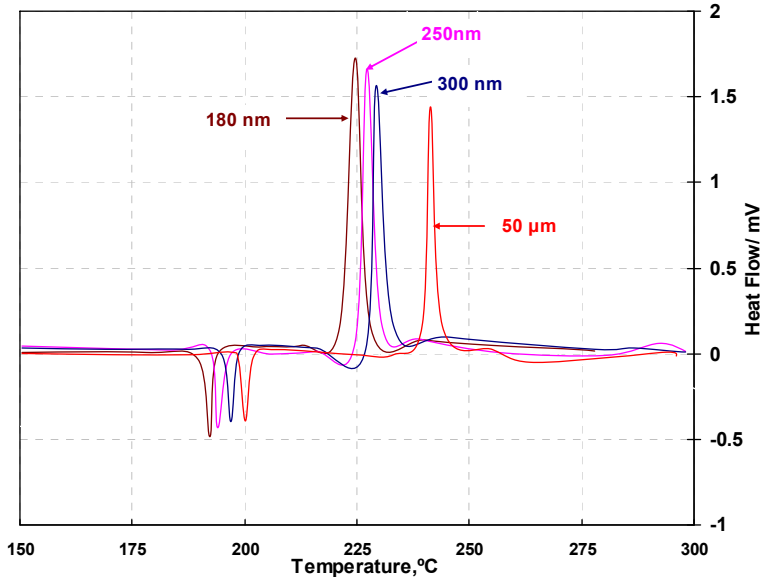

Effect of Particle size on Thermal Decomposition Behavior of RDX

References

[1] G. B. Manelis, G. M. Nazin, Y. I. Rubtsov, and V. A. Strunin, "Thermal decomposition and combustion of explosives and powders, " Moscow, Nauka, 1996.
[2] M. Fathollahi, S. M. Pourmotazavi, and S. G. Hosseini, "The effect of the particle size of potassium chlorate in pyrotechnic compositions" Combustion and Flame 138, 304-306 (2004).
[3] Y. Frolov, A. Pivkina, P. Ulyanova, and S. Zavyalov, "Nanomaterials and Nanostructures as Components for High-Energy Condensed Systems" Proceedings of 28th International Pyrotechnics Seminar, 5-9 November, Adelaide, Australia, 311-320 (2001).
[4] D. Render, R. Kapoor, M. Patel, and D. Martin, "Production and Characterization of Nano-RDX, " 18th ASC Conference 2006.
[5] Pivkina, P. Ulyanova, Y. Frolov, S. Zavyalov, and J. Schoonman, "Nanomaterials for Heterogeneous Combustion, " Propellants, Explosives, Pyrotechnics, (2003).
[6] M. Fathollahi; S. M. Pourmortazavi; S. G. Hosseini , " Particle Size Effects on Thermal

Decomposition of Energetic Material" Journal of Energetic Materials, Volume 26, Issue 1 January 2008 , pages 52 – 69
[7] S. G. Hosseini, S. M. Pourmortazavi, S. S. Hajimirsadeghi“ Thermal decomposition of pyrotechnic mixtures containing sucrose with either potassium chlorate or potassium perchlorate” Combustion and. Flame 141, 322- 326 (2005).
[8] J. S. Lee, C. K. Hsu “The thermal behaviors and safety characteristics of composition B explosive” Thermochimica Acta, 367-368, 371-374 (2001).
[9] Pratap, K.G. Raval, A. Gupta, S.K. Kulkarni, “A study on the thermal decomposition behaviors of PETN, RDX, HNS and HMX ” Bull. Mater. Sci 23, 185-188 (2000).
[10] H. Zhang, B. Mitchell, “A method for determining crystallization kinetic parameters from one nonisothermal calorimetric experiment” J. Mater. Res 15, 1000-1007 (2000).

14th Iranian Physical Chemistry Conference
University of Tehran, Kish, February 25-28, 2011

Electron Transfer Kinetic Theoretical and Quantitative Structural Relationship Studies of C_n@X-[HbA] (HbA=Hemoglobin A; X= α- and β-Fumarate Crosslinked Hemoglobins (αXL & βXL))Nanostructur Complexes

Avat (Arman) Taherpour* , Leila Fathiyan
Chemistry Department, Faculty of Science, Islamic Azad University,Arak Branch P. O. Box 38135-567, Arak, Iran. E-mail: avatarman.taherpour@ gmail.com and ataherpour@iau-arak.ac.ir

Keywords: Fullerenes; Hemoglobin A; Activated free energies of electron transfer; Kinetic constant of electron transfer; Marcus theory.

Introduction:

Various empty carbon fullerenes (C_n) with different carbon atoms have been obtained and investigated. The main component of the red blood cells, hemoglobin A (HbA) functions as an efficient oxygen carrier by reversibly binding oxygen at the ferrous ion of the heme groups[1]. Topological indices are purported to correlate chemical structures with various chemical and physical properties. They have been successfully used to construct effective and useful mathematical methods to establish clear relationships between structural data and physical properties of these materials [2].

Graphing and Mathematical Method:

All graphs were generated using the MATLAB-7.4.0(R2007) and *Microsoft Office Excel 2007* program. Using the number of carbon atoms contained within the C_n fullerenes, several valuable properties of the fullerenes can be calculated. The value of the electron transfer rate constant k_{et} is controlled by the activation free energy $\Delta G^{\#}_{et}$, which is a function of the reorganization energy and electron transfer driving force ΔG_{et} .

Result and Discussion:

The number of carbon atoms in the fullerenes was used as an index to establish a relationship between the structures of Hemoglobin A, HbA, αXL-[HbA] and βXL-[HbA],

respectively, **1-3** as the most well-known blood molecular systems and fullerenes C_n (n=60, 70, 76, 82 and 86) (figure1).The Calculations for the first oxidation potentials ($^{Ox.}E_1$) of fullerenes C_n and the first free-energies of electron transfer ($\Delta G_{et(1)}$) of supramolecular complexes for C_{60} to C_{300} were done. These were used to calculate the first free activation energies of electron transfer and kinetic rate constants of the electron transfers, $\Delta G_{et(1)}^{\#}$ and k_{et}, in accordance with the *Marcus* theory. The values of the first activated free energies of electron transfer, $\Delta G^{\#}_{et(1)}$ for the mentioned complexes, increase with increasing the $\Delta G_{et(n)}$ and the number of carbon atoms in the complexes, while the kinetic rate constants of the electron transfers $k_{et(1)}$, decrease with increasing $\Delta G_{et(1)}$ and $\Delta G_{et(1)}^{\#}$ for C_n@[HbA], C_n@ αXL-[HbA] and C_n@ βXL-[HbA].

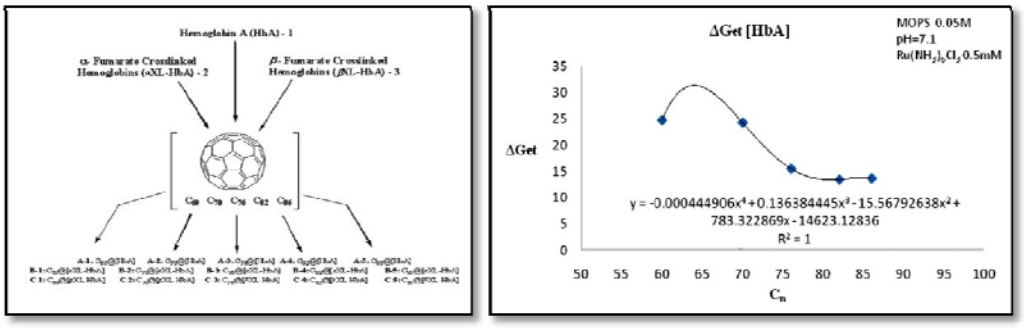

Figure.1.

Conclusion:

Hemoglobin A, α- and β-Fumarate Crosslinked Hemoglobins, **1-3** and fullerenes have important electron-transfer properties as the most well-known ox/redox systems and biomolecular systems. The results of this study could be utilized in nano-biochemistry and biotechnology studies related to these groups of biochemistry compound. The novel supramolecular complexes discussed have neither been synthesized nor reported previously.

References:

[1] S. A. Dragan, K. W. Olsen, E. G. Moore and A. Fitch, *Bioelectrochemistry,* 73 (2008) 55–63.

[2] A. A. Taherpour, *Fullerenes, Nanotubes and Carbon Nanostructures*, 17(1), 26 (2009).

Investigation of the photodegradation rate of methyl orange by synthetic flower ZnO/Au nanostructure

B. Fahimi Rad*, M. Arab Chamjangali, G. Bagherian, B. Bahramian
College of Chemistry. Shahrood University of Technology, Shahrood, Iran
E-mail:bahareh.fahimirad@Gmail.com

Keyword: Nanostructure; Au-ZnO; Photo-degradation; methyle orange

Introduction

Wastewaters contaminated with residual dyes from textile, paper and other industries are a source of environmental problems, especially in third world countries [1]. In particular, semiconductor mediated photocatalytic oxidation can be conveniently applied towards the degradation of dye pollutants. Zinc oxide (ZnO) is a semiconductor with a direct wide band gap (3.37 eV–387 nm, deep violet/borderline UV) and a large excitation-binding energy (60 meV) [2]. The combination of a semi-conductor substrate (TiO_2 or ZnO) and a metal cluster such as Ag, Au, Pd or Pt cluster has been reported to enhance the photo-catalytic activity by trapping the photo-induced charge carriers and thereby, improving the charge transfer processes [3].

This paper reports the photo-catalytic activity of synthesized Au-ZnO nanostructures using the PVP-coated Au/PANI precursors with flower morphology. All experimental factors affecting on the rate of photo-catalytic degradation of methyle orange (MO) were investigated. The reaction rates of the catalyzed and uncatalyzed reaction were calculated.

method

1.Synthesis of Au-ZnO nanostructures

A solution of Au nanoparticles (Au-NPs) was prepared using citritric acid according to Ref [4]. Then 1.0 mL of Au-NPs solution was heated in a 20-mL sample bottle at 60^0C and then, 10 mL of aqueous polyvinylpyrrolidone (PVP) was added. After 30 s, zinc acetate (1 mL) was added, followed by the addition of NaOH (1 mL) as to maintain a 1:5 Zn^{2+}:OH^- ratio. Heating

was continued for 1 h to get a clear supernatant with a white precipitate at the bottom of the bottle. The supernatant was removed and the white precipitate was washed a couple of times with both ethanol and water and was then kept in an oven for drying for 4 h.

2.Photodegradation procedure

The photo-reactivity experiments were carried out using a home made photo-reactor equipped with a 400W mercury lamp UV irradiation. For the irradiation experiment, MO (100 mL) was transferred into a sample vessel. A defined mass of the photo-catalyst was added to the dye solution, and the lamp was switched on to initiate the reaction, while the suspension was stirred magnetically. At fixed intervals of time, 2 mL of sample was withdrawn, and centrifuged to remove the catalyst particles before analysis of the solution spectrophtometrically at 464 nm.

3.Results and discussion

Two nanostructures were synthesized from the PVP-coated Au/PANI precursors. A part from PVP and Au-oligoaniline precursor concentrations, the ratio of Zn^{2+}: OH^- was the main parameter controlling the morphologies of the nanostructures prepared. The SEM images (Fig. 1) showed

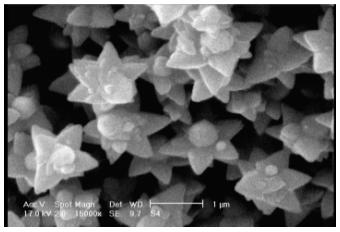

Fig. 1. SEM image

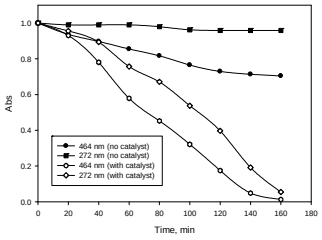

Fig. 2. Photo-degradation of (MO) in the presence of photo-catalyst

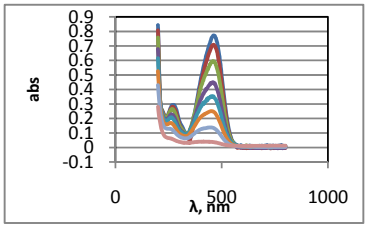

Fig. 2. Photo-degradation of (MO) in the presence of photo-catalyst

that at Zn^{2+}:OH^- ratio of ratio of 1:5, the flower-shaped structures were obtained.

The photo-catalytic activity of the synthesized Au-ZnO nanostructures was also studied. In this

study, the photo-degradation of methyl orange (10 mg L^{-1}) was investigated under the UV

irradiation in the presence of different amounts of 20 mg photo-catalysts. Fig. 3 shows the absorption spectra of MO at different times. The decrease in the absorbance at 464 nm shows the decolorization of MO and the decrease in the absorbane at 272 nm shows the degradation of MO in the presence of photocatalyst.

Fig. 2 shows the catalytic performances for MO photodegradation of the Au–ZnO nanostructure. According to the Fig. 2, irradiation in the absence of photocatalyst for 180 min showed no photodegradation of MO at 272 nm, confirming that the MO cannot be degraded by irradiation alone. Analysis of kinetic curves showed the rate constants of 1.16×10^{-2} min^{-1} and 2.6×10^{-3} min^{-1} for catalyzed and uncatalyzed decolorization reactions, respectively.

Refrence:

[1] R.W. Matthews, Water Res**. 25** (1991) 1169–1176.

[2] M.H. Huang, S. Mao, H. Feick, H. Yan, Y. Wu, H. Kind, E. Weber, R. Russo, P. Yang, Science **292** (2001) 1897.

[3] V. Subramanian, E.E. Wolf, P.V. Kamat, J. Phys. Chem. **B 107** (2003) 7479.

[4] Deepti Krishnan, T. Pradeep, Journal of Crystal Growth **311** (2009) 3889–3897.

Kinetic and Thermodynamic Studies in Removal of Nitrite from Aqueous Media by Application of Metalloporphyrin Functionalized Magnetite Nanoparticles as a New Adsorbents

Tahereh poursaberi[1*],sima Ghadernia[2],mostafa Hasanisadi[1],Kamran Torkestani[1],
Morteza Rezapour[1]and Maryam Abbasghorbani[3]

[1]Research Institute of petroleum Industry, Tehran, Iran

[2]Islamic Azad University, Shahre Ray Branch,Tehran, Iran

[3]Payame Noor University, Department of Chemistry, Mashhad, Iran

Keywords: metalloporphyrin functionalized magnetic NPs, nitrite, kinetic, thermodynamic study

Introduction

During the last few decades, magnetite (Fe_3O_4) nanoparticles (NPs) had attracted increasing research attentions in the field of environmental remediation [1]. For example, magnetic NPs have shown favorable activities for the adsorption of quite a few heavy metal ions (e.g. Ni^{2+}, $Cd^{2+}$and Cr^{6+} [2]). Nitrite is the famous contaminant anion in drinking and waste water. Its cancerous effects have been known since past decades. Therefore removing of excessive nitrite from aqueous environments could be considered as an alternative to elimination of its contamination. In the present work, we successfully synthesized metalloporphyrine functionalized magnetite NPs and investigated the adsorption feasibility of this nanomaterial for nitrite. Furthermore isotherm analysis, kinetic and thermodynamic studies were carried over. Kinetic parameters such as order of process and adsorption capacity were determined. Change in free energy (ΔG^0), enthalpy (ΔH^0) and entropy (ΔS^0) of adsorption process, under standard states, were calculated respectively.

Methods

The preparation of Fe_3O_4 nanoparticles was followed by a chemical co-precipitation of Fe(III) and Fe(II) ions. Then the nanoparticles were modified directly by 3-

aminopropyltrimethoxysilane to introduce reactive groups onto the particles' surface. Co(TCPP) [TCPP: 4,4',4",4"'- (21H,23H-porphine-5,10,15,20-tetrayl)tetrakis (benzoic acid)] was used as metalloporphirin ligand for immobilizing to nanoparticles. The final material was characterized by FT-IR spectroscopy, thermal analysis (TGA), SEM and XRD. Equilibrium isotherm experiments were conducted with initial nitrite concentrations ranging in 0–100 mgL^{-1} using batch procedure at 25±1°C with vigorous stirring in 1 hr. 2.5 mL of metalloporphyrin NPs suspension was added into nitrite solution. After a proper time, an strong magnet was used for deposition of NPs and the solution analyzed for the remaining nitrite concentration with ion chromatography. For kinetic study, the adsorption reactions were conducted by agitation at 300 rpm of the reaction mixture that was placed in water bath. Herein, 0.2 g of metalloporphirin NPs were thoroughly mixed with 200 mL of a nitrite solution with fixed initial nitrite concentrations (20, 40 and 60 mgL^{-1}). At a fixed preselected time interval from 0.1 to 240 min, 1 mL reaction mixture was withdrawn by a micropipette and analyzed for residual nitrite. The above adsorption reaction was conducted separately at a definite temperature (25, 40 and 50 °C).

Result and Discussions

The isotherm models of Langmuir and Freundlich were used to fit the experimental adsorption equilibrium data of nitrite on magnetic adsorbents. These models are represented mathematically as follows: Langmuir equ.: $q_e = \frac{q_m K_L C_m}{1 + K_L C_e}$ Freundlich equ.: $q_e = K_F C_e^{1/n}$

where C_e (mg L^{-1}) is the concentration of nitrite at equilibrium, K_L (L/mg), and q_m (mg g^{-1}) are the Langmuir constants related to the energy of adsorption and maximum capacity, respectively; K_F ($mg^{-(1/n)}L^{1/n}g^{-1}$) and 1/n are the Freundlich constants related to the adsorption capacity and intensity, respectively; and q_e (mg g^{-1}) is the mass of fluoride adsorbed per mass of adsorbent. Adsorption kinetic is one of the most important characters. Results indicated the kinetic of nitrite adsorption onto the magnetic adsorbents fit well with the pseudo-second-order kinetic model. The thermodynamic parameters for the adsorption process were calculated using the following relations: $\log\left(\frac{q_e}{C_e}\right) = \frac{\Delta S^0}{2.303R} - \left(\frac{\Delta H^0}{2.303R}\right)\frac{1}{T}$, $\Delta G^0 = \Delta H^0 - T\Delta S^0$

Where qe/Ce is the adsorption affinity. Results were summarized in table 1.

Table 1. Isotherm and thermodynamic analysis for nitrite adsorbtion on magnetic NPs.

Isotherm Analysis	Langmuir Isotherm Model			Freundlich Isotherm Model		
	q_m (mg g^{-1})	K_L (L/mg)	r^2	K_F	n	r^2
	48.2	0.08	0.981	8.5	2.7	0.978
Thermodynamic Analysis	ΔH^0(Kj mol^{-1})	ΔS^0(j mol^{-1} K^{-1})	r^2	ΔG^0(kj mol^{-1})		
				at 25 °C	at 40 °C	at 50 °C
	6.522	25.83	0.978	0.721	0.932	1.287

Conclusion

The metalloporphyrine functionalized magnetite NPs was synthesized successfully and applied for removing of nitrite from water samples. Kinetic and thermodynamic studies were carried over on adsorption process. Results indicated NPs have high capacity in adsorption of nitrite.

Reference

[1] A.F. Ngomsik, A. Bee,Comptes Rendus Chimie 8 (2005) 963–970.

[2] L.C.A. Oliveira, R.V.R.A. Rios, J.D. Fabris, Appl. Clay Sci. 22 (2003) 169–177.

14th Iranian Physical Chemistry Conference
University of Tehran, Kish, February 25-28, 2011

Synthesis and characterization iron oxide Nanoparticles and their Surface-Modified with Folic Acid

M.keshavarz*, Z.Ghasemi
Chemistry Department, Islamic Azad University-Shahreza Branch, pox311- 86145, Esfahan, Iran
E-mail:DMkeshavarz@yahoo.com

Keywords: nanoparticles, iron oxide, modify, folic acid

Introduction:

In recent years, the superparamagnetic iron oxide nanoparticles have attracted researchers from various fields such as physics, medicine, biology, and materials science due to their multifunctional properties such as small size, superparamagnetism and low toxicity [1–3]. Much research has been developed to the synthesis of iron oxide nanoparticles (NPs), and many reports have described efficient synthesis approaches to produce the shape controlled, stable, biocompatible, and monodispersed iron oxide NPs. The most common methods including co-precipitation, thermal decomposition, hydrothermal synthesis, microemulsion, sonochemical synthesis and electrochemical synthesis [4, 5].

Experimental section:

1. Materials:

The chemical reagents used in this work were $FeCl_2.4H_2O$, $FeCl_3.6H_2O$, ammonium hydroxide ($NH_3.H_2O$), Hexa trimethyl ammonium bromide (HTAB), (3-aminopropyl)-trimethoxysilane, toluene, folic acid, dimethylsulfoxide (DMSO), N-Hydroxysuccinimide (NHS) and1-[3-(Dimethylamino)propyl]- 3-ethylcarbodiimide (EDC). Distilled water was for preparation of the solutions after deoxygenation with dry N_2.

2. Synthesis iron oxide nanoparticles:

First, (0.01 mol) $FeCl_2.4H_2O$ (0.02 mol) $FeCl_3.6H_2O$ was dissolved in 25 mL distilled water, aqueous ammonium hydroxide solution (1.5 mol/L) was also obtained as this. Then, a certain surfactant (HTAB) was added to the former solutions to obtain Precursor solution II and Precursor solution I. Second, Precursor solution I was added into Precursor solution II

dropwise with strong stirring under the protection of dry nitrogen at the desired temperature. Just after mixing the solutions, the color of the solution changed from light brown to black, indicating the forming of Fe_3O_4 nanoparticles, which was allowed to crystallize completely for another 60 min under rapid stirring. The precipitate Fe_3O_4 nanoparticles were washed by repeated cycles of centrifugation and redispersion in distilled water. Washing was performed for five times in distilled water. Third, the precipitate Fe_3O_4 nanoparticles were redispersed in the same surfactant solution under the conditions of ultrasonic agitation for 30 min and strong stirring for another 40 min. The products (Fe_3O_4 nanoparticles) were also washed by repeated cycles of centrifugation and redispersion in distilled water. And washing was performed for four times in distilled water. Then, the final products were dried in a vacuum oven at room temperature for 24 h, and the Fe_3O_4 nanoparticles were finally obtained.

3. Modification of iron oxide with folic acid:

0.015 mg dried nanoparticles were dispersed in amount (3-aminopropyl)-trimethoxysilane in 5ml toluene. The mixture was sonicated, and put in water bath at 60ºC for 4h. The suspension was centrifuged and the precipitates were sonicated in toluene for 10 minutes, and washed with toluene and ethanol. The precipitates were added to the mixture of 1ml 0.01M folic acid solution in dimethylsulfoxide DMSO and certain amount NHS and EDC solution in water, using triethylamine as catalyst. The pH was adjusted to 9. After incubated at 37ºC for 4h, the suspension was centrifuged and the precipitate was washed by deionized water, and vacuum dried.

4. Characterization:

Scanning Electron Microscopy (SEM):

SEM was used to characterize the particle size and morphology of Fe_3O_4 particles.

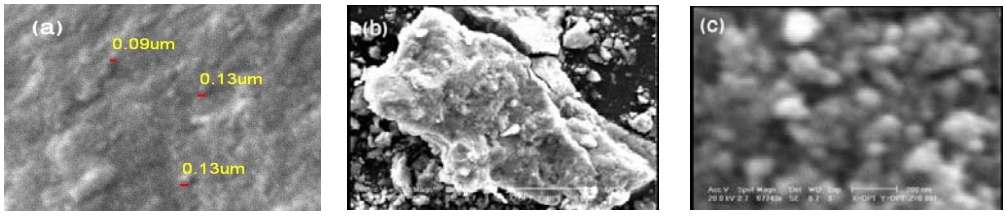

Fig1) a, b) nanoparticles iron oxide, c) nanoparticles iron oxide modify

Conclusions:

1) Ultrafine, uniform, nearly spherical, and high purity Fe_3O_4 nanoparticles could be prepared by the controlled chemical co-precipitation method from the solution of ferrous/ferric mixed salt-solution in aqueous ammonium hydroxide ($NH_3.H_2O$) solution when HTAB was chosen as the apt surfactant. The results (fig. 1) show that Fe_3O_4 nanoparticles can be produced in the sizes range from 8 to 20 nm by changing the operational parameters (i.e., concentration of HTAB, reaction temperature, solution pH, and stirring rate).

2) Folic acid was immobilized on magnetite nanoparticles to improve their biocompatibility, and to target the specific cells.

3) Fe3O4 nanoparticles coated with folic acid has a good biocompatibility and low toxicity.

Reference:

[1] Lian S, Wang E, Kang Z, Bai Y, Gao L, Jiang M, Hu C, Xu L."Synthesis of magnetite nanorods and porous hematite nanorods" *Solid State Commun*. 2004, 129, 485–490,.

[2] Zaitsev VS, Filimonov DS, Presnyakov IA, Gambino RJ, Chu B."Physical and chemical properties of magnetite and magnetite polymer nanoparticles and their colloidal dispersions" *J Colloid Interface Sci*. 1999, 212, 49–57,.

[3] L. Cabrera, S. Gutierrez, N. Menendezb, M.P. Morales, P. Herrasti, " Electro-precipitation of magnetite nanoparticles: An electrochemical study" *Electrochim. Acta*. 2008, 53, 3436

[4] C. Pascal, J.L. Pascal, F. Favier, M.L.E. Moubtassim, C. Payen, " ChemInform Abstract: Electrochemical Synthesis for the Control of γ-Fe2O3 Nanoparticle Size. Morphology, Microstructure, and Magnetic Behavior *Chem. Mate r* ". 1999, 11, 141.

14th Iranian Physical Chemistry Conference
University of Tehran, Kish, February 25-28, 2011

Tensile behavior of nano-size single crystalline Ni: A molecular dynamic simulation study

S. Ghasemi, A.R. Akbari*
Faculty of Materials Engineering, Sahand University of Technology, P.O. Box 51335-1996, Tabriz, Iran.
Email: akbari@sut.ac.ir

Introduction

Understanding the mechanical properties of nanophase materials is a challenging issue [1]. To determine mechanical properties, tensile test at nanoscale is extremely hard, if not impossible to conduct. An alternative approach is Molecular Dynamic (MD) Simulation [2] which provides better insight into the mechanical properties of nanocrystalline (nc) materials.

In this investigation, MD simulations were performed to execute tensile tests on defect-free nano single-crystalline Ni digital samples at the constant rate of loading (800m/s) in different directions ([111], [100], [110]). Actually we focused on studying effects of the crystal anisotropy on the nature of deformation, mechanical properties and fracture of the Ni nanocrystals.

Potential and simulation method

Three dimensional MD simulations have been performed to capture stress-strain response of nano single-crystal Ni samples. Digital sample constructed by including 1500 atoms with dimensions of 28*28*32 Å as shown schematically in figure 1. The samples were relaxed at 300K before loading. The boundary of atoms is fixed in the both sides of z-direction for loading and minimizing the edge effect. The motion of atoms is determined by Morse force-field.

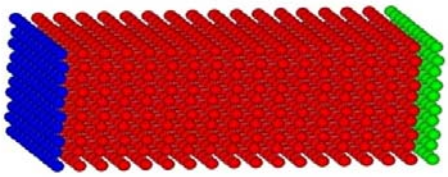

Figure 1) Atomic configuration of nano-single crystalline Ni sample.

Result and Discussion

Figure 2 shows the stress-strain curves of the nc Ni in different directions resulted from MD simulations of the tensile test. Unlike conventional tensile testing (bulk materials), where the stress–strain diagram is essentially smooth with a constant slope in the elastic region, in nano tensile testing, a series of fluctuations in the stress-strain curves in the both of the elastic and plastic (flow stress) regions are found. In earlier works [2] these fluctuations attributed to the strain hardening and subsequent softening of the material due to dislocation pileup and subsequent rapid motion of the dislocations. However, the dimensions of the studied samples were too small for lattice dislocations to be operative or dislocation pile up formation. It is thought that such fluctuations may be associated to the numerical methods. The tensile curves presented in Fig. 2 indicate a high strength and considerably high strain before failure, in all studied directions. Except for strains greater than 0.5 where the anisotropy effects are quit evident, the difference between stress-strain curves of different directions lies in the order magnitude of the fluctuations up to the ultimate strength.

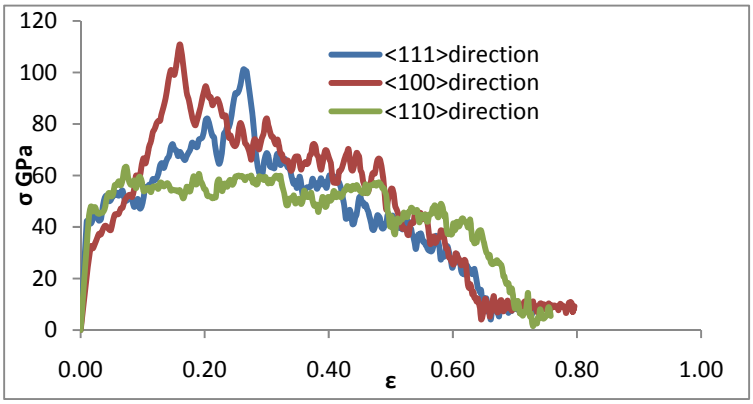

Figure2) Stress–strain curves of tensile deformation of nano-single crystalline Ni sample at different directions

Conclusion

According to the performed molecular dynamics simulations, defect-free nano size single crystalline Ni samples exhibit very high tensile strengths and considerably high strain before failure.

References

[1] H.Van Swygenhoven, A.Caro, Plastic behavior of nanophase metals studied by molecular dynamics, Physical Review B, Volume 58, Number 17,1998

[2] R. Komanduria, N. Chandrasekarana, L.M. Raff, Molecular dynamics (MD) simulation of uniaxial tension of some single-crystal cubic metals at nanolevel, International Journal of Mechanical Sciences 43 (2001) 2237–2260.

14th Iranian Physical Chemistry Conference
University of Tehran, Kish, February 25-28, 2011

Efficient Removal of Reactive Orange 12 by Multiwalled Carbon Nanotube

M. Ghaedi[a]*, F. Marahel[b], A. Amiri Pebdani[a] B. Sadeghian[a],

[a] Chemistry Department, Yasouj University Yasouj 75914-35, Iran

[b] Chemistry Department, Omidiyeh Azad University, Omidiyeh, Iran

Corresponding author E-mail: m_ghaedi@mail.yu.ac.ir

Abstract

Nano particle materials are unique one-dimensional macromolecules that possess outstanding thermal and chemical stability. These nano-materials have been proven to possess great potential as adsorbents for removing many kinds of environmental pollutants. For efficient removal of with high recovery the dye the influence of variables including pH, initial dye concentration, and temperature and sorption time on dye removal was studied. Following optimization of variables, the relation between concentrations of dye remained in aqueous and adsorbent has been evaluated using various adsorption isotherm models like, Langmuir, Freundlich, Tempkin. Evaluating and calculating the thermodynamic parameters including Gibb's free energy, entropy and enthalpy indicate the endothermic nature and feasibility of these days removal process. The kinetic studies suggest that the all process following pseudo second order kinetics and involvement of intera- particle diffusion mechanism.

Keywords: Adsorption; Reactive orange 12; Multiwalled Carbon Nanotube; Kinetic and Thermodynamics of Adsorption.

Introduction

It seems Multiwalled carbon Nanotube (MWCNT) be one of the best employed adsorbent for dye removal from aqueous solution because of its excellent adsorption properties that emerged from high surface and porous structure although the adsorption efficiency defend on the production of the MWCNT [1, 2]. The objective of the present work is to investigate the potential feasibility of MWCNT for the adsorption of RO-12. Reactive dyes in both ordinary

and hydrolyzed forms are not easily biodegradable, and thus, even after extensive treatment, colour may still remain in the effluent.

Experimental and results

The influence of variables including pH, contact time, initial dye concentration, amount of adsorbent, temperature required for efficient removal of RO-12 from 50 mL of 50 μg mL^{-1} sample has been investigated. The system is suitable for quantitative removal of this dye from such solution at pH 1 using 0.05 g MWCNT, equilibrium time 15 min even temperature of 50 ºC. The graphical correlation of various adsorption isotherm models like, Langmuir, Freundlich and Tempkin have been carried out for this adsorbent. Calculation of various thermodynamic parameters such as, Gibb's free energy, entropy and enthalpy of the on-going adsorption process indicate feasibility and endothermic nature or RO-12 adsorption on all adsorbent. The kinetic studies suggest the following pseudo second order kinetics and involvement of particle diffusion mechanism.

Conclusion

The MWCNT is identified to be an effective adsorbent for the removal of RO-12 from aqueous solutions. the kinetic study of RO-12 on MWCNT was investigated using pseudo-first-order, pseudo-second-order, Elovich and intraparticle diffusion equations. The results indicate that the adsorption kinetics for MWCNT follows the pseudo-second-order. the experimental data showed perfect fit with the Langmuir isotherm, which confirm that the adsorption process is homogeneous, specific and uniform in nature. Evaluating and calculating the thermodynamic parameters including Gibb's free energy, entropy and enthalpy indicate the endothermic nature and feasibility of these days removal process.

References

[1] E. Demirbas, M. Kobya, M.T. Sulak, Bioresour. Technol. 99 (2008) 5368–5373.

[2] D. Kavitha, C. Namasivayam, Chem. Eng. J. 139 (2008) 453–461.

14th Iranian Physical Chemistry Conference
University of Tehran, Kish, February 25-28, 2011

Kinetics, thermodynamic and equilibrium isotherms of Direct Yellow 12 adsorption on silver nano particle loaded on activated carbon

M. Ghaedi[a]*, B. Sadeghian[b], A. Amiri Pebdani[b], F. Marahel[b], J. Tashkhourian[c], M. Khirmand[a]

[a] Chemistry Department, Yasouj University Yasouj 75914-35, Iran

[b] Chemistry Department, Omidiyeh Azad University, Omidiyeh, Iran

[c] Chemistry Department, Persian Gulf University, Bushehr, Iran

*E-mail: m_ghaedi@mail.yu.ac.ir

Abstract

In this research, efficiency and performance of silver nano particle loaded on activated carbon (SNPC) adsorbent for the removal and recovery of Direct Yellow 12(DY 12) from wastewater has been compared. DY 12 was used as the model compound due to its wide range of applications and high stability in the environment. The maximum removal was 98% for 25 µg mL^{-1} of DY 12 concentration on 0.1 g L^{-1} carbon concentration. The influence of variables including pH, concentration of the dye, amount of adsorbent, contact time and temperature on the dye removal has been investigated in batch method by one at a time optimization method. The graphical correlation of various adsorption isotherm models like, Langmuir, Freundlich and Tempkin have been carried out for this adsorbent. Calculation of various thermodynamic parameters such as, Gibb's free energy, entropy and enthalpy of the on-going adsorption process indicate feasibility and endothermic nature of Direct Yellow 12 adsorption on all adsorbents. The kinetic studies suggest the process following pseudo second order kinetics and involvement of particle diffusion mechanism.

Keywords: Adsorption; Direct Yellow 12; Silver nano particle loaded on activated carbon (SNPC); Kinetic and Thermodynamics of Adsorption.

Introduction

Nano particle have very interesting physicochemical properties, such as ordered structure with high aspect ratio, ultra-light weight, high mechanical strength, high electrical conductivity, high thermal conductivity, metallic or semi-metallic behavior and high surface area [1, 2]. In this research, efficiency and performance of silver nano particle loaded on activated carbon (SNPC) adsorbent for the removal and recovery of Direct Yellow 12(DY 12) from wastewater has been compared. DY 12 was used as the model compound due to its wide range of applications and high stability in the environment.

Experimental and results

In the first SNPC was prepared by chemical plating method. Firstly,1.0 g purified and functionalized AC was mixed with 50 mL mixture solution of 38% (W/W) formaldehyde, absolute ethyl alcohol and double distilled water (volumetric ratio 3:10:10). Secondly, 50 mL mixture solution of 35 g L^{-1} silver nitrate (AgNO3) solution and 25 % ammonia solution (volumetric ratio1:2) was dropped one by one into the mixture of AC–formaldehyde–alcohol–water solution. Keeping the pH value of reacted solution is 8–9, the reaction is processed under strong stirring. After reaction, the product is centrifuged and washed by double distilled water, dried in vacuum oven at 60◦C. This new adsorbent was characterized scanning electron microscopy (SEM), while it surface functional groups was recognized by FTIR analysis. At nano-silver coated AC, the breadth of the tubes was a little broader. There are without the large size particles in the Ag/AC which mean the scale of Ag particles was at nanometer level. The influence of variables including pH, concentration of the dye, amount of adsorbent, contact time and temperature required for efficient removal of DY 12 from 50 mL of 25 µg mL^{-1} sample has been investigated. The system is suitable for quantitative removal of this dye from such solution at pH 1 using 0.005 g SNPC, equilibrium time of 9.5 min even temperature of 50 °C. The graphical correlation of various adsorption isotherm models like, Langmuir, Freundlich and Tempkin have been carried out for this adsorbent. Calculation of various thermodynamic parameters such as, Gibb's free energy, entropy and enthalpy of the on-going adsorption process indicate feasibility and endothermic nature of Direct Yellow 12 adsorption on all adsorbents. The kinetic studies suggest the process following pseudo second order kinetics and involvement of particle diffusion mechanism

Conclusion

The silver nano particle loaded on active carbon is identified to be an effective adsorbent for the removal of DY 12 from aqueous solutions. It was observed that batch sorption using SNPC was dependent on parameters such as initial concentration of dye, time, pH, dose of adsorbent and type of dye. The equilibrium and kinetic studies were made for the adsorption of dyes from aqueous solutions onto DY 12. Adsorption parameters for the Langmuir, Freundlich and Temkin isotherms were determined and the equilibrium data were best described by the Langmuir model. The process is endothermic in nature and its kinetics can be successfully fitted to pseudo-second-order kinetic model. The results of the intraparticle diffusion model suggested that intraparticle diffusion was not the only rate controlling step.

References

[1] M. Arami, N. Y. Limaee, N. M. Mahmoodi, N.S. Tabrizi, J. Colloid Interface Sci. 288 (2005) 371–376.

[2] F. D. Ardejani, K. H. Badii, N.Y. Limaee, N.M. Mahmoodi, M. Arami, S.Z. Shafaei, A.R. Mirhabibi, Dye Pigm. 73 (2007) 178–185.

14th Iranian Physical Chemistry Conference
University of Tehran, Kish, February 25-28, 2011

Synthesis of nanozeoliteNaX and application of it in photodegradation of mixture of methylen blue and rhodaminB dyes

A. Nezamzadeh-Ejhieh[a*] and M. karimi-shmsabadi[a]

[a]Department of chemistry, Islamic Azad University, Shahreza Branch

Email: Maryamkarimi54@yahoo.com

Keyword:Nanozeolite,CuO/X nanozeolite, photocatalyst.

Introduction

Zeolites are a class of microporouscrystallin solids and have been widely used as catalysts, adsorbents and ion-exchengers,because of their superior thermal/hedrothermal stability, stronga acidity, good shape-selectivity and high ion-exchange capacity.In recent years, zeolites have been used as efficient photocatalystsin the degradation of various environmental pollutants. The nanometer-dimension zeolite can have different properties than their micrometer sized counter parts. The reduction of the particle size from the micrometer to the nanometer scale can change the mass and heat transfer resistances in catalytic.Zeolite nanoparticles have large external surface areas and high surface activityThe treatment of highly colored wastewater containing hazardous industrial chemical effluents is one of the growing needs of the present time. Heterogeneous photocataiysis is abranch of advanced oxidation processes (AOPs) white transform the toxic organic pollutants in to nontoxic products like CO_2 and H_2O[1-5].

In this study CuO/X nanozeolite was synthesised and used as a heterogeneous photocatalyst in photodegradation of mixture of methylen blue and rhodaminB.

Experimental

1. Materials

$Cu(SO_4)_2 \cdot 6H_2O$, NaOH, TEOS and $Al(OH)_3$all from Merck were used as sources of catalyst synthesis.The methylene blue and rhodamin B were used as organic pollutants and purchased from Merck Company.

2. Preparation of photocatalyst and Characterization

The nanometer size faujasitezeoliteX was synthesized by hydrothermal crystalyzation. Aluminosilicate gel was prepared by mixing aluminate and silicate solusionstogather in the molar ratio,$5.5Na_2O$:$1.0Al_2O_3$:$4.0SiO_2$:$190H_2O$. First 250 ml plastic bottel containing freshly prepared sodiumaluminat solution and a stirring bar was immersed in to an ice-water bath. The mixture was cooled for 1h withstirring. Next a mesured amount of TEOS was added.Stirring was continued at $0^{\circ}C$ for 6h and then at room temperature for another 24h.Hydrothermal crystalyzation was conducted at $60^{\circ}C$ for 4 day. The powdered products were recovered with centrifugation,washed with DI water unitl pH <8 and then dried at room temperature for 24h[2].For ion-exchange experiments 4 g nanozeoliteNaX powder was added to 100 ml of 0.2 M Cu^{2+}solusion and shaked for 24h. The sample was filtered off, washed with water and dried at $100^{\circ}C$. For preparation of CuO/Xnanozeolite the obtained product was calcinated in air at $450^{\circ}C$ for 12h.

Synthesizednanozeolitewas characterized by X-ray powder diffraction (XRD) patterns, using a X-ray diffractometer and 2θ rang of 5-70.

3.Photocatalyticdecolorization experiments

Photodecolorization of MB and RB were conducted in the third months of summer under the direct irradiation of sunlight.Spectrophotometric analysis of samples before and after irradiation process was used to measure the decolorizationefficiency of the dyes.

Resultsand discussion

The XRD pattern of synthetic nanozeoliteNaXshow the characteristic lines at 2θ values of 6.2, 10, 15.6, 23.5, 26.8, 31.By use of Sherrer's equation the average particle size was foundto be5-10 nm.

The catalyst amount is one of the major kinetic factor of photocatalyticdecolorization reactions.To determine the optimal amount of catalyst, experiments were carried out with varying amount of CuO/Xnanozeolite (from 0.1g/l -10g/l).The opteinedreasults showed that, incresing in catalyst mass up to 10g/l, causes a decrease in degradationefficieny. Effect of other experimented parameters such as pH and concentration of dyes, was investigated and satisfactory resultes were optained.

Kinetic of reaction

In this reaserch the first order kinetic model was used to investigation of photodegradation kinetic as expressed in the following equation:

$$-\mathrm{Ln}(\frac{C_t}{C_o}) = K_p t$$

where C_o and $C_t$are respectivily the concentration of substrate at time zero and time t(s) and K_P the first-order rate constant (s^{-1}).

References

[1]Hang, Y.; Wang, K.; Dong, D.; Li, D. Micropor. Mesopor.Mater.**2010**, 127, 167-175.

[2]Zhan,B.; White, M.; Lumsden, M. Chem. Mater.**2002**, 14, 3636-3642.

[3]Vuong, G.; Hoang, V.; Nguyen, D.; Do, T.Appl. Catal. A. Gen. **2010**, 382, 231-239.

[4]Hsu, H.; Selvin, R.; Roselin, L, React. Kinet.Catal.Lett.**2009**, 98, 265-272.

[5]Nezamzadeh-Ejhieh, A.; Hushmandrad, Sh. Appl. Catal. A. Gen. **2010**, 388, 149-159.

14th Iranian Physical Chemistry Conference
University of Tehran, Kish, February 25-28, 2011

Structural, compositional, and optical properties of nanostructured SnS thin films prepared by chemical bath deposition method

R. Sahraei[a,*], A. Karimi[a,b], A. Daneshfar[a], N. Shokri[a,b] and S. Shahriyar[c]

[a]*Department of Chemistry, University of Ilam, Ilam ,Iran*

[b]*Department of Chemistry, Payam-e Nour University, Urmia, Iran*

[c]*Department of Chemistry, Science and Research Branch, Islamic Azad - Khozestan-Iran*

[*] *(Email: reza_sahrai@yahoo.com)*

Keywords: Nanostructures, SnS thin films, Chemical deposition, Optical properties

Introduction

Considerable efforts have been made in recent years in the search for low-cost materials for solar energy conversion [1]. Tin sulfide (SnS) is one of the promising materials for low cost thin film solar cells technology thanks to its optimum energy band gap (E_g) and a high absorption coefficient [2]. Chemical bath deposition (CBD) has been a more attractive technology which is well suited for large area coating, low temperature processing and low process cost [3]. In this work, we have used CBD method for obtaining nanostructured SnS thin film and investigated the composition, nanocrystalline structure, surface morphology and optical properties.

Experimental

The deposition bath contained 10 ml of 0.1 M Sn(II), 10 ml of 1M tartaric acid, 10 ml of 0.1 thioacetamide. The pH of the solution was adjusted to 8 by adding 1:1 NH_3. Final volume of the solution was made to 100 ml by adding distilled water. The time of deposition process was set for 7 h. The structural characterization of the film was performed by scanning 2θ in the range of 10-80˚. The morphology and composition of thin films were studied by a Cam Scan MV 2300 scanning electron microscope (SEM). Transmission and absorption spectra were obtained by means of Cary 300 Bio spectrophotometer.

Results and discussion

The XRD spectrum of the SnS film deposited in to the glass substrate is shown in figure 1 (left). The four peaks observed in the diffractogram at around 26.63˚, 30.87˚, 44.24˚ and 52.38˚ reveal a zinc blend lattice structure of SnS (α-SnS phase).

These peaks can be assigned to the planes (111), (200), (220) and (311), respectively, of the zinc blend phase. The average size of the nanocrystalline SnS has been calculated using the Debye-sherrer equation. The average size of the nanocrystalline SnS has been determined from the equation as about 45 nm. Chemical composition of SnS thin films were analyzed by energy-dispersive X-ray analyzer (EDX). EDX analysis indicated that the atomic ratio of S to Sn was ~1.02 for the entire layer deposited. SEM image of the film showed that the film consisted of small uniform grains free of pinholes (fig. 1 (right)). In addition this image shows that, the larger grains are formed from the aggregation of the small grains in surface of the SnS thin film.

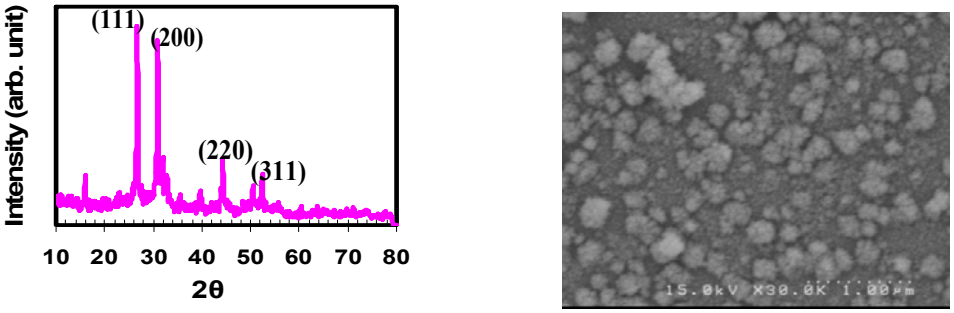

Fig.1: X-ray diffraction pattern of the SnS film deposited on glass substrate (Left) and SEM image of the nanocrystalline SnS thin film on glass substrate (Right).

Optical data show that, our band gap values of deposited SnS thin films are somewhat larger than the typical value of the bulk SnS (1.7 eV). This increase in E_g of SnS films can be attributed to the quantum size effect as expected from the nanocrystalline nature of the SnS thin films.

Conclusions

The salient conclusions arising from this study are summarized below: (i) The composition of the film is much close to the SnS stoichiometry. (ii) The deposited SnS films are nanocrystalline and have a zinc blend structure. (iii) Adherent, mirror like and uniform film with nanocrystalline grains are created on glass substrate.

References

[1] K.T. Ramakrishna Reddy, Materials Research Bulletin, 41 (2006) 414-422.

[2] G. Gordillo, M. Botero, J.S. Oyola, Microelectronics Journal, 39 (2008) 1351-1353.

[3] C.D. Lokhande, Oh-Shim Joo, Current Applied Physics, (2010) 1-45.

14th Iranian Physical Chemistry Conference
University of Tehran, Kish, February 25-28, 2011

Chemical deposition and characterization of nanostructured SnS thin films for application in solar cells absorber materials

R. Sahraei[a,*], A. Karimi[a,b], A. Daneshfar[a], N. Shokri[a,b] and S. Shahriyar[c], A. Goudarzi[d]

[a]*Department of Chemistry, University of Ilam, Ilam ,Iran*

[b]*Department of Chemistry, Payam-e Nour University, Urmia, Iran*

[c]*Department of Chemistry, Science and Research Branch, Islamic Azad - Khozestan-Iran*

[d]*Department of Engineering, University of Gholestan, Aliabad, Iran*

[*] *(Email: reza_sahrai@yahoo.com)*

Keywords: Absorber materials, Nanostructures, SnS thin films, Chemical deposition

Introduction

The synthesis of nanocrystalline metal chalcogenide thin films by chemical bath deposition (CBD) method is currently attracting considerable attention as it is relatively inexpensive, simple and convenient for large area deposition [1]. Tin sulphide (SnS) has a near optimum energy band gap. Therefore SnS films are suitable for absorber layers in solar cells [2, 3]. In this work, we prepared SnS thin films on glass substrates at 75˚ C. The resulting films had more than 70% absorbance in the high wavelengths.

Experimental

The deposition of SnS was carried out by a mixture of 10 ml of 0.1 M Sn(II), 15 ml of 3.7 M triethanolamine, 16 ml of 15 M ammonia, 10 ml of 0.1 M thioacetamide and distilled water. The deposition was carried out at 75˚ C for 45 min. Transmission, absorption and reflection spectra were obtained by means of a Cary 300 Bio spectrophotometer. The thin films thickness was measured by a Dektak profilometer. The X-ray diffraction (XRD) analysis was used to determine the nanocrystalline structure of SnS thin films and scanning electron microscope (SEM) was used to observe the microstructure of surface topology.

Results and discussion

Fig. 1 show the transmittance and SEM image of SnS thin films deposited on glass substrates. The average absorbance of SnS films is calculated to be 16, 30 and 70% respectively in the wavelength of 800 nm. Optical transmission spectra of the thin films are observed to be shifted towards the longer wavelength with increasing film thickness. SnS thin films grown here have the energy band gap in the range of 1.85 to 2.25 eV. Despite the high absorbance and appropriate thickness of the SnS thin films, these films had good nanocrystalline structure.

The XRD pattern was obtained by scanning 2θ in the range of 10-80˚. The four peaks observed in the diffractogram at around 26.63˚, 30.87˚, 44.24˚ and 52.38˚ reveal a zinc blend lattice structure of SnS. The thickness of the films was about 880 nm.

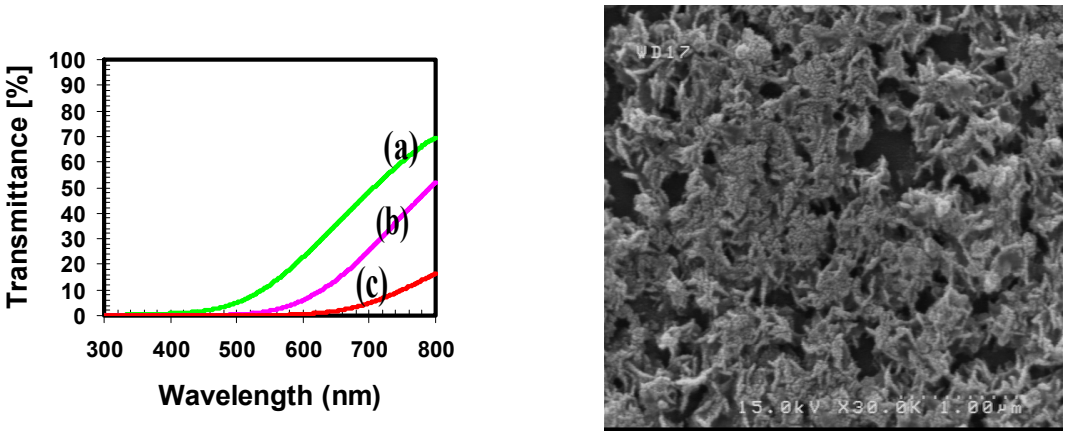

Fig.1: Optical transmittance spectra for the nanocrystalline SnS films deposited in 15 min (a), 30 min (b), and 45 min (c) (Left) and SEM image of the nanocrystalline SnS thin film with thickness 880 nm (Right).

Conclusions

Nanocrystalline SnS thin films with thickness of about 880 nm were deposited on glass substrate at 75˚ C by a chemical bath deposition technique. These thin films by having an optical absorbance about of 70% can be studied as absorber layers which are an important part of the solar cells.

References

[1] C.D. Lokhande, Oh-Shim Joo, Current Applied Physics, (2010) 1-45.

[2] C. Gumus, E. Guneri, C. Ulutas, Applied Surface Science, 257 (2010) 1189-1195.

[3] David Avellaneda, Guadalupe Delgado, Thin Solid Films, 515 (2007) 5771-5776.

ZnO nanoparticles: An efficient and versatile reagent for synthesis of triazole derivatives

Mohammad Kamali, Bahareh Sadeghi*
Department of Chemistry, Islamic Azad University, Yazd Branch, P.O. Box 89195-155, Yazd, Iran
Corresponding author E-Mail: bsadeghia@gmail.com

Keywords: Triazole, Solid acid, Nanoparticles, ZnO.

Introduction:

Click reaction established by Sharpless and co-workers is an efficient tool for the preparation of wide-ranging organic compounds [1,2]. The cycloaddition of azides to alkynes is one of the most important synthetic routs to 1H-[1,2,3]triazoles. N-heterocyclic compounds such as [1,2,3]-triazoles may display biological activities like anti-HIV, anti microbial activity and more [3]. [1,2,3]-Triazoles have also found wide use in industrial application such as dyes, corrosion inhibition, photo stabilizers, photographic materials and agrochemicals [4].

Methods:

Materials

All commercially available chemicals were obtained from Merck and Fluka companies, and used without further purifications.

Preparation of ZnO nanoparticle

Aqueous solutions of zinc nitrates and urea were added into a flask under vigorous stirring (300 rpm/min). The molar ratio of Zn^{2}+ to urea was about 1:4. In order to inhibit the growth of the ZnO crystallite during the course of precipitation, a certain amount of surfactant (SDS), was added into reaction system. Then the reaction system was heated to 95^{o}C and maintained at that temperature. After stirring for 2 h, a semitransparent zinc hydroxide colloid was obtained. The precipitates were then filtered, washed with distilled water and alcohol for three or four times, dried in air at 80^{o}C, and finally calcined at 350^{o}C for 2 h to achieve samples with 30-50nm particle size.

General procedure for triazoles synthesis

azides (1 mmol), phenylacetylene (1 mmol) and solvent (EtOH:H_2O, 1:1) in the presence of ZnO NPs (0.0009 g) were placed in a round bottom flask. The materials were mixed at room temprature. The progress of the reaction was followed by TLC (*n*-hexane:ethylacetate). After the completion of the reaction, the mixture was filtered to remove the catalyst. By evaporation of the solvent, the crude product was recrystallized from hot ethanol to obtain the pure compound. All products are known and were identified by comparison of their physical or spectral data with those of authentic samples.

Results and discussion:

In continution of our investigation about application of solid acids in organic synthesis [5,6] we investigated the synthesis of triazoles in the presence of ZnO NPs as a inorganic solid acid. To optimize the reaction conditions, the reaction of 4-nitrobenzoazide and phenylacetylene was used as a model reaction to triazoles synthesis . According to the obtained data, using the ZnO NPs (0.0009 g) under solvent (EtOH:H_2O) at room temprature is the best condition for the triazoles formation.

Therefore, some azides with phenylacetylene were subjected to triazoles (Scheme 1).

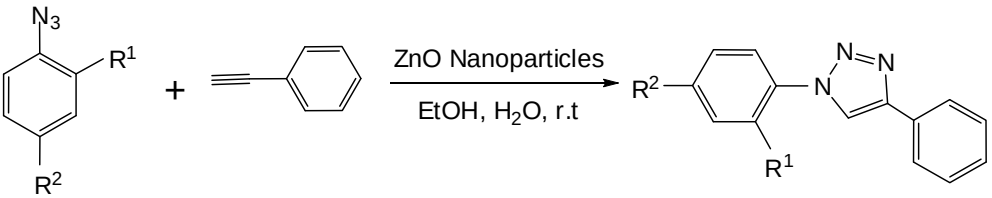

R^1:CH_3, H

R^2: NO_2, Cl, OCH_3, CH_3, H

Scheme 1

Conclusion:

In this work we report a mild procedure for the synthesis of different [1,2,3]-triazoles by solid phase acidic catalyst with improved yields. In summary, we have developed a new and high efficient, one-pot selective method for synthesis of [1,2,3]-triazoles in the presence of nano-catalyst with good to excellent yield of reaction.

References:

[1] Kolb, H. C.; Finn, M. G.; Sharpless K. B. *Angew Chem Int Ed.* **2001**,*40*, 2004.

[2] Rostovtsev, V. V.; Green, L.G.; Fokin, V.V.; Sharpless, K. B. *Angew Chem Int Ed.* **2002**, *41*, 2596.

[3] Velazquez, S.; Alvarez, R.; Perez, C. *Antivir. Chem. Chemother*. **1998**, *9*, 481.

[4] Fan, W. Q.; Katritzky, A. R. In comprehensive heterocyclic chemistry II; Katritzky, A. R.; Rees, C. W.; Scriven, E. F. V. Eds.; Elsevier Science; Oxford, **1996**; vol. *4*, pp 1-126.

[5] Sadeghi, B.; Mirjalili, B F.; Hashemi, M.M. *Tetrahedron Lett*. **2008**, *48*, 8554.

[6] Mirjalili, B F.; Hashemi, M.M.; Sadeghi, B.; Emtiazi, H. *J. Chin. Chem. Soc,*. **2009**, *56*, 386.

Chemically-deposited nanocrytalline CdTe films for solar cells

Azam Karimi[1], Ghaffar Motedayen Aval[1], Alireza Goudarzi[2*], Reza Sahraei[3]

[1]Department of Physical Chemistry, Tarbiat Moallem University, 49 Mofateh Ave., Tehran, Iran

[2]Department of Polymer Engineering, Golestan University, Gorgan, Iran

* Email address: a.goudarzi@gu.ac.ir

[3]Department of Chemistry, University of Ilam, Ilam, Iran

Introduction:

Thin film solar cells using CdTe semiconductor absorber Layers are one of the primary candidates for large-scale commercialization of photovoltaics. CdTe also is a very promising material for use in optoelectronic and photovoltaic devices because of its optimum band gap (ca. 1.45 eV) for energy solar conversion and its high optical absorption coefficient ($>10^4$ cm^{-1}). CdTe thin films can be fabricated by several methods, such as physical vapor deposition (PVD), electrodeposition, spray pyrolysis, R.F. sputtering, chemical bath deposition (CBD), and etc.[1-2]. Among these methods the chemical bath deposition (CBD) method has not lent itself to the preparation of CdTe thin films. M. Sotelo-Lerma and co-workers have mentioned that the main reasons for the lack of success in the preparation of CdTe films by chemical reaction in an aqueous solution have been the oxidative instability of aqueous solutions containing the telluride ion [2]. In this study, the CdTe thin film was prepared by CBD method in two steps and solved oxidation problem of telluride ion in aqueous solutions.

Method:

In a 250 ml beaker was added 20 ml of aqueous 1 M $CdCl_2.H_2O$, 37 ml of aqueous 5 M ammonia and pH was fixed on 11.1. Two clean microscope slides were immersed vertically into the solution and then the container solution was placed in a water bath and the temperature was adjusted on 70˚C. After approximately 20 min, the slides were coated by $Cd(OH)_2$ films. The prepared $Cd(OH)_2$ slides were dried in air for 24 h .In next step, we used NaHTe solution as the telluride source. The method for preparation of NaHTe solution was described elsewhere [3]. A Cd $(OH)_2$ coated slide was immersed in the prepared telluride

solution. The flask containing the coating solution and the slide is immediately transferred to a water bath kept at 70°C. In all steps, the N_2 bubbling was continued. The coated slide with Cadmium Telluride was removed after 5 min, washed with distilled water, dried in air atmosphere at. 150˚C for 24 h, and then characterized by XRD, ATR-FTIR, SEM, EDX, and Uv-Vis. spectrophotometer.

Results and discussion:

The XRD patterns of the annealed film showed four diffraction peaks at 2θ values of approximately 24, 40, 47, and 63, which correspond to the diffraction lines produced by the (111), (220), (311) and (331) crystalline planes of cubic CdTe. On the basis of the full width at half-maximum (FWHM) of (111) peak and applying the Debeye-Scherrer equation,[1] the average nanocrystallite size of the as-prepared and annealed CdTe films was estimated to be 4.4 and 7.7 nm, respectively. The film surface morphology was studied by SEM. The SEM image showed that the film compactness is high, the surface's uniformity is good, and the particle size distribution is also narrow. The prepared CdTe films had more quality than the CdTe films which had been prepared by others [3].The optical band gap value of the as-deposited CdTe thin film was obtained 1.46 eV by using the absorption data .The obtained band gap energy is in excellent agreement with reported values [3].For more investigation about the formation of CdTe film by CBD method, we have obtained the ATR_FTIR spectrum of one of the CdTe films in the region of 50-4000 cm^{-1} at room temperature. The attenuated total reflection-Fourier transform infrared (ATR-FTIR) spectrum of the prepared CdTe film revealed an strong and sharp band at 146.0 cm^{-1} which is assigned to the vibration frequency of CdTe nanocrystals.

Conclusions:

We have prepared successfully CdTe thin film on glass substrate by using CBD method in two steps. The prepared CdTe films were smooth and adhered tightly to the substrates.The XRD patterns exhibited the cubic zinc blend structure for CdTe thin films. The calculated band gap energy from optical absorbance date was 1.45 eV which is related to the direct band

gap of the CdTe. The ATR-FTIR spectrum showed a strong and sharp band related to vibrational mode of CdTe.

References:

[1] A. Goudarzi, G. Motedayen Aval, R. Sahraei, H. Ahmadpoor Thin Solid Films 516 (2008) 4953.

[2] M. Sotelo-Lerma, Ralph A. Zingaro, S.J. Castillo , J., Organometallic Chem., 623 (2001) 81–86

[3] V.B. Patil*, D.S. Sutrave, G.S. Shahane, L.P. Deshmukh, Thin Solid Films 401 (2001) 35–38

14th Iranian Physical Chemistry Conference
University of Tehran, Kish, February 25-28, 2011

GREEN SYNTHESIS, STRUCTURAL CHARACTERIZATION, AND OPTICAL PROPERTIES OF ZINC OXIDE NANOPARTICLES

Elaheh K. Goharshadi[1,2,*], Maryam Abareshi [1], Roya Mehrkhah[1], Sara Samiee[1], Majid Moosavi[3], Abbas Youssefi [4], and Paul Nancarrow [5]

[1] Dept. of Chemistry, Ferdowsi University of Mashhad, Mashhad 91779, Iran

Email: gohari@ferdowsi.um.ac.ir

[2] Center of Nano Research, Ferdowsi University of Mashhad, Mashhad 91779, Iran

[3] Dept. of Chemistry, Faculty of Sciences, University of Isfahan, Isfahan 81746-73441, Iran

[4] Par-e-Tavous Research Institute, Mashhad, Iran

[5] QUILL Research Centre and School of Chemistry and Chemical Engineering, Queen's University Belfast, UK

Keywords: Green synthesis, Ionic liquid, Nanomaterials, Zinc oxide, Semiconductor

Introduction

ZnO is an important wide band-gap (3.37 eV at room temperature) semiconductor with a large exciton binding energy (60 meV) [1]. As a versatile, multifunctional, and smart material, it has been extensively used in several industrial products such as white paints, ceramics, food additives, catalysts, electronic materials, spintronics, and biomedical applications [2].

By combining the advantages of both room temperature ionic liquid (RTILs) and microwave heating, we have developed a new microwave-assisted ionic liquid (MAIL) method for the fast controlled green synthesis of ZnONPs. The fabricated ZnONPs were characterized by X-Ray diffraction (XRD), transmission electron microscopy (TEM), UV-vis, and IR spectroscopy.

Results and discussion

Figure 1 shows the XRD pattern of ZnO nanopowders. All the peaks can be indexed to the known hexagonal wurtzite structure of ZnO with lattice constants of a = b = 3.242 Å, and c = 5.205 Å (JCPDS 89-1397). The strong intensity and narrow width of ZnO diffraction peaks

indicate that the resulting products are of high crystallinity. Figure 2 shows the TEM image of ZnONPs after 5 min irradiation with microwave.

Optical responses of the ZnO nanoparticles dispersed in ethylene glycol have been investigated via UV-vis absorption spectroscopy. The UV–vis absorption spectrum of the ZnO nanoparticles dispersed in EG exhibits an excitonic absorption feature at around 336 nm, which is blue shifted of about 39 nm with respect to the bulk absorption edge (appearing at 375 nm at room temperature). The direct interband transition energy of 3.40 eV was calculated using the UV-vis spectrum.

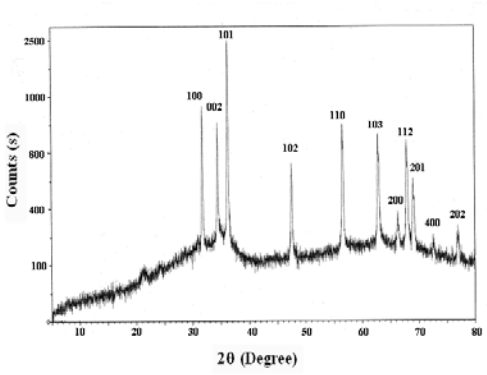

Fig. 1. XRD pattern of the ZnONPs.

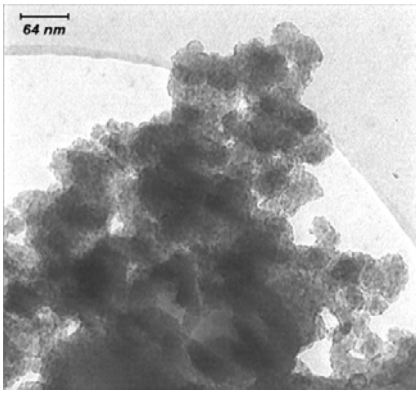

Fig. 2. TEM image of ZnONPs.

Conclusions

A convenient microwave method, which is friendly to environment, has been developed in preparation of ZnONPs. Microwave irradiation along with RTIL accelerate the formation of ZnO nanoparticles. The ZnONPs were characterized by XRD, TEM, UV-vis, and IR spectroscopy. The XRD pattern reveals that the ZnONPs have hexagonal wurtzite structure. The strong intensity and narrow width of ZnO diffraction peaks indicate that the resulting nanoparticles are of high crystallinity. The synthesized ZnONPs show direct band gap of 3.40 eV. The UV-visible absorption spectrum of ZnONPs dispersed in ethylene glycol at room temperature revealed a blue–shifted onset of absorption.

References

[1] Wan Q., Li Q. H., Chen Y. J., Wang T. H., He X. L., Li JP, Lin C. L. , *Appl. Phys. Lett*. **2004**; 84:3654.

[2] Ghule K., Ghule A. V., Chen B. J., Ling Y. C., *Green Chem.* **2006;**8:1034.

14th Iranian Physical Chemistry Conference
University of Tehran, Kish, February 25-28, 2011

Theoretical Study of Free Energies of Electron Transfer of *p*-Phenylenediamine Derivatives With Fullerenes in Nanostructure of [R].C_n Supramolecular Complexes

Avat (Arman) Taherpour* and Parastou Sadat Lajevardi
Chemistry Department, Faculty of Science, Islamic Azad University,Arak Branch
P. O. Box 38135-567, Arak, Iran
avatarman.taherpour@gmail.com & ataherpour@iau-arak.ac.ir

Abstract:

The *p*-phenylenediamine derivatives have shown the important electron-transfer properties. Topological indices are purported to correlate chemical structures with various chemical and physical properties. They have been successfully used to construct effective and useful mathematical methods to establish clear relationships between structural data and the physical properties of these materials. The relationship between the number of carbon atoms and the free energies of electron transfer ($\Delta G_{et(1)}$ to $\Delta G_{et(4)}$) are assessed using the electron transfer (ET) equation for **A-1** to **A-5** and **B-1** to **B-5** supramolecular [R].C_n (R= TMDAD and DHDAP) complexes.

Keywords: Fullerenes, *p*-Phenylenediamine, Electron transfer.

Introduction:

The *p*-phenylenediamine derivatives have important electron-transfer properties. The structures of four representative *p*-phenylenediamines to the discussion are: dodecahydro-3a,9a-diazaperylene (DHDAP) and *N,N,N,'N'*-tetramethyl-3,6-diaminodurene (TMDAD).[1] This class of compounds had been considered in electrochemical studies [1,2] and photoinduced electron transfer.[1] The various derivatives of *p*-phenylenediamine have demonstrated the typical pattern of lower redox potentials as the degree of methylation increases.[1]

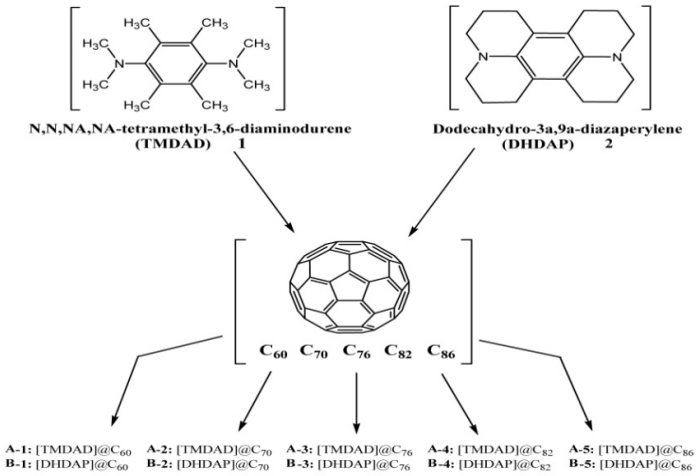

Mathematical Method:

All graphs were generated using the *Microsoft Office Excel 2003* program. Using the number of carbon atoms contained within the C_n fullerenes, several valuable properties of the fullerenes can be calculated. This study elaborates upon the relationship between the number of carbon atoms and the four free energies of electron transfer ($\Delta G_{et(1)}$ to $\Delta G_{et(4)}$) of fullerenes C_n (n= 60, 70, 76, 82 and 86) with TMDAD and DHDAP, on the basis of the four reduction potentials ($^{Red.}E_1$ to $^{Red.}E_4$) of the fullerenes, as assessed by applying the electron transfer (ET) equation. The ET equation estimates the free energy change between an electron donor (D) and an acceptor (A). There was good agreement between the calculated and the predicted values.

Results and Discussion:

Here, was calculated four free energies of electron transfer ($\Delta G_{et(1)}$ to $\Delta G_{et(4)}$) of other supramolecular complexes of this class of electron-transfer radicals, i.e. TMDAD and DHDAP, as the most well-known redox systems and fullerenes C_n (n=60, 70, 76, 82 and 86), which create [TMDAD].C_n, and [DHDAP].C_n. The related curves for [DHDAP].C_n, **B-1** to **B-5** have similar structures to Fig.1 (**a-d**) [TMDAD].C_n **A-1** to **A-5** .

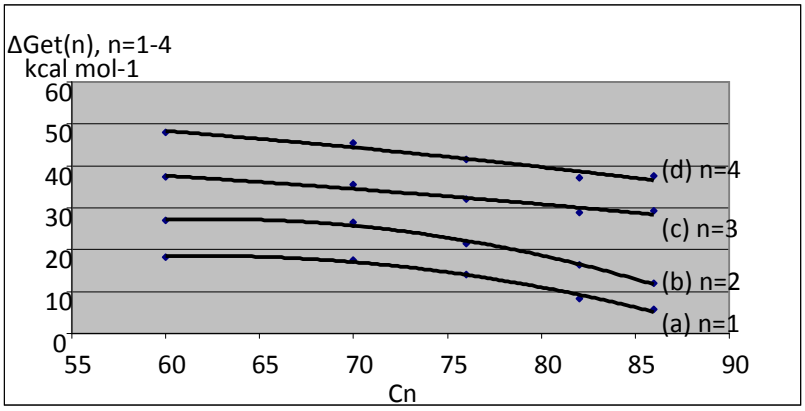

Figure-1: The relationship between the number of carbon atoms in the fullerenes and the free-energies of electron transfer of [TMDAD].C_n, compounds **A-1** to **A-5**.

Conclusion:

TMDAD and DHDAP with fullerenes have important electron-transfer properties as the most well-known redox systems and molecular conductors. The electrochemical data of selected *p*-phenylenediamine derivatives were reported here. These include the four free-energies of electron transfer ($\Delta G_{et(1)}$ to $\Delta G_{et(4)}$), calculated using the electron transfer (ET) equation. The novel supramolecular complexes discussed have neither been synthesized nor reported previously.

References:

[1] A. Monem, M. Rawashdeh, C. Sotiriou-Leventis, X. Gao and N. Leventis, *Chem. Commun.*, 2001, 1742–1743.

[2] B. A. Kowert, L. Marcoux and A. Bard, *J. Am. Chem. Soc.*, 1972, 94, 5538.

14th Iranian Physical Chemistry Conference
University of Tehran, Kish, February 25-28, 2011

DFT and ab initio study of Cycloaddition Reactions Between C_{28} and Buta-1, 3-diene

H. Mohammadzadeh Bahar*,S. Abedini Khorrami and Sh. Moradi
Faculty of Chemistry, Islamic Azad University, North Tehran Branch, Iran
Bahar.mohamadzadeh@gmail.com

Keywords: Nano structures of Fullerene; C_{28}; DFT calculations; cycloadditions, Ab initio

Introduction:

Cycloaddition reaction between C_{28} and buta-1, 3-diene was studied within the framework of DFT/B3LYP level. In cycloaddition reactions the [6,6] double bonds of C_{60} exhibit a dienophilic character [1]. A large variety of cycloadditions have carried out with C_{60} and the complete characterization of the products, mainly monoadducts, has greatly increased our knowledge of fullerene chemistry[2]. These chemical transformations also provide a powerful tool for the functionalization of the fullerene sphere. Almost any functional group can be covalently linked to C_{60} by the cycloaddition of suitable addends. Some types of cycloadducts exhibit a remarkable stability; for example, they can be thermally treated up to 400 °C without decomposition[3]. This is an important requirement for further side-chain chemistry as well as for possible applications of the new fullerene derivatives, which may be of interest due to their biological activity or as new materials[4-5].

The symmetrical structural of the C_{28} molecules and different position for cycloaddition cause choosing for these calculations. In this calculation cycloaddition reaction on some different position of double bond in C_{28} with butadiene (fig. 1) carried out and simulated by ab initio calculations. The stability of energy, reaction pathway, transition state and thermodynamics properties for these additions for all situations calculated in different temperatures .

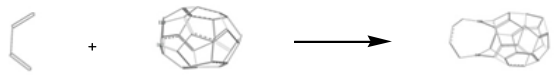

Fig.1. AM1 optimized geometry structures of product, C_{28} and Buta- 1, 3 –diene Methods:

In the present treatise, the geometry optimizations of all the structures leading to energy minima were achieved by using B3LYP self-consistent fields molecular orbital (SCF MO) method at the restricted DFT level. The initial geometry of butadiene and C_{28} structures was excerpted from Gauss View. All these calculations were performed by using Gaussian 98.

C_{28} have two valence isomers that we calculated reaction pathway and transition state and intermediate structure in cycloaddition reaction for each different position of double bond in each two valance isomer reaction pathway scanned step by addredundant key words.

Results and Discussion:

The pathaway reaction diagram and some thermodynamic geometry parameters of C_{28} and butadiene for a position at different temperatures are show in diagram 1 and Table 1.

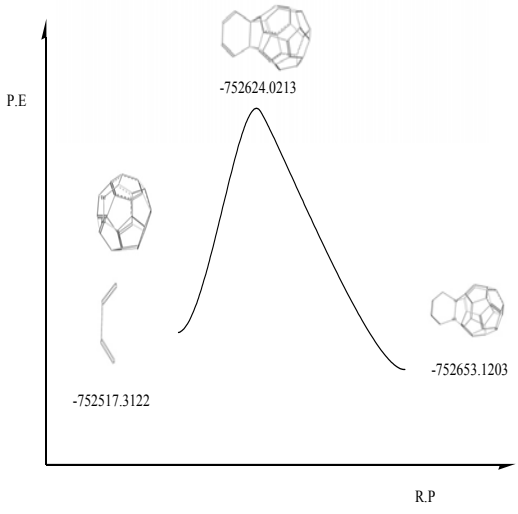

Diagram1: The pathaway reaction of C_{28} and butadiene

Table1. Some thermodynamic geometry parameters of the cycloadditions presently considered for a structure at different temperatures

	298.15	303.15	308.15	313.15	318.15
ΔG(Kcal/Mol)	-22.9298	-22.673	-22.4389	-22.2049	-21.9695
ΔH(Kcal/Mol)	-37.8281	-37.8434	-37.8648	-37.8979	-37.9132
ΔE(Kcal/Mol)	3.545	3.5237	3.5003	3.4771	3.4445
ΔS(Kcal/Mol.K)	-0.049968	-0.0499043	-0.04983195	-0.04974955	-0.04966721
ΔC_V(Kcal/Mol.K)	0.002547	0.002584	0.0026215	0.0026582	0.0026947
ΔZPVE(Kcal/Mol)	3.9390	3.9390	3.9390	3.9390	3.9390
ΔHF(Kcal/Mol)	-40.7812	-40.7812	-40.7812	-40.7812	-40.7812

Table 1 show that the ΔG increased with increasing the temperature and show that reaction between C_{28} and C_4H_6 at high temperatures are more exothermic and unstable.

Conclusion:

There are two status of double bond in structure of C_{28} that are completely different from each other. Cycloaddition is selected as a main part of reaction and addition process for single stage is considered. Thermodynamics parameters and stability energy are evaluated in different temperatures. The new cycle that produced after cycloaddition reaction was opened and created a new cycle with large size. two positions of double bond that lead to two products are strongly different. The structure that contain much resonance loop and the most double bond in resonance form was stable than that others, in the other hand these results completely Confirmed thermodynamics results that obtained from calculations.

References:

[1] F. Wudl, A. Hirsch, K. C. Khemani, T. Suzuki, P. M. Allemand, A. Koch, H. Eckert, G. Srdanov, H. M. Webb, ACS ymp. Ser. 1992, 486, 161.

[2] M. A. Yurovskaya, I. V. Trushkov, Russ. Chem. Bull. 2002, 51, 367. 3 S. R. Wilson, D. I. Schuster, B. Nuber,

[3] M. S. Meier, M. Maggini, M. Prato, R. Taylor, Full.: Chem., Phys. Technol. 2000, 91.

[4] B. Krcutler, J. Maynollo, Tetrahedron 1996, 52, 5033.

[5] F. Langa, P. de la Cruz, E. Espildora, J. J. Garcia, M. C. Perez, A. de la Hoz, Carbon 2000, 38, 1641.

Isothermal cure kinetics of epoxy silicone –nickel-diamine system

Hamid JavaherianNaghash, Monireh Mohammad Salehi Darani, Bahman johari
Dpartment of chemistry,Islamic Azad University,Shahrezal Branch
Email:salehi.monire@yahoo.com

Introduction:

Epoxy silicone resin is widely used for the matrix of compositesand electronic components owing to its excellent adhesive and dielectric properties. During curing, epoxy silicone resins display extensive branching, passing throughthe gel-point before the formation of macromolecular structures. During the isothermal reaction, two critical phenomena can take place gelation and vitrification.Vitrification is the transformation from liquid or rubbery material to a glassy state. At vitrification, the material solidifies, and the chemical reactions can be arrested.Cure kinetics models are generally developed by analyzing experimental results obtained by different thermal analysis techniques. In the first part of this work we have studied non-isothermal cure kinetics and mechanisms of epoxy silicone resin with the same curing agent. In this study we have reported kinetic and thermodynamic parameters on the epoxy silicone / (diethylenetriamine) 2NiI2 cure under isothermal conditions.

Experimental:

Synthesized a silicone containing diol by reaction of polybutylene glycol and dimethyl dichlorosilane in the presence of phosphoric acid and toluene at reflax temperature. Then the obtained silicone containing diol was reacted with diglycidyl ether of bisphenol A (DGEBA) in the presence of phosphoric acid at reflax temperature during 4h .when the epoxy silicone resin synthesis with (diethylenetriamine)2NiI2 were carefully mixed and stirred to produce a homogeneous mixture under nitrogen atmosphere. 4mg of the mixture was placed in an aluminium pan, sealedby using a press and stored in a refrigerator before introducing it into the calorimeter.

1.Kinetic Methods:

−ln tα,i = ln[A(α)/G(α)] − Ea/Rti Eqn (1). applied Eqn (1) to isothermal DSC data to indicate the dependence of Ea on conversion.used the Kamal autocatalytic model to estimate the rate constants and reaction orders of the studied epoxy silicone system. Thermodynamic parameters of curing reaction were calculated using thekinetic parameters and transition state (TS) theory.

Result and discution

Iso-conversional kinetic analysis

Figure 1. shows DSC curves recorded for epoxy silicone cured with (diethylenetriamine)2NiI2 complex at various isothermal temperatures .Table 1 listssome characteristics of the cured epoxysilicone systems. Theoriginal DSC data were transformed into the αi versustime curves at various isothermal temperatures and the corresponding plots are shown in Fig. 2. The reaction rate data were also calculated and plotted versus conversion values (Fig. 3). The maximum rates of reaction at the various isothermal temperatureswere in the conversion range of α = 0.4–0.5, which is characteristic of an autocatalytic reaction mechanism.Model-free iso-conversional analysis was applied totransform the DSC data (Fig. 2) by means of Eqn (1).The corresponding plot of Ea versus conversion is shown in Fig. 4.The average value of activation energy obtained from the isothermal data, 95.1kJmol−1 for the conversion range of α = 0.04–0.6, is ingood agreement with the value obtained undernon-isothermal conditions,102.6kJmol−1.

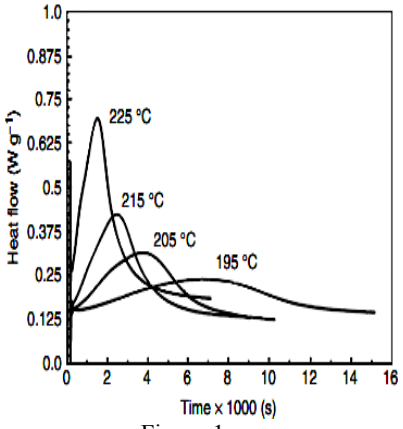

Figure 1.

Temperature (°C)	Cure onset (s)	Peak maximum (s)	ΔH (J g^{-1})
195	300	6913	683
205	270	3656	707
215	237	2480	687
225	226	1294	693

Table 1.

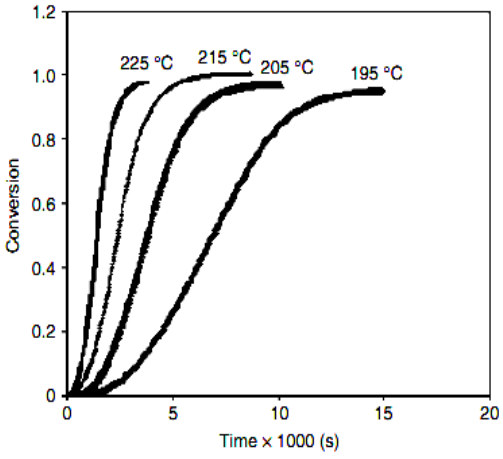

Figure 2.

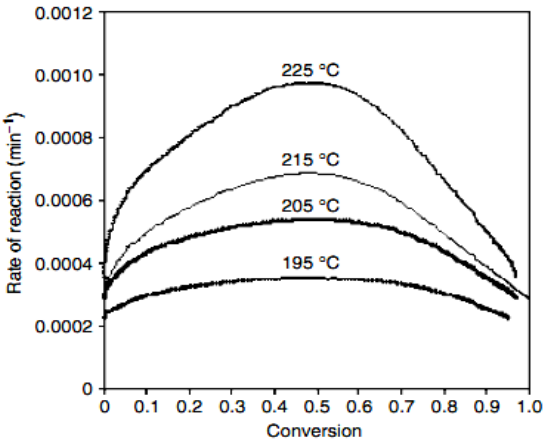

Figure3

Result and discution:

The kinetics and thermodynamic characteristics of a nickel-containing epoxy silicone polymer prepared through curing of epoxy silicone resin with bis-Ni(II)-diethylenetriamine- iodide inorganic curing agent were successfully studied by means of DSC techniques. The method used permitted us to regenerate consistent kinetics results in the form of similar Ea on α dependency derived from the dynamic data. The Kamal autocatalytic model was used to estimate the kinetic parameters of the examined epoxy silicone system [3]. Good agreement between the kinetics and thermodynamic results was also found, indicating that an

autocatalytic reaction mechanism was more favoured than the nth order path at the isothermal cure temperatures used.

Refrence:

[1]PrimeRB, Thermal Characterization of Polymer Academic Press, New York (1981)
[2] Jiang,J.; Zeng,Z.;Pearce,P.;Water,Air and soil pollution,2004,158,53-65.
[3] Kamal MR, Polym Eng Sci 14:231 (1974).
[4]Vyazovkin S andWight CA, Int Rev Phys Chem 17:2294 (1998).
[5]Kurnoskin AV, Polymer 34:1060 (1993).
[6] Kurnoskin AV, Polymer 34:1068 (1993).

14th Iranian Physical Chemistry Conference
University of Tehran, Kish, February 25-28, 2011

Comparison Study of Photocatalytic Properties of Sn doped TiO_2 and TiO_2 nanoparticles in Degradation of Methyl Orange

B. A. Maasoumi[1], M. Rabani [2], L. Ejlali[3], R. mohammadi[2*]

[1] *Organic Research Laboratory, Faculty of Chemistry, Payame noor University, Tabriz Branch, Tabriz, Iran*

[2] *Department of Applied Chemistry, Faculty of Chemistry, Islamic Azad University, North-Tehran Branch, Tehran, Iran*

[3] *Department of Organic Chemistry, Faculty of Chemistry, Islamic Azad University, Tabriz Branch, Tabriz, Iran*

∗ *Corresponding Author's E-mail: rb_mohammadi@yahoo.com*

KEYWORDS Photodegradation; Sn doped TiO_2 nanoparticles; Sol-gel method; Methyl orange

INTRODUCTION

The semiconductor TiO_2 has been proved to be an excellent catalyst in the photocatalytic degradation of organic pollutants. To enhance its photocatalytic activity, TiO_2 is often doped with various metal ions and oxides. [1,2]. In this contribution, Sn doped TiO_2 nanoparticles were synthesized by sol-gel method. The aim of this study was to determine the effects of Sn doping and wavelength of irradiation on the photocatalytic degradation of methyl orange under UV light.

2. EXPERIMENTAL

A mixture of 3 ml distilled H_2O and 6 ml ethanol was added to a mixture of 3 ml

Ti $(OC_4H_9)_4$ and 9 ml ethanol. After 3 h stirring, the sol was allowed to stand for 24 h, dried at 80 ºC for 12 h, and calcined at 450 ºC for 3 h. For the photodegradation studies, two lamps (15W, λ =254 nm and 36 W, λ = 365 nm) were used. Desired amounts of photocatalyst were used for degradation of MeO (0.05mM). Aliquots of the mixture were taken at periodic intervals during the irradiation and after centrifugation they were analyzed with the UV-Vis spectrophotometer at λ_{max} = 477 nm and a calibration curve to determine the residue concentration of methyl orange.

3. RESULTS AND DISCUSSION

3.1. Characterization results

The XRD patterns of synthesized TiO_2 and Sn doped TiO_2 photocatalysts are shown in Fig. 1. The XRD pattern of TiO_2 shows five primary peaks at 25.2^0, 38^0, 48.2^0, 55^0, 62.5^o,68.5^0 and 75^0 which can be attributed to different diffraction planes of anatase TiO_2.

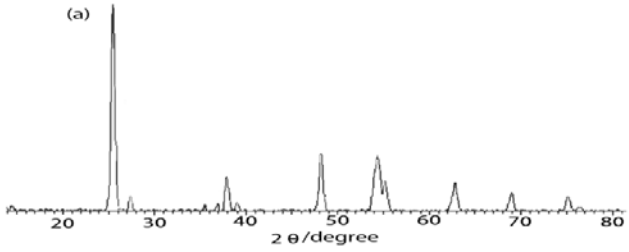

Fig.1. XRD patterns of 0.3mol% Sn doped TiO_2

3.2. The effect of Sn doping on the photocatalytic activity of TiO2 nanoparticles

Results in Fig.2 show that when the Sn content is 0.3mol%, the photocatalyst exhibits higher photocatalytic activity. If the Sn content continuously increases, the photocatalytic activity begins to fall down inversely. It can be reasonably explained by means of limits the amount of light reaching to the TiO_2 surface, reducing the number of photogenerated e^--h^+ pairs and consequently, lowering the TiO_2 photoactivity [3].

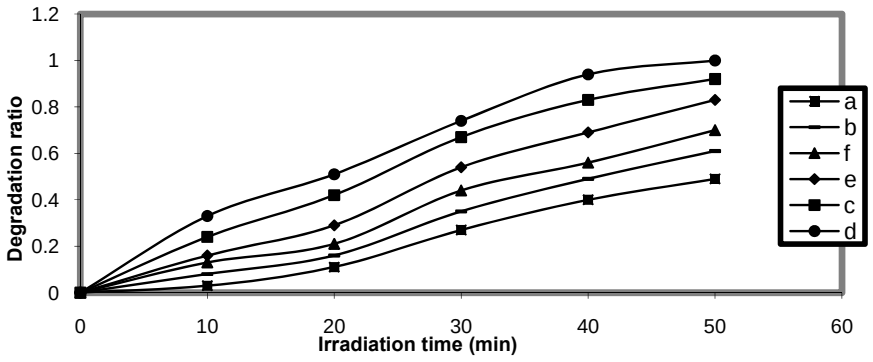

Fig. 2. Influence of Sn content on the photocatalytic activity of photocatalysts at wavelength 254 nm : a) undoped TiO_2, (b) 0.1%, (c) 0.2%, and (d) 0.3%, e) 0.5%, and f) 1% mol Sn doped TiO_2.

3.3. Effect of the source of irradiation

The semi-logarithmic graphs of the concentration of MeO in the presence of 400 mg l^{-1} of doped and undoped TiO_2 vs. irradiation time (Fig.3) yield straight lines indicating pseudo first order reaction. The results showed the MeO decolorization activity of Sn doped TiO2 under irradiation of 254 nm was much higher than irradiation of 365 nm [4].

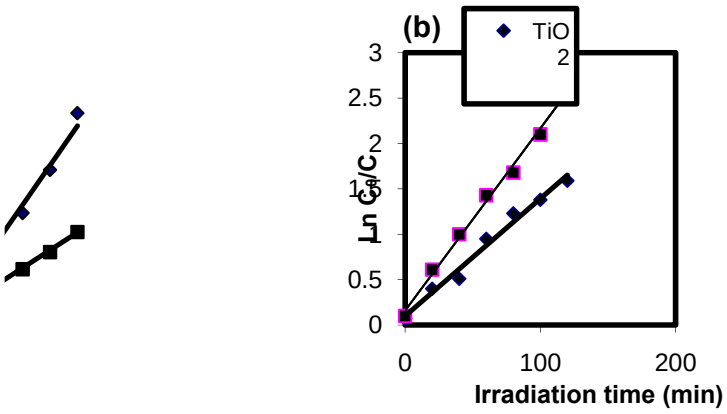

Fig.3. Semi-logarithmic graph of MeO concentration vs. irradiation time in the presence of undoped and Sn doped TiO_2 nanoparticles a) at wavelength 254 nm, b) at wavelength 365 nm.

4. CONCLUSIONS

The photodegradation of MeO has been studied using TiO_2 and Sn doped TiO_2 nanoparticles. Doping an appropriate amount of Sn can improve the photocatalytic activity of TiO_2. The reaction rate of MeO degradation depended on the wavelength of radiation.The shorter wavelength (254 nm) radiation can faster photo degraded MeO in comparison with the longer wavelength (365 nm) radiation.

REFERENCES

[1] L. Kumaresan, M. Mahalakshmi, Ind. Eng. Chem. Res: **49** (2010)1480.

[2] C. Liu, Y. Hsieh, P. Lai, C. Kao, Dyes and Pigments: **68** (2006) 191.

[3] X. Li, R. Xiong, G.Wei, Journal of Hazardous Materials; **164** (2009) 587.

[4] V. tengl1, S. Bakardjieva1, The Open Process Chemistry Journal: **1** (2008)

14th Iranian Physical Chemistry Conference
University of Tehran, Kish, February 25-28, 2011

Doping of Commercial TiO_2-P25 Nanoparticles with Urea and Investigation of Photocatalytic Activity under Visible Light

M.A. Behnajady, Z. Mahmodi* and N. Modirshahla

Department of Chemistry, Faculty of Science, Islamic Azad University, Tabriz Branch, Tabriz, Iran

(Email: z.mahmodi62@yahoo.com)

Keywords: *N-doped TiO_2, Photocatalytic Activity, Visible Light,* C.I. Acid Red 27

Introduction

Advanced oxidation processes (AOPs) are attractive alternatives to non destructive physical water treatment processes which can be applied for degradation of dyes and many organic pollutants in industrial wastewaters [1]. AOPs are able to mineralize aqueous organic contaminants [2]. Semiconductor photocatalysis is a newly developed method among advanced oxidation processes (AOPs), which can be conveniently applied for the degradation of dye pollutants. Many authors have reported that N-doped titanium dioxide, shows a significant catalytic activity in various reactions under visible light irradiation [3]. Sun is an economical and ecological sensible light source. Doping TiO_2 with nonmetals such as nitrogen and sulfur is promising method for enhancing photocatalytic performance of semiconductor nanoparticles under visible light [4]. Increasing photocatalytic activity of titanium dioxide nanoparticles under visible light can be useful for large scale applications of heterogeneous photocatalysis under solar light.

The aim of this study is doping of TiO_2-P25 nanoparticles with urea for preparing N-TiO_2 nanoparticles with high photocatalytic activity in the removal of a model contaminant from textile industry under visible light. Parameters such as weight ratio of urea to catalyst and calcination temperature were investigated for enhancing photocatalytic activity of N-TiO_2 nanoparticles under visible light.

Experimental details

For preparation of nitrogen-doped TiO_2, 1 g TiO_2-P25 powder obtained from Degussa Company was suspended in water; then a proper amount of urea was added at different weight ratio from catalyst to urea (1:1, 1:0.5, and 1:1.5). Prepared suspension was sonicated in an ultrasonic bath (T460H, Windaus) under frequency of 30 kHz for 15 min in order to improve the dispersion of TiO_2-P25 in water. The resultant slurry was refluxed and heated at 70-80˚C for 4 h. Then it was cooled to room temperature and washed several times by de-ionized water. The precipitate was centrifuged, dried at 80˚C for 10 h and finally annealed at 350, 450 and 550˚C for 1 h. Photocatalytic degradation was performed in a bath quartz photo reactor of 100 mL volume with Vis lamp in vertical array, which was placed in front of the quartz tube reactor.

Results

-The XRD patterns of TiO_2 nanoparticles (pure and doped with urea) were shown in figure 1. The XRD pattern of TiO_2 shows five primary peaks at 25.2°, 38°, 48.2°, 55° and 62.5° which can be attributed to different diffraction planes of anatase TiO_2. Four different peaks at 27.5°, 36°, 54°, and 69° can be attributed to different diffraction planes of rutile form of TiO_2. Results about crystallite size and phase content of TiO_2-P25 and N-doped TiO_2-P25 were reported in Table 1.

-The maximum photocatalytic activity of N-doped TiO_2-P25 under visible light irradiation was obtained at TiO_2/urea in weight ratio of 1:1 and calcination temperature of 350˚C.

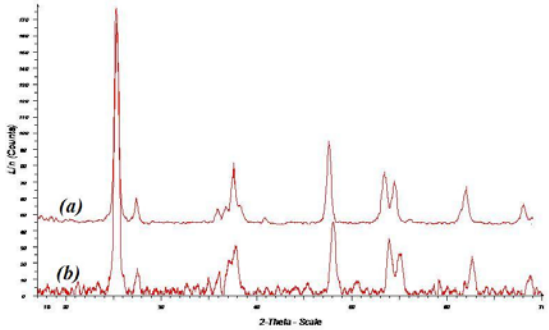

Figure 1: XRD pattern of (a) undoped TiO_2-P25, (b) N-doped TiO_2-P25.

Table 1: Effect of urea doping process on crystallite size and phase content of TiO_2-P25

Type	Phases	Crystallite size (nm)	Crystal structure (%)
TiO_2-P25	Anatase	13	89.36
	Rutile	13	10.64
N-doped TiO_2-P25	Anatase	14	87.36
	Rutile	14	12.64

Conclusion

Doping of TiO_2-P25 nanoparticles with urea produce N-TiO_2 nanoparticles with high photocatalytic activity under visible light. The effect of doping process on crystallite size and phase content of TiO_2-P25 nanoparticles is negligible. The photocatalytic activity of N-TiO_2 nanoparticles reached their maximum when the weight ratio of TiO_2/urea was 1:1 and calcination temperature was about 350˚C.

References

[1]O. Legrini, E. Oliveros & A.M. Braun, *Chem. Rev.* 93 (1993) 671.

[2] M.A. Behnajady, N. Modirshahla, N. Daneshvar & M. Rabbani, *Chem. Eng. J.* 127 (2007) 167.

[3] S. Sato, *Chem. Phys. Lett.* 123 (1986) 126.

[4] J.A. Rengifo-Herrera, E. Mielczarski, J. Mielczarski, N.C. Castillo, J. Kiwi & C. Pulgarin, *Appl. Catal. B* 84 (2008) 448.

Molecular Dynamics Simulation of Melting of Phase Change Materials on Carbon Nanotubes

M. Foroutan, M. Mokhtari

Department of Physical Chemistry, School of Chemistry, College of Science, University of Tehran, Tehran, Iran

mokhtari_mnano@yahoo.com

Keywords: Phase Change Materials, Molecular Dynamics Simulation, Carbon Nanotube, Aalkane.

Introduction

Phase change materials are substances with a high heat of fusion which, melting and solidifying at a certain temperature, is capable of storing and releasing large amounts of energy. It has been shown that paraffins can be considered as phase change materials. In the present work, the melting transition in monolayers of n-dodecane (n-$C_{12}H_{26}$) physisorbed onto the CNT is studied through use of molecular dynamics (MD) simulations.

Simulation details

MD simulations performed at different temperature for systems containing a CNT (5, 5) with length of 50 Å and dodecane alkane, using canonical ensemble. Since each simulation is performed in constant temperature, many simulations are required at different temperatures. Energy minimization was performed to find the thermal stable morphology and achieve a conformation with minimum potential energy for polymer molecules. The velocity form of Verlet algorithm method and the Nose-Hoover thermostat algorithm were used to integrate the equations of motion with a time step of 1.0 fs. A cutoff distance of 10 Å was used for the van der Waals potentials and Lorentz–Berthelot mixing rules were used for cross interactions. The CNT atoms to their initial positions have been fixed.

Results and Discussion

MD simulations performed at eight temperatures (235, 250, 260, 265, 270, 285, 300 and 350) K. Figure (1a) shows the configuration of simulated system in initial time of simulation at high temperature 350 K for mono layers of dodecan on CNT. Figure (1b) shows the high-temperature configuration in last simulation mono layers of dodecan on CNT. In this figures ordered structured disarrangement with this is due to interaction CNT with alkane.

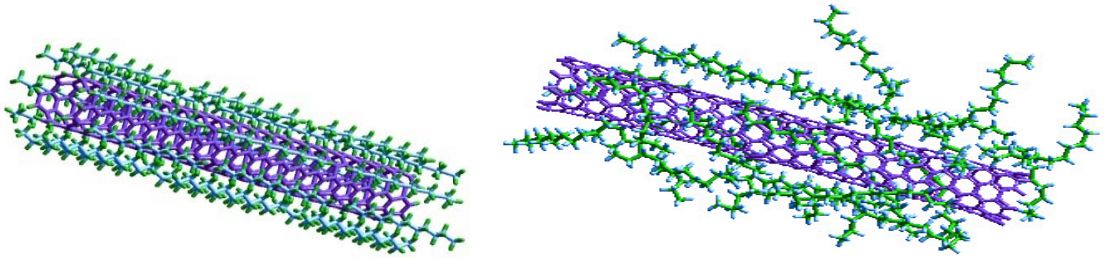

Figure 1-Configuration of simulated system at 350 K for (a) initial time (left) and (b) final time (right).

The values of the intermolecular energy are given for simulations at various temperatures in Figure 2. There is a discontinuous rise in intermolecular energy at the onset of melting. This temperature is taken as the melting point. We find that the melting point of dodecan on CNT system is T=250 K.

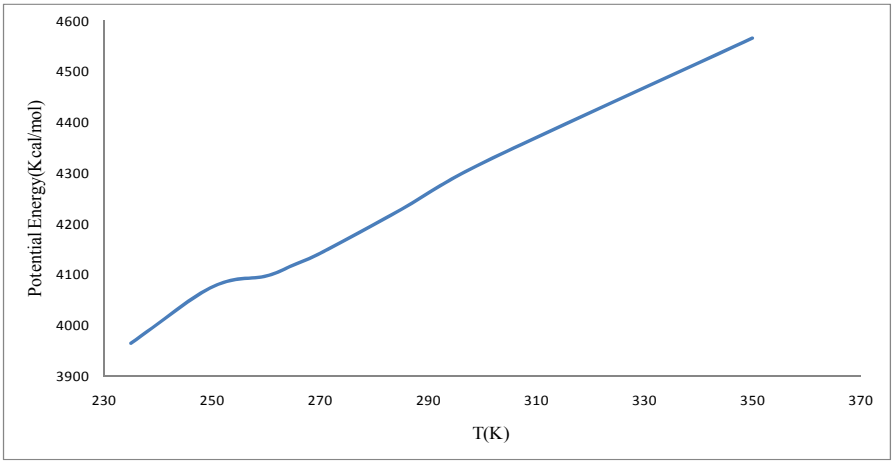

Figure 2- The variation of the potential energy as a function of the temperature for simulated system

References

[1]C. L. Pint. Surface Sci. 600(2006) 921-932.

[2] S. Alavi, D. L. Thompson, J. Phys. Chem. A, 110 (2006)1518-1523.

14th Iranian Physical Chemistry Conference
University of Tehran, Kish, February 25-28, 2011

Platinum-Graphene Nanoparticles Composite at Liquid-Liquid Interface

Mahnaz Maddahfar*[a], S. Jafar Hoseini[a], Mehdi Rashidi[b]

[a]*Department of Chemistry, Faculty of Sciences, Yasouj University, Yasouj, 74831, Iran*

[b]*Department of Chemistry, Faculty of Sciences, Shiraz University, Shiraz, 71454, Iran*

email: maddahfar2010@gmail.com

Keywords: Platinum, Graphene, Composite, nanoparticles

Recently graphene, a single-atom thick sheet of hexagonally arrayed sp^2-bonded carbon atoms has been discovered as "the thinnest material in our universe" and promises a diverse range of applications from composite materials to quantum dots [1,2].

Due to their unique nanostructure and extraordinary properties, graphene sheets are attractive as potential nanoscale building blocks for new materials. To explore the application potentials of graphene-based materials, an experiment using metal nanoparticles to decorate graphene sheets forming graphene-metal particle nanocomposites has been conducted [3].

The liquid-liquid (organic-aqueous) interface has been used for preparation of metals, semiconductors and oxides nanocrystals. The method used to prepare thin film at the organic-aqueous interface involves dissolving relevant precursor in organic layer and injecting appropriate reagent in the aqueous layer. The reaction occurs at the interface giving rise to a film at the interface. If the contact angle is 90°, then the nanoparticles will be located at the middle of the interface [4]. In this paper, we have used the liquid-liquid interface as a medium for synthesis of platinum-graphene composite with potential applications in supercapacitors and catalysis.

Methods:

Graphite oxide was prepared from purified graphite, purchased from Merck company, according to a modified method reported by Hummers and Offeman [5].

Graphite oxide powder (10 mg) was dispersed in 25 mL of water by sonication for 1 h, forming stable graphene oxide colloid. In a typical experiment, the platinum graphene nanoparticles composite was prepared by allowing a solution of $PtCl_2(SMe_2)_2$ in toluene

(1mM) to stand in contact with a solution of graphene oxide. Once the two layers were stabilized, appropriate volume of aqueous $NaBH_4$ was injected into the aqueous layer using a syringe with minimal disturbance to the toluene layer.

Results and Discussion

We have demonstrated a facile and efficient route for synthesis of platinum-graphene nanoparticles composite via a simple chemical reduction of $PtCl_2(SMe_2)_2$ and graphene oxide at toluene-water interface with $NaBH_4$ as reducing agent at room temperature.

Graphene oxide was characterized by XRD pattern and SEM image (Fig.1). Also, figures 2a and 2b show the overall morphology of the composite, indicating that the obtained product consists of spherical platinum nanoparticles. XRD characterization (Fig.2c) established synthesis of platinum-graphene composite.

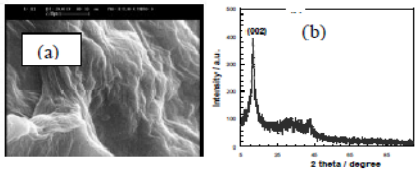

Fig.1 SEM image(a) and XRD pattern of graphene oxide (b).

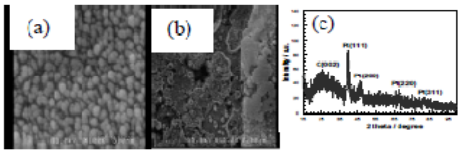

Fig.2 FE-SEM image (a,b) and XRD pattern of platinum-graphene nanoparticles composite (c).

Conclusion:

In summary, we have shown that graphene-platinum nanoparticles composite can be synthesized using graphene oxide sheets at the toluene-water interface.

This experiment generally has the following features: (i) formation of thin film at the interface between two immiscible liquids (ii) easy and simple separation of nanoparticles (iii) experiment is performed in a two phase system with no need to either burst nucleation or sequent separation of nucleation and growth.

References:

[1] C. N. R. Rao, A. K. Sood, K. S. Subrahmanyam and A. Govindaraj, *Angew. Chem. Int. Ed.* 2009, **48**, 7752.

[2] M. J. Allen, V. C. Tung and R. B. Kaner, *Chem. Rev.* 2010**, 110**, 132.

[3] Y. Si and E. T. Samulski, *Chem. Mater.* 2008**, 20**, 6792.

[4] C.N. R. Rao and K. P. Kalyanikutty, *Acc. Chem. Res*., 2008, **41**, 489.

[5] W. S. Hummers and R. E. Offeman, *J. Am. Chem. Soc.* 1958, **80**, 1339.

14th Iranian Physical Chemistry Conference
University of Tehran, Kish, February 25-28, 2011

Enhancement of hyperthermia effects by gold nanoparticles for cancer treatment; An in vitro study on melanoma cell line

R. Moradpoor[*a,b], **A . Sazgarnia**[c], **S.A. Aledavood**[b], **O. Rajabi**[d], **J. Chamani**[a]

a. Department Of Biology, Faculty of Sciences, Islamic Azad University-Mashhad Branch, Mashhad, Iran
b.Cancer Research Center , Mashhad University of Medical Sciences, Mashhad, Iran
c. Medical Physics Department, School Of Medicine, Mashhad University of Medical Sciences, Mashhad, Iran
d. Medical Chemistry Department, School Of Pharmacy, Mashhad University of Medical Sciences, Mashhad, Iran

Hyperthermia , either alone or combined with radiotherapy, immunotherapy or chemotherapy, can control tumor growth. Therapeutic hyperthermia is in practice by using laser light, microwave, focused ultrasound, and localized nanoparticle delivery. In the present study, we evaluated the effect of gold nanoparticles (GNPs) in human melanoma cancer cell line to determine : microwave hyperthermia induced heating of intracellular GNPs to produce thermal destruction of cancer cells.

Keywords: Gold nanoparticles, Microwave hyperthermia, Melanoma cell line.

Introduction

Recently the use of gold colloids and GNP_s has become an attactivve platform in biomedical applications. GNP_s have had a great impact on the medical field, are used for cancer diagnosis treatment , and as drug delivery vectors for biologic or pharmacological agents (Hirsch et al. 2005, Huang 2006, Niidome et al.2006, …). The use of GNP_s in medical fields is based on certain specific qualities such as: 1) they are easily fabricated and 2) the binding capacities of molecules with GNP_s to target cancer cells, antibodies, carbohydrates and pharmacological agents, is higher than other nanoparticles (Hirsch et al.2005, Ganon et al.2008).

Methods

MM200 cell line were initially cultured and proliferated.Then cells were treated with GNPs(50 nanometer diameter)at 37˚C and 43˚C. Cell viability was determined by MTT cell proliferation assay .

Results and discussion

Cytotoxicity of GNPs alone was determined according to the percentage of viable cells with varying concentrations of GNPs compared to the control. In Figure 1. it can be seen that a significant decrease in cell viability was observed when cells were incubated with .029mg/ml GNPs.

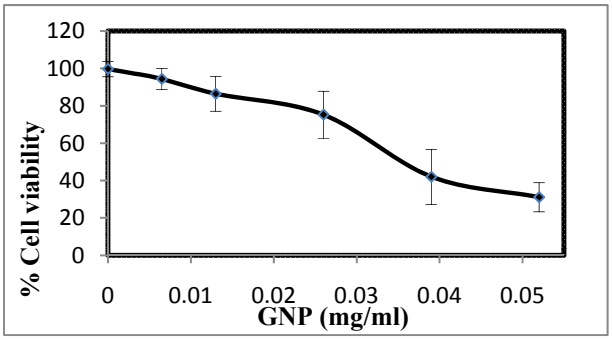

Fig 1. **MTT assay for viability of cells. Cell viability assay by MTT shows reduction in viability with variable concentrations of GNP-treated MM200 cells.**

Table 1. shows the effects of GNPs on cell survival fractions at different radiation microwave with and without GNPs. At 43˚C the cytotoxicity enhancement of GNP compared with hyperthermia alone (data not shown) had significant difference ($p<.001$). A concentration-response of cytotoxicity effect of GNP were shown(Table 1).

GNP concentration:	.013ml/ml	.019 mg/ml
37˚	86.44±9.25	80±9.25
43˚C	54.60±8.9	52.28±8.9

Table 1. antiprolifrative effect of concentration- response expriment of GNP. (mean ±SD)

Hyperthermia is a cancer therapy that relies on the localized heating of tumors above 43 °C for about 30 min[1]. tumor heating by placing multifunctional nanoparticles at tumor sites (hyperthermia) is emerging as an art of tumor treatment by ‘‘nanothermal therapy[2]. The

major approach of nanotechnology in tumor treatment includes: to develop less tissue resistance to nanoparticles, and enhanced energy deposition of microwave, light, magnetic, etc in tissue[3].

[1]. Magnetic nanoparticles for theragnostics; Veronica I. Shubayev a,c,*, Thomas R. Pisanic II d, Sungho Jin b; Advanced Drug Delivery Reviews 61 (2009) 467–477

[2]. Newer nanoparticles in hyperthermia treatment and thermometry; R. Sharma *. C. J. Chen; J Nanopart Res (2009) 11:671–689.

14th Iranian Physical Chemistry Conference
University of Tehran, Kish, February 25-28, 2011

Studies on Mechanical and Physical Properties Nanocomposite Polybutadiene of Nanoclay Modified by Quaternary Phosphonium

,Fatemeh Morad Tajari [b] , Davood Soudbar*[a], Hadi Irannezhad [b]

[a]. *Research and Development of Arak Petrochemical Company Complex*

[b]*Department of Chemistry, Azad Islamic University of Arak*

(Tajari_Fatemeh@Yahoo.Com)

Key word: Polybutadiene, Nanocomposites, Montmorillonite, Solution intercalation.

ABSTRACT

Polybutadiene rubber (PBR)/Nanocomposites was prepare by solution intercalation technique. Surface modification of the montmorillonite (MMT) was performed with trimethyl benzyl quaternary Phosphonium. The PBR-Nanocomposites morphology and clay dispersion were investigated by X-ray diffraction (XRD) and Scanning electron microscopy (SEM). The improvement of the tensile properties of BR with organoclay was less noticeable than inorganic-modified clay. Nevertheless, these mechanical properties were enhanced with addition of clay. The mechanical, physical properties and thermal stability of the PBR-Nanocomposites increasing as compared to the neat PBR but solvent uptake of these materials decreased as compared to the neat PBR indicating reduced permeability.

Introdution

Polymer clay mineral nanocomposites have attracted great interest both in industry and in science.The kind of nanocomposites exhibit improved properties compared to their micro or macro composites due to the fine phase dimensions and phase structure involved. In general, this kind of nanocomposites has superior mechanical properties, thermal stability, flame redundancy and gas barrier properties[1-3].

Experimental

The firste prepare organoclay modified with trimethyl benzyl quaternary Phosphonium and Then preparation of PBR-Nanocomposites. Organoclay was dispersed in the THF, and then added to the PBR solution.

Results and Discussion

XRD pattern of nanocomposite is typically with 5% nanoclay shown in figure 1. The basal spacing of the nanocomposite was increased to 34.78 nm relative to orgaoclay 31.50 nm (figure 1)that it proves structure of nanocomposite is intercalated. The microstructure of the fractured samples of PBR-Nanocomposite was investigated using SEM and the particle distribution of silica in the hybrid materials was recorded (Figure 2)

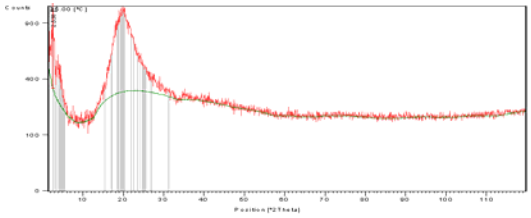

Fig. 1: X-ray diffraction patterns PBR- Nanocomposites Contents 5% organoclay.

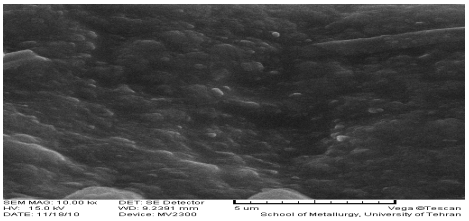

Fig. 2. Scanning electron micrographs of PBR- Nanocomposites Contents 5% organoclay.

The mechanical properties of the nanocomposite increasing as compared to the pure PBR(Table1) and also decreased swelling properties.

Table 1-the effect of organoclay on young s' modulus

No.	Analysis		Unit	Result
1	Modulus 300 %	25min	Kg/cm^2	92.5
		35min	Kg/cm^2	96
		50min	Kg/cm^2	90.5
2	Elongation (35 min)		%	455
3	Tensile (35 min)		Kg/cm^2	187.5
4	Hardness		Shore A	62

PBR- Nanocomposites were prepared by solution technique. XRD analysis indicated that the PBR chain were intercalated. The introduction of OMMT greatly improved the mechanical properties of nanocomposites. The PBR-Nanocomposites exhibited excellent thermal stability and swelling behavior, which is attributed to the improvement of the barrier properties of nanocomposites.

References

[1]. Li, Qingshan, Cong, Junying, Wang, Qingrui, 2004.Research advances in polymer/clay nano composites.Material Science and Technology 12,618-621.

[2]. J.h.;Koo. *Polymer Nanocomposites*. 2006. McGraw-Hill Companies.

[3]. Sartori, G.; Ballini, R.; Bigi, F.; Bosica, G.; Maggi, R.; Righi, P. *Chem. Rev.* 2004, *104*, 199

Synthesis and characterization of nanoclay modified by Quarternary phophonium for preparation of nanocomposite polybutadiene

,Fatemeh Morad Tajari [b] , Davood Soudbar*[a], Hadi Irannezhad [b]

[a]. *Research and Development of Arak Petrochemical Company Complex*

[b]*Department of Chemistry, Azad Islamic University of Arak*

(Tajari-Fatemeh@Yahoo.Com)

ABSTRAC

Polybutadiene rubber (PBR)/Nanocomposites was prepare by solution intercalation technique. Surface modification of the montmorillonite (MMT) was performed with trimethyl benzyl quaternary Phosphonium. The PBR-Nanocomposites morphology and clay dispersion were investigated by X-ray diffraction (XRD) and Scanning electron microscopy (SEM). The improvement of the tensile properties of BR with organoclay was less noticeable than inorganic-modified clay. Nevertheless, these mechanical properties were enhanced with addition of clay. The mechanical, physical properties and thermal stability of the PBR-Nanocomposites increasing as compared to the neat PBR but solvent uptake of these materials decreased as compared to the neat PBR indicating reduced permeability.

Key word: Polybutadiene, Nanocomposites, Montmorillonite, Solution intercalation.

Introdution

Polymer clay mineral nanocomposites have attracted great interest both in industry and in science.The kind of nanocomposites exhibit improved properties compared to their micro or macro composites due to the fine phase dimensions and phase structure involved. In general, this kind of nanocomposites has superior mechanical properties, thermal stability, flame redundancy and gas barrier properties[1-3].

Experimental

The firste prepare organoclay modified with triphenyl benzyl quaternary Phosphonium and Then preparation of PBR-Nanocomposites. Organoclay was dispersed in the THF, and then added to the PBR solution.

Results and Discussion

TGA pattern of nanocomposite is typically with 5% nanoclay shown in figure2. The microstructure of the fractured samples of PBR- Nanocomposite was investigated using SEM

and the particle distribution of silica in the hybrid materials was recorded (Figure1)

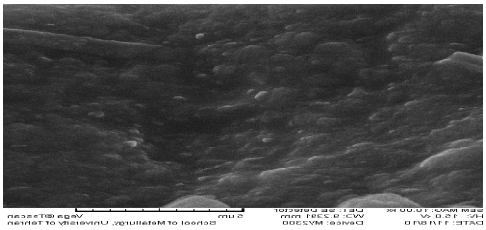

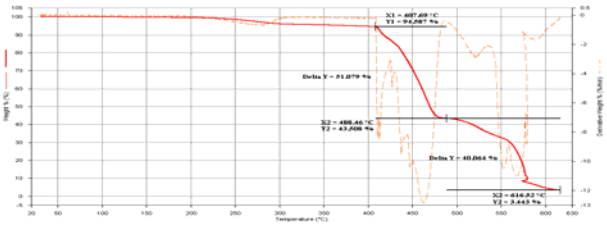

Fig.1. Scanning electron micrographs of PBR- Nanocomposites Contents 5% organoclay **Fig.2:** TGA

The solvent influence in to nanocomposit**es** increasing as compared to the pure PBR and also decreased swelling properties (Table1).

(Table1).Results solvent influence in to nanocomposit**es**

Time solvent influence	min	30	60	90	120	150	180	210	240	270
Nanocomposites Weight	0.3005	0.4960	0.6495	0.7270	0.7676	0.7984	0.8194	0.8343	0.8343	0.8343

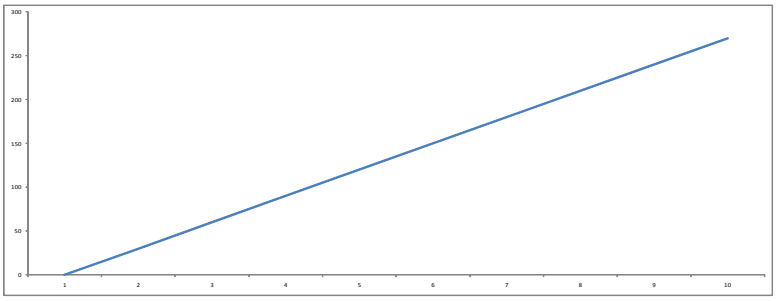

Fig3: Results solvent influence in to nanocomposit**es**

Conclusion

PBR- Nanocomposites were prepared by solution technique. XRD analysis indicated that the PBR chain were intercalated .The introduction of OMMT greatly improved the mechanical properties of nanocomposites. the PBR- Nanocomposites exhibited excellent thermal stability and swelling behavior ,which is attributed to the improvement of the barrier properties of nano composite.

References

[1]. Li, Qingshan, Cong, Junying, Wang, Qingrui, 2004.Research advances in polymer/clay nano composites.Material Science and Technology 12,618-621.

[2]. J.h.;Koo. *Polymer Nanocomposites*. 2006. McGraw-Hill Companies.

[3]. Sartori, G.; Ballini, R.; Bigi, F.; Bosica, G.; Maggi, R.; Righi, P. *Chem. Rev.* 2004, *104*, 199

14th Iranian Physical Chemistry Conference
University of Tehran, Kish, February 25-28, 2011

Modification of linear isotherm regularity equation of state (LIR) to long chain esters using group contribution

Z.Kalantar*, H.Nikoofard and A.Mortazavifar
School of Chemistry, Shahrood University of Technology, Shahrood, Iran
zkalantar@shahroodut.ac.ir , zahrakalantar@yahoo.com

Introduction:

The aliphatic esters are important materials in manufacturing processes connected with pharmaceutical, food, flavor and fragrance industries. *pVT* data of these fluids are important for efficient design of chemical processes but experimental of them are not available at all thermodynamic conditions . In this situation, equations of state are required for the calculation of thermodynamic properties needed in process engineering. A new equation of state (EOS) for dense liquids has been recently introduced by Parsafar and Kalantar (modified linear isotherm regularity "MLIR EOS") which has been found to be valid for different organic liquids such as *n*-alkanes, alcohols, ketones and 1-carboxylic acids [1].In the present work, we extended LIR EOS to esters using group contribution method.

Method:

According to contribution method each ester has been considered as a hypothetical mixture of their constituent groups, in which the interaction potential among any two groups is assumed to be the average effective pair potential. Then, based on the van der waals one-fluid approximation, the LIR equation of state is used for such a hypothetical mixture, but the new EOS parameters depend on group composition of the mixture. Hence, if the molar density of the fluid at temperature T is ρ, the total density for the hypothetical fluid is equal to $n\rho$, where n is number of carbonic groups of the molecule. Therefore, the LIR reduces to

$$\left[\frac{p}{n\rho RT}-1\right]/n^2\rho^2 = A_m + B_m n^2\rho^2 \rightarrow \left[\frac{Z}{n}-1\right]/\rho^2 = A_m n^2 + B_m n^4\rho^4 \qquad (1)$$

which we shall refer to it as the modified linear isotherm regularity (MLIR) from now on. Like the LIR, the MLIR is expected to be valid for dense fluids only ($\rho > \rho_B$). Also, the parameters of the new equation of state depend on temperature via the following equations:

$$A_m = \frac{a_1}{R} + a_2 \quad , \quad B_m = \frac{b_1}{R} + b_2 \qquad (2)$$

Result and Discussion

To investigate the accuracy of the MLIR EOS for different esters we have used the experimental *pvt* data for these fluids to plot $(Z/n-1)v^2$ against ρ^2 for each isotherm. We have found a quite good linearity for each isotherms of all esters, see figure 1. The line for each isotherm was used to determine intercept and slope to calculate A_m and B_m for that isotherm from Eq (1). Then, calculated values of A_m and B_m were plotted versus $1/T$ to obtain the values of a_1/R, a_2, b_1/R and b_2. These values are given in Table 1. Therefore having the values of the parameters given in Table 1 and using Eqs (2), the values of A_m and B_m of an ester may be calculated at any temperature. Then having the calculated A_m and B_m parameters along with Eq (1) the density of that ester at different pressure can be calculated.

Table1. The values of a_1/R , a_2,b_1/R and b_2. for different esters

fluid	$\frac{b_1}{R} \times 10^4$ ($L^4mol^{-4}K$)	$b_2 \times 10^7$ (L^4mol^{-4})	$\frac{a_1}{R}$ ($L^2mol^{-2}K$)	$a_2 \times 10^4$ (L^2mol^{-2})	Ref
Ethyl acetate	4.715	3.287	-1.322	6.924	2
Propyl acetate	4.869	0.242	-1.482	13.157	3
Butyl acetate	4.024	0.486	-1.311	10.239	3
Pentyl acetate	3.478	-0.337	-1.118	8.099	2
Ethyl butyrate	3.962	0.516	-1.399	10.343	4
Ethyl pentanoate	2.467	2.485	-0.918	2.624	5
Ethyl	4.720	0.502	-1.457	12.661	4

propionate					
Diethyl adipate	4.537	-3.525	-1.445	15.676	6

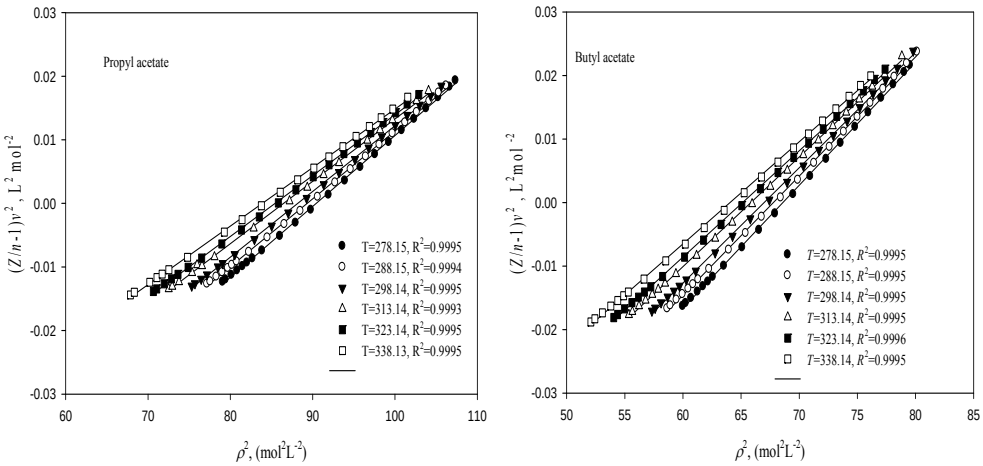

Fig. 1: plot $(Z/n-1)v^2$ against ρ^2 at different temperatures for propyl acetate and butyl acetate.

References

[1]. Parsafar, G. A., Kalantar, Z., *Fluid Phase Equilibria* **253** (2007) 108–117.

[2]. Gardas, R. L., *et al, J. Chem. Eng. Data*, **52** (2007) 737.

[3]. Molhotra, R., *Chem. Eng. Data,***41** (1996) 1366.

[4]. Malhotra, R., *J. Chem. Eng. Data,***41** (1996) 1371.

[5]. Costa, H. F., *et al, J. Chem. Eng. Data,***54** (2009) 256.

[6]. Meng, X., *et al*, *J. Chem. Eng. Data,* **53** (2008) 1474.

14th Iranian Physical Chemistry Conference
University of Tehran, Kish, February 25-28, 2011

Prediction of MLIR equation of state parameters for linear esters using group contribution method

Z.Kalantar*, H.Nikoofard and A.Mortazavifar
School of Chemistry, Shahrood University of Technology, Shahrood, Iran
zkalantar@shahroodut.ac.ir , zahrakalantar@yahoo.com

Introduction

The equation of states which are often used to predict thermodynamic properties requires pure fluid parameters as inputs. The prediction from EOS is very sensitive to such input parameter. Group contribution method has provided a high performance tool for predicting physical and thermodynamic properties from the chemical composition and state of matter. Recently this method is used to obtain the parameters of a few equation of state. The purpose of this work is to calculate the MLIR EOS parameters using group contribution method for esters.

Method

Using the group contribution method, the linear isotherm regularity equation of state (EOS) was recently modified for different organic compounds such as *n*-alkanes, primary, secondary and tertiary alcohols, ketons and 1- carboxylic acids and their mixtures [1 , 2]. Based on group contribution concept, an organic compound has been considered as a hypothetical mixture of their constituent groups. On the basis of the van der Waals one-fluid approximation, the LIR equation of state was used for such a hypothetical mixture. This equation of state which is named modified linear isotherm regularity equation of state (MLIR EOS) is as follows:

$$\left(\frac{Z}{n}-1\right)\Big/\rho^2 = A_{\mathrm{m}} + B_{\mathrm{m}} n^2 \rho^2 \qquad (1)$$

where, $Z = p/\rho RT$ is the compressibility factor, $\rho = 1/v$ is the number density, A_m and B_m are the MLIR parameters and n is the number of constituent groups of organic compound. According to MLIR EOS, plot of $(Z/n-1)v^2$ is linear against ρ^2 for each isotherm of these

dense fluids. Furthermore, the MLIR parameters were predicted using the contribution of 10 functional groups in the studied organic fluids. In this work we predicted the MLIR parameters (A_m and B_m) for esters using the group contribution method.

To do so, two basic compounds, namely propane and *n*-butane were used to obtain the contribution of methyl and terminal methylene groups (methylene groups each attached to one methyle group) in A_m and B_m from the following expressions:

$$\begin{cases} (B_m)_{propane} = \left(\frac{2}{3}\sqrt{B_{11}} + \frac{1}{3}\sqrt{B_{22}}\right)^2 \\ (B_m)_{n\text{-butane}} = \left(\frac{2}{4}\sqrt{B_{11}} + \frac{2}{4}\sqrt{B_{22}}\right)^2 \end{cases} \quad (2) \qquad \begin{cases} \left(\frac{A_m}{B_m}\right)_{propane} = \left(\frac{2}{3}\sqrt{\frac{A_{11}}{B_{11}}} + \frac{1}{3}\sqrt{\frac{A_{22}}{B_{22}}}\right)^2 \\ \left(\frac{A_m}{B_m}\right)_{n\text{-butane}} = \left(\frac{2}{4}\sqrt{\frac{A_{11}}{B_{11}}} + \frac{2}{4}\sqrt{\frac{A_{22}}{B_{22}}}\right)^2 \end{cases} \quad (3)$$

where A_{11} and B_{11} are the contributions of methyle groups in A_m and B_m and A_{22} and B_{22} are those for the terminal methylene groups, respectively. The cyclohexane was used to obtain the contribution of middle methylene groups. Middle methylene groups are methylene groups at the middle of chain which each of them attached to two methyle groups. If A_{33} and B_{33} are the contributions of the middle methylene groups in the A_m and B_m, the values of A_m and B_m of cyclohexane are the same as A_{33} and B_{33} for organic compounds. In esters, we consider $-COO-$ as a new functional group and use the values of A_m and B_m of ethyl propionate, to calculate the contribution of $-COO-$ group (A_{1111}, B_{1111}) from the following expressions at temperature of interest:

$$(B_m)_{ethylpropionate} = \left(\frac{1}{5}\sqrt{B_{11}} + \frac{2}{5}\sqrt{B_{22}} + \frac{1}{5}\sqrt{B_{33}} + \frac{1}{5}\sqrt{B_{1111}}\right)^2 \quad (4)$$

$$\left(\frac{A_m}{B_m}\right)_{ethylpropionate} = \left(\frac{1}{5}\sqrt{\frac{A_{11}}{B_{11}}} + \frac{2}{5}\sqrt{\frac{A_{22}}{B_{22}}} + \frac{1}{5}\sqrt{\frac{A_{33}}{B_{33}}} + \frac{1}{5}\sqrt{\frac{A_{1111}}{B_{1111}}}\right)^2 \quad (5)$$

where the mole fractions of the methyle, terminal methylene, middle methylene, and $-COO-$ groups in ethyl propionate are $\frac{1}{5}$, $\frac{2}{5}$, $\frac{1}{5}$, and $\frac{1}{5}$, respectively.

Having the contribution of constituent group in the EOS parameters along with dependencies of the LIR parameters to system composition, the MLIR parameters for each ester may be calculated from the following expressions:

$$(B_{\mathrm{m}})_{\mathrm{ester}} = \left(x_1\sqrt{B_{11}} + x_2\sqrt{B_{22}} + x_3\sqrt{B_{33}} + x_{11}\sqrt{B_{1111}}\right)^2 \tag{6}$$

$$\left(\frac{A_{\mathrm{m}}}{B_{\mathrm{m}}}\right)_{\mathrm{ester}} = \left(x_1\sqrt{\frac{A_{11}}{B_{11}}} + x_2\sqrt{\frac{A_{22}}{B_{22}}} + x_3\sqrt{\frac{A_{33}}{B_{33}}} + x_{11}\sqrt{\frac{A_{1111}}{B_{1111}}}\right)^2 \tag{7}$$

where

$$x_{\mathrm{i}} = \frac{\text{number of group i}}{\text{total number of groups}(n)} \quad . \tag{8}$$

We have calculated the contribution of three carbonic groups and the $-\mathrm{COO}-$ functional group at two different temperatures, 298.15 K and 323.15 K using Eqs (2) to (5). The values for the constituent groups were used, along with the Eqs (6) and (7) to calculate the MLIR parameters for the other esters. Then we were used the calculated values of A_{m} and B_{m} parameters at temperature of interest along with Eq. (1) for a given ester, to obtain its density at different pressures. Some of the calculated results are given in Table 1. The average percentage error and its maximum value for density were found to be lower than 2.16 and 2.27, respectively.

Table 1: Average absolute percent deviation of the calculated density for some esters at given temperatures and for the given pressure range (Δp), using the calculated values of A_m and B_m parameters along with Eq. (1)

fluid	T, K	Δp ,MPa	$100\left(\lvert\Delta\rho\rvert/\rho\right)_{av}^{a}$	ref
Ethyl acetate	298.15	0.1-35	2.16(2.24)	3
Ethyl acetate	323.15	0.1-35	2.17(2.27)	3
Propyl acetate	298.15	2.547-375.90	0.29(0.5)	4
Propyl acetate	323.15	2.547-376.34	0.28(0.55)	4
Butyl acetate	298.15	2.547-385.93	0.77(1.17)	4
Butyl acetate	323.15	2.547-372.09	0.60(1.03)	4
Pentyl acetate	298.15	0.1-35	1.12(1.25)	3
Pentyl acetate	323.15	0.1-35	0.87(1.03)	3
Ethyl pentanoate	298.15	0.1-35	1.01(1.15)	5
Ethyl pentanoate	323.15	0.1-35	1.03(1.24)	5
Ethyl butyrate	298.15	2.547-372.96	1.11(1.32)	6
Ethyl butyrate	323.15	2.547-375.18	0.71(1.46)	6
Di ethyl adipate	303.15	0.1-19.79	1.69(1.76)	7
Diethyl adipate	323.15	0.1-19.71	1.17(1.18)	7

References

[1] Parsafar, G.A., Kalantar, Z., *Iran. J. Chem. & Chem. Eng.*, **22** (2003) 1.

[2] Parsafar, G.A., Kalantar, Z., *Fluid Phase Equilibria*, **253** (2007) 108.

[3] Gardas, R. L., *et al, J. Chem. Eng. Data*, **52** (2007) 737.

[4] Malhotra,R. and Woolf, A. L., *Chem. Eng. Data, **41** (1996) 1366.*

[5] Costa, H. F., *et al, J. Chem. Eng. Data, **54** (2009) 256.*

[6] Malhotra,R. and Woolf, A. L., *J. Chem. Eng. Data, **41** (1996) 1371.*

[7]. Meng, X., et al, *J. Chem. Eng. Data, **53** (2008)* 1474.

14th Iranian Physical Chemistry Conference
University of Tehran, Kish, February 25-28, 2011

Modeling cohesive energy of nanosolid based on averaged coordination number

S. Morshedi*[a] , A. Yazdani [b] and M. R. Rostami[c]

[a]Department of physics، of Islamic Azad university north Tehran .Iran

(Sabah_morshedi@yahoo.com)

[b]Department of physics ،university of Tarbiat modares. Iran

Abstract

While the cohesive energy of material is well known to be the energy needed to divided the material into isolated atoms, but in the Nano-Structure it is still could be a question whether;

(i) The increased surface energy should be equal to the cohesive energy of the material, which results from the surface area difference (SAD) between the total atoms and the material[1].

(ii) In the metallic nanostructure it is decreased with the decreasing of the size of the particle[2].

Keywords: cohesive energy. coordination number. Nanostructure. . bond-energy.

Introduction

Since the surface-to-volume ratio is the effective parameter on the size and shape of the nano-structure the cohesive energy should be the functional of both the surface and interior atoms,(where it should depends of the strength and the angle of the chemical bond on which a large dangling bonds is exist).

Consequently the formation of the cohesive energy should be considered by functional of the, form factor, coordinate number and structural factor;

It is also suggested that the strength of the surface bond, due to the distribution of the bond-energy, degree of freedom, and as container, should be stronger than the interior bonds ($E_{\text{int}} \langle E_s$).

The model

If the ratio of this energy is suppose to be a constant $\gamma \geq 1$,which is supposed to be equal[3] $\gamma = 1$,the ratio of cohesive energy of nano metallic system to the bulk could be fined as follow:

$\frac{E_P}{E_b} = \frac{Z_{Lp}}{Z_{Lb}}\left\{1+\frac{(\gamma-1)n_s}{n_t}\right\}(1-2(1-q)\frac{D_0}{D+D_0})$ Where Z_{lp}, Z_{lb} are the number of nearest neishbour and D the size of Nano Particle with D_0 is the critical size on which the atoms are located on the surface and α is the form shape factor.and n_t, n_i, n_s are the number of total،interior and surface atomsin the nanostructures.

References:

[1] *W.H. Qi, M.P. Wang, Size and shape dependent melting temperature of metallic nanoparticles,* ***Mater. Chem. Phys.*** *2004, 88: 280.*

[2] K. K. Nanda, S. N. Sahu, and S. N. Behera, 2002. Liquid-drop model for the sizedependent

melting of low-dimensional systems, **Phys. Rev. A**, 66: 013208.

[3]*M. Attarian Shandiz, A. Safaei, S. Sanjabi, Z.H. Barber, "Modeling of the Cohesive Energy and Melting Temperature of Nanoparticles by Calculation of Average Coordination Number",SolidState Communications 145 (2008) 432*

14th Iranian Physical Chemistry Conference
University of Tehran, Kish, February 25-28, 2011

Synthesis and characterization of Ni-poly (vinylpyrrolidone)-KIT-6 nanocomposite as a highly efficient catalyst for the Suzuki-Miyaura reaction

Roozbeh Javad Kalbasi*, Neda Mosaddegh
Department of Chemistry, Islamic Azad University, Shahreza Branch, 311-86145, Shahreza, Isfahan, Iran
Corresponding Author E-mail: rkalbasi@iaush.ac.ir

Keywords: Poly vinylpyrrolidone, KIT-6, nanocomposite, Suzuki-Miyaura reaction, heterogeneous catalyst

Introduction

The Suzuki–Miyaura coupling reaction is a common and convenient tool for C–C bond formation during the construction of bi aryls. Because bi aryl moieties are used as the building block of a wide range of pharmaceuticals, herbicides, natural products, polymers, etc., much effort has been spent on the development of simple and practical conditions for the Suzuki–Miyaura coupling reaction [1]. Usually, the SM coupling is homogeneously catalyzed by palladium compound [2], but, the Ni catalysts have many advantages over the Pd catalyst and, for example, they are more reactive and often cheaper than the Pd complexes [3]. Ni Catalyzed reactions are more specific and are complementary to their Pd analogues. Their air stability, ease of preparation and separation of the catalyst mixture from the product at the end of the reaction sequence are some of the advantages of the Ni catalysts. Ni catalysts have been found to be better catalysts than their Pd counterparts because Ni is smaller in size compared to Pd. Consequently, Ni complexes can approach the aryl halides more easily than Pd during the oxidative addition step [4]. In addition Homogeneous catalysis is superior to heterogeneous catalysis, making possible highly active and selective organic transformations. However, the separation and recovery of homogeneous catalysts are not easy and so it is still significant to prepare more active heterogeneous catalysts and to find effective ways of heterogenizing homogeneous catalysts for industrial reaction processes [5].

Experimental

Catalyst synthesis

The large mesoporous silica with cubic *Ia3d* symmetry (KIT-6) is prepared in aqueous solution using a 1: 1 (wt %) mixture of Pluronic P123 (EO20PO70EO20) and butanol, around 0.5 M HCl concentrations at 25–35 °C. Either tetraethoxysilane (TEOS) or sodium silicate is acceptable as a silica source. In a typical synthesis batch with TEOS, P123 was dissolved in distilled water and conc. HCl (35%). To this, butanol was added under stirring at 35 °C. After 1 h stirring, TEOS was added at 35 °C. The mixture was left under stirring for 24 h at 35 °C, and subsequently heated for 24 h at 100 °C. The solid product was filtered, washed with distilled water and calcined at 550 °C or 5 h to get KIT-6. The nanocomposite catalyst was generated by post-synthesis method, which the poly (vinylpyrrolidone) was supported on the KIT-6 surface. Then, the nickel nanoparticles were synthesized by a simple method through chemical reduction reaction between hydrazine hydrate and vinyl pyrrolidone.

General procedure for Suzuki-Miyaura coupling reaction

The Suzuki-Miyaura carbon–carbon coupling reaction between iodobenzene and phenylbronic acid was performed using Ni-poly (vinylpyrrolidone)-KIT-6 (named as Ni-PNVP/KIT-6). To an organic reactor (Radleys Discovery Technologies) were added haloarene (1 mmol), arylboronic acid (1.5 mmol), catalyst (1 mmol), K_2CO_3 (3 mmol) and methanol (5 mL). The mixture was stirred at 70 °C for 12 h. The reaction mixture was cooled down to room temperature, poured into water and extracted with dichloromethane and water.

Results and discussion

Composite material Ni-PNVP/KIT-6, with polyvinylpyrrolidone (PNVP) chains encapsulated in the 3-D interconnected pore channels of mesoporous silica, KIT-6. The composite formation and the presence of PNVP inside the pore channels of KIT-6 were evidenced by FTIR, SEM, XRD, TGA, TEM and BET.

The main goal of this catalytic synthesis was to compare this organic-inorganic composite with other functional polymeric materials and to expand the use of these types of composites for organic reactions. In addition, the catalytic activity of this composite was compared to

show the advantages of Ni-PNVP/KIT-6 as a novel composite. In order to investigate the catalytic activity of this catalyst the Suzuki-Miyaura coupling reaction was chosen as a typical reaction. The effect of different parameters on Suzuki-Miyaura coupling reaction of phenylboronic acid with aryl halides was investigated.

Conclusion

A novel polymer–inorganic hybrid material (Ni-PNVP/KIT-6) is prepared by a very simple and inexpensive method without using any expensive Pd compounds (Ni catalysts have been found to be better catalysts than their Pd counterparts because Ni is smaller in size compared to Pd). This new solid catalyst become practical alternatives to soluble catalyst in view of the following advantages: a) high catalyst activity under mild reaction conditions; b) easy separation of the catalyst after the reaction; c) the existence of both organic and inorganic phases in this composite has critical effects on the catalyst activity; d) the merit of this methodology is that it is simple, fast, mild and efficient; e) the amount of used catalyst is so satisfied, f) reusability of the catalyst for several times without any loss in yield of the reaction. Finally, we believe that the new synthetic method reported here would greatly contribute to a process which is safe for the environmentally.

References:

[1] K.C. Nikolaou, P.G. Bulged, D. Sarlah, Angew. Chem. Int. Ed**. 2005**, 44, 4442.

[2] M. Beller (Ed.), Transition Metals for Organic Synthesis: Building Blocks and Fine Chemicals, VCH, Weinheim, **2004**.

[3] B.H. Lipshutz, J.A. Sclafani, P.A. Blomgren, Tetrahedron **2000,** 56, 2139.

[4] C. Griffiths, N.E. Leadbeater, Tetrahedron Lett. **2000**, 41, 2487.

[5] B.M. Bhanage, M. Arai, Catalyst product separation techniques in Heck reaction, Catal. Rev. Sci. Eng. **2001,** 43, 315.

14th Iranian Physical Chemistry Conference
University of Tehran, Kish, February 25-28, 2011

Molecular Dynamic Simulation of Fluids Confined between Graphite Layers

H. Mosaddeghi[a] , S. Alavi[b] , B. Najafi[a] and M.H. Kowsari[c]

[a]*Department of Chemistry, Isfahan University of Technology, Isfahan , Iran*

(Email:h.mosaddeghi@ch.iut.ac.ir)

[b]*Steacie Institute for Molecular Sciences, National Research Council of Canada*

[c]*Department of Chemistry, Institute for Advanced Studies in Basic Science (IASBS), Zanjan, Iran*

In this study we use classical molecular dynamic simulation to study structural and dynamic properties of water and methanol confined between graphite surfaces separated by various distance from 7 to 20 Å, at a constant density of 1 g/cm^3 for water and 0.8 g/cm^3 for methanol , at 300 K and 1Kbar. We used water as polar fluid and methanol as a polar fluid with a small CH_3- hydrophobic moiety. Results show the formation of a well-ordered structure of fluid layers parallel to the graphite surfaces. The fluid molecules in layers in contact with the surface have a tendency to orient their dipole parallel to the surface. Such ice-like structure may have, however, different structural and dynamical properties than those of ice.

Keywords: Confinement, Graphite layers, Water, Methanol, Z-density profile

Introduction:

The behavior of water confined in carbon nanostructures has many interesting implications in chemical, biological, and electrochemical fields, and several related applications have already been explored in the chemical, oil and gas, food, and pharmaceutical industries[1]. Our fundamental understanding of the behavior of confined water has been enriched by the study of water adsorption isotherms [2] and density distribution and water clustering growth[3] in carbon nanopores. Such behavior is influenced by water interactions with hydrophobic species in nano environments such as those arising in water channels present in living organisms.[3,4] In this work we used water and methanol as fluid and compared their behavior in the nanoconfined environment.

Methods:

We used slab model for graphite layers, see Figure1. And also used SPC/E model water and methanol with OPLS Force field. MD simulations are performed in the canonical NVT ensemble with the Nose-Hoover thermostat, using the DL_POLY 2.18 program.

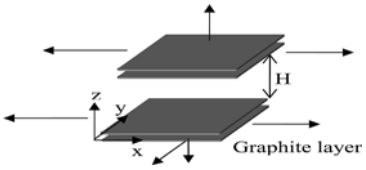

Fig1. Schematic of the slit pore model

Results and discussion:

In the water systems, most water molecules located in the layers next to the walls orient with both of the hydrogen atoms located nearly in the plane parallel to the surface [Figure2]. The z-density profile peaks show that the separation between the first peak and the wall is approximately 2.8 Å for H = 7 and 3.0 for H= 10 Å, and approximately 3.2 Å for H =14.5 Å. In the methanol system, the molecules are layered in similar manner position with different the separation between the first peak and the wall than the case of water, see Figure 3.

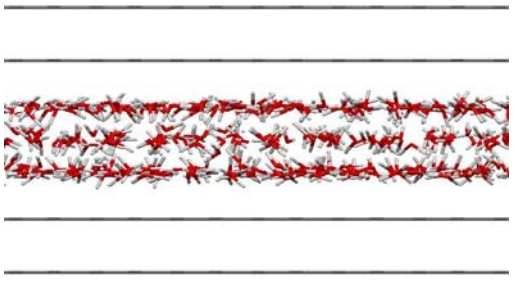

Fig.2. Water between graphite layers (H=10Å)

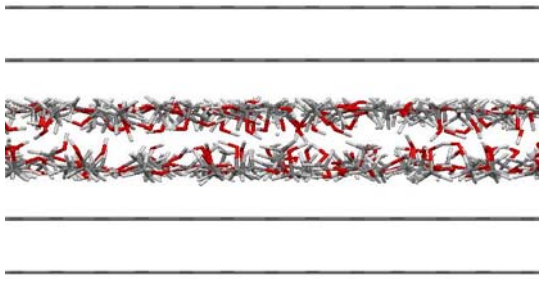

Fig.3. Methanol between graphite layers (H=10Å)

References:

[1] Brennan, J. K.; Bandosz, T. J.; Thomson, K. T.; Gubbins, K. E. Water in porous carbons. *Colloids Surfaces*, *A* **2001**, *187−188*, 539−568.

[2] Striolo, A.; Gubbins, K. E.; Chialvo, A. A.; Cummings, P. T. The Effect of Pore Connectivity on Water Adsorption Isotherms in Non-Activated Graphitic Nanopores. *Adsorption* **2005**, *11*, **337−341.**

[3] Ohba, T.; Kanoh, H.; Kaneko, K. Water Cluster Growth in Hydrophobic Solid Nanospaces. *Chem. Eur. J.* **2005**, *11*, 4890−4894.

[4] Choudhury, N.; Pettitt, B. M. On the mechanism of hydrophobic association of nanoscopic solutes. *J. Am. Chem. Soc.* **2005**, *127*, 3556−3567.

14th Iranian Physical Chemistry Conference
University of Tehran, Kish, February 25-28, 2011

NANOSILICA CATALYZED CONVERSION OF DIMETHYL 2-(5-BROMO-2-HYDROXYPHENYL)-(TRIPHENYLPHOSPHORANYLIDENE)BUTANEDIOATE TO METHYL 6-BROMO-2-OXO-2H-CHROMENE-4- CARBOXYLATE IN SOLVENT-FREE CONDITIONS

A. Souldozi[a]*, M. A. Mohammad Nezhady[a,b], H. Maadi[a,b]

[a]*Department of Science, Islamic Azad University–Urmia Branch, Urmia, Iran*

(Email:alisouldozi@yahoo.com)

[b]*Young Researchers Club of Islamic Azad University of Urmia Branch*

Coumarins are very well known natural products and many such compounds exhibited high levels of biological activity. They are used as anticoagulants, additives in food and cosmetics, and in the preparation of insecticides, optical brighteners, and dispersed fluorescent and laser dyes. Silica gel as an additive promotes the Wittig reactions of phosphorus ylides with aldehydes, including sterically hindered aldehydes to increase the rate and yields of alkenes. In the past we have established a convenient, one-pot method for preparing stabilized phosphorus ylides utilizing in situ generation of the phosphonium salts [1,2]. In this article, we report on the catalytic action of nanosilica powder in the conversion of dimethyl 2-(5-bromo-2-hydroxyphenyl)-3-(triphenylphosphoranylidene)butanedioate to methyl 6-bromo-2-oxo-2H-chromene-4-carboxylate in solvent-free conditions at 80°C in fairly high yield.

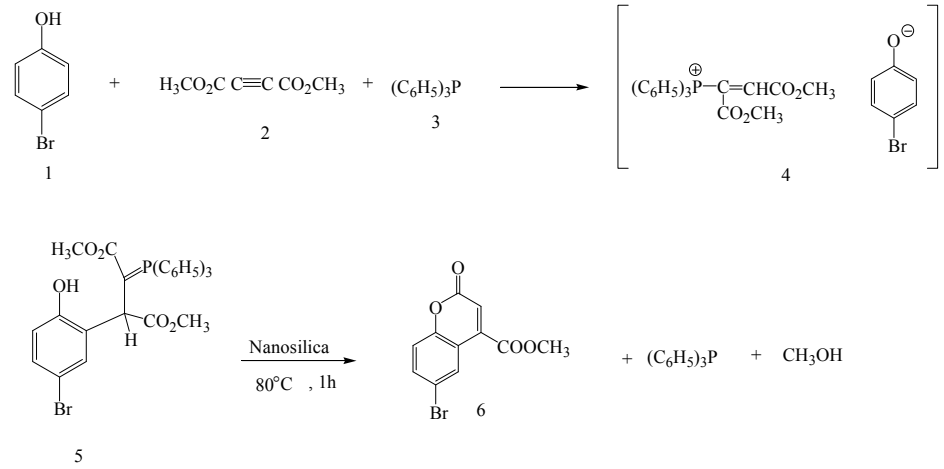

The ylide (5) may result from initial addition of triphenylphosphine 1 to the acetylenic ester 2 and concomitant protonation of the 1:1 adduct, followed by the electrophilic attack of the vinyltriphenylphosphonium cation to the aromatic ring at ortho-position relative to the strong activating group. TLC indicated formation of ylide 5 in CH_2Cl_2 . nanosilica powder was found to catalyze conversion of ylide 5 to methyl 6-bromo-2-oxo-2H-chromene-4-carboxylate (6) in solvent-free conditions at 80°C in fairly high yield. TLC indicated that the reaction was completed after 1 h. In the absence of nanosilica powder, this reaction was completed (6) at reflux temperature (CH_2Cl_2 as solvent) after 120 h. We also have used $MgSO_4$, $Mg(HSO_4)_2$, ZnO, $ZnSO_4$, Al_2O_3 , $Al_2(SO_4)_3$, $KAlSO_4$, $NaHSO_4$, $NaNO_2$, CuO, $Cu(NO_3)_2$ $CuSO_4$, $FeSO_4$, $Mn(NO_3)_2$, and MnO_2 powder instead of nanosilica in this reaction, but no correspounding product 6 was observed, and in all cases decomposition were observed. The structure 6 was deduced from its IR, UV, ^{1}H NMR, ^{13}C NMR spectra, and mass spectrometry.

In summary, we have found that nanosilica powder is able to catalyze conversion of ylide 5 to compound 6 in solvent-free conditions.

Keywords: 4-Bromophenol; chromene; dimethyl acetylenedicarboxylate; vinyltriphenylphosphonium salt , Nanosilica

References:

[1] A. Ramazani, A. R. Kazemizadeh, E. Ahmadi, N. Noshiranzadeh, and A. Souldozi, *Curr. Org.Chem.*, **12**, 59 (2008).

[2] A. Souldozi, A. Ramazani, N. Bouslimani and R. Welter, *Tetrahedron Lett.,* **48**, 2617 (2007).

Application of interpolymer complexes involving electrostatic intraction for delivery of fluoxetine

B. Vasheghani F , F. H. Rajabi , M. H. Ahmadi , A . Makvandi
Imam Khomeini International University, Faculty of Science, Department of Chemistry,
P.O.Box.: 288, Qazvin: 34149, I.R.Iran
E-mail: bvasheghanif@yahoo.com; Fax: +98 281 3780040

Introduction

Chitosan has attracted considerable interest because of their unique combination of properties, such as biocompatibility, biodegradability and antibacterial activity. Therefore, it is used widely in drug delivery applications.

Chitosan (CS) is a polysaccharide, similar in structure to cellulose. Both are made by linear β-(1→4)-linked monosaccharides. Chitosan is obtained from the deacetylation of chitin, applications of chitin are limited compared to CS because chitin is structurally similar to cellulose.

Chitosan has many advantages, specially for developing micro/nanoparticles. These include: its ability to control the release of active agents, it avoids the use of hazardous organic. while, reduced toxicity.

The purpose of this paper was to inspect the potential of chitosan as a carrier in drug delivery system. In order to, we studied for a typical interpolymer complexes between anionic-ationic polymers could lead to the formation of polyelectrolyte complexes.

Method

Chitosan (CS) is a polysaccharide, that made of 2-amino-2-deoxy-β-d-glucan combined with glycosidic linkages. Fig. (1)

Chitosan nano/microparticles can be prepared spontaneously through ionic crosslinking between positively charged amino group and counter ions like,sodium sulfate, tripoly

phosphate .22–25In either case, ionic interaction between oppositely charged ions is the key factor leading to gelation.

Briefly, the amount known of chitosan was dissolved in acetic acid under magnetic stirring at room temperature. then, the amount known of tripoly phosphate was dissolved in deionized water water, Then Nanoparticles were spontaneously obtained upon the addition dropwise of a tripoly phosphate aqueous basic solution to chitosan aqueous solution under magnetic stirring for 2h at room temperature. (rate of 1400 rpm). Then the solution was treated with super-filtration.The zone of opalescent suspension was further examined as nanoparticles. The drug (Floxetine) loaded chitosan nanoparticles were prepared. In vitro drug release study at 37 C in pH 7.4 phosphate buffer was examined with (UV) spectrophotometer .

Results and Discussion

The physicochemical properties of nano-particles were characterized by IR spectra, SEM,TEM and TGA analysis.

The effect of factors such as Floxetine concentration, Temperature, solution pH, and Stirring Rate on sorption kineties are studied.

encapsulation efficiency of Flouxetine have also been investigated.

The drug loading capacity (LC) and association efficiency (AE) of the nanoparticles were calculated according to the following equations:

$$LC = \frac{\text{Total amount Floxetin - Free amount Floxetin}}{\text{Nanoparticles weight}}$$

$$AE = \frac{\text{Total amount Floxetine - Free amount Floxetine}}{\text{Total amount Floxetine}}$$

Conclusion

In summary, novel ionic crosslinking nanoparticles composed of chitosan and poly anion.loaded with Floxetine were successfully prepared. The characterization of chitosan nanoparticles was investigated by different methods (IR, UV-vis, SEM, TG, TEM).

Particle size of nanoparticles was in the range of 300-500 nm. The nanoparticles were spherical shape and smooth surface. The formation of nanoparticles is confirmed with the FTIR spectrum.

The experiments results showed that chitosan nano-particles could adsorb Floxetine from aqueous solution effectively. The *in vitro* release studies nanoparticles was determined

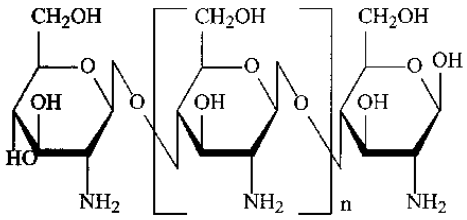

Chitosan

Fig (1) : Structure of chitosan

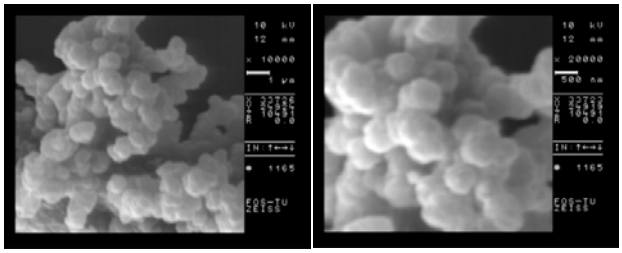

Fig (2): SEM micrograghs of the structure of chitosan nanoparticles

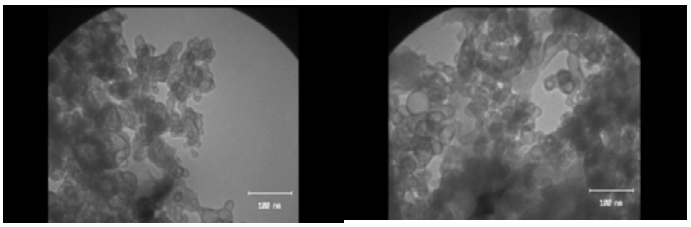

Fig (3): TEM image of Flouxetine-Chitosan nanoparticles.

References

[1] M. N. V. Kumar. J. Pharm. Pharmaceut. Sci., 3, No. 2, P. 234 - 258 (2000).

[2] Kas H.S. Chitosan: properties, preparation and application to microparticulate systems. J. Microencapsul. Vol. 14, p. 689-711, 1997.

[3] Singla A.K., Sharma M.L., Dhawan S. Nifedipine loaded chitosan microspheres: characterization of internal structure. Biotech. Histochem. Vol. 76, p. 165-171, 2001.

[4] Kato Y., Onishi H., Machida Y. Application of chitin and chitosan derivatives in the pharmaceutical field. Curr. Pharm. Biotechnol. Vol. 4, p. 303-309, 2003.

[5] Illum L., Chitosan and Its Use as a Pharmaceutical Excipient,*Pharm. Res.,* **15**, 1326-1331, 1998.

[6] Dodane V. and Vilivalam V.D., Pharmaceutical Applications of Chitosan, *Pharm. Sci. Technol. Today,* **1**, 246-253, 1998.

[7] Felt O., Buri P. and Gurny R., Chitosan: A Unique Polysaccharide for Drug Delivery, *Drug Dev. Ind. Pharm.,* **24**, 979-993,1998.

[8] P.C. Berscht, B. Nies, A. Liebendorfer, J. Kreuter, Incorporation of basic fibroblast growth factor into methylpyrrolidinone chitosan fleeces and determination of the in vitro release characteristics, Biomaterials 15 (1994) 593– 600.

[9] L. Illum, Chitosan and its use as a pharmaceutical excipient,Pharm. Res. 15 (1998) 1326–1331.

[10] V. Dodane, V.D. Vilivalam, Pharmaceutical applications of chitosan, Pharm. Sci. Technol. Today 1 (1998) 246–253.

[11] O. Felt, P. Buri, R. Gurny, Chitosan: a unique polysaccharide for drug delivery, Drug Dev. Ind. Pharm. 24 (1998) 979– 993.

[12] K.D. Yao, T. Peng, Y.J. Yin, M.X. Xu, Microcapsules/microspheres related to chitosan, J. Macromol. Sci., Rev.Macromol. Chem. Phys. C35 (1995) 155– 180.

14th Iranian Physical Chemistry Conference
University of Tehran, Kish, February 25-28, 2011

Free Activation Energies and kinetic Properties Study of Gadolinium Nitride Cluster Fullerenes $Gd_3N@C_n$ in[X-UT-Y][$Gd_3N@C_n$](n=80, 82, 84, 86 and 88) Supramolecular Complexes

Avat (Arman) Taherpour* and Maryam Maleki-Noureini
Chemistry Department, Facullty of science, Islamic Azad University Arak Branch
P.O.Box 38135-567,, Arak, Iran.
avatarman.taherpour@gmail.com & ataherpour@iau-arak.ac.ir

Abstract:

In this study, the relationships between this index and oxidation potential ($^{ox}E_1$) of **1-9**, as well as the first and second free energies of electron transfer ($\Delta G_{et(n)}$, for n=1, 2) between **1-9** and the nitride Gadolinium cluster $Gd_3N@C_{80}$ (n=80, 82, 84, 86 and 88) **10-14** derivatives as [X-UT-Y][$Gd_3N@C_n$](n=80, 82, 84, 86 and 88) **15a-i -19a-i** supramolecular complexes are presented and investigated. The first and second free activation energies of electron transfer and kinetic rate constants of the electron transfers, $\Delta G^{\#}_{et(n)}$ and k_{et} (n=1,2), respectively, were also calculated in this study for [X-UT-Y][$M_3N@C_{80}$-R] and in accordance with the *Marcus* theory.

Keywords: Nitride Gadolinium clusters; Marcus theory; free activation energies

Introduction:

Since 1985, metal-containing endohedral fullerenes (EMFs) have attracted special attention as a new class of technologically relevant materials due to their combined fullerene-like and metallic properties. A variety of endohedral metallofullerenes have been reported, but their investigations have been severely limited because they are typically formed in extremely low yields. Metallic nitride endohedral fullerenes (MNEFs) carbon cages that encapsulate trimetallic nitride clusters are one of the important classes of metallofullerenes due to their stability and their structures. The electron transfer process occurs between the metallic cluster and the fullerene cage. Paramagnetic clusters of Gd_3N permit MNEFs to be candidates in

applications such as molecular electronics, biomedical imaging, nonlinear optical devices, MRI imaging and may neutron absorber beside of radio-medicines.

Graphing and Mathematical Method:

All mathematical and graphing operations were performed using *MATLAB-7.4.0(R2007a)* and *Microsoft Office Excel-2003* programs. The value of the electron transfer rate constant k_{et} is controlled by the activation free energy $\Delta G^{\#}_{et}$, which is a function of the reorganization energy (l/4) and electron transfer driving force ΔG_{et} : $\Delta G^{\#}_{et} = (l/4)(1+\Delta G_{et}/l)^2$ $k_{et} = k_0 \exp(-\Delta G^{\#}_{et}/RT)$

Result and Discussion:

By using the equations which obtained in this modeling, it is possible to calculate the values of $\Delta G^{\#}_{et(1)}$ and $\Delta G^{\#}_{et(2)}$ of [X-UT-Y][M_3N@C_{80}-R] supramolecular complexes. The $\Delta G_{et(n)}$ (n=1,2) for [X-UT-Y][Gd_3N@C_n](n=80, 82, 84, 86 and 88) supramolecular complexes are predicted by using the appropriate equations. By utilizing these results, the electron transfer energies of $\Delta G_{et(n)}$ (n=1,2) of the complexes between nitride Gadolinium cluster derivatives with fullerenes (C_n=C_{80}, C_{82}, C_{84}, C_{86}, C_{88}) were approximated. The calculated values of the free electron transfer energies of $\Delta G_{et(n)}^{\#}$ (n=1,2) for selected [X-UT-Y][M_3N@C_{80}-R] supramolecular complexes in the equations were interpreted. There was good agreement between the calculated and the predicted values. In lieu of increasing the number of carbons atoms in the fullerene structure, the values of $\Delta G_{et(n)}^{\#}$ (n=1,2) decreased, while the kinetic rate constants of the electron transfers $k_{et(n)}$ (n=1,2) increased. The supramolecular complex structures which were discussed here and the calculated values of $\Delta G_{et(n)}^{\#}$ (n=1,2) and k_{et} (n=1,2) corresponding to these supramolecular complexes were neither synthesized nor reported before.

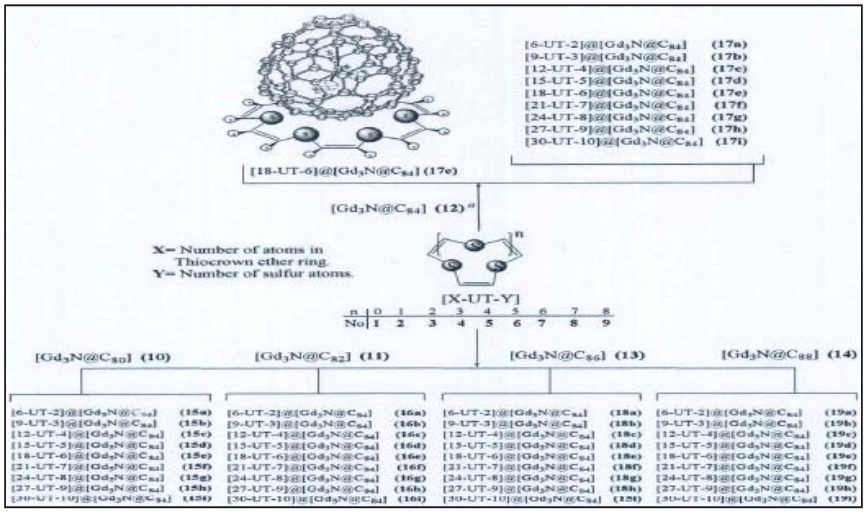

[a] The X-ray (ORTEP) structure of $[Gd_3N@C_{84}]$ was extracted from Ref.[1] directly and it is not the result of the present study.

References:

[1] M.N. Chaur, A. J. Athans, L. Echegoyen, Tetrahedron 64 (2008) 11387–11393.

[2] S. Stevenson, G. Rice, T. Glass, K. Harich, F. Cromer, M. R. Jordan, J. Craft, E. Hadju, R. Bible, M. M. Olmstead, K. Maitra, A. J. Fisher, A. L. Balch, H. C. Dorn, *Nature*, 401 (1999) 55–57.

Photo-assisted deposition of Au nanoparticles on TiO_2 and the effect of PH values.

M.Heravi[*a], E. Maleki[a], N. Reihani[a] M.

,Iran [a] Department of Chemistry Faculty of Science, Islamic Azad University,Mashhad branch

(Email:drmh@mshdiau.ac.ir) *

Keywords: Au, TiO_2, Photo-deposition, Gold catalysts

Introduction

Gold catalysts have gained due to their potential for many reactions.The Au particles prepared by photo-deposition on TiO_2 were smaller compared to those prepared by deposition-precipitation at similar Au loadings.[1-2].According to the literatures[3],gold catalysts supported on metal oxide semiconductor could be prepared by PD metiod.$AuCl_4^-$ ions adsorbed on the surface of TiO_2 particles can react with the photo generated e^- to from Au^{3+} and Au^0.In this study,a series of Au/TiO_2 catalysts were prepared by PD method under various PH values.The main objective of this study was to elucidate the effect of various PHs on the crystallite size of Au/TiO_2 catalysts.

Experimental

Catalyst preparation

Using $HAuCl_4$ solution as the gold precursor.The TiO_2 powder was synthesized using Hydrothermal method[4].$HAuCl_4$ and TiO_2 were adjusted at different PH values(PH 6,9,10,11)using 0.1M NH_4OH before illumination.The light source used was 16W UV(Philips) lamp.The time of irradiation was 10min.After irradiation,the solution was filtered and washed with deionized water until no Cl^- detected with $AgNO_3$ solution.

Characterization

Scanning electron microscopy(SEM) observation was performed with VEGATS-5136MM microscope at an accelerating voltage of 15.0KV and Transmission electron microscopy

(TEM) image was obtained using a (philips CM 120 kv) at an observe or determine the morphology and size of nanocrystal particles in Au/TiO_2 nanocrystalls.

Results and discussion

SEM images

Fig.1 shows images of Au/TiO_2 nanocatalysts and TiO_2.It can be seen that Au/TiO_2 nanocatalysts in different PH values have similar morphology with TiO_2.This suggests that different PH values have no obvious influence on their morphology.Further observation shows that Au/TiO_2 prepared at (PH=9) had the best size and morphology.The effect of PH on the crystal growth explains that the Au/TiO_2 nanocatalysts could be formed well at (PH=9).

TEM images

Fig.2 shows TEM images of Au/TiO2 nanocatalysts.It can be observed the Au/TiO_2 nanocatalysts consist of a large number of 50 nm.

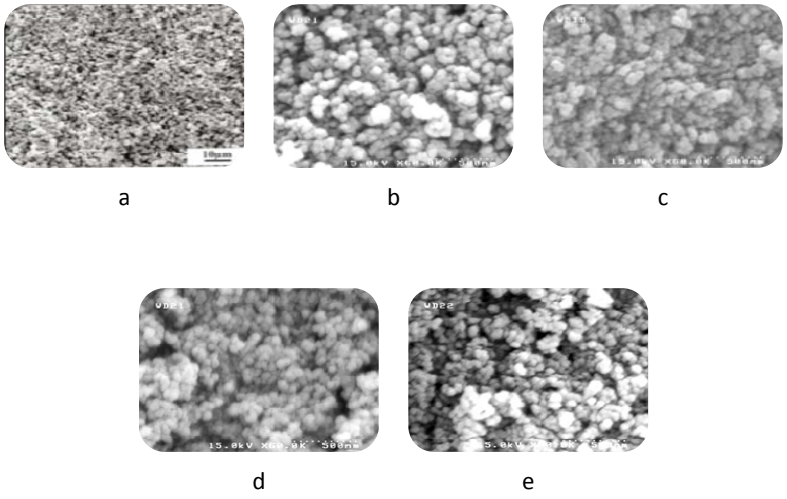

Fig.1.SEM images of TiO_2(a) and Au/TiO_2(b)PH=6,(c)PH=9,(d)PH=10,(e)PH=11.

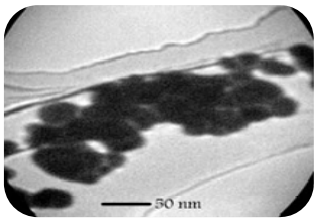

Fig.2.TEM image of Au/TiO_2 at PH=9.

References:

[1] Yi-Fen Yang.Palanivelu Sangeetha, Yu-Wen chen , Journal Energy 2009; 34:8912-8920.

[2] Cham SC,Barteau MA. Langmuir 2005; 21:5588-95.

[3] Wang CY. Zheng X.Chen.J shen T, A 1998;131:271-80.

[4] Hengboyin,Yuji Wada, Takayuki Kitamura, Shingo Kambe, Sadao Murasawa, Hirotaro Mori, Takao Sakata, and Shozo Yanagida.J.Mater.Chem 2001,11,1694-1703.

Adsorption characteristics of 4-chloro-2-nitrophenol from aqueous solutions onto nano-TiO_2

Parvin Gharbani[1], Ali Mehrizad[2]*, Samad M. Tabatabaei[1]

[1]Department of Chemistry, Islamic Azad University, Ahar Branch, Ahar, Iran

[2]Department of Chemistry, Science and Research Branch, Islamic Azad University, East Azarbayjan, Tabriz, Iran

e-mail: ali.mehrizad@yahoo.com

Keywords: Adsorption, 4-Chloro-2-nitrophenol, Nano-TiO_2

Phenols are pollutants of high priority concerns because of their toxicity and possible accumulation in the environment. Phenols are introduced into surface water from industrial effluents such as those from the coal tar, gasoline, plastic, rubber proofing, disinfectant, pharmaceutical and steel industries and domestic wastewaters, agricultural run-off and chemical spills [1]. Various methods such as UV [2], UV/ H_2O_2 [3], Photo catalysis [4], Ozonation [5], Adsorption [6] and etc., have been proposed for the treatment of wastewaters containing organic and inorganic pollutants. Adsorption technology is currently being used extensively for the removal of organic and inorganic micropollutants from aqueous solutions. There are many absorbents in use [1]. Nanoparticles have high adsorption capacity. In addition, the operation is simple and the adsorption process is rapid. In this paper, nano-TiO_2 adsorbents were used to separate 4-chloro-2-nitrophenol (4C2NP) from aqueous solutions. The effects of mixing device (shaker, ultrasonic or stirrer), contact time, adsorbent dose (0.005, 0.01, 0.05, 0.1 and 0.5 g), initial pH, temperature and initial concentration on adsorption capacity were investigated. Moreover, the adsorption data were fitted to various equations to obtain various constants related to the equilibrium of the adsorption phenomena. The batch adsorption experiments were carried out by varying initial pH, initial 4C2NP concentrations, temperature and adsorbent dosage. For each run, accurately weighed nano-TiO_2 was added to 250 mL of aqueous 4C2NP solution taken in a 500 mL erlenmeyer flask and the mixture was agitated in a waterbath shaker at constant RPM and temperature. Samples were withdrawn at regular time intervals and immediately centrifuged (Hettich) to separate

remaining adsorbent particles. Concentrations of the 4C2NP solutions were determined by measuring the absorbance of the solution at the characteristic wavelength of 4C2NP using a double beam UV-Vis. spectrophotometer (Shimadzu). The percentage of 4C2NP adsorbed to the nano-TiO_2 can be calculated using the following equation:

$$\% \text{ 4C2NP adsorbed} = \frac{(C_0 - C_t)}{C_0} \times 100 \qquad (1)$$

Where C_0 and C_t are the initial and time t liquid-phase concentration of 4C2NP (mg L^{1-}), respectively. It could be deduced that the performance of shaker is the best rather than ultrasonic and stirrer. Therefore, all of experiments fallowed by shaker. Adsorption studies were carried out for 3 h and it was observed that the amount of adsorbed 4C2NP increased linearly with time at the beginning of adsorption. A larger amount of 4C2NP was removed within the first 30 min of contact time and the equilibrium was established in 60 min. Effect of adsorbent mass on the adsorption of 4C2NP was investigated. Along with the increase of adsorbent dosage from 0.005 g to 0.01 g, the percentage of adsorbed increased from 27.5 - 31%. Above 0.01 g of adsorbent dose, the adsorption equilibria of 4C2NP decreased. So, 0.01g was considered as a optimum dosage of nano-TiO_2 to adsorption of 4C2NP. Effect of pH on adsorption of 4C2NP onto nano-TiO_2 was analyzed over a pH range from 2 to 12. 4C2NP was adsorbed onto the nano-TiO_2 surface remarkably at acidic pHs but scarcely at alkaline pHs. To study the effect of temperature on the adsorption, the experiments were performed at temperatures of 298, 308, 318 and 328 K. The equilibrium adsorption capacity of 4C2NP onto nano-TiO_2 was found to decrease with increasing temperature. To determine the impact of the concentration of 4C2NP on the adsorption in aqueous solution in contact with nano-TiO_2, the variation of the quantity of 4C2NP adsorbed with respect of the contact time has been examined for five initial concentrations: C_0 = 2, 4, 6, 8 and 10 mg L^{1-}. The adsorption capacity of the adsorbent, increases with increasing initial 4C2NP concentration because the initial adsorbate concentration provided an important driving force to overcome all mass transfer resistance. Equilibrium data were fitted to the Langmuir and Freundlich isotherm models and isotherm constants were determined. The equilibrium data were best represented by the Langmuir isotherm model.

References

[1] S.H. Lin and R.S Juan, J. Environ. Manag., 90 (2009) 1336-1349.

[2] M. Pera-Titus, V. Garcia-Molina, M.A. Banos, J. Gimenez and S. Esplugas, Appl. Cata. B: Environ., 47 (2004) 219-256.

[3] R. Andreozzi, V. Caprio, A. Insola and R. Marotta, Catal. Today, 53 (1999) 51-59.

[4] C. A. Emilio, W. F. Jardimm, M. I. Litter and H. D. Mansilla, J. Photochem. Photobio. A: chem., 151 (2002) 121-127.

[5] P. Gharbani, S. M. Tabatabaii and A. Mehrizad, I. J. Environ. Sci. Technol., 5 (2008) 495-500.

[6] V. Srihari and A. Das, Desalination, 225 (2008) 220-234.

14th Iranian Physical Chemistry Conference
University of Tehran, Kish, February 25-28, 2011

Molecular Dynamics Simulation of Diffusion Coefficient of Nano-Confined Lennard-Jones Fluid

Hossein Eslami and Neda Mousaviyan*
Departman of Chemistry, Persian Gulf University, Boushehr 75168, Iran.
E-mail:(salmosaviyan@yahoo.com)

Keywords: Nano-Confined Fluid, Molecular Dynamics Simulation, NAPT Ensemble, Lennard-Jones Fluids, Diffusion Coefficient.

Introduction

Understanding the properties of fluids at interfaces is of basic importance in many processes such as lubrication, adhesion, coating, chromatography, and membrane separation. Due to the nature of these systems, involving an interface between two many-body complex material phases, studies of such systems on atomic and molecular scales pose significant experimental and theoretical challenges. In fact, confining a fluid between two solid surfaces, whose separations are just a few molecular diameters affects significantly both equilibrium and nonequilibrium properties of fluids [1]. In this work we have calculated diffusion coefficient of nano-confined Lennard-Jones fluid according to Einstein relations and thereafter showed that the diffusion coefficient varies abruptly with decreasing intersurface separation.

Method

Recently we have proposed a simulation method [2] in which only the confined region is simulated at a constant number of confined molecules, N, constant surface area, A, constant temperature, T, and constant parallel component of the pressure, $P_{\|}$, which we call it *NAPT* ensemble simulation hereafter. In this method it is showed that the parallel component of pressure can be adjusted to bulk pressure by dynamically changing the intersurface separation. This method is employed in the present work to calculate the diffusion coefficient of a large number of confined systems (including LJ atoms confined between fcc (100) surfaces).

Results

The translational diffusion coefficients parallel to the confining surfaces for two sets of systems; one simulated at T=119.8 K and $P_{\|}$=20.37 MPa and another simulated at the same temperature and $P_{\|}$=167.5 MPa are plotted versus the gap width in figure1. Comparison of diffusion coefficient values as a function of separation between confining surfaces with solvation force (figure1) shows that the diffusion coefficient parallel to the confining surfaces oscillates out of phase with respect to the solvation force. The results of this study show that disordered films allow for larger diffusivities, while ordered films give smaller diffusivities. More illustratively, the high densities of ordered films leave limited free volume for fluid molecules and thus diminish the translational diffusivity. Since the fcc (100) surfaces in this work are in registry, films with 50, 150, 250, and 350 particles form commensurate layers with surfaces. Therefore the diffusion coefficients of such commensurate layers are much lower than the non commensurate ones.

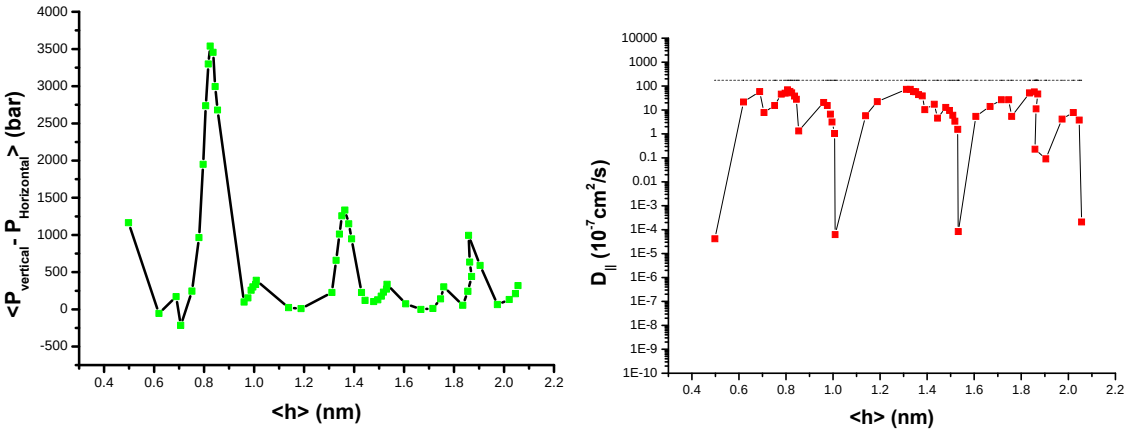

Figure1. Left panel: salvation force as a function of intersurface separation, h. Right panel: variation in the diffusion coefficient, parallel to the surfaces, with the pore size. The straight dashed line indicates the diffusion coefficient of bulk fluid.

References

[1] R. G. Horn, J. Am. Ceram. Soc. **73**, 1117 (1990).

[2] H. Eslami, F. Mozaffari, J. Moghadasi, F. Müller-Plathe, J. Chem. Phys. **129**, 194702, (2008).

Liquid Phase Selective Oxidation of Alcohols over NanoVPO Catalysts Supported on SBA-15

Vahid Mahdavi*, Farid mirhosseini
Department of Chemistry, Surface Chemistry and Catalysis Division, University of Arak,

Abstract

(5- 35 wt%)Nano vanadium phosphorous oxide (Nano VPO) catalysts supported on SBA-15 were prepared by Intercalation-Exfoliation-Reduction $VOPO_4$-$2H_2O$ in mixed alcohol (2-Butanol-Ethanol). The NanoVPO/SBA-15(wt%25)catalyst and the method are found to be suitable for the selective oxidation of benzyl alcohol to the corresponding aldehyde. The kinetic of benzyl alcohol oxidation with excess TBHP over NanoVPO/SBA-15(%wt25) catalyst at temperatures of 27, 58, and 90 °C was investigated .

Keywords: Nano Vanadium phosphorus oxide, SBA-15, Benzyl alcohol, alcohol Oxidation, supported Nano VPO catalyst

Introduction

Selective catalytic oxidation of alcohols to carbonyls is one of the most important chemical transformations in industrial chemistry.Intercalation, exfoliation, and reduction of $VOPO_4 \cdot 2H_2O$ were conducted in a mixed-alcohol solvent (2-butanol and ethanol). Whereas this processes produced crystallites of pure $VOHPO_4 \cdot 0.5H_2O$, much smaller and thinner crystallites were formed in the mixed alcohol compared pervious method. The nano$(VO)_2P_2O_7$ catalyst derived from nano-sized $VOHPO_4 \cdot 0.5H_2O$ crystallites exhibited extremely high selectivity[1] . The high surface area, large pore volume and large pore size of SBA-15[2], enable good dispersion of Nano VPO species in crystalline form[3].

Experimental

1. Preparation of catalysts

SBA-15 were synthesized using P123 ($EO_{20}PO_{70}EO_{20}$) as the template and (TEOS) at acidic

conditions in the presence of glycerol[4]. A mixture of $VOPO_4 \cdot 2H_2O$ [5], SBA-15 and 2-butanol was heated stepwise at 303, 323, 343, and 363 K for 1 h at each temperature under stirring to form a homogeneous solution .To the resulting homogeneous 2-butanol solution, ethanol was added at room temperature, and then this solution was refluxed for 20 h to form a light-blue precipitate. This precipitate was separated, washed, and dried at room temperature overnight to obtain nano-sized $VOHPO_4 \cdot 0.5H_2O$ crystallites. The dried precursors were heated from room temperature to 673K at a rate of 5 K/min in the air flow (30ml/min) and kept at this temperature for at 216h[6].

For the first time, in this study, we are going to report the use of mesoporous hexagonal molecular sieves (SBA-15) supported VPO catalyst (Nano VPO/SBA-15) for the oxidation of alcohols with tert-butylhydroperoxide (TBHP) in the liquid phase. Further, the oxidation kinetics of alcohols over (NanoVPO/SBA-15) catalyst is investigated. (Figs. 1-(a) and 1-(b)) .From the pseudo –first- order rate constants, the plot of In k´ vs. 1/T (Arrhenius plot) was drawn 1-(c)and the value of the apparent activation energy (Ea) was evaluated from the slope of the plot to be 35.69 kj mol^{-1}.

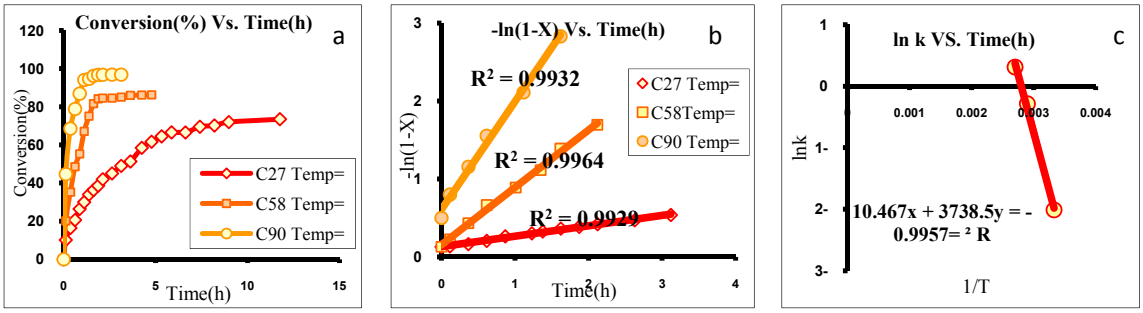

Fig1-(a) Conversion of benzyl alcohol as a function of time at 27, 58 and 90 °C with VPO/ SBA-15 (25wt %) catalyst in the presence of excess TBHP. **(b)** Pseudo-first order kinetics of benzyl alcohol oxidation with VPO/ SBA-15 (25wt %) catalyst in the presence of excess TBHP. Reaction condition: 15ml acetonitrile, 0.2g VPO/SBA-15(25wt%) catalyst with the grain size of 200–230 mesh; the rotation rate of the reaction mixture 750 cycle/min; benzyl alcohol 10mmol; Oxidant 150mmol.

Conclusions

Oxidation of benzyl alcohols is studied in the liquid phase over NanoVPO/SBA-15catalyst using tert-butylhydroperoxide (TBHP). The NanoVPO/SBA-15(25%) sample are found to be

suitable for the selective oxidation of alcohols than othre sample. The kinetic of benzyl alcohol oxidation using excess TBHP over NanoVPO/SBA-15 catalyst was investigated at temperatures of 27, 58, and 90 °C, and followed a pseudo- first order with respect to benzyl alcohol. The Nano VPO supported on SBA-15 showed high selectivity and activity compared to bulk NanoVPO catalyst. This may be due to highly dispersed nature of activephase (VPO) on high surface area SBA-15 support.

Refrence

[1]. Hiroyuki Imai, Yuichi Kamiya, Toshio Okuhara **,Journal of Catalysis**, 251 (2007) 195–203.

[2].Ying Wan and Dongyuan Zhao, **Chemical Reviews**, (2007), Vol. 107, No. 7,2822-2860.

[3].Xiu-Kai Li,Wei-JieJi, Jing Zhao, Zhi-Bing Zhang, Chak-Tong Au, **Journal of Catalysis** , 238 (2006) 232–241 .

[4].YangangWang, Fengyuan Zhang, YanqinWang, Jiawen Ren, Changlin Li, Xiaohui Liu, Yun Guo, Yanglong Guo, Guangzhong Lu, **Materials Chemistry and Physics**, 115 (2009) 649–655.

[5].Naoki Yamamoto, Norihito Hiyoshi, and Toshio Okuhara, **Chem. Mater**. (2002), 14, 3882- 3888.

[6].Hiroyuki Imai, Yuichi Kamiya, Toshio Okuhara, **Journal of Catalysis**, 255 (2008) 213–219.

14th Iranian Physical Chemistry Conference
University of Tehran, Kish, February 25-28, 2011

A new dinuclear mercury (II) complex nanoparticles of 5-Phenoxyl-1-H-Tetrazole: synthesis and characterization

Mohammad Mirzaie,[a*] Fatemeh Sarikhani,[b] Hafezeh Nabipour,[a,c] Ali Taherkhani,[a,c]

[a] *Islamic Azad University, Takestan Branch ,Department of Science, Takestan, Iran*

[b] *Department of Chemistry, University of Urmia, Iran.*

[c] *Member of Young Researchers Club, Islamic Azad University, Takestan, Iran .*

Corresponding Author E-mail: farinaz_94@yahoo.com

Keywords: tetrazoles**,** nanoparticles**,** ultrasonic treatment

Tetrazoles are an increasingly popular functionality with wide ranging applications [1]. This functional group has roles in coordination chemistry as a ligand, in medicinal chemistry as a metabolically stable surrogate for a carboxylic acid group [2], and in various materials science applications including propellants[3] and explosives [4]. Furthermore, tetrazole moieties are important synthons in synthetic organic chemistry [5]. Reaction of 5-Phenoxyl-1-H-Tetrazole with $Hg_2(NO_3)_2.2H_2O$ in the presence methanol and a withe microcrystalline precipitate formed which was collected on a fine grade fritted glass crucible and dried in *vacuo* over P_2O_5. The proposed reaction mechanism is discussed. All structures were characterized by ^1H-, ^{13}C NMR, IR and Elemental analysis. The ultrasonic treatment applied for preparation nanoparticles. The resulting nanoparticles were characterized by X-ray diffraction (XRD), infrared spectroscopy (IR) and scanning electron microscope (SEM)**.**

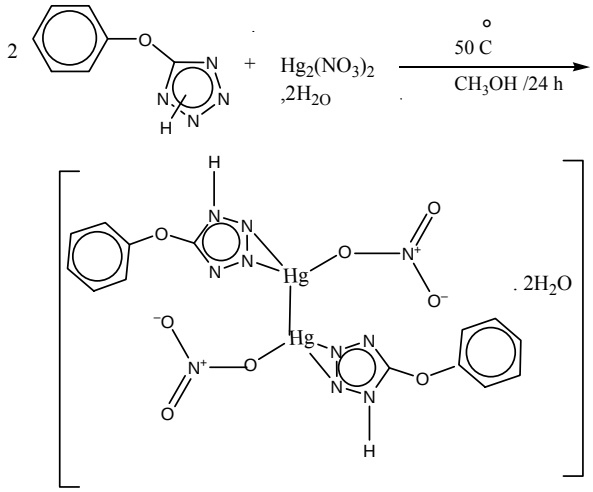

References

[1] R.N. Butler In: A.R. Katritzky, C.W. Rees and E.F.V. Scriven, Editors, *Comprehensive Heterocyclic Chemistry* **Vol. 4**, Pergamon, Oxford, UK (1996).

[2] H. Singh, A.S. Chawla, V.K. Kapoor, D. Paul and R.K. Malhotra, *Prog. Med. Chem.* **17** (1980), p. 151.

[3] Brown, M. U.S. Patent 3,338,915, 1967; *Chem. Abstr.* **1968**, 87299.

[4] (a)V.A. Ostrovskii, M.S. Pevzner, T.P. Kofmna, M.B. Shcherbinin and I.V. Tselinskii, *Targets Heterocycl. Syst.* **3** (1999), p. 467.

(b)M. Hiskey, D.E. Chavez, D.L. Naud, S.F. Son, H.L. Berghout and C.A. Bome, *Proc. Int. Pyrotech. Semin.* **27** (2000), p. 3.

[5] (a) A. Burger, *Prog. Drug Res.* **37** (1991), p. 287.

(b)T. Schelenz and W. Schafer, *J. Fuel Prakt. Chem.* **342** (2000), p. 91.

(c)H. Ruelke, A. Friedel, E. Martin, K. Kottke, I. Graefe and H. Kuehmstedt, *Pharmazie* (1991), p. 46.

14th Iranian Physical Chemistry Conference
University of Tehran, Kish, February 25-28, 2011

Synthesis, characterization and antibacterial activity of new sulfur complex nanoparticles

Ali Taherkhani, [1,2]* Hafezeh Nabipour, [1,2] Mohamad Mirzaie,[1] Ali Rahmani, [3] Mostafa Nabipour[4]

[1] *Islamic Azad University, Takestan Branch ,Department of Science, Takestan, Iran*

[2]*Member of Young Researchers Club, Islamic Azad University, Takestan, Iran.*

[3]*Student of Medicine, Tehran University of Medical Sciences, Tehran, Iran.*

[4]*Engineer of Islamic Repuplic of Iran Shipping Lines (IRISL).*

E-mail: ha.nabipour@gmail.com

Abstract

Dithiocarbamate formed an important class of biologically active ligands. An extremely large number of dithiocarbamate complexes with transition and non transition metal ions have been known. Dithiocarbamates as ligands are well known to bind strongly and selectively to many metal ions, so in the past few years self-assembly directed by metal–dithiocarbamate coordination have emerged as a useful supramolecular methodology for the preparation of macrocycles, cages, catenanes, and nanoparticles. Most of applications are based on complexation properties of DTC ligands with metal ions, especially with transition metal ions. The preparation of the metal complexes, benzaldehyde with 1,6-hexamethylenediamine in methanol followed by reduction of the Schiff base with $NaBH_4$ in methanol. One-pot syntheses from this amine, carbon disulfide, triethylamine and $CoCl_2.6H_2O$ gave colorless precipitates. The ultrasonic treatment applied for preparation of nanoparticles. The produced dithiocarbamate nanoparticles were characterized by X-ray diffraction (XRD), infrared spectroscopy (IR) and scanning electron microscope (SEM) and another techniques. The antibacterial activity of dithocarbamate nanoparticles derivatives tested against microorganism and compared with bulk (non-nano) forms conditions.

Keywords: nanoparticles**,** 1,6-hexamethylenediamine**,** dithiocarbamate

Introduction

The continuing discovery of the many pivotal roles played by anions in chemical, biological and environmental processes has stimulated the construction of molecular host systems capable of complexing anionic guests [1]. Dithiocarbamates are versatile ligands capable of forming complexes with most of the elements and able to stabilise transition metals in a variety of oxidation states [2]. Dithiocarbamate ligand were synthesized and characterized by using elemental analyses, FT-IR, NMR. The antibacterial activities of synthesized compounds were studied against two Gram-negative species, *Escherichia coli, Klebsiella pneumoniae* and two Gram-positive species, *Staphylococcus aureus* and *Bacillus subtilis*.

Experimental

The preparation of the metal complexes, benzaldehyde with 1,6-hexamethylenediamine in methanol followed by reduction of the Schiff base with $NaBH_4$ in methanol. One-pot syntheses from this amine, carbon disulfide, triethylamine and $CoCl_2.6H_2O$ gave colorless precipitates. A green powder precipitated that was filtered and recrystallized from chloroform.

Synthesis of dithiocarbamate nanoparticles

Ultrasonic device was employed to improve the dispersibility of the complex dithiocarbamate nanoparticles dispersed in aqueous solutions. The suspension dithicarbamte was ultrasonically irradiated with a high-density ultrasonic probe immersed directly into the solution. The obtained suspension was allowed to age for 120 min. The working parameters of the ultrasonic device were 70 kHz and 40 W/cm^2.

Result

1. Characterization of nanoparticles

X-ray diffraction (XRD) technique was used to determine the ingredients of the sample. The average crystallite size of the as-prepared dithiocarbamate complex nanoparticles is about 50 nm, according to the Debye-scherrer formula: $D = 0.9\lambda / \beta \cos\theta$ (Fig. 1) . The morphology of nanoparticles was observed using a scanning electron microscopy (Fig. 2). The obtained

samples were characterized and compared via FT-IR analysis with non-nano conditions. FT-IR spectrometer at room temperature in the range from 250 to 4000cm^{-1}.

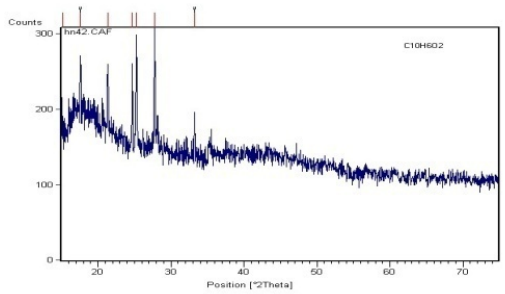

Fig. 1. The XRD pattern of complex dithiocarbamate nanoparticles.

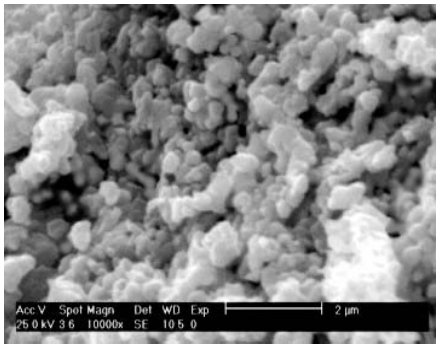

Fig. 2. SEM photographs of the sample dithiocarbamate (the scale bar is 2 µm).

2.In vitro antibacterial activity

The compounds have been screened in vitro against *Escherichia coli, Klebsiella pneumoniae* and *Staphylococcus aureus* , *Bacillus subtilis* various methods are available for the evaluation of the antibacterial activity of different types of drugs. Method disc diffusion assay applied for study antibacterial activity. Gentamycin was used as reference drug for bacteria. In general, the compounds showed significant antibacterial activity and the bacterial strains with the zone of inhibition (Table 1).

Table 1

No.	**Complexes**	**Zone of inhibitation (mm)**			
		Escherichia coli	Klebsiella pneumoniae	Staphylococcus aureus	Bacillus subtilis
1	dithiocarbamate complex	17	17	15	-
2	Nanodithiocarbamate complex	23	23	20	-

References

[1] G. Hogarth, Ebony-Jewel C.-R.C.R. Rainford-Brent, Shariff E. Kabir, I. Richards, James D.E.T. Wilton-Ely and Q. Zhang, (2009), Functionalised dithiocarbamate complexes: Synthesis and molecular structures of 2-diethylaminoethyl and 3-dimethylaminopropyl dithiocarbamate complexes[$M\{S_2CN(CH_2CH_2NEt_2)_2\}_n$]and [$M\{S_2CN\ (CH_2CH_2\ CH_2NMe_2\ )_2\}_n$] ($n$ = 2, M = Ni, Cu, Zn, Pd; n = 3, M = Co). Inorganica Chimica Acta. 362: 2020-2026.

[2] K. B. Pandeya, R. Singh, P. K. Mathur and R. P. Singh, (1986), E.s.r. spectra of mixed ligand manganese(II) dithiocarbamates. Transition Met. Chem. 11: 347-350.

14th Iranian Physical Chemistry Conference
University of Tehran, Kish, February 25-28, 2011

DFT study on the methane incorporation into the Si_{60} fullerene

M. D. Ganji [a,*], A. Mirnejad [b], M. Sobhani [a], M. Rezvani [c] and M. Shokry [a]

[a] Department of Chemistry, Islamic Azad University, Ghaemshahr Branch, Mazandaran, Iran
* Corresponding author. E-mail: ganji_md@yahoo.com, Tel: 98 911 113 7150.
[b] Young research club, Islamic Azad University, Ghaemshahr Branch, Mazandaran, Iran
[c] Young research club, Islamic Azad University, Tehran Central Branch, Tehran, Iran

***Keywords*:** Si_{60} fullerene; Methan; Energy storage; *ab initio* calculations

Introduction

Natural gas adsorbed on porous materials have been attracting an increasing interest since they are a promising alternative to compressed natural gas (at about 30 MPa) as a suitable nonpollution vehicular fuel and for bulk transportation [1]. There have been several works devoted to the possibility of formation of endohedral complexes between simple molecules, such as H_2, N_2 and NH_3, and fullerene nanocages [2, 3]. Here we present the results of our theoretical investigation on methane deposition into the Si_{60} fullerene, and its potential applications as a suitable material for energy storage.

Computational methods

The *ab initio* calculations based on the generalized gradient approximation (GGA) with the Perdew–Burke–Ernzerhof (PBE) functional [4] were performed in density functional theory (DFT) and the standard norm-conserving Troullier–Martins pseudo-potentials [5]. The calculations are done using a split-valence double-zeta plus polarization function (DZP) as basis set for all simulated atoms.

Results and discussion

We first examine the incorporation of methane molecule(s) inside C_{60} fullerene through calculating the formation energy (binding energy) of CH_4 molecules inserted into C_{60} cage. The formation energy is calculated from: $\Delta E = E_{C60\text{-}nCH4} - E_{C60} - nE_{CH4}$. After full structural optimization of the $n CH_4@C_{60}$ system we find that the formation energy value is negative for

only one encapsulated CH_4 molecule (-5.30 kcal/mol), similar to the experimental observation for diatomic molecules embedded inside the C_{60} fullerene [6].

Similar calculations have been performed for confined methane molecules in the Si_{60} nanocage. Our results reveal that up to eight methane molecules were encapsulated inside the Si_{60} cage can form the stable complex (have negative formation energies). It has been found that when methane molecules were incorporated into the cage the fullerene shape deviates from a sphere, as depicted in figure 1(a).

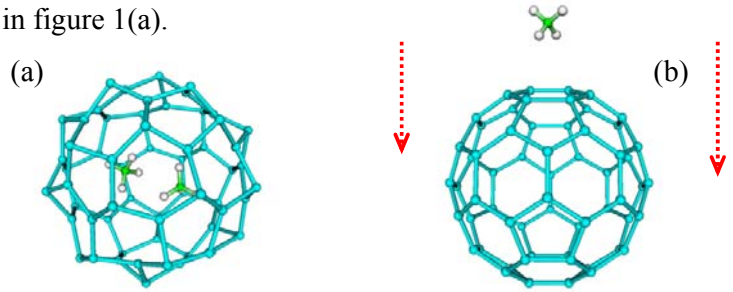

Figure 1. Schematic representation of two CH_4 molecules incorporated into Si_{60} fullerene and (a) corresponding optimized structure. Model for a CH_4 molecule pointing toward the side-wall of C_{60} fullerene and (b) Si_{60} fullerene with respect to the hexagon ring of the nanocage via its CH_2 groups.

We next investigate the insertion of a CH_4 molecule into the possible entry sites of the considered nanocages (Fig 1 (b)). The interaction of the CH_4 molecule with the nanocage skeleton was studied by performing single point energy (SPE) calculation. The result of present calculations show that CH_4 molecule prefers to penetrate into the Si_{60} through the six-membered ring via its C–H group with a barrier energy of about six time easier than that of the C_{60} cage one.

Conclusion

The calculated formation energies of the $n CH_4@X_{60}$ (X=Si, C) complexes showed that methane storage capacity of Si_{60} fullerene is three time higher than that of the C_{60} fullerene. Furthermore, the penetration of methane molecules into the Si_{60} nanocages is much easier than that of C_{60} one.

References

[1] Lozano-Castello, D., Alcaniz-Monge, J., de la Casa-Lillo, M.A., Cazorla-Amoros, D., and Linares-Solano, A. (2002) *Fuel* 81: 1777.

[2] Pupysheva, O.V., Farajian, A.A., and Yakobson, B.I. (2008) *Nano Lett.* 8: 3.

[3] Ganji, M.D., Mohseni, M., and Goli, O. (2009) *J. Mol. Structure: Theochem.* 913: 54.

[4] Perdew, J.P., Burke, K., Ernzerhof, M. (1996) *Phys. Rev. Lett*. 77: 3865.

[5] Troullier, N., Martins, J.L., (1991) *Phys. Rev. B* 43: 1993.

[6] Takenobu, T., Shiraishi, M., Yamada, A., Ata, M., Kataura, H., Iwasa, Y. (2003) *Synth. Met*. 135: 787.

14th Iranian Physical Chemistry Conference
University of Tehran, Kish, February 25-28, 2011

The Effect of Molar Ratio H_2O to TTIP on the Size and Quality of TiO_2 Nanoparticles Synthesized By Reflux Route

H. Milani Moghaddam[a,*]; H. Makhdoomi[a]

[a]*Physics department, Mazandaran University, Babolsar,Iran*

(Email: milani@umz.ac.ir), (Tel: 01125342486)

Abstract

In this study, TiO_2 nanoparticles were synthesized by reflux route. The crystallite sizes and their quality were investigated under effect of molar ratio H_2O to Titanium IV Isopropoxide (TTIP). Precursor used in this route is TTIP and pure ethanol, methanol and small amount of distilled water formed the alcoholic solution. All the resulting nanoparticles were in anatase phase. The quality and size of the particles changed with the molar ratio of H_2O to TTIP.

Keywords: TiO_2 nanoparticles, Reflux route, H_2O molar ratio effect.

Introduction

Titania is famous with its high Photocatalytic activity for the degradation of pollutant chemicals and hazardous organic compounds. It has three major phases: anatase, rutile and brookite. The anatase type has been selectively used for photocatalytic applications [1-2]. Having fine and homogeneous nanoparticles with controlled diameters is necessary for using these materials. It is therefore an important that the quality of prepared powder can be controlled with a molar ratio of reactants. In this work, we have tried to providing anatase TiO_2 nanoparticles by reflux method via changing the molar ratio of reactants.

Experimental

In the present work, ethanol, EtOH (absolute grade); methanol, MeOH (99.8% purity); TTIP (97% purity Sigma-Aldrich) and distilled water were used. In order to get nanostructured TiO_2, TTIP solution was dissolved in mixture of MeOH and EtOH with a molar ratio (1:1:10) and refluxed at 60 ^oC for 6 hours. Distilled water was added drop-wise into the hot solution. The obtained precipitate was isolated by a filter paper and washed several times with hot water and ethanol in order to remove large

aggregates from the product. That was then dried at 60 °C for 15 hours in ambient conditions. It is clear that the prepared sample is largly amorphous. The obtained powder was annealed at different temperatures by rate of 5 °C /min for 5 hours to the formation of the crystal structure.

Results and discussion

Effect of H_2O molar ratio based on a reaction formula of TTIP ($Ti(OC_3H_7)_4$) hydrolysis to obtain TiO_2 [3] is $Ti(OC_3H_7)_4 + 2H_2O \rightarrow TiO_2 + 4\ C_3H_7OH$.

A molar ratio of $[H_2O]/[TTIP]$ for completely hydrolysis of TTIP should be 2. For sake of study on effect of H_2O amount in the morphology and crystallite size of TiO_2 nanoparticles, $[H_2O]/[TTIP]$ ratio was changed from 5 to 10, 25 and 50 when all other parameters were fixed. The samples were calcined at 450 °C for 5 hours. The phase of synthesized structures was all anatase. According to the XRD patterns (see Fig. 1), general variation in the peaks intensity of anatase phase was not observed with a slowly increase of pure water to hot solution at reflux duration. SEM images of Fig. 2 indicate the morphology of nanostructures. In case of $[H_2O]/[TTIP]=5$, the morphology of particles on surface seems to be had a high uniformity. By increasing of $[H_2O]/[TTIP]$ ratios from 5,10,25 and 50, the size of the crystallites was 24, 22,22 and 17 nanometer, respectively.

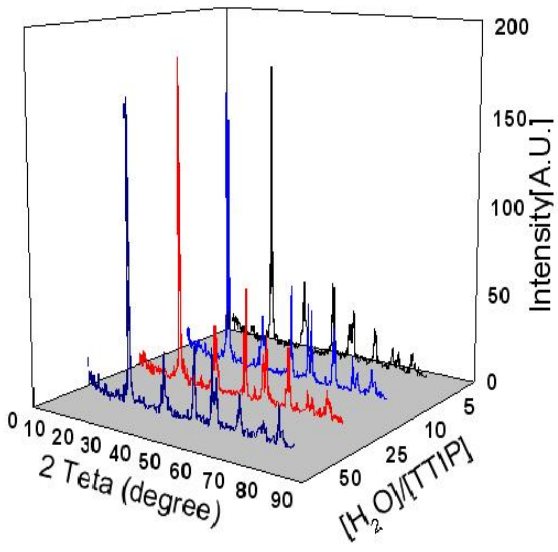

Fig. 1. XRD patterns of TiO_2 samples.

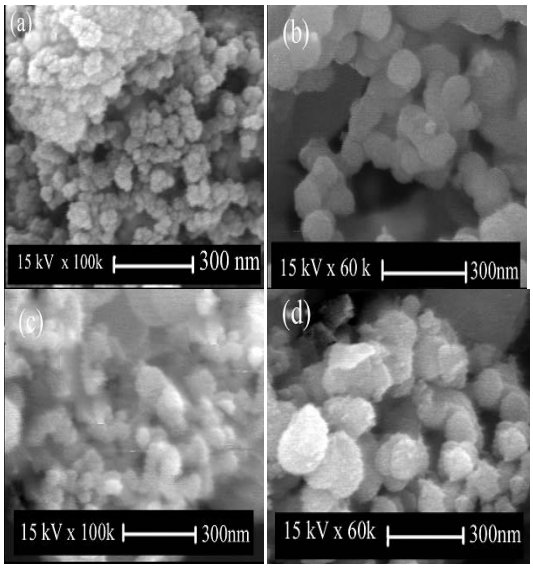

Fig. 2. SEM pictures of TiO_2 nanopowders. Those were calcined at 450 °C for 5 hours. $[H_2O]/[TTIP]$ ratio was: a) 5, b) 10, c) 25 and d) 50.

Concloution

In summary, titania pure nanoparticles have been successfully prepared using TTIP as precursor by a reflux route. The increase of $[H_2O]/[TTIP]$ molar ratio gives rise to better hydrolysis and the decrease of the size of TiO_2 nanocrystallites.

References

[1] Y. Liu *et al*., *J. Hazard. Mater*. **150** (2008) 153–157.

[2] F. Han *et al*, *Appl. Catal .A-Gen*. **359** (2009) 25–40.

[3] R.K. Wahi *et al. J. Colloid .Interface. Sci.* **302** (2006) 530–536.

The Effect of Molar Ratio H_2O to TTIP on the Size and Quality of TiO_2 Nanoparticles Synthesized By Reflux Route

H. Milani Moghaddam[a,*]; H. Makhdoomi[a]

[a]*Physics department, Mazandaran University, Babolsar,Iran*

(Email: milani@umz.ac.ir), (Tel: 01125342486)

Abstract

In this study, TiO_2 nanoparticles were synthesized by reflux route. The crystallite sizes and their quality were investigated under effect of molar ratio H_2O to Titanium IV Isopropoxide (TTIP). Precursor used in this route is TTIP and pure ethanol, methanol and small amount of distilled water formed the alcoholic solution. All the resulting nanoparticles were in anatase phase. The quality and size of the particles changed with the molar ratio of H_2O to TTIP.

Keywords: TiO_2 nanoparticles, Reflux route, H_2O molar ratio effect.

Introduction

Titania is famous with its high Photocatalytic activity for the degradation of pollutant chemicals and hazardous organic compounds. It has three major phases: anatase, rutile and brookite. The anatase type has been selectively used for photocatalytic applications [1-2]. Having fine and homogeneous nanoparticles with controlled diameters is necessary for using these materials. It is therefore an important that the quality of prepared powder can be controlled with a molar ratio of reactants. In this work, we have tried to providing anatase TiO_2 nanoparticles by reflux method via changing the molar ratio of reactants.

Experimental

In the present work, ethanol, EtOH (absolute grade); methanol, MeOH (99.8% purity); TTIP (97% purity Sigma-Aldrich) and distilled water were used. In order to get nanostructured TiO_2, TTIP solution was dissolved in mixture of MeOH and EtOH with a molar ratio (1:1:10) and refluxed at 60 ^oC for 6 hours. Distilled water was added drop-wise into the hot solution. The obtained precipitate was isolated by a filter paper and washed several times with hot water and ethanol in order to remove large aggregates from the product. That was then dried

at 60 °C for 15 hours in ambient conditions. It is clear that the prepared sample is largly amorphous. The obtained powder was annealed at different temperatures by rate of 5 °C /min for 5 hours to the formation of the crystal structure.

Results and discussion

Effect of H_2O molar ratio based on a reaction formula of TTIP ($Ti(OC_3H_7)_4$) hydrolysis to obtain TiO_2 [3] is $Ti(OC_3H_7)_4 + 2H_2O \rightarrow TiO_2 + 4\ C_3H_7OH$.

A molar ratio of $[H_2O]/[TTIP]$ for completely hydrolysis of TTIP should be 2. For sake of study on effect of H_2O amount in the morphology and crystallite size of TiO_2 nanoparticles, $[H_2O]/[TTIP]$ ratio was changed from 5 to 10, 25 and 50 when all other parameters were fixed. The samples were calcined at 450 °C for 5 hours. The phase of synthesized structures was all anatase. According to the XRD patterns (see Fig. 1), general variation in the peaks intensity of anatase phase was not observed with a slowly increase of pure water to hot solution at reflux duration. SEM images of Fig. 2 indicate the morphology of nanostructures. In case of $[H_2O]/[TTIP]=5$, the morphology of particles on surface seems to be had a high uniformity. By increasing of $[H_2O]/[TTIP]$ ratios from 5,10,25 and 50, the size of the crystallites was 24, 22,22 and 17 nanometer, respectively.

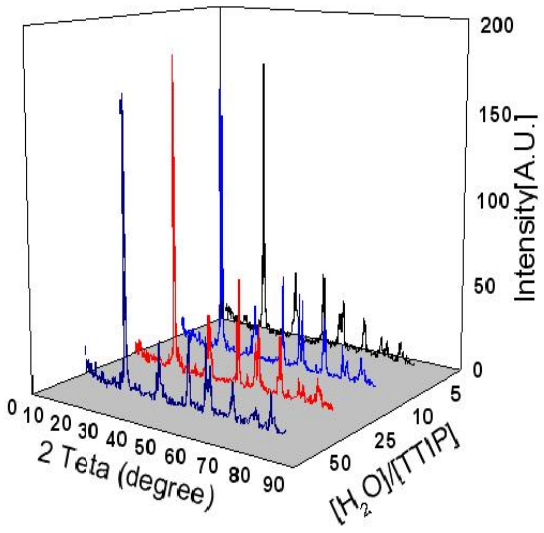

Fig. 1. XRD patterns of TiO_2 samples.

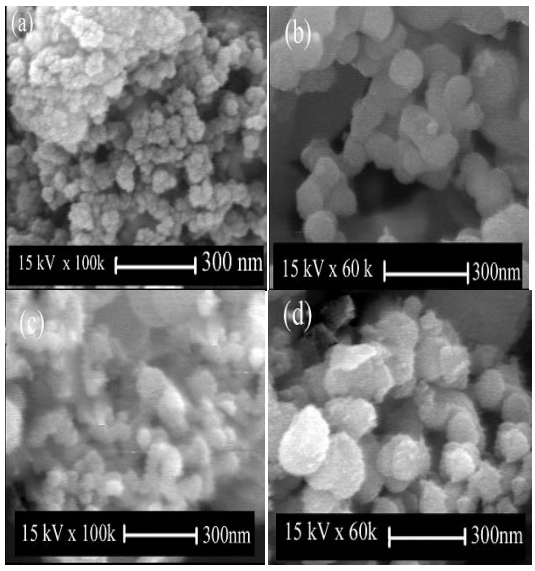

Fig. 2. SEM pictures of TiO_2 nanopowders. Those were calcined at 450 °C for 5 hours. $[H_2O]/[TTIP]$ ratio was: a) 5, b) 10, c) 25 and d) 50.

Concloution

In summary, titania pure nanoparticles have been successfully prepared using TTIP as precursor by a reflux route. The increase of $[H_2O]/[TTIP]$ molar ratio gives rise to better hydrolysis and the decrease of the size of TiO_2 nanocrystallites.

References

[1] Y. Liu *et al*., *J. Hazard. Mater*. **150** (2008) 153–157.

[2] F. Han *et al*, *Appl. Catal .A-Gen*. **359** (2009) 25–40.

[3] R.K. Wahi *et al. J. Colloid .Interface. Sci.* **302** (2006) 530–536.

Nanowire $Cd(OH)_2$ Thin Films Deposited by Chemical Solution Route

R. Sahraei[a,*], G. Nabiyouni [b], A. Mihandoost [b], L. Shiri[a], and A. Daneshfar[a]

[a]*Department of Chemistry, University of Ilam, Ilam ,Iran*

[b]*Department of Physics, University of Arak, Arak, Iran*

[*] *(Email: reza_sahrai@yahoo.com)*

Keywords: Nanowires, Thin films, Chemical solution deposition

Introduction

Thin films composed of randomly oriented nanowire have attracted tremendous interest in recent years. In recent years, nanostructures of metal hydroxides such as, $Ni(OH)_2$, $Cu(OH)_2$, $Mg(OH)_2$, and $Cd(OH)_2$ have been synthesized as potential templates or precursors for the corresponding oxide materials [1, 2]. Cadmium hydroxide ($Cd(OH)_2$) is a wide band gap (3.2 eV) semiconductor material [3]. Here, we present a one-step and template-free method for the selective growth of ultra-long nanowire bundles of crystalline $Cd(OH)_2$ on glass substrates at low temperature through a simple method involving controlled chemical precipitation based on principals of ionic and solubility products.

Experimental

An aqueous solution of 0.1 M $Cd(CH_3COO)_2$ was prepared, and to this solution aqueous NH_3 solution (25%) was added under constant stirring. A white precipitate was initially observed, which subsequently dissolved back into solution upon the further addition of the NH_3 solution. A pre-cleaned glass substrate was immersed and placed vertically in the solution. The solution was maintained at a PH of ca.12 and at room temperature, resulting in the direct growth of nanowire bundles on the glass substrate.

Results and discussion

Fig. 1 shows the XRD pattern and SEM image of nanowire $Cd(OH)_2$ thin films deposited on glass substrates. The six broad peaks observed in the diffractogram at around 23.81 º,

30.49 º, 35.65 º, 49.89 º, 61.57 º, and 75.01 º reveal a monoclinic lattice structure of $Cd(OH)_2$ [4]. The average crystallite calculated from reflection peaks was about 5 nm which clearly support nanocrystalline nature of nanowire.

. Figure 1 (right) show that the products consist of a large quantity of nanowires with lengths ranging up to several tens of micrometers. The wires are interconnected in a complex way, with porous structure of sample goes deep inside.

The optical properties of the $Cd(OH)_2$ nanowires were characterized. Uv-Vis absorption spectrum revels that as-deposited $Cd(OH)_2$ film has low absorbance in visible region. The band gap of the nanowires obtained was 3.3 eV which is in good agreement with the reported for the direct band gap of $Cd(OH)_2$ at 3.2 eV.

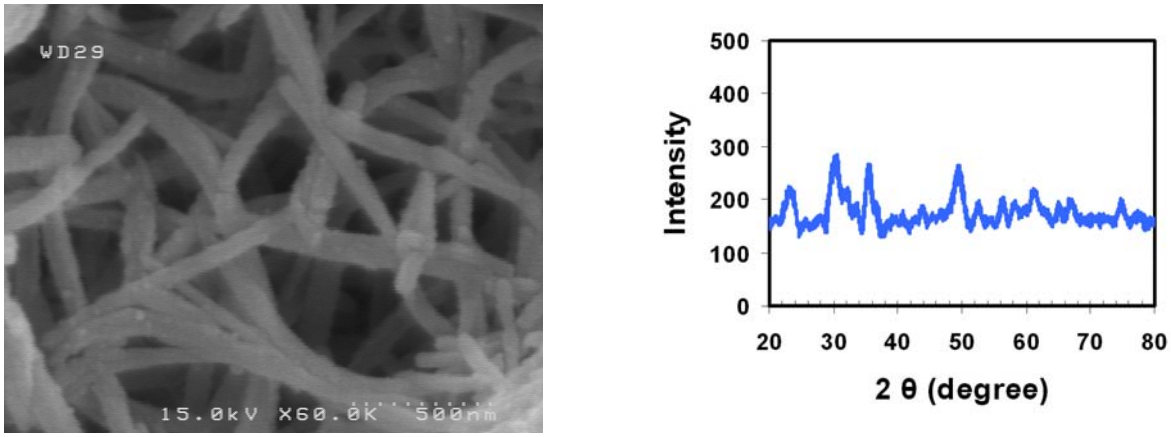

Fig.1: XRD pattern for the nanowire $Cd(OH)_2$ thin films (Left) and SEM image of the $Cd(OH)_2$ thin film (Right).

Conclusions

In this study, ultralong $Cd(OH)_2$ nanowires have been successfully synthesized directly onto the glass substrate using a simple, low-temperature, and economical soft solution chemical process. XRD revealed the films to consist of nanocrystalline $Cd(OH)_2$ ranging in size 5 nm. Also obtained nanowires are uniform and have monoclinic phase. FESEM image shows that

products consist of large quantity of nanowires with lengths ranging up to several tens of micrometers.

References

[1] S.-H. Park, H.J. Kim, J. Am. Chem. Soc. 126 (2004) 14368.
[2] P. Jeevanandam, Y. Koltypin, A. Gedanken, Nano Lett. 5 (2001) 263.
[3] R. S. Mane, S.-H. Han, Electrochem. Commun. 7 (2005) 205.
[4] R. R. Salunkhe, U. M. Patil, T. P. Gujar, C. D. Lokhande, Applied Surface Science 255 (2009) 3923.

Supercapacitive properties of MnO_2/Carbon black/Graphite nanocamposites prepared by sonochemistry method

H. Naderi*, A. Zolfaghari, H. Mortaheb, H. Sayahi, P. Samadi
Chemistry and Chemical Engineering Research Center of Iran
naderi.hamidreza7@gmail.com

Abstract

MnO_2/Carbon black/Graphite nanocomposites were prepared by a sonochemistry method. The structure of nanocomposites were characterized by X-ray diffraction (XRD) and scanning electron microscopy (SEM). Electrochemical performance of the nanocomposite electrodes with different MnO_2 content were studied by cyclic voltammetry, electrochemical impedance spectroscopy and charge/discharge measurements. The Electrochemical properties of the nanocomposites exhibited ideal capacitive. The nanocomposite has a high specific capacitance of 364 F g^{-1} at scan rate of 2 mVs^{-1}. The nanocomposites showed highe power density at high energy density.

Keywords: Supercapacitor, nanocamposite, MnO_2, Carbon black, Graphite, sonochemistry.

Introduction

Supercapacitors, are energy-storage devices which can be used for various electrical equipments, mobile devices and hybrid electric vehicles. Supercapacitors have higher power density and longer cycle life than batteries while energy density is lower that batteries[1]. On the basic these two mechanism supercapacitors classified as: Electric double-layer capacitors (EDLCs) that employ typical form carbons and pseudocapacitors that employ transitoin metal oxids compounds (e.g. RuO_2, NiO, MnO_2) or conducting polymers (polyaniline, polypyrrole,) [2]. supercapacitors based on MnO_2 as electroactive materials are attracting great attention due to low cost of the raw material, high theoretical specific capacitance (~1380 Fg^{-1}) and environmentally compatibility [3-4]. Recently, various types of carbonaceous compounds used as electrodes for SCs (e.g., activated carbon, carbon black, carbon fiber cloth, graphite powder, glassy carbon carbon aerogel and carbon nanotubes) They were used as sole electrode component in supercapacitor or as part of composite electrodes that contain pseudocapacitance materials [5].

Methods

Predetermined amounts of Carbon and Graphite, were added to Aqueous solutions of 0.25 M $MnSO_4$ (Merck, research grade) and 0.5 M $KBrO_3$ (Merck, research grade) with the total volume of 100 mL. The mixture was irradiated with high intensity ultrasound radiation with 480 Wcm^{-2} input power and working frequency of 24 kHz. The crystallographic structures of the MnO_2 and composites were determined by a X-ray diffractometer

(Bruker, D8-advance) at 2Θ=4-70° with monochromatized Cu Kα radiation (λ=1.541874 Å) operated at 40 kV/30 mA. The morphologies of the MnO_2 and nanocomposites powder were observed by scanning electron microscopy (SEM, philips, XL30).

Electrodes were prepared by mixing of the nonocomposites powder as active material with 5 wt% of PTFE dried powder (Merck). The resulting mixture was pasted on a steel grid (1 cm^2) and then pressed. All electrochemical measurements were performed using a potentiostat/galvanostat (PGSTAT100, Autolab, EchoChemie) in a three-electrode glass cell. The measurements were carried out in a 0.5 M Na_2SO_4 electrolyte.

Result and discusion

Typical XRD patterns for MnO_2 and MnO_2/Carbon/Graphite nanocomposites with diferent ratios are shown in Fig. 1. All these peaks can be indexed to pure orthorhombic γ-MnO2 (JCPDS card).

Fig. 2 shows the cyclic voltammogram MnO_2/Carbon/Graphite nanocomposite in aqueous 0.5M Na_2SO_4 electrolyte within a potential window of 0.0 to +1.0V versus Ag/AgCl at different scan rates. The specific capacitance (SC) can be calculated from CVs according to the equations:

$$SC = \frac{q}{\Delta V \times m}$$

where SC is the specific capacitance of active material (Fg^{-1}), q is the voltammetric charge (c), the ΔV is voltage difference and the m is the amount of active material (g). For the MnO_2/Carbon/Graphite nanocomposites with mass ratios 56/22/22, the initial specific capacitance based on MnO_2 is 358 and 175 Fg^{-1} at 2 and 200 mVs^{-1}, respectively, which is much higher than that of the other samples.

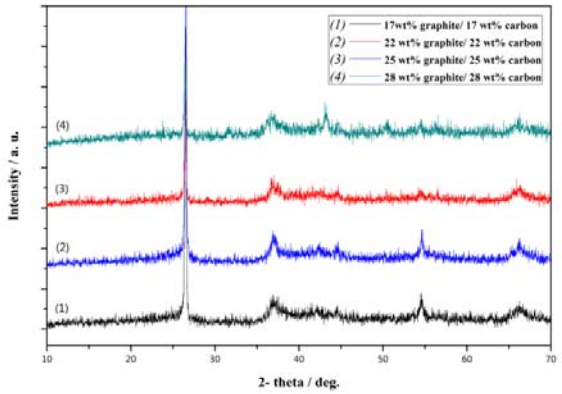

Fig. 1: Typical XRD patterns of the as-prepared MnO_2/Carbon nanocomposite samples.

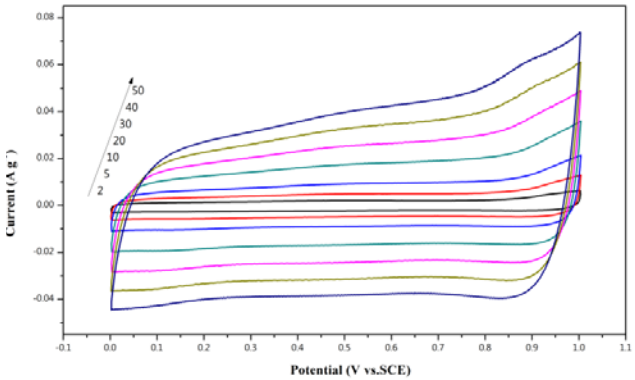

Fig. 2: CV curves of the nanocomposite electrode with at the various scan rates

Conclusions

MnO_2/Carbon/Graphite nanocomposites were synthesized using ultrasonic radiation. For the MnO_2/Carbon/Graphite nanocomposite with mass ratios 56/22/22 the specific capacitance based on MnO_2 is 364 at 2 mVs^{-1}. CV characterization indicates that this material shows fast kinetics for charge–discharge process as well as good kinetic reversibility. The nanocomposite demonstrate excellent reversibility and high power density. The nanocomposite material can be considered as promising materials in the application of supercapacitors.

References

[1] B.E. Conway, Electrochemical Supercapacitors, Kluwer-Plenum, New York, 1999.

[2] R. Kotz, M. Carlen, Electrochim. Acta 45(2000) 2483.

[3] M. Toupin, T. Brousse, D. Belanger, Chem Mater 16(2004) 3184.

[4] A. Zolfaghari, F. Ataherian, M. Ghaemi, A. Gholami, Electrochim. Acta 52 (2007) 2806.

[5] S. R. S. Prabaharan, R. Vimala, Z. Zulkarnian, J. Power Sources 161 (2006) 730.

Electron Transfer and Free Energies Theoretical Study of First-Generation Cephalosporin Antibiotics with Fullerenes in Nanostructure of [R].C_n Supramolecular Complexes

Avat (Arman) Taherpour* and Doreena Narian

Chemistry Department, Faculty of Science, Islamic Azad University,Arak Branch

P. O. Box 38135-567, Arak, Iran, Email: ataherpour iau-arak.ac.ir Gmail:avatarman.taherpour@gmail.com

Keywords: Fullerenes; Cephalosporin antibiotics; Electron transfer equation; Free energy of electron transfer.

Introduction:

The pharmacokinetic properties of cephalosporin antibiotics were reported and they are almost identical[1]. Cefadroxil and cephalexin has been shown activity broad-spectrum antibiotic of the cephalosporin type, effective in gram-positive bacterial infections. Cefadroxil is an antibacterial drug that is the *para*-hydroxy derivative of cefalexin. Since the discovery of fullerenes (C_n), one of the main classes of carbon compounds, the unusual structures and physiochemical properties of these molecules have been discovered. The numbers of carbon atoms at the structures of the fullerenes were utilized here. This study elaborates upon the relationship between the number of carbon atoms and the four free energies of electron transfer of fullerenes C_n with Cefadroxil and Cephalexin, on the basis of the four reduction potentials of the fullerenes, as assessed by applying the Electron transfer equation [2].

Graphing and Mathematical Method:

All graphs were generated using the *Microsoft Office Excel 2007* program. Using the number of carbon atoms contained within the C_n fullerenes, several valuable properties of the fullerenes can be calculated. The values were used to calculate the four free energies of electron transfer ($\Delta G_{et(1)}$ to $\Delta G_{et(4)}$), according to the Electron transfer equation.

Result and Discussion:

In this study, the number of carbon atoms in the fullerenes was used as an index to establish a relationship between the structures of Cefadroxil and Cephalexin, as well-known first-generation cephalosporins antibiotics and fullerenes C_n (n=60, 70, 76, 82 and 86). The relationship between the number of carbon atoms and the free energies of electron transfer ($\Delta G_{et(1)}$ to $\Delta G_{et(4)}$) are assessed using the Electron Transfer equation for these supramolecular complexes([Cefadroxil].C_n and [Cephalexin].C_n).

In 2000, the electrooxidation of cefadroxil was investigated by used a glassy carbon electrode by cyclic voltammetry. The electrooxidation of cefalexin at boron-doped diamond electrodes and glassy carbon electrodes was investigated by cyclic voltammetry [1]. The four reduction potentials of fullerenes C_n have been reported before[3]. The calculations are presented for the four reduction potentials ($^{Red.}E_1$ to $^{Red.}E_4$) of fullerenes C_n[2]. Fig 1(graphs *a-d*) demonstrate the relationships between the number of carbon atoms of fullerenes "n" and the first- fourth free-energy of electron transfer of [Cefadroxil].C_n (n = 60, 70, 76, 82 and 86). By using this graph, it is possible to calculate the values of $\Delta G_{et(1)}$ to $\Delta G_{et(4)}$ of [Cefadroxil].C_n. The related curves for [Cephalexin].C_n have similar structures to Fig. 1(**a-d**) [Cefadroxil].C_n . The results were used to calculate the four free-energies of electron transfer ($\Delta G_{et(1)}$ to $\Delta G_{et(4)}$) of supramolecular complexes for fullerenes C_{60} to C_{300}.

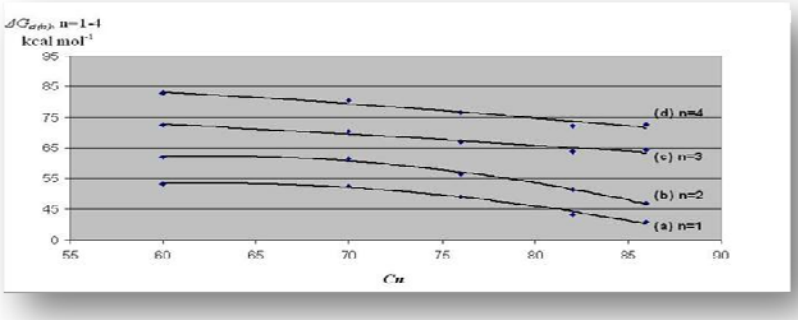

Fig 1

Conclusion:

Cefadroxil and Cephalexin with fullerenes have important electron-transfer properties as the most well-known first- generation cephalosporin antibiotics, and molecular conductors. The results of this study could be utilized in nano- pharmacokinetic studies related to these antibiotics. The novel supramolecular complexes discussed have neither been synthesized nor reported previously.

References:

[1] S. R. El-Shaboury, G. A. Saleh, F. A. Mohamed, A. H. Rageh, *Journal of Pharmaceutical and Biomedical Analysis 45 (2007) 1–19*.

[2] Taherpour. A. A., M. Maleki, Anal. Let. 43, 658 (2010).

[3] T. Suzuki, K. Kikuchi, F. Oguri, Y. Nakao, S. Suzuki, Y. Achiba, K. Yamamoto, H. Funasaka, and T. Takahashi, Tetrahedron, 52(14), 4973 (1996).

Preparation and characterization of NiO nanoparticle from new precursor

H. Najafgholi[a], A.R. Salehirad[b], M. Abedi[c], A.R. Rezvani[*d]
Department of Chemistry, University of Sistan & Baluchestan , Zahedan , Iran
(Rezvani2001ir@yahoo.ca)

Keywords: NiO nanoparticle, Heat treatment, Calcination, New precursor.

Introduction:

The synthesis of nanoparticles has been extensively attracted interests for their unique properties and quantum size effects [1]. Nickel oxide (NiO) nanoparticles are a very prosperous material extensively used in chemical catalysts [2], gas sensors [3] and magnetic materials [4]. Correspondingly, research into the synthesis of NiO nanoparticles has increased during the past decade with methods such as electrodeposition [5], sol–gel techniques [6] and precipitation [7]. In this study, NiO nanoparticles were successfully prepared with thermal decomposition method and characterized with several technique.

Methods:

In this work, NiO nanoparticle was prepared via thermal decomposition of simple precursor $(NH_4)_2[Ni(dipic)_2]$. The prepared precursor was heated in a crucible at 350, 450 and 550 °C for 2 h in air to get the NiO nanoparticles. Characterization of both precursor and nanoparticle was carried out using FT-IR, XRD, TEM and thermal analysis method TGA.

Results and Discussion:

The TGA shows that the temperature up to about 200 °C, there was a large amounts loss in weight which was due to loss of the evolution of water and carbon dioxide and no weight loss recorded when temperature increased to above 500 °C. On the basis of the TGA analysis, the precursor powders were calcinated between 350 °C and 550 °C for same time in air. The

XRD patterns of calcinated nickel oxide at 350 °C was shown a obvious peak that related to Crystalline phase of NiO. It indicates that the precursor was basically decomposed into NiO at this temperature. According to the Scherrer formula: $D=0.89\lambda/B\cos\theta$, the particle size is 30 nm. When the calcined temperature increased to 550 °C the intensity of the diffraction peak is increased with the increasing temperature. But, particle size of the as-prepared NiO increases from 30 to 38 nm with increasing temperature. In the FT-IR spectrum, the C=O vibration stretching modes occur at 1658 Cm^{-1} corresponding to two carboxylic groups of dipic. that disappear with increase of calcination temperature due to loss ligands. At calcination temperature (550 °C), the ligands decomposed and the FT-IR spectrum shows Ni=O peak at 454 Cm^{-1}. The Transmission electron microscopy (TEM) image of the NiO nanoparticles shows a uniform nanocrystalline NiO particles with spherical shapes with weak agglomeration. Its average size is about 33 nm, ranging from 30 nm to 38 nm.

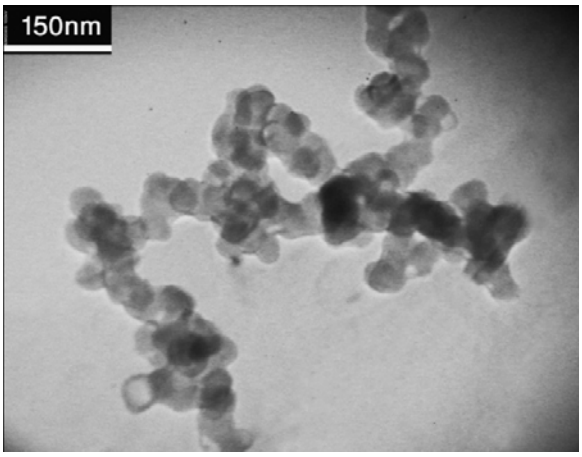

Conclusions:

Nanocrystalline NiO powder was prepared by thermal decomposition method, using $(NH_4)_2[Ni(dipic)_2]$ precursor. The obtained single-phase NiO powder has an average particle size of 33 nm after calcination the as-prepared precursor at 450 °C for 2 h. The sample exhibits narrow size distribution and weak agglomeration.

References:

[1] R.N. Bargava, J. Lumin. 70 (1996) 85.

[2] L.N. Lewis, Chem. Rev. 93 (1993) 2693-2730.

[3] H.X.Yang, Q.F.Dong, X.H. Hu, J. Power Sources 79 (1999) 256.

[4] Y. Wang, J. Ueyama, K. Ogura, J. Electonal. Chem. 408 (1996) 83.

[5] K. Nakaoka, J. Ueyama, K. Ogura, J. Electroanal. Chem. 571 (2004) 93.

[6] A. Surca, B. Orel, B. Pihlar, P. Bukovec, J. Electroanal. Chem. 408 (1996) 83.

[7] G.J. Li, X.X. Huang, Y. Shi, et al., Mater. Lett. 51 (2001) 325.

A novel green synthesis and characterization of citrate-capped CdSe nanostructures

R. Sahraei[a,*], M. Nosrati[a], L. Shiri[a]

[a]*Department of Chemistry, University of Ilam, Ilam , Iran*

[*] *(Email: reza_sahrai@yahoo.com)*

Introduction

Semiconductor nanocrystals synthesized by means of colloidal chemistry techniques attract considerable attention due to their size-tunable photoemission characteristics. Among the colloidal semiconductor nanocrystals, CdSe has shown almost full range visible light emission within an advantage of continuous tunability of the electronic and optical properties by changing the physical size of the nanocrystals [1-2] and thus it has been intensively studied for its distinguished role in technical applications such as light-emitting diodes, lasers, and biological labels [3]. In this article, a green facile room temperature synthesis of citrate-capped CdSe nanostructures via a novel method is reported. The as synthesized CdSe nanocrystals were characterized using UV-Vis spectrophotometry, scanning electron microscopy (SEM) and XRD techniques.

Experimental

A solution of selenium was prepared by a mixture of selenium powder, sodium thiosulfite and distilled water. The mixture was then stirred for 5 h, at 70 °C, for the entire selenium to dissolve in water giving rise to a colorless solution. In a typical procedure, 3 ml of an aqueous solution of $Cd(ClO_4).2H_2O$ (0.04 M) was added to an aqueous solution of citrate (20 mL, 0.1 wt%) at room temperature. This was followed by a slow addition of 3 mL (0.04 M) selenide ion solution, upon this addition, the color of the solution was changed from white to transparent red showing the formation of CdSe nanoparticles. The mixture was aged for 2 days. The transparent solution was filtered and red precipitate was obtained. The optical,

electronical and structural properties of these nanostructures were characterized using different techniques such as X-ray diffraction, Scanning electron microscopy (SEM) and UV-Vis spectrophotometry.

Result and Discussion

Figure 1 shows the SEM image of synthesized nanoneedles. These nanoneedles are formed upon nanocrystals growth at room temperature. The UV-Vis absorption spectra consist of an absorption shoulder at 498 nm. The electronic band gap was calculated to be 2.7 eV, while the corresponding gap of the bulk material is 1.7 eV. Therefore, it is possible to tune the electronical and optical properties of materials by reducing their size. The XRD pattern was obtained by scanning 2θ in the range of 10-80˚. The results showed that the citrate-capped CdSe nanocrystals are in hexagonal structure. Distinct diffraction peaks corresponding to (002), (102), (110), (103) and (112) crystalline planes of hexagonal structure.

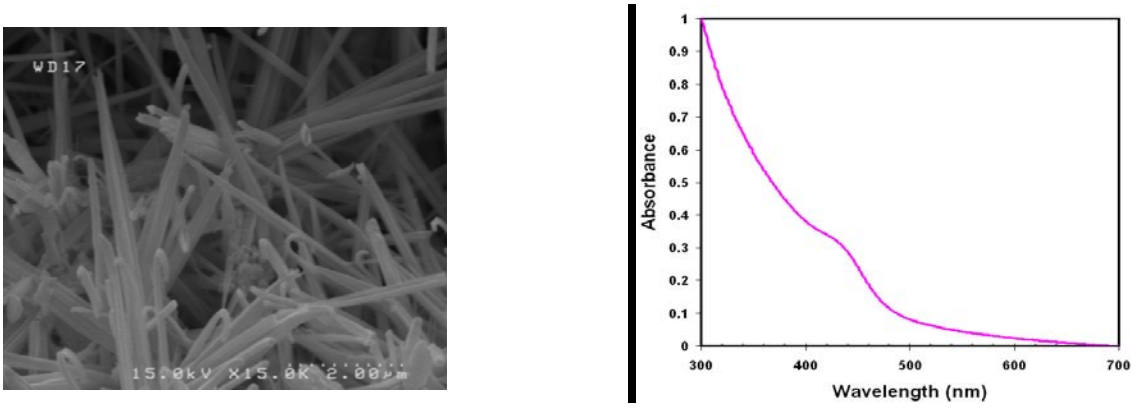

Fig1. SEM image of CdSe nanoneedles (Left) and UV-Vis absorption spectra of citrate-capped CdSe nanocrystals (Right)

Conclusion

The citrate-capped CdSe nanocrystals and nanoneedle were synthesized through a novel green facile room temperature method. The XRD analysis demonstrated that the nanocrystals have a hexagonal structure. The results obtained from UV-Vis absorption data showed that the energy band gap of the nanocrystals was increased by 1.0 eV respect to those the balk material.

Reference

[1] U. Woggon, *Optical Properties of Semiconductor Quantum Dots*; Springer-Verlag: Berlin, Germany, 1997.

[2] A. P. Alivisatos, Science 271 (1996) 933.

[3] Y. Xia, P. Yang, Y. Sun, Y. Wu, B. Mayers, B. Gates, Y. Yin, F. Kim, and H. Yan, Adv. Mater. 15 (2003) 353–89.

Facile Synthesis of Gold Nanoparticles in Aqueous Solutions and Nonlinear Optical Properties

H. Kavian[a], A. Daneshfar[a], M. Nosrati[a], M. H. Majles Ara[b], and R. Sahraei[a,*]

[a]*Department of Chemistry, University of Ilam, Ilam ,Iran*

[b]*Department of Physics, Tarbiat Moallem University, Tehran, Iran*

[*] *(Email: reza_sahrai@yahoo.com)*

Introduction

Metal nanoparticles have close-lying bands and electrons move quite freely. The oscillations of the free electrons in the conduction band occupying energy states near the Fermi level give rise to a surface plasmon absorption band which depends on both the size and chemical surrounding of the metal nanoparticles [1]. Their linear optical characteristics are recognized as being dominated by the surface plasmon resonance (SPR) that also enhances their nonlinear optical response [2].

Experimental

The Au nanoparticles were synthesized by the reduction of Au3- ions in the aqueous starch dispersion. The approach was quite simple and straightforward. In a typical preparation, a 200 µl aliquot of 0.1 M solution of HAuCl4.3H2O was added to 50 ml of a 0.2% (wt) aqueous solution of soluble starch. After complete dissolution of these components, an aqueous solution of NaOH 0.05 M was continuously added drop wise in the system and the pH of solution adjust at 7.0.

Results and discussion

The UV-Vis absorption spectrum of the Au nanoparticles after 5 h, showing the surface Plasmon absorption of these Au nanoparticles, is presented in Figure 1. The position and the width of the plasmon resonance peak can give information about the average diameter of the nanoparticles. The plasmon resonance peak at 520 nm and the low width of this peak can be related to the very small Au nanoparticles with narrow distribution of the particle size.

By properly monitoring the transmittance change through a small aperture placed at the far field position (closed aperture), one is able to determine the amplitude of the phase shift (Fig. 1). Experimental results of z-scan data with an aperture is divided by those without an aperture to obtain pure nonlinear refraction. The peak followed by a valley-normalized transmittance obtained from the closed aperture curves indicates that the sign of nonlinear refractive indices is negative, i.e. self-defocusing

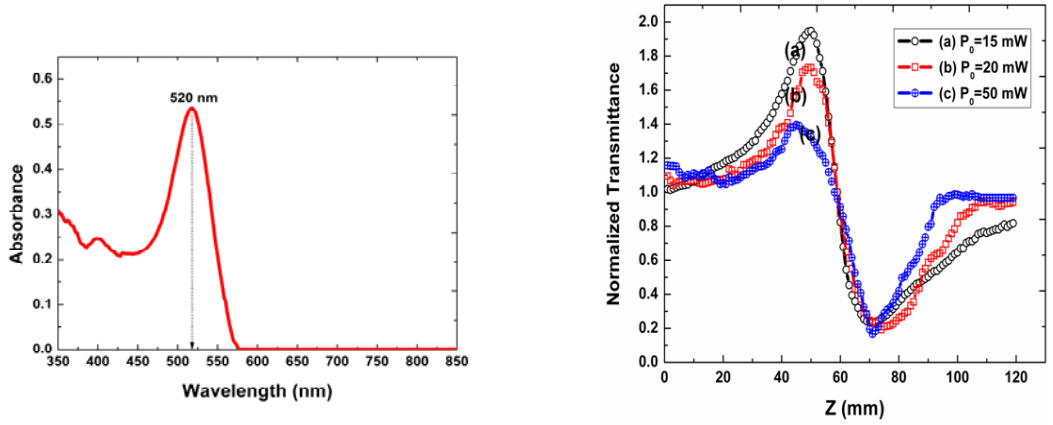

Fig.1: The surface plasmon absorbance spectrum of the gold nanoparticles stabilized in soluble starch solution (Left) and Close aperture z-scan experimental curves of the gold nanoparticles at three incident intensities (Right).

Conclusions

We have reported a simple route for the synthesis of relatively monodisperse gold nanoparticles, reduced and stabilized by soluble starch. The gold nanoparticles stabilized with soluble starch are found to be stable in solution over a period of six months at room temperature and show no signs of aggregation. The average nanoparticles size was obtained from TEM analysis is 16.8 nm that agreed fairly well with UV-Vis absorption spectroscopy results. The z-scan measurements, performed with CW He-Ne laser, revealed that the nonlinear refractive index in this crystal is in the range of 10^{-7} cm^2/W that mostly agrees with result of diffraction pattern.

Keywords

Nanomaterials, Gold nanoparticles, Non-linear optical properties,

References

[1] S. Qu, C. Zhao, X. Jiang, G. Fang, Y. Gao, H. Zeng, Y. Song, J. Qiu, C. Zhu, and K. Hirao, Chem. Phys. Lett. 368 (2003) 352 –358.

[2] Y. Zhang, M. Ma, X. Wang, D. Fu, H. Zhang, N. Gu, J. Liu, Z. Lu, L. Xu, and K. Chen, J. Phys. Chem. Solids 64 (2003) 927–931.

KF/nanoalumina or KF/nanosilica: Versatile catalysts in chemoselective desulfonylation of sulfonamides

Fatemeh Tamaddon,[*a] Fatemeh Aboie,[b] Alireza Nasiri,[b] Mohammad Hossein Moslemin,[b] Mohammad Mirjalili[c]

[a] *Department of Chemistry, Faculty of Science, Yazd University, Yazd, 89195-741, Iran.*

[b] *Department of Chemistry, Islamic Azad University, Yazd Branch, Yazd, Iran*

[c] *Department of Textile, Islamic Azad University, Yazd Branch, Yazd, Iran*

*Corresponding author: Tel.: 00983518122661; fax: 00983518210644

E-mail: ftamaddon@yazduni.ac.ir.

Abstract:

Sulfonylation and desulfonylation of amines and alcohols are fundamental process in organic synthesis which produces sulfonate esters as alkylating agents and sulfonamides as potent pharmaceutical and biological active compounds [1]. While, sulfonylation of amines or alcohols with sulfonyl chlorides requires basic conditions, deprotection of sulfonylated products is also occurred together with the formation of other side products under reaction conditions [2]. Thus, the reaction media is an influential factor governing the protection or deprotection by sulfonylation. It is usually helpful to control the surface area of catalyst, strength of base, solvent and reaction temperature.

Today, solvent-free heterogeneous reactions using nano catalysts are of much interest as eco-friendly and environmentally benign methods [3]. In the continuation of our researches, we report here the catalytic performances of supported KF on alumina or silica nanoparticles in desulfonylation reactions and *NH*- or *O*-sulfonylation under solvent-free conditions using microwave irradiation or thermal conditions (Scheme 1).

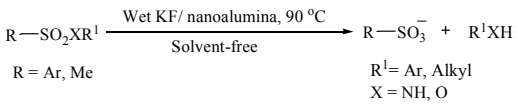

Scheme 1. Desulfonylation of sulfonamides using nano-catalysts

Desulfonylation of sulfonamides can be carried out under solvent-free conditions using preparative KF/nanoSiO_2 and KF/nanoAl_2O_3 as reusable basic heterogeneous catalysts. The

method offers several advantages such as excellent yields, chemoselectivity of the reaction and reusability of the catalysts.

References:

[1] (a) T. W. Green, P. G. M. Wuts, *Protecting Groups in Organic Synthesis*, Third ed., Wiely, NewYork, 1999. (b) A. Scozzafava, T. Owa, A. Mastrolorenzo, C. T. Supuran, *Curr. Med. Chem*. 10 (2003) 925.
[2] (a) A. Kamal, J. S. Reddy, E. V. Bharathi, D. Dastagiri, *Tetrahedron Lett*. 49 (2008) 348. (b) R. Sridhar, B. Srinivas, V. P. Kumar, M. Narender, K. R. Rao, *Adv. Synth. Catal*. 349 (2007) 1873.
[3] (a) A. Schatz, O. Reiser, W. J. Stark, *Chem. Eur. J*. 16 (2010) 8950. (b) Z. Wang, G. Chen, K. Ding, *Chem. Rev*. 109 (2009) 322. (c) J. M. Thomas, W. J. Thomas, *Principles and Practice of Heterogeneous Catalysis*, VCH, Weinheim, 1997.

KF/nanoalumina or KF/nanosilica: Versatile catalysts in chemoselective desulfonylation of sulfonamides

Fatemeh Tamaddon,[*a] Fatemeh Aboie,[b] Alireza Nasiri,[b] Mohammad Hossein Moslemin,[b] Mohammad Mirjalili[c]

[a] *Department of Chemistry, Faculty of Science, Yazd University, Yazd, 89195-741, Iran*

[b] *Department of Chemistry, Islamic Azad University, Yazd Branch, Yazd, Iran*

[c] *Department of Textile, Islamic Azad University, Yazd Branch, Yazd, Iran*

E-mail: ftamaddon@yazduni.ac.ir.

Abstract:

Sulfonylation and desulfonylation of amines and alcohols are fundamental process in organic synthesis which produces sulfonate esters as alkylating agents and sulfonamides as potent pharmaceutical and biological active compounds. In this research, we report the catalytic performances of supported KF on alumina or silica nanoparticles in desulfonylation reactions and *NH*- or *O*-sulfonylation under solvent-free conditions using microwave irradiation or thermal conditions.

Keywords: KF/nanoSiO_2, KF/nanoAl_2O_3, Desulfonylation, Chemoselectivity

Introduction:

Protection of amines and alcohols by sulfonylation is a fundamental process in organic synthesis which produces sulfonate esters as alkylating agents and sulfonamides as potent pharmaceutical and biological active compounds [1]. Sulfonate esters and sulfonamides have been used as protecting groups of *OH* or *NH* functionalities due to easy removal under mild conditions [2]. While, the most common synthetic approach for the sulfonylation of amines or alcohols with sulfonyl chlorides requires basic conditions [3-5], deprotection of sulfonate esters and sulfonamides is also occurred together with other side reactions in similar conditions. A number of basic and neutral catalysts have been reported for the sulfonylation of amines and alcohols, however the development of synthetic methods, enabling easy access to these compounds, are desirable.

Today, according to the progress of green chemistry, mineral supported heterogeneous reactions have been attracted much attention of synthetic chemists [6]. Among these reactions,

solvent-free reactions are of much interest as eco-friendly and environmentally benign methods [7-9].

In the continuation of our researches, we report here the catalytic performances of supported KF on alumina or silica nanoparticles in desulfonylation reactions and *NH*- or *O*-sulfonylation under solvent-free conditions using microwave irradiation or thermal conditions (Scheme 1).

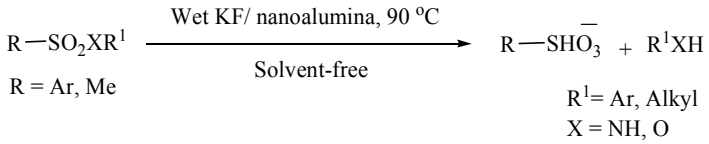

Scheme 1. Desulfonylation of sulfonamides using nano-catalysts

In conclusion, Desulfonylation of sulfonamides can be carried out under solvent-free conditions using preparative KF/nanoSiO_2 and KF/nanoAl_2O_3 as reusable basic heterogeneous catalysts. The method offers several advantages such as excellent yields, chemoselectivity of the reaction and reusability of the catalysts.

References:

[1]A. Scozzafava, T. Owa, A. Mastrolorenzo, C. T. Supuran, *Anticancer and Antiviral Sulfonamides*, 10 (2003) 925.

[2]W. Green, P. G. M. Wuts, *Protecting Groups in Organic Synthesis*, Third ed., Wiely, NewYork, 1999.

[3](a) Y. Wan, X. Wu, M. A. Kannan, M. Alterman, *Tetrahedron Lett*. 44 (2003) 4523, (b) J. Y. Q. Lai, Y. Ferguson, M. Jones, *Synth. Commun*. (2003) 3427.

[4]R. Sridhar, B. Srinivas, V. P. Kumar, M. Narender, K. R. Rao, *Adv. Synth. Catal*. 349 (2007) 1873.

[5](a) A. Kamal, J. S. Reddy, E. V. Bharathi, D. Dastagiri, *Tetrahedron Lett*. 49 (2008) 348, (b) J. I. Levin, M. T. Du, K. Park, *Synth. Commun*. 34 (2004) 2773.

[6] N. Ozbek, H. Katırcıoglu, N. Karacan, T. Baykal, *Bio. Med. Chem*. 15 (2007) 5105.

[7] M. Jafarpour, A. Rezaeifard, M. Aliabadi, *App. Catal. A*: *Gen*. 358 (2009) 49.

[1] A. R. Massah, H. Adibi, R. Khodarahmi, R. Abiri, M. B. Majnooni, S. Shahidi. B. Asadi, M. Mehrabi, M. A. Zolfigol, *Bio. Med. Chem*. 16 (2008) 5465.

G. A. Meshram, V. D. Patil, *Tetrahedron Lett*. 50 (2009) 1117.

One-pot Three Component Synthesis of Octahyroquinazolinone Derivatives Using Nano ZnO Catalyst

Zahra Nasirian, Bahareh Sadeghi*,SalehеZavar

Department of Chemistry, Islamic Azad University, Yazd Branch, Yazd, Iran
Corresponding author E-Mail: bsadeghia@gmail.com

Keywords: Nanoparticles**,** Dimedone, Aldehydes**,** Urea

Introduction:

In recent years, the development of efficient and environmentally benign chemical processes or methodologies for widely used recyclable catalyst and unharmful solvent is one of the major challenges for chemists in organic synthesis. Heterogeneous catalysts can be recovered and reused, whereas homogeneous catalysts are less stable and contaminate reaction mixtures [1]. systems are of great interest and importance due to their applications in industry and developing technologies [2]. The use of solid acids has many advantages over liquid acids such as ease of handling, decreasing reactor and plant corrosion problems, and environmentally safe disposal [3]. Also, wastes and by minimized or avoided by developing cleaner synthesis routes [4]. Octahyroquinazolinone first synthesized by the original multicomponent one Biginelli reaction [5] in 1893, and its derivatives show a diverse range of therapeutical properties and pharmacological activities. The simple and direct method for the synthesis of Octahyroquinazolinone involves the one-pot condensation of an aldehyde, α,β-ketoester and a urea under strongly acidic conditions.

Methods:

Preparation of ZnO nanoparticle:

Aqueous solutions of zinc nitrates and urea were added into a flask under vigorous stirring (300 rpm/min). The molar ratio of Zn^{2}+ to urea was about 1:4. In order to inhibit the growth of the ZnO crystallite during the course of precipitation, a certain amount of surfactant (SDS), was added into reaction system. Then the reaction system was heated to 95^{o}C and maintained at that temperature. After stirring for 2 h, a semitransparent zinc hydroxide colloid was obtained. The precipitates were then filtered, washed with distilled water and alcohol for three

or four times, dried in air at 80°C, and finally calcined at 350°C for 2 h to achieve samples with 30-50nm particle size.

A mixture of the aldehyde, the β-dicarbonyl compound, urea or thiourea and zinc oxide nanoparticles in ethanol was refluxed. The progress of the reaction was followed by TLC. After the completion of the reaction, the mixture was filtered to remove the catalyst. By evaporation of the solvent, the crude product was recrystallized from hot aq. ethanol to obtain the pure compound. All products are known and were identified by comparison of their physical or spectral data with those of authentic samples.

Results and discussion:

In continution of our investigation about application of solid acids in organic synthesis [6] we investigated the synthesis ofOctahyroquinazolinonein the presence of zinc oxide NPs as a inorganic solid acid. To optimize the reaction conditions, the reaction of benzaldehyde, dimedone and ureawas used as a model reaction. According to the obtained data, using the Nano ZnO (0.0009 g) under solvent (EtOH) in reflux is the best condition for the Octahyroquinazolinoneformation. Therefore, some benzaldehyde, dimedone and urea or thioureawere subjected toOctahyroquinazolinone(Scheme 1).

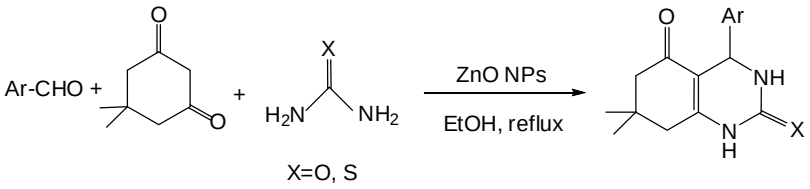

Scheme1. Nano ZnOcatalyzed synthesis of Octahyroquinazolinone.

Conclusion:

In this work we report a mild procedure for the synthesis of different Octahyroquinazolinone by solid phase acidic catalyst with improved yields.

References

[1] Minakata, S.; Komatsu, M. *Chem. Rev.* 711-724.

[2] Sheldon, R.A.; Downing, R.S. *Appl. Catal. A Gen.***1999,**189, 163.

[3] Corma, A.; Garcia, H. *Catal. Today* 308.

[4] Sikdar, S.K.; Howell, S.G. *J. Cleaner Production* **1998**, 253-259.

[5] Biginelli, P. *GazzChim Ital.***1893,** 23, 360.

[6] Sadeghi, B.; Mirjalili, B. F.; Hashemi, M. M. *Tetrahedron Lett.* **2008**, *49*, 2575.

Study of benzothiophene disulfurization by TiO_2 nanoparticles supported on clinptilolite

H.Faghihian[a*] and sh.Naeimib
Department of Chemistry, Islamic Azad University, Shahreza Branch
Email:naeimi_sh@yahoo.com

1.Introduction

Due to increasing environmental concern, special interest has been paid to the reduction of organosulfur compounds in transportation fuels [1]. Hydrodesulfurization (HDS), can remove most sulfur compounds, but some refractory sulfur compounds such as benzothiophene (BT) still stay in diesel oil. As a result, severe conditions such as higher temperature and more active catalysts are required to achieve ultra-low sulfur level of diesel oil [2].One idea that has drawn wide attention, as referred oxidative desulfurization (ODS), involves oxidizing the sulfur compounds [3]. TiO_2 nanoparticles as an photocatalyst can be fixed on an inert supports such as zeolite [4]. In this research, we examined oxidation of model sulfur compound (benzothiophene) in the presence of the photocatalyst synthesized by TiO_2 and clinoptilolite.

2.Experimental

2.1.preparation of TiO_2 nanoparticle

Titanium tetraisopropoxide (TTIP, 97%, Merck) was first mixed with isopropanol. A 250 ml solution of distilled water at various pH was used as the hydrolysis catalyst. Solutions were mixed together under vigorous stirring. The prepared precipitates were washed and dried at 100°C. Then yellow white powder was annealed at temperature from 200 to 800°C .The synthesized TiO_2 was deposited on the surface of clinoptilolite[5].

2.2.Desulfurization

N-hexan solution of BT with known amount of photocatalyst were placed in dark room undr UV irradiation for 0-10 h with magnetic stirring. Reactant samples were collected and analysed by HPLC.The effect of different parameters including amount of photocatalyst, TiO_2 content, irradiation time and initial concentration who studied and optimized.

3. Result and discussion

3.1. characterization materials

FTIR spectra and TEM image of the catalyst are shown in fig 1. It is clear that TiO_2 nanoparticle are immobilized on the surface of the zeolite and the structure of zeolite remaind intact after synthesis.

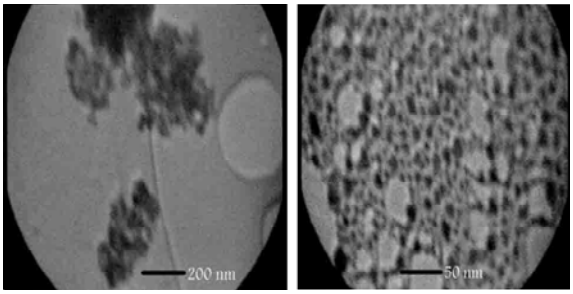

Figure1 (a). TEM image of photocatalyst

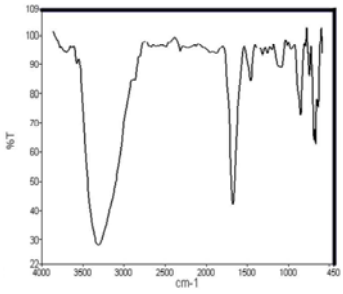

Figure1(b).FTIR spectra of photocatalyst

3.2. Optimization of Desulfurization

Degradation of BT at different experimental conditions were studied. Optimized reaction conditions are as follows: reaction time 300 min, amount of photocatalyst 0.4 g, initial concentration 200mg/L and percent of photocatalyst 20%. The degradation percentage of BT % 92 was obtained.

3.3.Kinetics of the reaction

The rate constant for the reaction was obtained from the pseudo first order equation :

$$-\ln(C_t/C_\circ) = k_p t$$

Where $C_\circ$ and Ct are respectively the concentrations of substrate at time zero and time t(s) and k_p the first-order rate constant (s^{-1}). Application of the equation to the results showed that the photocatalytic oxidation follows first-order kinetics..

4.Conclusion

Photocatalytic oxidation of BT in n-hexan by TiO_2-supported clinoptilolite showed that this photocatalyst is the most highly active catalyst for oxidation desulfurization of BT at UV light irradiation.

Refrences

[1] Lai J; Luo G; J. Petroleum Science and Technology. 27 **(2009)** 781-787

[2] Chao Y; Li H; Zhu W; Zhu G; Yan Y; J. Petroleum Science and Technology. 28 **(2010)** 1242-1249.

[3] Salari D; Rostamizadeh K; J. Petroleum Science and Technology. 26 **(2008)** 382-397.

[4] Li F; Jiang Y; Yu L; Yang Z; Hou T; Sun Sh; J. 252 **(2005)** 1410-1416.

[5] Mahshed S; Askari M; Sasani Ghamsari M; J. Materials Processing Technology. 189 **(2007)** 296-300

DFT Studies of C-doped Boron Nitride Nanocones

Azita Nouri [a,*], Arezu Nouri [b], Mahmoud Mirzaei [c]

[a] Department of Chemistry, Islamic Azad University, Shahr-e-Qods Branch, Shahr-e-Qods, Iran

[b] Central Laboratory, Iran Polymer and Petrochemical Institute, Tehran, Iran

[c] Young Researchers Club, Islamic Azad University, Shahr-e-Rey Branch, Shahr-e-Rey, Iran

E-mail: nouria244@yahoo.com

Keywords: Nanocone; Boron nitride; C-doped; DFT.

Introduction

Curved nanoscale structures such as carbon nanocones as either caps at the ends of carbon nanotubes (CNTs) or free-standing structures have arisen attentions due to their novel properties [1–5]. Another category of these materials are nanostructures composed by boron and nitrogen atoms, so called boron nitride (BN) [6]. Having characteristic property of semi-conducting made BN nanostructures as interesting topics for researchers [6]. In addition to hexagonal rings, pentagonal rings are also present in BN nanocones making the apex tip. Since the apex tip is important in determining the properties of nanaocones, it is important to examine the properties of this tip in pristine and doped conditions. Carbon atom is a common dopant in the chemical environments; hence, we have investigated the properties of pristine and carbon-doped (C-doped) BN nanocones through density functional theory (DFT) calculations.

Methodology

Within this work, the pristine BN nanocone contains 22 B and 22 N atoms and the C-doped model contains 21 B, 21 N and 2 carbon atoms. The mouths of both nanocones are saturated by hydrogen atoms due to avoiding dangling effects (Fig. 1). DFT calculations (B3LYP/6-31G*) are performed to optimize the structures and to calculate the EFG tensors in the optimized structures. The EFG tensors (q_{zz}) are then converted to quadrupole coupling constants (C_Q) employing C_Q (MHz) = $e^2Qq_{zz}h^{-1}$ [7]. All calculations are performed using the Gaussian 98 software [8].

Results and Discussions

Two sides of the C-doped BN nanocone are shown in Fig. 1 (panels a and b) and the obtained results are listed in Tables 1 and 2. One B and one N atom are doped by two C atoms at the apex tip. To make the analysis easier, the structure is divided into eight layers based on similarities of properties for atoms of each layer. The first layer is the mouth of nanocone and the eighth layer is the apex tip. As shown in Fig. 1, the atoms of mouths and apex tips are different in the two sides of nanocone. The optimization processes yield the averaged values of bond lengths as indicated by $d_{B\text{-}N}$=1.44 Å, $d_{B\text{-}C}$=1.54 Å, $d_{N\text{-}C}$=1.41 Å, and $d_{C\text{-}C}$=1.41 Å. The values of total energies indicate that the pristine model could be more stable than the C-doped model. The value of dipole moment is increased from 6.80 Debye in the pristine model to 7.91 Debye in the C-doped BN nanocone which means that the polarizability of the nanocone is increased due to the C-doped region. The values of gap energy are 5.66 and 5.31 eV for the pristine and the C-doped models, respectively, which indicates that the conducting property is slightly increased in the C-doped BN nanocone.

The C_Q properties for the ^{11}B and ^{14}N atoms are divided into layers due to similarities of properties for atoms of each layer. The results indicate that the largest magnitudes of the C_Q properties are for the atoms at mouth and at the apex tip of the pristine model which are important positions of nanocones in determining their properties. In the C-doped model, the mouth has still the largest value for the C_Q properties; however, the atoms of the seventh layers significantly detect the effects of the C-doped region as could be seen by changes of their C_Q properties with respect to the pristine nanocone. The properties of some other N atoms also detect the effects of the C-doped region; however, the properties of B atoms of other layers are remained unchanged.

Conclusion

The properties of the pristine and the C-doped models of the BN nanocone have been investigated by DFT calculations. The results of the optimization processes indicated different stabilities, polarizabilities, and conducting properties for the pristine and the C-doped BN nanocones. Moreover, the C_Q properties indicated that the apex tip and the atoms close to this tip are important in determining the properties of BN nanocones.

Table 1: Optimized properties for BN nanocones

Property	Pristine		C-Doped	
	B	N	B	N
Ptal energy (eV)	3.44	1.70	-47877	2.08
Gap energy (eV)	2.03	1.24	5.66	5.31
Dipole moment (Debye)	2.87	1.09	6.80	7.91

Table 2: C_Q properties /MHz for BN nanocones *

Layer	Pristine		C-Doped	
	B	N	B	N
Layer 1	3.44	1.70	-47877	2.08
Layer 2	2.03	1.24	5.66	5.31
Layer 3	2.87	1.09	6.80	7.91
Layer 4	2.98	1.04	2.98	1.04
Layer 5	2.86	1.08	2.87	1.09
Layer 6	3.16	1.75	3.09	1.86
Layer 7	2.90	0.98	3.00	2.38
Layer 8	3.09	1.70	C-Doped	C-Doped

* Averaged values for atoms of each layer are reported.

Figure 1. The 2D views of the C-Doped BN nanocone. The pristine model does not contain the C atoms.

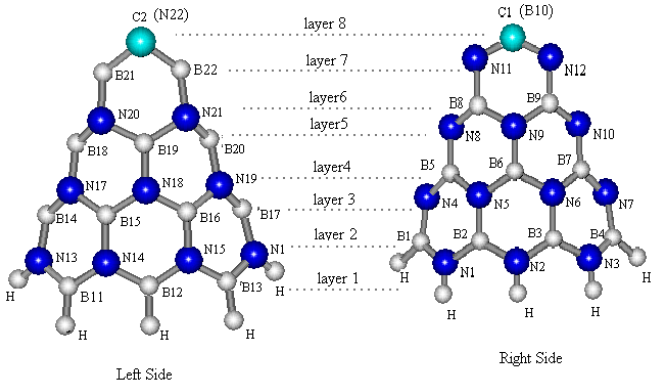

Refrences:

[1] S. Iijima, Nature 354 (1991) 56.

[2] G.N. Murthy, A. Auerbach, Phys. Rev. B 46 (1992) 331.

[3] S. Iijima, T. Ichihashi, Y. Ando, Nature 356 (1992) 776.

[4] M. Ge, K. Sattler, Appl. Phys. Lett. 64 (1994) 710.

[5] M. Ge, K. Sattler, Chem. Phys. Lett. 220 (1994) 192.

[6] A. Rubio, J.L. Corkill, M.L. Cohen, Phys. Rev. B 49 (1994) 5081.

[7] M. Mirzaei, A. Nouri, M. Giahi, M. Meskinfam, Monash. Chem. 141 (2010) 305.

[8] M.J. Frisch, et al., GAUSSIAN 98, Gaussian, Inc., Pittsburgh, PA, 1998.

Synthesis and Characterization of Oxidized Polyethylene wax of Arak Petrochemical Complex and Preparation of Nanocomposite Based on Organoclay

Davood Soudbar*[a], Zahra Hashemi [b], Hadi Irannezhad [b],Fatemeh moradtajari [b]

[a]. *Research and Development of Arak Petrochemical Company Complex*

[b]*Department of Chemistry, Azad Islamic University of Arak*

dsoudbar@yahoo.com& z_hashemi89@yahoo.com

Abstract:Low molecular weight polyethylene (wax) was produced as a byproduct during of polyethylene production by slurry – phase processes in hexane. This compound is soluble in hexane and isolated in separation section. Molecular weight fractionation of wax was performed by heptane as solvent then wax separated samples were oxidized at presence of air by benzoyl peroxide as catalyst at free solvent condition for production of oxidized wax. At finally in this research nanocomposite was prepared by solution technique based on oxidized wax and different concentration of organoclay.The microstructure of these composites was characterized by SEM and XRD. SEM and XRD confirmed the intercalated structure of nanocomposite and also thermal stability and swelling behaviour of nanocomposite were studied.

Keyword: Polyethylene wax, Benzoyl peroxide, Organoclay, Nanocomposite.

1-Introdution: Wax is valuable and applicable in widespread industrial applications such as coating, lubricating, and etc. Oxidized polyethylene wax (OPW) due to its polarity is used as lubricant for extrusion of PVC, polystyrene, polycarbonate, polymethylmethacrylate and other polar resins (pipes, sheets, profiles etc.) [1, 2]. Polymer clay mineral nanocomposites have attracted great interest both in industry and in science. The kind of nanocomposites exhibit improved properties compared to their micro or macro composites due to the fine phase dimensions and phase structure involved [3].Polymer /clay nanocomposite can be prepared by many methods. Including in situ polymerization intercalation, solution intercalation, melt intercalation and aqueous clay dispersions. The OMMT / OPW nanocomposites were prepared by solution intercalation in heptan solvent.In this research for

improvement in thermal property, barrier property and flame-retardant of oxidized wax, organo – montmorillonite (OMMT) was added to oxidized wax.

2-Experimental

2-1.Material

Polyethylene wax was prepared from ARPC(Arak Petrochemical Complex) and other materials were obtained and used from MERCK company without purification.

The organoclay (Cloisite15A) was obtained Rockwood Company.Cloisite15A is a nanoclay modified with dimethyl dehydrogenated tallow quaternary ammonium, specification of this compound is shown in(table1).

.

Modifier Concentration	**12 meq/100g Nanoclay**
Moisture%	**<2**
Density g/ml	**1.66**
X-Ray analysis	**d_{001}=31.5 A˙**

Table 1: Specification of Cloisite 15A

2-2. The preparation of OMMT/OPW nanocomposites

Oxidized polyethylene wax nanocomposites were obtained by the solution method.The organoclay modified layered (Closite15A) was dissolved in the heptane white continuous stirring, and then OPW solution in Heptane was added to the organoclay-heptanen solution. The mixture was vigorously stirred for 12 h.The amounts of added organoclay in OPW were 1,3,5 % .

3- Results and Discussion

XRD pattern of nanocomposite is typically with 5% nanoclay shown in(figure1).The basal spacing of the nanocomposite was increased to 102.36Å relative to orgaoclay 31.50Å(table 1),that it proves structure of nanocomposite is intercalated.

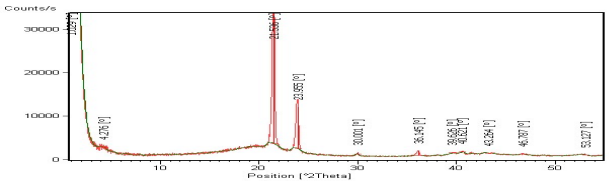

Fig.1-XRD pattern of OMMT/OPW nanocomposite

SEM micrograph (figure 2) showed that the layered silicates were dispersed informally in the OPW matrix at a nanoscal size,which indicated the formation of OPW nanocomposite.

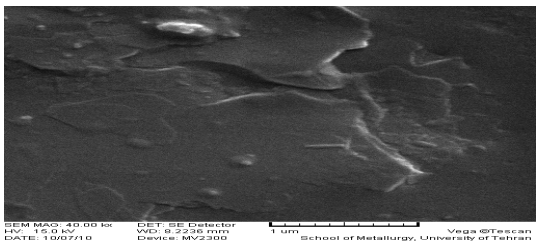

Fig.2-SEM micrograph of OMMT/OPW nanocomposite

(Fig3) shows the effects of organoclay on thermal stability of OPW, with increasing organoclay in OPW, thermal stability is improved.

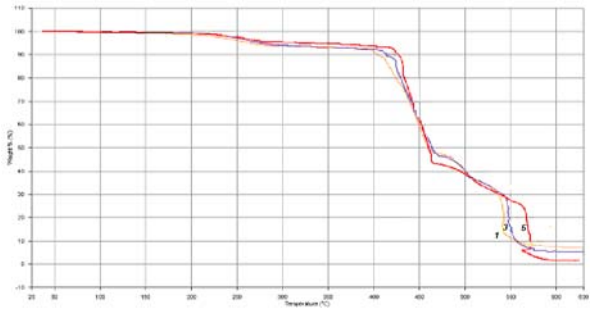

Fig .3- The effects of organoclay on thermal stability of OPW

(Fig.4) shows swelling behavior of nanocomposites in water media absorption decreased with increasing organs clay content. The precents of nano clay–dispersed impermeable OMMT layer with excellent barrier properties decreased the rate of transportation by Lengthening the average diffusion path length in WAX matrix .

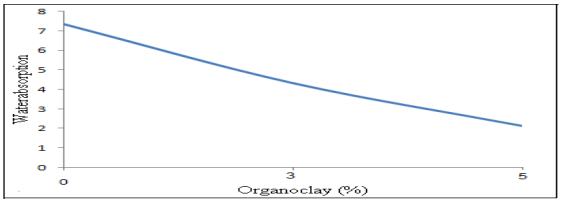

Fig.4 swelling behavior of nanocomposites In water

4-Conclusion: OMMT/OPW nanocomposites were prepared by solution technique.XRD analysis indicated that the OPW chain were intercalate. The OMMT/ OPW nanocomposites exhibited excellent thermal stability and swelling behavior, which is attributed to the improvement of the barrier properties of nana composites.

References:

[1]Basell, *The Technology Manual of High Density Polyethylene Plant* **2008**
[2]I. Krupa, *J. Polym*. **2003**, *42*, 7258
[3]Seng, Chai; Zhong, Yi Zhang. International Journal of Materials Engineering Innovation **2009**

Kinetics, thermodynamic and equilibrium isotherms of bromothymol blue adsorption on multi walled carbon nano tube and cadmium hydroxid nano particle loaded on activated carbon

M. Ghaedi[a]*, H. Khajesharifi[a], A. Hemati Yadkouri[a], A. Sahraei[b]

[a] Chemistry Department, Yasouj University, Yasouj, 75914-35, Iran

[b] Chemistry Department, Ilam University, Ilam, 65315-516, Iran

*E-mail: m_ghaedi@mail.yu.ac.ir

Abstract

In this research, efficiency and performance of multi walled nano tube carbon and cadmium hydroxide nano particle loaded on activated carbon (CNPC) adsorbents for the removal of bromothymol blue (BTB) from wastewater has been compared. BTB was used as the model compound due to its wide range of applications and high stability in the environment. The maximum removal was more than 98% for 25 μg mL^{-1} of BTB concentration on 0.1 g L^{-1} both adsorbents. The influence of variables including pH, concentration of the dye, amount of adsorbents, contact time and temperature on the BTB removal has been investigated in batch method by one at a time optimization method. The graphical correlation of various adsorption isotherm models like, Langmuir, Freundlich and Tempkin have been carried out for these adsorbents. Calculation of various thermodynamic parameters such as, Gibb's free energy, entropy and enthalpy of the on-going adsorption process indicate feasibility and endothermic nature of BTB adsorption on all adsorbents. The kinetic studies suggest the process following pseudo second order kinetics and involvement of particle diffusion mechanism.

Keywords: Adsorption; Bromothymol blue; Multi walled carbon nano tube; Cadmium hydroxide nanoparticle loaded on activated carbon (CNPC); Kinetic and Thermodynamics of Adsorption.

Introduction

Nano particle have very interesting physicochemical properties, such as ordered structure with high aspect ratio, ultra-light weight, high mechanical strength, high electrical

conductivity, high thermal conductivity, metallic or semi-metallic behavior and high surface area [1, 2]. In this research, efficiency and performance of multi walled nano tube carbon and cadmium hydroxide nanoparticle loaded on activated carbon (CNPC) adsorbents has been applied for BTB removal from wastewater and their efficincy was compared. BTB was used as the model compound due to its wide range of applications and high stability in the environment.

Experimental and results

In the first CNPC were prepared by chemical plating method. This new adsorbent was characterized scanning electron microscopy (SEM), while it surface functional groups was recognized by FTIR analysis.

The influence of variables including pH, concentration of the dye, amount of adsorbent, contact time and temperature required for efficient removal of BTB from 50 mL of 25 µg mL^{-1} sample has been investigated. The system is suitable for quantitative removal of this dye from such solution at pH 1 using 0.005 g CNPC, equilibrium time of 9.5 min even temperature of 50 °C. The graphical correlation of various adsorption isotherm models like, Langmuir, Freundlich and Tempkin have been carried out for this adsorbent. Calculation of various thermodynamic parameters such as, Gibb's free energy, entropy and enthalpy of the on-going adsorption process indicate feasibility and endothermic nature of Bromothymol blue adsorption on all adsorbents. The kinetic studies suggest the process following pseudo second order kinetics and involvement of particle diffusion mechanism

Conclusion

The cadmium hydroxide nano particle loaded on active carbon and multi walled carbon nano tube are identified to be an effective adsorbent for the removal of BTB from aqueous solutions. It was observed that batch sorption using multi walled nano tube carbon and CNPC were dependent on parameters such as initial concentration of dye, time, pH, dose of adsorbent and type of dye. The equilibrium and kinetic studies were made for the adsorption of dyes from aqueous solutions onto BTB. Adsorption parameters for the Langmuir, Freundlich and Tempkin isotherms were determined and the equilibrium data were best described by the Langmuir model. The process is endothermic in nature and its kinetics can

be successfully fitted to pseudo-second-order kinetic model. The results of the intraparticle diffusion model suggested that intraparticle diffusion was not the only rate controlling.

References

[1] M. Arami, N. Y. Limaee, N. M. Mahmoodi, N.S. Tabrizi, J. Colloid Interface Sci. 288(2005)371–376.

[2] F. D. Ardejani, K. H. Badii, N.Y. Limaee, N.M. Mahmoodi, M. Arami, S.Z. Shafaei, A.R. Mirhabibi, Dye Pigm. 73 (2007) 178–185.

Far-UV and Near-UV CD spectroscopic investigation of the interaction between Colchicine and Human serum albumin as a model for drug therapy

M.Vahidzadeh[1], M.Gharanfoli[2] and J. Chamani[1]

1. Department of Biology, Faculty of Sciences, Islamic Azad university–Mashhad Branch, Mashhad, Iran

2. Department of Development of Biology University of Science and Culture, Tehran, Iran

Abstract

Circular dichroism (CD) is being increasingly recognized as a valuable technique for examining the structure of proteins in solution. Change in structure of human serum albumin (HSA) in intraction of cochisine was studied by circular dichroism (CD) spectroscopy. Results show that in the presence of drug both secondary and tertiary structural changed.

Keywords: *Circular dichroism spectroscopic, Ligand binding, HSA, Colchicines*

Introduction

Human serum albumin (HSA) is the most abundant protein in human blood plasma and has high affinity to many endogenous and exogenous compounds, serving as a solubilizer and transporter for drugs and other organic molecules to their targets [1]. Colchicine, a plant alkaloid, is one such molecule that can bind tubulin and inhibit tubulin polymerization in animal cells, leading to mitotic arrest. Although colchicine itself is not used as an anti-mitotic drug due to its severe side effects, several synthetic anti-mitotic drugs, derived from colchicine, have immense pharmacy-logical importance [2]. Circular dichroism (CD) has become increasingly recognized as a valuable structural technique for addressing these issues. These CD contributions are very sensitive to changes in the environment of the chromophore and are therefore well suited to follow changes in the secondary and tertiary structure as well as the binding of ligand and protein–ligand interactions, provided that a conformational change occurs upon binding. Because the occurrence of aromatic side chains and disulfides is generally low compared to the total number of amino acids, the CD signal in the near UV-region is at least an order of magnitude lower than the far UV-CD signal. The aim of this

study is to analyze the interaction of COL with HSA; also the effect of drugs on the structure of protein was estimated.

Methods

Circular dichroism (CD) is an optical phenomenon resulting from the interaction of polarized light with chromophore that is either inherently chiral or placed in an asymmetric environment.

Results and discution

In proteins, the major optically active groups are the amide bonds of the polypeptide backbone and the aromatic side chains. Whereas the CD signal of the former can be monitored in the so-called far UV-region (i.e., at wavelengths below 260nm), the signal of the latter chromophore is observed in the near UV-region (260–310nm). The far UV-CD signal arises from the optical transitions of the amide bonds, which depend on the orientation of the peptide planes in the well-ordered secondary structure elements. Exploiting this phenomenon the overall secondary structure of proteins in solution can be determined, disclosing the main conformational motives such as α -helices, β -sheets, β -turns, and random coil (for reviews see [3]. In the near UV-region, aromatic side chains and cystines (disulfide bridges) exhibit absorption. Table 1 shows change in structure of HSA in absence and presence of COL by far-UV CD method. HSA shows a decrease in α -helical structure and an increase in β -sheet in the presence of COL, suggesting the interaction between COL and HSA has been occurred. The decrease of α -helix content suggests that the HSA molecules probably adopt a looser conformation with the extended polypeptide structures. Fig. 1(A,B) shows the near-UV CD spectra of HSA and HSA in the presence of COL, Fig. 7B shows in the presence of COL curve of HAS decresed, it means that presence of COL tertiary structural in the environment of the disulfide bonds and aromatic amino acid residues changed.

Table. 1. Secondary structure of HSA derived from the far-UV CD spectrum for binary and ternary systems.

system	α -helix %	β -sheet %	Turn %	Unordered coil %
HSA	53.88	18.35	13.50	14.27
HSA-COL	48.25	19.61	14.35	17.79

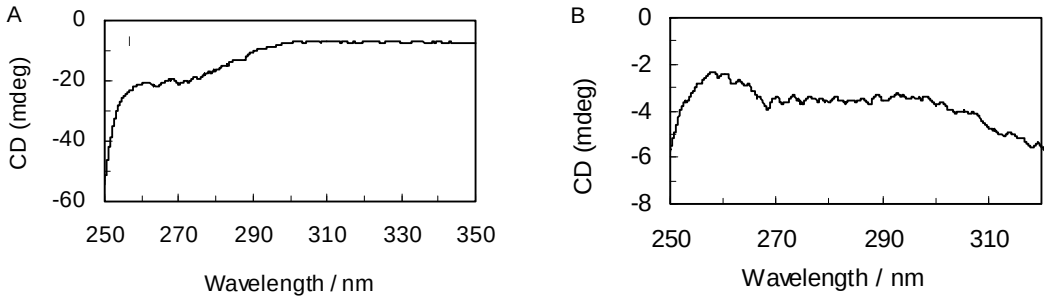

Fig.1. Near-UV CD spectra of HAS (A) and HSA-COL (B) were measured at pH 7.4.

Conclusion

The circular dichroism results evidenced partial unfolding of the protein and change in secondary an tertiary structure of HSA by binding COL.

Reference

[1] X. Hou, X. Tong, W. Dong, Sh. Shuang, Spectrochimica Acta Part A. 66 (2007) 552–556.

[2] M.Banerjee, D. Roy, B. Bhattacharyya, G. Basu, FEBS Letters. 581 (2007) 5019–5023.

[3] S.Y. Tetin, F.G. Prendergast, S.Y. Venyaminov, Analytical Biochemistry, 321 (2003) 183–187.

Investigation on adsorption capacity of TiO_2-P25 nanoparticles in the removal of a model contaminant from aqueous solutions.

M.A. Behnadjady[a], SH. Yavari[*b], N. Modirshahla[a], M. Eissanezhad Boushehri[b]

[a]*Department Chemistry, Faculty of Sciences, Islamic Azad University Tabriz Branch, Tabriz, I.R. Iran,* [b]*Member of chemistry scientific association, Department Chemistry, Faculty of Sciences, Islamic Azad University Tabriz Branch, Tabriz, I.R. Iran.*

[*]*E-mail:shahrzad.yavari@yahoo.com*

The decolourization of dye effluents has received increasing attention, thus various chemical, physical and biological treatment methods have developed for the removal dyes from aqueous solutions, including precipitation, coagulation-flocculation, reverse osmosis, oxidation with ozone, chlorine or hydrogen peroxide, use of anion exchange membranes and bacterial cells [1-3]. Adsorption has proven to be a reliable treatment methodology due to its low capital investment cost, simplicity of design, ease of operation and insensitivity to toxic substances, but its application is limited by the high price of some adsorbents and the large amounts of wastewater normally involved. Activated carbon [4,5], mesoporous carbon [6], clay minerals [7], hydrotalcite [8], biopolymers such as chitosan beads and quaternary chitosan and agriculture by-products are a few of the adsorptive materials that have been tested for the treatment of wastewaters. The aim of this work is to estimate Degussa TiO_2 P25 nanoparticles adsorption capacity in the removal of commercial monoazo dye C.I. Acid Red 27 in different conditions.

All adsorption experiments were carried out at the temperature of 25 ºC± 2. The variation of the AR27 concentration versus time in the supernatant aliquot has been observed under various conditions such as initial pH (3, natural and 9), initial dye concentration (10, 20, 40, 60 and 80 mg L^{-1}) and adsorbent amount (0. 2 and 1 g L^{-1}). A stock solution of AR27 dye was prepared in 200 mg/L concentration and then diluted to the presented concentrations. The initial pH was adjusted to the required value with small amount of HCl or NaOH solutions before mixing with the TiO_2 (Degussa P25). Samples were taken at 5 min intervals, centrifuged at 6000 rpm for 20 min and then analyzed by UV-Vis spectrophotometer.

In Fig. 1 the XRD pattern of TiO_2 nanoparticles (P25) for 2θ diffraction angles between 5 º and 70 º shows five primary peaks at 25.2 º, 38 º, 48.2 º, 55 º and 62.5 º which can be

attributed to different diffraction planes of anatase TiO_2 and four different peaks at 27.5 º, 36 º, 54 º and 69 º which can be attributed to different diffraction planes of rutile form of TiO_2. These results showed that TiO_2-P25 is almost 80% anatase and 20% rutile. The average particle size (D in nm) of TiO_2 nanoparticles was determined from XRD pattern according to the Scherrer's equation as 18 nm. These nanoparticles have high surface area (50 m^2 g^{-1}) and can be used for efficient adsorption of environmental pollutants with optimization of operational parameters.

The effect of initial pH on the adsorption yield of AR27 onto P25 at 25 ºC after 20 min equilibration, for adsorbent concentration 0.2 and 1 g L^{-1} and initial dye concentration 60 mg L^{-1} is depicted in Fig. 2.

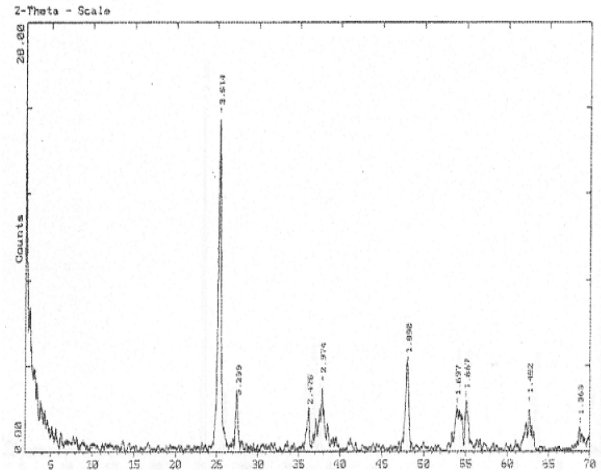

Fig. 1. XRD pattern of Degussa P25 TiO_2 nanoparticles.

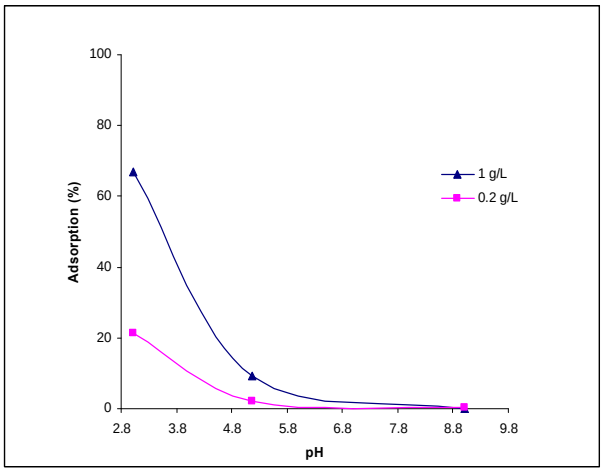

Fig. 2. Effect of initial pH on the adsorption of AR27 on Degussa P25 TiO_2.

The rate constant of adsorption was determined from pseudo-second order model calculated correlations are equal to unity that confirms this model for adsorption of AR27 onto TiO_2 P25 (Fig. 3).

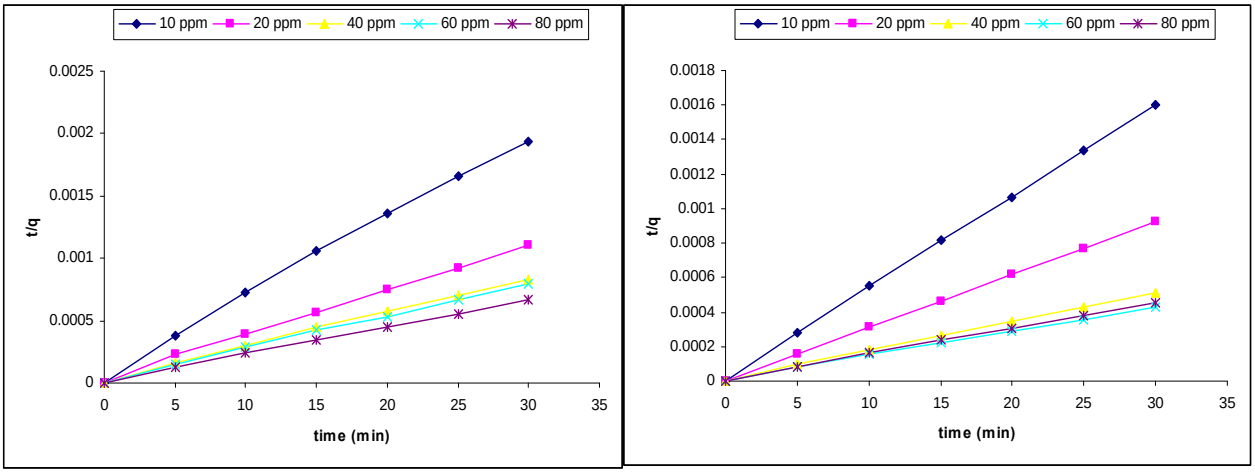

Fig. 3. Effect of dye cocentrations on the rate costant of TiO_2 P25 adsorption.A) 0.5 g L^{-1} and B) 1 g L^{-1} of catalyst

Results indicated that at acidic pH values high electrostatic attractions existed between the positively charged surface of the adsorbent and anionic dye. Optimal dye sorption occurred at pH 3. Adsorption of AR27 by P25 reached equilibrium within 20 min and results of adsorption showed that P25 nanoparticles can be effectively used as a sorbent for the removal of anionic dyes in solutions of a wide region of dye concentration. The kinetic model results show that the pseudo-second order constant decrease with increasing of initial dye concentration from 10 to 80 mg L^{-1}.

Keywords: TiO_2 P25 nanoparticles, Anionic dyes, Adsorption, AR27.

Reference:

[1] T. Robinson, G. McMullan, R. Marchant, P. Nigam, Remediation of dyes in textile effluent: a critical review on current treatment technologies with a proposed alternative, Bioresour. Technol. 77 (2001) 247–255.

[2] P. Cooper, Removing colour from dyehouse waste waters—a critical review of technology available, J. Soc. Dyers Colour. 109 (1993) 97–100.

[3] Y.M. Slokar, A.Majcen Le Marechal, Methods of decoloration of textile wastewaters, Dyes Pigments 37 (1998) 335–356.

[4] P.K. Malik, Dye removal from wastewater using activated carbon developed from sawdust: adsorption equilibrium and kinetics, J. Hazard. Mater. B113 (2004) 81–88.

[5] E. Demirbas, M. Kobya, M.T. Sulak, Adsorption kinetics of a basic dye fromaqueous solutions onto apricot stone activated carbon, Bioresour. Technol. 99 (2008) 5368–5373.

[6] D.D. Asouhidou, K.S. Triantafyllidis, N.K. Lazaridis, K.A.Matis, S.-S. Kim, T.J. Pinnavaia, Sorption of reactive dyes from aqueous solutions by ordered hexagonal and disordered mesoporous carbons, Micropor. Mesopor. Mater. 117 (2009) 257–267.

[7] S.D. Lambert, N.J.D. Graham, C.J. Sollars, G.D. Fowler, Evaluation of inorganic adsorbents for the removal of problematic textile dyes and pesticides, Water Sci. Technol. 36 (1997) 173–180.

[8] N.K. Lazaridis, T.D. Karapantsios, D. Georgantas, Kinetic analysis for the removal of a reactive dye fromaqueous solution onto hydrotalcite by adsorption,Water Res. 37 (2003) 3023–3033.

Nickel Nanowire Phase Transitions under Tensile Deformation: A Molecular Dynamics Approach

S. Yousefi [1,*], A. Akbari [1], M. Foroutan [2]

1- Department of Material Engineering, Sahand University of Technology, Tabriz, Iran.

2- Department of Physical Chemistry, School of Chemistry, College of Science, University of Tehran, Tehran, Iran.

syousefi81@gmail.com

Introduction

Nanowires have been studied intensely for nearly a decade due to their unique mechanical, electrical and optical properties that arise because of their nanometer size scale [1]. Among all nanowires, metal nanowires have attracted a lot of interest because of their appealing properties such as high thermal and electrical conductivity, and quantized conductance [2]. They can be used as nanoscale interconnects and active components of both optical electronic devices and nano electromechanical systems. In these applications, the electronic, magnetic, or optical properties of nanowire-based devices can be strongly affected by their deformation and shape changes, since they interact with each other mostly through surfaces.

In order to control their functionality, hence, the mechanical responses of nanowires need to be well characterized prior to any practical applications [3]. Atomistic and molecular dynamics (MD) simulations of nanowires have been utilized to give insight into the nanowire mechanical behavior and deformation mechanisms. This research is aimed at understanding the phase transitions behavior of metallic nanowires, through the use of molecular dynamics simulation.

Simulation Method

As shown in figure 1, a square cross-section nickel nanowire is created out of a bulk face-centered cubic fcc crystal with the dimension of 20a×9a×9a (a is lattice parameter, 0.352nm). The surface orientations are [100], [010] and [001] in X, Y and Z directions. The MD simulations performed in this work used the embedded atom method (EAM) [4], as the underlying atomic interaction model. For the EAM, the total energy U for a system of atoms can be written as

$$U = \sum_i^N (F_i(\rho_i) + \frac{1}{2}\sum_{ij} \phi_{ij}(r_{ij})) \quad , \quad \rho_i = \sum_j f(ij)$$

where the summations in above equation extend over the total number of atoms N in the system, F_i is the embedding function, ρ_i is the electron density at atom i, ϕ_{ij} is a pair interaction function, f is the contribution to the electron density at atom i due to atom j and r_{ij} is the distance between atoms i and j. In this simulation the time-step (Δt) was set at 1.0fs. The nanowire shown in figure 1 was first allowed to attain thermal equilibration at 300K based on Nose-Hoover thermostat.

Results and Discussion

During relaxation process, it was observed that there were some residual tensile stresses in the thermally equilibrated nanowire. From the simulation thermal equilibrium was achieved in about

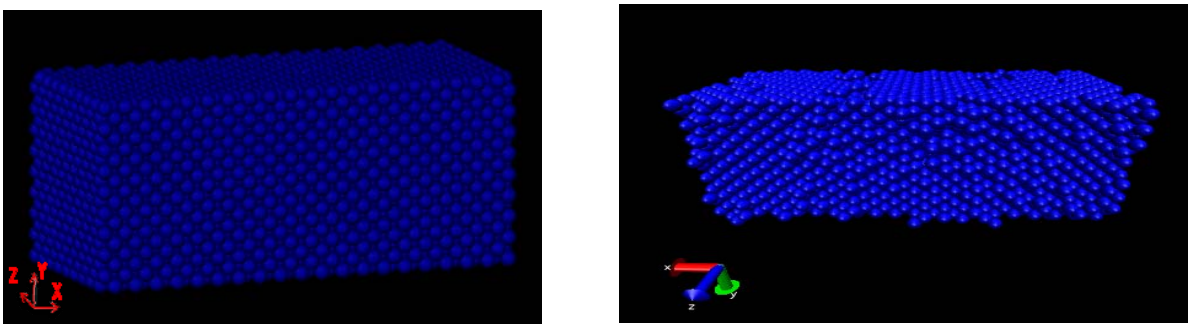

Figure 1. Left diagram shows the initial configuration and the right diagram shows thermally relaxed configuration of Ni nanowire.

130,000 time steps. Since the program has been restarted every 2000 to attain data, some data has been lost (figure 2). This process was continued until nanowire stress upon thermal equilibration was within a near-zero range of ±2MPa, which signifies total relaxation of nanowire was achieved.

The final results for phase transition after tensile loading of the nanowire will be added soon.

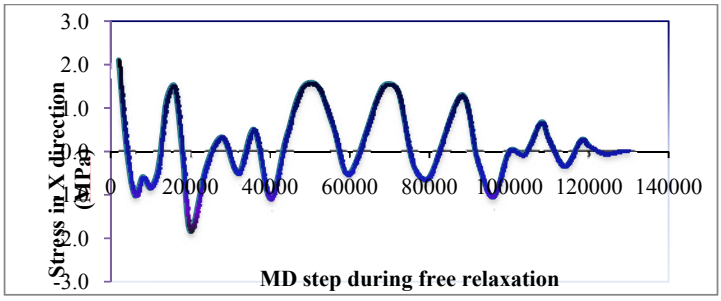

Figure 2. Variation of stress during relaxation process

References

[1] H. S. Park, K. Gall, J. A. Zimmerman, J. Mech. Phys. Solids 54 (2006) 1862.

[2] V. K. Sutrakar, D. R. Mahapatra, J. Phys. Condens. Matt. 20 (2008) 335206.

[3] Y. G. Zheng, H. W. Zhang, Z. Chen, L. Wang, Z. Q. Zhang, and J. B. Wang, Appl. Phys. Lett. 92 (2008) 041913.

[4] M.S. Daw, M. I. Baskes, Phys. Rev. B 29 (1984) 6443.

Quantum Mechanics

&

Spectroscopy

Synthesis, spectroscopy and quantum chemical calculation study of two novel 1,3,2-diazaphospholidine-2,4,5-triones

N. Oroujzadeh*[a], Kh. Gholivand[a], F. Afshar[b]

[a]Department of Chemistry, Tarbiat Modares University, Tehran, Iran

Email: N_oroujzadeh@yahoo.com

[b]Islamic Azad University, Garmsar Branch, Garmsar, Iran

Keywords: Diazaphospholidine, Dynamic NMR, Quantum chemical studies, Tautomeric interconversion

Carbacylamidophosphate compounds with general formula R'C(O)NHP(O)R2 have a decisive role in catalytic and metabolism processes [1–3], and many applications in agricultural and pharmacological industries [4–6]. This wide range of applications has stimulated a great research effort involving preparations and characterizations of compounds possessing the C(O)NHP(O) moiety [7–10]. In the present study, two new cyclic diazaphospholidine species, (**I**) and (**II**) (as below) have been synthesized by the reaction of $POCl_3$ with the carboxylic diamide (oxamide) salt. The characterization of the products was carried out by IR, ^{1}H, ^{13}C, ^{31}P NMR spectroscopy, elemental analysis and also mass spectrometry for compound (**I**).

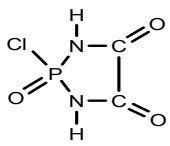

(I)

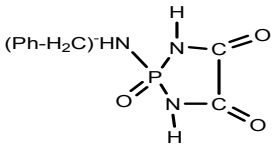

(II)

Both compounds show two signals at room temperature in the low field region of the ^{1}HNMR spectrum, which collapsed to a single peak when the temperature is increased. Dynamic NMR (^{1}H DNMR) and quantum chemical studies were performed to gain insight from this conversion process. The free activation energies, calculated at the coalescence temperatures are 18.51 and 17.45 kcal/mol for compounds (**I**) and (**II**), respectively, which are associated with a tautomeric interconversion process, most likely between the lactam and lactim forms.

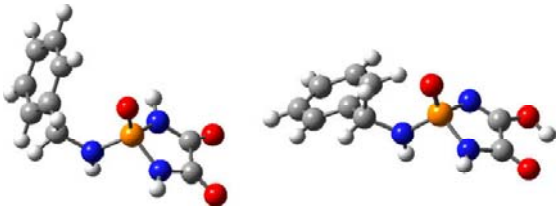

Molecular models for the most stable tautomeric forms of compound **II**

The relative energy, molecular geometry and vibrational properties of several plausible tautomers were analyzed by using quantum chemical calculations at the HF/6-311G** and B3LYP/6-311++G** levels of the theory.

Calculated relative energies (corrected by zero-point energy) in kcal mol^{-1} for the different tautomers and conformers of compound **I**

Tautomer	HF/6-311G**	B3LYP/6-311++G**	PCM/B3LYP /6-311++G** [a]
A	0.00	0.00	0.00
B	9.67	9.74	9.32
C	10.10	9.00	11.50
D	27.98	26.13	24.38
E	24.19	23.49	20.82
F	–[b]	37.46	30.92
G	26.04	24.65	21.08

[a] DMSO dielectric constant was used in the PCM calculations. [b]Converges to structure

References:

[1] C. Schultz, Bioorg. Med. Chem. 11 (2003) 885.

[2] L.Y. Wu, J.C. Do, M. Kazak, H. Page, Y. Toriyabe, M.O. Anderson, C.E. Berkman, Bioorg. Med. Chem. Lett. 18 (2008) 281.

[3] T.K. Venkatachalam, M. Sarquis, S. Qazi, F.M. Uckun, Bioorg. Med. Chem. 14 (2006) 6420.

[4] D.E.C. Corbridge, Phosphorus: An Outline of its Chemistry, fifth ed., Biochemistry and Technology, Elsevier, Amsterdam, 1995.

[5] C.-B. Xue, Y.-W. Yin, J. Chem. Soc. Perkin Trans. 2 (1990) 431.

[6] Kh. Gholivand, C.O. Della Védova, M.F. Erben, F. Mojahed, A.M. Alizadehgan, J. Mol. Struct. 840 (2007) 66.

[7] K.E. Gubina, V.A. Ovchynikov, V.M. Amirkhanov, T.Y.U. Silvia, V.V. Skopenko, T. Glowiak, H. Kozowski, Z. Naturforsch. 54B (1999) 1357.
[8] Kh. Gholivand, M. Pourayoubi, Z. Shariatinia, H. Mostaanzadeh, Polyhedron 24(2005) 655.
[9] K.E. Gubina, V.M. Amirkhanov, Z. Naturforsch. 55B (2000) 1015.
[10] T. Chivers, M. Krahn, G. Schatte, M. Parvez, Inorg. Chem. 42 (2003) 3994.

The Nature of Beryllium Bonds; a theoretical study based on the electron density and its Laplacian

K. Eskandari
School of Chemistry, Damghan University, Damghan
eskandari@du.ac.ir

Keywords: QTAIM, Beryllium bond, Electron density, Laplacian of electron density

Introduction

Noncovalent interactions play important roles in many different areas of chemistry. Although there are lots of types of noncovalent interactions, the hydrogen bond (HB) is, without doubt, the most important one. In fact in HBs, the principal role of interaction is played by the hydrogen atom. On the other hand, the beryllium atom has some similarities to hydrogen atom; it is electropositive and, when it is covalently bonded to a more electronegative atom, has low lying empty orbitals that allow it to behave as an electron acceptor (similar to what is happening for a hydrogen atom in hydrogen bonding). In other words, the Be is an element which may be regarded as a hydrogen that has a core of electrons! So, it is not surprising if Be participates in special type of interactions which share common characteristics with conventional HBs. Yáñez et. al. investigated the interactions between Be with different Lewis bases [1]. They showed that these "beryllium bonds" are in general very similar to HBs. In the present work, electron density and its Laplacian will be used to gain a deeper understanding of the nature of these bonds.

Computational details

Molecular geometries and their electronic wave functions were optimized at B3LYP/6-311+G(3df,2p) and CCSD/6-311+G(3df,2p) levels using Gaussian 03 program. Bader's Quantum Theory of Atoms in Molecules (QTAIM) [2] was used to study atomic and bond properties.

Results and discussions

The complexes formed between BeH_2 and some Lewis bases (NH_3, OH_2, PH3, HF and HBr) have been investigated in this work. Fig. 1a shows the distribution of the Laplacian of electron density for BeH_2. As it can be seen, there is a region of charge depletion (hole) in the Valence Shell Charge Concentration (VSCC) of Be, which, according to Laplacian complementary principal [3], can interact with a region of charge concentration (lump) of an atom in another molecule and form a "beryllium bond". As an example, the interaction between a hole in Be (in BeH_2) and a lump in N (in NH_3) has been indicated in Fig. 1b. The molecular graph (MG) of $H_2Be...NH_3$ has been also showed in Fig. 1b. As expected there is a bond critical point (BCP) and a bond path (BP) between Be and N atoms. Similar MGs (we have not presented here) have been observed for $H_2Be...OH_2$ and $H_2Be...PH_3$, but this is not the case for $H_2Be...FH$ and $H_2Be...BrH$ complexes. There is no BCP and BP between Be and Br(F) atoms instead, two BPs are formed between Br(F) and the hydrogens of BeH_2.

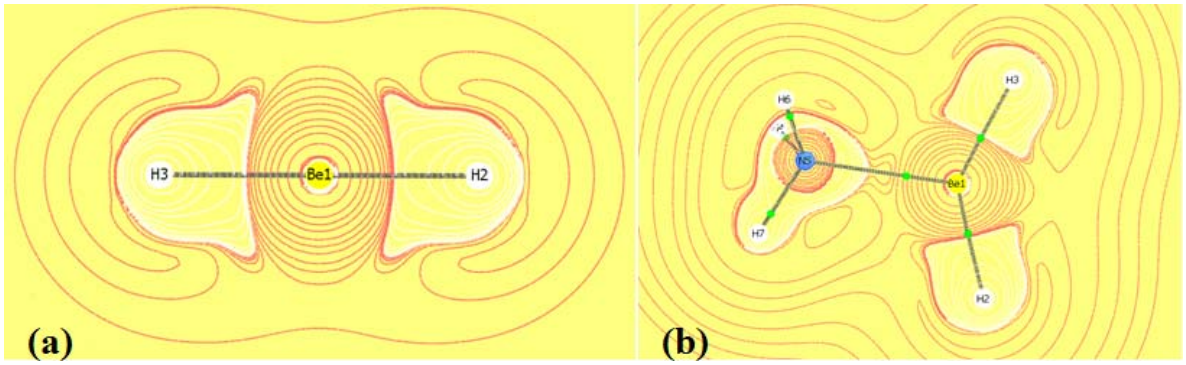

Fig. 1- The distribution of the Laplacian of electron density for a) BeH_2 and b) $H_2Be...NH_3$.

Conclusion

Complexes formed between BeH_2 and different Lewis bases were investigated. Eight criteria based on QTAIM properties, including the values of electron density and it's Laplacian at the BCP, penetration of beryllium and acceptor atom, charge, energy, volume and first atomic moment of beryllium atom, have been considered and compared with the corresponding ones in conventional HBs. Our results show that Be can form "beryllium bonds" with O, N and P but not with halogens. In addition QTAIM properties indicate that beryllium bonds and hydrogen bonds share many common features.

References

[1] M. Yáñez, P. Sanz, O. Mo, I. Alkorta, J. Elguero, J. Chem. Theory Comput. 2009 (5) 2763.

[2] R. F. W. Bader, *Atoms in Molecules: A Quantum Theory*; OUP, Oxford, U.K., 1990.

[3] P. Popelier, *Atoms in Molecules: An Introduction*; Prentice Hall, England, 2000.

Syntheses and Ab Initio Calculations of Two New Diazaphosphole And Diazaphosphorinane

F. Afshar[a], Z. Shariatinia[b], F. Ghaziani[c], and N. Oroujzadeh[d]

[a]*Islamic Azad University, Garmsar Branch, Garmsar, Iran, fzafshar@yahoo.com.*

[b]*Department of Chemistry, Amirkabir University of Technology, Tehran, Iran,*

[c]*Department of Animal Science, University College of Agriculture and Natural Resources, University of Tehran, Karaj, Iran*

[d]*Department of Chemistry, Faculty of Sciences, Tarbiat Modares University, Tehran, Iran.*

Keywords: Diazaphosphole; Diazaphosphorinane; NMR; Ab initio Calculations

Introduction:

Diazaphospholes and diazaphosphorinanes are considered as important compounds due to their great application in chemistry and medicine [1,2]. $^{2,3}J(P\text{-}X)$ [X = H,C] coupling constants dependency on the ring size, hybridization and substituents in some diazaphospholes and diazaphosphorinanes have been reported [3]. In this work, two new 1,3,2-diazaphosphole (**1**), $4\text{-}OCH_3\text{-}C_6H_4NHP(O)[4\text{-}CH_3\text{-}NH\text{-}C_6H_3\text{-}NH]$, and 1,3,2-diazaphosphorinane (**2**), $4\text{-}OCH_3\text{-}C_6H_4NHP(O)[NH\text{-}C_{10}H_6\text{-}NH]$, were synthesized and characterized by NMR and IR spectroscopic methods. Ab initio quantum chemical calculations were performed to optimize the structures of these molecules by density functional theory (B3LYP) and the Hartree-Fock (HF) methods, using the standard 6-31+G** basis set. The stabilization energies were calculated by the equation $\Delta E_{stabilization} = E_{molecule} - \sum E_i$, where i = atom. Moreover, NBO computations were done at B3LYP/6-31+G** level to obtain the atomic hybridizations.

Method:

N-4-methoxyphenyl phosphoramidic dichloride was prepared by the reaction of $POCl_3$ with 4-methoxyaniline in acetonitrile at -5 ºC according to the literature method [4]. The synthesis of compounds **1** and **2** were carried out from the reaction of N-4-methoxyphenyl

phosphoramidic dichloride with 4-methyl-1,2-phenylenediamine (for **1**) and 1,8-naphthalenediamine (for **2**) in the presence of an HCl scavenger, i.e. triethylamine.

Result and discussion:

A summary of spectroscopic data of these molecules is presented in Table 1.

Table 1. Some spectroscopic data for compounds **1** and **2**

Molecule	$^2J(PNH_{endocyclic})$(Hz)	$^2J(P,C)$(Hz)	$\delta(^{31}P)$(ppm)	$\bar{\nu}$(P=O)(cm^{-1})
1	17.0, 17.2	13.5, 12.2	12.63	1175
2	4.5	7.4, 10.1	-10.39	1100

The NMR spectra of compound **1** show high values for $^2J(PNH_{exocyclic})$ (17.0, 17.2 Hz) and $^2J(P,C)$ (13.5, 12.2 Hz), while for compound **2** these parameters show a drastically reduction ($^2J(PNH_{endocyclic})$= 4.5 Hz and $^2J(P,C)$ = 7.4 and 10.1 Hz). It seems that these differences of coupling constant values are related to the ring strain and ring's member. The IR spectra demonstrate that the $\bar{\nu}$(P=O) values for compounds **1** and **2** are 1175 and 1100 cm^{-1}, respectively, indicating a stronger P=O bond for molecule **1** relative to molecule **2**.

Optimized structures were obtained for molecules **1** and **2** by ab initio quantum chemical calculations. The calculated stabilization energies (kcal mol^{-1}) and dipole moments (Deby) are presented in Tables 2**.** The optimizations reveal nearly a planar plane for the five- and six-membered rings of molecules **1** and **2**. The P-N bond lengths are shorter than the P-N single bond (1.77 Å) [5].The exocyclic nitrogen atom of 4-methoxyaniline group in compound **1** is relatively planar, but the endocyclic nitrogen atoms are much deviated from planarity while all nitrogen atoms in compound **2** are nearly planar. This observation suggests the existence of partial multiple bond character between phosphorus and nitrogen.

Table 2. Calculated stabilization energies (kcal mole^{-1}) and dipole moments (Deby) for compounds **1** and **2**

	$\Delta E_{stabilization}$(kcal mole^{-1})		Dipole moments (Deby)	
Molecule	(HF/6-31+G**)	(B3LYP/6-31+G**)	HF/6-31+G**	B3LYP/6-31+G**
1	-3556.3641	-3902.7198	2.2224	1.8844
2	-4082.4713	-4391.7089	2.0966	1.7978

To more consider the atom hybridizations, NBO computations were made at B3LYP/6-31+G** level. The results exhibit that in both compounds **1** and **2** hybridization for P(1) atoms in P=O and P-N bonds are nearly sp^3 while N atoms have sp^2 hybrid. It is noticeable that the O(19) atom (in OCH_3) indicates sp^3 hybridization but the bond angles around it was about 120.0°.

References:

[1] Li Z., Han J., Jiang Y., Browne P., Knox R. J., Hu L. // Bioinorg. Med. Chem.- 2003. -**11** - 4171.

[2] Bauermeister S., Modro A. M., Modro T. A. // - Tetrahedron Lett. - 1989 - **30** - 2141.

[3] Gholivand K., Pourayoubi M., Shariatinia Z. // Polyhedron - 2007 - **26** - 837.

[4] Gholivand K., Ghadimi S., Forouzanfar A., Naderimanesh H. // Magn. Reson. Chem. - 2001 -**39** - 684.

[5] Corbridge D.E.C. Phosphorus, an outline of its Chemistry, Biochemistry and Technology - Fifth Edition, Elsevier, The Netherlands, 1995.

Syntheses and *Ab Initio* Calculations of Two New 1,3,2-Diazaphosphorinanes

F. Afshar[a], Z. Shariatinia[b], N. Oroujzadeh[c], and F. Ghaziani[d]

[a]*Islamic Azad University, Garmsar Branch, Garmsar, Iran, fzafshar@yahoo.com.*

[b]*Department of Chemistry, Amirkabir University of Technology, Tehran, Iran,*

[c]*Department of Chemistry, Faculty of Sciences, Tarbiat Modares University, Tehran, Iran.*

[d]*Department of Animal Science, University College of Agriculture and Natural Resources, University of Tehran, Karaj, Iran*

Keywords: 1,3,2-diazaphosphorinanes, NMR spectroscopy, *ab initio* calculations, Gaussian 98 program

Introduction:

Research on 1,3,2-diazaphosphorinanes that are important part of heterocyclic phosphorus chemistry is of interest because these ring systems are analogous compounds of antitumor drugs such as cyclophosphamide [1-3]. In this work, two new diazaphosphorinanes with formula $4-OCH_3-C_6H_4-NHP(O)[NHCH_2C(CH_3)_2CH_2NH]$ **(1)** and $4-OCH_3-C_6H_4NHP(O)[NH(CH_2)_3NH]$ (**2**) were synthesized and characterized by NMR and IR spectroscopic methods. *Ab initio* quantum chemical calculations with Gaussian 98 program [5] were done at HF level of theory to further investigate on the structures of these compounds. Results showed that the stabilization energy of a molecule highly increases when the level of the basis set increases

Method:

5,5-Dimethyl-2-(4-methoxyphenyl), 1,3,2-diazaphosphorinane-2-oxide (**1**) and 2-(4-methoxyphenyl), 1,3,2-diazaphosphorinane-2-oxide (**2**) were prepared by the reaction of 4-methoxyphenylphosphoramidic dichloride [4] with corresponding diamines.

Result and discussion:

A summary of the spectroscopic data of these molecules are given in Table 1.

Table 1. A summary of the spectroscopic data of compounds **1** and **2**.

Compound	$\delta(^{31}P)$ (ppm)	$^{2}J(PNH)_{exocyclic}$ (Hz)	$^{3}J(PNCH)$ (Hz)	$^{2}J(P,C)_{aliphatic}$ (Hz)	$^{3}J(P,C)_{aliphatic}$ (Hz)	$^{3}J(P,C)_{aromatic}$ (Hz)
1	9.16	---	23.9	2.3	6.3	6.4
2	6.08	10.0	---	3.3	7.7	6.4

The structures of compounds **1** and **2** were optimized using Gaussian 98 program with 6-31G*, 6-31G**, 6-31+G**, and 6-31++G** basis sets. Results showed that the stabilization energy of a molecule highly increases when the level of the basis set increases, Table 2.

Table 2. Calculated molecular stabilization energy (kcal mol^{-1}) for compounds **1**, **2**.

Compound	E(HF/6-31G*)	E(HF/6-31G**)	E(HF/6-31+G**)	E(HF/6-31++G**)
1	-702745.6616	-702770.4350	-702782.3654	-702782.7550
2	-653756.7284	-653777.5782	-653789.2571	-653789.6080
Compound	E(HF/6-311G*)	E(HF/6-311G**)	E(HF/6-311+G**)	E(HF/6-311++G**)
1	-702858.8937	-702880.5357	-702887.3291	-702887.6599
2	-653861.3302	-653879.7319	-653886.5224	-653886.8095

In order to find a more stable structure, calculations were performed using higher basis sets, 6-311G*, 6-311G**, 6-311+G**, and 6-311++G**, and the same result was observed. Selected calculated bond lengths and angles are presented in Table 3.

Table 3. Selected bond lengths (Å) and angles (°) of compounds **1**, **2** obtained from HF/6-311++G** optimization calculations.

1		**2**	
P(1)-O(1)	1.4592	P(1)-O(1)	1.4586
P(1)-N(1)	1.6603	P(1)-N(1)	1.6653
P(1)-N(2)	1.664	P(1)-N(2)	1.6579
P(1)-N(3)	1.6568	P(1)-N(3)	1.6607
O(1)-P(1)-N(1)	119.0453	O(1)-P(1)-N(1)	112.2695
O(1)-P(1)-N(2)	112.3068	O(1)-P(1)-N(2)	112.9516
O(1)-P(1)-N(3)	113.0646	O(1)-P(1)-N(3)	119.1425
N(1)-P(1)-N(2)	103.5922	N(1)-P(1)-N(2)	107.366
N(1)-P(1)-N(3)	100.4954	N(1)-P(1)-N(3)	103.4185
N(2)-P(1)-N(3)	106.9913	N(2)-P(1)-N(3)	100.3784

Single crystals of these compounds were obtained from a solution of methanol and acetonitrile after slow evaporation at room temperature. The selected bond lengths and angles are given in Table 4. Comparison of the calculated data with the corresponding

crystallographic parameters indicate that there are good agreement between the experimental data (from X-ray crystallography) and the theoretical ones.

Table 4. Selected bond lengths (Å) and angles (°) of compounds **1**, **2**.

5		**6**	
P(1)-O(1)	1.4872(10)	P(1)-O(1)	1.4877(14)
P(1)-N(1)	1.6479(12)	P(1)-N(1)	1.6558(16)
P(1)-N(2)	1.6501(12)	P(1)-N(2)	1.6313(15)
P(1)-N(3)	1.6371(12)	P(1)-N(3)	1.6589(15)
O(1)-P(1)-N(1)	111.31(6)	O(1)-P(1)-N(1)	111.89(8)
O(1)-P(1)-N(2)	109.37(6)	O(1)-P(1)-N(2)	114.18(8)
O(1)-P(1)-N(3)	115.34(6)	O(1)-P(1)-N(3)	112.39(8)
N(1)-P(1)-N(2)	110.70(6)	N(1)-P(1)-N(2)	105.18(8)
N(1)-P(1)-N(3)	104.51(6)	N(1)-P(1)-N(3)	106.78(8)
N(2)-P(1)-N(3)	105.37(6)	N(2)-P(1)-N(3)	105.83(8)

References

[1] R. F. Borch, G. W. Canute*J. Med. Chem*., **34**, 3044 (1991).

[2] S. M. Ludeman, G. Zon, W. Egan. *J. Med. Chem*., **22**, 151 (1979).

[3] Z. Li, J. Han, Y. Jiang, P. Browne, R. J. Knox, L. Hu. *Bioinorg. Med. Chem*., **11**, 4171 (2003).

[4] K. Gholivand, S. Ghadimi, H. Naderimanesh, A. Forouzanfar. *Magn. Reson. Chem.*, **39**, 684 (2001).

[5] M. J. Frisch et al. Gaussian 98, Revision A.9, Gaussian, Inc.; Pittsburgh, PA, 1998.

Investigation Energy level In Keto-Enol Tautomerism Of Structure 3-(cyclopenta-2,4-dienyl)-3-oxopropanoic acid Using Ab initio Quantum Mechanic Calculation

R.Soleymani*[a,b] , F.Afshari[a,c] and S.Obari[c]

[a] *Chemistry Department, Faculty of Sciences, Islamic Azad University, Touyserkan Branch, Young researchers Club, Touyserkan ,Iran*

(Email: nima_soleimany@yahoo.com)

[b] *Chemistry Department, Faculty of Sciences, Islamic Azad University Shahre-rey Branch, Tehran, Iran*

[c] *Chemistry Department, Faculty of Sciences, Islamic Azad University Touyserkan Branch, Touyserkan, Iran*

Keywords: Ab initio; DFT ; NBO ; Tautomerism Keto-Enol

Introduction

In fact tautomerism (isomeric reaction) is a special kind of isomerism which is derived from greek word tauto and merios. Each of isomers involved in the reaction is called tautomer and the difference of resonance forms is from the aspect of electron position. Also keto-enol tautomerism of carbonyl compositions are catalyzed by acids and bases[1].In this research we have investigated the energy levels of keto-enol tautomerism of structure 3-(cyclopenta-2,4-dienyl)-3-oxopropanoic acid and obtained IR spectrum ,Raman spectrum and ^{13}C,^{1}H –NMR and compare spectrum experimental obtained.

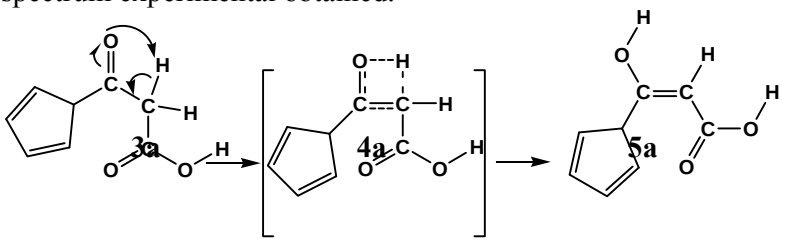

Methods

For investigation quantum mechanical calculation at theory of the level using DFT and UHF method with 6-311+G** basic set. The transition state simulated by using SADDLE keyword and calculation by winmopac software and final optimization calculated Gaussian 03w package program[2].Also in this research using pentum 4 computer with intel core i5 2.53 GHZ processor.

Result and discussion

The obtained results of Ab initio method for energy levels in tautomerism mechanism of structure 3-(cyclopenta-2,4-dienyl)-3-oxopropanoic acid are shown in table 1,2 .

Table1: Ab initio calculation compounds 3a,4a and 5a by B3LYP,HF/6-311+G** method (in the Hartree)

method	HF/6-311+G**				B3LYP/6-311+G**			
Structure	ZPE	Eele	E_0	ΔE_0	ZPE	Eele	E_0	ΔE_0
3a	0.156506	-532.3134752	-532.156970	0.110371 (69.2578)[a]	0.145015	-535.4648380	-535.319823	0.085657 (53.7497)[a]
4a	0.150365	-532.1969640	-532.046599		0.139317	-535.3734829	-535.234166	
5a	0.157427	-532.2979273	-532.140501		0.145771	-535.4554378	-535.309666	

[a]Number in parentheses are corresponding ΔE_0 values in kcal.mol^{-1}

Table 2 : Value parameter s total energy with using Ab initio calculation in theory of the level B3LYP/6-311+G** for temperature 298.15 K.

Geometry / Structure	Zero-point vibrational energy (Kcal/Mol)	CV (Cal/Mol-Kelvin)	S (Cal/Mol-Kelvin)	E (Thermal) (KCal/Mol)
3a	90.99825	36.907	103.988	97.194
4a	87.42289	36.548	100.262	93.616
5a	91.47299	37.536	102.047	97.793

Conclusion

Performed investigations on energy levels and comparing obtained IR-Raman-NMR spectrums using cuantum mechanic calculation showed that in Keto-Enol tautomerism reaction of structure 3-(cyclopenta-2,4-dienyl)-3-oxopropanoic acid is accompanied by a 53.7497675 Kcal/mol energy reagent and the balance tends more keton and keton state is during this reaction , pay electrons related to keton state are moved and form a new sigma bond between oxygen-hydrogen and cause forming enol form. Also the process of this reaction is completely endothermic and in transition state has structure between keton and enol state.

References

[1] John Mc Murry ,*Organic chemistry* ,5th ed ,**2000**

[2] M. j. Frisch et al. *GAUSSIAN 03*, Revision C. 01, Gaussian Inc.,Wallingford. CT, **2004**.

Calculation of rovibrational energy levels of rare gas dimers with Korona et al. potential function using Numerov and DVR methods

M. Elghaei*[a], M. Gharibi[a] and R. Islampour[a]
[a]Department of Chemistry, Tarbiat Moallem University, Tehran, Iran
E-mail: Mahdi.Elghaei@Gmail.com

Introduction

The potential energy function proposed by Korona et al. [1] for the homo- and hetero-nuclear rare gas dimers is used to solve the nuclear Schrodinger equation for these dimmers numerically. To this end, the Discrete Variable Representation (DVR) and Numerov numerical methods are employed.

Methods

The Numerov method *[2]***.** Let ψ_{n-1}, ψ_n, and ψ_{n+1} denote the values of ψ at the points $x_n - s$, x_n, and $x_n + s$, respectively (these are the endpoints of adjacent intervals and s is the length of interval)

$$\psi_{n-1} \equiv \psi(x_n - s), \quad \psi_n \equiv \psi(x_n), \quad \psi_{n+1} \equiv \psi(x_n + s) \tag{1}$$

By expanding $\psi(x_n + s)$ and $\psi(x_n - s)$ in Taylor series involving powers of s, adding these two expansion to eliminate odd powers of s, using the Schrodinger equation to express ψ'' and $\psi_n^{(iv)}$ in terms of ψ, and neglecting terms in s^6 and higher powers of s (an approximation that will be accurate if s is small), one finds that

$$\psi_{n+1} \approx \frac{2\psi_n - \psi_{n-1} + 5G_n\psi_n s^2/6 + G_{n-1}\psi_{n-1}s^2/12}{1 - G_{n+1}s^2/12} \tag{2}$$

where $G_n \equiv G(x_n) \equiv m\hbar^{-2}[2V(x) - 2E]$. Equation (2) allows us to calculate ψ_{n+1}, the value of ψ at point $x_n + s$, if we know ψ_n and ψ_{n-1}, the values of ψ at the preceding two points x_n and $x_n - s$. We use Excel 2007 for this method.

***The DVR method** [3].* DVR is a method for diagonalizing Hamiltonian matrix in a DVR basis set. The DVR basis functions $\{\Phi_\alpha(x)\}$ are expanded in terms of complete, orthonormal functions $\{\phi_\alpha(x)\}$:

$$\int_a^b dx\, \phi_\alpha^*(x)\phi_\beta(x) = \delta_{\alpha\beta} \tag{3}$$

as

$$\Phi_\alpha(x) = \sum_\beta \phi_\beta(x)\, T_{\alpha\beta}^\dagger \tag{4}$$

where the matrix $T_{\alpha\beta}^\dagger = \omega_\alpha^{1/2}\phi_\beta^*(x_\alpha)$ is defined for a set of N points $\{x_\alpha\}$ and weights $\{\omega_\alpha\}$.

From the orthonormality relation (3) we get

$$\delta_{kl} = (\mathbf{T}^\dagger\mathbf{T})_{kl} = \sum_{\alpha=1}^{N} \omega_\alpha^{1/2}\phi_k^*(x_\alpha)\,\omega_\alpha^{1/2}\phi_l(x_\alpha) \tag{5}$$

thereby, $\mathbf{T}^\dagger\mathbf{T} = \mathbf{T}\mathbf{T}^\dagger = \mathbf{I}$, so $\mathbf{T}$ is a unitary matrix. Indeed, $\mathbf{T}$ is the transformation matrix from the orthonormal basis functions onto the DVR basis functions.

In DVR basis, the matrix elements of the kinetic energy operator can be evaluated analytically and the potential energy matrix elements are approximately diagonal and equal to the values of the potential function at DVR points: $V_{\alpha\beta} = V(x_\alpha)\delta_{\alpha\beta}$. We use Mathematica 7 for this method.

Results and Discussion

The results are displayed in Table 1. Note that the results of Numerov and DVR methods are identical, if we use the appropriate grid points. It is also seen that there is a very good agreement between the calculated and the experimental results.

Table 1. Calculated and experimental rovibrational spacings (in cm^{-1}) in the ground vibrational state of $Ar-Ar$, $Ar-Kr$ and $Kr-Kr$

Dimers	$J'-J''$	DVR	Numerov	Expt
$Ar-Ar$	$2-1$	0.2313	0.2313	0.2310
$Ar-Ar$	$3-2$	0.3469	0.3467	0.3464
$Ar-Ar$	$4-3$	0.4624	0.4624	0.4618
$Ar-Kr$	$1-0$	0.0800	0.0800	0.0800
$Ar-Kr$	$2-1$	0.1600	0.1600	0.1599
$Ar-Kr$	$3-2$	0.2400	0.2400	0.2399
$Ar-Kr$	$4-3$	0.3200	0.3200	0.3198
$Kr-Kr$	$1-0$	0.0488	0.0488	0.0488
$Kr-Kr$	$2-1$	0.0977	0.0977	0.0976
$Kr-Kr$	$3-2$	0.1465	0.1465	0.1463
$Kr-Kr$	$4-3$	0.1953	0.1953	0.1951

References

[1] T. P. Haley and S. M. Cybulski, *J. Chem. Phys.***119** (2003) 5487.

[2] I. N. Levine, *Quantum Chemistry*, 6th ed., Prentice-Hall, 2009.

[3] W. Schweizer, *Numerical Quantum Dynamics,*Kluwer Academic Publishers, 2002.

A novel approach of HSA-ciprofloxacin interaction in the presence of Ag nano particles: Fluorescence spectroscopic approach

H. Iranfar*[1], R. Salari[2], O. Rajabi[2], J. Chamani[1]

1. Department of Biology, Faculty of Sciences, Islamic Azad University-Mashhad Branch, Mashhad, Iran (hediyehiranfar@gmail.com)

2. Medical Chemistry Department, School of Pharmacy, Mashhad University of Medical Sciences, Mashhad, Iran

Key words: *HSA, Ciprofloxacin, Ag nano particles, Fluorescence spectra,*

Introduction:

With the development of nanotechnology, nano particles are recognized to have potential applications in electronics, optics, genomics, proteomics and bio-analytical fields because of their larger surface area, enhanced chemical reactivity and easier penetration into cells [1]. Human serum albumin (HSA), serving as the major soluble protein with high affinity to many exogenous and endogenous compounds. HSA transfer many drugs and mineral materials in the blood so it uses as a model protein in the biological and chemical physics studies [2]. Ciprofloxacin (CIP) is a synthetic chemotherapeutic antibiotic of the fluoroquinolone drug class. It kills bacteria by interfering with the enzymes that cause DNA to rewind after being copied, which stops DNA and protein synthesis. HSA transfer CIP in the body to its target cells. In this study the interaction between HSA and CIP in presence of Ag nano particles at the physiological condition (pH=7.4) has been investigated by fluorescence spectroscopy.

Methods:

The fluorescence measurements were performed with F-6200 spectrofluorimeter (Jasco, Japan). Excitation and emission bandwidths were both set at 10 nm. pH meter Metrohm model. All experiments were carried out at room temperature.

Result and Discussion:

Fluorescence spectrum of HSA in the presence of CIP and Ag nano particles clearly shown that both CIP and Ag nano particles act as a quencher and with the increasing concentration

of them, the blue shift occurred in fluorescence spectrum which indicated the less polar environment. Fig.1 shows Fluorescence emission spectra for HSA-CIP in the presence of Ag nano particles at 280 nm excitation wavelength. For describing the fluorescence quenching by drug we used the Stern-Volmer equation. Figure 2 shows the Stern-Volmer plot of HSA-CIP and HSA-CIP-Ag nano particles at 280 nm excitation wavelenght Results indicate that there are two types of domain for CIP in presence of Ag nano particles. K_{sv} was calculated from Stern-Volmer equation and kq was determined by modified Stern-Volmer. Comparing kq in this experiment and kq polymer, shows that we have the static quenching in our experiment [$k_{q\ I} = 19.39x10^{13}\ M^{-1}s^{-1}$, $k_{q\ II} = 69.11x10^{13}\ M^{-1}s^{-1}$, kq polymer = $2 \times 10^{10}\ M^{-1}s^{-1}$].Table 1 shows K^{sv} and kq for two system.

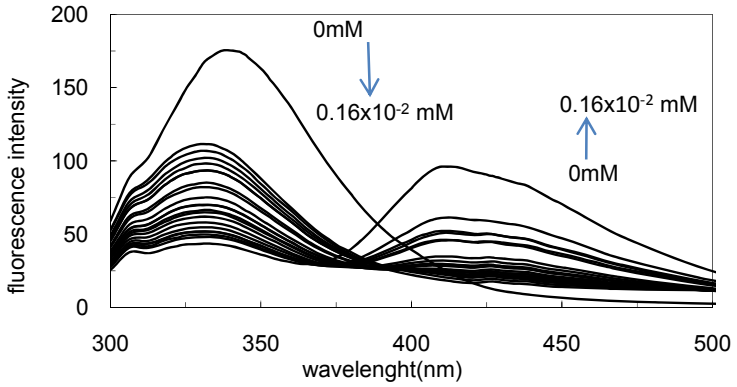

Fig 1. Fluorescence spectrum of HSA-CIP in presence of Ag nano particles

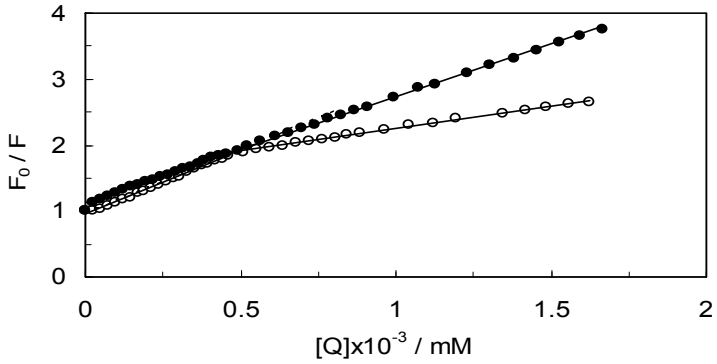

Fig 2. Stern -Volmer plot of HSA-CIP (●), HAS-CIP-Ag nano particles(○) at 280nm excitation wavelength.

Table 1. $K_{sv\ and}$ k_q calculated for HSA-CIP and HSA-CIP-Ag nano particles systems

System λ_{ex}=280nm	K_{sv}	K_{sv}	$kq_{(I)}$	$kq_{(II)}$
HSA-CIP-Ag nano particles	19.39×10^{5}	69.11×10^{5}	19.39×10^{13}	69.11×10^{13}
HSA-CIP	16.08×10^{5}	---------	16.08×10^{13}	---------

Conclusion:

The results revealed that binding of ciprofloxacin to HSA could induce conformational changes in macromolecule. Stern-Volmer plot showed that the mechanism of fluorescence quenching of HSA with ciprofloxacin is static. In the presence of Ag nano particles there are two domains for ciprofloxacin to bind HSA.

References:

[1] W. Sun, Y. Du, J. Chen, J. Kou, B. Yu, "Interaction between titanium dioxide nanoparticles and human serum albumin revealed by fluorescence spectroscopy in the absence of photoactivation", *J. Luminescence,* **129 (**2009) 778-783.

[2] Sh. Song, X. Hou, Y. Wu, Sh. Shuang, C. Yang, y. Inoue, C. Dong, "Study on the interaction between methyl blue and human serum albumin by fluorescence spectroscopy", *J. Luminescence*, **129 (**2009) 169-175.

Peak to Peak Repulsion in Ion Mobility Spectrometry

Vahideh. ILbeigi and Mahmoud. Tabrizchi*
Department of Chemistry, Isfahan University of Technology, Isfahan, Iran. 84156-83111
Vahide_2005vb@yahoo.com

Introduction

We recently introduced a novel method to increase the resolution of ion mobility spectrometry (IMS) [1]. The method is based on applying an inverse pulse to the shutter grid, i.e. instead of an ion packet, an empty space is traveling through a bath of ions. It is believed that, the space charge among the ions, especially at the edges, tends to narrow the gap, hence a better resolution. The space charge in IMS was also experimentally observed and proved to be important [2]. Spangler also showed that, the space charge is responsible for the higher resolution in the inverse-IMS [3]. We here introduce a method to accurately measure the space charge between the peaks in IMS.

Experimental

The method relies on generation of two consecutive ion packets close to each other by applying a double pulse, as shown in Fig.1 The initial spacing between the two packets is determined by the delay between the two applied pulses, which is adjustable from 10µs to 450µs. The two pulses push each other their separation increases with respect to their

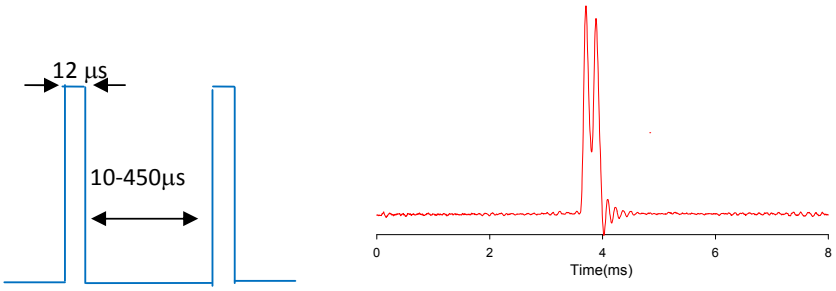

Fig.1. Generating two consecutive equal peaks by applying a double pulse to the shutter grid.

The increase in spacing can then be measured accurately. In addition, the ion density in the two packets can be varied by adjusting the widths of the two pulses. These experiments can

also be performed at the inverse mode of operation. Therefore, the change in spacing between two dips can be studied carefully.

Results and Discussion

The spacing was measured at a fixed delay between the two pulses while the pulse widths were increased. The experiment was performed at various delays. The results (Fig.2-a) show an increase in the distance between the two ion packets as a function of total charge of the two ion packets. In addition, the extent of increase depends on the initial spacing. However, the results for the inverse mode of operation shows that the two dips get closer together as they travel (Fig.2-b). The decrease depends on the intensity of the dips as well as their initial spacing.

Conclusion

The results are in well agreement with the Gause's and Coulomb's laws. Comparison between the results in the conventional and inverse mode of operation shows that, in the inverse mode, the ion bath expands due to repulsion among the ions. This is, therefore, the main cause for [illegible] inverse mode.

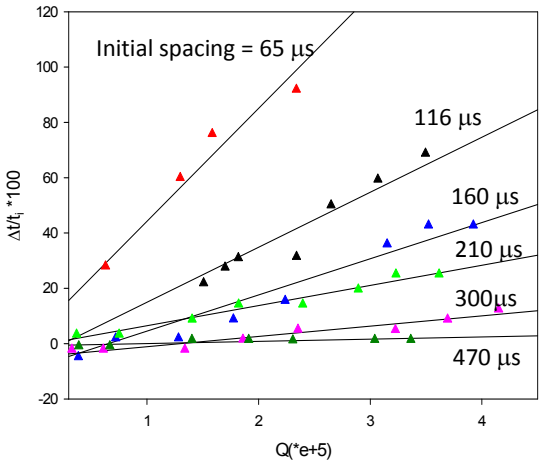

Fig.2-a

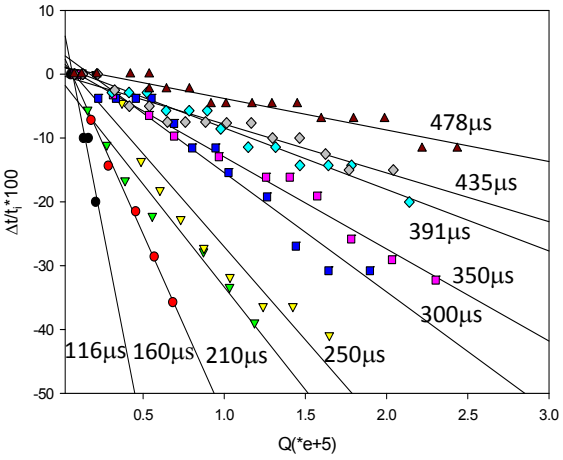

Fig.2-b

References

[1] "Inverse Ion Mobility Spectrometry" M. Tabrizchi, E. Jazan, *Anal. Chem*, 82 (2) (2010) 746–750.

[2] "Observation of Space Charge Effects in Ion Mobility Spectrometry*",*V. Ilbeigi, M. Tabrizchi, *13th Iranian Physical Chemistry Seminar, Shiraz University, Iran*, 2010.

[3] "Theory for Inverse Pulsing of The Shutter Grid in Ion Mobility Spectrometry", Glenn E. Spangler, *Anal. Chem.*, 2010, *82* (19), 8052–8059.

Conformational analysis, structure and vibrational assignment of hexafluoroacetone. A density functional theory study.

S.F. Tayyari, N. Khorshidi, S. Holakoee, S. Pozhhan, A.R. Berenji*
Department of Chemistry, Ferdowsi University of Mashhad, Mashhad 91779, Iran
(Email: berenji@staff.um.ac.ir)

Keywords: Vibrational spectra, Hexafluoroacetone, DFT methods, Conformational stability.

Introduction

Hexafluoroacetone, HFA, has been used as a stabilizer for peptide structures, as protecting and activating reagent, and as a structure modifier in proteins.

The vibrational spectra of HFA have been the subject of several studies [1-5]. Berney [1], based on the depolarization ratios of the Raman spectrum of HFA, concluded a C_s structure with two CF_3 groups staggered with respect to each other. Berney also, by considering the optional vibration of the CF_3 groups, estimated the barrier to rotation of the CF_3 groups of about 1000 cm^{-1}. Pace et al. [2] by assuming a C_{2v} structure for HFA reassigned the vibrational spectra of HFA. These authors, based on the calorimetric measurements in the gas phase, predicted a barrier to rotation for the CF_3 groups of about 1000-1500 cal/mol. Pertillä [3] by assuming a C_{2v} structure and using normal coordinate analysis reconsidered the vibrational spectra of HFA. Durig et al. [5], by considering the far infrared spectrum of HFA, a barrier to rotation of 777±5 cm^{-1} and a C_s structure concluded. Campton et al. [4], by using an *ab initio* SCF calculation, reconsidered the vibrational spectra assignment of HFA. The symmetry obtained by the SCF calculation of Compton et al. [4] is consistent with the two electron diffraction results, which conclude a C_2 symmetry for the HFA molecule [6,7]. The calculated energy difference between the C_{2V} and C_2 structures is 4.9 kJ/mol [4].

Theoretical Methods

The molecular equilibrium geometry and vibrational transitions of HFA were computed with the Gaussian 03. The B3LYP with the 6-31G*, 6-311G*, and 6-311+G(3df) basis sets were used for optimizing the structure and calculating the vibrational frequencies. To

compare the accuracy of several different computational methods, the geometry of HFA was further optimized at the HF and MP2 levels, using the 6-311G* basis set. The B3LYP/6-311G* level was used for calculating the Raman intensities of the vibrational frequencies.

In order to assign the observed vibrational transitions, anharmonic frequency calculations were performed for HFA using the B3LYP functional and 6-311G* basis set.

The size of the anharmonicity effect can be grasped from the difference between the harmonic and anharmonic frequencies.

Results and discussion

Theoretically, four conformers could be assumed for HFA, (1) C_{2v} (I) (both CF_3 groups are staggered with respect to the carbonyl groups, (2) C_{2V} (II) (both CF_3 groups are eclipsed with respect to the C=O), (3) C_2, and (4) C_s structure.

According to the calculated results, the C_2 structure is the most stable conformer, which is in agreement with the literature [6].

The energy difference between C_2 structure with other conformers, except for the C_{2v} (I), lies in the 2-3 kJ/mol. However, the calculated barrier to rotation for the CF_3 rotation is about 1400 cm^{-1} (about 17 kJ/mol) which is in agreement with the theoretical results [2].

The 1806, 363, and 192 cm^{-1} bands are assigned to the C=O stretching, in-plane C=O bending, which is strongly coupled to the asymmetric C-C-C stretching mode, and out-of-plane C=O bending vibrations, respectively. The C=O in-plane deformation has also considerably contribution in the 717 cm^{-1} band, which is mainly the CF_3 in-plane rocking mode belong to the B symmetry.

The 320 cm^{-1} band was assigned by Berney [1] to the C=O out-of-plane bending. According to our results this band is assigned to symmetric C-C-C stretching coupled to the CF_3 deformation.

The bands at 1272, 1254, 1157, 1252, 1215, and 972 cm^{-1} are mainly caused by C-F stretching movement. The first three bands are belong to the A symmetry species and others are due to the B symmetry species.

Conclusions

The vibrational spectra of hexafluoroacetone have been reassigned by aid of modern theoretical ab initio and density functional methods. The geometry and vibrational frequencies of HFA are calculated at the B3LYP level, using 6-31G*, 6-311G*, 6-311+G*, and 6-311+G(3df) basis sets. According to the calculated results, the C_2 structure is the most stable conformer.

References

[1] C. V. Berney, Spectrochim. Acta 21 (1965) 1809.

[2] E. L. Pace, A. C. Plaush, H. V. Samuelson, Spectrochim. Acta 22 (1966) 993.

[3] M. Perttilä, Acta Chem. Scand. A 28 (1974) 933.

[4] D. A. C. Compton, J. D. Goddard, S. C. Hsi, W. F. Murphy, D. M. Rayner, J. Phys. Chem. 88 (1984) 356.

[5] J. R. Durig, A. R. Fanning, T. G. Sheehan, G. A. Guirgis, Spectrochim. Acta 41 A (1991) 279.

[6] R. L. Hilderbrandt, A. L. Andreassen, S. H. Bauer, J. Phys. Chem. 74 (1970) 1586.

[7] G. A. Boulet, Ph.D. Thesis, University of Michigan, Ann Arbor, 1964.

Combined Photoionization and Corona Discharge Ionization Sources for Ion Mobility Spectrometry

M. Tabrizchi* and H. Bahrami

Department of Chemistry, Isfahan University of Technology, Isfahan ,Iran

(Email: m-tabriz@cc.iut.ac.ir)

Keywords: Ion mobility spectrometer, photo ionization, corona discharge.

Introduction

Ion mobility spectrometry (IMS) is a technique to detect ions in the gas phase separated on the basis of their mobility in an electrical field. Ions in IMS are often formed by ion-molecule reactions at atmospheric pressure. The choice of ionization method is vital for making an appropriate analysis. To achieve high sensitivity, one of the requirements is high ion flux through the IMS drift cell. Hence, developing new ion sources and/or improving the current systems are highly desirable. Most of the ion mobility spectrometers use radioactive material like ^{63}Ni as ionization source [1], which is favored due to its simplicity, stability and convenience. This source has deficiencies in limited linear range, inflexible selectivity and regulatory requirements associated with radioactive materials. In recent years non-radioactive ion sources have been of special interest.

In this study we present an ion mobility spectrometer equipped with two non radioactive ion sources, atmospheric pressure photoionization (APPI) [2] and corona discharge chemical ionization [3].

The Design

The principal components of the new ion mobility spectrometer are shown schematically in Fig. 1. It consists of three main parts: two ion sources, an ionization region and a drift tube. Ion sources are located in front of the reaction region. Electric field conducts the ions from both sources into the reaction region. Pulses of ions are then injected into the drift region where separation of ions occurs under the action of an external electric field and collisions with the countermoving drift gas. An ion collector is located at the end of the drift tube to register the arrival of the ions.

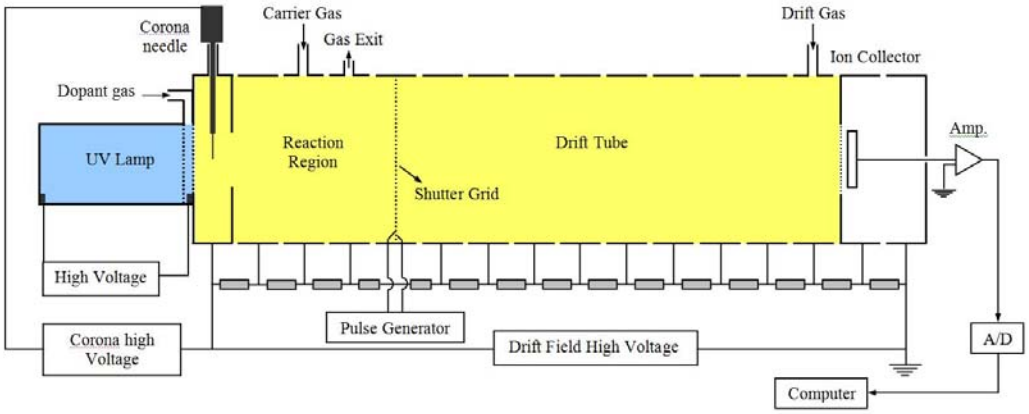

Fig. 1. The schematic view of the ion mobility spectrometer

A Krypton lamp, emitting UV light at 10.6 eV, was used as the UV source which is mounted in parallel with the axis of the reaction chamber and the drift tube. The lamp is powered by a 1.2kV DC power supply. The parallel design has the advantage of penetrating the UV light deeper in the ionization region, hence a better ionization efficiency. In addition, a curtain region is designed in front of the lamp to create a shield of gas, which could contain dopant to enhance ionization. The UV ligh could ionize the analyte directly or via charge transfer from a dopant ion. In fact, the dopant is used to covert photons to primary ions. It is an appropriate substance with ionization energy less than the photon energy such as toluene (IE= 8.828eV). Secondary ions are then formed via reaction with the ionized toluene. The corona needle has been mounted vertically not to obstacle the photoionization source.

Conclusion

In this new design an atmospheric pressure ionization IMS instrument whit two ion sources was developed. Corona discharge is a powerful ionization source that ionizes species with high proton affinity. On the other hand, UV photoionization is a primary ionization source which ionizes species with low ionization energy. Combination of the two sources covers the limitations of each other. The design enables fast and easy changing between the two ionization methods. This allows ionization and measurement of a wide range of analytes as well as study of ion molecule reactions.

In addition, the two ionization sources can operate simultaneously. Such combination provides the possibility of ionization of species with high ionization energy. The mechanism is expected to be excitation by the UV light followed by ionization in the discharge.

References

[1] G. A. Eiceman and Z. Karpas, Ion Mobility Spectrometry (CRC, Boca Raton, FL, 1993).

[2] Michael A. B., Randy L. E., Herbert H. Hill Jr., Ion mobility detector for gas chromatography with a direct photoionization source, *Anal. Chem.*, 1983, *55* (11), pp 1761–1766.

[3] M. Tabrizchi and A. Abedi, *A novel electron source for negative ion mobility spectrometry*, International Journal of Mass Spectrometry, Vol. 218, Issue 1, 2002, p. 75-85.

Correlation between ^{14}N chemical shielding tensors and antimalarial activity of quinoline derivatives

Hadi Behzadi*[a], Mehdi D. Esrafili[b], Javad Beheshtian[b], Nasser L. Hadipour[b]

[a]Islamic Azad university, Tehran Medical Branch, Tehran, Iran

(E-mail: behzadihadi@yahoo.com)

[b]Department of Chemistry, Tarbiat Modares University, Tehran, Iran

Keywords: Malaria, Quinoline, DFT, Chemical shielding tensors

Introduction:

Malaria is a serious health problem, particularly in tropical region. It is estimated there are between 300 and 500 million clinical cases of malaria annually, leading to 1.1-2.7 million deaths [1]. Current considerable evidences indicate that quinoline-based antimalarial agents such as chloroquine (Figure 1) probably act by forming toxic complexes with free hematin [2]. It seems that the investigation of electronic effect controlling the ability in some quinoline derivatives to inhibit β-hematin process provides an opportunity to test the activity of various quinolines in detail. Recently, Frosch and Popp investigated the relationship between molecular structure and Raman spectra of quinolines [3].

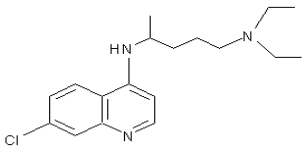

Figure1. Chloroquine

The present work includes the investigation of substitution effects on the calculated ^{15}N shielding tensors on various quinoline derivatives by DFT approach. The calculations were performed for two series of quinolines, series **A** (7-chloro 4-aminoalkyls quinolines compounds) and **B** (quinoline, 3-,5-,6-,8- amino quinolines and 4,8-dichloro quinoline). The calculated ^{15}N shielding tensors in this study are expected to lead to insights into structure-shielding relationships and substitution effects in quinolines.

Definitions and computational details:

All calculations were performed using *Gaussian 98* suite of programs [4] on a Pentium IV personal computer. The structure of quinolines were optimized using B3LYP/6-31G* [5] method. Then, the optimized structures were used to obtain shielding tensors by using GIAO method at B3LYP level with 6-311++G** basis set.

Results and discussion:

In the present study, we calculated the ^{15}N shielding tensors of some quinolines to investigate the relationship between electronic properties of these compounds and their ability to inhibit *β*-hematin formation. The calculated isotropic chemical shielding value for nitrogen nuclei in series **A** are remarkably consistent. It is also evident that the calculated σ_{iso} values for series **B** compounds (with the exception of **5b**) are not significantly differ. The σ_{11} and σ_{22} components as well as chemical shielding isotropy of the nitrogen nuclei for series **A** compounds significantly differ from those of the **B** series quinolines. In general, the σ_{33} component differs not significantly for two groups. Based on the calculated ^{15}N shielding tensors, the $\bar{\sigma}_{11}$ and $\bar{\sigma}_{22}$ from series **A** to series **B** are shielded,while $\bar{\sigma}_{33}$components is deshileded. The large changes in σ_{iso} values between two quinolines groups are due mainly to large changes in σ_{11} and σ_{22}. Due to the resonance effects of aminoalkyl substitutions in the para position to the nitrogen in series **A**, the nitrogen nucleus experiences large changes in π-electron density compared to bare quinoline and other quinolines in series **B**. This is in agreement with the ^{13}C shielding tensor orientation of quinolines and other aromatic systems [6].

Conclusions:

According to the results obtained in this study, we may draw the following conclusions:

1) Different aminoalkyl subsistent,-R, on the para position in series **A** compounds did not significantly affect the electron density of the nitrogen quinoline ring.

2) The results of isotropic ^{15}N shielding values in series **B** show that π-electron density of quinoline nitrogen is not significantly influenced by the presence of amino group in 3-,5-, 6-, 8-position and dichloro substituent in 4-,8- positions.

3) The ^{15}N shielding tensor components are appropriate parameters to examine the changes in π-electron density, where these results strongly support that the ^{15}N shielding tensor components of quinoline nitrogen are useful tool to compare the behavior of quinolines in relation to their *β*-hematin inhibition activity.

References:

[1] World Health Organization. The World Health Report: 2002: Reducing Risks, Promoting Healthy Life.

[2] T.J. Egan, Drug Design Reviews, 1 (2004) 93.

[3] T. Frosch, J. Popp, J. Mol. Struct., 924 (2009) 301.

[4] M.J. Frisch et al., Gaussian 98 (Revision A. 11), Gaussian, Inc, Pittsburgh, PA (2001).

[5] A. D. Becke, Phys. Rev. A 38 (1988) 3098.

[6] L.B. Casabianca, A.C. De Dios, J. Phys. Chem. A 110 (2006) 7787.

Covalent and ionic doorway states of H2 in ultrashort intense laser field

Mohsen Vafaee[a]*, Hassan Sabzyan[a]*, Behnaz Buzari[b]

[a]Department of Chemistry, University of Isfahan, Isfahan 81746-73441, I. R. Iran

[b]Laser-Plasma Research Institute, Shahid Beheshti University, Tehran, 19839-63113, I. R. Iran

*E-mails: sabzyan@sci.ui.ac.ir & MohsenVafaee@sci.ui.ac.ir

Keywords: Enhanced ionization; Gabor analysis; HHG; H_2; TDSE.

Introduction

Interaction of atomic or molecular systems with intense laser fields results in nonperturbative electron dynamics [1]. In the past decade, numerous works have been carried out on the one-electron H_2^+ molecular system [2-4], but a limited number of works is devoted to the two electron-H_2 system [5-6], with no reference to the HHG phenomena. In this work, The mechanism of enhanced ionization in the two–electron molecule H_2 subjected to an ultrashort intense laser pulse is investigated by solving exactly the 1-D electronic time-dependent Schrödinger equation including nuclear motion. Dynamics of adiabatic H^+H^+ and H^-H^+ states (doorway) are analyzed using time-dependent emission of three alternative forms of the high-order harmonic generation (HHG) spectra, obtained based on the Gabor analysis of the numerical data obtained obtained from the evolution of the central part of the two-electron wavepacket of H_2.

Computational method and results

The TDSE for the H_2 system considering two 1-D electrons and freed nuclei is solved numerically using the split-operator technique [7]. The space belonging to the H_2 subsystem is discretized to four areas on a generalized pseudospectral grid Fig. 1 and propagate the electronic wave function using a second-order split-operator method. Three alternative forms of harmonic spectra of adiabatic H^+H^+ and H^-H^+ states (doorway) are calculated and compared as functions of laser intensity, based on the dipole moment, dipole velocity, and dipole acceleration, using Gabor analysis [8]. The carrier frequency $\omega_\circ$ values correspond to the wavelengths of 390, 532 and 790 nm.The results of the λ= 532 nm and I= 5×10^{14} Wcm^{-2}

are represented. The results are plotted in Fig. 2. In each of the main panels of this Fig. 2, periodic population oscillation among molecular orbital levels are observable.

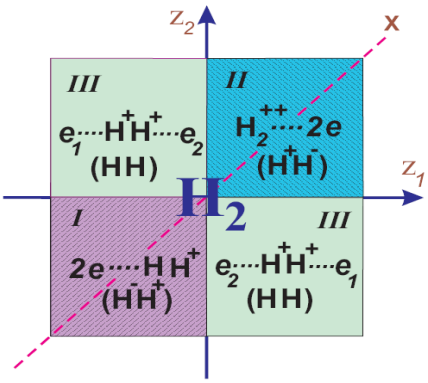

Figure 1. Details of the H_2 region pseudospectral grid simulation box divided into four sub-regions.

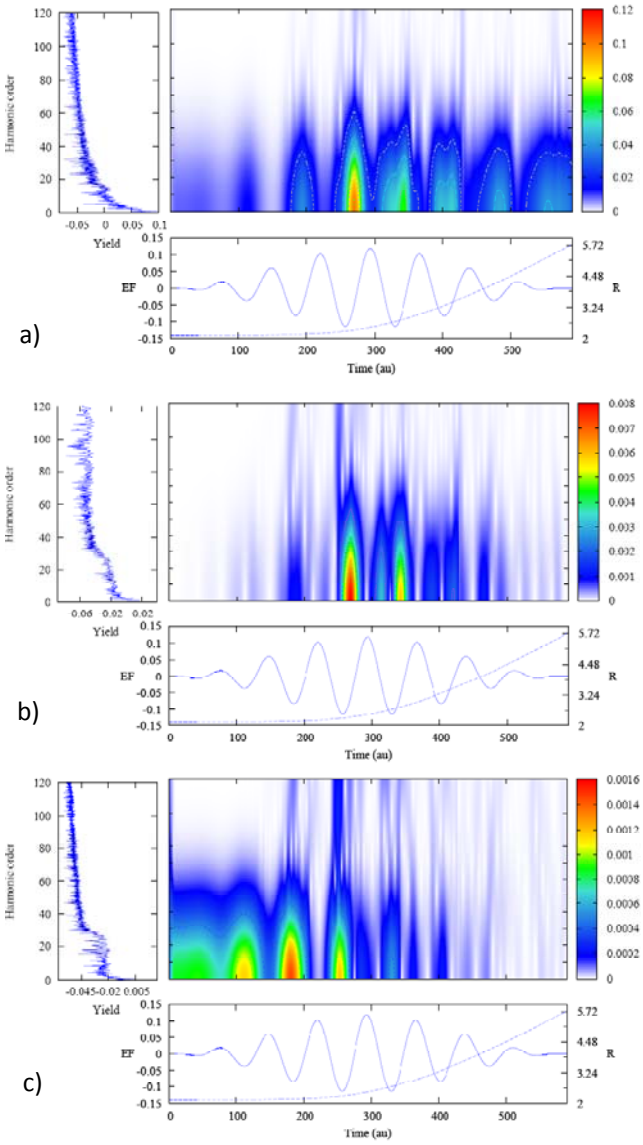

Figure 2. Time-frequency analysis of the a) dipole, b) velocity and c) acceleration responses belonging to the H_2–II zone of the central part of the wavepacket of 1-D H_2 system to a strong few-cycle laser pulse. The lower panel shows variation of the inter nuclei distance involved in the time dependenet electric field with $I=5\times10^{14}$ Wcm^{-2} and λ= 532 nm. The time-frequency analysis of the signal obtained by Fourier transforming with a Gaussian window function is given in the up panel. The overal harmonic spectrum is shown in the left inset.

Conclusions

In this work, HHG spectra of H^+H^+ and H^-H^+ states in the central part of the two-electron wavepacket of H_2 are investigated. The velocity HHG spectra follow the same scheme as the momentum HHG spectra but with more spectral detail and less intensity. The dynamics of the presented sub–systems before the enhanced ionization can be observed using the acceleration HHG spectra. Ionization is enhanced when the excited ionic state H^-H^+–II is most efficiently created from the covalent ground state HH–III, in the upper left of Fig. 1.

References

[1] Y.-J. Jin, et al., Phys. Rev. A 2010, 81,013408.

[2] Y.–M. Lee, et al., Chem, Phys Rev. A 2008, 77, 013414.

[3] M. Vafaee, Phys. Rev. A 2008, 78, 023410.

[4] M. Vafaee, H. Sabzyan J. Phys. B 2004, 37, 4143.

[5] A. D. Bandrauk, et al., J. Phys. B 2009, 42, 134001.

[6]K.-J. Yuan, et al., , Phys. Rev. A 2009, 80, 061403.

[7] M. D. Feit, et al., J. Comput. Phys. 1982, 47,412.

[8] C. C. Chirila, et al., Phys. Rev. A 2010, 81, 033412.

A new synthesized solvatochromic amino azo quinoline dye in pure and mixed binary solvents

A. Ghanadzadeh Gilani [a], E. Moradi [b], S. Binay [a]

Sedighe.Binay@gmail.com

[a]Department of Chemistry, Faculty of Science, University of Guilan, Rasht, Iran

[b]Department of Chemistry, Faculty of Science, Islamic Azad University, Lahijan-branch, Iran

Key word: Amino azo hydroxy-quinoline dye, Solvent-solute interactions, Linear solvation energy relationship, Solvent polarity scales

Introduction

It is well known that photo-physical behavior of a dissolved dye depends on the nature of its environment, i.e., the solvent influences the spectra characteristics of the solute molecules [1,2]. Several factors influence the visible spectral behavior of dye molecules, especially the solvent's polarity and its hydrogen-bond donor/acceptor capacities. In this work optical characteristic and the influence of solute–solvent interaction on the visible spectra of new amino azo hydroxy-quinoline dye (Fig. 1) was investigated.

Methods

Amino azo hydroxy-quinoline dye was synthesized in our laboratory. The absorption spectra of amino azo hydroxy-quinolines dye were recorded at room temperature in various pure and binary mixtures of organic solvents using UV-Vis Cary 100.

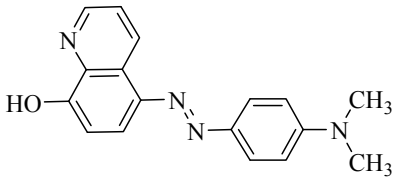

Fig. 1 The structure of amino azo hydroxy-quinolines dye

Results and discussion

It was found that solute-solvent interactions and solvent-solvent interactions plays an important role in determining the solvatochromic behavior and preferential solvation of

amino azo hydroxy-quinolines dye. As an example, Fig. 2a shows variation of maximum absorption wavelength (λ_{max}) of the dye in the mixed binary solvent (CCl_4 + EtOH). The plot of spectroscopic transition energy (E) with increasing solvent polarity was also shown in Fig. 2b. The investigated dye exhibits different spectroscopic behaviors with increasing of concentration of EtOH. The red shift in this mixed binary solvent might depend on either nonspecific or specific (e.g. hydrogen-bonding) solute–solvent interactions and preferential solvation**.** The solvent effect can be analyzed using multi-parameter solvatochromic scales [3,4].

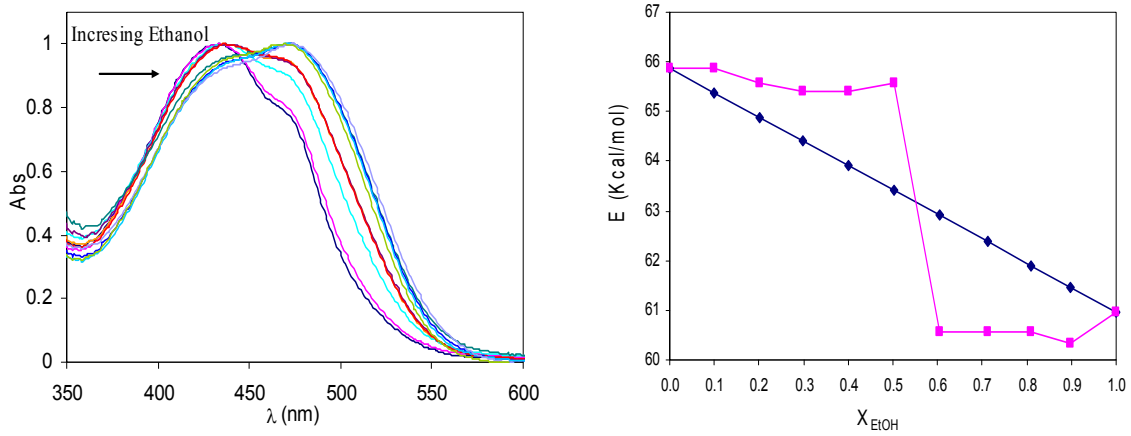

(a) (b)

Fig. 2 Absorption spectra and plot of spectroscopic transition energy (E) of amino azo hydroxy-quinolines in the (CCl_4 + Ethanol) binary mixtures

References:

[1] A. Ghanadzadeh, A. Zeini, A. Kashef , J. Mol. Liq., 133 (2007) 61–67.

[2] A. Ghanadzadeh, A. Zeini, A. Kashef, M. Moghadam, Spectrochimica Acta 73 (2009) 324–329.

[3] A.K. Laha, P. K. Das, S. Bagchi, 106 (2002) 3230-3234.

[4] A. R. Katritzky, D. C. Fara, H. Yang, and K. Tamm, Chem. Rev. 104 (2004) 75−198

Preferential Solvation of Sudan III and Sudan IV Dyes in Net and Mixed Binary Solvents

A.Ghanadzadeh[a], M.Parsaee[a]*

Matinparsaee63@yahoo.com

[a]*Department of chemistry, faculty of science, university of guilan, Rasht, Iran*

Keyword: Azo dyes; Solvent effect; Mixed solvents; Preferential solvation.

Introduction

Azo dyes are one of the important classes of colorants. Many studies have been carried out on the relationship between the structure, absorption spectra and photo stability of azo dyes [1]. When a polar molecule is dissolved in binary solvent mixture, it interacts differently with each of the solvent component. In mixtures of solvents of different polarity, a process of preferential solvation occurs [2-4].

Methods

Sudan dyes were purchase from Aldrich Chemical Co. The absorption spectra were recorded using UV-Vis Cary 100 spectrophotometer at room temperature. Samples for absorption measurements were prepared using a 1-cm quartz rectangular cell. The concentration of the solutions studied was about 1×10^{-5} M.

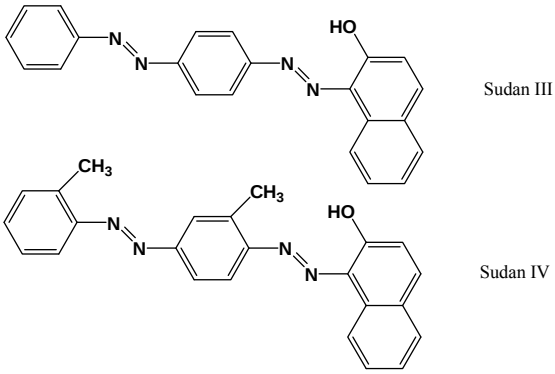

Fig. 1 The structure of Sudan dyes

Results and discussion

In this work, the solvatochromic behavior and preferential solvation of two Sudan dyes, Sudan III and Sudan IV, (Fig. 1) were investigated by studying their visible spectra in several pure and mixed organic solvents. As an example, the optical absorption spectra of Sudan III in (cyclohexane-butanol) binary mixtures and plot of spectroscopic transition energy (E) are shown in Fig. 2. By increasing solvent polarity, these compound exhibit different spectroscopic behaviors depending on the properties of the solubilizing media. The solvent dependent spectral shifts might be due to either nonspecific or specific (e.g. hydrogen-bonding) solute–solvent interactions and selective solvation in the solvation shell. The solvent effect can be analyzed using multi-parameter solvatochromic scales [5].

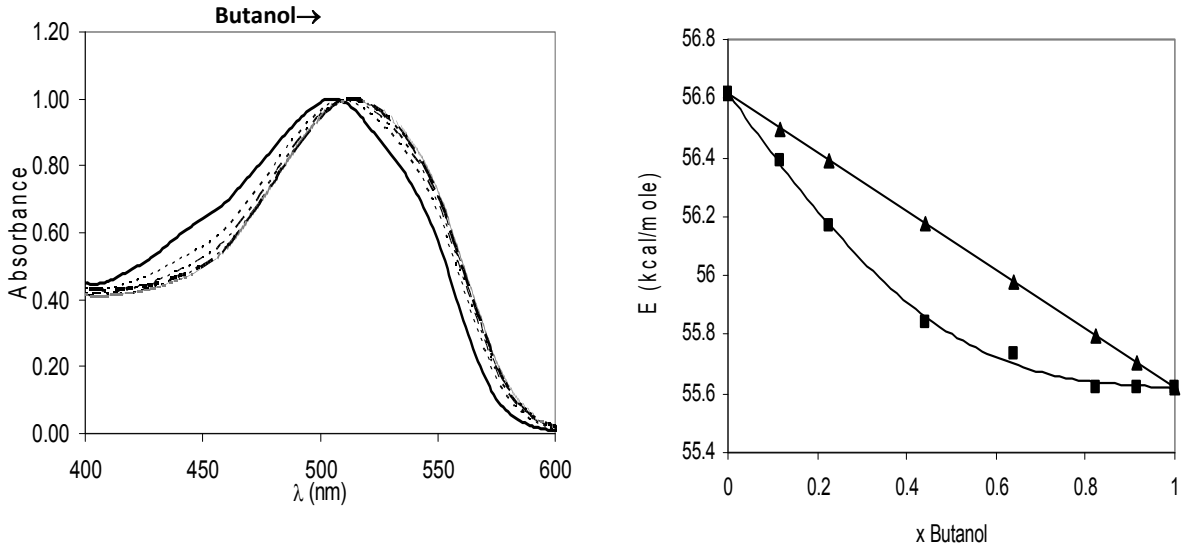

Fig. 2 Absorption spectra and plot of spectroscopic transition energy (E) of Sudan III in the (cyclohexane + 1-butanol) binary mixtures

References

[1] A. Ghanadzadeh, M.A. Shahzamanian, S. Shoarinejad, M.S. Zakerhamidi, M. Moghadam, J. Mol. Liq. 136 (2007) 22.

[2] P. Suppan, J. Chem. Soc., Faraday. Trans. 188 (1992) 963.

[3] N. Ghoneim, Spectrochim. Acta A 57(2001) 1877.

[4] T. Molotsky, D. Huppert, J. Phys. Chem. A107 (2003) 8449.

[5] A. Ghanadzadeh, M.S. Zakerhamidi, H. Tajalli, J. Mol. Liq. 109 (2004) 143.

Evaluation the origin of conformational and tautomeric preferences in N-acetylacetamide- a quantum chemical study

A. Nowroozi[a]*, M. Poorsargol[a], F. Naroei[a], S. Dahmardeh[a], F. Akbari[a]

[a] *Department of Chemistry, University of Sistan & Baluchestan, Zahedan, Iran*

(Email: Poorsargol.mahdiye@yahoo.com)

Keywords: N-acetylacetamide, Intramolecular hydrogen bond, Amide resonance, AIM and NBO.

Introduction:

Hydrogen bonding is one of the most important concepts in chemistry due to its profound influences on the chemistry of life, crystal packing, solvation, catalysis, chelation, and a host of other important phenomena [1-2]. The amide functional group is the fundamental unit of proteins, peptides, and other biologically important molecules and has been traditionally characterized by a restricted C-N bond rotation, coplanarity of the attached atoms, short C-N bond lengths, red-shifted carbonyl stretching frequencies, relative stability toward nucleophilic attack and protonation at oxygen rather than nitrogen [3]. N-acetylacetamide (NAA) as the simplest member of β-diacetamides compounds can participate in the amide↔imidic acid equilibrium (Fig. I).

In the present study the characterization of the equilibrium conformations, especially global minimum, and estimation of the intramolecular hydrogen bond (IHB) and π-electron delocalization strength were carried out.

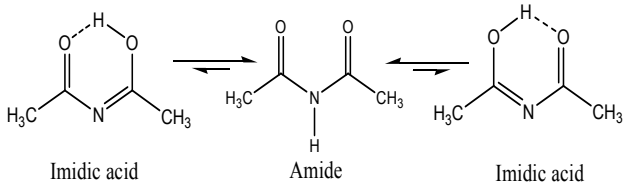

Fig I. Amid↔Imidic acid tautomeric equilibriums in NAA.

Methods:

All of the computations in the present study were performed by Gaussian 03 series of programs [4]. The geometry optimizations were carried out by B3LYP and MP2 methods with the most popular basis set, 6-311++G(d, p). The optimized structures at MP2/6-311++G(d, p) level of theory were used to obtained the appropriate wave function files for AIM and NBO analyses. The nature of the IHB in the most stable conformers has been studied using the AIM theory [5] and the NBO package included in Gaussian 03 [6].

Results and discussion:

Theoretically, NAA has about 11 different conformers, which systematically arranged in two tautomeric classes, DA and AI with 3 and 8 members, respectively. From the relative energies at all of the computational levels, we can easily conclude the following energy order: DA < HB-AI < non HB-AI

This order readily shows that the DA conformers are more stable than the others which followed by HB-AI and non HB-AI forms.

The Schuster energy of IHB for chelated enol forms of NAA and acetylaceton (AA) at all of the computational levels were obtained which signify the Schuster energy of hydrogen bond in NAA is lower than the corresponding value of AA. Unlike the HB energies, the electron densities and its Laplacian at BCPs signify that the IHB in NAA is stronger than the AA.

The results of NBO analysis also show that in chelated forms, one or two lone pairs of proton acceptor and the proton donor antibonds are involved and the corresponding stabilization energies of NAA and AA are about 42.17, 35.85 kcal/mol, respectively. These results again emphasized on the conclusion of geometrical parameters and AIM analyses.

From the Gillis parameters, $q_1=R_{C-N}-R_{C=N}$ and $q_2=R_{C-O}-R_{C=O}$, we can qualitatively estimate the greatness of resonance. The results reveal that the π-electron delocalization of AI-11 is much greater than the other AI conformers.

Conclusions:

1. At all of the theoretical levels, the DA forms have more stability with respect to the AI conformers. - DA-2 forms have greater stability with respect to the other forms and known as global minimum.

2. Theoretical calculations at all of the computational levels show that the IHB in AA is stronger than the NAA, however AIM and NBO analyses and geometrical parameters give the opposite result, $E_{HB}(NAA) > E_{HB}(AA)$.

3. A detail investigation of tautomeric equilibrium, hydrogen bond and resonance, explicitly show that the origin of tautomeric preference is mainly due to the electron delocalization in diamide tautomer, especially $LP(N) \rightarrow \pi^*_{C=O}$ charge transfer.

Refrences:

[1] Jeffrey, G.A.; an Introduction to Hydrogen Bonding. Oxford University Press, New York, 1997.

[2] Grabowski, S. J.; Hydrogen Bonding- New Insights, Springer, Berlin, 2006.

[3] Kemnitz, C. R.; Loeven, J. M.; J. Am. Chem. Soc. 2007, 129, 2521.

[4] Frisch, M. J. et al. Gaussian 03, Revision A.7, Gaussian, Inc., Pittsburgh PA, 1998.

[5] Biegler-König, F.; Schönbohm, J.; Bayles, D.; AIM2000-A Program to Analyze and Visualize Atoms in Molecules, J. Comp. Chem. 22 (2001) 545.

[6] Glendening, D. E.; Reed, A. E.; Carpenter, J. E.; Weinhold, F.; NBO, Version 3.1.

Measurement problem and a Critical approach on Decoherence theory

Arash Tirandaz[‡] and Afshin Shafiee[†]
Research Group on Foundation of Quantum Theory and Information,
Department of Chemistry, Sharif University of Technology,
P.O.Box 11365-9516, Tehran, Iran

Abstract:
Considering the decoherence theory we try to mention some conceptual problems of this theory in tackling the measurement problem The quantum to classical transition discussed in the framework of decoherence theory in section I. At the end, we survey some defects of the decoherence approach on measurement problem in the framework of *gedanken* experiments.

Introduction:

The main stream in quantum mechanics is the Copenhagen interpretation mechanics routed in the beliefs of Bohr that the quantum phenomena is a black box and it is impossible to represent a lucid description of its nature. Considering Copenhagen hegemony, quantum domain is not in the access of experimenter. Then, his knowledge about the micro world is based on the measurement results. What is happened in the black box, consisting of quantum system and apparatus, must be consider as a metaphysical and mysterious phenomena that has not any physical description in the theory.

I. Decoherene approach on measurement problem

Decoherence theory tries to explain the so-called transition from quantum to classical by considering the openness of quantum systems. Decoherence demands that realistic quantum systems are not isolated from their environment.

In spite of the classical physics, the environment has a crucial effect on the evolution of the system. The role of the environment is twofold: First the interaction with environment leads to the suppression of interference terms between quantum states of the system. It corresponds with the suppression of the off-diagonal elements of the reduced density matrix of the system under its interaction with surrounding. Then by the means of a non-unitary evolution which

[‡] tirandaz@mehr.sharif.ir
[†] shafiee@sharif.edu

results from the trace operation on the environment degrees of freedom decoherence shows that why interference terms due to the quantumness of the system, removes through the interaction with the environment. Second: during the ubiquitous interaction of system-environment, some preferred states of the system are selected known as pointer states. These are states which preserve their correlation under the decoherence phenomena.

Discussion:

Critical approach on Deceherence

In the theory of the classical statistics, mixed states are in relation with ignorance interpretation of probability. It means, the experimenter knows that every subsystem of the an ensemble is in definite states but she does not know exactly that which one is in which state. Then, it seems that mixed density matrix of the system results from decoherence phenomena, could be interpreted as classical ones. One should keep in mind that the improper mixed states results from trace operation on a pure density matrix of the system-environment. The whole is in a pure state and all of the possibilities exist simultaneously. Proper mixed state, in its classical sense, does not results from a pure density matrix. So, it is not accurate to say that improper mixed states could be considered as their classical counterparts. In addition, the interpretation of the proper mixed states is dependent on the interpretation of the quantum states. Before going further, suppose that we have an ensemble of a proper mixture with 30% of quantum systems in the state$|0_z\rangle$, 50% in $|0_x\rangle$ and 20% in the state$|1_y\rangle$. Where $|0\rangle and |1\rangle$ represents spin up and down respectively. If one carries out the spin measurement in the Z-direction what will be the results? One may think that the answer is that 20% of quantum particles in the ensemble reflected by the measuring apparatus in positive direction of the Z axis . However one can easily show that it is not correct! Since $|0_x\rangle and |1_y\rangle$ are in relation with $|0_z\rangle$ according to following relations:

$$|0_x\rangle = \frac{1}{\sqrt{2}}(|0_z\rangle + |1_z\rangle) \qquad .2$$

$$|1_y\rangle = \frac{1}{\sqrt{2}}(|0_z\rangle - i|1_z\rangle) \qquad .3$$

So, even if we have a proper mixture of states, still its interpretation is dependent rigorously on the interpretation of the isolated quantum states or the wave function. Obviously, the two description results from the formalism of standard quantum mechanics and the density matrix

approach are not in agreement. There is no evidence if the mixed state 3 could be results from the $|\psi\rangle$ in relation 4. As it is not possible to have a theory with two incompatible descriptions decoherence demands that if one takes the effect of the environment into account to describe the evolution of $|\psi\rangle$ and trace over the degrees of the environment the reduced density matrix 4 could be retrieved.

References:

[1]M. Schlosshauer, Decoherence, "the measurement problem, and interpretations of quantum mechanics", *Review Of Modern Physics* **76**, 1267–1305 (2004).

[2]W.H. Zurek, "Pointer basis of quantum apparatus: Into what mixture does the wave packet collapse?", *Physical Review.D* **24**, 1516–1525 (1981).

[3]W. H. Zurek, "Environment-induced superselection rules", *Phyical Reiewv.D* **26**, 1862–1880 (1982).

Synthesis, Structure, and vibrational assignment of 3-amino-1-phenyl-2-buten-1-one

M. Jamialahmadi[a*], M. Ghaffari[a], S. F. Tayyari[a]

[a]Chemistry Department, Ferdowsi University of Mashhad, Mashhad, 91775-1436, Iran

[*]Email: jamialahmadimina@yahoo.com

Keywords: 3-amino-1-phenyl-2-buten-1-one; Vibrational spectra; Density Functional Theory; X-ray crystalography.

Introduction

β-Enaminones have been extensively used as valuable precursors in organic synthesis[1, 2] and represent useful synthetic building blocks for the synthesis of amino acids, [3]peptides[4], alkaloids[5] and heterocyclic compounds[6].

The aim of the present work is the synthesis and full assignment of the vibrational spectra of 3-amino-1-phenyl-2-buten-1-one (AKBA) by means of density functional theory (DFT) studies. The calculated geometrical parameters for AKBA will be compared with the X-ray results and the calculated vibrational frequencies are compared with those observed experimentally.

Method of analysis

AKBA was synthesized according to [7] and after recrystallization from hexane/ethyl acetate (1:1), the white shining crystals were yielded.

The IR spectrum of AKBA was recorded by using Bomem MB-154 Fourier Transform Spectrophotometer in the region 500–4000 cm^{-1} in KBr pellet and in $CHCl_3$, CH_2Cl_2, and CH_3CN solution.

In this study, the molecular equilibrium geometry and vibrational transitions of AKBA were computed with the GAUSSIAN 03 software system [8] by using hybrid density functional B3LYP [9, 10] and 6-31G**, 6-311G**, and 6-311++ G** basis sets.

Results and discussion

The ORTEP and geometry of AKBA is given in Fig. 1, 2, respectively . The full optimized geometrical parameters of AKBA along with the experimental structural parameters of this compound are compared in Table 1.

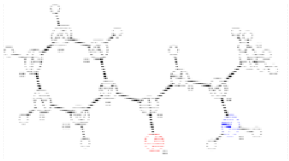

Fig 1

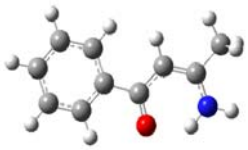

Fig 2

Table 1 calculated geometrical parameters for AKBA[a]
(bond lengths in Å, bond angles in °)

Bond lengths	**X-ray**	**A**	**B**	**C**	**APO** [b]
N…O	2.710	2.6375	2.6481	2.6479	2.658
N-H[7]	0.931	1.0210	1.0183	1.0183	1.021
N-H[8]	0.939	1.0061	1.0051	1.0051	-
C=O	1.254	1.2518	1.2447	1.2447	1.246
C-N	1.318	1.3471	1.3460	1.3460	1.349

[a]A: B3LYP/6-31G** B: B3LYP/6- 311G** C: B3LYP/6-311++G**
[b]: ref [11] calculated at B3LYP/ 6-31G**

Conclusions

Molecular structure and vibrational frequencies of 3-amino-1-phenyl-2-buten-1-one (AKBA) have been investigated by means of density functional theory (DFT) calculations. In addition, the geometry of this compound was also optimized at the B3LYP level and different basis sets. The results was compared with those of 4-amino-3-penten-2-one (APO). The main effect of phenyl substitution is shortening of the N· · ·O distance and lengthening of the N-H bond length, compared with the corresponding value for APO [17]. The structure of this compound was also confirmed by X-ray diffraction method.

References

[1] R.K. Vohra, J.L. Renaud, C. Bruneau, Collect. Czech. Chem. Commun. 70(2005) 1943.

[2] C.V. Stevens, B. Kesteleyn, E.R. Alonso, N. De Kimpe, Tetrahedron 57 (2001) 7685.

[3] Cimarelli, C.; Palmieri, G.; Volpini, E. *Synth. Commun.***2001**, *31*, 2943.

[4] Beholz, L. G.; Benovsky, R.;Ward, D. L.; Barta, N. S.; Stille, J. R. *J. Org. Chem*. **1997**, *62*, 1033.

[5] Michael, J. P.; Parsons, A. S. *Tetrahedron* **1999**, *55*, 10915.

[6] Alan, C.; Spivey, A. C.; Srikaran, R.; Diaper, C. M.; David, J.; Turner, D. J. *Org. Biomol. Chem.* **2003**, *1*, 1638.

[7] P. Simunek,V. Bertolasi, M. Peskova, V. Machaceka, A. Lyckac, Org. Biomol. Chem., 3 (2005) 1217.

[8] M. .J. Frisch, et al. GAUSSIAN03, Revision B.05, Gaussian, Inc., Pittsburgh PA, 2003.

[9] A. D. Becke, J. Chem. Phys. 98 (1993) 5648.

[10] C. Lee, W. Yang, R. G. Parr, Phys. Rev. B 37 (1988) 785.

[11] S.F. Tayyari, H. Raissi, F. Tayyari, Spectrosc. Chim. Acta Part A 58 (2002) 1681.

DFT-PCM Investigation of Hydrogen Bonding Strength of Different Configurations of Adenine- Thymine Base Pairs in Solution Phase

Behzad Chahkandi[1*], Nazanin Khodabakhsh[1], Tayebe Chahkandi[2]

1-Department of Chemistry, Islamic Azad University, Shahrood Branch, Shahrood, Iran

2- Assictant professor, Department of Pediatrics; instructor, Faculty of medicine, Birjand University of Medical Sciences, Birjand, Iran

Email: bchahkandi@gmail.com

Keywords : Hydrogen Bonding, Watson–Crick base pair, PCM, B3LYP, Solvent effect, BSSE

Introduction

The interaction between nucleotide bases is an important element in structure of DNA consequently, there have been numerous studies, experimental [1] and computational [2], concerned with the association of nucleotide base pairs. The computational studies rang from gas phase energy minimizations to Monte Carlo and molecular dynamics simulations in solution [3]. The work of Pohorille, Kollman, and co-workers is particularly notable. Porhorille et al. performed seminal Monte Carlo simulations of stacked and hydrogen-bonded base pairs in CCl_4 and in water [4]. The discovery of the hydrogen bonding between the bases Adenine (A) and Thymine (T) and between Guanine (G) and Cytosine (C) by Watson and Crick (1953), together with the crystal structure analyses of the protein hemoglobin and myoglobin by Perutz and Kendrew and their co-workers [5], initiated a new science, known as molecular biology, as described in Perutz (1963) and Kendrew (1963).

In the present work we try to calculate geometries, energies and other thermochemical properties of the hydrogen bonds in the Watson-crick DNA base pairs and other different configurations of A-T base pairs (See Fig 1) with DFT method in solution phase. And then we compared interaction energies, enthalpies, free energies, ΔG, and entropies of different orientations of A-T base pairs together.

Computational Methods

Nine different configurations of A-T base pairs have been studied in this paper (see Fig 1). All of calculations described in this paper were performed with the GAUSSIAN 98 , series of programs at $B_3LYP/6\text{-}31G(d)$ level of theory. The interaction energies, enthalpies, free energies, ΔG, and entropies, of hydrogen bonding between A-T base pairs were carried out in cyclohexane and chloroform solvents. PCM reaction field calculations are performing by using the polarizable dielectric model [6].

The basis set super position error (BSSE) was computed for all calculations using counterpoise method of Boys and Bernardi, employing the massage keyword in the Gaussian programs.

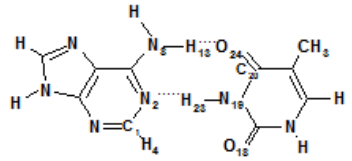

A-T(1) Watson-Crick

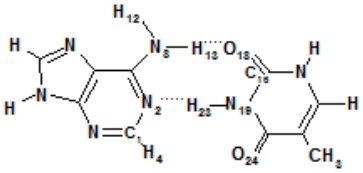

A-T(2)

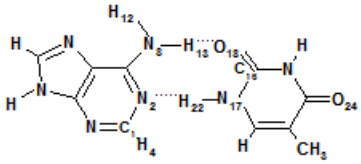

A-T(3)

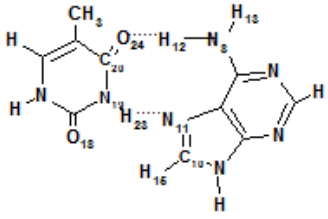

A-T(4)

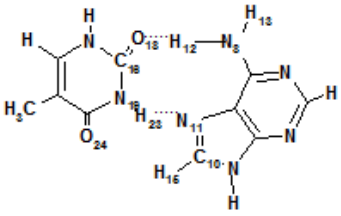

A-T(5)

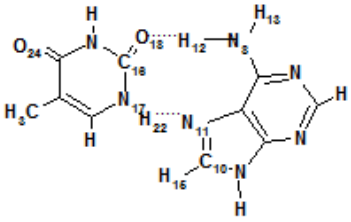

A-T(6)

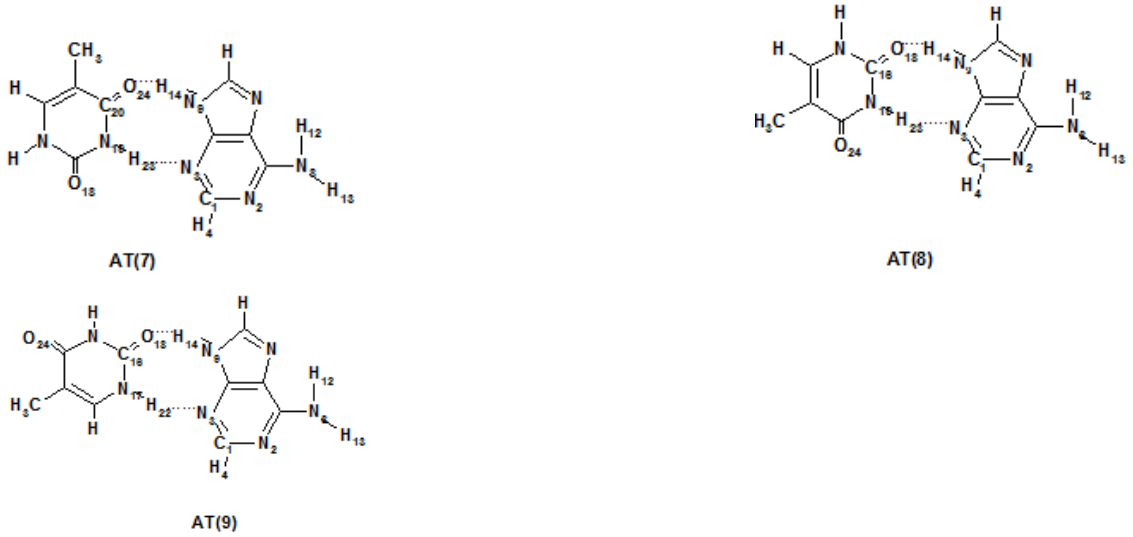

Fig 1. Watson -Crick geometry of adenine-thymine base pair and other different orientations of A-T.

Results and Discussion

The interaction energies of hydrogen bond in A-T base pairs and BSSE corrected interaction energies in cyclohexane (ε=2.023) and chloroform (ε=4.9) solvents were investigated. The effect of solvent on stabilization of A-T base pairs shows interesting results. The interaction energies of hydrogen bond in A-T complexes with increasing of dielectric constant of solvent decrease in agreement with our pervious work.[7] Our results turn out that the interaction energy (ΔE and $\Delta E_{BSSE)}$ for A-T (9) base pair is larger than others in the two solvents The values of ΔE_{BSSE} are significantly larger than ΔE which is due to correction of basis set super position error. The values of ΔH in the two solvents show that with decreasing dielectric constant of solvent bond enthalpies of each model of A-T base pairs increase and in both solvents the bond enthalpies of model (9) is larger than others. As can be seen, the ΔS values are quite similar for all complexes and for ΔG with decreasing dielectric constant of solvent the value of ΔG will decrease which shows complex stability increase.

Conclusion

1. DFT calculations indicate that A-T base pairs select different orientations that vary in energy and structures. This difference is reason of various hydrogen bonds between O, N and H atoms.

2. For different orientations of A-T base pairs, with increasing of dielectric constant of solvent, the energy decrease. AT (9) model is in lower level of energy and seems to be more stable than other models.

References

1. D. Voet and A. Rich, *The crystal structures of purines, pyrimidines and their intermolecular complexes*; *Prog. Nucleic Acid Res. Mol. Biol.* 1970, **10**, 183-265.

2. Y. Kyogoku, R. C. Lord and A. Rich, *Proc. Natl. Acad. Sci. U. S. A.* 1967, **57**, 250.

3. S. B. Petersen and J. J. Led, *J.Am. Chem. Soc*. 1981, **103**, 5308.

4. N. G. Williams, L. D. Williams and B. R. Shaw, *J. Am. Chem. Soc*. 1989, **111**, 7208.

5. B. Pullman, P, Claverie and J. Caillet, *Proc. Natl. Acad. Sci. U. S. A.* 1966, **55**, 904.

6. (a) P. Cieplak and P. A. Kollman, *J. Am. Chem. Soc*. 1988, **110**, 3734. (b) L. X. Dang and P. A. Kollman, *J. Am. Chem. Soc*. 1990, **112**, 503.

7. M. Monajjemi and B. Chahkandi, *J. Mol. Struct (THEOM)*. 2005, 714, 43.

Cloud Point Extraction and Spectrophotometric Determination of sulfide

S.F.Riazi[a] , M.Bahram[a],B. Hassanpour[b], S.Azimi[c]

[a]*Faculty of Chemistry urmia university, urmia, Iran*

(fardad.riazi@yahoo.com)

[b]*Faculty of Agricultural Engineering and Technology, University of Tehran, Karaj, Iran*

[c]*Faculty of Chemistry, Tarbiat Moallem University, Tehran, Iran*

Keywords: sulfide ion, cloud point, concentrate factor, beneficial factor

Introduction

One of the most important applications of surfactants in analytical chemistry is extraction and preconcentration based on cloud point [2]. Surfactants are inert molecules, which have two parts, head (Hydrophilic) and tail (Hydrophobic). When their concentration is more than their critical concentration (CMC), they get together and make micelles group [1]. Preconcentration methods through cloud point liquid-liquid extraction in comparison of common liquid-liquid preconcentration have a lot of advantages, such as: it's inexpensive and so stable reaction has minimal exposure to toxic organic solvents and satisfactory enrichments factors[3] .In this study, Cloud Point liquid-liquid Extraction method and UV detection are used for the determination of sulfide ion. Also, optimized factors that influence on the extraction efficiency have been found.

Method

1. Reagents and apparatus

Stock solution of para phenyl diamine (PPD), Fe^{+3}, sulfide ion were prepared and used daily. Several different factors such as nonionic surfactants concentration, temperature, and centrifuge speed affect on our results, and then we tried to optimize these factors. UV-vis absorption spectra were recorded using the spectrophotometer (PG mode T80) with 10mm quartz cell and centrifuge model Hettich Roto SILENTALL were used for extracting and dividing liquid phases.

2. Statistical Software

Microsoft Excel and Matlab7a for analyzing the results and chemo metrics method were used.

Results and discussion

1. Temperature and centrifuge speed optimization

They were don in a qualitative way, our optimized temperature and centrifuge speed for showing cloud point are about 45^{oC} - 70 ^{oC}, 3000 -4000(cycle per min) respectively.

2. Effect of nonionic surfactants (TX-114) concentration

For optimizing this factor at preconcentration step, several solutions with different concentrations of TX-114 were made. The results show at figure1.

The calibration graph under optimum conditions and different concentration of sulfide ion was plotted (figure 2).

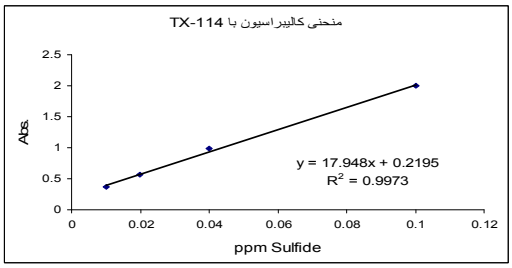

Figure2. Calibration graph under optimum condition

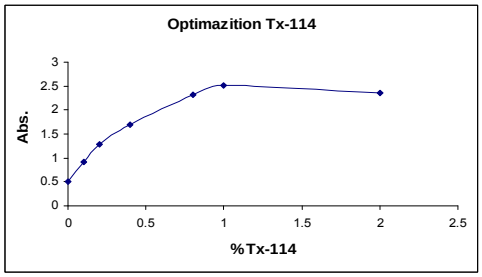

Figure1. Optimize value of TX-114 from spectrophotometeric results

3. Concentrate and beneficial factors

After comparing sample absorbance before and after preconcentration by triton x-100 and triton x-114, we can follow these formulas:

Concentration factor= final volume of sample without concentrate/final volume of concentrate sample

Concentrate factor= (15/0.5) =30

Calibration graph equation of no concentrate sample: y= 0.3435x+0.0385

Calibration graph equation of concentrate sample: y= 17.948x +0.2195

Beneficial factor= Calibration graph slope of concentrate sample/ calibration graph slope of no concentrate sample

Beneficial factor= 17.95/ 0.3435= 52.25

Conclusion

In this project cloud point liquid-liquid extraction was applied that it's concentrate and beneficial factors are 30, 52.25 respectively. It's so important to mention that in this method applying the system which they need hazardous and toxic organic solvents aren't necessary.

References

[1] Attwood D. and A. T. Florence (1983)Surfactant Systems, Chapman and Hall, London,

[2] Mashhadizadeh, M.H and L. Jafari (2009) Cloud Point Extraction and Spectrophotometric Determination of Codeine in Pharmaceutical and Biological Samples. JOURNAL OF THE Iranian Chemical Society. Vol. 7, No. 3, pp. 678-684

[3] Kaistha, K.K., Tadrus, R. (1978) J. Chromatogr 161 -287.

Investigation of structural and electronic properties of 3-alkoxythiophene

H. Nikoofard*, M. Khorrami
Faculty of chemistry, Shahrood University of Technology, Shahrood, Iran
monire.khorami@yahoo.com

Keywords: Alkoxythiophenes, Energy Gap, Charge Distribution, Conducting Polymers.

Introduction

Poly (3-alkoxythiophenes) (P3AOTs) have potential application in photoelectricity or micro-electronics field [1]. Especially, thiophene-based alternating donor–acceptor (D–A) conjugated polymers are particularly interesting because their electronic and optoelectronic properties can be tuned efficiently by intramolecular charge transfer (ICT), resulting from the efficiency conjugated sequence length (ECSL) of P3AOT can be changed by changing their electron distributing. The solubility, process ability, band gap and thermo stability of P3AOTs also can be adjusted by their side chains [2].In this work, we have studied structural and electronic properties of 3-alkoxythiophenes as candidate monomers for conducting polymers. We used quantum mechanical methods for calculations and then compare results with the corresponding values of 3-alkylthiophenes (ATHs).

Methods

All calculations were done with Gaussian 03 program. We calculated full optimization on, B3LYP level of theory with the 6-31G** basis set. We used these methods to find optimized geometries and electronic properties of 3-alkoxythiophenes and their radical cations.

Results and discussions

Using Mulliken population analysis, the net atomic electric charges and spin density distributions in the AOTs are calculated and summarized in Table1.

Table1.Electric charge (spin density) distributions calculated at B3LYP/6-31G**level of theory.

AOTs	C1(α)	C2(ά)	C3(β)
MeOTh	-0.3432(-0.2146)	-0.0798(0.0163)	-0.3066(-0.1773)
EtOTh	-0.3468(-0.2195)	-0.0793(0.0173)	-0.3078(-0.1790)
PrOTh	-0.3476(-0.2204)	-0.0786(0.0183)	-0.3081(-0.1795)
BuOTh	-0.348(-0.2209)	-0.0783(0.0186)	-0.3082(-0.1797)
PtOTh	-0.3482(-0.2211)	-0.0782(0.0188)	-0.3085(-0.1799)
HzOTh	-0.3482(-0.2212)	-0.0782(0.0188)	-0.3084(-0.1799)

As seen as in Table1, the electrical charge is more on α position of monomer rings and with addition of the length of the substituent increase, too. This manner had found about ATHs [3].

But electrical charges (spin densities) are more on similar positions of AOTs.

Consider of bond lengths of AOTs shows that the variations of bond lengths are too small and the same bonds of ATOs are shorter than of ATHs.

Electronic energies of ATOs are noticeably further than ATHs. The level of HOMO orbitals rise and the level of LUMO orbitals fall with growing the length of the substituent. The energy gap of ATOs and ATHs are presented on Table2.

Table2. The values of energy gaps (eV) of ATOs and ATHs at B3LYP/6-31G**.

Number of carbon atoms in the substituent	ATOs	ATHs
1	1.1205	1.1075
2	1.1243	1.13
3	1.117	1.1276
4	1.1184	1.1279
5	1.1183	1.1279
6	1.1181	1.1279

There are some fluctuations in variations of the energy gaps but it's obvious that the energy gaps reduce with adding the length of substituent. The values of band gap are less generally for ATOs in comparison the values of band gaps for ATHs.

Conclusions

Study properties of ATOs and comparison them with ATHs demonstrate that the bond lengths of ATOs are shorter than ATHs and the HOMO-LUMO Gaps (HLGs) are smaller and

electrical charge on different positions of heterocycle is more .It seems that addition atom of oxygen to the substituent of alkyl has good effects on properties of 3-alkylthiophenes. It's maybe related to influence of strong electron-donating of alkoxy group.

References

[1]. J.W. Jang, K.W. Lee, C.E. Lee, Solid State Commun, 131, (2004), 697.

[2]. D. Yanmao, J. Lu, Q. Xu, F. Yan, X. Xia, L. Wang, L. Hu, Syn. Met, 160, (2010), 409.

[3]. H. Nikoofard, Z. Kalantar, M. Khorrami, 13thIranian Physical Chemistry seminar, Shiraz, 2010.

Structural and electronic properties of 3-alkythiophenes terminated with formyl and consider of effects of a solvent on these characterization

H. Nikoofard*, M. Khorrami
Faculty of chemistry, Shahrood University of Technology, Shahrood, Iran
monire.khorami@yahoo.com

Keywords: DFT, Conducting Polymers, Alkylthiophene, Solvent Effects, HLG

Introduction

Conjugated oligomers have received broad interest recently in academic as well as in industrial research communities. The ease in obtaining compounds with high-purity and well-defined structures renders them promising active materials in thin film semiconductor devices such as organic field-effect transistors (OFETs), solar cells, nonlinear optical devices, and wave guides[1].

Polythiophene is one of conducting polymers that is been researched in many researching places. A variety of oligothiophene derivatives have been synthesized and their molecular and crystal structures, self-ordering, electrochemical, photophysical, optical, and electrical properties have all been studied. We have already investigated effects of substituent of alkyl on thiophene [2].In this study, we did two works to develop the previous results. At first, our researches had done in gas phase. It's clear without regarding effects of intramolecular forces; accordance of results with experimental data is not precise perfectly. So we use acetonitrile solvent and carried out quantum mechanical calculations in solution phase. The second is considering of properties of 3-alkythiophenes terminated with formyl to purpose enhancement of stability, fluorescence of this substance. Some oligoformyl-thiophenes derivatives have synthesized [3]. We inserted the substituent of alkyl on β position of end-capped formyl-thiophene and calculated structural and electronic properties of these materials.

Methods

All calculations were done with Gaussian 03 program. We calculated full optimization on, B3LYP level of theory with the 6-31G** basis set.

Results and discussion

Fig.1 shows the relation of the HLG changes with increasing length of the substituent. The HLG changes at gas phase and solution phase are shown and compared in Fig.1. The results indicate that a similar manner about both phase observe. On the other hand, with increasing the length of the substituent the energy gap and slope of the curve decrease and it is been flat finally. Some differences are obvious. The values of HLGs in gas phase are less for smaller substituents but this consequence is inverted about the later substituents.

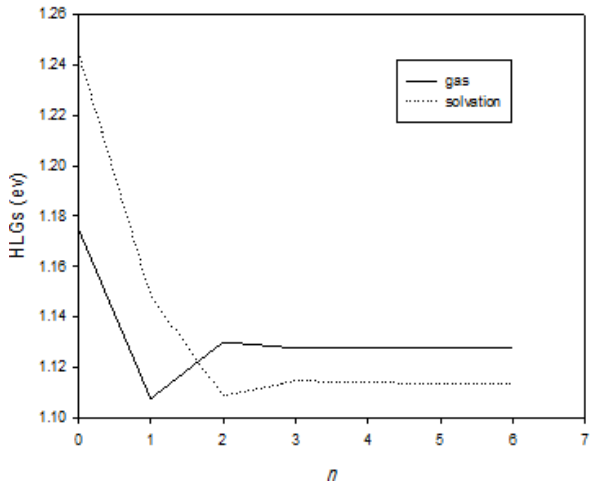

Fig1. Comparison the HLGs (eV) for two different phases.

Table1. shows some important geometric parameters. Adding alkyl group to thiophene increase all bond lengths and this effect is more about the bonds near to the substituent certainly. The similar bond lengths of 3-alkylthiophenes are longer in solution.

Table1. Some important bond lengths (Å) of ATHs in present of solvent at level B3LYP/6-31G**.

AThs	$R_1(C_\alpha\text{-H})$	$R_2(C_{\alpha'}\text{-H})$	$R_3(C_\beta\text{-R})$
Th	1.0846	1.0846	1.087
MTh	1.085	1.0847	1.5055
ETh	1.0831	1.0847	1.5122
PrTh	1.0834	1.0846	1.512
BTh	1.0833	1.0846	1.5121
PtTh	1.0833	1.0846	1.5121
HzTh	1.0833	1.0846	1.5121

Charge distribution and spin density for AThs terminated with formyl calculated and presented in Table2. It is obvious that equality of electrical charges on similar positions vary with attachment alkyl to ring of thiophene. Electrical charge is more on α position of heteroatom ring (α position near to the substituent) and increase with addition length of the substituent, too. Comparison the values of the electrical charge and spin density with the results related to calculations 3- alkylthiophenes (without formyl group) indicate that in present end-capped formyl the distribution of electrical charge is less on all studied positions of thiophene.

Consider of electronic energies show that addition of formyl causes rising the values of electronic energies and so the stability improves.

The calculations of energy gap demonstrate that the HLGs of studied molecules are more than the same values for 3-alkylthiophenes.

Table2. Electrical charge (spin density) distributions calculated for the B3LYP/6-31G** of ATHs terminated with formyl.

AThs	$C_1(\alpha)$	$C_2(\alpha')$	$C_3(\beta')$
Th	-0.2011(-0.2012)	-0.2011(-0.2012)	-0.0637(0.0551)
MTh	-0.2299(0.2499)	-0.2014(-0.2014)	-0.0881(0.0221)
ETh	-0.2550(-0.2550)	-0.2014(-0.2014)	-0.219(-0.0879)
PrTh	-0.2546(-0.2546)	-0.2024(-0.2024)	-0.2024(0.0226)
BTh	-0.2544(0.2544)	-0.2024(-0.2024)	-0.866(0.0228)
PtTh	-0.2546(-0.2546)	-0.2023(-0.2033)	-0.0864(0.023)
HzTh	-0.2546(-0.2045)	-0.2023(-0.2023)	-0.0864(0.0229)

Calculation of ionization potential indicates the ionization potential reduce when the length of the substituent grow.

Conclusion

Consider of energy gaps demonstrates that the values of energy gap in solution are less than gas. It's probably indicated effects of intramolecular forces. The bond lengths in solution are longer, but variations in the substituent length has no important effect on the bond length.

The growing of chain of polymer probably occurs on α position, because the electrical charge is more than other positions. The stability and charge distribution increase when formyl group use as end-capped specie in structure of 3-alkylthiophenes but the values of HLGs increase. The ionization potential fall with adding later methylene groups to the substituent and it means less potential is needed for polymerization of molecules with longer substituents.

References

[1]. H. Meng, J. Zheng, A. J. Lovinger, B. Wang,|P. Gregory Van Patten, Z. Bao ,Chem. Mater., Vol. 15, No. 9, 2003.

[2]. H. Nikoofard, Z. Kalantar, M. Khorrami, 13thIranian Physical Chemistry seminar, Shiraz, 2010.

[3]. B. Yin, C. Jiang, Y. Wang, M. La, P. Lu, W. Deng, Synthetic Metals 160 (2010) 432.

The calculation of vibrational energy levels inclusion anharmonic effect

M. Dehestani, Z. Kalantari,
Department of Chemistry, Shahid Bahonar University of Kerman, Kerman, Iran
dehestani2002@yahoo.com

Abstract

In this research we take the potential energy as a series expansion in dimensionless normal coordinates and consider terms through six-order. We use the contact transformation perturbed method to derive vibrational levels in terms of force constants. For illustration, a set of vibrational energies levels of SO_2 molecule has been calculated with inclusion of anharmonic effects.

Key words: Anharmonicity, vibrational levels, contact transformation perturbation method.

Introduction

The basic theory of anharmonicity in polyatomic molecules is well known. In previous literature, only the cubic and quartic parts of the potential function were considered as perturbation in calculation of vibrational energies levels. In the present work, we extend the development of the potential energies expression to higher terms. In this study, the zero-order Hamiltonian is taken to be the harmonic oscillator vibrational Hamiltonian. This paper consists of taking in the first-order Hamiltonian the cubic and quartic terms and the second-order Hamiltonian being a perturbation whose terms are of six-order. To facilitate the calculation of the second-order energy corrections, we use the contact transformation perturbation theory.

Computational method

A significant of the standard perturbation procedure is achieved by means of a contact transformation which changes the form of the perturbation Hamiltonian in such a way that the second order is reduced to a first order. These considerations show the convenience of transforming the Hamiltonian $\mathcal{H}$ into a new Hamiltonian $\mathcal{H}'$ through a similarity

Table (1). Energies (cm^{-1}) of the

transformation with a unitary function T as $\mathcal{H}' = T\mathcal{H}T^{-1}$ where T is $e^{i\lambda s}$[1]. If we write down the Hamiltonians $\mathcal{H}$ in order of magnitude as $\mathcal{H} = \mathcal{H}^{(0)} + \lambda\mathcal{H}^{(1)} + \lambda^2\mathcal{H}^{(2)}$ where

$$\mathcal{H}^{(1)} = \sum_i' k_{iii}q_i^3 + \sum_{i,j}' k_{iij}q_i^2 q_j + \sum_{i,j,k}' k_{ijk}q_i q_j q_k + \sum_{i,j}' k_{iiij}q_i^3 q_j + \sum_{i,j,k}' k_{iijk}q_i^2 q_j q_k + \sum_{i,j,k,l}' k_{ijkl}q_i q_j q_k q_l$$

$$\mathcal{H}^{(2)} = \sum_i k_{iiii}q_i^4 + \sum_{i,j}' k_{iijj}q_i^2 q_j^2 + \sum_i' k_{iiiiii}q_i^6 + \sum_{i,j,k}' k_{iijjkk}q_i^2 q_j^2 q_k^2 + \sum_{i,j}' k_{iiiijj}q_i^4 q_j^2$$

Where $\sum'$ means indices of summation are not same. Now we can obtain the energy

$$E = E_0 + hc\sum_i \omega_i\left(v_i + \frac{1}{2}\right) + hc\sum_{ij} x_{ij}\left(v_i + \frac{1}{2}\right)\left(v_j + \frac{1}{2}\right) + hc\sum_{ijk} x_{ijk}\left(v_i + \frac{1}{2}\right)\left(v_j + \frac{1}{2}\right)\left(v_k + \frac{1}{2}\right) + \cdots$$

Where

$$x_{iii} = \frac{5}{2}k_{iiiiii} + \frac{1}{2}\sum_j\left(\frac{41\omega_i^2\omega_j - 5\omega_j^3}{18\omega_i^4 - 20\omega_i^2\omega_j^2 + 2\omega_j^4}\right)k_{iiij}^2$$

$$x_{iij} = \frac{3}{2}k_{iiiijj} + \frac{3}{2}\left(\frac{3\omega_j}{\omega_i^2 - \omega_j^2}\right)k_{iiij}k_{jjji} - \frac{27}{4}\left(\frac{\omega_i}{\omega_i^2 - \omega_j^2}\right)k_{iiij}^2 + 3\sum_k\left(\frac{\omega_k}{\omega_i^2 - \omega_k^2}\right)k_{iiik}k_{jjik} + \sum_k\left(\frac{\omega_k\left(32\omega_i^4 + 3(\omega_j^2 - \omega_k^2)^2 - 4\omega_i^2(3\omega_j^2 + 5\omega_k^2)\right)}{(\omega_j^2 - \omega_k^2)\left(16\omega_i^4 + (\omega_j^2 - \omega_k^2)^2 - 8\omega_i^2(\omega_j^2 + \omega_k^2)\right)}\right)k_{iijk}^2$$

$$x_{ijk} = k_{iijjkk} - 6\left(\frac{\omega_i}{\omega_i^2 - \omega_j^2}\right)k_{iiij}k_{kkij} - 6\left(\frac{\omega_j}{\omega_j^2 - \omega_i^2}\right)k_{jjji}k_{kkij} - 6\left(\frac{\omega_i}{\omega_i^2 - \omega_k^2}\right)k_{iiik}k_{jjik} - 6\left(\frac{\omega_k}{\omega_k^2 - \omega_i^2}\right)k_{kkki}k_{jjik}$$
$$- 6\left(\frac{\omega_j}{\omega_j^2 - \omega_k^2}\right)k_{jjjk}k_{iijk} - 6\left(\frac{\omega_k}{\omega_k^2 - \omega_j^2}\right)k_{kkkj}k_{iijk} - 8\left(\frac{\omega_j(4\omega_j^2 - \omega_i^2 - \omega_k^2)}{16\omega_j^4 + (\omega_i^2 - \omega_k^2)^2 - 8\omega_j^2(\omega_i^2 + \omega_k^2)}\right)k_{jjik}^2$$
$$- 8\left(\frac{\omega_i(4\omega_i^2 - \omega_j^2 - \omega_k^2)}{16\omega_i^4 + (\omega_j^2 - \omega_k^2)^2 - 8\omega_i^2(\omega_j^2 + \omega_k^2)}\right)k_{iijk}^2 - 8\left(\frac{\omega_k(4\omega_k^2 - \omega_i^2 - \omega_j^2)}{16\omega_k^4 + (\omega_i^2 - \omega_j^2)^2 - 8\omega_k^2(\omega_i^2 + \omega_j^2)}\right)k_{kkij}^2$$
$$+ \frac{\hbar hc}{2}\sum_{l\neq ijk} M_{ijkl}e_7 k_{ijkl}^2$$

$$e_7 = -M_{ijkl}\left(\omega_l\left(-\omega_i^6 - \omega_j^6 + (\omega_l^2 - \omega_k^2)^3 + \omega_j^4(3\omega_l^2 + \omega_k^2) + \omega_i^4(\omega_j^2 + 3\omega_l^2 + \omega_k^2) + \omega_j^2(-3\omega_l^4 + 2\omega_l^2\omega_k^2 + \omega_k^4)\right.\right.$$
$$\left.\left. + \omega_i^2\left(\omega_j^4 - 3\omega_l^4 + 2\omega_l^2\omega_k^2 + \omega_l^4 + 2\omega_j^2(\omega_l^2 - 5\omega_k^2)\right)\right)\right)\hbar^2$$

$$M_{ijkl} = \left(\left(\omega_i^8 - 4\omega_i^6(\omega_j^2 + \omega_k^2 + \omega_l^2) + \left(\omega_j^4 + (\omega_l^2 - \omega_k^2)^2 - 2\omega_j^2(\omega_k^2 + \omega_l^2)\right)^2 + \omega_i^4\left(6\omega_j^4 + 6\omega_l^4 + 4\omega_l^2\omega_k^2 + 6\omega_k^2 + 4\omega_j^2(\omega_l^2 + \omega_k^2)\right)\right.\right.$$
$$\left.\left. - 4\omega_i^2\left(\omega_j^6 - \omega_j^4(\omega_k^2 + \omega_l^2) + (\omega_l^2 - \omega_k^2)^2(\omega_l^2 + \omega_k^2) - \omega_j^2(\omega_l^4 - 10\omega_l^2\omega_k^2 + \omega_k^4)\right)\right)\hbar^3 hc\right)^{-1}$$

vibrational levels of the ground states of SO_2: experimental [2] vs calculated energies.

Vibrational levels	E_{obs}	E_{ijk}
010	517.69	516.94
020	1029.38	1027.97
100	1151.38	1151.84
001	1361.76	1361.32
030	1535.06	1533.15
040	2034.74	2032.51
200	2295.88	2295.83
101	2499.55	2499.36
050	2528.41	2526.09
130	2674.44	2678.75
210	2805.57	2808.55

Conclusion

In Table (1) we present the results of our vibrational energies calculations corresponding to the expansion of the potential energy to sixth order. Comparing the calculated vibrational energies levels with the experimental energies shows acceptable agreement. In particular for the upper energy levels the agreement is very good. We note here that the effects of higher order anharmonicity constants on the upper levels are large.

References

[1] P. Jenson and P. R Bunker, Computational Molecular Spectroscopy, *John Wiley* (2000).

[2] S. Zelek, L. Cyrnek, J. Wasilewski, *J. Mol. Structure,* **629**, 61(2003).

Solutions of the Schrödinger equation for nuclear shell model with separation method

Seyed Hojatolaeh Rahimi, Mehri Deilam, and Vahid Moeini
Department of Chemistry, Payame Noor University, Behshahr Center, Behshahr, Iran
(Email: mehrideilam@yahoo.com)

Keywords: Schrödinger equation, Woods-Saxon potential, nuclear shell model, separation method

Introduction

The interactions between nuclei are commonly described by using a potential that consist of the Coulomb and the nuclear potentials. These potentials are usually taken to be of the Woods-Saxon form. [1]

Woods and Saxon introduced a potential to study elastic scattering of 20 MeV protons by a heavy nuclei [2] and The Woods-Saxon potential is a reasonable potential for nuclear shell model and hence attracts lots of attention in nuclear physics.[3,4,5,] The Woods-Saxon potential plays an essential role in microscopic physics, since it can be used to describe the interaction of a nucleon with the heavy nucleus.[6]

Methods

The Woods-Saxon potential can be introduce by the following relation

$$V(r) = \frac{-V_0}{1 + e^{\left(\frac{r-R}{a}\right)}} \qquad (1)$$

Where V_0 (having dimension of energy) represents the potential well depth, a is a length representing the "surface thickness" of the nucleus, and $R = r_0 A^{1/3}$ is the nuclear radius where r_0= 1.25 fm and A is the mass number.

The time- independent Schrödinger equation $\hat{H}\psi = E\psi$ is therefore

$$-\frac{h^2}{8\pi^2\mu}\nabla^2\psi-\frac{V_0}{1+e^{\left(\frac{r-R}{a}\right)}}\psi=E\psi \qquad (2)$$

Since the system is spherically symmetrical, it is most convenient to use spherical polar coordinates, which are related to Cartesian coordinates. When the Laplacian operator ∇^2 is converted to polar coordinates, the Schrödinger equation takes the form

$$\frac{1}{r^2}\frac{\partial}{\partial r}\left(r^2\frac{\partial\psi}{\partial r}\right)+\frac{1}{r^2\sin\theta}\frac{\partial}{\partial\theta}\left(\sin\theta\frac{\partial\psi}{\partial\theta}\right)+\frac{1}{r^2\sin^2\theta}\frac{\partial\psi}{\partial\phi^2}+\frac{8\pi^2\mu}{h^2}\left(E-\frac{V_0}{1+e^{\left(\frac{r-R}{a}\right)}}\right)\psi=0 \qquad (3)$$

This partial differential equation may be separated into three ordinary differential equation, in each of which we have only one of the variables r, θ, and ϕ. To do this we write the wave function ϕ, which is a function of r, θ, and ϕ, as the product of three function $R(r)$, $\Theta(\theta)$, and $\Phi(\phi)$:

$$\psi(r,\theta,\phi)=R(r)\Theta(\theta)\Phi(\phi) \qquad (4)$$

Substitution of this expression

$$\frac{1}{r^2R}\frac{\partial}{\partial r}\left(r^2\frac{\partial R}{\partial r}\right)+\frac{1}{r^2(\sin\theta)\Theta}\frac{\partial}{\partial\theta}\left(\sin\theta\frac{\partial\Theta}{\partial\theta}\right)+\frac{1}{r^2\sin^2\theta}\frac{1}{\Phi}\frac{\partial^2\Phi}{\partial\phi^2}+\frac{8\pi^2\mu}{h^2}\left(E-\frac{V_0}{1+e^{\left(\frac{r-R}{a}\right)}}\right)\psi=0 \qquad (5)$$

Therefore

$$\frac{\partial^2\psi}{\partial r^2}+\frac{2m}{\hbar^2}\left[E-\frac{V_0}{1+e^{\left(\frac{r-R}{a}\right)}}\right]\psi=0$$

Results and Discussion

By the using of this method we obtain the eigenvalues of energy of the Schrödinger equation:

$$E(n,m)=-(n-m+1)\left[\left(\frac{\delta(s)p'(s)}{p(s)}\right)'+\frac{1}{2}(n+m)\delta''(s)\right]$$

$$E(n,m)=-(n-m+1)\left[(\wp-2)+(n+m)\right]$$

Conclusions

In this paper, we will exactly solve the time-independent Schrödinger equation for the spherical woods-Saxon potential with the zero angular momentum and we obtained the eigenvalues of the Woods Saxon potential.

References

[1] A. Khare, B.P. Mandal, *Phys. Lett. A*, 2000, 272, 53

[1] H. Fakhri, and J. Sadeghi, Mod. *Phys. Lett. A*, 2004**,** 29, 615

[2] R. D. Woods, D. S. Saxon, *Phys. Rev*, 1954, 95, 577-57

[3] K. Abe & al., *Phys. Rev. Lett.*, 1996, 76, 587 - 591.

[4]. N.R.Pierson,et al,*phys.Rev*,. 1964, *B*133, 384

[5]. L.trache et al, *phys. REV.C*, 2000, 61

[6] S. Flugge, Springer - Verlag, Berlin, 1974.

Characterization of molecular toxic effects of nanoparticles in blood upon interaction with hemoglobin by using different spectroscopic methods

S. Zolghadri[a,b], A. A. Saboury[b]
(z.jahromi@ibb.ut.ac.ir)
[a] Department of Biology, Islamic Azad University of Jahrom, Jahrom, Iran
[b]Institute of Biochemistry and Biophysics, University of Tehran, Tehran, Iran

Keywords: Hemoglobin, spectroscopy, nanoparticle, Binding

Introduction

Due to their small size, nanoparticles have distinct properties compared with the bulk form of the same materials. These properties are rapidly revolutionizing many areas of medicine and technology. Despite the remarkable speed of development of nanoscience, relatively little is known about the interaction of nanoscale objects with living systems. Although more and more nanomaterials are available, only a few kinds of NP have been used in biological studies. Silver NPs, which are easy to synthesize, have attracted our attention due to their quantum characteristics of small granule diameter and large specific surface area as well as their ability to quickly transfer photo induced electrons at the surfaces of colloidal particles [1] As an oxygen-transport protein, hemoglobin (Hb), which has a molecular weight (MW) of 67 000, is often used as a model to study the structure and function of heme proteins. Hb is a physiologically important globular protein [2-5]. The Hb molecule contains four globin chins, of which two are α-chains and two are β-chains [4–7]. To explore the influence of different nanoparticles on the conformational structure of BHb, in this study, we have explored the interaction of nanoparticles with Hb by biophysical methods, mainly fluorescence, UV spectroscopy, and CD spectroscopy. This study may provide valuable answers to the growing concern regarding the effects of nanoparticles on the changes of secondary and tertiary structures in Hb conformation.

Methods

The UV-Visible absorption spectra were measured with a Cary spectrophotometer, 100 Bio-model, with jacketed cell holders. Spectral changes of 3 μM hemoglobin were monitored

after adding different concentration of iron oxide nanoparticles by recording the UV-Visible absorption (250-500 nm). All the experiments were run in phosphate buffer (0.1 M) at pH 7.0 in a conventional quartz cell thermostated to maintain the temperature at 20 ± 0.1 °C.

Intrinsic fluorescence intensity measurements were carried out using a Hitachi spectrofluorimeter, MPF-4 model, equipped with a thermostatically controlled cuvettecompartment. The working concentration of hemoglobin used was 3 μM so as to prevent quenching of Trp fluorescence by the neighboring heme group.

Results and discussion

In this work we will address the binding of Fe_2O_3, Cu and silver nanoparticles to Hemoglobin(Hb) and the effects of these particles on the structural and spectral properties of Hb, by UV-Visible, fluorescence and circular dichroism (CD) spectroscopic analyses.

From UV/Vis and fluorescence spectroscopy results, it can be suggested that owing to the binding of Fe_2O_3 nanoparticle to Hb, minor conformational changes at the tertiary structure are induced and Fe_2O_3 nanoparticle cause to partially unfolding of Hb. The CD spectrum of Hb showed that its secondary structure did not change as well.

The results of fluorescence spectroscopy and UV/Vis absorption spectroscopy indicated that the structure of the Trp residue environments was altered and the physiological functions of Hb were affected by silver nanoparticle.

Our results suggest that silver nanoparticle leads to a partial unfolding of Hb. Moreover, CD spectra demonstrate that silver nanoparticle binding leads to alpha beta transition.

cu nanoparticles induce hemoglobin to convert to hemichrome, which is confirmed by the peak position shifting from 405 to 410 nm, and by a new one appearing at 537 nm. we concluded that hemoglobin molecules absorbed on the Cu nanoparticle surface and the structure of the hemoglobin surface becomes loose, resulting in the decrease of α-helix content. Fe_2O_3 nanoparticle has not a major effects on the hemoglobin structure but the results show that silver and copper nanoparticles lead to unfolding of Hb. Hence, Fe_2O_3 nanoparticles may inject into the blood for drug delivery and the other applications but sliver and copper naoparticles have molecular toxic effects and cause to unfolding proteins.

References

[1] X.Chen, H.J.Schluesener. Toxicol Lett 176 (2008)1.

[2] J.M. Berg, T.L. Tymoczko, L. Stryer, Biochemistry, fifth ed., Freeman, San Francisco, 2002.

[3] A.L. Lehninger, D.L. Nelson, M.M. Cox, Principles of Biochemistry, CBS Publications, New Delhi, 1987.

[4] M.F. Perutz, Nature (London) 228 (1970) 726.

[5] M.F. Perutz, Sci. Am. 239 (1978) 92.

[6] R.E. Hirsch, R.S. Zukin, R.L. Nagel, Biochem. Biophys. Res. Commun. 93 (1980) 432.

[7] R.E. Hirsch, R.L. Nagel, J. Biol. Chem. 256 (1981) 1080.

Estimation of Franck-Condon factors for certain band systems of astrophysical molecule CN

Maryam Rasoolzadeh, *[a]and R. Islampour[b]

[a] *Young Researchers Club, Chemistry Department, Islamic Azad University- North Tehran Branch, Iran*

E-mail: Rasoolzadeh21@gmail.com

[b] Chemistry Department, Islamic Azad University- North Tehran Branch, Iran

Keywords: Franck-Condon factors, Numerov method, nuclear Schrodinger equation, CN molecule.

Introduction

The purpose of this investigation is to estimate Franck –Condon factors (FCFs) of CN radical, and to compare the results with the experimental values to find the ability of Numerov algorithm. To this end, Hulbert-Hirschfelder potential energy function is used to solve Schrodinger nuclear equation by the means of Numerov algorithm. The calculation of FCFs is based on the usage of vibrational wave functions.

Methods

Within the Condon approximation, the intensity of a vibronic transition between two Born-Oppenheimer vibronic states is proportional to the FCFs, which are defined as the square of the vibrational overlap integral $\int \psi_v^* \psi_{v''} dR$. The FCFs depend mainly on the shape and relative positions of the upper and lower potential curves. [1] In the absence of exact expressions for ψ_v, one may use the eigenfunctions derived from the same approximate potential function. Therefore, the methods for calculating FCFs depend on the choice of approximate vibrational wave functions ψ_v.

In this investigation, the Numerov method [2-3] is employed to solve nuclear Schrodinger equation for CN with five-parameter Hulbert-Hirschfelder empirical potential function [4] to obtain the vibrational energy levels and vibrational wave functions of CN to calculate FCFs. The results are compared with available experimental values.

The FCFs have been evaluated by the reliable numerical integration procedure for the bands of $A^2\prod_i - X^2\sum^+$ system of astrophysical molecule CN.

Results and Discussion

Our results are displayed in the following table. It is seen that the vibrational sum rule is roughly satisfied for v' and v'' progressions in the case of $A^2\prod_i - X^2\sum^+$ transition of CN molecule. (0,1) and (1,0) bands are found to be equal in magnitude which indicates that the bands are of roughly comparable intensities. (0,0) band is the stronger one compare to others. FCFs for the $A^2\prod_i - X^2\sum^+$ transition of CN molecule

(4,2) and (5,0) bands FC factors are small in comparison with others and hence they may not be observed experimentally. Table also reveals that the bands involving $v'=0$ with $v''\geq 2$ and those having $v'=3$ with $v''\geq 0$ have low intensities. The calculated FCFs agree quiet well with those obtained by McCallum et al. (1970), Sharp (1984), Melendez et al. (2002), and Reddy et al. (2003).

(v',v'')	McCallum et al., 1970 [5]	Sharp, 1984 [6]	Melendez et al., 2002 [7]	Reddy et al.2003 [8]	The Estimated Values
(0,0)	0.499	0.500	0.497	0.492	0.488
(0,1)	0.371	0.374	0.369	0.372	0.366
(0,2)	0.111	0.104	0.114	0.115	0.110
(0,3)	0.017	0.015	0.018	0.019	0.014
(1,0)	0.320	0.316	0.324	0.322	0.318
(1,1)	0.045	0.047	0.046	0.041	0.043
(1,2)	0.350	0.359	0.342	0.343	0.340
(1,3)	0.223	0.221	0.224	0.225	0.223
(2,0)	0.126	0.125	0.127	0.128	0.124
(2,1)	0.240	0.236	0.246	0.238	0.236
(2,2)	0.122	0.011	0.011	0.016	0.010
(3,0)	0.039	0.041	0.038	0.041	0.040
(3,1)	0.195	0.191	0.201	0.198	0.192
(3,2)	0.099	0.097	0.105	0.105	0.101
(4,0)	–	–	–	0.011	0.009
(4,1)	–	–	–	0.094	0.091
(4,2)	–	–	–	0.002	0.001
(5,0)	–	–	–	0.003	0.003
(5,1)	–	–	–	0.072	0.070

Conclusion

Our investigation shows that the Hulbert-Hirschfelder potential function accurately describes the vibrational states of CN and Numerov algorithm is a convenient method to estimate FCFs.

Reference

[1] J. M. Hollas, ***Modern Spectroscopy,*** 4thed. Wiley (2004)

[2] J. M. Blatt, ***J. Comp Phys.,*** 1, p382 (1967)

[3] I. N. Levine, ***Quantum Chemistry***, 5th ed. Prentice- Hall (2000)

[4] H. M. Hulburt and J. O. Hirschfelder, ***J. Chem. Phys.*** 9, 61 (1941)

[5] J.C. McCaluum, W.R. Jarmain, and R.W, Nicholls, ***Spectroscopic Report*** No. 1 (1970)

[6] C. Sharp, ***Astron. Astrophys. Suppl. Ser.*** 55, 33 (1984)

[7] F.M. Melendez, L. Sandoval, and A. Palma, ***J. Mol. Struct. (Theo. Chem.)*** 580, 91 (2002)

[8] R.R. Reddy, Y. Nazeer Ahammed, K. Rama Gopal, P. Abdul Azeem, and Rao, and D. BABA BASHA, ***Astrophysics and Space Science*** 286, 419–436 (2003)

The comparison between human serum albumin as a natural and artificial protein upon interaction with lomefloxacin : Synchronize fluorescence and Resonance reyleigh scattering investigation

R. Rasouli[1], H. Salari[1], M. R. Saberi[2], J. Chamani[1]

1-Department of Biology, Faculty of Sciences, Islamic Azad University–Mashhad Branch, Mahhad Iran

2-Medical Chemistry Department, School of Pharmacy, Mashhad University of Medical Sciences, Mashhad, Iran.

Keyword: Synchronous fluorescence spectra , HSA , Lomefloxacine , Heme ,Ternary system.

Introduction :

Serum albumin the most abundant protein in the blood circulatory system, plays an important role in the transport and deposition of a variety of endogenous and exogenous substances. Lomefloxacine(LMF) used to prevent urinary tract infections prior to surgery LMF is associated with phototoxicityand central nervous system advers effects.

Methods :

Fluorescence spectra was recorded by F-2500 Fluorescence Spectrophotometer (HITACHI Japan) and the widths of excitation and emission slit were set to 10 nm

Result and discussion :

By scanning both the excitation and emission monochromator of a common spectrofluorometer with $\Delta\lambda$= 0 nm, a resonance light scanning spectrum can be developed, which has been proved to be able to investigate the aggregation of small molecules and the long-range assembly and RLS technique is available to provide some insight into the process responsible for the formation of the complex,which is shown in Fig. 2. It can be seen that RLS intensityis obviously enhanced when Heme is added into HSA-LMF system, indicating the formation of the HSA-LMF-Heme ternary complex in the system[1].

When the (Δλ) between excitation wavelength and emission wavelength were set 60 nm, synchronous fluorescence indicates characteristic information ofTrp residues [2]. The shift of the λmax together with the fluorescence quenching of HSA implies the alteration of polarity microenvironment around Trp residues, and accordingly binding state of ligands in the protein can be deduced[2]. The spectra of Fig. 2 showed visible red shift with increasing of LMF and Heme, . The results suggested that LMF and Heme located in the vicinity of Trp residues and binding of LMF and Heme increased polarity of microenvironment around Trp residues. But binding of Heme increased the polarity more dramatically than binding of LMF and in prescence of Heme quenching and red shift was more evident than that of LMF, which could indicate that Heme was more close to Trp .

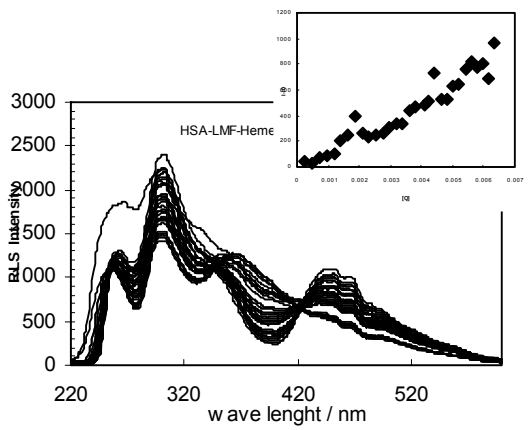

Fig1.RLS spectra of HAS-LMFin presence of Heme.

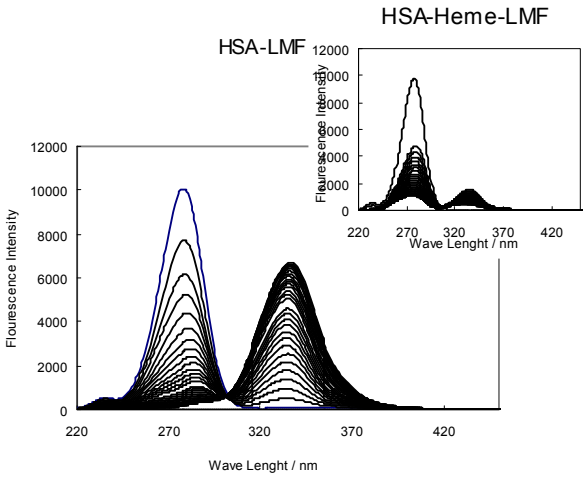

Fig. 2. Synchronous flurescence of HSA-LMF in the presence of Heme

Conclusion:

Under the determination conditions, the resonance light scattering spectra of HAS-LMF-Heme are tested and understand When Heme is added to HSA-LMF, the resonance light scattering intensity of the system increases in result of formation compelex [1]. By synchronize Flourescence , binding of the LMF and Heme toHSA had been investigated . The evident bindings of LMF and Heme to HSAwere resulted red shift , but , binding of Heme to HSA increased more drasticallypolarity of microenvironment around Trp residues than that of LMF [2].

Refrence :

[1] F. Wang, W. Huang and Y, Wang ," Flourescence enhancement effect for determination of curcumin with yttrium (III) – curcumin-sodium dodecyl benzene sulfanat system " Journal of Lumiscence , 128 (2008) 110-116

[2] J.L. Yuang, z. Lv, Z.G. Liu, Z. Hu and G.L. Zou " Study on interaction between apigenin and human serum albumin byspectroscopy and molecular modeling"Journal of photochemistry and photobiology A: Chemistry 191(2007) 104-113

Calculation of Vibrational Energy Levels of Alkali Hydrides with Empirical Potential Energy Functions Using DVR Method

Elham Ranjbari*[a], R. Islampour[b]

[a]Department of Chemistry, North Tehran Branch, Islamic Azad University, Tehran, Iran
(Elham_ph_chm@yahoo.com)

[b]Department of Chemistry, North Tehran Branch, Islamic Azad University, Tehran, Iran

Key Words: Alkali Hydrides, Nuclear Schrödinger Equation, DVR Method, Empirical Potential Function.

Introduction

Since 1980 there has been much interest in the alkali hydrides so as nearly all of the experimental advances occurred since then. Because an ionic-covalent avoided crossing between the $X^1\Sigma^+$ and $A^1\Sigma^+$ state potential energy curves is common to all the alkali hydrides, the behavior of each excited electronic state A is quite anomalous. The typical A state potential curve is flat-bottomed and highly anharmonic; the anharmonicity constant $\omega_e x_e$ is negative and the vibrational energy levels initially become more rather than less widely separated with increasing v. The shape of the ground electronic state X potential curve is also influenced by this ionic-covalent avoided crossing interaction.

For the four alkali hydride, NaH, KH, RbH, and CsH, spectroscopic constants and accurate RKR potential energy curves (typically $[G(v) + Y_{00}]$ values to $\leq 0.01\text{cm}^{-1}$ and $R_{v\pm}$ values to $\leq 0.001\text{A}^{\circ}$) for $X^1\Sigma^+$ and $A^1\Sigma^+$ states have been determined [1].

The nuclear Schrödinger equation is practical to establish characteristics of the diatomic molecules; however, this equation is not solvable for the four alkali hydrides, NaH, KH, RbH, and CsH, analytically. This work indicates that DVR method is employed to solve nuclear Schrödinger equation with various empirical potential functions such as, Hulbert-Hirschfelder, Levine, Lippincott, Rydberg,Varshni (III), and Varshni (VI). It results in calculated vibrational energies, which the first-six lower levels for NaH molecule are shown in the following table. Consequences are compared with the experimental energies which have been obtained by RKR energy potential curves.

DVR method

Discrete variable representation (DVR) is a representation in which coordinate operators are assumed diagonal and are approximated by their values at the DVR point. DVR's are highly advantageous to solve the nuclear Schrödinger equation in order to obtain vibration-rotation energies. They greatly simplify the evaluation of the Hamiltonian matrix: kinetic energy matrix elements are calculated simply, and potential matrix elements are merely the value of the potential at the DVR points. The standard DVR's are defined in terms of classical orthogonal polynomials, weight functions, and their related Gaussian quadratures [2,3]. The approximations in these DVR's are related directly to the approximations of the Gaussian quadratures associated with the polynomials used [4].

Results and discussion

The calculated vibrational energy levels of NaH molecule along with some empirical potential functions which are used to solve the nuclear Schrödinger equation are shown in the following table. It is obvious that Varshni (III) potential function has the least error value among the other functions, so it accurately describes NaH. Moreover, the outcomes which were obtained by using Varshni (VI), Lippincott and Levine functions show good agreement with experimental vibrational energies of NaH. Regarding the other three alkali hydrides, Lippincott, Levine and Varshni (VI) potential functions respectively for KH, RbH and CsH molecules are in the best agreement with their empirical vibrational energies.

Table- Energy values using empirical potential functions for the ground electronic state of NaH molecule ($\mathbf{cm^{-1}}$)

Vibrational Energy Levels		E0	E1	E2	E3	E4	E5	Mean absolute deviation (%)
Experimental energies (cm^{-1})		581.0138	1714.1155	2809.2263	3866.9889	4887.9646	5872.6067	0
Calculated energies using empirical potential functions (cm^{-1})	Hulbert-Hirschfelder	581.55783	1714.04648	2807.00439	3860.06156	4872.81216	5844.81559	0.186
	Levine	581.66579	1715.44931	2811.12301	3868.47142	4887.23629	5867.11311	0.056
	Lippincott	578.05826	1713.48658	2812.21713	3873.78987	4897.71017	5883.44441	0.024
	Rydberg	580.77721	1712.82614	2804.92439	3856.80712	4868.19387	5838.78703	0.21
	Varshni (III)	581.74391	1716.26313	2813.35033	3872.72775	4894.07271	5877.01369	0.003
	Varshni (VI)	579.97983	1715.01860	2812.85735	3872.97920	4894.83329	5877.83151	0.008

Conclusion

Generally the comparison of the results of the table implies that DVR-based estimation to solve the nuclear Schrödinger equation for diatomic molecules such as alkali hydrides depends on the potential function as well as the employed method. In addition, well defined representation, simplicity, and accuracy are the most advantages of the DVR method.

References

[1] W. C. Stwalley, W. T. Zemke and S. C. Yang, *J. Phys. Chem*., 20, 153, 1991.

[2] J. V. Lill, G. A. Parker and J. C. Light, *Chem. Phys. Lett*., 89, 483, 1982.

[3] J. C. Light, I. P. Hamilton and J. V. Lill, *J. Chem. Phys*., 82, 1400, 1985.

[4] J. C. Light and T. Carrington, Jr., *Adv. Chem. Phys*., 107, 2703, 2003.

A novel view of the interaction between lomefloxacin and human holo-transferrin in the presence of heme molecule: Investigation by Fluorescence Spectroscopy and Resonance Rayleigh Scattering techniques

H. Salari*[1], H. Vahedian-Movahed[1], M. R. Saberi[2], J. Chamani[1]

1. Department of Biology, Faculty of Sciences, Islamic Azad University Mashhad Branch, Mashhad, Iran
2. Medical Chemistry Department, School of Pharmacy, Mashhad University of Medical Sciences, Mashhad, Iran

Keywords: Human holo-transferrin, Lomefloxacin, Heme, Fluorescence spectroscopy,Resonance Rayleigh Scattering

Introduction:

Human holo-transferrin(HTf) as a kind of Carrier protein is in the human blood plasma, widely known as an iron-binding protein [1], however the drugs can be bound to HTf with a good affinity. This binding interaction results in a non-covalent protein-drug complex formation. In this study the interaction between lomefloxacin (LMF) and HTf in the presence and absence of heme molecule at the physiological condition (pH=7.4) has been investigated by fluorescence spectroscopy and Resonance Rayleigh Scattering (RRS) techniques. LMF is a fluoroquinolone with effective broad-spectrum antimicrobial activity. The clinic therapy and adverse effect of the drug has a good relationship to the concentration of the protein-drug complex, so the study for binding phenomena from different view will be important for interpretation of the metabolism and transported process [2,3]. The examinations also indicated the effect of heme molecule in the HTF-LMF interaction.

Methods:

The fluorescence measurements were performed with a F-2500 spectrofluorimeter (Hitachi, Japan). Excitation and emission bandwidths were both set at 10 nm. pH meter Metrohm model. All experiments were carried out at room temperature.

Result and Discussion:

Fluorescence spectrum of HTf in the presence of LMF and Heme molecule clearly shown that both LMF and Heme act as a quencher and with the increasing concentration of them, the red shift occurred in fluorescence spectrum which indicated the more polar environment. Fig1 shows Fluorescence emission specta for HTf,LMF in the presence of heme at 280 nm excitation wavelength. The Stern-Volmer plot is linear, indicating that only one type of quenching prosses occurs,either static or dynamic quenching [4].The result of comparing the kq in this experiment and kq polymer,shows that we have the static quenching in our experiment. [kq(exp)=6.2287*10^{12}, kq(polymer)=10^{10}]. Fig 2 shows the increase of RRS intensity with the increase of Heme concentration in ternary system of HTf-LMF and Heme.

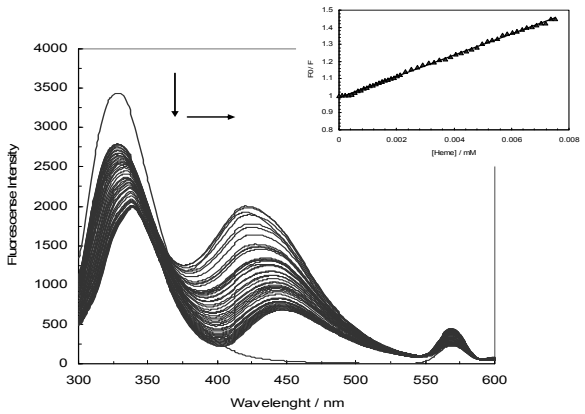

Fig.1. Fluorescense spectra of HTf-LMF-Heme.

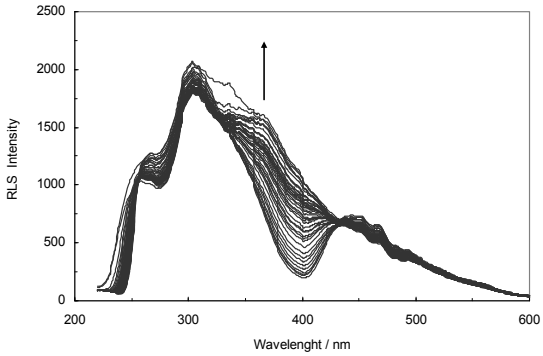

Fig. 2. RRS spectra of HTf-LMF-Heme.

Conclusion:

The compare of the Stern-Volmer constant of HTf-LMF, HTf-Heme and HTf-LMF-Heme systems, shows a competitive intraction between LMF and Heme with HTf. The RRS intensity was well proportional to the concentration of LMF that shown the form of HTf-LMF complex and increase the size of molecule and probability precipitation of the protein. In addition, RRS technique determined the critical aggregation concentration of LMF that inducing HTf aggregation.

References:

[1] P. T. Gomme, K. B. McCann, "Transferrin: Structure, function and potential therapeutic actions", Drug Discovery Today, 10 (**2005**) 267-273

[2] K. H. Ulrich, J. Pharmacol. Rev., **1981**, 33, 17.

[3] X. M. He, D. C. Carter, Nature, **1992**, 358, 209.

[4] J.R. Lakowicz, "Principles of Fluorescence Spectroscopy", Plenum Press, New York, **1983**, pp. 257–265.

Conformations and Intramolecular hydrogen bonding in 3-Bromodibenzoylmethane.

S. Salemi [a], A-R. Nekoei [b], S. F. Tayyari [c], S.Z.Banihashemi [a]

[a] *Department of Chemistry, Sabzevar Tarbiat Moallem University, Iran*

[b] *Department of Chemistry, Shiraz University of Technology, Shiraz, 71555-313, Iran*

[c] *Department of Chemistry, Ferdowsi University, Mashhad 91774-1436, Iran*

Keywords:2-bromo-1,3-diphenylpropane-1,3-dione;α-bromo-dibenzoylmethane;β-dicarbonyl; Intramolecular hydrogen bond; Density Functional Theory, vibrational study.

Introduction

The position of the keto-enol equilibrium and intramolecular hydrogen bond (IHB) strength in β-dicarbonyl compounds differ according to the electronic characteristics of the substituents, temperature and nature of the solvents [1]. 2-bromo-1,3-diphenylpropane-1,3-dione, which is also known as α-bromo-dibenzoylmethane, BrDBM, can be considered as representative example of a symmetric β-dicarbonyl. Since the DFT calculations and vibrational spectroscopy are highly sensitive methods to theoretically and experimentally examine the IHB strength, in addition to conformational analysis, we used these data as the empirical witness to study the conformations and IHB properties of BrDBM molecule. The obtained results then compare with those of dibenzoylmethane (DBM).

Experimental and method of analysis

BrDBM was purchased from Aldrich chemical company. The H^1-NMR spectra were obtained on a FTNMR Brucker at 100 MHz frequency using solution in $CDCl_3$ at 22°C. The FT-Infrared spectra were obtained by a Bomem MB-154 Fourier Transform Spectrophotometer. The spectra were considered in the solid and CCl_4 solution at room temperature. All calculations were performed using Gaussian 03W package program.

Results and Discussion

The structures and relative stabilities of all enol and keto forms of BrDBM, calculated at B3LYP/6-31G** level, and its atom numbering scheme are shown in Fig.1. For comparison,

the structures of enol and keto forms of DBM and their relative stabilities (in comparison to the most stable form of itself), calculated at the same level as BDBM, are also presented in Fig. 1. The *cis*-enol forms are designated as *I* and their corresponding *trans*-enol conformers are designated as *II*. Among 8 enol forms for each of DBM and BrDBM, only one (i.e. E1*(I)*) is engaged in a six-membered ring IHB system. Comparison between relative energies of BrDBM tautomers, clearly shows that its keto form (K3) is more stable than E1*(I)* *cis*-enol form, while for DBM the *cis*-enol form is the most stable. This is a good theoretical reason for more content of keto forms in BrDBM (100%), compared to that in DBM (0%), in CCl_4 solution, which are also concluded experimentally by ^{1}H-NMR and IR spectroscopy. We recently explained the relation of conformational relative stabilities and the keto and enol contents of β-dicarbonyls 2,2,6,6-tetramethyl-3,5-heptanedione, 5,5-Dimethyl-2,4-hexanedione, and Acetylacetone [1]. The H^1-NMR spectrum of BrDBM shows no band for enolic proton, while DBM spectrum shows a broad band at 16.8 ppm which is assigned to δOH proton chemical shift [2]. The IR vibrational spectroscopic study, also, confirm that BrDBM is completely in the keto form, while DBM is completely in the enol form. The IR spectrum of solid BrDBM shows two strong bands at 1700 and 1675 cm^{-1}, for two C=O stretching associated to keto forms, which are absent in the DBM solid spectrum. On the other hand, the IR band at about 1540 cm^{-1} of DBM spectrum (attributed to combined stretching of C=O and C=C bonds in the enol forms) is not observed for BrDBM. The IR spectra of BDBM and DBM in the region of 1750-1400 cm^{-1} are compared in Fig. 2. The fully optimized geometrical parameters of *cis*-enol E1 conformer for BrDBM and DBM calculated at the B3LYP/6-311++G** level, are given in Table 1. In a theoretical point of view, substitution of Br in α position of DBM decreases the O···O and O···H distances. Therefore the IHB strength in enol form of BrDBM seems to be more than that in DBM. In dihedral angle point of view, since the phenyl groups of DBM are nearer to be co-planar with the chelated ring (see Table 1), the IHB of DBM is more resonance assisted. Also, another interesting point is the difference between mentioned dihedral angles for keto and enol forms of BrDBM, which are 2.5 and 34.6 degrees (averaged values, calculated at B3LYP/6-31G** level). So, the conformational stabilization through resonance between double bonds of chelated ring and the phenyl group (which is impossible for the enol form of BrDBM) is very

proper for DBM keto form. This is why the keto form of BrDBM is more stable than the enol form.

Conclusion

The computational analysis and the experimental NMR and IR studies indicate that BrDBM, in the solid and solution phases, is completely in the keto form.

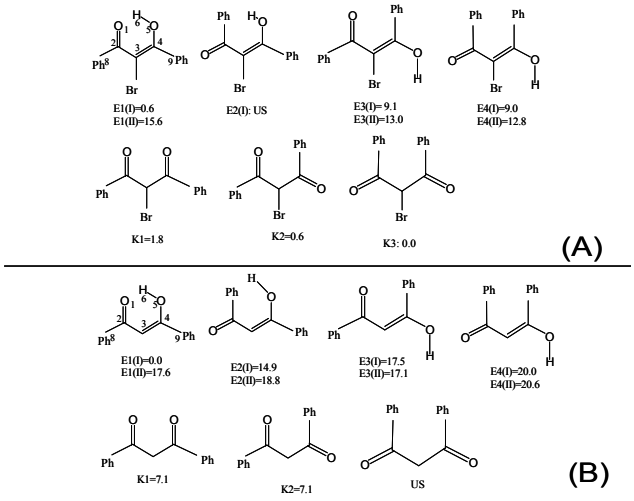

Fig 1: The atom numbering system, possible enol and keto tautomers of BrDBM (A) and DBM (B), and their relative stabilities (in kcal/mol), calculated at the B3LYP/6-31G** level. US; unstable.

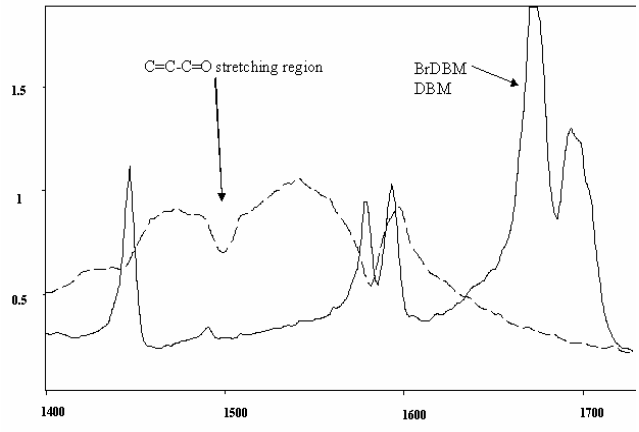

Fig 2: The IR spectra of DBM (···) and BrDBM (–) in neat liquid in the 1750- 1400 cm^{-1} region**.**

Table1. Geometrical parameters of BrDBM and DBM calculated at the B3LYP/6-311++G^{**} level.

bond distance (Å)	DBM	BDBM
O···O	2.502	2.470
O–H	1.010	1.011
C=O	1.254	1.251
C=C	1.378	1.387
C–O	1.326	1.326

References:

[1] M. Vakili, S.F. Tayyari, A-R. Nekoei, H. Miremad, S. Salemi, R. E. Sammelson; J. Mol. Struct., 970 (2010) 160.

[2] S.F. Tayyari, H. Rahemi, A.R. Nekoei, M. Zahedi-Tabrizi, Y.A. Wang; Spectrochimica Acta Part A 66 (2007) 394.

Interaction potential and Reduced Ion Mobility properties of Cl^- Ion in He Gas: Experimental and Theoretical Approaches

A. Abedi*[1], M. Gharibi[2], L. Sattar[3]

[1] *Islamic Azad University, Shahreza Branch, azraabedi@yahoo.com*

[2] *National Petrochemical Company-Research & Technology Co. (NPC-RT), m.gharibi@npc-rt.ir*

[3] *Islamic Azad University, Shareza Branch, Young Research Club, sattar_l2000@yahoo.com*

Key words: Ion Mobility, Cross Section, Interaction Potential, Halide Ions, Noble Gases.

Introduction

Ion mobility spectrometry (IMS) is a useful tool for detection of trace species, including industrial pollutants, narcotics, and explosives [1-2]. The detailed understanding of the origin of a signal relies on an understanding of the ion-molecule chemistry occurring, as well as the transport of the ions through the drift gas. Interactions between the closed-shell halide anions and the rare gas atoms are among the best-studied prototypes for understanding the details of ion-neutral forces [3-5]. In this work, the experimental measurements and theoretical calculations of the ion mobility coefficients of halide ions in noble gases are extended in a manner that allows comparison of theoretical and experimental mobility to serve the accuracy of *ab initio* potential data used in the calculations. The feasibility of these procedures is demonstrated with application of Cl^- halide ion in He noble gas.

Method

1. Experimental details

The IMS apparatus with the continuous corona discharge as ionization source has been used [6]. The chloroform that was used in this experiment had of purity about 99.9% and were obtained from Merck. The drift and carrier gases that were used in this work were helium. The temperature was changed from 27^0C to 100^0C and the electric field from 62.5V.cm^{-1} to 312.5 V.cm^{-1}.

2. Theoretical details

We calculated the Cl^-…He potential energy curve at the CCSD (T)/aug-cc-pvqz high level of theory using the Gaussian 98 package. Program PC is designed to work with uses a spline fit of the tabulated potentials for atomic ion- atom systems, where it varies as the inverse fourth power and to calculate transport cross sections, Fig 1. The cross sections were calculated from potential energy and then were used in program GC (Gram-Charlier approach) to compute the transport coefficients for the ion mobility coefficients to an electrostatic field.

Result and Discussion

The effects of temperature and electric field on mobility of Cl^- were investigated. As it is shown in Fig. 2 reduced mobility has positive temperature dependence, the reduced mobility in helium increases as the temperature is raised. In fact ions cluster with the water or other contaminant contained in the drift gas. As the temperature increases the clusters break down and cross-section and reduced mass decrease so, reduced ion mobility increases. The calculation results show a good agreement with experimental data of reduced ion mobility. In this work the maximum electric field was 312.5 $V.cm^{-1}$.

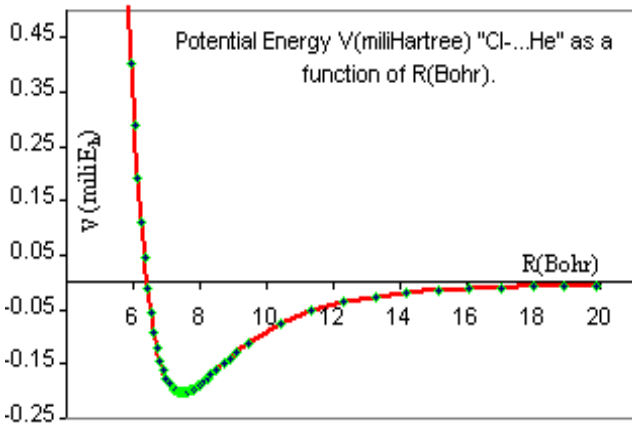

Figure 1: The CCSD (T)/aug-cc-pvqz potential curve for Cl…He system.

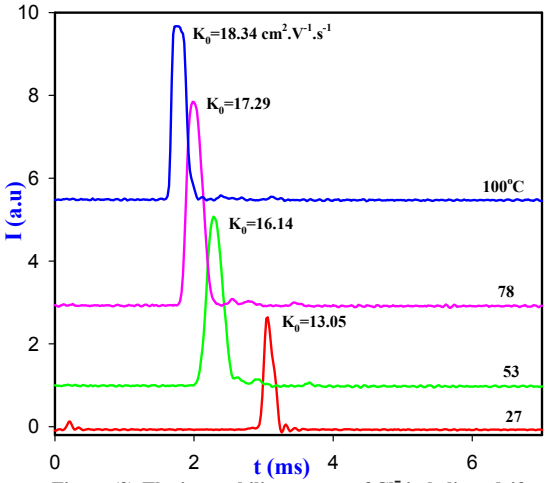

Figure (2):The ion mobility spectra of Cl^- in helium drif gas at 218.75 $V.cm^{-1}$ and different temperatures

Conclusion

The effect of temperature and electric field has been studied on mobility of Cl^- in noble gases. The reduced ion mobility was measured from experimental drift time. Also it was calculated from potential energy between ions and drift gases. The calculated ion mobility has a good agreement with experimental data.

References

[1] Eiceman, G. A.; Karpas, Z.; *Ion Mobility Spectrometry*, CRC Press, Boca Raton, second edition, **2005**.

[2] Ewing, R. G.; Atkinson, D. A.; Eiceman, G. A.; Ewing, G. J. Talanta; **2001**; Vol. 54; 515.

[3] Kita, A.; Noda, K.; Inouye, H., J. Chem. Phys. **1976**; Vol. 64; 3446.

[4] Diercksen, G. H. F.; Sadlej, A. J.; Chem. Phys. Lett.; **1989**; Vol. 156; No 2,3; 269

[5] Bera, N. C.; Das, A. K.; Chem. Phys. Lett ; **2008**; Vol. 460; 319.

[6] Tabrizchi, M.; Khayamian, T.; Taj, N., Rev. Sci. Instrum.; **2000**; Vol. 71; 2321

Analysis of IR , ^{13}C-NMR And ^{1}H-NMR Spectrums Of Structure 4-methoxyphenyl acetone Using Theoretical And Experimental Methods

R.Soleymani*[a,c] , A.Shamsali[b] ,A.Mousavi-Tashar

[a] *Chemistry Department, Faculty of Sciences, Islamic Azad University, Touyserkan Branch, Young researchers Club, Touyserkan ,Iran*
(Email: nima_soleimany@yahoo.com)
[b] *Chemistry Department, Faculty of Sciences, University Khoram abad Branch, Khoram abad, Iran*
[c] *Chemistry Department, Faculty of Sciences, Islamic Azad University Shahre-rey Branch, Tehran, Iran*

Keywords: Ab initio; DFT ; Nuclear Overhauser Enhancement ; 4-methoxyphenyl acetone

Introduction

Structure 4-methoxyphenyl acetone is synthesized experimentally in the laboratory. This structure has $C_{10}H_{12}O_2$ empirical formula and 3 group is identified for that a)methoxy group b)aromatic ring c) functional group keton. This structure are important material of industry[1].

Calculation method

^{1}H-NMR spectrum is obtained with 300 MHZ devicied and ^{13}C-NMR spectrum is obtained with 75 MHZ device using $CDCl_3$ solvent.

Also infrared spectrum is obtained using neat specimen (without solvent) on KBr salt plates. We used computer 4 pentum with intel core2duo 2.26 Ghz processor for Ab initio calculation and primary structure was draw using chemoffice 2010 software and the final optimization was performed using Gaussian software by B3LYP/6-311++G** method[2]. Also we used NMR-GIAO keyword for calculation spectrum NMR with theoretical method.

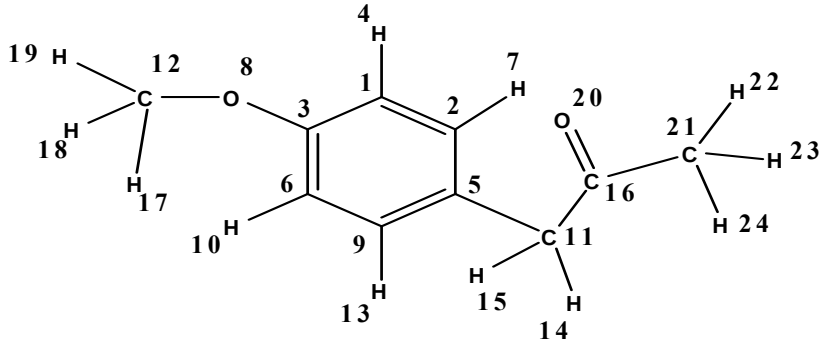

Result and discussion

The results a comparison between two theoretical and experimental methods which is reported following table.

Results Infrared Spectrum (IR)					
Method	Experimental		B3lyp/6-311++g**		Assignment
Important mode nos	Intensity	Wave number (cm^{-1})	Intensity	Wave number (cm^{-1})	
1	69.12	835	34.098	851.706	υ p-chain
2	78.03	1020	57.690	1061.85	υ C-O
3	62.50	1230	3.3810	1229.46	υ C-O
4	89.34	1275	98.741	1272.75	υ C-C
5	90.21	1490	36.596	1504.77	υ C=C
6	75.12	1610	54.874	1655.13	υ C=C
7	88.93	1711	83.089	1791.84	υ C=O
8	55.62	3000	33.240	2999.29	υ C-H
9	55.24	3080	59.547	3059.16	υ C-H

Results ^{13}C-NMR Spectrum		
Method	Experimental	B3lyp/6-311++g**
Kind atoms	Chemical Shifts(ppm)	Chemical Shifts(ppm)
C_1	130.2	126.732
C_2	114.4	114.383
C_3	28.30	26.9502
C_5	51.60	51.3463
C_6	130.7	121.260
C_9	114.0	112.927
C_{11}	126.9	131.177
C_{12}	123.3	128.281
C_{16}	207.1	227.351
C_{21}	159.2	152.900

Results ^{1}H-NMR Spectrum		
Method	Experimental	B3lyp/6-311++g**
Kind atoms	Chemical Shifts(ppm)	Chemical Shifts(ppm)
H_4	6.80	6.7824
H_7	6.80	6.5691
H_{10}	7.20	7.3273
H_{13}	7.20	7.0242
H_{14}	3.60	3.4387
H_{15}	3.60	3.3155
H_{17}	3.80	3.3626
H_{18}	3.80	3.3743
H_{19}	3.80	2.9545
H_{22}	2.10	2.6677
H_{23}	2.10	2.8483
H_{24}	2.10	3.0969

Conclusion

IR , ^{13}C-NMR and ^{1}H-NMR spectrums structure 4-methoxyphenyl acetone were obtained using quantum mechanic methods and it has compared with experimental spectrum which results showed that index of hydrogen deficiency for this structure is 5 and the obtained spectrum confirm the existence of aromatic ring. In infrared spectrum , the most important peaks are out of structure branch in 835 cm^{-1} and carbonyl group in 1711 cm^{-1} area. Even though we have 10 carbon but ^{13}C-NMR shows 8 peaks and the 4 peaks of 114 ppm , 130 ppm , 120 ppm and 159 ppm are showing an aromatic ring with para branch and also keton group shows off in 207 ppm which nuclear overhauser enhancement effect cause enlarging

some of the peak. ^{1}H-NMR shows field part above the spectrum has some H with 3:2:3 integrals and shows that the neighbor doesn't have any protons and CH_3 of low field in 3.3 ppm near to oxygen shows methoxy group.

References :

[1] Donald L. Pavia et al , *Introduction to spectroscopy*, Saunders golden sunburst series, Department of chemistry Washington university **(1996)**.

[2] M. j. Frisch et al. *GAUSSIAN 03*, Revision C. 01, Gaussian Inc.,Wallingford. CT, **(2004)**.

Quantum Non-locality

Afshin Shafiee[1] and Farhad T. Ghahramani[*2]

[1,2]Research Group On Foundations of Quantum Theory and Information
Department of Chemistry, Sharif University of Technology
P.O.Box 11365-9516, Tehran, Iran
farhadtq@mehr.sharif.edu

Abstract

Non-locality in quantum theory is implied into the global form of the wave function. In addition to manifesting itself through the well-known Bell's inequalities, non-locality also effects on the properties of condensed systems such as superconductors and superfluids. The aim of this article is to point out the significance of non-locality in quantum systems.

Keywords: Non-locality, Bell's inequality, Entangled State, Many-particle Quantum System

Introduction

The predictions of quantum theory often seem to contradict the intuitive, and apparently reasonable, assumptions about how the world should behave as described by classical theory. The principle of locality is one of the classical concepts that seems to fails at quantum level. Locality states that an object is influenced directly only by its immediate surroundings. So it's often stated that quantum mechanics is non-local. John S. Bell was the first who uncovered the inconsistency between the predictions of quantum mechanics and locality [1]. Now, Bell's demonstration is called Bell's theorem. On the other hand, Chemists adopted the notion of delocalized wave functions of electrons, e.g., in the description of molecular bonds. However, the relevance of quantum mechanics to chemistry goes far beyond this. The significance of non-locality on the macromolecular scale was already demonstrated in a diffraction experiment with fullerene (C_{60}) molecules [2]. The non-local aspect of quantum theory is also connected to the global form of the wave function. In classical theory, it is generally possible to decompose the system's description into that of various spatially separate subsystems in interaction. In quantum theory, however, the wave function is not spatially separable into that of product of subsystems, and so the special form of the wave

function plays a significant role. It is, to a good approximation, possible to treat a system of, for example, two protons and four electrons, as being reducible to a description of two helium atoms with a weak interaction between them. However, a collection of helium atoms can act in a noticeably different way, as a single coherent state, has been realized in superfluid. The nature of these coherent states is reflected in the non-local character of very special forms of their wave functions. In this article, we explore the connection between these two aspects of non-locality.

Discussion

First, we state an extensive disposition of Bell's theorem. All versions of Bell's theorem are usually generalizations of the original version published by Bell in 1964 [1]. The general framework of all of them is to consider an ensemble of pairs of particles prepared as an entangled state, so that statistical correlations may be expected between outcomes of experiments performed on the particles of each pair. Each pair in the ensemble is characterized by the same entangled state. For such an ensemble, the quantum mechanical predictions for correlations of the outcomes can be calculated. On the other hand, if it is assumed that the statistical character of the pairs is regulated by a theory which satisfies by certain Special Relativity based independence conditions, then it is possible to derive a constraint upon the statistical correlations of the outcomes of experiments. The constraint is stated as an inequality known as "Bell's Inequality". The quantum mechanical predictions violate Bell's Inequality. Experiments performed on the pairs confirm predictions of quantum mechanics and therefore reject Bell's Inequality.

The polarization of photons can be used to produce entangled particles. These photon pairs can be produced by $4p^2(^1S_0) \rightarrow 4p4s(^1P_1) \rightarrow 4s^2(^1S_0)$ cascade in Calcium (Fig. 1). Likewise, the spin of massive particles can be used to produce entangled particles. For massive particles, spin singlet entangled state can be written as:

$$\psi = \frac{1}{\sqrt{2}}(\alpha\beta - \beta\alpha) \qquad (1)$$

where α and β are eignstates of S_z correspond to eignvalues $+\hbar/2$ and $-\hbar/2$, respectively.

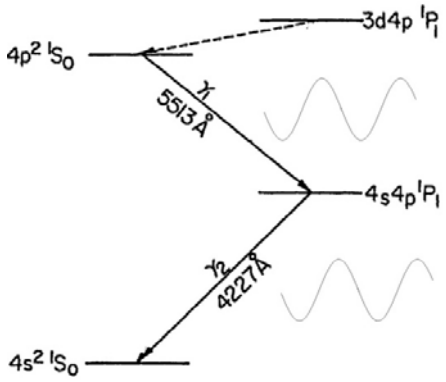

Fig. 1

Many experiments of Bell's inequality have been performed mostly by examining the correlation of linear polarization of photon pairs. In all these experiments, the analyzers are separated by such distances that no obvious mechanism would exist whereby locality condition would be violated. All experiments have violated Bell's inequality but were in good agreement with the predictions of quantum mechanics (e.g., [3]). These experiments constitute a spectacular demonstration that there is some non-locality in the physical world.

Conclusion

The global characteristics of the wave function are a feature unique to quantum theory. Information enfolded within the form of the wave function plays an important role in both the sort of non-local correlations discussed in Bell's inequalities and in the detailed behavior of condensed and coherent systems such as superconductors and superfluids. In fact, because of the non-separability of the general N-electron wave functions, the motion of each electron is related to the whole, not simply through a physical force but through non-local correlations. And so the fine details of the physical interactions between electrons is experienced within the whole system.

References

[1] Bell, J.S.: On the Einstein-Podolsky-Rosen Paradox. Physics **1**, 195-200 (1964)

[2] Arndt, M, et al: Wave-particle duality of C60 molecules. Nature **401**, 680-682 (1999)

[3] Aspect, A, et al: Experimental Test of Bell's Inequalities Using Time-Varying Analyzers. Phys. Rev. Lett. **49**, 1804–1807 (1982)

A novel approach of synchronize fluorescence and resonance light scattering studies of two anti-breast cancer drugs upon interaction with HAS

T. Zohoorian-Abootorabi*[a], H. Sanee[a], M.R. Saberi[b] , J. Chamani [a]

a. Department of Biology, Faculty of Sciences, Islamic Azad University-Mashhad Branch, Mashhad, Iran

b. Medical Chemistry Department, School of Pharmacy, Mashhad University of Medical Sciences, Mashhad, Iran

*Corresponding author. email address: zohoorian.toktam@yahoo.com, Tel: 09155154844

Keywords: Human serum albumin, RLS, Synchronous spectra, Fluoxymesterone, Cyclophosphamide

Introduction

The interaction of anti-cancer drugs with blood constituents, particularly with serum albumin may have a major influence on drug pharmacology and efficacy [1]. Human Serum albumin (66.5 kDa), is a monomeric protein comprising 585 amino acids. Cyclophosphamide is an anti-cancer chemotherapy drug that used for the treatment of several types of cancers. Fluoxymesterone is an anabolic steroid with strong androgenic properties that has been used in the treatment of breast neoplasms in women. Synchronous fluorescence spectroscopy provided narrow and sharp spectrum[3].The determination of protein using RLS technique mostly is based on the enhancement of RLS intensity, which attribute to the new complex formation [4].The aim of the present work was to determine the interaction of two anti-cancer drugs, Cyclophosphamide and Fluoxymesterone with HSA, as well as to evaluate the competition between the binding of one drug in the presence and absence of the other using the synchronous fluorescence spectroscopy and resonance light scattering methods.

Methods

The fluorescence spectra and measurements were recorded using a Hitachi F-2500 spectrofluorometer. The synchronous fluorescence scan spectra were measured at $\Delta\lambda$=60 and 15 nm. The RLS spectra were recorded by simultaneously scanning excitation and emission wavelengths ($\Delta\lambda$=0).

Results and discussion

1. Characteristics of RLS spectra

At physiological conditions (pH=7.4), the RLS spectra of protein-Fluoxymesterone system were recorded using from 220 to 600 nm with Δλ=0. The results are shown in fig1. The RLS intensities for only protein are very week and the coexistence of protein and a certain concentration of drug can lead to the enhancement of RLS intensity and the appearance of a new spectrum. According to this results and previous studies are concluded that the drug induced aggregation of protein leads to the enhancement of RLS intensity.

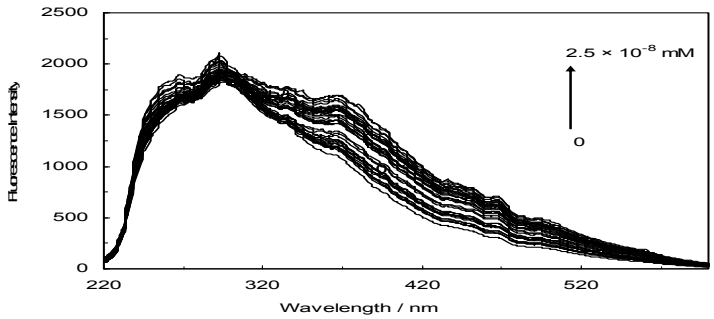

Figure 1. Effect of concentration of Flu on the intensity of RLS

2. Synchronous spectra

The effect of fluoxymesterone on the HSA synchronous fluorescence spectroscopy is shown in fig.2. It is apparent from fig.2 increasing concentration of the drug led to a dramatic decreased in the fluorescence.

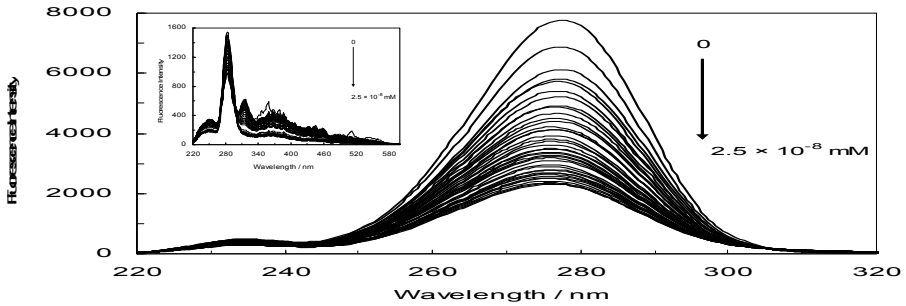

Figure 2. Synchronous fluorescence spectra of flu in the presence of various concentration of Flu .Δλ=60. **Inset**: Δλ=15.

Synchronous fluorescence spectra of Flu-HSA and Cyc-HSA-Flu in the various concentrations of Flu at room temperature were recorded in Δλ=60 nm and are displayed in Fig. 3. The peak intensity gradually decreased with increasing amounts of the Flu. It can be

noted that a complex was formed between the drugs and HSA. Furthermore Fig.3 has shown that Cyclophosphamide bound to HSA distinctly modifies the strong binding sites of fluoxymesterone.

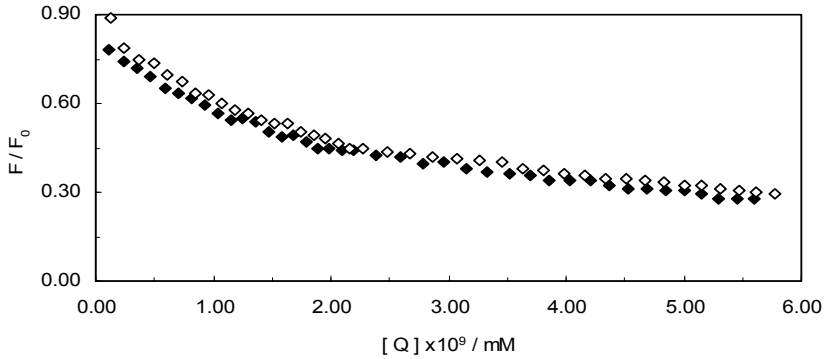

Figure 3. Synchrounous fluorescence changes in Δλ=60. ◊: binary system (HSA-FLU), ♦:Ternary system (HSA-CYC)FLU

Conclusion

The present work has explored the interaction and competitive binding of drugs with HSA through various spectroscopic techniques. Results presented in this paper indicate that fluoxymesterone binding to human serum albumin causes conformational changes. The partial blocking of specific binding sites in HSA molecule may have significant influence on drug availability thus leading to increased efficacy of multidrug therapy.

References:

[1] L. Trynda-Lemiesz, M. Luczkowski, " Human serum albumin: spectroscopic studies of the paclitaxel binding and proximity relationships with cisplatin and adriamycin", *Journal of Inorganic Biochemistry,* **98** (2004) 1851-1856 .

[2] F. Cui, X. Kong, G. Zhang, Q. Liu, B. Lei, X. Yao, " Specific interaction of 4'– o-(a-l-Cladinosyl) daunorubicin with human serum albumin: The binding site II on HSA molecular using spectroscopy and modeling ", *Journal of photochemistry and photobiology B: Biology,* **95** (2009) 162-169 .

[3] D. Patra, T.H. Ghaddar, " Aplication of synchronous fluorescence scan spectroscopy for size dependent simultaneous analysis of CdTe nanocrystals and their mixtures", *Talanta,* **77** (2009) 1549-1554.

[4] J. Wang, Z. Liu, S. Liu, W. Shen, " Study on the interaction between fluoroquinolones and erythrosine by absorption, fluorescence and resonance Rayleigh scattering spectra and their application", *Spectrochimica Acta Part A,* **69** (2008) 956-963.

Influence of structural features on ion mobility spectra of isomeric substituted benzene at atmospheric pressure and different temperature

A. Abedi*[1], M. Parsi[2]

[1] Department of science, Islamic Azad University, Shahreza Branch, abedi@iaush.ac.ir

[2] Department of science, Islamic Azad University, Shareza Branch, mp67307864@gmail.com

Key words: Ion Mobility Spectrometry, Structural Effects, Isomeric Compounds, Temperature Dependence , Electric Field.

Introduction

Usually recognizing of isomeric compounds from each other is difficult and needs special and expensive laboratory devices [1, 2]. Ion mobility spectrometry (IMS) permits the rapid and simple determination of these compounds. This instrument works at atmospheric pressure therefore the experiments are done very simple with this method in compare with other instruments such as mass spectrometry. The aim of this work is identification of some benzene substituted isomers by ion mobility spectrometry and investigation the temperature and the electric field effects on ion mobility spectra of these compounds in order to find the optimum condition for identification of them from each other by ion mobility spectrometry.

Experimental

The IMS apparatus with the continuous corona discharge as ionization source has been used [3, 4]. Corona discharge source is constructed from a stainless steel needle and an aluminum ring in front of it. The IMS cell has been made from 16 aluminum rings that were separated from each other by non-conductive Teflon sheets. The aluminum rings are connected to each other by a series of resistors in order to form a uniform electric field. The isomeric compounds that were investigated in this research are 2-nitro benzaldehyde, 3-nitro benzaldehyde, 4-nitro benzaldehyde, 2-nitro benzylalcohol, 3-nitro benzylalcohol, 4-nitro benzylalcohol, 1-choloro 2-nitro benzene, 1-choloro 3-nitro benzene, 1-choloro 4-nitro benzene. These materials had a purity of about 99% and were obtained from Fluka and Merck companies. The drift and carrier gas that was used in this work were Nitrogen. The temperature was changed from 25°C to 225°C and the electric field from 62.5V.cm^{-1} to 500 V.cm^{-1}. The follow rates of carrier and drift gas were 300 and 600 ml/min respectively.

Result and Discussion

Ion mobility is influenced by the molecular mass of analyt (M) and their collision cross-section in addition to the operational parameters such as temperature, drift gas composition and electric field. The collision cross-section (Ω_D) includes structural parameters (physical size and shape) and the resultant electronic factors describing the ion-neutral interaction forces. Therefore, ions with different mass and/or structure attain different drift velocities, providing a basis for the separation of ions in IMS analyzers. We investigated and compared isomeric compounds, that they have an identical molecular weight but different structures therefore it enables the mass effects to be ruled out and allows the structural effects to be examined. It is expected these processes lead to differences in the ion mobility spectra of different isomeric compounds. These differences can be caused either by various processes of ion formation at atmospheric pressure or during the motion of ions formed through the drift tube, due to the differences in interaction between drift gas molecules and ions.

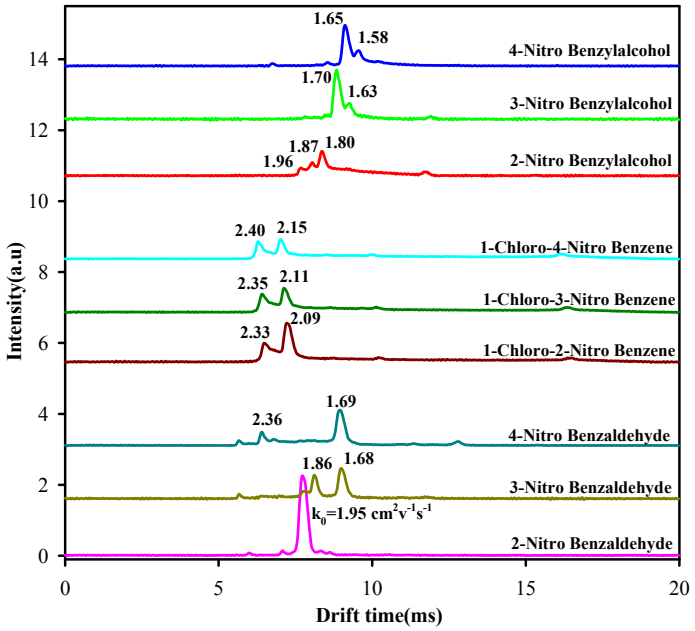

Figure 1: Ion mobility spectra of benzene substituted isomers at 125 ^{o}C and E= 437.5 Vcm^{-1} in N_2

Our studies on these substances using conventional IMS with corona discharge ionization source have provided differences in ion formation of isomeric compounds depending on their structure. The effects of temperature and electric field on mobility spectra of these isomeric compounds also were investigated.

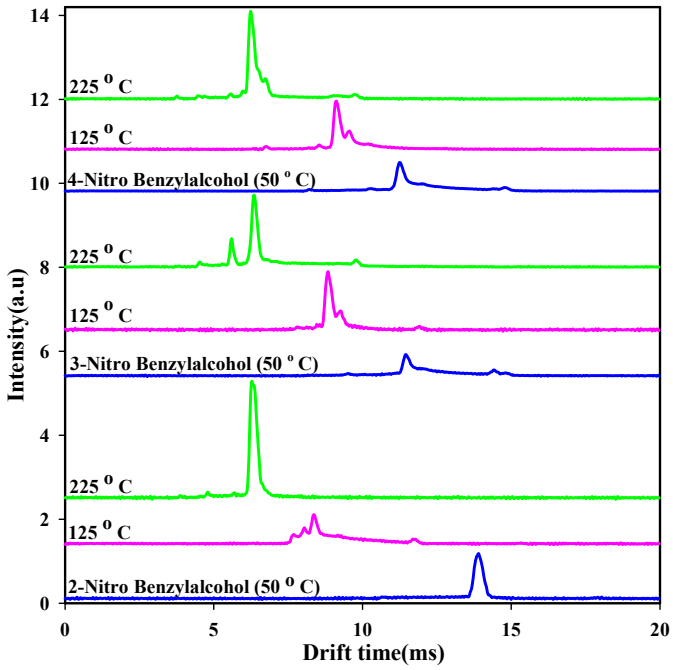

Figure 2: Ion mobility spectra of nitro benzyl alchol isomers at different temperature and E= 437.5 Vcm^{-1} in N_2

Figure 1 shows the ion mobility spectra of benzene substituted isomers that were studied in this research at 125 ^{o}C and 437.5 V.cm^{-1} in N_2. It shows that the ion mobility spectra of nitro benzaldehyde and nito benzylalcohol isomers have different ion pattern that related to different ion products with different reduced mobility (K_0). The chloro nitro benzene isomers have the same ion pattern but different reduced mobility that is probably related to different collision cross-section of ion-neutral molecules because of different physical size and shape of products. The effect of changing temperature in some isomers caused the production of different ions (figure 2) but increasing of the electric field only caused the increase of intensity and decrease of resolution. Therefore we chose 437.5 V.cm^{-1} as the optimum electric field.

Conclusion

In this research ion mobility spectrometer with corona discharge ionization source was applied for detection of several benzene substituted isomers at atmospheric pressure. The result showed the isomeric compounds had different ion mobility spectrum that arise from

different structure and different ion products. IMS can be introduced as a sensitive and selective method for identification of these compounds.

References

[1] Borsdorf, H., Neitshch, K., Eiceman, G.A., Stone, J.A., Talanta, 2009**, 78**, 1464-1475.

[2] Borsdorf, H., Int. J. Ion. Mobil. Spec, 2008, **11**, 27-33.

[3] M. Tabrizchi, T. Khayamian, N. Taj, Rev. Sci. Instrum., 2000, **71**,2321.

[4] M. Tabrizchi, A. Abedi, Int. J. Mass Spectrom., 2002, **218**, 75-85.

Theoretical Study of Group III-V (13-15) Composites

A. Mohajeri*, M. Ebadi
Department of Chemistry, College of Science, Shiraz University, Shiraz 71454, Iran
(Email: ebadi.mahsa@gmail.com)

Keywords: 13–15 composites, Clusters, Theoretical studies, Group 13 and 15 precursors

Introduction

Binary compounds of Group III–Group V elements and composites based on them are extensively used in modern microelectronics as light emitting diodes and solar battery elements [1]. It was shown that composite materials may be in principle obtained by deposition of different group 13 and 15 precursors [2]. In this research, we have studied group 13-15 ternary composites on the needle shaped of heptamer clusters. We consider two groups; first group with preserving nitrogen as non-metal elements and two different group 13 elements ;$[H_7M_lM'_KN_7H_7]$ {M,M′=B,Al,Ga},{(l,k)=(1,6),(2,5),(3,4)} and second group with gallium fixed in metal center and two different group 15 elements; $[H_7Ga_7Y_mY'_nH_7]$,{Y,Y′=N,P,As},{(m,n)=(1,6),(2,5),(3,4)}. The electronic properties and stability of these clusters have been studied. Indeed, we compare these ternary with binary compounds and investigate the effects of entering impurity in binary molecules.

Computational Details

The Calculations in this research have been performed by GAUSSIAN 03 [3] suite of program. The geometries of all compounds were optimized at the Becke's three-parameter hybrid functional (B3) with the nonlocal correlation of Lee-Yang-Parr (LYP) level of theory and the 6-311+G* basis set.

Results and discussion

Theoretical studies of mixed cluster compounds that lead to ternary alloys have been carried out. General structures of the considered species are given in Figure 1. The energies of formation of such species from constituent mixture of monomers are calculated for the reactions (1) and (2), respectively.

$$x(HMNH)+y(HM'NH)\rightarrow(H_7M_xM'_yN_7H_7)$$

(1)

$$x(HGaYH)+y(HGaY'H)\rightarrow(H_7Ga_7Y_xY'_yH_7)$$

(2)

In Table 1 the results according to reaction (1) are presented. The difference between the highest occupied molecular orbital and the lowest unoccupied molecular orbital known as HOMO-LUMO gap have been calculated for mentioned clusters.HLG is defined by formula below:

$$HLG= E_{HOMO}-E_{LUMO} \quad (3)$$

As an example the HLG values for $H_7Ga_7As_mM_lH_7$ clusters are given in Figure 2.

(a) $[HMYH]_7$ (b) $[(HM)_4(HM')_3(YH)_7]$ (c) $[(HM)_5(HM')_2(HY)_7]$ (d)$[(HM)_6(HM')(HY)_7]$

Figure 1 General structures of heptamer clusters: (a) homonuclear $[HMYH]_7$ heptamers; and mixed $[(HM)_x(HM')_y(YH)_7]$ clusters: (b) x = 4, y =3; (c) x =5, y =2; (d)x = 6, y =1.

Table 1 Energy of formation (kcal mol^{-1}) for clusters in reaction (1).

molecules	ΔE	molecules	ΔE
$H_7B_6AlN_7H_7$	-349.87	$H_7Al_6GaN_7H_7$	-682.28
$H_7B_5Al_2N_7H_7$	-402.31	$H_7Al_5Ga_2N_7H_7$	-657.60
$H_7B_4Al_3N_7H_7$	-459.59	$H_7Al_4Ga_3N_7H_7$	-632.71
$H_7B_6GaN_7H_7$	-327.86	$H_7Ga_6BN_7H_7$	-499.42
$H_7B_5Ga_2N_7H_7$	-356.26	$H_7Ga_5B_2N_7H_7$	-465.49
$H_7B_4Ga_3N_7H_7$	-389.31	$H_7Ga_4B_3N_7H_7$	-431.34
$H_7Al_6BN_7H_7$	-645.26	$H_7Ga_6AlN_7H_7$	-561.74
$H_7Al_5B_2N_7H_7$	-583.68	$H_7Ga_5Al_2N_7H_7$	-586.49
$H_7Al_4B_3N_7H_7$	-524.28	$H_7Ga_4Al_3N_7H_7$	-611.26

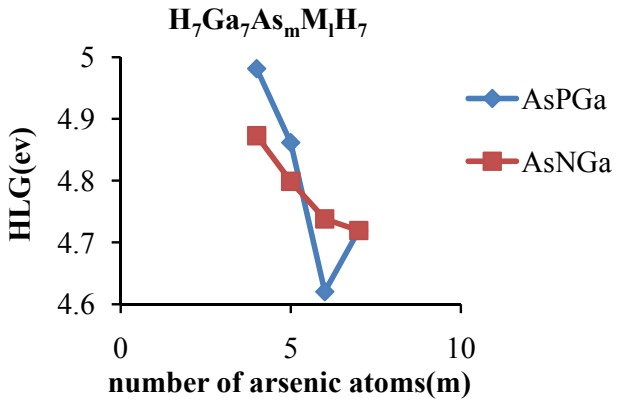

Figure 2 The HLG (eV) vs. the number of arsenic atoms (m).

Conclusion

The results predict that producing clusters from monomers are favorable in all species. We conclude that for first series compounds (nitrogen containing clusters) the observed trend for the reaction energy in ($H_7M_xM'_YN_7H_7$) compounds is: M: Al>Ga>B

The computed value of HLG for second series compounds lies within the expected values for semiconductors, especially for clusters containing more arsenic atoms.

References

[1] Timoshkin, A. Y. Russ J. Phys. Chem. A 2007, 81, 516.

[2] Den Baars SP, Keller S. Metalorganic chemical vapor deposition (MOCVD) of group III nitrides. Semicond Semimet 1998;50:11

[3] Frisch, M.J.et al.,Gaussian 03 ,revision B03,Gaussian Inc.,Pittsburgh PA,2003.

π-type halogen bonds; a theoretical study

Z. Abbasi, K. Eskandari
School of Chemistry, Damghan University, Damghan, Iran
(Email:abbasi_6382@yahoo.com)

Keywords: π-type Halogen Bond, QTAIM, Laplacian of Electron Density, Critical Point

Introduction

Halogen bond is a non-covalent interaction in which the halogen atom act as an electron acceptor and interact with various organic and inorganic electron donors [1]. These electron donors should have an available pair (lonepair or π) of electrons, and the resulting halogen bonds are usually called n-type or π-type, according to the nature of electron donor. Most of the recent studies of halogen bonds have devoted to n-type electron donors, while π-types have less considered.

Recently, distribution of Laplacian of the electron density has been used to study n-type halogen bonding interactions [2]. It has been shown that a halogen bond is an interaction between a region of charge depletion (hole) on the halogen atom and a region of charge concentration (lump) on an n-type electron donor. In the present work, Laplacian of electron density will be used to investigate π-type halogen bonds. Our focus will be on the properties of electron donor, i.e. the π-system.

Methods

Molecular geometries and their electronic wave functions were optimized at MP2/6-311++G(d, p)6d and CCSD/6-311++G(d, p)6d levels using Gaussian 03 program. Bader's Quantum Theory of Atoms in Molecules (QTAIM) [3] was used to analyze critical points in electron density and Laplacian fields.

Result and Discussion

In the present work π-type halogen bonds formed between Br_2 and different derivatives of butadiene have been investigated. Figure 1a indicates the molecular graph (MG) of complex between butadiene and Br_2. The MG indicates that, although Br_2 is positioned above the C-C

bond, it is slightly closer to the first carbon and connected to it via a curved bond path. To gain a deeper understanding of the nature of this interaction the distribution of the Laplacian of electron density has been considered. As stated in the introduction, a halogen bond can be described as a lump-hole interaction. Topologically, a lump corresponds to a (3,-3) critical point in Laplacian field. In n-type halogen bonds the lump is a non-bonded maximum in the valence shell charge concentration (VSCC) of donor atom, but the situation is different for π-type halogen bonds. Butadiene, for instance, does not have non-bonded maxima in the VSCC of its atoms, instead, it have several *bonded maxima*, as indicated in Fig 1b for a part of molecule. Therefore, it seems that in π-type halogen bonds, the interaction is between a hole in the VSCC of halogen atom and (two) bonded maxima at the C=C bond. Nevertheless, one question still remains; although the C-C single bond has also bonded maxima (Fig 1b), but why does not it participate in halogen bonding? Considering the QTAIM properties at these critical points reveal the differences between C=C and C-C bonds.

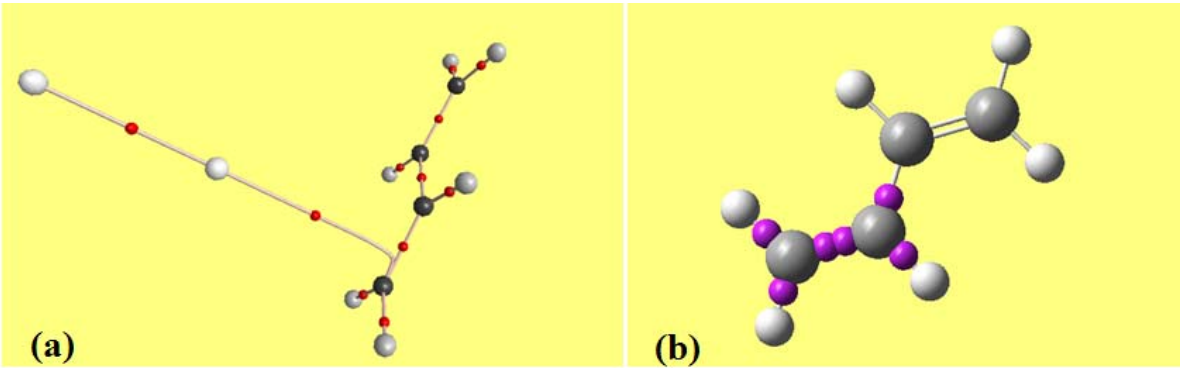

Figure 1- a) The molecular graph of butadiene-Br_2 complex. b) (3,-3) critical points (lumps) in Laplacian of electron density of butadiene.

Conclusion

Similar to n-type halogen bonds, π-types can also be described as a lump-hole interaction, but here the lumps are (3,-3) bonded maxima in double bonds. Although, C-C bond in butadiene has also two bonded maxima, but since the electron density at these critical points is low (in compare to maxima in C=C bond) it cannot act as an electron donor. In addition the differences between the potential energy density at the two bonded maxima of C=C, explain why the Br_2 is slightly closer to the first carbon.

References

[1] P. Metrangolo, G. Resnati, *Halogen Bonding; Fundamentals and applications*, Springer, Berlin, 2008.

[2] K. Eskandari, H. Zariny, Chem. Phys. Lett., 2010, 492, 9-13.

[3] R. F. W. Bader, *Atoms in Molecules; A Quantum Theory*, OUP, Oxford, UK, 1990.

Calculation of the vibrational frequencies for furan molecule and calculation of the Entropy for cubane molecule at the temperature of 298.15K

N. Abdollahi*[a]

[a] Department of Chemistry, Shahrood University of Technology, Shahrood, Iran

(E-mail: omiu110@yahoo.com)

Keywords : HF/6-31G , B3LYP/CEP-31G , vibrational frequencies , Entropy, Furan tetrahydro , cubane

Introduction

A molecule composed of n- atoms has 3n degrees of freedom. This leaves 3n-6 degrees of vibrational freedom (3n-5 if the molecule is linear). Vibrational modes are often given descriptive names, such as stretching, bending, scissoring, Rocking, and Twisting.

Some computational methods, particularly ab initio techniques, produce detailed molecular information, but no thermodynamic information directly. In the present study, we calculates entropy and integrated heat capacity of cubane molecule

Purpose of the research

Calculation of the vibrational frequencies for furan molecule By HF/6-31G* and calculation of the Entropy for cubane molecule By B_3LYP/CEP-31G*Method.

Methods

The vibrational frequencies produced by ab initio programs are often multiplied by a scale factor (in the range of 0.8 to 1) to better match experimental vibrational frequencies

In this study, the author, calculates molecular energy by B3LYP/CEP-31G* method, then molecular partition function Q is calculated, and finally by general relationships of statistical thermodynamic entropy and Integrated heat capacity is calculated

Results and discussion

Table1: HF/6-31G* Data

	calculation			Experimental		
Mode number	**symmetry**	**frequency**	**diff**	**symmetry**	**frequency**	**comment**
1	**A**	**2941**	**-21**	**A**	**2962**	
2	**A**	**2936**	**-5**	**A**	**2941**	
3	**A**	**2892**	**-21**	**A**	**2913**	
4	**A**	**2879**	**4**	**A**	**2875**	
5	**A**	**1523**	**35**	**A**	**1488**	
6	**A**	**1481**	**19**	**A**	**1462**	
7	**A**	**1401**	**36**	**A**	**1365**	
8	**A**	**1334**	**26**	**A**	**1308**	
9	**A**	**1241**	**14**	**A**	**1227**	
10	**A**	**1187**	**9**	**A**	**1178**	
11	**A**	**1156**	**14**	**A**	**1142**	
12	**A**	**1005**	**-24**	**A**	**1029**	
13	**A**	**919**	**-0**	**A**	**919**	
14	**A**	**888**	**-7**	**A**	**895**	
15	**A**	**825**	**-15**	**A**	**840**	
16	**A**	**652**	**-5**	**A**	**657**	
17	**A**	**235**	**-51**	**A**	**286**	
18	**B**	**2951**	**-21**	**B**	**2972**	
19	**B**	**2933**	**-1**	**B**	**2934**	

20	**B**	**2894**	**-18**	**B**	**2912**	
21	**B**	**2875**	**17**	**B**	**2858**	
22	**B**	**1511**	**34**	**B**	**1477**	
23	**B**	**1469**	**19**	**B**	**1450**	
24	**B**	**1359**	**25**	**B**	**1334**	
25	**B**	**1309**	**17**	**B**	**1292**	
26	**B**	**1242**	**-2**	**B**	**1244**	
27	**B**	**1180**	**18**	**B**	**1162**	
28	**B**	**1134**	**64**	**B**	**1070**	
29	**B**	**943**	**-12**	**B**	**955**	
30	**B**	**885**	**-25**	**B**	**910**	
31	**B**	**861**	**-4**	**B**	**865**	
32	**B**	**562**	**-29**	**B**	**591**	
33	**B**	**61**	**-76**	**B**	**137**	

Frequency in cm^{-1}. The calculated vibrational frequencies were scaled by 0.8985.

Table 2

shows calculated values of entropy and Integrated heat Capacity for Cubane molecule by B3LYP/CEP-31G* method. Note that the vibrational frequencies were scaled by 0.9657 .

	Entropy	Integrated heat capacity	Heat capacity
contribution	JK^{-1} mol^{-1}	KJ mol^{-1}	JK^{-1} mol^{-1}
Translation	166.80	6.197	20.79
Rotational	111.29	3.718	12.47
Vibrational	21.70	5.122	68.88
Electronic	0.00	0.000	0.00
Total	299.79	15.038	102.14

Conclusion

In the present study the vibrational frequencies obtained for furan, tetrahydro with HF methods using the 6-31G*basis sets were compared.the agreement between the calculated and experimental, In this paper the author, calculates thermodynamic properties from microscopic data. In the present context, statistical thermodynamics is meant to include the methods used to convert molecular energy levels in to macroscopic properties.

References

[1] Ab initio vibrational spectra and their use in the Identification of unusul molecules chem..Rev Vol.86.pages 709-730.1986

[2] calculations of molecular vibrational frequencies using semi- empirical methods J.comp.chem Vol12 pages 948-952.1991.

[3] Scott, A. P.; Radom, L. *J. Phys. Chem.* **1996**, *100*, 16502.

[4] Pitzer, K. S.; Gwinn, W. D. *J. Chem. Phys.* **1942**, *10*, 428.

Investigation of correlation between F & G parameters in some different potential energy functions

S. Noorizadeh*[a] and A. Askarynia [b]

[a]Department of Chemistry , University of Shahid Chamran , Ahvaz , Iran

[b]Department of Chemistry , University of Science and Research Branch-Khozestan , Ahvaz Iran

(Email : a.askarynia @gmail.com)

Keywords: Potential energy function, Spectroscopic constants, Diatomic molecules, F&G Parameters

Introduction

The potential energy of a set of atoms as a function of their relative positions is fundamental to all branches of chemistry. A good deal of information about the structure of molecule such as R_e , D_e , k_e ,α_e ,$\omega_e x_e$ are summarizes in the potential energy function(PEF). A number of workers have introduced various PEF for diatomic molecules such as Morse in 1923[1] till Norizadeh and Pourshams in 2004[2]. Examination of the function is done in two methods: comparing predicted spectroscopic constants with their known experimental value and fitting to experimental RKR data for evaluating goodness-of-fitting. There exist some relations between potential parameters and spectroscopic constants. Dunham [3] has shown relations between α_e ,$\omega_e x_e$ and derivatives of a PEF and varshni [4] has introduced two dimensionless functions, F and G , which depends on α_e and $\omega_e x_e$ .Because these parameters doesn't depend on PEF and are dimensionless and related to other spectroscopic quantities , finding a relationship between them can guide us to an estimation of other spectroscopic constants and we got them without any experimental work and simply by calculation.

We have introduced relation between F & G parameters for *Simon* $\left(U(r) = a_0\rho^2(1 + a_1\rho + a_2\rho^2 + a_3\rho^3 + a_4\rho^4 + a_5\rho^5 + a_5\rho^6 + ...)\right)$ and *Noorizadeh-Pourshams* $\left(U(r) = \frac{ar^b + m}{1 - e^{nr}}\right)$ functions where "a_i" is variational parameters and "ρ" equales to $\left(\rho = \frac{r - r_e}{r}\right)$ for the first function and a,b,m and n are variation parameters for the second.

Result and discussion

While these parameters (F&G) are related to the derivatives of PEF ,for two mentioned function , we calculate derivatives up to forth degree in equilibrium bond length bye Maple 6 software. We calculate values of F and G parameters from their frequently used relations that varshni introduced which are including derivatives of PEF.The obtained value of needed derivatives and F and G parameters are collected in Table 1.

As shown in Fig.1,study the change behavior of F&G and fitting their points with "Curve Expert" software for the Noorizadeh-Pourshams function give us: $G=28.15\ F^{1.43}$

molecule	d^2f				G
H_2	38.7229			5452	16.8746
I_2	12.4326			9192	200.93
HF	66.3573			0722	33.8553
N_2 $\sum g^+$	148.0501			7202	62.2623
N_2 $\sum u^+$	49.313			0422	77.7554
N_2 1a	73.4425			3669	66.6593
N_2 3B	78.7186			1648	83.6334
O_2 $\sum g^-$	77.0702	-544.404	3101.138	1.8393	62.4181
O_2 $\sum u^-$	78.6495	-597.751	3373.001	3.0240	134.690
O_2 $\sum u^+$	23.6321	-234.545	1740.21	3.9921	206.149
OH X^2	51.6207	-333.541	1616.687	1.0988	36.3372
OH A^2	38.2362	-263.005	1298.566	1.3230	46.0858
NO X^2	97.9644	-700.627	3775.842	1.7656	62.8574
NO B^2	29.4962	-145.85	592.9726	1.3487	41.9257
CO X^1	117.1063	-803.267	4437.432	1.5866	51.8643
CO a^3	91.6395	-488.942	1877.115	1.0120	34.5071
CO a'^3	39.7451	-242.829	1137.698	1.7654	61.9332
CO e^3	31.2028	-182.328	789.4457	1.7214	61.7014

We carry out this procedure for Simon function and readity get: $G=27.6\ F^{1.52}$

Table 1: Derivatives and F & G parameters of the Noorizadeh-Pourshams function

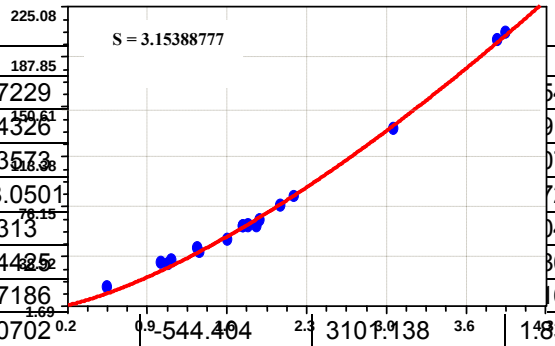

Fig 1: G via F of the Noorizadeh-Pourshams function

References:

[1] P.M. Morse, phys. Rev., 34, 57 (1929)

[2] S. Noorizadeh, G.R. Pourshams, J. Mol. Struct. (Theochem) 678 (2004) 207.

[3] J.L. Dunham, Phys .Rev. 41 (1932) 721.

4. Y. P. Varshni, J. Chem. Phys 353 (2008) 32.

Evolution of the free electron wavepacket into bound electron wave function

H. Sabzyan*[1], S.F. Alavi[1], M. Vafaee[2]

[1] Department of Chemistry, University of Isfahan, Isfahan 81746-73441, I. R. Iran

[2] Lasers-Plasma Research Institute, Shahid Beheshti University, Tehran 19839-63113, I. R. Iran

Keywords: Free electron, Bound electron, Spreading, Time evolution, Wavepacket

Introduction

During a collision between a thermal electron and an ionic core, the system can be assumed to be a quasi-atom with its outer electron in an extended orbit for a very short time, on the order of 10^{-15} s or shorter. The outcome of this collision is the simple scattering of electron which should, exchange energy and momentum with a third particle in order to remain in a bound state. Such a process is known as recombination [1] which has various types including radiative recombination [2], dielectronic recombination [2] and three-body recombination [1]. In particular, recombination experiment of electron-proton is carried out for the first time in 1991 by *Neumann* [4]. No study has been reported so far on the evolution of the bound electron wavefunction. In this research, this phenomenon has been studied by solving time-dependent Schrödinger equation (TDSE) numerically.

Computational method

The two-dimensional (2D) TDSE in Cartesian coordinate for the simulation of the evolution of free electron wavepacket (WP) into bound electron wavefunction around a proton, has the following form in atomic units (m_e=1, ħ=1, e=1)

$$i\frac{\partial\Psi(x,y,t)}{\partial t}=\hat{H}(x,y,t)\Psi(x,y,t) \qquad \hat{H}(x,y,t)=-\frac{m_e+m_p}{2m_e m_p}\left(\frac{\partial^2}{\partial x^2}+\frac{\partial^2}{\partial y^2}\right)+V_C(x,y,t) \qquad (1)$$

,

The coulomb potential, V_C, in the xy plane is given by $V_C=\left[(x-x_0)^2+(y-y_0)^2+q_e\right]^{-\frac{1}{2}}$ in which x_0 and y_0 are the positions of nucleus, x and y are coordinates of the WP center, and

q_e is the soft-core potential parameter that eliminates the singularity at nucleus. For a time-independent potential V_C, the time evolution operator has an exponential form [5]. The general solution of Eq. (1) is given by $\Psi(x,y,t+\partial t) = \exp(-i\partial t\hat{H})\Psi(x,y,t)$ which calculated by using split-operator [5] and padé approximation [6] for an 11-points finite difference method. In this simulation, for the optimization of the parameters, a 2D box of 10 au×10 au size, with a step size of 0.02 au has been used. The time step is set to 0.2.

Results, discussion and conclusion

Free electron WP consists of a 2D gaussian WP. Nucleus is fixed at the center of the box. Electron moves towards the nucleus at 45º angle with respect to the *x* axis. Calculation is carried out in two conditions; with a stationary (a), and moving (b) initial WPs. Electron WP is evolved by time-propagator operator and then position of the evolved WP has been moved classically based on Verlet algorithm. For the case (b), analysis of the simulated electron density at various time-steps shows fast evolution of the WP and spreading of electron by the nucleus field. Snapshots of this simulation have been shown in Fig. 1. Furthermore, the same simulation is carried out for the corresponding 1D system, and the kinetic energy, potential energy and the position expectation values are demonstrated in Fig. 2. Initial δ-function WP is transformed to a superposition of hydrogen-like wavefunctions. Symmetry behavior of electron WP with respect to the collision direction is due to the head-on collision setup. Effects of the reflection from the box walls are observable in the course of WP evolution. In the 1D system, the <x> shows clearly the movement of electron WP corresponding to its time evolution. Simulation of the evolution of a 3D δ-WP around the proton and study of the contribution of laser field to it are underway in this research group.

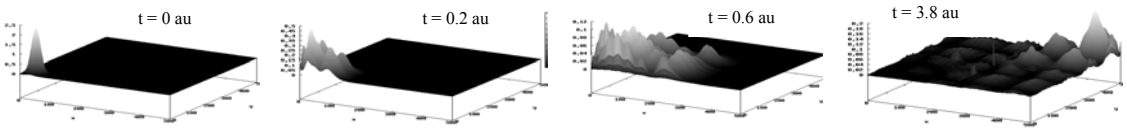

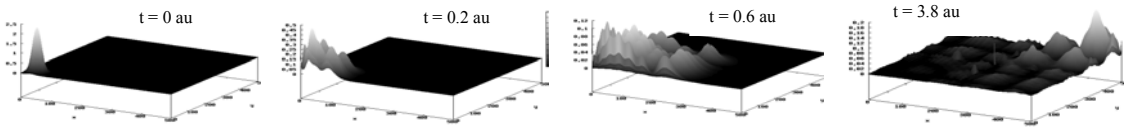

Fig. 1: Snapshots of the evolution of a standing (top) and moving (bottom) free electron δ-function wavepacket around the field of a proton.

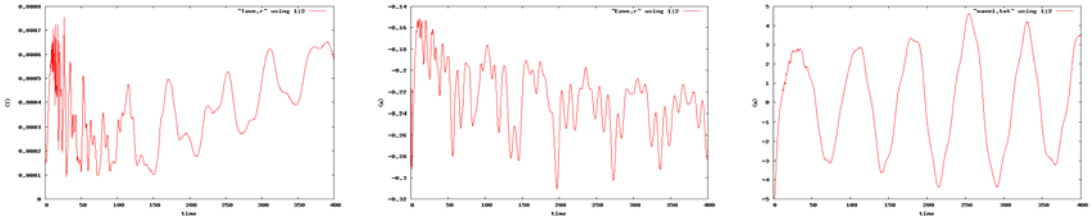

Fig. 2: Expectation values $< T >$ (left), $< V >$ (middle) and $< x >$ (right) during the evolution of a 1D electron δ-function wavepaket around a proton.

References

[1] M. Rogelstad et al, **J. Phys**. **B**. **1997**, 30, 3913.

[2] A. Muller et al, **Hyperfine Interact**. 1997, 109, 233.

[3] V.L. Jacobset et al, **Phys. Rev. Lett**. 1976, 37, 1390.

[4] U. Schramm et al, **Phys. Rev. Lett**. 1991, 67, 22.

[5] A.D. Bandrauk et al, **J. Chem. Phys**. 1993, 99, 1185.

[6] I. Kawata et al, **J. Chem. Phys**. 1999, 111, 9498.

Synthesis, Spectroscopic Study and *ab initio* Calculations Novel Chiral Diazaphospholanes

F. Ghaziani[a], K. Gholivand*[a], F.Afshar[b], N.Dorosti[a]

[a]*Department of Chemistry, Faculty of Sciences, Tarbiat Modares University, Tehran, Iran*

Email : ghaziany@modares.ac.ir

[b]*Islamic Azad University, Garmsar Branch, Garmsar, Iran,*

Keywords: diazaphospholane, diastereomers, NMR, *ab initio* calculations

Introduction

1,3,2-Diazaphospholanes and 1,3,2-diazaphosphorinanes constitute a class of interesting mimetics of aminoacids, whose importance derives from their promising and diverse biological activity[1,2]. In fact, the vicinal diamino functionality is a significant structural unit that can cause molecules to be biologically active [3]. In this work, some new diazaphospholanes **1-4** with formula $RPOX_2$, X_2=1,2-diaminopropane, (R= p-$NH_2SO_2C_6H_4NH$ **1**, R = *p*-$NO_2C_6H_4NH$ **2**, R= C_6H_5CONH **3**, R= *p*-$NO_2C_6H_4CONH$ **4**) were synthesized and characterized by multinuclear ^{1}H, ^{13}C, ^{31}P NMR and FTIR spectroscopy to investigate the effects of chirality and different substituents on the structures of diazaphospholanes. In addition, quantum chemical calculations were done using Gaussian 98 program to describe the structures of four possible diastereomers of **1** including **C1** (RR), **C2** (RS), **C3** (SR), **C4** (SS) and their corresponding enantiomeric mirror images **C5** (SS), **C6** (SR), **C7** (RS), **C8** (RR).

Method

To a solution of corresponding phosphoramidic dichloride [4] in dry acetonitrile, 20 mmol of related diamine (propane-1,2-diamine) was added dropwise at about 0°C (in an ice bath) and the mixture stirred for 8 h. Then the precipitate was filtered and the resulting solution was evaporated to yield the product which was washed with distilled water and ethylacetate and dried.

Result and discussion

Quantum mechanical calculations

In order to gain insight about the molecular structure and different conformations of the diazaphospholane **1**, *ab initio* calculations were performed by Gaussian 98 software at B3LYP levels. Several conformations are feasible depending on the orientation of the methyl group about five-membered ring. The presence of chiral diamino groups in compounds **1-4** produced various diastereomers, so that the $^{31}P\{^{1}H\}$ NMR spectra demonstrated two peaks with different ratios, respectively

Fiure .1 The conformational analysis can be approached using NMR spectroscopy especially $^{31}P\{^{1}H\}$ NMR spectra. In addition, the computational methods predict that the most stable conformers of **1** are those bearing Me group in equatorial position, i.e. **C1** (RR) and **C3** (SR).

References:

[1]. Kotti, S. R. S. S., Timmons, C., & Li, G. (2006) Vicinal Diamino Functionalities as Privileged Structural Elements in Biologically Active Compounds and Exploitation of their Synthetic Chemistry. *Chemical Biology & Drug Design*, 67, 101–114.

[2]. Lucet, D., Le Gall, T., & Mioskowski, C. (1998) The Chemistry of Vicinal Diamines. *Angewandte Chemie International Edition*, 37, 2580–2627.

[3]. Du, H. F., Zhao, B. G., & Shi, Y. (2008) *Journal of the American Chemical Society*, 130, 8590–8591.

[4]. Amirkhanov, V. M., Ovchynnikov, V. A., Glowiak, T., & Kozlowski, H. (1997). *Zeitschrift fur Naturforschung*, 52b, 1331-1336.

Two-Dimensional High Resolution Optogalvanic Spectroscopy

F. Fathi*, M. Tabrizchi, H. Farrokhpour,
Department of Chemistry, Isfahan University of Technology, Isfahan, 84156-83111, Iran
Email: fariman@ch.iut.ac.ir

Keywords: Optogalvanic effect, Temporal OG Signal, Hallow Cathode Lamp, Wavelength Calibration.

Introduction

Optogalvanic (OG) spectroscopy is an effective method and excellent tool for study of spices present in discharge media. In this technique, a pulsed laser beam, with wavelength in resonant with two electronic states of an atom, disturbs an existing discharge. As a consequence, the steady state populations of the electronic states are changed and a sudden rise or fall in the impedance of the discharge is observed. In practice, the wavelength is scanned over the transition while the change in the discharge current is recorded. This technique has a wide variety of uses such as wavelength calibration [1,2] as well as atomic and molecular spectroscopy [3]. The technique is though high resolution, we here report a method to further enhance the resolution by considering the time evolution of the optogalvanic signal as a second dimension. By this method, even two completely overlapped transitions may be separated.

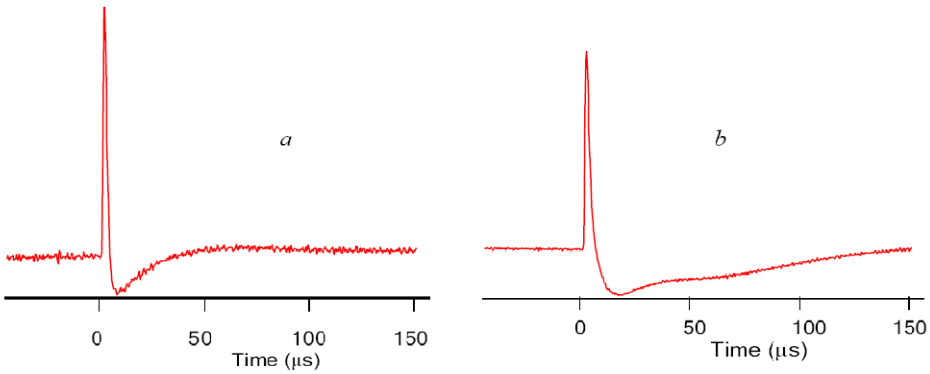

Fig.1. Typical shape of optogalvanic signals.

The Methods

Typical OG signals are demonstrated in Fig 1. Following the laser shot, a sudden increase in the discharge current is observed which follows by a sharp exponential decay to negative part. Then the current smoothly reaches its initial value. The wavelength is simply scanned to obtain a series of different OG signals at each wavelength, i.e. a three dimensional plot. The integration of the signal over a certain range of time at each wavelength yields a peak which corresponds to the transition between two electronic states. Careful investigation of Fig.1-*b*, reveals that an additional feature is presents between 40 to 100 μs range. The feature changes if the laser wavelength is scanned. This reveals that a second transition is contributing to this signal. The two transitions can be separated if the integration is made over different ranges of time. Fig.2. shows the integration for both traces *a* and *b* as a function of wavelength.

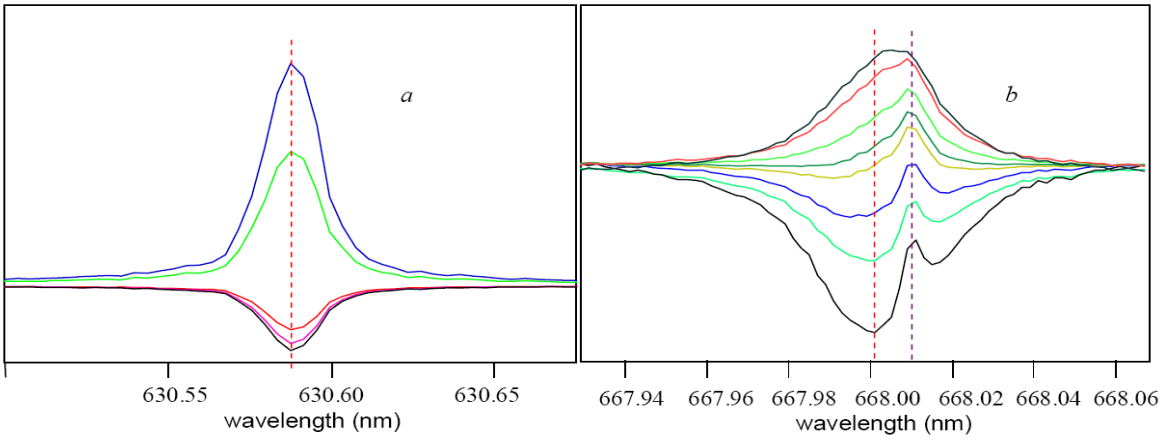

Fig.2. Integration of optogalvanic signal over different range of time as a function of wavelength for traces *a* and *b* in Fig.1.

As depicted, Fig.2-*a* shows only one peak at 630.58 nm but Fig.2-*b* which corresponds to the integration of trace *b* in Fig. 1, yields two opposite peaks with only 0.01 nm differences.

Conclusion

Optogalvanic spectroscopy of atoms is one of the best techniques in terms of resolution, which is often used for wavelength calibration. The line width could be as narrow as 0.025 nm. Using two dimensional optogalvanic spectroscopy, described in this work, it is possible

to further down to 0.01 nm resolution. Even, if two transitions are exactly coincident, they can be recognized if the have different behavior in time domain.

References

[1] N. J. Dovichi, D. S. Moore, R. A. Keller, Applied optics, 21 (1982) 1468.

[2] M. Hippler, J. Pfab, Optics Communications 97 (1993) 347.

[3] P. R. Sasi Kumar, V. P. N. Nampoori, C. P. G. Vallabhan, J. Phys. D: Appl. Phys. 26 (1993)

Ionic and Excited States of Hypoxanthine, Xanthine and Caffeine: A Theoretical Calculation of UV- photoelectron and Absorption Spectra using SAC/SAC-CI Method

F. Fathi[1]*, H. Farrokhpour[1,2]

[1] *Department of Chemistry, Isfahan University of Technology, Isfahan, 84156-83111, Iran*

[2] *Brazilian Synchrotron Light Laboratory, Campinas, Sao Paulo, Brazil*

E-mail: fariman@ch.iut.ac.ir

Keywords: Ionization, Photoelectron Spectroscopy, SAC-CI calculations

Introduction

Ultraviolet photoionization of hypoxanthine, xanthine and caffeine were first separately studied by Lin et al. and Dougherty et al. using He I lamp as radiation source, [1,2]. Recently, Feyer et al, reported the valance photoemission spectra of hypoxanthine, xanthine and caffeine at 100 eV photon energy, using the synchrotron radiation [3]. To the best of our knowledge, there is no high level theoretical calculation considering the electron correlations on the excitation and ionization spectrum of those compounds which play an important role in biochemistry and pharmacology. In this work, we used the Symmetry-adapted-cluster/Configuration Interaction (SAC-CI) method [4] to calculate several singlet, triplet and ionized states of hypoxanthine, xanthine and caffeine to predict the UV-photoelectron and excitation spectra of.those compounds.

Methodology

The Symmetry-adapted-cluster/Configuration Interaction (SAC-CI) calculations were carried out using direct SAC-CI program which is a new version of SAC-CI method. All singly excited or ionized configurations have been included in the calculations. In addition, the most important double excited configurations were considered via linked operators and. Triply and quadruply excited configurations were also considered by the products of singly and doubly configurations through unlinked operators. The D95+(d,p) basis set, with diffused function, was used for the geometry optimization. This geometry was then used for the SAC-CI calculations. The D95(d,p) basis set with *d* polarization function on C, N, O and *p* function on

hydrogen was used for the SAC/SAC-CI calculations. We have used frozen core approximation during SAC-CI calculations.

Results and Discussions

Calculations were performed for the ionized and the excited states up to 20 and 10 eV, respectively. The number of Hartee Fock molecular orbital used for the SAC-CI calculations were 130 for each compound. Vertical excitation and ionization energies, optical oscillator strengths and monopole intensities related to ionization intensities were all computed. Fig. (1) shows the calculated photoelectron spectrum of hypoxanthine and xanthine, respectvely at the SAC-CI level of theory using the D95 (d,p) basis set. As shown, there are good agreements between the calculated spectra and the reported experimental spectra in the literature. However, the calculations better agree with the spectra recorded by Lin et al.[1] in both cases in the range of 16 and 20 eV binding energy.

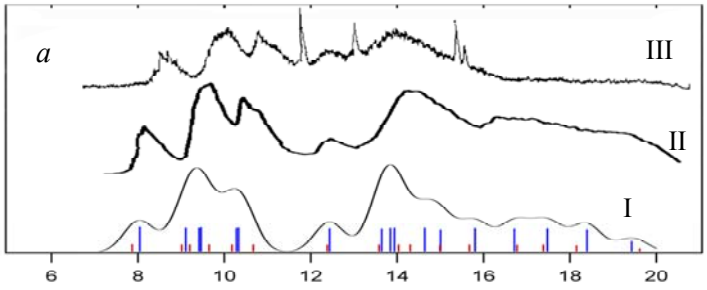

Hypoxanthine

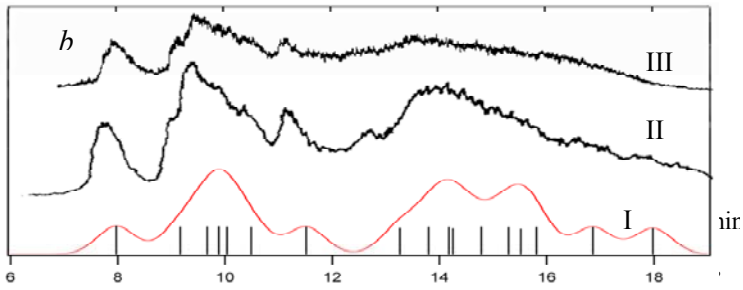

Xanthine

Fi ıir

ex

Binding Energy

respectively. The blue, gray and white

atoms represent N, C and H, respectively.

References

[1] J. Lin et al. *J. Phys. Chem*. 1980, 84, 1006-1012.

[2] D. Dougherty et al. *J. Elec. Spect. Rela. Phenom.* 1978, 13, 379-393.

[3] V. Feyer et al. *Chem. Phys*. 2009, 358, 33-38.

[4] H. Nakatsuji. *Chem. Phys.Lett.* 1979, 67, 329.

Valance Photoelectron Spectroscopy of DL-Valine Amino-Acid

F. Fathi[a,b], H. Farrokhpour*[a,b] Á. Miranda da Silva[c], A. Naves de Brito[b,c], M. Tabrizchi[a]

farrokhphossein@gmail.com

[a] Department of Chemistry, Isfahan University of Technology, Isfahan, 84156-83111, Iran

[b] Laboratório Nacional de Luz Síncrotron (LNLS), 13084-971, Campinas-SP Brazil

[c] Instituto de Física, Universidade de Brasília, 70910-900, Brasília-DF Brazil

Key Words: Photoelectron Spectroscopy, DL-Valine, thermodegradation, photon ion yield, OVGF

Introduction

The spectroscopic studies of amino acids, known as the building blocks of proteins, are important in understanding their properties in biological systems. Nevertheless, the intrinsic properties of bimolecules are usually masked by the complex medium of real biological systems. Those properties can be understood in an isolated environment i.e. gas phase. Here, we report a joint experimental and theoretical investigation of the He I valance photoelectron spectrum of DL-Valine amino acid.

Methods

The partial ion yield (PIY) measurements were performed in the range of 11.20 - 21.55 eV at the Toroidal Grating Monochromator Beam Line (D05-TGM) in the Laboratório Nacional de Luz Sincrotron (LNLS), in Campinas, Brazil using a time of flight mass spectrometer (TOF-MS). This experiment was performed to assure the thermal stability of the sample at different temperatures. A second chamber coupled with an electron analyzer (Scienta R4000) was used to record the photoelectron spectra. The gas jet was mounted perpendicularly to the plane formed by the He I lamp ($h\nu$=21.22 eV) and the entrance of the analyzer. The spectrum was obtained with an electron analyzer slit width of 0.2 mm and pass energy of 50 eV. The electron energy was calibrated with argon and xenon gas samples.

Results and Discussion

The experimental photoelectron spectrum of DL-Valine, recorded at 100ºC using the He I lamp as well as the spectrum recorded by Klasinc [1] are shown in Fig. 1 (trace *a* and *b*

,respectively). The theoretical photoelectron spectrum of DL-Valine was calculated by OVGF method using aug-cc-pVDZ basis set up to 18 eV, shown in Fig.1 (bottom). As seen, both experimental spectra have the same structures, although there are differences beyond 14 eV binding energy range. The theoretical spectrum agrees very well with that of the experimental one. Four structures is observed in the spectrum, among them, the first two represent the energies of the two most external orbitals HOMO and HOMO-1 correspond to 9.53 eV and 10.69 eV, respectively.

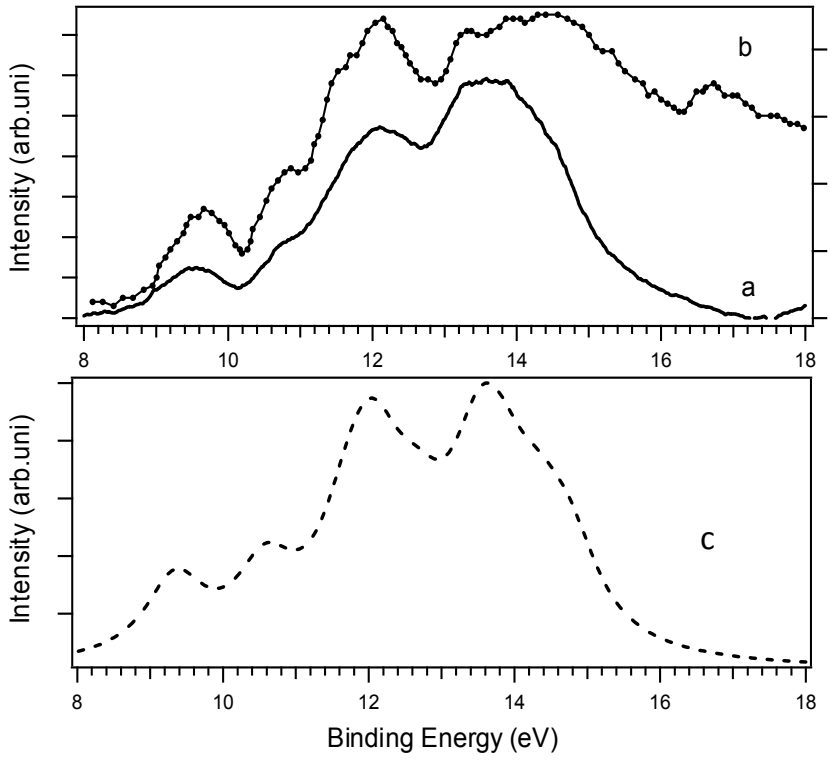

Figure 1: Top, the experimental photoelectron spectrum of DL-valine recorded in (a) this work and (b) recorded by Klasinc [1], bottom, the theoretical spectrum calculated by OVGF method in 3th order

References

[1] L. Klasinc, *J. Elec. Spec. Rel. Phenom.* 8 (1976) 161.

Quantum Chemical Study of Host-Guest Inclusion Complex Formation of Lidocaine and Salbutamol as Local Anesthetic Drugs with Cyclodextrins

Kh. Farzadnia[a], Z. B. Nojini[*b]

[a]Department of Chemistry, Islamic Azad University, Sciences and Researches Branch, Khuzestan, Ahvaz, Iran

[b]Department of Chemistry, Faculty of Science, Shahid Chamran University, Ahvaz, Iran

Email: khalilfarzadnia@yahoo.com

Keywords Cyclodextrin, Anesthetic drugs, Inclusion complexation

Introduction

Nowadays, Cyclodextrins are studied as carrior molecules to form complexes with some drugs to have a good efficiency. The α and β CDs consist of six and seven D glucopyranose residues, respectively [1]. The purpose of this research is to obtain the most stable complex.

Computational Method

In this research, Quantum mechanical (QM)calculations were carried out in order to study the host- guest inclusion complexes[2] of salbutamol and lidocaine with α and β-cyclodextrin(α and β- CDs). All the structures were optimized with HF method and 6-31G Basis set. The inclusion complexation was simulated by putting the guest at the end of CD cavity and allowing it to pass through the CD cavity by steps.

Results and discussion

For the complex of α-CD With Salbutamol, energy of the inclusion Complex vs the z coordinate is shown in Fig.1 The total energy of the α and β-CD/Lido and β-CD/Salbu were calculated. The complex formation energy, ΔE, was calculated using the following expression:

$$\Delta E = E_{(complex)} - (E_{CD} + E_{drug}) \quad (1)$$

The electronic chemical potential(μ) was calculated as half of the energy of the HOMO and LUMO as follows:

$$\mu = (E_{HOMO}+E_{LUMO})/2 \quad (2)$$

The energies of HOMO and LUMO and Stabilization energy values of Host-guest complexes are summarized in Table 1.The results indicate that the energy gaps between HOMO and LUMO for α –CD/Salbu is more than that of β-CD/Salbu and β-CD/Lido.

Table1. Electronic energies, HOMO, LUMO and Gap energy of the inclusion complexation of α and β-CDs with Lidocaine and Salbutamol of the HF optimized structures

Species	ΔE(kj/mol)	E_{HOMO}(eV)	E_{LUMO}(eV)	EnergyGap	μ(eV)	η(eV)	ω
Lidocaine	-	-11.36	5.28	16.65	-3.04	8.32	0.55
Salbtamol	-	-11.13	4.09	15.22	-3.51	7.61	0.80
α-CD	-	-8.43	3.50	11.94	-2.46	5.97	0.50
β-CD	-	-8.53	3.71	12.25	-2.41	6.12	0.47
α-CD/Lido	- 2000	-8.44	3.65	12.15	-2.41	6.07	0.48
β-CD/Lido	- 1000	-8.51	3.53	12.05	-2.41	6.02	0.51
α-CD/Salbu	- 9000	-8.72	3.53	12.25	-2.59	6.12	0.54
β-CD/Salbu	- 7000	-8.45	3.78	12.24	-2.33	6.12	0.44

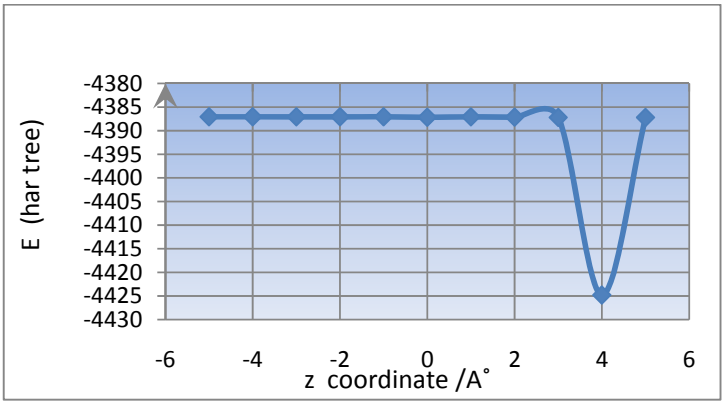

Fig.1 Graphic diagram for the emulation of the inclusion complexation of Salbutamol into α-CD

Conclusion

Owing to the results calculated by HF/6-31G, α-CD/Salbu complex with the most energies of HOMO and LUMO gap is the most stable complex.

References

[1] M. Farmeglia, M. Ferrone, A. Lodi, S. Pricl J. Carb.Poly 53 (2002) 15

[2] S. M. Hashemianzadeh, A. A. Rafati, Z. B. Nojini J. Mon.Chem 139 (2008) 763

Spectral studies on the interaction of tetrakis (N,N´,N´´,N´´´-tetramethyl tetra-3,4-pridino) porphyrazine cobalt(II) with anionic surfactants

H. Dezhampanah [a*], B. Ghalami[a], and R. Firouzi

[a] Department of Chemistry, Faculty of Science, University of Guilan P.O. Box 1914, Rasht 0098, Iran. (***e-mail**: h.dpanah@guilan.ac.ir)

Key word: porphyrazine, anionic surfactant, aggregation

Introduction

Cationic porphyrinic macrocycles (metallophthalocyanines, porphyrazines) represent a large and expanding class of compounds which have applications in biology, medicine, catalysis, and materials. Binding of porphyrins and metalloporphyrins to the simplest models for membranes (ionic surfactants) has attracted much interest due to the possibility of understanding many of their biological and photochemical processes, such as photosynthesis, oxygen transport, oxidation–reduction, and electron transport. The interaction of water-soluble porphyrin and metalloporphyrin with ionic surfactants has been widely demonstrated [1]. In the present paper we have investigated interactions of a series of anionic surfactants with different alkyl chain length; sodium dodecyl sulfate (SDS), sodium tetradecyl sulfonate (STS), sodium hexadecyl solfunate (SHS) with tetrakis (N, N´, N´´, N´´´-tetra methyl tetra-3, 4-pridino) porphyrazine Cobalt(II) ([Co (II) 3, 4-tmtppa] $^{4+}$) (scheme 1) in aqueous premicellar and micellar solutions by using optical absorption spectroscopy.

Methods:

Cobalt (II) complex of [Co (II) 3, 4-tmtppa] $^{4+}$ was prepared and purified according to literature methods [2]. Sodium do decyl sulfate (SDS), sodium tetra decyl sulfonate (STS), sodium hexa decyl sulfonate (SHS) were Sigma chemicals and were used without further purification. All experiments were run in phosphate buffer of pH 7.2. Aqueous solution of ([Co (II) 3, 4-tmtppa] $^{4+}$ (9.7×10^{-6} M) was titrated by adding appropriate volume concentrated solutions of SDS, STS and SHS, respectively. The absorbances were measured on the double beam absorbance spectrophotometer Cary 100 scan UV-vis-NIR after stirring for 30 min. The measurements were taken at 25 °C.

Results and discussion

The optical absorption spectrum of [Co (II) 3, 4-tmtppa] $^{4+}$shows a Soret band ($\lambda = 348\,nm$) and a Q-band ($\lambda = 656\,nm$) feature which is a characteristic of the base porphyrazine. The Q-band maximum of [Co (II) 3, 4- tmtppa] $^{4+}$ obeys beer's law over an extended concentration range between 2.0×10^{-6} to 3.0×10^{-5} M in water. From this observation we can conclude that [Co (II) 3, 4-tmtppa]$^{4+}$ does not show concentration dependent aggregation. The effect of NaCl solution on the absorption spectrum of [Co (II) 3, 4-tmtppa] $^{4+}$ in water is shown no new band appears even at high concentrations of the salt. This means that [Co(II)3,4-tmtppa]$^{4+}$does not form well defined aggregates (i.e. H or J type) even at high concentrations of the salt.

The UV–vis absorption spectra of [Co(II)3,4-tmtppa]$^{4+}$ in aqueous solution in the presence and the absence of SDS are displayed in Figure 1. It is observed that the addition of SDS changes the position, width, and intensity of the absorption spectra of [Co(II)3,4-tmtppa]$^{4+}$ at different concentrations of SDS. The most obvious change occurs in the Q-band region of the absorption spectrum, and no isobestic point is observed, which indicates significant aggregation of [Co(II)3,4-tmtppa]$^{4+}$ (including ordered J- and H-type). This aggregation can be attributed to the neutralization of the positive charges of [Co(II)3,4-tmtppa]$^{4+}$ by SDS, which decreases the electrostatic repulsive force between the porphyrazine monomer. Similar results were observed for other surfactants. With increasing alkyl chain length of surfactants, the interactions become stronger, which shows the importance of hydrophobic forces. Electrostatic interactions also play an important role, as shown by the effect of NaCl on binding process.

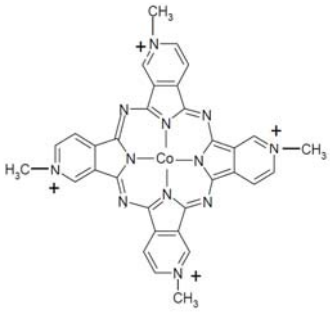

Scheme1: Chemical structures of [Co (II) 3, 4-tmtppa] $^{4+}$.

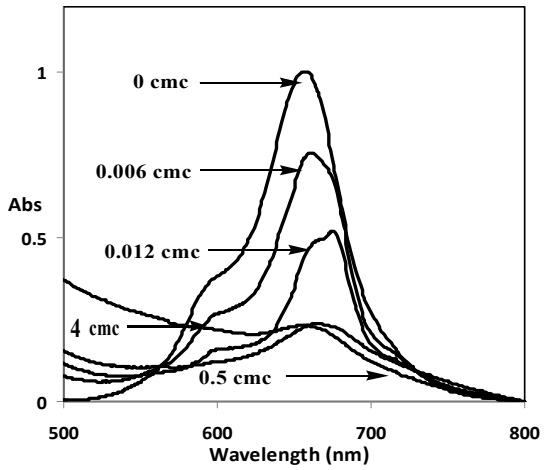

figure1. The UV-vis spectra of [Co (II) 3, 4-tmtppa] $^{4+}$ in the presence of various SDS concentrations at the buffer solutions.

References

[1] Yaffe, O. Korin, E. and Bettelheim, A. *Langmuir* **2008,** *24,* 11514-11517

[2] Bordbar, A. K. Dezhampanah, H., Asadi, M., Safaei, E., Sohrabi, N.and Khodadost, Y. *J. Porphyrins Phthalocyanines* **2007**, 11: 556–565.

Determination of Dunham constants and potential energy curves for BH from combined analysis of UV/visible and infrared spectra

E. Ghazizadeh, E. Masoumi, and A. Shayesteh*
School of Chemistry, College of Science, University of Tehran, Tehran, Iran
E-mail: shayesteh@khayam.ut.ac.ir

Keywords: Electronic spectroscopy, Dunham constants

Introduction

BH is one of the simplest diatomic molecules with only six electrons. Because of its simplicity, it has been the subject of many theoretical studies [1,2]. Experimental data on BH have been frequently used as benchmarks for testing the accuracy of various ab inito theoretical methods. Spectroscopic investigations on BH began in 1931, and so far, several electronic transitions involving the $X\ ^1\Sigma^+$ ground state and the low-lying excited states have been observed [3-8]. The $A\ ^1\Pi \rightarrow X\ ^1\Sigma^+$, $B\ ^1\Sigma^+ \rightarrow X\ ^1\Sigma^+$ and $C\ ^1\Sigma^+ \rightarrow A\ ^1\Sigma^+$ transitions appear near 23000, 52000 and 55000 cm^{-1}, respectively.

Data analysis and results

Spectroscopic constants were determined for the $X\ ^1\Sigma^+$, $A\ ^1\Pi$, $B\ ^1\Sigma^+$, $C\ ^1\Sigma^+$ and $C'\ ^1\Delta$ states of BH by least-squares fitting of rovibronic data. The experimental data listed in Tables 1 and 2 were used in our study [4-8].

Table 1. Electronic transitions of BH

Transition	v′ range	v″ range	Ref.
$A\ ^1\Pi \rightarrow X\ ^1\Sigma^+$	0 to 3	0 to 3	[5,7,8]
$B\ ^1\Sigma^+ \rightarrow X\ ^1\Sigma^+$	0 to 3	0 to 3	[6]
$C\ ^1\Sigma^+ \rightarrow X\ ^1\Sigma^+$	0	0	[6]
$C\ ^1\Sigma^+ \rightarrow A\ ^1\Pi$	0 to 2	0 to 2	[7]
$C'\ ^1\Delta \rightarrow A\ ^1\Pi$	0 to 2	0 to 2	[7]

Table 2. Vibration-rotation bands of BH

Electronic state	Infrared bands	Ref.
$X\ ^1\Sigma^+$	v = 1 → 0 v = 2 → 1 v = 3 → 2	[4]

All the observed transition wavenumbers were fitted using the Dunham expression:

$$E(\mathrm{v},J)=\sum_{m=0}\sum_{l=0}Y_{l,m}\left(\mathrm{v}+\tfrac{1}{2}\right)^{l}\left(J(J+1)-\Lambda^{2}\right)^{m}$$

for the $^1\Sigma^+$ and $^1\Delta$ states, while the Λ-doubling in the $^1\Pi$ states were taken into account by adding the following expression to the Dunham formula:

$$\delta E_{\Lambda}=\pm\frac{1}{2}\sum_{m=1}\sum_{l=0}q_{l,m}\left(\mathrm{v}+\tfrac{1}{2}\right)^{l}\left(J(J+1)-\Lambda^{2}\right)^{m}.$$

The preliminary equilibrium molecular constants for the low-lying electronic states of BH are listed in Table 3.

Table 3. Preliminary equilibrium molecular constants for BH (in cm^{-1})

State	T_e	ω_e	$\omega_e x_e$	B_e	r_e (Å)
$X\,^1\Sigma^+$	0	2366.730(9)	49.341(5)	12.0254(2)	1.232185(9)
$A\,^1\Pi$	23130.22(6)	2309.30(19)	113.73(19)	12.2015(19)	1.22326(9)
$B\,^1\Sigma^+$	52335.73(18)	2399.85(49)	69.53(39)	12.3475(25)	1.2160(1)
$C\,^1\Sigma^+$	55281.53(7)	2473.28(12)	53.37(4)	12.4164(17)	1.21263(8)
$C'\,^1\Delta$	46031.21(6)	2609.86(10)	46.57(3)	12.7609(10)	1.19615(5)

Work in progress

The RKR potential energy curves of BH have been obtained using the $Y_{l,0}$ and $Y_{l,1}$ constants from the Dunham fits. Accurate potential energy curves for the $X\,^1\Sigma^+$ and $A\,^1\Pi$ states will be obtained using the direct-potential-fit method.

References

[1] L. A. Curtis and J. A. Pople, *J. Chem. Phys.* 89, 614 (1988); 90, 2522 (1989).

[2] C. W. Bauschlicher, Jr., S. R. Langhoff, and P. R. Taylor, *J. Chem. Phys.* 93, 502 (1990).

[3] W. Lochte-Holtgreven and E. S. van der Vleugel, *Z. Phys.* 70, 188 (1931).

[4] F. S. Pianalto, L. C. O'Brien, P.C. Keller, and P. Barnath, *J. Mol. Spectrosc.* 129, 348 (1988).

[5] W. T. M. L. Fernando and P. F. Bernath, *J. Mol. Spectrosc.* 145, 392 (1991)

[6] S. H. Bauer, G. Herzberg, and J. W. C. Johns, *J. Mol. Spectrosc.* 13, 256 (1964).

[7] J. W. C. Johns, F. A. Grimm, and R. F. Porter, *J. Mol. Spectrosc.* 22, 435 (1967).

[8] J. Clark, M. Konopka, L.-.M. Zhang, and E. R. Grant, *Chem. Phys. Lett.* 340, 45 (2001).

Investigation of Temperature and Electric field effects on ion Mobility Spectra of Narcotic Druges

Azra Abedi*[a], Fariba Ghobadi[b]

[a]Islamic Azad University, Shahreza Branch, azraabedi@yahoo.com

[b]Islamic Azad University, Shahreza Branch, f_ghobadi62@yahoo.com

Keywords: Ion Mobility Spectrometry, Narcotic Drug, Electric Field Effect, Temperature Effect.

Introduction

Narcotics have been used for centuries for pain relief. Some of these compounds are also frequently abused as illicit drugs [1]. There is a growing need in the pharmaceutical industries for rapid, low cost, and sensitive analytical methods in quality assessment and cleaning verification for the quality control and production of narcotic drugs. Ion mobility spectrometry (IMS) is a simple, fast, inexpensive, highly selective and very sensitive technique for a wide range of compounds [2]. In this work, the corona discharge ion mobility spectrometry has been applied for identification of several narcotic compounds at different temperatures and electric fields.

Method

The IMS apparatus with the continuous corona discharge ionization source has been used [3]. The follow rates of carrier and drift gas were 400 and 600 ml/min respectively. Ion mobility spectra of codeine phosphate, oxycodone hydrochloride, papaverine hydrochloride, noscapine, methadone hydrochloride and cocaine have been investigated. All of these compounds are in solid state. In order to introduce them to ionization region a small amount of sample was placed on the tip of a needle and the needle was inserted into the injection port. By increasing the injection port temperature to 220^{o}C the vapor of sample was carried to the IMS cell by the carrier gas.

Results and discussion

The ion mobility spectra of several narcotic drugs were investigated in different electric fields, 340-470 V/cm, and different temperatures, 25-225 °C. Fig. 1 shows the ion mobility spectra of them at 225 °C and 406.25 V/cm. The results show that changing of electric filed did not have any effect on reduced mobility of ions. However, by increasing the electric filed the intensity increased. The effect of temperature on ion mobility spectra of codeine phosphate has been shown in Fig. 2. At low temperature the rate of proton transfer reaction from reactant ions (RIP) to sample molecules is slow therefore the intensity of sample ions is low. On the other hand production of dimer ion at low temperature is more probable than high temperature; therefore ion mobility spectrum of sample is more crowded. By increasing the temperature intensity of monomer ions of sample increased but intensity of reactant ions and dimer ions decreased and ion mobility spectra become clear.

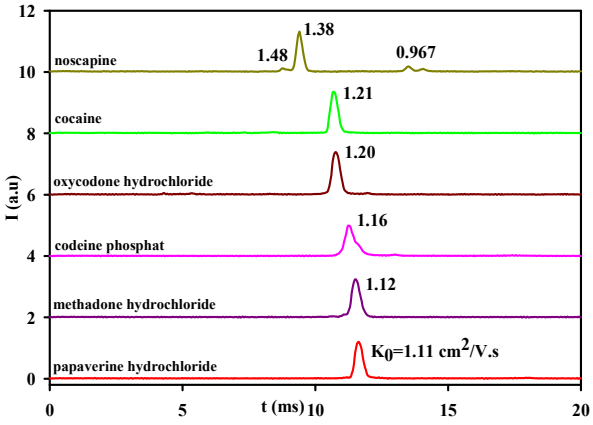

Figure 1: The ion mobility spectra of different narcotic drugs at 225 °C and E= 406.25 V/cm in N_2

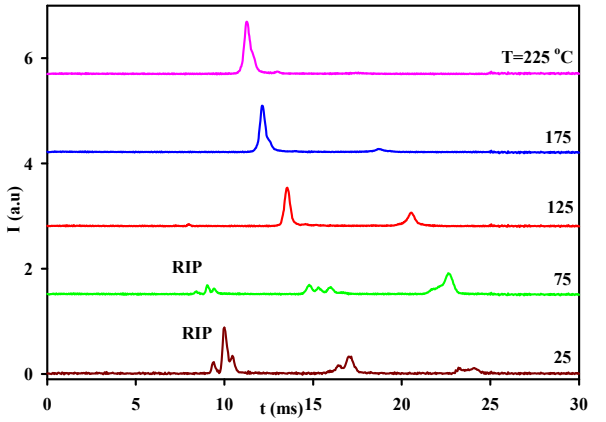

Figure 2: Ion mobility spectra of Codeine Phosphate at different temprature and E= 406.25 V/cm in N_2

Conclusion

Corona discharge ion mobility spectrometry has been used for investigation of narcotic drugs. This method could be a simple, fast, selective, and sensitive method for detection of these compounds as it is used for investigation of other compounds. The results show that optimum condition for study of narcotic drugs is high temperatures and electric field.

References

[1] F.E. Dussy, C. Berchtold, M. Bovens, Forensic Sci. Int., **177**, 2008, 105.

[2] Eiceman, G. A.; Karpas, Z.; Ion Mobility Spectrometry, CRC Press, Boca Raton, 2005.

[3] M. Tabrizchi, T. Khayamian, N. Taj, Rev. Sci. Instrum.,**71**, 2000, 2321.

Fluorine Bond; Is It Halogen Bond?

M. Lesani and K. Eskandari*
School of Chemistry, Damghan University, Damghan, Iran
(Email: mina_lesani@hotmail.com)

Keywords: QTAIM, Halogen Bond, Atomic Electrostatic Moment, Fluorine

Introduction

Non-covalent interactions play an important role in different areas of chemistry. And a halogen bond is a non-covalent interaction involving halogen atom as acceptor of electron density. The existence of halogen bonds have been proven, both theoretically and experimentally, for iodine, bromine and chlorine. But in the case of fluorine, it is usually believed that it does not participate in halogen bonding interactions. In recent years, on the other hand, some theoretical investigations raise doubts about this inability of fluorine atom [1]. Politzer and co-workers [2] showed that some fluorine containing molecules, such as NCF and FCCF, are able to interact with Lewis bases. Although, they classified these interactions as halogen bonds, but it seems that these bonds have fundamental differences with the traditional halogen bonds of chlorine, bromine and iodine.

Methods

Using the G03 program package, structures were fully optimized at MP2 theory level with 6-311++G(d,p) 6d basis functions. We analyzed the bonding characteristics by Bader's "Quantum Theory of Atoms in Molecules" (QTAIM) [3].

Result and Discussion

In this work we have investigated a series of complexes formed between ammonia and F2, NCF, NCCC-F, CF_3-CC-F and FCCF molecules. Furthermore, in addition to above mentioned molecules, their chlorine/bromine-containing analogous have been also considered. Our calculations show that these fluorine bonds differ from traditional halogen bonds. Some of these differences have been listed below.

Geometry. Except for F_2, all of the F…N distances are noticeably longer than the sum of van der Waals (vdW) radii of fluorine and nitrogen (3.02Å). In contrast, for all of the traditional halogen bonds, the X…N distances are substantially less than the vdW radii of the X and N atoms [4].

QTAIM. The anisotropic distribution of electron density around halogen atom is responsible for halogen bond formation. A covalently bonded halogen atom has two different radii, a shorter radius along R-X bond ($r_{\|}$), and a larger radius perpendicular to this bond ($r_{\perp}$). The values of $r_{\|}$ and $r_{\perp}$ has been calculated for F, Cl and Br (These values are correspond to the distance of nucleus of the X atoms to their non-bonded 0.001 au contour of the electron density in the isolated molecules). For chlorine and bromine the $r_{\|}$ values are considerably less than their corresponding $r_{\perp}$ values. But this is not the case for fluorine; the $r_{\|}$ and $r_{\perp}$ of fluorine are very close to each other which indicate a spherical electron density around fluorine.

Atomic properties also indicate that fluorine bonds differ from traditional halogen bonds. For instance, the atomic electrostatic moments (e.g. atomic monopole, dipole and quadrupole moments) has been used to calculate the electrostatic potential at a point in the vicinity of 3Å (a representative distance of halogen bonding) from the center of halogen atom. These results show that the attractive and repulsive terms in fluorine bonds differ from those of traditional halogen bonds.

Conclusion

The geometrical and QTAIM parameters show that there are some fundamental differences between the nature of traditional halogen bonds and these fluorine containing ones. Especially atomic properties of the halogen and the QTAIM values at the bond critical points in F…N bonds indicate that these bonds should be categorized as van der Waals interactions rather than halogen bonds.

References

[1] Lu, Y. Zou, J. Yu, Q. Jiang, Y. Zhao, W. *Chemical Physics Letters,* 449 (2007) 6-10.

[2] Politzer, P. Murray, J. S. Concha, M. C. *J. Mol. Model.,* 13 (2007) 643-650.

[3] Bader, R. W. F. (1990). *Atoms in Molecules, A Quantum Theory*. New York: OUP.

[4] Auffinger, P. Hays, F. A. Westhof, E. Ho, P. S. *Proc. Natl. acad. Sci. USA.*, 101 (2004) 16789–16794.

Three-particle quantum scattering via separable potentials

A Maghari and V.Moheb Maleki

Department of Physical Chemistry, College of Science, University of Tehran, Tehran, Iran
E-mail: maghari@khayam.ut.ac.ir; vahdat_mohebmaleki@yahoo.com

Keywords: Faddeev equation, Three-body scattering, uncoupled partial waves, thermophysical

Introduction

This work is another step forward in the development of our previous works [1-4], which has extended the analytical solution of Lippmann-Schwinger (LS) equation for three-body scattering via separable potential using the Faddeev approach [5-7]. For a system of three non-relativistic spinless particles we write down the total Hamiltonian in the form

$$\hat{H} = \hat{H}^0 + \hat{V} \tag{1}$$

where $\hat{H}^0$ is kinetic energy and $\hat{V}$ is the total potential interaction of three-body system. The transition operator $\hat{T}(z)$ for the system is the solution of the equation

$$\hat{T}(z) = \hat{V} + \hat{V}\hat{G}_0(z)\hat{T}(z) \tag{2}$$

where $\hat{G}_0(z)$ is the free three-body Green's function defined as $\hat{G}_0(z) = (z - \hat{H}_0)^{-1}$, in which z is complex energy parameter. Faddeev has shown that the three-body transition operator can be conveniently as a sum of separate terms corresponding to two-body forces as

$$\hat{T}(z) = \hat{T}^{(1)}(z) + \hat{T}^{(2)}(z) + \hat{T}^{(3)}(z) \tag{3}$$

in which $\hat{T}^{(i)}(z)$ satisfies the Faddeev equation for two-body scattering as:

$$\hat{T}^{(i)}(z) = \hat{T}_i(z) + \sum_{j \neq i} \hat{T}_j(z)\hat{G}_0(z)\hat{T}^{(j)}(z) \qquad i = 1,2,3 \tag{4}$$

The scattering matrix $\hat{T}_i(z)$ arising from two-body potential can be obtained by the LS equation:

$$\hat{T}_i(z) = \hat{V}_i + \hat{V}_i\hat{G}_0(z)\hat{T}_i(z) \tag{5}$$

where $\hat{V}_i \equiv \hat{V}_{jk}(j,k \neq i)$ is two-body potential..

Model separable potential

A separable potential model with uncoupled partial waves can be generally be written as

$$\hat{V} = \sum_{i=1}^{n} \sum_{\ell,\ell'} \sum_{m,m'} (2\ell+1)(2\ell'+1) v_i |\chi_i;\ell,m\rangle\langle\ell',m';\chi_i| \tag{6}$$

where n is the rank of the potential operator, v_i is the attractive (or repulsive) coupling strength and $|\chi_i;l\rangle$ is the state of the system with angular momentum quantum number l, which is a real number in the unitary case. The momentum representation of such a potential is

$$\hat{V}(\boldsymbol{p},\boldsymbol{p}') = \langle \boldsymbol{p}|\hat{V}|\boldsymbol{p}'\rangle = \sum_{i=1}^{n} \sum_{\ell,\ell'} \sum_{m,m'} v_i \chi_i^{(\ell,m)*}(\boldsymbol{p}) \chi_i^{(\ell',m')}(\boldsymbol{p}') \tag{7}$$

where $\chi_i^{(l)}(p) \equiv \langle p|\chi_i;l\rangle$. In this work, we use the form factor as a Yamaguchi model as

$$\chi_i^{(\ell)}(\boldsymbol{p}) = \frac{1}{\pi^{3/4}} \left[\frac{2^{2\ell}\,\ell!(2\ell+1)\,a_i^{2\ell+1}}{\Gamma(\ell+1/2)} \right]^{1/2} \frac{p^{\ell}}{(a_i^2+p^2)^{\ell+1}} \Im_{\ell,m}^{j}(\hat{\boldsymbol{p}}) \tag{8}$$

where $\Gamma(n)$ is the Gamma function and a_i plays the role of scale factor.

Results and discussion

The present model can be applied to obtain the elastic differential cross sections as well as total cross sections from the three-body potential model in the Faddeev approximation. The potential parameters are also adjusted to fit the two-body phase shift data and then applied to calculate the third virial coefficients of some appropriate systems. Further, we shall obtain the uncoupled partial-waves properties for some realistic three-body systems including partial waves scattering matrix and its corresponding phase shifts. Our motivation for calculating these scattering properties is continuing the previous work for obtaining the analytic expressions for both equilibrium and non-equilibrium thermophysical properties of fluids at moderately densities.

References

[1] Maghari, A. and Dargahi, M., *J. Phys. A: Math. Theor.* **41** (2008) 275306

[2] Maghari, A. and Dargahi, M., *J. Stat. Mech.* (2008) P10007

[3] Maghari, A. and Tahmasbi, N., *Physica A* **382** (2007) 537

[4] Maghari, A. and Tahmasbi, N. *J. Phys. A: Math. Gen.* **38** (2005) 4469

[5] Newton R G., Scattering *Theory of Waves and Particles* (New York: McGraw-Hill), 1966

[6] Phillips, A.C., *Phys. Rev*. **142** (1966) 985

[7] Ueta, K., Miyake, H. and Bund, G.W., *Phys. Rev*, **59C** (1999) 1806

Ab initio study of chemisorption of Hydrogen on Copper and Iron

F.Mokhles*[a] and A.A.Salari[a]and M.Shabani[b]and sara sayedi[a]

[a] Islamic Azad University, Shahr-e-rey Branch, Tehran- Iran

[b]Islamic Azad University, Varamin-Pishva Branch, Tehran- Iran

*Email: fmokhles61@yahoo.com

Keywords: Hydrogen, Heat of adsorption, Adsorption, Copper, Iron, Surface coverage.

Introduction:

Transition metals play an important role in catalytic processes. They adsorbed gases on their surfaces and make the chemical reactions easy [1-2].

Materials and Methods:

In this study, the adsorption of H atom on an eight-atom network of surface of Cu (001) and on a four- atom network of surface of Fe (001) in two rows is considered. Hydrogen atom put on each site and then the system was optimized in the B3LYP level of theory with lanl2dz basis set for Cu and Fe and 6-31G for hydrogen. The crystal parameters such as distance between Cu and Fe atom were fixed during optimization. In each case, heat of adsorption was measured by equation (1-1) and its dependency to surface coverage was studied.

$$\Delta H_{ads} = [E_{M-H} - E_M - E_{\frac{1}{2}H_2}] \quad (1-1)$$

Results and discussion:

The calculated energy for Cu metal, Hydrogen, metal-hydrogen and heat of adsorption in different surface coverage in three sites (top, bridge and hollow) are listed in tables 1, 2 and 3 respectively

Table 1: Calculated energy in different surfaces for top site.

No.H	*θ*	*EM-H*	E_{ad} (a.u)	E_{ad} (kcal/mol)	E_{ad} (kJ/mol)	*EM*	*EH2*
1	*0.25*	*-1569.934169*	*-0.0995911*	*-62.49341525*	*-267.472449*	*-1569.33430*	*-1.17548*
2	*0.5*	*-1570.506537*	*-0.08584295*	*-53.86645113*	*-225.377232*		
3	*0.75*	*-1571.055047*	*-0.73307967*	*-46.00074908*	*-192.467134*		
4	*1*	*-1571.61904*	*-0.0709108*	*-44.496527*	*-186.173469*		

Table2: Calculated energy in different surfaces for bridge site.

No.H	θ	EM-H	E_{ad} (a.u)	E_{ad} (kcal/mol)	E_{ad} (kJ/mol)	EM	E_{H2}
1	0.5	-1569.938173	-0.103595	-65.0058625	-271.984529	-1569.334305	-1.17548
2	1	-1570.514039	-0.08959405	-56.22026638	-235.225595		

Table3: Calculated energy in different surfaces for hollow site.

No.H	θ	EM-H	E_{ad} (a.u)	E_{ad} (kcal/mol)	E_{ad} (kJ/mol)	EM	E_{H2}
1	0.5	-1569.95407	-0.1194391	-74.94803525	-313.582579	-1569.2343	-1.17548
2	1	-1570.5058	-0.08547485	-53.63546838	-224.4108		

Figure 1 shows the three different sites top, bridge and hollow in different surface coverage

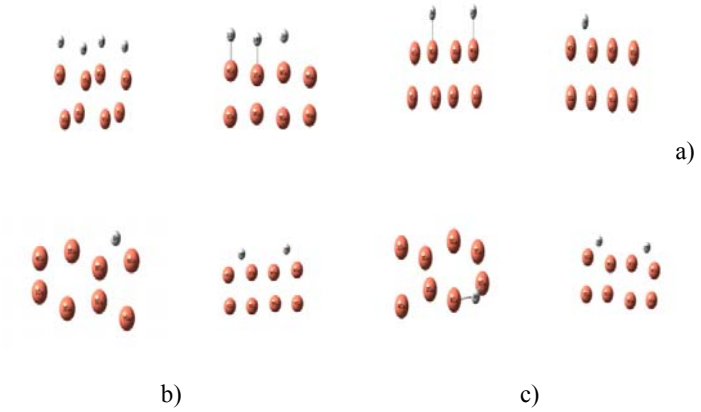

Figure 1: Adsorption of Hydrogen atom on three different sites top (a), bridge (b) and hollow (c) in different surface coverage for Cu.

The calculated energy for Fe metal, Hydrogen, metal-hydrogen and heat of adsorption in different surface coverage in two sites (top, bridge) are listed in tables4,5.

Table4: Calculated energy in different surfaces for top site

No.H	θ	EM-H	E_{ad} (a.u)	E_{ad} (kcal/mol)	E_{ad} (kJ/mol)	EM	E_{H2}
1	0.5	494.1542756-	-0.7125356	-447.116089	-1868.945252	-492.854	-1.17548
2	1	-494.0051038	-0.609298	-382.334495	-1598.15818		

Table5: Calculated energy in different surfaces for bridge site

No.H	θ	EM-H	E_{ad} (a.u)	E_{ad} (kcal/mol)	E_{ad} (kJ/mol)	EM	E_{H2}
1	0.5	-493.5057713	-0.0640313	-40.179640	-167.950898	-492.852	-1.17548

Figure 2 shows the two different sites top and bridge in different surface coverage.

Figure2: The adsorption of hydrogen atom on two different sites top (a) and bridge (b) in different surface coverage for Fe.

As we see, in Cu heat adsorption of hydrogen atom on hollow site is more negative than other sites and in Fe heat adsorption of hydrogen atom on bridge site is more negative than other sites. So these sites are more favorable. In each site, the interaction between adsorbed hydrogen atoms to Cu and Fe atoms caused decreases heat of adsorption heat of adsorption.

Conclusion:

In this paper, we study adsorption of atomic Hydrogen on Cu and Fe surface (001). Adsorption can occur in three sites: top, bridge and hollow. It was found that adsorption of

atomic hydrogen on hollow site on Cu is better than other sites and adsorption of atomic hydrogen on bridge site on Fe is better than other sites. The surface coverage dependence of heat adsorption of Hydrogen on has been investigated. It was found that the heat of adsorption decreases with increasing the surface coverage, and agrees with Freundlich isotherm.

References:

[1]J.w. Davenport and P.J. Estrup,in: The Chemical Physics of Solid Surfaces and heterogeneous catalysis,Vol.3A.Eds.D.A.King and D.P.Woodruff (Elsevier,Amstrdam,**1989**).

[**2]** K.Christmann, Surf. 103 (1981) 361.

DFT study on the mechanism of hydroalkoxylation catalyzed by Pd(II)

A. Morsali*[a], S. A. Beyramabadi [a] and M. R. Bozorgmehr[a]

[a] Faculty of Science, Department of Chemistry, Islamic Azad University–Mashhad Branch, Iran

* (Email: morsali@mshdiau.ac.ir)

Keywords: Hydroalkoxylation, Mechanism, Palladium, Density functional theory

Introduction

The palladium(II) complex is one of the most valuable metal complexes in various catalytic reactions and organic syntheses (Nobel prize 2010). Pd(II) coordination complexes catalyze the addition of alcohols to vinyl ketones to produce ethers. During the catalytic cycle, the alcohol adds selectively to the β-carbon (anti-Markovnikov). Mechanism for the reaction of Alcohol with methyl vinyl ketone (MVK), being catalyzed by Pd, has been experimentally reviewed in detail. Regarding the experimental evidence, Miller et al. proposed a mechanism, which are shown by Eqs. (1, 2) [1].

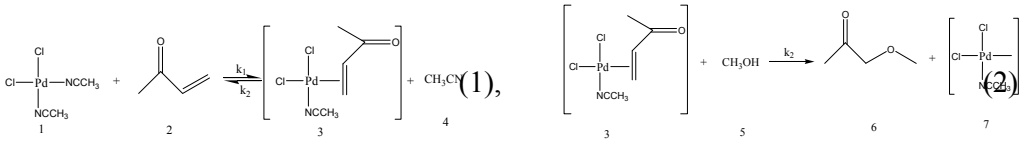

Miller et al. showed that Eq. (2) is the rds during which the alcohol OH bond is broken.

Computational details

All of the present calculations have been performed with the B3LYP [2] hybrid density functional level using the G03 package. The 6-311+G(d,p) basis set was employed except for Pd atom, in which the LANL2DZ [3] basis set was used with including effective core potential functions. The gas phase optimized geometries used to apply the solvent effects, where the valuable PCM [4] model was employed.

Results and discussion

Considering reactant (3+5) and product (6+7), a transition state is obtained which we call TS AA (Fig. 1). For this process, in gas phase, the high barrier (E_a) is 51.02 kcal/mol which are

much higher than the expected values, and therefore this probability is rejected. The following model is proposed. In the rate determining step, an enol product is created at first (species 8 in Eq. (4)) and in continuation is converted into a keto product (4-methoxy-2-butanone) which is much more stable (Eq. (5)).

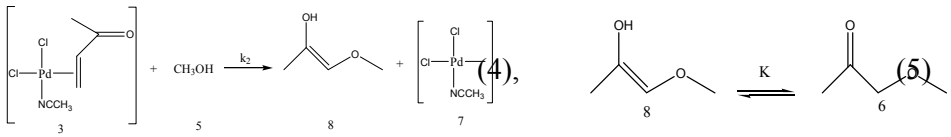

The optimized structure of transition state obtained from reactant (3+5) and product (8+7) has been shown in Fig. 2. By taking Solvent effects into consideration, $E_a = 16.32\ kcal/mol$. This shows that the model presented in this research is a suitable model for the methyl vinyl ketone hydroalkoxylation catalyzed by palladium(II) complex.

Conclusion

Using quantum mechanical method, methyl vinyl ketone hydroalkoxylation were investigated and ultimately a model was presented in which an enol form is produced in the rate determining step and in continuation is converted into keto form

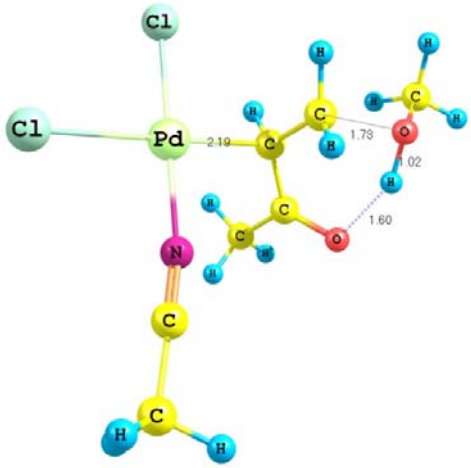

Fig 2. Optimized structure of the TS 2

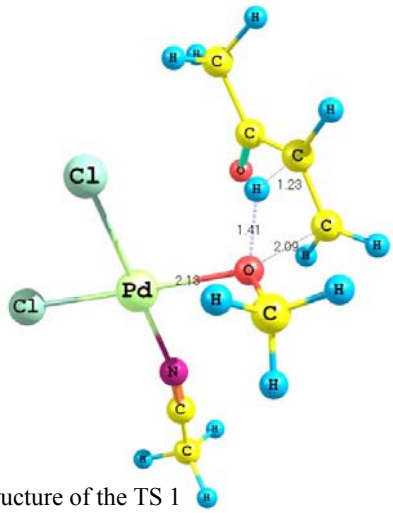

Fig 1. Optimized structure of the TS 1

References:

[1] K.J. Miller, T.T. Kitagawa, M.M. Abu-Omar, Organometallics, 20 (2001) 4403.

[2] A.D. Becke, Phys. Rev. A, 38 (1988) 3098.

[3] P.J. Hay, W.R. Wadt, J. Chem. Phys. 82 (1985) 299.

[4] S. Miertus, E. Scrocco, J. Tomasi, Chem. Phys. 55 (1981) 117.

Ground state potential energy curve of CN from direct-potential-fit analysis of spectroscopic data

E. Masoumi, and A. Shayesteh*

School of Chemistry, College of Science, University of Tehran, Tehran, Iran

E-mail: shayesteh@khayam.ut.ac.ir

Keywords: CN radical, Elcctronic spectroscopy, Direct-potential-fit

Introduction

The CN radical has been the subject of extensive studies because of its importance in chemical kinetics, flame diagnostics, and astrophysics. The CN radical is found in many extraterrestrial sources including the Sun, stellar atmospheres, comets, dark interstellar clouds and diffuse interstellar clouds [1-4]. The laboratory spectra of CN have been known for more than a century and are produced using a wide variety of sources such as arcs, flames, active nitrogen afterglows, shock tubes and electrical discharges of all types. Its spectra extend from the vacuum ultraviolet to the far infrared. Among the CN transitions, the $A\ ^2\Pi \rightarrow X\ ^2\Sigma^+$ and $B\ ^2\Sigma^+ \rightarrow X\ ^2\Sigma^+$ systems are the most prominent and have been studied extensively.

Overview of data

Data used in this analysis include transitions in the microwave, infrared and visible spectral regions [4, 5]. The visible spectra include several bands from the $B\ ^2\Sigma^+ \rightarrow X\ ^2\Sigma^+$ transition: Δv = -2,-1, 0, +1 and +2 sequences in which $v' = 0$ to 19 and $v'' = 0$ to 18. Infrared spectra include vibration-rotation transitions ($\Delta v = 1$ and 2) in which $v'' = 0$ to 7, and the microwave spectra contain pure rotational transitions in the v = 0 to 10 vibrational levels of the ground state.

Results

A few vibrational levels of the $X\ ^2\Sigma^+$ ground state (v = 11, 12 and 14) are perturbed by the nearby vibrational levels of the $A\ ^2\Pi$ and $B\ ^2\Sigma^+$ states. All the data involving the $v'' = 11$, 12 and 14 levels were deweighted, and Dunham-type energy expressions [Eqs. 1 and 2] were used for the $X\ ^2\Sigma^+$ ground state while the $B\ ^2\Sigma^+$ state levels were fitted as individual term values.

$$E^{e}(\mathrm{v},N)=\sum_{m=0}\sum_{l=0}Y_{l,m}\left(\mathrm{v}+\tfrac{1}{2}\right)^{l}\left(N(N+1)\right)^{m}+\frac{1}{2}(N)\sum_{l,m}\gamma_{l,m}\left(\mathrm{v}+\tfrac{1}{2}\right)^{l}\left(N(N+1)\right)^{m-1} \quad (1)$$

$$E^{f}(\mathrm{v},N)=\sum_{m=0}\sum_{l=0}Y_{l,m}\left(\mathrm{v}+\tfrac{1}{2}\right)^{l}\left(N(N+1)\right)^{m}-\frac{1}{2}(N+1)\sum_{l,m}\gamma_{l,m}\left(\mathrm{v}+\tfrac{1}{2}\right)^{l}\left(N(N+1)\right)^{m-1} \quad (2)$$

The leading Dunham constants for the ground state are listed in Table 1.

Table 1. Equilibrium molecular constants (in cm^{-1}) for the ground state of CN

State	ω_e	$\omega_e x_e$	B_e	r_e (Å)
$X\ ^2\Sigma^+$	2068.813(7)	13.278(7)	1.8997832(5)	1.1718074(2)

The RKR potential curve for the ground state was obtained using the $Y_{l,0}$ and $Y_{l,1}$ constants from the Dunham fit. Our preliminary results are shown below.

Table 2. RKR turning points for ground state CN CN

v	E(v) / cm^{-1}	r_{min} (Å)	r_{max} (Å)
0	1031.095	1.1243	1.2250
1	3073.517	1.0927	1.2681
2	5089.643	1.0725	1.3001
3	7079.441	1.0568	1.3277
4	9042.863	1.0439	1.3527
5	10979.868	1.0327	1.3760
6	12890.419	1.0229	1.3983
7	14774.471	1.0141	1.4197
8	16631.966	1.0061	1.4404
9	18462.842	0.9988	1.4607
10	20267.052	0.9921	1.4806
11	22044.570	0.9858	1.5002
12	23795.387	0.9800	1.5196
13	25519.482	0.9745	1.5388
14	27216.781	0.9694	1.5580
15	28887.124	0.9646	1.5771
16	30530.275	0.9600	1.5962
17	32146.055	0.9557	1.6153
18	33734.678	0.9516	1.6345

Figure 1. The RKR potential curve of ground state

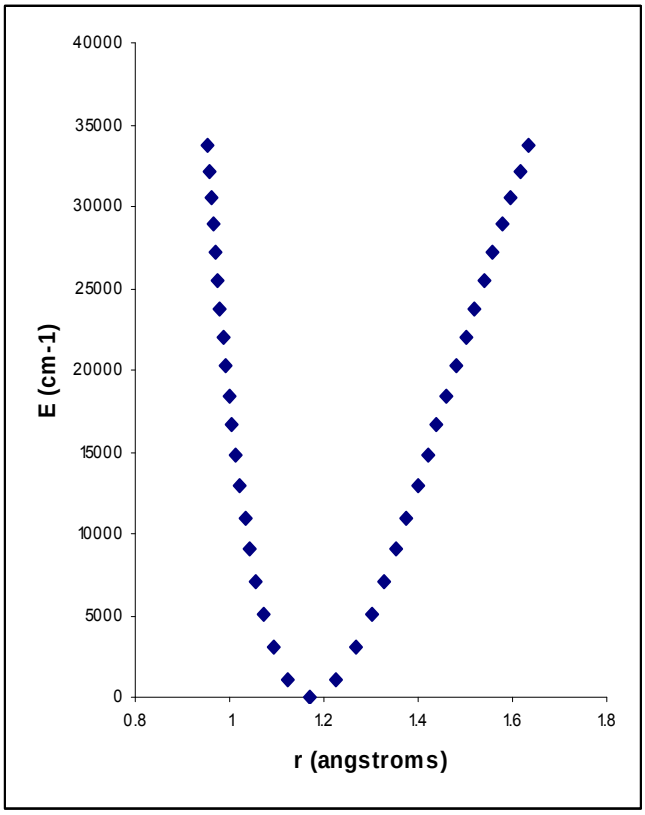

Work in progress

Accurate potential energy curve for the ground state of CN will be obtained by the direct-potential-fitting, and it will be followed by deperturbation analysis of the v = 11, 12 and 14 levels.

References

[1]. D.L. Lambert, J.A. Brown, K.H. Hinkle, H.R. Johnson, Astrophys. J. 284 (1984) 223–237.

[2]. J.R. Johnson, U. Fink, H.P. Larson, Astrophys. J. 270 (1983) 769–777.

[3]. B.E. Turner, R.H. Gammon, Astrophys. J. 198 (1975) 71–89.

[4]. P. Crane, D.J. Hegyi, N. Mandolesi, A.C. Danks, Astrophys. J. 309 (1986) 822–827

[5]. R.S. Ram, P.F. Bernath, Journal of Molecular Spectroscopy 237 (2006) 225–231.

[6]. H. Ito et al., J. Mol. Struct. 324 (1994) 29-43.

[7]. C.V.V. Prasad, P.F. Bernath, J. Mol. Spectrosc. 151 (1992) 459–473.

Vibrational assignment of ethyl benzoylacetate

Sepideh mehrani [a,*], Sayyed Faramarz Tayyari [b], Behzad Chahkandi [c]

[a] *Department of Chemistry, Golestan University, Gorgan, Iran*

sepideh_mehrani@yahoo.com

[b] *Department of Chemistry, Neyshabur Branch, Islamic Azad University, Neyshabur, Iran.*

[c] *Department of Chemistry, Shahroud Branch, Islamic Azad University, Shahroud, Iran.*

Key word: Ethyl benzoylacetate; Intramolecular hydrogen bond; Vibrational spectra; Density Functional Theory

Introduction

β-Dicarbonyl compounds, including β-diketones and β-ketoesters, are engaged in keto-enol tautomerisation and intramolecular hydrogen bonding. The simplest members of these compounds are malonaldehyde (MA) [1] and acetylacetone (AA) [2]. It is well known that the tautomerisation equilibrium and hydrogen bond strength in the β-dicarbonyl compounds are strongly affected by substitution in the terminal groups.

Ethyl benzoylacetate (EBA) is a β–ketoester, which is capable to be engaged in keto-enol tautomerisation. The study of tautomerisation and hydrogen bonding in EBA could be interesting since it seems to be similar to benzoylacetone (BA) except that the methyl group is replaced by an ethoxy groups (an electron donating group).

. The structure, hydrogen bonding, conformation analysis, and tautomerism in (MA) and acetylacetone (AA) have extensively studied by IR, Raman, NMR, X-ray, neutron, and electron diffraction methods [2-5].

The aim of the present paper is to predict the structure and vibrational spectra (harmonic wave numbers, and relative intensities for Raman and IR spectra) of EBA by means of density functional theory (DFT) levels. The calculated vibrational frequencies are compared with those observed experimentally.

Experiment

EBA is purchased from Merck compony and is used without further purification.

The mid-IR spectra of EBA and d2-EBA were recorded as liquid film and in CCl4, CS_2 and CH_3CN solutions by using a Bomem MB-154 Fourier transform spectrophotometer in the region 600–4000 cm^{-1}. The FT-Raman spectra in the region 3200-200 cm^{-1} were recorded employing a 180º back-scattering geometry and a Bomem MB-154 Fourier transform Raman spectrometer operating at the 1064 nm excitation line of a Nd:YAG laser.

Method of analysis

All calculations for EBA was performed with the Gaussian 03 program package. The full geometry optimization of the *cis*-enol form were performed at the B3LYP-DFT level using 6-31G** and 6-311G** basis sets.

Results and discussion

The calculated results indicate that EBA, at least theoretically, exists as several enol form (all engaged in intramolecular hydrogen bond) and two keto form. The vibrational spectra confirm coexisting of one enol form and two keto forms in the sample. However, the results of the NMR spectroscopy are consistent with the coexisting of one enol and one keto forms in the samples with the keto content of at least 50%.

As calculation suggests, the strength of the hydrogen bond in EBA is less than that in AA and BA. These results are confirmed by both NMR and vibrational spectroscopy techniques.

Conclusion

The conformation, hydrogen bonding and tautomerism in EBA have been studied by NMR, vibrational spectroscopy, and theoretical calculations. Both theoretical and experimental results supports coexisting of keto and enol tautomers and indicate that the intramolecular hydrogen bond in the cis enol forms of EBA are considerably weaker than that in AA and BA.

References

[1] F. Hibbert, J. Emsley, Hydrogen bonding and Chemical Reactivity, Advanced in Physical Chemistry, 26, Academic Press, London, 1990, p. 255.

[2] S.F. Tayyari, F. Milani-nejad, Spectrochim. Acta A 56 (2000) 2679.

[3]S.F. Tayyari, J.S. Emampour, M. Vakili, A.R. Nekoei, H. Eshghi, S. Salemi, M. Hassanpour, Journal of Molecular Structure 794 (2006) 204.

[4] E A.H. Lowrey, C. George, P. D'Antonio, J. Karle, J. Am. Chem. Soc. 93 (1971) 6399.

[5] T. Chiavassa, P. Verlaque, L. Pizalla, P. Roubin, Spectrochim. Acta A 50 (1994) 343.

Experimental and DFT determination of the reactivity sites, electronic structure and polarizability of benzothiazol and tetratiafulvalene

M. Oftadeh*[a] , S. Naseh[a], M. Hamadanian Khoozani[b]
[a]Department of Chemistry, Payame Noor University (PNU), Isfahan, I. R. Iran
[b]Department of chemistry, Kashan University, Kashan, I. R. Iran
(Email: m_odtafeh@pnu.ac.ir) (Email: sara_nasseh@yahoo.com)

Keywords: Benzothiazole, Tetratiafulvalene, Dipol Polarizability, Refractometry, DFT.

Introduction

Thiazole ring system are widely used structural elements in medicinal chemistry [1]. Azo compound constitute the largest class of compound amongst all known families of dyes. Benzothiazole-based disperse dyes are considered to be the first example of the successful commercial exploitation of hetrocyclic amines [2]. Thiazole and azobenzothiazole are applied in liquid crystal technology [3], reprography [4], non-linear optics (NLO) [5] and more recently have beeen investigated as potential sensitizers for photodynamic therapy (PDT) [6]. One of the important electronic properties is the electric dipole polarizability, which is a measure of the linear response of the electron density in the presence of an infinitesimal electric field, F, and represents a second-order variation in the energy, viz.:

$$\alpha = -(\frac{\partial^2 E}{\partial F_a \partial F_b}) \qquad \text{a,b = x,y,z} \qquad \langle\alpha\rangle = \frac{1}{3}(\alpha_{xx} + \alpha_{yy} + \alpha_{zz}) \qquad (1)$$

The experimental result is calculated by the Lorentz-Lorentz equation [7,8], viz;

$$\frac{n^2 - 1}{n^2 + 2} = \frac{N\langle\alpha\rangle}{3 \in_0 V} \qquad (2)$$

The goal of this work is the theoretical investigation of electronic structure, reactivity and dipole polarizability by DFT method and comparison with experimental result.

Theoretical Method

Theoretical calculations were performed at the B3LYP/6-31+G(3d,3p) level of theory using Gaussian 98. Calculated characters are including energy, dipole moment, total charge

on sulfur atom, energy gap, hardness and dipole polarizability.these values are showed in table 1 and 2. The highest occupied molecular orbital (HOMO) of benzothiazole and tetratiafulvalene is showed in fig. 1. that shows the active site for nucleophilic reaction [9].

Experimental Method

The average polarizability was determined experimentally by using the Lorentz-Lorentz equation and the refractometric technique, where the refractive index of molecule was measured with a DTM-1 refractometer at 50/60 HZ and 20 ^{o}C.. The experimental value of polarizability for molecule 1 is 1.5670 $\times 10^{-23}$ esu, which is exactly equal with calculational dipole polarizability value.

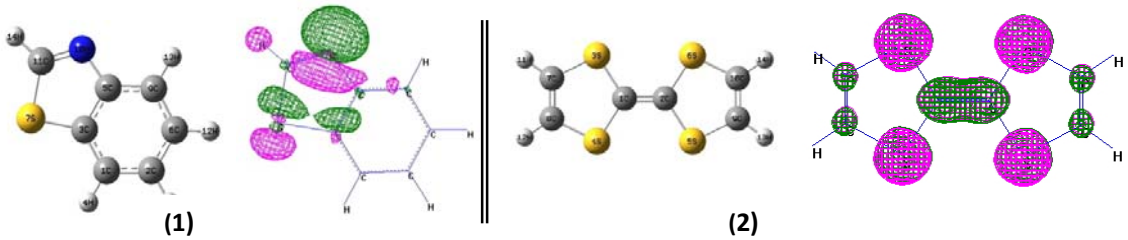

Fig. 1. Highest occupied molecular orbital (HOMO) of 1) benzothiazole and 2) tetratiafulvalene

Table 1. HF energy, E (hartree), dipole moment, μ (debay), charge on sulfur atom, Q (esu), energy gap (hartree) and hardness, η (hartree) at B3LYP/6-31+G(3d,3p) level.

NO.	E	μ	Q_S	E_{HOMO}	E_{LUMO}	$E_{LUMO-HOMO}$	η
1	-722.74405	1.3770	-0.19893	-024658	-0.05029	0.19629	0.09815
2	-1833.79610	0.0056	-0.16861	-0.17144	-0.04540	0.12604	0.06302

Table 2. calculated α_{ii} (i=x,y,z) and average of the dipole polarizability at B3LYP/6-31+G(3d,3p).

NO.	α_{xx} (au)	α_{yy} (au)	α_{zz} (au)	α_{ave} (au)	α_{ave} (10^{-23} esu)
1	148.777	112.375	61.483	107.545	1.5670
2	89.370	220.510	158.799	156.226	2.2764

Conclusions

We have found that dibenzothiophene molecule is an electron donor, based on the localization of the HOMO and that the nucleophilic attack will take place toward thiazole ring. Therefore this molecule can be applied in NLO materials. Also, tetratiafulvalene can be used as an electron donor because of resonance coming from delocalizing π electrons and

therefore its high polarizability. Agreement between theoretical and experimental polarizability showed that the theoretical method and selected basis set has been corrected.

References:

[1] Giran, L., Berenyi, S., Sipos, A. Tetrahedron. 64 (2008) 10388-10394.

[2] Faustino, H., El-Shishtawy, R. M., Reis, L. V., Santos, P. F., Almeida, P. Tetrahedron Lett. 49 (2008) 6907-6909.

[3] Belmar,J., Parra,M., Ziga,C., Pérez,C., Muoz,C. Liq. Cryst. 26 (1999) 389-396.

[4] Sharp. Japanese Patent 1036692, 1998, Chem.Abstr. 128, 193735m.

[5] Razus, A.C., Birzan, L., Surugiu, N.M., Corbu, A.C., Chiraleu, F. Dyes Pigments 74 (2007) 2633.

[6] Salvador, M.A., Reis, L.V., Almeida, P., Santos, P.F. Tetrahedron 64 (2008) 209-303.

[7] Hinchliffe, A., Soscun Machado, H. J. Int. J. Mol. Sci. 1 (2000) 8-16.

[8] Chattaraj, P.K. J. Phys. Chem. A 105 (2001) 511.

[9] Flores-Holguin, N., Glossman-Mitnik, D., J. Mol. Struc. (THEOCHEM).723 (2005) 231-234.

Theoretical studies on tautomerism of Tetrazole 5-thion

Alireza Najafi Chermahini, [a] Abbas Teimouri[b], Alireza Salimi Beni[a]

[a] *Department of Chemistry, Faculty of Science, Yasouj university, Yasouj, 75918-74831, Iran*

e-mail: najafi@mail.yu.ac.ir

[b]*Department of Chemistry, Payame Noor University, Isfahan, Iran*

Keywords: Tetrazole thion; Tautomersim; Solvent effect; Specific solvent Effect; Hydrogen bonding; DFT, MP2

Tetrazole compounds have a wide range of pharmaceutical applications, [1] where they act as stimulants or sedatives on the central nervous system. These compounds have antiinflammatory, antilipemic, antimicrobial, and antiallergic activities [2]. Moreover, such compounds are useful as oxidizers and effective agents for regulating plant growth and as explosives and rocket propellants [3]. In addition, tetrazole compounds have a significant role in medicinal chemical research [4].

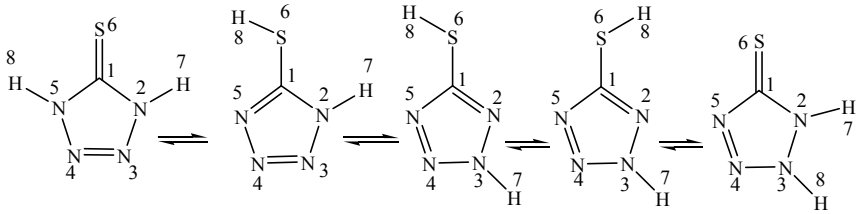

Scheme 1.

To systematically investigate all the possible tautomerisms from tetrazole thion (**A** and **E**) and its tetrazole forms (**B-D**) induced by proton transfer, we describe a study of structural tautomer interconversion in the gas phase, in a continuum solvent, and in a microhydrated environment with 1 explicit water molecule, using MP2, CBS-Q, CBS-QB3 and density functional theory (DFT) calculations by means of the B3LYP exchange functions. It was found that in the gas phase and solvent tetrazole thion is the most stable isomer. The r relative stability, ΔE, of a given tetrazole structure is defined as a difference between its total energy and that of the most stable one **A**. Relative enthalpies and free energies are also defined as the difference between the enthalpy or free energy of a given tautomer/rotamer and that of **A** form. MP2 and DFT calculations show that order of stability was found as **A** > **C**> **D**> **B**> **E**.

Based on MP2 calculations **B**, **C**, **D** and **E** isomers are higher than **A** form by 4.47, 0.21, 0.18, and 27.36 kcal/mol, respectively while DFT method predicts 9.53, 6.86, 7.39, 25.06 kcal/mol anstability for **B**-**E** forms, respectively. Addition of zero point energy (ZPE) does not affect the order of relative stabilities (See Table 1). In addition variation of dipole moments was studied in the gas phase and in the solvent. Water molecule was gradually put in different regions in the vicinity of five isomers. It was found that water can forms different hydrogen bonding with molecule.

Table 1
Relative thermodynamic data for the isomers of tetrazole thion in the gas phase calculated at various methods

	MP2[a]	ΔE[b]	ΔE_{ZPV}	ΔH	ΔG	DFT[a]	ΔE	ΔE_{ZPV}	ΔH	ΔG
A	-655.3268739[c]	0	0	0	0	-656.5536813	0.00	0.00	0.00	0.00
B	-655.3197565	4.47	2.29	1.81	0.93	-656.538496	9.53	2.58	7.24	6.68
C	-655.32654260	0.21	1.9	-2.02	-2.74	-656.5427556	6.86	2.10	4.96	4.57
D	-655.3265852	0.18	1.92	-1.50	-2.17	-656.5418976	7.39	2.13	5.47	5.06
E	-655.2821920	27.36	0.26	27.02	27.19	-656.5137513	25.06	0.70	24.39	24.33
	CBS-QB3					CBS-Q				
A	-655.6477306	0.0	0.0	0.0	0.0	-655.6446331	0.00	0.00	0.00	0.00
B	-655.6412731	4.05	2.53	4.34	3.78	-655.6378574	4.25	2.44	4.59	3.89
C	-655.6448680	1.80	2.11	2.01	1.60	-655.6419141	1.71	2.08	1.99	1.37
D	-655.6441801	2.23	2.13	2.44	2.03	-655.6411792	2.17	2.07	2.43	1.90
E	-655.	25.70	0.81	25.78	25.66	-655.6043696	25.26	0.65	25.34	25.20

[a] 6-311++G(d,p) basis set [b] Total Energies in Hartree, [c] Relative stabilities in kcal mol^{-1}

Conclusions

On the basis of our work, we summarize the following conclusions.

1. In the gas phase the tetrazole thion (**A** isomer) was found the most stable isomer. The order of stability was found as **A** > **C**> **D**> **B**> **E**.

2. The geometry, charges and dipole moments of isomers affected by solvent. With increase of the polarity of solvents the dipole moments were increased. In addition with increase of dielectric constant a regular variation was found.

3. In the interaction of different regions of mentioned molecule with a water molecule the most stable isomers was **A** but interaction can change the relative stability of different isomers of tetrazole thion molecule.

References

[1] Gilchrist TL (1992) Heterocyclic Chemistry, 2nd Ed.; John Wiley & Sons: New York,

[2] Herr RJ (2002) Bioorg. Med. Chem. 10: 3379-3393.

[3] John EO, Kirchmeier RL, Shreeve JM (1989) Inorg. Chem. 28: 4629-4633.

[4] Butler RN (1996) in: Katritzky AR, Rees CW, Scriven EFV (Eds.),Comprehensive Heterocyclic Chemistry II, vol. 4, Pergamon Press, New York.

Density functional efficiency in calculation of vibrational spectra of carbonyl compounds

F. Naghavi [*a], M. Zahedi-Tabrizi [b], S. F. Tayyari [c]

[a] Department of Chemistry, Shahrood University of Shahrood, Shahrood, Iran
(farnaz_naghavi@yahoo.com)

[b] Department of Chemistry, Alzahra University, Tehran, Iran

[c] Department of Chemistry, Ferdowsi University of Mashhad, Mashhad, Iran

Keywords: Density functional theory; Vibrational frequencies scaling factor; Infrared band intensities; Geometrical parameters; Dipole moment.

Introduction

Density Functional Theory (DFT) calculations have been extensively used as a powerful tool for predicting several molecular properties, such as geometry, vibrational frequencies, and their infrared and Raman intensities during the last decade. Understanding the efficiency and accuracy of these methods in predicting the molecular properties could be very useful for theoretical and practical chemists.

Knowledge about the efficiency and accuracy of these methods saves valuable time when selecting the most effective and economic method. Acetone, acetaldehyde, and ethyl-methyl ketone were selected because of the extensive experimental works on their vibrational frequency, and IR intensity.

Computational method

In the present study, the molecular equilibrium geometry, harmonic force field, and vibrational frequencies of carbonyl compounds were computed with the GAUSSIAN-03 software system by using a vast selection of modern density functionals and ab initio (MP2, MP3, and HF) methods. The B, B3 and G96 exchange functionals were combined with the PW91, VWN, PBE, LYP, P86, 971, and 972, non-local correlation functionals, resulting in the six different functionals: B3LYP, BLYP, G96LYP, BP86, B3P86, B3PW91, and B972. We have also implemented the Slater exchange functional and the VWN local correlation functional for the DFT calculation. With these DFT and ab initio levels the following basis

sets were used: (a) the split valance basis sets supplemented by polarization and diffuse functions, including 6-31G, 6-31G*, 6-31G**, 6-31++G**, 6-311G**, 6-311+G**, and 6-311++G**, SDD, CEP-4G, CEP-121G; (b) Double Zeta basis sets with polarization functions (D95**) and also with diffuse functions (D95++**), (c) double and triple zeta Dunning's correlation consistent basis sets including cc-PVDZ and cc-PVTZ. Calculations of regression parameters [R^2, standard deviation (SD), and scaling factor (α)] were performed on Excel program of Microsoft.

Results and Discussion

Regression parameters of the experimental vibrational frequencies on the theoretical data were obtained by the following equation: $\nu_{obs} = \alpha \nu_{Theo}$. Where ν_{Theo} and ν_{obs} are the *i*th calculated harmonic and *i*th experimental fundamental frequencies, in cm^{-1}, respectively (Experimental data for fundamental frequencies were taken from litratures [1-6], The mentioned Eqation is used for the experimental results in the gas phase. According to calculated results, over the entire region, superior results are obtained with B3LYP, resulting in SD=15 cm^{-1} for B3LYP/6-31G*. In the case of B972 and BLYP levels, the best results were obtained by the 6-31G** basis set. Our results also shows that the 6-31G* basis set in G96LYP and BP86 gives excellent agreement with the experimental values. Results obtained at the B3P86 level were very similar to those obtained at the BP86 level. The calculated results also indicate that the calculations at the B3PW91 and SVWN5 levels using the 6-31G and 6-31G* basis sets gives the best R^2 compared with other basis sets. To investigate the utility of separated scaling factors (dual scaling) for the two ranges <2000 cm^{-1} and >2000 cm^{-1}, we reanalyzed the agreement between theoretical harmonic frequencies and the experimental fundamentals for the two ranges separately. The obtained scaling factor, are in the 0.958-0.970 range for calculations at the B3LYP level with different basis sets using whole frequencies. The standard deviations obtained at the HF, MP2, and MP3 levels are quite high compared with the calculated results obtained at all DFT levels.

Conclusion

Vibrational spectra of carbonyl compounds were calculated and compared with the experimental results. Regression coefficient and standard deviation were calculated. The best results were obtained by calculation at the B3LYP level with the different basis sets.

References

[1] Allinger, N. L.; Chen. K.; Rahman, M.; Pathiaseril, A. J. Am. Chem. Soc. 1991, 113, 4505.

[2] Angeli, C.; Borini, S.; Ferrighi, L.; Cimiraglia, R. Theochem. 2005, 718, 55

[3] Smeyers, Y. G.; Senent, M. L.; Botella, V. J. Chem. Phys. 1993, 98, 2754.

[4] J. S. Crighton and S. Bell J. Mol. Spect., 112 (1985) 304.

[5] J.C. Evans, H.J. Bernstein, Can. J. Chem. 34 (1956) 1083.

[6] M.R. Anoop et al., J. Mol. Struct. 969 (2010) 48.

DFT Study stabilities and EPR of the Cupric Formate Dihydrate(II)

N. Noorani [*a], H. Rahemi [b]

Iran ,[a]Department of Chemistry, University of Payam Noor, Urmia
(Email:nnorani1@yahoo.com)
Iran ,[b]Department of Chemistry, University of Urmia

Keywords: Dibarium Cupric Formate Tetrahydrate, DFT, EPR, NMR/GIAO

Introduction

Dibarium Cupric Formate Tetra hydrate $CuBa_2(HCOO)_6 4H_2O$ is a paramagnetic crystal and of course an EPR interest, its structure is determined by the means of X-ray methods[1]. $[Cu(HCOO)_4.2H_2O]^{+2}$cation due to Jahn–Teller effect for a nonlinear molecule in a electronically degenerate state, distortion must occur to lower the symmetry, remove the degeneracy, and lower the energy has a distorted octahedral structure.EPR spectroscopy represents one of the most powerful experimental methods for investigating electronic and structural features of systems containing unpaired electrons, such as radicals, coordination compounds and paramagnetic sites in solids [2,3]. Since, the $[Cu(HCOO)_4.2H_2O]^{+2}$cation has the d^9 configuration, it possesses an unpaired electron, and can interact with an applied magnetic field, making it EPR active. Therefore, our other principal goal will be studying changes of the EPR g tensor parameters in the 108–375K temperature range using the available solid state bond lengths and bond angles of the complex.

Methods

All structures were fully optimized with the Gaussian 03W program at the B3LYP/6-311G, 6-31G**, BWP91/6-31G**levels. After the optimization, g values were calculated using the GIAO method [4,5].

Results and discussion

Geometry optimization of the $[Cu(HCOO)_4.2H_2O]^{+2}$cation is carried out at B3LYP/6-31G** and BPW91/6-31G** levels of calculations, which provide a chance to compare two basic methods B3LYP/6-31G** and BPW91/6-31G** with inclusion of polarization in the basis

sets. Bond angles and bond lengths were calculated in the gas phase; therefore it is expected that there will be a difference between experimental and calculated values. The B3LYP/6-31G** level of calculation provides a better agreement to corresponding experimental values. However, generally we expect by increasing the size of basis sets to approach the experimental values, but the level of calculation has a major effect in calculation. The g-tensor calculation was performed by using of NMR/GIAO option. The X-ray data in the temperature range of 108–375K is available, therefore there is a chance to use solid state experimental geometry data to calculate g values and inspect for possible phase transitions. We have used the temperature (108 K) experimental values in Fig 2, as the higher temperature values are a thermal average of a number of structural isomers (see below).

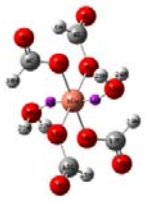

Fig. 1 The B3LYP/6-31G** optimized structure of the $[Cu(HCOO)_4.2H_2O]^{+2}$

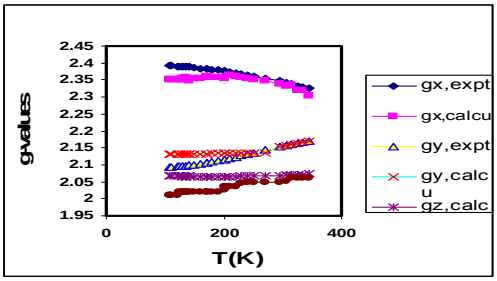

Fig. 2 The temperature dependence of the g- values

Conclusions

The structural optimization of $[Cu(HCOO)_4.2H_2O]^{+2}$cation has been carried out using B3LYP/6-31G** and BPW91/6-31G level of calculations Reasonable correlations between calculated and experimental determined values are obtained when the g tensor components are calculated using these geometries with a B3LYP/6-31G**approach, a good correlation between the experimental and calculated values is only obtained for the lowest g-value. This demonstrates that the temperature dependent structure and g-values of this complex are more complicated and we are pursuing additional structural and EPR measurements on this system

.

Reference

[1] K.Suwdaramma,K.Vedam ,R.V.G.Suwdararao,current Sci.26(1957)315-316.

[2] Atherton NM (1973) Electron spin resonance, theory and applications.Wiley, Chicheste.

[3] Abragam A, Bleaney B (1970) Electron paramagnetic resonance of transition metal ions, Clarendon, Oxford

[4] Tossell JA (1999) Chem Phys Lett 303:435–440

[5] Kintop JA, Machado WVM, Franco M, Toma HE (1999) Chem Phys Lett 309:90–94

Structure and EPR study of the Cu(II) ion in [CuL2][BF4]2 (L_2,6-dipyrazol-1-ylpyridine)

N. Noorani [*a], H. Rahemi [b]

[a]Department of Chemistry, University of Payam Noor, Urmia ,Iran

(Email:nnorani1@yahoo.com)

[b]Department of Chemistry, University of Urmia ,Iran

Keywords: 2,6-dipyrazol-1-ylpyridine, DFT,EPR, NMR/GIAO

Introduction

Six-coordinate copper (II) complexes invariably adopt geometries distorted from a regular octahedron, this normally being ascribed to Jahn–Teller (JT) vibronic coupling. The actual geometry and crystal packing is decided by a delicate balance between the JT coupling parameters, ligand characteristics and lattice interactions[1,2].As part of a general study of Cu(II) complexes with tridentate amine ligands, [Cu(L)2][BF4]2, L = 2,6-dipyrazol-1-ylpyridine:

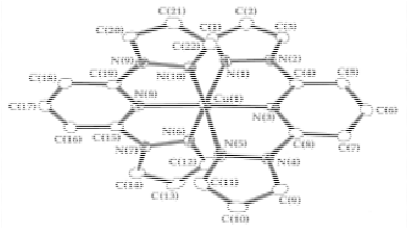

Fig 1 Crystallographic asymmetric Unit at 50 K

The coordination sphere of the Cu ion is rhombic at all the temperatures were determined by neutron diffraction and by X-ray diffraction at 5,40,50,120 and 290 k [3]. The (2,6-dipyrazol-1-ylpyridine)copper(II)complex has the d^9 configuration it possesses an unpaired electron, and can interact with an applied magnetic field, making it EPR active in the 5-290K temperature range using the available solid state bond lengths and bond angles of the complex.

Methods

The computer programs were used to the Gaussian view 3.01, Gaussian 03 and all calculations were carried out at DFT levels. All the structures were fully optimized with the Gaussian 03W program at the B3LYP/6-31G** level. The optimized structural parameters are saved for the next step of calculations. The g-tensor calculation was performed by using of NMR/GIAO [4,5] option.

Results and discussion

The structure, stability, and EPR spectroscopic properties of (2,6-dipyrazol-1-ylpyridine)copper(II)complex were studied theoretically using B3LYP/6-31G**method. The g-tensors are calculated using the NMR/GIAO computational method. The intention of the following investigation is to correlate the temperature dependence of the g-values with corresponding calculated values using the neutron diffraction and X-Ray measured Cartesian coordinates of all atoms, [3], which were available at the temperatures 5,40,50,120,290 k. In a series of calculations covering the temperature range 5-290 K the g tensor components are computed and diagonalized gx, gy, and gz are represented in Fig 2.

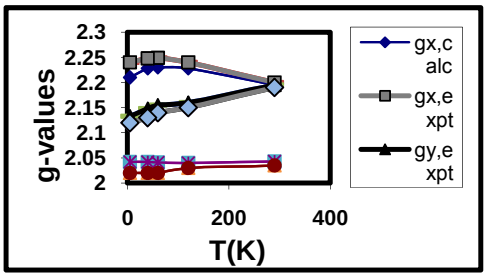

Fig. 2 The temperature dependence of the g- values

Conclusions

The crystallographically determined copper (II) coordination sphere varies with temperature, but when the g tensor components are calculated using these geometries with a B3LYP/6-31G**approach, a good correlation between the experimental and calculated values is obtained for the g-value.

Reference

[1] D. Reinen and M. A. Hitchman, *Z. Phys. Chem.*, 1997, **200**, 11;M. A. Hitchman, *Comments Inorg. Chem.*, 1994, **15**, 197.

[2] M. J. Riley, M. A. Hitchman and A. Wan Mohammed, *J. Chem.Phys.*, 1987, **87**, 3766.

[3] N.K. Solanki, M.A. Leech, E.J.L. McInnes, F.E. Mabbs, J.A.K. Howard, C.A. Kilner, J.M. Rawson and M.A. Halcrow,*J. Chem.Soc.Dalton Trans.* 2002, 1295.

[4] Orendt AM, Facelli JC, Grant DM (1999) Chem Phys Lett 302:499–504

[5] Wolinski K, Hilton KJF, Pulay P (1990) J Am Chem Soc112:8251

Study of third body effect on the potentials energy of F_2-F_2

M. R. Noorbala*[a], B. Noori [b], M. Namazian[a]
Email :Noorbala@yazduni.ac.ir
[a]Department of Chemistry, Yazd University, Yazd, I.R. Iran.
[b]Department of Physical Chemistry, Faculty of Chemistry, University of Kashan, I.R. Iran.

Keywords: Fluorine gas, Third body, Pairwise additivity approximation**,** Potential interaction energy

Introduction:

The properties of dense phases can be determined with intermolecular interaction. For first approximation, this can be explained by pairwise additivity interaction. Up to now, many studies that rely on pairwise additivity approximation is reported but in many cases this approximation is not sufficient for quantitative or qualitative agreement with experimental result. In the studies of solids and dense fluids properties pairwise nonadditivity, especially third body interaction is important. One of these properties is the crystal structure and solid binding energy. The experimental results show that fcc structure of rare gas solids is more stable than hcp structure [1]. Any way previous studies using pairwise additivity potentials do not show this trend but theoretical results in nonadditivity interaction of third body were in agreement with experimental values. In this research, in order to consider validity or nonvalidity pairwise additivity of potentials, third body effect of fluorine gas on interaction potentials energy F_2 system was studied.

Computational methods:

In order to study the third body effect, we have closed the third monomer to F_2-F_2 system at six different orientations (fig. 1) and we calculated the interaction of the third body. Calculation of potential energy was performed with MP2/aug-cc-pVTZ level of theory. For calculation of third body effect, we have used the following relation:

$E_3(N) = E(abc) - E(ab) - E(ac) - E(bc) + E(a) + E(b) + E(c)$

In which $E_3(N)$ is the energy of the third body effect and E(abc) is sum of the energy F_2-F_2 system and F_2 monomer for each values of distance between third monomer of F_2 and F_2-F_2.

E(a), E(b) and E(c) are the energy of each three monomers. E(ab) is the energy of dimer system.

Results and discussion:

Third body effect on potential interaction energy F_2-F_2 system at one orientation is shown in Fig. 2. It is observed that at near distances, the pairwise additivity of potentials is not valid, but in the distances about 7 angstrom of Cartesian coordinate origin, third body effect is closed to zero and we can use validity of pairwise potentials.

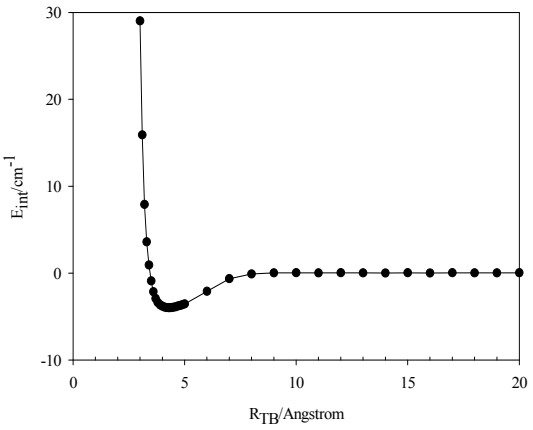

Fig. 2. Energy of third body effect in xy orientation

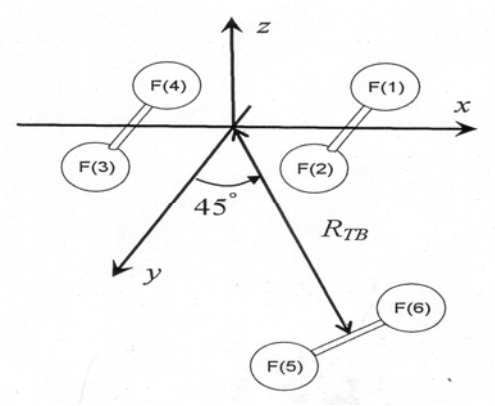

Fig. 1. The applied geometry in x-y plane for third F_2 monomer

References:

[1] K. Szalewicz, V.F. Lotrich, *J. Chem. Phys.* 106 (1997) 9668.

[2] V.F. Lotrich, K. Szalewicz, *J. Chem. Phys.* 112 (2000) 112-121.

[3] J.H. Dymond, E.B. Smith, *The Virial Coefficient of Pure Gases and Mixture*, Clarendon Press, Oxford, 1980.

Calculations of Structural and Electrical Properties of Oligo(3-alkylthiophene)

H. Nikoofard*, M. Khorrami
Faculty of chemistry, Shahrood University of Technology, Shahrood, Iran
monire.khorami@yahoo.com

Keywords: Conducting polymers, Polythiophene, Ionizational potential, HLGs

Introduction

Conductive polymers are new materials that have important role in modern industries. These substances apply in new generations of batteries, sensors, electrodes and different types intelligent materials. [1]. Polythiophene is one of conducting polymers that uses in many devices made by conducting polymers. Polymerization occurs in (α, α′) positions of monomer ring. Attachment of alkyl group in β position of ring improves some properties of polythiophene. We have already considered some characteristics of β-alkyl thiophenes as candidate for conducting materials [2]. In this work, we want to study some properties for (β-alkylthiophenes) using mechanical quantum methods. We considered the HT-HT regioregular oligomers (*n=1-6*) including methyl, ethyl and propyl substituent. We have done our calculations for neutral and radical cation oligomers.

Methods

All calculations were done with Gaussian 03 program. We calculated full optimization on two level of theory (HF, B3LYP) with the 6-31G** basis set. We used these methods to find optimized geometries and electrical and electronic properties of ATHs and their radical cations.

Results and discussion

There are some of essential structural parameters which should be attended in related to proper conducting polymers. Since the planarity and alignment of polymer chains are very important for conductivity of these materials, our results shown that no torsion observed oligo

(3-alkylthiophene) in polymer chain. Fig1. showes the bond lengths in hexa (3-alkylthiophene). The conjugated length is almost unit for all different types of substituent (1.4 Å). Calculation of the charge distribution and spin density of all oligomers that growth of polymer chain developed from α- position of heteroatom ring.

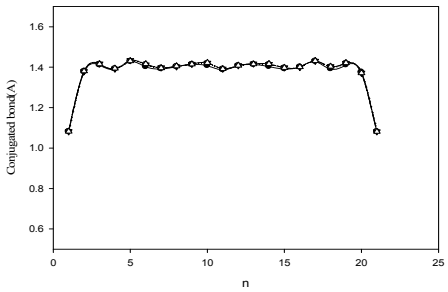

Fig1. The conjugated length of hexa (3-propylthiophene)

The HLGs decrease with growing the length of chain for all alkyl substituents and a falling trend in bond gaps is observed clearly. The IPs are presented in Table1. Also The IPs show that the ionization potential decreases when the length of chain increases.

Table1. IPs (Hartree) values at B3LYP/6-31G**for oligo (3-alkylthiophenes)

n	OligoMTh	OligoETh	OligoPrTh
1	0.3016	0.2988	0.2966
2	0.2514	0.2506	0.2941
3	0.2282	0.2264	0.2264
4	0.2152	0.2151	0.2152
5	0.206	0.207	0.2057
6	0.2	0.1978	0.196

Conclusions

Our calculations demonstrate the radical cation oligomers are completely planar, but the torsion exit in neutral oligomers. Also, the radical cation oligomers are aligned and have an unit length. The polymerization occurs in α position for all types of alkyl groups, so it's sure that possible of crossing bonds are too week with increasing length of oligomer chain, HLGs decrease, generally. Therefore conductivity increase with continuing polymerization process but the slope of changes will be low. The ionization potentials will be decreased too. It's shown that with adding next methylene groups to the chain the less potential will be needed.

References

[1]. T. A. Skothiem, R. Elsenbaumer, J. Reynolds, Handbook of Conducting Polymers, Marcel Dekker, New York, 1998.

[2] H. Nikoofard, Z. Kalantar, M. Khorrami, 13thIranian Physical Chemistry seminar,1389, Shiraz.

Intramolecular hydrogen bonding of 1,1,1-trifluoro-5,5-dimethyl-2,4-hexanedione. A vibrational spectroscopic study (Part II)

M. Vakili [a], A-R. Nekoei [b], A. Kanaani [c], S. F. Tayyari [a]

[a] *Department of Chemistry, Ferdowsi University, Mashhad 91774-1436, Iran*

[b] *Department of Chemistry, Shiraz University of Technology, Shiraz, 71555-313, Iran*

[c] *School of Chemistry, Damghan University of Basic Sciences, Iran*

Keywords:1,1,1-trifluoro-5,5-dimethyl-2,4-hexanedione; β-dicarbonyl; Intramolecular hydrogen bond; Vibrational assignment

Introduction

The *cis*-enol forms of *β*-dicarbonyls are stabilized by strong intramolecular hydrogen bonds (IHB) [1-3]. In the first part of this study [3], it has been theoretically concluded that the hydrogen bond strength of 1,1,1-trifluoro-5,5-dimethyl-2,4-hexanedione, TFMHD, is between those of trifluoroacetylacetone (TFAA) and 5,5-Dimethyl-2,4-hexanedione (DMHD). Since the vibrational spectroscopy is a highly sensitive technique to experimentally examine the hydrogen bonding, we used this data as the empirical witness. The goal in this part is to predict the hydrogen bond strength of TFMHD using spectroscopic methods and comparison with TFAA and DMHD. It will be showed that there is a good compliance between theoretical results and experimental data.

Experimental and Method of Analysis

TFMHD was purchased from Aldrich chemical company. D_2-TFMHD was prepared by mixing the non-deuterated sample with D_2O (3:1). The FT-IR, FT-Raman and Far-IR spectra were obtained on Bomem MB-154 Fourier Transform Spectrophotometer, Bomem MB-154 Fourier Transform Raman spectrometer, and Thermo Nicolet NEXUS 870 FT-IR spectrometer, respectively. All spectra were measured at room temperature. The spectra were considered in the neat liquid and CCl_4 solution.

Results and Discussion

The theoretical calculations have indicated that the IHB strength of TFMHD is stronger and weaker than those of TFAA and DMHD, respectively [3]. This result is excellently supported by the experimental NMR proton chemical shifts of 15.95, 14.24 and 15.0 ppm for DMHD, TFAA and TFMHD, respectively, which are tabled besides some other spectroscopic properties related to IHB strength in Table 1.

The IR spectra of TFMHD, D_2-TFMHD, DMHD and TFAA at regions of 3400-2200 and 1100-800 cm^{-1} are shown in Figs. 1 and 2, respectively. The mentioned trend in the IHB strength is also consistent with the experimental results of OH/OD and O···O stretching and OH/OD in-plane and out-of-plane bending frequencies. The *cis*-enol forms of *β*-dicarbonyls exhibit an extremely broad band of the OH stretching mode in the 3500-2200 cm^{-1} region of the IR spectrum, which upon deuteration of the enolic proton, appears as a new narrower but still broad band in the 2200-1800 cm^{-1} region. These bands in the IR spectra of DMHD, FTMHD and TFAA in CCl_4 are centered at about 2660, 2760 and 2900 cm^{-1}. Upon deuteration, these bands disappears and new bands with considerably narrower band widths appear at about 1976, 2070 and 2120 cm^{-1}, respectively (see Table 1). The position of these frequencies could well support the enhancement of IHB strength, going from TFAA to TFMHD, and from TFMHD to DMHD. The modes for out-of-plane bending deformation of OH and OD bonds are expected to be observed in the region below 1000 cm^{-1}. Considering the theoretical calculations and experimental spectra of TFMHD and D_2-TFMHD, the relatively weak and broad band at 905 cm^{-1} in the IR spectrum of TFMHD is assigned to its OH out-of-plane bending motion. The corresponding γOH bands in the IR spectra of DMHD and TFAA appear at 960 and 893 cm^{-1} (see Table 1), respectively. Another important band in this region is O···O stretching, which is attributed to the band at 365 cm^{-1}. The corresponding bands in DMHD and TFAA have been reported to occur at 397 and 264 cm^{-1}, respectively.

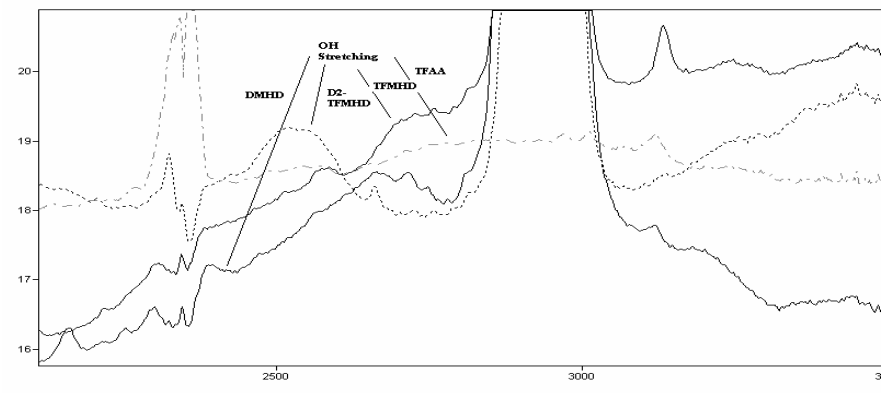

Fig. 1: The IR spectra of DMHD, TFMHD, D_2- FTMHD and TFAA in neat liquid phase at 2200-3400 cm^{-1} region.

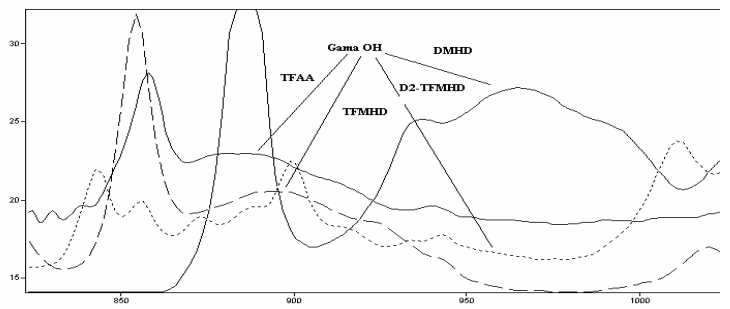

Fig. 2: The IR spectra of of DMHD, TFMHD, D_2- FTMHD and TFAA in neat liquid in the 1750- 850 cm^{-1} region.

Table1: Comparing several properties related to the hydrogen bond strength for TFMHD, DMHD and TFAA.

	DMHD	TFMHD	TFAA
δOH	15.95	15.0	14.24
νOH	2660	2760	2900
νOD	1976	2070	2120
γOH	960	905	893
νO···O	397	365	264
RO···O	2.525	2.535	2.566
θOHO	149.2	147.3	146.8

Conclusion

The comparisons of H^1-NMR chemical shifts and some observed vibrational frequencies, such as νOH, γOH and νO···O, and the calculated geometrical parameters confirm that the intramolecular hydrogen bond in TFMHD is stronger than that in TFAA, while it is weaker than that in DMHD.

References

[1]M. Zahedi-Tabrizi, F. Tayyari, Z. Moosavi-Tekyeh, A. Jalali, S.F.Tayyari, Spectrochim. Acta A 65 (2006) 387.

[2] S.F. Tayyari, A.R. Nekoei, M. Vakili, Y.A. Wang, J. Theor. Comp. Chem. 5 (2006) 647.

[3]A-R. Nekoei, M. Vakili, N. Sanati, A. kanaani, paper submitted to 14th Iran Physical Chemistry Seminar.

Effect of co-surfactant on the photo-physical properties of cresyl violet acetate

A.Ghanadzadeh[a], D.Ajloo[b], M.Peer[b]*

[b]*Department of chemistry, faculty of science, university of Damghan, Iran*

ahoo_gilan@yahoo.com

[a]*Department of chemistry, faculty of science, university of guilan, Rasht, Iran*

Keyword: Cresyl violet acetate, Surfactant effect, Premicellar region, Job method

Introduction

Cresyl violet acetate, CVA, (Fig. 1) is an ionic dye commonly used as organic chemical sensor [1, 2], photo-sensitizer in photodynamic therapy [3], and energy storage media [4] and as a photo-sensitizer in energy and electron transfer reactions [5]. It is a cationic oxazine dye which generally has properties similar to the related xanthane and rhodamine dyes [6]. Deeper understanding of the chemistry and photophysics of CVA would be of great interest.

Methods

The dye were obtained from Aldrich and used as received. The absorption spectra of the dye were recorded using UV-Vis Cary 100 spectrophotometer at room temperature. Sodium dodecylsulfate (SDS) and Sodium tetradecylsulfonate (STS), as anionic surfactants, and Hexadecyltrimethylammonium bromide (HTAB) as a cationic surfactant were obtained from Merck. The critical micelle concentrations (cmcs) of the surfactants are equal to 0.0009, 0.008, 0.0021 M for HTAB, SDS and STS, respectively.

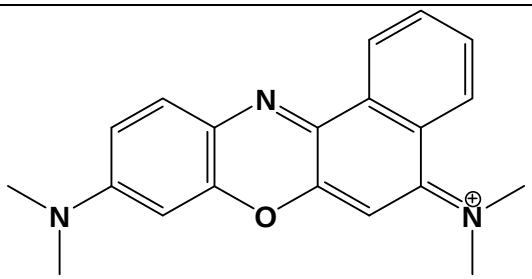

Fig.1.Structure of CVA

Results and discussion

In this work, the environmental and concentration effects on the photo-physical properties of CVA in aqueous, pre-micellar and micellar surfactant solutions (i.e. SDS, STS, and HTAB) were investigated. The Job method was applied for determination of stiochiometric ratio between the anionic surfactants and the dye (Fig.2). The spectral data demonstrate the importance of the hydrophobic force on the dye-surfactant interactions. Effect of addition of Para toluene sulfonate (PTS) and amino ethyl ethanolamine (AEEA) on pre-micellar properties of the surfactants was investigated. Finally, absorption spectrums of the dye in polymeric environments (PVA and Slime) were also explored and a new band, due to higher order aggregates, was detected in the polymeric medium.

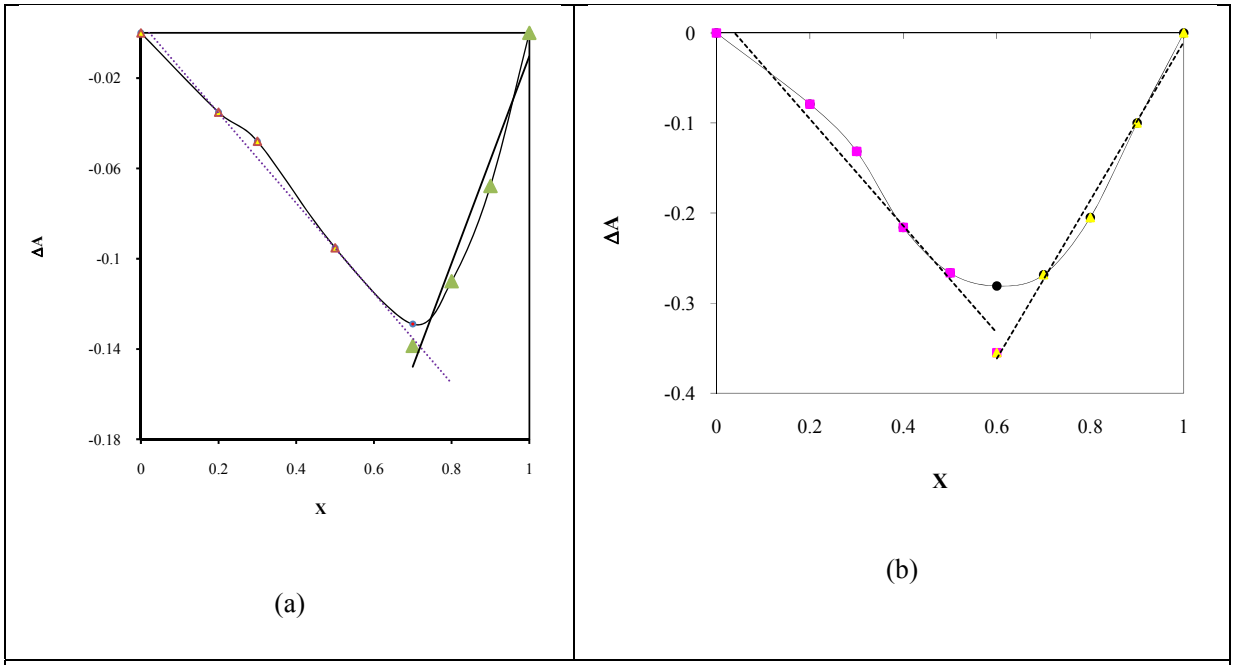

Fig.2. Diagram of job method with a) SDS b) STS

Reference

[1] Stefan J. Isak and Edward M. Eyring, cresyl violet chemistry and photophysics in various solvent and micell, J. Photochem. Photobiol. A: Chem., 64 (1992) 343-358.

[2] J. F. Giuliani, H. Wohltjen and N. L. Jarvis, Opt. Lett., 8 (1983) 54.

[3] L. Cincotta, J. W. Foley and A. H. Cincotta, Phtochem. Photobiol, 46 (1987) 751.

[4] J.S. Batchelder, A. H. Zewail and T. Cole, Appl. Opt., 20 (1981) 3733.

[5] D. I. Kreller and P. V. Kamat, J. Phys. Chem., 95 (1991) 4406.

[6] K. H. Drexhage, in F. P. Schafer (ed.), Dye Laser, Springer-Verlag, New York, 1977, Chapter 4.

Surface Chemistry

Adsorption of Nickel(II) from aqueous solution using palm leaf ash and kinetics,thermodynamics and isotherms studies

Elahe Ahmadi*,Nader Bahramifar and Fereydoun Ashrafi
Department of chemistry , Payame Noor University , Sari , Iran
E-mail: elahe1648@yahoo.com

Key word: Nickel ,Palm leaf ashe ,Adsorption ,Kinetic

Introduction

Environmental pollution due to technological developments is one of the most important problems of this century.Heavy metals such as chromium ,copper ,zink ,silver ,Nickel ,etc ,Present in waste water are hazardous to environmentent.Owing to their toxicity ,their polluting effects on our echo-system provide a possible human health risk. Nickel is a heavy metal that can cause water pollution [1] .Various methods has been used such as ion exchange , Sediment-making chemical, biological uptake, reverse osmosis, membrane and adsorption process using biomass to remove metals from aqueous environments[2]. Adsorption is one of common methods to remove heavy metals[3]. In this study, we considered the effect of solution pH, contact time, Nickel ion concentration, adsorbent dosage and temperature on the adsorption capacity of Palm leaf ash in order to analyze the adsorption kinetics and thermodynamic and determine the equilibrium time.

Materials and methods

Palm leaves washed several times and dried, then powdered using mixer.powder was burned,as result resume ashes were used as the absorbent to absorb heavy metals.In this study150ml metal solution of 100 ppm poured in bookherand and set pH, then we added 0.3g adsorbent to it and sampeled at (0,5,10,15,30,60,90,120,150,180 min).after this order we separated adsorbent from metal solution whit filter 0.2µm,then the concentration of metal ion in solution was measured by flame atomic absorption spectrometr (SensAA GBS) model.

Result and Discussion

The effect of pH on adsorption was investigated in the range (3-8) and optimum pH **w**as obtained also the amount of absorbent was studied at surfaces (1,1.5,2,2.5,3) and optimal

dose was obtained .Effet of various initital concentration was considerd at (50,100,150,200,250,300) mg/l .The result showed that the adsorption capacities of palm leaf ashe increased whit the initital Nickel concenteration. The results of adsorption experiments indicated that in metal Nickel adsorption using this adsorbent the optimum pH , adsorbent dosage and initital concentration of metal ion were 8 , 1g/li and 100mg/li Respectively,also kinetics and isotherms studies showed that Freundlich model was suitable to explain the experimental data(Fig1) and kinetic adsorption followed a pseudo-scond-kinetic(Fig2).

.

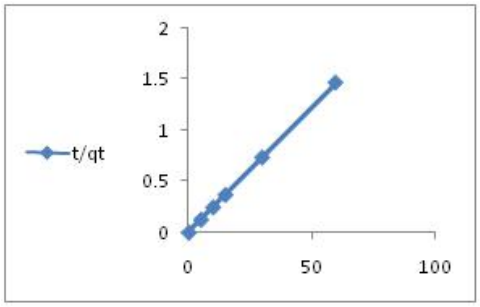

Fig2

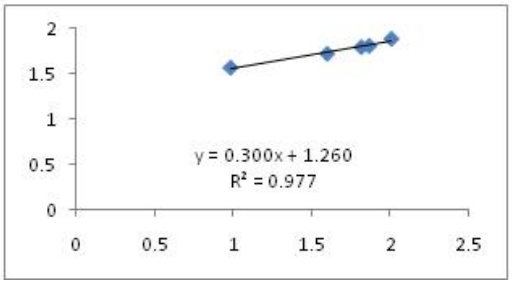

Fig1

Conclution

This study showed that palm leaf ash is a suitable adsorbent for removal heavy metal from waste water.. The obtained results showed that pH, sorbent amount, , initial metal concentration uptake time and solution temperature highly affected the uptake Ni(II) capacity of the the palm leaf ashe sorbent.

Refrence:

[1]Shukla SR, Pai RS. Adsorption of Cu (II), Ni (II)and Zn (II) on modified jute fibers . Bioresource Technology 2005; 96: 1430-1438

[2]Zhou D, Zhang L, Zhou J, Guo S. Cellulose/chitinbeads for adsorption of heavy metals in aqueous solution. Water Research. 2004; 38: 2643-2650.

[3] Wan Ngah WS, Hanafiah MAKM. Removal of heavymetal ions from wastewater by chemically modified plant wastes as adsorbents: A review. 2008; 99 (10): 3935-3943

Effect of the Support Al/P Ratio on Synthesis of the P4VP/$AlPO_4$-11 as a novel basic nanocomposite

Roozbeh Javad Kalbasi,* Hosseyn Faghihian and Elham Izadi
Department of Chemistry, Islamic Azad University, Shahreza Branch, 311-86145, Shahreza, Isfahan, Iran
Corresponding Author E-mail: rkalbasi@iaush.ac.ir

Keywords: Poly(4-vinyl pyridine)/$AlPO_4$-11, Nanocomposite, Knoevenagel condensation

Introduction

Nanoporous inorganic solids have found great utility as catalysts, because of their large internal surface area, and narrow pore size. They offer new opportunities in areas of guest-host synthesis and reaction in the nanoscale for making nanoparticles, and nanocomposites. According to IUPAC, porous materials classified in to three categories: microporous, mesoporous and macroporous. Microporous materials are exemplified by crystalline framework solids such as zeolites, whose crystal structure defines channels and cages. The largest known group of microporous materials is the aluminophosphate molecular sieves family, members of which were developed in 1982 by Wilson and co-workers. The aluminophosphate ($AlPO_4$-n) frameworks are formed from vertex-sharing AlO_4 and PO_4 tetrahedral [1]. The controllable pore size distributions are the main reasons for using inorganic solids $AlPO_4$ as support or hosts for organic molecules. The Al/P ratio is usually one, making the framework electrostatically neutral with no active sites present. Active sites for catalyst application can be seen, if organic species incorporated as a guest into the pores of $AlPO_4$ host. Organic–inorganic hybrid solids [2] with nanopores and channels have attracted much research interest because of their potential applications in molecular adsorption and catalysis. In this work, we wish to report the synthesis of poly(4-vinyl pyridine)/$AlPO_4$-11 nanocomposite by in situ polymerization of 4-vinyl pyridine (4VP) in the presence of $AlPO_4$-11 and investigation of Al/P ratio for selection the best surface of support. The basic catalytic activity of this novel organic-inorganic hybrid was tested for Knoevenagel [3] condensation reaction.

Experimental

(1) Synthesis of $AlPO_4$-11 from aqueous hydrothermal system and investigation of support Al/P ratio. (2) Synthesis of P4VP/$AlPO_4$-11 nanocomposite. (3) Knoevenagel condensation under solvent-free condition at room temperature.

Results and discussion

The catalyst was characterized by XRD, XRF, SEM, FT-IR, BET and TPD techniques. The $AlPO_4$-11 and P4VP/$AlPO_4$-11 samples showed the same XRD patterns, indicating that the crystalline structure of the $AlPO_4$-11 framework was retained after the hybridization. The presence of 4VP in the pores of $AlPO_4$-11 is demonstrated by FT- IR and BET specific surface areas. The morphology of the nanocomposite obtained from SEM photographs. The BJH pore size distribution was determined the size of nanoporous $AlPO_4$-11 and TPD of NH_3 was used to measure the number of acid sites in nanoporous inorganic solid ($AlPO_4$-11). In different basic catalyst tested (with different Al/P ratio), excellent yields (100%) and short reaction time (2 -5 min) at room temperature without solvent was achieved. It was observed that the activity of the catalyst was influenced directly by support Al/P ratio.

Conclusion

In summary, it was demonstrated that the P4VP/$AlPO_4$-11 nanocomposite could behave as recyclable catalyst for the solvent-free Knoevenagel condensation of aromatic aldehydes with malononitrile at room temperature offering the good yield. The large surface area of $AlPO_4$-11 causes this novel compound to act as an efficient basic catalyst. Green media for this reusability and simple work-up are the main advantages of this polymer material supported on a nanoporous inorganic surface.

References

[1] Q. Wang, G. Chen, S. Xu, Micropor. Mesopor. Mater, 119 (2009) 315–321

[2] S. Jaenicke, G.K. Chuah, X.H. Lin, X.C. Hu, Micropor. Mesopor. Mater, 35–36 (2000) 143–153

[3] K.M. Parida, S. Mallick, P.C. Sahoo, S.K. Rana, Appl. Catal. A: Gen, 381 (2010) 226–232

Prediction of Surface Tension and surface properties in the Binary Liquid Mixtures

A. A. Rafati[a], A. Bagheri[*a], A. R. Khanchi[b], E. Ghasemian[a] and L. Safdari Yekta[c]

[a]*Department of Physical Chemistry, Faculty of Chemistry, Bu-Ali Sina University, Hamedan, Iran*

[b]*Chemistry Research Department, School of Nuclear Science Research, Nuclear Science and Technology Research Institute, Tehran, Iran*

[c]*Department of Chemistry, Malayer University, Malayer, Iran*

Email: a_bagheri79@yahoo.com

Introduction

In this paper, we report experimental values of surface tension for binary mixtures of alkanol (methanol, ethanol, 2-propanol and 2-butanol) with acetonitrile obtained using the ring method and compared with predicted surface tension from the Suarez method [1, 2]. The activity coefficients were evaluated using the UNIFAC group contribution model [3]. Then, this model is used to derive surface mole (volume) fraction, surface activity coefficient.

Methods and Theory

The assumptions that bulk and surface phases are in equilibrium and the partial molar area of component *i* is the same as the molar area of *i* lead to the Sprow and Prausnitz equation for prediction of surface tension [1, 2]:

$$\sigma = \sigma_i + \frac{RT}{A_i} \ln \frac{x_i^s \gamma_i^s}{x_i^b \gamma_i^b} \qquad (1)$$

In Eq. (1), x_i is the mole fraction of component *i*, γ the activity coefficient of component *i*, σ the surface tension of the mixture and A_i is the molar surface area of component *i*. In this paper, two methods were used to calculate the molar surface area (Rasmussen and Paqueete model) [3]. Rasmussen molar surface areas have been estimated from experimental surface tension data:

$$A_i = 2.5 \times 10^9 \sum_k \upsilon_{k,i} Q_k \quad (2)$$

where Q_k is the UNIFAC area parameter of group k, and $\upsilon_{k,i}$ is the number of groups of type k in molecule i. The results also indicate that the best prediction is obtained for acetonitrile/ethanol system at two methods for calculation of surface area (see figure 1).

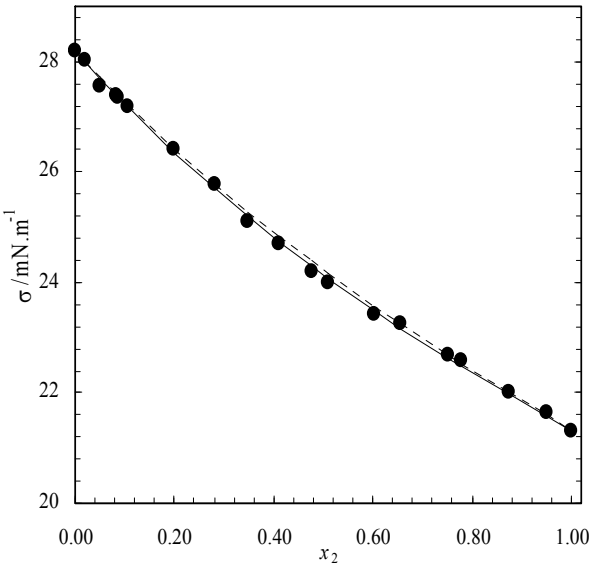

Fig. 1. Surface tension values, σ, versus x_2 for the binary system of acetonitrile(1)/ethanol(2): (•) experimental data, prediction using (—)Rasmussen, and (----)Paqueete molar surface area.

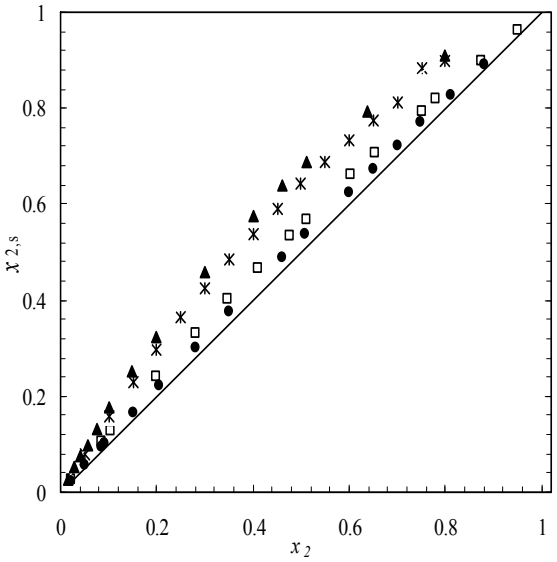

Fig. 2. Calculated concentration of alcohol at interface ($x_{2,s}$) as a function of (x_2) for the binary systems of alcohol(2)/acetonitrile(1): (•) methanol, (▯) ethanol, (▯) 2-propanol, and

We calculated surface mole fractions of components using Eq.(1) to investigate the relationship between surface layer concentrations and surface tensions(see figure 1).

Conclusion

The UNIFAC model is used for the calculation of activity coefficients in the bulk liquid mixture and in surface layer. Then, two techniques is used for calculation of molar surface areas**.** The surface tension predictions are found to be extremely sensitive to the values of the molar surface areas used in the computation. Calculated surface mole fraction values with this method show that the surface is enriched with alcohol molecules relative to bulk composition.

References

[1] J. T. Suarez, C. Torres-Marchal, P. Rasmussen, Chem. Eng. Sci. 44 (1989) 782–786.

[2] A. A. Rafati, E. Ghasemian, J. Colloid. Interface. Sci. 328 (2008) 385–390.

[3] S. J. Nath, J. Colloid. Interface. Sci. 209 (1999) 116–122.

Temperature dependent behavior of CTAB and Triton X-100 surfactants in relation to the Oil recovery enhancement efficiency

M.H. Ghatee*[a], M. Bahrami[a], N. Khanjari[a], Sh. Ayatollahi[b], O. Seiedi[b]

[a]Department of Chemistry, College of Science, Shiraz University, Shiraz, Iran, 71454

Email:ghatee@susc.ac.ir

[b]EOR Research Center, School of Chemical and Petroleum Engineering, Shiraz University

Keywords: Change in Solution Structure, Surfactant, Temperature Effect, Viscosity, UV and Flourescence Spectroscopy.

Introduction

The role of surfactant treatment has been widely investigated as an efficient method in Enhanced Oil Recovery. A surfactant either acts to reduce the interfacial tension (IFT) or to alter the wettability of reservoir rock. Therefore, the oil recovery enhancement is due to alternating the wettability of rock surface from oil-wet to more water-wet condition. The effect of cationic, anionic, and non-ionic surfactants on enhancing oil recovery has been studied.[1, 2]

Experiment has shown that the non-ionic surfactant/brine solution (Triton X-100) is more effective than the solution of cationic surfactant CTAB, Particularly as the temperature increases, the oil recovery by using Triton X-100 is appreciably increases.[3] Here, the interest is to understand the basic reason which makes Triton X-100 advantageous over CTAB in wattability alteration as the temperature is increased.[3] Certainly, the source of these differences is the physical properties specific to their chemical nature. Indeed we pursue the difference in the physical properties of the brine solution of these two surfactants and their behavior as temperature is raised. The physical property we study is the viscosity as a function of surfactant concentration at different temperature. Also, the temperature dependence of the structural behavior surfactants is probed using absorption and fluorescence spectroscopy.

Experimental

CTAB and Triton X-100 solutions were prepared in brine solution of usual concentration. The range of concentrations spans the critical micelle concentration (CMC), e.g. 0.03% for CTAB

and 0.015% for Triton X-100. The viscosity of each the solution was measured in the temperature range 25 to 80°C.

The structural behavior of Triton X-100 was probed as a function of temperature using pyrene. Further investigations are advancing to study the structural behavior as a function of change using fluorescence spectroscopy.

Results and Discussion

In Figure 1 and 2, the results of viscosities measurements are shown for CTAB and Triton X-100, respectively. As it can be seen, viscosity increases with concentration smoothly at all temperature. This is the case for CTAB too. Some fluctuations are seen close to CMC's. The fluctuations for TritonX-100 look to be different from those of CTAB, indicating the difference in the nature of these two surfactants. More importantly the fluctuation enhanced close to 60°C. These particular fluctuations are, however, absence in the case of CTAB. This can be interpreted in terms of salting out which occurs in the case of Triton X-100. Further investigations were performed by probing the particular structural changes as a function of temperature. Pyrene with the characteristics absorption spectra in the UV region was was found to be suitable (See Figure 3). It can be seen that as the temperature increases the base line of the spectra increases. From absorption spectra shown in Figure 3, a transition in the solution structure can be identified near 60 ^{o}C. Further investigations are in progress by fluorescence spectroscopy.

Conclusions

This study indicates that the preference of Triton X-100 over CTAB is due to the difference in their inherent structure. As the temperature increases there is a drastic change in the structure of Triton X-100. The high efficiency of it can be attributed to this.

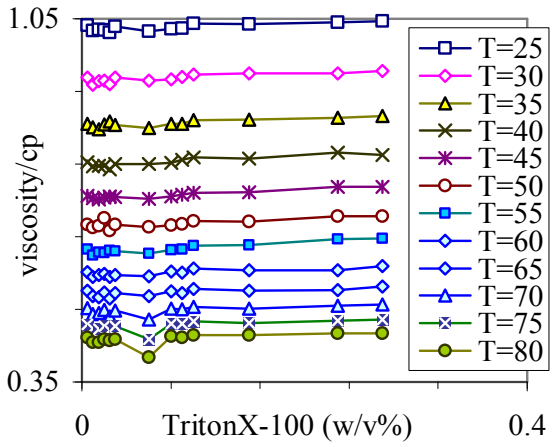

Figure 1. Viscosity versus concentration of Triton between 25-80 °C.

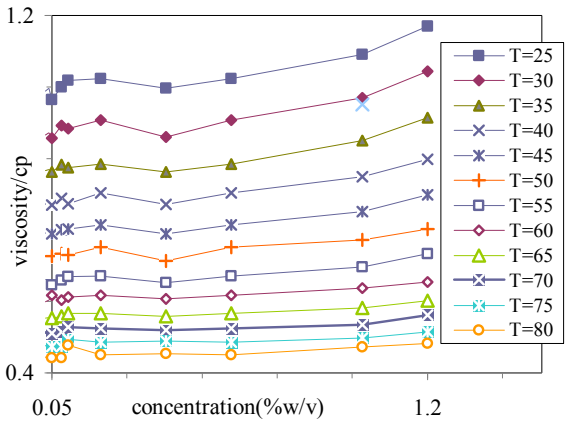

Figure 2. Viscosity versus concentration of CTAB between 25-80 °C.

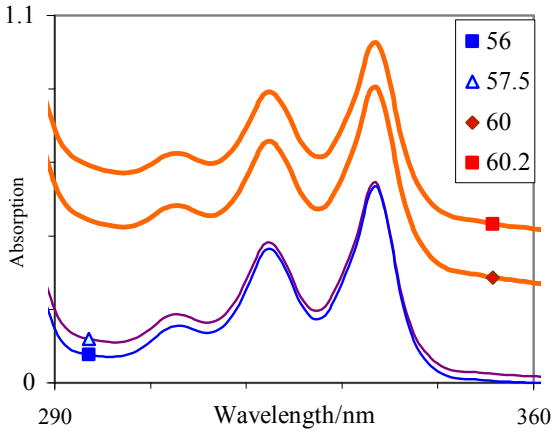

Figure 3. Absorption spectra of Triton solutions at different temperatures.

References:

[1]T. Austad, B. Matre, J. Milter, A. Sævareid, L. Øyno, Colloids and Surfaces A, 137 (1998) 117-129.

[2]D. Ch. Standnes, D.C., M.Sc. Thesis, University of Stavenger, Norway.

[3] O. Seiedi, M.Sc. Thesis, Shiraz University, July 2009.

Distribution coefficient of acetone between toluene / water in the presence of binary surfactants under different interfacial tension

Javad Saien , Somayeh Rezabeigy*,Mahboobe Behroozi
Department of Applied Chemistry, University of Bu- Ali Sina, Hamedan, 65174, Iran
(E-mail: somayye.rezabeigy@gmail.com)

Abstract:
Effect of binary mixtures of cationic and non–ionic surfactants, DTMAC, and Triton X–100, on distribution coefficient, K_d of acetone between toluene and water with variable mole fraction of mixed surfactants was investigated with interfacial tension was maintained constant. Gas chromatography (GC), with a high accuracy and repeatability in analysis, was used. Three constant interfacial tensions of 26.0, 28.0 and 30.0 $mN.m^{-1}$ were considered, and their appropriate distribution coefficient were examined. The equilibrium distribution of acetone between phases, shows linear variation. After surfactants addition, the system shows rise or fall of solute distribution between two phases. Results shows that, 1) Different Triton mole fractions provide different trends in the equilibrium curves and the value of distribution coefficient decrease with increasing the interfacial tension or with decreasing total concentration of surfactants. 2) At Triton bulk mole fraction of 0.1 the K_d finds the lowest value and there exists maximum K_d values at α=0.4 and α=0.1. It may be concluded that acetone can be well extracted by toluene in water in some points that $K_d$are great.

Keywords: distribution coefficient, surfactant mixture, DTMAC, Triton X-100

Introduction:

The selection of the solvent extraction as a separation technique depends greatly upon how the solute distributes between the extract and the rafinate phases[1]. Various means for altering this distribution in a desirable way exist but one of the most commonly used now-adays is what is termed the mixed surfactants. In this work, liquid–liquid equilibrium data have been obtained for water–acetone–toluene system in the presence of Triton X-100 and

DTMAC in aqueous phase at 298 K, natural pH and at atmospheric pressure at the 10 different bulk mole fraction of Triton X-100(α).

Experimental procedure:

A weighed amount of aqueous solution containing a known quantity of solute was mixed with a known quantity of solvent in a stoppered funnel[1]. The specified quantities of surfactants [2] were added to make corresponding mixtures of different bulk mole fraction of Triton X-100 from 0 to 1. These mixtures were maintained at constant temperature of 298 ± 0.1 K and agitated for an extended period of time and stirred on a plate magnetic stirrer (2h) until acetone distributes between tow phases. The thermodynamic equilibrium was achieved by letting the mixture rest for 4h. After quantitative gravity separation, concentration of acetone in the organic samples was measured using GC. Then remaining amount of acetone in the aqueous phase calculated from simple material balance since the initial amount is known [3]. This method more suitable for systems where the solvent pair is partially miscible as in a previous study carried out experimentally by the same authors the system water-ethyl acetate-ethanol [4]**.**

Results and Discussion:

Different Triton mole fractions provide different trends in the equilibrium distribution curves and the range of K_d is within (0.621 - 0.711) with coefficient of determination (R^2) values within (0.964 - 0.999) for $\gamma = 28$ mN.m^{-1} and (0.662 - 0.748) and (0.661-0.761) with R^2 values within (0.994 - 0.999) and (0.993-0.999) for $\gamma = 26$ and $\gamma = 24$ mN.m^{-1} respectively. The equilibrium distribution of acetone between phases for $\gamma = 26$ mN.m^{-1} is shown in Figure 1. Similar variation is appropriate for other interfacial tension. That plotted as C_{org} vs. C_{aq}. In this work, water and the organic solvent are totally immiscible. However the solute (acetone) present large affinity differences towards water.

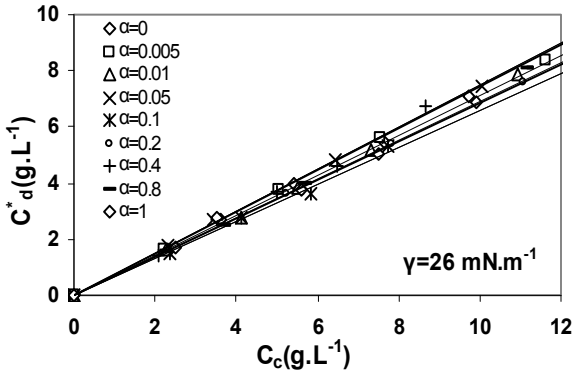

Fig. 1. Equilibrium distribution of acetone between phases in the presence of surfactants

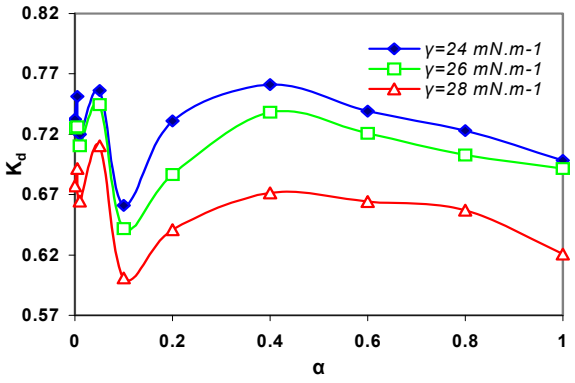

Fig. 2. K_d variation versus α for three interfacial tension.

The experimental results for various mole fraction of Triton X-100 are shown in Fig. 2 for $\gamma = 28$,24 and 26 mN.m^{-1}. Fig 2 shows variation of distribution coefficient K_d with α for three constant interfacial tension. From Fig. 2 it is also seen that K_d values are maximum in α=0.05 and minimum in α =0.1.

References:

[1] A. Hasseine, A.-H. Meniai, M. Korichi.. *Desalination*. 242 (2009) 264-276

[2] J. Saien, S. Asadabadi. *J. Chem. Eng. Data*. 55 (2010) 3817-3824.

[3] J. Saien, M. Riazikhah, S. N. Ashrafizadeh.. *Ind. Eng. Chem. Res*. 45 (2006) 1434-1440**.**

[4] G. Jia, G. Torri, M. Petruzzi. *Applied Radiation and Isotopes*. 61 (2004) 279–282.

Study on a Zinc-Manganese catalyst prepared from $[Zn(H_2O)_6]_2[Mn(NCS)_6]/SiO_2$ precursor for water gas shift reaction

A. R. Nowroozi*, M. Behzad Khoshgouei, A. R. Salehi Rad
Chemistry Department, University of Sistan & Baluchestan, Zahedan, Iran, P.O.Box 98135-674
(E-mail:*anowroozi@chem.usb.ac.ir*)

Keywords: water gas shift reaction, precursor, catalyst, complex

Introduction

Water gas shift (WGS) reaction is used to generate hydrogen and CO_2 from the reaction between carbon monoxide and water [1,2]. It is applied to increase the hydrogen production and remove CO before ammonia synthesis, refinery hydroprocesses and redistribution of hydrogen, or to adjust the H_2/CO ratio in the methanol production and the Fischer-Tropsch synthesis [3,4].

Experimental

In this study, Zn-Mn catalyst was prepared from precursor of $[Zn(H_2O)_6]_2[Mn(NCS)_6]$ supported on the silica and tested for water gas shift reaction.$[Zn(H_2O)_6]_2[Mn(NCS)_6]$ /SiO_2 was calcined at 773 K for 5 h. $[Zn(H_2O)_6]_2[Mn(NCS)_6]$ complex has been characterized by elemental analysis, XRD, FT- IR, UV-Vis spectroscopy. Characterization of both precursor and calcined catalyst were carried out using FT-TR, XRD, SEM, BET specific surface area and thermal analysis methods (TGA and DSC). The activity and selectivity of prepared catalyst has been studied under atmospheric pressure in a range of reactor temperatures using synthesis gas with H_2O/CO molar ratio of 2.

Results and discussion

The FT-IR spectrum of the $[Zn(H_2O)_6]_2[Mn(NCS)_6]$ complex shows two sets of vibrations due to the aqua and isothiocyanate ligands. In the FT-IR spectrum, the C=S stretching mode of free SCN^- is shifted to higher frequency in the corresponding complex which is consistent with nitrogen bonding to the manganese. The phase analysis of precursor and calcined

catalyst were done by XRD technique. The XRD patterns of both precursor and calcined catalyst showed crystalline phases. Characterization of both precursor and calcined catalyst was also carried out using scanning electron microscopy (SEM). All the electron micrographs were obtained from powder specimens of these materials. SEM observations have shown differences in morphology of both precursor and calcined catalyst.

The BET specific surface area measurements for both precursor and calcined catalyst were carried out and calcined catalyst showed a higher surface area than its precursor. This is in agreement with SEM results, which showed that the agglomerate size of the calcined catalyst is less than its precursor and therefore, leads to an increase in the BET specific surface area of the calcined sample.

The calcined catalyst was also characterized by FT-IR and due to thermal decomposition of isothiocyanate ligands, no vibration bands for C=S and C≡N stretching are seen. The catalyst showed high catalytic activity for WGS. In order to consider the stability of prepared catalyst using a novel method, it was tested for 60 h at 400 °C using H_2O/CO with molar ratio of 2. The obtained results indicate that this catalyst was highly stable and had retained its activity and selectivity for 60 h.

Conclusions

We have prepared alumina-supported Zinc-Manganese catalyst from $[Zn(H_2O)_6]_2[Mn(NCS)_6]$ /SiO_2 precursor. This preparation procedure is a novel suitable method to produce higher active catalysts for the different catalytic processes. During the calcination operation, the morphological features of calcined catalyst are quite different with the $[Zn(H_2O)_6]_2[Mn(NCS)_6]/SiO_2$. The Zinc-Manganese catalyst was studied for the water gas shift reaction. The catalyst exhibited appreciable water gas shift activity. This catalyst was also highly stable and had retained its activity and selectivity for 60 h. The reaction conditions were found to be 400 °C with molar feed ratio of H_2O/CO= 2:1 (GHSV= 5400 h^{-1}).

References

[1] S. H. Kim, J. H. Chung, Y. T. Kim, J. Han, S. P. Yoon, S. W. Nam, T. Lim, Int. J. Hydrogen Energy 35 (2010) 3136-3140.

[2] M. Laniecki, M. Ignacik, Catal. Today 116 (2006) 400-407.

[3] Y. Li, Q. Fu, M.F. Stephanopoulos, Appl. Catal. B: Environ. 27 (2000) 179-191.

[4] F. Huber, J. Walmsley, H. Venvik, A. Holmen, Appl. Catal. A: Gen. 349 (2008) 46-54.

Water gas shift reaction over Na-Mn/SiO_2 catalyst

M. Behzad Khoshgouei, A. R. Salehi Rad, A. R. Nowroozi*
Chemistry Department, University of Sistan & Baluchestan, Zahedan, Iran, P. O. Box 98135-674
(*E-mail:anowroozi@chem.usb.ac.ir*)

Keywords: precursor, $Na_4[Mn(NCS)_6]$ complex, water gas shift reaction, catalyst

Introduction

The water gas shift (WGS) reaction ,$CO+H_2O \leftrightarrow CO_2+H_2$, where converts carbon monoxide and water into hydrogen and carbon dioxide is one of the oldest and most important heterogeneous reactions [1,2]. It has been applied as an important industrial process for pure hydrogen production, e.g. for ammonia synthesis, and adjusting the CO/H_2 ratio in the production of methanol and the Fischer-Tropsch synthesis [3].

Methods

Na-Mn/SiO_2 catalyst was prepared by a novel method and studied for the water gas shift reaction.The catalyst was prepared from $Na_4[Mn(NCS)_6]/SiO_2$ precursor. $Na_4[Mn(NCS)_6]$ was supported on the silica and calcined at 500 °C. $Na_4[Mn(NCS)_6]$ complex was characterized by elemental analysis, FT-IR, UV-vis and XRD spectroscopy and cyclic voltammetry. The electrochemistry of this complex was investigated in DMF by cyclic voltammetry and differential pulse polarography. Characterization of both precursor and calcined catalyst were carried out using FT-IR, X-ray diffraction, thermal analysis method such as TGA and DSC, scanning electron microscopy (SEM) and BET specific surface area. The activity of prepared catalyst was studied in a fixed bed micro reactor in a range of reactor temperatures using H_2O/CO molar ratio of 2 at atmospheric pressure.

Results and discussion

The elemental analysis of the $Na_4[Mn(NCS)_6]$ complex is entirely consistent with its formulation as is the following spectroscopic characterization.In the FT-IR spectrum, the C=S stretching mode of free SCN^- at 749 cm^{-1} is shifted to 815 cm^{-1} in the corresponding

$Na_4[Mn(NCS)_6]$ complex which is in consistent with nitrogen bonding to the manganese. The C≡N stretching mode of free SCN^- was shifted to lower frequency in the corresponding complex.

The phase analysis of precursor and calcined catalyst were done by XRD technique. The XRD patterns of both precursor and calcined catalyst showed crystalline phases. The morphological features of calcined catalyst are quite different with the precursor and show that the agglomerate size is greatly reduced in compared to the precursor sample described above. Characterization of $Na_4[Mn(NCS)_6]/SiO_2$ precursor using TGA, generally have shown a three-stage decomposition. The first weight loss peak low-temperatures is associated to the removal of the physically adsorbed water from the precursor; the second weight loss is due to the decomposition of Mn−N and C=S bonds and the third weight loss peak at high-temperatures may be attributed to the decomposition of C≡N bond. The DSC pattern of the catalyst precursor, exhibited a peak at low-temperatures attributed to the removal of the physical adsorbed water and two endothermic peaks at mid-temperatures that are due to the various endothermic transition. The peaks at mid-temperatures may be attributed to the decomposition of Mn−N, C=S and C≡N bonds which were accompanied by different weight losses with changes only in rate of weight loss. The calcined catalyst was also characterized by FT-IR and due to thermal decomposition of isothiocyanate ligands, no vibration bands for C=S and C≡N stretching are seen. In order to study the stability of prepared catalyst, it was tested for 40 h at 300 °C using synthesis gas with molar ratio of $H_2O/CO = 2$.

Conclusions

We have reported a novel method to preparation of $Na\text{-}Mn/SiO_2$ catalyst for the water gas shift reaction. This catalyst showed high activity for the water gas shift reaction. Combining the results of the FT-IR spectra, TGA/DSC curves, classical identification method, and XRD patterns for $Na_4[Mn(NCS)_6]$ complex, precursor, and calcined catalyst showed that the complex decomposed to form an oxide of Mn as the solid product and a mixture of sulfur dioxide, carbon dioxide and nitrogen oxids as gaseous products.

References

[1] S. H. Kim, J. H. Chung, Y. T. Kim, J. Han, S. P. Yoon, S. W. Nam, T. Lim, Int. J. Hydrogen Energy 35 (2010) 3136-3140.

[2] M. Laniecki, M. Ignacik, Catal. Today 116 (2006) 400-407.

[3] Y. Li, Q. Fu, M.F. Stephanopoulos, Appl. Catal. B: Environ. 27 (2000) 179-191.

Study of silica-supported Copper-Nickel catalyst prepared from a novel precursor for CO hydrogenation and water gas shift reactions

A. R. Rezvani*, M. Behzad Khoshgouei, A. R. Salehi Rad
Chemistry Department, University of Sistan & Baluchestan, Zahedan, Iran, P. O. Box 98135-674
(E-mail:rezvani2001ir@yahoo.ca)

Keywords: Fischer-Tropsch synthesis, precursor, catalyst, complex

Introduction

Fischer-Tropsch synthesis (FTS), consisting of the CO hydrogenation to hydrocarbons, over transition metal catalysts has been studied extensively [1-3]. The Fischer-Tropsch synthesis can be simplified as a combination of the carbon monoxide hydrogenation (FT reaction) and the water gas shift (WGS) reaction [4]. Water gas shift (WGS) is used to generate hydrogen and CO_2 from the reaction between carbon monoxide and water [5].

Methods

Silica-supported copper-nickel bimetallic catalyst was prepared from $[Cu(H_2O)_6]_2[Ni(NCS)_6]$ precursor. The cationic-anionic complex ,$[Cu(H_2O)_6]_2[Ni(NCS)_6]$ was prepared from the reaction of $(NH_4)_4[Ni(NCS)_6]$ with $Cu(NO_3)_2.4H_2O$ in water and characterized by elemental analysis and various spectroscopy techniques such as FT-IR, UV-Vis and atomic absorption. The physicochemical characteristics of both precursor and calcined catalyst were carried out using X-ray diffraction, thermal analysis methods (TGA and DSC), FT-infrared, scanning electron microscopy and BET specific surface area. The catalyst was evaluated for CO hydrogenation and water gas shift reactions. The carbon monoxide hydrogenation was studied over prepared catalyst in the temperature range of 573-653 K, gas hourly space velocity (GHSV) of 3600 h^{-1} and H_2/CO molar ratio of 2 at atmospheric pressure.

Results and discussion

In the FT-IR spectrum of $[Cu(H_2O)_6]_2[Ni(NCS)_6]$ complex, the C=S stretching mode of free SCN^- is shifted to higher frequency which is consistent with nitrogen bonding to the nickel. The XRD pattern of the calcined catalyst exhibits characteristic peaks for NiO and CuO phases. Characterization of both precursor and calcined catalyst was also carried out using scanning electron microscopy (SEM). All the electron micrographs were obtained from powder specimens of these materials. SEM observations (Fig. 1) have shown differences in morphology of both precursor and calcined catalyst.

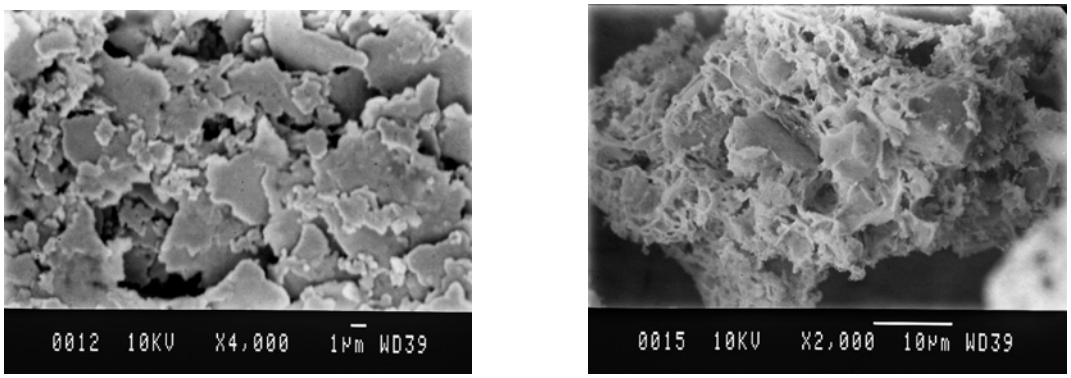

(a) (b)

Fig. 1. SEM micrographs of the $[Cu(H_2O)_6]_2[Ni(NCS)_6]/SiO_2$ precursor (a) and the calcined catalyst (b)

The BET specific surface area measurements for both precursor and calcined catalyst were carried out and calcined catalyst showed a higher surface area than its precursor. This is in agreement with SEM results, which showed that the agglomerate size of the calcined catalyst is less than its precursor and therefore, leads to an increase in the BET specific surface area of the calcined sample.

The calcined catalyst was also characterized by FT-IR and due to thermal decomposition of isothiocyanate ligands, no vibration bands for C=S and C≡N stretching are seen. In order to consider the stability of prepared catalyst using a novel method, it was tested for 40 h at 300 °C using synthesis gas with molar ratio of $H_2/CO=2:1$. The obtained results indicate that this catalyst was highly stable and had retained its activity and selectivity for 40 h.

Conclusions

The Cu-Ni/SiO_2 catalyst prepared by thermal decomposition of a new precursor, $[Cu(H_2O)_6]_2[Ni(NCS)_6]/SiO_2$. This method is a simple and suitable way to preparation of supported binary catalysts for different catalytic processes.The catalytic tests at 573-653 K (P = 1 atm, H_2/CO=2:1) showed that the catalyst has the high catalytic activity for methanation and water gas shift (WGS) reactions. The methanation reactivity increased with increasing temperature while a reverse trend was observed for the water gas shift reactivity.

References

[1] M. Janardanarao, Ind. Eng. Chem. Res. 29 (1990) 1735-1753.

[2] C. H. Bartholomew, Catal. Lett. 7 (1990) 303-316.

[3] L. Guczi, Catal. Lett. 7 (1990) 205-212.

[4] S. T. Hussain, M. A. Nadeem, M. Mazhar, Catal. Commun. 9 (2008) 2048-2052.

[5] G. P. v. Laan, A. A. C. M. Beenackers, Appl. Catal. A: Gen. 193 (2000) 39-53.

Adsorption of Chrysoidin G onto Al-MCM-41

Zeinab Pourghobadi*[a], Roghiyeh pourghobadi[b]

[a]Department of Chemistry, Faculty of Science, Islamic Azad University, Khorramabad Branch, Khorramabad, Iran

[b]Education Organization, Khorramabad, Lorestan, Iran

Email:zpourghobadi@gmail.com

Keywords: Adsorption, Langmuir isotherm, Al-MCM-41, Chrysoidin G

Introduction:

Some of dyes and pigments pollution corresponds to an important environmental problem due to its toxic effects and cummulation throughout the food chain and consequently in the human.There are a lot of ways that dyes and pigments removal from solution. Using molecular sieves is a good way for removal materials pollution[1].In this study, Al-MCM-41 is a molecular sieve as adsorbent. Such material as Al-MCM-41 is characterized by high surface area, high pore volume therefore can removal dyes from solution very well.

Materials and Methods:

Al-MCM-41 was prepared in hydrothermal condition by adding 2 g of sodium hydroxide that dissolved in 150ml of distilled water in a baker. Then 8 g of fumed silica was added to this solution at 75 $^{\circ}$C. The resulting mixture continuous stirring for 1h until a clear solution was obtained after that 3 g of cethyltrimethyl ammonium bromide (CTAB) was slowly added to this solution at room temperature under vigorous stirring. The resulting gel was stirring for 2h after the addition was completed. In the next stage 2 g aluminum choloride was dissolved in 100 ml of distilled water while adding 2.5 ml of concentrated H_2SO_4until a clear solution was obtained. This solution was added to resulting gel drop by drop. During the addition, the mixture was vigorously stirred for 2 h. the gel obtained was transferred into a Teflon-line stainless steel autoclave for a hydrothermal treatment at 100 $^{\circ}$C for 3 days. The resulting solid product was recovered by filtration and was washed for several times with deionized water. The white solid obtained was dried in air at 100 $^{\circ}$C for 5h. Finally, the sample was calcined at 6100 $^{\circ}$C for 16 h in air.

Dye solution preparation:

Solution of Chrysoidin G was prepared in double distilled water. Its concentration was determined by using absorbance values measured before and after the treatment, at 450nm with JENWAY UV-Vis spectrophotometer (Model 6505).

Results and Discussions:

We investigated effect of *p*H and amount of adsorbent for removal dye from solution. The adsorption of dye was increased at 2-4 pHs then it was constant in 4-7 pHs. So we selected *p*H = 4 for all studies. Then we investigated amount of adsorbent. Adsorption of dye increased with rising amount of adsorbent. We studied amount of 0.01-0.05 g of adsorbent. 0.05 is the best quantity for removal dye from solution.

Isotherms study:

Adsorption equilibrium data were correlated with the Langmuirand Freundlich isotherms. The isotherms fit Langmuire equation.

$$\frac{1}{q_e} = \frac{1}{qb}\left(\frac{1}{C}\right) + \frac{1}{q}$$

Where C_e is the equilibrium concentration of the adsorbate (mgL^{-1}), q_e is the amount of adsorbate adsorbed per unite mass of adsorbent(mgg^{-1}), q and b are Langmuire constants related to adsorption capacity and rate of adsorption, respectively (Fig.1).

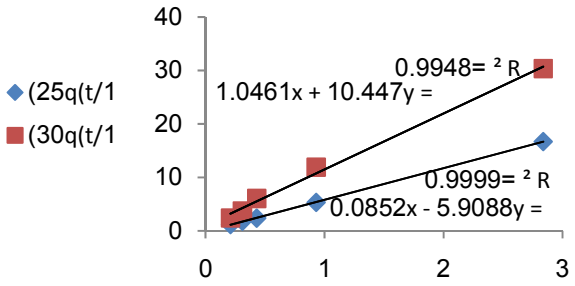

Fig. 1. Langmuir adsorption isotherm Chrysoidin G($1/q_e$ vs. 1/C)

Conclusion:

The present study shows that Al-MCM-41 is an effective adsorbent for removal dye solution. The optimum PH for adsorption was found to be up 4. The adsorption isotherm of Chrysoidin G was fitted by Langmuir model.

References:

[1] Esmaeili.A. et al.;"Evaluation of the activated carbon prepared from the algae Gracilaria for the biosorption of Cu(II) from aqueos solutions", African journal of biotechnology ,Vol.7(12),pp. 2034-2037,17june,2008.

[2] Han.R. et al .;"Biosorption of copper and lead ions by waste beer yeast", Journal of Hazardous B137.1569-1576,2006.

Adsorption Thermodynamic Studies of Cu (II) on Modified Multiwalled Carbon Nanotubes Using Glotarid-Dihydrazide

H. Tavallai[*a,b], M. Aalaee[a], D. Abdardideh[a]

[a] Department of chemistry, Payame Noor University (PNU), Shiraz, 711365 -944, Iran

[b] Islamic Azad University of Omidieh, Khozestan, Iran

(Tavallali@yahoo.com)

Abstract:

The present article reports on the application of modified multiwalled carbon nanotubes (MMWCNTs) as a new, easily prepared sensitive and stable solid sorbent for the adsorption of trace Cu(II) ion in aqueous solution. Multiwalled carbon nanotubes (MWCNTs) were modified using Glotarid-Dihydrazide Which characterized using different techniques. The equilibrium adsorption of copper on the functionalized MWCNTs was studied in various temperatures and the adsorption equilibrium was well described using different adsorption models. Then the thermodynamic parameters were obtained.

Introduction:

Many methods including physical and chemical have been used to treat the pollution caused by the heavy metals, of which adsorption is a most common adopted method because of its simplicity and facility [1]. Carbon nanotubes (CNTs) are relatively new adsorbents that have been proven to possess great potential for removing many kinds of metal ions. But, the selectivity of the raw or oxidized-MCWNTs for adsorption of metal ions is quite limited. MWCNTs modified with some organic compounds are expected to be more selective than untreated oxidized-MWCNTs for the adsorption [2]. In this paper, adsorption experiments of Cu (II) ion from aqueous solution by modified multiwalled carbon nanotubes (MWCNTs) were carried out. The thermodynamic and isotherm model of adsorption were studied systematically.

Methods:

To evaluate the thermodynamic properties, we first prepared various solutions with initial Cu (II) concentration ranging from 10 to 80 mg/L (100 ml, pH = 5), and then added 0.1 g CNTs to each solution. These samples were shaken continuously for 1 h at 280, 300 and 320 K, respectively. The suspensions were filtered and the filtrates were immediately measured using an atomic adsorption spectroscopy. The amount of copper adsorbed, q_e (mg g^{-1}) was computed by $q_e=(C_0-C_t)Vm^{-1}$, where C_0 and C_t are copper concentrations (mg L^{-1}) before and after adsorption, V is the volume of adsorbate (L) and m is the weight of the adsorbent (g).

Results and discussion:

Adsorption isotherm

This study employs the Langmuir and Freundlich isotherms to describe the equilibrium adsorption. The expression for the Langmuir isotherm is ($q_e = q_m[K_LC_e/(1 + K_LC_e)]$) models. Where where q_e is the amount of Cu^{2+} adsorbed per gram of MMWCNTs (mg/g) and Ce is the equilibrium concentration of metal ions (mg L^{-1}). The Freundlich isotherm is ($q_e =K_fCe^{1/n}$) that K_f and n are the Freundlich constants. Table 1 summarizes the coefficients of the Langmuir and Freundlich isotherms for different temperatures.

Table 1: Parameters of adsorption models for Cu (II) on modified MWCNTs

Temperature (K)	Langmuir model			Freundlich model		
	K_L(L/mg)	q_m(mg/g)	R^2	K_f	n	R^2
280	0.1386	44.64	0.998	9.897	2.893	0.870
300	2.9515	47.39	0.974	21.020	5.331	0.951
320	4.1925	51.81	0.933	29.540	7.716	0.872

Adsorption thermodynamics:

The thermodynamic parameters, the values of enthalpy,ΔH°, and entropy, ΔS°, and Gibbs free energy, ΔG°, of the sorption is defined as: $\Delta G^0 = - RT \ln K$ and $\ln K= - (\Delta H^\circ/RT)+(\Delta S^\circ/R)$. The equilibrium constants obtained from the best fitted model (Langmuir) at 280, 300 and 320 K were used to determine the Gibbs free energy changes as shown in Table 2.

Table 2: Thermodynamic parameters of Cu (II) adsorption by modified MWCNTs

Temperature (K)	ΔG° (kJ mol^{-1})	ΔH° (kJ mol^{-1})	ΔS° (JK^{-1} mol^{-1})
280	**−21.16**	**67.77**	**319.76**
300	**−30.30**		
320	**−33.26**		

Conclusion:

This study demonstrated that the modified multiwalled carbon nanotubes could be used as an effective adsorbent for the removal of Cu (II) ions. The isotherm study indicates that adsorption data correlated well with Langmuir isotherm model. The negative value of ΔG° indicates the feasibility and spontaneity of the adsorption process. The positive value of ΔH° suggests the endothermic nature of the adsorption.

References:

[1] Y.H. Li, S. Wang, J. Wei, X. Zhang, C. Xu, Chem. Phys. Lett, 357 (2002) 263.

[2] Z. Zang, Z. Hu, Z. Li, Q. He, X. Chang, Journal of Hazardous Materials 172 (2009) 958–963

Adsorption Characteristic of Functionalized Multiwalled Carbon Nanotube for Cd (II) in Aqueous Solution

H. Tavallai[*a,b], D.Abdardideh[a], M.Aalaee[a]

[a] *Department of chemistry, Payame Noor University (PNU), Shiraz, 711365 -944, Iran*

[b] *Islamic Azad University of Omidieh, Khozestan, Iran*

(Tavallali@yahoo.com)

Abstract:

The application of modified multiwalled carbon nanotubes (MMWCNTs) as a new, easily prepared sensitive and stable solid sorbent for the preconcentration of trace Cd (II) ions in aqueous solution was considerd. Multiwalled carbon nanotubes (MWCNTs) were modified using thiosemicarbazide were characterized using different techniques. The equilibrium adsorption of Cd (II) on the functionalized MWCNTs was studied in various temperatures and the adsorption equilibrium was achieved in freundlich isotherm which gave correlation in thermodynamic parameters.

Introduction:

In recent years, great attention has been paid to the application of nano-structure materials, especially carbon nanotubes (CNTs). CNTs are good anion and cation adsorption materials for wastewater treatment, as they exhibit exceptionally large specific surface areas which are easy to decorate [1, 2]. MWCNTs modified with some organic compounds are expected to be more selective than untreated and oxidized-MWCNTs for the adsorption of metal ions [3]. In this work, we will investigate the thermodynamic and isotherm of the Cd (II) adsorption onto modified MWCNTs, in order to obtain the adsorption capacity, thermodynamic parameters, and to establish the isotherm model of adsorption on MMWCNTs.

Method:

In general, the effects of pH, adsorbent dosage, and temperature on adsorption of Cd (II) ion were performed at room temperature (27±1 $^{\circ}$C) by stirring a mass of 0.3 g of MMWCNT with 150mL of 5mg L^{-1} copper solutions for 1 h. The study on effect of temperature was performed in various temperatures of 300, 310 and 320 K. For isotherm study, 0.1 g of MMWCNT was mixed with 50mL copper solutions at various concentrations (5–50 mg L^{-1}) and the mixtures were stirred for 1 h at room temperature. The amount of copper adsorbed, q_e

(mg g^{-1}) was computed by $q_e=(C_0-C_t)Vm^{-1}$, where C_0 and C_t are cadmium concentrations (mg L^{-1}) before and after adsorption, V is the volume of adsorbate (L) and m is the weight of the adsorbent (g).

Results and discussion:

Adsorption isotherm:

Adsorption isotherms are mathematical models that describe the distribution of the adsorbate species among liquid and adsorbent. The experimental data of Cd (II) adsorptions can be correlated with the Freundlich ($q_e = K_f Ce^{1/n}$) and Langmuir ($q_e = abC_e/(1 + bC_e)$) models. The Langmuir and Freundlich constants were obtained by fitting the adsorption equilibrium data to the isotherm models and are listed in Table 1.The results indicate that the Langmuir model fits the adsorption data better than the Langmuir model.

Table 1: Parameters of adsorption models for Cd (II) on modified MWCNTs

Temperature (K)	Langmuir model			Freundlich model		
	K_L(l/mg)	q_m(mg/g)	R^2	K_f	n	R^2
300	0.07	27.9	0.9968	3.30	1.83	0.9551
310	0.13	28.5	0.9879	4.62	2.10	0.9551
320	0.19	30.8	0.9825	5.63	2.13	0.9735

Adsorption thermodynamics:

The thermodynamic parameters, the values of enthalpy,ΔH°, and entropy, ΔS°, and Gibbs free energy, ΔG°, of the sorption is defined as: $\Delta G^0 = - RT \ln K$ and $\ln K= - (\Delta H^\circ/RT)+(\Delta S^\circ/R)$. The equilibrium constants obtained from the best fitted model (Langmuir) at 300, 310 and 320 K were used to determine the Gibbs free energy changes as shown in Table 2.

Table 2: Thermodynamic parameters of Cd (II) adsorption by modified MWCNTs

Temperature (K)	$-\Delta G^\circ$ (kJ mol^{-1})	ΔH° (kJ mol^{-1})	ΔS° (JK^{-1} mol^{-1})
300	1.66	41.68	0.143
310	3.37		
320	4.7		

Conclusion:

Adsorption thermodynamics and isotherms of copper on MMWCNTs have been studied. A positive value of the standard enthalpy change suggests that the interaction of Cd(II) adsorbed by MMWCNTs is endothermic. The negative adsorption standard free energy changes and positive standard entropy changes indicate that the adsorption reaction is spontaneous process.

The isotherm study indicates that adsorption data correlated well with Langmuir isotherm model.

References:

[1] Y.H. Li, S. Wang, Z. Luan, J. Ding, C. Xu, D. Wu, Carbon 41 (2003) 1057

[2] Li, Y.H., Wang, S.G., Luan, Z.K., Ding, J., Xu, C.L., Wu, D.H., 2003,Carbon, 41, 1057–1062

[3] Z. Zang, Z. Hu, Z. Li, Q. He, X. Chang, Journal of Hazardous Materials 172 (2009) 958–963

Adsorption of Zinc(II) from aqueous solution by mesoporous silica NH-MCM-41 and isotherm and kinetic studies

Nasim Jamshidi, Nader Bahramifar, Freydoon Ashrafi
Department of chemistry , Payam Noor University (PNU), sari unit , Mazandaran , Iran
E.mail: nasim_5989@yahoo.com
Phon number : 0123 3288852
Cell number : 09111261507

Keywords: Adsorption, Sliver, Mesoporous silica NH_2-MCM -41, Kinetic , Thermodynamic

Introduction

Zinc is one of the abundant metals which is used in steel production, alkaline batteries and anti-rust paint Several methods were used to remove and recycle this metal, including ion exchange, biosorption, electrolysis, reverse osmosis, coagulation, and solvent extraction, etc. (2). With increase of environmental pollution, there is a growing demand to develop novel adsorbents of higher efficiency for heavy metal ions removal from aqueous media than those commercially available mesoporous silica have received considerable attention because of their unique large surface area, well- defined pore size and pore shape Mesoporous silica NH_2-MCM-41 has been functionalized and employed to eliminate traces of toxic heavy metal from wastewater. Mostly, the functionalizations of mesoporous silica have been studied. In this study, NH2-MCM-41 mesoporous silica was prepared under basic condition by using hexadecyltrimethylammoniumbromide as template and fumed silica as the silica source by means of hydrothermal method. Then the effect of solution pH, contact time, Zinc ion concentration and adsorbent dosage on the adsorption capacity of NH_2-MCM-41 were studied in order to analyze the adsorption kinetics and determine the equilibrium time.

Materials and methods

Zinc (II) ions solution were obtained of chlorid salt of Zinc. (MERCK) . NH_2-MCM-41 was prepared according to refluxed for 6 h. the method of Ho *et al.* standard solution of 1000 mg/l were used for adsorption experiments. Experiments were performed with the NH_2-MCM-

41mesoporous adsorbent in batch system. This study was conducted by mixing known weight of solution of zinc ions of known concentration by the following experimental condition.

Initial metal ion concentration (mg/l)	50,100,150,200,250,300
Amount of NH2-MCM-41	0.25,0.5,1.0,1.25,1.5,2.0,2.5,3
pH	3-8
Contact time	5,10,20,30,60,90,120,150,180,210

Then the solid phase was separated by filtration through 0.2 μm microfilter. The concentration of Zinc was determined by GBC flame atomic adsorption spectrometr(Sens AA) and the sorbed amount was calculated.The percent of removed metal ions by the adsorbents were calculated by the following equation:

$$\mathrm{Re}moval = \frac{100(C_0 - C_e)}{C_0}$$

The equilibrium adsorption capacity of adsorbent was calculated by the following equation:

$$q_e = \frac{(C_0 - C_e)V}{W}$$

Results and discussion

The effects of initial pH on adsorption of Zn(II) ion onto NH_2-MCM-41 are investigated in a batch system. sorbent capacity, increased with an increase in sorbent dose for an initial zinc concentration of 100 mg/l. The equilibrium sorption capacity decrease from 84.11 to 32.84 mg/g when sorbent dose wase increased from 0.25-3.0 g/l. This shows that increasing the sorbent dosage increased the surface area available, hence the number of sites available for sorption increased. The initial metal ions concentration was varied from50 to 300 mg/L at temperature 22 ° C. Therefore, the percentage of ions adsorbed at higher concentration level shows a decreasing trend, whereas uptake of ions displays opposite trend The percent removal was increased as the initial Zn(II) concentration increased up to 50 mg/L but further increase in concentrations results in decrease in percent removal. Maximum percent removal of Zn(II) was observed 77.45 with NH_2-MCM-41 at 50 mg/L. This may be due to the saturation of the sorption sites and increase in the number of ions competing for the available binding sites in the biomass for complexation of Zn(II)ions at higher concentration . Maximum adsorption of Zn(II) were observed at pH 7.0 absorbent dose 2.0g/l ,metal concentration 200 mg/l in 210 min of contact time. The adsorption equilibria data has been fitted very well to Langmuir as

well as to freundlich adsorption model (Fig 1, Table 1).The sorption kinetics followed the pseudo – second order rate equation(Fig 2 , Table 2).

conclusions

The present study showed that the NH_2-MCM-41 can be considered as a technology for removal Zn(II) in batch process. The obtained results showed that pH, sorbent dose , initial metal concentration uptake time and solution temperature highly affected the uptake Zn(II) capacity of the the NH2-MCM-41 sorbent.

Table 1 Freundlich and Langmuir constants for Zn(II)

Langmuir constant			Freundlich constant		
Q(mg/g)	*b (l/mg)*	R^2	K_F *(mg/g(L/mg)1/n)*	*n*	R^2
۶۲,۵	۰,۴۷۰	۰,۹۸۳	۰,۰۰۷	۲۴,۹۴	۴,۹۰

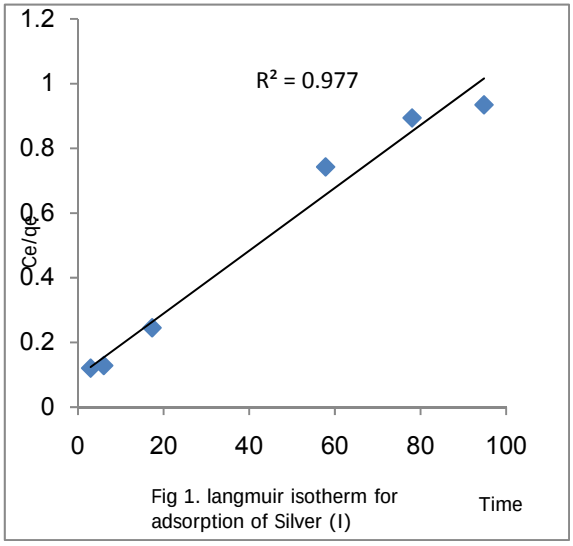

Fig 1. langmuir isotherm for adsorption of Silver (I)

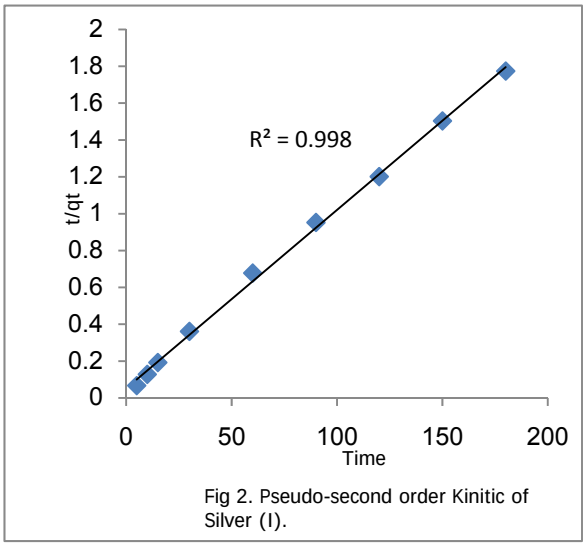

Fig 2. Pseudo-second order Kinitic of Silver (I).

References

[1] Butterman,W.C., Hilliar, H.E., 2005. Silver—mineral commodity profiles. U.S. Geological survey, Reston, Virginia.

[2] Wan, R.Y., Miller, J.D., 1986. Solvation extraction and electrodepotion of gold from cyanide solutions. J. Met. 38 (12), 35–40.

[3] H. Yoshitake, T. Yokoi, T. Tatsumi, Chem. Mater. 15 (2003) 1713-1721.

[4] *K.F. Lam, K.L. Yeung, G. McKay, The journal of physical chemistry. B110 (2006) 2187-2194.*

[5] M. Algarra, M.V. Jiménez, E. Rodríguez-Castellón, A. Jiménez-López, J. Jiménez-Jiménez, Chemosphere 59 (2005) 779-786. [6] R. Kumar, N. R. Bishnoi ∗, G., K. Bishnoi Chemical Eng. J. 135 (2008) 202–208

[7] V. Padmavathy * Bioresource Technology 99 (2008) 3100–3109

[8] A. Heidari, H.Younesi, Z. Mehraban *Chemical Eng. J.* (2008) 2-6

Role of Strain and Ligand Effects in the Modification of the Electronic and Chemical Properties of Au/M (M=Pt, Cu and Fe) Bimetallic Surfaces

S. Jalili[a], A. Zeini Isfahani[b], R. Habibpour*[c]

[a]Faculty of Sciences, Department of Chemistry, K. N. Toosi University of Technology, Tehran, Iran

[b]Azad University of Falavarjan, Falavarjan, Iran

[c]Faculty of Sciences, Department of Chemistry, University of Isfahan, Isfahan, Iran

(Email: razihabibi@gmail.com)

One of the main goals of the catalysis industry is to develop new materials that have novel catalytic properties. Bimetallic catalysts started to gain considerable commercial interest in the 1960's for their use in hydrocarbon reforming because they displayed reactivities unlike those of the monometallic catalysts [1]. The modification effect is especially important when the admetal coverage is in the submonolayer to monolayer regime. However, it is difficult to know a priori how the electronic and chemical properties of a particular bimetallic surface will be modified relative to the parent metals. There are two critical factors that contribute to the modification of the electronic and chemical properties of a metal in a bimetallic surface. First, the formation of the hetero-atom bonds changes the electronic environment of the metal surface, giving rise to modifications of its electronic structure through the ligand effect. Second, the geometry of the bimetallic structure is typically different from that of the parent metals, e.g. the average metal-metal bond lengths change. This gives rise to the strain effect that is known to modify the electronic structure of the metal through changes in orbital overlap [2].

Ab initio calculations offer the ability to identify parameters that correlate electronic and chemical properties, which in turn provide opportunities to predict how the properties of a metal surface are modified by alloying with other metals or promoters. For transition metal surfaces, the effect of substituting one metal for another can largely be attributed to the modification in the d-orbitals, which participate largely in the bonding interaction with adsorbates. It has been further shown that the d-orbitals on the surface of the catalyst of interest can be distinguished largely by characterizing the transition metal density of states (DOS) for the d-orbitals. Specifically, it is the location of the d-band center of the DOS in relation to the Fermi level that has been correlated for many bonding interactions [3].

The current work focuses on the general trends in the electronic and chemical properties of overlayer and submonolayer Au/M (M =Pt, Cu and Fe) bimetallic surfaces to demonstrate their unique electronic and chemical properties. We will then utilize the adsorption of atomic oxygen and O_2 to demonstrate the correlation between the surface d-band center and the binding energies of both atomic and molecular adsorbates for various bimetallic surfaces.

Calculations were performed within the framework of density functional theory (DFT) using the Quantum Espresso [4], which is a DFT code based on plane wave basis sets. Electron–ion interactions are described using the projectoraugmented wave (PAW) method, which was expanded within a plane wave basis setting up a cutoff energy of 50Ry (≈ 680.2 eV). Electron exchange and correlation effects were described by the general gradient approximation (GGA) of Perdew et al. are known as PW91. Brillouin zone integration was performed using 3×3×1 Monkhorst Pack grid. The Au and Au/M (M = Pt, Cu and Fe) surface calculations were performed with fcc(100) surfaces modeled by 2×2 unit cells of five substrate layers. A vacuum space equivalent to eight layers is used to separate the slab from the slabs of the upper and lower cells, thus ensuring that there were no interactions between the adsorbed intermediates and the bottom surface of the next slab. All metal layers were allowed to relax.

Keywords: Bimetallic Catalysis, Au Nanocatalysts, Strain Effects, Ligand Effects, DFT Calculation

References

[1] R. A. Campbell, J. A. Rodriguez, D.W. Goodman, Phys. Rev. B 46 (1992) 7077.

[2] A. Schlapka, M. Lischka, A. Gro, U. Ka¨sberger, P. Jakob, Phys. Rev. Lett. 91 (2003).

[3] M. A. Ortigoza, T. S. Rahman, Phys. Rev. B 77 (2008) 195404.

[4] User's Guide for Quantum ESPRESSO (version 4.1).

Effects of Electronic Structure Modifications on the Adsorption of Oxygen Reduction Reaction Intermediates on Au(100)/M (M=Pt, Cu and Fe) surfaces

S. Jalili[a], A. Zeini Isfahani[b], R. Habibpour*[c]

[a]Faculty of Sciences, Department of Chemistry, K. N. Toosi University of Technology, Tehran, Iran

[b]Azad University of Falavarjan, Falavarjan, Iran

[c]Faculty of Sciences, Department of Chemistry, University of Isfahan, Isfahan, Iran

(Email: razihabibi@gmail.com)

Supported gold nanoparticles have attracted intensive research interest in heterogeneous catalysis and fuel-cell electrocatalysis in the past two decades because of their exceptionally high activities for low-temperature CO oxidation and distinguished selectivities in a variety of redox reactions [1]. These unique features are very different from the traditional platinum group metals. One of the most important features of gold catalysis is the striking sizedependence. As bulk gold is highly noble, reactivity of goldbased catalysts is critically dependent on the particle size; only those particles with sizes below 5 nm show high reactivities [2].

Fuel cells enable the efficient production of electricity from hydrogen and oxygen. However, numerous challenges exist that prevent the viability of fuel cells. One area of intense research is the development of new cathode materials for catalyzing the oxygen reduction reaction (ORR). Since the electrocatalytic ORR began to receive significant attention in the 1960s, it has been known that platinum exhibits the best oxygen reduction kinetics among the noble metals. However, ORR rates on pure Pt are several orders of magnitude less than rates of the hydrogen oxidation reaction, the complementary reaction that takes place at fuel cell anodes. Additionally, cathodes require significantly higher Pt loadings than anodes, due to the decreasing ORR rates with increasing specific surface area [3]. The scarcity and cost of platinum have motivated the search for more efficient ORR catalysts.

Although it has suggested that the ORR activity depends on the atomic oxygen adsorption energy, rational catalyst design may benefit from an understanding of how alloys alter the adsorption of other species in the oxygen reduction. This involves identifying which

adsorbates are most important in determining ORR activity and determining if the activity can be predicted from the amount of strain and the identity of the alloying metal.

In this work, we report DFT calculations for exploring the effects of Au alloys. The electronic ligand effect can be isolated by substituting the second layer of a Au(100) slab with Pt, Cu and Fe transition metals, creating a AuMAu sandwich. Likewise, the strain effect induced in alloys through altering the lattice constant can be isolated by changing the lattice parameter of the Au(100) slab from its most stable value. Both effects can be combined in a pseudomorphic overlayer model in which a M (M = Pt, Cu and Fe) layer is placed over a Au(100) substrate.

Density functional theory (DFT) calculations were performed with the Quantum Espresso Simulation Package [4], using plane-wave basis sets based on the projector-augmented wave (PAW) method. Basis sets were made finite using a cutoff energy of 50Ry (≈ 680.2 eV). Brillouin zone integration was performed using 3×3×1 Monkhorst Pack grid. Surface calculations were performed with fcc(100) surfaces modeled by 2×2 unit cells of five substrate layers and vacuum space equivalent to eight metal layers. All metal layers were allowed to relax.

Keywords: Bimetallic Catalysis, Au Nanocatalysts, Oxygen Reduction, DFT Calculation

References

[1] M. Comotti, W. C. Li, B. Spliethoff, F. Schu¨th, J. Am. Chem. Soc. 128 (2006) 917.

[2] M. S. Chen, D. W. Goodman, Science 306 (2004) 252.

[3] D. B. Sepa, M. V. Vojnovic, L. M. Vracar, A. Damjanovic, Electrochim. Acta 32 (1987) 129.

[4] User's Guide for Quantum ESPRESSO (version 4.1).

Atomic Oxygen Adsorption on Au(100) and Au/M (M = Pt, Cu and Fe) Bimetallic Surfaces: Effects of Coverage

S. Jalili[a], A. Zeini Isfahani[b], R. Habibpour*[c]

[a]Faculty of Sciences, Department of Chemistry, K. N. Toosi University of Technology, Tehran, Iran

[b]Azad University of Falavarjan, Falavarjan, Iran

[c]Faculty of Sciences, Department of Chemistry, University of Isfahan, Isfahan, Iran

(Email: razihabibi@gmail.com)

Bulk gold is chemically inert and is regarded as a poor catalyst, but when gold is in the form of nanoparticles and is deposited on metal oxides or activated carbon it becomes surprisingly active, especially at low temperatures, for such reactions as CO oxidation and propene epoxidation [1]. A lot of studies have been carried out to understand the origin of such novel catalytic activity. Previous investigations proposed that the novel catalytic activity is originated from quantum size effects of Au nano-particles, from low-coordinated Au atoms of Au nano-particles, or from perimeter regions at the contact of Au nano-particles on oxide surfaces [2]. Effects of the interaction between Au nano-particles and oxide supports have been also investigated. It is considered that the interaction between oxygen and Au surfaces is also essential for the catalytic activity. The behavior of oxygen on or near Au nano-particles seems to play a key role in the catalytic reaction such as CO oxidation. One way to obtain an active gold catalyst on an inert support is to make nanoparticles of gold alloy with a second metal that plays the role of activating oxygen [3].

To understand the interaction between oxygen and Au surfaces, it is important to investigate the dependence of the adsorption states on the gold surface combination (effect of second metals) and on the coverage of oxygen.

Quantum Espresso program [4] based on Gradient-corrected periodic DFT (Density Functional Theory) slab calculations were used to determine all the structural, electronic and energetic results reported in this paper. The code gives an iterative solution of the Kohn–Sham equation for a system with periodic boundary conditions using plane-wave basis set. In order to represent the electron–ion core interaction, it uses the projector augmented wave (PAW) approach. The exchange and correlation potentials are described by the general gradient approximation (GGA) of Perdew et al. are known as PW91. In all the cases, the

plane-wave expansion was limited at a cutoff energy of 50Ry (≈ 680.2 eV) assuring a good convergence in energy. The Brillouin zone integration has been done on a grid of 3×3×1 using the Monkorst–Pack k-point. The Au and Au/M (M = Pt, Cu and Fe) Surface calculations were performed with fcc(100) surfaces modeled by 2×2 unit cells of five substrate layers. A vacuum gap equivalent to eight layers was set in order to separate two subsequent slabs and the adsorbates were placed on one side of the slab. All metal layers were allowed to relax.

Keywords: Bimetallic Catalysis, Oxygen Adsorption, Au Nanocatalysts, DFT Calculation

References

[1] A. Q. Wang, C. M. Chang, C. Y. Mou, J. Phys. Chem. B 109 (2005) 18860-18867.
[2] J. P. Chou, W. W. Pai, C. C. Kuo, J. D. Lee, C. H. Lin, C. M. Wei, J. Phys. Chem. C 113 (2009) 13151–13159.
[3] H. F. Wang, X. Q. Gong, Y. L. Guo, Y. Guo, G. Lu, P. Hu, J. Phys. Chem. C 113 (2009) 6124–6131
[4] User's Guide for Quantum ESPRESSO (version 4.1).

Removal of methylene blue and auramin from aqueous solutions with nanodimensional AlMCM-41: Thermodynamic and kinetic studies

S. Eftekhari, A. Habibi-Yangjeh*, Sh. Sohrabnezhad

Department of Chemistry, University of Mohaghegh Ardabili, P.O. Box 179, Ardabil, Iran. mail: ahabibi@uma.ac.ire

Keywords: AlMCM-41, Cationic dye, Adsorption, Kinetics, Thermodynamics

Introduction

The discharge of dye effluents to the environment, especially to water system, is becoming a major concern due to their toxicity. Therefore, adsorbents such as zeolites, mesoporous materials and pillared clays with higher surface areas are used in adsorption processes [1, 2]. In the present study, for a first time, we report single and binary component adsorption kinetic and thermodynamic studies for adsorption of methylene blue (MB) and auramine (AU) on AlMCM-41.

Experimental

The dyes were obtained from Merck and AlMCM-41 prepared by the method described in our previous paper [3]. Adsorption kinetics and isotherm experiments for the samples were undertaken in a batch reactor with 250 ml capacity provided with water circulation arrangement. Adsorption was performed by shaking 0.005 g of AlMCM-41 in 200 ml of the solutions with varying concentrations (10^{-6}–10^{-5} M) at 25 and 40 ˚C. Concentration of the dyes was determined spectrophotometrically by measuring absorbance at 664 and 432 nm for λ_{max} of MB and AU, respectively.

Results and discussion

Figure 1 demonstrates adsorption dynamic of MB onto AlMCM-41 at 25 and 40 º C. The adsorption capacity for adsorption of MB in initial concentration of 8×10^{-6} M at 25 ºC is 2.07×10^{-4} mol/g, respectively.

Fig. 1

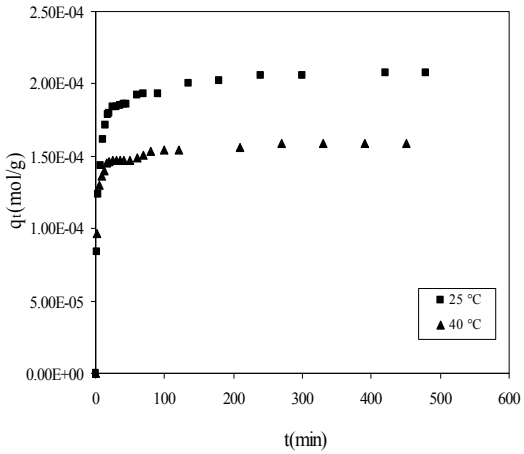

Fig. 2

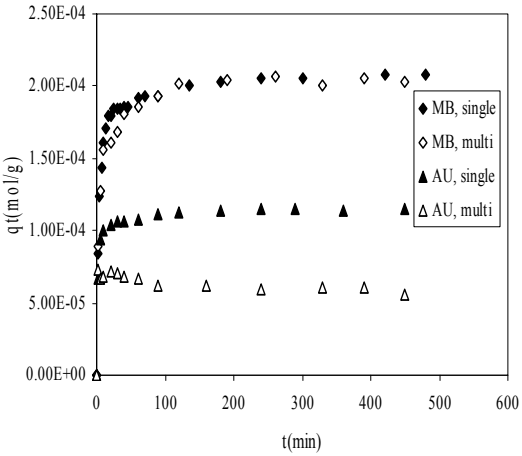

Figure 2 demonstrates a comparison of MB adsorption onto AlMCM-41 in single and binary component systems at 25 and 40 °C for initial concentration of 4×10^{-6} M. Thermodynamic parameters (ΔG°, ΔH° and ΔS°) for adsorption of MB and AU in binary component system were calculated. The results demonstrate that similar to single component systems, the adsorption is exothermic. Adsorption of the dyes on the adsorbent in binary component system follows the pseudo second-order kinetics. Also, the results demonstrate that the second-order rate constant for adsorption of AU is higher than that of MB. The intraparticle diffusion model was also applied to the adsorption kinetics of MB and AU in binary component system. It is clear that, similar to single component systems, the amount of MB and AU adsorption are greatly increasing as the pH is increasing. When pH of solution is changed from 6.5 to10, the adsorption capacity will change from 2.03×10^{-4} to 3.06×10^{-4} mol/g and from 5.56×10^{-5} to 1.08×10^{-4} mol/g for MB and AU, respectively.

References:

[1] V. K. Gupta, A. Mittal, L. Krishnan, J. Mittal, J. Colloid Interface Sci. 293, 16 (2006).

[2] P. P. Selvam, S. Preethi, P. Basakaralingam, N. Thinakaran, A. Sivasamy, S. Sivanesan, J. Hazard. Mater. 155, 39 (2008).

[3] S. Eftekhari, A. Habibi-Yangjeh, Sh. Sohrabnezhad, J. Hazard. Mater. 178, 349 (2010).

Adsorption of cationic and anionic dyes onto the activated carbon prepared from grapevine rhytidome: Kinetic and equilibrium studies

Saeid Azizian[1], Mahtab Hejazifar[1*]

[1]*Department of Physical Chemistry, Faculty of Chemistry, Bu-Ali Sina University, Hamedan, Iran*

(E-mail: Hejazi_64@yahoo.com)

Keywords: Adsorption, Activated carbon, Metylene blue, Methyl orange

Introduction

Dyes are important pollutants which are generally present in industrial wastewater. A simple method for removal of pollutants is adsorption, especially by activated carbon [1]. Although activated carbon has been used widely for pollutant removal, the disadvantage is its relatively high cost [2]. The objective of this work is study about the adsorption of cationic (methylene blue(MB)) and anionic (methyl orange (MO)) dyes onto the granular activated carbon prepared from grapevine rhytidome ,as an abundant and low-cost precursor, (AC-51) from both equilibrium and kinetic point of view. The results were compared with the commercial granular activated carbon (GAC).

Methods

In the equilibrium adsorption experiments, 2.0 mg of adsorbents were added into 5 ml of dyes aqueous solutions with different concentrations. Then, the samples were placed in a shaker with the speed of 150 rpm at 30.0 °C for 24 h. The residual concentrations of samples were determined with a UV/Vis spectrophotometer. In the kinetic adsorption experiments, 2.0 mg of adsorbents were added into 5 ml of 10 mg/l of MO and 5 mg/l of MB solutions. The samples were placed in a shaker (150 rpm, 30.0 °C) and the dye concentration at different time intervals was determined with UV/Vis spectrophotometer.

Results and discussion

Activated carbon was prepared from grapevine rhytidome using phosphoric acid and microwave radiation. The variation of the amount of adsorbed dyes as a function of time, q_t, onto commercial activated carbon (GAC) and the prepared activated carbon (AC-51) are shown in Fig. 1. To evaluate the kinetic mechanism that controls the adsorption process, three kinetic models (Table. 1) were tested. The results of non-linear fitting of different kinetic models to the experimental data are listed in Table 2. Based on the obtained correlation coefficients, r^2, for adsorption of MB and MO onto the GAC and AC-51 (except MO onto the GAC that fitted best with PFO model) the M-exp model fits the adsorption kinetic data and is better than the other models.

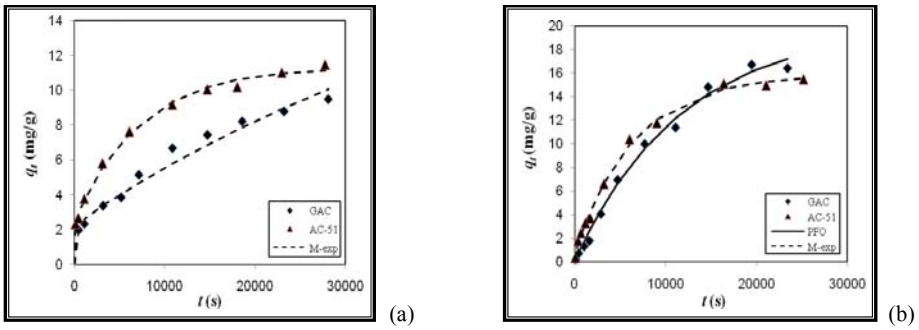

Fig. 1. Effect of contact time on the removal of dyes by GAC and AC-51 at T= 30.0 °C. (a) MB (b) MO. The solid line represents the predicted values by PFO model and the dashed lines by M-exp.

Table 1. Kinetic models [3].

Kinetic model	Abbreviation	Non-linear form
pseudo-first-order	PFO	$q_t = q_e(1 - \exp(-k_1 t))$
pseudo-second-order	PSO	$q_t = \frac{k_2 q_e^2 t}{1 + k_2 q_e t}$
multi-exponential equation	M-exp	$q_t = q_e(1 - \sum_{i=1}^{n} f_i \exp(-k_i t))$

Table 2. Parameters of different kinetic models for adsorption of MB and MO onto the GAC and AC-51.

MB	f_1	f_2	F_2	k_1	k_2	q_e	r^2
GAC							
PFO	-	-	-	1.16×10^{-4}	-	9.4	0.9564
PSO	-	-	-	-	9.0×10^{-5}	12.1	0.9651
M-exp	0.894	0.106	-	1.8×10^{-5}	2.992×10^{-3}	21.8	0.9804
AC-51							
PFO	-	-	-	2.70×10^{-4}	-	10.5	0.9347
PSO	-	-	-	-	3.1×10^{-5}	11.9	0.9607
M-exp	0.784	0.216	-	1.39×10^{-4}	2.5×10^{-6}	11.3	0.9968
MO							
GAC							
PFO	-	-	-	8.6×10^{-5}	-	19.8	0.9935
PSO	-	-	-	-	2.0×10^{-6}	29.4	0.9917
M-exp	0.999	1.0×10^{-5}	-	6.7×10^{-5}	-3.89×10^{-4}	23.5	0.9959
AC-51							
PFO	-	-	-	1.75×10^{-4}	-	15.6	0.9953
PSO	-	-	-	-	9.0×10^{-6}	19.6	0.9947
M-exp	0.954	4.6×10^{-2}	-	1.54×10^{-4}	6.859×10^{-3}	15.8	0.9972

Fig. 2 shows the adsorption isotherms of MB and MO onto the GAC and AC-51. The equilibrium adsorption data were analyzed with Langmuir (L) and Redlich-Peterson (R-P) isotherms (Table 3). The obtained constants of isotherms derived from linear fitting method are listed in Table 4. Based on the calculated correlation coefficients for both GAC and AC-51, it is found that R-P fits the adsorption equilibrium data better than L isotherm.

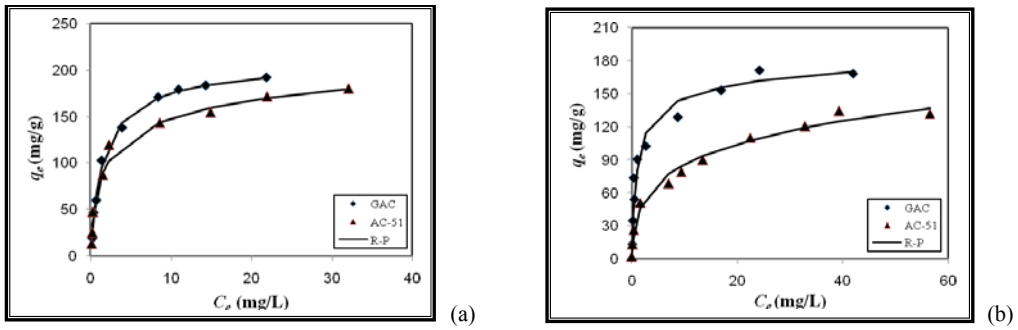

Fig. 2. Adsorption isotherms of (a) MB and (b) MO onto the GAC and AC-51 at 30.0 °C. Lines represent the predicted values by R-P isotherm.

Table 3. Isotherm models [3].

Isotherm	Abbreviation	Non-linear form	Linear form
Langmuir	L	$q_e = \frac{q_m K_L C_e}{1 + K_L C_e}$	$\frac{C_e}{q_e} = \frac{1}{K_L q_m} + \frac{C_e}{q_m}$
Redlich-Peterson	R-P	$q_e = \frac{K_R C_e}{1 + \alpha_R C_e^{\beta}}$	$\frac{C_e}{q_e} = \frac{1}{K_R} + \frac{\alpha_R}{K_R} C_e^{\beta}$

Table 4. Obtained isotherms parameters for adsorption of MB and MO onto the GAC and AC-51.

MB	q_m	K_L	K_F	K_R	K	$1/n$	α_R	β	a	r^2
GAC										
L	204.6	0.63	-	-	-	-	-	-	-	0.9989
R-P	-	-	-	138.89	-	-	0.74	0.97	-	0.9991
AC-51										
L	184.6	0.61	-	-	-	-	-	-	-	0.9963
R-P	-	-	-	180.02	-	-	1.47	0.88	-	0.9987
MO										
GAC										
L	172.5	0.83	-	-	-	-	-	-	-	0.9962
R-P	-	-	-	206.51	-	-	1.54	0.93	-	0.9974
AC-51										
L	138.3	0.26	-	-	-	-	-	-	-	0.9817
R-P	-	-	-	122.70	-	-	2.32	0.76	-	0.9947

Conclusions

The present study shows that the activated carbon prepared from low-cost grapevine rhytidome is an effective adsorbent for the removal of MB and MO from aqueous solution which is comparable with the commercial one. Based on the obtained results from both equilibrium and kinetic studies, GAC and AC-51 provide heterogeneous surface with at least two different sites for adsorption of MB and MO.

References

[1] A. Bhatnagar, A.K Jain, J. Colloid Interface Sci., 281 (2005) 49-55.

[2] R. Baccar, J. Bouzid, M. Feki, A. Montiel, J. Hazard. Mater., 162 (2009) 1522-1529.

[3] V.S. Mane, I.D. Mall, V.C. Srivastava, J. Environ. Manage., 84 (2007) 390–400.

A mesoporous poly(4-vinylpyridinium hydrochloride)-CrO_3 network as a purely organic heterogeneous nanocatalyst for the alcohols oxidation

Roozbeh Javad Kalbasi,* Majid kolahdoozan,* Seyed Mohsen Hosseini
Department of chemistry, Islamic Azad University, Shahreza Branch, 311-86145, Shahreza, Isfahan, Iran
Corresponding Author E-mail: rkalbasi@iaush.ac.ir, kolahdoozan@iaush.ac.ir

Introduction

The selective oxidation of alcohols to the corresponding aldehydes or ketones is a fundamental transformation in both laboratory synthesis and industrial production. Although many useful procedures for oxidation of different organic compounds have been reported [1], the main disadvantage of these reagents is the difficult working-up of the reaction mixture.

Functional polymers are specified as very efficient catalyst supports, since they provide the stabilizing steric bulk of their framework and several binding sites for simultaneous interactions with the particles and the substrates. Poly (4-vinylpyridine) (P4VP) is particularly attractive because of its ability for interacting with polar species through hydrogen bonding [2].

Mesoporous polymer networks are a class of materials that features the mentioned texturation [3,4], and works in this field recently succeeded in synthesizing mesoporous polymers with high thermal stability, namely highly cross-linked mesoporous poly(4-vinylpyridine) (mp-4-VP) [5], using silica nanospheres as hard templates [6]. The nanostructure of the mp-4VP network is not dependent on swelling effects, thus the material can be used in a variety of solvents without loss of the texturation. Since the pores are also well connected, the material is well suited for applications requiring good mass transport properties as it is the case for catalysis. Other features include possibility of tailoring the pore structure, framework composition, and morphologies over a wide range [7]. Many potential applications arise from the potential properties of these high surface area materials, including separation technology (chromatography, membranes, etc.), catalysis, nanoelectronics, sensors, and spatially defined host materials for substances or reactions [8]. In this work, mp-poly(4-vinylpyridinium hydrochloride)-CrO_3 network (mp-P4VP-CrO_3) was synthesized and fully characterized. Then, the properties of mp-P4VP-CrO_3 network on the oxidations of alcohols were tested.

Experimental

Fully cross-linked mp-P4VP-CrO_3 was synthesized using a SBA-15 as template. Then template was washed away. Then CrO_3 supported on it. A typical oxidation of aromatic alcohols was performed; the progress of reaction was monitored by Thin Layer Chromatography (TLC). After Completion of the reaction, for the reaction work-up, the catalyst was removed from the reaction mixture by the filtration.

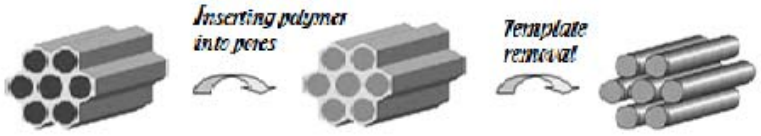

Results and discussion (TGA)

Obtained products were characterized by means of X-ray diffraction spectrophotometer (XRD), scanning electron microscopy (SEM), thermo gravimetric analysis (TGA), and brunauer emmet teller (BET). The etching of the formed nanocomposite of poly(4-vinylpyridine) and silica particles yielded a porous solid with a well defined and accessible porosity.

A narrow distributed average pore radius of about 60 Å was found which is consistent with the size of the template and the solid sample featured an average surface area of 180 $m^2\ g^{-1}$.

Conclusion

Our studies showed that P4VP-CrO_3 network serve as highly active heterogeneous oxidant nanocatalyst for the oxidation of benzyl alcohol and its substituted homologues. The existence of pure organic phase in this composite has had the critical effect on the catalytic activity. This methodology is simple, fast, mild, and efficient. Therefore it is believe that the synthetic method would be greatly contributed to the environmentally processes.

References

[1] Hudlicky, M. Oxidations in organic chemistry, American chemical society science, Washangton, DC, 1990.

[2] Tamami, B.; Parvanak Borujeni, K. Iran. Polym. J. 2009, 18, 191.

[3] J.S. Lee, A. Hirao, S. Nakahama, Macromolecules 21 (1988) 274.
[4] C.G. Göltner, M.C. Weissenberger, Acta Polym. 49 (1998) 704.
[5] J. Weber, M. Antonietti, A. Thomas, Macromolecules 40 (2007) 1299.
[6] A. Thomas, F. Goettmann, M. Antonietti, Chem. Mater. 20 (2008) 738.
[7] Kickelbick, G. Angew. Chem. Int. Ed. 2004, 43, 3102.
[8] Stein, A. Adv. Mater. 2003, 15, 763.

Preparation and Characterization of ZrO_2 Supported with $H_3SiW_9Mo_2VO_{40}$ and Its Application in Catalytic Esterification Reactions

M. Mirzaee*, B. Bahramian, M. Khosravi
Department of Chemistry, Shahrood University of Technology, Shahrood, Semnan, Iran
Email: mmirzaee@shahroodut.ac.ir

Keywords: Sol-gel method, $H_3SiW_9Mo_2VO_{40}$, Adsorption, Impregnation, Heterogeneous catalyst, Esterification reaction.

Introduction

The extensive application of supported heteropoly-acids (HPAs) as a heterogeneous catalyst for a wide variety of applications continues to thrive. Acidity of the HPAs for certain catalytic reactions can be adjusted by choosing a suitable support. Apparently, the surface area, particle size, pore structure and distribution of the protons of HPAs, which are usually referred to as the elements of tertiary structure, the nature of supports and interaction of HPAs with support is very influential on catalytic activity. In this research we have been investigated catalytic activity of $H_3SiW_9Mo_2VO_{40}$ supported on ZrO_2 for the esterification of n, s and t-butanol with acetic acid. Supporting of $H_3SiW_9Mo_2VO_{40}$ on the surface of ZrO_2 and the yield of organic reactions were investigated by IR, Uv-Vis Spectroscopies and GC respectively.

Methods

$H_3SiW_9Mo_2VO_{40}$ [1] and sol-gel derived ZrO_2 powder [2] were prepared according to the literature. $H_3SiW_9Mo_2VO_{40}$ was supported on hydrous zirconia by impregnation method. 1.0g ZrO_2 was impregnated with an aqueous solution of HPA (0.3g/30ml water). This suspension was mixed for 0.5-24hr, then centrifuged and the above aliquots were analyzed by uv-vis spectroscopy (Ray leigh UV-2601) in the wavelength range of 200 to 400 nm with quartz cell, to calculate the amount of adsorbed HPA on the surface of ZrO_2 powder; And the solid, analyzed with IR Spectroscopy (Shimadzo 470). The sample impregnated for 30min, after drying at 100˚C for 12hr, was used for the catalytic reaction. The esterification of n-butanol

(99.8mmol, 7.4 g) with acetic acid (199.8mmol, 12g) was investigated in round bottom flask provided with condenser containing different amount of catalyst at 60-100˚C up to 24hr. Founded optimum conditions were used for the esterification of 2-butanol and t-butanol with acetic acid. The product esters were analyzed on GC (Micro-Pars, FID detector, Silicon DC-200 column).

Results and Discussion

Uv-vis data shows that by stirring the ZrO_2 in HPA solution up to 30min, the concentration of the HPA in solution decreased, that means the amount of adsorbed $H_3SiW_9Mo_2VO_{40}$ on the surface of ZrO_2 was increased. But after 30min, up to 24hr, the concentration of HPA in solution was increased again and showed desorption of HPA from surface of ZrO_2. Because of this phenomenon, we stirred suspension of ZrO_2 in HPA solution for 30min in impregnation process for the preparation of heterogeneous catalyst. IR Spectroscopy proved that HPA was supported on the surface of ZrO_2 powder. GC analysis showed that in the esterification of n-butanol with acetic acid, increasing the amount of catalyst from 125mg to 250mg, increased the yield from 51.6 to 66% after 24hr. But further increasing of the amount of catalyst to 500mg lowered the yield of reaction to 47% after 24hr, maybe because of the inhomogeneous mixing during the process. On the other hand, by increasing the molar ratio of alcohol/acid from 1/2 to 1/1 and 2/1, the yield of reaction decreased from 66 to 51 and 34% after 24hr respectively. Furthermore, by increasing the reaction temperature from 60 to 80 and then 100˚C, the yield of reaction increased from 43 to 66 and then 81.6% after 24hr respectively. But in the esterification of s and t-butanol with acetic acid, with 250mg catalyst, alcohol/acid molar ratios of 1/2 at 80˚C after 24hr, the yield of reaction are 53 and 17% according to the GC analysis.

Conclusion

Results showed that the optimum conditions for the esterification of n-butanol with acetic acid in the presence of ZrO_2 Supported with $H_3SiW_9Mo_2VO_{40}$ are 250mg catalyst with alcohol/acid molar ratio of 1/2 at 100˚C. Also we can conclude that this catalyst is more efficient for esterification of first order alcohol with acetic acid in comparison by secondary or tertiary alcohols with acetic acid.

Reference:

[1] E. Cadot, R. Thouvenot, Inorg. Chem. 31 (1992) 4128-4133.

[2] N. Bhatt, A. Patel, J. Mol. Catal. A 238 (2005) 223-228.

Investigation of $H_3PW_{12}O_{40}$ and $H_4SiW_{12}O_{40}$ Adsorption on ZnO Powder

M. Mirzaee*, M. Khosravi, R. Doosti, M. Arefian
Department of Chemistry, Shahrood University of Technology, Shahrood, Semnan, Iran
Email: mmirzaee@shahroodut.ac.ir

Keywords: Heteropoly-acid, Adsorption, Uv-Vis Spectroscopy, Sol-gel method, nano-sized ZnO.

Introduction

The extensive application of supported heteropoly-acids (HPAs) as a heterogeneous catalyst for a wide variety of applications continues to thrive. Acidity of the HPAs for certain catalytic reactions can be adjusted by choosing a suitable support. Apparently, besides the surface area, particle size, pore structure and distribution of the protons of HPAs, which are usually referred to as the elements of tertiary structure, the nature of supports and interaction of HPAs with support is very influential on catalytic activity. In this research we have been investigated adsorption of different HPAs ($H_3PW_{12}O_{40}$, $H_4SiW_{12}O_{40}$) supported on different ZnO powders (commercial and nano-sized) by Uv-Vis Spectroscopy.

Methods

$H_3PW_{12}O_{40}$ [1] and $H_4SiW_{12}O_{40}$ [2] were prepared according to the literature. Commercial ZnO were purchased from Merck (108846) and nano-sized ZnO was prepared by sol-gel method with tow different precursors (salt [3] and alkoxide [4]) according to the literature. 0.015g ZnO was added to a 30 ml of 0.25 mg/ml HPAs solution in water (12.5 mg HPA dissolved in 50ml water) and stirred for 24hr. In different intervals, samples (4ml) of suspension were taken. The solid was separated by centrifuge and washed with cold and hot water respectively. The above aliquots were analyzed by uv-vis spectroscopy (Ray leigh UV-2601) in the wavelength range of 200 to 400 nm with quartz cell, to calculate the amount of adsorbed HPAs on the surface of ZnO powders.

Results and Discussion

Uv-vis data shows that the amount of adsorbed $H_3PW_{12}O_{40}$ on the surface of commercial ZnO powder, by increasing the processing time, increased up to 4 hr and then remained unchanged up to 24 hr. But the results of uv-vis data show that by adsorption of $H_4SiW_{12}O_{40}$ on the surface of commercial ZnO powder, the structure of HPA changed and destroyed. On the other hand by using nano-sized ZnO powders, the amount of adsorbed $H_3PW_{12}O_{40}$ increased up to 12 hr and then remained unchanged up to 24hr. This was attributed to the larger surface area of nano-sized ZnO powder in comparison with commercial ZnO powder. The loading percent of each sample was calculated and shows that it was increased by the order: nano-sized ZnO powder (alkoxide precursor, 10.6%), commercial ZnO powder (13.7%), nano-sized ZnO powder (salt precursor, 26.7%).

Conclusion

It was concluded that the ZnO preparation method has crucial effect on amount of HPAs adsorption on the surface of ZnO powders. In this way, commercial ZnO and nano-sized ZnO powder prepared from alkoxide precursor have lower capacity for the supporting HPAs than nano-sized ZnO powder prepared from salt precursor.

Reference:

[1] Booph, H. C. Inorganic Synthesis Vol. 1, 1939, Mc Grow Hill, New York.
[2] Hu C. W., Hashimota M., Okuhara T. J. Catal., 143 (1993) 437-448.
[3] N. Daneshvar, S. Aber, Separation and Purification Technology 58 (2007) 91-98.
[4] Cornes C. L., Klabunde K. J. Langmuir 16 (2000) 3764–3772.

Temperature dependent behavior of CTAB and Triton X-100 surfactants in relation to the Oil recovery enhancement efficiency

M.H. Ghatee*[a], M. Bahrami[a], N. Khanjari[a], Sh. Ayatollahi[b], O. Seiedi[b]

[a]Department of Chemistry, College of Science, Shiraz University, Shiraz, Iran, 71454

Email:ghatee@susc.ac.ir

[b]EOR Research Center, School of Chemical and Petroleum Engineering, Shiraz University

Keywords: Change in Solution Structure, Surfactant, Temperature Effect, Viscosity, UV and Flourescence Spectroscopy.

Introduction

The role of surfactant treatment has been widely investigated as an efficient method in Enhanced Oil Recovery. A surfactant either acts to reduce the interfacial tension (IFT) or to alter the wettability of reservoir rock. Therefore, the oil recovery enhancement is due to alternating the wettability of rock surface from oil-wet to more water-wet condition. The effect of cationic, anionic, and non-ionic surfactants on enhancing oil recovery has been studied.[1, 2]

Experiment has shown that the non-ionic surfactant/brine solution (Triton X-100) is more effective than the solution of cationic surfactant CTAB, Particularly as the temperature increases, the oil recovery by using Triton X-100 is appreciably increases.[3] Here, the interest is to understand the basic reason which makes Triton X-100 advantageous over CTAB in wattability alteration as the temperature is increased.[3] Certainly, the source of these differences is the physical properties specific to their chemical nature. Indeed we pursue the difference in the physical properties of the brine solution of these two surfactants and their behavior as temperature is raised. The physical property we study is the viscosity as a function of surfactant concentration at different temperature. Also, the temperature dependence of the structural behavior surfactants is probed using absorption and fluorescence spectroscopy.

Experimental

CTAB and Triton X-100 solutions were prepared in brine solution of usual concentration. The range of concentrations spans the critical micelle concentration (CMC), e.g. 0.03% for CTAB and 0.015% for Triton X-100. The viscosity of each the solution was measured in the temperature range 25 to 80 °C .

The structural behavior of Triton X-100 was probed as a function of temperature using pyrene. Further investigations are advancing to study the structural behavior as a function of change using fluorescence spectroscopy.

Results and Discussion

In Figure 1 and 2, the results of viscosities measurements are shown for CTAB and Triton X-100, respectively. As it can be seen, viscosity increases with concentration smoothly at all temperature. This is the case for CTAB too. Some fluctuations are seen close to CMC's. The fluctuations for TritonX-100 look to be different from those of CTAB, indicating the difference in the nature of these two surfactants. More importantly the fluctuation enhanced close to 60 °C . These particular fluctuations are, however, absence in the case of CTAB. This can be interpreted in terms of salting out which occurs in the case of Triton X-100. Further investigations were performed by probing the particular structural changes as a function of temperature. Pyrene with the characteristics adsorption spectra in the UV region was was found to be suitable (See Figure 3). It can be seen that as the temperature increases the base line of the spectra increases. From absorption spectra shown in Figure 3, a transition in the solution structure can be identified near 60 ^{o}C. Further investigations are in progress by fluorescence spectroscopy.

Conclusions

This study indicates that the preference of Triton X-100 over CTAB is due to the difference in their inherent structure. As the temperature increases there is a drastic change in the structure of Triton X-100. The high efficiency of it can be attributed to this.

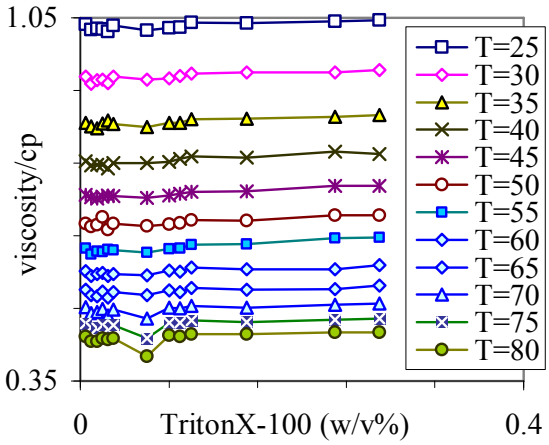

Figure 1. Viscosity versus concentration of Triton between 25-80 °C.

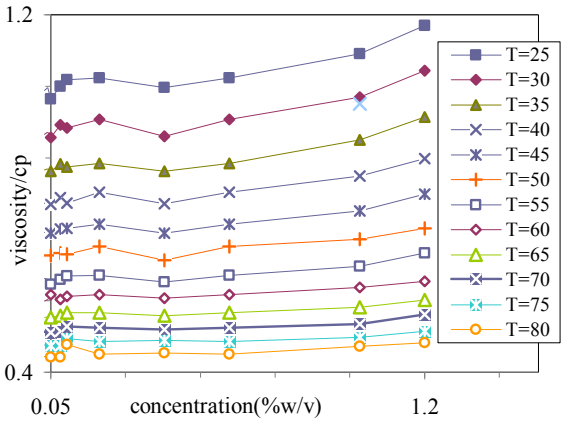

Figure 2. Viscosity versus concentration of CTAB between 25-80 °C.

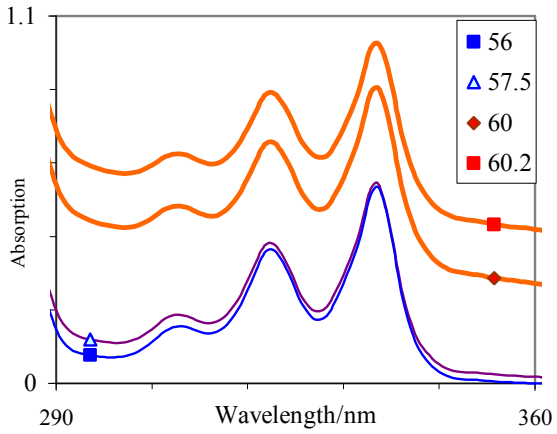

Figure 3. Absorption spectra of Triton solutions at different temperatures.

References:

[1]T. Austad, B. Matre, J. Milter, A. Sævareid, L. Øyno, Colloids and Surfaces A, 137 (1998) 117-129.

[2] D. Ch. Standnes, D.C., M.Sc. Thesis, University of Stavenger, Norway.

[3]O. Seiedi, M.Sc. Thesis, Shiraz University, July 2009.

Comparison the performance of MCM-41 and activated carbon for removal dye from solution

Zohreh Derikvand*, Ghazaleh Khochakzadeh

Department of Chemistry, Faculty of Science, Islamic Azad University, Khorramabad Branch, Khorramabad, Iran

zderik@yahoo.com

Keywords: Dye solution preparation, MCM-41, Activated Carbon,

Introduction:

Dye wastewaters are discharged by a wide variety of sources, such as textiles, printing, dyeing, dyestuff manufacturing, and food plants [1-3]. Dye can reduce light penetration into the water thereby decreasing the efficiency of photosynthesis in aquatic plants and hence having adverse impart on their growth. Adsorption is an effective method for lowering the concentration of such material in the environment especially if the adsorbent has high adsorption capacity. Adsorption using activated carbon is rapidly becoming a prominent method of treating aqueous effluents and has been used in industrial processes for variety of separation and purification process. In this regard activated carbon and MCM-41 were used for comparing the performance of both adsorbents for removal of dyes.

Methods and Materials:

The azo dye, safranine, activated carbon, GAC, were purchased from Merck. The concentration of safranine solution was 20, 25, 30, 35 and 40 mg/L. Maximum absorbance wavelength (λ_{max}) was recorded on a JELWAY 6505 UV-Vis spectrophotometer.

The mesoporous MCM-41 powder was crystallized from an alkaline solution containing cetyltrimethylammonium bromide (CTABr, 99%, Merck), sodium silicate solution and deionized water. After 72 h in hydrothermal treatment at 100 °C, the MCM-41 powder was filtered, washed, and dried then it was calcined at 600 °C for 16 h in air to remove the organic template.

Result and Discussion:

Fig. 1 shows *p*H effects on the adsorption capacity of safranine on the GAC and MCM-41. The amount of dye adsorbed on GAC decreases significantly at low (2-4) *p*Hs, then it increase and it is constant in *p*H = 6. However amount of dye adsorbed on MCM-41 increase at (2-6) pHs. In pH = 6 is nearly constant.

Dye removal efficiency:

The removal efficiency of safranine was calculated as follows:

$\%Removal = 100(C_i-C_e) / C_i$

Where C_i is initial dye concentration (mg/L), C_e is equilibrium dye concentration (mg/L)[4]. The result shows a lot of adsorption for adsorbent of MCM-41. Dye removal efficiency at the initial dye concentration of 30 (mg/L) on MCM-41 was calculated 99%, but dye removal efficiency in the same concentration on GAC was calculated 18%. So, dye removal efficiency from MCM-41 better than GAC because MCM-41 is a mesopore but GAC is a micr pore.

Enthalpy Adsorption:

Heat of adsorption dye was calculated as follows:

Where K is equilibrium constant, ΔH is heat of adsorption, R is gas constant and T is temperature. From slope of equation, ΔH in adsorption dye by GAC was calculated -22.87 KJ/mol and for adsorption dye by MCM-41 was -137.23 KJ/mol. We can say adsorption on MCM-41 is in the border line of physisorption-chemisorption and was named activated adsorption.

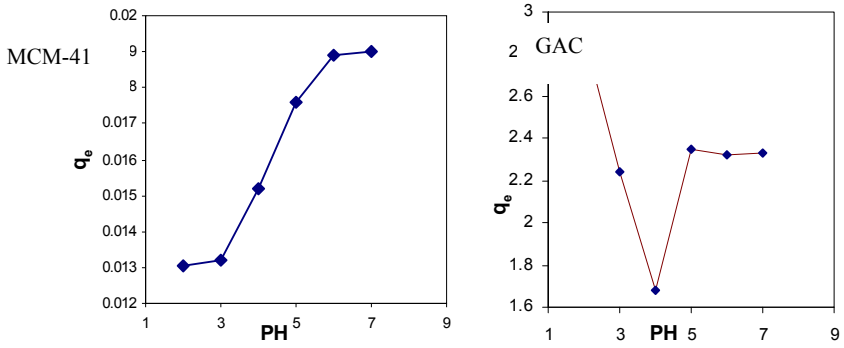

Fig.1 Effect of *p*H on adsorption capacity of safranine on GAC and MCM-41.

References

[1]D. Pokhrel, T. Viraraghavan, Sci. Total Environ. 333 (2004) 37–58.

[2] O. Tunay, I. Kabdasli, G. Eremektar, D. Orhon, 34 (1996) 9–16.

[3] A. Cassano, R. Molinari, M. Romano, E. Drioli, J.Membr. Sci. 181 (2001) 111–126.

[4] A. Babarinde, J. Appl. Sci. Research, 4(6) (2008) 716-721.

Comparison between different activity coefficient models in prediction of Surface tension and interfacial tension

M. Dadras, M. R. Dehghani

Chemical Engineering Department, Iran University of Science & Technology, Narmak, Tehran 16846, Iran

Abstract

A modified model has been proposed for the calculation of surface tension (ST) and interfacial tension (IFT) in electrolyte solutions. Based on the Gibbs dividing surface concept, the Langmuir adsorption equation was adopted for surface and interfacial tension in electrolyte solutions. Different activity coefficient model such as extended UNIQUAC model, Pitzer equation and Meissner method have been utilized for this purpose. In this work surface tension of single-electrolyte aqueous systems including NaCl, KCl, HCl, $NaNO_3$, HNO_3, KNO_3, NH_4NO_3, Na_2CO_3, Na_2SO_4, KOH, $BaCl_2$ have been estimated using modified model. The interfacial tension between NaCl and n-Dodecane, n-Hexane and Benzene, HCl and Tributyl phosphate & Solvesso, KCl and n-hexane have been estimated by mentioned activity models. The results showed that the modified model has been predicted surface and interfacial tension with overall absolute average deviation of 0.2 and 0.39 respectively.

Keywords: Surface Tension; Interfacial Tension; Prediction; Electrolyte; Extended Uniquac model; Activity coefficient.

Introduction

Surface properties such as surface tension and Interfacial tension have an important application in different processes such as separations and purifications in chemical engineering. In this regard Prediction of surface and interfacial tension has received more attention during recent years. In this work different activity models have been used for prediction surface and interfacial tension.

Theory

Gibbs adsorption equation is one of the most attractive methods in this field. The Gibbs adsorption equation states that the reversible surface energy change between the bulk vapor and liquid or two liquid phases at constant temperature and pressure can be introduced by [1]:

$$-d\sigma_{Int} = \Gamma_w d\mu_w^{Int} + \Gamma_{ca} d\mu_{ca}^{Int} \quad (1)$$

where, Γ_w and Γ_{ca} are described relative to an arbitrarily chosen dividing surface, it is feasible in principle to locate that surface, so that $\Gamma_w = 0$ and Eq. (1) is shrank in term of the activity of the electrolyte [2,3], a_{ca}, by

$$-d\sigma_{Int} = \Gamma_{ca}^{w} RTd \ln a_{ca} \quad (3)$$

In equilibrium the rate of adsorption and desorption of the electrolyte is equal. Using Langmuir adsorption model and coupling with equation following equation will derive:

$$-d\sigma_{Int} = \Gamma_{ca}^{w\infty} \frac{K_{ca} a_{ca}}{1 + K_{ca} a_{ca}} RTd \ln a_{ca} \quad (4)$$

Integration Eq. (4) from $a_{ca} = 0$ to a_{ca} leads us to following equation for estimating surface tension of aqueous single-electrolyte solution and IFT between an organic solvent and an aqueous single-electrolyte solution:

$$\sigma_{Int} = \sigma_{Int0} + RT\Gamma_{ca}^{w\infty} \ln \frac{1}{1 + K_{ca} a_{ca}} \quad (5)$$

In Eq. (5) σ_{Int0} is the surface tension of pure water or IFT between an organic solvent and pure water in absence of any electrolyte at the system temperature. Meanwhile activity of electrolyte can be substituted form different activity models such as Meissner, Pitzer and used Extended UNIQUAC model. In this work the capability of Extended UNIQUAC model has been investigated for the first time.

Result

In this work the capability of different activity models has been checked. The results showed that in overall, modified model can predict surface tension of inorganic salts accurate than acids. The model parameters have been determined by minimization of AARD. The results for different model have been presented in Table 1. It is shown that there are good agreements between experimental and model results. It can be concluded that the capability of different activity coefficient model are the same. This subject can be pointed to adjustable parameters in Gibbs adsorption model. As in each case two parameters should be adjusted. This matter has caused we cannot judge about ability of activity model. For better judgment this parameters must be utilized for prediction of surface tension in mixed electrolyte solution.

Table 1. The model parameters for Surface Tension with three models

			Extended UNIQUAC			Pitzer			Meissner		
Salt	**T(K)**	**m_{Max}**	$\Gamma_{ca}^{w\infty}$	**K**	**AAPD**	$\Gamma_{ca}^{w\infty}$	**K**	**AAPD**	$\Gamma_{ca}^{w\infty}$	**K**	**AAPD**
$NaNO_3$[2]	291.15	9.84	-1.5191e-6	1.5677	0.1828	-1.66e-6	1.25	0.22	-1.4243e-6	1.5827	0.2284
$NaNO_3$[5]	293.15	1.8	-7.6622e-7	5.5825	0.1117	-7.2098e-7	5.7032	0.114	-6.962e-7	6.4858	0.1114
HNO_3[2]	303.15	29.09	5.9872e-7	0.1082	0.5536	8.05e-7	0.106	1.04	5.0034e-7	0.1083	0.6776
$(NH_4)_2SO_4$[6]	295.15	1	-3.6450e-7	199.61	0.0683	-3.1546e-7	13.522	0.0692	-4.5272e-7	16.015	0.0559
KOH[2]	291.15	3.8	-5.6357e-7	8.5668	0.1896	-5.44e-7	8	0.31	…..	…..	…..
NaCl[7]	293.15	1	-3.0042e-7	15.536	0.0444	-2.8759e-7	15.591	0.0456	-2.8055e-7	16.573	0.0451
KCl[8]	293.15	1.84	-7.2325e-7	7.1981	0.1809	-7.4845e-7	6.3407	0.1899	-7.329e-7	6.7758	0.1901
$MgCl_2$[9]	298.15	0.81	-2.1905e-7	609.77	0.1098	-2.028e-7	400.59	0.1307	-1.7777e-7	559.14	0.1291
$BaCl_2$[4]	293.15	0.3	-3.6939e-6	25.961	0.2734	-2.7492e-6	23.924	0.2804	---	---	---
HCl[10]	293.15	14.9	5.4955e-7	0.0049	0.6409	4.12e-7	0.00468	0.51	5.0251e-6	0.0045	0.6128
KNO_3[5]	298.15	1.8	-1.3829e-6	3.8822	0.1503	-1.6676e-6	3.2216	0.1593	-1.3438e-6	4.4294	0.1493
NH_4NO_3[5]	293.15	1.9	-1.7836e-7	37.538	0.1196	-1.7547e-7	40.092	0.1192	-1.7899e-7	40.918	0.1182
Na_2CO_3[2]	303.15	0.465	-2.1315e-7	1035.5	0.0524	-1.9693e-7	1074.6	0.0537	-1.8133e-7	1420.5	0.0507
Na_2SO_4[2]	308.15	0.9	-3.2428e-7	268.44	0.0828	-3.1574e-7	312.562	0.0826	-2.8011e-7	389.27	0.0815
Overall AAPD					0.2			0.24			0.2

References

[1]A.W. Adamson and A.P. Gast, "Physical Chemistry of Surfaces", Journal of Wiley & Sons, New York, 1997.

[2] Z. Li, B.C.Y. Lu, Surface Tension of Aqueous electrolyte solutions at High Concentrations- Representation and Prediction, Chem. Eng. Sci., 2001, pp. 2879-2888.

[3]Z. Li, B.C.Y. Lu, Prediction of Interfacial Tension between an Organic Solvent and Aqueous Solution of Mixed Electrolytes, J. Fluid Phase Equilibria, 2002, 239-250.

[4]M. Kidokoro, The Interfacial Tension between Hexane and Aqueous Salt Solutions, Bulletin of Chemical Society of Japan, 1932, pp. 280-286.

[5]K. Ali, A.u.H. Ali Shah, S. Bilal and A.u. Haq, "Thermodynamic Parameters of Surface Formation of Some Aqueous Salt Solutions", Journal of Colloid Surfaces A: Physicochemistry Engineering Aspects, 2008, pp. 28-34.

[6]N. Matubayasi, K. Takayama and T. Ohata, "Thermodynamic Quantities of Surface Formation of Aqueous Electrolyte Solutions IX. Aqueous Solutions of Ammonium Salts", Journal of Colloid Interface Science, 2010, pp. 209-213.

[7]N. Matubayasi, H. Matsuo, K. Yamamoto,S.I. Yamaguchi and A. Matuzawa, "Thermodynamic Quantities of Surface Formation of Aqueous Electrolyte Solutions I.

Aqueous Solutions of NaCl, MgCl2, and LaCl3", Journal of Colloid Interface Science, 1999, pp. 398-402.

[8]K. Ali, A.u.H.A. Shah, S. Bilal, A.u.H.A. Shah, "Surface Tensions and Thermodynamic Parameters of Surface Formation of Aqueous Salt Solutions: III. Aqueous Solution of KCl, KBr and KI", Colloid Surface A: Physicochemistry Engineering Aspects, 2009, pp.194-199.

[9]N. Matubayasi, K. Yamamoto, S.I. Yamaguchi, H. Matsuo and N. Ikeda, "Thermodynamic Quantities of Surface Formation of Aqueous Electrolyte Solutions III. Aqueous Solutions of Alkali Metal Chloride", Journal of Colloid Interface Science, 1999, pp. 101-105.

[10]A.A. Abramzon and R. D. Gaukhberg, "Surface Tension of Salt Solutions", Russian Journal of Applied Chemistry, 1993, pp.1320.

Investigation of instability and relationship between instability and magnetic properties at ferrite magnetic single-domain region, MO-Fe_2O_3 (M=Cu,Ni)

M.R.Rostami*[a] , A.Yazdani[b] , S.Morshedi[a]

[a]*Department of Physics, University of Islamic Azad, North Tehran Branch, Tehran, Iran*

(Email:moosafere@yahoo.com)

[b]*Department of Physics, University of Tarbiat Modares, Tehran, Iran*

Keywords: Instability, Spinel, Ferrite, Magnetic, Coercivity, bond energy.

Introduction:

The ferrites are one type of spinel ceramics. These compounds have many applications for produce hydrogen and in medical science due to their soft magnetic properties and characteristics of their instability. Therefore, we study the instability and the magnetic properties of ferrites.

Results and discussions:

1. Study of thermal instability of ferrites:

In this study instability of thermal and its effect on the crystal structure of nickel ferrite and specially copper ferrite of prepared with co-precipitation method, has been considered. The effect of preparation conditions, the effect of environment at factors and the effect of cation distribution at ferrites have been taken for investigation of instability. In here, instability at two kind of gas has been investigated for nitrogen and methane gas (for effect of environmental conditions) and This result shows that the ferrites inside of gas space of CH_4 ,earlier become unstable. The results also shows that stability of $NiFe_2O_4$ is more than $CuFe_2O_4$[1]. Table 1, shows stability of prepared copper ferrite in T_a=1000°C is more than at T_a=800°C (for effect of preparation conditions).

Table 1. Mass loss of copper ferrite at various temperatures inside of gas space of Nitrogen (per persent).

T_b ($^{\circ}C$)	T_a=800 $^{\circ}C$	T_a=1000 $^{\circ}C$
900	1.4	-
1000	2.3	1.4
1100	2.9	2.4
1200	3.4	2.8

Effect of cation distribution indicated that for $NiFe_2O_4$ and $CuFe_2O_4$ that have inverse spinel structure, reduce their degree of inversion is causing instability. This is also true for nanoparticles and the degree of inversion is reduced for them because of reduced stability of particles in a nano-state. Then, Using Jahn-Teller effect, metallic property of ferrite in duration of thermal instability and WIEN2K software, change of crystal phase with creation of thermal instability has been investigated [2]. These results indicate that the crystal structure of copper ferrite during thermal instability is tilted and its structure becomes trigonal and triclinic. According to these results copper ferrite during thermal instability can not accept structures with degree of inversion x=0,0.5CM,0.25R3M , because these structures are not metallic.

2. Study of magnetic properties of nano ferrites:

In this study, bond-energy theory (about cohesive energy) is improved for thermal instability of ferrites of multi-element [3,4]. This equation shows the instability of ferrite depends on size of particl. Using this theory, relationship between magnetic coercivity ,H_C, saturation magnetization ,M_S, temperature instability of bulk ,T_{sb}, and temperature instability of nano ferrite ,$T_{sp,}$ is applied as follow:

$$H_C = \frac{2K_a}{M_S}\left[1 - \frac{1}{G}\left(\frac{Ln\left(\frac{\tau}{\tau_0}\right)(k_B T)}{K_a \pi}\right)^{\frac{1}{2}}\left(1 - \frac{T_{sp}}{T_{sb}}\right)\right]$$

Where ,$K_{a,}$ the constant of magnetic anisotropic ,τ, the spin relaxation time ,T, room temperature ,$k_{B,}$ Boltzman constant and ,G, is a coeffecient depends on ionic bond and the shape of particles of ferrite.

Conclusion:

1- Important factors for instability ferrites are include: preparation conditions, environmental conditions and cation distribution at ferrites.

2- Copper and nickel ferrites with inverse spinel structure are stable than normal spinel and partial-inverse spinel structures.

3- Any ratio of $\frac{T_{sp}}{T_{sb}}$ for ferrites to be more, we have stronger magnetic coercivity at magnetic single-domain region.

References:

[1] ZHANG Ping, YU Bo & ZHANG Lei "Mechanism of oxygen releasing of copper ferrite in the formation of the corresponding oxygen-deficient compound" Sci China Ser B-Chem, 101-108 (2009).

[2] Min Feng, Aria Yang, Xu Zuo, Carmine Vittoria, and Vincent G. Harris . "Ab initio study on copper ferrite" JOURNAL OF APPLIED PHYSICS 107, 09A521 (2010).

[3] W.H. Qi, M.P. Wang, G.Y. Xu, "The particle size dependence of cohesive energy of metallic nanoparticles" Chem. Phys. Lett. (2003), 372: 632.

[4] W.H. Qi, M.P. Wang "Size and shape dependent melting temperature of metallic nanoparticles" Mater. Chem. Phys. (2004), 88: 280.

Synthesis and characterization of nanoparticles of hematite (α-Fe_2O_3) and adsorption isotherms investigation of Cu (II) on hematite and the evaluations of thermodynamic and kinetic parameters

A. Farrokhnia* N. ramezani
Department of Chemistry, University of Chamran, Ahwaz, Iran
a.farookhnia@gmail.com
ramezaninasir@yahoo.com

Keywords: Hematite nanopasrticles, Adsorption isotherms, Thermodynamic parameters', Kineti parameters'.

Introduction

Iron oxide nano particle is a very important multifunctional material, which is extensively used in fine ceramics, pigments, catalysis and is the best of adsorbent for removal of heavy metals from aqueous solution. The presence of heavy metals in the environment is a major concern due to their toxicity for many life forms. Therefore, the elimination of heavy metals from water and
Waste water is important to protect public health.

Materials and methods

Iron chloride hexahydrate $FeCl_3 \cdot 6H_2O$, sodium hydroxide NaOH and distilled water were used in all experiments.

Hematite nanoparticles have been prepared by heating $Fe(OH)_3$ gel after adding trace Fe(II) catalyses in aqueous solution to reflux temperature [1]. The optimum conditions were obtained. α-Fe_2O_3 nanoparticles characterized by using X-ray diffraction (XRD), atomic force microscope (AFM), scanning electron microscope (SEM) and infrared spectroscopy (IR).The results are shows in Fig. 1and Fig. 2.

Results and discussion

The aim of the present work was the ability of hematite nanopaticles to removal of Cu(II) from aqueous solution and investigate thermodynamic and kinetic parameters of the adsorption process. In the thermodynamic study the adsorption isotherms Langmuir, Freundlich and Temkin were applied and standard enthalpy (ΔH°), standard entropy (ΔS°) and standard free energy (ΔG°) were calculated which are given in Table 1 and 2. In the kinetic study equilibrium constant (K) and order of reaction were calculated [2] are gathered in Table 3. The experimental data at five different temperatures (278 K, 291 K, 300 K, 317 K, and 339 K) were obtained. It is clear that these result have a significant correlation with Langmuir isotherm model; i.e. the best correlation coefficient is observed for Langmuir isotherm model (R^2= 0.996). The pseudo-second –order model was fitted for this adsorption system (K=0.0316).

Table 1. Calculated thermodynamic parameters (ΔS^0, ΔG^0) at different temperatures, in Kj/mol.

T(K)	**278**	**291**	**300**	**317**	**339**
ΔS°	**94.588**	**92.044**	**93.665**	**96.690**	**97.880**
ΔG^0	**- 2.5001**	**- 2.9904**	**- 4.3049**	**- 6.8576**	**- 9.3882**

Table 2. Calculated standard enthalpy (ΔH°)

Initial copper con. (mg/L)	ΔH° (**Kj/mol**)
20	**23.794**

Table 3. Calculated kinetic parameters in this study

Pseudo – first - order		**Pseudo – second - order**	
$q_{e(\exp)}$ (mg/g)	10.37	$q_{e(\exp)}$ (mg/g)	10.37
q_e (mg/g)	6.147	q_e (mg/g)	10.638
K_1 (1/min)	0.065	K_2 (g/mg.min)	0.0316
R^2	0.944	R^2	0.999

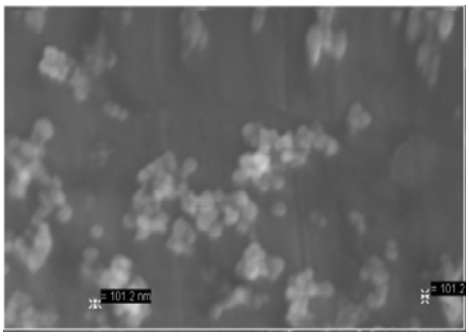

Fig 1. SEM of hematite nano particles

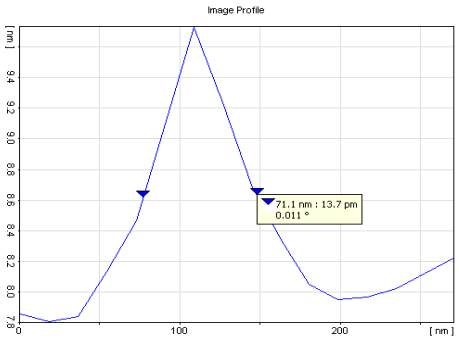

Fig 2. Profile of hematite nano particle

Conclusion

The results of this study indicate that hematite nanoparticle can be successfully used for the adsorption of cu (II) from aqueous solutions. Langmuir isotherm well fitted with the equilibrium data for adsorption of cu (II).

References:

[1] H. Liu, Y. Wei, P. Li, Y. Zhang, Y. Sun, Catalytic synthesis of nanosized hematite particles in solution, Mater. Chem. Phys. 102 (2007) 1-6.

[2] H. Uslu, Adsorption equilibrium of formic acid by weakly basic adsorbent Amberlite IRA-67: Equilibrium, Kinetics, thermodynamic, J. Chem. Eng. 155 (2009) 320-325.

Sodium dodecyl sulfate coated γ-Alumina: An alternative support for solid phase extraction of Pb^{2+} and Cu^{2+} ions after equilibrium study

Ardeshir Shokrollahi [a,*], HosseinTavallali[b], Batool zare khafri [b], Morteza Montazerozohori[a]

[a] Chemistry Department ,Yasouj university, Yasouj, Iran, ashokrollahi@mail.yu.ac.ir

[b] Chemistry Department , Shiraz payam nour University, shiraz, Iran : zare220@gmail.com

Keywords : Solid phase extraction ,Pb^{2+}& Cu^{2+}, γ-Alumina

Introduction

In this study primarily the complexation between the Bis(2-hydroxy acetophenon)-1,6-hexanediimine (BHAH) and metal ions such as $Pb^{2+}$and Cu^{2+} was investigated spectrophotometrically. Then this ligand was selected as a proper modifier for extraction of $Pb^{2+}$and Cu^{2+} ions on the γ-Alumina. The amount of extracted metal ions was determind by AAS.

The most prominent among the supports used are Amberlite XAD resins [1], activated carbon [2], modified chromosorb [3] and sepiolite[4].

Methods

About 1.0 g of γ-Alumina was added to 50 mg of SDS and was mixed with a magnetic stirrer. After addition of 20 mg BHAH ligand dissolved in 3 ml tetra hidro furan (THF) the pH was adjusted a approximately to 2.5 by addition of 1 M HCl. The solution was shaken for 30 min and filtered for preparation of the solid phase. The pH of the solution (250 mL) was adjusted to ~6.0 with hydrochloric acid and passed through the solid phase column at a flow rate of 2 mL min^{1-} with the aid of a suction pump. The analyte was then eluted with 6 mL of 4 M nitric acid. The metal ions content of the eluent was measured by flame-AAS. The same eluate was used to determine all analytes,

Results and discussion

Main factors such as pH, amount of ligand, γ-Alumina , surfactant and condition of eluting solutions on the sorption recovery have been investigated in detail. The method was successfully applied for the determination of these metal ions contents in real samples with satisfactory results.

1. Effect *of pH*

In the solid phase extraction studies, pH of the working solution is main factor for the quantitative adsorption of analytes on solid phase . In order to optimize the sorption conditions for the retention of the ions on modified γ-Alumina , the effects of pH was investigated in the pH range of 2–11 by using column packed with 1.0 g modified γ-Aloumina. Fig. 1 shows that the optimal pH value was in 6.0. Considering these results, the pH 6.0 has been recommended for subsequent experiments.

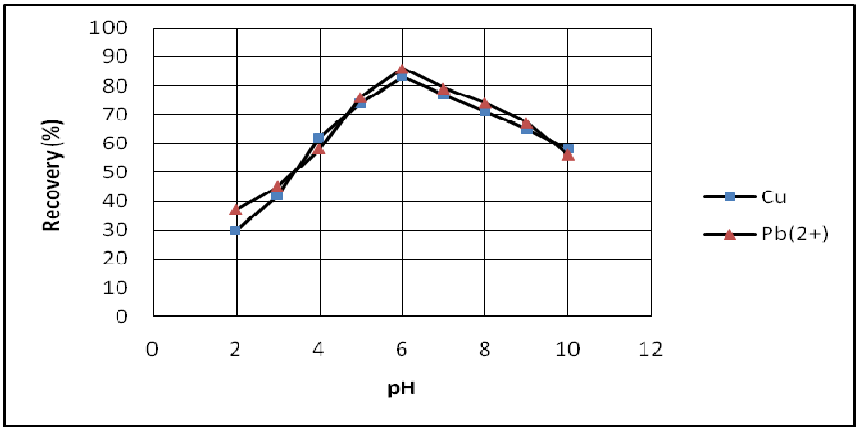

Fig. 1. Effect of pH on recovery of metal ions at optimum conditions

2. Effect of ligand concentration

The amount of ligand on the preconcentration studies is also another main factor. In order to investigate the optimum amount of ligand on the quantitative extraction of these ions by the γ-Alumina , these ions extraction was conducted by varying the amount of ligand from 2 to 70 mg. The recoveries of analyte ions without ligand were not quantitative. The results showed that with increasing amount of ligand up to 25 mg an increase in recoveries can be achieved and further increase does not mentionable change in efficiency.

Conclusion

The modified γ-Alumina by BHAH was used for the extraction and determination of Cu^{2+} and Pb^{2+} in low concentrations in various samples including vegetable, water and liver. This method is simple and there is no need for an elaborate cleanup procedure, since the adsorbed metals are simply eluted with 6 mL of 4 mol L^{-1} HNO_3.

The method due to advantages such as high reliability, reproducibility, sensitivity, and high tolerance limit of common ions and low detection limit is a powerful tool for rapid and sensitive determination of these ions in various media.

References

[1] S.L.C. Ferreira, C.F. Brito, A.F. Dantas, N.M.L. Araujo, A.C.S. Costa, Talanta 48 (1999) 1173–1179

[2] S. Cerutti, S. Moyano, J.A. G´asquez, J. Stripeikis, R.A. Olsina, L.D. Martinez, Spectrochim. Acta, Part B 58 (2003) 2015–2021.

[3] M. Ghaedi, M.R. Fathi, A. Shokrollahi, F. Shajarat, , Anal. Lett. 39 (2006) 1171–1185.

[4] M. Soylak, S. Saracoglu, L. Elci, M. Dogan, Kuwait J. Sci. Eng. 30 (2003)

Effect of calcination conditions on the catalytic performance of Co-Ni/Al_2O_3 catalyst used in FTS

A. A. Mirzaei, A. Zare*, M. Arsalanfar, S. Rezazade, S. Vahid
Department of Chemistry, University of Sistan & Baluchestan, Zahedan, Iran
(e-mail:a_zare87@yahoo.com)

Abstract

A Co-Ni-Al_2O_3 catalyst was prepared using the incipient wetness impregnation method in order to study its catalytic activity and selectivity in the Fischer-Tropsch synthesis. The effect of calcination temperature, time and atmosphere on the catalytic performance of 80%Co-20%Ni/90wt%Al_2O_3 catalyst was investigated. It was found that the optimum calcination temperature is 550˚C and the optimum calcinations time is a 6h at the air atmosphere.

Keywords: Co-Ni catalyst, Impregnation, Calcination conditions, Fischer-Tropsch synthesis.

Introduction

By Fischer-Tropsch (FT) reaction the synthesis gas is converted to a mixture of hydrocarbons. Then hydrocarbons undergo further treatment to yield distillates[1]. Fischer-Tropsch catalysts are mainly restricted to iron and cobalt and a lesser extent to nickel. The combination of Fe-Mn [2], Co-Mn [3,4] and Fe-Co catalyst [5] with or without promoters favors the formation of C_2-C_4 alkenes.

Method

All the tested catalysts in this study were prepared using an impregnation procedure and tested in a fixed bed stainless steel micro reactor.

Results and Discussion

1. Effect of calcination temperature

Cobalt nickel oxide catalysts were prepared by impregnation method, the catalyst precursor was calcined at different temperature between 500-800℃. It was found that the catalyst which was calcined at 550℃ has shown the best catalytic performance (Fig. 1).

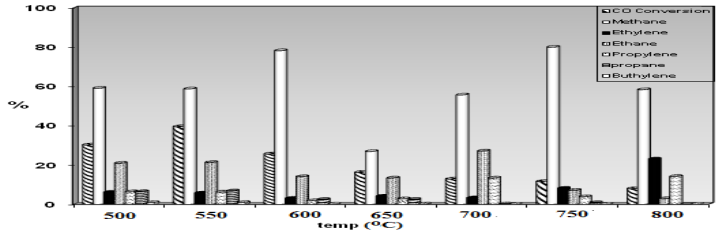

Figure 1. Effect of calcination temperature on the catalytic performance

2. Effect of calcination time

In order to investigate the effect of calcination time on the catalytic performance, the catalyst precursor was calcined for different time between 4-10h. It was observed that the catalyst which was calcined for 6h at 550℃ has shown the best catalytic performance. The morphology of this catalyst in the precursor and calcined states which are completely different are displayed in Fig. 2. These images showed that the morphological features and particles agglomerate were changed at different states.

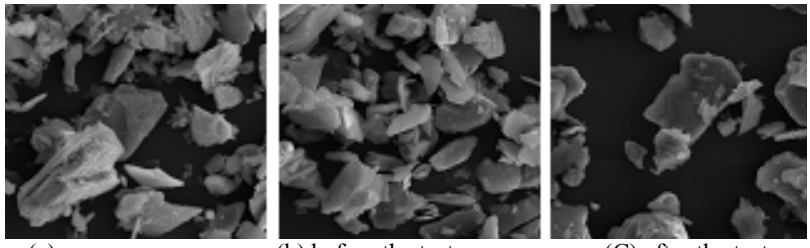

(a) precursor (b) before the test (C) after the test

Figure 2. The SEM images of the catalyst

3. Effect of calcination atmosphere

We also examined the effect of the calcination atmosphere, and calcination process was carried out at two different calcination atmospheres including N_2 and air. It was found that the catalyst which was calcined at air atmosphere has shown the best catalytic performance.

Conclusion

This study revealed that all the calcination conditions influenced the catalyst precursor texture and morphology of the calcined catalysts and also these conditions affect the catalytic performance of catalysts.

References:

[1] S. Jam, M. G. Ahangary, A. Tavasoli, K. Sadaghiani and A. Nakhaeipure, React. Kinet. Catal. Lett. 89(1) (2006) 71.

[2] R. Malesa, M. Bearns, Ind. Eng. Chem. Res. 27 (1988) 279.

[3] S. Colley, R. G. Coppertwaite, G. J. Hutchings, M. Vander Riet, Ind. Eng. Chem. Res. 27 (1998) 1339.

[4] M. J. Keyser, R. C. Everson, R. L. Espinoza , Appl. Catal. A: Gen. 171 (1998) 99.

[5] F. Tihay, A. C. Roger, A. Kiennemann and G. Pourroy, Catal. Today. 58 (2000) 263.

Effect of pretreatment conditions on the catalytic performance of impregnated Co/Ni/Al_2O_3 for FTS

A. A. Mirzaei, A. Zare*, M. Arsalanfar, S. Vahid, M. Fatemi
Department of Chemistry, University of Sistan & Baluchestan, Zahedan, Iran
(e-mail:a_zare87@yahoo.com)

Abstract

Cobalt nickel oxides, prepared using incipient wetness impregnation procedure, were studied as catalysts for the conversion of synthesis gas into light olefins. The effect of reduction temperature on the catalytic performance of an impregnated cobalt nickel catalyst (80%Co-20%Ni-90wt%Al_2O_3) during Fischer-Tropsch synthesis (FTS) was studied in a fixed bed micro reactor. Then the effect of the reduction time on the catalytic performance was studied. We also investigated effect of different reductant including H_2, CO and syngas (H_2/CO=1/1) on the catalytic performance. It was found that the catalyst which reduced using H_2 for 12h at 350˚C has shown the best catalytic performance, so that these conditions were chosen as the optimum conditions for pretreatment of this catalyst.

Keywords: Co-Ni/Al_2O_3 catalyst, Impregnation method, Light olefins, Pretreatment conditions**.**

Introduction

The Fischer-Tropsch synthesis leads to a wide variety of products, whose abundance depends on the catalysts employed, as well as operating conditions[1-3]. Although all VIII group metals[4] display some activity in C-C coupling reaction during CO hydrogenation, the most active metals for FTS are ruthenium, nickel, iron and cobalt[5].

Method

All the tested catalysts in this study were prepared using an impregnation procedure and tested in a fixed bed stainless steel micro reactor.

Results and Discussion

1. Effect of reduction temperature

Cobalt nickel oxide catalysts were prepared by impregnation method, were reduced at different temperature between 250-400℃. It was found that the catalyst which was reduced at 350℃ has shown the best catalytic performance.

2) Effect of reduction time

In order to investigate the effect of reduction time the Co-Ni/Al_2O_3 catalyst was reduced for different time between 2-24h. It was observed that the catalyst reduced for 12h has shown the best catalytic performance.

3) Effect of reductant agent

In the present study, we also examined the effect of the reductant agent, for this purpose the catalyst was reduced at different atmosphere including H_2, CO and H_2+CO. It was observed that the catalyst reduced using H_2 has shown the best catalytic performance. This catalyst was characterized using XRD method and the obtained XRD patterns are illustrated in Fig. 1. The catalyst precursor was found to be amorphous and the calcined sample before the test has different phases including Co_3O_4(cubic), NiO(cubic) and $NiCo_2O_4$ (cubic) and the calcined catalyst after the test has different phases including CoO(cubic), Co(cubic), and Ni (rhombohedral), C (hexagonal), Co_3C (orthorombic).

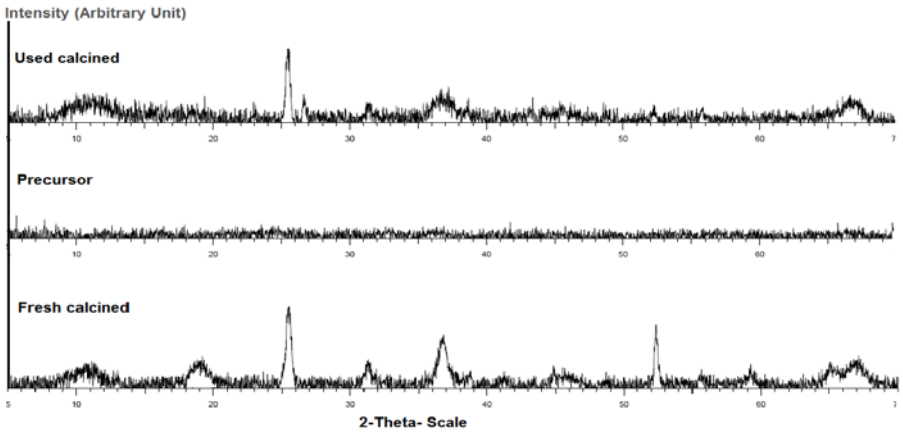

Conclusion

It was found that the pretreatment conditions influenced the catalyst precursor structure and morphology of the precursors and calcined catalysts and consequently the catalytic performance of catalysts.

References

[1] V. A. de la Pena O'Shea, M. C. Alvarez-Galvan, J. M. Campos-Martin, J. L. G. Fierro, Appl. Catal. A: Gen. 326 (2007) 65.

[2] H. Schulz, Appl. Catal. A: Gen. 186 (1999) 3.

[3] M. E. Dry, Catal. Today. 71 (2002) 227.

[4] M. A. Vannice, J. Catal. 37 (1975) 449.

[5] R. A. van Santen, Catal. Rev-Sci: Eng. 37 (1995) 557.

Effect of Zeolite support on the catalytic behavior and structure of the Co-Ce catalyst for FTS

M. Arsalanfar, A. A Mirzaei, S. Rezazade*, A. Zare and S. Vahid
Department of chemistry, Faculty of sciences, University of Sistan & Baluchestan, Zahedan, Iran.
(Email: rezazadeh.1363@Gmail.com)

Abstract

Cobalt cerium oxide catalyst, prepared using co-precipitation procedure was studied for the conversion of synthesis gas into light olefins (C_2-C_4). Effect of zeoilte support on the catalytic performance and structure of Co-Ce catalyst at the same operating conditions (T=450ºC, P=1atm and H_2/CO=2/1) was studied. The precursors and calcined catalysts (before and after the test) were characterized using different methods. It was found that zeolite has a marked influence on the catalytic performance, structure and morphology of Co-Ce catalyst.

Keywords: Co-Ce catalyst, Fischer-Tropsch synthesis, Light olefins, Zeolite

Introduction

Typically, FTS catalysts include VIII group based metals (Co, Ru, Fe) with Co-based ones ensuring a superior long-chain hydrocarbon yield and longer life time [1-3]. Co-Ce catalysts have been investigated for its selectivity to lower molecular weight olefins [4-6].

The aim of present work is to study the effect of the Zeolite support on the catalytic performance, surface area, structure, morphology and thermal behavior of Co-Ce catalyst.

Method

All the catalysts were prepared using the co-precipitation procedure and test of all of these catalysts were carried out in a fixed bed micro reactor.

Results and Discussion

1. Effect of Zeolite on the catalytic performance

In order to investigate the effect of zeolite on the catalytic performance, two separate catalyst were prepared which first one containing 20%Co-80%Co and the other sample containing 20%Ce-80%Co/15wt%Zeolite. Both of them were tested at the same reaction conditions for production of light olefins via Fischer-Tropsch synthesis. The obtained results are illustrated in Fig. 1.

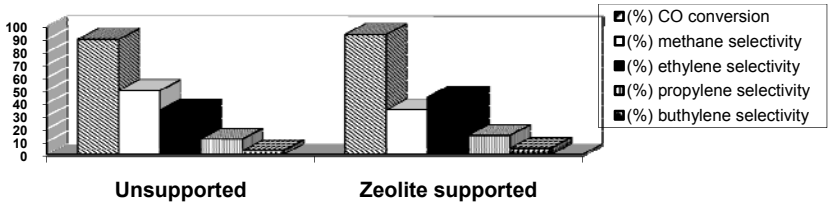

Figure 1. Effect of support on the catalytic performance

2. Effect of Zeolite on the catalyst structure

The scanning electron microscopy and BET surface area measurement techniques were used to investigate the texture and surface area of these two catalysts. The obtained results showed that the presence of zeolite has a great effect on the morphology and surface properties of the catalyst. The SEM images of unsupported and zeolite supported catalysts are displayed in Fig. 2 and the BET results are presented in Table 1.

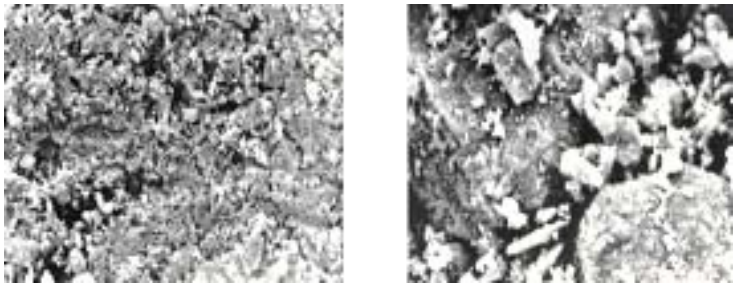

(a)Unsupported (b) Zeolite supported

Figure 2. SEM images of the different catalysts

Support	Specific surface area(m^2/gr)		
	Catalyst precursor	Calcined catalyst before test	Calcined catalyst after test
Unsupported	114	90	92
Zeolite	198	123	130

Table 1. BET results of different catalysts

Conclusion

The obtained results showed the presence of zeolite has great influence on the catalytic performance, morphology and the structure of the catalyst**.**

References:

[1] P. J. Van Berge, R. C. Everson, Stud. Surf. Sci. Catal. 107 (1997) 207.

[2] G. P. Van der Laan, A. A. C. M. Beenackers, Catal. Rev. Sci. Eng. 41 (1999) 255.

[3] P. Chaumette, Ph. Coutry, A. Kiennemann, B. Ernst, Top. Catal. 2 (1995) 117.

[4] L. A. Bruce, M. Hoong, A. E. Hughes, T. W. Turney, in: H. E. Curru-Hyde and R. F. Howe (Eds), Natural Gas Conversion II, Elsevier Science, 1994, pp 427-432

[5] J. Barault, A. Guilleminot, J. C. Achard, V. Paul-Boneour, A. Percheron Guegan, Appl. Catal. A: Gen. 22 (1986) 273.

[6] L. A. Bruce, M. Hoang, A. E. Hughes, T. W. Turney, Appl. Catal. A: Gen. 100 (1993) 51.

Dehydration of methanol over metal oxide catalysts supported on H-ZSM5 zeolite and study of the catalytic deactivation in a fixed bed reactor

V. Zarei[a]*. M. H. Peyrovi[b]

[b]Department of chemistry, Faculty of science, Shahid Beheshti University, Evin, Tehran, Iran

[a]Islamic azad university,arsanjan Branch,Iran

+982129902892,09176309527,vahid_zarei181@yahoo.com

Keywords: Dimetyl ether, Methanol, H-ZSM5 Zeolite , Catalytic activity, Si/Al ratio

Introduction

Dimetyl ether (DME) has recently been suggested as a clean alternative fuel for diesel engines instead of diesel, and as fuel additive and family cooking gas instead of liquefied petroleum gas (LPG) with much lower NOx emission, near-zero smoke production, and less engine noise compared with traditional diesel fuels [1,2]. In view of DME's potential as a clean alternative diesel fuel, much consideration should be given to the production of DME in large quantities. At present, DME is produced by methanol dehydration over solid acid catalysts such as γ –alumina, HY zeolite and H-ZSM5 zeolite:

$2CH_3OH \rightarrow CH_3OCH_3 + H_2O$ (ΔG = -12.1 kJ/mole at 250 ^oC)

It is known that the modified H-ZSM5 zeolite by various metals which has low acidic sites is the better catalyst than the pure H-ZSM5. In this study, we investigated the performance of catalytic activity of modified H-ZSM5 zeolites by different metals for production of the DME from methanol. Their catalytic activities were investigated at the several temperatures and two types compared for determination of the best condition for DME production.

Experimental

Catalytic reactions were carried out at atmospheric pressure in a continuous fixed-bed glass microreactor packed with 1.0 g catalyst. The catalyst was pretreated in a N_2 flow (20 ml min^{-1}) and then, methanol was introduced into the reactor with a space velocity of 2 ml/ (gcat h). The effluent from the reactor was analyzed on-line with Shimadzu 8A gas chromatograph equipped with Porapak-Q column and the thermal conductive detector (TCD). The main

products were DME and water. The reaction was carried in the temperature range of 250-450 ^{o}C to observe the effect of temperature on the conversion and various catalysts to determine the effect of the Si/Al ratio of zeolite and the type of impregnated metal on the catalytic activity.

H-ZSM5 modified by various metal oxides was prepared by wet impregnation with aqueous solutions of metal salts, followed by drying at 110 ^{o}C overnight and then calcined at 500 ^{o}C for 4 h in an air stream. By this method, 5 samples of modified zeolites: Na-H- ZSM5, Ni-H-ZSM5, Al-H-ZSM5, Zn-H-ZSM5, and Zr-H-ZSM5 catalysts were prepared [3,4].

Table: Results of catalytic deydration of methanol over H-ZSM5 and metal-modified H-ZSM5 at 400 ^{o}C (the best temperature for conversion).

Catalyst	Metal Oxide Content (%)	Si/Al Ratio	Conversion (%)	Selectivity (%)	
				DME	CO_x
H-ZSM5	10	15	39.5	88.5	11.5
		30	34.2	71.2	28.8
Na-H-ZSM5	10	15	67.6	97.1	2.9
		30	64.3	82.5	17.5
Ni-H-ZSM5	10	15	61.2	95.5	4.5
		30	58.7	80.3	19.6
Al-H-ZSM5	10	15	50.1	91.4	8.6
		30	46.9	75.2	24.8
Zn-H-ZSM5	10	15	41.3	90.2	9.8
		30	39.1	76.7	23.3
Zr-H-ZSM5	10	15	59.7	93.5	6.5
		30	56.5	79.3	207

Results and discussion

Table shows the results of conversion and selectivity of different catalyst for methanol deydration. Results indicate that the conversion and DME selectivity decreases with the increasing of Si/Al ratio in the all catalysts. Furthermore, adding of the metal in the surface of zeolite increases the catalytic activity of the methanol dehydration. Maximum activity is reached by using Na-H-ZSM5 catalyst. For others, the activity is decrease by the respect of Ni> Zr> Al> Zn.

It is well known that by increasing the Si/Al ratio, the strong acidic sites of zeolite convert into supper-acid sites. That this lead to increase of coke deposition and deactivation of the catalyst, ultimately with increasing the Si/Al ratio the conversion and DME selectivity are reduced.

From the above results, we think that methanol dehydration proceeds easily on the surfaces of H-ZSM5 and of each metal modified H-ZSM5, while the activity of these samples depends strongly on their acidity strength, H-ZSM5 and Zn-and AL-modified H-ZSM5, which possess higher proportions of strong acid sites, deactivate easily due to the carbon deposition. That is, carbon deposition occurs mainly on strong acid sites and the formed carbon deactivates the dehydration ability of the catalysts. Zr-, Na-,and Ni-modified H-ZSM5 zeolites exhibited a higher activity for methanol dehydration.large amount of carbon was detected on Zn– H-ZSM5, AL– H-ZSM5, and H-ZSM5, which would be the main reason for their deactivation. On Na– H-ZSM5 Ni- H-ZSM5 and Zr– H-ZSM5, the detected amount of carbon formed is limited. Thus methanol dehydration arises on all kinds of acid sites, but that strong acid sites should be depressed in order to prevent carbon deposition.

Ultimately, it was determined that Na-modified H-ZSM5 zeolite is an optimum catalyst for dehydration of methanol to DME with high conversion, selectivity and stability.

References

[1] Vishwanathan V, Jun KW, Kim JW, Roh HS., Appl Catal A 2004;276(1–2):251–5.

[2] Arkharov AM, Glukhov SD, Grekhov LV, Zherdev AA, Ivashchenko NA, Kalinin N,Chem Petro Eng 2003; 39(5–6):330–6.

[3] Shan Jiang,a,b Jin-Soo Hwang,a,* Taihuan Jin,a Tianxi Cai,b Wonihl Cho,c Young soon Baek,c and Sang-Eon Parkd,*bull.koreanchem soc 2004,25,185-189

[4] I. Sierra, J. Ereña, A. T. Aguayo, J. M. Arandes, A. G. Gayubo, J. Bilbao,ECCE.2007

Kinetics and thermodynamic parameters for Cr^{3+} adsorption by *1-(2-pyridylazo)-2-naphtol* immobilized on surfactant-coated alumina

Ebrahim sabokrooh *[1] and Hossein Faghihian [2]

[1]Shahrekord University of Medical Sciences, [2] Department of chemistry, Islamic Azad University Shahreza Branch, faghihian@iaush.ac.ir

*Corresponding author: sabokrooh 206 @ yahoo com

Key words: 1-(2-Pyridylazo)-2-naphtol, sodium dodecyle sulfate

Introduction:

Ionic or nonionic surfactant molecules from self-aggregate called “micelles” above the critical micelle concentrations. It is well known that the hydrocarbons cores of the micelles solubilize many hydrophobic compounds in aqueos solutions. Similarly, surfactants can form their aggregates on solid surfaces, which are called “admicelles” or “hemimicells”. The use of admicelles in trace analysis has recently reported [1]. Typical chelating agents, such as dithizone and PAN, can be incorporated into the inner hydrophobic part of admicelles. The dithizone - impregnated admicelles can be used for separation of cations [2-3]. In this research the kinetic and thermodynamic parameters for removal Cr^{3+} by *a micro column of alumina modified with sodium dodecyl sulfate (SDS) and 1-(2-pyridylazo)-2-naphtol (PAN)* was investigated.

Experimental:

1-Immobilization of PAN on SDS – coated alumina

The reagent solution was prepared by dissolving 0.25 g of PAN [1-(2-pyridylazo)-2-naphthol] in 100 ml of 95% ethanol. Two gram of alumina was added to 75 ml of water containing 100mg of SDS and the solution was magnetically stirred. After addition of 4 ml of PAN solution, the pH was adjusted to 2.5 with 1M hydrocholoric acid. The suspension was stirred for 15 min and transferred to Millipore filter holder for the preparation of a column (15 mm in diameter × 9 mm in height). Under optimized conditions (pH; flow rate) cations were retained on the column. The cations collected on the column were eluted with nitric acid. Recoveries greater than 96% was obtained for most cations.

Result and discussion:

***1-Adsorption isotherms**:*

Tow isotherms were tested for their ability to describe the experimental result, namely the Langmuire and the Freundlich isotherms. As can be seen in table 1. The Langmuire isotherm has good regression coefficient that shows the adsorption obeys the model.

Table1: Compression of Langmuire and Freundlich isotherm.

"Isotherms	parameters	R2	Sample
Langmuire	Q_0=21.82mg/g b=.0141L/mg	0.9991	Alumina modified PAN/SDS
Freundlich	$K_{f=1.9828}$ n=2.9231	0.8392	

2-Thermodynamic parameters:

The effect of temperature on the adsorption of $Cr^{3+}$by alumina modified PAN/SDS was carried out in the temperature range from 25 to 50^0C. The results showed that the adsorption capacity increased with increasing temperature which indicates that the adsorption process is endothermic in nature. For alumina modified PAN/SDS, adsorption process is exothermic which indicates that the entropy of Cr^{3+}ions adsorbing by sorbent is higher than the hydrated lattice in solution phase. The calculate Gibbs free energy at 298^0, 308^0 and 328^0K was negative which indicate that the adsorption process is spontaneous.

3-Adsorption Kinetics:

The modeling of the kinetics of adsorption of $Cr^{3+}$by modified alumina was investigated by two common models, namely the Lagergren pseudo-first-order model and pseudo-second-order model. Adsorption kinetics $Cr^{3+}$by alumina modified PAN/SDS can be described by pseudo- second -order.

Refrences:

[1] K. T. Valsaraj, Sep. Sci. Technol, 27, 1633, 1992

[2] J. L. Manzoori, H. Sorouradin, A. M. Haji Shabani, "Atomic Absorption Determination of Cobalt after preconcenteration by 1-(2-pyridylazo)-2-naphtol Immobilized on surfactant-Alumina" Micro chemical, 295–301, 63, 1999 .

[3] G. Absalan, A.Aghaei Goudi, "Optimizing the immobilized dithizone on surfactant-coated alumina as a new sorbent for determination of silver", Separation Purification technology, 209-214, 38, 2004.

The inhibiting effect of organic compounds on corrosion behavior of stainless steel in acidic solution

E.Sedghamiz[a],A.Dolatabadi[b], F.Rezaei[a] and S.M.A.Hosseini[a*]

[a]*Department of chemistry,Shahid Bahonar university of kerman, kerman 76169,Iran*

[b]*Department of chemistry,payame noor university of kerman,Iran*

(E-mail:s.m.a.hosseini@uk.ac.ir)

Keywords: corrosion, organic compounds, stainless steel, acidic solution.

Introduction:

Acid solutions are widely used in industry and due to their general aggression, inhibitors are commonly employed to reduce the corrosive attack on metallic materials [1].In this work three synthesized organic compounds have been investigated as corrosion inhibitors (fig.1).The inhibition properties of these compounds on stainless steel was tested in sulfuric acid 0.5 M containing 100 ppm of inhibitor in different temperatures. These compounds contain heteroatoms such as N,O and S which causes greater adsorption of the inhibitor molecules into the surface of the steel[2]. Since oxygen have negative charge and easily donates electron to Fe atoms, the inhibitors attack from the oxygen sides of the carbonyl group.

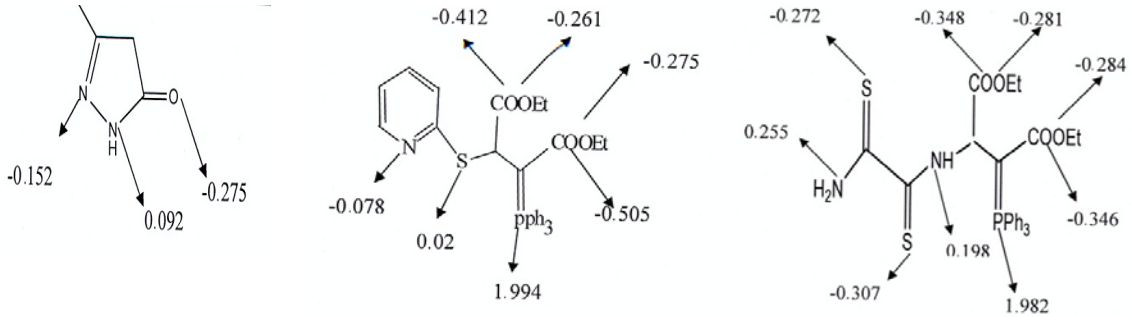

A **B** **C**

Fig.1. Determination of charges by quantum mechanical calculations

Method:

All experiments were performed potentiodynamically in 0.5 M H_2SO_4 .Initially the cell was filled with desired solution and after regulating the temperature,working,counter and reference electrodes were inserted in the solution .The potential range was 700-1500 mV with scanning rate of 4mV/s. all tests were done with respect to saturated calomel electrode in the absence and presence of inhibitors. Finally SEM micrographs were taken from the surface of the exposed samples to see the performance of the inhibitors.

Results and discussion:

The polarization curves (not shown) for stainless steel in 0.5 M H_2 SO_4 in the absence and presence of the various concentrations of compounds A,B and C indicate that addition of either compound induces a decrease in both anodic and cathodic current densities and result in shift of the corrosion potentials to positive direction compared to uninhibited steel.So it can be concluded that these compounds are acting as mixed-type inhibitor but dominantly suppressing anodic portion of the curves. Corrosion inhibition efficiencies increase as the inhibitors concentration increase.Fig 2 shows the effect of temperature on the polarization curve of compound B which exhibited the maximum efficiency at a concentration of 100 ppm. B molecule has bigger size and covers the surface better than others and is less soluble so it's adsorption on steel surface increases compare to two other inhibtors.Temperature variations don't have any effect on general shapes of polarization curves.

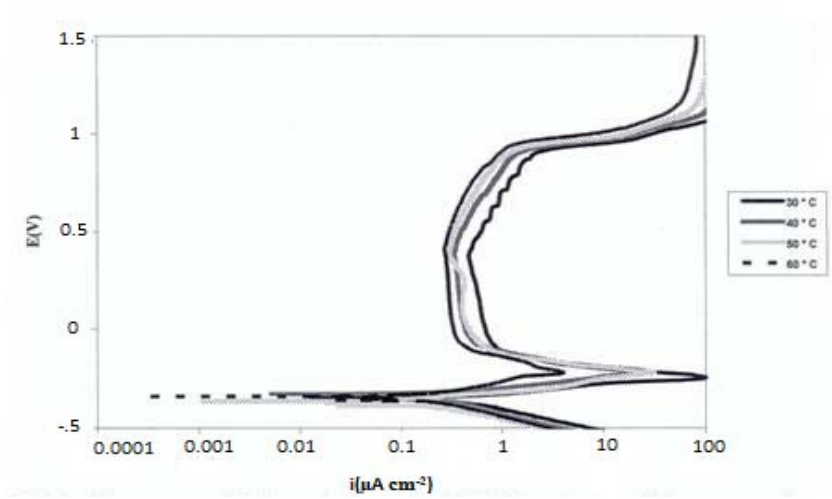

Fig.2.polarization curves of stainless steel recorded in 0.5M H_2SO_4 in presence of 100ppm of B at different temperatures (30-60)

Conclusion:

The investigated compounds A,B and C are good inhibitors and are of the mixed-type.The adsorption of these inhibitors obeys the Temkin adsorption isotherm.Icorr increases and inhibition efficiency decreases(Especially compound A lose its inhibition effect faster than B and C) as the temperature increases which suggests a physical adsorption mechanism. The corrosion efficiencies are in order B>C>A. The negative values of ΔG indicate the spontaneous adsorption of the inhibitor on the surface of stainless steel.Theoritical findings reveal that the differences in inhibitor's efficiencies can be explained in terms of the value of sum of electron charges.Determination of oxygen,sulfure and nitrogen charges by quantum mechanical calculations satisfactorily correlate with experimental results,validate the method employed here.

Refrences:

[1].B.Mernari,H.Elattari,M.Traisnel,F.Bentiss,M.Legrence,Corros.Sci.40(1998)391.

[2].W.Machu,3rd European Symp,Corrosion inhibitors,University of Ferrara Italy,Ferrara,Italy,(1971)107.

Characterization of Co-Ce catalysts using XRD, BET, TGA and DSC

M. Arsalanfar, A. A Mirzaei, S. Rezazade*, A. Zare, M. Fatemi

Department of chemistry, Faculty of sciences, University of Sistan & Baluchestan, Zahedan, Iran.

(Email: rezazadeh.1363@Gmail.com)

Abstract

The effect of a range of preparation variables on the composition and morphology of cobalt-cerium oxide catalysts prepared using a co-precipitation method is described and the optimum preparation conditions were identified with respect to the catalyst activity for the Fischer-Tropsch reaction. Characterization of catalysts was carried out using different methods including XRD, TGA, DSC, TPR, BET and SEM.

Keywords: Characterization, Cobalt-cerium oxide, Fischer-Tropsch synthesis, Morphology.

Introduction

Group VIII metals, such as Fe, Co, Ni and Ru, are the most popular Fischer-Tropsch synthesis (FTS) catalysts[1]. Cobalt containing catalysts are known to be effective in CO hydrogenation[2]. It has suggested that on cobalt catalysts, FTS is a structural-insensitive reaction and the active phase is cobalt metal[3].

Method

All the catalysts were prepared using the co-precipitation procedure and test of all of these catalysts were carried out in a fixed bed micro reactor.

Results and Discussion

1. Effect of ageing time on the morphology of catalysts

A series of mixed cobalt cerium oxide catalysts were prepared by co-precipitation procedure with a range of ageing times between 0-5h; then these catalysts were tested for hydrogenation of CO. The obtained results showed that the sample aged for 2h gave the best performance. All of these catalysts were characterized using XRD and the actual phases identified in these

catalysts under the specified preparation conditions were CeO_2 (cubic) and Co_3O_4 (cubic) (Fig. 1).

2. Effect of solution [Co]/[Ce] ratio on the morphology of catalysts

According to the obtained results, the catalyst containing 80%Co/20%Ce was chosen as the optimum catalyst for the conversion of synthesis gas to light olefins. This optimum calcined catalyst was characterized using TPR method. The TPR profile of this catalyst revealed four distinct reduction peaks at 180ºC, 300ºC, 420ºC and 540ºC (Fig. 2). The precursor of this catalyst was characterized using TGA and DSC method and the obtained curves are illustrated in Fig. 3. The precursor shows three main thermal effects.

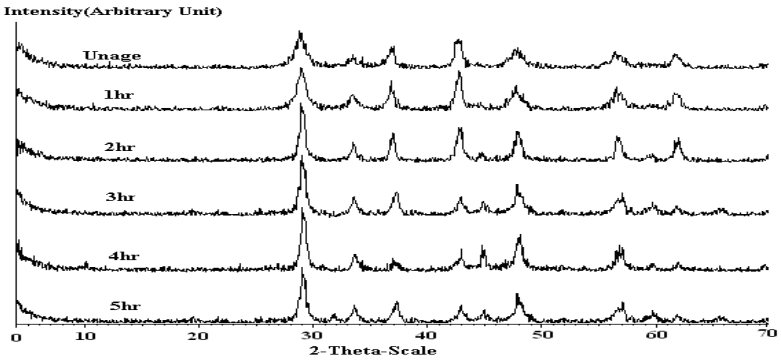

Figure 1. XRD patterns of the aged calcined catalyst before the test

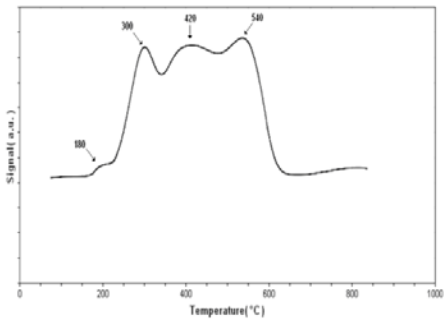

Figure 2. TPR profile of calcined catalyst

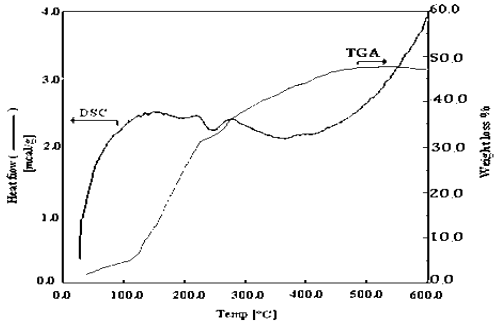

Figure 3. TGA and DSC curves of the catalyst precursor

Conclusion

Characterization of both precursors and calcined catalysts by XRD, SEM, BET, TGA and DSC methods, showed that the catalyst precursors are sensitive to the preparation conditions,

so that these parameters should be incorporated into the design of experimental programs involving precipitation as the method of catalyst preparation.

References

[1] M. E. Dry, in: J R Ander, Boudart (Eds.), "The Fischer-Tropsch synthesis",
Catalysis-Science and Technology, Vol. 1, Springer- Verlag, New York, 1981

[2] V. A. Pena O'Shea, M. C. Alvarez-Galvan, J. M. Campos-Martin, J. L. G. Fierro, Appl. Catal. A: Gene. 326 (2007)65.

[3] E. Iglesia, Appl. Catal. A: Gene. 161 (1997) 59.

Effect of operating conditions on the catalytic behavior of Fe-Co FT catalyst

M. Arsalanfar*, A. A. Mirzaei, M. Fatemi, A. Zare, S. Rezazade
Department of Chemistry, University of Sistan & Baluchestan, Zahedan, Iran
(e-mail: maryam_galavy@yahoo.com)

Abstract

The catalyst containing 40%Fe/60%Co/15wt%SiO_2/1.5wt%K was prepared using fusion procedure and studied for the conversion of synthesis gas to light olefins. The effect of a range of operating variables such as the pressure, temperature and H_2/CO molar feed ratio on the catalytic performance of fused catalyst was investigated. It was found that the best operating conditions is H_2/CO=2/1, T=350˚C and P=5 bar.

Keywords: Fe-Co catalyst, Fusion method, Light olefins, Operating conditions**.**

Introduction

The Fischer-Tropsch (FT) reaction entails the conversion of CO and H_2 to a spectrum of product mainly comprising alkenes and alkanes[1-3]. Both Co and Fe are typically used when combined with a range of supports and promoters that permit further control over the product spectrum[4].

Method

In the present study, a catalyst with 40%Fe/60%Co/15wt%SiO_2/1.5wt%K composition was prepared using fusion method.

Results and Discussion

The operating conditions were investigated to identify and optimize the operation variables, such as H_2/CO molar feed ratios, reaction temperatures and reaction pressures that have a marked effect on the catalytic performance.

1) Effect of H_2/CO feed ratio

The influence of the reaction H_2/CO molar feed ratio on the steady state catalytic performance of the catalyst containing 40%Fe/60%Co/15wt%SiO_2/1.5wt%K prepared using fusion method for the Fischer-Tropsch reaction at 350˚C under atmospheric pressure was investigated and it was found that the catalyst has shown the best catalytic performance at H_2/CO=2/1. Characterization of this catalyst was carried out using SEM and the obtained images of different stages of precursor, fresh calcined catalyst (before the test)& used calcined catalyst (after the test) at H_2/CO=2/1 are shown in Fig. 1. As it can be seen the morphological features of these samples are quite different and they have different aggregation and particles size.

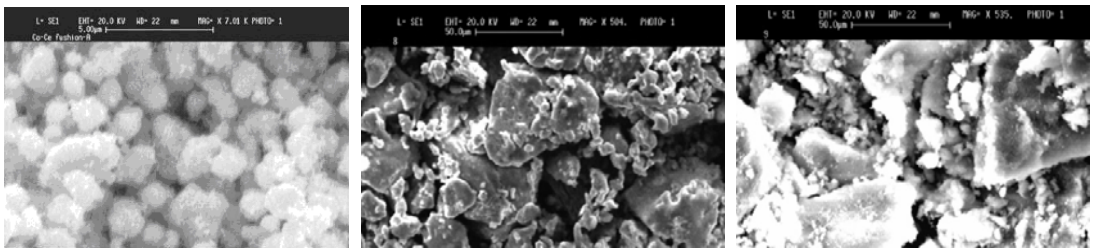

(a) precursor **(b) fresh calcined** **(c) used calcined**

Figure 1. SEM images of the 40%Co/60%Ce/15wt%SiO_2/1.5wt%K catalyst

2) Effect of reaction temperature

The effect of reaction temperature, ranging from 300-450ºC on the catalytic performance of this catalyst was studied. According to the obtained results (Fig. 2), the optimum reaction temperature was 350 ºC, at which temperature the total selectivity of light olefins products was higher than those at the other reaction temperatures under the same operating conditions.

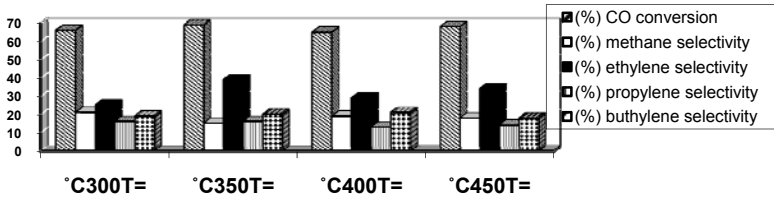

Figure 2. Effect of different reaction temperatures on the catalytic performance.

3) Effect of total reaction pressure

The effect of reaction pressure, ranging from 1-10 bar on the catalytic performance of this catalyst was studied (T=350˚C and H_2/CO=2/1). According to the obtained results, the optimum reaction pressure was 5bar, at which pressure the total selectivity of light olefins

products was higher than those at the other reaction pressure under the same operating conditions.

Conclusion

The obtained results showed that the catalyst is sensitive to the operating conditions. These operating parameters should be incorporated into achieve the highest selectivity toward light olefins from the catalyst containing 40%Fe/60%Co/15wt%SiO_2/1.5wt%K prepared using fusion procedure.

References

[1] M. E. Dry, Catal. Sci. Technol. 1 (1981) 1159.
[2] H. Schulz, Appl. Catal. A: Gen. 186 (1999) 3.
[3] D. J. Duvenhage, N. J. Coville, Appl. Catal. A: Gen. 289 (2005) 231.
[4] M. Luo, R. O'Brien, B. H. Davis, Catal. Lett. 98 (2004) 17.

Evaluation of kinetics and thermodynamics parameters of adsorption of methylene blue from aqueous solution onto α-alumina

M.Amirzehni* , N. Ghalebsaz-Jeddi , A. Shamel, L. Fathollahi , H.Eskandari
Department of Chemistry, Faculty of Science, Islamic Azad University-Tabriz Branch
* Corresponding Author E-mail: maliheamirzehni@yahoo.com

Keywords: Adsorption, Methylene blue, α-alumina, Kinetics,Thermodynamic

Introduction

The excessive release of color in to the environment is a major concern worldwide[1]. Methylen blue has wider application,which inclde coloring paper, temporary hair colorant, dyeing cotton, wools, coating for paper stock, medical purpose, ets [2]. Methylen blue (MB) is selected as a model compound in order to evaluate its capasity for the removal of methylem blue from aqueous solution. Adsorption techniques have been widly applid to the treatment of water solution containing dyes [3-5]. Therefore, this study was carried out to understand the adsorption behavior of methylene blue from aquous system onto α-alumina. The effect of various experimental parameters, such as initial MB concentration, adsorbent dosage, pH, contact time and stirring rate were investigated.

Method:

The experiments were performed on MB solutions with concetration of 1.75 mg l^{-1} . At the beginning of each run 15 mL, solution of desired concentration of the dye was fed into a 150 mL pyrex glass reactor and then 0.2 g of adsorbent was introduced and stirred for certain times at known speeds , then filtered for spectrophotometric analysis.

Results and discussion:

The effects of initial MB concenration, adsorbent dosage, pH, contact time and stirring rate were studied in a batch mode.The desired conditions for decolorization of 70.57% were obtained to be 30 min of contact time, stirring rat of 50 spm with 13 gL^{-1} of adsorbent. The kinetics and thermodynamics of MB adsorption onto the α-alumina in aqueuos solution were

investigated. The kinetic of adsorption process was best described by the pseudo-second-order kinetic model (Fig.1). The negative value , the Gibbs free energy change confirms the feasibility of the process and spontaneousadsorption of methylene blue onto α-alumina.

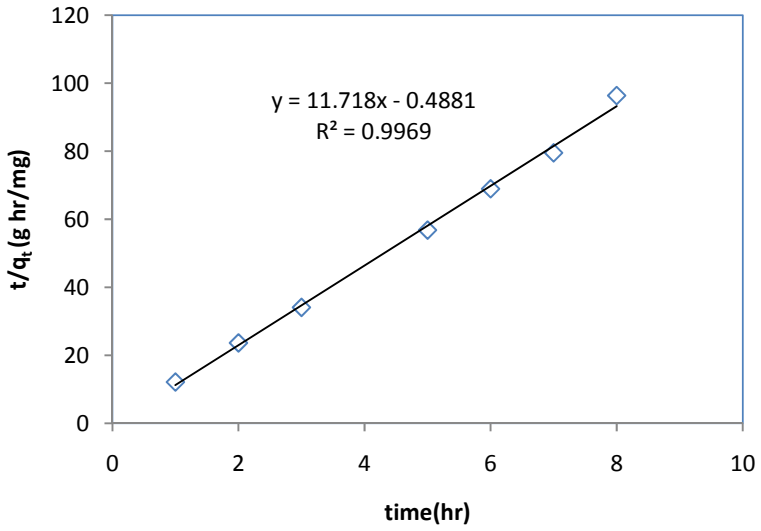

Fig.1. pseudo-second-order kinetic plots for adsorption of Methylene blue

Conclusions:

The results was shown that optimum uptake capacity was found at pH 9 . Kinetic data was well described by pseudo-second-order kinetic model. The amount adsorption increased with the increasing temperature. The thermodynamic analysis was indicated that adsorption is endotermic prosses (enthalpy 18149.462 $kjmol^{-1}$) and the amount Gibbs free energy was shown that adsorption MB on to α-alumina is the spontaneous prosses. The obtained results were indicated that the entropy is 58.82 $jmol^{-1}k^{-1}$.

References:

[1] Mall, I., Srivastava, Dayes Pigments., 2005, 69, 210-223.

[2] Dogan, M., Abak, A., J. Hazar. Mater., 2009, 164, 172-181.

[3] Abramian, L., Rassy, H., Chem. Eng. J. 2009, 150, 403-410.

[4] Das, R.. M., Mahiuddin, S., Colloid. Surf., 2005, 264, 90-100.

[5] You, L., Wu, Z., J. Colloid. Interface. Sci., 2006, 300, 526-535.

Photodegradation Thermodynamics study of Acid yellow 36 in aqueous suspension

R.Fazaeli*[a], Z. Emadian Razavi[b], M.Yousefi[b]

[a] Modeling and Optimization Research Center in Science and Engineering, Islamic Azad University-South Tehran Branch, Tehran, Iran

E-mail: r_fazaeli@azad.ac.ir

[b]Department of Chemistry, Islamic Azad University-Shahr-e- Rey Branch, Tehran, Iran

Abstract

Nowadays the large amounts of dyes can be synthesized and used for many industries such as textiles, paper, leather,plastics, etc.. The colored effluents ofwaste water from these industries can be mixed in surfacewater and ground water systems, and then they may alsotransfer to drinking water and bring a chief threat to humanhealth due to either toxic or mutagenic and carcinogenicfor most of dyes .

The main problem for dyestuff manufactures is the removal of colour, to reduce the quantity of colour in effluent and water sources [1], since at the present time there is no single process capable of adequate treatment, mainly due to the complex nature of these effluents [2]. Most of the existing processes include an initial step of activated sludge treatment to remove the organic matter, followed by oxidation (with ozone [3], or Fenton's reactant [4], or hydrogen peroxide plus UV radiation [8]), or by membrane separation [5], or by adsorption, usually with AC [6].

The experimental data was analyzed by photodegradation of Acid Yellow 36 into the photochemical reactor at the presence of TiO_2 /PZT/ $FeCl_3$ and $K_2S_2O_8$. Aqueous AY36 solution was prepared at the concentration of 10^{-4}M. The sample was enclosed in cylindrical, quartz cell and exposed to the UV irradiation.

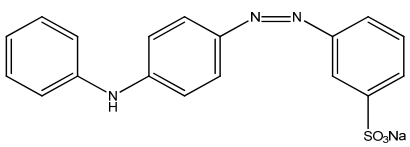

Fig.1. Acid Yellow 36

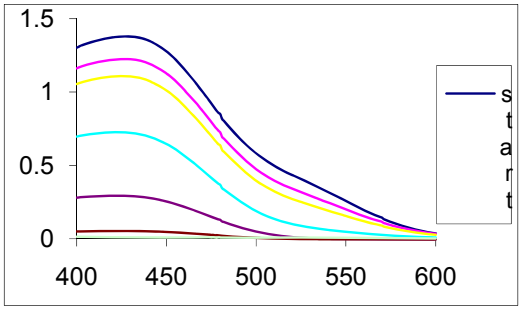

This Fig. shows the degradation time of Acid Yellow 36.

In this section, some representative isotherm equations were discussed with a special focus on theoretical derivation of the combined Langmuir, Freundlich, Temkin, Dobinin-Radoshkevich isotherm equation, also known as the Sips isotherm.

This table shows the Thermodynamic isotherm of Acid Yellow 36

Isotherm	General formula	Regression equation	R^2
Langmuir	$\frac{1}{qe}=\frac{1}{q\max}+\frac{1}{Kq_{\max}}.\frac{1}{C_e}$	y = 1E-06X-8E-07	R^2=0.972
Freundlich	$\log q_e=\log k_f+\frac{1}{n}\log C_e$	Y=0.7638X-2.0769	R^2=0.852
Temkin	$q_e=\frac{RT}{b}\ln A+\frac{RT}{b}\ln C_e$	Y=2E-06X+2E-05	R^2=0.813
Dobinin-Radoshkeuich	$\ln q_e=\ln Q_m-k\varepsilon^2$	Y=-0.0034X-4.78	R^2=0.852

Keywords: Thermodynamic isotherms, Photodegradation, UV irradiation.

References

[1] [4] M.F.R. Pereira, S.F. Soares, J.J.M. Orfao, J.L. Figueiredo, Carbon41 (2003) 811.

[2] P. Cooper, J. Soc. Dyers Colour. 109 (1993) 97.

[3] W.S. Perkins, W.K. Walsh, I.E. Reed, C.G. Namboodri, Text. Chem.Color. 7 (1995) 28.

[4] F. Ferrero, Color. Technol. 116 (2000) 148.

[5] A. Uygur, E. Ko¨k, J. Soc. Dyers Colour. 115 (1999) 350.

[6] G. Ciardelli, L. Corsi, M. Marcucci, Resour Conserv Recy 31 (2000)189.

[7] U. Rott, R. Minke, Water Sci. Technol. 40 (1999) 137.

Predicting Surface Composition of Organic Binary Mixtures Based on Sprow- Prausnitz Model

Ensieh Ghasemian*
Email: Eghasemian@ymail.com
Department of Chemistry, Faculty of Science, Ilam University, Ilam, Iran.

Abstract

Among thermodynamic properties, surface tension is an important physical property that shows information about surface composition and exerts a considerable influence on the transfer of mass and energy across interface [1]. Surface tension of mixtures is often very sensitive to small changes in composition of the mixtures, and a detailed knowledge of this dependency is important for many fields [2]. In this study, we predicted surface mole fraction of some organic binary mixtures by Sprow- Prausnitz model [3] and different relations between surface mole fraction and bulk mole fraction of studied system have been considered.

Keywords: Surface mole fraction, Surface tension prediction, Binary mixtures, Sprow- Prausnitz model

Method

Experimental density and surface tension data available from the open literatures was used in the present work [4].

Results and discussion

The assumptions that bulk and surface phases are in equilibrium and the partial molar area of component *i* is the same as the molar area of *i* lead to the Sprow and Prausnitz equation for prediction of surface tension and surface mole fraction. In the present work, we calculated surface mole fractions of components using eq 1 .

$$\sigma = \sigma_i + \frac{RT}{A_i} \ln \frac{x_{i,s}\gamma_{i,s}}{x_{i,B}\gamma_{i,B}} \qquad (1)$$

In this equation σ and σ_i refer to the surface tension for the mixture and the pure component i, A_i is the molar surface area of pure component i, R and T are the gas constant and absolute temperature, $x_{i,B}$ and $x_{i,s}$ are the mole fractions in the bulk and surface liquid phases, and also $\gamma_{i,B}$ and $\gamma_{i,s}$ are the corresponding activity coefficients, respectively. The variation of $x_{2,s}$ versus x_2 for 1,4-dioxane/*n*-alkyl acetate mixtures is given in Figure 1 typically. This figure shows that the mole fraction of *n*-alkyl acetate at the surface is greater than its mole fraction in the bulk at all concentration ranges.

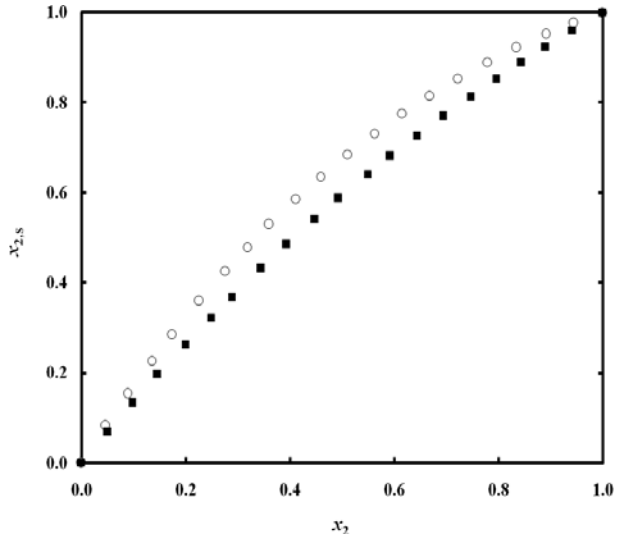

Figure 1: variation of $x_{2,s}$ versus x_2 for 1,4-dioxane/*n*-alkyl acetate :(○) hexyl (■) butyl

Conclusion

In this work we calculated the values of surface mole fractions of solute using the Sprow and Prausnitz model. In addition parameters such as molecular structure and dipole moment of molecules considered in order to get more information about relation between surface mole fraction and bulk mole fraction.

References:

[1] Nath, S. *J. Colloid Interface Sci.* **1999**, *209*, 116

[2] Skapski, A.S. *J. Chem. Phys.* **1948**, *16*, 386.

[3] Sprow, F. B. Prausnitz, *J. Trans. Faraday Soc.* **1966**, *62*, 1105

[4] Lechner, Physical Chemistry,Volume 24, Surface Tension of Pure Liquids and Binary Liquid Mixtures, **2008**.Springer.

The Study of Temperature Effects on Heat of Adsorption in Some Textile Pigments from Aqueous Solution onto Activated Carbon

M. H. Ghorbani[a], R. Fazaeli[*, a], R. Kazemi[b], N. Niksirat[a]

a. *Modeling and Optimization Research Center in Science and Engineering, Islamic Azad University-South Tehran Branch, Tehran, Iran*

E-mail: r_fazaeli@azad.ac.ir

b. *Department of Chemistry, Islamic Azad University – Shahr-e-Rey Branch, Tehran, Iran*

In this work the adsorption of some textile pigments (such as acid yellow 199, reactive black 8, direct red 264, and direct blue 308) from aqueous solution onto activated carbon has been studied. The adsorption isotherm at temperatures 298-325 K and at pH=2 have been described by the Longmuir equation. The characteristic curves of the adsorption process have been determined. It was found out that the temperature dependence of the adsorption equilibrium was described well by the Longmuir model [1]. In this study, the effects of various experimental parameters such as temperature and pH have been investigated, Which concentrations of Acid yellow 199, Reactive black 8, Direct red 264, Direct blue 308 in the solution before and after adsorption were determined using a double beam UV–visible spectrophotometer respectively at λ_{max} [396 nm, 594 nm, 487 nm, 591 nm]. Each experiment was duplicated under identical conditions. The amount of adsorption at equilibrium, q_e (mg/g), was calculate by $q_e = (C_0 - C_e)V/W$ where C_0 and C_e (mg/L) are the liquid-phase concentrations of dye initially and at equilibrium, respectively. V is the volume of the solution and W is the mass of dry adsorbent used (g). The equilibrium data were then fitted using model of Langmuir isotherm, which describes the dependence of Longmuir equilibrium constant on temperature and the adsorption capacity of activated carbon decreases when temperature solution increase [2-3]. The amount of adsorption equilibrium constant K_L (L/mol), was calculated by $\frac{1}{q_e} = \frac{1}{q_m} + \frac{1}{q_m K_L^2} \cdot \frac{1}{C_e}$. Where q_m (mg/g) is monolayer adsorption capacity.

Dye	Temp (°C)	K_L (L/mol)	ΔH (kcal/mol)
Acid yellow 199	25	23.67	-28.41
	33	4.75	
	47.5	0.79	
Reactive black 8	33	25.55	-32.19
	42.5	6.61	
	47.5	2.24	
Direct red 264	33	1.51	-10.99
	47.5	0.8	
	53	0.47	
Direct blue 308	33	8.12	-16.29
	47.5	7.51	
	53	1.04	

By plotting $\ln(K_L)$ vs. 1/T(K) based on Van't Hoff equation, ΔH_{ads} can be obtained. The values of ΔH_{ads} for each dye in the relevant temperature range are shown in the table. With notice to the obtained results all reactions are exothermic but there is no specific relation between ΔH and the number of $-SO_3^-Na^+$ groups in each chemical structure.

Keywords: Temperature, Longmuir Isotherm, Adsorption, Activated carbon

References:

[1] I.A.W. Tan, A.L. Ahmad, B.H. Hameed, Journal of Hazardous Materials 154 (2008) 337–346

[2] V. Garcia-Cuello, etall. Microporous and Mesoporous Materials 120 (2009) 239–245

[3] D.A. Blanco-Martinez, etall. Journal of Hazardous Materials 169 (2009) 291–296

Investigation of Thermodynamic Properties and Isotherm Adsorptions Cd adsorption on to RHA

J.Gheisarinfard*[a], M.bahadori[b]
[a,b] Research & Development Center, South Pars Gas Complex, Asalloyeh, Iran
Javad.gheisarian@spgc.ir

Abstract

The adsorption behavior of rice husk ash for cadmium ions from aqueous solutions has been investigated as a function of appropriate equilibrium time, adsorbent dose, temperature, particle size, adsorbate concentrations and pH in a batch system. Studies showed that the pH of aqueous solutions affected cadmium removal with the result that removal efficiency increased with increasing solution pH. The experimental data were analyzed by the Langmuir and Freundlich models of adsorption. The characteristic parameters for each isotherm and related correlation coefficients have been determined. Thermodynamic parameters such as ΔG°, ΔH° and ΔS° have also been evaluated and it has been found that the sorption process was feasible, spontaneous and exothermic in nature.

Keywords: Rice husk ash; Cadmium; Isotherms; Thermodynamics.

Introduction

In recent years, special attention has been focused on the use of natural adsorbents as an alternative to replace the conventional adsorbents, based on both the environmental and the economical points of view [1]. The RHA has good adsorptive properties and has been used previously for the adsorptive removal of metal ions and dye, and filtration of arsenic from water [2]. In the present paper, rice husk ash was examined for their sorption properties towards cadmium cations. The influence of several operating parameters for adsorption of cadmium, such as contact time, pH, initial concentration, particle size, temperature, adsorbent dose, Thermodynamic Properties and Isotherm Adsorptions was investigated.

Materials and Methods

The rice husk ash obtained from burning of rice husk in electrical oven at 700 °C for 1 hour. The entire chemical used in the study was of analytical reagent grade, cadmium nitrate, NaOH and HCl.

Adsorption experiments were conducted by varying pH, contact time, particle size, adsorbent dose, temperature, and adsorbate concentration. For the thermodynamic and Adsorption Isotherms study, the experiments were performed using various concentrations of cadmium solutions. The filtrate samples were analyzed by Atomic absorption spectrometry.

Results and Discussion

The result shows that the adsorption of cadmium decreased with the increase in initial concentration of cadmium, particle size of sorbent and temperature. With the increase in adsorbent dose the adsorption of cadmium is increase. The percentage removal of cadmium by rice husk ash increased as the pH of the solution increased and reached a maximum value at pH 6. The increasing contact time increased the cadmium adsorption and it remained constant after equilibrium was reached. Thermodynamic parameters such as ΔG, enthalpy ΔH and entropy ΔS changes during adsorption can be determined from the slope and the intercept of the plots of plots of log K_c versus 1/T (Fig.١).

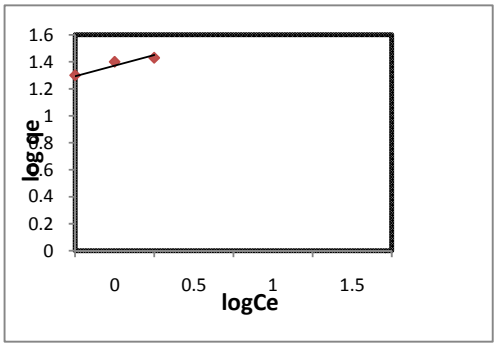

Figure1: Thermodynamic study

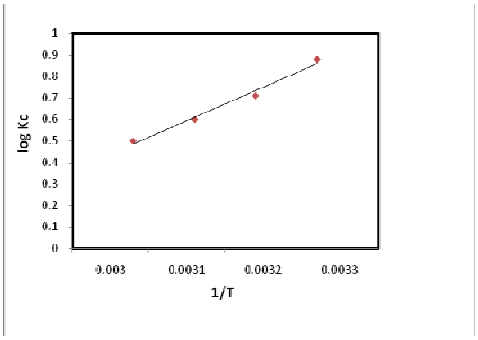

Figure2: Freundlich adsorption isotherm

The Freundlich isotherm is obeyed better than the Langmuir isotherms, as is evident from the values of the regression coefficients (Fig.2).

Conclusion

The goal for this work is to develop inexpensive, highly available, effective metal ion adsorbents from natural waste as alternative to existing commercial adsorbents. A simple and cost effective treatment procedure was proposed for the removal of heavy metals through adsorption on rice husk ash. The

rice husk ash investigated in this study showed good potential for the removal of cadmium from aqueous solutions.

References

[1]. S.E. Bailey, T.I.Olin, M. Bricka, D. Adrian, (1999). Areview of potentially low-cost sorbents for heavy metals, Water Res. 33, 2469- 2479.

[2]. V. Mane, I. D. Mall, V. C. Srivastava, (2007). Kinetic and equilibrium isotherm studies for the adsorptive removal of Brilliant Green dye from aqueous solution by rice husk ash , J. Environ. Manage. , 84(4) , 390-400

Preparation, structure and surface properties of Salen Schiff base complex-poly vinyl amine/SBA-15 nanocomposite

Roozbeh Javad Kalbasi,* Ahmad Reza Massah, Somayeh Kavyani
Department of chemistry, Islamic Azad University, Shahreza Branch, 311-86145, Shahreza, Isfahan, Iran
Corresponding Author E-mail: rkalbasi@iaush.ac.ir

Keywords: Surface properties, Mesoporous molecular sieve, Composite materials, heterogeneous catalyst.

Introduction

Organic–inorganic hybridizing materials, especially the composites consisting of nano-inorganic particles and polymer resin, have received considerable attention recently due to the resultant materials are supposed to have better mechanical and/or thermal properties [1].

On the other hand, a novel porous material, i. e. mesoporous molecular sieve has attracted a great deal of interests for its particular characteristics such as large internal surface area, uniform framework and easily controlled pore diameter [2]. Thus some of their application including catalysts, sorbent, and separating materials are expected [3]. Furthermore, several researchers published finding on the host–guest polymerization of organic molecules in such inorganic mesoporous materials [4].

Experimental

In this study, poly(vinyl amine)/mesoporous SBA-15 (PVAm/SBA-15) nanocomposite were prepared by in–situ polymerization within the nano-channels of SBA-15, This nanocomposite developed by incorporation of salicylaldehyde Schiff base complex in poly(vinyl amine) and applied as heterogeneous catalyst by large internal surface area for oxidation of alcohols.

Results and discussion

The structural feature of composite was studied by BET, XRD, SEM and TGA techniques and the Surface properties was investigated. The specific area and the pore size have been calculated using Brunauer–Emmett–Teller(BET) and Barrett–Joyner– Halenda (BJH) methods, respectively. The structure data of all these mesoporous materials (BET surface area, total pore volume and pore size, etc.) were summarized in Table 1.

Table1 Surface data of salen Schiff base complex-supported PVAm/SBA-15.

Sample	BET surface area ($m^2\ g^{-1}$)	Pore volume ($cm^3\ g^{-1}$)	Pore diameter (nm)
Mesoporous silica SBA-15	1430	1.90	9.90
PVAm/SBA-15	856	1.08	8.81
salen Schiff base ligand–PVAm/SBA-15	442	0.39	4.63
salen Schiff base complex–PVAm/SBA-15.	104	0.25	1.22

It is clear that calcined SBA-15 has a high BET surface area (1430 m^2/g), a large pore volume (1.9 cm^3/g) and a pore size (9.9 nm), indicative of its potential application as a host in organic materials. After hybridization with PVAm through in-situ polymerization, PVAm/SBA-15 exhibits a smaller specific area, pore size and pore volume in comparison with those of pure SBA-15, which might be due to the presence of polymer on the surface of the SBA-15. Although these textural properties are smaller than those found for mesoporous silica SBA-15, PVAm/SBA-15 still has mesoporous form and does not block the pores of the SBA-15, hence suitable to function then grafting schiff base complex on poly(vinyl amine) specific area were decreased but hence suitable to function as a oxidation catalyst for oxidation of alcohols.

The scanning electron microscopy (SEM) photographs of SBA-15 and PVAm/SBA-15 is obvious that before hybridization, the surface of SBA-15 is somewhat coarse and after hybridization, the surface of SBA-15 becomes smooth. These results show that surfaces of SBA-15 are filled with PVAm. The effect of mole ratio of salicylaldehyde, metal ion and amount of mesoporous molecular sieve for synthesis of catalyst was studied. The amounts of catalyst in the reaction were investigated and the product obtained in high yield (100 %).

Conclusion

In this work we report the efficient heterogeneous catalyst for selective oxidation of alcohols to aldehyde by TBHP. The large surface area of SBA-15 causes this novel compound to act as an efficient oxidation catalyst.

References:

[1] Run, M.T.; Wu, S.Z.; Zhang, D.Y.; Wu, G. *Mater. Chem. Phys*. **2007**, *105,* 341.

[2] Li, X.F.; Guan, W.C.; Yan, H.B. Huang, L. *Mater. Chem. Phys*.**2004**, *88*, 53.

[3] Kickelbick, Guido. *Prog. Polym. Sci*.**2003**, *28*, 83.

[4] Shanbhag, G.V.; Choi, M.; Kim, J.; Ryoo, R. J. Catal. **2009**, *264*, 88.

Synthesis and characterization of zinc oxide nanoparticles via a hydrothermal method and investigation of adsorption isotherms and evaluation of thermodynamic parameters of ammonia adsorption on zinc oxide

A. Farrokhnia [a] , A. Kajbaf Vala [a]

[a] *Department of chemistry, University of Shahid Chamran, Khusestan, Ahvaz*

(a.farrokhnia@gmail.com)

In this study, zinc oxide nanoparticles synthesis in a mild hydrothermal process was studied. The ZnO powders were characterized by Scanning Electron Microscopy (SEM), X-Ray diffraction (XRD), and Fourier transform infrared (FT-IR) spectroscopy. The aim of the present work was to investigate the ability of zinc oxide to remove ammonia from aqueous solution. For this purpose, batch adsorption experiments were carried out. The effect of contact time, temperature, adsorbent dosage and adsorbate concentration on this process has been investigated. The Langmuir, Freundhich. Temkin and D-R isotherms were applied to fit the experimental results. The results showed that experimental data was best fitted with Freundlich isotherm with $r^2 = 0.994$.

The thermodynamic parameters such as standard enthalpy change (ΔH^0), standard entropy change(ΔS^0) and standard Gibbs free energy change (ΔG^0) were evaluated. These parameters indicated that adsorption of ammonia was spontaneous and exothermic process in nature.

Key Words: zinc oxide, hydrothermal, adsorption isotherms, thermodynamic parameters.

References:

[1] J. Lee, A.J. Easteal, U. Pal, D. Bhattacharyya, Curr. Appl. Phys., 9 (2009) 792–796.

[2] Kadir Saltalı, Ahmet Sarı, Mehmet Aydın, J. Hazard. Mater., 141 (2007) 258–263.

[3] Alias Mohd Yusof, Lee Kian Keat, Zaharah Ibrahim, Zaiton Abdul Majid, Nik Ahmad Nizam, J. Hazard. Mater., 174 (2010) 380–385.

Dye removal from solution by using MCM-41 as adsorbent

Ghazaleh Koutchakzadeh

Department of chemistry , Science Faculty , Islamic Azad University ,Khorramabad Branch , Khorramabad , Iran

Email:gh_kouchakzadeh@yahoo.com.

Keywords : Adsorption , Safranine , MCM-41 , Langmuire isotherm

Introduction

The adsorption process is one of the effective methods for removal dyes from the waste effluent. Adsorption can produce high quality products while also being a process that is economically feasible. In the study we selected MCM-41. It provides exciting opportunities for fundamental and applied studies on mesoporous materials. Such material is characterized by high surface area, high pore volume, as well as parallel and ideally shaped pore structures without the complications of a network. The goal of present work was to test the ability of adsorption a zeolite such as MCM-41 that removal dye from aqueous solution[1].

Materials and Methods

***Preparation of adsorbent**:*

Mesoporous MCM-41 has been successfully prepared using different synthesis procedures and conditions. For preparation MCM-41, Fumed silica (8 g) was added to a solution of sodium hydroxide (2g) in distilled water (150 mL) in a baker at 80 °C. The resulting mixture continuously stirred until a clear solution was obtained. Then cethyltrimethyl ammonium bromide (CTAB) (3 g) was slowly added to this solution under vigorous stirring at room temperature. The resulting gel was additionally stirred for 2 h. The obtained gel was transferred into a teflon-line stainless steel autoclave for a hydrothermal treatment at 100 °C for 3 days. The resulting solid product was recovered by filtration and washing with deionized water for several times. The obtained white solid was dried in air at 100 °C for 5 h. Finally, the sample was calcined at 600 °C for 16 h in air.

Dye solution preparation:

For this study, safranine was used and it was obtained from Merck. Solution of safranine were prepared in double distilled water. Dye concentration was determined by using absorbance values measured before and after the treatment, at 48 nm with JENWAY UV-Vis spectrometer (Model 6505).

Result and Discussion

The effect PH:

The amount of dye adsorbed increases with increase in PH.The dye adsorption was significantly change over the PH value of 4 to 6. At the PH renge up to 6, The percentage of removal was almost remains constant**.**

Isotherms study:

Adsorption equilibrium data were correlated with the Langmuire and Freundlich isotherms . The isotherms fit the Langmuire equation (1) and to some extent Freundlich equation (2) .

$$\frac{1}{q_e} = \frac{1}{qb}\left(\frac{1}{C_e}\right) + \frac{1}{q} \qquad (1)$$

$$\log q_e = \log K_f + \frac{1}{n}\log C_e \qquad (۲)$$

Where C_e is the equilibrium concentration of the adsorbate (mgL^{-1}), q_e is the amount of adsorbate adsorbed per unite mass of adsorbent (mgg^{-1}), q and b are Langmuir constants related to adsorption capacity and rate of adsorption, respectively and K_f and n are the Freundlich constants [2].

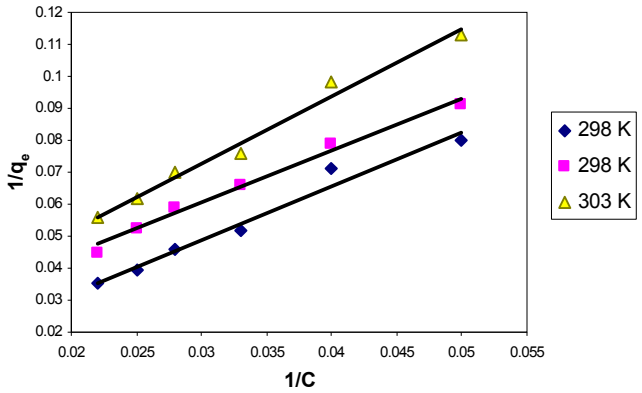

Figure 1. Plot of $1/q_e$ vs. 1/C safranine (Langmuir equation)

Conclusion

In this study, MCM-41 is able to adsorbed safranine from aqueous solutions. It was noted that an increase in the temperature resulted the decrease of the adsorption.

The equilibrium adsorption isotherm was followed, Langmuir and Freundlich isotherms, thus correlation coefficient for fitting the Langmuir equation was significantly better than Freundlich equation.

References

[1]Lain-Chuen,J. et al. "Adsorption of basic dyes onto MCM-41"; J. Chemosphere, 64(2006),1920-1928.

[2]Han,R. et al. "Equilibrium biosorption isotherm for lead ion on chaff"; J. Hazardous Materials,B125(2005),266-271.

N-doped TiO_2 thin films by chemical method

S. Kimiagar[1]*; M. R. Mohammadizadeh[2]

[1] Department of Physics, Islamic Azad University, Central Tehran Branch, Tehran,

[2] Superconductivity Research Lab (SRL), Department of Physics, University of Tehran, Tehran

Keywords: Chemical method, Thin film, Tio2, Photocatalytic, Superhydrophilicity.

Titanium dioxide is extensively used in antibacterial surfaces and solar cells [1]. TiO_2-anatase leads to the degradation of a great number of pollution in air or water [2]. Moreover, the photo-induced superhydrophilicity of TiO_2 films has also been achieved under UV light [3]. TiO_2 films can decompose atmospheric pollutants present on its surface and get self cleaning from any dust and organic residues.

The improvement of visible light photocatalytic activity of nitrogen doped TiO_2 was usually attributed to the decrease of the band gap through hybridization of the N 2p states with O 2p states on the top of the valence band[4].

Doping of nitrogen into titanium dioxide was discovered to induce photocatalytic activity under visible light irradiation [5]. Various techniques have been employed to incorporate nitrogen to TiO_2, either based on chemical reactivity (sol–gel synthesis[6], chemical treatment of the bare dioxide [7]and oxidation of titanium nitride (TiN) [8]) or on physical methods (laser ablation [9], electron beam evaporation [10] and magnetron sputtering [11]). N-TiO_2 films have been prepared by various techniques. Among the methods sol-gel technique is widely used because of its low processing cost, simplicity and ability to produce thin and uniform films and easily can be repeated.

In this work N-TiO_2 sample was prepared by chemical sol-gel method. The sol was saturated by doping N. The doping effect was measured on improving the hydrophilicity and photocatalytic activity. The biggest advantage of N doped TiO_2 samples, compared to pure TiO_2, is their lower excitation energy, which allows the absorbance of the UV portion and the visible portion of solar light.

Experiment

The process of preparing sol-gel was such as below. Container included 20 cm^3 Ethanol and magnetic stir. All of these were inside ice-water bath. We added 2 cm^3 $Ticl_4$ drop by drop. When the result vapor vanished, the composition of the 20 cm^3 distillate water and 20 gr urea powder $(NH_2)_2CO$ ( ) were added drop by drop. Spray Pyrolysis deposition method started after 5 minutes aging. Substrate was at 300^{oC} and deposition time was 45 minutes. Annealing temperature was one hour at 150 ^{oC}, one hour at 300 ^{oC} and one hour at 450^{oC}. Hydrophilicity activity was studied by measuring angle of distillate water drop of 20 µl volume . UV light was used with 1mw strength. Photoactivity was measured in the case of Methylene blue ($C_{16}H_{18}N_3SCL$) with 0.01 molar density was covered the sample at a dark place for 48 hours. Transition spectrums were studied after 10 minutes irradiating under the UV light. The maximum absorption of Methylene blue is in wavelength 660 nm and consequently maximum decomposition. Methylene blue concentration at time t (C), over Methylene blue concentration at time t=0 (C_0) is calculated by:

$$C/C_0=Ln(T_0/T_m)/Ln(T_0/T_i) \qquad (1)$$

Where T_0 is the transition coefficient before pollution with Methylene blue at time=0, T_i is the transition coefficient after pollution with Methylene blue at time=0 and T_m is the transition coefficient after pollution with Methylene blue at time t.

Therefore by measuring the transition coefficient each 10 minutes and using equation (1), decomposition as a function of time is evaluated.

Results

Fig 1 and 2 show the contact angle of water for glass and N-Tio_2 substrates. The decreasing of angle for N-Tio_2 is clear and the sample shows superhydrophilicity activity. The angles for different UV irradiation time have been shown in Fig 3. Photoactivity was studied by measuring the transition coefficient at different times and using equation 1. Fig 4 demonstrates that N-Tio_2 is better photocatalytic than the glass. It means the recombination of electron and hole is slow and band gap decreases.

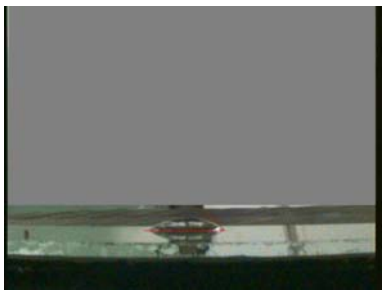

Fig 1: Water drop contact angle for glass substrate.

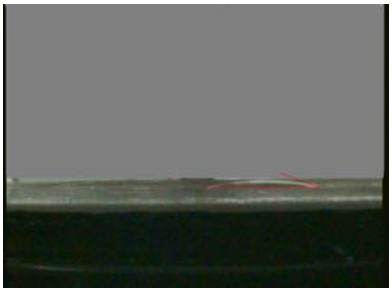

Fig 2: Water drop contact angle for N-Tio$_2$ substrate.

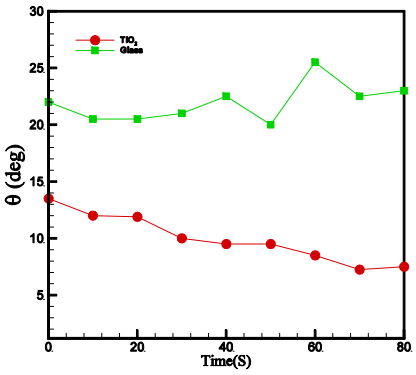

Fig 3: Water drop contact angle for two substrates.

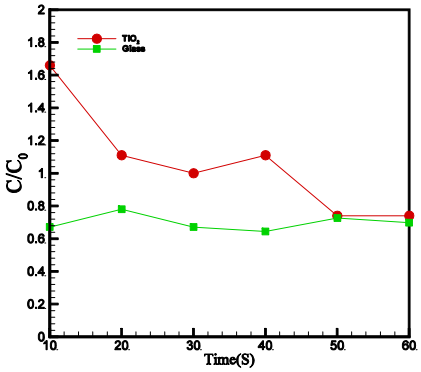

Fig 4: Photocatalytic activity for two substrates.

Refferences

[1] L. Schmidt-Mende, M. Grätzel, Thin Solid Films 500 (2006) 296.

[2] A. Fujishima, K. Hashimoto, T. Watanabe, TiO2 Photocatalysis: Fundaments and Applications, BKC, Tokyo, May 1999.

[3] T. Watanabe, A. Nakajima, R. Wang, M. Minabe, S. Koizumi, A. Fujishima, K. Hashimoto, Thin Solid Films 351 (1999) 260.

[4] R. Asahi, T. Morikawa, T. Ohwaki, K. Aoki, Y. Taga, Visible-light photocatalysis in nitrogen-doped titanium oxides, Science 293 (2001) 269–271.

[5] R. Asahi, T. Morkawa, T. Ohwaki, K. Aoki, Y. Taga, Science 293 (2001) 269.

[6] Z. Lin, A. Orlov, R.M. Lambert, M.C. Payne, J. Phys. Chem. B 109 (2005) 20948.

[7] H. Ire, Y. Watanabe, K. Hashimoto, J. Phys. Chem. B 107 (2003) 5483.

[8] Z. Wu, F. Dong, W. Zhao, S. Guo, J. Hazard. Mater. 157 (2008) 57.

[9] B. Farkas, J. Budai, I. Kabalci, P. Heszler, Zs. Geretovszky, Appl. Surf. Sci. 254 (2008) 3484.

[10] P.G. Wu, C.H. Ma, J.K. Shang, Appl. Phys. A 81 (2005) 1411.

[11] Y. Nakano, T. Morikawa, T. Ohwhi, Y. Taga, Chem. Phys. 339 (2007) 20.

Efect of solution pH and temperature on adsorption behavior of direct dyes on activated carbon

E. Mosaddegh Ardebili*[a], A. Parchehbaf jadid[a], A. Shamel[a], S. Babashpour[b],M. Alem[b], R. Rahimi[a]

[a]Department of Chemistry, Faculty of Science, Islamic Azad University, Ardabil Branch, Ardabil, Iran

[b]Department of Chemistry, Islamic Azad University, Young Researchers club, Ardabil Branch, Ardabil, Iran

(E-mail: elhammosadeg@ymail.com)

Keywords: Activated Carbon,Dye,Spectrophotometry,Adsorption,Langmuir_ Frendlich Isotherms

Introduction

There are more than 100000 types dyes of commercially available. In aqueous solution anionic dyes carry a net negative charge due to the presence of sulphonate group while cationic dyes carry a net positive charge due to the presence of protonated amine or sulfur containing groups [2]. A considerable amount of research on wastewater treatment has focused on the elimination of direct dyes essentially for three reasons firstly direct dyes represent 20-30% of the total dye market, secondly large fraction of direct dyes are wasted during the dying process [3] thirdly conventional wastewater treatment methods which rely on adsorption and aerobic biodegradation were found to be inefficient for complete elimination of many direct dyes [1]. In this study the removal of three problematic direct dyes from water has been investigated using a highly porous high surface area activated carbon. Adsorption isotherms for the direct dyes were undertaken at 25°C to study the effects of solution pH and temperature.

Experimental

Activated carbon was purchased from Merck .The bulk density and the porosity of the adsorbent were 0.64 g/cm^3 and 0.4 respectively. There direct dyes which have a wide industrial application were selected, namely; Red3BS. The chemical structures of the dye is illustrated in Fig.1.

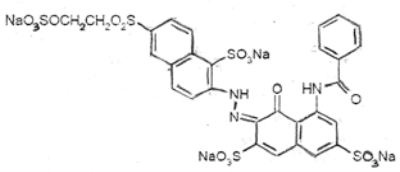

Fig1: RED3BS

The effect of solution pH on dye adsorption was investigated according to the following procedure. 0.250 g of dried activated carbon was added to a 250 cm^3 glass bottles containing 100 cm^3 of 6.0×10^{-4} mol /dm^3 dye solution. The pH of the dye solutions was adjusted over the range pH (2- 10) using 0.5 M HCl or 0.5 M NaOH solutions.

5×10^{-3} of Red3BS solution was added into active carbon (0.2g) until doing surface absorb. The adsorption process was done at the wavelength of 542 nm.

For surface absorb degree by using activated carbon was calculated according to the initial and final concentration in the solution:

$$q_e = \frac{(C_0 - C_e)V}{W}$$

Results and Discussion

Effect of solution pH on dye adsorption

A large decrease in adsorption capacity for this dye was observed under basic condition (i.e. a decrease to 40

% removal at pH 10). Similar adsorption behavior with variation in solution pH has been reported in the

Literature [2,4].

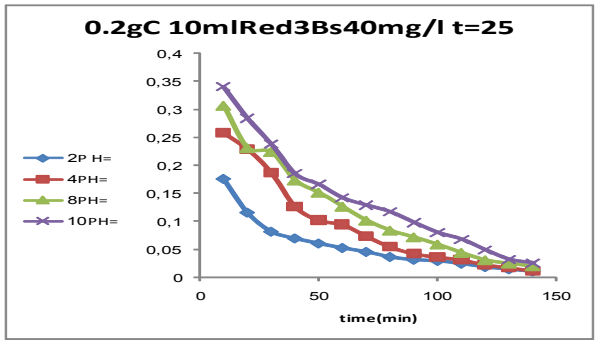

Fig. 2: Effect of solution pH on dye adsorption

Effect of temperature on dye adsorption

The adsorption of red 3BS on activated carbon was studied at temperatures of 298,308,318,328 K

With these adsorption isotherms being shown in Fig.

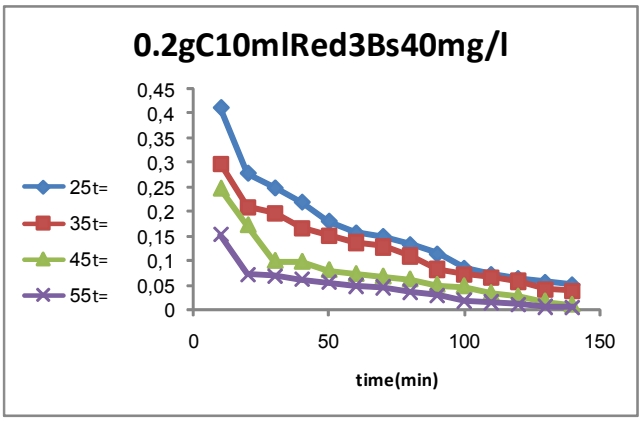

Fig. 3: Effect of solution temperature on dye adsorption

Conclusions

At 298 K the maximum adsorption values as described using the Langmuir equilibrium isotherm model was 40 mg/L for Red3BS. The adsorption capacity of the dyes on activated carbon increased in acidic solution, but decreased in basic solution. Adsorption of direct dye was found to be spontaneous at the temperatures under investigation (298-328K) as indicated from the negative values of free energy .

References

[1] Robinson T,McMullan G,bioresource Technology 2001;77:247-55.

[2] Netpadit S,Thiravetyan p;Journal of Collid and Interface Science 2004;270;255-61.

[3] Al Duri B,Khader K, Journal of Chemical Technology 1992;53:345-52.

[4] Namassivayam C,Kalttha D.Dyes and pigments 2002,54;47-58.

Synthesis and characterization of mesoporous poly(4-methyl vinylpyridinium hydroxide) as a purely organic heterogeneous catalyst for the Knoevenagel reaction

Roozbeh Javad Kalbasi*, Sedigheh Mozafari Vanani
Department of Chemistry, Islamic Azad University, Shahreza Branch, 311-86145, Shahreza, Isfahan, Iran
Corresponding Author E-mail: rkalbasi@gmail.com

Introduction

Mesoporous silica materials prepared with the aid of surfactants have been widely used as sacrificial templates to obtain a variety of porous materials with well-controlled textural properties such as carbons, metals, inorganic compounds, polymers, etc. On the other hand, only a few works have been focused on the synthesis of mesoporous materials with an organic framework. To date, mesoporous polymers have attracted a great deal of attention owing to their diverse range of applications, including such areas of purification, separation, catalysis, and energy storage. Most synthetic strategies for fabricating mesoporous polymers have been dependent on the hard template approach. The template mesoporous polymeric replicas were obtained after the selective removal of the silica framework in the polymer/silica composites. In this way, a porous polymeric material was obtained [1-3].

The main purpose of the present work is to investigate strategies to control the structural characteristics of porous polymers fabricated by using porous silica materials as sacrificial templates. In this paper, it was attempted to report the synthesis of poly (4-methyl vinylpyridinium hydroxide) mesoporous polymer (mp-P4MVPH) and used in the Knoevenagel condensation as a basic catalyst.

Experimental

Mp-P4MVPH was synthesized using a SBA-15 as template. In the first step, the porosity of the silica is filled with a monomer 4-vinylpyridine, which is polymerized in situ and then quaternized by CH_3I and the iodide ion was exchanged with NaOH. Subsequently, the silica framework is selectively removed by an etching agent (NaOH), which allows a porous polymer to be retrieved. The catalytic activity of mp-P4MVPH was investigated for the Knoevenagel condensation of various aldehydes with active methylene. The reaction performed in solvent-free conditions and completion of the reaction was monitored by TLC. The product obtained in high yield and purity after a simple work-up.

Results and discussion

This novel composite was synthesized and fully characterized with different methods. The specific area and the pore size of mesoporous silica SBA-15, P4VP/SBA-15 and P4MVPH/SBA-15 and mp-P4MVPH had been calculated using BET and BJH methods, respectively. It was known that calcined SBA-15 had a high BET surface area (1430 m^2/g), a large pore volume (1.9 cm^3/g) and pore size (9.9 nm). It was clear that P4VP/SBA-15 and P4MVPH/SBA-15 exhibit a smaller specific area, pore size and volume in comparison with those of pure SBA-15, which might be due to the presence of polymer on the surface of the SBA-15. It was indicated that mp-P4MVPH was exhibited a smaller specific area ($594 m^2 g^{-1}$) in contrast to a larger pore size (44.3 nm) and volume ($6.5 cm^3 g^{-1}$) in comparison with those of pure P4MVPH/SBA-15 which was obtained after the selective removal of the silica framework.

Powder X-ray diffraction patterns of SBA-15 showed a typical mesoporous structure with three sharp peaks, including one strong peak (100) and two weak peaks (110) and (200) at 2θ ranging between 0.5° and 3°. The P4MVPH/SBA-15 sample showed the same pattern, indicating that the long-range order of the SBA-15 framework was well retained after immobilizing. However, this peak almost disappeared after the removal of template showing the destruction of the ordered structure.

Conclusion

In this paper, it was shown that a clean, efficient, and simple method had been developed for the synthesis of mesoporous polymer using inexpensive materials as a good catalyst for Knoevenagel condensation. The reactions proceeded with high yield selectivity (100%) under solvent-free conditions at room temperature. The catalyst mp-P4MVPH is recyclable and can be reused more than seven times without significant loss of activity and selectivity.

References

[1] A. B. Fuertes, M. Sevilla, S. Alvarez, T. Valdes-Solis, Micropor. Mesopor. Mater,112 (2008) 319–326.

[2] M. Fujiwara, K. Shiokawa, Y. Zhu, J. Mol. Catal. A: Chem, 264 (2007) 153–161.

[3] F. Liu, X. Meng, Y. Zhang, L. Ren, F. Nawa, F. S. Xiao, J. Catal. 271 (2010) 52–58.

Investigation of interaction between anionic azo dye – cationic surfactant in aqueous solutions

S. Fazeli[a*], M.Moallemi[a], B. Sohrabi[a] A. R. Tehrani Bagha[b]

[a]Department of chemistry, Surface Chemistry Research Laboratory, Iran University of Science and Technology, P.O. Box 16765-163, Tehran, Iran.

[b]Institute For Color Science And Technology, Tehran, Iran

Email: sarafazeli@gmail.com

Abstract

The association of an anionic azo dye, sunset yellow, and cationic surfactant dodecyl trimethyl ammoniom bromide (DTAB) has been investigated using tensiometry and UV-vis spectrophotometer. Sunset yellow can form complex structures with cationic surfactant species in solutions at very low concentrations of the surfactant. The results show hypsochromic shift for the azo dye followed by significant decrease in the λ_{max} at the optimum concentrations of this surfactants. However, when the concentration of surfactant is above their critical micelle concentration, the dye can redissolve and dissociate into molecular or ionic forms. The importance is discussed of both hydrophobic and electrostatic interactions in the binding process.

Keywords: cationic surfactant; azo dye; dye-surfactant interaction; Spectral studies

Introduction

Interaction between surfactant and dye are important in various dyeing process as textile dyeing, photography, inhabitation of dye transfer in detergency. Surfactants act as wetting agent, leveling agent, solubilizers for water insoluble dye, suspending agent and etc [1-3]. Strong complex formation was found between cationic surfactant and anionic azo sunset yellow dye [2].The reported results in this paper are the results of investigation on the interfacial and micellar properties of anionic azo dye sunset yellow with cationic surfactant dodecyl trimethyl ammonium bromide.

Method

Surface tension measurements were carried out a PC-controlled KSV Sigma 700 tension balance that employs the DuNouy ring-detachment method at 298K.The absorbance measurements of dye-surfactant solutions were carried out by Shimatzu UV-mini spectrophotometer had a one quartz cells (10.0 mm in light pass length).

Results and discussion

In aqueous solutions sunset yellow exist anionic forms. Fig. 1 presents the visible spectra of aqueous sunset yellow at 0.04 mM for several concentrations DTAB surfactant. Aqueous solution of the dye exhibits a maximum absorption band at 480 nm. In the presence of dodecyl trimethyl ammonim bromide up to 1mM the absorbance band decrease weakly and a new band at 470 nm appear (hypsochromic shift) [3]. The equilibrium surface tension is further studied in mixture of dye and surfactant. The adsorbtion at air – water interface cause reduction of surface tension.

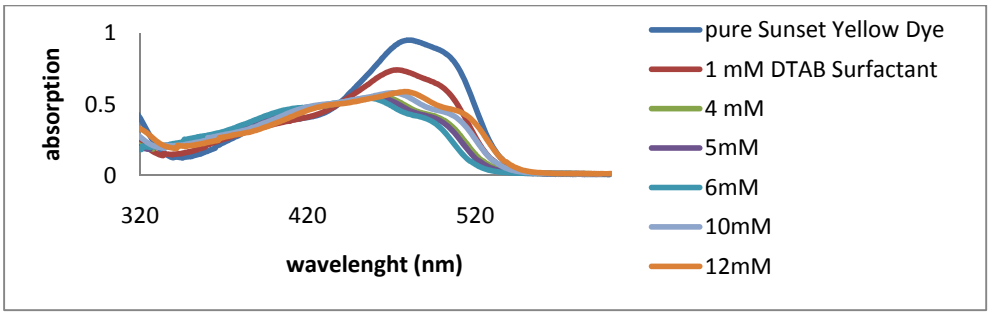

Fig.1. Absorption spectra of 0.04 mM Sunset Yellow solution at various concentrations of DTAB.

Conclusion

The present study shows that the closed packed dye – surfactant ion pairs are formed between sunset yellow and cationic surfactant in submicellar aqueous solutions due to the prevailing hydrophobic and electrostatic forces in the systems.

Reference

[1] Jiang YangJournal of Colloid and Interface Science 274 (2004) 237–243

[2] Halide Akba¸s and Melike Aydemir , Colloid Journal 70 (2008) 541-548

[3] Ma1gorzata Bielska, Anna Sobczyn ska, Dyes and Pigments 80 (2009) 201–205

Intermicellar interaction in catanionic mixtures in presence of electrolyte

M.Moallemi*[a], S.Fazeli, P.Moradi, B.Sohrabi

[a] *Department of chemistry, Surface Chemistry Research Laboratory, Iran University of Science and Technology, P.O. Box 16765-163, Tehran, Iran.*

(Email:m.moallemy@Gmail.com)

Abstract

Micellization and adsorption at liquid-air interface are investigated for mixture of cetyl trimethyl ammonium bromide (CTAB) and sodium dodecyl sulfate (SDS) at different concenteration of inorganic salt by surface tension and cyclic voltammetry (CV) measurements. The data based on plotting of surface tension(γ) as a function of solution composition and total surfactant concentration enable us to determine critical micelle concentration (CMC) and also from plots of surface tension (γ) as a function of total surfactant concentration, we have determined the surface excess (Γ_{max}) and mean molecular surface area (A_{min}). The electrochemical behavior of cationic-anionic (catanionic) mixed surfactant and self-assembled solutions at Pt wire electrode has been studied by cyclic voltametry [1].

Key words: Mixed surfactant, Electrolyte, Cyclic voltametry, Surface tension

Introduction

Mixtures of oppositely charged surfactants exhibit novel solution and interface properties; the aggregation in aqueous mixtures of cationic and anionic surfactants occurs at considerably lower concentrations than the critical micelle concentration (CMC) of individual surfactant[2, 3]. In the present study, we investigated the mixed micelle and adsorption properties of binary surfactant systems containing the cationic surfactant (CTAB) and the anionic surfactant SDS in the absence and presence of various concentrations of sodium bromide.

Experimental and Methods

CTAB and SDS (99%), Sodium bromide (98%). Ferrocen (98%) were obtained from Merck. Surface tension measurements were carried out at 298.15 K by the ring method. Cyclic Voltametry (CV) was performed by using an electrochemical analyzer, SAMA 500. A three-electrode system consisting of a working Pt electrode and saturated Ag/AgCl reference electrode with a salt bridge containing 3M aqueous NaCl solution and the counter electrode.

Results and Discussion

Fig.1 shows the plots of surface tension (γ) measurement of CTAB/SDS mixture in presence of NaBr in cationic-rich regions. The concentration corresponding to the break in the plot represents the CMC in all the systems.

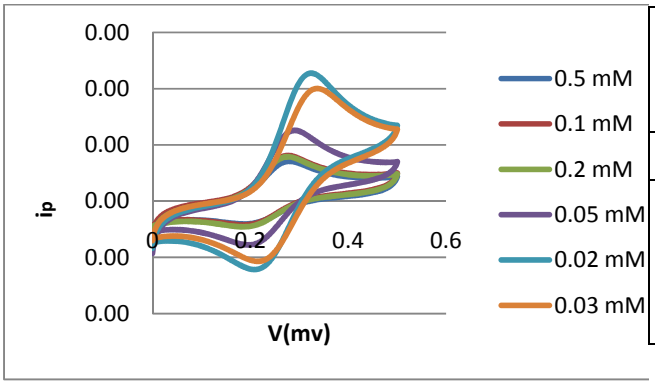

TABLE 1: Obtained values of *CMC* the mixed system CTAB/SDS by cyclic-voltammetery and surface tension methods in cationic-rich in C_{NaBr}=0.05M.

	method	CTAB99/SDS1	CTAB97,SDS3
Cationic-rich	CV	0.131	0.156
	Surface-tension	0.119	0.131

The values of CMC determined from the cyclic-voltametery and surface tension plots are listed in the Table 1. The agreement of the CMC derived from these two methods seems satisfactory.

Also, we determined minimum surface tension at CMC (γ_{cmc}), maximum surface excess concentration (Γ_{max}), the minimum area per molecule at the aqueous solution/air interface (A_{min}), and the effectiveness of surface tension reduction (Π_{cmc}) in the various percents of NaBr.

Conclusion

The results of surface tension show that the size of mixed micelles and vesicles change with the increase of NaBr to surfactant mixtures. voltammetric measurements have been carried out to calculate the micellar self-diffusion coefficient (D_s) and intermicellar interaction parameter (K_d) of catanionic surfactant in aqueous NaBr solutions at 298.15 K. the results

indicate that K_d and N_{agg} in anionic rich region is more than in cationic rich, this effect attributed to the distribution of charges on head group surface of SDS.

References

[1] Rakesh Kumar Mahajan, N. K., Mandeep Singh Bakshi, *Colloids and Surfaces A: Physicochem. Eng. Aspects* **2006,** 276, 221–227

[2] Yuan, Z.; Dong, S.; Liu, W.; Hao, J.*Langmuir* **2009,** 25, (16), 8974-8981.

[3]Piela, K.; Djojorahardjo, E.; Koper, G. J. M.; Ooms, G., *Chemical Engineering Research and Design* **2009,** 87, (11), 1466-1470.

Adsorption of SDS on Various oil-Water Interfaces in the presence of salt

P. Moradi Shahrbabak[a,*], B.Sohrabi[a], ,M.Moallemi[a] ,M. Najafi[b]

[a]*Department of chemistry, Surface Chemistry Research Laboratory, Iran University of Science and Technology, P.O. Box 16765-163, Tehran, Iran.*

[b]*Department of chemistry, Faculty of science, Imam hossein university, Tehran, Iran*

(parviz.moradi.sh@gmail.com)

Abstract

Interfacial tension data and adsorption thermodynamic parameters for sodium dodecyl sulfate from aqueous solutions on the oil-water interface in the presence of salt have been investigated. Also the results are compared with data for water-air interface. In this work critical micelle concentration (CMC), the surface excess (Γ_{max}) and mean molecular surface area (A_{min}) are determined.

Keyword: Surfactant, Adsorption, Oil, Interfacial

Introduction

Although much works has been performed on the adsorption of surfactant on air-water interface [1,2], comparatively less work has been done on the adsorption of surfactant on oil-water interface [3,4]. Surfactants adsorption on oil-water interface, along with the resulting lowering of the interfacial tension, plays an important role in controlling the desired interfacial tension properties in many applications involving surfactants. These applications range from large scale industrial operations, such as the enhanced recovery of crude oil from reservoirs.

Experimental and Methods

SDS (99%), Sodium bromide (98%) were obtained from Merck. toluene, n-hexane, n-heptane and n-nonane were used as oils, The concentration of salt was varied from 0.008 M to 0.05 M. The interfacial tension of the samples was measured using a PC-controlled KSV Sigma 700 tension balance that employs the DuNouy ring-detachment method at 298K. Measurements of the surface tension of pure water at 298.15 K were used to calibrate the tensiometer and to

check the cleanliness of the glassware. In all cases, more than three successive measurements were carried out, and the standard deviation did not exceed ±0.1 $mN.m^{-1}$. The temperature was controlled to within ±0.1°C by circulating thermostated water through the jacketed glass cell.

Results and discussion

The interfacial tension measurements were used to determine interface data. The addition of salt decreased interfacial tension significantly The addition of salt reduced the electrostatic double layer repulsion between the SDS ions, which augmented their adsorption at the interface. The critical micelle concentration where the concentration of surfactants above which micelles are spontaneously formed. For the case of aliphatic alkanes, the CMC decreases as the chain length is decreased. A decrease in the CMC due to the presence of unsaturation in the hydrocarbon is illustrated also by the lower CMC found for toluene [3]. The decrease in the CMC was found to be related to the water solubility of the hydrocarbons. The aromatic hydrocarbon, toluene, is solubilized in the palisade layer of the micelle, which spreads out the surfactant molecules considerably, thus lowering the CMC of the SDS in comparison with aliphatic hydrocarbons[4].

Conclusion

The results are compared and discussed in view of the role of the salt and the type of the oil phase. On the oil-water interface the adsorption is always lower than that on air-water interface. Addition of salt increases the adsorption of the surfactant and decreases CMC values on both interface.

References

[1] Prosser, A. J.; Franses, E. I. *Colloids Surf. A***2001**, 178, 1-40.

[2] Svitova, T. F.; Wetherbee, M. J.; Radke, C. J. *J. Colloid Interface Sci*.**2003**, 261, 170-179.

[3] Rehfeld, S. J. *J. Phys. Chem***. 1967, 71,** 738-745

[4] Murphy, D. S.; Rosen, M. J. *J. Phys. Chem.***1988,**92, 2870-2873.

Photocatalytic degradation of azo dye acid red 14 in water with ZnO/Bentonite as a catalyst

Hossean Malekhosseani [*1], Kazem Mahanpoor [2], Aboalfazl Soufi [3]
1,2, 3) Department of Chemistry, Faculty of Science, Islamic Azad Univrsity, Arak Branch,
kazem_mahanpoor@yahoo.com E-mail:

Abstract:
In this study, The Acid Red14 was used as a typical revealed organic dye. The results of this study show that was degradable in the presence of oxygon solution in water under UV-C irradiation and ZnO/Bentonite catalyst. Investigation of the kinetics prosess showd that the log plot of the dye concentration versus time was liner, suggesting a first order reaction. Furthermore, the effect of some operational parameters in the prosses such as pH, Initial concentration of AR14, amount of catalyst and temperature of reaction were investigated.

Key Word: ZnO/Bentonite, Photocatalyst, Acid Red 14

Introduction:
From the viewpoint of green chemistry, the photocatalytic decomposition of organic compounds in wastewater has attracted a great deal of attention [1]. Many researchers have examined some methods for fixing ZnO on supporting materials including glass beads [2], silica and zeolite [3]. When using zeolite as ZnO support, care should be taken that ZnO does not loose its photo activity and adsorption properties of zeolite is not affected. In this work ZnO was supported on a zeolite without loosing photoefficiency and affecting the adsorption properties of zeolite. This mixture was used for degradation of aqueous AR 14.

Method :
Zeolite-based photocatalysts were prepared by solid state dispersion (SSD) of ZnO. SSD initially involves mixing of ZnO and zeolite thoroughly using ethanol in agate pestle and mortar; the solvent was then removed by evaporation while mixing. Samples prepared by this method were dried at 110°C and calcined in air at 400°C for 6 h to obtain ZnO-supported zeolite catalysts. ZnO weight was maintained to obtain 5-100 wt.% in the finished forms of

the catalyst. For UV/photocatalyst process, irradiation was performed in a batch photoreactor of 2 liter in volume with a mercury lamp 48W (UV-C manufactured by Philips, Holland). UV-VIS Spectrophotometer, Perkin-Elmer lambda25 was employed for absorbance measurements using silica cells of path length 1 cm.

Results and discussion:

The changes in the absorption spectra of AR14 solution during the photocatalytic process at initial and after 2.5 h irradiation times are shown in the Fig. 1.

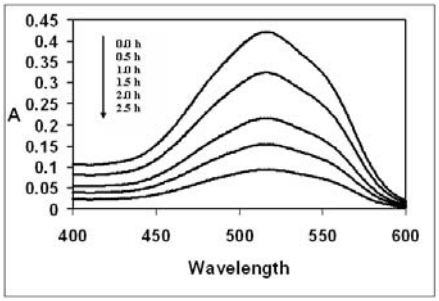

Fig. 1: UV-Vis spectra of AR14 (30 ppm) in aqueous photocatalyst (ZnO 10% +BEN 90%) dispersion with concentration of 250 ppm, irradiated with a mercury lamp light atpH =7, T = 298 K.

The decrease of absorption peaks of AR14 at λmax =515nm in this figure indicates a rapid degradation of azo dye.

Kinetics of photcatalytic degradation of AR14 :The photo oxidation reaction is pseudo-ferst order with respect to dye concentration. The plot Ln[dye] versus irradiation time for AR14 was linear suggesting that the photodegradation reaction approximately follows the first order kinetics (Fig. 4). Rate constant ($K = 7.1 \times 10^{-3}$ min^{-1}) was estimated from the slope of the Ln[dye] versus time plot in the optimized conditions.

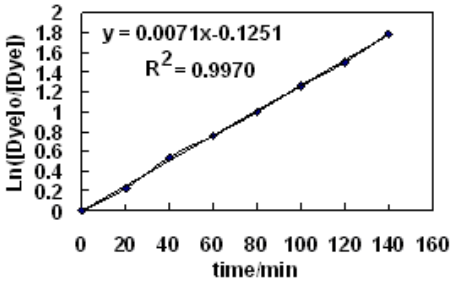

Fig. 2: Plot of reciprocal of pseudo-first order rate constant against initial concentration of AR 14=50 ppm, concentration of photocatalyst (10%ZnO + 90% BEN) = 40 ppm, T = 298 K, pH=7.

References

[1] D.F. Ollis, Photocatalytic Purification and Treatment of Water and Air, Elsevier, Amsterdam, 1993.

[2] Y. Xu, X. Chen, Chem. Ind. (London) 6 (1990) 497.

[3] A. Maurino, C. Guillard, J. M. Marinas, A. Fernandez, A. Aguera, J. M. Herrmann, Appl. Catal. B : Environ. 34(2001)241.

Removal of Reactive Black 5 (RB5) from aqueous solution by a combined method of ultrasound and sorption process

S. Hozhabr Araghi*, M.H. Entezari, M. Chamsaz,
(samira.hozhabr@yahoo.com)
Department of Chemistry, Ferdowsi University of Mashhad, 91775 Mashhad, Iran

Keywords: Sono-sorption، Reactive Black 5، Azo dye، Cavitation، Langmuir model، Freundlich model.

Introduction

Synthetic dyestuffs are used extensively by several industries. The pollution caused by dyestuffs has been a serious environmental problem for years [1] .Therefore, it is necessary to remove the dyes from waste water. Traditional techniques used for treating dye effluents include adsorption [2], coagulation [3], etc. In the recent decades ultrasound as a new method has been used alone or combined with other methods for the removal of dyes and other pollutants [4]. The main objective of this study is de-colorization of RB5 by the combination of ultrasound and the sorption process.

Methods

The sorbent used in this study was $NiCo_2O_4$ spinel which synthesized by citrate gel method [5] and characterized by X-ray diffraction. In all experiments, conventional and combination (sono-sorption) methods were compared. In combination method, ultrasonic horn was inserted to a depth of 10 mm into the Rosett cell containing 50 ml solution of pollutant with different concentrations and different amounts of sorbent. A circulating bath was used to maintain constant temperature during the sonication but conventional experiments were performed in a jar cell with a double cylindrical jacket in which the temperature was controlled by the circulating water through the jacket and stirring speed was fixed without ultrasonic irradiation The sorbent and solution were separated by centrifuge .After each run, the concentration of pollutant was determined by UV–vis spectrophotometer.

Results and discussion

In this study, sono-sortion of dye on surface of sorbent was studied in range of different amount of pH and results released that the maximum adsorption occurred in the range of pH 11- 12. Different parameters such as amount of sorbent, effects of contact time, temperature, initial concentration, ultrasonic irradiation intensity were investigated. In both methods sorption increased with increasing of sorbent dose due to the increase of surface area of sorbent. Also, sorption efficiency increased with increase of temperature in both methods. In all experiments, amount of removal and rate of removal was higher in the presence of ultrasound than conventional method. The major factors for this behavior are probably related to the increase of surface area of the solid phase from cavitation-induced particle size reduction and improve of mass transport of liquid solution to the solid surface via acoustic streaming. The sorption process in combination method was studied at three selected intensity. The result indicated that the sorption efficiency increased with increasing of intensity from 30% to 60%. It is suggested that in the higher intensity, there are more bubbles and also more violently bubbles collapse. Adsorption isotherms Langmuir and Frundlich models were studied and both models fitted by experimental data. Also, the removal kinetics of RB5 followed pseudo-second-order kinetic model.

Conclusion

The present study clearly shows that the spinel $NiCo_2O_4$ is an effective sorbent for RB5 removal from aqueous solution. This removal was enhanced in the presence of ultrasound. The experimental data was fitted by Langmuir and Freundlich modeles. The kinetics of sorption was obeyed the pseudo-second-order.

References

[1] A. A. Attia, W.E.Rashwan, S.A.Khedr, DyesPigments 69 (2006) 128.

[2] Z. Aksu, Process Biochem. 40 (2005) 997.

[3] A. Reife, D. Betowski, H.S. Freeman, "Dyes and pigments, environmental chemistry, in: R. A. Meyers (Ed.), Environmental Analysis and Remediation", Wiley, 1998. And Remediation, Wiley, NewYork, 1998.

[4] M. Inoue, F. Okada, A. Sakurai, M. Sakakibara, Ultrason. Sonochem. 13 (2006) 313.

[5] T. Swathi, G. Buvaneswari. Materials Letters 62 (2008) 3900.

Statistical Thermodynamics

Transport properties of $Ar - H_2S$ plasma

G. Afsahi*[a], H. Behnejad[a], A.H. Jalili[b]
[a]Department of Chemistry, University of Tehran, Tehran, Iran
[b]Gas science Department, Research institute of Petroleum Industry, Tehran ,Iran
(Behnejad@gmail.com)

Introduction:

Nowadays Transport properties in fluids and fluids mixture are one of the paid intentioned topics in physics and chemistry and have been of interest to scientists over many decades because of its adoption in industry as a potential plasma forming gas [1]. Plasma is a state of matter similar to gas in which a certain portion of the particles are ionized, the basic premise is that heating a gas dissociates its molecular bonds and changing it into its constituent atoms. Further heating leads to ionization and turning it into a plasma which contains charged particles, positive ions and negative electrons.[2]

In present work we have investigated composition of $Ar - H_2S$ plasma, in order to obtain equilibrium transport properties of mentioned plasma, such as equilibrium constant and then the viscosity, diffusion coefficient and the other transport properties of mixture are computed in the 4th approximation of the Chapman-Enskog method. This theory presents accurate formulas for the multi component gas mixture under thermal and chemical equilibrium [2]. The obtained results are compared with the literature and the agreement is quite good.

Keywords: Transport properties, Plasma, Chapman-Enskog, equilibrium constant.

Methodology

At first step, we studied the possible chemical reactions in $Ar - H_2S$ plasma and tabulated the corresponding chemical reaction in table 1, it is assumed that seven different species are existed in the Argon and Hydrogen Sulfide plasma so using statistical mechanic and definition of the partition functions the equilibrium constants for the mentioned reactions are obtained. For partition function, the calculation was carried out including all energy levels provided by NIST[3]. Values of individual partition functions have significant effect on plasma composition, which causes influence the transport properties of the plasma.

Table 1. Reactions and the corresponding equilibrium constants

Reactions	log K
$\mathbf{Ar + \bar{e} \rightarrow Ar^+ + 2\bar{e}}$	4.7139
$\mathbf{Ar + H_2S^+ \rightarrow Ar^+ + H_2S}$	10.3899
$\mathbf{HS + H \rightarrow H_2S^+ + \bar{e}}$	1.4799
$\mathbf{HS + H + \bar{e} \rightarrow H_2S + \bar{e}}$	6.5837
$\mathbf{H_2S + \bar{e} \rightarrow H_2S^+ + 2\bar{e}}$	5.1038

Then the transport coefficient of the mixture are obtained following the perturbation technique in the solution of Chapman Enskog [2] for the Boltzmann equation, the transport properties were obtained by its first order perturbation method. The Chapman-Enskog solution of Boltzmann transport equation leads to the expression for transport properties based on a series of collision integrals $\Omega^{(l,s)}$, that depend on the intermolecular potential energy $U(r)$, which is defined as:

$$\Omega_{ij}^{(l,s)} = \sqrt{\frac{2\pi k_B T*}{m_{ij}^*}} \int_0^\infty \int_0^\infty exp(-\gamma_{ij}^2)\gamma_{ij}^{2s+3}(1 - cos^l\chi)bdbd\,\gamma_{ij}$$

(1)

where, k_B is the Boltzmann constant, m_{ij}^* and T^* are the effective mass and the effective temperature of the colliding particle, b is the impact parameter and γ_{ij} is related to the relative velocity. he first approximation, diffusion and viscosity coefficient for pure substances depend only on $\Omega_{ij}^{(1,1)}$ and $\Omega_{ij}^{(2,2)}$ respectively.

Following the kinetic theory of dilute gases, the binary diffusion coefficient involving particle i and j is computed

$$D_{ij}^b = \frac{3k_B^2\, T_i\, T_j}{16\, p\, m_{ij}^*\, T_{ij}^* \Omega_{ij}^{(1,1)}}$$

(2)

where T_i and T_j are temperature of ith and jth particle respectively and T_{ij}^* is the effective temperature. Similar expression can be written for the other transport properties and also these equations can be extended for a multicomponent system.

Conclusion

In this work we studied a method for evaluating thermophysical properties for various species in the $Ar - H_2S$ plasma, As a matter of fact results for thermophysical properties of pure

Argon can be compared with works of many other authors [4] which are in satisfactory agreement with them. Thermophysical properties including equilibrium and non equilibrium properties for various species in Argon and Hydrogen Sulfide plasma are expressed by the different values of the heavy particle temperature and electron temperature ratio. No published data exist for comparison but these data will become a useful data for calculating plasma characteristics of arc in a gas mixture containing the mentioned species in high electron temperatures.

References:

[1] A. H. Jalili, A. Abbaspour, H. Behnejad and L. A. Viehland; Mol.phys., 108 (2010)35-40.

[2] S. Chapman , T.G. Cowling (1952), The mathematical theory of non-equilibrium gases, Cambridge University press, Cambridge.

[3] NIST Atomic Spectra database, http://physcs.nist.gov.

[4] E. A. Mason, R.J. Munn, F.J. Smith, Phys Fluids, 10(1967)1827.

The Changes in Free Energies from Analytical Radial Distribution Functions

A. Morsali[a]*, J. S. Emampour[b], M. Sarvghadi[a] and N. Beyzaie[b]

[a] Faculty of Science, Department of Chemistry, Islamic Azad University–Mashhad Branch, Iran

b Department of Chemistry, Ferdowsi University of Mashhad 91779, Iran

* (Email: morsali@mshdiau.ac.ir)

Keywords: Radial distribution function, Helmholtz free energy, Entropy, Statistical mechanics

Introduction

If radial distribution functions (RDFs) are available as a function of interparticle distance (r), density (ρ), and temperature (T), then the entropic properties such as changes in free energies ($\Delta A, \Delta G$) and entropies (ΔS) could be calculated. In this project, the entropic properties will be calculated using three analytical RDF (MGMA [1], Goldman [2] and MM [3])

Theory: Statistical mechanical equations for ΔA and ΔS

Using thermodynamic fundamental equations ($\Delta A = \int_{\rho_1}^{\rho_2} (P/\rho^2)\, d\rho$), we can write:

$$\Delta A = kT \int_{\rho_1}^{\rho_2} (1/\rho)\, d\rho \; - (2\pi/3) \int_0^{\infty} \int_{\rho_1}^{\rho_2} \left(du(r)/dr\right) g(r,\rho,T) r^3 \, d\rho \, dr \qquad (1)$$

where k and u(r) are the Boltzmann's constant and interparticle pair potential, respectively. The first expression on the right hand side of equation (1) is related to ideal gas. ΔS is obtained from $\Delta S = (\Delta E - \Delta A)/T$ where $\Delta E = E(\rho_2) - E(\rho_1)$ and

$$E = E^{ig} + 2\pi N \rho \int_0^{\infty} u(r)\, g(r,\rho,T)\, r^2 dr \qquad (2)$$

where E^{ig} is internal energy for ideal gas.

Results and discussion

Using Goldman, MM and MGMA expressions, theoretical values of $\Delta A^*/T^*$ and ΔS^* are obtained. These quantities are compared with the experimental data. Table 1 shows the numerical values of $\Delta A_{ex}^*/T^*$ and ΔS_{ex}^* at reduced temperature $T^* = kT/\varepsilon = 2.087$ and different densities. In this table, theoretical values obtained from Goldman, MM, and MGMA expressions have been compared with those of Exp. and an accurate analytic equation of state for the L-J fluid (Mecke et al. EOS) [4].

The AAD values related to $\Delta A_{ex}^*/T^*(\Delta S_{ex}^*)$ in connection with Goldman, MM, and MGMA expressions at the range of applied temperatures and densities are 10.44(6.85), 73.14(26.7) and 3.81(3.01), respectively.

Table 1. Comparison of numerical values of $\Delta A_{ex}^*/T^*$ and ΔS_{ex}^* at $T^* = 2.087$

ρ_2^*	$\Delta A_{ex}^*/T^*$ Exp.	$\Delta A_{ex}^*/T^*$ Mecke et al. EOS	$\Delta A_{ex}^*/T^*$ MGMA	$\Delta A_{ex}^*/T^*$ Goldman	$\Delta A_{ex}^*/T^*$ MM	ΔS_{ex}^* Exp.	ΔS_{ex}^* Mecke et al. EOS	ΔS_{ex}^* MGMA	ΔS_{ex}^* Goldman	ΔS_{ex}^* MM
0.498	-0.189	-0.189	-0.171	-0.242	-0.557	0.708	0.738	0.721	0.771	1.068
0.538	-0.173	-0.174	-0.160	-0.219	-0.468	0.583	0.608	0.594	0.637	0.874
0.598	-0.132	-0.133	-0.125	-0.163	-0.316	0.384	0.398	0.390	0.420	0.569
0.642	-0.086	-0.087	-0.082	-0.104	-0.189	0.226	0.232	0.229	0.247	0.332
0.719	0.035	0.036	0.034	0.041	0.066	-0.078	-0.080	-0.079	-0.085	-0.112
0.773	0.155	0.159	0.153	0.176	0.269	-0.308	-0.317	-0.312	-0.336	-0.443
0.815	0.273	0.280	0.271	0.304	0.439	-0.499	-0.512	-0.505	-0.543	-0.712
0.850	0.388	0.400	0.387	0.426	0.588	-0.663	-0.682	-0.670	-0.718	-0.940
0.880	0.500	0.518	0.500	0.543	0.721	-0.808	-0.833	-0.816	-0.873	-1.140
0.906	0.610	0.633	0.612	0.657	0.842	-0.939	-0.968	-0.948	-1.010	-1.319
0.929	0.718	0.745	0.722	0.768	0.953	-1.058	-1.090	-1.067	-1.134	-1.482
0.949	0.824	0.850	0.830	0.877	1.057	-1.168	-1.199	-1.178	-1.248	-1.631
0.968	0.927	0.958	0.936	0.984	1.153	-1.270	-1.304	-1.280	-1.352	-1.769
0.986	1.029	1.067	1.041	1.088	1.244	-1.366	-1.405	-1.376	-1.448	-1.898
1.017	1.229	1.272	1.246	1.293	1.411	-1.540	-1.583	-1.553	-1.620	-2.133
1.044	1.423	1.469	1.445	1.494	1.563	-1.697	-1.741	-1.713	-1.770	-2.344
1.069	1.613	1.668	1.641	1.691	1.703	-1.839	-1.889	-1.861	-1.903	-2.536

Conclusion

The Goldman and MGMA expressions both predict the values of $\Delta A^*/T^*, \Delta S^*$, $\Delta A_{ex}^*/T^*$ and ΔS_{ex}^* with acceptable errors, but MM expression is not suitable for this purpose. Among the three expressions, MGMA expression predicts these properties with less error.

References

[1] A. Morsali, E. K. Goharshadi, G. A. Mansoori, and M. Abbaspour, Chem. Phys. **310,** 11 (2005).

[2] S. Goldman, J. Phys. Chem. **83**, 3033 (1979)..

[3] E. Matteoli and G. A. Mansoori, J. Chem. Phys.**103**, 4672 (1995).

[4] (a) M. Mecke, A. Muller, J. Winkelmann, J. Vrabec, J. Fischer, R. Span, and W. Wagner, Int. J. Thermophys. **17**, 391 (1996). (b) M. Mecke, A. Muller, J. Winkelmann, J. Vrabec, J. Fischer, R. Span, and W. Wagner, Int. J. Thermophys. **19**, 1439 (1998).

Molecular orientation at liquid/vapor interface by the study of surface thermodynamic functions

M. H. Ghatee*, L. Pakdel
Department of Chemistry, Shiraz University , Shiraz 71454, Iran
(E-mail: ghatee@susc.ac.ir)
(E-mail: niloofarpakdel@yahoo.com)

Keywords: Molecular orientation, surface entropy, surface tension, surface energy, dipole moment.

Introduction

A detailed understanding of molecular orientation at liquid/vapor interface is of great importance in chemical engineering, chemistry, and biology. Plenty experimental methods has been devoted to study the surface orientation [1,2]. Also molecular dynamics has been shown to be very specific in determination of orientation [3]. Interfacial Surface tension (σ) and surface energy (E^s) are practically and theoretically important factors in determination of the solubility. The correlation between surface entropy (S^s), surface energy, surface tension, with the liquid dipole moment (μ) support molecular orientation at the liquid/vapor interface.
In this study the relation between the surface tension, surface entropy and the surface energies of a model solvent is investigated to provide evidences and to establish a relative molecular orientation at the liquid/vapor interface.

Method

Surface tension is inherently can be measured accurately. It turns out that surface tension is a strong and reliable method of studying the liquid surface energetics, surface energy and surface entropy. By accurate measuring surface tension thus these two important surface thermodynamic functions can be determined accurately. At the microscopic level an estimate of the molecular surface structure in particular the molecular orientation at liquid/vapor interface**,** can be studied. Model liquids, pyridine (Py) and its alkyl derivatives methyl (MPy), ethyl (EPy), propyl (PPy) and butyl (BPy) substituted for which surface tension data is available [4] are employed. Gaussian 2003 program is used to calculate the gas and liquid

phase dipole moments of these materials by DFT method [5]. The correlation of molecular dipole moment to S^s, E^s, and σ at the freezing point are studied.

Results and Discussion

Pyridine and its alkyl derivatives, the class of reagent nominated for the preparation of pyridinium ionic liquids, are chosen as the model liquids. Certainly the differences in physical and chemical properties of these compounds arise from their structural details. Then what can be said about the orientation of the molecules at the interface from experimental S^s, E^s, σ and the calculated liquid dipole moment is as the following. First it should be noted that model compounds are consisted of a polar part involving the nitrogen atom and a non-polar part consisting the rings carbon atoms and the alkyl group. Both parts contribute to the surface thermodynamic functions. Therefore, the most probable orientation must be consistent with the surface energy and surface tension as well as the surface entropy. Since both surface tension and surface energy of methyl derivatives are decreasing function of dipole moment (Fig.1 and Fig.2) it can be concluded that the trend is in the order of decreasing component of dipole moments normal to the liquid surface. This implies that the contribution of pyridinium nitrogen is decreased by the increase of the dipole moment and conversely the contribution of the methyl group to the surface microstructure is increased. For this we have to use the principle of independent surface action. Based on this principle each part of the molecule contributes to the surface tension independently. For instance the most probable orientation of the 4MPy is the one that has the most symmetric orientation with respect to the surface. That is, among methyl derivatives, 4MPy with the largest dipole moment and the smallest surface tension can take an orientation with its nitrogen exposing less than its methyl group to the surface. This means that as the molecular dipole moment among an alkyl analogue increases the molecules oriented at surface in such a way to decrease the surface tension. This could be attained by exposing the alkyl group, rather nitrogen atom, to the surface which accordingly decrease the force exerted on the atoms on the surface. At the same time this will restrict the motion of the surface molecules, specially the rotation, and hence the surface entropy.

Conclusions

In this study we have explored the use of σ and its temperature dependence as well as S^s , E^s, to establish correlation with the calculated liquid and gas dipole moments to determine the relative orientation of molecules at the interface for model liquid pyridine and its alkyl derivatives.

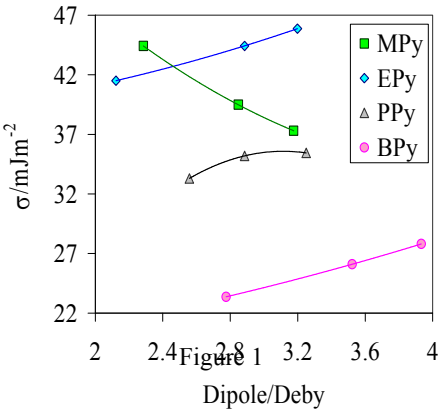

Figure 1

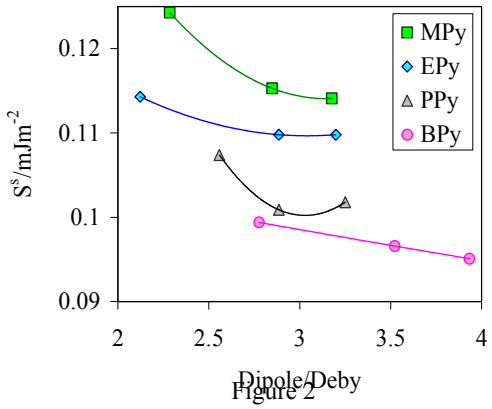

Figure 2

References

[1] D. K. Hore, D. K. Beaman, and G. L. Richmond, J. Am. Chem. Soc. **127**, 9356 (2005).

[2] G. Law and P. R.Watson, Langmuir **17**, 6138 (2001).

[3] M.A. Amat and G. C. Rutledge, J. Chem. Phys. **132**, 114704 (2010).

[4] J.J. Jasper, J. Phys. Chem. Ref. Data **1**, 841 (1972).

[5] Gaussian 03, Revision B.03, J. A. Pople, Gaussian, Inc., Pittsburgh PA, (2003).

Equilibrium and Transport Properties of Acetone and Poly (methyl methacrylate) Solution by Molecular Dynamics Simulation

M. H. Ghatee*, S. Taslimian
Department of Chemistry, Shiraz University, Shiraz, 71454, Iran
(Email: ghatee@susc.ac.ir)

Keywords: Acetone; Molecular dynamics simulation; OPLS; Thermodynamics and transport property; Poly(methyl methacrylate).

Introduction

Molecular dynamics (MD) simulation is an indispensable tool for investigating the behavior of liquid [1]. The outcome of the simulations is primarily controlled by the expressions for the total energy, which are collectively referred to as the force field [2]. The ability to accurately investigate the properties of different solution by using the suitable force field will provide an increased understanding of the thermodynamics and properties of these systems [3]. In this work we will predict density, viscosity and structure of pure acetone, which is largely used in chemistry, by molecular dynamic using a general force field such as OPLS. Using the acetone as the solvent, we will simulate the structural properties of poly (methyl methacrylate) (PMMA) solution.

Method

Properties of acetone, PMMA, and the acetone/PMMA were carried out using the DLPOLY2 program. The calculations were performed in the NPT ensemble. Periodical boundary conditions were applied. All bonds were constrained using Shake algorithm. The Berendsen algorithm was used for constant temperature and pressure simulations. The DLPOLY package contains the computation of the configurational part of the internal energy, by a direct averaging of the pair interactions over the whole cell for Lennard-Jones interaction, and by the Ewald summation techniques for Coulomb part, because of the long range nature of this interaction. The energy and pressure contributions from the long range part of the Lennard-

Jones interactions were corrected as usual by analytically expressed contributions beyond the cutoff.

Results and Discussion

Density of the liquid is important measure of the size of the molecules and the strength of their interaction. The accuracy of simulated density is quite good with the maximum deviation 1.99 % with respect to the experimental [4], which is also a test for the accuracy of the force field used.

Transport properties such as diffusion (D) and viscosity (η) of acetone were predicted by using the Eq. 1 and 2 . For this, we use the simulated mean square displacement, MSD, (Fig. 1).

$$D = \frac{1}{6N\tau}\left\langle \left| r(t) - r \right|^2 \right\rangle \quad (1)\,, \qquad \eta = \frac{kT}{6\pi r D} \quad (2)$$

which $r(t)$ is the position at time t, τ is the simulation time, r is the radius of molecule. The value r was determined by using Gaussian program with MP2/6-311++g** level.

The structure of liquid acetone can be characterized well by RDF, $g(r)[x-y]$ which is the probability of finding atom y located at distance r from atom x. The $g(r)[C_c - C_c]$ and $g(r)[C_m - O_c]$ obtained by MD simulation using OPLS force field are shown in Fig. 2. From all atoms correlations considered, C_c-C_c and C_m-O_c show the highest regular correlation both at short- and long-range. The simulated structural properties of PMMA in acetone involves interesting features. The acetone molecule does not interact deep into the polymer backbone but interact regularly with the side chain. Also the backbones interact in a particular way, but the side chains interaction is an indication of regular molecular system. Fig. 3 and 4.

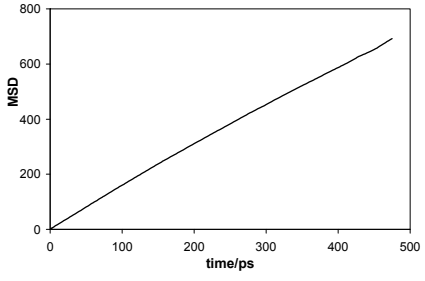

Fig. 1

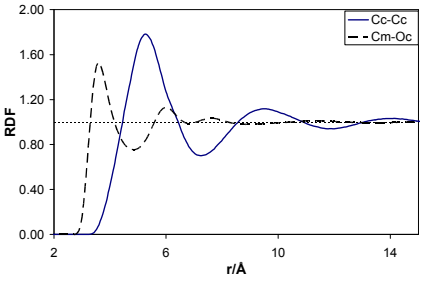

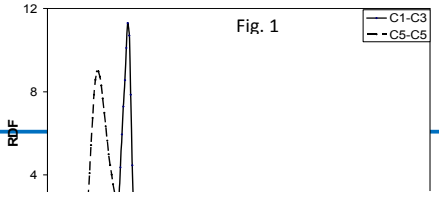

Fig. 2

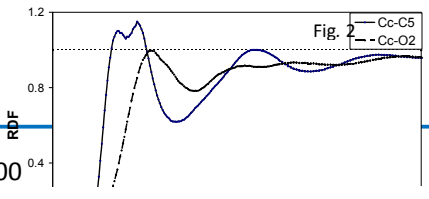

References:

[1] W. Liang, H. Li, Y. Lei, S. Han, J. Molecular Structure (Theochem) **686**, 109 (2004).

[2] W. L. Jorgensen, D. S. Maxwell, J. Tirado-Rives, Am. Chem. Soc. **118**, 11225 (1996).

[3] S. Weerasinghe, P. E. Smith, J. Chem. Phys. **118**, 10663 (2003).

[4] L. p. Yang, T. L. Luo, H. L. Lian, G. J. Liu, J. Chem. Eng. Data **55**, 1364 (2010).

Prediction of The thermodynamic properties of n-alkanols using the statistical associating fluid theory

*S. Hosseini[a] ,A. Maghari[b]

[a]Department of chemistry, University of Payamenoor, Zahedan, Iran

(Email: s.hosseini_60@yahoo.com)

[b]Department of chemistry, University of Tehran, Tehran, Iran

Abstract:

Equations of state (EOSs) are generally used to estimate thermodynamic properties of gases, liquids and solids. In most of the EOSs critical properties or intermolecular potential energy parameters are needed as input data to estimate constants in the equations. Measured values of critical properties are available for some compounds, but for such data can not accurately be predicted. statistical associating fluid theory (SAFT) has been proposed by Chapman et al that it based on thermodynamic perturbation theory of Wertheim. In this research our aim is to predict sound velocity and heat capacities with the Simplified PC-SAFT.

Keywords: Simplified PC-SAFT, Equation of state, Sound velocity, heat capacities

Introduction:

The thermodynamic properties of n-alkanols are a problem of great practical interest. Among all of the EOSs proposed by different investigators, only a few are based on a fundamental theory, but the majority has been developed as a result of the mathematical processing of experimental data. Two theoretical treatments commonly used in chemical engineering for n-alkanols are (SPHCT) and (SAFT) [1]. For years, SAFT has been extensively used to calculate the phase behavior of associating and non-associating fluids. In SAFT a molecule is composed of m segments correspond to atoms, functional groups or complete molecules. the contribution to Helmholtz free energy of bonding between segments can be calculated from the background correlation function for segments.

SAFT EOS can be represented as a sum of Helmholtz energies:

$$A = A_{\text{ideal gas}} + A_{\text{hard sphere}} + A_{\text{dispersion}} + A_{\text{association}}$$

where A and A^{ideal} are the total Helmholtz energy and the ideal gas Helmholtz energy

$$\tilde{A}^{hs} = \frac{4\eta - 3\eta^2}{(1-\eta)^2}$$

Term of hard sphere:

The packing factor η is defined as

$$\eta \equiv \frac{1}{6}\pi N_{AV} m \rho d^3$$

Term of association:

$$A^{assoc}=(2Log[x]-x+1)N_{Av}.k.T$$

Term of dispertion:

The dispersion term is expressed also with the results of Alder et al.

$$\frac{A_{dis}}{NkT} = \frac{A_1}{NkT} + \frac{A_2}{NkT}$$

$$A_1 = -2\pi\rho m^2 n_{Av} \sigma^3 \left(\varepsilon / kT\right) w$$

$$A_2 = -\pi\rho m \left(1 + m\frac{8\eta - 2\eta^2}{(1-\eta)^4} + (1-m)\frac{20\eta - 27\eta^2 + 12\eta^3 - 2\eta^4}{(1-\eta)^2(2-\eta)^2}\right)^{-1}$$

Speed of sound:

the Speed of sound calculations from: $V_s = \left[\left(\frac{\gamma}{M}\right)\left(\frac{\partial p}{\partial \rho}\right)_T\right]^{1/2}$

Heat capacities:

the specific heats at constant pressure C_p and volume C_V, given by the derivative of the Helmholtz energy and the pressure, which are direct calculations from the Simplified PC – SAFT:

$$C_V = C_V^{ideal} - T\left(\frac{\partial^2 A^{res}}{\partial T^2}\right)$$

$$C_p = C_V + \left(T/\rho^2\right)\frac{(\partial p/\partial T)_\rho^2}{(\partial p/\partial \rho)_T}$$

Results and discussion:

The results of Chen and Mi have shown that the Simplified PC – SAFT EOS predicts accurate phase envelope of chain fluids. In this work, the Speed of sound and Heat capacity calculated on the basis of the Simplified PC – SAFT EOS over the wide density and temperature ranges including critical temperature. In Figs. 1, 2 we compare correlated values of Speed of sound and Heat capacities for methanol with the values calculated with the Simplified PC – SAFT EOS. Very good predictions are obtained for both at three different temperatures, including liquid and supercritical regions.

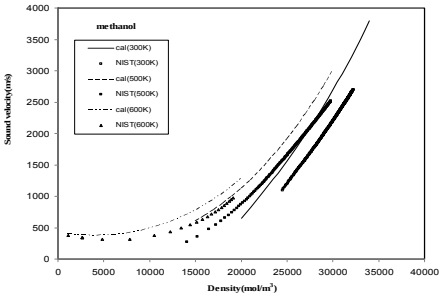

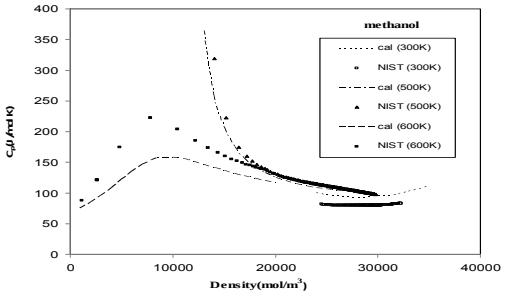

References:

[1]J. Gross, G. Sadowski, Ind. Eng. Chem. Res. 40:1244 (2001).

[2] D. A. McQuarrie, Statistical Mechanics, Harper & Row (1976).

[3] T. M. Reed and K. E. Gubbins, Applied Statistical Mechanics, McGraw-Hill, Inc (1973).

Thermophysical properties from a recent methane, ethane and propane dimers ab initio potential energy surfaces

A. Maghari and M. Hamzehloo

Department of Physical Chemistry, School of Chemistry, University College of Science, University of Tehran, Tehran, Iran

Keywords:thermophysical properties**,** potential energy surfaces**,** propane**,** ethane**,** methane**,** Mason-Monchick Approximation**,** collision integrals**.**

Introduction

In this work, a recently intermolecular potential energy surfaces for methane, ethane and propane dimers [1-3], derived from the quantum-mechanical *ab initio* calculations at MP2/6-3111G(2*d f* ,2*pd*) level, have been used to calculate the cross-sections and transport collision integrals of ethane and propane governed by two-body interactions. To calculate the low-density viscosity and diffusion coefficients, we have used the procedure known as the Mason-Monchick Approximation (MMA) [4], which is the classical counterpart of the infinite-order-sudden (IOS) approximation of quantal inelastic scattering. The potential energy obtained for complete site-site interactions for each different type of selected hydrocarbons. For calculating the ab initio potential interactions, several data points are used to calculate the main routes.

Transport cross-sections and collision integrals

According to the kinetic theory of gases at low-densities, the scattering angle $\chi(\omega)$, the transport cross section $Q^{(l)}(E,\chi)$ and the collision integral $\Omega^{(l,s)}(T,\omega)$ can be calculated from the intermolecular potential interaction as follow:

$$\chi(\omega) = \pi - 2b\int_{R_0}^{\infty} \frac{R^{-2}dR}{\left\{1-\left(b^2/R^2\right)-\left[U(R,\omega)/E\right]\right\}^{1/2}} \qquad (1)$$

$$Q^{(l)}(E,\omega) = 2\pi\left[1-\frac{1+(-1)^l}{2(1+l)}\right]^{-1}\int_0^{\infty}\left(1-\cos^l\chi\right)b\,db \qquad (2)$$

$$\Omega^{(l,s)}(T,\omega)=\left[(s+1)!(k_BT)^{s+2}\right]^{-1}\int_0^{\infty}Q^{(l)}(E)\exp\left(\frac{-E}{k_BT}\right)E^{s+1}dE \qquad (3)$$

where b is the impact parameter, E is the relative kinetic energy of colliding molecules and R_0 is the closest approach of two molecules. The superscripts l and s appearing in the collision integral Ω denotes weighting factors that account for the mechanism of transport by molecular collision. Thus three successive numerical integrations are required to obtain the collision integrals.

For polyatomic molecules, the theory is complicated, which a simple approximation has been proposed by Monchick and Mason, who assumes that the Chapman-Enskog theory of non-spherical molecules retains its original form, but the collision integrals as a function of reduced temperature $T^* \equiv k_B T/\varepsilon$, must be averaged over all possible relative orientations occurring in collisions as :

$$\left\langle \Omega^{(l,s)*}(T^*)\right\rangle = \frac{1}{8\pi}\int d\omega\, \Omega^{(l,s)*}(T^*) \qquad (4)$$

Results and Discussion

In this work, we have examined a recently proposed *ab initio* PES of methane, ethane and propane dimmers with calculating the transport properties. The Numerical values of $\Omega^{(1,1)*}$ and the defined ratios A^*, B^*, C^* and E^* are obtained in this work. The temperature behavior of $\Omega^{(2,2)*}$ for propane, as an example, is shown in Fig. 1. Further, calculated viscosity coefficient of propane from the MMA approach has been compared with the experimental results, which has shown in Fig. 1. The overall agreement between the experimental data and those obtained from the *ab initio* surface is reasonable under the MMA assumptions.

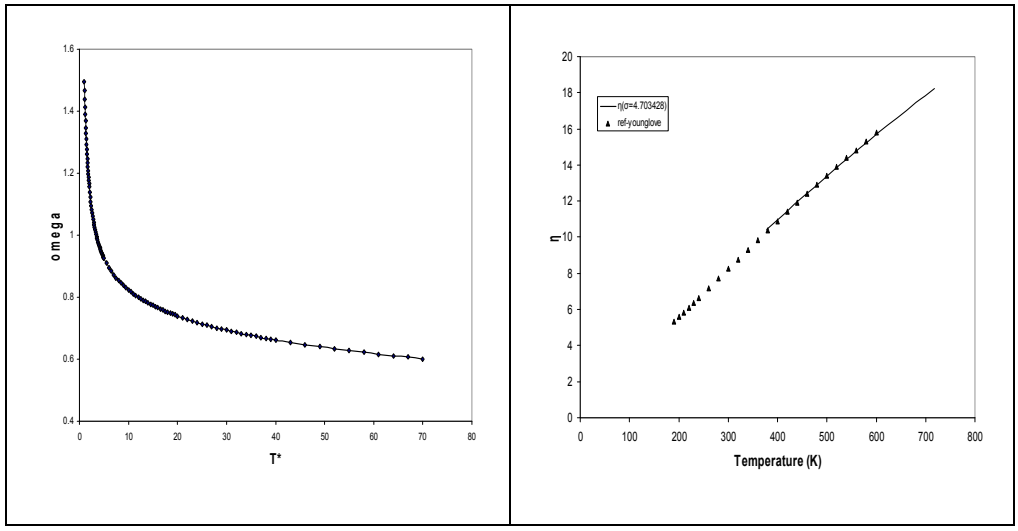

Fig. 1,2: Temperature behavior of calculated $\Omega^{(2,2)*}$ and η from the MMA approach in comparison of experimental data for propane.

References:

[1] R. L. Rowley and T. Pakkanen, *J. Chem. Phys*. **110** (1999) 3368.

[2] R. L. Rowley, Y. Yang and T. A. Pakkanen, *J. Chem. Phys*. **114** (2001) 6058.

[3] J. P. Jalkanen, R. Mahlanen, T. A. Pakkanen and R. L. Rowley, *J. Chem. Phy* **116** (2002) 1303.

[4] L. Monchick and E.A. Mason, *J. Chem. Phys.* **35** (1961) 1676.

Investigation Of Self-Diffusion Of Trichlorofluorocarbon In Faujasite Zeolites: A Molecular Dynamics Stady

R.Rabiei[*a], S.Alavi[b], and B.Najafi[a]

[a]Department of chemistry, Isfahan University of Technology, Isfahan, Iran

(e-mail:rzh.rabiei@gmail.com)

[b]Department of chemistry, University of Ottawa, Ottawa, Canada

Introduction

In recent years, there has been increased interest in aluminosilicate zeolites containing extra framework alkali cations. In the basic zeolites, aluminum is substituted for silicon in the framework. Alkali metal cations, such as sodium and litium, compensate the net negative charge left by the substitution of silicon by aluminum and are located in distinct sites in the zeolite pore system. The cations are bound at these sites mainly by electrostatic forces, although they are often conveniently described as being coordinated to one or more oxygen atoms. The common location of the cations in dry faujasite-structure zeolites (such as X or Y) are shown in figure1.[1,2,3]

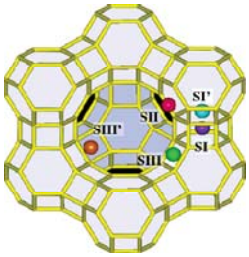

Figure1. Cation sites in FAU type zeolite

Many previous studies, both experimental and computational, have focused on the adsorption of halocarbons in faujasite-structured zeolites. Vibrational spectroscopy and molecular simulations carried out by Mellot, Davidson, and others[4,5] have shed light on the mode of bonding of chlorofluorocarbos (CFCs) and hydrofluorocarbons (HFCs) in siliceous FAU, NaY, and NaX. Also, the basic NaY and NaX faujasites can be used to separate various hydrofluorocarbons during the manufacture of CFCs substitutes.[6] This paper deals with the self-diffusion of $CFCl_3$ in siliceous faujasite and NaY zeolites.

Methods

The total host-guest interaction energy was taken as the sum of a short-range terms modeled with a (6-12) Lennard-Jones potential, and long-range columbic term. The Zeolite hosts were modeled as follows: (i) Siliceous faujasite, $Si_{192}O_{384}$, with q(Si)=+2.4 and q(O)=-1.2; (ii) $Na_{56}Al_{56}Si_{136}O_{384}$. The NaY zeolite framework was built in accordance with Lowenstein ' s Al-O-Al avoidance rule.[7] ,and then was placed n 56 Na cations in especial sites as showed in figure1. Charges for guest molecule ($CFCl_3$) consist of : q(C)=0.616, q(F)=-0.176, q(Cl)=-0.086.[5] All our molecular dynamic simulations carry out in the DL_POLY program in the NVT and then NVE ensemble. All self-diffusion coefficients were obtained over 5×10^6 iterations, after an equilibration periods of 3×10^6 steps, with a cutoff radius of 13Å. The simulations spanned a range of temperatures between 200 and 700K. The trajectory was recorded every 20000 steps during the production stage. The mean square displacements (MSDs) of $CFCl_3$ molecules at different temperatures in siliceous faujasite and NaY zeolite were evaluated by means of the following classical equation:[7]

$$MSD(t) = \langle \Delta r_j^2(t) \rangle = \frac{1}{N}\sum_{j=1}^{N} \Delta r_j^2(t) = \frac{1}{N}\sum_{j=1}^{N} [r_j(t) - r_j(0)]^2$$

where N corresponds to the number of $CFCl_3$ molecules considered in the computation of the MSD. The self-diffusion coefficients were obtained from the long-time limit of the MSD using the following Eintein relation:[7]

$$MSD(t) = A + 6Dt$$

The activation energies corresponding to the self-diffusion processes were calculated from the Arrhenius relation:[7]

$$D = D_0 \exp\left(-E_a / RT\right)$$

3. Result and discussion

Figures 2 and 3 illustrate MSD plots for $CFCl_3$ in siliceous faujasite and NaY zeolites as a function of temperature. Table 1 reports the self-diffusion coefficients in various temperatures (200-700K) and activation energies. As is shown, the MSDs and self-diffusion coefficient for $CFCl_3$ in both of zeolites increase with temperature because of increase of kinetic energy of particles.

Table 1: Diffusion Coefficients and activation energies calculated for $CFCl_3$ in FAU and NaY

Temp (K)	D_{CFCl3} in FAU (m^2/s)	D_{CFCl3} in NaY (m^2/s)

200	1.091×10^{-9}	0.1092×10^{-9}
298	2.913×10^{-9}	0.4393×10^{-9}
400	7.363×10^{-9}	1.040×10^{-9}
500	9.291×10^{-9}	4.340×10^{-9}
600	10.350×10^{-9}	5.054×10^{-9}
700	13.996×10^{-9}	8.347×10^{-9}
Activation energies (KJ/mol)	5.959	10.200

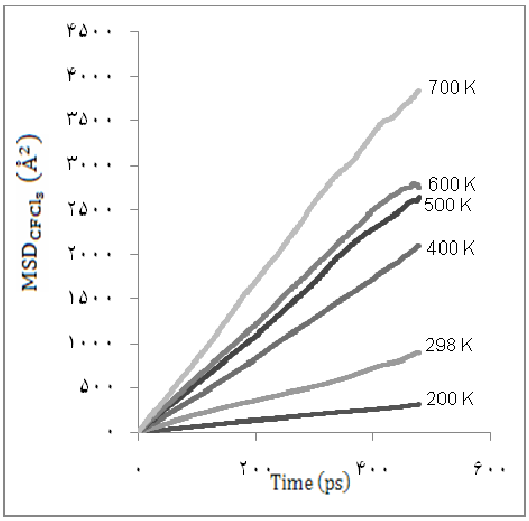

Figure 2. MSD plots for $CFCl_3$ in siliceous zeolite

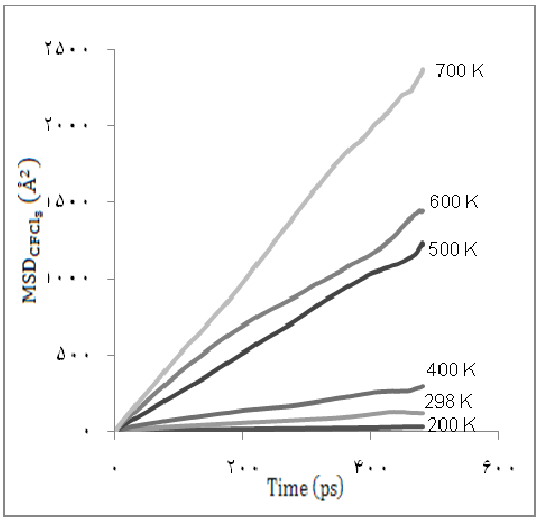

Figure 3. MSD plots for $CFCl_3$ in NaY zeolite

In the case of $CFCl_3$ diffusion in NaY, the presence of extra framework cations gives rise to additional host/guest electrostatic interactions. Because of this reason, self-diffusion coefficient of $CFCl_3$ in NaY zeolite is less than in siliceous faujasite zeolite in each temperature. Also activation energy of $CFCl_3$ in NaY zeolite is more than in siliceous faujasite.

Reference

[1] N. A. Ramsahye and R. G. Bell, J. Phys. Chem. 109 (2005) 4738.

[2] R. J. Davis, Catal. 216 (2003) 396.

[3] D. Barthomeuf, Catal. Rev.-Sci. Eng. 38 (1996) 521.

[4] A. M. Davidson, C. F. Mellot, J. Eckert, A. K. Cheetham, J. Phys. Chem. 104 (2000) 432.

[5] C. F. Mellot, A. K. Cheetham, J. Phys. Chem. 103 (1999) 3864.
[6] D. R. Corbin, B. A. Mahler, World Patent, W. O. 94/02440 (1994).
[7] D. F. Plant, G. Maurin, R. G. Bell, J. Phys. Chem. 111 (2007) 2836.

Prediction of the low-*k* behavior of structure factor for xenon fluid by definition of direct correlation function

H. Nikoofard*,T. Rezayie
Department of chemistry, industrial university of shahroud, shahroud, Iran
(Email:toktamrezayie@yahoo.com)

Key words: Xenon fluid, Structure factor, Direct correlation function, Attractive and repulsive forces.

Introduction

It is well known that the main feature of structure factor, S (k), in the large values of k are almost completely determined by the short-range repulsive part of the inter atomic forces that its range develops with density. But the behavior of S(k) in low-k is correctly determined only by using long-range attractive forces. Since the attractive forces have a crucial role in determining the thermodynamic properties of a liquid, there is a considerable interest to study of S(k) in the low-k [1]. In this work we use the model based on the definition of DCF to calculate S(k) of xenon fluid in low-k. This definition is [2]:

$$c(r) = \begin{cases} c_0 \left(1 - 0.127\ \rho^2 \sigma^6\right) & r \le \sigma \\ \frac{B}{r} \exp\left(20\left(1 - \frac{r}{\sigma}\right)\right) & r > \sigma \end{cases}$$

c_0 is direct correlation function of hard sphere fluid. ρ is density. σ and B are molecular diameter and adjustable parameter that must be obtain in different thermodynamic states.

Methods

By having direct correlation function we may calculate the structural factor of xenon fluid as:

$$S(k) = \frac{1}{(1 - \rho\, c(k))}$$

c(k) is Fourier transformation of c(r)

$$c(k) = 4\pi \int_0^\infty c(r) \frac{\sin kr}{kr} r^2 dr$$

Results and discussion

We calculated structural factor of xenon fluid and shown this result in Fig.1. In this way we investigate the behavior of $S(k_{\min})$ for xenon fluid in other thermodynamic states. This result is shown in Fig.2. It is clear we observe the qualified behavior of $S(k_{\min})$ in which the increasing in density leads to decrease in $S(k_{\min})$.

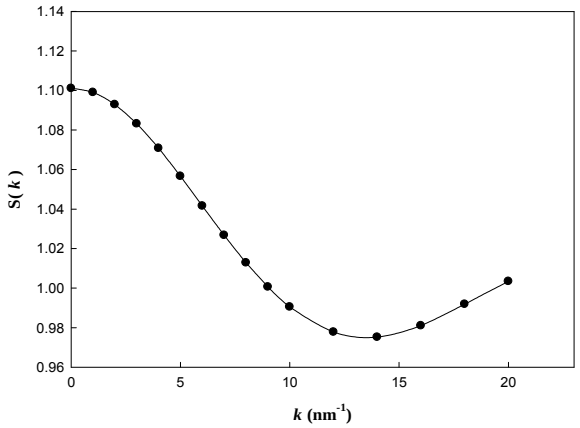

Fig.1. Structure factor of xenon fluid in T=285 and $\rho = 0.33\, mol\ /\ L$.

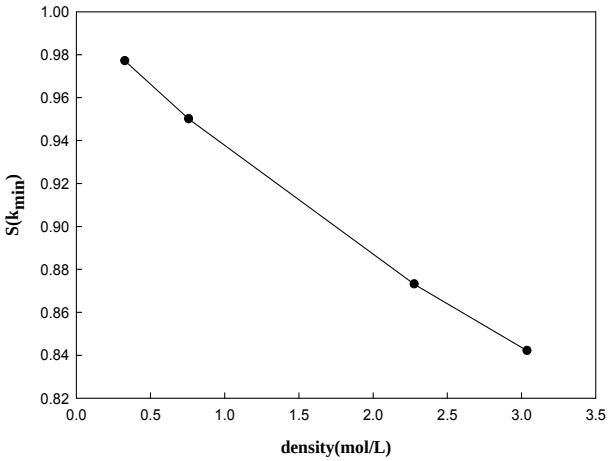

Fig.2. Variation of $S(k_{\min})$ versus density at T=300K.

Conclusions

By using the expression of the direct correlation function, an analytic solution for the calculation of structural factor, S(k), for xenon fluid was obtained. The good behavior of

structural factor, S(k), observed in low densities. The approach here for structure factor, S(k), of xenon can be used for showing the linear relation of S(k_{min}) with density.

References

[1]- R. Evans, W. Schirmacher, Phys. C 11 (1978) 2437.

[2]- D. Henderson, E.W. Grundke, Chemical Physics 63 (1975) 601.

Theoretical Study of the Effect of C/Si Exchange on the Properties of n-Pentane

M. H. Ghatee* and M. Zare
Department of Chemistry, Shiraz University, Shiraz, 71454, Iran
(E-mail:ghatee@susc.ac.ir)

Keywords: Diffusion, n-pentane, Molecular dynamics simulation, Density functional theory.

Introduction

Properties of compound containing the heavier group 14 elements, Si, Ge, Sn, and Pb are very different compared to the corresponding carbon compounds. Si-containing molecular systems have attracted great attention because of their interesting mechanical and electronic properties [1]. Shirota and Castner [2] have studied the effect of C replacement by Si on viscosity of ILs and found that the viscosities of the ionic liquids (ILs) are substantially reduced by this replacement.

To understand the effect of silicon substitution on the dynamic properties of hydrocarbons, we study the properties of pentane **(1)** and its Si-containing analogous **(2)** (Figure 1) by ab initio molecular dynamics simulation and gas phase density functional theory (DFT).

Methods

Geometry optimization and harmonic normal mode vibrational analysis for **(1)** and **(2)** were carried out with the Gaussian03 program at the B3LYP/6-311+G(d,p) level. For *ab initio* molecular dynamics simulations we used the version 3.11.1 of the computational CPMD code. Simulations were performed for 19.35 ps on the gas phase **(1)** and **(2)**, using periodic cubic box at 273.15 K and local density approximation (LDA) functional with the Goedecker-Teter-Hutter pseudopotentials was applied. The plane wave basis energy cutoff was set to 150 Ry. The MD time-step was 4 a.u. and the electron mass is set to be 800 a.u.

Results and discussion

The mean square displacement (*MSD*) [3] obtained by simulations is relevant to transport processes (e.g. diffusivity and viscosity) in the material, and thus this allows comparison, recognition and an estimate of the difference of the transport properties based on the molecular specifications. In spite of the fact that *MSD* obtained do not represents true diffusion of the system in liquid bulk, the outcome is quite evident by the difference within 19.35 ps of the simulation (Figure 2). The slope of the *MSD* considered in time for **(2)** is more than **(1)** and this is evidence for higher diffusion in compound that contains Si.

Harmonic normal mode vibrational analysis is performed for **(1)** and **(2)**. They both have

Figure 1. Chemical structures of n-Pentane and Si-substituted.

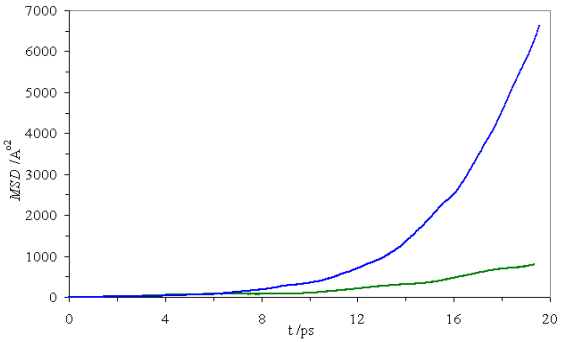

Figure 2. *MSD*s for the n-pentane (green line) and its Si-containing analogous (blue line) versus simulation time t obtained by ab initio CPMD.

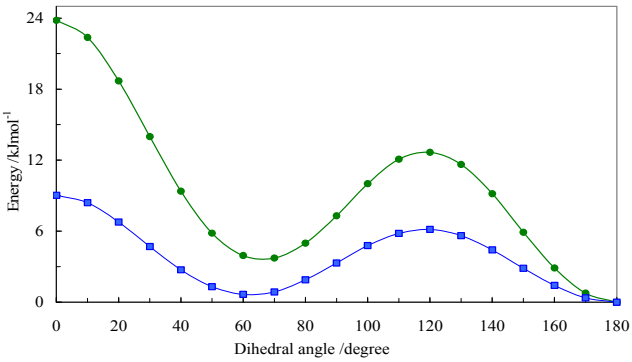

Figure 3. Barrier to rotation about the dihedral angle τ = C1–C2–X3–C4 (X=C and Si), green line for n-pentane and blue line for the Si analog.

(1) **(2)**

45 fundamental frequencies. Comparison of the vibrational frequencies shows 30 mimicking vibrational modes undergo a reduction in their frequency (red shift) due to replacement of C

by Si, while a blue shift is obtained for other 12 mimicking vibrational modes. These red-shifted frequencies are in the range of 2.07 cm^{-1} to 825.5 cm^{-1} and the values of blue shift are between 1.02 cm^{-1} and 12.12 cm^{-1}. The shift in frequency can be followed by changes in the reduced mass and force constant. The decrease in force constant and /or the increase in reduced mass lead to a reduction in vibrational frequency. The reduction in force constants in these stretching modes is related to weakening of the Si–H bond and elongation of this bond, compared to C–H bond.

Transport phenomena may be affected by the rotational barrier for interconversion of these minima. For determination of the rotational barriers, the relaxed potential energy surface was scanned for dihedral angle τ, e. g. C^1–C^2–X^3–C^4 (X=C and Si), Figure 3. The maximum barriers to rotation for **(1)** and **(2)** are 23.81 and 9.03 $kJ.mol^{-1}$, respectively. The maximum barrier for **(2)** is lower by about 15 $kJ.mol^{-1}$ than **(1)**. It seems this is due to elongation of the Si–C bond relative to C–C bond, which reduces steric interactions and facilitates rotation about the dihedral angle τ. Thus, we can infer this more easier rotational motion leads to the interconversion of conformers become more plausible and this causes the *MSD* of the Si-analog is more than n-pentane.

Conclusions

In accord to these results, insight can be gained into the molecular basis for observed higher diffusivity and less viscosity of silicon containing hydrocarbon, which in particular shown for pentane.

References

[1] Sigal, N. *Organometallics* **2002**, *21*, 5486.

[2] Shirota, H.; Castner E. W. *J. Phys. Chem. B* **2005**, *109*, 21576.

[3] Frenkel, D.; Smith, B. *Understanding Molecular Simulation: From Algorithms to Applications*, 2nd ed.; Academic Press: New York, **2002**.

Transport properties in mixtures involving Nitrogen at low and moderate density

F. Zargari*, D. Mohammad Aghaiee, M. M. Papari

Department of Chemistry, Shiraz University of Technology, Shiraz, 71555-313, Iran
Email: papari@sutech.ac.ir, Fax: +98-711-726-1288

Keywords: interaction potential, collision integrals, direct inversion method, extended principle of corresponding states

Introduction

Dilute gas transport properties have been proven to be quite useful for testing and refining intermolecular potentials [1]. Direct inversion of the data of any of these properties gives an effective isotropic interaction potential energy .In the present work the unlike interaction energy are employed to calculate the low density as well as high density transport properties of several mixtures containing nitrogen using Chapman-Enskog and Vesovic-Wakeham[2] methods through the exact form of Lebowitz's solution of the Percus-Yevick equation [3], respectively.

Results and discussion

In this work we obtain transport properties of N_2 and noble gas mixtures. Figure 1 shows deviation plot for the viscosity of He-N_2, Ne-N_2, and Ar-N_2 at high density from the experimental data [4, 5].

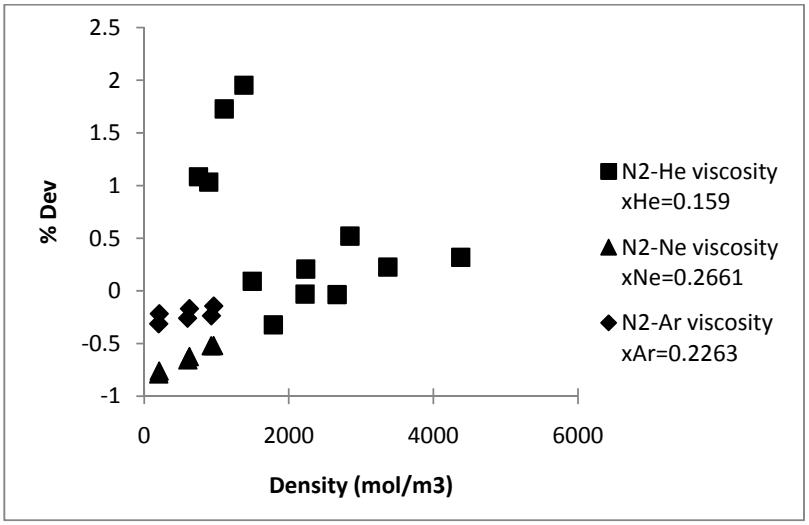

Our estimated accuracies are within 1% for the dilute viscosity, 2% for the dilute binary diffusion coefficient, 25% for the dilute thermal diffusion factor, and 7% for dilute thermal

conductivity. The accuracies of the calculated viscosity at high density were found to be within ±2%.

References

[1] Najafi B, Ghayeb Y, Parsafar GA, *Int .J .Thermophys* , **2000,** 21, 1011–1031.

[2] Royal D D, Vesovic V, Trusler J P M, Wakeham W A, *Mol. Phys* ,**2003**,101**,**339-352.

[3] Moghadasi J, Yousefi F, Papari M. M, Faghihi M. A and Mohsenipour A. A, *Heat and Mass Transfer*, **2009** , 45, 1453-1466.

[4] J. T. F. Kao and R. Kobayashi, *J. Chem. Phys*. **1967**, 47, 2836 .

[5] DiPippo R., Kestin J., AND OGUCHI , *J. Chem. Phys* , **1967**,46,4758

Crossover modified SAFT-BACK equation of state for pure *n*-alkanes

Z. Biglari, M. Setareh and A. Maghari
Department of Physical Chemistry, College of Science, University of Tehran, Tehran, Iran
(E-mail: m.setareh@khayam.ut.ac.ir)

Keywords: Modified SAFT-BACK; Crossover EOS; *n*-Alkane; Critical point.

Introduction

It is well known that none of the classical analytical equations of state (EOS) can represent the thermodynamic properties of fluids near the critical point accurately. However, an analytical equation of state can be developed to a universal model for describing the crossover from classical to non-classical critical behavior upon approach of the critical point [1]. The original crossover (CR) EOS, introduced by Kiselev, obtained from a general procedure for transforming a classical EOS into a crossover model, which reproduces the scaling laws in the asymptotic critical region and is transformed into the original classical EOS in a wide range around the critical point [2].

In recent years, several works have been made to construct a classical EOS with a crossover treatment that is able to describe with equal accuracy the critical region as well as the uncritical region**.** For this purpose, several molecular-based EOS have been proposed; among those equations the statistical associating fluid theory (SAFT) EOS is one of the most powerful predictive tools for the study of thermophysical properties of fluids. At present several versions of the SAFT EOS are available, most of them differing in the reference term. An analytical version of SAFT, the so-called modified SAFT-BACK EOS, developed by Maghari et al., has been developed to predict the second-order thermodynamic derivative properties of *n*-alkane in the wide density and temperature ranges [3].

In this work, we developed a crossover theory combined with the modified SAFT-BACK EOS to calculate thermodynamic properties of *n*-alkanes near and far from critical region and comprised with classical modified SAFT-BACK model and experimental data.

Equation of state

Within the statistical associating fluid theory framework, following the SAFT-BACK EOS, Helmholtz energy for a fluid is written as a sum of the separate contributions to the energy. The residual Helmholtz free energy for a non-association chain fluid is written as:

$$A^{\text{res}} \equiv A - A^{\text{ideal}} = A^{\text{seg}} + A^{\text{chain}} \quad (1)$$

where A and A^{ideal} are the total Helmholtz energy and the ideal gas Helmholtz energy at the same temperature and density, $A^{\text{seg}} = A^{\text{hcb}} + A^{\text{dis}}$ is the contribution due to segment-segment interactions and A^{chain} is the contribution due to the formation of a chain of m segments. In this model the reference term is selected as hard-convex-body (hcb), which is different with most versions of SAFT:

$$\frac{A^{\text{hcb}}}{Nk_{\text{B}}T} = m\left[\frac{\alpha^2}{(1-\eta)^2} - \frac{\alpha^2 - 3\alpha}{1-\eta} - (1-\alpha^2)\ln(1-\eta) - 3\alpha\right] \quad (2)$$

Where m is segment number, α is considered the segment shape by a non-spherical degree, which is related directly and rigorously to the geometry of the hard convex body and η is packing fraction. By introducing the reduced form of Helmholtz energy $a(T,v) \equiv \frac{A}{Nk_{\text{B}}T}$, the critical parameters for the classical EOS can be found through the conditions [3]

$$P_{0C} = -\left(\frac{\partial A}{\partial v}\right)_{T_{0C}}; \qquad \left(\frac{\partial^2 A}{\partial v^2}\right)_{T_{0C}} = 0; \qquad \left(\frac{\partial^3 A}{\partial v^3}\right)_{T_{0C}} = 0 \quad (3)$$

Crossover modified SAFT-BACK EOS

In order to obtain the CR SAFT EOS, we must firstly represent the classical expression for the dimensionless Helmholtz free energy as:

$$\Delta a(\Delta T, \Delta v) = a^{res}(\Delta T, \Delta v) - a^{res}(\Delta T, 0) - \ln(\Delta v + 1) + \Delta v P_0(\Delta T) \quad (4)$$

where $\Delta T \equiv (T - T_{0c})/T_{0c}$, $\Delta v \equiv (v - v_{0c})/v_{0c}$ and $a^{res}(\Delta T, \Delta v)$ is the dimensionless residual part of the Helmholtz free energy. Secondly, on the basis of the renormalization-group calculations [4,5], one must replace the classical dimensionless temperature ΔT and Δv in $\Delta a(\Delta T, \Delta v)$ equation with renormalized values:

$$\bar{\tau} \equiv \tau Y^{-a/2\Delta} + (1+\tau)\Delta\tau_c Y^{-2(2-a)/3\Delta}; \quad \bar{\varphi} \equiv \varphi Y^{-(\gamma-2\beta)/4\Delta} + (1+\varphi)\Delta v_c Y^{(2-a)/2\Delta} \qquad (5)$$

where a, β, γ and Δ are the current best estimates of the non-classical critical exponents and $\tau \equiv (T-T_c)/T_c$, $\varphi \equiv (v-v_c)/v_c$, $\Delta\tau_c \equiv (T_c - T_{0c})/T_{0c}$, $\Delta v_c \equiv (v_c - v_{0c})/v_{0c}$ and Y is crossover function, which can be written in the parametric form $Y(q) = \left(\frac{q}{1+q}\right)^{2\Delta}$.

Results and Discussion

Critical parameters for the first four n-alkanes are calculated through the modified SAFT-BACK EOS and are listed in **Table 1**. As shown in this table, calculated parameters are in good satisfaction with experimental values which are given in NIST Chemistry WebBook.

Table 1. Experimental and calculated values of the critical parameters

Alkanes	T_c^{exp} / K	T_c^{cal} / K	V_c^{exp} / m^3	V_c^{cal} / m^3	ρ_c^{exp} (mol/m^3)	ρ_c^{cal} (mol/m^3)
CH4	190.564	190.3	9.86×10^{-5}	9.30×10^{-5}	10139.00	10752.70
C2H6	305.330	305.0	1.45×10^{-4}	1.76×10^{-4}	6870.00	5672. 15
C3H8	369.825	369.7	2.00×10^{-4}	1.99×10^{-4}	5000.00	5128.21
C4H10	425.125	423.9	2.55×10^{-4}	2.48×10^{-4}	3923.00	4032.26

Furthermore, **Figs. 1** and **2** represent the 3D graphs of critical part of classical and crossover the Helmholtz free energy, respectively for n-Butane.

It must be noted that the graphs for Methane, Ethane and Prapane are similar to Buthane's graph

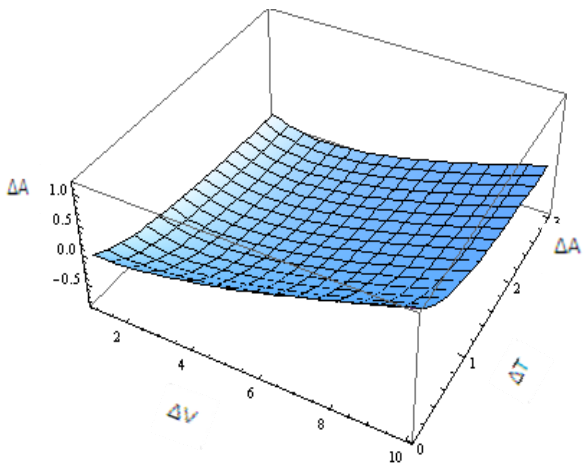

Figure 2: Critical part of the crossover Helamoltz free energy versus renormalized parameters

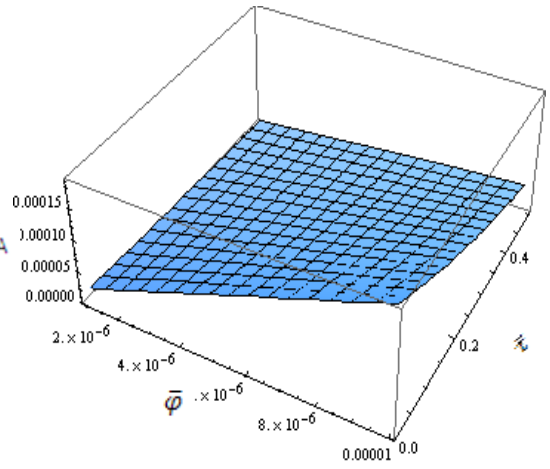

Figure 1: Critical part of the classical Helamoltz free energy versus dimentionless parameters

Refrences

[1] J.M.H. Levelt-Sengers, Fluid Phase Equilib. 158–160 (1999) 3.

[2] S.B. Kiselev, Fluid Phase Equilib. 147 (1998) 7.

[3] A.Maghari, M. Sadeghi, Fluid Phase Equilib. 252 (2007) 152.

[4] T. Boublık, J. Chem. Phys. 63 (1975) 4084.

[5] Z.Y. Chen, P.C. Albright, J.V. Sengers, Phys. Rev. A 41 (1990) 3161.

Studies of Asphaltene Aggregation and Solvation Mechanisms by Molecular Dynamic Simulation

M.H. Ghatee*[a], T. Sedghamiz[a] and A. R. Zolghadr[a]

[a]*Department of Chemistry, Shiraz University, Shiraz, Iran, 71454*

(E-mail: ghatee@susc.ac.ir)

(E-mail: tsedghamiz@shirazu.ac.ir)

Keywords: Asphaltene, Simulation, Molecular dynamics, Aggregation

Introduction

Asphaltenes are molecular substances that are found in crude oil, along with resins, aromatic hydrocarbons, and alkanes. Asphaltenes consist primarily of carbon, hydrogen, nitrogen, oxygen, and sulfur, as well as trace amounts of vanadium and nickel atoms. Asphaltenes are believed to be suspended as a microcolloid in the crude oil [1]. The molecules are believed to be held together with π-bonds, hydrogen bonds, and electron donor-acceptor bonds [2]. In this work the classical molecular dynamic simulation was used to study the mechanism of aggregation of a typical crude oil asphaltene. The aggregation and solubility of asphaltene which are important issue in industry are studied by molecular dynamic (MD) simulation.

Methods

We carried out the simulations by using a computer cluster in parallel mode. All MD simulations were done by DL-POLY version 2.17. The initial ensemble was constructed form eight asphaltene molecules by duplication of this molecule in a cubic box of sides 73.01 Å (Figure 1). The ensemble was initially simulated as NVE ensemble at zero pressure with a time step of 0.0001 ps for 5000 steps. Then, the simulation was carried out in the canonical NVT ensemble by the Verlet leapfrog algorithem at 300 K using Berendsen thermostat. The intramolecular potential parameters were chosen from DRIEDING force field. Figures 1 (a)-(c) can be used to deduce the mechanism of the aggregation processes.

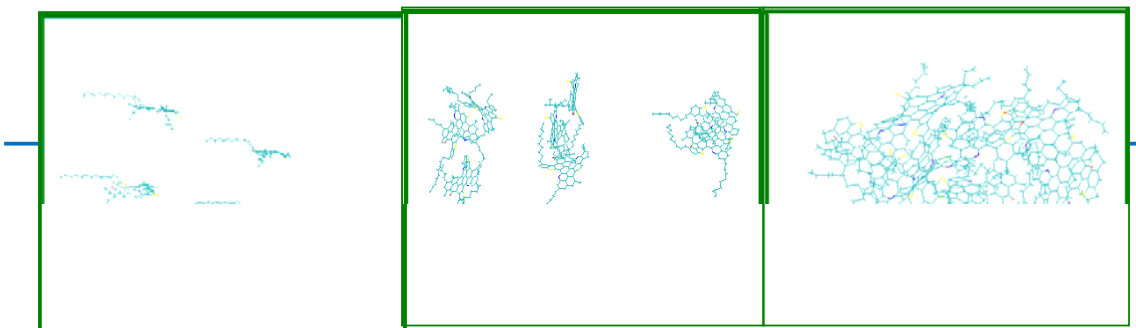

Figure 1: a) Initial NVT ensemble, b) after 20000 steps, c) after 50000 steps.

Results and discussions

By the energy profile it is found that the final equilibrium configuration is adequately attained, at time steps 0.001 ps, after 1.4 ns.Two group of three and one group of two asphaltene molecules were put in a 3-3-2 matrix. It was noticed that, at first, asphaltenes molecules in each group stack together producing aggregate comprising closely packed asphaltene molecules. Then the packed asphaltene at the middle move toward each other and a pack of four and eventually all molecules stack together. The best way of characterization of the relative structure of fused ring is to use the pair correlation functions and identify the site-site correlation of the fused ring plane using heteroatom as the particular site. In addition to considering heteroatoms, four carbon atoms are labeled almost symmetrically at corners of the fused ring plane, C_a, C_b, C_c, and C_d as the corresponding appropriate sites. In the same plots comparisons are made with the simulation when the simulation box is filled with Toluene as the solvent (Total 750 Toluene molecules)(Fig.2 and 3). The density of the box content is 0.86 gr/cm^3.

Conclusion

Mechanism of solvation has been followed by addition of solvent. Accordingly, part of the fused ring plane next to the long alkyl chain gain a higher momentum than the opposite side of the plane with short chains. The height of the peaks corresponding to correlation function of this part diminishes drastically and since a shift in the position of the first and subsequent peak, either to higher or to small distances with respect to aggregated asphaltenes occurs, indicates the planes take apart from this part. The fact that the opposite parts of the plane to which short alkyl chain attack remain almost "intact", in either solvated and aggregated asphaltene, it can be seen that plans may take positions intact in pairs, which is evident by the fact that almost all peak are doubly over laid.

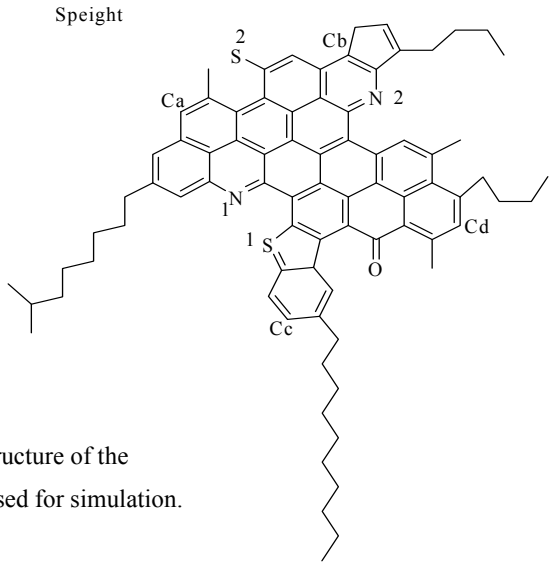

Schem 1. Chemical structure of the asphaltene molecule used for simulation.

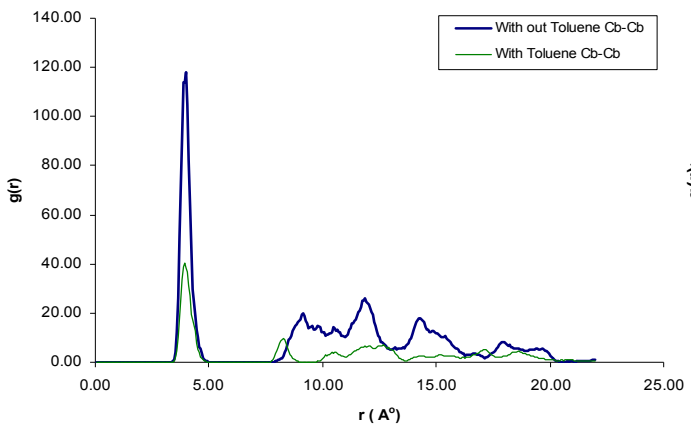

Figure 2 Pair correlation of Cb-Cb

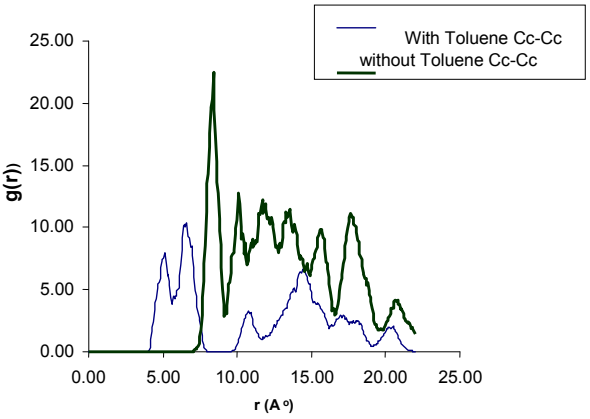

Figure 3 Pair correlation of Cc-Cc

References

[1] Sheu, E. Y.; Mullins, O. C. (1995). Asphaltene: Fundamental and Applications; Plenum Press: New York.

[2] Spiecker, P. M. Ph. D. thesis, North Carolina State University, Raleigh, 2001.

Thermodynamics properties of some ionic liquids from the SAFT equation of state

A. Maghari and F. Ziamajidi
Department of Chemistry, University of Tehran, Tehran, Iran
Email:ziamajidi@khayam.ut.ac.ir

Key words:Ionic liquid, SAFT, PVT, sound velocity.

Introduction

Ionic liquids are attracted a widely important application in many fields of science and technology such as liquid/liquid extraction and polymerization processes. They are liquid at room temperature, but in fact have an enormous liquid range of organic and polymeric materials. In this work, the statistical associating fluid theory (SAFT) is developed for prediction of thermodynamic properties of imidazolium-based ionic liquids (ILs) by fitting PVT data over a wide temperature range (313.15 K to 472.15 K) at both liquid and supercritical state. The results in agreement with recent experimental evidence.

Model description

In this work, an equation of state (EOS) is developed to predict accurately the PVT properties as well as sound velocity of ILs based on the SAFT EOS. Our model is described as:

$$a^{res}(T,\rho) = a^{hs}(T,\rho) + a^{chain}(T,\rho) + a^{disp}(T,\rho) + a^{polar}(T,\rho)$$

$$a^{hs} = \frac{4\eta - 3\eta^2}{(1-\eta)^2}$$

$$a^{chain} = (1-m)\ln\frac{1-0.5\eta}{(1-\eta)^3}$$

$$a^{dis} = m\sum_{i}\sum_{j} D_{ij}\left(\frac{u}{RT}\right)^{i}\left(\frac{\eta}{\tau}\right)^{j}$$

$$a^{polar} = m\frac{a_2^{polar}}{1-\frac{a_3^{polar}}{a_2^{polar}}}$$

The residual Helmholtz energy (a^{res}) is a sum of four terms representing contribution from different intermolecular forces. The first term a^{hs} ,hard sphere, second term (a^{chain}) is due to

the presence of covalent chain-forming bonds among the segments, third term dispersion and last term a^{polar} ,which includes dipole-dipole interactions. a_2^{polar} , a_3^{polar} are the second and third order perturbation polar terms, respectively[1,2]. The model contains six pure-component parameters: (i) three parameters for nonassociating nonpolar compounds (i.e., the segment number *m*, the temperature-independent segment volume v_{00}, and the segment dispersive energy parameter *u/k*),(ii) two additional parameters for association and one additional parameter for polar interactions (i.e., the effective polar interaction diameter v_p).

Result and Discussion

In this work, the model parameters for pure ILs are estimated by fitting the PVT data available over a wide temperature range.[4]. We have calculated the PVT as well as second derivative properties of some selected ILs. As an example, the PVT properties of $[Hmim]^+[BF4]^-$ at different densities and temperatures are shown in Fig. 1. Comparisons of the pressures obtained in this work and literature data are shown in Fig. 2.

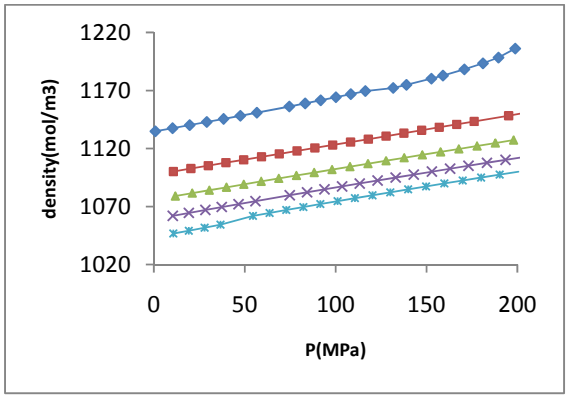

Figure 1. Pressure data of$[Hmim]^+[BF4]$- at different densities and temperatures(♦,313.15; ■,352.15; ▲,393.15; ×432.15; *,472.15).

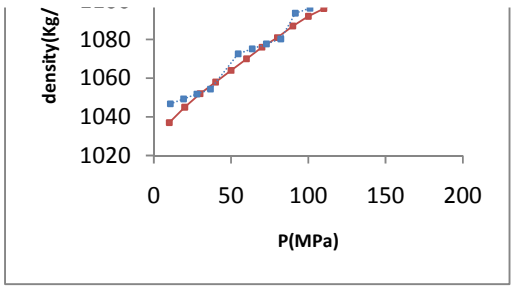

Figure2.Comparisons of the pressures measured in this work (■) and literature

Reference

[1] Kroon, M. C.; Karakatsani, E. K.; Economou, I. G.; Witkamp, G. J.; Peters, C. J. J. Phys. Chem. C (2007)111, 15487.

[2] M. C. Kroon, E. K. Karakatsani, I. G. Economou, G. Witkamp and C. J. Peters, J. Phys. Chem. B (2006) 110, 9262.

[3] Gross, J; Sadowski, G. Ind. Eng. Chem. Res (2002) 41, 5510.

[4] R. Taguchi, H. Machida, Y. Sato and R. L. Smith, Jr. J. Chem. Eng. Data 22 (2009) 54, 22.

[5] Karakatsani, E. K.; Economou, I. G;Fluid Phase Equilib(2007)261,265.

Theoretical investigation of toxicity effect of PAHs on photosynthesis process in plants and photosynthetic bacteria

S.Faramarzi*, Gh.A. Parsafar*
*Department of Chemistry, Sharif University of Technology, Tehran, Iran
faramarzi@mehr.sharif.ir

Keywords. Phototoxicity- PAH- Computational Chemistry- Electronic Structure

Introduction

Some organic compounds such as polycyclic aromatic hydrocarbons (PAHs) exert photoinduced toxicity to numerous plants and bacterias in the presence of solar radiation [1]. The mechanism of photoinduced toxicity can be generally classified as photosensitization (generation of reactive oxygen species) and photomodification to more toxic photoproducts [2,3]. The detailed mechanism of PAHs action on these species hasn't completely been understood yet. In this study we will calculate molecular and thermodynamic parameters for some PAHs to investigate probable mechanisms by using quantum mechanical methods.

Methods

We have used Density Functional Theory (DFT) and Time Dependant Density Functional Theory (TD-DFT) methods to calculate electronic and vibrational energy levels of some PAHs to predict transition states of their oxidation/reduction reactions. The calculations are carried out by Gaussian 03 and Firefly packages.

Results and discussion

Interpreting the results from mentioned calculations, we will describe the probable mechanisms of PAHs. The energy gap between the highest occupied molecular orbital (HOMO), and the lowest unoccupied molecular orbital (LUMO) is an important parameter to indicate the extent of toxicity of PAHs.The reason for that is the phototoxicity of these compounds is based on electronic excitation due to absorption of photons from solar radiation. Hence, almost none of them are toxic in dark.

Conclusion

Inferring the detailed reaction pathway and mechanism of PAHs require the knowledge about electronic structure of PAHs as well as electronic structure of the molecules in plant and bacteria infected by them. This goal can be achieved by using computational chemistry softwares. In this study we show that PAHs could inhibit photosynthesis with a competitional reduction-oxidation reaction in plants and bacteria.

References

[1] Ying Wang et.al., Dyes and Pigments 2009:83:276-280

[2] Ali Mallakin et.al., Ecotoxiocology and Environmental Safety 1999:43:204-212

[3] Ali Mallakin et.al., Chemosphere 2000:40:1435-1441

Long range corrections to the vapor–liquid equilibrium and surface tension of methane with NVT molecular dynamics simulations

Mehrangiz Sheikhabbasi and Farazneh Feyzi[1]
Thermodynamics Research Laboratory, School of Chemical Engineering,
Iran University of Science and Technology, Tehran 16846-13114, Iran

Keywords: Molecular dynamic simulations, Inhomogeneous systems, Long range corrections

Introduction

Molecular Dynamics (MD) simulations have been used extensively during the past few decades to study the properties of inhomogeneous systems [1-4].

Lower computation time is achieved by applying smaller values for cut–off radius which, in turn, results in less accuracy. The execution of the long range corrections in order to overcome the inaccuracy resulting from using small values of cut–off radius is affected by the non uniform distribution of density profile of inhomogeneous systems along the direction normal to the interface. Many studies are concerned with performing long range corrections for inhomogeneous fluids [4-7].

Theory

During our MD simulations, the non bonded interactions between united atoms are described with a lennard–Jones potential. We used a truncated potential in our simulations, and calculated the forces acting on any particle *i* inside its cut–off distance. To consider long range corrections an extra contribution is added to the *z*-component of the force affecting particle *i*. In fact, this contribution accounts for those forces acting on any particle from outside its cut–off distance[4].

In this work, to consider long range corrections to the direction perpendicular to the interface, we have added the slab based long range corrections to the diagonal components of pressure tensor and also to the forces acting on each particle in the form similar to Eq. 1.

$$f_{LRC}(z_k) = 2\pi \int_{R_c}^{\infty} f(r)dr \int_{-r}^{r} \rho(z)\Delta z d\Delta z \qquad (1)$$

[1] Corresponding author email: feyzi@iust.ac.ir

Where $\Delta z = z - z_k$ and z_k is the position of the kth slab, r is the distance between the centers of interaction sites, R_c is the cut−off radius, $\rho(r)$ is the number density and $f(r)$ is the force.

We first performed a number of simulation runs for methane by the cut−off distance equals to 5.5σ without using long range corrections. We then adjusted the obtained values of the density to a hyperbolic tangent function [2]. This function is then replaced in Eq. 1 to obtain the long range correction expressions in our MD simulations of inhomogeneous methane.

Results and discussion

We performed a series of MD simulations at seven values of reduced temperature in the interval T^*=0.7-1.127 in NVT ensemble to study the vapor-liquid thermodynamic properties of methane using DL_POLY_2.20 simulation package[8].

In the case of simulations with cut-off radius equals to 5.5σ, the average absolute deviation (AAD) of calculated liquid densities from the experimental values is 2.54%, while liquid densities are predicted with AAD equals to 1.33% with the application of long range corrections for cut-off radius R_c=2.5σ. The AAD in the prediction of vapor pressure is 2.47% with small cut off distance and using long range corrections, while the vapor pressures with R_c=5.5σ without the application of long range corrections show large deviations from experimental data[9]. The values of the surface tension with smaller cut-off radius have large deviations from experimental data but the long range correction contributions have significantly reduced the error. On average, the calculated uncertainties, using the block average method, for simulations with small cut-off distance including long range corrections was about 0.0281.

Conclusions

The effects of truncation of intermolecular forces in inhomogeneous systems are treated in this study. By employing new long range corrections, more accurate results by the cut-off radius R_c=2.5σ for the values of the coexisting densities and the surface tension are observed. The time required for the simulations with R_c=2.5σ, applying corrections of this work, is 5 times lower than the time required with R_c=5.5σ without the application of the corrections.

Refrences

[1] Blokhuis, E.M., et al., Mole. Phys., **85,** 665 (1995).

[2] Chapela, G.A., et al., J. Chem. Soc., Faraday Trans 2, **73,** 1133 (1977).

[3] Holcomb, C.D., P. Clancy, and J.A. Zollweg, Mol. Phys., **78,** 437 (1993).

[4] Mecke, M., J. Winkelmann, and J. Fischer, J. Chem. Phys, **107,** 9264 (1997).

[5]Guo, M. and B.C.Y. Lu, J. Chem. Phys., **106,** 3688 (1997).

[6] Janeček, J.Ã., J. Phys. Chem B., **110,** 6264 (2006).

[7] Lotfi, A., J. Vrabec, and J. Fischer, Mol. Sim., **5,** 233 (1990).

[8]Smith, W., T.R. Forester, and I.T. Todorov., Available from:
http://www.ccp5.ac.uk/DL_POLY/.

[9] Lemmon, E.W., M.O. McLinden, and D.G. Friend., Available from:
http://webbook.nist.gov.

Prediction osmotic pressure of protein solutions using Flory- Huggins Theory

F. Kermanpour*, S. Sharifi

*Faculty of Chemistry, Bu- Ali Sina University, Hamadan, 65178-38695, Iran

In this work, the Flory- Huggins theory [1] has been applied for investigating phase equilibrium behavior of protein solutions. Based on such a model, we can obtain the following relations for chemical potential of solvent (0) and solute (1) molecules, respectively,

$$\mu_0 = \mu_0^0 + RT[\ln(1-\varphi_1) + (1-P_1^{-1})\varphi_1 + \chi\varphi_1^2] \quad (1)$$

$$\mu_1 = \mu_1^0 + RT[\ln\varphi_1 - (P_1-1)(1-\varphi_1) + P_1\chi(1-\varphi_1)^2] \quad (2)$$

where, $\chi = z\Delta u/k$ is Flory- Huggins parameter, φ_0 and φ_1 are volume fractions. The liquid-liquid phase equilibrium can be predicted by converting φ_1 to x_1 in Eq. (2) and using the thermodynamic relation $\left(\frac{\partial\mu_1}{\partial x_1}\right)_{T,p} = 0$. So, for the spinodal line we have,

$$\varphi_1^2 - \left(1 - \frac{P_1-1}{2P_1\chi}\right)\varphi_1 + \frac{1}{2P_1\chi} = 0 \quad (3)$$

Denoting the compositions of two phases φ_1 by and $\acute{\varphi}_1$, we have the condition for phase equilibrium bianodal as,

$$ln(1-\varphi_1) + (1-P_1^{-1})\varphi_1 + \chi(\varphi_1)^2 = ln\left(1-\acute{\varphi}_1\right) + (1-P_1^{-1})\acute{\varphi}_1 + \chi\left(\acute{\varphi}_1\right)^2 \quad (4)$$

$$ln\varphi_1 - (P_1-1)(1-\varphi_1) + P_1\chi(1-\varphi_1)^2 = ln\acute{\varphi}_1 - (P_1-1)\left(1-\acute{\varphi}_1\right) + P_1\chi\left(1-\acute{\varphi}_1\right)^2 \quad (5)$$

The osmotic pressure, π, can also be obtained by deriving the activity a_0 from Eq. (2) and the relation between activity and pressure, $\pi = -(RT/V_0^0)lna_0(T,p,x)$, as

$$\pi = -\left(\frac{RT}{V_0^0}\right)\left[P_1^{-1}\varphi_1 + \left(\frac{1}{2} - \chi\right)\varphi_1^2 + \frac{1}{3}\varphi_1^3\right] \quad (6)$$

By rearranging Eq. (3) we will have, $\chi = \frac{(1-P_1)\varphi_1 - 1}{2P_1\varphi_1(P_1-1)}$. This is the relation between spinodal data with the parameter, χ. It is also possible to use the bionodal data for calculating the χ parameter at any temperature. To do that, Eqs. (4) and (5) should be solved simultaneously, which tends to the relation,

$$ln(\varphi_1/\acute{\varphi_1}) - P_1 ln\left[\frac{(1-\varphi_1)}{(1-\acute{\varphi_1})}\right] + 2P_1\chi(\acute{\varphi_1} - \varphi_1) = 0$$

(7)

Such calculations have been done for some protein solutions and the obtained χ parameters have been indicated that the behavior of the χ parameter in terms of inverse temperature, 1/ *T*, can be expressed in a linear relation as$\chi = a + b/T$. Following figure shows this linear dependency for behavior of χ in terms of 1/ *T* for some given mixtures.

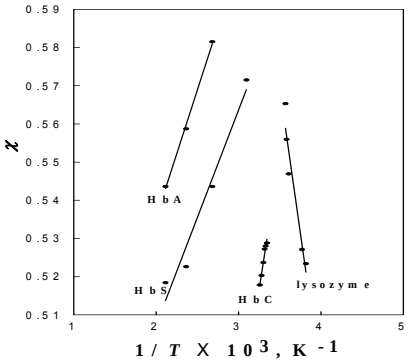

Eq. (6) predicts the osmotic pressure of a mixture at any concentration by having the spinodal or bianodal data. So, we can replace the parameter χ in Eq. (6) to obtain the osmotic pressure, π. Such a calculation has been done for some protein solutions and the results are shown in the following figure. The predicted linearity of osmotic pressure via concentration in Flory theory can be considered in this figure obviously.

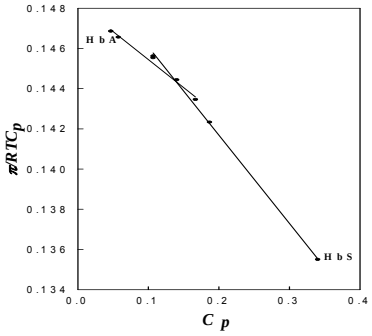

Keywords: Flory- Huggins theory, phase equilibrium, bianodal line, spinodal line, osmotic pressure, protein mixtures

References

[1] Michio Kurata, Thermodynamics of Polymer Solutions, MMI PRESS, 1982.

[2] Qiuying Chen, et al, Biophysical Journal, 86 (2004) 1702- 1712.

[3] Wei Li, et al, Chemical Engineering Journal, 78 (2000) 179- 185.

A Thermodynamic Model for the Crowding Effect on Biochemical Reaction Equilibria

F. Kermanpour*

*Faculty of Chemistry, Bu-Ali Sina University, Hamdana, 65178-38695, Iran, fakhri.kermanpour@gmail.com

Introduction

Many of reactions occurring in the biological systems such as biological cells, are taken place in the situations that include species like crowding molecules. So, it is necessary for such reactions to take into account the role of crowding molecules on the thermodynamic properties. In this work, using statistical thermodynamics the equilibrium concentrations of a typical biochemical reaction has been calculated.

Molecular thermodynamic formulation

We can consider the typical biochemical reaction as,

n $R \overset{\leftarrow}{\rightarrow} P$

(1)

where R is the reactant and P is the product that are distributed in a sea of crowder, denotes as C with the concentration of c_C. The initial concentrations of R and P are denoted by c_R^0 and c_P^0 , respectively. If we consider the degree of reaction by α, so the concentrations of R and P at equilibrium are $c_R^0(1-\alpha)$ and $c_P^0(1-\alpha)$, respectively.the thermodynamic equilibrium constant K is then,

$$K = \frac{(c_R^0 \alpha/n)}{[c_P^0(1-\alpha)]^n}$$

(2)

Based on a statistical thermodynamic model we represent the reactant, product, and crowder as chain molecules with number density, chain length , and segment diameter (i= R, P, C). In addition, the short range interactions between the nonbonded segments is modeled by the SW potential,

$$u_{ij}(r) = \begin{cases} \infty & r < \sigma_{ij} \\ -\varepsilon_{ij} & \sigma_{ij} < r < \lambda_{ij}\sigma_{ij} \\ o & r > \sigma_{ij} \end{cases}$$

(3)

where $\sigma_{ij} = (\sigma_i + \sigma_j)/2$ is the additive HS diameter, $\varepsilon_{ij} = \sqrt{\varepsilon_i \varepsilon_j}$ is the cross well depth, and $\lambda_{ij} = (\lambda_i \sigma_i + \lambda_j \sigma_j)/(\sigma_i + \sigma_j)$ is the cross well width.

The Helmholtz free energy of such a system can be obtained by adding three contributions from a) hard-sphere (HS) interactions, b) the attractive square-well (SW) interactions, and c) chain formation contributions to the ideal contribution as,

$$A = A^{ideal} + A^{hs} + A^{sw} + A^{chain}$$

(4)

The HS contribution can be written [1],

$$\frac{\beta A^{hs}}{V} = \left(\frac{\zeta_2^3}{\zeta_3^2} - \zeta_0\right) ln\Delta + \frac{(\pi\zeta_1\zeta_2/2) - (\zeta_2^3/\zeta_3^2)}{\Delta} + \frac{\zeta_2^3/\zeta_3^2}{\Delta^2}$$

(5)

where $\zeta_l = \sum_i m_i \rho_i \sigma_i^l$ and $\Delta = 1 - \pi\zeta_3/6$. The SW contribution can be obtained using the second order Barker- Henderson perturbation theory [2],

$$\frac{\beta A^{sw}}{V} = \frac{1}{\zeta_0} \sum_i \sum_j m_i m_j \rho_i \rho_j \left(\beta a_1^{ij} + \beta^2 a_2^{ij}\right)$$

(6)

where,

$$\beta a_1^{ij} = -\tfrac{2}{3}\pi\zeta_0 \sigma_{ij}^3 (\beta\varepsilon_{ij})(\lambda_{ij}^3 - 1) g_{ij}^{hs}(\sigma_{ij}, \zeta_3^{eff})$$

(7)

$$\beta^2 a_2^{ij} = \frac{\zeta_0^2 \Delta^4 (\beta\varepsilon_{ij})}{2(\zeta_0\Delta^2 + \pi\zeta_1\zeta_2\Delta + \pi^2\zeta_2^3/4)} \frac{\partial(\beta a_1^{ij})}{\partial\zeta_0}$$

(8)

and ζ_3^{eff} is an effective packing factor, and $g_{ij}^{hs}(\sigma_{ij})$ is the pair correlation function of hard spheres at contact which defines as,

$$g_{ij}^{hs}(\sigma_{ij}) = \frac{1}{\Delta} + \frac{\pi\sigma_i\sigma_j\zeta_2}{4\Delta^2\sigma_{ij}} + \frac{\pi^2\sigma_i^2\sigma_j^2\zeta_2^2}{72\Delta^3\sigma_{ij}^2}$$

(9)

The contribution from chain connectivity has been obtained in the statistical associating fluid theory (SAFT) [3] and equation of state for chain fluids [4] as,

$$\frac{\beta A^{chain}}{V} = \sum_i \rho_i (1 - m_i) ln y_{ii}^{sw}(\sigma_i)$$

(10)

where the cavity correlation function at contact, $y_{ii}^{sw}(\sigma_i)$, is defined by,

$$y_{ii}^{sw}(\sigma_i) = g_{ii}^{sw}(\sigma_i)exp(-\beta\varepsilon_i)$$

(11)

with

$$g_{ii}^{sw}(\sigma_i) = g_{ii}^{hs}(\sigma_i) + \frac{1}{2\pi\zeta_0\sigma_i^3}\left(3\zeta_0\frac{\partial(\beta a_1^{ii})}{\partial\zeta_0} - \lambda_i\frac{\partial(\beta a_1^{ii})}{\partial\lambda_i}\right)$$

(12)

Finally, the degree of reaction, α, can be obtained from,

$$\left(\frac{\partial(\beta A/V)}{\partial\alpha}\right)_{T,V,\rho_j} = 0$$

(13)

Results and Discussion

The degree of reaction can be calculated at various molecular structure conditions for *R*, *P*, and *C*. One sample of such calculations has been shown in the Fig. 1. As one can see, size of the protein can affect degree of reaction, since increasing protein size will decrease the volume accessible to the crowders as folding occurs, and it would then decrease the degree of reaction. Overlay, we can get the results that are definitely similar with the results that have been reported for crowding effect via the activity coefficient model [5].

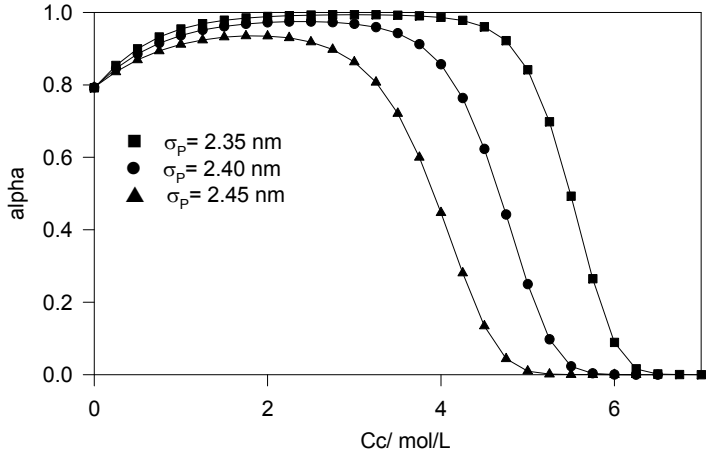

Fig. 1: Degree of reaction α for folding $R_{76}\overrightleftarrows P$ as a function of the molecular concentration of crowder *C*, for c_R^0=0.013 mol/l, $\sigma_P = 0.38\ nm, \sigma_C = 0.5\ nm,\ \ m_P = 1, m_C = 1.$

References

[1] G.A. Mansoori, et al, J. Chem. Phys., 54 (1971) 1523.

[2] J.A. Barker, D. Henderson, J. Chem. Phys., 47 (1967) 2856.

[3] A.A. Gill Villegas, et al, J. Chem. Phys., 106 (1997) 4168.

[4] J.W. Jiang, J.M. Prausnitz, J. Chem.Phys., 111 (1999) 5964.

[5] J.W. Jiang, et al, Biophysical J., 93 (2007) 1464.

Molecular dynamics simulation of water effect on structure and dynamics of poly(ethylene terephthalate)

Hossein Eslami[a,b] and Mojghan Karimi[b*]

[a]Department of Chemistry, College of Sciences, Shiraz University, Shiraz 71454, Iran.

[b]Department of Chemistry, College of Sciences, Persian Gulf University, Boushehr 75168, Iran.

E-mail: (m.karimi_3000@yahoo.com)

Keywords: Poly(ethylene therphthalate), Molecular dynamics, wet polymer simulation, Dynamic Properties.

Introduction

Poly(ethylene terephthalate) (PET) is the most important polyester, used for many applications such as food packaging for ovenable food trays and beverage packaging, due to its superior barrier properties in comparison with polyolefins, polycarbonates, polystyrene, and other polymers.[1] Among all plastics, PET is of particular attention in terms of possibility of recycling of PET bottles. Despite the existence of large experimental data on the properties of PET, computer simulation studies of this polymer are scarce. This is due to the fact that the rigid structure of PET does not allow the use of advanced Monte Carlo methods. Moreover, molecular dynamics simulation studies of PET are difficult due to the high relaxation times of polymer, especially in the glassy state.

Very recently Eslami and Muller-Plathe[2] have developed an accurate force-field for PET. The force field has been employed to simulate a long chain, consisting of 120 repeat units, of PET over a wide temperature (from 280 to 600 K) and pressure range, for long time scales (30 ns).

The force field is validated against the experimental results for the PVT properties, the characteristic ratio, the dipolar ratio, and the population of ethylene glycol bond conformer. In all cases the agreement with experiment is shown to be quite good.[2] The local dynamics of the chain has also been investigated by calculating phenylene reorientation, collective dipole moment, and individual dipole moment correlation functions.

In this work we aim to perform detailed atomistic molecular dynamics simulation of water effect on the structure and dynamics of PET in the NPT ensemble.

Method

We use the force field reported by Eslami and Müller-Plathe[2] and simulated a long chain, consisting of 120 repeat units with different weight percents of water (0.5%, 1.0%, and 1.5%), over a wide temperature range (280 to 600K). To include water molecules in the simulation box, we used a recently developed grand canonical ensemble simulation method.[3] Setting a high values for the target chemical potential of water molecules, fractional water molecules were inserted in the simulation box and grown up to full water molecules. This procedure has been repeated till getting a fixed composition of water-polymer mixture. The prepared polymer-water samples were relaxed for about 5 ns. After this initial equilibration period, long simulation runs were performed to study the effect of water on the static and dynamics of polymer in the presence of water.

Results

Static Properties

Local structure of chain in the presence of water has been examined by looking at the immediate neighborhood of CO groups. Our results show that initially added water molecules to the polymer matrix are more probable to be found in the vicinity of polymer CO groups. Addition of more water molecules to the polymer matrix causes the formation of small-size clusters among water molecules.

Dynamic Properties

Analysis of the chain dynamics in the presence of water is performed by looking at the local dynamics of phenylene groups. In Figure (1) we have shown the autocorrelation functions, at

300 K, for vectors normal to the phenylen groups. The results indicate that added water molecules to the polymer significantly enhance the polymer mobility.

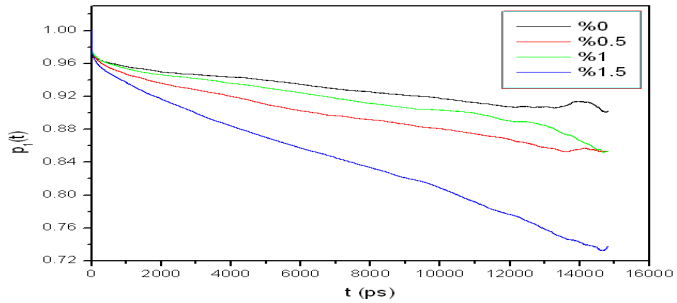

Figure 1. Autocorrelation function for vectors normal to phenylene groups at 300 K.

Refrance:

[1] D. Mastio, Plastics World 1997, 55, 59.

[2] H. Eslami, F. Müller-Plathe, Macromolecules 2009, 42, 8241.

[3] H. Eslami, F. Müller-Plathe, *J. Comput. Chem.* **2007**, 28, 1763.

Three dimensional structure of a hard sphere fluid confined within a nanoslit using Density Functional Theory

Azin Shahsavar, Mohammad Kamalvand* and Mohammad Reza Noorbala

Department of Chemistry, Faculty of Science, Yazd University, Yazd, Iran

* *Email address: kamalvand@gmail.com*

Keywords: Confined Fluid, Density Functional Theory, Nanoslit, Hard Sphere, Tarazona, Three Dimensional Structure.

Introduction

A property of central interest for theoretical study of confined fluids is the density distribution of the molecules. In a macroscopic thermodynamic system, the density distribution of molecules about a central molecule has a spherical symmetry and therefore, one-body density profile, $\rho(\mathbf{r})$ is only a function of intermolecular distance, r, and hence $\rho(\mathbf{r})=\rho(r)$. In a confined fluid system, like a fluid confined between two parallel plates (nanoslit), the density profile only changes against the walls [1]. Therefore, for a nanoslit $\rho(\mathbf{r})=\rho(z)$ which z is the normal distance from one of slit walls. This is noticeable that all average thermodynamic properties of the confined fluid can be obtained using this density profile, if the intermolecular interactions are known. However, some thermodynamic properties, like normal and lateral pressures, have a local behavior and for calculation of these properties, we need to three dimensional density profile of the fluid around a confined molecule inside the nanoslit [2]. To calculate the three dimensional structure of a hard sphere fluid within a nanoslit, we used density-functional theory, as a powerful approach to study the structure and the phase behavior of nano confined fluids [3].

Density Functional Theory

In a density functional theory for an inhomogeneous fluid, the grand potential functional energy is related to the Helmholtz free energy functional as follows [4]:

$$\Omega[\rho(\mathbf{r})] = F[\rho(\mathbf{r})] + \int d\mathbf{r}\rho(\mathbf{r})\{V_{ext}(\mathbf{r}) - \mu\} \qquad (1)$$

Where μ is the chemical potential of the system and $V_{ext}(\mathbf{r})$ is the external field. In the Tarazona version of the non-local weighted density approximation [3], the Helmholtz free energy divides to ideal and excess parts. According to the variational principle, the equilibrium density distribution function of the non-uniform fluid corresponds to the minimum of the grand potential [4],

$$\rho(\mathbf{r})\Lambda^3 = exp\left(\beta\mu - \beta\frac{\partial F_{ex}[\rho(\mathbf{r})]}{\partial\rho(\mathbf{r})} - \beta V_{ext}(\mathbf{r})\right) \quad (2)$$

Results and Discussion

In this work, to obtain three dimension density profile of a hard sphere fluid around one of fluid molecules, V_{ext} in cylindrical coordinate is as follows:

$$V_{ext}(\mathbf{r}) = \begin{cases} 0 & (R^2 + z^2) > \sigma \\ \infty & (R^2 + z^2) \leq \sigma \\ \infty & z > H_1 - \sigma/2 \\ \infty & z < -H_2 + \sigma/2 \end{cases} \quad (3)$$

where σ is the diameter of the hard sphere molecule and H_1 and H_2 are the normal distances of central molecule from walls 1 and 2, respectively. While the external field is non-spherical, the density profile is non-spherical and a function of R and z. In Fig. 1 (a), the three dimensional density profile of a hard sphere fluid with bulk density $\rho\sigma^3$=0.6, confined inside a nanoslit with H=8σ is showed. In this Figure, H_1=4.5σ and H_2=3.5σ. The unsymmetrical behavior of density profile around a confined molecule is clear from this Figure. In addition, in Fig. 1(b) the density profile of the mentioned fluid is showed when R=0. As is shown in this Figure, the slit walls change the radial symmetry of density profile about a molecule and density profile in left and right hand sides of molecule is different.

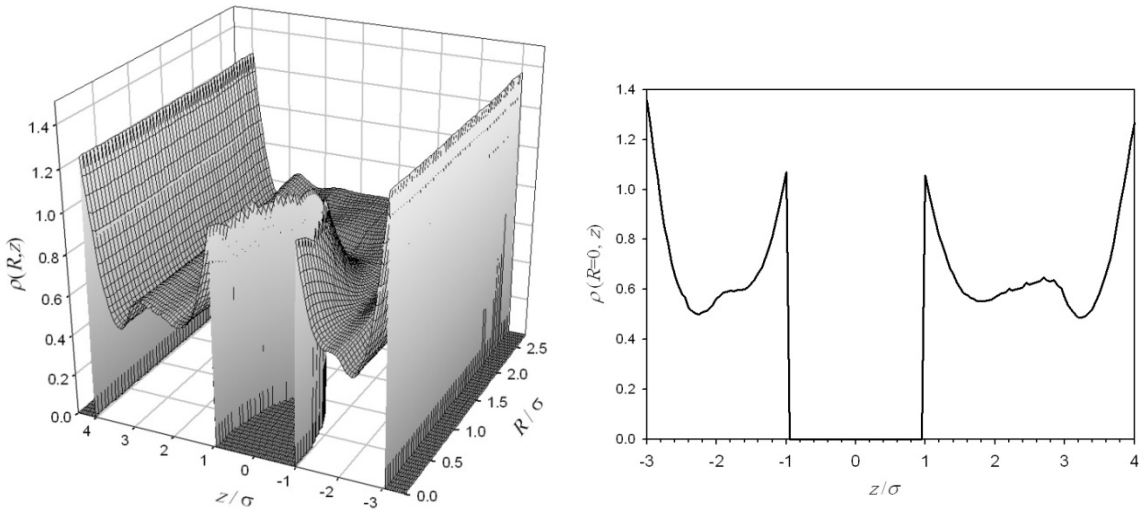

(a) (b)

Fig. 1 (a) Three dimensional density profile of hard sphere fluid with $\rho\sigma^3$=0.6 about one of molecules inside a nanoslit with H=8σ. The distance of central molecule from left and right hand side walls is 3.5 σ and 4.5σ respectively. (b) Density profile of the mentioned fluid when R=0.

References

[1] Keshavarzi, E., Kamalvand, M., *J. Phys. Chem. B*, **2009**, 113, 5493.

[2] Keshavarzi, E., Sedaghat, F., Mansoori, G.A., *Microfluids-Nanofluids*, **2010**, 8, 97.

[3] Roth, R., Evans, R., Lang, A., Kahl, G., *J. Phys.: Condens. Matter*, **2002**, 14, 12063.

[4] Tarazona, P., *Phys. Rev. A*, **1985**, 31, 2672.

Dependency of total adsorption and thermal conductivity enhancement in nanofluids

Mohsen Karami and Mohammad Kamalvand*
Department of Chemistry, Faculty of Science, Yazd University, Yazd, Iran
* Email address: kamalvand@gmail.com

Keywords: Nanofluid, Thermal Conductivity, Density Functional Theory, Nanoparticle.

Introduction

Nanofluids are dispersions of solid or liquid nanoparticles in a liquid. These fluids have attracted considerable attention recently because of their potential as high performance heat transfer fluids. This is known that the thermal conductivity of base fluids will enhanced by suspending nano or larger sized solid particles in fluids, since the thermal conductivity of solid is typically higher than the base fluid [1]. To explain the reasons for the anomalous increase of the thermal conductivity in nanofluids, four possible mechanisms are proposed. These possible mechanisms are Brownian motion of the nanoparticles, the nature of heat transport in the nanoparticles, the effects of nanoparticle clustering and molecular layering of the liquid at the liquid-particle interface [1]. From these four mechanisms, some researches show that the layering structure of the based fluid around nanoparticle has the dominant role [2]. In all these researches assumed that the base fluid aggregate about nanoparticle and create a layer with homogeneous density. In the other hand, statistical mechanical results show that the density profile of fluid about a nanoparticle has an inhomogeneous feature, i.e. the structure of fluid around nanoparticle has a layering form [3]. The main goal of this work is to investigate the role of depletion of fluid molecules around nanoparticles. To do this, we used Density Functional Theory for obtaining accurate density profile of fluid around nanoparticles.

Fundamental Measure Density Functional Theory (FMDFT)

In a density functional theory for an inhomogeneous fluid, the grand potential functional energy is related to the Helmholtz free energy functional as follows:

$$\Omega[\rho(\mathbf{r})] = F[\rho(\mathbf{r})] + \int d\mathbf{r}\rho(\mathbf{r})\{V_{ext}(\mathbf{r}) - \mu\} \quad (1)$$

Where μ is the chemical potential of the system and $V_{ext}(\mathbf{r})$ is the external field. According to the variational principle, the equilibrium density distribution function of the non-uniform fluid corresponds to the minimum of the grand potential,

$$\rho(\mathbf{r})\Lambda^3 = exp\left(\beta\mu - \beta\frac{\partial F_{ex}[\rho(\mathbf{r})]}{\partial\rho(\mathbf{r})} - \beta V_{ext}(\mathbf{r})\right) \quad (2)$$

In FMDFT the Helmholtz free energy splits to ideal and excess parts and Eq. (2) can be solved using a standard Picard iterative method.

Results and Discussion

While the repulsion forces have the main role in structure of fluids, and while nanopaticles can be assumed as colloidal particles with hard sphere field, we used a hard sphere model to obtain density profile of the base fluid around nanoparticles. However, this is well known that if the fine structure of soft spheres has minor deviation from density profile of hard spheres, but their averaged properties such as excess adsorption are close together. Therefore, we have used density profile of a hard sphere fluid around nanoparticles, obtained using FMDFT. To do this, while the distance between nanoparticles in nanofluid is very large, we assumed that the suspended nanoparticles are independent. Therefore, the total excess adsorption is equal to the number of nanoparticles multiply to the excess adsorption about each nanoparticle. This should be noted that excess adsorption defines as $\int[\rho(\mathbf{r})-\rho_b]d\mathbf{r}$ where ρ_b is the base fluid density. Our results show that the total excess adsorption increases with decreasing the size of nanoparticle which is similar to the behavior of the thermal conductivity enhancement of nanofluids with decreasing the nanoparticle diameter. These behaviors for Al_2O_3-water nanofluid are compared in Fig. 1. In addition, in Fig. 2 the variation of total excess adsorption versus thermal conductivity enhancement is showed for Al_2O_3-water nanofluid. The linear correlation (R^2=0.992) between total excess adsorption and thermal conductivity approved the strong dependency between them.

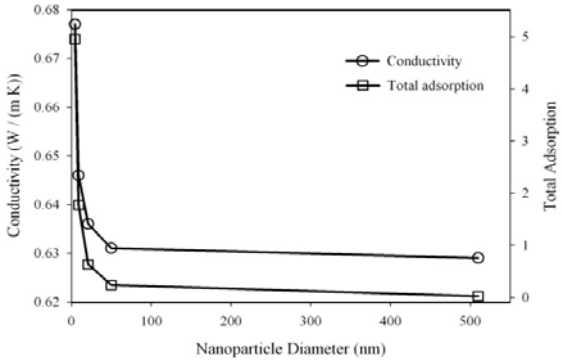

Fig. 1 Dependence of effective thermal conductivity for water–Al_2O_3 nanofluid [4] and total adsorption to the nanoparticle size.

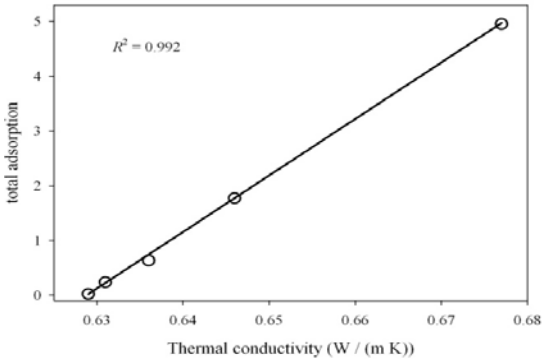

Fig. 2 Dependence of effective thermal conductivity for water–Al_2O_3 nanofluid [4] to total adsorption.

References

[1] Wang, X.-Q., Mujumdar, A.S., *Int. J. of Therm. Sci.,* 2007, 46, 1.

[2] Tillman, P., Hill, J.M., *Int. Commun.in Heat and Mass Trans*. 2007, 34, 399.

[3] Kamalvand, M., and Keshavarzi, E., *J. Iran. Chem. Soc.,* 2010, 7, S34.

[4] Mokmeli, A., Saffar-Avval, M., *Int. J. of Therm. Sci*., 2010, 49, 471.

Equation of state for polymers based on glass transition data

M. Kiani[1,2,*], M. M. Papari[1], R. Behjatmanesh[2], J. Moghadasi[3]

[1]Department of Chemistry, Shiraz University of Technology, Shiraz, 71555-313, Iran

[2]Department of Chemistry, Payame noor University (PNU), Ardakan, Iran

(Email: Masoumehkiani@gmail.com)

[3]Department of Chemistry, Shiraz University, Shiraz, 71454, Iran

Keywords: Corresponding states principle, Equation of state; Polymer melts; Statistical mechanics; Surface tension, Volumetric Properties

Introduction:

Macromolecular science has had a major impact on the way people live over the world. Polymeric liquids are widely used for industrial and residential purposes. A parameter of particular interest in synthetic polymer is the glass temperature, which describes the temperature at which amorphous polymers undergo a second-order phase transition.

Methods:

In 1994, Tao and Mason [1] calculated a perturbation correction term related to the effect of attractive forces. The final form of the original TM EOS is expressed as follows:

$$\frac{P}{\rho kT} = 1 + (B_2(T) - \bar{\alpha}(T))\rho + \frac{\bar{\alpha}(T)\rho}{1 - \rho b(T)\lambda} + A_1(\bar{\alpha}(T) - B_2(T))b(T)\rho^2 \frac{(e^{kTc/T} - A_2)}{1 + 1.8(\rho b(T))^4} \qquad (1)$$

where P is the pressure, kT has its usual meaning, B_2 is the second virial coefficient, α is the scaling factor, b is the effective Van der Waals co-volume, and ρ is the number density. The parameters A_1, A_2, and κ are defined by: $A_1 = 0.143$; $A_2 = 1.64 + 2.65[e^{(\kappa - 1.093)} - 1]$;

$$\kappa = 1.093 + 0.26[(\omega + 0.002)^{1/2} + 4.50(\omega + 0.002)] \qquad (2)$$

In which ω denotes the Pitzer acentric factor. These parameters in the EOS are not accessible for polymers. We decided to investigate about a new corresponding states correlation in order that TM EOS could be applied to polymers. In this respect, the following correlation equation for B_2 using new scaling parameters, such as the surface tension γ_g and the molar density ρ_g,

both at the glass transition point has been developed. The resulting correlation for the second virial coefficient reads as follows:

$$B_2^* = \rho_g B_2(T) = 0.0804 - 2.1288T^{*-1} - 8.5597T^{*-2} + 7.4294T^{*-3} - 3.3494T^{*-4} \quad (3)$$

with $T^* = [T^{3/2}/T_{ref}T_g^{1/2}]^{3/4}$ and $T_{ref} = \gamma_g \rho_g^{-2/3} N^{1/3}/R$.

where ρ_g is the density at glassing point, T_g the glassing temperature, N the Avogadro number, and γ_g the surface tension at glassing point. The other two functions, α and b, were correlated by way of the following pair of equations:

$$\rho_g \alpha = a_1[\exp(-c_1 T^*)] + a_2[1 - \exp(-c_2/T^{*1/4})] \text{ and } \rho_g b = a_1[(1 - c_1 T^*)\exp(-c_1 T^*)] + a_2[1 - (1 + 0.25c_2/T^{*1/4})\exp(-c_2/T^{*1/4})] \quad (4)$$

Where $a_1 = -0.01054$, $a_2 = 2.9387$, $c_1 = 0.7613$, and $c_2 = 1.3227$. We were able to obtain λ from PVT data at a high density. The physical properties of all six polymers were taken from Refs. 4-7 and are listed in Table 1.

Table 1. Parameters for the polymer liquids.

Substance	MMW[g]	T_g (K)	ρ_g (kg/m^3)	γ_g (mN/m)
a-PP	42	260[a]	842.85[b]	31.23[c]
PEO	44	232[a]	1192.90[b]	49.20[d]
PDMS	74	150[a]	1114.04[b]	28.45[c]
PS	104	373[a]	1022.97[b]	34.94[c]
PVME	58	239[a]	1066.44[b]	35.77[c]
PC	254	459[c]	1192.66[c]	32.94[c]

[a] taken from Ref. 4; [b] taken from Ref. 5; [c] taken from Ref. 6; [d] taken from Ref. 7; [g]Monomer molecular weight.

Results and discussion:

At first, a correlation equation for the second virial coefficient was developed using the surface tension and the liquid state density at the glass transition temperature. This modification is important because it delivers two advantages: 1) it relieved us from the usage of critical constants and acentric factors as appeared in the Tsonopoulos correlation [2], 2) glass transition temperature is an important property in plastics applications, because it provides information about how the polymer behaves under ambient conditions. This property is more important than the melting and critical point of polymers. In the present study, we have empirically found that κ in Eq. 2 is a weak function of the acentric factor so that we can approximate κ to 1.093. Moreover, the parameter Tc in the exponential term that appears in the TM EOS was changed to T_g. We performed the calculation of molar volume of all six

aforementioned polymers using the modified TM EOS. We have compared our correlation with one proposed by Ghatee and Boushehri (GB) correlation [3]. Table 2 contains the AAD of the calculated molar volumes using the TM EOS along with these two correlations.

Table 2. Percent deviation means of the calculated specific volume with reference to literature data [8].

polymer	class	NP	ΔP(bar)	ΔT(k)	AAD (%) density	
					With using our correlation	With using GB
a-PP	Poly(α-olefins)	55	1-1000	353.15-393.15	0.11	0.14
PEO	Polyethers	45	1-400	353.15-393.45	0.05	0.14
PDMS	Polysiloxanes	95	1-2025	291.25-338.15	0.30	0.65
PS	Vinyl polymers	189	1-2000	391.45-557.25	0.61	0.58
PVME	Polyesters	84	1-1200	311.5-415.5	0.25	0.26
PC	Polyesters	48	1-1500	443.7-603.4	1.35	1.49

Generally speaking, the present work convincingly demonstrates that the modified TM EOS along with the input parameters at the glassing point is capable of providing reliable information on the PVT properties of polymer melts.

Conclusions:

In the present work, the surface tension and the liquid density at the glass transition temperature were employed to construct a new corresponding states correlation of second virial coefficient for polymer melts.

References:

[1] Tao, F.M.; Mason, E. A. Statistical-Mechanical Equation of State for Nanpolar Fluids: Prediction of Phase Boundaries. *J. Chem. Phys.* **1994**, *100*, 9075.

[2] Tsonopoulos, C. An Empirical Correlation of Second Virial Coefficients. *AIChE J.* **1974**, *20*, 263.

[3] M. H. Ghatee, A. Boushehri, Equation of State for Compressed Liquids from Surface Tension *Int. J. Thermophys.***1996***, 17*, 945.

[4] Mark, J. E. *Polymer Data Handbook*. Oxford University Press: New York, 1999.

[5] Brandrup, J.; Immergut, E. H.; Grulke, E. A. *Polymer Handbook.* John Wiley & Sons: New York, 2005.

[6] Mark, J. E. *Physical Properties of Polymers Handbook. Springer*, New York, 2007.

[7] Ryong-Joon, R. Surface Tension of Polymer Liquids. *J. Phys. Chem.* **1968**, *72*, 2013.

[8] Wohlfarth, C. *CRC Handbook of Thermodynamic Data of Polymer Solutions at Elevated Pressures.* Taylor & Francis: New York, 2005.

Equation of State for Fluids Based on Minimum Input Information

Nargess Mehdipour and Taheheh Ansari
Department of Chemistry, College of Sciences, Persian Gulf University, Boushehr 75168, Iran
email: mnargess@hotmail.com

Keywords: Equation of state; Fluids; Fluid Mixtures; Hard sphere; Thermodynamics

Introduction and Theory

In the perturbed hard-sphere chain (PHSC) theory a chain molecule is modeled by a series of freely jointed tangent hard spheres, and the influence of attractive forces is taken in to account by adding a van der Waals attractive term. Following the introduction of a new form for the radial distribution function [1] into the reference system of the PHSC equation of state, by Song *et al.* [2], a much better agreement with the computer simulation data was obtained. The resulting equation of state [3], has three input parameters; an energy parameter, a size parameter, and a parameter representing the number of chains per molecule. Recently, Eslami [4] proposed a corresponding states correlation, based on minimum input information, for calculating the temperature-dependent parameters of the PHSC equation of state. In this work this equation of state has been extended to mixtures and tested against the experimental data for a large number of multicomponent mixtures.

In the simplest form, the PHSC equation of state developed by Eslami [4] reads as:

$$\frac{P}{\rho kT} = 1 + r^2 b\rho g(d^+) - (r-1)\frac{\eta(5-2\eta)}{(2-\eta)(1-\eta)} - (q_a + q_b\eta)\frac{a\rho}{kT} \qquad (1)$$

where P is the pressure, ρ is the number (molar) density, d is the hard-sphere diameter, $g(d^+)$ is the pair radial distribution function of hard spheres at contact, kT is the thermal energy per one molecule, and q_a and q_b are constants for each chain. The temperature-dependent parameters, $a(T)$ and $b(T)$, are expressed in terms of the critical constants [4]. In this work, by applying suitable mixing and combining rules, this equation of state has been extended to mixtures (the results are not shown here). The final equation of state for mixtures is expressed

Results and discussions

The experimental *PVT* data of a large number of fluid mixtures; including mixtures of liquid noble gases, nitrogen and carbon dioxide with hydrocarbons, hydrocarbons, olefins,

aromatics, and refrigerants, are employed to check the prerdictive power of the equation of state for mixture. The results for a few typical mixtures are compared with experimental data in Figure 1. The results in Figure 1show that knowing just the critical constants of pure components is sufficient to calculate the *PVT* properties of mixtures of varieties of molecular shapes, sizes, and polarities. Even in the case of mixtures with different sizes the results are quite good; there is no need to introduce the binary interaction parameters in the equation of state. In the case of mixtures of long-chain alkanes, the deviations are higher than the others. This is expected, as the equation of state of pure components [4], and the original perturbed hard-sphere-chain equation [2,3] also show higher deviations for long-chain hydrocarbons, compared to light components. Even for the mixtures of long-chain alkanes the predications of the present equation of state are shown, see Figure 1, to agree very well with experimental data.

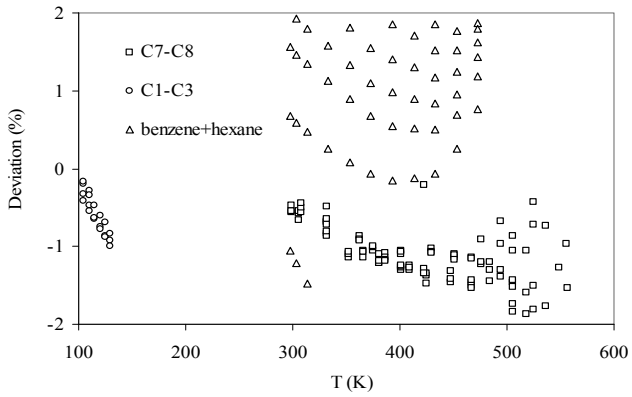

Figure 1. Deviation plot for the density of mixtures, compared to experimental data, as function of temperature.

References

[1] W. G. Chapman, G. Jackson, K. E. Gubbins, Mol. Phys. 65 (1988) 1057–1062.

[2] Y. Song, T. Hino, S. M. Lambert, J. M. Prausnitz, Fluid Phase Equilib. 117 (1996) 69–76.

[3] I. H. Kim, Y. C. Bae, Chem. Phys. 260 (2000) 337–345.

[4] H. Eslami, Fluid Phase Equilib. 216 (2004) 21–26.

The Correlation of Interaction Energy with Critical Point Temperature of Ionic Liquids obtained from Surface Tension

M. H. Ghatee*, F. Moosavi, A. R. Zolghadr, and R. Jahromi
Department of Chemistry, Shiraz University, Shiraz 71454, Iran
(E-mail: ghatee@susc.ac.ir)

Keywords: Critical point temperature, Interaction energy, Ionic liquid, Surface tension at vapor-liquid equilibrium

Introduction

The inherent possibility of accurate measurement of the liquid surface tension (γ) turns into a strong and reliable method of studying the liquid surface energetic and surface microstructure [1]. Liquid surface tension linearly decreases at low temperatures close to the freezing point and vanishes non-linearly as the critical point approaches. The existing empirical scaling laws elucidate the surface tension close to the critical temperature as a function of temperature scaled distance from the critical temperature.

As a part of systematic studies on liquid surface properties [2,3] first we use the temperature dependence data of the experimental surface tension over a wide range of temperature to estimate the critical temperature of different ILs based on imidazolium, phosphonium, and ammonium cations. The use of surface tension values measured under liquid-vapor equilibration has a meaningful feature of producing critical point temperature.

Evaluation of Critical Temperature

According to Guggenheim [4], a certain exponent describes the vanishing of surface tension with the temperature irrespective to their chemical nature:

$$\gamma = a(T_c - T)^{11/9} \qquad (1)$$

Using the experimental surface tension data measure at equilibrated liquid/vapor was used to determine the critical point of the ILs.

Computational Details

The usual procedure of the quantum mechanical density functional theory was performed to determine the interaction energy between the cation and the anion, using the Gaussian 03 package [5] at B3LYP/6-311G** level of theory. The calculations were performed on twelve ILs: $[C_n mim]BF_4$, $[C_n mim]PF_6$, $[C_n mim]I$, and $[C_n mim]Cl$, where n is 4, 6, and 8.

Results and Discussion

The available surface tension data for imidazolium-, phosphonium-, and ammonium-based ILs having different anions show that the predicted critical temperature by scaling law, Guggenheim, and Eötvös approaches is a function of cation type and its alkyl chain length as well as the anion type as shown in Figure 1.

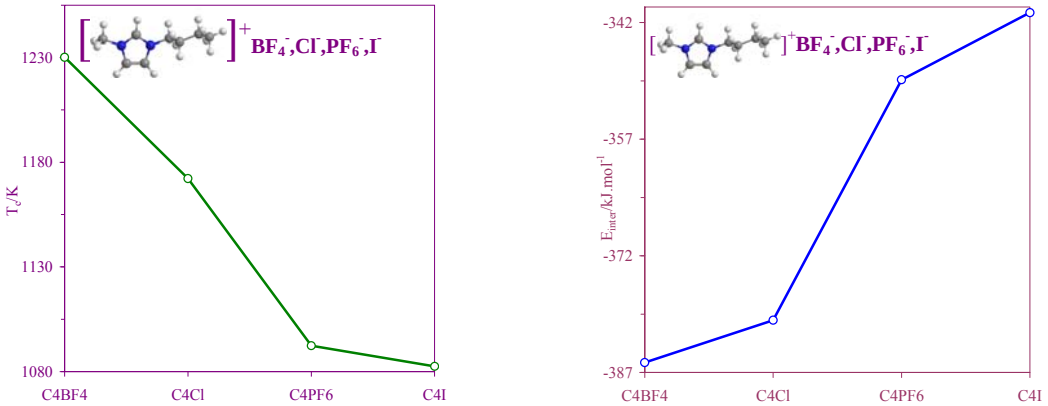

Figure 1. Critical point temperature of ILs, predicted using surface tension data measured at liquid-vapor equilibrium.

According to this dependence on the nature of IL, the anion-cation interaction energy (E_{inter}) was calculated and the correlation with the predicted critical temperature was studied. The predicted critical temperature has a direct relation to the absolute value of E_{inter}. The ILs with BF_4^- anion, which have the highest critical point temperature consistently, have the largest absolute value of E_{inter}. As the alkyl chain length increases, the critical temperature decreases.

Conclusions

Ionic liquids with BF_4^- anion have small surface entropies [2] and show high critical point temperatures, which decreases with the alkyl chain length. The cation-anion interaction

energy, calculated by quantum chemical method, has been correlated with the predicted critical temperature. IL having a stronger cation-anion interaction has a higher critical temperature.

References

[1] Wu, X. Z.; Ocko, B. M.; Sirota, E. B.; Sinha, S. K.; Deutsch, M.; Cao, B. H.; Kim, M. W. Science 1993, 261, 1018-1021.

[2] Ghatee, M. H.; Zolghadr, A. R. Fluid Phase Equilib. 2008, 263, 168-175.

[3] Ghatee, M. H.; Maleki, A.; Ghaed-Sharaf, H. Langmuir 2003, 19, 211-213.

[4] Guggenheim, E. A. J. Chem. Phys. 1945, 13, 253-261.

[5] Pople, J. A.; Gaussian, Inc., Wallingford CT, 2004.